UNIVERSITY OF ADELAIDE LIBRARY
1.2.90

# PLANT PHYSIOLOGY:
# TRANSPORT PROCESSES IN PLANTS

A Thesis submitted to

The University of Adelaide

as a requirement for the

Degree of Doctor of Science

in the Faculty of Science

by

WILLIAM J. LUCAS, B.Sc. (Hons.), Ph.D.

Professor

Department of Botany
University of California
Davis, California, USA

January, 1989

awarded 9.1.90

## PREFACE

The published works contained within this Thesis represent original research conducted during the various phases of my academic development. The first seven papers (1A-7A) represent the research conducted during my Ph.D. period in the laboratory of Dr. F. Andrew Smith, in the Department of Botany, at the University of Adelaide. As a Postdoctoral Fellow in the laboratory of Professor Jack Dainty, Department of Botany, University of Toronto, Ontario, Canada, I extended my research on membrane transport processes in the giant fresh water algal system of Chara corallina. Although much of the work was conducted on my own, I did avail myself of the opportunity to collaborate with other scientists on several research projects; the most profitable association was with Dr. Jack Ferrier, who was also a Postdoctoral Fellow in the same laboratory. During this two year postdoctoral period, my main focus was on the spatial aspects of membrane transport in Chara, and from the research conducted at the University of Toronto papers 8A-13A were published.

In September of 1977 I moved to the University of California, Davis Campus, to take up a junior faculty position in the Department of Botany. In view of the agricultural focus of the UC Davis campus, I established an integrated research program to study the physiology, cytology and biophysics of transport processes in plants. Although we still continued to work on Chara as a model system, we expanded our focus to include ion transport into roots, and sugar transport in terms of phloem physiology. Over the last eighteen months we have further expanded our program to encompass both the role played by plasmodesmata in plant-related transport processes, and the use of molecular biology to further probe the physiology and biophysics of the above-mentioned transport systems.

Over the ensuing twelve years I have had the pleasure of training and working with a large number of outstanding graduate students

(candidates for both the M.S. and Ph.D. degrees), Postdoctoral Fellows and Visiting Scientists. Except for a few instances, all of these scientists have worked in my laboratory on research projects funded by grants from the National Science Foundation. Although the conceptual and technological developments required for these grants were generally my responsibility, the collective intellectual resources of my laboratory group provided the academic ambiance that was so essential for success. Thus, in evaluating papers numbered 14A-43A, 1B-20B and 1C-8C, the reader should be very much aware of the valuable contributions made by each laboratory member. It is impossible for me to say to what extent my academic development would have been curtailed had I not been afforded the pleasure of my students!

William J. Lucas
Department of Botany
University of California
Davis, California
January 6th, 1989

# TABLE OF CONTENTS

Preface 1

Published Works on Plant Physiology: Transport Processes in Plants

**Section A:**

Published Works on Chara Physiology, Cytology & Biophysics 4

**Section B:**

Published Works on Phloem Transport 9

**Section C:**

Published Works on $K^+$ Transport in Roots 11

Explanation of Coauthorship and Relative Contribution

**Section A:**

Published Works on Chara Physiology, Cytology & Biophysics 12

**Section B:**

Published Works on Phloem Transport 17

**Section C:**

Published Works on $K^+$ Transport in Roots 19

Acknowledgements 21

Published Works

**SECTION A:**

**PUBLISHED WORKS ON CHARA PHYSIOLOGY, CYTOLOGY & BIOPHYSICS**

1A. Lucas, W.J. 1975. Analysis of the diffusion symmetry developed by the alkaline and acid bands which form at the surface of Chara corallina cells. Journal of Experimental Botany 26:271-286.

2A. Lucas, W.J. 1975. Photosynthetic fixation of $^{14}$carbon by internodal cells of Chara corallina. Journal of Experimental Botany 26:331-346.

3A. Lucas, W.J. 1975. The influence of light intensity on the activation and operation of the hydroxyl efflux system of Chara corallina. Journal of Experimental Botany 26:347-360.

4A. Lucas, W.J. 1976. Plasmalemma transport of $HCO_3^-$ and $OH^-$ in Chara corallina: Non-antiporter systems. Journal of Experimental Botany 27:19-31.

5A. Lucas, W.J. 1976. The influence of $Ca^{2+}$ and $K^+$ on $H^{14}CO_3^-$ influx in internodal cells of Chara corallina. Journal of Experimental Botany 27:32-42.

6A. Lucas, W.J. and F.A. Smith. 1976. Influence of irradiance of $H^+$ efflux and $Cl^-$ influx in Chara corallina: An investigation aimed at testing two $Cl^-$ transport models. Australian Journal of Plant Physiology 3:443-456.

7A. Lucas, W.J. 1977. Plasmalemma transport of $HCO_3^-$ and $OH^-$ in Chara corallina: Inhibitory effect of ammonium sulphate. Journal of Experimental Botany 28:1307-1320.

8A. Lucas, W.J. 1977. Analogue inhibition of the active $HCO_3^-$ transport site in the Characean plasma membrane. Journal of Experimental Botany 28:1321-1336.

9A. Lucas, W.J. and J. Dainty. 1977. Spatial distribution of functional $OH^-$ carriers along a Characean internodal cell: Determined by the effect of cytochalasin B on $H^{14}CO_3^-$ assimilation. Journal of Membrane Biology 32:75-92.

10A. Lucas, W.J. and J. Dainty. 1977. $HCO_3^-$ influx across the plasmalemma of Chara corallina. Divalent cation requirement. Plant Physiology 60:862-867.

11A. Lucas, W.J., J. M. Ferrier, and J. Dainty. 1977. Plasmalemma transport of $OH^-$ in Chara corallina: Dynamics of activation and deactivation. Journal of Membrane Biology 32:49-73.

12A. Lucas, W.J., R.M. Spanswick, and J. Dainty. 1978. $HCO_3^-$ influx across the plasmalemma of Chara corallina. Physiological and biophysical influence of 10 mM $K^+$. Plant Physiology 61:487-493.

13A. Lucas, W.J., M.T. Tyree, and A. Petrov. 1978. Characterization of photosynthetic $^{14}$Carbon assimilation by Potamogeton lucens L. Journal of Experimental Botany 29:1409-1421.

14A. Lucas, W.J. 1979. Alkaline band formation in Chara corallina: Due to $OH^-$ efflux or $H^+$ influx. Plant Physiology 63:248-254.

15A. Ferrier, J.M., C. Morvan, W.J. Lucas, and J. Dainty. 1979. Plasmalemma voltage noise in Chara corallina. Plant Physiology 63:709-714.

16A. Ferrier, J.M. and W.J. Lucas. 1979. Plasmalemma transport of $OH^-$ in Chara corallina. II. Further analysis of the diffusion system associated with $OH^-$ efflux. Journal of Experimental Botany 30:705-718.

17A. Lucas, W.J. and J.M. Alexander. 1980. Sulfhydryl group involvement in plasmalemma transport of $HCO_3^-$ and $OH^-$ in Chara corallina. Plant

Physiology 65:274-280.

18A. Lucas, W.J. and J.M Ferrier. 1980. Plasmalemma transport of $OH^-$ in Chara corallina. III. Further studies on transport substrate and directionality. Plant Physiology 66:46-50.

19A. Franceschi, V.R. and W.J. Lucas. 1980. Structure and possible function(s) of charasomes; complex plasmalemma-cell wall elaborations present in some characean species. Protoplasma 104:253-271.

20A. Lucas, W.J. and R. Nuccitelli. 1980. $HCO_3^-$ and $OH^-$ transport across the plasmalemma of Chara: spatial resolution obtained using extracellular vibrating probe. Planta 150:120-131.

21A. Lucas, W.J. and T. Shimmen. 1981. Intracellular perfusion and cell centrifugation studies on plasmalemma transport processes in Chara corallina. Journal of Membrane Biology 58:227-237.

22A. Franceschi, V.R. and W.J. Lucas. 1981. The glycosome of Chara: ultrastructure, development, and composition. Journal of Ultrastructural Research 75:218-228.

23A. Lucas, W.J. and J.M. Alexander. 1981. Influence of turgor pressure manipulation on plasmalemma transport of $HCO_3^-$ and $OH^-$ in Chara corallina. Plant Physiology 68:553-559.

24A. Lichtner, F.T., W.J. Lucas, and R.M. Spanswick. 1981. Effect of sulfhydryl reagents on the biophysical properties of the plasmalemma of Chara corallina. Plant Physiology 68:899-904.

25A. Lucas, W.J. and V.R. Franceschi. 1981. Characean charasome-complex and plasmalemma vesicle development. Protoplasma 107:255-267.

26A. Franceschi, V.R. and W.J. Lucas. 1981. The Charasome periplasmic space. Protoplasma 107:269-284.

27A. Keifer, D.W. and W.J. Lucas. 1982. Potassium channels in Chara corallina: Control and interaction with the electrogenic $H^+$ pump. Plant Physiology 69:781-788.

28A. Franceschi, V.R. and W.J. Lucas. 1982. The relationship of the charasome to chloride uptake in Chara corallina: physiological and histochemical investigations. Planta 154:525-537.

29A. Keifer, D.W., V.R. Franceschi and W.J. Lucas. 1982. Plasmalemma chloride transport in Chara corallina: Inhibition by 4,4'-diisothiocyano-2,2'-disulfonic acid stilbene. Plant Physiology 70: 1327-1334.

30A. Lucas, W.J. 1982. Mechanism of acquisition of exogenous bicarbonate by internodal cells of Chara corallina. Planta 156: 181-192.

31A. Lucas, W.J. 1983. Photosynthetic assimilation of exogenous $HCO_3^-$ by aquatic plants. Annual Review of Plant Physiology 34:71-104.

32A. Lucas, W.J., D.W. Keifer and D. Sanders. 1983. Bicarbonate transport in Chara corallina: Evidence for cotransport of $HCO_3^-$ with $H^+$. Journal of Membrane Biology 73:263-274.

33A. Lucas, W.J., C. Wilson and J.P. Wright. 1984. Perturbation of Chara plasmalemma transport function by 2[4(2',4'-Dichlorophenoxy)phenoxy] propionic acid. Plant Physiology 74:61-66.

34A. Wille, A.C. and W.J. Lucas. 1984. Ultrastructural and histochemical studies on guard cells. Planta 160:129-142.

35A. Pesacreta, T.C. and W.J. Lucas. 1984. The plasma membrane coat and a coated vesicle-associated reticulum: Their structure and possible interrelationship in Chara corallina. Journal of Cell Biology 98:1537-1545.

36A. Pesacreta, T.C. and W.J. Lucas. 1985. Presence of a partially-coated reticulum in angiosperms. Protoplasma 125:173-184.

37A. Lucas, W.J. 1985. Bicarbonate utilization by Chara: A re-analysis. In: Inorganic Carbon Uptake by Aquatic Photosynthetic Organisms, eds., W.J. Lucas and J.A. Berry, American Society of Plant Physiologists, Rockville, MD, pp. 229-254.

38A. Lucas, W.J. and K. Ogata. 1985. Hydroxyl- and bicarbonate-associated transport processes in Chara corallina: Studies on the light-dark regulation mechanism. Journal of Experimental Botany 36:1947-1958.

39A. Lucas, W.J. and J.A. Berry. 1986. Inorganic carbon transport in aquatic photosynthetic organisms. Physiologia Plantarum 65:539-543.

40A. Lucas, W.J., D.W. Keifer and T.C. Pesacreta. 1986. Influence of culture medium pH on charasome development and chloride transport in Chara corallina. Protoplasma 130:5-11.

41A. Ferrier, J. and W.J. Lucas. 1986. Ion transport and the vibrating probe. Biophysics Journal 49:803-807.

42A. Brechignac, F. and W.J. Lucas. 1987. Photorespiration and internal $CO_2$ accumulation in Chara corallina as inferred from the influence of DIC and $O_2$ on photosynthesis. Plant Physiology 83:163-169.

43A. Lucas, W.J. and D. Sanders. 1988. Ion transport in Chara cells. Methods in Enzymology 4(75):(In press).

**SECTION B:**

## PUBLISHED WORKS ON PHLOEM TRANSPORT

1B. Maynard, J.W. and W.J. Lucas. 1982. A reanalysis of the two-component phloem loading system in Beta vulgaris. Plant Physiology 69:734-739.

2B. Maynard, J.W. and W.J. Lucas. 1982. Sucrose and glucose uptake into Beta vulgaris leaf tissues: A case for general (apoplastic) retrieval systems. Plant Physiology 70:1436-1443.

3B. Lucas, W.J. and V.R. Franceschi. 1982. Organization of the sieve-element walls of leaf minor veins. Journal of Ultrastructural Research 81:209-221.

4B. Grusak, M.A. and W.J. Lucas. 1984. Recovery of cold-inhibited phloem translocation in sugar beet. I. Experimental analysis of an existing mathematical model. Journal of Experimental Botany 35:389-402.

5B. Grusak, M.A. and W.J. Lucas. 1985. Cold-inhibited phloem translocation in sugar beet. II. Characterization and localization of the slow-cooling response. Journal of Experimental Botany 36:745-755.

6B. Wilson, C., J.W. Oross and W.J. Lucas. 1985. Sugar uptake into Allium cepa leaf tissue: an integrated approach. Planta 164:227-240.

7B. Lucas, W.J. 1985. Phloem loading: A metaphysical phenomenon? In: Regulation of Carbon Partitioning in Photosynthetic Tissue, eds., R.L. Heath and J. Preiss. American Society of Plant Physiologists, Monograph Series, Rockville, MD, pp. 254-271.

8B. Oross, J.W. and W.J. Lucas. 1985. Sugar beet petiole structure: vascular anastomoses and phloem ultrastructure. Canadian Journal of Botany 63:2295-2304.

9B. Pesacreta, T.C., A.B. Bennett and W.J. Lucas. 1986. Spectrophotometric and cytochemical analyses of phosphatase activity in Beta vulgaris L. Journal of Histochemistry and Cytochemistry 34:327-338.

10B. Grusak, M.A. and W.J. Lucas. 1986. Cold-inhibited phloem translocation in sugar beet. III. The involvement of the phloem pathway in source-sink partitioning. Journal of Experimental Botany 37:277-288.

11B. Wilson, C. and W.J. Lucas. 1986. Kinetic analysis of sugar transport: From yesterday to tomorrow. In: Phloem Transport, eds. J. Cronshaw, W.J. Lucas and R. Giaquinta. Alan R. Liss, New York, pp. 3-15.

12B. Oross, J.W., M.A. Grusak, and W.J. Lucas. 1986. Regulation of long-distance translocation in sugar beet: Structural aspects. In: Phloem Transport, eds., J. Cronshaw, W.J. Lucas and R. Giaquinta. Alan R. Liss, New York, pp. 477-486.

13B. Morrow, D.L. and W.J. Lucas. 1986. (1->3)-β-D-Glucan synthase from sugar beet. I. Isolation and solubilization. Plant Physiology 81:171-176.

14B. Madore, M.A., J.W. Oross and W.J. Lucas. 1986. Symplastic transport in Ipomoea tricolor source leaves: Demonstration of functional symplastic connections from mesophyll to minor veins by a novel dye-tracer method. Plant Physiology 82:432-442.

15B. Madore, M.A. and W.J. Lucas. 1987. Control of photoassimilate movement in source leaf tissues of Ipomoea tricolor Cav. Planta

171:197-204.

16B. Morrow, D.L. and W.J. Lucas. 1987. (1->3)-β-D-Glucan synthase from sugar beet. II. Product inhibition by UDP. Plant Physiology 84:565-567.

17B. Wilson, C. and W.J. Lucas. 1987. Influence of internal sugar levels on apoplasmic retrieval of exogenous sucrose in source leaf tissue. Plant Physiology 84:1088-1095.

18B. Lucas, W.J. and C. Wilson. 1987. Influence of mannose on the apoplasmic retrieval systems of source leaves. Plant Physiology 85:423-429.

19B. Lucas, W.J. and M.A. Madore. 1988. Recent advances in sugar transport. In: The Biochemistry of Plants: A Comprehensive Treatise, Volume 12: Carbohydrates, ed., J. Preiss, Academic Press, New York, pp. 35-84.

20B. Wilson, C. and W.J. Lucas. 1988. Wounding and the regulation of apoplasmic retrieval in source leaf tissue of Spinacia oleracea L. Journal of Experimental Botany 39:529-542.

**SECTION C:**

**PUBLISHED WORKS ON $K^+$ TRANSPORT IN ROOTS**

1C. Kochian, L.V. and W.J. Lucas. 1982. Potassium transport in corn roots. I. Resolution of kinetics into a saturable and linear component. Plant Physiology 70:1723-1731.

2C. Kochian, L.V. and W.J. Lucas. 1982. A re-evaluation of the carrier-kinetic approach to transport in roots of higher plants. What's New in Plant Physiology 13:45-48.

3C. Kochian, L.V. and W.J. Lucas. 1983. Potassium transport in corn roots. II. The significance of the root periphery. Plant Physiology 73:208-215.

4C. Kochian, L.V. and W.J. Lucas. 1985. Potassium transport in corn roots. III. Perturbation by exogenous NADH and Ferricyanide. Plant Physiology 77:429-436.

5C. Kochian, L.V., J. Xin-Zhi and W.J. Lucas. 1985. Potassium transport in corn roots. IV. Characterization of the linear component. Plant Physiology 79:771-776.

6C. Newman, I.A., L.V. Kochian, M.A. Grusak, and W.J. Lucas. 1987. Fluxes of $H^+$ and $K^+$ in corn roots: Characterization and stoichiometries using ion-selective microelectrodes. Plant Physiology 84:1177-1184.

7C. Lucas, W.J. 1987. Functional aspects of cells in root apices. In: Root Development and Function, eds., J.V. Lake, D.A. Rose and P.J. Gregory, Society for Experimental Biology Seminar Series, vol. 30, pp. 27-52, Cambridge University Press.

8C. Kochian, L.V. and W.J. Lucas. 1988. Potassium transport in roots. Advances in Botanical Research 15:93-178.

**EXPLANATION OF COAUTHORSHIP & RELATIVE CONTRIBUTION**

**SECTION A:**

**PUBLISHED PAPERS ON CHARA PHYSIOLOGY, CYTOLOGY & BIOPHYSICS**

1A-7A: Papers originating from my Ph.D. Dissertation entitled, "**Ionic Relations of Chara corallina: Studies on the Transport of $HCO_3^-$, $OH^-$ and $H^+$ Across the Plasma Membrane,**" accepted by the University of Adelaide in 1975.

8A: Part of this work formed a section of my Ph. D. Dissertation, the remainder was performed at the University of Toronto. (100%)

9A: Experiments conducted by W.J. Lucas (as a postdoctoral fellow). Prof. Jack Dainty provided the necessary grant support. (95%)

10A: Experiments conducted by W.J. Lucas. Prof. Jack Dainty provided necessary grant support. (95%)

11A: Experiments and model developed jointly by W.J. Lucas and J.M. Ferrier and Prof. Jack Dainty provided grant support. (50%)

12A: Major portion of experiments conducted by W.J. Lucas, R.M. Spanswick helped with some of the electrophysiology experiments, and Prof. Jack Dainty provided grant support. ((85%)

13A: Experiments designed and analyzed by W.J. Lucas and conducted by A. Petrov (M.S. student). (50%)

14A: Experiments designed and conducted by W.J. Lucas. (100%)

15A: Experiments designed and conducted jointly by J.M. Ferrier, C. Morvan and W.J. Lucas. W.J. Lucas and J.M. Ferrier prepared grant proposal that was awarded to support this work. (40%)

16A: Theory developed jointly by W.J. Lucas and J.M. Ferrier and experiments conducted by W.J. Lucas. (50%)

17A: Experiments designed by W.J. Lucas and performed by W.J. Lucas and J.M. Alexander (undergraduate student). Project supported by a National Science Foundation (USA) grant to W.J. Lucas. (85%)

18A: Theory and experiments developed jointly by W.J. Lucas and J.M. Ferrier. Chara experiments conducted by W.J. Lucas. Project supported by an NSF grant to W.J. Lucas and an NRC grant to Prof. Jack Dainty. (50%)

19A: Project developed as an NSF proposal by W.J. Lucas, protocols for fixation of Chara for TEM developed jointly by W.J. Lucas and V.R. Franceschi, electron microscopy performed by V.R. Franceschi as a Ph.D. student in laboratory of W.J. Lucas. Project funded by an NSF grant to W.J. Lucas. (40%)

20A: Experiments designed and executed jointly by W.J. Lucas and R. Nuccitelli. Project supported by NSF grants to W.J. Lucas and R. Nuccitelli. (50%)

21A: Experiments designed and executed jointly by W.J. Lucas and T. Shimmen (Visiting Assistant Prof. from Tokyo University). Project supported by an NSF grant to W.J. Lucas. (50%)

22A: Experiments designed and executed by V.R. Franceschi in consultation with W.J. Lucas. Project supported by an NSF grant to W.J. Lucas. (30%)

23A: Experiments designed by W.J. Lucas and conducted jointly by W.J. Lucas and J.M. Alexander. (75%)

24A: Experiments designed by W.J. Lucas and conducted jointly by F.T. Lichtner, W.J. Lucas and R.M. Spanswick. All work conducted in W.J. Lucas' laboratory and supported by an NSF grant to W.J. Lucas. (35%)

25A: Protocol development, and conceptual development of models of the charasome were a joint effort between W.J. Lucas and V.R. Franceschi. Electron microscope work conducted by V.R. Franceschi. Project supported jointly by an NSF grant and a

UC Davis research grant to W.J. Lucas. (50%)

26A: Protocol development, and conceptual development of models of the charasome were a joint effort between W.J. Lucas and V.R. Franceschi. Electron microscope work conducted by V.R. Franceschi. Project supported jointly by an NSF grant and a UC Davis research grant to W.J. Lucas. (50%)

27A: Experiments performed jointly by W.J. Lucas and D.W. Keifer (NSF Postdoctoral Fellow) and the study was supported by an NSF grant awarded to W.J. Lucas and D.W. Keifer. (50%)

28A: Physiological experiments designed and executed jointly by W.J. Lucas and V.R. Franceschi. TEM component conducted by V.R. Franceschi. Project supported by an NSF grant to W.J. Lucas. (50%)

29A: Experiments designed and conducted jointly by W.J. Lucas, D.W. Keifer and V.R. Franceschi. Project supported by a joint NSF grant to W.J. Lucas and D.W. Keifer. (30%)

30A: Experiments designed and conducted by W.J. Lucas. (100%)

31A: Invited review article. (100%)

32A: Experiments designed by W.J. Lucas and D. Sanders (Visiting Postdoctoral Fellow) and conducted by all three authors. Project was supported by two NSF grants awarded to W.J. Lucas. (35%)

33A: Experiments designed by W.J. Lucas and conducted jointly by W.J. Lucas, J.P. Wright (Visiting Scientist) and C. Wilson (Ph.D. student). Project supported by an NSF grant to W.J. Lucas. (50%)

34A: Experimental work performed by A.C. Wille (M.S. student). (35%)

35A: Project was an extension of our earlier work on the charasome. TEM work conducted primarily by T.C. Pesacreta (Postdoctoral Fellow), and data/model development joint effort between W.J. Lucas and T.C. Pesacreta. Project supported by an NSF grant to W.J. Lucas. (35%)

36A: Experimental work performed by W.J. Lucas and T.C. Pesacreta. Project concept and support developed by W.J. Lucas through an NSF grant. (45%)

37A: Experiments designed by W.J. Lucas and conducted by W.J. Lucas, K. Ogata (Visiting Associate Professor) and M.E. Bassett (Visiting Ph.D. student). (90%)

38A: Experiments conducted jointly by W.J. Lucas and K. Ogata (Visiting Associate Professor). Project supported by an NSF grant to W.J. Lucas. (55%)

39A: Review commissioned to W.J. Lucas; invited J.A. Berry to coauthor this work. (50%)

40A: Experiments designed by W.J. Lucas and conducted jointly by all authors. T.C. Pesacreta performed the TEM portion of this work. Project supported by an NSF grant to W.J. Lucas. (40%)

41A: Theory developed jointly by W.J. Lucas and J.M. Ferrier. Project supported by an NSF grant to W.J. Lucas and a Medical Research Council of Canada grant to J.M. Ferrier. (50%)

42A: Experimental system designed and constructed under supervision of W.J. Lucas. Experiments performed by F. Brechignac (Visiting Scientist from France). Project supported by an NSF grant to W.J. Lucas. (45%)

43A: Article commissioned to W.J. Lucas; invited D. Sanders (faculty member of York University, U.K.) to coauthor this work. (50%)

SECTION B:

**PUBLISHED PAPERS ON PHLOEM TRANSPORT**

1B: Conceptual framework developed by W.J. Lucas in an NSF grant proposal. Experiments conducted by J.W. Maynard (Ph.D. student) with help from W.J. Lucas. Project supported by an NSF grant awarded to W.J. Lucas. (35%)

2B: Experiments conducted by J.W. Maynard (Ph.D. student) and W.J. Lucas. Project supported by an NSF grant to W.J. Lucas. (40%)

3B: Experiments designed and conducted jointly by W.J. Lucas and V.R. Franceschi. Project supported by an NSF grant to W.J. Lucas. (50%)

4B: Experimental system developed by W.J. Lucas (and technician A.C. Wille). Theoretical background and experimental protocols developed by W.J. Lucas. Experiments conducted by M.A. Grusak (Ph.D. student) and W.J. Lucas. Project supported by NSF grants to W.J. Lucas. (40%)

5B: Experiments designed, executed and analyzed jointly by M.A. Grusak and W.J. Lucas. Project supported by an NSF grant to W.J. Lucas. (40%)

6B: Experiments designed and supervised by W.J. Lucas. Kinetic experiments conducted by C. Wilson (Ph.D. student) and W.J. Lucas. TEM work performed by J.W. Oross (Postdoctoral Fellow). Project funded by NSF grants to W.J. Lucas. (35%)

7B: Invited review of phloem loading. (100%)

8B: Experimental framework developed as part of an NSF grant to W.J. Lucas. Microscopy conducted by J.W. Oross under the supervision of W.J. Lucas. (50%)

9B: Experiments designed and executed by T.C. Pesacreta, W.J. Lucas and A.B. Bennett. Project supported by NSF grants to W.J. Lucas. (30%)

10B: Experimental system developed by W.J. Lucas. Theoretical background and experimental protocols developed by W.J. Lucas, with most experiments being run by M.A. Grusak. Project supported by NSF grants to W.J. Lucas. (40%)

11B: Conceptual development and data analysis performed by W.J. Lucas and C. Wilson (Ph.D. student). Project supported by an NSF grant to W.J. Lucas. (50%)

12B: Experimental design and execution joint effort of all authors. Project supported by an NSF grant to W. J. Lucas. (30%)

13B: Conceptual framework developed by W.J. Lucas under an Industry-University grant awarded by Chevron Chemical Company, Richmond, California. Experiments performed by D.L. Morrow (Postdoctoral Fellow). (30%)

14B: Conceptual framework and experimental protocol developed by W.J. Lucas in an NSF grant proposal. Experiments conducted jointly by W.J. Lucas, M.A. Madore (Canadian National Research Council Postdoctoral Fellow) and J.W. Oross (Postdoctoral Fellow). Project supported by an NSF grant to W.J. Lucas. (40%)

15B: Experiments designed and executed jointly by W.J. Lucas and M.A. Madore. Project supported by an NSF grant to W.J. Lucas.

16B: Continuation of 13B, but with funding now provided by an NSF grant to W.J. Lucas. (50%)

17B: Experiments designed and executed jointly by W.J. Lucas and C. Wilson. Project supported by an NSF grant to W.J. Lucas. (50%)

18B: Experiments designed and executed jointly by W.J. Lucas and C. Wilson. Project supported by an NSF grant to W.J. Lucas. (50%)

19B: Review commissioned to W. Lucas; invited M.A. Madore to coauthor this work. (50%)

20B: Experiments designed, executed and analyzed jointly by W.J. Lucas and C. Wilson (Postdoctoral Fellow). Project supported by an NSF grant to W.J. Lucas. (50%)

**SECTION C:**

**PUBLISHED PAPERS ON $K^+$ TRANSPORT IN ROOTS**

1C: Experimental approach developed by W.J. Lucas and L.V. Kochian (Ph.D. student). Most experiments conducted by L.V. Kochian, with some assistance from W.J. Lucas. Project supported by an NSF grant to W.J. Lucas. (40%)

2C: Review commissioned to W.J. Lucas; invited L. Kochian to coauthor this work. (50%)

3C: As in 1C, except that experiments were conducted jointly by L.V. Kochian and W.J. Lucas. (40%)

4C: As in 1C, except that experiments were conducted jointly by L.V. Kochian and W.J. Lucas. (40%)

5C: Experiments designed by W.J. Lucas and L.V. Kochian, and conducted by J. Xin-Zhi (Visiting Scientist from Academica Sinica, China) and L.V. Kochian. Project supported by an NSF grant to W.J. Lucas. (35%)

6C: Experimental system was developed by W.J. Lucas and L.V. Kochian, while ion-specific electrode and electrical measurements were contributed to by all authors. Project was supported by an NSF grant to W.J. Lucas. I.A. Newman (Visiting Scientist) was on sabbatical leave from the Physics Department, the University of Tasmania. (35%)

7C: Invited review article. (100%)

8C: Review commissioned to W.J. Lucas; invited L.V. Kochian to coauthor this work. (50%)

**ACKNOWLEDGEMENTS**

I would like to express my thanks to the University of California for providing me with the ideal academic environment in which to develop my research program. I am especially grateful to the UC Davis Administration for its positive responses to my many requests for financial support. Of course my gratitude to the Program Directors at the National Science Foundation cannot be over stressed. Clearly, without the UC Davis and extramural support that I have received, much of the research embodied in the publications enclosed in this Thesis would not have been possible.

To the valued colleagues in my present department, and the numerous coworkers in the laboratories around the world in which I have had the pleasure of working, I would like to extend a special note of appreciation; the support afforded by true collegial interactions can never be forgotten. This sentiment is also applicable to the members of my laboratory, past and present; I think of you often and take pleasure in your continued achievements.

Finally, I would like to thank my family, and especially Diana, my wife and companion through all of these scientific experiences, for without their love, patience and encouragement, I would not have had the energy to pursue my scientific " passion".

*Journal of Experimental Botany, Vol. 26, No. 91, pp. 271–286, April 1975*

# Analysis of the Diffusion Symmetry Developed by the Alkaline and Acid Bands which form at the Surface of *Chara corallina* Cells

W. J. LUCAS

*Department of Botany, University of Adelaide, Adelaide, South Australia 5001*

Received 21 July 1974

## ABSTRACT

The diffusion symmetry developed by the alkaline and acid bands of *Chara corallina* was studied. The alkaline system developed a diffusion pattern which could not be fitted to the equation for a continuous point-source efflux. However, good correlation was obtained between experimental data and the diffusion equation for a hollow sphere. The calculated $OH^-$ efflux values, obtained using the equation of a continuous spherical-surface source, were checked against the influx values of $H^{14}CO_3^-$ obtained under the same experimental conditions. Individual $OH^-$ band efflux values ranged from 0·07 to 5·95 pmol $s^{-1}$ and total cell fluxes of 25 pmol $cm^{-2}$ $s^{-1}$ for $OH^-$ and $HCO_3^-$ were obtained (in the presence of 0·5 mM $NaHCO_3$).

The acid system developed a cylindrical diffusion pattern, but this could not be fitted to a mathematical equation. Numerical analysis will have to be employed to obtain values of $H^+$ efflux.

## INTRODUCTION

The electrical response of Characean plasma membranes to illumination has received considerable attention (Nishizaki, 1968; Andrianov, Kurella, and Litvin, 1969; Volkov and Misyuk, 1969; Andrianov, Bulychev, and Kurella, 1970; Spanswick, 1972; Volkov, 1973; Saito and Senda, 1973*a*, *b*). This is a complex response because it depends on the ionic composition of the bathing solution and the pre-illumination history of the cell (Nishizaki, 1968).

The involvement of photosynthesis is shown by the sensitivity of the plasmalemma response to photosynthetic inhibitors, which reduce or eliminate the plasmalemma response to light (Volkov, 1973; Saito and Senda, 1973*a*, *b*). The electrical changes produced by light have an action spectrum similar to that of photosynthesis (Walker, 1962) and it has been suggested that the resistance change produced by light may be due to an increase in permeability of the membrane to one or more ions. Walker (1962) suggested this ion might be $HCO_3^-$, but the involvement of this ion is controversial because its electrogenic action, postulated by Hope (1965), has been refuted by Spanswick (1970). Spanswick claimed the electrical potential change was independent of the chemical nature of the buffer and that $HCO_3^-$ produced the hyperpolarization *via* its buffering action. However,

it should be pointed out that the solutions used by Spanswick were not free of $HCO_3^-$ and therefore did not eliminate a specific role for this anion.

Attempts to match light-induced electrical changes to ionic fluxes ($K^+$, $Na^+$, and $Cl^-$) have been unsuccessful (Walker and Hope, 1969). Walker and Hope (1969) considered proton fluxes to be low and excluded them from the membrane conductance calculations. $HCO_3^-$ fluxes (1–5 pmol $cm^{-2}$ $s^{-1}$ for several Characeae: Smith, 1968) were also excluded from the conductance calculation. The main point of contention appears to be the magnitude of the $H^+$ flux, but $HCO_3^-$ and $OH^-$ ions may also be important. Kitasato (1968) suggested that a large, passive $H^+$ influx accounted for most of the electrical conductance of the plasmalemma.

Spear, Barr, and Barr (1969) observed light-dependent acid and alkaline bands, at the surface of *Nitella clavata* cells. By making various assumptions they calculated a $H^+$ flux approximating that inferred by Kitasato (1968). Some support was given to this value by Rent, Johnson, and Barr (1972). Lucas and Smith (1973), on the other hand, measured the pH of the acid and alkaline bands that developed at the surface of *Chara corallina* cells, but could obtain only approximate values of the $HCO_3^-$ and $OH^-$ fluxes and were unable to evaluate $H^+$ fluxes associated with the acid bands. It is important that these fluxes be measured. Firstly, it is essential to check the values obtained by Kitasato (1968), Spear *et al.* (1969), and Rent *et al.* (1972). Secondly, a more complete understanding of the properties of this banding phenomenon may help to determine the contribution, if any, that it plays in affecting the electrical properties of the plasma membrane.

This paper reports the results of an investigation into the diffusion symmetry established by the $OH^-$ and $H^+$ systems. As a result, a complete solution to the alkaline system is obtained. Unfortunately the acid system cannot be solved completely; however the relative magnitudes of the two processes could be inferred. The mechanism of alkaline band formation is refined beyond that originally proposed by Lucas and Smith (1973).

## MATERIALS AND METHODS

The measurement of pH along the cell wall of a *Chara corallina* cell has been previously reported (see Lucas and Smith, 1973, especially Figs 1 and 2). Cells were grown in the laboratory under artificial light and only cells whose walls were free of visible $CaCO_3$ were used in experiments. Bathing solutions (which contained 1·0 mM NaCl, 0·2 mM KCl, and 0·5 mM $CaSO_4$ unless otherwise specified) were maintained at 25 °C. A larger Perspex holder (Lucas and Smith, 1973) was used to perform the diffusion experiments, the agar held within the perspex being 1·4 cm wide, 3·0 cm high, and 8·0 cm long.

The cell to be investigated was inserted into the centrally located hole in the agar gel (made with a stainless steel tube of 1 mm outer diameter) and the pH electrode placed above one of the pre-located alkaline band centres. After the required illumination period, the electrode was slowly racked down, in a stepwise manner, onto the surface of the cell, using a Leitz micromanipulator, which had a vertical movement adjustable to ±0·01 mm. In this way vertical scans onto the cell were performed for each alkaline band.

When the bathing solution contained $NaHCO_3$, the following procedure was adopted. The bathing solution, containing 0·7 per cent agar, was boiled until the agar powder dissolved. It was then transferred to a measuring cylinder and hot distilled water added to replace that lost during the boiling process. The solution was then cooled to 40 °C in a water bath. Simultaneously a fresh stock solution of 20 mM $Na_2CO_3$ was prepared and used to obtain the required concentration of $NaHCO_3$. The pH of the bathing solution containing $Na_2CO_3$ was adjusted

to the desired value using 100 mM $H_2SO_4$. The required aliquot of stock $Na_2CO_3$ was added to the agar solution (40 °C) and titrated immediately to the pH of the bathing solution. The agar solution was allowed to gel in a sealed Petri dish and the agar block (inside the Perspex holder) cut and removed. After locating the *Chara* cell in the block, it was immersed into 250 ml of bathing solution in the thermostatted test vessel. A liquid paraffin seal (10 mm thick) was poured over the surface of the bathing solution to isolate it from atmospheric $CO_2$. Using this procedure the bathing solution and agar block pH values agreed to within $\pm 0{\cdot}01$ pH units and the pH of the bathing solution remained constant for the duration of the experiment.

$HCO_3^-$ influx values were obtained using $^{14}C$. All stock and experimental solutions required for $H^{14}CO_3^-$ experiments were prepared just before they were required in the experiment. Experimental solutions and cells were sealed in test tubes during the $H^{14}CO_3^-$ treatments. At the conclusion of an experiment, cells were washed with non-radioactive solutions for 3–5 min before being dried on planchettes. The planchettes were then treated with 0·5 ml of 100 mM propionic acid to remove any precipitated $CaCO_3$ and unfixed $^{14}CO_2$. After a minimum acidification period of 3 h, the planchettes were dried and the activity counted using a thin end-window GM tube, to determine $HCO_3^-$ uptake.

It should be emphasized that when $H^{14}CO_3$ experiments were performed, the pH of the bathing solution was initially 8·6 and usually rose to 8·9 by the conclusion of the experiment, and at this pH no significant amount of $CO_2$ is present. Under these conditions fixation of $H^{14}CO_3^-$ is considered equal to influx.

## RESULTS

Lucas and Smith (1973) considered the development of an alkaline band to be due to the localized efflux of $OH^-$ from a point on the cell surface, accumulation of $OH^-$ near the surface eventually forming a band. Such a system can be analysed, using the equation of a continuous point source, to obtain the actual $OH^-$ efflux. Fig. 1A illustrates a normal cell wall pH scan of an alkaline band. The vertical pH scan locations are indicated on this figure and the actual results of the six vertical pH scans are shown in Fig. 1B and C. From these horizontal and vertical pH scans a two-dimensional diffusion pattern can be mapped using iso-concentration lines (Fig. 2). The mismatch with the 1·0 and 10 (mol $cm^{-3} \times 10^{-10}$) iso-concentration lines was due to the elapsed time between scan 1 and 6 (at least 40 min per scan). Fig. 2 indicates that an alkaline band establishes a diffusion pattern which approximates to that of a spherical coordinate system. However, the band or diffusion centre is wider (0·05 cm) than would be expected for a point source efflux of $OH^-$ ions.

### *Point source or band surface source*

To test the OH ion$^-$ distribution around the complete band, a cell was located in an agar block with its single nodal orientation cell (see Lucas and Smith, 1973) in the vertical (upright) position. This orientation is referred to as the 0° position. The cell was illuminated (using a light intensity of 10 W $m^{-2}$) for 2 h and a cell wall pH scan performed. After completing the scan, the cell was carefully transferred to another agar block which had been equilibrated with the bathing solution. The nodal orientation cell was rotated to the horizontal or 90° position and the procedure repeated. The entire sequence was repeated for the 180° position. A typical pattern of pH values obtained from such a sequence of scans is shown in Fig. 3 on which, for simplicity, only the 0° and 180° values have been plotted. These results indicated that there was very little change in the concentration of $OH^-$

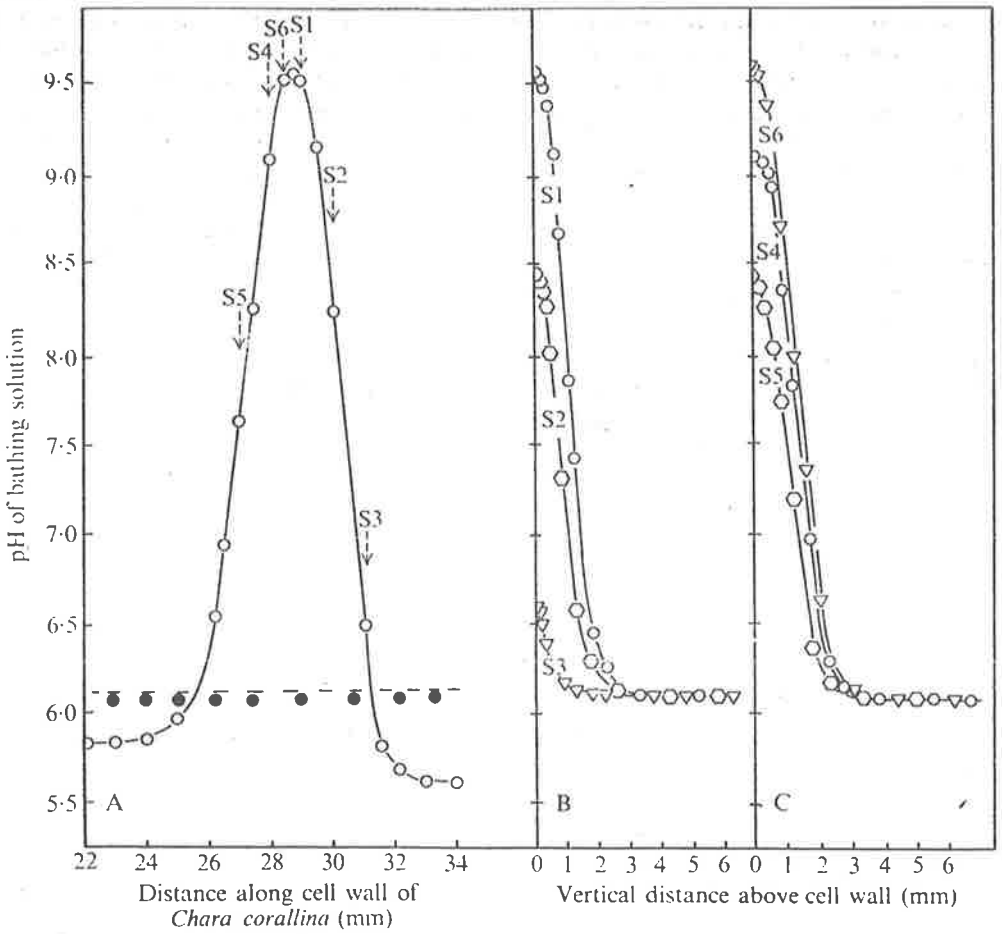


FIG. 1. Two-dimensional analysis of the pH values in the vicinity of an alkaline band. The cell was held in an agar block (normal bathing solution) and illuminated (10 W $m^{-2}$) for 4 h before measurements were made. Fig. 1A represents the pH values developed along the cell wall. The arrows represent the positions of the vertical scans conducted from the bulk solution onto the cell wall. The vertical scans S1, S2, and S3 are shown in Fig. 1B and S4, S5 and S6 in Fig. 1C. Each scan took approximately 40 min to perform and they were conducted in the order S1 to S6. The broken line represents the pH of the bathing solution, and ●, the dark, cell wall values.

ions around the surface of the cell, within any particular band. The small band, illustrated on the extreme left of Fig. 3, is an exception and demonstrates the presence of the occasional very small localized $OH^-$ efflux system.

It was found that the alkaline band centres had attained the steady-state situation within the 2-h pre-scan illumination period. If it is assumed that for a particular band the point source efflux is located at the 0° position, the time required to establish the steady state $OH^-$ concentration at the 180° position can be obtained from the continuous point source equation (Carslaw and Jaeger, 1959, p. 261, (2)),

$$C = \frac{q}{4\Pi DR} \operatorname{erfc} \frac{R}{(4Dt)^{1/2}}, \tag{1}$$

where $C$ is the concentration of $OH^-$ ions at a radial distance of $R$ cm from the point source, $D$ is the diffusion coefficient for $OH^-$ ions, $q$ is the steady state rate at which $OH^-$ ions are flowing out through the point source, and $t$ is the time during

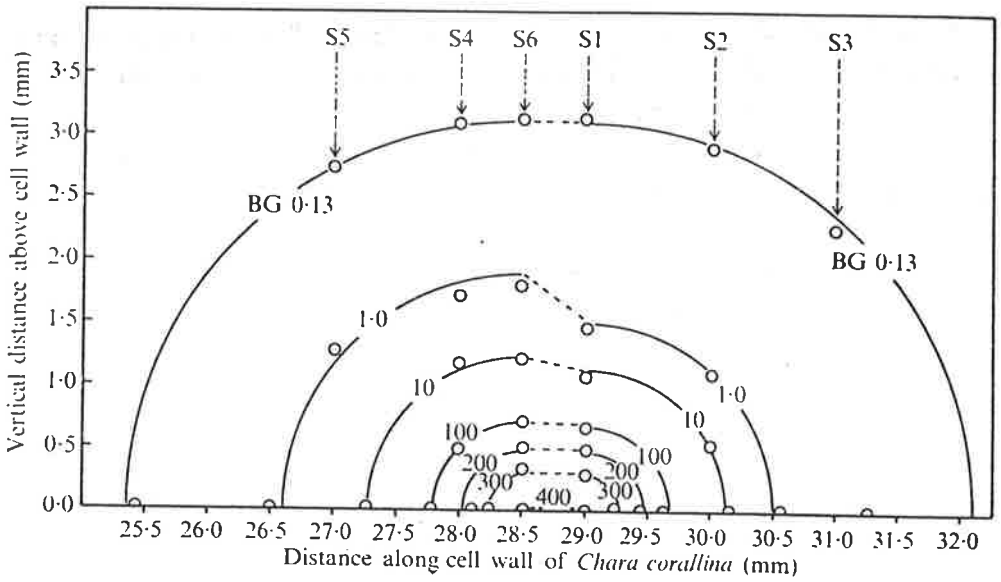


FIG. 2. The two-dimensional iso-concentration pattern, of an $OH^-$ band, constructed using the results presented in Fig. 1. The $OH^-$ band centre extends from 28·5 to 29·0 mm. The number associated with each iso-concentration line is its actual $OH^-$ ion concentration in mol $cm^{-3} \times 10^{-10}$. BG 0·13 indicates the background value of the bathing solution.

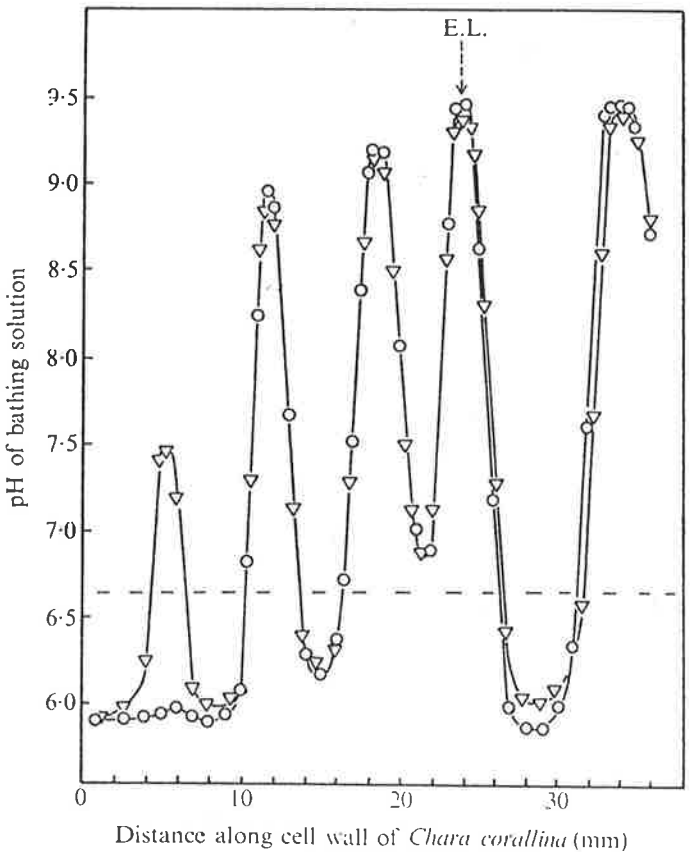


FIG. 3. Cell wall pH values obtained after 2 h illumination (10 W $m^{-2}$) in normal bathing solution; ○, indicates values obtained when the cell was in the 0° position, and, ▽, the 180° position (see text for full details). E.L. refers to the pH electrode position used to obtain the results presented in Fig. 4.

which the point source has been in action. The diffusion distance for the above situation would be $\Pi R_{Chara}$ (where $R_{Chara}$ is the radius of the cell in question) and this could be substituted into equation (1). This would result in a steady-state time actually shorter than the true time required, because equation (1) assumes radial flow, whereas the $OH^-$ diffusion being considered would be around the cell wall.

For large values of time $t$, erfc $R/(4Dt)^{1/2}$ tends to 1·0 and the result at position $R$ is the steady-state concentration, i.e.

$$C = \frac{q}{4\Pi DR}. \tag{2}$$

The way in which the steady state is approached depends on the distance $R$ from the source. Hence $C$ will have attained 95 per cent of the steady value given by equation (2) when erfc $R/(4Dt)^{1/2} = 0{\cdot}95$ or $R/(4Dt)^{1/2} = 0{\cdot}044$ (value obtained from Appendix II of Carslaw and Jaeger (1959). So the time to attain 95 per cent of the steady value at $R$ is

$$t = \frac{R^2}{4(0{\cdot}044)^2\,\mathrm{D}}. \tag{3}$$

Substituting values of $2{\cdot}129 \times 10^{-5}$ cm$^2$ s$^{-1}$ for $D$ and $R = 4{\cdot}62 \times 10^{-2}$ $\Pi = 1{\cdot}451 \times 10^{-1}$ cm a value of 35·5 h is obtained for $t$.

This conclusion was supported by time-course experiments in which $OH^-$ band activation and steady-state establishment were recorded. It was found that the response of a particular $OH^-$ band to illumination was the same whether observed from the 0°, 90°, or 180° positions (Fig. 4). In Fig. 4, traces 1 and 3 were obtained when the cell was held in the 0° position and traces 2 and 4 in the 180° position. (The $OH^-$ band and pH electrode location, employed in the experiment associated with Fig. 4, are indicated in Fig. 3; the same cell was used for both experiments.) The attainment of the steady-state $OH^-$ ion concentration, around the surface of the $OH^-$ band, within a period of 12–14 min (see Fig. 4) could not possibly occur if a point-source $OH^-$ efflux was operating.

It would appear that most alkaline bands are formed *via* efflux of $OH^-$ ions over a band surface whose width is usually less than 0·05 cm. An inspection of Fig. 2 suggests that the diffusion symmetry of an alkaline band should fit the equation for a spherical-surface source of radius $R_{Chara}$, provided radial values close to the surface of the cell are not used.

*Limiting $OH^-$ ion capture*

Any attempt to analyse the diffusion pattern of $OH^-$ ions, with the ultimate aim of obtaining an absolute value of the flux crossing that particular band surface, must ensure that $OH^-$ ion capture is minimal. The bathing solutions employed in these experiments had $HCO_3^-$ concentrations of 0·2 or 0·5 mM. Consequently within a normal band centre (pH of at least 9·9 and with 0·5 mM $HCO_3^-$ present) the equilibrium

$$HCO_3^- + OH^- \rightleftharpoons H_2O + CO_3^{2-}$$

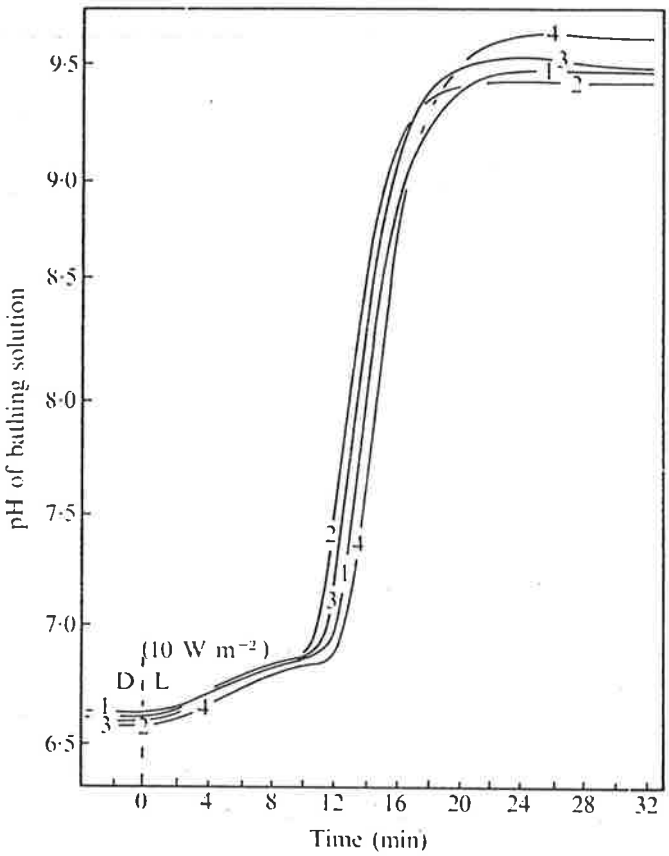


FIG. 4. An alkaline band response to 10 W $m^{-2}$ illumination. Each trace is part of the band response to 1-h dark treatment (D) followed by a 1-h light treatment (L). The band used and the electrode location is indicated by E.L. on Fig. 3. Traces 1 and 3 represent the alkaline band response when the cell was in the 0° position and traces 2 and 4 the response when the cell was in the 180° position.

would establish a $CO_3^{2-}$ level of 0·136 mM. If the $Ca^{2+}$ concentration was left at 0·5 mM, the ionic product $[Ca^{2+}][CO_3^{2-}]$ would be $6{\cdot}8 \times 10^{-8}$ which is greater than the solubility product for these ions at 25 °C ($0{\cdot}87 \times 10^{-8}$). This level of $Ca^{2+}$ could not be employed, for it would result in the precipitation of $CaCO_3$ and hence the continued removal of $OH^-$ at the cell surface. $Ca^{2+}$ at 0·06 mM would be low enough to prevent $CaCO_3$ precipitation.

A series of $HCO_3^-$ influx experiments was performed, at various $Ca^{2+}$ concentrations, to determine whether the influx remained unaffected at $Ca^{2+}$ levels of 0·06 or lower. *Chara* cells were cut and allowed 2 h recovery time in their culture tank water. During this period the cells were illuminated by a bank of fluorescent lamps, the intensity at the solution surface being 8·3 W $m^{-2}$. At the end of the recovery period the cells were washed with $Ca^{2+}$-free bathing solution and pre-treated for 1 h in their respective bathing solutions, which contained $Ca^{2+}$ levels ranging from 0 to 0·5 mM and 0·5 mM $NaHCO_3$. The pH of all solutions was adjusted to 8·6 and no other buffer was employed. The light intensity, during the 1 h pre-treatment and 1 h experimental periods (when $H^{14}CO_3^-$ was present) was 15·0 W $m^{-2}$. The results of this series of experiments (Fig. 5) show that $Ca^{2+}$ levels as low as 0·02 mM did not reduce the $HCO_3^-$ uptake.

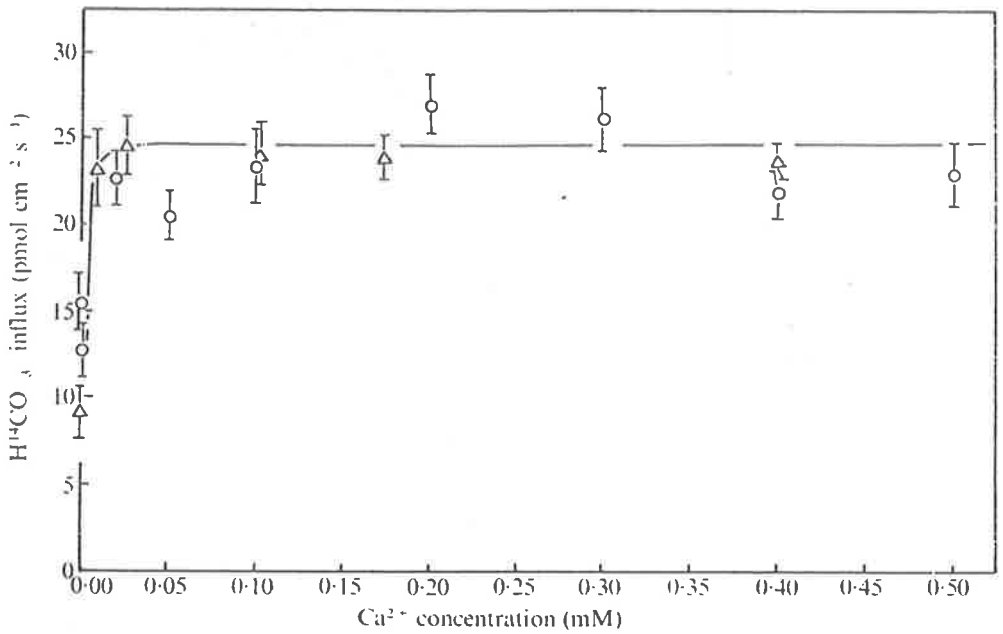


FIG. 5. Influence of $Ca^{2+}$ concentration, in the bathing solution, on $H^{14}CO_3^-$ uptake. Light intensity was 15 W $m^{-2}$. Two experimental sequences were used; ○, represents the sequence: 2 h recovery period after cutting (in natural tank water) followed by 1 h pre-treatment in experimental solutions and a further 1 h in the $H^{14}CO_3^-$ solutions. The second sequence, △, included a 10 h pre-treatment in 0·02 mM $CaSO_4$ bathing solution. This was incorporated between the 2 h recovery phase and the 1 h experimental pre-treatment. Solutions contained 0–0·5 mM $CaSO_4$, 1·0 mM NaCl, 0·2 mM KCl, and 0·5 mM $NaHCO_3$ and were at pH 8·6. Vertical lines indicate standard error of the means.

Longer exposure times to low $Ca^{2+}$ levels were required for a diffusion experiment, since preliminary studies indicated that at least 6 h were required to establish the steady state situation at distances of up to 7 mm radially out from the cell surface. A series of experiments, similar to those previously described, was performed to test the effect of prolonged low $Ca^{2+}$ exposure on $HCO_3^-$ influx. After the 2 h recovery period, the cells were bathed in a solution which contained 0·02 mM $CaSO_4$, 0·5 mM $NaHCO_3$, 1·0 mM NaCl, and 0·2 mM KCl (pH 8·6). The cells were treated in this solution for 10 h (6 h light, 8·3 W $m^{-2}$; 4 h dark). The 1 h pre-treatment and 1 h $H^{14}CO_3$ treatment were as previously described. These results (see Fig. 5) supported the conclusion that prolonged contact with low-$Ca^{2+}$ solutions does not reduce the $HCO_3^-$ influx.

*Hollow sphere diffusion analysis*

The steady-state (radial flow) diffusion pattern established by a hollow sphere, with boundary conditions $a < r < b$, $C = C_1$ at $r = a$, and $C = C_2$ at $r = b$, can be described by the equation

$$C_{(r)} = \frac{aC_1(b-r) + bC_2(r-a)}{r(b-a)} \tag{4}$$

(Carslaw and Jaeger, 1959, p. 231, (3)). Where $C_{(r)}$ is the concentration at the radial distance $r$, $a$ is the radius of the hollow sphere, and $C_1$ is the concentration at the surface of the hollow sphere; $b$ is the radial distance at which $C_2$ is equal to the

concentration of the bulk solution. Since $a$, $b$, $C_1$, and $C_2$ are constant for each particular alkaline band, it can be shown that

$$C_{(r)} = K\frac{1}{r} - B, \tag{5}$$

where $K$ and $B$ are numerical constants which can be derived when the boundary conditions are known. It should be pointed out that the value of $r$ appearing in equation (4) is equal to $(R_{Chara} + R)$ where $R$ is the radial distance from the surface of the cell to a particular point in the bulk solution.

A *Chara* cell, whose alkaline band centres had previously been mapped, was placed in a large agar block which contained 0·02 mM $CaSO_4$, 0·2 mM $NaHCO_3$, 1·0 mM NaCl, and 0·2 KCl (full details given in Materials and Methods). Vertical

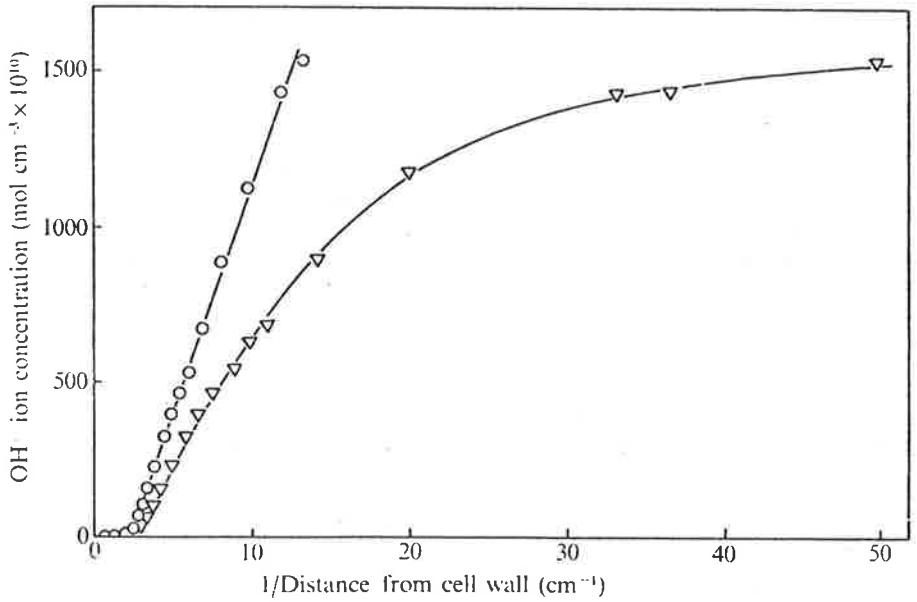


FIG. 6. Analysis of $OH^-$ ion concentrations as a function of distance from the cell wall, using equations (2), ▽, and (5), ○.

pH scans of the bands were performed after 6 h illumination (15 W $m^{-2}$). Analysis of these scans, based on equations (2) and (5), are shown for one band, in Fig. 6. A linear relationship was observed between $C_{OH^-}$ and $(R_{Chara} + R)^{-1}$ which indicated that the alkaline band closely approximates a hollow sphere diffusion system. Consequently the equation for a continuous spherical-surface source can be used to evaluate, using experimental data, the efflux rate of $OH^-$ for each alkaline band and hence the complete cell.

Several experiments were conducted to test this correlation between alkaline band symmetry ($OH^-$ concentration profiles) and the hollow sphere geometry. Fig. 7 illustrates a typical cell response to 15·0 W $m^{-2}$ illumination and 0·2 mM $NaHCO_3$. The solid line represents the banding pattern developed after 2 h illumination and was performed to locate the band centres. At the completion of this scan, the cell was given a 4-h dark treatment followed by re-illumination for 2 h. The subsequent banding pattern, which redeveloped, is indicated by the open

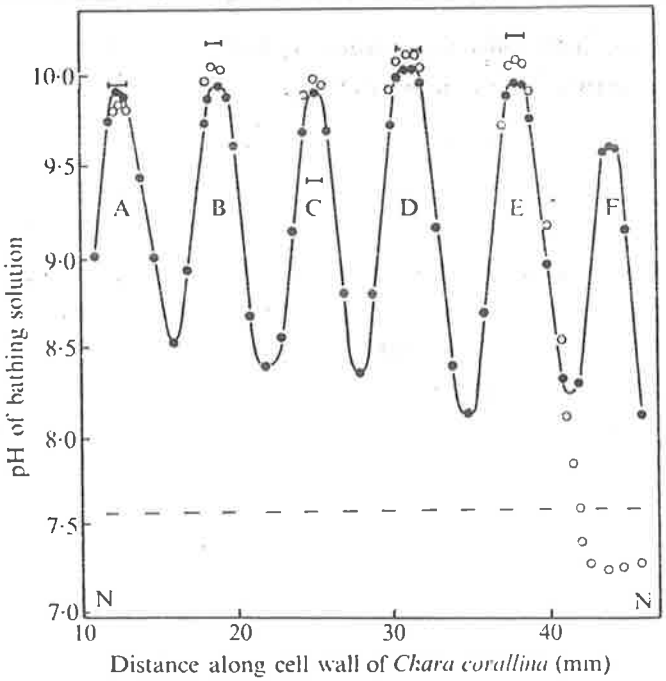


FIG. 7. Typical cell response to 15 W $m^{-2}$ illumination. Bathing solution contained 1·0 mM NaCl, 0·2 mM KCl, 0·02 mM $CaSO_4$, and 0·2 mM $NaHCO_3$. The banding pattern developed after 2 h, ●, was checked after a 4-h dark period followed by re-illumination for 2 h, ○. The nodal positions are represented by N, the broken line represents the pH of the bathing solution, and the horizontal bars represent the peak heights developed after 6 h illumination (see Fig. 8 for an analysis of these bands).

circles. A stable banding pattern of this type enabled this cell to be used to obtain vertical scans through the axes of symmetry of the alkaline bands. The results of these scans are shown in an analysed form (based on equation (5)) in Fig. 8.

The equation for a continuous spherical-surface source (Carslaw and Jaeger, 1959, p. 231) was used to obtain values of $Q_t$, the steady state efflux of $OH^-$ ions (mol $s^{-1}$), for each of these bands. The equation used was:

$$Q_t = 4\Pi D \frac{r_1 r_2 (C_1 - C_2)}{r_2 - r_1} \qquad (6)$$

where $r_1$ is equivalent to $(R_{Chara} + R_1)$, $r_2$ is $(R_{Chara} + R_2)$, $C_1$ and $C_2$ are the respective $OH^-$ concentrations, and $D$ is the $OH^-$ ion diffusion coefficient. The values obtained for the experimental data given in Fig. 8, are tabulated in Table 1b under the Expt. No. 1 column. This table also contains the results of several repeat experiments conducted in exactly the same way to test the accuracy of this procedure. The agreement between different cells, in terms of their total $OH^-$ efflux, is excellent.

*Correlation between* $\Sigma Q_t$ *for* $OH^-$ *and the influx of* $H^{14}CO_3^-$

An internal test, which could be applied to check the validity of this diffusion analysis model, was to evaluate the total $OH^-$ efflux as before and then determine the $HCO_3^-$ influx, by this cell, under the same conditions. This was done using

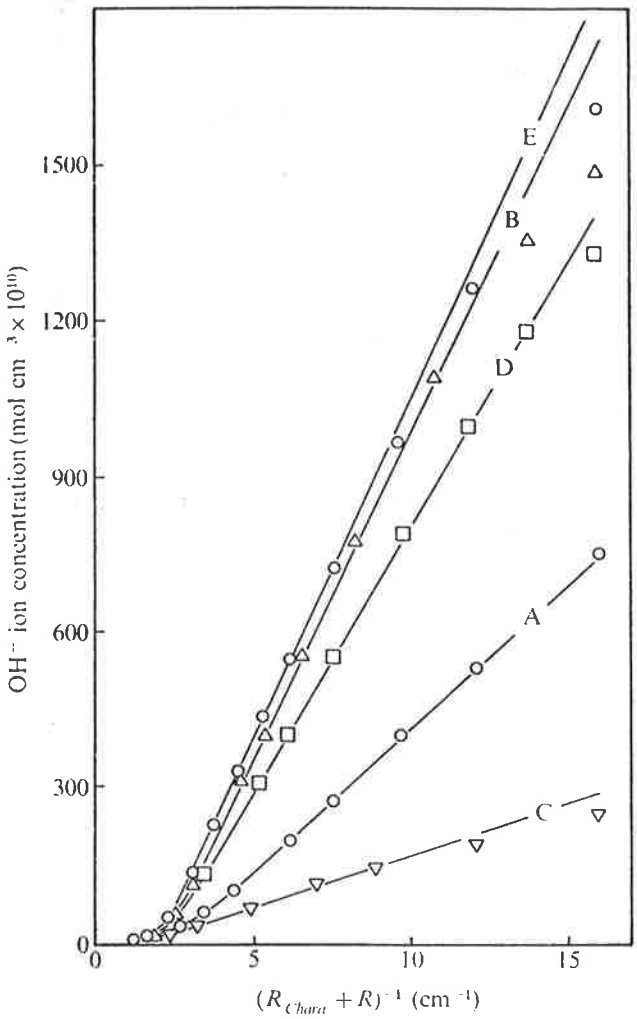


FIG. 8. A complete, $OH^-$ ion band analysis. The $OH^-$ ion concentration values obtained from the vertical scans, onto the five band centres, are plotted against the reciprocal of $(R_{Chara} + R)$. $R_{Chara}$ is the radius of the *Chara* cell involved and $R$ is the radial distance from the *Chara* cell wall to the point in the solution where the $OH^-$ ion concentration was measured. (The letters refer to the bands represented on Fig. 7.)

0·5 mM $NaHCO_3$ in the low-$Ca^{2+}$ bathing medium and the complete set of results is presented in Table 2. The correlation between calculated total $OH^-$ efflux and $HCO_3^-$ influx is excellent. The values are also in excellent agreement with those presented in Fig. 4.

*Acid band diffusion pattern*

The diffusion pattern established by the acid bands was investigated using the same techniques described for the alkaline band analysis. Fig. 9A illustrates the pH scan along the cell wall, in the vicinity of an acid band, with $OH^-$ bands present on either side. The results of the five vertical pH scans are presented in Fig. 9B, C, and D. As in the alkaline band analysis, these results were used to construct a two-dimensional acid iso-concentration pattern, the result of which is illustrated in Fig. 10. It is apparent that an acid band approximates to the diffusion pattern developed by a continuous cylindrical-surface source. This case is dealt with in

TABLE 1. *Tabulation of* $Q_t$ *values for each* $OH^-$ *band obtained using equation* (6) *and the summation of* $Q_t$ *to give total* $OH^-$ *efflux per cell*

| Expt. No. | Band No. | | | | | | | $\sum Q_t$ (pmol $s^{-1}$) | $\frac{\sum Q_t}{\text{Surface area}}$ (pmol $cm^{-2} s^{-1}$) | Chlorophyll concentration ($\mu$g Chl $cm^{-2}$)[a] |
|---|---|---|---|---|---|---|---|---|---|---|
| | A | B | C | D | E | F | G | | | |
| 1 | 1·51[b] | 3·02 | 0·57 | 2·76 | 3·53 | | | 11·39 | 12·95 | |
| 2 | 1·0 | 2·10 | 2·10 | 1·78 | 5·98 | 0·35 | 0·07 | 13·38 | 10·40 | 10·82 |
| 4 | 1·25 | 1·43 | 2·79 | 0·80 | 2·54 | | | 8·81 | 11·49 | 8·71 |
| 5 | 5·64 | 4·78 | 1·43 | | | | | 11·85 | 13·62 | 8·90 |
| 6 | 1·51 | 3·02 | 0·57 | 2·76 | 3·53 | | | 11·39 | 12·95 | 10·62 |
| 8 | 1·73 | 1·74 | 1·41 | 1·61 | 1·48 | 1·74 | 1·70 | 11·41 | 13·85 | |

Experimental conditions were 15 W $m^-$ illumination for 6 h before commencing the vertical scans and the bathing solutions contained 0·2 mM $NaHCO_3$, 0·02 mM $CaSO_4$, 1·0 mM NaCl, and 0·2 mM KCl.

[a] Determined using the equations derived by Arnon (1949).

[b] Values of $Q_t$ for each band in pmol $s^{-1}$.

TABLE 2. *Correlation between total $OH^-$ efflux calculated using the diffusion analysis and $H^{14}CO_3^-$ influx obtained on the same cell*

| Expt. No. | Band No. | | | | | $\sum Q_t$ (pmol $s^{-1}$) | $\frac{\sum Q_t}{\text{surface area}}$ (pmol $cm^{-2}$ $s^{-1}$) | $HCO_3^-$ influx (pmol $cm^{-2}$ $s^{-1}$) |
|---|---|---|---|---|---|---|---|---|
| 16 | 2·15[a] | 4·54 | 5·35 | .. | .. | 12·04 | 25·40 | 28·60 |
| 18 | 5·13 | 1·39 | 1·49 | 1·92 | 2·67 | 12·60 | 24·43 | 25·14 |
| 20 | 2·72 | 5·95 | 4·60 | 3·99 | .. | 17·26 | 27·62 | 25·93 |

Experimental conditions were 15 W $m^{-2}$ illumination for 6 h before commencing the vertical scans and the bathing solutions contained 0·5 mM $NaHCO_3$, 0·02 mM $CaSO_4$, 1·0 mM NaCl, and 0·2 mM KCl.

[a] Values of $Q_t$ for each band (pmol $s^{-1}$).

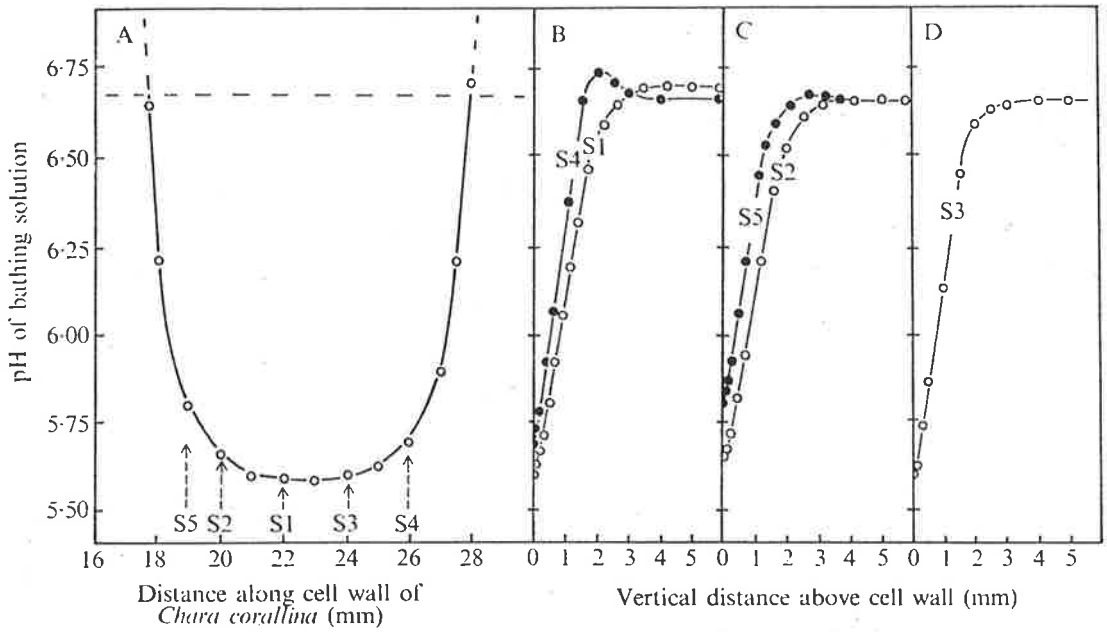


FIG. 9. Two-dimensional analysis of the pH values in the vicinity of an acid band. The cell was held in an agar block (normal bathing solution) and illuminated (10 W $m^{-2}$) for 6 h before measurements were made Fig. 9A represents the pH values developed along the cell wall. The arrows represent the positions of the vertical pH scans conducted from the bulk solution onto the cell wall. These cans are shown in Fig. 9B, C, and D. Each scan took approximately 30 min to perform and they were conducted in the order S1 to S5. The broken line represents the pH of the bathing solution.

Carslaw and Jaeger (1959, p. 262), where it is stated that this system cannot be expressed in terms of tabulated functions. Numerical integration may be the only way of obtaining efflux values for the acid bands.

## DISCUSSION

### *The nature of the two bonding systems*

It is clear that the basic mechanisms of the acid and alkaline systems differ. The numerous, localized band surface sources of $OH^-$ ions are obviously acting as

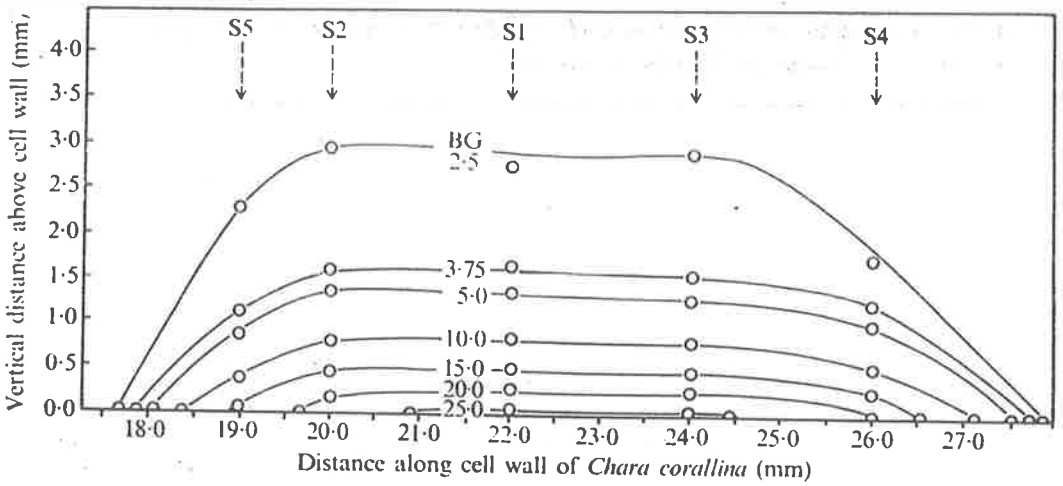


FIG. 10. The two-dimensional iso-concentration pattern of an acid band, constructed using the results presented in Fig. 9. The number associated with each iso-concentration line is its actual $H^+$ concentration in mol $cm^{-3} \times 10^{-10}$. BG 2·5 indicates the background value of the bathing solution.

disposal sites for the internally generated $OH^-$ ions. These ions result when $CO_2$, supplied as $HCO_3^-$, is fixed photosynthetically. The plasmalemma mechanism which operates to transport these $OH^-$ ions is unresolved. However this study does enable some comment on the properties of these bands. The variation in individual $Q_t$ values, compared with the uniformity of total $OH^-$ efflux observed between cells, suggests that on the cytoplasmic/plasmalemma level there exists a preferential $OH^-$ supply system. If this was not so, all bands would be expected to operate at an equal efflux rate. The nature of this *band status* will be described in a later paper.

The acid bands appear to form as a result of uniform acid efflux over the cell surface in regions where alkaline bands are not active. The source of these protons is not known, nor is the mechanism by which they cross the plasmalemma. It is unfortunate that the geometry of the acid bands (Fig. 10) cannot be analysed by any available mathematical relationship; this situation is further complicated by the interaction with alkaline bands at the acid boundaries. Since the presence of the alkaline bands complicates the numerical analysis it would be more effective if these bands could be inhibited in a manner which does not affect the acid efflux. This is at present under investigation.

*Inferred magnitude of acid efflux*

It was found that in the presence of 0·2 mM $NaHCO_3$ very little net efflux of acid occurred (see Fig. 7) since, in the experimental scans conducted, few regions became sufficiently acidic to depress the cell wall pH value below that of the bulk solution. If acid effluxes of the magnitude reported by Spear, Barr, and Barr (1969) were present, they would certainly have been observed. Fig. 2 also indicates that the acid efflux system does not operate in the vicinity of the alkaline band because the $OH^-$ concentration values along the surface of the cell (away

from the band centre) are not seriously distorted from the spherical diffusion pattern.

*Connection between the alkaline system and other membrane properties*

The $HCO_3^-$ influx and $OH^-$ efflux values reported in this paper are much larger than those reported by Smith (1968). The value of approximately 25 pmol $cm^{-2}$ $s^{-1}$, when 0·5 mM $NaHCO_3$ was present, suggests that this alkaline system may influence the membrane properties in the light, for these are the largest anion fluxes reported for any Characean cell. If the $HCO_3^-$ and $OH^-$ ions are transported across the membrane on an obligate coupled non-electrogenic system, the system could not contribute either to the membrane conductance or the potential. The $H^{14}CO_3$ results, which indicate the accuracy of the analysis used to evaluate the total $OH^-$ efflux for each cell, do not indicate the manner in which the $HCO_3^-$ enters the cell, i.e. it is not possible to say whether the $HCO_3^-$ enters only in the $OH^-$ efflux regions or in fact uniformly over the entire cell surface. (The latter may in fact be the expected situation.) Hence, because the nature of these transporters is not known, their contribution to the electrical properties of the plasmalemma should not be rejected (cf. Richards and Hope, 1974).

The successful analysis of the alkaline banding system will enable an investigation to be conducted on the response of the $OH^-$ efflux to illumination (cf. Fig. 4). This response can now be fitted to the continuous spherical-surface source equation (see Carslaw and Jaeger, 1959, p. 263, (10)), and the manner in which $Q_t$ activates and approaches the steady-state value after illumination will be obtained. These data can be compared with the response of the membrane potential and resistance to illumination.

ACKNOWLEDGEMENTS

This work was done while the author held an Australian Commonwealth Postgraduate Scholarship. I wish to thank Drs. J. T. Wiskich and B. J. Steel for critical readings of the manuscript. Thanks are also due to Prof. J. C. Jaeger for his valuable guidance in relation to the mathematics of the diffusion systems.

LITERATURE CITED

ANDRIANOV, V. K., BULYCHEV, A. A., and KURELLA, G. A., 1970. *Biophysics*, **15**, 199–200.
—— KURELLA, G. A., and LITVIN, F. F., 1969. *Tsitologiya*, **11**, 1014–20.
ARNON, D. I., 1949. *Pl. Physiol., Lancaster*, **24**, 1–15.
CARSLAW, H. S., and JAEGER, J. C., 1959. *Conduction of heat in solids*. Second edn, Clarendon Press, Oxford.
HOPE, A. B., 1965. *Aust. J. biol. Sci.* **18**, 789–801.
KITASATO, H., 1968. *J. gen. Physiol.* **52**, 60–87.
LUCAS, W. J., and SMITH, F. A., 1973. *J. exp. Bot.* **24**, 1–14.
NISHIZAKI, Y., 1968. *Pl. Cell. Physiol., Tokyo*, **9**, 377–87.
RENT, R. K., JOHNSON, R. A., and BARR, C. E., 1972. *J. Membrane Biol.* **7**, 231–44.
RICHARDS, J. L., and HOPE, A. B., 1974. Ibid. **16**, 121–44.
SAITO, K., and SENDA, M., 1973a. *Pl. Cell. Physiol., Tokyo*, **14**, 147–56.
—— —— 1973b. Ibid. **14**, 1045–52.
SMITH, F. A., 1968. *J. exp. Bot.* **19**, 207–17.

SPANSWICK, R. M., 1970. *J. Membrane Biol.* **2**, 59–70.
—— 1972. *Biochim. biophys. Acta*, **288**, 73–89.
SPEAR, D. G., BARR, J. K., and BARR, C. E., 1969. *J. gen. Physiol.* **54**, 397–414.
VOLKOV, G. A., and MISYUK, L. A., 1969. *Tsitologiya*, **11**, 998–1006.
—— 1973. *Biochim. biophys. Acta*, **314**, 83–92.
WALKER, N. A., 1962. *A. Rep. Div. Pl. Ind. C.S.I.R.O.* p. 80.
—— and HOPE, A. B., 1969. *Aust. J. biol. Sci.* **22**, 1179–95.

*Journal of Experimental Botany, Vol. 26, No. 92, pp. 331–346, June 1975*

# Photosynthetic Fixation of $^{14}$Carbon by Internodal Cells of *Chara corallina*

W. J. LUCAS[1]

*Department of Botany, University of Adelaide, Adelaide, South Australia* 5001

Received 2 September 1974

## ABSTRACT

Maximum fixation rates of 120 and 60 pmol cm$^{-2}$ s$^{-1}$ were obtained when exogenous carbon was supplied as $^{14}CO_2$ and $H^{14}CO_3^-$ respectively. These values are considerably higher than those previously reported for this species. A kinetic analysis was performed on this data. Substrate saturation in the concentration range 1·0–1·5 mM was observed for both $CO_2$ and $HCO_3^-$.

In the presence of exogenous $CO_2$, a linear relationship was observed between light intensity and fixation while the $HCO_3^-$ relationship was slightly sigmoidal. Fixation saturated at intensities of 15–20 W m$^{-2}$ and 13–15 W m$^{-2}$ for exogenous $^{14}CO_2$ and $H^{14}CO_3^-$ respectively.

The presence, in this species, of an extremely active $HCO_3^-$ transport system, situated in the plasmalemma, demonstrates that when alkaline solutions are employed the involvement of this ion cannot be ignored during electrical studies on this membrane. The maximum $H^{14}CO_3^-$ influxes obtained during this study are the largest ionic fluxes measured for any Characean species.

It was demonstrated that $CO_2$ for fixation can be supplied simultaneously by gaseous diffusion and $HCO_3^-$ transport (cf. Raven, 1968). Inhibition of $H^{14}CO_3^-$ influx was observed in the presence of Tris, Tricine, and borate buffers, and $CO_3^{2-}$ also appeared to act as a strong inhibitor. The possible mechanism(s) by which this inhibition occurs is discussed.

## INTRODUCTION

Extensive biophysical studies have been conducted on *Chara corallina* in an attempt to describe the observed membrane properties in terms of measurable ionic fluxes. Several of these ionic fluxes are light-stimulated (see Findlay, Hope, Pitman, Smith, and Walker, 1969; and Smith and Raven, 1974). Electrical changes of the plasmalemma, which occur in response to cell illumination, have been shown to have an action spectrum similar to that of photosynthesis (Walker, 1962). It is surprising, therefore, that limited attention has been focused on the photosynthetic properties of *Chara corallina*.

If photosynthetic light reactions supply all, or part, of the energy required by the light-activated ionic fluxes, competition for ATP and/or reducing power may exist between these fluxes and the photosynthetic fixation reactions. In this respect, knowledge of the kinetics of photosynthesis may be valuable in understanding the response of *Chara corallina* cells to illumination.

Smith (1968) demonstrated that several Characeae (including *Chara corallina*) fixed $^{14}CO_2$ at 30–40 pmol cm$^{-2}$ s$^{-1}$, or $H^{14}CO_3^-$ at 1–9 pmol cm$^{-2}$ s$^{-1}$. Previous work

[1]Present address; Department of Botany, University of Toronto, Toronto, Ontario, M5S 1A1, Canada.

with *Nitella translucens* (Smith, 1967) had suggested that experimental conditions of 1·0 mM total carbon (pH 6·5) and a light intensity of 13 W $m^{-2}$ would give maximal fixation rates. There is disagreement between these values and other reports in the literature. Fixation rates for $^{14}CO_2$ of 50 and 95 pmol $cm^{-2}$ $s^{-1}$ were obtained by Robinson (1969) and Smith and Raven (1974) respectively. The $H^{14}CO_3^-$ value of 25 pmol $cm^{-2}$ $s^{-1}$ (0·5 mM $HCO_3^-$, pH 8·6) reported by Lucas (1975*a*) is considerably larger than the value of 6·4 pmol $cm^{-2}$ $s^{-1}$, reported for this species by Smith (1968).

The aim of this study was to investigate, in detail, $^{14}CO_2$ fixation in *Chara corallina* cells when the exogenous $^{14}C$ was supplied as either $^{14}CO_2$ or $H^{14}CO_3^-$. The results show that differences in the concentration and nature of the exogenous carbon, as well as light intensity and the cellular photosynthetic capacity, may account for part of the variation in light effects reported by workers in this field (cf. Nagai and Tazawa, 1962; Nishizaki, 1963, 1968; Barr and Broyer, 1964; Hope, 1965; Andrianov, Kurella, and Litvin, 1969; Saito and Senda, 1973*a*; Volkov, 1973; Spanswick, 1972, 1974; Richards and Hope, 1974).

The presence of a $HCO_3^-$ transport system at the plasmalemma demonstrates that when solutions of alkaline pH are employed, the involvement of this ion, with respect to the electrical properties of the plasmalemma, cannot be ignored (see Lucas, 1975*b*).

## MATERIALS AND METHODS

During the summer growing season experiments were performed on cells cultured in the laboratory under artificial (12 h light : 12 h dark) or window light. Optimal growth rate ensured that uniform mature cells were obtained. Experimental cells were cut from the third to fifth internodal region and in many cases the fourth and fifth internodal cells were used as pairs. The average cell length and surface area was 2–2·5 cm and 0·5–0·7 $cm^2$ respectively. Field cells, collected from the River Murray (Mannum), were used in some experiments as a comparison with laboratory cultured cells.

The bathing solution contained 1·0 mM NaCl, 0·2 mM KCl, and 0·5 mM $CaSO_4$ (unless otherwise specified) and all fixation experiments were conducted at 25 °C. $CO_2$ fixation and $HCO_3^-$ influx were determined using $^{14}C$. Fixation at pH values >8·6 were assumed equivalent to $H^{14}CO_3^-$ influx since it has been shown (Lucas, 1975*a*) that above this pH value there is extremely close correlation between $^{14}C$ fixation and $OH^-$ efflux. This indicates that there is very little loss, to the bathing solution, of $^{14}CO_2$ generated in the cytoplasm *via* equilibration with transported $H^{14}CO_3^-$. Stock bicarbonate and experimental solutions were prepared just before they were required in the experiment. Exposure to the atmosphere was minimized and all treatments were conducted in sealed test tubes (25 ml). The pH values were measured at the commencement and conclusion of each experiment.

Chlorophyll concentrations were determined using the technique of Arnon (1949).

Ionic composition of the culture solutions was measured using an EEL flame photometer ($Na^+$, $K^+$, and $Ca^{2+}$), an Orion solid-state halide electrode ($Cl^-$), a Radiometer pH meter ($H^+$), and $HCO_3^-$ was determined by titration.

Details of the light system have been previously reported (Lucas, 1975*b*). Except for time-course experiments, cells were cut and pre-treated for 90 min in normal bathing solution (8·3 W $m^{-2}$ fluorescent illumination), followed by a 1 h dark pre-treatment. Cells were then pre-treated for 30 min in the light, in non-radioactive experimental solutions, followed by 1 h exposure to $^{14}C$ solutions.

At the conclusion of experiments, cells were washed with non-radioactive solutions (5 min) before being cut and dried onto planchettes. Planchettes were treated with 0·5 ml of 100 mM propionic acid to remove precipitated $Ca^{14}CO_3$ and unfixed $^{14}CO_2$; a minimum acidification period of 3 h was employed. Specific activities were determined on 0·1 ml samples of experimental solution, 0·2 ml of fresh 100 mM NaOH was used to precipitate the $NaH^{14}CO_3$ as

$Na_2{}^{14}CO_3$, and the activity was counted immediately after drying. (Aluminium planchettes were treated with heat-resistant polyurethane to prevent the NaOH reacting with the metal.) Activity was counted using a thin end-window GM-tube system.

Results are expressed as mean ± s.e. mean for each treatment; 14–16 cells were used per treatment. Values are expressed in pmol $cm^{-2}$ $s^{-1}$ so that direct comparison could be made with earlier results.

## RESULTS

### *Culture tank conditions*

Table 1 gives the chlorophyll concentrations of the cells and ionic composition and pH of the culture tanks used during this series of experiments.

TABLE 1. Chara corallina *culture tank conditions*

| Tank | Illumination | Average chlorophyll[b] conc. ($\mu$g chl. $cm^{-2}$) | Ionic composition[c] (mM) | | | | | |
|---|---|---|---|---|---|---|---|---|
| | | | $Na^+$ | $K^+$ | $Ca^{2+}$ | $Cl^-$ | $HCO_3^-$ | pH[d] |
| Delta | Full sunlight | 5·2 ± 0·3 | .. | .. | .. | .. | 2·05 | 9·3–9·5 |
| Delta | Diffuse sunlight | 8·9 ± 0·5 | 2·2 | 0·17 | 0·26 | 1·2 | 2·13 | 9·3–9·5 |
| E′ | Artificial[a] | 9·1 ± 0·6 | 1·0 | 0·22 | 0·64 | 0·7 | 1·56 | 9·4 |
| A | Artificial | 11·2 ± 0·6 | 1·7 | 0·25 | 0·92 | .. | 3·63 | 8·5 |
| xG-2 | Artificial | 14·0 ± 1·0 | 2·2 | 0·2 | 0·56 | 1·0 | 3·54 | 8·6 |
| Mannum cells | Full sunlight | 5·0 ± 0·5 | 2·5 | 0·22 | 0·50 | .. | 2·16 | 7·4 |

[a] Light was provided by Osram MCFE Daylight Fluorescent tubes, giving an intensity, at the solution surface, of 15–17 W $m^{-2}$.

[b] Chlorophyll concentration expressed as [(Chl. a + Chl. b) + Chl. 652] ÷ 2.

[c] Only the ions listed in this table were monitored.

[d] pH values were measured after 6 h illumination.

### *Time-course of $^{14}C$ fixation*

Initial experiments showed linearity of $^{14}CO_2$ fixation with time (Fig. 1). It was assumed that a 1·5 h experimental period was suitable for all other experiments. The $H^{14}CO_3^-$ results, using low light intensities of 2 and 3 W $m^{-2}$, indicated that under these experimental conditions there was not a long lag period associated with $H^{14}CO_3^-$ influx.

### *Concentration and light intensity results obtained using exogenous $^{14}CO_2$*

During exogenous $^{14}CO_2$ experiments the normal bathing solution was buffered at 5·3 with 5 mM 2-(N-morpholino)ethanesulfonic acid (MES). At this pH value 92 per cent of the added $NaH^{14}CO_3$ existed as $^{14}CO_2$ and it was assumed that no $H^{14}CO_3^-$ influx occurred. Measured $^{14}CO_2$ fixation rates, in response to various levels of exogenous $^{14}CO_2$, are presented in Fig. 2. The substrate ($^{14}CO_2$) values were calculated according to Buch (1960, Equation 10 and tabulated constants). The fixation rates of tank delta and River Murray cells are included for comparison.

The influence of light intensity on $^{14}CO_2$ fixation, in the presence of saturating $CO_2$, was observed for three different cell cultures (Fig. 3).

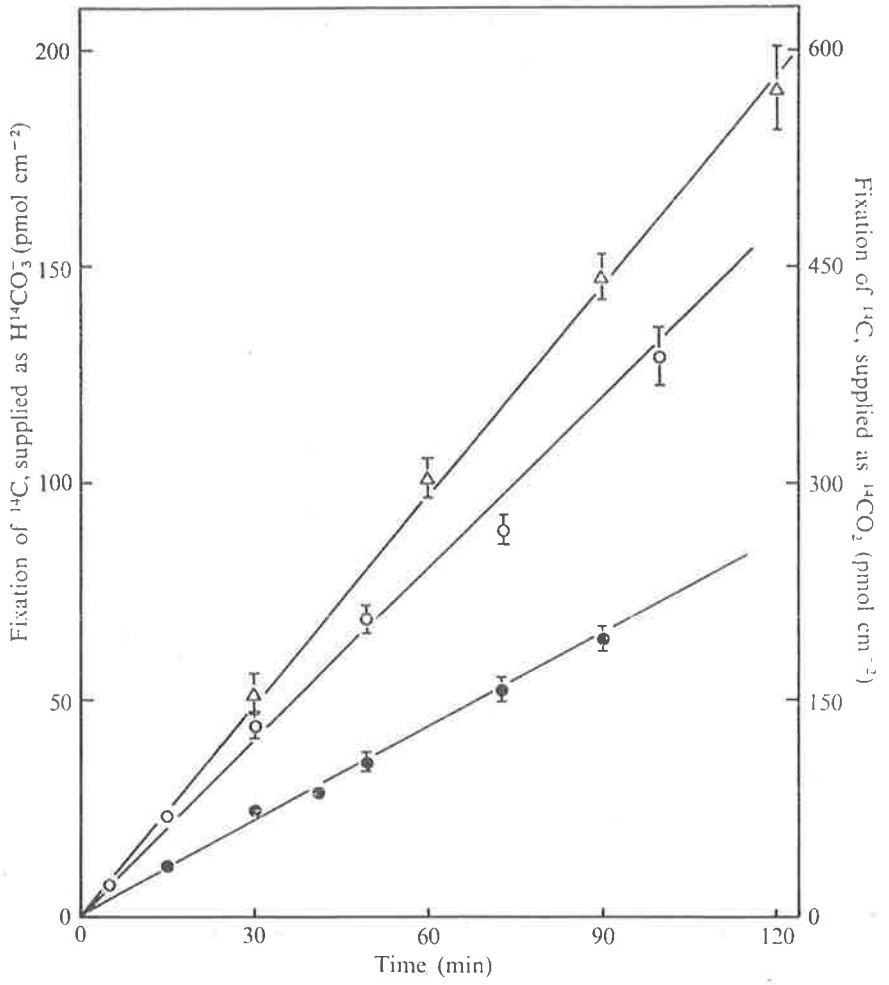


FIG. 1. Time-course of $^{14}C$ fixation. $^{14}CO_2$ fixation (△) was determined in the presence of 2 mM total carbon, pH 5·3, and 5 mM MES buffer; the light intensity was 12 W m$^{-2}$. $H^{14}CO_3^-$ uptake was determined in the presence of 2 mM total carbon, pH 8·6, and 5 mM TES buffer. The $H^{14}CO_3^-$ time-courses (●) and (○) were obtained using light intensities of 2 and 3 W m$^{-2}$ respectively.

*$H^{14}CO_3^-$ Influx: the influence of exogenous $H^{14}CO_3^-$ concentrations and light intensity*

Preliminary experiments indicated that the buffers tris(hydroxymethyl)aminomethane (Tris), N-tris(hydroxymethyl)methylglycine (Tricine), and disodium borate-boric acid all significantly reduced the influx of $H^{14}CO_3^-$ (Table 2). Only N-tris(hydroxymethyl)methyl-2-aminoethanesulfonic acid (TES) appeared to act as an inert buffer; however its buffer range did not extend to pH 9·0. For a sealed system, the pH value at which an insignificant amount of $CO_2$ existed was 9·0–9·2. In this pH range, with experimental levels of $HCO_3^-$ to buffer the solutions, only slight pH increases were observed, e.g. an initial pH value of 9·0 would rise by only 0·2 pH units after a 1 h fixation period. Because of the influence of the artificial buffer, it was decided to conduct $H^{14}CO_3^-$ experiments at an initial pH value of 9·0 and to omit artificial buffers from the solutions. Fig. 4 indicates the relationship between $H^{14}CO_3^-$ influx and exogenous $H^{14}CO_3^-$ concentration; a saturating light intensity of 25 W m$^{-2}$ was used for these experiments. (As in Fig. 2, the $H^{14}CO_3^-$ substrate concentrations were calculated according to Buch (1960, Equation 9 and tabulated constants)).

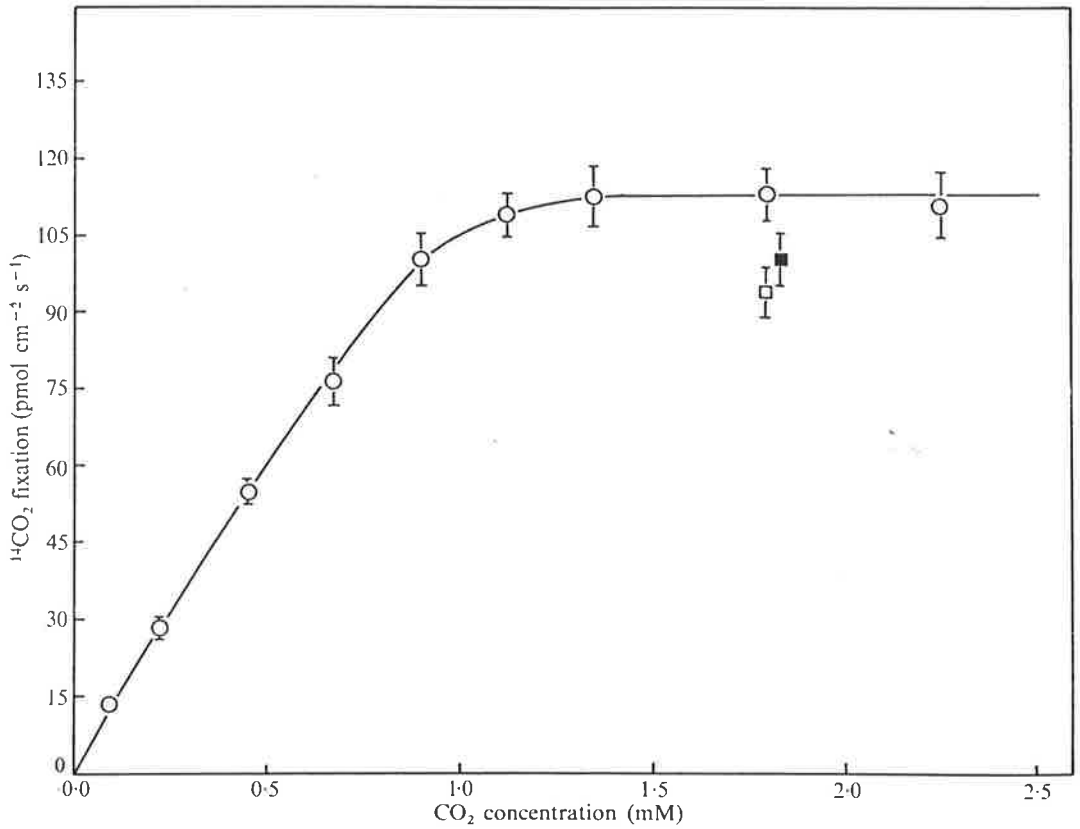


FIG. 2. $^{14}CO_2$ fixation in response to increasing substrate concentration. The bathing solution was buffered at pH 5·3 with 5 mM MES buffer and a light intensity of 25 W m$^{-2}$ was used throughout. ○, Rates using cells cultured in tank ×G-2; ■, Mannum cells; and □, cells cultured in tank delta.

The concentration curve marked A was obtained using cells from tank delta cultured under full sunlight, while curves B and C were obtained with cells from tank delta cultured under diffuse sunlight (see Table 1). The removal of precipitated $Ca^{14}CO_3$ and unfixed $^{14}CO_2$ by propionic acid is represented by the difference between curves B and C. The results presented in curve A have been corrected for $Ca^{14}CO_3$ and unfixed $^{14}CO_2$. The cell chlorophyll concentration was lower when culture conditions of full sunlight were employed (Table 1) and this may be due to photo-oxidation.

The influence of light intensity on $H^{14}CO_3^-$ influx is expressed, for cells from tank delta, in Fig. 5.

*The relationship between $^{14}CO_2$ supplied by diffusion and $H^{14}CO_3^-$ transport*

Raven (1968, 1970) suggested *Hydrodictyon africanum* 'only displays the characteristics of bicarbonate use when bicarbonate is present at more than ten times the concentration of $CO_2$'. Fixation experiments, conducted at pH values 4·8–10·8 (Fig. 6A), in the presence of saturating substrate (3 mM total carbon) and light intensity (32 W m$^{-2}$), revealed that *Chara corallina* does not require a $CO_2$:$HCO_3^-$ ratio of 1:10 before the bicarbonate system operates. The actual change in concentration of $CO_2$, $HCO_3^-$, and $CO_3^{2-}$, as the pH is increased, is presented in Fig. 6B. An analysis of these results (Fig. 6A and B) is given in the discussion.

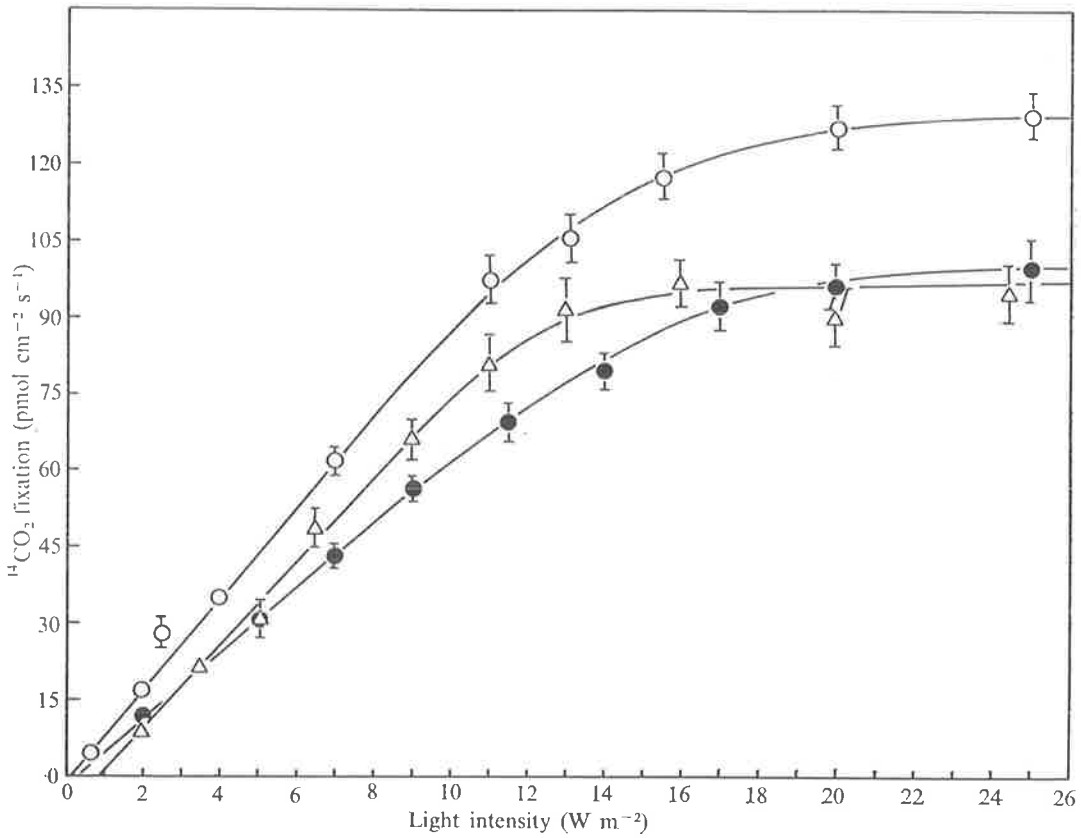


FIG. 3. The effect of light intensity on $^{14}CO_2$ fixation. Bathing solutions as in Fig. 2 except that 2 mM total carbon was used throughout. The symbols ○, △, and ● represent the responses obtained using xG-2, delta, and Mannum cells respectively.

TABLE 2. *Effects of various buffers on* $H^{14}CO_3^-$ *influx*

| Solution[a] | $H^{14}CO_3^-$ influx (pmol cm$^{-2}$ s$^{-1}$) Culture tank | | | | pH of experimental solution |
|---|---|---|---|---|---|
| | E′ | Delta | xG-2 | A | |
| Control | 59·3 ± 3·6 | 58·9 ± 2·6 | 55·5 ± 3·0 | 51·6 ± 2·4 | 9·0, 9·2[b] |
| Tricine (5 mM) | 5·85 ± 0·37 | 18·3 ± 1·0 | 5·28 ± 0·56 | 3·99 ± 0·35 | 9·0 |
| Tris (5 mM) | .. | 4·03 ± 0·21 | 4·6 ± 0·33 | .. | 9·2 |
| Borate (5 mM) | 4·18 ± 0·40 | 6·81 ± 0·45 | .. | .. | 9·0 |
| TES (5 mM) | .. | .. | .. | 52·6 ± 2·6 | 8·34 |
| Control | 91·7 ± 7·1 | | | | 7·35, 7·7[b] |
| TES (5 mM) | 98·5 ± 5·9 | | | | 7·4 |

[a] Normal bathing solution with 2mM $NaHCO_3$ added. A saturating light intensity of 25W m$^{-2}$ was employed.

[b] Initial and final pH values respectively.

## DISCUSSION

### *Apparent* $K_m$ *and theoretical* $V_{max}$ *values for* $^{14}CO_2$ *fixation*

In this study the apparent $K_m$ is used in the operational sense of the substrate concentration (either $^{14}CO_2$ or $H^{14}CO_3^-$) required to give half maximal velocity.

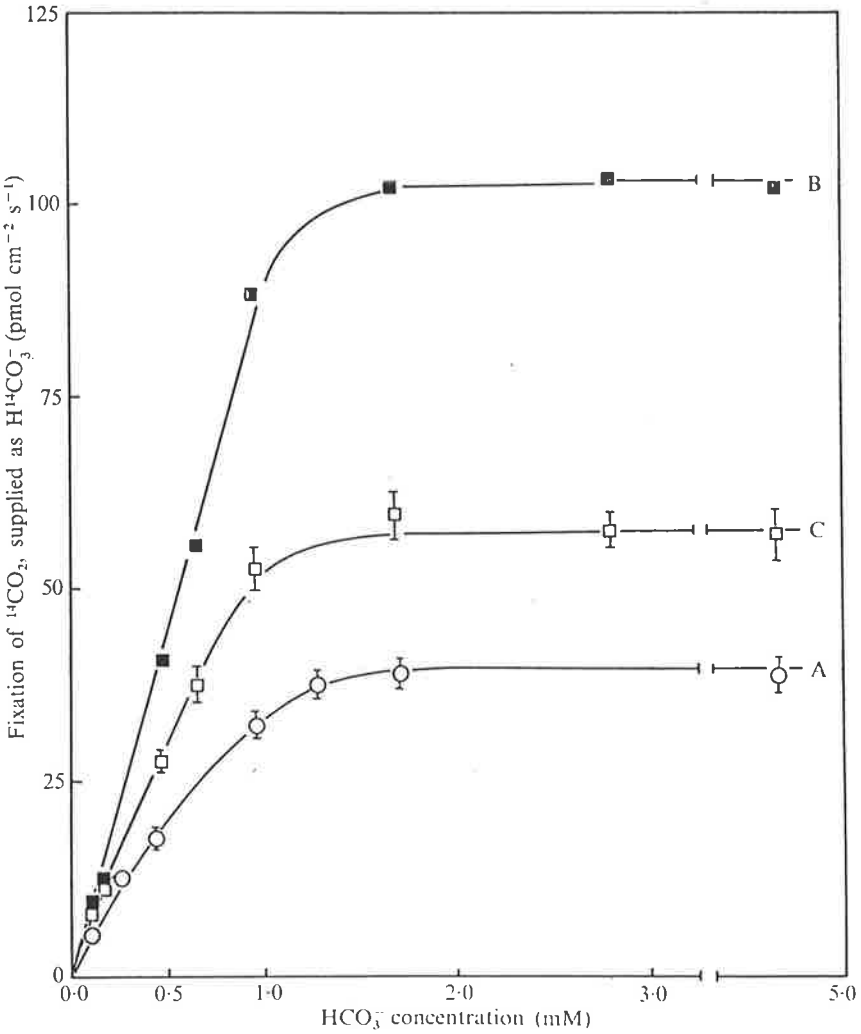


FIG. 4. $H^{14}CO_3^-$ influx in response to increasing substrate concentration. The bathing solution pH was controlled by the buffering effect of the added $NaHCO_3$ and experimental pH values were held between 9·0 and 9·2. A light intensity of 25 W m$^{-2}$ was used throughout. Curve A represents the response of cells cultured in tank delta under full sunlight; the values have been corrected for unfixed $^{14}CO_2$ and precipitated $Ca^{14}CO_3$. Curve B represents the response of tank delta cells cultured under diffuse sunlight. The difference in values between curves B and C represents the removal of unfixed $^{14}CO_2$ and precipitated $Ca^{14}CO_3$ by propionic acid.

The values were obtained using a computer programme developed by Cleland (1963) which eliminates the unconscious bias associated with graphical analysis.

$^{14}CO_2$ fixation at pH 5·3 gave an apparent $K_m$ of 0·71 ± 0·20 mM and a $V_{max}$ of 159·5 ± 17·6 (pmol cm$^{-2}$ s$^{-1}$). The values when $H^{14}CO_3^-$ was the carbon species (pH 9·0–9·2) were $K_m$, 0·59 ± 0·16 mM and $V_{max}$, 71·2 ± 6·2 (pmol cm$^{-2}$ s$^{-1}$) for the 8·9 $\mu$g chl. cm$^{-2}$ cells from tank delta, and a $K_m$, 0·58 ± 0·19 mM and $V_{max}$, 46·9 ± 4·6 (pmol cm$^{-2}$ s$^{-1}$) for the 5·2 $\mu$g chl. cm$^{-2}$ cells from tank delta.

These fixation rates are considerably higher than those previously reported for $^{14}CO_2$ or $H^{14}CO_3^-$ except for the one value of 95 pmol cm$^{-2}$ s$^{-1}$ (Smith and Raven, 1974). The bicarbonate results are important, for they demonstrate that *Chara corallina* cells are capable of very large anionic fluxes when alkaline solutions, containing $HCO_3^-$, are employed. A theoretical consideration of the maximum rate at which $HCO_3^-$ can be converted to $CO_2$ is presented in the Appendix. The values

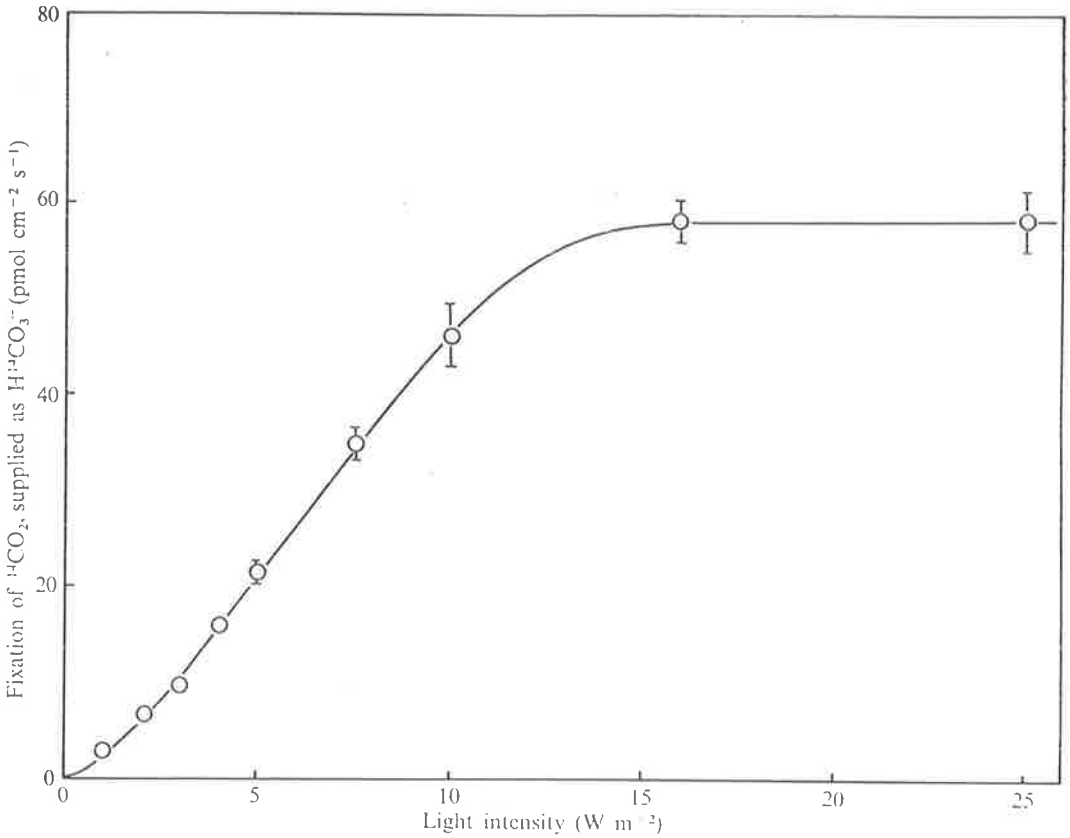


FIG. 5. The effect of light intensity on $H^{14}CO_3^-$ influx. The bathing solution contained 3 mM $NaHCO_3$ and the pH values were as in Fig. 4.

obtained indicate that at pH 9·0 and in the presence of 1 mM total carbon, the maximized rate of supply of $CO_2$ cannot account for the observed rate of $^{14}C$ fixation. Under the experimental conditions employed, the free $CO_2$ contribution would be small; the discrepancy between the calculated $CO_2$ and experimentally observed rates demonstrates beyond doubt that cells of this species can assimilate $HCO_3^-$.

The discrepancy between these high $H^{14}CO_3^-$ influx rates and those of Smith (1968) cannot be due to differences in chlorophyll concentration (cf. Smith, 1968: 11 $\mu$g chl. cm$^{-2}$, with Table 1). A possible explanation is that the cells used by Smith were very much older than those used in this study. The experiments were also performed during the winter months (F. A. Smith, personal communication).

Experiments were performed, during the mid-winter period, on cultures that had been allowed to grow from autumn to mid-winter. Cells used for $^{14}CO_2$ fixation (3·0 mM $NaHCO_3$, 5 mM MES, pH 5·3, 25 W m$^{-2}$ light intensity) gave rates of 107·3 $\pm$ 13·9 pmol cm$^{-2}$ s$^{-1}$–values which are equivalent to those obtained during the summer months. However, the $H^{14}CO_3^-$ influx values (3 mM $NaHCO_3$, pH 9·0, and 25 W m$^{-2}$ light intensity) were lower, with an average influx of 17·8 $\pm$ 2·10 pmol cm$^{-2}$ s$^{-1}$. It would appear that part of the discrepancy for $H^{14}CO_3^-$ results can be explained on the basis of seasonal variations, but this does not hold for $^{14}CO_2$ fixation values.

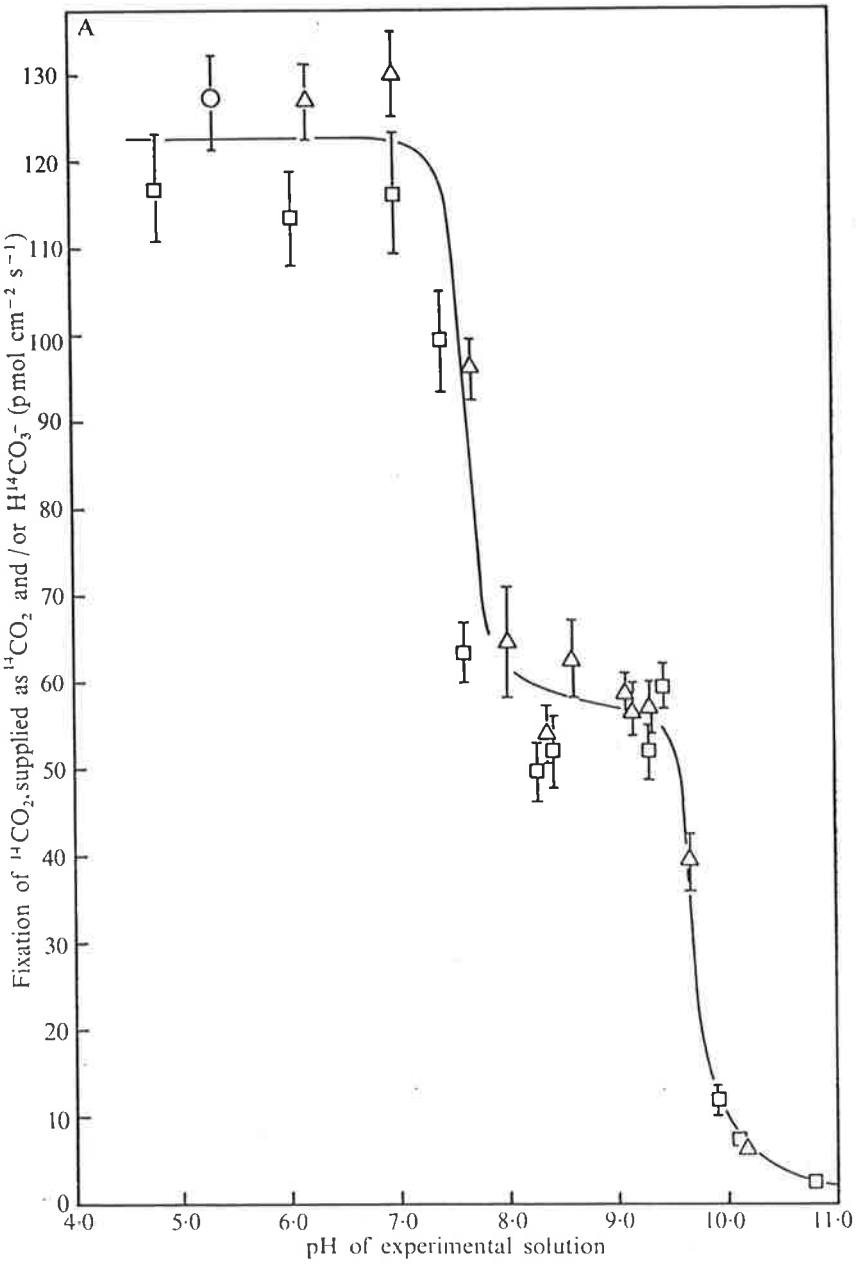


FIG. 6A. The effect of increasing pH on $^{14}C$ fixation. A total $^{14}C$ concentration of 3 mM and a 25 W m$^{-2}$ light intensity were employed for each experiment. The pH region 5·0–6·2 was buffered by 5 mM MES, the region 7·0–8·6 by 5 mM TES, and the region 9·0–10·8 by the 3 mM $HCO_3^-/CO_3^{2-}$ buffer. Culture cells used were: ○, xG-2 tank; △, delta tank, and □, E′ tank.

*Interpretation of the kinetic data*

It is not possible to categorically assign the observed apparent $K_m$ values to specific binding sites. Under conditions of light saturation, the photosynthetic fixation rate, when only exogenous $^{14}CO_2$ is present, is a function of $CO_2$ diffusion and the carboxylating reaction (see Raven, 1970). Consequently the apparent $K_m$, obtained with solutions buffered at pH 5·3, is almost certain to be associated with the ribulose diphosphate carboxylase. The value of 0·7 mM is in reasonable agreement with the adjusted value of 0·45–0·54 mM obtained for the enzyme *in vitro* (see Cooper, Filmer, Wishnick, and Lane, 1969; and Walker, 1973).

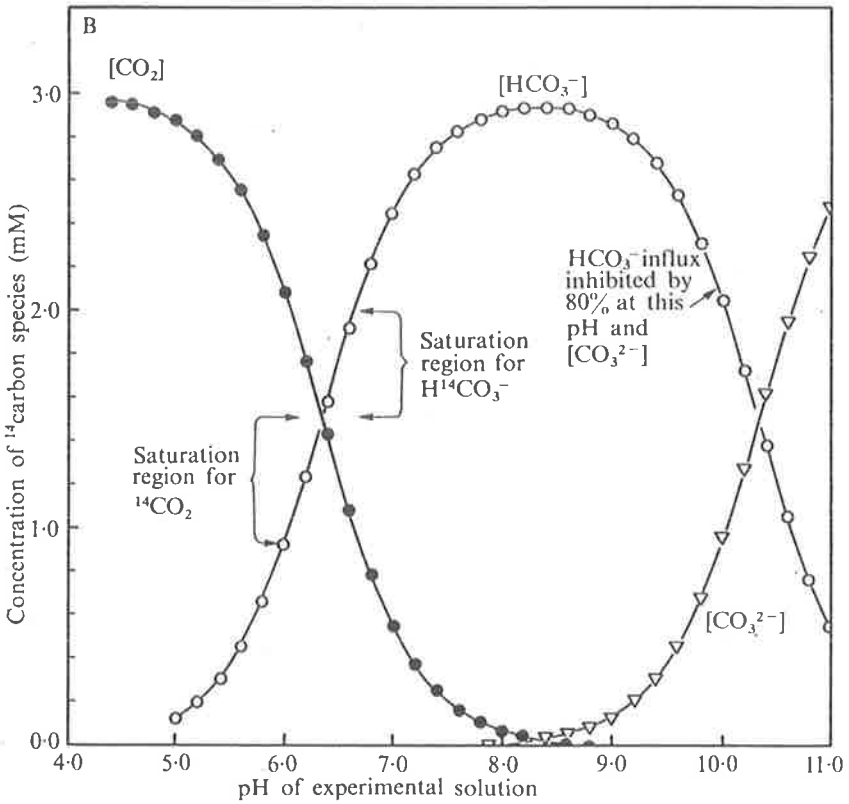


FIG. 6B. Calculated concentrations of $CO_2$, $HCO_3^-$, and $CO_3^{2-}$ present over the experimentally employed pH range. The values were calculated according to Buch (1960).

The exogenous $H^{14}CO_3^-$ situation is more complex; the photosynthetic fixation rate will depend upon the properties associated with the $HCO_3^-$ carrier system situated in the plasmalemma, the concentration of these carriers, the diffusion of $HCO_3^-$ to the chloroplasts, and finally the carboxylating reaction. The apparent $K_m$ associated with the exogenous $H^{14}CO_3^-$ system is not significantly different from that obtained for exogenous $^{14}CO_2$. However, the fixation rates in the presence of $HCO_3^-$ are always lower than observed under the same concentration of $CO_2$, i.e. the $V_{max}$ values are always lower when $H^{14}CO_3^-$ is the exogenous carbon species. A similar situation was observed for *Hydrodictyon africanum* (Raven, 1968).

The difference between $^{14}CO_2$ and $H^{14}CO_3^-$ fixation rates cannot be due to differences in chlorophyll concentrations. This is demonstrated by the results presented in Fig. 6A, where it is shown that uniform cells cultured in tanks delta and E′ fixed exogenous $CO_2$ at maximum values of approximately 130 pmol $cm^{-2}$ $s^{-1}$, but for the same cells the $H^{14}CO_3^-$ maximum was 60 pmol $cm^{-2}$ $s^{-1}$. This implies that the fixation rate, when only $H^{14}CO_3^-$ is present, is limited by a process other than the carboxylating reaction. The limiting process may be the transport of $HCO_3^-$ across the plasmalemma, and would explain the differences in $V_{max}$, because the maximum rate of bicarbonate transport would be proportioned to the number of operational carriers in the plasmalemma. If this process requires photosynthetic energy (Raven, 1968; Lucas, 1975*b*) it would provide a link between $H^{14}CO_3^-$ influx rates and chlorophyll concentration. The apparent $K_m$, obtained using exogenous

$H^{14}CO_3^-$, may therefore be associated with the $HCO_3^-$ carrier system situated in the plasmalemma.

*Influence of light intensity in the presence of saturating substrate*

Over a significant range of light intensities the $^{14}CO_2$ fixation rate is directly proportional to the light intensity (Fig. 3). A similar response was observed by Raven (1969) and Rabinowitch (1951) pointed out that it is the most common photosynthetic response. With low light intensities and saturating $CO_2$ levels, the rate limiting step is most likely the production of ribulose diphosphate, this would give the observed pseudo-first-order reaction. Under light and substrate saturation the maximum fixation rate will be determined by the ribulose diphosphate carboxylase concentration (Fig. 3).

The $H^{14}CO_3^-$ light intensity response is slightly sigmoidal; the significance of this is not known. A comparison of fixation rates, at a particular light intensity, for exogenous $^{14}CO_2$ and $H^{14}CO_3^-$ reveal that the value is always greater in the presence of $^{14}CO_2$. This situation has been reported for *Myriophyllum* leaves (Steemann Nielsen, 1947) and for *Hydrodictyon africanum* (Raven, 1968). This lower rate, in the presence of $H^{14}CO_3^-$, indicates that more light is required to fix a mole of carbon, supplied as $H^{14}CO_3^-$, than is needed for a mole supplied as $^{14}CO_2$. Steemann Nielsen considered that this extra energy was required for the excretion of $OH^-$ after the $^{14}CO_2$ from the $H^{14}CO_3^-$ had been fixed. Raven concluded that passive $HCO_3^-$ entry was unlikely and this was supported by Lucas (1975*a*, *b*). It is possible that energy is required both for $HCO_3^-$ and $OH^-$ transport across the plasmalemma. This difference in energy requirement between $^{14}CO_2$ fixation from exogenous $^{14}CO_2$ and exogenous $H^{14}CO_3^-$ may explain the results obtained by others who conduct their experiments under light-limiting conditions (Spear, Barr, and Barr, 1969; Richards and Hope, 1974).

*Compensation-point light intensities in relation to the $OH^-$ efflux system*

The respiration rate for *Chara corallina* is in the range 1–3 pmol $O_2$ $cm^{-2}$ $s^{-1}$ (Smith, 1968) so that compensation intensity would be approximately 0·3–0·5 W $m^{-2}$ for high chlorophyll cells and 1·0–1·3 W $m^{-2}$ for the lower chlorophyll cells. These values are close to the primary hydroxyl critical intensities reported previously (see Lucas, 1975*b*).

*Comparison between field- and laboratory-cultured cells*

There appears to be no significant difference in fixation rates between field cells and cells cultured in the laboratory (tank delta) under full sunlight (Fig. 3). The total exogenous carbon required to saturate the photosynthetic system appears to be between 1·0 and 1·5 mM, and both field and culture tank systems had $HCO_3^-$ in excess of this amount (see Table 1). The summer light intensity in the field situation may be in excess of the saturation level, but would depend to some extent upon the density of surface-floating vegetation. It would seem, therefore, that the rates obtained in this study are realistic in terms of the natural growth of this species.

It should be stressed that some species, particularly those growing in naturally acidic waters, may not possess the ability to utilize $HCO_3^-$. Smith (1968) demonstrated that the $HCO_3^-$ influx of collected *Nitella translucens* cells was considerably lower than the value obtained with cultured cells.

*Buffer effects at alkaline pH*

The experiments with the various buffers (see Table 2) showed that their presence interfered with the cellular utilization of bicarbonate. The pronounced inhibition of $H^{14}CO_3^-$ influx by Tris and Tricine buffers is particularly noteworthy, because these buffers are used in membrane potential studies (see Kitasato, 1968; and Saito and Senda, 1973*a* and *b*) and in artificial culture media (see Rent, Johnson, and Barr, 1972). Lannoye, Tarr, and Dainty (1970) reported that 'Tris buffer, in particular, had a secondary effect on the membrane potential not due to pH'. The secondary effect was not detailed, but may have been associated with an effect on $HCO_3^-$ influx. Of the four buffers used, only TES was found not to interfere with the $HCO_3^-$ influx system.

In this respect it is interesting to note that Spanswick (1970, Fig. 4) used TES buffer, at pH 7·1, to investigate the electrogenic bicarbonate hypothesis proposed by Hope (1965). The parallel in response when TES or 0·1 mM $HCO_3^-$ was used, would be expected because TES does not inhibit the $HCO_3^-$ influx, and the buffer at pH 7·1 would contain 0·072 mM $HCO_3^-$ if the solution was equilibrated with the atmosphere.

The mode of action, by which the Tricine, Tris, and borate buffers inhibit $HCO_3^-$ influx, is not known. However, it may be that the Tricine buffer acts as a competitive inhibitor at the $HCO_3^-$ plasmalemma binding site, i.e. the carboxyl group may act as an analogue for $HCO_3^-$. TES, in this respect, would be inert because the sulphonate group of this buffer could not act as an analogue of bicarbonate.

Ammonium sulphate has been found to specifically inhibit the $OH^-$ efflux system of *Chara corallina* (Lucas, unpublished results). It is possible that Tris buffer acts in the same way; inactivation of the $OH^-$ efflux system would prevent the $HCO_3^-$ transport system from operating normally. From these results it is clear that the buffers Tris and Tricine should not be employed as buffers in future membrane potential studies.

*Simultaneous supply of $^{14}C$ by diffusion of $^{14}CO_2$ and transport of $H^{14}CO_3^-$*

Lucas and Smith (1973) demonstrated that alkaline bands, which have been correlated with $HCO_3^-$ transport, develop at pH values as low as 5·8–6·0. At this pH range the $CO_2$:$HCO_3^-$ relationship proposed by Raven (1968, 1970) would not hold, and so it would appear that the control of $HCO_3^-$ utilization in *Chara corallina* is different from that in *Hydrodictyon africanum*. Evidence that both gaseous diffusion and $HCO_3^-$ transport are operating simultaneously is found in the results presented in Fig. 6A. Using the calculated data of Fig. 6B, it is obvious that saturating $CO_2$ concentrations are present until pH values higher than 6·7 are employed (cf. Fig. 2, $CO_2$ saturation approx. 1 mM). At pH values above 6·7 the $CO_2$ decreases, but the resultant $HCO_3^-$ increase is not significant because the $HCO_3^-$ saturating

concentration has been exceeded. The observed fixation value of 120 pmol $cm^{-2}$ $s^{-1}$ at pH 7·0 cannot be due simply to $^{14}CO_2$ supplied by diffusion for, at this pH 0·54 mM $CO_2$ is present and this $CO_2$ level would only support a fixation rate of 62 pmol $cm^{-2}$ $s^{-1}$ (see Fig. 2). However, exogenous $HCO_3^-$ is present at a concentration greater than that required for saturation and consequently the $^{14}C$ supplied *via* this $H^{14}CO_3^-$ transport process would be 60 pmol $cm^{-2}$ $s^{-1}$ (see Fig. 4). The agreement between the combined rates and the experimentally observed value must be taken as conclusive evidence for the simultaneous supply of $^{14}C$ by diffusion of $^{14}CO_2$ and $HCO_3^-$ transport to maintain the maximum possible rate. This maximization, governed by the prevailing external conditions, is demonstrated by the decline in fixation from 120 to 60 pmol $cm^{-2}$ $s^{-1}$ over the pH range 7·0 to 8·4. Over this same pH range the $CO_2$ level falls from 0·54 to 0·03 mM (Fig. 6B).

*Decrease in $H^{14}CO_3^-$ influx in pH range* 9·5 *to* 10·8

It was assumed that $H^{14}CO_3^-$ fixation would remain constant from pH 8.4 ($HCO_3^-$ concentration 2·93 mM) to 10·33 ($HCO_3^-$ concentration 1·50 mM). Above pH 10·33 exogenous $HCO_3^-$ would be limiting and a decline in fixation was expected. Experimental results did not confirm this assumption (Fig. 6A); at pH values $\geqslant$9·5 considerable inhibition of $HCO_3^-$ influx occurred.

It is interesting to note that a decrease of this nature, at a slightly lower pH, was also observed by Smith (1968). The inhibition could be due to either the influence of high pH *per se* on the membrane properties or to the presence of $CO_3^{2-}$ which may interfere with the $HCO_3^-$ transport system. Because cells grow in culture tanks in which the pH can exceed 9·5 (Smith, 1968), and since the hydroxyl bands develop localized pH regions of values > 10·0, it would appear that the $CO_3^{2-}$ inhibition is the more likely explanation of this decline in $H^{14}CO_3^-$ influx.

Figure 6B gives the actual change in concentrations of $HCO_3^-$ and $CO_3^{2-}$ caused by this pH manipulation (9·5–10·8 in particular), and it was found that when 0·8 mM $CO_3^{2-}$ was present the $H^{14}CO_3^-$ influx was inhibited by 80 per cent, even though a saturating $HCO_3^-$ concentration was present. Raven (1968) conducted his bicarbonate experiments at pH 9·6 and 10·2–10·4, in consequence the low fixation rates obtained may have been due to the experimental conditions used and not to the inability of *Hydrodictyon africanum* to utilize $H^{14}CO_3^-$ at higher rates.

## APPENDIX

*A calculation of the maximum rate at which $CO_2$ could be supplied by the dehydration of $H_2CO_3$*

The supply of $CO_2$ by the uncatalysed reactions (i.e. carbonic anhydrase assumed to be absent):

$$2H^+ + CO_3^{2-} \underset{\text{(i)}}{\rightleftharpoons} H^+ + HCO_3^- \underset{\text{(ii)}}{\rightleftharpoons} H_2CO_3 \underset{\text{(iii)}}{\rightleftharpoons} CO_2 + H_2O \qquad (1)$$

would be limited by reaction (iii) since (i) and (ii) are ionic in nature and hence almost instantaneous (Sirs, 1958). The equilibrium constants for these reactions

(25 °C) are $K_{(i)} = 4{\cdot}69 \times 10^{-11}$ (Harned and Scholes, 1941), $K = K_{(ii)}K_{(iii)} = 4{\cdot}45 \times 10^{-7}$ (Harned and Davis, 1943) and $K_{(iii)} = 2{\cdot}59 \times 10^{-3}$ (Wissburn, French, and Patterson, 1954). The consequence of the almost instantaneous nature of (i) and (ii) is that $H_2CO_3$ can be considered to be in equilibrium with $HCO_3^-$ and $CO_3^{2-}$. As a result, the formation of $CO_2$, from added $NaHCO_3$, can be obtained by solving the rate equation for the reaction:

$$H_2CO_3 \underset{k^b}{\overset{k^f}{\rightleftharpoons}} CO_2 + H_2O \tag{2}$$

where $k_f$ and $k_b$ are the first order forward and backward rate coefficients respectively. It is important to note that reaction (2) would be catalyzed by $OH^-$ ions at pH values above 8·0 (Faurholt, 1924; Brinkman, Margaria, and Roughton, 1933; and Kiese and Hastings, 1940). To allow for this catalysis, Watt and Paasche (1963) employed a slightly higher value for the forward rate coefficient, namely $k_f = 24\ s^{-1}$ (25 °C) (cf. $k_f = 20\ s^{-1}$ quoted in the review by Kern, 1960). The higher $k_f$ value of Watt and Paasche (1963) will be employed in the following calculations.

The rate equation for the production of $CO_2$ would be

$$\frac{d[CO_2]}{dt} = k_b\,[CO_2] + k_f[H_2CO_3] \tag{3}$$

To obtain an absolute maximum rate at which $CO_2$ could be supplied to the *Chara* cells, it was assumed that $[CO_2]$ tended to zero. This would not only provide a maximal rate, but also greatly simplifies the solution of the rate equation. Thus (3) becomes:

$$\frac{d[CO_2]}{dt} = k_f[H_2CO_3] \tag{4}$$

Since $H_2CO_3$ is in equilibrium with $HCO_3^-$ and $CO_3^{2-}$, its concentration can be expressed as:

$$[H_2CO_3] = \frac{[HCO_3^-][H^+]}{K_{(ii)}} \tag{5}$$

By substitution of

$$[HCO_3^-] = \frac{[\text{Total added carbon}]}{\left(1 + \dfrac{[H^+]}{K} + \dfrac{K_{(i)}}{H^+}\right)}$$

(after Buch, 1960) into (5) and re-expressing (4) gives:

$$\frac{d\,[CO_2]}{dt} = k_f\,\frac{K_{(iii)}}{K}\cdot[H^+]\cdot\frac{[\text{Total added carbon}]}{\left(1 + \dfrac{[H^+]}{K} + \dfrac{K_{(i)}}{[H^+]}\right)} \tag{6}$$

Under experimental conditions where the total added carbon existed almost entirely as exogenous $H^{14}CO_3^-$ (1 mM $NaHCO_3$, pH 9·0), the observed $^{14}C$ assimilation rate was approximately 53 pmol $cm^{-2}\ s^{-1}$ (see Fig. 4). Substituting these values (1 mM total carbon and $[H^+] = 10^{-9}$ mol $l^{-1}$) into equation (6) and solving gives:

$$\frac{d[CO_2]}{dt} = 1{\cdot}331 \times 10^{-10}\ \text{mol}\ cm^{-3}\ s^{-1}.$$

To determine the contribution of this $CO_2$ supply in terms of the observed $^{14}C$ assimilation rate required that this value be converted to the same units employed to express the rate of carbon fixation in *Chara* cells. This necessitated several assumptions concerning the physical system in which the $CO_2$ was considered to be generated. The most simple assumption which could be applied was that the $CO_2$ was being formed in a cylindrical volume element. The length of this cylindrical volume element was equivalent to that of the *Chara* cell concerned and it was considered to extend from the plasmalemma into the bathing solution, by an amount $dr$. It was also assumed that within this volume element:

(a) $HCO_3^-$ was supplied from the bathing solution such that $d[HCO_3^-]/dt = 0$,

(b) as soon as a molecule of $CO_2$ was formed, it was immediately transferred across the plasmalemma, i.e. $[CO_2]$ remained at or near zero. (This assumption greatly simplifies the physical diffusion system which would otherwise have had to have been solved, in order to obtain a value for $d[CO_2]/dt$. However, it is clear that this assumption will result in a rate much greater than that present during a $^{14}C$ assimilation experiment).

(c) For the purpose of calculating the volume element, $r_1 = R_{Chara} = 0{\cdot}045$ cm and $dr$ was increased from 20 $\mu$m up to 1000 $\mu$m. The cell surface area of a 1 cm length of cylinder was equivalent to 0·2827 $cm^2$.

Hence the value of $d[CO_2]/dt$ could be converted from mol $cm^{-3}$ $s^{-1}$ to mol $cm^{-2}$ $s^{-1}$ by the following:

$$\frac{d[CO_2]}{dt} \times \frac{\pi l(r_2^2 - r_1^2)}{\text{(Surface area per unit length of cylinder)}} \qquad (7)$$

where $l$ = unit length of cylinder in this case and $r_2 = r_1 + dr$. Substituting the value of $1{\cdot}331 \times 10^{-10}$ mol $cm^{-3}$ $s^{-1}$ into (7) and solving for various values of $\pi l(r_2^2 - r_2^1)$ gives an indication of the relative order of magnitude of the maximal supply of $CO_2$ at the cell surface. The values obtained are listed below.

| $dr$ ($\mu$m) | Volume element $\pi l(r_2^2 - r_1^2)$ ($cm^3$) | $\frac{d[CO_2]}{dt} \times \pi l(r_2^2 - r_1^2)$ (surface area per unit length of cylinder) (pmol $cm^{-2}$ $s^{-1}$) |
|---|---|---|
| 20 | $5{\cdot}78 \times 10^{-4}$ | 0·27 |
| 40 | $1{\cdot}18 \times 10^{-3}$ | 0·56 |
| 100 | $3{\cdot}14 \times 10^{-3}$ | 1·47 |
| 300 | $1{\cdot}13 \times 10^{-2}$ | 5·33 |
| 1000 | $5{\cdot}97 \times 10^{-2}$ | 28·11 |

It should be emphasized that all of the above assumptions were such that the value obtained was considerably higher than would be obtained in the true experimental situation. Even under the influence of these assumptions the calculated rate remained less than the observed $^{14}C$ value (50–60 pmol $cm^{-2}$ $s^{-1}$) obtained using these cells. It can therefore be concluded that internodal cells of this species can assimilate exogenous $HCO_3^-$.

ACKNOWLEDGEMENTS

I wish to thank Drs. J. T. Wiskich and F. A. Smith for critically reading the manuscript and also the latter for his advice on the techniques adopted in these experiments.

LITERATURE CITED

ANDRIANOV, V. K., KURELLA, G. A., and LITVIN, F. F., 1969. *Tsitologiya*, **11**, 1014–20.
ARNON, D. I., 1949. *Pl. Physiol., Lancaster*, **24**, 1–15.
BARR, C. T., and BROYER, T. C., 1964. Ibid. **39**, 48–52.
BRINKMAN, R., MARGARIA, R., and ROUGHTON, F. J. W., 1933. *Phil. Trans. R. Soc.* **A, 232**, 65–97.
BUCH, K., 1960. In *Encyclopedia of plant physiology*. Ed. W. Ruhland. Berlin, Springer. Vol. 5/1, pp. 1–11.
COOPER, T. G., FILMER, D., WISHNICK, M., and LANE, M. D., 1969. *J. biol. Chem.* **244**, 1081–3.
FAURHOLT, C., 1924. *J. Chim. phys.* **21**, 400–55.
FINDLAY, G. P., HOPE, A. B., PITMAN, M. G., SMITH, F. A., and WALKER, N. A., 1969. *Biochim. biophys. Acta*, **183**, 565–76.
HARNED, H. S., and SCHOLES, S. R., 1941. *J. Am. chem. Soc.* **63**, 1706–9.
—— and DAVIS, R., 1943. Ibid. **65**, 2030–7.
HOPE, A. B., 1965. *Aust. J. biol. Sci.* **18**, 789–801.
KERN, D. M., 1960. *J. chem. Educ.* **37**, 14–23.
KIESE, M., and HASTINGS, A. B., 1940. *J. biol. Chem.* **132**, 267–80.
KITASATO, H., 1968. *J. gen. Physiol.* **52**, 60–87.
LANNOYE, R. J., TARR, S. E., and DAINTY, J., 1970. *J. exp. Bot.* **21**, 543–51.
LUCAS, W. J., 1975*a*. Ibid. **26**, 271–86.
—— 1975*b*. Ibid. (In the press).
—— and SMITH, F. A., 1973. Ibid. **24**, 1–14.
NAGAI, R., and TAZAWA, M., 1962. *Pl. Cell Physiol., Tokyo*, **3**, 323–39.
NISHIZAKI, Y., 1963. Ibid. **4**, 353–6.
—— 1968. Ibid. **9**, 377–87.
RABINOWITCH, E. I., 1951. *Photosynthesis*. Interscience Publishers, New York. Vol. II.
RAVEN, J. A., 1968. *J. exp. Bot.* **19**, 193–206.
—— 1969. *New Phytol.* **68**, 1089–113.
—— 1970. *Biol. Rev.* **45**, 167–221.
RENT, R. K., JOHNSON, R. A., and BARR, C. E., 1972. *J. Membrane Biol.* **7**, 231–44.
RICHARDS, J. L., and HOPE, A. B., 1974. Ibid. **16**, 121–44.
ROBINSON, J. B., 1969. *J. exp. Bot.* **20**, 212–20.
SAITO, K., and SENDA, M., 1973*a*. *Pl. Cell Physiol., Tokyo*, **14**, 147–56.
—— —— 1973*b*. Ibid. **14**, 1045–52.
SIRS, J. A., 1958. *Trans. Faraday Soc.* **54**, 207–12.
SMITH, F. A., 1967. *J. exp. Bot.* **18**, 509–17.
—— 1968. Ibid. **19**, 207–17.
—— and RAVEN, J. A., 1974. *New Phytol.* **73**, 1–12.
SPANSWICK, R. M., 1970. *J. Membrane Biol.* **2**, 59–70.
—— 1972. *Biochim. biophys. Acta*, **288**, 73–89.
—— 1974. Ibid. **332**, 387–98.
SPEAR, D. G., BARR, J. K., and BARR, C. E., 1969. *J. gen. Physiol.* **54**, 397–414.
STEEMANN NIELSEN, E., 1947. *Dansk. bot. Ark.* **12**, 1–71.
VOLKOV, G. A., 1973. *Biochim. biophys. Acta*, **314**, 83–92.
WALKER, D. A., 1973. *New Phytol.* **72**, 209–35.
WALKER, N. A., 1962. *A. Rept. Div. Pl. Ind. C.S.I.R.O.* P. 80.
WATT, W. D., and PAASCHE, E., 1963. *Physiologia Pl.* **16**, 674–81.
WISSBURN, K. F., FRENCH, D. M., and PATTERSON, A., 1954. *J. phys. Chem., Ithaca*. **58**, 693–5.

*Journal of Experimental Botany, Vol. 26, No. 92, pp. 347–360, June 1975*

# The Influence of Light Intensity on the Activation and Operation of the Hydroxyl Efflux System of *Chara corallina*

W. J. LUCAS[1]
*Department of Botany, University of Adelaide, Adelaide, South Australia* 5001

Received 3 September 1974

## ABSTRACT

The interrelationships between light intensity and the activation of $OH^-$ bands was investigated. The lag period prior to $OH^-$ efflux activation was longer than the photosynthetic induction period. It was found that this lag period depended upon the light regime employed as well as the photosynthetic capacity of the cell.

The response of the cell to low light intensities revealed that all $OH^-$ bands were not of equal status. Below a critical light intensity the cell did not develop any bands even after prolonged illumination. An hypothesis is presented to account for these results, in terms of total cell $OH^-$ band activation and the regulation of the $HCO_3^-$ and $OH^-$ transport systems. It is proposed that the electrical properties of the *Chara corallina* plasmalemma, observed at high pH values, can be explained on the basis of the hypothesis presented in this paper.

## INTRODUCTION

Alkaline bands develop on the outer surface of *Chara corallina* cells when they photosynthetically fix $CO_2$, supplied as $HCO_3^-$ (Lucas and Smith, 1973). These bands originate from the localized export of $OH^-$, produced during $CO_2$ fixation. The origin of these bands is completely dependent on light.

This paper investigates the interrelationships between light energy and the activation and regulation of the $OH^-$ transport system.

## MATERIALS AND METHODS

The measurement of pH along the cell wall of a *Chara corallina* cell has been previously reported (see Lucas and Smith, 1973; especially Figs 1 and 2). Cells were grown in the laboratory under artificial light and only cells whose walls were free of visible $CaCO_3$ were used in experiments. In general the third to fifth internodal cells were used. All experimental bathing solutions contained 1·0 mM NaCl, 0·2 mM KCl, 0·5 mM $CaSO_4$, and 0·1 mM $NaHCO_3$ and were thermostatted at 25 °C. Complete details of the procedure involved in measuring the response of an alkaline band to illumination are given in Lucas (1975*a*).

Light intensities (Rank-Aldis 24 V, 150 W Quartz-Iodide) were attenuated using a range of nickel–nicron neutral density filters (prepared by the Department of Physics, University of Adelaide); the infrared component was removed using a water filter.

A silicon solar cell (IRC, Type No. S0510E 7PL) was placed in the bathing solution so that it measured the light intensity at the cell surface, (the silicon solar cell was calibrated using a miniature Middleton pyranometer, Model CN6). A mirrored surface, immediately behind the cell (approx. 2 cm), and perpendicular to the light path, enabled illumination of the entire cell surface. The light intensity was monitored during experiments.

[1] Present address: Department of Botany, University of Toronto, Toronto, Ontario, M5S 1A1, Canada.

RESULTS

Fig. 1 shows that illumination of the cell (10 W $m^{-2}$), after a 1 h dark period, gave a lag[1] of 8·6 min before the $OH^-$ band activated. Initial results failed to show a simple relationship between this $OH^-$ lag period and light intensity. When a cell was placed in low light intensities, the banding pattern was not uniform and not all bands were activated.

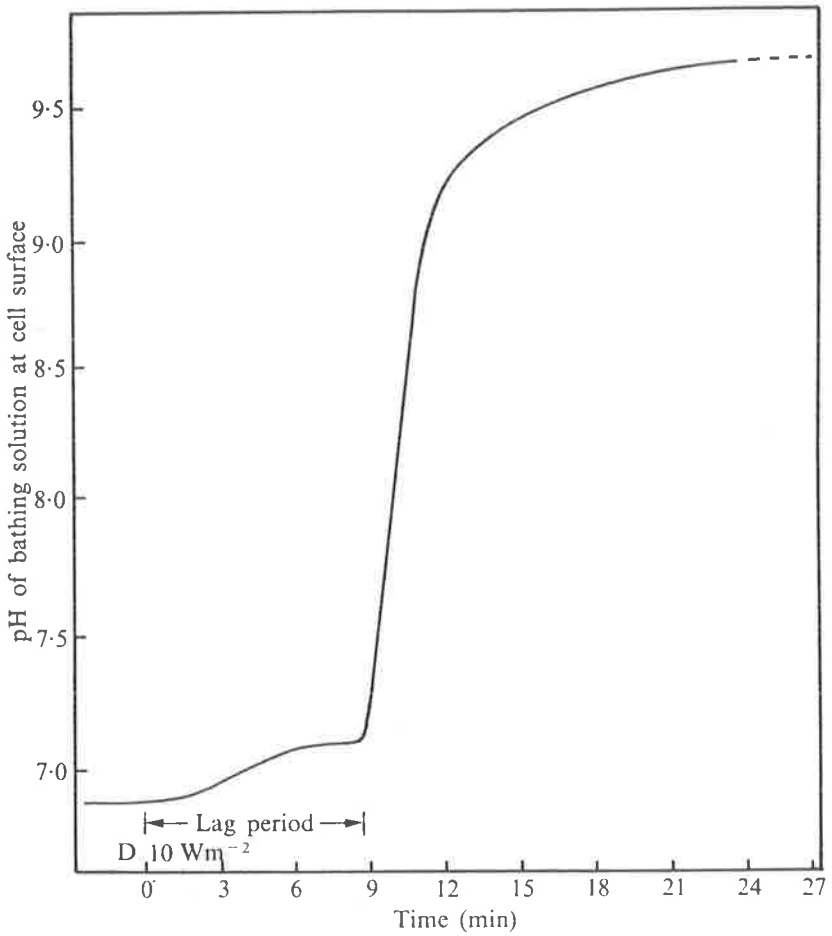


FIG. 1. An alkaline band response to 10 W $m^{-2}$ illumination following a 1 h dark (D) pre-treatment. The $OH^-$ lag period for this band was 8·6 min.

*Primary and subsidiary $OH^-$ band status*

Stable alkaline banding patterns developed under different light intensities are shown in Fig. 2. A light intensity of 10 W $m^{-2}$ caused six $OH^-$ bands to develop, but under 1·6 W $m^{-2}$ only three formed (Fig. 2A), i.e. the six bands did not reactivate and operate at a lower $OH^-$ efflux rate; this would have been reflected in lower band-centre pH values. Band 2 and band 6 actually increased their $OH^-$ efflux rates under 1·6 W $m^{-2}$. An intensity of 1·1 W $m^{-2}$ also caused three bands to develop, but band 5 replaced band 4 and bands 2 and 6 remained the more active sites of $OH^-$ efflux (Fig. 2B). At a lower intensity (0·8 W $m^{-2}$) only band 2 activated and

[1] This lag will be called the $OH^-$ lag period.

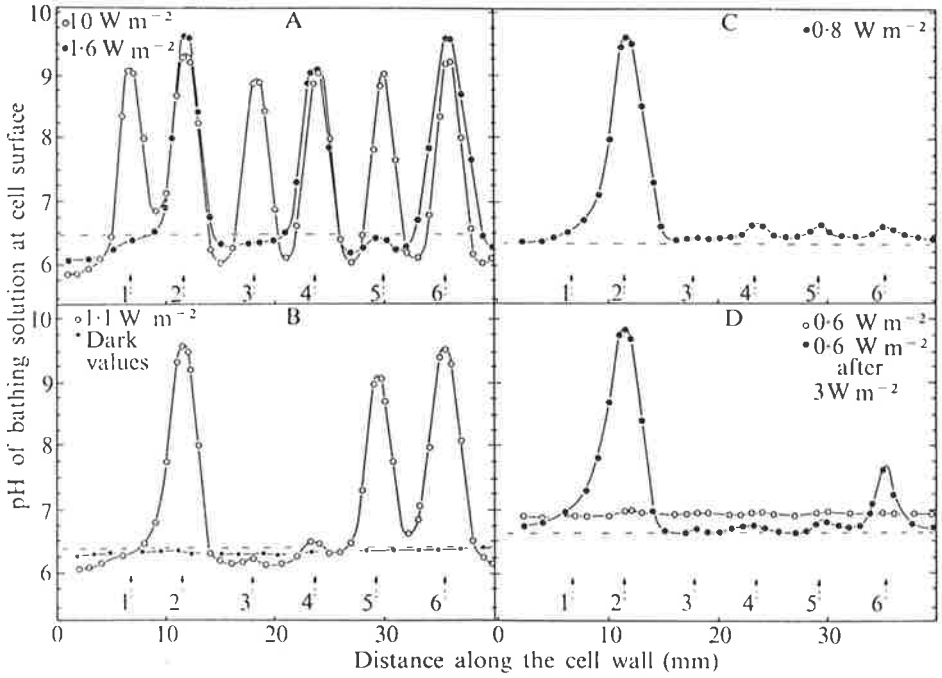


FIG. 2. Cell wall pH values obtained after 2 h illumination. The light intensity employed for each situation is indicated on the Figure. A dark treatment of 1 h was employed between different light intensities. The arrows and their respective numbers indicate the positions of the six $OH^-$ bands. The broken line represents the pH value of the bathing solution. The results in this Figure form part of Expt. No. 10. In Fig. 2D, ○ represents the cell response to 0·6 W $m^{-2}$ after 2 h (the actual time-course is shown in Fig. 3A) and ● represents the cell response after 2 h at 0·6 W $m^{-2}$ following activation of this band by 3 W $m^{-2}$ (this activation is shown in Fig. 3A).

no reduction in efflux activity was observed (Fig. 2C). Repeated illumination at this low intensity always caused only this band to activate.

Light intensities below a certain value would not activate any bands (Fig. 2D), unless the $OH^-$ efflux system was previously established using a higher intensity (Fig. 2D). Thus the $OH^-$ bands developed by a cell are not equivalent in status. The most permanent band (e.g. band 2 of Fig. 2) is also the main $OH^-$ efflux site and the other bands develop when the efflux capacity of the main band is saturated. This main $OH^-$ band was termed the *primary* $OH^-$ system. Another band (e.g. band 6 of Fig. 2) which increased in activity under lower light intensities, but deactivated before the *primary* band was termed the *sub-primary* $OH^-$ band. All other bands were termed *subsidiary* $OH^-$ bands.

*Primary band lag period as a function of light intensity*

Following identification of the primary $OH^-$ band, the cell was treated for 1 h in the dark and the primary band response to a particular light intensity was recorded. This dark to light sequence was repeated using a range of light intensities (Fig. 3A and B). The results show that as the light intensity was decreased the $OH^-$ lag period increased. Fig. 3A and B also demonstrates that with primary bands (as with sub-primary bands) the band-centre pH value increased as the light intensity was reduced.

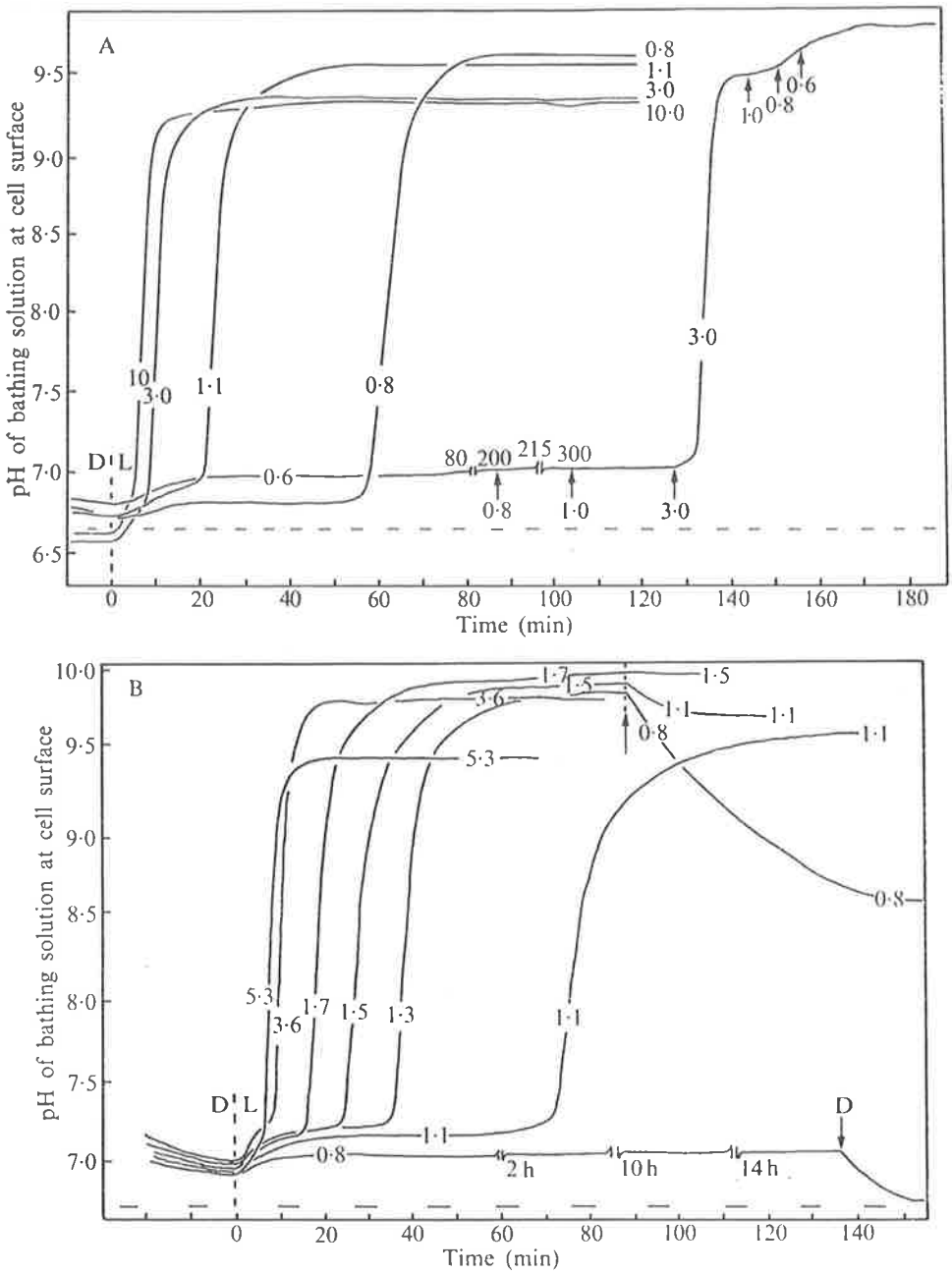


FIG. 3. $OH^-$ (primary) band response to illumination. Each trace is the cell response, following a 1 h dark treatment, to illumination; the respective light intensities are indicated on the traces. The broken line represents the pH value of the bathing solution. Fig. 3A (Expt. No. 10) also illustrates the cell response to sub-critical illumination; 0·6 W $m^{-2}$ did not activate the primary band and a subsequent increase in intensity to 0·8 W $m^{-2}$ did not cause the expected activation (cf. 56·5 min, Table 1). (See Text for full details.) In Fig. 3B (Expt. No. 9), 0·8 W $m^{-2}$ is a test of the prediction, based on the experimentally determined critical light intensity (0·9 W $m^{-2}$), that activation will not result when intensities < 0·9 W $m^{-2}$ are employed. Arrows indicate a change in the light intensity after the initial dark to light transition.

*Subsidiary $OH^-$ band response to decreasing light intensity*

Deactivation of any subsidiary band occurred abruptly over a relatively short decrease in light intensity (Fig. 4). In Fig. 4 a decrease of light intensity from 14 to 1·5 W $m^{-2}$ resulted in a decrease in efflux activity. However, this decrease was slow, and required a period greater than 1 h for the new steady state to be established.

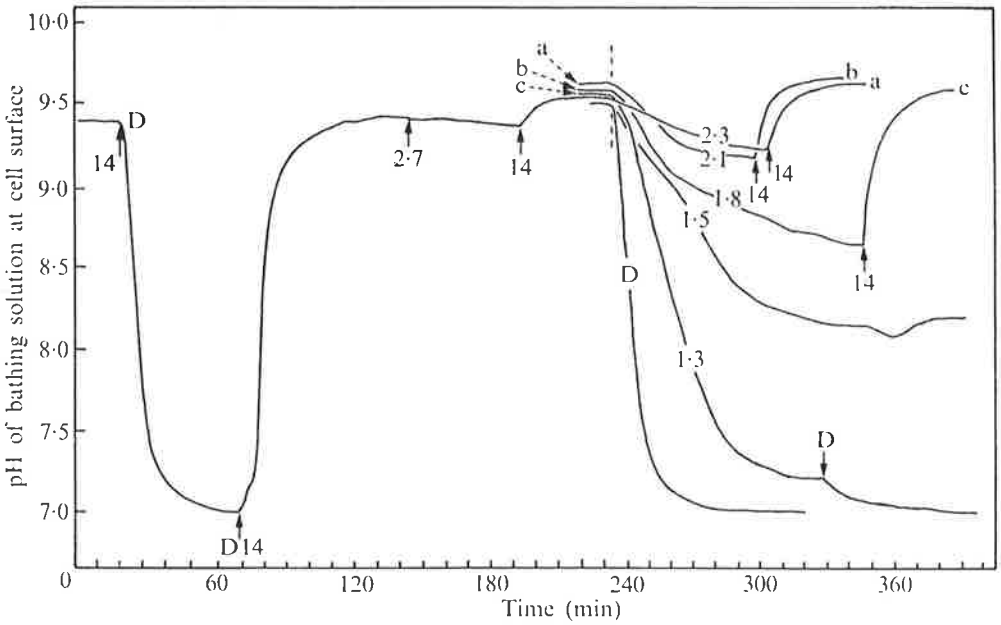


FIG. 4. Subsidiary $OH^-$ band response to decreasing light intensity. Arrows and vertical broken lines indicate changes in light intensities and the actual intensities are indicated on each trace; the units are W $m^{-2}$ and D represents a dark treatment. On each return to 14 W $m^{-2}$ the cell was given a 40 min equilibration period.

This slow response was due to some aspect of cellular activity, because the response of the measuring system was shown to be much faster (see Fig. 4, 14 W $m^{-2}$ to dark response). In transferring the cell from a 14 to a 1·5 W $m^{-2}$ light regime the photosynthetic process is changed from a substrate- to a light-limited condition. The slow response of the subsidiary band suggests that either there is a slow readjustment of the rate of $CO_2$ fixation or that a 'pool' of $OH^-$ is present in the cytoplasm.

The observed rise in activity of primary and sub-primary bands, when the light intensity was reduced, may reflect the transfer of $OH^-$ efflux function on the deactivation of a subsidiary band (Fig. 3A and B).

*Analysis of the lag in activation of the primary $OH^-$ band*

$OH^-$ lag periods of four primary bands, in response to a range of light intensities, are presented in Table 1. The reciprocal plot of these $OH^-$ lag periods against light intensity (Fig. 5) shows two linear regions. Light intensities greater than 5 W $m^{-2}$ (approx.) do not cause an increase in the reciprocal of the $OH^-$ lag period; the lag period had a minimum value determined by factors other than light intensity. The linear region observed for light intensities generally less than 3 W $m^{-2}$ is informative. It implies that light produces a substrate (i.e. for the $OH^-$ efflux system) at a rate proportional to light intensity and this substrate is required at a specific level before the primary $OH^-$ band can activate. The intercept on the 'X' axis could be interpreted as the light intensity which would take infinite time to establish this activating condition. This intercept value was termed the critical light intensity and values below it should not cause activation of the primary band. The validity of this prediction was tested, e.g. in Expt. 9 the critical value was obtained (0·9 ± 0·05 W $m^{-2}$, see Fig. 5) and an intensity of 0·8 W $m^{-2}$ was tested for a period greater

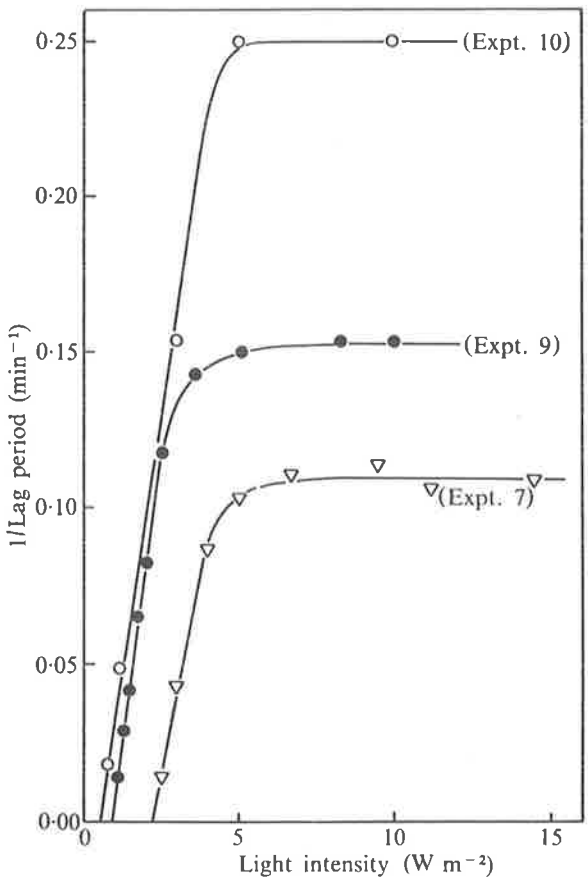


FIG. 5. Reciprocal plot of primary $OH^-$ lag period against light intensity. The experimental numbers in parenthesis refer to Table 1. The critical activation intensities obtained from this analysis were $2{\cdot}2 \pm 0{\cdot}05$ W m$^{-2}$, $0{\cdot}9 \pm 0{\cdot}05$ W m$^{-2}$, and $0{\cdot}7 \pm 0{\cdot}05$ W m$^{-2}$ for Expts. 7, 9, and 10 respectively.

TABLE 1. *Lag period for primary $OH^-$ bands in response to different light intensities*

| Experiment No. | | | | | | | | | | | |
|---|---|---|---|---|---|---|---|---|---|---|---|
| 5 | | | 7 | | | 9 | | | 10 | | |
| LI[a] | AT[b] | AT$^{-1}$[c] | LI[a] | AT[b] | AT$^{-1}$[c] | LI[a] | AT[b] | AT$^{-1}$[c] | LI[a] | AT[b] | AT$^{-1}$[c] |
| 2·3 | >300 | .. | | | | 0·8 | >14 h | .. | 0·6 | >205 | .. |
| 2·5 | 90 | 0·011 | 2·5 | 70 | 0·014 | 1·1 | 71·5 | 0·014 | 0·8 | 56·5 | 0·018 |
| 2·9 | 26 | 0·038 | 3·0 | 23 | 0·043 | 1·3 | 35·5 | 0·029 | 1·1 | 20·5 | 0·049 |
| 3·2 | 25 | 0·040 | 4·0 | 11·5 | 0·087 | 1·5 | 24·0 | 0·042 | 3·0 | 6·5 | 0·154 |
| 4·0 | 13·5 | 0·074 | 5·0 | 9·7 | 0·103 | 1·7 | 15·5 | 0·065 | 5·0 | 4·0 | 0·250 |
| 6·7 | 9·0 | 0·111 | 6·7 | 9·0 | 0·111 | 2·0 | 12·0 | 0·083 | 10·0 | 4·0 | 0·250 |
| 9·5 | 9·0 | 0·111 | 9·5 | 8·8 | 0·114 | 2·5 | 8·5 | 0·118 | | | |
| 11·2 | 7·0 | 0·143 | 11·2 | 9·5 | 0·105 | 3·6 | 7·0 | 0·143 | | | |
| 14·5 | 8·5 | 0·118 | 14·5 | 9·2 | 0·109 | 5·3 | 6·7 | 0·149 | | | |
| 17·0 | 8·0 | 0·125 | | | | 8·3 | 6·5 | 0·154 | | | |
| | | | | | | 10·0 | 6·5 | 0·154 | | | |

[a] LI is the light intensity in W m$^{-2}$.
[b] AT is the lag period (see Fig. 1) (min).
[c] AT$^{-1}$ is the reciprocal of the lag period (min$^{-1}$).

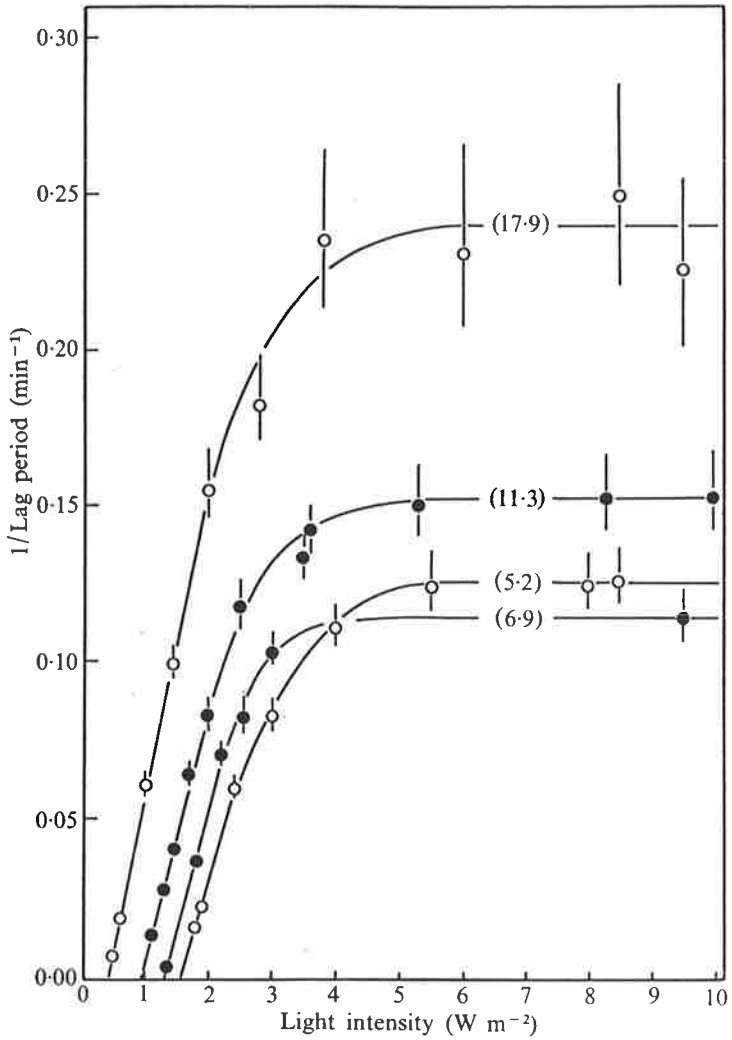


FIG. 6. Reciprocal plot of primary $OH^-$ lag period against light intensity. The values in parenthesis are the chlorophyll concentrations of the cell in $\mu$g chl. cm$^{-2}$ (determined using the method developed by Arnon, 1949).

than 14 h (see Fig. 3B) with no primary band activation resulting. In all other experiments where sub-critical illumination was employed, no bands were activated. However, an interesting feature is that once the primary band is activated, a sub-critical intensity will maintain it in the active state (Figs 2D, 3A and B, 7A and B).

The reciprocal plot of $OH^-$ lag period against light intensity was obtained for a group of cells whose chlorophyll concentrations were determined at the conclusion of each experiment (Fig. 6). Higher chlorophyll concentration appeared to correlate with a shorter $OH^-$ lag period and with a lower critical light intensity. Consequently part of the variation between cells may be due to different chlorophyll concentrations.

*Deactivation of primary $OH^-$ bands being maintained by sub-critical light intensities*

Fig. 7A presents the results of an experiment conducted on a cell whose critical illumination value was 0·9 W m$^{-2}$; in Fig. 7B the cell had a critical illumination value of 0·5 W m$^{-2}$. Reduction from 1·3 or 1·1 W m$^{-2}$ to 0·8 W m$^{-2}$ (Fig. 7A) caused the

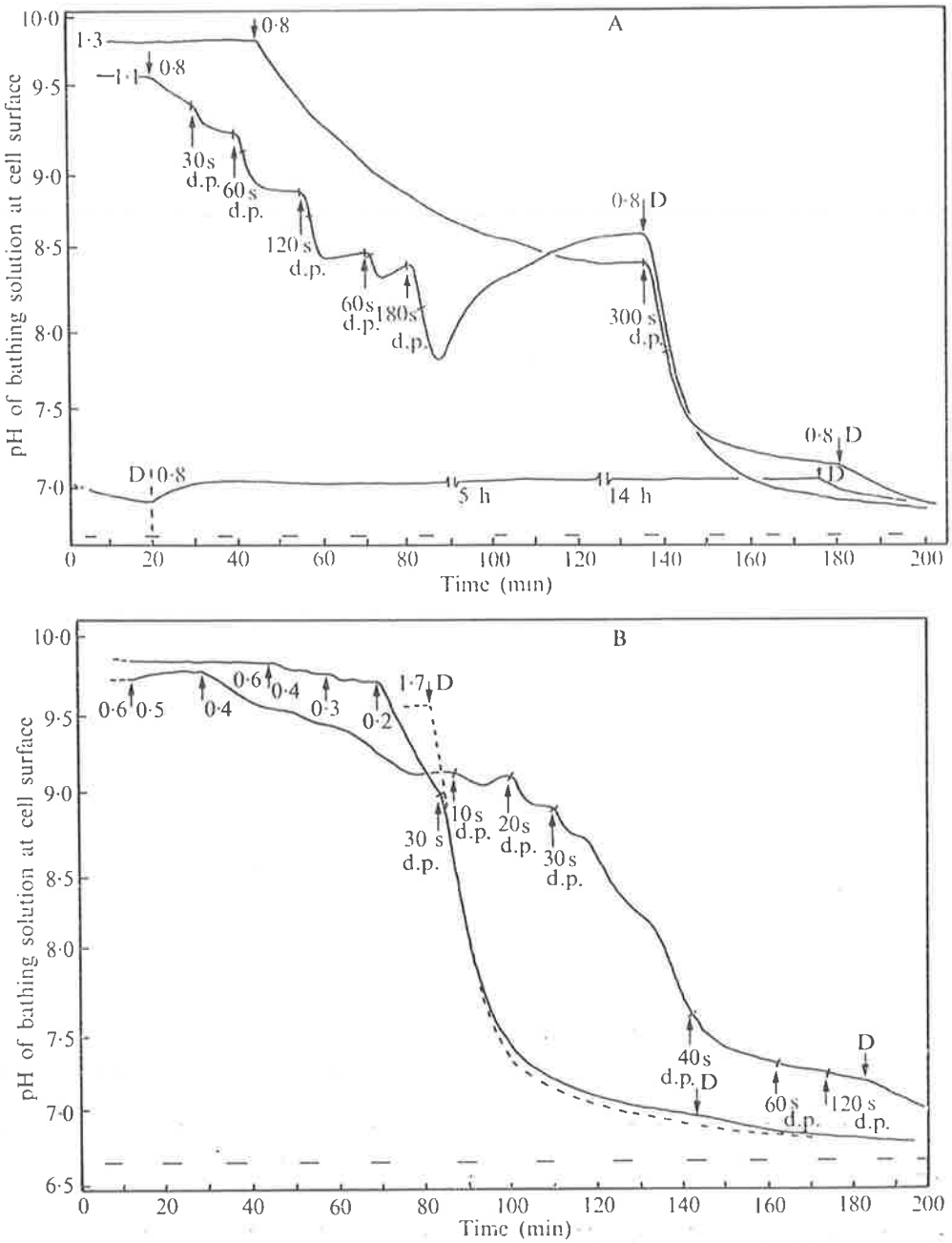


FIG. 7. Deactivation of primary $OH^-$ bands being maintained by sub-critical light intensities. In Fig. 7A and B the critical light intensities were 0·9 and 0·5 W $m^{-2}$ respectively. The primary band was active (at the light intensity indicated on the individual traces) for 1 h prior to the commencement of the experiment. The horizontal broken line represents the pH value of the bathing solution, the broken trace in Fig. 7B is a superimposed response of this primary band to a dark treatment, and 30 s d.p. indicates the application of a 30 s dark period.

primary band to decrease its band-centre pH value. This suggested that at this intensity the rate of photosynthetic $OH^-$ generation was considerably lower than the saturating $OH^-$ efflux rate of this primary band. During the establishment of this new level, dark periods of up to 3 min duration did not cause the band to deactivate, but a 5 min dark period caused almost complete deactivation. However, the band was still operating because complete deactivation was only obtained on transferring the cell to the dark (see Fig. 7A). A similar situation was observed in

Fig. 7B, where two sub-critical intensities were employed (0·2 and 0·4 W $m^{-2}$) and a 0·5 min dark period was sufficient to reduce the activity to a very low level in the case of the 0·4 W $m^{-2}$ intensity and in the presence of 0·2 W $m^{-2}$ the band appeared to deactivate completely.

## DISCUSSION

### *Photosynthetic induction in relation to the $OH^-$ lag period*

Photosynthetic fixation of $CO_2$ often requires an induction period of between 1 and 2 min before a maximum rate, governed by the prevailing conditions, is attained (Osterhout and Haas, 1918; Rabinowitch, 1956; Heber and Willenbrink, 1964; Walker, 1973). A deficiency in the level of ribulose-1,5-diphosphate, at the beginning of a light period, may explain this induction period. Wildner and Criddle (1969), however, suggested that the ribulose-1,5-diphosphate carboxylase requires photoactivation (see also Bassham, 1971). Further evidence of the involvement of light as a requirement for the activation of Calvin cycle enzymes was presented by Pedersen, Kirk, and Bassham (1966) and Buchanan, Kalberer, and Arnon (1967).

Regardless of its actual mechanism, the induction period could account for at least part of the lag period associated with the $OH^-$ bands. Since the induction period does not increase with decreasing light intensity (Walker, 1973) it cannot account for the linear relationship observed in the low light intensity region of Fig. 5. Walker (1973) also demonstrated that an increase in chlorophyll concentration did not result in a shortening of the induction period. This condition did not apply to the $OH^-$ bands (see Fig. 6); it was evident that under identical experimental conditions the cell with a higher chlorophyll concentration had a shorter $OH^-$ lag period.

### *The relationship between cytoplasmic $CO_2$ and $HCO_3^-$ and the $OH^-$ efflux system*

An obvious factor, which would influence the length of the $OH^-$ lag period, is the $CO_2$ level of the cytoplasm. Fig. 8A outlines the equilibria and diffusion and transport processes which would be involved in determining cytoplasmic $CO_2$ values. After the induction phase, when light is non-limiting, the value of $R_5$ will be governed primarily by the concentration of $CO_2$ in the cytoplasm. If the combined rates of $R_1$ and $R_2$ balanced $R_5$, $OH^-$ would not be generated; for this situation there is no requirement for an $OH^-$ efflux system. However, when $R_2 + R_1 < R_5$, a situation which would occur when the bathing solution contained $HCO_3^-$ rather than $CO_2$, fixation of $CO_2$ from the cytoplasmic pool would cause the equilibria (Fig. 8A) to move to the left, with the consequent generation of $OH^-$. The rate of $OH^-$ generation, at a fixed value of $R_2$, will depend on the cellular levels of $HCO_3^-$, and the rate of $CO_2$ fixation, i.e. $OH^-$ generation may be proportional to the level of chlorophyll in the cell at maximum rates of photosynthesis.

If the activation of all $OH^-$ bands required a specific substrate level (e.g. this may be reflected in a particular pH value) this would provide a link between photosynthesis and the observed $OH^-$ lag period. The existence of a critical cytoplasmic substrate (e.g. $OH^-$) level is inferred from the lag periods of $OH^-$ activation greater than required for the induction of photosynthesis (Fig. 3A and B).

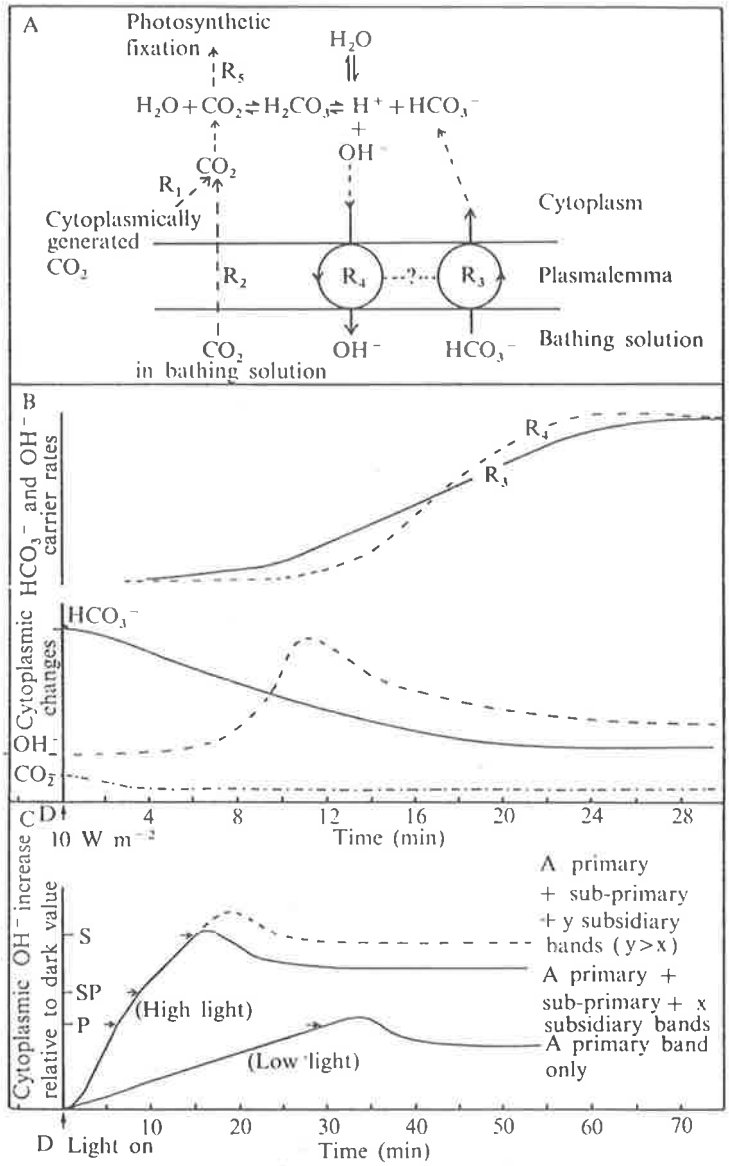


FIG. 8A. Schematic representation of the equilibria, diffusion processes, and carriers associated with the operation of the $OH^-$ and $HCO_3^-$ transport system in *Chara corallina*. $R_1$ is the rate at which $CO_2$ is supplied, *via* respiration and photorespiration, to the cytoplasmic pool of $CO_2$; $R_2$ is the rate of diffusion of $CO_2$ from the bathing solution; $R_3$ is the rate of supply of $HCO_3^-$, *via* a plasmalemma carrier system, from the bathing solution to the cytoplasm; $R_4$ is the rate of $OH^-$ efflux, *via* plasmalemma carriers, from the cytoplasm to the bathing solution. The coupling between $HCO_3^-$ and $OH^-$ carriers is doubtful (see text). $R_4$ is the cumulative result of the operation of several $OH^-$ bands (e.g. a primary, a sub-primary, and several subsidiary bands); $R_3$ is the result of $HCO_3^-$ carriers which are thought to be distributed evenly over the plasmalemma surface. B. Hypothetical responses of cytoplasmic $HCO_3^-$, $CO_2$, and $OH^-$ 'pools' to 10 W $m^{-2}$ illumination and the development of the $HCO_3^-$ and $OH^-$ transport systems in response to this light intensity. In this Figure it is considered that $OH^-_{cytoplasm}$ must reach a critical value prior to activation of the $OH^-$ efflux system. C. Hypothetical responses of cytoplasmic $OH^-$ to illumination using high or low light intensities. In this Figure it is considered that there exist different sets of $OH^-$ carriers, and each set is activated at a specific $OH^-_{cytoplasm}$ level; P, SP, and S represent the levels for the primary, sub-primary, and subsidiary transport systems respectively. (See text, points (1)–(3)).

*Total $OH^-$ efflux activation under high light intensities*

Recent experimental results (Lucas, unpublished results) indicate that the obligatory $HCO_3^-/OH^-$ transport system, as considered by Lucas and Smith (1973), may not occur. For this reason, the coupling between the $HCO_3^-$ and $OH^-$ transport systems in the plasmalemma, is represented by a question-mark (Fig. 8A). The relationship between $HCO_3^-$ influx and $OH^-$ efflux activation may depend upon the internal level of $HCO_3^-$ relative to the buffering capacity of the cytoplasm. Regarding this relationship, it is obvious that the $HCO_3^-$ transport system could not operate at high rates, before the $OH^-$ transport system is activated, because large membrane potentials would be generated. (The steady-state rate of $R_4$ will be assumed to be dependent upon $R_3$.)

To activate the total cell $OH^-$ system (i.e. all $OH^-$ bands) the following sequence may occur: $R_5 > R_1 + R_2$ results in a lowering of $[HCO_3^-]_{cytoplasm}$ and this increases $[OH^-]_{cytoplasm}$, $R_3$ operates because of the reduction in $[HCO_3^-]_{cytoplasm}$, and when $[OH^-]_{cytoplasm}$ reaches a critical level $R_4$ is activated allowing $R_3$ to increase; in the steady-state, $R_4$ will equal $R_3$. A hypothetical representation of this sequence is demonstrated in Fig. 8B.

A comment is necessary concerning the initial pH rise, which is observed along the entire cell surface, when the cell is first illuminated (see Figs. 1, 2D, 3A and B). This change in pH may be due to the removal of $CO_2$ (*via* $R_2$) from the solution. It is also possible that the $OH^-$ system can operate at a very low rate even before the critical activating condition is established. Evidence which supports the latter possibility is obtained from prolonged sub-critical illumination (see Fig. 2D) and from deactivation of the subsidiary bands by reducing the light intensity (see Fig. 4 and Fig. 5A and B).

*The primary, sub-primary, and subsidiary band hypothesis*

In the previous section a sequence was proposed to account for the activation of the $OH^-$ system. It is proposed that the following properties and conditions operate within the total cell $OH^-$ system:

(1) There exists a set of $OH^-$ carriers (one band) whose critical activation level is lower than that of all the other carriers. These carriers have a greater affinity for $OH^-$ than the other carriers; i.e. the Michaelis-Menten $K_m$ is much lower for this set of carriers.

This set of carriers constitutes what has been termed a *primary* $OH^-$ band.

(2) A second set of carriers exists which has a slightly higher activation level and whose affinity for $OH^-$ is slightly lower than (1), i.e. the $K_m$ for this system is greater than that proposed for (1). This constitutes a *sub-primary* $OH^-$ band.

(3) Numerous sets of carriers exist which have activation levels > (1) and (2) and similarly have lower affinities for $OH^-$ and higher $K_m$ values. These would be *subsidary* $OH^-$ bands. There are considered to exist, in the plasmalemma, particular functional groups which impart, to the $OH^-$ carriers, this observed

range of affinities, activation levels, etc. A hypothetical sequence, using these properties, is demonstrated in Fig. 8C, and may explain the results observed in Fig. 2 and Fig. 3.

*Subsidiary band deactivation as light intensity is reduced*

Fig. 4 demonstrates that, for a particular subsidiary band, there exists a light intensity below which its activity is reduced before finally becoming inactive. This suggests that not only is there a critical activation level of substrate, but that there is also a substrate level at which this band deactivates. Loss of activity of this subsidiary band would result in a slight rise in substrate level and the operational primary and sub-primary systems would respond by slightly increasing their rates (see Fig. 3A and B).

Under conditions where light is limiting, the critical activation level of the primary band may be reached and the steady-state efflux rate of this band may be such that it maintains the cytoplasmic 'pool' below the sub-primary critical level. Hence, at this light and $[HCO_3^-]_{\text{bathing solution}}$ level only one band would operate. The critical light intensity can now be defined as the intensity which would cause the cell to take an infinite time to raise the cytoplasmic substrate ($OH^-$) to the critical level of the primary $OH^-$ system.

Sub-critical illumination following dark treatment, appeared to modify the substrate ($OH^-$) system because on the subsequent application of higher intensities a much longer $OH^-$ lag period than expected was observed. Fig. 3A indicated that for an intensity of 0·8 W $m^{-2}$ the primary $OH^-$ lag period was 56·5 min; however after 200 min of sub-critical illumination (0·6 W $m^{-2}$) the increase in light intensity to 0·8 W $m^{-2}$ did not result in primary $OH^-$ band activation even after 100 min. This low-light regime may result in different photosynthetic products which may change the buffering capacity of the cytoplasm.

*Further evidence for critical activating and deactivating substrate levels*

Strong support is obtained, for the existence of a critical activation level, from the results which show that the primary $OH^-$ band, once activated, can be maintained in an active form, in the presence of sub-critical light intensities.

The deactivation of the subsidiary bands has already been dealt with; however a similar situation appears to exist for the primary band. When a dark period was given (see Fig. 5A and B) it had to be of a certain duration before it caused band deactivation. In the initial phase of the dark period, it is possible that $CO_2$ was still being fixed (see Gaffron and Fager, 1951; and Togasaki and Gibbs, 1967); $t_{1/2}$ for this fixation could vary from 15 to 120 s. Hence the deactivating period would be determined by the amount of dark fixation as well as the amount by which the $OH^-$ level had to be reduced for it to fall below the deactivating value. It is considered that the reduction of $[OH^-]$ during this dark period occurs primarily by $HCO_3^-$ formation *via* $R_1$ and $R_2$. Deactivation would not be due to a re-introduction of a photosynthetic induction lag (Walker, 1973). It therefore seems that a further property must be added to points (1)–(3) to complete the characterization of the total $OH^-$ efflux system. The final point is:

(4) Each specific $OH^-$ carrier system has a critical level of substrate, which will result in deactivation. The levels being in the order, subsidiary > sub-primary > the primary system.

*$HCO_3^-$ and $OH^-$ transport systems and their energy requirement*

It is difficult to demonstrate categorically that these systems require an energy-dependent reaction during the transport of $HCO_3^-$ into and $OH^-$ out of the cell. The rates at which they operate (maximum value of 50–60 pmol $cm^{-2}$ $s^{-1}$; Lucas, 1975*b*) suggest that $HCO_3^-$ transport would be an energy-dependent process. For the $HCO_3^-$ system to operate as a facilitated diffusion system the internal $HCO_3^-$ level would have to be extremely low. The situation which would favour facilitated $OH^-$ transport would be high cytoplasmic $OH^-$ levels and low concentrations in the bathing solution. This situation is not observed, for the $OH^-$ ions are transported over a small area of the plasmalemma (see Lucas, 1975*a*) and the pH in the band centre can be as high as 10·3.

If photosynthetic energy is required for both processes, part of the $OH^-$ lag period could be due to the time required for the production of this energy substrate within the chloroplasts and its diffusion to the plasmalemma. Hence, it is possible that the critical cytoplasmic substrate discussed previously is a complex system involving energy and $OH^-$ levels.

*Electrical properties of the plasmalemma*

The proposed $OH^-$ and $HCO_3^-$ transport systems would certainly produce membrane potential fluctuations during their activation stages. If the $HCO_3^-$ system activated before the $OH^-$ efflux system the membrane would become more negative (hyperpolarize) at a rate governed by the imbalance of the two transport systems. This hyperpolarization is likely to be transient because the $OH^-$ efflux, once activated, may exceed $HCO_3^-$ influx for a short period thus reducing the previously established imbalance of negative charge.

The main effect of the proposed system would be on the resistance of the membrane. If the cell is supplied with $HCO_3^-$ and it has the capacity to utilize this substrate the membrane resistance should decrease significantly. In the presence of $CO_2$ no such resistance change would occur since the $HCO_3^-$ and $OH^-$ systems should not operate. Walker (1962) reported a light-induced decrease in *Chara corallina* plasmalemma resistance at high pH; the response had an action spectrum suggesting the involvement of chlorophyll. Hope (1965), Nishizaki (1968), and Spanswick (1972) have also reported light-mediated resistance decreases at high pH. Therefore, the explanation of these light-mediated resistance changes, at high pH, may be due to the $OH^-$ and $HCO_3^-$ transport as discussed above.

ACKNOWLEDGEMENTS

I wish to thank the Department of Physics, University of Adelaide, for its generous donation of the nickel-nicron neutral density filters. Thanks are also due to Dr. J. T. Wiskich, F. A. Smith and Mr. D. A. Day for critical readings of the manuscript.

## LITERATURE CITED

ARNON, D. I., 1949. *Pl. Physiol., Lancaster*, **24**, 1–15.
BASSHAM, J. A., 1971. *Science, N.Y.* **172**, 526–34.
BUCHANAN, B. B., KALBERER, P. P., and ARNON, D. I., 1967. *Biochem. biophys. Res. Commun.* **29**, 74–9.
GAFFRON, H., and FAGER, E. W., 1951. *A. Rev. Pl. Physiol.* **2**, 87–114.
HEBER, U., and WILLENBRINK, J., 1964. *Biochim. biophys. Acta*, **82**, 313–24.
HOPE, A. B., 1965. *Aust. J. biol. Sci.* **18**, 789–801.
LUCAS, W. J., 1975*a*. *J. exp. Bot.* **26**, 271–86.
——, 1975*b*. *J. exp. Bot.* **26**, 331–46.
—— and SMITH, F. A., 1973. Ibid. **24**, 1–14.
NISHIZAKI, Y., 1968. *Pl. Cell. Physiol., Tokyo*, **9**, 377–87.
OSTERHOUT, W. J. V., and HAAS, A. R. C., 1918. *J. gen. Physiol.* **1**, 1–16.
PEDERSEN, T. A., KIRK, M., and BASSHAM, J. A., 1966. *Physiologia Pl.* **19**, 219–31.
RABINOWITCH, E. I., 1956. *Photosynthesis and regulated processes*. Interscience, New York. Vol. II, Pt 2, p. 1313.
SPANSWICK, R. M., 1972. *Biochim. biophys. Acta*, **288**, 73–89.
TOGASAKI, R. K., and GIBBS, M., 1967. *Pl. Physiol., Lancaster*, **42**, 991–6.
WALKER, D. A., 1973. *New Phytol.* **72**, 209–35.
WALKER, N. A., 1962. *A. Rept. Div. Pl. Ind. C.S.I.R.O.* P. 80.
WILDNER, G. F., and CRIDDLE, R. S., 1969. *Biochem. biophys. Res. Commun.* **37**, 952–60.

*Journal of Experimental Botany, Vol. 27, No. 96, pp. 19–31, February 1976*

# Plasmalemma Transport of $HCO_3^-$ and $OH^-$ in *Chara corallina*: Non-antiporter Systems

W. J. LUCAS

*Department of Botany, University of Toronto, Toronto, M5S 1A1, Ontario, Canada*

Received 3 August 1975

## ABSTRACT

An experimental system was designed to test the obligate coupling between $HCO_3^-$ and $OH^-$ fluxes (i.e. a 'Mitchell-type' antiporter) proposed by Lucas and Smith (1973). The results of these experiments demonstrated categorically that the $OH^-$ efflux process can function in the absence of exogenous $HCO_3^-$ at the actual $OH^-$ efflux site. Hence, the obligate coupling hypothesis is invalid. It is proposed that $HCO_3^-$ and $OH^-$ are transported across the plasmalemma 'independently', on quite distinct carriers. It is possible, therefore, that these fluxes contribute towards determining the electrical properties of this membrane when the bathing solution pH value is $\geqslant 6{\cdot}5$. It was also found that $HCO_3^-$ can be transported across the dark segment of a partly illuminated cell. The observed rates were always much less than those obtained in the illuminated cell segment. The significance of this result is discussed.

## INTRODUCTION

It has been suggested that the $HCO_3^-$ influx and $OH^-$ efflux, across the plasmalemma of *Chara corallina*, is mediated *via* a 'Mitchell-type' antiporter (see Lucas and Smith, 1973). However, as stressed by Lucas (1975*c*), experimental support for this hypothesis is still lacking. It is important that this obligate coupled non-electrogenic antiporter hypothesis be tested, since if it is valid the $HCO_3^-/OH^-$ system could not contribute either to the membrane conductance or potential. In contrast, invalidation would suggest that these very active $HCO_3^-$ and $OH^-$ transport systems (Lucas, 1975*a*,*b*) may contribute to the electrical properties of the plasmalemma (see Lucas, 1975*c*).

This paper investigates the relationship between the influx of $HCO_3^-$ and the efflux of $OH^-$ in the internodal cells of *Chara corallina*.

## MATERIALS AND METHODS

The measurement of pH along the cell wall of *Chara corallina*, and the procedure involved in measuring the response of an alkaline band to illumination, have been previously reported (Lucas and Smith, 1973; Lucas, 1975*a*). Cells were grown in the laboratory under artificial light and experimental cells were pre-treated for 6 h in a bathing solution containing 10 mM 2-(*N*-morpholino)ethanesulphonic acid, pH 5·0, to remove $CaCO_3$ deposits. (Normal bathing solutions contained 1·0 mM NaCl, 0·2 mM KCl, and 0·5 mM $CaSO_4$ unless otherwise specified.)

The experimental apparatus used to isolate an operational primary $OH^-$ band (see Lucas, 1975*c*) is shown in Fig. 1. It consisted basically of two clear[1] perspex blocks. The bottom of the smaller, movable block was machined so that it seated, with precision, into the channel of the basal block (see Fig. 1c). A cylindrical chamber, diam. 6 mm, was cut through this movable block such that it centred over the smaller channel of the basal block. Two stainless steel tubes were set into the smaller block; these acted as inlet and outlet tubes for the experimental solutions. An adjustable volume Manostat Mini-Pet syringe system was used to inject solutions into the isolating chamber. The expelled solutions were drawn off using a vacuum line connected to the outlet tube. Screw clips were employed on the inlet and outlet tubes to seal the system, thereby preventing movement of solutions during an experimental sequence.

The experimental procedure, employed during the use of this isolating chamber, was as follows:

(i) A *Chara* cell was investigated (under a light intensity of 10 W $m^{-2}$) using the agar block technique described by Lucas and Smith (1973) and Lucas (1975*c*). From this pH scan, the exact location of each $OH^-$ band, on the cell surface, was determined. At the conclusion of this mapping sequence, the light intensity was decreased in a stepwise manner until an intensity was reached at which only the primary $OH^-$ band remained operational. (All experiments reported in this paper were conducted on the primary $OH^-$ band of the cell under investigation.)

(ii) The *Chara* cell was removed from the agar block and the cell wall was dried in the region surrounding the primary $OH^-$ band. A small quantity of silicon grease was injected into the small channel at a distance of 5 mm on either side of the site at which the $OH^-$ band was to be centred. The cell was then placed into this small channel such that the primary $OH^-$ band was located centrally between the two greased regions.

(iii) The entire lower surface of the small movable block was covered with a uniform layer of silicon grease prior to the performance of (ii). This enabled the small block to be quickly sealed into place over the top of the $OH^-$ band. The unit was then transferred to a thermostatted (25 °C) experimental chamber (see Lucas and Smith, 1973).

(iv) The bathing solution level, in the experimental chamber, was adjusted so that it was just below the outlet tube. The same experimental bathing solution was injected into the isolating chamber.

(v) Using a micromanipulator (see Lucas, 1975*a*), an experimental pH electrode was lowered into the isolating chamber until the pH tip was located approx. 3–4 mm directly above the cell wall. At this stage an agar bridge was lowered into the isolating chamber (see Fig. 1B). (This agar bridge was necessary to complete the electrical circuit between the solution in the isolating chamber and the calomel reference electrode in the outer solution.) Thirty min was allowed (under 10 W $m^{-2}$) for the cell to recover from the isolating process.

(vi) Following the recovery period, the pH electrode was lowered onto the cell wall; the $OH^-$ band centre was then located. The system was then ready for experimentation.

For some experiments a $CO_2$-free form of the standard bathing solution was required. This was obtained by scrubbing the solution with air from which $CO_2$ had been removed by pumping it through two Drechsel bottles (sintered dome pore size 40–60 $\mu$m) which contained freshly prepared 10 M NaOH solution. The glass scrubbing vessel was gas-tight except for the entrance and exit sites for the $CO_2$-free air. A 250 ml volume of bathing solution was scrubbed by $CO_2$-free air, flowing at 0·6 l $min^{-1}$, through a sintered glass bubbler (pore size 40–60 $\mu$m); the solution was stirred continuously *via* a 'magnetic flea' system. The pH value was monitored and it was found that at least 1 h was required before the pH of the solution rose from 5·7 to 7·0 ($\pm$0·05). As an added precaution, all $CO_2$-free solutions were scrubbed for 2 h before being employed in an experimental sequence.

## RESULTS

The obligate coupling of the $HCO_3^-/OH^-$ transport system proposed by Lucas and Smith (1973) was tested by isolating the cell's primary $OH^-$ band within a special

[1] All surfaces of these perspex blocks were highly polished so that, when the apparatus was immersed in the experimental solution, very little light was prevented from reaching the cell surface.

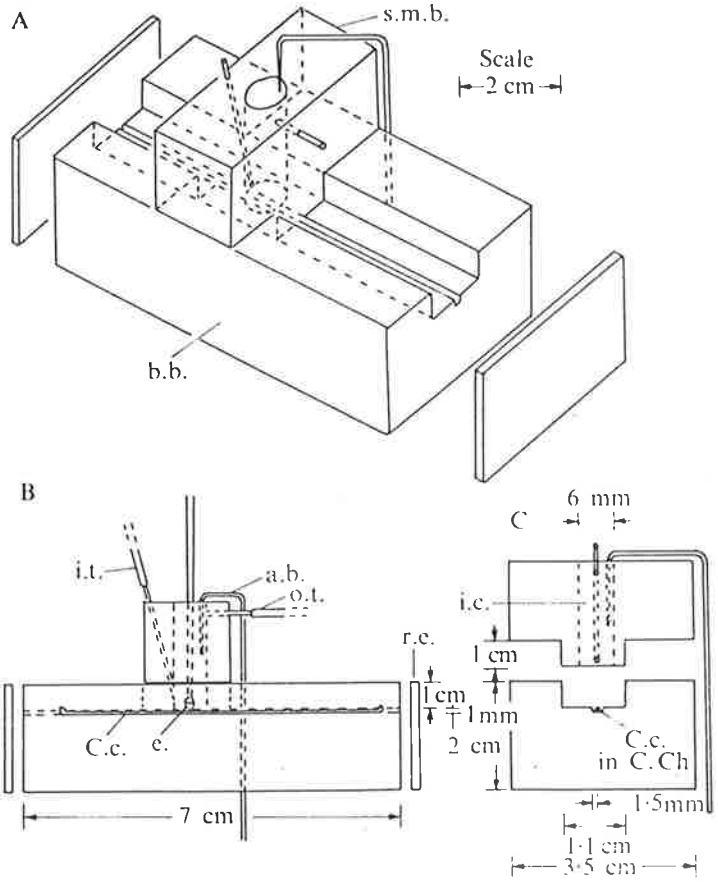


FIG. 1. Apparatus for isolating *Chara* cell segments. This apparatus was used to isolate, from the rest of the bathing solution, an external segment of a cell which contained an operational $OH^-$ band. Abbreviations are as follows: agar bridge, a.b.; basal block, b.b.; *Chara* cell, C.c.; *Chara* cell located in the central channel, C.c. in C. Ch.; pH electrode, e.; isolating chamber, i.c.; inlet tube, i.t.; outlet tube, o.t.; removable end, r.e.; small movable block, s.m.b.

experimental chamber (see Fig. 1). (The primary $OH^-$ band was selected since it would always be the last $OH^-$ efflux site to deactivate (Lucas, 1975*c*).) On the basis of the above hypothesis, cessation of $OH^-$ efflux would be expected when the isolating chamber was flushed with a solution 'totally' free of inorganic carbon (this solution will be called $CO_2$-free). A typical result obtained under such an experimental situation is presented in Fig. 2. (The syringe–flushing system changed the solution within the isolating chamber four times a minute, and the normal period of flushing was 5 min. At the end of each flushing sequence the surface of the isolating chamber was resealed, to a depth of 6 mm, with liquid paraffin.)

Figure 2 shows that removing $HCO_3^-$ from the isolated $OH^-$ band had little or no effect on its efflux activity, i.e. the increase in alkaline band centre pH value, following the flushing sequence, followed the same time course irrespective of whether $CO_2$-free or 0·2 mM $NaHCO_3$ solutions were employed. This efflux activity could be maintained over prolonged periods of time, provided the outer cell segment was in contact with exogenous $HCO_3^-$. When the outer cell segment was immersed in liquid paraffin (following irrigation with $CO_2$-free solution) the $OH^-$ activity was immediately influenced and the primary band eventually deactivated (see Fig. 2).

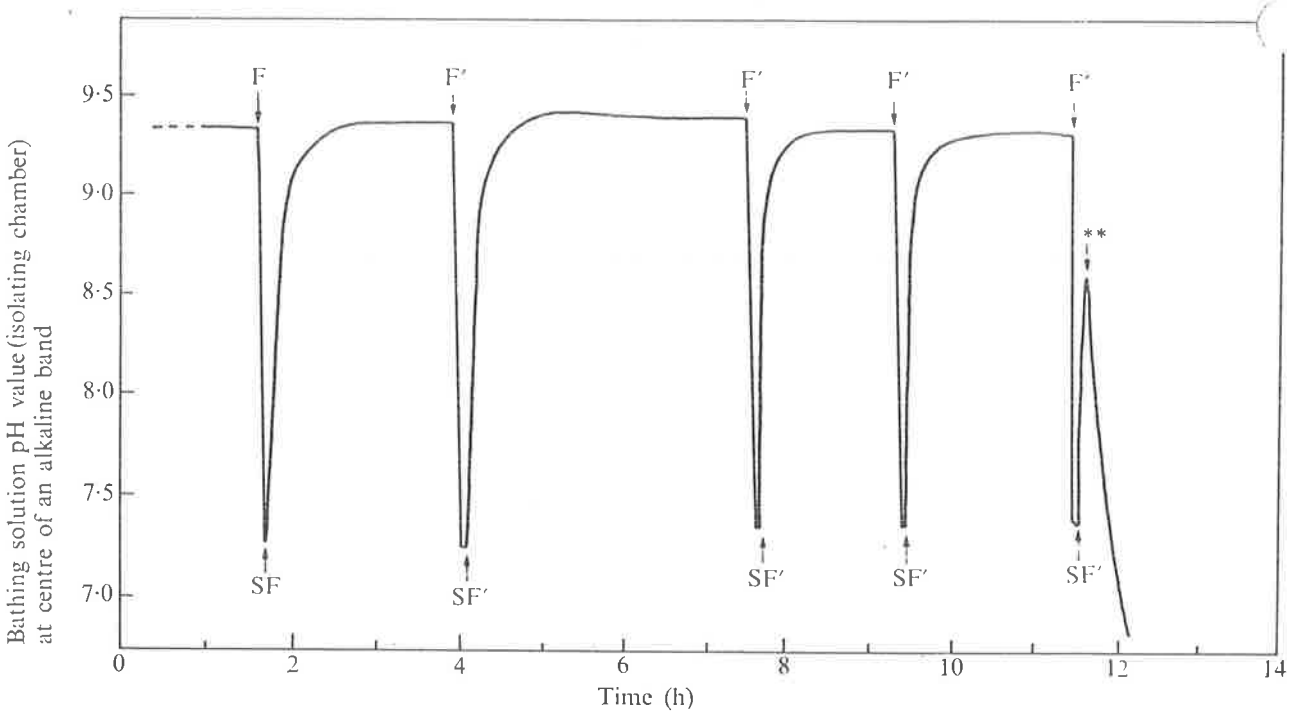


FIG. 2. Hydroxyl band activity in the presence of $CO_2$-free bathing solution. A primary $OH^-$ band was located in the isolating chamber (see Fig. 1) and the chamber flushed with normal solution containing 0·2 mM $NaHCO_3$ (F) or $CO_2$-free solution (F′). The symbols SF and SF′ indicate when the flushing with the $NaHCO_3$ and $CO_2$-free solution, respectively, was stopped; ** indicates when the outer cell segment was sealed in liquid paraffin after irrigation with $CO_2$-free solution.

It was considered that a result of this nature demonstrates that the $OH^-$ transport system can operate in the absence of exogenous $HCO_3^-$ at the actual effluxing site.

When the liquid paraffin seal in the outer chamber was replaced by a bathing solution which contained 0·2 mM $NaHCO_3$, the primary $OH^-$ band was re-established (Fig. 3). (The results presented in Fig. 3 form a continuation of the experimental sequence illustrated in Fig. 2.) To ensure that deactivation of $OH^-$ efflux was not caused by the effect of liquid paraffin *per se* the reverse experimental sequence was investigated. Figure 4 shows that sealing the outer cell segment in liquid paraffin, whilst the inner chamber still contained $HCO_3^-$, did not result in deactivation of the isolated $OH^-$ band. The resultant decrease in the alkaline band centre pH value is a reflection of the reduction in available $HCO_3^-$ to the photosynthetic system. (A similar reduction, under equivalent conditions, is shown in Fig. 3.) However, as soon as the $HCO_3^-$ within the isolating chamber was replaced by a $CO_2$-free solution, the $OH^-$ efflux activity was affected. Immediate deactivation did not occur; rather a gradual decline in $OH^-$ efflux activity was observed which suggested that the $OH^-$ system was operating on a cytoplasmic 'pool' (see also Lucas, 1975*c*). Figure 4 also shows that, when the $OH^-$ efflux system became inactive, the influence of the net $H^+$ efflux system could be discerned, i.e. the $OH^-$ and $H^+$ systems derive from entirely different cellular processes (cf. Spear, Barr, and Barr, 1969).

The relationship between the deactivation of the $OH^-$ efflux site and the pH value of the cell surface within the isolating chamber was obtained to ensure that the

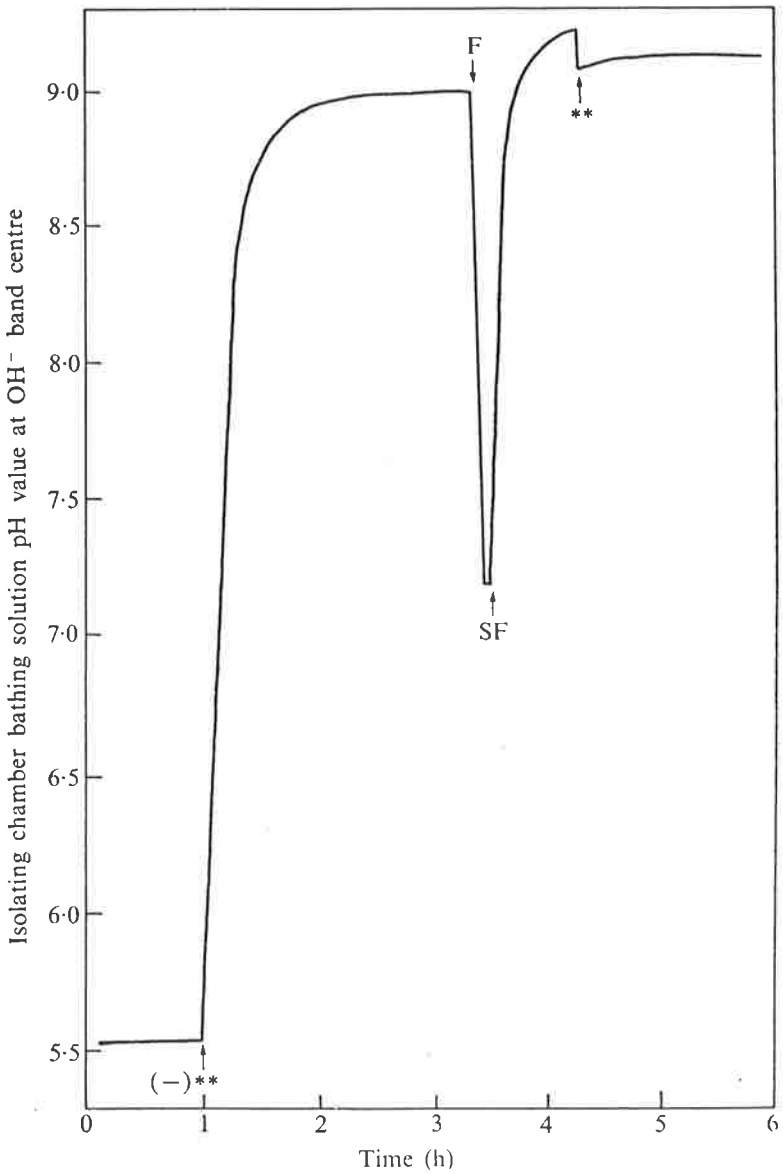


FIG. 3. Reactivation of the isolated primary $OH^-$ band. This trace is a continuation of the results presented in Fig. 2. The symbol (−)** indicates the removal of the liquid paraffin seal from the outer cell segment and replacement by bathing solution containing 0·2 mM $NaHCO_3$; other symbols as in Fig. 2.

actual $OH^-$ band centre remained stationary during the deactivation process. A typical result is presented in Fig. 5, and it is clear that the decrease in band centre pH value did not result as a consequence of migration of the alkaline band centre. This figure also shows that the initial decline in $OH^-$ efflux activity, which resulted when the outer cell segment was immersed in liquid paraffin, was similar in form to that obtained by transferring the cell from light to dark.

*Influence of* 0·2 *mM* $CO_2$ (*pH* 5·0)

The influence of 0·2 mM $CO_2$ (pH 5·0), in the outer chamber bathing solution, on the activity of the primary $OH^-$ system was investigated to determine whether

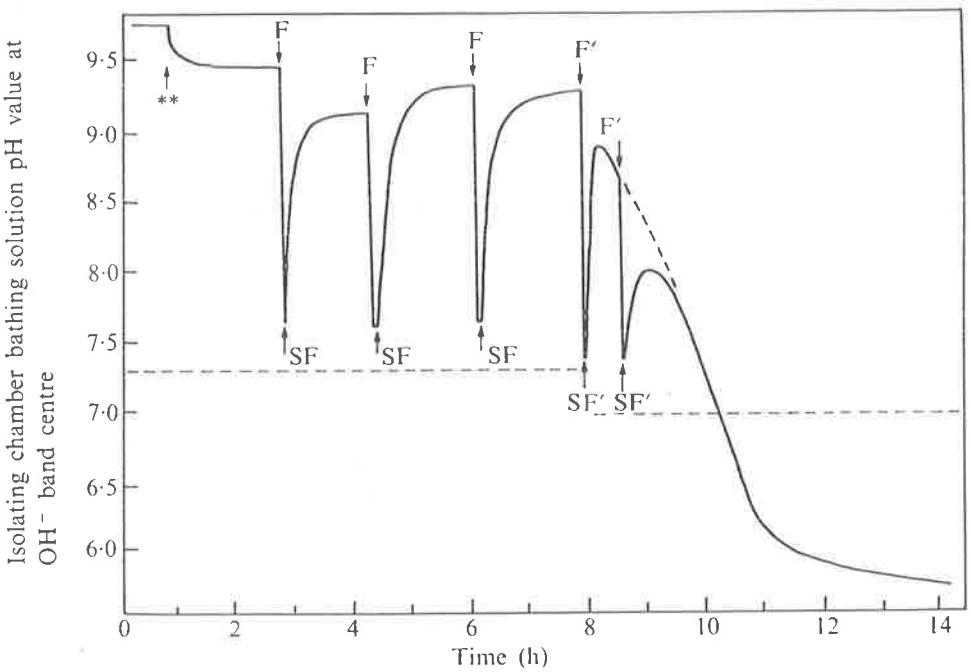


FIG. 4. Hydroxyl band activity in the presence of $CO_2$-free bathing solution. The sequence was reversed in this experiment, i.e. the outer cell segment was sealed in liquid paraffin (**) before the isolating chamber was flushed with $CO_2$-free solution (F′). The symbols are as in Fig. 2, and the horizontal broken line represents the background pH value within the isolating chamber.

$OH^-$ efflux would cease when the isolating chamber was flushed with $CO_2$-free solution. It was found (see Fig. 6) that exogenous $CO_2$, in the outer bathing solution, could not maintain the activity of the isolated $OH^-$ efflux system. During these particular experiments the solutions in the outer chamber also contained 0·1 mM phenol red (an acid/base indicator, see Spear *et al.*, 1969). In this way it was possible to ascertain whether $OH^-$ efflux bands were present on the outer cell segment; it was found that no alkaline bands developed when 0·2 mM $CO_2$ (pH 5·0) was employed.

*Transfer of $OH^-$ efflux function*

The influence, on the isolated $OH^-$ efflux activity, of transferring the outer cell segment to the dark was also examined. For this series of experiments the cells were placed in the apparatus in such a way that approx. half the cell surface was projecting into the outer chamber; the other half was sealed within the isolating chamber system. Darkening of the outer cell segment was achieved by slipping a black polythene sleeve (filled with outer chamber solution) over this half of the cell. The type of response recorded when the outer cell segment was darkened and re-illuminated in this manner is shown in Fig. 7. Re-illumination of the darkened cell surface caused a decline in the primary $OH^-$ peak height. This was interpreted as resulting from reactivation of $OH^-$ efflux sites located on the outer cell segment, and the subsequent transfer of $OH^-$ efflux function to these particular sites. This interpretation was supported by the primary band response to darkening and re-illuminating the outer cell segment when the outer bathing solution contained 0·2 mM $CO_2$ (pH 5·0).

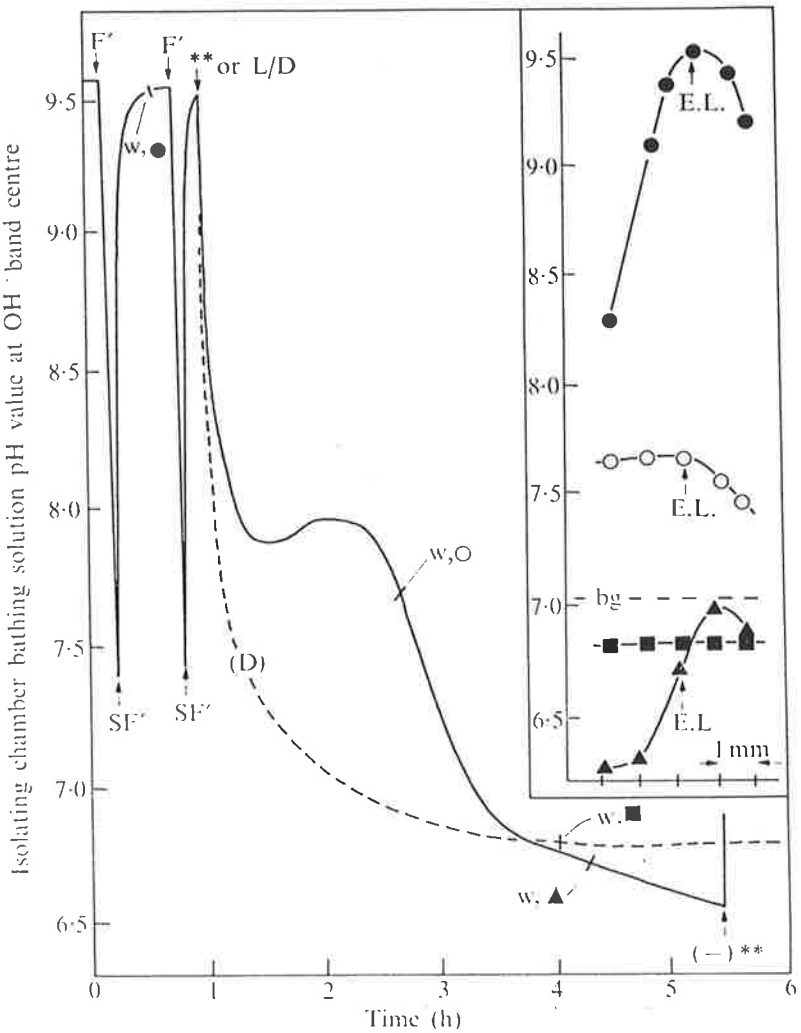


FIG. 5. Relationship between $OH^-$ band deactivation and the pH values of the cell segment within the isolating chamber. Both chambers contained 0·2 mM $NaHCO_3$ for 30 min prior to the first F′, at the indicated points the cell wall within the isolating chamber was scanned, and the pH values recorded; namely w, ●; w, ○; w, ▲; and w, ■; the latter being conducted during the dark response (D). Symbols as in Figs 2 and 3, except the E.L. represents the electrode location during the experiment, and L/D indicates the transfer of the cell from 10 W $m^{-2}$ to the dark. The background value of the $CO_2$-free solution in the isolating chamber is represented by bg.

A slight drop (cf. the previously recorded increase) in the steady-state peak height, when the cell was darkened, implied that the chloroplasts in the outer segment were fixing a small component of the $HCO_3^-$ being influxed from the solution within the isolating chamber. (It should be remembered that 0·2 mM $CO_2$, pH 5·0, will not supply $OH^-$ to the isolated $OH^-$ band.)

Figure 8 illustrates the response observed when the above sequence was repeated using firstly 0·2 mM $NaHCO_3$ within the isolating chamber, and then $CO_2$-free solutions; the outer chamber contained 0·2 mM $NaHCO_3$ throughout. Figure 8A indicates that $OH^-$ efflux activity remained when the outer cell segment was darkened and the inner chamber contained $CO_2$-free solutions. Had the continued $OH^-$ efflux been due to a cytoplasmic 'pool' of $OH^-$ (or $HCO_3^-$), the peak height would have decayed within 1–2 h (cf. Figs 4, 5, and 6). Over a prolonged dark period (outer

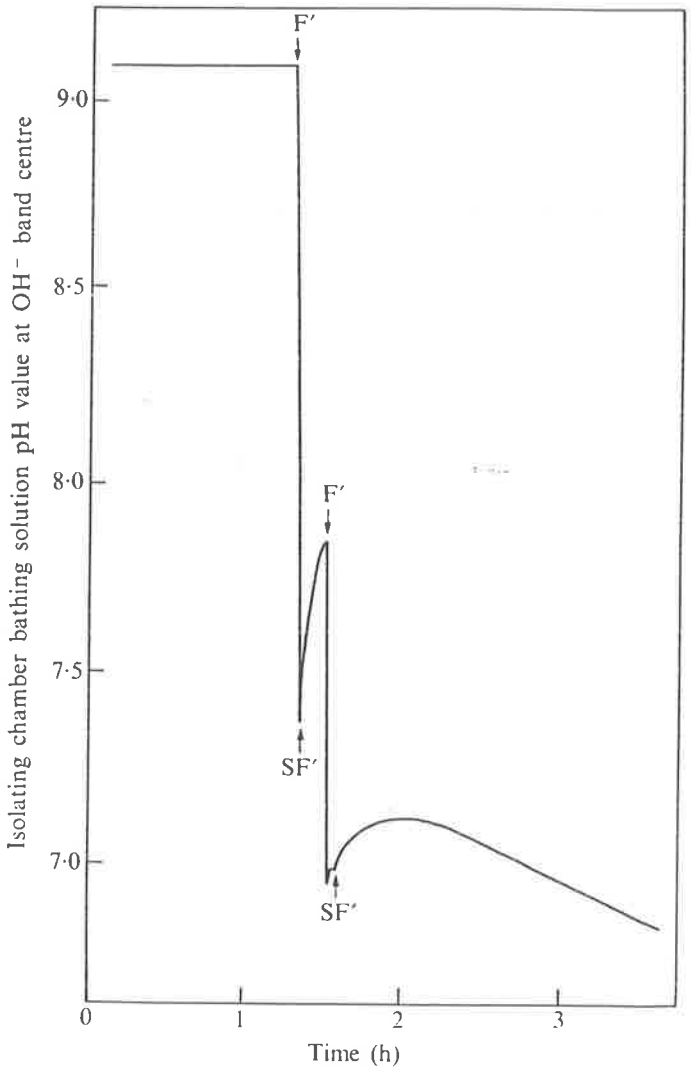


FIG. 6. Influence of $CO_2$ in the outer chamber. The cell was treated with 0·2 mM $CO_2$, pH 5·0, in the outer chamber and a solution containing 0·2 mM $NaHCO_3$ in the isolating chamber for 1½ h prior to flushing the inner chamber with $CO_2$-free solution. The outer chamber contained 0·2 mM $CO_2$, pH 5·0, for the entire experiment.

cell segment only) a fall in $OH^-$ peak height to a new steady state was observed (see Fig. 8A), but it should be stressed that activity was retained. This suggested that $HCO_3^-$ could be supplied *via* the dark cell segment. However, almost immediately the entire cell surface was darkened, the primary $OH^-$ site deactivated (Fig. 8B).

An accurate estimate of the actual $OH^-$ efflux through the primary $OH^-$ band, under these prolonged dark periods to the outer cell segment, could not be obtained because the cell was resting directly on the perspex. Hence, the $OH^-$ effluxed over the band surface which was in contact with the perspex would be reflected back over the cell, in order for it to diffuse into the bathing solution of the isolating chamber. However, based on knowledge gained during diffusion analysis experiments (Lucas, 1975*a*), it was considered that the steady-state $OH^-$ efflux associated with Fig. 8A would be of the order of 0·6 pmol $s^{-1}$. Assuming that this was the only active $OH^-$ efflux site, the $HCO_3^-$ influx across the darkened cell surface could have been 0·75 pmol $cm^{-2}$ $s^{-1}$ for this particular cell (surface area in the outer chamber

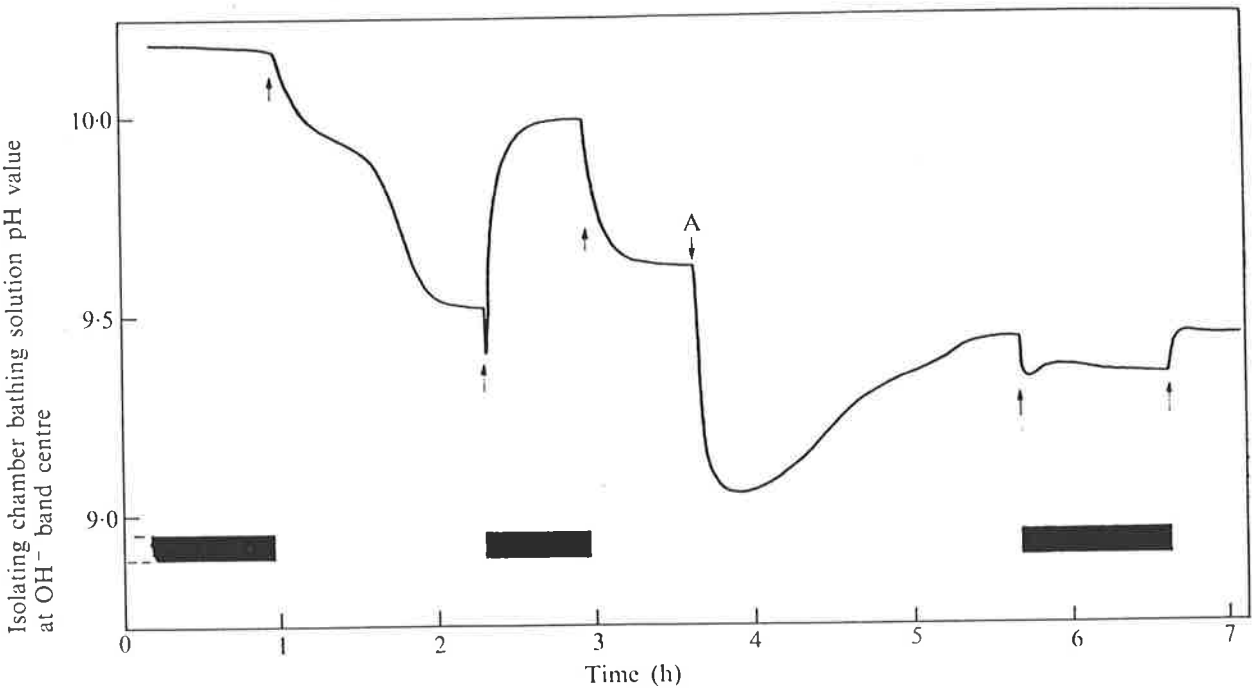


FIG. 7. Dark treatments on the outer cell segment and their influence on the $OH^-$ efflux activity within the isolating chamber. Both chambers contained 0·2 mM $NaHCO_3$ solutions initially, and the outer chamber was changed to 0·2 mM $CO_2$, pH 5·0, at A. The dark bars and arrows indicate dark treatments applied to the outer chamber only (see text for full details).

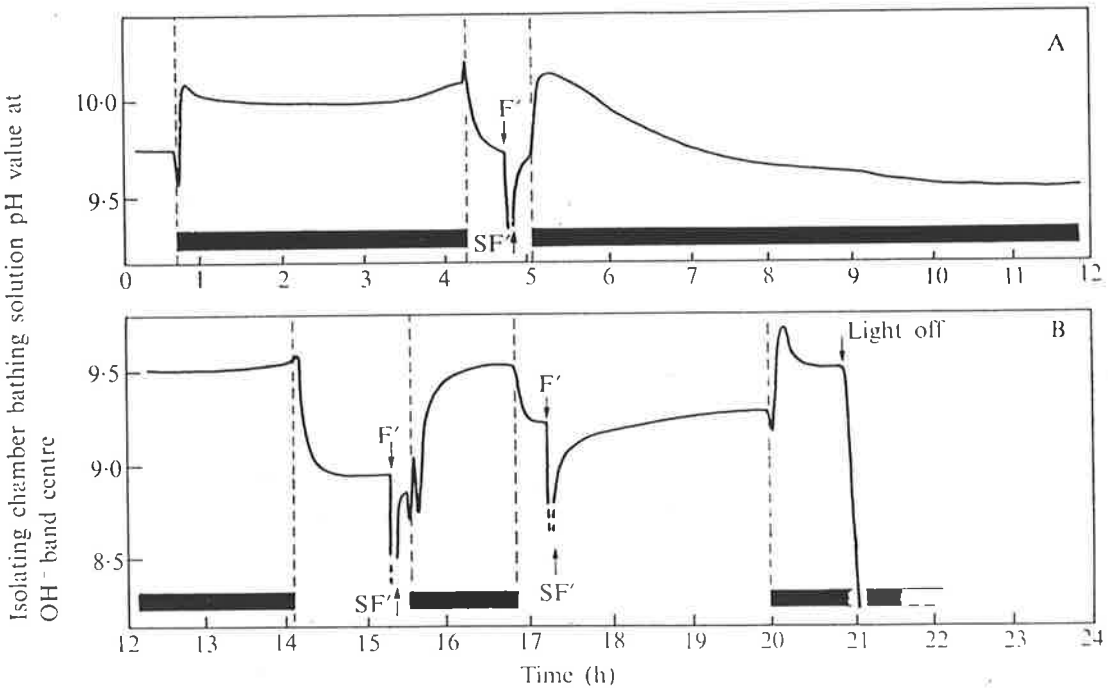


FIG. 8. Dark treatments on the outer cell segment and their influence on the $OH^-$ efflux activity within the isolating chamber. The outer chamber contained a 0·2 mM $NaHCO_3$ bathing solution throughout, and the inner chamber the same until it was flushed with $CO_2$-free solution. Figure 8B is a continuation of A; the experimental features are as described in Fig. 7.

TABLE 1. *Investigation of $H^{14}CO_3^-$ influx using a cell-partitioning apparatus*

| Tank | Expt. No. | Experimental conditions | | | | | $H^{14}CO_3^-$ influx (pmol $cm^{-2}$ $s^{-1}$) | | |
|---|---|---|---|---|---|---|---|---|---|
| | | Chamber A | | Chamber B | | Duration of pre-treatment (h) | Based on partitioned cell surface area exposed to radioisotope | | Control[a] cells |
| | | Solution | Treatment | Solution | Treatment | | Chamber A | Chamber B | |
| E′ | 1 | $NaH^{14}CO_3$[c] | L[b] | $NaH^{14}CO_3$ | L | 2 | 32·9 ± 1·7 | 33·0 ± 2·1 | 38·2 ± 3·1 |
| E′ | 2 | $NaH^{14}CO_3$ | L | BS[d] | D[b] | 2 | 32·2 ± 2·1 | — | 33·7 ± 0·5 |
| E′ | 3 | BS | L | $NaH^{14}CO_3$ | D | 2 | — | 0·50 ± 0·07 | 0·11 ± 0·01 |
| XG-2 | 4 | $NaH^{14}CO_3$ | L | $NaH^{14}CO_3$ | L | 1 | 17·7 ± 2·2 | 18·3 ± 1·6 | 19·1 ± 1·8 |
| XG-2 | 5 | BS | L | $NaH^{14}CO_3$ | D | 1 | — | 1·12 ± 0.04 | 0·49 ± 0·02 |
| XG-2 | 6 | NBS[d] | L | $NaH^{14}CO_3$ | D | 1 | — | 0·62 ± 0·04 | 0·412 ± 0·01 |

[a] Cells placed free in chamber containing the radioactive $HCO_3^-$.

[b] Symbol L represents a light treatment of 10 W $m^{-2}$, while the symbol D represents a dark treatment.

[c] The $NaHCO_3$ solutions were at a concentration of 0·5 mM and the pH value was 9·2.

[d] The symbol BS represented bathing solution titrated to pH 9·2 using freshly prepared NaOH, and NBS indicates normal bathing solution, pH value 5·75.

was 0·8 $cm^{-2}$). Estimates of the rates obtained during other experiments gave dark $HCO_3^-$ influx rates of between 0·4 and 1·0 pmol $cm^{-2}$ $s^{-1}$.

*Measurement of dark $H^{14}CO_3^-$ transport*

An experimental system was constructed which simulated the conditions used to obtain results typified by Fig. 8. A perspex holder was used in which cells could be partitioned into two equal halves such that each half was located in a separate chamber. The sides of the holder were constructed of black perspex and hence one or both chambers could be darkened or illuminated simply by employing black or clear perspex tops and bottoms to the respective chamber.

Using this holder, experiments were performed to investigate the magnitude of the dark $H^{14}CO_3^-$ influx when one half of the cell was located in the dark and the other in the light. The results obtained using cells cultured in tanks E′ and XG-2 (see Lucas, 1975*b*) are presented in Table 1. Experiments 1 and 4 indicated that holding the cells in the stocks did not interfere with the process of $H^{14}CO_3^-$ influx and its subsequent assimilation. (In terms of $H^{14}CO_3^-$ influx rates, these experiments revealed that tank E′ cells were particularly active (cf. Fig. 4 of Lucas, 1975*b*).) Bicarbonate influx rates equivalent to control rates were obtained when $H^{14}CO_3^-$ was supplied to only one half of the cell surface and the other half was darkened (see expt. 2 of Table 1). At the conclusion of the experiment the $^{14}C$ fixation products were distributed between the light and dark regions of the cell in approx. proportions of 2:1 respectively. (The mobility of these products is in agreement with the observations of Smith, 1965; see also Heber, 1974.)

The dark $H^{14}CO_3^-$ results presented in Table 1 (expts. 3, 5, and 6) support the estimated values obtained using the small isolating chamber apparatus. For tank E′ cells, the average dark $H^{14}CO_3^-$ influx, associated with the cells partitioned into dark and light segments, was approx. four times higher than the value obtained for cells which were darkened along their entire length (i.e. 0·50 ± 0·07 cf. 0·11 ± 0·01 pmol $cm^{-2}$ $s^{-1}$). Results obtained using tank XG-2 cells indicated that the dark $H^{14}CO_3^-$ influx for the partitioned cells was also higher than the control cells. However, it appeared that bathing the illuminated cell segments in normal bathing solution (pH 5·75) was not as effective in facilitating this stimulated dark influx (cf. expts. 5 and 6).

## DISCUSSION

*The coupled $HCO_3^-/OH^-$ transport hypothesis*

The results presented in this paper demonstrate categorically that the $OH^-$ efflux process can function in the absence of exogenous $HCO_3^-$ at the actual $OH^-$ efflux site. Collectively they invalidate the obligate $HCO_3^-/OH^-$ transport hypothesis proposed by Lucas and Smith (1973). It must therefore be assumed that the transports of $HCO_3^-$ and $OH^-$ are independent, insofar as the two processes can be spatially separated. It seems probable that quite distinct carriers are involved in the respective transport of $HCO_3^-$ and $OH^-$ across the plasmalemma.

A further interesting feature of these results is that, although $HCO_3^-$ can be transported across the plasmalemma in the dark cell segment, this influx value is always

much lower than the rate obtained when $H^{14}CO_3^-$ is added to the illuminated chamber. (A similar situation was found for $^{36}Cl^-$ influx into *Nitella flexillis* by Takeda and Senda, 1974.) This low value may indicate that photosynthetic 'energy' cannot be transported effectively over the involved distances. This seems unlikely, especially as the products of fixation were distributed in the streaming cytoplasm. Hence, it may be that the energy required for the $H^{14}CO_3^-$ transport system is present, but that other properties of the darkened cytoplasm prevent the effective operation of this system. Net production of $CO_2$ within this region, *via* respiration, may prevent the establishment of a 'critical' $HCO_3^-$ concentration gradient across the plasmalemma. Alternatively, this gradient may be required at the interface between the plasmalemma carrier site and the cytoplasm.

*Electrical implications*

The spatially separate and 'independent' operation of the $HCO_3^-$ and $OH^-$ transport systems should establish a situation in the plasmalemma whereby, during the initial illumination of the cell, any imbalance between the influx of $HCO_3^-$ and the efflux of $OH^-$ should result in fluctuations in the membrane potential. This is of course provided the movements of $HCO_3^-$ and $OH^-$ are not coupled to cationic fluxes. (The large fluxes involved suggest that this is not so.) The form of the membrane potential response under these conditions is discussed by Lucas (1975*c*). It should be stressed, however, that the main electrical influence of the fluxes through these particular transport systems is likely to be *via* their contribution to the electrical conductance of the plasmalemma. This will be particularly so at pH values where a supply of exogenous $HCO_3^-$ exists. It is possible that $HCO_3^-$ and $OH^-$ fluxes can account for a large proportion of the observed rise in conductance which occurs when the pH of the bathing solution is increased (Walker, 1962; Hope, 1965; Nishizaki, 1968; Spanswick, 1972; Saito and Senda, 1974; but see also Volkov, 1973).

The relationship between these fluxes and the electrical resistance of the plasmalemma of this species is at present under investigation.

ACKNOWLEDGEMENTS

This work was conducted in the Department of Botany, University of Adelaide, South Australia, while the author held an Australian Commonwealth Postgraduate Scholarship. I wish to thank Prof. J. Dainty for reading the mansucript.

LITERATURE CITED

Heber, U., 1974. *A. Rev. Pl. Physiol.* **25**, 393–421.
Hope, A. B., 1965. *Aust. J. biol. Sci.* **18**, 789–801.
Lucas, W. J., 1975*a*. *J. exp. Bot.* **26**, 271–86.
—— 1975*b*. Ibid. **26**, 331–46.
—— 1975*c*. Ibid. **26**, 347–60.
—— and Smith, F. A., 1973. Ibid. **24**, 1–14.
Nishizaki, Y., 1968. *Pl. Cell. Physiol., Tokyo*, **9**, 377–87.
Saito, K., and Senda, M., 1974. Ibid. **15**, 1007–16.

SMITH, F. A., 1965. *Links between solute uptake and metabolism in Characean cells*. Ph.D. thesis, University of Cambridge.
SPANSWICK, R. M., 1972. *Biochim. biophys. Acta*, **288**, 73–89.
SPEAR, D. G., BARR, J. K., and BARR, C. E., 1969. *J. gen. Physiol.* **54**, 397–414.
TAKEDA, J., and SENDA, M., 1974. *Pl. Cell. Physiol., Tokyo*, **15**, 957–64.
VOLKOV, G. A., 1973. *Biochim. biophys. Acta*, **314**, 83–92.
WALKER, N. A., 1962. *A. Rep. Div. Pl. Ind. C.S.I.R.O.* P. 80.

*Journal of Experimental Botany, Vol. 27, No. 96, pp. 32–42, February 1976*

# The Influence of $Ca^{2+}$ and $K^+$ on $H^{14}CO_3^-$ Influx in Internodal Cells of *Chara corallina*

W. J. LUCAS

*Department of Botany, University of Toronto, Toronto M5S 1A1, Ontario, Canada*

Received 4 August 1975

## ABSTRACT

The influences of $Ca^{2+}$-free solutions and increasing $K^+$ concentrations on the $H^{14}CO_3^-$ influx capacity of *Chara corallina* were investigated. It was found that contact with $Ca^{2+}$-free solutions resulted in a gradual reduction in the $H^{14}CO_3^-$ influx capacity of these cells. Recovery of this influx capacity, following the return of $Ca^{2+}$ to the experimental solution, followed a 'mirror-image' of the time course of decay.

Potassium concentrations above a certain critical value (2 mM) induced a rapid reduction in $H^{14}CO_3^-$ influx capacity. Normal activity was recovered within 60–90 min following the return to 0·2 mM $K^+$ solutions. It was also shown that 10 mM $K^+$ can be used to determine the relative contribution of $^{14}C$ supplied by diffusion of $^{14}CO_2$ and transport of $H^{14}CO_3^-$. The $Ca^{2+}$ and $K^+$ results are discussed in relation to the effects of these treatments on the electrical properties of the plasmalemma.

## INTRODUCTION

The membrane potential of Characean cells can be partially described by the Hodgkin and Katz passive diffusion equation, after cells have been exposed to $Ca^{2+}$-free solutions (Osterhout, 1949; Kishimoto, 1959; Hope and Walker, 1961; Spanswick, Stolarek, and Williams, 1967; Kitasato, 1968; Gillet and Lefebvre, 1973). It has also been shown that, in the presence of $Ca^{2+}$ ions, once the concentration of $K^+$ in the bathing solution has been raised above a certain value, the membrane appears to function as a '$K^+$ electrode' system (Kishimoto, 1959; Kishimoto, Nagai, and Tazawa, 1965; Kitasato, 1968; Spanswick, 1972; Saito and Senda, 1973, 1974; Volkov, 1973).

Kitasato (1968), Lefebvre and Gillet (1973), and Richards and Hope (1974) also demonstrated that the '$K^+$ sensitivity' of the membrane was influenced by the pH value of the bathing solution. These results implied that the removal of $Ca^{2+}$, or alternatively an increase in the $K^+$ concentration, affected the electrogenic component of the membrane potential, i.e. the electrogenic system either becomes inoperative or is in some way short-circuited by these treatments.

Since it has been proposed that at, or above, bathing solution pH values of 6·5 the influx of $HCO_3^-$ and efflux of $OH^-$ may contribute towards determining the membrane potential and resistance (see Lucas, 1975c, 1976), it was of interest to deter-

mine the effect of these cationic treatments on the influx of $H^{14}CO_3^-$. The results of an investigation of this nature are reported in this paper.

## MATERIALS AND METHODS

Culture material of *Chara corallina* was grown in the laboratory under artificial light. Full details of the procedures and experimental apparatus employed in the analysis of $^{14}C$ fixation, in the internodal cells of this species, have been previously reported (Lucas, 1975*a*,*b*). All experimental solutions contained 1·0 mM NaCl, 0·2 mM KCl, and 0·5 mM $CaSO_4$ (unless otherwise specified) and all fixation experiments were conducted at 25 °C, under a light intensity of 15 W $m^{-2}$.

## RESULTS

### *Effect of removing $Ca^{2+}$ from the bathing solution*

It was shown previously that prolonged (10 h) exposure to low $Ca^{2+}$ solutions (0·02 mM) did not cause a decrease in $H^{14}CO_3^-$ influx (Lucas, 1975*a*). However, in this same work it was shown that a decrease in $H^{14}CO_3^-$ influx was observed when $Ca^{2+}$-free solutions were employed. The time course of decay in $H^{14}CO_3^-$ influx capacity, which resulted following the exclusion of $Ca^{2+}$ from the bathing solution, is shown in Figs 1 and 2. Cells used for these experiments were pre-treated for 2 h in normal bathing solution which contained 10 mM 2-(N-morpholino)ethanesulphonic acid (MES) (pH 5·0), to ensure that $CaCO_3$ deposits were removed from the cell wall. The decay curve for Fig. 1 was obtained by the following experimental procedure: at the conclusion of a 12 h dark recovery period (normal bathing solution +0·5 mM $NaHCO_3$, pH 8·8), the cells were divided into two batches. One batch was simultaneously illuminated (15 W $m^{-2}$) and transferred to a modified bathing solution which contained 5 mM NaCl, 0·2 mM KCl, 0·5 mM $NaHCO_3$, and no $Ca^{2+}$ (pH 9·0). The second batch of cells was employed for control treatments; they were

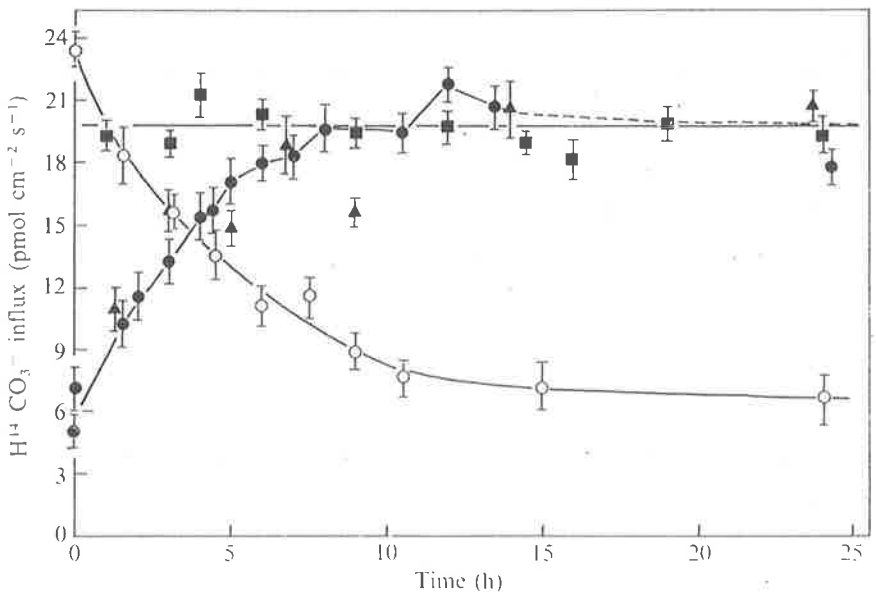


FIG. 1. Influence of $Ca^{2+}$ on $H^{14}CO_3^-$ influx. See text for full details of experimental treatments. The response to $Ca^{2+}$-free solutions is represented by the symbol ○, while ■ is the control treatment. The recovery of $H^{14}CO_3^-$ influx capacity following a 12 h $Ca^{2+}$-free exposure is shown by ● (light) and ▲ (dark). The dark treatments were given a 30 min light pre-treatment before exposure to $H^{14}CO_3^-$ solutions. The error bars represent the s.e. mean.

illuminated under the same light intensity, but the bathing solution contained 1·0 mM NaCl, 0·2 mM KCl, 0·25 mM $CaSO_4$, and 0·5 mM $NaHCO_3$ (pH 9·0). Solutions for both treatments were changed at 2-hourly intervals, and a normal $H^{14}CO_3^-$ exposure period of 1 h was employed. Under these conditions the $H^{14}CO_3^-$ influx appeared to decrease slowly until the 10th hour of contact with $Ca^{2+}$-free solution, when the rate had dropped to a new steady value. This value was approximately 38 per cent of the control.

Figure 1 also shows the effect upon $H^{14}CO_3^-$ influx of returning $Ca^{2+}$ to the experimental solution. These cells were given a similar decalcification treatment. A 12 h dark treatment using the 5 mM NaCl solution was then employed, the solutions being changed every 4 h. It was found that the cellular recovery of $H^{14}CO_3^-$ influx capacity followed almost the mirror image of its decline. Recovery appeared to follow the same time course irrespective of whether dark or light treatments were employed.

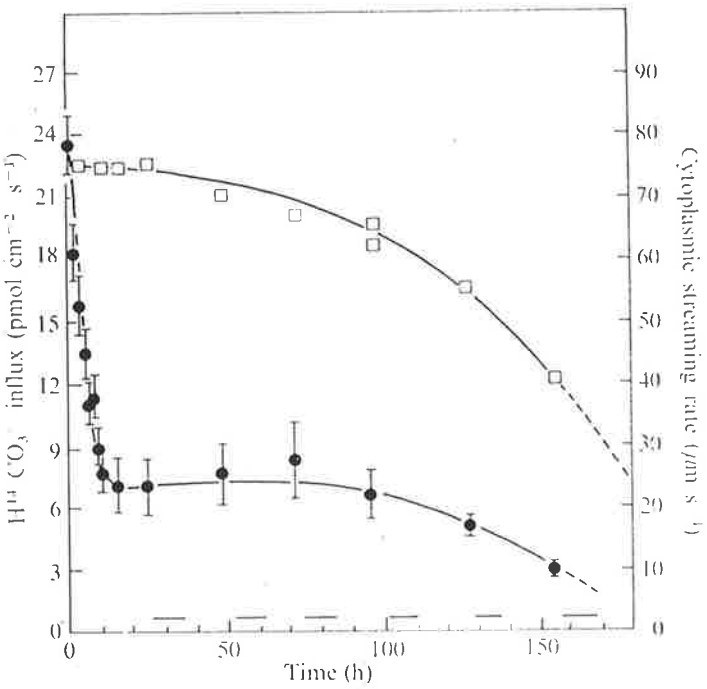


FIG. 2. Effect on $H^{14}CO_3^-$ influx and cyclosis of prolonged exposure to $Ca^{2+}$-free solutions. The experimental details are as for Fig. 1, and the solid bars along the abscissa indicate the employment of dark periods. The symbols are ●, $H^{14}CO_3^-$ influx; □, cytoplasmic streaming rate. The s.e. mean for the cytoplasmic streaming rate was approximately ± 1·5 $\mu m\ s^{-1}$ for all treatments; this value was too small for inclusion on the individual experimental points.

The influence of extremely long exposure periods to $Ca^{2+}$-free solutions is shown in Fig. 2. It can be seen that a further decrease in cellular $H^{14}CO_3^-$ transport capacity was not observed until cells had been exposed to these solutions for approximately 127 h. Cyclosis was also measured on each $H^{14}CO_3^-$ treatment. These results (included on Fig. 2) showed that after the initial 24 h exposure to $Ca^{2+}$-free solutions, the streaming rate began to decrease. It should be noted that the period over which cyclosis declined most rapidly also coincided with the second phase in the reduction of $H^{14}CO_3^-$ influx. These results indicated that prolonged exposure to $Ca^{2+}$-free

solutions eventually depressed both $H^{14}CO_3^-$ influx and cyclosis, and this effect culminated in the death of the experimental cells.

*Effect of decalcification treatments on fixation of exogenous $^{14}CO_2$*

Table 1 indicates that the 10 mM MES buffer treatment did not alter significantly the cellular ability to utilize exogenous carbon (either $^{14}CO_2$ or $H^{14}CO_3^-$). (The $^{14}CO_2$ fixation rate actually increased slightly above that of the control cells.) Similarly, exposure to $Ca^{2+}$-free solutions did not reduce the $^{14}C$ fixation rate in the presence

TABLE 1. *$^{14}CO_2$ and $H^{14}CO_3^-$ assimilation following MES buffer and $Ca^{2+}$-free solution treatments*

| Pre-treatment | Experimental treatment | $H^{14}CO_3^-$ influx (pmol cm$^{-2}$ s$^{-1}$) | $^{14}CO_2$ fixation (pmol cm$^{-2}$ s$^{-1}$) |
|---|---|---|---|
| Control: | | | |
| 10 h in normal bathing solution which contained 0·5 mM $NaHCO_3$, pH 8·8. | A[a] | 25·35 ± 1·05 | |
| | B[a] | | 58·37 ± 4·21 |
| (i) 2 h in normal bathing solution which contained 10 mM MES buffer, pH 5·0. | A[a] | 25·13 ± 1·13 | |
| (ii) 8 h in normal bathing solution + 0·5 mM $NaHCO_3$, pH 8·8. | B[a] | | 68·03 ± 4·29 |
| (i) 2 h in normal bathing solution + 10 mM MES buffer, pH 5·0. | A[b] | 7·01 ± 1·25 | |
| (ii) 4 h in 5·0 mM NaCl + 0·2 mM KCl, pH 5·75. | | | |
| (iii) 4 h in 5·0 mM NaCl + 0·2 mM KCl + 0·5 mM $NaHCO_3$, pH 8·8. | B[b] | | 64·28 ± 3·45 |

[a] A represents the employment of normal bathing solution + 0·5 mM $NaH^{14}CO_3$, pH 9·0; B, normal bathing solution + 0·5 mM $NaH^{14}CO_3$ + 5 mM MES buffer, pH 5·3.

[b] Both A and B as above except that the bathing solution did not contain $Ca^{2+}$.

of exogenous $^{14}CO_2$. The exogenous $H^{14}CO_3^-$ treatment, however, resulted in a decrease in $^{14}C$ assimilation in accorance with the results presented in Fig. 1. These results were taken as supporting evidence that the reduction in cellular ability to assimilate $H^{14}CO_3^-$, under $Ca^{2+}$-free conditions, was due to an effect at the plasmalemma rather than on the chloroplasts.

*Increasing $K^+$ concentration: its influence on $^{14}C$ assimilation*

Figure 3 shows that when the $K^+$ concentration was increased above 2·0 mM, the $^{14}HCO_3^-$ influx rate was depressed from approximately 20 to 3·5 pmol cm$^{-2}$ s$^{-1}$. Further reduction in the $H^{14}CO_3^-$ influx rate was not observed when higher $K^+$ levels were employed. A parallel reduction in $^{14}C$ fixation in the presence of exogenous $^{14}CO_2$ fixation was only observed at $K^+$ concentrations approximately ten times higher than those required to affect $H^{14}CO_3^-$ influx. Even at this concentration, the reduction in fixation rate was relatively small. It would seem, therefore, that the reduction in $H^{14}CO_3^-$ influx and $^{14}CO_2$ fixation reflect two separate modes of action of the $K^+$ ion. The reduction in $H^{14}CO_3^-$ influx, which was elicited by increasing the $K^+$ concentration above 2 mM, was considered to result from the effect of

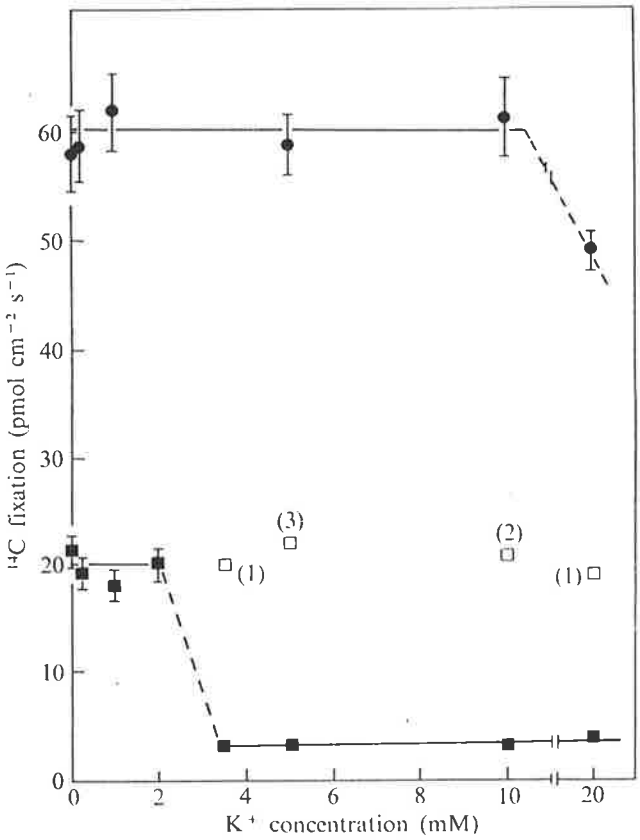


FIG. 3. The influence of $K^+$ concentration on $^{14}C$ fixation. The experimental solutions all contained 0·5 mM $NaHCO_3$; ■ and □ treatments were conducted at pH 9·0; ●, at pH 5·3 and at this pH value the solution was buffered by 5 mM MES. The $K^+$ concentration was increased by adding KCl to obtain the required value. The symbol □ represents experimental values which deviated significantly from the mean obtained for the particular treatment, and the values in parenthesis indicate the number of cells.

$K^+$ either on the general structure of the plasmalemma or directly upon the $HCO_3^-$ carrier system.

Some cells did not show a reduction in $H^{14}CO_3^-$ influx when $K^+$ was increased to concentrations above 2·0 mM (see Fig. 3). This phenomenon was further investigated by conducting an experiment in which 50 cells were treated in 10 mM $K^+$ solutions, and 30 control cells were treated in 0·2 mM $K^+$ solutions. Frequency histograms of the results obtained from this experiment are presented in Fig. 4. From the distribution of the control $H^{14}CO_3^-$ influx values, it was assumed that $K^+$-treated cells which had influx values $\geqslant$10 pmol cm$^{-2}$ s$^{-1}$ had not been affected by the high $K^-$ concentration. This was unquestionably so for the five cells having values $\geqslant$18 pmol cm$^{-2}$ s$^{-1}$; however, one cannot be as certain of the three values in the influx range 10–12 pmol cm$^{-2}$ s$^{-1}$. Collectively the results presented in Figs 3 and 4 suggest that the reduction in $H^{14}CO_3^-$ influx, in response to $K^+$ concentrations $\geqslant$2·0 mM, is an 'all or none' phenomenon.

Experiments in which $K^+$ was held constant at 0·2 mM and the $Na^-$ concentration increased revealed that the influx of $H^{14}CO_3^-$ remained unaffected even at a concentration of 10 mM $Na^+$ (cf. 18·6 ± 1·5 pmol cm$^{-2}$ s$^{-1}$ (1·0 mM NaCl, 0·2 mM KCl, 0·5 mM $NaHCO_3$, 0·5 mM $CaSO_4$, pH 9·0) with 20·6 ± 1·3 pmol cm$^{-2}$ s$^{-1}$ (as above

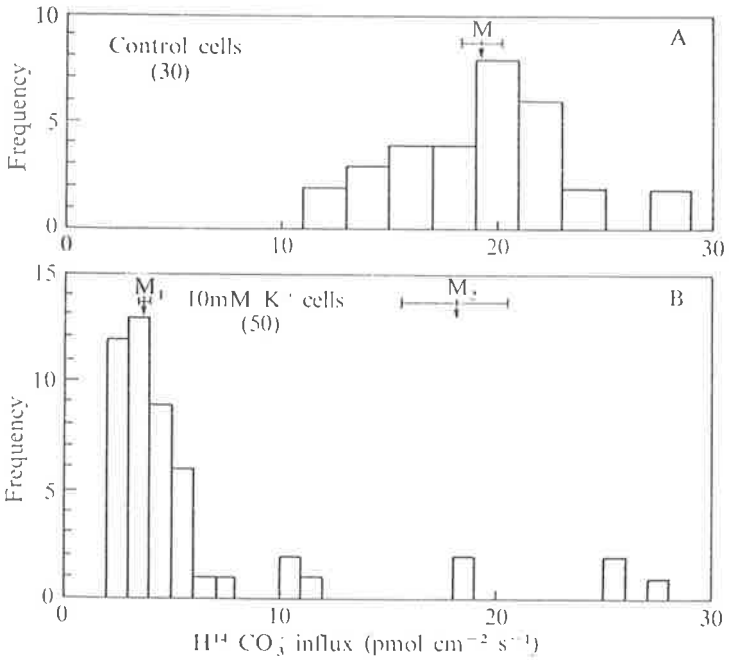


FIG. 4. Histograms of the $H^{14}CO_3^-$ influx values obtained in the presence and absence of 10 mM $K^+$. The control treatment (30 cells) was conducted in normal solution + 0·5 mM $NaHCO_3$, pH 9·0; the 10 mM $K^+$ treatment was in an identical solution except that it contained 10 mM $K^+$. The symbol M and the accompanying arrow indicate the mean and the error bar is the associated s.e. mean. In Fig. 4B, $M_1$ is the mean calculated by including only values $\leqslant 8$ pmol $cm^{-2}$ $s^{-1}$, and $M_2$ is the mean for $H^{14}CO_3^-$ influx values $\geqslant 8$ pmol $cm^{-2}$ $s^{-1}$.

except 10 mM NaCl)). The absence of an effect of $Na^+$ on the $H^{14}CO_3^-$ influx process is in agreement with the relative insensitivity of the membrane potential to changes in the concentration of this ion (see for example Spanswick, 1972, Table 1).

*Recovery of $H^{14}CO_3^-$ influx capacity following removal of 10 mM $K^+$ solution*

Figure 5 illustrates the recovery of $H^{14}CO_3^-$ influx capacity following the transfer of cells from a solution containing 10 mM KCl (plus 0·5 mM $NaHCO_3$, pH 9·1) to normal bathing solution (plus 0·5 mM $NaHCO_3$, pH 9·1). The 10 mM $K^+$ pre-treatment was given for 1 h under a light intensity of 15 W $m^{-2}$. The $H^{14}CO_3^-$ influx values (of Fig. 5) were obtained using a 15 min radioactive exposure period. Time course treatments of duration greater than 15 min were in non-radioactive solutions until the final 15 min of the particular experiment. The recovery of activity was more rapid than was observed in the $Ca^{2+}$-free solution experiments, i.e. whereas 7–9 h were required to regain full activity in the $Ca^{2+}$ experiments, this period was only 1–1½ h for $K^+$ experiments.

*Increasing $HCO_3^-$ concentration in the presence of 10 mM $K^+$*

Figure 6 indicates that increasing the $HCO_3^-$ concentration, in the presence of a fixed concentration of $K^+$ (10 mM), did not result in the recovery of normal $H^{14}CO_3^-$ influx capacity. The apparent linear response is suggestive of a passive diffusion process. Alternatively it could be that the 10 mM $K^+$ treatment affected the binding properties of the $HCO_3^-$ carrier such that its $K_m$ was increased to a much larger value. This large $K_m$ would then give an approximately linear response between influx and

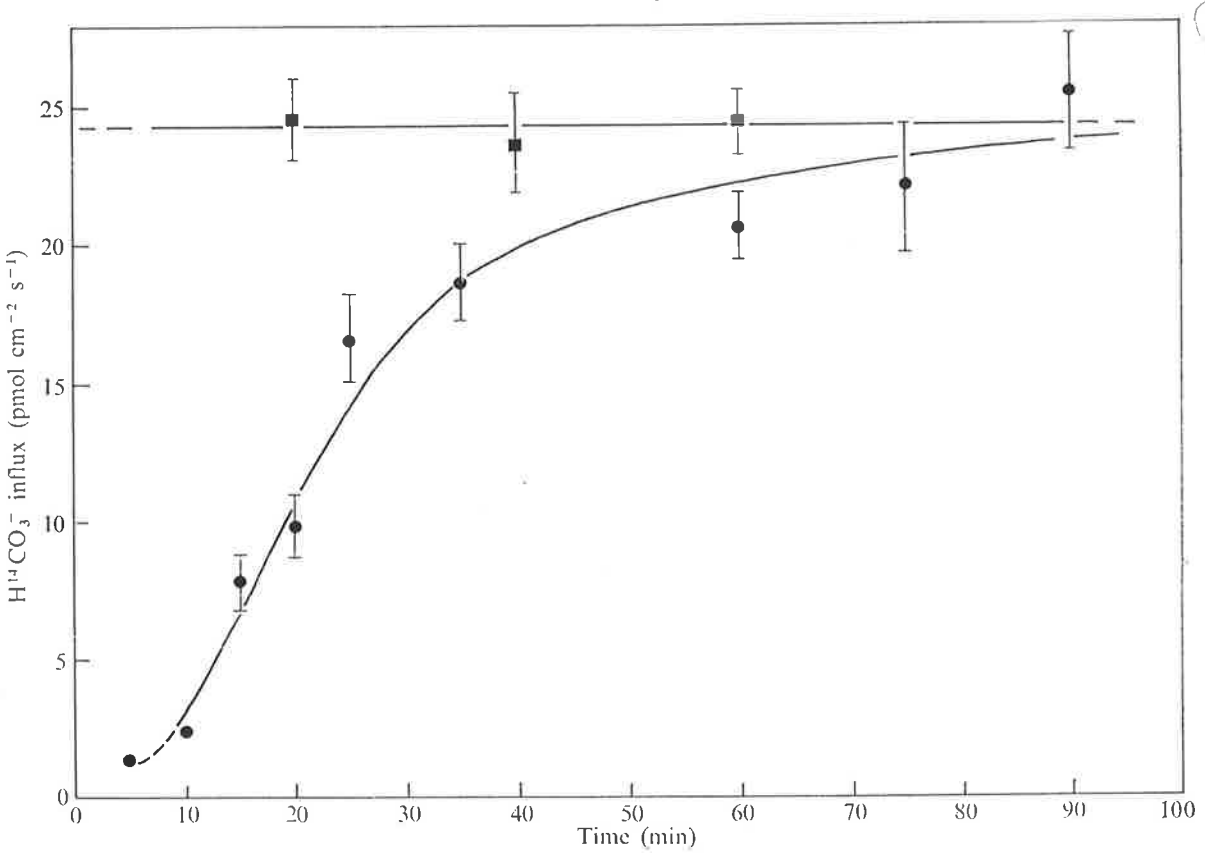


FIG. 5. Recovery of $H^{14}CO_3^-$ influx capacity following the removal of 10 mM $K^+$ from the experimental solution. See text for full details of experimental sequences. The symbol ● represents the $H^{14}CO_3^-$ influx value obtained following the transfer of the cells from a 10 to a 0·2 mM $K^+$ solution; ■ represents the control $H^{14}CO_3^-$ influx values (cells not treated with 10 mM $K^+$ solutions).

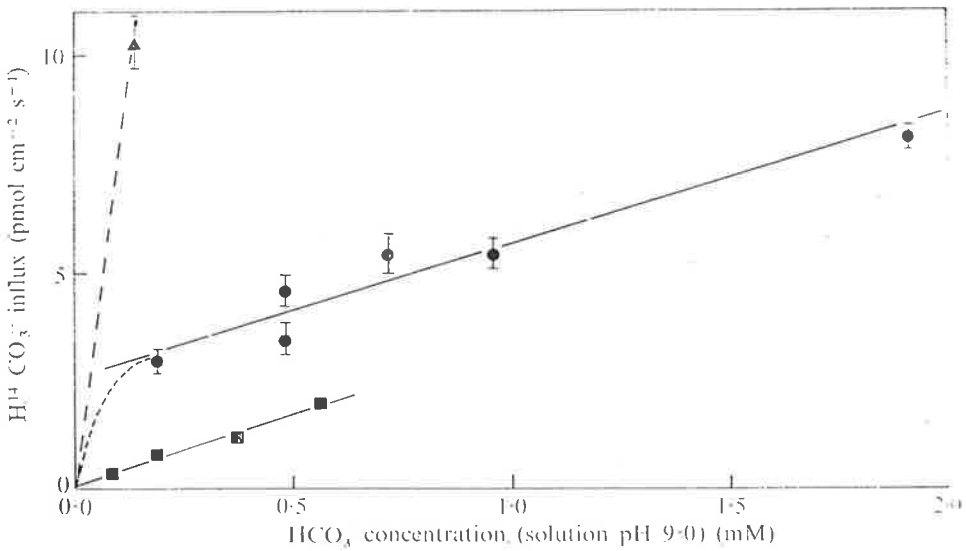


FIG. 6. Effect of increasing $HCO_3^-$ concentration in the presence of 10 mM $K^+$. Normal $H^{14}CO_3^-$ procedures were followed for these experiments; the initial pH value was 9·0 for each treatment. The symbol ● represents the 10 mM $K^+$ treatments; ■ represents $H^{14}CO_3^-$ influx in the presence of 0·3 mM $(NH_4)_2SO_4$ (0·2 mM $K^+$); and ▲ the controls.

substrate concentration. The effect of 0·3 mM $(NH_4)_2SO_4$ was included to demonstrate that other inhibitory processes can depress the $H^{14}CO_3^-$ influx value even further. The inhibitory effect of $(NH_4)_2SO_4$ on $H^{14}CO_3^-$ assimilation will be given in detail in a forthcoming paper.

*Influence of* 10 *mM* $K^+$ *on* $^{14}C$ *fixation at pH* 7·5

When 10 mM $K^+$ was employed in the experimental solution at pH 7·5, the $^{14}C$ assimilation rate was considerably reduced (Fig. 7). This was to be expected if $H^{14}CO_3^-$ influx was making a significant contribution to the total $^{14}C$ fixation rate at this pH value. When the $^{14}C$ fixation values, obtained in the presence of 10 mM $K^+$, were corrected for the residual 'concentration response' (using the data presented in Fig. 6), the values were considered to represent the $^{14}CO_2$ component of fixation.

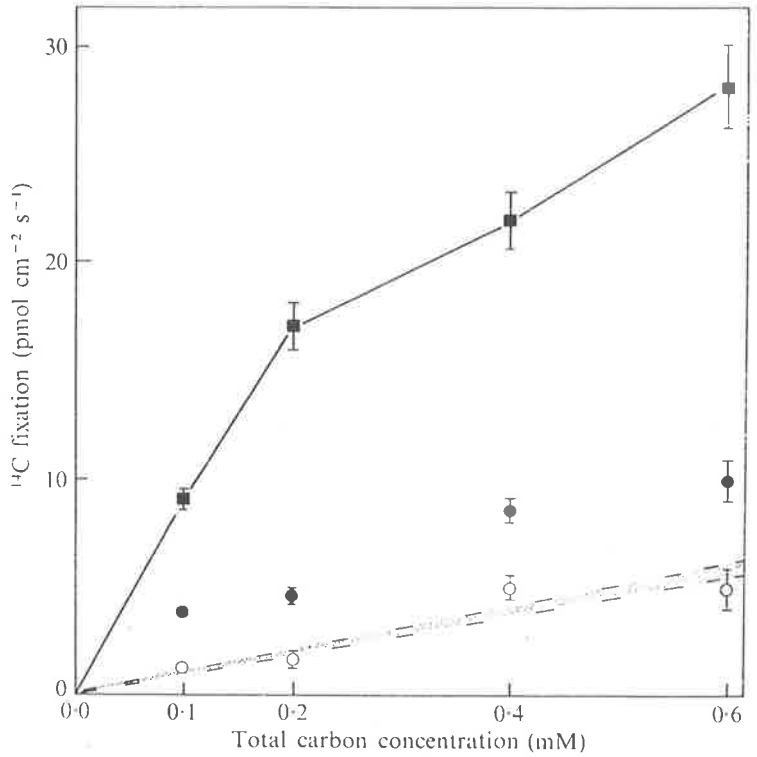


FIG. 7. Influence of 10 mM $K^+$ on $^{14}C$ fixation at pH 7·5. Symbols are as follows: ■, control treatments; ●, $^{14}C$ fixation in the presence of 10 mM $K^+$; ○, values corrected for $H^{14}CO_3^-$ influence using the data presented in Fig. 6. The broken lines represent the estimated $^{14}CO_2$ contribution at this pH value and the value was determined using the results of Lucas (1975*b*, Fig. 2); the stippled region is equivalent to the s.e. mean.

It was calculated that at a total carbon concentration of 0·6 mM and a pH value of 7·5, the level of $CO_2$ would have been 0·040 mM. From an earlier series of experiments it was estimated that this concentration of $CO_2$ would support a fixation rate of 5·3–6·2 pmol $cm^{-2}$ $s^{-1}$ (see Lucas, 1975*b*, Fig. 2). Assuming a linear relationship between $^{14}CO_2$ fixation and exogenous $^{14}CO_2$ over this concentration range, two straight lines were constructed through the origin. (The stippled region represents the expected s.e. mean.) The agreement between the experimental values (i.e. 10 mM $K^+$, subtracting the residual $HCO_3^-$ influx) and this graph was taken as

extremely strong support for the fact that these corrected values do represent the $^{14}CO_2$ contribution to fixation under these experimental conditions. It is considered, therefore, that the results presented in Fig. 7 give further support to the hypothesis presented by Lucas (1975*b*), namely that diffusion of $^{14}CO_2$ and $H^{14}CO_3^-$ transport operate simultaneously to give maximum possible rates of fixation (cf. Raven, 1968, 1970).

## DISCUSSION

### *The influence of $Ca^{2+}$ on $H^{14}CO_3^-$ influx activity*

Dainty and Hope (1959) reported that the removal of $Ca^{2+}$ from the ion-exchange component of the cell wall of *Chara corallina* could be separated into two fractions, one fast and the other slow. They found that the slow fraction had a $t_{\frac{1}{2}}$ of approximately 15 d. In the present series of experiments, the employment of a 10 mM MES treatment and a 5 mM $Na^+$ level would be likely to produce a much faster elution of $Ca^{2+}$ from the cell wall and possibly from the plasmalemma and cytoplasmic phases.

The slow decrease in $HCO_3^-$ influx capacity in response to cellular exposure to $Ca^{2+}$-free solutions implies that either $Ca^{2+}$ is being eluted slowly from the plasmalemma or that the reduction in $HCO_3^-$ influx involves several stages. Calcium may be required to maintain the integrity (or structural conformation) of the plasmalemma such that all membrane-bound processes can function normally. It may also be, however, that $Ca^{2+}$ *per se* acts as an integral component of the functional $HCO_3^-$ transport system. If this were so, elution of $Ca^{2+}$ from the membrane would result in the gradual deactivation of the operational $HCO_3^-$ carriers. This process would be expected to be slow, since under normal conditions the fluxes of $Ca^{2+}$ are small (Spanswick and Williams, 1965). The almost identical 'mirror image' recovery phase of $HCO_3^-$ influx capacity, following the re-introduction of $Ca^{2+}$, suggests that $Ca^{2+}$ is an integral component of the $HCO_3^-$ carrier system. (The second stage of the $H^{14}CO_3^-$ influx decay curve (see Fig. 2) may have been related to the depletion of $Ca^{2+}$ from the cytoplasmic phase.) Further experiments, on the influence of other divalent cations (for example $Mg^{2+}$) on the recovery phase of the $H^{14}CO_3^-$ influx capacity, should demonstrate whether there is a specific requirement for $Ca^{2+}$ associated with the transport of $HCO_3^-$.

### *The influence of $K^+$ on $H^{14}CO_3^-$ influx activity*

The time course in decay of $H^{14}CO_3^-$ influx activity was not investigated in detail. However, it was found that in general an exposure of 1 h to critical $K^+$ concentrations (i.e. $\geqslant$2 mM) was sufficient to deactivate the carrier system. In fact the normal mode of operation of the $H^{14}CO_3^-$ carrier must have been impaired almost immediately the cell was exposed to higher $K^+$ levels. If this were not so, the s.e. mean in each case would have been very large (see Fig. 3). Hence the mode of action of $K^+$, on the $H^{14}CO_3^-$ carrier system, must be quite different from that of $Ca^{2+}$-free solutions. This is also suggested by the very different recovery curves (cf. Figs 1 and 5). It was anticipated that the recovery of $H^{14}CO_3^-$ influx capacity, following the re-

moval of $K^+$, would have been much more rapid than was observed, since the membrane is relatively permeable to $K^+$ at this stage. The slower response perhaps suggests that there is a requirement for metabolic repair to the membrane before the return of normal activity.

Nevertheless, the parallel between the effect of high $K^+$ concentration on $H^{14}CO_3^-$ influx capacity and the reported effects of this ion ($K^+$) on the membrane potential (see for example Spanswick, 1972; Saito and Senda, 1973) indicates that the two phenomena probably share some common feature. Support is given to this conclusion by the paralleled ineffectiveness of increasing $Na^+$ concentrations on both the membrane potential (see Kitasato, 1968; Hope and Richards, 1971; Spanswick, 1972) and $H^{14}CO_3^-$ influx capacity.

It is also important to note that the apparent insensitivity of the membrane potential, 'when a large electrogenic component of potential is present' (Richards and Hope, 1974) may not have held, had the authors increased their $K^+$ concentration above 1 mM. On the basis of the results presented in Figs 3 and 7, 10 mM $K^+$ should have given a response similar to that observed by Spanswick (1972).

The 'all or none' effect of $K^+$ on $H^{14}CO_3^-$ influx capacity (Fig. 4) also has a parallel in that similar effects have been observed during studies on the membrane potential (Richards and Hope, 1974, Table 1; Lucas, unpublished results). Hence, since both cationic treatments ($Ca^{2+}$ and $K^+$) influence the influx of $HCO_3^-$ in a manner virtually identical to their electrical effects, this parallel must give weight to the proposal that $HCO_3^-$ assimilation contributes towards determining the electrical properties of the plasmalemma. Studies to test this hypothesis (see Lucas, 1975*c*, 1976) are at present in progress in this laboratory.

ACKNOWLEDGEMENTS

This work was conducted in the Botany Department, University of Adelaide, South Australia, during the author's tenure of an Australian Commonwealth Postgraduate Scholarship.

LITERATURE CITED

Dainty, J., and Hope, A. B., 1959. *Aust. J. biol. Sci.* **12**, 395–411.
Gillet, C., and Lefebvre, J., 1973. In *Ion transport in plants*. Ed. W. P. Anderson. New York, Academic Press. Pp. 101–12.
Hope, A. B., and Richards, J. L., 1971. *Proc. 1st eur. biophys. Congr.* Eds E. Broda, A. Locker, and H. Springer-Lederer. Wein, Verlang Wein Med. Akad. Vol. 3, p. 105.
—— and Walker, N. A., 1961. *Aust. J. biol. Sci.* **14**, 26–44.
Kishimoto, U., 1959. *Ann. Rep. Sci. Works*. Faculty of Sci., Osaka Univ. Vol. 7, pp. 115–30.
—— Nagai, R., and Tazawa, M., 1965. *Pl. Cell Physiol., Tokyo*, **6**, 519–27.
Kitasato, H., 1968. *J. gen. Physiol.* **52**, 60–87.
Lefebvre, J., and Gillet, C., 1973. *J. exp. Bot.* **24**, 1024–30.
Lucas, W. J., 1975*a*. Ibid. **26**, 271–86.
—— 1975*b*. Ibid. **26**, 331–46.
—— 1975*c*. Ibid. **26**, 347–60.
—— 1976. Ibid. **27**, 19–31.
Osterhout, W. J. V., 1949. *Proc. natn. Acad. Sci. U.S.A.* **35**, 548–58.
Raven, J. A., 1968. *J. exp. Bot.* **19**, 193–206.
—— 1970. *Biol. Rev.* **45**, 167–221.
Richards, J. L., and Hope, A. B., 1974. *J. Membrane Biol.* **16**, 121–44.

SAITO, K., and SENDA, M., 1973. *Pl. Cell Physiol., Tokyo*, **14**, 147–56.
—— —— 1974. Ibid. **15**, 1007–16.
SPANSWICK, R. M., 1972. *Biochim. biophys. Acta*, **288**, 73–89.
—— STOLAREK, J., and WILLIAMS, E. J., 1967. *J. exp. Bot.* **18**, 1–16.
—— WILLIAMS, E. J., 1965. Ibid. **16**, 463–73.
VOLKOV, G. A., 1973. *Biochim. biophys. Acta*, **314**, 83–92.

*Aust. J. Plant Physiol.*, 1976, 3, 443–56

# Influence of Irradiance on $H^+$ Efflux and $Cl^-$ Influx in *Chara corallina*: An Investigation Aimed at Testing Two $Cl^-$ Transport Models

*W. J. Lucas*[AB] *and F. A. Smith*[A]

[A] Department of Botany, University of Adelaide, Adelaide, S.A. 5001.
[B] Present address: Department of Botany, University of Toronto, Toronto, Ontario, M5S 1A1, Canada.

*Abstract*

Parallel studies on the influence of irradiance on net $H^+$ efflux and $^{36}Cl^-$ uptake were conducted on *C. corallina*. Following the dark-to-light transition, a lag period of 8–15 min was observed before net $H^+$ efflux activity could be discerned experimentally. Decreasing the irradiance did not significantly lengthen this lag period. Studies on $^{36}Cl^-$ uptake revealed that a lag period of 40–60 min was required before the $Cl^-$ transport system attained maximum activity, governed by the prevailing experimental conditions.

These results are discussed in relation to the $Cl^-$ transport hypotheses proposed by Spear *et al.* and by Smith. It would seem that the hypothesis of Spear *et al.*, in its present form, is invalid for *Chara corallina*. The results were inconclusive in terms of support (or otherwise) for a $Cl^-/OH^-$ antiporter. However, the $Cl^-/OH^-$ antiporter hypothesis originally proposed by Smith will require significant modification, especially in terms of the energy supply.

## Introduction

Spear *et al.* (1969) demonstrated that $Cl^-$ uptake into *Nitella clavata* was restricted primarily to the acidic regions of the cell surface. Since the acidification phenomenon and the major portion of the $Cl^-$ influx were light-dependent, these workers proposed that $Cl^-$ influx might be 'mechanistically' linked to $H^+$ efflux. Spear *et al.* (1969) interpreted the localized alkaline regions at the cell surface as the result of passive $H^+$ entry balancing the $H^+$ efflux, rather than $OH^-$ efflux associated with $HCO_3^-$ assimilation (see Smith 1970; Lucas and Smith 1973; Lucas 1975*a*, 1975*b*). The possibility of a coupled $Cl^-/OH^-$ transport system was rejected by these workers (cf. Smith 1970).

Spear *et al.* did, however, propose three possible mechanisms by which $Cl^-$ could be accumulated; their main hypothesis concerned the selective movement of $Cl^-$, via a $Cl^-$-specific channel, into an intramembrane (plasmalemma) region where $H^+$ was being formed. Molecular HCl was considered to partition into the lipid phase of the membrane and preferential inward diffusion of HCl to the cytoplasm was proposed. For diffusion to be restricted to this direction, it was necessary for these workers to postulate that the outer portion of the membrane functions as a barrier to the diffusion of HCl. Also, to account for the observed net $H^+$ efflux, Spear *et al.* were forced to include a specific channel for $H^+$ movement between the intramembrane space and the external solution. It is difficult to see how these 'channels' can function and yet exclude the HCl ion-pair (MacRobbie 1970).

However, the above hypothesis is, in fact, a simple form of a cotransport system. With respect to the characteristics proposed by Spear *et al.*, the light-stimulated

component of $Cl^-$ uptake should become operational almost simultaneously with the appearance of acid at the cell surface, provided that $H^+$ extrusion significantly exceeds $Cl^-$ influx. Hence, it should be possible to test this hypothesis.

Smith (1970) has also proposed an hypothesis for $Cl^-$ transport which was aimed specifically at the influx of this ion into *Chara corallina*. (For excellent reviews on the topic of $Cl^-$ transport in the Characeae, the reader is referred to MacRobbie 1970, 1974.) Smith suggested that an active 'Mitchell-type' $H^+$ and $OH^-$ charge-separating mechanism may be located in the plasmalemma (see Smith 1970, figure 4). (Supporting evidence for the existence of this transport system was gained from the observation of the development of light-dependent acid regions on the cell surface.) The secondary transport processes of $Na^+$ and $K^+$ influx, both of which are passive in this species, were considered to result from the electrogenic nature of the $H^+/OH^-$ separation. That is, the increased negative value of the membrane potential increased the electrochemical potential driving force for these ions, in the direction which stimulated cation influx. The operation of an electrically neutral $Cl^-/OH^-$ antiporter was considered to be the more important secondary process associated with this proposed $H^+/OH^-$ system. Smith proposed that this antiporter was driven 'energetically' by the pH gradient across the plasmalemma, and he further stipulated that $Cl^-$ influx would be limited by the rate of $H^+$ extrusion.

There are numerous examples of antiporters of this general form in the literature: see, for example, Chappell and Crofts (1966) and Harold and Baarda (1968). However, it should be stressed that the $Cl^-/OH^-$ antiporter is operationally equivalent to a $H^+$ cotransport system for $Cl^-$ (Slayman 1974).

The most noteworthy aspect of the $Cl^-$ transport models proposed by Spear *et al.* (1969) and Smith (1970) is that both hypotheses relate $Cl^-$ influx to the observed acidification of the cell surface. Thus, both models suggest, implicitly, that the light-activated $Cl^-$ uptake process should follow quite closely the activation response of the acid bands. Since both are based on the electrogenic movement of $H^+$, there may also be a correlation between the light-stimulated hyperpolarization of the membrane potential and $Cl^-$ influx.

The experiments described in this paper were designed to investigate the relationship between $H^+$ efflux and $Cl^-$ uptake. It was hoped that information of this nature would provide an experimental test of the above-mentioned hypotheses (see MacRobbie 1974).

## Materials and Methods

### *Culture Material*

*Chara corallina* cells were grown in large plastic containers in solutions containing 1·0–2·0 mM $Na^+$, 0·2 mM $K^+$, 0·5 mM $Ca^{2+}$, 1·0 mM $Cl^-$ and approximately 2 mM $HCO_3^-$. Full details of the culture techniques have been previously reported (Lucas 1975*b*). Experiments reported in this paper were performed during the summer growing season, when optimal growth rate ensured that uniform mature cells were obtained.

### *Techniques and Procedures Employed in $^{36}Cl^-$ Experiments*

Experiments were performed in a thermostatted (25°C) water bath. The light source was a Rank–Aldis 24-V 150-W quartz–iodide projector. Irradiances were attenuated using a range of nickel–Nicron neutral-density filters prepared by the Department of Physics, University of Adelaide. Irradiance was measured using a silicon solar cell (IRC, type No. S 0510E 7PL) which was calibrated against a miniature Middleton pyranometer, model CN 6.

A map of the irradiances within the experimental plane (i.e. the plane in which the test tubes were to be held) was constructed, and it was found that a uniform irradiance band 7 cm high by 10 cm wide could be obtained. All $^{36}Cl^-$ experiments were conducted within this uniform irradiance band. A mirrored surface perpendicular to the incident light path was placed in position slightly behind the experimental test tubes. This was included to improve the light regime of the *Chara* cell surfaces that faced away from the light beam of the lamp. As a further attempt at obtaining a sample of uniformly illuminated cells, the test tubes were rotated through 180° every 10–15 min.

*General $^{36}Cl^-$ Experimental Sequence*

The general experimental sequence followed to determine $^{36}Cl^-$ uptake under a given set of experimental conditions, was as follows:

(i) Mature internodal cells were cut from the third to fifth internodal region and trimmed of whorl cells. Only cells having normal whorl cell development were used in these experiments. Dead cell wall segments of adjacent internodal cells were used in handling individual cells.

(ii) A 90-min recovery period was employed after the cells had been cut. During this period, cells were bathed in normal experimental solution (20°C) and illuminated by fluorescent lighting (8·3 W $m^{-2}$).

(iii) Following the recovery phase, cells were 'batched' for the various experimental treatments; 14–16 cells were used per treatment. Diameters and lengths were measured to compute individual cell surface areas. Cytoplasmic streaming was also checked and, in general, it was found that cells recovered normal cyclosis (50–70 $\mu m\ s^{-1}$) within 15 min of being cut from the culture.

(iv) Experiments were performed in sealed test tubes (25 ml) and a 1-h dark treatment was employed. Specific details of the various $^{36}Cl^-$ treatments (in terms of substitution times for radioactive solutions, irradiances and duration of light treatment) will be given in the text. It is important to note that stirring of the experimental solution was considered undesirable, because it was found that unless cells were held by some form of rigid support, spontaneous action potentials were induced by the flowing solution. Hence, all $^{36}Cl^-$ experiments were conducted in unstirred solutions.

(v) At the conclusion of each experiment, cells were washed with non-radioactive solutions (5 min) before being cut and dried onto planchets. Activity was counted using a thin end-window Geiger–Müller tube system. Results were expressed as mean ± standard error of the mean for each treatment (14–16 cells per treatment).

*pH Measurement at the Surface of* Chara *cells*

Experimental procedures involved in the measurement of pH at the cell surface of the *Chara* cells have been previously reported (Lucas and Smith 1973; Lucas 1975*a*).

*Experimental Solutions*

The standard experimental solution, which was prepared using glass-distilled water (specific conductivity $1{\cdot}1 \times 10^{-6}$ S $cm^{-1}$), contained 1·0 mM NaCl, 0·2 mM KCl and 0·5 mM $CaSO_4$ unless otherwise specified. All chemicals used were of Analar Reagent grade. Some $^{36}Cl^-$ experimental solutions were buffered using *N*-2-hydroxyethylpiperazine-*N'*-2-ethanesulphonic acid (HEPES) at 5 mM concentration.

Radioactive $^{36}Cl^-$ was obtained from Radiochemical Centre, Amersham, U.K., as HCl. This solution was neutralized with 0·1 M NaOH and diluted with glass-distilled water to give a final volume of 100 ml. Experimental solutions were obtained using 0·6 mM non-radioactive NaCl and an aliquot of $Na^{36}Cl$ was added to give a final NaCl concentration of 1·0 mM. The specific activity was 50 $\mu$Ci/mmol.

## Results

### *Time Course of Net $H^+$ Efflux*

Net $H^+$ efflux time course experiments were conducted along the same lines as the $OH^-$ efflux experiments described by Lucas (1975*c*). Acidification time courses, obtained when a particular cell was transferred from the dark to four different

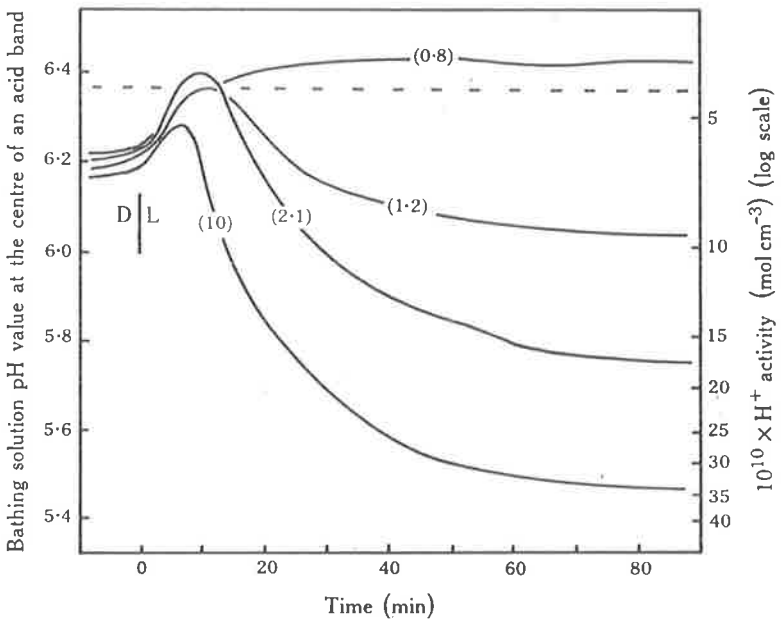


**Fig. 1.** Acidification time courses obtained under a range of irradiances. Traces were recorded by placing the pH-sensitive tip of the electrode onto the cell wall, within the central region of an acid band. Actual irradiance values (W m$^{-2}$) are indicated on the respective traces. The broken line represents the pH value of the bathing solution; *D*, *L* indicate the transition from dark to light. The experimental solution did not contain $NaHCO_3$; the pH value was adjusted with 100 mM NaOH.

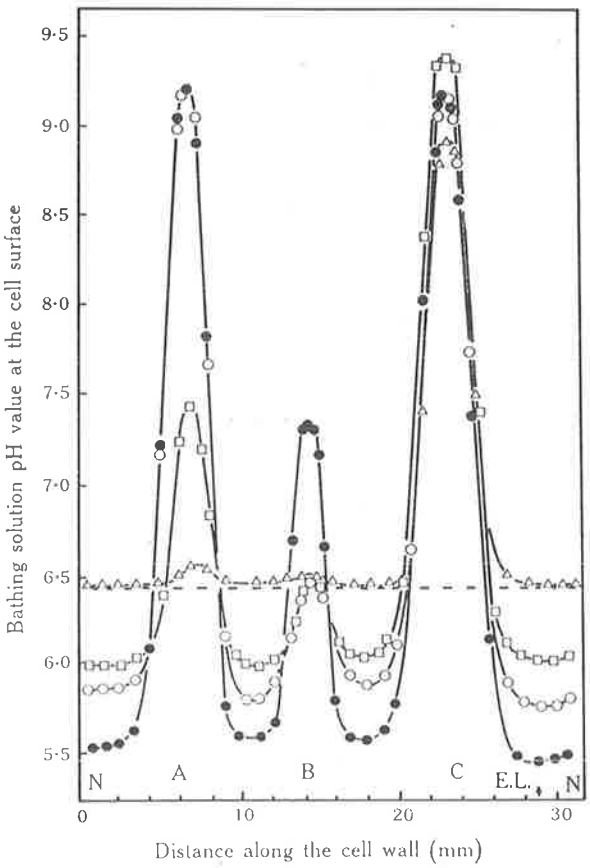


**Fig. 2.** pH values established at the cell wall surface following a 90-min illumination period. ●, ○, □, △, the values obtained under 10, 2·1, 1·2 and 0·8 W m$^{-2}$ irradiance, respectively. The nodal locations are indicated by *N*. *E.L.*, the electrode location and acid band studied in the results presented in Fig. 1. Alkaline bands *C*, *A*, and *B* were the primary, subprimary and subsidiary bands respectively (Lucas 1975*c*). Note that the acid bands approach the same pH value under the respective irradiance levels.

irradiance levels, are presented in Fig. 1. The dark period in each case was 1 h, and because the acid bands require a considerable time to return to the steady dark value, the dark sections of the pH traces in Figs 1 are in fact still rising towards the dark steady state. At each irradiance level, following a 90-min illumination period, a pH scan was performed along the cell wall. Figs 1 and 2 represent a complete acid band time course and cell surface steady state analysis for a particular cell. These results are typical of the responses obtained when cells were illuminated over a range of irradiances.

**Table 1. Acid and alkaline band lag periods prior to activation**

| Irradiance ($W\ m^{-2}$) | Experiment A Primary $OH^-$ lag period (min) | Acid band lag period (min) | Irradiance ($W\ m^{-2}$) | Experiment B Primary $OH^-$ lag period (min) | Acid band lag period (min) |
|---|---|---|---|---|---|
| 10·0 | 4·5 | 6·0 | | | |
| 8·0 | 4·5 | 6·0 | 9·5 | 6·3 | 8·5 |
| 2·1 | 6·5 | 10·0 | 5·0 | 8·4 | —[A] |
| 1·6 | 12·5 | —[A] | 3·0 | 9·8 | 11·0 |
| 1·2 | 20·0 | 12·0 | 1·9 | 13·0 | 14·0 |
| 0·8 | 44·5 | n.a.[B] | 1·2 | 53·0 | n.a.[B] |

[A] An acid time course was not conducted. [B] The acid efflux system remained inactive.

On the day after an acid band experiment had been conducted, the primary $OH^-$ band system (Lucas 1975*c*) was investigated so that a comparison could be made between the acid and alkaline lag periods. The acid lag period was defined as the time required, following illumination, for the cell surface pH value to reach the inflection point associated with the change from alkalinization to acidification (see Fig. 1). Table 1 contains experimental data for two such consecutive acid and primary $OH^-$ band studies (experiment A refers to the results presented in Figs 1 and 2). For a detailed account of the nature of the $OH^-$ lag period, see Lucas (1975*c*). This comparison revealed that, although the lag periods were comparable under high irradiances, the similarity did not extend to the situation where very low irradiances were employed. As the irradiance was reduced, both the $H^+$ and $OH^-$ lag periods increased; however, under low irradiances (approximately $1\ W\ m^{-2}$) the acid efflux system did not appear to activate at all (see also Fig. 3). Under the same conditions, the primary $OH^-$ efflux system did activate after a prolonged lag period. Under low irradiances, it would appear that, of the two light-dependent efflux processes, the $OH^-$ efflux is more critical to the maintenance of cellular cytoplasmic pH.

Figs 1 and 2 also demonstrated that the actual depression of the pH of the bathing solution increased in a regular sequence once the irradiance was raised above a certain 'critical' value. Further experimental support for this correlation between irradiance and the rate of acid extrusion is presented in Fig. 3. Here, the results of four experiments have been summarized by presenting the response of a single acid band from each cell. These results were included not only to illustrate the increase of acidity with increasing irradiance, but also to give some indication of the variability in the degree of acidification of the cell surface observed between different cells. It should be noted that there is a direct correlation between the level of acidification,

in terms of the external cell surface pH value, and the value of net acid efflux from the cell. Variation in individual cell acid efflux activity depicted by Figs 2*a*, 2*b* and 2*d* was frequently observed. For most cells, net acid efflux appeared to saturate under an irradiance of approximately 3–4 W $m^{-2}$.

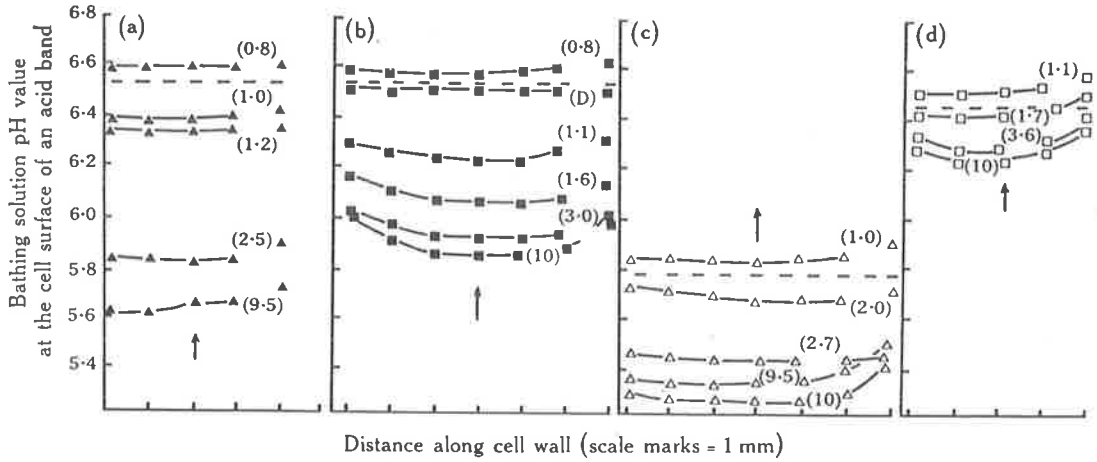


**Fig. 3.** Approximate steady-state acid values obtained under a range of irradiances. (*a*), (*b*), (*c*), (*d*), the responses of four different cells; the values were recorded as for Figs 1 and 2. The broken lines represent the pH values of the bathing solutions; (*a*), (*b*) and (*d*) values were raised above 5·75 with freshly prepared NaOH; (*c*) is the normal, unaltered pH value. The values in parentheses are the respective irradiance levels in W $m^{-2}$. The arrows indicate the location of the acid band centres.

### *$^{36}Cl^-$ Uptake Time Course in Relation to the Measured Net $H^+$ Efflux Lag Period*

The results presented in Fig. 1 indicate that after an initial rise in the pH value at the acid band centre, it was possible to discern net acid efflux within 8–10 min after the dark-to-light transition. This lag period was for an irradiance of 10 W $m^{-2}$; however, the results presented in Fig. 1 and Table 1 indicate that although this lag period increased under lower light levels, the increase was not as significant as that observed for the $OH^-$ efflux system. Hence, if the transport of $Cl^-$ is coupled to the pH gradient set up by $H^+$ efflux, the time course for the light-promoted uptake of this ion should exhibit a lag of at least 10–20 min over a wide range of irradiances.

Preliminary $^{36}Cl^-$ experiments, conducted to determine whether a lag of this nature existed, were performed using unbuffered solutions. A 1-h dark period was employed so that the conditions would be consistent with those of the $H^+$ efflux experiments, and $^{36}Cl^-$-labelled solution was substituted immediately before the commencement of the light period. Results obtained using this experimental sequence are presented in Fig. 4*a*. A lag in $^{36}Cl^-$ uptake was in fact observed. Uptake did not attain a steady state value, however, until the cells had been illuminated for a period greater than 40 min.

This lag in $^{36}Cl^-$ uptake may have been a reflection of cellular disturbance caused by solution substitution just before illumination of the cells. This possibility was tested by substituting the radioactive solutions 30 min before the cells were illuminated (Fig. 4*b*, 10 W $m^{-2}$). Again it was found that $^{36}Cl^-$ uptake was only slightly stimulated above the dark level for the first 30–40 min of the illumination period. At the end of this period, the uptake increased significantly. This procedure was repeated using

solutions which were buffered at pH 5·8 by 5 mM HEPES [Smith (1970) showed that HEPES buffer did not affect $^{36}Cl^-$ uptake]. The results were identical in form to the unbuffered treatments (cf. Fig. 4*b*, 14·4 W $m^{-2}$ with 10 W $m^{-2}$).

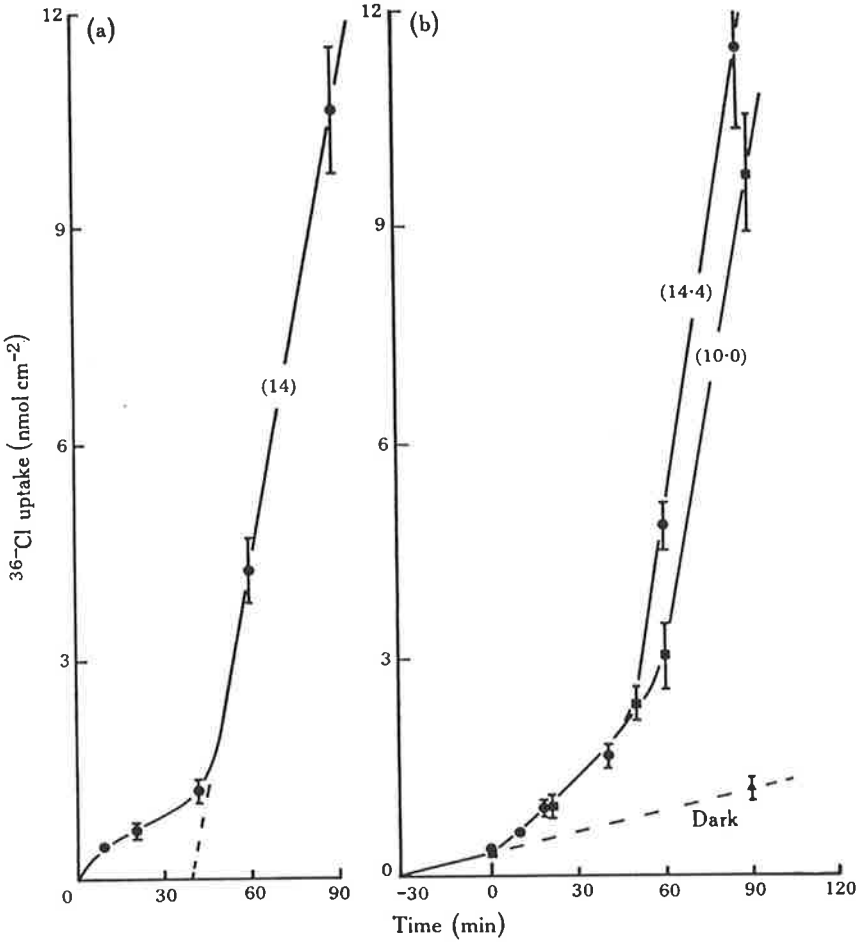


**Fig. 4.** Time course of $^{36}Cl^-$ uptake into culture tank Δ *C. corallina* cells. (*a*) Experiments conducted in unbuffered bathing solution, pH 5·8. (*b*) Time course at 10 W $m^{-2}$, as in (*a*), except that $^{36}Cl^-$ was substituted 30 min before the light treatment was commenced. Irradiance levels (W $m^{-2}$) are shown in parentheses. The 14·4 W $m^{-2}$ treatments were buffered by 5 mM HEPES, pH 5·8, and also included a 30-min dark pretreatment in $^{36}Cl^-$ solutions. All values are expressed as mean ± s.e.m., for 14 cells per treatment. In (*b*), the light period commenced at time 0.

### $^{36}Cl^-$ *Uptake: Influence of Irradiance*

Experiments at different irradiance values were conducted in an identical manner to that employed in Fig. 4*b*. The solutions were buffered at pH 5·8 (5 mM HEPES) to reduce the influence of the $OH^-$ efflux system associated with the cellular assimilation of $HCO_3^-$. It was argued that, since similar results were obtained in the presence and absence of this buffer, it could not be having an effect on the functioning of the $^{36}Cl^-$ uptake system. Results obtained using cells from two different culture tanks (tanks Δ and E′) are presented in Figs 5 and 6 respectively. In Fig. 5 the $^{36}Cl^-$ uptake values have not been corrected for dark $^{36}Cl^-$ uptake. Since the experiments were conducted over several days, at least one dark treatment was included in each

irradiance series. Following the completion of the series, an average dark $^{36}Cl^-$ influx value of $0{\cdot}26 \pm 0{\cdot}03$ pmol $cm^{-2}$ $s^{-1}$ was computed from the collective results. This value was then used to construct the 'mean averaged' dark uptake line marked on Fig. 5. The same procedure was employed for the results presented in Fig. 6, except that the $^{36}Cl^-$ uptake values were corrected for this dark uptake component.

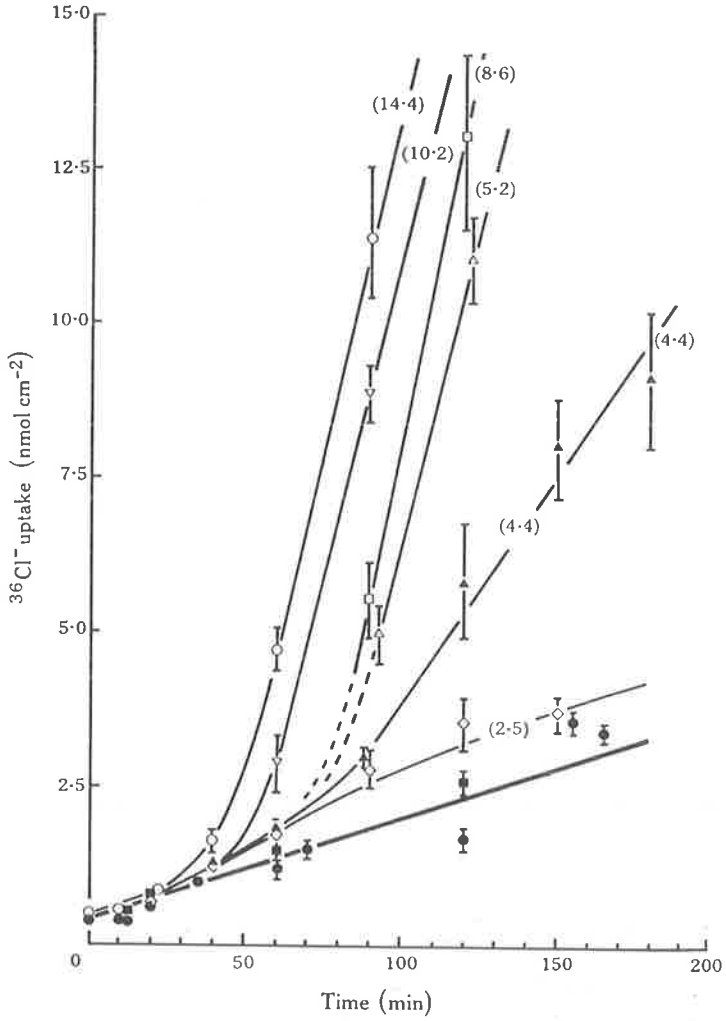


**Fig. 5.** Time course of $^{36}Cl^-$ uptake by tank Δ cells. Cells were given a 1-h dark pretreatment, 30 min of which was in normal solutions and an equal period in $^{36}Cl^-$. All solutions were buffered at pH 5·8 using 5 mM HEPES. Irradiance levels (W $m^{-2}$) are shown in parentheses. The heavy line represents the 'mean averaged' dark uptake rate; ■, ●, the uptake values measured under 1·4 W $m^{-2}$ and dark conditions, respectively. To avoid congestion, not all experimental points in the region 0–50 min have been included. Values are expressed as mean ± s.e.m.

The results from these experiments were used to calculate $^{36}Cl^-$ influx values present under the respective irradiances; the values are presented in Fig. 7. Some influx values included in Fig. 7 were determined by preilluminating the cells for 2 h, under the specified irradiance, before substituting radioactive solutions. The $^{36}Cl^-$ uptake and influx values were determined over a 1-h experimental period. The shape of these $^{36}Cl^-$ influx versus irradiance graphs (Fig. 7) is interesting in two respects. Firstly, they show that the maximum $^{36}Cl^-$ influx rate of 4 pmol $cm^{-2}$ $s^{-1}$ was obtained under irradiances in excess of 6–7 W $m^{-2}$; this irradiance is higher than that required to saturate the net $H^+$ efflux system. This maximum influx value is equal to or greater than the $^{36}Cl^-$ influx reported by Smith (1970, e.g. figure 1*a*). Secondly, they indicate that experiments conducted in the irradiance region of 2–5 W $m^{-2}$ could give variable influx results if a stable, uniform light system was not employed.

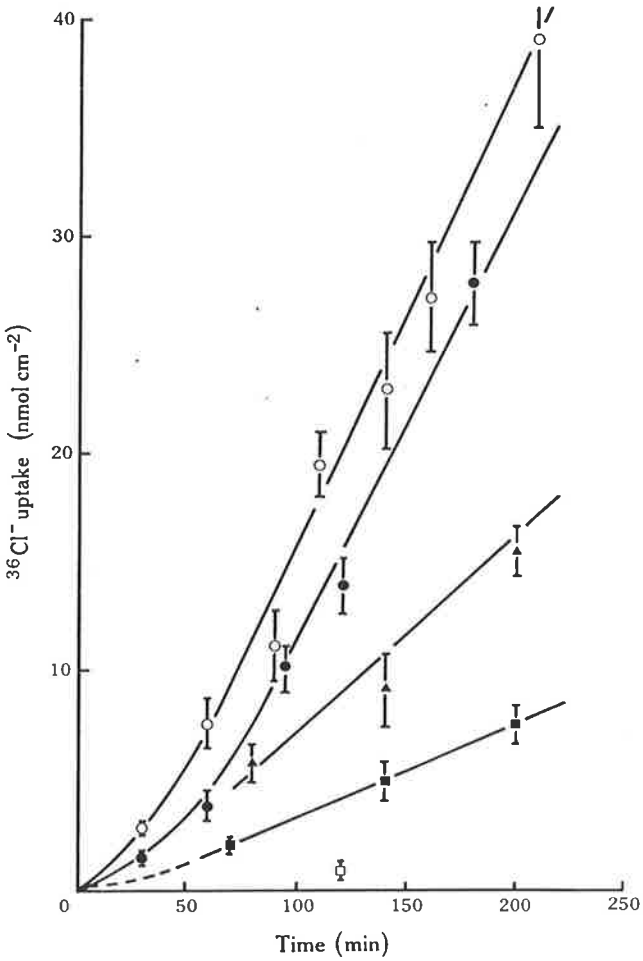


Fig. 6. Time course of $^{36}Cl^-$ uptake by tank E′ cells. Solutions and treatments as in Fig. 5. □, ■, ▲, ●, ○, the uptake values measured under irradiances of 1·0, 2·0, 3·0, 6·0 and 10·2 W m$^{-2}$, respectively. Values are expressed as mean ±s.e.m.

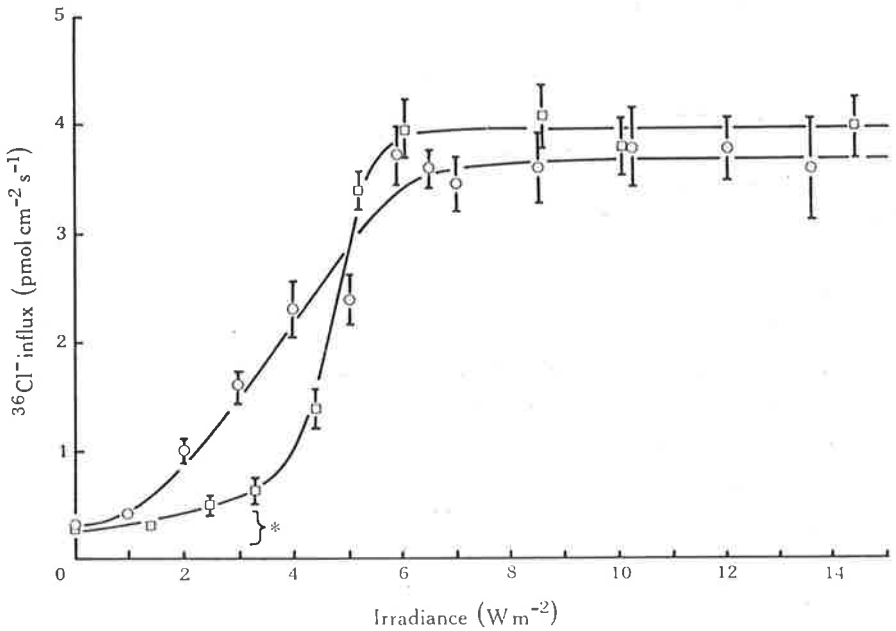


Fig. 7. $^{36}Cl^-$ influx as a function of irradiance. The influx values were determined from the results used to construct Figs 5 and 6. Additional values were measured over a 1-h radioactive contact time, following a preillumination period of 2 h. □, ○, influx values for culture tanks △ and E′ respectively; * represents the dark influx value which may be attributable to exchange diffusion. Values are expressed as mean ±s.e.m.

## Discussion

### *The $Cl^-$ Hypothesis of Spear* et al. *(1969)*

According to the $Cl^-$ transport hypothesis of Spear *et al.* (1969), the uptake of this ion should commence at least as soon as, and possibly before, net $H^+$ efflux is discernable at the cell surface. Since the observed lag in $Cl^-$ uptake (Figs 5 and 6) was greater than the lag associated with net $H^+$ efflux (Fig. 1), it is felt that this hypothesis (at least in its present form) is invalid for internodal cells of *C. corallina*.

### *The $Cl^-/OH^-$ Antiporter Hypothesis of Smith (1970)*

During the lag in $^{36}Cl^-$ uptake, the value in the light was only just stimulated above the dark value. This was particularly so for tank Δ cells (Fig. 5). The duration of this lag was approximately 40–50 min for tank Δ cells and 20–30 min for tank E′ cells. For cells from either culture, under a particular irradiance, the $^{36}Cl^-$ influx did not attain the steady state value until a period of greater than 50–60 min had elapsed. These lags are similar in magnitude to those reported for *Griffithsia flabelliformis* (Lilley and Hope 1971) and slightly longer than the lag these workers reported for *G. monile* (see also Raven 1974).

There appears to be, nevertheless, some degree of correlation between the lags observed in $^{36}Cl^-$ uptake and net $H^+$ efflux. (The $H^+$ efflux experiments were performed on cells cut from culture tank E′.) It would appear that the true light stimulation of $^{36}Cl^-$ uptake (E′ tank cells) began approximately 20 min after the cells were illuminated by an irradiance of 10·2 W $m^{-2}$ (Fig. 6). The same cells would have commenced net $H^+$ efflux at approximately 6–10 min after the onset of illumination (Fig. 1), and the external pH became steady after at least 60 min. The delay in attaining the maximum $Cl^-$ influx may have been related to the establishment across the plasmalemma of a critical energy gradient (i.e. the pH gradient as proposed by Smith 1970). If this 'activating' energy gradient required 20–30 min for its establishment, it may account for the pattern of the external pH changes. Once the activating condition is established, the $Cl^-/OH^-$ antiporter would tend to limit the observed acidification process at the cell wall. An alternative explanation is that the slow approach of the $H^+$ system towards the steady state is a consequence of the cylindrical diffusion system established by these bands (see Lucas 1975*a*). The acidification of the cell surface may also be limited by the passive influx of $H^+$ into the cell.

The strongest evidence against the activation of $Cl^-$ transport by a critical external pH level was obtained from the $^{36}Cl^-$ uptake experiments with buffered solutions. The presence of 5 mM HEPES buffer did not appear to influence the length of the lag period (Fig. 4*b*). This buffering capacity prevented the establishment of acid and alkaline bands at the cell surface (Lucas, unpublished data). The external surface of the plasmalemma may not be buffered to the same extent as the bathing solution because of Donnan effects in this regions. If the fixed negative charge distribution follows the pattern proposed by Dainty and Hope (1959), the free space region near the plasmalemma would be quite strongly buffered. There remains, however, the possibility of local pH gradients within the surface organelles reported by Barton (1965) and Crawley (1965).

Further evidence against the concept of an external pH value critical for light-induced uptake is the fact that the lag period appears to be almost independent of irradiance. Walker (1973) demonstrated that the photosynthetic induction period

in plant cells is also independent of the irradiance employed. Since most of the cells employed would have had irradiance acid time course responses similar to those presented in Fig. 1, the time to establish a particular acid pH value (at least at the cell surface) would have increased as the irradiance was reduced.

The above evidence suggests that the activation of $Cl^-$ influx is controlled by events within the cytoplasm (or plasmalemma). The dependence of $Cl^-$ influx on the pH of the bathing solution (see Smith 1970) may after all be explicable in terms of an effect of pH *per se* on the $K_m$ of the antiporter system (see Komor and Tanner 1974). However, this would not explain stimulation of $Cl^-$ influx at low pH following pretreatment at high pH (Smith 1972).

This study has been concerned with only one 'product' of the $H^+$ pump, namely the localized pH values developed at the cell surface. At the present time, we have no knowledge about pH changes (over the short term) within the cytoplasm, which might result from $H^+$ extrusion. Furthermore, it is difficult to correlate the $H^+$ efflux and $Cl^-$ influx systems with changes in the membrane potential. It is currently considered that the steady-state membrane potential reflects the balance between the electrogenic $H^+$ efflux and the other passive ion fluxes (see Kitasato 1968; Spanswick 1972). The times required for the establishment of the hyperpolarized state following illumination appear to lie between 10 and 20 min in various charophyte species, including *Chara corallina* (see Nagai and Tazawa 1962; Hope 1965; Andrianov *et al.* 1968; Nishizaki 1968; Spanswick 1972; Volkov 1973; also Lucas, unpublished results with *Chara corallina*). In other words, the membrane p.d. would stabilize before the external pH (cf. Fig. 1) and before the $Cl^-$ influx is fully stimulated (cf. Figs 4–6). Based on these collective results, the $Cl^-/OH^-$ antiporter would by itself appear to play a very insignificant role in the determination of the membrane potential of *Chara* [compare the large effect of the glucose–proton cotransport system on the membrane potential of *Neurospora* (Slayman and Slayman 1974)]. This is supported by the work of Findlay *et al.* (1969) and Pickard (1973), who showed that replacing $Cl^-$ by $SO_4^{2-}$ had very little effect on the resting potential. It should not be forgotten that changes in $H^+$ extrusion accompanying (or causing) changes in $Cl^-/OH^-$ exchange would be balanced by changes in influx of cations (e.g. $K^+$ and $Na^+$). If the stoichiometry for $Cl^-/OH^-$ is not one-for-one [see Walker and Smith (1975) who suggested a $1Cl^-/2OH^-$ exchange], larger effects of the system on the membrane p.d. might be expected. Again, this would depend on the interactive nature (feedback) of the $Cl^-$ transport system on the primary electrogenic $H^+$ extrusion system. It would also depend on the absolute magnitude of $H^+$ efflux compared with the rate of $Cl^-/OH^-$ exchange. As yet, there is no direct method available by which $H^+$ efflux can be distinguished from the net flux, which must include all 'back fluxes' of $H^+$ or exchange fluxes of $OH^-$.

### *Energetics of the $Cl^-/OH^-$ Transport Process*

The Gibbs free energy involved in the coupled transfer of a mole of $Cl^-$ from the bathing solution to the cytoplasm ($Cl^o \rightarrow Cl^i$), in exchange for a mole of $OH^-$ being transferred in the opposite direction ($OH^o \leftarrow OH^i$), can be calculated from the following equation:

$$\Delta G = RT \ln[(a^i_{Cl} \cdot a^o_{OH})/(a^o_{Cl} \cdot a^i_{OH})],$$

where the superscripts o and i refer to the bathing solution and cytoplasmic phases respectively, $a_{Cl}$ and $a_{OH}$ are the activities of $Cl^-$ and $OH^-$ respectively, $R$ is the gas constant and $T$ the absolute temperature (K).

From this equation, it can be calculated that the $OH^-$ gradient would provide sufficient energy for the coupled transport system to move spontaneously in the forward direction in the light and dark. As shown in Table 2, $\Delta G$ is negative in both

**Table 2. Energetics of the $Cl^-/OH^-$ transport process**

Gibbs free energy values were calculated by substitution into the equation presented in the text. All values of activity are given in moles per litre

| $10^3 \times a^o_{Cl}$ | $10^9 \times a^o_{OH}$ | $pH^o$ | $10^2 \times a^i_{Cl}$ | $10^7 \times a^i_{OH}$ | $pH^i$ | $\Delta G_{Cl/OH}$ (kJ $mol^{-1}$) |
|---|---|---|---|---|---|---|
| 1·2 | 6·31 | 5·8 | 1·0[A] | 5·13[B] | 7·71 | −5·65 |
| | | | | 2·88[C] | 7·46 | −4·23 |
| 1·2 | 6·31 | 5·8 | 2[D] | 5·13[B] | 7·71 | −3·93 |
| | | | | 2·88[C] | 7·46 | −2·51 |

[A] From Coster (1966). [B] Cytoplasmic pH (steady state) reported for *Chara corallina* when cells were illuminated (Walker and Smith 1975). [C] As for [B], except cells were darkened. [D] From Walker (1974).

these situations. (The $\Delta G$ values for a coupled $H^+$–$Cl^-$ cotransport would of course, be identical.) Hence, on the basis of the results presented in this paper and those of Walker and Smith (1975), it would appear that the uptake of $Cl^-$ is not linked to $H^+$ efflux in as simple a manner as was originally proposed by Smith (1970). Theoretically, the energy supply for the $Cl^-/OH^-$ system (i.e. $\Delta pH$) appears to exist across the plasmalemma in the dark. This suggests that the observed delay in $Cl^-$ uptake is not associated with a time-dependent process involved in the establishment of such an energy gradient. It is still possible that the cytoplasmic pH plays a specific role in triggering the exchange in the light. The slight differences in cytoplasmic pH between light and darkness (at most 0·2 pH units) reported by Walker and Smith (1975) may be significant here. It is also possible (and perhaps more likely) that the lag is due to the slow cytoplasmic build-up of an energy substrate produced by the chloroplasts, such as $NADPH_2$ or ATP or both (Lilley and Hope 1971; Smith and Raven 1974). Although levels of these compounds ought to be sufficient to provide the energy for $Cl^-$ transport in the dark as well as the light, it is possible that they may mediate in the binding of ions to the carrier. Alternatively, it may be necessary to activate the carrier system over a relatively large energy of activation barrier.

Unfortunately, the results presented in this paper do not allow a firm conclusion to be drawn as to the validity of the $Cl^-/OH^-$ antiporter hypothesis proposed by Smith (1970). However, it is now obvious that the original hypothesis needs to be modified, especially with respect to the energy requirements of the actual transport system.

**Acknowledgments**

This work was done while W. J. Lucas held an Australian Commonwealth Postgraduate Scholarship. Additional support was provided by an Australian Research Grants Committee award to F. A. Smith. Thanks are also due to Professor J. Dainty for his helpful discussions and Dr R. M. Spanswick for reading the manuscript.

## References

Andrianov, V. K., Kurella, G. A., and Litvin, F. F. (1968). Influence of light on the electrical activity of *Nitella* cells. In 'Transport and Distribution of Matter in Cells of Higher Plants'. (Eds K. Mothes, E. Müller, A. Nelles and D. Neumann.) pp. 187–96. (Akademie-Verlag: Berlin.)

Barton, R. G. (1965). An unusual organelle in the peripheral cytoplasm of *Chara* cells. *Nature (Lond.)* **205**, 201.

Chappell, J. B., and Crofts, A. R. (1966). Ion transport and reversible volume changes of isolated mitochondria. In 'Regulation of Metabolic Processes in Mitochondria'. (Eds J. M. Tager, S. Papa, E. Quagliariello and E. C. Slater.) pp. 293–314. (Elsevier: Amsterdam.)

Coster, H. G. L. (1966). Chloride in cells of *Chara australis*. *Aust. J. Biol. Sci.* **19**, 545–54.

Crawley, J. C. W. (1965). A cytoplasmic organelle associated with cell walls of *Chara* and *Nitella*. *Nature (Lond.)* **205**, 200–1.

Dainty, J., and Hope, A. B. (1959). Ionic relations of cells of *Chara australis*. I. Ion exchange in the cell wall. *Aust. J. Biol. Sci.* **12**, 395–411.

Findlay, G. P., Hope, A. B., Pitman, M. G., Smith, F. A., and Walker, N. A. (1969). Ionic fluxes in cells of *Chara corallina*. *Biochim. Biophys. Acta* **183**, 565–76.

Harold, F. M., and Baarda, J. R. (1968). Inhibition of membrane transport in *Streptococcus faecalis* by uncouplers of oxidative phosphorylation and its relationship to proton conduction. *J. Bacteriol.* **96**, 2025–34.

Hope, A. B. (1965). Ionic relations of *Chara australis*. X. Effects of bicarbonate ions on electrical properties. *Aust. J. Biol. Sci.* **16**, 429–41.

Kitasato, H. (1968). The influence of $H^+$ on the membrane potential and ion fluxes of *Nitella*. *J. Gen. Physiol.* **52**, 60–87.

Komor, E., and Tanner, W. (1974). Proton movements associated with hexose transport in *Chlorella vulgaris*. In 'Membrane Transport in Plants'. (Eds U. Zimmermann and J. Dainty.) pp. 209–15. (Springer-Verlag: Berlin, Heidelberg and New York.)

Lilley, R. McC., and Hope, A. B. (1971). Chloride transport and photosynthesis in cells of *Griffithsia*. *Biochim. Biophys. Acta* **226**, 161–71.

Lucas, W. J. (1975*a*). Analysis of the diffusion symmetry developed by the alkaline and acid bands which form at the surface of *Chara corallina* cells. *J. Exp. Bot.* **26**, 271–86.

Lucas, W. J. (1975*b*). Photosynthetic fixation of $^{14}$Carbon by internodal cells of *Chara corallina*. *J. Exp. Bot.* **26**, 331–46.

Lucas, W. J. (1975*c*). The influence of light intensity on the activation and operation of the hydroxyl efflux system of *Chara corallina*. *J. Exp. Bot.* **26**, 347–60.

Lucas, W. J., and Smith, F. A. (1973). The formation of alkaline and acid regions at the surface of *Chara corallina* cells. *J. Exp. Bot.* **24**, 1–14.

MacRobbie, E. A. C. (1970). The active transport of ions in plant cells. *Q. Rev. Biophys.* **3**, 251–94.

MacRobbie, E. A. C. (1974). Ion uptake. In 'Algal Physiology and Biochemistry'. (Ed. W. D. P. Stewart.) pp. 676–713. (Blackwell: Oxford.)

Nagai, R., and Tazawa, M. (1962). Changes in resting potential and ion absorption induced by light in a single plant cell. *Plant Cell Physiol.* **3**, 323–39.

Nishizaki, Y. (1968). Light-induced changes of bioelectric potential in *Chara*. *Plant Cell Physiol.* **9**, 377–87.

Pickard, W. F. (1973). Does the resting potential of *Chara braunii* have an electrogenic component? *Can. J. Bot.* **51**, 715–24.

Raven, J. A. (1974). Time course of chloride fluxes in *Hydrodictyon africanum* during alternating light and darkness. In 'Membrane Transport in Plants'. (Eds U. Zimmermann and J. Dainty.) pp. 167–72. (Springer-Verlag: Berlin, Heidelberg and New York.)

Slayman, C. L. (1974). Proton pumping and generalized energetics of transport: a review. In 'Membrane Transport in Plants'. (Eds U. Zimmermann and J. Dainty.) pp. 107–19. (Springer-Verlag: Berlin, Heidelberg and New York.)

Slayman, C. L., and Slayman, C. W. (1974). Depolarization of the plasma membrane of *Neurospora* during active transport of glucose: evidence for a proton-dependent cotransport system. *Proc. Natl Acad. Sci. U.S.A.* **71**, 1935–9.

Smith, F. A. (1970). The mechanism of chloride transport in Characean cells. *New Phytol.* **69**, 903–17.

Smith, F. A. (1972). Stimulation of chloride transport in *Chara* by external pH changes. *New Phytol.* **71**, 595–601.

Smith, F. A., and Raven, J. A. (1974). Energy-dependent processes in *Chara corallina*: absence of light stimulation when only photo-system one is operative. *New Phytol.* **73**, 1–12.

Spanswick, R. M. (1972). Evidence for an electrogenic ion pump in *Nitella translucens*. I. The effects of pH, $K,^{+}$ $Na^{+}$, light and temperature on the membrane potential and resistance. *Biochim. Biophys. Acta* **288**, 73–89.

Spear, D. G., Barr, J. K., and Barr, C. E. (1969). Localization of hydrogen ion and chloride ion fluxes in *Nitella*. *J. Gen. Physiol.* **54**, 397–44.

Volkov, G. A. (1973). Bioelectrical response of the *Nitella flexilis* cell to illumination: a new possible state of plasmalemma in a plant cell. *Biochem. Biophys. Acta* **314**, 83–92.

Walker, D. A. (1973). Photosynthetic induction phenomena and the light activation of ribulose diphosphate carboxylase. *New Phytol.* **72**, 209–35.

Walker, N. A. (1974). Chloride transport to the Charophyte vacuole. In 'Membrane Transport in Plants'. (Eds U. Zimmermann and J. Dainty.) pp. 173–9. (Springer-Verlag: Berlin, Heidelberg and New York.)

Walker, N. A., and Smith, F. A. (1975). Intracellular pH in *Chara corallina* measured by DMO distribution. *Plant. Sci. Lett.* **4**, 125–32.

Manuscript received 16 September 1975

*Journal of Experimental Botany, Vol. 28, No. 107, pp. 1307–1320, December 1977*

# Plasmalemma Transport of $HCO_3^-$ and $OH^-$ in *Chara corallina*: Inhibitory Effect of Ammonium Sulphate

W. J. LUCAS[1]
*Department of Botany, University of Toronto, Toronto, Ontario M5S 1A1, Canada*

Received 21 March 1977

## ABSTRACT

The influence of $(NH_4)_2SO_4$ on $^{14}C$ assimilation and cyclosis in internodal cells of *Chara corallina* was investigated. Severe inhibition of $^{14}C$ assimilation was found at pH values above 7·0, this inhibition being correlated with the exogenous level of $NH_3$ rather than $NH_4^+$. Cyclosis was also affected at higher concentrations of $(NH_4)_2SO_4$. This effect was similarly correlated with exogenous levels of $NH_3$.

$^{14}C$ assimilation was inhibited non-competitively by $(NH_4)_2SO_4$, the apparent $K_m$ being increased from 0·55 to 1·5 mM. The results suggest that the site(s) of inhibition is located at the plasmalemma, rather than at the chloroplasts. (Evidence in support of *in vivo* uncoupling of photophosphorylation, by low concentrations of $(NH_4)_2SO_4$, was not obtained).

Significant perturbation of the $OH^-$ efflux pattern was observed as the level of $(NH_4)_2SO_4$ was increased. Induced migration of efflux sites indicates that $NH_3$ may interfere with the cellular mechanism that controls $OH^-$ transport. Using a cell-segment isolating chamber it was shown that $(NH_4)_2SO_4$ inhibited $OH^-$ efflux rather than $HCO_3^-$ transport. This inhibitory effect was readily reversible.

These data are discussed in terms of a possible relationship between the observed $(NH_4)_2SO_4$ stimulation of $^{36}Cl^-$ influx and the effect of this compound on $^{14}C$ assimilation.

## INTRODUCTION

Photophosphorylation in isolated chloroplasts can be effectively uncoupled by amines (Ohmura, 1958; Krogmann, Jagendorf, and Avron, 1959; Good, 1960) and nitrogenous bases (Hind and Whittingham, 1963). The differential effect of imidazole (and ammonium) on the active influx of $K^+$ and $Cl^-$ in *Nitella translucens* was interpreted by MacRobbie (1965, 1966) on the basis of *in vivo* uncoupling of photophosphorylation by this amino compound. (Pronounced inhibition of $K^+$ influx suggested a requirement for photosynthetically generated ATP, whereas the slight stimulatory effect on $Cl^-$ influx suggested a reductive energy requirement associated with non-cyclic electron flow.) These amino compounds also inhibited the light-mediated active flux of phosphate and D-glucose in these cells (Smith, 1965).

However, the apparent insensitivity of *in vivo* $^{14}CO_2$ fixation to imidazole or ammonium sulphate (Smith, 1967) did not appear to support MacRobbie's hypothesis concerning the *in vivo* uncoupling of photophosphorylation. Subsequent studies on *Chara corallina* appeared to confirm this view. Parallel *in vivo* and *in vitro* experiments revealed that, whereas imidazole stimulated the light-promoted influx

[1] Present address: Department of Botany, University of California, Davis, California 95616, U.S.A.

of $Cl^-$ and uncoupled photophosphorylation (*in vitro*), it had no observable effect on *in vivo* $^{14}CO_2$ assimilation (Smith and West, 1969). Similar results were obtained using ammonium sulphate (Smith and West, 1969; Smith, 1970).

An alternative hypothesis to account for the stimulatory influence of imidazole, ammonium sulphate, and also tris(hydroxymethyl)methyl ammonium chloride, on the influx of $Cl^-$ into *Chara corallina*, was proposed by Smith (1970, 1972). He suggested that the cytoplasmic pH may be affected by an influx of these compounds. Imidazole, for example, could traverse the plasmalemma either as the neutral molecule, which would then react with protons in the cytoplasmic phase to form the cationic species, or it could possibly penetrate as the cation in an exchange process for $H^+$. In either case, the net result would be an increase in the pH value of the cytoplasm. This pH gradient was considered to act as a driving force on a $Cl^-/OH^-$ exchange system (Smith, 1970; see also Lucas and Smith, 1976; Smith and Walker, 1976).

Again, experimental confirmation of this proposal was not obtained. Walker and Smith (1975) determined cytoplasmic pH values in *Chara corallina* under a range of conditions, in the presence and absence of ammonium sulphate. Rather than increase, the cytoplasmic pH value appeared to decrease slightly in the presence of ammonium sulphate. The slight increase in cytoplasmic pH that was observed in the presence of imidazole (Smith and Walker, 1976) was considered by these authors to be inadequate to explain the observed effect of this compound on $Cl^-$ transport.

Photosynthesis, in *Chara corallina*, is maximized by the simultaneous supply of exogenous carbon by diffusion of $CO_2$ and transport of $HCO_3^-$ across the plasmalemma (Lucas, 1975*a*). Bicarbonate transport dominates at pH values above 7·0. It was within this pH region (and higher) that MacRobbie (1965) and Smith (1970, 1972) observed the stimulatory effect of these amino compounds on $Cl^-$ influx. In the presence of $HCO_3^-$ assimilation the transport of $HCO_3^-$ appears to competitively inhibit $Cl^-$ influx (Van Lookeren Campagne, 1957; Smith, 1965; Raven, 1968). Hence, these compounds may partially inhibit $HCO_3^-$ or $OH^-$ transport in such a way that the competitive inhibition of $Cl^-$ transport is relieved. Since the rate of $H^{14}CO_3^-$ transport is high (60 pmol $cm^{-2}$ $s^{-1}$; Lucas, 1975*a*) compared with the 'normal' or 'stimulated' $Cl^-$ influx values (1·0–4·0 pmol $cm^{-2}$ $s^{-1}$, Smith, 1970, 1972; but see Lucas and Smith, 1976), this stimulation may occur with very little affect on the observed rate of photosynthesis.

In an attempt to elucidate this problem, the present study was conducted to determine the effect(s) of ammonium sulphate on the $H^{14}CO_3^-$ assimilating system of *Chara corallina*.

## MATERIALS AND METHODS

### *Culture material*

Culture material of *Chara corallina* Klein ex Willd., em. R.D.W. (=*C. australis* R. Br.) (Wood and Imahori, 1965) was grown in the laboratory under artificial light. Culture details and methods used to cut internodal cells from the culture have been previously reported (Lucas and Smith, 1973; Lucas, 1975*a*). In general, mature third to fifth internodal cells were used.

*Experimental solutions*

All chemicals used were of Analar Reagent grade and glass-distilled water having an approximate specific conductivity of $1{\cdot}2 \times 10^{-6}$ s $cm^{-1}$ was employed for solution preparation. The standard experimental solution contained 1·0 mM NaCl, 0·2 mM KCl, and 0·5 mM $CaSO_4$, unless otherwise specified. Some $^{14}C$ experimental solutions were buffered using 2-(*N*-morpholino)ethanesulphonic acid (MES) or *N*-tris(hydroxymethyl)methyl-2-aminoethanesulphonic acid (TES) at 5 mM concentration.

Radioactive $NaH^{14}CO_3$ was obtained from New England Nuclear, Boston, as a sterile aqueous solution, and aliquots were added to the experimental solutions to give the required specific activity.

*Experimental system*

Experiments were performed in a thermostatted (25 °C) system. The light source was a Leitz-Pradovit 24 V, 150 W quartz-iodide projector. Irradiances were attenuated using a range of nickel-Nicron neutral density filters prepared by the Department of Physics, University of Adelaide. Irradiance was measured using a silicon solar cell (IRC, type No. S 0510E 7PL) which was calibrated against a Kipp and Zonen Compensated Thermopile (Model CA1). Actual irradiances employed are specified in the text.

Cytoplasmic streaming, cell well pH scans, and radioisotope ($NaH^{14}CO_3$) studies were performed on cells cut one day prior to the performance of the experiment. These cells were pre treated in experimental solutions which contained 1·0 mM $NaHCO_3$ (pH 9·0). The light regime employed for the cultures (13 h light : 11 h dark) was maintained during this pretreatment period, and all cells were illuminated under fluorescent lights (10 W $m^{-2}$) for 2 h before the start of an experiment. The radioisotope techniques employed have been detailed by Lucas (1975*a*). Cyclosis was measured with a binocular microscope having an ocular micrometer. The time required for a standard-sized cytoplasmic particle to traverse 1000 μm was measured with a stopwatch.

*pH measurement at the surface of* Chara *cells*

The pH values, along the cell surface of *C. corallina* internodal cells, were measured using the technique developed by Lucas and Smith (1973). To prepare agar blocks (0·7%, w/v) containing $(NH_4)_2SO_4$ and/or $NaHCO_3$, the following procedure was employed. Agar powder (Difco, Bacto-agar) was dissolved by boiling a known volume of standard experimental solution. This solution was then cooled to 39 °C, at which temperature the required amounts of stock $(NH_4)_2SO_4$ and/or $NaHCO_3$ solutions were added. The pH value was checked and titrated to the required value. Experimental agar blocks were then set within special Perspex holders (see Lucas and Smith, 1973, for full details).

Following a 90 min illumination period, a Leitz micromanipulator was used to move a miniature pH electrode (Microelectrodes Inc., Model MI-405) along the cell well. A Beckman Model 4500 digital pH meter was used in conjunction with the miniature pH electrode. From the values obtained the pH pattern established at the cell surface was mapped.

## RESULTS

### *Influence of $(NH_4)_2SO_4$ on $H^{14}CO_3^-$ assimilation*

The effect of various concentrations of $(NH_4)_2SO_4$ on $H^{14}CO_3^-$ assimilation was investigated. Experiments were conducted at pH 9·1, and all experimental solutions contained 3 mM total carbon (added as $Na_2CO_3$ and titrated to pH 9·1 using $H_2SO_4$). The results indicated that $^{14}C$ assimilation was inhibited even at the lowest $(NH_4)_2SO_4$ concentration employed (Table 1). The $(NH_4)_2SO_4$ concentration range 0·05–0·5 mM spans that employed by MacRobbie (1966), Smith (1967, 1970, 1972), and Smith and Walker (1976); but note that these authors conducted their experiments over a range of pH values (7·0–9·2).

Cells were examined under the microscope, at the conclusion of $^{14}C$ experiments, to ensure that cyclosis remained unaffected. It was found that $(NH_4)_2SO_4$ con-

TABLE 1. *Influence of $(NH_4)_2SO_4$ on $H^{14}CO_3^-$ assimilation*

| Experimental solutions[a] | | Photosynthetic $^{14}C$ assimilation (pmol $cm^{-2}$ $s^{-1}$) | Inhibition (%) |
|---|---|---|---|
| $(NH_4)_2SO_4$ added (mM) | $NH_3$[b] (mM) | | |
| — | — | 60·7 ± 3·0 | Control |
| 0·05 | 0·04 | 44·9 ± 3·6 | 26·0 |
| 0·10 | 0·08 | 20·5 ± 2·6 | 66·2 |
| 0·25 | 0·21 | 11·4 ± 0·5 | 81·2 |
| 0·50 | 0·41 | 10·7 ± 0·5 | 82·4 |
| 0·75 | 0·62 | 7·7 ± 0·6 | 87·3 |
| 1·25 | 1·03 | 3·5 ± 0·2 | 94·3 |

[a] All $^{14}C$ fixation experiments were conducted under an irradiance of 25 $Wm^{-2}$. A period of 1 h was employed both for pretreatment and $^{14}C$ exposure, and 3·0 mM total carbon (pH 9·1) was used throughout. Values are expressed as mean ± s.e. mean; ten cells were used per treatment and some treatments were duplicated.

[b] Equilibrium concentrations of $NH_3$ calculated using the equilibrium constant $K_b = 1{\cdot}77 \times 10^{-5}$ (Bates and Pinching, 1949).

centrations above 0·5 mM (pH 9·1) induced the formation of large cytoplasmic inclusions in the vacuole and cyclosis also appeared to be reduced. At high $(NH_4)_2SO_4$ concentrations (1·25–1·5 mM) some chloroplast rupture was observed.

*Cyclosis in the presence of $(NH_4)_2SO_4$*

The effect of $(NH_4)_2SO_4$ on cyclosis is illustrated in Fig. 1. These experiments were conducted at pH 8·0 and 9·0 in the presence of 2·0 mM total carbon. The correlation between cyclosis inhibition and the level of ammonia ($NH_3$) in the solution is demonstrated in Fig. 1B. The formation of spherical cytoplasmic inclusions in the vacuole was also correlated with the second, abrupt phase in the reduction of cyclosis. It would appear, therefore, that the partial 'precipitation' of the streaming cytoplasm into spherical inclusions is induced once the level of $NH_3$ (rather than $NH_4^+$) in the experimental medium exceeds a concentration of approximately 0·5 mM. Ammonia concentrations above this level always resulted in the eventual death of the cells. However, prolonged exposure (>24 h) of internodal cells to $NH_3$ concentrations below 0·4–0·45 mM did not result in further reduction of cyclosis. Similarly, chloroplast rupture was not in evidence at this $NH_3$ concentration.

A comparison of the results presented in Table 1 and Fig. 1 revealed that, whereas cyclosis was only slightly affected at $NH_3$ concentrations below 0·45 mM, $H^{14}CO_3^-$ assimilation was severely inhibited within this same $NH_3$ concentration range. Cyclosis may be reduced due to an effect of $NH_3$ (or $NH_4^+$) on either the energy supply (Chappell and Haarhoff, 1967; Matsumoto, Wakiuchi, and Takahashi, 1971) for cyclosis or the mechanism that imparts the motive force to the cytoplasm. The observed inhibition of photosynthesis, in the presence of $(NH_4)_2SO_4$, may have resulted from the action of $NH_3$ (or $NH_4^+$) at either the plasmalemma or the chloroplasts.

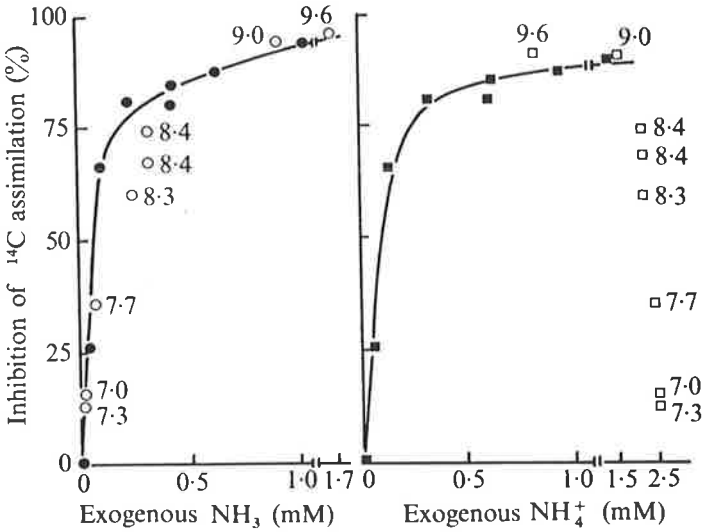


FIG. 2. Relationship between percentage inhibition of $^{14}C$ assimilation and the exogenous concentration of $NH_4^+$ and $NH_3$ present. Data from Tables 1 and 2 represented by solid and open symbols respectively. For the latter, experimental pH values are indicated by the points.

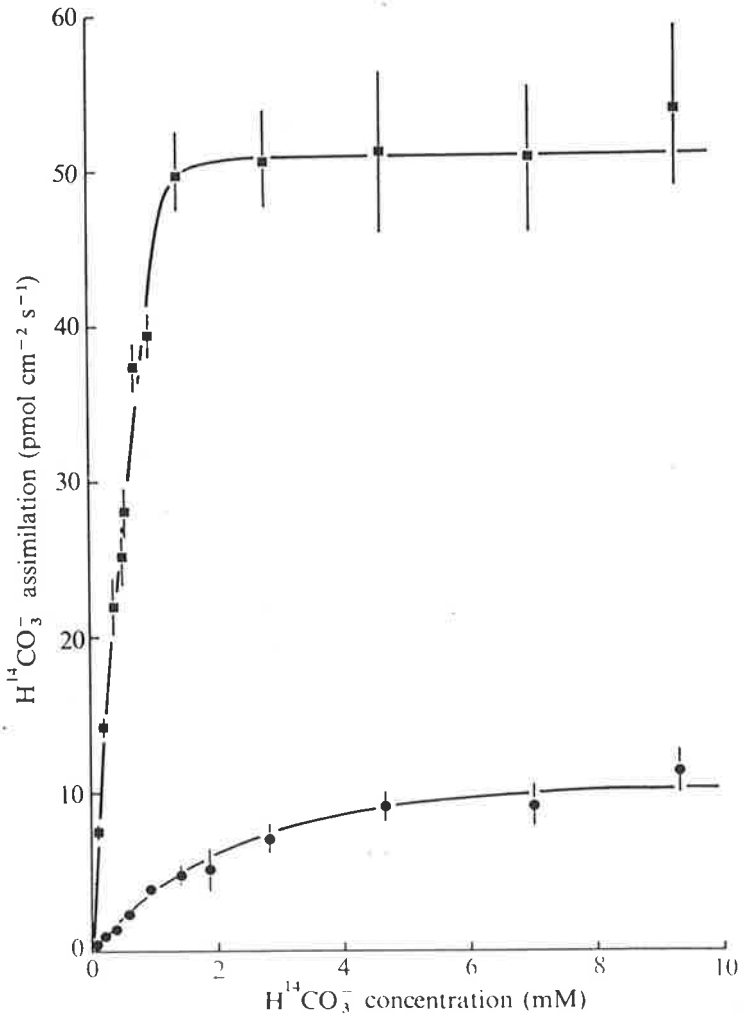


FIG. 3. $H^{14}CO_3^-$ assimilation in response to increasing substrate concentration, in the presence of a constant concentration (0·3 mM) of $(NH_4)_2SO_4$. ■, control treatments; ●, $(NH_4)_2SO_4$ treated cells. Normal 1 h pretreatment and $^{14}C$ exposure periods were employed and cells were illuminated with an irradiance of 20 W $m^{-2}$. Values express mean ± s.e. mean for 10 cells.

0·55 mM (control value) to 1·5 mM. Uncoupling of the chloroplasts by $NH_3$ would limit the amount of ATP available for $CO_2$ fixation. This would reduce the rate of fixation, but the apparent $K_m$ may remain unaltered, i.e. providing $NH_3$ does not have any secondary effect on any of the Calvin cycle enzymes. Ribulose diphosphate carboxylase is an allosteric enzyme, whose $K_m$ is affected by such factors as the concentration of $Mg^{2+}$ and the pH value within the stroma (Walker, 1973). There is therefore the slight possibility that the observed increase in apparent $K_m$ may be related to an effect of $NH_3$ on this enzyme, either directly or via an effect on stromal pH.

Alternatively the site of $NH_3$ inhibition of $H^{14}CO_3^-$ assimilation may be located at the plasmalemma. This interpretation was supported by the observation that chloroplast rupture, which represents swelling induced by the penetration of $NH_3$, does not occur until higher (lethal) $(NH_4)_2SO_4$ concentrations are employed.

Although the $H^{14}CO_3^-$ and $OH^-$ transport systems operate at spatially separate sites within the plasmalemma (Lucas, 1976) their rates of operation are coupled by the steady state requirement of electrical neutrality. If $NH_3$ partially inhibited the functioning of the $OH^-$ efflux system, $OH^-$ transport would become the rate-determining step in the overall process of $H^{14}CO_3^-$ assimilation. (We recently reported a situation of this nature that resulted when cyclosis was inhibited by cytochalasin B (Lucas and Dainty, 1977).)

*Hydroxyl transport affected by $(NH_4)_2SO_4$*

A study of the $OH^-$ efflux pattern, established under various $(NH_4)_2SO_4$ concentrations, was conducted to investigate this possibility. Control pH scans were performed on each cell, using 1·0 and 0·25 mM total carbon, prior to employing a range of $(NH_4)_2SO_4$ concentrations. Figure 4A indicates the manner in which the pH pattern, established at the cell surface, altered as the cell responded to varying rates of photosynthetic assimilation. Based on the diffusion analysis techniques developed by Lucas (1975*b*) and Lucas, Ferrier, and Dainty (1977), the $OH^-$ efflux rate for the 1·0 and 0·25 mM $HCO_3^-$ controls would have been approximately 45 and 15 pmol $cm^{-2}$ $s^{-1}$, respectively. (These values are in agreement with the rates of $^{14}C$ fixation presented in Fig. 3.)

The important feature illustrated in Fig. 4A is that, as the $OH^-$ efflux 'load' is reduced, the transport rate is lowered; this is reflected in the decrease in pH value at the $OH^-$ band centres (Lucas *et al.*, 1977). The adjustment in the $OH^-$ transport rate is achieved by narrowing the pumping width of the operational $OH^-$ band as well as reducing the rate, *per se*, within this transport band (see Lucas *et al.* 1977).

The results presented in Fig. 4B typify the $OH^-$ efflux response observed in the presence of $(NH_4)_2SO_4$. At very low $(NH_4)_2SO_4$ concentrations ($\leqslant$0·1 mM) the pH values were reduced, but the location of the $OH^-$ efflux sites remained stable with respect to the control sites. However, a significant perturbation of the $OH^-$ efflux pattern was observed as the level of $(NH_4)_2SO_4$ was increased (see Fig. 4B, 0·2–0·5 mM $(NH_4)_2SO_4$). From Fig. 3 it can be seen that in the presence of 0·3 mM $(NH_4)_2SO_4$ and 1·0 mM $HCO_3^-$, the $^{14}C$ fixation rate would have been 4–5 pmol $cm^{-2}$ $s^{-1}$. If $NH_3$ had been acting at the $HCO_3^-$ transport site (or at the chloroplast

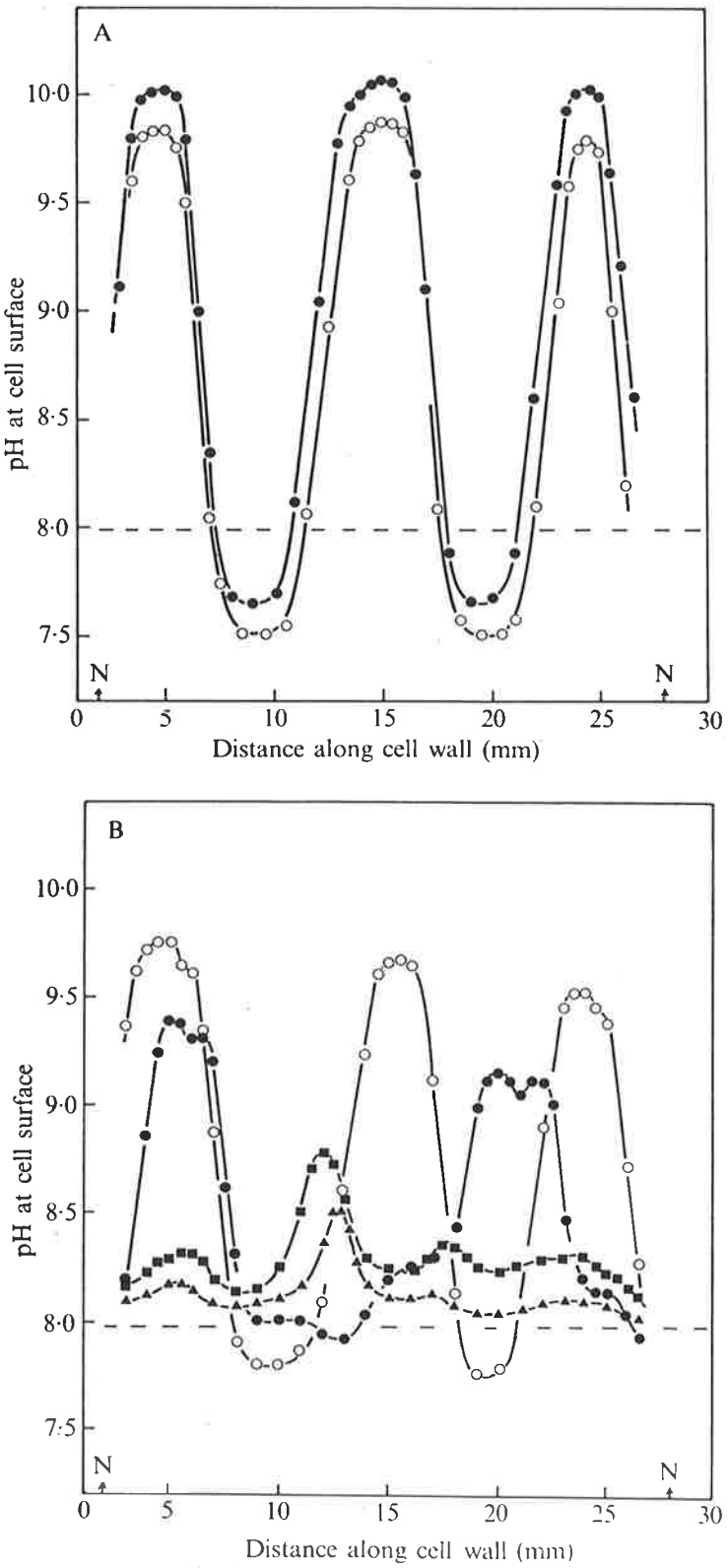


FIG. 4. Influence of $(NH_4)_2SO_4$ on the $OH^-$ efflux pattern established on the internodal cell surface of *Chara corallina*. The pH value of the agar block and bathing solution was adjusted to approximately 8·0 and contained 1·0 mM $NaHCO_3$ except for (○) of Fig. 4A where a level of 0·25 mM was employed. Each pH trace was conducted after 90 min illumination (15 W $m^{-2}$). A Control pH traces. B pH traces conducted in the presence of $(NH_4)_2SO_4$; ○, 0·1 mM; ●, 0·2 mM; ■, 0·3 mM; and ▲, 0·5 mM. (This effect was reversible provided high ammonium concentrations were not employed.) N = node.

level for that matter) the cell would have disposed of the 4–5 pmol $cm^{-2}$ $s^{-1}$ of $OH^-$, generated by $^{14}C$ fixation, through its primary and sub-primary $OH^-$ efflux sites (Lucas, 1975*c*). The loss in $OH^-$ efflux activity and the observed migration (or instability) of the efflux sites suggests that $NH_3$ 'interferes' with the cellular control of $OH^-$ efflux. (As indicated in Fig. 4, the dramatic perturbation of the $OH^-$ efflux pattern occurred in the absence of a significant effect on cyclosis.)

*Isolated $OH^-$ efflux site experiments*

It has been shown previously that the $OH^-$ transport system can operate in the absence of exogenous $HCO_3^-$ at the actual effluxing site, provided $HCO_3^-$ is supplied to some segment of the internodal cell (see Lucas, 1976). This 'isolating chamber' technique was employed to test the hypothesis that $NH_3$ inhibits $OH^-$ rather than $HCO_3^-$ transport. A typical result, obtained using this $OH^-$ band isolating system, is presented in Fig. 5. In accord with the data of Fig. 4, $OH^-$ efflux was progressively reduced as the concentration of $(NH_4)_2SO_4$ increased. Ammonia inhibition of $HCO_3^-$ transport, across the plasmalemma of this isolated cell segment, would not have eliminated the supply of $OH^-$ to this efflux site. Over short time periods the low concentration of $NH_3$ in contact with the small isolated cell segment (pH 7·7 and 0·7 mM $(NH_4)_2SO_4$, $NH_3$ 0·04 mM) would not permit sufficient $NH_3$ to penetrate

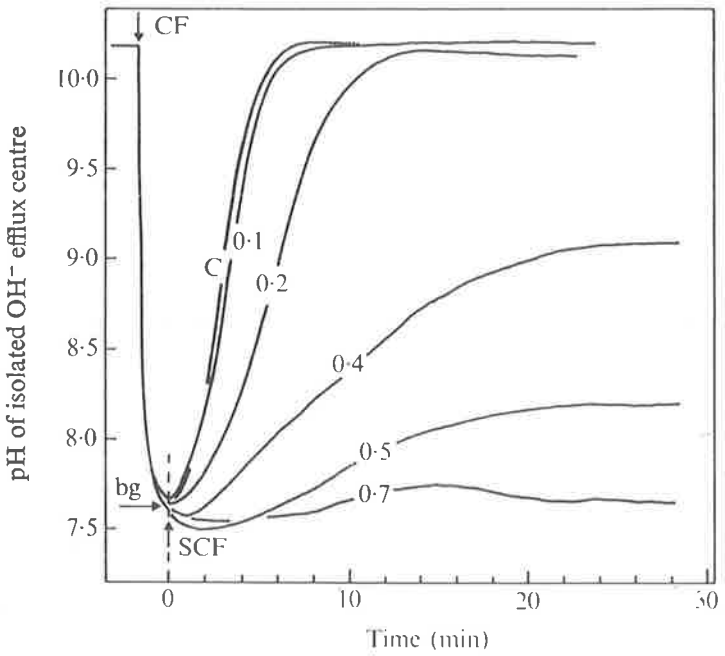


FIG. 5. Isolated $OH^-$ band activity in the presence of a range of $(NH_4)_2SO_4$ concentrations. A pretreatment period of 2 h was employed during which the isolated and outer internodal cell segments were bathed in normal solution containing 1·0 mM $NaHCO_3$, pH 8·0, under an irradiance of 15 W $m^{-2}$. The response to solutions containing 1·0 mM $NaHCO_3$ (pH 7·7 approx.) and various concentrations of $(NH_4)_2SO_4$ (values indicated on the traces in mM) was then investigated. During these experiments the outer cell segment was bathed in the control solution. A 20–25 min recovery (control) treatment was employed between the various $(NH_4)_2SO_4$ treatments. Symbols are as follows: bg, background pH value of isolating chamber solution; C, control trace; CF, flushing of isolating chamber with the required experimental solution; SCF, end of flushing sequence. (Note, the $OH^-$ efflux band centre did migrate slightly during this experiment, but its movement was slight enough to permit the performance of the experiment.)

into the cell to cause a significant reduction in $HCO_3^-$ transport. Fixation of this $HCO_3^-$ influxed across the outer cell segment would generate $OH^-$ in the cytoplasm (Lucas and Dainty, 1977). Hence, these results support the hypothesis that $NH_3$ is acting on the $OH^-$ transport system.

Because of its nucleophilic property, ammonia (within the non-aqueous phase of the plasmalemma) may react with an electrophilic group on individual $OH^-$ transport complexes. In this way it could act as an allosteric effector, preventing the transport of $OH^-$ ions. If a large number of transport complexes exist within one $OH^-$ efflux band, this would account for the dependence of inhibition on the concentration of ammonia.

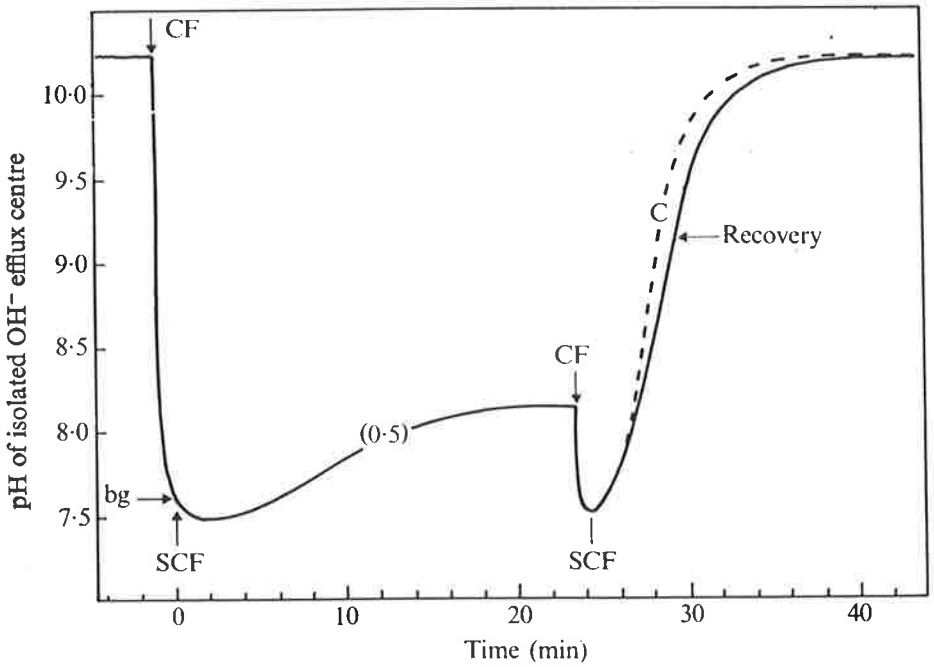


FIG. 6. Recovery of $OH^-$ efflux activity following the removal of exogenous $(NH_4)_2SO_4$. Experimental details and symbols as described for Fig. 5.

The labile nature of the $OH^-$ efflux inhibition is demonstrated in Fig. 6; recovery of efflux function, following removal of exogenous $(NH_4)_2SO_4$, was extremely rapid. The time course for the re-establishment of the steady state pH value, at the $OH^-$ band centre, differed by less than 1 min for the control and ammonia-recovery experiments. This similarly in response adds weight to the hypothesis that $NH_3$ is acting at the plasmalemma and, more specifically, on the $OH^-$ transport system. (Similarly, removal of exogenous $(NH_4)_2SO_4$ following the inhibition of $OH^-$ efflux along the entire internodal cell surface always resulted in the re-establishment of the control $OH^-$ efflux pattern.)

## DISCUSSION

### *Ammonium toxicity*

The toxic effect of ammonium on higher plant cell metabolism has been known for some time (Chibnall, 1939). Respiratory metabolism is considered to be affected by ammonia either via its effect on the activity of the mitochondrial enzymes (Vines

and Wedding, 1960; Matsumoto *et al.*, 1971) or by uncoupling of mitochondrial phosphorylation (Chappell and Haarhoff, 1967). The results presented in this paper demonstrate that $(NH_4)_2SO_4$ can influence total cellular metabolism in the internodal cells of the Characean species, *Chara corallina*. Above a certain concentration of ammonia, this influence becomes deleterious and is often lethal in nature. Whether this deleterious effect is related to the uncoupling of mitochondrial function remains to be investigated. This work indicates that caution should be taken when employing $(NH_4)_2SO_4$ in ion transport experiments involving the Characeae.

Low concentrations (0·15 mM) of $(NH_4)_2SO_4$ appeared to have a slight influence on cytoplasmic streaming. Within this same concentration (and pH) range, Smith and Walker (1976) could not detect any influence of $(NH_4)_2SO_4$ on the pH value of the cytoplasm. This suggests that the $(NH_4)_2SO_4$ mode of action, on cyclosis, does not involve a significant interaction with protons (buffering capacity) in the cytoplasm. Alternatively, it may be that the DMO[1] method of cytoplasmic pH determination is insensitive to pH perturbations occurring within small compartments or at membrane interfaces. If the latter is the case, 'bulk' cytoplasmic pH determinations may be of little value in elucidating the mechanics of certain ion transport systems that putatively involve $H^+$ or $OH^-$ ions (Smith, 1970; Lucas, 1975*c*).

*$H^{14}CO_3^-$ transport in the presence of $(NH_4)_2SO_4$*

From the results presented, it would appear that $NH_3$ inhibits the functioning of the $OH^-$ efflux system. Hence, $HCO_3^-$ transport may be restricted by the absence of a charge balance mechanism. The small $H^{14}CO_3^-$ influx, measured in the presence of 0·4–0·5 mM $(NH_4)_2SO_4$ (pH 9·0), could be due to residual $OH^-$ efflux activity (see Fig. 4). In addition, the plasmalemma may be slightly permeable to $NH_4^+$. Influx of this cationic species would not only neutralize the negative charge carried by the $HCO_3^-$, but also the $OH^-$ generated by its photo-assimilation. The $NH_3$ so produced may be assimilated by the cell, or it may diffuse back across the plasmalemma.

A similar residual $H^{14}CO_3^-$ influx was measured when the plasmalemma was perturbed by 10 mM $K^+$ (Lucas, 1975*d*). Under these conditions the electrical resistance of the plasmalemma decreased dramatically, and the majority of the passive membrane current was carried by $K^+$ ions. Presumably localized passive $K^+$ fluxes balanced the charge associated with the small influx of $HCO_3^-$.

Under both $(NH_4)_2SO_4$ and 10 mM $K^+$ treatment the apparent $K_m$ of $H^{14}CO_3^-$ assimilation increased to 1·5–2·0 mM. This increase may be a reflection of the utilization of a less effective method of maintaining charge balance across the plasmalemma. Parallel measurements of plasmalemma fluxes ($H^{14}CO_3^-$, $NH_4^+$, and $K^+$) and electrical potential and conductance will be required to test this hypothesis.

*$(NH_4)_2SO_4$ inhibition of $H^{14}CO_3^-$ assimilation in relation to $Cl^-$ influx*

There appears to be no evidence in support of MacRobbie's (1965) hypothesis that *in vivo* photophosphorylation is being uncoupled by low exogenous $(NH_4)_2SO_4$

[1] DMO; 5,5-dimethyloxazolidine-2,4-dione.

concentrations. The characteristics of $(NH_4)_2SO_4$ inhibition of $^{14}C$ fixation, at pH values above 7·0, were interpreted on the basis of a selective effect of this compound on the $OH^-$ transport system. If competition for a common energy substrate does exist between the $Cl^-$, $OH^-$, and $HCO_3^-$ transporters, the inhibition of $OH^-$ transport and the resultant retarding effect on the influx of $HCO_3^-$ would mean that more energy should become available for $Cl^-$ transport (provided, of course, that the chloroplast and mitochondrial systems remain unaffected).

Whether this form of energy substrate competition exists may be difficult to verify. Lucas and Smith (1976) demonstrated the existence of a lag in $^{36}Cl^-$ transport; uptake did not attain a steady state value until the cells had been illuminated for a period greater than 40 min. The possibility that this lag was due to the slow cytoplasmic build-up of an energy substrate required by the $Cl^-$ transport system was proposed by these workers (see also Lilley and Hope, 1971; Smith and Raven, 1974). The above hypothesis, and in effect the competitive energy substrate hypothesis, could be tested by examining the influence of $(NH_4)_2SO_4$ on this lag associated with $^{36}Cl^-$ uptake. (A reduction, or complete abolition, of the lag would offer support for the above hypothesis.)

Bicarbonate influx in the dark is quite low (Lucas, 1976) and the mechanism of $OH^-$ efflux appears to be deactivated after a 30 min dark period (Lucas *et al.*, 1977). In contrast, $^{36}Cl^-$ influx can be stimulated in the dark by low levels of $(NH_4)_2SO_4$ (Smith, 1972). Under these conditions, energy competition between these systems cannot exist. This discrepancy suggests that $(NH_4)_2SO_4$ may influence $Cl^-$ transport in some other way. Unfortunately this aspect of the present study remains unresolved.

Finally, it should be mentioned that migration of the $OH^-$ efflux sites, under 0·3–0·5 mM $(NH_4)_2SO_4$, indicates that the cellular mechanism controlling the location of these efflux bands is also affected (see Lucas and Dainty, 1977). Further $(NH_4)_2SO_4$ experiments are presently being conducted in an attempt to discover more about the mechanism of cytoplasmic control over the $OH^-$ efflux system of *Chara corallina*.

ACKNOWLEDGEMENTS

This work was supported jointly by grants from the National Research Council of Canada and the Connaught Fund (University of Toronto) to Professor J. Dainty, Department of Botany, University of Toronto.

LITERATURE CITED

Bates, R. G., and Pinching, G. D., 1949. *J. Res. natn. Bur. Stand.* **42**, 419–30.

Chappell, J. B., and Haarhoff, K. N., 1967. In *Biochemistry of mitochondria*. Ed. E. C. Slater, Z. Kaniuga, and L. Wojtczak. Academic Press, New York. Pp. 75–91.

Chibnall, A. C., 1939. *Protein metabolism in the plant*. Yale University Press, New Haven. Pp. 1–306.

Good, N. E., 1960. *Biochim. biophys. Acta*. **40**, 502–17.

Hind, G., and Whittingham, C. P., 1963. Ibid. **75**, 194–204.

Krogmann, D. W., Jagendorf, A. T., and Avron, M., 1959. *Pl. Physiol., Lancaster*, **34**, 272–7.

Lilley, R. Mc., and Hope, A. B., 1971. *Biochim. biophys. Acta*, **226**, 161–71.

LUCAS, W. J., 1975*a*. *J. exp. Bot.* **26**, 331–46.
—— 1975*b*. Ibid. **26**, 271–86.
—— 1975*c*. Ibid. **26**, 347–60.
—— 1975*d*. Ph. D. thesis, University of Adelaide.
—— 1976. *J. exp. Bot.* **27**, 19–31.
—— and DAINTY, J., 1977. *J. membrane Biol.* **32**, 75–92.
—— FERRIER, J. M., and DAINTY, J., 1977. Ibid. **32**, 49–73.
—— and SMITH, F. A., 1973. *J. exp. Bot.* **24**, 1–14.
—— —— 1976. *Aust. J. Pl. Physiol.* **3**, 443–56.
MACROBBIE, E. A. C., 1965. *Biochim. biophys. Acta*, **94**, 65–73.
—— 1966. *Aust. J. biol. Sci.* **19**, 363–70.
MATSUMOTO, N., WAKIUCHI, N., and TAKAHASHI, E., 1971. *Physiologia Pl.* **25**, 353–7.
OHMURA, T., 1958. *J. Biochem., Tokyo*, **45**, 319–31.
RAVEN, J. A., 1968. *J. exp. Bot.* **19**, 193–206.
SMITH, F. A., 1965. Ph. D. thesis, University of Cambridge.
—— 1967. *J. exp. Bot.* **18**, 509–17.
—— 1970. *New Phytol.* **69**, 903–17.
—— 1972. Ibid. **71**, 595–601.
—— and RAVEN, J. A., 1974. *New Phytol.* **73**, 1–12.
—— and WEST, K. R., 1969. *Aust. J. biol. Sci.* **22**, 351–63.
—— and WALKER, N. A., 1976. *J. exp. Bot.* **27**, 451–9.
VAN LOOKEREN CAMPAGNE, R. N., 1957. *Acta bot. neerl.* **6**, 543–82.
VINES, H. M., and WEDDING, R. T., 1960. *Pl. Physiol., Lancaster*, **35**, 820–5.
WALKER, D. A., 1973. *New Phytol.* **72**, 209–35.
WALKER, N. A., and SMITH, F. A., 1975. *Pl. Sci. Lett.* **4**, 125–32.
WOOD, R. D., and IMAHORI, K., 1965. *A revision of the Characeae*. Weinham, J. Cramer.

*Journal of Experimental Botany, Vol. 28, No. 107, pp. 1321–1336, December 1977*

# Analogue Inhibition of the Active $HCO_3^-$ Transport Site in the Characean Plasma Membrane

W. J. LUCAS[1]
*Department of Botany, University of Toronto, Toronto, Ontario M5S 1A1, Canada*

Received 28 May 1977

ABSTRACT

Competitive inhibition of the $HCO_3^-$ transport site, at the plasmalemma of *Chara corallina*, by the $CO_3^{2-}$ ion is demonstrated. This $CO_3^{2-}$ inhibition was used to demonstrate that $HCO_3^-$ ions enter the cell by facilitated 'diffusion' when the $HCO_3^-$ transport system has been inactivated by treatment with 10 mM $K^+$. Use of $CO_3^{2-}$ as a $HCO_3^-$ analogue is limited, however, because of the necessity to employ solutions of high pH. Inhibition was not observed in the presence of a range of organic and inorganic acid anions. These results demonstrate the stereospecific nature of the $HCO_3^-$ binding site.

A variety of amino compounds were found to inhibit $H^{14}CO_3^-$ influx. Inhibition appeared to be competitive, being completely relieved at higher substrate ($HCO_3^-$) concentrations. A simple correlation was not found between the degree of inhibition and the concentration of neutral base. A combination of the presence of neutral base and experimental pH values of at least 8·0 was required to produce the reactive species that inhibited $HCO_3^-$ transport. This species is considered to be the amino carbamate. These results are discussed with respect to further $HCO_3^-$ analogue experiments.

## INTRODUCTION

Internodal cells of *Chara corallina* can photosynthetically assimilate exogenous $HCO_3^-$ at rates of up to 50–60 pmol $cm^{-2}$ $s^{-1}$ (Lucas, 1975*b*). These high fixation rates are facilitated by the $HCO_3^-$ (influx) and $OH^-$ (efflux) transport systems that are located in the plasmalemma of this species (Lucas and Smith, 1973; Lucas, 1975*b*, 1976*a*). Photosynthetic fixation of carbon supplied by $HCO_3^-$ results in the production of one $OH^-$ for each $CO_2$ molecule fixed. This 'waste product' ($OH^-$) is exported from the cytoplasmic phase, across the plasmalemma, by the $OH^-$ efflux system (Lucas and Smith, 1973; Lucas, 1975*a*; Lucas and Dainty, 1977).

The ability of this species to assimilate exogenous $HCO_3^-$ can be impaired considerably by employing experimental solutions whose pH values are higher than 9·5 (Smith, 1968; Lucas, 1975*b*). We suggested (Lucas, 1975*b*) that this inhibition resulted from competitive binding of $CO_3^{2-}$ to the $HCO_3^-$ site on the $HCO_3^-$ transport system. The reduction in $HCO_3^-$ influx, that was observed in the presence of Tris and Tricine buffers, was also considered to result from competitive inhibition at the $HCO_3^-$ binding site (Lucas, 1975*b*).

This paper reports the results of experiments designed to test these proposals. The effects of some organic, inorganic, and amino-acid compounds on $H^{14}CO_3^-$

[1] Present address: Department of Botany, University of California, Davis, California 95616, U.S.A.

transport were also examined, in an attempt to find an artificial $HCO_3^-$ analogue. A highly competitive analogue would be of considerable value in examining the electrical properties of the plasmalemma with respect to the possible electrical involvement of $HCO_3^-$ transport.

## MATERIALS AND METHODS

### *Culture material*

Culture material of *Chara corallina* Klein ex Willd., em. R. D. W. (= *C. australis* R. Br.) was grown in the laboratory under artificial light. Culture details and methods used to cut internodal cells from the cultures have been previously reported (Lucas and Smith, 1973; Lucas, 1975*b*). Mature third to fourth internodal cells were used, and experiments reported in this paper were conducted on cells cut from two culture tanks.

### *Experimental solutions*

Solutions were prepared from Analar Reagent grade chemicals using glass-distilled water (approximate specific conductivity $1{\cdot}2 \times 10^{-6}$ mho $cm^{-1}$). The standard experimental solution contained 1·0 mM NaCl, 0·2 mM KCl, and 0·2 mM $CaSO_4$, unless otherwise specified. Inorganic carbon was added as $Na_2CO_3$, and the required pH value was obtained by titration with 100 mM $H_2SO_4$.

Stock solutions (100 mM) of the buffers *N*-tris(hydroxymethyl)methyl-2-aminoethanesulphonic acid (TES), *N*-tris(hydroxymethyl)methyl-3-aminopropanesulphonic acid (TAPS), tris(hydroxymethyl)methylammonium chloride (Tris), and *N*-tris(hydroxymethyl)-methylglycine (Tricine) were prepared and titrated to pH 7·0 using freshly prepared 100 mM NaOH. The same procedure was adopted for all other acids studied (inorganic, organic, and amino) except for formic and acetic acid which were prepared directly from their sodium salts.

Radioactive $NaH^{14}CO_3$ was obtained from New England Nuclear, Boston, as a sterile aqueous solution, and aliquots were added to the experimental solutions to give the required specific activity. Specific activities were determined using the method described by Lucas (1975*b*).

### *Experimental procedure*

Radioisotope ($NaH^{14}CO_3$) studies were performed on cells cut 1 d prior to the actual performance of the experiment. Cells were cut and pretreated in standard solution which contained 1·0 mM $NaHCO_3$ (pH 9·0). The light regime employed for the cultures (13 h light : 11 h dark) was maintained during this recovery pretreatment. Following the 11 h dark period, cells were illuminated (fluorescent lights, 10 W $m^{-2}$) for 1 h prior to the commencement of an experiment.

All experiments were performed in a thermostatted (25 °C) system. Full details of the radioisotope techniques employed have been previously described (Lucas, 1975*b*; Lucas and Smith, 1976). Unless otherwise specified, experimental pretreatment and $^{14}C$ periods were of 1 h duration. The light source used for fixation experiments was a Leitz-Pradovit 24 V 150 W quartz-iodide projector. The light intensity was attenuated using nickel-Nicron neutral density filters (prepared by the Department of Physics, University of Adelaide); the infrared component was removed using a water filter (20 cm). A light intensity of 20 W $m^{-2}$ was used throughout.

Results are expressed as mean ± s.e. mean for each treatment (10–12 cells per treatment).

## RESULTS

### *Competitive inhibition of $H^{14}CO_3^-$ transport by $CO_3^{2-}$ ions*

The inorganic carbon that is added to the experimental solution exists in its various forms; namely $CO_2$, $H_2CO_3$, $HCO_3^-$, and $CO_3^{2-}$. In alkaline solutions (pH > 9·0) $HCO_3^-$ and $CO_3^-$ predominate, the equilibrium between the two forms being

$$HCO_3^- \rightleftharpoons CO_3^{2-} + H^+ \qquad (1)$$

with an equilibrium constant ($K$) of $4{\cdot}69 \times 10^{-11}$ (Harned and Scholes, 1941) or $pK_a$ of 10·33. The concentration of $HCO_3^-$, at a particular pH value, is given by the equation

$$[HCO_3^-] = \text{total added carbon}/(1 + K/a_{H^+}) \quad (2)$$

where $a_{H^+}$ is the activity of protons in the solution. From equation (2) it can be seen that the level of $CO_3^{2-}$ can be increased, while the concentration of $HCO_3^-$ is held constant, simply by manipulating both the level of total added inorganic carbon and the pH of the solution.

Experiments of this nature were performed to ascertain whether the $CO_3^{2-}$ ion competitively inhibits the $HCO_3^-$ transport system of *Chara*. Figure 1 indicates that $H^{14}CO_3^-$ influx was reduced, linearly, when the $CO_3^{2-}$ concentration was increased ($HCO_3^-$ concentration kept constant at 0·25, 0·50, and 0·80 mM). From these results

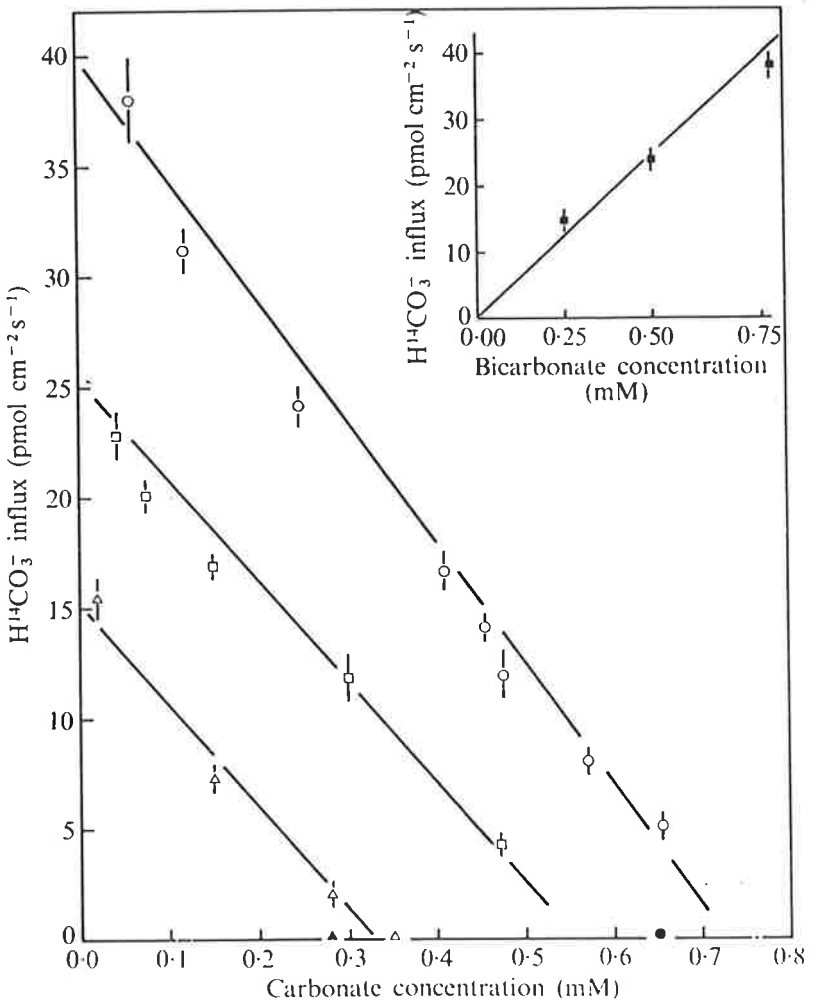


FIG. 1. Competitive inhibition of $H^{14}CO_3^-$ influx by $CO_3^{2-}$ ions. Three series of experiments were conducted in the presence of 0·25 (△), 0·50 (□), and 0·80 mM $HCO_3^-$ (○). The $CO_3^{2-}$ concentrations were obtained by manipulating the total added inorganic carbon and the experimental pH value. The pH of the experimental point at the lowest $CO_3^{2-}$ concentration employed was always 9·2. The highest pH in each series was 10·5, 10·3, and 10·26 for the 0·25, 0·50, and 0·8 mM $HCO_3^-$ series, respectively. The symbols (▲) and (●) represent $H^{14}CO_3^-$ influx measured in the presence of 10 mM $K^+$ and 0·25 and 0·8 mM $HCO_3^-$, respectively. The inset represents $H^{14}CO_3^-$ influx (measured at pH 9·2) plotted against $HCO_3^-$ concentration.

it can be seen that, for a particular $CO_3^{2-}$ concentration, this inhibition could be relieved by raising the substrate ($HCO_3^-$) concentration. These results clearly demonstrate that $CO_3^{2-}$ does compete competitively for the binding site on the $HCO_3^-$ transport system. Presumably the extra negative charge on the $CO_3^{2-}$ ion prevents its successful transport.

The experiments presented in Fig. 1 were performed using $HCO_3^-$ concentrations that were within the linear portion of the $HCO_3^-$ concentration curve (see inset Fig. 1; Lucas, 1975*b*). The negative, linear, relationship between $H^{14}CO_3^-$ influx and $CO_3^{2-}$ concentration was, therefore, to be expected. The $CO_3^{2-}$ ion appears to have a high affinity for the $HCO_3^-$ binding site. The $CO_3^{2-}$ concentrations ($K_1$) that reduced the $H^{14}CO_3^-$ influx to 50% of the control value were 0·16, 0·28, and 0·36 mM for the 0·25, 0·50, and 0·80 mM $H^{14}CO_3^-$ experiments, respectively. At equal $HCO_3^-$ and $CO_3^{2-}$ concentrations, the calculated percentage inhibition was 76, 88, and approximately 100 respectively, for the 0·25, 0·50 and 0·8 mM experiments. The apparent increase in affinity of $CO_3^{2-}$ for the binding site, which was observed

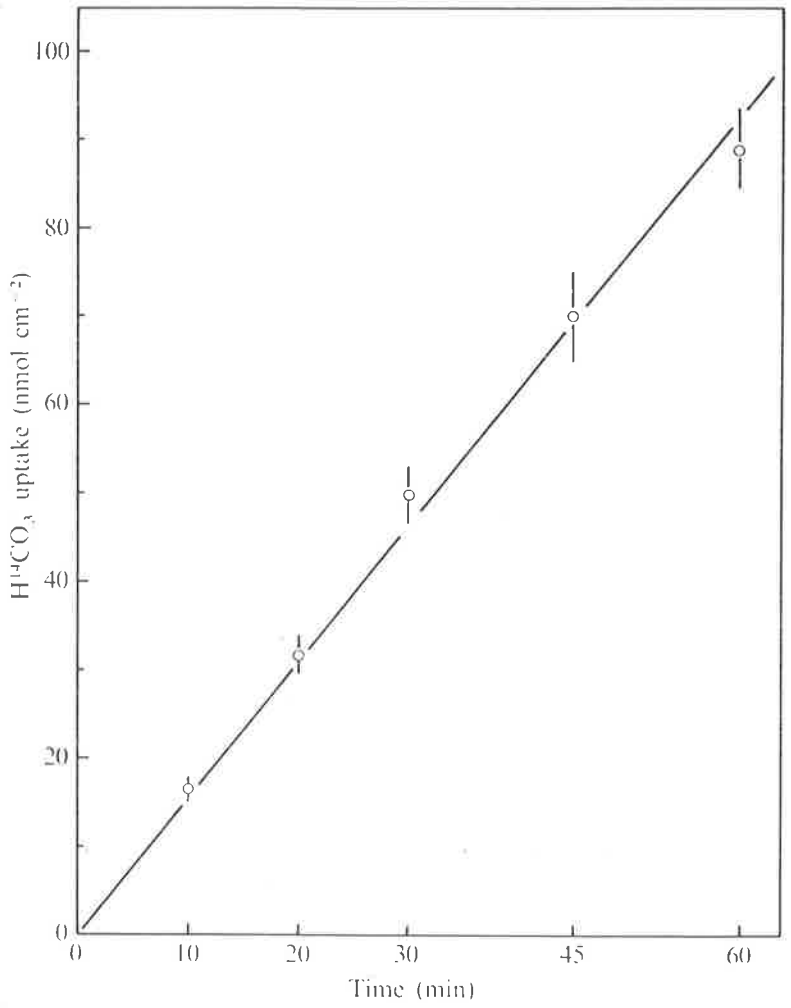


FIG. 2. $H^{14}CO_3^-$ uptake, following a 90 min high pH (10·3) treatment. Radioisotope experiments were conducted in standard solutions containing 0·5 mM $HCO_3^-$, pH 9·2, after the cells had been exposed to high pH solutions, 0·5 mM total carbon, pH 10·3. The linear response indicates that high pH treatment did not cause any permanent perturbation of the $HCO_3^-$ transport system.

as the $HCO_3^-$ concentration was increased, may have been due to a combined effect of $CO_3^{2-}$ concentration and high pH.

The possibility that pH, *per se*, was modifying the membrane structure, in a manner deleterious to transport, was examined (see Coster and Kaplin, 1973). Cells were bathed for 90 min in pretreatment solutions containing 0·5 mM total inorganic carbon, pH 10·3. Immediately following this high pH treatment, $H^{14}CO_3^-$ uptake was measured at pH 9·2. Figure 2 demonstrates that if any pH-induced perturbation of the $HCO_3^-$ transport system existed at pH 10·3 it was abolished immediately the cells were returned to pH 9·2. (The slope of this line gave a $H^{14}CO_3^-$ influx value of 26·4 ± 1·7 pmol $cm^{-2}$ $s^{-1}$, a value slightly higher than that obtained for the experiments presented in Fig. 1.) A 60–90 min recovery period was required before normal $HCO_3^-$ transport rates were established, following a high $K^+$ (10 mM) treatment (Lucas, 1976*b*). The complete absence of any lag, associated with cellular treatment at high pH, and the negative linear relationship between $H^{14}CO_3^-$ influx and $CO_3^{2-}$ concentration, strongly suggest that any pH interference must be of minor importance.

*$K^+$ (10 mM) inactivation of $HCO_3^-$ transport*

We demonstrated previously that increasing the $HCO_3^-$ concentration, in the presence of 10 mM $K^+$, resulted in a linear increase in $^{14}C$ assimilation (Lucas, 1976*b*). This response suggested that, following the inactivation of the $HCO_3^-$ transport system by 10 mM $K^+$, $HCO_3^-$ entered the cell by passive or facilitated diffusion. This facilitated diffusion may occur by the random thermal motion of the inactivated $HCO_3^-$ transport system.

This hypothesis was tested by examining the combined effects of 10 mM $K^+$ treatment and $CO_3^{2-}$ competition on the influx of $H^{14}CO_3^-$. The results of these experiments are presented in Fig. 3. The initial linear decline in $H^{14}CO_3^-$ influx, observed in the presence of increasing $CO_3^{2-}$ concentration, had a negative slope of 42 pmol $cm^{-2}$ $s^{-1}$ per mM $CO_3^{2-}$. This value is close to those obtained in the absence of 10 mM $K^+$; 46 (0·25 and 0·50 mM $HCO_3^-$) and 44 pmol $cm^{-2}$ $s^{-1}$ $mM^{-1}$ $CO_3^{2-}$ (0·8 mM $HCO_3^-$). This similarity in slope can be interpreted in terms of $CO_3^{2-}$ binding to the same $HCO_3^-$ transport site. The result, therefore, offers support for the facilitated diffusion hypothesis. At high $CO_3^{2-}$ concentrations a residual $H^{14}CO_3^-$ influx was observed, its value being between 0·4 and 0·5 pmol $cm^{-2}$ $s^{-1}$. It is felt that this value reflects the passive permeation of $H^{14}CO_3^-$ across the plasmalemma.

*Possible organic acid anion analogues for $HCO_3^-$*

Although the $CO_3^{2-}$ ion functions as a very effective analogue for $HCO_3^-$, its usefulness is restricted, because it can only be employed at high pH values. The anions of several organic acids were tested to determine whether any functioned as analogues for $HCO_3^-$. The results of this study are presented in Table 1. The influx in the presence of 0·5 mM $HCO_3^-$ served as the control, and the data relating to the $CO_3^{2-}$ ion were included for comparative purposes. (It should be mentioned that the results presented in Tables 1–3 and Figs 4–7 were obtained on cells cut from

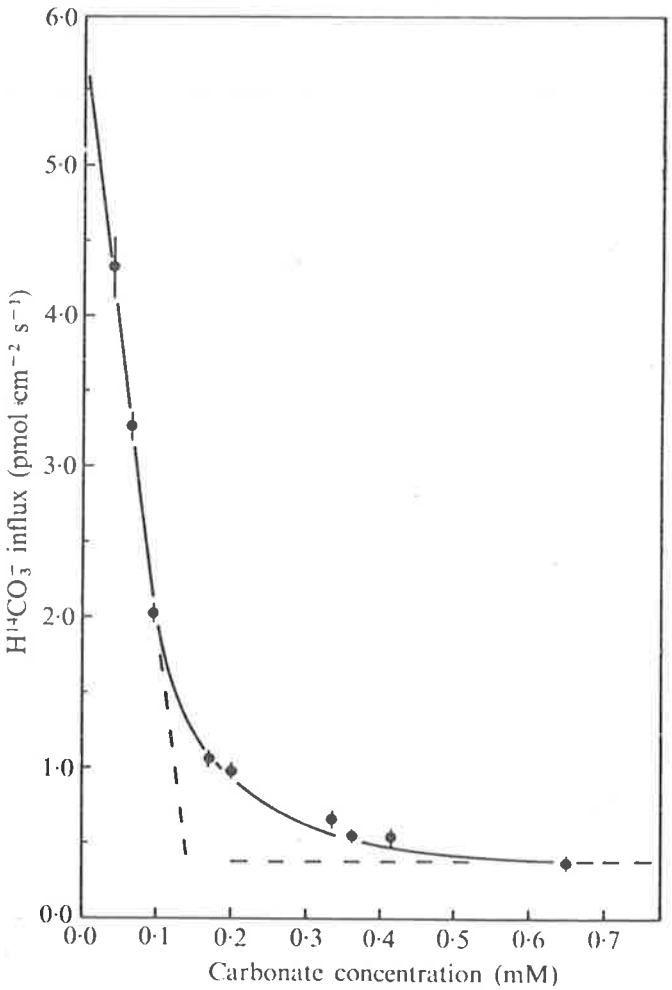


FIG. 3. Carbonate inhibition of $H^{14}CO_3^-$ transport in the presence of 10 mM $K^+$. Experimental solutions contained 0·8 mM $HCO_3^-$, 10 mM $K^+$, and the indicated concentrations of $CO_3^{2-}$. One hour pretreatment and 30 min $^{14}C$ exposure periods were employed for all experiments. The horizontal broken line is considered to represent the rate of passive permeation of $H^{14}CO_3^-$ across the plasmalemma. (The 0·8 mM $HCO_3^-$ results presented in Fig. 1 represent the controls for these experiments.)

culture tank L. Cells from this tank exhibited high rates of $H^{14}CO_3^-$ assimilation at 0·5 mM $HCO_3^-$.)

Based on the similarity in structure between $HCO_3^-$ and acetate the latter was expected to inhibit $H^{14}CO_3^-$ influx. However, inhibition was not observed (see Table 1). Either the methyl group prevented the acetate ion from approaching the binding site, or there is a specific O—H requirement for successful binding of the substrate. However, the absence of the proton, on the $CO_3^{2-}$ ion, did not prevent it from binding to the $HCO_3^-$ transport site. The formate ion did not appear to bind to the $HCO_3^-$ site either. In this case the size of the ion would not have prevented it from approaching the binding site. The hydrogen atom of the C–H bond would not be able to participate in hydrogen bonding. Also, the length of this bond would be too short to allow the hydrogen atom to approach the putative O—H binding site.

Glycolate was investigated because it was thought that the OH group, at the methyl position, may have been able to approach the putative OH specific site on

TABLE 1. *Effect of organic acid anions on $H^{14}CO_3^-$ transport across the plasmalemma of* Chara corallina

| Anion[b] | p$K_a$ | Structure | $H^{14}CO_3^-$ influx[a] (pmol $cm^{-2}$ $s^{-1}$) |
|---|---|---|---|
| Bicarbonate | 6·35 | 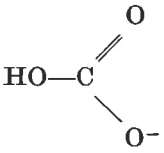 | 33·0 ± 2·0 |
| Carbonate | 10·33 | 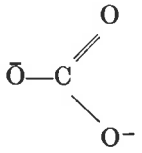 | 2·5[c] |
| Formate | 3·75 | 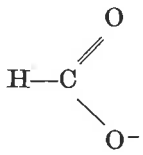 | 34·3 ± 1·8 |
| Acetate | 4·75 | 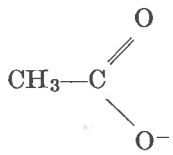 | 35·4 ± 2·1 |
| Glycolate | 3·83 | 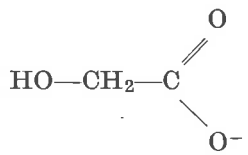 | 37·1 ± 1·2 |
| Propionate | 4·87 | 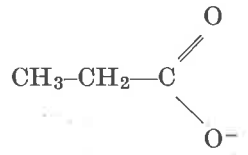 | 36·6 ± 1·3 |
| Isobutyrate | 4·86 | 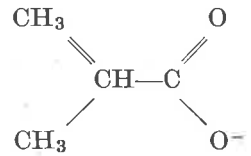 | 40·2 ± 2·1 |
| Oxalate | 1·27, 4·28 | 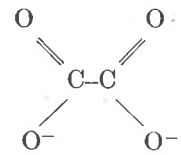 | 35·2 ± 2·6 |

[a] Influx values were determined using a $HCO_3^-$ concentration of 0·5 mM (pH 9·2) and a light intensity of 20 W $m^{-2}$. The bicarbonate result represents the control situation; other values indicate the effect of a 0·5 mM concentration of the respective anion.

[b] All anions were employed as the $Na^+$ salt.

[c] Value taken from Fig. 1.

TABLE 2. *Effect of inorganic acid anions on* $H^{14}CO_3^-$ *transport*

| Inorganic acid[a] anion (0·5 mM) | Formula | $H^{14}CO_3^-$ influx[b] (pmol $cm^{-2}$ $s^{-1}$) |
|---|---|---|
| Control | | 36·0 ± 0·9 |
| Bisulphite | $HSO_3^-$ | 36·2 ± 1·0 |
| Borate | $B(OH)_4^-$ | 29·6 ± 1·9 |
| Nitrate | $NO_3^-$ | 32·8 ± 1·9 |
| Phosphate | $HPO_4^{2-}$ | 31·1 ± 1·0 |

[a] All anions were employed as the $Na^+$ salt.
[b] $H^{14}CO_3^-$ influx experimental details as described in Table 1.

TABLE 3. *Influence of some amino acids on* $H^{14}CO_3^-$ *influx*

| Amino acid (0·5 mM) | Structural formula | $pK'_{a(NH_3)}$ | $H^{14}CO_3^-$ influx (pmol $cm^{-2}$ $s^{-1}$) |
|---|---|---|---|
| Control[a] | — | — | 37·3 ± 1·5<br>35·6 ± 2·3 |
| Tris | $(CH_2OH)_3C—NH_3^+$ | 8·10[b] | 25·1 ± 1·5 |
| Tricine | $(CH_2OH)_3C—N^+H_2—CH_2—COO^-$ | 8·15 | 25·0 ± 1·9 |
| α, β-Diamino-propionic acid | $H_2N—CH_2—CH(N^+H_3)—COO^-$ | 6·73<br>(9·56) | 28·5 ± 0·9 |
| α-Aminosuccinamic acid | $H_2N—CO—CH_2—CH(N^+H_3)COO^-$ | 8·80 | 24·3 ± 1·4 |
| α-Aminoglutaramic acid | $H_2N—CO—(CH_2)_2—CH(N^+H_3)—COO^-$ | 9·13 | 23·6 ± 1·4 |
| α-Aminoacetic acid | $N^+H_3—CH_2—COO^-$ | 9·60 | 41·1 ± 1·1 |
| α-Aminobutyric acid | $CH_3—CH_2—CH(N^+H_3)—COO^-$ | 9·60 | 33·5 ± 1·8 |
| β-Aminobutyric acid | $N^+H_3—(CH_2)_3—COO^-$ | 10·43 | 37·3 ± 1·7 |
| Iminodiacetic acid | $N^+H_2(CH_2—COO^-)_2$ | 9·89 | 36·8 ± 2·7 |

[a] Control experiments were conducted, under a light intensity of 20 W $m^{-2}$, in normal bathing solutions which contained 0·5 mM total inorganic carbon, pH 9·2. A period of 1 h was employed for pretreatment and $^{14}C$ exposure. Amino acid experiments were conducted under identical conditions except that solutions contained 0·5 mM amino acid.
[b] Amino acid $pK'_a$ values taken from Jencks and Regenstein (1970).

the transport complex. The absence of inhibition indicates that either the size of the $CH_2OH$ group prevented the ion from penetrating to the site, or insufficient degrees of freedom were available, within its ionic structure, to allow successful binding of the OH group. The influence of increasing the length of the alkyl group was investigated using propionate and isobutyrate. Rather than inhibition, a slight stimulation of $H^{14}CO_3^-$ influx occurred in the presence of isobutyrate. We have no explanation as to the nature of this stimulation.

Provided one of the carboxyl groups of a dicarboxylic acid could penetrate and partially bind to the $HCO_3^-$ site, the close proximity of the negative charge, associated with the second carboxyl group, may induce a conformational change in the transport complex. A modification of this nature was not observed in the presence of sodium oxalate (Table 1).

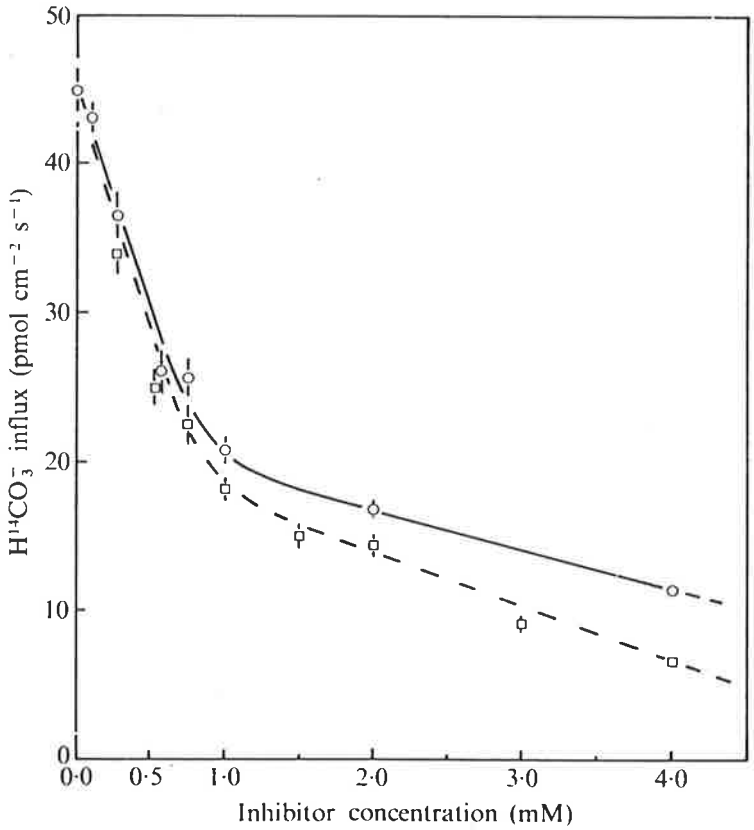


FIG. 4. Concentration dependence of $H^{14}CO_3^-$ influx inhibition by Tricine and Tris buffers. Experiments were conducted in the presence of 0·5 mM total added carbon, pH 9·2, and the indicated concentrations of Tricine (○) and Tris (□). Inhibitor concentrations are expressed as total concentration of buffer added.

*$HCO_3^-$ analogue studies: inorganic acid anions*

The effect, on $H^{14}CO_3^-$ influx, of several inorganic acid anions was also investigated. Except for nitrate, the molecular structure of these acids differed from the planar nature of the $HCO_3^-$ ion (phosphate and borate, tetrahedral; bisulphite, pyramidal; nitrate, planar). The probability that these anions would act as effective $HCO_3^-$ analogues was therefore very slight. The bisulphite ion was found to be completely ineffective (Table 2). Borate inhibited $H^{14}CO_3^-$ influx by approximately 17%, and lower rates of inhibition were observed with nitrate and phosphate. We are not certain whether the inhibitions observed were due to the competitive binding of these ions to the $HCO_3^-$ site or to competitive effects between different transport systems (e.g. phosphate transport; Smith, 1966). In any event, the level of inhibition was too slight for these compounds to be of use as $HCO_3^-$ analogues.

*Influence of tricine and tris buffers on $H^{14}CO_3^-$ transport*

Lucas (1975*b*) suggested that the pronounced inhibition of $HCO_3^-$ assimilation, that was observed in the presence of 5 mM Tricine or Tris, may have been due to their competitive binding action at the $HCO_3^-$ transport site. To test this hypothesis, the influence of these buffers was examined in more detail. Figure 4 indicates that, at low concentrations, both Tricine and Tris act as quite effective inhibitors of $H^{14}CO_3^-$ influx. The respective $K_i$ values for Tricine and Tris were 0·85 and 0·75

mM (cf. the $CO_3^{2-}$ $K_1$ of 0·28 mM). The slope inhibition was approximately the same for both compounds, having a negative value of 31 pmol $cm^{-2}$ $s^{-1}$ $mM^{-1}$ Tricine (or Tris). At higher concentrations, however, neither compound appeared to be very effective. (This aspect will be expanded in a later section.)

Bicarbonate concentration experiments were conducted, in the presence of a constant concentration of Tris (1 mM), to determine whether this inhibition was competitive. Under increased substrate concentrations ($HCO_3^-$) the inhibition was relieved (Fig. 5). A similar response was found for Tricine. Thus, both compounds reduce $H^{14}CO_3^-$ influx by competitive inhibition.

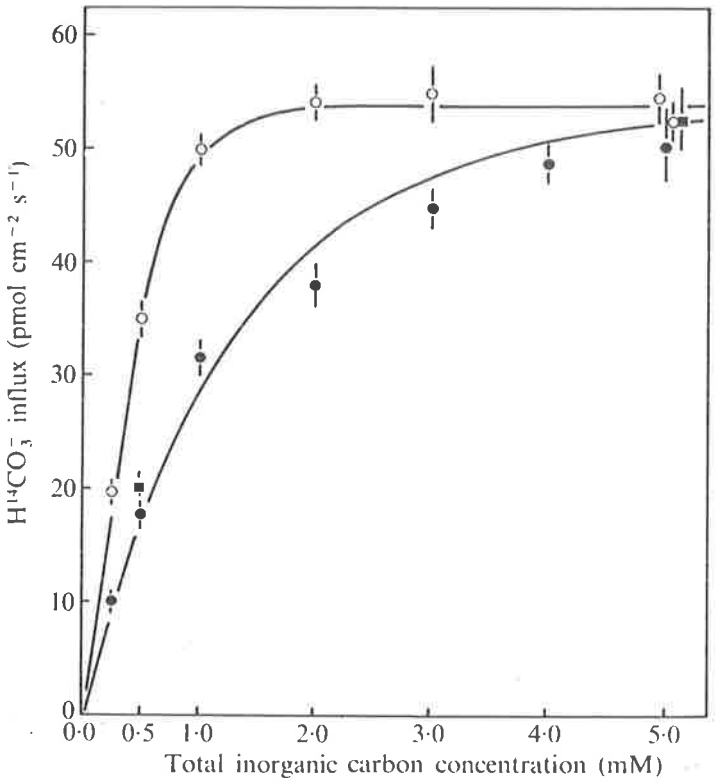


FIG. 5. Competitive inhibition of $H^{14}CO_3^-$ transport by Tris and Tricine. Experiments were conducted in the absence (○) and presence of 1 mM Tris (●) or Tricine (■), under the indicated levels of total inorganic carbon (pH 9·1).

The structure of Tris and Tricine is shown in Table 3. It is possible that the terminal carboxyl group of Tricine may bind to the $HCO_3^-$ transport site. However, it is more likely that these two compounds share a common mode, by which they competitively inhibit $HCO_3^-$ influx. The neutral form of amino compounds can react with $CO_2$ to form the carbamate (Edsall and Wyman, 1958; Jensen and Faurholt, 1952), according to the reaction:

$$R{-}NH{-}R^1 + CO_2 \underset{k_b}{\overset{k_f}{\rightleftharpoons}} R{-}NR^1{-}COOH \rightleftharpoons R{-}NR^1{-}COO^- + H^+ \qquad (3)$$

where R and $R^1$ represent, respectively, $(CH_2OH)_3C$, and H for Tris and $(CH_2OH)_3$ and $CH_2COO^-$ for Tricine ($k_f$ and $k_b$ are the forward and backward rate coefficients). The reaction is rapid, but occurs only with the uncharged amino group. The carbamate formed is stable only in alkaline solutions (Edsall and Wyman, 1958). Under

the conditions of the present experiments (0·5 mM total inorganic carbon and pH 9·1–9·2) sufficient R—$NR^1COOH$ may exist, within the proximity of the $HCO_3^-$ binding site, to competitively bind with the carrier.

*Influence of amino acids on $H^{14}CO_3^-$ influx*

If the carbamate hypothesis is correct, inhibition of $HCO_3^-$ influx will be strongly dependent upon the $pK'_a$ value of the amino acid present. Table 3 represents $HCO_3^-$ influx results obtained in the presence of a range of amino acids. It is clear that inhibition of $HCO_3^-$ influx does not occur, provided the $pK'_a$ value of the amino acid is at least 0·4 units greater than the pH value of the experimental solution. Under these conditions, the concentration of neutral amine would be quite low, and hence insufficient quantities of carbamate would form. These results (Table 3) appear to support the carbamate hypothesis.

The buffers TES and TAPS are similar in chemical structure to Tricine, except that the $CH_2CO_2^-$ group is replaced by $(CH_2)_2SO_3^-$ in TES, and $(CH_2)_3SO_3^-$ in TAPS. The $pK'_a$ values, for the $RR^1NH_2^+$ group, are 7·5 (TES) and 8·4 (TAPS). In the presence of 2 mM $NaHCO_3$ (pH 8·34), 5 mM TES buffer did not inhibit $H^{14}CO_3^-$ influx (Lucas, 1975*b*). At this pH value and $HCO_3^-$ concentration, TES-carbamate should have been formed. The absence of any inhibition may have been due to steric hinderance imposed by the large $SO_3^-$ group. Alternatively, a substrate level of 2 mM $HCO_3^-$ may have been sufficient to mask the presence of competitive inhibition. Table 4 indicates that 5 mM TES does inhibit $H^{14}CO_3^-$ influx when the level of exogenous $HCO_3^-$ was 0·5 mM, pH 9·2. The level of inhibition was only

TABLE 4. *Competitive inhibition of $H^{14}CO_3^-$ transport by the buffers TES and TAPS*

| pH | $HCO_3^-$ concentration (mM) | Buffer and concentration (mM) | $H^{14}CO_3^-$ influx[a] (pmol $cm^{-2}$ $s^{-1}$) | Inhibition (%) |
|---|---|---|---|---|
| 9·2 | 0·5 | — | 25·7 ± 0·6 | — |
| | | TAPS[b], 1·0 | 18·9 ± 0·8 | 26·5 |
| | | TAPS, 2·5 | 15·8 ± 0·9 | 38·5 |
| | | TAPS, 5·0 | 12·5 ± 0·8 | 51·4 |
| | | TES, 5·0 | 14·9 ± 0·9 | 42 |
| 9·2 | 3·0 | — | 52·0 ± 3·2 | — |
| | | TAPS, 5·0 | 39·8 ± 1·0 | 23·4 |
| 9·2 | 6·0 | — | 51·1 ± 4·6 | — |
| | | TAPS, 5·0 | 47·1 ± 2·4 | 7·8 |
| | | TES, 5·0 | 49·2 ± 3·4 | 0 — 3·7 |
| 8·2 | 0·5 | — | 29·6 ± 1·5 | — |
| | | TAPS, 5·0 | 19·8 ± 1·3 | 31·1 |
| | | TES, 5·0 | 18·2 ± 0·6 | 38·5 |
| 8·2 | 3·0 | — | 57·6 ± 2·4 | — |
| | | TES, 5·0 | 59·4 ± 21·0 | 0 |

[a] Standard 1 h pretreatment and $^{14}C$ periods were employed.
[b] The $pK'_{a(NH_3^+)}$ values of TES and TAPS are 7·5 and 8·4, respectively.

slightly less at pH 8·2. However, in agreement with the previous results of Lucas (1975*b*), this inhibition was completely relieved by increasing the $HCO_3^-$ level to 3·0 mM (pH 8·2). A similar reversal was observed using 6·0 mM $HCO_3^-$ at pH 9·2. As shown in Table 4, a similar response was found when TAPS buffer was investigated. It would appear, therefore, that at solution pH values above 8·0 both these buffers form a reactive species that competitively inhibits $HCO_3^-$ transport. It is presumed that this reactive species is the undissociated carbamate of TES and TAPS.

*$H^{14}CO_3^-$ inhibition by Tricine and Tris: influence of pH*

We recently reported that inhibition of $HCO_3^-$ assimilation, which occurred in the presence of $(NH_4)_2SO_4$, was strongly correlated with the level of neutral $NH_3$ (Lucas, 1977). This correlation held over a wide pH range (7·0–9·6). Ammonia appeared to interfere with the cellular mechanism that controls the $OH^-$ efflux system in *Chara*.

If the neutral forms of Tricine and Tris (and all the other amino acid compounds investigated) were involved in the inhibition of $^{14}C$ assimilation, rather than the undissociated carbamates, a similar correlation should exist between the concentration of neutral base and the degree of inhibition. This possibility was tested by

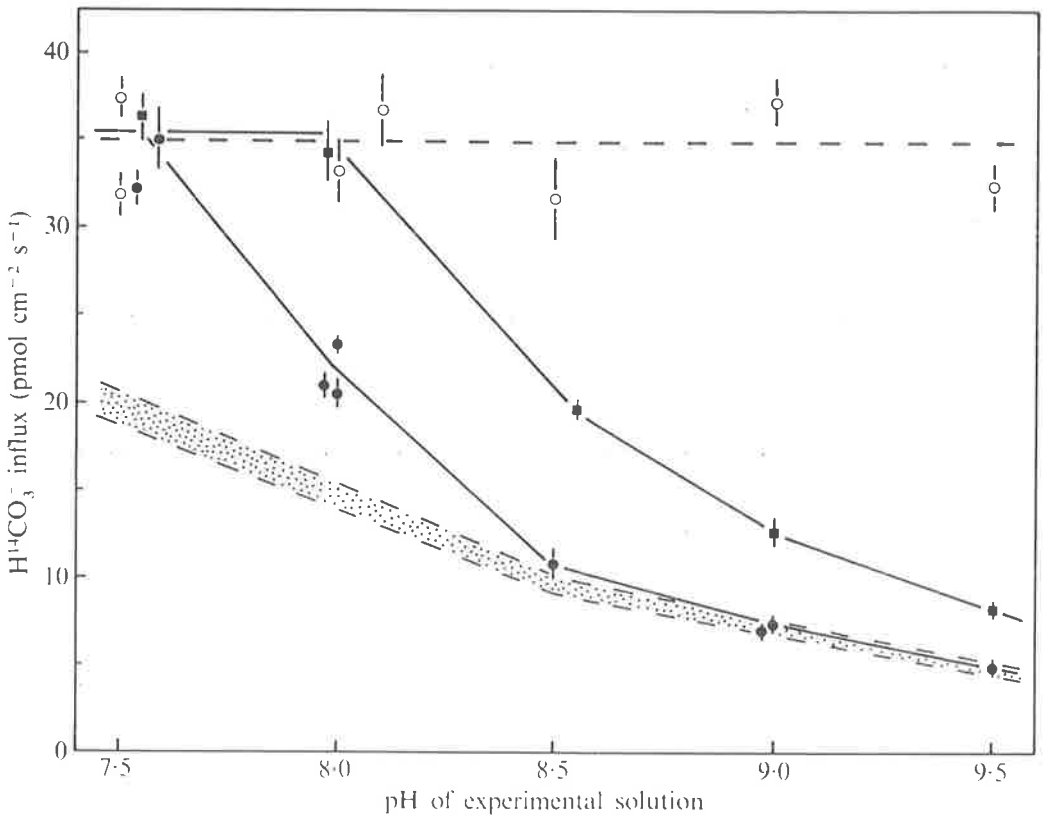


FIG. 6. Influence of experimental pH on Tris and Tricine inhibition of $H^{14}CO_3^-$ influx. Control experiments (○) were conducted in standard solutions containing 0·5 mM total added inorganic carbon. The horizontal broken line represents the mean control influx of 35 pmol cm$^{-2}$ s$^{-1}$. The influence of 4 mM Tris (●) and Tricine (■) was investigated in the presence of the same level of total carbon. The stippled region represents the expected degree of inhibition that 4 mM Tris would cause, assuming that this inhibition is caused by the neutral form of Tris (see text for full details).

conducting $H^{14}CO_3^-$ influx experiments over a range of pH values (7·5–9·5). A constant concentration (4 mM) of Tricine or Tris was employed in each treatment. Neither compound inhibited $H^{14}CO_3^-$ influx at pH 7·5; pH values higher than 8·0 were required before the influence of Tricine was observed (Fig. 6).

From the results presented in Fig. 4 (conducted at pH 9·2), the per cent inhibition at a particular concentration of neutral (base) Tricine or Tris was calculated. Using the equation:

$$RNH_2^+R^1 \rightleftharpoons RNHR^1 + H^+ \qquad (4)$$

and the respective equilibrium constants (see Table 3), the concentrations of neutral Tricine and Tris (base) were calculated at each pH value employed in Fig. 6. From these values the expected per cent inhibition, at a particular pH value, was obtained. Conversion of these per cent inhibition values to expected rates of $HCO_3^-$ influx was performed using a control rate of 35 pmol $cm^{-2}$ $s^{-1}$. The stippled region on Fig. 6 represents the expected $H^{14}CO_3^-$ influx values for experiments conducted in the presence of 4 mM Tris. The discrepancy between the experimental and expected values, at pH 7·5 and 8·0, indicates that the inhibitory effect of Tris is not correlated in a simple manner with the level of base present. A similar result was obtained for Tricine but, to simplify Fig. 6, the expected values were not included.

As previously stated, the formation of stable carbamate occurs only at alkaline pH values. Based on the results presented in Fig. 6, it would appear that this stable pH value is 8·0 for the carbamates of Tris and Tricine. The obligate, combined requirement, of neutral base and alkaline pH values necessary to produce the inhibitory complex is illustrated in Fig. 7. In these experiments the concentration of added inorganic carbon was held constant at 0·5 mM. At pH 7·5, no inhibition of $H^{14}CO_3^-$ influx was observed, even in the presence of 4 mM Tris base (20 mM total concentration of Tris). An initial linear relationship between the concentration of Tris (base) and per cent inhibition was observed at pH 8·0. However, increasing the Tris (base) concentration beyond 1·5 mM did not result in further inhibition. The degree of inhibition could only be increased by raising the pH value of the experimental solution (see Fig. 7, pH 9·0 and 9·5).

As suggested by Edsall and Wyman (1958), the values for the rate coefficients, $k_f$ and $k_b$ of reaction (3), are pH-dependent. Presumably as the pH increases, $k_f$ increases and $k_b$ either decreases or remains unaltered. The concentration of $R—NR^1—COOH$ will depend, therefore, upon several factors. The most important will be the pH of the solution, for this will determine the relative values of $k_f$ and $k_b$, and the concentrations of $CO_2$ and neutral $R—NHR^1$ present. Although the exogenous $CO_2$ concentration will decrease as the pH is increased, this reduction in substrate must be more than compensated for by the relative increase in $k_f$. A value for the carbamate acid dissociation constant does not appear to have been determined. It is unlikely, however, that its value will deviate significantly from those observed for other amino acids. If this is the case, most of the carbamate would exist as $R—NR^1COO^-$, and the amount of $R—NR^1COOH$ would be small. Since significant inhibition of $H^{14}CO_3^-$ influx was observed, it would appear that

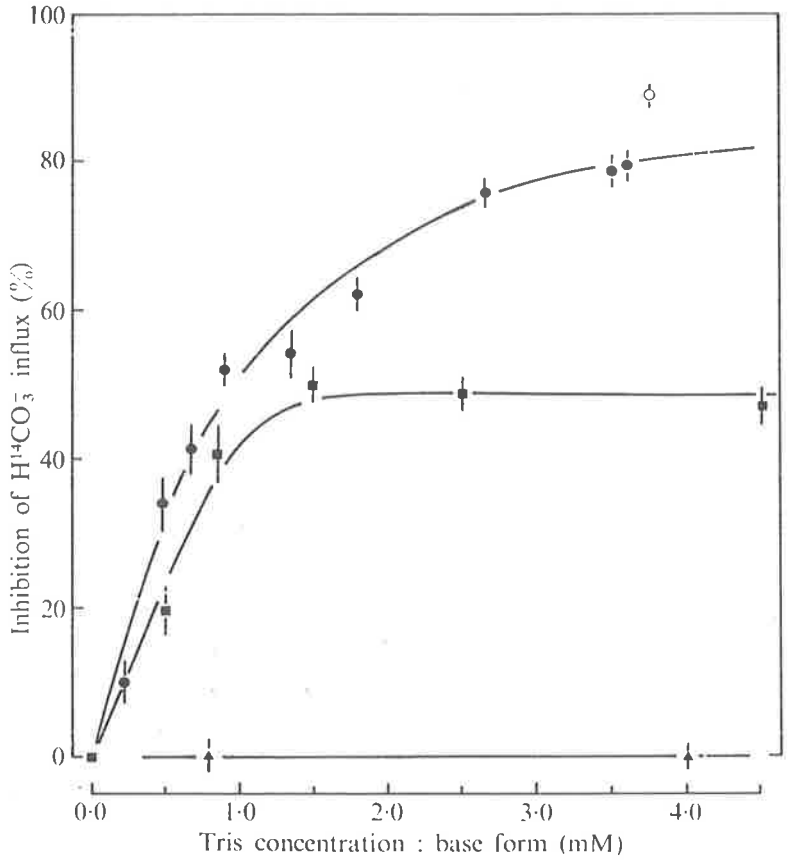


FIG. 7. Percentage inhibition of $H^{14}CO_3^-$ influx as a function of the concentration of neutral Tris (base) and the experimental pH. Control and Tris experiments were conducted in the presence of 0·5 mM total added inorganic carbon. pH values: 7·5, ▲; 8·0, ■, 9·0, ●; 9·45, ○.

R—$NR^1COOH$ has a high affinity for the binding site, provided, of course, that the reactive species is actually R—$NR^1COOH$.

## DISCUSSION

The results presented in this paper confirm our hypothesis that $CO_3^{2-}$ ions competitively inhibit $H^{14}CO_3^-$ influx in cells of *Chara corallina* (Lucas, 1975*b*). Similarly, competitive inhibition by Tricine and Tris has now been confirmed and the range of competitive compounds has been extended to include amino acids whose $pK'_a$ ($NH_3^+$) values fall in the range 7·5–9·3. The formation of the carbamate, and its subsequent competitive inhibition of the $HCO_3^-$ site, seems to be the simplest interpretation of the amino acid results. Provided that the $HCO_3^-$ transport system contributes to either the electrical potential or conductance of the plasmalemma, electrophysiological experiments should indicate whether our present interpretation is correct.

### *Functional groups involved in substrate binding*

The $CO_3^{2-}$ ion was quite effective in competing for the $HCO_3^-$ site on the transport complex. This suggested that the functional groups, involved with the binding of $HCO_3^-$ to the transport site, may be C=O and C—$O^-$. However, if this was the

case, formate, acetate, and propionate should have been effective inhibitors. These ions could not have been excluded from the site by virtue of their size, because much larger compounds were found to be capable of competitive inhibition (Tricine, Tris, TES, TAPS, etc.).

It would appear, therefore, that to bind successfully the functional groups on the substrate must be either:

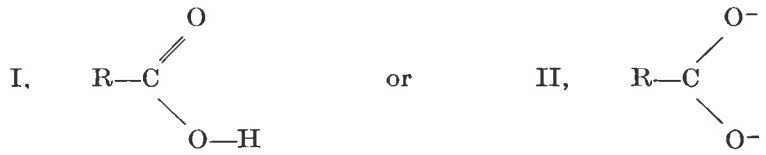


where the R group represents the non-specific part of the ion. In form I, R may be $O^-$ ($HCO_3^-$ ion) or the structure of Tris, Tricine, etc. (carbamates). Form II is the special case of the $CO_3^{2-}$ ion, where the =O group is represented by R. Although these two forms provide an explanation for the observed experimental results, the significant difference between the structures is disconcerting. Accommodation of these differences, at the molecular level of the $HCO_3^-$ binding site, would almost certainly be impossible.

In view of the carbamate results, we feel that form I is more likely to represent the functional binding groups. It may be that, in the partially bound state, the two negatively charged oxygen atoms on the $CO_3^{2-}$ ion may induce a slight conformational change in the $HCO_3^-$ binding site. Under these conditions, both the presence of the $CO_3^{2-}$ ion at the binding site and the induced conformational change may prevent the approach of $HCO_3^-$ ions. Unfortunately, with the exception of $HCO_3^-$, all the simple mono- and dicarboxylic acids have $pK_a$ values in the range 1·5–6·0 (Jenck and Regenstein 1970). This means that a suitable, stable, protonated carboxylic acid is not available to test the validity of our hypothesis. Future experiments will investigate the possibility of the existence of a suitable analogue for the O—H group on the carboxylic acid.

ACKNOWLEDGEMENTS

This work was supported jointly by grants from the National Research Council of Canada and the Connaught Fund (University of Toronto) to Prof. J. Dainty, Department of Botany, University of Toronto.

LITERATURE CITED

Coster, H. G. L., and Kaplin, I. J., 1973. *Biochim biophys. Acta*, **330**, 141–6.

Edsall, J. T., and Wyman, J., 1958. *Biophysical chemistry*. Academic Press, New York. Pp. 571–8.

Harned, H. S., and Scholes, S. R., 1941. *J. Am. chem. Soc.* **65**, 2030–7.

Jenck, W. P., and Regenstein, J., 1970. In *Handbook of biochemistry, selected data for molecular biology*. Ed. H. A. Sober, Second edition. The Chemical Rubber Company, Cleveland Pp. J 187–226.

Jensen, A., and Faurholt, C., 1952. *Acta chem. scand.* **6**, 385–94.

Lucas, W. J., 1975*a*. *J. exp. Bot.* **26**, 271–86.

—— 1975*b*. Ibid. **26**, 331–46.

—— 1976*a*. Ibid. **27**, 19–31.

—— 1976*b*. Ibid. **27**, 32–42.

—— 1977. Ibid. **28**, 1307–1320.
—— and Dainty, J., 1977. *J. Membrane Biol.* **32**, 75–92.
—— and Smith, F. A., 1973. *J. exp. Bot.* **24**, 1–14.
—— —— 1976. *Aust. J. Pl. Physiol.* **3**, 443–56.
Smith, F. A., 1966. *Biochim. biophys. Acta*, **126**, 94–9.
—— 1968. *J. exp. Bot.* **19**, 207–17.

J. Membrane Biol. 32, 75–92 (1977)
© by Springer-Verlag New York Inc. 1977

# Spatial Distribution of Functional $OH^-$ Carriers Along a Characean Internodal Cell: Determined by the Effect of Cytochalasin B on $H^{14}CO_3^-$ Assimilation

William J. Lucas and Jack Dainty

Department of Botany, University of Toronto, Toronto M5S 1A1, Ontario, Canada

Received 30 June 1976

*Summary.* The present study was aimed at testing an hypothesis relating to the $OH^-$ efflux pattern developed on internodal cells of *Chara corallina*. It was suggested that $OH^-$ efflux carriers were restricted to a limited number of sites along the internodal cell. Hydroxyl ions were considered to be delivered to these sites via the streaming cytoplasm. To test this hypothesis, cytochalasin B was used to inhibit cyclosis. Under these conditions $OH^-$ efflux and $H^{14}CO_3^-$ assimilation should have been inhibited.

Our results indicated that cyclosis was inhibited within 60 min in the presence of 30 μg/ml cytochalasin B. When $^{14}CO_2$ (pH 5.0) fixation experiments were conducted under these conditions, no inhibition of photosynthesis was observed. Cytochalasin B was shown, therefore, to inhibit cyclosis without affecting the *in vivo* reactions of photosynthesis.

A parallel study on the effect of increasing cytochalasin B concentrations on cyclosis and $H^{14}CO_3^-$ assimilation revealed that there was a limiting velocity of cyclosis below which $H^{14}CO_3^-$ assimilation was inhibited. These results were interpreted in terms of a rate-limiting step associated with the supply of $OH^-$ to the operational efflux sites.

At cytochalasin B concentrations below 15–20 μg/ml, no effect was observed on $H^{14}CO_3^-$ assimilation. This suggested that cytochalasin B does not interfere with the membrane-bound $HCO_3^-$ and $OH^-$ transport systems of this species.

The $OH^-$ efflux pattern underwent significant modification following cyclosis inhibition. A change from discrete band efflux sites to a network of numerous small, localized, disc-shaped efflux sites was observed. The discovery of this modified $OH^-$ efflux system provided an explanation for the observed limited sensitivity of $H^{14}CO_3^-$ influx to cessation of cyclosis.

These results invalidated part of our hypothesis, since they revealed that the $OH^-$ carriers are uniformly distributed over the plasmalemma surface. A modified hypothesis to account for the spatial distribution of the $OH^-$ efflux sites is presented.

Several Characean species (giant fresh water algae cells) develop light-dependent acid and alkaline bands along their cell walls [20, 19, 15]. The alkalinization phenomenon depends upon the presence of exogenous $HCO_3^-$ in the experimental solution [15]. Photosynthetic assimilation of the carbon supplied by $HCO_3^-$ results in the production of one $OH^-$ for each $CO_2$ molecule fixed. This "waste product" ($OH^-$) is exported

from the cytoplasm, across the plasmalemma, at discrete $OH^-$ efflux sites [11, 12]. Each alkaline band is formed by the transport of $OH^-$ over a small cylindrical band of plasmalemma surface [11], the length of which is approximately 0.05 cm (cf. 4–5 cm total cell length). Accumulation of $OH^-$ at the cell surface, and its diffusion into the neighboring bathing solution, gives rise to the observed alkaline banding phenomenon [15, 11].

Under $HCO_3^-$ assimilating conditions, the $OH^-$ bands are spaced at somewhat regular intervals along the length of the internodal cell. The number of bands per cell and their efflux activities depend on the level of exogenous $HCO_3^-$, the incident light intensity and the length of the actual cell [15, 11, 12]. Recent progress in this field has revealed that the $OH^-$ efflux system of *Chara corallina* is, however, a more complex phenomenon than would appear at first sight [11, 12, 14]. There exists an hierarchy of functional $OH^-$ efflux sites within the plasmalemma. The three operationally distinct forms of $OH^-$ bands that have been observed were termed the primary, sub-primary and subsidiary $OH^-$ efflux systems [12]. Within this hierarchy the primary $OH^-$ efflux site always activates first and is the last to deactivate, under a given set of experimental conditions; the sub-primary behaves in an almost identical manner. It is thought the subsidiary sites activate only when the $OH^-$ production rate, at the chloroplast layer, exceeds the combined efflux rates of the primary and sub-primary systems. Under these conditions subsidiary sites activate at various positions along the internodal cell, until the combined $OH^-$ efflux activity of the operational bands equals the photosynthetic production of $OH^-$ [12]. This system is a unique example of cytoplasmic substrate regulation on a macroscopic scale, i.e., the distribution of the $OH^-$ efflux sites along the cell appears to be related to their capacity to efflux the photosynthetically generated $OH^-$ from the chloroplast layer. (In these cells the chloroplasts are uniformly distributed in a single layer in the outer, nonstreaming cytoplasmic layer.)

As a result of these recent studies, we became interested in the question of the cellular mechanism controlling the spatial distribution of the primary, sub-primary and subsidiary $OH^-$ bands along an internodal cell. This interest increased when it was discovered that the $HCO_3^-$ and $OH^-$ transport systems function independently, in that the respective ions are transported across the plasmalemma by different sets of carriers [14]. This suggested to us that in order to maximize photosynthesis, the $HCO_3^-$ carriers would probably be uniformly distributed over the

cell membrane surface. A situation of this nature would involve complex electrical and transport interactions between the two systems, especially as the $OH^-$ efflux system is so highly localized.

This system was investigated in the present study, and on the basis of our results we have formulated a model which we feel can account for the spatial distribution of the $OH^-$ efflux sites of *C. corallina*.

## Materials and Methods

*Chara corallina* cells were cultured in the laboratory under artificial light. Culture details and the method used to cut internodal cells from the culture have been previously reported [15, 13]. In general, mature third to fifth internodal cells were used.

The standard experimental solution contained 1.0 mM NaCl, 0.2 mM KCl and 0.5 mM $CaSO_4$, unless otherwise specified. The pH values of some solutions were controlled by artificial buffers. All chemicals used were of Analar Reagent grade.

Radioactive $NaH^{14}CO_3$ was obtained from New England Nuclear, Boston, as a sterile aqueous solution, and aliquots were added to the experimental solutions to give a final specific activity of 1 mCi per mmole.

Cytochalasin B was obtained from Aldrich Chemical Company, Milwaukee, Wisconsin. A stock solution (3 mg/ml) in dimethyl sulphoxide (spectroscopic grade) was stored at 4 °C until used. This stock solution was added to experimental media to give the concentrations described in the text. Unless otherwise specified, the final dimethyl sulphoxide concentration in experimental and control solutions was 1% (v/v).

Cytoplasmic streaming and radioisotope ($NaH^{14}CO_3$) studies were performed on cells cut one day prior to the actual performance of the experiment. These cells were pre-treated in experimental solution which contained 1.0 mM $NaHCO_3$ (pH 9.0). The light regime employed for the cultures (13L:11D) was maintained during this pre-treatment period, and all cells were illuminated under fluorescent lights (10 $Wm^{-2}$) for 2 hr prior to the commencement of an experiment. For experiments associated with cytochalasin B, a 1 hr pre-treatment in 1% dimethyl sulphoxide was employed. The actual duration and radioactive exposure period for each experiment is indicated in the text. The radioisotope techniques employed have been detailed by Lucas [13]. Cyclosis was measured with a binocular microscope having an ocular micrometer. The time required for a standard sized cytoplasmic particle to traverse 1000 μm was measured with a stopwatch; 10 cells were used per treatment. (When cyclosis was severely retarded, the traverse distance was reduced to 100 μm.)

Details of the illumination and experimental systems have been previously reported [12].

The pH values along the cell surface of *C. corallina* internodal cells were measured using the technique developed by Lucas and Smith [15]. To prepare agar blocks (0.7% w/v) containing cytochalasin B and/or 1.0 mM $NaHCO_3$, the following procedure was employed. Agar powder (Difco, Bacto-agar) was dissolved by boiling a known volume of standard experimental solution. This solution was then cooled to 39 °C, at which temperature the required amounts of stock $NaHCO_3$ and cytochalasin B solutions were added. The pH value was checked and titrated to the required value. Agar blocks were then set within perspex holders. Channels designed specifically to hold experimental *Chara* cells, were made in the agar blocks [13] and cells subsequently located in them. The blocks were then placed in thermostatted experimental solutions. Following a 2 hr illumination period, a Leitz micromanipulator was used to traverse a miniature pH electrode (Microelectrodes, Inc., Model MI-405) along the cell wall. From the values obtained the pH pattern established was mapped.

## Results and Discussion

### *A Working Hypothesis*

The simplest explanation for the localized, regular pattern of $OH^-$ efflux sites along a particular *Chara* cell was that the transport entities (carriers) are restricted to a limited number of sites along the length of the plasmalemma. In addition, we also considered that the $HCO_3^-$ transport system was uniformly distributed (on a macroscopic scale) over the entire plasmalemma surface.

At this point it should be stressed that these cells are, to a good approximation, right circular cylinders of macroscopic dimensions (diameter 0.6–1.0 mm, length 40–80 mm), having their chloroplasts restricted to a single uniform layer in the outer region of the cortical (gel) cytoplasm. The distance from the plasmalemma to the chloroplast layer is approximately 4–6 μm [5]. Consequently, the time associated with the diffusion of $HCO_3^-$ from the carriers to the chloroplasts would be extremely short (approximately 50–200 msec). However, the lateral diffusion path from the site of $OH^-$ generation, within the chloroplast layer, to the nearest operational $OH^-$ efflux site can be quite long. The distance between neighboring operational $OH^-$ efflux sites, under maximal $HCO_3^-$ assimilating conditions, ranges from 6 to 10 mm (*see* Fig. 6A). The maximum lateral diffusion path for $OH^-$ under these conditions would be 3–5 mm. But, when only the primary site is functioning, this distance can be 30 mm of more [12]. Free diffusion of $OH^-$ over these distances would take a considerable time (approximately 1–50 hr respectively). It therefore seemed most likely that $OH^-$ ions are not moved exclusively by free diffusion, but rather are rapidly transported around the cell by the streaming layer of the cytoplasm. (For a streaming rate of 60 μm per sec, the time to cover 5 and 20 mm is approximately 1.4 and 5.6 min, respectively.)

A prediction, based on the above, is that if cytoplasmic streaming is stopped, the rate of $HCO_3^-$ assimilation should be greatly reduced. The $OH^-$ efflux process would be expected to be rate-limiting under these conditions, since $HCO_3^-$ influx cannot proceed for long in the absence of $OH^-$ efflux.

### *Influence of Dimethyl Sulphoxide on Cyclosis and Photosynthesis*

Cytochalasin B, an alkaloid metabolite of the fungus *Helminthosporium dematioideum* [1] inhibits cyclosis in the Characeae [21–23, 2, 4].

Table 1. Influence of Dimethyl Sulphoxide on $^{14}C$ assimilation[a]

| pH Value of experimental solution | Exogenous substrate | Assimilation of $^{14}C$ (pmole $cm^{-2}$ $sec^{-1}$) | |
|---|---|---|---|
| | | Control | 1% Dimethyl sulphoxide |
| 5.01 | $^{14}CO_2$ | 116.4 ± 5.0 | 123.1 ± 5.9 |
| 9.00 | $H^{14}CO_3^-$ | 62.2 ± 1.9 | 60.2 ± 2.3 |

[a] Radioactive $^{14}C$ assimilation was measured using a 1 hr pre-treatment, followed by a 1 hr exposure to the radioisotope solution. A concentration of 1.0 mM total carbon was employed at the two pH values. Experimental solutions at pH 5.01 were buffered by 5 mM 2-(N-morpholino) ethanesulphonic acid (MES); at pH 9.0 no artificial buffers were used. Values given are mean ± SEM (15 cells per treatment).

Although the recent literature relating to this compound indicates that it is not as specific in its action as previously thought [6], it was considered more reliable than compounds like *p*-chloromercuribenzoate [7] or 8-Hydroxyquinoline (W.J. Lucas, *unpublished*) and was consequently used in the present study.

Preliminary experiments were conducted to ensure that dimethyl sulphoxide, the solvent used for cytochalasin B, did not have a deleterious effect on either cyclosis or photosynthesis. Table 1 shows that 1% (v/v) dimethyl sulphoxide does not affect either $^{14}CO_2$ or $H^{14}CO_3^-$ assimilation. Similarly no effect was observed on cyclosis; this agrees with the findings of Williamson [22] and Bradley [2].

### *Inhibition of Cyclosis by Cytochalasin B*

The nature of the time course of cyclosis inhibition by various cytochalasin B concentrations is shown in Fig. 1. The slow, linear phase of these time courses is indicative of a diffusion limited system. This is readily accounted for in this experimental system since stagnant solutions were employed throughout [16], and this would cause a diffusional limitation on the rate of entry of cytochalasin B to the cytoplasm. However, the results presented in Fig. 2 demonstrate that the time course of cyclosis inhibition is also strongly influenced by the level of dimethyl sulphoxide employed. Hence, since dimethyl sulphoxide probably acts both as a solvating agent and as a carrier for cytochalasin B across the plasmalemma, it would appear that the entry of cytochalasin B into the cell is limited by its permeation across the plasmalemma as well as by diffusion in the aqueous and cytoplasmic phases.

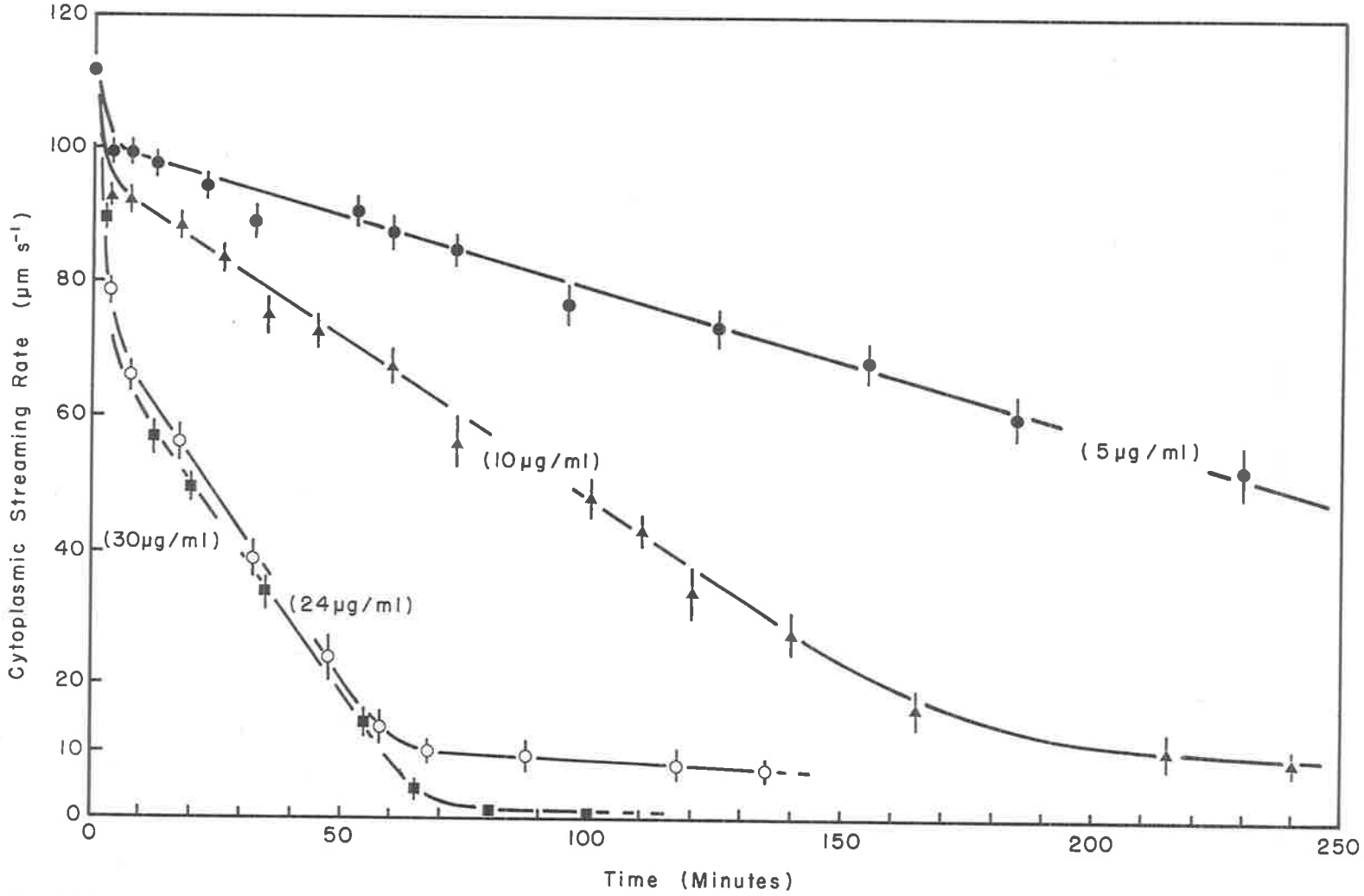


Fig. 1. Time course of cyclosis inhibition by cytochalasin B. Experiments were conducted in standard solutions, containing 1.0 mM $NaHCO_3$ (pH 9.0) and 1% (v/v) dimethyl sulphoxide, for 1 hr prior to transferring to solutions containing cytochalasin B. The actual cytochalasin B concentrations employed are indicated on the respective time courses. Ten cells were used for each time course and the values presented are the mean ± SEM

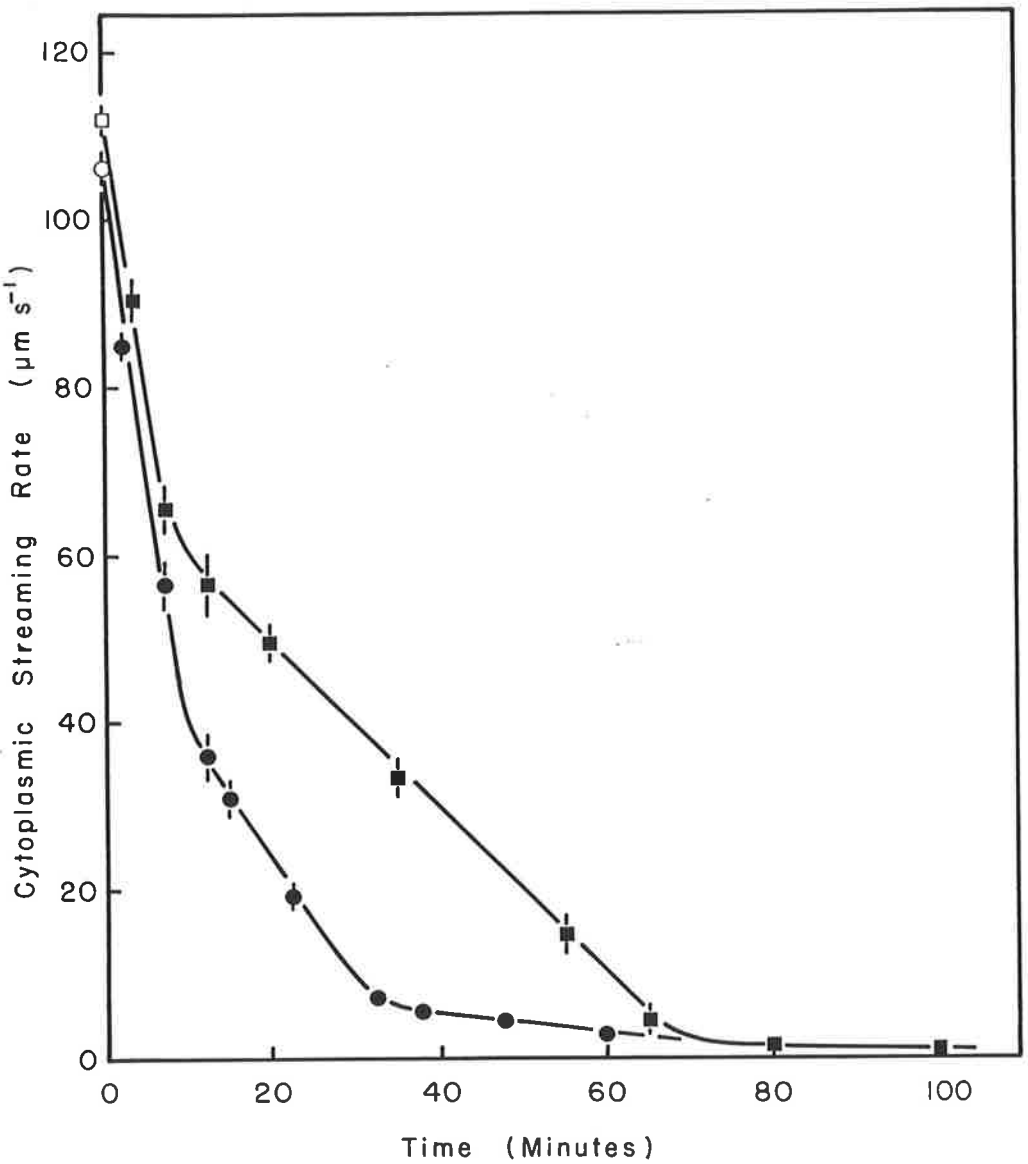


Fig. 2. Influence of dimethyl sulphoxide level on cytochalasin B mediated inhibition of cytoplasmic streaming. Experimental details are as in Fig. 1. The levels of dimethyl sulphoxide employed were 1% (■) and 2% (●) (v/v) and both treatments were conducted in the presence of 30 μg/ml cytochalasin B

Figs. 1 and 2 show that after a 70 min exposure to 30 μg/ml cytochalasin B, cytoplasmic streaming is reduced to a very low level. This concentration seemed suitable for investigating the effect of cytoplasmic streaming on $H^{14}CO_3^-$ assimilation. But, since exposure to this alkaloid during radioisotope and pH scanning experiments may extend to 100 min or longer, it was essential to ascertain whether the effect caused at this concentration was reversible. Fig. 3 demonstrates that it was reversible. Inhibition of streaming by 30 μg/ml cytochalasin B was found to be

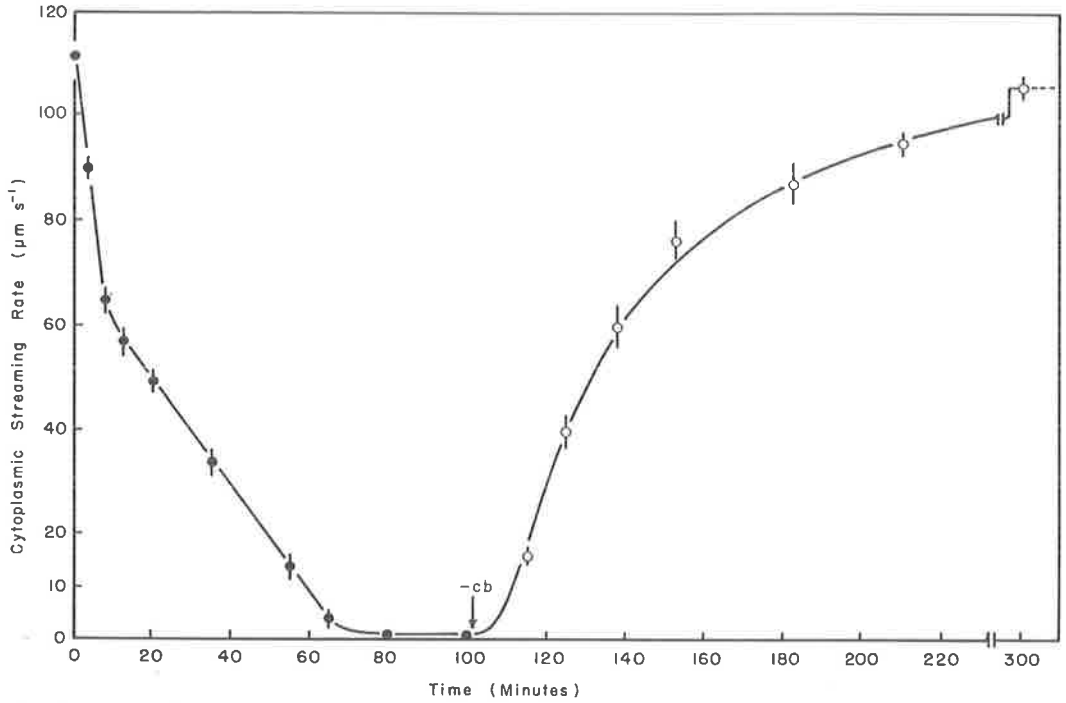


Fig. 3. Reversibility of cyclosis inhibition caused by cytochalasin B. Experimental details are as in Fig. 1. The experimental medium contained 30 μg/ml cytochalasin B (1%, v/v, dimethyl sulphoxide) for 102 min, a cytochalasin B-free medium was then substituted (−cb). This solution was changed three times in the first 10 min and then hourly

reversible for periods of up to 180 min, provided 1% (v/v) dimethyl sulphoxide was used. (Higher levels of dimethyl sulphoxide tended to decrease the reversibility.)

### *Effect of Cytochalasin B on $^{14}CO_2$ fixation*

*Exogenous* $CO_2$ moves by passive diffusion from the external medium, through the plasmalemma and cortical (gel) cytoplasmic layer, to the chloroplasts. Consequently, over short periods when cyclosis is inhibited, the rate of $CO_2$ fixation should not be influenced by the inhibition of streaming, *per se*. Table 2 indicates that for periods up to 80 min, $^{14}CO_2$ fixation was not altered even though cyclosis was almost completely stopped. Therefore it can be assumed that cytochalasin B can inhibit streaming in *Chara* cells without affecting the reactions of photosynthesis.

### *Bicarbonate Assimilation in the Presence of Cytochalasin B*

Fig. 4*A* and *B* represent the results of cyclosis and $H^{14}CO_3^-$ assimilation experiments conducted in parallel. An experimental cytochalasin

Table 2. Influence of 25 μg/ml Cytochalasin B on $^{14}CO_2$ fixation [a]

| Experimental duration (min) | $^{14}CO_2$ fixation (pmole $cm^{-2}$ $sec^{-1}$) | | Cyclosis (Percentage inhibition in presence of Cytochalasin B) |
|---|---|---|---|
| | Control | + Cytochalasin B | |
| 20 | 126.3 ± 4.2 | 123.6 ± 6.2 | 80.1 |
| 40 | 120.0 ± 4.0 | 115.9 ± 4.7 | 94.8 |
| 60 | 120.1 ± 9.0 | 127.1 ± 6.1 | 98.1 |
| 80 | 130.8 ± 3.4 | 123.1 ± 5.6 | 98.1 |

[a] Experimental solutions were buffered with 5 mM MES (pH 5.02) and contained 1.0 mM total carbon and 2% (v/v) dimethyl sulphoxide. Cytochalasin B concentration employed was 25 μg/ml. Following a 1 hr pre-treatment, nonradioactive experimental solutions were substituted until the final 20 min period of each treatment. Values are mean ± SEM (15 cells per treatment).

B exposure period of 1 hr was employed for this series of experiments. This period was chosen as it offered, by the use of various cytochalasin B concentrations, a wide range of cytoplasmic streaming rates, while all treatments would remain well within the reversible period of this drug (*see* Fig. 1). A decrease in cyclosis with increasing cytochalasin B concentrations was expected; however, the linear nature of the decline was not anticipated (Fig. 4*A*). We do not have a satisfactory explanation for this relationship.

Fig. 4*B* indicates that incomplete inhibition of $H^{14}CO_3^-$ assimilation (approximately 50%) occurred at high cytochalasin B concentrations, where cyclosis was completely inhibited. This aspect of the results will be discussed and expanded in a later section. The insensitivity of $H^{14}CO_3^-$ assimilation to cytochalasin B concentrations of up to 15 μg/ml is of importance, since it tends to eliminate the possibility that cytochalasin B caused the observed $H^{14}CO_3^-$ inhibition by an effect on the $HCO_3^-$ transport system of the plasmalemma (*see* Fig. 4*B*). We interpreted the decrease in $H^{14}CO_3^-$ influx, under 20–35 μg/ml cytochalasin B, as resulting from the reduction of cyclosis below a "limiting velocity", i.e., below this "limiting velocity" the rate at which $OH^-$ ions are supplied to the efflux sites becomes the limiting step in the overall process of $H^{14}CO_3^-$ assimilation. Based on the results presented in Fig. 4, the "limiting velocity" for these cells would be 38 ± 8 μm per sec.

To test this "limiting velocity" proposal, $H^{14}CO_3^-$ assimilation time course experiments were conducted at a 30 μg/ml cytochalasin B concentration in the presence of 2% (v/v) dimethyl sulphoxide. The higher

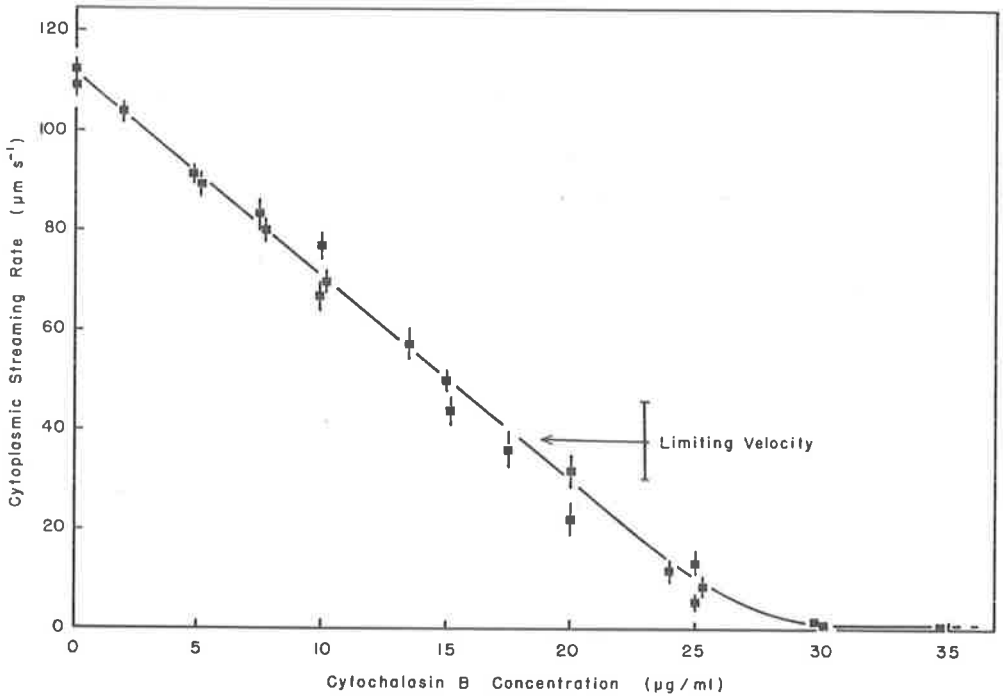


Fig. 4*A*

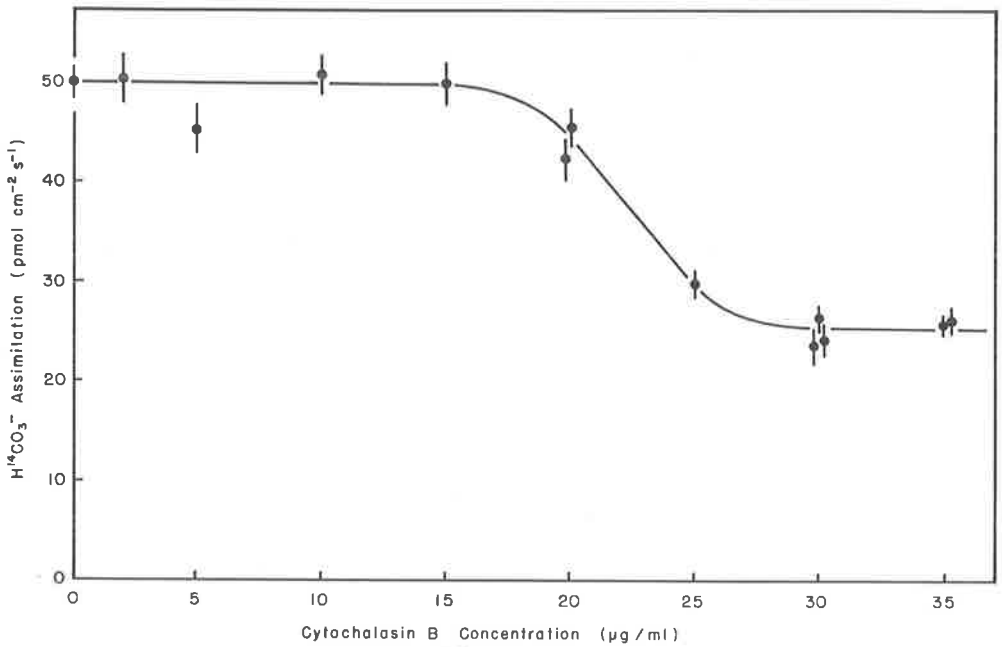


Fig. 4*B*

Fig. 4. Parallel study on the effect of increasing cytochalasin B concentration on cyclosis and $H^{14}CO_3^-$ influx. Experiments were conducted in standard solutions containing 1.0 mM $NaHCO_3$ (pH 9.0), 1% (v/v) dimethyl sulphoxide and the indicated cytochalasin B concentration. All treatments were given 1 hr pre-treatment and experimental periods. Cyclosis (Fig. 4*A*) was measured over the final 10 min of the 1 hr experimental period. Similarly $H^{14}CO_3^-$ was not substituted until this final 10 min period. A check on the cytoplasmic streaming rate was made at the end of $H^{14}CO_3^-$ influx experiments to ensure that rates were compatible with those presented in Fig. 4*A*. The significance of the limiting velocity is explained in the text. All values are expressed as mean ± SEM (10 cells per treatment)

dimethyl sulphoxide level was employed to accelerate the decline in cyclosis. Under these conditions the "limiting streaming velocity" would be attained within $12 \pm 3$ min compared with $32 \pm 8$ min associated with the 1% (v/v) dimethyl suphoxide situation (*see* Fig. 2). A theoretical time course of $H^{14}CO_3^-$ influx inhibition in the presence of 2% (v/v) dimethyl sulphoxide was obtained as follows:

(i) From Fig. 4*A* and *B* the percentage inhibition of $H^{14}CO_3^-$ influx was calculated over a range of cyclosis values.

(ii) From the 2% (v/v) dimethyl sulphoxide results presented in Fig.2, and a control $H^{14}CO_3^-$ influx value of 60 pmole per $cm^2$ per sec, an inhibition curve was computed.

Close agreement between the predicted and experimental curves was obtained (*see* Fig. 5). The depression of $H^{14}CO_3^-$ influx below the predicted level, in the 60–90 min region, may have been due to the increase in dimethyl sulphoxide, *per se*. We consider that these results add weight to our concept of a "limiting cytoplasmic streaming velocity" in relation to the supply of $OH^-$ ions to operational efflux sites.

These results also support our earlier conclusion that cytochalasin B does not affect the membrane-bound $H^{14}CO_3^-$ transport system. This is a significant finding in view of recent reports that indicate cytochalasin B can affect certain membrane-bound active transport processes [3, 8–10]. If the proposal is correct that the cytochalasins inhibit ATP-mediated active transport systems [3, 8], our results imply that $H^{14}CO_3^-$ transport in *C. corallina* may not be energized by ATP.

### *Partial Inhibition of $H^{14}CO_3^-$ Assimilation by Cytochalasin B*

Figs. 4*B* and 5 revealed that when cyclosis was stopped, $H^{14}CO_3^-$ influx and assimilation was only partially inhibited. On the basis of our working hypothesis we expected a close parallel between both the inhibition of cyclosis and $H^{14}CO_3^-$ assimilation. This limited sensitivity of $H^{14}CO_3^-$ assimilation, to the cessation of cyclosis, suggested to us that the normal $OH^-$ efflux system must undergo a modification under these conditions. We conducted cell wall pH scanning experiments to investigate this possibility.

A proliferation of $OH^-$ efflux sites was observed following a 2 hr pretreatment with 30 μg/ml cytochalasin B (Fig. 6*A*). These $OH^-$ efflux sites were considerably smaller and less active when compared with the normal sites developed by the same cell under control conditions. However, the presence of these new $OH^-$ efflux sites explained why $H^{14}CO_3^-$ assimilation was not completely inhibited when cyclosis was stopped.

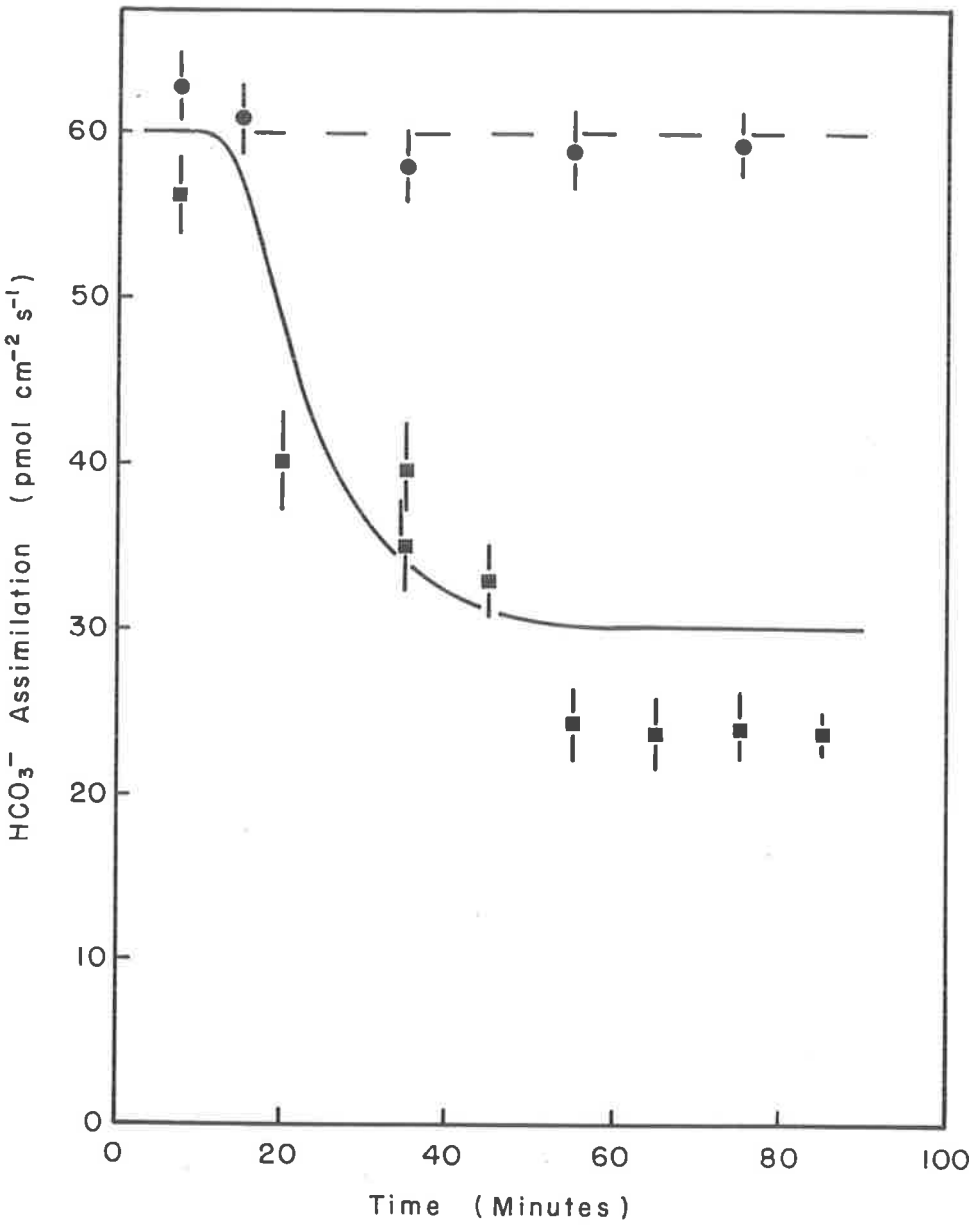


Fig. 5. Comparison between predicted and experimental time courses for $H^{14}CO_3^-$ influx inhibition, in the presence of 30 μg/ml cytochalasin B and 2% (v/v) dimethyl sulphoxide. Experiments were conducted in standard solutions containing 2.0 mM $NaHCO_3$ (pH 9.0). Radioactive $H^{14}CO_3^-$ solutions were employed over the final 10 min experimental period. The symbol (●) and broken line represent the control treatments, conducted in the absence of cytochalasin B. The solid line represents the predicted decay curve based on the limiting cyclosis hypothesis; the values used for its construction were obtained from Figs. 2 and 4 (*see* text for full details). The symbol (■) represents the experimental points. All values are expressed as mean ± SEM (10 cells per treatment)

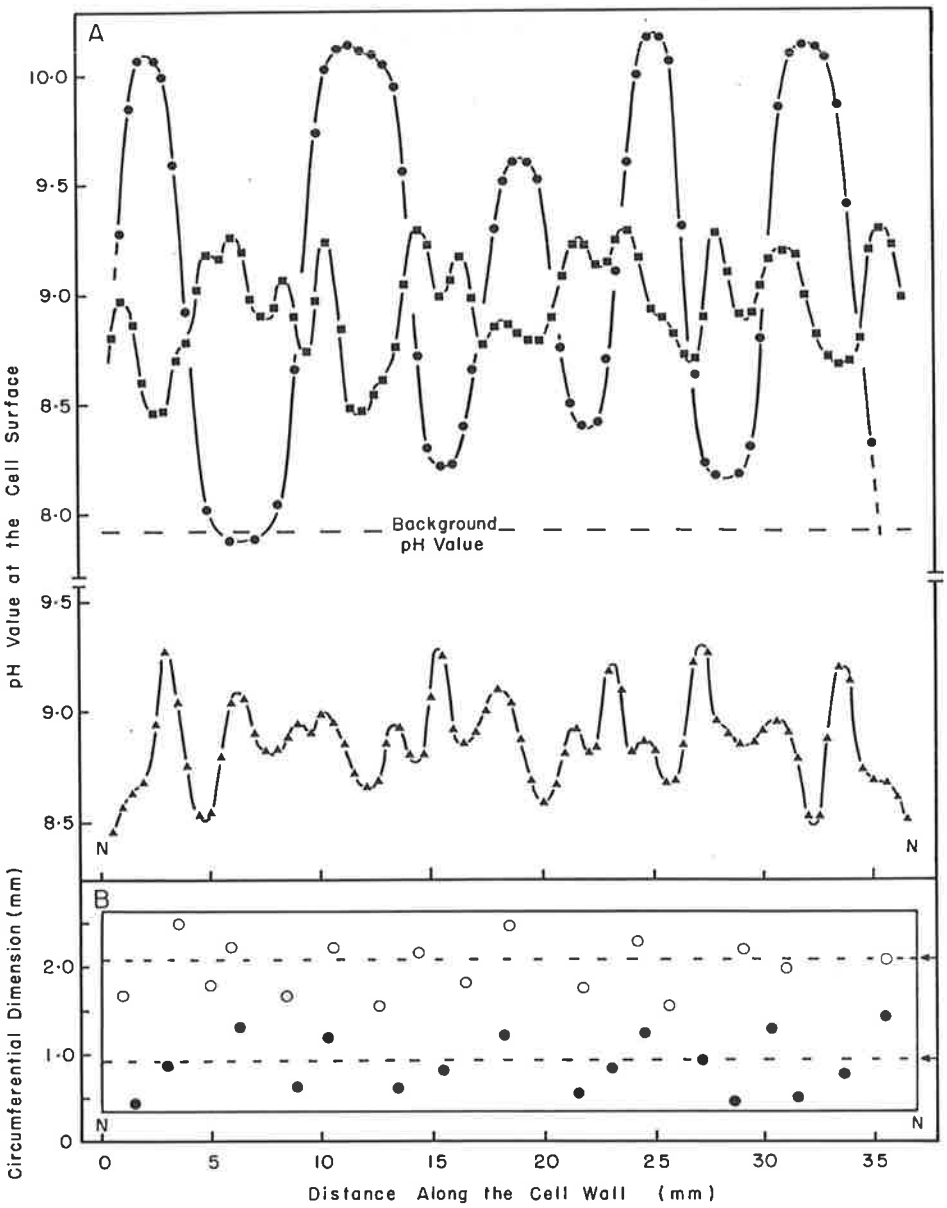


Fig. 6. Influence of 30 μg/ml cytochalasin B on the $OH^-$ efflux pattern established on the internodal cell surface of *C. corallina*. (*A*) The pH value of the agar block and bathing solution was adjusted to 7.9 and the experimental system contained 1.0 mM $NaHCO_3$. Each pH trace was conducted after a 2 hr illumination period (15 $Wm^{-2}$). The control (●) was conducted and then the cell was transferred to solutions containing 30 μg/ml cytochalasin B. The two cytochalasin B-affected traces, (■) and (▲), were conducted on diametrically opposite cell wall surfaces. Following the completion of the first cytochalasin B trace (■), the experimental cell was transferred to a second identical agar block, and in this block the opposite cell surface was exposed for scanning. The symbol *N* refers to the location of the nodes at the end of this internodal cell. (*B*) The pH pattern developed when cyclosis was stopped by cytochalasin B has been interpreted, and presented in this Fig, in terms of small localized "disc" shaped $OH^-$ efflux sites scattered almost uniformly over the cell surface. The open and closed "discs" are associated with traces (■) and (▲), respectively (*see* text for full details). The arrowed broken lines refer to the two pH scan lines and the rectangle is a two dimensional plan of the internodal cell surface. (The circumference of this internodal cell was 2.3 mm)

It was also found that the location of these new efflux sites bore no relationship to the $OH^-$ efflux sites established during control treatments (*see* Fig. 6*A*). By conducting pH scans along diametrically opposite cell wall surfaces of cytochalasin B treated cells, it was established that these newly developed $OH^-$ efflux sites were very localized indeed. From the two traces presented in Fig. 6*A*, it can be seen that the new sites did not form efflux bands. That is, there was not continuity of the $OH^-$ efflux pattern around the entire cell surface (*cf.* Lucas [11]). Rather, it appeared that the sites exist as small patches of isolated operational carriers (perhaps disc-shaped). If the small pH electrode was traversed through, or close to, the center of an operational "disc" a sharp pH maximum would be registered. However, if the "disc" was to the side of the pH scan line (*see* Fig. 6*B*) a broad peak or shoulder would be registered. The elevation of the pH value above background would also depend upon the distance of the disc from the scan line. The cytochalasin B results of Fig 6*A* have been interpreted in this manner and a possible cell surface distribution of small "disc" $OH^-$ efflux sites is presented in Fig. 6*B*. We wish to stress that we consider this pattern to be very approximate indeed. Since we are uncertain of the circumferential distances over which we can sense these small $OH^-$ efflux sites, it may be that there were many more present than we have shown.

This pattern of small, localized, $OH^-$ efflux sites was confirmed by visual observations using phenol red, an acid/base indicator, in the experimental medium [20]. These experiments were performed by firstly treating internodal cells in a control medium, containing 1.0 mM $NaHCO_3$ (pH 9.0) and 1% (v/v) dimethyl sulphoxide, for 2 hr. Cells were then transferred to an identical solution except that it contained 0.1 mM phenol red and the pH value had been titrated to 5.0. In this medium the normal $OH^-$ banding pattern could be observed as red bands on a yellow background. After recording this pattern, cells were transferred to a solution containing 30 μg/ml cytochalasin B (plus 1.0 mM $NaHCO_3$, pH 9.0 and 1% dimethyl sulphoxide). Following a 2 hr treatment in this solution the streaming rate was checked to ensure cyclosis had been inhibited and then the cells were transferred to an identical solution (containing 0.1 mM phenol red), pH value 5.0. Under these conditions the pattern of small localized $OH^-$ efflux sites could be readily observed and the number of sites recorded. As many as 30–50 sites could be counted on a cell of length 3–4 cm.

The ability of these cells to establish this new $OH^-$ efflux pattern, when cyclosis is stopped, demonstrates that the $OH^-$ carriers cannot

be restricted to a limited number of discrete bands along the plasmalemma length. Consequently we had to modify our working hypothesis. Our experimental results suggest the $OH^-$ efflux carriers are rather uniformly distributed within the cell's total plasmalemma surface, i.e., in a similar manner to that proposed for the $HCO_3^-$ carriers. At any one time, however, only a small fraction of these carriers are operational. Undoubtedly the cellular mechanism that determines which carriers become operational will also determine the location and form of these sites along the cell surface.

### *A Possible Cytoplasmic Mechanism for Determining the Spatial Distribution of Operational $OH^-$ Sites Along the Cell Length*

As yet we have no information regarding the molecular nature of the $OH^-$ carriers or their operational sites within the plasmalemma. Consequently our model is formulated on very generalized concepts of possible interactions between the cellular processes of photosynthesis, cyclosis and $OH^-$ efflux. The model is presented in terms of a description of the sequential events which are considered to occur in the cytoplasmic phase following cell illumination.

(i) The commencement of photosynthesis generates $OH^-$ ions within the chloroplast layer.

(ii) These $OH^-$ ions diffuse into the cortical (gel) and streaming cytoplasm. Cyclosis and the short diffusion time between the two cytoplasmic phases results in a uniform "concentration" of $OH^-$ throughout the nonmembrane bounded regions of the cytoplasm. (It should be noted that we do not wish to specify, at this stage, $OH^-$ *per se* or a substrate which generates $OH^-$ at the efflux carrier site.)

(iii) The $OH^-$ "concentration" increases until the activating level of the primary $OH^-$ efflux site is reached [12]. (There must be a cellular mechanism which, under normal cyclosis conditions, imparts not only this hierarchical status to these respective sites, but also causes the operational entities to exist in the form of $OH^-$ efflux bands. This mechanism has not been fully elucidated [12].)

(iv) Activation of the primary site reduces the $OH^-$ "concentration" in its immediate vicinity. The localized concentration decrease will, however, be relatively small due to the coupling between this region and the larger "pool" of $OH^-$ in the streaming cytoplasm.

(v) If the efflux rate through the primary site is less than the total cellular rate $OH^-$ generation by the chloroplasts, the cytoplasmic $OH^-$

"concentration" will increase with time. This increase will be slightly greater in the cortical cytoplasmic regions farthest from the primary efflux site. It is in this region that the sub-primary site is generally found (*see* Lucas [12], Fig. 2), and it will activate once its activating concentration has been attained.

(vi) Further $OH^-$ efflux sites will activate only if the cytoplasmic $OH^-$ "concentration" continues to increase. The plasmalemma contains a macroscopic continuum of $OH^-$ efflux carriers which can, under the correct conditions, form subsidiary efflux sites. Hence, subsidiary sites will become activated at those locations along the cell length where the $OH^-$ "concentration" has increased to the subsidiary activating level.

(vii) In conjunction with (vi), it should be stressed that the increase in $OH^-$ "concentration" will be greatest in the cortical cytoplasmic regions having the greatest distance separating consecutive operational $OH^-$ efflux sites. This physical feature of the system will cause the $OH^-$ efflux sites to be spaced at almost regular intervals along the cell length.

(viii) The number of operational $OH^-$ efflux sites increases until the efflux through these sites establishes a steady state $OH^-$ "concentration" in the cytoplasmic phase. There is, however, a limit to the number of $OH^-$ sites that can operate along any one cell. This limit is related to the inhibition of the $HCO_3^-$ carriers by $CO_3^{2-}$, at pH values above 9.6 [13]. Since the pH value within the immediate cell wall region of an operational $OH^-$ band is generally 9.5–10.1, it is obvious that this region of plasmalemma would not be available for $HCO_3^-$ transport. Hence, the more bands operating, the smaller is the area available for $HCO_3^-$ transport. In the steady state, under saturating exogenous $HCO_3^-$ conditions, there exists a balance between maximizing $HCO_3^-$ influx and the area of plasmalemma required to dispose of the $OH^-$ generated by this $HCO_3^-$ influx.

When cyclosis is stopped, or reduced to a very low level, the cell loses its fine control over cytoplasmic pH regulation. Under these conditions one might expect the $OH^-$ "concentration" in the cytoplasm to increase to such a level that a "continuum" of subsidiary bands (sites) would become activated along the entire cell length. The fact that this was not observed experimentally suggests that when cyclosis was inhibited, the cellular mechanism that imparts status, etc., to these sites is also impaired. The network of small "disc" efflux sites which was established appeared, however, to cope quite adequately with the imposed

limitations of $OH^-$ diffusion. This network pattern may reflect an attempt to minimize the $OH^-$ diffusion path whilst leaving a reasonable area of plasmalemma available for $HCO_3^-$ transport.

A network pattern of this nature is in fact rather reminiscent of $CaCO_3$ deposition in the more primitive members of the Characeae (genus Tolypella [17]). Future studies relating to the implications of this change in basic $OH^-$ efflux pattern, in terms of the phylogeny of the Characeae, may provide independent support for phylogenetic arguments presently based on anatomical and cytological data [17, 18, 24].

## Conclusions

In this study we have shown that the $OH^-$ transport system of *C. corallina* is not localized at discrete sites along the plasmalemma. A macroscopic continuum of potentially operational $OH^-$ carriers within the cell's plasmalemma appears to be a more accurate description of this $OH^-$ efflux system. The experiments described also firmly established that the streaming cytoplasm is the mode by which the $OH^-$ are delivered from the chloroplasts to the operational efflux sites, under normal conditions.

We feel that our descriptive model can account for the experimentally observed features of the total $OH^-$ efflux system of *C. corallina*. However, the limitations of this model are all too apparent. We will not have a complete characterization of this phenomenon until we have elucidated the features of this system at the molecular level. This will certainly provide an interesting avenue for future research.

This work was supported jointly by grants from the National Research Council of Canada (grant No. A6459) and the Connaught Fund (University of Toronto).

## References

1. Aldridge, D.C., Armstrong, J.J., Speake, R.N., Turner, W.B. 1967. The structure of cytochalasins A and B. *J. Chem. Soc. C* **2**:1667
2. Bradley, M.O. 1973. Microfilaments and cytoplasmic streaming: Inhibition of streaming with cytochalasin. *J. Cell Sci.* **12**:327
3. Bos, C.J., Emmelot, P. 1974. Studies on plasma membranes: XXI. Inhibition of liver plasma membrane enzymes by tumor-promoting phorbolester, mitotic inhibitors and cytochalasin B. *Chem. Biol. Interact.* **8**:349
4. Chen, J.C.W. 1973. Observations of protoplasmic behaviour and motile protoplasmic fibrils in cytochalasin B treated *Nitella* rhizoid. *Protoplasma* **77**:427
5. Costerton, J.W.F., MacRobbie, E.A.C. 1970. Ultrastructure of *Nitella translucens* in relation to ion transport. *J. Exp. Bot.* **21**:535

6. Hepler, P.K., Palevitz, B.A. 1974. Microtubules and microfilaments. *Annu. Rev. Plant Physiol.* **25**:309
7. Kamiya, N. 1960. Physics and chemistry of protoplasmic streaming. *Annu. Rev. Plant Physiol.* **11**:323
98. Kuo, S.C., Lampen, J.O. 1975. Action of cytochalasin A, a sulfhydryl-reactive agent, on sugar metabolism and membrane-bound adenosine triphosphatase of yeast. *Biochim. Biophys. Acta* **389**:145
9. Lin, S., Spudich, J.A. 1974. Biochemical studies on the mode of action of cytochalasin B: Cytochalasin B binding to red cell membranes in relation to glucose transport. *J. Biol. Chem.* **249**:5778
10. Lin, S., Spudich, J.A. 1974. Binding of cytochalasin B to a red cell membrane protein. *Biochem. Biophys. Res. Commun.* **61**:1471
11. Lucas, W.J. 1975. Analysis of the diffusion symmetry developed by the alkaline and acid bands which form at the surface of *Chara corallina* cells. *J. Exp. Bot.* **26**:271
12. Lucas, W.J. 1975. The influence of light intensity on the activation and operation of the hydroxyl efflux system of *Chara corallina*. *J. Exp. Bot.* **26**:347
13. Lucas, W.J. 1975. Photosynthetic fixation of $^{14}$carbon by internodal cells of *Chara corallina*. *J. Exp. Bot.* **26**:331
14. Lucas, W.J. 1976. Plasmalemma transport of $HCO_3^-$ and $OH^-$ in *Chara corallina:* Nonantiporter systems. *J. Exp. Bot.* **27**:19
15. Lucas, W.J., Smith, F.A. 1973. The formation of alkaline and acid regions at the surface of *Chara corallina* cells. *J. Exp. Bot.* **24**:1
16. Lucas, W.J., Smith, F.A. 1976. Influence of irradiance on $H^+$ efflux and $Cl^-$ influx in *Chara corallina:* An investigation aimed at testing two $Cl^-$ transport models. *Aust. J. Plant Physiol.* **3**:1
17. Sawa, T. 1974. New chromosome numbers for the genus *Tolypella* (Characeae). *Bull. Torrey Bot. Club* **101**:21
18. Sawa, T., Frame, P.W. 1974. Comparative anatomy of Charophyta: I. Oogonia and Oospores of *Tolypella,* with special references to the sterile Oogonial cell. *Bull. Torrey Bot. Club* **101**:136
19. Smith, F.A. 1970. The mechanism of chloride transport in Characean cells. *New Phytol.* **69**:903
20. Spear, D.G., Barr, J.K., Barr, C.E. 1969. Localization of hydrogen ion and chloride ion fluxes in *Nitella*. *J. Gen. Physiol.* **54**:397
21. Wessell, N.K., Spooner, B.S., Ash, J.F., Bradley, M.O., Luduena, M.A., Taylor, E.L., Wrenn, J.T., Yamada, K.M. 1971. Microfilaments in cellular and developmental processes. *Science* **171**:135
22. Williamson, R.E. 1972. A light-microscope study of the action of cytochalasin B on the cells and isolated cytoplasm of the Characeae. *J. Cell Sci.* **10**:811
23. Williamson, R.E. 1975. Cytoplasmic streaming in *Chara:* A cell model activated by ATP and inhibited by cytochalasin B. *J. Cell Sci.* **17**:655
24. Wood, R.D., Imahori, K. 1965. A revision of the Characeae, Part I. J. Cramer, Weinheim

Plant Physiol. (1977) 60, 862-867

# $HCO_3^-$ Influx Across the Plasmalemma of *Chara corallina*

## DIVALENT CATION REQUIREMENT[1]

Received for publication April 26, 1977 and in revised form August 8, 1977

WILLIAM J. LUCAS[2] AND JACK DAINTY
*Department of Botany, University of Toronto, Toronto, Ontario, M5S 1A1, Canada*

### ABSTRACT

**An absolute requirement for divalent cations is reported for $H^{14}CO_3^-$ influx in *Chara corallina*. Effective substitution of eluted $Ca^{2+}$ by $Mg^{2+}$ and $Sr^{2+}$ was observed, but $Mn^{2+}$ was completely ineffective in restoring $H^{14}CO_3^-$ transport activity. Similarly, $La^{3+}$ could not substitute for $Ca^{2+}$ in this system. Low concentrations of ethylenediaminetetraacetate (0.01 to 0.06 mM) significantly enhanced the rate at which $H^{14}CO_3^-$ transport capacity was lost.**

**Examination of the response of $OH^-$ efflux, during $Ca^{2+}$-free treatment, indicated that the cellular control over $OH^-$ efflux remained unaffected until membrane integrity became severely affected. This conclusion was supported by the response of $OH^-$ efflux to 10 mM $K^+$. Therefore, assimilation of $H^{14}CO_3^-$ is not rate-limited by an effect of $Ca^{2+}$ elution on the $OH^-$ transport system. Kinetic experiments indicated that $Ca^{2+}$ removal from the membrane resulted in noncompetitive inhibition of $H^{14}CO_3^-$ assimilation; the apparent Michaelis constant remained unaltered over a wide range of conditions. An hypothesis is presented which suggests that membrane integrity is necessary for $HCO_3^-$ transport to occur, but $Ca^{2+}$ ($Mg^{2+}$, $Sr^{2+}$), *per se*, must be bound to the transport complex before activity is established.**

Exposure of Characean internodal cells to $Ca^{2+}$-free solutions results in several physiological changes. Electrophysiological studies on the Characean plasma membrane have revealed that, under normal physiological conditions, the electrical properties of this membrane indicate the presence of at least one electrogenic ion transport system (7, 30). Calcium-free solutions perturb the membrane to such an extent that its electrical characteristics can be described by the Hodgkin and Katz passive diffusion equation (6, 7, 24, 31). Electrogenicity is lost in the absence of $Ca^{2+}$. Operation of the $HCO_3^+$ transport system, located in the plasmalemma of *Chara corallina*, is also depressed in the absence of exogenous $Ca^{2+}$ (14). This study showed that the reduction in cellular ability to assimilate $HCO_3^-$, under $Ca^{2+}$-free conditions, was due to an effect at the plasmalemma rather than the chloroplasts (14, 23).

The presence of $Ca^{2+}$ appears essential for the maintenance of plant and animal membrane integrity (1, 5, 19-21, 25, 27, 34-36). Calcium may therefore be required to maintain plasmalemma integrity, such that all membrane-bound processes can function normally. It may also be that, in addition to controlling membrane integrity, $Ca^{2+}$ *per se* may be required as an integral component of the functional $HCO_3^-$ (or $OH^-$) transport system(s) in *C. corallina*. Results relating to this proposal, and to the influence of other divalent and trivalent cations on $HCO_3^-$ assimilation, are presented in this report.

[1] This work was supported jointly by grants from the National Research Council of Canada (No. A6459) and the Connaught Fund (University of Toronto).

[2] Present address: Department of Botany, University of California, Davis, California 95616.

### MATERIALS AND METHODS

**Culture Material.** Culture material of *C. corallina* Klein ex Willd., em. R.D.W. (=*C. australis* R. Br.) was grown in the laboratory in 120 liter containers in solutions containing (mM): 1.0 to 2.0 $Na^+$, 0.2 $K^+$, 0.1 to 0.5 $Ca^{2+}$, 1.0 $Cl^-$, and approximately 2.0 $HCO_3^-$. Artificial fluorescent lighting was employed; the intensity at the solution surface was 17 w $m^{-2}$. (Full details of the culture techniques and the methods used to cut experimental cells have been previously reported [11, 18].)

**General $NaH^{14}CO_3$ Experimental Sequence.** Bicarbonate influx was determined using $^{14}C$. (When inorganic carbon is present as $HCO_3^-$, photosynthesis in *C. corallina* is rate-limited by the influx of this ion across the plasmalemma.) Radioactive $NaH^{14}CO_3$ was obtained from New England Nuclear as a sterile aqueous solution, and aliquots were added to the experimental solutions to give the required specific radioactivity. All $H^{14}CO_3^-$ experiments were performed using the following sequence: (*a*) Mature internodal cells were cut from the third to fifth internodal region and trimmed of whorl cells. (*b*) A 1-hr recovery period was employed after the cells had been cut. During this period cells were bathed in their respective culture solution (20 C) and illuminated by fluorescent lighting (10 w $m^{-2}$). (*c*) A 3-hr cell wall decalcification treatment was then given in bathing solution (basic chara pond water composition [CPW]; 1.0 mM NaCl, 0.2 mM KCl) containing 0.2 mM $CaSO_4$ and 10 mM MES, (pH 5.1 ± 0.1). (This treatment was employed to remove precipitated $CaCO_3$, it did not affect the $Ca^{2+}$ bound in the Donnan phase.) (*d*) Following decalcification cells were "batched" for the various treatment, 10 cells/treatment. Diameters and lengths were measured to compute individual cell surface areas. Cyclosis was also checked. (*e*) A 12-hr dark treatment (overnight) followed; cells bathed in CPW containing 0.2 mM $CaSO_4$ and 1.0 mM $NaHCO_3$ (pH 9.2). (*f*) A 2-hr illumination period (10 w $m^{-2}$) was used prior to commencement of experiment. (*g*) $Ca^{2+}$-free experiments were conducted as described by Lucas (14). (Solutions were prepared using double glass-distilled $H_2O$.)

Experiments were conducted at 25 C, under a light intensity of 20 w $m^{-2}$. Details of the illumination and experimental systems have been previously reported (11). At the conclusion of experiments, cells were washed with nonradioactive solution for 5 min. Planchets containing individual cells were treated with 0.5 ml of 0.1 M propionic acid to remove precipitated $Ca^{14}CO_3$ and unfixed $^{14}CO_2$. After 3 hr acidification planchets were dried and activity counted (using a Nuclear-Chicago gas flow system) to determine $HCO_3^-$ influx. Results are expressed as mean ± SEM.

**pH Measurement of $OH^-$ Band Pattern.** The pH values

along the cell surface of *C. corallina* internodal cells were measured using the technique developed by Lucas and Smith (18). Agar blocks, that were used as embedding media for experimental cells, were prepared in the manner described by Lucas and Dainty (16). For $Ca^{2+}$-free scanning experiments, preweighed samples of agar powder were washed in 5 mM NaCl for 2 days to remove endogenous $Ca^{2+}$. Cell pretreatment, prior to conducting scanning experiments, was as detailed in (*a*)-(*f*) above. Experiments were conducted at 25 C, and a light intensity of 20 w $m^{-2}$ was employed. Details relating to individual scanning experiments will be specified in the text.

The pH measurements were made using a miniature pH electrode (Microelectrodes model MI-405) in conjunction with a Beckman model 4500 digital pH meter. A Leitz micromanipulator was used to position the electrode on the *Chara* cell wall. From the values obtained the pH pattern established at the cell surface was mapped.

## RESULTS

**Cation Substitution Experiments.** It was shown previously that 24-hr exposure to $Ca^{2+}$-free solutions resulted in a decrease in $H^{14}CO_3^-$ influx (14). When 0.2 mM $Mg^{2+}$ was substituted for $Ca^{2+}$, no decline in $H^{14}CO_3^-$ influx was observed (Table I). Bicarbonate transport was maintained, by $Mg^{2+}$, over a wide $HCO_3^-$ concentration range, with no significant difference being detected between the $Ca^{2+}$ control and $Mg^{2+}$ treatments. Apparently $Mg^{2+}$ can substitute for $Ca^{2+}$ in maintaining membrane integrity or $HCO_3^-$ ($OH^-$) transport function. However, the presence of a divalent cation ($Mg^{2+}$) *per se* may have significantly reduced the elution of $Ca^{2+}$ from the $HCO_3^-$ (or $OH^-$) transport complex.

This possibility was investigated by observing the effect of divalent cations on the restoration of $H^{14}CO_3^-$ transport capacity, following 24-hr exposure to $Ca^{2+}$-free solutions. The results presented in Table II show that $Mg^{2+}$ and $Sr^{2+}$ are equally as effective as $Ca^{2+}$ in restoring the rate of $H^{14}CO_3^-$ influx to the control level. Hence, irrespective of its specific role(s) in maintaining $HCO_3^-$ transport, $Ca^{2+}$ can be replaced by $Mg^{2+}$ or $Sr^{2+}$. Manganese, however, was ineffective in the restoration of transport; there was no significant difference between the $Ca^{2+}$-free and $Mn^{2+}$ treatments (Table II). The relatively slight decrease in $H^{14}CO_3^-$ transport capacity, observed between the 24- and 48-hr $Ca^{2+}$-free treatments is in agreement with our earlier results (14).

**Divalent/Trivalent Cation Substitution.** The trivalent cation, $La^{3+}$, has been reported to bind competitively to $Ca^{2+}$ sites on the plasmalemma of roots (9) and to inhibit the $Ca^{2+}$ transporter in the mitochondrial membrane (22, 26). Substitution experiments were performed using $La^{3+}$ to ascertain whether it could bind to the two putative $Ca^{2+}$ sites.

Table I. Protective Effect of $Mg^{2+}$ on $H^{14}CO_3^-$ Influx in the Absence of Exogenous $Ca^{2+}$

| Treatment[1] | $HCO_3^-$ Concn (mM) | | |
|---|---|---|---|
| | 0.5 | 1.0 | 3.0 |
| $Ca^{2+}$ | 27.1±2.3[2] | 44.3±1.7 | 55.0±3.9 |
| $Ca^{2+}$-Free | 11.6±1.3 | 14.2±1.6 | 18.1±1.8 |
| $Mg^{2+}$ | 24.4±0.5 | 36.7±2.0 | 60.9±3.7 |

[1]All cells were given a 3 hr decalcification treatment in CPW containing 0.2 mM $CaSO_4$ and 10 mM MES buffer (pH 5.0). Experimental solutions contained 1.0 mM NaCl, 0.2 mM KCl, 1.0 mM $NaHCO_3$ (pH 9.2) and, where appropriate, the respective divalent cation (0.2 mM) as the sulphate.
[2]$H^{14}CO_3^-$ influx values (pmol $cm^{-2}$ $sec^{-1}$ measured after 24 hr exposure to the respective experimental solutions.
[V]alues are expressed as mean ± SEM; ten cells were used per treatment.

Table II. Divalent Cation Restoration of $H^{14}CO_3^-$ Influx Following $Ca^{2+}$-free Treatment

| Control I[2] (A→C)[1] | $Ca^{2+}$-Free (A→B) | Control II[2] (A→D) | $H^{14}CO_3^-$ Influx Cation (0.2 mM) (A→B→C) | |
|---|---|---|---|---|
| 44.8±2.0 | 9.2±2.2 | 35.0±1.6 | $Ca^{2+}$ | 34.4±1.6 |
| | | | $Mg^{2+}$ | 34.9±1.4 |
| 41.6±3.2 | 14.1±2.9 | ... | $Ca^{2+}$ | 31.6±1.6 |
| | | | $Mn^{2+}$ | 11.7±0.4 |
| 40.6±2.1 | 11.4±1.3 | 34.8±2.9 | $Ca^{2+}$ | 32.6±1.6 |
| | | | $Sr^{2+}$ | 35.7±2.6 |
| | | | ... | (10.9±0.9)[3] |

[1]Experimental sequences, indicated in parentheses, are as follows: A, 3 hr decalcification as in Table I; B, 24 hr exposure to $Ca^{2+}$-Free CPW containing 1.0 mM $NaHCO_3$ (pH 9.2); C, 24 hr exposure to CPW containing 1.0 mM $NaHCO_3$ (pH 9.2) and the respective divalent cation; D, as in C except that a 48 hr period was employed.
[2]Experiments performed in the presence of 0.2 mM $Ca^{2+}$
[3]48 hr $Ca^{2+}$-Free experiment

Normal $H^{14}CO_3^-$ influx values were obtained when cells were exposed for 2 hr to $Ca^{2+}$-free solutions containing $La^{3+}$ (Table III). This suggested that $La^{3+}$ may have been able to substitute for $Ca^{2+}$. However, following 12-hr exposure to $Ca^{2+}$-free solutions (Table III, column 4) $H^{14}CO_3^-$ influx decreased. The influx values for the $Ca^{2+}$-free solutions were the same in the presence or absence of $La^{3+}$. The results obtained for recovery experiments also suggested that $La^{3+}$ could not bind to the $Ca^{2+}$ site(s) associated with $HCO_3^-$ (or $OH^-$) transport. Normal recovery was observed in the presence of 0.2 mM $Ca^{2+}$, however, in the $La^{3+}$ treatment the decline in $H^{14}CO_3^-$ influx capacity paralleled that observed in the $Ca^{2+}$-free treatment (Table III, column 5).

Leonard *et al.* (9) suggested that $La^{3+}$ does not penetrate the plasmalemma, but mediates its effect (as does $Ca^{2+}$) by binding to exposed sites on the outer surface of the membrane. If the present results are interpreted in this manner, it seems that at least one of the $Ca^{2+}$ sites, presumably that associated with the $HCO_3^-$ (or $OH^-$) transport system, is located within the plasmalemma and in consequence access is not afforded to the $La^{3+}$ ion. Alternatively, if $Ca^{2+}$ is an integral part of the $HCO_3^-$ (or $OH^-$) transport complex, substitution at this site by $La^{3+}$ would be expected to inhibit transport due to the added positive charge associated with the $La^{3+}$ ion. Support for this hypothesis is lacking, in that competitive inhibition of $H^{14}CO_3^-$ transport, during 2-hr exposure experiments (Table III, lines 3-6), was not observed. The similarity between the results obtained in the presence and absence of $La^{3+}$ (in $Ca^{2+}$-free solutions) both for the 12-hr exposure and 24-hr recovery experiments also suggest that $La^{3+}$ cannot bind to the transport complex.

The short term ability of $La^{3+}$ to support $H^{14}CO_3^-$ transport, observed in the absence of added $Ca^{2+}$, may result from a transient increase in $Ca^{2+}$ concentration in the free space. This increase may occur by the displacement of $Ca^{2+}$, from the negative charge groups in the cell wall, by the $La^{3+}$ ion. Similarly, $Ca^{2+}$ may be made available by $La^{3+}$ displacement of this ion from the $Ca^{2+}$-binding sites that are associated with the maintenance of membrane structure or integrity. This source of $Ca^{2+}$ would be temporary, due to the employment of a large solution volume which was replaced hourly.

**Effect of EDTA on $H^{14}CO_3^-$ Transport.** Low concentrations of the $Ca^{2+}$-chelating agent, EDTA, in the experimental solution significantly decreased the rate of $H^{14}CO_3^-$ transport. Table IV shows that a 24-hr exposure to an EDTA concentration as low as 0.06 mM was in fact lethal. A time course of the inhibition of

Table III. Influence of $La^{3+}$ on $H^{14}CO_3^-$ Influx

| $La^{3+}$ Concn (mM) | $Ca^{2+}$ Concn (mM) | $H^{14}CO_3^-$ Influx (pmol $cm^{-2}$ $sec^{-1}$) | | |
|---|---|---|---|---|
| | | Experimental Duration[1] | | Recovery Experiment[2] |
| | | 2 hr | 12 hr | 24 hr |
| ... | 0.20 | 42.6±2.9 | 40.6±1.3 | 35.4±1.5 |
| ... | 0.0 | 34.2±2.3 | 17.0±1.7 | (11.4±2.0) |
| 0.10 | 0.0 | 43.9±2.9 | 15.8±0.9 | 9.9±2.4 |
| 0.05 | 0.20 | 43.2±1.6 | | |
| 0.10 | 0.20 | 41.8±2.2 | | |
| 0.20 | 0.20 | 42.7±2.1 | | |

[1]Experimental pretreatment procedures as described in Table I. Cells were then bathed in their respective solutions for 2 or 12 hr. Solutions contained 1.0 mM NaCl, 0.2 mM KCl, 1.0 mM $NaHCO_3$ (pH 9.2) and the indicated cation(s).
[2]Following a 12 hr $Ca^{2+}$-Free treatment, cells were given a 24 hr recovery period. Solution composition as detailed above. Value in parentheses indicates $H^{14}CO_3^-$ influx after 36 hr exposure to $Ca^{2+}$-Free solutions.

Table IV. Inhibition of $H^{14}CO_3^-$ Influx by EDTA in $Ca^{2+}$-Free Solutions

| EDTA Concn (mM) | $H^{14}CO_3^-$ Influx (pmol $cm^{-2}$ $sec^{-1}$) |
|---|---|
| ... | 40.6±2.6[1] |
| ... | 12.9±1.9 |
| 0.01 | 9.5±1.1 |
| 0.02 | 5.7±0.6 |
| 0.04 | 3.3±0.9 |
| 0.06 | Lethal |

[1]This experiment was conducted in a solution which contained: 1.0 mM NaCl, 0.2 mM KCl, 0.2 mM $CaSO_4$, 1.0 mM $NaHCO_3$ (pH 9.2). All other experiments were conducted in identical solutions except they were $Ca^{2+}$-Free and, where appropriate, contained EDTA. $H^{14}CO_3^-$ influx was measured after 24 hr exposure to the respective solutions. (As in Table I, cells were decalcified, as a pretreatment, using 10 mM MES buffer.)

$H^{14}CO_3^-$ transport by EDTA is illustrated in Fig. 1. For comparison, results obtained in the absence of EDTA are included. (Note the difference in slope between the two treatments.) This concentration of 0.02 mM EDTA became lethal if exposures were longer than 36 to 48 hr. For the $Ca^{2+}$-free treatment to become lethal, approximately 130 hr were required in the absence of EDTA (14).

**Influence of $Ca^{2+}$-free Treatments on $HCO_3^-$ Transport *Km*.** Apparent *Km* values, associated with $H^{14}CO_3^-$ assimilation, were determined under control and various $Ca^{2+}$-free conditions (Fig. 2). Figure 2A shows that a 24 hr $Ca^{2+}$-free treatment reduced the $V_{max}$ but left the apparent *Km* unaltered; the *Km* values were: control: 0.45 ± 0.10 mM; $Ca^{2+}$-free: 0.40 ± 0.10 mM. These values, although slightly lower, are in agreement with the values reported by Lucas (11). Similarly, under the influence of $Ca^{2+}$-free conditions and 0.02 mM EDTA the $V_{max}$ was reduced, but the apparent *Km* did not differ significantly from the control value (Fig. 2B). The apparent *Km* value determined after 5-hr exposure to $Ca^{2+}$-free solutions (0.02 mM EDTA) was 0.55 ± 0.11 mM, and after 24 hr the value was 0.40 ± 0.10 mM. These results indicate that the $Ca^{2+}$-free treatment inhibits $H^{14}CO_3^-$ assimilation noncompetitively. The site of this inhibition is at the plasmalemma (14) and the interaction between $Ca^{2+}$ and $H^{14}CO_3^-$ influx is heterotropic in nature (4) *i.e.* at least two dissimilar ligand-binding sites appear to be involved). Calcium appears to act as an allosteric effector (activator) of the $HCO_3^-$ transport system (4, 19).

**$OH^-$ Efflux Pattern: Influence of $Ca^{2+}$-free Treatment.** Although the $H^{14}CO_3^-$ and $OH^-$ transport systems operate at spatially separate sites, within the plasmalemma (13), their rates of operation are coupled by the steady-state requirement of electrical neutrality. If the $Ca^{2+}$-free treatment affected the functioning of the $OH^-$ efflux system, rather than $HCO_3^-$ transport, $OH^-$ transport would become the rate-determining step in the over-all process of $H^{14}CO_3^-$ assimilation. We have

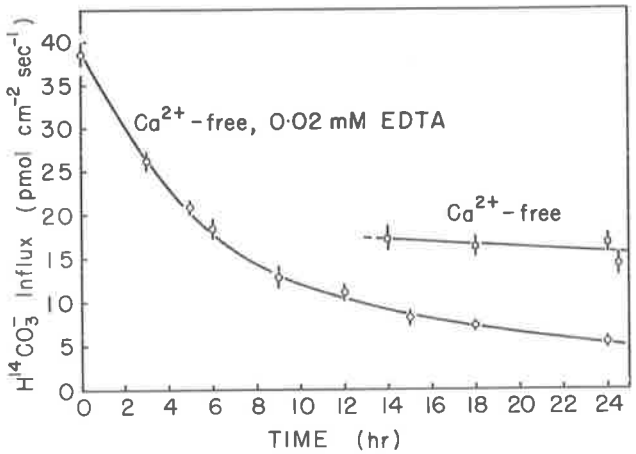


FIG. 1. Inhibition of $H^{14}CO_3^-$ transport by $Ca^{2+}$-free treatments containing 0.02 mM EDTA. $H^{14}CO_3^-$ influx was measured in an experimental medium containing 1.0 mM NaCl, 0.2 mM KCl, 1.0 mM $NaHCO_3$, 0.02 mM EDTA (pH 9.2) (○); the control value (at 0 hr) also contained 0.2 mM $CaSO_4$ (□); identical conditions except that EDTA was omitted.

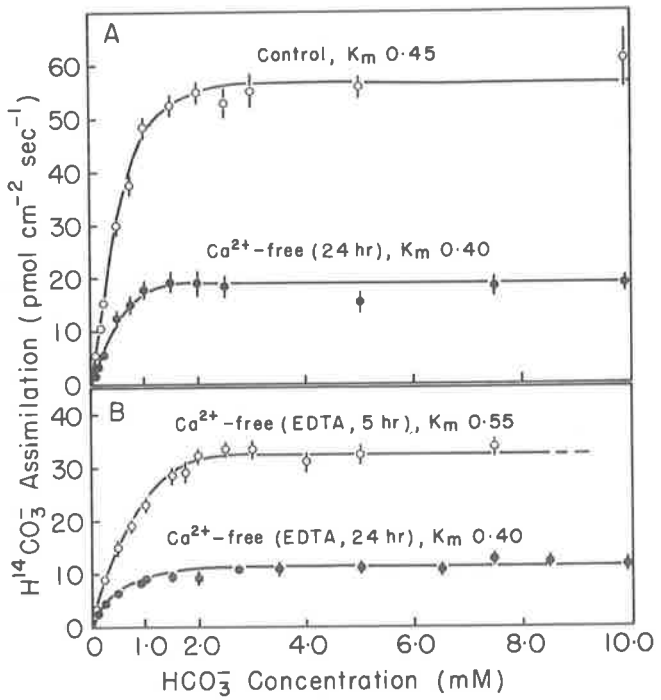


FIG. 2. Influence of $Ca^{2+}$-free treatments on the apparent *Km* of $H^{14}CO_3^-$ assimilation. All experiments were performed on cells cut from the same culture tank. Cells were pretreated in control (1.0 mM NaCl, 0.2 mM KCl, 0.2 mM $CaSO_4$, 1.0 mM $NaHCO_3$, [pH 9.2]) and $Ca^{2+}$-free (1.0 mM NaCl, 0.2 mM KCl, ±0.02 mM EDTA, 1.0 mM $NaHCO_3$ [pH 9.2]) solutions for 22 hr (or 3 hr, B[0]) before being transferred for 1 hr to nonradioactive experimental solutions. Experimental solutions were identical except that the $NaHCO_3$ concentration was varied. Standard 1-hr $^{14}C$ experimental period was employed (10).

recently reported two situations in which $OH^-$ efflux *per se* acted as the rate-limiting process; one being when cyclosis was inhibited by cytochalasin B (16) and the second being when cells were treated with low concentrations of $(NH_4)_2SO_4$ (15).

A study of the $OH^-$ efflux pattern, established after various periods of exposure to $Ca^{2+}$-free solutions, was conducted to investigate whether this treatment perturbed the cellular control of $OH^-$ efflux. Control pH scans were performed on each cell, using substrate levels of 1.0 and 0.1 mM $HCO_3^-$, prior to commencing the $Ca^{2+}$-free treatment. Figure 3A illustrates how the pH pattern altered as the cell responded to varying rates of photosynthetic assimilation of exogenous $HCO_3^-$. Lucas (10) demonstrated, by diffusion analysis of the $OH^-$ efflux bands, that in the steady-state a direct 1:1 correlation existed between the rates of $H^{14}CO_3^-$ influx and $OH^-$ efflux. Hence, using $H^{14}CO_3^-$ assimilation values obtained from Figure 2, the pH patterns developed under 1.0 and 0.1 mM $NaHCO_3$ represent $HCO_3^-$ assimilation rates of 47 and 6 pmol $cm^{-2}$ $sec^{-1}$, respectively. A control pH scan was conducted at 0.1 mM $NaHCO_3$ since the efflux rate, under these conditions, would be very close to that observed after 24-hr exposure to $Ca^{2+}$-free solutions containing 0.02 mM EDTA (see Table IV and Fig. 1). A comparison of these two pH patterns should demonstrate whether $Ca^{2+}$-free treatment perturbs the $OH^-$ efflux system of *C. corallina*.

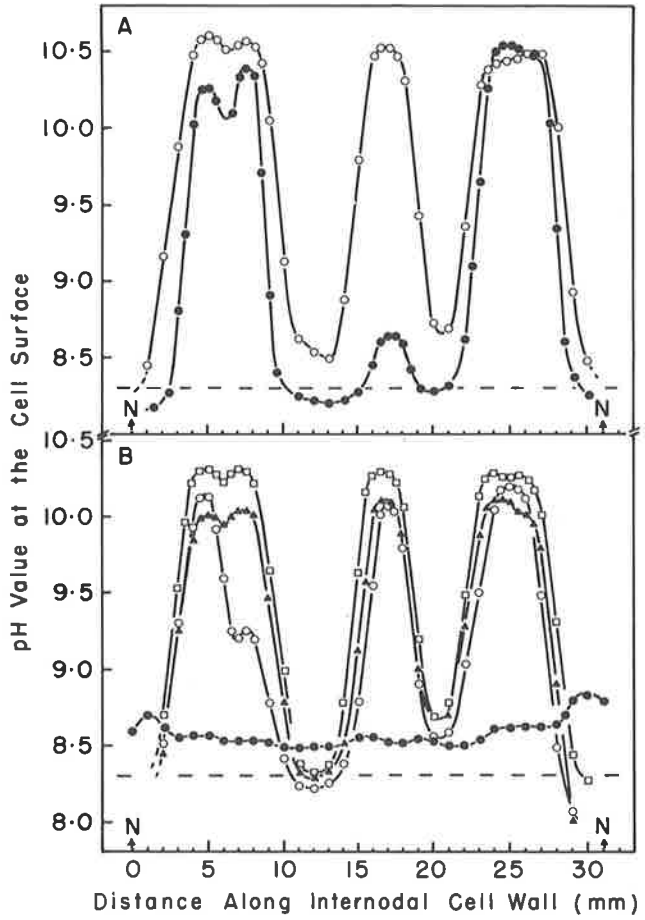


FIG. 3. Influence of $Ca^{2+}$-free treatment on $OH^-$ efflux from *Chara corallina*. Cell pretreatment was as described under "Materials and Methods." Control pH scans (A) were conducted in the presence of 1.0 (○) and 0.1 mM (●) $NaHCO_3$ (these solutions also contained 1.0 mM NaCl, 0.2 mM KCl, 0.2 mM $CaSO_4$, 0.02 mM EDTA). Solutions employed for $Ca^{2+}$-free treatments (B) were as above, except that $Ca^{2+}$ was omitted and 1.0 mM $NaHCO_3$ was used. Broken line indicates background pH value (8.3) and the arrowed symbol N indicates the cell nodal location. All pH scans were conducted following a 2-hr illumination period (20 w $m^{-2}$). The light (L)/dark (D) regime employed after the commencement of the $Ca^{2+}$-free treatment was: 3L:2D:3L:4D:3L:7D: 3 hr L. B: scans conducted after 2- (□), 7- (▲), 24- (○), and 36-hr (●) exposure to $Ca^{2+}$-free solutions.

The important feature illustrated in Figure 3A is that as the $HCO_3^-$ concentration was reduced, $OH^-$ efflux was lowered as shown by the decrease in pH value at the $OH^-$ band centers (17). The cellular adjustment in $OH^-$ transport was achieved by a narrowing of the pumping width of the $OH^-$ bands as well as a reduction of the rate, *per se,* within these bands (Fig. 3A, [17]). The effux is also often adjusted by deactivating subsidiary efflux bands (12) as illustrated in Figure 3A.

The results presented in Figure 3B typify the response of $OH^-$ efflux to $Ca^{2+}$-free treatment. (These experiments were conducted in the presence of 1.0 mM $NaHCO_3$ and 0.02 mM EDTA. The EDTA was employed to minimize the influence of any residual $Ca^{2+}$ that may have been bound to the agar.) A gradual decline in net $OH^-$ efflux with time was observed, but no significant perturbation of the $OH^-$ efflux pattern was found, until the $Ca^{2+}$-free treatment had been in effect for 24 hr or longer (*cf.* 24- and 36-hr scans, Fig. 3B). Within 3 hr of commencing the $Ca^{2+}$-free treatment, the pH values within the $OH^-$ band centers had begun to fall and the bands had also become narrower. However, migration of instability of the $OH^-$ efflux sites was not observed (*cf.* cytochalasin B [16] and $(NH_4)_2SO_4$ [15] experiments). Comparison of the pH scans conducted after 7- and 24-hr $Ca^{2+}$-free periods indicates that cellular control of $OH^-$ efflux is still in evidence. The efflux band locations are still stable, with respect to the controls, and the total cellular $OH^-$ efflux appears to be reduced mainly by narrowing the widths of the individual bands.

Although the central subsidiary band (15- to 19-mm site) did not deactivate following 24-hr exposure to $Ca^{2+}$-free solutions, the activity of the subsidiary band located in the 6- to 9-mm region was significantly reduced. In all experiments conducted there was a similarity between the 0.1 mM $NaHCO_3$ control and 24-hr $Ca^{2+}$-free pH scans. Following the 24-hr $Ca^{2+}$-free pH scanning sequence, $H^{14}CO_3^-$ assimilation was measured on several cells to verify that their rates were typical of those presented in Figures 1 and 2. Table V shows that this was so.

After scanning at the 36-hr period, cells were returned to control solutions and within 24 hr pH values like the control were observed (results not shown). It seems that the reduction

Table V. Comparative $H^{14}CO_3^-$ Assimilation Results
Assimilation ($H^{14}CO_3^-$) rates were measured under control, normal $Ca^{2+}$-free and following 24 hr $Ca^{2+}$-free pH scanning sequence. Experimental details are as described in Table IV, except that all treatments had 0.02 mM EDTA and the experimental duration was 26 hr.

| | $HCO_3^-$ Influx (pmol $cm^{-2}sec^{-1}$) | | |
|---|---|---|---|
| Cell No. | Control | $Ca^{2+}$-Free | $Ca^{2+}$-free pH Scan cells[1] |
| 1 | 32.6 | 14.3 | 10.3 |
| 2 | 42.9 | 8.2 | 10.8 |
| 3 | 44.1 | 11.9 | 14.7 |
| 4 | 37.4 | 4.7 | 5.2 |
| 5 | 35.8 | 10.5 | |
| 6 | 39.9 | 7.8 | |
| 7 | 48.1 | 10.6 | |
| 8 | 30.3 | 4.7 | |
| 9 | 42.5 | 8.9 | |
| 10 | 38.8 | 5.5 | |
| Average | 39.2±1.7 | 8.7±1.0 | |

[1] $H^{14}CO_3^-$ influx measured after the 24 hr $Ca^{2+}$-free pH scanning sequence.

in $H^{14}CO_3^-$ assimilation, which results in response to cellular exposure to $Ca^{2+}$-free solutions, is caused by an effect of this treatment on a site other than the $OH^-$ efflux process.

**Manipulation of Membrane Permeability by Treatment with 10 mM $K^+$.** Spanswick (30) demonstrated that a 10 mM $K^+$ treatment seriously affected the electrical properties of the plasmalemma in *Nitella translucens*. The membrane potential depolarized to that of the Nernst potential for $K^+$ and appeared to function as a $K^+$ electrode. The electrical resistance (passive permeability) of the membrane was also drastically reduced. (This effect of $K^+$ on the membrane is considered to result from the displacement of membrane-bound $Ca^{2+}$ by $K^+$ ions [33].) Lucas (14) also showed that a 10 mM $K^+$ treatment caused almost total inhibition of $H^{14}CO_3^-$ assimilation in *C. corallina*.

The effect of 10 mM $K^+$ on the $OH^-$ efflux system is typified by the response presented in Figure 4. In both the prolonged $Ca^{2+}$-free (36 hr) and 10 mM $K^+$ situations the cell surface became slightly alkaline. However, no correlation existed between the control sites of $OH^-$ efflux and the irregular pH pattern observed under the $Ca^{2+}$-free and 10 mM $K^+$ situations. This similarity in effect between the 10 mM $K^+$ (Fig. 4) and prolonged $Ca^{2+}$-free (Fig. 3B, ●) treatments on the $OH^-$ efflux pattern strongly suggests that the cellular control over $OH^-$ efflux is lost only when membrane integrity (passive permeability) is severely affected.

## DISCUSSION

The evidence presented in this paper confirms and extends our earlier report (14) that $H^{14}CO_3^-$ assimilation has an absolute divalent cation requirement. We demonstrated previously that this $Ca^{2+}$ requirement was associated with $HCO_3^-$ transport across the plasmalemma (14). Figure 5 presents a schematic representation of the possible sites, within the plasmalemma, where this $Ca^{2+}$ control might be mediated.

$Ca^{2+}$-free and 10 mM $K^+$ pH scanning experiments demonstrated fairly conclusively that the initial decline in $H^{14}CO_3^-$ assimilation, observed in $Ca^{2+}$-free solutions, was not a result of rate limitation imposed by an effect of $Ca^{2+}$ elution on the $OH^-$ efflux system. We therefore consider that the involvement of $Ca^{2+}$ site [3] (OH transport) can be discounted.

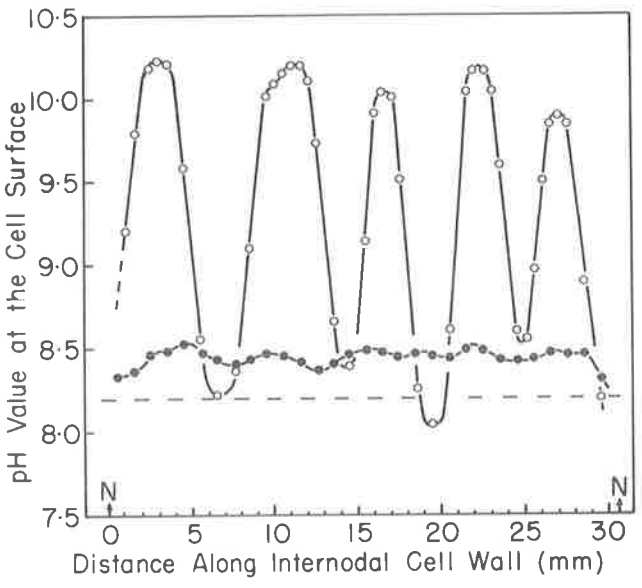


FIG. 4. Perturbation of $OH^-$ efflux activity by 10 mM $K^+$ treatment. The control experiment (○) was conducted in a solution containing 10 mM NaCl, 0.2 mM KCl, 0.2 mM $CaSO_4$, 1.0 mM $NaHCO_3$. Following the control scan (conducted after 1-hr illumination), the cell was given a 30-min dark pretreatment in the 10 mM $K^+$ solution (as above, except NaCl 0.2 mM, KCl 10 mM). Again the pH pattern (●) was mapped after 1-hr illunination (20 w $m^{-2}$). (Over this short period cyclosis remained unaffected, having a value of 91 $\mu$m $sec^{-1}$ at the conclusion of the 10 mM $K^+$ scan.)

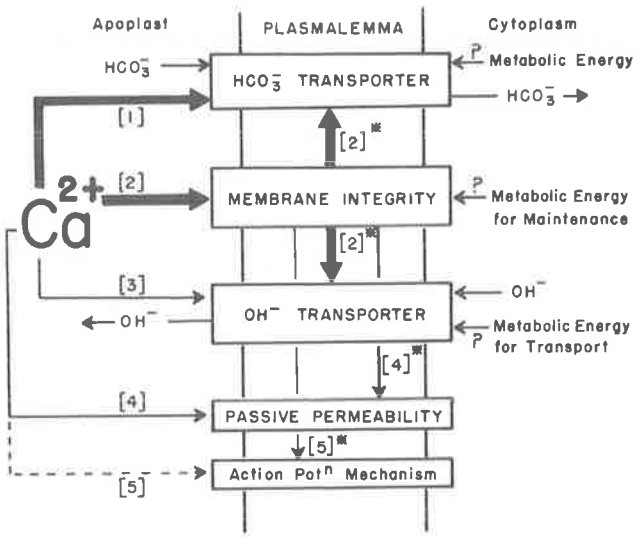


FIG. 5. Schematic representation of the possible sites of $Ca^{2+}$ involvement in controlling $H^{14}CO_3^-$ assimilation. Direct sites of involvement are numbered [1] to [5], and indirect control via membrane integrity is denoted by an asterisk. The slight possibility that $Ca^{2+}$ elution from the membrane limits the supply of metabolic energy, to the various systems, is represented by a question mark.

A decline in $H^{14}CO_3^-$ assimilation appeared to occur prior to the loss in membrane integrity. This hypothesis could be tested by performing hydraulic conductivity experiments on $Ca^{2+}$-free treated cells (20). If the initial effect is localized at $Ca^{2+}$ site [1], the hydraulic conductivity of the membrane should remain unaltered. Only when the integrity of the membrane becomes affected should hydraulic conductivity increase. The $La^{3+}$ results suggested that the putative $Ca^{2+}$ site [1], on the $HCO_3^-$ transport complex, is within the membrane, *i.e.* $Ca^{2+}$ binding to an intrinsic protein may be involved. This interpretation would be strengthened if it could be shown that $La^{3+}$ can substitute for $Ca^{2+}$ at site [2]. Biophysical measurements of plasmalemma membrane potential, electrical conductance, and hydraulic conductivity may similarly provide an answer to this question.

It is difficult to envisage how a gradual elution of $Ca^{2+}$ could have the apparent *Km* value unaffected, if the $Ca^{2+}$ control over $HCO_3^-$ transport is mediated through its maintenance of general membrane integrity (*i.e.* sites [2] + [2]*). An alternate hypothesis is that a specific divalent cation requirement exists within the $HCO_3^-$ transport complex. The cation may serve as a transport (enzyme) activator, possibly in a manner similar to that observed for membrane-bound ATPase systems (8, 29, 36) or as proposed by Epstein (3) in terms of imparting transport specificity (see also 19, 20). In the absence of bound $Ca^{2+}$ individual transport complexes would remain inoperative. (A variation of this hypothesis would be that $Ca^{2+}$ mediates in the transfer of metabolic energy to the $HCO_3^-$ transport complex.)

Calcium-binding site [1] does not appear to exhibit divalent cation specificity, with respect to $Ca^{2+}$, $Mg^{2+}$, or $Sr^{2+}$ since, at the concentrations employed, these ions appeared equally effective in supporting $HCO_3^-$ influx. The difference in binding specificity between $Ca^{2+}$ and $Mn^{2+}$ has been frequently encountered (8, 19, 25, 28). Dainty *et al.* (2) and Tarr *et al.* (32) demonstrated that $Mg^{2+}$ could substitute for $Ca^{2+}$ at site [4] or [4]*, thereby restoring passive permeability to the Characean membrane. These experiments suggest an equivalence between $Ca^{2+}$ sites [4] and [2]+[4]* (see Fig. 5). In the absence of $Ca^{2+}$,

however, $Mg^{2+}$ could not re-establish electrical excitability (2, 32). Site [5] appears to be $Ca^{2+}$-specific. Although membrane integrity, *per se,* is certain to be an essential factor in the control of the action potential mechanism, its mere existence, however, does not establish excitability. We consider that our present results provide a further example of this form, *i.e.* membrane integrity is necessary for transport to occur, but that $Ca^{2+}$ *per se* is required to establish transport activity.

## LITERATURE CITED


1. Benedetti EL, P Emmelot 1968 Structure and function of plasma membranes isolated from liver. *In* AJ Dalton, F Haguenau, ed, The Membranes. Academic Press, New York, pp 33–120
2. Dainty JR, J Lannoye, SE Tarr 1970 Voltage-current characteristics of *Chara australis* during changes of pH and exchange of Ca-Mg in the external medium. J Exp Bot 21: 558–565
3. Epstein E 1961 The essential role of calcium in selective cation transport by plant cells. Plant Physiol 36: 437–444
4. Hammes GG, C-W Wu 1974 Kinetics of allosteric enzymes. Annu Rev Biophys Bioengin 3: 1–33
5. Hill TL 1967 Electric fields and the cooperativity of biological membranes. Proc Nat Acad Sci USA 58: 111–114
6. Hope AB, NA Walker 1961 Ionic relations of cells of *Chara australis* R. Br. IV. Membrane potential differences and resistances. Aust J Biol Sci 14: 26–44
7. Kitasato H 1968 The influence of $H^+$ on the membrane potential and ion fluxes of *Nitella*. J Gen Physiol 52: 60–87
8. Leonard RT, CW Hotchkiss 1976 Cation-stimulated adenosine triphosphatase activity and cation transport in corn roots. Plant Physiol 58: 331–335
9. Leonard RT, G Nagahashi, WW Thomson 1975 Effect of lanthanum on ion absorption in corn roots. Plant Physiol 55: 542–546
10. Lucas WJ 1975 Analysis of the diffusion symmetry developed by the alkaline and acid bands which form at the surface of *Chara corallina* cells. J Exp Bot 26: 271–286
11. Lucas WJ 1975 Photosynthetic fixation of $^{14}$carbon by internodal cells of *Chara corallina*. J Exp Bot 26: 331–346
12. Lucas WJ 1975 The influence of light intensity on the activation and operation of the hydroxyl efflux system of *Chara corallina*. J Exp Bot 26: 347–360
13. Lucas WJ 1976 Plasmalemma transport of $HCO_3^-$ and $OH^-$ in *Chara corallina: non-antiporter systems*. J Exp Bot 27: 19–31
14. Lucas WJ 1976 The influence of $Ca^{2+}$ and $K^+$ on $H^{14}CO_3^-$ influx in internodal cells of *Chara corallina*. J Exp Bot **27:** 32–42
15. Lucas WJ 1977 Plasmalemma transport of $HCO_3^-$ and $OH^-$ in *Clara corallina:* inhibitory effect of ammonium sulphate. J Exp Bot, in press
16. Lucas WJ, J Dainty 1977 Spatial distribution of functional $OH^-$ carriers along a Characean internodal cell: determined by the effect of cytochalasin B on $H^{14}CO_3^-$ assimilation. J Membr Biol 32: 75–92
17. Lucas WJ, JM Ferrier, J Dainty 1977 Plasmalemma transport of $OH^-$ in *Chara corallina:* dynamics of activation and deactivation. J Membr Biol 32: 49–73
18. Lucas WJ, FA Smith 1973 The formation of alkaline and acid regions at the surface of *Chara corallina* cells. J Exp Bot 24: 1–14
19. Maas EV, DP Moore, BJ Mason 1969 Influence of calcium and magnesium on manganese absorption. Plant Physiol 44: 796–800
20. Manery JF 1966 Effects of Ca ions on membranes. Fed Proc 25: 1804–1810
21. Marinos NG 1962 Studies on submicroscopic aspects of mineral deficiencies. I. Calcium deficiency in the shoot apex of barley. Am J Bot 49: 834–841
22. Mela L 1968 Interactions of $La^{3+}$ and local anesthetic drugs with mitrochondrial $Ca^{2+}$ and $Mn^{2+}$ uptake. Arch Biochem Biophys 123: 286–293
23. Murakami S, L Packer 1971 The role of cations in the organization of chloroplast membranes. Arch Biochem Biophys 146: 337–347
24. Osterhout WJV 1949 Some bioelectric problems. Proc Nat Acad Sci USA 35: 548–558
25. Poovaiah BW, AC Leopold 1976 Effects of inorganic salts on tissue permeability. Plant Physiol 58: 182–185
26. Pressman BC 1970 Energy-linked transport in mitochondria. *In* E Racker, ed, Membranes of Mitochondria and Chloroplasts. Van Nostrand Reinhold Co, New York, pp 213–250
27. Romero PJ, R Whittam 1971 The control by internal calcium of membrane permeability to sodium and potassium. J Physiol 214: 481–507
28. Rubinstein B, KD Johnson, DL Rayle 1977 Calcium-enchanced acidification in oat coleoptiles. *In* E Marrè, O Ciferri, eds, Regulation of Cell Membrane Activities in Plants. North-Holland, Amsterdam pp 307–316
29. Scharff O 1976 $Ca^{2+}$ activation of membrane-bound ($Ca^{2+}$-$Mg^{2+}$)-dependent ATPase from human erythrocytes prepared in the presence or absence of $Ca^{2+}$. Biochim Biophys Acta 443: 206–218
30. Spanswick RM 1972 Evidence for an electrogenic pump in *Nitella translucens*. I. The effect of pH, $K^+$, $Na^+$, light and temperature on the membrane potential and resistance. Biochim Biophys Acta 288: 73–89
31. Spanswick RM, J Stolarek, EJ Williams 1967 The membrane potential of *Nitella translucens*. J Exp Bot 18: 1–16
32. Tarr SE, RJ Lannoye, J Dainty 1970 Changes of ionic and electrical properties of *Chara australis* when the external Ca is replaced by Mg. J Exp Bot 21: 552–557
33. Tobias JM 1964 A chemically specified molecular mechanism underlying excitation in nerve: a hypothesis. Nature 203: 13–17
34. Van Steveninck RFM 1965 The significance of calcium on the apparent permeability of cell membranes and the effects of substitution with other divalent ions. Physiol Plant 18: 54–69
35. Wildes RA, TF Neales 1971 Maintenance of viability of carrot tissue slices in washing after cutting. Aust J Biol Sci 24: 297–402
36. Wyn Jones RG, OR Lunt 1967 The function of calcium in plants. Bot Rev 33: 407–426

J. Membrane Biol. 32, 49–73 (1977)
© by Springer-Verlag New York Inc. 1977

# Plasmalemma Transport of $OH^-$ in *Chara corallina*

## Dynamics of Activation and Deactivation

W.J. Lucas, J.M. Ferrier, and J. Dainty

Department of Botany, University of Toronto, Toronto, Ontario, Canada

Received 1 June 1976; revised 2 September 1976

*Summary.* The light-mediated, time-dependent rise in the pH value at the center of an alkaline band was analyzed using the methods of numerical analysis. From this analysis an expression of the time-dependent build-up of $OH^-$ efflux was obtained for these bands. This information can now be employed to determine whether the light-activated transport of $OH^-$ and $HCO_3^-$ influences the electrical properties of the plasmalemma. The dark-induced deactivation of $OH^-$ transport was also characterized, revealing a transition from efflux to a transient influx phase during deactivation.

Numerical analysis of the steady-state $OH^-$ diffusion pattern, established along the surface of an alkaline band, revealed that the $OH^-$ efflux width was wider than previously envisaged. It was also found that $OH^-$ sink regions exist on either side of the efflux zone. These, and other characteristics revealed by the numerical analysis, enabled us to extend the $OH^-$ transport model proposed by Lucas (*J. Exp. Bot.* 1975, **26**:347).

Electrophysiological studies on the Characean plasmalemma have revealed that the observed electrical properties of this membrane require the presence of an electrogenic ion transport system (Kitasato, 1968; Spanswick, 1972, 1974; Saito & Senda, 1973, 1974; Volkov, 1973; Richards & Hope, 1974). The main point of contention appears to be whether the putative $H^+$ transport system (Kitasato, 1968) is the sole electrogenic component, over the investigated pH range of 5.0–10.0. It is possible that when a Characean species can photosynthetically assimilate $HCO_3^-$ the transport of this species may also be electrogenic (Walker, 1962; Hope, 1965; Volkov, 1973; Lucas, 1975*a*,*c*). However, it has been generally accepted that the $OH^-$ ions, generated in the cytoplasm as a result of $CO_2$ fixation from $HCO_3^-$ uptake, were exported across the plasmalemma on a $HCO_3^-/OH^-$ antiporter (Lucas & Smith, 1973). A system of this nature would not have been electrogenic.

The recent finding that the $HCO_3^-$ and $OH^-$ transport systems function independently, the respective ions being transported across the plas-

malemma by different transporters and at spatially separate regions (Lucas, 1976), suggested that the electrical involvement of $HCO_3^-$ and also $OH^-$ should be further investigated. It is possible that the activation of the transport systems of these ions, at alkaline pH values, is responsible for the observed light-mediated increase in membrane conductance (Walker, 1962; Hope, 1965; Nishizaki, 1968; Spanswick, 1972; Saito & Senda, 1974).

One method of testing the involvement of $HCO_3^-$ assimilation, in terms of its possible electrical contribution at the plasmalemma, would be to compare the time courses of photo-activated $HCO_3^-$ and $OH^-$ transport with the time course of membrane conductance. A close parallel between these respective time courses would be strong evidence for the electrical involvement of these ions.

The experimental difficulty is, however, in obtaining the $HCO_3^-$ and $OH^-$ time courses. Ideally these should be obtained on the same cell, simultaneously with the membrane potential and conductance measurements. It is impossible to obtain a $H^{14}CO_3^-$ uptake time course from a single cell, but, since $OH^-$ efflux only occurs during $HCO_3^-$ uptake, it may suffice to have simply the time course for the activation of the $OH^-$ efflux system.

The time-dependent rise in the pH value at the center of an alkaline band has been fully characterized (Lucas, 1975*c*). We had hoped that this experimental information could be analyzed using time-dependent analytical diffusion equations to elucidate the manner in which $OH^-$ efflux activates and approaches the steady-state. However, we found that these equations are at present insoluble. Only by methods of numerical analysis have we been able to successfully analyze the experimental data. This paper presents the results of this numerical analysis in terms of the dynamics of the $OH^-$ transport activation and deactivation processes. This analysis also revealed further operational features of this system and based on these findings, the model presented by Lucas (1975*c*) has been extended.

## Materials and Methods

### *Culture Material*

*Chara corallina* cells were grown in large plastic containers in solutions containing (mM): 1.0–2.0 $Na^+$, 0.2 $K^+$, 0.1–0.5 $Ca^{++}$, 1.0 $Cl^-$ and approximately 2 $HCO_3^-$. Full details of the culture techniques and the methods used to cut experimental cells have been previously reported (Lucas, 1975*b*).

### *Experimental Solutions*

All experimental solutions contained (mM): 1.0 NaCl, 0.2 KCl, 0.2 $CaSO_4$ and 0.5 $NaHCO_3$ and were prepared using Analar Reagent grade chemicals.

### *pH Measurement of the $OH^-$ Band*

The pH values along the cell surface and radially away from the cell at the $OH^-$ band center were measured using the techniques developed by Lucas and Smith (1973, *see* especially Figs. 1 and 2) and Lucas (1975*a*). Similarly, the procedures employed in measuring the response of an alkaline band to illumination were those described by Lucas (1975*a* and *c*). The pH measurements were made using a miniature pH electrode (Microelectrodes, Inc., Model MI-405) and a Leitz micromanipulator was used to position the electrode on the *Chara* cell wall.

Details of the illumination system have been previously reported (Lucas, 1975*c*).

All experiments were performed in the following sequence:

(*i*) Cells were illuminated (10 $Wm^{-2}$) for 1 hr and following this period the pH pattern along the entire cell wall was mapped.

(*ii*) Of the operational $OH^-$ bands, one was selected for detailed study. The pH electrode was located on this alkaline band center.

(*iii*) Following a one-hour dark pretreatment, the light activation of this $OH^-$ band was followed over a 30-min period; the cellular response to darkness was then recorded.

(*iv*) Sequence (*iii*) was repeated except that the respective light and dark responses were followed for 1 hr.

(*v*) At the end of the one-hour dark period the pH electrode was moved to a position on the cell surface 4 mm to the right of the $OH^-$ band center. After a further one-hour illumination period the pH values within the vicinity of this particular $OH^-$ band were measured.

(*vi*) The pH electrode was then raised to a position 4 mm vertically above the $OH^-$ band center. After consecutive one-hour dark and light treatments, the vertical pH profile onto the $OH^-$ band center was measured.

These pH measurements gave a comprehensive picture of the experimental system, with respect to a particular $OH^-$ band. The numerical analysis was based on these measurements.

### *Numerical Analysis*

The numerical calculation used a Fortran program on an IBM 370/165 computer. The time-dependent diffusion of $OH^-$, $HCO_3^-$ and $CO_3^{2-}$ was calculated in a two-dimensional system; the two dimensions being the direction of the axis of the cylindrical *Chara* cell and perpendicular to this axis (*see* Fig. 1). This system was spatially divided into 100 μm sections (in each direction), each section being a cylindrical ring 100 μm wide and thick. In the axial direction, the system originated at the center of an $OH^-$ efflux band (the center of symmetry for this system) and extended over a distance of 4 mm. The radial coordinates commenced at the cell surface and similarly extended over a distance of 4 mm.

A boundary condition of zero net flux was imposed along the plane of symmetry cutting through the center of the $OH^-$ efflux band (perpendicular to the axial direction). The boundary conditions imposed at the extremities of the system were, in general, that the concentrations at these planes equaled those of the background medium. However,

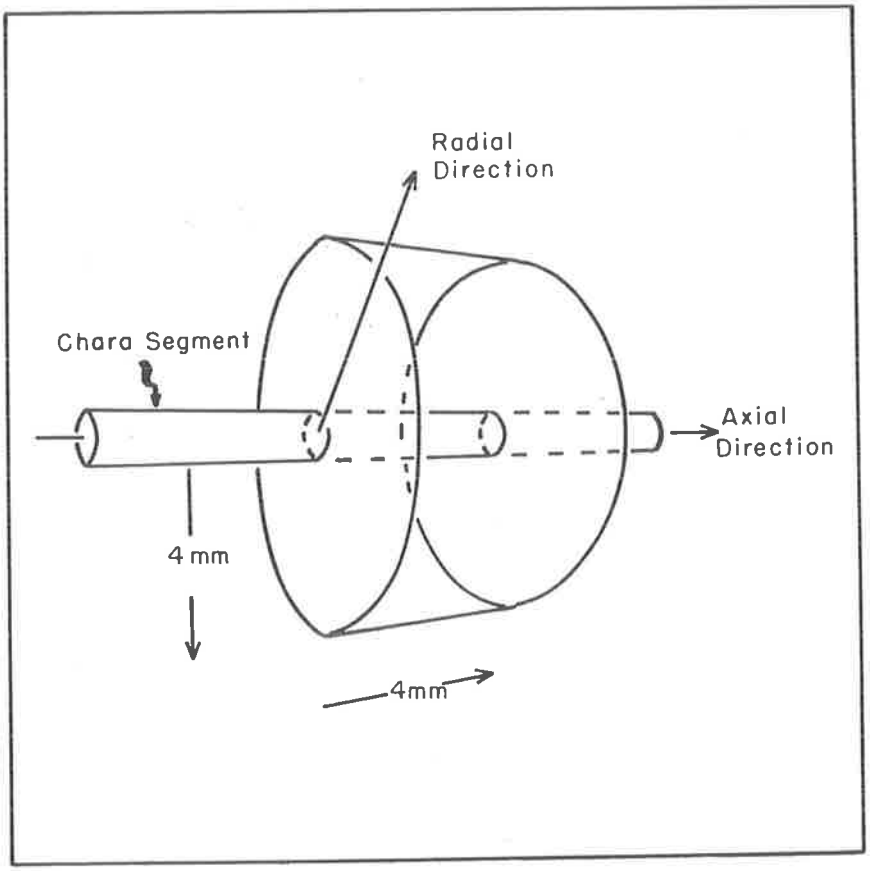


Fig. 1. Segment of *Chara* cell with boundaries of numerical diffusion region shown. One of the planes perpendicular to the axial direction of the cell cuts through the center of symmetry of the $OH^-$ efflux band. Zero $OH^-$ flux was the boundary condition on this plane. On the other plane, perpendicular to the axial direction, two alternative boundary conditions were used: $OH^-$ concentration equal to the initial background concentration, or zero $OH^-$ flux. This latter boundary condition corresponded to this plane being a plane of symmetry half-way between two $OH^-$ efflux bands. The boundary condition on the surface 4 mm out and parallel to the cell surface was that of $OH^-$ concentration equal to the initial background concentration

we also investigated the effect of imposing zero net flux along the plane cutting perpendicularly through the cell at a distance of 4 mm from the $OH^-$ efflux center. (This case simulates the experimental condition of two $OH^-$ efflux sites whose band centers are separated by a distance of 8 mm.)

To ensure stability within the calculation, it was neccessary to maintain the condition $4D\Delta t < (\Delta X)^2$, where D is the largest diffusion coefficient of the ionic species involved, $\Delta t$ is the time interval used for each iteration and $\Delta X$ is the smallest spatial interval employed. For our calculations, where $\Delta X = 100$ μm and $D_{OH^-} = 2.129 \times 10^{-5}$ cm$^2$ sec$^{-1}$, a $\Delta t$ value of 1 sec was employed. To verify mathematical accuracy of the calculation a limited number of runs were performed using smaller values of $\Delta X$ and $\Delta t$. In order to minimize computing time these checks were performed assuming symmetry in the axial direction. The agreement between the results obtained using $\Delta X = 10$ μm and $\Delta t = 0.01$ sec and those of the $\Delta X = 100$ μm, $\Delta t = 1$ sec case, was within 5%. For the case of $\Delta X = 50$ μm.

$\Delta t = 1$ sec, the agreement was within 3%. Because of the computing expense involved (cost increased inversely with $(\Delta X)^2$ and $\Delta t$), we were forced to accept, for the results presented in this paper, the 95% accuracy limits imposed by employing $\Delta X = 100$ μm, $\Delta t = 1$ sec. It should be stressed that we feel these limits do not detract from the predictive nature of this analysis.

Since $HCO_3^-$ is a fundamental requirement for $OH^-$ efflux (Lucas & Smith, 1973) all $OH^-$ efflux experiments had to be performed in the presence of $NaHCO_3$. This meant that the chemical reaction

$$HCO_3^- + OH^- \rightleftharpoons H_2O + CO_3^{2-}$$

would occur within the immediate vicinity of the alkaline band. Hence we had to incorporate into the numerical analysis not only the diffusion of $OH^-$ away from the efflux site but also the associated diffusion of $HCO_3^-$ and $CO_3^{2-}$. To solve this system numerically it was necessary to make the basic assumption that chemical equilibrium was established in each section, following every iteration. [This appeared to be a valid assumption since the above reaction is almost instantaneous (Sirs, 1958).] Again, the added computing cost associated with the incorporation of this $HCO_3^-$ buffering effect, forced us to do the majority of the calculations on the "simple unbuffered" system. However, sufficient cross-checks were made to ensure that the same general time-dependent diffusion pattern existed in both cases.

### *$OH^-$ Efflux Activation Time Course*

Initial attempts to fit the experimental pH data, associated with the light-mediated activation of the $OH^-$ efflux band, involved calculating the time-dependent diffusion pattern using various "trial functions" for the activation of the plasmalemma transport rate. The experimental steady-state $OH^-$ efflux value obtained using the spherical analysis technique employed by Lucas (1975*a*) gave the rate in units of moles $sec^{-1}$. Performing a similar cylindrical analysis on data from measurements close to the cell surface gave an equivalent rate in moles $sec^{-1}$ per unit cell length. Hence, division of the spherical rate by the cylindrical value gave an estimate of the $OH^-$ band pumping width. This width, along with the experimentally deduced steady-state plasmalemma efflux rate (moles $cm^{-2}$ $sec^{-1}$), was used to define the required steady-state conditions in the numerical calculation.

The "trial function" that gave the best fit between experimental and numerical data was that of an exponential build-up of $OH^-$ efflux (*see* Fig. 4). This "trial function" was rather limited, however, so the procedure was refined. The experimental pH values (60-sec intervals) were put into the program and used as "target" values. The difference between diffusion away from the central section of the $OH^-$ band and the plasmalemma efflux rate was compared with the rate of $OH^-$ build-up that was required to meet the next "target" pH value. This was done every second, and the plasmalemma transport rate adjusted accordingly. This procedure resulted in a fairly smooth, second by second, time curve for the efflux rate which produced a build-up (or decline) of pH at the cell surface in exact conformity with the experimental values (further details are given in the Appendix).

A similar procedure was developed for ensuring that the calculated pH values along the cell surface conformed with those obtained experimentally.

Complete details of the computational procedures associated with this $OH^-$ efflux analysis are available from the authors.

## Results

### *Spherical and Cylindrical Diffusion Analysis*

It was essential to verify that the two-dimensional $OH^-$ diffusion pattern, established by the numerical analysis, was comparable to the experimentally obtained data. We used the steady-state spherical and cylindrical diffusion analysis for this purpose (Lucas, 1975*a*). In the spherical system, the steady-state $OH^-$ concentration at any radial point ($C_R$) is related to the radial distance ($R$) by the equation,

$$C_R = K\frac{1}{R} - B \tag{1}$$

where $K$ and $B$ are numerical constants whose values are defined by the boundary conditions. (It should be pointed out that the value of $R$ appearing in Eq. (1) is equal to $(R_{Chara}+r)$ where $r$ is the vertical distance from the cell surface.)

Fig. 2 is typical of the numerical results obtained and demonstrates that there was indeed close agreement between the experimental and numerical results. This was especially so for the "unbuffered" case. The slight discrepancy observed at the highest $OH^-$ concentrates resulted from a 0.02 pH unit difference between the one-hour light activation and vertical scan experiments. (The light activation data were employed for the numerical analysis.) The fact that the "buffered" values did not fit as well as the simple "unbuffered" $OH^-$ system was not really surprising. The complexity of the actual experimental system is perceived when one realizes that $HCO_3^-$ uptake is also occurring along the cell surface. Because of this simultaneous $HCO_3^-$ uptake, it is difficult to estimate the actual concentration of $HCO_3^-$ within the immediate system. However, the numerical results expressed in Fig. 2 suggest that the $HCO_3^-$ "buffering" effect is of rather limited importance in this diffusion system.

As previously shown, linearity of the analysis based on the spherical diffusion system was not observed close to the cell surface (*see* Lucas, 1975*a*). We considered that within this region (0.5 mm) the diffusion system may be closer to that of a cylindrical coordinate system. The steady-state diffusion equation of a hollow cylinder can be simplified to

$$C_R = G \ln R + A \tag{2}$$

where $A$ and $G$ are numerical constants whose values are defined by the boundary conditions. The results of a cylindrical analysis of the

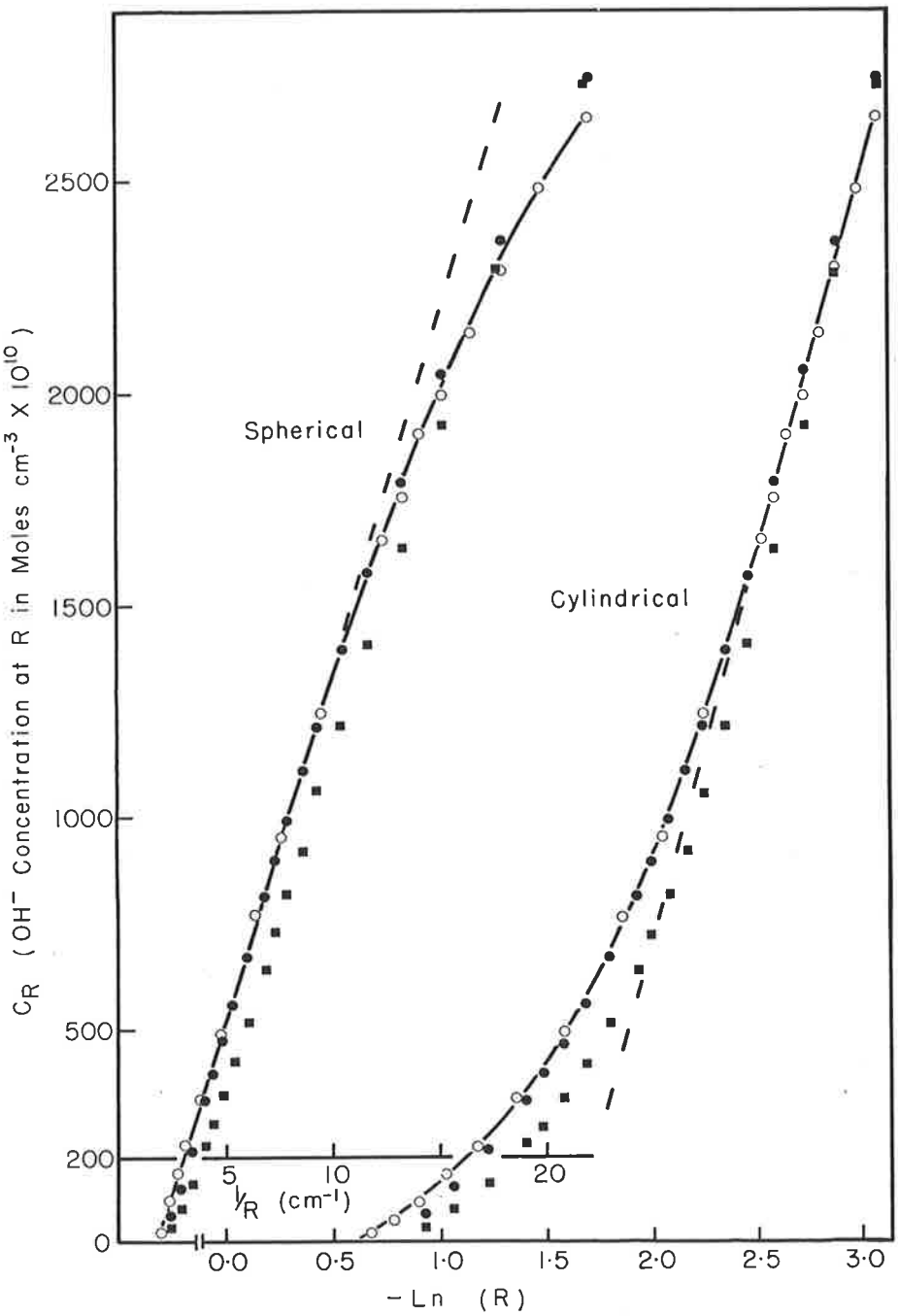


Fig. 2. Steady-state spherical and cylindrical diffusion analysis of the $OH^-$ concentration distribution in the plane which cuts through the center of the OH efflux region. Symbols used: ○, experimental values; ●, calculated values; ■, calculated values with $HCO_3^-$ buffering effect incorporated. R is the radial distance from the central axis of the cell (i.e. the cell radius plus the distance from the cell surface)

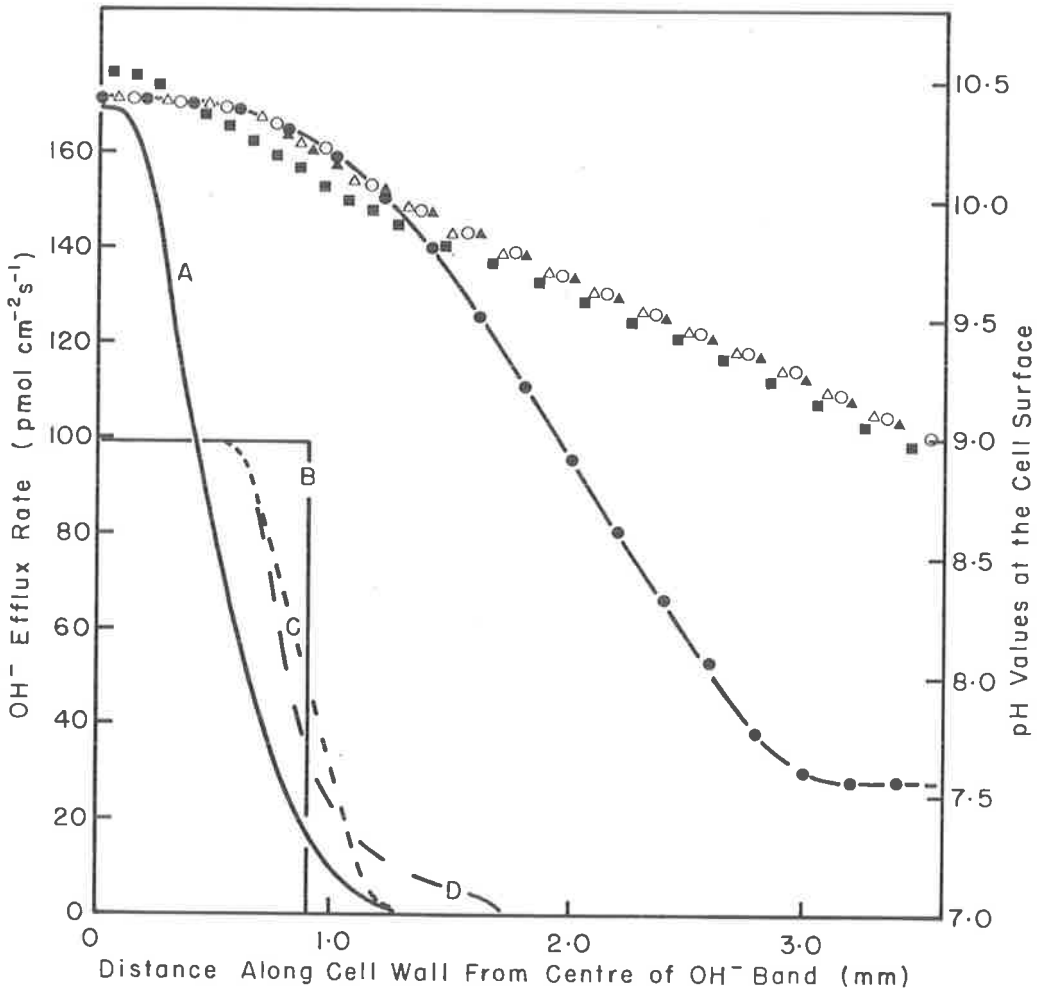


Fig. 3. Steady-state pH and $OH^-$ efflux values along the cell surface, commencing at the efflux band center. The experimental pH values are represented by the symbol, ●. Various forms of $OH^-$ efflux are illustrated, and the pH values calculated using the respective forms are as follows: ■, form *A* (a Gaussian distribution); △, form *B*; ○, form *C*; and ▲, form *D*

experimental and numerical values, based on Eq. (2), are presented in Fig. 2. The linear results verify our assumption concerning the $OH^-$ diffusion pattern in the region close to the cell surface. The cylindrical analysis also revealed very close agreement between experimental and numerical results.

Some experiments were conducted over longer periods and these results showed that quasi-steady-state diffusion was established approximately 1 hr after the cell was illuminated. Again, the numerical results were in agreement with this finding.

### *Spatial Distribution of $OH^-$ Efflux Activity*

To obtain information relating to the actual spatial distribution of the $OH^-$ efflux activity associated with an $OH^-$ band, we investigated a range of efflux forms. In each case, the total $OH^-$ efflux was the same, only the distribution of the spatial activity was varied. Fig. 3 illustrates some of the forms investigated. The Gaussian efflux distribution deviated noticeably from the observed experimental pattern. It is also apparent from Fig. 3 that the calculated pH values, for all forms investigated, deviated from the experimental data significantly as the distance from the $OH^-$ band center increased. This feature was observed with all efflux bands studied, and its significance will be discussed in detail in a later section. At present we will confine our attention to the cell surface within 1.5 mm of the band center. From the results presented in Fig. 3, it can be seen that close agreement between experimental and numerical results was obtained with either a uniform step-function (*B*) or a uniform ramp-function (*C*). Although this analysis does not enable us to differentiate between these two generalized forms, we feel that the ramp-function is more likely to be representative of the actual $OH^-$ efflux pattern. It should also be stressed that Fig. 3 represents only one-half of the actual $OH^-$ efflux band, hence the total length over which $OH^-$ was being effluxed is approximately 2.0–2.4 mm. In general, $OH^-$ efflux widths of 1.9 to 2.2 mm were observed (*see* Table 1); this is considerably larger than the previously envisaged pumping width (Lucas & Smith, 1973; Lucas, 1975*a*).

### *Activation of $OH^-$ Efflux*

Fig. 4 shows the build-up of pH at the centers of two $OH^-$ bands, as measured with the pH electrode just touching the cell surface. These data were first fitted using the "trial function" method, where it was found that the pH build-up could be closely approximated if an exponential build-up of $OH^-$ efflux was used (*see* lower curves of Fig. 4*A* and *B*). Virtually an exact fit was obtained by using the "target pH" method, in which the difference between the efflux rate and the rate of diffusion away from the center of the efflux band was compared with the rate of build-up of $OH^-$ required to match the observed experimental pH change. It should be emphasized that the resultant time course for the

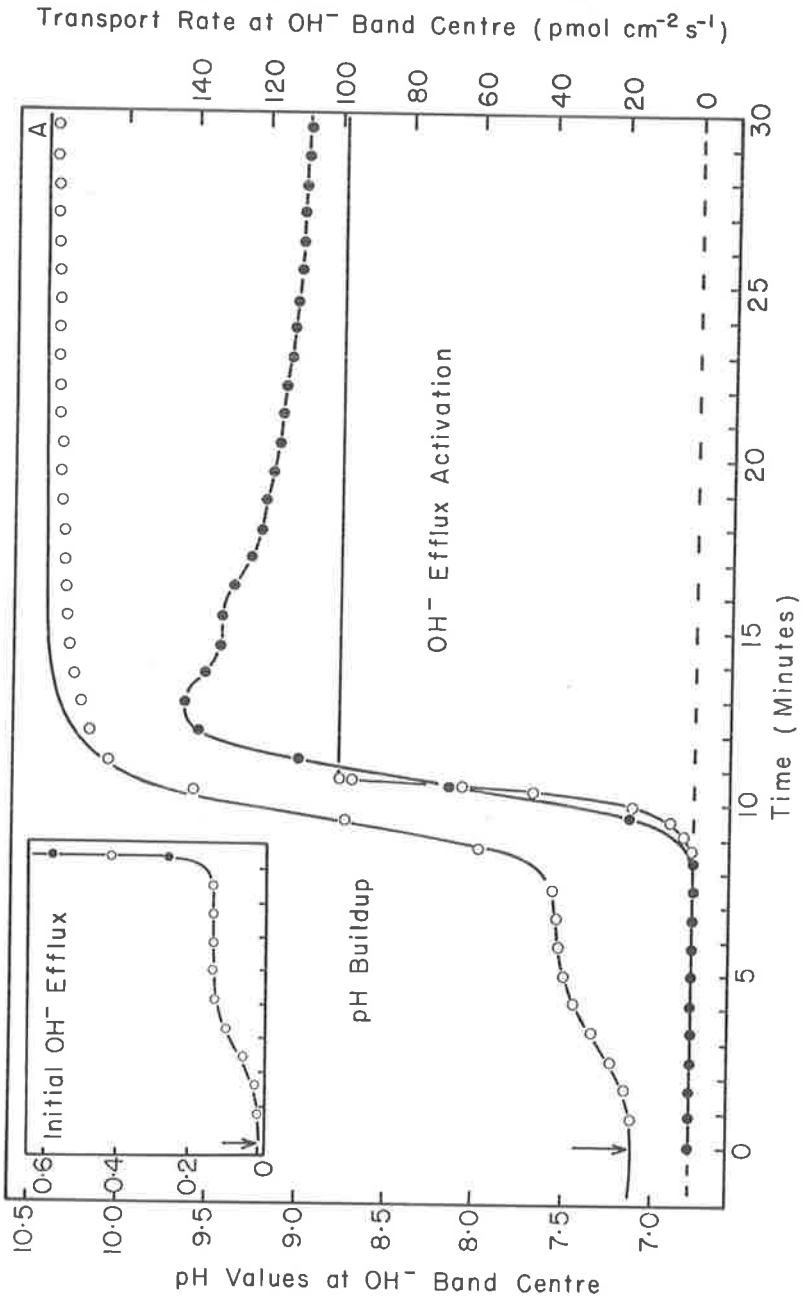


$OH^-$ efflux build-up, obtained from this numerical procedure, is not dependent on any assumptions or parameters except the value(s) of the diffusion coefficient(s) and the background concentrations of $OH^-$, $HCO_3^-$ and $CO_3^{2-}$.

The $OH^-$ efflux build-up follows an exponential curve until approximately one-half of the maximum value is attained. The two general forms of $OH^-$ efflux activation depicted in Fig. 4 are representative

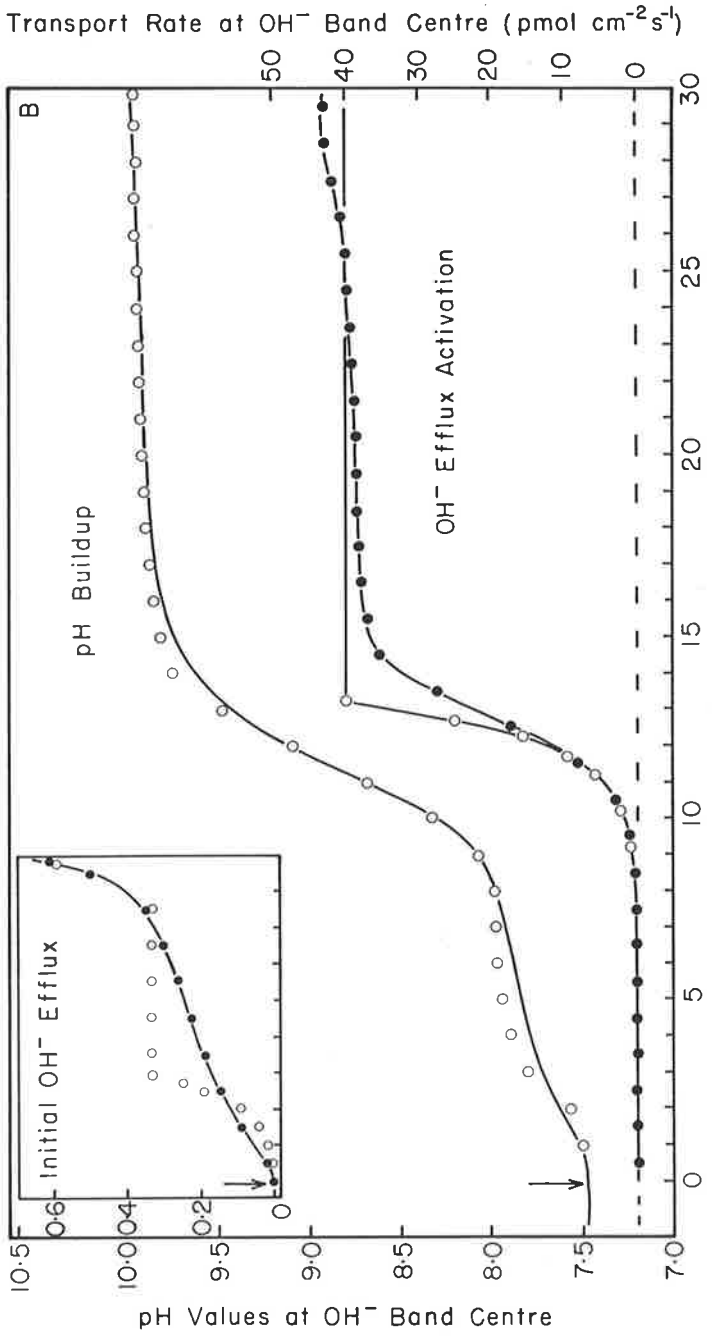


Fig. 4. pH build-up and $OH^-$ efflux activation curves. The upper curves in *A* and *B* are experimental pH values, obtained as a function of time, at the efflux band centers. The symbol ○, associated with these pH curves, represents the numerical values obtained using exponential "trial" functions for $OH^-$ efflux activation. The same symbol was employed, on the $OH^-$ efflux curves, to present the exponential "trial" function $OH^-$ efflux values. (The time constants for these exponential curves were 170 and 300 sec for *A* and *B*, respectively.) The curves associated with the solid circles (●) are the $OH^-$ efflux activations required to give an exact fit of the respective experimental pH build-up. The inserts show, on a magnified scale, exponential (○) and "exact fit" (●) efflux activation curves for the small, initial, pH build-up. The scales on the ordinate and abscissa represent $OH^-$ transport rate in pmole $cm^{-2}$ $sec^{-1}$ and time in minutes, respectively. (In *A*, these two methods gave almost the same values.) The arrows indicate the commencement of the illumination period

of the most frequently observed forms. The overshoot characteristic illustrated in Fig. 4*A* can possibly be explained using the model of Lucas (1975*c*). The reduction in efflux rate may be due to the activation of other efflux bands, which is thought to be in response to the establishment of critical activation levels of a substrate in the cytoplasm. Several cases were also observed in which the efflux rate was found to increase after activation and establishment of a quasi-steady-state. The change observed

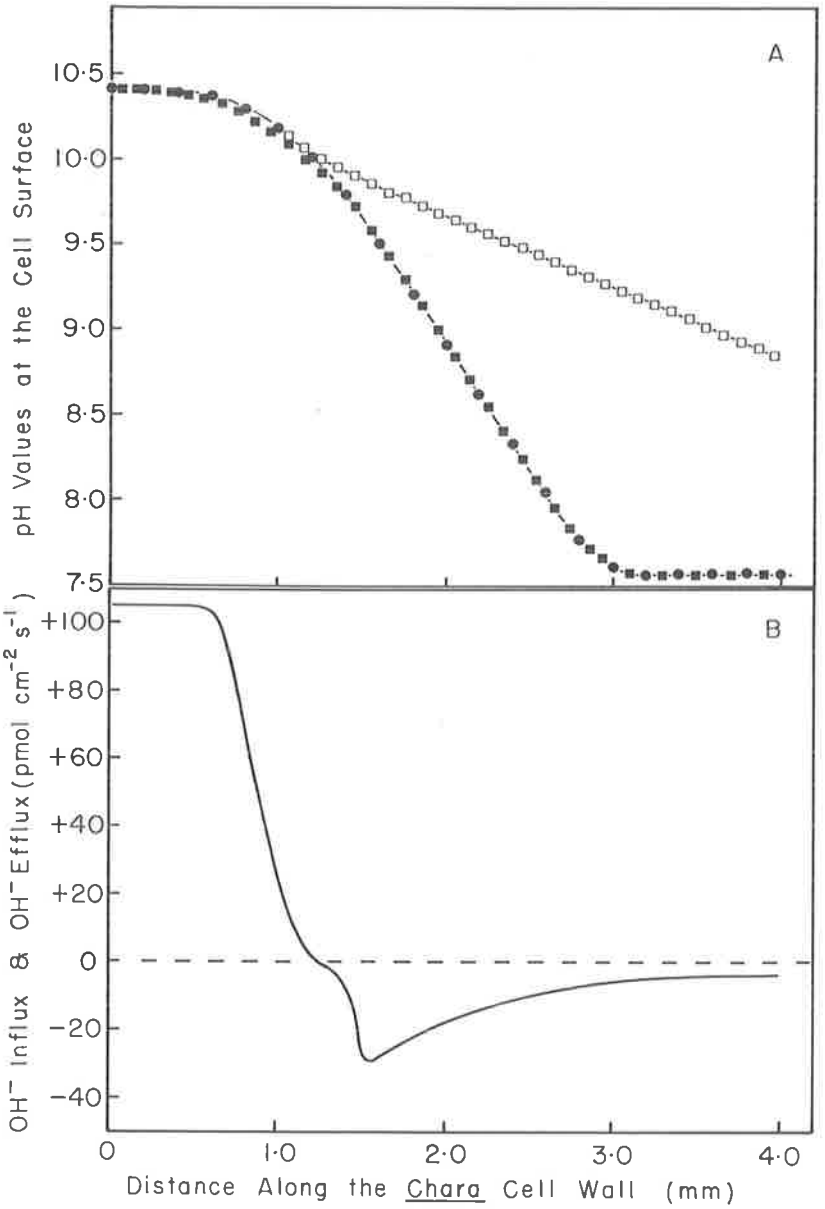


Fig. 5. Steady-state pH and $OH^-$ efflux values along the cell surface. The solid circles (●) are experimental pH values. The solid squares (■) are pH values calculated with the $OH^-$ efflux and sink pattern shown in the lower curve. The open squares (□) are pH values calculated with the $OH^-$ efflux pattern shown in the lower curve, but without the lateral sink region

in the latter phase of the results presented in Fig. 4*B* is an example of this form. Hydroxyl efflux regulation, or "feedback", is in agreement with the observed $OH^-$ efflux characteristics and models propounded by Lucas (1975*c*) and Lucas and Dainty (1976).

The inserts in Fig. 4*A* and *B* show the very small initial $OH^-$ efflux rate which is required to produce the initial pH step that precedes the

main activation. In general, this initial efflux process fits a simple exponential form (*see* Fig. 4*A*) but as shown in Fig. 4*B*, this is not always observed. However, this small initial efflux is always present during the activation of $OH^-$ bands in *Chara corallina*, and its possible significance as a clue to the mechanism of $OH^-$ transport will be discussed in a later section.

### *Lateral $OH^-$ Sink Requirement*

When the numerical calculation was performed with zero $OH^-$ back flux, through the cell surface adjacent to the $OH^-$ efflux band, the experimental pH values were always substantially lower than those obtained from the numerical calculation (*see* Fig. 3 and Fig. 5*A*). To correct for this discrepancy, the computational procedure was modified so that the calculated pH values were prevented from going above their respective experimental value by incorporating an $OH^-$ sink (influx). The strength of this sink was matched to the increase in diffusional flux, into a given section, once the respective pH value was reached. A typical band with the related $OH^-$ efflux and sink regions is shown in Fig. 5*B*. (Since *Chara corallina* has a light-activated $H^+$ efflux system (Lucas & Smith, 1973), it should be realized that part of this $OH^-$ sink may be associated with this phenomenon.)

Although the magnitude of individual sinks varied (*see* Table 1), all bands studies had $OH^-$ sinks typified by the general shape illustrated in Fig. 5*B*. The possible significance of the lateral sink, in helping to elucidate the mechanism of $OH^-$ transport, will be discussed later.

### *General Features of the $OH^-$ Band*

The numerical results presented in Table 1 were drawn from calculations performed on steady-state experimental data obtained from five $OH^-$ bands on three cells. [These experimental data reflected typical $OH^-$ efflux band characteristics (Lucas & Smith, 1973; Lucas, 1975*a* and *c*, 1976).] Experiments were conducted on internodal cells except for experiment 2, in which a whorl cell was used. Experiments 3, 4 and 5 were conducted on different bands on the same cell.

Some general features of the $OH^-$ band are apparent. The width of the $OH^-$ efflux region ranged from 1.9 to 2.2 mm. The rate of $OH^-$

Table 1. Steady-state hydroxyl band characteristics[a]

| Computational aspects | Exp. No. | Band center pH | Efflux width (mm) | Band center efflux rate (pmol $cm^{-2}$ $sec^{-1}$) | Maximum lateral sink flux (pmol $cm^{-2}$ $sec^{-1}$) | Efflux[b] rate (pmol $sec^{-1}$) | Lateral sink flux rate (pmol $sec^{-1}$) | Net efflux (efflux − sink) (pmol $sec^{-1}$) | Efflux from spherical analysis of numerical results (pmol $sec^{-1}$) | |
|---|---|---|---|---|---|---|---|---|---|---|
| | | | | | | | | | $OH^-$ | $CO_3^-$ |
| $D_{OH}=2.13\times10^{-5}$ $cm^2$ $sec^{-1}$ | 1 | 10.44 | 2.2 | 105.4 | 29.7 | 5.40 | 1.72 | 3.68 | 5.05 | |
| | 2 | 9.96 | 1.9 | 42.4 | 7.1 | 1.89 | 0.33 | 1.56 | 1.88 | |
| | 3 | 10.18 | 2.0 | 64.9 | 26.1 | 2.70 | 0.97 | 1.73 | 2.41 | |
| | 4 | 10.22 | 2.2 | 66.2 | 18.1 | 3.10 | 0.94 | 2.16 | 2.81 | |
| | 5 | 10.08 | 2.2 | 49.3 | 21.8 | 2.30 | 0.85 | 1.45 | 2.03 | |
| $D_{OH}=2.13\times10^{-5}$ $cm^2$ $sec^{-1}$ | 1 | 10.44 | 2.2 | 157.1 | 40.4 | 8.04 | 2.40 | 5.64 | 4.43 | 2.92 |
| $HCO_3^-$ buffering | 2 | 9.96 | 1.9 | 79.5 | 11.6 | 3.54 | 0.59 | 2.95 | 1.63 | 1.84 |
| $D_{OH}=5.32\times10^{-5}$ $cm^2$ $sec^{-1}$ | 1 | 10.44 | 2.2 | 262.5 | 75.4 | 13.42 | 4.46 | 8.96 | 12.18 (4.87)[c] | |
| | 2 | 9.96 | 1.9 | 105.9 | 17.9 | 4.72 | 0.84 | 3.88 | 4.58 (1.84)[c] | |
| $D_{OH}=5.32\times10^{-5}$ $cm^2$ $sec^{-1}$ $HCO_3^-$ buffering | 1 | 10.44 | 2.2 | 315.2 | 111.2 | 16.14 | 5.54 | 10.60 | 11.63 (4.65)[c] | 3.08 |

[a] The values presented in this Table were obtained by numerical analysis of the experimental data, using the "target" pH method of analysis

[b] Each $OH^-$ efflux band was divided into a number of 100 μm efflux units. The efflux rate was obtained by summation of the rates associated with these units.

[c] Efflux calculated assuming $D_{OH}=2.13\times10^{-5}$ $cm^2$ $sec^{-1}$.

uptake by the lateral sink was approximately one-third of the rate of $OH^-$ efflux for internodal cell bands. For the single whorl cell investigated, the uptake rate was about one-sixth the efflux rate.

The effect of including $HCO_3^-$ buffering in the calculation was to increase the efflux and lateral sink rates by almost the same factor (Experiment 1, efflux increased by 1.49×, lateral sink by 1.40×; Experiment 2, efflux increased by 1.87×, lateral sink by 1.79×). The $OH^-$ efflux calculated from the steady-state spherical diffusion analysis was slightly reduced. However, under these conditions there was a significant movement of alkalinity in the form of $CO_3^{2-}$.

Because of the presence of the lateral sink, net $OH^-$ efflux was always smaller than that from the efflux region. For the unbuffered situation it can be seen that the value obtained from the spherical analysis was always larger than that of net efflux, but smaller than from the efflux region. In the buffering calculations the situation was different, the value obtained for $OH^-$ efflux by spherical analysis was in fact smaller than the net efflux. However, we consider that the buffering influence in the numerical calculation is probably greater than exists in the experimental situation. It is possible that the true buffering level is near the "flux cross-over point", namely where the net $OH^-$ efflux value is equivalent to that calculated on the basis of the spherical analysis. This would be consistent with the earlier work of Lucas (1975*a*), where a close correlation was observed between $H^{14}CO_3^-$ uptake and $OH^-$ efflux (spherical analysis).

The diffusion coefficient most frequently used for $OH^-$ was $2.129\times 10^{-5}$ $cm^2$ $sec^{-1}$ and is the limiting diffusion coefficient for NaOH. This value was used by Lucas (1975*a*) in his steady-state spherical diffusion analysis. The value was obtained using the limiting ionic conductances for $Na^+$ and $OH^-$ in the Nernst-Hartley relationship (Robinson & Stokes, 1965, pp. 286–288, 465). However, since in these experiments the concentration of $OH^-$ was considerably lower than that of $Na^+$, it is possible that the correct relation between conductivity and the diffusion coefficient is that of Onsager for the case of self- or tracer-diffusion (Onsager, 1945). This relationship becomes the Nernst-Einstein relation for low total concentrations. If this relation held for the experimental situation, the $OH^-$ diffusion coefficient would be increased by a factor of 2.5 above that of the limiting NaOH case. The value for $CO_3^{2-}$ would be increased by 1.6, while that for $HCO_3^-$ would be decreased by 0.95. (We also theoretically investigated the possibility that there were no cations accompanying the $OH^-$ diffusion, finding a negligible effect on

the Onsager self-diffusion relation. We similarly found that the $HCO_3^-$ and $CO_3^{2-}$ fluxes would have a negligible effect on the $OH^-$ diffusion.)

Using the modified diffusion coefficient in the unbuffered calculations increased the values of $OH^-$ efflux and sink flux by the same factor as the diffusion coefficient was increased. In the buffering calculation these two fluxes were also increased, but to a lesser extent than the increase in the value of the diffusion coefficient. The $OH^-$ efflux which one could calculate from the steady-state spherical diffusion analysis of this buffered data, was almost the same as that obtained in the calculation with the NaOH diffusion coefficient, provided that the NaOH diffusion coefficient was used in the analysis. Of course if the modified coefficient was used, the result would be much larger.

It is important to note that the only assumptions or parameters in the numerical diffusion calculation are those concerning the $HCO_3^-$ buffering and the diffusion coefficients. Hence, since the essential features of the $OH^-$ bands were insensitive to the level of $HCO_3^-$ buffering and the absolute value of the diffusion coefficient, we consider the existence of the lateral $OH^-$ sink region to be as firmly established as the existence of the $OH^-$ efflux region.

### *Dynamics of $OH^-$ Transport Deactivation*

The photosynthetic assimilation of $HCO_3^-$ is totally light dependent and consequently, following the initiation of a dark period, the pH value at the $OH^-$ band center begins to decline (Fig. 6 and *also see* Lucas, 1975*c*). Previously it was not possible to obtain further information from the dark pH time course, because of the complexity of the time-dependent diffusion system. However, with the aid of numerical analysis, a complete characterization of the $OH^-$ transport deactivation process was possible.

Fig. 6*A* illustrates that even with the incorporation of the $HCO_3^-$ buffering effect, the continued operation of the lateral $OH^-$ sink in the dark, and an increase in the respective diffusion coefficients, it was not possible to obtain results that even approximated to the shape of the experimental pH time course. The influence of an $OH^-$ influx (sink), of various magnitudes, activated simultaneously with the light off event, is illustrated in Fig. 6*A*. This revealed that a pH decline having at least some general characteristics in common with the experimental system, could be obtained using a dark sink flux somewhere between 10 and

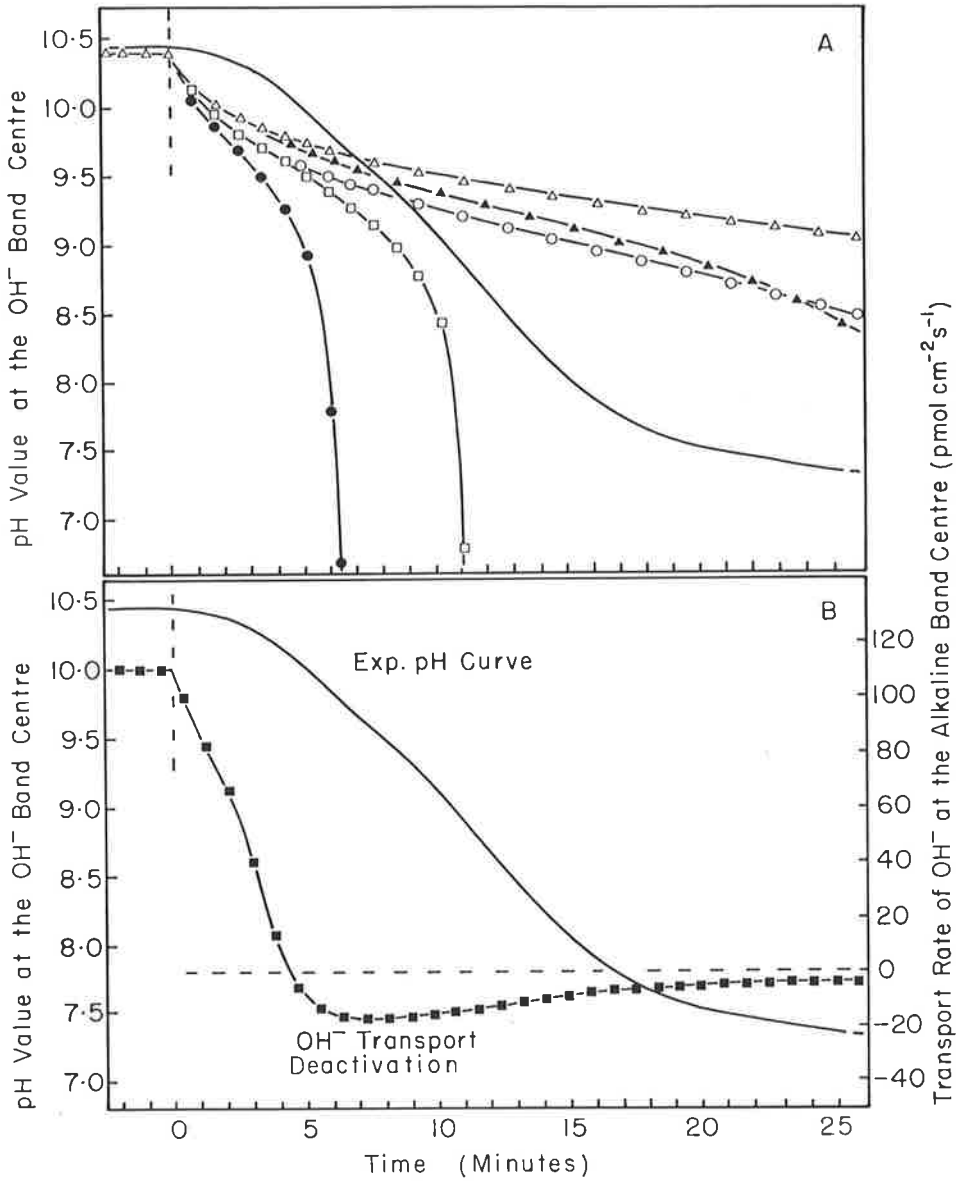


Fig. 6. Hydroxyl transport deactivation curves. The unbroken line in *A* and *B* represents the experimentally observed pH decay associated with experiment 1. The pH values were measured with the electrode on the cell surface at the $OH^-$ band center. The other curves in *A* show calculated pH decay curves obtained for various conditions. With $OH^-$ transport switched off at time zero, almost identical results were obtained under a range of conditions, which included the presence and absence of both a lateral sink and $HCO_3^-$ buffering. (The lateral sink employed was equivalent to that established in the steady-state during illumination.) The results from these calculations are represented by the symbol, △. The influence of doubling the diffusion coefficient for $OH^-$, in the presence of a lateral sink, is also shown (○). Calculations were also done in which $OH^-$ transport was switched to a constant influx upon cessation of illumination (these calculations also incorporated the influence of a lateral sink). A range of dark sink fluxes was investigated: ▲, 2.5 pmol $cm^{-2}$ $sec^{-1}$; □, 10 pmol $cm^{-2}$ $sec^{-1}$; ●, 20 pmol $cm^{-2}$ $sec^{-1}$. Fig. 6*B* presents the actual $OH^-$ transport (■), at the band center, required to generate a pH decay curve identical to the experimental case. The vertical broken line indicates the light to dark transition

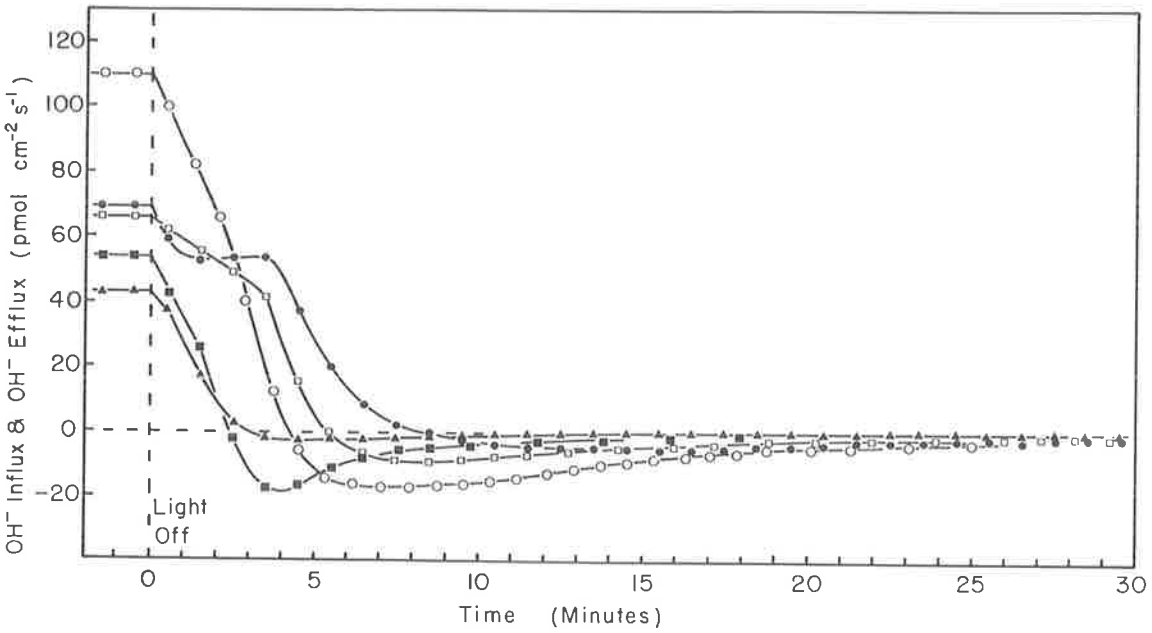


Fig. 7. Dark deactivation of $OH^-$ transport. This Figure presents the dark deactivation results of the experiments detailed in Table 1. The individual characteristics of these curves were elucidated using the "target" calculation method. The symbols ○, ▲, □, ● and ■ represent experiments 1 through 5, respectively

20 pmole $cm^{-2}$ $sec^{-1}$. However, in all the numerical results obtained for the various conditions, it can be seen that in the initial dark phase, the numerical values always fell below the experimental time course (Fig. 6*A*). This indicates that the $OH^-$ efflux system does not deactivate immediately upon darkening.

To obtain the best estimate of the time-dependent change in $OH^-$ transport, following the dark treatment, we employed the "target pH" method that was used to characterize the $OH^-$ transport activation phenomenon. The results obtained using this procedure are presented in Fig. 6*B*. Following the commencement of the dark period, the $OH^-$ efflux rate declined with what appeared to be a biphasic response. After 5 min the rate had fallen to zero efflux and, as can be seen in Fig. 6*B*, the cell surface then began to function as an $OH^-$ sink. These general features are supported by the results presented in Fig. 7. Apparently the dark $OH^-$ sink flux commences somewhere between 2 and 10 min after the cell is darkened, and is reduced to a very low level within a period of 30 min.

Numerical calculations were also performed to investigate the possible effect of the $HCO_3^-$ "buffer" on the shape of the time course of $OH^-$

transport deactivation. Incorporation of the "buffering" effect did not change the general characteristics of the deactivation process, it merely increased the required strength of the dark sink flux. Similar results were obtained when the numerical calculations were performed using the larger $OH^-$ diffusion coefficient. We are therefore confident that the dark $OH^-$ deactivation phenomenon, as revealed by numerical analysis, is a realistic representation of the time course of events that actually occur in these *Chara* cells.

## Discussion

The results presented above may be summarized as follows. Numerical analysis of the experimental pH data, obtained on cells of *Chara corallina,* has revealed certain important operational characteristics of the plasmalemma $OH^-$ transport system. The initial exponential nature of the $OH^-$ activation curve is an important discovery, for it must surely be a physical expression of a fundamental characteristic of at least one component of the $OH^-$ transport system. A comprehensive $OH^-$ transport "model" must incorporate this exponential phase and also explain its limited duration. We have not, as yet, formulated such a sophisticated description of the system. However, in terms of elucidating the possible electrical contribution of $OH^-$ and $HCO_3^-$ transport at the plasmalemma, this exponential characteristic will be an extremely useful marker.

The presence of a relatively wide, uniform $OH^-$ efflux region and the probable ramp decline in efflux at the boundaries is of interest with respect to the recent finding by Lucas and Dainty (1977) that the $OH^-$ transporters are uniformly distributed over the plasmalemma surface. Lucas and Dainty (1977) showed that at any one time, only a small fraction of the total number of transporters are operational. The cellular mechanism that determines the $OH^-$ band location may also determine the density of operational transporters as a function of distance from the center of the band. If, on a molecular scale, the release of $OH^-$ at the outer surface of the plasmalemma takes place at specific localized "enzymic transport sites", it may be possible to identify these sites and their spatial distribution using electron microscopy.

There are several possible explanations that may account for the $OH^-$ sink in the lateral regions adjacent to the $OH^-$ efflux zone. It may be that in this region a pH-energized transport system is operating. To function as an $OH^-$ sink would require either the movement of $OH^-$ into, or $H^+$ out of the cell. The only active transport system

proposed for this cell that involves the coupled movement of $OH^-$ is the $Cl^-/OH^-$ antiporter of Smith (1970). However, this system would operate in the reverse direction to that required. [In addition, this hypothesis has received only limited experimental support (Lucas & Smith, 1976.] A proton co-transport or antiport system may have more credence since this cell has a light-mediated $H^+$ efflux system. Spear, Barr and Barr (1969) proposed a simple HCl co-transport model for *Nitella clavata,* but this system has not gained experimental support (Lucas & Smith, 1976).

Part of the $OH^-$ sink may be directly associated with the operation of the $H^+$ efflux system. We feel, however, that the characteristic shape of the $OH^-$ sink, in terms of the spatial distribution of its relative strengths, suggests that any contribution from the $H^+$ efflux system is probably limited to the outer zone of the sink.

Another possibility is that there may be an efflux of $CO_2$ generated by the $HCO_3^-$ influx to the cytoplasm. (Reaction of $CO_2$ with $OH^-$ yields $HCO_3^-$, and in this manner the $CO_2$ efflux acts to remove $OH^-$ from the region close to the cell surface.) Although analysis of the relation between $CO_2$ concentration at the cell surface and $OH^-$ sink strength failed to reveal a simple relationship, a small contribution from this effect cannot be discounted. The possibility of passive $OH^-$ diffusion into the cell in the lateral sink region is untenable, since this would involve movement against the electrochemical gradient for this ion. [Plasmalemma electrical potential difference is $-180$ to $-190$ mV (Lucas, 1975*d*); the pH difference is not great enough to balance this electrical potential difference.] A tentative hypothesis that we wish to forward is that the $OH^-$ sink flux relates to an imperfection in the overall regulating mechanism controlling the cellular efflux of $OH^-$. Details of this hypothesis will be presented in the following section.

The biphasic deactivation response of the $OH^-$ transport system may reflect the existence of a critical substrate level, in the cytoplasm, below which the transport system loses its efflux activity. Experimental support for the existence of critical activation and deactivation levels of an essential substrate in the cytoplasm has already been reported by Lucas (1975*c*). With the aid of numerical analysis it should be possible to design experiments to test this "critical substrate" hypothesis.

### *An Extension of the $OH^-$ Transport Model*

The control of $OH^-$ transport at the molecular level is no doubt a complex process. However, it is possible to propose a fairly simple

model which accounts for the main features of the activation, steady-state, and deactivation of $OH^-$ transport.

The first feature to be explained is the small flux which activates within 60 sec of illuminating the cell. (We consider that the linkage between cell illumination and this small $OH^-$ efflux process is via the photosynthetic reactions occurring in the chloroplasts, The chloroplasts may provide energy to the transport system, or alternatively these reactions may be required to generate a compound that is essential for transport activity. This "compound" may also be involved in the establishment of $OH^-$ efflux band centers.) The proposed model will assume that activation of the $OH^-$ transporters occurs in such a way that they will actively transport $OH^-$ in both directions across the plasmalemma. (We consider that the active nature of this process largely eliminates the influence of the membrane potential on the influx phase of this process.) Thus, in the presence of a higher pH value inside the cell than outside, a small net efflux would occur.

The activation of the undirected active transport will spread out along the cell surface in both directions from the band center. The mechanism which selects (or imparts) the location of the band center is unknown, but by experimentation we know that, once selected, the band center location is stable over a series of activations and deactivations.

The next step in the activation process is the initiation of the main efflux build-up, which occurs in the band center region as an exponential function of time, until the efflux is about one-half the maximum value. According to the proposed model, this efflux build-up is due to the cooperative effect of two events. Firstly, the imposition of directionality on the active transport process, and secondly the establishment of a critical concentration of a cytoplasmic substrate that is generated by photosynthesis (Lucas, 1975*c*). (It should be noted that we do not wish to specify, at this stage, $OH^-$ *per se* or a substrate which generates $OH^-$ at the transport site.) It is obvious that there are many ways in which directionality could be imparted to this membrane-bound transport system. One tentative proposal is that a conformational change, at the cytoplasm-plasmalemma interface, increases the binding affinity of the enzyme transport site for $OH^-$ at this inner membrane surface. Similarly, a conformational change within the $OH^-$ transport "complex" may increase the availability of energy (say ATP or $NADPH_2$) to the reactions associated with the efflux process. Whatever the molecular mechanism involved may be, it is clear that the activation of directionality does not extend as far along the plasmalemma surface, from the band

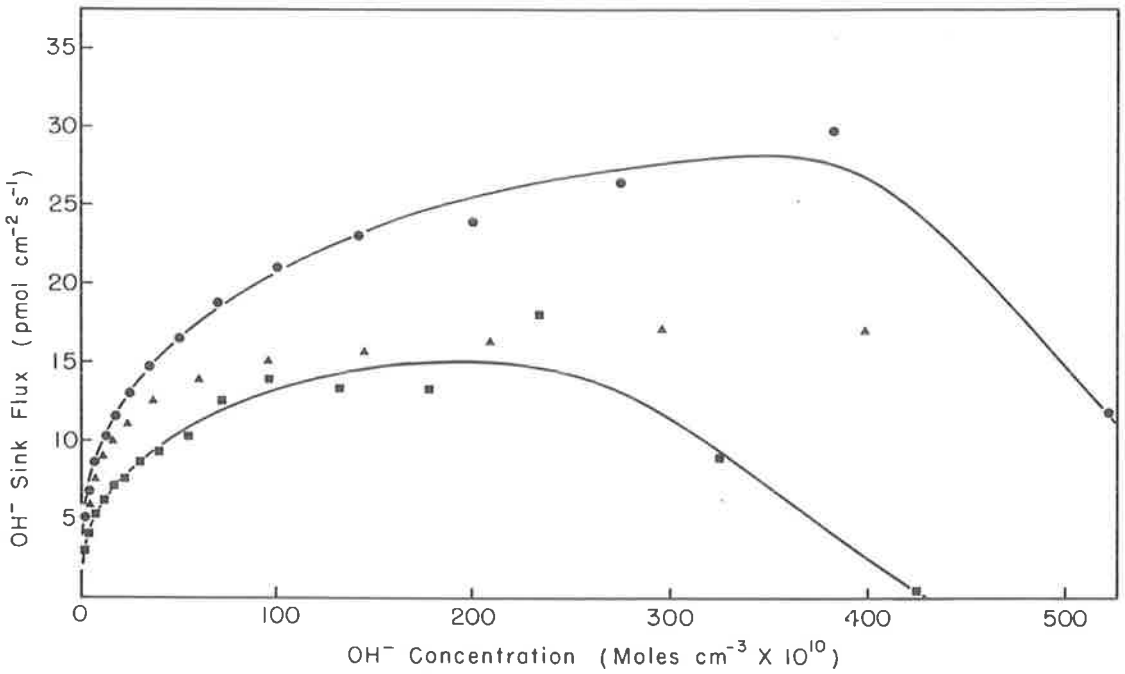


Fig. 8. Steady-state sink and dark sink flux as a function of $OH^-$ concentration. Calculated steady-state lateral sink fluxes are plotted for experiments 1 (●) and 4 (■). Other experimental lateral sink fluxes followed similar curves. The calculated dark sink flux values (experiment 1), at the center of this $OH^-$ band, are also given (▲). These values remained almost constant (14–17 pmole $cm^{-2}$ $sec^{-1}$) for $OH^-$ concentrations between $60 \times 10^{-10}$ and $800 \times 10^{-10}$ mole $cm^{-3}$

center, as does the activation of undirected transport. This lack of complete matching of the regions covered by the two activation processes results in the observed phenomenon of the lateral sink. That the lateral sink behaves like a simple enzymic carrier system is shown by the results presented in Fig. 8, which shows the relationship between $OH^-$ sink flux and $OH^-$ concentration for two $OH^-$ bands. The influence of the directionality factor becomes apparent at higher $OH^-$ concentrations where the sink flux falls to zero. In a similar manner, the proposed model accounts for the dark sink that is observed during the deactivation process. Photosynthetic assimilation of $HCO_3^-$ ceases shortly after the light is turned off. Following this there is a decline in $OH^-$ efflux, as a result of the reduction in substrate available to the transporters. A faster decay of efflux rate occurs once the directionality component is lost. The latter stage of the biphasic dark deactivation process may be an expression of the gradual loss of this directionality factor (*see* Fig. 7).

There ensues a longer period during which only the undirected transport remains. A graph of dark sink flux against $OH^-$ concentration again follows a pattern which fits that of facilitated diffusion (Fig. 8). The concentration-limited part of the dark sink flux curve correlates closely with that of the lateral sink flux. The carrier-limited part of the dark sink flux is lower than the corresponding lateral sink flux. This can be interpreted, according to the proposed model, as indicating that the number of undirected activated transporters is decreasing in the dark case. The existence of the dark sink would thus be due to a difference in decay rate of the control process for directionality and the undirected transport, with the directionality component having the faster decay rate.

It must be emphasized that we do not claim this model as a unique solution for the observed characteristics of the $OH^-$ transport system. We realize the limitations of this, and earlier models (Lucas, 1975*c*; Lucas & Dainty, 1977) at the molecular level. However, the successful application of numerical analysis to this $OH^-$ efflux system now means that we are in a position to investigate the involvement of $HCO_3^-$ and $OH^-$ transport on the electrical properties of the plasmalemma. This study may facilitate the further refinement of the present model.

This work was supported jointly by grants from the National Research Council of Canada (Grant No. A6459) and the Connaught Fund (University of Toronto).

## Appendix

### *Numerical Calculation of $OH^-$ Diffusion*

In the computer program, the spatial region was divided into sections designated by the subscripts $i$ and $m$. The subscript $i$ designated the annular layers concentric with the cell axis, starting with $i=1$ at the cell surface. The subscript $m$ designated the layers that were perpendicular to the axial direction, commencing with $m=1$ at the center of symmetry of the $OH^-$ efflux band.

The quantity $Y_i = DA_i \Delta t / \Delta x$ was first calculated, where $D$ is the diffusion coefficient for $OH^-$, $\Delta t$ the time interval used for each iteration, $\Delta x$ the spatial size of the sections and $A_i$ the area perpendicular to the radial direction, between section $i, m$ and section $i+1, m$. The quantity $W_m = DB_m \Delta t / \Delta x$ was also calculated, where $B_m$ is the area perpendicular to the axial direction between sections $i, m$ and $i, m+1$.

The next step was to calculate $Q_{i,m}=(C_{i,m}-C_{i+1,m})\ Y_i$, where $C_{i,m}$ is the $OH^-$ concentration in section $i,m$. $Q_{i,m}$ is the number of moles of $OH^-$ moving in the radial direction from section $i,m$ to section $i+1,m$, in time $\Delta t$. Similarly, the number of moles of $OH^-$ moving in the axial direction ($S_{i,m}$) from section $i,m$ to section $i,m+1$, in time $\Delta t$, was calculated using $S_{i,m}=(C_{i,m}-C_{i,m+1})\ W_m$. The number of moles of $OH^-$ moving across the cell surface into section 1, $m$ in time $\Delta t$, was designated $Q_{0,m}$, and was controlled by a subroutine in the program. $Q$ and $S$ at the other boundaries of the spatial region of the numerical calculation were controlled by other subroutines, which imposed boundary conditions closely approximating to those existing in the experimental system.

The new $OH^-$ concentrations, in each section, were then calculated using:

$C_{i,m}=C_{i,m}+(Q_{i-1,m}-Q_{i,m}+S_{i,m-1}-S_{i,m})/V_{i,m}$, where $V_{i,m}$ is the volume of section $i,m$. The new values for $C_{i,m}$ were then used to calculate new $Q$ and $S$ values. This procedure was repeated many times, yielding the numerical approximation to the time-dependent diffusion process.

### *Target pH Method*

Experimental pH values, obtained by placing the pH electrode on the cell surface and in the center of symmetry of an $OH^-$ efflux band ("target pH" values), were put into the program (60-sec intervals) and converted to $OH^-$ concentrations, $CT$ ("target concentrations"). The change in the number of moles of $OH^-$ in section 1,1 (at the cell surface, at the center of $OH^-$ efflux band symmetry), in time $\Delta t$, was calculated using $R=Q_{0,1}-Q_{1,1}-S_{1,1}$, (and $S_{1,0}=0$). The change in the number of moles of $OH^-$ in section 1,1 that should occur in $\Delta t$, if the target pH is to be matched in the calculation, is $U=(CT-C_{1,1})\ V_{1,1}/(T/\Delta t)$, where $T$ is the time remaining until $CT$ should be matched by $C_{1,1}$. A new value for $Q_{0,1}$ was then calculated, using $Q_{0,1}=Q_{0,1}+U-R$. This process was repeated at the beginning of every time interval ($\Delta t$) in the calculation, and was quite successful in producing a smooth sequence of calculated $C_{1,1}$ values which almost exactly matched the experimental values.

The other values of $Q$ along the cell surface, $Q_{0,m}$, $m=2$, 3, etc., were set equal to $Q_{0,1}$ multiplied by a weighting factor. This weighting factor could be set by a subroutine which ensured that the calculated values of $C_{1,m}$ matched the measured (experimental) $OH^-$ concentration along the cell surface.

## References


Hope, A.B. 1965. Ionic relations of cells of *Chara australis*. X. Effects of bicarbonate ions on electrical properties. *Aust. J. Biol. Sci.* **18**:789

Kitasato, H. 1968. The influence of $H^+$ on the membrane potential and ion fluxes of *Nitella*. *J. Gen. Physiol.* **52**:60

Lucas, W.J. 1975*a*. Analysis of the diffusion symmetry developed by the alkaline and acid bands which form at the surface of *Chara corallina* cells. *J. Exp. Bot.* **26**:271

Lucas, W.J. 1975*b*. Photosynthetic fixation of $^{14}$carbon by internodal cells of *Chara corallina*. *J. Exp. Bot.* **26**:331

Lucas, W.J. 1975*c*. The influence of light intensity on the activation and operation of the hydroxyl efflux system of *Chara corallina*. *J. Exp. Bot.* **26**:347

Lucas, W.J. 1975*d*. Ionic relations of *Chara corallina*: Studies on transport of $HCO_3^-$, $OH^-$ and $H^+$ across the plasma membrane. Ph.D. Thesis. University of Adelaide, South Australia

Lucas, W.J. 1976. Plasmalemma transport of $HCO_3^-$ and $OH^-$ in *Chara corallina*: Non-antiporter systems. *J. Exp. Bot.* **27**:19

Lucas, W.J., Dainty, J. 1977. Spatial distribution of functional $OH^-$ carriers along a Characean internodal cell: Determined by the effect of cytochalasin B on $H^{14}CO_3^-$ assimilation. *J. Membrane Biol.* **32**:75

Lucas, W.J., Smith, F.A. 1973. The formation of alkaline and acid regions at the surface of *Chara corallina* cells. *J. Exp. Bot.* **24**:1

Lucas, W.J., Smith, F.A. 1976. Influence of irradiance on $H^+$ efflux and $Cl^-$ influx in *Chara corallina*: An investigation aimed at testing two $Cl^-$ transport models. *Aust. J. Plant Physiol.* **3**:1

Nishizaki, Y. 1968. Light-induced changes of bioelectric potentials in *Chara*. *Plant Cell Physiol.* **9**:377

Onsager, L. 1945. Theory and problems of liquid diffusion. *Ann. N.Y. Acad. Sci.* **46**:241

Richards, J.L., Hope, A.B. 1974. The role of protons in determining membrane electrical characteristics in *Chara corallina*. *J. Membrane Biol.* **16**:121

Robinson, R.A., Stokes, R.H. 1965. Electrolyte Solutions. Second edition, Butterworths, London

Saito, K., Senda, M. 1973. The light-dependent effect of external pH on the membrane potential of *Nitella*. *Plant Cell Physiol.* **14**:147

Saito, K., Senda, M. 1974. The electrogenic ion pump revealed by the external pH effect on the membrane potential of *Nitella*. Influences of external ions and electric current on the pH effect. *Plant Cell Physiol.* **15**:1007

Sirs, J.A. 1958. Electrometric stopped flow measurements of rapid reactions in solution: Part 2. Glass electrode pH measurements. *Trans. Faraday Soc.* **54**:207

Smith, F.A. 1970. The mechanism of chloride transport in Characean cells. *New Phytol.* **69**:903

Spanswick, R.M. 1972. Evidence for an electrogenic ion pump in *Nitella translucens*. I. The effects of pH, $K^+$, $Na^+$, light and temperature on the membrane potential and resistance. *Biochim. Biophys. Acta* **288**:73

Spanswick, R.M. 1974. Evidence for an electrogenic ion pump in *Nitella translucens*. II. Control of the light-stimulated component of the membrane potential. *Biochim. Biophys. Acta* **332**:387

Spear, D.G., Barr, J.K., Barr, C.E. 1969. Localization of hydrogen ion and chloride ion fluxes in *Nitella*. *J. Gen. Physiol.* **54**:397

Volkov, G.A. 1973. Bioelectrical response of the *Nitella flexilis* cell to illumination: A new possible state of plasmalemma in a plant cell. *Biochim. Biophys. Acta* **314**:83

Walker, N.A. 1962. Effect of light on the plasmalemma of *Chara* cells. *Annu. Rep. Div. Plant Ind. C.S.I.R.O.*, p. 80

Plant Physiol. (1978) 61, 487–493

# $HCO_3^-$ Influx across the Plasmalemma of *Chara corallina*[1]

## PHYSIOLOGICAL AND BIOPHYSICAL INFLUENCE OF 10 mM $K^+$

Received for publication September 21, 1977 and in revised form November 4, 1977

WILLIAM J. LUCAS
*Department of Botany, University of California, Davis, California 95616*
ROGER M. SPANSWICK
*Division of Biological Sciences, Cornell University, Ithaca, New York 14853*
JACK DAINTY
*Department of Botany, University of Toronto, Toronto, Ontario, M5S 1A1, Canada*

### ABSTRACT

**The effect of 10 mM $K^+$ on the $HCO_3^-$ influx in *Chara corallina* has been used to distinguish a $Ca^{2+}$-dependent membrane integrity site from the $HCO_3^-$ transport site which is also $Ca^{2+}$-dependent (Lucas and Dainty, Plant Physiology 1977 60: 862–867).**

**In the presence of 0.2 mM $Ca^{2+}$ at pH 9, 10 mM $K^+$ inhibits the $HCO_3^-$ influx and depolarizes the membrane potential. Inhibition of the $HCO_3^-$ influx may be prevented by raising the $Ca^{2+}$ concentration in the solution or by addition of $Mg^{2+}$, $Sr^{2+}$, or $Mn^{2+}$. Protection is also afforded by 20 mM $Na^+$ and $Cs^+$ but not by $Rb^+$ which acts as a weak analog of $K^+$ in producing inhibition of the $HCO_3^-$ influx and depolarization of the membrane potential. With the exception of $Na^+$, ions which prevent inhibition of the influx also prevent depolarization of the membrane potential.**

**Once inhibited by 10 mM $K^+$, $HCO_3^-$ transport cannot be restored by addition of $Ca^{2+}$, $Mg^{2+}$, or $Sr^{2+}$ in less than 3 hours. Addition of $Mn^{2+}$, however, results in a progressive restoration of the proportion of cells with influxes equal to the control value. $Mn^{2+}$ also produces an increase in the membrane potential with a sharp hyperpolarization occurring at a threshold of about −180 mv. This sudden recovery of the $HCO_3^-$ influx in individual cells contrasts with the gradual recovery observed when the $K^+$ concentration is reduced to 0.2 mM. Since $Mn^{2+}$ cannot substitute for $Ca^{2+}$ at the $HCO_3^-$ transport site, restoration of $HCO_3^-$ transport by $Mn^{2+}$ involving the membrane integrity site, as evidenced by the effect on the membrane potential and resistance, is clearly separate. The other divalent cations were able to restore $HCO_3^-$ transport if applied at a concentration of 2 mM for 14 hours.**

**The $OH^-$ efflux is also inhibited by 10 mM KCl. It is postulated that voltage dependency of the $OH^-$ or $HCO_3^-$ transport systems may account for the observed effects of 10 mM $K^+$ on the $HCO_3^-$ influx.**

The fresh water algal species *Chara corallina* can photosynthetically assimilate exogenous $HCO_3^-$ (6). The $HCO_3^-$ ion is transported across the plasmalemma and the subsequent fixation of this carbon results in the production of 1 $OH^-$ for each $CO_2$ molecule fixed. The $OH^-$ ions are exported from the cytoplasm via the active $OH^-$ transport system located in the plasmalemma of this species (7, 8).

The ability to assimilate $HCO_3^-$ can be impaired considerably by employing experimental solutions from which $Ca^{2+}$ has been excluded (9, 12). From the commencement of the $Ca^{2+}$-free treatment $HCO_3^-$ assimilation began to decrease steadily. The hydroxyl efflux pattern, which reflects the cellular control over $OH^-$ efflux, remained unaffected until cells had been exposed to $Ca^{2+}$-free solutions for a considerable period (36 hr). Kinetic experiments revealed that $Ca^{2+}$ removal from the membrane resulted in noncompetitive inhibition of $HCO_3^-$ assimilation. The $V_{max}$ was progressively reduced as the exposure period lengthened, but the apparent $K_m$ remained unaltered over a wide range of experimental conditions.

Based on these results we proposed that, in addition to controlling membrane integrity, $Ca^{2+}$ *per se* may be required as an integral component of the functional $HCO_3^-$ transport system of *C. corallina* (12).

Membrane integrity can also be influenced by other treatments; *e.g.* it has been suggested that $K^+$ can displace $Ca^{2+}$ from the $Ca^{2+}$-binding sites on the membrane surface (19, 20). Displacement of sufficient $Ca^{2+}$ would affect membrane structure and hence membrane integrity or permeability. In this respect it is of interest to note that $HCO_3^-$ assimilation, by internodal cells of *C. corallina*, can be drastically reduced by bathing cells in a solution which has a $K^+$ concentration greater than 2 to 3 mM (9). Under these conditions the $OH^-$ efflux pattern, established at the cell surface, closely resembled that observed when the integrity of the plasmalemma was affected by prolonged $Ca^{2+}$-free exposure (12).

Electrophysiological properties of the Characean membrane are also affected by these high $K^+$ concentrations. Following depolarization by 10 mM $K^+$, the Characean membrane appears to function as a $K^+$ electrode (18), *i.e.* beyond a critical $K^+$ concentration the membrane suddenly becomes quite permeable to $K^+$ ions.

We have recently demonstrated that when the plasmalemma is in the $K^+$-induced depolarized state $HCO_3^-$ ions still bind to their transporter with the same affinity (10). This implied that $K^+$ did not displace the $Ca^{2+}$ putatively involved in the activation of the $HCO_3^-$ transport system.

The present study was conducted to investigate further the relationship between membrane integrity and the proposed divalent cation requirement of the $HCO_3^-$ transport system (12). We have now shown that high concentrations of $Ca^{2+}$, $Mg^{2+}$, $Sr^{2+}$, and $Mn^{2+}$ can restore $HCO_3^-$ transport activity in the presence of high $K^+$ concentrations. Electrophysiological studies using these high divalent cation concentrations also revealed that the $K^+$-induced depolarization of the plasmalemma could be prevented, or reversed, by these ions. These results support the proposal that high $K^+$ concentrations affect the properties of the membrane by the displacement of $Ca^{2+}$.

In the presence of low $K^+$ concentrations (0.2 mM), $Mn^{2+}$ could not restore $HCO_3^-$ transport activity when $Ca^{2+}$ was eluted from the plasmalemma (12). The present results, however, indicate that

[1] This study was supported in part by National Research Council of Canada Grant A6459 to J. D. and National Science Foundation Grant BMS 75-15277 to R. M. S.

$Mn^{2+}$ can bind to the $Ca^{2+}$ site associated with the establishment of membrane integrity. Collectively, these results provide strong support for the hypothesis that $Ca^{2+}$ (or a divalent cation) is required at both the membrane integrity and $HCO_3^-$ transport sites.

## MATERIALS AND METHODS

**Culture Material.** Culture material of *C. corallina* Klein ex Willd., em. R.D.W. (=*C. australis* R. Br.) employed in $^{14}C$ experiments was grown in the laboratory (Toronto) in large plastic containers in solutions containing (mM): 1 to 2 $Na^+$, 0.2 $K^+$, 0.1 to 0.5 $Ca^{2+}$, 1 $Cl^-$, and approximately 2 $HCO_3^-$. Artificial fluorescent lighting was employed; the intensity at the solution surface was 17 w $m^{-2}$. Cells used for electrophysiological experiments (Cornell) were cultured under similar conditions; details concerning this culture medium have been described by Fischer *et al.* (1).

**General $NaH^{14}CO_3$ Experimental Sequence.** Bicarbonate influx was measured using the procedures detailed by Lucas (6) and Lucas and Dainty (13). Radioactive $NaH^{14}CO_3$ was obtained from New England Nuclear as a sterile aqueous solution, and aliquots were added to the experimental solutions to give the required specific radioactivity. *Chara* cells that were to be used in photosynthetic fixation experiments were given the following pretreatment. (*a*) Mature internodal cells were cut from the third to fifth internodal region and trimmed of whorl cells. (*b*) A 1-hr recovery period was employed after the cells had been cut. During this period cells were bathed in their respective culture solutions (20 C) and illuminated by fluorescent light (10 w $m^{-2}$). (*c*) Following the recovery period, cells were transferred to a pretreatment solution containing (mM) 1 NaCl, 0.2 KCl, 0.2 $CaSO_4$, and 1 $NaHCO_3$ (pH 9.2). Cell diameters and lengths were measured to compute individual cell surface areas. (*d*) A 12-hr dark (overnight) treatment in the above solution followed. (*e*) Unless otherwise specified, a 1-hr illumination period (10 w $m^{-2}$) was employed prior to the commencement of an experiment. (*f*) All experiments were conducted at 25 C, under a light intensity of 20 w $m^{-2}$. Under these conditions, the pretreatment and radioactive $H^{14}CO_3^-$ treatment were each of 1-hr duration, unless otherwise specified. Details of individual experimental treatments are specified in the text. Values are expressed as the mean ± SEM.

**pH Measurement of $OH^-$ Band Pattern.** The pH values along the cell surface of *C. corallina* internodal cells were measured using the technique developed by Lucas and Smith (14). Agar blocks that were used as embedding media for experimental cells were prepared in the manner described by Lucas and Dainty (13). Cells used in pH-scanning experiments were pretreated in the same manner as that detailed for photosynthetic experiments. Following insertion into its agar block, the *Chara* cell to be scanned was placed in the thermostatted (25 C) experimental solution (see ref. 14 for details of experimental chamber). Cells were illuminated (20 w $m^{-2}$) for 1 hr prior to conducting the pH scan. A Leitz micromanipulator was used to traverse a miniature pH electrode (Microelectrodes, Inc., model MI-405) along the cell wall. From the pH values obtained the pH pattern established was mapped.

**Electrophysiological Measurements.** Membrane potentials were measured using WPI model 750 amplifiers (WPI Instruments, New Haven, Conn.) and microelectrodes made from Omega Dot glass (Frederick Haer and Co., Ann Arbor, Mich.). The microelectrodes were filled with 3 M KCl, adjusted to pH 2 to reduce tip potentials (17).

Membrane resistances were measured using the single voltage probe method (2). This method is an approximation which is accurate only when the space constant, $\lambda$, is comparable with or larger than the half-length, $l$, of the internodal cell. ($\lambda$ is a measure of the attenuation of the voltage change induced along the cell in response to an imposed current pulse.) Because the membrane resistance of these cells in the light at high pH values is low, and hence $\lambda$ is small, it was necessary to use short cells (2–3 cm) for experiments in which resistance was to be measured. The very low resistances measured in the presence of 10 mM KCl may be slightly underestimated. Time courses for the membrane resistance were obtained by delivering a 4-sec current pulse (0.5 $\mu$amp) derived from a Pulsar 4I pulse generator (Frederick Haer and Co.) at 100-sec intervals. This current was passed between a microelectrode inserted at the center of the cell and a Ag/AgCl wire placed parallel to the cell in the external solution. The current-induced change in membrane potential was measured using a microelectrode inserted at a distance 0.42 $l$ from the current microelectrode. Using the measured voltage change and the known current, the membrane resistance may be calculated from Ohm's law and converted to specific resistance by multiplying by the surface area of the cell.

## RESULTS AND DISCUSSION

**Effect of Divalent Cation Concentration on the Inhibition of $HCO_3^-$ Influx by 10 mM $K^+$.** Tobias (20) and Tasaki (19) have suggested that $K^+$ can displace $Ca^{2+}$ from the fixed negative charges at the external surface of the plasma membrane. Displacement of sufficient $Ca^{2+}$, such that membrane integrity becomes affected, should depend upon the relative concentrations of $Ca^{2+}$ and $K^+$ in the vicinity of these negative binding sites.

Increasing the level of $Ca^{2+}$, in the presence of a fixed $K^+$ concentration, should eventually result in $Ca^{2+}$ saturation of these negative sites. Under this $Ca^{2+}$ concentration, the membrane integrity would be protected against the influence of the $K^+$ ions. Experiments of this nature, conducted on internodal cells of *C. corallina*, revealed that the $K^+$-induced inhibition of $HCO_3^-$ influx could be prevented by increasing the level of $Ca^{2+}$ in the experimental solution (Table I). As the concentration of $Ca^{2+}$ was increased, fewer cells lost the ability to assimilate exogenous $HCO_3^-$.

A similar protective effect was found when $Mg^{2+}$, $Sr^{2+}$, and $Mn^{2+}$ were employed. These results suggest that $Mg^{2+}$, $Sr^{2+}$, and $Mn^{2+}$ can bind to the putative $Ca^{2+}$ sites on the membrane surface, thereby maintaining the integrity of the plasmalemma. In $Ca^{2+}$-free experiments, $Mn^{2+}$ could not maintain $HCO_3^-$ influx by substituting for the $Ca^{2+}$ that was being eluted from the cell (12). The fact that $Mn^{2+}$ prevented the $K^+$-mediated inhibition of $HCO_3^-$ influx offers support for our hypothesis that two separate $Ca^{2+}$-binding sites are involved in the control of $HCO_3^-$ influx. The $Mn^{2+}$ results certainly suggest that 10 mM $K^+$ does not displace the $Ca^{2+}$ associated with the activation of the $HCO_3^-$ transport system.

**Protection Afforded by $Na^+$ Ions.** The possible protective influence of various NaCl concentrations was also investigated. Table II shows that the number of cells in which $HCO_3^-$ influx was inhibited, by 10 mM $K^+$, was reduced as the $Na^+$ level increased. The control experiments indicated that these high levels of $Na^+$ did not affect $HCO_3^-$ influx. At the concentrations employed, $Na^+$ ions did not appear to displace $Ca^{2+}$ from the membrane surface. Thus, when the concentration of $Na^+$ in the free space is high, these ions must tend to lower the effective $K^+$ concentration within the vicinity of the fixed negative charges. The probability that sufficient $Ca^{2+}$ will be displaced to influence membrane integrity will be diminished in consequence.

The reduced effectiveness of $Na^+$, when added as $Na_2SO_4$ (Table II), may reflect the influence of the double negative charge on the $SO_4^{2-}$ ion. In comparison to $Cl^-$, $SO_4^{2-}$ will be more strongly excluded from the negatively charged region of the cell wall. This anion exclusion will tend to lower the cation concentration within the free space. Experiments were also conducted using the organic cation choline$^+$. The fact that this cation offered the membrane almost no protection against the 10 mM $K^+$ (Table II)

Table I. 10 mM $K^+$ Inhibition of $HCO_3^-$ Influx: Protective Effect of Divalent Cations

| Total Divalent Cation Concn (mM)[1] | $H^{14}CO_3^-$ Influx (pmol $cm^{-2}$ $s^{-1}$) | | | | | | | |
|---|---|---|---|---|---|---|---|---|
| | $Ca^{2+}$ | | $Mg^{2+}$ | | $Sr^{2+}$ | | $Mn^{2+}$ | |
| | I[3] | N | I | N | I | N | I | N |
| 0.2 | 3.7±0.3(12) | ... | ... | | ... | | ... | |
| 0.5 | 4.4±0.3(11) | 30.9(1) | 4.6±1.2(10) | 27.3(2) | 3.04±1.0(9) | 35.8(3) | 4.6±0.8(5) | 30.3±2.4(7) |
| 1.0 | 3.9±1.0(9) | 33.1(3) | 4.2±1.8(7) | 27.4±1.5(5) | 3.4±0.9(8) | 33.4±3.0(4) | 8.1(2) | 35.7±1.8(10) |
| 1.5 | --(0) | 32.0±2.2(12) | 5.8±1.6(6) | 28.6±1.5(6) | --(0) | 31.8±1.9(12) | --(0) | 33.8±1.4(12) |
| 2.0 | 2.4(2) | 36.2±1.2(10) | 5.9(2) | 32.2±2.2(10) | --(0) | 31.9±1.6(12) | --(0) | 32.9±0.9(12) |
| 2.0[2] | | | ... | 31.4±1.5(12) | ... | 34.0±1.5(12) | ... | 31.5±0.8(12) |

[1] Experimental solutions contained 1.0 mM NaCl, 10 mM KCl, 0.5 mM $NaHCO_3$ (pH 9.1). All solutions contained 0.2 mM $CaSO_4$, the total divalent cation concentration was increased by addition of the respective cation as the chloride.
[2] Control $H^{14}CO_3^-$ influx values obtained using identical solutions except that the 10 mM KCl was replaced by 10 mM NaCl.
[3] Cellular response to 10 mM $K^+$ treatment is indicated by the symbol I for inhibited and N for normal $HCO_3^-$ influx. Twelve cells were used per treatment. The number of cells in which $H^{14}CO_3^-$ influx remained normal or was inhibited is indicated in parentheses.

Table II. Inhibition of $H^{14}CO_3^-$ Influx by 10 mM $K^+$: Protective Influence of $Na^+$ Ions

| Experimental Conditions | Control | 10 mM $K^+$ Treated Cells | |
|---|---|---|---|
| | | I | N |
| Basic Solution[1] | | 2.09±0.14 (12) | --(0) |
| 10 mM NaCl | 25.6±0.9[2] | 2.04±0.4 (9) | 23.8±(3) |
| 20 mM NaCl | 25.9±1.3 | 2.70 (1) | 26.0±2.5 (11) |
| 20 mM $Na^+$, as $Na_2SO_4$ | 25.2±1.4 | 1.70±0.3 (5) | 27.8±2.4 (7) |
| 2 mM Choline Chloride | 26.4±1.4 | 2.87±0.2 (11) | 25.2 (1) |
| 4 mM Choline$^+$ $Cl^-$ | ... | 2.22±0.3 (9) | 26.5 (3) |
| 6 mM Choline$^+$ $Cl^-$ | ... | 2.60±0.1 (12) | --(0) |
| 10 mM Choline$^+$ $Cl^-$ | ... | 2.53±0.2 (10) | 25.1 (2) |
| 20 mM Choline$^+$ $Cl^-$ | 25.7±1.2 | 2.70±0.3 (10) | 23.5 (2) |

[1] Solutions contained, unless indicated otherwise, (mM): 1.0 NaCl, 0.2 KCl, 0.5 $NaHCO_3$ (pH 9.1), 0.2 $CaSO_4$. In the $K^+$ experiments the level of KCl was 10 mM.
[2] $H^{14}CO_3^-$ influx (pmol $cm^{-2}$ $sec^{-1}$). Symbols I and N as defined in Table I.

Table III. Inhibition of $H^{14}CO_3^-$ Influx by 10 mM $K^+$: Protective Influence of Monovalent Cations

| Cation | 'Control' | | 10 mM $K^+$ Treated Cells | |
|---|---|---|---|---|
| | I | N | I | N |
| Basic solution[1] | --(0) | 23.9±0.9 (12) | 2.35±0.10 (12) | --(0) |
| 20 mM $Li^+$ | --(0) | 26.4±1.7 (12) | 2.03±0.11 (10) | 18.0 (2) |
| 20 mM $Na^+$ | --(0) | 26.4±1.4 (12) | 2.70 (1) | 26.0±2.5 (11) |
| 30 mM $Na^+$ | --(0) | 26.6±1.6 (12) | 1.50 (1) | 25.3±1.5 (11) |
| 10 mM $Rb^+$ | --(0) | 25.0±1.8 (12) | ... | ... |
| 20 mM $Rb^+$ | 1.7 (2) | 26.3±1.8 (10) | 3.51±0.32 (11) | 29.6 (1) |
| 30 mM $Rb^+$ | 2.42±0.12(10) | 27.9 (2) | ... | ... |
| 20 mM $Cs^+$ | --(0) | 25.9±1.9 (12) | --(0) | 25.2±1.3 (12) |

[1] The basic solution contained (mM): 0.5 $NaHCO_3$ (pH 9.1), 0.2 $CaSO_4$, 1.0 NaCl and 0.2 KCl. Other solutions contained the indicated cations, added as the chloride. All other conditions and details as described for Table I.

Table IV. Depolarization of the Membrane Potential by 10mM $K^+$: Protective Influence of Monovalent and Divalent Cations

| Cation | Control | | 10 mM $K^+$ Treated Cells | |
|---|---|---|---|---|
| | Depolarized | Hyperpolarized[1] | Depolarized | Hyperpolarized |
| Basic solution[2] | --(0) | -210±13(10)[3] | -76±7(9) | -208(1) |
| 2 mM $Ca^{2+}$ | --(0) | -182±13(10) | -67(3) | -202±8(7) |
| 2 mM $Sr^{2+}$ | --(0) | -225±9(10) | --(0) | -209±10(10) |
| 20 mM $Na^+$ | --(0) | -232±7(14) | -94±5(12) | -221(2) |
| 30 mM $Na^+$ | --(0) | -217±7(6) | -62±13(6) | --(0) |
| 20 mM $Cs^+$ | --(0) | -239±8(10) | --(0) | -191±8(10) |
| 10 mM $Rb^+$ plus 20 mM $Na^+$ | --(0) | -213±8(8) | | |
| 20 mM $Rb^+$ plus 10 mM $Na^+$ | -84±9(5) | -206(3) | | |
| 30 mM $Rb^+$ | -60±10(6) | -189(2) | | |

[1] Membrane potential in mV, values expressed as mean ± S.E.M. Numbers in parentheses represent the number of cells in each category.
[2] Basic solution as described in Table I, the indicated cationic additions were made using the chloride.
[3] Steady state membrane potential values obtained after approximately 90 min in the respective experimental solutions.

suggests that the size and/or charge density of the cation may be of importance.

**Influence of Monovalent Cations on 10 mM $K^+$ Effect.** The influence of the alkali metals, in terms of their prevention of the $K^+$-induced inhibition of $HCO_3^-$ influx, is illustrated by the results presented in Table III. With the exception of $Rb^+$, a correlation exists between the number of cells protected and the cationic radius. The smallest cation ($Li^+$) gave the weakest degree of protection, while $Cs^+$, being the largest cation employed, completely prevented the 10 mM $K^+$ inhibition.

The $Rb^+$ results are of special importance, since this cation has been employed extensively as a radioisotope analog for $K^+$. Although $Rb^+$ did cause the inhibition of $HCO_3^-$ influx (30 mM $Rb^+$, Table III), the concentration at which this occurred was approximately 10 times greater than the observed 3 mM $K^+$ threshold (9). In this example as an analog for $K^+$, $Rb^+$ appears to have a much lower affinity than $K^+$ for the negative binding sites on the membrane surface.

**Depolarization of the Membrane by 10 mM $K^+$.** Electrophysiological studies were performed on these cells to determine whether the membrane potential would respond to 10 mM $K^+$ in a similar manner to that observed for $HCO_3^-$ influx. Most cells depolarized when their membrane was exposed to 10 mM $K^+$ solutions (Table IV, basic solution). (The hyperpolarized state represents the normal state of the membrane, and the depolarized condition is when the membrane has become $K^+$-sensitive [4, 16, 18].) A similar $K^+$-induced depolarization of the plasmalemma in *Nitella translucens* was observed by Spanswick (18). In the presence of 2 mM $Ca^{2+}$ or $Sr^{2+}$ the membrane potential was prevented from depolarizing. These results are in excellent agreement with the observed protective influence of these divalent cations on $HCO_3^-$ influx (*cf.* Table I).

Of the monovalent cations investigated, only $Cs^+$ protected the membrane potential from depolarization by 10 mM $K^+$. The control values presented in Table IV indicate that 20 to 30 mM $Na^+$ did not perturb the membrane potential. However, we have no explanation as to why these high $Na^+$ levels did not protect the membrane potential as they did $HCO_3^-$ influx. Depolarization of the membrane potential was observed in the presence of 20 and 30 mM $Rb^+$ (Table IV). The similarity between the $Rb^+$-induced inhibition of $HCO_3^-$ influx and depolarization of the membrane potential offers support for the proposal that this ion functions as a weak analog for $K^+$.

The general agreement between the $HCO_3^-$ influx results and the membrane response to the various $K^+$ treatments adds further support to the hypothesis that $K^+$ mediates its effect via the displacement of membrane-bound $Ca^{2+}$.

**$K^+$-induced Inhibition of $HCO_3^-$ Influx: Effect of $HCO_3^-$ Concentration.** We demonstrated previously that increasing the $HCO_3^-$ concentration in the presence of 10 mM $K^+$ resulted in a linear increase in $HCO_3^-$ influx (9). We have now performed these experiments over a much wider $HCO_3^-$ concentration range; a linear response was similarly obtained (Fig. 1). This linear response suggests that in the presence of 10 mM $K^+$, $HCO_3^-$ assimilation may be rate-limited by a diffusive process. When the plasmalemma is depolarized to the $K^+$-sensitive state it is possible that the perturbation in membrane permeability (or integrity)

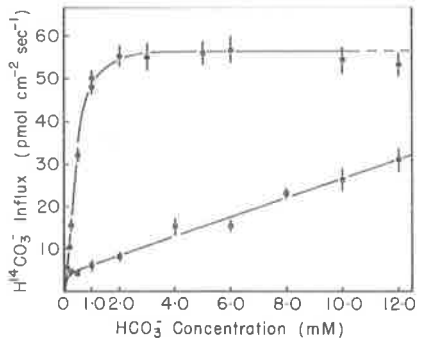


FIG. 1. Effect on $H^{14}CO_3^-$ influx of increasing $HCO_3^-$ concentration in the presence of 10 mM $K^+$. The $HCO_3^-$ was added as $NaHCO_3$ to reduce the level of $Na^+$ in the experimental solution. The control treatments (●) contained (mM): 1 NaCl, 0.2 KCl, 0.2 $CaSO_4$, and the indicated level of $NaHCO_3$ (pH 9). Potassium inhibition treatments (■) were identical except that the KCl was increased to 10 mM. Values are expressed as mean ± SEM; 12 cells were used per treatment.

deactivates the $HCO_3^-$ transport system. In the deactivated state this transport system may then act only as a facilitative diffusion system for $HCO_3^-$.

To maintain electrical neutrality, the influx of $HCO_3^-$ and the efflux of $OH^-$ ions, across the plasmalemma, must be balanced. Since the $HCO_3^-$ and $OH^-$ ions are transported across the plasmalemma on separate carriers (8), inhibition of the $OH^-$ efflux system results in a reduction of $HCO_3^-$ influx (11, 13). Thus, if the 10 mM $K^+$ treatment inhibited the $OH^-$ efflux system alone, a reduction in $HCO_3^-$ influx would still be observed. To investigate this possibility we examined the alkaline banding patterns established on the cell surface, in response to 10 mM $K^+$ and various $HCO_3^-$ concentrations. The perturbation of the $OH^-$ efflux pattern which occurred when cells were treated with 10 mM $K^+$ is typified by the results presented in Figure 2. Since the $OH^-$ and $HCO_3^-$ fluxes are balanced (5), the control $OH^-$ efflux pattern (Fig. 2) must represent an efflux of approximately 50 pmol cm$^{-2}$ sec$^{-1}$ (see Fig. 1, 1 mM $NaHCO_3$). When 10 mM $K^+$ was included in the solution, the measured pH values indicated a marked inhibition in $OH^-$ efflux. This pH pattern (●, Fig. 2) must represent an $OH^-$ efflux of approximately 4 to 5 pmol cm$^{-2}$ sec$^{-1}$ (see Fig. 1, 10 mM $K^+$ + 1 mM $NaHCO_3$). Increasing the $HCO_3^-$ concentration from 1 to 6 or 12 mM did not alter this $OH^-$ efflux pattern. The increased buffering capacity of the 6 and 12 mM $HCO_3^-$ solutions simply prevented the pH values at the cell surface from rising significantly.

The pH pattern established under the influence of 10 mM $K^+$ is very similar to that observed when cells have been exposed to $Ca^{2+}$-free solutions for prolonged periods (36–48 hr) (12). This suggests that both treatments may have a common effect, in that they both drastically modify the permeability (or integrity) of the membrane. From the results presented in Figures 1 and 2, we cannot say categorically which transport process acts as the rate-limiting step in the assimilation of $HCO_3^-$ (when cells have been treated with 10 mM $K^+$). Certainly the $OH^-$ efflux process could be reduced to operating as a facilitative diffusion system, but the same may also be true of the $HCO_3^-$ transport system.

**Restoration of $HCO_3^-$ Influx by Divalent Cations.** When cells were treated simultaneously with 10 mM $K^+$ and a divalent cation concentration of 2 mM, $HCO_3^-$ influx was not inhibited. However, when cells were treated initially (1 hr) with 10 mM $K^+$ and then transferred to 10 mM $K^+$ plus 2 mM divalent cations, $HCO_3^-$ influx was not restored when $Ca^{2+}$, $Mg^{2+}$, or $Sr^{2+}$ were employed (Table V).

An entirely different result was obtained when the influence of 2 mM $Mn^{2+}$ was investigated. As shown in Figure 3A, $Mn^{2+}$ induced an "all-or-none" transition from the inhibited back to the normal $HCO_3^-$ influx state. This response is in marked contrast to the smooth recovery pattern of $HCO_3^-$ influx observed following the removal of 10 mM $K^+$ from the experimental solution (Fig. 3B). The time course results presented in Figure 3A were obtained using 20-min radioactive $H^{14}CO_3^-$ exposure periods. The fact that intermediate $H^{14}CO_3^-$ influx values were not obtained suggested that the combination of 2 mM $Mn^{2+}$, in conjunction with the mechanical vibration of the cells which results during the change of solutions, was sufficient to initiate the recovery process. Once initiated, the recovery process must have returned cells to the normal state in a short period (2–3 min), otherwise a range of $H^{14}CO_3^-$ influx values would have been observed (*cf.* Fig. 3A).

The probability of initiating the recovery process spontaneously may be much lower when $Ca^{2+}$, $Mg^{2+}$, or $Sr^{2+}$ are employed. The 1- and 2-hr exposure periods employed in Table V may have been too short to allow the recovery of any cells. A 14-hr exposure to 2 mM $Ca^{2+}$, $Mg^{2+}$, or $Sr^{2+}$ (plus 10 mM $K^+$) resulted in a significant increase in the number of cells that exhibited normal $H^{14}CO_3^-$ influx values (Table VI). The probability of the recovery process occurring must depend upon the divalent cation concentration, because after 14 hr in the presence of 0.2 mM $Ca^{2+}$ no cells had recovered.

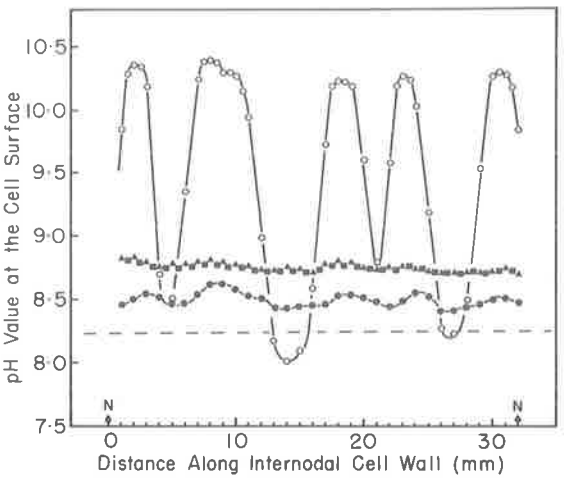


FIG. 2. Perturbation of $OH^-$ efflux activity by 10 mM $K^+$ treatment. The control experiment (○) was conducted in a solution containing 10 mM NaCl, 0.2 mM KCl, 0.2 mM $CaSO_4$, 1 mM $NaHCO_3$. Following the control scan (conducted after 1-hr illumination, 20 w m$^{-2}$), the cell was transferred to an identical solution except that it contained 1 mM NaCl and 10 mM KCl. The pH pattern established under these conditions was mapped after 1-hr illumination (●). The pH patterns established in the presence of 6 (▲) and 12 mM (■) $NaHCO_3$ (plus 10 mM $K^+$) were mapped in the same way. (The background pH value of the experimental solutions is represented by the horizontal broken line.)

Table V. Apparent Inability of Divalent Cations to Restore $HCO_3^-$ Influx Following Deactivation by 10 mM $K^+$

| Pre-treatment | Cation (mM) | $H^{14}CO_3^-$ Influx (pmol cm$^{-2}$ s$^{-1}$) A | B |
|---|---|---|---|
| Control[1] | $Ca^{2+}$(2.0) | 26.9±1.8 | 26.0±0.8 |
| 10 mM $K^+$ Treatment[2] | $Ca^{2+}$(0.2) | 2.69±0.17 | ... |
| | $Ca^{2+}$(2.0) | 2.98±0.24 | 3.77±0.33 |
| | $Mg^{2+}$(2.0) | 3.16±0.42 | 5.03±0.62 |
| | $Sr^{2+}$(2.0) | 5.31±0.32 | 6.50±0.78 |

[1] Control cells pre-treated (1 hr) in solutions containing 10 mM NaCl, 0.2 mM KCl, 2.0 mM $CaSO_4$, 0.5 mM $NaHCO_3$ (pH 9.1). $H^{14}CO_3^-$ influx measured after a further 1 hr (A) or 2 hr (B) illumination period. Experimental conditions were as in pre-treatment.

[2] Cells pre-treated (1 hr) in solutions containing 10 mM KCl, 1.0 mM NaCl, 0.2 mM $CaSO_4$, 0.5 mM $NaHCO_3$ (pH 9.1). Following pre-treatment, cells were transferred to solutions containing 10 mM KCl, 1.0 mM NaCl, 0.5 mM $NaHCO_3$ (pH 9.1) and the indicated concentration of the respective divalent cation (added as the chloride). $H^{14}CO_3^-$ influx was measured after 1 hr (A) and 2 hr (B) exposure to these solutions.

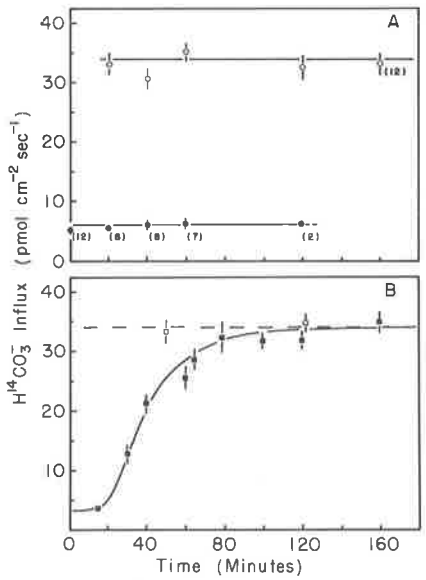


FIG. 3. Recovery of $H^{14}CO_3^-$ influx following the substitution of 10 mM $K^+$ plus 2 mM $Mn^{2+}$ (A) and 0.2 mM $K^+$ (B) solutions. Experimental cells were pretreated for 1 hr in 10 mM $K^+$ solutions (mM: 0.5 $NaHCO_3$ [pH 9.2], 1 NaCl, 0.2 $CaSO_4$, 10 KCl). They were then transferred to similar solutions, except that either 2 mM $MnCl_2$ was incorporated (A) or the KCl level was reduced to 0.2 (B, ■). (The symbol, □, represents control $H^{14}CO_3^-$ influx values obtained in the absence of a 10 mM $K^+$ pretreatment.) $H^{14}CO_3^-$ values were obtained using a 20-min radioactive exposure period. Twelve cells were used per treatment; the values in parentheses (A) indicate the number of cells in the inactive (●) and normal (○) influx states.

Table VI. Restoration of $H^{14}CO_3^-$ Influx by Divalent Cations

A 14 hr recovery period, in the respective solutions, was employed following 10 mM $K^+$ treatment (1 hr). Cells were illuminated (20 $Wm^{-2}$) during the 10 $K^+$ treatment, and for the initial 6 hr of the recovery period. At the 13 hr period cells were re-illuminated for 1 hr prior to measuring $H^{14}CO_3^-$ influx (20 min exposure).

| Divalent Cation (mM) | $H^{14}CO_3^-$ Influx (pmol $cm^{-2}$ $sec^{-1}$) | |
|---|---|---|
| | Inactive | Normal |
| Control[1] | --(0) | 34.5±1.8 (12) |
| $Ca^{2+}$ (0.2) | 4.08±0.48 (12) | --(0) |
| $Ca^{2+}$ (2.0) | 3.63 (3) | 34.9±2.9 (9) |
| $Mg^{2+}$ (2.0) | 2.30 (1) | 32.7±2.7 (11) |
| $Sr^{2+}$ (2.0) | 2.60 (1) | 32.5±1.3 (11) |

[1] Control solutions contained 1.0 mM NaCl, 0.2 mM KCl, 0.2 mM $CaSO_4$, 0.5 mM $NaHCO_3$ (pH 9.1). All other treatments were conducted in identical solutions, except that they contained 10 mM KCl, and the indicated concentrations of the respective divalent cations (added as the chloride).

**Membrane Potential Recovery in the Presence of 2 mM $Mn^{2+}$.** The influence of 2 mM $Mn^{2+}$ on the depolarized membrane was investigated to ascertain whether the membrane potential would exhibit a similar recovery phenomenon. After membrane depolarization by 10 mM $K^+$, cells were exposed to solutions that contained both 10 mM $K^+$ and 2 mM $Mn^{2+}$. The four traces presented in Figure 4 typify the membrane potential response to the $Mn^{2+}$ treatment. Complete recovery of the potential was observed in the eight cells studied. In the hyperpolarized state prior to depolarization by 10 mM $K^+$, the mean potential was −220 ± 9 mv and following the $Mn^{2+}$-induced recovery, the mean value was −225 ± 6 mv. The observed minimum and maximum recovery times were 48 and 100 min, respectively; this range is similar to that observed for the $Mn^{2+}$-mediated recovery of $HCO_3^-$ influx (Fig. 3A).

The most significant feature of the membrane potential response to 2 mM $Mn^{2+}$ was that once the value of the potential had risen to approximately −180 mv, the final rise was extremely rapid (Fig. 4). Mechanical vibration of the cell may in some way accelerate the initial rise in membrane potential to this −180 mv region. If this was the case, complete recovery would take only a few min. Unfortunately membrane resistance could not be measured during these $Mn^{2+}$ experiments, because the injection of current into the cell appeared to prevent the $Mn^{2+}$-induced recovery. Details of the changes in membrane resistance may have given us a clearer picture of the mode by which $Mn^{2+}$ effects this repolarization of the membrane.

**Recovery of $H^{14}CO_3^-$ Influx Induced by Mechanical Stimulation of the Cell.** Experiments were performed to test whether mechanically disturbing the internodal cells would increase the probability of initiating the recovery process. These experiments were similar to those described for Table V. When cells were left unperturbed, except for making the necessary solution changes, the $H^{14}CO_3^-$ influx values were identical to those presented in Table V and Figure 3A (see Table VII). However, when the experimental solutions were mixed at 5-min intervals, by gently inverting the experimental test tubes, the number of cells that exhibited normal $H^{14}CO_3^-$ influx values was greatly increased. This increase was observed for all divalent cations studied, but it was most pronounced in the presence of $Mn^{2+}$ and $Sr^{2+}$ (Table VII). The effect on $H^{14}CO_3^-$ influx of changing the 2 mM $Mn^{2+}$ solution, at 5-min intervals, is also presented in Table VII. This

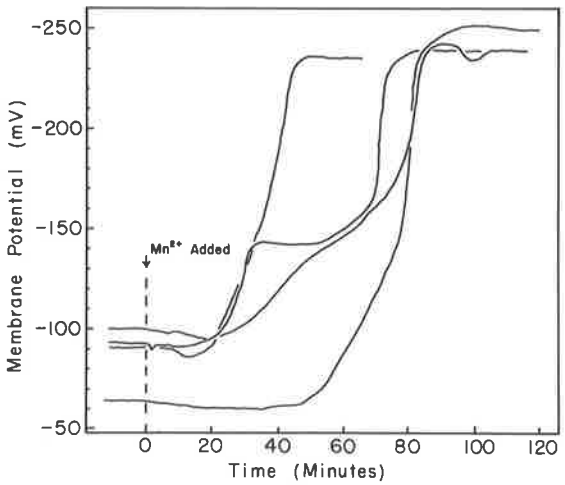


FIG. 4. Membrane potential repolarization in response to 2 mM $Mn^{2+}$. During electrode insertion cells were bathed in solutions containing (mM): 1 NaCl, 0.2 KCl, 0.2 $CaSO_4$, 0.5 $NaHCO_3$ (pH 9.1). After the membrane potential had stabilized, the KCl in the above solution was increased to 10 mM. When the membrane had depolarized and a new steady potential had been established, the 10 mM $K^+$ solution was modified to include 2 mM $Mn^{2+}$.

Table VII. $H^{14}CO_3^-$ Influx Recovery in the Presence of 2 mM Divalent Cations: Mechanical Induction

| Divalent Cation (2 mM) | Induction Treatment[2] | $H^{14}CO_3^-$ Influx (pmol $cm^{-2}$ $sec^{-1}$)[1] | |
|---|---|---|---|
| | | Inactive | Normal |
| $Mn^{2+}$ | U.P. | 7.01±0.9 (8) | 30.7±2.8 (4) |
| | C. | 6.00±0.9 (7) | 34.0±0.8 (5) |
| | M. | 7.03±0.8 (3) | 32.1±2.8 (9) |
| $Ca^{2+}$ | U.P. | 3.85±0.56(11) | 21.9 (1) |
| | M. | 2.94±0.27(9) | 32.9 (3) |
| $Mg^{2+}$ | M. | 3.58±0.35(9) | 30.9 (3) |
| $Sr^{2+}$ | U.P. | 4.28±0.38(12) | --(0) |
| | M. | 5.75±1.13 (6) | 35.9±2.5 (6) |

[1] All experiments were pre-treated for 1 hr in 10 mM $K^+$ solutions (1.0 mM NaCl, 0.2 mM $CaSO_4$, 0.5 mM $NaHCO_3$, pH 9.1 and 10 mM KCl). Cells were then transferred to identical solutions except they contained the respective divalent cation (2 mM, as the chloride).

[2] Treatments were as follows: U.P., unperturbed or stagnant experimental solution; C., solution changed at 5 min intervals for the initial 20 mins; M., solution mixed by gentle inversion of the test tube.

treatment must have been too severe, for it was less effective in restoring $HCO_3^-$ transport than the mild treatment of mixing the experimental solution by inverting the test tube.

**Recovery of $HCO_3^-$ Influx in the Presence of 0.2 mM $K^+$.** The results presented in Table VIII indicate that the recovery of $H^{14}CO_3^-$ influx, in 0.2 mM $K^+$ solutions, was not stimulated by increasing the level of $Ca^{2+}$ or $Mn^{2+}$. Substitution of 10 mM NaCl for the 10 mM KCl also had no effect on the rate of recovery. We also found that the recovery of $H^{14}CO_3^-$ influx could not be mechanically initiated after the 10 mM $K^+$ was replaced by 0.2 mM $K^+$. Similar values were obtained for all of these treatments (Table VIII); the values were consistent with those presented in Figure 3B (40-min recovery period).

This slow recovery of $H^{14}CO_3^-$ influx, observed in the presence of 0.2 mM $K^+$ and a high divalent cation concentration, was quite unexpected. Following the removal of 10 mM $K^+$, the negatively charged sites that are occupied by $K^+$ ions may become less accessible to the ions in the free space. This would account for the ineffectiveness of both the high divalent cation and mechanical perturbation treatments. It remains to be shown whether the recovery of $HCO_3^-$ influx, under these conditions, is limited by a much slower exchange of $Ca^{2+}$ for bound $K^+$, or whether metabolic repair to the membrane is also required (9).

**Membrane Potential, Resistance, and $H^{14}CO_3^-$ Influx: Recovery Under Light and Dark Conditions.** Figure 3B indicates that the reestablishment of normal rates of $H^{14}CO_3^-$ assimilation, following 10 mM $K^+$ treatment, requires approximately 60 to 80 min in 0.2 mM $K^+$ solutions. If this recovery is controlled by the slow exchange of $Ca^{2+}$ for bound $K^+$, the ability to transport $HCO_3^-$ should be reestablished in the dark.

Bicarbonate uptake experiments were performed on cells that had been dark-pretreated initially in 10 mM $K^+$ (1 hr), followed by 1 hr in 0.2 mM $K^+$ solutions. These cells took approximately 50 min to establish linear uptake (data not shown). This value is longer than the 10 min required by the control cells (2-hr dark pretreatment in 0.2 mM $K^+$). These results suggest, therefore, that membrane recovery proceeds at a much slower rate in the dark.

The recovery of membrane potential and resistance, from 10 mM $K^+$ treatment, was also investigated under light and dark conditions. In the light, the recovery of both membrane potential and resistance appeared to require approximately 60 to 80 min (Fig. 5A) before the values approached those of the controls (246 ± 9 mv, 17.3 ± 3.1 kΩ $cm^2$). This time scale is similar to that required for the full recovery of $H^{14}CO_3^-$ influx (*cf.* Fig. 3B). A shorter period (approximately 30–40 min) was required when these experiments were performed in the dark (Fig. 5B). (The higher potential and lower resistance values recorded in the light are in agreement with the previously reported influence of light on the Characean membrane [3, 15, 18].)

Since the electrical properties are reestablished in the dark, it would seem that the $HCO_3^-$ and/or $OH^-$ transport system(s) require(s) light for complete reactivation. Further studies will be required to determine the nature of this light requirement.

Table VIII. Recovery of $H^{14}CO_3^-$ Influx Following the Removal of 10 mM $K^+$ from the Experimental Solution

| Recovery solution | Induction[1] treatment | $H^{14}CO_3^-$ Influx[2] (pmol $cm^{-2}$ $sec^{-1}$) |
|---|---|---|
| Basic solution contained (mM) 0.5 $HCO_3^-$, pH 9.1, 0.2 KCl, 0.2 $CaSO_4$ plus: | | |
| 1.0 NaCl | U.P. | 21.3±1.9(12) |
| 1.0 NaCl + 2.0 $CaCl_2$ | U.P. | 21.7±2.1(12) |
| 10 NaCl + 2.0 $CaCl_2$ | M. | 18.7±1.5(12) |
| 1.0 NaCl + 2.0 $MnCl_2$ | U.P. | 19.1±1.6(12) |
| 10 NaCl + 2.0 $MnCl_2$ | U.P. | 20.0±1.5(12) 18.8±1.9(12) |
| 10 NaCl + 2.0 $MnCl_2$ | M. | 22.5±1.7(12) |

[1] Induction treatments as described in Table VII.
[2] Cells were treated for 1 hr in 10 mM $K^+$ solutions (mM: 1.0 NaCl, 0.2 $CaSO_4$, 10 KCl, 0.5 $NaHCO_3$, pH 9.1) and then transferred to their respective recovery solutions. For the initial 20 min of the recovery period the cells were bathed in non-radioactive solutions. $H^{14}CO_3^-$ influx was measured over the 20-40 min recovery period.

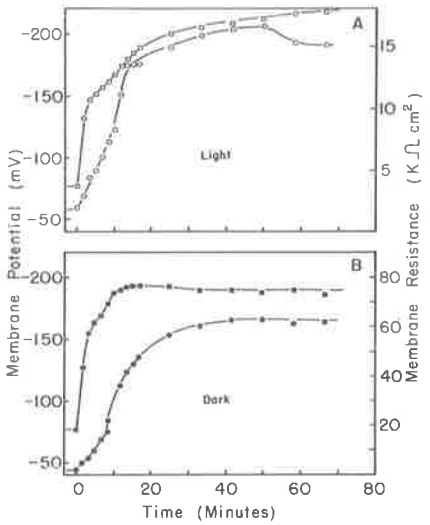


FIG. 5. Recovery of membrane potential and resistance following the transfer of cells from 10 to 0.2 mM $K^+$ solutions. Cells were pretreated in 10 mM $K^+$ solutions in the light (A), and the dark (B), for 1 hr before being transferred to 0.2 mM $K^+$ solutions. (The $K^+$ solutions were identical to those described in Fig. 5.) The membrane potential (□) and resistance (○) values in the light are the means obtained using 10 cells. The values in the dark (■, potential; ●, resistance) were obtained using five cells. (Note the difference in membrane resistance scales between light and dark treatments.)

## CONCLUSIONS

The strong correlation between the $K^+$-induced inhibition of $HCO_3^-$ influx and depolarization of the membrane, and their similar, paralleled protection and recovery responses, when treated with various mono- and divalent cations, suggests that in the presence of 10 mM $K^+$ both $HCO_3^-$ influx and the electrical properties of the membrane are affected by a common event. We consider this event to be the loss of membrane integrity, which results when $K^+$ displaces a critical amount of bound $Ca^{2+}$ from the plasmalemma.

Our most pertinent result was the discovery that $Mn^{2+}$ could protect, and reverse, the effect of 10 mM $K^+$ on both $HCO_3^-$ influx and membrane potential. It would appear, therefore, that $Mn^{2+}$ can bind to the $Ca^{2+}$ site associated with the maintenance of membrane integrity (*i.e.* $Ca^{2+}$ site [2] proposed by Lucas and Dainty [12]). Since Lucas and Dainty (12) demonstrated that $Mn^{2+}$ could not substitute for the $Ca^{2+}$ ions putatively involved in establishing the activation of the $HCO_3^-$ transport system, our present results offer strong support for the hypothesis that for normal $HCO_3^-$ influx to occur, $Ca^{2+}$ ions are required at both the membrane integrity and $HCO_3^-$ transport sites.

Finally, on a speculative note, perhaps the relationship between the final rapid recovery phase of the membrane potential and the all-or-none phenomenon of $HCO_3^-$ influx recovery (both observed in the presence of 2 mM $Mn^{2+}$) is that either (or both) $HCO_3^-$ or $OH^-$ transport may be voltage-dependent. This possibility will be investigated in a future study.

### LITERATURE CITED

1. FISCHER RA, J DAINTY, MT TYREE 1974 A quantitative investigation of symplasmic transport in *Chara corallina*. I. Ultrastructure of the nodal complex cell walls. Can J Bot 52: 1209–1214
2. HOGG J, EJ WILLIAMS, RJ JOHNSTON 1968 A simplified method for measuring membrane resistances in *Nitella translucens*. Biochim Biophys Acta 150: 518–520
3. HOPE AB 1965 Ionic relations of cells of *Chara australis*. X. Effects of bicarbonate ions on electrical properties. Aust J Biol Sci 18: 789–801

4. KITASATO H 1968 The influence of $H^+$ on the membrane potential and ion fluxes of *Nitella*. J Gen Physiol 52: 60–87
5. LUCAS WJ 1975 Analysis of the diffusion symmetry developed by the alkaline and acid bands which form at the surface of *Chara corallina* cells. J Exp Bot 26: 271–286
6. LUCAS WJ 1975 Photosynthetic fixation of $^{14}$carbon by internodal cells of *Chara corallina*. J Exp Bot 26: 331–346
7. LUCAS WJ 1975 The influence of light intensity on the activation and operation of the hydroxyl efflux system of *Chara corallina*. J Exp Bot 26: 347–360
8. LUCAS WJ 1976 Plasmalemma transport of $HCO_3^-$ and $OH^-$ in *Chara corallina*: non-antiporter systems. J Exp Bot 27: 19–31
9. LUCAS WJ 1976 The influence of $Ca^{2+}$ and $K^+$ on $H^{14}CO_3^-$ influx in internodal cells of *Chara corallina*. J Exp Bot 27: 32–42
10. LUCAS WJ 1977 Analogue inhibition of the active $HCO_3^-$ transport site in the Characean plasma membrane. J Exp Bot. In press
11. LUCAS WJ 1977 Plasmalemma transport of $HCO_3^-$ and $OH^-$ in *Chara corallina*: inhibitory effect of ammonium sulphate. J Exp Bot. In press
12. LUCAS WJ, J DAINTY 1977 $HCO_3^-$ influx across the plasmalemma of *Chara corallina*: divalent cation requirement. Plant Physiol 60: 862–867
13. LUCAS WJ, J DAINTY 1977 Spatial distribution of functional $OH^-$ carriers along a Characean internodal cell: determined by the effect of cytochalasin B on $H^{14}CO_3^-$ assimilation. J Membr Biol 32: 75–92
14. LUCAS WJ, FA SMITH 1973 The formation of alkaline and acid regions at the surface of *Chara corallina* cells. J Exp Bot 24: 1–14
15. NISHIZAKI Y 1968 Light-induced changes of bioelectric potential in *Chara*. Plant Cell Physiol 9: 377–387
16. ODA K 1962 Polarized and depolarized states of the membrane in *Chara braunii*, with special reference to the transition between the two states. Sci Rep Tohoku Univ Ser IV (Biol) 28: 1–16
17. OKADA Y, A INOUYE 1975 Tip potential and fixed charges on the glass wall of microelectrode. Experimentia 31: 545–546
18. SPANSWICK RM 1972 Evidence for an electrogenic ion pump in *Nitella translucens*. I. The effects of pH, $K^+$, $Na^+$, light and temperature on the membrane potential and resistance. Biochim Biophys Acta 288: 73–89
19. TASAKI I 1968 Nerve Excitation. Charles C Thomas, Springfield Ill
20. TOBIAS JM 1964 A chemically specified molecular mechanism underlying excitation in nerve: a hypothesis. Nature 203: 13–17

*Journal of Experimental Botany, Vol. 29, No. 113, pp. 1409–1421, December 1978*

# Characterization of Photosynthetic $^{14}$Carbon Assimilation by *Potamogeton lucens* L.

W. J. LUCAS

*Department of Botany, University of California, Davis, California 95616, U.S.A.*

AND

M. T. TYREE AND A. PETROV

*Department of Botany, University of Toronto, Toronto, Ontario, Canada M5S 1A1*

Received 4 April 1978

## ABSTRACT

Photosynthetic assimilation of exogenous $^{14}CO_2$ and $H^{14}CO_3^-$ by the aquatic angiosperm *Potamogeton lucens* L. is reported. Equivalent maximum rates of assimilation (1·5 $\mu$mol $s^{-1}$ $m^{-2}$) were obtained in the presence of saturating levels of $^{14}CO_2$ (1·0 mol $m^{-3}$, pH 5·3) or $H^{14}CO_3^-$ (1·5 mol $m^{-3}$, pH, 9·2). Under subsaturating $^{14}CO_2$ levels, both gaseous diffusion and $H^{14}CO_3^-$ transport were shown to operate simultaneously, such that maximal photosynthetic rates were established.

An induction lag of approximately 3 min was observed when exogenous $^{14}CO_2$ was assimilated. A longer lag of approximately 12 min was required, however, before linear assimilation rates were established when $H^{14}CO_3^-$ acted as the carbon source. The light-activated $H^{14}CO_3^-$ transport system was found to be quite labile. A brief (5 min) dark treatment returned the system to the inactive state.

Bicarbonate transport was shown to be competitively inhibited by $CO_3^{2-}$ ions. The possibility is discussed that this form of inhibition may be common to many $HCO_3^-$ assimilators.

Preliminary polar cation transport studies (from lower to upper leaf surface) indicated an almost exact one to one relationship between the rates of $Na^+$ influx and efflux and $H^{14}CO_3^-$ assimilation. The possible relationship(s) between these transport processes and the requirement for electrical neutrality is briefly discussed.

## INTRODUCTION

An extensive literature exists pertaining to the ability, or inability of aquatic plants to photosynthetically assimilate exogenous $HCO_3^-$ (see e.g. Steemann Nielsen, 1947, 1960; Österlind, 1949; Raven, 1970). One of the early species to be studied was the aquatic angiosperm *Potamogeton lucens*. The initial studies of Arens (1933, 1936), and the later more rigorous experiments of Steemann Nielsen (1947), indicated that this species could photosynthetically assimilate exogenous $HCO_3^-$. Although there is a slight discrepancy in the literature, the results of these workers revealed that leaves of *P. lucens* can acquire exogenous $HCO_3^-$ from only the lower surface.

Photosynthetic fixation of the carbon supplied by $HCO_3^-$ results in the production of one $OH^-$ for each $HCO_3^-$ converted to $CO_2$. These $OH^-$ ions are exported from the cells that form the upper surface of the leaf (Steemann Nielsen, 1947). (Similar examples of spatially separate $HCO_3^-$ and $OH^-$ transporting sites have been demonstrated in *Elodea* (Arens, 1938; Ruttner, 1947), *Vallisneria* (Ruttner, 1947), and *Myriophyllum* (Steemann Nielsen, 1947).)

It has also been shown that polar cation transport occurs across the leaves of *P. lucens* (i.e. cation transport from the lower to the upper leaf surface) during assimilation of exogenous $HCO_3^-$ (Arens, 1933; Steemann Nielsen, 1947; Helder and Boerma, 1972, 1973). This phenomenon of polar cation transport is light-mediated and exhibits a specific requirement for the presence of $HCO_3^-$ at the lower-leaf surface (Helder and Boerma, 1972).

Numerous hypotheses have been presented regarding the nature and inter-relationship(s) between the $HCO_3^-$, $OH^-$, and polar cation fluxes. Serious disagreement exists, however, between the various proposals. Steemann Nielsen (1947, 1960) proposed that $HCO_3^-$ entry was passive. He considered the active process associated with $HCO_3^-$ assimilation to be the excretion of $OH^-$ ions from the upper leaf surface. The cationic fluxes which were observed during $HCO_3^-$ assimilation were assumed to be passive (Arens, 1936; Steemann Nielsen, 1947). In contrast, Lowenhaupt (1956, 1958) suggested that it was the polar cation transport process that was active. Helder and Boerma (1972) supported this proposal. In addition, they suggested that the polarity observed in relation to the fluxes of $HCO_3^-$ and $OH^-$ may result from a difference in specific anion permeability between the lower and upper layers of the leaf tissue. Helder (1975*a*, *b*) later suggested that the polar cation fluxes may result from either a cation pump, or via some form of coupling to the transport of $HCO_3^-$ or $OH^-$ ions.

Obviously, to resolve the exact relationship between these various fluxes, a complete characterization of both the $HCO_3^-$ assimilation and polar cation transport systems will be required. This paper presents the results of a study aimed at elucidating the operational characteristics of $HCO_3^-$ assimilation in *P. lucens*.

## MATERIALS AND METHODS

### *Culture material and conditions*

Plant material of *Potamogeton lucens* L. was obtained from Dr. R. J. Helder (Biology Centre, University of Groningen, The Netherlands). Shoots were planted in a sandy loam soil and tap water was used as the basic culture medium (see Table 1). Sodium bicarbonate was added to ensure an initial minimum concentration of 2 mol $m^{-3}$ (= 2 mM, pH 8·3).

The main culture was established in a large concrete tank (volume approx. 1·5 $m^3$). This tank was located inside the departmental greenhouse. Shading at this site resulted in low incident radiation provided by sunlight. The summer midday irradiance was less than 100 W $m^{-2}$ at the water surface. Plant morphology was found to alter in response to this low irradiance level. The internodal distance increased from 30–60 mm to 100–150 mm, and the few totally submerged leaves were much smaller than the surface leaves. A much closer morphological correlation existed between the surface leaves and leaves observed under field conditions. Only larger surface leaves were employed during the initial experiments.

A supplementary light source (mercury halide lamp) was employed during the latter stages of the project. This provided an irradiance of 250 W $m^{-2}$ and the illumination period was from 0600 to 2230. Under these conditions plants returned to their normal morphology. For both lighting conditions the summer temperature of the culture remained at approximately 18–20 °C.

TABLE 1. Potamogeton lucens *L. culture conditions*

| Culture | Ionic composition[a] (mol $m^{-3}$) | | | | | |
|---|---|---|---|---|---|---|
| | $Na^+$ | $K^+$ | $Ca^{2+}$ | $Cl^-$ | $HCO_3^-$ | pH |
| Main culture inside greenhouse | 0·88 | 0·10 | 0·44 | 1·3 | 1·80 | 8·2–8·3 |
| Smaller culture outside (full sunlight) | 1·65 | 0·54 | 0·56 | 1·3 | 1·85 | 8·2–8·3 |

[a] Only the ions listed were monitored. Cations were measured using a Unicam SP 191 atomic absorption spectrophotometer, $Cl^-$ was determined by electrometric titration, and $HCO_3^-$ by pH titration.

A second smaller culture (volume 59 l) was established in the outside area of the greenhouse complex. During the summer these plants received direct sunlight from 1000 to approx. 1730. Although the pH value remained almost constant at 8·2, the temperature fluctuated from 20–25 °C (night) to 30–35 °C (midday).

Even though the plants in the second culture site received direct sunlight, the plant morphology was different from that found in nature. The internodal distance was typical (30–60 mm), but the leaf size was smaller (10–20 mm wide and 40–50 mm long). This influence on leaf size may have resulted from the limited culture volume or the temperature fluctuations.

### *$^{14}C$ assimilation experiments*

Measurements of assimilation rates under exogenous $CO_2$ and $HCO_3^-$ were performed using $^{14}C$. Radioactive $NaH^{14}CO_3$ was obtained from New England Nuclear, Boston, as a sterile aqueous solution. The experimental $^{14}C$ procedures of Lucas (1975*a*, *b*) and Lucas and Dainty (1977) were adopted. Experimental solutions were prepared using steam-distilled water, and all chemicals were of Analar Reagent grade. All experiments were performed at 20 °C, under a light intensity of 30–35 W $m^{-2}$. (A Leitz pradovit projector (24 V, 150 W Quartz-Iodide) was used as a light source; the intensity was attenuated using nickel–nicron neutral density filters.)

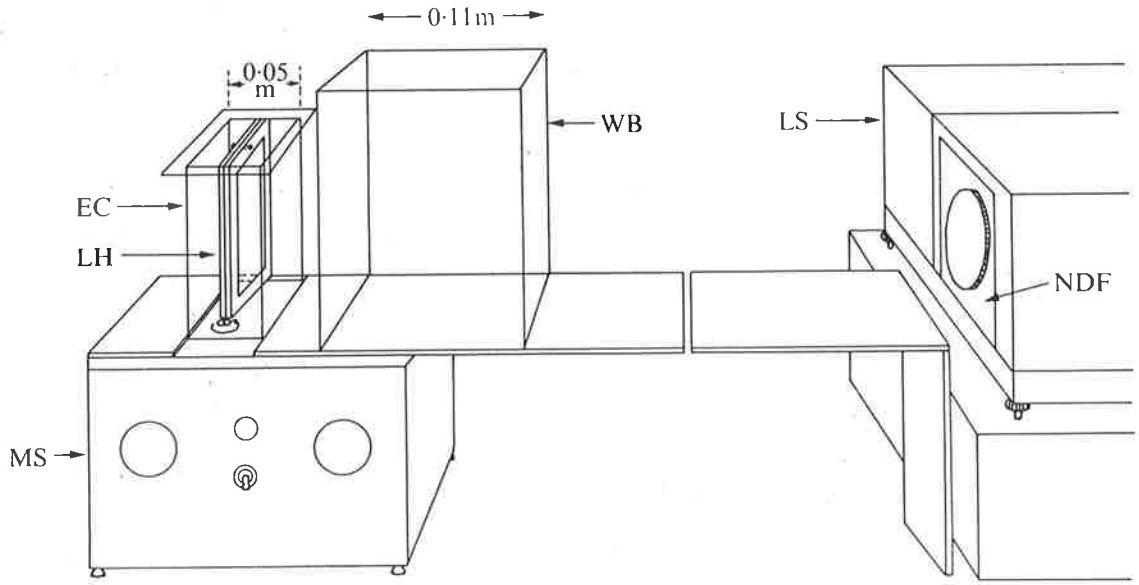


FIG. 1. Schematic diagram of experimental system used for photosynthetic $^{14}C$ measurements on leaves of *Potamogeton lucens*. In these experiments excised leaves were held in a centrally located perspex holder such that both leaf surfaces were exposed to the radioactive solution. Vigorous stirring ensured that a uniform $^{14}C$ concentration existed within this system. Abbreviations: EC, experimental chamber; LH, leaf holder; LS, light source (Leitz–Pradovit 24 V, 150 W quartz–iodide projector); MS, magnetic stirring system; NDF, nickel–nicron neutral density filters; WB, water bath to remove infrared component.

Bicarbonate assimilation experiments were performed at pH 9·1 ± 0·1, the pH value being adjusted with either 10 mol $m^{-3}$ or 100 mol $m^{-3}$ $H_2SO_4$. Although both leaf surfaces were in contact with $H^{14}CO_3^-$, it was assumed that this ion was transported across only the lower leaf surface. Thus all $H^{14}CO_3^-$ fluxes are expressed on the basis of lower leaf surface area. For $^{14}CO_2$ experiments, the pH value was adjusted to 5·2 ± 0·1 using 2–5 mol $m^{-3}$ MES buffer and 10 mol $m^{-3}$ $H_2SO_4$. In all experiments, except those presented in Fig. 5, $^{14}CO_2$ fluxes were calculated assuming that $CO_2$ could enter through both leaf surfaces. For experiments performed within the pH range 7·0–8·5, TES buffer was used to titrate the solutions to the required pH value. For experiments reported in this paper, the only cation *added* to the solution was $Na^+$, added as $Na_2CO_3$.

Before being placed in the experimental chamber (see Fig. 1), leaves were washed several times to remove epiphytic algae and $CaCO_3$ deposits. A dark pretreatment period (30–45 min) was used for all experiments. Subsequent light pretreatment periods of 1–2 h and 2–3 h were employed for $^{14}CO_2$ and $H^{14}CO_3^-$ experiments, respectively. Except for time course experiments, a 45 min radioactive exposure period was always employed. At the conclusion of experiments, leaves were washed with non-radioactive solution for 5 min. Planchets, containing leaf discs of known surface area, were treated with 5 × $10^{-7}$ $m^3$ of 100 mol $m^{-3}$ propionic acid to remove unfixed $^{14}CO_2$ and $Ca^{14}CO_3$ that may have precipitated in the cell wall. After 12 h acidification, planchets were dried and activity counted (using a Nuclear–Chicago gas slow system) to determine the rate of $^{14}C$ assimilation. No fewer than 3 leaves were used per treatment, 5–10 leaves being used in most cases. Results are expressed as mean ± s.e. mean.

*Polar cation transport*

Polar cation transport experiments were performed using the apparatus and techniques described by Helder and Boerma (1972, 1973). For these experiments $10^{-5}$ ml $m^3$ of the required $NaHCO_3$ solution (pH 9·2) was placed on each side of the leaf. (These solutions were prepared in the same manner as that described for $^{14}C$ experiments.) Following a 3 h light pretreatment, fresh solutions were placed in the chambers. These solutions were replaced after 45 min and the eluted solutions analysed for their cationic content. All cation analyses were performed using a Unicam SP191 atomic absorption spectrophotometer.

## RESULTS

### *Preliminary experiments*

Despite the morphological differences observed between plants growing at the two culture locations, their chlorophyll content was very similar (see Table 2). Consequently, we feel it justifiable to express photosynthetic rates based on leaf surface area.

Experiments were performed to determine whether the direction of illumination had any influence on the rate of $HCO_3^-$ assimilation. We found similar rates, irrespective of which leaf surface was being illuminated (date not shown). This finding is in agreement with the earlier results on polar cation transport (Arens, 1936; Steemann Nielsen, 1947; Helder and Boerma, 1972).

TABLE 2. *A comparison of chlorophyll levels determined on leaves of* Potamogeton lucens *obtained from two culture locations*

| Culture | Natural sunlight | | Artificial lighting |
|---|---|---|---|
| | Summer | Winter | Summer |
| Main culture inside greenhouse | 190 ± 0·3[a] | — | 194 ± 0·4 |
| Small culture outside area | 177 ± 0·1 | 189 ± 1 | — |

[a] Values were determined using the techniques of Arnon (1949) and are quoted as mean ± s.e. mean (mmol total chlorophyll $m^{-2}$)

TABLE 3. *Comparison of $H^{14}CO_3^-$ influx values obtained using leaf samples that included and excluded the midrib vein*

All experiments were performed at 32 ± 2 W $m^{-2}$ and pH 9·2, using a 2–3 h light pretreatment period.

| $H^{14}CO_3^-$ influx ($\mu$mol $s^{-1}$ $m^{-2}$) | | $HCO_3^-$ concentration (mol $m^{-3}$) |
|---|---|---|
| Vein included | Vein excluded | |
| 0·25 | 0·27 ± 0·06 | 0·25 |
| 0·79 | 0·74 ± 0·08 | 0·75 |
| 1·38 | 1·36 ± 0·12 | 1·50 |
| 1·46 | 1·43 ± 0·03 | 2·5 |
| 1·22 | 1·26 ± 0·04 | 5·0 |

In order to obtain the maximum number of subsamples from each experimental leaf, it was sometimes necessary to include part of the prominent midrib. Experiments were performed to compare $H^{14}CO_3^-$ influx over equal subsample areas in which this vein was either present or absent. Typical results are presented

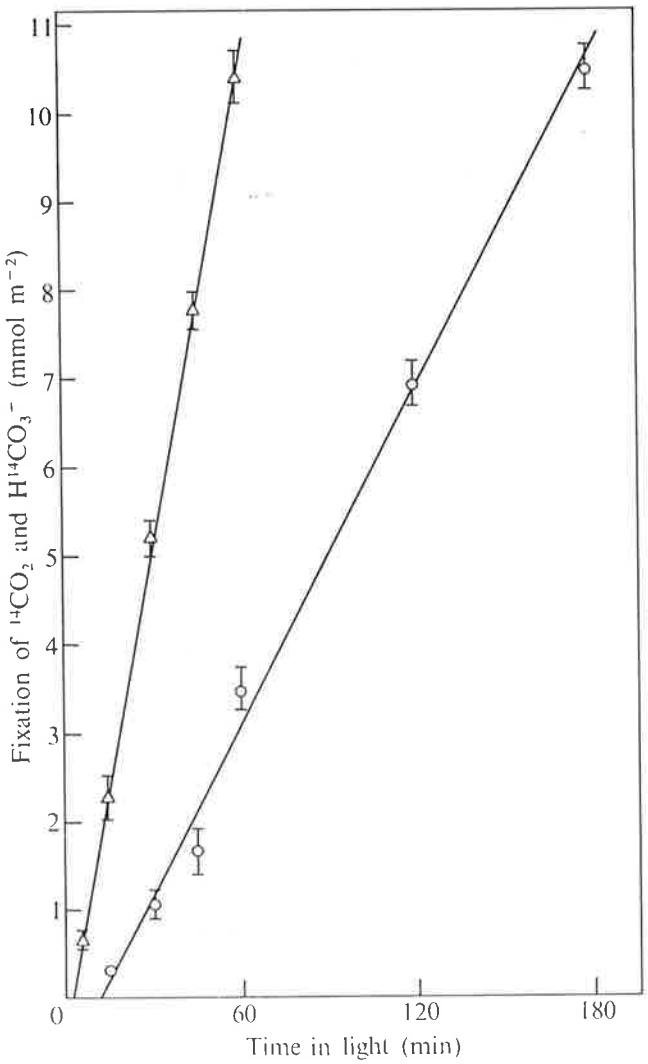


FIG. 2. Time course of $^{14}C$ fixation. Experiments performed in presence of 1·0 mol $m^{-3}$ total carbon; △, $^{14}CO_4$ (pH 5·2); ○, $H^{14}CO_3^-$ (pH 9·1).

in Table 3, and they demonstrate that the midrib vein had no discernible effect on $H^{14}CO_3^-$ influx.

*Time course of $^{14}C$ fixation*

Activation time-course experiments were performed to determine whether there was a lag between the onset of illumination and the establishment of the steady state rate of photosynthetic assimilation. In these experiments, leaves were cut 12 h prior to the $^{14}C$ treatment and they were stored, in the dark, in filtered culture solution. Following a 30–40 min dark pretreatment in non-radioactive solutions (1·0 mol $m^{-3}$ total carbon), leaves were simultaneously illuminated and exposed to their respective $^{14}C$ solutions. The results of this study are presented in Fig. 2. In the presence of exogenous $^{14}CO_2$, a lag of approximately 3 min was observed. When leaves were exposed to exogenous $H^{14}CO_3^-$, this lag was increased to approximately 12 min. The dark-induced deactivation of the $H^{14}CO_3^-$ assimilation system was also examined. Following a 12 h dark pretreatment, leaves were illuminated for 2–3 h to fully activate $HCO_3^-$ assimilation. Prescribed dark periods were then administered, after which leaves were simultaneously illuminated and exposed to $H^{14}CO_3^-$ solutions for 15 min. The results of these experiments are presented in Fig. 3. The dashed line represents the response of control leaves that were given 15 min $H^{14}CO_3^-$ exposure immediately after the 12 h dark pretreatment. From Fig. 3 it can be seen that a dark period of only 5 min was sufficient to completely deactive the $HCO_3^-$ assimilating system. During the first 30 min of darkness, not only was the $H^{14}CO_3^-$ assimilating system deactivated, but its reactivation also appeared to be suppressed to a fraction of 0·7 × the control. This

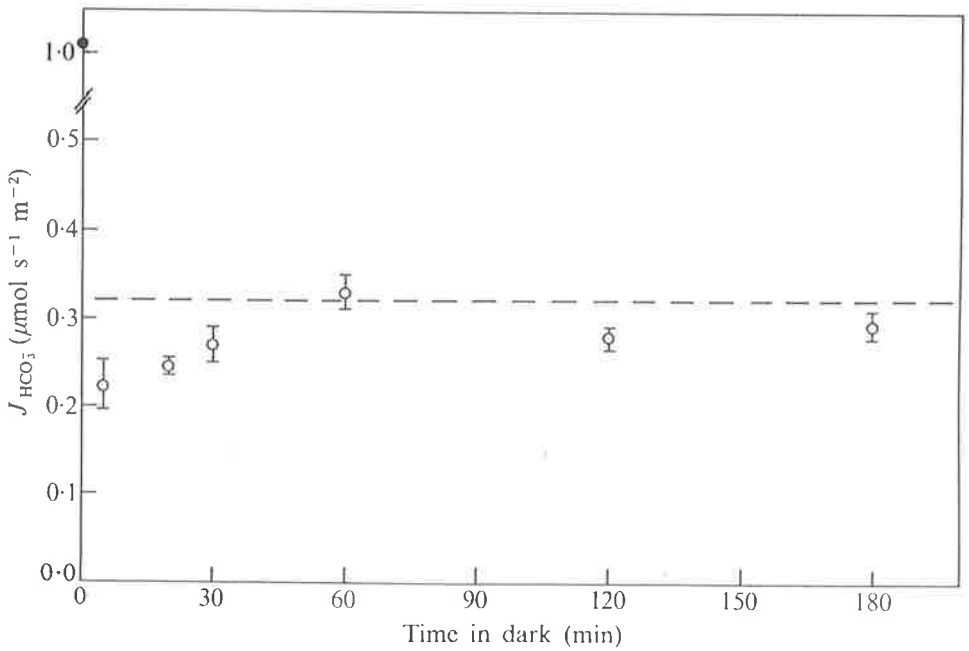


FIG. 3. Dark-induced deactivation of $H^{14}CO_3^-$ assimilation in *P. lucens*. Control rate obtained after 2 h illumination (●); dashed line represents leaf response to 15 min illumination following 12 h dark pretreatment. (All experiments conducted in presence of 1·0 mol $m^{-3}$ $NaHCO_3$.)

rapid deactivation was not expected. Osterlind (1951), using *Scenedesmus quadricauda*, found no effect of short (10 min) dark periods on the rate of $HCO_3^-$ assimilation. Similarly, Walker (1973) also demonstrated that short dark periods did not result in a renewed photoinduction period.

*Kinetics of $^{14}C$ assimilation*

The time course experiments demonstrated that a difference exists between the behaviour of the $^{14}CO_2$ and $H^{14}CO_3^-$ assimilating systems. These experiments suggested that a factor, either a membrane carrier(s) or some other cellular property, is required before exogenous $HCO_3^-$ can be photosynthetically assimilated. This difference may also be expressed by different kinetic parameters observed under conditions of exogenous $^{14}CO_2$ and $H^{14}CO_3^-$.

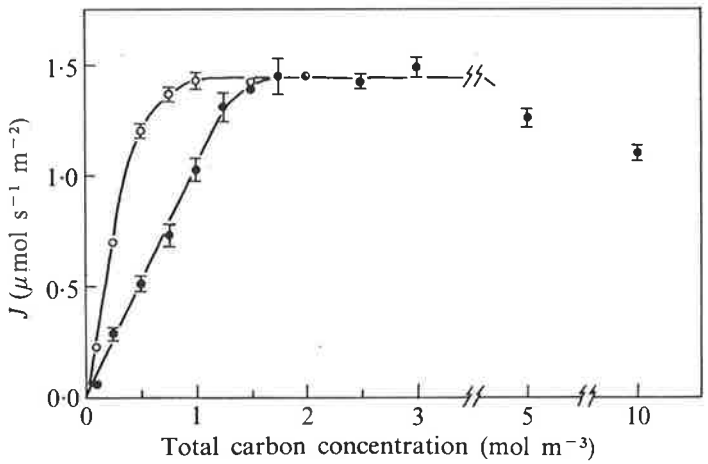


FIG. 4. Influence of substrate concentration on the rate of photosynthetic assimilation of exogenous $^{14}CO_2$ (○) and $H^{14}CO_3^-$ (●).

Substrate kinetic results for $^{14}CO_2$ and $H^{14}CO_3^-$ are presented in Fig. 4. Rates of assimilation were plotted against concentration of total inorganic carbon added. This was done to stress the fact that even though $CO_2$ is the dominant carbon species at pH 5·3, and $HCO_3^-$ the dominant form at pH 9·2, there is still an equilibrium established with the other forms of inorganic carbon. The fixation rates measured in the presence of exogenous $^{14}CO_2$ and $H^{14}CO_3^-$ were calculated assuming that $^{14}CO_2$ was able to enter through both leaf surfaces, whereas $H^{14}CO_3^-$ was assumed to enter through only the lower leaf surface.

Figure 4 indicates that photosynthesis, in the presence of exogenous $^{14}CO_2$, saturated at approximately 1 mol $m^{-3}$, having an apparent $V_{max}$ of 1·45 μmol $s^{-1}$ $m^{-2}$. In the presence of exogenous $H^{14}CO_3^-$, photosynthesis saturated at approximately 1·5–2 mol $m^{-3}$ (ignoring the points at 5 and 10 mol $m^{-3}$) with an apparent $V_{max}$ of 1·47 μmol $s^{-1}$ $m^{-2}$. Interestingly enough, the $V_{max}$ for photosynthesis was identical for both forms of inorganic carbon (i.e. $CO_2$ *and* $HCO_3^-$), but the shapes of the kinetic curves were different. This suggests that different limiting processes are involved under the two substrate conditions.

*Simultaneous assimilation of $^{14}CO_2$ and $H^{14}CO_3^-$*

Evidence that both exogenous $^{14}CO_2$ and $H^{14}CO_3^-$ are assimilated simultaneously, to maximize the photosynthetic rate, is presented in Fig. 5. These experiments were conducted in the presence of saturating 2·5 mol $m^{-3}$ total carbon; over the pH range 7·1–8·5 solutions were buffered with 3 mol $m^{-3}$ TES (pH adjusted with 10 mol $m^{-3}$ $H_2SO_4$). Over the pH range 7·0–8·5 significant amounts of $^{14}CO_2$ and $H^{14}CO_3^-$ were available simultaneously to the leaf. This complicated the flux calculation, since the individual contributions made by $^{14}CO_2$ and $H^{14}CO_3^-$ could not be separated. This situation was further complicated by the fact that $^{14}CO_2$ could enter across both leaf surfaces, whereas $H^{14}CO_3^-$ can enter only across the lower surface. Because of these complications, the total $^{14}C$ fixation rate was expressed on the basis of the area of one leaf surface (Fig. 5).

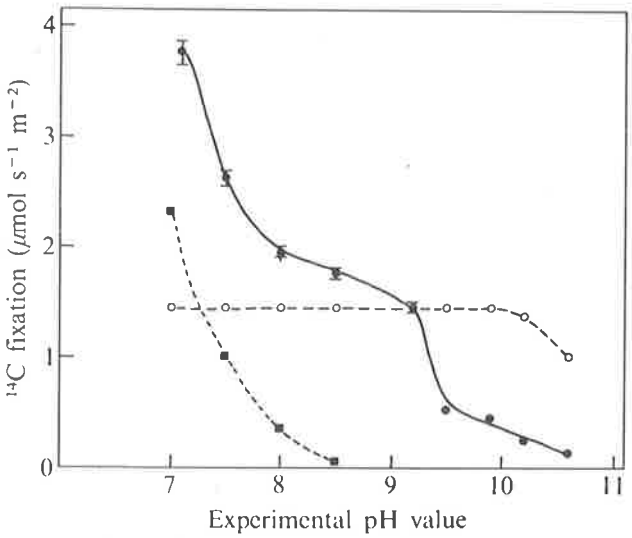


FIG. 5. Effect of solution pH on $^{14}C$ fixation. Experiments were conducted in the presence of saturating 2·5 mol $m^{-3}$ total carbon. Experimental values (●) are expressed on the basis of the area of one leaf surface only. This was necessitated by the fact that $HCO_3^-$ is transported only across the lower leaf surface, hence, the $^{14}CO_2$ and $H^{14}CO_3^-$ contributions could not be determined exactly. Theoretical contributions made by $^{14}CO_2$ (■) and $H^{14}CO_3^-$ (○) are also plotted (see text for full details).

The theoretical contributions made by $^{14}CO_2$ (passive diffusion) and $H^{14}CO_3^-$ (plasmalemma transport) are also presented in Fig. 5. These values were determined by calculating the equilibrium $CO_2$ and $HCO_3^-$ concentrations at the respective pH values. The theoretical fixation rate for each carbon species was then obtained using the calculated concentration values and the data presented in Fig. 4. The values for $CO_2$ were doubled to allow for the fact that this carbon species can penetrate across both leaf surfaces.

Reasonable agreement was found between the total theoretical rate of fixation ($CO_2$ and $HCO_3^-$) and the experimental data, except for the results obtained at pH values above 9·2. In this pH region, $H^{14}CO_3^-$ influx was found to decrease much more rapidly than predicted by our theoretical $HCO_3^-$ curve. An inhibition of this nature was also observed for $H^{14}CO_3^-$ influx in *Chara corallina* (Lucas, 1975*b*). Some form of inhibition must occur, therefore, at these pH values. It was also

noticed, however, that $H^{14}CO_3^-$ influx was inhibited when high substrate levels were employed at pH 9·2 (see Fig. 4). Both forms of inhibition could be due to the presence of $CO_3^{2-}$, which may act as a competitive inhibitor of $HCO_3^-$ transport.

Carbonate inhibition studies were conducted by maintaining a constant $HCO_3^-$ concentration in the presence of varying levels of $CO_3^{2-}$. (This was achieved by manipulating the level of total inorganic carbon and the solution pH value.) The results of these experiments, performed on winter leaves grown under artificial light, are presented in Fig. 6. Unfortunately we found that winter leaves assimilated $H^{14}CO_3^-$ at much lower rates compared with summer cultures. (A similar seasonal trend was observed by Lucas, 1975*b*.) However, regardless of this lower assimilation rate, a clear correlation was observed between $CO_3^{2-}$

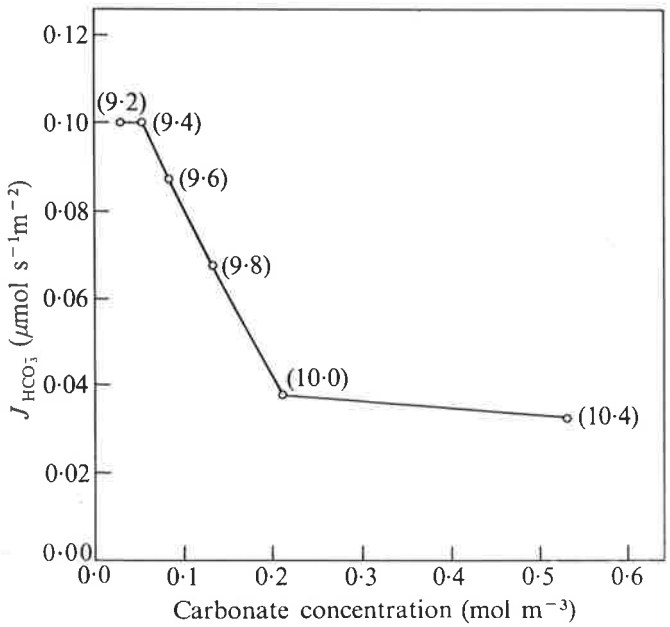


FIG. 6. Competitive inhibition of $H^{14}CO_3^-$ influx by $CO_3^{2-}$ ions. These experiments were conducted in the presence of 0·5 mol m$^{-3}$ $NaHCO_3$. The $CO_3^{2-}$ concentrations were obtained by manipulating the total added inorganic carbon and the experimental pH value (given in parentheses). (S.e. mean values for these data were smaller than symbols used.)

concentration and the degree of $H^{14}CO_3^-$ influx inhibition. The initial linear decline in $H^{14}CO_3^-$ influx, observed in the presence of increasing $CO_3^{2-}$ concentration, had a negative slope of 0·4 μmol s$^{-1}$ m$^{-2}$ per mol m$^{-3}$ $CO_3^{2-}$. This result is very similar to that presented by Lucas (1977). He obtained a negative slope of 0·46 μmol s$^{-1}$ m$^{-2}$ per mol m$^{-3}$ $CO_3^{2-}$, for *C. corallina* (0·5 mol m$^{-3}$ $HCO_3^-$). Collectively, these results add considerable weight to the hypothesis that the $CO_3^{2-}$ ion binds competitively to the $HCO_3^-$ site of this particular transporter.

This form of inhibition may be widespread amongst $HCO_3^-$ assimilators. The species distribution of $HCO_3^-$ assimilators, within the Scottish lochs, may reflect the influence of $CO_3^{2-}$ inhibition. The species *Chara papillosa, Potamogeton lucens*, and *Ceratophyllum demersum* appear to be restricted to alkaline lochs, the waters of which have pH values up to 8·7 (Spence, 1967). Only *Myriophyllum spicatum* appears to be able to utilize exogenous $HCO_3^-$ in non-calcareous lochs, in which the

pH value may exceed 10·0. Bicarbonate assimilation in marine seagrasses also exhibited a range of species-specific sensitivities to experimental pH (Beer, Eshel, and Waisel, 1977). Of the four species that Beer *et al.* studied, only *Halophila stipulacea* could assimilate exogenous $HCO_3^-$, at appreciable rates, when pH values above 9·0 were employed.

Assuming it has been demonstrated that a particular species can assimilate exogenous $HCO_3^-$, we suggest that an observed sensitivity, of this assimilation process, to pH values above 8·7, indicates a $HCO_3^-$ transport system that can be competitively inhibited by $CO_3^{2-}$. Insensitivity to pH may reflect an evolutionary adaptation to the $HCO_3^-$ transport system that reduces, or prevents, competitive binding of $CO_3^{2-}$. In this regard, *M. spicatum* may be a species that has evolved such a protective adaptation.

*Polar cation transport*

Substrate kinetics of polar $Na^+$ transport were investigated to determine whether a close correlation exists between the rate of $H^{14}CO_3^-$ assimilation and $Na^+$ transport. For these experiments a 3 h light pretreatment period was employed; hence $HCO_3^-$ assimilation was operating under steady state conditions. The results for these experiments are presented in Fig. 7. A comparison between these data and the $H^{14}CO_3^-$ influx results (see Fig. 4) demonstrates an almost exact 1:1 relationship between the two processes. Since $HCO_3^-$ was available to both leaf surfaces, during polar cation transport and $HCO_3^-$ assimilation experiments, this

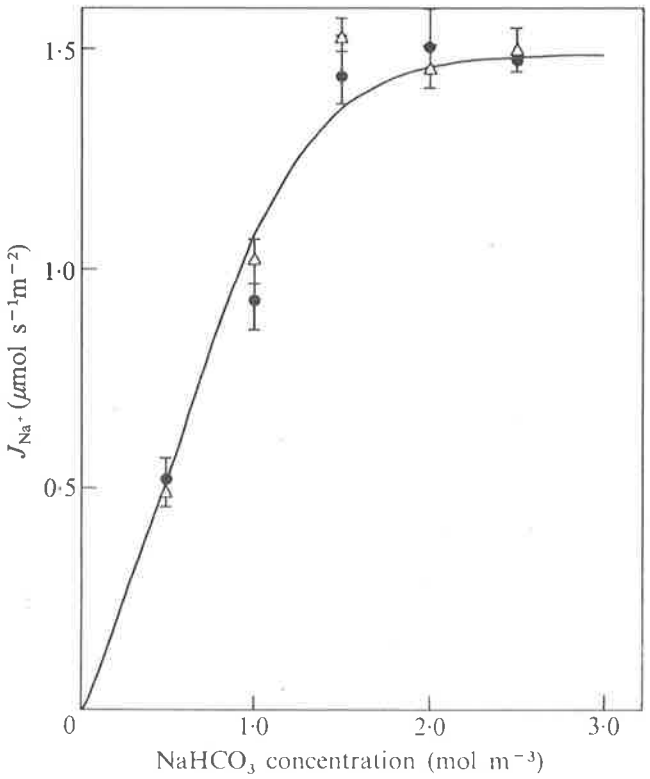


FIG. 7. Relationship between polar $Na^+$ transport and $NaHCO_3$ concentration. Uptake of $Na^+$ across lower leaf surface represented by symbol (●) and efflux across upper leaf surface by (△).

close correlation between the respective transport rates offers strong support for the hypothesis that $HCO_3^-$ is only transported across the lower leaf surface (Arens, 1933, 1936). Polar cation transport is probably necessary to maintain charge neutrality during polar anion ($HCO_3^- + OH^-$) transport. If, however, some $HCO_3^-$ was being assimilated from the upper leaf surface, polar cation transport would be less than the net rate of $HCO_3^-$ assimilation.

## DISCUSSION

Our present results confirm that *P. lucens* can photosynthetically assimilate exogenous $HCO_3^-$. In this respect, it was interesting to observe that the lower leaf surface attained equivalent maximum rates of photosynthesis, irrespecitve of whether carbon was supplied as exogenous $^{14}CO_2$ (pH 5·2) or $H^{14}CO_3^-$ (pH 9·1). This aspect of $^{14}C$ fixation is different from that observed for *C. corallina*, where the $^{14}CO_2$ fixation $V_{max}$ was approximately double the $H^{14}CO_3^-$ $V_{max}$ value (Lucas, 1975*b*). The difference between these two $HCO_3^-$ assimilators may lie in the complete spatial separation of the $HCO_3^-$ and $OH^-$ transport sites in *P. lucens*. Under these conditions the potential for $HCO_3^-$ transport inhibition by $CO_3^{2-}$ would be minimized. Although the operational $OH^-$ transporters are localized in discrete efflux bands, along the cylindrical internodal cells of *C. corallina* (Lucas, 1976), the $OH^-$ diffusion pattern associated with these efflux sites extends over much of the cell surace area. This pH influence could tend to give an artificially low $H^{14}CO_3^-$ $V_{max}$ value, since a proportion of the $HCO_3^-$ transporters would be inhibited by the $CO_3^{2-}$ that is produced by the reaction between $OH^-$ and $HCO_3^-$.

Exclusion of $Ca^{2+}$ from our experimental medium may have resulted in a suppression of $H^{14}CO_3^-$ assimilation (Lucas and Dainty, 1977). However, an unknown quantity of $Ca^{2+}$ would have been retained, for many hours, by the apoplast of the leaves, especially since a limited volume of low ionic strength solution was employed. Comparative $^{14}CO_2$ and $H^{14}CO_3^-$ $V_{max}$ values (Fig. 4), and the observed constant rate of $H^{14}CO_3^-$ assimilation (over a 3 h period, Fig. 2) suggest that for short-term experiments the exclusion of $Ca^{2+}$ may not be deleterious.

### *Kinetic analysis*

Kinetic analysis of the $^{14}C$ fixation data (see Fig. 4) revealed that neither system ($^{14}CO_2$ or $H^{14}CO_3^-$) conformed to simple Michaelis–Menten-type kinetics. Since the reaction chamber used for $^{14}C$ experiments was well stirred, it seems unlikely that an unstirred layer effect could be the cause of this deviation from Michaelis–Menten kinetics. (For an unstirred layer of 100 $\mu$m thickness, diffusion would requite a decrease in concentration of 0·14 mol $m^{-3}$ for $CO_2$ and about 0·18 mol $m^{-3}$ for $NaHCO_3$, at maximum assimilation rates.)

When the $^{14}C$ fixation data were analysed using the Hill equation, a linear relationship was observed for both $^{14}CO_2$ and $H^{14}CO_3^-$ assimilation. The Hill coefficients ($n$) were 2·06 and 1·66 for $^{14}CO_2$ and $H^{14}CO_3$, respectively (a value of $n = 1$ would have been obtained for simple Michaelis–Menten kinetics). A value of $n$ greater than unity is generally thought to indicate the involvement of an allosteric

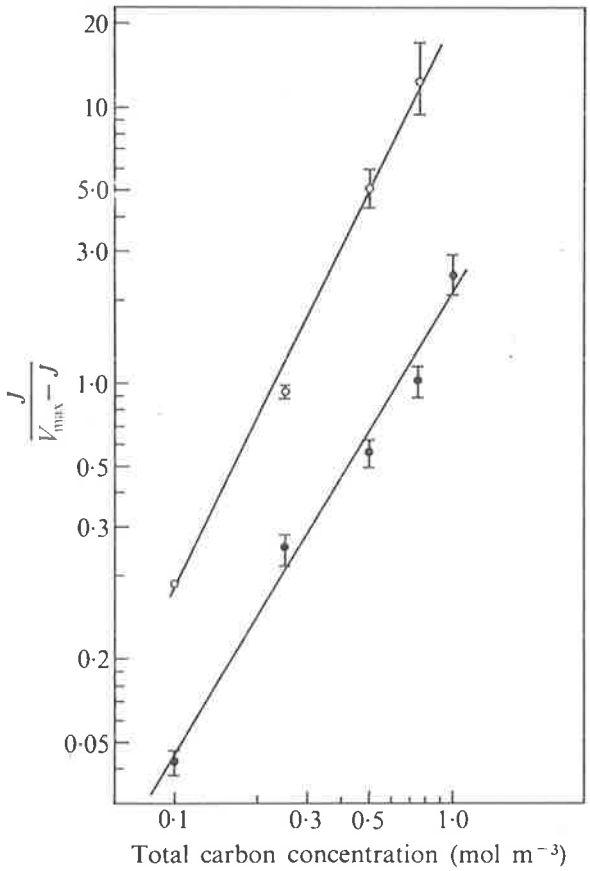


FIG. 8. Hill plots of photosynthetic $^{14}C$ assimilation data obtained on leaves of *P. lucens*. ○, $CO_2$; ●, $HCO_3^-$.

enzyme. On this basis, the $^{14}CO_2$ data imply that ribulose bisphosphate carboxylase may be an allosteric enzyme, having at least two binding sites for $CO_2$. The lower $n$ value observed for $H^{14}CO_3^-$ would be consistent with this interpretation, since the $HCO_3^-$ transport site appears to have a higher apparent $K_m$ value (see Fig. 4). However, because of the complex nature of this system, the above conclusions associated with the kinetic analysis should be viewed with caution.

*Possible relationship between polar cation transport and $HCO_3^-$ assimilation*

The close agreement between the influx of $Na^+$ and $H^{14}CO_3^-$ across the lower leaf surface, and the efflux of $Na^+$ across the upper leaf surface, certainly suggests that the role of one of these transport systems is concerned primarily with the maintenance of charge neutrality. It would appear that this charge neutrality must be maintained both across the cell membrane and between the leaf surfaces. Although our present results do not indicate which transport process occurs as the primary (initial) event, the light activation and dark deactivation results provide a basis upon which future experiments may be designed to elucidate this relationship. In these experiments we will also examine the mono- and divalent cation specificity of this polar cation transport phenomenon.

ACKNOWLEDGEMENTS

This work was supported by a grant from the National Research Council of Canada (NRCC A 6919). One of us, M.T.T., wishes to acknowledge a grant from the Netherlands (Z.W.O.) which permitted him to study cation transport in *Potamogeton* with Dr. R. J. Helder.

LITERATURE CITED

ARENS, K., 1933. *Planta*, **20,** 621–58.
—— 1936. *Jb. wiss. Bot.* **83,** 561–6.
—— 1938. *Protoplasma*, **30,** 104–29.
ARNON, D. I., 1949. *Pl. Physiol., Lancaster*, **24,** 1–15.
BEER, S., ESCHEL, A., and WAISEL, Y., 1977. *J. exp. Bot.* **28,** 1180–89.
HELDER, R. J., 1975*a*. *Proc. K. ned. Akad Wet.* (Ser. C biol. med. Sci.) **78,** 189–97.
—— 1975*b*. Ibid. **78,** 376–88.
—— and BOERMA, J., 1972. *Acta bot. neerl.* **21,** 211–18.
—— —— 1973. Ibid. **22,** 686–93.
LUCAS, W. J., 1975*a*. *J. exp. Bot.* **26,** 271–86.
—— 1975*b*. Ibid. **26,** 331–46.
—— 1976. Ibid. **27,** 19–31.
—— 1977. Ibid. **28,** 1321–36.
—— and DAINTY, J., 1977. *Pl. Physiol., Lancaster*, **60,** 862–7.
LOWENHAUPT, B., 1956. *Biol. Rev.* **31,** 371–95.
—— 1958. *J. cell. comp. Physiol.* **51,** 199–208.
ÖSTERLIND, S., 1949. *Symb. bot. upsal.* **10,** 1–141.
—— 1951. *Physiologia Pl.* **4,** 514–27.
RAVEN, J. A., 1970. *Biol. Rev.* **45,** 167–221.
RUTTNER, F., 1947. *Öst. bot. Z.* **94,** 265–94.
SPENCE, D. H. N., 1967. *J. Ecol.* **55,** 147–70.
STEEMANN NIELSEN, E., 1947. *Dansk. bot. Ark.* **12,** 1–71.
—— 1960. In *Encyclopedia of plant physiology*, Ed. W. Ruhland. Berlin, Springer. Vol. 5/1, pp. 70–84.
WALKER, D. A., 1973. *New Phytol.* **72,** 209–35.

Plant Physiol. (1979) 63, 248–254
0032-0889/79/63/0248/07/$00.50/0

# Alkaline Band Formation in *Chara corallina*

## DUE TO $OH^-$ EFFLUX OR $H^+$ INFLUX?

Received for publication July 24, 1978 and in revised form September 27, 1978

WILLIAM J. LUCAS
*Department of Botany, University of California, Davis, California 95616*

### ABSTRACT

**The nature of the transport system responsible for the establishment of alkaline bands on cells of *Chara corallina* was investigated. The transport process was found to be insensitive to external pH, provided the value was above a certain threshold. At this threshold (pH 5.1 to 4.8) the transport process was inactivated. Transport function could be recovered by raising the pH value of the external solution. The fastest rate of recovery was always obtained in the presence of exogenous $HCO_3^-$.**

**Experiments in which plasmalemma integrity was modified using 10 millimolar $K^+$ treatment were also performed. Alkaline band transport was significantly reduced in the presence of 10 millimolar $K^+$, but the system did not recover, following return to 0.2 millimolar $K^+$ solutions, until the transport site was reexposed to exogenous $HCO_3^-$.**

**The influence of presence and absence of various cations on both alkaline band transport and total $H^{14}CO_3^-$ assimilation was examined. No specific cation requirement (mono- or divalent) was found for either process, except the previously established role of $Ca^{2+}$ at the $HCO_3^-$ transport site. The alkaline band transport process exhibited a general requirement for cations. This transport system could be partially or completely stalled in low cation solutions, or glass-distilled water, respectively. The results indicate that no cationic flux occurs across the plasmalemma in direct association with either the alkaline band or $HCO_3^-$ transport systems.**

**It is felt that the present results offer support for the hypothesis that an $OH^-$ efflux transport system (rather than a $H^+$ influx system) is responsible for alkaline band development in *C. corallina*. The results support the hypothesis that $OH^-$ efflux is an electrogenic process. This $OH^-$ transport system also appears to contain two allosteric effector sites, involving an acidic group and a $HCO_3^-$ ion.**

Bicarbonate assimilation in the fresh water algal species *Chara corallina* has been well characterized (4, 9). A plasmalemma-bound $HCO_3^-$ transport system enables this species to transport exogenous $HCO_3^-$ to the cytoplasm (9). During photosynthetic assimilation of the $CO_2$ that is supplied via this $HCO_3^-$ transport system, internodal cells develop localized regions of alkalinity on their cell surface (11). These regions of alkalinity form the now well known alkaline-banding phenomenon observed in several of the Characean species (1, 11, 17). These alkaline bands form only when cells are exposed to exogenous $HCO_3^-$, and their existence is completely light-dependent.

It has been assumed that these alkaline bands result from the operation of an $OH^-$ transport system (efflux), located in the plasmalemma of this species (6, 8). The requirements of charge balance across the plasmalemma and cytoplasmic pH regulation (during $HCO_3^-$ assimilation) could also be fulfilled by a $H^+$ transport system (influx) (17, 19). A schematic representation of these two alternative methods of alkaline band formation is presented in Figure 1. The possibility that monovalent cations may move in a coupled manner with the various fluxes is also included in this scheme.

The present study was conducted in an attempt to resolve the nature of the transport process responsible for the generation of alkalinity at the surface of *C. corallina* cells.

## MATERIALS AND METHODS

**Cultural Material.** Culture material of *C. corallina* Klein ex Willd., em. R.D.W. (= *C. australis* R.Br.) was grown in the laboratory in 120-liter containers in solutions containing (mM): 3.0 $Na^+$, 0.2 $K^+$, 0.2 $Ca^{2+}$, 1.0 $Cl^-$ and approximately 2.0 $HCO_3^-$ (pH 9.0). Artificial fluorescent lighting was employed; the intensity at the solution surface was 17 w $m^{-2}$. (Full details of the culture techniques and the methods used to cut experimental cells have been previously reported [4, 11].)

**pH Measurement of Alkalinity Developed on Cell Walls of *Chara*.** Experimental cells were cut from the culture 16 hr prior to being used in an experiment. During this period cells were bathed in a solution containing (mM): 1.0 NaCl, 0.2 KCl, 0.2 $CaSO_4$, 1.0 $NaHCO_3$ (pH 9.2) (CPW/B),[1] and were illuminated by fluorescent lighting (10 w $m^{-2}$) for the first 3 and last hr of the pretreatment period.

The alkaline-banding pattern established along the surface of a particular *Chara* cell was determined using the pH-scanning technique developed by Lucas and Smith (11). Initial pH-mapping experiments were conducted at 25 C in CPW/B (B = 0.5 mM $NaHCO_3$) under 20 w $m^{-2}$ illumination. These pH scans enabled us to determine the number of alkaline bands present and their spatial distribution along the particular internodal cell. This information was then used to locate a small Plexiglas chamber over one of the operational alkaline bands. The apparatus used to perform this physical isolation is illustrated in Figure 2. With this system, the solution that is in contact with one particular alkaline band can be physically separated from the control solution that bathes the rest of the internodal cell suface. (Full details of this technique have been described by Lucas [8]).

After sealing the Plexiglas isolating block in place, both the isolated and control cell wall segments were bathed in CPW/B (B = 0.5 mM $NaHCO_3$, pH 8.1) for a 30-min recovery period, under 20 w $m^{-2}$ illumination. A Leitz micromanipulator was then used to lower a miniature pH electrode (Microelectrode Inc. model MI-405) down into the isolating chamber until the electrode tip just touched the cell surface. The electrode was then located at the center of the alkaline band (*i.e.* at the position having the highest pH value).

A 10-ml Manostat Mini-Pet syringe system was used to inject experimental solution into the isolating chamber. The expelled

[1] Abbreviations: GDW: glass-distilled water; CPW: *Chara* pond water; CPW/B: *Chara* pond water containing added sodium bicarbonate.

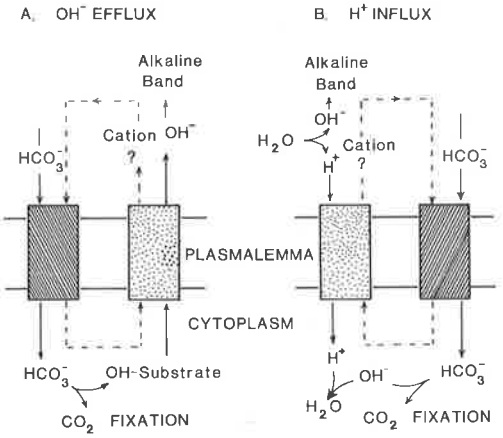


FIG. 1. Schematic representation of two modes by which alkaline bands may be formed on the surface of *C. corallina* cells. $HCO_3^-$ and $OH^-$ (or $H^+$) transporters exist at spatially separate sites within the plasmalemma (8).

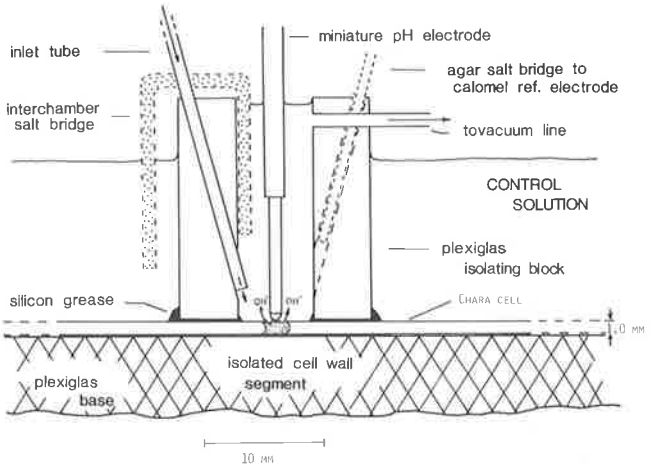


FIG. 2. Physical arrangement of a *Chara* internodal cell held within the special alkaline band isolating chamber system (constructed of clear Plexiglas). Experimental solution was pumped into the small isolated chamber using a 10-ml Manostat Mini-Pet syringe system. Salt bridges consisted of 0.7% (w/v) agar and 200 mM NaCl.

solution was drawn off using a vacuum line connected to the outlet tube (Fig. 2). Screw clips were used on the inlet and outlet tubes to seal the system, thereby preventing movement of solution during an experimental sequence. With a system of this nature, we could study the response of an alkaline band to a range of experimental conditions. It should be stressed that for the duration of the experiments, the majority of the cell's surface remained exposed to the control solution (CPW/B; B = 0.5 mM $NaHCO_3$).

**Cation Requirement for $HCO_3^-$ Assimilation.** Bicarbonate assimilation was determined using $^{14}C$. Radioactive $NaH^{14}CO_3$ was obtained from New England Nuclear as a sterile aqueous solution, and aliquots were added to the experimental solutions to give the required specific radioactivity. All $H^{14}CO_3^-$ and alkaline band experiments were performed using solutions prepared from GDW having a specific conductivity of $\leq 5.0 \times 10^{-7}\ \Omega^{-1}\ cm^{-1}$. Cell wall decalcification and recovery pretreatment procedures were as described by Lucas and Dainty (10).

Choline bicarbonate was obtained as a 45% (approximately) aqueous solution from Sigma Chemical Company. The stock choline bicarbonate solution was stored at 2 C and, immediately prior to being used to prepare experimental solutions, the actual $HCO_3^-$ concentration was determined by pH titration. The solution was also tested for $K^+$, $Na^+$, and $Ca^{2+}$, using flame photometry; no detectable amounts of these cations were found.

Radioactive experiments were conducted at 25 C and 20 w $m^{-2}$ illumination. Details of the illumination, experimental, and radioactivity assay systems have been previously reported (4, 10, 12). Results are expressed as mean ±SE, (12 cells used/treatment).

## RESULTS

**Alkaline Band Response to Low pH Treatment.** If the alkaline bands of *C. corallina* develop as a result of localized $H^+$ influx (Fig. 1B), it should be possible to manipulate the transport rate, through an isolated band, by changing the proton concentration at the outer plasmalemma surface. Within certain limitations, an increase in proton concentration (*i.e.* lowering bathing solution pH value) would be expected to cause at least a transient increase in $H^+$ influx. This concept was examined using the alkaline band isolating system developed by Lucas (8). (See Fig. 2 for the physical arrangement of the cell within this system.)

When the solution in the isolating chamber was changed from CPW/B (B = 0.5 mM $NaHCO_3$, pH 8.1) to unbuffered CPW (*i.e.* no added $HCO_3^-$, pH 5.8) the transport activity of the alkaline band continued (Fig. 3). (In some experiments the new steady-state pH value was lower in CPW compared with CPW/B [see Fig. 3], but in others the values were the same or even higher.) This response is in agreement with the earlier results presented by Lucas (8), where it was shown that $HCO_3^-$ and $OH^-$ (?) are not transported on an antiport system, but rather via their own specific transport systems that are located at spatially separate sites within the plasmalemma.

The Manostat syringe system was used to pump experimental solution from an external reservoir to the isolating chamber. The pH value of the CPW in this reservoir was titrated (using 20 mM $H_2SO_4$), in a stepwise manner, to successively lower values, and the alkaline band response to these pH treatments was examined.

Provided that the pH of the flushing solution was above a certain threshold value, the pH traces always recovered toward the control value. Representative traces are presented in Figures

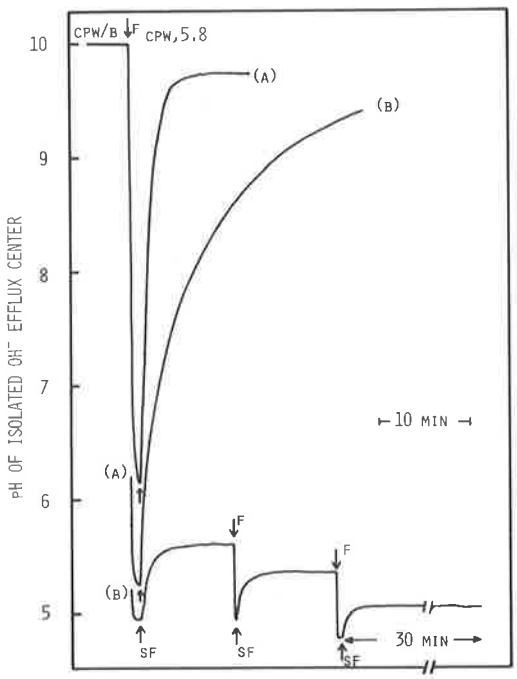


FIG. 3. Alkaline band response to low pH treatment. F: commencement of a chamber flushing sequence; SF: end of flushing sequence; letters in parentheses indicate chronological sequence of respective traces; CPW/B: 1.0 mM NaCl, 0.2 mM KCl, 0.2 mM $CaSO_4$, 0.5 mM $NaHCO_3$ (pH 8.1); CPW 5.8: 1.0 mM NaCl, 0.2 mM KCl, 0.2 mM $CaSO_4$ (pH 5.8).

3 (traces A and B) and 4 (traces A–E). At the conclusion of each flushing sequence there was an immediate response of the pH traces, with no discernible lag, or indeed any significant deviation in the initial response between the various treatments. (See, in particular, the flushing sequences presented in Fig. 4.) If the alkaline band was being generated by $H^+$ influx, it would seem logical to suppose that changing the $H^+$ concentration from $10^{-10}$ molar (*i.e.* a steady-state pH of 10.0) to $10^{-5}$ to $10^{-6}$ molar (pH 5–6.0) would come close to saturating the putative $H^+$ transport system. If this were the case, the "saturating" supply of $H^+$ would "buffer" the alkalinization process. Proton transport would need to occur for a period before the system would generate $OH^-$ at a significant rate at the cell surface. The absence of a discernible lag means that alkaline bands are probably not formed as a result of $H^+$ influx.

Figures 3 and 4 also demonstrate that a threshold pH value existed, and that within this critical pH region the transport function associated with the development of alkalinity was affected dramatically. When pH values just slightly above the threshold value were employed, the shape of the pH trace was affected. The reestablishment of a steady-state diffusion system took a long time. This suggested that the near-threshold pH treatment caused a dramatic reduction in alkaline band transport function, and that this reduction was only temporary. This interpretation was supported by the fact that complete recovery to the control level was always observed, following such a treatment, provided the system was given a 60- to 90-min recovery period (Fig. 4).

Alkalinity was not reestablished at the cell surface when a solution having a threshold pH value was employed. The threshold value varied between cells, but was generally in the pH range 4.8 to 5.1 (or slightly higher). Apparently, following threshold pH inactivation, the alkalinization transport process remains inactivated. The small apparent flux that still occurred through the system (as evidenced by the slight pH rise) was probably associated with the light-inactive transport state (6).

**Alkaline Band Recovery following Low pH Inactivation.** Recovery of alkalinity production, following 30-min low pH inactivation treatment, is illustrated in Figure 5. In the presence of unbuffered CPW (pH 5.8, no added $HCO_3^-$), recovery was slow. After 60 min the isolating chamber was reflushed with CPW (pH 5.8) and the resultant trace compared with the control trace obtained prior to the low pH inactivation treatment. Full transport capacity was not reestablished after 1 hr (Fig. 5).

Titrating the CPW to pH 8.1 (using 100 mM NaOH) accelerated the recovery of transport function compared with the CPW (pH 5.8) response. Fastest recovery was always observed in the presence of $HCO_3^-$ (Fig. 5). After a 20-min 0.5 mM $NaHCO_3$ (pH 8.1) recovery treatment there was no difference between the alkalinization pH traces observed for the control and $HCO_3^-$ recovery situation. Complete transport capacity appeared to be reestablished after approximately 20 min. (A further example of this $HCO_3^-$-mediated transport recovery is demonstrated in Fig. 4.)

After low pH inactivation and subsequent reactivation, the location of the alkaline band center was almost always reestablished in the control position. This band center stability indicates that the low pH treatment does not perturb the cytoplasmic mechanism that controls the location of the alkaline bands.

**Alkaline Band Recovery following 10 mM $K^+$ Treatment.** When $Ca^{2+}$ is displaced from the membrane integrity sites of *C. corallina* (10), several membrane-associated functions are perturbed. Lucas *et al.* (13) have presented recent evidence that suggests 10 mM $K^+$ displaces $Ca^{2+}$ from the plasmalemma integrity sites. In response to this $K^+$-mediated loss of "integrity," the $HCO_3^-$ transport system was converted to a facilitated diffusion system, the alkaline-banding pattern was seriously perturbed, the membrane potential depolarized to a value that was in close agreement with the calculated passive diffusion potential, and the membrane electrical resistance was decreased to a low value.

To ensure that the observed threshold pH inactivation was not due to a $H^+$ effect, *per se*, on membrane integrity, the alkaline band response to and recovery from $K^+$ was investigated. Normal transport function occurred in the presence of 10 mM $Na^+$, but as expected, alkaline band-associated transport function was significantly reduced in the presence of 10 mM $K^+$ (10 mM KCl, 1.0 mM NaCl, 0.2 mM $CaSO_4$, pH adjusted to 5.8) (Fig. 6). The most important aspect of the 10 mM $K^+$ experiments was the discovery that transport function was not reestablished following reexposure to normal $K^+$ (0.2 mM) levels. The recovery time courses, following low pH and 10 mM $K^+$ inactivation, have entirely different forms

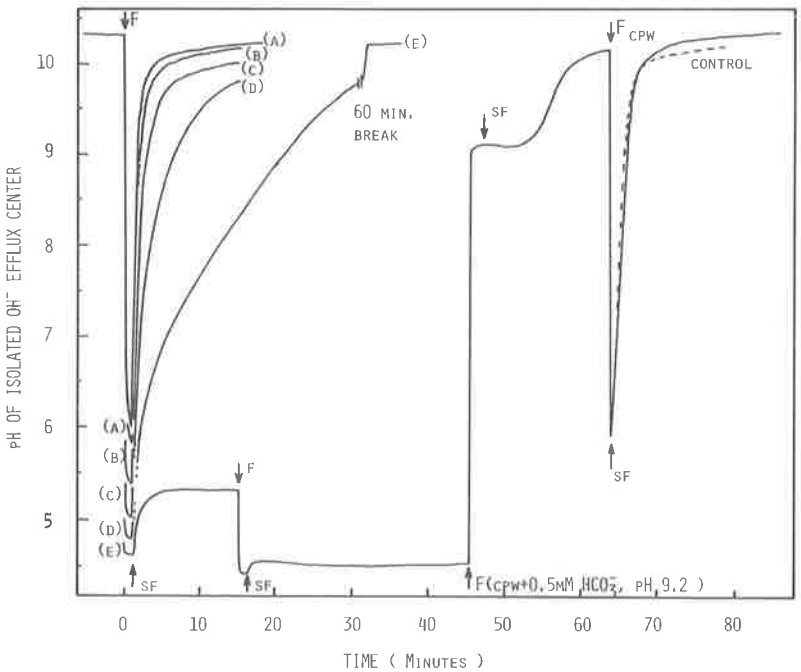


FIG. 4. Alkaline band response to low pH treatment. Symbols as in Figure 3. pH trace represented by broken line illustrates control response measured prior to low pH inactivation.

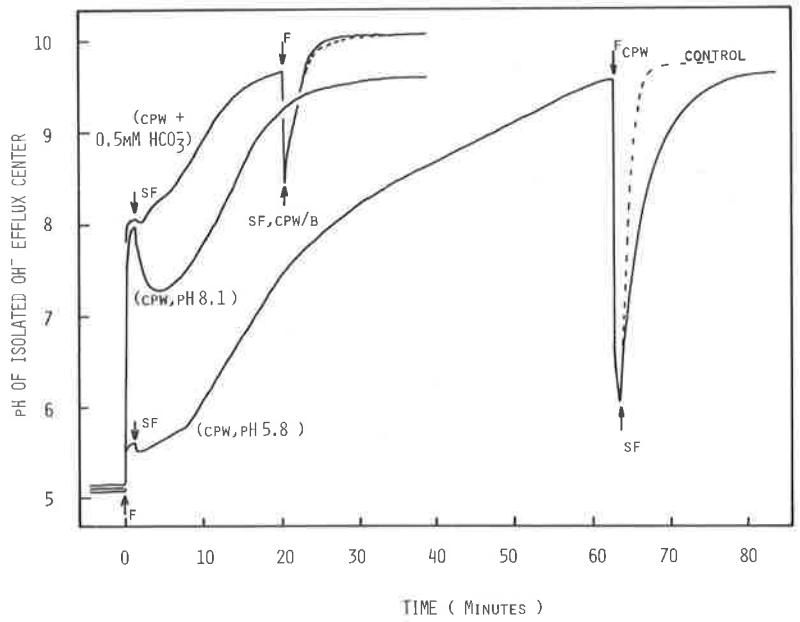


FIG. 5. Alkaline band recovery following 30-min low pH inactivation treatment. Symbols as in Figures 3 and 4. (See text for full details.)

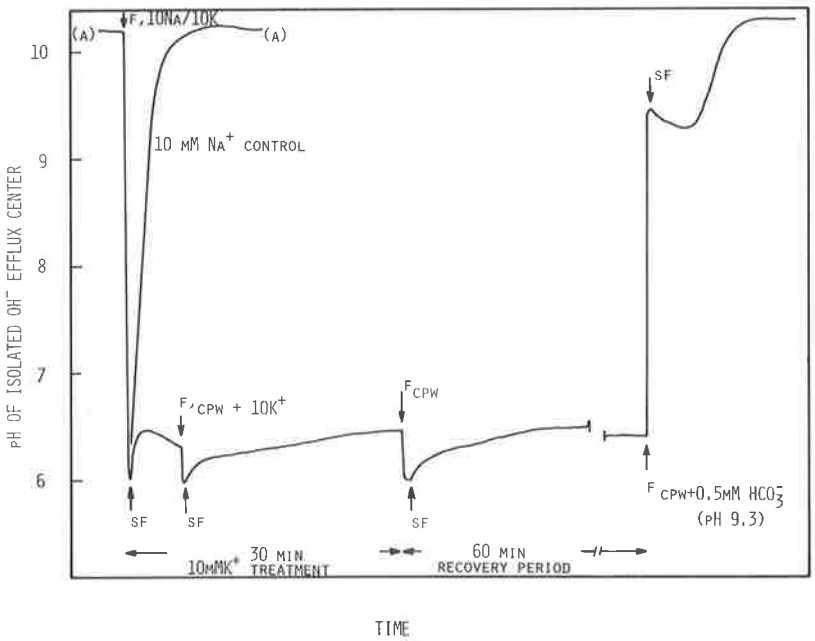


FIG. 6. Alkaline band response to and recovery from 10 mM $K^+$ treatment. Control 10 mM $Na^+$ treatment contained (mM): 10 NaCl, 0.2 KCl, 0.2 $CaSO_4$ (pH 5.8); CPW 10 mM $K^+$ treatment contained (mM): 10 KCl, 1.0 NaCl, 0.2 $CaSO_4$ (pH 5.8); other symbols as in Figure 1.

(*cf.* Figs. 5 and 6), implying that the low pH treatment acts on a site other than membrane integrity.

Although transport function did not return during a 60-min recovery period, the alkaline band could be reestablished by flushing the isolating chamber with $HCO_3^-$ solution (Fig. 6). The implications of this response will be dealt with in the discussion section.

**Cation Requirement for Alkaline Band Formation.** Experiments were conducted both with the isolating chamber technique and $H^{14}CO_3^-$ assimilation system to determine whether monovalent cations are required for photosynthetic assimilation of exogenous $HCO_3^-$. Figure 7 indicates that the transport process associated with the alkaline band was influenced by the general cation content of the flushing solution. No specific cation requirement was observed. The isolated alkaline band remained operational in the presence of any of the following species: NaCl, $Na_2SO_4$, choline chloride, or $CaCl_2$. Collectively, these results suggest that the observed cation requirement (mono- or divalent) is associated with a process that occurs at the outer membrane surface, rather than a transmembrane cationic flux.

Lucas and Dainty (10) demonstrated that the transport process responsible for the formation of alkaline bands did not have a transport-specific requirement for $Ca^{2+}$, other than the role this ion plays in maintaining membrane integrity. An influence at the integrity site was not observed until after approximately 36 hr exposure to $Ca^{2+}$-free solutions (7, 10). The almost immediate "stalling" of the alkalinization process observed in GDW cannot be due to an effect on membrane integrity associated with the removal of $Ca^{2+}$ from the solution (Fig. 7). Again, these results suggest that the cation requirement is associated with a process that is occurring at the outer cell surface. The GDW "stalling" results allow us to conclude that the cationic requirement cannot

be associated with a flux of cations that originates from within the cytoplasm (Fig. 1).

Bicarbonate assimilation experiments were conducted in the presence and absence of various cations (Table I). Assimilation was reduced when the experimental solution contained only choline bicarbonate. But, as shown in the appropriate $Ca^{2+}$-free control, this reduction was due to the influence of a 2-hr $Ca^{2+}$-free exposure, rather than expressing an imposed cation-dependent limitation. No evidence of a specific cation requirement for $^{14}CO_3^-$ assimilation was found.

**Influence of GDW Stalling on Alkaline Band Transport System.** Exposure of an isolated alkaline band to low ionic strength solutions apparently influences not only the transport rate (as evidenced by the reduction in the steady-state pH value), but also the transport capacity of the band (Fig. 8). When partially stalled alkaline bands were reexposed to control solutions, the recovery pH traces had a different shape than, and lagged behind, their respective controls. These differences are probably a reflection of a reduction in the number of operational transporters that existed within the transport band. A period of 15 to 20 min appeared to be required before the band regained its control transport capacity.

Transport recovery, following 30-min GDW treatment, is illustrated in Figure 9. Experiments of this nature revealed that stalling the system in GDW inactivated the transport complex, returning it to the light-inactive state. Subsequent recovery of transport function closely resembled the observed light-induced activation response.

## DISCUSSION

**Question of $OH^-$ Efflux *Versus* $H^+$ Influx.** Although the present results do not categorically refute the existence of $H^+$ influx system, they tend to offer stronger support for the $OH^-$ efflux hypothesis. The apparent insensitivity of the transport process to external pH, provided the values were above a certain threshold, suggests that substrate regulation occurs at the inner, rather than the outer, membrane surface. A further argument against the $H^+$ influx hypothesis can be presented based on the statistical problem of the $H^+$ concentration that would exist in the vicinity of the putative transport system. Under normal $HCO_3^-$-assimilating conditions (1–2 mM $HCO_3^-$), alkaline bands develop pH values of 10 to 10.5 at their centers (10, 13). These values are measured at the cell surface (actually at a distance of 10 to 20 $\mu$m from the cell wall), hence the values at the transport site would be even higher. Consequently the proton-substrate concentration would be extremely low, being approximately 0.3 to 1.0 $\times$ $10^{-10}$ molar. This would require a system with an extremely low $K_m$, in the nano-

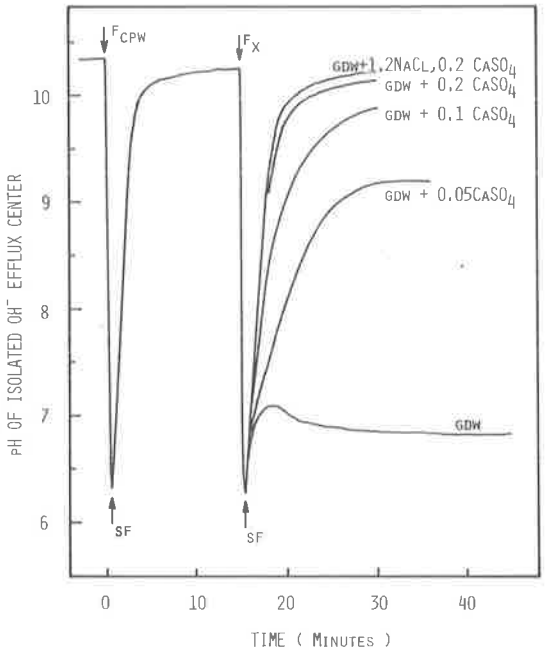


FIG. 7. Influence of cation concentration on the development of alkalinity as measured at the center of an isolated alkaline band. $F_x$: flushing the isolating chamber with solutions of indicated compositions (mM).

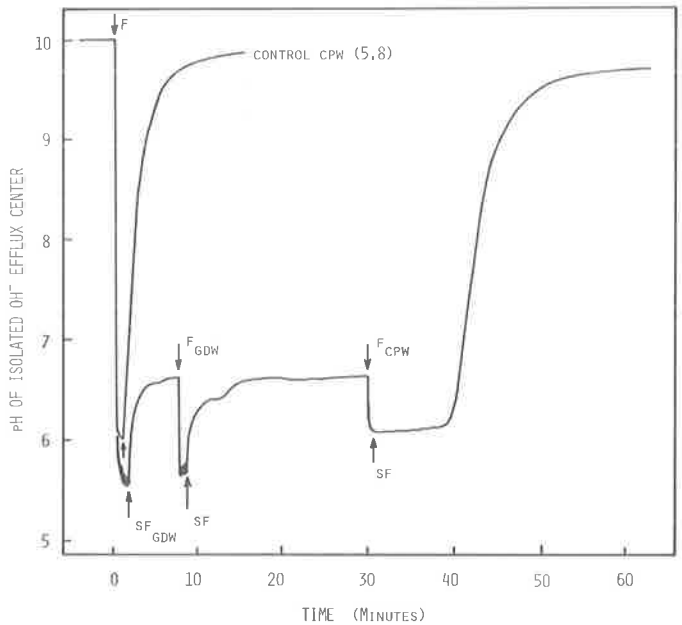


FIG. 8. Alkaline band transport recovery following partial stalling by low cation concentration solution. Symbols and conditions as described in Figures 3 and 7.

Table I. Cation Requirement for $H^{14}CO_3^-$ Assimilation in *C. corallina*

| Ionic Conditions (mM) | $H^{14}CO_3^-$ Assimilation[1] (pmol $cm^{-2}$ $s^{-1}$) |
|---|---|
| 1.0 Choline$^+$ $HCO_3^-$ + NaCl, 0.2 KCl, 0.2 $CaSO_4$ | 40.4 ± 1.6 |
| 1.0 Choline$^+$ $HCO_3^-$ + 0.2 $CaSO_4$ | 39.9 ± 2.6 |
| 1.0 $Na^+$ $HCO_3^-$ + 1.0 NaCl, 0.2 KCl, 0.02 $CaSO_4$ | 44.8 ± 1.5 |
| 1.0 Choline$^+$ $HCO_3^-$ + 0.02 $CaSO_4$ | 37.5 ± 1.8 |
| 1.0 Choline$^+$ $HCO_3^-$ (no other additions, $Ca^{2+}$-free) | 31.7 ± 1.6 |
| 1.0 Choline$^+$ $HCO_3^-$ + 1.0 NaCl, 0.2 KCl, $Ca^{2+}$-free | 33.9 ± 1.3 |

[1] All treatments given two rinses (5 min duration) in GDW (± 0.2 or 0.02 mM $CaSO_4$); cells then transferred to pretreatment (1 h) and $^{14}C$ solutions (1 h). pH of experimental solutions was 9.1.

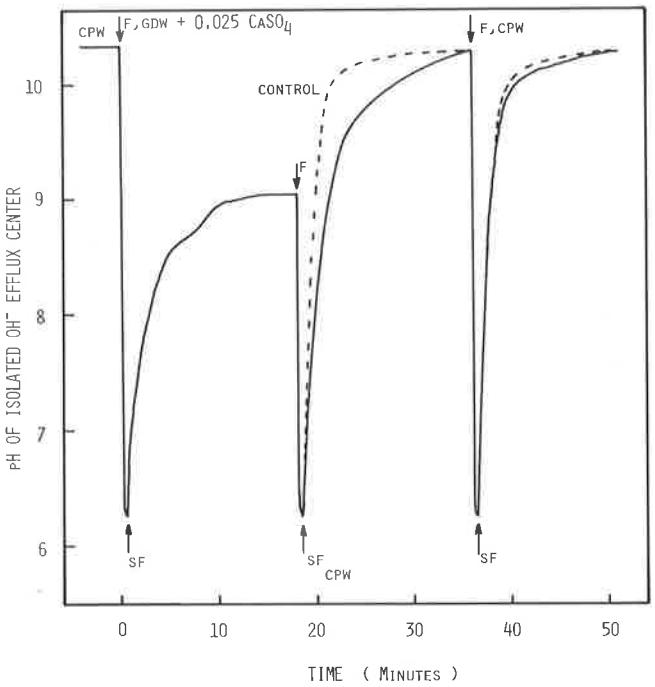


FIG. 9. Recovery of transport function following a 30-min stalling treatment in GDW. Symbols as described in Figures 3 and 7.

molar range or lower, and the feasibility of a transport system functioning effectively within this range seems rather unlikely. Furthermore, following activation of an alkaline band, the pH value at the cell surface rises very rapidly and, in consequence, the available substrate for the putative $H^+$ influx system would be drastically reduced. It should be recalled that $H^+$ influx (or $OH^-$ efflux) is required to maintain charge balance (and cytoplasmic pH control) across the plasmalemma during the $HCO_3^-$ transport (and assimilation). When $HCO_3^-$ influx has reached a steady-state, the physical conditions at the outer membrane surface, in the vicinity of the alkaline bands, are such that it seems extremely unlikely that a $H^+$ influx system could operate at a rate sufficient to balance the very high rate of $HCO_3^-$ influx.

These substrate limitations would not be as serious for an $OH^-$ efflux system. During $HCO_3^-$ assimilation the cytoplasmic pH is probably 8.1 to 8.4 (18), and thus the $OH^-$ concentration would be about 1.3 to 2.5 $\mu$M. In contrast to the $HCO_3^-$-$H^+$ influx system, there would be a positive cooperative effect between $HCO_3^-$ influx and $OH^-$ efflux. An increase in $HCO_3^-$ influx would result in a paralleled increase in $OH^-$ in the cytoplasm. As indicated in Figure 1 (see also ref. 6), we have proposed that the binding substrate for $OH^-$ transport is not $OH^-$, *per se,* but an OH-substrate. The OH-substrate would serve to shuttle $OH^-$, released from the $HCO_3^-$ during $CO_2$ fixation, from the chloroplasts to the transport sites. Admittedly this is a speculative hypothesis, but the implications of its effect on the problem of substrate-transport control are quite apparent.

Apart from the remote possibility that the $H^+$ influx system binds and splits $H_2O$, the above discussion suggests that an $OH^-$ transport system would be more effective in maintaining charge balance and cytoplasmic pH control during $HCO_3^-$ assimilation.

**Threshold pH Inactivation of Transport Function.** The existence of a threshold pH value, at which transport function is inactivated, suggests that on the outer surface of the transport complex there may be an allosteric control site that contains either a carboxyl or a phosphate group. Presumably in the negative (dissociated) form the group functions as a transport activator. Protonation of this charged group may result in a conformational change in a transport-related protein. Such a change, for example, may prevent the release of $OH^-$ at the outer membrane surface.

This hypothesis provides an explanation of the alkaline band response to pH values just above the threshold. At these pH values a proportion of the total transporters that constitute an alkaline band would have their allosteric sites protonated, and would thus be inactivated. The remaining transport sites, which would presumably be found within the central region of the alkaline band, would remain operational. Their continued activity would raise the pH along the membrane surface, and those protonated sites that remained exposed to this surface would be reactivated by deprotonation. The slow return to full transport capacity (Fig. 3 and 4) suggests that most of the protonated sites are no longer permanently exposed at this outer surface. However, they must become exposed periodically, and when this happens the probability of deprotonation would depend upon the pH value in their immediate vicinity. Exposure to a threshold pH solution would allow all allosteric sites to be protonated and thus the entire transport complex would be converted to the inactive form.

The range of threshold values observed between different cells is possibly a reflection of the variation in cell wall-buffering capacities of the experimental cells. It should be stressed that the pH value at the membrane surface will certainly be lower than the value measured at the cell surface (14), but the degree to which it will be lowered is not known with any certainty. There will also probably be a relationship between the threshold pH value and both the number of operational transporters and the spatial dimensions of the transport complex forming the alkaline band.

These cells possess a $H^+$ excretion system (11, 12) and from the recent studies of Métraux *et al.* (14) it seems there is a functional relationship between the acid zones and cell wall extension (growth). The existence of a low pH-inactivating "switch" (associated with alkaline band formation) would certainly place the phenomenon of growth, in these cells, under greater cytoplasmic control. In this way the cell could prevent an alkaline band from being established in a region in which cell extension was about to occur.

**Alternative Interpretation of Transport Inactivation at Low pH.** Richards and Hope (15) suggested that passive (?) membrane conductance (presumably associated with $H^+$) increases at low pH (4.0–5.0). In addition, Walker and Smith (19) have shown that cytoplasmic pH is influenced by the pH of the bathing solution. The possibility also exists that when low pH solutions are employed passive $H^+$ influx may lower the cytoplasmic pH in the vicinity of the isolated cell wall segments. This change in cytoplasmic pH could reduce the $OH^-$, or OH-substrate level to below the critical level required to maintain the transport system in its operational state. (Evidence for the existence of a critical substrate level was found by Lucas [6] during a study of the light-mediated activation process of these alkaline bands.)

The same reasoning could also be applied to the $H^+$ influx hypothesis. A stimulation of the $H^+$ influx transport system, under conditions of low external pH, could lower the local cytoplasmic pH value at this transport site. This may activate a feedback signal which could stop the $H^+$ transport process.

The main argument against this low cytoplasmic pH response is based on the physical arrangement of the *Chara* cell within the isolating system. In these experiments only a small section of cell's surface was exposed to these low pH solutions; the majority of the surface being bathed in control CPW/B. Both the high rate of cyclosis and the short diffusion distance (10 $\mu$m) involved between the streaming cytoplasm and the plasmalemma would tend to reduce the magnitude of any localized cytoplasmic pH changes. (This argument would be invalid, however, if a membrane-bound compartment was involved with the alkaline band transport process.) A cytoplasmic pH effect would also be less likely to respond in the observed manner of an abrupt threshold pH response.

The Characean membrane potential is also influenced by the external pH (3, 15, 16). The potential becomes less negative at lower pH values. There is also the possibility that the transport process involved in alkaline band formation has a voltage-de-

pendent aspect; a threshold voltage may exist below which the system inactivates. This possibility will be investigated by conducting voltage clamp experiments on an alkaline band.

**Transport Recovery following Low pH or 10 mM $K^+$ Inactivation.** The acceleration of transport recovery in the presence of $HCO_3^-$ was an important finding. There are at least two ways that $HCO_3^-$ could effect this acceleration. First, the alkaline transport system may contain an additional allosteric binding site involving $HCO_3^-$. The conformational change associated with the protonation of the acidic allosteric site may expose, or cause the release of, the $HCO_3^-$ ion. The slow recovery observed in the absence of $HCO_3^-$ (in the isolating chamber) may be due to a very slow rebinding of $HCO_3^-$ at (or across) the cytoplasmic interface. It is also possible that $HCO_3^-$ is the carboxyl group involved in the acidic allosteric site. Under the observed threshold pH value, $HCO_3^-$ would be converted to $H_2CO_3$ and this species would dissociate to $CO_2$ and $H_2O$.

The second possibility is that $HCO_3^-$ transport, in the immediate vicinity of the inactive alkaline transport system, may relieve some limitation imposed by the physical presence of the isolating system. The relationship between $HCO_3^-$ transport and the alkaline transport system may also be via an effect on the local electric potential.

Lucas (7) has shown that the effect of 10 mM $K^+$ treatment on $H^{14}CO_3^-$ assimilation, in *C. corallina,* was almost completely reversed following a 60-min recovery period. Lucas *et al.* (13) have also demonstrated that the effect of 10 mM $K^+$ on membrane potential and conductance was completely reversed within a 60-min recovery period. In both of these studies, the entire cell surface was exposed to $HCO_3^-$ during the recovery process. The present results, in which a lack of transport recovery was observed until the system was exposed to $HCO_3^-$, offers strong additional support for the proposal that $HCO_3^-$ is required at some site associated specifically with the alkaline transport system. The fact that the transport system did not recover (*cf* Figs. 5 and 6) in the absence of $HCO_3^-$ implies that the 10 mM $K^+$ treatment exposed all of the $HCO_3^-$-binding sites at the outer membrane surface. The sites must have remained at this surface during the initial 60-min recovery period, otherwise some $HCO_3^-$ binding would have occurred across the inner membrane surface.

**Cation Requirement for Normal Alkaline Band Activity.** We have now clearly demonstrated that no cationic flux occurs across the plasmalemma in direct association with either the $HCO_3^-$ or alkaline band transport sites. The observed nonspecific cation requirement must be associated with the movement of $HCO_3^-$ toward and $OH^-$ away from the outer membrane surface. Walker and Smith (19) have shown that large ionic currents circulate between alkaline bands and the regions on the cell surface between adjacent alkaline bands. Our present findings, in conjunction with the ionic current results of Walker and Smith (19) offer strong support for our hypothesis that $HCO_3^-$ and $OH^-$ are transported across the membrane in an electrogenic manner. Electrogenic transport of $OH^-$ from the cytoplasm to the outer solution can occur only if the general condition of charge neutrality can be maintained. The observed nonspecific cation requirement must be associated with the necessity of charge balance of the $OH^-$ transport site. This aspect of charge balance will be discussed in detail in a forthcoming paper (2).

In the presence of GDW, the cation concentration would be so low that very few of the transported $OH^-$ could move away from the membrane surface. This accumulation of $OH^-$ would develop a localized region of negative charge on the outer membrane surface. This charge may be the feedback signal that causes the inactivation of the alkaline band. We will investigate the possible nature of this feedback signal in a future study.

## LITERATURE CITED


1. ARENS K 1939 Physiologische Multipolarität der Zelle von *Nitella* während der Photosynthese. Protoplasma 33: 295–300
2. FERRIER JM, WJ LUCAS 1978 Plasmalemma transport of $OH^-$ in *Chara corallina*. II. Further analysis of the diffusion system associated with $OH^-$ efflux. J Exp Bot. In press
3. KITASATO H 1968 The influence of $H^+$ on the membrane potential and ion fluxes of *Nitella*. J Gen Physiol 52: 60–87
4. LUCAS WJ 1975 Photosynthetic fixation of $^{14}$carbon by internodal cells of *Chara corallina*. J Exp Bot 26: 331–346
5. LUCAS WJ 1975 Ionic relations of *Chara corallina*: studies on the transport of $HCO_3^-$, $OH^-$ and $H^+$ across the plasma membrane. PhD thesis. University of Adelaide, South Australia, pp 184–190
6. LUCAS WJ 1975 The influence of light intensity on the activation and operation of the hydroxyl efflux system of *Chara corallina*. J Exp Bot 26: 347–360
7. LUCAS WJ 1976 Influence of $Ca^{2+}$ and $K^+$ on $H^{14}CO_3^-$ influx in internodal cells of *Chara corallina*. J Exp Bot 27: 32–42
8. LUCAS WJ 1976 Plasmalemma transport of $HCO_3^-$ and $OH^-$ in *Chara corallina*: non-antiporter systems. J Exp Bot 27: 19–31
9. LUCAS WJ 1977 Analogue inhibition of the active $HCO_3^-$ transport site in the Characean plasma membrane. J Exp Bot 28: 1321–1336
10. LUCAS WJ, J DAINTY 1977 $HCO_3^-$ influx across the plasmalemma of *Chara corallina*: divalent cation requirement. Plant Physiol 60: 862–867
11. LUCAS WJ, FA SMITH 1973 The formation of alkaline and acid regions at the surface of *Chara corallina* cells. J Exp Bot 24: 1–14
12. LUCAS WJ, FA SMITH 1976 Influence of irradiance on $H^+$ efflux and $Cl^-$ influx in *Chara corallina*: an investigation aimed at testing two $Cl^-$ transport models. Aust J Plant Physiol 3: 443–456
13. LUCAS WJ, RM SPANSWICK, J DAINTY 1978 $HCO_3^-$ influx across the plasmalemma of *Chara corallina*: physiological and biophysical influence of 10 mM $K^+$. Plant Physiol 61: 487–493
14. MÉTRAUX J-P, PA RICHMOND, L TAIZ 1978 Multiaxial cell wall extension and acid growth in *Nitella*. Plant Physiol 61: S-237
15. RICHARDS JL, AB HOPE 1974 The role of protons in determining membrane electrical characteristics in *Chara corallina*. J Membr Biol 16: 121–144
16. SPANSWICK RM 1972 Evidence for an electrogenic ion pump in *Nitella translucens*. I. The effects of pH, $K^+$, $Na^+$, light and temperature on the membrane potential and resistance. Biochim Biophys Acta 288: 73–89
17. SPEAR DG, JK BARR, CE BARR 1969 Localization of hydrogen ion and chloride ion fluxes in *Nitella*. J Gen Physiol 54: 397–414
18. WALKER NA, FA SMITH 1975 Intracellular pH in *Chara corallina* measured by DMO distribution. Plant Sci Lett 4: 125–132
19. WALKER NA, FA SMITH 1977 Circulating electric currents between acid and alkaline zones associated with $HCO_3^-$ assimilation in *Chara*. J Exp Bot 28: 1190–1206

Plant Physiol. (1979) *63*, 709–714
0032-0889/79/63/0709/06/$00.50/0

# Plasmalemma Voltage Noise in *Chara corallina*[1]

Received for publication August 3, 1978 and in revised form November 27, 1978

JACK M. FERRIER AND CLAUDINE MORVAN[2]
*Department of Botany, University of Toronto, Ontario M5S 1A1 Canada*
WILLIAM J. LUCAS
*Department of Botany, University of California, Davis, California 95616*
JACK DAINTY
*Department of Botany, University of Toronto*

## ABSTRACT

**Voltage noise analysis is applied to plasmalemma ion transport in *Chara corallina*. There is a component in the noise power spectrum that is probably associated with current fluctuations within passive transport channels, and another component that may be associated either with fluctuations in the number of open channels, or with active transport. The data allow the calculation of time constants that may be attributable to molecular level events in these transport processes.**

The analysis of random fluctuations in membrane current or potential difference has proven to be useful in studying the molecular aspects of ion transport. When applied to passive currents in axons and end plates, this method has provided estimates for transport channel lifetimes and densities, and allowed some testing of molecular level models (1, 4, 6, 9, 19). This method of analysis has also been applied to active transport in toad bladder (23), in frog skin (20), and in the cells of the plants *Chara braunii* (17, 18) and *Neurospora crassa* (24). In these last three systems it has not been established whether the measured noise is produced directly by the processes of active transport, or by associated passive fluxes.

In this paper we report an analysis of voltage fluctuations across the plasmalemma of *Chara corallina*. There are large transport fluxes that may be active and electrogenic in these algal cells. These fluxes have been well characterized by tracer and diffusion analysis (11–14).

## MATERIALS AND METHODS

Culture cells of *C. corallina* were grown in solutions containing (mM): 1 to 2 $Na^+$, 0.2 $K^+$, 0.1 to 0.5 $Ca^{2+}$, 1.0 $Cl^-$, and 2 $HCO_3^-$ at about pH 9 (11). Except where otherwise indicated, measurements were made in a standard solution containing (mM): 1.0 NaCl, 0.2 KCl, 0.2 $CaSO_4$, and 1.5 $NaHCO_3$. The pH value of the solution was generally between 8 and 9. Cell illumination (10 $wm^{-2}$) was provided by a quartz-iodide lamp powered by a 12-v battery (required to eliminate the 60-Hz signal from a standard AC powered light source).

Measurements of electrical potential ($V$) and random potential fluctuations ($\delta V$) were made between a Ag-AgCl: 3 M KCl-filled glass microelectrode that was inserted into the cell, and a similar electrode outside the cell. The microelectrodes had tip diameters and resistances of about 1 $\mu$m and 5 m$\Omega$, respectively. Each electrode was connected to a voltage follower (a WPI 725 and a WPI VF-1) to increase stability and impedance of the measuring circuit. These fed into a Kiethley 604 differential electrometer. A low pass frequency filter on the Kiethley was used to attentuate signals above the range of interest. This helped to prevent aliasing, a mathematical artifact in the noise analysis in which higher frequency fluctuations are mistaken for lower frequency ones. The measuring system was electrically shielded by a Faraday cage, and mechanical vibrations were damped by a spring and hydraulic system.

Data were digitized and stored on a flexible magnetic disk on a PDP 11/03 microcomputer system. Typically, the output of the measuring circuit was sampled at a rate of 1,000, 100, or 10 Hz and stored in blocks of 4,096 points. The following calculations were performed. The mean square voltage fluctuation (variance) was calculated both with and without removal of linear trends from the data. Power spectra were calculated on blocks of 512 points with linear trend removed using the autocorrelation-Fourier transform algorithm (2). The mean and standard error were calculated for the 8 power spectra thus produced. This procedure provided total noise and noise as a function of frequency within certain frequency ranges, as well as a measure of stationarity. The frequency ranges were 10 to 300 Hz for the 1,000-Hz sample rate, 1 to 30 Hz for the 100-Hz sample rate, and 0.1 to 3 Hz for the 10-Hz sample rate. The overlap between the ranges allowed a spectrum to be obtained from 0.1 to 300 Hz for a process of good stationarity. One measure of stationarity was provided by the effect of removing linear trends in the variance calculation; another was provided by comparing the theoretical statistical stability of the power spectrum (2) to the calculated standard error. The data reported in this paper exhibited signs of good stationarity.

Membrane impedance as a function of frequency was measured as follows. Sinusoidal current at $10^{-6}$ to $10^{-7}$ amp was injected into the cell through a separate electrode. Injected current was measured by oscilloscope, and the root-mean-square voltage response was measured using the microcomputer system. At least 10 periods with a total of 4,096 data points were included in each measurement at a given frequency. These results were not corrected for the cable effect. We are interested in the existence of peaks (at low frequency) and bumps (at any frequency) in the impedance. Such features in the measured absolute value of impedance *versus* frequency function would not be influenced by the cable effect.

The noise produced by the electrodes prior to insertion into the cell was characterized over a period of time and was found to be quite stable. An electrode was then inserted into a *C. corallina* internodal cell and the noise measured over a period of time under various conditions. The electrode noise was again characterized after the intracellular electrode had been withdrawn from the cell.

[1] This work was supported by Connaught Fund (University of Toronto) and National Research Council of Canada (A6459) grants to J. D.

[2] Present address: Laboratoire de Nutrition minérale, Faculté des Sciences de Rouen, 76130 Mont-Saint-Aignon, France.

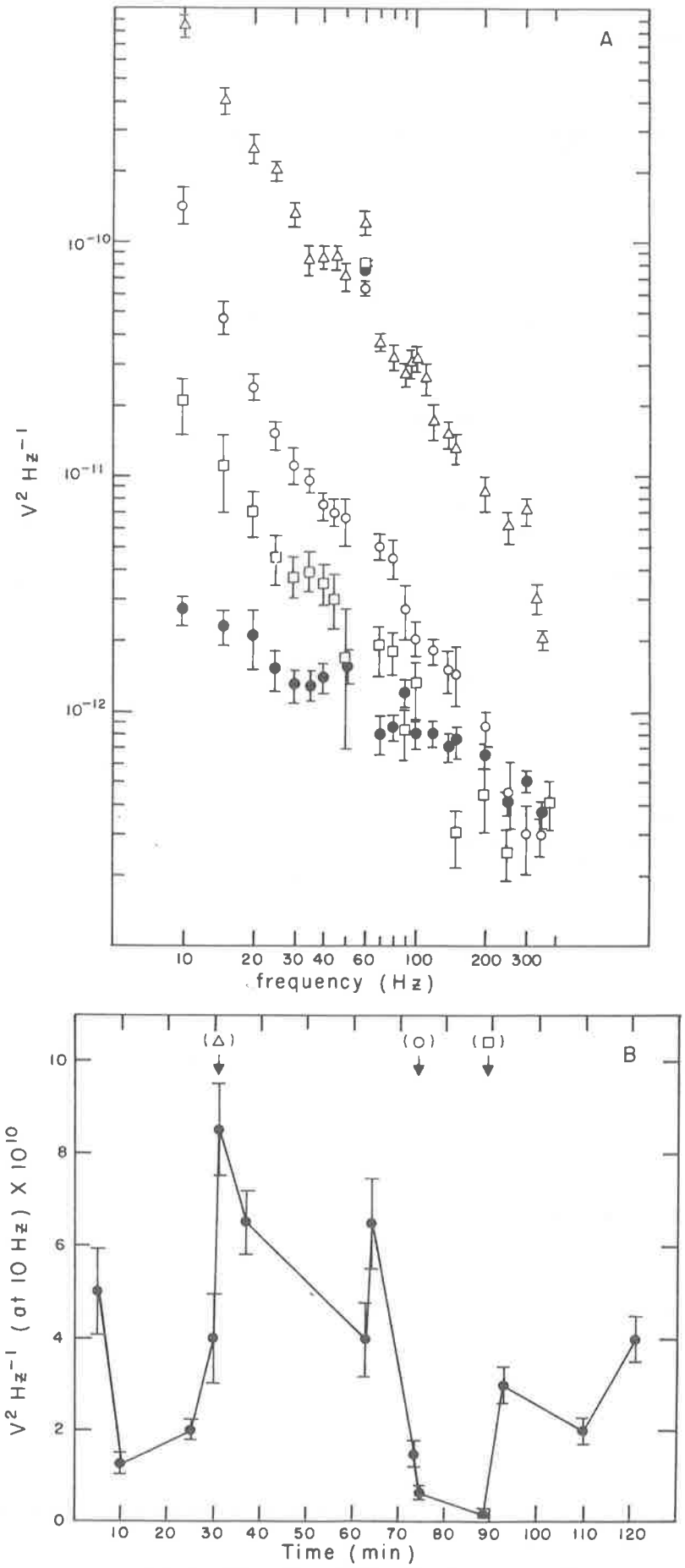


FIG. 1. A: voltage fluctuation power spectra measured at different times. The lowest power spectrum (●) represents noise produced by the electrodes. There is a narrow peak at 60 Hz produced by leakage from the power line into the measuring circuit. Each spectrum is an average of eight spectra which are based on 512 data points each. The error bars represent the standard error of the mean for the eight averaged spectra. B: time course of the voltage fluctuation power at 10 Hz.

The electrode resistance was also checked during the measurements, to see that there was not a large increase that would increase electrode noise.

## RESULTS

At least six measurements of plasmalemma voltage noise were made per cell on 20 *C. corallina* cells under standard conditions, and on 10 cells under high external $K^+$ concentration (10 mM). The magnitude of the measurable noise was quite variable. Some cells showed little measurable noise even though they had a high magnitude of membrane potential (about −200 mv) and exhibited normal cyclosis. Other cells showed relatively large noise levels, the magnitude of which had a time-dependent variation of irregular period (Fig. 1).

The measurable plasmalemma noise power spectrum generally has a slope of −2 on a log-log plot in the range of 5 to 300 Hz.

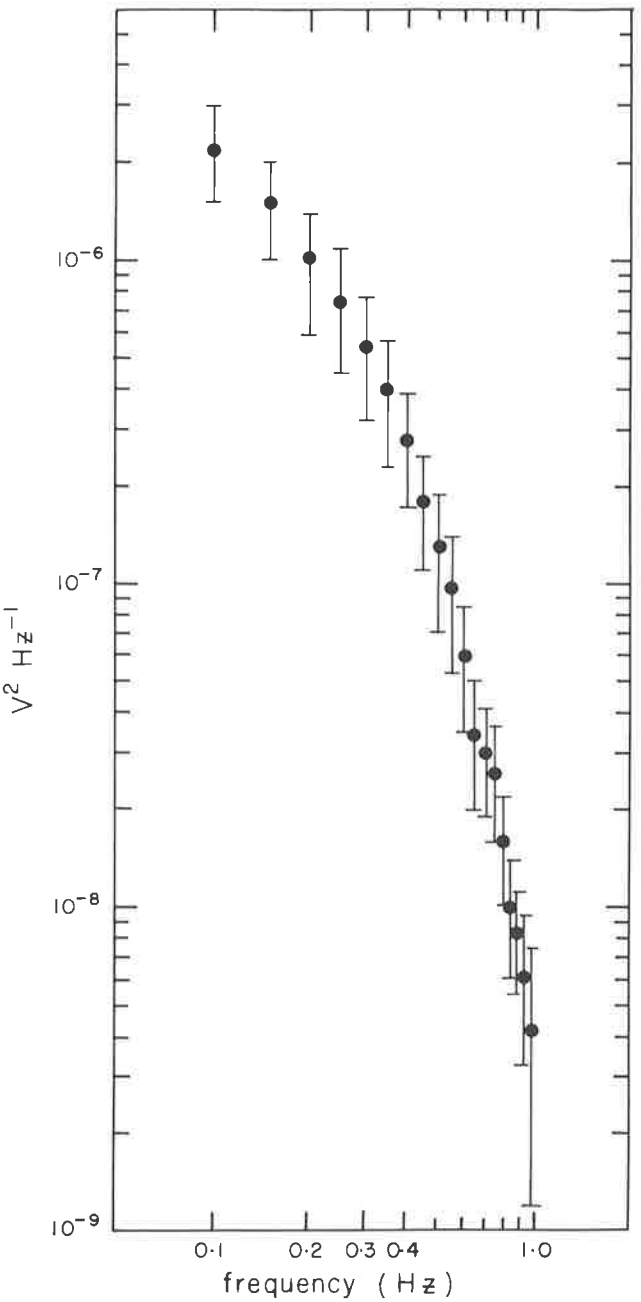


FIG. 2. Low frequency voltage fluctuation power spectrum.

Below 5 Hz the slope can become as steep as −4. This is in contrast to the slope of the power spectrum from the electrodes alone, which is between 0 and 1 in the 5- to 300-Hz range and may be as steep as −2 at lower frequencies. A representative low frequency power spectrum for plasmalemma noise is shown in Figure 2.

The most interesting feature of the noise spectra is the existence of "peaks" or "bumps" in the range of 20 to 55 Hz. These bumps were found under conditions which promote high rates of $HCO_3^-$ and $OH^-$ transport. The bumps show up above the −2 slope and have characteristic frequencies that shift slightly from measurement to measurement (Fig. 3). These bumps persist in the dark, but disappear when the cell is exposed to high external $K^+$ concentration (10 mM) for 16 h.

The −2 slope between 5 and 300 Hz is essentially unchanged under dark or high $K^+$ condition (Fig. 4). The −2 slope noise under dark or high $K^+$ is generally of the same order of magnitude as under normal conditions, but can be somewhat higher or lower than under normal conditions. The low frequency (0.1–5 Hz) slope under high $K^+$ is generally lower than under normal conditions, usually near −2.

## DISCUSSION

**Interpretation of Voltage Noise.** All real processes produce noise because of the probabilistic nature of molecular interactions, which results in fluctuations of concentration and transport rates. The purpose of noise analysis is 2-fold. The first aim is to help produce and test meaningful models for processes at the molecular level. The second aim is to characterize different processes by their noise spectra, so that the effects of various treatments on such processes can be studied.

Fluctuations can be analyzed mathematically in terms of total noise, or in terms of noise as a function of frequency. The former measure of noise consists simply of calculating the variance of the measured quantity. The data points are collected at a uniform sampling rate, and linear trends are usually removed before calculating the variance. The second method of noise analysis involves calculating the strength of the fluctuations at different frequencies. Random fluctuations occur in the form of perturbations of a quantity away from its time-average mean value. These perturbations decay toward the mean value with a lifetime that depends on the molecular interactions of the process. If this lifetime is very long, only very low frequencies will appear in the spectrum. The shorter the fluctuation lifetime, the greater the frequency to which the spectrum extends before falling toward zero. The decay of the fluctuations can be mathematically analyzed as the autocorrelation (or autocovariance) function, which involves calculating the covariance of a time series of data points with the same series of points which has been shifted along the time axis (with mean and linear drift removed from the data). This covariance as a function of time is the autocorrelation function. A Fourier analysis of the autocorrelation function yields the power spectrum, which shows the noise energy as a function of frequency. We used a maximum time shift ("lag time") in the autocorrelation function of $10^2$/sampling rate, and an averaging procedure known as a "hanning window," which ensures that points in the power spectrum that are (sample rate)/$10^2$ apart are nearly statistically independent.

The voltage noise measured with an electrode in the cell is attributable to fluctuations in ion transport rate across the plasmalemma, since the plasmalemma provides the highest resistance between the electrode tips. The voltage fluctuation power spectrum, $S_V(f)$, is equal to the power spectrum for current fluctuations, $S_I(f)$, multiplied by $|Z(f)|^2$, where $Z(f)$ is plasmalemma impedance and $f$ is frequency (see refs. 9, 19, and 23 for discussions on this point). Using the results of Coster and Smith (7) $|Z(f)|$ for *C. corallina* whorl cells can be calculated. It is a concave function, decreasing monotonically with frequency. Below 5 Hz $|Z|$ is

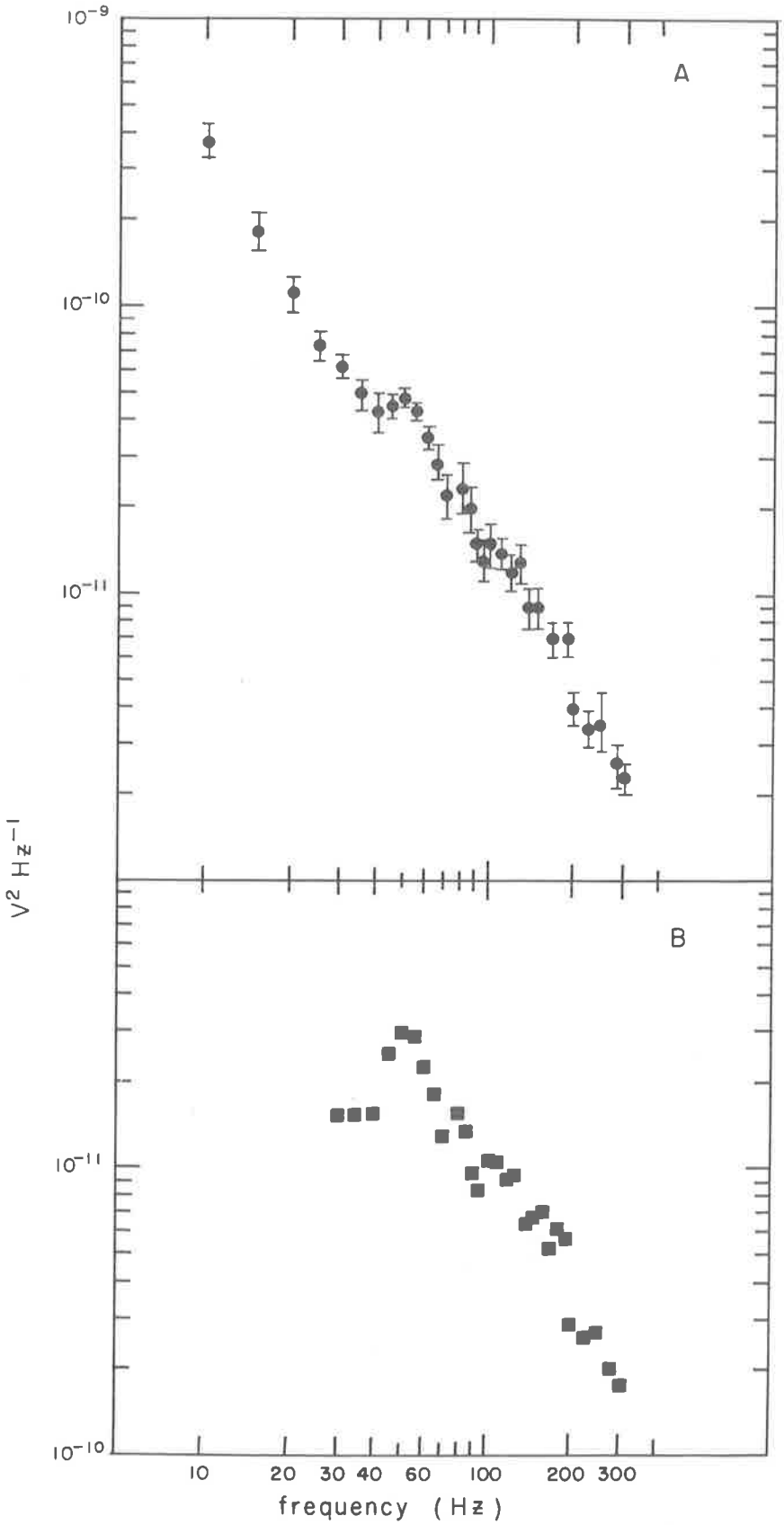


FIG. 3. A typical power spectrum measured under standard conditions. B: spectrum resulting from fitting a straight line with −2 slope to the first four points in the spectrum in part A, and subtracting this line from the other points in part A.

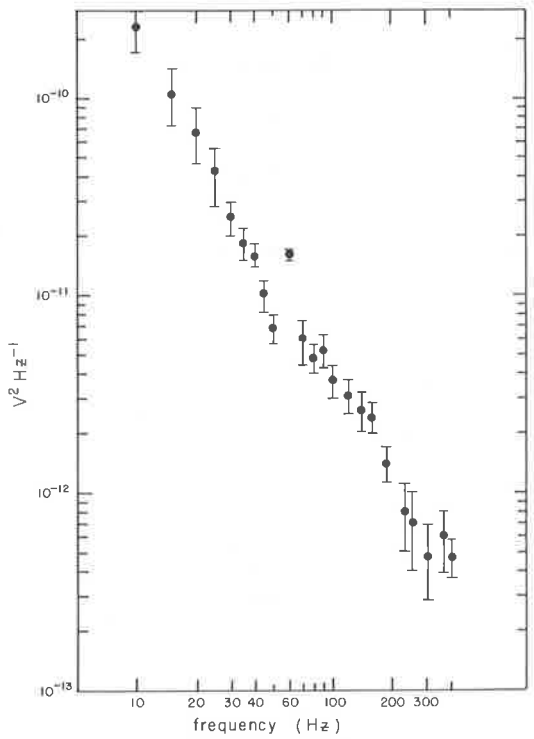


FIG. 4. Typical power spectrum measured with the cell in 10 mM $K^+$ for 16 h.

essentially constant, while between 10 and 100 Hz $|Z|$ has a slope on a log-log plot of about $-0.60 \pm 0.07$. This is less of a slope than expected from a purely passive membrane with constant resistance and capacitance. According to Coster and Smith (7) these parameters are functions of frequency. The membrane time constant ranges from 11.7 ms at 10 Hz to 4.7 ms at 100 Hz. This may include a frequency dependence for the pump conductance.

Coster and Smith used short cells (~2 mm), that were "space-clamped" with an internal current injection electrode running the length of the cell. This method provides a correct measurement of impedance, without having to correct for the cable effects (see ref. 25 for a discussion of the cable effect). Our measurements of impedance show less of a slope than do the results of Coster and Smith, probably because our long cylindrical cells partially offset the effect of capacitance. The relation between the voltage spectrum and the current spectrum should be given by the impedance as measured by Coster and Smith, *i.e.* the cable effect should not have a large effect on voltage noise. (The cable effect produces an increase in impedance with frequency, but the effect of this on voltage noise will be largely offset by a greater attenuation of voltage noise with distance from the current fluctuation.) Our results and those of Coster and Smith show an absence of peaks or bumps in the impedance between 0.1 and 300 Hz.

There are a number of plasmalemma transport processes in *C. corallina*. Lucas (11) has provided evidence for a large $HCO_3^-$ influx. According to a model proposed by Lucas (13) the $HCO_3^-$ transport would be active and electrogenic. It would be closely linked to photosynthesis, and would be expected to shut down in the dark. There is also a strong possibility of considerable $OH^-$ active transport (12) which would shut down after 10 min under dark conditions. There may be smaller $H^+$, $Cl^-$, and $Na^+$ active fluxes and there are almost certainly passive fluxes of $Cl^-$, $K^+$, $Na^+$, and $Ca^{2+}$ (8, 15). All of these ionic fluxes could contribute to the noise power spectrum.

All theoretical interpretations of noise spectra rest on the assumption of stationarity, but it is unlikely that any real process is perfectly stationary. A stationary process is one in which the underlying stochastic transition probabilities are not changing with time. If the potential or current values averaged over a few seconds are changing with time, the underlying processes are probably not stationary. If the change of such a time-averaged potential is small over the time period required to collect enough data to calculate a noise spectrum, and if the spectra calculated over neighboring time intervals are similar, then we are probably close enough to stationarity for practical purposes.

**Low Frequency Noise.** The low frequency noise (Fig. 2) is similar to that measured in *C. braunii* by Roa and Pickard (17, 18). Inasmuch as our measurements and those of Coster and Smith (7) show that the impedance is a fairly flat function of frequency in the range of 0.1 to 5 Hz, the steep slope in the voltage noise power spectrum is probably a real feature of the current power spectrum, and not a result of a steep slope for $|Z(f)|^2$. Rather than representing noise produced by random fluctuations of current associated with individual channels or carriers, it seems likely that the low frequency spectrum results from the kind of small oscillations in plasmalemma potential measured in *Nitella pulchella* by Ogato and Kishimoto (16), which we also observe in *C. corallina*, which have a period of minutes to tens of minutes.

**Interpretation of the −2 slope.** Two kinds of noise have been found in spectra measured in axons (6, 9, 22). These are characterized by their frequency dependence, either as $1/f$ or $1/f^2$, which give slopes of $-1$ and $-2$ on a log-log plot. Fluctuations in the number of open channels should give a current noise power spectrum with a slope of $-2$ on a log-log plot, except at sufficiently low frequencies where it would have a zero slope (this assumes that the closing of an open channel is a Poisson process, *i.e.* that the probability of closing is not time-dependent). However, the slope for $|Z|$ of approximately $-0.5$ above 10 Hz implies that the current noise actually has a slope of about $-1$. This is similar to the component of the current noise measured in squid axon which is usually attributed to fluctuations of $K^+$ current *within* individual channels (9), rather than to fluctuations in channel number.

According to a model proposed by F. N. Hooge and applied by Stevens (22) to $1/f$ noise in membranes, noise produced by a given ion species should be proportional to the conductance attributable to that species, and to the square of the driving force on that species. The conductance associated with passive transport of $K^+$ in *Chara* is not known with any precision, nor is the driving force. It is known that under high external $K^+$, the membrane conductance is greatly increased ($\sim \times 10$) relative to standard conditions, the membrane potential depolarizes, and the cell behaves like a $K^+$ electrode (10, 21). Although the driving force on $K^+$ transport is presumably small, the $K^+$ conductance must be quite large, so the "return current" for any electrogenic pumping which persists is probably carried by $K^+$ under such conditions. Even though the passive conductance for other ion species is almost certainly much lower than that for $K^+$ in the depolarized state, the driving force may be larger, so a contribution from other species to $1/f$ noise cannot be ruled out. Under standard conditions, the $K^+$ conductance will be lower than in the depolarized state, but the effect of this on voltage noise should be more than offset by the increase in $|Z|^2$. The driving force on $K^+$ under normal conditions is probably higher than in the depolarized state, possibly as high as $-20$ mv, so that an increase in the $K^+$ contribution to $1/f$ noise would be expected.

**Interpretation of Bumps in the Spectrum.** The possibility that the bumps in the voltage spectrum could be explained as the result of an impedance with similar bumps can be ruled out. There is no hint of such a $|Z(f)|$ behavior in the results of Coster and Smith (7) or in our measurements of impedance.

Since our results showing a $1/f^2$ dependence of the voltage noise spectrum represent an approximately $1/f$ dependence of the current noise, the bumps seen in the voltage spectrum between 20

and 55 Hz (Figs. 1 and 3) may actually represent a $1/f^2$ component of the current noise. Fishman (9) and Conti *et al.* (6) have found both a $1/f$ and $1/f^2$ component for current noise in squid axon. The $1/f^2$ component is seen after the $1/f$ component is subtracted from the current power spectrum.

In our results, subtracting a line with $-2$ slope from the voltage power spectrum, is equivalent to first subtracting a $-1$ slope line to correct for $|Z|^2$, and then subtracting another $-1$ slope line to remove the $1/f$ current noise. Figure 3B shows that this results in a bump with a $1/f^2$ dependence on the high frequency side. As mentioned above, such a power spectrum can result from fluctuations in the number of open channels.

If we adopt such an interpretation, and assume that the peak of the bump can be taken to be the corner frequency of such a spectrum, then we can calculate a lifetime for the closing open channels. This would be $1/(2\pi \times$ corner frequency), or 3 to 8 ms. These values are similar to those obtained for $K^+$ channel lifetimes in axon (6, 9).

The amplitude of such a spectrum would be equal to $4I^2\tau/N$, where $I$ is current, $\tau$ is the lifetime, and $N$ is the number of open channels (22, 23). The amplitude of the bump in Figure 3B translates to about $3 \times 10^{-19}$ amp$^2$ Hz$^{-1}$, using $|Z|^2 \simeq 10^8\ \Omega^2$. Using the measured unidirectional flux (8) as an upper bound for net current, $I \leq 10^{-7}$ amp, and we have $N < 10^3$ for a cell with 1 cm$^2$ surface area, under normal conditions. The conductance per channel would be greater than $5 \times 10^{-9}\ \Omega^{-1}$ for $K^+$, at least $10^2$ times larger than the values obtained for $K^+$ and $Na^+$ channels in axons and end plates (1, 6, 19).

The bumps may be associated with active transport. They can persist for at least 2 h in high $K^+$ concentration, but following 16 h there are no measurable bumps in the 20- to 55-Hz range. A decrease in transport rate for the system producing the bumps, and the decrease in plasmalemma impedance which occurs under high external $K^+$ concentration (10, 21), could both contribute to the decreased magnitude of the bumps. High $K^+$ concentration has been shown to reduce substantially net $H^{14}CO_3^-$ tracer uptake in an "all-or-none" fashion. This treatment appears to convert the $HCO_3^-$ transport system into a facilitated diffusion process with a much lower transport rate (14).

If the bumps are associated with $HCO_3^-$ or $OH^-$ transport, the magnitude of the bumps would be expected to decrease in the dark, when $HCO_3^-$ and $OH^-$ transport are expected to decrease. However, the time scale for $HCO_3^-$ transport shut-down in the dark has not been established. The plasmalemma impedance is known to increase in the dark (15), which would tend to counteract the effect on voltage noise of a change in transport rates.

A possible explanation for such bumps is that there is a periodically correlated random variable which contributes to the fluctuations. Another way of saying this is that the exponential decay type of autocorrelation expected of a Poisson process is somehow modulated by a sinusoidal variation. It can be easily shown using the modulation theorem of Fourier analysis (2) that such a process would lead to a power spectrum with a bump. The frequency at the center of the bump would be equal to that of the sinusoidal modulation, while the half-width of the bump would be related to the lifetime of the Poisson process. Chen (3) has shown that a steady-state cycling process in which detailed balancing does not hold is one way to obtain such a power spectrum. Chen (5) has also shown that the presence of such a bump implies that the system is not at thermodynamic equilibrium. This does not imply that the particular process directly responsible for the bump is "active," but that it is associated in some way with an active process.

The frequency at the center of the largest bump varies between 20 and 55 Hz, while the half-power frequency of the bump varies between 10 and 20 Hz. Thus, the time constants are $5 \pm 2$ ms and $12 \pm 4$ ms. The identification of these time constants with particular molecular steps in an active transport process must of cours wait on future work.

**Time Dependence of the Noise.** The time dependence of th noise is difficult to explain. It would seem that the time depenc ence of the noise should be related to a time dependence of io flux rate. However, the entire spectrum seems to be time-depenc ent. This means that if different processes produce the $-2$ slop and the bumps, these different processes must have the same tim dependence for their flux rates. There is no evidence that larg time-dependent oscillations in impedance occur under stable cor ditions.

The measured voltage fluctuations associated with ion transpo across the plasmalemma of *C. corallina* are complex, varying fror cell to cell, but showing characteristic patterns. The low frequenc spectrum is probably not associated with random fluctuations, bu rather with small oscillations of fairly regular period in the mem brane potential. The $-2$ slope in the 5- to 300-Hz range is probabl associated with current fluctuations within passive ion transpo channels. Bumps in the power spectrum in the 20- to 55-Hz rang may be associated with fluctuations in the number of open chan nels, or alternatively with active transport, possibly of $HCO_3^-$ o $OH^-$. Further use of noise analysis in conjunction with precis inhibition of the various transport systems should provide infor mation regarding the molecular level aspects of these systems.

## LITERATURE CITED


1. Anderson CR, CF Stevens 1973 Voltage clamp analysis of acetylcholine produced end-pla current fluctuations at frog neuromuscular junction. J Physiol 235: 655–691
2. Blackman RB, JW Tukey 1959 The Measurement of Power Spectra from the Point of Vie of Communications Engineering. Dover, New York
3. Chen Y 1975 Fluctuations and noise in kinetic systems. III. Cycling steady state models. Theor Biol 55: 229–243
4. Chen Y 1976 Differentiation of channel models by noise analysis. Biophys J 16: 965–971
5. Chen Y 1978 Differentiation between equilibrium and nonequilibrium kinetic systems b noise analysis. Biophys J 21: 279–285
6. Conti F, LJ De Felice, E Wanke 1975 Potassium and sodium ion current noise in th membrane of the squid giant axon. J Physiol 248: 45–82
7. Coster HGL, JR Smith 1977 Low-frequency impedance of *Chara corallina*: simultaneou measurements of the separate plasmalemma and tonoplast capacitance and conductanc Aust J Plant Physiol 4: 667–674
8. Findlay GP, AB Hope, MG Pitman, FA Smith, NA Walker 1969 Ionic fluxes in cells c *Chara corallina*. Biochim Biophys Acta 183: 565–576
9. Fishman HM 1973 Relaxation spectra of potassium noise from squid axon membranes. Pro Nat Acad Sci USA 70: 876–879
10. Hope AB, NA Walker 1961 Ionic relations of cells of *Chara australis* RBR. IV. Membran potential differences and resistances. Aust J Biol Sci 14: 26–44
11. Lucas WJ 1975 Photosynthetic fixation of $^{11}$carbon by internodal cells of *Chara corallina*. Exp Bot 26: 331–346
12. Lucas WJ 1975 The influence of light intensity on the activation and operation of the hydroxy efflux system of *Chara corallina*. J Exp Bot 26: 347–360
13. Lucas WJ, JM Ferrier, J Dainty 1977 Plasmalemma transport of $OH^-$ in *Chara corallina* Dynamics of activation and deactivation. J Membr Biol 32: 42–73
14. Lucas WJ, RM Spanswick, J Dainty 1978 $HCO_3^-$ influx across the plasmalemma of *Char corallina*. Plant Physiol 61: 487–493
15. MacRobbie EAC 1970 Active transport of ions in plant cells. Q Rev Biophys 3: 252–293
16. Ogata K, U Kishimoto 1976 Rhythmic change of membrane potential and cyclosis of *Nitell* internode. Plant Cell Physiol 17: 201–207
17. Roa RL, WF Pickard 1976 The use of membrane electrical noise in the study of Characea electrophysiology. J. Exp Bot 27: 460–472
18. Roa RL, WF Pickard 1977 Further experiments on the low frequency excess noise in th vacuolar resting potential of *Chara braunii*. J Exp Bot 28: 1–16
19. Sachs F, H Lecar 1973 Acetycholine noise in tissue culture muscle cells. Nature New Bio 246: 214–216
20. Segal JR 1972 Electrical fluctuations associated with active transport. Biophys J 12: 1371 1390
21. Spanswick RM 1972 Evidence for an electrogenic ion pump in *Nitella translucens*. I. Th effects of pH, $K^+$, $Na^+$, light and temperature on the membrane potential and resistance Biochim Biophys Acta 288: 73–89
22. Stevens CF 1972 Inferences about membrane properties from electrical noise measurements Biophys J 12: 1028–1047
23. Strandberg MWP, EL Hammer 1975 Current-fluctuation noise in toad urinary bladde during active transport of sodium ions. J Appl Phys 46: 3661–3671
24. Warncke J, CL Slayman 1978 Voltage noise of $H^+$ transport in *Neurospora*. Biophys J 21 128a
25. Williams EJ, RJ Johnston, J Dainty 1964 The electrical resistance and capacitance of th membrane of *Nitella translucens*. J Exp Bot 15: 1–14

*Journal of Experimental Botany, Vol. 30, No. 117, pp. 705–718, August 1979*

# Plasmalemma Transport of $OH^-$ in *Chara corallina*

## II. FURTHER ANALYSIS OF THE DIFFUSION SYSTEM ASSOCIATED WITH $OH^-$ EFFLUX

J. M. FERRIER

*Department of Botany, University of Toronto, Toronto, Ontario, Canada M5S 1A1*

AND

W. J. LUCAS

*Department of Botany, University of California, Davis, California 95616, U.S.A.*

Received 18 December 1978

ABSTRACT

The dynamic and steady state aspects of the pH and electric potential ($\psi$) profiles, that develop in the experimental medium in association with the photosynthetic assimilation of exogenous $HCO_3^-$ by internodal cells of *Chara corallina*, were investigated. A theoretical treatment is presented which explains the origin of the $\psi$ phenomenon. This theory was tested by comparing the pH and $\psi$ values generated by a numerical analysis model (which simulated the experimental system) against experimental data. Verification of our model indicates that the steady state ionic fluxes, associated with $HCO_3^-$ assimilation ($HCO_3^-$, $OH^-$, and $CO_3^{2-}$), are not significantly influenced by the electric potential gradients. The main driving force causing the observed fluxes is the diffusion gradient associated with the respective ion.

By simultaneous measurement of $\psi$ and pH, at the centre of an alkaline band, a direct correlation was established between light-activation and dark-deactivation of the $OH^-$ transport system and the light-mediated changes in $\psi$ at the cell surface. In addition, under steady state conditions, an almost perfect correlation was observed between alkaline band pH centres and the negative electric potential maxima. These data offer strong support for the hypothesis that $OH^-$ efflux, in this system, is an electrogenic process.

Based on our present analysis, the $\psi$ profile along the cell indicates that, in terms of the spatial aspect of $HCO_3^-$ transport, the rate of $HCO_3^-$ influx varies quite dramatically along the length of an internodal cell. This aspect is discussed in terms of the cellular integration of $OH^-$ and $HCO_3^-$ transport in this species.

## INTRODUCTION

In the presence of exogenous $HCO_3^-$, internodal cells of *Chara corallina* develop light-dependent alkaline regions on their cell surface (Lucas and Smith, 1973). These alkaline regions have been investigated quite extensively in recent years.

Lucas (1975*a*) and Lucas, Ferrier, and Dainty (1977) analysed the transport of $OH^-$ away from the *Chara corallina* cell surface, into the experimental bathing medium, in terms of a diffusional process. These authors reported measurements of pH profiles both along and perpendicular to the cell surface. Based on these experi-

mentally measured profiles, they presented results of theoretical diffusion calculations that related the observed gradients to ionic flux rates at the cell surface, both at steady state and for the time-dependent processes that are associated with light/dark transitions. The numerical analysis programme which was used to model the diffusion system took into account not only the movement of $OH^-$, but also the interrelated fluxes of $HCO_3^-$ and $CO_3^{2-}$.

Walker and Smith (1977) measured electric currents and electric potential gradients in the bathing medium around cells of *C. corallina*. They interpreted their results in terms of the electrical influence imposed on the system by the transport of $HCO_3^-$ and $H^+$ ($OH^-$?) across the plasmalemma. However, their theoretical calculation of electric current in the bathing medium, based on their $\psi$ measurements, is in error.

Walker and Smith (1977) assumed that the electric current in the bathing medium was driven by the gradient of electric potential. That is, they assumed that $I = -\sigma\nabla\psi$, where $I$ is the current density, $\sigma$ is the electrical conductivity of the medium, and $\nabla\psi$ is the gradient of electric potential. This is correct only if the main driving force for the current is the gradient of electric potential, and if all ions carry current in proportion to their respective concentrations and mobilities. However, the measured electric potential gradient (Walker and Smith, 1977) is small compared to the chemical potential gradient represented by the measured pH gradient (Lucas, 1975*a*; Lucas *et al.*, 1977). Thus the contribution of the electrical driving force to the transport of $OH^-$ must be small. The theoretical calculations of Walker and Smith (1977) can only be valid for a time of the order of a few minutes after activation of $HCO_3^-$ and $OH^-$ transport across the plasmalemma. After this time the process of diffusion establishes the concentration profiles required to carry the ionic current.

In the present paper we develop the correct theoretical analysis for the electric potential measurements associated with this experimental system. This electric potential component was incorporated into our previous $OH^-$ diffusion model (Lucas *et al.*, 1977) and the theoretical results compared to experimental data obtained by simultaneous measurement of both $\psi$ and pH. These studies verified our previous diffusion model. The results are discussed in terms of this process of diffusion and the spatial distribution of the $HCO_3^-$ and $OH^-$ transporters, along the giant internodal cells of this species.

## MATERIALS AND METHODS

### *Culture material*

Culture material of *Chara corallina* Klein ex Willd., em. R.D.W. (= *C. australis* R. Br.) was grown in the laboratory under artificial light. Mature cells (third to fourth internodal cells) were cut from the culture 24 h prior to being used in an experiment. During this recovery period cells were bathed in a pretreatment solution containing (mM): NaCl, 1·0; KCl, 0·2; $CaSO_4$, 0·2; and $NaHCO_3$, 0·5 (initial pH 7·7).

### *Simultaneous measurement of pH values and electric potential*

A special perspex holder was employed which held a miniature pH electrode (Microelectrodes Inc., Model MI-405) and a glass microelectrode (tip diameter 50–80 $\mu$m), in an orientation such

that the two sensing tips were as close together as physically possible. The two electrode centres were held within the same plane perpendicular to the cell axis; however, the relative position of the two tips was such that they touched the cell surface at slightly different circumferential positions. This circumferential separation was approximately 300 $\mu$m. A Leitz micromanipulator was used to move the electrode pair along the cell wall.

The pH values along the *Chara* cell surface, and in the radial direction away from the cell surface, were measured using the techniques developed by Lucas and Smith (1973) and Lucas (1975*a*). Agar blocks, that were used as embedding media for experimental cells, were prepared in the manner described by Lucas and Dainty (1977). All experimental solutions contained (mM): NaCl, 1·0; KCl, 0·2; $CaSO_4$, 0·2; $NaHCO_3$, 0·5 (pH 7·7), unless otherwise specified. The response of the miniature pH electrode was measured using a Beckman Model 4500 digital pH meter in conjunction with a Radiometer (Model K 401) calomel reference electrode.

Electrical potential measurements were made using a Keithley 604 electrometer in the differential mode. Glass electrodes were filled with a solution containing 0·7% (w/v) agar and 10 mM KCl. Electrical contact between the electrode and a calomel reference junction was made using tygon tubing filled with identical solution. The signal from the calomel reference junction was fed to the high input of the electrometer. The low input was connected to the same calomel reference electrode used for the pH measuring circuit. This input was connected to a common ground for the system. This system was tested and found to be light-insensitive.

All experiments were performed in a thermostatted (25 °C) experimental chamber. Spurious electrical noise generated by the thermostatting fluid was significantly reduced by using high purity, low viscosity, liquid paraffin. The light source was a Leitz-Pradovit 24 V, 150 W quartz-iodide projector. The irradiance value was adjusted to 20 W $m^{-2}$ using nickel-Nicron neutral density filters, and was measured before and after an experiment using a silicon solar cell (IRC, type No. S 05 10E 7PL).

*Theoretical treatment*

We consider the correct theoretical interpretation of the external electric potential phenomenon to be as follows. The transport of $OH^-$, $HCO_3^-$, and $CO_3^{2-}$ (produced by the titration of $HCO_3^-$ by $OH^-$), in the bathing medium surrounding an illuminated *Chara* cell, is largely a diffusion process. We will assume in accordance with the measured flux values (Lucas, 1975*a*; Lucas *et al.*, 1977) that the transport of $OH^-$, $HCO_3^-$, and $CO_3^{2-}$ is considerably greater than the transport of other species. Hydroxyl, $HCO_3^-$, and $CO_3^{2-}$ will be referred to as the 'transported species', while the other species, which for the present system would include $Na^+$, $K^+$, $Ca^{2+}$, $Cl^-$, and $SO_4^{2-}$, will be referred to as the 'non-transported species'.

The existence of the concentration gradients for the transported species requires that the non-transported species develop concentration gradients to achieve charge neutrality. This, in turn, requires a small $\psi$ gradient produced by a very small net charge to balance the concentration gradients of the non-transported species. Hence, the $\psi$ gradient is somewhat analogous to a diffusion potential. The net charge distribution responsible for the $\psi$ gradient will be so small that charge neutrality will hold to an excellent approximation at all times. During the time-dependent build-up or depletion of the concentration gradients of the transported species (which would occur upon transferring a cell either to the light or the dark), the non-transported species will undergo a small, but continuous, adjustment of concentration distribution to maintain charge neutrality.

The flux of an ionic species in the external medium surrounding an experimental *Chara* cell will be the result of two 'driving forces', namely the electric potential gradient and the concentration gradient for that species. This can be represented mathematically by the following general equation:

$$J_i = -\lambda_i z_i e C_i \nabla\psi - \lambda_i kT \nabla C_i \qquad (1)$$

where $J_i$ is the flux of species $i$ (mol $cm^{-2}$ $s^{-1}$), $\lambda_i$ is its mobility (cm $s^{-1}$ $dyne^{-1}$), $z_i$ is its valency, $e$ is the electron charge (coulombs), $kT$ is the product of the Boltzmann constant and the absolute temperature (ergs), $\nabla$ represents the gradient of either electric potential or concentration, $C_i$ is the concentration of the species $i$ (mol $cm^{-3}$), and $\psi$ is the electric potential (V).

The condition of charge neutrality, at any point in the experimental medium, can be expressed as:

$$\sum_{i=1}^{n} z_i C_i = 0 \qquad (2)$$

where there are a total of $n$ ionic species. If there are $k$ species of transported ions, and we designate these as the first through $k$th species, we can write

$$\sum_{i=k+1}^{n} z_i C_i = -\sum_{i=1}^{k} z_i C_i. \tag{3}$$

Equation 3 can be rewritten as

$$\sum_{i=k+1}^{n} z_i \frac{\delta C_i}{\delta t} = -\sum_{i=1}^{k} z_i \frac{\delta C_i}{\delta t}. \tag{4}$$

Then, since $-\nabla . J_i = \delta C_i/\delta t$, equations 1 and 4 can be combined to give

$$\sum_{i=k+1}^{n} z_i(\lambda_i z_i e C_i \nabla^2 \psi + \lambda_i z_i e \nabla C_i . \nabla \psi + \lambda_i kT \nabla^2 C_i) = -\sum_{i=1}^{k} z_i \frac{\delta C_i}{\delta t}. \tag{5}$$

Of the terms on the left-hand side of equation 5 the second is small, compared to the others, and will be ignored. To facilitate the numerical calculation, and also for conceptual reasons, we will split the electric potential into two terms, so that $\psi = \psi_0 + \psi_1$. Equation 5 can be satisfied by the following equations for $\psi_0$ and $\psi_1$:

$$\sum_{i=k+1}^{n} \lambda_i z_i^2 e C_i \nabla^2 \psi_0 = -\sum_{i=k+1}^{n} \lambda_i z_i kT \nabla^2 C_i \tag{6}$$

$$\sum_{i=k+1}^{n} \lambda_i z_i^2 e C_i \nabla^2 \psi_1 = -\sum_{i=1}^{k} z_i \frac{\delta C_i}{\delta t}. \tag{7}$$

Equation 3 can be combined with equation 6, and, since $\lambda_i$ will be approximately equal to $\lambda_j$ for all non-transported species, the result can be integrated to yield

$$\nabla \psi_0 = \left(\frac{kT}{e}\right) \frac{\sum_{i=1}^{k} z_i \nabla C_i}{\sum_{i=k+1}^{n} z_i^2 C_i}. \tag{8}$$

In obtaining equation 8, we have set the constant of integration equal to zero. This means that $\nabla\psi_0$ is the gradient of electric potential that balances the gradient of concentration of the non-transported species. Alternatively, equation 8 could have been obtained by setting $J_1 = 0$ for each non-transported species, and combining equations 1 and 3. Equation 8 will also satisfy (at steady state) the 'small' second term of the left-hand side of equation 5. The second term, $\psi_1$, is the component of electric potential that is responsible for producing the small flux, of the non-transported ions, that is required to match the build-up or depletion in the concentration of transported ions. Following light-activation of $OH^-$ efflux, $\psi_1$ will be about as important as $\psi_0$, i.e. it will be important during the build-up of the concentration gradients required to carry $OH^-$ and $CO_3^{2-}$ away from the cell, and will diminish to zero as the steady state situation is established. In the steady state only $\psi_0$ will be important.

*Numerical calculation*

Theoretical values of $\psi$ can be obtained using the numerical diffusion calculation of Lucas *et al.* (1977). The concentrations of the transported species, $OH^-$, $HCO_3^-$, and $CO_3^{2-}$, can be calculated as a function of position in the external bathing medium. Equation 8 can then be integrated numerically from one diffusional volume element to the next to obtain $\psi_0$. Equation 7 can be solved by an iterative method which calculates new values of $\lambda_1$ from old values using difference equations to approximate $\nabla^2 \psi_1$. In performing these calculations we found that 3 cycles of such an iterative procedure, per time step (0·5 s) of the numerical diffusion calculation, were sufficient to produce a smooth, stable solution for $\psi_1$. (Increasing the cycle number, per time step, to 5 changed the resultant $\psi_1$ value by less than 3%.)

Two other simplifying assumptions were made in performing the present calculations. Since the concentration differences of the non-transported species are small, in comparison to their absolute concentrations, we found that, to an accuracy of about 5%, we could assume that the absolute concentrations of these species remained constant when using equations 7 and 8. We also found that we could ignore the electrically driven term in the flux equation for the transported species. It was found in preliminary studies that including this term resulted in less than a 4% change in the calculated concentration profiles of the transported species.

## RESULTS

### *Simultaneous measurement of $\psi$ and pH values*

Experimental cells were illuminated (20 W $m^{-2}$) for 2 h prior to measuring the pH and $\psi$ profiles along the cell wall. (This period allows the establishment of the steady state condition within the vicinity of the cell surface (Lucas *et al.*, 1977).) For simultaneous $\psi$ and pH measurements, the electrode pair was positioned 6 cm vertically above the cell wall of the experimental cell and the differential electrometer output nulled to zero. The sensing tips were then lowered onto the cell wall, at a position 1·0–1·5 mm from the node and then traversed along the cell wall to map the pH and electric potential profiles. Figure 1 illustrates the observed pH and $\psi$ profiles. These data indicate an almost perfect correlation between the alkaline band pH centres and the negative $\psi$ maxima. There appears to be a

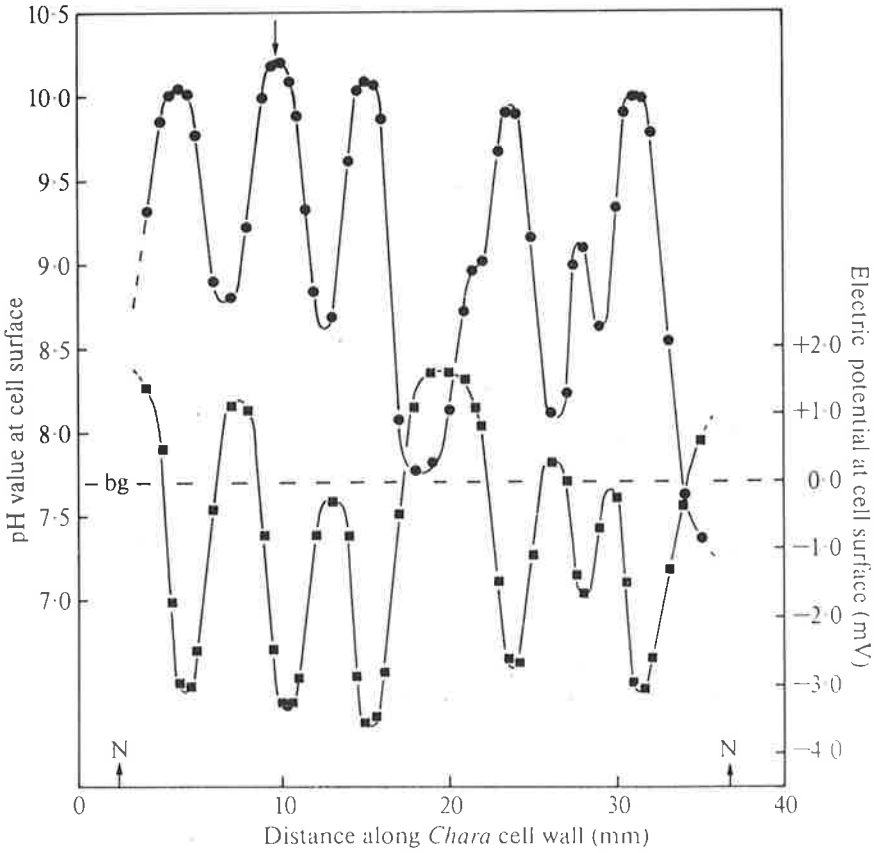


FIG. 1. Steady state electric potential (■) and pH (●) profiles measured along the surface of an internodal cell of *Chara corallina*. The $\psi$ and pH values were measured simultaneously using a special dual electrode holding system. The vertical arrow indicates the band centre of the $OH^-$ efflux system studied in the computer simulation. The symbol bg represents the background pH value of the bathing medium, and N represents the physical location of each node.

correlation not only of spatial position, but also of transport strength and the actual negative $\psi$ value. (The higher the band-centre pH value the greater the transport rate associated with that band (Lucas *et al.*, 1977).) Our results provide strong support for the proposal (Walker and Smith, 1977) that the negative $\psi$ values are generated by the alkaline band transport system. (We consider that an alkaline band is formed as the result of an $OH^-$ efflux process (Lucas, 1979; cf. Walker and Smith, 1977, and also Raven and Smith, 1978).)

This conclusion was further confirmed by the results obtained from alkaline band light-activation and dark-deactivation studies. In these experiments, the $\psi$ and pH sensing tips were located at the centre of an operational alkaline band, and then

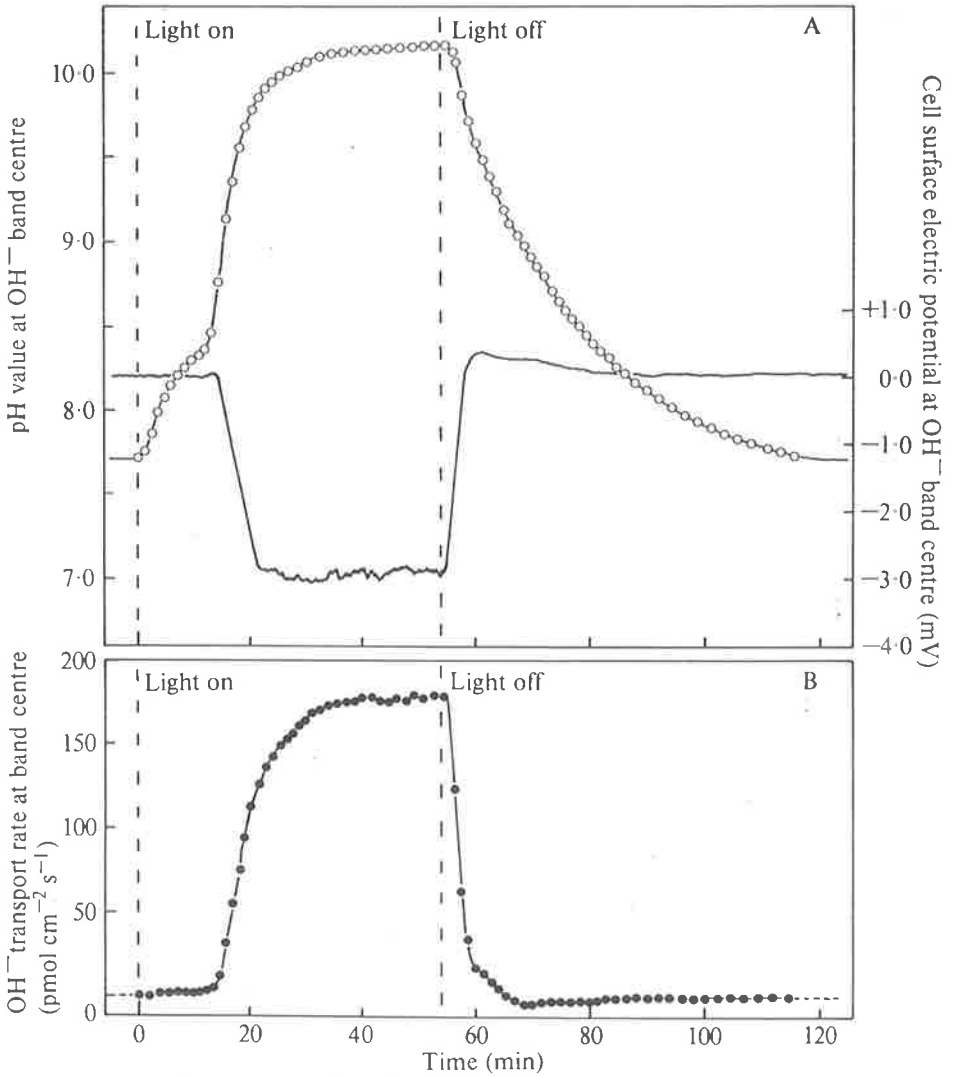


FIG. 2. Light-induced changes in cell wall pH and $\psi$ values and $OH^-$ transport function. Following a 2 h dark treatment the time course of pH and $\psi$ were measured (simultaneously) in response to cell illumination (20 W $m^{-2}$) and darkening (Fig. 2A). (The pH and $\psi$ sensing tips were located on the cell wall in the centre of an alkaline band.) The pH data and the steady state cell wall pH profile presented in Fig. 1 were used in the numerical programme of Lucas *et al.* (1977) to determine the time course of $OH^-$ efflux activation and deactivation (Fig. 2B). These calculations employed the self-diffusion coefficient for $OH^-$, $5{\cdot}32 \times 10^{-5}$ $cm^2$ $s^{-1}$. (The symbol, O, represents the target pH values generated by the numerical analysis programme.)

the cell was given a 2 h dark pretreatment. Upon reillumination the alkaline band always activated with its normal biphasic characteristic (Lucas, 1975*b*; Lucas *et al.*, 1977). The $\psi$ (at the cell surface), however, did not change until the alkaline band transport system entered its second exponential transport mode (Lucas *et al.*, 1977), i.e. where the actual transport rate increased dramatically as a function of time. This correlation between the activation of $OH^-$ transport and the light-induced change in $\psi$, at the cell surface, is illustrated in Fig. 2. The $OH^-$ efflux data presented in Fig. 2B were calculated using the target-pH programme (Lucas *et al.*, 1977), modified to include the electric potential phenomenon. The computed $OH^-$ efflux values depend upon the value of the $OH^-$ diffusion coefficient ($D_{OH^-}$) employed. This is an extremely important aspect, and will be dealt with extensively in the following sections.

As shown in Fig. 2, the light-induced electric potential decayed quite rapidly when the light was turned off. Again there was excellent correlation between the time course of the decline in $\psi$ and the deactivation of the $OH^-$ transport system.

*Computed electric potential profiles*

Initially it was hoped to perform a computer simulation of the $OH^-$ transport and $\psi$ profile along the entire length of an internodal cell. The size and complexity of the computer programme made the cost of such a simulation quite prohibitive. As a consequence we performed an in-detail simulation of a cell wall segment that contained a typical alkaline band. (This band was located within the 7–13 mm region of Fig. 1.) The region of calculation extended 28 mm along the cell surface from the centre of band symmetry, and 40 mm in the radial direction perpendicular to the cell surface. The region of $HCO_3^-$ uptake was taken to extend over the 13 mm segment furthest from the $OH^-$ efflux band centre. This corresponded to a shutdown of $HCO_3^-$ influx for surface pH values greater than 9·5.

The pH data associated with this band (light-activation, dark deactivation, and steady state cell wall pH profile) were used in the computer analysis, and the resultant profiles compared with the experimental data.

A close correlation was observed between the radial $OH^-$ concentration profile determined in the diffusion model and that measured experimentally (Fig. 3A). The $OH^-$ profile was insensitive to both the value of $D_{OH^-}$ (Fig. 3A) and the magnitude of $HCO_3^-$ influx (results not shown). The radial $\psi$ profile also exhibited spherical symmetry, however, its computed shape depended markedly upon the values of $D_{OH^-}$ and $HCO_3^-$ influx employed (Fig. 3B). The discrepancy between the experimental and calculated profiles was greatest when the $D_{OH^-}$ for self-diffusion was used. This deviation strongly suggests that the $OH^-$ and $CO_3^{2-}$ ions do not move by a purely self-diffusional process. The closest agreement between the experimental and computed radial $\psi$ profiles was observed when a numerical value equivalent to the limiting $D_{NaOH}$ was used, however, in all cases there was a difference in magnitude between experimental and computed $\psi$ values. This discrepancy (less negative calculated compared with the measured values) was a common feature observed for all aspects of the computer simulation.

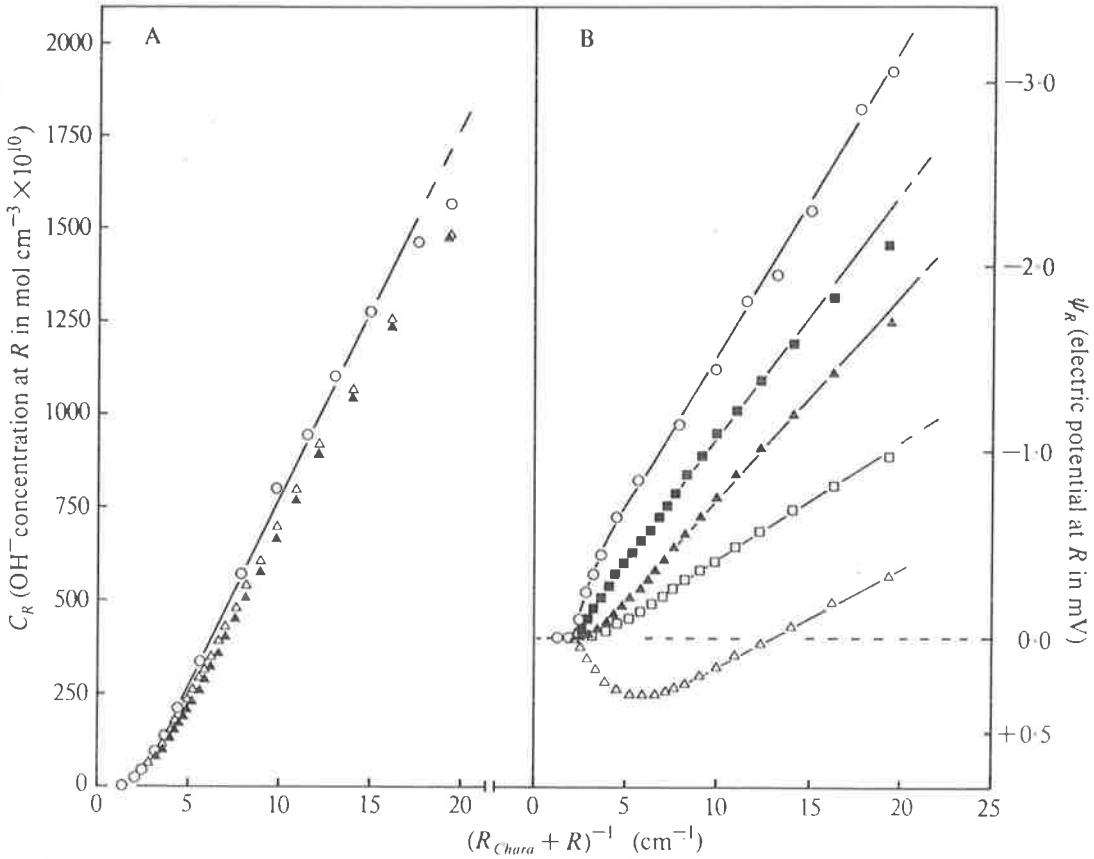


FIG. 3. Spherical diffusion analysis of experimental and theoretically determined radial values of pH and $\psi$. Symbols are as follows: $R_{Chara}$, radius of the experimental *Chara* cell; $R$. radial distance vertically above the cell surface; ○, experimental data; solid symbols represent values calculated using $D_{OH^-} = 2{\cdot}13 \times 10^{-5}$ $cm^2$ $s^{-1}$ (NaOH limiting diffusion coefficient) and for open symbols $D_{OH^-} = 5{\cdot}32 \times 10^{-5}$ $cm^2$ $s^{-1}$ ($OH^-$ self-diffusion coefficient) was used; the symbols △, and □ represent computer values determined assuming ratios of total $OH^-$ efflux : total $HCO_3^-$ influx of 1·0 and 2·5, respectively.

The sensitivity of the radial $\psi$ profile upon the strength of the $HCO_3^-$ uptake process, that occurs in the lateral regions of the OH band, indicates quite clearly the complexity of this physical system. This sensitivity enabled elucidation of certain basic features of the spatial distribution of $HCO_3^-$ transport (see Discussion).

*Light/dark-mediated changes in $\psi$ at cell surface*

Computed values of $\psi$ for the centre of the $OH^-$ efflux system were compared with experimental data. Various time courses for the response of $\psi$ to cell illumination and darkening are presented in Fig. 4. Again, the greatest discrepancy between theoretical and experimental data was observed when $D_{OH^-}$ for self-diffusion was employed (Fig. 4, △). (In this calculation the total $HCO_3^-$ flux, occurring on both sides of the alkaline band, was set equal to the $OH^-$ efflux.) This discrepancy could be partially reduced by lowering the $HCO_3^-/OH^-$ flux ratio (see Fig. 4). Excellent agreement was found between the shape of the calculated and experimental time courses when the smaller $D_{OH^-}$ was employed ($D_{OH^-}$ value equal to limiting $D_{NaOH}$ and $OH^-$ efflux across the membrane set equal to $HCO_3^-$ influx).

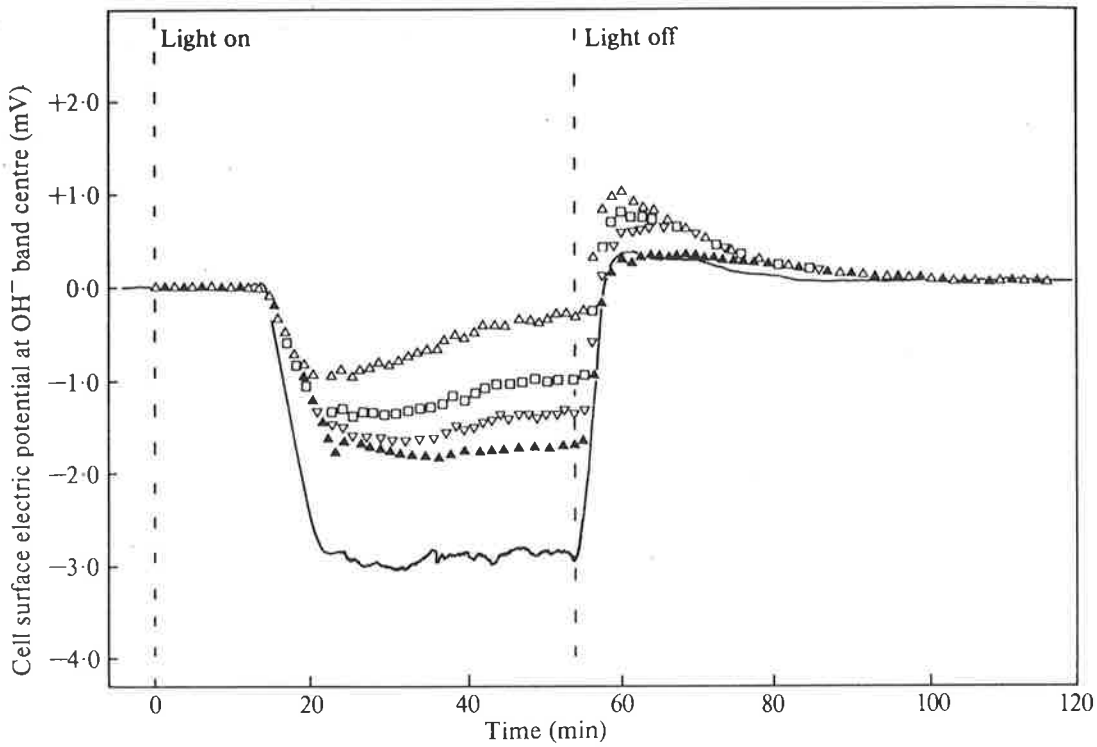


FIG. 4. Comparison between experimental and computed $\psi$ values that are associated with an alkaline band transport system. The experimental trace is replotted from the data presented in Fig. 2. Solid and open symbols, and the geometric shapes, have the same meaning as in Fig. 3, except that (▽) represents a $OH^-$ to $HCO_3^-$ flux ratio of 12·5.

*Influence of $HCO_3^-$ flux on calculated cell wall $\psi$ profile*

Experimental cell wall pH data, and the pH profile from which interpolated values were obtained for the computer programme, are presented in Fig. 5A. Measured $\psi$ values are also presented in Fig. 5A (●), and we have illustrated the necessity of moving these values slightly to the left to obtain coincidence between pH and $\psi$ maxima. Discrepancies of this nature were found when the small glass electrode became slightly displaced during an experimental scan. (A modification to the original dual electrode holder prevented this form of displacement from occurring in our later experiments (see e.g. data presented in Fig. 7).)

Three versions of the computer programme were run in which the self-diffusion value of $D_{OH^-}$ was used and $OH^-$ to $HCO_3^-$ flux ratios of 1·0, 2·5, and 12·5, were employed (Fig. 5B, C, and D, respectively). These data indicate that the best agreement between the experimental and computed data was obtained under the condition where the $OH^-$ and $HCO_3^-$ fluxes were equal. As $HCO_3^-$ transport was progressively reduced, the discrepancy became more pronounced. This trend was in direct contrast to that found for both the radial and light-mediated time course studies, where a reduction in $HCO_3^-$ uptake improved the fit between experimental and computed results (cf. Figs 3, 4, and 5B, C, and D).

A similar set of programmes were run, except that a $D_{OH^-}$ having a numerical value equivalent to the limiting diffusion coefficient for NaOH was employed. The same basic trend was also observed under these conditions (Fig. 6. ▲, ■). We still

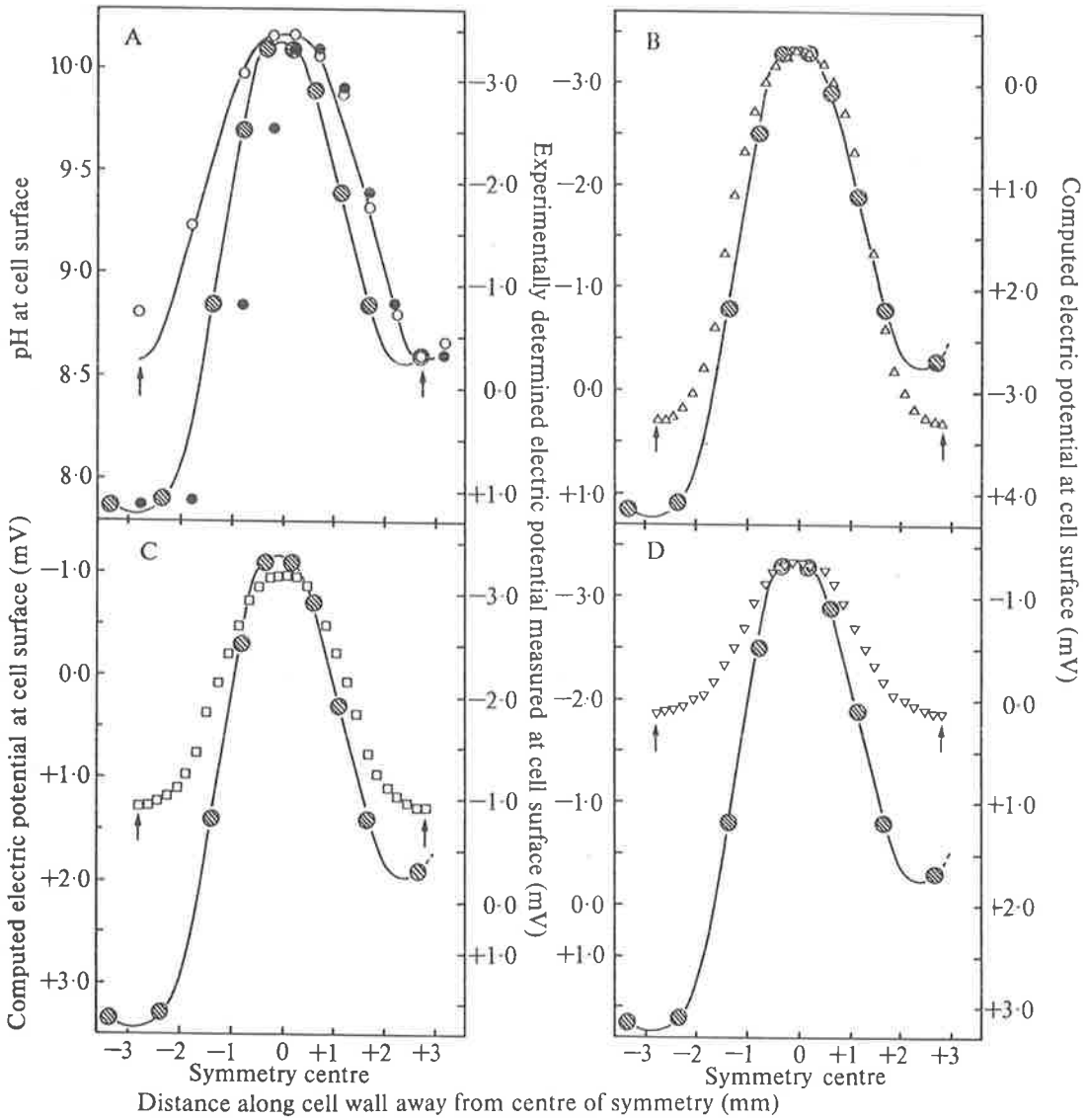


FIG. 5. Comparison between the steady state cell wall profile of $\psi$ measured experimentally (● replotted to give ⊘) and that calculated for various $OH^-$:$HCO_3^-$ flux ratios (△, □, and ▽). Except for Fig. 5A (see text for details), all symbols have the same meaning as in Fig. 4. ○ = pH at cell surface. (The vertical arrows indicate the spatial limits of the theoretical calculations.)

observed a discrepancy in terms of the absolute $\psi$ values, but the agreement between the experimental and computed (equal $OH^-$ and $HCO_3^-$ fluxes) cell wall profiles was excellent.

Since the computed $\psi$ values demonstrated a dependence upon the magnitude of $HCO_3^-$ transport, it was thought that the $\psi$ values may also be influenced by the spatial profile of $HCO_3^-$ uptake along the cell wall. This possibility was investigated by modifying the $HCO_3^-$ transport profile from the previously employed uniform pumping situation, to a mirror-image of the $OH^-$ transport profile (Lucas *et al.*, 1977, Fig. 5). However, a modification of this nature did not significantly affect the $\psi$ values generated within the centre of the $OH^-$ band (Fig. 6).

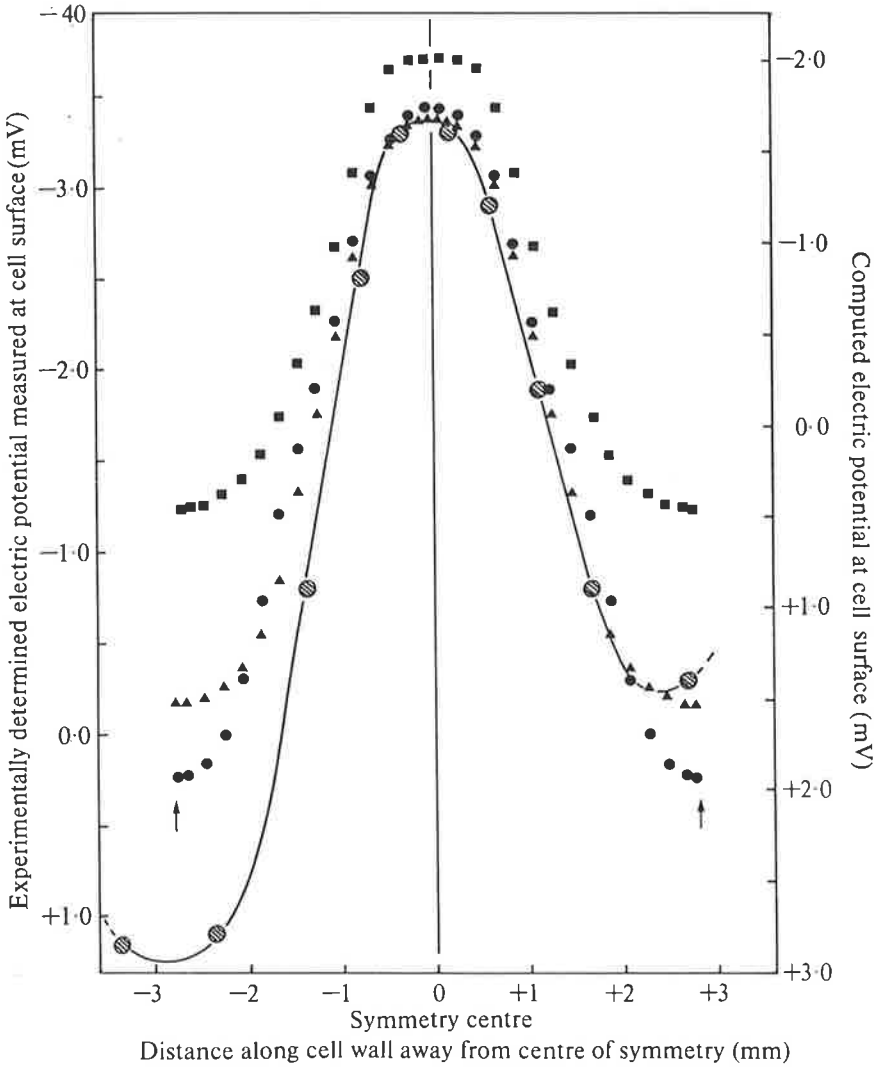


FIG. 6. Steady state cell wall profiles of $\psi$ determined experimentally (⦸) or computed (closed symbols) using a $D_{OH^-}$ equivalent in numerical value to the limiting diffusion coefficient for NaOH. Symbols have the same meaning as in Fig. 3 except that (●) represents a simulation in which the $OH^-$:$HCO_3^-$ flux ratio was set equal to one, but a non-linear distribution of $HCO_3^-$ transport function was investigated (see text for full details).

*Influence of ionic strength on $\psi$*

To further verify our diffusion model, we investigated the effect, on $\psi$, of increasing the ionic strength of 'non-transported' species in the bathing medium. In these experiments a cell was scanned (after 2 h illumination) firstly in control medium and then in an identical medium except that the NaCl concentration was increased from 1·0 to 10·0 mM. Under the new conditions, the denominator in the term on the right-hand side of equation 8 would be increased by a factor of 5·0. Thus the electric potential gradient under these conditions should be reduced by a factor of 5, compared with the control situation. As can be seen from Fig. 7, the $\psi$ differences along the cell wall were reduced by almost exactly a factor of 5. The pH profile, however, was not reduced under the 10 mM NaCl condition; in fact, for the data presented in Fig. 7, a slight stimulation in $OH^-$ transport activity was

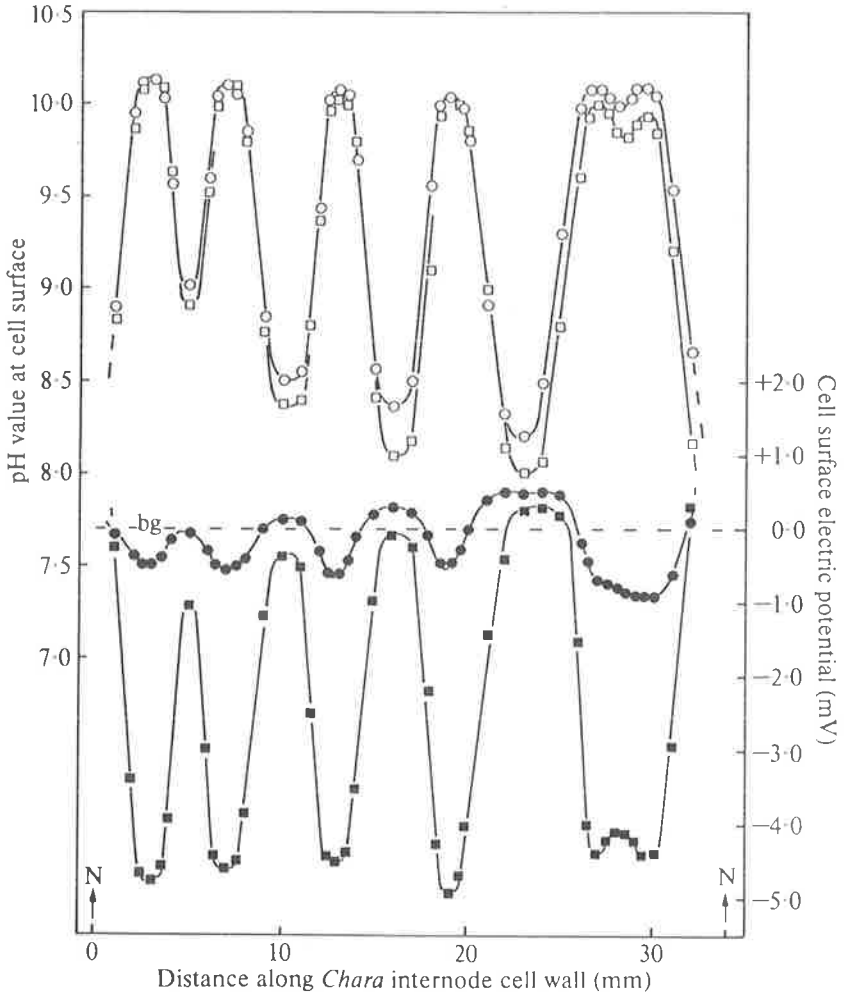


FIG. 7. Influence on $\psi$ and pH of increasing the ionic strength of the 'non-transported' species in the medium. The symbols □ (pH) and ■ ($\psi$) represent the steady state values measured in the experimental medium which contained (mM): NaCl, 1·0; KCl, 0·2; $CaSO_4$, 0·2; $NaHCO_3$, 0·5 (pH 7·7); ○ (pH) and ● ($\psi$) are the values measured in an identical solution, except that NaCl was increased to 10 mM.

observed. These data offer strong support for our theoretical interpretation of this complex multi-species diffusion system.

## DISCUSSION

### *Diffusion-mediated transport*

The present electric potential data are in agreement with the experimental results of Walker and Smith (1977). Collectively these results offer extremely strong experimental support for the concept that the membrane-associated transport processes involved ($HCO_3^-$ influx and $OH^-$ efflux) are electrogenic. The recent report (Lucas, 1979) that neither alkaline band transport nor total $H^{14}CO_3^-$ assimilation have a specific cation requirement (except for the previously established role of $Ca^{2+}$ at the $HCO_3^-$ transport site) also supports this electrogenic transport hypothesis.

In terms of the nature of the transport processes occurring in the bathing medium, the general correlation between the present theoretical and experimental

data offers extremely strong support for our diffusion model. Our analysis of the system indicates that Walker and Smith (1977) were incorrect in attributing the electric potential gradient as the basic driving force responsible for the measured ionic fluxes. There are still, however, several discrepancies between the experimental and theoretically calculated values that need to be discussed. Firstly, the calculated negative values of the maxima are always smaller than the measured values. We can find no theoretical explanation for this difference. It may be due, therefore, to some physical aspect of the experimental system which is not included in the numerical model. Since Lucas (1975*a*) demonstrated that within the centre of an alkaline band the $OH^-$ concentration did not vary as a function of circumferential position, it is unlikely that this difference in $\psi$ is due to the circumferential separation of the pH and $\psi$ sensing tips. It is possible, however, that the agar matrix may be having an effect on the $\psi$ profile. This aspect will require further investigation.

More serious in nature is the conceptual problem of why the $OH^-$ ions do not move at the rate predicted by the self-diffusion coefficient. What physical force(s) retards the diffusion of $OH^-$ away from the efflux site, such that its 'effective' self-diffusion coefficient is close to the numerical value of the limiting diffusion coefficient (obtained for infinitely dilute solutions of NaOH)? Presently we have no explanation for this phenomenon.

*Spatial distribution of $HCO_3^-$ transport along the cell surface*

From the data presented in Fig. 6 it can be seen that an equality between $OH^-$ efflux and $HCO_3^-$ influx gives a calculated $\psi$ profile in almost perfect agreement with the experimental $\psi$ values measured on the right-hand side of the alkaline band. However, on the left-hand side, a discrepancy between the values develops as the distance from the $OH^-$ efflux centre increases. At the 'positive' $\psi$ maximum position the experimental value was 1·4 mV more positive than the theoretically calculated value. Based on the sensitivity of the cell wall $\psi$ value to the relative $HCO_3^-$ pumping strength, one can see that this discrepancy would be diminished by increasing the rate of $HCO_3^-$ transport above the $OH^-$ efflux value that exists within the central $OH^-$ pumping region. We estimate that, within this particular region, the rate of $HCO_3^-$ transport would therefore be 2–3 times higher than the central $OH^-$ efflux value. From the computer calculation this would give a $HCO_3^-$ flux of approximately 250 pmol $cm^{-2}$ $s^{-1}$.

If this interpretation of the data is correct, we can see from the $\psi$ profiles presented in Figs 1 and 7 that, in terms of the spatial aspect of transport, the rate of $HCO_3^-$ influx varies quite dramatically along the length of an internodal cell. This is an interesting discovery, since it suggests that $HCO_3^-$ transport may be under cytoplasmic control, perhaps in a manner similar to that involved in controlling $OH^-$ efflux.

*Relation between $OH^-$ efflux and $HCO_3^-$ influx*

In his initial diffusion analysis of the alkaline band phenomenon Lucas (1975*a*) obtained steady state flux values for $OH^-$ (by diffusion analysis) and $HCO_3^-$

($H^{14}CO_3^-$ measured on experimental diffusion cells). There appeared to be a 1:1 correlation between these fluxes. In a further analysis of this system, Lucas *et al.* (1977) demonstrated that $CO_3^{2-}$ ions can carry from 30 to 40% of the total flux (alkalinity) away from the $OH^-$ efflux centre. Consequently $OH^-$ efflux values determined solely on $OH^-$ concentration profiles underestimate the absolute flux. In the present calculations (see also Lucas *et al.*, 1977) we estimated that, of the total $OH^-$ efflux, approximately 30% of the alkalinity was back-fluxed into the cell in the lateral sink regions. Fortuitously, or otherwise, this lateral sink flux into the cell tends to reduce the value of the net flux to that which would be determined in the absence of a $CO_3^{2-}$ flux. Thus we again have the situation where net $OH^-$ efflux would be equivalent to $H^{14}CO_3^-$ assimilation. But this relationship would only hold if 'effective' $D_{OH^-}$ and $D_{CO_3^{2-}}$ values were closer to the numerical values of the limiting-diffusion rather than the self-diffusion.

It is important that future studies be conducted to resolve the exact nature of this $OH^-$ sink flux. Lucas *et al.* (1977) suggested that $CO_2$, generated within the cytoplasm from recently transported $HCO_3^-$, may diffuse back across the plasmalemma and react with $OH^-$ in the bathing medium to produce $HCO_3^-$ (see also Walker and Smith, 1977). This process would not only act as a sink for $OH^-$ but it would also short-circuit the $HCO_3^-$ influx process. If this situation exists, there will be a serious discrepancy between $HCO_3^-$ influx and the measured value of $H^{14}CO_3^-$ assimilation. Alternatively, if the lateral sink reflects an influx of $OH^-$, this would raise the question of cytoplasmic control over $OH^-$ pumping, in relation to the control of the electric currents circulating through this complex system. This aspect gains in importance when viewed in relation to the probable asymmetric spatial distribution of $HCO_3^-$ transport function that also appears to be present in these giant internodal cells.

## LITERATURE CITED

LUCAS, W. J., 1975*a*. *J. exp. Bot.* **26,** 271–86.
—— 1975*b*. Ibid. **26,** 347–60.
—— 1979. *Pl. Physiol., Lancaster,* **63,** 248–54.
—— and DAINTY, J., 1977. Ibid. **60,** 862–7.
—— FERRIER, J. M., and DAINTY, J., 1977. *J. Membr. Biol.* **32,** 49–73.
—— and SMITH, F. A., 1973. *J. exp. Bot.* **24,** 1–14.
RAVEN, J. A., and SMITH, F. A., 1978. Ibid. **29,** 853–66.
WALKER, N. A., and SMITH, F. A., 1977. Ibid. **28,** 1190–206.

Plant Physiol. (1980) 65, 274–280
0032-0889/80/65/0274/07/$00.50/0

# Sulfhydryl Group Involvement in Plasmalemma Transport of $HCO_3^-$ and $OH^-$ in *Chara corallina*[1]

Received for publication July 20, 1979 and in revised form September 20, 1979

WILLIAM J. LUCAS AND JON M. ALEXANDER
*Department of Botany, University of California, Davis, California 95616*

## ABSTRACT

**The effect of the sulfhydryl reagents (—SH) *p*-chloromercuribenzenesulfonic acid (PCMBS), *N*-ethylmaleimide (NEM), and inorganic mercury on $H^{14}CO_3^-$ assimilation in *Chara corallina* is reported. Commercial grade PCMBS caused severe inhibition of $H^{14}CO_3^-$ assimilation. Results obtained using purified PCMBS (stock solution passed through a chelating resin) indicated that inhibition observed using unpurified PCMBS was due predominantly to the presence of inorganic mercury (as a contaminant). The inhibitory role of inorganic mercury was verified using $HgCl_2$. This chemical caused a dramatic inhibition of $H^{14}CO_3^-$ assimilation, while it had little effect on cellular $^{14}CO_2$ fixation. Reversal of the $Hg^{2+}$ inhibition of $H^{14}CO_3^-$ assimilation (in presence of 1.0 millimolar dithioerythritol) was extremely slow, requiring 2 to 3 hours for the reestablishment of control rates. This slow recovery may reflect *de novo* synthesis of transport proteins.**

**Almost complete (irreversible) inhibition of $H^{14}CO_3^-$ assimilation was observed after cells were briefly (2 min) exposed to 0.1 to 0.3 millimolar NEM. At critical concentrations, both inorganic mercury and NEM perturbed the $HCO_3^-$ transport system to such an extent that the $H^{14}CO_3^-$ assimilation *versus* $HCO_3$ concentration profiles changed shape. This could reflect a conversion of the transport system to a facilitated diffusion mode. Alternatively, the efficiency of the transport system may have been affected such that $HCO_3^-$ efflux increased significantly.**

**The influence of these —SH reagents on the $OH^-$ efflux system was also investigated. The $H^{14}CO_3^-$ assimilation and $OH^-$ efflux results demonstrate the involvement of —SH groups in the plasmalemma transport of both $HCO_3^-$ and $OH^-$ in *C. corallina*. Greater transport susceptibility to inorganic mercury and NEM compared to purified PCMBS suggested that the sulfhydryl groups were not located on the peripheral surface of the plasmalemma.**

Chemical agents specific for protein sulfhydryl groups (—SH) have been used quite extensively to investigate functional aspects of enzyme action and membrane transport phenomena (10, 14, 16). Although the use of these compounds, in intact tissue studies, has not always allowed an unequivocal interpretation of results (3, 15), they still, nonetheless, provide a valuable tool for probing the interrelationships that may exist between plasmalemma-bound transport systems.

In the present study we investigated the effects of NEM[2], PCMBS, and $Hg^{2+}$ on $HCO_3^-$ assimilation in *Chara corallina*. We speculated that the $HCO_3^-$ (influx) and $OH^-$ (efflux) transport systems would exhibit differential sensitivity to —SH reagents. This would have provided an extremely valuable tool for further electrophysiological studies into the electrogenic nature of the $HCO_3^-$ and $OH^-$ transporters (2, 6, 13). However, both transport systems exhibited —SH reagent sensitivity.

## MATERIALS AND METHODS

**Culture Material.** Culture material of *C. corallina* Klein ex Willd., em. R. D. W. (=*C. australis* R. Br.) was grown in the laboratory in large plastic containers in a culture medium containing (mM): 1–2 $Na^+$, 0.2 $K^+$, 0.2 $Ca^{2+}$, 1–2 $Cl^-$, and 2 $HCO_3^-$. Artificial fluorescent lighting was employed; the intensity at the solution surface was 17–20 w $m^{-2}$. Full details of the culture techniques and the methods used to cut and pretreat experimental cells have been previously reported (4, 7, 8).

**Experimental Solutions.** Solutions were prepared using high purity glass-distilled $H_2O$. The basic experimental solution (CPW) contained (mM): 1.0 NaCl, 0.2 KCl, 0.2 $CaSO_4$; modifications to this medium will be detailed in the text. All chemicals were of Analar reagent grade and, except for PCMBS, were not purified further. Stock (100 mM) NEM and DTE solutions were titrated to pH 7 using fresh NaOH solution and stored at 4 C for a maximum of 4 days. Because hydrolytic ring opening in the NEM molecule occurs at alkaline pH (14), experimental NEM solutions were prepared immediately (2 min) before use.

Purification of commercial PCMBS (Sigma Chemical Co.) was achieved using the procedure of Will and Hopfer (15). Inorganic mercury in the stock PCMBS solution was removed with a column (0.5 × 4.0 cm) of Bio-Rad analytical grade chelating resin (Chelex 100 in $H^+$ form). Eluted PCMBS was titrated to pH 7.5 and its concentration determined spectrophotometrically ($A$ at 265 nm). Purified PCMBS was prepared 10 min before use.

**General $H^{14}CO_3^-$ Experimental Sequence.** Bicarbonate and $CO_2$ assimilation experiments were performed using the procedures detailed by Lucas (4), Lucas and Dainty (7), and Lucas *et al.* (9). Radioactive $NaH^{14}CO_3$ was obtained from New England Nuclear as a sterile aqueous solution, and aliquots were added to the experimental solution to give the required specific radioactivity. Sample radioactivity was determined using a Nuclear-Chicago gas flow system (9). Experiments were conducted at 25 C, under a light intensity of 20 w $m^{-2}$. Results are expressed as mean ± SEM; 10–12 cells/treatment.

**pH Measurement of $OH^-$ Band Pattern.** The pH values along the surface of *C. corallina* internodal cells were measured using the techniques developed by Lucas and Smith (8) and Lucas and Dainty (7). Details relating to individual scanning experiments will be specified in the text.

## RESULTS AND DISCUSSION

**Influence of Unpurified and Purified PCMBS on $H^{14}CO_3$ Assimilation.** Initial experiments were conducted with the widely used nonpenetrating —SH reagent, PCMBS. In the course of our

[1] This research was supported by National Science Foundation Grant PCM 78-10474.

[2] Abbreviations: NEM: *N*-ethylmaleimide; PCMBS: *p*-chloromercuribenzenesulfonic acid; CPW: *Chara* pondwater; DTE: dithioerythritol.

preliminary experiments we used several different batch lots of unpurified PCMBS. Bicarbonate assimilation was inhibited significantly in each case; however, different batch lots gave very different inhibition profiles (Fig. 1). Purification of the PCMBS prior to use changed the inhibition profile dramatically (Fig. 1). The significant reduction in inhibition could be due only to the removal of inorganic mercury from the solution ($Hg^{2+}$ is a potent —SH reagent).

Will and Hopfer (15) reported that PCMBS can contain as much as 0.5% (by weight) inorganic mercury. Using this value as an upper limit, an unpurified 0.5 mM PCMBS solution would have an inorganic mercury concentration of approximately 5 μM. $H^{14}CO_3^-$ assimilation was extremely sensitive to inorganic mercury, and almost complete inhibition was observed at a concentration much lower than the estimated upper limit of 5 μM (Fig. 2).

**Influence of Unpurified PCMBS and Inorganic Mercury on Cyclosis.** Cytoplasmic streaming studies indicated that at pH 9 unpurified PCMBS caused a slight reduction in the streaming rate. Transferring cells from pH 9 to 5.4 (an experimental procedure used to examine the influence of a particular treatment on *in vivo* chloroplastic $^{14}CO_2$ fixation) resulted in immediate cessation of cyclosis (Fig. 3). Returning the cells to pH 9 did not elicit recovery (data not shown) and cells subjected to this 9.0/5.4 pH pulse always died. Treatment with 1.0 mM DTE appeared to protect the plasmalemma. Purified PCMBS and NEM (0.3 mM) had no such effect on cyclosis (data not shown). A similar effect on cyclosis could be achieved with an inorganic mercury concentration of 0.7 μM (Fig. 4). In these experiments the cells also died, and the effect could be prevented by pretreating with 1.0 mM DTE. We feel that these data confirm our hypothesis that the observed sensitivity of $H^{14}CO_3^-$ assimilation to unpurified PCMBS is due predominantly to the effect of inorganic mercury (present as a breakdown contaminant).

The nature of the perturbative effect that inorganic mercury is having on the membrane, to make the pH 9 to 5.4 pulse lethal, we cannot say with any certainty. Proton permeability of the plas-

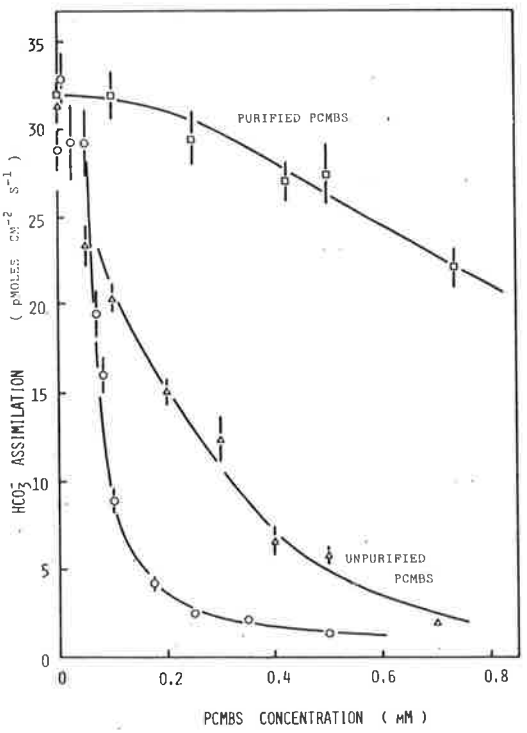


FIG. 1. Influence of unpurified (○, △) and purified (□) PCMBS on $H^{14}CO_3^-$ assimilation in *C. corallina*. Cells were given a 30-min pretreatment in CPW + 0.5 mM $HCO_3^-$ + indicated concentrations of PCMBS (pH 9.2, 20 w $m^{-2}$ illumination) before being transferred to identical $^{14}C$ solutions (1-h $^{14}C$ exposure). Symbols ○ and △ represent results obtained using two different commercial PCMBS batch lots obtained from Sigma Chemical Co.

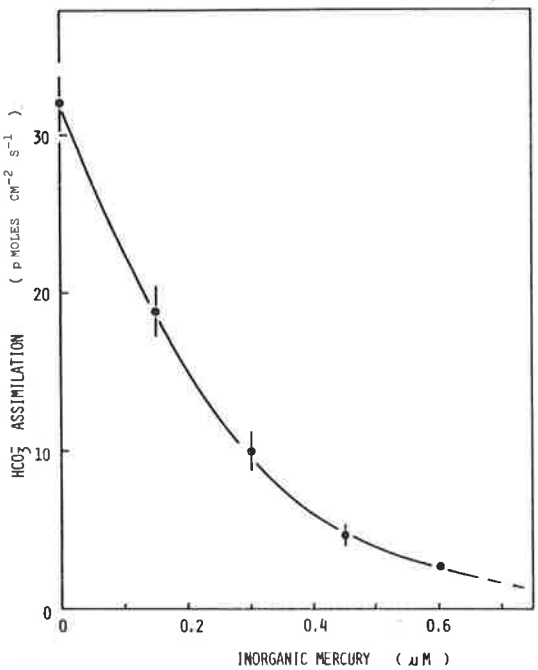


FIG. 2. Inhibition of $H^{14}CO_3^-$ assimilation by inorganic mercury (added as $HgCl_2$). Experimental details as described in Figure 1.

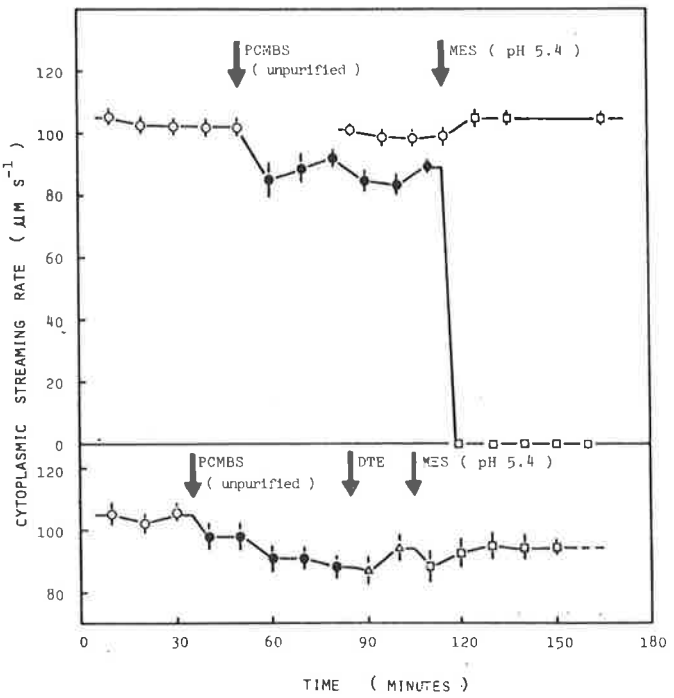


FIG. 3. Effect of unpurified PCMBS on cyclosis in *C. corallina*. Cyclosis was measured with a binocular microscope having an ocular micrometer. Time required for a standard sized cytoplasmic particle to traverse 1,000 μm was measured with a stopwatch. Control solutions (○) contained: CPW + 0.5 mM $HCO_3^-$ pH 9; unpurified PCMBS (batch lot ○ of Fig. 1) and DTE solutions were identical except for inclusion of 0.5 mM PCMBS (●) and 1 mM DTE (△); Mes solutions (△) contained: CPW + 0.5 mM total added carbon + 5 mM Mes (pH 5.4).

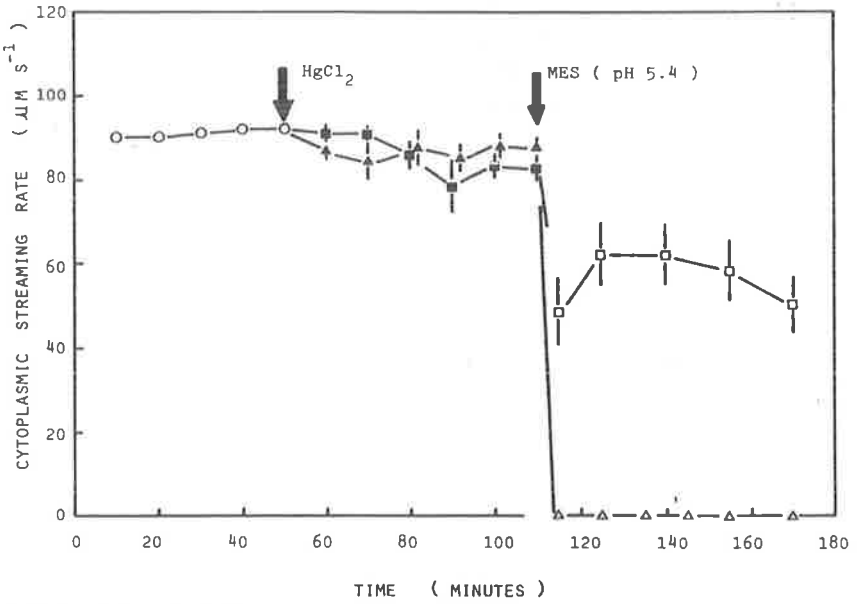


FIG. 4. Effect of inorganic mercury on cyclosis in *C. corallina*. Control (○) and Mes (□, △) solutions were as described in Figure 3 (in these treatments SEM values were smaller than symbols used). Inorganic mercury solutions contained: CPW + 0.5 mM $HCO_3^-$ (pH 9) + 0.3 μM $HgCl_2$ (■) or 0.7 μM $HgCl_2$ (▲).

Table I. *Influence of Purified PCMBS and Inorganic Mercury on $^{14}$Carbon Assimilation*

The control cells were given 60-min pretreatment in CPW + 0.5 mM $HCO_3^-$ (pH 9.2) (20 w $m^{-2}$); $HgCl_2$ and PCMBS cells were pretreated in the same manner in solutions containing indicated concentrations of the respective —SH reagent. All treatments were given 10-min exposure to CPW + 0.5 mM $HCO_3^-$ + 1.0 mM DTE (pH 9.2) prior to introducing $^{14}$C solutions. The $H^{14}CO_3^-$ experimental solutions contained CPW + 0.5 mM total added carbon (pH 9.2) (1-h exposure). $^{14}CO_3$ experimental solutions contained CPW + 0.5 mM total added carbon + 5 mM Mes (pH 5.4) (1-h exposure).

| Exogenous $^{14}$C Species | Experimental Treatment | | | | |
|---|---|---|---|---|---|
| | Control | $HgCl_2$ | | PCMBS | |
| | | 0.45 μM | 0.6 μM | 0.4 mM | 0.73 mM |
| | | | *pmol $cm^{-2}$ $s^{-1}$* | | |
| $H^{14}CO_3^-$ | 32.0 ± 0.88 | 4.7 ± 0.66 | 2.75 ± 0.14 | 26.9 ± 1.22 | 22.1 ± 1.08 |
| $^{14}CO_2$ | 85.8 ± 3.8 | 84.7 ± 2.9 | 82.8 ± 3.7 | 84.3 ± 3.7 | 78.1 ± 3.4 |

malemma may be affected, or the pH pulse may in some way cause the release of mercury into the cytoplasm. In any event, these data indicate that inorganic mercury is having an additional effect on the plasmalemma not found in the presence of NEM or purified PCMBS.

**$^{14}CO_2$ Fixation Unaffected by Inorganic Mercury or Purified PCMBS.** Pretreatment, at pH 9.2, with inorganic mercury concentrations that severely inhibited $H^{14}CO_3^-$ assimilation, did not cause a reduction in cellular $CO_2$ fixation capacity (Table I). Purified PCMBS had only a slightly inhibitory effect on $H^{14}CO_3^-$ fixation and, as with $Hg^{2+}$, cellular $^{14}CO_2$ fixation also remained little affected. These results support the interpretation that inhibition of $H^{14}CO_3^-$ assimilation is due to an effect of inorganic mercury and PCMBS at the plasmalemma.

**$HCO_3^-$ Concentration Curves Obtained under Various Inorganic Mercury Levels.** Our results thus far have demonstrated the involvement of a $Hg^{2+}$-sensitive —SH group that affects $H^{14}CO_3^-$ assimilation in *C. corallina*. Bicarbonate concentration experiments were conducted in the presence of various inorganic mercury levels to see if we could further resolve the nature of this inhibition. In the presence of low $HgCl_2$ concentrations (0.1–0.2 μM), only the maximum rate of $^{14}$C assimilation was affected (Fig. 5). At higher concentrations (0.45 μM $HgCl_2$), however, the shape of the assimilation curve change dramatically. (For comparison, the effect on $H^{14}CO_3^-$ assimilation of 0.5 mM unpurified PCMBS is also included in Fig. 5. As expected, an identical linear response was obtained.)

The reduction in $V_{max}$, at low $HgCl_2$ levels, may indicate the presence of an —SH group that, upon binding $Hg^{2+}$, modified the microenvironment of the $HCO_3^-$-binding site to an extent that substrate cannot bind. At higher $HgCl_2$ concentrations other —SH groups (or even amino or carboxyl groups) could be affected. The resultant perturbation of the $HCO_3^-$ transport system may allow $HCO_3^-$ to bind again, but the transporter itself may have become uncoupled from cellular energy metabolism. This condition may allow it to function as a facilitated diffusion system (having a very high $K_m$). Alternately, the efficiency of the $HCO_3^-$ transport system may have been affected, *i.e.* influx may have continued, but a change within the transporter may have allowed a dramatic increase in $H^{14}CO_3^-$ efflux. If this were the case, the plasmalemma would appear to be leaky to $HCO_3^-$. Transport conversion to what appeared to be a facilitated diffusion mode was reported for *Chlorella* by Komor *et al.* (3) using the antibiotic nystatin. However, in this system NEM appeared to inhibit the operation of the nystatin-affected hexose transporter. We have previously shown that high $K^+$ (>3 mM) also converts the *C. corallina* $HCO_3^-$ transport system to an apparent facilitated diffusion system (9). (This aspect will be further discussed in relation to the effect of —SH reagents on the $OH^-$ efflux system.)

**NEM Inhibition of $H^{14}CO_3^-$ Assimilation.** Figure 6 illustrates

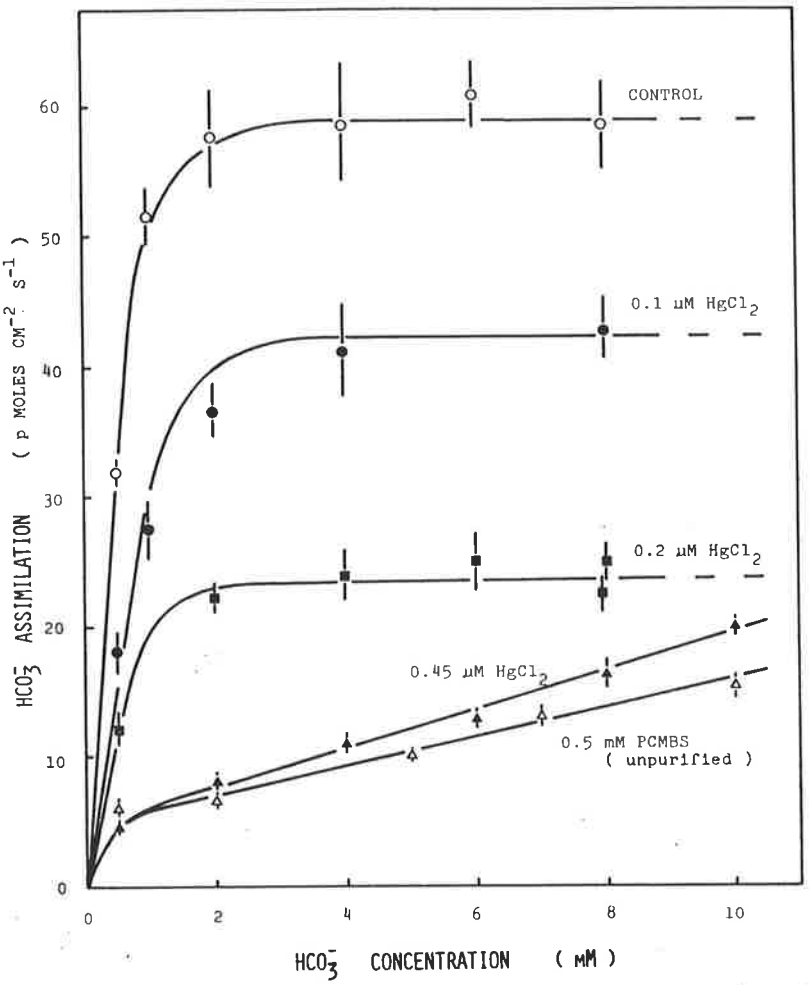


FIG. 5. $H^{14}CO_3^-$ assimilation concentration profiles obtained in the presence and absence of $HgCl_2$ and unpurified PCMBS. Cells were pretreated for 30 min in CPW plus the indicated $HCO_3^-$ and —SH reagent concentrations (pH 9.2, 20 w $m^{-2}$), prior to the introduction of $^{14}C$ (1-h exposure). (Unpurified PCMBS was batch lot [Δ] of Fig. 1.)

the $H^{14}CO_3^-$ assimilation inhibition time-courses for cells exposed to 0.1 and 0.3 mM NEM. This irreversible —SH reagent was a rapid and potent inhibitor of $H^{14}CO_3^-$ assimilation. Because NEM penetrates through the plasma membrane (10), we examined its effect on *in vivo* chloroplast $^{14}CO_2$ fixation to determine whether NEM could be sensibly employed in studying $HCO_3^-$ transport. Table II indicates that NEM inhibited assimilation of exogenous $H^{14}CO_3^-$ and $^{14}CO_2$; however, $H^{14}CO_3^-$ assimilation appeared to be affected to a greater extent than $^{14}CO_2$. After a 2-min exposure to 0.3 mM NEM, cells would still have the cellular photosynthetic capacity to fix $CO_2$ at a rate equal to, or greater than, the control rate observed in the presence of exogenous $H^{14}CO_3^-$. Unless NEM has influenced the mechanism by which $HCO_3^-$ moves from the plasmalemma to the chloroplast stroma, we can assume that NEM inhibition of $H^{14}CO_3^-$ assimilation is predominantly the result of NEM binding to —SH groups that influence $HCO_3^-$ transport at the plasmalemma.

When cells were pretreated for 1 or 2 min in 0.1 mM NEM, they exhibited the same substrate characteristics as the low concentration $HgCl_2$-treated cells, namely, a successive reduction in $V_{max}$ (Fig. 7). After a 2-min pretreatment in 0.3 mM NEM, the transport system exhibited a linear substrate response comparable to that observed with 0.45 µM $HgCl_2$ (*cf.* Figs. 5 and 7). The similarity between the $Hg^{2+}$ and NEM results suggested that both —SH reagents are acting at the membrane, rather than the cytoplasmic level. Presumably, NEM and inorganic mercury can both penetrate sufficiently into the plasmalemma to react with the same —SH groups. In this regard, the limited inhibition, observed in the presence of purified PCMBS (Fig. 1), may be due to its molecular dimensions imposing a limitation on its penetration to the —SH sites.

**Recovery of $H^{14}CO_3^-$ Assimilation.** Cells treated with unpurified PCMBS (inhibition due to $Hg^{2+}$) exhibited a very slow recovery response to treatment with DTE (1.0–2.0 mM). A period of 2–2.5 h was required before full $H^{14}CO_3^-$ assimilation was reestablished (Fig. 8). This slow response is in contrast to the generally rapid reversal of inhibition by thiol reagents (10). However, some workers using PCMBS have also reported irreversibility after 1 h (11) and this may reflect transport systems that undergo structural changes within the membrane transport system. Changes of this nature may be a reasonable explanation because of the report by Carter (1) that PCMBS caused the elution of proteins from the erythrocyte membrane. Furthermore, Trump *et al.* (12, and refs. contained therein) have recently demonstrated acute structural perturbation of the plasma membrane of Ehrlich ascites tumor cells caused by 1 mM PCMBS.

In Figure 8 the degree of $H^{14}CO_3^-$ transport inhibition was such that the system would definitely have been converted to the facilitated diffusion (or $HCO_3^-$-leaky) mode. Conversion to this transport mode may be due to the elution, from the plasmalemma,

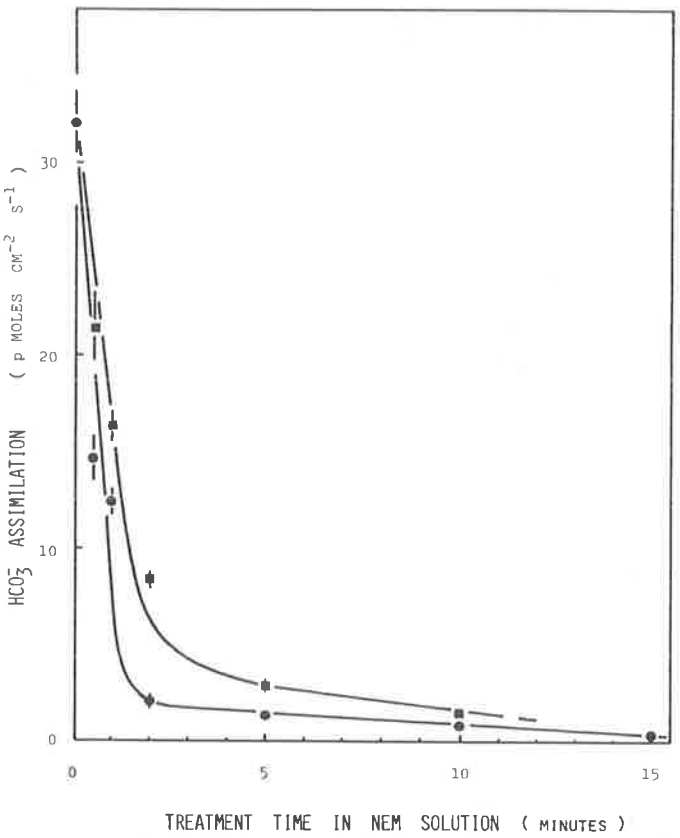


FIG. 6. NEM-induced inhibition of $H^{14}CO_3^-$ assimilation. Sequence of experimental treatments was as follows; (*a*) pretreatment in CPW + 0.5 mM $HCO_3^-$ (pH 9.2) for 30 min; (*b*) NEM exposure (0.1 mM, ■; 0.3 mM, ●) for indicated time; (*c*) 5-min wash in CPW + 0.5 mM $HCO_3^-$ + 1.0 mM DTE; (*d*) 30-min $^{14}C$ fixation period in CPW + 0.5 mM $HCO_3^-$ (pH 9.2). (For controls treatment (*b*) was omitted.)

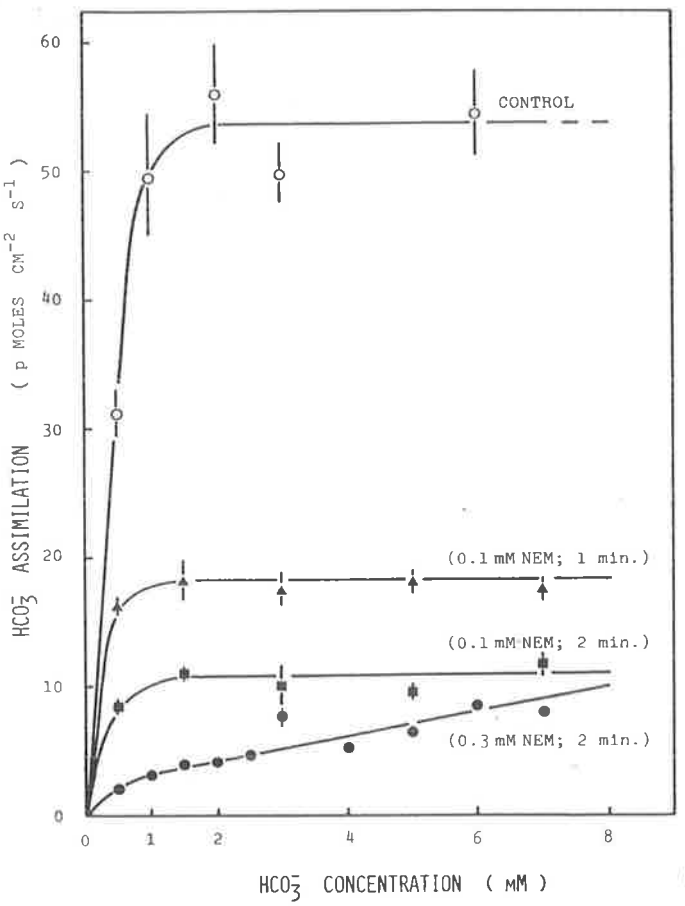


FIG. 7. $H^{14}CO_3^-$ assimilation concentration profiles obtained following pretreatment with NEM. Experimental details are as described in Figure 6, except that $HCO_3^-$ concentrations were varied from 0.5 to 7.0 mM.

Table II. *Effect of NEM on $^{14}C$ Assimilation*

The experimental cells were given 30-min pretreatment in CPW + 0.5 mM $HCO_3^-$ (pH 9.2) (20 w $m^{-2}$) then indicated exposure to NEM in same solution plus 0.3 mM NEM. Following NEM treatment cells given were 5-min wash in CPW + 0.5 mM $HCO_3^-$ pH 9.2 + 1.0 mM DTE prior to introduction of $^{14}C$ solutions. The $H^{14}CO_3^-$ experimental solutions contained CPW + 0.5 mM total added carbon (pH 9.2). $^{14}CO_2$ experimental solutions contained CPW + 0.5 mM total added carbon + 5 mM Mes (pH 5.4).

| Carbon Species | Control | 0.3 mM NEM Treatment | |
|---|---|---|---|
| | | 2 min | 10 min |
| | | *pmol $cm^{-2}$ $s^{-1}$* | |
| $H^{14}CO_3^-$ | 25.2 ± 1.5 | 7.36 ± 0.7 | 0.75 ± 0.06 |
| $^{14}CO_2$ | 78.3 ± 2.9 | 37.2 ± 2.8 | 10.3 ± 0.9 |

of a protein subunit of the $HCO_3^-$ transport system. Reactivation in this instance would require *de novo* synthesis of the subunit.

Experiments are presently being conducted to examine the effect(s) of PCMBS, inorganic mercury, and NEM on the plasmalemma of *C. corallina*. Future work will investigate the involvement of protein synthesis in the recovery process.

**Effect of —SH Reagents on $OH^-$ Efflux.** A perturbation of the $OH^-$ transport system by PCMBS, inorganic mercury, or NEM would also cause a reduction in $H^{14}CO_3^-$ assimilation, since both $HCO_3^-$ and $OH^-$ transport must work in synchrony (5, 7, 9). Figures 9, 10, and 11 illustrate the effects of PCMBS (unpurified), $HgCl_2$, and NEM, respectively. All cells scanned showed the same general trend, irrespective of the —SH reagent employed. Following exposure to 0.5 mM unpurified PCMBS (Fig. 9) and 0.45 μM $HgCl_2$ (Fig. 10), the subsequent pH values of the steady-state $OH^-$ efflux patterns were depressed below their control values. (This was expected inasmuch as $HCO_3^-$ influx was drastically reduced by these treatments.) Of more importance was the finding that new $OH^-$ efflux sites were always activated, even though the control efflux sites almost always remained operational and fixed in position. This suggested that the cells were responding to a reduction in the transport ability of the efflux sites established under control conditions.

The NEM-scanning studies also supported this interpretation, The pH scan conducted following 1-min exposure to 0.1 mM NEM (Fig. 11, ●) revealed that even though $HCO_3^-$ transport would have been reduced from 30 to approximately 16 pmol $cm^{-2}s^{-1}$ (see Figures 6 and 7), two further efflux sites were added to cope with this reduced generation of alkalinity within the cytoplasm. Subsequent exposures to NEM reduced the rate of $OH^-$ efflux from each transport site, without further activation of new sites.

Based on the pH scanning data, we feel sure that there is at least one functional —SH group associated with the operation of the $OH^-$ transport system.

## CONCLUSIONS

The present results have demonstrated the involvement of —SH groups in the plasmalemma transport of both $HCO_3^-$ and $OH^-$ in *C. corallina*. Since these sites were more susceptible to inorganic mercury ($HgCl_2$) and NEM compared to purified PCMBS, we suggest that the —SH groups are not located on the peripheral surface of the plasmalemma.

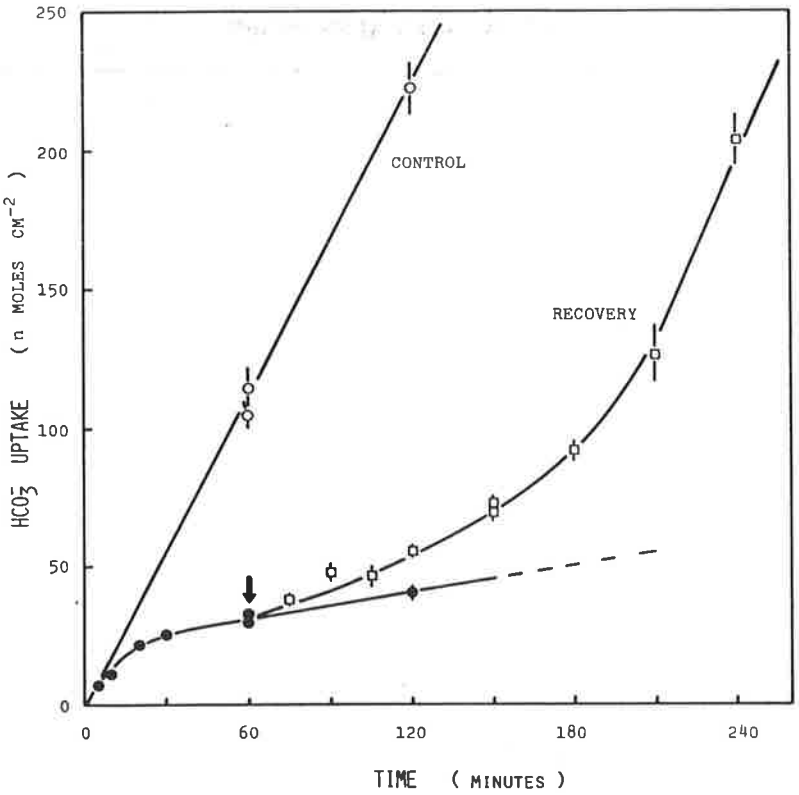


FIG. 8. $H^{14}CO_3^-$ assimilation inhibition by (–) and recovery from PCMBS treatment. Symbols are as follows; ○: control, CPW + 0.5 mM $HCO_3^-$ (pH 9.2); ●: unpurified PCMBS (batch lot ○ of Fig. 1), solution composition as control + 0.3 mM PCMBS; □: DTE recovery, solution composition as control + 1.0 mM DTE. (Solutions used for ● and □ had identical $^{14}C$ specific radioactivities.)

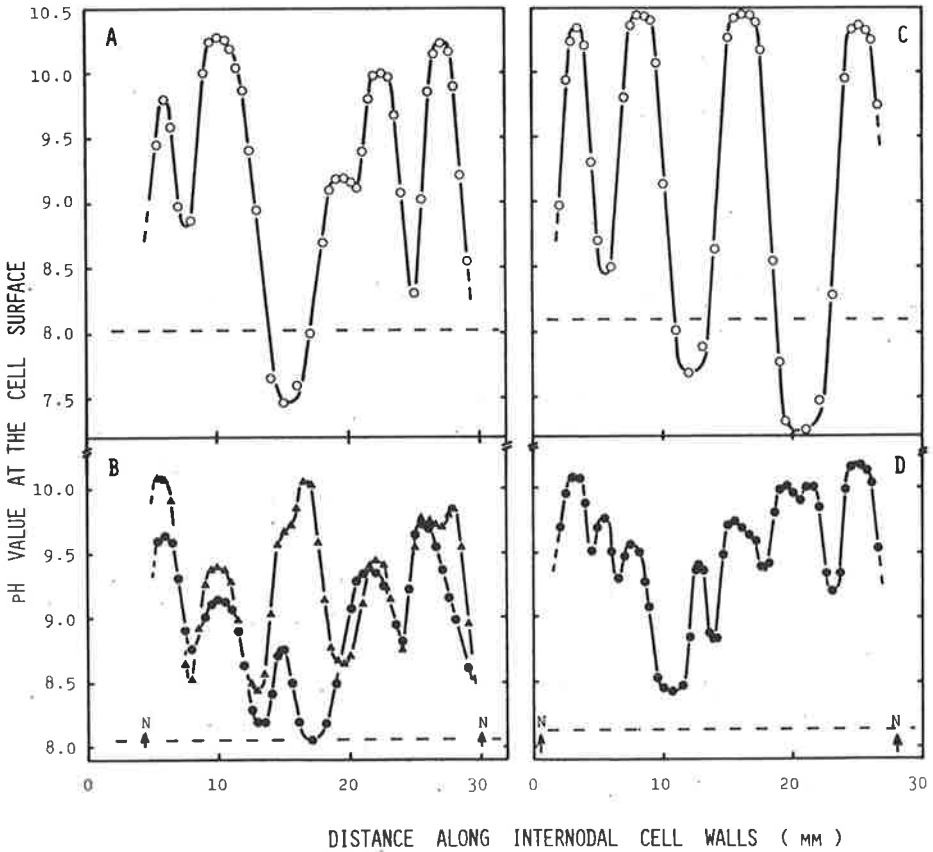


FIG. 9. Influence of unpurified PCMBS on $OH^-$ efflux from *C. corallina*. Control (○) pH scans (A, C) were conducted (after 1-h illumination (20 w $m^{-2}$)) in agar scanning blocks containing CPW + 0.5 mM $HCO_3^-$. Cells were then removed from the scanning block and given a 90-min treatment in CPW + 0.5 mM $HCO_3^-$ + 0.5 mM PCMBS (unpurified batch lot [△] of Fig. 1). Following PCMBS treatment, cells were returned to new identical scanning blocks and the pH patterns established 1 h (●) and 3 h (▲) later were mapped. Broken lines indicate background pH values and the arrowed N symbols indicate the nodal locations.

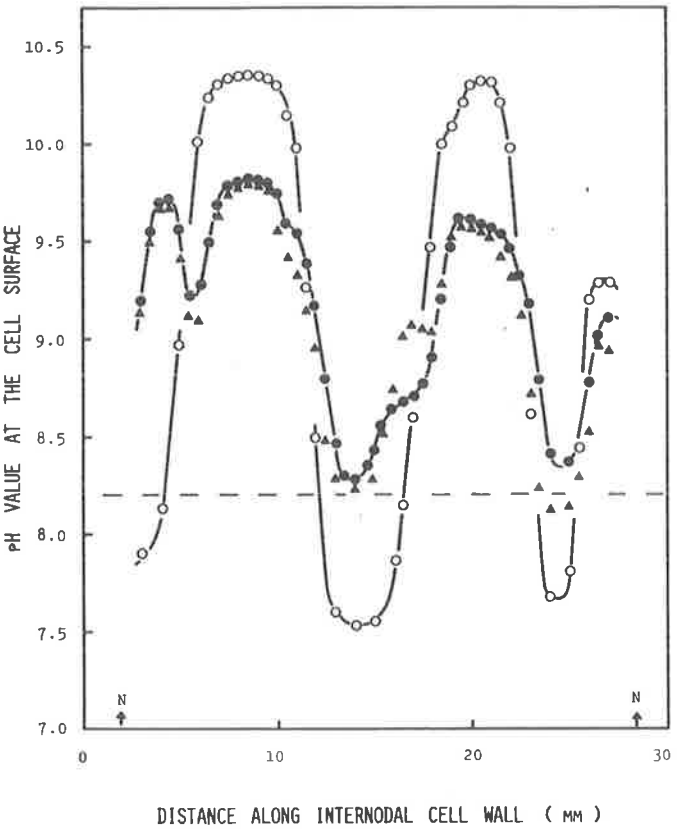


FIG. 10. Influence of inorganic mercury on the $OH^-$ efflux system of *C. corallina*. Experimental details are as described in Figure 9. ○: control pH scan; ●: pH pattern established 1 h after a 90-min treatment in CPW + 0.5 mM $HCO_3^-$ + 0.45 μM $HgCl_2$ (pH 9.2); ▲: pH pattern established 3 h after $HgCl_2$ treatment.

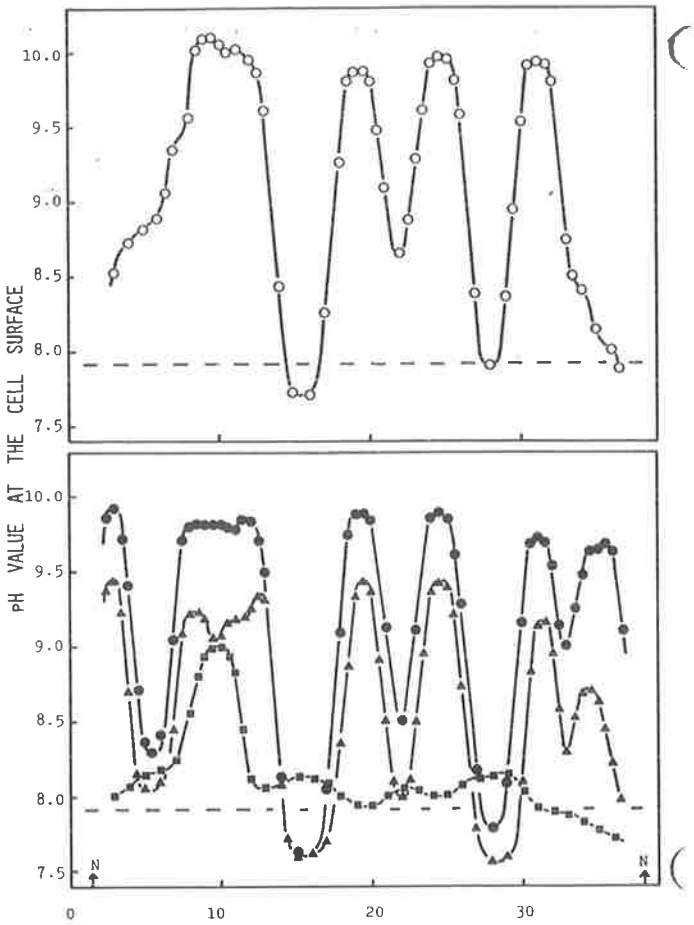


FIG. 11. Influence of NEM on $OH^-$ efflux system of *C. corallina*. Experimental details are as described in Figure 9. ○: control pH scan; ●: pH pattern established 1 h after a 1-min treatment in CPW + 0.5 mM $HCO_3^-$ + 0.1 mM NEM (pH 9.2); ▲: pH pattern established (1 h) after a further 1 min 0.1 mM NEM treatment; ■: pH pattern established (1 h) after a further 3-min 0.1 mM NEM treatment.

Both NEM and inorganic mercury can be used to "titrate" the activity of the $HCO_3^-$ and $OH^-$ transport systems. Under conditions of increasing concentrations of either NEM or $HgCl_2$, the $HCO_3^-$ transport system was eventually converted to a facilitated diffusion, or $HCO_3^-$-leaky system. At —SH reagent concentrations where this occurred, the $OH^-$ transport system did not reflect the efflux pattern found when membrane integrity, *per se*, was affected (as found, *e.g.* in 10 mM $K^+$ or $Ca^{2+}$-free experiments [7, 9]). This suggested that the microenvironment in the vicinity of the individual $OH^-$ transport sites was not being perturbed to the same extent as that experienced by the $HCO_3^-$ transport system. Whether this enhanced $HCO_3^-$ transport perturbation is due to elution of a transport subunit from the membrane, or some other structural change within the membrane, will be investigated in future experiments.

Finally, the inorganic mercury contamination of commercial PCMBS is of serious concern. The degree to which this will affect the interpretation of previous work that involved this compound is impossible to predict. We can only recommend that in all future work PCMBS be purified immediately before use.

## LITERATURE CITED


1. CARTER JR 1973 Role of sulfhydryl groups in erythrocyte membrane structure. Biochemistry 12: 171–176
2. FERRIER JM, WJ LUCAS 1979 Plasmalemma transport of $OH^-$ in *Chara corallina*. II. Further analysis of the diffusion system associated with $OH^-$ efflux. J Exp Bot. In press
3. KOMOR E, H WEBER, W TANNER 1978 Essential sulfhydryl group in the transport-catalyzing protein of the hexose-proton co-transport system of *Chlorella*. Plant Physiol 61: 785–786
4. LUCAS WJ 1975 Photosynthetic fixation of $^{14}$carbon by internodal cells of *Chara corallina*. J Exp Bot 26: 331–346
5. LUCAS WJ 1977 Plasmalemma transport of $HCO_3^-$ and $OH^-$ in *Chara corallina*: inhibitory effect of ammonium sulphate. J Exp Bot 28: 1307–1320
6. LUCAS WJ 1979 Alkaline band formation in *Chara corallina* due to $OH^-$ efflux or $H^+$ influx? Plant Physiol 63: 248–254
7. LUCAS WJ, J DAINTY 1977 $HCO_3^-$ influx across the plasmalemma of *Chara corallina*: divalent cation requirement. Plant Physiol 60: 862–867
8. LUCAS WJ, FA SMITH 1973 The formation of alkaline and acid regions at the surface of *Chara corallina* cells. J Exp Bot 24: 1–14
9. LUCAS WJ, RM SPANSWICK, J DAINTY 1978 $HCO_3^-$ influx across the plasmalemma of *Chara corallina*: physiological and biophysical influence of 10 mM $K^+$. Plant Physiol 61: 487–493
10. ROTHSTEIN A 1970 Sulfhydryl groups in membrane structure and function. *In* F Bronner, A Kleinzeller, eds. Current Topics in Membranes and Transport, Vol 1. Academic Press, New York, pp 135–176
11. SCARBOROUGH GA 1977 Properties of the *Neurospora crassa* plasma membrane ATPase. Arch Biochem Biophys 180: 384–393
12. TRUMP BF, A PENTTILA, IK BEREZESKY 1979 Studies on cell surface conformation following injury. I. Scanning and transmission electron microscopy of cell surfaces changes following *p*-chloromercuribenzene sulfonic acid (PCMBS)-induced injury of Ehrlich ascites tumor cells. Virchows Arch B Cell Path 29: 281–296
13. WALKER NA, FA SMITH 1977 Circulating electric currents between acid and alkaline zones associated with $HCO_3^-$ assimilation in *Chara*. J Exp Bot 28: 1190–1206
14. WEBB JL 1966 Enzyme and Metabolic Inhibitors. Vol 2. Academic Press, New York, pp 337–365, 635–653, 729–651
15. WILL PC, U HOPFER 1979 Apparent inhibition of active non-electrolyte transport by an increased sodium permeability of the plasma membrane. Mechanism of action of *p*-chloromercuribenzene sulfonate. J Biol Chem 25: 3806–3811
16. WISKICH JT 1977 Mitochondrial metabolite transport. Annu Rev Plant Physiol 28: 45–69

Plant Physiol. (1980) 66, 46–50
0032-0889/80/66/0046/05/$00.50/0

# Plasmalemma Transport of $OH^-$ in *Chara corallina*

## III. FURTHER STUDIES ON TRANSPORT SUBSTRATE AND DIRECTIONALITY[1]

Received for publication November 19, 1979 and in revised form February 25, 1980

WILLIAM J. LUCAS
*Department of Botany, University of California Davis, California, 95616*

JACK M. FERRIER
*Department of Botany, University of Toronto, Toronto, Ontario M5S 1A1 Canada*

### ABSTRACT

**The identity of the plasmalemma-transported species that develops the alkaline bands of *Chara corallina* was investigated. The effect of fusicoccin on the rate of $HCO_3^-$ assimilation, and on the time-dependent alkaline band pH buildup following low pH flushing, was found to be small, with no stimulatory effect. Computer simulation of the flushing experiments showed that in the experimental situation the alkaline band transport system was slowed down, rather than speeded up, by low pH flushing. A detailed theoretical examination of the maximum rate of proton production from water showed that measured alkaline band fluxes are too large to be explicable in terms of an $H^+$ influx system. The experimental and theoretical results indicate that the plasmalemma transport of $OH^-$ ions is responsible for the measured negative external electric potential and alkalinity flux which are associated with the alkaline band phenomenon. Consequently, $HCO_3^-$ influx across the characean plasmalemma must be charge-balanced by the efflux of $OH^-$ ions.**

Following the inception of the Chemiosmotic theory (12, 13) numerous plant transport systems have been linked with the vectorial movement of protons across various membranes (14). In these transport systems it is assumed that $H^+$ is the chemical species which moves, not $OH^-$. In line with this general philosophy, Walker and Smith (16) suggested that the light (photosynthetic)-dependent alkalinity that develops on the cell wall surface of *C. corallina* (4) is formed by $H^+$ influx, via the operation of a simple $H^+$ uniport.

Recently Lucas (5) presented evidence which, although it did not categorically refute the existence of a $H^+$ influx system, tended to offer stronger support for the $OH^-$ efflux hypothesis. Supporting evidence against the operation of a $H^+$ uniport was claimed based on the very low $K_m$ requirement of such a system (nM range). Also, the apparent insensitivity of the alkalinization process to external pH (from 10 down to 5.0) was thought to be inconsistent with the operation of a $H^+$ uniport.

To study the synchronization mechanism which functions in these giant algal cells to integrate $HCO_3^-$ influx and the necessary charge-balancing transport process (6), it would be of advantage to know the chemical nature of the charge-balancing species. This study was conducted to test whether, physicochemically, exogenous $H^+$ ions could fill this charge-balancing role. As a result of these studies we are now almost certain that $HCO_3^-$ influx is charge-balanced by $OH^-$ efflux.

[1] Supported by National Science Foundation Grant PCM 78-10474 (to W. J. L.), and National Research Council of Canada Grant A6459 (to J. Dainty).

## MATERIALS AND METHODS

**Culture Material.** Culture material of *Chara corallina* Klein ex Willd., em. R.D.W. (= *Chara australis* R. Br.) was grown in the laboratory under artificial light. Cells were cut from the culture 16 h prior to use in an experiment. During this recovery period cells were bathed in a pretreatment solution containing (mM): NaCl, 1.0; KCl, 0.2; $CaSO_4$, 0.2; and $NaHCO_3$, 0.5 (initial pH 7.7).

**Photosynthetic $H^{14}CO_3^-$ Assimilation.** Assimilation of exogenous $H^{14}CO_3^-$ was measured using radioactive $NaH^{14}CO_3^-$ (New England Nuclear, sterile aqueous solution). These experiments were performed in the manner detailed by Lucas and Dainty (7). Individual experimental details are given in the text.

**pH Measurement of Alkaline Band Activity.** The pH values along the cell surface of *C. corallina* internodal cells were measured using the procedures of Lucas and Smith (9) and Lucas and Dainty (7). For experiments in which FC[2] was employed, cells were mounted in a small Plexiglas chamber instead of an agar diffusion block.

**Numerical Analysis Modeling.** Various theoretical pH profiles were obtained using the expanded numerical analysis (diffusion) program of Ferrier and Lucas (2). These programs were run on an IBM 370 Computer (University of Toronto).

## RESULTS

**Influence of FC on $HCO_3^-$ Assimilation.** Marrè has suggested that FC stimulates $H^+$ efflux in the Characeae (10, 11). If Walker and Smith (16) are correct, in that the light-dependent alkaline bands are produced by an $H^+$ influx system, it may be that the $H^+$ efflux and influx transport systems of the Characeae are identical in all respects except for their spatial location on the plasmalemma and their direction of net transport. If this were so, FC may well act to stimulate the alkaline band transport system; stimulation of $H^+$ influx would result in increased alkalinity at the cell surface.

This possibility was investigated using the isolating chamber technique developed by Lucas (5). In these experiments, 0.5 mM exogenous $HCO_3^-$ was employed (apparent $K_m$ for assimilation) to ensure the alkaline band transport system was operating well below saturation. The response of an alkaline band to ethanol (0.5%) and ethanol plus 10 μM FC-containing solutions is typified by the data presented in Figure 1. Provided the isolating chamber solution contained $HCO_3^-$, the alkaline band transport system was

[2] Abbreviations: CPW/B: *Chara* pond water containing added bicarbonate; FC: fusicoccin.

not perturbed by the introduction of 0.5% ethanol. The addition of FC did not elicit a consistent response in terms of affecting transport activity (Fig. 1). We found that the presence of FC frequently caused the transport center to migrate (Figs. 1 and 2). The same type of FC response was observed when $HCO_3^-$ was excluded from the isolating chamber solution (data not shown). The variability of the results and the FC-induced mobility of the band center limited the usefulness of the isolating chamber technique.

The effect of exposing entire internodal cells to FC was examined. In these experiments, internodal cells of varying maturation

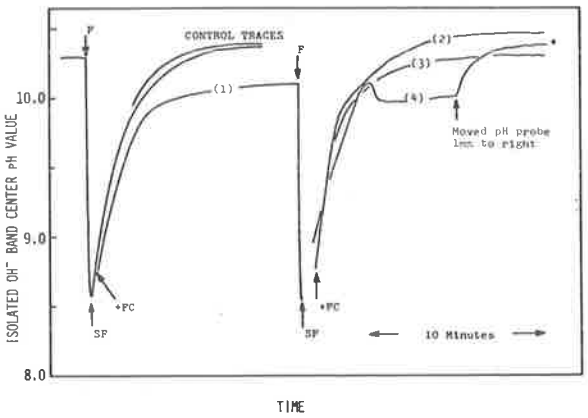


FIG. 1. Influence of ethanol and FC on the alkaline band transport system of *C. corallina*. Isolating chamber located over operational transport site and then cell allowed 30-min recovery, bathed in a solution containing (mM) 1.0 NaCl, 0.2 KCl, 0.2 $CaSO_4$, 0.5 $NaHCO_3$ (30 w $m^{-2}$ light intensity) [CPW/B]. Solution within the isolating chamber was changed (F: chamber flush) to CPW/B plus 0.5% ethanol (SF: end of flushing sequence). After repeating this treatment, the isolating chamber solution was replaced by CPW/B + 0.5% ethanol + 10 μM (+FC). Four FC recovery responses were obtained (*, rechecked band center and verified its position approximately 1 mm from previous location).

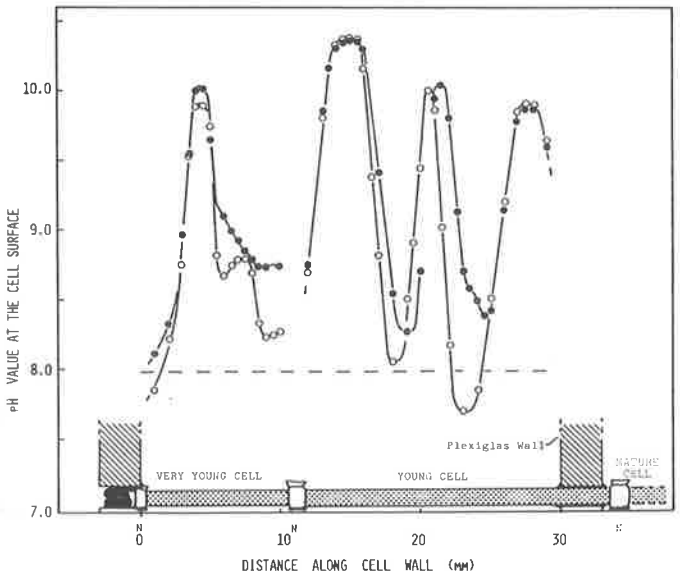


FIG. 2. Effect of FC on the light-dependent pH pattern established on the cell surface of *C. corallina*. Cells were bathed in CPW/B (20 w $m^{-2}$) for 1 h before being scanned (data not shown). The CPW/B + 0.5% ethanol (○) and CPW/B + 0.5% ethanol + 10 μM FC (●) scans were also conducted after 1 h pre-equilibration. -----, Represents the pH value of the background solutions; N, represents the nodal location.

were employed. This approach gave consistent results. In all experiments in which young or mature cells were used, alkaline band transport activity was not enhanced by FC. This was also the case for very young cells, and the response shown in Figure 2 was selected because it was the largest effect obtained for all cells studied.

In the presence of FC, the steady state pH values in the regions between the alkaline bands were always more alkaline compared with the control situation. Inasmuch as this region is thought to be involved in $HCO_3^-$ transport (2), the possible influence of FC on $H^{14}CO_3^-$ assimilation was studied. Table I indicates that 10 and 20 μM FC had a slight inhibitory effect on net $H^{14}CO_3^-$ assimilation. However, when $K^+$ was either absent or present at higher than control levels, 20 μM FC caused a slight stimulation of $H^{14}CO_3^-$ assimilation. The observed effects were all quite small, and it is doubtful whether they demonstrate a significant influence of FC on the $H^{14}CO_3^-$ assimilating processes ($HCO_3^-$ influx, in particular).

The pH scanning and $H^{14}CO_3^-$ assimilation data do not provide support for the hypothesis that an $H^+$ influx system is responsible for the formation of the alkaline bands of *Chara*. The present data are also at variance with the proposal that FC stimulates $H^+$ efflux in the Characeae (10, 11).

**Computer Simulation of pH Pulse Experiments.** Lucas (5) suggested that if localized $H^+$ influx systems were generating the alkaline bands, it should be possible to saturate the carriers involved by exposing the localized site to low pH values. Under this substrate-saturation condition, it was suggested that the redevelopment of alkalinity (on the cell surface) would be delayed, due to the enhanced level of available substrate ($H^+$). However, no such delay was observed experimentally (5).

The validity of this delay hypothesis was investigated using our numerical analysis computer model (2, 8). The basic mechanics of the program remained unaltered except that we expanded the treatment to account for the diffusion of $OH^-$ away from, and $H^+$ toward, the alkaline band site. The flushing solutions did not contain $HCO_3^-$, hence, the numerical analysis program did not have to include the $HCO_3^-$ buffering effect. We simply simulated the pH flushing technique, whereby the $OH^-$ diffusion gradient established near the cell wall surface (by the alkaline band) was eliminated, and replaced by a new solution having a low pH value (5.0–7.0). In these studies a 100-μm spatial increment was used for the diffusion calculations. During the simulation, chemical equilibrium between $H^+$, $OH^-$, and $H_2O$ was imposed within the 100-μm volume element every 0.5 s.

As a control we examined the response of a simulated $OH^-$ efflux system to this external pH change. When the same program was run, except that $H^+$ ions were pumped into the cell (at a rate identical to that used for the $OH^-$ efflux program), an identical recovery pH response was generated (Fig. 3). A delay in the reestablishment of alkalinity was absent in both simulations. These

Table I. *Effect of Fusicoccin on $H^{14}CO_3^-$ Assimilation in C. corallina*

Control cells were pretreated for 30 min in a solution containing (mM): 1.0 NaCl, 0.2 KCl, 0.2 $CaSO_4$, 0.5 $NaHCO_3$ ([pH 9.0] 25 C and 20 w $m^{-2}$) followed by 1 h $^{14}C$ exposure. All other treatments were identical except the control solution which was modified as indicated.

| Treatment | Net $H^{14}CO_3^-$ Assimilation | Control |
|---|---|---|
| | *pmol $cm^{-2}$ $s^{-1}$* | *%* |
| Control | 27.6 ± 1.7 | |
| +0.5% (v/v) Ethanol | 27.9 ± 2.1 | 100 |
| +0.5% Ethanol + 10 μM FC | 25.0 ± 2.03 | 91 |
| +0.5% Ethanol + 20 μM FC | 24.7 ± 2.25 | 90 |
| +0.5% Ethanol + 20 μM FC − KCl | 30.8 ± 1.62 | 111 |
| +0.5% Ethanol + 20 μM FC + 0.5 mM KCl | 30.4 ± 1.78 | 110 |

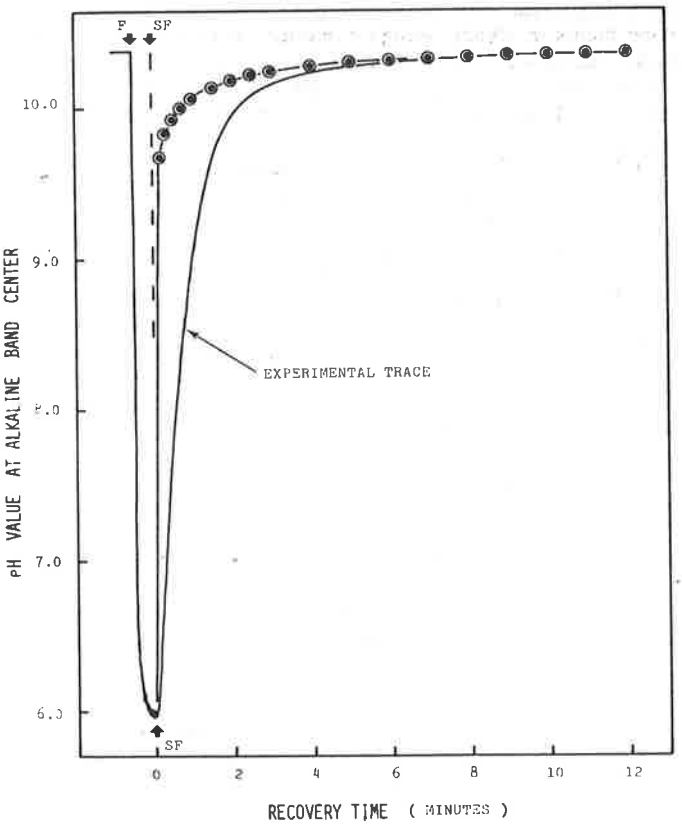


FIG. 3. Experimental and simulated recovery pH traces generated following the elimination of the $OH^-$ diffusion pattern, established near the cell surface by the alkaline band transport system. In the experimental situation the diffusion pattern was eliminated by flushing new solution into the chamber (solution composition (mM): 1.0 NaCl, 0.2 KCl, 0.2 $CaSO_4$). F and SF represent the commencement and cessation of this flushing procedure, respectively. In the numerical analysis program the diffusion pattern was eliminated by resetting the pH values in all the spatial increments to the predetermined value (pH 6.0 in the case illustrated). The symbol (○) represents a simulated recovery response in which $OH^-$ ions were the transported species and the $OH^-$ efflux within the band center was 100 pmol $cm^{-2}$ $s^{-1}$. ●, Represents an identical computer simulation, except that $H^+$ ions were transported into the cell, with an equivalent band-center influx value.

results appear to invalidate the delay hypothesis proposed by Lucas (5).

The data in Figure 3 also indicate that for comparable steady-state fluxes, the pH responses obtained by computer simulation were more rapid than the experimental situation. Since we adjusted the steady-state experimental and simulation fluxes to the same value, this difference most probably reflects a slight perturbation of the characean alkaline band transport system during the flushing sequence.

**Chemical $H^+$ Production.** The accuracy of the numerical analysis data obtained for $H^+$ influx will depend to a marked degree on whether a suitable spatial increment was employed in the program and on whether a reasonable limit was placed on the rate of proton production within these spatial increments. We investigated this aspect by examining the kinetics of $H_3O^+$ production from $H_2O$.

An estimate of the maximum possible rate of $H^+$ influx at the plasmalemma surface can be obtained in the following manner. The net rate of $H_3O^+$ production from $H_2O$ per unit volume of solution ($Q_r$) can be written as:

$$Q_r = k_f[H_2O]^2 - k_b[H_3O^+][OH^-] \quad (1)$$

where $k_f$ ($5 \times 10^{-7}$ $mol^{-1}$ liter $s^{-1}$) and $k_b$ ($1.3 \times 10^{11}$ $mol^{-1}$ liter $s^{-1}$) are the forward and backward rate coefficients, respectively, for the dissociation of water (3). By continuity we can write, at steady-state:

$$Q_r = -D_H \cdot \nabla^2[H_3O^+] \quad (2)$$

where $D_H$ is the proton diffusion coefficient (positive sign, of $H^+$, omitted to avoid confusion within the equations).

An absolute upper limit for $Q_r$ can be obtained by dropping the back reaction term in equation 1. Also, near the plasmalemma surface, the $H^+$ ($OH^-$) gradient will closely approximate that of a one-dimensional diffusion system. By employing these conditions, equations 1 and 2 can be combined to give:

$$-C''(x) = k_f[H_2O]^2/D_H$$

or (3)

$$-C''(x) = K$$

where $C = [H_3O^+]$, $K = k_f[H_2O]^2/D_H$, and a prime sign indicates partial differentiation with respect to $x$, the distance from the plasmalemma.

Integration of equation 3 yields:

$$C(x) = -(K/2)x^2 + C'(O)x + C(O) \quad (4)$$

where $C(x)$ is the proton concentration at $x$, and $C(O)$ and $C'(O)$ are, respectively, the proton concentration and gradient at the plasmalemma surface.

Equation 4 can be rearranged to give:

$$C'(O) = \{C(x) - C(O)\}/x + (K/2)x \quad (5)$$

Now the proton flux at $x = 0$ is given by:

$$J_H(O) = -D_H \cdot C'(O) \quad (6)$$

To obtain a solution for equation 6 it was necessary to determine the upper limit for $C'(O)$. To achieve this solution for equation 5 we had to establish realistic boundary limits and conditions. This entailed setting an upper limit for $x$ (*i.e.* $x_{max}$) and performing a sensitivity analysis with respect to $C(O)$ and $C(x_{max})$.

An initial value for $x_{max}$ was estimated by invoking the following condition: proton half-life = proton diffusion time to the plasmalemma. For a second order reaction where one reactant is present in excess, the half-life of the reaction ($\tau$) is given by the equation:

$$\tau = -\ln 2/k_b(a - b) \quad (7)$$

where a and b are the initial reactant concentrations. In this situation where ($b \gg a$) equation 7 reduces to:

$$\tau_a = \ln 2/k_b(b) \quad (8)$$

This is the case in our experimental system, where the steady state pH values (at the cell surface) range from 10 to 10.5; hence, $[OH^-] \gg [H^+]$.

Since an approximate diffusion time for a one-dimensional system is given by:

$$T = x^2/2D \quad (9)$$

equations 8 and 9 can be combined to give a first order upper limit for $x$. Thus:

$$x_{max} = \{2D_H \ln 2/k_b[OH^-]\}^{1/2} \quad (10)$$

Equations 5 and 10 were substituted into equation 6 and values for $J_H(O)_{max}$ calculated for a range of $C(x_{max})$ values. [The value of $C(O)$ was held constant at $10^{-14}$ mol liter$^{-1}$.]

Data pertinent to these calculations are presented in Table II. Theoretical concentration profiles that would be established for

Table II. *Physico-chemical Limits to the Production and Supply (by Diffusion) of $H_3O^+$ to a Putative $H^+$ Influx System in the Plasmalemma of Chara corallina*

| $(H_3O^+)_{max}$ | $^{\tau}H_3O^+$ | $\chi_{max}$ | C′ (O) | $^{J}H_3O^+$ $(O)_{max}$ |
|---|---|---|---|---|
| *mol liter$^{-1}$* | *s* | *cm × 10$^6$* | *mol liter$^{-1}$ cm$^{-1}$* | *pmol cm$^{-2}$ s$^{-1}$* |
| $10^{-10}$ | $5.33 \times 10^{-8}$ | 1.88 (3.15)[a] | $9.58 \times 10^{-5}$ ($5.73 \times 10^{-5}$) | 3.22 (5.33) |
| $10^{-9}$ | $5.33 \times 10^{-7}$ | 5.96 (9.96) | $3.03 \times 10^{-4}$ ($1.81 \times 10^{-4}$) | 10.2 (16.8) |
| $10^{-8}$ | $5.33 \times 10^{-6}$ | 18.9 (31.5) | $9.58 \times 10^{-4}$ ($5.73 \times 10^{-4}$) | 32.2 (53.3) |

[a] Values were calculated using equations 5, 6 and 10 and $[H_3O^+]$ (O) of $10^{-14}$ mol liter$^{-1}$. Solutions to equations obtained using $D^o_{H^+}$ (self diffusion coefficient, $9.308 \times 10^{-5}$ cm$^2$ s$^{-1}$) are given in parenthesis, all other solutions were obtained using $D^l_{HCl}$ (limiting diffusion coefficient, $3.335 \times 10^{-5}$ cm$^2$ s$^{-1}$).

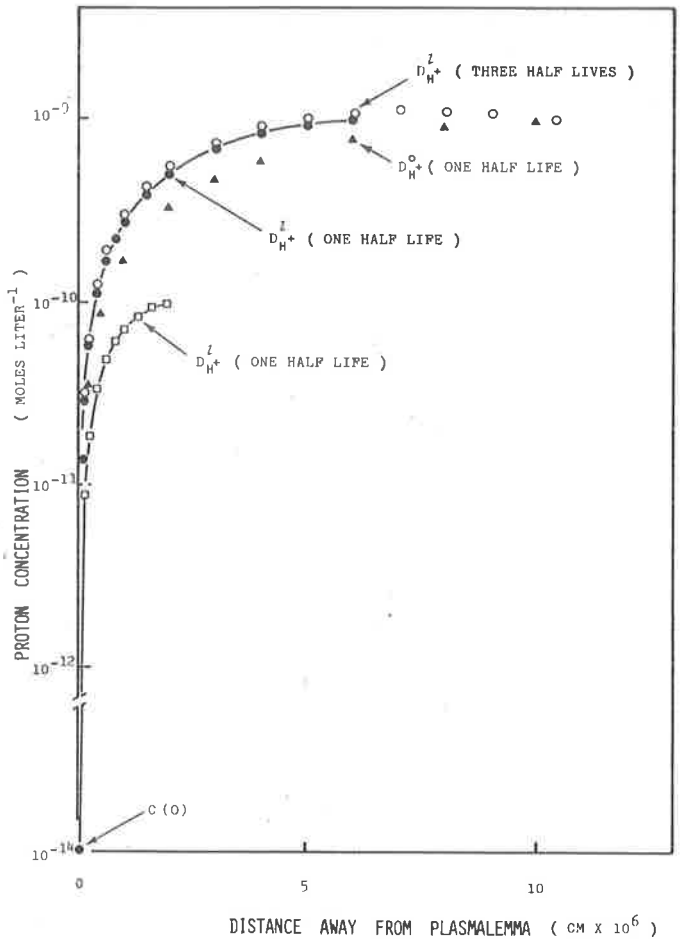


FIG. 4. Theoretical $H^+$ concentration profiles generated from equations 4, 5 and 10. The symbols $D^l_{H^+}$ and $D^o_{H^+}$ represent values computed using the limiting and self diffusion coefficients for protons, respectively.

different $C(x_{max})$ and $D_H$ values are also illustrated in Figure 4. The values obtained for $x_{max}$ indicate that the 100 $\mu$m diffusional increment used in the numerical analysis program was too large for $H^+$ calculations by several orders of magnitude. The computer program also allowed an unlimited rate of $H_3O^+$ production from water. The values obtained for the maximum proton flux were dependent upon the diffusion coefficient employed (Table II). However, irrespective of whether the limiting or the self diffusion coefficient was used, the maximum theoretical computed $H^+$ influx was smaller than the range of values obtained from diffusion studies (100–300 pmol cm$^{-2}$ s$^{-1}$; see Table I in ref. 8).

**Possible Electrophoretic Contributions.** There are two sources of electric fields that could also conceivably help to drive the putative (theoretical) proton influx. These fields originate from the fixed changes on the outer plasmalemma surface, and also as a result of ionic fluxes that are being carried by self diffusion (2).

The Debye length ($\lambda$) for the field resulting from the plasmalemma surface charge can be calculated by Gouy-Chapman theory, provided that the surface potential is not too high. (This procedure will overestimate the potential gradient away from the plasmalemma because the theory ignores the existence of surface-adsorbed ions.) In the present study, $\lambda$ was calculated using the following equation:

$$\lambda = [(\kappa\epsilon_0 RT)/(F^2\Sigma_i C_i Z_i^2)]^{1/2} \quad (11)$$

where $\kappa$ is the dielectric coefficient of the solution, $\epsilon_0$ the permittivity of the free space, R the gas constant, T the absolute temperature, F the Faraday, and $\Sigma_i C_i Z_i^2$ is the ionic strength of the wall solution. To determine a value for the wall solution ionic strength, we assumed a Donnan potential of −60 mv. This gave $\Sigma_i C_i Z_i^2$ equal to 97 mM (using the standard ionic strengths employed in the experimental bathing solutions). Substitution of this value (97 mM) into equation (11) gave a $\lambda$ value of 1.4 nm.

Under our present conditions and assumptions the value of the surface potential can be calculated from the equation:

$$\psi(o) = \lambda q/\kappa\epsilon_0 \quad (12)$$

where q is the surface charge density. Using $-8 \times 10^{-7}$ coulombs cm$^{-2}$ as a reasonable estimate for q (1) a value of $\psi(o) = -16$ mv was obtained. This value is low enough that the Debye length is a meaningful quantity, and we can write:

$$\psi'(x) = \psi'(o) \exp(-\chi/\lambda) \quad (13)$$

where $\psi'(o)$ is the electric potential gradient at the membrane surface, given by:

$$\psi'(o) = q/\kappa\epsilon_0 \quad (14)$$

Using the given value for q, $\psi'(o)$ would be $10^5$ v cm$^{-1}$. At a distance $7\lambda$ away from the membrane (9.8 nm), $\psi'(x)$ would be reduced to 100 v cm$^{-1}$.

The electrically driven (electrophoretic) proton flux at this distance would then be given by:

$$J_H(x) = -(D_H F/RT)\, C(x)\psi'(x) \quad (15)$$

Using the self diffusion coefficient for protons, C (9.8 nm) equal to $10^{-12}$ mol cm$^{-3}$ and a $\psi'$ (9.8 nm) of 100 v cm$^{-1}$, one obtains an electrophoretic proton flux [$J_H$ (9.8 nm)] of 0.4 pmol cm$^{-2}$ s$^{-1}$. A comparison of this value with the diffusion-mediated fluxes presented in Table II indicates that this surface-potential electrophoretic flux could not make a significant contribution to the total putative proton flux.

Electrogenic transport of either $H^+$ into, or $OH^-$ out of, the *Chara* cell will establish a negative electric potential gradient within the external cell wall solution (2, 16). To determine the electrophoretic effect that this electric potential gradient would have on the total putative $H^+$ influx requires that we know the magnitude of this potential gradient ($\psi_e'$). The following equation, derived by Ferrier and Lucas (2), gives the relationship between

the electric and proton activity gradients:

$$\psi_e' = (RT/F)C'(x)/\Sigma_i C_i Z_i^2. \quad (16)$$

The ratio of the electrophoretic and self diffusion fluxes can be used to determine their relative importance. Hence:

$$\frac{J_{electrophoretic}}{J_{self\ diffusion}} = (D_H F/RT)C(x)\psi_e'(x)/D_H C'(x) = C(x)/\Sigma_i C_i Z_i^2 \quad (17)$$

Substitution of $C(x) = 10^{-9}$ M and $\Sigma_i C_i Z_i^2 = 0.097$ M into equation 17 gives a flux ratio of $1.03 \times 10^{-8}$. Again we see that the flux contribution derived from this electric potential gradient would be negligible.

## DISCUSSION

At the center of alkaline bands, measured pH values can be as high as 10.5 (7). This represents a value measured slightly away from the cell wall surface. It is difficult to know exactly what the related value would be within the wall, or more pertinent to this analysis, what the pH would be against the plasmalemma surface. The Donnan potential of the cell wall, which may be as high as −80 mv (15), would have a definite effect on the $OH^-$ concentration within the wall. This effect may reduce the "local" pH of the wall from 10.5 to a value of approximately 9.0. However, it must be stressed that the distribution of these fixed negative charges within the wall is as yet not known. If the negative charge density of the wall is asymmetrically distributed such that the charges are concentrated near the plasmalemma, the negative charges may function as stabilizing sites for the protons produced from water. However, the $x_{max}$ values listed in Table II indicate that unless the majority of the negative charges are concentrated within the inner 0.2 $\mu$m of the wall, they would not play a direct role in reducing the back reaction of $H_3O^+$ and $OH^-$ to form $H_2O$.

A reliable value for $C(x_{max})$ within the wall solution is probably close to $10^{-10}$ mol liter$^{-1}$. Based on this value, the results presented in Table II clearly demonstrate that from a physico-chemical standpoint the maximum theoretical $H^+$ influx is much smaller than the range of experimentally observed fluxes. The values are too small by at least an order of magnitude.

At this point it should be stressed that the $J_{H_3O^+}$ values in Table II represent our attempt to obtain a theoretical absolute upper limit. Because the back reaction is not negligible (see $\tau_{H_3O^+}$ values in Table II), realistic $J_{H_3O^+}$ (max) values would be much smaller. Similarly, if we allowed for the physical effect of the cell wall material on both the effective proton diffusion coefficient and volume of water available in which the dissociation reaction could proceed, we would obtain flux values below those presented in Table II.

The values of C(O) and $x_{max}$ have different degrees of influence on the calculations. The value of C(O) was set at $10^{-14}$ mol liter$^{-1}$; firstly, because we wanted to set the value lower than known $pK_b$ values for an amino group, and secondly, values smaller than $10^{-14}$ had no further influence on $J_{H^+}$ (max). If $x_{max}$ is recalculated allowing for a three half-life situation, the value for $J_{H_3O^+}(O)$ changes from 10.2 (Tables II, C(O) = $10^{-9}$ mol liter$^{-1}$) to 10.9 pmol cm$^{-2}$ s$^{-1}$. This change is almost insignificant, indicating that the determined values are not highly sensitive to the spatial conditions imposed.

This aspect can be examined another way. The observed fluxes associated with the center of the alkaline band often fall into the range of 150–200 pmol cm$^{-2}$ s$^{-1}$. Using a value of 150 pmol cm$^{-2}$ s$^{-1}$, C'(O) would have to be $4.43 \times 10^{-3}$ mol liter$^{-1}$ cm$^{-1}$ (using $D_{H^+}^f$ in the calculation). A value of 2 $\mu$m for $x_{max}$ would be obtained from equation 5. For a proton flux of this magnitude to occur, the $H_3O^+$ ions produced from the dissociation of water within this volume would have to be stabilized within this cell wall solution for a period in excess of 1,000 half-lives.

We feel that the present results indicate that from a physico-chemical standpoint, the alkalinity which develops on the surface of *Chara* internodal cells cannot be produced by a transport system moving $H^+$ from the cell wall solution to the cytoplasm. The evidence most strongly favors the existence of an $OH^-$ efflux system. However, there is one possibility that cannot be discounted. It is possible, theoretically, that the observed alkalinity is generated by a transport system that initially binds $H_2O$ and then splits this substrate, vectorially, into $H^+$ (influx) and $OH^-$ (diffuses away from the plasmalemma).

*Acknowledgments*—The authors would like to thank Professor E. Marrè for the supply of fusicoccin used in this study and Professor J. Dainty for the use of the University of Toronto computer facilities.

## LITERATURE CITED

1. ELUL R 1967 Fixed charge in the cell membrane. J Physiol 189: 351–365
2. FERRIER JM, WJ LUCAS 1979 Plasmalemma transport of $OH^-$ in *Chara corallina*. II. Further analysis of the diffusion system associated with $OH^-$ efflux. J Exp Bot 30: 705–718
3. FROST AA, RG PEARSON 1961 Kinetics and Mechanism. Ed 2. John Wiley & Sons, New York, pp 209–210
4. LUCAS WJ 1975 The influence of light intensity on the activation and operation of the hydroxyl efflux system of *Chara corallina*. J Exp Bot 26: 347–360
5. LUCAS WJ 1979 Alkaline band formation in *Chara corallina*: due to $OH^-$ efflux or $H^+$ influx? Plant Physiol 63: 248–254
6. LUCAS WJ 1980 Control and synchronization of $HCO_3^-$ and $OH^-$ transport during photosynthetic assimilation of exogenous $HCO_3^-$. *In* RM Spanswick, WJ Lucas, J Dainty, eds, Membrane Transport in Plants: Current Conceptual Issues. Elsevier, Amsterdam, pp 317–330
7. LUCAS WJ, J DAINTY 1977 $HCO_3^-$ influx across the plasmalemma of *Chara corallina*: divalent cation requirement. Plant Physiol 60: 862–867
8. LUCAS WJ, JM FERRIER, J DAINTY 1977 Plasmalemma transport of $OH^-$ in *Chara corallina*: Dynamics of activation and deactivation. J Membr Biol 32: 49–73
9. LUCAS WJ, FA SMITH 1973 The formation of alkaline and acid regions at the surface of *Chara corallina* cells. J Exp Bot 24: 1–14
10. MARRÈ E 1978 Membrane activities as regulating factors for plant cell functions. Biol Cellulaire 32: 19–24
11. MARRÈ E 1979 Fusicoccin: a tool in plant physiology. Annu Rev Plant Physiol 30: 273–288
12. MITCHELL P 1966 Chemiosmotic coupling in oxidative and photosynthetic phosphorylation. Biol Rev 41: 445–502
13. MITCHELL P 1967 Translocations through natural membranes. Adv Enzymol 29: 33–87
14. POOLE RJ 1978 Energy coupling for membrane transport. Annu Rev Plant Physiol 29: 437–460
15. SPANSWICK RM, J STOLAREK, EJ WILLIAMS 1967 The membrane potential of *Nitella translucens*. J Exp Bot 18: 1–16
16. WALKER NA, FA SMITH 1977 Circulating electric currents between acid and alkaline zones associated with $HCO_3^-$ assimilation in *Chara*. J Exp Bot 28: 119–120

Protoplasma 104, 253—271 (1980)

PROTOPLASMA
© by Springer-Verlag 1980

# Structure and Possible Function(s) of Charasomes; Complex Plasmalemma-Cell Wall Elaborations Present in Some Characean Species

V. R. Franceschi and W. J. Lucas *

Department of Botany, University of California, Davis, California

Received April 2, 1980
Accepted June 12, 1980

## Summary

Charasomes, complex membrane structures, were found along the longitudinal walls of internodal and lateral branch cells of *Chara corallina* and *C. braunii*, but not along their transverse walls or in other cell types. Charasome-complexes were larger and more numerous in the lateral branch cells than in internodal cells. In *C. corallina*, a dioecious species, especially large elaboration of charasome material occurs in the lateral branch cells of the female plant, sometimes reaching a cross-sectional width which is as great as that of the adjacent cell wall.

*Chara* internodes transport hydroxyl ($OH^-$) out of the cell and bicarbonate ($HCO_3^-$) into the cell. Spatial distribution of charasomes along the cell was examined with respect to these transport phenomena, which occur at specific identifiable regions along the cell. Charasome-complexes were always found in regions in which $HCO_3^-$ transport occurs but were often fewer, reduced in size or absent in areas of $OH^-$ efflux. *Nitella flexilis* exhibited similar patterns of $OH^-$ and $HCO_3^-$ transport along the cell; however, there was a complete absence of charasomes. Ultrastructural examinations on *Nitella translucens* indicated that charasomes were also absent in this species. The observation that charasomes are present in both transport regions of *Chara* but are totally lacking in the two *Nitella* spp. indicates that the charasome-complex is not involved in transport of either substance. Other possible functions for the charasomes, including a role in osmoregulation, are discussed.

Charasome substructure is the same in both *Chara* species, consisting of a mass of short (50 nm average length) anastomosing tubules (30 nm average diameter) derived from the plasmalemma. The interior of the tubules is open to the cytoplasm while the area surrounding the tubules is ultimately open to the wall and thus can be considered to be wall space. Charasomes are quite variable in size and shape, but are roughly globular, with the bulk of the structure projecting into the cell cytoplasm. Tubular components of the charasome

* Correspondence and Reprints: Department of Botany, University of California, Davis, CA 95616, U.S.A.

0033-183X/80/0104/0253/$ 03.80

were sometimes seen to extend into the microfibrillar wall matrix. A three dimensional model of the charasome-complex presented details the great complexity of this membrane system.

*Keywords:* Bicarbonate transport; *Chara;* Charasome-complex; *Nitella;* Plasmalemma invaginations.

## 1. Introduction

There are numerous reports of the occurrence of membranous structures in plant cells that are produced by the elaboration of areas of the plasmalemma, or other membrane systems (see Bracker 1967, Marchant and Robards 1968, Pate and Gunning 1972, Marchant and Moore 1973). The resulting structures have been variously termed lomasomes (Moore and McAlear 1961), plasmalemmasomes (Edwards 1962), or more generally, paramural bodies (Marchant and Robards 1968). In higher plants, cells having an increase in plasmalemma surface area are called transfer cells (Pate and Gunning 1972). However, in this situation the increase in membrane area is achieved by specific wall ingrowth.

Membranous structures at the plasmalemma/cell wall interface of some *Chara* and *Nitella* species were reported by Barton (1965 a) and Crawley (1965) and were considered by them to be organelles. They consisted of masses of anastomosing membranous tubules, surrounded by a seemingly continuous unit membrane possibly derived from the plasmalemma. Barton (1965 b) called these structures "charasomes" and later (Barton 1968), using autoradiography, examined them for involvement in cell wall synthesis, but could find no indication of such a function.

*Chara* and *Nitella* species have been used extensively for ion transport studies. In *C. corallina* $HCO_3^-$ assimilation is mediated by spatially separated $HCO_3^-$ (influx) and $OH^-$ (efflux) transport systems (Lucas 1976, Ferrier and Lucas 1979, Lucas and Nuccitelli 1980). Under normal conditions, identical transport profiles occur on both internodal and lateral branch cells (Lucas, Ferrier, and Dainty 1977, Lucas and Nuccitelli 1980). In the absence of mechanical or chemical perturbation, mature cells maintain very stable (spatial location and transport rate) transport profiles. Modification of the plasmalemma to produce charasomes could be a factor in the location, intensity,

---

Figs. 1–4. *C. corallina.* Charasome-complex (*C*), mitochondrion (*M*), Chloroplast (*P*), vacuole (*V*), cell wall (*W*)

Fig. 1. Very young internode (X. S.). No charasomes. ×10,500

Fig. 2. Mature male lateral branch cell (L.S.). Charasome material and associated mitochondria are apparent. ×14,000

Fig. 3. Chloroplast closely appressed to plasmalemma in male lateral branch cell, and surrounded by charasome material (L.S.). ×14,000

Fig. 4. Massive charasome formation in mature female lateral branch cell (X.S.). ×24,000

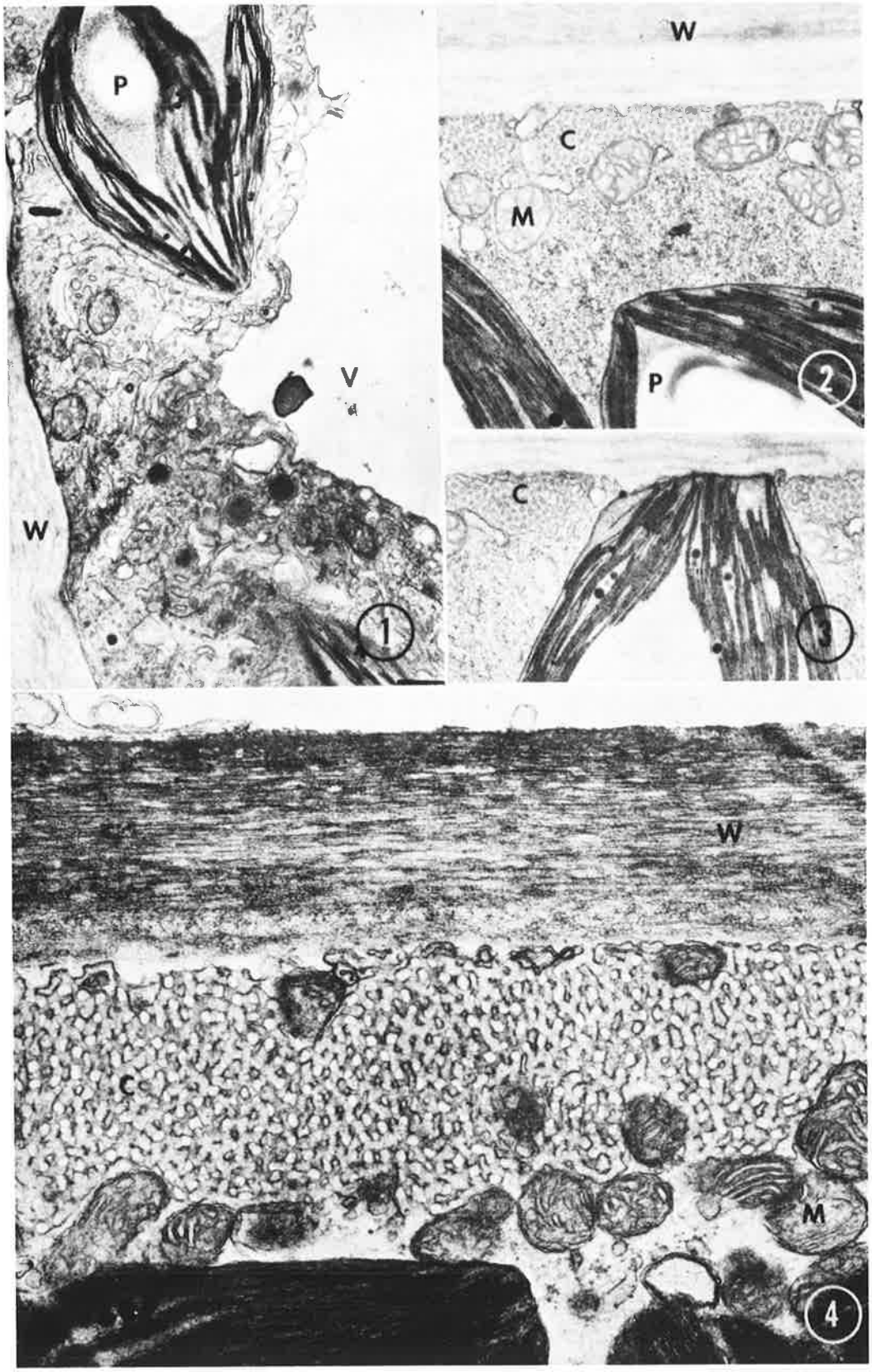
P
V
W
1
W
C
M
P
2
C
3
W
C
M
4

and/or mechanism of such transport phenomena. We report here the results of our examination of two *Chara* and two *Nitella* species for the presence of charasomes, and on our investigation to determine whether a correlation exists between charasome distribution and the spatial distribution of $HCO_3^-$ or $OH^-$ transport. We have closely re-examined the ultrastructural aspects of the charasome and report some new observations. Based on these studies we present a three dimensional interpretation of the charasome-complex.

## 2. Materials and Methods

### *2.1. Organisms*

The *Chara* species examined were *C. corallina* Klein ex Willd., em. R. D. W. (= *C. australis* R. Br.), a dioecious species, which was grown in the laboratory under conditions previously described (LUCAS 1975), and *C. braunii f. novi-mexicana* (A. Br.) R. D. W., a monoecious species, collected in Fresno County, California, U.S.A., during October, 1979. The *Nitella* species used were *N. flexilis f. longifolia* (A. Br. ex. Mig. Vilh.) collected at the same time and locations as *C. braunii*, and *N. translucens*, which was provided by Dr. R. M. SPANSWICK (Cornell University).

### *2.2. Transmission Electron Microscopy (TEM)*

Cells at various stages of maturity from very young to mature (fully expanded) were used. Emphasis was placed upon internodal cells of the main axis and lateral branches, however, other cell types (nodal, antheridial, etc.) were also examined to some extent. Cells from both male and female plants of *C. corallina* were prepared for TEM.

Cells were immersed in a very slightly hypotonic fixative solution (1.25% glutaraldehyde, 0.05 M sodium cacodylate, 1 mM CaCl; pH 7.2). Solution temperature was then lowered from 22 to 4 °C by refrigeration. Fixation was carried out for 12–16 hours followed by a 1 hour wash in several changes of the fixative buffer. Cells were postfixed for 2 hours in 1% osmium tetroxide (22 °C), rinsed thoroughly with distilled water and dehydrated in a graded acetone series. Material was embedded in Spurr's Resin (SPURR 1969), sectioned with a diamond knife and examined on a JEOL 100S TEM.

During cell preparation for TEM an interesting observation was made. Osmium tetroxide fixation caused *Nitella* cells to become very densely black, in comparison to cells of the *Chara* spp. which did not stain intensely. TEM examination of *Nitella* cells usually revealed large amounts of a fine granular material within the vacuole. This material, which was apparently responsible for the density of staining of whole cells fixed in osmium, was not observed in *Chara* cells.

### *2.3. Mapping of pH Along the Cell Surface*

Mature internodal cells of the main axis and lateral branches of male *C. corallina* plants were used for pH scan experiments. The surface of these cells was scanned with a pH electrode as previously described by LUCAS and SMITH (1973), generating pH values which were used to produce a "map" of changes in pH along the cell wall. The scanned cells were prepared for electron microscopy as described above. On internodal cells the first branch cell was left attached. The junction between these two cells was used as a reference point to obtain a spatial correlation between the pH scans and sections cut for TEM. In the branch cell situation the junction between the nodal complex and the first nodal (branch) cell served as this reference point. Cross-sections were made along each cell within areas of maximum and minimum pH (corresponding to areas of peak $OH^-$ and $HCO_3^-$ transport, respectively;

see Ferrier and Lucas 1979; Lucas and Nuccitelli 1980) and examined by TEM for ultrastructural differences. A similar study was also performed on an internodal cell of *Nitella flexilis*.

## 3. Observations

Charasomes were found in both *Chara* species examined, but were not seen in either *Nitella* species. Our observations on the occurrence of charasomes in *C. corallina* and *C. braunii* will be given first, followed by an account of their distribution with respect to cell wall pH and an examination of the general and fine structure of the charasomes. A brief account of our observations on the two *Nitella* species will be given last.

### *3.1. Chara corallina*

Charasomes were found in mature internodal cells of the main axis and lateral branches of both male and female *C. corallina* plants. They were absent in young internodal cells of up to 2 mm in length (Fig. 1), which are already vacuolated. Charasomes were found only on the longitudinal walls of internodal cells and were not present along any of the cross-walls which exist between the cells of the thallus.

Charasomes were both larger and more numerous in lateral branch cells compared with those found in internodal cells. In the male lateral branch cells the charasomes were typically as large as, or larger than the numerous mitochondria which were always present (Figs. 2 and 3). Massive charasome arrays were observed in the female lateral branch cells examined (Figs. 4 and 5). Mitochondria were often seen to be enveloped by the arrays, an observation which was especially evident in oblique sections (Fig. 5). In some areas of the female lateral branch cells the cross-sectional thickness of the charasome material was as great as that of the adjacent cell wall (2–5 μm, Fig. 4). In contrast to the lateral branch cells, charasomes of the internodal cells of the main axis were about the same size or much smaller than the mitochondria (see Fig. 19).

A close association between mitochondria and the plasmalemma and charasomes was a consistent feature in mature cells. The mitochondria were generally concentrated just below the plasmalemma and charasomes (Figs. 2, 4, and 5). No such arrangement was observed in young internodes without

---

Figs. 6–9. *C. braunii*. Charasome (*C*), cell wall (*W*), spherosome (*S*)

Fig. 6. Tip region of mature lateral branch cell with numerous charasomes (X.S.). ×14,000

Fig. 7. Mature internode, oblique section. Note small charasome and microtubules associated with the plasmalemma (arrows). ×17,500

Fig. 8. Developing antheridial cells with pockets of membranous tubules (arrows). ×10,500

Fig. 9. Section near surface of antheridial cells. Tubules can be seen to be extensions of the protoplast (arrows). ×10,500

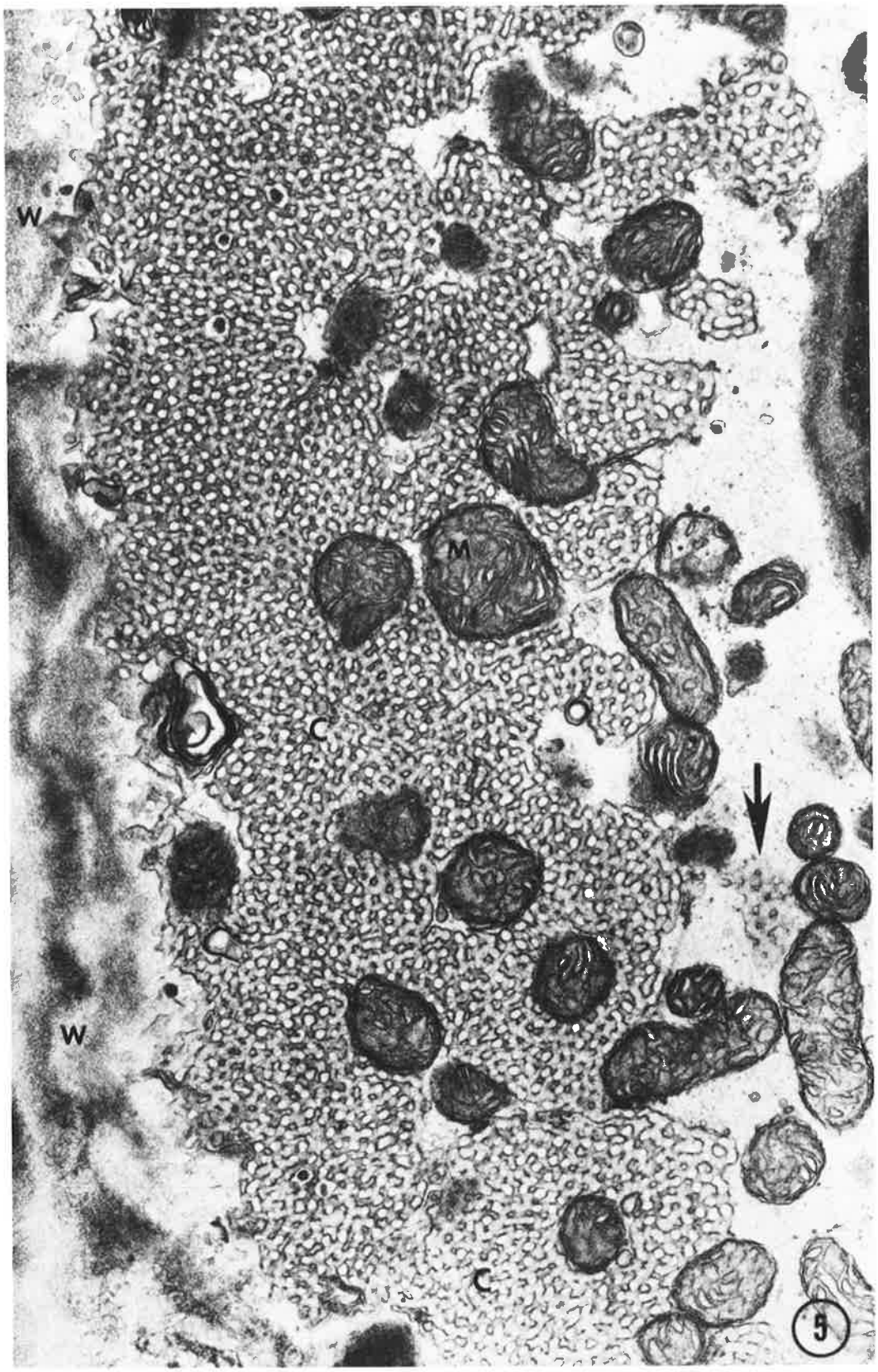


Fig. 5. Oblique section from mature female lateral branch cell. Numerous mitochondria (*M*) are embedded within charasome material (*C*). Note glancing section of surface of charasome (arrow). Cell wall (*W*). ×21,500

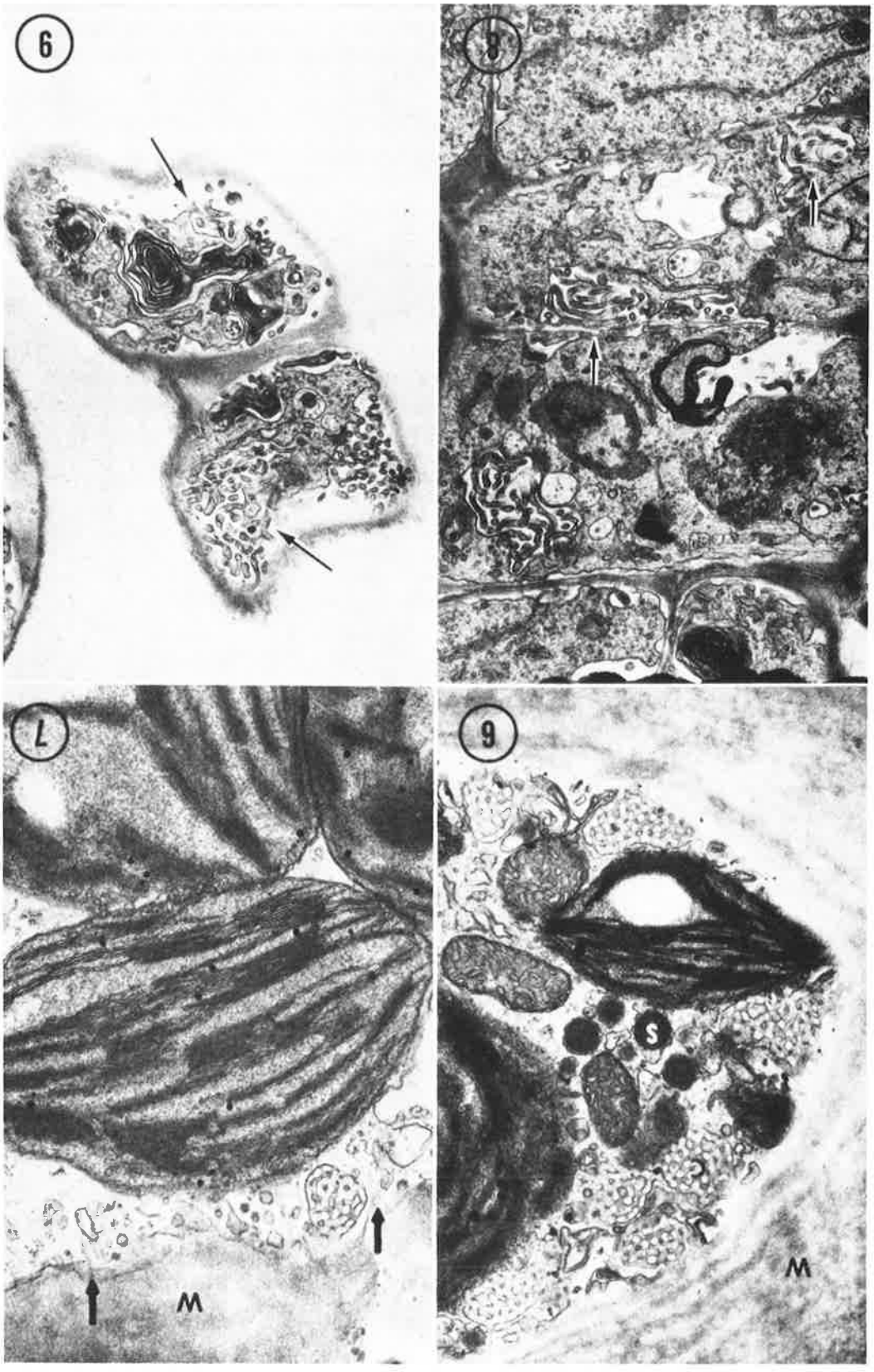
6
8
L
M
9
S
M

charasomes (Fig. 1). Another interesting feature of mature cells was the occasional chloroplast which was closely appressed to the plasmalemma (Fig. 3). This phenomenon occurred often enough in most cells examined to indicate it is not artifactual. In some instances 2 or 3 adjacent chloroplasts exhibited this behavior.

The observed arrangement of structures in the non-streaming portion of the cytoplasm (cortex or gel layer: from chloroplasts to plasmalemma) of the mature internode cells thus appears fairly well ordered. Beginning at the cell

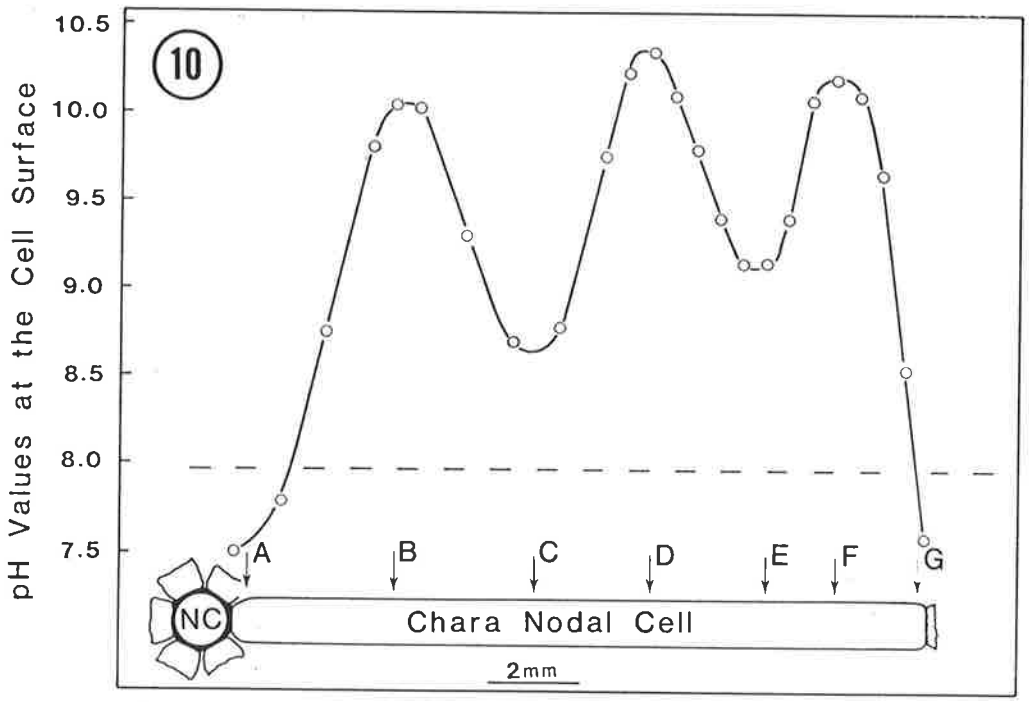


Fig. 10. Cell surface pH scan of a mature, male, *C. corallina* lateral branch cell. *A*, *C*, *E*, and *G* are $HCO_3^-$ transport regions; *B*, *D*, and *F* are $OH^-$ transport regions. *NC* is nodal complex

surface are the plasmalemma and charasomes, internal to which is an area of numerous mitochondria, and internal to these are the chloroplasts. Microbodies, spherosomes and lipid bodies are also occasionally seen in the general region occupied by mitochondria and chloroplasts (Figs. 6 and 18) and are abundant in the streaming portion of the cytoplasm.

### *3.2. Chara braunii*

Charasomes were also present in this species, showing the same structure and distribution as in *C. corallina*. Charasomes were fairly large and numerous in the lateral branch cells (Fig. 6) and fewer and reduced in size in the internode cells of the main axis (Fig. 7). Again they were not present at the cross-walls between adjacent internodal and nodal (branch) cells.

Although charasomes were found only in internodal and branch cells, tubular proliferations of the plasmalemma were seen in young antheridia. They appeared as long, simple tubular extensions of the plasmalemma (and cytoplasm) lacking anastomoses (Figs. 8 and 9). The tubules were slightly larger in diameter than the charasome tubules, and of a much longer, but indeterminate length. The resulting structure is a pocket of intertwining tubules.

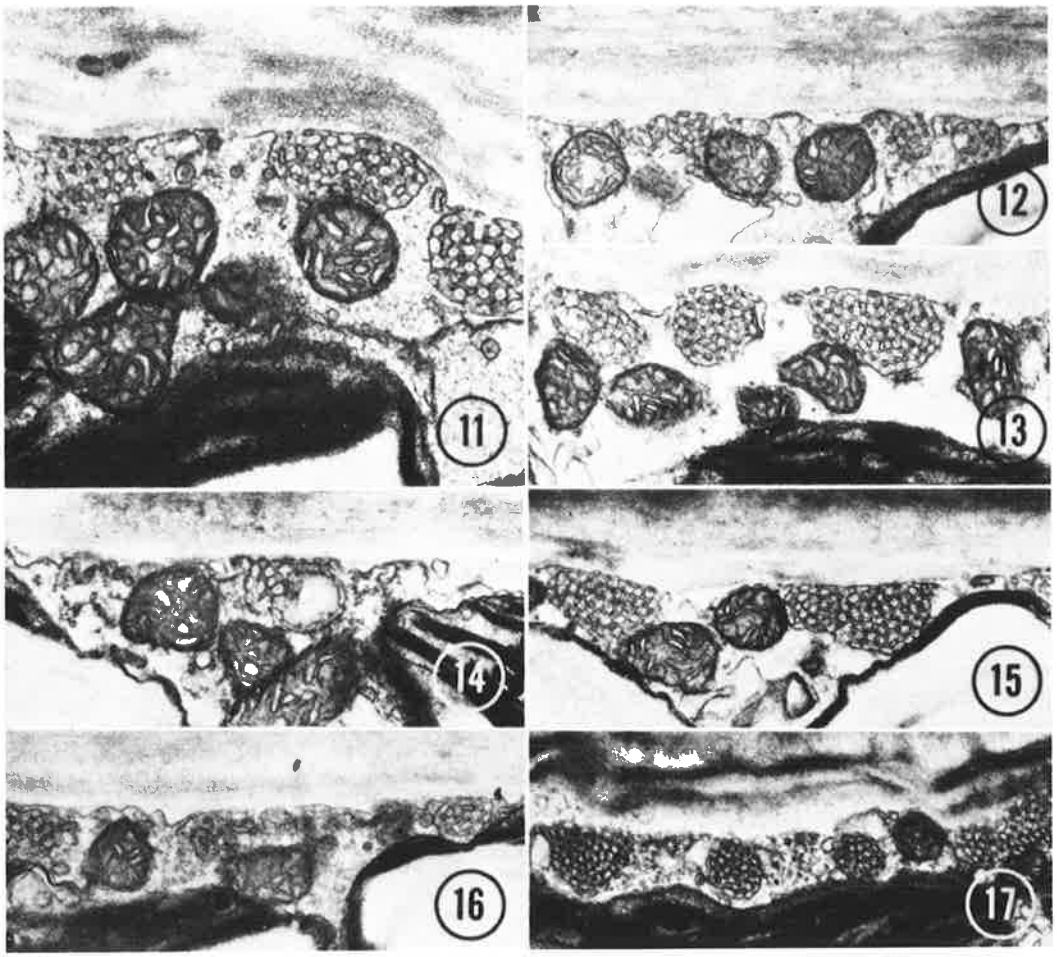


Figs. 11–17. Sections (X.S.) from peak transport regions of cell scanned in Fig. 10. Fig. 11 = A (×21,000), Fig. 12 = B (×14,000), Fig. 13 = C (×14,000), Fig. 14 = D (×17,500), Fig. 15 = E (×14,000), Fig. 16 = F (×14,000), Fig. 17 = G (×10,500). Use size of charasomes with respect to mitochondria to compare between $OH^-$ and $HCO_3^-$ regions

Although at times these pockets can be completely surrounded by cytoplasm (Fig. 8), they ultimately open to the cell wall (see Figs. 8 and 9). Later stages of antheridial development were not observed during this study.

### *3.3. pH Scans of C. corallina*

A number of mature cells from both the main axis (internodal) and lateral branches (nodal) of male *C. corallina* plants were scanned. Lateral branch cells are generally shorter in length than cells of the main axis; however, pH scan

patterns are similar in both cell types. A typical pH scan is reproduced in Fig. 10. Figs. 11–17 are micrographs from areas corresponding to the peaks and troughs from the pH scan. Charasome-complexes were always seen in areas of the cell having the lowest surface pH values (Figs. 11, 13, 15, and 17), which can be correlated to areas of $HCO_3^-$ transport into the cell (Ferrier and Lucas 1979, Lucas and Nuccitelli 1980). They were generally well formed and numerous in lateral branch cells but slightly smaller in the cells of the main axis. In regions of high pH, which corresponds to areas of $OH^-$ efflux, charasomes were fewer and generally much reduced in size, or absent altogether (Figs. 12, 14, and 16). The total absence of charasomes was especially prominent in cells of the main axis, and when charasomes were present in these cells they were often very rudimentary (see Fig. 23). It should be stressed that micrographs shown for the high pH regions represent areas of greater charasome frequency than is often seen when a cross section of the entire region of the cell is examined. These data are presented to indicate the difference in size, and complexity of charasomes (when they are present) in these regions, as compared to the larger, more complex charasomes present in the low pH regions of the same cell.

### *3.4. Charasome Structure*

The charasome-complexes of *C. corallina* und *C. braunii* exhibit the same basic structure. The bulk of the structure projects into the cell cytoplasm, however, they do not extend beyond the chloroplast layer. Charasomes do sometimes extend down between the chloroplasts (Fig. 18) but this is only seen when the chloroplasts are very close to the plasmalemma (Figs. 3 and 6). At its outer surface the charasome-complex is bounded by the cell wall. Continuity between the plasmalemma and charasome membranes can be seen at this surface (Figs. 11, 12, and 23). The charasome membrane facing the wall often appears discontinuous, having openings into the wall area (Figs. 4, 6, 23, and 24) and part of the charasome can be embedded within the cell wall matrix. In

---

Figs. 18–22. *C. corallina*. Charasome tubules (*T*), cell wall matrix (*W*), cytoplasm (*ct*), lipid body (*L*), microbody (*m*)

Fig. 18. Mature male lateral branch cell; plane of section parallel to cell wall. Charasomes can be seen to extend between chloroplasts. ×5,600

Fig. 19. Charasome tubules extending into cell wall matrix of mature male internode (X.S.). Plasmolysis of cell emphasizes connection. ×25,000

Fig. 20. Section through wall near plasmalemma of mature female lateral branch cell. Charasome tubules are seen within the cell wall matrix. ×28,000

Fig. 21. Oblique section through wall and part of cytoplasm of male lateral branch cell. Extension of charasome tubules into the wall matrix is evident. ×17,500

Fig. 22. Mature male lateral branch cells with charasome tubules and dense material (arrows) within the cell wall. ×14,000

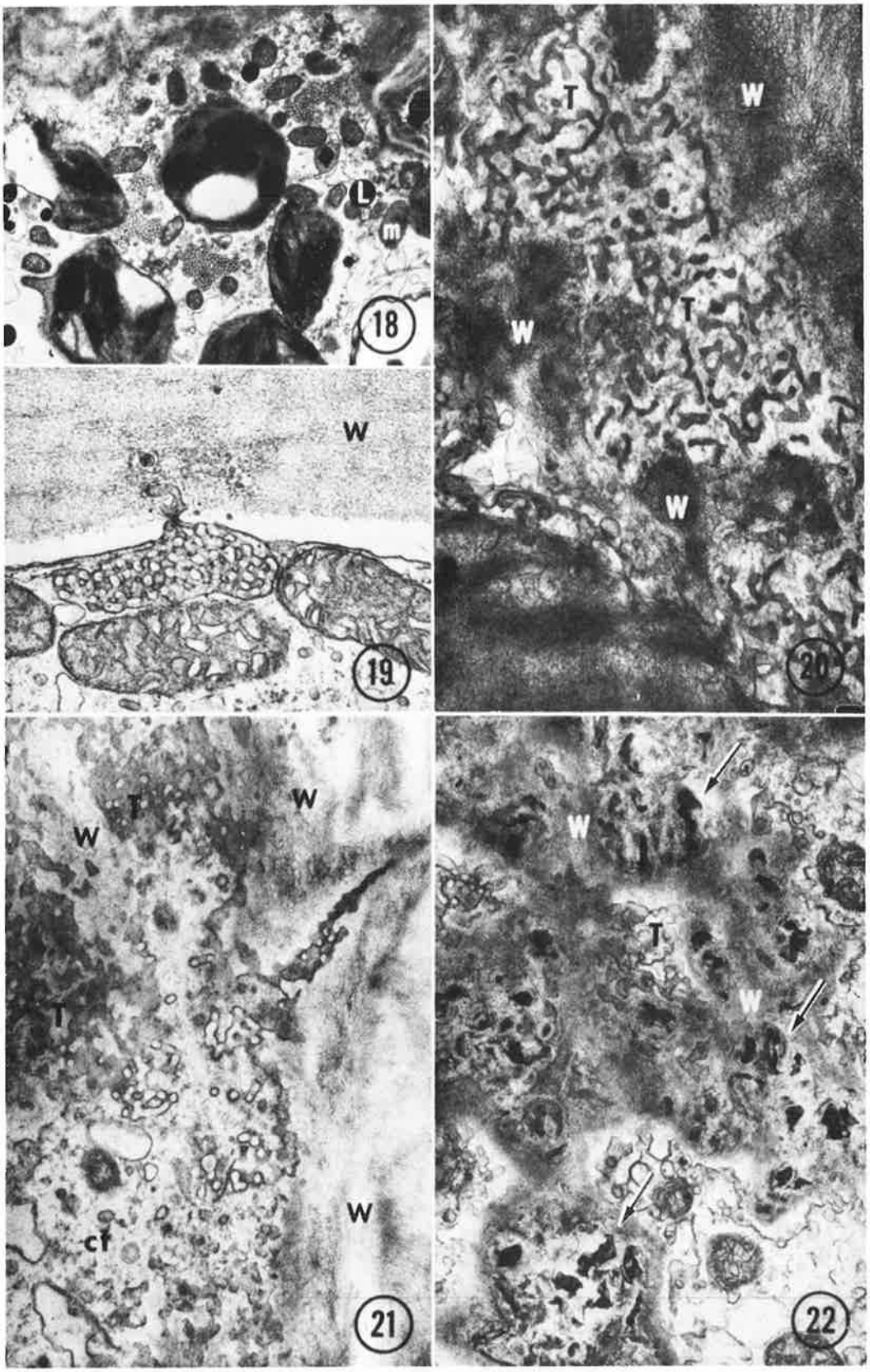
L
m
18
W
19
T
W
T
W
W
20
T
W
W
T
W
ct
21
T
W
T
W
22

longitudinal and cross sections tubules can sometimes be seen extending from the charasome-complex into the wall (Fig. 19). Sections through the cell wall that are parallel to it and close to the plasmalemma give further proof that tubules from the charasomes are embedded within the wall matrix (Figs. 20–22). The charasome material within the wall shows a lesser degree and uniformity of branching and in some areas stains more densely than its cytoplasmic counterpart (Fig. 20). At times, dense charasome-associated deposits were found within the wall (Fig. 22). These deposits ranged from membranous to semimembranous in nature.

Although the size, shape, and complexity of the charasomes vary greatly, they all share the same basic substructure. The simplest charasomes which can be found in mature cells are very useful in understanding this basic substructure. A typical example is shown in Fig. 23. In cross section it appears as a membrane-bound ring which is interrupted at intervals by cross connections. Upon careful examination the cross connections are seen to be membrane tubules with diameters ranging from 20 to 40 nm and lengths of between 40 to 60 nm. In the more complex charasomes, 3 to 6 tubules radiate from a single point within the charasome and, in turn, each interconnects with other tubules except for those that lead directly to the cytoplasmic surface of the charasome (Fig. 24).

### *3.5. Nitella translucens* and *N. flexilis*

Developing and mature cells from both the main axis and lateral branches were examined; however, charasomes were not found at any stage of development. The ultrastructural features of the two *Nitella* species were otherwise very similar to those seen in the *Chara* species. In the mature cells mitochondria are often closely associated with the plasmalemma (Figs. 25–27) as are the chloroplasts in some instances (Figs. 25 and 28). Lipid bodies and microbodies are also quite common in the gel layer (Figs. 26–29).

The pH pattern along the cell wall of *N. flexilis* (Fig. 30) was found to be similar to that obtained for *C. corallina*. Cross sections were examined from

---

Fig. 23. Simple charasome from mature male internode of *C. corallina*. Cell partially plasmolyzed so that the plasmalemma (*P*) is pulled away from wall area (*W*). Note tubules open to cytoplasm (arrowheads), invagination of plasmalemma (open arrows) and wall space of charasome (*s*). ×91,400

Fig. 24. Small charasome-complex from *C. braunii*. Note tubules open to cytoplasm (arrows) and tubules cut in cross-section (arrowheads). Cell wall (*W*), wall space of charasome (*s*). ×51,000

Fig. 25. Mature lateral branch cell from *N. translucens* (X.S.). ×14,000

Figs. 26–29. Cross-sections through mature *N. flexilis* internodal cell at areas of peak $OH^-$ and $HCO_3^-$ transport. (pH scan of this cell appears in Fig. 30.) Fig. 26. $HCO_3^-$, ×14,000. Fig. 27. $OH^-$, ×7,000. Fig. 28. $HCO_3^-$, ×7,000. Fig. 29. $OH^-$, ×7,000

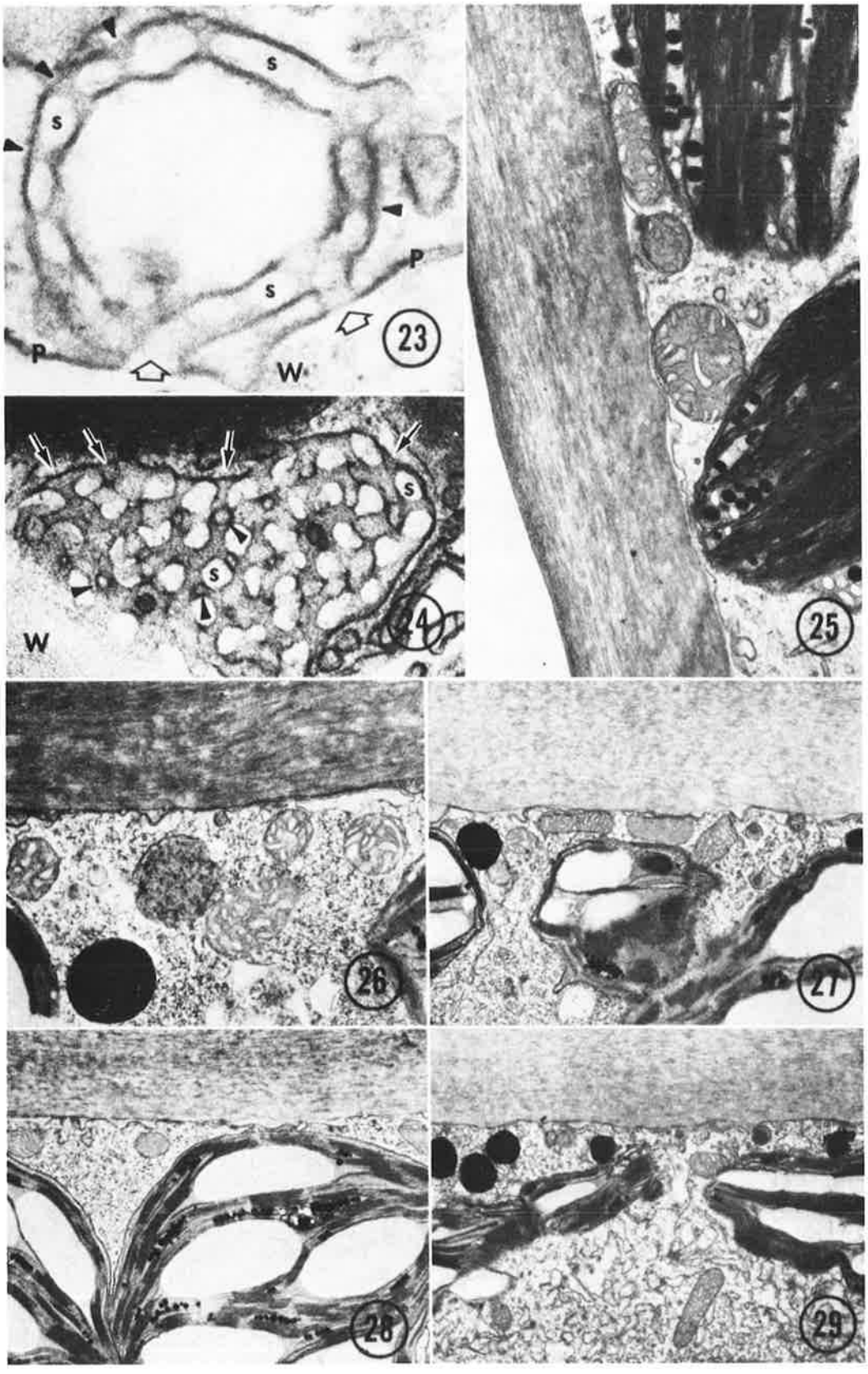
S
S
S
P
P
W
23
W
S
S
24
25
26
27
28
29

areas of the cell of maximum and minimum pH, but no ultrastructural differences could be detected (*cf.*, Figs. 26 and 28, low pH, with Figs. 27 and 29, high pH).

## 4. Discussion

Paramural bodies, membranous structures associated with the plasmalemma and cell wall, are found throughout the plant kingdom (Marchant and Robards 1968). Those reported have generally been simple structures con-

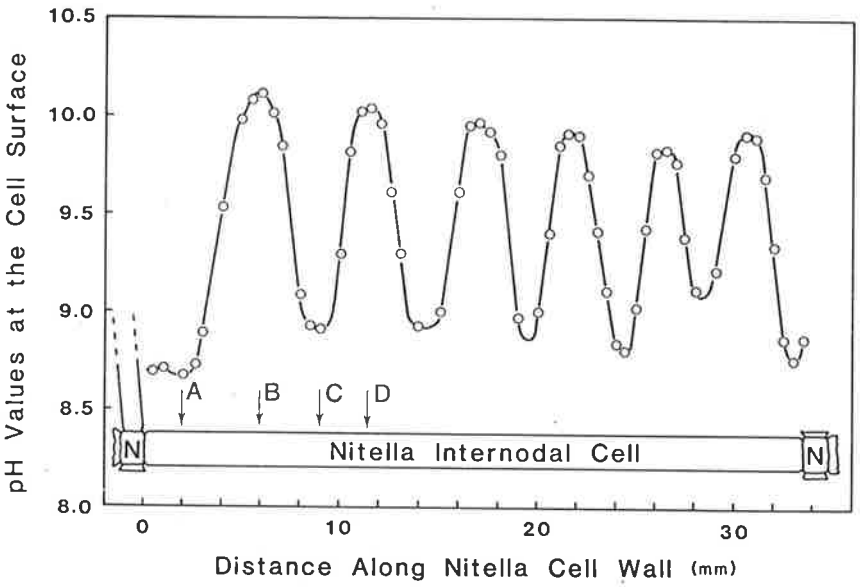


Fig. 30. pH scan of *N. flexilis internode*. *A–D* refer to Figs. 26–29, respectively

sisting of pockets of membranous vesicles and tubules, or concentric membrane rings. The charasome-complex, which falls within the definition of a paramural body, represents the most intricate and highly ordered of such membrane systems. There is little doubt that the charasome-complex is derived from the plasmalemma. Not only can one see direct connections of the plasmalemma and charasome-complex membranes, but it has been shown that charasomes stain with phosphotungstic acid-chromic acid, a plasmalemma-specific stain (Sundberg and Lembi 1976). Developmental studies will further confirm this point.

The pockets of tubules observed within the developing antheridia are not considered here as charasomes. Their structure is quite different from that of the charasome-complex. Indeed, these structures more closely resemble some of the lomasomes seen in the fungus *Pythium* (Bracker 1967). Since they usually appear at the periphery of young antheridia they are probably of a transitory nature. Similar tubular proliferations can be seen in micrographs of developing plurilocular male gametangia of *Cutleria* (la Claire and West

1979). In comparison to these structures the charasome-complex shows a much higher degree of organization.

Ultrastructurally, the charasome-complex is unique among plasma membrane structures. Its complexity is such that its three-dimensional structure is difficult to envision when looking at the two-dimensional micrographs presented. Through close examination of numerous micrographs of charasomes of vary-

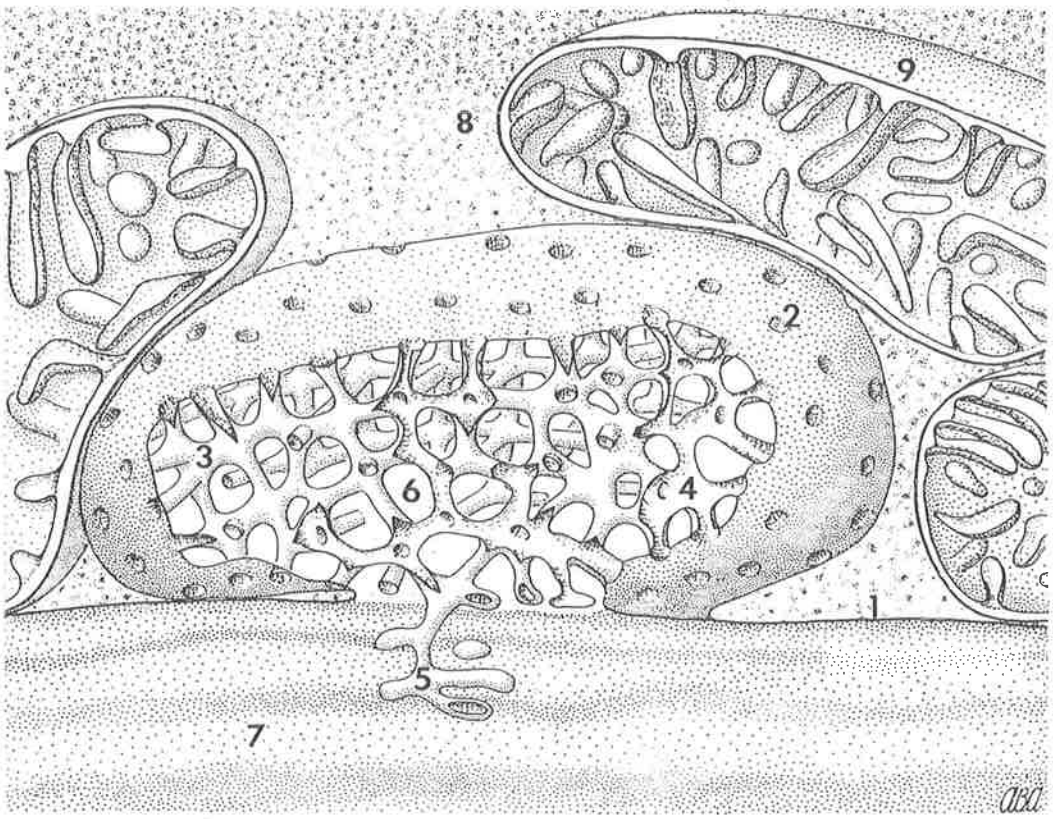


Fig. 31. Model reconstruction of a small charasome-complex comparable to that of Fig. 24. In order to present a clear picture only a few of the anastomosing membrane tubules have been presented. *1* plasmalemma; *2* opening of tubule to cytoplasm; *3* whole tubules; *4* sectioned tubules; *5* tubules in wall; *6* wall space (periplasmic space); *7* cell wall; *8* cytoplasmic gel layer; *9* mitochondrion

ing complexity we have constructed a three-dimensional structural model (Fig. 31). Examination of cross, longitudinal and oblique sections show that the charasome-complex is roughly globular in shape, although the exact shape and size varies greatly. (The massive material in female branch cells is apparently made of numerous large, closely appressed, charasome-complexes.) If one could look down upon a charasome its surface would appear as a membrane sheet perforated by many small openings. Glancing sections of charasomes show such a view (Fig. 5, arrow). The perforations are the openings to the cytoplasm of the tubules near the surface of the charasome. Based on our model one would expect to find, on occasion, regions near the surface of

the charasomes which give only cross-sections through a number of tubules. These would appear as circular profiles surrounded by the clear area of the charasome (wall or periplasmic space). However, this is not seen in our sections because the section thickness is greater than the average tubule length, thus background tubules are always seen. Generally three to six tubules radiate in various directions from a central point and each in turn connects with other tubules or the charasome surface. The tubules in sectioned material appear as amorphous dense areas because they are smaller in diameter than the section thickness. As a result, at least one surface of a tubule cut in the longitudinal plane is always present. Because tubules project in different directions, in three dimensional space, direct cross-sections of tubules are also often seen (Fig. 24). Again, because section thickness is greater than average tubule length, they are always observed against a background of anastomosing tubules.

The area surrounding the tubules is considered wall space since it ultimately opens to the inner cell wall surface (Figs. 23 and 24). This wall space appears electron lucent in our micrographs, lacking the fibrillar structure of the cell wall proper. In the absence of cellular support structures, we have assumed that the wall space contains solid material which would prevent the turgor pressure-collapse of the charasome-complex. Lack of staining does not rule out a solid phase since some wall materials (*e.g.*, callose) do not stain under the preparative technique used. It is interesting to note that what we refer to here as wall space may in fact be a true periplasmic space.

The significance of the tubules embedded in the microfibrillar wall matrix remains to be determined. This phenomenon was seen only occasionally (Fig. 19), which indicates either that it occurs only along a small area of the charasome-complex, and hence will not be seen in many sections, or alternatively it does not occur in all charasomes. The tubules within the wall show a lower frequency of anastomoses than those in the charasome material which projects into the cytoplasm. The small amount of less complex tubules seen within the cell wall is perhaps indicative of intrusive tubule growth, rather than wall formation around existing tubules.

The structure of the charasome produces a tremendous increase in surface area between the cell and its environment. This increase could serve to amplify the capacity for transmembrane fluxes of important substances, a function hypothesized for plant transfer cells (Pate and Gunning 1972). The charasome-complex, with its large surface area, might seem especially suited to the spatial arrangement and large fluxes involved in $OH^-$ (and $HCO_3^-$) transport in *Chara* and *Nitella*. However, our results indicate that they are not involved in transport of these ions (as a major function). Although charasome-complexes were usually present in $HCO_3^-$ transport regions, they were always fewer or absent in areas of $OH^-$ transport. Also, the amount of charasome material was generally much less in internodal cells than in lateral

branch cells, but ion fluxes are similar in each. Thus $HCO_3^-$ and $OH^-$ transport appear to be independent of the amount of charasome material present. Furthermore, *Nitella* cells which show the same transport phenomena, with similarly large fluxes, do not have charasomes. One note must be added concerning the charasomes in $OH^-$ transport regions. It is possible that the variability in number and size of charasomes seen in these areas may be due to inaccuracy in obtaining the area of peak $OH^-$ efflux during sectioning. Charasome number and size may be least within the $OH^-$ transport band-center and increase on either side of the peak (see LUCAS *et al.* 1977, and LUCAS and NUCCITELLI 1980, for a description of the spatial aspects of $HCO_3^-$ and $OH^-$ transport distribution).

Growth of *C. corallina* in our cultures is extremely rapid. The charasome-complex could conceivably contain, or be, a mechanism for the generation of osmoticum during rapid extension growth. Such a mechanism could involve active chloride ($Cl^-$) transport with charge-balance being achieved by a passive potassium ($K^+$) flux. The lateral branch cells mature very quickly and much sooner than the internode cell immediately above the respective nodal complex. The branch cells, with their large amount of charasome material, would be a likely site for generation of osmoticum necessary for extension growth of the developing internodal cells. WALKER (1976) noted that measured transmembrane $Cl^-$ fluxes (across the plasmalemma of internodal cells) were insufficient to account for rates of consumption observed in growing *Chara* cells (internodes). Translocation of $Cl^-$ (and the balancing cation) appears to be necessary. This would occur by symplasmic transport from cell to cell via plasmodesmata. Indeed, plasmodesmata are numerous between nodal cells and nodal and internodal cells in *Chara* and *Nitella* (SPANSWICK and COSTERTON 1967, FISCHER *et al.* 1974, and personal observations). Considering the number of plasmodesmata and their importance in solute transport, WALKER (1976), in agreement with SPANSWICK and COSTERTON (1967) concluded that the *Chara* plant functions as a syncytium. According to this argument, $Cl^-$ (and $K^+$) taken up in the already mature lateral branch cells could be readily translocated (via the symplasm) to the node and finally to the young, rapidly expanding internode.

DUCREUX (1975) found that removal of lateral branches in young, growing regions of *C. vulgaris* which have charasomes (BARTON 1965 b) inhibits expansion of the young internodes, resulting in a progressive decrease in their successive size. We have seen the same phenomenon in *C. corallina* (unpublished results). Such observations are perhaps supportive of a role for the charasome, and branch cells, in generation of osmoticum for extension growth. However, morphogenetic development in *Chara* is controlled by interactions at the organ and cellular level which are not fully understood (DUCREUX 1975). Hormonal or nutrient effects could also account for the above observations.

We are not familiar with the growth rate or pattern of the two *Nitella* species studied, thus we cannot relate their lack of charasomes to the osmotic requirements of extension growth. *Nitella* internodes do show osmotic regulation; however, it is fairly slow, occurring over a matter of days (Kamiya and Kuroda 1956, Nakagawa *et al.* 1974). Osmoregulation in *Chara* has been poorly documented. Experiments on internodes with attached lateral branch cells would perhaps be more indicative of true osmoregulatory phenomena than experiments on isolated internodes. The plant does approach a syncytium in its organization, and, thus, such phenomena as osmoregulation should be looked at with respect to possible interactions on a whole plant level.

The charasome-complex is a unique and interesting structure which presents some important implications in the field of characean transport studies (see Walker 1980, and session discussion following). The formation of such a complex structure is, in itself, intriguing, and developmental studies to elucidate this process are underway. The physiological function of the charasome-complex remains conjectural. Future studies will examine its possible role in terms of $Cl^-$ and $K^+$ transport, and their putative function in extension growth.

## Acknowledgements

This work was supported by a grant from the National Science Foundation (PCM 78-10474). Thanks are due to Dr. T. Sawa (University of Toronto) for his advice on preparation of *Chara* cells for T.E.M. We would also like to thanks Drs. N. J. Lang and A. Läuchli for critically reading the manuscript, and Drs. R. R. Jeo (University of California, Davis), and R. M. Spanswick (Cornell University) for supplying us with several of the characean species used in the present study.

## References

Barton, R., 1965 a: An unusual organelle in the peripheral cytoplasm of *Chara* cells. Nature **205**, 201.

— 1965 b: Electron microscope studies on surface activity in cells of *Chara vulgaris*. Planta **66**, 95—105.

— 1968: Autoradiographic studies on wall formation in *Chara*. Planta **82**, 302—306.

Bracker, C. E., 1967: Ultrastructure of fungi. Ann. Rev. Phytopath. **5**, 343—374.

Crawley, J. C. W., 1965: A cytoplasmic organelle in association with the cell walls of *Chara* and *Nitella* cells. Nature **205**, 200—201.

Ducreux, G., 1975: Corrélations et morphogenèse chez le *Chara vulgaris* L. cultivé *in vitro*. Rev. gén. Bot. **82**, 215—357.

Edwards, M. R., 1962: Plasmalemma and plasmalemmasomes of *Listeria monocytogenes*. 8th Int. Congr. Microbiol., Montreal. Abst., p. 31.

Ferrier, J. M., Lucas, W. J., 1979: Plasmalemma transport of $OH^-$ in *Chara corallina*. II. Further analysis of the diffusion system associated with $OH^-$ efflux. J. exp. Bot. **117**, 705—718.

Fischer, R. A., Dainty, J., Tyree, M. T., 1974: A quantitative investigation of symplasmic transport in *Chara corallina*. I. Ultrastructure of the nodal complex cell walls. Can. J. Bot. **52**, 1209—1214.

KAMIYA, N., KURODA, K., 1956: Artificial modification of the osmotic pressure of the plant cell. Protoplasma **46**, 423—436.

LACLAIRE II, J. W., WEST, J. A., 1979: Light and electron-microscopic studies of growth and reproduction in *Cutleria* (*Phaeophyta*). II. Gametogenesis in the male plant of *C. hancockii*. Protoplasma **101**, 247—267.

LUCAS, W. J., 1976: Plasmalemma transport of $HCO_3^-$ and $OH^-$ in *Chara corallina:* non-antiporter systems. J. exp. Bot. **27**, 19—31.

— FERRIER, J. M., DAINTY, J., 1977: Plasmalemma transport of $OH^-$ in *Chara corallina*. Dynamics of activation and deactivation. J. Membrane Biol. **32**, 49—73.

— NUCCITELLI, R., 1980: $HCO_3^-$ and $OH^-$ transport across the plasmalemma of *Chara:* spatial resolution obtained using extracellular vibrating probe. Planta (submitted for publication).

— SMITH, F. A., 1973: The formation of alkaline and acid regions at the surface of *Chara corallina* cells. J. exp. Bot. **24**, 1—14.

MARCHANT, R., MOORE, R. T., 1973: Lomasomes and plasmalemmasomes in fungi. Protoplasma **76**, 235—247.

— ROBARDS, A. W., 1968: Membrane systems associated with the plasmalemma of plant cells. Ann. Bot. **32**, 457—471.

MOORE, R. T., MCALEAR, J. H., 1961: Fine structure of *Mycota*. 5. Lomasomes—previously uncharacterized hyphal structures. Mycologia **53**, 194—200.

NAKAGAWA, S., KATAOKA, H., TAZAWA, M., 1974: Osmotic and ionic regulation in *Nitella*. Plant Cell Physiol. **15**, 457—468.

PATE, J. S., GUNNING, B. E. S., 1972: Transfer cells. Ann. Rev. Plant Physiol. **23**, 173—196.

SPANSWICK, R. M., COSTERTON, J. W. F., 1967: Plasmodesmata in *Nitella translucens:* structure and electrical resistance. J. Cell Sci. **2**, 451—464.

SPURR, A. R., 1969: A low-viscosity epoxy resin embedding medium for electron microscopy. J. Ultrastruct. Res. **26**, 31—43.

SUNDBERG, I., LEMBI, C. A., 1976: Phosphotungstic acid-chromic acid: a selective stain for algal plasma membranes. J. Phycol. **12**, 48—54.

WALKER, N. A., 1976: Transport of solutes through the plasmodesmata of *Chara* nodes. In: Intercellular communication in plants: studies on plasmodesmata (GUNNING, B. E. S., ROBARDS, A. W., eds.), pp. 165—199. Berlin-Heidelberg-New York: Springer.

— 1980: The transport systems of charophyte and chlorophyte giant algae and their integration into modes of behavior. In: Plant membrane transport: current conceptual issues (SPANSWICK, R. M., LUCAS, W. J., DAINTY, J., eds.), pp. 287—304. Amsterdam: Elsevier North Holland.

Printed in Austria

Planta 150, 120–131 (1980)

Planta
© by Springer-Verlag 1980

# $HCO_3^-$ and $OH^-$ Transport Across the Plasmalemma of *Chara*

## Spatial Resolution Obtained Using Extracellular Vibrating Probe

William J. Lucas [1] and Richard Nuccitelli [2]
Departments of [1]Botany and of [2]Zoology, University of California, Davis, CA 95616, USA

**Abstract.** Internodal and whorl (branch) cells of the green alga, *Chara corallina* Klein ex Willd., em. R.D.W., were studied with the extracellular vibrating probe for measuring transmembrane ion currents, and with an extracellular pH microprobe for measuring the surface pH profile. Bands of positive inward current ($OH^-$ efflux) 1–3 mm wide were separated by wider bands of outward current ($HCO_3^-$ influx) along the length of the cell. The measured peaks of inward current ranged from 20 to 60 μA $cm^{-2}$ (98 μm from the cell surface) which would correspond to a surface ionic flux of 270–800 pmol $cm^{-2}$ $s^{-1}$. The peaks of outward current ($HCO_3^-$ influx) ranged from 10 to 30 μA $cm^{-2}$ which would correspond to a surface ionic flux of 140–400 pmol $cm^{-2}$ $s^{-1}$. The inward current bands matched the regions of surface alkalinity very well. The outward current ($HCO_3^-$ influx) was reduced at least 10-fold in low-$HCO_3^-$ medium, with a commensurate readjustment in the strength and pattern of inward current ($OH^-$ efflux). (Although these experiments involved a manipulation of the external pH, it is felt that the main adjustment in current patterns was in response to the reduction in exogenous $HCO_3^-$). The presence of the vibrating probe perturbed the inward current region when vibrating with a 26-μm amplitude, but this perturbation was eliminated when a 7-μm amplitude was used. The perturbation was usually observed as a reduction in the number of inward current peaks with an increase (approximate doubling) in the amplitudes of the one or two remaining peaks. Both the inward and outward currents were light-dependent, falling off within seconds of light removal.

**Key words:** *Chara* – Electric currents, extracellular – $HCO_3^-$ and $OH^-$ Plasmalemma transport – Vibrating probe

## Introduction

The light-dependent alkaline banding phenomenon of *Chara corallina*, and the related photosynthetic assimilation of exogenous $HCO_3^-$, by these giant algal cells, have been the subject of extensive research. Bicarbonate and $OH^-$ ions are transported across the plasmalemma by systems that can be spatially separated (Lucas 1976). Both transport systems appear to be electrogenic in nature (Lucas et al. 1977; Walker and Smith 1977; Ferrier and Lucas 1979), and no cationic requirement has been observed under conditions of steady-state assimilation (Lucas 1979).

In general, $OH^-$ efflux is restricted to specialized regions or zones which are called alkaline bands (Lucas and Smith 1973). $OH^-$ efflux rather than $H^+$ influx is thought to be involved because band formation is independent of external pH between 5.5 and 10 (Lucas 1979). Lucas and Ferrier (1980) have also recently presented theoretical calculations which demonstrate that maximum $H^+$ production, from the dissociation of $H_2O$ within the cell wall, would be much less than the known rates of alkalinization. Based on this evidence we will assume that external cell surface alkalinity is generated by $OH^-$ efflux. The spatial aspects of $OH^-$ transport, within these bands, has been modeled using diffusion and numerical analysis techniques (Lucas et al. 1977; Ferrier and Lucas 1979). Limited computer simulation studies have been conducted on the spatial distribution of $HCO_3^-$ transport in this system. Based on their external electric potential studies, and also those of Walker and Smith (1977), Ferrier and Lucas (1979) have suggested that the rate of $HCO_3^-$ influx may vary quite dramatically along the length of individual cells.

This macroscopic spatial separation of electrogenic $HCO_3^-$ influx and $OH^-$ efflux presents an excellent system in which to examine the concepts of transport control and synchronization. Under steady-state pho-

0032-0935/80/0150/0120/$02.40

tosynthetic conditions, where exogenous $HCO_3^-$ is being utilized, it is axiomatic that the spatially integrated net current crossing the plasmalemma must be zero. Knowledge concerning the biophysical and biochemical mechanisms utilized by these cells to achieve this current regulation appears to us basic to our general understanding of membrane transport.

In the present study, the extracellular vibrating probe technique (Jaffe and Nuccitelli 1974) was used to resolve the spatial distribution of both the $HCO_3^-$ and $OH^-$ transport along the entire surface of internodal and whorl cells. The results confirmed both the details relating to the $OH^-$ transport system presented by Lucas et al. (1977) and the variation in $HCO_3^-$ transport strength proposed by Ferrier and Lucas (1979). Additionally, we gained further insight into the complex mechanism of cellular control over $OH^-$ efflux.

## Material and Methods

*Culture Material.* Culture material of *Chara corallina* Klein ex Willd., em. R.D.W. (=*C. australis* R. Br) was grown in the laboratory in 120-liter containers in solutions containing (mM): 3.0 $Na^+$, 0.3 $K^+$, 0.2 $Ca^{2+}$, 1.5 $Cl^-$ and approx. 2.0 $HCO_3^-$ (pH 9.0). Light from fluorescent lamps (cool-white, Lifeline; Sylvania, Seneca Falls, N.Y., USA) was employed; the irradiance at the solution surface was 20 $Wm^{-2}$ (measured using a silicon solar cell, Type No SO510E 7PL; International Rectifier Corp., Los Angeles, Cal., USA).

*Cell-Surface pH-Mapping.* Experimental cells were cut from the culture 16 h prior to being used in an experiment. During this period the cells were bathed in a medium (CPW/B) containing (mM): 1.0 NaCl, 0.2 KCl, 0.2 $CaSO_4$, 1.0 $NaHCO_3$ (pH 8.0), and were illuminated by light from fluorescent lamps (10 $W m^{-2}$) for the first 3 and the last hour of the pretreatment period. The resistivity of this medium was $3{,}500 \pm 50\ \Omega$ cm.

The pH values along the cell surface of internodal and whorl cells were measured using the technique developed by Lucas and Smith (1973). The agar blocks which served as embedding media for experimental cells, were prepared as described in Lucas and Dainty (1977a). For experiments in which $HCO_3^-$ was not added to the system, the agar blocks were set and preequilibrated for 24 h in CPW (mM: 1.0 NaCl, 0.2 KCl, 0.2 $CaSO_4$; pH 5.7) to establish equilibrium between the agar and the experimental medium. Cell-surface pH-mapping experiments were conducted at 25° C in CPW/B under 20 $W m^{-2}$ illumination (near-maximum $HCO_3^-$ assimilation will be obtained under these conditions). Following a 2-h illumination period, a micromanipulator (Leitz, Rockleigh, N.J.; model 520–138) was used to traverse a miniature pH electrode (Microelectrodes, Londonderry, N.H., USA; model MI-405) along the cell wall. Measurements were made with the dome of the electrode just touching the cell wall. From the values obtained, the pH pattern established at (near) the cell surface was mapped. Details relating to individual experiments will be specified in the text.

*External Current Measurements.* *Chara* cells were placed in a 3-mm-deep dish (Plexiglas, 36 mm diameter) with a coverslip glass bottom. They were held down to the bottom by sandwiching extending pieces of neighboring cell wall under small pieces of glass coverslip which were, in turn, stuck to the bottom of the dish with silicone grease. The cells were observed with a compound inverted microscope (Zeiss, New York, USA; model IM 35) from below as the probe was brought down into solution from above and positioned near the cell at the equatorial plane.

Since the vibrating probe sometimes disturbed the distribution of the ion transport site(s) on the cell surface, we mapped the extracellular current pattern rapidly by moving the cell past the probe at 0.3 mm/s. This was accomplished by attaching a motorized micromanipulator (Narishige, Tokyo, Japan; model MM-3) to the sliding microscope stage. The probe was then vibrated perpendicular to the longitudinal axis of the cell with a 67-μm gap between the cell wall and the probe so that the perpendicular component of the membrane current could be detected.

This cell-scanning procedure was a two-man operation. One operator viewed the cell through the inverted microscope and, using the X component of an X-Y-Z micropositioner (Line-Tool, Allen Town, Pa., USA; model H-2), maintained the probe at a distance of $70 \pm 20$ μm from the wall. The second operator adjusted the Z component of the micropositioner to keep the probe in the equatorial plane of the cell.

*Instrumentation.* The sensor of our extracellular current-measuring system (Vibrating Probe Company, Davis, Calif., USA) is a vibrating metal-filled microelectrode (probe) with a spherical platinum-black electrode at its tip (diameter 26 μm) (Jaffe and Nuccitelli 1974). The oscillating voltage between this tip and a grounded coaxial reference electrode 3 mm behind the tip is measured while the probe is vibrated at a predetermined frequency (100–900 Hz) in a horizontal plane between two extracellular points 30 μm apart. In some experiments, the probe was vibrated over a reduced distance of 7–9 μm. Vibration between these points converts any steady voltage between them into a sinusoidal output, the amplitude of which is measured with the aid of a lock-in amplifier (Princeton Applied Research, N.J., USA; model 5101) tuned to the vibration frequency. This conversion of a direct voltage to an alternating one serves to eliminate any drift or low-frequency noise originating at the probe's surface. Furthermore, at the probe's vibration frequency, its impedance and hence its thermal or Johnson noise are greatly reduced compared to the static impedance. The measured local voltage difference, $\Delta V$, can be directly converted to I, the local current density in the vibration direction, because the electrical field, E, is practically constant over the relatively small vibration distance, d (it varies by 23% over a 26-μm interval near $OH^-$ efflux regions, and by 6% near $HCO_3^-$ influx regions). Ohm's law gives:

$$I = \frac{E}{\rho} = \Delta V / \rho d \qquad (1)$$

where $\rho$ is the resistivity of the medium. For example, a measurement of 10 μV while vibrating over 26 μm in 3,600 Ω-cm *Chara* pond water, indicates a current density of $10\ \mu V/(0.0026\ cm \times 3{,}600\ \Omega\text{-cm}) = 1.07\ \mu A\ cm^{-2}$ in the center and direction of vibration. The ion flux to which this current density corresponds can be calculated by dividing by Faraday's constant (i.e. 11.0 pmol $cm^{-2}\ s^{-1}$).

We have assumed here that the local medium resistivity 98 μm from the surface is the same as the bulk resistivity. However, with very high ion-transport rates by the *Chara* plasmalemma in these low-ionic-strength media, one might suspect that the local resistivity could be modified by ion activity gradients. Local stirring by the vibrating probe should minimize such effects, but we tested this possibility directly by measuring the current density at both an $OH^-$ and a $HCO_3^-$ transport site in two solutions of different ionic strength. After measuring an extracellular current scan (de-

scribed below) three times in normal (1 mM NaCl) medium (380 Hz), the NaCl concentration was increased to 10 mM (a 4.5-fold decrease in resistivity from 3,400 to 763 Ω-cm) and three more scans were made. The average peak values for the various inward and outward current bands in these two media were then compared. If $OH^-$ efflux significantly lowered the local resistivity, the measured current density would be an understimate so that one might expect the measured current density in the 1 mM-NaCl solution to be smaller than in 10 mM NaCl. When five such $OH^-$ efflux regions were compared, the average current density was indeed smaller in 1 mM NaCl by an average of $14 \pm 16\%$ (N = 5). However, this is clearly not a major change. The current density variation at the $HCO_3^-$ influx region was also small, averaging $1 \pm 6\%$ (N = 2) greater in 1 mM-NaCl medium. We therefore conclude that there is sufficient local stirring to eliminate any ion activity gradients which might alter the local solution resistivity.

The piezoelectric vibrator has been modified as described previously (Nuccitelli et al. 1977) so that the driving voltage is applied to the metal center strip and the entire outer surface is grounded. This greatly reduces barrier artifacts; however, control measurements were made near glass rods each day to assure that no such artifacts were present.

A lock-in amplifier time-constant of 30 ms was used in all experiments, and this allowed us to measure the true signal amplitude at the rapid scan rate employed. The probe was moved to a reference position approx. 1 cm away from the cell before and after each scan and this reference level is indicated on all figures as the zero current level.

*Extrapolation to the Surface of the Cell.* The probe measures the current density at the center of its vibration, which was 98 μm from the cell surface when a 26-μm vibration amplitude was used, and 91 μm away when a 7-μm amplitude was used [i.e. gap + 1/2 probe diameter + 1/2 probe vibrating amplitude + cell-wall thickness (5 μm)]. In order to determine the current density crossing the membrane, we must extrapolate the measured current densities to the surface on the basis of the field's fall-off with distance from the surface. Several measurements were made of the current density at a variety of distances from the membrane for both inward and outward current regions using both 7- and 26-μm vibration amplitudes. These data are plotted in Fig. 1. We then empirically determined the curve which best fitted the data in order to calculate the surface current value. Surprisingly, for the inward current ($OH^-$ efflux) regions, the field fall-off depended on the vibration amplitude. For a 26-μm vibration amplitude an inverse cube fall-off, with the field center lying 350 μm below the cell surface, gave the best fit. The extrapolation factor which this equation provides to estimate the surface current density from that measured 98 μm from the surface is given by $[(350+98)/350)]^3 = 2.1$. However, when a 7-μm vibration amplitude is used the field falls of more slowly; the best fit being proportional to 1/r, with the field center lying 275 μm below the surface. This equation yields an extrapolation factor of $(275+91)/275 = 1.33$. The reason for this discrepancy is not clear, but may be a function of the reduced stirring at the smaller amplitude. The smaller amplitude provides a more accurate approximation to the field gradient and indeed indicates the fall-off theoretically expected outside a hollow cylinder (Lucas et al. 1977; Walker and Smith 1977). Therefore, we feel that the most reliable extrapolation factor is 1.3. The outward current ($HCO_3^-$ influx) also falls off in a manner proportional to 1/r, regardless of vibration amplitude. For both the 26- and 7-μm vibration amplitudes an extrapolation factor of 1.3 was obtained (Fig. 1, A and B). The field centers for both the inward and outward current regions must be below the cell surface, because the plasmalemma of this giant algal cell has the shape of a hollow cylinder. The location of the empirical field center is within the vacuole, but the currents actually originate at the plasmalemma.

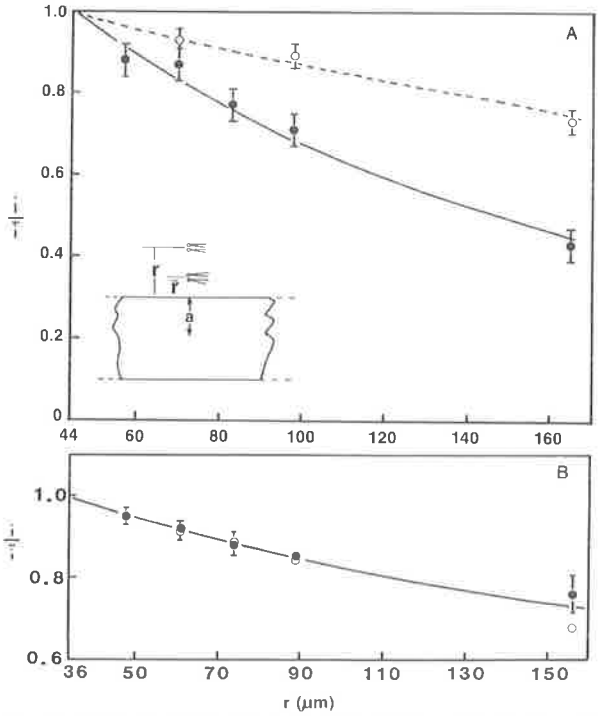


**Fig. 1A and B.** Relative current density versus radial distance from the *Chara corallina* cell surface. Reference-current density, $\bar{i}$, was measured at a distance $\bar{r}$ from the surface. Solid dots are the data points for fall-off near inward current regions; open circles are the data for outward current regions. **A** $\bar{r} = 44$ μm, vibration amplitude 26 μm. The solid line is a plot of $i/\bar{i} = [(a+r)/(a+\bar{r})]^{-3}$ for a = 350 μm. The dotted line is a plot of $i/\bar{i} = [(a+r)/(a+\bar{r})]^{-1}$ for a = 325 μm. (As indicated in the inset figure, "*a*" is the distance between the plasmalemma surface and the empirical "origin" of the field within the cell.) **B** $\bar{r} = 36$ μm, vibration amplitude 7 μm. The line is a plot of $i/\bar{i} = [(a+r)/(a+\bar{r})]^{-1}$ for $a = 275$ μm

## Results

*Magnitude and Spatial Resolution of $HCO_3^-$ and $OH^-$ Transport.* Initial experiments with the extracellular vibrating probe were conducted on short, semi-mature (50–60% final length) internodal cells. These cells were used because the maximum cell length which the probe could scan was 2 cm. As found in earlier work (Lucas and Smith 1973), the $OH^-$-transport system of these young cells exhibited a high degree of instability (Fig. 2A). The pH profile changed substantially over a 24-h period.

The scan of a second young internodal cell is shown in Fig. 2B. Here the extracellular current measurements were made on two opposite sides of the cell and, while the inward current regions match up quite well, they differ greatly in amplitude. This would indicate that the membrane ion-fluxes do not necessarily exhibit cylindrical symmetry in these young cells as they do for the more mature whorl cells which were next studied. Despite the instability of these

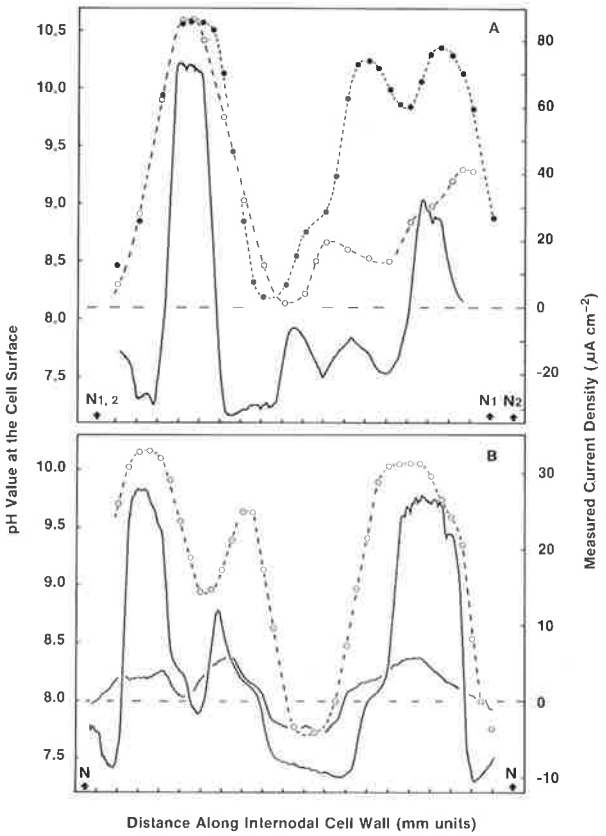


**Fig. 2 A and B.** Extracellular current measurements (solid line) and surface pH profiles (dotted lines) along the length of two semi-mature internodal cells of *Chara corallina*. A positive current density represents the flow of positive current into the cell. **A** The cell surface pH profile was measured 3 h before (○) and again 20 h after (●) the extracellular current measurement was made with the probe vibrating at 478 Hz perpendicular to the membrane surface, and with 98 μm between the membrane and center of vibration (see inset to Fig. 1). The cell's basal node (N) was positioned at the left arrow on the abscissa and the apical node at the right arrow. Since the apical end is growing, two arrows appear on the right to mark the node position at the two times when the pH scans were performed. **B** A second internodal cell scanned on two opposite sides with the vibrating probe (two solid lines). The surface pH profile was measured 3 h before the current measurements

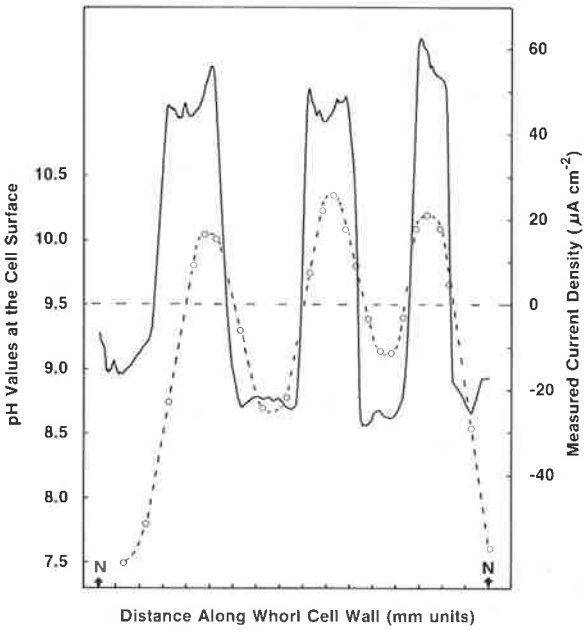


**Fig. 3.** Extracellular current scan (solid line) and surface pH (dotted line) along the length of a whorl cell of *Chara corallina*. The positions of the cell nodes (N) are marked by the arrows the basal end on the left. The background pH of the surrounding medium was 7.95. The probe was vibrated with a 26 μm amplitude perpendicular to the membrane surface, 98 μm to the center of vibration (478 Hz)

growing cells we consistently found a good correlation between the inward current regions ($OH^-$ efflux) and the alkaline pH bands.

Experiments conducted on mature whorl or branch cells showed an excellent correlation between the pH and vibrating-probe data. Positive inward current ($OH^-$ efflux) was found in regions where the cell-surface pH was approx. 9.5 or greater (Fig. 3). The transition zones between inward and outward current were extremely sharp, and in most cases where stable transport systems were observed, current profiles obtained from opposite sides of the cell showed a high degree of circumferential and lateral symmetry.

The magnitude of the measured current densities was remarkably large. The $OH^-$ efflux peaks generally ranged from 20 to 60 μA $cm^{-2}$ 98 μm from the cell surface, which corresponds to a cell-surface current density range of 26–78 μA $cm^{-2}$ (using the extrapolation factor of 1.3 derived empirically in Material and Methods). If $OH^-$ efflux were carrying this entire current, efflux values would range between 270 and 800 pmol $cm^{-2}$ $s^{-1}$. The $HCO_3^-$ influx peaks ranged from 10 to 30 μA $cm^{-2}$ 98 μm from the surface, and the extrapolation factor of 1.3 for this region predicts surface current density values ranging from 13 to 39 μA $cm^{-2}$. If $HCO_3^-$ influx were the sole current carrier, this would predict peak influx rates of 140–400 pmol $cm^{-2}$ $s^{-1}$. The outward current profiles indicated that $HCO_3^-$ transport does vary along the length of the cell (Figs. 2, 3, 4B, 7B).

In order to determine if the total inward current equaled the outward current, the areas under the $OH^-$ and $HCO_3^-$ profiles were measured for three different symmetrical scans. The outward current was consistently slightly larger than the inward current, with an average ratio of $0.84 \pm 0.13$. This ratio indicates that we may have been scanning slightly too fast to measure the entire $OH^-$ signal, but is sufficiently close to assure us that the measurements are reliable.

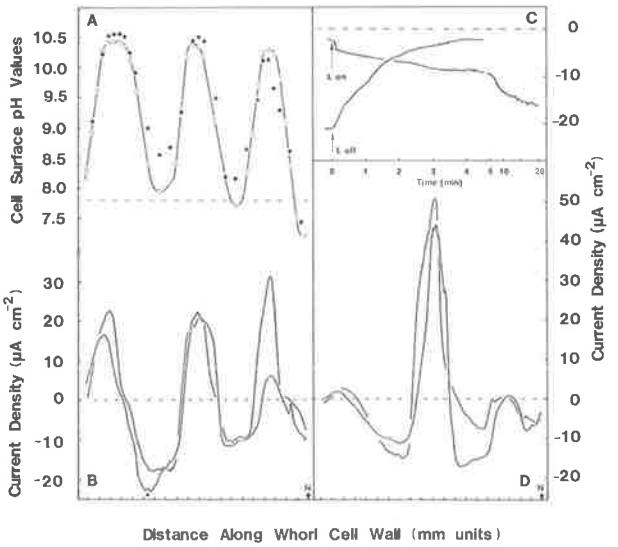


**Fig. 4A–D.** Surface pH profile along a whorl cell of *Chara corallina*, with basal end on the left. The horizontal dotted line marks the background pH of the external solutions. **A** Scans conducted 4 h before (○) and 14 h after (●) vibrating probe experiments. **B** Extracellular current scans along the cell's length on two opposite sides. The probe was vibrating at 478 Hz perpendicular to the cell surface, 98 μm to the center of vibration. Asterisk marks the outward current position in which the light dependence was investigated in Fig. 4C. **C** Light dependence of the outward current. The probe was positioned at the outward current peak marked by the asterisk in 4B and the light was turned off. The cell was reilluminated 4.5 min later. This record was moved over to line up with the light off time so that the two response times could be more easily compared. **D** Extracellular current scans along two opposite sides of the same cell which were taken after the probe had been vibrating near the outward current region (*of B) for 25 min (which included a 4.5-min dark period)

*Perturbative Influence of the Vibrating Probe.* During the course of these studies we found that the presence of the vibrating probe could perturb the $OH^-$-transport system under certain conditions. Under constant illumination, the perturbation could be eliminated by reducing the vibration amplitude from 26 to 7 μm. Using a 7-μm vibration amplitude, no change in the current profile occurred while the probe was vibrating near a $OH^-$ peak for as long as 70 min. However, when short dark periods were introduced even the 7 μm amplitude disturbed the restablishment of the current profile. Either the site of maximum $OH^-$ efflux shifted slightly to the left or right of the probe, or its amplitude decreased greatly with an increase in the amplitude of another $OH^-$ band. A typical example of this transport perturbation phenomenon is illustrated in Fig. 4 where a 26-μm vibration amplitude was used. After obtaining current profiles on opposite sides of the whorl cell (Fig. 4B), the vibrating probe was located within the center of the most active $HCO_3^-$-transport region (see Fig. 4B, *). The influence of a short dark treatment (4.5 min) on $HCO_3^-$ transport was then investigated (Fig. 4C). Upon reillumination, the $HCO_3^-$-transport site exhibited quite a rapid initial response; this was followed by a very gradual increase in transport activity. Slow $HCO_3^-$ transport reactivation was not expected since the photosynthetic induction lag for this system is usually less than 1 min (Lucas, 1975a) and also this lag period should not be reintroduced by a short dark period. After monitoring the $HCO_3^-$-transport site for 20 min (Fig. 4C), the current profiles on both sides of the cell were remapped. Only one $OH^-$-transport band remained operational; however, the transport rate associated with this site had increased to almost twice its original value (Fig. 4D). Apparently the probe vibration somehow interferes with the cellular control mechanism that regulates the complex $OH^-$-transport system.

A further illustration of the effect of the vibrating probe, on the $OH^-$ transport system, is shown in Figs. 5 and 6. (Figures 4, 5, 6 illustrate experiments conducted on the same cell.) When the probe was located at the center of $OH^-$-efflux activity and vibrated at 26 μm amplitude, the transport rate went through a characteristic decline (Fig. 5A). The current profiles presented in Fig. 5B indicate that this decline was the consequence in part, of a lateral migration of the $OH^-$-efflux center to a position further away from the probe. The width of the transport band also appeared to be reduced.

Imposing a brief dark period, while the current probe was located near the $OH^-$ efflux center, resulted in almost complete disappearance of transport activity within that region (Fig. 6). Since $HCO_3^-$ transport was not reduced to an equivalent extent by these treatments, we must assume that limited $OH^-$-efflux activity was occurring on the cell surfaces not directly exposed to the probe. Although the vibrating probe elicited dramatic changes in the cell's ability to control and operate its $OH^-$-transport system, these perturbations were not permanent. Figure 4A illustrates that 16 h after the cellular system had been perturbed, the pH banding pattern was equivalent to the control pattern measured before the current experiments were performed.

*Currents Measured in the Presence and Absence of Added $HCO_3^-$.* The influence of added exogenous $HCO_3^-$ on the extracellular current profiles was examined. In these experiments the whorl cell to be used was cut from the culture and, after a 1-h recovery period in CPW/B medium, was pretreated over night in CPW. (Cells used in the present study did not contain $CaCO_3$ encrustations, so no attempt was made to free these cells of exogenous $CaCO_3$.) The

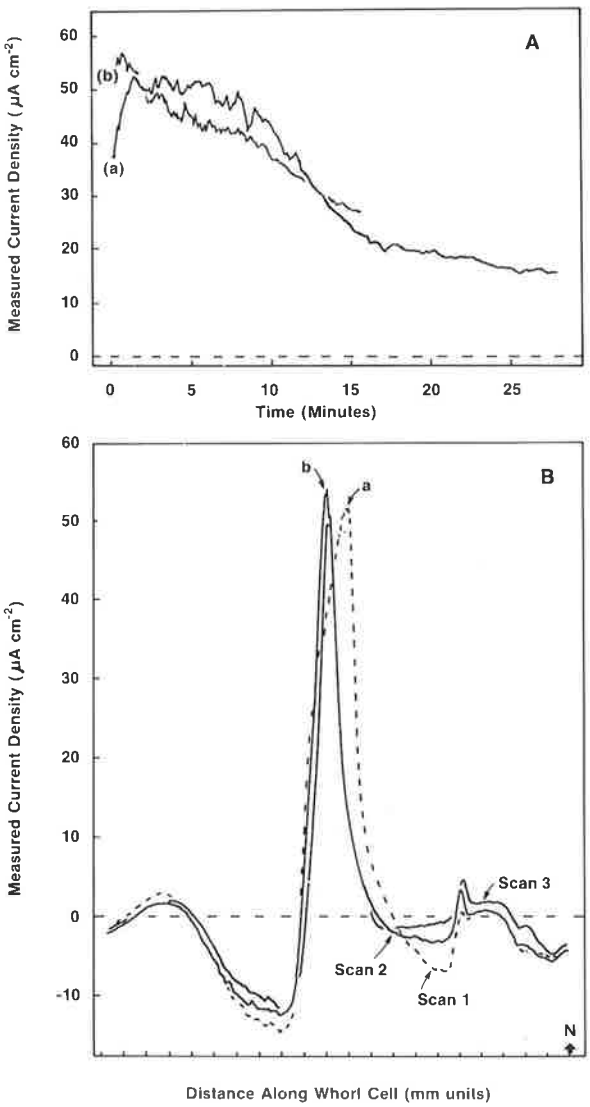


**Fig. 5 A and B.** Perturbation of inward current region by the vibrating probe in whorl cells of *Chara corallina*. After extracellular current scan 1 was made in **B** (same as record shown in Fig. 4D), the probe (vibrating at 478 Hz) was positioned over the inward current peak "*a*" in **B**. The current time course there is shown in **A** as record "*a*". The cell was then scanned again (scan 2) showing that the inward current peak had shifted 1 mm to the left. The probe was then positioned over the new peak at "*b*" and the current time course there is shown in **A** as record "*b*". Scan 3 of **B** was then performed indicating another slight shift in peak position and amplitude

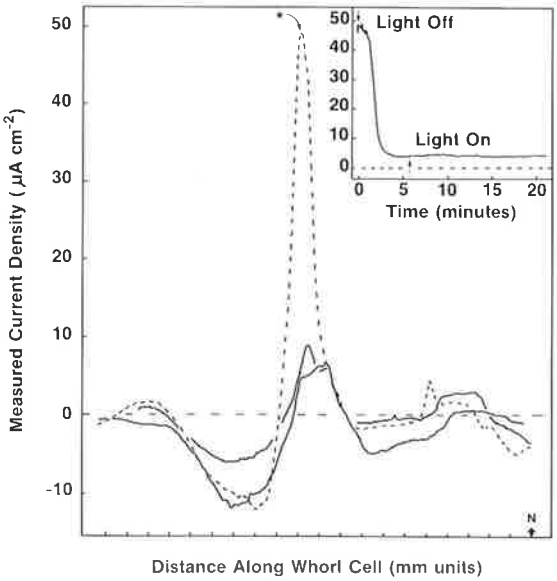


**Fig. 6.** Combined effect of the probe's presence and a short dark period on $OH^-$ efflux activity in *Chara corallina*. Probe vibrated (478 Hz) 98 μm away from the peak of inward current (*). Extracellular current scan, indicated by broken line, was obtained before the short dark period. Solid lines represent scans (opposite sides of the cell) conducted after 15 min reillumination. (Light and dark treatments indicated on inset)

pH profile in this almost $HCO_3^-$-free system (13 μM $HCO_3^-$ from solution equilibration with atmospheric $CO_2$) was mapped and then the cellular response to 1.0 mM $NaHCO_3$ (CPW/B) was recorded (see Fig. 7A, C). In these experiments it was necessary to use media having different pH values. Lucas (1975a) demonstrated that these cells are not physiologically perturbed by exposure to pH values ranging from 5.0 to 10.3. By manipulating total exogenous inorganic carbon and media pH, he also showed that the $HCO_3^-$-assimilating system operated over the pH range 5.7–9.5 in a manner which could be predicted based on $^{14}CO_2$ and $H^{14}CO_3^-$ transport rates obtained at pH 5.3 and 9.2, respectively. We feel, therefore, that the major cell response to the imposed media changes will be due to a reduction in available $HCO_3^-$ and not to pH, per se.

The experimental cell was then transferred to the current probe system and pretreated in an identical manner to that employed for the experiments with CPW and CPW/B media. Current profiles along the surface of dark-adapted cells indicated almost complete absence of transport activity (Fig. 7D). The small inward current (0.27 μA $cm^{-2}$) observed in the dark under CPW conditions may be the result of diffusion of respiratory $CO_2$ away from the cell (converted to $HCO_3^-$ by solution equilibria). In CPW/B medium the buffering capacity of the solution would eliminate this effect.

The relationship between cell-surface pH and current profiles, obtained in the presence of CPW medium, is shown in Fig. 7C and D, respectively. Under these conditions of extremely low exogenous $HCO_3^-$, only one $OH^-$-transport band was activated. (This response is consistent with the earlier results published by Lucas and Smith 1973, and Lucas 1975b.) Figure 7D indicates that, under these conditions, the out-

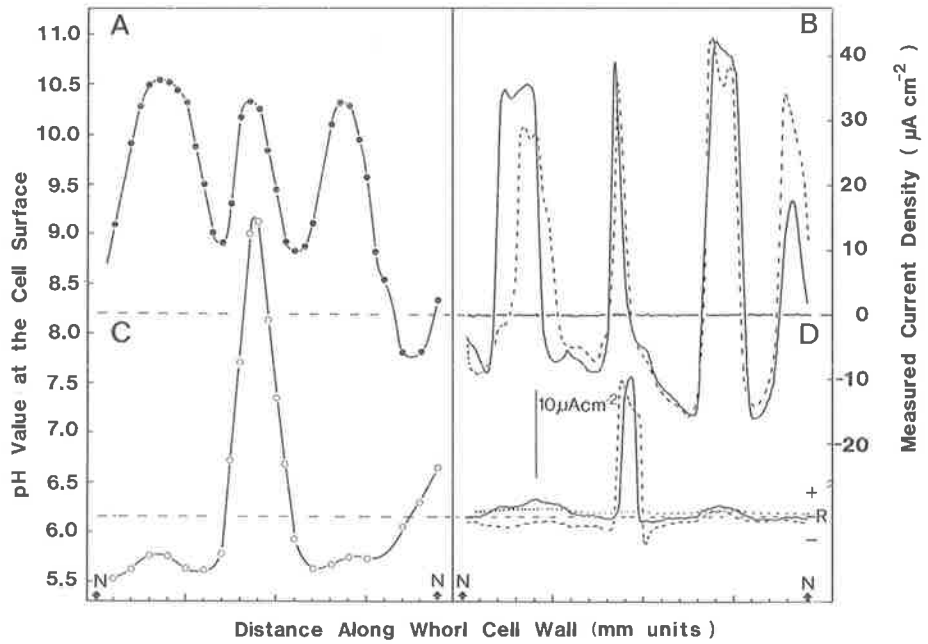


**Fig. 7A–D.** Surface pH profiles and extracellular current scans of *Chara corallina* obtained in the presence and absence ($\leqq 13$ μM $HCO_3^-$) of extracellular $HCO_3^-$. In all scans, the probe was vibrated at 380 Hz perpendicular to the cell, 98 μm to the center of vibration. **A** Surface pH profile in 1 mM $HCO_3^-$, medium. Basal end of cell is on left. Dotted line marks background pH of medium. **B** Extracellular current scans on same cell 24 h later in 1 mM $HCO_3^-$ medium. The trace which appears along the zero current level was a scan measured after 81 min of darkness. A green filter (transmission peak 525 nm) was used on the microscope illuminator during the scan. No significant current could be detected. After 80 min in the light the other two scans were made on opposite sides of the cell. **C** Surface pH profile of the same cell in 13 μM $HCO_3^-$ medium after overnight pretreatment in this medium. Horizontal dotted line marks the background pH level of the medium. **D** Extracellular current scans on the same cell in 13 μM $HCO_3^-$ medium after overnight pretreatment in this medium. The dotted trace which appears along the zero current level was a scan measured after 15 h in the dark. The peak inward current here was 0.27 μA $cm^{-2}$. A green filter was again used. After 80 min in the light the other two scans were made on opposite sides of the cell

ward current profile along the cell was variable and quite asymmetric (compare Fig. 7B, D). We should stress that a component of the current profile (both positive and negative) will almost certainly be associated with other electrogenic transport systems that operate across the plasmalemma of this species. Likely candidates are $H^+$ efflux (Kitasato 1968; Spanswick 1972; Keifer and Spanswick 1978, 1979) and $Cl^-$ influx (Sanders 1980), and these possibilities will be investigated in future experiments with this system. On this note, it is important to realize that for *Chara* the fluxes associated with $HCO_3^-$ and $OH^-$ transport are much larger than any of the other presently known ionic fluxes. This means, of course, that when current experiments are conducted in CPW/B medium, any "fine detail" that may be associated with these other electrogenic transport systems will be masked by the $HCO_3^-$ and $OH^-$ systems.

When the same cell was then placed in 1 mM $HCO_3^-$ medium, the current and pH profiles followed the expected trends. The positive inward current profiles obtained on the left hand side alkaline band of Fig. 7B illustrate a degree of circumferential and lateral asymmetry. We feel that this is a real reflection of $OH^-$ transport asymmetry that does exist at some alkaline bands. The positive inward current region that is depicted on the right hand extremity of the cell was not activated during the pH scan experiment (compare Fig. 7A). This transport site exhibited a high degree of variability during the CPW/B experiments. It may have been activated as a result of the cell's response to the presence of the vibrating probe.

If the positive outward current is carried mainly by $HCO_3^-$ influx there should be good agreement between uptake measurements with tracer $H^{14}CO_3^-$ and the outward current magnitude. When three cells with symmetrical current profiles on the top and bottom scans were averaged, the surface outward current was 200 pmol $cm^{-2}$ $s^{-1}$. Since the outward current region comprises 55–62% of the total surface area this would predict a total surface $HCO_3^-$ influx of 110–124 pmol $cm^{-2}$ $s^{-1}$. This is about two times greater than the tracer measurements of 50–60 pmol $cm^{-2}$ $s^{-1}$ (Lucas 1975a). Considering all the variables involved, this level of agreement is close enough to support the hypothesis that $HCO_3^-$ influx carries most

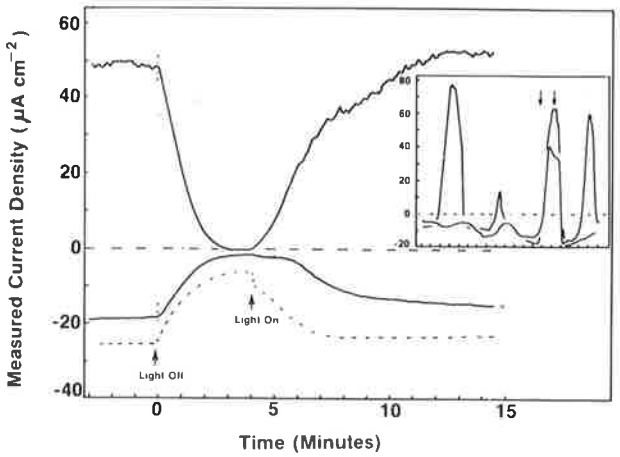


**Fig. 8.** Light dependence of inward current peak in a whorl cell of *Chara corallina*. One h after making the scan shown in Fig. 7B, the probe was positioned 98 µm from the cell over the next-to-last inward current peak (see inset) and the light was turned off for 4 min at the arrow. The inward current fell rapidly as shown in the upper trace. After reillumination the probe was positioned near an adjacent outward current peak and the same 4-min dark period was applied (bottom solid trace). The dotted curve was the response of a second cell to this same treatment. The inset shows the extracellular current scans on two opposite sides of the cell after the two light off-on studies of this figure. The vibration frequency was 380 Hz

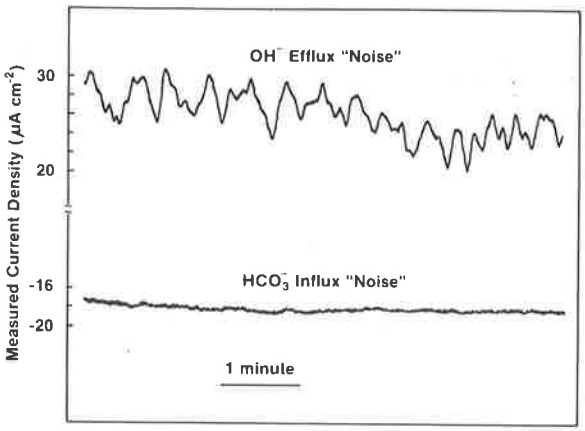


**Fig. 9.** Extracellular current "noise" recorded at an inward current peak (top) and outward current peak (bottom) of *Chara corallina* show at a greater amplification. The vibration frequency was 478 Hz

of the outward current. It is also worth pointing out that the $H^{14}CO_3^-$ measurements were made under conditions where a large unstirred layer was present. Removal of this diffusion limitation may give almost equivalent $HCO_3^-$ influx values. Experiments are presently being conducted to test the effect, on $H^{14}CO_3^-$ assimilation, of reducing the unstirred layer.

The only other ion variation we studied was increasing the NaCl concentration to determine the current dependence on resistivity. A ten fold increase in NaCl had no major effect on the magnitude of either the inward or outward current (see Material and Methods).

*Activation and Deactivation of $HCO_3^-$ and $OH^-$ Transport.* The light dependence of the $HCO_3^-$ and $OH^-$ currents was also investigated. These were difficult experiments to perform because the $OH^-$ profile did not always return to normal when the probe was nearby. Figure 8 represents a good example of a cell which displayed greater transport stability, yet it still responded by readjusting its transport profiles. In this example it can be seen that the $OH^-$ efflux site did not decline in activity in the presence of the probe (compare Figs. 5A and 8). The $OH^-$ transport site was also not deactivated in response to a short dark period (compare Figs. 6 and 8).

A comparison between the time-courses of $HCO_3^-$ and $OH^-$ transport inactivation, in response to two separately imposed dark treatments, indicates that neighboring transport regions respond in a highly correlated manner. The characteristics of the $OH^-$ current, observed during the light-off and light-on manipulations, are similar in nature to earlier reports using extracellular pH and voltage measuring microprobes (Lucas et al. 1977; Walker and Smith 1977; Ferrier and Lucas 1979). The discrepancy between the time courses of $HCO_3^-$ and $OH^-$-transport activation, following reillumination, may be result of a complex cellular control over $HCO_3^-$ transport. We feel, however, that a more reasonable interpretation is that the cell reacted to the probe, and the $HCO_3^-$ reactivation is atypical. Current scans on two sides of the cell indicated that, during the period of the experiment, the current profiles had changed (compare Fig. 8, inset, and Fig. 7B). This view was also supported by time courses obtained from other cells which were treated in the same manner (see broken trace on Fig. 8; this $HCO_3^-$ reactivation followed a time course more similar to the $OH^-$ reactivation). Note that in both examples the $HCO_3^-$ current did not go to zero within this short dark period.

*Transport Current Noise.* During current scan experiments, we noticed that $OH^-$ efflux, at any one location, often exhibited quite marked fluctuations. Examples of this "noise" can be seen in Figs. 5A and 8. We examined this aspect further by collecting data from neighbouring $HCO_3^-$- and $OH^-$-transport areas. Typical "noise" profiles are illustrated in Fig. 9. In general, the current measured in the $HCO_3^-$-transport regions was more uniform than the $OH^-$ current.

The high degree of similarity between the form of the "noise" associated with the $OH^-$ current and the fluctuations observed during external electric potential measurements (Ferrier and Lucas 1979), indicates that the "noise" is not induced by the perturbative effect of the probe.

*Increasing Extracellular Viscosity.* Since the vibrating probe greatly stirs the medium, one would expect that the surface $OH^-$ bands would have a lower concentration than in the unstirred agar diffusion system. This would lead to a much steeper $OH^-$-activity gradient from the plasmalemma to the outer cell-wall surface, which would, in turn, lead to a lower $OH^-$ activity at the plasmalemma surface. Such a lowered $OH^-$ activity may influence the rate of $OH^-$ efflux. In order to test for the influence of stirring, a commercial viscogen (15,000 centipoise K15MS Methocel; Dow Chemical USA, Midland, Mich, USA) was added to the medium at a concentration of 1.2%. This raised the viscosity from 1 to 1,500 centipoise. This increase in viscosity slowed down the velocity of 0.8 μm polystyrene latex spheres by 500-fold (3,000 $\mu m\ s^{-1}$ in CPW/B to 6 $\mu m\ s^{-1}$ in 1.2% Methocel) and would, therefore, greatly reduce the mixing effect of the probe (Jaffe and Nuccitelli 1974). After 4d in this medium *Chara* cells were still streaming normally, so the Methocel itself was not harmful, yet, after just a few minutes in this high-viscosity medium the current amplitude fell sharply (Fig. 10). The peak $OH^-$ current was reduced about fivefold and the $HCO_3^-$ peaks fell by twofold. This may indicate the presence of some extracellular feedback on these transporters which can be influenced by extracellular stirring. One likely candidate is the local $OH^-$ concentration which may inhibit $OH^-$ efflux. Reducing the band concentration by stirring would remove this inhibition and increase the transport rate as observed in low viscosity media.

An alternative explanation of the high-viscosity effect relates to the different modes by which the $OH^-$ and $HCO_3^-$ ions move under the two viscosity conditions. The increase in viscosity would greatly extend the unstirred layer associated with the cell wall. This would impose a limitation on the rate of $HCO_3^-$ diffusion and this could easily reduce the influx of $HCO_3^-$ by the observed factor of two. Ferrier and Lucas (1979) developed the theoretical transport equations for the $OH^-$ transport system, and their treatment indicated that the external electric field became an insignificant component of the driving force when a large $OH^-$ activity gradient was established. This would be the situation in the high-viscosity medium. A direct consequence of this is that the vibrating probe will not measure the large diffusion-driven component of the $OH^-$ efflux. This, and the feedback influence of the higher cell-surface $OH^-$ activity, may account for the measured fivefold reduction in $OH^-$ current.

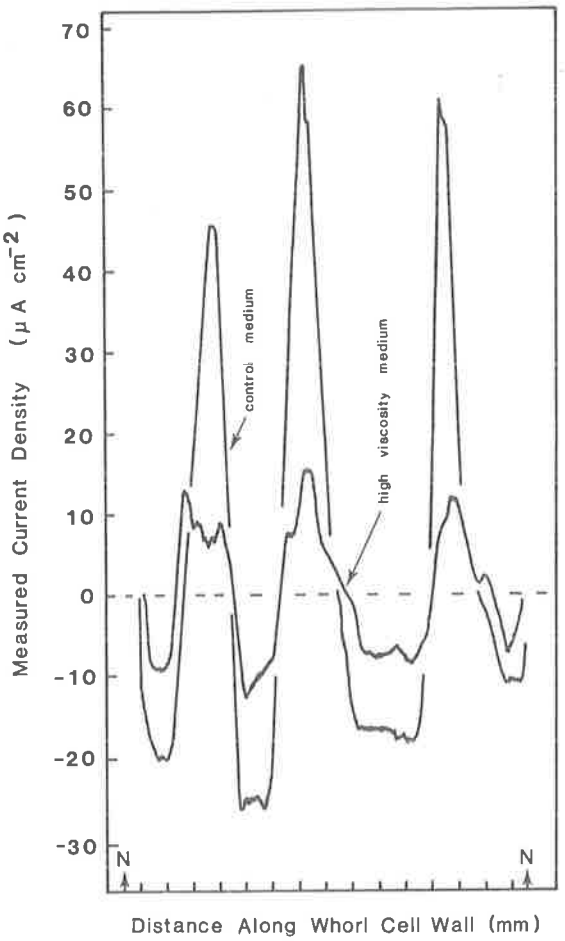


**Fig. 10.** Influence of media viscosity on the $HCO_3^-$ and $OH^-$ current profiles. Control and high viscosity media had viscosities of 1 and 1500 centipoise, respectively. See text for full details

## Discussion

*New Findings.* The greatly improved spatial and temporal resolution provided by the vibrating probe technique has led to several important new findings which will be discussed in detail below: 1) The magnitude of the inward and outward current densities is 10- to 100-fold larger than previously reported (Walker and Smith 1977). 2) The detail of transport activity within single $OH^-$ and $HCO_3^-$ bands has demonstrated important differences between the two transport systems as well as their dynamic nature. 3) Large $OH^-$ current fluctuations or "noise" have been un-

covered. 4) The average $OH^-$ current in an alkaline band is well below its potential maximum.

*Measured $OH^-$ and $HCO_3^-$ Currents.* At first sight, the current values measured in the $OH^-$-transport regions seem remarkably high. Based on experimental data collected using the diffusion-limited system, Lucas et al. (1977) used a numerical analyis model to obtain efflux values for $OH^-$ bands. They reported values ranging from 100 to 300 pmol $cm^{-2}$ $s^{-1}$ (i.e. 10–30 μA $cm^{-2}$). It should be stressed, however, that these values were obtained using 0.5 mM $HCO_3^-$, a concentration specifically employed to limit the problem of $HCO_3^-$-buffering within the system. In the present experiments we selected a $HCO_3^-$ level (1.0 mM) that would give near-maximum assimilation rates. Our higher substrate level would give an approximate doubling of the fluxes.

An earlier report of circulating currents between "acid" and "alkaline"zones in *Chara* was made by Walker and Smith (1977) using agar contact electrodes 2–17 mm apart. Their short-circuit current measurements indicated current densities of approx. 7.5 μA $cm^{-2}$ in the same general direction as the currents reported here. These authors used lower $HCO_3^-$ concentrations (0.2–0.5 mM) which would, of course, result in lower flux values. However, their contact regions were 2–12 mm wide so that they may have underestimated the current by spanning both an inward and outward current region at the contact points. The spatial separation between the agar contact electrodes (a necessity for short-circuit current measurements) may also have imposed an unnatural physiological condition along the membrane length. If this were the case, it would almost certainly result in an underestimation of the "true" current densities.

As discussed earlier, the further possibility exists that vigorous mixing of the experimental solution near the cell surface may facilitate higher $HCO_3^-$ and hence higher $OH^-$ fluxes. In the vibrating probe system, the pH values at the surface of the $OH^-$ bands will be lower than those present in the agar system. Consequently, there will be a much steeper $OH^-$-activity gradient from the plasmalemma to the outer cell wall surface. This would establish a lower $OH^-$ activity at the plasmalemma surface, compared with the agar-diffusion situation. In this regard, the high $OH^-$-efflux values may reflect transport stimulation, per se, in response to lower $OH^-$ activities in the cell wall. An interpretation of this nature would indicate some form of feedback between the apoplast and the cytoplasm.

Bicarbonate currents were not as large as those associated with $OH^-$ transport. Surprisingly enough, the range of measured values was quite close to those predicted by Ferrier and Lucas (1979). No strong correlation was found between the absolute pH values along the inter-alkaline band regions and the $HCO_3^-$ current strengths measured in these locations (see e.g. Figs. 3, 7A and B). This was true even for regions where the surface pH value was depressed below the background value, a phenomenon previously interpreted as representing a site of strong $HCO_3^-$ transport. We are uncertain as to the reason for the differences; however, important differences exist between the conditions used for pH-mapping and experiments with the extracellular vibrating probe. *Chara* cells positioned in the center of an agar diffusion block (see Fig. 2 of Lucas and Smith 1973) are in a convection-free environment. This situation maximizes the diffusion profiles that develop in association with the $HCO_3^-$- and $OH^-$-transport systems. Quite the opposite situation exists for experiments with the extracellular vibrating probe. Both the shallow solution and the mixing action of the vibrating probe tend to minimize diffusional gradients near the cell surface.

*Transport Profiles.* The transport profiles associated with $OH^-$ efflux are very similar to those computed by Lucas et al. (1977) and Ferrier and Lucas (1979). These authors used pH and external electric potential measurements to test their numerical analysis model of the $OH^-$- and $HCO_3^-$-transport systems. The most striking difference between our measured and their computed profiles was the irregular nature of the transport rate within the central $OH^-$-efflux region. Presumably the origin of this discrepancy is the difference between the time constants of the pH and vibrating probe systems (30 and 0.03 s, respectively). By moving the probe rapidly past each $OH^-$ band, an "instantaneous" transport profile is recorded. Typical $OH^-$ efflux "noise" variations of 10 μA $cm^{-2}$ would impose that much variability on the current scan profile. The pH electrode, on the other hand, averages over a 1,000-fold longer time interval so that these $OH^-$ fluctuations would be averaged out. This averaging effect would also be enhanced by the buffering effect of exogenous $HCO_3^-$. Localized rapid changes in the $OH^-$ activity would titrate $HCO_3^-$ to $CO_3^{2-}$. The current probe world still measure the $CO_3^{2-}$-associated component of the current, whereas the pH system would show a high degree of insensitivity. This pH insensitivity would be enhanced as the cell-surface pH value approached 10.3 (pKa of $HCO_3^-/CO_3^{2-}$).

The dynamic nature of the $OH^-$-transport bands was particularly evident with the vibrating probe technique. The site of peak efflux would often shift away from the probe, or even turn off completely in response to large vibration amplitudes. The dynamic response not only indicates the involvement of some

feedback from the extracellular environment, but implies that the $OH^-$-transporters can operate over a very wide range of rates within the same band.

The present results form only a preliminary study of the characteristics of $HCO_3^-$ transport. An extensive study will be conducted to examine the $HCO_3^-$ transport profiles established under a range of both exogenous $HCO_3^-$ levels and light intensities.

*Transport Control and $OH^-$ Current Fluctuation.* Perhaps the most interesting aspect of the present work was the discovery that cytoplasmic control over $OH^-$ efflux, at each of the functional bands, modulates the transport rates at values well below their potential maxima. This feature was clearly demonstrated in experiments in which probe-induced transport perturbations occurred. Under these conditions, cellular control over $OH^-$ transport is impaired in some way, and this often results in a doubling of transport rates at specific membrane locations (see Figs. 4D, 8).

Synchronization of $HCO_3^-$ and $OH^-$ transport, to obtain charge balance across the plasmalemma, must be very finely controlled in this system. Recently, Lucas and Shimmen (1980) presented clear evidence that an organelle within the streaming cytoplasmic phase is responsible for the spatial location and control over $OH^-$ transport. Presumably a complex feedback mechanism is involved. The existence of low frequency "noise" associated with the $OH^-$ current (see Fig. 9) may reflect the operation of such a feedback system (Hansen 1978). A low-frequency noise component has also been reported from experiments on the electric potential of the *Chara* plasmalemma (Rao and Pickard 1976, 1977; Ferrier et al. 1979). Ogata and Kishimoto (1976) have also reported small oscillations in the membrane potential of *Nitella pulchella*. In their experiments, the period of oscillation was highly correlated with the rate of cytoplasmic streaming. Since Lucas and Dainty (1977b) found a close relationship between the presence of a stable $OH^-$ efflux pattern and the existence of a critical rate of streaming, it is conceivable that these phenomena will be explicable in terms of a feedback process which controls $HCO_3^-$ and $OH^-$ synchronization.

Finally, it was our experience during this work that great care was needed in the handling and pretreatment of the *Chara* cells. Quite minor mechanical manipulations of the cells often caused an almost complete shut-down of both $HCO_3^-$- and $OH^-$-transport function. This sensitivity is probably a reflection of the absolute necessity for membrane-transport synchronization, which must be established over such a large membrane area (typical cells 4–6 cm in length and 0.8–1.2 mm in diameter). This is an important feature, and until we know more about the spatial aspects of $HCO_3^-$- and $OH^-$-transport synchronization, great care should be taken in designing experiments in which specific segments of the cell surface are being isolated, in a physical manner, from the rest of the cell (see Tazawa et al. 1975; Ueda et al. 1975; Lucas 1976; Ogata and Kishimoto 1976; Walker and Smith 1977). This will be particularly important when attempts are made at measuring absolute efflux values (e.g. see the physical system used by Walker and Smith 1977, to measure short-circuit $HCO_3^-/OH^-$ currents).

This work was supported jointly by National Science Foundation grants PCM 78-10474 (W.J.L.) and PCM 78-26022 (R.N.).

## References

Ferrier, J.M., Lucas, W.J. (1979) Plasmalemma transport of $OH^-$ in *Chara corallina*. II. Further analysis of the diffusion system associated with $OH^-$ efflux. J. Exp. Bot. **30**, 705–718

Ferrier, J.M., Morvan, C., Lucas, W.J., Dainty, J. (1979) Plasmalemma voltage noise in *Chara corallina*. Plant Physiol. **63**, 709–714

Hansen, U.P. (1978) Do light-induced changes in the membrane potential of *Nitella* reflect the feed-back regulation of a cytoplasmic parameter? J. Membr. Biol. **41**, 197–224

Jaffe, L.F., Nuccitelli, R. (1974) An ultrasensitive vibrating probe for measuring extracellular currents. J. Cell Biol. **63**, 614–628

Keifer, D.W., Spanswick, R.M. (1978) Activity of the electrogenic pump in *Chara corallina* as inferred from measurements of the membrane potential, conductance and potassium permeability. Plant Physiol. **62**, 653–661

Keifer, D.W., Spanswick, R.M. (1979) Correlation of adenosine triphosphate levels in *Chara corallina* with the activity of the electrogenic pump. Plant Physiol. **64**, 165–168

Kitasato, H. (1968) The influence of $H^+$ on the membrane potential and ion fluxes of *Nitella*. J. Gen. Physiol. **52**, 60–87

Lucas, W.J. (1975a) Photosynthetic fixation of $^{14}$Carbon by internodal cells of *Chara corallina*. J. Exp. Bot. **26**, 331–346

Lucas, W.J. (1975b) The influence of light intensity on the activation and operation of the hydroxyl efflux system of *Chara corallina*. J. Exp. Bot. **26**, 347–360

Lucas, W.J. (1976) Plasmalemma transport of $HCO_3^-$ and $OH^-$ in *Chara corallina*: non-antiporter systems. J. Exp. Bot. **27**, 19–31

Lucas, W.J. (1979) Alkaline band formation in *Chara corallina*: due to $OH^-$ efflux or $H^+$ influx? Plant Physiol. **63**, 248–254

Lucas, W.J., Dainty, J. (1977a) $HCO_3^-$ influx across the plasmalemma of *Chara corallina*: divalent cation requirement. Plant Physiol. **60**, 862–867

Lucas, W.J., Dainty, J. (1977b) Spatial distribution of functional $OH^-$ carriers along a characean internodal cell: determined by the effect of cytochalasin B on $H^{14}CO_3^-$ assimilation. J. Membr. Biol. **32**, 75–92

Lucas, W.J., Ferrier, J.M. (1980) Plasmalemma transport of $OH^-$ in *Chara corallina*. III. Further studies on transport substrate and directionality. Plant Physiol. **66**, 46–50

Lucas, W.J., Ferrier, J.M., Dainty, J. (1977) Plasmalemma transport of $OH^-$ in *Chara corallina*: dynamics of activation and deactivation. J. Membr. Biol. **32**, 49–73

Lucas, W.J., Shimmen, T. (in press) Intracellular perfusion and cell centrifugation studies on plasmalemma transport processes in *Chara corallina*. J. Membr. Biol.

Lucas, W.J., Smith, F.A. (1973) The formation of alkaline and acid regions at the surface of *Chara corallina* cells. J. Exp. Bot. **24**, 1–14

Nuccitelli, R., Poo, M.-M., Jaffe, L.F. (1977) Relations between ameboid movements and membrane-controlled electrical currents. J. Gen. Physiol. **69**, 743–763

Ogata, K., Kishimoto, U. (1976) Rhythmic change of membrane potential and cyclosis of *Nitella* internode. Plant Cell Physiol. **17**, 201–207

Rao, R.L., Pickard, W.F. (1976) The use of membrane electric noise in the study of characean electrophysiology. J. Exp. Bot. **27**, 460–472

Rao, R.L., Pickard, W.F. (1977) Further experiments on the low frequency excess noise in the vacuolar resting potential of *Chara braunii*. J. Exp. Bot. **28**, 1–16

Sanders, D. (1980) The mechanism of $Cl^-$ transport at the plasma membrane of *Chara corallina*. I. Co-transport with $H^+$. J. Membr. Biol. **53**, 129–141

Spanswick, R.M. (1972) Evidence for an electrogenic ion pump in *Nitella translucens*. I. The effects of pH, $K^+$, $Na^+$, light and temperature on the membrane potential and resistance. Biochim. Biophys. Acta **288**, 73–89

Tazawa, M., Kikuyama, M., Nakagawa, S. (1975) Open-vacuole method for measuring membrane potential and membrane resistance of Characeae cells. Plant Cell Physiol. **16**, 611–622

Ueda, T., Kurihara, K., Kobatake, Y. (1975) Response of *Nitella* internodal cell to chemical stimulation: a model for olfactory receptor system. J. Membr. Biol. **25**, 271–284

Walker, N.A., Smith, F.A. (1977) Circulating electric currents between acid and alkaline zones associated with $HCO_3^-$ assimilation in *Chara*. J. Exp. Bot. **28**, 1190–1206

Received 26 February; accepted 20 August 1980

J. Membrane Biol. 58, 227–237 (1981)

The Journal of
Membrane Biology

# Intracellular Perfusion and Cell Centrifugation Studies on Plasmalemma Transport Processes in *Chara corallina*

William J. Lucas and Teruo Shimmen*
Department of Botany, University of California, Davis, California 95616

**Summary.** The $OH^-$ transport system of *Chara corallina* was studied using the techniques of intracellular perfusion and cell centrifugation. Application of silk ligatures to internodal cells had quite a perturbative effect on the $OH^-$ transport activity. Approximately 12 hr were required before normal pH profiles were reestablished.

Tonoplast-free internodal cells developed rather weak, uniform alkalinity along the cell surface. Redevelopment of control pH patterns was never observed in these experiments. Surface pH profiles similar to those observed on tonoplast-free cells could also be obtained by subjecting cells to mild centrifugation ($180 \times g$). Organelles of the streaming cytoplasm were contained within the centrifugal cell segment by applying a ligature near the cell center. Normal pH profiles were observed along the centrifugal segment, while the centripetal segment developed weak, rather uniform alkaline profiles. Upon redistribution of the cytoplasmic organelles, normal pH profiles were established along the entire cell length.

These results indicate that an organelle within the streaming cytoplasmic phase is responsible for the spatial location and control over $OH^-$ transport. This explains the absence of control pH profiles in tonoplast-free cells, since during the disintegration of the tonoplast, most of the streaming cytoplasm coagulates at one end of the cell.

Parallel pH mapping and electrophysiological studies indicated that the plasmalemma of this species contains an ATP-dependent electrogenic $H^+$ transport system. Also, experiments conducted in the presence and absence of cellular ATP demonstrated that $OH^-$ efflux can be driven passively by the membrane potential. Whether $OH^-$ transport is strictly a passive process in normal cells remains to be resolved.

* : *Permanent address:* Department of Botany, Faculty of Science, University of Tokyo, Hongo, Tokyo 113, Japan.

Perfusion of the plant vacuole with an artificial sap was first attempted by Blinks (1935); he used the marine alga *Halicystis*. The giant internodal cells of the Characeae were also amenable to this type of experimental manipulation. Kamiya and Kuroda (1957) and later Tazawa (1964) developed the technique for perfusing the vacuole of Characean cells. Using this procedure Tazawa and his collaborators were able to examine the influence of vacuolar ionic composition adjustment (Nakagawa, Kataoka and Tazawa, 1974; Tazawa, 1975), the resting membrane potential, and membrane excitability (Tazawa & Kishimoto, 1964).

The tonoplast in these perfused cells remained intact, and as such it imposed a barrier to the movement of certain chemical agents between the artificial vacuole and the cytoplasm. This limited the usefulness of the vacuolar perfusion technique. Tazawa, Kikuyama and Shimmen (1976) overcame this problem by incorporating 5 mM EGTA into the perfusion medium; the presence of this $Ca^{2+}$-chelator caused the disruption of the tonoplast. Williamson (1975) reported that the tonoplast could also be removed by rapid perfusion using a medium containing 50 mM EGTA.

Extensive use is now being made of this tonoplast-free *Chara* cell system. Thus far the technique has been used to demonstrate the ATP and $Mg^{2+}$ dependency of cyclosis (Williamson, 1975; Tazawa et al. 1976; Shimmen, 1978). Progress has also been made towards understanding the physiological requirements necessary for normal maintenance of membrane potential. Shimmen and Tazawa (1977) demonstrated that approximately one half the resting membrane potential is supported by Mg-ATP. A similar dependence of membrane excitability has also been established (Shimmen, Kikuyama & Tazawa, 1976). Recent progress using this technique has been reviewed by Tazawa and Shimmen (1980*a*, *b*).

In some situations, results have been obtained on

0022-2631/81/0058-0227 $02.20
© 1981 Springer-Verlag New York Inc.

perfused cells that are atypical of those found using normal intact cells. Cessation of cytoplasmic streaming, which occurs in normal Characean cells upon membrane excitation (Tazawa & Kishimoto, 1968), is not observed in tonoplast-free cells (Tazawa et al., 1976). In his investigation on the effect of internal $Cl^-$ concentration on $Cl^-$ influx into *Chara corallina*, Sanders (1980*a*) cautioned that the membrane potential of his perfused cells was low (−95 to −110 mV). Of equal importance was the pH insensitivity of the membrane potential in these perfused cells. Walker (1980) also presented current-voltage curves, obtained using perfused *Chara* cells, which indicated that the addition of ATP caused a hyperpolarizing current, but did not generally restore the original membrane conductance. These results suggest that the perfusion procedure may perturb certain aspects of membrane function. Since the number of laboratories employing this technique is increasing, it seemed essential to determine whether or not the procedure was seriously perturbative.

The plasmalemma-bound $HCO_3^-$ and $OH^-$ (alkaline band) transport systems of *C. corallina* have been extensively characterized (Lucas & Dainty, 1977*a*, Lucas, 1980). The purpose of the present study was, therefore, to determine whether tonoplast-free perfused *Chara* cells could develop normal alkaline bands, under conditions of $HCO_3^-$ assimilation.

## Materials and Methods

### *Culture Material*

Culture material of *Chara corallina* Klein ex Willd., em. R.D.W. (=*C.australis* R.Br.) was grown in the laboratory in 120-liter containers in solutions containing (mM): 3.0 $Na^+$, 0.2 $K^+$, 0.2 $Ca^{2+}$, 1.0 $Cl^-$, and approximately 2.0 $HCO_3^-$ (pH 9.0). Artificial fluorescent lighting was employed; the intensity at the solution surface was 17–20 W $m^{-2}$. *Chara* internodal cells were cut from the culture at least 24 hr prior to being used in experiments. During this pretreatment period cells were bathed in a modified pond water (CPW/B) containing (mM) 1.0 NaCl, 0.2 KCl, 0.2 $CaSO_4$, and 1.0 $NaHCO_3$ (pH 8.0).

### *Experimental Solutions*

All experimental solutions were prepared from Analar Reagent grade chemicals using glass distilled water (Corning Mega-Pure automatic still, model 3513). Composition and pH ($pH_i$) of the various perfusion media (PM) is detailed in Table 1. Buffers used in these media were prepared and stored as 0.5-M stock solutions. Stock solutions of glucose (100 mM), sorbitol (1 M), EGTA (100 mM), $MgCl_2$ (100 mM) and $K_2SO_4$ (100 mM) were also stored under refrigeration. ATP (purchased as the dipotassium salt from Sigma, St. Louis, Mo.) was prepared as a stock solution immediately before daily PM preparation. Hexokinase (Sigma, Type III) was preweighed to give 1 mg/ml of PM, and was added to the PM immediately prior to cell perfusion. Ficoll (Sigma, Type 70) solution (approx. 30% wt/vol) was dialyzed (benzolated tubing) at 4 °C for two days against glass distilled water (changed daily). An accurate stock solution (20% wt/vol) was then prepared and stored at 4 °C.

Bathing solutions used for electrophysiology experiments contained CPW/B and were buffered (2 mM) at pH 7.0 with NaOH-HEPES, pH 8.0 and 8.25 with NaOH-Tricine, and pH 8.5 and 9.0 with NaOH-TAPS.

### *Intracellular Perfusion*

The perfusion technique employed was similar to that of Tazawa, Kikuyama and Shimmen (1976). For the present experiments long internodal cells were employed (8 to 12 cm in length and approximately 0.7 mm in diameter). Surface water was blotted from the cell wall before it was placed on a Plexiglas block. One of the nodal complexes was then immediately irrigated with a small

**Table 1.** Perfusion media composition

| Component | pH of ATP/ATP-free (H.K.) media | | | | | | | | | | | |
|---|---|---|---|---|---|---|---|---|---|---|---|---|
| | 7.0(ATP) | 7.0(HK) | 7.5(ATP) | 7.5(HK) | 8.0(ATP) | 8.0(HK) | 8.25(ATP) | 8.25(HK) | 8.5(ATP) | 8.5(HK) | 9.0(ATP) | 9.0(HK) |
| Buffer (100 mM) | HEPES | HEPES | HEPES | HEPES | Tricine | Tricine | Tricine | Tricine | TAPS | TAPS | TAPS | TAPS |
| ATP (mM) | 2 | – | 2 | – | 2 | – | 2 | – | 2 | – | 2 | – |
| Glucose (mM) | – | 5 | – | 5 | – | 5 | – | 5 | – | 5 | – | 5 |
| Hexokinase(mg/ml) | – | 1 | – | 1 | – | 1 | – | 1 | – | 1 | – | 1 |
| $K^+$ (mM) | 45 | 41 | 78 | 73 | 75 | 71 | 100 | 88 | 89 | 79 | 105 | 101 |
| $MgCl_2$ (mM) | 6 | 6 | 6 | 6 | 6 | 6 | 6 | 6 | 6 | 6 | 6 | 6 |
| EGTA (mM) | 5 | 5 | 5 | 5 | 5 | 5 | 5 | 5 | 5 | 5 | 5 | 5 |
| Sorbitol (mM) | 60 | 60 | 50 | 35 | 20 | 20 | 10 | 30 | 35 | 35 | 10 | 0 |
| Ficoll-70 (wt/vol%) | 5 | 5 | 5 | 5 | 5 | 5 | 5 | 5 | 5 | 5 | 5 | 5 |

Sorbitol was used to adjust perfusion media osmotic pressure to 545 kPa (220 mOsM)

amount of perfusion medium. Loss of water vapor from the internodal cell wall eventually reduced the turgor to zero. During this drying process six silk threads (Kanagawa Co. Ltd., Kanagawa, Japan, Type: Orizuru 9 and 50) were positioned at the required places along the cell surface and loosely tied. It was essential to complete this operation before the cell became flaccid.

Upon wilting, the PM-bathed nodal complex was removed by carefully cutting the internodal cell wall with a pair of fine-pointed scissors. The opposite nodal complex was then irrigated and removed in the same way. A reservoir (approx. 0.5 ml) of PM was then placed over this open cell end prior to raising the end of the Plexiglas block. (A gradient of 1 in 40 mm was generally applied). An absorbent paper "wick" was used to draw PM through the cell until the vacuolar volume had been replaced at least three times. This step took between 30 to 60 sec, depending on the cell length. Post-perfusion cell ligation was performed in the following manner. An initial set of ligatures was placed approximately 1 cm in from each cut end of the cell. The cell was then irrigated with a CPW/B solution containing 180 mM sorbitol. A second set of ligatures was then applied to the turgid section of the cell. After a period of 2 min, a single ligature was applied at one end of the cell, and, after a further 2 min, the final ligature was applied at the opposite end. The cell wall was then cut between the second and third sets of ligatures using fine-pointed scissors. The spacing between the three sets of ligatures was adjusted such that the final perfused cell segment was approximately 2 cm in length, for cells used in pH mapping experiments, and 3 cm in length for electrophysiological studies. Full turgor was restored by irrigating the ligated cell segment with CPW/B.

Cyclosis and the ligatured ends of the cell were examined using a binocular microscope (100 to 400× magnification). The areas of ligation were checked both for leakage and symmetry. Cells with nonsymmetrically ligatured walls were discarded, as these had a much greater tendency to either leak or rupture during the course of an experiment. (It is perhaps worth mentioning that the greatest frequency of symmetrical ligatures were obtained by applying an half-reef knot. If applied with sufficient tension, this silk knot does not loosen.) Inclusion of 5 mM EGTA in the PM (*see* Table 1 for composition of various perfusion media employed) caused the destruction of the tonoplast (Tazawa et al., 1976). Establishment of the tonoplast-free state was easily identified under the microscope. A normal cyclosis pattern was always observed until the tonoplast disintegrated, then, upon its disruption it collected, along with other cytoplasmic organelles, near one end of the perfused cell. In general, the tonoplast was destroyed within 5 min of PM entry into the vacuole. When ATP was included in the PM, cyclosis continued at the control rate after EGTA-induced membrane coagulation; however, only small "granular" particles remained in the streaming phase. Depletion of endogenous ATP by perfusion with glucose and hexokinase (Shimmen & Tazawa, 1977; Kikuyama, et al., 1979) resulted in complete stoppage of streaming within 5 to 10 min of perfusion.

At the end of each experiment cells were re-examined for chloroplast appearance and cyclosis. At this stage a general check was also made on cell turgor. This was done by observing the cell's response to a bending force. Cells that deformed under this force had lost the ability to maintain turgor. Results obtained on cells in which either streaming, or normal turgidity was not observed were discarded.

### *Cell Centrifugation*

Distribution of streaming cytoplasm was manipulated using a bench-top centrifuge (International Clinical Centrifuge, model CL). A silk thread was attached to one end of the experimental cell and this thread was used to suspend the cell in a test tube containing CPW/B. An ice bath was used to lower the temperature of the centrifugation medium. The reduced temperature slowed the rate at which cytoplasmic streaming redistributed the centrifuged cell contents. After four minutes of centrifugation ($180 \times g$) cells were transferred to the Plexiglas perfusion block and irrigated with CPW/B containing 180 mM sorbitol (4 °C). A single ligature was then applied to the cell center. For these experiments, ligatures were tied rather weakly so that the plasmalemma on opposite sides of the cell did not fuse. Cyclosis was then observed in CPW/B. In successful experiments, the centrifuged half of the cell contained the larger organelles of the streaming cytoplasm, while the streaming phase of the centripetal segment contained only small "granules".

### *pH Measurement Along the Chara Cell Wall*

The pH profile along the cell surface of *C. corallina* internodal cells was measured using the technique developed by Lucas and Smith (1973). Agar blocks, that we used as embedding media for experimental cells, were prepared in the manner described by Lucas and Dainty (1977*b*). Perfused cells were found to be much more sensitive to mechanical manipulation during insertion into the agar blocks. To overcome this problem, we cut wider channnels (3–4 mm) in the agar block, and, in addition, a new procedure was used to position the cell in the diffusion channel. This involved the following sequence: (i) the diffusion channel was filled with CPW/B, (ii) the perfused cell was floated on top of the block, (iii) one end of the block was then raised to allow the CPW/B to drain; this pulled the cell down into the diffusion channel, and (iv) the agar block was then positioned into the experimental chamber. All experiments were performed in CPW/B media at 25 °C under a light intensity of 20 W $m^{-2}$.

The pH measurements were made using a miniature pH electrode (Microelectrodes, Londondery, N.H., model MI-405) in conjunction with a Beckman model 4500 digital pH meter. A micromanipulator (Leitz) was used to position the electrode on the cell wall. In experiments using perfused cells, the electrode was positioned approximately 5 μm away from the cell wall to prevent possible mechanical disturbance. From the values obtained the pH pattern established at the cell surface was mapped. Details relating to individual scanning experiments will be specified in the text.

### *Electrophysiological Measurements*

Membrane potential and resistance measurements were made in a similar manner to that reported by Lucas, Spanswick and Dainty (1978). The potential between the vacuole and the bathing solution (or across the plasmalemma in tonoplast-free cells) was measured (WPI model 750 amplifiers; WPI Instruments, New Haven, Conn.) using an inserted microelectrode (1 μm tip diameter) and an external reference electrode (10–20 μm tip diameter). Microelectrodes were filled with 3 M KCl, adjusted to pH 2 to reduce tip potentials (Okada & Inouye, 1975). Membrane resistance was calculated from the deviation of the membrane potential that occurred when a square current pulse (0.5 to 1.0 μA, 1 sec duration) was injected into the cell (*see* Lucas et al., 1978, for full details).

## Results

### *Influence of Ligation and Perfusion on $OH^-$ Band Pattern*

Potentially, any one of the steps or conditions necessary to obtain a tonoplast-free perfused cell could

perturb the $OH^-$ (and/or $HCO_3^-$) transport system. The first aspect to be examined was the procedure of cell ligation. Experimental cells were illuminated (10 W $m^{-2}$) in CPW/B containing phenol red (acid/base indicator: 5 mg/liter) for 30 min to ensure that normal $HCO_3^-$ assimilation was occurring, as evidenced by the presence of strong alkaline bands. Cells were then dried down and ligated in the manner detailed in the Materials and Methods, except that the nodal complexes were not removed and the vacuole was not replaced. Ligated cells were either returned to CPW/B (plus phenol red) or positioned in agar blocks for pH mapping. The alkaline banding pattern response to this treatment is typified by the results presented in Fig. 1. Immediately after ligation (30–60 min) only very weak $OH^-$ efflux activity was observed. Transport activity then increased gradually with time, and within 10 to 14 hr normal pH banding patterns were recorded. Complete agreement was found between the pH mapping data and the visual observations made on cells placed in phenol red solutions. Once recovered, these cells exhibited stable alkaline bands for weeks.

Hydroxyl transport perturbation occurred whether or not the nodal complexes were cut from the ligated cell (data not shown). This indicated that the perturbation was not caused by injury resulting from cutting, *per se*. Recent studies (J.M. Alexander and W.J. Lucas, *unpublished results*) have also shown that the procedure adopted to reduce and then return cell turgor does not significantly affect the $OH^-$ transport system.

Experiments on cells in which the vacuolar sap had been replaced by a simple PM (110 mM KCl and 5 mM $CaCl_2$) gave $OH^-$ transport perturbation and recovery profiles identical to those observed for ligation-only experiments (data not shown). However, long term pH scan experiments, conducted on cells in which the tonoplast had been destroyed, gave quite different results. In the initial period immediately after perfusion and ligation, the entire cell surface became alkalinized, exhibiting rather uniform pH profiles (Fig. 2, 30–60 min scan). Generally, these pH profiles varied little with time during the first 3 to 4 hr after perfusion. With prolonged periods (4 to 6 hr after perfusion) the profiles often became irregular, with some regions on the cell surface becoming slightly more acidic than the background (*see* Fig. 2). However, the alkaline regions always remained rather broad and were relatively weak in $OH^-$ transport activity. Indeed, in these tonoplast-free experiments, redevelopment towards the control pH pattern was never observed. Measurement of cyclosis, at the conclusion of each experiment, indicated that the streaming mechanism was still functioning; rates were always above the critical level necessary for maintenance of normal alkaline bands (Lucas & Dainty, 1977*b*).

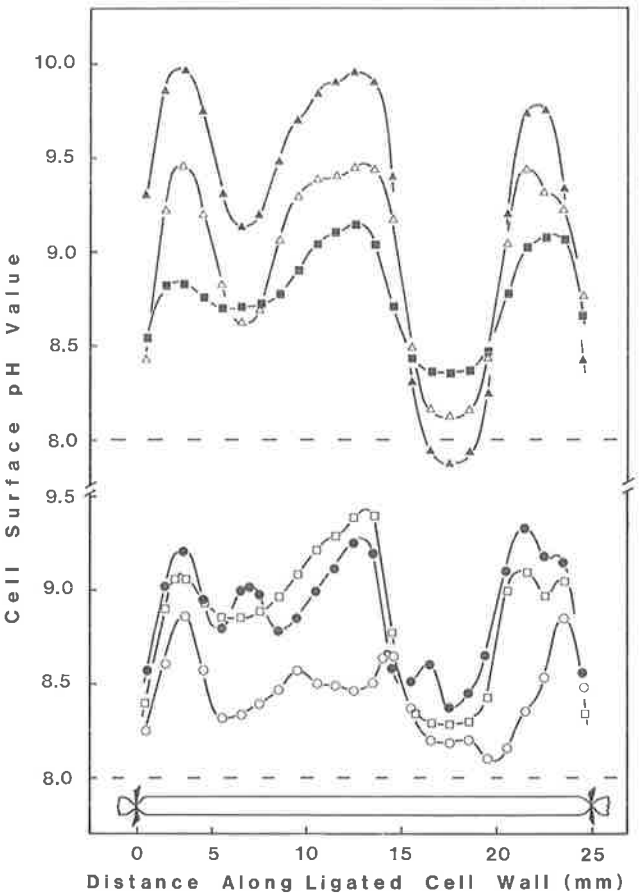


**Fig. 1.** Time-dependent recovery of $OH^-$ efflux activity following cell ligation. Silk ligatures were applied (*see* Materials and Methods), and then, in this particular experiment, the nodal complexes were cut away. The vacuole was not replaced by perfusion. Cell surface pH scans were conducted at 0.5 (○), 1.5 (●), 3.0 (□), 5.5 (■), 8.0 (△) and 12 (▲) hr after cell ligation. (Horizontal broken lines represent background pH value.)

### *Centrifugation of Organelles within Streaming Cytoplasm*

Removal of the tonoplast may have impaired, in same way, the characean cellular mechanism which is believed to control and synchronize the spatially separated $HCO_3^-$ and $OH^-$ transport systems (Lucas, 1980). Certainly, including 5 mM EGTA in the PM caused significant ultrastructural changes to the streaming phase of the cytoplasm (*see* Materials and Methods for details). Recent electrophysiological (Ogata & Kishimoto, 1976) and plasmalemma transport studies (Lucas & Nuccitelli, 1980) on the Chara-

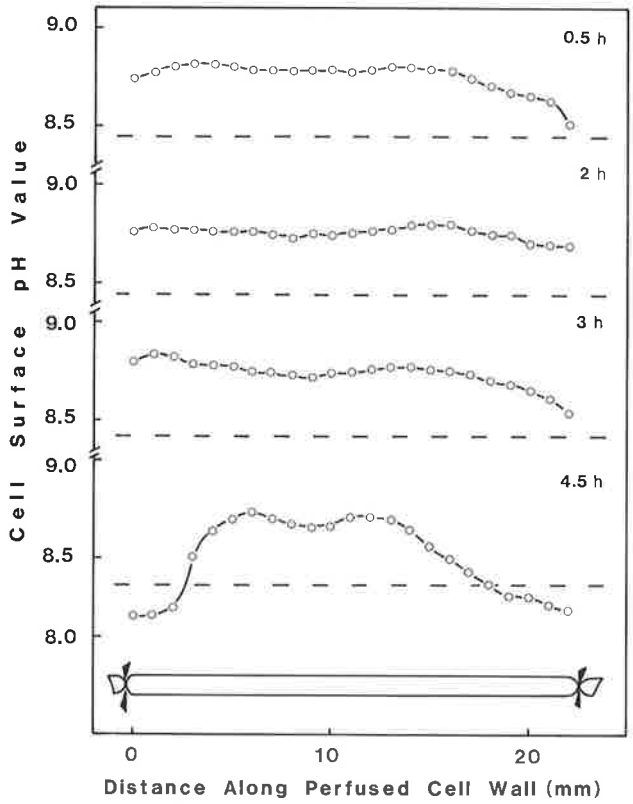


**Fig. 2.** pH profiles developed at various periods after establishing the tonoplast-free condition. Scans were commenced at the indicated times and each took approximately 30 min to complete. The perfusion medium used in this experiment contained 2 mM ATP and its $pH_i$ was 8.5 (*see* Table 1 for full details). At the conclusion of the experiment the cell $pH_i$ had decreased to 8.05. (Background pH values are indicated by horizontal broken lines.)

ceae have indicated that a membrane-associated control signal(s) (feedback) may orginate from within the streaming cytoplasm. If the control signal(s) that regulates $OH^-$ and $HCO_3^-$ transport is produced by an organelle within the streaming phase, 5 mM EGTA may also destroy it, along with the tonoplast.

This possibility was examined using the technique of cell centrifugation. By employing the correct combination of centrifugation time and speed (*g*-force), we were able to concentrate in the centrifuged end of the cell all the large organelles of the streaming phase. When the organelles were allowed to redistribute throughout the cell, it was found that the centrifugation treatment had little overall effect on the $OH^-$ transport pattern. Within 30 min after centrifugation there were only slight differences between the pre- and post-centrifugation pH profiles (Fig. 3). By 2.5 hr, the only remaining differences involved a slight positional rearrangement of the bands and minor reallocation of $OH^-$ transport activity (e.g., *see* the central bands of Fig. 3).

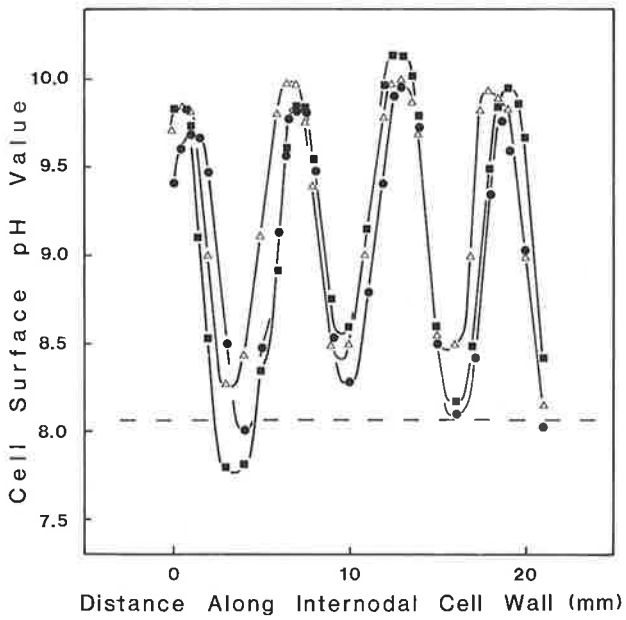


**Fig. 3.** Effect of cell centrifugation on the spatial arrangement of the $OH^-$ efflux bands. A control pH scan (△) was conduced (2 hr preillumination, 20 W $m^{-2}$) prior to cell centrifugation. Recovery profiles were mapped 0.5 hr (●) and 2.5 hr (■) after the cell had been centrifuged for 4 min at $180 \times g$

An entirely different result was obtained when the redistribution of the organelles was restricted to the centrifuged half of the cell (Fig. 4). A normal pH banding pattern was always observed along the centrifugal segment, but the centripetal segment in which the cytoplasmic streaming phase contained only small "granules", developed rather weak diffuse regions of alkalinity (Fig. 4*A*). These profiles were very similar to those obtained from perfused, tonoplast-free cells (*cf.* Figs. 2 and 5). An important feature of the ligation technique used to partition the cytoplasm of the centrifuged cell was that the imposed blockage was reversible with time. In general, cells took 8 to 24 hr to remove the blockage. After ligation, the streaming within the two segments was monitored. It was found that when the blockage was removed, the large organelles of the centrifugal segment became redistributed throughout the cell. Although the time at which the blockage was removed was extremely variable, once it had occurred the redistribution of organelles and the recommencement of normal alkaline banding along the centripetal segment was rapid (approximately 5 to 10 min). Figure 4*B* indicates that when the larger cytoplasmic organelles were again present in both cell segments, normal alkaline bands were distributed along the entire cell length. These results clearly indicate that a cytoplasmic organelle (yet to be identified) is involved in regulating $OH^-$ (and possibly $HCO_3^-$) transport

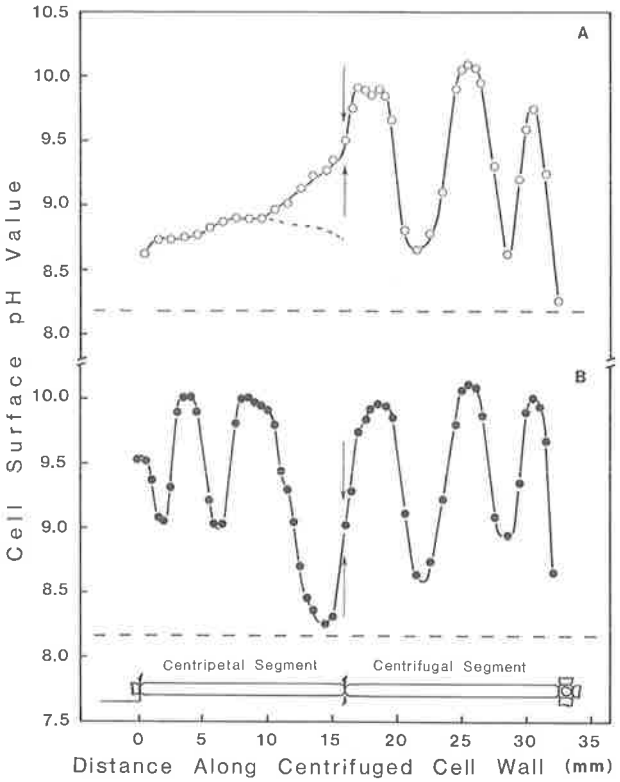


**Fig. 4.** Influence of streaming cytoplasmic organelle distribution on the alkaline banding phenomenon. Following centrifugation a weakly applied silk ligature was used to partition the cell into centrifugal (containing all large organelles present in streaming phase) and centripetal (containing only small "granules") segments. Banding pattern established in presence of asymmetric organelle distribution (Fig. 4*A*) and after the blockage had been removed and the organelles were streaming in both cell segments (Fig. 4*B*)

at the plasmalemma. We feel that the absence of the $OH^-$ banding pattern in perfused cells is due, therefore, to the EGTA-induced destruction of that organelle, rather than a direct effect of the PM on the transport systems of the plasmalemma.

*ATP and Hexokinase Perfused Cells*

Experiments were performed to investigate the effect of the presence and absence of ATP on the pH profile established at the surface of perfused, tonoplast-free *Chara* cells. An alkalinization of the entire cell surface of ATP-free (depleted) cells was observed over a $pH_i$ range of 7.0 to 9.0 (Fig. 5, ○). A much more complex situation was observed when the perfused cells contained 2 mM ATP. At $pH_i$ values of 8.5 and 9.0, no significant differences were observed between the pH profiles established by ATP and ATP-free cells. However, for $pH_i$ values ranging from 7.0 to 8.25, the cells containing ATP developed more acidic (less alkaline) pH profiles than ATP-free cells having the same $pH_i$ value. This was particularly significant at $pH_i$ values of 7.5 and 8.0; here the cell surface pH values were depressed below the background medium (Fig. 5). The difference between ATP and ATP-free pH profiles presumably reflects the operation of an ATP-dependent acidification processes (proton pump?).

The situation seemed to be even more complex when the $pH_i$ was 7.0. In the presence of ATP we expected the cell surface to go more acidic than the 7.5 and 8.0 $pH_i$ conditions. An indication that greater membrane transport complexity was being introduced at $pH_i$ values near neutrality was also obtained from light/dark studies. Figure 6*A* and *B* illustrate the pH profiles established in the light and dark, respectively (30 min after perfusion, $pH_i = 7.0$, 2 mM ATP). Dark treated cells developed slightly acidic wall profiles, while those of the illuminated cells were weakly alkaline. Acidic profiles, established in the dark, could be reduced appreciably by 30 min of illumination (Fig. 6*C*). This light/dark sensitivity was not observed when $pH_i$ values of 8.5 and 9.0 were employed (data not shown).

Parallel experiments, identical to those illustrated

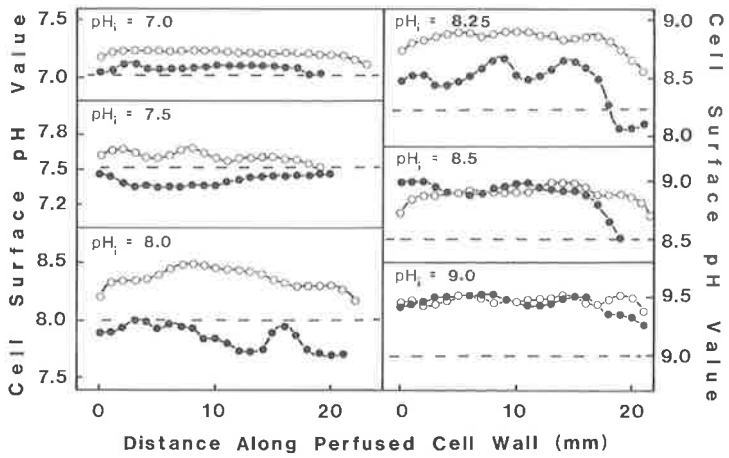


**Fig. 5.** Development of pH profiles by perfused cells in which either 2 mM ATP (●) or 1 mg/ml hexokinase plus 5 mM glucose (○) was included in the PM. A range of $pH_i$ values was investigated, and, in each situation, the pH of the external medium ($pH_o$, indicated by horizontal broken line) was adjusted to the same value as the PM $pH_i$ using either 100 mM NaOH or 100 mM $H_2SO_4$. Cells were illuminated (20 W $m^{-2}$) in CPW/B ($pH_o$ as indicated) for 30 min before scanning. Between 4 and 5 perfused cells were scanned for each treatment; representative pH profiles are presented

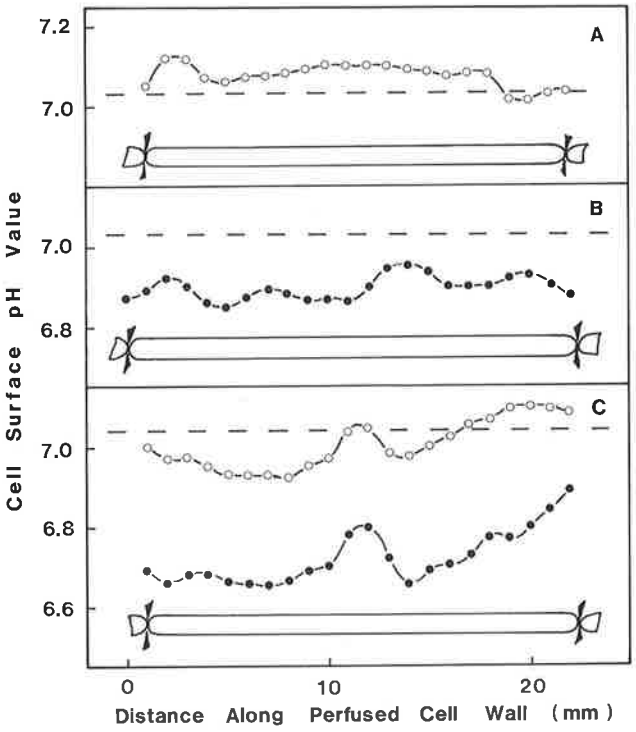


**Fig. 6.** Comparison between pH profiles obtained under light and dark conditions for cells in which the ATP perfusion medium $pH_i$ was 7.0. (*A*): Profile obtained after 30 min illumination (20 W $m^{-2}$); (*B*): pH profile after 30 min dark treatment; (*C*): ●, 30 min dark treatment, cell then illuminated for 30 min (○)

in Fig. 5, were conducted in which the $pH_i$ values were measured after 2 hr illumination. The perfusion medium was withdrawn from the cell using the technique of Fujii, Shimmen and Tazawa (1979), and the $pH_i$ was measured with a micro combination pH electrode (Microelectrodes Inc., model 410). For cells containing ATP, the changes in $pH_i$ followed a simple trend; values higher than 8.0 were reduced, while lower values were increased (Table 2). This response suggests that a pH-stat mechanism is operating in these perfused cells. In ATP-free (depleted) cells the general trend was a reduction in $pH_i$, with the change being greatest at the highest $pH_i$ values. This trend would be consistent with a reduction in passive $OH^-$ efflux which would be due to diminished $OH^-$ availability at lower $pH_i$ values, provided the membrane potential remained constant over the $pH_i$ range examined.

Included in Table 2 are the changes in $pH_i$ that occurred during a 2-hr dark treatment. Cells containing ATP raised their $pH_i$ in the dark, while the $pH_i$ of ATP-free cells did not appear to change. The relationship between these data and the results presented in Fig. 6 will be discussed in a later section.

### *Electrophysiological Properties of Perfused Cells*

The influence of $pH_i$ on the membrane potential of perfused *Chara* cells is illustrated in Fig. 7. Illuminated cells that contained ATP exhibited highly negative potentials when the $pH_i$ was 7.0 to 8.0. Indeed, these values were quite similar to normal control cells ($-210 \pm 4.9$ mV). Figure 7 also indicates that within this $pH_i$ region the potential responded to light/dark changes. At $pH_i$ values above 8.0, the potential depolarized to a level similar to that observed for ATP-free cells. In this depolarized state, as with the ATP-free situation, the potential was no longer light-responsive. Related membrane resistance values which were measured under these various perfusion conditions, are presented in Fig. 8. Again, as with the membrane potential, the resistance values for ATP- and ATP-free cells converged at $pH_i$ values above 8.0, and, under these conditions, sensitivity to light was also lost.

The response of the membrane potential to changes in the pH of the external medium ($pH_o$) was

**Table 2.** Tonoplast-free *Chara* cell $pH_i$ values measured after 2 hr light pretreatment

| Medium | Initial perfusion medium $pH_i$ values | | | | | |
|---|---|---|---|---|---|---|
| | 7.0 | 7.5 | 8.0 | 8.25 | 8.5 | 9.0 |
| ATP (2 mM) | $7.14 \pm 0.14(3)$<br>$\Delta pH = +0.14$<br>$[7.18 \pm 0.02(3)]$ | $7.60 + 0.06(5)$<br>$\Delta pH = +0.10$ | $7.83 + 0.06(4)$<br>$\Delta pH = -0.17$ | $8.14 \pm 0.08(7)$<br>$\Delta pH = -0.11$ | $8.22 \pm 0.12(5)$<br>$\Delta pH = -0.27$ | $8.75 \pm 0.07(3)$<br>$\Delta pH = -0.25$ |
| Hexokinase (1 mg/ml) | $7.07 \pm 0.02(3)$<br>$\Delta pH = +0.07$<br>$[7.01 \pm 0.13(4)]$ | $7.43 \pm 0.06(4)$<br>$\Delta pH = -0.07$ | $7.83 \pm 0.11(4)$<br>$\Delta pH = -0.17$ | $7.99 \pm 0.01(3)$<br>$\Delta pH = -0.26$ | $8.18 \pm 0.09(8)$<br>$\Delta pH = -0.32$ | $8.68 \pm 0.12(3)$<br>$\Delta pH = -0.32$ |

Perfused cells were pretreated for 2 hr in CPW/B; $pH_o$ adjusted to particular $pH_i$ value. Full details of the respective perfusion medium composition for each $pH_i$ value is given in Table 1. Mean ± SEM, number of duplicates indicated in parenthesis. [ ], values obtained on cells given 2 hr dark treatment.

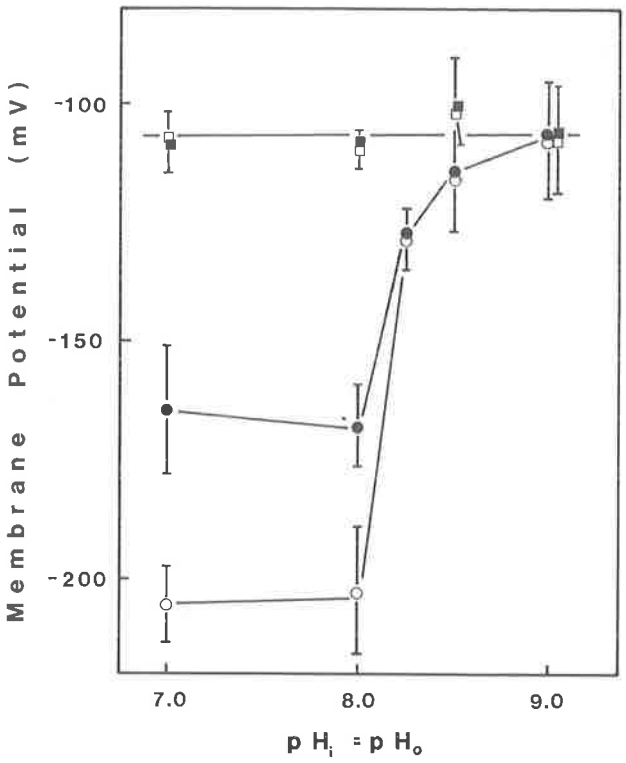


**Fig. 7.** Membrane potential of perfused, tonoplast-free *Chara* cells. In individual experiments, the pH of the external medium ($pH_o$) was adjusted to the perfusion medium value ($pH_i$). Stable values in the light (open symbols, 20 W $m^{-2}$) and the dark (filled-symbols) were obtained on each perfused cell: ○, ATP-perfused; □, hexokinase-perfused cells. (Experimental duration was usually 2 hr)

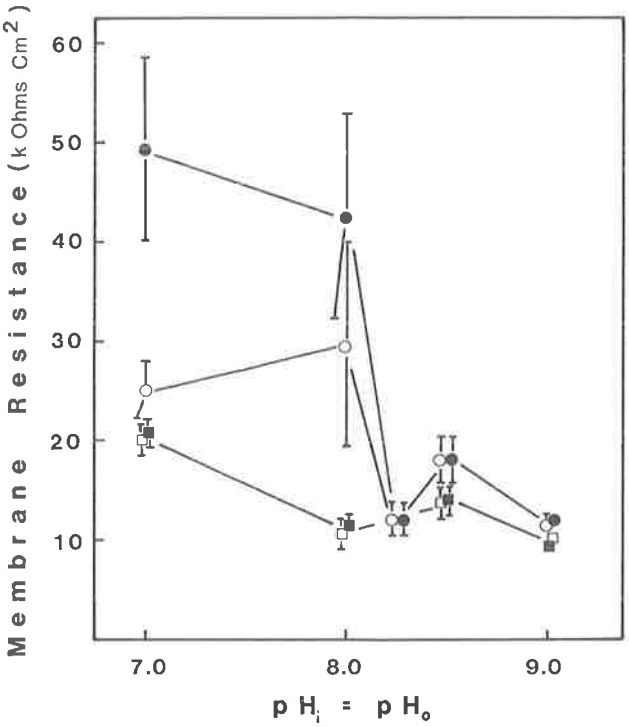


**Fig. 8.** Membrane resistance of perfused tonoplast-free *Chara* cells. Details are as in Fig. 7

also investigated. Normal sensitivity to $pH_o$ was observed when the perfused cells contained ATP and the $pH_i$ was in the 7.0 to 8.0 region (*see* Fig. 9). These data also serve to illustrate the observed stability of the membrane potential in these perfused cells. The present results on the effects of $pH_i$ and $pH_o$ on the membrane potential and the membrane resistance were similar to those obtained previously in perfused cells of *Chara australis* (Fujii et al., 1979, Kawamura et al., 1980).

## Discussion

### *Regulation of $OH^-$ Transport by a Cytoplasmic Organelle*

One of the most important features of the present study was the clear demonstration that control over the $OH^-$ transport system originates within the streaming phase of the cytoplasm. In these giant cells, the chloroplasts are fixed in position and uniformly distributed along the inner boundary of the gel layer. Also, the mitochondria, endoplasmic reticula, and Golgi are rather uniformly distributed in the gel matrix (Franceschi & Lucas, 1980). Hence, unless there are functionally different types of these organelles within the cell, they cannot be directly involved in the transport regulation processes. The main organelles that are most probably removed by either EGTA-perfusion or centrifugation are the nuclei (multinucleate cells), microbodies, spheresomes, and mini-vacuoles. At this point it would be pure speculation to suggest which of these organelles is involved. However, ultrastructural studies are presently being conducted, on centrifuged cells, in an attempt to identify the "control" organelle(s) whose redistribution into the centripetal segment is necessary for banding to reoccur. Organelle isolation and purification, using continuous sucrose density gradient centrifugation, will also be employed in an attempt to identify the organelle involved. We may be able to reinstate control $OH^-$ transport function by perfusing the purified organelle(s) back into tonoplast-free cells.

Certainly the removal (destruction) of this organelle in tonoplast-free cells would offer a reasonable explanation for their observed pH profiles. However, the origin of the ligation-induced perturbation of the

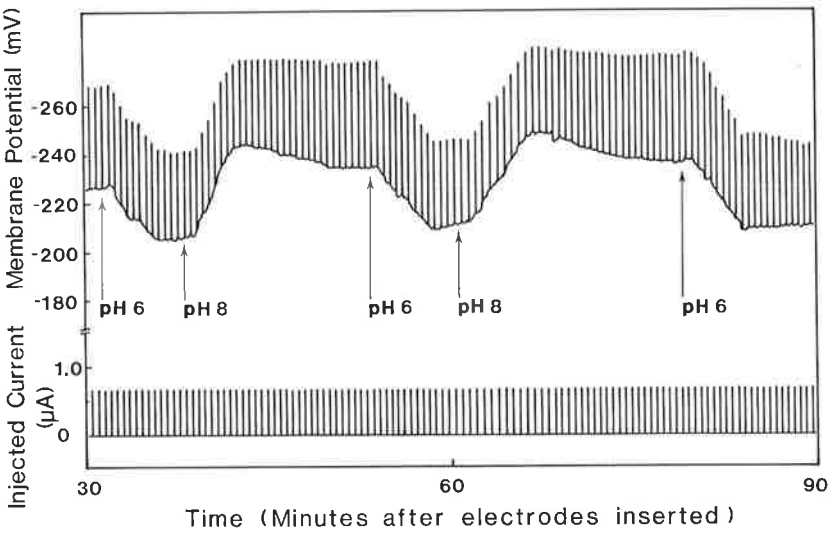


**Fig. 9.** Membrane potential response to changes in $pH_o$. Perfused cell (2 mM ATP, $pH_i = 7.0$) was allowed a 30-min recovery period after electrodes were inserted. The $pH_o$ was then changed from its initial value of 7.0 to 6.0 and 8.0

$OH^-$ efflux pattern remains unknown. Mechanical damage to a local region of the membrane may impair transmission of the control signal. This could be either via a direct effect transmitted along the entire membrane surface, or indirectly through a perturbation of cellular metabolism. Whatever the mechanism, the peturbation is long-lasting, and its existence must serve as a cautionary note to those using the perfusion technique to study ion transport processes.

### *Energy Relations of $OH^-$ Transport*

Although tonoplast-free *Chara* cells did not establish normal $OH^-$ transport bands they did, however, alkalinize the cell surface. This rather weak alkalinization appeared to be ATP-independent. The membrane potential of hexokinase perfused cells was approx. −106 mV (Fig. 7), and this could easily act as the sole driving force for the passive efflux of $OH^-$. Presumably the $OH^-$ ions cross the plasmalemma by carrier-mediated facilitated diffusion. However, it should be stressed that in normal cells, where the $OH^-$ transport control system is functioning, much higher $OH^-$ efflux values are obtained. Extrapolation of the ATP-independence of $OH^-$ transport to the control cell situation should be performed with caution.

### *ATP-Dependency of Membrane Potential in Relation to External pH Profiles*

Cells perfused with ATP-PM of $pH_i$ between 7.5 and 8.25 had surface pH values that went below that of the background value (Fig. 5). This result differs significantly from that observed for ATP-free cells, where a rather simple alkalinization was observed. We suggest that the external pH differences between the ATP and ATP-free cells reflect the operation of an ATP-dependent external acidifying process. The most simple mechanism for this acidification would be an ATP-dependent $H^+$ transport system.

Based on this interpretation of the external pH profiles, one would predict that if the putative ATP-dependent $H^+$ efflux system was the dominant electrical component of the plasmalemma (Kitasato, 1968; Spanswick, 1972; Shimmen & Tazawa, 1977; Keifer & Spanswick, 1978, 1979), at $pH_i$ values above 8.25 the membrane potential should be reduced, since no $H^+$ efflux activity could be detected under these conditions. The results presented in Figs. 5 and 7 indicate that an extremely close correlation was observed between the $pH_i$-induced changes in membrane potential and the external pH profiles. These results are consistent with the earlier reports that the membrane potential (Shimmen & Tazawa, 1977) is dependent on intracellular ATP. Collectively, these results provide extremely strong evidence in support of the electrogenic $H^+$ transport hypothesis (Kitasato, 1968).

### *pH-Stat Hypothesis*

The data presented in Table 2 indicate that in the presence of ATP, the processes occurring within the cytoplasm and at the plasmalemma tend to regulate $pH_i$ towards the region 7.7 to 7.8. This region falls within the range of measured (25 °C) cytoplasmic pH values for internodal cells of *C. corallina* (Raven & Smith, 1978). These data offer general support for the proposed biophysical pH-stat mechanism in *Chara* (*see* Smith & Raven, 1979). In the presence

of ATP, efflux of both $H^+$ and $OH^-$ occurred simultaneously; however, in the absence of ATP, only $OH^-$ efflux occurred. In this latter situation the cytoplasmic pH tended to decline. This may indicate that in normal cells only the efflux of $H^+$ is utilized to regulate the internal pH through some, as yet unidentified sensing mechanism. Alternatively, the removal of $OH^-$ transport control in the tonoplast-free cell could prevent the operation of a cytoplasmic pH regulating signal. Whether two pH stat signals ($H^+$ *and* $OH^-$) exist must remain conjectural.

At, or above, $pH_i$ 8.5 net $H^+$ efflux was not detectable (Fig. 5). Such a response could be due to $pH_i$ inactivation of the ATP-dependent $H^+$ transport system. Alternatively, under these $pH_i$ values the passive $OH^-$ transport component may dominate the electrical properties of the plasmalemma. Since membrane potential and resistance both changed dramatically at slightly lower $pH_i$ values ($>8.0$ and $<8.25$) both alternatives remain possible. With respect to this issue, long-term pH scans indicated that, although $H^+$ efflux was not observed during the first few hours after $pH_i$ 8.5 perfusion, acid regions did eventually develop (Fig. 2). Presumably the passive $OH^-$ efflux system lowered the $pH_i$ value sufficiently to either reduce the $OH^-$ contribution or reactivate the $H^+$ efflux system. In any event, this type of response indicates that the ATP-dependent $H^+$ efflux system is not permanently inactivated by high $pH_i$ treatment.

### *Complex $pH_i$ 7.0 Situation*

The external pH profiles obtained for $pH_i$ 7.0 (Figs. 5 and 6) suggest that a more complex transport situation may exist under these conditions. Since under these conditions the membrane potential has hyperpolarized at $-206 \pm 9$ mV (2 mM ATP-PM 20 $Wm^{-2}$), the reduction in the acidifying trend (*cf.* $pH_i$ 7.5 and 8 of Fig. 5) is presumably not due to an inactivation of $H^+$ transport activity. It is possible that other transport processes, which utilize $H^+$ as a co-substrate, may increase in activity at near neutral $pH_o$ values. Sanders (1980*c*) has recently presented rather compelling evidence in support of a Cl-$2H^+$ cotransport system in *C. corallina*. Chloride transport in normal *Chara* cells has a $pH_o$ optimum around 6.5; influx of this ion may therefore complicate the external pH profile at $pH_o$ 7.5 to 7.0. Presumably $Cl^-$ influx does not occur in the dark (Lucas & Smith, 1976; Sanders, 1980*b*) and this would explain both the more acidic profiles and the enhanced alkalinization of the cytoplasm observed in the dark. This aspect will be further investigated by manipulating external ionic composition (e.g., removal of external $Cl^-$ may remove the light/dark effect on the pH profiles). It should also be noted that alkalization was also accelerated, to some extent, by light in hexokinase-perfused cells ($pH_i$ 7.0) (data not shown).

### *Stability of the Membrane Potential*

Membrane potential measurements indicated that stable potential and resistance values were obtained when the cells were in the hyperpolarized state. These values were stable over periods of more than two hours, and if the perfused cells were given light-to-dark and dark-to-light treatments, the membrane potential (hyperpolarized state only) and resistance responded in a regular manner. Given the acceptance that the pH and electrical data of the present study provide irrefutable evidence for the existence (and function) of an ATP-dependent electrogenic $H^+$ transport system, this stability in membrane potential must indicate that the control process(es), that regulates the $H^+$ efflux activity, has remained intact in the tonoplast-free cell system. This control process may not possess an EGTA-sensitive site. Alternatively, insufficient EGTA may have penetrated into the gel layer to prevent its operation. This aspect could be tested by perfusing cells with a range of EGTA concentrations.

Perhaps a more appealing explanation is that the control process is intimately associated with the inner surface of the membrane; it may form an integral component of the ATP-dependent $H^+$ transport system. This would suggest that quite different regulatory mechanisms exist for what may otherwise appear as closely related phenomena (i.e., $H^+$ efflux and $OH^-$ efflux – which by some is considered to be $H^+$ influx).

### *Perfused Cells as a Physiological Tool*

The results presented in the present study indicate that perfused cells can be used to elucidate important biophysical aspects of the characean cell. However, the perturbative effect of ligation, and the EGTA-induced destruction of at least one transport regulating system, indicates that extreme caution must be used when interpreting data obtained on tonoplast-free cells. We suggest that in future studies an hyperpolarized membrane potential (equivalent to control values) be used as an initial screening criterion for cell usefulness. Many secondary membrane transport processes (e.g., $Cl^-$ influx) may be difficult to investigate using this technique, unless of course they are controlled and regulated in a much simpler manner than that evolved for the $OH^-$ transport process.

This study was supported by a National Science Foundation Grant (PCM 78-10474). The authors wish to thank Professor Masashi Tazawa (Tokyo University) for fostering this cooperation and also for critically reading the manuscript. Preliminary experiments on the occurrence of $OH^-$ extrusion in tonoplast-free cells were done by Tazawa and Shimmen in Tokyo University.

## References

Blinks, L.R. 1935. Protoplasmic potentials in *Halicystis*. IV. Vacuolar perfusion with artificial sap and sea water. *J. Gen. Physiol.* **18**:409

Franceschi, V.R., Lucas, W.J. 1980. Structure and possible function(s) of charasomes; complex plasmalemma-cell wall elaborations present in some characean species. *Protoplasma* **104**:253

Fujii, S., Shimmen, T., Tazawa, M. 1979. Effect of intracellular pH on the light-induced potential change and electrogenic activity in tonoplast-free cells of *Chara australis*. *Plant Cell Physiol.* **20**:1315

Kamiya, N., Kuroda, K. 1957. Cell operation in *Nitella*. I. Cell amputation and effusion of the endoplasm. *Proc. Jpn. Acad.* **33**:149

Kawamura, G., Shimmen, T., Tazawa, M. 1980. Dependence of the membrane potential of *Chara* cells on external pH in the presence or absence of internal Mg.ATP. *Planta (in press)*

Keifer, D.W., Spanswick, R.M. 1978. Activity of electrogenic pump in *Chara corallina* as inferred from measurements of membrane potential, conductance and potassium permeability. *Plant Physiol.* **62**:653

Keifer, D.W., Spanswick, R.M. 1979. Correlation of adenosine triphosphate levels in *Chara corallina* with the activity of the electrogenic pump. *Plant Physiol.* **64**:165

Kikuyama, M., Hamaya, T., Fujii, S., Tazawa, M. 1979. Relationship between light-induced potential change and internal ATP concentration in tonoplast-free *Chara* cells. *Plant Cell Physiol.* **5**:993

Kitasato, H. 1968. The influence of $H^+$ on the membrane potential and ion fluxes of *Nitella*. *J. Gen. Physiol.* **52**:60

Lucas, W.J. 1980. Control and synchronization of $HCO_3^-$ and $OH^-$ transport during photosynthetic assimilation of exogenous $HCO_3^-$. *In:* Plant Membrane Transport: Current Conceptual Issues. R.M. Spanswick, W.J. Lucas, and J. Dianty, editors. p. 317. Elsevier, Amsterdam

Lucas, W.J., Dainty, J. 1977*a*. Bicarbonate assimilation and $HCO_3^-/OH^-$ exchange in *Chara corallina*. *In:* Regulation of Cell Membrane Activities in Plants. E. Marre and O. Ciferri, editors. p. 43. North-Holland, Amsterdam

Lucas, W.J., Dainty, J. 1977*b*. Spatial distribution of functional $OH^-$ carriers along a characean internodal cell: Determined by the effect of cytochalasin B on $H^{14}CO_3^-$ assimilation. *J. Membrane Biol.* **32**:75

Lucas, W.J., Nuccitelli, R. 1980. $HCO_3^-$ and $OH^-$ transport across the plasmalemma of *Chara:* Spatial resolution obtained using extracellular vibrating probe. *Planta (in press)*

Lucas, W.J., Smith, F.A. 1973. The formation of alkaline and acid regions at the surface of *Chara corallina* cells. *J. Exp. Bot.* **24**:1

Lucas, W.J., Smith, F.A. 1976. Influence of irradiance on $H^+$ efflux and $Cl^-$ influx in *Chara corallina:* An investigation aimed at testing two $Cl^-$ transport models. *Aust. J. Plant Physiol.* **3**:443

Lucas, W.J., Spanswick, R.M. Dainty, J. 1978. $HCO_3^-$ influx across the plasmalemma of *Chara corallina:* Physiological and biophysical influence of 10 mM $K^+$. *Plant Physiol.* **61**:487

Nakagawa, S., Kataoka, H., Tazawa, M. 1974. Osmotic and ionic regulation in *Nitella*. *Plant Cell Physiol.* **15**:457

Ogata, K., Kishimoto, U. 1976. Rhythmic change in membrane potential and cyclosis of *Nitella* internode. *Plant Cell Physiol.* **17**:201

Okada, Y., Inouye, A. 1975. Tip potentials and fixed charges on the glass wall of microelectrode. *Experimentia* **31**:545

Raven, J.A., Smith, F.A. 1978. Effect of temperature and external pH on the cytoplasmic pH of *Chara corallina*. *J. Exp. Bot.* **29**:853

Sanders, D. 1980*a*. Control of $Cl^-$ influx in *Chara* by cytoplasmic $Cl^-$ concentration. *J. Membrane Biol.* **52**:51

Sanders, D. 1980*b*. Control of plasma membrane $Cl^-$ fluxes in *Chara corallina* by external $Cl^-$ and light. *J. Exp. Bot.* **31**:105

Sanders, D. 1980*c*. The mechanism of $Cl^-$ transport at the plasma membrane of *Chara corallina*. I. Cotransport with $H^+$. *J. Membrane Biol.* **53**:129

Shimmen, T. 1978. Dependency of cytoplasmic streaming on intracellular ATP and $Mg^{2+}$ concentrations. *Cell Struct. Funct.* **3**:113

Shimmen, T., Kikuyama, M., Tazawa, M. 1976. Demonstration of two stable potential states of plasmalemma of *Chara* without tonoplast. *J. Membrane Biol.* **30**:249

Shimmen, T., Tazawa, M. 1977. Control of membrane potential and excitability of *Chara* cells with ATP and $Mg^{2+}$. *J. Membrane Biol.* **37**:167

Smith, F.A., Raven, J.A. 1979. Intracellular pH and its regulation. *Annu. Rev. Plant Physiol.* **30**:289

Spanswick, R.M. 1972. Evidence for an electrogenic ion pump in *Nitella translucens*. I. The effect of pH, $K^+$, $Na^+$, light and temperature on the membrane potential and resistance. *Biochim. Biophys. Acta* **288**:73

Tazawa, M. 1964. Studies on *Nitella* having artificial cell sap. I. Replacement of cell sap with artificial solutions. *Plant Cell Physiol.* **5**:33

Tazawa, M. 1975. Cytoplasmic streaming and ionic regulation in *Nitella flexilis* having artificial cell saps of a low ionic strength. *Bot. Mag. Tokyo* **88**:219

Tazawa, M., Kikuyama, M., Shimmen, T. 1976. Electric characteristics and cytoplasmic streaming of characean cells lacking tonoplast. *Cell Struct. Funct.* **1**:165

Tazawa, M., Kishimoto, U. 1964. Studies on *Nitella* having artificial cell sap. II. Rate of cyclosis and electric potential. *Plant Cell Physiol.* **5**:45

Tazawa, M., Kishimoto, U. 1968. Cessation of cytoplasmic streaming of *Chara* internodes during action potential. *Plant Cell Physiol.* **9**:361

Tazawa, M., Shimmen, T. 1980*a*. Action potential in Characeae: Some characteristics revealed by internal perfusion studies. *In:* Plant Membrane Transport: Current Conceptual Issues. R.M. Spanswick, W.J. Lucas, and J. Dainty, editors. p. 349. Elsevier, Amsterdam

Tazawa, M., Shimmen, T. 1980*b*. Control of electrogenesis by ATP, $Mg^{2+}$, $H^+$ and light in perfused cells of *Chara*. *In:* Electrogenic Ion Pumps. C.L. Slayman, editor. Academic Press, New York (*in press*)

Walker, N.A. 1980. The transport systems of Charophyte and Chlorophyte giant algae and their integration into modes of behavior. *In:* Plant Membrane Transport: Current Conceptual Issues. R.M. Spanswick, W.J. Lucas, and J. Dainty, editors. p. 287. Elsevier, Amsterdam

Williamson, R.E. 1975. Cytoplasmic streaming in *Chara:* A cell model activated by ATP and inhibited by cytochalasin B. *J. Cell Sci.* **17**:655

Received 8 July 1980; revised 30 September 1980

JOURNAL OF ULTRASTRUCTURE RESEARCH 75, 218–228 (1981)

# The Glycosome of *Chara*: Ultrastructure, Development, and Composition

V. R. FRANCESCHI AND W. J. LUCAS[1]

*Department of Botany, University of California, Davis, California 95616*

*Received January 6, 1981*

Certain membrane-bound inclusions which we have called glycosomes are a common feature of both young and mature cells of *Chara corallina*. Glycosomes are spherical in form, bound by a unit membrane, and contain a fine, granular, electron-opaque material. The glycosomes are derived from dictyosomes, initially as large vesicles containing a granular material. They apparently reach their full size some time after release from the dictyosome cisternae. Addition of material through fusion of smaller dictyosome-derived vesicles to the young glycosome is indicated by TEM observations. The silver methenamine staining technique for polysaccharides gives positive proof of the polysaccharide nature of the material within the glycosome. The contents of the glycosome stained intensely for polysaccharides, as did the contents of some of the associated dictyosome vesicles. Staining did not occur in sections of nonosmicated tissues which were not oxidized or in oxidized sections treated with an aldehyde blocking reagent (dimedone) prior to staining.

The giant alga *Chara* is often used for physiological experimentation due to the large size of individual cells. Knowledge of the ultrastructural features of this alga is essential in developing a more complete understanding of its physiology. Some very good developmental ultrastructural work has been done with young tissues of *Chara fibrosa* by Pickett-Heaps (1967a, b, 1968a, b). However, because of the difficulty in preparing this alga for TEM observation, many questions remain unanswered regarding the structure–function relationships of some of the unique ultrastructural features observed. The charasome, perhaps one of the most unusual ultrastructural features unique to *Chara*, has only recently been described in detail (Franceschi and Lucas, 1980, 1981, Lucas and Franceschi, 1981). This complex plasma membrane structure has special significance with respect to the numerous transmembrane transport studies carried out on this alga, which emphasizes the need for a more complete characterization of the ultrastructure of the Characeae.

During our recent investigations on the charasome, unusual membrane-bound inclusions were found to be a prominent feature of *Chara* tissues. Similar structures were reported by Pickett-Heaps (1967a) which he referred to as spherosome-like inclusions. The origin and composition of these structures has not previously been determined. We have recently found that these bodies contain a polysaccharide material. The following is a report of our examination of the structure, development, and composition of this body, which, based on its glycan composition, we will call a glycosome.

## MATERIALS AND METHODS

*TEM preparation.* Shoots, branches, and internodal cells of *Chara corallina* from laboratory cultures were fixed for electron microscopy as previously described (Franceschi and Lucas, 1980). Some tissues to be used for polysaccharide localization were not given an osmium tetroxide postfixation. Thin sections were stained with saturated methanolic uranyl acetate for routine observation and examined on a JEOL JSM 100S TEM.

*Polysaccharide localization.* Localization of polysaccharide in sectioned tissue was done using the silver methenamine method as outlined by Hayat (1975). This stain reacts with aldehydes, produced by periodic

[1] To whom reprint requests and correspondence should be addressed.



0022-5320/81/050218-11$02.00/0
Copyright © 1981 by Academic Press, Inc.
All rights of reproduction in any form reserved.

acid oxidation of vicinal hydroxyl groups of sugars (in polysaccharides), to form an electron-dense silver deposit. The stain solution was made fresh just prior to use by mixing 0.3 g of hexamethylenetetramine in 12 ml of glass-distilled water with 8 ml of 5% sodium borate and 10 ml of 0.25% silver nitrate (all percentage values given as w/v). Sections on nickel grids were stained by floating on the stain solution for 1 hr at 60°C in the dark. After staining, the grids were washed with glass-distilled water, floated on drops of 0.5% sodium thiosulfate for 5 min at 22°C to remove nonspecific silver deposits, and then washed thoroughly with distilled water. Sections of osmicated tissue were prepared as follows prior to staining: (1) No pretreatment, (2) periodic acid oxidation, (3) $H_2O_2$ oxidation, (4) $H_2O_2$ oxidation followed by dimedone blocking. Sections of nonosmicated tissue were prepared as follows prior to staining: (1) No pretreatment, (2) periodic acid oxidation, (3) periodic acid oxidation followed by dimedone blocking. Oxidations were done by floating the grids on drops of 10% $H_2O_2$ or 1% periodic acid for 30 min at 22°C. Following thorough washing, some of the sections were incubated in a saturated solution of dimedone (5,5-dimethyl-1,3-cyclohexanedione) in 1% acetic acid for 1 hr at 60°C to block aldehyde groups prior to staining.

## RESULTS

### *Ultrastructure*

Spherical bodies of various types are common in almost all cells of the *Chara* thallus (Fig. 1). A distinction shall be made between the three most common bodies, other than the mitochondria and chloroplasts. One type of spherical body has a homogeneous appearance and no limiting membrane (Figs. 1 and 2) and is assumed here to be lipoidal in nature. The lipid bodies become much larger than the other spherical bodies which shall be described. A second type of spherical body is identical in appearance to higher plant microbodies. This body is membrane bound and has a coarse granular matrix (Fig. 1) often containing a crystalline structure. The third type of spherical body, the glycosome, which is the subject of this paper, is also membrane bound and has an electron-dense matrix of variable appearance (Figs. 1–3). The membrane of the glycosome has a distinct wavy appearance and stains quite intensely (Fig. 3). The enclosed material has a fine granular texture and there is usually an electron-lucent space between this material and the bounding membrane. (This space is thought not to be due to an artifact of fixation.) This material stains quite homogeneously in mature glycosomes but can show regions of varying density in younger glycosomes. Glycosomes are very numerous in nodal, branch, and internodal cells of all ages and they reach a maximum diameter of about 1.2 $\mu$m (range 0.4–1.2 $\mu$m).

### *Development*

Glycosome development was followed and found to be the same in both young internodal and nodal cells. In young cells, identifiable glycosomes are most often associated with the numerous dictyosomes

FIG. 1. Section through seven glycosomes (G), microbody (MB), lipid droplet (L), and mitochondrion (M) in the streaming cytoplasm of an internodal *Chara* cell. × 33 000.

FIG. 2. Lipid droplet (L) and glycosome (G). Note lipid drop has no limiting membrane and stains less intensely than the glycosome. × 72 000.

FIG. 3. Large glycosome showing characteristic waviness of limiting membrane and space between membrane and enclosed material. Note membrane appears thicker and stains more intensely than that of the ER (arrows). × 72 000.

FIG. 4. Glycosome (G) associated with dictyosome and vesicles containing material that appears to be loosely fibrillar in nature (open arrows) and some vesicles that appear to be of a more dense, granular nature (closed arrows). × 36 000.

FIG. 5. Swollen dictyosome cisternal end (arrow) containing material similar to that of adjacent small glycosome (G). × 59 000.

FIG. 6. Oblique section through dictyosome showing reticulate pattern and fibrils within associated vesicles. × 59 000.

FIG. 7. Coated vesicles containing fine granular material similar to that in nearby glycosomes (G). Larger granules can be distinguished within matrix of glycosome in upper left. × 82 000.

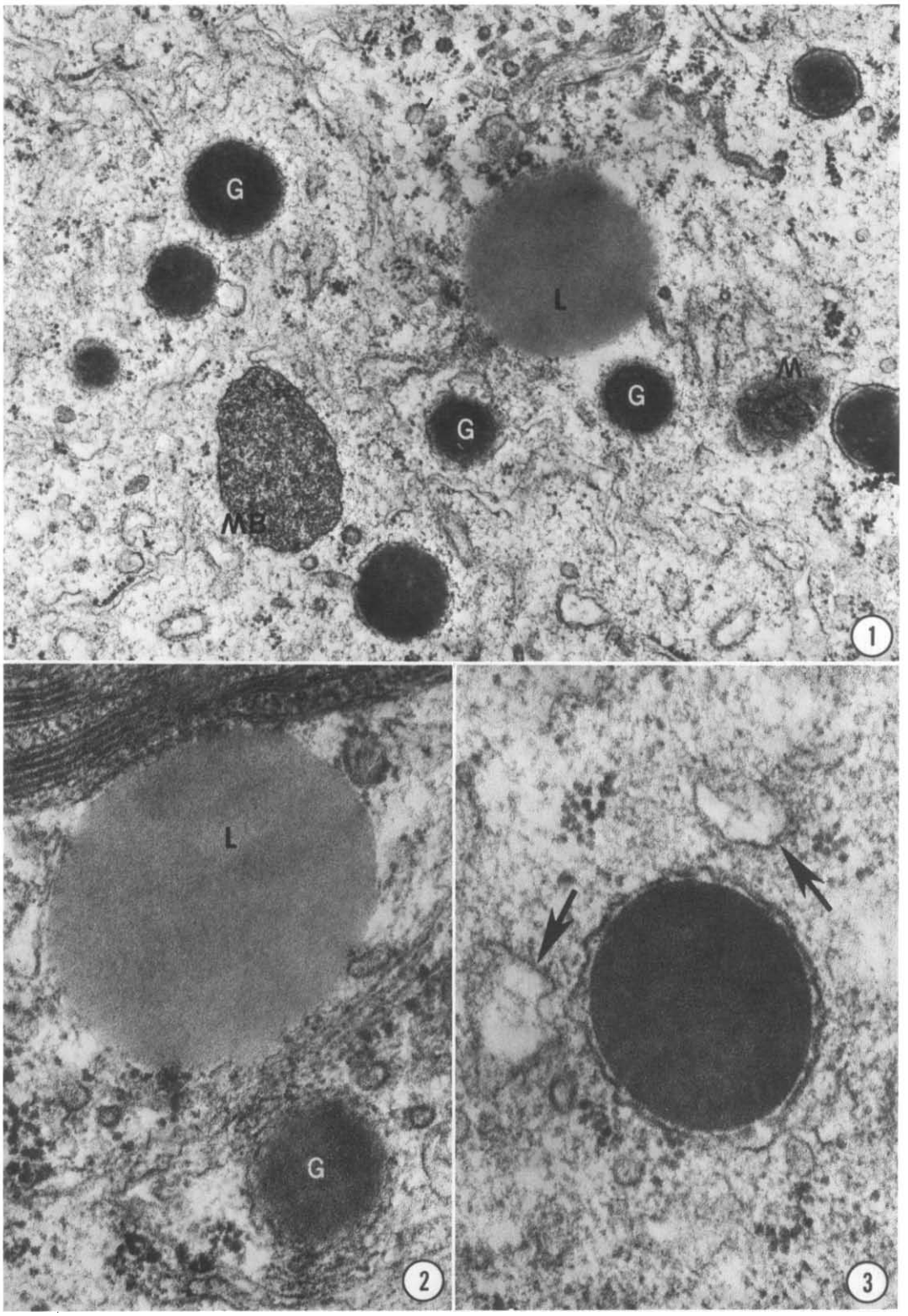
G
L
G
G
M
MB
1
L
G
2
3

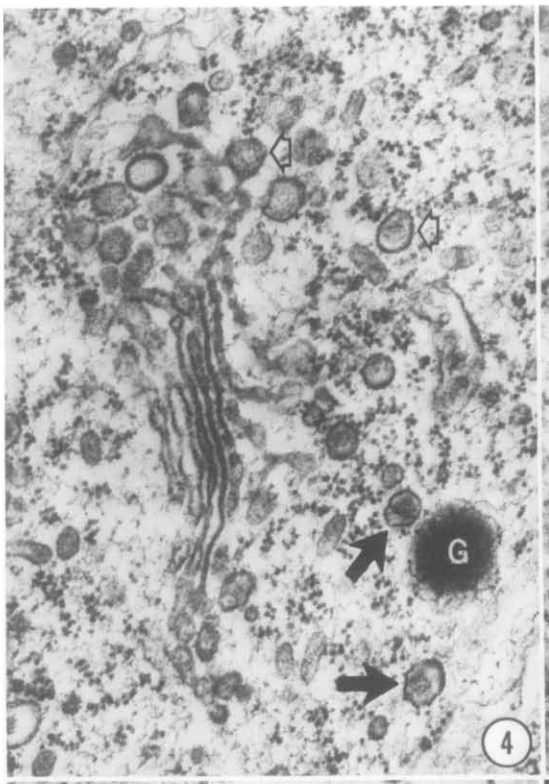
G
4

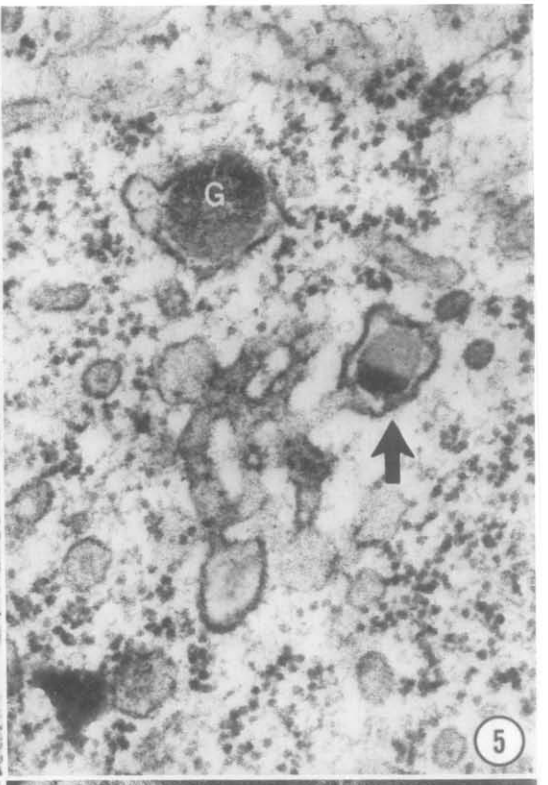
G
5

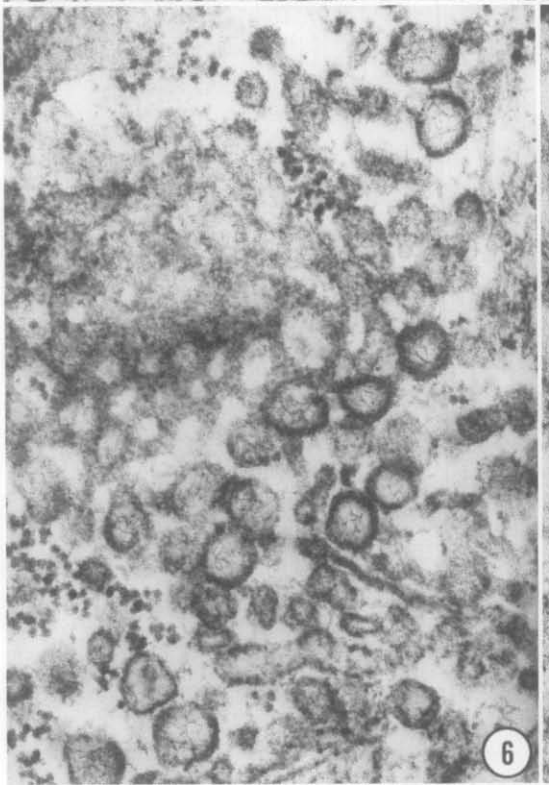
6

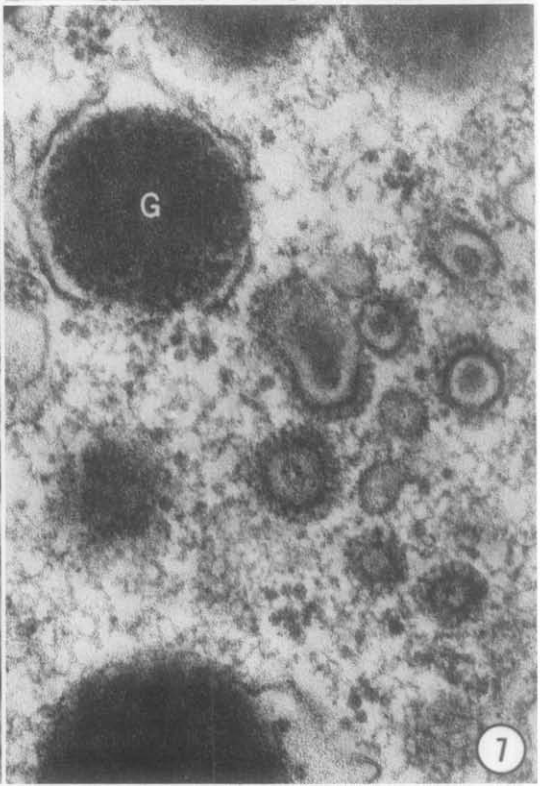
G
7

present (Fig. 4). The glycosomes were found to originate from the dictyosomes. Vesicles produced by many of the dictyosomes could be seen to contain a substance similar in appearance to that in the mature glycosome (Fig. 4). Larger vesicles containing such material could sometimes be found still connected to the dictyosome (Fig. 5). Such large vesicles have a space between the membrane and enclosed material and also have a wavy membrane profile, features which we feel are characteristic of the glycosome. The glycosome membrane and dictyosome vesicle membrane have the same thickness and density of staining. These membranes appear thicker than the membranes of other organelles, including the endoplasmic reticulum (Fig. 3), an observation which supports the concept of a dictyosomal origin of the glycosome. While vesicles derived from a particular dictyosome can contain either fibrillar (Figs. 4 and 6) or granular (Figs. 4 and 5) material, it must be noted that the material in the glycosomes has a distinct granular appearance in all planes of section. Occasionally the material appears to be made of distinct large granules (Fig. 7) which may be compacted to form the homogeneous matrix normally observed in the mature glycosome. It is not known whether the fibrillar material seen in some dictyosome vesicles is incorporated into the glycosome material. In some instances coated vesicles containing dense material were found associated with the glycosomes (Fig. 7). These vesicles are not the same as the much smaller coated vesicles commonly found associated with the dictyosomes and plasma membrane (Lucas and Franceschi, 1981).

Developing glycosomes probably become detached from the dictyosome at an early stage in their formation. We base this statement on the observations that small glycosomes can be found in regions of cytoplasm remote from dictyosomes and in no instance was a large glycosome seen still attached to a dictyosome. TEM observations indicate that addition of material to the glycosome is most likely to be by fusion of small dictyosome-derived vesicles to the developing glycosome (Figs. 8–10). Often the glycosomal membrane has a profile which could easily be envisioned as the result of fusion to it of small vesicles (Figs. 9 and 10); budding of the glycosome membrane could give similar profiles. Such glycosomes generally have regions of varying density (Figs. 8–10). A few observations indicative of fusion of more mature glycosomes were made (Fig. 11), but were rare.

*Composition*

Glycosomes stain intensely for polysaccharide when the silver methenamine staining technique is used. When controls were run to determine the specificity of the reaction, it became apparent that osmium tetroxide fixation causes certain structures to become reactive to the stain prior to oxidation with periodic acid. In nonoxidized osmicated sections the glycosomes stain intensely (Fig. 12). This staining can be partially reduced if the sections are treated with hydrogen peroxide prior to staining (Fig. 13), which removes osmium from the sections. When sections are treated with $H_2O_2$ and dimedone (an aldehyde blocking agent) prior to staining, reactivity of the glycosomes to the stain is further reduced (Fig. 14). Glycosomes in sections of nonosmicated tissue show virtually no staining when the tissue has not been oxidized with periodic acid (Fig. 15). If the sections are oxidized with periodic acid, the glycosomes become very reactive to the polysaccharide stain (Fig. 16). This reactivity is completely blocked by treatment of the sections with dimedone after periodate oxidation, but prior to staining (Fig. 17). These results show that the glycosome is indeed composed of polysaccharide material. The staining seen in nonperiodated osmicated tissues is probably due partly to oxidation of polysaccharides by $OsO_4$ and partly to reaction of osmium with the polysaccharide stain. One further comment must be made

concerning the use of osmicated tissue with this technique. While the mature glycosomes stain intensely after periodation the lipid bodies, which are osmiophilic, show no staining (Fig. 18). Periodic acid oxidation removes osmium from the sections, but unlike $H_2O_2$ it also oxidizes the polysaccharides. The fact that in osmicated sections the lipid bodies do not stain after periodation while the glycosomes do, is further proof of the specificity of the silver methenamine stain.

The polysaccharide staining technique was used to further study developmental aspects of the glycosome. Osmicated tissue was used because nonosmicated tissue showed poor ultrastructural preservation. Dictyosomes in close association with glycosomes were examined carefully to determine distribution of polysaccharide material (Fig. 19). Many of the vesicles attached to, or closely associated with the dictyosomes, contained reactive material (Fig. 19). The larger vesicles, sometimes still attached to the dictyosome cisternae, were especially reactive (Fig. 20). Such vesicles are almost certainly the early glycosome precursors. One can compare Figs. 19 and 20 with Figs. 4 and 5, respectively, to see this relationship. The results of the polysaccharide staining are consistent with the previously introduced developmental aspects of the glycosomes.

## DISCUSSION

Our present results have helped to partially characterize an ultrastructural feature of *Chara* whose function and composition was formerly unknown. We feel that the term glycosome is most appropriate for this structure. This term refers to a body or structure which is primarily involved in some way with glycans. The silver methenamine method for polysaccharide localization has shown quite clearly that this structure contains polysaccharides with glycol groups, as do certain glycans. The glycosome has been referred to as a spherosome (Franceschi and Lucas, 1980) or as spherosome-like (Pickett-Heaps, 1967a) due to structural similarities to other plant spherosomes. These appear to be misnomers, in this case, since plant spherosomes are normally considered to be involved in fat metabolism (Robards, 1970) and are thought to be derived from the ER (Frey-Wyssling *et al.*, 1963) and not from the dictyosome as is seen with the glycosome.

It is often difficult to reconstruct dynamic developmental sequences from static micrographs. However, the observations made during this study provide quite convincing evidence for the role of the dictyosome in glycosome formation. Dictyosome vesicles, some still attached to cisternae, and glycosomes both contain material of

FIG. 8. Close association of glycosome and vesicles containing dense material. Note heterogeneity of material within the glycosome. × 84 000.

FIG. 9. Membrane profile of this glycosome shows three bulges similar in size to vesicles associated with glycosome in Fig. 8. × 84 000.

FIG. 10. Glycosome with bulge in membrane. In close proximity to the bulge is a small vesicle containing material similar to that in the glycosome. × 84 000.

FIG. 11. Irregular shaped glycosome apparently formed by fusion of three separate, smaller glycosomes. Continuity of membranes surrounding the three parts is evident (arrow). × 84 000.

FIGS. 12–17. Thin sections of *Chara* stained by the silver methenamine technique. No other poststain. × 79 000.

FIG. 12. Osmicated; no oxidation.

FIG. 13. Osmicated; $H_2O_2$ oxidation.

FIG. 14. Osmicated; $H_2O_2$ oxidation and dimedone blocking.

FIG. 15. Nonosmicated; no oxidation.

FIG. 16. Nonosmicated; periodic acid oxidation.

FIG. 17. Nonosmicated; periodic acid oxidation and dimedone blocking.

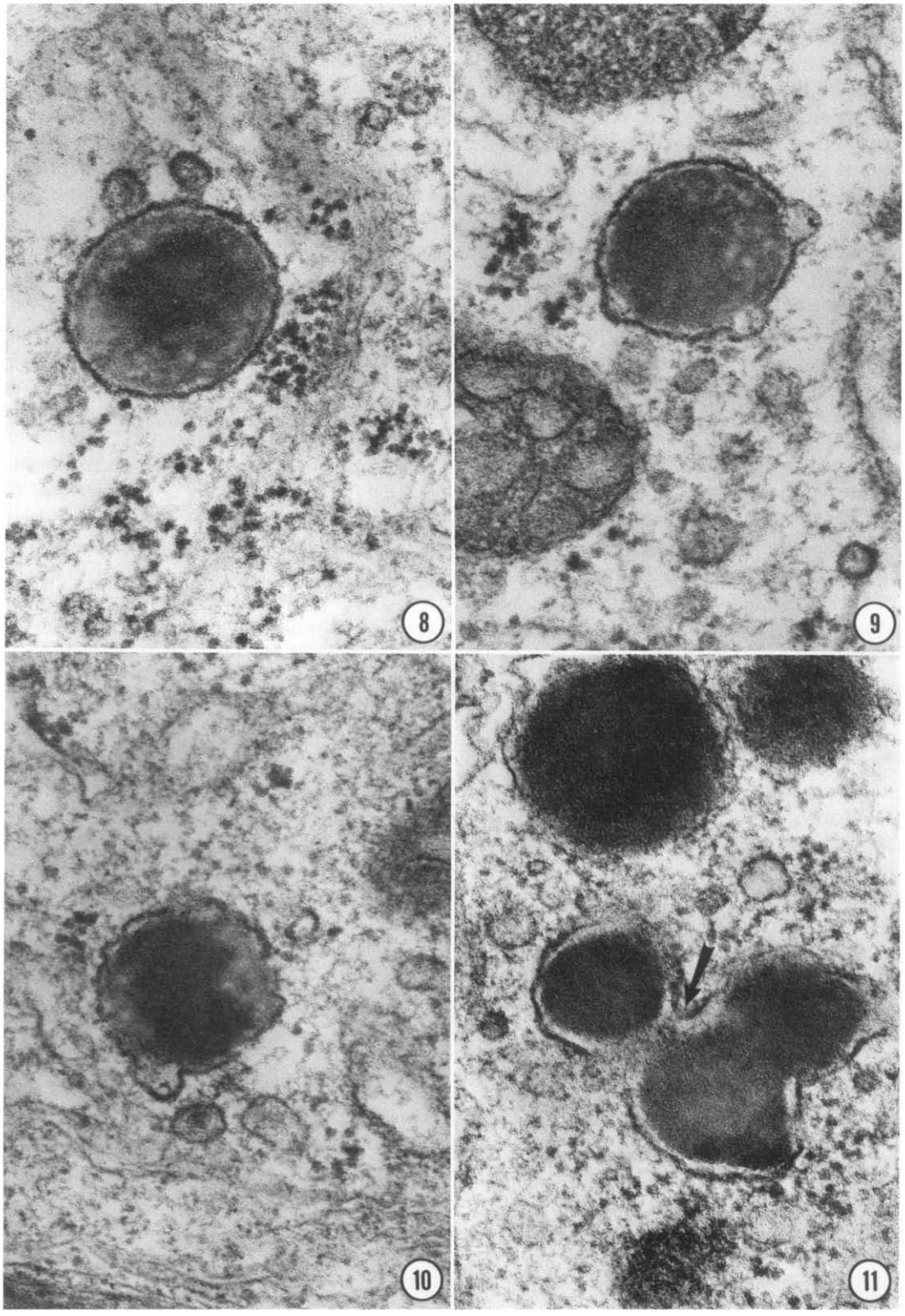
8
9
10
11

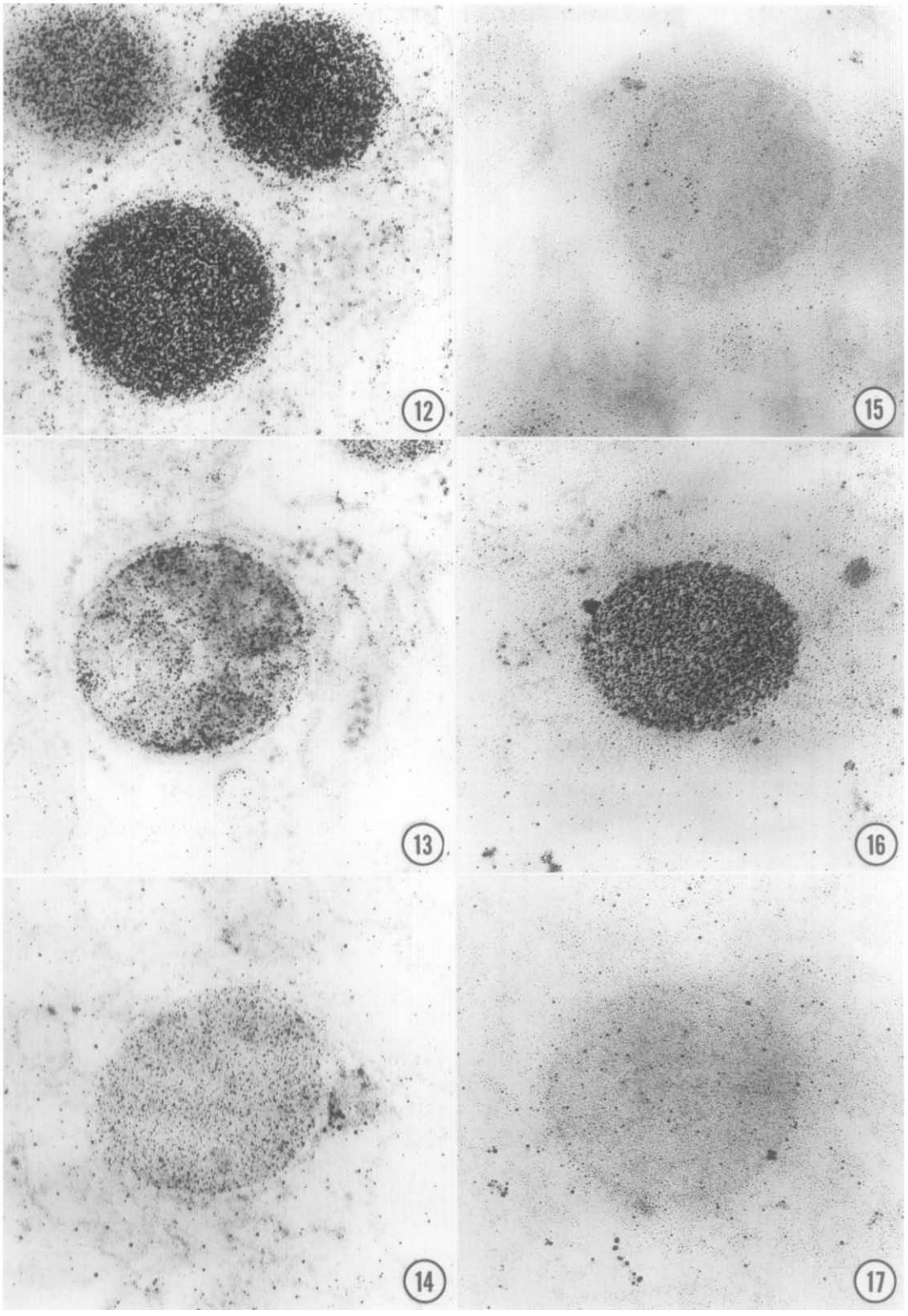
12
15
13
16
14
17

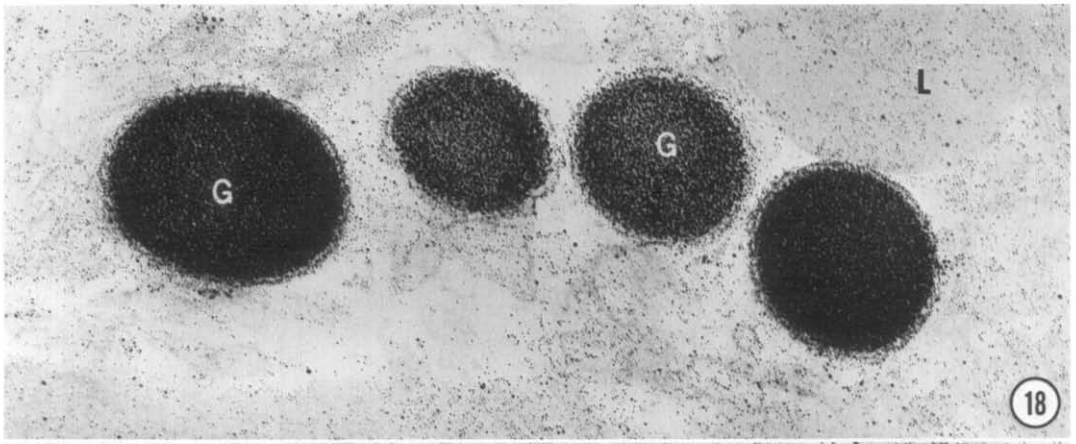
G
G
L
18

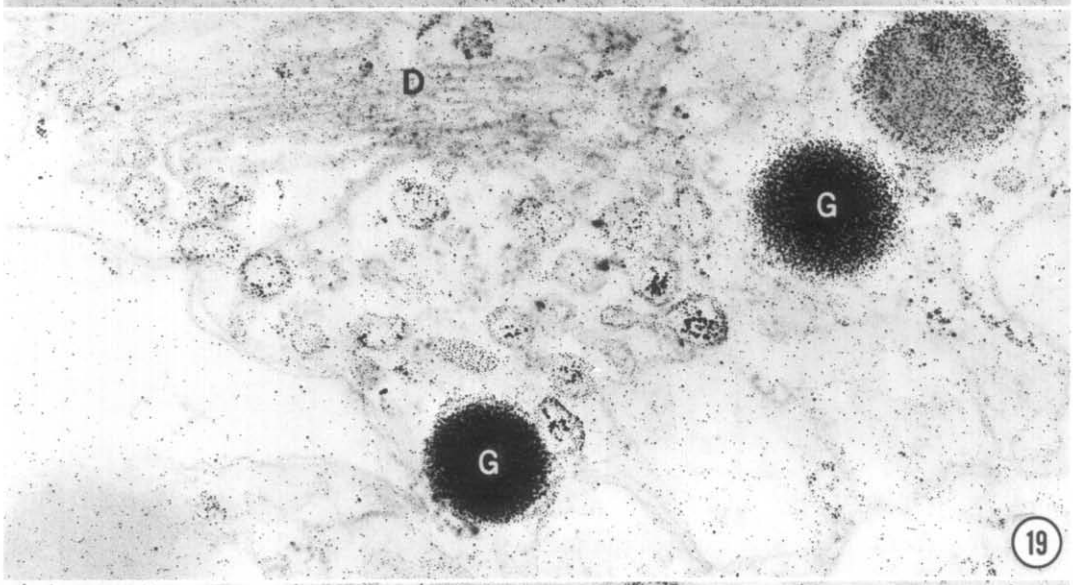
D
G
G
19

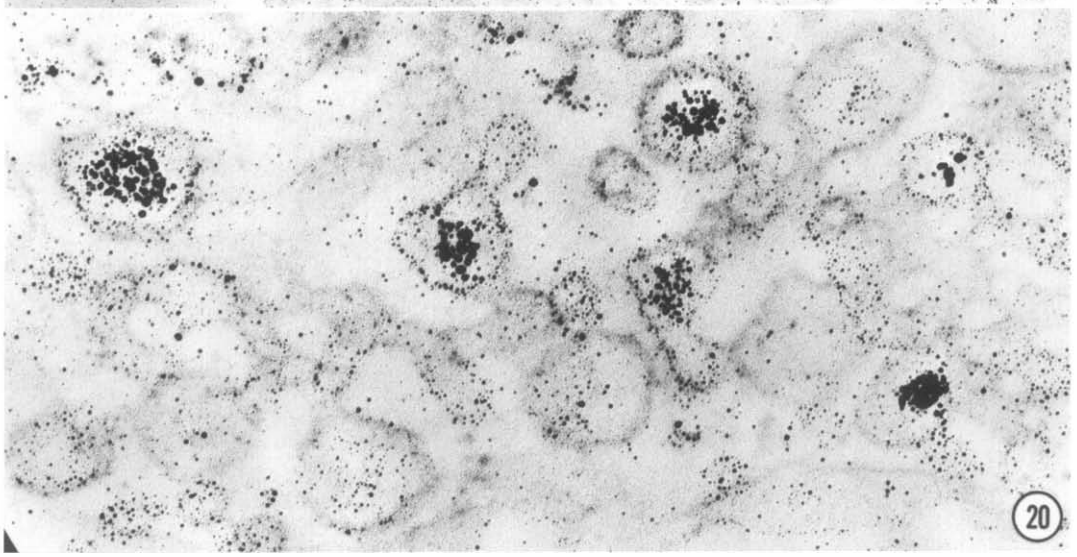
20

similar appearance when stained with uranyl acetate and of similar composition as shown by the silver methenamine technique. Additionally, the membranes of the dictyosome vesicles and glycosomes are of the same thickness and density of staining while other membranes, including the ER, appear thinner.

The glycosomes do not appear to acquire full size while attached to the dictyosomes. During examination of hundreds of glycosomes, connections between dictyosomes and mature glycosomes were never observed. It is more likely that once detached from the dictyosome, large vesicles which are to become glycosomes acquire more material by fusion of smaller dictyosomal-derived vesicles to their surfaces. It is possible that the developing glycosomes contain the enzymes necessary for uptake and polymerization of sugars into polysaccharides.

Although we can say that the glycosome does contain polysaccharide material, the complete function of this organelle is not known at this time. The glycosome is found in mature internodal cells and in such instances may be considered as a storage body. It may play a far more dynamic role in the rapidly growing young cells of the vegetative shoot. In these cells glycosomes are often found in very high concentrations, usually as groups of many glycosomes rather than evenly distributed throughout the cytoplasm. Perhaps the glycosomes provide a means of concentrating material for wall precursors to be used during the later rapid expansion which these cells undergo. But again it must be emphasized that glycosomes are numerous in cells of all ages and no evidence of their breakdown has been observed during the present investigation.

Membrane-bound bodies of a somewhat similar appearance to the glycosome have been found to be involved in release of material from manubrial cells into the antheridium of *Chara* (Pickett-Heaps, 1968b). A similar membrane-bound body is seen during the development of the zoospore of *Oedogonium,* but this body was not particularly reactive to polysaccharide stains (Pickett-Heaps, 1971). In both instances these bodies appeared to be derived from the dictyosome. This is not surprising, considering the known role of dictyosomes in formation or packaging of wall precursors, mucilage, and protein substances; the product being highly dependent upon cell type. We feel the glycosome is not the same structure as seen in the developing manubrial cells. Release of glycosome contents into the wall was never seen in meristematic, developing, or mature cells of the nodal complex or internodes. Also, the mature glycosome is generally larger than the bodies of the manubrial cells.

The glycosome has been shown here to be derived from the dictyosome and contain a polysaccharide matrix. It is possible that the glycosome is a storage body for polysaccharides. Further work must be done to determine the actual function of this body. Attention will be focused on examining cells cultured under various conditions. If the glycosomes are storage bodies, conditions which stress the cells for carbohydrate should reduce glycosome formation.

This work was supported by a grant from the National Science Foundation (PCM 78-10474). V. R. Franceschi also gratefully acknowledges the support of a University of California Regents Fellowship.

FIGS. 18–20. Osmicated tissue sections oxidized with periodic acid and stained by the silver methenamine technique. No other poststain was employed.

FIG. 18. Electron-opaque material of the glycosomes (G) stains intensely but lipid bodies (L) show only slight nonspecific silver precipitation. × 53 000.

FIG. 19. A dictyosome (D) with associated vesicles and three glycosomes (G). Reaction product is clearly localized in the dictyosomal vesicles and within the glycosomes. Compare with Fig. 4. × 53 000.

FIG. 20. Section through a portion of a dictyosome. Heavy staining is found within the larger vesicles. Section is comparable with that presented in Fig. 5. × 106 000.

## REFERENCES

FRANCESCHI, V. R., AND LUCAS, W. J. (1980) *Protoplasma* **104,** 253–271.

FRANCESCHI, V. R., AND LUCAS, W. J. (1981) *Protoplasma,* in press.

FREY-WYSSLING, A., GRIESHABER, E., AND MÜHLETHALER, K. (1963) *J. Ultrastruct. Res.* **8,** 506–516.

HAYAT, M. A. (1975) Positive Staining for Electron Microscopy, Van Nostrand Reinhold, New York.

LUCAS, W. J., AND FRANCESCHI, V. R. (1981) *Protoplasma*, in press.

PICKETT-HEAPS, J. D. (1967a) *Aust. J. Biol. Sci.* **20,** 539–551.

PICKETT-HEAPS, J. D. (1967b) *Aust. J. Biol. Sci.* **20,** 883–894.

PICKETT-HEAPS, J. D. (1968a) *Aust. J. Biol. Sci.* **21,** 255–274.

PICKETT-HEAPS, J. D. (1968b) *Aust. J. Biol. Sci.* **21,** 655–690.

PICKETT-HEAPS, J. D. (1971) *Protoplasma* **72,** 275–314.

ROBARDS, A. W. (1970) Electron Microscopy and Plant Ultrastructure, McGraw-Hill, London.

Plant Physiol. (1981) 68, 553–559
0032-0889/81/68/0553/07/$00.50/0

# Influence of Turgor Pressure Manipulation on Plasmalemma Transport of $HCO_3^-$ and $OH^-$ in *Chara corallina*[1]

Received for publication December 30, 1980 and in revised form March 23, 1981

WILLIAM J. LUCAS AND JON M. ALEXANDER
*Department of Botany, University of California, Davis, California 95616*

## ABSTRACT

**A modified version of the osmotic shock technique was used to investigate $HCO_3^-$ and $OH^-$ transport in the alga *Chara corallina*. Cell turgor was brought close to zero and then restored. When turgor was reduced to near the plasmolytic point using an osmoticum, little effect was observed on $H^{14}CO_3^-$ assimilation and $OH^-$ transport. However, when turgor was recovered in these cells, there was a large reduction in $HCO_3^-$ and $OH^-$ transport activity. In contrast, when cells were air-dried to zero turgor, and rewetted to restore turgor, no significant effect on $OH^-$ transport was observed.**

**The effect of plasmolysis was also studied. When *Chara* cells were plasmolyzed, in most cases, all $OH^-$ transport activity was lost and acidification was observed along the cell surface.**

**None of the above treatments had any long term effect on cyclosis. These results are discussed with respect to present concepts of turgor-induced changes in membrane functions.**

In recent years, several research groups have focused their attention on the manner in which plant cells regulate their turgor pressure. Zimmermann and his colleagues (7, 8, 23, 24) have presented an hypothesis which suggests that the main turgor-sensing mechanism involves changes in the thickness of the plasmalemma. According to these workers, there is a "normal" thickness, at which there are no corrections for turgor; however, when the membrane is too thin, the cell will attempt to relieve the turgor. Alternatively, when it is too thick, signals are generated that result in an increase in turgor. Thickness-dependent interactions between intrinsic and extrinsic membrane proteins are suggested as a likely mechanism by which absolute membrane thickness is transduced into a biological signal. If the membrane were too thin, more sites would be exposed on the intrinsic proteins as they are not as "submerged" within the lipid portion of the membrane, and these would be involved in turgor reduction. Alternatively, if the membrane were too thick, the functional sites on the intrinsic proteins would be covered by lipid, and this would induce the activation of transport or other processes involved in developing an increase in turgor (via an increase in the osmotic pressure of the cell).

The main supporting evidence for this hypothesis was obtained from dielectric breakdown studies conducted on biological membranes. Zimmermann *et al.* (23) noted that as the turgor in *Valonia*, a marine alga, was increased, the voltage required for dielectric breakdown decreased, and vice versa. Inasmuch as they assumed that the membrane was essentially a uniform insulator, these results implied that the membrane thickness was changing and that the resulting insulatory properties were also changing. A clear implication of this hypothesis is that there must be responses when the membrane reaches certain critical thickness.

Bisson and Gutknecht (3) present an alternative hypothesis concerning possible turgor-sensing mechanisms. They suggest that in the normal state of turgor the membrane is not a planar surface, but that it is pressed against and stretched across the cell wall microfibrils. This would give rise to a convoluted surface, with tension in the membrane in the regions between the microfibrils and compression at the microfibrils of the cell wall.

In the marine algal system *Valonia* that these workers used, an increase in the external osmotic pressure would lower the turgor pressure and reduce the stresses experienced by the plasmalemma. As the turgor pressure approached zero, the membrane would become more planar in nature. Bisson and Gutknecht (3) present several ways in which various turgor-related changes in the membrane/cell wall environment could result in an error signal which would bring about turgor regulation.

Both of these general turgor regulation hypotheses involve changes in the physical forces that act across and within the plasmalemma. We felt it important to determine whether the effect of such changes act specifically on transport processes that are directly linked to osmotic adjustment, or whether a more general modulation of membrane transport occurs. We decided to investigate the influence of turgor pressure manipulation on plasmalemma-bound transport systems that are unlikely to be directly involved in cellular osmotic pressure adjustment (*i.e.* turgor regulation). In the present study we report the effect of such changes on $HCO_3^-$ assimilation by internodal cells of the giant alga, *Chara corallina*. We found that reduction of turgor by air drying the cells and subsequent rehydration did not cause significant changes in the transport of either $HCO_3^-$ or $OH^-$. When an osmoticum was used to reduce the turgor and the turgor was subsequently restored, a large reduction in transport ability of these ions occurred. These results are discussed with respect to the present concepts on turgor-induced changes in membrane functions.

## MATERIALS AND METHODS

**Culture Material.** The culture material of *C. corallina* Klein ex Willd., em, R.D.W. (*C. australis* R. Br.) was grown in the laboratory in 100-liter Nalgene containers with Plexiglas lids. The culture medium contained 1 to 2 mM $Na^+$, 0.2 mM $K^+$, 0.2 mM $Ca^{2+}$, 1 to 2 mM $Cl^-$, and 2 mM $HCO_3^-$. Fluorescent lighting (Sylvania Lifeline, 30 w) was used with the intensity at the surface of the culture medium being between 17 and 20 w $m^{-2}$. A light regime of 13 h light, 11 h dark was employed, and the tanks were housed in a thermostated laboratory in which the temperature was 25 C (±3).

On the afternoon prior to an experiment, the third to fifth internodal cells were cut free from the rest of the plant body, and the whorl (branch) cells removed to give single or double inter-

[1] Supported by National Science Foundation Grant PCM 78-10474.

nodal cell sets. These isolated cells were placed in a CPW/B[2] solution (see below for composition) having a pH value of either 8.0 or 9.2, depending on the type of experiment in which the cells were to be used. After a 1-h recovery in this solution, cells were rinsed in at least three changes of the solution and then left under fluorescent lights (10 w $m^{-2}$) for the remainder of the afternoon. Cut cells were given a normal dark period and at least 1 h of illumination before an experiment was begun the next morning.

**Experimental Solutions.** All solutions were prepared using double glass-distilled water. The CPW/B contained 1 mM NaCl, 0.2 mM $CaSO_4$, 0.2 mM KCl, and 1 mM $NaHCO_3$. Sorbitol, mannitol, and sucrose were used as osmotica. The osmolality of all solutions was determined using a vapor pressure osmometer (Wescor, Inc., model 5130, Logan, UT). This instrument was calibrated daily using standard NaCl solutions. All chemicals used were Analar reagent grade and were not further purified.

**Cytoplasmic Streaming Procedure.** After 1 h illumination under fluorescent lights, cells were placed in experimental solutions and the rate of streaming monitored every 10 min. The rate was determined by timing one of the particles in the streaming cytosol over a distance of 1 mm while being observed at × 30 magnification under a dissecting microscope (Bausch and Lomb, zoom binocular type). All rates are expressed in meters $s^{-1}$. After cytoplasmic streaming had stabilized (as evidenced by a constant rate), the bathing solution was changed to that required by the particular experiment, and the rate monitored until it restabilized.

**General $^{14}$Carbon Experimental Procedure.** Bicarbonate and $CO_2$ assimilation studies were performed using techniques developed by Lucas (13) and Lucas and Dainty (14). Experimental cells were cut and washed as detailed above. Following this recovery, cells were separated into groups of 10 and their diameters and lengths measured so that the surface area of each cell could be computed. A normal overnight pretreatment was then employed.

Experimental cells were placed in vials and given a 1 h or 0.5 h pretreatment in nonradioactive solutions. After the pretreatment period, cells were placed in a solution containing $H^{14}CO_3^-$ adjusted to an appropriate specific activity (0.8–8 mCi/mmol). For $^{14}CO_2$ experiments, solutions were buffered with 5 mM Mes (pH 5.4). Radioactive $^{14}$C was obtained from New England Nuclear as a sterile aqueous $NaHCO_3$ solution.

During an experiment, vials were illuminated using a 150 w quartz-iodide lamp (Leitz-Pradovit projector, model C1500). Light intensity was attenuated to 20 w $m^{-2}$ using nickel-Nicron neutral density filters. All experiments were conducted at 25 C.

At the end of the $^{14}$C treatments, cells were rinsed with nonradioactive solution (same composition), identified, and killed on aluminum planchets. Discs of Kodak lens paper were used to absorb and disperse the cell solution (the nodal-complexes were always removed). Propionic acid (0.5 ml, 100 mM) was used to drive off unfixed $H^{14}CO_3^-$ and $Ca^{14}CO_3$ precipitate. After at least 6 h propionic acid treatment, the planchets were dried on electric hot plates. During this drying procedure, 2 drops of 95% ethanol were added to enhance solubilization of $^{14}$C-labeled compounds from the cell. A small amount of sucrose (2 drops of a 2% w/v solution) was also added as an adhesive agent, thereby sticking the cell wall and the lens paper to the planchet.

Aliquots of the experimental radioactive solutions were used to determine the solution activity. Sample radioactivity was determined using a Nuclear Chicago gas flow system (model 8703 decade scaler, model 1073 automatic planchet changer). Results are expressed as mean ± SE.

***Chara* Cell Surface pH Measurement.** Cell surface pH values were determined using the procedures of Lucas and Smith (18), Lucas and Dainty (14, 15), and Lucas *et al.* (19). In preparing the agar diffusion blocks, all chemical additions (*e.g.* $NaHCO_3$, sorbitol, etc.) were made once the agar had cooled to 40 C. The pH pattern established along the cell surface was mapped using a miniature pH electrode (Microelectrodes, Inc., model MI-405), in conjunction with a Leitz micromanipulator.

After a control scan had been performed, the agar block containing the cell was removed from the experimental chamber and the bathing solution was changed. The cell was carefully transferred to a block prepared to have the chemical composition identical with the new bathing solution. Following a 1-h reequilibration period, the pH-banding pattern was remapped.

**Protein Determination.** Cells (approximate surface area 40 $cm^2$ in 25 ml CPW/B) were pretreated for 2 h (20 w $m^{-2}$, 25 C), then the solution was changed to a 235 mosmol (sorbitol) CPW/B solution; the control solution was kept for protein analysis. After 2 h reduced turgor treatment, the cells were returned to a control solution. Again the reduced turgor solution was kept for protein determination. This was also true for the solution from the recovery phase of the experiment. The Bradford (5) method of protein determination (Bio-Rad, 500-0002) was used to measure the quantity of protein released.

**Cell Sap Osmolality.** Cell sap osmolality was determined at the conclusion of some pH scan experiments. Vacuolar sap was collected using the technique of Fujii *et al.* (10). These samples (10 μl) were analyzed using a Wescor vapor pressure osmometer.

## RESULTS

**Effect of Turgor Reduction and Turgor Recovery on Cyclosis.** Because it is known that $H^{14}CO_3^-$ assimilation and $OH^-$ efflux in *Chara* are sensitive to the rate of cytoplasmic streaming (15), we first investigated the effect of turgor reduction on cyclosis. In experiments in which a cell wall-penetrating osmoticum was used, a reduction in streaming rate was observed when the turgor was reduced. However, cyclosis recovered somewhat and the rate steadied after approximately 20 min (Fig. 1, A and B). When the turgor pressure was returned to its normal value, by changing to control solution, the streaming rate was again reduced, but returned within 20 min to the rate established at reduced turgor (Fig. 1A). The physical appearance of the cells was not affected by these treatments, as evidenced by the form, color, and arrangement of the chloroplasts.

When cells were plasmolyzed using a solution with a slightly greater osmolality than the cell sap, the plasmalemma pulled away from the cell wall in patches, resembling the "dimples" on a golf ball. Increasing the osmolality of the plasmolyzing solution caused the membrane to separate completely from the wall and the protoplasm became "ribbon-like" in some areas. In both cases, some of the chloroplasts lysed, especially near the "neutral line" (line of demarcation between the directions of cyclosis in these giant cells). The more severely plasmolyzed cells usually died fairly rapidly, while the less severely plasmolyzed cells survived until at least the next day.

Upon transferring cells from a control to a plasmolyzing solution, cyclosis was inhibited at least 60%, but after 60 min, the rate was almost fully recovered to the control value (Fig. 1C). However, when cells were plasmolyzed after already having had their turgor reduced, the decrease in cyclosis was much less than observed for cells that were plasmolyzed directly from control solutions (Fig. 1, B and C). When plasmolyzed cells were returned to control solutions in order to recover their turgor, the shrunken protoplasm rapidly rehydrated to fill the cell wall. Usually, some of the chloroplast arrays split apart while this was occurring, leaving damaged areas which persisted for several days. In these treatments, when *Chara* cells were deplasmolyzed, cyclosis recovered to the control rate in approximately 20 min (Fig. 1C).

In the above experiments, none of the treatments caused cyclosis

[2] Abbreviations: CPW/B, *Chara* pond water containing bicarbonate; $E_{Cl^-}$, Nernst equilibrium potential for $Cl^-$; $P_{Cl^-}$, membrane permeability for $Cl^-$.

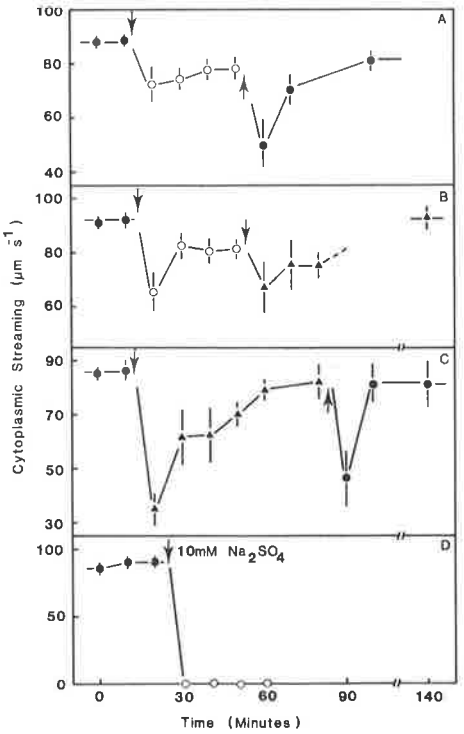


FIG. 1. Effect of reduced turgor, turgor recovery and plasmolysis on cyclosis. Cyclosis was measured with a binocular microscope with an ocular micrometer. The time required for cytoplasmic particles to traverse 1 mm was measured with a stopwatch. Solutions were CPW/B (●), 210 mosmol CPW/B (sorbitol) (○), and plasmolyzing CPW/B (about 250 mosmol) (▲). Arrows indicate time of solution changes. All experiments were performed at 25 C and 10 w $m^{-2}$ illumination. Solutions were at pH 8.

Table I. *Effect of Reduced Turgor on $H^{14}CO_3^-$ Assimilation Using Different Osmotica*

All cells were given a 1-h pretreatment in their respective solutions before exposure to $H^{14}CO_3^-$ (1 h). All solutions contained CPW/B, and experiments were performed at 25 C and 20 w $m^{-2}$ illumination.

| Osmoticum Used | Treatment | |
|---|---|---|
| | Control | 210 mosmol turgor reduction |
| | *pmol $cm^{-2}$ $s^{-1}$* | |
| Sorbitol | 34.8 ± 1.2 | 33.7 ± 4.0 |
| Sorbitol | 24.8 ± 0.8 | 34.5 ± 2.2 |
| Mannitol | 24.8 ± 0.8 | 31.3 ± 3.2 |
| Sucrose | 24.8 ± 0.8 | 24.9 ± 1.3 |
| Sorbitol | 29.2 ± 1.6 | 37.3 ± 2.8 |

to be reduced below the critical streaming rate found by Lucas and Dainty (15). However, during these studies, we found that a combination of turgor reduction (205 mosmol) and $Na^+$ levels of 20 mM rapidly and permanently stopped cyclosis and the cells died (Fig. 1D). An interesting feature of this effect was that the cell contents settled rapidly to the lower cell surface, and it appeared that the plasmalemma had disintegrated. Lower $Na^+$ levels did not affect cyclosis at all (data not shown).

**Effect of Turgor Reduction and Recovery on $H^{14}CO_3^-$ Assimilation.** The influence of turgor reduction on $H^{14}CO_3^-$ assimilation was studied next. Slight changes in $H^{14}CO_3^-$ assimilation were noted when cells were transferred to 210 mosmol solutions (Table I). Given the level of variability observed between the various controls, little difference was found between control and reduced turgor assimilation rates; this response was independent of the osmoticum used.

A significant drop in $H^{14}CO_3^-$ assimilation occurred when cells were transferred from 210 mosmol to control solutions (Table II). An 8-h recovery period was required to restore assimilation to control levels. When this experiment was performed in the presence of 20 mM $CaCl_2$, the loss of transport was slightly less than observed in 0.2 mM $Ca^{2+}$ solutions, but full transport recovery still had the same time course (Table II). It was hoped that $Ca^{2+}$ would protect the membrane from the loss of transport activity (20). However, the present results are in agreement with the work of Amar and Reinhold (1).

**Effect of Turgor Reduction and Recovery on $^{14}CO_2$ Assimilation.** As can be seen in Table III, $^{14}CO_2$ assimilation was not decreased by turgor reduction and subsequent recovery, unlike the $H^{14}CO_3^-$ situation. This indicates that turgor manipulation had no effect on photosynthesis at the chloroplast level.

**Effect of Turgor Reduction and Recovery on $OH^-$ Efflux.** In pH scans performed 1 h after cell turgor had been reduced using an osmoticum, there was generally a small reduction in $OH^-$ efflux activity (Fig. 2). In some cases, at least one of the $OH^-$ peaks increased its pH value, a situation reflecting higher $OH^-$ transport activity. In a few experiments, we found that one of the $OH^-$ peaks was lost (Fig. 4). In this situation, one of the remaining peaks usually increased its transport activity. It should be noted that the position of the $OH^-$ bands was constant (stable) at reduced turgor.

When cell turgor was recovered after having been reduced by at least 205 mosmol, and 1 h was allowed for stabilization of the pH profile, the transport activity of the $OH^-$ bands was found to be dramatically reduced. Based on the results of approximately 30

Table II. *Recovery of $H^{14}CO_3^-$ Assimilation after Turgor Reduction*

All cells were given a 1-h pretreatment in CPW/B (25 C and 10 w $m^{-2}$ illumination). Solutions were then changed to CPW/B, 20 mM $CaCl_2$ + CPW/B, 235 mosmol CPW/B, and 235 mosmol + 20 mM $CaCl_2$ + CPW/B for 2 h. Cells with reduced turgor were returned to either CPW/B or 20 mM $CaCl_2$ + CPW/B. One h before radioisotope exposure cells were transferred to a waterbath thermostatted at 25 C and 20 w $m^{-2}$ illumination. The radioisotope solution consisted of 1 mM [$H^{14}CO_3^-$]CPW (pH = 9.2). Exposure was for 1 h.

| Treatment | Time after Turgor Recovery | | | |
|---|---|---|---|---|
| | 1 h | 2 h | 4 h | 8 h |
| | *pmol $cm^{-2}$ $s^{-1}$* | | | |
| Control | | | 39.9 ± 1.4 | 40.6 ± 3.1 |
| Reduced turgor | 9.1 ± 1.9 | 10.2 ± 1.0 | 18.8 ± 3.0 | 40.5 ± 3.0 |
| $Ca^{2+}$ control | | 28.0 ± 1.9 | 33.7 ± 2.1 | 31.7 ± 1.4 |
| $Ca^{2+}$ reduced turgor | 18.1 ± 1.7 | 13.4 ± 1.0 | 24.5 ± 2.3 | 33.3 ± 3.1 |

Table III. *Effect of Turgor Reduction and Recovery on $^{14}CO_2$ and $H^{14}CO_3^-$ Assimilation*

After 1-h pretreatment in CPW/B, cells were given a 1-h exposure in a 212 mosmol CPW/B (pH = 9.2) solution. Cells were then returned to CPW/B solutions and given 1-h exposure to $^{14}C$ at the indicated pH values.

| Treatment ($^{14}C$) | Control[a] | After Turgor Recovery | % Control |
|---|---|---|---|
| $^{14}CO_2$ (5 mM Mes [pH = 5.4]) | 95.1 ± 5.6[b] | 109.1 ± 6.0 | 115 |
| $H^{14}CO_3^-$ (pH = 9.2) | 35.4 ± 2.7 | 9.3 ± 1.3 | 26 |

[a] Control cells were given identical treatments except for the 212 mosmol reduction in turgor.

[b] Assimilation in pmol $cm^{-2}$ $s^{-1}$.

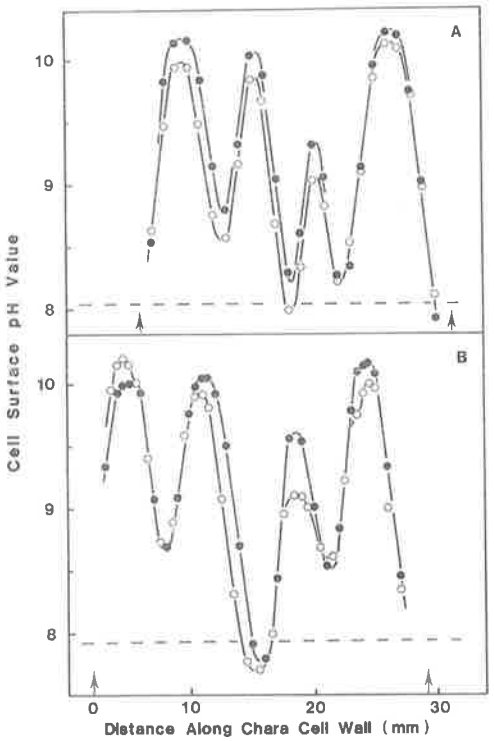


FIG. 2. Effect of reduced turgor pressure on $OH^-$ banding pattern. A control pH scan was performed with a CPW/B bathing solution (●). Solution was then changed to one with an osmolality of 210 to 230 mosmol. After 1 h in these 210 mosmol media, the cell surface pH pattern was remapped (○). Horizontal broken lines represent pH values of background media. Typical data from two experiments are presented in A and B.

pH scan experiments, we found that there was a threshold for the induction of this perturbation. For the full effect, there had to be a difference of less than 30 mosmol between the osmolality of the bathing solution and that of the cell sap, determined at the completion of the experiment (Fig. 3, B and C).

Re-establishment of normal $OH^-$ transport activity, following a turgor threshold treatment, took a considerable time (Fig. 4). After 16 h of recovery, the overall magnitude of $OH^-$ efflux approached that of the control, but the pH pattern was often different (cf. Fig. 4, △ and ●).

**Effect of Drying and Rehydration on $OH^-$ Efflux.** In these giant algal cells, turgor can also be reduced by allowing evaporation of the cell wall water. This approach was used to investigate further the perturbative effect of turgor restoration. The collective results presented in Figure 5 illustrate that when turgor was reduced in this way, subsequent rehydration of the cell had little effect on $OH^-$ efflux activity. In general, there appeared to be a slight loss of $OH^-$ efflux activity, with little effect on band position. In one experiment, one peak was lost, but again other peaks increased in activity to compensate (Fig. 5A). This response is in marked contrast to the effect obtained using a cell wall-penetrating osmoticum like sorbitol (*cf.* Figs. 3 and 5).

**Effect of Plasmolysis on pH Banding Pattern.** The pH pattern of most plasmolyzed cells showed a complete loss of $OH^-$ efflux activity. From the representative data presented in Figure 6, it can be seen that, under plasmolyzing conditions, almost the entire cell surface became acidified. In some cells slight $OH^-$ efflux activity remained (Fig. 6B).

**Protein Release after Turgor Manipulation.** It has been reported that there is a release of protein from osmotically shocked (plasmolysis and subsequent turgor recovery) tissue (1, 11, 21). Inasmuch as the procedures used were similar to osmotic shock,

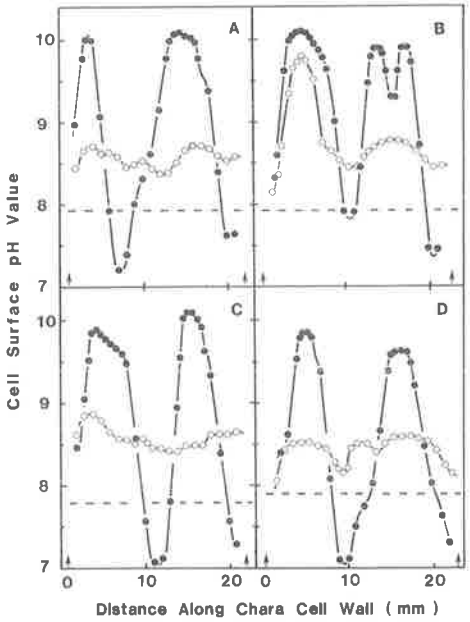


FIG. 3. Effect of turgor recovery on cells with reduced turgor. The cells were scanned in a CPW/B solution with an osmolality of at least 205 mosmol (●). The cells were placed in a CPW/B solution and allowed to recover for 1 h before the next scan was performed (○). A: solution 230 mosmol; cell not measured; B: solution 208 mosmol; cell, 243 mosmol; C: solution, 235 mosmol; cell, 261 mosmol; D: solution, 240 mosmol; cell, 246 mosmol.

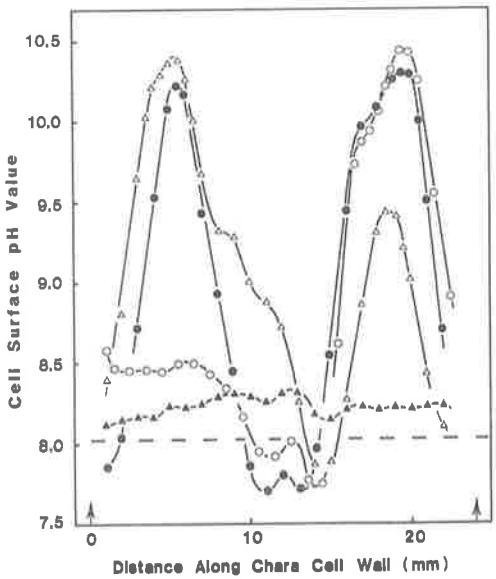


FIG. 4. Effect of turgor reduction and recovery on $OH^-$ banding pattern. A control scan was performed (●). The solution was then changed to a 215 mosmol CPW/B solution, and after 1 h, the surface was rescanned (○). The turgor was then restored (CPW/B), and a scan performed after 3.5 h. (▲). Sixteen h after turgor recovery another scan was performed (△).

protein determinations were performed on *Chara* cells. After a 2-h control treatment, there was no measureable release of protein. The same was true after a 2-h treatment in 235 mosmol solution, and after a 2-h recovery in control solution (data not shown).

Significant protein release has only been observed after plasmolysis. As *Chara* cells were not plasmolyzed in the experiments where transport activity was reduced, insufficient protein may

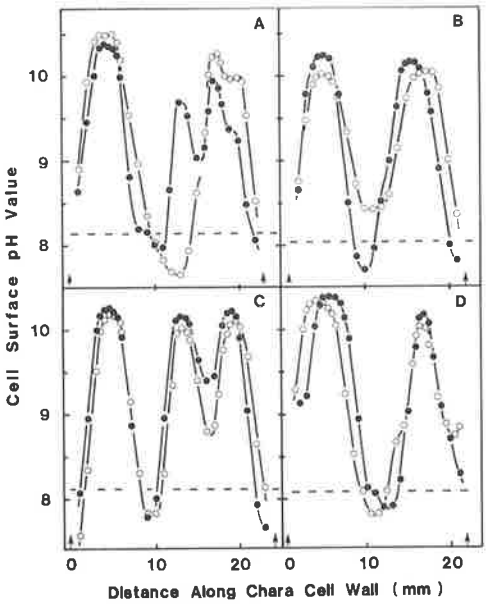


FIG. 5. Effect of cell drying and rehydration on $OH^-$ efflux activity in *C. corallina*. A control pH scan was performed in CPW/B (●). Individual cells were then removed from the experimental chamber and placed on a glass slide and allowed to dry until the volume of the cell was roughly half of the original volume. Turgor was restored by irrigating the cell with CPW/B and the cell was then placed back into the chamber. After 1 h, a second pH scan was performed (○).

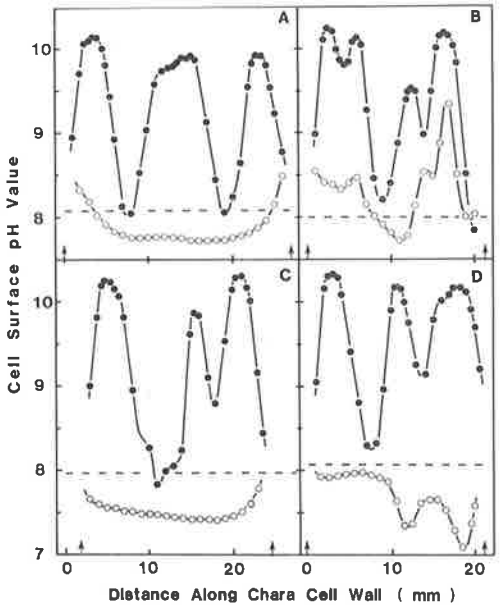


FIG. 6. Effect on the pH banding pattern of plasmolyzing *Chara* cells with an osmoticum. Representative profiles are presented in A to D. Control pH scans were conducted (●) in CPW/B before the system was changed to one close to the plasmolytic point (about 250 mosmol). Small amounts of a 350 mosmol mannitol solution were added to the bathing solution until the cells plasmolyzed. After 1 h, the pH pattern was remapped (○).

have been released to allow its detection by the method employed. Alternatively, the *Chara* cell wall may have prevented the escape of the released protein.

## DISCUSSION

**Effect of Turgor Manipulation on Cyclosis.** From the data on cytoplasmic streaming, it can be seen that turgor reduction, recovery, and mild plasmolysis does not have any long term effect on general cell viability. Turgor manipulation may induce an action potential, which is known to stop cyclosis momentarily (12). Work by Barry (2) suggests that this may be caused by an influx of $Ca^{2+}$. If the membrane is made slightly more permeable to $Ca^{2+}$ by turgor reduction, this could explain the transient effects on streaming observed at reduced turgor. Presumably enough $Ca^{2+}$ can then enter the cytoplasm to slow, but not stop streaming.

The dimpled appearance of slightly plasmolyzed *Chara* cells probably arises from the membrane-cell wall interaction at the charasome sites (9). Further plasmolysis probably ruptures the plasmalemma at the charasome sites, thereby destroying its physical integrity. This would explain why severely plasmolyzed cells die.

**Influence of $Na^+$ on Turgor-Reduced Cells.** Twenty mM $CaCl_2$ had no detrimental effect on *Chara* cells with reduced turgor (Table II), while under the same conditions, 20 mM $Na^+$ was lethal 1D). Also, 10 mM $Na^+$ had no effect under reduced turgor conditions (data not shown). This may be explained by a change in membrane permeability to $Na^+$. Under normal turgor conditions, this $Na^+$ level did not affect cell functions (19). If the $Na^+$ permeability was increased at reduced turgor, a large influx of $Na^+$ would result in response to the negative membrane potential (−200 to −260 mv; [19]). The $Na^+$ content might then increase to the point where it becomes lethal. Lower $Na^+$ concentrations may not kill the cell because the $Na^+$ efflux pump has not become overloaded. An overload would allow a rapid and lethal build-up of $Na^+$ in the cytoplasm.

**Effect of Turgor Reduction.** Turgor reduction had little effect on $H^{14}CO_3^-$ assimilation *per se*. The pH scans performed on cells with reduced turgor closely resembled the control scans, but had slightly reduced over-all $OH^-$ efflux activity. The $OH^-$ bands were in the same position and the bandwidths (16) were generally invariant. When efflux activity was reduced at one or more sites, the remaining $OH^-$ site(s) increased transport activity to compensate (Figs. 2B and 4). This alteration of transport activity at the $OH^-$ sites suggests that there is an effect on them, but this effect does not reduce the over-all $OH^-$ efflux capacity of the cell. These data indicate that turgor reduction and the putative physical changes within the membrane have little effect on the $HCO_3^-$ and $OH^-$ transport systems. These results would appear consistent with the previously mentioned hypotheses on turgor regulation, since neither $HCO_3^-$ nor $OH^-$ would be directly involved in osmotic adjustment.

**Effect of Turgor Recovery.** The significant loss of $HCO_3^-$ and $OH^-$ transport activity after turgor restoration, following reduction below a threshold value, indicates an unexpected degree of complexity. From the $^{14}CO_2$ data (Table III), it can be seen that reduced $H^{14}CO_3^-$ influx was not a result of impaired chloroplast function, since $^{14}CO_2$ assimilation was actually slightly enhanced by the turgor reduction and recovery treatments. Hence, the reduction of $HCO_3^-$ influx, and/or $OH^-$ efflux, must be due to either a direct effect on the plasmalemma or an indirect effect elicited via rapid osmotic changes within the cell. The involvement of the plasmalemma in the reduction of transport is indicated by the experiments in which cells were dried and then rehydrated. This treatment reduced the turgor to zero, without the plasmalemma pulling free from the wall, or an osmoticum permeating to the membrane-wall interface. After a 1-h recovery, there was almost no difference between the control pH pattern and that established after the cell had been dried and rehydrated (Fig. 5). Since the cytoplasm in these experiments was concentrated to a greater level than in any other experiment, the lack of perturbation shows clearly that rapid osmotic changes within the cell were not responsible for the transport inhibition observed after "turgor

recovery." Consequently, the plasmalemma appears to be the only site at which this "turgor recovery" effect can occur. In addition, it would appear that there must be an osmoticum present for inhibition to occur. Apparently, turgor pressure, *per se*, is not involved, since the air-dried cells were reduced to zero turgor (*i.e.* zero internal hydrostatic pressure). This is an extremely important point, and we will return to it later in the discussion.

**Effect of Plasmolysis on pH Banding Pattern.** The mechanism of $OH^-$ efflux inactivation and the observed acidification of the cell surface in response to plasmolysis is not clear. It should be stressed that the different responses illustrated by Figures 2 and 6 were obtained by increasing the solution osmolality by only 30 to 40 mosmol. The effect, therefore, appears to have its origin in the plasmolytic event rather than in a change in cell turgor. It is possible that components on the cell wall are required for transport of $HCO_3^-$ and $OH^-$ and that after plasmolysis these were no longer in contact with the plasmalemma. This interpretation is unlikely, since in the plasmolyzed state, many areas of the wall remained in contact with the plasmalemma. If wall contact was an essential feature for transport, we would have expected an irregular alkalinization pattern similar to that observed when cyclosis is stopped by cytochalasin B (15).

The electric potential across the plasmalemma is normally negative (cytoplasm with respect to apoplast). However, there are varying reports as to the sign of the membrane potential in plants cells in which no turgor exists (6, 22). In our present system the plasmolytic event may have preferentially increased the permeability of the membrane to $Cl^-$. This would cause the potential to reset at $E_{Cl^-}$ (Nernst potential for $Cl^-$), which would be a positive value in this system. Such a change in sign would have a profound effect on the $OH^-$ transport system; it is presently thought that this process may be driven passively by the negative membrane potential (4, 17). This explanation could account for the degree of $OH^-$ transport variability observed in response to plasmolysis. The incomplete inactivation of $OH^-$ transport shown in Figure 6B may be due to a lesser influence on $P_{Cl^-}$ in this cell and thus the potential may not have depolarized to a positive value.

Acidification of the cell surface, in response to plasmolysis, could be caused by several different processes. The putative proton transport system of the plasmalemma may not be affected by plasmolysis, and the observed acidification may be a result of its activity; an event which would be easily discernable in the absence of $OH^-$ efflux.

**Theoretical Considerations Concerning Turgor.** By carefully examining not only the results, but also the physical systems used in these experiments, we have unraveled a new aspect which we feel has a profound effect on all work relating to osmotic adjustment in terrestrial plants. In any marine algal system, as for example those studied by the groups of Gutknecht and Zimmermann, the cell turgor can legitimately be adjusted by manipulating the external concentration of the ions normally present in sea water. This legitimacy does not, however, extend to the aerial portions of terrestrial plants, and it is doubtful whether it can be extended to root systems. This is because, under water stress conditions, the main component of the water potential within the cell walls is the matrix ($\psi_\tau$) not the osmotic component ($\psi_\pi$). This is an extremely important difference as we will proceed to demonstrate using the drying *Chara* cell situation.

In its normal culture solution, *Chara* internodal cells develop an osmotic pressure of approximately 0.6 MPa which is balanced by an equal turgor pressure. If a cell is cut from the culture and transferred to a clean, dry Petri dish, the following sequence occurs:

1. Initially, there will be no change in cellular osmotic or turgor pressures, because excess water is evaporating from the cell wall surface.
2. As this surface water becomes exhausted, the air-water interface recedes into the outer region of the wall. The strong forces of adhesion between the wall material and the water molecules, and the high surface tension of water (due to the high cohesive force of water) prevent the air-water interface from being easily distended into the microfibrillar matrix of the wall.
3. Water continues to evaporate across the air-water interface, but now, because the surface resists being stretched, the tension that develops at this surface is transmitted to the body of the water within the wall. This tensional component ($\psi_\tau$) tends to pull water from deeper within the wall, and eventually from within the cell.
4. At this point, we will assume that water is crossing the plasmalemma via water-filled channels (pores). When sufficient water has evaporated from the cell, such that turgor has been reduced to zero, the membrane will not move away from the inner region of the wall, *i.e.* the cell will not be plasmolyzed. This is because, even though there is no net hydrostatic pressure remaining within the cell, the tension in the apoplastic water is transmitted, via the water in the pores, to the interior of the cell. Hence, water is still being pulled out of the cell, and the positive hydrostatic pressure gradient that existed before drying has been replaced by an equal and opposite (in sign) tensional gradient. It is this tensional gradient that holds the membrane up against the inner microfibrils of the wall.
5. Since the *Chara* cell wall has very little compressive strength, which is also true for plant primary cell walls, continued water loss will cause an inward collapse of the wall. The plasmalemma will continue to be held against the wall by the tension developed at the air-water interface. It appears to us that, as the cell continues to dry, the increased tension across the membrane may result in membrane thinning rather than a thickening.
6. Irrigation of the dried cell will result in a rapid rehydration of the cell wall, such that the tensional component is reduced to zero within a few seconds. Because the hydraulic conductivity of the plasmalemma is much lower than that of the wall, rehydration of the protoplasm will be much slower (30–60 s). There will, therefore, be a very brief period in which, during the change from a tensional to a compressive situation, the membrane may have the chance to thicken. (As this treatment did not influence $HCO_3^-$ and $OH^-$ transport [Fig. 5], we deduce that transient membrane thickening and subsequent thinning is not perturbative unless it occurs in the presence of an osmoticum.) It should also be stressed that rapid cell wall rehydration would not occur in leaves of terrestrial plants.

Use of a cell wall-penetrating osmoticum will, on the other hand, give an entirely different result, since the osmotic effect will be expressed across only the plasmalemma. At a high enough external osmotic pressure, cell turgor will be reduced to zero and, under these conditions, there will be no compressive force acting within the membrane. Hence, the membrane may thicken, and it is also possible for the membrane to move away from the wall. In our assessment, this situation will only occur in marine systems and perhaps in root cells found in saline soils.

Our results indicate that turgor reduction, *per se*, has almost no effect on $HCO_3^-$ and $OH^-$ transport in *Chara*, until the cell becomes plasmolyzed. However, restoration of turgor is detrimental to transport function, but only when a penetrating osmoticum is used to lower the turgor. These results, and especially those obtained using the cell evaporation technique, indicate that an effect on membrane transport may be elicited via the technique used, rather than as a direct result on the parameter of interest, turgor pressure in this situation. Since mannitol and sorbitol are commonly used to manipulate cell water relations parameters, the present results indicate that they must be employed with extreme caution.

Finally, if our theoretical analysis of this situation is correct, it would appear that the plasmalemma does not undergo thickening as the water potential of the tissue is reduced. This would mean

that the turgor adjustment hypotheses propounded for the *Valonia* situation (3, 7, 24) have little direct relevance to leaf tissue, etc. The plasmalemma may thin under extreme water stress, but it appears unlikely that the membrane-microfibrillar interactions, as outlined by Bisson and Gutknecht (3), will occur in anything but the marine or aquatic situation.

*Acknowledgments*—We wish to thank Drs. A. Läuchli and T. M. Murphy for their helpful discussions during this work.

## LITERATURE CITED


1. Amar L, L Reinhold 1973 Loss of membrane transport ability in leaf cells and release of protein as a result of osmotic shock. Plant Physiol 51: 620–625
2. Barry WH 1968 Coupling of excitation and cessation of cyclosis in *Nitella*: role of divalent cations. J Cell Physiol 72: 153–160
3. Bisson MA, J Gutknecht 1980 Osmotic regulation in algae. *In* RM Spanswick, WJ Lucas, J Dainty, eds, Plant Membrane Transport: Current Conceptual Issues. Elsevier/North Holland, Amsterdam. pp 131–146
4. Bisson MA, NA Walker 1980 The *Chara* plasmalemma at high pH. Electrical measurements show rapid specific passive uniport of $H^+$ or $OH^-$. J Membr Biol 56: 1–7
5. Bradford MM 1976 A rapid and sensitive method for the quantitation of microgram quantities of protein utilizing the principle of protein-dye binding. Anal Biochem 72: 248–254
6. Briskin DP, RT Leonard 1979 Ion transport in isolated protoplast from tobacco suspension cells. III: membrane potential. Plant Physiol 64: 959–962
7. Coster HGL, U Zimmermann 1976 Transduction of turgor pressure by cell membrane compression. Z Naturforsch 31c: 461–463
8. Coster HGL, E Steudle, U Zimmermann 1976 Turgor pressure sensing in plant cell membranes. Plant Physiol 58: 636–643
9. Franceschi VR, WJ Lucas 1980 Structure and possible function(s) of Charasomes; complex plasmalemma-cell wall elaborations present in some characean species. Protoplasma 104: 253–271
10. Fujii S, T Shimmen, M Tazawa 1979 Effect of intracellular pH on the light-induced potential change and electrogenic activity in tonoplast-free cells of *Chara australis*. Plant Cell Physiol 20: 1315–1328
11. Grunwaldt G, R Ehwald, H Göring 1978 Suitability of the osmotic shock procedure for the analysis of membrane transport in root tips of *Zea mays* L. J Exp Bot 29: 97–106
12. Hope AB, NA Walker 1975 The Physiology of Giant Algal Cells. Cambridge University Press, London
13. Lucas WJ 1975 Photosynthetic fixation of $^{14}$carbon by internodal cells of *Chara corallina*. J Exp Bot 26: 331–346
14. Lucas WJ, J Dainty 1977 $HCO_3^-$ influx across the plasmalemma of *Chara corallina*: divalent cation requirement. Plant Physiol 60: 862–867
15. Lucas WJ, J Dainty 1977 Spatial distribution of functional $OH^-$ carriers along a characean internodal cell: determined by the effect of cytochalasin B on $H^{14}CO_3^-$ assimilation. J Membr Biol 32: 75–92
16. Lucas WJ, JM Ferrier, J Dainty 1977 Plasmalemma transport of $OH^-$ in *Chara corallina*: dynamics of activation and deactivation. J Membr Biol 32: 49–73
17. Lucas WJ, T Shimmen 1981 Intracellular perfusion and cell centrifugation studies on plasmalemma transport processes in *Chara corallina*. J Membr Biol 58: 227–237
18. Lucas WJ, FA Smith 1973 The formation of alkaline and acid regions at the surface of *Chara corallina* cells. J Exp Bot 24: 1–14
19. Lucas WJ, RM Spanswick, J Dainty 1978 $HCO_3^-$ influx across the plasmalemma of *Chara corallina*: physiological and biophysical influence of 10 mM $K^+$. Plant Physiol 61: 487–493
20. Nakane PK, GE Nichoalds, DL Oxender 1968 Cellular localization of leucine-binding protein from *Escherichia coli*. Science 161: 182–183
21. Neu HC, LA Heppel 1965 The release of enzymes from *Escherichia coli* by osmotic shock and during the formation of sphaeroplasts. J Biol Chem 240: 3685–3692
22. Racusen RH, AM Kinnersley, AW Galston 1977 Osmotically induced changes in electrical properties of plant protoplast membranes. Science 198: 405–407
23. Zimmermann U, F Beckers, HGL Coster 1977 The effect of pressure on the electrical breakdown in the membranes of *Valonia utricularis*. Biochim Biophys Acta 464: 399–416
24. Zimmermann U, E Steudle 1980 Fundamental water relations parameters. *In* RM Spanswick, WJ Lucas, J Dainty, eds, Plant Membrane Transport: Current Conceptual Issues. Elsevier/North Holland, Amsterdam. pp 113–130

Plant Physiol. (1981) 68, 899–904
0032-0889/81/68/0899/06/$00.50/0

# Effect of Sulfhydryl Reagents on the Biophysical Properties of the Plasmalemma of *Chara corallina*[1]

Received for publication December 15, 1980 and in revised form April 15, 1981

FRANCIS T. LICHTNER, WILLIAM J. LUCAS, AND ROGER M. SPANSWICK[2]
*Department of Botany, University of California, Davis, California 95616*

## ABSTRACT

**The administration of the sulfhydryl reagent *N*-ethyl-maleimide (NEM) to internodal cells of *Chara corallina* caused alterations in the biophysical properties of the plasmalemma, as measured with electrophysiological and radioactive tracer techniques. The membrane potential depolarized to, or near, the calculated Nernst potential for potassium ($E_K$) after 30 seconds' exposure to 0.1 millimolar NEM. During this time, the ATP level did not decrease below the control value, and the specific membrane resistance did not increase; only upon further exposure to NEM did the resistance approach the value observed in the dark. In the depolarized state, the membrane potential responded to changes in the external potassium concentration in the manner of a $K^+$-electrode, but it retained it's relative insensitivity to external sodium.**

**These results are interpreted in the following manner: NEM causes a) an increase in the membrane permeability to $K^+$ (*i.e.* an increase in $K^+$ conductance); and b) perturbation of the electrogenic transport system(s) of the plasma membrane. The latter effect is manifested in a manner that is not consistent with an inhibition of ATP catalysis by a voltage-dependent ATPase possessing conductance. The nonpermeant sulfhydryl modifier, *p*-chloromercuribenzenesulfonic acid, appeared to affect membrane properties in a similar, but reversible, way.**

The biochemical and biophysical properties of the plasmalemma play an undisputed key role in the organization and function of membrane transport phenomena. Increasingly, heavy metals and sulfhydryl reagents have been used to probe the interrelationships of these processes (4–6, 12, 18, 31). Whereas the action of these disulfide- and thiol-reactive compounds (such as NEM[3], $Hg^{2+}$, and organic mercurials) may sometimes be interpreted as specific for protein-mediated transport processes (12), these chemical agents may also modify general membrane permeability characteristics, especially at elevated inhibitor concentrations (*e.g.* see Ref. 25).

Modification of the permeability characteristics of the plasma membrane leads to changes in the response of membrane potential and membrane resistance to manipulations of the ionic composition of the external medium. Because the electrophysiology and ionic relations of *Chara corallina* are relatively well understood and since certain transport processes in this alga appear to be differentially susceptible to -SH reactive agents (18), we investigated the biophysical properties in *C. corallina* before and after treatment with thiol-modifying reagents. This approach has allowed us to conclude that sulfhydryl reagents affect the passive permeability of the membrane by increasing potassium conductance and act upon the electrogenic transport processes of the cell membrane.

## MATERIALS AND METHODS

**Culture Material.** Culture material of *C. corallina* Klein ex Willd., em R. D. W. (=*C. australis* R. Br.) was grown in the laboratory in large plastic containers in a culture medium containing 1 to 2 mM $Na^+$, 0.2 mM $K^+$, 0.2 mM $Ca^{2+}$, 1 to 2 mM $Cl^-$, and 2 mM $HCO_3^-$. Artificial fluorescent lighting was employed; the intensity at the solution surface was 17–20 w $m^{-2}$. Full details of the culture techniques and the methods used to cut and pretreat experimental cells have been reported previously (16, 20). Cells (Cornell University) used for ATP determinations were cultured under similar conditions (8).

**Experimental Solutions.** Solutions were prepared using high purity glass-distilled $H_2O$. The CPW contained 1.0 mM NaCl, 0.2 mM KCl, 0.2 mM $CaSO_4$, 1.0 mM TAPS (pH 8.0); modifications to this medium will be detailed in the text. Bicarbonate-free solutions were prepared by bubbling solutions with air that had been passed through $CO_2$-absorbent material (Ascarite; Arthur H. Thomas Co.). All chemicals were of Analar reagent grade and, except for PCMBS, were not purified further. Stock (100 mM) NEM solutions were titrated to pH 7, using fresh NaOH solution, and stored at 4 C for a maximum of 4 days. Because hydrolytic ring opening in the NEM molecule occurs at alkaline pH, experimental NEM solutions were prepared immediately (2 min) before use.

Removal of inorganic mercury from commercial PCMBS (Sigma Chemical Co.) was achieved using a modification of the procedure of Willard *et al.* (32). Dowex chelating resin (Sigma Chemical Co.) was converted to the acid form by washing in 0.1 M HCl, followed by suspension in glass-distilled $H_2O$ for 24 h at 4 C. Unpurified PCMBS (about 0.2 g) was dissolved in a minimum amount of unbuffered CPW and then added to 10 ml (packed volume) Dowex chelating resin ($H^+$-form) and 20 ml CPW. The mixture, maintained in darkness, was agitated for 20 min; PCMBS concentration in the supernatant was determined spectrophotometrically (after allowing the resin to settle by gravity). Experimental solutions containing purified PCMBS were prepared immediately prior to use.

**Electrophysiological Measurements.** Membrane potentials were measured using WPI model 750 amplifiers (WP Instruments, New Haven, CT) and microelectrodes made from Omega Dot glass (Frederick Haer and Co., Ann Arbor, MI). The microelectrodes were filled with 3 M KCl (adjusted to pH 2 to reduce tip potentials)

[1] Supported by National Science Foundation grants PCM 78-10474 (to W. J. L.) and PCM 78-12119 (to R. M. S.).

[2] Permanent address: Section of Plant Biology, Division of Biological Sciences, Cornell University, Ithaca, NY 14853.

[3] Abbreviations: NEM, *N*-ethyl maleimide; CPW, basic experimental solution; TAPS, Tris (hydroxymethyl) methylaminopropanesulfonic acid; PCMBS, *p*-chloromercuribenzenesulfonic acid; $E_K$, $E_{Na}$, $E_{Cl}$, etc., Nernst potential for $K^+$, $Na^+$, $Cl^-$; $E_m$, membrane potential (in mv); ANDA, 7-amino-1,3-naphthalene disulfonic acid; $R_m$, specific membrane resistance (K Ω-$cm^2$); $g_m$, total membrane conductance; $P_K$, potassium permeability.

(24).

Membrane resistance was measured using the single voltage probe method (7). This method is an approximation which is accurate only when the space constant, $\lambda$, is comparable with or larger than the half-length, $\ell$, of the internodal cell. ($\lambda$ is a measure of the attenuation of the voltage change induced along the cell in response to an imposed current pulse.) Because the membrane resistance of these cells in the light at high pH values is low (and, hence, $\lambda$ is small), it was necessary to use short cells (2–3 cm) in all of our experiments. The very low resistances measured in the presence of high KCl may be slightly underestimated. Time courses for the membrane resistance were obtained by delivering a 4-s current pulse (0.4 $\mu$amp) derived from a Pulsar 4i pulse generator (Frederick Haer and Co.) at 60-s intervals. This current was passed between a microelectrode inserted at the center of the cell and a Ag/AgCl wire placed parallel to the cell in the external solution. The current-induced change in membrane potential was measured using a microelectrode inserted at a distance of 0.42 $\ell$ from the current microelectrode. Using the measured voltage change and the known current, the membrane resistance was calculated from Ohm's law and converted to specific resistance using individual cell surface areas.

Determination of $E_K$ was accomplished by establishing the value for the membrane potential in CPW (pH 8) + 10 mM $K^+$, *i.e.* when the membrane potential is dominated by the $K^+$ term in the Goldman equation. Provided the internal $K^+$ levels do not change significantly during this high $K^+$ treatment, $E_K$ values can then be calculated for the respective $K^+$ concentrations, assuming a 59 mv per decade response (29).

Electrophysiological experiments were conducted under a light intensity of 20 $wm^{-2}$. This irradiance was obtained using a Leitz Pradovitz projector (quartz iodide lamp, 150 w, 12 v). The beam was attenuated using nickel-Nicron neutral density filters, and the IR component was removed using a 10-cm water filter. The temperature of the system was 25 ± 2 C. Representative data for each species of treatments is depicted in "Results." Each experiment was repeated a minimum of three times (except for PCMBS experiments, which were replicated twice).

**$^{42}K^+$ Influx Measurements.** Cells used for short-term influx studies were cut and their surface area determined and then pretreated overnight in CPW (pH 8). On the day of the experiment, control cells were pretreated in their respective $K^+$ solutions for 30 min (irradiance 20 $wm^{-2}$, thermostatted at 25 C). $^{42}K^+$ (as KCl; New England Nuclear Corp.) was added for either 30 min (0.2, 0.8, and 1.8 mM $K^+$) or 15 min (10.8 mM $K^+$). NEM-treated cells were pretreated for 15 min in CPW (pH 8.0) then exposed two times to pulses of 0.5 min NEM (0.1 mM) solution per 12 min pretreatment solution. This schedule was followed by a 15 min exposure to $^{42}K^+$ at concentrations indicated in Table II. All cells were rinsed briefly (2–5 min) in nonradioactive solution (1–2 C) and placed into scintillation vials; radiation was counted in the presence of 10 ml of 5 mM ANDA (14). Light emission was measured by a Beckman LS8000 Liquid Scintillation Counter.

Determination of cell wall binding was accomplished by removing intracellular material from *Chara* internodes of known surface area, incubating the cell walls in the respective uptake solution for the appropriate time, and then counting the material as described above. These values were subtracted from the gross counts obtained with intact cells after accounting for $^{42}K^+$ decay. Corrected results are expressed as mean ± SE for 10 cells per treatment (units in pmol $cm^{-2}s^{-1}$.)

**ATP Determination.** Cellular ATP content was measured by the luciferin-luciferase assay, according to the method described by Keifer and Spanswick (9).

## RESULTS

**Initial Response of the $E_m$ to NEM.** Administration of *N*-ethyl maleimide, at a concentration of 0.1 mM, caused a differential effect on the membrane potential and resistance depending on the presence or absence of exogenous $HCO_3^-$. In the presence of 1.0 mM $HCO_3^-$ (Fig. 1A), the membrane potential transiently hyperpolarized as much as 25 to 30 mv and then proceeded to return to, or near, the original resting level. Subsequent pulses of NEM caused a depolarization of the potential to, or below the calculated Nernst potential for potassium ($E_K$), with a concomitant decrease in resistance at the time of maximum depolarization. After a short time, typically within 3 to 5 min following each pulse, the potential repolarized to and remained steady at $E_K$.

In the absence of exogenous bicarbonate, the initial hyperpolarization resulting from the addition of NEM was not present (Fig. 1B). Treatment with NEM caused an immediate depolarization of the membrane potential. In the case illustrated in Figure 1B, a single 30-s pulse of 0.1 mM NEM was sufficient to decrease $E_m$ to $E_K$; in some experiments, an additional NEM pulse was required to depolarize $E_m$ to $E_K$.

Under both bicarbonate-free conditions and in the presence of 1 mM bicarbonate, a small (2-fold) change in membrane resistance was noted after initial treatments with NEM (Fig. 2). By treating the cells with successive short (10-s) pulses of NEM, the effects of NEM on the time dependence of changes in $E_m$ and $R_m$ are clearly resolvable. In this series of experiments, the potassium concentration was maintained at 20 $\mu$M; this allows a minimum conductance through the NEM-sensitive potassium channels in the membrane, so that the total membrane conductance should be approximated by the conductance through the electrogenic pumps. Depolarization of the membrane potential below $E_K$ was completed within 30 s; only upon further treatment (30–40 additional s) did the membrane resistance begin to increase. After a total of 120 s of exposure to 0.1 mM NEM, the specific resistance approached that found in the dark.

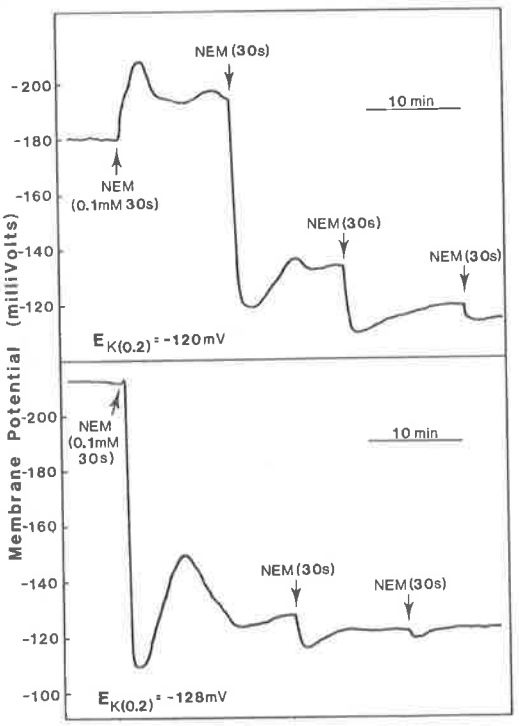


FIG. 1. Response of the membrane potential to NEM in the presence of 1.0 mM $HCO_3^-$ and in $HCO_3^-$-free solution. Membrane potentials were measured as described in "Materials and Methods." Composition and preparation of experimental solutions are as described in "Materials and Methods." NEM (0.1 mM) was administered by rapidly flowing solution across the length of the cell for the prescribed time, followed by a rinse in experimental solution.

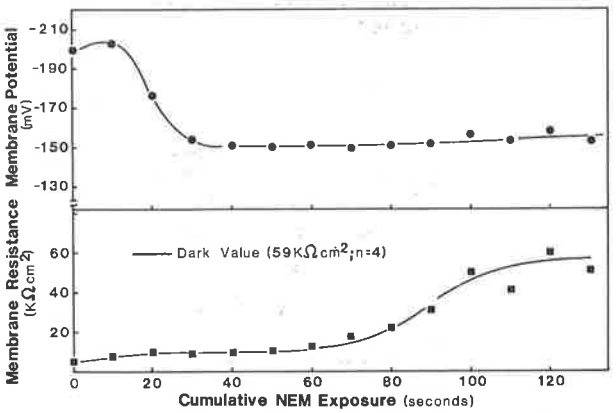


FIG. 2. Response of the membrane potential and resistance to exposure to NEM. Measurements of membrane potential and resistance were made as described in "Materials and Methods." Experimental solution contained 1.0 mM NaCl, 0.02 mM KCl, 0.2 mM $CaSO_4$, 1.0 mM TAPS (pH 8.0), and no added bicarbonate. Results are the average of three cells. Abscissa represents cumulative exposure (s) to 0.1 mM NEM. Each 10-s pulse was followed by a 12-min period in control experimental solution; data represents the values for $E_m$ and $R_m$ at the end of the 12-min recovery period. $E_{K(0.02)}$ was estimated at −180 mv, as described in "Materials and Methods."

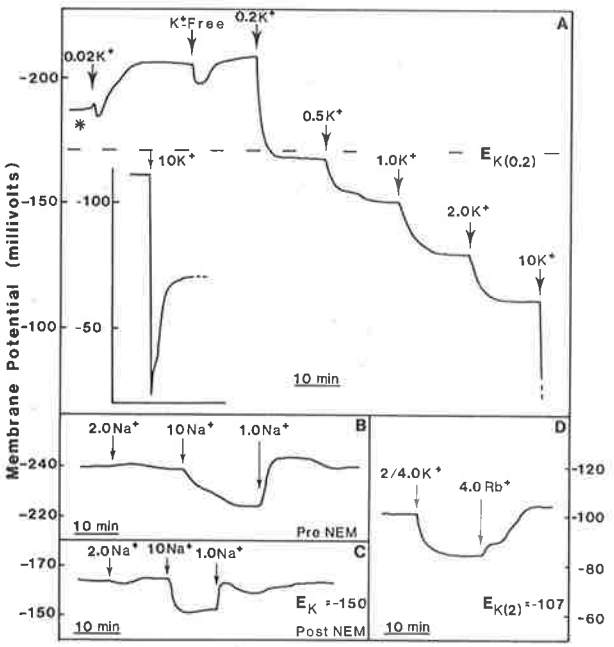


FIG. 3. Response of the membrane potential to the ionic composition of external media. Membrane potentials were measured as described in "Materials and Methods." A, Effect of potassium concentration on $E_m$ following exposure to four 30-s exposures to NEM (0.1 mM), each separated by a 12-min wash in CPW plus 1.0 TAPS (pH 8). Asterisk represents the end of the last 12-min rinse. (– – –), Calculated Nernst potential for potassium at 0.2 mM $[K^+]_0$ (=$E_{K(0.2)}$). Inset, Action potential elicited by exposure to 10 mM $[K^+]_0$. B, Effect of 2.0 and 10.0 mM $Na^+$ on $E_m$ before NEM treatment. C, Effect of 2.0 and 10.0 mM $Na^+$ on NEM-treated cells (schedule of treatment as described for A). Potassium concentration was 0.2 mM $K^+$. D, Effect of the replacement of 4.0 mM $K^+$ with 4.0 mM $Rb^+$ (NEM-pretreatment as described for A).

**Effect of External Cations on the Membrane Potential and Resistance of NEM-Treated Cells.** Under normal conditions, the membrane potential and resistance of Characean cells in the light respond minimally to potassium at a concentration below 1.0 mM (30); above this concentration (typically 2–3 mM $[K^+]$), the membrane behaves as a $K^+$ 'electrode' (20, 29). After treatment with NEM, the membrane potential changed with respect to external $[K^+]$ with a 59 mv per decade response (Fig. 3A). In this state, membrane resistance behaved as a function of external $K^+$ concentration (data not shown). This was observed even in the presence of 2 mM $Sr^{2+}$, an agent which has been found to prevent the $K^+$-induced inhibition of $HCO_3^-$ influx in *Chara*, presumably through protection of the normal potassium channels (20).

External potassium at a concentration greater than 2 to 3 mM in pre- or post-NEM treated cells often elicited action potentials (Fig. 3A, inset). The shape and duration of the action potentials were similar under both control and inhibited conditions, although no systematic investigation of this phenomena was undertaken.

As was found previously for *Nitella translucens* (29), the membrane potential did not respond dramatically to changes in the external sodium concentration (Fig. 3B). In the post-NEM, depolarized state, the sodium effect remained unaltered (Fig. 3C).

Substitution of $K^+$ with an equal concentration of rubidium in cells treated with NEM caused a partial repolarization of the membrane potential (Fig. 3D) and an increase in the resistance of greater than 7-fold (data not shown).

In experiments where $SO_4^{2-}$ anion completely replaced $Cl^-$ ($Cl^-$-free media), no change in pattern or magnitude of the above-mentioned responses was noted.

**Effect of pH on the Membrane Potential and Resistance.** In control cells, the membrane potential depolarized by about 40 mv when pH was changed from 8.0 to 6.0. A return to pH 8.0 resulted in the repolarization of the membrane potential (Fig. 4A). The hyperpolarizing response was often accompanied by an overshoot of the potential. Resistance remained constant during these pH shifts.

Treatment with NEM altered this pH response. While the original direction of the change in membrane potential was conserved, the magnitude of the peak depolarization and hyperpolarization was reduced. In addition, the initial rapid change in potential associated with the pH shift was transient. Within 1 to 2 min, the membrane potential returned to $E_K$ (Fig. 4B). Increasing the external potassium concentration depolarized the cells further (Fig. 4, C and D) and eliminated the sensitivity of the cells to external pH. (Three spontaneous action potentials are depicted in Fig. 4C.)

**Effect of PCMBS on $E_m$ and $R_m$.** The nonpermeant sulfhydryl modifier, PCMBS, also caused a decrease in $E_m$ towards $E_K$ when applied at a concentration of 0.5 or 1.0 mM (Fig. 5, A and B). Removal of PCMBS from the experimental medium allowed the potential to recover towards the preinhibition value. A small decrease in resistance values was noted between the control and depolarized states (data not shown).

In the depolarized state and in the presence of PCMBS, the membrane potential was sensitive to external $K^+$ concentration, responding with a depolarization of 35 mv per 10-fold increase in $[K^+]_0$ (Fig. 5B). Under these conditions, changes in $Na^+$ concentration produced a negligible effect on $E_m$ (Fig. 5B).

**Effect of NEM on the ATP Level of *Chara* Cells.** After a 15-min exposure to 0.1 mM NEM, ATP levels remained unaffected with respect to the control (Table I). After 15 min in 1.0 mM NEM, a 10-fold higher concentration than was used in electrophysiological experiments, the ATP level was reduced to about one-half of that found in normal cells.

**$^{42}K^+$ Influx into NEM-Treated and Control Cells.** $^{42}K^+$ absorption by *Chara* internodal cells was measured to assess the effect of NEM on potassium influx. Control cells showed increasing $K^+$ influx with increasing external potassium concentration (Table II). At low (0.2 and 0.8 mM) potassium levels, treatment with NEM caused an increase of greater than 2-fold in potassium influx. At higher $[K^+]_0$, influx was marginally affected by NEM treatment (Table II).

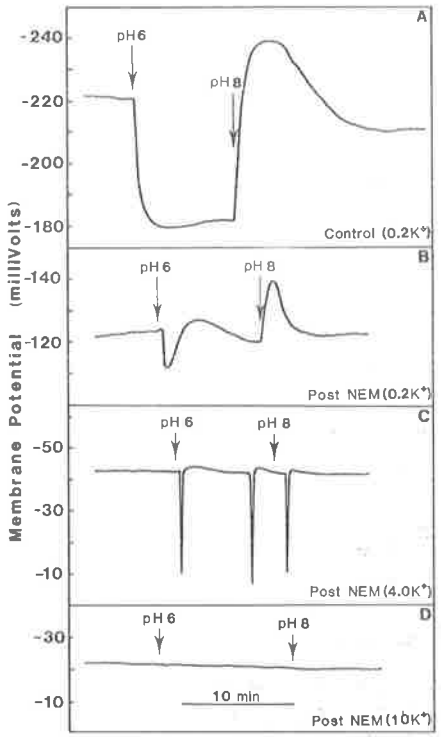


FIG. 4. Effect of $pH_0$ on the membrane potential of *C. corallina* before and after NEM treatment. Measurements of membrane potentials and preparation and composition of experimental media were as described in "Materials and Methods." For pH 6 solutions, 1.0 mM Mes replaced 1.0 mM TAPS. A, Effect of $pH_0$ on control cells. B, Effect of $pH_0$ on cells treated four times with a schedule of 0.5-min exposure to NEM (0.1 mM) /12-min CPW plus 1.9 TAPS. $[K^+]_0$ = 0.2 mM. C, Effect of $pH_0$ on cells treated with NEM as described in B; $[K^+]_0$ = 4.0 mM. D, Effect of $pH_0$ on cells treated with NEM as described in B; $[K^+]_0$ = 10 mM.

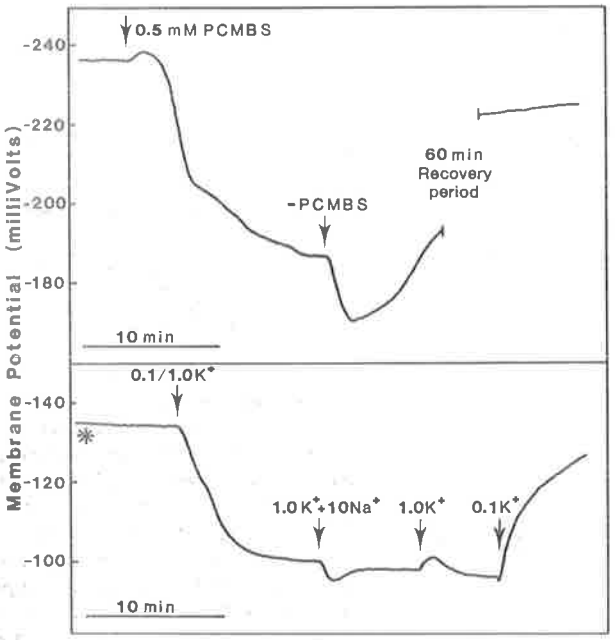


FIG. 5. Effect of PCMBS on the membrane potential and its response to cations in the bathing solution. Measurements of membrane potentials are described in "Materials and Methods." A, Effect of 0.5 mM PCMBS. B, Effect of 1.0 mM PCMBS. Asterisk indicates 70-min exposure to PCMBS. Subsequent $K^+$ and $Na^+$ concentration changes were made in the presence of 1.0 mM PCMBS.

Table I. *Effect of NEM on ATP Levels in C. Corallina*

Control cells were illuminated (20 w $m^{-2}$) for 87 min (25 C). NEM-treated cells were pretreated for 60 min in the light, exposed to NEM for 15 min, and placed in NEM-free solutions for 12 min. ATP concentrations were calculated assuming that the cytoplasm occupies 5% of the total cell volume.

| Treatment | ATP Level | Control |
|---|---|---|
| | *mM* | % |
| Control | 6.47 ± 0.61 (9)[a] | 100 |
| NEM, 0.1 mM | 5.89 ± 0.78 (8) | 91 |
| NEM, 1.0 mM | 3.08 ± 0.58 (9) | 48 |

[a] Number of samples.

## DISCUSSION

In Characean cells, under normal conditions and in the light or dark, the measured membrane potential is more negative than is the value of the diffusion potential, as predicted by the Goldman equation (8). This hyperpolarized condition is the result of at least two electrogenic ion transport processes (pumps) operating across the plasmalemma: the proton extrusion mechanism, most likely a $H^+$-ATPase (8, 10, 27, 29) and the $HCO_3^-$ and $OH^-$ transport processes (16, 17). In the presence of bicarbonate at a pH above 7 and $[K^+]_0 < 2$ mM, both of these systems contribute to, and dominate, the total membrane conductance (since the measured conductance is at least an order of magnitude larger than that predicted from diffusion through the passive channels), and, hence, set the value at which the membrane potential rests. It is presently assumed that $g_m$ can be represented as the sum of that through the passive channels, $g_D$, and that through the pump, $g_p$ (29). The value for the membrane potential may be changed by altering the relative contribution of the individual components to the total membrane conductance. Thus, a decrease in the membrane potential from the hyperpolarized state to that predicted by the Goldman equation may be accomplished by the inhibition of the electrogenic process(es) or by an increase in the conductance of the passive ionic channels or by a combination of both.

The administration of NEM to *C. corallina* in the absence of added bicarbonate causes a decrease in $E_m$ to, or below, $E_K$ (Fig. 1, A and B; Fig. 2). In experiments designed to minimize the contribution of passive conductance by decreasing the external potassium concentration to 20 μM (results presented in Fig. 2), $E_m$ is controlled in the nontreated state by the electrogenic pumps, since values of $E_m$ are more negative than those of $E_K$. During NEM exposure, electrogenicity is lost as $E_m$ becomes depolarized below the theoretically calculated $E_{K(0.02)}$ of −180 mv. In this regard, the concentration of potassium in the experimental medium (20 μM) probably represents an underestimate of actual $K^+$ level within the cell wall, since leakage of $K^+$ from the cell during depolarization would tend to deplete $K^+$ from the vicinity of the cytoplasmic face of the plasmalemma and increase $K^+$ concentration immediately external to the membrane (where potassium movement through the wall into the bulk solution would be limited by diffusion). This would tend to reduce the $K^+$ concentration profile and make the measured $E_K$ less negative than predicted. The conductance of the membrane remained essentially unchanged from pre-NEM values. These results may be explained by two mechanisms of action by NEM.

First, NEM may alter the functionality of the electrogenic proton pump by separating pump conductance from ATP hydrolysis. This would be consistent with the observation that NEM treatment for 15 min at 1.0 mM concentration did not inhibit membrane ATPase activity, as detected microscopically by visualization of the reaction of the ATPase with Mg·ATP, followed by precipitation of the reaction product (Pi) with lead (Franceschi

Table II. *Effect of NEM on $^{42}K^+$ Influx into C. Corallina*

Control cells were pretreated (20 w $m^{-2}$, 25 C) in their respective $K^+$ solutions for 30 min, and the $^{42}K^+$ was added for either 30 min (0.2, 0.8, and 1.8 $K^+$) or 15 min (10.8 $K^+$). Following a 15-min pretreatment in 0.2 $K^+$ control solution, NEM-transport cells were given two 0.5-min NEM (0.1 mM) per 12 min control solution pulses before being exposed to the indicated $^{42}K^+$ treatment (15-min duration). All cells were given a brief (2–5 min) wash in nonradioactive medium (1–2 C). See "Materials and Methods" for details relating to correction for cell wall binding.

| | $K^+$ Concentration[a] | | | |
|---|---|---|---|---|
| | 0.2 | 0.8 | 1.8 | 10.8 |
| | mM | | | |
| Control | 1.81 ± 0.2 | 6.4 ± 0.4 | 22.3 ± 1.6 | 103 ± 6.3 |
| NEM | 4.5 ± 0.4 (250%)[b] | 13.2 ± 1.4 (206%) | 28.1 ± 1.6 (126%) | 119 ± 11 (116%) |

[a] Experimental solutions contained 1.0 mM NaCl, 0.2 mM $CaSO_4$, 1.0 mM TAPS (pH 8.0) plus the indicated levels of $K^+$.

[b] Per cent stimulation.

and Lucas, unpublished) as well as with our results presented in Table I, where ATP levels were unaffected during brief exposure to 0.1 mM NEM. This uncoupling of potential and conductance may be caused by a perturbation of the enzyme structure itself or of the microenvironment in close proximity to the proton channel. Such an effect, of separating proton current from ATP synthase activity (termed 'energy transfer inhibition' by Moroney *et al.* [22]) is seen also in isolated chloroplasts exposed to sulfhydryl reagents (23, 30). The value to which $E_m$ would fall under this condition would be of complex origin, depending on the contributions of the relative conductances of the active and passive ion channels and the concentrations of the ionic species involved. The eventual decrease in conductance seen with increased NEM exposure may be due to a blockage of the conductance pathway of the electrogenic pump as well as the inhibition of other transport systems in the membrane, such as $Cl^-$ influx (26), $OH^-$ efflux (17, 18), and $Na^+$ extrusion (21). It is also of interest to note that these latter systems are light-stimulated; if they represent major conductance pathways in the membrane, then the regulation of transport by light may account for the rise of the membrane resistance in the dark.

A second interpretation is that the electrogenic $H^+$-translocator is without conductance, acting as a constant current source in a manner similar to the plasmalemma $H^+$-ATPase of *Neurospora crassa* (28). In this case, elimination of the potential derived from the electrogenic pump may be due to short-circuiting the pump through an increased $K^+$ conductance (results discussed below). The potential would then fall to $E_K$ which, for reasons stated above, may be less negative than predicted for 20 $\mu$M $K_o^+$. If the $H^+$-translocator is without conductance, then the rise in resistance seen later during NEM exposure must be due to the inhibition of other ion transport systems that operate in an electrogenic manner across this membrane (see above).

Regardless of the mechanism by which the electrogenic component of the potential is lost, it is clear that NEM treatment causes an increase in $K^+$ membrane conductance, since the membrane potential becomes very sensitive to $[K^+]_o$ after NEM treatment (Fig. 3A) while retaining its relative insensitivity to $[Na^+]_o$ (Fig. 3, A and B). This sensitivity to potassium is retained even in the presence of 2 mM $Sr^{2+}$, which protects the membrane from calcium displacement and is thereby thought to maintain the normal function of the $K^+$ channels (20). Changes in chloride permeability are not likely to be involved, since replacement of $Cl_o^-$ by $SO_4^{2-}$ does not alter the effect of NEM, and the value to which the membrane potential moves is $E_K$ rather than $E_{Cl}$.

This interpretation of the effect of NEM on passive $K^+$ conductance is strengthened by $^{42}K^+$ influx studies (Table II). Under conditions where the membrane is normally freely permeable to $K^+$ (*i.e.* at 1.8 and 10.8 mM $[K^+]_o$), only a small increase in potassium permeability can be seen after treatment with NEM. However, at low $[K^+]_o$ of 0.2 and 0.8 mM, where the membrane is normally in a potassium-insensitive state, NEM causes a greater than 2-fold stimulation of $^{42}K^+$ influx.

Our interpretation that NEM causes increased $P_K$ can be used to present a possible explanation for the effect of pH on the membrane potential. Under normal conditions, changing external pH causes a change in membrane potential (Fig. 4A). This potential at pH 8 or pH 6 is always more negative than $E_K$, providing a driving force for passive potassium influx. In the period after NEM-exposure, the membrane is made more permeable to potassium, and $E_m$ decreases to $E_K$. Changing external pH from 8 to 6 initially displaces the membrane potential towards a more positive value, forcing a temporary net $K^+$ efflux until $E_m$ returns to $E_K$ (Fig. 4B). Similarly, increasing pH from 6 to 8 causes a hyperpolarization favoring a net $K^+$ influx which resets the membrane potential to $E_K$. Increasing the external potassium concentration increases the magnitude of the unidirectional $K^+$ fluxes (Table II) such that the pH-induced shifts in $E_m$ become increasingly reduced (Fig. 4, C and D). At 10 mM $[K^+]_o$, the $K^+$ fluxes dominate the unidirectional fluxes crossing the membrane, and, thus, there are no discernible pH transients.

PCMBS-treated cells also exhibit an increased $P_K$, as evidenced by the decrease in membrane potential to $E_K$ (Fig. 5, A and B) and the increased sensitivity of the membrane potential of these cells to external potassium concentrations (Fig. 5B). As with NEM treatment, PCMBS had no discernible effect on $P_{Na}$ (as judged from the effect of sodium on the membrane potential, Fig. 5B) or membrane resistance (data not shown).

Our results support the hypothesis that NEM and PCMBS affect the generation or maintenance of the electrogenic potential as well as the potassium permeability of the plasmalemma of *C. corallina.* This latter finding is in accordance with conclusions reached by Bogucka and Wojtczak (2) for mitochondrial membranes, Knauf and Rothstein (11) for red blood cells, and others (reviewed in Rothstein, Ref. 25). In other systems, the permeability of the cell membranes to other cations, especially sodium, has also been enhanced (1, 31).

The initial hyperpolarizing effect of NEM on *Chara* in the presence of $HCO_3^-$ is consistent with the observations of Lucas and Alexander (18), where both $OH^-$ efflux activity and $HCO_3^-$ assimilation were found to be reduced by NEM. Inasmuch as these systems work in synchrony (19), a decrease in the capacity of one system demands a corresponding change in the second. Under NEM inhibition, a reduction in $OH^-$ efflux would initially allow a net transfer of negative charge into the cell, causing a hyperpolarization of the membrane potential (Fig. 1A). The increase in alkalinity generated by continued $HCO_3^-$ assimilation must eventually be countered by $OH^-$ extrusion, possibly by the generation of new $OH^-$ efflux sites as suggested by Lucas and Alexander (18). This increased $OH^-$ extrusion would lead to a depolarization of the membrane potential and a return to the original resting value, consistent with our observations.

As mentioned in "Results," the peak depolarization occurring with NEM exposure is below $E_K$; this is accompanied by a sharp decrease in $R_m$. Both the depolarization below $E_K$ and the decrease in $R_m$ are transient as the membrane potential repolarizes and remains steady at $E_K$, and $R_m$ stabilizes close to, or above, the original value. This suggests that the membrane becomes temporarily permeable to other ion(s) in the presence of NEM. At pH 8 and in CPW, $E_{Na}$, $E_{Cl}$, $E_H$, and $E_{Ca}$ are all more positive than $E_K$; transient increases in the permeabilities of any of these ions may be responsible for this phenomenon.

The increase in permeability to potassium subsequent to NEM

and PCMBS exposure and the corresponding depolarization of the membrane potential offers an alternative interpretation to recent work involving effects of sulfhydryls on secondary active transport processes. For example, in $HCO_3^-$ and $OH^-$ transport in *Chara*, the transition to the facilitated diffusion (or $HCO_3^-$-leaky) mode (18) after NEM treatment may result from a short circuit of the driving force for $HCO_3^-$ uptake or, perhaps, from the depolarization of $E_m$ below a critical level that is needed to drive $OH^-$ efflux. Indeed, this situation may be similar to that postulated by Lanyi and Silverman (13) for *Halobacterium halobium* transport systems. These investigators proposed that the transmembrane electrochemical gradients act both as components of the driving force in the transport of electrically-charged substrates ($H^+/Na^+$ exchange; $Na^+$/amino acid cotransport) and as regulators of these processes. Modulation of transport activity is achieved as values for these gradients reach a threshold, beyond which the transporters function in an altered fashion. As an example, they have shown that $Na^+$-coupled amino acid fluxes exhibit different stoichiometries as a function of the membrane potential and, thus, are voltage-gated.

The sulfhydryl-mediated decrease in transport ability of the sucrose carrier involved in phloem loading (5) may also be due to a depolarization of $E_m$ to $E_K$, since it is presently thought that the membrane potential provides an important component of the driving force for proton-coupled cotransport systems. Lichtner and Spanswick (15) have demonstrated that NEM and PCMBS depolarize the membrane potential to $E_K$ in developing soybean cotyledons and eliminate sucrose-induced transient depolarizations of the membrane potential. Buffer washes following administration of PCMBS, but not of NEM, allow a repolarization of $E_m$ to its original hyperpolarized state, consistent with results presented here. However, in the soybean system, the mechanism of PCMBS inhibition of sucrose cotransport appears to involve a modification of the sucrose carrier itself. PCMBS-induced depolarization of $E_m$ also is observed in *Lemna* fronds (4). Here, $E_m$ is depolarized to a value that is approximately 15 mv more positive than is the calculated $E_K$ (23). However, transient depolarization of the membrane potential upon administration of the amino acid glycine was not eliminated by PCMBS treatment.

Transport mechanisms responsible for substrate movement across the plasmalemma in higher plant cells may also be differentially sensitive to sulfhydryl reagents. However, the lack of a reliable method for measurement of cell resistance (3) makes the interpretation of data from higher plant systems difficult and speculative.

In conclusion, the sulfhydryl reagents NEM and PCMBS have complex effects on the electrical characteristics of the *C. corallina* plasmalemma. These reagents depolarize $E_m$ to, or below, $E_K$ in a manner not consistent with a simple inhibition of a voltage-dependent electrogenic pump having conductance. In addition, NEM and PCMBS alter potassium permeability. These results suggest that inhibition of transport function by sulfhydryl reagents in both algae and higher plants may be explained by mechanisms other than direct interaction with the carrier protein. In view of these results, a reevaluation of the effects of these reagents on membrane transport processes seems warranted.

## LITERATURE CITED


1. Biber J, H Hauser 1979 The role of SH-groups in the concentrative transport of D-glucose into brush border membrane vesicles. FEBS Lett 108: 451–456
2. Bogucka K, L Wojtczak 1979 On the mechanism of mercurial-induced permeability of the mitochondrial membrane to $K^+$. FEBS Lett 100: 301–304
3. Etherton B, DW Keifer, RM Spanswick 1977 Comparison of three methods for measuring electrical resistances of plant cell membranes. Plant Physiol 60: 684–688
4. Fischer E, A Novacky 1980 Effect of PCMBS and DCCD on membrane potential of *Lemna gibba* G1. *In* RM Spanswick, WJ Lucas, J Dainty, eds, Plant Membrane Transport: Current Conceptual Issues. Elsevier/North Holland, Amsterdam, pp 553–554
5. Giaquinta RT 1976 Evidence for phloem loading from the apoplast. Chemical modification of membrane sulfhydryl groups. Plant Physiol 57: 872–875
6. Hendrix DL, N Higinbotham 1974 Heavy metals and sulphhydryl reagents as probes of ion uptake in pea stem. *In* U. Zimmermann, J Dainty, eds, Membrane Transport in Plants. Springer-Verlag, New York, pp 412–417
7. Hogg J, EJ Williams, RJ Johnston 1968 A simplified method for measuring membrane resistances in *Nitella translucens*. Biochim Biophys Acta 150: 518–520
8. Keifer DW, RM Spanswick 1978 Activity of the electrogenic pump in *Chara corallina* as inferred from measurements of the membrane potential, conductance and potassium permeability. Plant Physiol 62: 653–661
9. Keifer DW, RM Spanswick 1979 Correlation of adenosine triphosphate levels in *Chara corallina* with the activity of the electrogenic pump. Plant Physiol 64: 165–168
10. Kishimoto U, N Kami-Ike, Y Takeuchi 1980 The role of electrogenic pump in *Chara corallina*. J Membr Biol 55: 149–156
11. Knauf PA, A Rothstein 1971 Chemical modification of membranes. I. Effects of sulfhydryl and amino reactive reagents on anion and cation permeability of the human red blood cell. J Gen Physiol 58: 190–210
12. Komor E, H Weber, W Tanner 1978 Essential sulfhydryl group in the transport-catalyzing protein of the hexose-proton cotransport system of *Chlorella*. Plant Physiol 61: 785–786
13. Lanyi JK, MP Silverman 1979 Gating effects in *Halobacterium halobium* membrane transport. J Biol Chem 254: 4750–4755
14. Läuchli A 1969 Radioassay for $\beta$-emitters in biological materials using Cerenkov radiation. Int J Appl Radiat Isot 20: 265–270
15. Lichtner FT, RM Spanswick 1981 Electrogenic sucrose transport in developing soybean cotyledons. Plant Physiol 67: 869–874
16. Lucas WJ 1975 Photosynthetic fixation of $^{14}$carbon by internodal cells of *Chara corallina*. J Exp Bot 26: 331–346
17. Lucas WJ 1976 Plasmalemma transport of $HCO_3^-$ and $OH^-$ in *Chara corallina*: non-antiporter systems. J Exp Bot 27: 19–31
18. Lucas WJ, JM Alexander 1980 Sulfhydryl group involvement in plasmalemma transport of $HCO_3^-$ and $OH^-$ in *Chara corallina*. Plant Physiol 65: 274–280
19. Lucas WJ, R Nuccitelli 1980 $HCO_3^-$ and $OH^-$ transport across the plasmalemma of *Chara*: spatial resolution obtained using extracellular vibrating probe. Planta 150: 120–131
20. Lucas WJ, RM Spanswick, J Dainty 1978 $HCO_3^-$ influx across the plasmalemma of *Chara corallina*: physiological and biophysical influence of 10 mM $K^+$. Plant Physiol 61: 487–493
21. MacRobbie EAC 1970 The active transport of ions in plant cells. Quarterly Rev Biophys 3: 251–294
22. Moroney JV, CS Andreo, RH Vallejos, RE McCarty 1980 Uncoupling and energy transfer inhibition of photophosphorylation by sulfhydryl reagents. J Biol Chem 255: 6670–6674
23. Novacky A, CI Ullrich-Eberius, U Lüttge 1978 Membrane potential changes during transport of hexoses in *Lemna gibba* G1. Planta 138: 263–270
24. Okada V, A Inouye 1975 Tip potential and fixed charges on the glass wall of microelectrode. Experimentia 31: 545–546
25. Rothstein A 1970 Sulfhydryl groups in membrane structure and function. *In* F Bronner, A Kleinzeller, eds, Current Topics in Membranes and Transport, Vol 1. Academic Press, New York, pp 135–176
26. Sanders D 1980 Control of plasma membrane $Cl^-$ fluxes in *Chara corallina* by external $Cl^-$ and light. J Exp Bot 31: 105–118
27. Shimmen T, M Tazawa 1977 Control of membrane potential and excitability of *Chara* cells with ATP and $Mg^{2+}$. J Memb Biol 37: 167–192
28. Slayman CL, WS Long, Cy-H Lu 1973 The relationship between ATP and an electrogenic pump in the plasma membrane of *Neurospora crassa*. J Memb Biol 14: 305–338
29. Spanswick RM 1972 Evidence for an electrogenic ion pump in *Nitella translucens*. I. The effects of pH, $K^+$, $Na^+$, light and temperature on the membrane potential and resistance. Biochim Biophys Acta 288: 73–89
30. Underwood C, JM Gould 1980 Proton efflux through the chloroplast ATP synthase ($CF_0 \cdot CF_1$) in the presence of sulfhydryl-modifying agents. Biochim Biophys Acta 589: 287–298
31. Will PC, U Hopfer 1979 Apparent inhibition of active non-electrolyte transport by an increased sodium permeability of the plasma membrane. Mechanism of action of *p*-chloromercuribenzene sulfonate. J Biol Chem 254: 3806–3811
32. Willard JM, JJ Davis, HG Wood 1969 Phosphoenolpyruvate carboxytransphosphorylase. IV. Requirement for metal cations. Biochemistry 8: 3137–3144

Protoplasma 107, 255—267 (1981

PROTOPLASMA
© by Springer-Verlag 1981

# Characean Charasome-Complex and Plasmalemma Vesicle Development

W. J. Lucas * and V. R. Franceschi

Department of Botany, University of California, Davis, California

Received January 16, 1981
Accepted May 5, 1981

## Summary

We report on an unusual phenomenon which occurs in some characean algae as a normal plasma membrane activity and also in association with charasome formation. The phenomenon of formation of coated invaginations of the plasma membrane was observed in two *Chara* and 6 *Nitella* species. These invaginations are coated on their cytoplasmic surface, are 50–60 nm in diameter and rarely exceed 60 nm in length. They are abundant in the young cells of *Chara* and *Nitella* and also occur in mature cells, but at a lower frequency. *N. translucens* is an exception in that coated invaginations were few in the young cells and absent in mature cells. Coated vesicles (50–60 nm diameter) were closely associated with these invaginations. Our observations suggest the vesicles may be derived from the invaginations by endocytosis.

A close relationship was noted between the development of charasomes (plasmalemma modifications) and coated invaginations. Numerous coated invaginations are seen along the membranes of young charasomes; these invaginations appear to be associated with growth of the charasomes. Coated vesicles were not associated with the coated invaginations of the charasome membrane. The tubular network of cytoplasm and wall space seen in the mature charasome may be formed by fusion of coated invaginations of the developing charasomes, leaving cytoplasmic strands between the fused portions. Coated invaginations were not present along charasomes of the mature cells.

*Keywords: Chara;* Charasome development; Coated membrane vesicles; Endocytosis; *Nitella;* Plasmalemma invaginations.

## 1. Introduction

The giant algae of the genera *Chara* and *Nitella* have been used extensively in studies of membrane transport phenomena; however, very little correlative structural works has been done on the mature cells. In two brief publications,

* Correspondence and Reprints: Department of Botany, University of California, Davis, CA 95616, U.S.A.

0033-183X/81/0107/0255/$ 02.60

Barton (1965 a) and Crawley (1965) independently reported the occurrence of unusual membranous structures along the plasmalemma in some *Chara* and *Nitella* species. Barton (1965 b) called these structures "charasomes". The structure of the charasome was not well defined in these early papers and its origin also remained unresolved. In a recent paper (Franceschi and Lucas 1980) we described in detail the structural and morphological features of the charasome and found that the charasome is actually an elaborate extension of the plasmalemma. This complex membranous structure can be quite variable in size and shape but its ultrastructural features are constant. The charasome-complex consists of a mass of anastomosing membrane tubules of approximately 50 nm in length and 30 nm in diameter. The tubules enclose cytoplasmic material, are ultimately open to the cytoplasm, and are surrounded by a nonmicrofibrillar wall space or periplasmic space (Franceschi and Lucas 1981). The tremendous increase in plasmalemma surface area and the formation of a periplasmic space within the charasome hold special significance in relation to transmembrane transport processes.

The function of the charasome-complex remains unknown. Barton (1968), using autoradiography, could find no association of charasomes with wall formation. We examined the hypothesis that charasomes are related to the spatially separated $OH^-$ and $HCO_3^-$ transport sites in *Chara* and *Nitella* internodes (see Lucas 1980), but could find no such relationship (Franceschi and Lucas 1980). We then hypothesized that the charasome-complex may be involved in transport of $Cl^-$ as osmoticium for expansion growth. This present paper is a report of our investigations into the formation and development of this complex system. We also report on a membrane phenomenon, invagination of the plasmalemma, which is associated with developing charasomes but which also occurs in cells in which charasomes have not, or will not be, formed. This phenomenon closely resembles the pinocytotic process (endocytosis) reported in animal tissues (Silverstein, Steinman and Cohn 1977) but thought to be nonexistant in plants (Cram 1980). Our explorations of this possibility are presented.

## 2. Materials and Methods

The algae used in this study were *Chara corallina*, *C. braunii*, *C. globularis*, *Nitella axillaris*, *N. clavata*, *N. dualis*, *N. flexilis*, *N. furcata*, and *N. translucens*. *C. braunii*, *C. globularis*, *N. dualis*, and *N. furcata* were collected from a small fresh water pond in Napa county, California, U.S.A. *C. corallina* came from cultures grown in our laboratory and *N. clavata* and *N. axillaris* were provided from the laboratory cultures of Dr. C. E. Barr (State University College, Brockport, N.Y.) and Dr. J. P. Metraux (University of California, Berkeley). Portions of plants of various stages of maturity were prepared for transmission electron microscopy (TEM) as previously described (Franceschi and Lucas 1980). The TEM unit used was a JEOL JSM 100S. The algae were examined for the presence of charasomes and, in those which had charasomes, developmental details were resolved.

*2.1.* $^{14}$*C-Sorbitol Uptake*

Sorbitol uptake experiments were performed using radioactively labeled sorbitol ($^{14}$C-sorbitol obtained from New England Nuclear, Boston, MA). Experimental tissue was cut from the main culture and given an overnight pretreatment in a solution containing 1.0 mM $NaHCO_3$, 1.0 mM NaCl, 0.2 mM KCl, and 0.2 mM $CaSO_4$ (pH 8.0). Sorbitol experiments were conducted (10 $Wm^{-2}$, 25 °C) in an identical solution except that it contained 3 µM sorbitol (specific activity 325 mCi/mMole). Radioactivity was determined using liquid scintillation counting on a Beckman LS8000 scintillation spectrophotometer set for $^{14}$C counting.

*2.2. Paper Chromatography*

*Chara* cell sap and various standards, both radioactive and non-radioactive were spotted onto Whatman No. 1 filter paper (55 cm length) and developed for 10 hours with 3 : 3 : 2 butanol : acetic acid : water (descending). For labelling experiments, strips were scanned with a Packard Radiochromatogram Scanner (0.5 min/cm, 30 s time constant, 1.2 kVolts, 300 $cm^3$/min gas flow).

## 3. Results

Charasome formation was studied in detail in *C. corallina* and *C. braunii* and found to be the same in both species. The following results concerning structural aspects of charasome formation pertain equally to both species, unless otherwise noted. *C. globularis*, a corticated species, was found to have charasomes at those surfaces of the cortical cells facing the environment. Although this species was not examined in detail, preliminary studies suggest that charasome formation is similar to that seen in *C. corallina* and *C. braunii*. Charasomes were not found in any of the *Nitella* species examined.

*3.1. Charasome Development*

The stage of cell development during which charasome formation begins is probably variable and depends upon the culture conditions and the cells examined (internodes or first, second or third branch cell from the node). In our laboratory cultures, the second branch cell from the node of the main axis of the female plant of *Chara corallina* reaches a length of about 5 mm at maturity. This cell was used to investigate the relationship between charasome formation and cell elongation.

Cells 0.5 mm in length or less lack charasomes but contain numerous coated invaginations of the plasma membrane (Fig. 1), which will be described more fully in a following section. Coated invaginations are still quite common in 1 mm long cells, however, they are sometimes elongate in appearance (Fig. 2). When the cell reaches a length of 1–2 mm, small charasomes are numerous (Figs. 3–5). Coated invaginations of the charasome membrane have also been observed at this stage (Fig. 7).

The developing charasomes often contain cytoplasmic pockets lacking the network of membrane tubules (Figs. 6 and 7). Coated invaginations can often be seen protruding from the charasome membrane into the cytoplasmic

pockets (Fig. 6). These cytoplasmic pockets are uncommon in the mature charasomes, except for the poorly formed charasomes sometimes found in the hydroxyl ion efflux regions of the mature internode cells, as previously described (Franceschi and Lucas 1980). Coated invaginations of the charasome membranes are common in cells of 2 mm in length and less frequent in cells of 3 mm length, at which point the charasomes are quite large. The charasomes of the mature branch cell (5 mm long) may form a continuous mass along large portions of the plasma membrane (Fig. 8). Coated invaginations of the charasome membrane are absent in these mature cells.

The coated invaginations of the charasome membranes are apparently dynamic structures associated with the process of charasome formation. The membrane invaginations are "coated" at their cytoplasmic surface and have a diameter of 50–60 nm. The length of the coated portion of the invagination is variable, depending upon the stage of its formation, but rarely exceeds 60 nm. In the earliest clearly distinguishable developing charasomes there appear to be many coated invaginations protruding in different directions (Fig. 9). Occasionally, they can be seen protruding toward or around organelles such as mitochondria (Fig. 10). It must be noted that the coating is found only on the invaginations and not along any other part of the charasome membrane.

The interior of the coated invaginations is open to the wall space and thus these structures are apparently related to the formation of the periplasmic space. The cytoplasmic tubules apparent in the mature charasome must be formed by a different process. Although the complete details have not been resolved, it would appear that the cytoplasmic tubules are formed as a result

---

Figs. 1–8. Reconstruction of a possible charasome developmental sequence. All sections from female *Chara corallina* branch cells, second from the node, at various stages of elongation. Charasome (*C*), mitochondrion (*M*), cell wall (*W*). All ×50,000

Fig. 1. Cell 0.5 mm long. Arrow indicates coated invagination of plasma membrane and associated coated vesicle

Fig. 2. Cell 1.0 mm long. Arrow indicates elongated coated invagination

Fig. 3. Cell 1.5 mm long. Heavy arrow indicates very small, simple charasome. Smooth dictysome vesicles (small arrows)

Fig. 4. Cell 1.5 mm long. Arrow indicates slightly larger charasome than that of Fig. 3

Fig. 5. Cell 1.0 mm long. This small charasome (solid arrow) has a coated invagination at its surface in the plane of section (open arrow)

Fig. 6. Cell 2.0 mm long. Oblique section through a young charasome with a coated invagination protruding into a small enclosed cytoplasmic pocket (open arrow)

Fig. 7. Cell 1.5 mm long. Section through two young charasomes, one fairly large, but with a coated invagination at one end (heavy arrow) and a smaller charasome with 2 small cytoplasmic pockets. Smooth dictyosome vesicles (small arrows)

Fig. 8. Cell 5.0 mm long. Portion of a large charasome formation in a mature cell. Notice close association of mitochondria and charasome

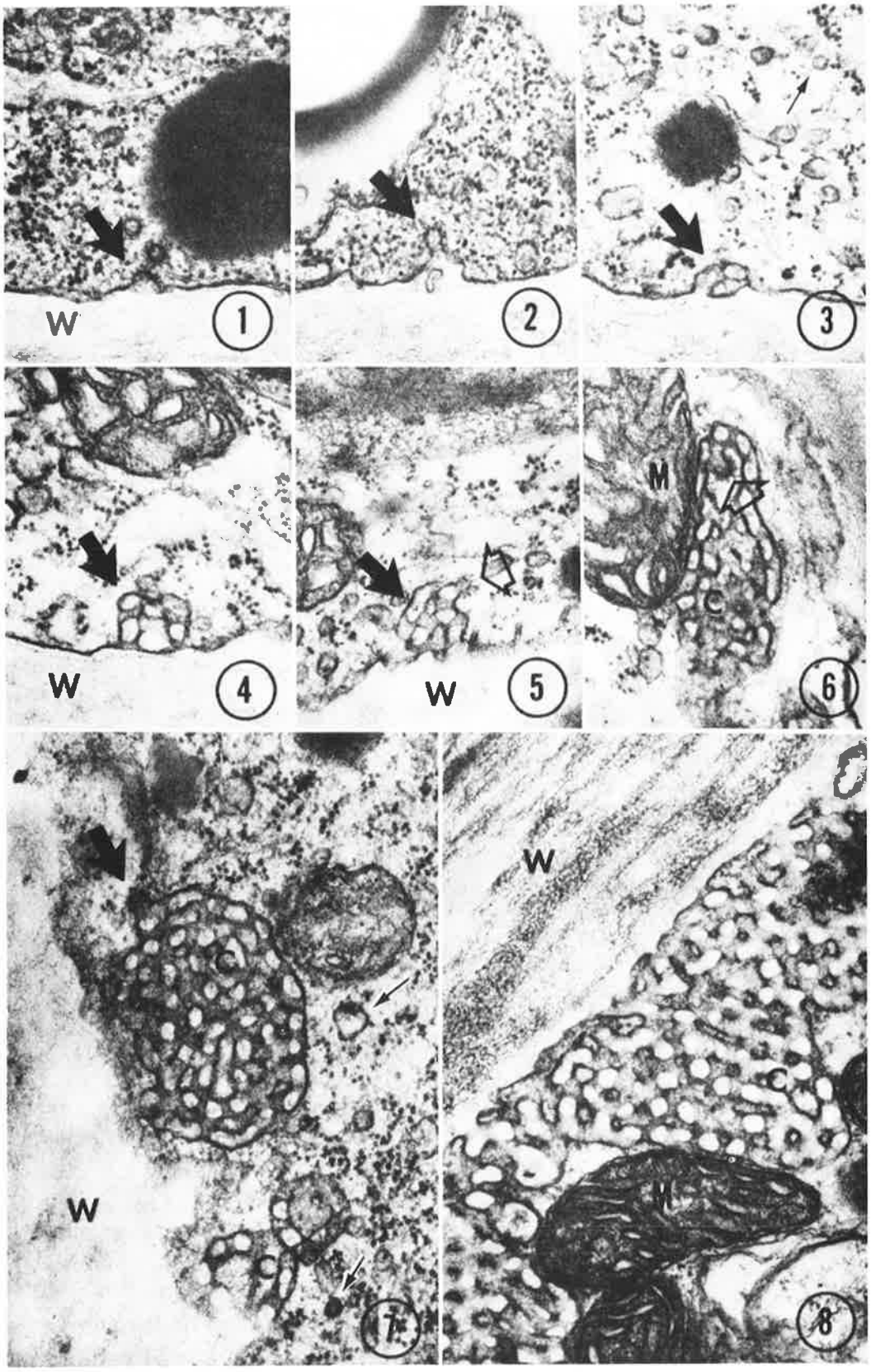
W
1
2
3
W
4
W
5
M
C
6
W
7
W
8

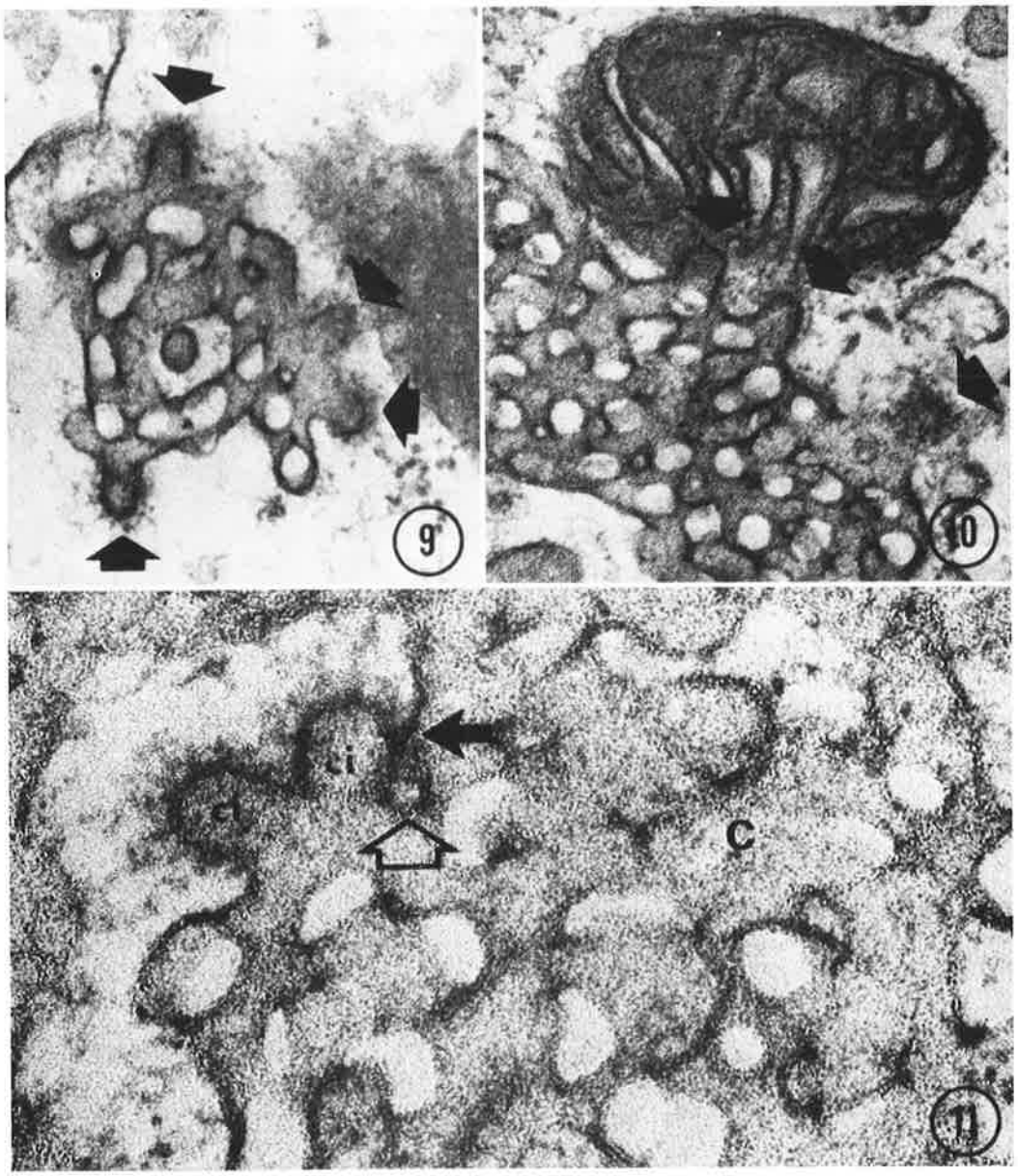


Fig. 9. Tangential section through a developing charasome from a very young branch cell (1.5 mm long). Four coated invaginations of the charasome membrane can be seen (arrows). ×70,000

Fig. 10. Tangential section through a developing charasome with three coated invaginations (arrows), two of which are growing along a mitochondrion. ×70,000

Fig. 11. Tangential section of charasome with two coated invaginations (*ci*). Portion of one invagination appears to be fusing with previously formed charasome membrane (dark arrow). This fusion may result in the formation of a cytoplasmic tubule (open arrow). ×147,600

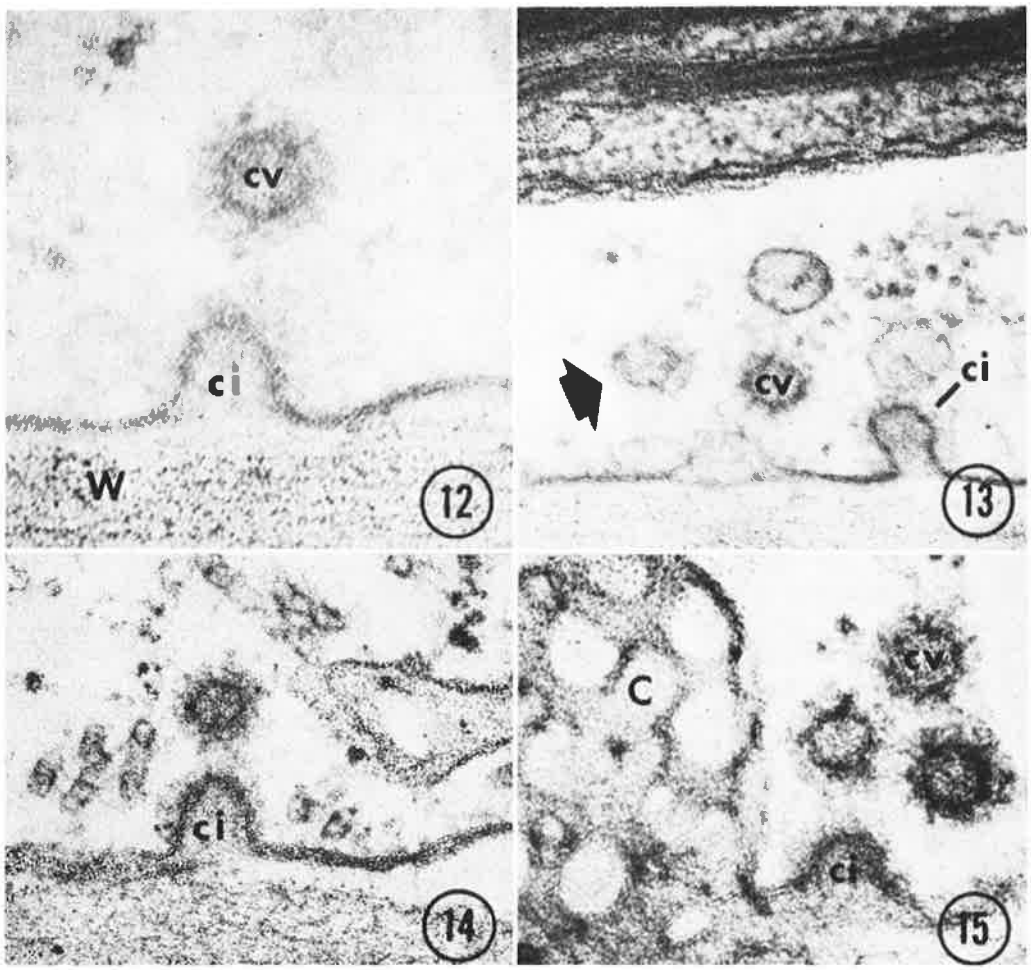


Figs. 12–15. Coated invaginations and coated vesicles. Charasome (C), coated invagination (*ci*), coated vesicle (*cv*), wall (*W*)

Fig. 12. Coated invagination with coated vesicle above it. ×176,100

Fig. 13. Coated invagination and 2 coated vesicles. Note shape and size of invagination compared to that of vesicles. Also vesicle furthest from invagination is only partially coated (arrow). ×107,500

Fig. 14. Coated invagination and vesicle. Vesicle appears hexagonal in section. ×105,100

Fig. 15. Coated invagination and vesicles closely associated with a charasome. From a section thicker (dark gold/brown) than those normally used. ×131,800

of fusion of one coated invagination with another, or with some other part of a charasome, leaving a cytoplasmic strand between the fused membranes. An example of this fusion process is indicated in Fig. 11.

### *3.2. Plasmalemma Invaginations*

Simple invaginations of the plasmalemma are also a consistent feature of young vegetative cells of *C. corallina, C. braunii, N. axillaris, N. clavata, N. dualis, N. flexilis,* and *N. translucens.* These invaginations are approximately 50–60 nm in diameter and are coated on their cytoplasmic surface.

Fig. 16. Two coated invaginations (arrows) surrounded by a charasome (C). The invaginations appear to have filled the cytoplasmic pocket within the young charasome with vesicles (*V*). The density of the central region of these spherical structures indicates that they are, in fact, vesicles and not cross-sections of tubules, which would have an electron lucent center. The nearby dictyosome (*D*) does not appear to be involved in coated vesicle formation. Mitochondrion (*M*). ×97,700

Cytoplasmic coated vesicles (50–60 nm) are generally found in association with the invaginations (Figs. 12–15). Coated vesicles are not associated with the coated invaginations of the charasome membranes. The vesicles furthest away from the invaginations are often uncoated or only partially coated (Fig. 13). When sectioned, these coated vesicles may appear 5 or 6 sided (Fig. 14). This is probably due to the coating itself which in glancing sections of coated vesicles appears as a polygonal network of material.

As mentioned above, the coated invaginations appear to be associated with charasome formation in growing cells of *Chara*. Developing charasomes and invaginations of the plasmalemma (with associated coated vesicles) can be found adjacent to each other during certain developmental stages of the cell (Fig. 15). In some instances we have found coated invaginations and vesicles surrounded by the membranes of a developing charasome (Fig. 16). Such observations suggest that the coated vesicles may well be formed from the coated invaginations of the plasmalemma.

The close association of dictyosomal vesicles with the plasmalemma is documented in numerous systems. This also seems to be the case in *Chara*, however, the vesicles are of the uncoated type and of various sizes (see Figs. 3, 7, and 16). Coated vesicles are found associated with dictyosomes of young cells but the dictyosomes were rarely seen in the vicinity of the plasmalemma or coated invaginations. In the few instances where we saw dictyosomes near the plasmalemma they did not appear to be involved in coated vesicle formation, although they did appear to be active in formation of smooth vesicles (Fig. 16).

Physiological studies using $^{14}$C-sorbitol indicated that it entered the cell in a manner consistent with an endocytotic mode. However, chromatograms indicated cellular metabolism of the sorbitol, and thus the results remain inconclusive (data not shown).

Colloidal gold was also used to test for the presence of endocytosis. These experiments were inconclusive, because the gold droplets did not penetrate through the cell wall. Lanthanum was also used and although it penetrated the cell wall it appeared to be excluded from both the coated invagination lumen and the periplasmic space of the charasomes (data not shown).

## 4. Discussion

The ultrastructural aspects of charasome formation are very interesting in the light of current concepts of membrane formation (MORRÉ and MOLLENHAUER 1974). Our observations leave no doubt that the charasome membrane and plasmalemma are one contiguous membrane network. Further evidence that the charasome membrane and plasmalemma are structurally similar is indicated by the fact that both are stained by the plasmalemma-specific stain, PTA-$CrO_3$ (SUNDBERG and LEMBI 1976). Growth of the charasome, or addition of membrane material, may occur at the coated areas seen with

TEM (see Figs. 1–4). Formation of a coated invagination of the plasmalemma appears to be the initial step in charasome development, and eventually produces the complex network observed in the mature structure. Coated invaginations are often found within cytoplasmic pockets in the body of a developing charasome, further evidence that the invaginations are the site of membrane addition and not formed by fusion of coated vesicles with the charasome membrane. The envelopment of organelles by charasome material is likely due, in part, to growth of the charasome at many discrete points, leading to growth around organelles, and partly to fusion or compaction of separately initiated charasomes.

The area interior to the coated surface of the invaginations is open to the wall space and, thus, formation of the coated invaginations does not in itself result in development of the cytoplasmic tubules found in the charasome. Such tubules appear to arise from the fusion of coated regions of the developing charasome, leaving a cytoplasmic strand between part of the fused invaginations. Occasionally, we have seen evidence of such a process (see Fig. 11). The coated invaginations have a diameter of approximately the same dimension as the length of the cytoplasmic tubules in the mature charasome (50–60 nm). Thus, the fusion mechanism described would result in the same length of cytoplasmic tubule as is observed. Random budding and fusion of the developing charasome membrane can, likewise, result in the isolation of small cytoplasmic areas by the charasome membrane. These cytoplasmic pockets are later filled in by further coated invagination formation; a common phenomenon at certain stages of formation.

The apparent mode of formation of the charasome (via coated membrane invaginations) is, to our knowledge, unique among membrane organelle formation. The coating which occurs on the cytoplasmic surface of the membrane invaginations may provide mechanical support for the developing membrane until it is fully stabilized against the pressure gradient across the membrane, due to the internal hydrostatic pressure. Stabilization of the charasome membrane may be through equalization of the osmotic pressures across the membrane, or by formation of a mechanically incompressible structural entity within the developing periplasmic space. These possibilities are further investigated and expanded upon elsewhere (Franceschi and Lucas 1981). Coating of the membrane is also found in certain vesicles derived from dictyosomes. The coating may serve a similar mechanical function. Such vesicles may contain material at a concentration different enough from the surrounding cytoplasm that without the mechanical support of the coating rupture or collapse of the vesicle may occur.

Although coated invaginations of the plasmalemma were found to be related to charasome formation, they also appear to be associated with the formation of coated vesicles. It can be argued that fusion of coated vesicles with the plasmalemma is giving rise to the invaginations; however, our results indicate

that the opposite could also be occurring. The size and shape of the invagination is often inconsistent with what it should be if it were formed by vesicle fusion. Coated invaginations are seen which have a coated vesicle-sized portion on an elongated coated neck (see, for example, Fig. 13). This is a profile which is unlikely to arise as a result of vesicle fusion with the plasmalemma. In addition, one or more vesicles are often observed lined up directly beneath a coated invagination, indicating that they may have been formed from it. A further observation that appears to be consistent with the endocytosis hypothesis is that vesicles found further away from the coated invaginations often lack part or all of their coating. It must be noted that, even for dictyosome-derived coated vesicles, the coating is laid down as the vesicle is formed; thus loss of the coating, or part of it, is probably an ageing or breakdown process. Dictyosomes, the supposed source of coated vesicles in plants (NEWCOMB 1980) are generally not associated with the plasmalemma and, when they were found near the plasmalemma, they were very seldom involved with coated vesicle formation.

Coated invaginations and associated vesicles were often found enveloped by charasome membranes (Fig. 16). Our interpretation of such an observation is that the coated invaginations have developed within a cytoplasmic pocket surrounded by charasome material and have, subsequently, produced vesicles which become trapped within the charasome. If this interpretation of the data (Fig. 16) is correct, the present results would offer strong support for the hypothesis that endocytosis occurs in this plant system.

The manner in which charasomes are formed also supports the hypothesis that the plasmalemma can form invaginations. The charasome is part of the plasmalemma and the coated invaginations of the developing charasome seldom, if ever, have coated vesicles associated with them. The coated invaginations of the charasome portion of the plasmalemma must be formed by modification and growth of the plasmalemma and not by coated vesicle fusion. If such a process can occur at the charasome membrane, there is no reason that it could not occur at other plasma membrane areas.

Many animal tissues contain coated vesicles and, in a number of instances, have been clearly shown to be of endocytotic origin (ROTH and PORTER 1964, FRIEND and FARQUHAR 1967, LANGUNOFF and CURRAN 1972, and others). Coated vesicles have also been reported in growing plant tissues, including several *Chara* species (PICKETT-HEAPS 1967, SIEVERS 1967), roots (BONNETT and NEWCOMB 1966, HEPLER and NEWCOMB 1967, STELZER 1977) and protoplasts (DOOHAN and PALEVITZ 1980). However, they have usually been assumed to be dictyosome-derived. In most instances, it is thought that these vesicles are involved in cell-wall formation (BONNETT and NEWCOMB 1966, HEPLER and NEWCOMB 1967, CRONSHAW and ESAU 1968, O'BRIEN 1972, FRANKE and HERTH 1974). As pointed out, however, by O'BRIEN (1972), the static systems with which we are working (fixed plant tissues) makes it

difficult to determine in which direction the vesicles are going, and so an endocytotic origin of coated vesicles in plants can not be totally excluded.
The putative function of the endocytotic vesicles remains obscure (Woodward and Roth 1978, Doohan and Palevitz 1980, Newcomb 1980). Their formation may serve to recycle plasma membrane (Heuser and Reese 1973, Bretscher 1976). Alternatively, they may represent the remnants of a primitive and energetically inefficient ion transport mechanism (see Cram 1980, for the rationale on the energetics of this process). Cram (1980) analyzed the theoretical aspects of a possible endocytotic process in plant cells and concluded that such a process "could not occur in plant cells". We agree that endocytosis is unlikely to function as "the principal means of transporting major nutrients across the plasmalemma" (Cram 1980). The main point of controversy concerning the formation of endocytotic vesicles appears to be the pressure-volume work which must be done against the cell turgor (hydrostatic) pressure. The cell must also contend with this pressure-volume work during formation of the charasome complex (Franceschi and Lucas 1981). However, the mere existence of the charasome is unequivocal proof that a mechanism does, indeed, exist in *Chara* for dealing with this problem. Our present data offer support for the hypothesis that endocytosis occurs in *Chara* and *Nitella* cells. The challenge now becomes one of understanding how and why such a mechanism would operate.

## Acknowledgements

This work was supported by a grant from the National Science Foundation (PCM 78-10474). We would also like to thank Dr. C. E. Barr (State Univ. College, Brockport, N.Y.), Dr. J.-P. Metraux (Univ. of California, Berkeley) and Mr. P. Doud (Elder Valley Ranch, Napa County, Calif.) for kindly supplying us with plant material. Thanks are also due to Dr. B. A. Palevitz (Univ. of Georgia, Athens) for making their manuscript available before publication.

## References

Barton, R., 1965 a: An unusual organelle in the peripheral cytoplasm of *Chara* cells. Nature **205**, 201.

— 1965 b: Electron microscope studies on surface activity in cells of *Chara vulgaris*. Planta **66**, 95—105.

— 1968: Autoradiographic studies on wall formation in *Chara*. Planta **82**, 302—306.

Bonnett, H. T., Newcomb, E. H., 1966: Coated vesicles and other cytoplasmic components of growing root hairs of radish. Protoplasma **62**, 59—75.

Bretscher, M. S., 1976: Directed lipid flow in cell membranes. Nature **260**, 21—23.

Cram, W. J., 1980: Pinocytosis in plants. New Phytol. **84**, 1—17.

Crawley, J. C. W., 1965: A cytoplasmic organelle associated with the cell walls of *Chara* and *Nitella*. Nature **205**, 200—201.

Cronshaw, J., Esau, K., 1968: Cell division in leaves of *Nicotiana*. Protoplasma **65**, 1—24.

Doohan, M. E., Palevitz, B. A., 1980: Microtubules and coated vesicles in guard-cell protoplasts of *Allium cepa* L. Planta **149**, 389—401.

FRANCESCHI, V. R., LUCAS, W. J., 1980: Structure and possible function(s) of charasomes; complex plasmalemma-cell wall elaborations present in some Characean species. Protoplasma **104**, 253—271.

— — 1981: The charasome periplasmic space. Protoplasma **107**, 269—284.

FRANKE, W. W., HERTH, W., 1974: Morphological evidence for *de novo* formation of plasma membrane from coated vesicles in exponentially growing cultured plant cells. Exp. Cell Res. **89**, 447—451.

FRIEND, D. S., FARQUHAR, M. G., 1967: Functions of coated vesicles during protein absorption in the rat vas deferens. J. Cell Biol. **35**, 357—376.

HEPLER, P. K., NEWCOMB, E. H., 1967: Fine structure of cell plate formation in the apical meristem of *Phaseolus* roots. J. Ultrastruct. Res. **19**, 498—513.

HEUSER, J. E., REESE, T. S., 1973: Evidence for recycling of synaptic vesicle membrane during transmitter release at the frog neuromuscular junction. J. Cell Biol. **57**, 315—344.

LAGUNOFF, D., CURRAN, D. E., 1972: Role of bristle-coated membrane in the uptake of ferritin by rat macrophages. Exp. Cell Res. **75**, 337—346.

LUCAS, W. J., 1980: Control and synchronization of $HCO_3^-$ and $OH^-$ transport during photosynthetic assimilation of exogenous $HCO_3^-$. In: Plant Membrane Transport: Current Conceptual Issues (SPANSWICK, R. M., LUCAS, W. J., DAINTY, J., eds.), pp. 317—328. Amsterdam: Elsevier.

MORRÈ, D. J., MOLLENHAUER, H. H., 1974: The endomembrane concept: a functional integration of endoplasmic reticulum and Golgi apparatus. In: Dynamic aspects of plant ultrastructure (ROBARDS, A. W., ed.), pp. 84—137. New York: McGraw Hill.

NEWCOMB, E. H., 1980: Coated vesicles: their occurrence in different plant cell types. In: Coated vesicles (OCKLEFORD, C. D., WHYTE, A., eds.), pp. 55—68. Cambridge: University Press.

O'BRIEN, T. P., 1972: The cytology of cell-wall formation in some eukaryotic cells. Bot. Rev. **38**, 87—118.

PICKETT-HEAPS, J. D., 1967: Ultrastructure and differentiation in *Chara* sp. I. Vegetative cells. Aust. J. biol. Sci. **20**, 539—551.

ROTH, T. F., PORTER, K. R., 1964: Yolk protein uptake in the oocyte of the mosquito *Aedes aegypti* L. J. Cell Biol. **20**, 313—332.

SIEVERS, A., 1967: Elektronenmikroskopische Untersuchungen zur geotropischen Reaktion. II. Die polare Organisation des normal wachsenden Rhizoids von *Chara foetida*. Protoplasma **64**, 225—253.

SILVERSTEIN, S. C., STEINMAN, R. M., COHN, Z. A., 1977: Endocytosis. Ann. Rev. Biochem. **46**, 669—722.

STELZER, R., 1977: Salz- und Überflutungstoleranz von *Puccinella peisonis:* Physiologisch-Anatomische Anpassungen von Poaceen-Wurzeln an Salinität und Überflutung. Ph.D. Dissertation, Technische Hochschule, Darmstadt, W. Germany.

SUNDBERG, I., LEMBI, C. A., 1976: Phosphotungstic acid-chromic acid: a selective stain for algal plasma membranes. J. Phycol. **12**, 48—54.

WOODWARD, M. P., ROTH, T. F., 1978: Coated vesicles: Characterization, selective dissociation, and reassembly. Proc. Natl. Acad. Sci. U.S.A. **75**, 4394—4398.

Printed in Austria

Protoplasma 107, 269—284 (1981)

PROTOPLASMA
© by Springer-Verlag 1981

# The Charasome Periplasmic Space

V. R. Franceschi and W. J. Lucas *

Department of Botany, University of California, Davis, California

Received January 16, 1981
Accepted May 5, 1981

## Summary

Charasome structure, with special attention to the periplasmic space, is examined using various techniques. The periplasmic space appears electron lucent in sections stained with 2% aqueous uranyl acetate and lead citrate. When sections are stained with saturated methanolic uranyl acetate a densely staining central core can be seen within the periplasmic space. The region surrounding the core does not stain. If tannic acid is added to the fixative and rinse solutions during preparation of the tissue for TEM, the entire periplasmic space becomes stained. This space appears to be filled with a fine granular material. Charasomes prepared in this way appear as negatives of those stained with uranyl acetate. The periplasmic space does not contain polysaccharides of the type having *vic*-glycol groups, as indicated by lack of staining by the silver methenamine technique.

Severe plasmolysis of cells by treatment with 350 mM mannitol prior to fixation resulted in disruption of charasomes, but did not cause collapse of the structure. The periplasmic space of freeze-fractured charasomes contains a distinct granular material, while negatively stained isolated charasomes retain their structural configuration, even after air drying.

The results give us new insight into the nature of the periplasmic space and confirm our earlier description of the charasome structure. This information is used to construct a model which attempts to explain how a structure such as the charasome can be formed along the plasmalemma of a cell having a high internal hydrostatic pressure.

*Keywords: Chara;* Charasome-complex; Freeze-fracture; Negative staining; Periplasmic space; Tannic acid.

## 1. Introduction

The charasome is an interesting ultrastructural feature of certain cells of the *Chara* thallus. The structure and development of the charasome has been described elsewhere (Franceschi and Lucas 1980, Lucas and Franceschi 1981). The charasome consists of a mass of anastomosing membrane tubules filled with cytoplasm and surrounded by a specialized wall space, which we call a periplasmic space. One consequence of the structural features of the

* Correspondence and Reprints: Department of Botany, University of California, Davis, CA 95616, U.S.A.

0033-183X/81/0107/0269/$ 03.20

charasome is a phenomenal increase in the surface area of the plasmalemma. Of equal importance to the above is the formation of a periplasmic space within the charasome, which is non-protoplasmic, yet is distinct from the cell wall. It is clear that the charasome provides a special interface between cytoplasm and external environment which does not exist where the plasmalemma abuts directly against the cell wall.

The nature of the periplasmic space is of importance to an understanding of the function of the charasome. The charasome-complex must be maintained against a high internal hydrostatic pressure. This indicates that the periplasmic space must contain a material having structural properties or an osmotic pressure great enough to offset the turgor pressure of the cell. In transmission electron micrographs of charasomes stained with aqueous uranyl acetate and lead citrate the periplasmic space appears electron lucent, showing no ultrastructural detail. A a continuation of our previous study, we have used various TEM staining procedures in an attempt to elucidate the structure and character of the periplasmic space. Freeze-fracture and negative staining techniques have also been employed. This work has provided some interesting information about the charasome periplasmic space which will be presented here. We have also developed a model from this and previous information to explain the formation and existence (against a hydrostatic pressure) of the periplasmic space.

## 2. Materials and Methods

### *2.1. TEM Preparation and Staining*

Shoots, branches, and internodal cells of *Chara corallina* and *C. braunii* were fixed as previously described (Franceschi and Lucas 1980). Some cells were incubated in 350 mM mannitol in CPW (mM: 1.0 NaCl, 0.2 KCl, 0.2 $CaSO_4$, pH 5.7) for 10 minutes to plasmolyse them prior to fixation. (Cells from our laboratory culture have an osmolality in the range 240–280 mOSm). They were further processed as above, except that fixatives and rinses were brought to 350 mOSm with mannitol. Sections of resin-embedded cells were stained with 2% lead citrate (30 minutes) and 2% aqueous uranyl acetate (30 minutes) or with saturated methanolic uranyl acetate (30–60 minutes). Staining with tannic acid (TA; Mallinckrodt) was done by making all fixative and rinse solutions 0.1% (w/v) with respect to stain content. Whole shoots and branches of *C. corallina* were used.

### *2.2. Polysaccharide Localization*

Localization of polysaccharides in sectioned material was done by the silver methenamine method (Rambourg 1967). Sections on nickel grids were incubated on drops of 1% periodic acid for 30 minutes at 22 °C, washed with distilled water and stained with freshly prepared silver methenamine solution at 60 °C for 1 hour in the dark. The stain was prepared by mixing 0.3 g hexamethylenetetramine in 12 ml glass distilled water with 10 ml of 0.25% silver nitrate and 8 ml of 5% sodium borate (Hayat 1975). After staining, the grids were washed with glass distilled water, incubated on drops of 0.5% sodium thiosulfate for 5 minutes at 22 °C and then washed with water. Controls were run for specificity of staining as described elsewhere (Franceschi and Lucas 1981) but are not important to the results presented.

*2.3. Freeze-Fracture*

Small branch cells of female *C. corallina* plants were mounted on stubs with polyvinyl alcohol and immediately frozen by plunging into Freon 22 cooled with liquid nitrogen (LN). The cells were trimmed under LN, then freeze-fractured at — 120 °C in a Balzers Freeze-fracture unit. Two coatings of carbon were necessary to stabilize the replica. Replicas were cleaned with 40% chromic acid, washed with glass distilled water and picked up on Formvar coated grids for TEM examination. Some cells were fixed in glutaraldehyde (1.25% in 0.05 M sodium cacodylate; pH 7.2) for 30 minutes prior to freezing. No difference could be seen between charasomes in unfixed or prefixed cells.

*2.4. Negative Staining*

Shoots from female *C. corallina* plants were macerated by chopping with scissors until a fine pulp resulted. This material was strained through nylon mesh to remove wall fragments. The resulting homogenate was mixed with an equal volume of 2% aqueous phosphotungstic acid (pH adjusted to 7.0 with NaOH) and applied to Formvar coated grids. Excess liquid was removed with a piece of filter paper and the grids were allowed to air dry, then immediately examined in the TEM.

## 3. Results

*3.1. Uranyl Acetate Staining*

Our previous TEM observations of the charasome were made on sections stained with 2% aqueous uranyl acetate and lead citrate. Fig. 1 is a TEM micrograph of a charasome from a section stained in this manner. The dark tubules are open to the cytoplasm at the inner surface of the charasome and the area surrounding the tubules is periplasmic space. The periplasmic space is devoid of any electron dense material when stained in this manner.

Intensity of staining with uranyl acetate is dependent upon the amount of stain which is able to bind to a given component within a section. The use of saturated methanolic uranyl acetate should allow better penetration and staining of thin sections, and possibly stain material present within the periplasmic space. When thin sections were stained for 30 minutes, at room temperature, by immersion in saturated methanolic uranyl acetate, staining was found to be much more intense compared with the level observed in aqueous stain. Under such staining procedures the charasome membranes stained intensely and the periplasmic space was also found to contain a stainable element (Fig. 2). This material appeared as a core within the center of the periplasmic space and was surrounded by a nonstaining region. When cut in cross-section the core has a circular profile, while in longitudinal sections it appears as a strand running through the periplasmic space (Fig. 2, inset). The core was of similar size in all charasomes viewed. Charasomes of different stages of development were examined and all were found to contain this periplasmic component.

*3.2. Tannic Acid Staining*

Tannic acid, as used here, did not appear to penetrate the cell to any extent as indicated by lack of staining of cytoplasmic membranes. This was further

evidenced by the more intense staining of the plasmalemma leaflet facing the periplasmic space (Figs. 3 and 5), as compared to the plasmalemma surface facing the cytoplasm. The periplasmic space of the charasome stained intensely by this technique (Fig. 3). The staining is considered to be due to reaction of TA with material within the periplasmic space and not due to "backwall" staining. A comparison of Figs. 3 and 4 shows that in most instances the periplasmic space in thin sections is devoid of background membrane due to the thinness of the sections. Staining of the periplasmic space was not intensified by post-staining of sections with aqueous uranyl acetate, although such poststaining did increase membrane staining.

The image presented by TA staining is almost a negative of that shown with uranyl acetate staining. This makes the TA staining difficult to interpret and to clarify the effect of such staining it is necessary to directly compare similar sections of charasomes stained by the two techniques. Such a comparison is given in Figs. 3 and 4. With TA staining the periplasmic space has a fine granular density, while the cytoplasmic regions of the charasome appear electron lucent. Thus, the periplasmic space is well defined and appears tubular, while the cytoplasmic regions are indistinct (Fig. 3). Connections of the periplasmic space to the wall are apparent in cross-sections of TA stained charasomes. Openings of the cytoplasmic tubules to the cytoplasm can also be identified (Fig. 3). The periplasmic space stains more intensely than the cell wall (Fig. 5), indicating a quite different structural component.

### *3.3. Polysaccharide Localization*

The silver methenamine technique will stain polysaccharides with *vic*-glycol groups when these groups are oxidised to aldehydes. Periodic acid oxidised sections of *Chara* show intense staining for polysaccharides within the cell wall (Fig. 6). The plasmalemma and charasome membrane also stain, probably due to glycoproteins and exposed sulfhydryl groups. The periplasmic space shows no staining by this technique (Fig. 6); an observation that rules out the presence of a certain group of polysaccharides. The specificity of this technique, when used with *Chara*, has been demonstrated elsewhere (Franceschi and Lucas 1981), and was also found to hold in this

---

Fig. 1. Mature charasome stained with aqueous uranyl acetate and lead citrate. Cytoplasm (*C*), plasmalemma (*P*), periplasmic space (*S*), charasome cytoplasmic tubules (*T*), wall (*W*). Continuity between periplasmic space and wall is indicated by open arrows. Solid arrows point to openings of tubules to the cytoplasm. ×67,000

Fig. 2. Oblique section through charasome stained with saturated methanolic uranyl acetate. Note dense core within periplasmic space (solid arrows). Two growing points (open arrows) are present, one in cross-section (upper) and one in longi-section (lower). ×178,000. Inset: periplasmic space with strand of core material (arrows). ×103,000

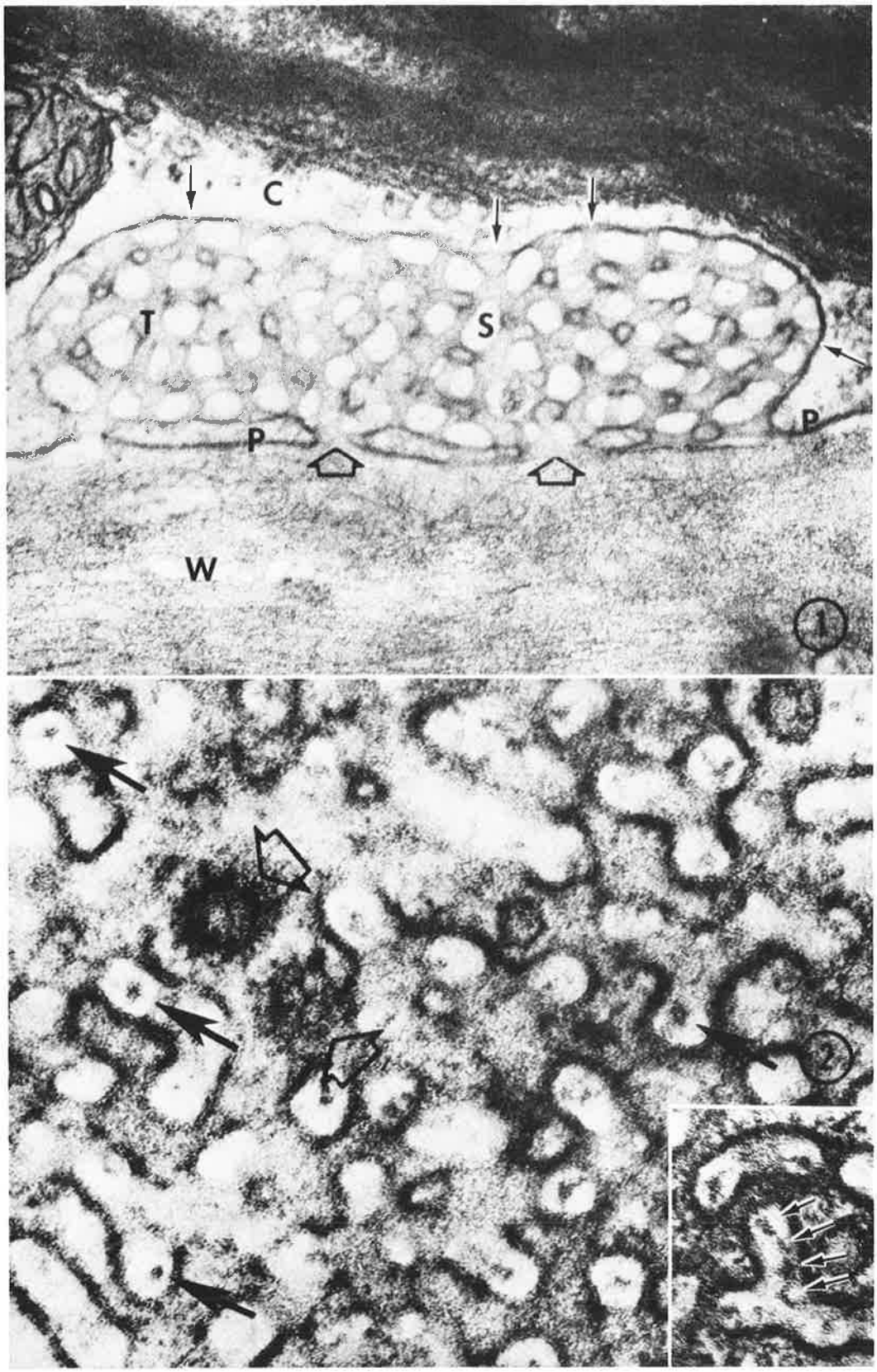
C
T
S
P
P
W
1
2

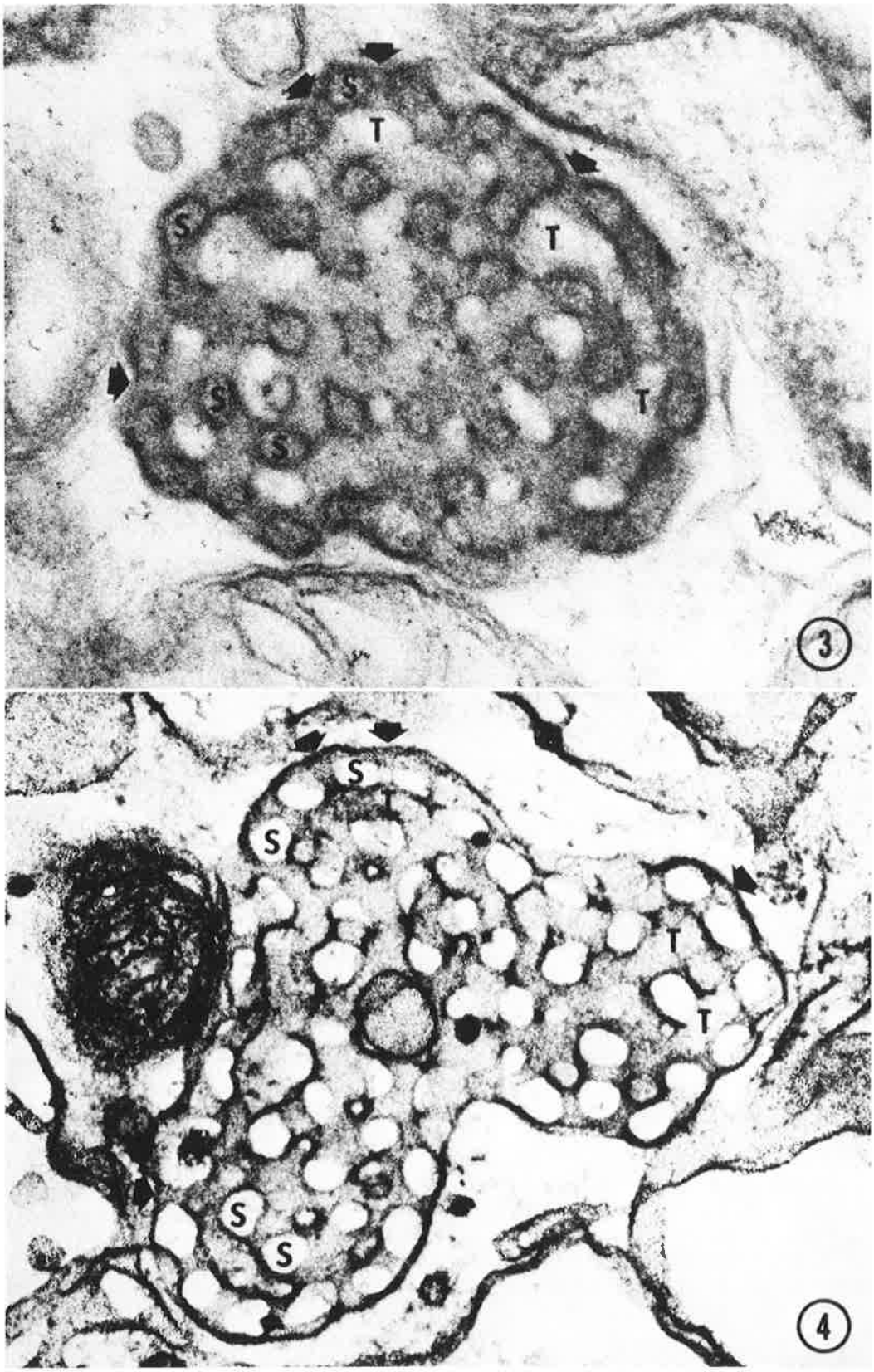


Figs. 3 and 4. A comparison of oblique sections through charasomes stained with TA (Fig. 3) and with aqueous uranyl acetate and lead citrate (Fig. 4). TA treatment results in staining of periplasmic space (*S*), but not material within cytoplasmic tubules (*T*). Arrows indicate openings of tubules to the cytoplasm. Fig. 3 ×106,000; Fig. 4 ×88,500

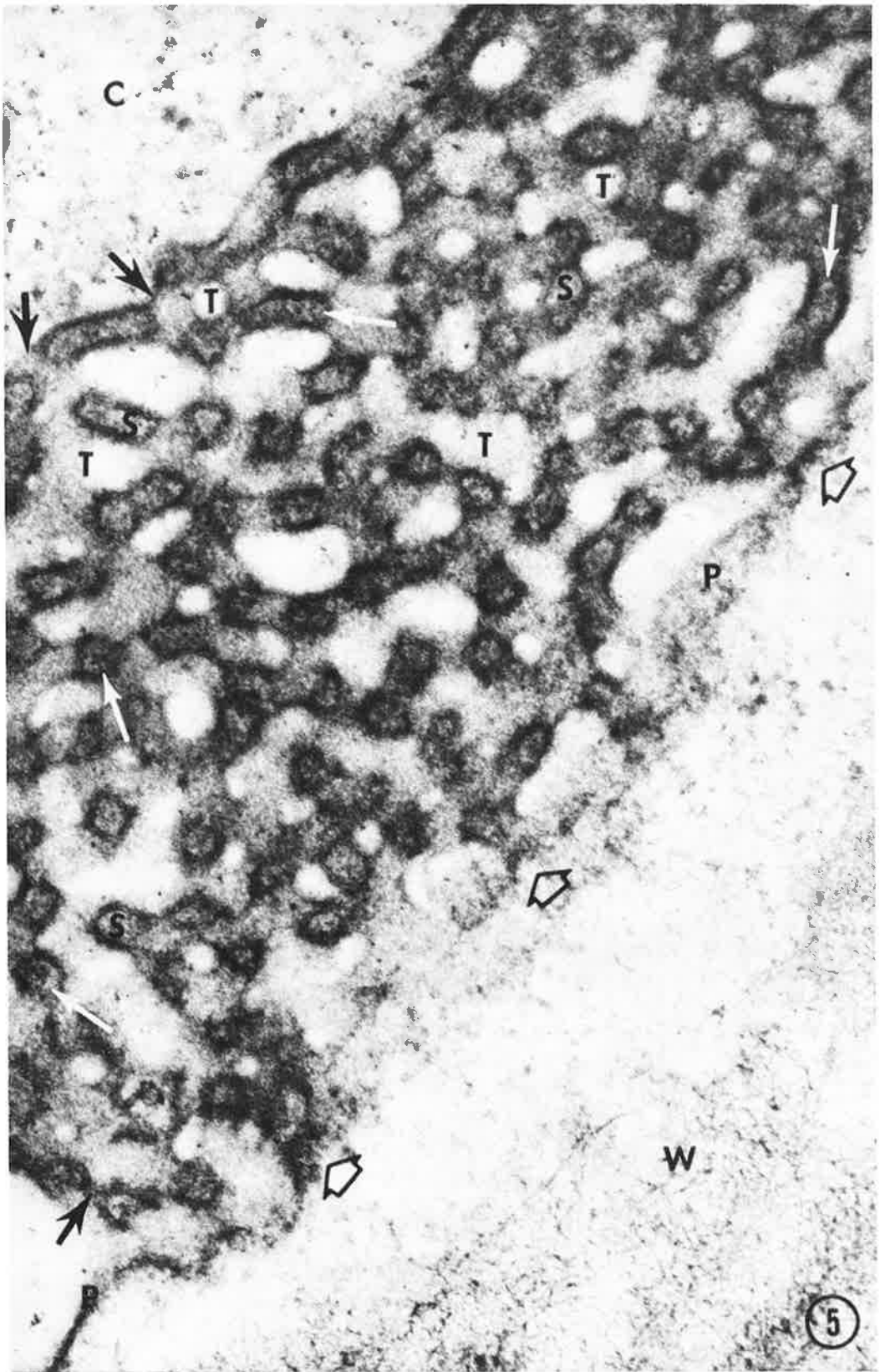


Fig. 5. Tannic acid stained charasome. Note material within periplasmic space (*S*), continuity between the wall and periplasmic space (open arrows) and openings of cytoplasmic tubules (*T*) at the inner charasome surface (solid arrows). Periplasmic material appears granular in some areas (white arrows). The plasmalemma is sectioned obliquely in some areas. ×98,700

instance. Staining of wall and membrane could be reduced or eliminated by incubation of sections in aldehyde blocking agents prior to silver staining (data not shown).

### *3.4. Plasmolysis*

Incubation of cells in a 350 mM mannitol solution resulted in severe plasmolysis of branch and internodal cells (Fig. 7). However, the tubules of the charasome were not collapsed against each other. The charasomes appear as if they have been pulled apart, leaving large spaces between some of the tubules. The innermost membrane of the charasome (see Fig. 31 in Franceschi and Lucas 1980) is detached from the charasome tubules in many areas (Fig. 7) as if it has been subjected to the brunt of the forces experienced during plasmolysis. Disruption of the charasome, as evidenced by the pulling apart of the tubules and innermost membrane, probably occurs during the initial phase of plasmolysis. When the osmotic barrier presented by the charasome membrane is thus disrupted, rapid equilibration between periplasmic space and cytoplasm can occur and so the charasome tubules do not collapse against each other (Fig. 7).

### *3.5. Negative Staining*

Fresh homogenates of *Chara* cells were found to contain charasomes or charasome fractions. The isolated charasomes retained their anastomosing tubular structure after negative staining and air drying (Fig. 8). However, the innermost membrane of the charasome, that facing the cytoplasm, was apparently not preserved except in small areas. This was probably due to massive osmotic changes and shearing forces induced during homogenization or mixing of homogenate with the stain solution. Our interpretation of the micrographs is that the stain penetrates the periplasmic space but not the cytoplasmic tubules. This staining technique helps to portray the intricate interconnections of the charasome tubules. No substructure could be seen within the periplasmic space (Fig. 8). This region of the charasome appears black in negatively stained preparations, except for the faint outlines of underlying tubules.

---

Fig. 6. Portion of a section which has been oxidised with periodic acid and stained for polysaccharides with silver methenamine. The wall (*W*) stains intensely. The plasmalemma and charasome membrane also stain but the periplasmic space (*S*) does not. Cytoplasm (*C*), charasome tubules (*T*). ×99,000

Fig. 7. Part of a cell that has been plasmolysed in 350 mM mannitol prior to fixation. The charasome complex is partially disrupted but the tubules (*T*) are not collapsed against each other. The innermost membrane of the charasome has been pulled away in many areas (arrows). Mitochondrion (*M*), wall (*W*). ×17,800

Fig. 8. Portion of a negatively stained isolated charasome. The anastomosing of tubules is clearly seen at this magnification. No substructure can be identified within the periplasmic space. Periplasmic space (*S*), charasome cytoplasmic tubules (*T*). ×180,700

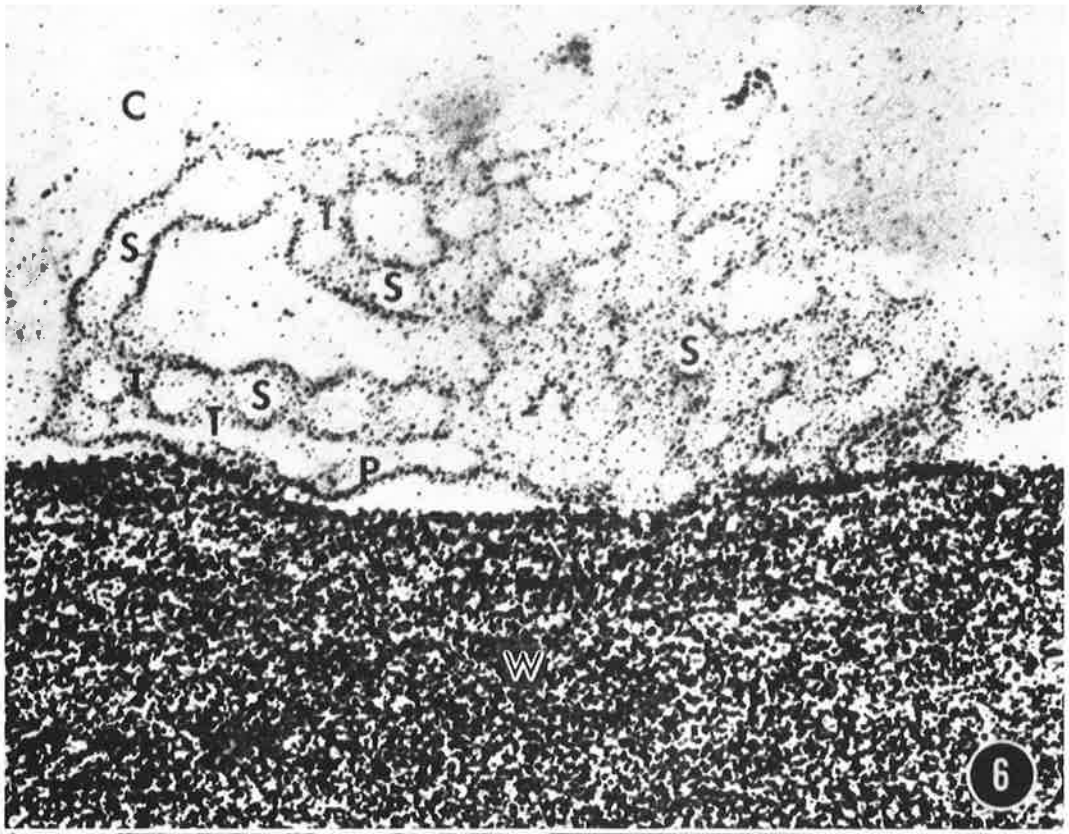
C
S
T
S
S
T
T
S
P
W
6

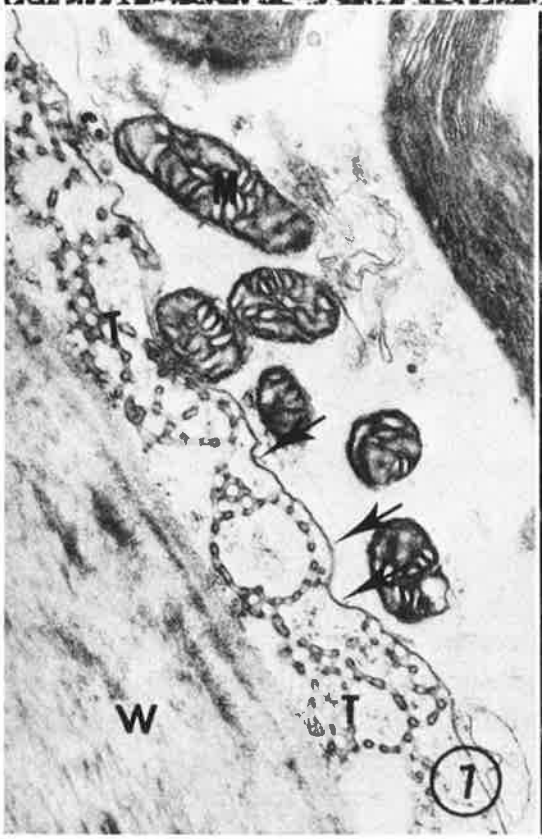
M
T
W
T
7

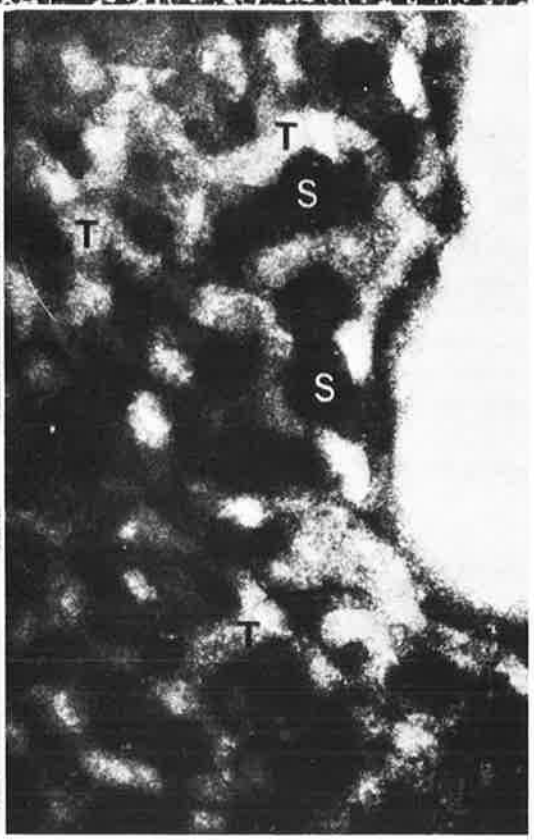
T
S
T
S
T

*3.6. Freeze-fracture*

Freeze-fracturing branch or internodal cells proved to be technically very difficult with the equipment available. The size and shape of the branch cells used made it difficult to anchor them securely to the specimen stubs. Additionally, the large vacuolar portion of the replica usually became detached during cleaning, even when a double coating of carbon was used.

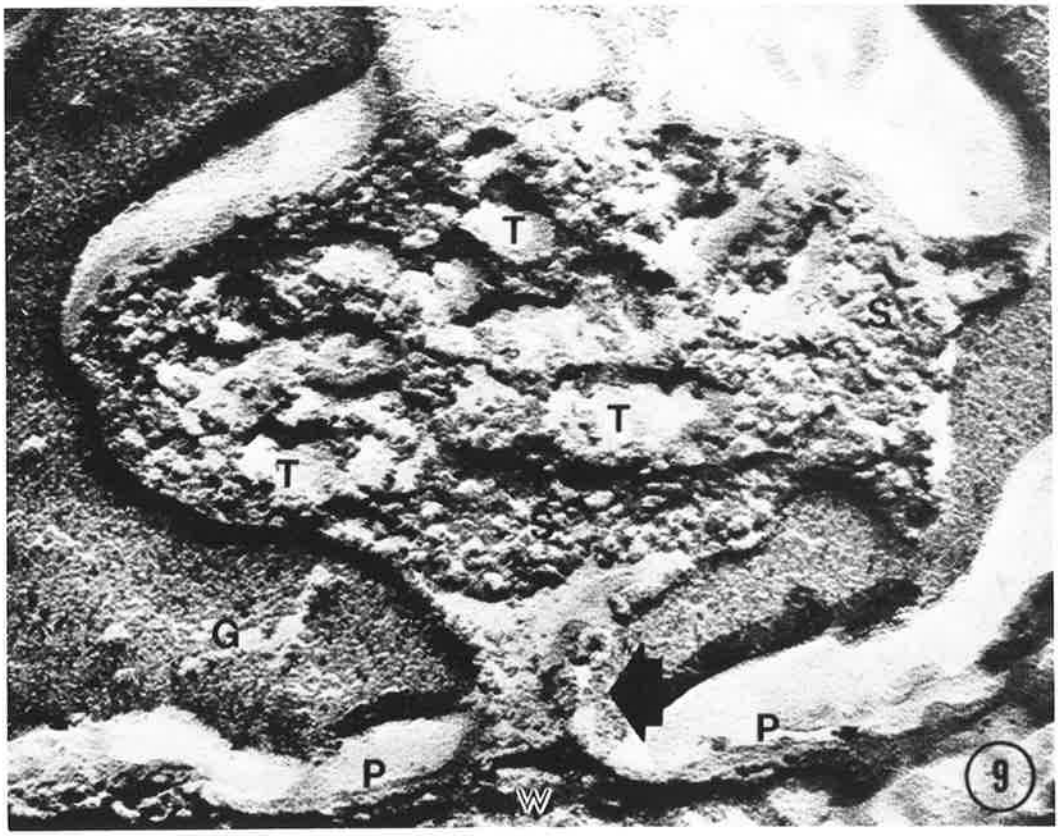


Fig. 9. Young, freeze-fractured charasome. The arrow indicates an area where the periplasmic space (*S*) opens into the wall (*W*). The granular periplasmic material was removed from the connection during fracturing exposing the inner surface of the membrane surrounding the periplasmic space. Continuity of plasmalemma (*P*) and charasome membrane is especially evident. Gel layer (*G*), tubules (*T*). ×197,000

However, fractions of replicas were obtained and fractures through charasomes were observed. The cytoplasmic tubules of young charasomes appear as smooth circular or cylindrical areas in these preparations. Definite interconnections of tubules can be identified and the overall appearance is consistent with thin section TEM preparations. The most interesting observation is that the periplasmic space has a distinct granular appearance when freeze-fractured (Fig. 9). This was quite different from the fine, smooth appearance of the cytoplasmic tubules or the surrounding cytoplasm of the

gel layer. No indication of a separate central region of the periplasmic space could be seen. The continuity of the periplasmic space with the cell wall region was especially apparent in these preparations (Fig. 9).

## 4. Discussion

Membrane structures associated with the plasmalemma of plant cells are frequently observed with electron microscopy. Such structures fall into two broad categories, lomasomes and plasmalemmasomes (MARCHANT and ROBARDS 1968, MARCHANT and MOORE 1973). Lomasomes are supposedly formed by ejection of material from the cytoplasm to the region between the plasma membrane and cell wall (MOORE and MCALEAR 1961). Plasmalemmasomes are considered to be elaborations of the plasma membrane (MARCHANT and ROBARDS 1968). The consistent presence of such structures in cells fixed by many different techniques (HEATH and GREENWOOD 1970, LEIVA and CARBONELL 1970, MARCHANT and MOORE 1973) and in freeze fractured cells in which fixatives are avoided (BROWN and WEIER 1970, MARCHANT and MOORE 1973 and references therein) provide strong evidence that in many instances such structures are real and not artifactual.

The charasome falls within the plasmalemmasome category because it is a modification of the plasma membrane. The highly ordered structure of the charasome, consisting of an intricate anastomosing network of membrane tubules of constant length and diameter, is unique among the reports of plasmalemmasomes known to us. Such structures which have been reported, generally lack such complexity, and consist of concentric membrane rings or pockets of tubules of various length or combinations of such structures with no apparent order. Unlike most reported plasmalemmasomes which show great variability in substructure within a cell and from cell to cell, the charasome tubular substructure is constant among charasomes within a single cell and between charasomes of different species examined (*C. corallina, C. braunii, C. globularis;* personal observations). The only variability seen in the charasome is in its overall size and shape in mature cells.

We contend that the charasome is a real ultrastructural feature of *Chara* and not artifact. Observations which support this statement can be summarized as follows. 1. Charasomes having the exact same structure were found in all three *Chara* spp. examined, including collected specimens and those grown in laboratory cultures, but in none of six *Nitella* spp. examined (LUCAS and FRANCESCHI 1981). The ultrastructural features of these two genera are otherwise indistinguishable. Artifact induced in one would be expected to occur in the other. 2. The charasome shows a highly specific spatial distribution along the internode cells (FRANCESCHI and LUCAS 1980). It is found in the acid band regions, but is reduced or absent in the alkaline bands. Charasomes are also more numerous in branch cells than in internodal cells of the main axis of the plant, and are much larger in branch cells of

female *C. corallina* plants than in male plants. Such a distribution is difficult to explain as an artifact. 3. When plant shoots are plasmolysed prior to fixation, charasomes are still found within the cells, but are torn apart (see Fig. 7). This is a strong indication that the charasomes are present prior to processing for TEM and are an integral part of the living cells. 4. Charasomes can be isolated from fresh, unfixed living plants (Fig. 8). 5. Charasomes are present in cells prepared with various fixatives (glutaraldehyde; glutaraldehyde/$OsO_4$; $OsO_4$) and buffers (cacodylate; phosphate). They are also present in freeze-fractured cells whether fixed or unfixed prior to freezing. 6. A characteristic developmental sequence for charasome formation has been observed (Lucas and Franceschi 1981). Charasome development is related to cell development and involves formation of specialized structures not found in charasomes of mature cells.

The charasome retains its unique structure and cytoplasm/external environment relationship despite the presence of the cell's hydrostatic pressure, which would tend to work towards a collapse of this structure. The implication is that the periplasmic space contains some material which either acts as a structural framework to support the charasome or develops an osmotic pressure which offsets the cell turgor pressure. Our previous work on the charasome gave us little information on the nature of the periplasmic space. The results presented here, however, give evidence of material within this region. The increased intensity of staining made possible by the use of methanolic uranyl acetate, reveals the presence of what appears to be a strand of material running through the center of the periplasmic space. When tannic acid (TA) is used during tissue preparation, the periplasmic space stains densely throughout. However, the central core is not generally apparent in these preparations. Perhaps this is an indication that two distinct components exist within the periplasmic space. One component has an affinity for TA and appears as a fine granular material distributed throughout the periplasmic space, while the other component forms a central core and is only stained after long incubation in saturated methanolic uranyl acetate.

The periplasmic space is, in effect, part of the wall space of the cell, and, as such, may be expected to contain polysaccharide material. As determined by the silver methenamine technique, the periplasmic space does not contain polysaccharides which have *vic*-glycol groups. However, this does not mean that the periplasmic space material is not polysaccharide in nature. There are many polysaccharides which do not stain by this technique (no *vic*-glycol groups). Callose is one such polysaccharide which also does not stain with uranyl acetate.

Tannic acid has been found to increase the contrast of extracellular structures and spaces in animal tissues, possibly by binding to serum proteins (Futaesaku *et al.* 1972, Rodewald and Karnovsky 1974, van Deurs 1975). However, TA has been demonstrated to be a general mordant which induces high

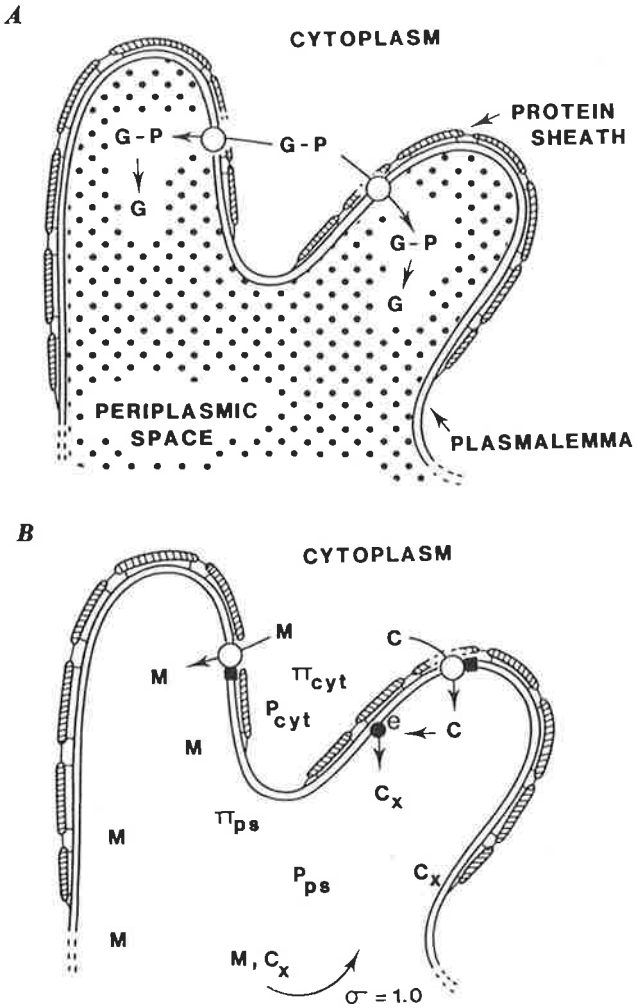


Fig. 10. Schematic representation of the manner in which the developing charasome may stabilize its periplasmic space against the turgor pressure of the cell. Only the region of the coated invaginations (LUCAS and FRANCESCHI 1981) is represented in these models. *A* = Periplasmic structural-matrix situation. Transport of a granular-precursor (*G-P*) across the charasome plasmalemma may result in the synthesis of a granular-like material (*G*) within the periplasmic space. The granular material could fill this space, thereby preventing its collapse under the influence of the cell's turgor pressure. *B* = Osmotic pressure adjustment. Development of an osmotic pressure within the periplasmic space ($\pi_{ps}$) could be achieved by transporting a molecule of medium molecular weight (*M*) into this space. Alternatively, a carbohydrate subunit (C) may be transported across the plasmalemma and then polymerized (at *e*) to $C_x$. The constraint on the chemical species (*M* or $C_x$) would be that it could not penetrate the cell wall proper (*i.e.*, *M* or $C_x$ would have a reflection coefficient [$\sigma$] for the wall equal to one). The transport of *M*, or the production of $C_x$ would raise $\pi_{ps}$ such that it would balance the osmotic pressure of the cytoplasm ($\pi_{cyt}$). In this situation, the hydrostatic pressures in the periplasmic space ($P_{ps}$) and the cytoplasm ($P_{cyt}$) would be equalized. For such a system to work, the transport system responsible for establishing $\pi_{ps}$ must have a turgor pressure sensing component (represented in the model as ■)

contrast in many different types of cellular structures and, thus, is not specific for protein (Simionescu and Simionescu 1976 a, b). The staining of the periplasmic space by TA is therefore not indicative of a certain chemical identity. At this time there is little that we can say concerning the chemical nature of the periplasmic space material, although we feel that oligo- or polysaccharides still remain a likely possibility.

The freeze-fracture, negative staining, and plasmolysis studies are important from two viewpoints. First, they show clearly and conclusively that our earlier structural model is correct. The negative staining makes the spatial aspects of the charasome especially apparent. This study also gives an indication that charasomes can perhaps be isolated for more extensive biochemical analysis. Secondly, the techniques give us some idea of the possible nature of the material within the periplasmic space. When freeze-fractured, the periplasmic space has a granular appearance quite different from other regions of the cell. This granular appearance, also indicated by TA staining, may be representative of small distinct particles making up the periplasmic material. No such appearance was noted in negatively stained isolated charasomes. In fact, no substructure could be seen within the periplasmic space of charasomes thus prepared. It is possible that the material within the periplasmic space was lost during homogenization and staining. This would be especially true if the material in this space consisted of small particles. Furthermore, the tubules of negatively stained charasomes often appear to be resting upon each other (Fig. 8), which is indicative of a lack or loss of mechanically supportive material within the periplasmic space. The plasmolysis studies can similarly be interpreted as showing the lack of a structurally continuous material within the periplasmic space. The charasome tubules would not be pulled apart during plasmolysis (see Fig. 7) if the material within this space formed a polymerized structural continuum throughout, although separation of the innermost membrane could still occur.

The results presented here are consistent with the presence of small distinct particles within the periplasmic space, as opposed to a structurally continuous matrix. To enable charasome growth, and also maintenance of its mature structure, these particles must either form an inelastic matrix or be osmotically active. If this were not the case, the turgor of the cell would crush the entire charasome membrane-complex against the true cell wall. Fig. 10 represents, in a diagrammatic sense, the manner in which these two alternatives may function in this system. The structural-matrix situation is presented in Fig. 10 *A*. Based on presented TEM results, this matrix would consist of small packed granules. (As previously mentioned, the specific nature of this matrix is yet to be determined.) Since growth of the charasome does not appear to involve fusion of cytoplasmically generated vesicles (Lucas and Franceschi 1981), we suggest that the structural granules are synthesized

*in situ*. This synthesis would occur within the newly forming periplasmic space of the charasome coated invaginations (see LUCAS and FRANCESCHI 1981).

The osmotic pressure situation is illustrated in Fig. 10 *B*. Since, by itself, the plasmalemma can withstand only the slightest of pressure gradients, the osmotic pressure of the periplasmic space ($\pi_{ps}$) must be adjusted to match that of the cell ($\pi_{cyt}$). This could be accomplished by a plasmalemma transport system moving either a medium molecular weight polymer (M in Fig. 10 *B*), or a carbohydrate subunit (C) which would then be polymerized ($C_x$) at an extrinsic enzyme site on the outer membrane surface. The important constraint here is that M or $C_x$ must be large enough so that it cannot penetrate the cell wall. In this way the cell wall would function as the osmotic barrier and the periplasmic space could develop an hydrostatic pressure ($P_{ps}$) equivalent to the cell's turgor pressure ($P_{cyt}$). The protein "coat" or "sheath" that has been observed on the invaginations of the developing charasome (LUCAS and FRANCESCHI 1981) may permit the existence of a slight disequilibrium between $P_{ps}$ and $P_{cyt}$.

The function of the charasome remains unresolved. The tremendous increase in plasmalemma surface area, together with the periplasmic space created by the charasome structure would obviously provide favorable conditions for certain transmembrane transport processes. Our future studies will focus on the possible transport role played by the charasome.

## Acknowledgements

This work was supported by a grant from the National Science Foundation (PCM 78-10474) and by a University of California (Davis) Intramural Research Award (D-1309). V. R. FRANCESCHI also gratefully acknowledges the support of a University of California Regents Fellowship.

## References

BROWN, D. L., WEIER, T. E., 1970: Ultrastructure of the freshwater alga *Batrachosperum*. I. Thin-section and freeze-etch analysis of juvenile and photosynthetic filament vegetative cells. Phycologia **9**, 217—235.

FRANCESCHI, V. R., LUCAS, W. J., 1980: Structure and possible function(s) of charasomes; complex plasmalemma-cell wall elaborations present in some Characean species. Protoplasma **104**, 253—271.

— — 1981: The glycosome of *Chara:* ultrastructure, development, and composition. J. Ultrastruct. Res. in press.

FUTAESAKU, Y., MIZUHIRA, V., NAKAMURA, H., 1972: A new fixation method using tannic acid for electron microscopy and some observations of biological specimens. Proc. Int. Congr. Histochem. Cytochem. **4**, 155—156.

HAYAT, M. A., 1975: Positive Staining for Electron Microscopy. New York: Van Nostrand Reinhold Company.

HEATH, I. B., GREENWOOD, A. D., 1970: The structure and formation of lomasomes. J. gen. Microbiol. **62**, 129—137.

LEIVA, S., CARBONELL, L. M., 1970: Demonstration of succinic dehydrogenase in the mesosomes of the mycelial phase of *Paracoccidioides brasiliensis*. J. gen. Microbiol. **62**, 43—47.

LUCAS, W. J., FRANCESCHI, V. R., 1981: Characean charasome-complex and plasmalemma vesicle development. Protoplasma **107**, 255—267.

MARCHANT, R., MOORE, R. T., 1973: Lomasomes and plasmalemmasomes in fungi. Protoplasma **76**, 235—247.

— ROBARDS, A. W., 1968: Membrane systems associated with the plasmalemma of plant cells. Ann. Bot. **32**, 457—471.

MOORE, R. T., MCALEAR, J. H., 1961: Fine structure of Mycota. 5. Lomasomes—previously uncharacterized hyphal structures. Mycologia **53**, 194—200.

RAMBOURG, A., 1967: An improved silver methenamine technique for the detection of periodic acid-reactive complex carbohydrates with the electron microscope. J. Histochem. Cytochem. **15**, 409—412.

RODEWALD, R., KARNOVSKY, M. J., 1974: Porous substructure of the glomerular slit diaphragm in the rat and mouse. J. Cell Biol. **60**, 423—433.

SIMIONESCU, N., SIMIONESCU, M., 1976 a: Galloylglucoses of low molecular weight as mordant in electron microscopy. I. Procedure and evidence for mordanting effect. J. Cell Biol. **70**, 608—621.

— — 1976 b: Galloylglucoses of low molecular weight as mordant in electron microscopy. II. The moiety and functional groups possibly involved in the mordanting effect. J. Cell Biol. **70**, 622—633.

VAN DEURS, B., 1975: The use of a tannic acid-glutaraldehyde fixative to visualize gap and tight junctions. J. Ultrastruct. Res. **50**, 185—192.

Printed in Austria

Plant Physiol. (1982) 69, 781–788
0032-0889/82/69/0781/08/$00.50/0

# Potassium Channels in *Chara corallina*[1]

## CONTROL AND INTERACTION WITH THE ELECTROGENIC $H^+$ PUMP

Received for publication June 25, 1981 and in revised form December 2, 1981

DAVID W. KEIFER AND WILLIAM J. LUCAS
*Department of Botany, University of California at Davis, Davis, California 95616*

### ABSTRACT

**Plasmalemma electrical properties were used to investigate $K^+$ transport and its control in internodal cells of *Chara corallina* Klein ex Willd., em R.D.W. Cell exposure to solutions containing 10 mM KCl caused the potential, normally −250 millivolts (average), to depolarize in two steps. The first step was a 21 millivolt depolarization that lasted from 1 to 40 minutes. The second step started with an action potential and left the membrane potential at −91 millivolts, with a 10-fold reduction in resistance. We suggest that the second step was caused by the opening of $K^+$-channels in the membrane. This lowered the resistance and provided a current pathway that partially short-circuited the electrogenic pump. Although largely short-circuited, the electrogenic pump was still operating as indicated by: (a) the depolarized potential of −91 millivolts was more negative than $E_K$ (= −42 millivolts in 10 mM $K^+$); (b) a large net $K^+$ uptake occurred while the cell was depolarized; (c) both the electrogenic pump inhibitor, diethylstilbestrol, and the sulfhydryl-reagent *N*-ethylmaleimide (which increased the passive membrane permeability) further depolarized the potential in 10 mM KCl.**

**A two-phase recovery back to normal cell potentials occurred upon lowering the $K^+$ concentration from 10 to 0.2 mM. The first phase was an apparent Nernst potential response to the change in external $K^+$ concentration. The second phase was a sudden hyperpolarization accompanied by a large increase in membrane resistance. We attribute the second phase to the closing of $K^+$-channels and the removal of the associated short-circuiting effect on the electrogenic pump, thereby allowing the membrane to hyperpolarize. Further experiments indicated that the $K^+$-channel required $Ca^{2+}$ for normal closure, but other ions could substitute, including: $Na^+$, tetraethylammonium, and 2,4,6-triaminopyrimidine. Apparently, $K^+$-channel conductance is determined by competition between $Ca^{2+}$ and $K^+$ for a control (gating ?) binding site.**

Transport processes through the plasmalemma play a key role in the functioning of the cell (1). In the characean cells, these transport processes and their interactions have been extensively studied. The membrane potential of both *Chara* and *Nitella* cells is much more negative than any possible diffusion potential and is probably due to the operation of an ATP-dependent electrogenic $H^+$ efflux system (8, 18, 19). In these plant cells, $K^+$ has the highest passive ionic permeability across the plasmalemma (2); its partial conductance being 0.15 Semen-$m^{-2}$ compared to 0.01 and 0.02 Semen-$m^{-2}$ for $Na^+$ and $Cl^-$, respectively (7). Thus, in the observed hyperpolarized state, there would be net passive movement of $K^+$ into these cells, which would tend to depolarize the potential. If this passive $K^+$ influx were not controlled, not only would the system lose potential energy that would otherwise be available to drive, for example, $Cl^-$ influx (17) but, in addition, cytoplasmic $K^+$ levels may increase beyond physiological limits.

Previous work has shown that the *Chara* cell can exist in two different potential states; termed polarized and depolarized states by Oda (15). A transition between these two states can be caused by changing the external $K^+$ concentration, or by passing current through the membrane (15, 18). The membrane potential in the polarized state was relatively insensitive to changes in $K^+$ concentration, while in the depolarized state it changed by 42 mv for a 10-fold $K^+$ concentration change (15).

The $K^+$ permeability in *Chara* is influenced by the exogenous $Ca^{2+}$/monovalent cation ratio. In the presence of $Ca^{2+}$, the characean membrane electrical properties are essentially independent of $K^+$ concentration, but in the absence of $Ca^{2+}$ the membrane behaves like a $K^+$ electrode (6, 10, 20). If there is a $Ca^{2+}$ binding site for this effect, it is possible that other ions may also bind to it. Recent work suggests that $Mg^{2+}$, $Sr^{2+}$, or $Mn^{2+}$ can substitute for $Ca^{2+}$ under some circumstances (13, 14). It is also possible that other cations may bind to this site, but without having the $Ca^{2+}$ effect. $K^+$ may compete for $Ca^{2+}$ binding sites in nerves (21, 24), and a similar possibility has been suggested for *Chara* (14).

In the present study, we further examined some of the interactions of various ions with the $K^+$-channels in order to advance our understanding of how $K^+$ permeability is controlled. The interaction between the $K^+$-channels and the electrogenic pump was also investigated. The evidence presented is consistent with the hypothesis that in the $K^+$-induced depolarized state, the electrogenic $H^+$ pump remains operational. However, the influence of the $H^+$ pump is masked by the short-circuiting effect of the open $K^+$-channels.

### MATERIALS AND METHODS

**Culture Material.** *Chara corallina* Klein ex Willd., em R.D.W. (= *Chara australis* R.Br.) was grown in a plastic container with 8 to 10 cm of lake mud (Lone Star Lake, Kansas) and 120 liters of solution which initially contained (mM): 3 $Na^+$, 0.2 $K^+$, 0.2 $Ca^{2+}$, 0.2 $SO_4^{2-}$, 1.2 $Cl^-$, and 2 $HCO_3^-$. Fluorescent lights provided 16 h of illumination at an intensity of 17 to 20 w $m^{-2}$ at the solution surface. Internodal cells (about 2–3 cm for electrophysiology and 3–5 cm for $K^+$ determinations) were cut the day before the experiments and incubated overnight in a solution containing (mM): 1.0 NaCl, 0.2 KCl, 0.2 $CaSO_4$, and 1.0 $NaHCO_3$.

**Experimental Solutions.** The basic experimental solution, CPW7[2], was prepared using high purity glass-distilled $H_2O$ and contained (mM): 1.0 NaCl, 0.2 KCl, 0.2 $CaSO_4$, 1.0 Hepes, and

[1] Supported by National Science Foundation Grant PCM 8003133 to W. J. L. and D. W. K.

[2] Abbreviations: CPW, *Chara* pond water; TEA, tetraethylammonium; NEM, *N*-ethylmaleimide; DES, diethylstilbestrol; $E_K$, Nernst potential for potassium; DCCD, dicyclohexylcarbodiimide; AP, 4-aminopyridine; TAP, 2,4,6-triaminopyrimidine; MA, methylamine.

was adjusted to pH 7 using freshly dissolved NaOH. Ca-free CPW7 was as above but without $CaSO_4$. All modifications to this medium are detailed in the text. TEA (Matheson, Coleman, and Bell) was purified by recrystallization from chloroform and vacuum dried in the presence of a liquid $N_2$ cold finger, or used as received (Aldrich). Inorganic chemicals were from Mallinckrodt; all other chemicals were from Sigma. NEM was prepared as a 100 mM stock solution (pH 3.3), stored at 4°C for, at most, 36 h, and diluted into the experimental solution just before use. The DES (40 mM) was dissolved in absolute ethanol and then diluted just before use to 40 μM in the experimental solution. Solutions were flowed through the chamber at a rate of 15 to 25 ml/min.

**Measurements of Membrane Potential and Resistance.** The basic details of the electrical measurement methods have been published previously (8). For these experiments, WPI model 750 amplifiers with a differential input (WP Instruments, New Haven, CT) were used. Electrodes were pulled from glass fiber-filled capillary tubing (WPI or Frederick Haer) on a Kopf puller (David Kopf Instruments, Tujunga, CA) to a taper length of 0.5 to 0.8 cm (2–5 Mohm). Contact with the 3M KCl (pH 2) filling solution was made using holders containing AgCl plugs (WPI). Cell resistances were determined by the method of Hogg *et al.* (5) using a Pulsar 4i pulse generator (Frederick Haer and Co., Brunswick, ME) connected to the current electrode through a $10^8$ ohm resistor (0.4 μamp current injected into the cells).

Light was from a Leitz Pradovit projector (quartz iodide lamp; 150 w, 12 v), with the beam attenuated to 20 w $m^{-2}$ using a neutral density filter and 10 cm of water.

**Potassium Concentration.** Potassium concentration in the vacuole was measured by atomic emission spectrophotometry using a Varian model 1200 Atomic Absorption Spectrophotometer. Vacuolar sap (10 μl) was extracted using the technique of Fujii *et al.* (3) and diluted with 10 ml of $H_2O$. $K^+$ standards contained only KCl.

## RESULTS

**Internal Potassium Concentrations.** Table I presents the measured $K^+$ concentrations of extracted vacuolar sap for three different pretreatment conditions. These values, along with other known parameters, can be substituted into the Goldman equation to obtain a value for the diffusion potential. However, in *Chara* the dominant term in this equation is that of $K^+$, resulting in the value of the Goldman equation being only slightly more positive than the value of $E_K$. Thus, $E_K$ provides a negative limit on the diffusion potential and this has been tabulated in Table I for two different external $K^+$ concentrations.

**Membrane Potential and Resistance during and following Exposure to 10 mM KCl.** *Chara* cells in CPW7 ($K^+$ = 0.2 mM) had membrane potentials (mean, −250 mv; range, −220 to −290 mv), that were only slightly altered by changes in external $K^+$. On exposure to 10 mM $K^+$, the potential initially depolarized by 10 to 30 mv (Fig. 1) and then, following an action potential, the potential restabilized at −91 mv (range, −60 to −118 mv). This transition to the depolarized state occurred 1 to 40 min (mean, 16 ± 3 [$n$ = 19] min) after exposure to 10 mM KCl. After this transition, the membrane resistance, originally 10 to 20 kohm-$cm^2$, was 1/10 to 1/20 of the original value, and the potential responded to changes in external $K^+$ as if the membrane were a $K^+$ electrode (99% of theoretical response). The potential stayed in this depolarized state as long as the cell was in the 10 mM KCl solution. When the cell was transferred back into control solution (0.2 mM $K^+$), the membrane potential hyperpolarized (Fig. 1). This recovery exhibited two phases, with a definable break point (Figs. 1 and 2).

Table I. *Vacuolar $K^+$ Level and Nernst Potential for Potassium, $E_K$, in Cells of Chara corallina after Various Pretreatments*

| Pretreatment | Vacuolar Potassium | $E_K$[a] | |
|---|---|---|---|
| | | 0.2 mM External $K^+$ | 10 mM External $K^+$ |
| | *mM* | *mv* | |
| Freshly cut cells | 49 ± 3 ($n$ = 16) | −141 | −41 |
| 16–18 h in CPW + 1.0 mM $NaHCO_3$ | 51 ± 2 ($n$ = 29) | −143 | −42 |
| 16–18 h in CWP7 + 10 mM KCl | 77 ± 3 ($n$ = 18) | −153 | −53 |

[a] $E_K$ was calculated for two different external potassium concentrations.

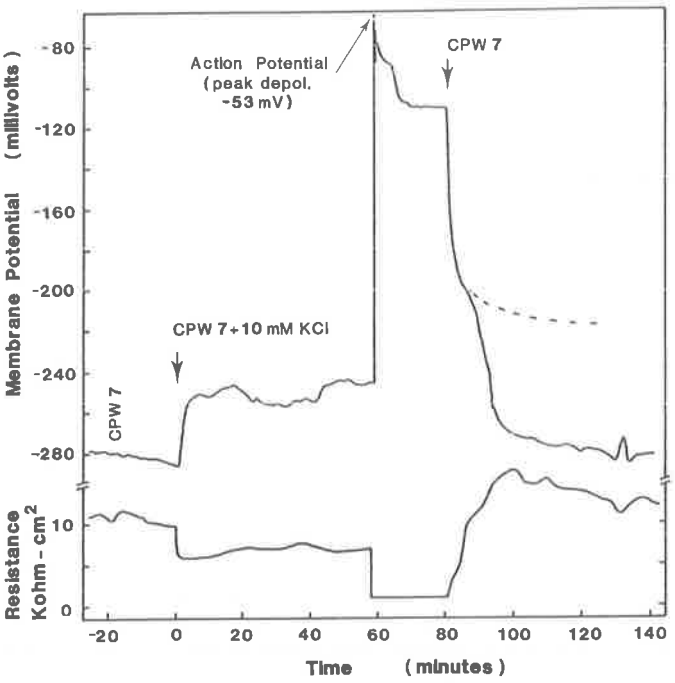


FIG. 1. Membrane potential and resistance changes accompanying exposure of the cell to CPW7 + 10 mM KCl and the later recovery in CPW7. Resistance values were measured once per min; the line on this graph is a fit through these individual points (Fig. 2 has the individual points represented). On return to CPW7, the potential recovered in two phases, the first phase was extrapolated with a dashed line.

In the first phase, which began with the solution change, the potential rapidly approached the break point (−168 ± 3 [$n$ = 22] mv); only toward the end of this first phase did the resistance begin to increase. The first phase was extrapolated to find its asymptote, a value of −191 ± 3 ($n$ = 22) mv was obtained. The change in potential from the 10 mM KCl solution, $E_m$ = −91 ± 3 ($n$ = 22), to the asymptotic value was 100 mv, the same difference as between the $E_K$ values in these two solutions (Table I, line 2). However, both the potential in 10 mM KCl and the asymptotic value were 48 to 49 mv more negative than $E_K$, in the respective solutions.

The second phase of recovery involved a further hyperpolarization of the membrane that started very rapidly and was simultaneous with a sudden increase in membrane resistance (Fig. 2). The resistance increase seen towards the end of the first phase may indicate the imminent onset of this second phase. During the second phase, the membrane hyperpolarized to a value similar to, but often slightly more negative than, the initial control potential. Both the response of the cell to changes in the external $K^+$ while in the state induced by 10 mM KCl, and the first phase of the recovery, indicate that the $K^+$ permeability of the membrane is much higher in the depolarized state than in the control.

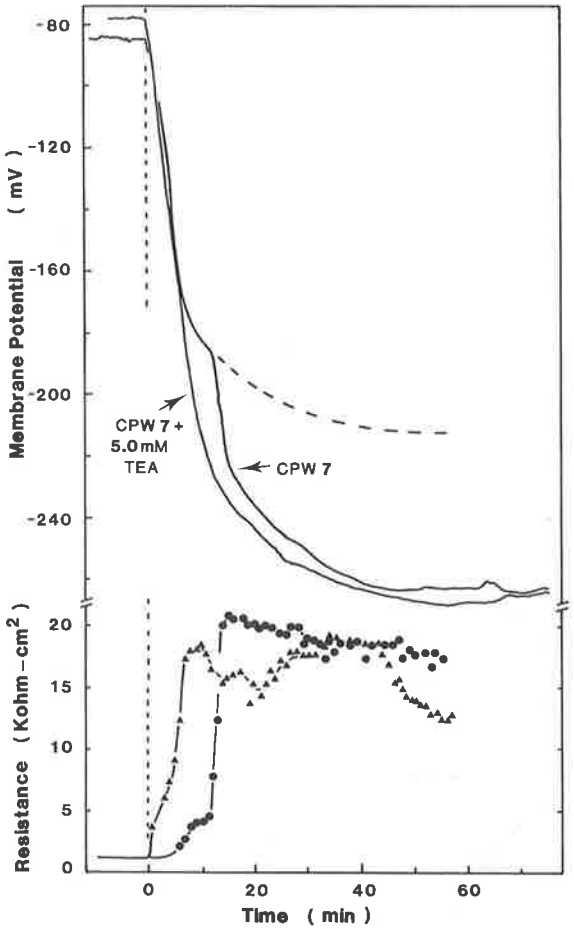


FIG. 2. Recovery time course of potential and resistance following exposure to 10 mM KCl. Prior to the time shown here, cells had been depolarized by exposure to CPW7 + 10 mM KCl (see Fig. 1). At time zero, the solution was changed to either CPW7 or to CPW7 + 5.0 mM TEA. The resistance values were measured once per min in CPW7 (●) or CPW7 + 5.0 mM TEA (▲).

The resistance increase on recovery from the 10 mM KCl solutions occurred with a shorter lag time if 5 mM TEA was present in the solution (Fig. 2). This caused the two phases of recovery to merge into one.

**Experiments under Ca-free Conditions.** Hope and Walker (6) pretreated their *Chara* cells for 2 to 6 h in 5 mM NaCl before inserting microelectrodes, and a similar treatment was used by Spanswick *et al.* (20) on *Nitella*, to produce a membrane that responded to $K^+$ as if the membrane were a $K^+$ electrode. In some experiments, cells were exposed to Ca-free CPW7 + 5 mM NaCl (high NaCl solution) for 6 h following electrode insertion, and the time course of the membrane potential was followed (Fig. 3A). (Increasing the $Na^+$ level enhanced the removal of bound $Ca^{2+}$ from the cell wall and plasmalemma.)

During exposure to high NaCl solutions, the cells did not make a transition, either suddenly or gradually, from the normal hyperpolarized to the depolarized potassium-sensitive state. Upon initial exposure to the high NaCl solution, there was a depolarization of about 20 mv, followed, during the next few h, by a gradual hyperpolarization of about the same magnitude (Fig. 3A). Following an action potential, induced by passing current through the membrane, the potential quickly recovered back to its original, or even more hyperpolarized value when the solution contained 6 mM NaCl (Fig. 3A). Upon changing the solution to Ca-free CPW7, a 20 mv hyperpolarization was seen as the NaCl concentration decreased; the reversal of the depolarization observed on exposure to the high NaCl concentration. The potential would usually stay at this hyperpolarized value (about −280 mv); but, in seven cases (out of 20 experiments), a spontaneous action potential was observed after the cell had been in Ca-free CPW7 for 30 min or more. After an action potential, whether spontaneous or induced by current injection, the potential did not recover back to the extremely hyperpolarized state (−280 mv), but instead, recovered only to −190 to −200 mv. In this new state, the membrane initially exhibited (with one exception out of 20 experiments) a series of spontaneous transient depolarizations to −130 to −150 mv, with a rapid recovery back to −190 to −200 mv. The frequency of these transient depolarizations slowly decreased and finally they ceased completely, leaving the potential steady at −190 to −200 mv.

A transition from the potential level of −190 to −200 back to the extremely hyperpolarized state (−250 mv) occurred when various ions were added to the bathing solution (Fig. 3B): $Na^+$ (5.0 mM addition), $Ca^{2+}$ (0.2–5.0 mM), and TEA (5 mM). Following recovery in either $Na^+$ or TEA, changing back and forth between these two solutions (Fig. 3B) had little effect on the value of the membrane potential (≤5 mv). After any of these treatments ($Na^+$, TEA, or $Ca^{2+}$), switching to Ca-free CPW7 caused the membrane to hyperpolarize a further 20 mv where it remained. In this latter state, an induced action potential given within 2 to 3 h of the previous depolarization in Ca-free CPW7 usually did not cause a transition to the −190 to −200 mv state (data not shown). However, if the cell was left in Ca-free CPW7 until the next morning (8–9 h), then the cell readily made this transition.

When cells were in the hyperpolarized state (−250 mv) in Ca-free CPW7, irrespective of whether or not they had previously made the transition to −200 mv, exposure to Ca-free CPW7 + 10 mM KCl had the same results as found for exposure of normal cells to CPW7 + 10 mM KCl: a depolarization of 20 to 30 mv, followed, after a variable lag time (but shorter than that observed in $Ca^{2+}$-containing solutions), by an action potential that marked the transition to a depolarized state of −90 to −110 mv. Now, in the absence of $Ca^{2+}$, on return to normal levels of $K^+$ (0.2 mM), there was only a one phase recovery to approximately −180 mv (Fig. 4) with only a small increase in resistance. The potential could by hyperpolarized further (−250 mv) by exposing the cell to 0.2 mM $CaCl_2$ or 5 mM TEA.

**Effects of NEM and DES.** When cells in CPW7 + 10 mM KCl and with $E_m$ of −91 mv (Fig. 1) were exposed to one to four 30-s pulses of CPW7 + 10 mM KCl + 0.1 mM NEM solution, the potential depolarized by 15 to 30 mv, leaving the cells with a potential of −65 to −80 mv, a value much closer to the calculated diffusion potential of −42 mv, (Table I) than before (Fig. 5A, inset). Exposure of other cells to CPW7 + 10 mM KCl + 40 μM DES caused the potential to depolarize by 10 to 30 mv, often with a transient hyperpolarization following the initial depolarization (Fig. 5A). This treatment significantly increased the resistance over that observed in CPW7 + 10 mM KCl. When 10 mM KCl + DES-inhibited cells were exposed to CPW7 + 40 μM DES (reduction in $K^+$ to 0.2 mM), the potential hyperpolarized to about −160 mv and the resistance increased dramatically.

Although the application of DES depolarized the membrane, it was still more negative than $E_K$. Since it was thought that the high KCl concentration could have been interfering with the operation of DES, three alternate experiments were performed. (a) The $K^+$ concentration was lowered from 10 to 2 mM before DES was applied. This did not increase the DES inhibition. (b) Another inhibitor, DCCD, was used. DCCD (50 μM) depolarized the membrane (20 to 40 mv) somewhat more than did DES. (c) DES was applied first, then cells were exposed to 10 mM KCl (Fig. 5B). This caused a depolarization to about −60 mv, less negative than when DES was applied last, and often the depolarization was in two steps as seen in Figure 5B. This last combination came the

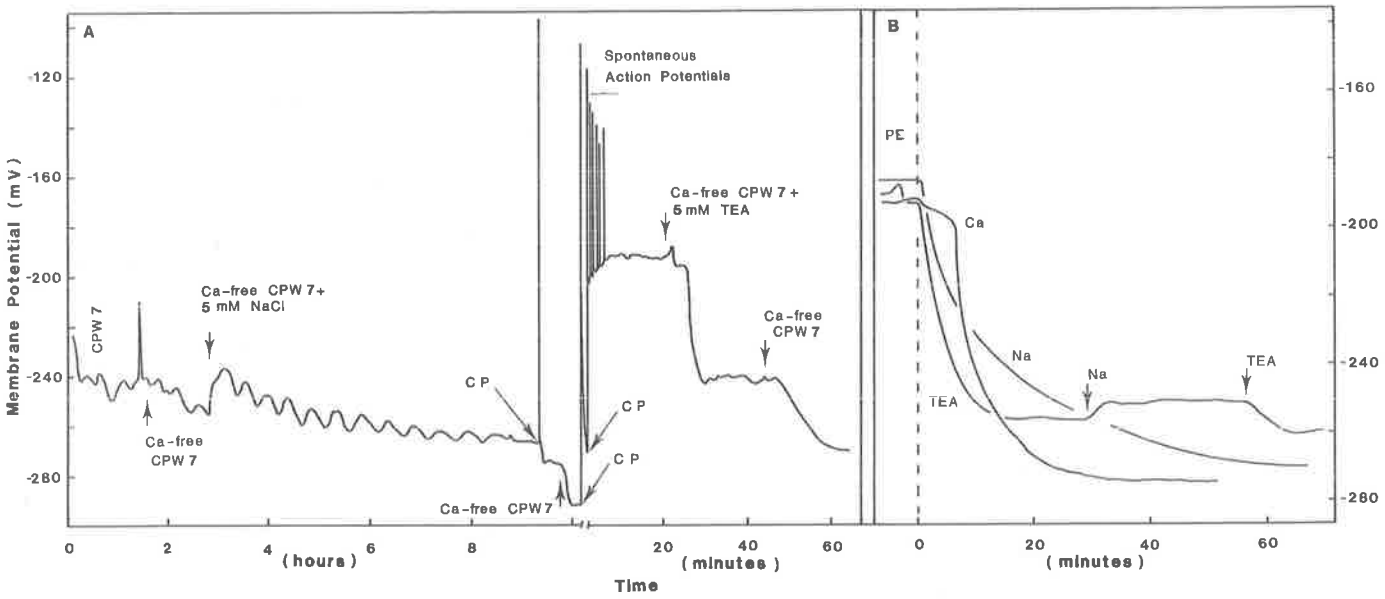


FIG. 3. Time course of the membrane potential in a Ca-free experiment. A, Cell pretreated by a long exposure to Ca-free conditions to remove $Ca^{2+}$ from the wall; to speed this process, the ionic strength of the solution was increased with NaCl (Ca-free CPW7 + 5 mM NaCl). On a few occasions (as shown here) the potential exhibited a slow oscillation. In both the high NaCl solution and in the Ca-free CPW7, current was passed through the membrane (CP) to stimulate an action potential. In Ca-free CPW7, this stimulated action potential (CP) caused the transition to the depolarized state during which a number of experiments were done, one of which appears in A, and three others in B.

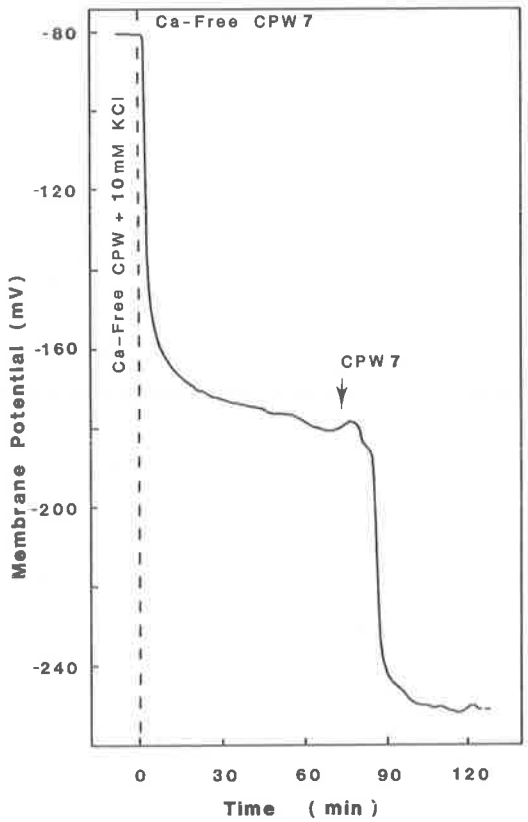


FIG. 4. Membrane potential recovery from a depolarized state induced by Ca-free + 10 mM KCl conditions. Cell pretreatment was similar to Figure 3; following long exposure to Ca-free conditions, the cell was depolarized with Ca-free CPW7 + 10 mM KCl. Reducing the $K^+$ concentration from 10 to 0.2 mM (Ca-free CPW) resulted in a Nernst response of 100 mv. Addition of $Ca^{2+}$ (CPW7) allowed the re-establishment of a control potential.

closest to depolarizing the cell to $E_K$ (= −42 mv).

Inhibitor experiments were also performed on cells that had been depolarized to −180 to −200 mv by an induced action potential following several h in Ca-free solutions (Fig. 3A). For these cells, one 30-s exposure to 0.1 mM NEM caused the potential to begin an immediate depolarization; in about 30 min, a stable value of about −140 mv was reached (Fig. 5C). After this NEM exposure, increasing NaCl by 5 mM, depolarized the membrane reversibly by about 38 mv (compared to the maximal Nernst response of 46 mv). (In this state, a 10-fold increase in $K^+$ concentration depolarized the membrane by 28–30 mv.) During these treatments, NEM decreased the resistance by a factor of 2 to 3. Both the high $Na^+$ and $K^+$ treatments also decreased the resistance.

A DES treatment, to cells in Ca-free CPW7 following an action potential (Fig. 3A), initially depolarized the membrane by 20 to 40 mv (Fig. 5D), and at times was followed by a transient hyperpolarization (Fig. 5D).

**Reputed $K^+$-Channel Blocking Agents.** Compounds known to block $K^+$-channels in animal tissue were also used: TEA (22), previously discussed, AP (23), and TAP (16). When cells were exposed to 5 mM AP, the membrane depolarized in about 10 min from its normal state (−250 mv) to −150 mv (Fig. 6). This AP-induced depolarization was accompanied by a 5-fold decrease in membrane resistance. Lower concentrations of 0.1 to 0.5 mM AP caused a hyperpolarization of the membrane, the size of which was a function of the AP concentration; in 0.5 mM AP, this hyperpolarization was about 20 mv (Fig. 6). At higher AP concentrations (1.0–1.5 mM), a threshold was reached where, after an initial hyperpolarization, the membrane rapidly depolarized. The rate of this depolarization was a function of the AP concentration, but the final potential in 0.2 mM KCl was −140 to −150 mv, irrespective of the AP concentration, as long as it was greater than the threshold. In this state, with 1.0 mM AP, the potential was sensitive to $K^+$ concentration; increasing $K^+$ concentration to 2.0 mM, a 10-fold increase, depolarized the cell by 40 to 45 mv (data not shown), compared to the theoretical Nernst response of 59 mv. However, a 10-fold reduction of the $K^+$ concentration, to 0.02 mM, hyperpolarized the membrane by only 7 to 10 mv. The resistance

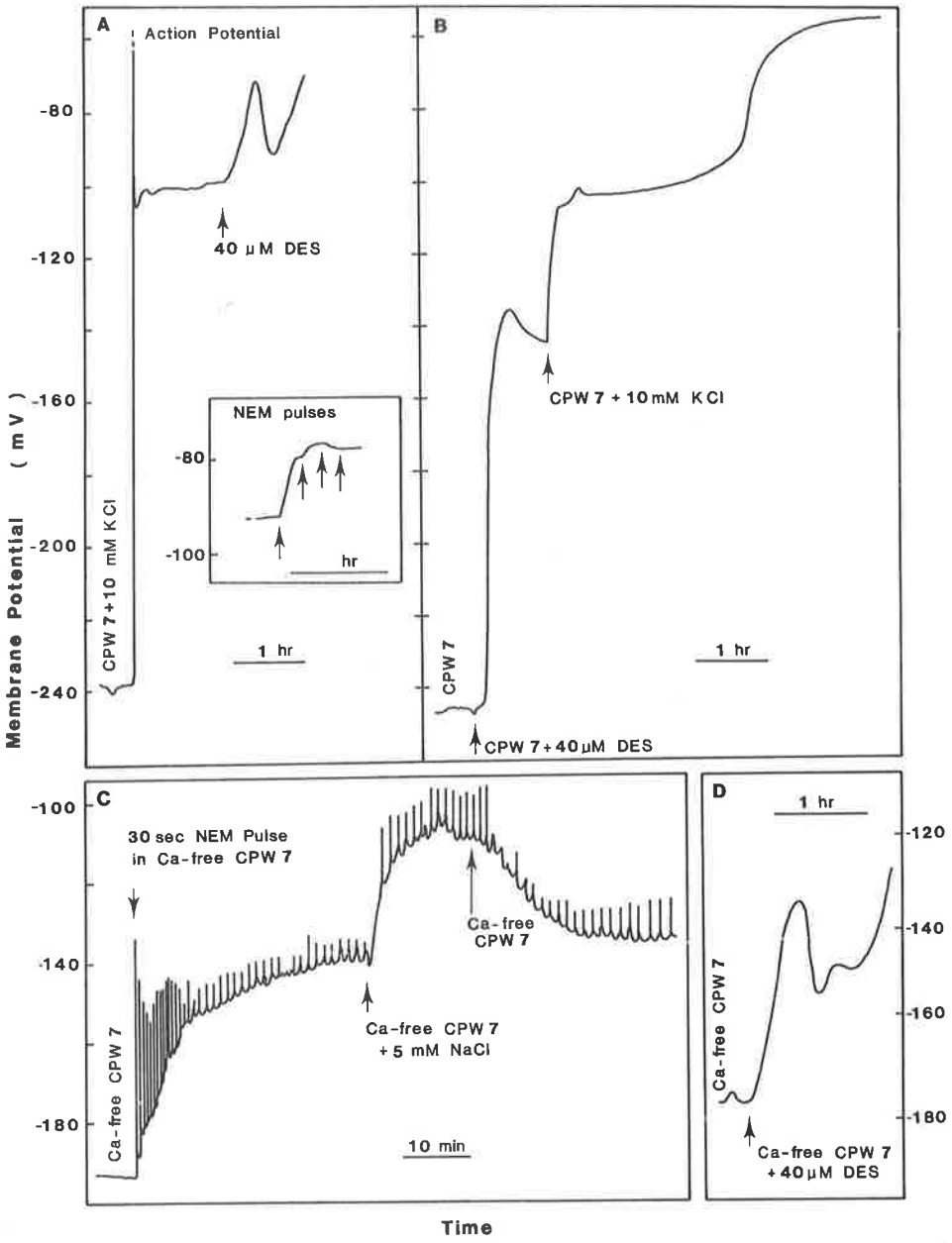


FIG. 5. Effect of NEM and DES on the cell potential. After the cell had been depolarized by exposure to CPW7 + 10 mM KCl, the potential could be further depolarized by treatment with CPW7 + 10 mM KCl + 40 μM DES or with several 30-s exposures to CPW7 + 10 mM KCl + 0.1 mM NEM (at arrows in insert) (A). We reversed the order of treatment, exposing the cell to CPW7 + 40 M DES to inhibit the electrogenic pump(s) before changing to CPW7 + 10 mM KCl (B). Following depolarization with a stimulated action potential in Ca-free CPW7 (see Fig. 3), the potential was further depolarized by a 30-s exposure to Ca-free CPW7 + 0.1 mM NEM (C) or Ca-free CPW7 + 40 μM DES (D). NEM treatment in Ca-free media leaves the cell very sensitive to changes in $Na^+$ concentration (C).

observed in these AP solutions was larger the lower the KCl concentration.

When cells were recovering from 10 mM $K^+$ exposure (Fig. 1), the presence of 1.0 mM TAP caused the recovery to occur in one phase, as did 5.0 mM TEA. The initial rates of hyperpolarization were similar to those obtained with TEA. When applied to an undisturbed cell, TAP caused a slight hyperpolarization (20 mv with 0.5 mM TAP) just as AP did at low concentrations. Unlike AP, even at 1.0 mM, TAP never caused the cell to depolarize.

TAP had no observable effect on the potential or resistance when the cell was in a depolarized state in CPW7 + 5 mM KCl (following a depolarization in a prior exposure to 10 mM KCl). This contrasts with 5.0 mM TEA, which could restore cells to their hyperpolarized state about 50% of the time when they were in CPW7 + 5.0 mM KCl.

Exposure of the cell to a solution containing 5 mM TEA + 1.0 mM AP, after an exposure to 1.0 mM AP, caused a depolarization of about 40 mv. In this new state, with both TEA and AP present in the solution, the potential was relatively insensitive to changes in $K^+$ concentration; a change from 0.2 to 1.0 mM KCl caused a potential change of 7 to 10 mv.

**Methylamine.** At pH 7, MA is a cation which could also interact with $K^+$-channels. Cell exposure to 0.05 mM MA caused a rapid depolarization of 20 to 25 mv. At higher concentrations, 0.2 mM MA, the depolarization was 60 to 80 mv (Fig. 7A). This exposure reduced the resistance to one-half to one-third of the control,

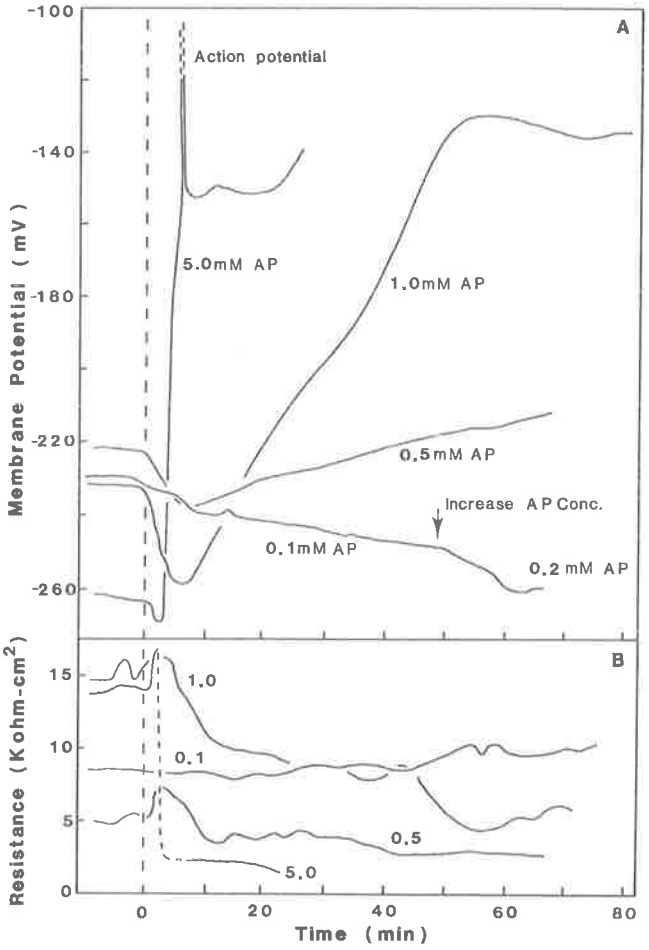


FIG. 6. Membrane potential (A) and resistance (B) changes caused by exposure to different concentrations of AP at time zero.

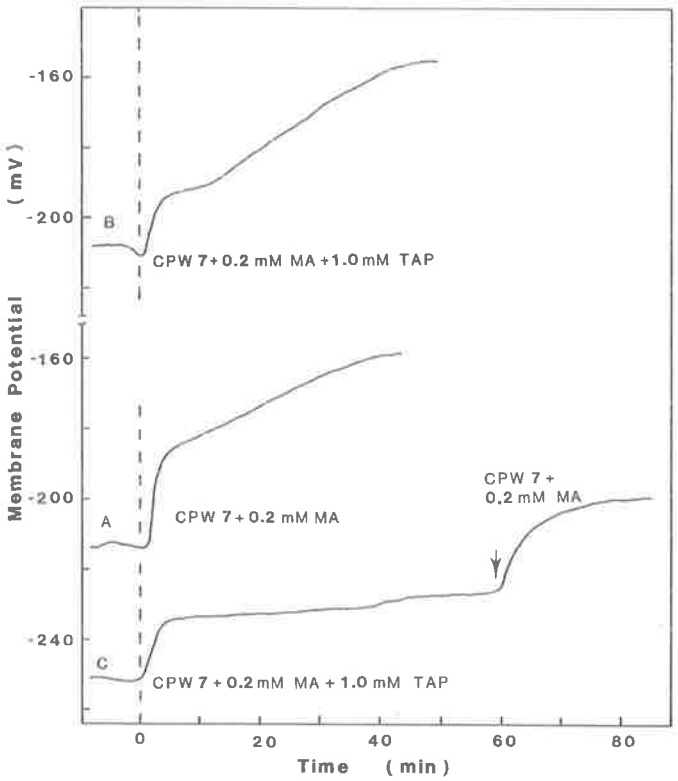


FIG. 7. Effect of MA and TAP on the membrane potential. A, Effect of MA on control (CPW7) cells. B, Cell pretreated with CPW7 + 1.0 mM TAP prior to MA treatment. C, Cell given a complex pretreatment (preexposed to CPW7 + 10 mM KCl to open $K^+$-channels, and then introduction of CPW7 + 10 mM KCl + 1.0 mM TAP, followed by recovery from high KCl, in CPW7 + 1.0 mM TAP) before introducing MA. TAP removal caused a further depolarization such that the total depolarization was similar to the control (A).

consistent with charge movement through the membrane.

If the cell was exposed to TAP (1.0 mM) prior to the MA (0.2 mM) exposure, this depolarization (Fig. 7B) was reduced about 20% compared to the control (Fig. 7A). However, if the prior exposure to TAP began while cells were depolarized in 10 mM KCl, then the depolarization on exposure to MA (Fig. 7C) was reduced to about 55% of the control depolarization.

**Action Potential Initiation.** Exposure of *Chara* to 10 mM $K^+$ caused an action potential to occur, with a lag time of typically 10 to 20 min. At lower $K^+$ concentrations the lag time was longer, until at a threshold concentration of 2 to 3 mM $K^+$, no action potential occurred (12). When this experiment was repeated in the presence of 0.2 mM MA, 2.0 mM $K^+$ routinely initiated action potentials with a lag time of 5 to 30 min. In the presence of 0.2 mM MA, changing from 0.02 to 0.2 mM KCl caused, at most, a 5 to 6 mv change in potential, about one-tenth of the theoretical Nernst response.

## DISCUSSION

**Effect of, and Recovery from, 10 mM KCl Treatment.** Two phases of membrane potential change were observed, both when the cell depolarized on exposure to 10 mM KCl and later when it repolarized after the exposure was terminated. The transition between these two phases was correlated with a large change in membrane resistance and in the sensitivity of the membrane to changes in external $K^+$ concentrations. It is believed that these phenomena indicate the operation of a gated $K^+$-channel across the plasmalemma. On exposure to 10 mM KCl, the membrane initially depolarized slightly, then after a variable lag time, the resistance decreased as these $K^+$-channels opened, providing a large conductance through the membrane. This $K^+$ conductance depolarized the membrane potential by short-circuiting the electrogenic pump in the plasmalemma (8).

The first phase of recovery from the 10 mM KCl exposure is assumed to be the voltage change expected if the membrane were responding as a $K^+$ electrode to the reduction in external $K^+$ from 10 mM ($E_K = -42$ mv; Table I, line 2) to 0.2 mM ($E_K = -143$ mv). The difference between these two calculated Nernst potentials is 101 mv, which compares closely with the potential change of 100 mv measured when the first phase of recovery was extrapolated (Figs. 1 and 2). This first phase of recovery is initially accompanied by only a small resistance change which can be attritubed to the reduction of available charge carriers when the $K^+$ concentration is lowered.

The increase in membrane resistance that occurred at the transition from the first to the second phase of recovery could be accounted for by a closure of $K^+$-channels. This explanation would be consistent with the observed decrease in $K^+$ permeability following recovery from a high $K^+$ treatment. The sudden hyperpolarization that accompanied the resistance increase could also be explained in terms of $K^+$-channel closure. Open $K^+$-channels would short-circuit the electrogenic pump, thereby reducing the maximum observable electrogenic component of the membrane potential. As these $K^+$-channels close (and the resistance increases), this short-circuit would be eliminated and the electrogenic component of the potential would become more apparent, thus the sudden hyperpolarization.

The two phases of potential recovery from 10 mM KCl exposure were completely separated in the $Ca^{2+}$-free experiments (Fig. 4). In the first phase, the membrane is still responsive to $K^+$, due to open $K^+$-channels, and, hence, the potential change is that due to readjustment in the diffusion potential. When the $K^+$-channels were closed by introduction of $Ca^{2+}$ (0.2 mM), the membrane became relatively insensitive to $K^+$; a state reflected by an increase in membrane resistance. Under these conditions, the second phase of membrane potential recovery, back to the control state, was observed (Fig. 4).

**Electrogenic Potentials.** The potential of −91 mv observed in the depolarized state in the presence of 10 mM KCl was much more negative than any diffusion potential ($E_K$ = −42 mv, and $E_K$ is more negative than the Goldman diffusion potential for $K^+$, $Na^+$, and $Cl^-$). This potential in 10 mM KCl probably reflects the operation of an electrogenic pump in the membrane, just as was observed for the normal state of the cell (8). Further evidence for an electrogenic potential was provided by the large increase in internal $K^+$ concentration following an overnight incubation in 10 mM KCl (Table I). During most of the 16 to 18 h uptake period, the cell would be in the depolarized (−91 mv) state since this state is established within 40 min. For this large net accumulation, there must be a substantial driving force on $K^+$; for passive $K^+$ movement, this would be provided by the membrane potential (−91 mv) that is more negative than $E_K$ (= −42 mv). Our present results, which indicate that the electrogenic pump is still operating in the high $K^+$ depolarized state, is counter to the hypothesis of Walker and his collaborators (25, 27). These workers postulated that the electrogenic proton pump was inactivated when the membrane was depolarized by high $K^+$ treatment.

The potential observed in Ca-free solutions (−190 to −200 mv) was more negative than $E_K$ (= −143 mv since external $K^+$ = 0.2 mM); hence, in this state, there must also be an electrogenic component. Further evidence for both this state and that in 10 mM KCl being electrogenic was provided by the ability of DES and NEM to depolarize the membrane. DES inhibits the electrogenic pump of *Chara* (8, 9) either directly or through a reduction of ATP levels. By inhibiting the electrogenic pump, the membrane should depolarize towards a diffusion potential, and it did for both of these cases (Fig. 5). NEM increases the $K^+$ permeability of *Chara* (11) and should further short-circuit the electrogenic pump, depolarizing the membrane to a value nearer to $E_K$, which was observed for both cases (Fig. 5). If, however, the membrane potential were only a diffusion potential prior to NEM exposure, then increasing the $K^+$ permeability would have had little effect, since the $K^+$-permeability would already have been the dominant influence in the diffusion potential. The sensitivity of the membrane potential to $Na^+$ concentration changes in the Ca-free experiments, after NEM exposure, indicates that NEM probably alters both the $Na^+$ and $K^+$ permeability.

**Reputed $K^+$-Channel Blocking Agents.** The presence of 5 mM TEA caused the recovery from the 10 mM KCl exposure to occur with only one phase, and a shorter lag time before the resistance increased. This suggests that TEA causes the $K^+$-channels to close much sooner, accounting for the earlier resistance increase and merging of the two recovery phases. TEA appears to function as a gate on the $K^+$-channel.

The agents, which reputedly block the $K^+$-channels of animal cells, did not all have the same effect in *Chara*. Our results are consistent with both TEA and TAP blocking $K^+$-channels once the channels have been opened. But, AP apparently opens the normally closed $K^+$-channels, depolarizing the membrane to a value near $E_K$. AP could work by competing for binding sites, displacing $Ca^{2+}$, and yet not blocking the channels when bound.

Because of the different effects of TEA and AP, cells were exposed to solutions containing both of these agents, following an initial AP exposure to open $K^+$-channels. The membrane potential was now relatively insensitive to $K^+$ as if TEA had closed the channels. However, the combination of these two agents depolarized the membrane as if the electrogenic pump had been further short-circuited, instead of the hyperpolarization expected if the $K^+$-channels had been closed and the short-circuit on the electrogenic pump removed.

**Calcium.** We interpreted the results of the Ca-free experiments as showing that $Ca^{2+}$ is the normal substrate required to close the $K^+$-channels. Long exposures to Ca-free conditions do not by themselves open these channels, probably because (a) the $Ca^{2+}$ that closes the channel is bound too tightly to be removed by this treatment alone or (b) the $Ca^{2+}$ does leave the channel binding sites, but the channels remain closed until they are stimulated to open by either an action potential or exposure to high levels of KCl (10 mM) (which stimulates an action potential as well). In cells in which the $K^+$-channels are open, the potential developed by the electrogenic pump would be at least partially short-circuited; thus, the potential would be depolarized by these open channels to a value that is intermediate between the normal hyperpolarized electrogenic potential and the diffusion potential. Under normal conditions, the passive diffusion potential is given by the Goldman equation and is slightly more positive than $E_K$. In cells in which the $K^+$-channels are open, the $K^+$ permeability is much larger so the importance of $K^+$ is increased and the diffusion potential would be essentially equal to $E_K$. In a solution containing 0.2 mM $K^+$, $E_K$ in the cells would be near −143 mv. In the Ca-free experiments described above, where either an action potential or a brief exposure to high KCl placed the cell in a depolarized state, the potential in 0.2 mM $K^+$ is always more negative than −143 mv, suggesting that the electrogenic pump is operating and able to hyperpolarize the membrane to values of −180 to −200 mv, even with the load of open $K^+$-channels. When the $K^+$-channels are closed by $Na^+$, $Ca^{2+}$, or TEA, the short-circuit load on the pump is removed, and the membrane rapidly hyperpolarizes to values of −250 to −290 mv (Fig. 3B). A $K^+$-sensitive membrane potential, observed in either *Chara* or *Nitella* (6, 20) under $Ca^{2+}$-free conditions, probably represents a state in which the $K^+$-channels have been opened.

**Methylamine.** It has been suggested that MA enters *Chara* as does $NH_4^+$ and $K^+$ (4, 26). The inhibition of MA entry by TAP is the predicted result of TAP blocking $K^+$-channels if MA enters through the $K^+$-channels. The TAP inhibition was larger (40–50%) if TAP was applied when the $K^+$-channels had been opened by 10 mM KCl than if TAP was applied to a normal cell (20% inhibition). This is consistent with the ability of TAP to block $K^+$ movement; TAP is relatively ineffective at reaching the blocking sites unless the channels have been opened. Thus, this TAP inhibition provides further evidence for MA movement through $K^+$-channels. Blockage by TAP may involve first removing $Ca^{2+}$ from the binding sites with 10 mM KCl, and then binding TAP to block the channel. Thus, TAP protection against the depolarization by MA is effective only when TAP is applied while the $K^+$-channels are open.

The interaction between MA and $K^+$ could be explained in two ways: (a) MA acts directly by opening $K^+$-channels, thus potentiating the ability of $K^+$ to initiate action potentials; or (b) MA acts indirectly through its known depolarization of the membrane, and this depolarization then alters the action of $K^+$ on the $K^+$-channels. The first explanation is supported by the observation that MA reduces the membrane resistance to one-half to one-third of the control. The second explanation is supported by voltage clamp experiments (D. W. Keifer and W. J. Lucas, unpublished observations) in which the voltage for action potential initiation was found to be dependent upon the exogenous $K^+$ level. At higher concentrations of $K^+$, the membrane has to be depolarized less to initiate an action potential; the action potential occurs at more negative values of the membrane potential. The first expla-

nation would require that in the presence of MA the membrane potential be more responsive to changes in the external $K^+$ concentration; but, in fact, it was found to respond by only about one-tenth of the theoretical Nernst response. We feel, therefore, that it is more likely that MA interacts with $K^+$ only indirectly through the depolarization of the membrane by MA.

**Speculative Model.** The $K^+$-channel in the plasmalemma of *Chara* has a cation binding site associated with it, presumably at the exterior entrance to the channel. When this site is occupied by $Ca^{2+}$, the channel is closed, and when the site is occupied by $K^+$, the channel is open. The membrane, which presumably contains a large population of channels, has a non-zero $K^+$ permeability even when substantial amounts of $Ca^{2+}$ are available. At least three explanations are possible: (a) there are two populations of channels, only one of which is blocked by $Ca^{2+}$; (b) a given channel is only partially blocked by $Ca^{2+}$, and at any given time some amount of $K^+$ can pass through the channels; (c) $Ca^{2+}$ totally blocks the channel, but $Ca^{2+}$ bound to the channel is in equilibrium with free-$Ca^{2+}$, so that in a population of channels some will not have a $Ca^{2+}$ bound and will thus be open.

This binding site may have its highest affinity for $Ca^{2+}$, but it is not entirely specific for $Ca^{2+}$. Other ions will compete for this site and displace $Ca^{2+}$, including: $K^+$, $Na^+$, TEA, TAP, and AP. The concentration of the various exogenous ions that it takes to displace $Ca^{2+}$ varies widely; some of these differences in concentrations could be due to the cation exchange properties of the cell wall which would concentrate divalent cations more than it would monovalent cations. Concentrations in the following discussion will refer to those in the external solution. $Ca^{2+}$ (0.2 mM) can be displaced by 10 mM $K^+$ (with a probable threshold of 2–3 mM $K^+$), leaving the channels open. In zero $Ca^{2+}$, 6 mM $Na^+$ can fill the sites displacing 0.2 mM $K^+$ and close the channels. If the $K^+$ is reduced to 5 mM, 5 mM TEA can sometimes displace the $K^+$ to close the channels, but it is a slow process. $K^+$ can always be displaced by 2.0 mM $Ca^{2+}$, but again it is slow. While all the possibilities and combinations have not been investigated, our data suggest the following series: $Ca^{2+} \gg TAP > K^+ \simeq TEA > Na^+$, for the binding affinity. All of these ions close the channel except $K^+$, which allows $K^+$ passage through the channel. Of these ions, $K^+$ is also the one with the smallest hydrated radius, so it may be able to bind to the site at the channel mouth and not obstruct $K^+$ access to the channel itself.

The state of the $K^+$-channel, whether open or closed, plays a substantial role in determining the membrane potential. Probably, the best example is during the Ca-free experiments where the $K^+$-channels opened without any change in $K^+$ concentration. The membrane potential changes from typically −280 mv when the $K^+$-channels are closed, to −190 mv when they are open. In the state with the open $K^+$-channels, the electrogenic pump is still operating, keeping the potential substantially more negative than $E_K$ (= −143 mv). Further evidence for this is (a) the depolarization of this potential by inhibiting the electrogenic pump with DES or by short-circuiting the pump by further increasing $K^+$ permeability with NEM and (b) the large uptake of potassium driven by this potential.

*Acknowledgment*—We thank Alison Wille for doing preliminary experiments with TEA.

## LITERATURE CITED


1. Clarkson DT 1974 Ion Transport and Cell Structure in Plants. McGraw-Hill, Maidenhead, England
2. Findlay GP, AB Hope, MG Pitman, FA Smith, NA Walker 1969 Ionic fluxes in cells of *Chara corallina*. Biochim Biophys Acta 183: 565–576
3. Fujii S, T Shimmen, M Tazawa 1979 Effect of intracellular pH on the light-induced potential change and electrogenic activity in tonoplast-free cells of *Chara australis*. Plant Cell Physiol 20: 1315–1328
4. Hille B 1973 Potassium channels in myelinated nerve: selective permeability to small cations. J Gen Physiol 61: 669–686
5. Hogg J, EJ Williams, RJ Johnston 1968 A simplified method for measuring membrane resistance in *Nitella translucens*. Biochim Biophys Acta 150: 518–520
6. Hope AB, NA Walker 1961 Ionic relations of cells of *Chara australis* R. Br. IV. Membrane potential differences and resistances. Aust J Biol Sci 14: 26–44
7. Hope AB, NA Walker 1975 The Physiology of Giant Algal Cells. Cambridge University Press, Aberdeen, Great Britain
8. Keifer DW, RM Spanswick 1978 Activity of the electrogenic pump in *Chara corallina* as inferred from measurements of the membrane potential, conductance and potassium permeability. Plant Physiol 62: 653–661
9. Keifer DW, RM Spanswick 1979 Correlation of adenosine triphosphate levels in *Chara corallina* with the activity of the electrogenic pump. Plant Physiol 64: 165–168
10. Kishimoto, U 1959 Electrical characteristics of *Chara corallina*. Annu Rep Sci Work Fac Sci Osaka Univ 7: 115–146
11. Lichtner FT, WJ Lucas, RM Spanswick 1981 Effect of sulfhydryl reagents on the biophysical properties of the plasmalemma of *Chara corallina*. Plant Physiol 68: 899–904
12. Lucas WJ 1976 The influence of $Ca^{2+}$ and $K^+$ on $H^{14}CO_3^-$ influx in internodal cells of *Chara corallina*. J Exp Bot 27: 32–42
13. Lucas WJ, J Dainty 1977 $HCO_3^-$ influx across the plasmalemma of *Chara corallina*. Divalent cation requirement. Plant Physiol 60: 862–867
14. Lucas WJ, RM Spanswick, J Dainty 1978 $HCO_3^-$ influx across the plasmalemma of *Chara corallina*: physiological and biophysical influence of 10 mM $K^+$. Plant Physiol 61: 487–493
15. Oda K 1962 Polarized and depolarized states of the membrane in *Chara braunii*, with special reference to the transition between the two states. Sci Rep Tahoku Univ Fourth Ser (Biol) 28: 1–16
16. Reuss L, TP Grady 1979 Triaminopyrimidinium ($TAP^+$) blocks luminal membrane K conductance in *Necturus* gallbladder epithelium. J Membr Biol 48: 285–298
17. Sanders D 1980 The mechanism of $Cl^-$ transport at the plasma membrane of *Chara corallina*. I. Cotransport with $H^+$. J Membr Biol 53: 129–141
18. Spanswick RM 1972 Evidence for an electrogenic ion pump in *Nitella translucens*, I. The effects of pH, $K^+$, $Na^+$, light and temperature on the membrane potential and resistance. Biochim Biophys Acta 288: 73–89
19. Spanswick RM 1974 Evidence for an electrogenic ion pump in *Nitella translucens*, II. Control of the light-stimulated component of the membrane potential. Biochim Biophys Acta 332: 387–398
20. Spanswick RM, J Stolarek, EJ Williams 1967 The membrane potential of *Nitella translucens*. J Exp Bot 18: 1–16
21. Tasaki I 1968 Nerve Excitation. Charles C Thomas, Springfield, IL
22. Tasaki I, S Hagiwara 1957 Demonstration of two stable potential states in the squid giant axon under tetraethylammonium chloride. J Gen Physiol 40: 859–885
23. Thompson SH 1977 Three pharmacologically distinct potassium channels in molluscan neurons. J Physiol (Lond) 265: 465–488
24. Tobias JM 1964 A chemically specified molecular mechanism underlying excitation in nerve: a hypothesis. Nature (Lond) 203: 13–17
25. Walker NA 1980 The transport system of charophyte and chlorophyte giant algae and their integration into modes of behavior. *In:* RM Spanswick, WJ Lucas, J Dainty, eds, Plant Membrane Transport: Current Conceptual Issues. Elsevier/North-Holland, Amsterdam, pp 287–300
26. Walker NA, MJ Beilby, FA Smith 1979 Amine uniport at the plasmalemma of charophyte cells: I. Current-voltage curves, saturation kinetics, and effects of unstirred layers. J Membr Biol 49: 21–55
27. Walker NA, FA Smith, IR Cathers 1980 Bicarbonate assimilation by freshwater charophytes and higher plants: I. Membrane transport of bicarbonate ions is not proven. J Membr Biol 57: 51–58

Planta (1982) 154:525–537

Planta
© Springer-Verlag 1982

# The relationship of the charasome to chloride uptake in *Chara corallina*: physiological and histochemical investigations

Vincent R. Franceschi and William J. Lucas
Department of Botany, University of California, Davis, CA 95616, USA

**Abstract.** A possible role of the charasome in terms of chloride transport into *Chara corallina* Klein ex. Willd., em. R.D.W. is examined. The branches of *Chara* contain the most charasome material and are shown to be very effective in acquiring $Cl^-$ to support continued shoot growth. The early maturation of the branches, the rather large $Cl^-$ fluxes into these cells, and their ability to translocate $Cl^-$ to growing cells of the shoot indicate a special role of these branches in $Cl^-$ accumulation. The structure of the charasome, with its extensive periplasmic space, appears especially suited as a site for $H^+ - Cl^-$ cotransport (influx). We show, by histochemical assay, that the charasomes of mature cells contain ATPase activity; such activity is absent in growing charasomes of very young cells. ATPase activity is also associated with the plasmodesmata of *C. corallina*. Charasome ATPase activity and $Cl^-$ uptake are both inhibited by *p*-chloromercuribenzenesulfonic acid (1 mM) or diethylstilbestrol (40 μM; 45 min). The anion transport inhibitor, 4,4-diisothiocyano-2,2-disulfonic acid stilbene (1 mM) had no effect on $Cl^-$ transport and inhibited ATPase activity only when applied after chemical fixation of the cells. Results of an attempt to demonstrate the presence of $Cl^-$ within the cytoplasmic tubules of the charasome, using a silver precipitation technique, proved difficult to interpret because of a reaction between the silver and a cellular substance produced in the light.

**Key words:** ATPase localization – *Chara* – Charasome – Chloride transport – Plasmalemma ($Cl^-$ transport).

## Introduction

Until recently, both the structure and physiological function of the charasome were unresolved. Ultrastructural details of the charasome and the manner in which this complex plasmalemma modification is formed have now been described (Franceschi and Lucas 1980, 1981; Lucas and Franceschi 1981). The charasome is composed of an intricate network of anastomosing membrane tubules that are continuous with the plasmalemma. The membrane tubules contain cytoplasm and are surrounded by a non-cytoplasmic region (periplasmic space) which is distinct from the cell wall. This compact, membranous structure gives rise to a tremendous increase in membrane surface area; approx. 27 $\mu m^2$ of membrane per $\mu m^3$ of charasome (Franceschi 1981).

Barton (1968) examined the charasome with respect to a role in cell-wall formation, but could find no evidence for such a function. *Chara* internode cells exhibit distinct acid and alkaline bands (see Lucas and Smith 1973) and charasomes occur primarily in the acid bands (Franceschi and Lucas 1980). However, a major role of the charasome in $HCO_3^-$ uptake, which occurs in the acid band regions, can be disregarded since *Nitella*, which has banding patterns and $HCO_3^-$ fluxes similar to those seen in *Chara*, does not contain charasomes (Franceschi and Lucas 1980). Chloride uptake also occurs primarily in the acid band regions of characean internodes (Spear et al. 1969) and it is possible that the charasome is involved in uptake of this ion. Chloride is generally the major anion found in the vacuole of *Chara*, an indication of its importance, although a strict requirement for $Cl^-$ as vacuolar osmoticum has apparently not yet been demonstrated.

We report here on our investigations into the possibility of the involvement of the charasome in $Cl^-$ uptake. Charasomes are most numerous in the internodes of the branches (Franceschi and Lucas 1980) and if they are involved in $Cl^-$ uptake, the branches of *Chara* should play a major role in $Cl^-$ accumulation. This hypothesis is tested by various means. Chloride fluxes into isolated cells and into cells still attached to growing shoots are determined and com-

*Abbreviations:* CPW = *Chara* pond water; DES = diethylstilbestrol; DIDS = 4,4-diisothiocyano-2,2-disulfonic acid stilbene; Mops = 3-(N-morpholino)propanesulfonic acid; PCMBS = *p*-chloromercuribenzenesulfonic acid

0032-0935/82/0154/0525/$02.60

pared, and $Cl^-$ partitioning in the growing shoot when the ion is supplied to a single branch, is examined.

Chloride uptake may be coupled to plasmalemma-associated ATPase activity (associated with proton pumping). We demonstrate ATPase activity within the charasome by a histochemical technique, examine the effect of enzyme inhibitors on this activity, and compare it with the effect of such inhibitors on $Cl^-$ influx. An attempt to show the presence of $Cl^-$ within the charasome cytoplasmic tubules, by a $Cl^-$ precipitation technique, although not conclusive is also described.

## Materials and methods

*Culture material.* Culture material of *Chara corallina* Klein ex Willd., em. R.D.W. (= *C. australis* R.Br.) was grown in the laboratory in 120-l containers. Details of the culture conditions have been described in Lucas and Nuccitelli (1980). Dr. J.-P. Métraux, University of California, Berkeley, provided *Nitella clavata* Kutz., em. from his laboratory cultures.

*Chemical solutions.* N-ethyl maleamide (NEM) was prepared as a 100 mM stock solution in glass-distilled water. This stock was stored at 4° C in the dark and used for 2–3 d. The NEM concentration of the experimental solution was checked spectrophotometrically (absorbance read at 302 nm; extinction coefficient = 620 $M^{-1}$ $cm^{-1}$). *p*-Chloromercuribenzenesulfonic acid (PCMBS) was prepared as a 20 mM stock solution in glass-distilled water, then purified on an ion-exchange resin (see Lucas and Alexander 1980, for procedure). The final concentration of the stock solution was determined spectrophotometrically (absorbance read at 265 nm; extinction coefficient = 611 $M^{-1}$ $cm^{-1}$). The PCMBS solutions were used immediately after preparation. Solutions containing 4,4-diisothiocyano-2,2-disulfonic acid stilbene (DIDS) were prepared by dissolving the proper amount of the reagent in the appropriately buffered *Chara* pond water (CPW-Mops; 1.0 mM NaCl, 0.2 mM KCl, 0.2 mM $CaSO_4$, 5 mM Mops; pH 6.5) to give the concentration desired for a given experiment. Diethylstilbestrol (DES) was prepared as a 40 mM stock solution in 100% ethanol. Experimental solutions were made by slow mixing of stock solution with CPW-Mops.

*Growth experiments.* Vegetative apices of *Chara corallina* were cut from laboratory cultures and trimmed such that only the three youngest internodes remained. All the branch cells of the nodal complex between the second and third internodes were removed except two opposite branches. The terminal nodal complex was also trimmed of all its branch cells. The shoots were rinsed twice with $Cl^-$-free CPW (0.5 mM $Na_2SO_4$, 0.2 mM $CaSO_4$, 0.1 mM $K_2SO_4$, 1.0 mM $NaHCO_3$; pH 8.0), then placed in a large glass Petri dish (diameter 14 cm, height 2 cm), and the two mature branches isolated from the shoot with two metal triangular frames (1.5 cm deep) notched at one point for passage of the branch. During these manipulations, the cells were kept wet with $Cl^-$-free CPW. The triangles were sealed to the bottom of the Petri dish, and around the branches, with either paraffin or lanolin. This resulted in three isolated compartments as shown in Fig. 1. Using this arrangement, various experimental solutions could be applied to the mature branches (still attached to the growing apex). *Chara* pond water of varying $Cl^-$ concentration was added to the branch chambers; actual concentrations used were 0 ($Cl^-$-free), 5, 10, 50, 100, 500 µM and 5, 10, 20 mM ($Cl^-$ present as NaCl). Chloride-free CPW (adjusted to the osmotic activity of the solution in the branch compartments using sorbitol) or 5 mM $Cl^-$ CPW was added to the compartment containing the young internodes. Solutions were changed after 12 h, at which time the lengths of the two youngest internodes were measured. Subsequent measurements were generally taken every 24 h and solutions changed at the same time. In one experiment, shoots from *C. corallina* (three internodes) and *N. clavata* (four internodes) were placed together in a large Petri dish containing $Cl^-$-free medium. During the initial 12-h period of this experiment, the $Cl^-$-free bathing solution was changed three times. All internodes were then measured for length. Subsequent measurements and solution changes were made at 24-h intervals. All growth experiments were conducted under 13 h light–11 h dark daily at 25° C and an energy fluence rate of 20 W $m^{-2}$.

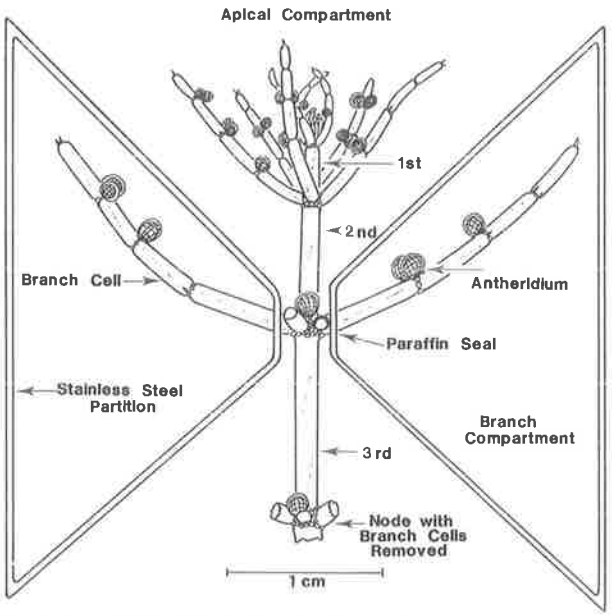


**Fig. 1.** Experimental setup for growth experiments

*Studies with radioactive chloride ($^{36}Cl^-$).* Plasmalemma transport of $Cl^-$ into internodal and branch cells of *C. corallina* was studied using $^{36}Cl^-$. Radioisotope was obtained from ICN (Irvine, Cal., USA) as a sterile aqueous solution of NaCl. Experimental solutions were prepared such that they contained 1.2 mM total $Cl^-$, with a specific activity of approx. $4 \cdot 10^6$ Bq $mmol^{-1}$ chloride.

For experiments in which mature internodal cells were employed, the following protocol was adopted: 1) Internodal cells were cut from the culture and, after a 1-h recovery in culture solution, were washed in CPW-Mops, pH 6.5. All subsequent pretreatments and experiments were conducted in the same solution except where noted otherwise. 2) Cells were randomly sorted into groups of 10, their diameters and lengths measured for surface-area computation, and the cells then given an 18-h pretreatment before being used in an experiment. 3) Experiments to measure $^{36}Cl^-$-fluxes were conducted at 25° C under an irradiance of 20 W $m^{-2}$ and were terminated by transferring cells to identical nonradioactive solutions. A 1-min, followed by a 5-min wash was used to remove $^{36}Cl^-$ present in the cell wall. 4) During the second wash, the cells were examined microscopically (100-fold magnification) to determine the state of cytoplasmic streaming. 5) The cells were then transferred to scintillation vials and treated with 0.1 ml of 7% (v/v) perchloric acid and 0.1 ml of 30% (v/v) $H_2O_2$ to digest the tissue and prevent chlorophyll quenching during scintillation counting. After 15 min the tissue was suspended in a toluene-based

scintillation fluid (containing 30% (v/v) Triton X-100, 4% (v/v) ethanol, 2,5-diphenyloxazole, 2.5 g per 500 ml final volume, and 1,4-bis(2-[5-phenyl-1,3-oxazoyl])-benzene, 0.05 g per 500 ml final volume) and radioactivity measured in a Beckman (LS 8000) liquid scintillation counter. In some experiments the cells were treated with PCMBS (1 mM), NEM (0.1 mM), DIDS (2 mM) or DES (40 μM) for various amounts of time prior to exposure to $^{36}Cl^-$.

Transport into, and subsequent translocation from intact branch cells was examined using a modification of the above protocol. Shoots with three internodes were used and the branches at the base of the oldest internode were removed as were all but two opposite branches at each of the next two nodes of the shoot. The shoots were first washed in culture solution for 1 h, then in CPW plus 1 mM $NaHCO_3$ for 3 d. A stainless-steel chamber was sealed (with paraffin) around one of the two branches between the first and second or second and third internode and CPW-Mops (pH 6.5), or $Cl^-$-free CPW-Mops, was placed in the chamber and region surrounding the rest of the shoot. The shoots were allowed to remain 18 h in this solution for recovery from handling, the last 3.5 h being in the light. Experiments were started by replacing the chamber solution with $^{36}Cl^-$ CPW-Mops, pH 6.5, and terminated by rinsing the chamber for 4 min with CPW-Mops (four changes). In some experiments samples of solution around the labelling chamber were taken periodically and examined by scintillation counting, but no chamber leaks were ever detected. The shoots were frozen on dry ice and broken up into various regions which were placed into separate vials and prepared for counting as above. For autoradiographic studies the frozen shoots were freeze-dried and then placed on Blue Brand X-ray film (Eastman-Kodak, Rochester, N.Y., USA) for exposures of 1–5 d.

*ATPase localization.* Freshly cut shoots from laboratory cultures of *C. corallina* were incubated in CPW for 3–4 h. They were then fixed in 1.25% glutaraldehyde in 50 mM sodium-cacodylate buffer (pH 7.2) for 2 h at 4° C. Chemical fixation was followed by a 2-h rinse in 50 mM sodium-cacodylate buffer and a 15-min rinse in tris(hydroxymethyl)aminomethane(Tris)-maleate buffer (50 mM, pH 7.2). The shoots were then incubated in a medium containing 3.6 mM $Pb(NO_3)_2$, 2 mM ATP and 2 mM $Ca(NO_3)_2$ in 50 mM Tris-maleate buffer (pH 7.2), or 2 mM $Pb(NO_3)_2$, 2 mM ATP and 2 mM $Mg(NO_3)_2$ in 50 mM Tris-maleate buffer (pH 7.2). The second medium was used for most studies, although both media gave similar results. Incubations were run for 0.5, 1 or 2 h at 23° C in the dark, and 1–2 h was found to give adequate reaction product for localization. Control shoots were incubated in media without ATP or without $Pb(NO_3)_2$. The shoots were washed with Tris-maleate buffer for 15–30 min, followed by a 30-min wash with cacodylate buffer. Postfixation was for 1 h at 23° C in 1% $OsO_4$ (25 mM cacodylate buffer, pH 7.2). The tissue was then washed with distilled water, dehydrated in an acetone series, and embedded in Spurr's resin. Thin sections were examined and photographed unstained, using a JEOL (Tokyo, Japan) model JEM 100S transmission electron microscope.

In some experiments the shoots were exposed to the following reagents prior to fixation: $HgCl_2$ (5 μM, 2 h), DES (40 μM, 15, 20 and 45 min), DIDS (2 mM, 90 min). Both DIDS and DES were prepared in CPW-Mops, pH 6.5. After treatment with the reagents the shoots were rinsed with CPW, placed into fixative solution and further processed as outlined above. The following reagents were used after fixation, by addition to the Tris-maleate-buffer rinse and ATPase incubation medium: PCMBS (1 mM), $HgCl_2$ (2 mM), DIDS (2 mM), NaF (2 mM).

The specificity of the phosphatase activity localized with this technique was tested by substituting various substrates in place of ATP. The substrates used were uridine, guanosine, inosine 5′-triphosphates and ADP; all substrates were used at a concentration of 2 mM.

*Chloride localization.* A number of shoots of *C. corallina* approx. 3–4 cm long were cut from the culture and placed in $Cl^-$-free medium in the dark for 10 h. The solution was changed hourly for the first 4 h and every 2 h for the next 6 h. Shoots were then divided into three batches. One batch was continued in the same medium for 4 h in the dark, then put into $HCO_3^-$- and $Cl^-$-free medium (0.5 mM $Na_2SO_4$, 0.1 mM $K_2SO_4$, 0.2 mM $CaSO_4$, 5.0 mM 2-(N-morpholino)ethanesulphonic acid (Mes) pH 6.0) in the dark for 15 min with frequent changes of solution. After this, the shoots were placed in chloride precipitation-fixative containing 0.3% Ag acetate, 0.5% Ag lactate, 1% $OsO_4$, 0.2 M Na cacodylate, 0.02 M Na acetate, pH 6.9 and, in some cases, 0.1% picric acid was included; Stelzer et al. (1978). Fixation was for 1 h at room temperature in the dark. The cells were then washed with distilled water and prepared for transmission electron microscopy. Nitric acid at 0.1 N was included in the 50% acetone step to remove nonspecific silver deposits. The other two batches of cells were incubated for 2 h in the light in $Cl^-$-free medium. Then one batch was incubated for 2 h (in the light) in $HCO_3^-$-free and $Cl^-$-free medium while the other was incubated for 2 h (in the light) in $HCO_3^-$-free medium containing 1.2 mM $Cl^-$ (1.0 mM NaCl, 0.2 mM KCl, 0.2 mM $CaSO_4$, 5 mM Mes; pH 6.0). The cells were then treated with the chloride precipitation-fixative as above and prepared for transmission electron microscopy.

## Results

*Growth experiments.* Chloride is a major ion found in the vacuole of *Chara* cells (Hope and Walker 1960) and may act as an important osmoticum for extension growth. This is indicated by the observation that when shoots from laboratory-grown cultures of *C. corallina* and *N. clavata* were grown together in $Cl^-$-free medium only the *Nitella* species grew (Table 1) rapidly, resulting in the formation of two new internodes on the main axis, plus three more internodes at lateral shoots. The only time appreciable growth occurred in *Chara* under these conditions was when an antheridium ruptured or a cell died; growth is probably the result of the tissue scavenging the released $Cl^-$. Although *Nitella* was still growing well after 11 d

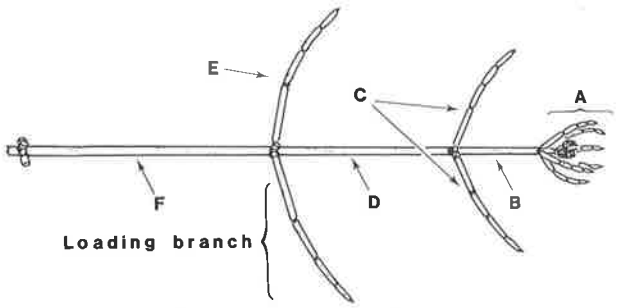


**Fig. 2.** Diagram of the shoot region of *Chara corallina* tested for the presence of $^{36}Cl$ after label was applied at one branch (loading branch). The letters correspond to the "Position" letters of Table 4. In the case where the young branches at the base of the first internode were placed in the labelling chamber, E became the branch opposite the loading branch and C became the branches at the base of the second internodal cell

**Table 1.** Growth of *Chara corallina* and *Nitella clavata* shoots in $Cl^-$-free CPW

| Time (d) | Increase over initial length (%) | | | | | | | | |
|---|---|---|---|---|---|---|---|---|---|
| | *C. corallina* | | | *N. clavata* | | | | | |
| | A[a] | B | C | A | B | C | D | E | F |
| 1 | 3 | 1 | 0 | | | 13 | 15 | 0 | 16 |
| 2 | 8 | 1 | 0 | | – | 50 | 28 | 0 | 18 |
| 3 | 8 | 1 | 0 | – | 200 | 100 | 31 | 0 | 18 |
| 4 | 10[b] | 1 | 2 | [c] | 230 | 125 | 44 | 0 | 18 |
| 5 | 10 | 1 | 2 | 50[d] | 320 | 192 | 50 | 6 | 18 |
| 6 | 20[b] | 2 | 4 | [c] | 320 | 230 | 59 | 6 | 18 |
| 8 | 33[b] | 3 | 4 | 50 | 600 | 300 | 73 | 6 | 18 |
| 9 | 33 | 3 | 4 | 90 | 860 | 342 | 73 | 6 | 18 |
| 10 | 37 | 3 | 4 | 100 | 1,000 | 365 | 75 | 6 | 18 |
| 11 | 67[d] | 3 | 4 | 120[d] | 1,150 | 365 | 75 | 6 | 18 |

[a] Letters A–C and A–F represent individual internodal cells, in order of increasing age
[b] Antheridia found ruptured
[c] Growth of branch cell obstructed view such that youngest internodal cell could not be reliably measured
[d] Branch cells on oldest nodal complex beginning to die

in $Cl^-$-free medium, a number of the older branch cells were dying and so the experiment was terminated.

Next, experiments were performed to determine the effectiveness of *C. corallina* branch cells in $Cl^-$ uptake and subsequent symplastic transport to the growing apex. The results of growth experiments are presented in Tables 2 and 3. In all cases the absence of exogenous $Cl^-$ inhibited shoot growth. The only growth which occurred in shoots not supplied with $Cl^-$ was when antheridia burst or cells died, presumably releasing $Cl^-$ into the medium. When $Cl^-$ was supplied to the branch cells of shoots grown in the absence of $Cl^-$ for 10 d, growth immediately resumed (see Table 3). When $Cl^-$ was supplied to the two mature branch cells (see Fig. 1) at concentrations greater than 50 μM, but not to the rest of the shoot, growth of the shoot was sustained. Growth was more rapid at $Cl^-$ concentrations in the milli- than in the micromolar range; however, there was very little difference in the rate of growth at $Cl^-$ concentrations of 5–20 mM (Table 2). With concentrations of $Cl^-$ at the branches of 50 μM or below, growth of the shoot was very slow or inhibited altogether, except when antheridia ruptured (Table 3). In one experiment where 5 mM $Cl^-$ was supplied to the shoot and $Cl^-$-free solutions applied to the branch compartments, growth of the shoot occurred but at a slightly lower rate than when $Cl^-$ was supplied only to the branches (Table 2).

After 10–11 d mature cells of the shoot began to die. This was probably the consequence of accelerated senescence induced by lack of nitrogen and other micronutrients. The growth experiments were conducted twice at each set of $Cl^-$ concentrations with similar results, except that the absolute values of the changes in growth varied.

*$^{36}Cl$ uptake by branches of intact shoots.* These studies confirm a role of the branches in $Cl^-$ uptake, as indicated by the growth experiments. Chloride taken up by the branches of the shoot is subsequently distributed throughout the shoot, but primarily to growing regions. This is clearly indicated by autoradiographs (data not shown) and $^{36}Cl^-$ distribution studies (Table 4). Another interesting aspect of $Cl^-$ uptake in shoots which is shown by the autoradiographs is that the antheridia are a major sink for $Cl^-$. This is further evidence that the growth seen in $Cl^-$-starved

**Table 2.** Effect on shoot growth of differential supply of $Cl^-$ to branches or shoot of *Chara corallina*

| Time (d) | Increase, over initial length, of 1st and 2nd internodes (%) | | | | | | | | | |
|---|---|---|---|---|---|---|---|---|---|---|
| | [a]0 $Cl^-$/0 $Cl^-$ | | 0 $Cl^-$/5 mM $Cl^-$ | | 0 $Cl^-$/10 mM $Cl^-$ | | 0 $Cl^-$/20 mM Cl | | 5 mM $Cl^-$/0 $Cl^-$ | |
| 1 | 0 | 3 | 18 | 5 | 10 | 3 | 13 | 7 | 20 | 3 |
| 2 | 0 | 3 | 27 | 10 | 30 | 10 | 25 | 10 | 20 | 15 |
| 3 | 0 | 3 | 36 | 11 | 30 | 15 | 25 | 10 | 30 | 15 |
| 4 | 0 | 3 | 45 | 14 | 30 | 15 | 38 | 10 | 30 | 16 |
| 5 | 0 | 3 | 54 | 21 | 40 | 21 | 50 | 10 | 40 | 18 |
| 6 | 0 | 3 | 64 | 25 | 40 | 24 | [c] | 13 | 40 | 22 |
| 7 | 7.1 | 5 | 82 | 28 | 70 | 27 | [c] | 13 | 50 | 23 |
| 8 | 29[b] | 10 | 100 | 33 | 100[b] | 42 | 75 | 14 | 60 | 26 |
| 10 | 64[b] | 18 | 173 | 39 | [b,c] | 59 | 150[b] | 31 | 110 | 27 |
| 11 | – | – | 218 | 44 | 190 | 66 | 175 | 36 | 110 | 38 |

[a] $Cl^-$ content of the medium bathing the shoot and the two mature branches, respectively
[b] Antheridia found ruptured
[c] Branch cell obstructing view such that reliable internode measurement could not be made

**Table 3.** Effect on shoot growth of differential supply of $Cl^-$ to branches of *Chara corallina*

| Time (d) | Increase, over initial length, of 1st and 2nd internodes (%) | | | | | | | | | | | |
|---|---|---|---|---|---|---|---|---|---|---|---|---|
| | [a]0 $Cl^-$/0 $Cl^-$ | | 0 $Cl^-$/5 μM $Cl^-$ | | 0 $Cl^-$/10 μM $Cl^-$ | | 0 $Cl^-$/50 μM Cl | | 0 $Cl^-$/100 μM $Cl^-$ | | 0 $Cl^-$/500 μM $Cl^-$ | |
| 1 | 0 | 0 | 0 | 0 | 0 | 0 | 8 | 1 | 10 | 4 | 10 | 3 |
| 2 | 0 [b(1)] | 0 | 0 [b(1)] | 0 | 0 | 0 | 10 | 6 | 12 [b(1)] | 7 | 12 | 4 |
| 3 | 0 | 0 | 0 [b(1)] | 0 | 0 | 0 | 10 | 6 | 20 [b(1)] | 9 | 15 | 4 |
| 4 | 0 [b(1)] | 0 | 0 | 0 | 3 [b(2)] | 1 | 10 | 7 | 25 | 11 | 22 | 4 |
| 5 | 13 [b(2)] | 4 | 2 [b(2)] | 0 | 5 [b(1)] | 1 | 19 | 8 | 35 | 11 | 41 | 5 |
| 6 | 13 | 4 | 2 | 0 | 5 | 2 | 20 [b(1)] | 9 | 38 | 12 | 51 | 6 |
| 7 | 17 [b(1)] | 5 | 5 [b(4)] | 0 | 7 [b(1)] | 2 | 20 | 10 | 0 [c] 38 | 13 | 61 | 6 |
| 8 | 17 | 5 | 6 [b(2)] | 2 | 7 [b(1)] | 2 | 20 | 10 | 33 40 | 13 | 71 | 6 |
| 9 | 17 [b(2)] | 5 | 8 [b(3)] | 2 | 14 [b(1)] | 2 | 25 | 10 | 80 50 [b(2)] | 13 | 83 | 7 |
| 10 | 33 [b(2)] | 5 | 8 | 2 | 17 [b(1)] | 2 | 30 | 10 | 107 60 | 14 | 98 | 7 |
| 11 | 167 [d] | 14 | | | | | | | | | | |
| 12 | 217 | 17 | | | | | | | | | | |

[a] $Cl^-$ content of the medium bathing the shoot and the two mature branches, respectively
[b] Antheridia found ruptured. Number in parenthesis indicates number of antheridia ruptured
[c] New internode visible at shoot apex
[d] Chloride (500 μM) added to the $Cl^-$-free branch cell chambers on day 10

**Table 4.** Chloride uptake by branch cells of *Chara corallina* attached to growing shoot

See Fig. 2 for diagramatic representation of position of labelling chamber along the shoot. After termination of labelling and subsequent rinsing, the shoots were frozen on dry ice and broken up into various regions (A–F), as indicated in Fig. 2, for scintillation counting. Flux calculations were normalized to the surface area of the branch cells in the labelling chamber. Each value is the mean for 5 shoots

| Conditions and position of labelling chamber | Influx (pmol $cm^{-2}$ $s^{-1}$) | Location of isotope as % of total isotope in shoot | | | | | | |
|---|---|---|---|---|---|---|---|---|
| | | Loading branch | Position | | | | | |
| | | | A | B | C | D | E | F |
| CPW-Mops, pH 6.5 Branch at base of 1st internode below apex | 2.77 | 49 | 12 | 8 | 3 | 13 | 5 | 8 |
| CPW-Mops, pH 6.5 Branch at base of 2nd internode below apex | 3.96 | 47 | 5 | 6 | 6 | 17 | 4 | 14 |
| $Cl^-$-free CPW-Mops, pH 6.5 Branch at base of 2nd internode below apex | 10.60 | 35 | 7 | 10 | 5 | 20 | 3 | 19 |

cells after rupture of antheridia is the result of scavanging of released $Cl^-$.

Chloride fluxes across branch cells attached to shoots were determined under different conditions and are presented in Table 4, along with the distribution of the label within the shoot. Chloride uptake in almost fully expanded branch cells was about 2.77 pmol $cm^{-2}$ $s^{-1}$. In more mature branch cells the value was about 3.96 pmol $cm^{-2}$ $s^{-1}$. Chloride uptake into branch cells of $Cl^-$-starved shoots showed a value of 10.6 pmol $cm^{-2}$ $s^{-1}$. This is more than seven times greater than uptake into isolated internodal cells in the presence of $Cl^-$ (see Table 5), and about three times greater than uptake by mature branches of shoots not $Cl^-$ starved. Approximately 50% of the label was found in the branches in the

**Table 5.** Effect of some chemical agents on chloride influx into *Chara corallina*

All chemical agents were in CPW-Mops, pH 6.5. Each value is the mean ± SE of ten cells

| Treatment | $Cl^-$ influx (pmol $cm^{-2}$ $s^{-1}$) | Inhibition (%) |
|---|---|---|
| DES (40 μM) | | |
| Control | 1.45 ± 0.17 | |
| DES, 15 min | 0.26 ± 0.03 | 82% |
| PCMBS (1 mM) | | |
| Control | 1.43 ± 0.15 | |
| PCMBS, 80 min | 0.29 ± 0.02 | 80% |
| DIDS (2 mM) | | |
| Control | 1.48 ± 0.23 | |
| DIDS, 90 min | 1.35 ± 0.08 | – |

labelling chamber of shoots incubated in CPW. In the $Cl^-$-starved shoots about 34% of the label was in the branch exposed to the isotope. Surprisingly, very little isotope was translocated from the labelled branch to other mature branches of the shoot in any of the experiments. Most of the isotope translocated out of the branch in the labelling chamber appeared to be moving up the shoot. This is more apparent when one remembers that many of the cells of the apical end of the shoot are very small or not fully expanded. Thus, the percentages given in Table 4 do not reflect concentrations of isotope in each region since cell size was not taken into account.

*$^{36}Cl$ uptake by isolated internodal cells.* Chloride flux in isolated *Chara* internodal cells averaged about 1.45 pmol $cm^{-2}$ $s^{-1}$ (Table 5) which is in agreement with values reported in the literature. The effect of DES, PCMBS and DIDS on $Cl^-$ uptake was examined and is presented in Table 5. A 15-min pretreatment of cells with 40 μM DES and 80-min pretreatment with 1 mM PCMBS resulted in about 80% inhibition in $Cl^-$ uptake, but did not affect streaming. A 90-min pretreatment of cells with 2 mM DIDS had no significant effect on $Cl^-$ uptake.

*Localization of ATPase activity.* The charasomes were found to contain dense deposits of reaction product after incubation of cells in the complete ATPase medium (Figs. 3, 4). The reaction product was limited to the cytoplasmic tubules of the charasome and the surface of the charasome membrane facing the cytoplasm (Fig. 4). It was not present within the periplasmic space. Some reaction product could be seen along the plasmalemma, within the chloroplast envelope (Figs. 20, 21) and, to a lesser degree, along the chloroplast thylakoids. Mitochondria showed little or no reaction product while microbodies of developing cells often were reactive (Fig. 21). Control shoots incubated in the absence of lead or ATP were free of reaction product (Figs. 5, 6).

The specificity of the phosphatase activity in the preparations used was not absolute for ATP. Guanosine 5′-triphosphate (GTP) gave a similar amount of reaction product in charasomes to that seen with ATP as substrate (data not shown). With uridine 5′-triphosphate (UTP) in the reaction medium, some reaction product was seen but appeared to be restricted to the outer regions of the charasome (Fig. 7). When inosine 5′-triphosphate (ITP) was used as substrate, no or occasional small isolated deposits of reaction product were seen in the charasome (data not shown). Little reaction product was seen in charasomes of cells incubated in reaction medium containing ADP as substrate (Fig. 8). However, when reaction product was present, it was found in isolated patches. The term "ATPase activity" will be used here for the description of experiments in which ATP was employed as substrate.

The effect of various sulfhydryl reagents on the charasome ATPase activity was examined. Mercuric chloride is a very potent, penetrating, sulfhydryl-binding reagent. At 5 μM, $HgCl_2$ stopped streaming in mature branch and internodal cells of *Chara* within 15 min. Cells lost turgor after 2 h incubation in 5 μM $HgCl_2$ and coagulation of the cytoplasm began. Figure 9 is from a cell pretreated with 5 μM $HgCl_2$. The charasomes showed no ATPase activity and the chloroplasts appear disrupted. If $HgCl_2$ is added to the incubation medium, instead of being used as a pretreatment, cellular detail is better preserved. The charasome ATPase activity is, again, mostly inhibited, although there are occasional patches of reaction product seen (Fig. 10). When the non-penetrating

**Figs. 3–10.** Localization of ATPase activity in mature *C. corallina* branch cells. Unstained sections. Charasome (*C*), chloroplast (*Ch*), mitochondrion (*M*), starch (*St*), wall (*W*). Bars = 1 μm

**Fig. 3.** Complete ATPase medium. Reaction product is seen along the plasmalemma and within charasomes (arrows). ×5,100

**Fig. 4.** Complete medium. Reaction product is within cytoplasmic tubules of the charasome and not within the periplasmic space. Reaction product also at the cytoplasmic surface of the charasome (arrows). ×25,000

**Fig. 5.** No-lead control. ×25,000

**Fig. 6.** No-ATP control. ×25,000

**Fig. 7.** Uridine 5′-triphosphate as substrate. ×25,000

**Fig. 8.** Adenosine 5′-diphosphate as substrate. ×25,000

**Fig. 9.** Shoot incubated in 5 μM $HgCl_2$ for 2 h prior to chemical fixation. No ATPase reaction product in charasome. ×20,000

**Fig. 10.** 2 mM $HgCl_2$ added to ATPase incubation medium. ×25,000

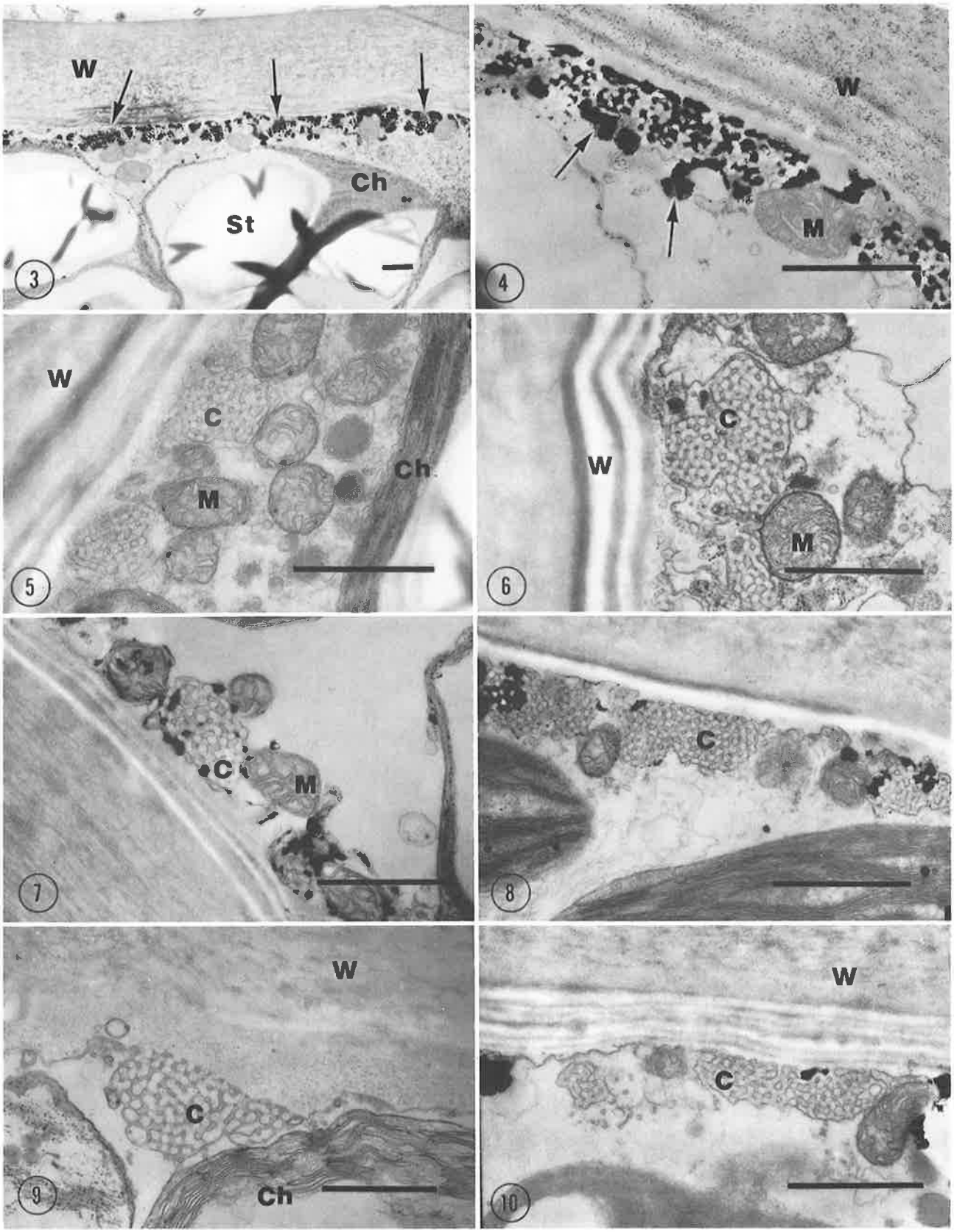
W
Ch
St
3
W
M
4
W
C
Ch
M
5
W
C
M
6
C
M
7
C
8
W
C
Ch
9
W
C
10

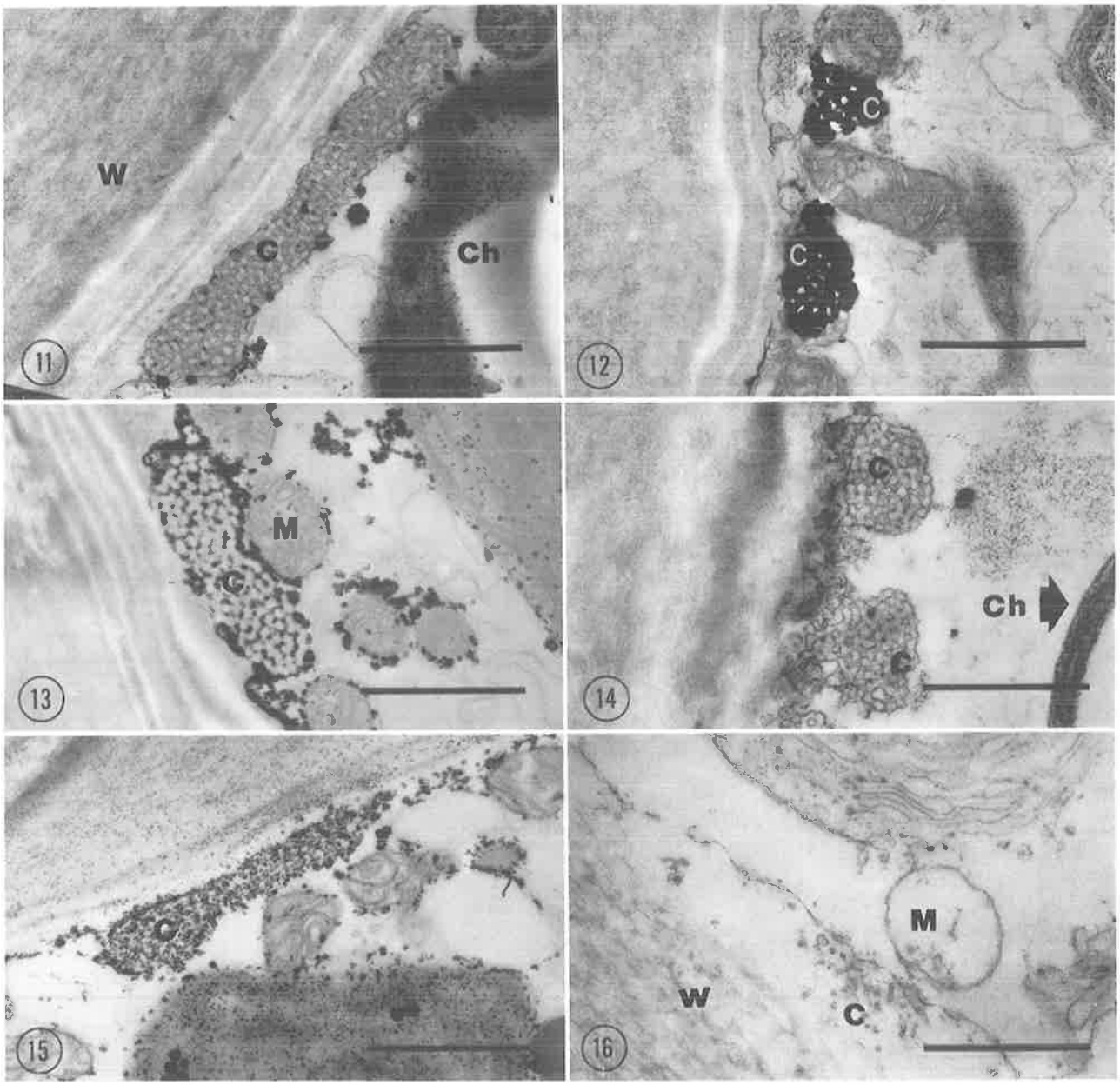


**Figs. 11–16.** Localization of ATPase activity in mature *C. corallina* branch cells. Unstained sections. Charasome (*C*), chloroplast (*Ch*), mitochondrion (*M*), wall (*W*). Bars = 1 μm

**Fig. 11.** Shoots incubated in 1 mM p-chloromercuribenzenesulfonic acid (PCMBS) after chemical fixation. ×25,000

**Fig. 12.** 2 mM NaF added to ATPase medium. ×25,000

**Fig. 13.** Shoot incubated in 2 mM 4,4-diisothiocyano-2,2-disulfonic acid stilbene (DIDS) prior to chemical fixation. ×25,000

**Fig. 14.** 2 mM DIDS added to ATPase medium. ×25,000

**Fig. 15.** Shoot incubated 20 min in 40 μM diethylstilbestrol (DES) prior to fixation. ×25,000

**Fig. 16.** Shoot incubated 45 min in 40 μM DES prior to fixation. ×25,000

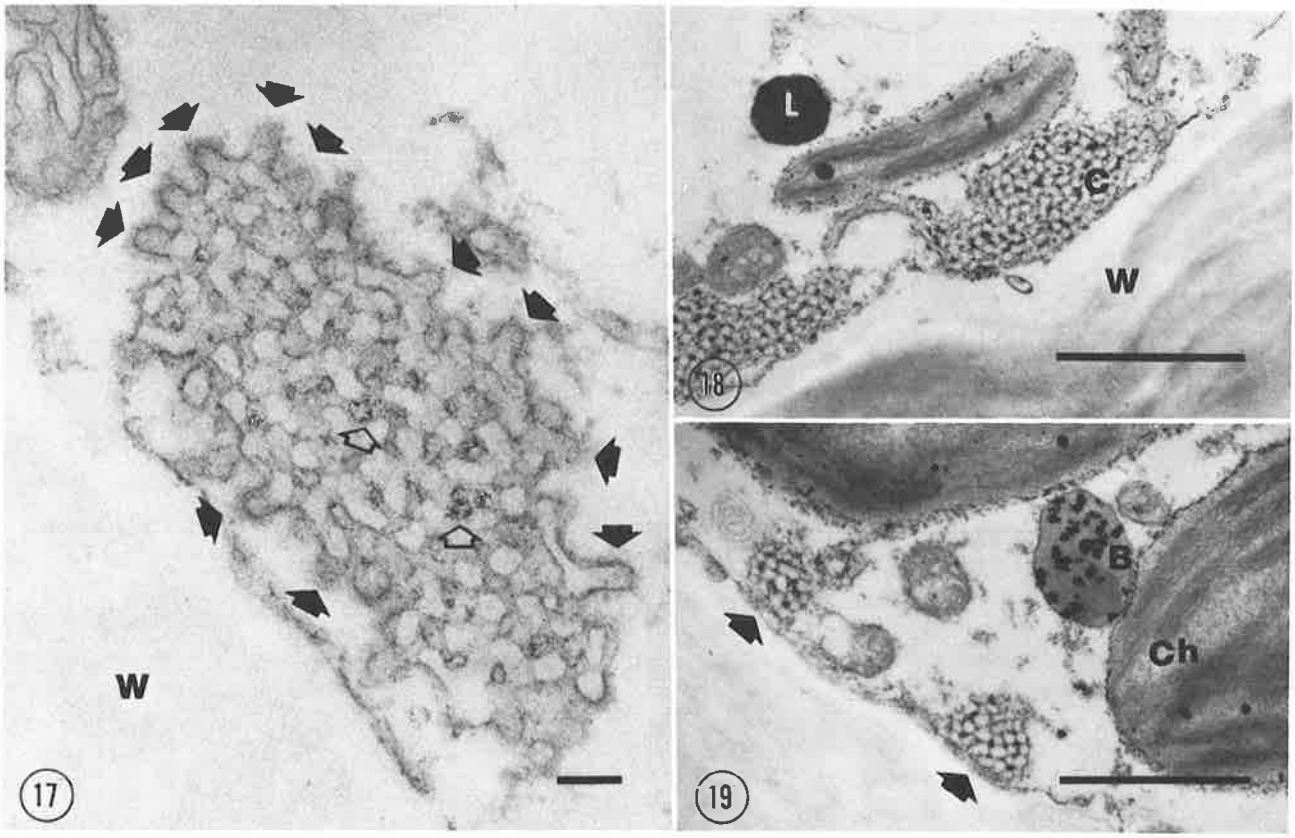


**Figs. 17–19.** Localization of ATPase activity in young, growing branch cells of *C. corallina*. Unstained sections. Microbody (*B*), charasome (*C*), chloroplast (*Ch*), lipid drop (*L*), wall (*W*)

**Fig. 17.** Charasome in 1.5-mm-long branch cell. Numerous growing points are visible (solid arrows). Only sparse ATPase reaction product is present (open arrows). Bar = 0.1 μm; ×84,000

**Fig. 18.** Charasomes in 3-mm-long branch cell. Appreciable reaction product can be seen within the cytoplasmic tubules. No growing points are visible. Bar = 1 μm; ×25,000

**Fig. 19.** Charasomes in 3-mm-long branch cell. Although the charasomes are very small, there is still appreciable reaction product within the cytoplasmic tubules. Note reaction product within microbody and along chloroplast envelope. Bar = 1 μm; ×25,000

sulfhydryl reagent PCMBS was included in the ATP reaction-medium little reaction product was observed within the charasomes, although there was often some reaction product at the cytoplasmic surface of the charasome (Fig. 11).

A number of other transport or enzyme inhibitors were also used. Sodium fluoride, when used in the reaction medium at a concentration of 2 mM, had no effect on the charasome ATPase activity (Fig. 12). A 90-min pretreatment of shoots with DIDS had no effect on charasome ATPase activity (Fig. 13). However, when DIDS was used in the reaction medium, after fixation, the ATPase activity was inhibited (Fig. 14). Diethylstilbestrol (DES), at a concentration of 40 μM, had no effect on the ATPase activity when shoots were exposed to the reagent for 15 or 20 min prior to fixation (Fig. 15). A 45-min pretreatment with DES did inhibit ATPase activity but also had very drastic effects on cellular integrity (Fig. 16). The cells lost turgor after subsequent fixation in glutaraldehyde, and observations of such cells by transmission electron microscope indicated severe disruption of membranous components (Fig. 16). The charasomes, when recognizable, were completely disrupted and consisted of masses of short tubules and vesicles (Fig. 16).

Young cells were also examined for charasome ATPase activity. Formation of charasomes in branch cells begins when the cells are about 1 mm long (Lucas and Franceschi 1981) and proceeds rapidly until the cells are about 3 mm long. At this point, charasome growth slows down although the cells may reach a length of 0.5–1.0 cm in the cultures used. Figure 17 shows a section through a rapidly developing chara-

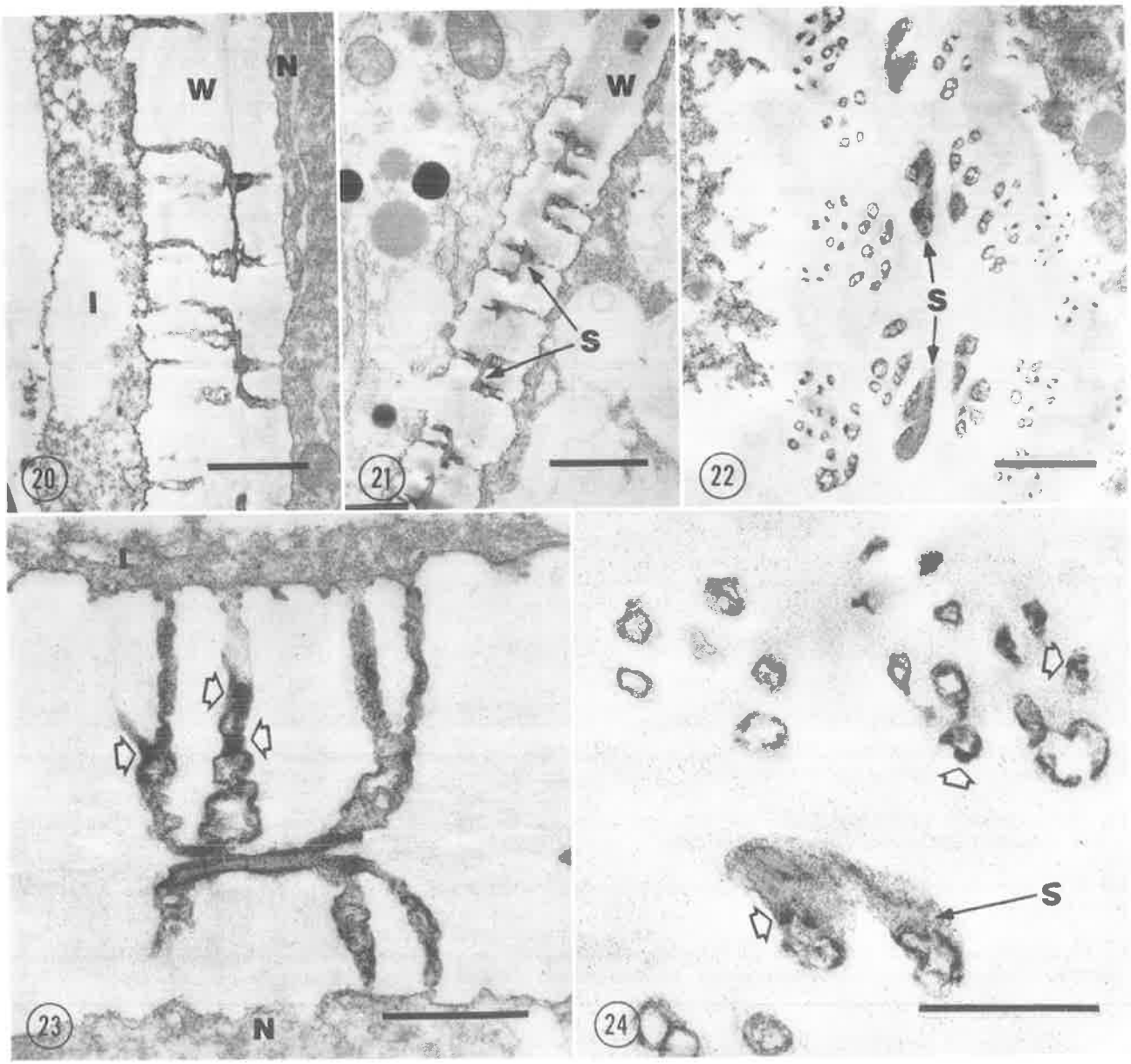


**Figs. 20–24.** Localization of ATPase activity in plasmodesmata of *C. corallina*. Unstained sections. Internodal cell (*I*), nodal cell (*N*), sinuses (*S*), wall (*W*). Bars = 1 μm (Figs. 20–22) and 0.5 μm (Figs. 23–24)

**Fig. 20.** Crosswall between branch internodal and nodal cells. Reaction product occurs along plasmalemma and plasmodesmata. × 15,000

**Fig. 21.** Cross wall between two nodal cells. Reaction product is evident in the plasmodesmata. × 15,000

**Fig. 22.** Tangential section through cross-wall between two nodal cells. ATPase activity occurs in the plasmodesmata. × 15,000

**Fig. 23.** Plasmodesmata between branch internodal and nodal cells. Reaction product is along plasmodesmatal membrane and within lumen in some areas (open arrows). × 44,600

**Fig. 24.** Tangential section through plasmodesmata in cross wall between nodal cells. Heavy deposits of reaction product can be seen (open arrows). × 53,700

some from a branch cell of 1.5 mm length. Growth is presumed to be occurring at the numerous, coated invaginations along the surface of the charasome (Lucas and Franceschi 1981). Such young, growing charasomes show little ATPase reaction product. When present at all, the reaction product is generally near the center of the charasome in the cytoplasmic tubules (Fig. 17). Figure 18 is a section from a 3-mm-long branch cell. The cell is still elongating at this stage but the charasomes already show appreciable ATPase activity. That the ATPase activity is not related strictly to size of the charasome is indicated by Fig. 19. The two small charasomes present have appreciable reaction product in them, although they are very small and from a cell which is still expanding (approx. 3 mm in length).

*ATPase activity along plasmodesmata.* Very complex plasmodesmata occur between branch cells and nodal cells, and between some nodal cells of the nodal complex (Figs. 20–24). The plasmodesmata often contain large sinuses within the central portion of the cell wall, from which numerous tubules project to the plasmalemma of the adjacent cells. Tangential sections through the wall of nodal cells indicate that clusters of tubules may connect to each sinus (Figs. 22, 24). During this study it was found that ATPase reaction product was consistently localized within these complex plasmodesmata. The reaction product occurs along the membrane of the plasmodesmata at both the tubular portion and sinuses (Figs. 23, 24). The importance of this observation to transport in *Chara* will be discussed later.

*Chloride localization.* The results of the $Cl^-$-localization experiments were inconclusive. Shoots which were incubated in $Cl^-$-free medium, in the dark, gave slight amounts of silver precipitate along the coated invaginations of the plasmalemma and in association with coated vesicles, but the cyroplasm was free of silver precipitate (Fig. 25). Shoots incubated in $Cl^-$-free medium in the light had heavy silver precipitation in the cytoplasm but little or no precipitate in the charasomes (Fig. 26). Shoots which were incubated in $Cl^-$ medium in the light also had heavy silver precipitation in the cytoplasm and the same amount of, or slightly more, precipitate in the charasomes, as compared to shoots treated in $Cl^-$-free medium in the light (Fig. 27). When the silver precipitate was found in charasomes it was associated with the cytoplasmic tubules. This silver precipitation technique has inherent problems that are difficult to overcome, thereby limiting its usefulness (see discussion following, Van Steveninck 1976).

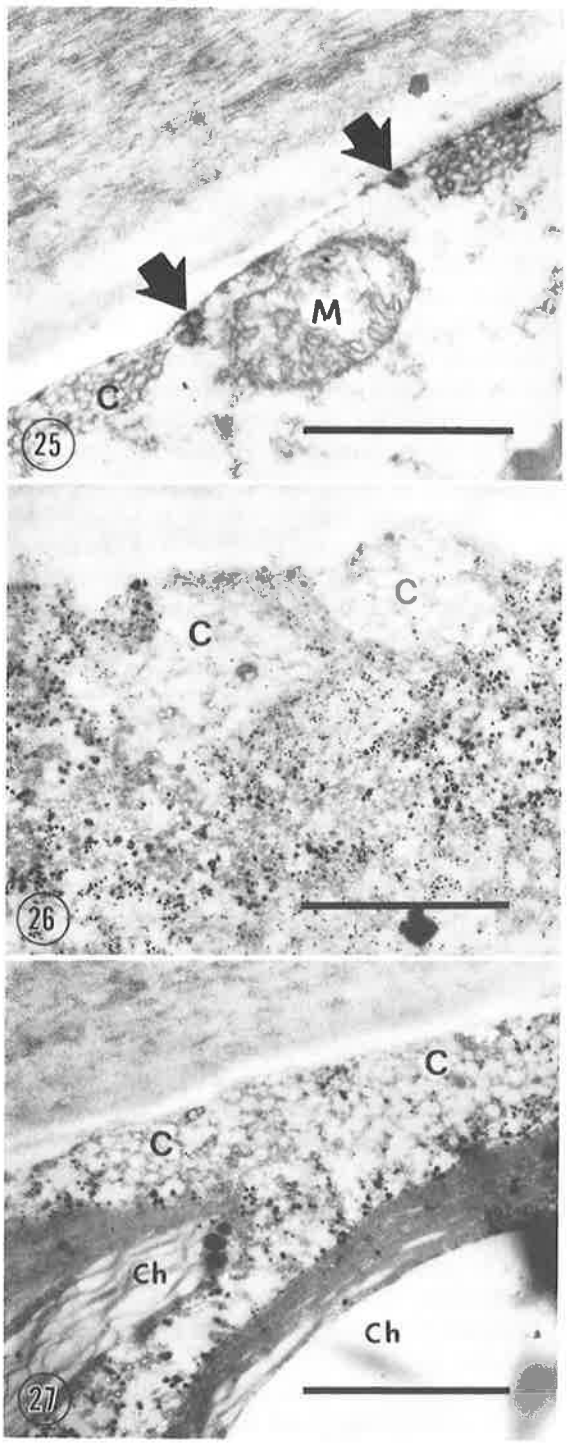


**Figs. 25–27.** *C. corallina* cells prepared for $Cl^-$ localization. Lead citrate staining only. Charasome (*C*), chloroplast (*Ch*), mitochondrion (*M*). Bars = 1 μm; all ×27,500. **Fig. 25.** Chloride-free cell incubated in the dark. Precipitate is only along the membrane of coated invaginations and vesicles (arrows). **Fig. 26.** Chloride-free cell after light incubation. Heavy precipitation in cytoplasm and slight precipitation along charasome tubules. **Fig. 27.** Cell incubated in $Cl^-$ medium in the light prior to incubation in $Cl^-$ precipitation medium. Heavy precipitation in cytoplasm and some large deposits along charasome tubules

## Discussion

The branch cells of *Chara* from cultures used in this study contain considerably more charasome material than the internodal cells of the main axis of the thallus (Franceschi and Lucas 1980). If the charasome is involved in $Cl^-$ uptake, the branches would be expected to have a very special role in $Cl^-$ accumulation and in growth of the plant. The branches certainly play an important role in the development of the plant. They mature much earlier than the internode directly above the node to which they are attached, and removal of the branches results in an inhibition of elongation of the immature internodal cells of the shoot (DuCreux 1975). It thus appears that the branches are supplying the growing shoot with some required substance. We suggest this substance is $Cl^-$, which we have shown to be essential for growth of the shoot. Evidence for this is seen when a shoot is placed in $Cl^-$-free medium, which inhibits growth; but supplying just two branches of the shoot with $Cl^-$, while keeping all other nutrients the same, results in resumption of growth.

Isotope distribution experiments and related autoradiography show that the branches are instrumental in $Cl^-$ uptake and subsequent distribution to the shoot. The young, expanding vegetative apex appears to be the main destination for $Cl^-$ taken up by the branches. Chloride acquired by the branches is transported down the shoot to the mature cells to a much lesser degree, except when these cells have been $Cl^-$-starved.

The observation that $Cl^-$ is not transported to any extent from one branch to another, even between opposite branches on a node, is intriguing. We feel that this may be an indication of the efficiency of these structures in removing $Cl^-$ from the bathing medium. It is possible that the branch cells are so effective at scavenging $Cl^-$ from the medium that very little $Cl^-$ is actually lost from them during the period in $Cl^-$-free medium. The vast network created by the charasome material present in the branches would facilitate recapture of $Cl^-$ lost by any passive efflux process.

Chloride fluxes into cells that are still attached to the shoot are approx. twice those of isolated cells (both internodal and branch). This probably reflects, in part, a response of the tissue to regions that require $Cl^-$ as an osmoticum for growth; i.e., the growing apex or developing antheridia. In $Cl^-$-starved shoots the flux across branch cells was about seven fold greater than in isolated internodal cells. This is in contrast to the maximum three-fold increase which Sanders (1980a) saw in $Cl^-$-starved, isolated internodal cells. The better than two-fold difference between $Cl^-$-starved stimulation in branch cells attached to a shoot as opposed to isolated internodes may be related to the amount of charasome material present in each. An involvement of the charasomes in $Cl^-$ transport would explain the greater rates of $Cl^-$ uptake possible in the branches as compared to internodal cells.

As pointed out earlier, the charasome is ideally suited for the $Cl^- - H^+$ cotransport system which has been suggested to exist in *Chara* (Beilby and Walker 1981; Sanders 1980b). The charasome is shown here to contain ATPase activity which could participate in proton pumping necessary to energize $Cl^-$ uptake. It is also closely associated with numerous mitochondria, which could supply the necessary ATP. Limited ATPase activity is observed in developing charasomes of young tissue in which a high demand for metabolic energy would exist for the synthesis of membrane components and other substances needed for growth of these rapidly expanding cells.

We have also been able to obtain partial correlation between inhibition of the charasome ATPase activity and inhibition of $Cl^-$ uptake. Both *p*-chloromercuribenzenesulfonic acid and diethylstilbestrol (long exposures) inhibited the ATPase activity and strongly inhibited $Cl^-$ uptake. The observation that 15- to 20-min exposures to DES did not inhibit the ATPase activity while they did inhibit $Cl^-$ uptake is interesting. Diethylstilbestrol has previously been found to increase membrane resistance in *Chara* (Keifer and Spanswick 1978, 1979). The resistance increase and inhibition of $Cl^-$ transport caused by DES may thus be consequences of an effect of DES on the $Cl^- - H^+$ pump and not the $H^+$ translocating ATPase.

The demonstration of ATPase activity in the plasmodesmata of *Chara* is interesting and must be commented upon. Adenosine triphosphatase activity has been seen in plasmodesmata of various higher plants (Hall 1969; Robards and Kidwai 1969; Coulomb and Coulomb 1972; Gilder and Cronshaw 1973a, b) and it has been suggested that it may be involved with a regulatory capacity or active transport capability of the plasmodesmata (Van Steveninck 1976). Van Steveninck proposed that there may be a distinction between plasmodesmata with internal structures (desmotubules) such as are found in higher plants, and the more simple, open plasmodesmata of characean algae. Those which contain structural units may have a regulatory effect on transport of materials through them while the open type may provide a simple diffusion pathway. However, the demonstration of ATPase activity in *Chara* plasmodesmata may be an

indication of possible regulation of solute transport through these structures. Thus, classification of plasmodesmata into two types according to their possible ability to regulate transport, as proposed by Van Steveninck (1976), cannot be based simply on the presence or absence of a desmotubule or other structural feature in the plasmodesmatal lumen.

*In summary,* the results presented are consistent with a role of the charasome in $Cl^-$ transport. The structure of the charasome is ideal for the $H^-/Cl^+$ co-transport system hypothesized for $Cl^-$ uptake, and the charasome and $Cl^-$ transport occur at the same spatially distinct regions of the cell. The charasome contains ATPase activity which could be involved in proton pumping necessary to energize $Cl^-$ uptake. Some correlation between inhibition of charasome ATPase activity and $Cl^-$ uptake has been demonstrated. The branches, which contain the largest amount of charasome material, are especially effective in $Cl^-$ uptake. In this respect, it is interesting to note that Walker (1976) found that measured transmembrane $Cl^-$ fluxes of internodal cells were insufficient to account for rates of consumption observed in growing *Chara* cells, and translocation of $Cl^-$ from other parts of the thallus appears to be necessary. The early maturation of the branches, the rather large $Cl^-$ fluxes possible across branch cells and the ability to translocate $Cl^-$ from branches to growing cells of the shoot indicate a special role of the branches in $Cl^-$ accumulation. Since much of the surface of the branch cells is covered with charasome material, it is very likely that these structures are involved in $Cl^-$ transport.

This research was supported by National Science Foundation grants PCM 80-03133 and PCM 81-17721, and V.R.F. gratefully acknowledges the support of a University of California Regents Fellowship.

## References

Barton, R. (1968) Autoradiographic studies on wall formation in *Chara*. Planta **82**, 302–306

Beilby, M.J., Walker, N.A. (1981) Chloride transport in *Chara*: I. Kinetics and current voltage curves for probable proton symport. J. Exp. Bot. **32**, 43–54

Coulomb, P., Coulomb, C. (1972) Localisation cytochimique ultrastructurale d'une adenosine triphosphatase-$Mg^{++}$ dépendent dans cellules de méristèmes radicularies de la courge (*Cucurbita pepo* L. Cucurbitacée). C.R. Acad. Sci. Ser. D **275**, 1035–1038

DuCreux, G. (1975) Corrélations et morphogenèse chez le *Chara vulgaris* L. cultivé in vitro. Rev. Gen. Bot. **82**, 215–357

Franceschi, V.R. (1981) Membrane structure-function relationships in several characean species. Ph. D. dissert., University of California, Davis, USA

Franceschi, V.R., Lucas, W.J. (1980) Structure and possible function(s) of charasomes: complex plasmalemma-cell wall elaborations present in some characean species. Protoplasma **104**, 253–271

Franceschi, V.R., Lucas, W.J. (1981) The charasome periplasmic space. Protoplasma **107**, 269–284

Gilder, J., Cronshaw, J. (1973a) Adenosine triphosphatase in the phloem of *Cucurbita*. Planta **110**, 189–204

Gilder, J., Cronshaw, J. (1973b) The distribution of adenosine triphosphatase activity in differentiating and mature phloem cells of *Nicotiana tabacum* and its relationship to phloem transport. J. Ultrastruct. Res. **44**, 388–404

Hall, J.L. (1969) Localization of cell surface adenosine triphosphatase activity in maize roots. Planta **85**, 105–107

Hope, A.B., Walker, N.A. (1960) Ionic relations of cells of *Chara australis*. III. Vacuolar fluxes of sodium. Aust. J. Biol. Sci. **13**, 277–291

Keifer, D.W., Spanswick, R.M. (1978) Activity of the electrogenic pump in *Chara corallina* as inferred from measurements of the membrane potential, conductance, and potassium permeability. Plant Physiol. **62**, 653–661

Keifer, D.W., Spanswick, R.M. (1979) Correlation of adenosine triphosphate levels in *Chara corallina* with the activity of the electrogenic pump. Plant Physiol. **64**, 165–168

Lucas, W.J., Alexander, J.M. (1980) Sulfhydryl group involvement in plasmalemma transport of $HCO_3^-$ and $OH^-$ in *Chara corallina*. Plant Physiol. **65**, 274–280

Lucas, W.J., Franceschi, V.R. (1981) Characean charasome-complex and plasmalemma vesicle development. Protoplasma **107**, 255–267

Lucas, W.J., Nuccitelli, R. (1980) $HCO_3^-$ and $OH^-$ transport across the plasmalemma of *Chara*. Spatial resolution obtained using extracellular vibrating probe. Planta **150**, 120–131

Lucas, W.J., Smith, F.A. (1973) The formation of alkaline and acid regions at the surface of *Chara corallina* cells. J. Exp. Bot. **24**, 1–14

Robards, A.W., Kidwai, P. (1969) Cytochemical localization of phosphatase in differentiating secondary vascular cells. Planta **87**, 227–238

Sanders, D. (1980a) Control of $Cl^-$ influx in *Chara* by cytoplasmic $Cl^-$ concentration. J. Membr. Biol. **52**, 51–60

Sanders, D. (1980b) The mechanism of $Cl^-$ transport at the plasma membrane of *Chara corallina*. I. Cotransport with $H^+$. J. Membr. Biol. **53**, 129–141

Spear, D.G., Barr, J.K., Barr, C.E. (1969) Localization of hydrogen ion and chloride ion fluxes in *Nitella*. J. Gen. Physiol. **54**, 397–414

Stelzer, R., Läuchli, A., Kramer, D. (1978) An improved precipitation technique for $Cl^-$ localization in plant tissues by use of picric acid. J. Exp. Bot. **29**, 729–733

Steveninck, R.F.M. van (1976) Cytochemical evidence for ion transport through plasmodesmata. In: Intercellular communication in plants: Studies on plasmodesmata, pp. 137–147, Gunning, B.E.S., Robards, A.W., eds. Springer, Berlin Heidelberg New York

Walker, N.A. (1976) Transport of solutes through the plasmodesmata of *Chara* nodes. In: Intercellular communication in plants: Studies on plasmodesmata, pp. 165–199, Gunning, B.E.S., Robards, A.W., eds. Springer, Berlin Heidelberg New York

Received 17 August 1981; accepted 15 February 1982

Plant Physiol. (1982) 70, 1327–1334
0032-0889/82/70/1327/08/$00.50/0

# Plasmalemma Chloride Transport in *Chara corallina*[1]

## INHIBITION BY 4,4′-DIISOTHIOCYANO-2,2′-DISULFONIC ACID STILBENE

Received for publication March 30, 1982 and in revised form July 13, 1982

DAVID W. KEIFER, VINCENT R. FRANCESCHI[2], AND WILLIAM J. LUCAS
*Department of Botany, University of California, Davis, California 95616 (D. W. K., W. J. L.); and Central Research and Development Department, E. I. DuPont DeNemours and Company, Experiment Station (V. R. F.), Wilmington, Delaware 19801*

### ABSTRACT

**Chloride transport, presumably via a $Cl^-$-$2H^+$ co-transport system, was investigated in *Chara corallina*. At pH 6.5, the control influx (3.1 picomoles per centimeter$^2$ per second) was stimulated 4-fold by an 18-hour $Cl^-$ starvation. The stimulated influx was inhibited to 4.7 picomoles per centimeter$^2$ per second after a 60-minute pre-exposure to 0.5 millimolar 4,4′-diisothiocyano-2,2′-disulfonic acid stilbene (DIDS). This compares with a nonsignificant inhibition of the control under similar conditions. At 2 millimolar DIDS, both stimulated and control influx were inhibited to values of 1.1 and 2.2 picomoles per centimeter$^2$ per second, respectively; in all cases, DIDS inhibition was reversible. Over the pH range 4.8 to 8.5, the control and DIDS-inhibited influx showed only slight pH sensitivity; in contrast, the stimulated flux was strongly pH dependent (pH 6.5 optimum). Inasmuch as changes in pH alter membrane potential, *N*-ethylmaleimide was used to depolarize the membrane; this had no effect on $Cl^-$ influx. A transient depolarization of the membrane (about 20 millivolts) was observed on restoration of $Cl^-$ to starved cells. The membrane also depolarized transiently when starved cells were exposed to 0.5 millimolar DIDS, but the depolarization associated with $Cl^-$ restoration was inhibited by a 40-minute pretreatment with DIDS. Exposure of control cells to DIDS caused only a small hyperpolarization (about 7 millivolts). DIDS may have blocked $Cl^-$ influx by inhibiting the putative plasmalemma $H^+$-translocating ATPase. Histochemical studies on intact cells revealed no observable effect of DIDS on plasmalemma ATPase activity. However, DIDS application after fixation resulted in complete inhibition of ATPase activity.**

**The differential sensitivity of the stimulated and control flux to inhibition by DIDS may reflect an alteration of transport upon stimulation, but could also result from differences in pretreatment. The stimulated cells were pretreated with DIDS in the absence of $Cl^-$, in contrast to the presence of $Cl^-$ during pretreatment of controls. The differential effect could result from competition between $Cl^-$ and DIDS for a common binding site. Our histochemical ATPase results indicate that $Cl^-$ transport and membrane ATPase are separate systems, and the latter is only inhibited by DIDS from the inside of the cell.**

In *Chara corallina,* as in other plants, chloride is actively accumulated against a large electrochemical potential gradient. The electric potential across the *Chara* plasmalemma usually falls within the range −190 to −250 mv (cytoplasm negative), depending on media conditions (10, 11). In external solutions of 1 mM $Cl^-$, it has been estimated that cytoplasmic $Cl^-$ is 7 to 10 mM (17). Although fewer measurements are available for the potential across the tonoplast, the value is probably somewhere near +20 mv, the vacuole being positive with respect to the cytoplasm (9). In *C. corallina,* vacuolar $Cl^-$ is about 106 mM (8). Since the vacuole constitutes approximately 95% of the cell volume, substantial amounts of $Cl^-$ must be transported across both the plasmalemma and tonoplast in order to provide the osmotic activity necessary for cell expansion (7).

Transport across both these membranes may involve the indirect coupling of $Cl^-$ movement to an ATP-dependent electrogenic $H^+$ current. Considerable evidence exists in support of the hypothesis that an electrogenic $H^+$ efflux system operates across the *Chara* plasmalemma (for a review, see Ref. 23). The concept that $Cl^-$ transport may be coupled to the resulting proton gradient was first postulated by Spear *et al.* (24) and subsequently developed by Smith (21) and Smith and Walker (22). It has been proposed that the transport stoichiometry for $Cl^-$ uptake is $2H^+/Cl^-$ transported across the plasmalemma (22). Only recently has transport into the vacuole been examined in terms of the possible mechanism(s) involved. Using isolated plant membrane fractions, Bennett and Spanswick (1) have obtained results consistent with the operation of an electrogenic $H^+$ ATPase located in the tonoplast. This ATPase appears to be $Cl^-$-dependent and may be the system responsible for driving $Cl^-$ transport into the vacuole.

In his recent studies on $Cl^-$ transport into *C. corallina,* Sanders (16–18) found that rates of transport across the plasmalemma were not controlled by the actual thermodynamic driving force, but were under kinetic control. The transport model, proposed by Sanders and Hansen (19) to explain their experimental data, suggests that a depletion of the cytoplasmic $Cl^-$ level acts in a kinetic sense to greatly enhance the flux across the plasmalemma. Despite these details, little is known about the spatial and/or mechanistic relationship(s) between the $Cl^-$-$2H^+$ co-transport process and the $H^+$-translocating ATPase of the plasmalemma.

Anion transport processes in animal cell membranes (*e.g.* into red blood cells [3]) can be inhibited irreversibly by the membrane-impermeable aminoreactive agent, DIDS[3] (2, 3, 20). Recently, Lin (13) showed that DIDS was an effective inhibitor of $Cl^-$ and $SO^{2-}_4$ transport into isolated corn root protoplasts. Lin also reported that DIDS inhibited the ATPase activity of isolated corn root plasma membranes; this result is consistent with the work of Churchill and Sze (4).

In the present paper, we report on the inhibitory effect of DIDS on $Cl^-$ transport into *Chara corallina.* We found that DIDS was

[1] Supported by National Science Foundation Grant PCM 8003133 to W. J. L. and D. W. K.

[2] Current address: Department of Botany, Washington State University, Pullman, WA 99164.

[3] Abbreviations: DIDS, 4,4′-diisothiocyano-2,2′-disulfonic acid stilbene; APW, artificial pond water; NEM, *N*-ethylmaleamide; CPW, *Chara* pond water.

very effective in inhibiting the stimulated component of $Cl^-$ influx, *i.e.* the enhanced component that was obtained by an 18-h pretreatment of cells in $Cl^-$-free medium. However, unlike the animal anion transport systems, the DIDS inhibition could be reversed, indicating that an irreversible covalent bond had not been formed. Plasma membrane ATPase activity (as evidenced by histochemical studies) was not affected by DIDS, except when this aminoreagent was included in the reaction medium following tissue fixation for electron microscopy. Our results are consistent with DIDS acting as a competitor for the $Cl^-$ binding site, presumably on the membrane carrier.

## MATERIALS AND METHODS

**Culture Material.** *Chara corallina* Klein ex Willd., em R.D.W. (= *Chara australis* R. Br.) was cultured in the laboratory (10). Internodal cells (2–3 cm for electrophysiology; or 4–8 cm long, containing 1–3 cells, for flux studies) were cut the day before the experiments. After measuring their surface areas, cells were preincubated (overnight) in either APW-6.5 or $Cl^-$-free APW-6.5 under continuous light (10 w $m^{-2}$, approximately 18 h). Cells used to investigate the effect of NEM on $^{36}Cl^-$ influx were pretreated in CPW-6.5 and given an 8-h dark period, followed by 3-h illumination (10 w $m^{-2}$) before being used in an experiment.

**Experimental Solutions.** The basic solution used for the DIDS experiments, APW-6.5, was prepared using high purity, glass-distilled $H_2O$ and contained (mM): 1.0 NaCl, 0.2 $K_2SO_4$, 1.0 $CaSO_4$, 2.0 Mes, adjusted to pH 6.5 with freshly dissolved NaOH. Chloride-free APW-6.5 was as above but with 0.5 mM $Na_2SO_4$ substituting for the 1.0 mM NaCl. The DIDS (Calbiochem) was added to the experimental solutions just before use and the solution pH was adjusted to the desired value. In some experiments, solution pH values other than 6.5 were used. In those cases, the pH and buffers used were: pH 4.8, Mes; pH 5.7, Mes; pH 7.5, Hepes; and pH 8.5, 3-{[tris(hydroxymethyl)methyl]amino} propanesulfonic acid (Taps); all at 2.0 mM.

In experiments with NEM, a slightly different basic solution was used, CPW, which contained (mM): 1.0 NaCl, 0.2 KCl, 0.2 $CaSO_4$, and either 5 mM 3-(*N*-morpholino)propanesulfonic acid (Mops) at pH 6.5 or 5 mM 3-{[tris(hydroxymethyl)methyl]amino} propanesulfonic acid at pH 8.0. A 100 mM stock solution of NEM was prepared and stored at 4°C for up to 3 d. The concentration (0.1 mM) of NEM in the experimental solution was assayed spectrophotometrically (at *A* 302 nm; extinction coefficient = 620 $M^{-1}$ $cm^{-1}$).

**Electrophysiological Measurements.** The equipment, electrodes, and methods used in these experiments have been previously described (10). However, most DIDS experiments were performed in nonflowing solutions to reduce the amount of reagent utilized per experiment.

**Measurements of $^{36}Cl^-$ Influx.** Radioactive $^{36}Cl$ was obtained from ICN (Irvine, CA) as a sterile aqueous solution of NaCl. Experimental solutions were prepared such that they contained 1.0 mM total $Cl^-$ for the DIDS experiments and 1.2 mM $Cl^-$ for the NEM experiments; all solutions had a specific activity of approximately 80 $\mu$Ci/mmol chloride. Following the prescribed pretreatment, cells were transferred from Petri dishes into sealed tubes that were placed in a thermostated water bath (25°C) in the light (20 w $m^{-2}$) for a 1- to 2-h equilibration period. Solutions used for this pretreatment will be specified in the text. In experiments in which we examined the effects of pH, the pretreatments were done at the same pH values used during uptake. A $^{36}Cl^-$ uptake period of 10 min was employed because the stimulation in $Cl^-$ influx, caused by cell exposure to $Cl^-$-free conditions, decreases rapidly (17). A 1-min wash, followed by a second 5-min wash, was used to remove $^{36}Cl^-$ present in the cell wall. Individual cells were then blotted and placed into scintillation vials where they were treated (15 min) with 0.1 ml of 30% $H_2O_2$ and 0.1 ml of 7% $HClO_4$ to digest the tissue and prevent Chl quenching during scintillation counting. Tissue was suspended in 10 ml of a toluene-based scintillation fluid (containing 300 ml Triton X-100, 40 ml ethanol, 5 g 2,5-diphenyloxazole, and 0.1 g POPOP plus toluene to make 1 L final volume) and radioactivity was measured in a Beckman (LS 9800) liquid scintillation system. Influx into each cell was calculated using its measured surface area. Typically, each treatment consisted of 12 cells; in some cases, treatments were pooled. Results are reported as average ± SE ($n$ = total number of cells measured).

**ATPase Localization.** Shoots were cut from the *Chara* cultures and incubated in APW-6.5 or $Cl^-$-free APW-6.5 for 18 h (continuous light, 10 w $m^{-2}$). Some $Cl^-$-starved shoots were incubated in 0.5 mM DIDS (80 min) and fixed directly, or the 0.5 mM DIDS treatment was followed by a 1- or 15-min wash with $Cl^-$-free APW-6.5 prior to tissue fixation. Primary fixation was in 1.25% glutaraldehyde in 50 mM sodium cacodylate buffer (pH 7.2) for 2 h at 4°C. This was followed by a 2-h rinse in 50 mM sodium cacodylate buffer (three changes) and a 15-min rinse in 50 mM Tris-maleate buffer (pH 7.2). The shoots were then incubated for 2 h (in dark; room temperature) in reaction medium containing 2 mM $Pb(NO_3)_2$, 2 mM ATP, and 2 mM $Mg(NO_3)_2$ in 50 mM Tris-maleate buffer (pH 7.2). They were then washed with Tris-maleate buffer for 15 min followed by a 30-min wash with sodium cacodylate buffer. Postfixation was for 1 h at 23°C in 1% $OsO_4$ (25 mM cacodylate buffer, pH 7.2). Shoots were then rinsed with distilled $H_2O$, dehydrated with an acetone series, and embedded in Spurr's resin (25). Thin sections were examined, unstained, using a JEOL 100S or Zeiss 10 transmission electron microscope.

In one experiment, DIDS was added both to the Tris-maleate wash (15-min) and the following ATPase reaction medium. Controls for the specificity of the ATPase reaction in this tissue have been previously described (7).

For our NEM studies, cells were cut and pretreated as described under "Culture Material." In some experiments, *Chara* cells were exposed, for 15 min, to 1 mM NEM (CPW-6.5) prior to primary fixation. The tissue was then rinsed with CPW-6.5, placed into fixative solution, and further processed as outlined above. The effect of including 1 mM NEM in both the Tris-maleate buffer rinse and the ATPase incubation medium was also examined.

## RESULTS

**Electrophysiological Measurements.** Representative membrane potential changes are illustrated in Figure 1; the potentials represent values measured between the vacuole and the bathing medium. Because the potential across the tonoplast is small, we will refer to our measured potentials as representing the value across the plasmalemma. Reintroducing $Cl^-$ to cells that had been pretreated for 18 h in $Cl^-$-free APW-6.5 elicited a large transient depolarization in the potential across the plasmalemma (Fig. 1A). This response is similar to that reported by Sanders (18); however, the magnitude of our depolarization was larger, being 20 ± 4 ($n$ = 5) mv (*cf.* 9.8 ± 1.3 mv [18]). Treatment of control (*i.e.* not $Cl^-$-starved) cells with 0.5 mM DIDS resulted in a small, 4- to 10-mv hyperpolarization of the potential (Fig. 1B). When DIDS was applied to cells that had been treated in $Cl^-$-free APW-6.5 for approximately 18 h, the membrane potential depolarized by 10 to 20 mv, but then quickly hyperpolarized to a value 21 ± 6 ($n$ = 9) mv more negative than the initial potential (Fig. 1C). After 40 to 60 min in DIDS solution, we introduced $Cl^-$ in the presence of DIDS. As shown in Figure 1D, this introduction of $Cl^-$ had little effect on the potential.

In the experiments outlined above, the treatments had, at most, only a small influence on measured values of membrane resistance.

**DIDS Inhibition of $^{36}Cl^-$ Influx.** The results presented in Figure 1 suggest that DIDS may have an inhibitory effect on $Cl^-$ transport

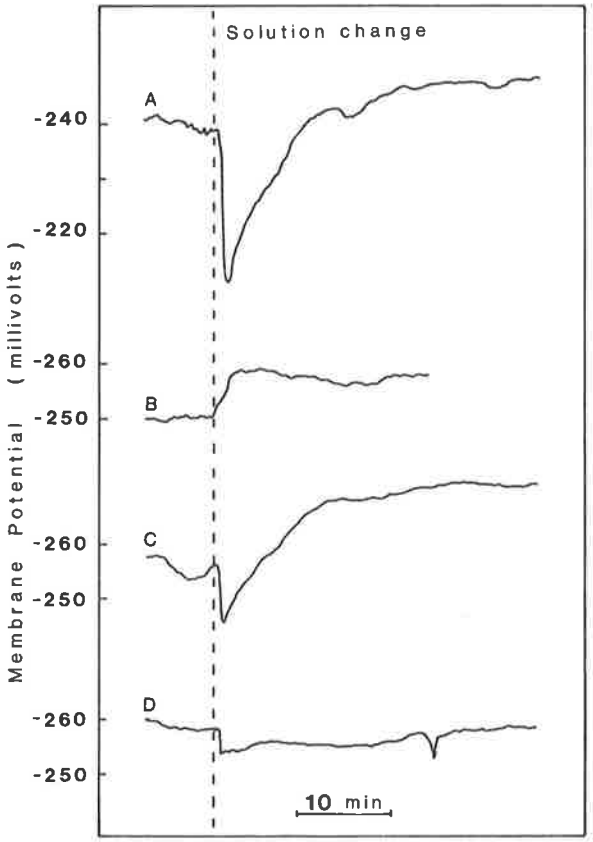


FIG. 1. Membrane potential measurements in *Chara*. A, Cell pretreated for 18 h in $Cl^-$-free APW-6.5; then, at the dashed line, the experimental medium was changed to APW-6.5 containing 1.0 mM $Cl^-$. B, The cell was pretreated for 18 h in APW-6.5; this cell was then exposed to APW-6.5 + 0.5 mM DIDS. C, After an 18-h treatment in $Cl^-$-free APW-6.5, cells were exposed to $Cl^-$-free APW-6.5 + 0.5 mM DIDS. D, following 40 to 60 min in the solution in C, the medium was changed to APW-6.5 + 0.5 mM DIDS.

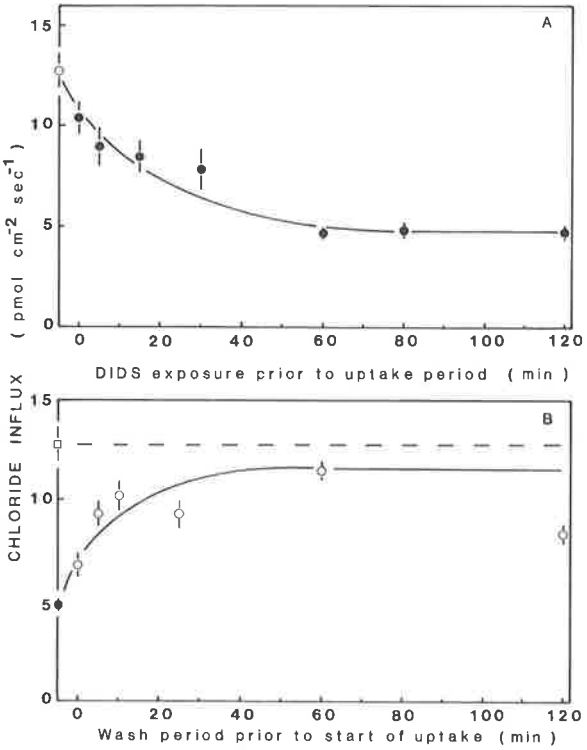


FIG. 2. Measurement of $^{36}Cl^-$ influx following an 18-h treatment in $Cl^-$-free media. A, Chloride uptake was measured in APW-6.5 + 0.5 mM DIDS following increasing periods of pre-exposure to 0.5 mM DIDS under $Cl^-$-free conditions (●), with a control (○) in the absence of DIDS. B, After a 60-min exposure to 0.5 mM DIDS (●), $^{36}Cl^-$ influx was measured following increasing periods of exposure to DIDS-free solution ($Cl^-$-free APW-6.5) (○), and compared with a control (□) that was not exposed to DIDS.

in *Chara*. To investigate this further, we examined the effect of 0.5 mM DIDS treatment (60 min) on $^{36}Cl^-$ uptake. Influx into control cells (APW-6.5, no $Cl^-$-free treatment) was 3.1 ± 0.3 ($n$ = 22) pmol $cm^{-2}$ $s^{-1}$, whereas in the presence of DIDS, the value was 3.0 ± 0.3 ($n$ = 12) pmol $cm^{-2}$ $s^{-1}$. However, $Cl^-$-starved cells showed a much greater level of DIDS sensitivity. A time course for DIDS inhibition of $Cl^-$ influx into $Cl^-$-starved cells is presented in Figure 2A. As a comparison, our stimulated influx, in the absence of DIDS, was 12.7 ± 0.9 ($n$ = 32) pmol $cm^{-2}$ $s^{-1}$, a value 2 to 3 times larger than that reported by Sanders (18).

The inhibition of $Cl^-$ uptake by DIDS could be reversed by its removal from the experimental medium (Fig. 2B); this result is at variance with the irreversible effect observed on animal anion transport systems.

**pH Effects on $Cl^-$ Influx.** Figure 3 shows the pH dependence of $Cl^-$ influx in control cells and cells that were starved for approximately 18 h in $Cl^-$-free media. The inhibitory effect of 0.5 mM DIDS on $Cl^-$-starved cells is also shown. This DIDS treatment inhibited the stimulated $Cl^-$ influx to values close to those obtained for control cells (not $Cl^-$-starved). Since 0.5 mM DIDS had little effect on control influx (see earlier section), the DIDS concentration was increased to 2.0 mM to determine whether the stimulated influx could be inhibited to a value below that of the control. At pH 6.5 and in the presence of 2 mM DIDS, the stimulated $Cl^-$ influx was inhibited to 1.1 ± 0.1 ($n$ = 12) pmol $cm^{-2}$ $s^{-1}$. For a comparison, $^{36}Cl^-$ influx into 2 mM DIDS-treated control cells (*i.e.* not $Cl^-$-starved) was 2.2 ± 0.2 ($n$ = 12) pmol $cm^{-2}$ $s^{-1}$.

The pH dependence of 2.0 mM DIDS inhibition on the stimulated influx is also illustrated in Figure 3. The degree of inhibition becomes more apparent when the inhibited flux is given as a percentage of the noninhibited flux; these values are 3% at pH 4.8, 13% at pH 5.7, 9% at pH 6.5, 26% at pH 7.5, and 35% at pH 8.5.

**DIDS Inhibition at Different External $Cl^-$ Concentrations.** The effectiveness with which 2.0 mM DIDS inhibited $Cl^-$ influx (measured always in 1.0 mM total $Cl^-$) was determined after a 60-min DIDS pretreatment in the presence of various external $Cl^-$ concentrations (0, 0.5, 0.1, 0.2, and 1.0 mM). The results of two experiments are shown in Figure 4, along with the relevant controls in which cells were given a 60-min pretreatment at the specified $Cl^-$ concentrations, but in the absence of DIDS. The control treatments illustrate the stimulatory effect of pretreatment of reduced exogenous $Cl^-$ levels on $^{36}Cl^-$ influx and serve to demonstrate the complexity of the observed inhibition.

**Cation Effects on DIDS Inhibition.** Inhibition of the stimulated $Cl^-$ influx by DIDS became more effective at higher $H^+$ concentrations (Fig. 3). Experiments were performed in the presence of higher $Na^+$ and $Ca^{2+}$ levels to ascertain whether this increased inhibition was due to a screening of the fixed negative charges in the cell wall. When 5 mM $Na_2SO_4$ or 5 mM $CaSO_4$ was added to the pretreatment and uptake solutions, we observed no significant influence on either the stimulated $Cl^-$ influx or its inhibition by DIDS (Table I).

**Plasma Membrane ATPase Activity.** In a recent study, Franceschi and Lucas (7) suggested that the charasome (for structure and development, see Refs. 5, 6, and 14) may be a special plasma membrane modification adapted to function as a site for $Cl^-$-$2H^+$

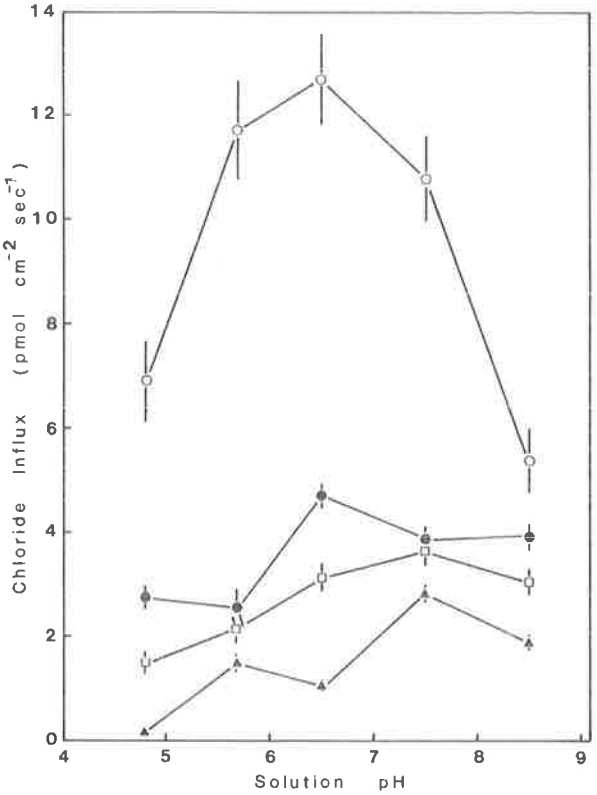


FIG. 3. Chloride influx measured as a function of external pH. All $^{36}Cl^-$ fluxes were measured after overnight pretreatment in the following solutions: APW-6.5 (□); $Cl^-$-free APW-6.5 (○); $Cl^-$-free APW-6.5 for 18 h plus 60 min in either $Cl^-$-free APW-6.5 + 0.5 mM DIDS (●); or $Cl^-$-free APW-6.5 + 2.0 mM DIDS (▲).

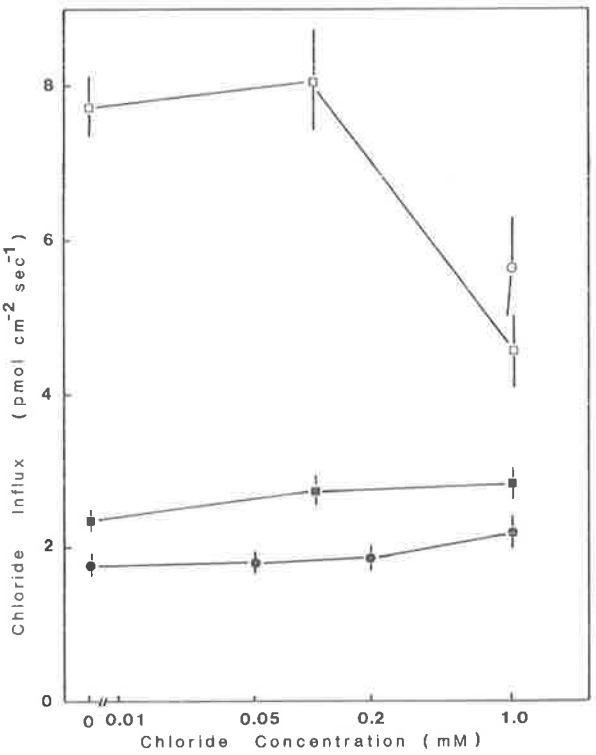


FIG. 4. Chloride influx measured following a 60-min pretreatment in solutions of different $Cl^-$ concentration. Controls (○, □) and, following 60-min exposure to 0.5 mM DIDS, simultaneous with $Cl^-$ pretreatment (●, ■).

co-transport. We used a histochemical approach to investigate the influence of DIDS on the ATPase activity along the *Chara* plasma membrane. ATPase activity reaction product was abundant in the charasomes of $Cl^-$-starved cells (Fig. 5). No detectable difference in the amount of reaction product within the charasomes could be discerned between $Cl^-$-starved cells and cells that were not starved of $Cl^-$. The reaction product often occurred as very dense patches within the cytoplasmic tubules of the charasomes and at the inferface of the charasome and the gel layer of the cytoplasm. The same distribution pattern was found in $Cl^-$-starved shoots treated with DIDS (Fig. 6) or with DIDS followed by a 1- or 15-min wash (Fig. 7). The mitochondria of cells exposed to the above conditions were generally devoid of reaction product (Figs. 5–7), while the chloroplasts always contained slight amounts of reaction product (Figs. 5–8). Charasomes in cells exposed to DIDS after fixation (included in both reaction medium and prior buffer rinse) were almost completely devoid of reaction product (Fig. 8). However, we observed that the mitochondria in these cells now contained reaction product. Under these conditions, the chloroplasts also contained reaction product at a level similar to that seen after the other treatments previously described. Ultrastructural preservation of charasomes, mitochondria, and chloroplasts of cells treated with DIDS after fixation was the same as for all other experimental treatments examined.

**Influence of NEM on $^{36}Cl^-$ Influx and Charasome ATPase Activity.** The results presented in Figure 3 indicate that $^{36}Cl^-$ influx into our control cells was not markedly sensitive to external pH. Inasmuch as the membrane potential of *Chara* is extremely pH-sensitive (11, 23), this implied that the transport process responsible for $Cl^-$ influx must be relatively insensitive to the potential across the plasmalemma. This aspect was investigated by using the permeant sulfhydryl reagent NEM, which has been shown to open the $K^+$ channels in the plasmalemma of *Chara* (12). Since Lichtner *et al.* (12) did their experiments at pH 8.0, we exposed cells to NEM at both pH 8.0 and 6.5. Cells that were given 1- or 2-min pretreatment in 0.1 mM NEM had $^{36}Cl^-$ influx values similar to those of the controls (Table II).

Table I. *Cation Effect on DIDS Inhibition of $^{36}Cl^-$ Uptake into Chara corallina*

After an 18-h treatment in $Cl^-$-free APW-6.5, in continuous light, the cells received a 1-h pretreatment in $Cl^-$-free APW-6.5 containing the additions as indicated. Chloride influx was measured in APW-6.5 (10-min uptake period) containing the same cation concentration as the pretreatment. The results are the mean for 12 cells ± SE.

| Solution Additions | $Cl^-$ Influx |
|---|---|
| | *pmol cm$^{-2}$ s$^{-1}$* |
| No addition | 11.5 ± 1.1 |
| 0.5 mM DIDS | 4.4 ± 0.5 |
| 5.0 mM $Na_2SO_4$ | 13.9 ± 1.1 |
| 5.0 mM $Na_2SO_4$ + 0.5 mM DIDS | 4.8 ± 0.4 |
| 5.0 mM $CaSO_4$ | 11.2 ± 1.1 |
| 5.0 mM $CaSO_4$ ± 0.5 mM DIDS | 4.4 ± 0.3 |

In our histochemical study, we found that NEM did not inhibit the charasome ATPase activity when used either prior to tissue fixation (Fig. 9) or in the ATPase incubation medium (Fig. 10). However, NEM did appear to inhibit most of the ATPase activity that was associated with the chloroplast membranes (compare Figs. 5, 6, and 10).

## DISCUSSION

**Electrophysiology.** Figure 1A shows the transient depolarization that results when $Cl^-$ is restored to the cell following a period of $Cl^-$ starvation. Sanders (16) attributed this depolarization to the

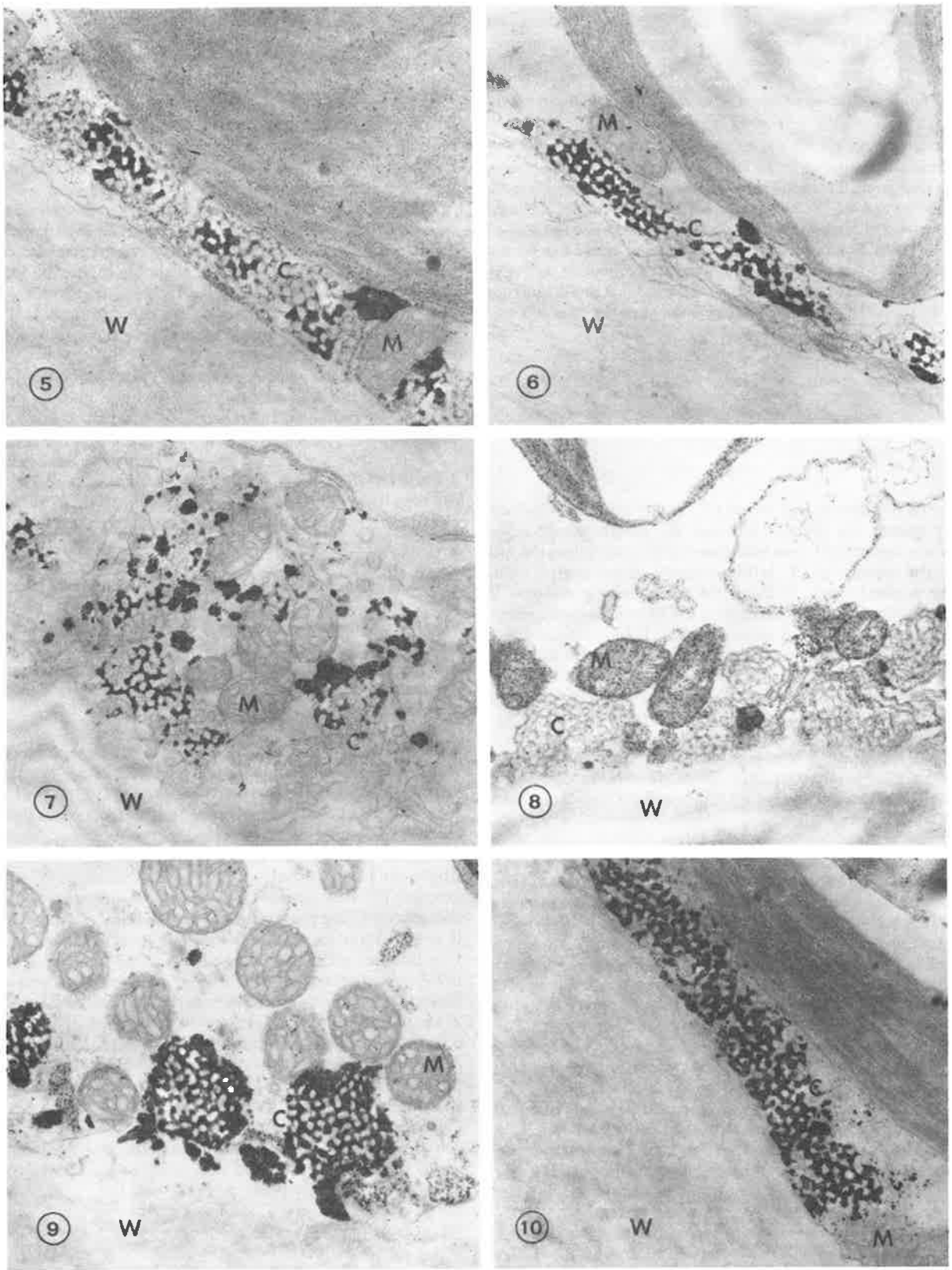


FIGS. 5–10. ATPase localization along the cortical region of branch internodal cells of *Chara corallina*. No poststaining was employed. Charasome (C), mitochondrion (M), cell wall (W).

FIG. 5. ATPase reaction product observed in cells pretreated in $Cl^-$-free APW-6.5 for approximately 18 h. × 24,000.

FIG. 6. Reaction product pattern observed after pretreatment as in Figure 5, except that cells were also given an 80-min exposure to 0.5 mM DIDS $Cl^-$-free APW-6.5, prior to chemical fixation. × 24,000.

FIG. 7. Pretreatment and DIDS exposure as in Figure 6. Tissue was washed in $Cl^-$-free APW-6.5 for 15 min before chemical fixation. Section shown is tangential to the wall. × 24,000.

FIG. 8. Tissue treated as above, except that 0.5 mM DIDS was applied after fixation and during incubation in the ATPase reaction medium. × 24,000.

FIG. 9. Section from shoot incubated in 1 mM NEM for 15 min prior to chemical fixation. × 23,200.

FIG. 10. Reaction product pattern observed when 1 mM NEM was included in the ATPase incubation medium. × 28,700.

Table II. *Influx of $^{36}Cl^-$ into Chara Cells following Pretreatment with 0.1 mM NEM*

In pretreatment A, cells were given 60 min in control medium (CPW-6.5). The indicated exposure to an identical solution containing 0.1 mM NEM was then given; this treatment was stopped by returning cells to the control solution and the $^{36}Cl^-$ uptake period (30 min) was initiated after a further 5 min. For pretreatment B, cells were given 30 min in CPW-6.5 and then a further 20 min in CPW-8.0 before being exposed to 0.1 mM NEM (pH 8.0); a 1-min rinse in CPW-8.0 was used to remove the NEM. Cells were then returned to CPW-6.5 for 10 min prior to initiating the $^{36}Cl^-$ uptake period (30 min). The results are the mean for 10 cells ± SE.

| Pretreatment | $^{36}Cl^-$ Influx | | |
|---|---|---|---|
| | Control (0 NEM) | 1-min NEM | 2-min NEM |
| | *pmol cm$^{-2}$ s$^{-1}$* | | |
| A | 1.68 ± 0.20 | 1.89 ± 0.14 | 1.47 ± 0.11 |
| B | 1.38 ± 0.23 | | 1.40 ± 0.12 |

net entry of positive charge when $Cl^-$ enters on a $Cl^-$-$2H^+$ co-transport system. He pointed out that the membrane potential recovery was faster (5–10 min half-time for recovery) than the rate at which the stimulated $Cl^-$ influx returned to the control value (half-time approximately 30 min). He attributed the recovery in membrane potential to a stimulation of the $H^+$ electrogenic pump. Figure 1B shows that DIDS caused a small hyperpolarization of the membrane potential when applied to control cells (not $Cl^-$-starved). This could be attributed to DIDS inhibiting the $Cl^-$ co-transport system, thereby reducing the return current of $H^+$ across the membrane and, thus, allowing the electrogenic pump to hyperpolarize the membrane slightly. However, this explanation is unlikely as DIDS, at 0.5 mM, has an insignificant effect on $Cl^-$ influx, even after a 60-min pretreatment. It may be that DIDS affects, to some extent, passive leakage currents associated with either $H^+$ or $K^+$ influx.

In contrast to the above treatments, DIDS had a dramatic effect on the potential when applied in the absence of $Cl^-$ (Fig. 1C). This is difficult to explain, inasmuch as the $Cl^-$ co-transport system should not have been operating in the absence of substrate and as DIDS had no apparent effect on the ATPase activity when applied to the outer surface of the plasmalemma. Although it seems unlikely, the similarity between the depolarizing and hyperpolarizing responses observed in Figure 1, A and C, suggests that DIDS may have been entering the cell. However, it would seem more likely that under external $Cl^-$-free conditions, sufficient $Cl^-$ may leak into the inner cell wall space to provide substrate for the transport system, and it was this activity that was then inhibited. When $Cl^-$ was restored to a DIDS-inhibited, $Cl^-$-starved cell, the effect on the membrane potential was minimal, compared to restoring $Cl^-$ to a $Cl^-$-starved cell (compare Fig. 1, A and D). This effect is consistent with a DIDS inhibition of $Cl^-$ influx and, hence, the large transient depolarization was prevented. This interpretation is also supported by the inhibitory effect of DIDS on the stimulated $Cl^-$ influx system (Fig. 2A). It would appear that for DIDS inhibition to occur, exogenous $Cl^-$ must either be absent or present in very low concentrations. The small effect of these treatments on membrane resistance can also be rationalized on the basis that the major conductance through the membrane is associated with the electrogenic $H^+$ pump and that the conductance of the $Cl^-$-$2H^+$ co-transport is small in comparison.

**Reversibility of DIDS Inhibition.** In the present study, we found that the DIDS inhibition of $Cl^-$ influx was reversible (*cf.* Fig. 2, A and B). This is in contrast to the case in red blood cells where DIDS irreversibly inhibits anion transport (3). In red blood cells, it is thought that DIDS binds reversibly to the anion transport site, which places DIDS in a position to react, covalently, with the ε-amino group of two lysine residues on the transport protein (2, 20). In other situations, the likelihood of this geometry for DIDS binding is low, and may account for the reversibility we observed. Since the inhibition is reversible, we cannot use this molecule to label the proteins involved with $Cl^-$ transport.

**Effect of the Plant Cell Wall.** The slowness with which DIDS acts in *Chara* (60 min to saturate) and the high concentrations needed (0.5–2.0 mM), as compared to the micromolar concentrations used in red blood cells (3), probably reflect the influence of the plant cell wall. Lin (13) also reported that inhibition of $Cl^-$ and $SO_4^{2-}$ transport into root segments required higher DIDS concentrations than were necessary to achieve similar inhibition in root protoplasts.

Given that DIDS is quite a large divalent anion (mol wt of 456) and that the cell wall contains fixed negative charges, the ion may have some difficulty in penetrating the cell wall to the outer plasmalemma surface. Evidence suggesting that the cell wall may act as a barrier is obtained from the larger per cent inhibition by 2.0 mM DIDS at lower pH values. As the solution pH is lowered, the negative charge sites in the cell wall are either titrated or are electrically shielded by the increased $H^+$ concentration, thereby making it easier for the DIDS anion to enter and cross the cell wall.

Our experiments in which we increased the level of $Na^+$ (by 10 mM) or $Ca^{2+}$ (by 5 mM) do not offer support for the hypothesis that the dominant wall effect is due to the influence of the fixed negative charges. Such a high concentration of $Ca^{2+}$ would reduce the negative Donnan potential of the wall, but, under these conditions, we found no enhancement of DIDS inhibition on $Cl^-$ influx (Table I).

DIDS could have been acting as a weak acid, where the concentration of the reactive species is pH-dependent. However, titration indicated that its pK value is well below 1.3. Hence, it is very unlikely that the increased sensitivity to DIDS, at lower pH values, is due to the presence of the undissociated form of this reactive molecule. The observed pH effect may, nevertheless, reflect the involvement of more than one complex process occurring at the plasmalemma of these cells. Also, the absolute effect of external pH may actually be masked, in this system, due to the complexity of the plasmalemma-cell wall interface. In this regard, it is important to point out that our control $Cl^-$ fluxes showed very little pH sensitivity from pH 6.5 to 8.5 (see Fig. 3, □). In this pH region, our control fluxes were maximal; this response is in direct contrast with the earlier work of Smith (see Fig. 1 of Ref. 21) and the recent work of Sanders (see Fig. 6 of Ref. 16). These differences may reflect variations in culture conditions, and experiments are presently underway in our laboratory to investigate the effect of culture medium pH on charasome development and Cl transport.

**External Buffering and $Cl^-$ Transport.** The present model for active $Cl^-$ transport into *Chara* proposes that this anion moves across the plasmalemma via a $Cl^-$-$2H^+$ co-transport system, with the necessary energy being derived from the $H^+$ electrochemical potential gradient (16–19). The operation of a $H^+$-translocating ATPase is thought to maintain this energy gradient. In this regard, it is of interest to consider the influence of an external buffer which may act in a competitive manner, against the co-transport system for $H^+$. Various workers have used a range of buffer conditions in their studies on $Cl^-$ transport (15, 21), and, except for the amine-type buffers, $Cl^-$ influx does not appear to be sensitive to exogenous buffer. (However, in some experiments, buffers were used at pH values well below their pK, and so there would have been little chance for the conjugate base to compete for $H^+$ [15].) This insensitivity to exogenous buffer may be due, in part, to the anion-screening effect of the cell wall. Additionally, if the charasome plays a role in $Cl^-$ uptake, its specialized periplasmic space may confine the protons such that they are not

readily accessible to the buffer.

**DIDS Competition with $Cl^-$.** The stimulated component of $Cl^-$ influx that was elicited by $Cl^-$ starvation could be almost completely eliminated by pretreatment with 0.5 mM DIDS. However, DIDS at the same concentration had no significant effect on the control $Cl^-$ transport process. This suggested to us that there may be two $Cl^-$ transport mechanisms—the normal transporter and another mechanism that carries the stimulated flux—with only the latter being sensitive to DIDS. Inasmuch as increasing the DIDS concentration to 2.0 mM caused a significant inhibition of normal $Cl^-$ influx, this interpretation seems unlikely. Yet we must explain why 2.0 mM DIDS always produced a much greater inhibition of $Cl^-$ transport into $Cl^-$-starved *versus* control cells (not $Cl^-$-starved). The basic difference between these two experiments is that, for DIDS inhibition of the stimulated $Cl^-$ influx, DIDS was always applied for the last 60 min of the $Cl^-$-free pretreatment. In control experiments, DIDS was applied for 60 min, but it was always in the presence of 1.0 mM $Cl^-$. On a speculative note, the differential effect of DIDS may indicate that $Cl^-$ and DIDS are competing for the same binding site. If competition with $Cl^-$ was actually preventing DIDS from effectively reaching the binding site, then a 60-min pretreatment with DIDS, under conditions of reduced exogenous $Cl^-$, should increase its ability to inhibit transport. These competition experiments were complicated by the stimulatory effect of even a short period of $Cl^-$ starvation (16), so controls (no DIDS) were run for each pretreatment concentration of $Cl^-$. The pretreatment with DIDS at lower $Cl^-$ concentration gave absolute flux values that were slightly lower, but with only a marginal level of significance (Fig. 4). However, the important point to note is that the relative inhibition by DIDS, compared to the control, is significantly larger at lower $Cl^-$ pretreatment concentrations. Inasmuch as any effort to reduce competition between $Cl^-$ and DIDS also stimulates $Cl^-$ influx, the possibility still exists that there are two $Cl^-$ transport mechanisms, with DIDS being more effective at inhibiting the mechanism associated with the stimulated $Cl^-$ influx.

**Membrane ATPase Activity.** The apparent insensitivity of the *Chara* plasma membrane ATPase to DIDS, in both control and $Cl^-$-starved situations, suggests that $Cl^-$ inhibition by DIDS is not due to an indirect effect on the electrogenic $H^+$ pump. This interpretation is also supported by the observation that in control cells the membrane potential actually hyperpolarized in the presence of DIDS (Fig. 1B). Electrogenic $H^+$ pump inhibition would have resulted in a depolarization of the potential to the diffusion potential (11, 23).

The plasmalemma ATPase activity was inhibited, however, by including DIDS in the reaction medium (after tissue fixation). Thus, once DIDS can penetrate the tissue, it presumably finds reactive sites (lysine residues?) on the inner surface of the plasmalemma to which it binds, thereby inhibiting the ATPase system. This result and interpretation are in agreement with studies on isolated plasma membrane preparations in which ATPase sensitivity to DIDS was also observed (4, 13). In these membrane preparations, the microsomal vesicles are usually everted and, hence, the inner plasma membrane surface is accessible to the DIDS molecule. Bennett and Spanswick (1) also reported that their putative tonoplast vesicles derived from corn roots contained a $H^+$-translocating ATPase that was partially sensitive to DIDS. However, they interpreted this DIDS inhibition in terms of DIDS acting at a $Cl^-$ transport site that was thought to be intimately associated with the $H^+$-translocating ATPase. *Chara* cell perfusion studies must now be performed to determine whether, in unfixed tissue, DIDS can inhibit the electrogenic $H^+$ ATPase of the plasmalemma; depolarization of the membrane potential in such cells would offer support for the above hypothesis.

**Insensitivity of $Cl^-$ Transport to Membrane Potential.** A brief exposure of *Chara* cells to NEM results in an opening of $K^+$ channels within the plasmalemma (12). Thus, in our NEM-pretreated cells, the membrane potential would have been depolarized from −250 mv down to −150 mv (12). However, under these conditions, $^{36}Cl^-$ influx was not significantly different from values obtained with control cells (Table II). This result supports the hypothesis of Sanders and Hansen that $Cl^-$ influx is under kinetic, rather than thermodynamic control (19). The limits of $Cl^-$ transport insensitivity to membrane potential will be investigated in the near future.

The insensitivity of both $Cl^-$ influx and plasmalemma-charasome ATPase activity to NEM also supports our recent hypothesis that the plasmalemma $H^+$-translocating ATPase remains operational in the presence of open $K^+$ channels (10).

**Conclusions.** DIDS is an effective inhibitor of the *Chara* plasma membrane $Cl^-$ transport system, a system presently thought to operate as an electrogenic $Cl^-$-$2H^+$ co-transport process. Transport inhibition appears to result from competition between DIDS and $Cl^-$ for an external binding site, although a more complex form of interaction between DIDS and the transport system cannot be discounted. The ability of DIDS to form covalent bonds with the $\epsilon$-amino group of lysine plays no role in its inhibition in *Chara*, suggesting that there are no lysine residues in the vicinity of the external binding site of the $Cl^-$ transport system.

*Acknowledgments*—We wish to thank Drs. A. B. Bennett and R. M. Spanswick for making their manuscript available prior to publication.

## LITERATURE CITED


1. Bennett AB, RM Spanswick 1982 Optical measurements of $\Delta pH$ and $\Delta\psi$ in corn root membrane vesicles. Kinetic analysis of $Cl^-$ effects on a proton-translocating ATPase. J Membr Biol In press
2. Cabantchik ZI, PA Knauf, A Rothstein 1978 The anion transport system of the red blood cell. The role of membrane protein evaluated by the use of 'probes.' Biochim Biophys Acta 515: 239–302
3. Cabantchik ZI, A Rothstein 1974 Membrane proteins related to anion permeability of human red blood cells. I. Localization of disulfonic stilbene sites in proteins involved in permeation. J Membr Biol 15: 207–226
4. Churchill KA, H Sze 1981 Anion sensitivity of the electrogenic ATPase from tobacco callus plasmalemma. Plant Physiol 67: S-162
5. Franceschi VR, WJ Lucas 1980 Structure and possible function(s) of charasomes; complex plasmalemma-cell wall elaborations present in some characean species. Protoplasma 104: 253–271
6. Franceschi VR, WJ Lucas 1981 The charasome periplasmic space. Protoplasma 107: 269–284
7. Franceschi, VR, WJ Lucas 1982 The relationship of the charasome to chloride uptake in *Chara corallina:* physiological and histochemical investigations. Planta 154: 525–537
8. Hope AB, NA Walker 1960 Ionic relations of cells of *Chara australis.* III. Vacuolar fluxes of sodium. Aust J Biol Sci 13: 277–291
9. Hope AB, NA Walker 1975 The Physiology of Giant Algal Cells. Cambridge University Press, London
10. Keifer DW, WJ Lucas 1982 Potassium channels in *Chara corallina:* control and interaction with the electrogenic $H^+$ pump. Plant Physiol 69: 781–788
11. Keifer DW, RM Spanswick 1978 Activity of the electrogenic pump in *Chara corallina* as inferred from measurements of the membrane potential, conductance, and potassium permeability. Plant Physiol 62: 653–661
12. Lichtner FT, WJ Lucas, RM Spanswick 1981 Effect of sulfhydryl reagents on the biophysical properties of the plasmalemma of *Chara corallina.* Plant Physiol 68: 899–904
13. Lin W 1981 Inhibition of anion transport in corn root protoplasts. Plant Physiol 68: 435–438
14. Lucas WJ, VR Franceschi 1981 Characean charasome-complex and plasmalemma vesicle development. Protoplasma 107: 255–267
15. Lucas WJ, FA Smith 1976 Influence of irradiance on $H^+$ efflux and $Cl^-$ influx in *Chara corallina:* an investigation aimed at testing two $Cl^-$ transport models. Aust J Plant Physiol 3: 443–456
16. Sanders D 1980 Control of plasma membrane $Cl^-$ fluxes in *Chara corallina* by external $Cl^-$ and light. J Exp Bot 31: 105–118
17. Sanders D 1980 Control of $Cl^-$ influx in *Chara* by cytoplasmic $Cl^-$ concentration. J Membr Biol 52: 51–60
18. Sanders D 1980 The mechanism of $Cl^-$ transport at the plasma membrane of *Chara corallina.* I. Cotransport with $H^+$. J Membr Biol 53: 129–141
19. Sanders D, U-P Hansen 1981 Mechanism of $Cl^-$ transport at the plasma membrane of *Chara corallina.* II. Transinhibition and the determination of $H^+/Cl^-$ binding order for a reaction kinetic model. J Membr Biol 58: 139–153
20. Shami Y, A Rothstein, PA Knauf 1978 Identification of the $Cl^-$ transport site

of human red blood cells by a kinetic analysis of the inhibitory effects of a chemical probe, Biochim Biophys Acta 508: 357–363
21. SMITH FA 1970 The mechanism of chloride transport in characean cells. New Phytol 69: 903–917
22. SMITH FA, NA WALKER 1976 Chloride transport in *Chara corallina* and the electrochemical potential difference for hydrogen ions. J Exp Bot 27: 451–459
23. SPANSWICK RM 1981 Electrogenic ion pumps. Annu Rev Plant Physiol 32: 267–289
24. SPEAR DG, JK BARR, CE BARR 1969 Localization of hydrogen ion and chloride ion fluxes in *Nitella*. J Gen Physiol 54: 397–414
25. SPURR AR 1969 A low-viscosity epoxy resin embedding medium for electron microscopy. J Ultrastruct Res 26: 31–43

Planta (1982) 156:181–192

Planta
© Springer-Verlag 1982

# Mechanism of acquisition of exogenous bicarbonate by internodal cells of *Chara corallina*

William J. Lucas
Department of Botany, University of California, Davis, CA 95616, USA

**Abstract.** Electrophysiological measurements on internodal cells of the alga, *Chara corallina* Klein ex Willd., em. R.D.W., showed that the potential across the plasmalemma was sensitive to the level of exogenous $HCO_3^-$. In alkaline solutions (pH 8) the membrane potential depolarized by 50–75 mV when exogenous $HCO_3^-$ was removed from the bathing medium. In the presence of exogenous $HCO_3^-$, the membrane potential rapidly hyperpolarized when the cell was given a brief dark treatment; in the light the potential was approx. −240 mV; after the cell had been in the dark for 3–6 min the potential was −330 to −350 mV. In the absence of exogenous $HCO_3^-$ the potential only hyperpolarized slowly and to a much smaller extent when cells were placed in the dark. Upon re-illuminating the cell, the potential further hyperpolarized, transiently, and then rapidly depolarized back towards the light-adapted value. (These responses were only obtained when cells were not perturbed by microelectrode insertion into the vacuole.) Analysis of membrane potential and experiments with the extracellular vibrating electrode indicated a high level of correlation between the light- and dark-induced changes in membrane potential and extracellular currents. However, when experiments were conducted in $HCO_3^-$-free media that contained 1.0 mM phosphate buffer, pH 8, it was found that the dark-induced hyperpolarization of the membrane potential and the light-dependent extracellular currents could be maintained in the absence of exogenous $HCO_3^-$. These results are interpreted in terms of two basic models by which internodal cells of *C. corallina* may acquire exogenous $HCO_3^-$ for photosynthesis. They are consistent with $HCO_3^-$ being transported across the plasmalemma via an electrically neutral $HCO_3^- - H^+$ cotransport system. The hyperpolarizing response is thought to be the consequence of the operation of an electrogenic $H^+$-translocating ATPase that has a transport stoichiometry of 1 $H^+$ per ATP hydrolyzed.

**Key words:** *Chara* – Electric current (extracellular) – Electrogenic $H^+$-translocating ATPase – Membrane potential – Plasmalemma transport ($H^+$–$HCO_3^-$–$OH^-$).

## Introduction

The cell membrane potential of many green plants appears to be sensitive to light (for a review, see Higinbotham 1973). The phenomenon of the electrical response of the characean plasmalemma to illumination has been investigated by numerous workers. The response is complex, with some studies indicating a light-induced hyperpolarization of the membrane potential (Nagai and Tazawa 1962; Nishizaki 1968), while others report a depolarization (Andrianov et al. 1968). The electrical changes produced by light have an action spectrum similar to that of photosynthesis (Walker 1962; Volkov 1973). Andrianov et al. (1968) also found a close correlation between the shape of the light-induced change in membrane potential and the induction of photosynthesis. The involvement of photosynthesis has also been shown by the sensitivity of the plasmalemma response to photosynthetic inhibitors (Volkov and Petrushenko 1969; Volkov 1973; Saito and Senda 1973a, b). Excellent conformation of the coupling between changes in membrane potential and photosynthesis was also obtained by Andrianov et al. (1970). These

*Abbreviation:* CPW/B = artificial *Chara* pond water containing exogenous bicarbonate

0032-0935/82/0156/0181/$02.40

workers demonstrated that when the rhizoids of *Nitella flexilis* were free of chlorophyll, no light-induced changes occurred in the resting potential. However, as the rhizoids developed chloroplasts, the membrane potential became sensitive to light.

The nature of the coupling between the chloroplasts and the plasmalemma is still speculative. The involvement of $HCO_3^-$, in an electrogenic sense, was first proposed by Hope (1965). Subsequently, numerous workers have implied that $HCO_3^-$ may play an important role in coupling the observed light-dependent membrane phenomena to the photosynthetic reactions occurring within the chloroplasts (Nishizaki 1968; Saito and Senda 1973a; Volkov 1973; Lucas 1976a). However, the actual mechanism by which exogenous $HCO_3^-$ crosses the plasmalemma remains controversial. Experimental evidence provided by Lucas (1976a), Walker and Smith (1977) and Ferrier and Lucas (1979) indicated that the $HCO_3^-$ transport process may be electrogenic in nature. More recently, Walker (1980), Ferrier (1980) and Walker et al. (1980) have presented theoretical arguments against electrogenic $HCO_3^-$ transport in *Chara*.

In the present study we show that for *Chara corallina* in alkaline media (pH 8), the changes in membrane potential, elicited by transfer to light or dark conditions, are not totally dependent upon the level of exogenous $HCO_3^-$. Our results are consistent with $HCO_3^-$ being transported across the plasmalemma via an electrical neutral $H^+$-$HCO_3^-$ cotransport system. Under alkaline conditions the changes in the membrane potential that can be elicited by light-dark manipulations are the result of complex interactions between the electrogenic, plasmalemma-bound, $H^+$- and $OH^-$-efflux systems.

## Material and methods

### *Plant material*

*Chara corallina* Klein ex Willd., em. R.D.W. (= *C. australis* R. Br.) was grown in the laboratory in 120-l containers in solutions containing (mM): 3.0 $Na^+$, 0.2 $K^+$, 0.1–0.2 $Ca^{2+}$, 1.5 $Cl^-$ and approx. 2.0 $HCO_3^-$ (pH 8.5–9.5). For full details see Lucas and Nuccitelli (1980). All experiments were performed on mature male internodal cells that were cut from the main axis of the vegetative shoot the day prior to being used in an experiment.

In all cases, cells were cut at noon and given a 1-h pretreatment in their culture solution prior to being transferred to an artificial *Chara* pond water (CPW/B) containing (mM): 1.0 NaCl, 0.2 KCl, 0.2 $CaSO_4$, 1.0 $NaHCO_3$ (pH 8.0). Cells used in electrophysiology experiments were pretreated, overnight, in CPW/B in 2-cm-deep, 9-cm-diameter Petri dishes. For vibrating-probe experiments a more complex protocol was involved.

The internodal cells were rinsed in CPW/B and then cellular debris was removed from the cut ends of the branch- and adjoining internodal-cells using a Pasteur pipette to which a partial vacuum had been applied. A silk thread (type: Orizuru 9; Kanagawa Co., Kanagawa, Japan) was then attached to each end of the internodal cell (actually tied to the dead cell-wall fragment of the adjoining internodal cells). These silk threads were then used to suspend the *Chara* internodal cell in the center of a 9-mm-deep, 30-mm-wide and 56-mm-long Plexiglas chamber filled with CPW/B. Small blocks of Plexiglas (height 4.5 mm) were placed beneath the threads near the ends of the cell to stabilize the cell's position. Cells mounted in this manner were stored in covered Petri dishes to minimize solution evaporation.

All experiments were performed in temperature-controlled rooms with the temperature being $25 \pm 2°$ C.

### *Electrophysiological measurements*

Membrane potential measurements were made in a similar manner to that reported by Keifer and Lucas (1982). The potential between the vacuole and the bathing solution was measured (WPI model 750 amplifiers; WPI Instruments, New Haven, Conn., USA) using an inserted microelectrode (1 μm tip diameter) and an external reference electrode (tip diameter approx. 10 μm). The inserted microelectrode was positioned at the half-length of the internodal cell. (In most experiments membrane resistance was not measured, since this required an additional microelectrode insertion.) Cells were illuminated using a Leitz Pradovit projector (Model C1500, 150-W quartz-iodide lamp; E. Leitz, Rockleigh, N.J., USA), the irradiance was attenuated to either 20 or 2 W $m^{-2}$ using neutral density filters (Balzers, Type No. 106613; PTR Optics Corp., Waltham, Mass., USA).

In some experiments, "$HCO_3^-$-free" solutions were required and these were prepared using the protocol detailed by Lucas (1976a). When a pH-8 solution was to be buffer-free (CPW/B), it contained (mM): 2.0 NaCl, 0.2 KCl, 0.2 $CaSO_4$. After 1 h of bubbling with $CO_2$-free air, the solution pH was adjusted to 8.2 with freshly prepared 100 mM NaOH. The solution was then further bubbled for at least 1 h before being used in an experiment. A second "$HCO_3^-$-free" solution (CPW/P) (pH 8) contained phosphate buffer (mM): 1.0 NaCl, 0.2 KCl, 0.2 $CaSO_4$, 1.0 $Na_2HPO_4$. With these solutions, we prepared a 100 mM $Na_2HPO_4$ stock solution at the commencement of each experiment and, prior to the 2-h scrubbing, the CPW/P solution was titrated to pH 8.0 using 100 mM HCl.

### *External-current measurements*

Extracellular currents near the cell wall of *Chara* internodal cells were measured using the vibrating probe system developed by Jaffe and Nuccitelli (1974). Full details of the application of this technique to the *Chara* system have been reported by Lucas and Nuccitelli (1980). In the present study we followed the same basic procedures, with the following exceptions. All measurements were made using a spherical platinum-black electrode with a tip diameter of approx. 10 μm. The electrode was vibrated at 328 Hz and we reduced the distance over which the electrode was vibrated from 30 μm (Lucas and Nuccitelli 1980) to 12.5 μm. These modifications, in conjunction with the above-detailed protocol for suspending the *Chara* cell within the experimental solution via silk threads, completely eliminated the perturbations associated with the vibrating probe that we previously reported (Lucas and Nuccitelli 1980).

The Plexiglas chamber containing the suspended *Chara* internodal cell was placed on the stage of a compound inverted microscope (Invertoscope D; Zeiss, New York, N.Y., USA)

and the cell illuminated (20 W $m^{-2}$) using a bifurcated fiber optic light source (Model MK II; Ehrenreigh Photo Optical Industries, Garden City, N.Y., USA). The microscope stage was motorized (stepping motor, Model KD 3402-004; Hurst Manufacturing Corp., Princeton, Ind., USA, coupled to a Model SL 10 adjustable speed controller; Minarik Electric Co., Los Angeles, Cal., USA) so that the entire length of a *Chara* cell could be traversed past the vibrating electrode. In all experiments the vibrating probe was maintained at a distance of $50 \pm 5$ µm from the cell surface. The speed of the motor was adjusted such that we traversed 1 cm of cell length per minute.

The local current densities (µA $cm^{-2}$) were converted to flux densities by dividing by Faraday's constant (see Lucas and Nuccitelli 1980). We have presented all vibrating probe data in terms of flux densities, in units of pmol $cm^{-2}$ $s^{-1}$. The convention followed was to display inward current ($OH^-$ efflux), which occurs in the alkaline regions (Lucas and Smith 1973; Lucas and Nuccitelli 1980), as positive fluxes, and the outward current ($HCO_3^-$ influx) as negative fluxes.

## Results

### *Effects of light and dark treatments on the* Chara *membrane potential*

Under conditions where *C. corallina* internodal cells were assimilating exogenous $HCO_3^-$, the membrane potential was extremely responsive to brief periods of darkness. Transferring the cell from light (20 W $m^{-2}$) to the dark resulted in a rapid hyperpolarization of the membrane potential, which reached a plateau after 3–7 min (Fig. 1). Upon re-illumination the potential further hyperpolarized, in a transient manner, and then rapidly depolarized, eventually stabilizing at or near the original light-adapted value. If longer dark periods were employed, the membrane potential reached a plateau and then began to decline back towards the value established under illumination. After a 40-min dark treatment, the cell responded to illumination in a manner similar to that observed after the cessation of short dark periods, with the exception that the initial transient hyperpolarization was reduced in magnitude and the onset of membrane potential depolarization was delayed (Fig. 1).

In some experiments cytoplasmic streaming was stopped, momentarily, as the microelectrode was inserted into the vacuole. Although the membrane potential of these cells stabilized within the $-240$ to $-260$ mV region, their responses to light-dark transitions were different. A typical example is presented in Fig. 2. Only after an overnight recovery period did these cells exhibit membrane potential responses consistent with those depicted in Fig. 1.

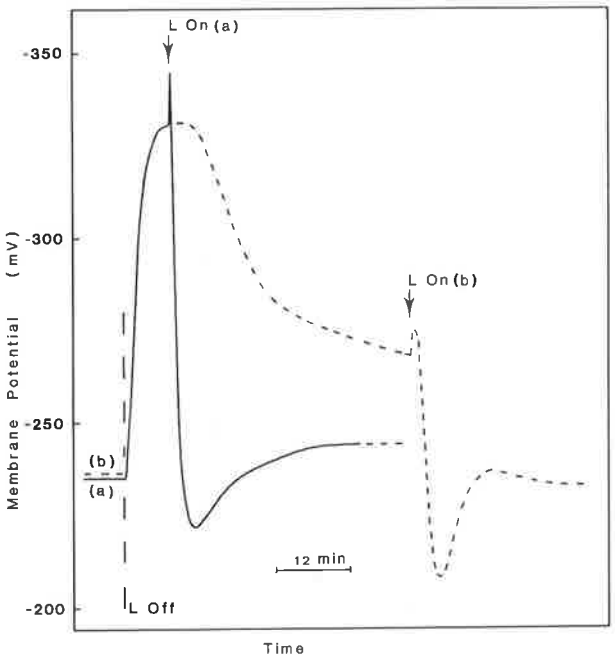


**Fig. 1.** Influence of light and dark treatments on the *Chara* membrane potential when internodal cells were assimilating exogenous $HCO_3^-$. Following electrode insertion into the vacuole, the cell was given a 2-h recovery period in CPW/B (20 $Wm^{-2}$, 25° C) before the application of a brief dark period (**a**: L Off). The influence on the membrane potential of a longer dark treatment (40 min) was then investigated (**b**)

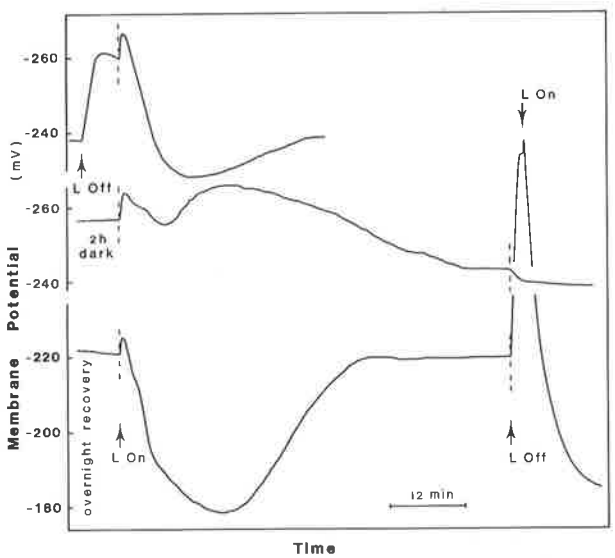


**Fig. 2.** Light- and dark-induced changes in the membrane potential obtained on a *Chara* cell that showed temporary perturbation to cytoplasmic streaming upon insertion of the microelectrode into the vacuole. The cell was given a 2-h recovery period in CPW/B (20 $Wm^{-2}$, 25° C) and then the response of the membrane potential to a short dark period was recorded. A 2-h dark treatment was then utilized in an attempt to return the cell to the control state (middle trace). After an overnight recovery period (electrode remained in the vacuole) the cell exhibited normal responses to light and dark treatments

*Bicarbonate involvement in the membrane potential response*

After steady-state photosynthetic conditions had been established (CPW/B, 20 W $m^{-2}$) the membrane potential of the *Chara* cells responded to changes in the level of exogenous $HCO_3^-$. In these experiments we made every attempt to keep the pH of the experimental medium constant, because the membrane potential, per se, is very pH-sensitive (Spanswick 1972; Richards and Hope 1974). By monitoring the pH value of the solution as it entered and left the electrophysiological chamber, we were able to obtain the desired pH value to within $\pm 0.1$ units. Figure 3 illustrates that when the exogenous $HCO_3^-$ level was lowered from 1.0 to 0.2 mM, the potential depolarized by approx. 20 mV. Exposure of cells to "$HCO_3^-$-free" media further depolarized the membrane potential. In our experiments, with the solution pH remaining constant at $8.0 \pm 0.1$, we could obtain a 50–75 mV depolarization of the membrane potential by removing the exogenous $HCO_3^-$ (see also Fig. 5).

When cells were bathed in $HCO_3^-$-free medium (pH 8), the application of a brief dark period (3–6 min) elicited a much smaller and slower hyperpolarization of the membrane potential. Figure 3 illustrates the typical responses observed, on the same cell, when a dark treatment was applied in the presence and then in the absence of exogenous $HCO_3^-$. Upon returning $HCO_3^-$ to the bathing medium, the membrane potential underwent a rapid hyperpolarization, and in this state the cell once again exhibited the normal response to cell darkening (Fig. 3).

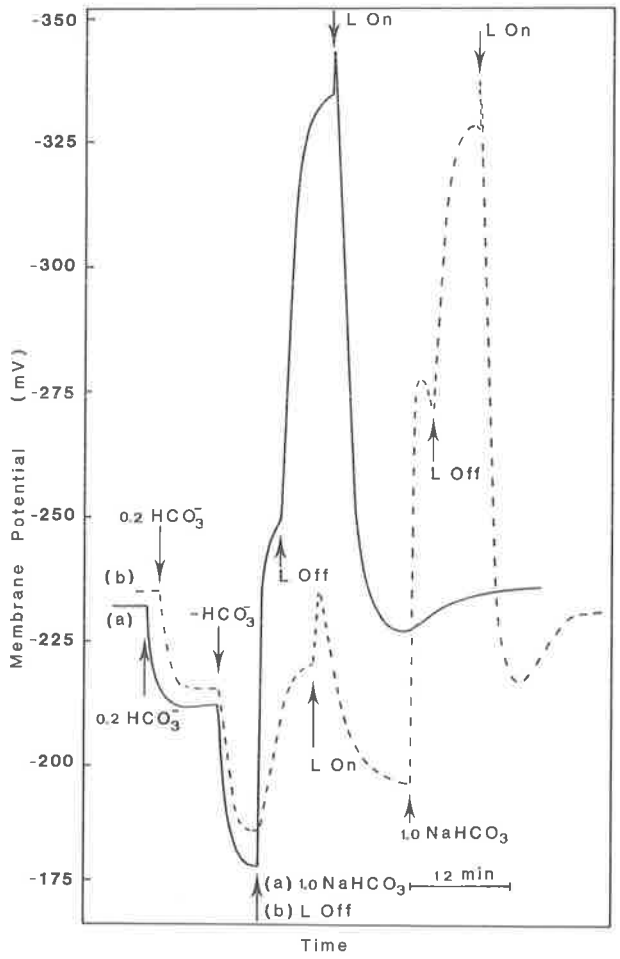


**Fig. 3.** Involvement of exogenous $HCO_3^-$ in the membrane potential response of *Chara*. In traces (**a**) and (**b**) the level of exogenous $HCO_3^-$ was reduced from 1.0 to 0.2 mM, and then the cell was exposed to $HCO_3^-$-free media. In trace (**a**), 1.0 mM $HCO_3^-$ was returned to enable a direct comparison to be made between the dark responses obtained in the presence (trace (**a**)) and absence (trace (**b**)) of $HCO_3^-$. (Trace (**b**) is an immediate continuation of trace (**a**))

*Effects of the brief dark pulse on $HCO_3^-$ and $OH^-$ transport*

The depolarization of the *Chara* membrane potential upon reduction of exogenous $HCO_3^-$, and the hyperpolarization either upon return of $HCO_3^-$ or cell darkening, presumably reflect differential changes in the rates of $HCO_3^-$ and $OH^-$ transport across the plasmalemma. We used the vibrating-probe technique to examine the influence of brief dark periods on the $HCO_3^-$-associated extracellular currents that develop along the internodal cells of *C. corallina* (Walker and Smith 1977; Lucas and Nuccitelli 1980). For these studies a new protocol was developed to hold the *Chara* cells so that they could be scanned without perturbing the transport activity of the plasmalemma (see Material and methods). Figure 4 illustrates both the spatial aspect of the currents along a typical internodal cell and the manner in which these currents responded to a 3-min dark treatment. These data were obtained by scanning the cell until the vibrating probe was in the position(s) indicated in Fig. 4B. The scan was then stopped and the dark-light response recorded; the numbers 1–7 indicate both the position on the cell surface and the sequence in which we made the measurements. From these experiments we found that the $HCO_3^-$-transport regions, along the cell, responded with very similar time courses to a dark pulse; however, the $OH^-$-transport regions responded in a more complex manner. Lucas (1975b) has previously reported on the hierarchical nature of the alkaline bands ($OH^-$-transport regions), and the dark-induced deactivation, followed by the light-mediated reactivation of the

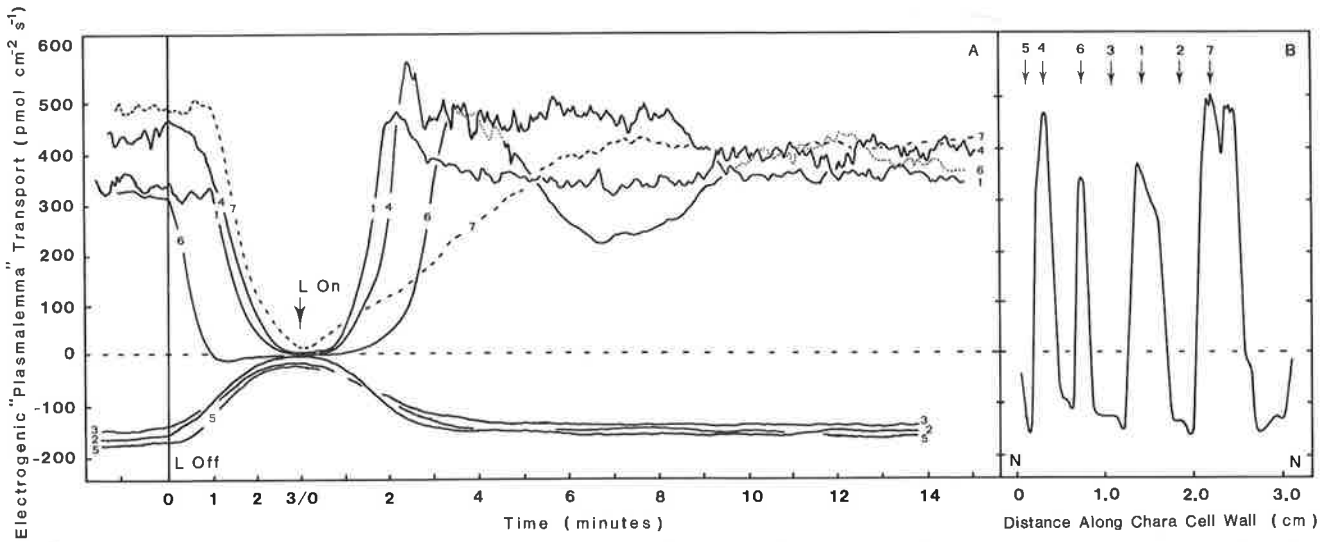


**Fig. 4A, B.** Extracellular vibrating probe measurements on the light-dependent currents that develop near the *Chara* cell wall as a result of electrogenic plasmalemma transport. After a 2-h equilibration period (CPW/B, 20 W m$^{-2}$ and 25° C) the current pattern was mapped along the entire cell length (**B**). The vibrating electrode was then located at various centers of $HCO_3^-$ and $OH^-$ transport, and the extracellular current responses to short dark pulses were recorded. The actual location, along the cell surface, at which the traces of **A** were recorded are shown in **B**. The numbering sequence represents the chronological order in which the sites were investigated. (Measurements were made using a 10-μm-diameter platinum-black electrode positioned 50 μm from the cell surface and a vibrating at 328 Hz over a distance of 12.5 μm)

$OH^-$-transport regions is a further illustration of this complex phenomenon. In general, after a dark period of 3–6 min, $OH^-$ transport was reduced to values very close to zero. On the other hand, some regions of $HCO_3^-$ transport still exhibited activity after equivalent dark periods (see Fig. 4A, traces 3 and 5). Although the differential in the rate of deactivation of $HCO_3^-$ and $OH^-$ transport was small, it may account for the observed hyperpolarization of the membrane potential (Figs. 1, 3 and 5). In any event, the time courses of the two phenomena were very similar.

The $HCO_3^-$ and $OH^-$ systems also exhibited a differential in transport reactivation following illumination. A rather smooth, apparently synchronized reactivation occurred at the various $HCO_3^-$-transporting regions along the cell, with a steady-state condition being established within 4 min of re-illumination. As with its deactivation, the $OH^-$-transport system demonstrated a complex interplay between the reactivation of the various regions along the cell that engage in transport of this ion. Approximately 1 min after reillumination, the primary and sub-primary $OH^-$-transporting regions on the cell surface (terminology formulated by Lucas 1975b) began to increase their rates of transport in an exponential manner (Fig. 4A, traces 1 and 4). These regions (bands) always exhibited an "overshoot" in their activation and, by the third minute, their rates had begun to decline back towards the values observed prior to the dark treatment. A period of approx. 10 min was required before the $OH^-$-transport sites re-established their steady-state rates.

### *Is the dark-induced hyperpolarization the result of $HCO_3^-$ transport?*

In the absence of exogenous $HCO_3^-$ we found that the membrane potential was less responsive to dark treatments (Fig. 3). Although in these experiments the pH value was kept close to 8, the medium was devoid of buffering capacity. This aspect was investigated by substituting $Na_2HPO_4$ for the 1.0 mM $NaHCO_3$ present in CPW/B. Figure 5 shows that when this was done the membrane potential depolarized, but the extent of the depolarization was less than that obtained when cells were given a $HCO_3^-$- and buffer-free treatment. Returning the exogenous $HCO_3^-$ caused the expected hyperpolarization of the membrane potential.

We were surprised to find that in $Na_2HPO_4$-buffered, $HCO_3^-$-free medium the membrane potential hyperpolarized in a manner similar to that observed in the presence of $HCO_3^-$. After a brief dark pulse (3–6 min), the membrane potential showed the same transient hyperpolarization and rapid depolarization as recorded in CPW/B media

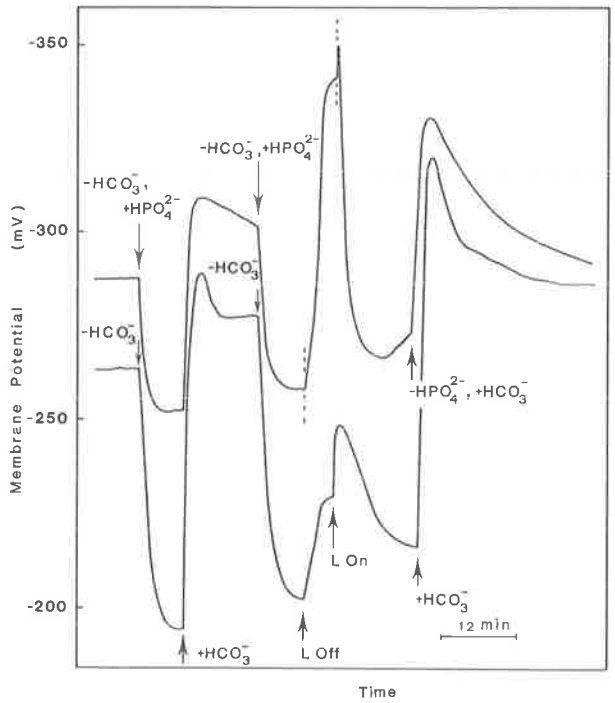


**Fig. 5.** Response of the *Chara* membrane potential to an experimental medium that was buffered by 1.0 mM $Na_2HPO_4$, but "free" of exogenous $HCO_3^-$. Experimental details for the lower trace are as in Figs. 1 and 3, and this trace represents the control for the $Na_2HPO_4$-buffered experiment (upper trace) which was then conducted on the same cell. The composition of the experimental solutions used was as follows (mM): $+HCO_3^-$, 1.0 NaCl, 0.2 KCl, 0.2 $CaSO_4$, 1.0 $NaHCO_3$ (pH 8); $-HCO_3^-$, 2.0 NaCl, 0.2 KCl, 0.2 $CaSO_4$, plus NaOH to adjust to pH 8; $-HCO_3^- + HPO_4^{2-}$, 1.0 NaCl, 0.2 KCl, 0.2 $CaSO_4$, 1.0 $Na_2HPO_4$ (pH 8)

(compare Figs. 1 and 5). Results of this nature indicated that the dark-light elicited transients in the membrane potential were influenced by the presence of exogenous $HCO_3^-$, but that under certain conditions $HCO_3^-$ was not essential. Since resubstituting $HCO_3^-$ (1 mM) for $Na_2HPO_4$ always resulted in a rapid, but transient hyperpolarization of the membrane potential (Fig. 5), we concluded that the electrogenic transport process that caused this response must have some preference, in a kinetic sense, for $HCO_3^-$ over $HPO_4^{2-}$.

*Extracellular current profiles in the presence of $Na_2HPO_4$*

Vibrating-probe experiments were next performed in which we investigated the current profiles that were developed along the *Chara* internode in the presence of either $HCO_3^-$ or $HPO_4^{2-}$. In these experiments the bathing medium of the vibrating probe chamber had to be changed several times to ensure removal of $HCO_3^-$ from the system. No effect of solution manipulation, per se, was found on the steady-state transport profiles, when CPW/B was changed repeatedly. Profiles measured 1–4 min after the solution had been replaced were identical to the profiles mapped after 15 and 30 min (data not shown).

The results presented in Fig. 6A were obtained by pretreating a *Chara* internodal cell for 2 h, in CPW/B (20 $Wm^{-2}$), prior to performing a vibrating-probe scan of the cell surface. The control scan was repeated three times to verify the stability (and reproducibility) of the system. The CPW/B was then replaced by CPW + 1.0 mM $Na_2HPO_4$ (pH 8.05) and the *Chara* cell was then scanned, repeatedly, for 30 min. Although there were minor differences between the transport profiles observed in the $HCO_3^-$- and $HPO_4^{2-}$-containing solutions, the results presented in Fig. 6A indicate, unequivocally, that once photosynthetic $HCO_3^-$ assimilation was established, the extracellular current profiles could be maintained in the absence of exogenous $HCO_3^-$. At this point it should be stressed that although the CPW + 1.0 mM $Na_2HPO_4$ solution was initially $HCO_3^-$-free, this condition could not be maintained because the solution at (pH 8) was in direct contact with the atmosphere. Entering atmospheric $CO_2$ would be converted to $HCO_3^-$, and the buffering effect of the $Na_2HPO_4$ would minimize the reduction in solution pH.

The same problems were amplified when we conducted vibrating-probe experiments on cells exposed to $HCO_3^-$- and buffer-free media. In this situation we changed the experimental solution every 10–12 min. Figure 6B illustrates that upon removal of both exogenous $HCO_3^-$ and the buffering capacity of the medium, the extracellular currents were significantly reduced. Internodal cells could be maintained in this stalled state or, upon return of $HCO_3^-$, control profiles could again be established. (The details of the manner in which the substrate-stalled cells returned to the control state will be the subject of a later communication.)

A series of experiments was also performed to investigate the effect of dark treatments, of various durations, on the extracellular transport profiles of cells bathed in CPW + 1.0 mM $Na_2HPO_4$. As described previously (see Fig. 6A), a 2-h pretreatment was used to ensure that the internodal cells were in the steady-state phase of $HCO_3^-$ assimilation before the $HCO_3^-$ was exchanged for $HPO_4^{2-}$. Dark pulses of 3–6 min duration caused a small reduction in the magnitude of the extracellular currents (data not shown). Longer dark treatments of 15, 30 and 60 min caused a significant reduction

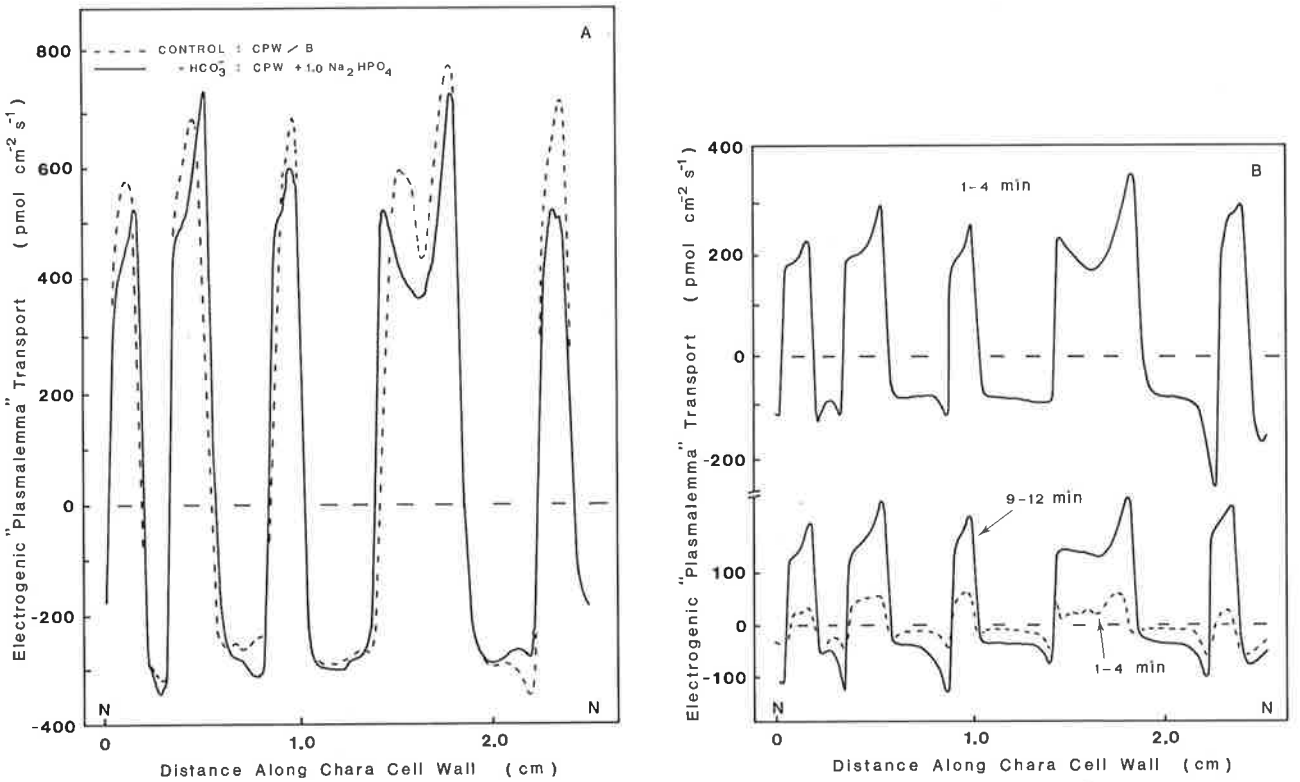


**Fig. 6A, B.** Effect of $Na_2HPO_4$ buffered and $HCO_3^-$-free media on the extracellular currents of *Chara* internodal cells. **A** Control scans (CPW/B) were conducted after a 2-h equilibration period, and a representative profile is presented. The experimental medium was then changed to an $HCO_3^-$-free, but $Na_2HPO_4^-$ buffered solution (1 mM, pH 8.05); four volume replacements were used in order to remove the preexisting exogenous $HCO_3^-$. The extracellular current profile in the $Na_2HPO_4$-buffered medium was investigated for 1 h and a typical profile is illustrated, after which time the cell was returned to CPW/B and the profile followed for a further 1 h. **B** The cell was then transferred to $HCO_3^-$- and buffer-free media (adjusted to pH 8) and the current profiles mapped almost continuously. The upper trace represents the profile established during the first 4 min of exposure to this $HCO_3^-$-free and unbuffered solution. The lower trace (solid line) illustrates how the extracellular currents had declined by the 9–12 min period. Because the medium in the vibrating probe chamber had contact with the air, the solution was changed every 10–12 min to reduce the influence of atmospheric $CO_2$. The lower trace (broken line) was obtained after the first such solution replacement, and this profile then remained until the internodal cell was again exposed to CPW/B

in the transport profile (Fig. 7). Thus, once the membrane transport system responsible for $HCO_3^-$ assimilation becomes dark-adapted (see Lucas 1975b), inorganic $HPO_4^{2-}$ cannot substitute for $HCO_3^-$ to cause its complete reactivation. Indeed, the reduced activity illustrated in Fig. 7 may be related to $HCO_3^-$ derived from atmospheric $CO_2$.

### *Influence of exogenous $HCO_3^-$ as a buffer*

In a recent, related series of experiments we found that the extracellular current patterns were not changed by including 5 mM $Na_2HPO_4$ or 5 mM 4-(2-hydroxyethyl)-1-piperazineethanesulfonic acid (Hepes) buffer in the CPW/B medium (Lucas W.J., Keifer, D.W., Sanders, D., unpublished results). However, since in these cells $HCO_3^-$ assimilation is saturated at or near 1.0 mM exogenous $HCO_3^-$, we investigated the effect of higher $HCO_3^-$ concentrations on the electrical response of the plasmalemma. Application of a 5 mM $HCO_3^-$ solution to cells that had been treated in $HCO_3^-$-free media elicited a hyperpolarizing response which was similar to that obtained when the cell was given a dark-pulse (Fig. 8A).

A comparison of the hyperpolarizing responses elicited by either darkness or a tenfold reduction in irradiance showed that they were almost identical (Fig. 8B). Thus, the dark-induced hyperpolarization of the membrane potential was not dependent upon darkness, per se, but on an abrupt reduction in the rate of photosynthesis.

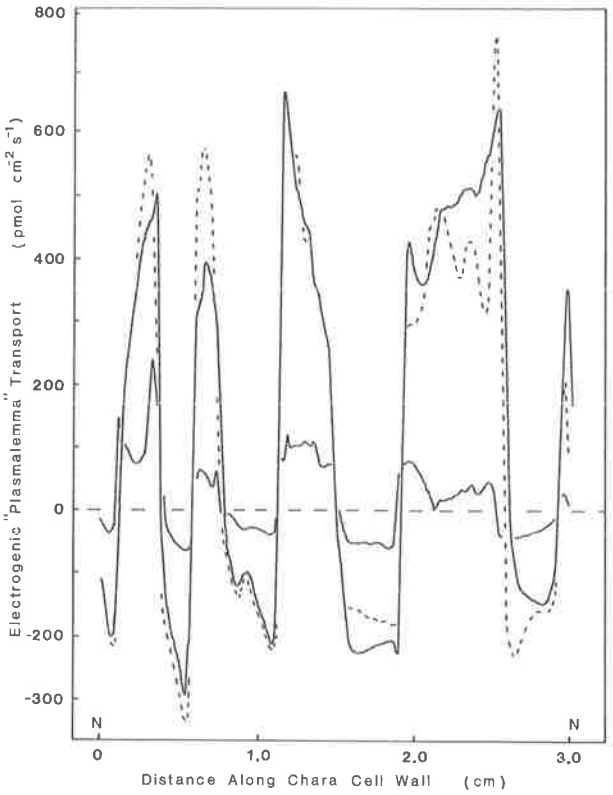


**Fig. 7.** Inability of $Na_2HPO_4$ to substitute for exogenous $HCO_3^-$ following dark-adaptation of the *Chara* $HCO_3^-$-assimilating system. After control (CPW/B, broken line) and $Na_2HPO_4$ ($HCO_3^-$-free) profiles were measured, the cell was given dark pulses of various duration while the cell was exposed to $HCO_3^-$-free conditions. As in Fig. 6B, the medium was changed every 10–12 min. After 30–60 min of treatment, the current profile (following 1 h re-illumination) was measured (current profile greatly reduced)

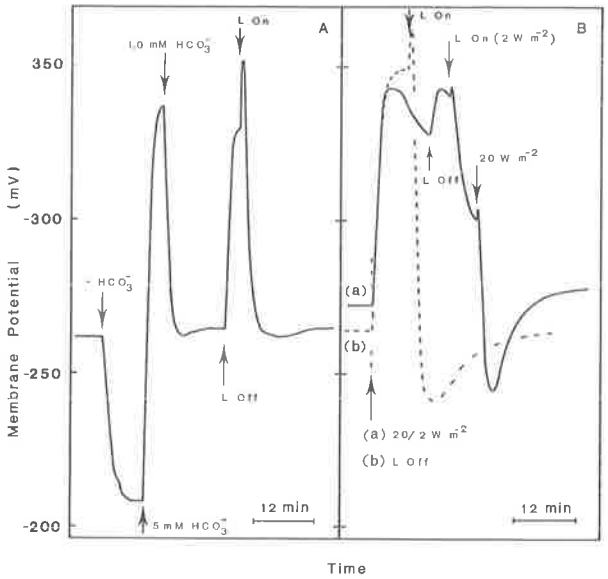


**Fig. 8 A, B.** Response of the membrane potential to super-saturating levels of exogenous $HCO_3^-$ and sub-optimal light intensity. **A** *Chara* internodal cell pretreated as in Figs. 1 and 3. Following a brief $HCO_3^-$-free treatment, the cell was exposed to CPW containing 5 mM $NaHCO_3$. The elicited membrane-potential response was then compared with the response obtained when the cell was given a brief dark pulse in CPW/B. **B** Comparison between a dark-pulse-induced hyperpolarization of the membrane potential and the effect of reducing the light intensity from a level that saturates photosynthesis in this system (20 W m$^{-2}$), to a sub-optimal value (2 W m$^{-2}$)

## Discussion

### *Relationship between exogenous $HCO_3^-$, membrane potential and extracellular currents*

The present results clearly indicate that under optimal physiological conditions (i.e. healthy cells preadapted to $HCO_3^-$ assimilation) the membrane potential of *C. corallina* is sensitive to the level of exogenous $HCO_3^-$. This confirms the early report by Hope (1965), but is inconsistent with the data of Spanswick (1970). However, it should be stressed that Hope used *C. corallina*, while Spanswick did his experiments on *Nitella translucens*. There is no reason why species from these two genera should behave in an identical manner, especially when one considers the difference in culture conditions employed. The wide-ranging responses reported in the literature concerning the sensitivity of the characean membrane potential to light-dark treatments can, in all probability, be explained on the basis of cellular conditions (age, storage after cutting, culture conditions, etc.) and slight perturbation due to electrode insertion through the plasmalemma and tonoplast (compare Figs. 1 and 2).

Analysis of the electrical and vibrating probe experiments conducted on *Chara* internodal cells (Figs. 1, 3, 4) indicates an excellent level of correlation between the light- and dark-induced changes in extracellular currents and membrane potential. The presence of a plasmalemma-bound electrogenic $HCO_3^-$ influx system, in association with an electrogenic $OH^-$-efflux process, could explain the observed electrical responses. However, the electrogenic $HCO_3^-$-transport model is not supported by the data presented in Fig. 5. In the presence of $HPO_4^{2-}$ (as an external buffer) and the absence of $HCO_3^-$, the membrane potential still hyperpolarized when cells were given a brief dark pulse. Certainly we could take the standpoint that the $HPO_4^{2-}$ buffer solution (pH 8.0) was slightly contaminated with $HCO_3^-$, and that this level of substrate was sufficient to give the necessary negatively charged flux imbalance, during deactivation, to

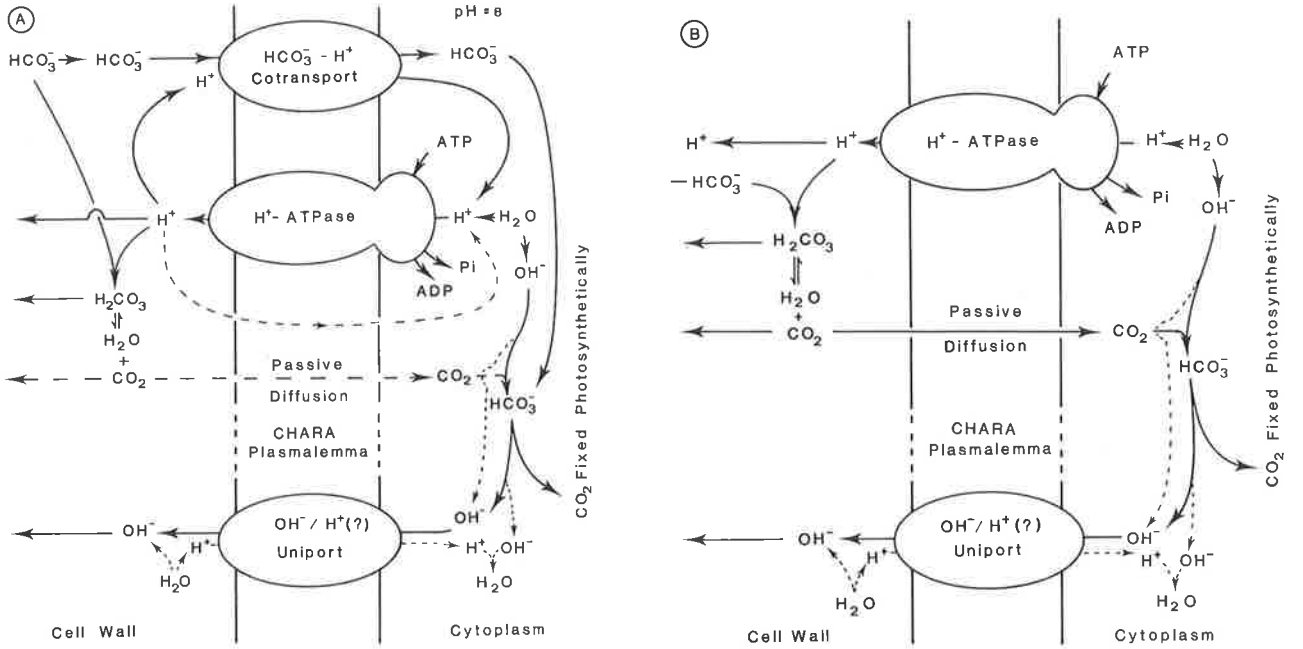


**Fig. 9A, B.** Schematic representation of the plasmalemma-bound transport complexes that may enable internodal cells of *Chara corallina* to acquire exogenous $HCO_3^-$ for photosynthetic fixation. **A** The $HCO_3^- - H^+$ Cotransport Mechanism: An electrogenic $H^+$-translocating ATPase provides the thermodynamic driving force to energize an electrically neutral $HCO_3^- - H^+$ cotransport system. The combination of the $H^+$-translocating ATPase and the nearby $HCO_3^- - H^+$ cotransport system would form an $H^+$-current loop. Photosynthetic assimilation of $CO_2$ would cause $HCO_3^-$ to dissociate to provide further $CO_2$ and thereby generate alkalinity ($OH^-$) within the cytoplasm. This alkalinity would be removed either by an efflux of $OH^-$ or influx of $H^+$ (represented in broken lines) via an electrogenic uniport system. Passive movement of $CO_2$ could also occur by either of two processes. First, conversion of $HCO_3^-$ to $H_2CO_3$, and its subsequent dissociation at the outer surface of the plasmalemma, could provide a supply of $CO_2$ which would diffuse down its gradients of concentration (i.e. into the cell and the surrounding bathing medium). Second, the $HCO_3^- - H^+$ cotransport system may raise the $HCO_3^-$ concentration within the cytoplasm such that $CO_2$ would diffuse from the cytoplasm to the bathing medium. **B** $CO_2$-diffusion: Differs from A only insofar as there is no $HCO_3^- - H^+$ cotransport mechanism

produce the observed membrane hyperpolarization. But this line of reasoning cannot explain the extracellular current-scan data presented in Figs, 6 and 7. Hence, the hyperpolarizing response does not appear to be explicable on the basis of a primary, electrogenic $HCO_3^-$-influx process. These findings give experimental support to the theoretical models developed by Ferrier (1980) and Walker et al. (1980).

### *Extracellular currents in the absence of exogenous $HCO_3^-$*

The experimental finding that the extracellular currents in the $HCO_3^-$-transporting region of the cell membrane can be maintained in the absence of exogenous $HCO_3^-$ (Figs. 6A, 7), is exciting, and of paramount importance in terms of our development of a more accurate model of this complex transport process. This finding indicates that the loop between $HCO_3^-$ assimilation and $OH^-$ efflux can be opened. In Fig. 9 we have illustrated two possible plasma-membrane transport associations that can explain all of our experimental data; in essence, Fig. 9A is the $H^+ - HCO_3^-$ cotransport system proposed by Walker et al. (i.e. their model IIa), and Fig. 9B is their $H_2CO_3 - CO_2$ model.

Our present experimental evidence is equivocal in terms of offering support for either $H^+ - HCO_3^-$ cotransport or extracellular $CO_2$ production (which diffuses into the cytoplasm where it is converted to $HCO_3^-$). We will therefore interpret our results in terms of Fig. 9A, with the clear understanding that the same arguments could equally well be applied to Fig. 9B. Under normal $HCO_3^-$-assimilating conditions, the $H^+$-translocating ATPase of the *Chara* plasmalemma provides a supply of protons to the outer surface of this membrane. (Whether this ATPase is the same as the one which is thought to drive $Cl^-$ transport into these cells remains to be elucidated.) These protons are used to drive the $HCO_3^-$-$H^+$ cotransport sys-

tem; the re-entering protons are again cycled through the ATPase, thereby forming an $H^+$ current loop. Some of the protons will also react with $HCO_3^-$ to produce $H_2CO_3$, which will dissociate to provide $CO_2$. The $CO_2$, so produced, will diffuse both into the cytoplasm and the bathing medium. Because the cytoplasmic pH is close to 8 (Walker and Smith 1975), the entering $CO_2$ will be converted to $HCO_3^-$. Photosynthetic $CO_2$ fixation produces $OH^-$ by causing $HCO_3^-$ to dissociate and the resulting alkalinity is removed from the cell through the $OH^-$-transporting regions of the plasmalemma.

Application of an abrupt dark treatment stalls the photosynthetic light reactions and, as a consequence, $OH^-$ production is quickly reduced (1 to 3 min). However, under the conditions used in our experiments, photosynthesis was maximal and thus the level of $HCO_3^-$ in the cytoplasm may have been lowered. Consequently, the $H^+$-ATPase and $HCO_3^-$-$H^+$ cotransport system may not be so rapidly inactivated. If this were the case, it would provide an explanation for the observed rapid hyperpolarization of the membrane potential when cells were given a brief dark treatment.

Our explanation of the $HPO_4^{2-}$ experiments would be as follows. Substituting $HPO_4^{2-}$ for $HCO_3^-$ provided an apoplastic buffer that could penetrate to the plasmalemma, be converted to $H_2PO_4^-$ (pKa 7.2) and then diffuse back into the bathing medium where it would dissociate to $HPO_4^{2-}$. Thus, the $HPO_4^{2-}$ provided an $H^+$-shuttle as well as an extracellular ionic flux that was electrogenic in nature. The $HPO_4^{2-}$ also prevented the pH at the outer plasma-membrane surface from dropping, and so the ATPase continued to pump $H^+$. In this way, the production of $OH^-$, via $HCO_3^-$ assimilation, was eliminated and the $OH^-$ ions could only be supplied as a direct result of the $H^+$-translocating ATPase. It would appear that it is possible to open the $H^+$ circuit.

The results presented in Fig. 7 indicate that the controls on the entire membrane system must be quite complex. After a 1-h dark treatment in $HPO_4^{2-}$ buffer ($HCO_3^-$-free) the extracellular currents did not return to the pre-dark-adapted levels. This indicates that the rate of $H^+$ translocation through the ATPase may be regulated by the exogenous and-or cytoplasmic level(s) of $HCO_3^-$. Evidence in support of this idea is provided by the results presented in Fig. 8A, where it was demonstrated that application of 5 mM $HCO_3^-$ caused the membrane potential to hyperpolarize rather dramatically. Under stagnant solution conditions, photosynthetic assimilation of exogenous $HCO_3^-$ saturates at approx. 1.0–1.5 mM $HCO_3^-$ (Lucas 1975a). In the rapid flow system used for electrophysiological experiments, the influence of unstirred layers would be reduced, and hence assimilation would saturate at even lower levels of $HCO_3^-$. In consequence, returning a super-saturating level of $HCO_3^-$ to an operating, but stalled system, appeared to elicit enhanced transport activity from the $H^+$ – ATPase.

### *Question of $HCO_3^-$ versus $CO_2$ movement across the* Chara *plasmalemma*

The above discussion could equally well have been applied to the transport model presented in Fig. 9B. The question is, then, do we have any other evidence which allows us to separate these two models? Lucas and Dainty (1977) showed that $Ca^{2+}$-free conditions resulted in a gradual reduction in the $HCO_3^-$ assimilating capacity of *Chara* internodal cells. It was quite clear from this work that the removal of $Ca^{2+}$ had its effect on the $HCO_3^-$ transport processes rather than on the $OH^-$ efflux system. According to Walker et al. (1980), removal of $Ca^{2+}$ inhibits the $H^+$-translocating ATPase, and thus $HCO_3^-$ assimilation would be affected, whether $HCO_3^- - H^+$ or $CO_2$ was moving across the membrane. However, recent results from our laboratory do not support the interference that under $Ca^{2+}$-free conditions the electrogenic $H^+$-ATPase is inhibited (Keifer and Lucas 1982). Membrane potentials of $-260$ to $-280$ mV were maintained under prolonged (5–7 h) $Ca^{2+}$-free treatment (see Fig. 3 of Keifer and Lucas 1982). Under equivalent conditions, $HCO_3^-$ assimilation would have been inhibited by approx. 50% (Lucas 1976b). Keifer and Lucas (1982) also showed that even when the membrane potential did depolarize, the electrogenic $H^+$-ATPase was still operating; the depolarization was the consequence of a short-circuiting effect of opened $K^+$ channels. Collectively, these results tend to favor the existence of a $HCO_3^- - H^+$ cotransport system that has a divalent cationic ($Ca^{2+}$, $Mg^{2+}$, $Sr^{2+}$) requirement.

Exposure of the characean plasmalemma to $K^+$ levels above about 3 mM causes the potential to depolarize (Spanswick 1972; Lucas et al. 1978; Keifer and Lucas 1982). Under these conditions, $HCO_3^-$ assimilation is also affected. Walker et al. (1980) suggest that "the effect of raising the concentration of $K^+$ in the medium is to produce a transition to the depolarized state in which, it is reasonable to postulate, the pump does not run". However, the result is not a complete inhibition

of assimilation, but rather an effect on the shape of the substrate curve (see Fig. 1 of Lucas et al. 1978). In addition, we have now shown that a 10 mM $K^+$ treatment opens the $K^+$ channels, but that the $H^+$-ATPase continues to operate (Keifer and Lucas 1982). Finally, we need to return to the earlier $Ca^{2+}$-free experiments, in which Lucas and Dainty (1977) found that $Mn^{2+}$ could not substitute for $Ca^{2+}$ to reinstate the cellular ability to acquire exogenous $HCO_3^-$. In the present context, this is a very important finding because $Mn^{2+}$ could reverse the effect of a 10 mM $K^+$ treatment, both with respect to $HCO_3^-$ assimilation *and* membrane potential restoration, provided the cells were depolarized in 0.2 mM $Ca^{2+}$ (Lucas et al. 1978). This provides further strong experimental evidence for the existence of a divalent cation-binding site on the outer plasma-membrane surface that is not closely associated with the $H^+$-ATPase, but which can influence the cells ability to utilize exogenous $HCO_3^-$. The simplest interpretation is that this binding site is associated with a $HCO_3^- - H^+$ co-transport system in *C. corallina*. Experiments are presently being conducted to further investigate this hypothesis.

### *Two $H^+$-translocating ATPases or variable transport stoichiometry?*

The thermodynamics of the plasma-membrane $H^+$-translocating ATPase of characean cells have been discussed by various workers (see Spanswick 1972; Walker and Smith 1975). Walker and Smith (1975) showed that, based on the operation of a $2H^+$-translocating ATPase (i.e. $2H^+$ per ATP hydrolysed) the maximum membrane potential that could be established in *Chara* was −268 mV (pH 8). (To derive these maximum values, the assumption was made that the ATPase was at equilibrium.) During the present study we routinely measured membrane potentials in the vicinity of −350 mV when either the cell was given a dark pulse, or $HCO_3^-$ was returned to the medium. The most negative potential actually measured to date was −373 mV, and it should be stressed that these measurements give vacuolar to outside values, thus the value across the plasmalemma would be approx. −383 to −393 mV. Hence, the $H^+$-translocating ATPase that operates under conditions of exogenous $HCO_3^-$ assimilation must be a $1H^+$ per ATP hydrolysed. This system is far from thermodynamic equilibrium (theoretical value approx. −560 mV; see Walker and Smith 1975) and must be rate-controlled by other parameters.

The question now to be answered is whether the plasma membrane of *C. corallina* has a single ATPase that can change (switch) its $H^+$ translocating stoichiometry under different physiological conditions, or whether there are at least two different ATPases having $2H^+$: 1 ATP and $1H^+$:1 ATP transport stoichiometries.

### *Membrane conductance*

In the present work no attempt was made to measure changes in membrane conductance. The decision not to make these measurements was based on the desire to inflict as minor a perturbation on the membrane system as possible, and the problem surrounding the measurement and interpretation of this parameter. At present we know that the extracellular currents along the cell wall can vary quite dramatically, both as a function of position and time. If these currents truly reflect plasmalemma transport, then the conductance along the membrane will not be uniform, but rather, it will vary as a function of the specific processes operating at any point along the cell. In further studies we will need to measure membrane conductance using a region-specific method, rather than by applying general cable theory.

This work was supported by National Science Foundation grant PCM 81-17721. We wish to dedicate this work to Dr. E.B. Romanoff on the occasion of his retirement from the National Science Foundation.

## References

Andrianov, V.K., Kurella, G.A., Litvin, F.F. (1968) Influence of light on the electrical activity of *Nitella* cells. In: Transport and distribution of matter in cells of higher plants, pp. 187–196, Mothes, K., Müller, E., Nelles, A., Neumann, D., eds. Akademie, Berlin

Andrianov, V.K., Bulychev, A.A., Kurella, G.A. (1970) Connection between photo-induced changes in the resting potential and the presence of the chloroplasts in *Nitella* cells. Biophysics **15**, 199–200

Ferrier, J.M. (1980) Apparent bicarbonate uptake and possible plasmalemma proton efflux in *Chara corallina*. Plant Physiol. **66**, 1198–1199

Ferrier, J.M., Lucas, W.J. (1979) Plasmalemma transport of $OH^-$ in *Chara corallina*. II. Further analysis of the diffusion system associated with $OH^-$ efflux. J. Exp. Bot. **30**, 705–718

Higinbotham, N. (1973) Electropotentials of plant cells. Ann. Rev. Plant Physiol. **24**, 25–46

Hope, A.B. (1965) Ionic relations of cells of *Chara australis*. X. Effects of bicarbonate ions on electrical properties. Aust. J. Biol. Sci. **18**, 789–801

Jaffe, L.F., Nuccitelli, R. (1974) An ultrasensitive vibrating probe for measuring extracellular currents. J. Cell Biol. **63**, 614–628

Keifer, D.W., Lucas, W.J. (1982) Potassium channels in *Chara corallina:* control and interaction with the electrogenic $H^+$ pump. Plant Physiol. **69**, 781–788

Lucas, W.J. (1975a) Photosynthetic fixation of $^{14}$carbon by internodal cells of *Chara corallina*. J. Exp. Bot. **26**, 331–346

Lucas, W.J. (1975b) The influence of light intensity on the activation and operation of the hydroxyl efflux system of *Chara corallina*. J. Exp. Bot. **26**, 347–360

Lucas, W.J. (1976a) Plasmalemma transport of $HCO_3^-$ and $OH^-$ in *Chara corallina*: non-antiporter systems. J. Exp. Bot. **27**, 19–31

Lucas, W.J. (1976b) The influence of $Ca^{2+}$ and $K^+$ on $H^{14}CO_3^-$ influx in internodal cells of *Chara corallina*. J. Exp. Bot. **27**, 32–42

Lucas, W.J., Dainty, J. (1977) $HCO_3^-$ influx across the plasmalemma of *Chara corallina*: divalent cation requirement. Plant Physiol. **60**, 862–867

Lucas, W.J., Nuccitelli, R. (1980) $HCO_3^-$ and $OH^-$ transport across the plasmalemma of *Chara*: spatial resolution obtained using extracellular vibrating probe. Planta **150**, 120–131

Lucas, W.J., Smith, F.A. (1973) The formation of alkaline and acid regions at the surface of *Chara corallina* cells. J. Exp. Bot. **24**, 1–14

Lucas, W.J., Spanswick, R.M., Dainty, J. (1978) $HCO_3^-$ influx across the plasmalemma of *Chara corallina*: physiological and biophysical influence of 10 mM $K^+$. Plant Physiol. **61**, 487–493

Nagai, R., Tazawa, M. (1962) Changes in resting potential and ion absorption induced by light in a single cell. Plant Cell Physiol. **3**, 323 339

Nishizaki, Y. (1968) Light-induced changes of bioelectric potentials in *Chara*. Plant Cell Physiol. **9**, 377–387

Richards, J.L., Hope, A.B. (1974) The role of protons in determining membrane electrical characteristics in *Chara corallina*. J. Membr. Biol. **16**, 121–144

Saito, K., Senda, M. (1973a) The light-dependent effect of external pH on the membrane potential of *Nitella*. Plant Cell Physiol. **14**, 147–156

Saito, K., Senda, M. (1973b) The effect of external pH on the membrane potential of *Nitella* and its linkage to metabolism. Plant Cell Physiol. **14**, 1045–1052

Spanswick, R.M. (1970) The effects of bicarbonate and external pH on the membrane potential and resistance of *Nitella translucens*. J. Membr. Biol. **2**, 59 70

Spanswick, R.M. (1972) Evidence for an electrogenic ion pump in *Nitella translucens*. I. The effects of pH, $K^+$, $Na^+$, light and temperature on the membrane potential and resistance. Biochim. Biophys. Acta **288**, 73–89

Volkov, G.A. (1973) Bioelectrical response of the *Nitella flexilis* cell to illumination: a new possible state of plasmalemma in a plant cell. Biochim. Biophys. Acta **314**, 83–92

Volkov, G.A., Petrushenko, V.V. (1969) Studies of the resting potential of a single cell of the alga *Nitella flexilis*. IV. The correlation between the cell response to light and the photosynthesis process. Tsitologiya **11**, 1007–1013

Walker, N.A. (1962) Effect of light on the plasmalemma of *Chara* cells. Ann. Rept. Div. Plant. Industry, CSIRO, p. 80

Walker, N.A. (1980) The transport systems of Charophyte and Chlorophyte giant algae and their integration into modes of behaviour. In: Plant membrane transport: current conceptual issues, pp. 287–300, Spanswick, R.M., Lucas, W.J., Dainty, J., eds. Elsevier North-Holland, Amsterdam New York Oxford

Walker, N.A., Smith, F.A. (1975) Intracellular pH in *Chara corallina* measured by DMO distribution. Plant Sci. Lett. **4**, 125–132

Walker, N.A., Smith, F.A. (1977) Circulating electric currents between acid and alkaline zones associated with $HCO_3^-$ assimilation in *Chara*. J. Exp. Bot. **28**, 1190–1206

Walker, N.A., Smith, F.A., Cathers, I.R. (1980) Bicarbonate assimilation by fresh-water charophytes and higher plants: I. Membrane transport of bicarbonate ions is not proven. J. Membr. Biol. **57**, 51–58

Received 2 June; accepted 17 June 1982

*Ann. Rev. Plant Physiol. 1983. 34:71–104*
*Copyright © 1983 by Annual Reviews Inc. All rights reserved*

# PHOTOSYNTHETIC ASSIMILATION OF EXOGENOUS $HCO_3^-$ BY AQUATIC PLANTS

*William J. Lucas*

Department of Botany, University of California, Davis, California 95616

## CONTENTS

INTRODUCTION ..... 71
STRATEGIES USED FOR $HCO_3^-$ ACQUISITION ..... 72
*Polarized Transport Across Aquatic Leaves* ..... 73
*$HCO_3^-/OH^-$ Antiport?* ..... 75
*Electrogenic Transport of $HCO_3^-$ and $OH^-$* ..... 76
A NEW HYPOTHESIS/CONTROVERSY FOR CARBON ACQUISITION ..... 83
*Aquatic Angiosperms* ..... 83
*Characean Cells* ..... 84
*Further Tests of the $CO_2$-Production Hypothesis* ..... 86
$HCO_3^-H^+$ COTRANSPORT OR $HCO_3^-$ UNIPORT? ..... 89
*Electrophysiological Evidence* ..... 90
*Transport Stoichiometry of the $H^+$-ATPase?* ..... 92
ELECTROGENIC $OH^-$ TRANSPORT ..... 92
*Spatial and Temporal Regulation* ..... 93
*Active or Passive Process?* ..... 96
BENEFITS OF BICARBONATE TRANSPORT ..... 98
CONCLUDING REMARKS ..... 98

## INTRODUCTION

The topic of photosynthetic assimilation of exogenous $HCO_3^-$ by aquatic plants (algae and aquatic angiosperms) has been, and still is, controversial. In the present review, our attention will be confined to freshwater species. Much of the early work in this field focused on the influence of inorganic carbon availability on organismal growth (85–88). These studies revealed that many aquatic species can grow very effectively under culture conditions where the available inorganic carbon exists almost entirely as $HCO_3^-$. This led to the conclusion that these species could utilize the exoge-



0066-4294/83/0601-0071-$02.00

nous inorganic carbon of both $CO_2$ and $HCO_3^-$ for photosynthesis. Prior reviews have dealt with the problems of interpreting such experiments (99, 120).

Raven (99) developed a more rigorous form of analysis to ascertain whether a species could utilize exogenous $HCO_3^-$. This approach consisted of comparing photosynthetic carbon fixation at high and low external pH values. If the species is *unable* to utilize $HCO_3^-$ (i.e. transport it into the cell), fixation is predicted to vary in proportion to the external $H^+$ concentration, because this parameter determines the concentration of $CO_2$ within the medium (sealed systems are generally used). An excellent example of such a response is seen with high $CO_2$-grown cells of *Scenedesmus obliquus* (25). However, following adaptation to normal air levels of $CO_2$, *S. obliquus* can utilize exogenous $HCO_3^-$. Numerous species appear to be capable of higher levels of fixation, at alkaline pH, than would be predicted by the presumed concentration of $CO_2$ present under these conditions (10, 14, 23, 29, 51, 59, 80, 110). These data have been rather widely accepted as demonstrating that certain aquatic plants have the ability to transport $HCO_3^-$ from the external medium into the cytoplasm.

A further difficulty in interpreting results pertaining to $HCO_3^-$ assimilation is caused by the fact that $HCO_3^-$ may (can) act as a reservoir for extracellular $CO_2$ (see Figure 1). In recent years, several investigators have addressed this issue by developing theoretical analyses of the rate(s) at which $CO_2$ could be produced from $HCO_3^-$. Lucas (60) was able to show that the maximum rate at which $CO_2$ could be supplied, from the equilibrium reactions involving $HCO_3^-$, was insufficient to account for $^{14}C$-fixation in *Chara corallina* as measured in alkaline media. Similar analyses have indicated that *Microcystis aeruginosa, Ceratium hirudinella* (121), *Chlamydomonas reinhardtii* (55), *Egeria densa* (14), *Scenedesmus obliquus* (96) and *Coccochloris peniocystis* (80) can assimilate exogenous inorganic carbon at rates in excess of those possible by $HCO_3^-$ to $CO_2$ conversion (cf 34, 35, 95). Thus, there is a growing body of evidence which supports the contention that numerous aquatic species can utilize both $CO_2$ and $HCO_3^-$ for photosynthesis. It should be stressed, however, that $CO_2$ is the chemical species utilized by the ribulose bisphosphate carboxylase (15).

## STRATEGIES USED FOR $HCO_3^-$ ACQUISITION

In a morphological sense, the photosynthetic tissues which utilize exogenous $HCO_3^-$ are extremely variable, ranging from single cells (6, 10, 24, 28, 50, 79) to the submerged leaves of aquatic angiosperms (14, 38, 94, 119). Within this range of cellular complexity, it is possible to elucidate certain basic strategies that appear to have been adopted to enable the tissue to acquire exogenous $HCO_3^-$. At this point it is important to stress that follow-

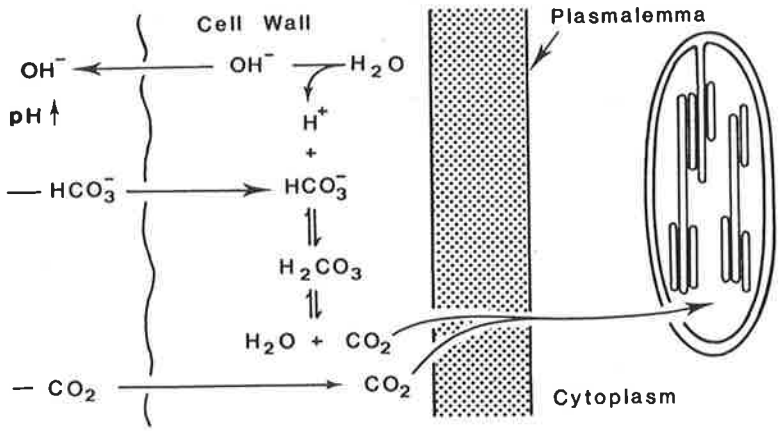


*Figure 1* Diffusion of inorganic carbon ($CO_2$ and $HCO_3^-$) from the medium up to the plasmalemma. Conversion of $HCO_3^-$ to $CO_2$ at the outer surface of the membrane enhances the flux into the cell.

ing $HCO_3^-$ transport into the cell, $CO_2$ is fixed via the photosynthetic reactions and, as a result of this removal of $CO_2$, alkalinity ($OH^-$) is produced in near stoichiometric quantities. To control the cytoplasmic pH during this assimilation process, this alkalinity must be disposed of via $OH^-$ efflux to the bathing medium. It is the operation and spatial location of the $HCO_3^-$ and $OH^-$ transport systems that will now be examined.

## *Polarized Transport Across Aquatic Leaves*

Arens, an early pioneer in the field of $HCO_3^-$ assimilation, was one of the first to develop the concept of a spatial separation of physiological events associated with $HCO_3^-$ assimilation. Arens talked of the submerged leaves of *Potamogeton* and *Elodea* as being polarized (3, 4), in that only the lower surface appeared to be able to transport exogenous $HCO_3^-$ while the upper surface became very alkaline, presumably due to $OH^-$ excretion. Extensive research on the species *Potamogeton lucens* by Steemann Nielsen (119; see also 120), Helder & co-workers (38–42), and others (75, 92–94) has confirmed Aren's hypothesis. Similar examples of spatially separate (polar) $HCO_3^-$ and $OH^-$ transporting systems have been demonstrated in *Elodea* (5, 102) and *Myriophyllum* (119). However, in a recent report, Helder et al (41) showed that the upper leaf surface of *P. lucens* could be "induced" to take up $HCO_3^-$. Whether this involved true induction of transport capacity at the upper surface or apoplastic transfer of $HCO_3^-$ to the lower leaf surface remains to be elucidated.

During assimilation of $HCO_3^-$, polar cation transport also occurs across the leaves of *P. lucens,* i.e. cations are transported from the lower to the upper leaf surface (3, 39, 40, 119). This phenemenon is light-mediated and

exhibits a specific requirement for the presence of $HCO_3^-$ at the lower leaf surface (39). It has also been found that during this process an electrical potential gradient of approximately 15 to 20 mV is established across the leaf (38, 40, 42, 94). A potential of this magnitude could only be developed if at least one of the transported species is moved via an active electrogenic mechanism. (Electrogenic transport involves the movement of unbalanced charge.) This polar transport system is illustrated schematically in Figure 2A.

Numerous hypotheses have been presented regarding the nature and interrelationship(s) between $HCO_3^-$, $OH^-$, and polar cation fluxes. Serious

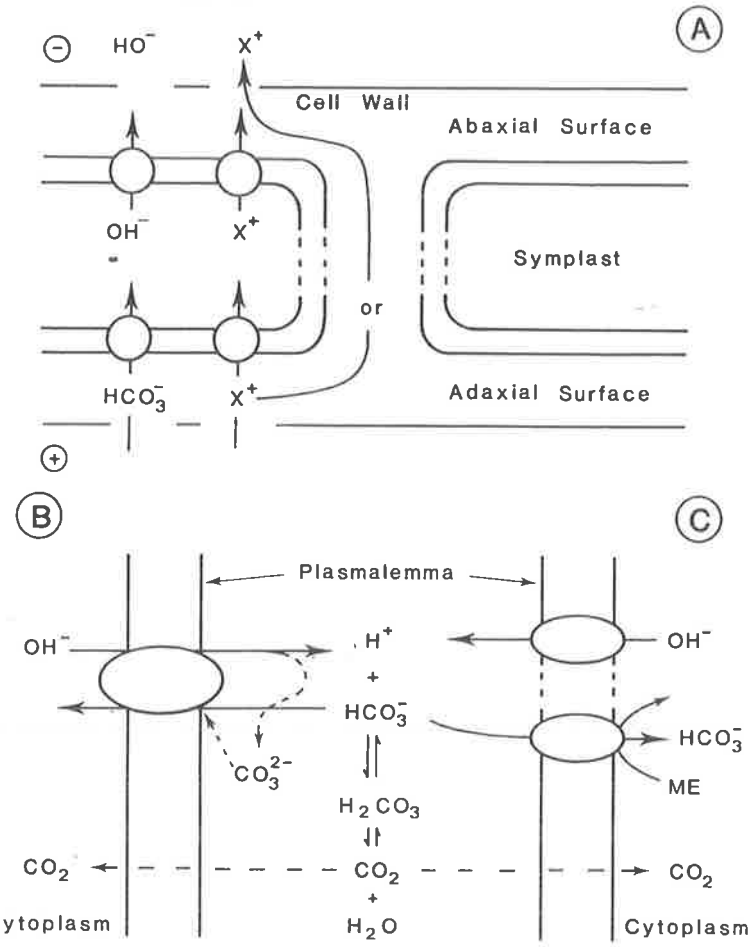


*Figure 2* Possible mechanisms by which exogenous $HCO_3^-$ may be transported into the cytoplasm. A: Polar transport situation observed in *Potamogeton* and *Elodea;* $X^+$ represents cations that are transported either through the apoplast or symplast. B: Mitchell-type antiporter; extracellular production of $CO_3^{2-}$ may inhibit $HCO_3^-$ transport via competitive binding to the $HCO_3^-$-binding site. C: Electrogenic $HCO_3^-$ and $OH^-$ transport systems that are spatially separated along the plasmalemma; ME represents the investment of metabolic energy.

disagreement exists, however, between the various proposals. Steemann Nielsen (120) proposed that $HCO_3^-$ entry was passive, with the active process being the excretion of $OH^-$ from the upper leaf surface. The polar cation fluxes were thought to be passive (4, 119). Lowenhaupt (57, 58), and later Helder & Boerma (39), proposed that it was the polar cation transport process that was active. Helder (38) later suggested that the polar fluxes may result from either a cation pump or via some form of coupling to the transport of $HCO_3^-$ and $OH^-$ ions.

Since an electric potential is established across the leaf during $HCO_3^-$ assimilation, this potential could explain in part the polar cation flux. A completely apoplastic pathway for the cations could be tested using $HCO_3^-$ solutions containing large cations that could not be transported across the plasmalemma. Further developments concerning the energetics of $HCO_3^-$ and $OH^-$ transport will be dealt with in later sections.

### *$HCO_3^-/OH^-$ Antiport?*

In contrast to the polar transport situation found in *Potamogeton, Elodea,* and *Myriophyllum,* it has been suggested that in *Chara* (74) and *Scenedesmus* (24, 28) the $HCO_3^-$ and $OH^-$ ions may move on a "Mitchell-type" antiporter. In this situation, $HCO_3^-$ and $OH^-$ transport would occur at the same location on the plasmalemma and involve a single transport entity (see Figure 2B). Provided $HCO_3^-$ influx and $OH^-$ efflux were balanced, such a transport system would be electrically neutral, thereby eliminating any effect of the membrane potential on either flux. If this were the case, photosynthesis could develop a sufficient $HCO_3^-$ concentration gradient to facilitate the influx of $HCO_3^-$ and efflux of $OH^-$.

During photosynthesis, when exogenous $HCO_3^-$ is utilized, alternating acid and alkaline bands (zones) develop along the internodal cells of *Chara corallina* (74, 111). Diffusion analysis of the alkaline bands indicated an equivalence between $OH^-$ efflux from these regions and the rate of $H^{14}CO_3^-$ fixation by the internodal cells (59), a result consistent with the antiporter hypothesis. However, Lucas (62) later invalidated this hypothesis by showing that when the solution bathing a particular alkaline band (region of $OH^-$ efflux) was $HCO_3^-$-free, $OH^-$ efflux continued. This result demonstrated categorically that the $OH^-$ efflux process could function in the absence of exogenous $HCO_3^-$ at the actual efflux site. Thus, in *Chara,* the transport of $HCO_3^-$ and $OH^-$ appears to be independent insofar as the two processes can be spatially separated (62, 72). This conclusion has been verified by results obtained using a range of techniques (21, 65, 69, 72, 128), and will be discussed further in a later section.

High $CO_2$-grown (2%) cells of *Scenedesmus obliquus* cannot utilize exogenous $HCO_3^-$; however, after 2–3 hr adaptation to 0.03% $CO_2$, cells appear

to be able to utilize the exogenous inorganic carbon in proportion to the levels of $CO_2$ and $HCO_3^-$ present in the bathing medium (26, 28). Findenegg has shown that during this period of adaptation, cells develop carbonic anhydrase activity (23, 25), and it has been suggested that this enzyme may act as a permease for $HCO_3^-$ at the plasmalemma of *Scenedesmus* (24). However, carbonic anhydrase is essential for $HCO_3^-$ assimilation at low pH (5.7–7.0) but not at pH 9–9.5 (26–28). This finding is inconsistent with a direct role of carbonic anhydrase in the transport of $HCO_3^-$ across the plasmalemma of *Scenedesmus* (27).

Nonetheless, in assaying carbonic anhydrase activity, which was identified as being within the cytoplasm of *S. obliquus,* Findenegg obtained evidence consistent with there being extremely large plasmalemma fluxes (200 nmol $cm^{-2}s^{-1}$) of $HCO_3^-$ and $OH^-$ (28). These high rates were obtained at 3°C and were independent of metabolism. *Scenedesmus* may, therefore, possess a $HCO_3^-/OH^-$ antiport system which is not metabolically driven at low pH, but becomes energy dependent under high pH conditions (28). This hypothesis should be tested by utilizing microprobe techniques, as has been done for *Chara* (71, 72, 128). If the transport of $HCO_3^-$ is electrogenic, it may be possible to detect local electric fields within the region where this ion is being transported. Although these cells are small (diameter approximately 10–15 $\mu$m), it should be possible to use extracellular voltage electrodes (tip diameter 0.5 $\mu$m) and/or the vibrating probe technique (46, 72) to confirm or refute the above hypothesis.

## *Electrogenic Transport of $HCO_3^-$ and $OH^-$*

RELATIONSHIP BETWEEN LIGHT, MEMBRANE POTENTIAL, AND $HCO_3^-$ TRANSPORT The cell membrane potential of many green plants appears to be sensitive to light [for a general review see (43)]. This phenomenon has been studied in only a limited number of aquatic plant species, with most research having been done on the giant cells of the Characeae. Much of the early work is quite confusing, the light-response being obviously complex, with more than one transport system (both active and passive) influencing the direction in which the potential changes upon cell illumination. In some cases, a light-induced hyperpolarization (transient or stable) of the membrane potential was observed (82, 83, 123), while other workers reported a depolarization (2). However, in *Chara* and *Nitella,* it has been shown that the electrical changes produced by light have an action spectrum similar to that of photosynthesis (123, 125). Andrianov and co-workers (1) also found a close correlation between the shape of the light-induced change in membrane potential and the induction of photosynthesis. The involvement of photosynthesis has also been shown by the sensitivity of the

plasmalemma response to photosynthetic inhibitors (103, 104, 123, 124). Excellent confirmation of the coupling between changes in membrane potential and photosynthesis was obtained by Andrianov et al (1). These workers were able to demonstrate that when the rhizoids of *Nitella flexilis* were free of chlorophyll, no light-induced changes occurred in the membrane potential. However, as the rhizoids developed chloroplasts, the membrane potential became sensitive to light.

The nature of the coupling between the chloroplasts and the plasmalemma is still speculative. An electrogenic role for $HCO_3^-$ (see Figure 2C) was first proposed by Hope (45), who showed that the membrane potential of *Chara* became hyperpolarized upon the addition of $HCO_3^-$, and this response was light-sensitive, as was the decrease in the membrane resistance, which occurred upon addition of $HCO_3^-$. Spanswick (114) refuted this role of $HCO_3^-$; he claimed that the electrical potential change was independent of the chemical nature of the buffer employed, i.e. $HCO_3^-$ produced a hyperpolarization via its buffering action. However, the conditions used by Spanswick were not $HCO_3^-$-free and, therefore, his results did not eliminate a specific role for$HCO_3^-$. Reports of the influence of $HCO_3^-$ on the membrane potential have been presented by other workers (16, 65, 83, 103, 123).

Saito & Senda (103), using *Nitella flexilis* and *Nitella axilliformis,* found that addition of $NaHCO_3$ to the medium caused a small hyperpolarization (approximately 20 mV) when added in the dark, and illumination then caused a further stable hyperpolarization of about 40 mV. This response is similar to that reported by Hope (45). However, Nishizaki's (83) results with *Chara* were quite different from those obtained by Hope. He found that illumination in the presence of 0.2 mM $NaHCO_3$ caused a slight hyperpolarization, followed by a rapid depolarization; in the dark, the potential again hyperpolarized. This result is quite similar to that obtained on submerged leaves of *Potamogeton schweinfurthii* (16), and is also consistent with the recent results obtained by Lucas (65).

Much of the early work relied almost entirely on electrophysiological measurements to elucidate the influence of $HCO_3^-$ on the electrical properties of the plasmalemma. As illustrated above, many of these results were either inconsistent or contradictory, and this is probably attributable to the complexity of the transport processes which reside in the plant plasma membrane (see 76, 91, 117 for reviews of this literature). In addition, the ability of a particular species to assimilate $HCO_3^-$ can vary quite dramatically as a function of season (47, 60), age (81, 88, 89), and storage after tissue excision (W. J. Lucas, unpublished results), and this variation most surely contributed toward impeding progress in this area. Thus, until the mid-1970s, the hypothesis that $HCO_3^-$ was being transported across the plasmalemma of photosynthesizing (aquatic) cells in an electrogenic manner received only equivocal support.

EXTRACELLULAR pH AND ELECTRICAL MEASUREMENTS Following the demonstration that *Chara corallina* could assimilate exogenous $HCO_3^-$ at quite high rates (60) via transport processes that were not coupled in the form of an antiporter (62), considerable attention was focused on this system to further elucidate its characteristics. In studies where both the pH and the external electric potential were measured at the cell surface, an excellent correlation was observed between alkaline band pH centers and the negative electric potential maxima (21, 128). In the regions between the alkaline bands, where $HCO_3^-$ transport was thought to occur, positive external electric potentials were observed. These results clearly demonstrated that electric currents circulate between the alkaline and "acid" zones of the *Chara* internodal cell. In general, these currents were dependent upon cell illumination and the presence, within the bathing medium, of $HCO_3^-$. These findings offered strong experimental support for the hypothesis that $HCO_3^-$ transport (in this system) was electrogenic and that the alkaline bands were being formed by electrogenic efflux of $OH^-$ (or $H^+$ influx).

Using their theoretical numerical analysis model, Ferrier & Lucas (21) were able to use their experimental values of pH and electric potential to compute the magnitude of the putative $HCO_3^-$ fluxes. As a result of this analysis, they suggested that along the length of a particular *Chara* cell, the actual $HCO_3^-$ fluxes may vary quite significantly. This prediction was later confirmed by Lucas & Nuccitelli (72) when they used the Jaffe-Nuccitelli vibrating probe (46) to further investigate these extracellular currents. This technique, in which a small (10 $\mu$m) platinum spherical probe is vibrated over a known distance (usually 10 to 20 $\mu$m) at a particular frequency (300 to 500Hz), enables an accurate measurement of local voltage gradients that are established near the cell wall. The local voltage gradient can be converted to local current density or ionic flux (both in the direction of vibration). Using this technique, these authors found that extracellular bands of positive inward current ($OH^-$ efflux) 1–3 mm wide were separated by wider bands of outward current ($HCO_3^-$ influx) along the length of the cell. The measured peaks of inward current ranged from 20 to 60 $\mu A\ cm^{-2}$, which would correspond to an ionic flux across the cell surface of 270–800 pmol $cm^{-2}s^{-1}$. The peaks of outward current ($HCO_3^-$ influx) ranged from 10 to 30 $\mu A\ cm^-$, or 140–400 pmol $cm^{-2}s^{-1}$. The inward current bands matched the regions of surface alkalinity very well. The $HCO_3^-$–associated current declined when the exogenous $HCO_3^-$ level was reduced; a commensurate readjustment in the strength and pattern of the $OH^-$ current was always observed under these conditions.

The greatly improved spatial and temporal resolution provided by this vibrating probe technique enabled Lucas & Nuccitelli (72) to detect details of transport activity within single $HCO_3^-$ or $OH^-$ bands. Bicarbonate-

associated currents were much more stable than those measured in the alkaline bands, and the $HCO_3^-$ currents were surprisingly close to those predicted by Ferrier & Lucas (21). A further point of importance was that no strong correlation was found between the absolute pH values along the interalkaline band regions and the $HCO_3^-$ current strengths measured in these locations. This was true even for regions where the surface pH was depressed below the background value, a phenomenon which was often used as representing a site of strong $HCO_3^-$ transport (72). We will return to this point in a later section.

It will be of considerable interest to see what details this technique can elucidate when it is applied to the polar $HCO_3^-$ transport situation of *Potamogeton* and *Elodea* leaves.

$HCO_3^-$ TRANSPORT IN UNICELLULAR SYSTEMS A considerable amount of elegant work has been published during the past few years which shows that many unicellular algal species and certain blue-green algae (Cyanobacteria) can assimilate exogenous $HCO_3^-$ (7, 8, 10, 23, 48, 50, 79). General aspects of nutrient transport (including $HCO_3^-$) in the microalgae have been reviewed recently (100). Some of the most outstanding work has been done on the Cyanobacteria, where, although their smallness of size precludes the attainment of spatial details possible with the Characeae, the simplified cytoplasmic phase (no cellular compartmentation) has enabled the measurement of $HCO_3^-$ accumulation ratios, internal pH, and membrane potentials under $HCO_3^-$-assimilating conditions (50, 51).

Badger et al (7) used the silicone oil centrifugation technique to separate low $CO_2$-grown cells of *Anabaena variabilis* and *Chlamydomonas reinhardtii* rapidly from a $H^{14}CO_3^-$-incubation medium. This separation could be achieved in 2 sec or less (7). Analysis of the acid-labile and -stable components within these two cell types revealed that inorganic carbon concentrations within the cytoplasm were as much as 1000 times that of the incubation medium; i.e. the values were far in excess of those possible by passive equilibration across the plasmalemma. Similar results have now been obtained on a variety of microalgal species, including *Coccochloris peniocystis* (79, 80), *Chlorella emersonii* (10), *Dunaliella salina* (130), and *Spirulina platensis* (48). Using $^{14}$C-dimethyloxazolidinedione, Badger et al (7, 8) were able to measure the cytoplasmic pH, and this parameter enabled a calculation of the extent to which internal $CO_2$ was raised above the level of the bathing medium. In *C. reinhardtii,* low $CO_2$-grown cells were able to concentrate $CO_2$ up to 40-fold in relation to the external medium (8). Similar or somewhat smaller $CO_2$ concentration ratios have been reported for *Anabaena* (50, 78), *Coccochloris* (79, 80), *Chlorella* (10), and *Dunaliella*

(130). In the above-mentioned studies, various metabolic inhibitors were shown to reduce severely the accumulation of inorganic carbon.

The ability of certain low $CO_2$-grown microalgae to concentrate $CO_2$ within the cell has been generally attributed to an increased capacity by these cells to utilize exogenous $HCO_3^-$. This conclusion is consistent with the analysis of photosynthesis with respect to the theoretical rate of $CO_2$ production from $HCO_3^-$. Talling (121) showed that both *Microcystis aeruginosa* and *Ceratium hirudinella* have photosynthetic rates, at pH values of 10 or greater, that are in excess of the rates that could be supported by the spontaneous dehydration of $HCO_3^-$ within the medium. Similarly, Miller & Colman (80) have shown, in an elegant study on *Coccochloris peniocystis,* that the rate of $CO_2$ fixation at alkaline pH is as much as 50-fold the maximum rate of $CO_2$ production from $HCO_3^-$ dehydration.

The observed accumulation ratios in the microalgae could be caused by facilitated diffusion of $HCO_3^-$ across the plasmalemma. However, as pointed out by Kaplan et al (50), this would require that the membrane potential be positive; the value for *Anabaena* would have to be approximately +150 mV (inside positive). In a recent study (51) it was shown that during $HCO_3^-$ assimilation, the membrane potential of *Anabaena* was negative, having a value of approximately –100 mV. Negative membrane potentials are a common feature of plant cells (43), and thus it is probably safe to conclude that in many microalgae there is an active $HCO_3^-$ transport system.

The relationship between $O_2$ evolution and $OH^-$ efflux has been studied in *Anabaena* (49) and *Coccochloris* (80). In both cases a close equivalance was observed between $O_2$ evolution and $OH^-$ efflux. In the *Anabaena* system, however, Kaplan (49) found that addition of $NaHCO_3$ to cells which had previously depleted the inorganic carbon in the medium resulted in an almost immediate evolution of $O_2$, whereas a lag of approximately 20 to 40 sec was observed before $OH^-$ efflux reached its steady state. This temporal separation in $O_2$ and $OH^-$ efflux suggests that the transport of $HCO_3^-$ and $OH^-$ may not be coupled in a compulsory manner (49). Thus, $HCO_3^-$ transport in this system may also be electrogenic in nature. Since no inner membranes enclose the photosynthetic system in the Cyanobacteria, the location of such an electrogenic $HCO_3^-$ transport system would be at the plasmalemma. Beardall & Raven (10) have argued, albeit not all that convincingly, that in *Chlorella* and *Chlamydomonas* the site of $HCO_3^-$ transport may be the chloroplast envelope rather than the plasmalemma.

In a recent study, Kaplan and co-workers (51) investigated the influence of $HCO_3^-$ transport on the membrane potential of *A. variabilis.* To do this they used the lipid-soluble cation tetraphenyl phosphonium ($TPP^+$). They found that when 1.0 mM $NaHCO_3$ (pH 8.0) was added to cells bathed in a $CO_2$-depleted medium, the membrane potential immediately hyperpola-

rized, with a maximum value being established after 90 to 120 sec. Approximately the same time was required for similarly treated cells of *A. variabilis* to reach a steady state with respect to accumulation of inorganic carbon (50). An important point to note concerning this work was that the membrane potential hyperpolarized quite rapidly and then remained in this state for up to 20 min. The correlation between inorganic carbon uptake and the development of a stable hyperpolarized membrane potential is certainly consistent with the involvement (operation) of an electrogenic $HCO_3^-$ transport system.

The question of monovalent cation coupling to the movement of $HCO_3^-$ has also been examined in *A. variabilis* (51). Addition of $NaHCO_3$ to $CO_2$-depleted cells resulted in an immediate uptake of $K^+$ from the bathing medium which ceased after 2 min, and, shortly thereafter, $K^+$ began to be released from the cells. Approximately 9 min after the addition of $NaHCO_3$ there was no further net flux of $K^+$, but $O_2$ evolution continued in a linear manner. These results could be explicable in terms of a symport of $K^+$ with $HCO_3^-$, followed by a coupled release of $K^+$ and $OH^-$. If this were the case, photosynthesis in *A. variabilis* should be influenced by the presence or absence of $K^+$ in the bathing medium. Kaplan and co-workers (50) have demonstrated that only under low levels of exogenous $HCO_3^-$ is photosynthesis limited by the transport capacity of the $HCO_3^-$ accumulating system. Thus, the critical $K^+$ concentration experiments were performed under low levels of exogenous $HCO_3^-$. From these experiments it was clear that photosynthetic assimilation of exogenous $HCO_3^-$ was independent of external $K^+$ concentration (51). A similar independence on the external monovalent cation concentration was observed in *Chara* (64). In his studies on *Chara,* Lucas used choline bicarbonate so that there would be no transportable cation available. It would have been of interest to see the effect of choline bicarbonate on the *Anabaena* system.

In view of the observed insensitivity to $K^+$ availability, and since the membrane potential appeared to hyperpolarize and remain in this state, it is intriguing to speculate as to the reasons for the observed $K^+$ fluxes. Uptake of $K^+$, upon addition of $NaHCO_3$, could be due to the passive movement of this ion down its electrochemical potential gradient. However, $K^+$ efflux cannot be explained on this basis, since the membrane potential did not decline and thus a net $K^+$ loss from the cells should not have occurred. It would appear that events occurring across the plasmalemma are more complex than can be resolved using a single probe like $TPP^+$.

Any model proposed to explain $HCO_3^-$ uptake and accumulation in the microalgae must take account of the experimental findings outlined above. Beardall & Raven (10) favor the operation of a primary, electrogenic $HCO_3^-$ transport system; however, they speculated that this pump may be

present in the chloroplast envelope of eukaryotes. Miller & Colman (80) discuss the possibility that electroneutrality could be maintained by an equivalent uptake of $H^+$ with $HCO_3^-$, the protons coming from the dissociation of $H_2O$; the resultant $OH^-$ ions would cause an alkalinization of the medium. They rejected this model on the basis that photosynthesis in *Coccochloris* was as rapid at pH 10 as it was at pH 8; i.e. a 100-fold reduction in $H^+$ concentration had no observable effect on $HCO_3^-$ transport. Since the cytoplasmic pH in the Cyanobacteria appears to be between 7 and 8 (6, 49), Miller and Colman rationalized that electroneutrality could more reasonably be maintained via the operation of an $OH^-$ efflux system. (The concentration of $OH^-$ ions available to the cytoplasmic face of the plasmalemma would be approximately 1.0 $\mu$M compared with a $H^+$ concentration of 0.1 nM at the outer surface.) Based on the available evidence, these workers could not distinguish between a tightly coupled obligate exchange of $OH^-$ for $HCO_3^-$ or separate electrogenic transport components.

A $HCO_3^-/OH^-$ antiport system could not explain the hyperpolarizing response observed in *Anabaena* (51). Such a transport system is also at variance with the lag between onset of $O_2$ evolution and $OH^-$ efflux that was observed when $HCO_3^-$ was introduced to $CO_2$-depleted cells of *Anabaena* (49). Similarly, unless such an antiporter had a variable stoichiometry, it could not account for the change in the $O_2$ to $OH^-$ ratio that Kaplan (49) observed when cells of *Anabaena* were exposed to pH values above 9.5.

Two possibilities remain: first, a $HCO_3^-$-$H^+$ cotransport system driven by the $H^+$ electrochemical potential gradient, which could be maintained by a plasmalemma-bound $H^+$-translocating ATPase; and second, a primary, active, electrogenic $HCO_3^-$ transport system. Beardall & Raven (10) regarded $HCO_3^-$-$H^+$ transport as unlikely because, on energetic grounds, 2 $H^+$ per $HCO_3^-$ may be required to account for movement against the measured inorganic carbon accumulation ratios. Such a transport system would tend to depolarize the membrane potential upon addition of $NaHCO_3$. However, as pointed out by Kaplan et al (51), a $HCO_3^-$-$2H^+$ cotransport system could be operative and still be consistent with the observed membrane potential hyperpolarization, provided the $H^+$ current through the putative ATPase is sufficiently stimulated by the addition of $HCO_3^-$. In other words, the $H^+$-translocating ATPase would have to be stimulated, by addition of $NaHCO_3$, in advance of the activation of the putative $HCO_3^-$-$2H^+$ transport system. In both models the efflux of $OH^-$ could occur via a passive $OH^-$ uniport system (51). (This aspect of $HCO_3^-$ assimilation will be discussed in a separate section on $OH^-$ transport.) Experimental evidence presently available does not permit us to select between these two possibilities, but some workers favor the electrogenic $HCO_3^-$ transport hypothesis (51).

## A NEW HYPOTHESIS/CONTROVERSY FOR CARBON ACQUISITION

Following the pioneering work of Kitasato on the involvement of an electrogenic $H^+$ pump in the plasmalemma of *Nitella* (52), innumerable plant systems have been examined with respect to the operation of such an efflux system. The existence of this $H^+$ pump is now widely accepted (91, 117).

### *Aquatic Angiosperms*

The operation of this pump recently has become entwined in a novel way with photosynthetic utilization of exogenous $HCO_3^-$. Prins and co-workers (92–94) have suggested that the cells of the lower surface of *Elodea* and *Potamogeton* leaves contain $H^+$ pumps that act to acidify the wall. It has been claimed that the cells of the lower epidermis are transfer cells and that the wall ingrowths act to retain the protons within the wall. As a consequence of $H^+$ pump activity, $HCO_3^-$ would be converted to $CO_2$. It is suggested that the increased plasmalemma surface area of the transfer cells allows for an efficient "capture" of the $CO_2$ molecules so produced. This hypothesis suggests that a $HCO_3^-$ transport system does not exist; carbon transfer occurs via diffusion of $CO_2$. A model of this system is presented in Figure 3. According to this model, $H^+$ efflux at the lower epidermis is balanced by $OH^-$ efflux (or $H^+$ influx) across the plasmalemma of the upper epidermal cells. These fluxes would form a current of negative charges, moving from the lower to the upper leaf surface, which would create an electric potential difference across the leaf (see earlier section and Figure 2A). The current would have to be balanced by a polar cation flux ($Na^+$ or $K^+$) and the cations could move either apoplastically or through the symplasm.

Using miniature pH electrodes placed on both leaf surfaces, Prins and co-workers (92–94) have shown that upon illumination, the lower surface of both *Elodea canadensis* and *Potamogeton lucens* (previously established to be $HCO_3^-$ assimilators) became acidified. Acidification could have been due to $H^+$ escape from the transfer cell wall labyrinth or, alternatively, $HCO_3^-$ transport into the cytoplasm could have raised the internal level of $CO_2$ above that of the bathing medium. In this situation, back diffusion of $CO_2$ would cause an acidification near the leaf surface.

This second possibility was investigated by examining the pH changes at the leaf surface in the "absence" of exogenous inorganic carbon (94). The results were most intriguing. Following illumination, the pH value at both surfaces remained rather stationary until, after approximately 20 min, the upper surface began a gradual alkalinization and the lower surface acidified. In the absence of exogenous buffer the pH at the lower surface approached values as low as pH 4.5. The changes at both surfaces were more or less in

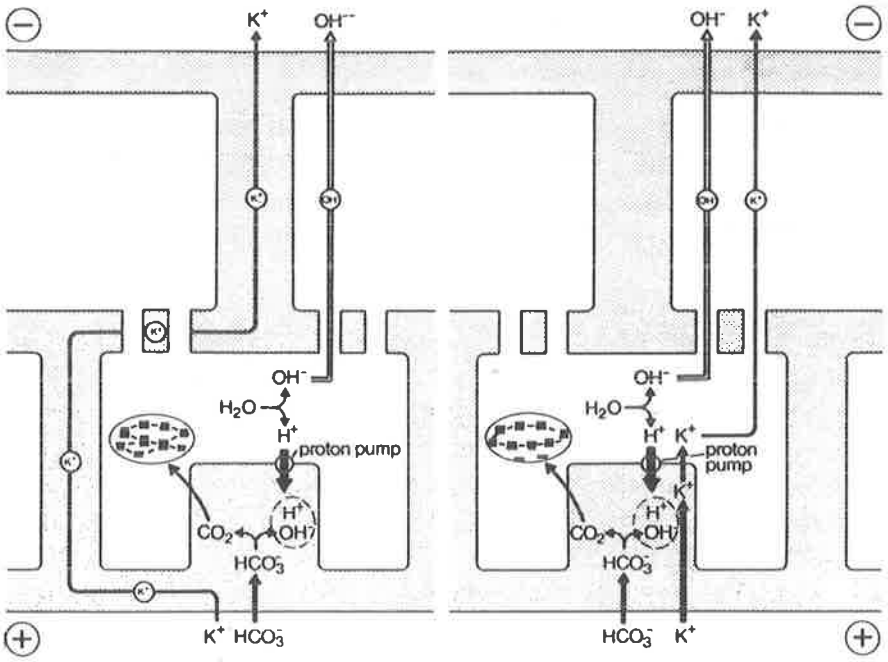


*Figure 3* Model for exogenous $HCO_3^-$ utilization through the action of a proton pump. Two possible pathways are given for $K^+$ transport: in the left half through the cell wall and in the right half via the symplast (from Ref. 94).

phase. After a further 30–40 min the pH values at both leaf surfaces returned toward the dark-adapted value, and then 2 hr later the entire cycle started again. When the leaf was kept in continuous light these oscillations in pH continued until the light was turned off (94). These data indicate that the acidification and alkalinization phenomena are coupled, but it is not possible to determine from the pH data alone whether the associated $H^+$ and $OH^-$ fluxes are stoichiometric. It would be difficult to analyze these fluxes using diffusion analysis (see 59), but the vibrating probe technique (72) may be useful to further study this system.

At present the available data from *Potamogeton* and *Elodea* are consistent with the hypothesis as outlined in Figure 3. Whether other species have also adopted this strategy remains to be shown.

## *Characean Cells*

It has long been known that *Nitella* and *Chara* develop regions of acidity and alkalinity along their internodal cells (74, 111, 118). The acid bands are easily detectable when the *Chara* cells are bathed in media low in total inorganic carbon (74). In analyzing the kinetics of $H^{14}CO_3^-$ fixation obtained on *Chara corallina,* Walker and co-workers stressed the influence that the unstirred layer near the cell wall would have on the supply of inorganic carbon to these cells (113, 126, 129). As a result of their evaluation of the

data available for Characean cells, Walker and co-workers (129) put forward an hypothesis not unlike that of Prins et al (92–94). They suggested that the unstirred layer, in conjunction with the plasmalemma elaboration made possible by the charasome (see 30, 31, 70), would permit a $H^+$ efflux system to generate $H_2CO_3$ at a sufficient rate to account for the observed $^{14}C$-fixation data (60). They stress that a specific $HCO_3^-$ transport system may not be necessary; the $H_2CO_3$ produced in the unstirred layer-cell wall-periplasmic space could diffuse across the plasmalemma, being driven by its concentration gradient.

Ferrier & Lucas (69) were also aware that during $HCO_3^-$ assimilation in *C. corallina,* the interalkaline regions appeared as sinks for $OH^-$. They suggested that these "sinks," detected using numerical analysis of diffusion profiles for $OH^-$ ($H^+$), could be caused by $OH^-$ influx, $H^+$ efflux, or $CO_2$ diffusion (leakage) from the cytoplasm following $HCO_3^-$ transport into the cell. Ferrier also raised the question of whether the action of a $H^+$ efflux pump could generate molecular $CO_2$ at a rate sufficient to explain photosynthesis in *Chara* (20). Figure 4 represents the basic details of the new

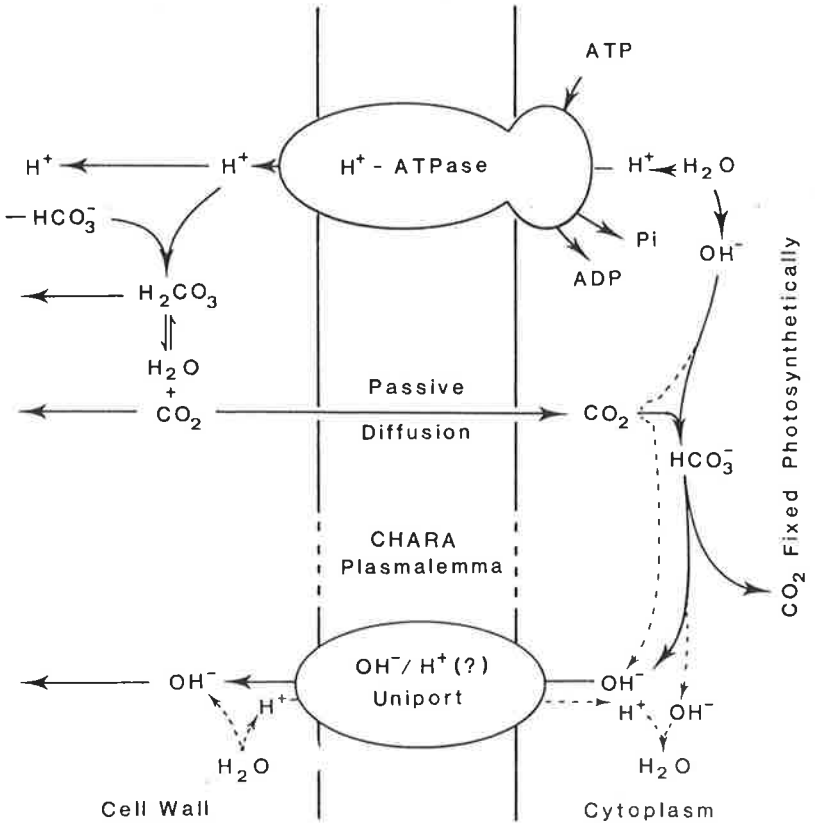


*Figure 4* Model for extracellular $CO_2$-production in *Chara* (from Ref. 62; see text for details).

hypothesis by which *Chara* may acquire inorganic carbon for photosynthesis.

The theoretical models developed to examine the $H^+$ efflux-extracellular $CO_2$ production hypothesis predict that the pH at or near the cell surface should be at least as low as pH 6.0 in order to achieve the experimentally observed rates of $^{14}C$-fixation. The conditions used in the models were those which Lucas used to achieve near maximum rates of fixation; i.e. 1.0 mM $NaHCO_3$, pH 8–9. An examination of the pH profiles obtained on *Chara* under these conditions indicates that the measured pH values in the $HCO_3^-$-acquiring regions of the cell never approach this value of pH 6. In most of the profiles published by Lucas, the pH value in the interalkaline regions was above that of the background bathing medium, but below that which would be established by diffusion of $OH^-$ along the cell from the neighboring alkaline bands (69).

Walker et al (129) explained that the discrepancy between the measured pH values and the predicted value of 6.0 might be attributed to the physical dimensions of the miniature pH electrodes used in these experiments; it was argued that the pH-sensitive area of these electrodes was as large as the unstirred layer itself. In a recent study on the *Chara* system, a comparison was made between the pH profiles obtained using miniature and recessed-tip pH microelectrodes (tip diameter approximately 0.5 $\mu$m). A dramatic difference was observed between the pH profiles measured by the two electrode systems; in the alkaline regions the profiles were quite similar, but in the $HCO_3^-$-transporting regions, only the recessed-tip pH microelectrode detected acidification of the medium at the cell surface (71).

Although the pH dropped below that of the background medium (pH 8.2), it did not approach the theoretical values generated by the models. Even as close as 2 $\mu$m from the wall the pH was generally between 7.2 and 7.6. Thus, although Walker et al (129) were correct in their assessment that the miniature pH electrode was unable to measure accurately the pH within the unstirred layer, the values obtained using the appropriate technique did not provide supporting evidence for their hypothesis.

## *Further Tests of the $CO_2$-Production Hypothesis*

The $CO_2$-production model proposed that the outward current measured in the acid regions (72) was due to (or generated by) electrogenic $H^+$ efflux. If this hypothesis were correct, one should find a correlation between the electrogenic fluxes (currents) and the level of cell surface acidification measured in these "acid" regions; similar correlations should exist from cell to cell. However, as mentioned previously, no such correlation has been observed, either with the external electric potential work (21) or with the more recent combined recessed-tip pH microelectrode-vibrating probe studies (71).

Since the charasome has been implicated in the acquisition of $HCO_3^-$ in *Chara* (126), and transfer cells may be involved in *Elodea* and *Potamogeton* (94), it is possible that these structures mask the true events that are occurring within the vicinity of the wall. The spatial distribution of charasomes along the cell has been examined with respect to the position of the alkaline and $HCO_3^-$-acquiring (acid) regions (30). Charasomes were always found in the "acid" regions, but were fewer in number or absent in the areas engaged in $OH^-$ efflux. The observed distribution is consistent with their involvement in some way with $HCO_3^-$ acquisition. However, since *Nitella flexilis* exhibited the same acid and alkaline banding pattern but did not possess the charasome structure along its plasmalemma, Franceschi & Lucas (30) concluded that the charasome must be involved in the transport of some other species, perhaps $Cl^-$ (32).

Doubt has also been cast on the involvement in $HCO_3^-$ acquisition of the transfer cell wall ingrowth in *Elodea* and *Potamogeton.* Prins et al (94) have recently reported that these "membrane foldings are not always present" in the leaves of species which are still capable of $HCO_3^-$ utilization. They suggest that the wall ingrowth may not be essential for extracellular $CO_2$ production, but may increase the efficiency of the process. Further experiments should, therefore, be conducted on species which can assimilate exogenous $HCO_3^-$ but which do not possess complex plasmalemma structures. In these species the predicted correlations between electrogenic currents and surface acidification may be found. (Experiments of this nature are presently being conducted in our laboratory.)

Walker et al (129) found that their theoretical model was relatively insensitive to the presence of the cell wall. Thus, almost all of their computations and predictions ignored the influence of the wall. It is possible that the wall may develop specific properties in response to localized membrane transport function. This view is supported by the recent report that the cell wall of *Anabaena variabilis* undergoes ultrastructural modification when cells are grown under low $CO_2$ culture conditions (78). There are other reports of changes in the cytoplasmic ultrastructure that occur during adaptation to $HCO_3^-$ utilization (54). It would seem that further studies of this nature may provide valuable insight into the mechanism of cellular utilization of exogenous $HCO_3^-$.

UNSTIRRED LAYER MANIPULATION Walker et al (129) suggested that extracellular production of $CO_2$ would be highly efficient "because the diffusion resistance of the unstirred layer retains the $CO_2$ that is produced near the cell surface, and the $H^+$ that flow out from the cell." An explicit prediction of their model is, therefore, that a reduction in the unstirred layer should cause a decline in the rate of photosynthesis. This prediction was tested by measuring $^{14}C$-fixation in *Chara* as a function of the rate of

solution flow (71). Again, contradictory results were obtained; photosynthesis was found to increase, not decrease, as the unstirred layer was reduced in thickness. Although this result appears to be incompatible with the extracellular $CO_2$-production hypothesis for *Chara,* it should be stressed that interpretation of these data is complex. Flowing the solutions past the cell surface would sweep away the $OH^-$ ions that are released across the plasmalemma within the alkaline bands. This would contain the alkaline band-associated pH increase which would otherwise occur along the cell wall. A larger membrane surface area would therefore be available to engage in $HCO_3^-$ acquisition, which may offset a reduction in efficiency due to the sweeping away of $H^+$ and $CO_2$ (71).

BUFFER EXPERIMENTS A further prediction of the extracellular $CO_2$-production hypothesis is that the addition of buffer to the bathing medium should reduce the rate of photosynthesis. The reduction would occur because the buffer would compete with $HCO_3^-$ for the transported $H^+$, thereby reducing the level of $CO_2$ available. It has been suggested that the well-documented inhibitory effect of high pH on $^{14}C$-assimilation (60, 99, 101) could be caused by $OH^-$ ions competing with $HCO_3^-/CO_3^{2-}$ for transported $H^+$ (129).

In *C. corallina,* $H^{14}CO_3^-$ assimilation is inhibited in what appears to be a competitive manner by the presence of certain amino-type buffers (63). Lucas interpreted the inhibition as being caused by the formation of carbamate, which then competed with $HCO_3^-$ at the binding site on the transport system. Walker and co-workers (129) interpreted the inhibition as resulting from a nonspecific buffer effect in which competition for $H^+$ was occurring. However, it should be stressed that other workers have reported inhibitory buffer effects (49, 94), and in at least one case there is clear evidence for competitive inhibition. Photosynthesis in *A. variabilis* was drastically reduced in the presence of 10mM 3-[cyclohexylamino]-1-propanesulfonic acid (CAPS); the $V_{max}$ was unchanged but the $K_m$ was raised by a factor of 100 (49). Since the $pK_a$ of this buffer is 10.4, and these experiments were conducted in the presence of 50 mM Hepes, pH 8.0, this effect must be explained by the chemical nature of the buffer rather than via competition for $H^+$.

In a recent study on *Chara,* the effect of artificial buffer on the pH and extracellular current profiles and $H^{14}CO_3^-$ fixation was investigated (71). In the presence of 5 mM phosphate buffer (or Hepes), the pH profiles were significantly reduced, with the acid regions being more affected than the alkaline bands. This level of buffer almost completely dissipated the radial pH gradients within the "acid" regions of the cell surface. Raising the pH value at the cell surface in this way would reduce the $CO_2$ concentration

and, according to the $CO_2$-production hypothesis, photosynthesis should therefore be dramatically reduced. Photosynthesis was reduced, but only by about 30% (71). When the extracellular currents were measured under the same conditions, they were found to be completely unaffected by the presence of the buffer. (This result will be discussed in the next section.)

Collectively, these results indicate that in *Chara* the extracellular production of $CO_2$ is unlikely to account for the ability of these cells to assimilate exogenous $HCO_3^-$.

## $HCO_3^-$-$H^+$ COTRANSPORT OR $HCO_3^-$ UNIPORT?

Plasmalemma transport of $HCO_3^-$ via either electrogenic uniport or a $HCO_3^-$-$H^+$ contransport mode could also result in acidification of the external medium near the *Chara* cell wall. These systems were modeled by Walker et al (129), and reasonable agreement has been found between their predicted radial pH profile for the $HCO_3^-$-$H^+$ cotransport model and the experimental results obtained using the recessed-tip pH microelectrode system (71). However, since there may well be insufficient resolution in the theoretical model to distinguish between these two transport modes, the observed correlation should be viewed only as offering support for the $HCO_3^-$-$H^+$ cotransport hypothesis and not as diagnostic proof.

At pH 8–9, a $HCO_3^-$ uniport system should not be influenced by the presence of exogenous buffer. The partial sensitivity to phosphate or Hepes buffer that was observed in *C. corallina* (71) is consistent, therefore, with the operation of a $HCO_3^-$-$H^+$ cotransport system in this species. Although data on the extent of inhibition were not presented, Prins et al (94) reported that photosynthesis in *E. densa* was affected by artificial buffers (phosphate, Taps, and Tris). This effect was claimed to support the hypothesis that an extracellular $CO_2$-generating mechanism operates in this species; however, it is also consistent with transport via $HCO_3^-$-$H^+$ cotransport.

If we follow this line of reasoning for the *A. variabilis* data, the apparent insensitivity to 50 mM Hepes would offer support for the hypothesis that inorganic carbon in *Anabaena* is accumulated via a primary electrogenic $HCO_3^-$ transport system. Further support for this conclusion may be obtained by applying CAPS buffer to cells which have been preincubated in $TPP^+$ (pH 8) but starved of inorganic carbon. Application of $HCO_3^-$ should cause one of two possible responses: a hyperpolarization of the membrane potential, which would be consistent with a $HCO_3^-$-$H^+$ system, or little change in the potential, which would indicate the operation of a $HCO_3^-$ uniport that has been competitively blocked by CAPS.

## *Electrophysiological Evidence*

In a recent study, the effects of light/dark and $HCO_3^-$ were reexamined on the *Chara* system (65). It was found that when an internodal cell was assimilating exogenous $HCO_3^-$ (pH 8.2), the membrane potential was extremely sensitive to changes in the level of exogenous $HCO_3^-$. Removal of $HCO_3^-$ resulted in a rapid 50 to 70 mV depolarization of the potential; returning $HCO_3^-$ to the bathing medium elicited an equivalent hyperpolarization. Since the pH of the bathing medium was constant during these experiments, the results invalidate Spanswick's (114) claim that $HCO_3^-$ does not have a direct effect on the electrical properties of the Characean plasmalemma.

Using light/dark transitions as a probe, Lucas (65) found that in the presence of exogenous $HCO_3^-$, the potential rapidly hyperpolarized when the *Chara* cell was given a brief dark treatment. In the light the resting (stable) membrane potential was approximately –240 mV, whereas after the cell had been in the dark for 3–6 min, the potential was –330 to –350 mV. Upon reilluminating the cell, the potential further hyperpolarized transiently (–375 mV), and then rapidly depolarized back toward the light-adapted value. Analysis of electrophysiological and vibrating probe experiments conducted on *Chara* cells indicated an excellent level of correlation between the light- and dark-induced changes in extracellular currents and membrane potential. The presence of a plasmalemma-bound electrogenic $HCO_3^-$ influx system in association with an electrogenic $OH^-$ efflux process could explain the observed electrical responses.

In the presence of phosphate buffer (1 mM) and the absence of $HCO_3^-$, however, the membrane potential still hyperpolarized when cells were given a brief dark pulse. In addition, the extracellular currents that are associated with $HCO_3^-$ assimilation in *C. corallina* (71, 72, 128) could also be maintained in the absence of $HCO_3^-$, provided the bathing medium contained 1.0 mM phosphate buffer. These results demonstrate conclusively that the hyperpolarizing response cannot be explained on the basis of a $HCO_3^-$ uniport system. The simplest explanation is that the hyperpolarizing response is caused by an electrogenic $H^+$-translocating ATPase. Experimental evidence outlined in the above sections indicates that the extracellular $CO_2$-production model is almost certainly invalid *for this species,* and thus it would appear that $HCO_3^-$ is transported via a $HCO_3^-$-$H^+$ cotransport system. Lucas (65) suggested that this system may be electrically neutral, but the possibility of a $HCO_3^-$-$2H^+$ cotransport mechanism cannot be discounted. If such a system exists, the transport of $HCO_3^-$ would be electrogenic, but in this situation the membrane might respond by depolarizing. The actual change in membrane potential upon activating the $HCO_3^-$ as-

similating system would depend upon the relative time-dependent change in conductance of each of the transport elements involved—namely, $H^+$ efflux, $HCO_3^-$-$2H^+$ cotransport, and $OH^-$ efflux.

The finding that the extracellular currents in the $HCO_3^-$ transporting region of the cell membrane can be maintained in the absence of exogenous $HCO_3^-$ is of paramount importance. It indicates that in *Chara* the loop between $HCO_3^-$ assimilation and $OH^-$ efflux can be opened. A summary of this system is now possible and is presented in model form in Figure 5. Under normal $HCO_3^-$-assimilating conditions, the $H^+$-translocating ATPase of the *Chara* plasmalemma provides a supply of protons to the outer surface of this membrane. These protons are used to drive the $HCO_3^-$-$H^+$ cotransport system; the reentering protons are again cycled through the ATPase, thereby forming a $H^+$ current loop. Some of the $H^+$ will also react with $HCO_3^-$ to produce $H_2CO_3$ and thereby $CO_2$, which will diffuse both into the cytoplasm and the bathing medium. Photosynthetic

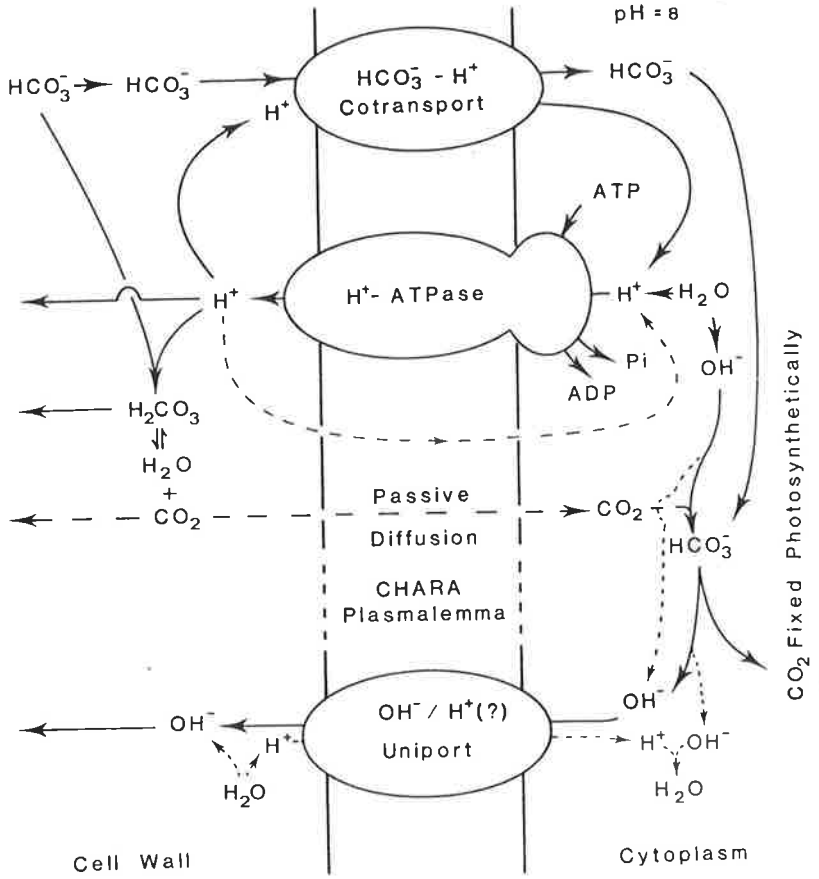


*Figure 5* Schematic representation of the plasmalemma-bound transport complexes that may enable internodal cells of *Chara* to acquire exogenous $HCO_3^-$ for photosynthesis (from Ref. 62; see text for details).

$CO_2$ fixation produces $OH^-$ by causing $HCO_3^-$ to dissociate and the $OH^-$-transporting regions of the plasmalemma serve to dispose of this alkalinity.

Substitution of phosphate ($HPO_4^{2-}$) for $HCO_3^-$ (65, 71) provided an apoplastic buffer that could penetrate to the plasmalemma, be converted to $H_2PO_4^-$ ($pK_a$ 7.2), and then diffuse back into the bathing medium where it would dissociate to $HPO_4^{2-}$. Thus, phosphate (and Hepes) can provide a $H^+$-shuttle which is sensed by the vibrating probe as an electrogenic current. Earlier theoretical treatments have addressed this role for exogenously applied buffers (19), but the implications have been largely ignored. Clearly, since many recent studies have indicated a central role for protons in energizing substrate cotransport systems (9, 33, 53, 77, 105), the standard approach of buffering a tissue to maintain a desired pH value will have to be reassessed. It may even be necessary to develop a new series of buffers which are larger, or at least less mobile in nature, so that their ability to transfer $H^+$ away from the site of transport would be reduced, yet the ability to buffer the system would be maintained.

### *Transport Stoichiometry of the $H^+$-ATPase*

The thermodynamics of the *Chara* $H^+$-translocating ATPase have been discussed by various workers (115, 127). Walker & Smith (127) showed that, based on the operation of a $2H^+$-translocating ATPase (i.e. $2H^+$ per ATP hydrolyzed), the maximum membrane potential that could be established in *Chara* was –268 mV (pH 8). However, Lucas has now measured membrane potentials in the vicinity of –350 mV; correcting for the positive tonoplast potential would raise this value to a maximum of approximately –390 mV. Lucas (65) concluded, therefore, that the $H^+$-translocating ATPase that operates during $HCO_3^-$ assimilation must be a $1H^+$ per ATP hydrolyzed. This system would be far from thermodynamic equilibrium and must therefore be rate-controlled by other parameters.

The question now to be addressed is whether the plasmalemma of *Chara,* and other plants, has a single ATPase that can change (switch) its $H^+$ translocating stoichiometry under different physiological conditions, or whether there are at least two different ATPases having $2H^+$:1ATP and $1H^+$:1ATP transport stoichiometries. This will form an extremely valuable avenue for future research in terms of providing basic information on the control processes which regulate membrane transport. The technique presently being pioneered by Hansen and co-workers (36, 37) may be particularly valuable in helping to elucidate these details.

## ELECTROGENIC $OH^-$ TRANSPORT

The main $OH^-$ transport systems that have been studied with respect to $HCO_3^-$ assimilation are those of *Chara corallina, Potamogeton lucens,*

*Elodea canadensis, and Anabaena variabilis*. Although other systems have been examined, the main features can be demonstrated by drawing from the information available for the above species. Obviously, if $HCO_3^-$ transport occurs via either a uniport, in cotransport with $H^+$, or by extracellular $CO_2$ production, alkalinity will be produced within the cytoplasm and $OH^-$ ions will need to be excreted both to maintain cytoplasmic pH and electrical balance across the plasmalemma. The area of cytoplasmic pH regulation has been reviewed recently (112).

## *Spatial and Temporal Regulation*

The reason for spatially separating the $OH^-$ efflux region from that of $HCO_3^-$ uptake is all too apparent for the systems that appear to utilize $H^+$ efflux to energize the transport of $HCO_3^-$. From the macroalgae and the aquatic angiosperms it can be seen that spatial separation was achieved by regulating the location of transport processes either along the plasmalemma of each single cell, as in *C. corallina* (62, 72), or on the plasmalemma of cells forming the opposite surface of the leaf, as in *P. lucens* and *E. canadensis* (38, 41, 42, 92–94). Whether the microalgae and Cyanobacteria follow the strategy adopted in the Characean cells remains to be elucidated, but if $HCO_3^-$ enters via a primary, active uniport mechanism, the necessity for separation would not be as important. However, $OH^-$ efflux produces $CO_3^{2-}$ near the plasmalemma, and if this form of inorganic carbon competitively inhibits the uptake of $HCO_3^-$, then spatial separation of $HCO_3^-$ uptake and $CO_3^{2-}$ production may be of value. Considering the size of the Cyanobacteria, a spatial separation of these sites may have been of little value. In this regard, Kaplan (49) considers that in *A. variabilis*, the inhibition of photosynthesis at high pH is attributable to a rise in cytoplasmic pH rather than an effect of carbonate.

It should also be stressed that not all $HCO_3^-$ assimilators have separated the $HCO_3^-$ and $OH^-$ transport sites; for example, *Vallisneria* appears to transport both ions across the upper and lower leaf surface (93). Whether different cells are involved in these processes is not yet known.

The question of what controls the spatial positioning of either transport system is intriguing. In the aquatic angiosperms it may be a matter of cellular development in which tissue (cell) specialization is expressed. However, it should be recalled that recent results indicate that the upper leaf surface of *P. lucens* may be induced to accumulate exogenous $HCO_3^-$ (41). The situation in the Characeae appears to be more complex. Lucas & Dainty (67) have investigated the question of whether the discrete location of the $OH^-$ bands was caused by a restricted distribution of the $OH^-$ transport entities along the *Chara* plasmalemma. When cytoplasmic streaming was reduced (using cytochalasin B) below a threshold value, the normal pattern of $OH^-$ efflux disintegrated, and numerous small discs of

$OH^-$ efflux activity appeared to operate over the entire cell surface. The rate of collapse and subsequent establishment of this new mode of transport was too rapid to have been caused by lateral migration of membrane proteins. This process was reversible; removal of the cytochalasin B caused a restoration of cyclosis and subsequently the control $OH^-$ efflux pattern was reestablished.

It would seem, therefore, that the $OH^-$ transporters are distributed over the entire surface of the *Chara* plasmalemma, but that a regulating mechanism operates to control which of the transporters actually function. This concept of spatial control of $OH^-$ efflux is also supported by the transport profiles computed using numerical analysis of the $OH^-$ diffusion profiles generated by these alkaline bands (69). For those who are skeptical of the numerical analysis technique, further conformation of the $OH^-$ transport profiles along the plasmalemma surface was obtained using the vibrating probe technique (72). In the central region of the alkaline band, $OH^-$ efflux is uniform (in a time-averaged sense), and the width of this region depends upon the $HCO_3^-$ concentration present, the light intensity, and the status of the band (see below). At the margins of this central region the rate of $OH^-$ transport declines to zero quite rapidly. This is the region, along the cell surface, where the transition occurs from $OH^-$ efflux to $HCO_3^-$ influx. Under constant conditions, where photosynthesis is stable over many hours, the position of these transition zones is extremely stable.

In experiments on tonoplast-free *C. corallina* cells, $OH^-$ efflux did not occur in its normal pattern (73). Preparation of these cells resulted in the destruction of certain organelles within the streaming cytoplasm. Lucas & Shimmen (73) demonstrated that $OH^-$ efflux patterns equivalent to those obtained with perfused cells were established on the centripetal segment of centrifuged cells. In these centrifugation experiments very low gravitational forces (X180) were used, and only heavy organelles like the nuclei were displaced to the centrifugal end. Ligation of the cell at its midpoint prevented these organelles from being redistributed throughout the length of the cell. The cell segment at the centrifugal end developed normal alkaline bands. Upon redistribution of the larger cytoplasmic organelles, normal pH profiles (bands) were established along the entire cell length. These results are consistent with the hypothesis that an organelle within the streaming phase of the cytoplasm is ultimately responsible for the spatial location and control over $OH^-$ transport. The identity of this putative organelle and the nature of the control signal(s) is an area worthy of future research. On a speculative note, the nucleus has been implicated and a protein has been suggested as being part of the control signal (73).

In terms of temporal regulation, *Chara, Potamogeton, Elodea,* and *Anabaena* appear to have evolved certain common attributes. Following

tissue illumination, there is always a lag prior to activation of the $OH^-$ efflux process (49, 61, 93). In *Chara,* a precise relationship was found between light intensity and the lag period. This suggested that it is necessary to establish a threshold condition within the cytoplasm before $OH^-$ transport can be activated. A preliminary model to explain this phenomenon has been presented in which the threshold condition is dealt with in terms of changes in cytoplasmic pH (61).

The steady state pH value at the upper leaf surface of *P. lucens* declines as lower light intensities are employed. This suggests a simple relationship between photosynthesis, production of alkalinity, and competition for $OH^-$ by the transporters at the upper leaf surface. Such a system was not found in *Chara;* here a complex hierarchy of $OH^-$ transport exists (61). The $OH^-$ efflux bands which develop along a particular cell are not equivalent in status. The terms *primary, sub-primary,* and *subsidiary* bands were established by Lucas (61) to explain his findings that as the light intensity was reduced, the number of alkaline bands diminished, with the remaining bands being somewhat unaffected in their rates of $OH^-$ transport. At very low light intensities, only one $OH^-$ band would become activated, and this was given the status of the *primary* band. Although this hierarchical status has been clearly established at the phenomenological level, its explanation at the molecular level awaits further work.

Further insight into the complexity of the control or regulatory processes operating on the $OH^-$ transport system of *Chara* was obtained in studies using the vibrating probe technique. In their initial study, Lucas & Nuccitelli (72) found that the presence of the vibrating probe caused a perturbation of the $OH^-$ transport system. The perturbation was usually observed as a reduction in the number of operational $OH^-$ efflux bands, with an approximate doubling of the transport rate through the one or two remaining bands. This suggested that cytoplasmic control over $OH^-$ efflux at each of the functional bands modulates the transport rates at values well below their potential maxima. Whether this form of rate control is a part of the hierarchial system in these cells must await further investigation.

Another feature concerning the temporal relationship between $HCO_3^-$ and $OH^-$ transport was also discovered in experiments using the vibrating probe. The extracellular currents in the $HCO_3^-$ transport regions were very steady with time, and synchronized with respect to the cellular response to cell darkening or illumination (65). This was not true for the extracellular currents in the alkaline bands; here the currents often exhibited quite marked, but low-frequency, fluctuations. Fluctuations of a similar form were observed during external electric potential measurements (21). A low-frequency noise component has also been reported from experiments on the *Chara* membrane potential (22, 97, 98). Ogata & Kishimoto (84) have

reported small oscillations in the membrane potential of *N. pulchella,* and the period of these oscillations was highly correlated with the rate of cytoplasmic streaming. Since a close relationship between the presence of a stable $OH^-$ efflux pattern and the existence of a critical rate of streaming has been found (67), it is conceivable that these phenomena reflect the operation of a feedback process which controls $HCO_3^-$ and $OH^-$ transport synchronization (see 36).

## *Active or Passive Process?*

Extensive research has shown that $OH^-$ ions accumulate at the cell surface during photosynthetic assimilation of $HCO_3^-$, but it should be realized that external alkalinity could be generated by at least two different mechanisms, i.e. $OH^-$ efflux or $H^+$ influx. This issue has been addressed by several workers, but little agreement has been achieved (12, 13, 64, 68). Lucas and co-workers have argued from experimental and theoretical grounds that in *Chara* the rate of $H^+$ production from the dissociation of $H_2O$ within the cell wall is much too slow to account for the measured rates of $OH^-$ efflux. However, they pointed out that if $H_2O$ was the initial species involved in binding to the transport entity, then the theoretical computations would no longer hold (see also 109). Based on the response of the *Chara* membrane potential to high pH (9.0 to 12.0), it has been proposed that the membrane changes its state under these conditions ($pH > 10.5$), becoming very permeable, in a passive manner, to $H^+$ (12). Bisson & Walker (12) point out that their results could be discussed equally well in terms of a pH-induced change in $OH^-$ permeability. Miller & Colman (80) have also concluded that for *Coccohloris* the relatively higher concentration of $OH^-$ (in the cytoplasm) compared with $H^+$ (in the cell wall) makes the $OH^-$ the more likely candidate responsible for charge and pH balance.

Since the exact nature of the transported species remains somewhat equivocal, both possibilities were included in Figures 4 and 5. The following section will focus on the question of passive $OH^-$ efflux; the arguments could equally well have been applied to passive $H^+$ influx. To establish that $OH^-$ efflux is *not* a passive process, it is necessary to show that $OH^-$ ions move against their electrochemical potential gradient. This requires the measurement of both the activity and electric gradients that are "sensed" by these ions. In many situations these parameters have not been accurately determined, and so definitive conclusions cannot be drawn.

In the Cyanobacteria, the cytoplasmic pH has been measured, but under alkaline conditions the values must be considered to be only approximate. Also, only few measurements of the membrane potential are available for species which can assimilate exogenous $HCO_3^-$. In any event, it is possible to use a general approach to examine the nature of $OH^-$ efflux in these cells.

Kaplan (49) and Miller & Colman (80) have shown that *Anabaena* and *Coccochloris* can assimilate exogenous $HCO_3^-$ at external pH values in excess of 10.0. Under these conditions the internal pH of these cells may be close to 8.0. Thus, a membrane potential of at least –120 mV would be needed to drive the passive efflux of $OH^-$. Potentials of approximately –100 mV were recently reported (51), and in view of the errors involved in making these measurements, it may well be that in the Cyanobacteria $OH^-$ efflux is passive.

In *Potamogeton,* pH values as high as 11.8 have been observed on the upper leaf surface (42); however, values of cytoplasmic pH under these conditions are not available. If we assume a value of 8.0, a membrane potential of approximately –240 mV would be required to drive passive $OH^-$ efflux. We are unaware of such negative values being measured across the upper leaf cells of this plant, but such values have been recorded in leaves of *Elodea* (116). In the absence of experimental data to the contrary, it would appear that $OH^-$ efflux in *Potamogeton* and *Elodea* is also passive.

For Characean cells, the membrane potential, cell surface pH, and cytoplasmic pH have been measured over a wide range of experimental conditions. Under $HCO_3^-$ assimilating conditions the central region of the alkaline band can reach a pH of 10.5, with the value at the plasmalemma being higher. The cytoplasmic pH value under these conditions would be about 8 (112, 127). For passive $OH^-$ efflux a membrane potential of –150 to –180 mV would be required; such values are now obtained routinely (65). This value is of interest with respect to recent work, where it was found that removal of exogenous $HCO_3^-$ caused the *Chara* membrane potential to depolarize quite dramatically. It was noticed that the potential never went below –175 mV (65), which may indicate passive $OH^-$ efflux. However, this conclusion should be viewed with reservation, since it has been shown that brief treatment of *Chara* cells with *N*-ethyl maleimide (0.1 mM, 1 min) caused the membrane potential to depolarize to approximately –125 mV (56), yet the alkaline bands were only marginally affected (66), the pH at the cell surface being about 10.0.

Since the plasmalemma of *Chara* is extremely heterogenous with respect to the spatial distribution of various transport processes, etc, it would seem unwise to apply a simple thermodynamic approach to these cells. Bisson & Walker (12, 13) have clearly demonstrated the complexity of this situation. However, at present it would appear that $OH^-$ efflux in Characean cells, as well as in other $HCO_3^-$-assimilating species, occurs via a passive mechanism. To change this conclusion, it will be necessary to find an experimental condition which will reduce the membrane potential without influencing $OH^-$ efflux.

## BENEFITS OF BICARBONATE TRANSPORT

Any aquatic species that can fully exploit its environment with respect to exogenous inorganic carbon acquisition has the potential to establish photosynthetic dominance. A species which can utilize both exogenous $CO_2$ and $HCO_3^-$ may also have available a wider range of ecological habitats. Certainly for some of the microalgae and Cyanobacteria, in which the internal levels of inorganic carbon can be raised by as much as 1000 over that of the medium, the advantage must be considerable. An outcome of inorganic carbon utilization is an alkalinization of the medium, and this must also aid in conferring species dominance to $HCO_3^-$ assimilators; this would be especially so in bodies of water which undergo rather slow mixing. However, since metabolic energy must be expended to achieve this level of carbon accumulation, there is an additional cost associated with this aspect of photosynthetic carbon production. A vigorous analysis of the cost:benefit ratio should now be possible on some species, because many of the details relating to transport mechanisms appear to have been resolved.

In recent years considerable attention has been focused on the question of whether all aquatic plants utilize the $C_3$ pathway of photosynthesis (17, 18, 44, 90). One of the main issues is whether algae undergo photorespiration, since many species exhibit the $C_4$ characteristic of extremely low photosynthetic compensation points (see 11). Considerable controversy developed over this issue (see 106–108), and the literature pertaining to the subject is quite extensive and warrants a review in its own right. It is now generally believed that algae do possess the photorespiration pathway (122). This being the case, there is a further advantage for a species which has an effective $CO_2$-concentrating mechanism, because this mechanism can serve to reduce the effect of $O_2$ on photosynthesis in an analogous way to that seen in $C_4$ plants. At present there is little information available on whether the macroalgae (like *Chara*) and aquatic angiosperms (like *Potamogeton* and *Elodea*) use a carbon-concentrating mechanism to modulate the influence of photorespiration.

## CONCLUDING REMARKS

Over the past few years considerable progress has been made toward elucidating the mechanism(s) by which aquatic plants acquire exogenous $HCO_3^-$ for photosynthetic assimilation. Most species studied fall into the category of electrogenic $HCO_3^-$ transport or $HCO_3^-H^+$ cotransporting systems, with a few examples of extracellular $CO_2$-production and $HCO_3^-/OH^-$ antiport. Thus, it appears that various species may have evolved different mechanism by which they energize the transport of $HCO_3^-$ across the

plasmalemma. Many of the aquatic angiosperm, algal and cyanobacterial systems which have been established as "$HCO_3^-$ assimilators" have not been investigated to ascertain the specific effect of buffers on photosynthesis. This will form an important area for future research, the result of which may test the hypothesis that all microalgae and cyanobacteria possess a similar transport mechanism (8). Similarly, the effect of CAPS buffer may also prove to be informative with respect to identifying "classes" of $HCO_3^-$ transport-binding sites.

Finally, although the phenomenon of spatially separate transport sites for $HCO_3^-$ and $OH^-$ has now been well documented, little is known about the biophysical and biochemical mechanisms utilized by the tissue to maintain electrical and pH balance. Parallel studies on intact and isolated membrane systems may enable the resolution of some of these details.

## ACKNOWLEDGMENTS

We thank the National Science Foundation for its continuing support of research in our laboratory through Grants PCM 78-10474, PCM 80-03133, and PCM 81-17721. Our special thanks go to Roswitha Burchardt for technical assistance and Barbara Shaneyfelt for typing the manuscript.

*Literature Cited*

1. Andrianov, V. K., Bulychev, A. A., Kurella, G. A. 1970. Connection between photo-induced changes in the resting potential and the presence of the chloroplasts in *Nitella* cells. *Biophysics* 15:199–200
2. Andrianov, V. K., Kurella, G. A., Litvin, F. F. 1968. Influence of light on the electrical activity of *Nitella* cells. In *Transport and Distribution of Matter in Cells of Higher Plants,* ed. K. Mothes, E. Müller, A. Nelles, D. Neuman, pp. 187–96. Berlin: Akademie-Verlag
3. Arens, K. 1933. Physiologisch polarisierter Massenaustausch und Photosynthese bei submersen Wasserpflanzen I. *Planta* 20:621–58
4. Arens, K. 1936. Physiologisch polarisierter Massenaustausch und Photosynthese bei submersen Wasserpflanzen. II. Die $Ca(HCO_3^-)_2$-assimilation. *Jahrb. Wiss. Bot.* 83:513–60
5. Arens, K. 1938. Manganablagerungen bei Wasserpflanzen als Folge des physiologisch polarisierten Massenaustausches. *Protoplasma* 30:104–29
6. Badger, M. R., Kaplan, A., Berry, J. A. 1977. The internal $CO_2$ pool of *Chlamydomonas reinhardtii:* response to external $CO_2$. *Carnegie Inst. Washington Yearb.* 76:362–66
7. Badger, M. R., Kaplan, A., Berry, J. A. 1978. A mechanism for concentrating $CO_2$ in *Chlamydomonas reinhardtii* and *Anabaena variabilis* and its role in photosynthetic $CO_2$ fixation. *Carnegie Inst. Washington Yearb.* 77:251–61
8. Badger, M. R., Kaplan, A., Berry, J. A. 1980. Internal inorganic carbon pool of *Chlamydomonas reinhardtii:* Evidence for a carbon dioxide-concentrating mechanism. *Plant Physiol.* 66:407–13
9. Baker, D. A. 1978. Proton co-transport of organic solutes by plant cells. *New Phytol.* 81:485–97
10. Beardall, J., Raven, J. A. 1981. Transport of inorganic carbon and the '$CO_2$ concentrating mechanism' in *Chlorella emersonii* (Chlorophyceae). *J. Phycol.* 17:134–41
11. Birmingham, B. C., Colman, B. 1979. Measurement of carbon dioxide compensation points of freshwater algae. *Plant Physiol.* 64:892–95
12. Bisson, M. A., Walker, N. A. 1980. The *Chara* plasmalemma at high pH. Electrical measurements show rapid specific passive uniport of $H^+$ or $OH^-$. *J. Membr. Biol.* 56:1–7

13. Bisson, M. A., Walker, N. A. 1982. Control of passive permeability in the *Chara* plasmalemma. *J. Exp. Bot.* 33:520–32
14. Browse, J. A., Dromgoole, F. I., Brown, J. M. A. 1979. Photosynthesis in the aquatic macrophyte *Egeria densa.* III. Gas exchange studies. *Aust. J. Plant Physiol.* 6:499–512
15. Cooper, T. G., Filmer, D., Wishnick, M., Lane, M. D. 1969. *J. Biol. Chem.* 244:1081–83
16. Denny, P., Weeks, D. C. 1970. Effects of light and bicarbonate on membrane potential in *Potamogeton schweinfurthii* (Benn.). *Ann. Bot.* 34:483–96
17. Döhler, G. 1974. $C_4$-pathway of photosynthesis in the blue-green alga *Anacystis nidulans. Planta* 118:259–69
18. Döhler, G. 1974. Effect of growth conditions on the photosynthetic pathway of *Chlorella vulgaris. Z. Pflanzenphysiol.* 71:144–53
19. Engasser, J., Horvath, C. 1974. Dynamic role of buffers: Facilitated transport of protons, weak acids and bases. *Physiol. Chem. Phys.* 6:541–43
20. Ferrier, J. M. 1980. Apparent bicarbonate uptake and possible plasmalemma proton efflux in *Chara corallina. Plant Physiol.* 66:1198–99
21. Ferrier, J. M., Lucas, W. J. 1979. Plasmalemma transport of $OH^-$ in *Chara corallina.* II. Further analysis of the diffusion system associated with $OH^-$ efflux. *J. Exp. Bot.* 30:705–18
22. Ferrier, J. M., Morvan, C., Lucas, W. J., Dainty, J. 1979. Plasmalemma voltage noise in *Chara corallina. Plant Physiol.* 63:709–14
23. Findenegg, G. R. 1974. Relations between carbonic anhydrase activity and uptake of $HCO_3^-$ and $Cl^-$ in photosynthesis by *Scenedesmus obliquus. Planta* 116:123–31
24. Findenegg, G. R. 1974. Carbonic anhydrase and the driving force of light-dependent uptake $Cl^-$ and $HCO_3^-$ by *Scenedesmus.* In *Membrane Transport in Plants,* ed. U. Zimmerman, J. Dainty, pp. 192–96. Berlin/Heidelberg/New York: Springer, 473 pp.
25. Findenegg, G. R. 1976. Correlation between accessibility of carbonic anhydrase for external substrate and regulation of photosynthetic use of $CO^2$ and $HCO_3^-$ by *Scenedesmus obliquus. Z. Pflanzenphysiol.* 79:428–37
26. Findenegg, G. R. 1976. Zur Frage eines $HCO_3^-/OH^-$-Austausches im Plasmalemma von *Scenedesmus obliquus. Ber. Dtsch. Bot. Ges.* 89:277-84
27. Findenegg, G. R. 1977. Estimation of bicarbonate fluxes in *Scenedesmus obliquus.* In *Ionic Exchange in Plants,* eds. M. Thellier, A. Monnier, M. Demanty, J. Dainty, pp. 275–81. Paris: Univ. Rouen; CNRS Publ. No. 258
28. Findenegg, G. R. 1979. Inorganic carbon transport in microalgae. I: Location of carbonic anhydrase and $HCO_3^-$ / $OH^-$ exchange. *Plant Sci. Lett.* 17:101–8
29. Findenegg, G. R. 1980. Inorganic carbon transport in microalgae. II: Uptake of $HCO_3^-$ ions during photosynthesis of five microalgal species. *Plant Sci. Lett.* 18:289–97
30. Franceschi, V. R., Lucas, W. J. 1980. Structure and possible function(s) of charasomes; complex plasmalemma-cell wall elaborations present in some Characean species. *Protoplasma* 104:253–71
31. Franceschi, V. R., Lucas, W. J. 1981. The charasome periplasmic space. *Protoplasma* 107:269–84
32. Franceschi, V. R., Lucas, W. J. 1982. The relationship of the charasome to chloride uptake in *Chara corallina:* Physiological and histochemical investigations. *Planta* 154:525–37
33. Giaquinta, R. T. 1980. Mechanism and control of phloem loading of sucrose. *Ber. Dtsch. Bot. Ges.* 93:187–201
34. Goldman, J. C., Oswald, W. J., Jenkins, D. 1974. The kinetics of inorganic carbon limited algal growth. *J. Water Pollut. Control Fed.* 46:554–74
35. Goldman, J. C., Porcella, D. B., Middlebrooks, E. J., Toerien, D. F. 1972. The effects of carbon on algal growth—its relationship to eutrophication. *Water Res.* 6:637–79
36. Hansen, U-P. 1978. Do light-induced changes in the membrane potential of *Nitella* reflect the feed-back regulation of a cytoplasmic parameter? *J. Membr. Biol.* 41:197–224
37. Hansen, U-P., Keunecke, P. 1977. The parallel pathways of the action of light on membrane potential in *Nitella.* See Ref. 27, pp. 333–40
38. Helder, R. J. 1975. Polar potassium transport and electrical potential difference across the leaf of *Potamogeton lucens* L. *Proc. Kon. Ned. Akad. Wet. Ser. C* 78:189–97
39. Helder, R. J., Boerma, J. 1972. Polar transport of labelled rubidium ions across the leaf of *Potamogeton lucens. Acta Bot. Neerl.* 21:211–28
40. Helder, R. J., Boerma, J. 1973. Exchange and polar transport of rubidium

ions across the leaves of *Potamogeton lucens. Acta Bot. Neerl.* 22:686–93
41. Helder, R. J., Boerma, J., Zanstra, P. E. 1980. Uptake pattern of carbon dioxide and bicarbonate by leaves of *Potamogeton lucens* L. *Proc. Kon. Ned. Akad. Wet. Ser. C* 83:151–66
42. Helder, R. J., Zanstra, P. E. 1977. Changes of the pH at the upper and lower surface of bicarbonate assimilating leaves of *Potamogeton lucens* L. *Proc. Kon. Ned. Akad. Wet. Ser. C* 80:421–36
43. Higinbotham, N. 1973. Electropotentials of plant cells. *Ann. Rev. Plant Physiol.* 24:25–46
44. Hogetsu, D., Miyachi, S. 1979. Operation of the reductive pentose phosphate cycle during the induction period of photosynthesis in *Chlorella. Plant Cell Physiol.* 20:1427–32
45. Hope, A. B. 1965. Ionic relations of cells of *Chara australis. Aust. J. Biol. Sci.* 18:789–801
46. Jaffe, L., Nuccitelli, R. 1974. An ultrasensitive vibrating probe for measuring extracellular currents. *J. Cell Biol.* 63:614–28
47. Kadono, Y. 1980. Photosynthetic carbon sources in some *Potamogeton* species. *Bot. Mag.* 93:185–94
48. Kaplan, A. 1981. Photoinhibition in *Spirulina platensis:* response of photosynthesis and $HCO_3^-$ uptake capability to $CO_2$-depleted conditions. *J. Exp. Bot.* 32:669–77
49. Kaplan, A. 1981. Photosynthetic response to alkaline pH in *Anabaena variabilis. Plant Physiol.* 67:201–4
50. Kaplan, A., Badger, M. R., Berry, J. A. 1980. Photosynthesis and the intracellular inorganic carbon pool in the bluegreen alga *Anabaena variabilis:* Response to external $CO_2$ concentration. *Planta* 149:219–26
51. Kaplan, A., Zenvirth, D., Reinhold, L., Berry, J. A., 1982. Involvement of a primary electrogenic pump in the mechanism for $HCO_3^-$ uptake by the cyanobacterium *Anabaena variabilis*. *Plant Physiol.* 69:978–82
52. Kitasato, J. 1968. The influence of $H^+$ on the membrane potential and ion fluxes of *Nitella. J. Gen. Physiol.* 52:60–87
53. Komor, E., Tanner, W. 1974. The hexose-proton cotransport system in *Chlorella:* pH-dependent change in $K_m$ values and translocation constants of the uptake system. *J. Gen. Physiol.* 64:568–81
54. Kramer, D., Findenegg, G. R. 1978. Variations in the ultrastructure of *Scenedesmus obliquus* during adaptation to low $CO_2$ level. *Z. Pflanzenphysiol.* 89:407–10
55. Lehman, J. T. 1978. Enhanced transport of inorganic carbon into algal cells and its implications for the biological fixation of carbon. *J. Phycol.* 14:33–42
56. Lichtner, F. T., Lucas, W. J., Spanswick, R. M. 1981. Effect of sulfhydryl reagents on the biophysical properties of the plasmalemma of *Chara corallina. Plant Physiol.* 68:899–904
57. Lowenhaupt, B. 1956. The transport of calcium and other cations in submerged aquatic plants. *Biol. Rev.* 31:371–95
58. Lowenhaupt, B. 1958. Active cation transport in submerged aquatic plants. I. Effect of light upon the absorption and excretion of calcium by *Potamogeton crispus* (L.) leaves. *J. Cell Comp. Physiol.* 51:199–208
59. Lucas, W. J. 1975. Analysis of the diffusion symmetry developed by the alkaline and acid bands which form at the surface of *Chara corallina* cells. *J. Exp. Bot.* 26:271–86
60. Lucas, W. J. 1975. Photosynthetic fixation of $^{14}$carbon by internodal cells of *Chara corallina. J. Exp. Bot.* 26:331–46
61. Lucas, W. J. 1975. The influnce of light intensity on the activation and operation of the hydroxyl efflux system of *Chara corallina*. *J. Exp. Bot.* 26:347–60
62. Lucas, W. J. 1976. Plasmalemma transport of $HCO_3^-$ and $OH^-$ in *Chara corallina:* non-antiporter systems. *J. Exp. Bot.* 27:19–31
63. Lucas, W. J. 1977. Analogue inhibition of the active $HCO_3^-$ transport site in the characean plasma membrane. *J. Exp. Bot.* 28:1321–36
64. Lucas, W. J. 1979. Alkaline band formation in *Chara corallina:* Due to $OH^-$ efflux or $H^+$ influx? *Plant Physiol.* 63:248–54
65. Lucas, W. J. 1982. Mechanism of acquisition of exogenous $HCO_3^-$ by internodal cells of *Chara corallina*. *Planta* 156:181–92
66. Lucas, W. J., Alexander, J. M. 1980. Sulfhydryl group involvement in plasmalemma transport of $HCO_3^-$ and $OH^-$ in *Chara corallina*. *Plant Physiol.* 65:274–80
67. Lucas, W. J., Dainty, J. 1977. Spatial distribution of functional $OH^-$ carriers along a characean internodal cell: Determined by the effect of cytochalasin B on $H^{14}CO_3^-$ assimilation. *J. Membr. Biol.* 32:75–92

68. Lucas, W. J., Ferrier, J. M. 1980. Plasmalemma transport of $OH^-$ in *Chara corallina.* III. Further studies on transport substrate and directionality. *Plant Physiol.* 65:46–50
69. Lucas, W. J., Ferrier, J. M., Dainty, J. 1977. Plasmalemma transport of $OH^-$ in *Chara corallina:* Dynamics of activation and deactivation. *J. Membr. Biol.* 32:49–73
70. Lucas, W. J., Franceschi, V. R. 1981. Characean charasome-complex and plasmalemma vesicle development. *Protoplasma* 107:255–67
71. Lucas, W. J., Keifer, D. W., Sanders, D. 1983. Bicarbonate transport in *Chara corallina:* Evidence for cotransport of $HCO_3^-$ with $H^+$. *J. Membr. Biol.* In press
72. Lucas, W. J., Nuccitelli, R. 1980. $HCO_3^-$ and $OH^-$ transport across the plasmalemma of *Chara corallina:* Spatial resolution obtained using extracellular vibrating probe. *Planta* 150:120–31
73. Lucas, W. J., Shimmen, T. 1981. Intracellular perfusion and cell centrifugation studies on plasmalemma transport processes in *Chara corallina. J. Membr. Biol.* 58:227–37
74. Lucas, W. J., Smith, F. A. 1973. The formation of alkaline and acid regions at the surface of *Chara corallina* cells. *J. Exp. Bot.* 24:1–14
75. Lucas, W. J., Tyree, M. T., Petrov, A. 1978. Characterization of photosynthetic $^{14}$carbon assimilation by *Potamogeton lucens* L. *J. Exp. Bot.* 29:1409–21
76. MacRobbie, E. A. C. 1970. The active transport of ions in plant cells. *Q. Rev. Biophys.* 3:251–94
77. Malek, F., Baker, D. A. 1977. Proton cotransport of sugars in phloem loading. *Planta* 135:297–99
78. Marcus, Y., Zenvirth, D., Harel, E., Kaplan, A. 1982. Induction of $HCO_3^-$ transporting capability and high photosynthetic affinity to inorganic carbon by low concentration of $CO_2$ in *Anabaena variabilis. Plant Physiol.* 69:1008–12
79. Miller, A. G., Colman, B. 1980. Active transport and accumulation of bicarbonate by a unicellular cyanobacterium. *J. Bacteriol.* 143:1253–59
80. Miller, A. G., Colman, B. 1980. Evidence for $HCO_3^-$ transport by the blue-green alga (Cyanobacterium) *Coccochloris peniocystis. Plant Physiol.* 65: 397–402
81. Mukerji, D., Glover, H. E., Morris, I. 1978. Diversity in the mechanism of carbon dioxide fixation in *Dunaliella tertiolecta* (Chlorophyceae). *J. Phycol.* 14:137–42
82. Nagai, R., Tazawa, M. 1962. Changes in resting potential and ion absorption induced by light in a single plant cell. *Plant Cell Physiol.* 3:323–39
83. Nishizaki, Y. 1968. Light-induced changes of bioelectric potentials in *Chara. Plant Cell Physiol.* 9:377–87
84. Ogata, K., Kishimoto, U. 1976. Rhythmic change of membrane potential and cyclosis of *Nitella* internode. *Plant Cell Physiol.* 17:201–7
85. Österlind, S. 1949. Growth conditions of the algal *Scenedesmus quadricauda* with special reference to the inorganic carbon sources. *Symb. Bot. Ups.* 10:1–141
86. Österlind, S. 1950. Inorganic carbon sources of green algae. I. Growth experiments with *Scenedesmus quadricauda* and *Chlorella pyrenoidosa. Physiol. Plant.* 3:353–60
87. Österlind, S. 1950. Inorganic carbon sources of green algae. II. Carbonic anhydrase in *Scenedesmus quadricauda* and *Chlorella pyrenoidosa. Physiol. Plant* 3:430–34
88. Österlind, S. 1951. Inorganic carbon sources of green algae. III. Measurements of photosynthesis in *Scenedesmus quadricauda* and *Chlorella pyrenoidosa. Physiol. Plant.* 4:242–54
89. Österlind, S. 1951. Inorganic carbon sources of green algae. IV. Photoactivation of some factor necessary for bicarbonate assimilation. *Physiol. Plant.* 4:514–27
90. Ouellet, C., Benson, A. A. 1952. The path of carbon in photosynthesis. XIII. pH effects in $^{14}CO_2$ fixation by *Scenedesmus. J. Exp. Bot.* 3:237–45
91. Poole, R. J. 1978. Energy coupling for membrane transport. *Ann. Rev. Plant Physiol.* 29:437–60
92. Prins, H. B. A., Snel, J. F. H., Helder, R. J., Zanstra, P. E. 1979. Photosynthetic bicarbonate utilization in the aquatic angiosperms *Potamogeton* and *Elodea. Hydrobiol. Bull.* 13:106–11
93. Prins, H. B. A., Snel, J. F. H., Helder, R. J., Zanstra, P. E., 1980. Photosynthetic $HCO_3^-$ utilization and $OH^-$ excretion in aquatic angiosperms: Light-induced pH changes at the leaf surface. *Plant Physiol.* 66:818-22
94. Prins, H. B. A., Snel, J. F. H., Zanstra, P. E., Helder, R. J. 1982. The mechanism of bicarbonate assimilation by the polar leaves of *Potamogeton* and *Elo-*

*dea.* $CO_2$ concentrations at the leaf surface. *Plant Cell Environ.* 5:207–14
95. Rabinowitch, E. I. 1951. *Photosynthesis and Related Processes,* Vol. 2, Part 1. New York: Interscience. 1208 pp.
96. Radmer, R., Ollinger, O. 1980. Light-driven uptake by oxygen, carbon dioxide, and bicarbonate by the green alga *Scenedesmus. Plant Physiol.* 65:723–29
97. Rao, R. L., Pickard, W. F. 1976. The use of membrane electric noise in the study of characean electrophysiology. *J. Exp. Bot.* 27:460–72
98. Rao, R. L., Pickard, W. F. 1977. Further experiments on low frequency excess noise in the vacuolar resting potential of *Chara braunii. J. Exp. Bot.* 28:1–16
99. Raven, J. A. 1970. Exogenous inorganic carbon sources in plant photosynthesis. *Biol. Rev.* 45:167–221
100. Raven, J. A. 1980. Nutrient transport in microalgae. *Adv. Microb. Physiol.* 21: 47–226
101. Raven, J. A., Glidewell, S. M. 1978. $C_4$ characteristics of photosynthesis in the $C_3$ alga *Hydrodictyon africanum. Plant Cell Environ.* 1:185–97
102. Ruttner, F. 1947. Zur frage der karbonatassimilation der wasserpflanzen. I. Teil: Die beiden haupttypen der kohlenstoffaufnahme. *Oesterr. Bot. Z.* 94: 265–94
103. Saito, K., Senda, M. 1973. Light-dependent effect of external pH on the membrane potential in *Nitella. Plant Cell Physiol.* 14:147–56
104. Saito, K., Senda, M. 1973. The effect of external pH on the membrane potential of *Nitella* and its linkage to metabolism. *Plant Cell Physiol.* 14:1045–52
105. Sanders, D. 1980. The mechanism of $Cl^-$ transport at the plasma membrane of *Chara corallina.* I. Cotransport with $H^+$. *J. Membr. Biol.* 53:129–41
106. Shelp, B. J., Canvin, D. T. 1980. Photorespiration and oxygen inhibition of photosynthesis in *Chlorella pyrenoidosa. Plant Physiol.* 65:780–84
107. Shelp, B. J., Canvin, D. T. 1980. Utilization of exogenous inorganic carbon species in photosynthesis by *Chlorella pyrenoidosa. Plant Physiol.* 65:774–79
108. Shelp, B. J., Canvin, D. T. 1981. Photorespiration in air and high $CO_2$-grown *Chlorella pyrenoidosa. Plant Physiol.* 68:1500–3
109. Simons, R. 1979. Strong electric field effects on proton transfer between membrane-bound amines and water. *Nature* 280:824–26
110. Smith, F. A. 1968. Rates of photosynthesis in characean cells. II. Photosynthetic $^{14}CO_2$ fixation and $^{14}C$-bicarbonate uptake by Characean cells. *J. Exp. Bot.* 19:207–17
111. Smith, F. A. 1970. The mechanism of chloride transport in Characean cells. *New Phytol.* 69:903–17
112. Smith, F. A., Raven, J. A. 1979. Intracellular pH and its regulation. *Ann. Rev. Plant Physiol.* 30:289–311
113. Smith, F. A., Walker, N. A. 1980. Photosynthesis by aquatic plants: effects of unstirred layers in relation to assimilation of $CO_2$ and $HCO_3^-$ and to carbon isotope discrimination. *New Phytol.* 86:245–59
114. Spanswick, R. M. 1970. Bicarbonate pH and membrane potentials. *J. Membr. Biol.* 2:59–70
115. Spanswick, R. M. 1972. Evidence for an electrogenic ion pump in *Nitella translucens.* I. The effects of pH, $K^+$, $Na^+$, light and temperature on the membrane potential and resistance. *Biochim. Biophys. Acta* 288:73–89
116. Spanswick, R. M. 1973. Electrogenesis in photosynthetic tissues. In *Ion Transport in Plants,* ed. W. P. Anderson, pp. 113–39. London/New York: Academic. 630 pp.
117. Spanswick, R. M. 1981. Electrogenic ion pumps. *Ann. Rev. Plant Physiol.* 32:267–89
118. Spear, D. G., Barr, J. K., Barr, C. E. 1979. Localization of hydrogen ion and chloride ion fluxes in *Nitella. J. Gen. Physiol.* 54:397–414
119. Steemann Nielsen, E. 1947. Photosynthesis of aquatic plants with special reference to the carbon-sources. *Dan. Bot. Ark.* 12:1–71
120. Steemann Nielsen, E. 1960. Uptake of $CO_2$ by the plant. In *Encyclopedia of Plant Physiology, Vol. V, The Assimilation of Carbon Dioxide,* ed. W. Ruhland, pp. 70–84. Berlin: Springer. 1013 pp.
121. Talling, J. F. 1976. The depletion of carbon dioxide from lake water by phytoplankton. *J. Ecol.* 64:79–121
122. Tolbert, N. E. 1979. Glycolate metabolism by higher plants and algae. In *Encyclopedia of Plant Physiology,* New Ser. ed. M. Gibbs, E. Latzko, 6:338–52. Berlin: Springer. 578 pp.
123. Volkov, G. A. 1973. Bioelectrical response of the *Nitella flexilis* cell to illumination: A new possible state of plasmalemma in a plant cell. *Biochim. Biophys. Acta* 314:83–92

124. Volkov, G. A., Petrushenko, V. V. 1969. Studies of the resting potential of a single cell of the alga *Nitella flexilis*. IV. The correlation between the cell response to light and the photosynthesis process. *Tsitologiya* 11:1007–13
125. Walker, N. A. 1962. Effect of light on the plasmalemma of *Chara cells*. *Ann. Rep. Div. Plant Ind.*, CSIRO
126. Walker, N. A. 1980. The transport systems of charophyte and chlorophyte giant algae and their integration into modes of behaviour. In *Plant Membrane Transport: Current Conceptual Issues*, ed. R. M. Spanswick, W. J. Lucas, J. Dainty, pp. 287–300. Amsterdam: Elsevier/North Holland. 670 pp.
127. Walker, N. A., Smith, F. A. 1975. Intracellular pH in *Chara corallina* measured by DMO distribution. *Plant Sci. Lett.* 4:125–32
128. Walker, N. A., Smith, F. A. 1977. Circulating electric currents between acid and alkaline zones associated with $HCO_3^-$ assimilation in *Chara*. *J. Exp. Bot.* 28:1190–1206
129. Walker, N. A., Smith, F. A., Cathers, I. R. 1980. Bicarbonate assimilation by fresh-water charophytes and higher plants: I. Membrane transport of bicarbonate ions is not proven. *J. Membr. Biol.* 57:51–58
130. Zenvirth, D., Kaplan, A. 1981. Uptake and efflux of inorganic carbon in *Dunaliella salina*. *Planta* 152:8–12

J. Membrane Biol. 73, 263–274 (1983)

The Journal of
Membrane Biology
© Springer-Verlag 1983

# Bicarbonate Transport in *Chara corallina*: Evidence for Cotransport of $HCO_3^-$ with $H^+$

William J. Lucas, David W. Keifer and Dale Sanders*
Department of Botany, University of California, Davis, California 95616

**Summary.** Experiments were undertaken on the fresh water alga *Chara corallina* to determine the form of inorganic carbon ($CO_2$ or $HCO_3^-$) which enters the cell during photosynthesis at alkaline pH. Recent proposals have centered on the possibility that proton efflux in alkaline solution is able to generate, in the immediate vicinity of the cell, a sufficiently low pH to raise the partial pressure of $CO_2$, and hence facilitate its passive permeation into the cell. Predictions have been made by modelling this situation (N.A. Walker, F.A. Smith & I.R. Cathers, 1980, *J. Membrane Biol.* **57**:51–58, J.M. Ferrier, 1980, *Plant Physiol.* **66**:1198–1199), and these were tested by placing recessed-tip pH microelectrodes in the unstirred layer surrounding cells in stagnant solution (bulk pH 8.2, buffered only with 1 mM $HCO_3^-$). Even as close as 2 μm from the cell wall, the pH was typically 7.2 to 7.6 in the acid band center – over 1 pH unit *greater* than that suggested by the models for $CO_2$ entry at the necessary rate for C-fixation. Further evidence for the entry of $HCO_3^-$, rather than $CO_2$, at high solution pH was obtained from experiments in which the radial pH gradient in the unstirred layer was reduced. Buffer solutions containing 5 mM phosphate or 5 mM HEPES, raised the pH at the cell surface in the acid regions from around 7.2 to 7.8 or higher. This pH increase (reduction in acid gradient) would have greatly reduced the $CO_2$ level at the cell surface and should, therefore, have greatly reduced the $CO_2$-related $^{14}C$-influx. However, $^{14}C$-fixation was reduced by only 31% (phosphate) or 15% (HEPES), compared with buffer-free controls. Reduction of the unstirred layer thickness by fast solution flow resulted in a stimulation, and not a reduction, of $^{14}C$-fixation. The similarity of our radial pH profiles near the wall with that predicted by the model (Walker et al., 1980) assuming $H^+ - HCO_3^-$ cotransport, together with the effects of buffer, and the results of increased solution flow rate, lead to the conclusion that cotransport of $HCO_3^-$ with $H^+$ is the likely method of entry of inorganic carbon. Longitudinal pH profiles of the *Chara* cell were obtained at a distance of 25 μm from the wall. These revealed much sharper delineation of the acid and alkaline bands than has previously been possible with miniature pH electrodes. Profiles of local electric field, obtained with a vibrating probe, were in excellent agreement with the high resolution pH profiles. This supports the hypothesis that membrane proton transport has a role (direct) in the generation of the extracellular currents.

**Key Words** *Chara* · bicarbonate transport · extracellular pH · recessed-tip pH microelectrodes

* *Current address:* Department of Physiology, Yale University School of Medicine, New Haven, Connecticut 06510.

## Introduction

The topic of photosynthetic assimilation of exogenous $HCO_3^-$ by aquatic plants has indeed been controversial. However, there are numerous reports in the literature which purport to demonstrate that certain algae and aquatic angiosperms can utilize the inorganic carbon of exogenous $HCO_3^-$ for photosynthesis (Arens, 1933, 1936; Ruttner, 1947; Steemann-Nielsen, 1947, 1960; Österlind, 1949; Raven, 1968, 1970; Lucas, 1975). The main difficulty in the interpretation of the results pertaining to $HCO_3^-$ assimilation is the fact that $HCO_3^-$ may act as a reservoir for extracellular $CO_2$. Hood and Park (1962) attempted to remove the $CO_2$ from the $HCO_3^-$ solution and hence determine whether photosynthetic fixation still proceeded. This approach was justifiably criticized by Watt and Paasche (1963) and Steemann-Nielsen (1963).

Raven (1968, 1970) developed a more rigorous form of analysis to ascertain whether a species could utilize exogenous $HCO_3^-$. The approach consisted of comparing fixation at high external pH (where membrane transport appears to be the rate-limiting step) with that at low pH, where most of the inorganic carbon is in the molecular form. If the cell is unable to transport bicarbonate, then at a given total carbon concentration fixation should vary with the external proton concentration, since this parameter will determine the concentration of $CO_2$ present. In fact, much higher levels of fixation were found at alkaline pH than could be accounted for by the presumed concentration of molecular $CO_2$, and this led Smith (1968), and later Lucas (1975) to propose that internodal cells of *Chara corallina* could transport $HCO_3^-$. Lucas (1975) also showed, on theoretical grounds, that the rate of $CO_2$ supply from the pool of $HCO_3^-$ could not match the rates of $^{14}C$-fixation

observed in alkaline media. Similar theoretical analyses have been reported for *Microcystis aeruginosa* and *Ceratium hirudinella* (Talling, 1976), *Egeria densa* (Browse, Dromgoole & Brown, 1979) and *Coccochloris peniocystis* (Miller & Colman, 1980).

However, the above approach does not take into consideration the possibility that an acidic unstirred layer might exist around the cell, even in alkaline media, due to the activity of the outwardly directed $H^+$ pump (Spanswick, 1981). This has prompted several groups to suggest that in this locally acidic region, the molecular $CO_2$ concentration may be significantly higher than that estimated from measurements in the bulk medium, and that in reality, aquatic angiosperms and Characean algae may not have the capability to transport $HCO_3^-$ (Prins et al., 1979, 1980, 1982; Ferrier, 1980; Smith & Walker, 1980; Walker et al., 1980). Two independent attempts to quantify these ideas have led to the notion that the pH at the membrane (cell surface) should be about 6.0 or lower in order to attain the observed rates of $^{14}C$-fixation in media of bulk pH 8.2 or above (Ferrier, 1980; Walker et al., 1980).

It is clear that a critical discrimination between these hypotheses must come from measurement of the pH in the unstirred layer, and as close as possible to the cell wall. Until recently, good spatial resolution of the radial pH profile has not been possible, because the miniature pH electrodes used for such studies had pH-sensitive areas about as large as the unstirred layer itself. However, with the advent of pH microelectrodes, it has now become possible to measure the pH inside the unstirred layer. From these observations, we have been able to conclude that in *Chara* $HCO_3^-$ transport, and not permeation of molecular $CO_2$, appears to be the major mode of carbon uptake under alkaline conditions.

Besides the possibility that $CO_2$ is the predominant permeant species at all external pH values, Walker et al. (1980) also considered, quantitatively, the effects of two alternative modes of $HCO_3^-$ transport on the pH of the unstirred layer. For both $HCO_3^-$ uniport and for $HCO_3^- - H^+$ cotransport, some acidification near the cell wall is expected, although low pH in the unstirred layer is a consequence of, and not a requirement for, transport in either case. On the other hand, changing the pH of the unstirred layer should have a different effect on the $HCO_3^-$ flux depending on the mode of entry. For a uniport mechanism, raising the pH of the unstirred layer from 7.2 to 7.8 should slightly *increase* the $HCO_3^-$ flux, whereas a more complex effect is expected for $HCO_3^- - H^+$ cotransport. In the present work, we have tried to discriminate between these two possibilities by adjusting the pH in the unstirred layer either with buffers, or with fast flowing solutions.

## Materials and Methods

### *Plant Material*

Culture material of *Chara corallina* Klein ex Willd., em. R.D.W. (= *C. australis* R. Br.) was grown in the laboratory in two large containers (A: 80 liters, B: 45 liters). The solution in A initially contained (mM): 3.0 $Na^+$, 0.2 $K^+$, 0.2 $Ca^{2+}$, 0.2 $SO_4^{2-}$, 1.2 $Cl^-$ and 2.0 $HCO_3^-$, pH 8.5 to 9.5; the solution in B contained: 6.0 $Na^+$, 0.2 $K^+$, 0.2 $Ca^{2+}$, 0.2 $SO_4^{2-}$, 1.2 $Cl^-$, 2.0 $HCO_3^-$ and 2 mM N-2-hydroxyethyl-piperazine-N′-2-ethanesulfonic acid (HEPES) at pH 7.5. Both systems were illuminated (14 h light) with fluorescent lighting (Sylvania, Lifeline, F30T12-CW-RS or F48-CW-RS) with the intensity at the solution surface being 17 to 20 W $m^{-2}$. All experiments were performed on mature male internodal cells that were cut from the main axis of the vegetative shoot one or two days prior to being used in an experiment.

### *Recessed-Tip pH and Extracellular Current Measurements*

Excised internodal cells were rinsed in an artificial pond medium [CPW/B, containing (mM): 1.0 NaCl, 0.2 KCl, 0.2 $CaSO_4$, 1.0 $NaHCO_3$ (pH 8.0 to 8.2)] and then cellular debris was removed from the cut ends of the branch- and adjoining internodal-cells using a Pasteur pipette to which a partial vacuum had been applied. During initial experiments with the miniature pH electrode we used the agar-block technique (Lucas & Smith, 1973) to measure the steady-state pH profile along the *Chara* cell wall. [The agar blocks were used as embedding media for experimental cells, and were prepared in a manner similar to that described by Lucas and Dainty (1977).] Cells were pretreated in CPW/B (20 W $m^{-2}$) for 1 to 2 h to establish a stable pH profile near the cell wall. It should be mentioned that we conducted all surface pH experiments in the presence of 1 mM total inorganic carbon to allow a direct comparison between our results and the theoretical data obtained by Walker et al. (1980) and Ferrier (1980). For the agar-block system, the pH measurements were made using a miniature pH electrode (Microelectrodes, Inc., Londondery, New Hampshire, Model MI-405) in conjunction with a Beckman 4500 digital pH meter. A Leitz micromanipulator was used to position, and traverse, the pH electrode along the *Chara* cell wall. From the values obtained the pH pattern established near the cell surface was mapped.

The *Chara* internodal cell was then removed from the agar block and silk threads (Type: Orizuru 9; Kanagawa Co. Ltd., Kanagawa, Japan) were attached to the dead cell wall-fragments of the adjoining internodal cells. These silk threads were then used to suspend the cell in the center of a 9-mm-deep, 30-mm-wide and 56-mm-long Plexiglas chamber filled with CPW/B. Small Plexiglas blocks (height 4.5 mm) were placed beneath the threads near the ends of the cell to stabilize the cell's position. (A mature antheridium was used to orient the internodal cell such that the same cell wall regions could be scanned with both the miniature and micro pH electrodes.) Cells mounted in this manner were stored, overnight, in a covered petri dish.

On the following day, the Plexiglas chamber containing the suspended *Chara* cell was placed on the stage of a compound inverted microscope (Invertoscope D; Zeiss, New York) and the cell illuminated (20 W $m^{-2}$) using a bifurcated fiber optic light source (model MK II; Ehrenreigh Photo Optical Industries, Inc., Garden City, New York). The microscope stage was motorized (stepping motor, model KD 3402-004; Hurst Manufacturing Corp., Princeton, Indiana, coupled to a model SL 10 adjustable speed controller; Minarik Electric Co., Los Angeles, Calif.) so that the entire length of the *Chara* cell could be traversed past either the vibrating electrode or recessed-tip pH microelectrode.

After a 2-h illumination period the extracellular currents near the cell wall were measured using the vibrating probe system developed by Jaffe and Nuccitelli (1974). Full details of the application of this technique to the *Chara* system have been reported by Lucas and Nuccitelli (1980). In the present study we adopted the same basic procedures, with the following exceptions. All measurements were made using a spherical platinum-black electrode with a tip diameter of approximately 10 μm. The electrode was vibrated over a distance of 12.5 μm at a frequency of 328 Hz; the vibrating electrode was maintained at a distance of $50 \pm 5$ μm from the cell surface.

Using the measured conductivity of the solution, the potentials obtained from the vibrating probe were converted to local current densities (μA $cm^{-2}$), and these were converted to flux densities by dividing by Faraday's constant (*see* Lucas & Nuccitelli, 1980). All vibrating probe data are presented in terms of flux densities, in units of pmol $cm^{-2}$ $s^{-1}$. The convention followed was to display inward current, which occurred in the alkaline regions, as positive fluxes, and the outward current which occurred in the acid regions as negative fluxes.

After current scans were completed, the vibrating probe assembly was removed and replaced by the recessed-tip pH microelectrode system; *Chara* cells were allowed approximately 1 h to re-equilibrate before making pH measurements. The motorized stage was used to position the *Chara* cell, and a micromanipulator (Model H-2; Line-Tool, Allentown, Pa.) was used to adjust the position of the pH microelectrode. Recessed-tip electrodes were fabricated according to the method of Thomas (1978) with their dimensions optimized for rapid response (*see* Sanders & Slayman, 1982). Generally, the time constants of the electrodes in response to a step change in pH in buffered solutions were on the order of 5 to 20 s, with a sensitivity of greater than 55 mV/pH unit. The length of exposed pH glass in most cases was 35 μm, and the tip diameter was 0.5 μm. The reference electrode was a broken-tipped microelectrode (tip diameter, about 10 μm), filled with 1 M KCl in 2% agar. In order to prevent perturbation by leaking KCl under these stagnant conditions the reference electrode was positioned at least 2 cm from the cell. The output from the pH electrode was fed into a high impedence ($10^{14}$ ohm) amplifier (constructed by Bob Sind, Washington University Medical School, St. Louis, Missouri) and readings were made from a digital meter. Since, in these experiments, we were only interested in steady-state pH gradients, a single pH value was recorded for each position of the electrode after the reading had stabilized, as determined from recordings on a Hewlett-Packard (Model 7132A) chart recorder. Usually, stabilization required a few minutes, probably due to slight solution mixing during the movement of the electrode. Periodically during an experiment, the electrode was repositioned to a site for which the pH had already been determined, in order to check for time-dependent drift. However, in spite of the rather lengthy duration of the experiments (about 3 to 4 h), the measured values and patterns were quite stable. All manipulations were observed under 200 × magnification. Longitudinal scans of extracellular pH were performed with the electrode tip 25 μm from the cell surface. In some experiments, radial scans were then made at specific locations along the cell, pH values being obtained as close as 2 μm from the cell wall. During all pH microelectrode measurements the upper solution surface was partially covered. with the aid of several large glass coverslips, to reduce convection currents and $CO_2$ loss from the solution.

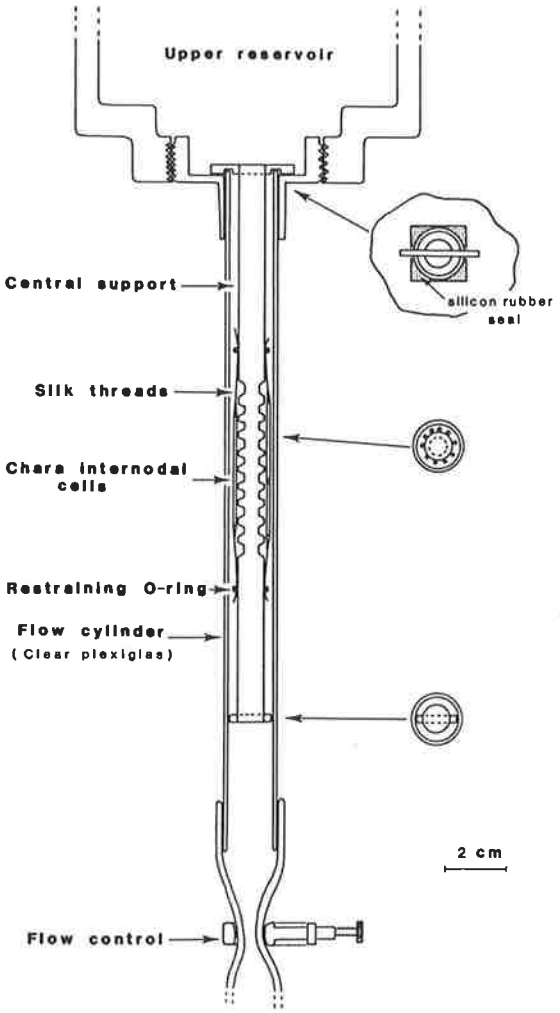


**Fig. 1.** Schematic representation of the apparatus used to vary the width of the *Chara* cell unstirred layer. The *Chara* internodal cells were attached to a clear Plexiglas central support via silk threads and restraining O-rings. This support fitted into a flow cylinder which screwed into an upper reservoir and was connected, via Tygon tubing, to a lower reservoir (4.5 liter total volume). Experimental solution was pumped from the lower to the upper reservoir and the flow rate past the cells was adjusted using a screw clamp; excess volume within the upper cylinder was returned via a bypass. The position of the bypass valve was such that a constant hydrostatic head of 80 cms was maintained for all experiments

## *Flowing Solution Experiments*

The apparatus illustrated in Fig. 1 was used to investigate the effect of the unstirred layer thickness on the rate of $H^{14}CO_3^-$ assimilation. For these experiments, cells were cut from the

culture and their lengths and diameter measured to enable surface area computation. Silk threads were then attached to the cells (*see above*) and these threads were used to anchor the cells onto the central support (*see* Fig. 1). The mounted cells were given an overnight pretreatment in CPW/B (0.5 $HCO_3^-$) before being used in flow experiments. The general procedure used in these experiments was as follows. The central support, with the mounted cells, was transferred to the flow cylinder, which contained solution, and this unit was quickly screwed into the upper reservoir housing (*see* Fig. 1). The lower reservoir originally contained 3 liters of CPW/0.5 $NaHCO_3$ and this was circulated through the system by means of a Teflon-sealed impeller-driven pump (model 1P681 Teel; Dayton Electric Manufacturing Co., Chicago, Ill.). All cells were pretreated for 1 h under 20 W $m^{-2}$, 25 °C at the flow rate used during the $^{14}C$ uptake experiment. The period of $H^{14}CO_3^-$ exposure (30 min) was initiated by injecting 50 µl of stock $NaH^{14}CO_3$ solution (47 mCi/mmol; New England Nuclear) into the lower reservoir. Preliminary experiments indicated that the upper and lower reservoirs become uniformly labeled in less than 30 s at high flow rates; at lower flow rates stirring within the two reservoirs accomplished this uniform mixing.

The specific activity of the solution did not change significantly throughout the course of an experiment, as determined from aliquots of the $^{14}C$-solution obtained about 2 min after adding isotope and just before uptake was terminated. The solution pH, 8.4 at the start of the experiment, decreased by 0.4 units, or less, over the 90-min experimental period.

At the end of an isotope treatment the cells were removed from the flow cylinder, the silk threads severed, and the cells rinsed before being bathed for 5 min in CPW/B to remove external $^{14}C$. Individual cells were then blotted and placed in scintillation vials where they were treated (60 min) with 0.1 ml of 30% $H_2O_2$ and 0.1 ml of 7% perchloric acid to digest the tissue, prevent chlorophyll quenching during scintillation counting and remove unfixed $^{14}C$. Tissue was suspended in 10 ml of Beckman Filtersolv and radioactivity measured in a Beckman LS 9800 liquid scintillation system. Influx into each cell was calculated using its measured surface area. Each treatment consisted of 10 cells. Results are reported as: average ± SE.

## Results

### *Miniature Versus Micro pH Electrode Measurements*

Our initial experiments were directed towards comparing the *Chara* cell wall pH profiles that were measured with a miniature pH electrode and a recessed-tip pH microelectrode. Figure 2 illustrates the striking difference observed between the pH profiles measured by the two pH electrodes; in the alkaline regions the profiles were quite similar, but in the $HCO_3^-$-transporting regions, only the recessed-tip pH microelectrode detected acidification of the medium to values below the pH of the bulk solution. Clearly, Walker et al. (1980) were corrected in their assessment that the miniature electrode was too large to accurately measure the localized pH gradients that develop within the immediate vicinity of the cell surface.

Experiments were also conducted in which we utilized the vibrating probe technique in conjunction with the miniature and micro pH electrodes

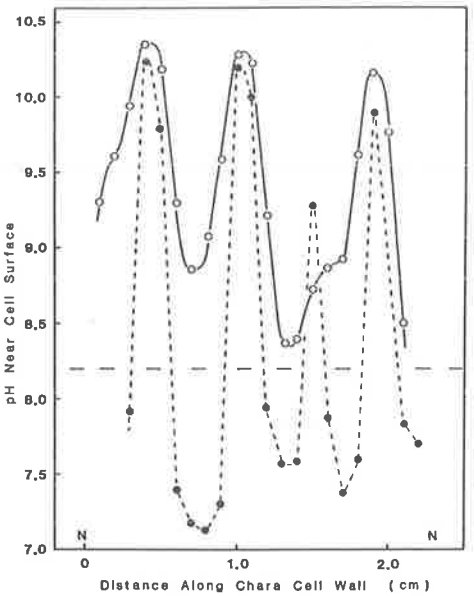


**Fig. 2.** Comparative pH profiles measured near the surface of *Chara* internodal cells during photosynthetic assimilation of exogenous $HCO_3^-$. Measurements were made using a miniature pH electrode (○) and a recessed-tip pH microelectrode (●). The miniature pH electrode was positioned such that the tip of the hemispherical electrode just touched the cell surface, while the tip of the pH microelectrode was maintained at a distance of 25 µm from the cell wall. The horizontal broken line represents the pH value of the bathing medium and the symbol *N* indicates the position of the nodes

(Fig. 3). From these studies we found an excellent correlation, within any given cell, between the profiles of current density and of pH, measured with the microelectrode (*cf.* Fig. 3*A* & *B*). For the cell in Fig. 3, for example, the current density in the acid bands indicates electrogenic fluxes of 120 to 170 pmol $cm^{-2}$ $s^{-1}$. If this current were entirely due to $H^+$ efflux, then this would be slightly larger than the $H^+$ efflux of 100 pmol $cm^{-2}$ $s^{-1}$ used in the models for formation of sufficient extracellular $CO_2$ (Ferrier, 1980; Walker et al., 1980) for uptake solely as $CO_2$. However, even if $H^+$ efflux is solely responsible for this electrogenic activity, it is clear that the pH value 25 µm from the cell wall (7.2 to 7.6) is substantially higher than the theoretical value (about 6.0) obtained from the models of Walker et al. (1980) and Ferrier (1980). Indeed, as the radial pH profile in Fig. 3*C* shows, we were unable to measure a pH value of less than 7.2 with the pH microelectrode positioned only 2 µm from the cell wall. In only one experiment of all those conducted did we measure a lower pH value. A major conclusion is, therefore, that the proton concentration at the cell wall appears to be at least 10-fold too low to yield sufficient $CO_2$ for the observed rates of photosynthesis at this pH value.

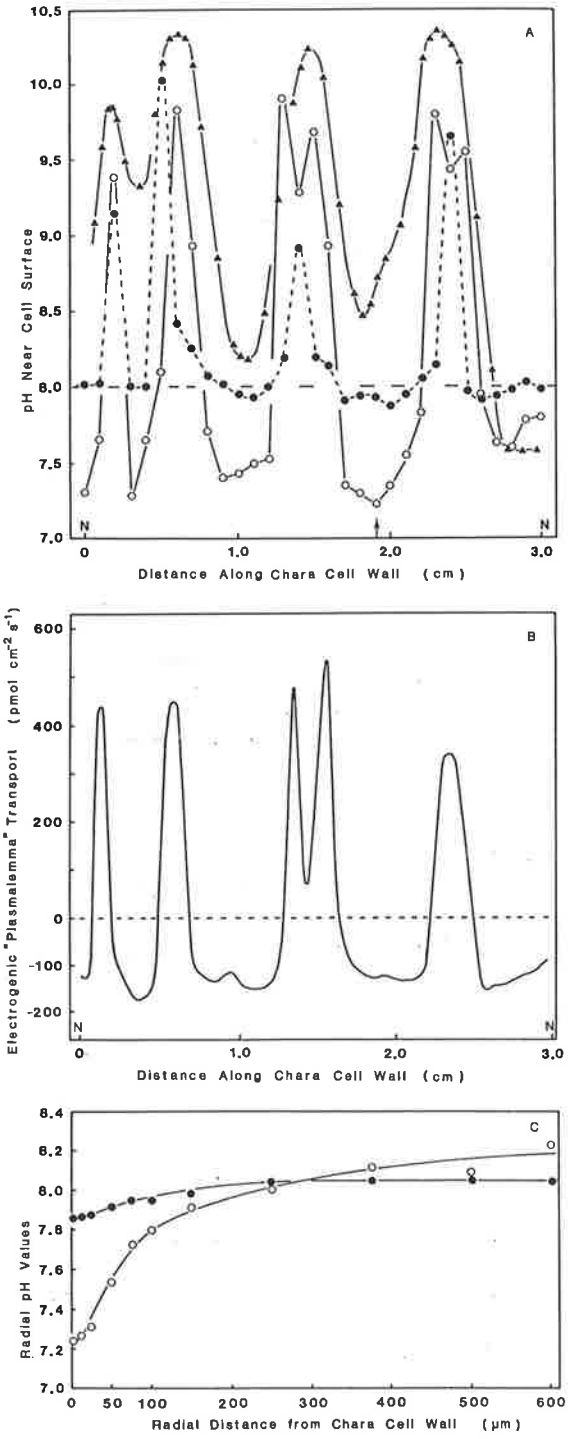


**Fig. 3.** Correlation between cell surface and radial pH profiles obtained along a *Chara* cell and the extracellular currents that were measured using the vibrating probe technique. *A:* Cell surface pH profiles measured using either a miniature pH electrode (▲) or a recessed-tip pH microelectrode (○). Micro pH electrode measurements were also made in CPW/B medium containing 5 mM phosphate buffer (●). Arrow indicates the position at which radial pH profiles were obtained (*see C*). *B:* Extracellular vibrating probe scan conducted on the same cell. *C:* Radial pH scans obtained using a recessed-tip pH microelectrode; ○, medium contained CPW/B; ●, CPW/B medium buffered by 5 mM phosphate

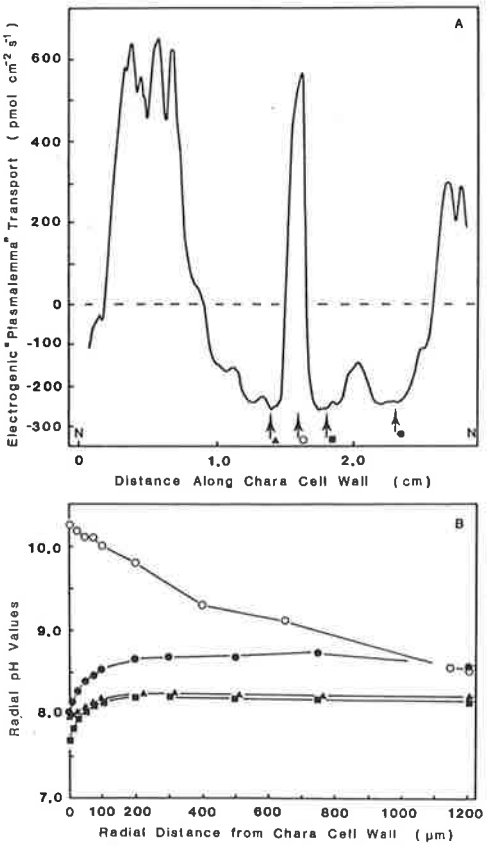


**Fig. 4.** Extracellular current (*A*) and radial pH profiles (*B*) measured on a *Chara* internodal cell bathed in CPW/B. The spatial positions along the cell at which the radial profiles were obtained are indicated by arrows in *A*

If the $CO_2$ permeation hypothesis were correct, then the observed currents in the acid bands (which would be due to $H^+$ efflux across the plasmalemma) should be positively correlated with the pH value at the cell surface. Comparison of the radial pH profiles and current scans for the two cells in Figs. 3 and 4 shows that this is not the case. In Fig. 3*C*, the pH value of the cell surface was 7.22, in a region where the outward current indicates the presence of an electrogenic flux of 130 pmol $cm^{-2}$ $s^{-1}$, whereas in Fig. 4*B*, the pH was never below 7.65 and yet the electrogenic flux was 250 pmol $cm^{-2}$ $s^{-1}$. However, the interpretation of these pH values is complicated by the increase in pH that would be caused by $CO_2$ leaving the $HCO_3^-$ solution and entering the cell. The ionic identity of this outward current is considered in the Discussion.

### *Influence of Artificial Buffers on the pH and Extracellular Current Profiles*

Inclusion of 5 mM $HPO_4^{2-}$ (pK = 7.2) or HEPES (pK = 7.55) buffer in the CPW/B significantly

**Table 1.** Effect of exogenous buffers on $^{14}C$-fixation in *Chara corallina*[a]

| Treatment | $^{14}C$ Fixation (pmol $cm^{-2}$ $s^{-1}$) | % of Control |
|---|---|---|
| Control, unbuffered (except for 1.0 mM $NaHCO_3$) | 39±2 | – |
| 5 mM Phosphate buffer | 27±1 | 69 |
| 10 mM Phosphate buffer | 27±2 | 69 |
| 5 mM HEPES | 33±2 | 85 |
| 10 mM HEPES | 28±1 | 71 |

[a] Photosynthetic fixation was measured from $^{14}C$ incorporated during a 10-min uptake period in CPW/B, pH 8.2 (25 C and 20 W $m^{-2}$). In addition, the solution contained the buffer indicated in the Table. Values represent the mean ±SE; twelve cells were used per treatment

reduced the cell surface pH profiles, with the acid regions being influenced more so than the alkaline regions (Fig. 3*A*). As expected, this level of buffer significantly dissipated the radial pH gradients (Fig. 3*C*). According to the $CO_2$-production model, raising the pH value at the cell surface would reduce the concentration (and hence the flux) of $CO_2$ (Walker et al., 1980, Fig. 6). Therefore, the buffer should dramatically reduce the rate of $^{14}C$ fixation. The results presented in Table 1 indicate that photosynthesis was reduced when *Chara* cells were bathed in artificial buffer. However, levels of buffer which caused the proton concentration at the cell surface to be reduced by a factor greater than 4 (pH change from 7.22 to 7.84 in Fig. 3*C*) resulted in only a 30% reduction in $^{14}C$ fixation. The origins of this reduction are considered in the Discussion.

The influence of buffering the bathing medium on the extracellular currents was next examined. Since photosynthesis was reduced when cells were exposed to buffered medium, we anticipated that the extracellular currents would reflect this inhibition. A comparison of vibrating probe scans obtained under control (CPW/B) and buffered (CPW/B, plus 5 mM $HPO_4^{2-}$) conditions revealed that this was not the case (Fig. 5). The extracellular currents in the acid regions were unaffected by the presence or absence of buffer (either $HPO_4^{2-}$ or HEPES at 5 to 10 mM). The total $OH^-$ current of the cell was also unaffected, but at times there seemed to be a slight redistribution of the $OH^-$ fluxes between the various alkaline bands.

### *Reduction of the Unstirred Layer*

Walker et al. (1980) suggested that extracellular production of $CO_2$ would be highly efficient in the environment of the *Chara* cell, "because the

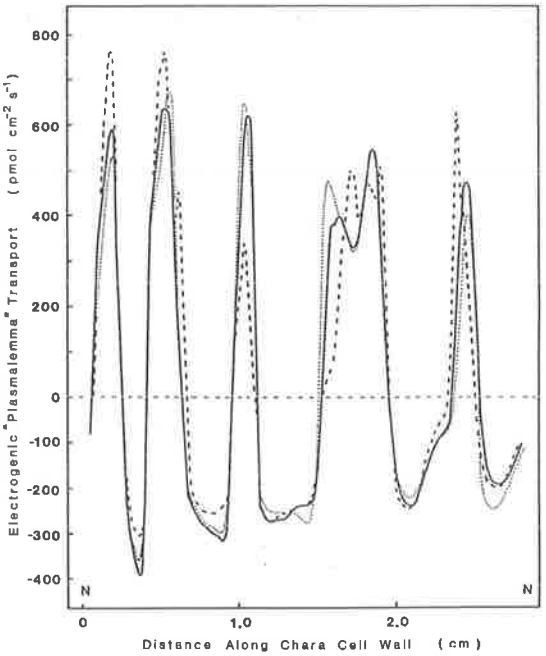


**Fig. 5.** Influence of artificial buffer on the extracellular currents that develop along the *Chara* cell during $HCO_3^-$ assimilation. The solid and dotted traces are representative control scans obtained when the cell was bathed in CPW/B. The broken trace is a typical scan obtained when the medium was buffered by 5 mM $Na_2HPO_4$

diffusion resistance of the unstirred layer retains the $CO_2$ that is produced near the cell surface, and the $H^+$ that flow out from the cell." Hence, an explicit prediction of the $CO_2$-production model would be that a reduction in the unstirred layer could cause a decline in the rate of photosynthesis. To test this prediction, we built a system that allowed us to vary the rate at which the experimental solution flowed past the *Chara* cell surface (*see* Fig. 1). Since we knew that $HCO_3^-$ assimilation in *C. corallina* is easily perturbed (*see*, e.g., Lucas & Nuccitelli, 1980), we took considerable care in the development of the protocol used in these experiments (*see* Materials and Methods). The results of these experiments are presented in Fig. 6. Under stagnant solution conditions we found the same rate of $H^{14}CO_3^-$ assimilation as obtained when we used our previous system (Lucas, 1975; Lucas & Dainty, 1977). The influence of solution flow, as a pretreatment, was investigated in a control experiment by exposing cells to a flow rate of 1.76 liters per min for 1 h and then measuring $^{14}C$ assimilation under stagnant conditions (Fig. 6, △). There did appear to be a slight perturbative effect on assimilation, but it was not serious. As the flow of experimental solution was increased, the rate of $^{14}C$ assimilation underwent an increase, not a

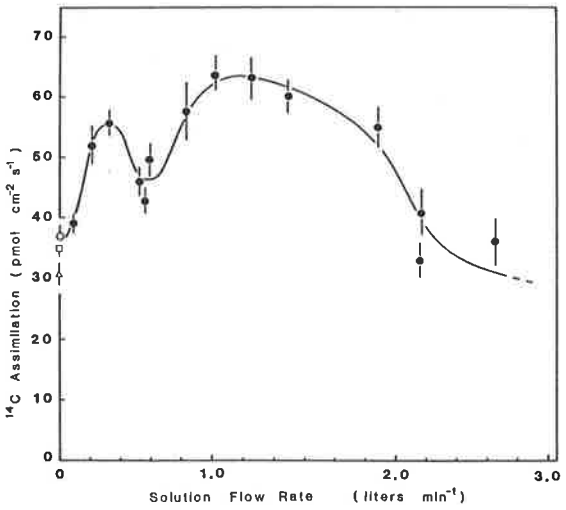


**Fig. 6.** Effect of reducing the unstirred layer on $^{14}C$ assimilation in *Chara* internodal cells. The apparatus illustrated in Fig. 1 was used to conduct experiment under both stagnant (○) and flowing (●) solution conditions. All measurements were performed in the presence of 0.5 mM total inorganic carbon. The symbol, □, represents $^{14}C$ assimilation measured using the technique of Lucas (1975). In one experiment (△), cells were pretreated for 1 h in flowing solution (1.76 liters per min) and then $^{14}C$ assimilation was measured in a stagnant solution. In all other experiments, pretreatment (1 h) and $H^{14}CO_3^-$ exposure (30 min) were at the indicated rate of solution flow. (Values represent the mean and SE for 10 cells.)

decrease. Intermediate flow rates resulted in a transient decrease in $^{14}C$ fixation, back towards the stagnant-solution values, with a subsequent recovery at the higher flow rates; at very high flow rates $^{14}C$ fixation again declined.

*Flow Velocity Near the Cell Wall*

In correlating the $^{14}C$-fixation rate with the rate of volume flow through the experimental system (Fig. 6), it is important to know the actual flow velocities near the cell surface. By making the assumption that the cells mounted in the fast flow chamber do not significantly alter the chamber geometry, our system can be approximated as fluid flow through the annulus between two concentric round tubes. This geometry has been treated in many texts on fluid dynamics (*see*, e.g., Streeter, 1958) and from the equations so derived the velocity ($U$) of fluid flow, at a distance $x$ from the inner surface, can be given in terms of the fluid volume flow rate $Q$:

$$\frac{U(x)}{Q}=\frac{2}{\pi}\frac{a^2-b^2-2bx-x^2+\dfrac{a^2-b^2}{\ln b/a}\ln\dfrac{a}{(b+x)}}{(a^2-b^2)(a^2+b^2)-(a^2-b^2)^2/\ln a/b} \quad (1)$$

where $a$ and $b$ are the radii of the inner and outer surfaces, respectively. In our system $a=0.47$ cm and $b=0.79$ cm, thus for $U(x)$ in cm/s, $Q$ needs to be in ml/s. For small values of $x$ ($<0.01$ cm), this relationship can be reduced to: $U(x)/Q=16.4x$. This says, for example, that if the flow rate through the chamber is 1 liter/min (16.7 ml/s) the fluid flow 50 μm from the cell surface is 1.34 cm/s. These calculations apply, of course, only to the surface of the cell facing the fluid flow; the flow rate on the side facing the central support would be greatly reduced. Relating this flow velocity to an unstirred layer thickness is difficult, because the unstirred layer thickness is not defined in terms of the flow rate. But if we assume that the unstirred layer thickness would be the distance from the cell where the permeability rate ($P$) by diffusion through that layer is comparable to the flow velocity component perpendicular to the cell at that point, then we can define such a thickness. Further, if the fluid flow has a component of flow perpendicular to the cell that is 1% of the flow parallel to the surface, $U(x)$, (probably an underestimate), then: $P=D/x=0.01\ U(x)=(0.01)\ (16.4)\,Q\,x$, where $D$ = diffusion coefficient $=1.1\times10^{-5}$ cm/s for $HCO_3^-$ in aqueous solution (Walker et al., 1980), with the other terms as defined above. This can be rearranged to give:

$$x=\left(\frac{D}{0.16\,Q}\right)^{\frac{1}{2}}. \quad (2)$$

We see that the unstirred layer thickness is inversely proportional to the square root of the flow rate. For the above example (1 liter/min flow rate), this gives an unstirred layer thickness of approximately 20 μm. If the perpendicular component of flow were larger, say 4% of the parallel flow, then the unstirred layer thickness would be reduced to 10 μm in this example.

## Discussion

*Evidence Against the $CO_2$ Model*

The present results clearly indicate that in alkaline media (pH 8 to 9) *Chara* internodal cells acidify regions along the cell wall, and these regions are coincident with the areas along the wall where we detected $HCO_3^-$-associated currents (Fig. 3 *A* & *B*). At first sight these findings appear to offer experimental support for the theoretical $CO_2$-generating model forwarded by Ferrier (1980) and Walker et al. (1980). However, a detailed comparison between our experimental findings and the predictions of the theoretical model(s) indicate that the

model is invalid. First, the $CO_2$ model suggests that the pH value at the *Chara* cell should be 6.0 in order for $CO_2$ to be produced at rates consistent with experimentally determined rates of photosynthesis (i.e. rates under alkaline conditions). We were unable to detect this level of acidification. Indeed, the pH value 2 μm from the cell wall was seldom lower than 7.2 (*compare* Fig. 3*C* with Fig. 3 of Walker et al., 1980). Second, the $CO_2$ model proposes that the outward current in the acid regions is due to electrogenic $H^+$ efflux. If this were the case, we would expect to find a relationship between the electrogenic fluxes (currents) in the acid regions and the level of surface acidification (only slightly complicated by the proposed entry of $CO_2$ into the cell), when comparing different cells. However, as shown in Figs. 3 and 4, we could find no such correlation. Although the $HCO_3^-$-associated currents were stable, the degree of cell surface acidification was quite variable. Third, raising the pH value within the unstirred layer, by means of a buffer did not result in a dramatic reduction in $^{14}C$-fixation (Table). The $CO_2$ model predicts that production of exogenous $CO_2$, and hence $^{14}C$-fixation, would be sensitive to alteration of cell surface pH by exogenous buffer. The reason for the partial inhibition of photosynthesis, observed in the presence of buffer, will be discussed in a later section. Finally, if $CO_2$ molecules were actually being produced in the unstirred layer, then flowing solution past the cell surface should deplete the $CO_2$ available for diffusion into the cell; i.e. photosynthesis should be reduced under flowing-solution conditions. Photosynthesis was actually enhanced under these conditions (Fig. 6), a result quite incompatible with the exogenous $CO_2$ production model.

### *Mitigating Circumstances for the $CO_2$ Model*

There are several possibilities as to the reason(s) for the discrepancies between our experimental findings and the predictions of the $CO_2$ model. Basic differences exist between our experimental system and the numerical model used by Walker et al. (1980). In the theoretical model the boundary layer thickness was set at 1.0 mm, while in our system analysis of the radial pH profile suggests that the boundary layer was approximately 200 μm in width. The narrower unstirred layer should cause the radial pH profile to be both steeper and reduced in magnitude. Whereas our experimental gradients were reduced in magnitude, the gradients were not steeper. Walker et al. (1980) obtained a theoretical gradient of 1.3 pH units over the initial 100 μm distance out from the cell surface, and this value was for a $H^+$ pump rate of 100 pmol $cm^{-2}$ $s^{-1}$. In our experiments, the measured pH gradients over this same distance were much less; e.g. in Fig. 3*C* the value was 0.55, and in Fig. 4*B* the values were approximately 0.25. The extracellular currents, in the region where these radial pH profiles were measured, were 130 (Fig. 3*C*) and 250 (Fig. 4*B*) pmol $cm^{-2}$ $s^{-1}$; these values reinforce our point concerning the lack of correlation between the observed currents and pH gradients.

Walker et al. (1980) reported that if in their model "the conditions are modified to include a representation of the cell wall, the results are very similar." Thus, almost all of their computations ignored the influence of the wall. In the absence of evidence of the contrary, it would seem unwise for us to assume that the cell wall of this species is homogenous throughout its width and length. Actually, the level of heterogeneity of the plasmalemma with respect to both the frequency and complexity of the charasomes (Franceschi & Lucas, 1980) suggests that changes in cell wall properties, in response to localize membrane transport function, may indeed be possible. This view is supported by the recent report that the cell wall of *Anabaena variabilis* undergoes sub-structural modification when cells are grown under low $CO_2$ culture conditions (Marcus et al., 1982).

### *Mechanism of $HCO_3^-$ Transport*

Under alkaline conditions, exogenous carbon does not appear to cross the plasmalemma of *Chara* solely via a $CO_2$ diffusion mechanism. The issue to be dealt with now concerns the discrimination between electrogenic $HCO_3^-$ uniport and the possibility of cotransport with $H^+$. The similarity between our measured surface pH and radial pH profiles (Figs. 3*C* and 4*B*) and those computed by Walker et al. (1980), assuming $HCO_3^- - H^+$ cotransport, offer support for the latter hypothesis. The partial inhibition of photosynthesis, observed when 5 or 10 mM buffer ($HPO_4^{2-}$ or HEPES) was included in the medium (Table 1), is also consistent with a $HCO_3^- - H^+$ cotransport mechanism. Given that the pH value within the cell wall is near the pK of the buffers used, the conjugate base of the buffer could inhibit $H^{14}CO_3^-$ transport by competing for $H^+$. Walker et al. (1980) offered a similar explanation to account for the inhibition of photosynthesis that Lucas (1975) found at pH values above 9.5, and in the presence of such buffers as

Tris, tricine and TES (Lucas, 1977). A $HCO_3^-$ uniport system should be stimulated by exogenous buffer, as the buffer would reduce the draw-down of the surface pH as $HCO_3^-$ is taken up, and the buffer would facilitate diffusion of $HCO_3^-$ through the unstirred layer. Hence, the observed inhibition appears to indicate that primary electrogenic $HCO_3^-$ transport does not occur in *Chara* (Lucas, 1976; Walker & Smith, 1977; Ferrier & Lucas, 1979).

*Interpreting the Flowing Solution Experiments*

A $HCO_3^- - H^+$ cotransport system or a $HCO_3^-$ electrogenic uniport system would respond to flowing solutions in at least three ways. First, a reduction in the unstirred layer would increase net photosynthesis by reducing the diffusion-limitation on the movement of substrate from the bathing medium to the plasmalemma. Second, flowing solutions would sweep away the $OH^-$ ions that were being released across the plasmalemma within the alkaline bands. This would serve to contain the alkaline band-associated pH increase along the cell wall and, thereby, allow a larger membrane surface area to engage in $HCO_3^-$ acquisition. Third, flowing solutions would keep the surface pH closer to that of the bulk pH. If cell surface acidification represents protons that have escaped being captured by the cotransport process(es), then flowing solution, by sweeping away protons, should reduce the efficiency of the $HCO_3^- - H^+$ cotransport process. It may be that relatively few protons are lost to the bulk solution, possibly due to confinement in the cell wall or within membrane structures like the charasomes (Franceschi & Lucas, 1980), where these protons are quickly transferred from the $H^+$-electrogenic pump to the $HCO_3^- - H^+$ cotransport system. Or alternatively, the $H^+$-translocating ATPase may not be the rate-limiting step in $^{14}C$-acquisition. On the other hand, if the cell surface acidification represents a draw-down of solution pH as $HCO_3^-$ is transported into the cell by a uniport mechanism, then flowing solution would stimulate uptake by reducing this pH draw-down. It is likely that the first two of these ways are more important than the third, so that the results of the flowing solution experiments, while clearly supporting $HCO_3^-$ uptake, are at least consistent with the proposed $HCO_3^- - H^+$ cotransport process.

The shape of the $^{14}C$-photosynthesis versus solution flow rate is intriguing. We have no simple explanation as to why the stimulation in photosynthesis decreased in the region of 0.5 liters per min, only to recover at higher flow rates. Although the cells were securely anchored to the central support, the flowing solutions could still induce individual cells to vibrate. Lucas and Nuccitelli (1980) found that *Chara* cells could be perturbed by certain frequency-amplitude combinations of the vibrating probe. The perturbing influence of the vibrating probe manifested itself in a dramatic change in the $OH^-$ efflux pattern along the *Chara* cell surface. If, at a certain flow rate, the *Chara* cells responded in a similar manner to that observed by Lucas and Nuccitelli (1980), the reduction in photosynthesis may reflect a limit on photosynthesis imposed by a reduction or alteration of $OH^-$ efflux.

*Nature of the Extracellular Current(s) in the Acid Bands*

Lucas and Nuccitelli (1980) showed that the extracellular current, in the acid regions of the *Chara* cell wall, was dependent upon the presence of exogenous $HCO_3^-$. If an electrogenic $HCO_3^-$ uniport system were operating across the plasmalemma, the outward extracellular current in the steady state would be carried almost entirely by this anion. However, our present data is more consistent with the operation of a $HCO_3^- - H^+$ cotransport process, and, thus, the nature of the ionic fluxes responsible for the extracellular current in the acid region becomes a little more complex.

In the presence of 5 or 10 mM $HPO_4^{2-}$ (or HEPES) buffer the extracellular current patterns were not reduced (Fig. 5), although photosynthesis, *per se*, was inhibited by approximately 30% (Table 1). Our interpretation is that competition for $H^+$ between the $HCO_3^- - H^+$ cotransport system and the exogenous buffer reduced $HCO_3^-$ transport into the cells, so that photosynthesis was depressed. But $H^+$ efflux was not affected as the protons were carried away from the $H^+$-electrogenic pump by diffusion of the buffer. The buffer facilitates the movement of $H^+$ away from the cell surface by diffusing away from the membrane, through the unstirred layer, in the protonated form (Gutknecht & Tosteson, 1973). The result is a net flow of positive charge away from the cell. If the limitation on photosynthesis is the rate of the $H^+$-electrogenic pump, then the buffer, by carrying $H^+$ away from the cell, would reduce $HCO_3^-$ uptake. But in the unstirred layer no change would be observed in the current, as the vibrating probe can not distinguish between a current of $HCO_3^-$ and

a current of protonated buffer. This process depends on the rate of diffusion of the buffer; if a less mobile buffer were used, then it should be less effective at inhibiting $^{14}C$-fixation. That is borne out by our data: at a concentration of 5 mM, HEPES (mol wt = 238) is less effective than is phosphate (mol wt = 96). With phosphate the inhibitory effect is already saturated by a 5 mM concentration; with HEPES it takes 10 mM to reach equivalent levels of inhibition.

In a recent study, Lucas (1982) found that the extracellular current in the $HCO_3^-$-transporting region of the cell can be maintained in the absence of exogenous $HCO_3^-$, provided the $HCO_3^-$ is replaced with 1 mM $HPO_4^{2-}$. Lucas (1982) concluded from this that the $H^+$translocating ATPase must be separate from the $HCO_3^- - H^+$ cotransport system and that it is possible to effectively decouple the two systems.

### *The Problems of Modelling this System*

Throughout this paper we have constantly compared our experimental results with the mathematical modelling done by Ferrier (1980) and by Walker et al. (1980). Walker et al. (1980) specifically modelled the proposed $HCO_3^- - H^+$ cotransport system. In comparing our experimental data with their predicted radial pH profiles, we noted the similarities but the fit was less than perfect. There are at least two simplifying assumptions in their model(s) that could be the cause of these differences. First is the elimination of the cell wall from most of their modelling. Not only does the cell wall provide a reaction space where $H^+$ would be restricted from free exchange with the bulk solution, but there are the charasome structures (Francheschi & Lucas, 1980) that may be important. These charasomes are found at higher density in the acid bands (Franceschi & Lucas, 1980), the region where $HCO_3^-$ (Lucas, 1976) and $Cl^-$ (Spear, Barr & Barr, 1969) are taken up into Characean cells. Since *Nitella flexilis* exhibited the same acid and alkaline banding pattern but did not possess the charasome structure, Franceschi and Lucas (1980) suggested that the charasome may not be involved in $HCO_3^-$ transport. It will be of considerable interest to conduct recessed-tip micro pH electrode studies on *Nitella* species to further test this hypothesis.

In the present study, we provide evidence that $HCO_3^-$ is taken up by a $H^+$-cotransport system, as has been shown for $Cl^-$ (Sanders, 1980). It could be that the charasome is a structure which makes these cotransport systems much more efficient (*see* Franceschi & Lucas, 1982). If this is so, then the analysis in Walker et al. (1980) of the relative efficiency of the transport models versus unstirred layer (Fig. 4) (Walker et al., 1980) could be an underestimate. This is supported by our finding that reduction of the unstirred layer stimulates $^{14}C$-fixation (Fig. 6) rather than inhibiting it. It may be that accurate modelling will have to incorporate both the charasome volume and the cell wall space.

Second, although the external electric potentials measured in the acid and alkaline regions (Walker & Smith, 1977) have been shown to be of little consequence in driving the fluxes of $OH^-$ (Ferrier & Lucas, 1979), it should not be concluded that this is also true for the $HCO_3^-$ situation, especially within the wall. These potentials will influence the diffusion of $HCO_3^-/CO_2$ and charged buffers; that this is an important effect has been shown both experimentally and theoretically by Meldon, Smith and Colton (1977). Although Ferrier (1980) suggested that the influence of this external potential and the surface potential of the membrane had little effect, this aspect warrants further investigation. While it may not be easy or possible, at present, to incorporate these changes into the computer models, it certainly makes clear the complexity of biological systems.

### *Why Does Chara Maintain Acid and Alkaline Regions?*

We feel that our present results invalidate the proposal that *Chara* establishes discrete acid and alkaline regions along the cell wall to enable the acquisition of exogenous carbon by $CO_2$ diffusion. A more valid interpretation appears to be that the cell establishes localized regions of acidity to provide a high enough $H^+$ concentration to drive the cotransport of $HCO_3^-$ and $Cl^-$. (For evidence in support of $Cl^- - 2H^+$ cotransport *see* Sanders, 1980.) Under the alkaline conditions in which this species grows it may also be necessary to establish acid regions along the cell to enable cell wall extension.

On a more general note, it should be realized that for many aquatic organisms there is considerable evidence in support of the hypothesis that these species can utilize exogenous $HCO_3^-$, *per se*, rather than $CO_2$. (For an analysis of this literature, *see* Lucas, 1983.) The point of interest in the future will be to determine if all $HCO_3^-$ assimilators utilize a $HCO_3^- - H^+$ cotransport mechanism, or

whether, in some species, a primary active electrogenic $HCO_3^-$ transport system actually exists (*see*, for example, Kaplan et al., 1982). Obtaining unequivocal evidence in support of the latter mechanism may be difficult.

This study was supported by National Science Foundation Grants PCM 81-17721 and PCM 80-03133. D.S. was supported by Grant GM 15858, National Institutes of General Medical Sciences, awarded to C.L. Slayman. Thanks are also due to Ms. Carol Whitman for assistance in performing some of the pH scan experiments, and to Messrs. Young and Tallon of our Physical Plant Workshop for their excellent technical assistance.

## References

Arens, K. 1933. Physiologisch polarisierter massenaustausch und photosynthese bei submersen wasserpflanzen I. *Planta* **20**:621–658

Arens, K. 1936. Physiologisch polarisierter massenaustausch und photosynthese bei submersen wasserpflanzen. II. Die Ca $(HCO_3^-)_2$-assimilation. *Jahrb. Wiss. Bot.* **83**:513–560

Browse, J.A., Dromgoole, F.I., Brown, J.M.A. 1979. Photosynthesis in the acquatic macrophyte *Egeria densa*. III. Gas exchange studies. *Aust. J. Plant Physiol.* **6**:499–512

Ferrier, J.M. 1980. Apparent bicarbonate uptake and possible plasmalemma proton efflux in *Chara corallina*. *Plant Physiol.* **66**:1198–1199

Ferrier, J.M., Lucas, W.J. 1979. Plasmalemma transport of $OH^-$ in *Chara corallina*. II. Further analysis of the diffusion system associated with $OH^-$ efflux. *J. Exp. Bot.* **30**:705–718

Franceschi, V.R., Lucas, W.J. 1980. Structure and possible function(s) of charasomes; complex plasmalemma-cell wall elaborations present in some Characean species. *Protoplasma* **104**:253–271

Franceschi, V.R., Lucas, W.J. 1982. The relationship of the charasome to chloride uptake in *Chara corallina:* Physiological and histochemical investigations. *Planta* **154**:525–537

Gutknecht, J., Tosteson, D.C. 1973. Diffusion of weak acids across lipid bilayer membranes: Effects of chemical reactions in the unstirred layers. *Science* **182**:1258–1260

Hood, D.W., Park, K. 1962. Bicarbonate utilization by marine phytoplankton in photosynthesis. *Physiol. Plant.* **15**:273–282

Jaffe, L.F., Nuccitelli, R. 1974. An ultrasensitive vibrating probe for measuring extracellular currents. *J. Cell Biol.* **63**:614–628

Kaplan, A., Zenvirth, D., Reinhold, L., Berry, J.A. 1982. Involvement of a primary electrogenic pump in the mechanism for $HCO_3^-$ uptake by the Cyanobacterium *Anabaena variabilis*. *Plant Physiol.* **69**:978–982

Lucas, W.J. 1975. Photosynthetic fixation of $^{14}$carbon by internodal cells of *Chara corallina*. *J. Exp. Bot.* **26**:331–346

Lucas, W.J. 1976. Plasmalemma transport of $HCO_3^-$ and $OH^-$ in *Chara corallina:* non-antiporter systems. *J. Exp. Bot.* **27**:19–31

Lucas, W.J. 1977. Analogue inhibition of the active $HCO_3^-$ transport site in the characean plasma membrane. *J. Exp. Bot.* **28**:1321–1336

Lucas, W.J. 1982. Mechanism of acquisition of exogenous $HCO_3^-$ by internodal cells of *Chara corallina*. *Planta* **156**:181–192

Lucas, W.J. 1983. Photosynthetic assimilation of exogenous $HCO_3^-$ by aquatic plants. *Annu. Rev. Plant Physiol.* **34**:71–104

Lucas, W.J., Dainty, J. 1977. $HCO_3^-$ influx across the plasmalemma of *Chara corallina:* Divalent cation requirement. *Plant Physiol.* **60**:862–867

Lucas, W.J., Nuccitelli, R. 1980. $HCO_3^-$ and $OH^-$ transport across the plasmalemma of *Chara corallina:* Spatial resolution obtained using extracellular vibrating probe. *Planta* **150**:120–131

Lucas, W.J., Smith, F.A. 1973. The formation of alkaline and acid regions at the surface of *Chara corallina* cells. *J. Exp. Bot.* **24**:1–14

Marcus, Y., Zenvirth, D., Harel, E., Kaplan, A. 1982. Induction of $HCO_3^-$ transporting capability and high photosynthetic affinity to inorganic carbon by low concentration of $CO_2$ in *Anabaena variabilis*. *Plant Physiol.* **69**:1008–1012

Meldon, J.H., Smith, K.A., Colton, C.K. 1977. The effect of weak acids upon the transport of carbon dioxide in alkaline solutions. *Chem. Eng. Sci.* **32**:939–950

Miller, A.G., Colman, B. 1980. Evidence for $HCO_3^-$ transport by the blue-green alga (Cyanobacterium) *Coccochloris peniocystis*. *Plant Physiol.* **65**:397–402

Österlind, S. 1949. Growth conditions of the alga *Scenedesmus quadricauda* with special reference to the inorganic carbon sources. *Symb. Bot. Ups.* **10**:1–141

Prins, H.B.A, Snel, J.F.H., Helder, R.J., Zanstra, P.E. 1979. Photosynthetic bicarbonate utilization in the aquatic angiosperms *Potamogeton* and *Elodea*. *Hydrobiol. Bull.* **13**:106–111

Prins, H.B.A., Snel, J.F.H., Helder, R.J., Zanstra, P.E. 1980. Photosynthetic $HCO_3^-$ utilization and $OH^-$ excretion in aquatic angiosperms: Light-induced pH changes at the leaf surface. *Plant Physiol.* **66**:818–822

Prins, H.B.A., Snel, J.F.H., Zanstra, P.E., Helder, R.J. 1982. The mechanism of bicarbonate assimilation by the polar leaves of *Potamogeton* and *Elodea*. $CO_2$ concentrations at the leaf surface. *Plant Cell Environ.* **5**:207–214

Raven, J.A. 1968. The mechanism of photosynthetic use of bicarbonate by *Hydrodictyon africanum*. *J. Exp. Bot.* **19**:193–206

Raven, J.A. 1970. Exogenous inorganic carbon sources in plant photosynthesis. *Biol. Rev.* **45**:167–221

Ruttner, F. 1947. Zur frage der karbonatassimilation der wasserpflanzen. I. Teil: Die beiden haupttypen der kohlenstoffaufnahme. *Oesterr. Bot. Z.* **94**:265–294

Sanders, D. 1980. The mechanism of $Cl^-$ transport at the plasma membrane of *Chara corallina:* I. Cotransport with $H^+$. *J. Membrane Biol.* **53**:129–141

Sanders, D., Slayman, C.L. 1982. Control of intracellular pH: Predominate role of oxidative metabolism, not proton transport in the eukaryotic microorganism *Neurospora*. *J. Gen. Physiol.* **80**:377–402

Smith, F.A. 1968. Rates of photosynthesis in Characean cells. II. Photosynthetic $^{14}CO_2$ fixation and $^{14}$C-bicarbonate uptake by Characean cells. *J. Exp. Bot.* **19**:207–217

Smith, F.A., Walker, N.A. 1980. Photosynthesis by aquatic plants: Effects of unstirred layers in relation to assimilation of $CO_2$ and $HCO_3^-$ and to carbon isotopic discrimination. *New Phytol.* **86**:245–259

Spanswick, R.M. 1981. Electrogenic ion pumps. *Annu. Rev. Plant Physiol.* **32**:267–289

Spear, D.G., Barr, J.K., Barr, C.E. 1969. Localization of hydrogen ion and chloride ion fluxes in *Nitella*. *J. Gen. Physiol.* **54**:397–414

Steemann-Nielsen, E. 1947. Photosynthesis of aquatic plants

with special reference to the carbon sources. *Dan. Bot. Ark.* **12**:1–71

Steemann-Nielsen, E. 1960. Uptake of carbon dioxide by the plant. *In:* Encyclopedia of Plant Physiology. W. Ruhland, editor. Vol. 5/1, pp. 70–84. Springer-Verlag, Berlin

Steemann-Nielsen, E. 1963. On bicarbonate utilization by marine phytoplankton in photosynthesis. With a note on carbamino carboxylic acids as a carbon source. *Physiol. Plant.* **16**:466–469

Streeter, V.L. 1958. Fluid Mechanics. McGraw-Hill, New York

Talling, J.F. 1976. The depletion of carbon dioxide from lake water by phytoplankton. *J. Ecol.* **64**:79–121

Thomas, R.C. 1978. Ion-Sensitive Intracellular Microelectrodes: How to Make and Use Them. Academic Press, London, pp. 32–44

Walker, N.A., Smith, F.A. 1977. Circulating electric currents between acid and alkaline zones associated with $HCO_3^-$ assimilation in *Chara*. *J. Exp. Bot.* **28**:1190–1206

Walker, N.A., Smith, F.A., Cathers, I.R. 1980. Bicarbonate assimilation by fresh-water charophytes and higher plants: I. Membrane transport of bicarbonate ions is not proven. *J. Membrane Biol.* **57**:51–58

Watt, W.D., Paasche, E. 1963. An investigation of the conditions for distinguishing between $CO_2$ and bicarbonate utilization by algae according to the methods of Hood and Park. *Physiol. Plant.* **16**:674–681

Received 24 August 1982; revised 3 December 1982

Plant Physiol. (1984) 74, 61–66
0032-0889/84/74/0061/06/$01.00/0

# Perturbation of *Chara* Plasmalemma Transport Function by 2[4(2′,4′-Dichlorophenoxy)phenoxy]propionic Acid[1]

Received for publication July 14, 1983 and in revised form September 15, 1983

WILLIAM J. LUCAS*, CLYDE WILSON, AND JOHN P. WRIGHT
*Department of Botany, University of California, Davis, California 95616 (W. J. L., C. W.); and Metabolism and Radiation Research Laboratory United States Department of Agriculture, Science and Education Administration, Agricultural Research Service, and Botany Department, North Dakota State University, Fargo, North Dakota 58105 (J. P. W.)*

## ABSTRACT

**Electrophysiological measurements on internodal cells of *Chara corallina* Klein ex Willd., em. R.D.W. revealed that in the presence of (2-[4-(2′,4′-dichlorophenoxy)phenoxy]propionic acid) (diclofop) the membrane potential was very sensitive to the pH of the bathing medium. At pH 5.7, 100 micromolar diclofop caused a slow reduction in the electrogenic component of the membrane potential to the value of −123 ± 5 millivolts. Membrane resistance initially decreased, recovered transiently, then stabilized at approximately 65% of the control value. At pH 7.0, the potential appeared to plateau around −200 millivolts before rapidly declining to −140 ± 4 millivolts; removal of diclofop resulted in recovery of the electrogenic component. Diclofop reduced cytoplasmic ATP levels by 96.4% and 36.6% at pH 5.7 and 7.0, respectively. At pH 8.2, diclofop did not change the ATP concentration significantly, but induced a hyperpolarization of the membrane potential to near −250 millivolts, and also reduced or inhibited the dark-induced hyperpolarization; the light-induced depolarization was reduced to a lesser extent. DCMU applied in the light elicited the same response at the plasmalemma as placing cells in the dark. When $K^+$ channels were opened and cells depolarized with 10 millimolar $K^+$, diclofop induced a further depolarization of approximately 30 millivolts. Cells decoupled with $HPO_4^{-2}$ were still sensitive to diclofop. Currents associated with $OH^-$ efflux and $HCO_3^-$ influx, as measured with a vibrating probe technique, became spatially destabilized and reduced in magnitude in the presence of diclofop. After 60 minutes, most of the cell surface was engaged in a low level of $OH^-$ efflux activity. The results indicate that diclofop may be a proton ionophore at pH 7.0 and 5.7. At pH 8.2, diclofop may inhibit the operation of the $H^+$-ATPase and $OH^-$ efflux systems associated with $HCO_3^-$ transport by perturbing the control processes that integrate the two, without a reduction in ATP concentration.**

The phytotoxic effects of diclofop,[2] the primary metabolite of the herbicide diclofop-methyl (methyl-2-[4-(2′,4′-dichlorophenoxy)phenoxy]propanoate, Hoelon) (34), include chlorosis of treated areas (6), antagonism of IAA-induced growth and proton extrusion (34), increased leakage of electrolytes from treated leaves (5), and severe ultrastructural damage (3). These toxic symptoms may represent secondary responses to diclofop's primary effect of increasing the proton permeability of the plasma membrane with the subsequent collapse of the proton electrochemical potential gradient, alteration of cytoplasmic pH, and loss of membrane transport activity. However, the effects of diclofop acting as a weak acid or proton ionophore explain neither the previously observed differences in herbicidal activity between stereoisomers of this and related compounds (1) nor the differences in activity seen for various phenoxypropionic acid derivatives (28). The structural requirements for activity suggest that diclofop may also interfere with specific, membrane-bound, enzyme-mediated processes.

In recent herbicide mode of action studies, Wright and Shimabukuro (39) found that diclofop rapidly abolished the electrogenic component of the membrane potential of oat and wheat coleoptile cells. A 100 $\mu$M solution was sufficient to depolarize the membrane potential ($E_m$) of these cells to the diffusion potential ($E_D$) with a half-time of 15 to 20 min in oats and 35 to 40 min in wheat. The depolarizing response was not caused by an increase in the permeability of the plasmalemma to $K^+$, $Na^+$, $Cl^-$, or $SO_4^{2-}$ since the $E_m$ response to changes in the external concentrations of these ions was unaltered by pretreatment with diclofop, and because the $E_D$ remained unchanged in the presence of this chemical. In both oats and wheat, diclofop did increase the membrane permeability to protons, making the $E_m$ strongly dependent upon the external pH in the range of 5.5 to 8.5. Diclofop also appeared to increase the $K^+$-stimulated ATPase activity (pH 6) of oat roots; this activity is thought to be associated with the proton pump of the plasmalemma (Wright and Shimabukuro, unpublished).

As a result of extensive physiological and biophysical studies on the Characeae (8, 37, 19), much is known concerning the plasma membrane transport properties of these giant cells. The present study was therefore conducted to investigate the influence of diclofop on the *Chara* system.

## MATERIALS AND METHODS

**Culture Material.** *Chara corallina* Klein ex Willd., em. R.D.W. (= *C. australis* R. Br.) was grown in the laboratory in 120-L containers in solutions containing (mM): 3.0 $Na^+$, 0.2 $K^+$, 0.1 to 0.2 $Ca^{2+}$, 1.5 $Cl^-$, and approximately 2.0 $HCO_3^-$ (pH 8.0–9.0). For full details, see Keifer and Lucas (10). All experiments were performed on mature male internodal cells that were cut from the main axis of the vegetative shoot 1 or 2 d prior to being used in an experiment. During this pretreatment period, cells were bathed in an artificial *Chara* pond medium (CPW) containing (mM) 1.0 NaCl, 0.2 KCl, 0.2 $CaSO_4$, to which 1.0 $NaHCO_3$ (pH 8.2) had been added (CPW/B).

**Electrophysiological Experiments.** The equipment, electrodes,

[1] Supported by National Science Foundation Grant PCM 81-17721.

[2] Abbreviations: diclofop, 2-[4-(2′,4′-dichlorophenoxy)phenoxy]propionic acid; CPW, artificial *Chara* culture media; DNP, 2,4-dinitrophenol; CCCP, carbonyl cyanide *m*-chlorophenylhydrazone.

and methods used in these experiments have been previously described (10, 18). Membrane resistance was measured by the method of Hogg *et al.* (7), using a Pulsar 4i[3] pulse generator (Haer and Co., Brunswick, ME) connected to the inserted microelectrode through a $10^8$-ohm resistor. At 1- or 2-min intervals, 0.4 $\mu$amp of current was injected into the cell and the induced change in membrane potential was used to compute the specific resistance.

In some electrophysiology experiments, "$HCO_3^-$-free" solutions were employed, and these were prepared using the protocol detailed by Lucas (17, 18). The $NaHCO_3$ in the CPW/B solution was replaced by 1 mM $Na_2HPO_4$ (pH 8.2) and this solution was bubbled with $CO_2$-free air to remove residual inorganic carbon.

All electrophysiology experiments were conducted at 25°C under a 20 w $m^{-2}$ light intensity.

**External Current Measurements.** Extracellular currents near the cell wall of *Chara* internodal cells were measured using the vibrating probe system developed by Jaffe and Nuccitelli (9). Full details of the application of this technique to the *Chara* system have been reported by Lucas and Nuccitelli (22) and Lucas (18).

Local current densities ($\mu$amp $cm^{-2}$) were converted to flux densities by dividing by the faraday. All vibrating probe data are presented in terms of flux densities, in units of pmol $cm^{-2}$ $s^{-1}$. The convention followed was to display inward current ($OH^-$ efflux), which occurs in the alkaline regions (22, 23), as positive fluxes, and the outward current ($HCO_3^-$ influx) as negative fluxes.

**ATP Determination.** In order to extract many samples quickly and efficiently, we modified the procedure of Lee *et al.* (15). *Chara* cells were plunged into liquid $N_2$ and stored at −70°C for 1 to 2 d. The frozen *Chara* cells were transferred to culture tubes (1.2 × 10 cm) containing 3 ml of prechilled extraction media (0.2 N $H_2SO_4$, 25% [w/v] ethanol, and 15 mg Dowex chelating resin, dry mesh: 50–100). $H_2SO_4$ was preferred over $HClO_4$ since perchlorate has been shown to inhibit the luciferase reaction (4). Ethanol was included both to permeabilize the plasmalemma and depress the freezing point of the extraction medium to below −15°C. Dowex chelating resin was added to remove any heavy metal contaminants which could shift the emission peak of the firefly luminescence (33).

Tissue was incubated at −10°C for 3 h, after which the extract solution was decanted into chilled 25-ml beakers. A small volume (2 ml) of 200 mM Hepes buffer (pH 7.5) was used to rinse each culture tube and was combined with the extract. The resultant mixture was neutralized to pH 7.5 ± 0.1 with 130 $\mu$l of 5 N KOH, and then diluted 1:10 in preparation for the ATP assay. (Incubation of known amounts of ATP in the extraction medium, for 3 h at −10°C, indicated that ATP was not hydrolyzed under the above conditions.)

ATP content was determined using the luciferin-luciferase assay as described by Kimmich *et al.* (14). Firefly lantern extracts (luciferin-luciferase, Sigma FLE-50) were reconstituted with 5 ml $H_2O$ and then the background activity of this solution was allowed to decay (see [25]) over 4 h (24°C in dark). Debris was then removed from this preparation by centrifugation (10 min, 18,000*g*) and the enzyme was then treated with $Ca_3(PO_4)_2$ (14). Assays were performed on a Beckman LS 9800 liquid scintillation spectrometer using the coincident mode. Our protocol for ATP standards and cell extracts was as follows: 1825 to 1855 $\mu$l of assay medium (50 mM Hepes, 10 mM $MgSO_4$, 0.1 mM EDTA, 3.75 mM sodium arsenate, and 125 $\mu$l of luciferin-luciferase mixture) was placed into a plastic scintillation vial (5 ml); the reaction was initiated by introducing 20 to 50 $\mu$l of ATP standard or cell extract via the vial cap; a counting period (30 s) was initiated 15 s after starting the reaction. In agreement with Kimmich *et al.* (14), we obtained a linear relationship ($r^2 = 0.99$) between the rate of photons emitted and the square of the ATP content (0.5–4 pmol range).

ATP standards were interspersed along with cell extracts to monitor decay of enzyme activity. We report ATP levels as cytoplasmic concentrations; the cytoplasm was assumed to occupy 5% of the cell volume (29).

**Purification of Diclofop.** A quantity (220 ml) of formulated diclofop-methyl (360/g/l; Hoelson, HOE 23408 OH 225, Farbwerke Hoechst AG, Frankfurt) was evaporated in a rotary evaporator until approximately one-half of the organic solvents were removed. The remaining formulation was diluted with 10 L of distilled $H_2O$ and allowed to stand at room temperature for 4 d. Crystals of diclofop-methyl were recovered by filtration (Whatman 50 filter paper). The crystals were then washed with ice-cold water before being dried.

Diclofop (acid form) was obtained by hydrolyzing diclofop-methyl in 1 N KOH overnight at room temperature. Unhydrolyzed material was removed by partitioning the hydrolysate with methylene chloride. Diclofop was recovered from the aqueous phase by acidifying to pH 2 and repartitioning with methylene chloride. The organic fraction was evaporated to yield white fluffy crystals of diclofop which were twice purified by recrystallization from ether. The purified diclofop had a melting point of 121.5 to 122.3°C. The purity of the compound was also established using HPLC. A single, UV-absorbing peak was observed on a linear gradient of 25 to 100% $CH_3CN$:$H_2O$ acidified with acetic acid (1%), and its retention time was identical with that of a diclofop standard.

**Diclofop $pK_a$ Determination by $^1H$ NMR Spectroscopy.** Because of the limited aqueous solubility of diclofop, we had to employ proton NMR spectroscopy to determine the $pK_a$ of diclofop. A stock solution of diclofop was prepared in deuterated acetone and from this a 100 $\mu$M solution was prepared in $D_2O$. The pH value of the solution was adjusted, during the spectral scan, using either 0.1 N DCl or 0.1 N NaOD. $^1H$ NMR spectra were obtained at 360 MHz on a Nicolet-360 narrow bore spectrometer employing a Nicolet 293′ pulse programmer. The procedures employed were those described by Benisek and Ogez (2). Although we experienced slight difficulties in acidifying the solution, we obtained sufficient data. Our computed $pK_a$ for diclofop was 3.57 ± 0.08.

## RESULTS

**Diclofop-Induced Membrane Depolarization.** The influence of diclofop on the *Chara* membrane potential was very sensitive to the pH value of the bathing medium. At pH 5.7, 100 $\mu$M diclofop caused a slow but complex reduction in the electrogenic component(s) of the membrane potential; within 1 h the potential had stabilized at a value of −123 ± 5 mv (Fig. 1). Membrane resistance also exhibited a complex response to diclofop exposure: initially, the value decreased but then recovered transiently; finally, the value restabilized at approximately 65% of the control (pH 5.7) value. Generally, removal of diclofop from the pH 5.7 medium did not result in recovery of the electrogenic component (data not shown). When the bathing medium pH was raised to 7.0, we observed a similar response of the membrane potential to diclofop, except that the final phase of depolarization towards the diffusion level was even more complex. The potential appeared to plateau at around −200 mv, from which it eventually declined quite rapidly to −140 ± 4 mv (Fig. 2). Although the initial membrane resistance response to diclofop was the same at both pH 5.7 and 7.0, the final increase in resistance was much more pronounced at pH 7.0. The increase in resistance occurred

[3] Mention of a trademark or proprietary product does not constitute a guarantee or warranty of the product by the United States Department of Agriculture and does not imply its approval to the exclusion of other products that may also be suitable.

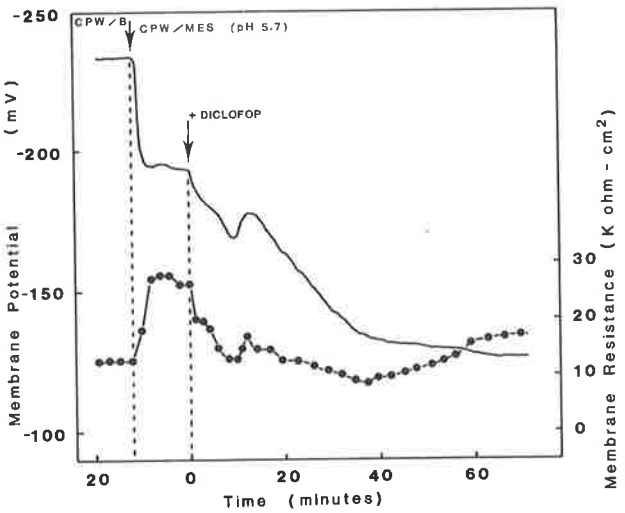


FIG. 1. Influence of 100 μM diclofop on the membrane potential and resistance (●) in *Chara corallina*. Cells were pretreated for 1 h in CPW/B (pH 8.2) before being exposed to CPW containing 1 mM Mes (pH 5.7); diclofop was introduced at pH 5.7.

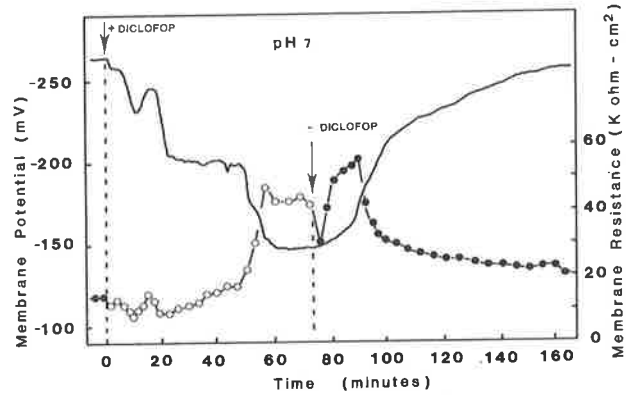


FIG. 2. Response of membrane potential and resistance (○, ●) to addition and removal of 100 μM diclofop, pH 7.0. A 1-h CPW/B pretreatment was employed before bathing the *Chara* cells in CPW plus 1 mM Hepes buffer, pH 7.0. Diclofop was introduced after a 30-min pH 7.0 pretreatment.

at the same time as the membrane potential declined to the diffusion level (Fig. 2). At pH 7.0, removal of diclofop always resulted in recovery of the electrogenic component of the membrane potential.

At alkaline pH (8.2), and in the presence of exogenous $HCO_3^-$, diclofop had a very different effect on *Chara*. The two types of responses that we observed are shown in Figure 3; the potential hyperpolarized and then stabilized near −250 mv. No loss of the electrogenic component was observed, even after prolonged exposure to 100 μM diclofop.

**Perturbation of $HCO_3^-$ Assimilation.** The influence of diclofop upon the sensitivity of the membrane potential to dark/light transitions was next studied. Diclofop appeared to reduce (Fig. 3A) or prevent (Fig. 3B) the hyperpolarization of the membrane potential which occurs when *Chara* internodal cells are transferred from light to dark (see [18]). However, the depolarizing phase associated with re-illumination did not appear to be as sensitive to diclofop (Fig. 3).

*Chara* cells that had been photosynthetically "decoupled" (18), by replacing $HPO_4^{2-}$ for the $HCO_3^-$, were still found to be sensitive to diclofop. In these decoupled cells, a brief dark treatment still elicited the rapid hyperpolarizing and depolarizing responses

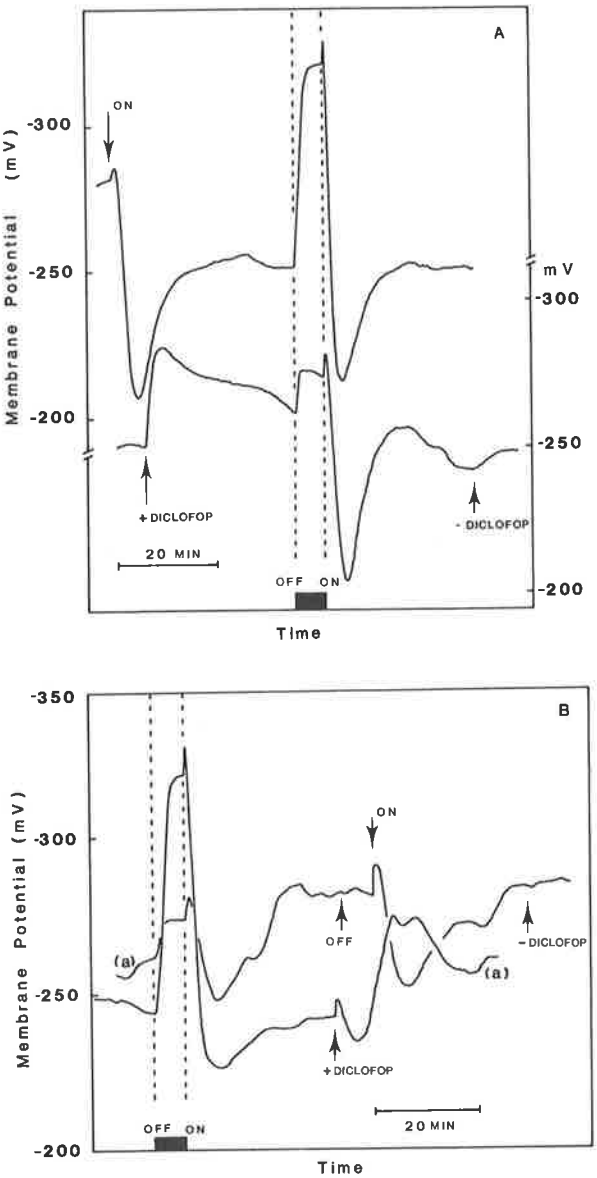


FIG. 3. Effect of 100 μM diclofop on the light sensitivity of the *Chara* membrane potential when the cell was bathed in CPW/B. A: Upper trace illustrates first the influence of light (20 w $m^{-2}$) on a cell that was given a 12-h dark pretreatment and second the effect of a short dark pulse (6 min) on the membrane potential. Lower trace shows the influence that diclofop had on both the membrane potential and its sensitivity to brief dark pulses. B: Conditions as in A, except that the cell was not given an overnight pretreatment in the dark. (a): indicates continuation of the experimental trace.

observed for control (+ $HCO_3^-$) cells (*cf.* Figs. 3 and 4). However, after 30-min exposure to diclofop, the magnitude of these responses was much reduced (Fig. 4).

Although we had recently found that isolated spinach chloroplasts were insensitive to diclofop (J. P. Wright, unpublished results), we further investigated this aspect by examining the effect of DCMU on the membrane potential of $HCO_3^-$-assimilating cells (Fig. 5). Inhibition of electron transport within the chloroplasts resulted in a hyperpolarization of the membrane potential with a time course identical with that obtained by a dark treatment. This DCMU effect on the membrane potential was completely reversible.

In an endeavor to correlate the electrophysiological responses

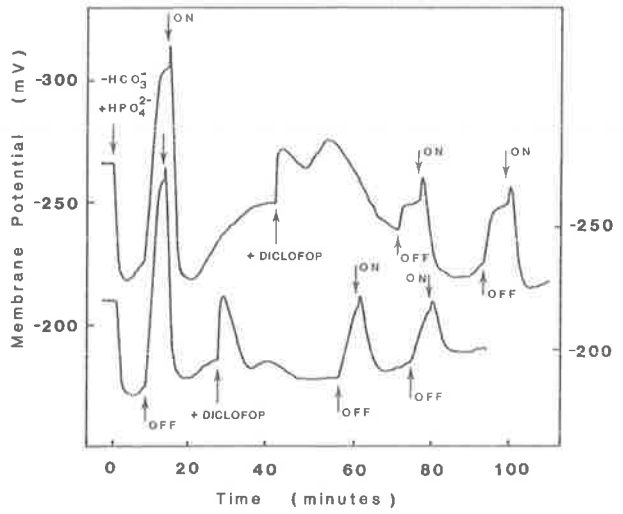


FIG. 4. Effect of diclofop (100 $\mu$M) on the membrane potential of "decoupled" *Chara* cells. For these experiments, the medium was buffered by 1 mM $Na_2HPO_4$ (8.2), but was "free" of exogenous $HCO_3^-$. Two experiments have been presented; scales for the upper and lower traces are on the left and right ordinates, respectively.

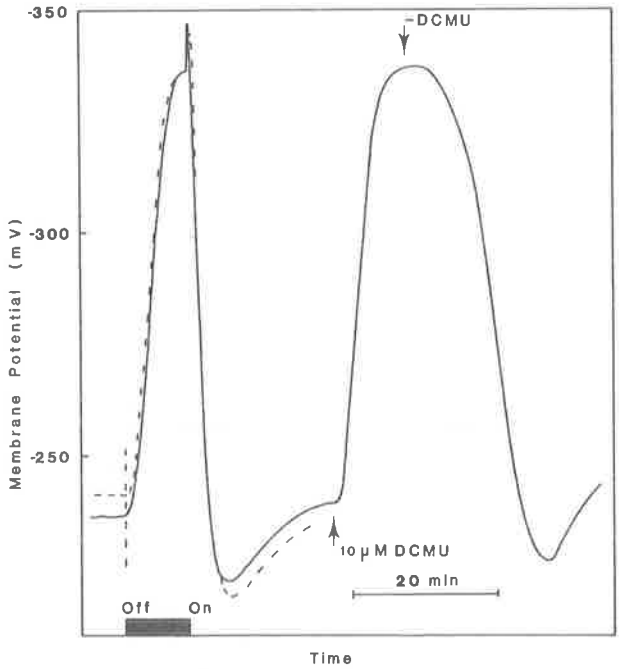


FIG. 5. Comparison between the influence of a dark pulse and 10 $\mu$M DCMU on the membrane potential of *Chara*. The experimental medium was CPW/B (pH 8.2) and the broken trace represents the cellular response to a brief dark pulse 60 min after DCMU was removed from the bathing medium.

with the physiological transport processes occurring across the plasmalemma, we next used the vibrating probe technique to examine the influence of diclofop on the $HCO_3^-$-associated extracellular currents that develop along the internodal cells of *Chara* (18, 21, 22, 38). Figure 6 illustrates both the spatial aspect of the currents along a typical *Chara* cell and the manner in which these currents responded to diclofop treatment. The $OH^-$ efflux regions appeared to be most influenced by the presence of diclofop. The position of the $OH^-$ efflux sites became destabilized and, in addition, the extracellular currents were quite erratic in nature. After 30 min in diclofop, the extracellular currents were

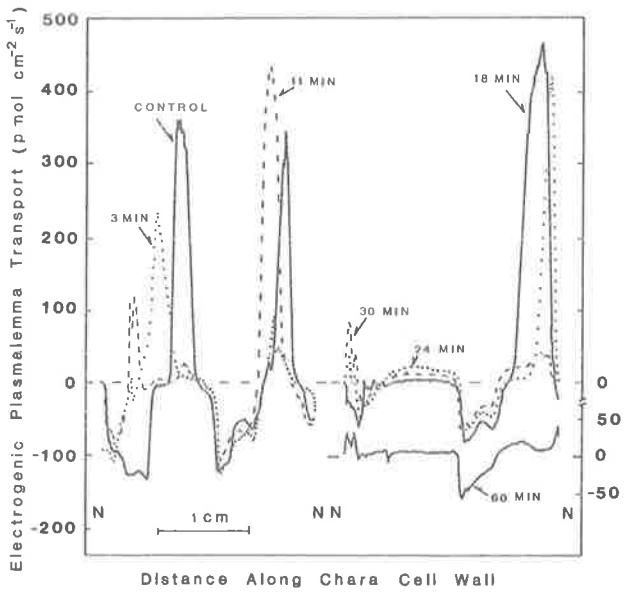


FIG. 6. Perturbative effect of 100 $\mu$M diclofop on the extracellular current patterns that develop along the *Chara* cell during $HCO_3^-$ assimilation. Current patterns were measured before (control) and after the introduction of diclofop and the times at which the respective traces were made is indicated. Note the change in scale position for the 60-min trace. N represents the position of each nodal complex.

dramatically reduced and, by 60 min, most of the cell surface was associated with a low level of inward current (assumed to represent reduced $OH^-$ efflux activity).

**$K^+$ Conductance Experiments.** Keifer and Lucas (10) recently demonstrated that the electrogenic $H^+$-translocating ATPase of the *Chara* plasmalemma continues to function in the presence of open $K^+$ channels. In this high $K^+$ permeability state, $HCO_3^-$ assimilation is perturbed and the photosynthetic rate is reduced to 15% of the control value (20, 24). We investigated the effect of diclofop on the depolarized *Chara* membrane at pH 8.2, and found that it consistently caused a depolarization of approximately 30 mv (Fig. 7). Under these conditions, removal of the high $K^+$ level in the bathing medium resulted in a rapid rehyperpolarization of the membrane potential. Whether diclofop was present or absent during the initial recovery caused little difference in the rise in potential. However, in the latter stage of recovery, a lower potential was established in the presence of diclofop (Fig. 7B). During this recovery phase, the membrane potential exhibited very reduced sensitivity to brief dark treatments (Fig. 7A). This may indicate that the $HCO_3^-/OH^-$ transport processes have not yet fully recovered from the 10 mM $K^+$ treatment.

**Diclofop Influence on Cellular ATP Levels.** Cellular ATP levels were measured to ascertain whether diclofop influenced membrane transport processes via a reduction in available energy. Table I indicates that at pH 5.7, 90-min exposure to diclofop caused a dramatic reduction in the cytoplasmic ATP level in *C. corallina*. As the treatment pH value was raised, the reduction in ATP level became less and at pH 8.2 the value did not differ from that of the control. It was also interesting to note that the control ATP levels were influenced by the pH value of the bathing medium (Table I).

## DISCUSSION

**Diclofop Effect: Weak Acid or Proton Ionophore?** Diclofop is a weak acid ($pK_a$ 3.57) that is very lipid soluble. Thus, in the undissociated form it may facilitate the movement of $H^+$ into

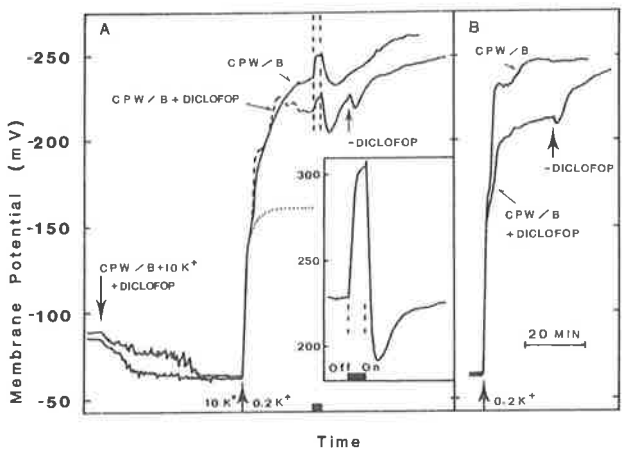


FIG. 7. Influence of diclofop (100 $\mu$M) on 10 mM $K^+$-depolarized *Chara* cells. A: Light/dark membrane sensitivity was established (see inset) prior to exposing cells to CPW/B + 10 mM KCl. The dotted line represents the passive phase of the membrane potential response to a reduction in external $K^+$ from 10 to 0.2 mM (see Keifer and Lucas, [10]). B: Membrane potential response to a reduction in $K^+$ (from 10 to 0.2 mM) following a 50-min pretreatment in CPW/B + 10 mM KCl + 100 $\mu$M diclofop; the response was observed in the presence and absence of diclofop.

Table I. *Influence of Diclofop and Solution pH on Cellular ATP Levels in C. corallina*

*Chara* cells were pretreated (20 w $m^{-2}$, 25°C) for 15 min in control solutions of the respective pH value before being exposed to 100 $\mu$M diclofop. Control and diclofop treatment solutions were changed at 10-min intervals, with the duration of diclofop exposure being 90 min. Cells were then transferred to test tubes filled with liquid $N_2$ and cellular ATP content was assayed as described in "Materials and Methods." Values presented are mean ± SE (10 cells/treatment).

| Solution pH Value[a] | ATP Content | |
|---|---|---|
| | Control | +100 $\mu$M Diclofop |
| | *mM* | |
| 5.7 | 5.28 ± 0.33 | 0.19 ± 0.04 (3.6%)[b] |
| 7.0 | 3.03 ± 0.28 | 1.92 ± 0.14 (63.4%) |
| 8.2 | 2.42 ± 0.26 | 2.74 ± 0.17 (100%)[c] |

[a] Solution composition was: pH 8.2, CPW/B; pH 7.0, CPW + 1.0 mM Hepes; pH 5.7, CPW + 1.0 mM Mes; 0.5% acetone was included in all media.

[b] Percentage of control value.

[c] Not statistically different.

the cytoplasm. Based on the weak acid effects observed in *Neurospora*, acidification of the cytoplasm would give rise to a transient hyperpolarization of the membrane potential (31, 32). We have found that 1.0 mM propionic acid ($pK_a$ 4.87) caused a 10 to 12 mv hyperpolarization (stable, half-time 5 min) of the *Chara* membrane potential when the bathing medium pH was 5.7. As expected, at pH 7.0 the response was reduced to about 2 mv (W. J. Lucas, unpublished results). However, the initial response to diclofop, at both pH 5.7 and 7.0, was a depolarization of the potential (Figs. 1 and 2). After approximately 10 min, the potential did undergo a transient hyperpolarization, but this response was the same at pH 5.7 and 7.0 and seems, therefore, not to be due to a weak acid effect. (The absence of such an effect could be due to the low concentration of diclofop used, which was set by its aqueous solubility.)

Lipid-soluble weak acids that can cross membranes in both the dissociated and undissociated forms often function as proton ionophores (eg. DNP, CCCP). Keifer and Spanswick (11, 12) made a thorough investigation of the effect of these agents on the *Chara* system. Certain similarities were observed between the diclofop effects and those found for DNP and CCCP. (a) The membrane potential depolarized towards the diffusion potential (in our cells $E_K$, the most negative passive membrane component, has a value of −143 mv [10] under the present media conditions). A close correlation between the time course of this depolarization in the presence of either diclofop or DNP (both 100 $\mu$M and pH 5.7 to 6.0) suggests a common function. (b) Membrane resistance exhibited transients before commencing a slow increase towards the dark-adapted value. (c) Cytoplasmic ATP levels declined in the presence of diclofop, DNP, and CCCP (*cf.* Table I and [12]). These correlations indicate that diclofop may function as a proton ionophore.

The transient hyperpolarization of the membrane potential and the related increase in resistance (see Figs. 1 and 2) indicate that the diclofop response is more complex than a simple effect on ATP levels. Changes in the actual rates of individual transport processes have been shown to cause transients in the membrane potential (16, 30). It is possible that diclofop influences other membrane transport processes (*e.g.* $Cl^-$ influx, $Na^+$ efflux, etc.) either directly, or via cell metabolism.

**Diclofop Perturbation of $HCO_3^-$ Assimilation.** Based on our recent studies (18, 21), it appears that exogenous $HCO_3^-$ is transported into *C. corallina* by the operation of a $H^+$–$HCO_3^-$ cotransport mechanism. The protons appear to be supplied through the operation of a $H^+$-translocating ATPase having a $1H^+$/ATP transport stoichiometry. Under $HCO_3^-$-assimilating conditions, the membrane potential is very sensitive to light/dark manipulations; brief dark periods cause the potential to rapidly hyperpolarize to −330 mv (Fig. 3). Lucas (18) has suggested that this dark response is due to a differential reduction in the transport rates of the $H^+$-ATPase and the $OH^-$ efflux ($H^+$ influx) systems.

In our present experiments, diclofop had a pronounced effect on the dark-induced hyperpolarization of the potential; the magnitude of this response was either reduced or entirely abolished (Fig. 3, A and B). However, the depolarizing phase associated with reillumination was influenced to a lesser degree. Based on our present $HCO_3^-$ transport model, it would appear that diclofop is either (a) directly inhibiting the operation of the $H^+$-ATPase or, (b) perturbing the control process(es) that integrates the spatially separate $HCO_3^-$ and $OH^-$ transport processes or, (c) inhibiting photosynthesis.

First, at pH 8.2, diclofop did not cause any reduction in the ATP levels within these cells (Table I). Hence, the absence of a dark-induced hyperpolarizing response and the reduction in the extracellular currents cannot be due to an ATP limitation on membrane transport processes. Second, it seems unlikely that diclofop is acting directly to inhibit the $H^+$-translocating ATPase, because over the time course of these pH 8.2 experiments such an effect would have caused the membrane potential to depolarize. At this stage, more complex interactions between diclofop and the $H^+$-ATPase seem unwarranted, but that the situation may be more complex is indicated by the diclofop effect at pH 8.2 in the presence of 10 mM $K^+$ (Fig. 7). Third, an effect on photosynthesis seems unlikely, due to the lack of effect of diclofop on isolated chloroplasts and the basic difference found in the present study between the effects of diclofop and DCMU (*cf.* Figs. 3 and 5). This conclusion is also supported by the results obtained using decoupled cells (18, 21) in which $HCO_3^-$ was replaced by $HPO_4^{2-}$. In this $HCO_3^-$-decoupled state, photosynthetic carbon fixation is limited to respiratory $CO_2$ and $H^+$-$HCO_3^-$ cotransport would not be expected to act as a rate-limiting step in this complex process. Under these conditions, diclofop still caused a reduction in the light/dark sensitivity of the mem-

brane potential (Fig. 4). This response implicates the plasmalemma as the site of diclofop action.

An evaluation of the extracellular current patterns associated with $HCO_3^-$ and $OH^-$ transport revealed that both systems were influenced by diclofop; however, the $OH^-$ transport system appeared to be more dramatically perturbed (Fig. 6). Greater diclofop sensitivity of the $OH^-$ efflux system would provide an explanation for the membrane hyperpolarizing response observed when diclofop is introduced under alkaline pH conditions (Fig. 3). Inhibition of $OH^-$ transport would cause an imbalance between $H^+$ efflux and $OH^-$ efflux which would hyperpolarize the membrane.

The erratic nature of the $OH^-$-associated currents and the observed instability of the actual transport sites may reflect not only an inhibition of transport *per se* but also an effect on the synchronization process that regulates these currents.

**ATP Levels and Membrane Depolarization.** Numerous studies using perfused internodal cells of *Chara*, *Nitella*, and *Nitellopsis* have confirmed the relationship between cytoplasmic ATP levels and the electrogenic component of the membrane potential (13, 27, 35, 36). Based on these results, it has been suggested that the $K_m$ of the $H^+$-translocating ATPase is in the range of 30 to 70 $\mu$M. An inconsistency exists between these estimates and our observation that at pH 5.7 the electrogenic component was completely inhibited in the presence of 0.2 mM ATP (Table I). Our results obtained at pH 7 are even more at variance with such a low $K_m$. Under these conditions, the membrane potential was at, or near, the diffusion potential for $K^+$ and yet the ATP concentration was 1.9 mM. Either Diclofop interacts with the $H^+$-ATPase to decrease its affinity for ATP or the ATPase becomes very sensitive to ADP levels (see also [13, 26, 36]). Alternatively, the $K_m$ obtained using perfused *Chara* cells may not be directly applicable to the intact cell system.

## LITERATURE CITED


1. ABERG B 1980 Plant growth regulators. XL. Some halogeno- and alkylphenoxyacetic and optically active phenoxypropionic acids. Swed J Agric Res 10: 107–114
2. BENISEK WF, JR OGEZ 1982 Proton nuclear magnetic resonance studies of *Pseudomonas testosteroni* 3-oxo-5-steroid isomerase and its interaction with 17$\beta$-estradiol. Biochemistry 21: 5816–5825
3. BREZEANU AG, DG DAVIS, RH SHIMABUKURO 1976 Ultrastructural effects and translocation of methyl-2-[4-(2,4-dichlorophenoxy)phenoxy]proponoate in wheat (*Triticum aestivum*) and wild oat (*Avena fatua*). Can J Bot 54: 2038–2048
4. CHAPMAN AG, L FALL, DE ATKINSON 1971 Adenylate energy charge in *Escherichia coli* during growth and starvation. J Bacteriol 108: 1072–1086
5. CROWLEY JC, GN PRENDEVILLE 1979 Effect of diclofop-methyl on leaf-cell membrane permeability in wild oat, barley and wheat. Can J Plant Sci 59: 275–277
6. HEORAUF RA, RH SHIMABUKURO 1979 The response of resistant and susceptible plants to diclofop-methyl. Weed Res 19: 293–299
7. HOGG J, EJ WILLIAMS, RJ JOHNSON 1968 A simplified method for measuring membrane resistance in *Nitella translucens*. Biochim Biophys Acta 150: 518–520
8. HOPE AB, NA WALKER 1975 The Physiology of Giant Algal Cells. Cambridge University Press, Aberdeen, Great Britain
9. JAFFE LF, R NUCCITELLI 1974 An ultrasensitive vibrating probe for measuring extracellular currents. J Cell Biol 63: 614–628
10. KEIFER DW, WJ LUCAS 1982 Potassium channels in *Chara*: control and interaction with the electrogenic $H^+$ pump. Plant Physiol 69: 781–788
11. KEIFER DW, RM SPANSWICK 1978 Activity of the electrogenic pump in *Chara corallina* as inferred from measurements of the membrane potential, conductance, and potassium permeability. Plant Physiol 62: 653–661
12. KEIFER DW, RM SPANSWICK 1979 Correlation of adenosine triphosphate levels in *Chara corallina* with the activity of the electrogenic pump. Plant Physiol 64: 165–168
13. KIKUYAMA M, T HAYAMA, S FUJII, M TAZAWA 1979 Relationships between light-induced potential change and internal ATP concentration in tonoplast-free *Chara* cells. Plant Cell Physiol 20: 993–1002
14. KIMMICH GA, JR RANDLES, JS BRAND 1975 Assay of picomole amounts of ATP, ADP and AMP using the luciferase enzyme system. Anal Biochem 69: 187–206
15. LEE CC, RF HARRIS, JDH WILLIAMS, DE ARMSTRONG, JK SYERS 1971 Adenosine triphosphate in lake sediments. I. Determinations. Soil Sci Soc Am Proc 35: 82–86
16. LICHTNER FT, RM SPANSWICK 1981 Electrogenic sucrose transport in developing soybean cotyledons. Plant Physiol 67: 869–874
17. LUCAS WJ 1976 Plasmalemma transport of $HCO_3^-$ and $OH^-$ in *Chara corallina*: non-antiporter systems. J Exp Bot 27: 19–31
18. LUCAS WJ 1982 Mechanism of acquisition of exogenous bicarbonate by internodal cells of *Chara corralina*. Planta 156: 181–192
19. LUCAS WJ 1983 Photosynthetic assimilation of exogenous $HCO_3^-$ by aquatic plants. Annu Rev Plant Physiol 34: 71–104
20. LUCAS WJ, J DAINTY 1977 $HCO_3^-$ influx across the plasmalemma of *Chara corallina*: divalent cation requirement. Plant Physiol 60: 862–867
21. LUCAS WJ, DW KEIFER, D SANDERS 1983 Bicarbonate transport in *Chara corallina*: evidence for cotransport of $HCO_3^-$ with $H^+$. J Membr Biol 73: 263–274
22. LUCAS WJ, R NUCCITELLI 1980 $HCO_3^-$ and $OH^-$ transport across the plasmalemma of *Chara*: spatial resolution obtained using extracellular vibrating probe. Planta 150: 120–131
23. LUCAS WJ, FA SMITH 1973 The formation of alkaline and acid regions at the surface of *Chara corallina* cells. J Exp Bot 24: 1–14
24. LUCAS WJ, RM SPANSWICK, J DAINTY 1978 $HCO_3^-$ influx across the plasmalemma of *Chara corallina*: physiological and biophysical influence of 10 mM $K^+$. Plant Physiol 61: 487–493
25. MCELROY WD, HH SELIGER 1961 Mechanisms of bioluminescent reactions. In: WD McElróy, B Glass eds, Light and Life, The John Hopkins Press, Baltimore, pp 219–257
26. MIMURA T, T SHIMMEN, M TAZAWA 1982 Respiration-dependent membrane hyperpolarization in tonoplast-free cells of *Nitella axilliformis*. Plant Cell Physiol 23: 1419–1425
27. MIMURA T, T SHIMMEN, M TAZAWA 1983 Dependence of the membrane potential on extracellular ATP concentration in tonoplast-free cells of *Nitellopsis obtusa*. Planta 157: 97–104
28. NESTLER JH, P LANGELUDDEKE, H SCHONOWSKY, F SCHWERDTLE 1979 Phenoxyphenoxy-propionic acids and derivatives as grass herbicides. In: H Geissbuhler, GT Brooks, PC Kearney, eds, Advances in Pesticide Science, Part 2. Pergamon Press, New York, pp 248–255
29. PEEBLES MJ, FV MERCER, TC CHAMBER 1964 Studies on the comparative physiology of *Chara australis*. I. Growth pattern and gross cytology of the internodal cell. Aust J Biol Sci : 49–61
30. SANDERS D 1980 The mechanism of $Cl^-$ transport at the plasma membrane of *Chara corallina*. I. Cotransport with $H^+$. J Membr Biol 53: 129–141
31. SANDERS D, U-P HANSEN, CL SLAYMAN 1981 Role of the plasma membrane proton pump in pH regulation in non-animal cells. Proc Natl Acad Sci USA 78: 5903–5907
32. SANDERS D, CL SLAYMAN 1982 Control of cytoplasmic pH. Predominant role of oxidative metabolism, not proton transport, in the eukaryotic microorganism *Neurospora*. J Gen Physiol 80: 377–402
33. SELINGER H, WD MCELROY 1964 The colors of firefly bioluminescence: enzyme configuration and species specificity. Proc Natl Acad Sci USA 52: 75–81
34. SHIMABUKURO MA, RH SHIMABUKURO, WC WALSH 1982 The antagonism of IAA induced hydrogen ion extrusion and coleoptile growth by diclofop-methyl. Physiol Plant 56: 444–452
35. SHIMMEN T, M TAZAWA 1977 Control of membrane potential and excitability of *Chara* cells with ATP and $Mg^{2+}$. J Membr Biol 37: 167–192
36. SMITH PT, NA WALKER 1981 Studies on the perfused plasmalemma of *Chara corallina*. I. Current-voltage curves: ATP and potassium dependence. J Membr Biol 60: 223–236
37. SPANSWICK RM 1981 Electrogenic ion pumps. Annu Rev Plant Physiol 32: 267–289
38. WALKER NA, FA SMITH 1977 Circulating electric currents between acid and alkaline zones associated with $HCO_3^-$ assimilation in *Chara*. J Exp Bot 28: 1190–1206
39. WRIGHT JP, RH SHIMABUKURO 1982 Effect of diclofop-methyl and diclofop on the membrane potentials of wheat and oat coleoptiles. Plant Physiol 69: S-524

Planta (1984) 160:129–142

Planta
© Springer-Verlag 1984

# Ultrastructural and histochemical studies on guard cells

Alison C. Wille and William J. Lucas
Department of Botany, University of California, Davis, CA 95616, USA

**Abstract.** Serial thick sections of guard cells from *Vicia faba* L., *Nicotiana tabacum* L., *Allium cepa* L., *Zea mays* L. and *Beta vulgaris* L. were obtained systematically (600–800 nm) and viewed with the transmission electron microscope in an effort to demonstrate the presence or absence of a symplastic transport pathway within the stomatal complex. Eight to ten stomata from each species were examined, and no continuous plasmodesmata were found connecting guard cells to sister guard cells or to adjacent epidermal or subsidiary cells. Continuous plasmodesmata were observed in immature guard cells, but were sealed (truncated) during the development of the mature cell wall. Histochemical stains, phosphotungstic acid and silver methenamine, were used to demonstrate differentiation within the mature guard-cell wall. The structural differentiation of the stomatal apoplastic region is discussed in relation to functional specialization. Plasma-membrane elaborations or plasmalemmasomes were identified in the guard cells of *Zea*, and it is suggested that these structures may function in ion transport.

**Key words:** Cell wall structure – Guard cell – Stoma – Plasmalemmasome – Plasmodesma.

## Introduction

Studies on symplastic connection between guard cells and adjacent subsidiary or epidermal cells have produced conflicting reports, and the structure of the guard-cell wall and its possible influence on apoplastic ion transport have not been investigated. Plasmodesmatal connections between guard cells and adjacent cells were first reported on the basis of light-microscopic studies (Waterkeyn and Bienfait 1966; Litz and Kimmins 1968; Inamdar et al. 1973). The presence of pit callose, fluorescent when stained with aniline blue, was taken as evidence for plasmodesmata in one study (Peterson and Hambleton 1978). The improved resolution available with transmission electron microscopy provides direct means for visualizing plasmodesmata, but most ultrastructural studies reported the absence of cytoplasmic connections in mature guard cells (Brown and Johnson 1962; Srivastava and Singh 1972; Singh and Srivastava 1972; Allaway and Setterfield 1972; Ziegler et al. 1974; Peterson and Hambleton 1978; Rutter and Willmer 1979; Galatis and Mitrakos 1980). Plasmodesmata have been identified in the guard cells of three species, *Vicia faba* and *Nicotiana tabacum* (Pallas and Mollenhauer 1972a, b) and *Commelina communis* (Fujino and Jinno 1972), but these reports are not entirely convincing. In the former study, there is reason to believe, based on the thickness of the cell walls and absence of a well-developed vacuolar system, that the guard cells in which continuous plasmodesmata were demonstrated were, in fact, immature. In the latter study, the quality of the micrographs was insufficient to interpret accurately the images of the alleged plasmodesmata. Continuous plasmodesmata have been observed to connect developing guard cells with adjacent cells, and plasmodesmata that appear truncated have been observed in the walls of mature guard cells (Willmer and Sexton 1979). However, no published micrographs contain both continuous plasmodesmata and a view of the stomatal pore that demonstrates that it had opened for the first time.

The resolution of the light microscope is not sufficient for the accurate visualization of plasmo-

*Abbreviations:* PTA-HCl = phosphotungstic acid and hydrochloric acid; SM = silver methenamine; UA-LC = uranyl acetate and lead citrate

desmata, while the high resolution obtained with the transmission electron microscope requires sections so thin that several hundred must be observed in order to inspect an entire cell. Serial thick sections have been shown to provide sufficient contrast and resolution to visualize plasmodesmata. Through this technique, it has been possible to carry out a thorough search for plasmodesmata in 20–30 stomata in five plant species. The fact that not a single continuous plasmodesma was encountered provides strong evidence that plasmodesmatal communication does not play an important role in stomatal function.

The absence of cytoplasmic communication between guard cells and adjacent cells has important implications in relation to the mechanism of stomatal ion transport. With plasmodesmata being absent, transport of ions and carbohydrates to and from guard cells must be entirely apoplastic. It follows that the guard-cell wall may be involved in specialized interactions with ions as they are transported between guard cells and adjacent cells.

Histochemical reagents have been used to demonstrate the differentiation of sieve-element walls into regions with distinct structure and composition (Lucas and Franceschi 1982). We have applied similar techniques to the walls of guard cells to demonstrate structural specialization of various apoplastic regions. We propose that the specific structure of the guard-cell wall has functional implications with respect to intercellular communication between guard cells and epidermal cells, and merits further study.

## Materials and methods

*Plant materials and culture techniques. Allium cepa* L. (grown from bulb sets; Coast Brand, Aurora, Ore., USA), *Beta vulgaris* L. cv. USH10 (Spreckels Sugar Co., Woodland, Cal., USA; Lot 3102) and *Vicia faba* L. cv. Long Pod (W. Atlee Burpee Co., Warmister, Penn., USA; Lot 517602) were maintained in a growth chamber under the following conditions: 27° C day-17° C night temperatures, 75%–100% relative humidity and a 16-h photoperiod at 180 μmol $m^{-2}$ $s^{-1}$. The soil used was a 2:1:1 (by vol.) mixture of medium vermiculite, peatmoss and sand, and the plants were watered daily and fertilized with full-strength Hoagland's solution (Hoagland and Arnon 1950) once per week. Fully expanded leaves were harvested when the plants were four to eight weeks old. In addition, young leaves of *B. vulgaris* were harvested when less than 2 cm long for observation of developing guard cells.

*Allium cepa* L. cv. White Lisbon (Northrup King Seeds, Fresno, Cal., USA) was grown from seed in vermiculite, and the seedlings were maintained under constant light at 52 μmol $m^{-2}$ $s^{-1}$. Cotyledons were harvested after 5 d, and the region between the hook and the terminally attached seed coat was prepared for observation of developing guard cells (Palevitz and Hepler 1976).

*Phaseolus vulgaris* L. cv. Light Red Kidney (University of California, Davis, California Crop Improvement), *Nicotiana rustica* L. (U.C. Davis, Botany Department Greenhouse Facility), *Commelina coelistis* L. (Kew Gardens, Richmond, Surrey, UK), and *Zea mays* L. (A632 × [C3640 × Ohio 43]; Crow's Hybrid Corn Co., Milford, Ill., USA), and *Allium porrum* L. (grown from bulbs) were grown and maintained in our greenhouse facility where they were watered three times per week with 0.5-strength Hoagland's solution.

*Tissue preparation.* Tissue from fully expanded leaves was cut with a tissue slicer (Mickle Laboratory Engineering Co.; Gomshall, Surrey, UK) into 1.0 mm × 0.3 mm sections. After cutting, the tissue was immersed immediately, at room temperature, in a fixative containing glutaraldehyde (2%), depolymerized paraformaldehyde (3%, for *Allium* spp.) and sodium-cacodylate buffer (50 mM, pH 7.2). Vacuum infiltration was occasionally employed to facilitate penetration of the fixative. Following fixation (3–10 h, 4° C), tissue was post-fixed with 1% osmium tetroxide in sodium-cacocylate buffer (25 mM, pH 7.2) for 1–3 h, dehydrated through a graded acetone series, and embedded in Spurr's resin (Spurr 1969).

*Serial thick sectioning.* To determine with certainty the presence or absence of plasmodesmata, guard cells were serial-sectioned, and each section was carefully examined for plasmodesmata. To decrease the number of sections required to serial-section a pair of guard cells completely, sections were cut at a thickness which produced green to red interference colors (approx. 600–800 nm). The stomata of *Vicia faba, Nicotiana tabacum, Allium cepa, Zea mays,* and *Beta vulgaris* were serial-sectioned with a diamond knife on a Porter-Blum MT-2 ultramicrotome (Ivan Sorvall, Newton, Conn., USA). After sectioning, the specimens were mounted on 0.5 mm × 2.0 mm slotted Cu-Rh,

**Figs. 1–9.** Plasmodesmata between leaf cells of various species. Sections were cut at a thickness that produced red-green interference colors (600–800 nm) and were viewed unstained at 100 kV. **Fig. 1.** Plasmodesmata in primary pit field between mesophyll cell (*above*) and epidermal cell (*below*) in *Allium cepa*. × 15,000; bar = 1 μm. **Fig. 2.** Plasmodesma between epidermal cells of *Vicia faba*. × 40,000; bar = 0.25 μm. **Fig. 3.** Plasmodesmata in a primary pit field between subsidiary cell (*above*) and epidermal cell (*below*) of *Zea mays*. × 40,000; bar = 0.25 μm. **Fig. 4.** Truncated plasmodesmata between guard cell (*below*) and epidermal cell (*above*) of *V. faba*. × 40,000; bar = 0.25 μm. **Fig. 5.** Truncated plasmodesmata between guard cell (*below*) an epidermal cell (*above*) of *Nicotiana tabacum*. × 25,000; bar = 0.5 μm. **Fig. 6.** Truncated plasmodesmata between guard cell (*below*) and epidermal cell (*above*) of *Beta vulgaris*. × 25,000; bar = 0.5 μm. **Figs. 7–9.** Serial thick sections of the guard cell wall of *V. faba* demonstrating that plasmodesmata are indeed truncated. × 15,000; bars = 1 μm

**Figs. 10–12.** Truncated plasmodesmata between epidermal cells (*top*) and guard cells (*below*) in various species. Sections post-stained with uranyl acetate and lead citrate; bars = 0.1 μm. **Fig. 10.** Truncated plasmodesma in guard-cell wall of *Beta vulgaris*. × 100,000. **Fig. 11.** Guard-cell plasmodesmata in *V. faba*. × 100,000. **Fig. 12.** Guard-cell plasmodesmata in *N. tabacum*. × 80,000

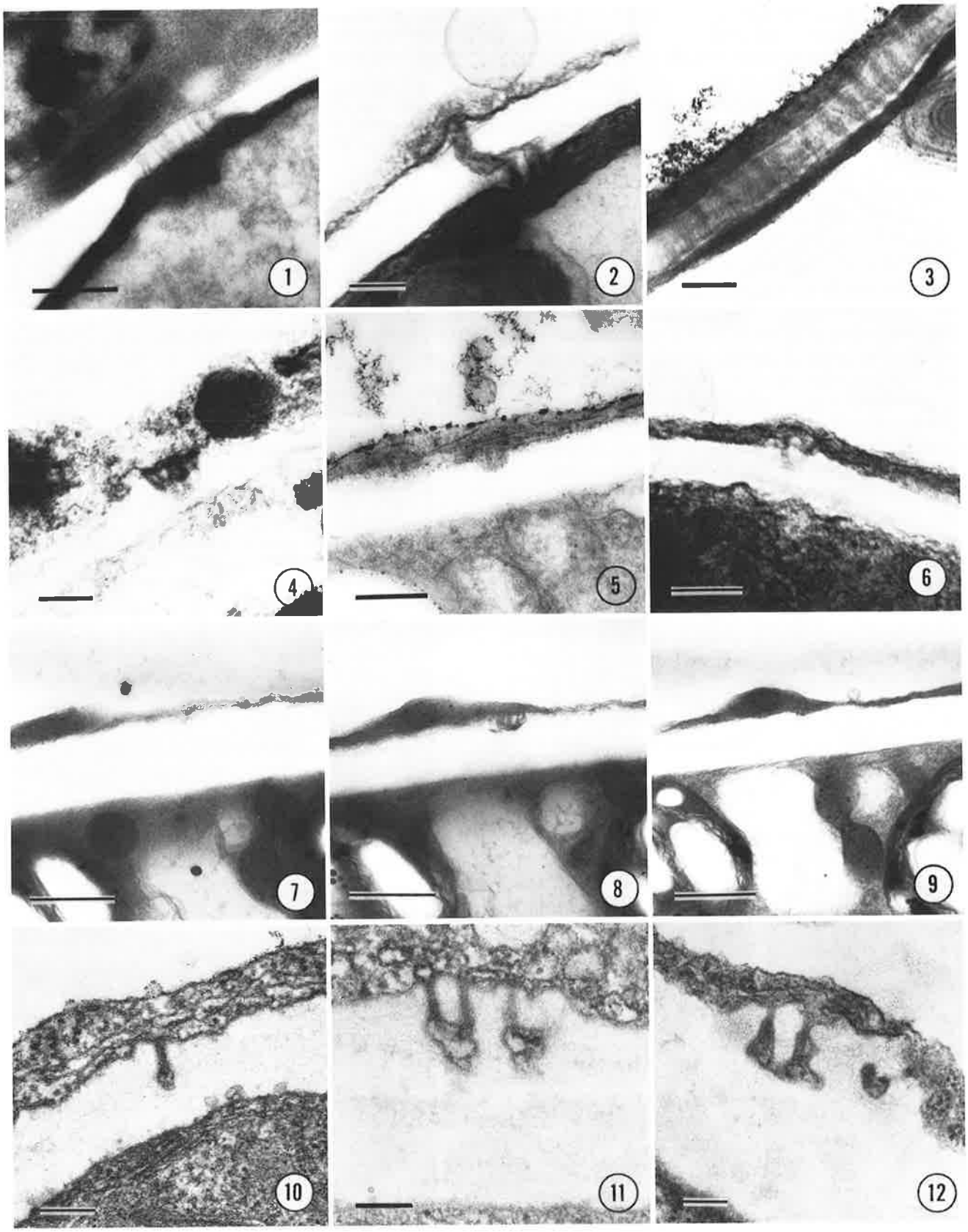
1
2
3
4
5
6
7
8
9
10
11
12

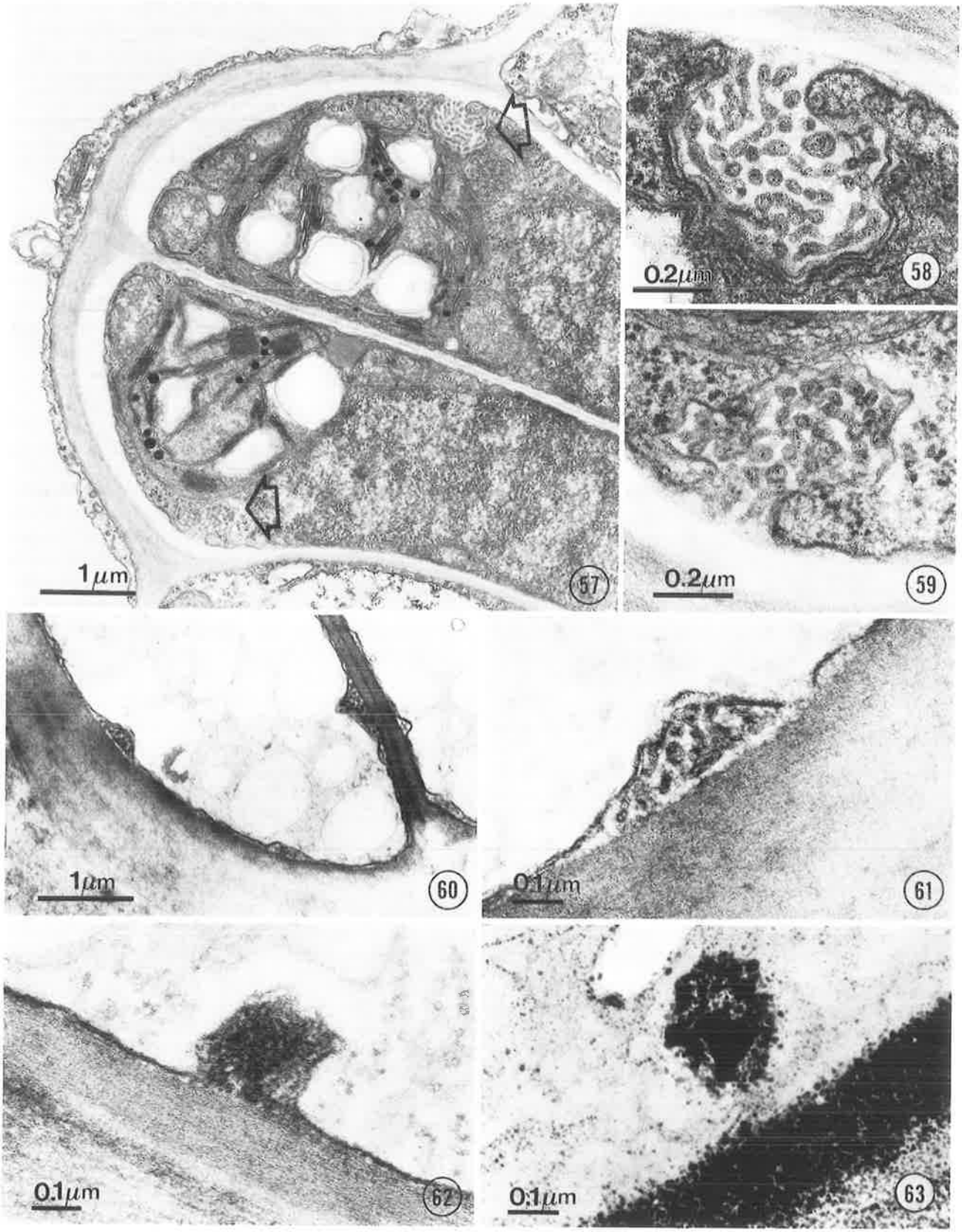
1 μm
57
0.2μm
58
0.2μm
59
1μm
60
0.1μm
61
0.1μm
62
0.1μm
63

this reason, histochemical stains were applied in an effort to distinguish different regions of the guard-cell wall.

*Structure and function of the guard-cell wall.* While it is impossible to ascertain the precise molecular interactions of histochemical stains with materials as structurally and chemically complex as cell walls, staining patterns observed with various reagents can be correlated to help us elucidate the structure and differentiation of guard-cell walls.

Silver methenamine is a derivative of the periodic acid-Shiff's reaction in which *vic*-hydroxyl groups, present in the subunits of polysaccharides, are oxidized to aldehyde groups by periodic acid and allowed to react with silver. Cellulose, hemicellulose and pectin are all composed of *vic*-hydroxyl-containing sub-units; therefore, the density of the reaction product should correlate with the relative density of carbohydrates in particular wall regions. In sieve-element walls, which show a SM staining pattern similar to that of guard-cell walls, enzymatic digestion and subsequent staining with SM have demonstrated that the heavily staining region is composed primarily of cellulose with a pectin-rich region directly adjacent to the sieve-element plasmalemma (Lucas and Franceschi 1982). Pectinase digestion of guard-cell walls may demonstrate a close structural similarity between guard-cell and sieve-element walls.

A PTA radical consists of a $PO_4$ group surrounded by twelve $WO_6$ groups, each of which contains a double-bonded oxygen atom. It has been proposed that the affinity of PTA for carbohydrates results from its ability to form numerous hydrogen bonds with the exposed hydroxyl, carboxyl and amino groups of these compounds (Pease 1966). The selectivity of PTA staining is thought to result from the high hydrogen-bonding potential of polysaccharides relative to other cellular macromolecules. Pease also suggested that PTA produces only surface staining and does not penetrate thin sections, noting the large size of the PTA radical and the tendency of sections which have been exposed to PTA on both sides to show twice the density of those exposed on only one side.

The epidermal wall regions that stain most densely with PTA-HCl are located at the junctions where walls of different cells come together and also in a ring that encircles the guard cells. These regions can be interpreted as the primary wall which was laid down prior to deposition of the specialized thickenings which form the mature guard-cell wall. A similar staining pattern observed in sieve element walls has been interpreted as indicating the primary wall (Lucas and Franceschi 1982). Wall layering has also been noted in the guard cells of *Funaria hygrometrica* (Sack and Paolilo 1983). *Funaria* guard-cells walls are apparently differentiated into three layers which can be recognized by microfibrillar texture. The relatively thick electron-lucent region between the primary wall and the guard-cell protoplast (also stains densely with SM) is indicative of special thickening of the guard-cell wall. To the epidermal cell side of the primary wall, little thickening appears to have occurred. This, along with the thinness of walls between adjacent epidermal cells, indicates that the epidermal cells do not undergo extensive wall thickening. Further support for this comes from the appearance of truncated plasmodesmata which are preserved in the epidermal cell wall. The length of these plasmodesmata remains equal to the thickness of the primary wall in spite of the fact that the guard-cell wall doubles or triples in thickness during development.

*Plasmalemmasomes.* In at least one species, *Z. mays*, specialized plasmalemma elaborations, or plasmalemmasomes, were observed in some of the guard cells. Plasmalemmasomes have been described in a number of plant species, and they have been proposed to function in solute transport (Robards and Kidwai 1969; Wangermann and Withers 1978). Investigations into the function of these plasma-membrane elaborations have been carried out on plasmalemmasome-like structures in the genus *Chara* (charasomes), and these studies impli-

**Figs. 57–59.** Paradermal sections of guard cells from mature leaves of *Zea mays* post-stained with uranyl acetate and lead citrate. **Fig. 57.** Bulbous end of guard cell showing two plasmalemmasomes indicated by *arrows*. ×17,500. **Fig. 58.** High magnification view of plasmalemmasome in upper guard cell. Note surrounding membrane and internal tubules. ×69,000. **Fig. 59.** High magnification view of plasmalemmasome in lower guard cell. ×69,000

**Figs. 60–62.** Paradermal sections of *Z. mays* guard cells pretreated with $H_2O_2$ and post-stained with PTA-HCl. **Fig. 60.** Bulbous end of guard cell showing two plasmalemmasomes. 18,000. **Fig. 61.** Plasmalemmasome. Note the dense staining of plasmalemma and internal tubules. 90,000. **Fig. 62.** Glancing section of plasmalemmasome. Electron density is probably the consequence of intense staining of the plasmalemma. ×90,000. **Fig. 63.** Possible plasmalemmasome stained with SM. Membrane structure is obscured, making interpretation tentative. ×90,000

cate the involvement of charasomes in $Cl^-$ transport (Franceschi and Lucas 1982). Rapid movement of $Cl^-$ from subsidiary cells to guard cells during stomatal opening has been described in corn (Raschke and Fellows 1971), and the plasmalemmasomes may be involved in this process.

*Conclusions.* The importance of establishing with certainty whether or not cytoplasmic transport occurs between guard cells and epidermal cells is clear. The present work confirms that guard-cell cytoplasm is physically, and hence, electrically isolated from all other epidermal and mesophyll cells. We can now focus on the problems associated with the release of ions into the apoplast and the mechanisms by which these ions are accumulated in guard cells during stomatal opening and in epidermal cells during the closing phase.

Finally, much remains to be learned about the importance of the structure and composition of the apoplast in terms of its influence on the movement of solutes between guard cells and adjacent cells. The composition of the guard-cell wall may be more precisely determined by the use of purified digestive enzymes. Also, plasmalemmasomes of the type seen in *Z. mays* may be an important specialization for transport. Further characterization of these structures may offer important insight into guard-cell function.

This work was supported by National Science Foundation grant Pcm 81–17721. We also thank Dr. Norma Lang for her most valuable advice during this study.

## References

Allaway, W.G., Setterfield, G. (1972) Ultrastructural observations on guard cells of *Vicia faba* and *Allium porrum*. Can. J. Bot. **50**, 1405–1413

Brown, W.V., Johnson, Sr.C. (1962) The fine structure of the grass guard cell. Am. J. Bot. **49**, 110–115

Franceschi, V.R., Lucas, W.J. (1982) The relationship of the charasome to chloride uptake in *Chara corallina*: physiological and histochemical investigations. Planta **154**, 525–537

Fujino, M., Jinno, N. (1972) The fine structure of the guard cell of *Commelina communis* L. Sci. Bull. Fac. Educ., Nagasaki Univ. **23**, 101–111

Galatis, B., Mitrakos, K. (1980) The ultrastructural cytology of the differentiating guard cells of *Vigna sinensis*. Am J. Bot. **67**, 1243–1261

Hayat, M.A. (1975) Positive staining for electron microscopy. Van Nostrand Reinhold, New York

Hoagland, D.R., Arnon, D.I. (1950) The water-culture method for growing plants without soil. Calif. Agric. Exp. Stn., Circ. No. 347

Inamdar, J.A., Patel, R.C., Bhatt, D.C. (1971) Structure and development of stomata in some leptosporangiate ferns. Ann. Bot. (London) **35**, 643–651

Litz, R.E., Kimmins, W.C. (1968) Plasmodesmata between guard cells and accessory cells. Can. J. Bot. **46**, 1603–1604

Lucas, W.J., Franceschi, V.R. (1982) Organization of the sieve-element walls of leaf minor veins. J. Ultrastruct. Res. **81**, 209–221

Palevitz, B.A., Hepler, P.K. (1976) Cellulose microfibril orientation and cell shaping in developing guard cells of *Allium*: the role of microtubules and ion accumulation. Planta **132**, 71–93

Pallas, J.E., Jr., Mollenhauer, H.H. (1972a) Physiological implications of *Vicia faba* and *Nicotiana tabacum* guard-cell ultrastructure. Am. J. Bot. **59**, 504–514

Pallas, J.E., Jr., Mollenhauer, H.H. (1972b) Electron microscopic evidence for plasmodesmata in dicotyledonous guard cells. Science **175**, 1275–1276

Pease, D.C. (1966) Polysaccharides associated with the exterior surface of epithelial cells: kidney, intestine, brain. J. Ultrastruct. Res. **15**, 555–588

Peterson, R.L., Hambleton, S. (1978) Guard cell ontogeny in leaf stomata of the fern *Ophioglossum petiolatum*. Can. J. Bot. **56**, 2836–2852

Rambourg, A. (1967) An improved silver methenamine technique for the detection of periodic acid-reactive complex carbohydrates with the electron microscope. J. Histochem. Cytochem. **15**, 409–412

Raschke, K. (1979) Movements of stomata. In: Encyclopedia of plant physiology, N.S., vol. 7: Physiology of movements, pp. 383–441, Haupt, W., Feinleib, M.E., eds. Springer, Berlin Heidelberg New York

Raschke, K., Fellows, M.P. (1971) Stomatal movement in *Zea mays*: shuttle of potassium and chloride between guard cells and subsidiary cells. Planta **101**, 296–316

Reynolds, E.S. (1963) The use of lead citrate at high pH as an electron-opaque stain in electron microscopy. J. Cell Biol. **17**, 208–213

Robards, A.W., Kidwai, P. (1969) Vesicular involvement in differentiating plant vascular cells. New Phytol. **68**, 343–349

Rutter, J.C., Willmer, C.M. (1979) A light and electron microscopy study of the epidermis of *Paphiopedilum* spp. with emphasis on stomatal ultrastructure. Plant Cell Environ. **2**, 211–219

Sack, F., Paolillo, D.J., Jr (1983) Structure and development of walls in *Funaria* stomata. Am. J. Bot. **70**, 1019–1030

Singh, A.P., Srivastava, L.M. (1973) The fine structure of pea stomata. Protoplasma **76**, 61–82

Spurr A.R. (1969) A low-viscosity epoxy resin embedding medium for electron microscopy. J. Ultrastruct. Res. **26**, 31–43

Srivastava, L.M., Singh, A.P. (1972) Stomatal structure in corn leaves. J. Ultrastruct. Res. **39**, 345–363

Wangermann, E., Withers, L.A. (1978) Auxin transport characteristics and cellular ultrastructure of different types of parenchyma. New Phytol. **81**, 1–17

Waterkeyn, L., Bienfait, A. (1966) Production et degradation successives de callose membranaire dans les stomates en formation, chez quelque Fougeres. C.R. Acad. Sci. Paris D **262**, 251–254

Willmer, C.M., Sexton, R. (1979) Stomata and plasmodesmata. Protoplasma **100**, 113–124

Ziegler, H., Shmueli, E., Lange, G. (1974) Structure and function of the stomata of *Zea mays*. I. The development. Cytobiologie **9**, 162–168

Received 6 July; accepted 3 October 1983

# Plasma Membrane Coat and a Coated Vesicle-associated Reticulum of Membranes: Their Structure and Possible Interrelationship in *Chara corallina*

THOMAS C. PESACRETA and WILLIAM J. LUCAS
*Department of Botany, University of California, Davis, California 95616*

ABSTRACT Primary fixation with buffered glutaraldehyde plus 2.0 mM $CaCl_2$ and 0.1% tannic acid results in the preservation of certain portions of the plasma membrane coat of *Chara* when seen with the electron microscope. Such a coat is not observable after fixation with glutaraldehyde alone. The coat appears to be present on all the above ground, vegetative cells of the male plant. Within complex invaginations of the plasma membrane, which are known as charasomes, the coat has two structural components, a central core that is either tubular or solid and a fibrous or granular peripheral region that surrounds the core. The coat material appears to be at least partially derived, via exocytosis, from the contents of single membrane-bound organelles known as glycosomes. Glycosomes seem to originate from within an assemblage of membranes and coated vesicles that can be described, in purely structural terms, as a partially coated reticulum. Such a reticulum is distinguishable from Golgi stacks because the reticulum (*a*) is not composed of stacked membranes, (*b*) is extensively involved with large, clearly detailed coated vesicles and coated invaginations, (*c*) is closely associated with glycosomes, and (*d*) is only slightly stained by the zinc-iodide-osmium tetraoxide reagent.

*Chara corallina* is a member of the Characeae, a family of large-celled algae that have been studied by many investigators with regard to processes such as ion transport (1), cyclosis (2), and cell wall growth (3). In an earlier series of articles from our laboratory (4–6), the ultrastructure of *Chara* was examined with special attention being given to studying the development of the charasomes. Barton originated the term charasome (7) to denote a multi-tiered complex of anastomosing tubules that are part of the plasma membrane of *Chara*. Periplasm is an ancillary term that refers to the apoplastic space that is present within the charasome. Instead of being evenly distributed over the entire cell surface, charasomes are located in a series of circumferential bands along the length of these cylindrical cells (4). Given the proper conditions (8), such bands will acidify the surrounding solution; between bands, the solution that is adjacent to the cell will become alkaline. The precise function of charasomes is not presently understood. However, it has been shown that enzymes that are capable of using ATP are present in the charasome membrane (9) and it has been suggested that proteins that are involved with chloride transport may be present as well (9).

One of the questions regarding the charasome concerns its ability to maintain an anastomosing tubular form while being compressed by a turgor pressure of ~0.7 mPa. While the plant cell wall can resist turgor pressure along the "smooth" portions of the plasma membrane, it is doubtful that a conventional cell wall is present in the periplasm of the charasome (6). Preliminary evidence that the periplasm of *Chara* does contain some structural components has been presented (6). Such work did not consider the influence of divalent cations on the structure of the charasome, nor was the structure of other portions of the plasma membrane considered. In animal cells, proteoglycans in the extracellular matrix are associated with the plasma membrane and absorb compressive loads (10). However, to our knowledge, little information is available concerning the existence of a plasma membrane associated extracellular matrix (which we shall refer to as a "plasma membrane coat" to distinguish it from the plant cell wall) of plant cells. Robards (11), Levering and Thomson (12), and Olesen (13) have published micrographs of plant cell plasma membranes that have either dense particles or linings that are associated with the membrane to some degree. Robards (11) and Olesen (13) hypothesized that such particles were cellulose synthesizing enzymes. Levering and Thomson (12) showed an extensive lining with a circular substructure that was located within invaginations of the plasma membrane and

THE JOURNAL OF CELL BIOLOGY · VOLUME 98 APRIL 1984 1537–1545
© The Rockefeller University Press · 0021-9525/84/04/1537/09 $1.00

that was heavily stained when compared to the cell wall. Such a paucity of information may have been brought about by the existence of factors similar to those that made visualization of the lamina rara of animal cells difficult, until the proper fixation techniques were discovered (14).

In animal cells, proteoglycans of the extracellular matrix are synthesized within the endoplasmic reticulum and the Golgi complex, and are then further processed after exocytosis (10). Supportive evidence for the existence of a generally similar delivery system, in other plant cells, comes from studies that show that exocytosis of Golgi vesicles that contain wall scales (15) and mucilage (16) can occur. It should be noted that some ambiguity is present in contemporary scientific literature concerning the implication of the phrase "Golgi vesicles." Such ambiguity mainly stems from the studies of Novikoff et al. (17), who have interposed the concept of a GERL into previously constructed schemes of endomembrane flow. The GERL contains an assemblage of vesicles and lamellae that are structurally similar to, but which sometimes differ in their enzyme content from, the immediately adjacent vesicles and lamellae of the Golgi complex. While usage of the term GERL is becoming common in the scientific literature, some workers still prefer to think of the GERL as being part of the Golgi complex (18).

Here we describe the effect of fixative composition on the complex structure of the plasma membrane coat of *Chara*. In addition, we present micrographs that support the contention that at least some of the material of the plasma membrane coat is derived from a partially coated reticulum of membranes rather than being directly derived from the Golgi stacks. Finally, we describe the distinctive structure and staining characteristics of the partially coated reticulum and show its close association with both coated vesicles and glycosomes.

## MATERIALS AND METHODS

*Material and Growing Conditions:* Plants of *Chara corallina* Klein ex Wild., em. R.D.W. (= C. australis R. Br.), obtained from subcultures that had been maintained in our laboratory for more than 5.0 years, were grown in the laboratory under fluorescent lamps at 21.0–23.0°C in 120-l containers in solutions containing 3.0 mM $Na^+$, 0.2 mM $K^+$, 0.1–0.2 mM $Ca^{2+}$, 1.5 mM $Cl^-$, and ~2.0 $HCO_3^-$ (pH 8.5–9.5). Only male plants were used. In all cases, cells were exised from the parent plants during the afternoon, incubated in culture media for 1.0 h and then were transferred to our laboratory's standard physiological testing solution that was composed of 1.0 mM NaCl, 0.2 mM KCl, 0.2 mM $CaSO_4$, and 1.0 mM $NaHCO_3$ (pH 8.0). Extensive testing by one of us (W. J. Lucas) has shown that *Chara* cells remain viable when exposed to pH values ranging from pH 5.5 to 9.5 (19). The incubation period after excision v as necessary to allow recovery of the cells from both the action potential and the cessation of cyclosis that occur following excision from the parent plant. Primary fixation for electron microscopy was begun during the afternoon of the next day.

*Techniques for Electron Microscopy:* Cells were immersed in a very slightly hypotonic fixative solution composed of 1.25% glutaraldehyde, 0.05 M sodium cacodylate, 2.0 mM $CaCl_2$, and 0.1% tannic acid. The temperature of the primary fixative was initially 21–23°C. After the cells had been immersed in the fixative for 5.0 min, they were then transferred to a refrigerator at 4°C. The pH of the primary fixative and the buffer washes was adjusted to pH 7.2 by using HCl or NaOH. The use of more alkaline fixatives was not possible because of the tendency of calcium and tannic acid to precipitate in alkaline solutions. After 12–16 h, the cells were removed from the refrigerator, washed three times in buffer, and then placed in 1.0% $O_8O_4$ in 25.0 mM sodium cacodylate buffer, pH 7.2, for 2.0 h at 21–23°C. Next, the cells were washed in buffer and then dehydrated with acetone and embedded in Spurr's resin. Serial sections for transmission electron microscopy were placed on formvar coated, single-slot rhodium grids.

The zinc-iodide-osmium (ZIO)[1] technique was carried out with cells that were fixed in a solution that contained 3.0% formaldehyde (freshly made from paraformaldehyde), 0.5% glutaraldehyde, 10.0 mM $CaCl_2$, and 50.0 mM sodium cacodylate with the pH adjusted to 6.8 by adding a few drops of 1.0 N HCl. After a postaldehyde wash in distilled water they were placed in the ZIO solution described by Parker and Hawes (20), except that the temperature of the solution was kept at 30.0°C for 18.0 h. For osmium impregnation the cells were placed in 2.0% $O_8O_4$ at 30.0°C for 18.0 h. Sections were viewed without poststaining.

[1] *Abbreviations used in this paper:* PCR, partially coated reticulum; PMC, plasma membrane coat; ZIO, zinc-iodide-osmium.

## RESULTS

### Preservation of the Plasma Membrane Coat

While primary fixation with glutaraldehyde alone results in the absence of visible material within the periplasm (4–6), the inclusion of tannic acid and calcium chloride in the fixative results in the preservation of the plasma membrane coat (PMC) both within the periplasm and on the external surface of the plasma membrane outside the charasome (Fig. 1). Because the PMC has been preserved, the periplasmic tubules appear to be denser than the symplastic tubules; this is the reverse of the image that is seen after fixation with glutaraldehyde alone.

Two structural components, a core and a matrix that surrounds the core, comprise the PMC (Fig. 1). In some instances, the core appears as a discrete rod or tube with a diameter of ~130.0–180.0 Å. Frequently, the core is associated with radial extensions that bridge the space between the core and the plasma membrane. Matrix materials of variable structure always surround the core. Discrete particles are evident in some areas of the matrix. In other cases, the matrix is simply a dense, amorphous material that in some places obscures the structure of the core.

Outside the charasome, the matrix appears as a dense fibrogranular material that is attached to the external surface of the plasma membrane; core material is only occasionally observed (Fig. 1). In areas where charasomes are not present and the plasma membrane is closely appressed to the cell wall, it is difficult to perceive any structural distinction between the PMC and the wall. But, when the cell is intentionally plasmolysed during fixation, the presence of the PMC and its attachment to the plasma membrane are evident (Fig. 2). Such a PMC is present on all the cell types of vegetative, male *Chara* plants (with the possible exception of rhizoids, which we have not studied).

We found that the preservation of PMC core material is quite sensitive to the presence of calcium in the fixative. Concentrations of calcium as low as 0.2 mM, without any tannic acid being added, are sufficient to preserve small, but faintly discernable amounts of core material (micrographs not shown). Also, we noted that if 4.0 mM NaCl is substituted for 2.0 mM $CaCl_2$ in the fixative, no core material is present. Such a result indicates that the chloride in the fixative is not responsible for the preservation of the core. The addition of 4.0 mM sodium was assumed to have a negligible effect on the fixation process because 50.0 mM sodium was already present in the buffer.

*Chara corallina* is a long-lived, multi-cellular alga and so it is possible to harvest cells from the same populations over periods of many months. In old cultures of *Chara*, the growth rate of the alga slows because of depletion of bicarbonate and other nutrients from the culture solution. We observed that when cells from young, rapidly growing cultures are fixed, they always respond to the presence or absence of calcium and tannic acid in the manner that we have indicated. However, in either young or old cells taken from old cultures, in

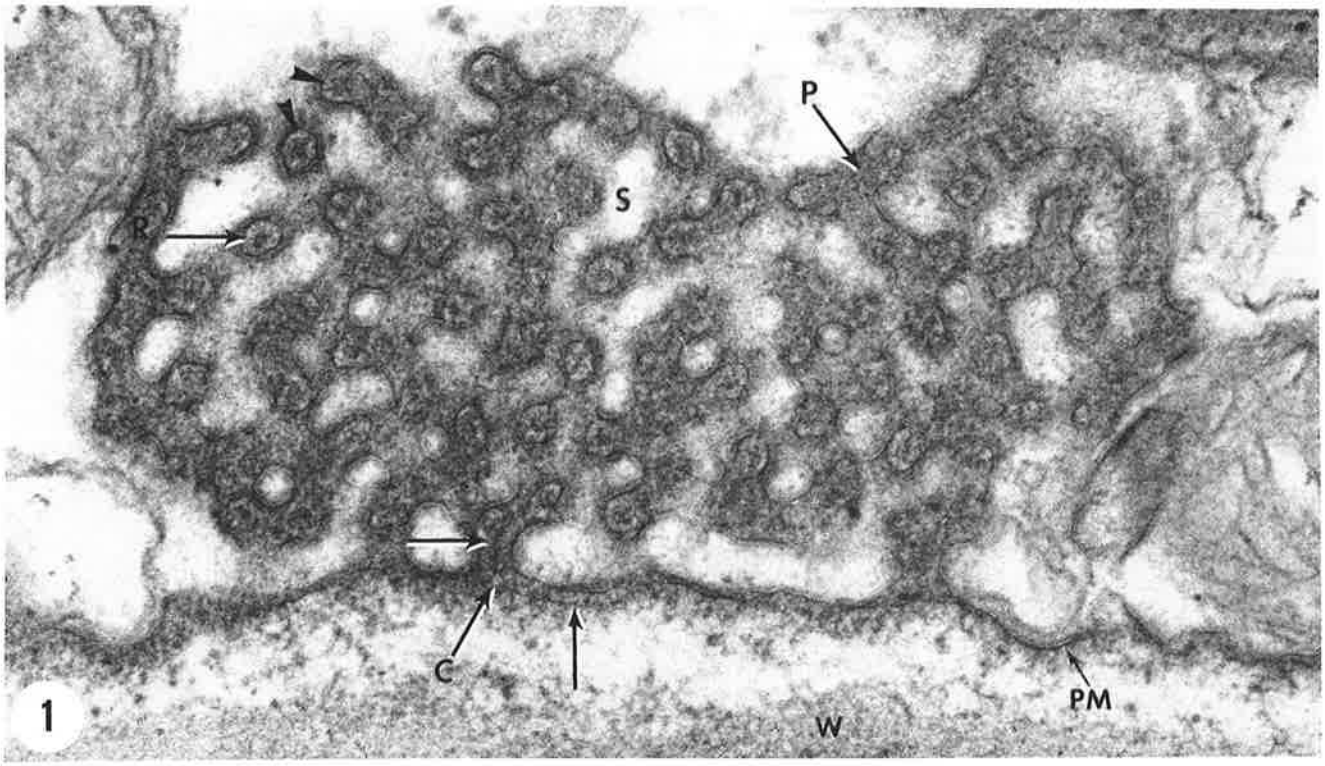


FIGURE 1 Plasma membrane (*PM*). Cell wall (*W*). Periplasm (*P*) is quite dense compared to symplast (*S*). Core (unlabeled arrows) is present throughout the periplasm and also along some areas of the plasma membrane outside the charasome. When cut in cross-section, the core appears either as a discrete rod (*R*) surrounded by a particulate matrix or as a rod with radial extensions attached to it (unlabeled darts). Although a slight plasmolysis has occurred during specimen preparation, the PMC outside the charasome is still continuous (*C*) with the PMC in the periplasm and also remains attached to the external surface of the plasma membrane. × 112,500.

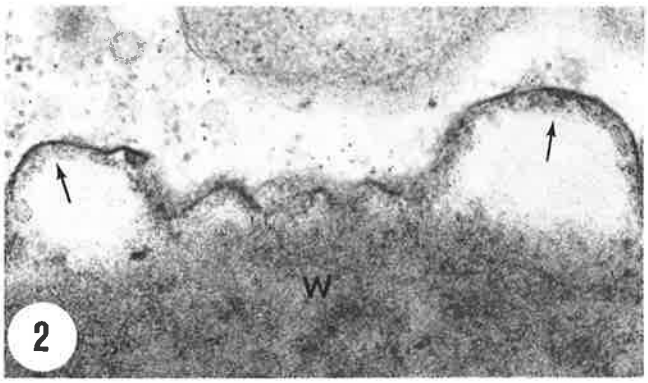


FIGURE 2 Smooth portion of plasma membrane. Space between plasma membrane and wall is artifact of plasmolysis. Unlabeled arrows indicate PMC still attached to portions of plasma membrane that have moved away from the wall as a result of plasmolysis. Wall (*W*). × 53,500.

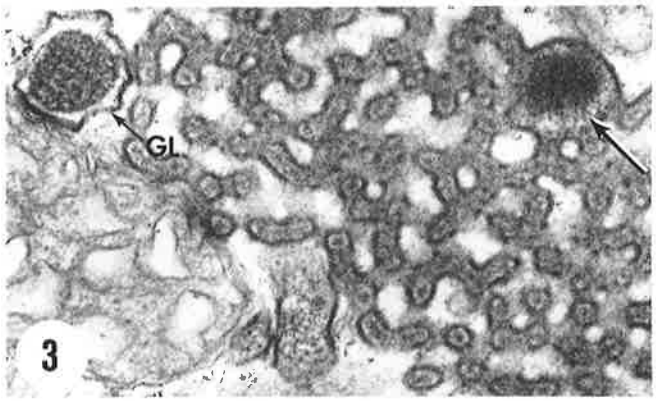


FIGURE 3 Glycosome (*GL*) adjacent to charasome with glycosome-like dense body (unlabeled arrow) within the periplasm. × 64,500.

which the starch grains are small or absent, the density of the PMC is markedly diminished.

## *Transport of PMC Materials to the Plasma Membrane*

Several types of vesicles appear to physically interact with the plasma membrane of *Chara*. Frequently, coated pits were observed on portions of the plasma membrane of mature and immature cells. Presumably such coated pits are the result of some type of interaction between coated vesicles and the plasma membrane. The possible relationship of coated pits to the transport of PMC material will become evident in the following section that concerns coated vesicles in the cytoplasm.

At least one other type of vesicle, the glycosome, seems to interact with the plasma membrane. Glycosomes are polysaccharide containing, single membrane bound organelles (21) that occur in all cells of *Chara* that we studied. The diameter of glycosomes varies within the range of 0.1 $\mu$m to 1.4 $\mu$m (Figs. 3, 4, and 10). Characteristically, each glycosome contains a central mass of dense material that is separated from the membrane by a nonstaining space. Structures which appear to be similar to glycosomes occur in the periplasm of charasomes (Fig. 3). In most cases, the presumptive former contents of the glycosome partially resemble the PMC in

form. We note that the apparent fusion of glycosomes with the plasma membrane occurs more frequently in some cells than in others, irrespective of either the cell size or cell type. Also, the observed frequency of apparent fusions of glycosomes with the plasma membrane is generally lower than that observed for coated vesicles.

## Coated Vesicles and Glycosomes in the Cytoplasm

Both glycosomes and coated vesicles with large, clearly detailed coats are frequently observed in the cytoplasm (Figs. 4 and 5). Often, coated vesicles and glycosomes are in close association with a loosely organized reticulum of membranes which we will refer to as a partially coated reticulum (PCR) (Figs. 4–6). Initially, we believed that the PCR was part of a Golgi stack. However, we have never observed the Golgi stack membranes to contain structures that resemble the contents of glycosomes, nor have we observed clearly detailed coated invaginations of the Golgi stack membranes. The only vesicles with which the Golgi stacks of *Chara* are closely associated are either smooth vesicles, which do not resemble glycosomes, or vesicles with small coats that are so faintly detailed as to be only tentatively identifiable. Even when the PCR and the Golgi stacks are laterally adjacent to each other in the same section (Fig. 6), the PCR is structurally distinguishable from the Golgi stacks. Such structural dissimilarities are further emphasized by the results of serial sectioning (Figs. 7–10). While the PCR has overall dimensions which are similar to those of the Golgi stack, the membranes of the PCR do not overlay each other in the stacked configuration that is characteristic of the Golgi complex. Instead, the PCR is an assemblage of interconnected membranes having no apparent structural symmetry.

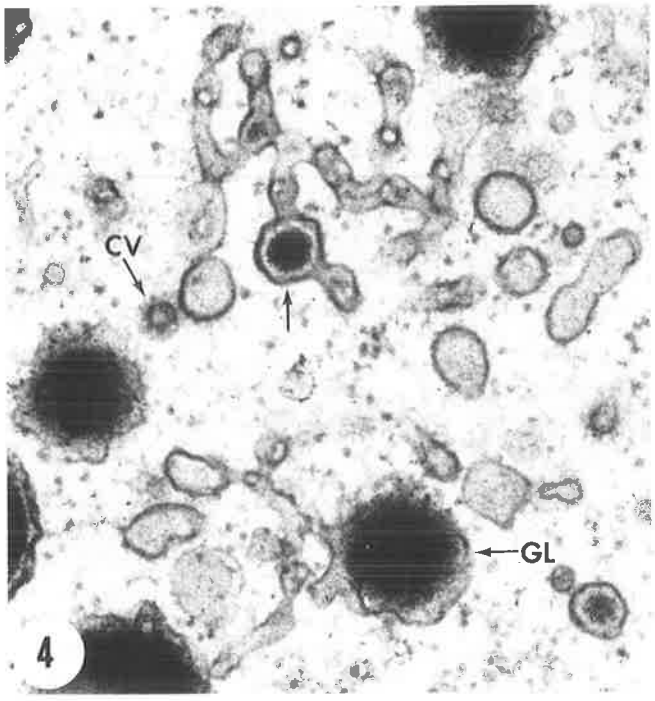


FIGURE 4 Unlabeled arrow indicates presumed nascent glycosome located within reticulum of membranes. Glycosome (*GL*) and coated vesicle (*CV*) are closely associated with reticulum. × 65,500.

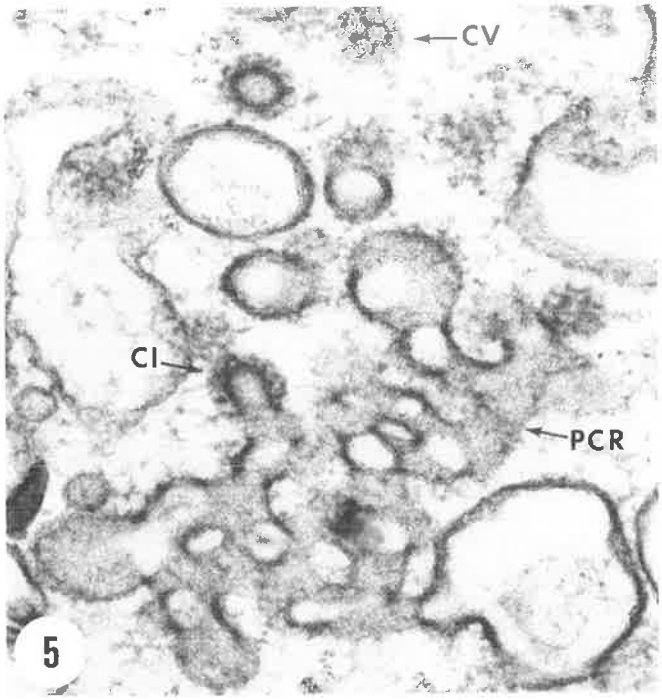


FIGURE 5 Coated vesicles (*CV*) closely associated with partially coated reticulum (*PCR*) of membranes. Coated invagination (*CI*). × 110,300.

Occasionally, some degree of association between the PCR and the Golgi is evident. Figs. 7–10 are serial thin sections that show an area in which one of the PCRs may connect with a Golgi; but it is also possible that these figures represent an instance in which the membranes are located near each other but are not physically connected. Indeed, we examined serial sections of a number of other PCRs in *Chara* and have not found either a physical connection or even a spatial association with the Golgi. It seemed possible that shear forces within the streaming cytoplasm of *Chara* might separate the PCR from the Golgi. We obtained evidence against such an hypothesis by noting that, in very young cell types in which cyclosis does not occur (according to our observations), the PCR and Golgi stacks are no more closely related to each other (Fig. 6) than they are in streaming cells.

The general morphological asymmetry of the PCR is accentuated by the variety of structures that compose it. Tubules, lamellae, fenestrated lamellae, smooth vesicles, coated vesicles, and coated invaginations are all frequently part of, or are located very near, the PCR (Figs. 4–10). We did not observe the presence of ribosomes on any PCR membranes. Coated vesicles are more frequently associated with PCR than with any other structure in the cell except the plasma membrane. In some sections (Fig. 7), we observed few coated vesicles or coated invaginations either near or on the PCR. However, serial sections have always shown that coated vesicles or invaginations are present near or on at least some portion of the PCR (Figs. 8–10). Glycosome-like structures occur within the PCR more frequently in some cells than in others, irrespective of either cell size or cell type. Thus it appears that the processes that control the formation of glycosomes have the same intermittent temporal characteristics as do the processes that control the exocytosis of glycosomes.

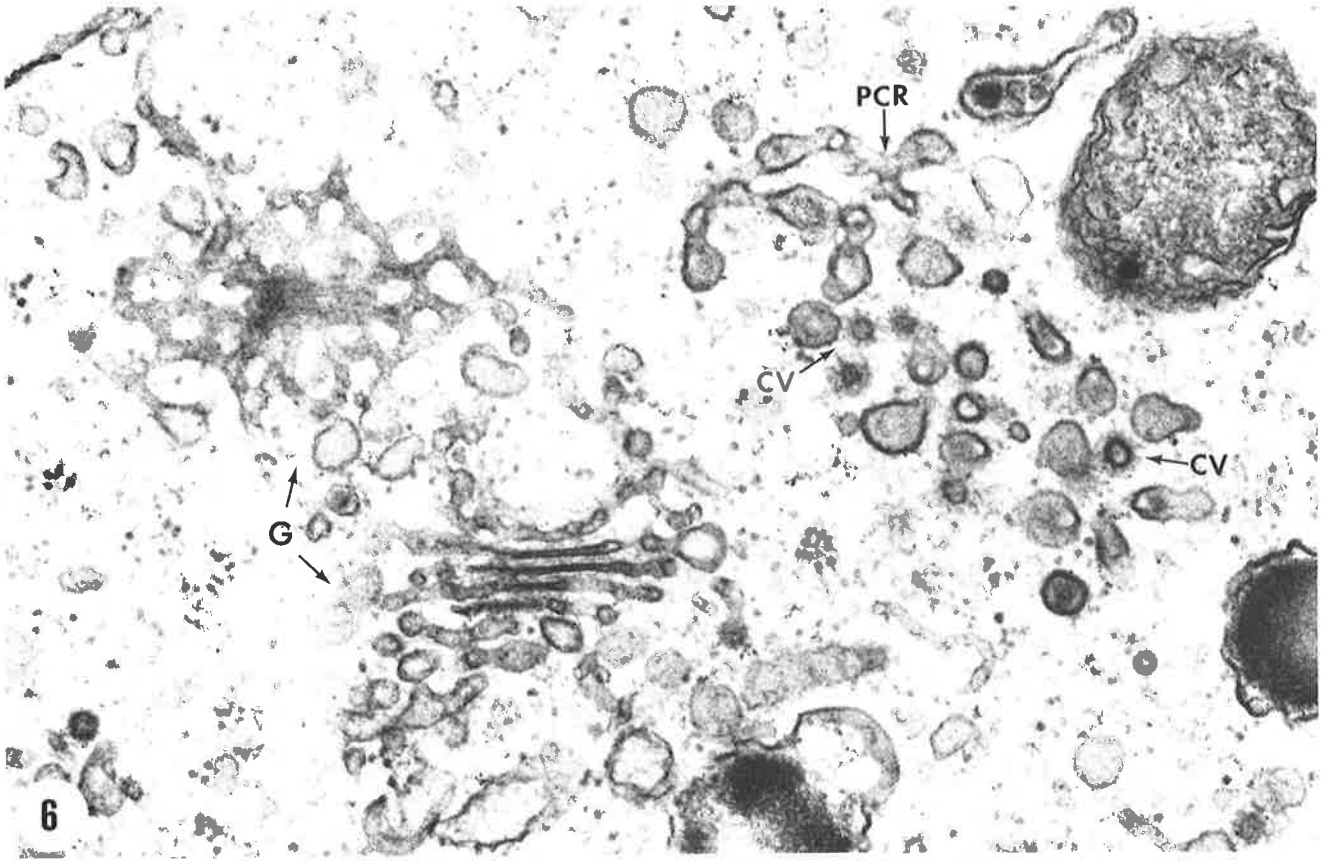


FIGURE 6 Two Golgi complexes (G) that are laterally adjacent to a partially coated reticulum (*PCR*) in a young, nonstreaming cell of the vegetative apex. Note that while the Golgi are surrounded by many apparent vesicles, the only vesicles with clearly defined coats (*CV*) are located next to the PCR. × 67,500.

### *Endomembrane Histochemistry*

The chemical nature of the PCR and the other membranes in young cells was examined by using both osmium impregnation and ZIO. After osmium impregnation, the only cellular structures that showed increased density when compared with controls were some cisternae of the endoplasmic reticulum (micrographs not shown). In contrast, after ZIO many components of the cell, including the endoplasmic reticulum, Golgi, and nuclear envelope, showed greatly increased density (Figs. 11–13). It appeared that much of the Golgi complex was stained and often membranes that were similar in form to those designated as GERL in cotyledon cells (22) were stained (Fig. 11). In no case was an unstained Golgi stack observed, but in some instances a few cisternae of the Golgi or endoplasmic reticulum were unreactive. Additionally, in a few cells an apparent overreaction occurred and the entire cytoplasm of such cells was filled with dense precipitates. However, in no case in which specific staining of cell components was observed were any of the PCR or glycosome membranes stained with much intensity.

Many attempts were made to localize acid phosphatase activity in *Chara* by using techniques that were similar to those of Novikoff and Novikoff (23). However, in no case were we able to observe an indication that acid phosphatase activity was present either in or near the Golgi complex. Instead, we observed that the membranes of the Golgi complexes of both the controls (incubated without substrate) and the tests (incubated with either nitrophenyl phosphate or $\beta$-glycerol phosphate at pH 5.0–5.5) showed numerous lead deposits (micrographs not shown).

## DISCUSSION

### *Plasma Membrane Coat*

The precise structure of the plasma membrane coat is far from clear at present. It is probable that the core within the periplasm of the charasome is a continuous tubule and that the instances of solid, rod-like cores are artifacts caused by either the thickness of, or plane of, the section. However, it may be that the core is both tubular and solid, depending on the location of the core within the anastomosing tubules of the charasomes. From transverse sections, it appears that the core is always surrounded by radial arrays of particulate and fibrous structures. These structures may represent images of helices wound around the core. To either confirm or refute such an hypothesis it will be necessary to understand the precise details of the distribution of these structures both around and along the core.

In an earlier study on *Chara* (6), it was proposed that the periplasmic space was filled with "small distinct particles . . ., as opposed to a structurally continuous matrix." In contrast, the results of the present report support the concept that the periplasm contains a complex array of interconnected structures that are also connected to the plasma membrane. Our results do not necessarily preclude the existence of distinct particles in the periplasm. However, we now believe that such particles may have resulted from the relatively extended period of tannic acid application that was used in previous fixations (6).

We have also shown that the external surface of the plasma membrane outside the charasome is connected to a substantial

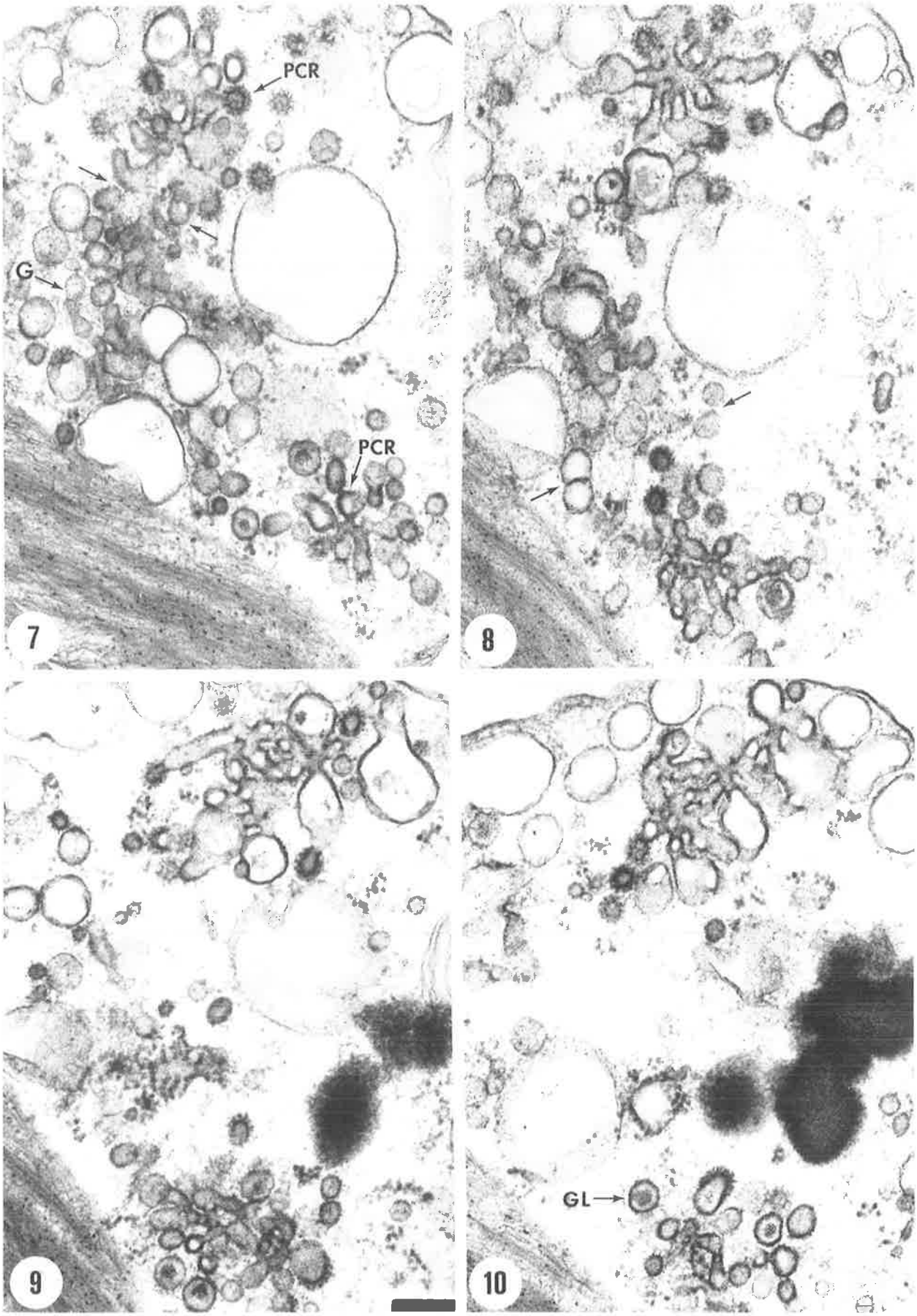


FIGURES 7–10 Serial sections. Chloroplast (*CL*), Golgi complex (*G*), glycosome (*GL*), and partially coated reticulum (*PCR*). Figs. 7–9 show an apparent Golgi complex located in the central portion of the figure. Two PCRs are present near the lateral margins of the Golgi at the top and bottom of each figure. The uppermost PCR could be connected to the Golgi (unlabeled arrows; Fig. 7) while the lower PCR does not appear to be in close contact with the Golgi (unlabeled arrows, Fig. 8). It is possible that the membranes of the upper PCR merely overlay the Golgi without actually merging. × 58,000.

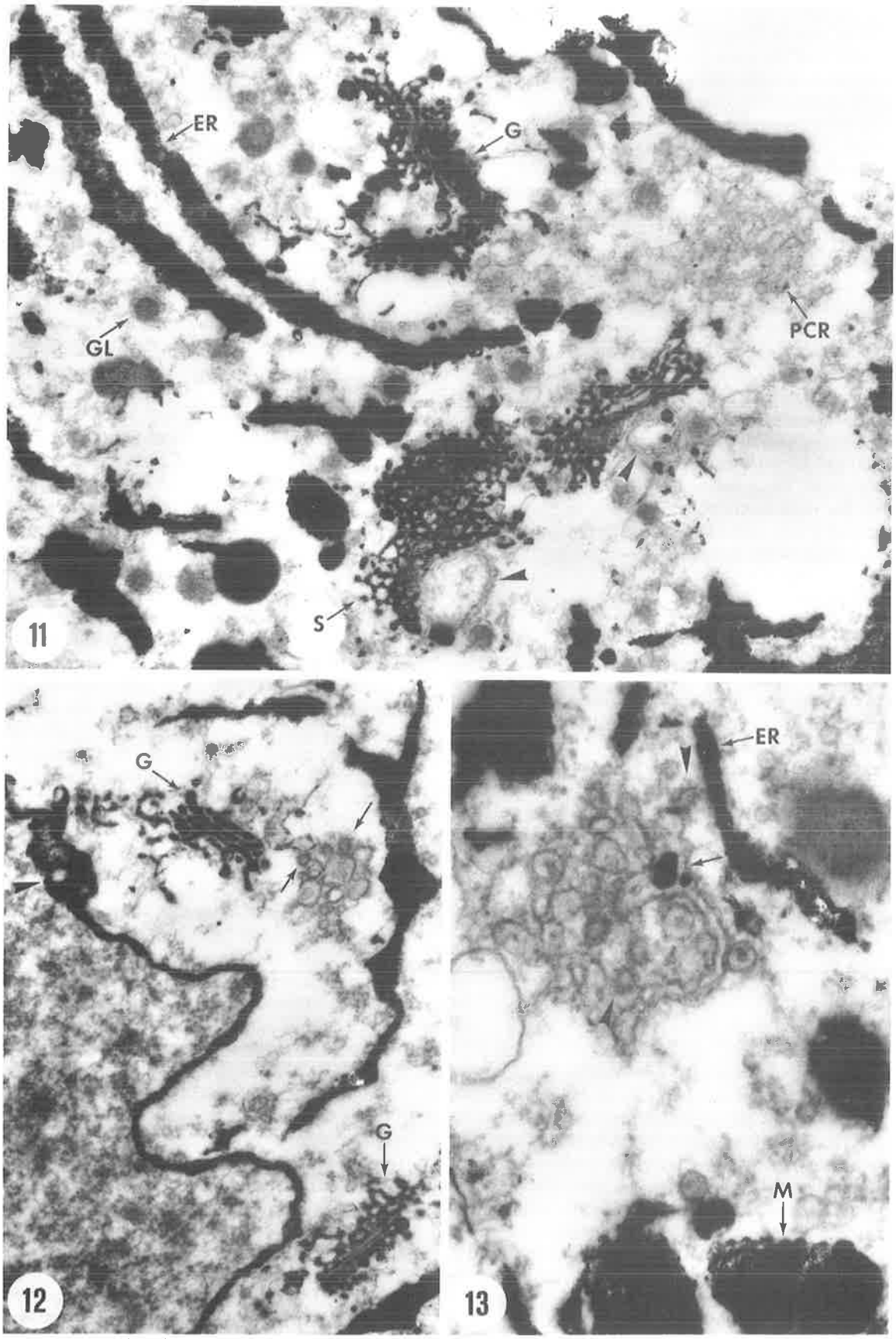


FIGURES 11–13 Results of ZIO staining technique. Golgi (*G*), partially coated reticulum (*PCR*), endoplasmic reticulum (*ER*), glycosome (*GL*), and mitochondria (*M*). Fig. 11: A few cisternae of the Golgi are unreactive (unlabeled darts) as are the PCR membranes and the glycosomes. The extended, fenestrated sheet of Golgi membranes (*S*) resembles the GERL in cotyledon cells (23). × 24,000. Fig. 12: Pore in nuclear envelope (unlabeled dart) is evident as are stained Golgi and unstained PCR. Lack of poststaining makes coated regions on PCR difficult to discern (unlabeled arrows) at this relatively low magnification. × 24,000. Fig. 13: Coated regions (unlabeled darts) on PCR are evident as is small amount of ZIO staining within PCR tubules (unlabeled arrow). In contrast, ER and mitochondrion are almost completely stained. × 55,000.

extracellular matrix. Such an observation is at variance with the conventional ultrastructural image of plant plasma membranes as being smooth, tripartite structures with little material being connected to the external surface. The literature already contains some recent information regarding the existence of projections on the internal surface of plant plasma membranes in association with microtubules (24). Thus, it seems that while the complex structure of the plant plasma membrane is becoming more thoroughly understood, its limits are becoming less clearly defined.

Franceschi and Lucas (6) have advanced the hypothesis that the electron-dense material within the periplasm serves to stabilize the structure of the charasome against turgor pressure. Our results support their hypothesis by showing that in the periplasm there exists an abundance of structures that could conceivably form a continuous internal scaffolding to support the charasome membrane against turgor pressure. It also seems possible that the structural continuum of the plasma membrane coat might support the plasma membrane against turgor pressure during a coated vesicle-mediated endocytotic event. The presence of a plasma membrane coat on areas of the plasma membrane other than the charasome suggests that a compressive cushion may function around the entire periphery of the protoplast.

### Composition

Commercial tannic acid is a heterogeneous mixture, thus it is difficult to fully understand the nature of its reaction with the plasma membrane coat. However, tannic acid has been used to enhance the contrast and/or preservation of many structures such as microfilaments (25), microtubules (26), the cytoplasmic matrix (27), and the extracellular matrix of animal cells (28). The common attribute of these structures is that they are proteinaceous in nature. Calcium is known to decrease the amount of lipid that is lost during fixation (29). This could stabilize proteins which are linked to lipids in the plasma membrane and PMC. Calcium may also be binding to acidic polysaccharides in the PMC in a manner similar to the binding of calcium to pectins, a class of carbohydrates present in the plant cell wall. It seems reasonable to propose that the PMC is composed of proteoglycans similar to those which are known to be present in the extracellular matrix of animal cells (30).

### Formation

The plasma membrane coat is present in all the cell types of *Chara* that we investigated. However, images both of apparent fusions of glycosomes with the plasma membrane and of glycosome production in the PCR are not visible in all cells. It seems probable that either the production and exocytosis of glycosomes is a periodic phenomenon, or that variations in the metabolic rates of particular cells allow us to observe events that occur either more rapidly or slowly in other cells. A further complication is that at present we have not determined which, if any, of the other types of smooth or coated vesicles in *Chara* may be capable of, or necessary for, the formation of the plasma membrane coat. The frequent and close association of coated vesicles with the PCR and nascent glycosomes may indicate that the vesicles are involved in the processing of glycosome-like material. Speculatively, it is suggested that either coated vesicles or small, smooth vesicles that are derived from coated vesicles may represent the most frequently used route for the transfer of coat materials to the plasma membrane.

### The Partially Coated Reticulum

The PCR has been previously identified as being a part of a dictyosome or Golgi complex (21). Such an identification is understandable because of the fenestrations that are present in membranes of both the PCR and the Golgi complex. However, it should be noted that the fenestrated configuration is not restricted to Golgi membranes. Recently, Harris and Oparka (22) have shown the existence of fenestrated endoplasmic reticulum membranes in cotyledonous cells. They have also observed membranes having a fenestrated morphology that they believe may be a GERL. The GERL in cotyledons is connected to the Golgi stack by extended tubules; this may be the case in *Chara* as well. In the future we intend to search for the existence of such tubules in *Chara* by examining the cytoplasm with high-voltage electron microscopy. However, the results of the present investigation lead us to conclude that in most cases the PCR in *Chara* possesses a high degree of structural autonomy from the Golgi complex.

It is somewhat difficult to understand why, to our knowledge, a PCR has not been observed in other organisms. In this regard it is interesting to note that, in many cases, coated vesicles or coated invaginations having large, clearly detailed coats are frequently observed to be associated with membranes that are located near Golgi stacks (18 and 31) rather than being directly attached to the lamellae of the Golgi stacks. We propose that the PCR structure in *Chara* has undergone hyperplasic development; in other organisms, the PCR may be composed only of a few coated vesicles and a relatively small amount of membrane. An additional distinction is that in many cases, in *Chara*, the PCR does not appear to be specifically associated with the Golgi stacks.

The results of our cytochemical tests clearly differentiate the PCR and the glycosome from both the Golgi and much of the ER. Given the many instances in the literature of a close association between the Golgi complex of plant cells and coated vesicles (31), we were surprised that the PCR differed so much from the Golgi. To our knowledge, no previous studies of plant cells have documented the reaction of the ZIO reagents with membranes that contain coated regions. As far as the other membranes of the cell are concerned, our results were quite consistent with those obtained for cotyledon cells by Harris and Oparka (22). While in many cases we observed structures that were quite similar to those identified morphologically as the GERL in cotyledon cells (22), our inability to demonstrate acid phosphatase activity in the Golgi makes the use of the term GERL questionable in the case of *Chara*.

The lack of ZIO staining in both the glycosomes and the PCR strengthens our earlier assumption that the glycosomes are directly derived from the PCR. Additionally, such results offer little support for the existence of either membranous connections or membrane flow from the Golgi to the PCR. Instead, it seems more plausible to postulate that the PCR functions as part of a plasma membrane retrieval system using coated or smooth vesicles in a manner similar to that reported by Farquhar (32) for somatotrophs. As such, by monitoring the rate and condition of retrieved membranes, the PCR may apportion plasma membrane coat material into either a storage form (glycosomes) or a form that is immediately used (coated or smooth vesicles). The relationship of the

PCR to the Golgi in such a scheme is unclear, although the evidence does not preclude the eventual passage of membrane from the PCR to the Golgi.

This work was supported by National Science Foundation Grant PCM 81-17721.

*Received for publication 20 June 1983, and in revised form 16 January 1984.*

## REFERENCES

1. Lucas, W. J. 1982. Mechanism of acquisition of exogenous bicarbonate by internodal cells of *Chara corallina*. *Planta* (*Berl.*). 156:181–192.
2. Kamiya, N., and K. Kuroda. 1965. Rotational protoplasmic streaming in *Nitella* and some physical properties of the endoplasm. *In* Proceedings of the Fourth International Congress on Rheology. John Wiley & Sons, New York. Pp. 157–171.
3. Green, P. B., and A. King. 1966. A mechanism for the origin of specifically oriented textures in development with special reference to *Nitella* wall texture. *Aust. J. Biol. Sci.* 19:421–437.
4. Franceschi, V. R., and W. J. Lucas. 1980. Structure and possible functions of charasomes: complex plasmalemma-cell wall elaborations present in some Characean species. *Protoplasma*. 104:253–271.
5. Lucas, W. J., and V. R. Franceschi. 1981. Characean charasome-complex and plasmalemma vesicle development. *Protoplasma*. 107:255–267.
6. Franceschi, V. R., and W. J. Lucas. 1981. The charasome periplasmic space. *Protoplasma*. 107:269–284.
7. Barton, R. 1965. Electron microscope studies on surface activity in cells of *Chara vulgaris*. *Planta* (*Berl.*). 66:95–105.
8. Smith, F. A. 1970. The mechanism of chloride transport in characean cells. *New Phytologist*. 69:903–917.
9. Franceschi, V. R., and W. J. Lucas. 1982. The relationship of the charasome to chloride uptake in *Chara corallina*: physiological and histochemical investigations. *Planta* (*Berl.*). 154:525–537.
10. Hascall, V. C., and G. K. Hascall. 1981. Proteoglycans. *In* Cell Biology of Extracellular Matrix. E. Hay, editor. Plenum Press, New York. Pp. 39–63.
11. Robards, A. W. 1969. Particles associated with developing plant cell walls. *Planta* (*Berl.*). 88:376–379.
12. Levering, C. A., and W. W. Thomson. 1971. The ultrastructure of the salt gland of *Spartina foliosa*. *Planta* (*Berl.*). 97:183–196.
13. Olesen, P. 1980. The visualization of wall-associated granules in thin sections of higher plant cells: occurrence, distribution, morphology and possible role in cell wall biogenesis. *Z. Pflanzenphysiol.* 96:35–48.
14. Farquhar, M. G. 1981. The glomerular basement membrane. *In* Cell Biology of Extracellular Matrix. E. Hay, editor. Plenum Press, New York. pp. 335–378.
15. Manton, I. 1967. Further observations on the fine structure of *Chrysochromulina chiton* with special reference to the haptonema, peculiar Golgi structure and scale production. *J. Cell Sci.* 2:265–272.
16. Whaley, W. G. 1975. The Golgi apparatus. Cell Biology Monographs. Vol. 2. Springer-Verlag, Berlin and New York.
17. Novikoff, P. M., A. B. Novikoff, N. Quintana, and J.-J. Hauw. 1971. Golgi apparatus, GERL, lysosomes and neurons in rat dorsal ganglia, studied by thick section and thin section cytochemistry. *J. Cell Biol.* 50:859–886.
18. Farquhar, M. G., and G. E. Palade. 1981. The Golgi apparatus (complex)—(1954–1981)—from artifact to center stage. *J. Cell Biol.* 91(3, Pt. 2):775s–1035s.
19. Lucas, W. J., and F. A. Smith. 1973. The formation of alkaline and acid regions at the surface of *Chara corallina* cells. *J. Exp. Bot.* 24:1–14.
20. Parker, M. L., and C. R. Hawes. 1982. The Golgi apparatus in developing endosperm of wheat (*Triticum aestivum* L.). *Planta* (*Berl.*) 154:277–283.
21. Franceschi, V. R., and W. J. Lucas. 1981. The glycosome of *Chara*: ultrastructure, development and composition. *J. Ultrastruct. Res.* 75:218–228.
22. Harris, N., and K. J. Oparka. 1983. Connections between dictyosomes, ER, and GERL in cotyledons of mung bean (*Vigna radiata* L.). *Protoplasma*. 114:93–102.
23. Novikoff, A. B., and P. M. Novikoff. 1977. Cytochemical contributions to differentiating GERL from the Golgi apparatus. *Histochem. J.* 9:525–551.
24. Oross, J. W., and W. W. Thomson. 1982. The ultrastructure of the salt glands of *Cynodon* and *Distichlis* (Poaceae). *Am. J. Bot.* 69:939–949.
25. Seagull, R. W., and J. B. Heath. 1979. The effects of tannic acid on the *in vivo* preservation of microfilaments. *Eur. J. Cell Biol.* 20:184–188.
26. Tilney, L. G., J. Bryan, D. J. Bush, K. Fujiwara, M. S. Mooseker, D. B. Murphy, and D. H. Snyder. 1973. Microtubules: evidence for 13 protofilaments. *J. Cell Biol.* 59:267–275.
27. Maupin, P., and T. D. Pollard. 1983. Improved preservation and staining of HeLa cell actin filaments, clathrin-coated membranes, and other cytoplasmic structures by tannic acid-glutaraldehyde-saponin fixation. *J. Cell Biol.* 96:51–62.
28. Rodewald, R., and M. J. Karnovsky. 1974. Porous substructure of the glomerula slit diaphragm in the rat and mouse. *J. Cell Biol.* 60:423–433.
29. Glauert, A. M. 1975. Fixation, Dehydration and Embedding of Biological Specimens. American Elsevier Publishing Co., New York. Pp. 24–25.
30. Hay, E. D. 1981. Extracellular matrix. *J. Cell Biol.* 91(3, Pt. 2):205s–223s.
31. Newcomb, E. H. 1980. Coated vesicles: their occurrence in different plant cell types. *In* Coated Vesicles. C. D. Ockleford and A. Whyte, editors. Cambridge University Press, Cambridge. Pp. 55–68.
32. Farquhar, M. G. 1978. Recovery of surface membranes in anterior pituitary cells. *J. Cell Biol.* 77:R35–R42.

Protoplasma 125, 173—184 (1985)

PROTOPLASMA

© by Springer-Verlag 1985

# Presence of a Partially-Coated Reticulum in Angiosperms

TH. C. PESACRETA[1,*] and W. J. LUCAS

Received May 30, 1984
Accepted October 23, 1984

Department of Botany, University of California, Davis, California

## Summary

The form and distribution of partially-coated membrane systems and coated vesicles in the leaf glands of *Phaseolus* and the root cortical cells of *Zea* were investigated. Partially-coated membranes exist as a reticulum which is either sparsely branched or extensively anastomosed. Coated vesicles and coated membrane regions may occur at all points that are in the vicinity of such a reticulum. Golgi stack membranes, though associated with the partially-coated reticulum in many cases, show no consistent orientation to it. Occasionally, the reticulum and the associated coated vesicles are located away from any Golgi stack. We examined other plant tissues from such species as *Allium cepa, Beta vulgaris* and *Nicotiana tabacum* and the partially-coated reticulum was observed in all material. We suggest that membrane flow may be occurring from the partially-coated reticulum to either the Golgi stack or to other intracellular compartments.

*Keywords:* Coated vesicles; Endomembrane flow; Endosomes; Golgi complex.

## 1. Introduction

Coated vesicles of various diameters are known to exist in a wide variety of plant and animal cell types (for a review, see OCKLEFORD and WHYTE 1980). Each coated vesicle is composed of a membrane that is surrounded by a polygonal network (OCKLEFORD 1976) of interconnected triskelions. Clathrin, a 180,000–190,000 MW protein, is the major constituent of triskelions (PEARSE 1975, MERSEY *et al.* 1982). Presumably, the formation of coated vesicles occurs when triskelions aggregate to form supramolecular complexes that then are able to "pinch-off" specific portions of membranes (KANASEKI and KADOTA 1969). Recently, it has been demonstrated that coated vesicle membranes contain ATPases which can cause the acidification of the vesicle lumen (FORGAC *et al.* 1983), and also that interactions between clathrin, pH and various associated proteins can affect the size and formation of coated vesicles (ZAREMBA and KEEN 1983).

Most of the information concerning coated vesicle function has come from studies of animal cells. Numerous pulications have documented the involvement of coated vesicles with the receptor-mediated endocytosis of molecules such as immunoglobulins (RODEWALD 1980), insulin (PILCH *et al.* 1983), and transferrin (HARDING *et al.* 1983). In addition, many results indicate that coated vesicles are part of an endocytotic system which is concerned with the recycling of plasma membrane (FARQUHAR 1978, HEUSER and REESE 1973, HARDING *et al.* 1983). Less frequently suggested but equally credible roles which have been proposed for coated vesicle function include bulk-phase uptake (ROBERTS *et al.* 1977) and the secretion of molecules such as acetylcholine receptors (BURSZTAJN and FISCHBACH 1984).

Coated vesicle function in plant cells has been widely assumed to involve exocytotic events, primarily the delivery of Golgi-derived membranes and their con-

[1] Present address: The Biological Laboratories, Harvard University, 16 Divinity Ave., Cambridge, MA 02138, U.S.A.
* Correspondence and Reprints: The Biological Laboratories, Harvard University, 16 Divinity Ave., Cambridge, MA 02138, U.S.A.

tents to the plasma membrane. Marker-particle evidence for such exocytosis is lacking. However, factors such as the presence of large numbers of coated membranes in regions where cell walls form after the competition of mitosis (FRANKE and HERTH 1974) and the often-noted association of coated vesicles with both the Golgi and the plasma membrane of interphase cells (BONNETT and NEWCOMB 1966) have been viewed as supportive evidence for an exocytotic, as opposed to an endocytotic, role for coated vesicle mediated transport. In addition, while it has been suggested that endocytosis may occur in plant cells (MACROBBIE 1969), CRAM (1980) has described some of the biophysical obstacles to endocytosis in plants. However, recently we have reported the existence of a structure which is attached to the external surface of the plasma membrane and which we term the plasma membrane coat (PMC) in the green alga *Chara* (PESACRETA and LUCAS 1984). We suspect that the PMC is a structural component which, among other things, functions to support wall-less portions of the plasma membrane against turgor pressure, thereby facilitating endocytosis. Even more recently, results with plant protoplasts indicate that coated vesicle-mediated endocytosis may occur in turgorless plant systems (JOACHIM and ROBINSON 1984, TANCHAK *et al.* 1984).

Remarkably few detailed structural considerations of plant coated vesicles have been published. In a review article, NEWCOMB (1980) cites instances in which coated regions have been observed on the surface of algal Golgi stack lamellae and on the "tubate peripheries" of isolated, negatively stained *Allium* Golgi. In addition, he notes that coated vesicles and coated membrane regions were present either near or on vesicles "in the neighborhood of" *Raphanus* Golgi. MOLLENHAUER and MORRÉ (1966), in a diagrammatic representation of the plant Golgi apparatus, showed coated membrane regions connected to the ends of tubules which themselves were connected to the Golgi stack lamellae; the details of this diagram were derived from studies of negatively-stained membrane isolates (CUNNINGHAM *et al.* 1966).

Investigations in this laboratory have indicated that, in the alga *Chara corallina,* coated vesicles are most frequently present amongst a partially coated reticulum (PCR) of membranes which are distinct from the Golgi stack (PESACRETA and LUCAS 1984). After noting the resemblance of the PCR in *Chara* to partially-coated membranes which are involved with endocytosis and recycling in various animal cell types (FARQUHAR 1978, HEUSER and REESE 1973), we were prompted to speculate that the characean PCR was involved in similar processes. As such, the PCR would be a type of endosome (for a review of endosomes, see HELENIUS *et al.* 1983): polymorphic assemblages of membranes in the cytoplasm which mediate various pathways of membrane flow and recycling.

In this article we present our findings concerning the presence of the partially coated reticulum in several cell types of higher plants. Our investigations show that the PCR possesses a considerable degree of structural complexity beyond that reported in the previous literature; features which are easily interpretable in terms of membrane flow to, as well as from, the Golgi stack.

## 2. Materials and Methods

*Phaseolus vulgaris* var. Red Kidney was grown in a greenhouse during the winter and spring months. *Zea mays* (A 632 X [C 3640 X Oh 43], Crows Hybrid Corn Co., Milford, IL.) was grown hydroponically in aerated solutions as described by KOCHIAN and LUCAS (1982). *Allium cepa* var. Stockton Yellow Globe and *Beta vulgaris* var. SSBN 1, VSH 11, Lot 82312, were grown in growth chambers at 25 °C. *Nicotiana tabacum* var. Wisconsin 38, was grown in a greenhouse during summer months. *Phaseolus* leaves were placed into fixative and then immediately cut into pieces having a surface area of 4.0 $mm^2$, with the length of the intact leaf being approximately 1.0 cm. *Zea* roots were placed in the fixative while intact and then cut into smaller portions after approximately 30 minutes had elapsed; all solutions were at room temperature (21–24 °C). Primary fixative solutions were composed of 25.0 mM sodium cacodylate buffer plus 5% glutaraldehyde. In some cases, 0.5% tannic acid plus 2.0 mM calcium chloride was added. Primary fixative pH was 6.6–6.9. After 3 hours in glutaraldehyde, the samples were given three washes in buffer, post fixed in 1% $OsO_4$ for 12–20 hours on ice, washed three times in distilled water, dehydrated in an acetone series, and then infiltrated and embedded in Epon-Araldite. Sections were cut on a diamond knife, picked up on Formvar-coated 0.2 × 1.5 mm slot grids, and viewed with a JEOL 100-S transmission electron microscope.

For the purposes of the present report, the following terminology will be employed. "Coated membranes" will refer both to coated vesicles and to regions of otherwise smooth membranes which have coated vesicle-like structures attached to some portions of their surface. To specifically refer to the latter sub-class, the term "coated membrane region" will be used. Golgi stacks represent a special terminological problem, because many of the currently-used Golgi-related terms are meant to convey a particular direction of transport which is presumably occurring within the Golgi; however, numerous and sometimes divergent views of intra-Golgi transport are present in the contemporary literature (FARQUHAR and PALADE 1981), and so we feel that it is advisable for us to remain neutral in this matter. Therefore, in the present report we will employ a strictly morphological terminology of our own. Assuming that the overall form of a Golgi stack generally resembles that of a short cylinder, we will refer to the flat ends of the cylinder as being the "horizontal faces" of the Golgi, while the remainder of the surface of the cylinder will be referred to as the "circumferential face" of the Golgi.

## 3. Results

### *3.1. Coated Membranes in the Cytoplasm of Phaseolus vulgaris Gland Cells*

In young *P. vulgaris* leaves, coated vesicles were present in all cell types examined but occurred most frequently in gland cells that were located on the abaxial surface (see Figs. 1 and 2). Often, coated vesicles appeared in groups (Fig. 2) which were located near Golgi stacks. However, coated vesicles were also commonly associated with a partially coated reticulum (PCR) of irregularly shaped membranes (Fig. 3). Physical continuities between the PCR and Golgi stack membranes were not evident in most cases (Fig. 4) or were problematic (Fig. 5). Only occasionally did the PCR seem to be directly connected to the Golgi stack (Fig. 6). Coated membranes were located in many areas that were either on or around the PCR (Figs. 2–6) and only in a few cases were coated membranes not observed in the zone between the Golgi stack and the PCR (Fig. 6). PCRs were observed to be adjacent to either the horizontal (Figs. 4 and 5) or the circumferential (Figs. 2 and 6) faces of the Golgi.

With regard to overall spatial relationships within the cell, PCRs could be found either near the plasma membrane or in the interior of the cell. Similarly, no particular spatial arrangements of the PCR, Golgi and plasma membrane with each other seemed to be favored.

Serial sectioning (Figs. 7–18) revealed that a PCR could contain a much more extensive assemblage of membranes than one might have imagined from looking at single section images alone; great diversity in the size and form of other serially-sectioned PCRs was encountered and so this particular series should not be construed to represent more than one of a number of possibilities. In this series, PCR 1 was approximately the same size as the nearby Golgi stack, a common circumstance. As was seen in the single sections, no obvious symmetry of placement was evident with regard to the location of the coated membranes that were either on or around the PCR. Also, several coated vesicles were present in the zones between each PCR and the Golgi stack (Figs. 14 and 18). Connections between the PCRs and the Golgi were problematic (Figs. 11–15) and the membranes of both PCRs were most concentrated in regions of the cell which were spatially distinct from the Golgi stack (Figs. 13 and 17). It should be emphasized that in serial sections of other gland cells which we examined, the degree of association which existed between the PCR and the Golgi was occasionally less extensive than is seen in Figs. 7–18; such a circumstance will be documented in the following description of *Zea mays* cortical cells.

### *3.2. Coated Membranes in the Cytoplasm of Zea mays Root Cortical Cells*

In *Zea* root cortical cells (Fig. 19), many of the structural features of the PCRs resembled those already described for *Phaseolus*. For example, the PCRs of *Zea* could occupy a position that was opposite to either a circumferential or a horizontal face of the Golgi (Fig. 20) and coated vesicles were frequently interposed between the Golgi and the PCR. However, the morphology of the PCRs in cortical cells (Figs. 21 und 22) was usually less complex than that observed in the serial sections of *Phaseolus*. In *Z. mays,* the PCR was frequently comprised of a single, sparsely branched, fenestrated membrane, although, in some cases, it was difficult to use such a generalization with confidence (Fig. 20).

Serial sectioning showed that even this relatively simple form of the PCR could develop an elongate system extending from the Golgi stack into other portions of the cytoplasm (Figs. 23–25). In certain areas, this simple PCR was associated with small, dense zones of membrane that appeared to be either greatly anastomosed or vesiculated (Figs. 23, 26, and 27). These small, dense zones of PCR membrane were more frequently observed in instances where the PCR was not closely associated with the Golgi (Figs. 26 and 27). In cases in which the PCR was predominantly composed of dense aggregates of membranes and was not at all associated with Golgi (Figs. 28–42), only small regions of the PCR (Figs. 30, 32–34, and 37) resembled the distinct, single membranes seen in Figs. 21, 22, 25, and 26.

Approximately 10% of the PCRs that we examined in serial sections were not closely associated with Golgi. However, our confidence in this estimate is limited given that our serial section sample size included only 100 PCRs in *Zea* and *Phaseolus*. Further, no one cell was examined in its entirety to determine the total number of PCRs and Golgi which were present. In both species, organelles other than Golgi were often located near the PCR. Most frequently, elements of both the rough and the smooth endoplasmic reticulum were adjacent to the PCR (Figs, 3, 6, 9, 21, 22, 31, 32, and 35).

### *3.3. Coated Membranes in Other Cell Types and Species*

Virtually every cell type in the young primary tissues of both *Zea* roots and *Phaseolus* leaves contained PCRs.

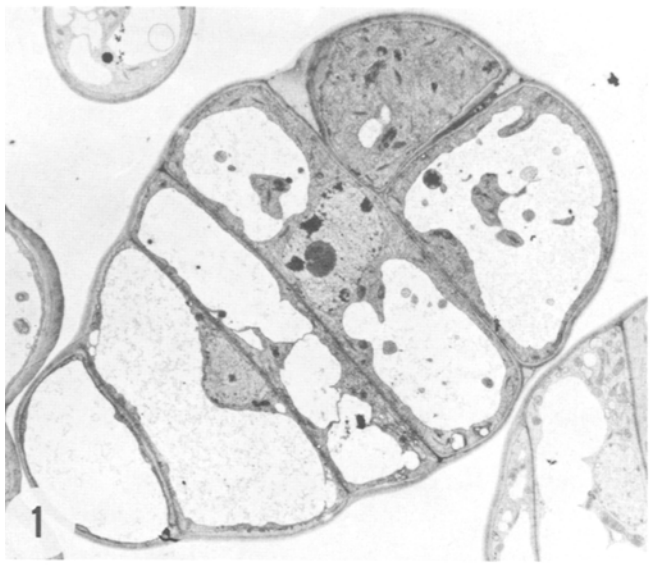
1

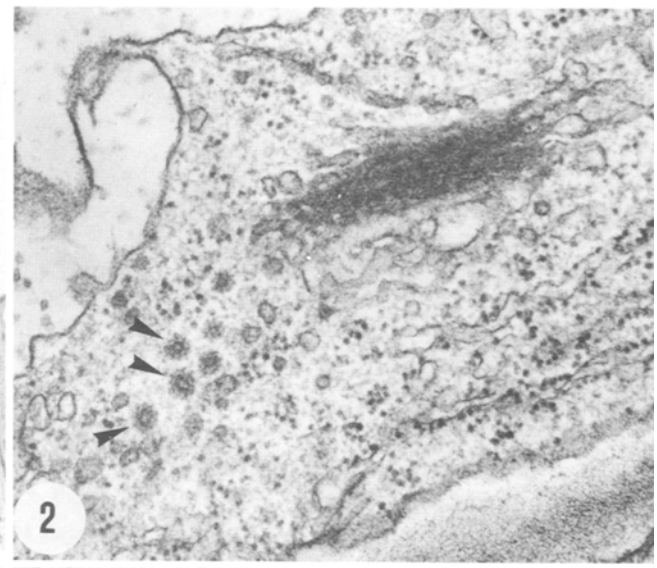
2

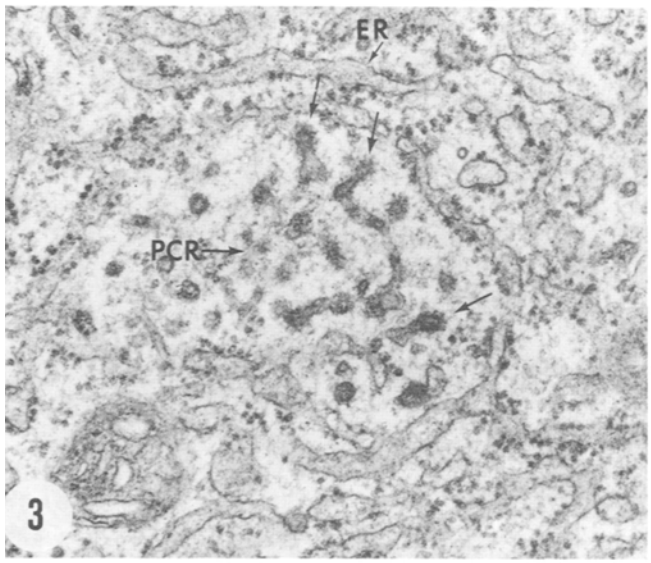
ER
PCR
3

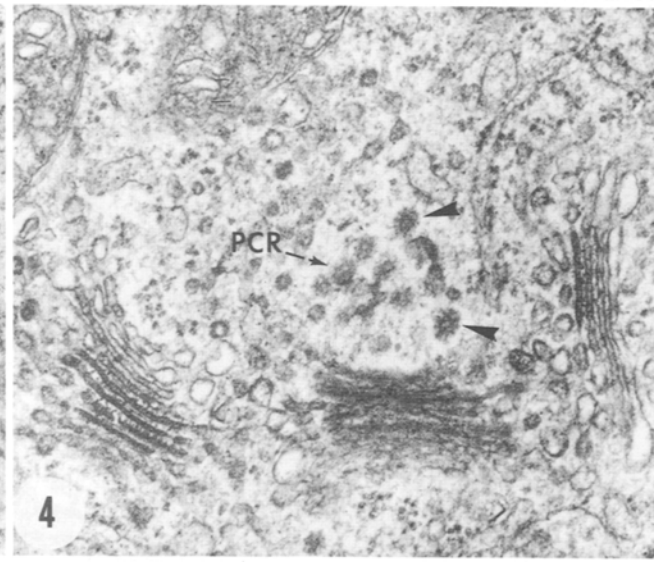
PCR
4

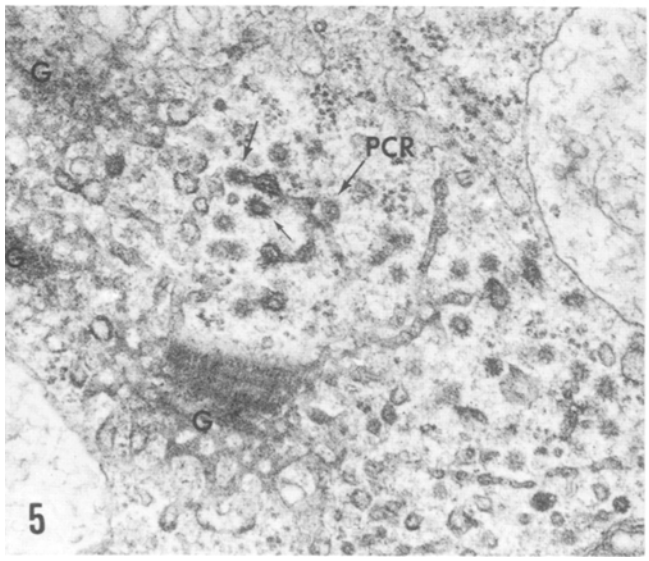
G
PCR
G
5

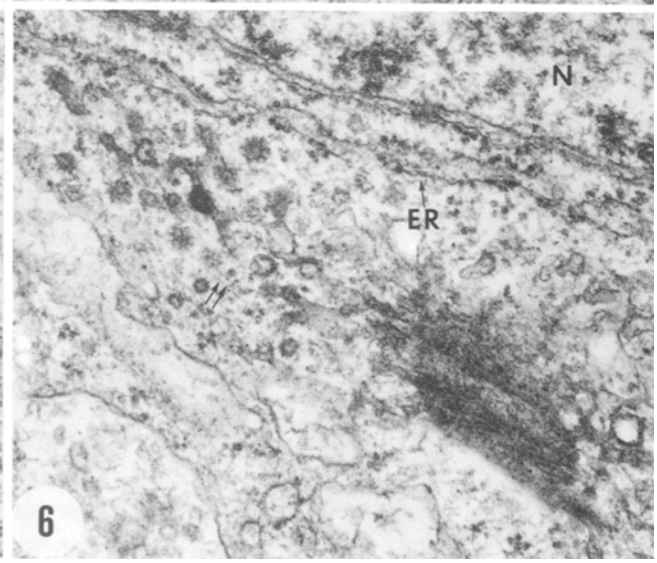
N
ER
6

These organelles varied in their frequency of occurrence, not only between cell types in a given section but also between tissue pieces, thus causing us to suspect that the stage of cellular differentiation could be an important determinant of the number and size of PCRs. Leaves of *Beta vulgaris, Allium cepa* and *Zea mays* contained approximately as many PCRs as did those of *Phaseolus vulgaris*. However, we were unable to observe the presence of PCRs in young *Nicotiana tabacum* leaves; Golgi stacks and coated vesicles were present. While the overall fixation image of *N. tabacum* was excellent, some features, specifically microtubules, were lacking.

## 4. Discussion

### *4.1. Partially-Coated Reticulum*

Our results indicate that, in many cases, the morphology of cytoplasmic coated membranes in higher plants is different from that observed by previous investigators. In both *Zea* and *Phaseolus*, the PCR can be more complex than the small number of coated and partially-coated vesicles which BONNETT and NEWCOMB (1966) observed to be associated with the Golgi in *Raphanus*. Additionally, the PCR has a number of structural features, such as its frequent lack of a clearly evident connection with the Golgi and the presence of coated membranes between it and the Golgi, which are features that are not found in the model of MOLLENHAUER and MORRÉ (1966). Finally, the presence of PCRs which apparently are not associated with Golgi is, to our knowledge, a previously unreported phenomenon.

There are, however, many similarities between our observations and those of previous investigators. For example, we believe that the lack of a PCR in *Nicotiana* approximates the situation in *Raphanus*, where no PCR as such was evident. Likewise, the occasional instances of physical continuities between the PCR and the Golgi in *Phaseolus* probably resemble situations which influenced the form of MOLLENHAUER and MORRÉ's model of the Golgi complex.

As an initial approximation, we suggest that our understanding of these different assemblages of coated membranes that are near the Golgi may be facilitated if we think of them as being parts of an ultrastructural series. The first and simplest case in such a series would be the one in which only a few, small coated membranes are grouped together; the next case would involve instances in which a larger but still relatively distinct membrane system is present (*i.e.*, the PCR which we have most commonly observed), and the final case would be the one in which extensive physical continuities between the PCR and the Golgi are evident. Such a series, while obviously simplistic, is useful in that it not only provides a framework for the classification of structural types, but it also must reflect physiological differences in the rate, type, and extent of interactions between the PCR and the Golgi. It should be emphasized that we do not intend to infer that only one particular type of coated membrane system exists in each species. For example, in contrast to our present results that concern *Nicotiana*, CRONSHAW and ESAU (1968) have published micrographs which show the presence of PCR-like organelles in meristematic *Nicotiana* cells. Thus, it appears that parameters such as

---

Abbreviations: *C* coated vesicle, *ER* endoplasmic reticulum, *G* Golgi stack, *M* microtubule, *Mi* microbody, *N* nucleus, *P* plasma membrane, *PCR* partially coated reticulum, *R* coated membrane region, *V* vacuole membrane.

Figs. 1–18. Sections of bulbous glands which were located on the abaxial surface of *Phaseolus* leaves

Fig. 1. Bulbous gland. × 2,050

Fig. 2. Coated vesicles (unlabeled darts) in a group and near a Golgi stack. × 50,000

Fig. 3. Coated membrane regions associated with a PCR. Unlabeled arrow indicates a coated membrane region. × 46,400

Fig. 4. Irregular, reticulate morphology of a PCR is evident as is its position near to a horizontal face of a Golgi stack. Coated membranes are present in the zone which is between the PCR and the Golgi and also on the side of the PCR which is furthest from the Golgi (unlabeled darts). × 51,200

Fig. 5. PCR bordered by and possibly connected to the membranes of three nearby Golgi stacks. Numerous coated membrane regions (unlabeled arrows) are evident on the PCR. × 42,800

Fig. 6. Double arrows indicate zone in which PCR appears to be connected to a Golgi stack. × 54,700

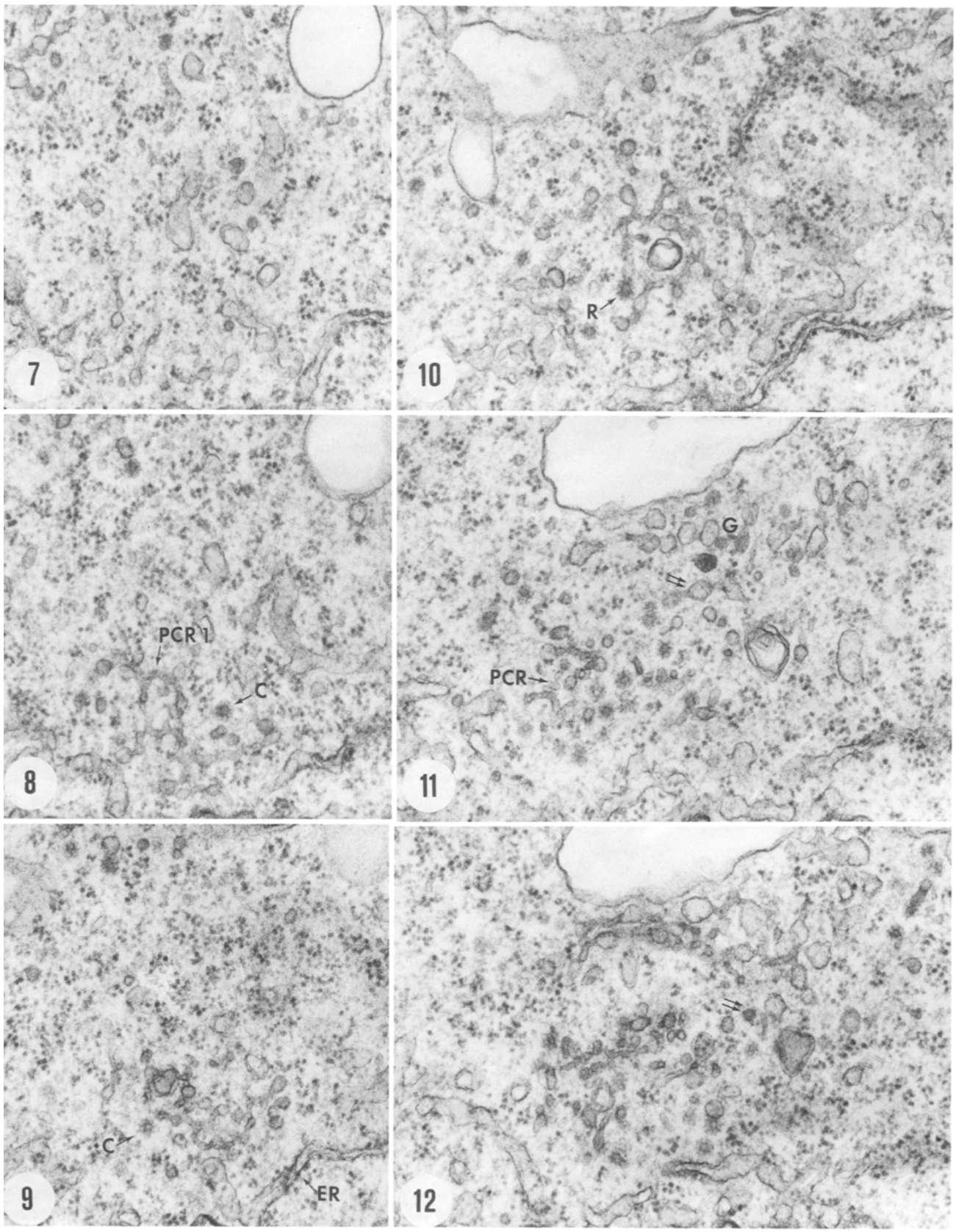


Figs. 7–18. Semi-serial sections taken from a complete series. While some small portion of the PCR may be present in Fig. 7, the four sections that were taken previous to Fig. 7 contained neither PCR-like membranes nor Golgi stack membranes. PCR nr. 1 membranes are first evident in Fig. 8 where they form a reticulum which is associated with a coated vesicle. A coated membrane region is present in Fig. 10. Note that the reticulated form of the PCR is clearly evident in Figs. 8–14. One section deleted between Figs. 10 and 11. In Fig. 11 the peripheral region of a Golgi stack can be seen, and in Figs. 11–14 the double arrows indicate a zone in which the membranes of the PCR are near but do not clearly connect with the

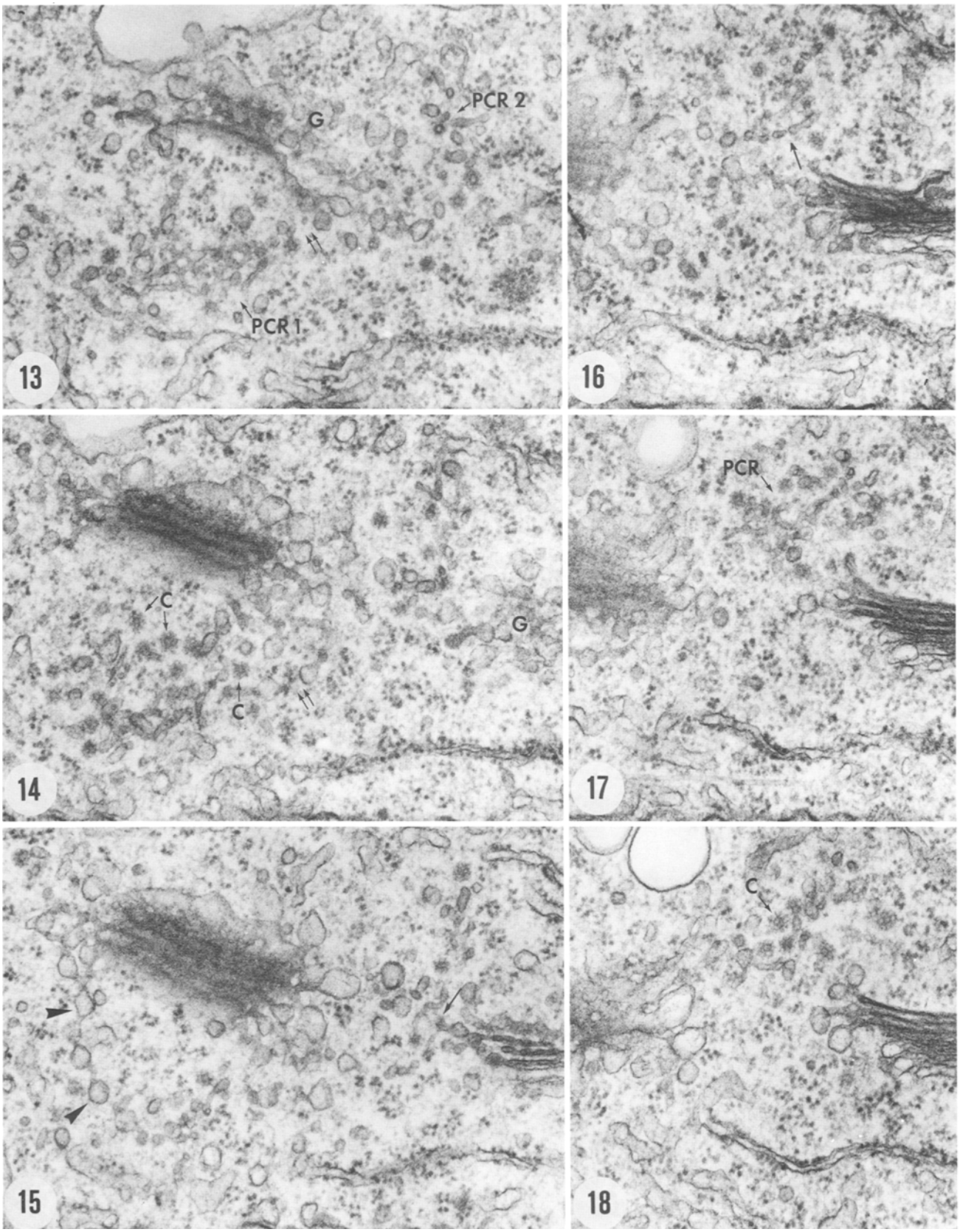


Golgi membranes. Note the relatively high concentration of coated membranes in Fig. 14 where the PCR is near the Golgi stack. PCR nr. 1 "ends" in Fig. 15 where the Golgi stack membranes, which have been sectioned obliquely, begin to overlie the former PCR zone (unlabeled darts). PCR nr. 2 is first clearly evident in Fig. 13, and in Fig. 15 it may connect to the Golgi stack (unlabeled arrow). Fig. 16 shows the fenestrated structure of the PCR membrane (unlabeled arrow), and the reticulum is evident in Fig. 17. × 51,400

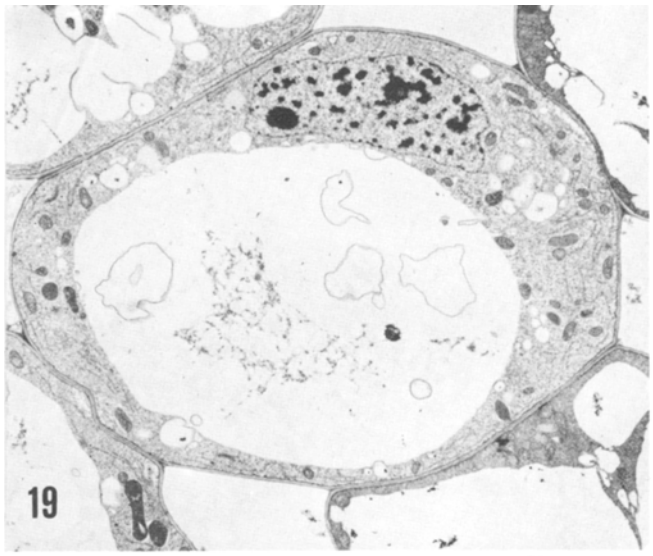
19

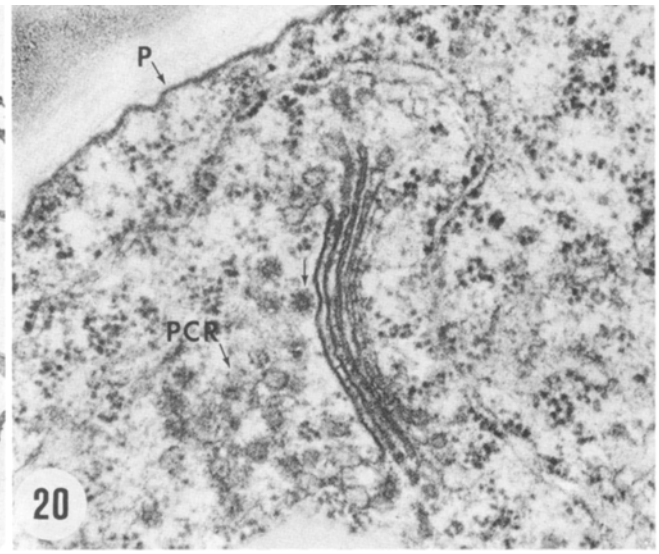
P
PCR
20

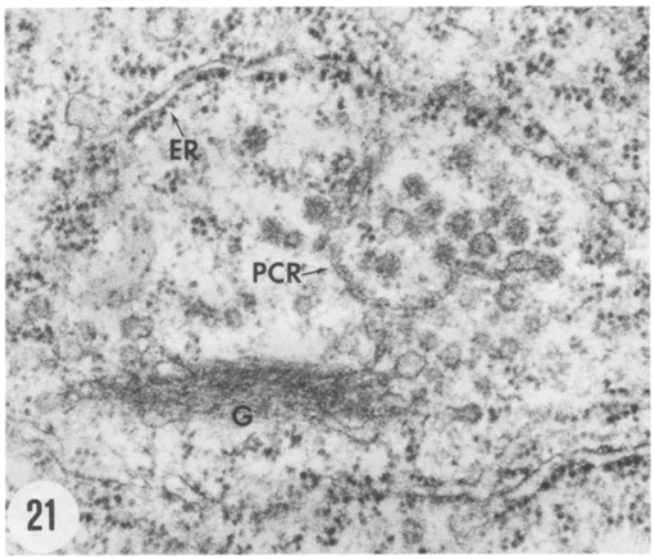
ER
PCR
G
21

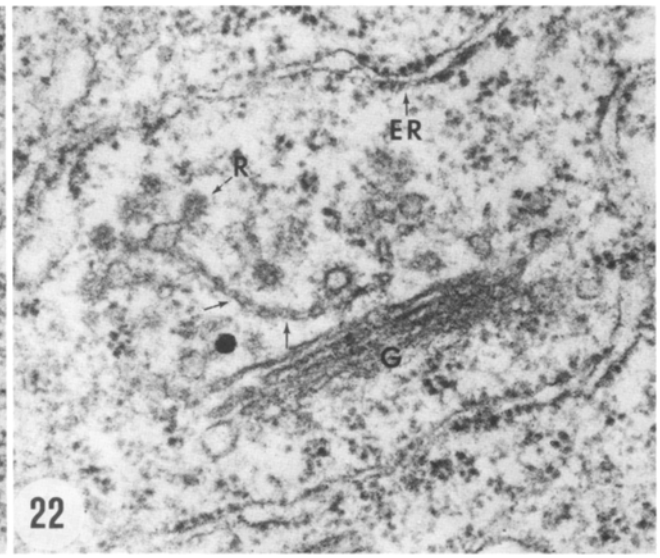
ER
R
G
22

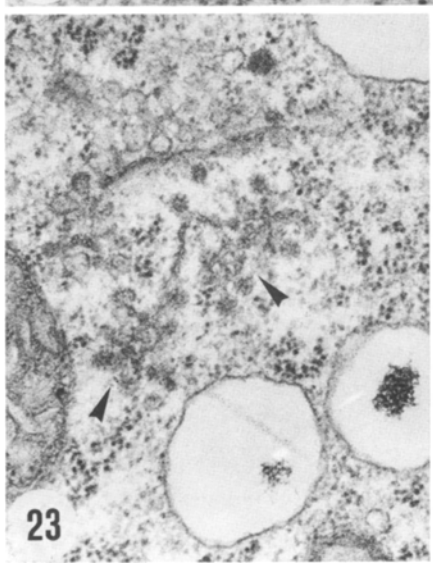
23

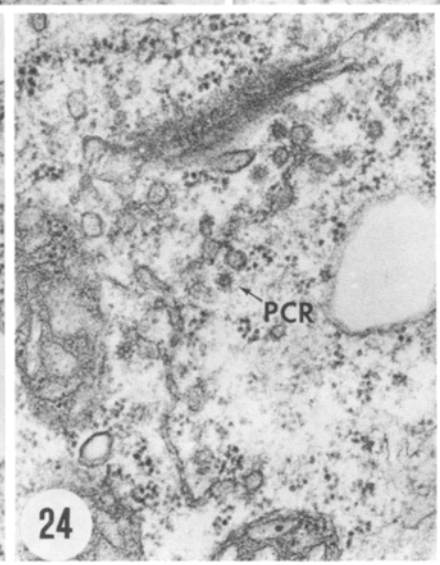
PCR
24

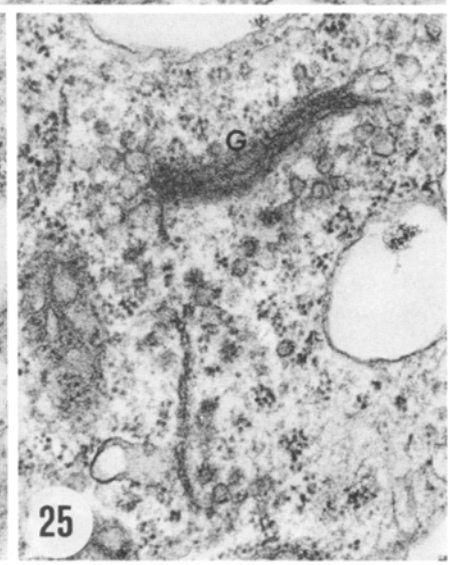
G
25

fixation conditions, growth environment, and cell type may affect the form of intracellular coated membrane systems.

Perhaps the most interesting aspect of PCR function which our structural investigation has revealed concerns the frequent presence of coated membranes that are near various areas around the periphery of the Golgi stack. Given the veracity of the current "pinching-off" models of coated vesicle formation, it appears to be likely that coated vesicles are forming on the membranes of the PCR and then possibly being transported to specific portions of either the horizontal or circumferential faces of the adjacent Golgi stack. Such a direction of transport would be the opposite of that which is commonly proposed for plant coated vesicles (*i.e.*, exocytosis from the Golgi). An alternative interpretation would be that the region in which the PCR and the Golgi adjoin each other is both a structural and metabolic interface from which coated vesicles arise during the transport of newly-synthesized molecules to other regions of the cell. This interpretation is somewhat complicated by the frequent presence of coated membranes on the portions of the PCR which are farther from the Golgi.

In those cases in which PCRs are not adjacent to the Golgi, the destination of coated vesicles which are presumably forming on the PCR is rather difficult to infer. While relatively long-range interactions with the Golgi could still exist, or these two membrane systems might eventually move closer to each other, it also seems equally likely that interactions with the PCR and other compartments, such as the ER, could be occurring. PEARSE and BRETSCHER (1981) have speculated that animal cells might contain a processing system which involves coated vesicle-mediated lipid recycling from the Golgi and plasma membrane to the ER.

If the PCR did mediate the endocytotic transfer of membranes, then it would be an endosome-like organelle. However, at present we know of no direct evidence concerning the flow of membrane through the PCR in turgid plant cells. TANCHAK *et al.* (1984) have demonstrated that the PCR is involved with endocytotic processes in protoplasts. However, these authors also pointed out the possibility that such a system might to not operate in the presence of turgor. Therefore, we intend to continue the use of the morphologically-defined term "PCR" until some compelling evidence regarding its function might suggest a more precise descriptive term.

While it was obviously impossible for us to examine all of the previous ultrastructural literature concerning endomembranes, we have been able to note instances in which other authors have observed PCR-like structures in ferns (Figs. 28 and 29 in GALATIS *et al.* 1983), palms (Fig. 5 in PARTHASARATHY and PESACRETA 1980), primitive angiosperms (Figs. 9 and 14 in BEHNKE and KIRITSIS 1983), and in cotton (Figs. 2, 7, and 8 in RYSER 1979). In the first, third, and fourth cases which are listed above, the authors noted the presence of coated vesicles/membranes and assumed them to be, respectively, derived from, portions of, or associated with, dictyosomes. RYSER focused his attention on coated vesicle distribution during cell wall growth. His observations indicated that the plasma membrane-associated population of coated vesicles and coated pits differed in its chemical composition from those which he observed in the vicinity of a PCR-like organelle. Further, he speculated that the plasma membrane-associated coated vesicles and pits were involved in endocytosis (rather than exocytosis). It occurs to us that his observations also suggest, as do ours as well, that coated vesicles located near the PCR are not involved in exocytosis but instead are concerned with membrane flow processes which do not directly involve the plasma membrane.

---

Figs. 19–42. Sections of *Zea* root cortical cells

Fig. 19. Cortical cell. × 3,800

Fig. 20. A PCR that is adjacent to the horizontal face of a Golgi stack. In this case, the form of the PCR is indistinct. Unlabeled arrow indicates a coated membrane. × 50,500

Fig. 21. A PCR which exhibits the relatively simple type of membrane morphology that is frequently observed in *Zea*. In this figure, no coated membranes are evident between the PCR and the Golgi stack. × 54,100

Fig. 22. A PCR which generally resembles that seen in Fig. 21 but also shows the fenestrated aspect of its membrane structure (unlabeled arrows). × 60,000

Figs. 23–25. Sections taken from a series. These sections show an elongate PCR with coated membranes distributed around it. While the PCR membranes in Figs. 24 and 25 are tubular or lamellar, in Fig. 23 compact regions of dense, somewhat indistinct, PCR membranes are present (unlabeled darts). × 42,100

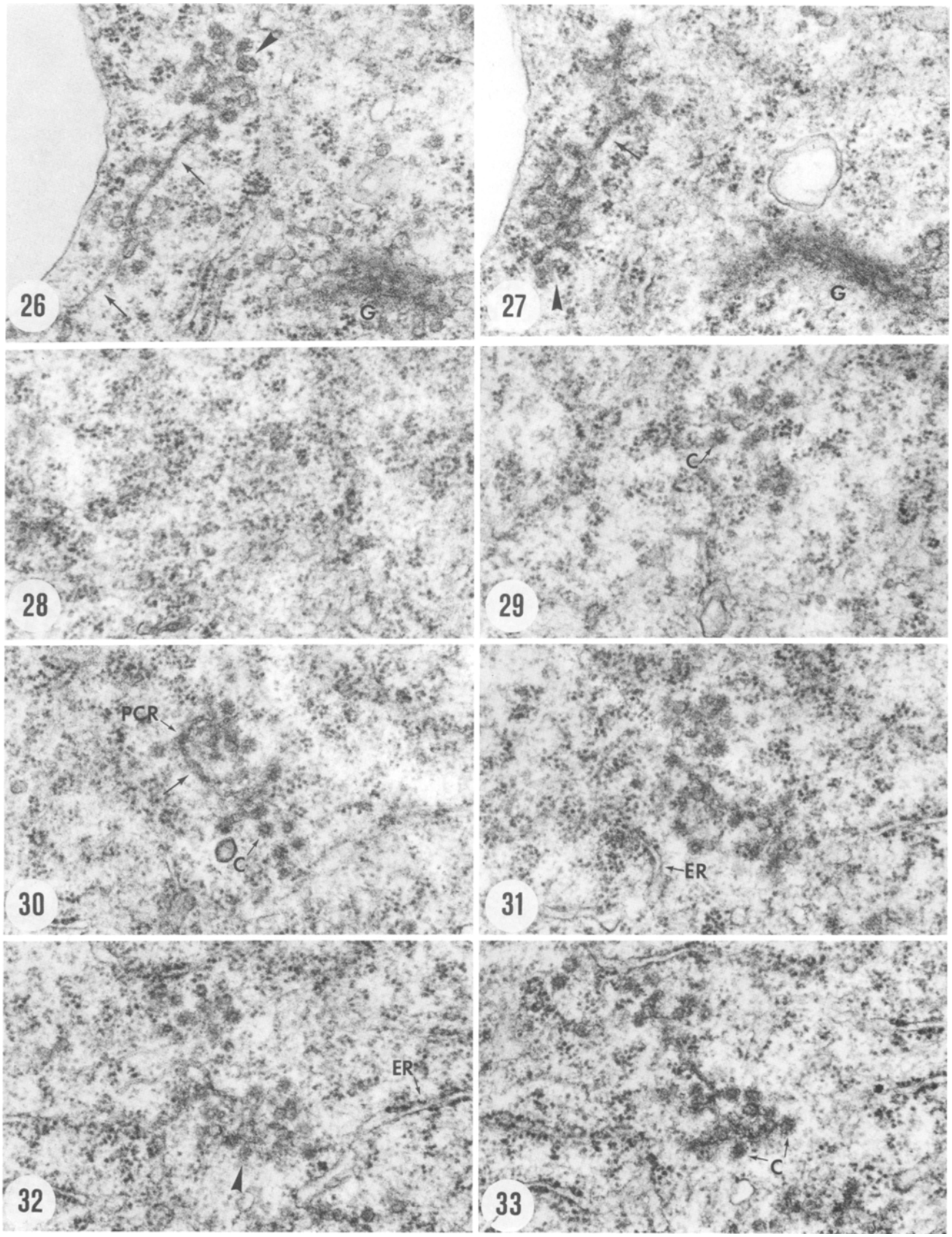


Figs. 26 and 27. Sections taken from a series. This PCR was not closely associated with any Golgi membranes and appeared to be composed of roughly equal amounts of membranes which were either simple (unlabeled arrows) or densely compacted (unlabeled darts) in form. × 44,700

Figs. 28–42. Serial sections of a PCR which was not closely associated with a Golgi stack (4 additional sections that were on each end of this series

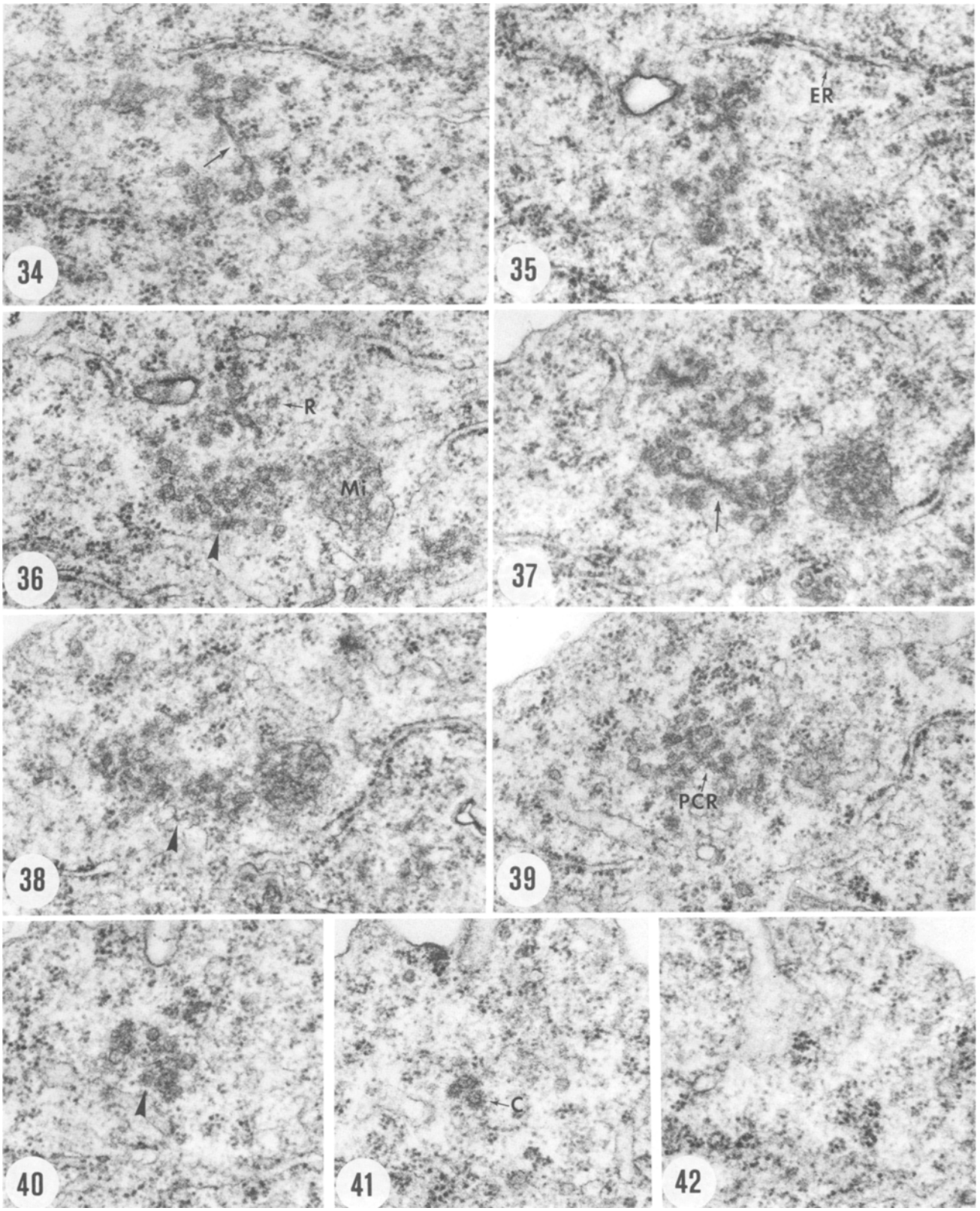


were examined as well and showed no evidence of Golgi stack membranes). Segments of the endoplasmic reticulum (Figs. 31, 32, and 35) and a microbody (Fig. 36) are near the PCR. While some small regions of distinct PCR membranes are evident (unlabeled arrows in Figs. 30, 34, and 37), much of the PCR is composed of dense aggregates (unlabeled darts in Figs. 32, 36, 38, and 40) which are difficult to morphologically characterize. × 44,100

## Acknowledgements

This work was supported by a National Science Foundation Grant (PCM 81-17721) to W. J. L. We thank Dr. L. R. GRIFFING for providing us with a copy of TANCHAK *et al.* 1984 prior to its publication.

## References

BEHNKE, H.-D., KIRITSIS, U., 1983: Ultrastructure and differentiation of sieve elements in primitive angiosperms. I. *Winteraceae*. Protoplasma **118**, 148—156.

BONNETT, H. T., JR., NEWCOMB, E. H., 1966: Coated vesicles and other cytoplasmic components of growing root hairs of radish. Protoplasma **62**, 59—75.

BURSZTAJN, S., FISCHBACH, G. D., 1984: Evidence that coated vesicles transport acetylcholine receptors to the surface membrane of chick myotubes. J. Cell Biol. **98**, 498—506.

CRAM, W. J., 1980: Pinocytosis in plants. New Phytol. **84**, 1—17.

CRONSHAW, J., ESAU, K., 1968: Cell division in leaves of *Nicotiana*. Protoplasma **65**, 1—24.

CUNNINGHAM, W. P., MORRÉ, D. J., MOLLENHAUER, H. H., 1966: Structure of isolated plant Golgi apparatus revealed by negative staining. J. Cell Biol. **28**, 169—179.

FARQUHAR, M. G., 1978: Recovery of surface membranes in anterior pituitary cells. J. Cell Biol. **77**, R 35—42.

— PALADE, G. E., 1981: The Golgi apparatus (Complex)—(1954–1981)—from artifact to center stage. J. Cell Biol. **91**, 775—1035.

FORGAC, M., CANTLEY, L., WIEDERMANN, B., ALTSTIEL, L., BRANTON, D., 1983: Clathrin-coated vesicles contain an ATP-dependent proton pump. Proc. Nat. Acad. Sci. U.S.A. **80**, 1300—1303.

FRANKE, W. W., HERTH, W., 1974: Morphological evidence for de novo formation of plasma membrane from coated vesicles in exponentially growing cultured plant cells. Exp. Cell Res. **89**, 447—451.

GALATIS, B., APOSTOLAKOS, P., KATSAROS, C., 1983: Microtubules and their organizing centers in differentiating guard cells of *Adiantum capillus veneris*. Protoplasma **115**, 176—192.

HARDING, C., HEUSER, J., STAHL, P., 1983: Receptor-mediated endocytosis of transferrin and recycling of the transferrin receptor in rat reticulocytes. J. Cell Biol. **97**, 329—339.

HELENIUS, A., MELLMAN, I., WALL, D., HUBBARD, A., 1983: Endosomes. Trends in Biochem. Sci. **8**, 245—250.

HEUSER, J. E., REESE, T. S., 1973: Evidence for recycling of synaptic vesicle membrane during transmitter release at the frog neuromuscular junction. J. Cell Biol. **57**, 315—344.

JOACHIM, S., ROBINSON, D. G., 1984: Endocytosis of cationic ferritin by bean leaf protoplasts. Eur. J. Cell Biol. **34**, 212—216.

KANASEKI, T., KADOTA, K., 1969: The "vesicle in a basket." A morphological study of the coated vesicle isolated from the nerve endings of the guinea pig brain, with special reference to the mechanism of membrane movements. J. Cell Biol. **42**, 202—220.

KOCHIAN, L., LUCAS, W. J., 1982: Potassium transport in corn roots. Plant Physiol. **70**, 1723—1731.

MACROBBIE, E. A. C., 1969: Ion fluxes to the vacuole of *Nitella translucens*. J. exp. Bot. **20**, 236—256.

MERSEY, B. G., FOWKE, L. C., CONSTABEL, F., NEWCOMB, E. H., 1982: Preparation of a coated vesicle-enriched fraction from plant cells. Exp. Cell Res. **141**, 459—463.

MOLLENHAUER, H. H., MORRÉ, D. J., 1966: Golgi apparatus and plant secretion. Ann. Rev. Plant Physiol. **17**, 27—46.

NEWCOMB, E. H., 1980: Coated vesicles: their occurrence in different plant cell types. In: Coated vesicles (OCKLEFORD, C. D., WHYTE, A., eds.), pp. 55—68. Cambridge: Cambridge University Press.

OCKLEFORD, C. D., 1976: A three-dimensional reconstruction of the polygonal pattern on placental coated vesicle membranes. J. Cell Science **21**, 83—91.

— WHYTE, A., 1980: Coated vesicles. Cambridge: Cambridge University Press.

PARTHASARATHY, M. V., PESACRETA, T. C., 1980: Microfilaments in plant vascular cells. Canad. J. Bot. **58**, 807—815.

PEARSE, B. M. F., 1975: Coated vesicles from pig brain: purification and biochemical characterization. J. mol. Biol. **97**, 93—98.

— BRETSCHER, M. S., 1981: Membrane recycling by coated vesicles. Ann. Rev. Biochem. **50**, 85—101.

PESACRETA, T. C., LUCAS, W. J., 1984: The plasma membrane coat and a coated vesicle-associated reticulum of membranes: their structures and possible interrelationship in *Chara corallina*. J. Cell Biol. **98**, 1537—1545.

PILCH, P. F., SHIA, M. A., BENSON, R. J. J., FINE, R. E., 1983: Coated vesicles participate in the receptor-mediated endocytosis of insulin. J. Cell Biol. **93**, 133—138.

ROBERTS, A. V. S., WILLIAMS, K. E., LLOYD, J. B., 1977: The pinocytosis of $^{125}$I-labelled poly(vinylpyrrolidone), [$^{14}$C] sucrose and colloidal [$^{198}$Au] gold by rat yolk sac cultured *in vitro*. Biochemical J. **168**, 239—244.

RODEWALD, R., 1980: Immunoglobulin transmission in mammalian young and the involvement of coated vesicles. In: Coated vesicles (OCKLEFORD, C. D., WHYTE, A., eds.), pp. 69—101. Cambridge: Cambridge University Press.

RYSER, U., 1979: Cotton fibre differentiation: occurrence and distribution of coated and smooth vesicles during primary and secondary wall formation. Protoplasma **98**, 223—239.

TANCHAK, M. A., GRIFFING, L. R., MERSEY, B. G., FOWKE, L. C., 1984: Endocytosis of cationized ferritin by coated vesicles of higher plant protoplasts. Planta, submitted for publication.

WILD, A. E., 1980: Coated vesicles: a morphologically-distinct subclass of endocytic vesicles. In: Coated vesicles (OCKLEFORD, C. D., WHYTE, A., eds.), pp. 1—22. Cambridge: Cambridge University Press.

ZAREMBA, S., KEEN, J. H., 1983: Assembly polypeptides from coated vesicles mediate reassembly of unique clathrin coats. J. Cell Biol. **97**, 1339—1347.

Inorganic Carbon Uptake by Aquatic Photosynthetic Organisms WJ Lucas and JA Berry Eds Copyright ©1985, the American Society of Plant Physiologists

CHAPTER 16

# BICARBONATE UTILIZATION BY *CHARA*: A RE-ANALYSIS

*William J. Lucas*

Department of Botany, University of California Davis, CA 95616

## INTRODUCTION

During this workshop, numerous workers have reflected on their past research and have been able to share with us new insights and interpretations. I would like to follow in this tradition and attempt to 'set the scene' by quoting from our first publication on photosynthetic utilization of $HCO_3^-$. In 1973, we concluded that "*external alkalinity (on the surface of Chara) results from* $HCO_3^-$ *uptake, and it is considered that the processes of acidification and alkalinization are separate phenomena. This is supported by the evidence that different Characean species have different abilities to utilize* $HCO_3^-$, *whereas their basic electrical properties, which Kitasato (1968; see 12) has related to* $H^+$ *extrusion, show considerable similarity. An obvious extension of this view is that* $HCO_3^-$ *uptake cannot be electrogenic and that there must be an obligate linkage with* $OH^-$ *efflux*" (see Lucas and Smith (25), page 11). It will be obvious to the reader that over the following decade we have been forced to modify our initial interpretation of the *Chara* pH banding phenomenon.

The controversial issue that has plagued these studies, both in the past and present situation, is whether or not $HCO_3^-$, *per se*, enters the cytoplasm. In *Chara*, the development of the 'revived' controversy certainly acted as a fulcrum for progress.

## $HCO_3^-/OH^-$ ANTIPORT *VERSUS* PRIMARY $HCO_3^-$ TRANSPORT

The physical size of the *Chara* internodal cell (right-circular cylinder, length ranging from 3-10 cm, diameter approximately 1.0 mm) made it possible for us to test our $HCO_3^-/OH_-$ antiporter hypothesis (see Fig. 1A). We did this by constructing an experimental system that allowed us to physically isolate, from the rest of the cell, a region of the *Chara* cell wall along which an alkaline band had developed. The experimental solution bathing this region of the cell wall could be changed such that it no longer contained $HCO_3^-$ (see Fig. 1 of 15). Under these conditions ($-HCO_3^-$), $OH^-$ efflux continued; only when $HCO_3^-$ was removed from the medium bathing the entire cell did $OH^-$ efflux cease (15). This result demonstrated that the $OH^-$ efflux process could function in the absence of $HCO_3^-$ at the actual efflux site. Thus, we were forced to 'abandon' our antiporter hypothesis. We next proposed that the transport of $HCO_3^-$ and $OH^-$ occurred at spatially separate sites, with both being electrogenic in nature and $HCO_3^-$ uptake being energy dependent (14, 15).

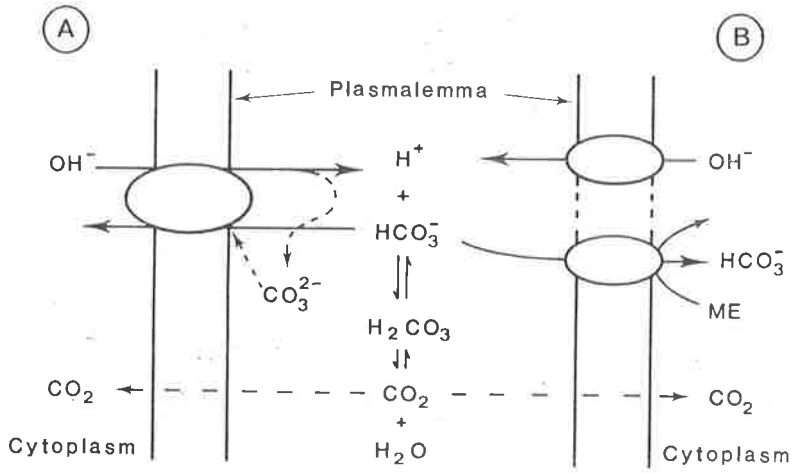


**Figure 1.** Our early models depicting the mechanisms by which $HCO_3^-$ was thought to cross the *Chara* plasmalemma. Both the $HCO_3^-/OH^-$ antiporter hypothesis of Lucas and Smith (25). and the spatially separated transport systems of $HCO_3^-$ and $OH^-$ were proposed to be electrogenic, and $HCO_3^-$ was a primary, active process (after 14, 15).

Strong experimental support for our electrogenic $HCO_3^-$ and $OH^-$ transport hypothesis was obtained from studies in which both the pH

and the external electric potential were measured at the *Chara* cell surface. An excellent correlation was observed between alkaline band pH centers and the negative electric potential maxima (3, 37). In the regions between the alkaline bands, where we postulated that $HCO_3^-$ transport was occurring, positive external electric potentials were observed. Using these experimentally obtained pH and electric potential data, we were able to compute, through the application of our numerical analysis model (20), the magnitude of the putative $HCO_3^-$ fluxes. Values in the range of 100 to 250 pmol $cm^{-2}$ $s^{-1}$ were obtained.

As a result of these studies, Jack Ferrier and I claimed that these results offered strong support for the electrogenic $HCO_3^-$ and $OH^-$ transport hypothesis. We also advanced the notion that the actual magnitude of the $HCO_3^-$ influx may vary quite significantly along the length of a particular cell. This aspect was investigated using the Jaffe-Nuccitelli vibrating probe (23). Under $HCO_3^-$ assimilating conditions, we found that along the length of the cell, extracellular bands of positive inward current ($OH^-$ efflux) 1-3mm in width were separated by wider bands of outward current ($HCO_3^-$ influx). The measured peaks of inward current ranged from 20 to 60 $\mu$A $cm^{-2}$ (i.e. an $OH^-$ efflux of 270-800 pmol $cm^{-2}$ $s^{-1}$, while the outward current ranged from 10 to 30 $\mu$A $cm^{-2}$ (i.e. a $HCO_3^-$ influx of 140-400 pmol $cm^{-2}$ $s^{-1}$). Again, these results appeared to offer support for both aspects of our hypothesis, namely the spatial asymmetry of the fluxes associated with these two transport processes and their electrogenic nature.

## PRIMARY $HCO_3^-$ TRANSPORT OR $H^+$-MEDIATED EXTRACELLULAR $CO_2$ PRODUCTION

One of the basic problems associated with studies involving the photosynthetic assimilation of exogenous $HCO_3^-$ is that it is quite difficult to establish that $HCO_3^-$, *per se*, is being transported into the cytoplasm. The alternative to $HCO_3^-$ transport is the extracellular production of $CO_2$ from the exogenous $HCO_3^-$. Several investigators have addressed this issue by developing theoretical analyses of the rate(s) at which $CO_2$ could be produced from $HCO_3^-$ (see 18 and Chapter 2). Using the reaction kinetic approach, we were able to show that the maximum rate at which $CO_2$ could be supplied was insufficient to account for $^{14}C$-fixation in *Chara corallina*, as measured in alkaline media (13).

The one feature that was missing from these earlier reaction kinetic approaches was the notion that the cell may actually take an 'active' role in driving the equilibrium reactions by 'brute force.' This could be achieved by the operation of a $H^+$ translocating ATPase; such an

outwardly directed pump would acidify the cell wall and surrounding medium, thereby converting $HCO_3^-$ into $H_2CO_3$ and, thus, $CO_2$. Prins and coworkers were the first to realize that such a situation may exist in the aquatic angiosperms, *Potamogeton* and *Elodea* (see 32-35 and Chapter 18). Jack Ferrier also realized that in *Chara* the operation of a $H^+$–ATPase could generate $CO_2$ at a rate sufficient to explain the measured rate of photosynthesis. Jack did this simulation in 1978 when we were expanding our numerical analysis model to include the external electric potential and the spatial asymmetry of $HCO_3^-$ uptake along the cell (3). I must admit that when he told me of his hypothesis, I thought the idea not worthy of serious consideration. After all, the available experimental data was totally consistent with the operation of a primary, electrogenic $HCO_3^-$ system.

Both Jack Ferrier (2) and Alan Walker and his coworkers (36, 38) pursued this avenue of thought, and 'collectively' they suggested that the unstirred layer, in conjunction with a plasmalemma-bound $H^+$ efflux system, would permit the generation of extracellular $H_2CO_3$ (or $CO_2$) such that inorganic carbon would be provided by diffusion of $H_2CO_3$ rather than via the operation of a specific $HCO_3^-$ carrier. Figure 2 illustrates the basic scheme; note the absence of a primary $HCO_3^-$ transport system. The model was consistent with the then available experimental data; the $H^+$–ATPase would develop a positive electric potential on the outer surface of the cell wall.

Walker *et al.* (38) suggested that extracellular production of $CO_2$ would be highly efficient "*because the diffusion resistance of the unstirred layer retains the* $CO_2$ *that is produced near the cell surface.*" An explicit prediction of their model was, therefore, that a reduction in the unstirred layer would cause an inhibition of photosynthesis. We tested this prediction by measuring [$^{14}$C]-fixation in *Chara* as a function of the solution flow rate; photosynthesis was found to increase, not decrease, as the unstirred layer was reduced (22).

An additional prediction of the extracellular $CO_2$ production model was that the pH at the surface of the *Chara* cell, in the acid zones, should be quite low. For a localized flux density of 100 pmol $cm^{-2}$ $s^{-1}$, the required pH value was 6.0. Walker *et al.* (38) suggested that the discrepancy between the measured pH values (usually more alkaline than the bathing medium) and the predicted acidification, may have been due to the physical size of the miniature pH electodes used for these studies. The electrodes were as large as the calculated unstirred layers. We investigated this by comparing the pH profiles detected by miniature and micro (0.5$\mu$m)-pH electrodes. Indeed, the two profiles were strikingly different, with only the recessed-tip micro-pH electrode

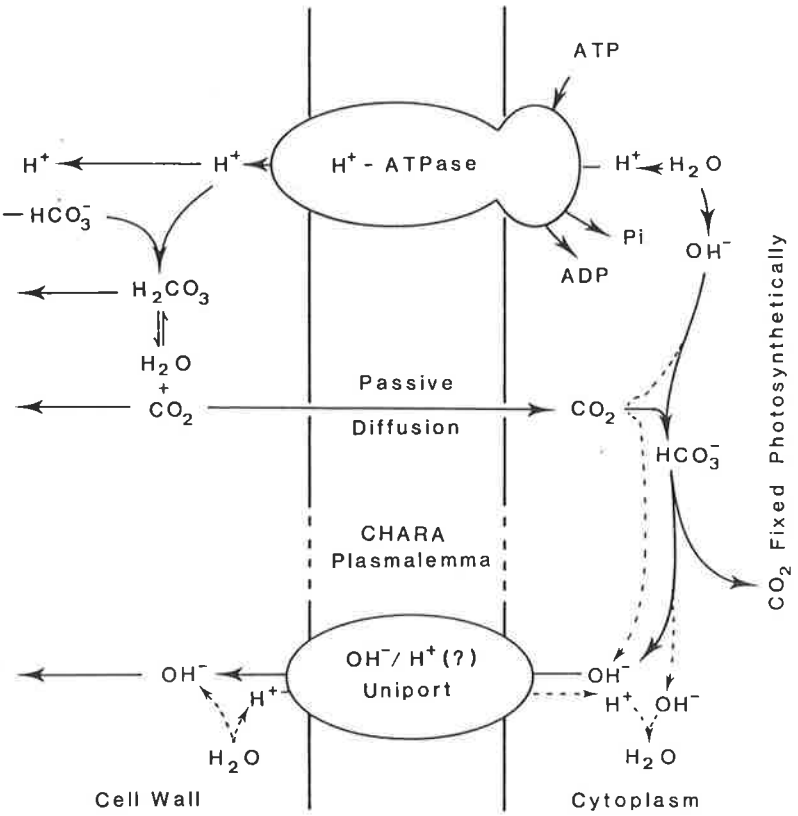


**Figure 2.** Model for extracellular $CO_2$ production in *Chara* (from 17). This hypothesis was advanced by Ferrier (2) and Walker and his coworkers (36, 38); see text for full details. A later development of this model suggested that the $CO_2$ production occurred within the periplasmic space of the Charasome, and that extracellular CA was involved in producing $CO_2$ (30).

being able to detect acidification near the cell surface (see Fig. 2 of (22)). However, the detected pH values, at a distance of 2 $\mu$m from the wall. were generally between 7.2 and 7.6, i.e. they were not low enough to provide support for the extracellular $CO_2$ production hypothesis. (The actual reduction in pH could have been caused by 'back-diffusion' of $CO_2$ from the cytoplasm.) An additional finding, which did not support the $CO_2$ production hypothesis, was that we could not obtain any correlation between the $HCO_3^-$-associated extracellular currents (detected using the vibrating probe) and the degree of cell surface acidification in the same regions.

A final prediction of the extracellular $CO_2$ production hypothesis was that artificial buffers should compete with $HCO_3^-$ for $H^+$ and thereby

reduce the level of $CO_2$ available. Hence, addition of a buffer should significantly inhibit photosynthesis. We found that addition of 5 mM phosphate (or HEPES) buffer almost completely reduced the radial pH profiles in the 'acid' regions of the cell surface. Under these conditions, [$^{14}$C]-photosynthesis was reduced, but only by 30% (22). This level of reduction had a double edge; it did not support the Walker-Ferrier model, but nor was it consistent with a primary $HCO_3^-$ transport system, which at pH 8.0 should not have been sensitive to the presence of phosphate buffer.

## METAMORPHOSIS OF THE PRIMARY $HCO_3^-$ TRANSPORT HYPOTHESIS

Our next piece of experimental evidence that was not consistent with the operation of a primary electrogenic $HCO_3^-$ system was obtained using the vibrating probe. In the presence of 1.0 mM $HCO_3^-$ and 5 mM exogenous buffer (HEPES or phosphate) the rate of photosynthesis was reduced, but we could not detect any commensurate reduction in the extracellular currents under these same conditions (22). This suggested that something was happening between the cell surface and the chloroplasts which could generate this additional 'current.' The situation became somewhat clearer when we conducted the obvious experiment, i.e., measure the extracellular currents in the presence of buffer and in the absence of $HCO_3^-$. Much to our surprise, the current pattern remained, provided the cell was illuminated and was bathed by either $HCO_3^-$ or phosphate buffer (see Fig. 3).

At about the same time we did these experiments, we were also conducting electrophysiological experiments in which we were examining the light/dark sensitivity of the membrane potential. When an internodal cell was assimilating exogenous $HCO_3^-$, the potential would rapidly hyperpolarize when a brief dark treatment was employed (17). In the light, the resting potential was approximately -240 mV, whereas after the cell had been in the dark for 3-6 min., the potential was -330 to -350 mV. Upon reillumination, the cell's potential further hyperpolarized transiently and then rapidly depolarized towards the light-adapted value. In the absence of $HCO_3^-$ (i.e., no buffer or substrate present) these dark/light transients were dramatically reduced. However, when $HCO_3^-$ was *replaced* by phosphate or HEPES buffer, almost identical transients in the membrane potential were induced by dark/light transitions. These results were of paramount importance because they showed us that $HCO_3^-$, *per se*, is not responsible for the trans-membrane or extracellular currents!! A re-analysis of all the experimental data available

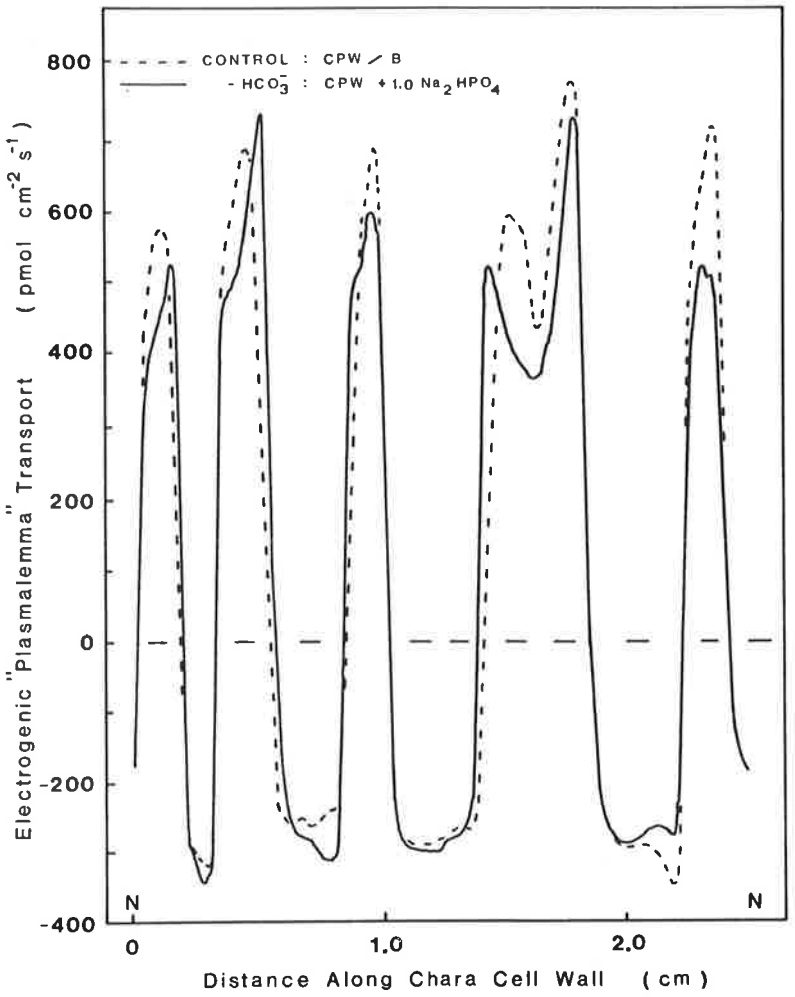


**Figure 3.** Effect of $Na_2HPO_4$-buffered and $HCO_3^-$-free media on the extracellular 'currents' of *Chara* internodal cells. Control scans were conducted in a medium containing mM; 1.0 $NaHCO_3$, 0.2 $CaS0_4$, 0.2 KCl, and 1.0 NaCl, pH 8.2. The experimental medium was then changed to a $HCO_3^-$-free, but $Na_2HPO_4$-buffered solution (1.0mM, pH 8.2), and the extracellular 'current' pattern was investigated for 1 h. Data from Lucas (17).

for *Chara* indicated that under alkaline conditions, inorganic carbon is most probably being transported via a $H^+$–$HCO_3^-$ cotransport system. Figure 4 illustrates what we presently consider to be a viable hypothesis. The reader can see that we have completely reversed our position with respect to our original statement. Now the 'processes of acidification and alkalinization' are *related* to the *same* phenomenon, i.e., the process

of $HCO_3^-$ assimilation. The nature of the putative $H^+$–$HCO_3^-$ cotransport system remains to be elucidated; at present we cannot say whether the process is electroneutral or electrogenic (i.e., $2H^+ / HCO_3^-$).

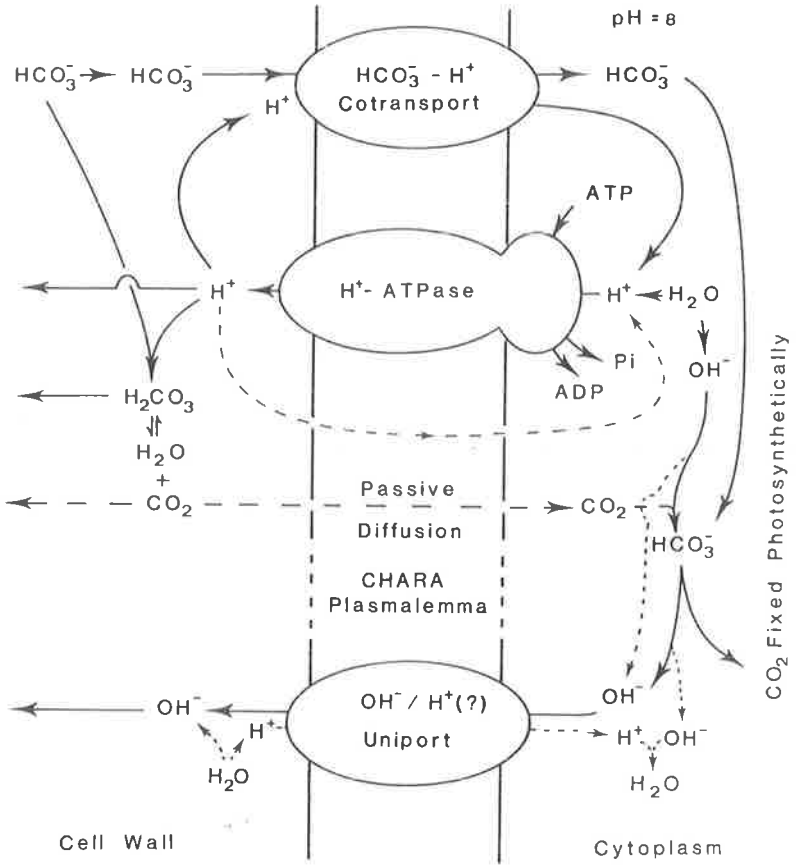


**Figure 4.** Schematic representation of the plasmalemma-bound transport complexes that may function to enable internodal cells of *Chara* to aquire exogenous $HCO_3^-$ for photosynthesis. It is suggested that under normal $HCO_3^-$-assimilating conditions, the $H^+$-translocating ATPase provides a supply of protons to the outer surface of the plasmalemma. These $H^+$ are used to drive the $H^+$–$HCO_3^-$ cotransport system; the re-entering $H^+$ are again cycled through the ATPase, thereby forming a $H^+$ 'current' loop. Some of the $H^+$ will also react with $HCO_3^-$ to produce $H_2CO_3$ and thereby $C0_2$, which will diffuse both into the bathing medium and into the cytoplasm (if the appropriate concentration gradient exists). Photosynthetic $CO_2$ fixation produces $OH^-$ by causing $HCO_3^-$ to dissociate and the $OH^-$ transport regions serve to dispose of this alkalinity. (From 17).

## A RENEWED CHALLENGE: POSSIBLE INVOLVEMENT OF CARBONIC ANHYDRASE

### (a) Ethoxyzolamide effects on photosynthesis as measured with $^{14}C$ or an $O_2$ electrode.

Although most workers would agree that the experimental evidence, obtained using *Chara*, does not support the 'brute force' extracellular $CO_2$ production hypothesis, some presently consider that this $CO_2$ production may occur within the periplasmic space of the charasome (see 4, 5, 21, 31). Because of the slow rate of the dehydration step ($H_2CO_3 \rightarrow CO_2 + H_2O$), a role for extracellular carbonic anhydrase (CA) has been invoked (30). Figure 2 could be modified to incorporate this hypothesis simply by adding the influence of extracellular CA. For additional discussion of this topic the reader is referred to Chapter 3 of this volume.

Mary Bassett, a Ph.D. exchange student from the Australian National University, recently joined our laboratory to investigate the role of carbonic anhydrase on $H^{14}CO_3^-$ assimilation in *Chara corallina*. In a previous study, she and Dean Price had used an $O_2$ electrode to investigate the effect of ethoxyzolamide (EZ), an inhibitor of CA, on photosynthesis (30). They found that at a concentration of about 20 $\mu$M, EZ caused a 30–40% inhibition of $O_2$ evolution at pH 8.2 and 60% or more at pH 9.3; there was no inhibition detected at pH 5.0.

Our results obtained using $^{14}C$ are presented in Table I. We also found no inhibition at pH 5.5, which suggests that CA does not play a significant role in $^{14}CO_2$ assimilation at the chloroplast level. At pH 8.2 we detected a 10.7% decrease in photosynthesis when 1.0 mM DIC was employed. There was a definite effect of DIC concentration on this EZ-induced inhibition; at 5 mM DIC the inhibition of [$^{14}C$]-fixation was completely relieved. When Mary Bassett used an $O_2$ electrode system to investigate the influence of EZ on our tissue, she obtained a variable effect, but the average degree of inhibition was about 40%, which was in agreement with her earlier work done in Canberra. The effect of EZ at pH 9.2 was even more interesting in that the degree of inhibition did not increase as dramatically as might have been expected from her earlier $O_2$ electrode studies, and increasing the DIC level did not relieve the inhibition (see Table I).

The basic difference between the $O_2$ electrode and $^{14}C$ experiments is that in the former, the experimental medium must be well-stirred, while in the latter we have traditionally used stagnant conditions. Hence, in the $O_2$ electrode the unstirred layer next to the *Chara* cell wall will be about 50 $\mu$m, while in the $^{14}C$ system this layer may be very large (possibly greater that 500-1000 $\mu$m; see Chapter 3). The explanation

**Table I.** Influence of 20 $\mu$M Ethoxyzolamide (EZ) on $^{14}C$ Fixation at Different DIC Concentrations and pH Values. *Chara* internodal cells were pretreated for 60 min under the appropriate DIC level and pH value prior to the introduction of [$^{14}C$]-labelled solutions. In experiments where EZ was employed, it was added to the pretreatment solution for the final 30 min of the pretreatment period. Since the EZ was dissolved in ethanol, all treatments contained 0.1% (v/v) ethanol. All experiments were conducted at 25°C under 22 W $m^{-2}$ irradiance.

| pH | [DIC], mM | −EZ | +EZ | % Inhibition[a] |
|---|---|---|---|---|
| 5.5 | 0.25 | 50.8 ± 3.1[b] | 53.5 ± 3.4 | No Effect |
| | 0.5 | 90.3 ± 3.7 | 100.0 ± 2.6 | No Effect |
| | 1.0 | 111.1 ± 2.5 | 117.8 ± 5.2 | No Effect |
| 8.2 | 0.25 | 5.7 ± 0.5 | 4.2 ± 0.3 | 26.5 |
| | 0.5 | 40.1 ± 2.8 | 33.2 ± 1.8 | 17.3 |
| | 1.0 | 44.2 ± 1.4 | 39.5 ± 1.5 | 10.7 |
| | 5.0 | 54.1 ± 2.9 | 51.2 ± 2.1 | No Effect |
| 9.2 | 0.5 | 37.2 ± 2.5 | 31.1 ± 1.4 | 16.4 |
| | 1.0 | 44.2 ± 1.2 | 34.6 ± 1.1 | 21.8 |
| | 2.5 | 58.9 ± 3.2 | 46.8 ± 2.1 | 20.5 |

[a]All inhibitions are significant to the 95% confidence level.

[b]Net photosynthetic fixation in units of pmol $cm^{-2}s^{-1}$.

as to the differences obtained using EZ in these two systems will, in all probability, be found in the influence of the unstirred layers. If periplasmic $CO_2$ production is dependent upon the combined action of CA and $H^+$ efflux, inhibition of CA would slow down the conversion of $H_2CO_3$ to $CO_2$. Under these conditions, the associated reactions would probably extend beyond the cell wall into the unstirred layer. This would establish a situation analogous to the $CO_2$ model originally envisioned by Walker and his colleagues (38). Hence, in an experimental system where a large unstirred layer is present, net photosynthesis may show a moderate sensitivity to CA inhibition because of the 'buffering effect' of the unstirred layer; such a situation would be present in our $^{14}C$ experiments (see Table I). The opposite situation would exist in the $O_2$ electrode system: here rapid mixing would create a small unstirred layer. and so the diffusion gradients would be enhanced for all species involved (i.e. $H^+$, $H_2CO_3$ and $CO_2$). In this situation, much of the $CO_2$ that would have been generated near the cell wall would not enter the cy-

toplasm and, hence, net photosynthesis would be much reduced. This was what Price *et al.* (30) observed at high pH, and one could argue that the difference that they found between pH 8.2 and 9.3 was due to a steepening of the $H^+$ gradient and an increase in the rate of the back reaction, $CO_2 + OH^- \rightarrow HCO_3^-$.

**(b) Electrophysiolgical studies.**

As discussed in an earlier section, we recently showed that under $HCO_3^-$-assimilating conditions the *Chara* membrane potential is extremely sensitive to the level of exogenous $HCO_3^-$ (17). It should be recalled that this sensitivity could be maintained in the presence of an artificial buffer, with $HCO_3^-$ being absent or present at a very low level. The experimental chamber in which these experiments were conducted was designed to give a rapid flow rate past the *Chara* cell surface. Mary Bassett used normal flowing solutions, as well as stagnant conditions, to investigate the effect of EZ on the membrane potential of *Chara*. Addition of EZ (at 20 to 30 $\mu$M) always caused a depolarization in the membrane potential of about 15-20 mV. A similar result could be obtained by reducing the level of exogenous $HCO_3^-$ from 1.0 to about 0.5 mM. Based on the hypothesis presented in Fig. 2, this depolarization could be explained on the basis of a feedback effect of $H^+$ on the $H^+$–translocating ATPase; i.e., inhibition of CA by EZ would reduce the rate of consumption of $H^+$ via the conversion of $HCO_3^-$ to $CO_2$ and the putative increase of $H^+$ in the periplasmic space would partially inhibit the $H^+$ pump. (An analysis of the $H^+$–$HCO_3^-$ cotransport hypothesis will be given in a later section. See Fig. 4.)

Since, in these experiments, the solution was flowing past the cell, the reduced unstirred layer would tend to facilitate the removal of $H^+$ from the cell surface and thereby act to reduce the influence of EZ on the putative $H^+$ increase. The prediction would be, therefore, that the dark-induced hyperpolarization of the membrane potential would be reduced only slightly by the effect of EZ. Mary's experiments confirmed this prediction (see Fig. 5). However, the effect of EZ was not reduced when the $HCO_3^-$ level was raised from 1.0 to 5.0 mM.

One could argue that under stagnant solution conditions, the control dark-induced transient should be much larger than that obtained in the presence of EZ, because the inhibition of CA activity and the presence of the large unstirred layer should cause a greater reduction in the activity of the $H^+$ pump. Alternatively, since in the presence of added CA, the pH profile becomes contracted towards the cell surface and more sharply defined (Lucas, unpublished results), the presence of CA under stagnant solution conditions should result in a larger dark-

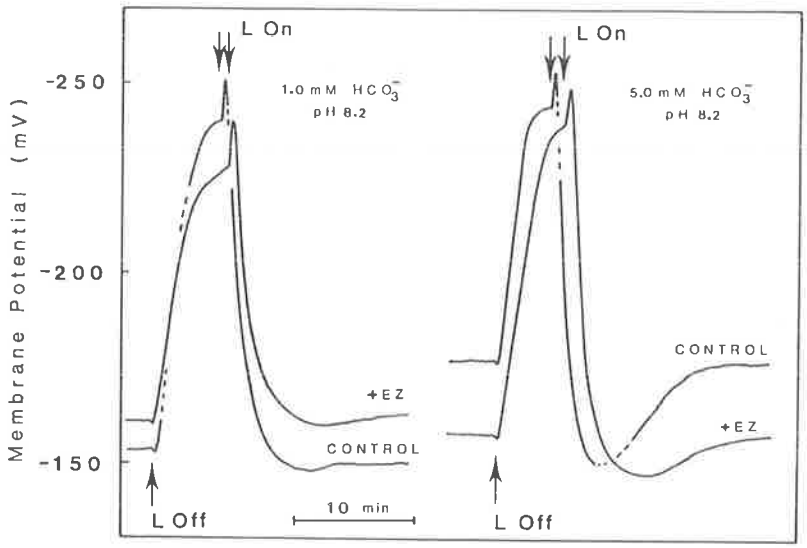


**Figure 5.** Influence of 20 $\mu$M EZ on the dark/light-induced transients in the membrane potential of *Chara corallina*. Experiments were conducted under a light intensity of 20 W $m^{-2}$ and at a temperature of 26°C. The experimental medium contained (mM) 1.0 NaCl, 0.2 $CaSO_4$, 0.2 KCl, and the indicated level of $NaHCO_3$, pH 8.2.

induced transient than the control (-CA). When we conducted this type of experiment we could not detect any influence of CA on the initial rate at which the membrane potential hyperpolarized upon darkening the cell (see Fig. 6). The observed traces (+CA), although slightly displaced, were almost identical to the response obtained under flowing solution conditions, the only difference being in the absolute magnitude of the induced hyperpolarization. This suggests that the conditions on the cell surface have little influence over the processes that occur across the plasmalemma to generate these membrane potential transients.

### (c) Extracellular potentials and currents.

The extracellular 'currents' that are associated with $HCO_3^-$ assimilation were also found to be affected by EZ treatment, although, as shown in Fig. 7, the degree of inhibition was not very large. The interesting feature to note from Fig. 7 is that EZ caused a reduction in the 'currents' in both the alkaline and acid (or $HCO_3^-$ acquiring) regions (or bands). This result can be interpreted on the basis of EZ reducing either the amount of inorganic carbon available for photosynthesis, or the integrated rate of $H^+$ efflux which would cause a proportional reduction in total $OH^-$ efflux.

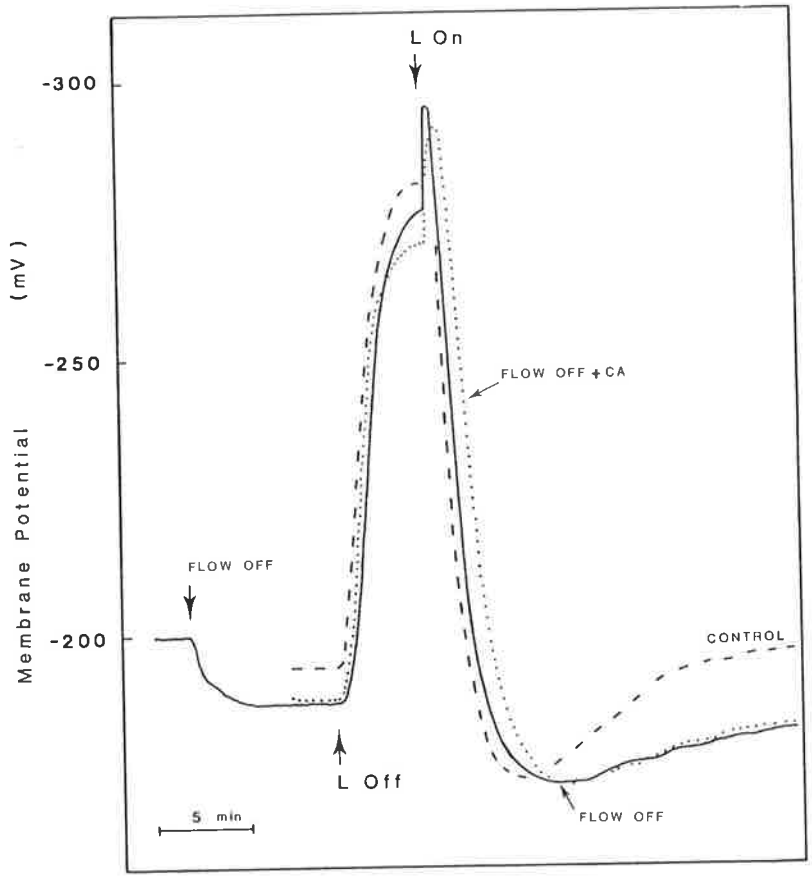


**Figure 6.** Influence of stagnant solution conditions on the dark/light induced transients in the membrane potential of *C. corallina*. The induced transients, obtained in the presence of flowing solution (control), are compared with those obtained in stagnant solutions, with and without added CA. Experimental details as in Fig. 5. $NaHCO_3$ concentration was 1.0 mM, pH 8.2.

During these vibrating probe experiments, we noticed that following EZ treatment the *Chara* internodal cells were particularly sensitive to any form of handling. Simply replacing the medium within the experimental chamber was enough to cause a perturbation of the $HCO_3^-$ and $OH^-$-associated transport systems (see Fig. 7). Following such a perturbation, the cells always re-established 'control' patterns, even if they were left in medium containing EZ. This suggests that CA does not play a central role in the $HCO_3^-$-assimilating system of *Chara*.

During our preparations for the $HCO_3^-$ workshop, Dr. Koreaki Ogata from Osaka, Japan, was visiting our laboratory to collaborate on some experiments in which we needed to use his ingenious water-film tech-

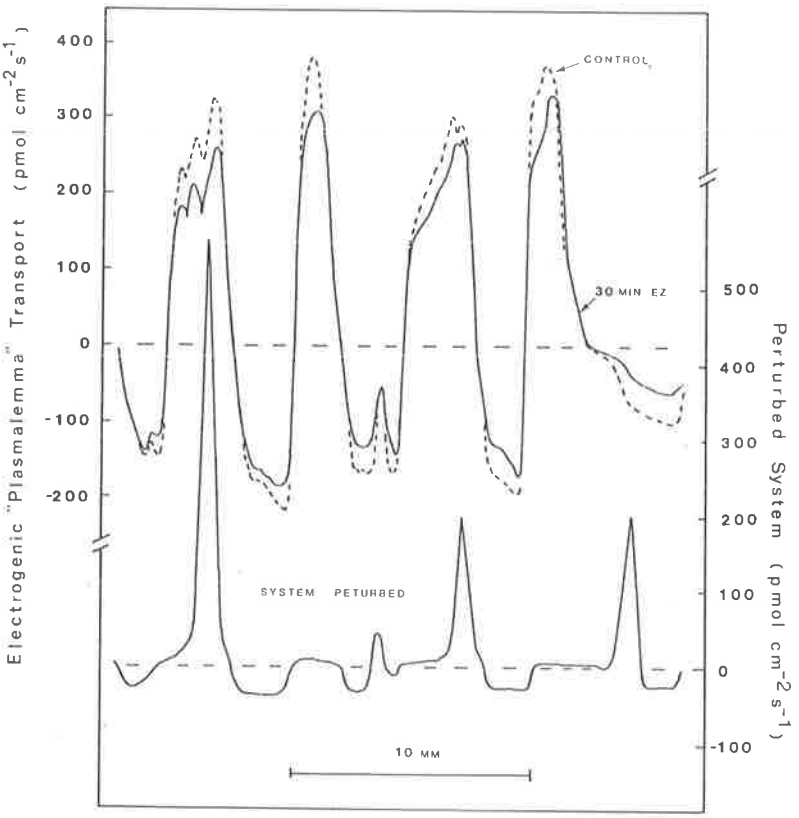


**Figure 7.** $HCO_3^-$ and $OH^-$-associated extracellular 'currents' measured 50 $\mu$m from the *Chara* cell surface by using the vibrating probe technique. Experimental conditions as in Fig. 5, except that the experimental solution was not flowing. EZ concentration used was 20 $\mu$M.

nique (1, 28, 29). In brief, his system allows the measurement of both the trans-membrane electric potential and the extracellular electric potential as a function of position along the length of an internodal cell. In addition, by injecting a sinusoidal current pulse across the plasmalemma, it is also possible to measure the membrane conductance as a function of position. (For a discussion of this technique and the problems associated with data interpretation, the reader is referred to Chapter 17, and references therein).

Experiments conducted with this water-film technique showed that EZ (at 18–20 $\mu$M) had almost no detectable effect on the extracellular electric potential profiles when the medium contained 1.0 mM $NaHCO_3$, pH 8.2. A typical result is presented in Fig. 8. Apparently, in this 'open-circuit' condition, the EZ response is too small to cause a detectable

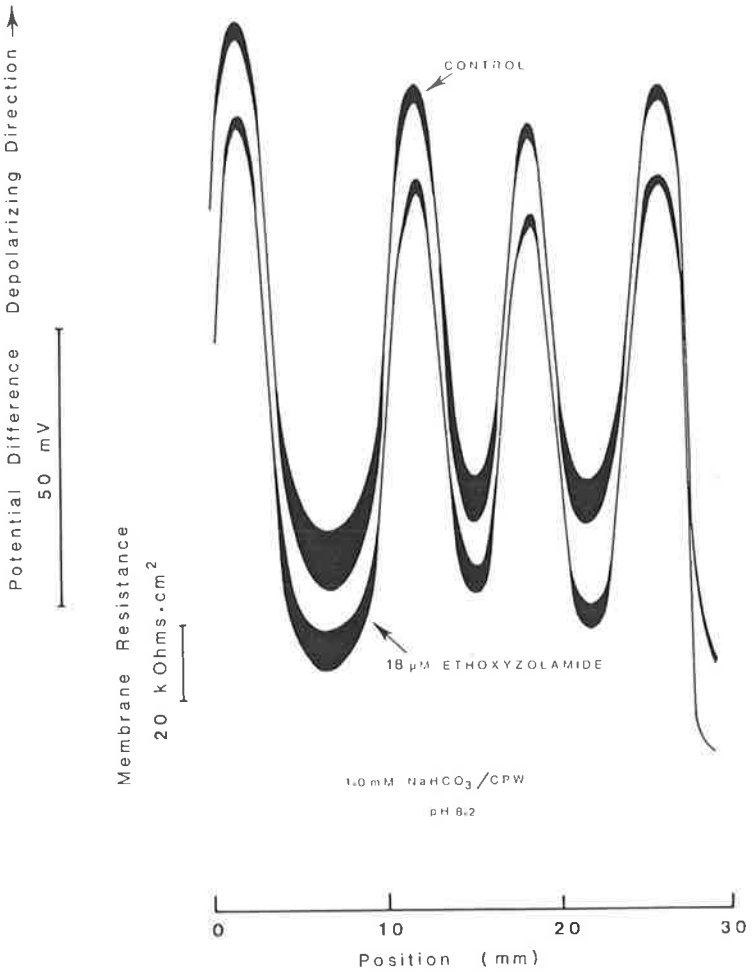


**Figure 8.** *Chara* extracellular electric potential profiles obtained in the presence and absence of EZ using the water-film electrode technique developed by Ogata (28). Experimental details were as follows: light intensity at the surface of the humidity chamber was 17W $m^{-2}$; temperature 25°C; experimental medium in the bottom of the chamber contained (mM) 1.0 $NaHCO_3$, 1.0 NaCl, 0.2 KCl, 0.2 $CaSO_4$, initial pH adjusted to 8.2; humidifying gas stream was air. EZ was introduced to the experimental medium via the base of the humidity chamber and the level of this solution was raised such that the entire length of the cell was submerged. After 10 min of EZ treatment, the solution level was lowered and the voltage scans performed. (This cell immersion technique was used to introduce and remove specific chemical treatments.) Control and EZ solutions contained 0.5% (v/v) ethanol. Plasmalemma resistance (shaded area) was measured by injecting current as the water-film was moved down the cell length.

effect on the transport processes. By increasing the EZ concentration to 30 $\mu$M and raising the medium pH value to 9.2, we could obtain an effect on the acid or $HCO_3^-$ regions of the cell; here the electric potential was reduced in magnitude (see Fig. 9). For a comparison, Fig. 9 also illustrates the effect of 0.1 $\mu$M DCMU on the external electric potential profile. This level of DCMU would cause an approximate 20% inhibition of photosynthesis. Thus, the effect observed at pH 9.2 must represent quite a significant inhibition of the $HCO_3^-$-associated transport process(es).

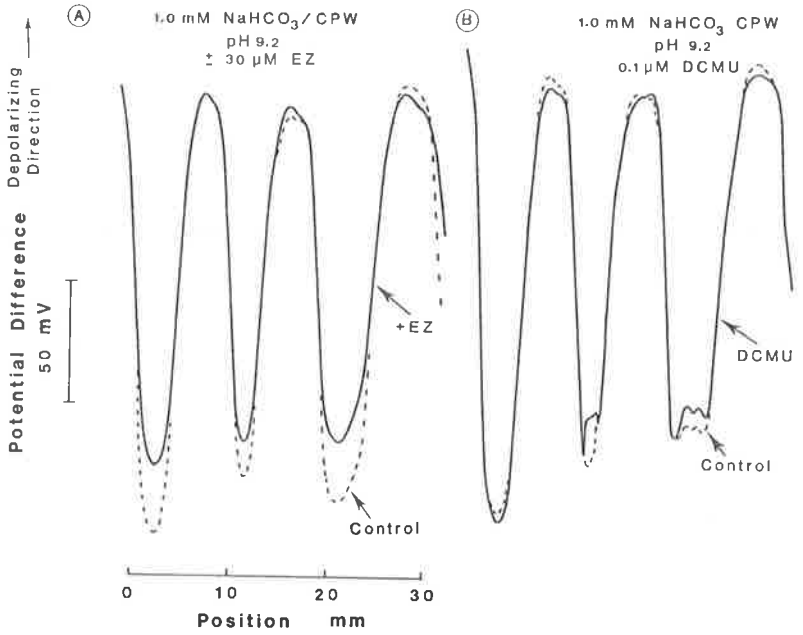


**Figure 9.** Influence of EZ (30 $\mu$M) and DCMU (0.1 $\mu$M) on the extracellular electric potential profiles of *Chara* under high pH conditions (pH 9.2). Experimental details as in Fig. 8. Following the EZ experiment, this chemical was removed, and once control profiles had been re-established, the DCMU was introduced.

We continued these water-film experiments using our technique of 'decoupling' the membrane transport processes from $HCO_3^-$ uptake (see 17); i.e., we removed the $HCO_3^-$ from the system and replaced it by a non-transportable buffer analog like HEPES. Under $HCO_3^-$-decoupled conditions, the extracellular electric potential profiles were the same as those obtained in the presence of $HCO_3^-$. However, when we introduced EZ at pH 8.2, the external electric potentials in both the alkaline and acid regions were affected, and generally the magnitude of the potentials

was reduced more in the central region of the cell (see Fig. 10). This result certainly complicates the picture of the EZ effect since there was, in essence, no inorganic carbon available to the cells during these decoupled experiments. We conclude that EZ may have effects other than those directly related to the inhibition of CA.

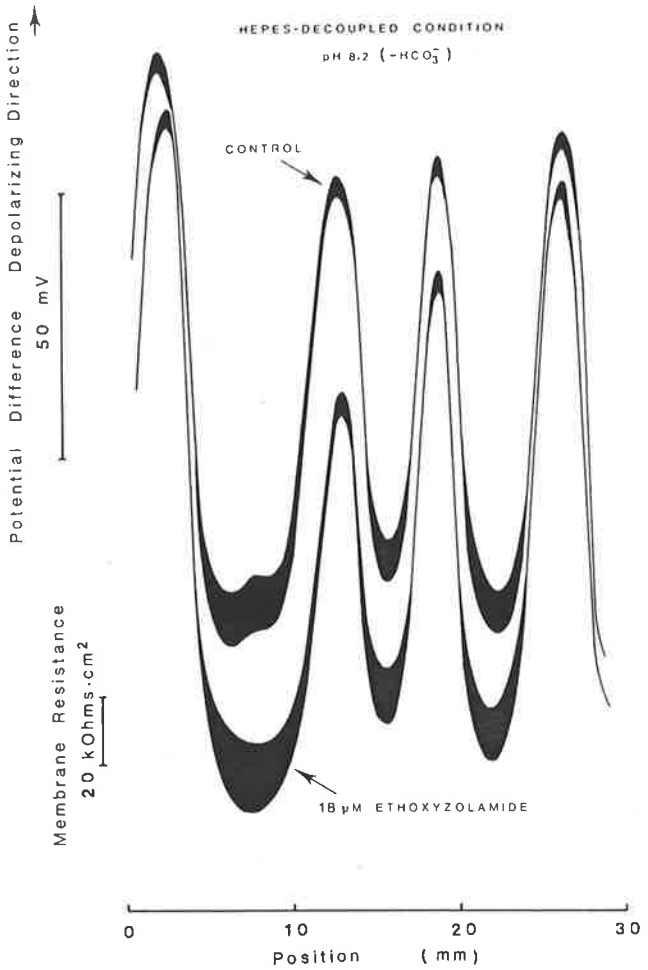


**Figure 10.** Influence of 18 $\mu$M EZ on the extracellular electric potential and plasmalemma conductance profiles of *Chara* under '$HCO_3^-$-free' HEPES-decoupled conditions. Experimental details as in Fig. 8.

## AN ALTERNATIVE ROLE FOR EXTRACELLULAR CA

The results obtained using EZ provide some support for the periplasmic $CO_2$ production hypothesis (i.e. a CA-modified Fig. 2). We would now like to include an alternative model that can equally-well explain the CA/EZ results. If *Chara* does possess a $H^+$–$HCO_3^-$ cotransport mechanism that is driven by a $H^+$–translocating ATPase, then this process may be able to significantly raise the cytoplasmic level of $HCO_3^-$ above that in the bathing medium. *Chara* may be able to raise the cytoplasmic DIC level to an extent similar to that observed in certain microalgae and cyanobacteria (see Chapters 4, 6, 7, 9 and 21). If this were the case, the $CO_2$ within the cytoplasm would be considerably out of equilibrium with that present in the cell wall; leakage of $CO_2$ out of the cell would occur under these conditions. Of course, this $CO_2$ leakage would act as a DIC shunt, reducing the effectiveness of the $H^+$–$HCO_3^-$ cotransport mechanism. Now we propose that the presence of periplasmic extracellular CA could greatly reduce the influence of this $CO_2$ shunt. Our model is presented in Fig. 11. Basically, CA is involved in enhancing the hydration of $CO_2$ to form $H_2CO_3$, which upon dissociation, gives back the $HCO_3^-$ and $H^+$ originally utilized to transport the inorganic carbon into the cytoplasm. In this model, then, the role of extracellular CA is not central to the actual acquisition of DIC by the *Chara* cell, but it is an important, albeit not essential component in that it increases the efficacy of the overall process.

Needless to say, all the arguments that were applied to the EZ/CA data could equally-well be applied to the model presented in Fig. 11. It will be necessary to measure the DIC level in the *Chara* cytoplasm to distinguish between the two hypotheses. This will be an extremely difficult experiment to perform. One might say then that we are in a position of 'check,' and we await, with great interest, to see what will be the next 'move.'

## CHARASOME INVOLVEMENT IN MEMBRANE TRANSPORT

The elaborate plasmalemma structure, the charasome, that develops in the genus *Chara*, has been ascribed a role in the transport of $Cl^-$ (6) as well as in $HCO_3^-$ uptake (30, 36). The experimental result that led our laboratory to conclude that the charasome does not play a central role in $HCO_3^-$ acquisition was the finding that although certain species in the genus *Nitella* exhibit identical pH banding patterns, they were found not to contain charasomes. In view of the recent developments relating to extracellular CA, and to the finding in the aquatic angiosperms

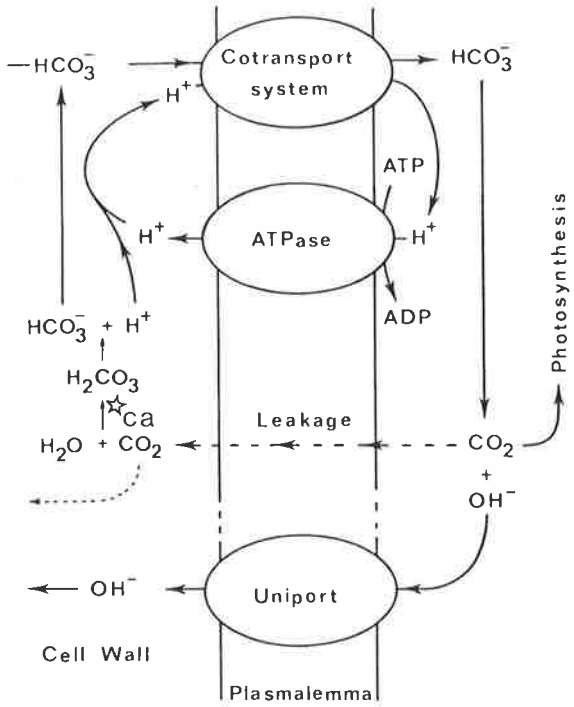


**Figure 11.** Modification of the $HCO_3^-$ assimilation model presented in Fig. 4 to incorporate the action of extracellular CA. In this version of our model, we have assumed that the $H^+ - HCO_3^-$ cotransport system raises the cytoplasmic DIC levels such that $CO_2$ leaks back out of the cell. In contrast with the CA role proposed by Price *et al.* (30), we suggest that this enzyme functions to recapture the $CO_2$ that has leaked out (by diffusion) from the cytoplasm.

that transfer cell wall characteristics are not essential for assimilation of exogenous $HCO_3^-$ (35), we should be extremely cautious about extrapolating from one cell system to another. Clearly, we need to do extensive parallel studies on *Chara corallina* and *Nitella flexilis* (or, indeed, any robust *Nitella* sp that forms acid and alkaline bands). These comparative studies should investigate:

(a) the radial pH profiles in the acid and alkaline regions;
(b) the extracellular fluxes ('current') and their relationship to changes in DIC;
(c) sensitivity of photosynthesis to solution flow and to inhibitors of CA;
(d) manipulation of charasome development to determine if *Chara* can be made analogous to *Nitella* in its characteristics;

(e) whether CA is present in the periplasm using histochemical and immunocytochemical techniques;
(f) if it is possible to block, in a specific manner, the synthesis of CA in both *Nitella* and *Chara*; and
(g) the transport of other ions and their relationship to the development/presence of the charasome.

Although there is some debate about the ability of the charasome to act as a capture site for $H^+$ (see Chapter 3), we consider that this specialized 'organelle' will be involved in enhancing the transport capability of those processes that utilize $\Delta\tilde{\mu}_{H^+}$ as their driving force.

Finally, aside from the need to understand their role in membrane transport, the charasome presents a unique developmental system for further study. The actual centers where the charasome will develop are established when the growing cell is about 2 mm in length. (Remember that the relative spatial aspect will be maintained during expansion growth, and the cell will have a final length of about 40–50 mm.) Now that we have been able to modulate the extent to which the Charasome develops (see 30, and Lucas, Keifer and Pesacreta, unpublished results), it should be possible to study the cytological processes that orchestrate this phenomenon of the charasome.

## THE PROBLEM OF SPATIAL AND TEMPORAL REGULATION

Many of the details of our present model(s) that explain the phenomenon of $HCO_3^-$ assimilation in *Chara* are based on the interpretation of membrane potential transients and extracellular 'current' patterns. As an example, take the dark-induced hyperpolarization of the membrane potential which is observed when *Chara* cells are in the $HCO_3^-$-assimilating mode. We have developed a model, presented in Fig. 4 (see also Fig. 11), which can explain this hyperpolarization. If the $H^+$-$HCO_3^-$ cotransport system is a neutral carrier system, then only the $H^+$–translocating ATPase and the $OH^-$ uniport system will have an influence on the membrane potential. (Other known electrogenic systems will be ignored for the present discussion, primarily because we consider that their influence is likely to be small in comparison with the $H^+$ and $OH^-$ systems.)

Both the $H^+$ efflux and $OH^-$ efflux systems must operate under a rather complex regulatory network that is responsible for both spatial and temporal control. We have almost no information as to the biochemical/biophysical nature of the control signals used to effect spatial control along the length of the cell (but see 24, and Chapter 17). Based on experiments done using photosynthetic inhibitors (19) and modulated

light intensities (7-10), we are beginning to unravel the details pertaining to the temporal regulation. At the present time it would appear that the $H^+$–ATPase and the $OH^-$ efflux system both receive at least one set of control signals that originate from within the chloroplasts. This light-dependent signal could account for the hyperpolarization phenomenon as follows. Modulation of the light reactions within the chloroplasts, e.g., by reducing the light intensity or by introducing DCMU, causes a change in the putative signal(s) such that the $OH^-$ efflux system (the feedback system in this situation) begins to inactivate more rapidly than does the $H^+$–ATPase. The temporary imbalance in the currents associated with these two systems gives rise to the transient hyperpolarization. The nature of this putative signal is presently under investigation in our laboratory, but at present, all we can say is that it is not a photorespiratory metabolite.

During some of our recent studies (27), we found that we could pretreat cells in such a way that we could no longer obtain this dark-induced hyperpolarization. This could be achieved by opening the $K^+$ channels in the *Chara* plasmalemma by imposing a 10 mM $K^+$ treatment. Keifer and Lucas (11) showed that even when the $K^+$ channels were opened and the potential was 'short-circuited' to a value close to the $K^+$ diffusion potential, the $H^+$–ATPase continued to operate. In addition, in earlier studies, we had shown that under these $K^+$–depolarized conditions, $HCO_3^-$ assimilation was not stopped, but rather the entire system was perturbed. In this perturbed state, the 'kinetics' of $HCO_3^-$ assimilation exhibited a linear dependence upon $HCO_3^-$ concentration (26).

Closure of the $K^+$ channels results in a rapid repolarization of the membrane potential, with a normal resting potential being established within 60 min. Lucas studied the time course of the re-establishment of normal $H^{14}CO_3^-$ assimilation in 10 mM $K^+$-pretreated *Chara* cells and found that near-control values of photosynthesis were obtained after 60 min (see Fig. 5 in 16, and Fig. 3 in 26). In addition, vibrating probe data also established that the extracellular 'current' pattern had returned within 90 min of closing the $K^+$ channels (Lucas, unpublished results). However, even though all the characteristics of the membrane potential appeared to be normal after a 1 h recovery, and $H^{14}CO_3^-$-assimilating capacity had been returned, we could not obtain the normal dark/light transients. As shown in Fig 12, the normal hyperpolarizing effect of darkness was only obtained several hours after recovery from the $K^+$ depolarized condition.

Results of this nature suggest that the apparent phase difference in the control signals that function to inactivate (as well as activate) the $OH^-$ and $H^+$ efflux systems can be adjusted, such that they become

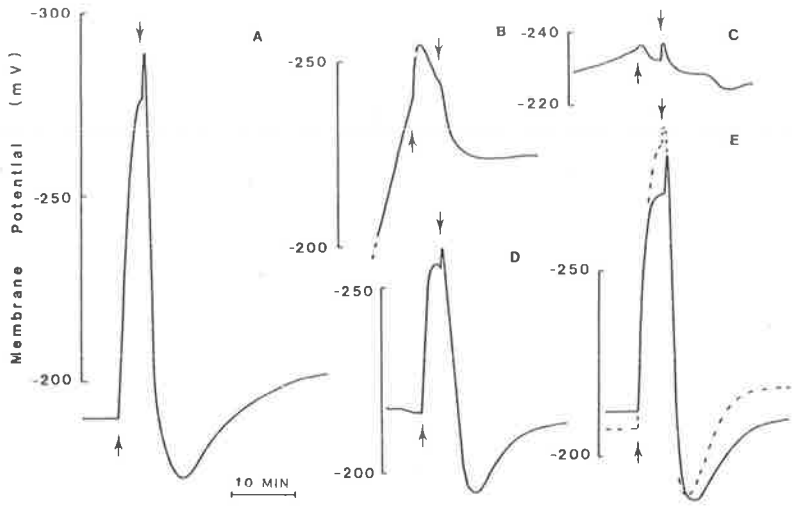


**Figure 12.** Re-establishment of the dark/light-induced membrane potential transients following $K^+$channel closure in *C. coralina*. Control response was obtained prior to depolarizing the membrane potential by the application of 10mM $K^+$. Control solution contained (mM) 1.0 $NaHCO_3$, 0.2 KCl, 0.2 $CaSO_4$, 1.0 NaCl, pH 8.2. Upward pointing arrows = light off; downward pointing arrows = light on (20 $Wm^{-2}$). Following a 1 h depolarization in solution in which the 0.2 KCl had been increased to 10mM KCl, the $K^+$ channels were closed by returning the cell to the 0.2mM KCl solution. The response of the membrane potential to dark/light treatments was investigated at various times in the recovery phase: 12 min; 1 h; 1.5 h; 3.5 h (solid line); and 5.5h (broken line).

totally in phase with each other. Since we have very limited information concerning the nature of these regulatory processes and, in view of the above results suggesting that the signals themselves may be capable of changing, we should exercise extreme caution in terms of interpreting membrane transients. It has now become essential that we coordinate the simultaneous use of numerous independent techniques to further study the $HCO_3^-$ assimilation phenomenon of *Chara*.

The results presented in Fig. 13 further serve to illustrate the difficulty associated with interpreting membrane transients on the basis of presumed mechanisms. This particular result was obtained by Mary Bassett: trace 'a' was obtained prior to the microelectrode being sealed out by the cell; trace 'b' was obtained 1 h after the microelectrode was re-inserted. Clearly, the light/dark/light-induced transients in the membrane potential are almost identical, yet the absolute values of the

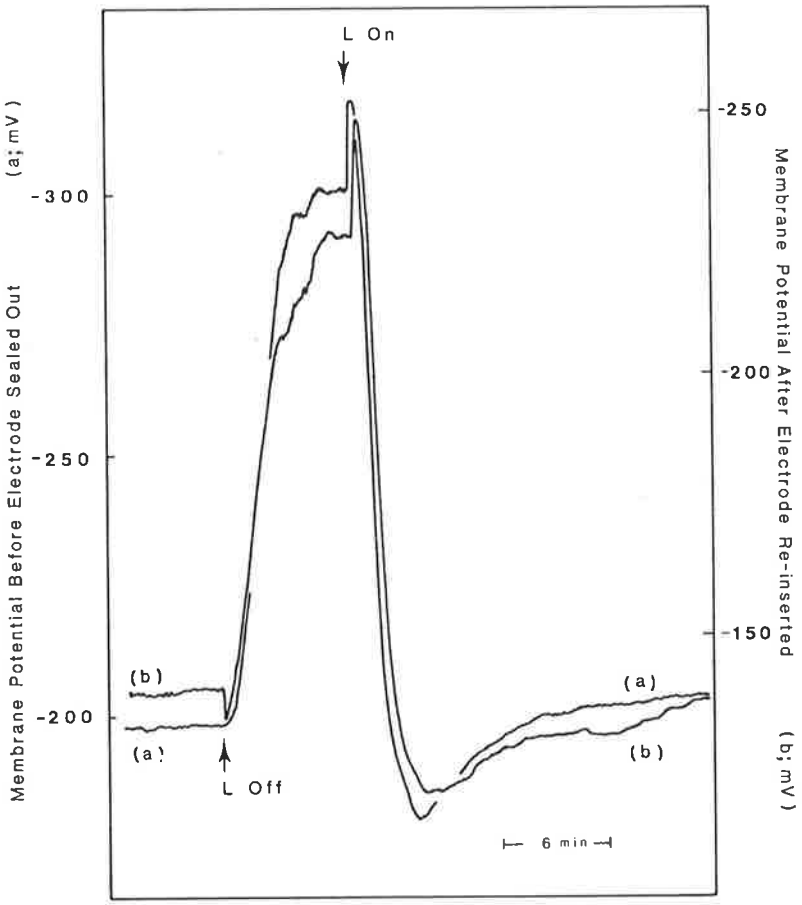


**Figure 13.** Membrane potential transients induced by a short dark treatment. Experimental details as in Fig. 5; 1.0 mM $NaHCO_3$, pH 8.2. Trace (a) represents a dark-induced transient obtained just before the cell sealed out the microelectrode that was inserted into the vacuole to measure the membrane potential. Trace (b) was recorded 1 h after the same electrode was unsealed by further insertion of the electrode tip. Note that although the transients are similar in form, the absolute values of the membrane potentials differ by about 70 mV.

potential differ by about 70 mV. We have observed this phenomenon for quite some time; i.e., the general form and magnitude of the induced transients are quite similar whether the resulting potential is -150 or -280mV. This observation is difficult to reconcile with the involvement of two electrogenic transport systems, with one being active and the other passive (i.e. the $OH^-$ efflux system). The apparent voltage-insensitive hyperpolarizing trend could be rationalized in terms of the operation of

control signals limiting the influence of the $1H^+/ATP$ system. However, it is difficult to explain the voltage-insensitivity of the depolarizing trend as reflecting the influence of the electrogenic $OH^-$ efflux system. One cannot help but wonder what new set of experimental conditions will allow us to unravel this particular problem.

## ACKNOWLEDGEMENTS

Much of the work presented in this chapter was conducted with the support of National Science Foundation Grants PCM 78-10474, PCM 80-03133, and PCM 81-17721. Mary Bassett was supported in part by an Australian National University Postgraduate Fellowship and the University of California–Australian National University Exchange Program.

## LITERATURE CITED

1. CHILCOTT TC, HGL COSTER, K OGATA, JR SMITH 1983 Spatial variation of the electrical properties of *Chara australis*. II Membrane capacitance and conductance as a function of frequency. Aust J Plant Physiol 10: 353–362
2. FERRIER JM 1980 Apparent bicarbonate uptake and possible plasmalemma proton efflux in *Chara corallina*. Plant Physiol 66: 1198–1199
3. FERRIER JM, WJ LUCAS 1979 Plasmalemma transport of $OH^-$ in *Chara corallina*. II Further analysis of the diffusion system associated with $OH^-$ efflux. J Exp Bot 30: 705–718
4. FRANCESCHI VR, WJ LUCAS 1980 Structure and possible function(s) of Charasomes; complex plasmalemma-cell wall elaborations present in some Characean species. Protoplasma 104: 253–271
5. FRANCESCHI VR, WJ LUCAS 1981 The charasome periplasmic space. Protoplasma 107: 269–284
6. FRANCESCHI VR, WJ LUCAS 1982 The relationship of the Charasome to chloride uptake in *Chara corallina*: Physiological and histochemical investigations. Planta 154: 525–537
7. HANSEN U-P 1978 Do light-induced changes in the membrane potential of *Nitella* reflect the feedback regulation of a cytoplasmic parameter? J Membr Biol 41: 197–224
8. HANSEN U-P 1980 Homeostasis in *Nitella*: Adaptation of $H^+$ transport to the photosynthetic load. *In* RM Spanswick, WJ Lucas, J Dainty, eds, Plant Membrane Transport: Current Conceptual Issues. Elsevier/North Holland Biomedical Press, Amsterdam, pp 587–588
9. HANSEN U-P, D SANDERS, D GRADMANN, J TITTOR, CL SLAYMAN 1984 Steady-state and nonsteady-state models of membrane transport. *In* WJ Cram, K Janáček, R Rybová, K Sigler, eds, Membrane Transport in Plants. Academia, Praha, pp 33–38
10. HANSEN U-P, P KENUNECKE 1977 The parallel pathways of the action of light on membrane potential of *Nitella*. *In* M Thellier, A Monnier, M Demarty. J Dainty, eds, Ionic Exchange in Plants. Paris, Univ Rouen, CNRS Publ No 258. pp 333–340

11. KEIFER DW, WJ LUCAS 1982 Potassium channels in *Chara corallina*: Control and interaction with the electrogenic $H^+$ pump. Plant Physiol 69: 781–788

12. KITASATO H 1968 The influence of $H^+$ on the membrane potential and ion fluxes of *Nitella*. J Gen Physiol 52: 60–87

13. LUCAS WJ 1975 Photosynthetic fixation of $^{14}$Carbon by internodal cells of *Chara corallina*. J Exp Bot 26: 331–346

14. LUCAS WJ 1975 The influence of light intensity on the activation and operation of the hydroxyl efflux system of *Chara corallina*. J Exp Bot 26:347–360.

15. LUCAS, WJ 1976. Plasmalemma transport of $HCO_3^-$ and $OH^-$ in *Chara corallina*: Non-antiporter systems. J Exp Bot 27: 19–31

16. LUCAS WJ 1976 The influence of $Ca^{2+}$ and $K^+$ on $H^{14}CO_3^-$ influx in internodal cells of *Chara corallina*. J Exp Bot 27: 32–42

17. LUCAS, WJ 1982. Mechanism of acquisition of exogenous $HCO_3^-$ by internodal cells of *Chara corallina*. Planta 165:181–192.

18. LUCAS WJ 1983 Photosynthetic assimilation of exogenous $HCO_3^-$ by aquatic plants. Annu Rev Pl Physiol 34: 71–104

19. LUCAS WJ 1984 How are the plasmalemma transport processes of *Chara* regulated? *In* WJ Cram, K Janáček, R Rybová, K Sigler, eds, Membrane Transport in Plants. Academia, Praha, pp 459–465

20. LUCAS WJ, JM FERRIER, J DAINTY 1977 Plasmalemma transport of $OH^-$ in *Chara corallina*: Dynamics of activation and deactivation. J Membr Biol 32: 49–73

21. LUCAS WJ, VR FRANCESCHI 1981 Characean charasome-complex and plasmalemma vesicle development. Protoplasma 107: 255–267

22. LUCAS WJ, DW KEIFFER, D SANDERS 1983 Bicarbonate transport in *Chara corallina*: Evidence for cotransport of $HCO_3^-$ with $H^+$. J Membr Biol 73: 263–274

23. LUCAS WJ, R NUCCITELLI 1980 $HCO_3^-$ and $OH^-$ transport across the plasmalemma of *Chara corallina*: Spatial resolution obtained using extracellular vibrating probe. Planta 150: 120–131

24. LUCAS WJ, T SHIMMEN 1981 Intracellular perfusion and cell centrifugation studies on plasmalemma transport processes in *Chara corallina*. J Membr Biol 58: 227–237

25. LUCAS WJ, FA SMITH 1973 The formation of alkaline and acid regions at the surface of *Chara corallina* cells. J Exp Bot 24: 1–14

26. LUCAS WJ, RM SPANSWICK, J DAINTY 1978 $HCO_3^-$ influx across the plasmalemma of *Chara corallina*: Physiolgical and biophysical influence of 10 mM $K^+$. Plant Physiol 61: 487–493

27. LUCAS WJ, C WILSON, JP WRIGHT 1984 Perturbation of *Chara* plasmalemma transport function by 2[4(2', 4'-Dichlorphenoxy)-phenoxy]propionic acid. Plant Physiol 74: 61–66

28. OGATA K 1983 The water-film electrode: A new device for measuring the Characean electro-potential and-conductance distributions along the length of the internode. Plant Cell Physiol 24: 695–703

29. OGATA K, TC CHILCOTT, HGL COSTER 1983 Spatial variation of the electrical properties of *Chara australis*. I Electrical potentials and membrane conductance. Aust J Pl Physiol 10: 339–351

30. PRICE, GD, MR BADGER, ME BASSETT, MI WHITECROSS 1985 Involvement of plasmalemmasomes and carbonic anhydrase in photosynthetic utilisation of bicarbonate in *Chara corallina*. Aust J Pl Physiol, in press.

31. PRICE GD, MI WHITECROSS 1983 Cytochemical localization of ATPase activity on the plasmalemma of *Chara corallina*. Protoplasma 116: 65–74

32. PRINS HBA, RJ HELDER 1980 Photosynthetic use of $HCO_3^-$ by *Elodea* and *Potamogeton*, pH changes induced by $HCO_3^-$, $CO_2$, $K^+$ and $H^+/OH^-$ transport. *In* RM Spanswick, WJ Lucas, J Dainty, eds, Plant Membrane Transport: Current Conceptual Issues. Elsevier/North Holland Biomedical Press, Amsterdam, pp 625–626

33. PRINS HBA, JFH SNEL, RJ HELDER, PE ZANSTRA 1979 Photosynthetic bicarbonate utilization in the aquatic angiosperms *Potamogeton* and *Elodea*. Hydrobiol Bull 13: 106–111

34. PRINS, HBA, JFH SNEL, PE ZANSTRA, RJ HELDER 1980 Photosynthetic $HCO_3^-$ utilization and $OH^-$ excretion in the aquatic angiosperms: Light-induced pH changes at the leaf surface. Plant Physiol 66: 818–822

35. PRINS HBA, JFH SNEL, PE ZANSTRA, RJ HELDER 1982 The mechanism of bicarbonate assimilation by the polar leaves of *Potamogeton* and *Elodea*: $C0_2$ concentrations at the lower leaf surface. Plant Cell Environ 5: 207–214

36. WALKER NA 1980 The transport systems of charophyte and chlorophyte giant algae and their integration into modes of behaviour. *In* RM Spanswick, WJ Lucas, J Dainty eds, Plant Membrane Transport: Current Conceptual Issues. Elsevier/North Holland Biomedical Press, Amsterdam, pp 287–300

37. WALKER NA, FA SMITH 1977 Circulating electric currents between acid and alkaline zones associated with $HCO_3^-$ assimilation in *Chara*. J Expt Bot 28: 1190–1206

38. WALKER NA, FA SMITH, IR CATHERS 1980 Bicarbonate assimilation by freshwater charophytes and higher plants: I Membrane transport of bicarbonate ions is not proven. J Membr Biol 57: 51–58

*Journal of Experimental Botany, Vol. 36, No. 173, pp. 1947–1958, December 1985*

# Hydroxyl- and Bicarbonate-Associated Transport Processes in *Chara corallina*: Studies on the Light–Dark Regulation Mechanism

WILLIAM J. LUCAS[1] AND KOREAKI OGATA[2]

[1]*Department of Botany, University of California, Davis, California 95616, U.S.A.*

[2]*Department of Physiology, College of Medical Technology, Kansai, 660, Hyogo, Japan*

Received 5 March 1985

ABSTRACT

Lucas, W. J. and Ogata, K. 1985. Hydroxyl- and bicarbonate-associated transport processes in *Chara corallina*: Studies on the light–dark regulation mechanism.—J. exp. Bot. 36: 1947–1958.

Experiments were undertaken on the fresh water alga *Chara corallina* to investigate the nature of the coupling between the chloroplasts and the light-dependent $OH^-$ and $HCO_3^-$-associated plasmalemma transport systems. Electrophysiological experiments, in which DCMU was employed, revealed that this chemical could elicit a hyperpolarization of the membrane potential that was *identical* to that normally obtained by turning off the light. This DCMU-induced hyperpolarization was obtained under control ($+HCO_3^-$) and phosphate-decoupled conditions ($-HCO_3^-$). Measurements of the extracellular electric potentials which are associated with the acidic ($HCO_3^-$) and alkaline ($OH^-$) regions, indicated that, in the presence of control ($+HCO_3^-$) or phosphate-decoupled conditions, normal profiles were established under air, oxygen *or* nitrogen environments. These results indicate that the generation of the control signal(s) is related to events associated with chloroplast electron transport, rather than to changes in the flow or levels of carbon intermediates within the reductive pentose phosphate or photorespiratory cycles. Although the level of oxygen was found to have no effect on the light-induced activation of the $OH^-$ regions, we found that in pure oxygen the dark-induced inactivation of the $OH^-$ efflux system was delayed, and that partial transport function could be maintained in the dark. The possible involvement of changes in either the ratio of oxidized to reduced ferridoxin or $NADP^+$ to NADPH, as part of this light-mediated control signal, is discussed.

*Key words*—*Chara corallina*, plasma membrane transport, $OH^-$ and $HCO_3^-$, regulation.

*Correspondence to: Department of Botany, University of California, Davis, California 95616, U.S.A.*

## INTRODUCTION

Under photosynthesizing conditions, and in the presence of exogenous $HCO_3^-$, the freshwater alga, *Chara corallina*, develops alternating alkaline and acid regions along its internodal cells (Lucas and Smith, 1973; Lucas, 1975). Extracellular electric potential and vibrating probe experiments have shown that the alkaline and acid zones are associated with negative and positive potentials, respectively (Walker and Smith, 1977; Ferrier and Lucas, 1979; Lucas and Nuccitelli, 1980). Initially, these results were interpreted in terms of electrogenic $HCO_3^-$ and $OH^-$ transport systems operating across the *Chara* plasmalemma. However, recent experiments indicate that $HCO_3^-$, *per se*, is not essential for the presence of

© Oxford University Press 1985

these extracellular currents; pH buffers (Hepes, phosphate) can substitute for $HCO_3^-$, once the cell is photosynthetically assimilating exogenous $HCO_3^-$ (Lucas, 1982).

At present, the *Chara* pH banding phenomenon is thought to represent the operation of spatially separated $H^+$ and $OH^-$ efflux systems, with the function of the $H^+$ system being controversial. The involvement of protons in producing $CO_2$ within the unstirred layers (Ferrier, 1980; Walker, Smith, and Cathers, 1980) received little experimental support (Lucas, Keifer, and Sanders, 1983). However, it is not possible to discount the notion that extracellular carbonic anhydrase is involved in mediating the $H^+$-driven production of $CO_2$ within the cell wall or periplasmic space of *Chara* (Price, Badger, Bassett, and Whitecross, 1985). Alternatively, Lucas (1982) and Lucas *et al.* (1983) suggest that the $H^+$ efflux system may drive a $H^+$-$HCO_3^-$ cotransport mechanism which could provide inorganic carbon for photosynthesis (but see also Lucas, 1985).

Irrespective of the actual inorganic carbon species crossing the plasmalemma, activation and operation of the involved transport processes requires light (Lucas, 1975, 1982). The involvement of the chloroplasts and photosynthesis has been established by the sensitivity of the plasmalemma response to photosynthetic inhibitors (Volkov and Petrushenko, 1969; Volkov, 1973; Saito and Senda, 1973*a*, *b*) and the similarity between the action spectra of photosynthesis and the light-induced electrical transients (Walker, 1962; Volkov, 1973).

The nature of the coupling between the chloroplasts and the plasmalemma is still poorly resolved. Hansen (1978, 1980) has used kinetic analysis to help elucidate the components of this system. From these studies it would appear that light acts via three reaction pathways; membrane potential hyperpolarizing and depolarizing pathways and a third pathway that forms a feedback loop. This interpretation is consistent with the light-dark-induced membrane potential transients observed by Lucas (1982), but information on the chemical nature of these signals is still lacking.

Since Lucas (1982) found that $HCO_3^-$ could be removed, once the transport systems had been activated, it would appear that changes in the level of normal products of photosynthesis do not function as components in this control system. In the present study we show that light, *per se*, is not required, but that non-cyclic electron flow through the chloroplasts is essential to maintain normal transport function. Also, using the Ogata (1983) water-film technique, we have established that photorespiration is not involved in producing the light-mediated signals. However, we found that increasing the $O_2$ level serves to slow down the dark-induced deactivation of the transport processes. Under these conditions, we could achieve partial transport activation in the dark.

## MATERIALS AND METHODS

### *Plant material*

Culture material of *Chara corallina* Klein ex Willd., em. R.D.W. (= *C. australis* R.Br.) was grown in the laboratory in 80 $dm^3$ containers in solutions containing (mol $m^{-3}$): 3·0 $Na^+$, 0·2 $K^+$, 0·1 $Ca^{2+}$, 1·5 $Cl^-$ and approximately 2·0 $HCO_3^-$ (pH 9·0–9·5). Cells were illuminated (14 h light) with fluorescent lighting (Sylvania, Lifeline, F) with the intensity at the solution surface being 17–20 W $m^{-2}$. All experiments were performed on mature male internodal cells that were cut from the main axis of the vegetative shoot one or two days prior to being used in an experiment. During this period cells were bathed in an artificial *Chara* pond water (CPW) that contained (mol $m^{-3}$): 2·0 $Na^+$, 0·2 $K^+$, 0·2 $Ca^{2+}$, 1·2 $Cl^-$, 0·2 $SO_4^{2-}$ and 1·0 $HCO_3^-$ (pH 8·2). The illumination and photoperiod was identical to that used for the cultures, except that the intensity was reduced to 10 W $m^{-2}$.

Unless otherwise indicated, all experiments were conducted at 25 ± 1 °C under a photosynthetically saturating light intensity (16–20 W $m^{-2}$). When lower light intensities were required, the output of the Leitz Pradovit projector (Model C1500, 150 W quartz-iodide lamp) was further attenuated using neutral density filters (Balzers, Type No. 106613).

*Electrophysiological measurements*

Membrane potential measurements were made using the equipment, electrodes, and methods of Keifer and Lucas (1982) and Lucas (1982). In some experiments, '$HCO_3^-$-free' CPW solutions were employed. The 1·0 mol $m^{-3}$ $NaHCO_3$ was replaced by 1·0 mol $m^{-3}$ $Na_2HPO_4$ and the medium bubbled for 1 h with $CO_2$-free air before adjusting the pH to 8·2 with freshly prepared 100 mol $m^{-3}$ NaOH. The solution was then further bubbled for at least 1 h before being used in an experiment: $CO_2$-purging was continued during the experiment.

*Water-film technique*

The spatial variation of the membrane electric potential along the *C. corallina* internodal cells was measured using the modified loop-electrode water-film technique developed by Ogata (1983; see also Ogata, Chilcott, and Coster, 1983). In brief, two internodal cells, in series, were held vertically within a humidity chamber such that the lower portion (approximately 5·0 mm) of the test cell dipped into CPW (containing 0·01% of Tween-80) and most of the upper cell was sealed into a silicon rubber cup which acted as a reservoir for CPW. The CPW in this reservoir contained 20 mol $m^{-3}$ $K_2SO_4$ which was included to open the $K^+$ channels in the plasmalemma of the upper cell (Keifer and Lucas, 1982). With the $K^+$ channels opened, the membrane has a very high conductance and, in the presence of 40 mol $m^{-3}$ $K^+$, the membrane potential of this cell is close to zero. Electrical contact with the external surface of the lower cell was achieved by using an agar-encased (3% w/v in CPW) loop of Ag/AgCl wire; withdrawing the loop from the lower CPW reservoir produced a thin film of solution that formed a bridge from the cell to the agar surface of the loop. A constant bipolar sinusoidal current ($2·0 \times 10^{-8}$ Amp, 1·0 Hz) was injected from this loop electrode to an Ag/AgCl electrode positioned in the lower CPW reservoir; this allowed the measurement of membrane conductance as a function of position along the *Chara* cell. Potential measurements were made between two micropipette electrodes ($2 \times 10^2$ mol $m^{-2}$ KCl in 3% agar) with one being positioned in the agar of the wire loop and the other in the CPW of the upper reservoir. A motor-driven micromanipulator was used to move the loop electrode up and down the cell.

The solution within the lower reservoir contained (mol $m^{-3}$): 2·0 $Na^+$, 0·2 $K^+$, 0·2 $Ca^{2+}$, 1·2 $Cl^-$, 0·2 $SO_4^{2-}$ and 1·0 $HCO_3^-$ (pH 9·2) and could be exchanged via a three-way valve mechanism. In addition, the level of this reservoir could be raised to an extent that almost all of the lower cell was submerged in solution. This allowed us to establish a control photosynthetic condition, on each specimen, before commencing the 'open-circuit' or low electrical shunt experiments. The composition of the gas phase was also manipulated via an inlet port that delivered the humidified gas stream to a position just above the surface of the lower CPW reservoir. Under control conditions, humidified air (supplied from a compressed air cylinder) was passed through the chamber; in some experiments the influence of pure (humidified) $N_2$ or $O_2$ was investigated.

## RESULTS

*Inhibition of chloroplast electron transport*

Lucas (1982) showed that a hyperpolarizing response of the membrane potential could be elicited by transferring the *C. corallina* cell from conditions of saturating light intensity (20 W $m^{-2}$) to low intensities (2·0 W $m^{-2}$). This suggested that a change in the rate of a photosynthetic process was involved in controlling membrane transport of $H^+$ and $OH^-$ efflux. In the present study we examined the influence of a range of DCMU concentrations on the membrane potential. Figure 1 indicates that the initial rate and the actual degree of hyperpolarization of the membrane potential increased in the presence of higher DCMU concentrations. When 10 mmol $m^{-3}$ DCMU was employed, the potential hyperpolarized more rapidly than the dark-induced response, although the extent of the response was the same. Removal of DCMU from the medium resulted in a rapid depolarization of the potential, but the return to the resting potential was quite complex in its form. The membrane potential also became insensitive to light–dark transitions following a 30 min pretreatment with 10 mmol $m^{-3}$ DCMU (Fig. 1).

Experiments conducted using phosphate-decoupled ($-HCO_3^-$) cells indicated that the normal control signals functioned in the absence of exogenous $HCO_3^-$. Under these conditions, DCMU elicited an identical hyperpolarizing response to that obtained by

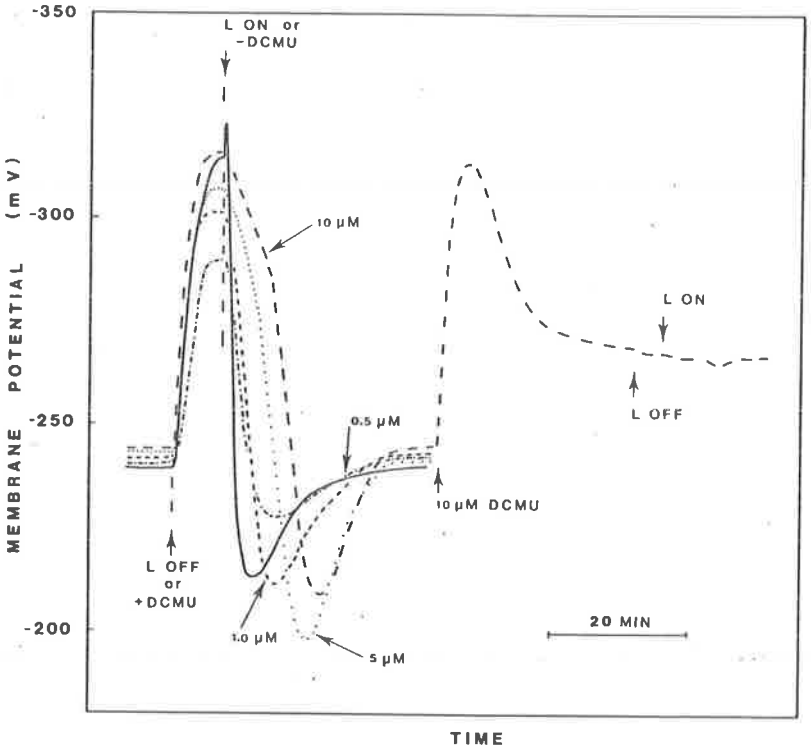


FIG. 1. Response of the *Chara* membrane potential to various concentrations of DCMU and to short dark periods. Experiments were conducted under a light intensity of 20 W $m^{-2}$. (Symbol L represents light.)

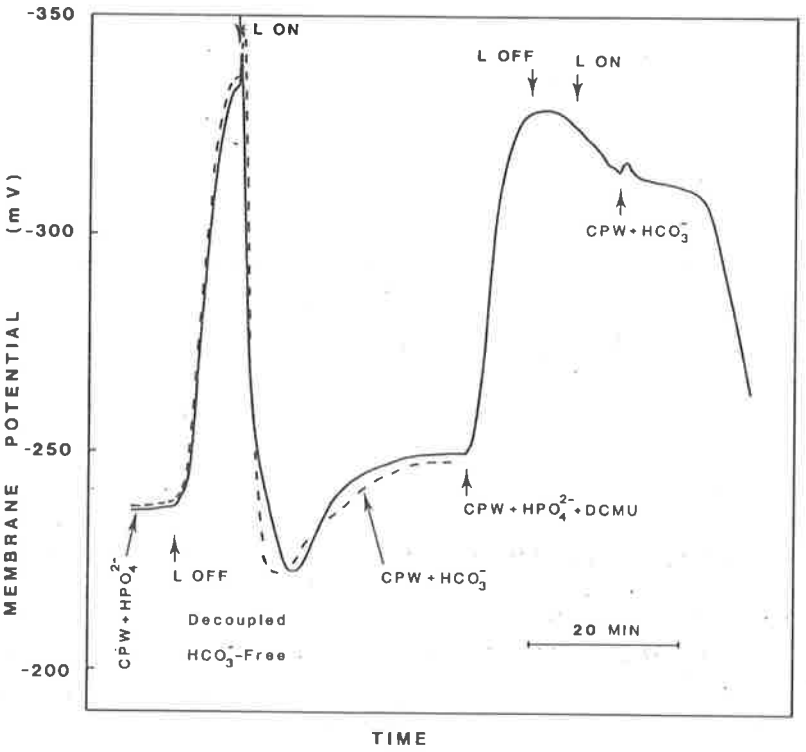


FIG. 2. Effect on the *Chara* membrane potential of 10 mmol $m^{-3}$ DCMU when applied to phosphate-decoupled cells. The following pretreatments were conducted on each cell prior to DCMU application. Control responses to light/dark transitions were obtained in the presence of CPW that contained 1·0 mol $m^{-3}$ $NaHCO_3^-$, pH 8·2 (---). A $HCO_3^-$-free CPW bathing medium was then introduced which contained 1·0 mol $m^{-3}$ $Na_2HPO_4$, pH 8·2 (phosphate-decoupled), and their response to light/dark transitions were recorded prior to applying 10 mmol $m^{-3}$ DCMU. (L represents light).

turning off the light (Fig. 2). This suggests that the generation of the control signals is related to chloroplast electron transport, rather than to changes in the flow of products within the reductive pentose phosphate cycle. Removal of DCMU from phosphate-decoupled cells did not result in an immediate depolarization of the membrane potential, but following a lag period of approximately 10 min the potential began to depolarize in the expected manner (cf. Figs 1 and 2). Repeated DCMU or light off/on treatments on these decoupled cells indicated that the control signals were stable under these conditions (data not shown); it was only the reactivation of the depolarizing signal that appeared to be affected.

*Water-film electrode experiments*

Photorespiration would still be occurring in *Chara* cells that had been phosphate-decoupled. Indeed, the atmospheric levels of $O_2$ and the dramatic reduction in the inorganic

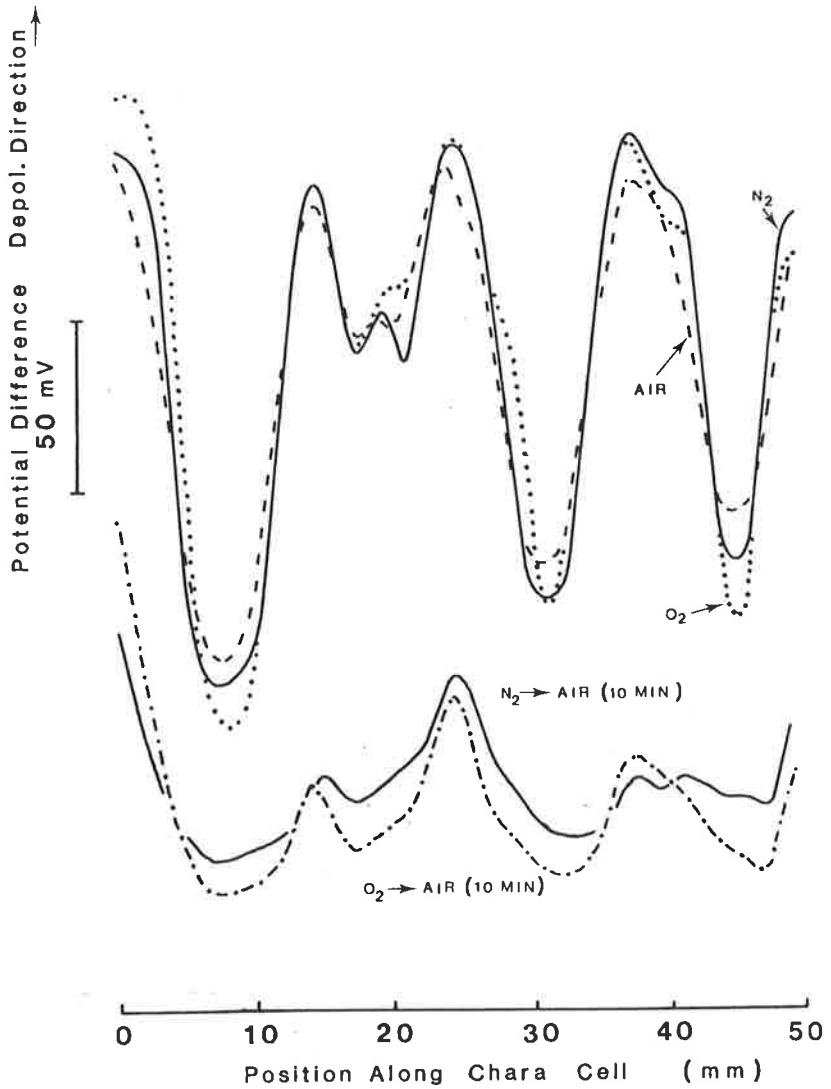


FIG. 3. Extracellular electric potentials measured along a *Chara* internodal cell using the Ogata (1983) water-film technique. The peaks in the depolarizing and hyperpolarizing directions represent the centres of the alkaline and acid bands, respectively. The electric potential profiles were obtained while the *Chara* cell was exposed to an atmospheric environment of firstly air, then pure nitrogen, followed by pure oxygen. The lower profiles were recorded 10 min after the gas phase flowing past the cell was changed from either oxygen or nitrogen back to normal air.

carbon supply would favour this process. We used the Ogata water-film technique (Ogata, 1983; Ogata *et al.*, 1983) to investigate the possible involvement of the photorespiratory pathway in signal generation. (This system was selected because of the ease with which the gaseous environment of the cell could be manipulated.) Control experiments were conducted with the *Chara* internodal cell being suspended in air. Upon stabilization of the external electric potential profiles, the inflowing gas stream was switched to humidified pure nitrogen. Under these conditions, photorespiration should cease, however, as evidenced by the lack of change in the external electric potential profile, there appeared to be no change in activity of the plasmalemma transport systems (Fig. 3). Stable external electric potential profiles could be obtained under air, or either pure nitrogen or oxygen. However, in either air, oxygen or nitrogen, introduction of 1·0 mmol $m^{-3}$ DCMU always caused the dissipation of these electric potential profiles (data not shown).

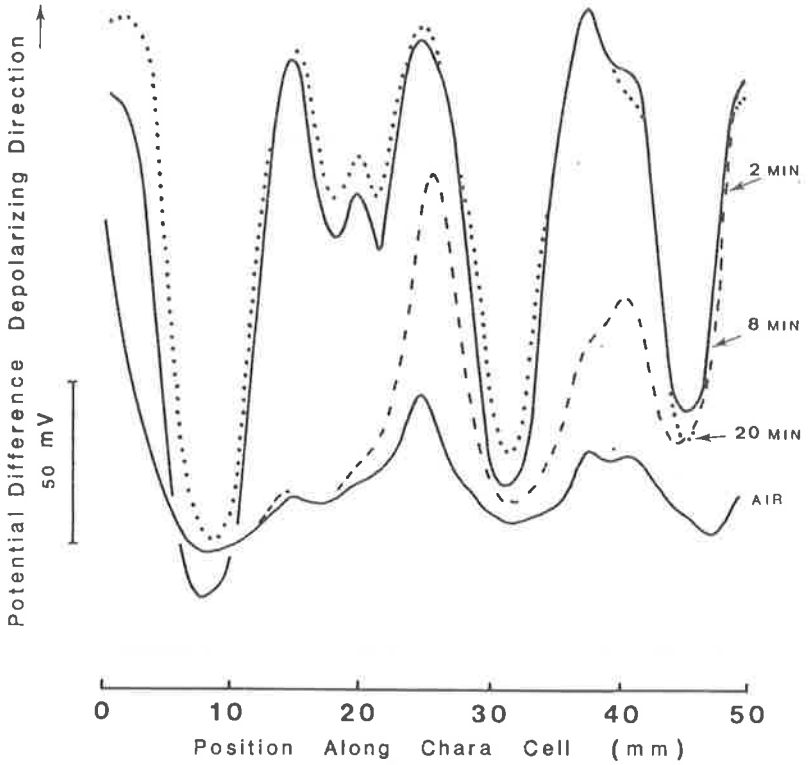


FIG. 4. Time-dependent recovery of the extracellular electric potential profile along a *Chara* internodal cell following the cell's return to an oxygen environment. These results were obtained on the same cell as used for the experiments presented in Fig. 3. After monitoring (for 30 min) the oxygen-to-air associated perturbation of the electric potential profile, the gas stream was switched back to pure oxygen and the recovery of the profile was recorded after 2, 8 and 20 min.

Although stable electric potential profiles could be obtained when the atmosphere was changed from oxygen to nitrogen, and *vice versa*, returning the cells to normal air almost always resulted in a pronounced reduction in the magnitude of the external electric potential profiles. A typical response is presented in Fig. 3. This apparent inhibition of membrane transport was not relieved with time in air. However, immediately the cell was returned to either an oxygen or a nitrogen environment the external electric potential profiles began to return to the 'control' pattern and values. As illustrated in Fig. 4, this reactivation was rapid, requiring less than 8 min for full recovery.

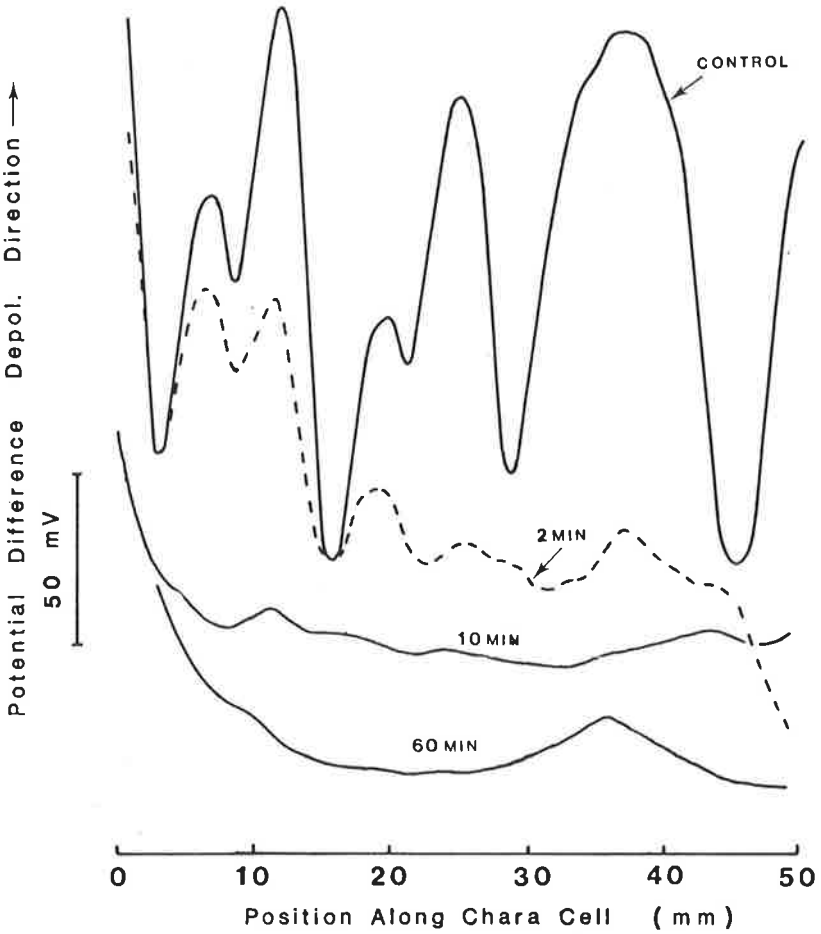


FIG. 5. Decay of the extracellular electric potential profile upon transferring the *Chara* internodal cell to darkness. Control profile was measured immediately before the light was switched off. Profiles presented were measured 2, 10, and 60 min after the cell was placed in the dark.

*Delay in dark-induced inactivation of transport by oxygen*

Lucas (1975) showed that the light-induced activation of the $OH^-$ transport system is complex and involves some form of threshold phenomenon. On the other hand, the deactivation of a particular $OH^-$ band appeared to be dependent only upon the available level of exogenous $HCO_3^-$ and the light intensity. Our initial experiments, therefore, were aimed at maintaining transport activity in the dark.

Ogata (1983) previously found that for cells being examined by the water-film technique, the complete dark-induced deactivation took much longer (40–60 min) than the 3–6 min usually observed for cells immersed in experimental medium (Lucas, 1982). However, in the present experiments, control (air-bathed) cells took less than 10 min in the dark to deactivate the $H^+$- and $OH^-$-associated transport systems (Fig. 5). The same time course for dark-induced deactivation was observed when cells were exposed to pure nitrogen (data not shown). When air was replaced by oxygen, not only was the deactivation process slowed down, but as shown in Fig. 6, partial recovery of the extracellular electric potential profile was observed. Within 60 min in the dark, a stable oxygen-mediated transport system was established.

In the light ($O_2$ atmosphere) the conductance values in the centres of the $OH^-$ and $H^+$ regions were 4·4 and 0·9 S $m^{-2}$, respectively. After 60 min in the dark the values in the $OH^-$

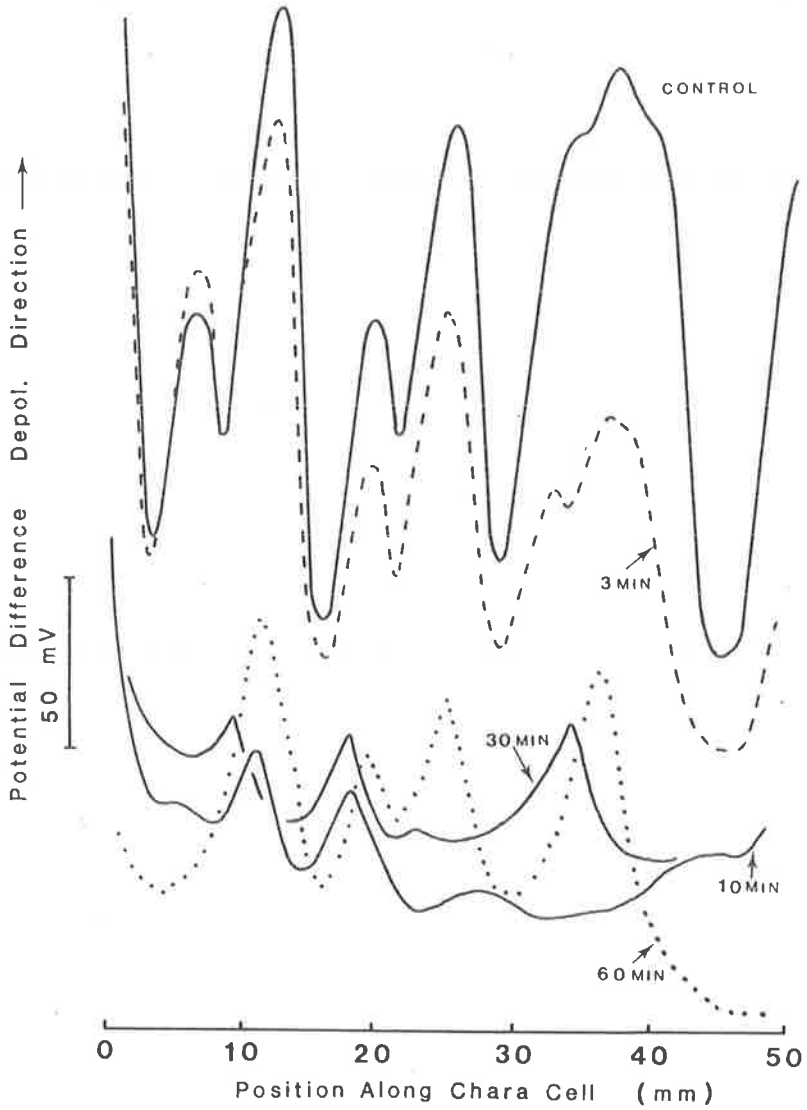


FIG. 6. Influence of an oxygen environment on the dark-induced decay of the extracellular electric potential profile. Data were obtained on the same cell as used in the experiments presented in Fig. 5. Control trace was measured after the cell had been exposed to an oxygen environment for 1 h; the light was then switched off and the change in profiles monitored. Profiles after 3, 10, 30 and 60 min in the dark have been presented. (Other details as in Fig. 5.)

and $H^+$ centres were 0·27 and 0·15 S $m^{-2}$, respectively for the oxygen experiment (Fig. 6) and 0·11 and 0·15 S $m^{-2}$, respectively for the dark control (Fig. 5).

Since oxygen appears to influence the deactivation process, we investigated its effect on the light-induced activation phenomenon. Lucas (1975) established that a relationship exists between light intensity and the lag period which occurs prior to $OH^-$ efflux activation. The critical light intensity can be deduced from this relationship; i.e., the intensity at which the $OH^-$ system will never activate. Light intensity experiments using the water-film technique indicated that the same phenomenon was present in air-suspended cells with the critical light intensity being in the range of 0·6–0·8 W $m^{-2}$.

Our approach in these experiments was to determine whether the critical light intensity could be lowered in the presence of $O_2$. Having determined this value in nitrogen, the cell under study was given a 60 min dark treatment and then illuminated with this intensity for

30–60 min to establish that activation could not occur. The nitrogen was then replaced by oxygen and the electric potentials were monitored in a routine manner. If the activation curve had been displaced to lower intensities by an oxygen environment, the $OH^-$ transport system should have activated within a short time (see Figs 5 and 6 of Lucas, 1975). In no experiment of this nature did we ever observe activation, but raising the intensity above the critical value resulted in the development of normal external electric potential profiles (data not shown).

## DISCUSSION

### *Light-mediated control signals*

The results using DCMU, and in particular those with phosphate-decoupled ($-HCO_3^-$) cells, indicate that membrane transport control, in *Chara* in the light, is via electron transport and not by modulation of carbon intermediates of the reductive pentose phosphate cycle. In the presence of low concentrations of DCMU (0·1–1·0 mmol $m^{-3}$), cyclic photophosphorylation can still occur and so, although $CO_2$ fixation is reduced, ATP levels do not decline (Keifer and Spanswick, 1979). Thus, since the same basic hyperpolarizing response was obtained in the presence of 0·5, 1·0, 5·0 and 10 mmol $m^{-3}$ DCMU, it would appear that changes in the stromal ATP content are unlikely to be involved in this signalling process.

In addition, the extracellular electric potential profiles, which reflect the transport of $H^+$ and $OH^-$ across the plasmalemma, did not change when oxygen was replaced with nitrogen in the experimental system. This indicates that photorespiratory substrates are also unlikely to be involved in the process of transport regulation.

It is well recognized that light modulation of post-transcriptional chloroplast enzymes is a complex phenomenon and involves numerous enzymes. In most of these activation processes light is thought to act via a redox reaction involving ferredoxin/thioredoxin (Anderson, Mohamed, Ashton, Scheibe, Brennan, and Ben-Bassat, 1981; Buchanan, 1980). However, as pointed out by Buchanan (1980), little is known about the processes involved in deactivation of these regulatory enzymes. It could be that a reduction in either the ratio of reduced to oxidized ferridoxin or $NADPH/NADP^+$, or both, may be involved. The hyperpolarizing response elicited by DCMU may be explicable in these terms, since it blocks non-cyclic electron flow, and this would cause a decline in the production of reduced ferredoxin and NADPH.

The involvement of $NADP^+$, as a component in the signalling system, would be consistent with recent findings on $HCO_3^-$ transport into cyanobacteria. Ogawa, Omata, Miyano, and Inoue (1985) found that DCMU blocked $HCO_3^-$ uptake into *Anacystis nidulans*, but in the presence of iodoacetamide (a specific inhibitor of $CO_2$ fixation; see Calo and Gibbs, 1960) and DCMU, $HCO_3^-$ uptake still occurred. They showed that uptake was correlated with the levels of $NADP^+$, which were high in both darkness and in the presence of DCMU, and low in the light and in the presence of iodoacetamide plus DCMU. Ogawa *et al.* (1985) concluded that in *A. nidulans*, $HCO_3^-$ uptake may be driven by ATP, but that this process only occurs when the $NADPH/NADP^+$ ratio is high.

The biochemical mechanism(s) by which such changes in the $NADPH/NADP^+$ ratio could be transduced to modulate $OH^-$ and $H^+$ transport across the plasmalemma are at present unknown. However, numerous possibilities exist, and it may be that enzymes like phosphofructokinase, which are activated under reduced levels of NADPH (Cséke, Nishizawa, and Buchanan, 1982), could function even when *Chara* cells have been deprived of a $CO_2$ source for photosynthesis (Fig. 2). One approach to elucidating the processes

involved would be to focus on chloroplastic and cytosolic enzyme/substrate changes that occur following the removal of DCMU. Since the lag phase, prior to transport reactivation, is greater and more pronounced in phosphate-decoupled cells (Fig. 2), this system would be most suitable for the initial studies.

*Transport perturbation following oxygen or nitrogen pretreatment*

Stable extracellular electric potential profiles could be observed when *Chara* cells were exposed to air, oxygen or nitrogen. In these water-film experiments, the bathing medium in the lower reservoir contained 1·0 mol $m^{-3}$ $NaHCO_3^-$ (pH 9·2) and saturating light intensities were employed. Thus, even though $CO_2$ was excluded from the atmosphere in the oxygen and nitrogen experiments, dissolved inorganic carbon was still being supplied via the moving water film and so photosynthetic activity would have continued under all conditions. Consequently, it is difficult to explain why the *Chara* cell deactivated its transport systems when its was returned to air, following pretreatment in either oxygen or nitrogen.

Clearly, the perturbative signal must be associated with the transition from oxygen (or nitrogen) to air, since air, *per se*, provides a suitable environment for transport function. Since both the oxygen and nitrogen atmospheres were $CO_2$-free, it may be the return of gaseous $CO_2$ that acts to disturb the transport signals. It seems unlikely that this level of $CO_2$ could supply sufficient inorganic carbon for photosynthesis to eliminate the physiological need for a $HCO_3^-$ transport mechanism. If this were the case, the transport systems would have deactivated when the cell was first exposed to air. The putative $CO_2$ effect, therefore, would more likely be due to a $CO_2$ pulse perhaps affecting a regulatory process at the plasmalemma.

A further interesting feature of these results was that once transport function was perturbed, it remained in this state until the *Chara* cell was re-exposed to either oxygen or nitrogen (Fig. 4). We will further examine this phenomenon by conducting experiments in which we will use air that contains various levels of $CO_2$.

*Oxygen affects membrane transport deactivation*

Although we could find no effect of an oxygen environment on the light-dependent activation of the $OH^-$ and $HCO_3^-$-associated transport processes, we did find that oxygen delayed the dark-induced deactivation (Fig. 6). Indeed, oxygen actually prevented *full* dark-induced deactivation from occurring. After a 60 min dark treatment, in the presence of oxygen, the magnitude of the extracellular potentials was still as large, or larger, than those previously reported by Ogata (1983) and Ogata *et al.* (1983) for illuminated *Chara* cells. In their studies, the magnitude of the resting potential, measured in the acidic regions, was generally below −240 mV, which is much smaller than that routinely recorded in the present study; i.e., larger than −300 mV. The difference in the culture material, which presumably is reflected in this difference in membrane potential recorded across the plasmalemma, is also the cause of the observed differences between the measured external electric potential profiles. However, the magnitude of our potential profiles established in the dark, under oxygen, were still only 42% of the values established in the light. In addition, membrane conductance measurements indicated that in the presence of oxygen, the normal dark-induced decrease in conductance was only slightly affected in the $OH^-$ bands (cf. 0·27 and 0·11 S $m^{-2}$ for oxygen and air, respectively) while in the acidic regions the membrane conductance decreased to the *same* value (0·15 S $m^{-2}$). These results indicate that enhanced levels of oxygen can, in some way, prevent the complete dark-induced decay of a cytosolic constituent (signal?) that is essential for transport function. However, the conductance results indicate that oxygen, alone, cannot prevent the dark-induced decrease in membrane

conductance. In future experiments, perfused *Chara* cells will be used in our attempt to elucidate the putative chloroplast signals.

Our present results are encouraging for, although they illustrate the complexity of the regulatory processes involved in controlling plasmalemma transport, they suggest that with further work we may eventually be able to completely override the control that the chloroplasts have on *Chara* transport processes. Such a 'chloroplast-decoupled' system would permit the biophysical characterization of the $OH^-$ and $HCO_3^-$ ($H^+$)-associated transport systems without the problems of the complexity introduced by cellularly-mediated kinetic control.

## ACKNOWLEDGEMENTS

This research was supported by National Science Foundation Grant PCM 81-17721. We would also like to thank David Deamer and Richard Nuccitelli of the Zoology Department, University of California, Davis, for the loan of electronic and data recording equipment.

## LITERATURE CITED

ANDERSON, L. E., MOHAMED, A. H., ASHTON, A. R., SCHEIBE, R., BRENNAN, T., and BEN-BASSAT, D., 1981. Light modulation: the light effect mediator (LEM) system. In *Photosynthesis. IV. Regulation of carbon metabolism.* Ed. G. Akoyunoglou. Balaban International Science Services, Philadelphia. Pp. 293-302.

BUCHANAN, B. B., 1980. Role of light in the regulation of chloroplast enzymes. *Annual Review of Plant Physiology*, **31,** 341-74.

CALO, N., and GIBBS, M., 1960. The site of inhibition of iodoacetamide in photosynthesis studied with chloroplasts and cell-free preparations of spinach. *Zeitschrift für Naturforschung*, **156,** 287-91.

CSÉKE, C., NISHIZAWA, A. N., and BUCHANAN, B., 1982. Modulation of chloroplast phosphofructokinase by NADH: A mechanism for linking light to the regulation of glycolysis. *Plant Physiology*, **70,** 658-61.

FERRIER, J. M., 1980. Apparent bicarbonate uptake and possible plasmalemma proton efflux in *Chara corallina.* Ibid. **66,** 1198-9.

——and LUCAS, W. J., 1979. Plasmalemma transport of $OH^-$ in *Chara corallina.* II. Further analysis of the diffusion system associated with $OH^-$ efflux. *Journal of Experimental Botany*, **30,** 705-18.

HANSEN, U.-P., 1978. Do light-induced changes in the membrane potential of *Nitella* reflect the feedback regulation of a cytoplasmic parameter? *Journal of Membrane Biology*, **41,** 197-224.

——1980. Homeostasis in *Nitella*: Adaptation of $H^+$ transport to the photosynthetic load. In *Plant membrane transport: current conceptual issues.* Eds R. M. Spanswick, W. J. Lucas and J. Dainty. Elsevier/North Holland Biomedical Press, Amsterdam. Pp. 587-8.

KEIFER, D. W., and LUCAS, W. J., 1982. Potassium channels in *Chara corallina*: Control and interaction with the electrogenic $H^+$ pump. *Plant Physiology*, **69,** 781-8.

——and SPANSWICK, R. M., 1979. Correlation of adenosine triphosphate levels in *Chara corallina* with the activity of the electrogenic pump. Ibid. **64,** 165-8.

LUCAS, W. J., 1975. The influence of light intensity on the activation and operation of the hydroxyl efflux system of *Chara corallina. Journal of Experimental Botany*, **26,** 347-60.

——1982. Mechanism of acquisition of exogenous $HCO_3^-$ by internodal cells of *Chara corallina. Planta*, **165,** 181-92.

——1985. Bicarbonate utilization by *Chara*: A re-analysis. In *Inorganic carbon uptake by aquatic photosynthetic organisms.* Eds W. J. Lucas and J. A. Berry. American Society of Plant Physiologists Monograph Series, Rockville. Pp. 229-54.

——KEIFER, D. W., and SANDERS, D., 1983. Bicarbonate transport in *Chara corallina*: Evidence for cotransport of $HCO_3^-$ with $H^+$. *Journal of Membrane Biology*, **73,** 263-74.

——and NUCCITELLI, R., 1980. $HCO_3^-$ and $OH^-$ transport across the plasmalemma of *Chara corallina*: Spatial resolution obtained using extracellular vibrating probe. *Planta*, **150,** 120-31.

——and SMITH, F. A., 1973. The formation of alkaline and acid regions at the surface of *Chara corallina* cells. *Journal of Experimental Botany*, **24,** 1-14.

OGATA, K., 1983. The water-film electrode: A new device for measuring the characean electro-potential and -conductance distributions along the length of the internode. *Plant and Cell Physiology*, **24,** 695-703.

OGATA, K., CHILCOTT, T. C., and COSTER, H. G. L., 1983. Spatial variation of the electrical properties of *Chara australis*. I. Electrical potentials and membrane conductance. *Australian Journal of Plant Physiology*, **10,** 339–51.

OGAWA, T., OMATA, T., MIYANO, A., and INOUE, Y., 1985. Photosynthetic reactions involved in the $CO_2$-concentrating mechanism in the cyanobacterium, *Anacystis nidulans*. In *Inorganic carbon transport by aquatic photosynthetic organisms*. Eds W. J. Lucas and J. A. Berry. American Society of Plant Physiologists Monograph Series, Rockville. Pp. 287–304.

PRICE, G. D., BADGER, M. R., BASSETT, M. E., and WHITECROSS, M. I., 1985. Involvement of plasmalemmasomes and carbonic anhydrase in photosynthetic utilization of bicarbonate in *Chara corallina*. *Australian Journal of Plant Physiology*, (In press.)

SAITO, K., and SENDA, M., 1973*a*. The light-dependent effect of external pH on the membrane potential of *Nitella*. *Plant and Cell Physiology*. **14,** 147–56.

——— 1973*b*. The effect of external pH on the membrane potential of *Nitella* and its linkage to metabolism. Ibid. **14,** 1045–52.

VOLKOV, G. A., 1973. Bioelectrical response of the *Nitella flexilis* cell to illumination: A new possible state of plasmalemma in a plant cell. *Biochimica et biophysica acta*, **314,** 83–92.

——and PETRUSHENKO, V. V., 1969. Studies of the resting potential of a single cell of the alga *Nitella flexilis*. IV. The correlation between the cell response to light and the photosynthesis process. *Tsitologiya*, **11,** 1007–13.

WALKER, N. A., 1962. Effect of light on the plasmalemma of *Chara* cells. *Annual Report of Division of Plant Industry, CSIRO*. Pp. 80.

——and SMITH, F. A., 1977. Circulating electric currents between acid and alkaline zones associated with $HCO_3^-$ assimilation in *Chara*. *Journal of Experimental Botany*, **28,** 1190–1206.

——— and CATHERS, I. R., 1980. Bicarbonate assimilation by fresh-water charophytes and higher plants. I. Membrane transport of bicarbonate ions is not proven. *Journal of Membrane Biology*, **57,** 51–8.

PHYSIOL. PLANT. 65: 539–543. Copenhagen 1985



# Inorganic carbon transport in aquatic photosynthetic organisms

**William J. Lucas and Joseph A. Berry**

Lucas, W. J. and Berry, J. A. 1985. Inorganic carbon transport in aquatic photosynthetic organisms. – Physiol. Plant. 65: 539–543.

*Additional key words* – Aquatic angiosperms, macroalgae, microalgae.

*W. J. Lucas (reprint requests), Dept of Botany, Univ. of California, Davis, CA 95616, USA, and J. A. Berry, Dept of Plant Biology, Carnegie Institution of Washington, Stanford, CA 94305, USA.*

## Introduction

Carbon dioxide is an obligatory intermediate in the fixation of inorganic carbon by photosynthetic organisms, since this is the substrate for the RuBP carboxylase reaction. Terrestrial plants obtain $CO_2$ directly from the atmosphere, but aquatic photosynthetic organisms must obtain their $CO_2$ from the dissolved inorganic carbon in the surrounding water. Bicarbonate, rather than $CO_2$, is usually the major form of dissolved inorganic carbon (DIC). Even if the equilibrium concentration of $CO_2$ were adequate, diffusion of $CO_2$ in water is much slower than in air, and the interconversion of $CO_2$ and other forms of DIC, in the absence of carbonic anhydrase (CA), is so slow that these may restrict the supply of $CO_2$ if its rate of uptake is rapid. (Note: CA catalyzes the interconversion of $CO_2$ and $H_2CO_3$: $CO_2 + H_2O \rightleftharpoons H_2CO_3$; the dissociation of $H_2CO_3$ to $HCO_3^-$ and $H^+$ is extremely rapid). All of these factors complicate inorganic carbon uptake in aqueous media, and aquatic organisms (cyanobacteria, microalgae, macroalgae and aquatic angiosperms) have evolved physiological specializations adapting them to obtain $CO_2$ for photosynthesis from their environments.

Active transport of DIC across cellular membranes and the enzyme CA, that speeds interconversion of $CO_2$ and other forms of DIC, play important roles in these processes. The mechanism(s) of DIC uptake of some aquatic organisms results in a high apparent affinity for $CO_2$, reduced photorespiration and a low $CO_2$ compensation point, giving them functional similarities to $C_4$ species of terrestrial higher plants. The DIC transport mechanism(s), like the $C_4$ mechanisms, may have important implications for improving plant performance under $CO_2$-limiting conditions.

The question of whether certain photosynthetic aquatic organisms can utilize exogenous $HCO_3^-$, as well as $CO_2$, has been the subject of considerable research. Progress in this field was recently reviewed (Lucas 1983) and the topic was also the subject of a recent international workshop (Lucas and Berry 1985). In the following sections we will show that, although the phenomenon of DIC utilization is well established, there is still considerable controversy with respect to both the chemical species that crosses the plasma membrane and the mechanism(s) used.

*Abbreviations* – CA, carbonic anhydrase; DIC, dissolved inorganic carbon; HEPES, N-2-hydroxyethylpiperazine-N'-2-ethanesulfonic acid; RuBP, ribulose-1,5-bisphosphate.

## Microalgae and cyanobacteria

We will first deal with some important features illustrated by the cyanobacteria and microalgae *before* we discuss the macroalgae and aquatic angiosperms. We do this because recent studies with these organisms have illustrated certain important features associated with utilization of exogenous DIC by photosynthetic aquatic organisms.

When a culture of microalgae is transferred from high-$CO_2$ (5%) to low $CO_2$ (0.03%) growth conditions, the rate of photosynthesis is strongly depressed, but

Received 12 August 1985

over several hours the culture adapts to these conditions in such a way as to permit the cells to re-establish a high photosynthetic rate in the presence of low $CO_2$. Low $CO_2$-adapted cells have many similarities to $C_4$ plants. In Österlind's (1951) pioneering studies on the low $CO_2$-associated induction of photosynthesis in *Scenedesmus*, he concluded that "the factor to be activated is either connected to the absorption of bicarbonate ions or is carbonic anhydrase." Some 30 years later we now know that *both* CA and inorganic carbon transport across the plasma membrane (or across the chloroplast envelope, as thought by some workers) are involved in the expression of the induction phenomenon.

#### Induction of DIC transport by low $CO_2$ conditions

A group at the Carnegie Institution (Stanford, CA, USA) investigated this adaptation phenomenon in two organisms [a microalga, *Chlamydomonas reinhardtii* (Badger et al. 1978) and a blue-green alga (a cyanobacterium) *Anabaena variabilis* (Kaplan et al. 1980)] by using the silicone oil centrifugation technique. As with plant organelles, very small algal cells were incubated in a small volume of reaction medium containing $H^{14}CO_3^-$ and then separated from the medium, rapidly, by centrifugation through a silicone oil layer, into a "killing" medium. Analysis of the concentration of $^{14}C$-labelled DIC (acid-labile) and fixed carbon (acid-stable) contained within these adapted cells revealed that the internal DIC concentration was much higher than in non-adapted cells, or that present in the incubation medium. Also, by measuring the internal or cytoplasmic pH of *C. reinhardtii* it was possible to calculate that the low $CO_2$-grown cells could concentrate $CO_2$ up to 40-fold, in relation to that which would be in passive equilibrium with the bathing medium. High $CO_2$-grown cells lacked the ability to concentrate $CO_2$; in these cells the internal $CO_2$ concentration was in passive equilibrium with the bathing medium (Badger et al. 1980).

From kinetic studies of the rate of photosynthesis and the rate at which $CO_2$ could be formed from $HCO_3^-$ (in the absence of CA), Miller and Colman (1980) concluded that the $CO_2$-concentrating ability was associated with an increased capacity of these microalgal cells to utilize exogenous $HCO_3^-$. These observed accumulation ratios could be caused by facilitated diffusion of $HCO_3^-$ across the plasma membrane (e.g., down an electrochemical gradient). However, as pointed out by Kaplan et al. (1980), the accumulation observed in *Anabaena* would require a potential of +150 mV (inside positive). During $HCO_3^-$ assimilation the membrane potential in *A. variabilis* is approximately – 100 mV (Kaplan et al. 1982). Negative membrane potentials are a common feature of plant cells, and thus, it seems reasonable to conclude that there is an *active* $HCO_3^-$ transport system. Indeed, Badger et al. (1978) showed that the accumulation of intracellular DIC was sensitive to a number of metabolic inhibitors. Elegant studies, conducted by Ogawa et al. (1985) on *Anabaena* and *Anacystis* (both cyanobacteria), have provided evidence that the DIC transporting system of the cyanobacteria may be linked, in an energetic sense, to cyclic electron flow driven by photosystem I. Although they obtained contradictory results with respect to the involvement of ATP, their findings were consistent with a complex interaction between the thylakoid and plasma membranes; the ratio of $NADP^+$/NADPH may be involved in a regulating capacity.

At this point it is important to mention that many recent results indicate a more complex situation for some of the unicellular systems that possess the DIC accumulating mechanism. For the cyanobacteria, Kaplan (1985, and references therein) has presented evidence that in *A. variabilis* there may be a carrier in the plasma membrane that binds both $CO_2$ *and* $HCO_3^-$. Consistent with this is the finding that internal DIC in *Synecoccus* spp. (another cyanobacterium) accumulates at a faster rate when exogenous $CO_2$, rather than $HCO_3^-$, is given at the same concentration (Badger and Andrews 1982). In the microalgae, Tsuzuki et al. (1985) showed very conclusively, using the isotopic disequilibrium approach, that at neutral pH *Chlorella vulgaris* 11h (the term 11h here denotes a particular genotype) accumulates DIC when either $CO_2$ or $HCO_3^-$ is supplied. *However,* in their particular microalgal species, exogenous $CO_2$ was the preferred substrate for DIC accumulation. These results, and those of other laboratories, have forced workers in this field to re-evaluate the concept of a molecular $CO_2$ transporting system. If such a system exists, it would be very interesting to see what strategies have been adopted to limit the back diffusion, or leakage of the transported $CO_2$, since membranes normally have a high passive permeability to this form of inorganic carbon.

#### Carbonic anhydrase induction by low $CO_2$ conditions

The activity of CA may increase many fold during the adaptation of microalgae to low $CO_2$-growth conditions (Coleman et al. 1984, and references therein). The inducible protein associated with this activity in *C. reinhardtii* has been identified, and its major CA location in these cells is within the periplasmic space (i.e., the space between the plasma membrane and the cell wall; Coleman and Grossman 1984, Miyachi et al. 1985). Translatable RNA for CA is found only in induced cells, and the primary translation product has a higher molecular weight than the mature polypeptide (Coleman and Grossman 1984). Molecular analysis of the induction of CA may reveal how the gene encoding CA is activated under low $CO_2$ growth conditions. Indeed, similar approaches may also lead to identification of the inducible components of the DIC transport system.

The presumed function of CA is to facilitate the production of $CO_2$ from $HCO_3^-$ at the site of the RuBP carboxylase reaction (see Fig. 1). Miyachi et al. (1985 and

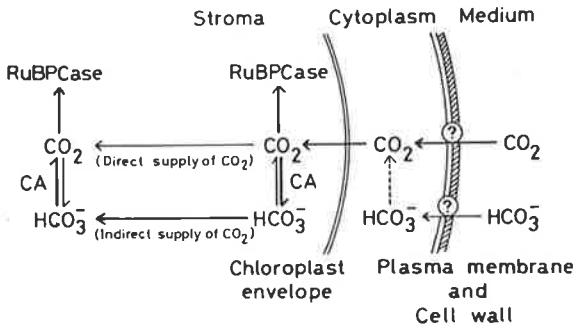


Fig. 1. Direct and indirect supply of $CO_2$ to RuBP carboxylase of microalgae. Circles with question marks represent hypothetical DIC transport systems and sites of carbonic anhydrase activity are marked by CA. From Miyachi et al. (1985) with permission.

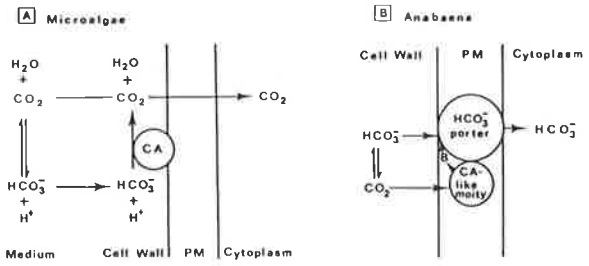


Fig. 2. Possible roles of extracellular CA in DIC acquisition. A, Proposed by Miyachi et al. (1985) for microalgae; B, proposed by Kaplan (1985) for the cyanobacterium, *Anabaena variabilis*. In this scheme, B in the PM represents $HCO_3^-$ released from the CA-like moiety which then binds directly to the transport binding site labeled "$HCO_3^-$ porter" (PM, plasma membrane; CA, carbonic anhydrase). From Miyachi et al. (1985) and Kaplan et al. (1985) with permission.

references therein) have provided valuable information on the low $CO_2$-induced synthesis of CA. Consistent with its function, CA is found within the cells of all algae, presumably in the chloroplast; but, as mentioned above, in some microalgae CA activity is *also* detected outside the cell in association with the cell wall/periplasmic space. That there is more than one function of CA, has been shown by the recent work of Spalding et al. (1985 and references therein). In these studies Spalding and coworkers used photosynthetically-defective mutants of *Chlamydomonas reinhardtii*. One mutant of *C. reinhardtii*, designated *ca-1*, failed to grow under low $CO_2$ culture conditions, but it could develop the ability to transport and accumulate DIC to very high levels. Photosynthetic carbon fixation was low and RuBP carboxylase sensitive to the level of $O_2$ in the medium suggested that the internal $CO_2$ concentration was low. However, the detected extracellular CA activity in the cells of the induced mutant did not differ from that present in wild-type *C. reinhardtii* cells. These results are consistent with the hypothesis that cytoplasmic CA activity, associated with the production of $CO_2$ for photosynthesis, was lacking in this particular mutant (*ca-1*). The role of the extra-cellular CA is not yet fully elucidated; Fig. 2 illustrates two quite different hypotheses as to its possible function in DIC transport.

#### Physiological advantages of the DIC-accumulating system

Whatever the mechanism(s), the $CO_2$ concentrating ability of the microalgae and cyanobacteria enables them to develop an apparent high photosynthetic affinity for $CO_2$, such that they have near zero $CO_2$ compensation points. In addition, as with $C_4$ plants, they develop a reduced sensitivity to $O_2$ inhibition of photosynthesis, with commensurate reduction in synthesis of photorespiratory products (Badger et al. 1978). An understanding of the ecophysiological aspects of these photosynthetic advantages has yet to be fully developed. However, the work by Turpin and coworkers using DIC-limiting and non-limiting conditions in controlled chemostats will provide valuable information (see Lucas and Berry 1985).

#### Macroalgae and aquatic angiosperms

Many of the early studies on the ability of aquatic plants to assimilate exogenous $HCO_3^-$ photosynthetically were conducted on the algal cells of the Characeae and on such aquatic angiosperms as *Potamogeton, Elodea, Vallisneria,* etc. (see Steemann Nielsen 1960). The early studies (1880's–1950's) focused on the ability of these photosynthetic tissues to raise the pH value of the experimental medium; the higher the final pH (9.5–10.5), the greater the presumed ability to utilize exogenous $HCO_3^-$.

Although the large size of the thallus and the highly vacuolated nature of the cells were not conducive to the study of DIC accumulation within the cytoplasm, the characteristics of these macrophytes did permit the study of spatial aspects of $HCO_3^-$ assimilation. It is now well recognized that the leaves of the aquatic angiosperms are "polarized," in that DIC, perhaps in the form of $HCO_3^-$, enters the lower leaf surface and $OH^-$, the waste produce of $HCO_3^-$ assimilation, is excreted at the upper surface. A polar movement of cations was found to be coupled to this net movement of anions (first $HCO_3^-$ and then $OH^-$) across the leaf. Various hypotheses have been presented to explain the plasma membrane-associated transport processes involved in $HCO_3^-$ assimilation in these plants. Figure 3 illustrates the latest model developed by Prins et al. (1982; also see Lucas and Berry 1985). Clearly the most important feature of this model is the hypothesis that $HCO_3^-$, per se, does not cross the plasma membrane. Rather, the activity of a $H^+$-translocating ATPase is thought to titrate $HCO_3^-$ to $H_2CO_3$; this could then produce a very localized increase in the concentration of $CO_2$ in the periplasmic space of cells within the lower leaf surface. DIC would move into the cytosol, and subsequently into the chloroplasts, by *diffusion* of $CO_2$. In this model, $OH^-$ ions are a consequence of $H^+$ pumping and the

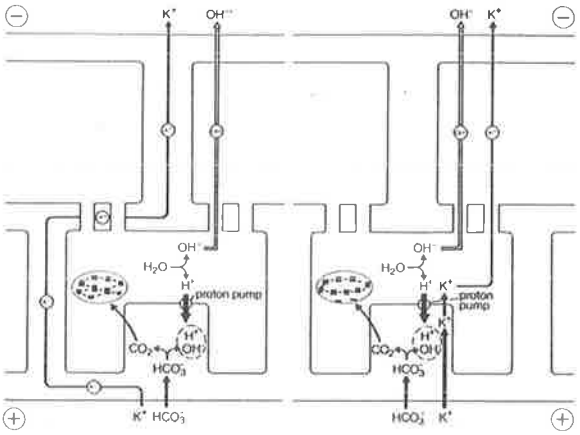


Fig. 3. The model of Prins et al. (1982) for exogenous $HCO_3^-$ utilization in *Potamogeton* and *Elodea* through the action of a proton pump. Two polar transport pathways are given for $K^+$; through the cell wall on the left, and via the symplast on the right. See text for details. Chloroplasts are represented by ovals that contain solid squares (grana). From Prins et al. (1982) with permission.

polar aspect of the leaf is clearly necessary to allow the localized development of an enhanced $CO_2$ partial pressure.

At present the available experimental data from *Potamogeton* and *Elodea* are consistent with the model presented in Fig. 3. Whether other aquatic angiosperms have also adopted this strategy remains to be shown.

#### Characean cells

The giant internodal cells of many *Chara* and *Nitella* species can also utilize exogenous $HCO_3^-$ for photosynthesis. Like the aquatic angiosperms, they too have spatially specialized regions on their plasma membrane that are involved in $HCO_3^-$ acquisition and $OH^-$ excretion. In the characean internodal cells, these regions alternate along the length of the cell and can be identified as acid ($HCO_3^-$ acquiring) and alkaline ($OH^-$ excretion) bands (or regions) by the use of pH indicator dyes (Spear et al. 1969).

Numerous techniques have been used to study $HCO_3^-$ assimilation in these cells, with most of the work having been done on one species, *Chara corallina*. Extracellular electric potential and miniature pH electrode measurements indicated that the alkaline and acid bands were associated with negative and positive potentials, respectively (see Lucas 1983). Use of a specialized vibrating probe [a very small tipped (10 μm diameter) platinum-black electrode that measures the localized gradient in the electric field] showed that $HCO_3^-$-associated *"currents"* flowed through the cell and the nearby bathing medium. Finally, the membrane potential of *C. corallina* (measured via microelectrodes inserted into the vacuole) was shown to be light- and $HCO_3^-$-dependent (Lucas 1982).

Initially, these results were interpreted in terms of *electrogenic* (i.e., charge generating) $HCO_3^-$ and $OH^-$ transport, with $HCO_3^-$ moving on a primary, active transport system and $OH^-$ efflux being passive (see Lucas 1983). However, recent results have indicated that $HCO_3^-$, per se, is *not essential* for the presence of either the extracellular potentials (and currents) or the light sensitivity of the membrane potential; artificial buffers (HEPES or $NA_2HPO_4$) can substitute for $HCO_3^-$, once the cell is photosynthetically assimilating exogenous $HCO_3^-$ (Lucas 1982). In addition, use of pH microelectrodes (tip diameters of 0.5–1.0 μm) revealed that the pH values within the center of the "acid" bands were lower than previously measured (Lucas et al. 1983).

Ferrier (1980) and Walker et al. (1980) put forward a hypothesis similar to that developed by Prins et al. (1982; see also Fig. 3), but in the case of *Chara* the production of $CO_2$ was thought to occur in the large unstirred layers next to the cell wall. In this situation, the currents would be associated with $H^+$ and $OH^-$ fluxes across the plasma membrane. However, experiments conducted to test this hypothesis provided little support (see Lucas 1983, 1985); one aspect that could not be discounted was the possibility that extracellular CA is involved in mediating the $H^+$-driven production of $CO_2$ within the cell wall or periplasmic space of *Chara*.

Although very recent results indicated that inhibitors of CA activity do reduce the photosynthetic capacity of these cells, the effect was variable (Lucas 1985 and references therein). Because of this, and numerous other

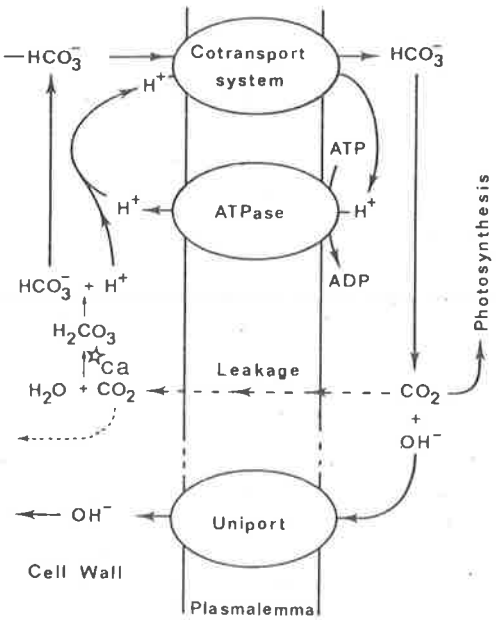


Fig. 4. Schematic representation of the plasma membrane-bound transport complexes that *may* function to enable internodal cells of *Chara* to acquire exogenous $HCO_3^-$ for photosynthesis. Extracellular carbonic anhydrase (denoted as ca) is thought to help reduce the leakage of $CO_2$. Inhibition of this carbonic anhydrase function (☆) would result in a build-up of $CO_2$. From Lucas (1985).

findings, it is presently thought, by some, that $HCO_3^-$ enters the *Chara* cell via a $H^+$-ATPase. Figure 4 illustrates the proposed system; its operation may raise the DIC level in the cytoplasm to an extent similar to that observed in the microalgae and cyanobacteria. If such a situation exists, leakage of $CO_2$ out of the cell would occur, and this would act as a partial shunt on the DIC accumulation mechanism. As shown schematically in Fig. 4, the presence of extracellular/periplasmic CA activity could greatly reduce the influence of this $CO_2$ shunt by enhancing the rehydration of $CO_2$; dissociation of $H_2CO_3$ would return the initial starting products of $H^+$ and $HCO_3^-$. In this model the role of extracellular CA is not central to the actual acquisition of DIC by *Chara,* but it would be important in terms of the efficiency of the overall process.

## Concluding remarks

The phenomenon of $CO_2$ and $HCO_3^-$ utilization by various photosynthetic aquatic organisms is now well established. Although the membrane transport models that explain these phenomena are constistent with much of the experimental data, they are still seriously deficient with respect to molecular details. In addition, very little information is available concerning the actual energetic costs of these various DIC accumulating mechanisms. On the same note, although we have some preliminary data concerning the cellular events involved in spatial and temporal control of the specific membrane-bound transport protein, there is much information yet to be gleaned from these systems.

Application of the techniques of cellular and molecular biology to the study of the processes involved in the low $CO_2$-induction phenomenon will provide valuable information concerning the control signals, their initiation and transduction.

## References


Badger, M. R. & Andrews, T. J. 1982. Photosynthesis and inorganic carbon usage by the marine cyanobacterium, *Synechococcus* sp. – Plant Physiol. 70: 517–523.

– , Kaplan, A. & Berry, J. A. 1978. A mechanism for concentrating $CO_2$ in *Chlamydomonas reinhardtii* and *Anabaena variabilis* and its role in photosynthetic $CO_2$ fixation. – Carnegie Inst. Washington Yearb. 77: 251–261.

– , Kaplan, A. & Berry, J. A. 1980. Internal inorganic carbon pool of *Chlamydominas reinhardtii:* Evidence for a carbon dioxide-concentrating mechanism. – Plant Physiol. 66: 407–413.

Coleman, J. R. & Grossman, A. R. 1984. The biosynthesis of carbonic anhydrase in *Chlamydomonas reinhardtii* during adaptation to low $CO_2$. – Proc. Natl. Acad. Sci. USA 81: 6049–6053.

– , Berry, J. A., Togasaki, R. K. & Grossman, A. R. 1984. Identification of extracellular carbonic anhydrase of *Chlamydomonas reinhardtii.* – Plant Physiol. 76: 472–477.

Ferrier, J. M. 1980. Apparent bicarbonate uptake and possible plasmalemma proton efflux in *Chara corallina.* – Plant Physiol. 66: 1198–1199.

Kaplan, A. 1985. Adaptation to $CO_2$ levels: Induction and the mechanism for inorganic carbon uptake. – *In* Inorganic Carbon Uptake by Aquatic Photosynthetic Organisms (W. J. Lucas and J. A. Berry, eds), Chapter 21, American Society of Plant Physiologists: Symposium Series, Rockville, MD, pp. 325–338.

– , Badger, M. R. & Berry, J. A. 1980. Photosynthesis and the intracellular inorganic carbon pool in the blue-green alga *Anabaena variabilis:* Response to external $CO_2$ concentration. – Planta 149: 219–226.

– , Zenvirth, D., Reinhold, L. & Berry, J. 1982. Involvement of a primary electrogenic pump in the mechanism for uptake by the cyanobacterium *Anabaena variabilis.* – Plant Physiol. 69: 978–982.

Lucas, W. J. 1982. Mechanism of acquisition of exogenous $HCO_3^-$ by internodal cells of *Chara corallina.* – Planta 156: 181–192.

– 1983. Photosynthetic assimilation of exogenous $HCO_3^-$ by aquatic plants. – Annu. Rev. Plant Physiol. 34: 71–104.

– 1985. Bicarbonate utilization by *Chara:* A re-analysis. – *In* Inorganic Carbon Uptake by Aquatic Photosynthetic Organisms (W. J. Lucas and J. A. Berry, eds), Chapter 16, American Society of Plant Physiologists: Symposium Series, Rockville, MD, pp. 229–254.

– & Berry, J. A. (eds) 1985. Inorganic Carbon Uptake by Aquatic Photosynthetic Organisms. – American Society of Plant Physiologists: Symposium Series, Rockville, MD, p. 494.

– , Keifer, D. W. & Sanders, D. 1983. Bicarbonate transport in *Chara corallina:* Evidence for cotransport of $HCO_3^-$ with $H^+$. – J. Membr. Biol. 73: 263–274.

Miller, A. G. & Colman, B. 1980. Evidence for transport by the blue-green alga (Cyanobacterium) *Coccochloris peniocystis.* – Plant Physiol. 65: 397–402.

Miyachi, S., Tsuzuki M. & Yagawa, Y. 1985. Carbonic anhydrase in various microalgae. – *In* Inorganic Carbon Uptake by Aquatic Photosynthetic Organisms (W. J. Lucas and J. A. Berry, eds), Chapter 11, American Society of Plant Physiologists: Symposium Series, Rockville, MD. pp. 145–154.

Ogawa, T., Omata, T., Miyano, A. & Inoue Y. 1985. Photosynthetic reactions involved in the $CO_2$-concentrating mechanism in the cyanobacterium, *Anacystis nidulans.* – *In* Inorganic Carbon Uptake by Aquatic Photosynthetic Organisms (W. J. Lucas and J. A. Berry, eds), Chapter 19, American Society of Plant Physiologists: Symposium Series, Rockville, MD. pp. 287–304.

Österlind, S. 1951. Inorganic carbon sources of green algae. IV. Photoactivation of some factor necessary for bicarbonate assimilation. – Physiol. Plant. 4: 514–527.

Prins, H. B. A., Snel, J. F. H., Zanstra, P. E. & Helder, R. J. 1982. The mechanism of bicarbonate assimilation by the polar leaves of *Potamogeton* and *Elodea.* $CO_2$ concentrations at the leaf surface. – Plant Cell Environ. 5: 207–214.

Spalding, M. H., Spreitzer, R. J. & Ogren, W. L. 1985. Use of mutants in analysis of the $CO_2$-concentrating pathway of *Chlamydomonas reinhardtii.* – *In* Inorganic Carbon Uptake by Aquatic Photosynthetic Organisms (W. J. Lucas and J. A. Berry, eds), Chapter 23, American Society of Plant Physiologists: Symposium Series, Rockville, MD. pp. 361–376.

Spear, D. G., Barr, J. K. & Barr, C. E. 1969. Localization of hydrogen ion and chloride ion fluxes in *Nitella.* – J. Gen. Physiol. 54: 397–414.

Steemann Nielsen, E. 1960. Uptake of $CO_2$ by the plant. – *In* Encyclopedia of Plant Physiology (W. Ruhland, ed.), Vol. V, pp. 70–84. Springer, Berlin.

Tsuzuki, M., Miyachi, S. & Berry, J. A. 1985. Intracellular accumulation of inorganic carbon and its active species taken up by *Chlorella vulgaris* 11h. – *In* Inorganic Carbon Uptake by Aquatic Photosynthetic Organisms (W. J. Lucas and J. A. Berry, eds), Chapter 5, American Society of Plant Physiologists: Symposium Series, Rockville, MD. pp. 53–66.

Walker, N. A., Smith, F. A. & Cathers, I. 1980. Bicarbonate assimilation by fresh-water charophytes and higher plants: I. Membrane transport of bicarbonate ions is not proven. – J. Membr. Biol. 57: 51–58.


Edited by G. Fritz

Protoplasma 130, 5–11 (1986)

PROTOPLASMA
© by Springer-Verlag 1986

# Influence of Culture Medium pH on Charasome Development and Chloride Transport in *Chara corallina*

W. J. Lucas *, D. W. Keifer[1], and T. C. Pesacreta[2]

Department of Botany, University of California, Davis, California

Received February 18, 1985
Accepted August 9, 1985

## Summary

Internodal cells of *Chara*, grown in culture either at pH 5.7, 6.5 or 7.5, were studied to determine their chloride influx capability, the quantitative aspects of charasome morphology and the degree to which these two parameters could be correlated. In cells grown at pH 5.7 the charasomes were relatively small, were widely spaced on the plasma membrane, and contributed only a 0.6% increase to the surface area of the plasma membrane in the acid region of the cell. In contrast, the charasome membrane surface area of cells grown at pH 7.5 had increased × 19, the density of charasomes on the cell surface increased × 42, thus producing a × 3.57 increase in the acid region plasma membrane surface area. Chloride influx in cells grown at pH 7.5 was × 8.7–12.7 greater than in cells grown at pH 5.7. Cells that had been starved of chloride exhibited a × 2.4 average increase in the rate of chloride influx. Our observations establish the existence of a positive correlation between the rate of chloride influx and the increase in membrane surface area due to charasomes, although other factors, such as the effect of pH on transport-related enzymes, and the effect of charasome structure on chemical equilibria, may also be of importance.

*Keywords:* *Chara corallina*; Charasome development; Chloride transport; Electron microscopy.

## 1. Introduction

Various algal species of the freshwater genus, *Chara*, have been shown to develop complex anastomosing plasma membrane structures that have been called charasomes (Barton 1965, Crawley 1965, Franceschi and Lucas 1980). These structures establish a specialized region, between the plasma membrane and the true space of the cell wall, termed the periplasm. In addition, the anastomosing network greatly increases the surface area of the plasma membrane. Although the mechanism by which this intricate structure is constructed remains to be fully elucidated, there appears to be an involvement of coated membranes (Lucas and Franceschi 1981, Franceschi and Lucas 1981b), and the matrix of the periplasm seems to be delivered via special membrane-bounded structures termed glycosomes (Franceschi and Lucas 1981a, Pesacreta and Lucas 1984).

In mature internodal cells of *Chara corallina*, the charasomes are asymmetrically distributed along the cell length. Franceschi and Lucas (1980) showed that the highest charasome density was coincident with the regions of the cell surface that become acidified during photosynthetic $HCO_3^-$ utilization (see Lucas 1983). Although the charasomes are not entirely absent from the alkaline band regions of the cell, their frequency and size are greatly reduced.

The physiological role of the charasome is still under investigation. Histochemical analysis of the development of ATPase activity associated with the membranes of the charasome indicated the appearance of such activity when the internodal cells and the charasomes approached maturity. Various membrane transport hypotheses have implicated the involvement of plasmalemma-bound $H^+$ - translocating ATPase, and

[1] Present address: Agricultural Chemicals Group, FMC Corporation, Box 8, Princeton, NJ 08540, U.S.A.
[2] Present address: The Biology Laboratories, Harvard University, 16 Divinity Avenue, Cambridge, MA 02138, U.S.A.
* Correspondence and Reprints: Department of Botany, University of California, Davis, CA 95616, U.S.A.

it has been suggested that similar systems may function within the charasome (Franceschi and Lucas 1982, Price and Whitecross 1983, Price *et al.* 1985). Initially, the correlation between the position of the charasomes and the regions of the cell wall where $HCO_3^-$ uptake was thought to occur, implicated the charasome in the transport of this ion. However, charasomes have not been found in *Nitella* cells, but they, too, develop the acid and alkaline zones that are thought to reflect photosynthetic assimilation of exogenous $HCO_3^-$ (Franceschi and Lucas 1980). Thus, either the charasomes are not involved in $HCO_3^-$ acquisition, or their role may be associated with enhancing the efficiency of $HCO_3^-$ transport in *Chara* relative to *Nitella*.

The concept that $Cl^-$ transport may be coupled to $H^+$ fluxes was first postulated by Spear *et al.* (1969) who found that in *Nitella*, $Cl^-$ transport occurred predominantly in the acid bands. Later Smith (1976), Smith and Walker (1976), Sanders (1980 a and b), and Beilby and Walker (1981) developed the hypothesis that $Cl^-$ uptake was driven by a $H^+$-ATPase and that the transport stoichiometry of the $H^+/Cl^-$ cotransport mechanism was $2\,H^+$ per $Cl^-$. Franceschi and Lucas (1982) suggested that the periplasmic space of the charasome may enhance the utilization of such a $2\,H^+/Cl^-$ transport system. Consistent with this idea, they found that the highest rates of $Cl^-$ transport were obtained on branch cells; these cells had the highest density of charasome material.

We reported here on studies in which we investigated the effect of culture medium pH on the development of the charasomes. Since most of our studies have been conducted on tissue cultured under alkaline (pH 8.5) or very alkaline (pH 9.5–10.0) conditions, we examined *Chara* cells grown at pH 5.7, 6.5, and 7.5. Under low pH conditions (5.7 and 6.5) normal charasomes developed, but their density along the plasma membrane was significantly reduced. At pH 7.5, we observed the same density and distribution as previously reported. Chloride influx experiments were conducted on these different cultures, and we found a good correlation between the extent of charasome development and density and the ability of the cells to transport chloride.

## 2. Materials and Methods

### 2.1. Culture Material and Conditions

Vegetative shoots of *Chara corallina* Klein ex Wild., em. R.D.W. (= *C. australis* R. Br.) were cut from our main culture and transplanted into sub-culture tanks (Nalgene drums, diam approx. 37 cm, height 60 cms) in which the pH values were controlled by the addition of artificial buffers. Each tank contained approximately 2.5 liters of soil that was covered by 1.5 liters of sand (both autoclaved twice) and 45 liters of culture solution. The ionic composition was kept the same as that used for our normal cultures (mM: 2 $NaHCO_3$, 1.0 NaCl, 0.2 KCl, 0.2 $CaSO_4$) except for the inclusion of buffer (2 mM: pH 5.7, Mes; pH 6.5, Mops; pH 7.5, Hepes). The surface of the low pH tanks (5.7 and 6.5) was covered by 1.5 cm of liquid paraffin to prevent the exchange of $CO_2$ with the atmosphere. Although this gave us better control over the culture pH value, it did give us some problems with maintaining the supply of dissolved inorganic carbon. At first we did not realize how fast the culture could deplete the medium of inorganic carbon. This was corrected for by addition of $NaHCO_3$.

Once the *Chara* had started to grow vigorously, the pH value was checked about every 5 days and adjusted by addition of either 0.5 M NaOH or 2.0 M HCl. Experimental material was harvested after 2.5 months and used in our electron microscopy and $^{36}Cl^-$ uptake studies. We also measured the chlorophyll content using the procedures of Arnon (1949). We found little difference between the various cultures, with the actual values being $12.0 \pm 1.2$, $10.7 \pm 1.5$, and $13.7 \pm 1.0$ mg chlorophyll $\cdot$ cm$^{-2}$ for pH values 5.7, 6.5, and 7.5 respectively.

### 2.2. Analysis of Charasome Development

Cells were immersed in a very slightly hypotonic fixative solution composed of 1.25% glutaraldehyde, 0.05 M sodium cacodylate, 2.0 mM $CaCl_2$, and 0.1% tannic acid, pH 7.2. The temperature of the primary fixative was initially 21–23 °C. After the cells had been immersed in the fixative for 5.0 minutes, they were carefully transferred to a refrigerator at 4 °C. After 12–16 hours, the tissue was washed three times in buffer and then placed for 2 hours in 1.0% $OsO_4$ in 25 mM sodium cacodylate buffer, pH 7.2 (21–23 °C). Next, the cells were washed in buffer, then dehydrated with acetone and embedded, intact, in Spurr's resin (Spurr 1969). Embedded cells were cut, transversely, into sequentially numbered pieces that were then trimmed to the approximate median longitudinal plane, prior to thin-sectioning. In some cases, cells were sectioned both longitudinally and transversely in order to determine the three-dimensional shape of the charasomes.

For quantitative analysis, our JEOL 100 S TEM was calibrated by using a diffraction grating at the beginning and end of each period of use. Quantitative data were obtained by measuring distances with an ocular micrometer. In order to determine, and compare, the amount of charasomal membrane surface area that the cells developed under the different pH values, we employed the Franceschi (1981) "standard charasome unit" of material (see Fig. 1).

### 2.3. Measurement of $^{36}Cl^-$ Influx

Radioactive $^{36}Cl^-$ was obtained from ICN (Irvine, CA) as a sterile aqueous solution of NaCl. Experimental solutions were prepared such that they contained 1.0 mM total $Cl^-$ having a specific activity of approximately $3 \times 10^6$ Bq mmol$^{-1}$.

Experimental protocols were as previously described by Keifer *et al.* (1982). In brief, cells from the three cultures were pretreated, overnight, in either control or $Cl^-$-free media containing: mM; 1.0 NaCl, 0.2 $K_2SO_4$, 1.0 $CaSO_4$, or 0.5 $Na_2SO_4$, 0.2 $K_2SO_4$, 1.0 $CaSO_4$, respectively. Pretreatment and experimental solutions were buffered (2 mM) at the indicated pH value with the following: Mes, pH 4.8, 5.7, 6.5; Hepes, pH 7.5; Taps, pH 8.5. Following the prescribed pretreatment, cells were transferred from Petri dishes into sealed tubes that were placed in a thermostatted water bath (25 °C) in the light (20 Wm$^{-2}$) for a 1-hour equilibration period. A 10 minute $^{36}Cl^-$ uptake period was employed, because the stimulation in $Cl^-$ influx,

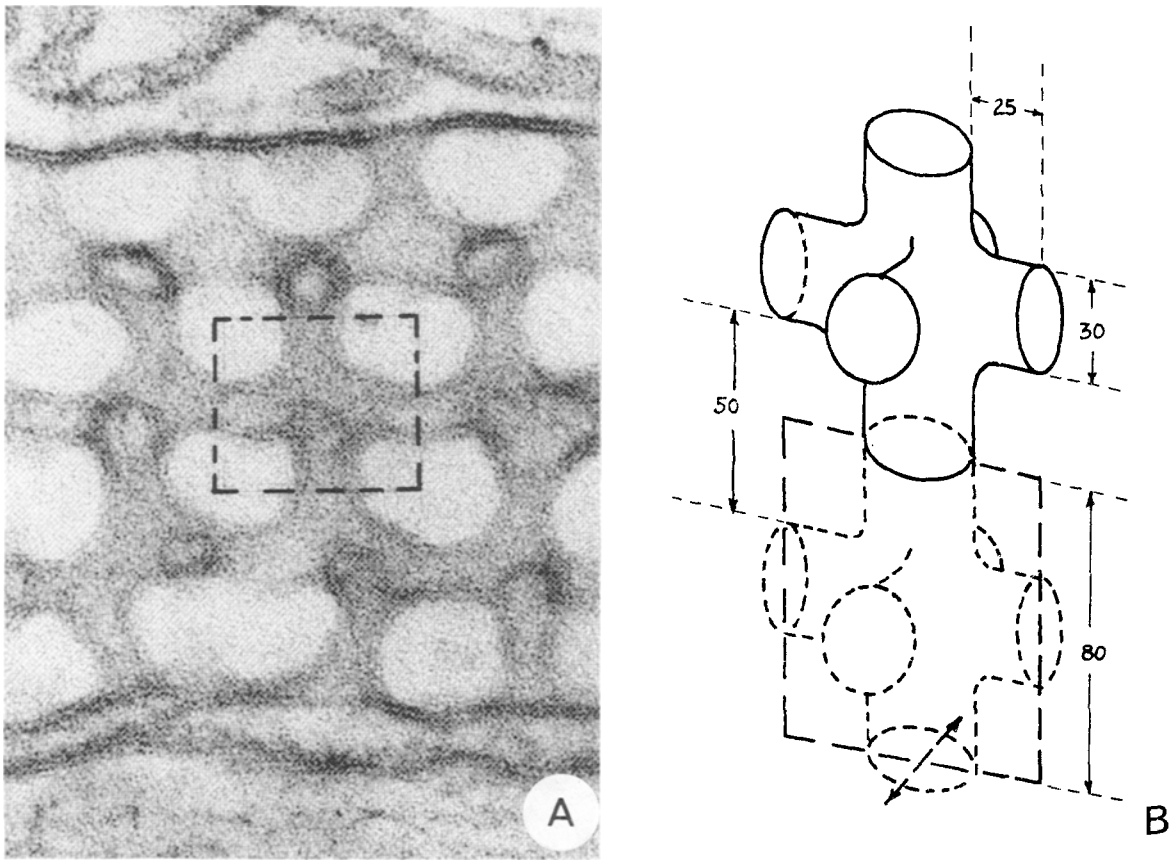


Fig. 1. Electron micrographic (*A*, mag. × 330,000) and diagrammatic illustration (*B*) of a "standard unit of charasome material." The unit (see area outlined by broken line on micrograph) is based on the average charasome tubule (cytoplasmic) length of 50 nm and outside diameter of 30 nm, as determined from electron micrographs. The diagrammatic representation of the "standard unit" assumes that each tubule intersects at a common point with 5 other tubules. Based on these dimensions and morphology, one can calculate that the average "standard charasome unit" has a volume of $5.12 \times 10^{-4}$ μm³, a membrane surface area of $1.41 \times 10^{-2}$ μm², and 27.6 μm² of membrane surface area per μm³ of charasome material. [Reproduced from FRANCESCHI (1981), with permission]

caused by exposing *Chara* cells to $Cl^-$-free conditions, has been found to decrease rapidly (SANDERS 1980 a). A 1 minute wash, followed by a 5 minutes wash in the appropriate non-radioactive experimental medium, was used to remove $^{36}Cl^-$ present in the cell wall. Cells were processed for scintillation counting as previously described (KEIFER *et al.* 1982). Twelve cells were used per treatment, and influx into each cell was calculated using its measured surface area. Results are reported as average ± SE.

## 3. Results

### *3.1. Charasome Development Under Culture pH 5.7 and 7.5*

Normal charasomes were observed in material examined from the cultures buffered at pH 5.7, 6.5, and 7.5 (*cf.*, Fig. 2 with FRANCESCHI and LUCAS 1980, KEIFER *et al.* 1982, FRANCESCHI and LUCAS 1982). However, although the anastomosing nature of the membrane, the presence of the periplasmic core, and the spatial distribution of the charasomes were similar, the *absolute* amount of charasome material was very much reduced under the low pH culture conditions (*cf.* Figs. 2, A and B). Since we found the same reduction in the amount of charasome material developed under pH 5.7 and 6.5, we present here a detailed comparison between the pH 5.7 and 7.5 culture material. The data presented in Table 1 provide a quantitative basis in support of the general features illustrated in Fig. 2. Thus, although the charasomes were actually distributed over a greater proportion of the cell length in the pH 5.7 culture, only 2% of that length was covered by charasomes, in comparison with 42% in the pH 7.5 *Chara* cells. A three-dimensional examination of the pH 5.7- and 7.5-grown cells indicated that the charasomes frequency, or density (*i.e.*, number of charasomes per μm² of plasma membrane surface) was reduced by a factor of 42 in the pH 5.7 material (see Table 1).

The *average* charasome developed under pH 5.7 con-

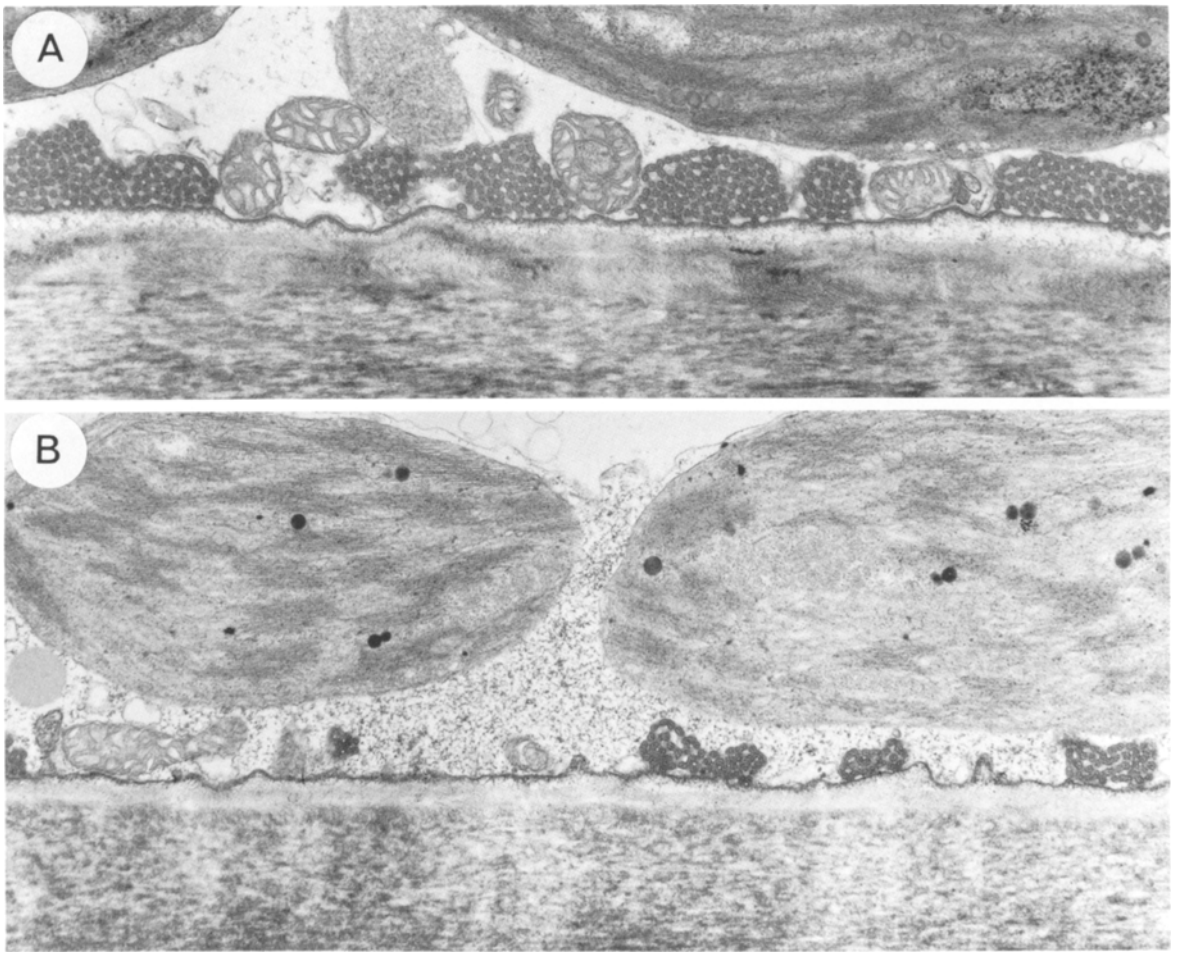


Fig. 2. Influence of culture medium pH value on the relative distribution of charasomes within the acid regions of the internodal cells of *Chara corallina*. *A* Representative micrograph of charasomes (longitudinal section) developed under a culture medium pH of 7.5 (× 18,000). *B* As in *A*, except culture medium pH was 5.7 (× 18,000)

ditions was found to be isodiametric, while those of the pH 7.5 culture were 1 μm in length and projected into the cytoplasm a distance of approximately 0.6 μm. These differences in length and width translate into a 6-fold reduction, in the pH 5.7 tissue, in the longitudinal cross-sectional area. When we performed the three-dimensional analysis on the charasomes, the difference between the pH 7.5 and 5.7 material was found to be even greater. Using the "standard charasome unit" (see Fig. 1 adopted from FRANCESCHI 1981), we converted the volume of the charasome into the area of membrane surface contained within the charasome. Analysis of the pH 5.7 and 7.5 data indicated that the total membrane surface area of the average pH 5.7 charasome was smaller, by a factor of 19, when compared with the average pH 7.5 charasome (Table 1).

By using the data on the density of charasomes, the relative length of the acid and alkaline regions and the volume-total membrane surface area per charasome, we computed the percentage increase in total membrane surface area, in the acid regions, due to the charasomes. This form of analysis indicated that, in comparison with the pH 7.5 cells, the pH 5.7 tissue underwent a dramatic 590-fold reduction in the amount of membrane surface area present within the acid regions of the *Chara* cell.

### *3.2. Influence of Culture Media pH on Chloride Transport Capability*

To fully examine the effect of culture media pH on the ability of *Chara* to transport $Cl^-$, we conducted two types of experiments. In the first, *Chara* cells from the three cultures (pH 5.7, 6.5, and 7.5) were pretreated, for approximately 16 hours, in buffered media (pH values were 4.8, 5.7, 6.5, 7.5, and 8.5) that did not contain chloride. SANDERS (1980 a and b) has shown that under these conditions, the kinetic controls acting on the

Table 1. *Influence of culture medium pH on charasome development in Chara corallina*

| Average charasome-related parameter | Culture pH value | | Ratio $\frac{7.5}{5.7}$ |
|---|---|---|---|
| | 5.7 | 7.5 | |
| Distances between charasomes[a] (μm) | 14.6 ± 0.01 | 1.34 ± 0.02 | 0.09 |
| Ratio of length of acid to length of alkaline region | 4.2 | 2.7 | 0.6 |
| Length of acid region covered by charasome[b] (%) | 2.0 | 42 | 21 |
| Charasome density in acid region (number/$\mu m^2$)[c] | 0.0043 | 0.18 | 42 |
| Charasome height (μm) | 0.34 ± 0.01 | 0.58 ± 0.02 | 1.7 |
| Charasome diameter (μm) | 0.34 ± 0.01 | 1.0 ± 0.02 | 2.9 |
| Charasome area in longitudinal section ($\mu m^2$) | 0.10 | 0.59 | 5.9 |
| Membrane surface area per charasome ($\mu m^2$)[c, d] | 1.05 ± 0.06 | 20 ± 0.5 | 19 |
| Increase in total membrane surface area, in acid region, due to charasomes (%) | 0.6 | 357 | 590 |

[a] Values represent mean ± SEM; for cells from culture pH 5.7 and 7.5 the number of charasomes measured were 320 and 1,730, respectively.
[b] Determine on one representative cell from each culture.
[c] Parameters determined by conducting a three-dimensional analysis of the material. See Materials and Methods for full details.
[d] Surface area and volume relationships computed using the FRANCESCHI unit charasome concept illustrated in Fig. 1.

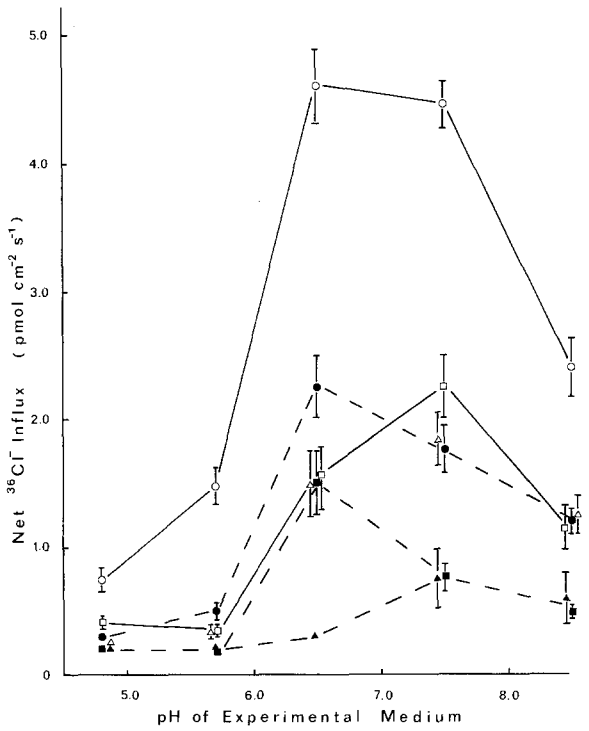


Fig. 3. Chloride influx into main axis internodal cells of *Chara corallina* that were cultured at different pH values. Symbols are as follows: ○, ●: cells cultured at pH 7.5; □, ■: cells cultured at pH 6.5; △, ▲: cells cultured at pH 5.7. Solid symbols represent $^{36}Cl^-$ influx into cells that were pretreated in the presence of 1.0 mM $Cl^-$, while open symbols represent influx into cells that were pretreated in the absence of $Cl^-$. See text for full details

*Chara* $Cl^-$ transport system are relieved, and so it should be possible to measure the transport capacity of the different cell types (see also SANDERS and HANSEN 1981). Figure 3 illustrates that, under such a $Cl^-$-free pretreatment, the highest values for $Cl^-$ influx were obtained on *Chara* cells cultured at pH 7.5. At each *experimental* pH value, the stimulated $Cl^-$ influx values were the same (given the SE values) for cells grown at pH 6.5 and 5.7.

In the second type of experiment, we followed the same protocol, except that 1.0 mM $Cl^-$ was included in all pretreatment solutions. Similar trends were observed, in that the pH 7.5 culture had the highest influx values and except for one anomalous point, similar values were obtained for the pH 6.5 and 5.7-grown cells (Fig. 3).

## 4. Discussion

### *4.1. Control of Charasome Growth by Culture Medium pH*

Our results presented in Fig. 2 and Table 1 confirm the recent findings of PRICE *et al.* (1985), namely that the pH value of the culture medium has an influence on the extent to which the charasome network develops. The development of individual charasomes, with their attendant ultrastructural details, does not seem to be

affected by the pH value of the culture medium. Thus, the dramatic reduction in charasome density, observed in the pH 5.7- (and 6.5) grown *Chara* cells, must be due to an effect on the cellular process(es), which controls the rate of charasome growth, rather than via a pH-mediated influence on the actual processes involved in forming these complex anastomosing structures. Since we have only documented the ultrastructural details involved in the phenomenon of charasome development (see LUCAS and FRANCESCHI 1981), it is difficult to present a more detailed analysis of these findings. However, it should be mentioned that the pH effect on charasome density could be due to an enhanced level of cell expansion under the more acid culture conditions. If the sites of charasome initiation were slow in forming, or slowed by the lower pH values, then the cell may extend to its mature length in a much shorter time than that required for normal (*i.e.*, pH values $> 7.5$) charasome growth. For this to be the case, further charasome growth would have to cease once the individual *Chara* cell attained its mature length.

At present we have little information on the dynamic aspects of the mature charasomes. Use of the culture medium pH value should provide a valuable means of studying the time-dependent turnover of the charasome membrane. In future studies we will transfer mature culture material from pH 5.7 to 7.5 and then monitor the charasome-related parameters to see whether further growth is possible in mature cells.

### *4.2. Relationship Between $Cl^-$ Transport Capability and Charasome Development*

A positive correlation exists between the measured values of $Cl^-$ influx and the extent of charasome development within the tissue obtained from the three pH culture conditions. In the control $Cl^-$ influx experiments (*i.e.*, *Chara* cells always kept in the presence of $Cl^-$) the value obtained, at pH 7.5, by the pH 7.5 culture material, was 8.7 times greater than the value obtained, at pH 5.7, by the pH 5.7 culture material. For the $Cl^-$-starved cells (*i.e.*, kept in $Cl^-$-free media), the ratio of the stimulated fluxes at 7.5 and 5.7 (measured at the respective pH values) was 12.7. These relative $Cl^-$ transport capabilities fall within the same general range as the values obtained for the ratio (pH 7.5/5.7) of such charasome-related parameters as the cross-sectional area ($\times 5.9$), and the membrane area per charasome ($\times 19$). However, since the total amount of membrane added to the acid region by the charasomes in pH 5.7 cells is negligible, then the $\times 3.57$ or 357% increase of acid region plasma membrane in pH 7.5 cells becomes the crucial value to consider. Obviously, this value is smaller than the 8.7 to 12.7-fold increase in chloride influx in pH 7.5 cells compared to pH 5.7 cells. This 2.4 to 3.7-fold disparity may not be as significant as it first appears. It is possible that the anastomosing structure of the charasome and the materials in the periplasmic space are able to slow the diffusion of protons or other substances into the apoplast, thus stimulating chloride influx to a greater extent than would be expected if the amplification of plasma membrane surface area were the only relevant factor involved.

An alternative explanation of these data is that the charasome is engaged in effecting numerous $H^+$-mediated transport processes, not just $Cl^-$ uptake. In a recent study, PRICE *et al.* (1985) correlated the change in pH-induced charasome development with the ability of the *Chara* cells to utilize exogenous $HCO_3^-$. They suggested that the limited photosynthetic ability at alkaline pH, of charasome-deficient cells, may have been due to the decreased efficiency of $HCO_3^-$ to $CO_2$ conversion in the limited periplasmic space. The basic problem with their experiments is that PRICE *et al.* (1985) cut the cells from their pH 6.8 culture and used them *immediately* in experiments to measure photosynthetic capacity at acid and alkaline pH conditions. It is well known that microalgal cells grown under high $CO_2$ conditions require, at a minimum, 4–6 hours to induce the ability to utilize exogenous $HCO_3^-$ (see ÖSTERLIND 1951, STEELMANN NIELSEN 1960). Thus, before we can accept this correlation between the extent of the charasome material and the ability to utilize $HCO_3^-$, it remains to be established that these cells were not in the process of $HCO_3^-$ transport induction.

### *4.3. Effect of Culture Medium pH on $Cl^-$ Transport per se*

The broad pH optimum of 6.5 to 7.5 in both control and $Cl^-$-starved tissues is in agreement with our previous findings (KEIFER *et al.* 1982); however, the maximum stimulated values in the present study are about half those reported by KEIFER *et al.* (1982), but close to those reported by SANDERS (1980 a). An interesting feature of the present results is that the ratio of the stimulated value of $Cl^-$ influx, relative to the control value, remained rather constant, irrespective of culture medium pH value, or the actual experimental pH value employed. For the pH 7.5, 6.5 and 5.7 cultures, the average values of this ratio were 2.40 (or a stimulation of 240%), 2.33 and 2.46, respectively. That the percentage stimulation of $Cl^-$ influx was independent of

bathing medium pH was an unexpected finding, especially for the pH 5.7 and 6.5 culture material, where the extent of the charasomes was so much reduced. It was also interesting to observe that, except for the one anomalous point, both pH 5.7 and 6.5 cultured cells transported $Cl^-$ more effectively when they were bathed in high pH (7.5 and 8.5) media (see Fig. 3). If a $H^+$-translocating ATPase is involved in supplying the energy ($\Delta\mu_{H^+}$) needed to drive $Cl^-$ uptake, this response could be ascribed to the alkaline pH optimum of the ATPase. At pH 5.7, or lower, there may be an equivalent $\Delta\mu_{H^+}$ available to drive $Cl^-$ uptake, but the kinetic limitations on the rate of $H^+$ pumping may set this lower limit on uptake. If this were the case, the higher rates of $Cl^-$ transport observed in pH 7.5- (and higher) cultured cells may be due to the combined effects of higher $H^+$ pumping, by the plasmalemma-bound ATPase, and enhanced $H^+$ capture afforded by the more elaborate periplasm of the charasomes that develop under these conditions.

Alternatively, this stimulation in $^{36}Cl^-$ influx observed under alkaline bathing conditions may be due to the influence of external pH, *per se*, on the cytoplasmic pH value. SANDERS and HANSEN (1981) suggested that such an effect on the cytoplasmic pH value may relieve a major kinetic control on $Cl^-$ uptake in *Chara* cells.

## Acknowledgements

We thank Dr. VINCENT FRANCESCHI for allowing us to reproduce Fig. 1 (from Appendix V of his Ph. D. Dissertation) and DEAN PRICE for making his manuscript available to us prior to publication. This work was supported by National Science Foundation grant PCM 81-17721.

## References

ARNON, D. I., 1949: Copper enzymes in isolated chloroplasts. Polyphenoloxidase in *Beta vulgaris*. Plant Physiology **24**, 1–15.

BARTON, R., 1965: An unusual organelle in the peripheral cytoplasm of *Chara* cells. Nature **205**, 201.

BEILBY, M. J., WALKER, N. A., 1981: Chloride transport in *Chara*: I. Kinetics and current voltage curves for probable proton symport. J. exp. Bot. **32**, 43–54.

CRAWLEY, J. A. C., 1965: A cytoplasmic organelle in association with the cell walls of *Chara* and *Nitella* cells. Nature **205**, 200–201.

FRANCESCHI, V. R., 1981: Membrane structure-function relationships in several characean species. Ph. D. Dissertation, University of California, Davis, U.S.A.

FRANCESCHI, V. R., LUCAS, W. J., 1980: Structure and possible function(s) of charasomes; complex plasmalemma-cell wall elaborations present in some characean species. Protoplasma **104**, 253–271.

— — 1981 a: The glycosome of *Chara*: Ultrastructure, development, and composition. J. Ultrastruct. Res. **75**, 218–228.

— — 1981 b: The charasome periplasmic space. Protoplasma **107**, 269–284.

— — 1982: The relationship of the charasome to chloride uptake in *Chara corallina*: physiological and histochemical investigations. Planta **154**, 525–537.

KEIFER, D. W., FRANCESCHI, V. R., LUCAS, W. J., 1982: Plasmalemma chloride transport in *Chara corallina*: inhibition by 4,4′-Diisothiocyano-2,2′-disulfonic acid stilbene. Plant Physiol. **70**, 1327–1334.

LUCAS, W. J., 1983: Photosynthetic assimilation of exogenous $HCO_3^-$ by aquatic plants. Ann. Rev. Plant Physiol. **34**, 71–104.

— FRANCESCHI, V. R., 1981: Characean charasome-complex and plasmalemma vesicle development. Protoplasma **107**, 255–267.

ÖSTERLIND, S., 1951: Inorganic carbon sources of green algae. IV. Photoactivation of some factor necessary for bicarbonate assimilation. Physiol. Plant. **4**, 514–527.

PESACRETA, T. C., LUCAS, W. J., 1984: Plasma membrane coat and a coated vesicle-associated reticulum of membranes: their structure and possible interrelationship in *Chara corallina*. J. Cell Biol. **98**, 1537–1545.

PRICE, G. D., BADGER, M. R., BASSETT, M. E., WHITECROSS, M. I., 1985: Involvement of plasmalemmasomes and carbonic anhydrase in photosynthetic utilization of bicarbonate in *Chara corallina*. Aust. J. Plant Physiol., in press.

— WHITECROSS, M. I., 1983: Cytochemical localization of ATPase activity on the plasmalemma of *Chara corallina*. Protoplasma **116**, 65–74.

SANDERS, D., 1980 a: Control of $Cl^-$ influx in *Chara* by cytoplasmic $Cl^-$ concentration. J. Membrane Biol. **52**, 51–60.

— 1980 b: The mechanism of $Cl^-$ transport at the plasma membrane of *Chara corallina*. I. Cotransport with $H^+$. J. Membrane Biol. **53**, 129–141.

— HANSEN, U.-P., 1981: Mechanism of $Cl^-$ transport at the plasma membrane of *Chara corallina*. II. Transinhibition and the determination of $H^+/Cl^-$ binding order for a reaction kinetic model. J. Membrane Biol. **58**, 139–153.

SMITH, F. A., 1970: The mechanism of chloride transport in characean cells. New Phytol. **69**, 903–917.

— WALKER, N. A., 1976: Chloride transport in *Chara corallina* and the electrochemical potential difference for hydrogen ions. J. exp. Bot. **27**, 451–459.

SPEAR, D. G., BARR, J. K., BARR, C. E., 1969: Localization of hydrogen ion and chloride ion fluxes in *Nitella*. J. gen. Physiol. **54**, 397–414.

SPURR, A. R., 1969: A low-viscosity epoxy resin embedding medium for electron microscopy. J. Ultrastruct. Res. **26**, 31–43.

STEELMANN NIELSEN, E., 1960: Uptake of $CO_2$ by the plant. In: Encyclopedia of Plant Physiology, Vol. V, The Assimilation of Carbon Dioxide (RUHLAND, W., ed.), pp. 70–84. Berlin-Göttingen-Heidelberg: Springer.

# ION TRANSPORT AND THE VIBRATING PROBE

JACK FERRIER* AND WILLIAM J. LUCAS‡
*Medical Research Council Group in Periodontal Physiology, University of Toronto, Toronto, Ontario M5S 1A8, Canada; and ‡Department of Botany, University of California, Davis, California 95616

ABSTRACT The theory of ion transport in the vicinity of a vibrating probe is developed. It is shown that the convection loops produced by the probe will not affect the electrical current density, assuming that the action of the probe does not affect the sources of the current in the biological system. However, the convection loops will significantly alter the ion concentration gradients in the unstirred layer near a tissue or cell surface. The concentration gradients within each convection loop will be reduced, while the concentration gradients between the loops and outside of the loops will be increased relative to the gradients existing without the probe. As a consequence, the electrical potential gradients can be changed relative to the potential gradients existing in the absence of the convection caused by the probe. If the mobility of the ion species carrying the electrical current is greater than the average ion mobility in the medium, then a decrease in ion concentration gradient will be accompanied by an increase in electrical potential gradient, while an increase in concentration gradient will be accompanied by a decrease or even a reversal of electrical potential gradient. Thus, the electrical potential gradient measured by the probe will depend on the concentration gradient in the vicinity of the probe, which will depend in turn on the spatial relation of the convection loops to the probe. An example of the effect of the convection loops on ion concentration and electrical potential is obtained from the theory via a numerical computer calculation. Experimental tests of this theory are discussed.

## INTRODUCTION

The vibrating probe has been used to measure electrical currents produced by a number of biological systems (e.g., Jaffe and Nuccitelli, 1974, 1977; Lucas and Nuccitelli, 1980; Nuccitelli, 1983). However, the vibrating probe is thought to actually measure the electrical potential gradient. The current density is then calculated by assuming that it is related to the potential gradient by the electrical conductivity of the medium and Ohm's law. That the relationship between current and the electrical potential gradient is not governed by Ohm's law in many systems is well known. For example, in a wide range of solid state systems the existence of charge carrier concentration gradients leads to drastic departures from Ohm's law (e.g., Wannier, 1966; Ferrier, 1973). For ion transport in electrolytic solutions, the conducting system in which the vibrating probe is used, it has also been shown that there can be significant deviations from Ohm's law in the unstirred layer near tissue and cell surfaces (Ferrier and Lucas, 1979; Ferrier, 1980, 1981*a*, 1981*b*, 1983; Ferrier et al., 1985).

In this paper, we show that the current density is not affected by the convection loops produced by the vibrating probe. In addition, we develop a relationship between current density, the ion concentration gradients, and the electrical potential gradient. This relationship is not affected by the convection loops that are generated by the vibrating probe. As a consequence, it can be used to show the conditions under which Ohm's law does not hold, and can also be used to investigate the effect of the convection loops on the electrical potential gradient.

## THEORY

The results of Ferrier (1980, 1981*b*) for extracellular ion transport at steady state, and the investigations in this paper, are based in part on the mathematical property of a vector field that, if the divergence and curl of the vector are zero everywhere inside a closed boundary (i.e., if there are no sources, sinks, or closed loops), then there is a unique solution for the vector inside the boundary that depends only on the normal component of the vector on that boundary (e.g., Jackson, 1962). The flux vector of ion species $k$ can be written as the sum of three terms, involving the concentration gradient, the electrical potential gradient, and the convection velocity

$$J_k = -D_k \mathrm{grad} C_k - (D_k C_k z_k F/RT)\mathrm{grad} V + v C_k, \quad (1)$$

where $D_k$ is the diffusion coefficient for species $k$, $C_k$ is the concentration, $z_k$ is the valency, $V$ is the electrical potential, $v$ is the convection velocity, and $F$, $R$, and $T$ have their usual thermodynamic meanings. At steady state, the divergence of $J_k$ must equal zero (otherwise $C_k$ will change with time). Furthermore, the curl of a gradient is identically zero. Thus, if the curl of $v$ is zero inside the boundary, then the curl of $J_k$ will be zero, and there must be a unique vector field, $J_k$, which depends only on the normal component of $J_k$ on the boundary. This means that if the boundary is drawn to include the cell membranes, plus an

outer boundary at some distance from the cells, then the $J_k$ for species not transported across the cell membranes will depend only on the normal component of $J_k$ for those species at the outer boundary. If this boundary is sufficiently far from the cells so that ion transport there is not affected by membrane ion transport, then transport of these species anywhere within the boundary will be unaffected by membrane transport at steady state.

On the other hand, an ion species that is membrane-transported will have a nonzero normal component of flux at the membrane, and hence the vector field for its flux within the boundary will be clearly dependent on membrane transport. This implies that at steady state an electric current that results from membrane ion transport will be carried only by those ion species that are membrane-transported. Furthermore, it is clear that a species will contribute to carrying the current in the extracellular medium in proportion to its contribution to carrying the current across the membrane. However, these results hold only if the curl of the convection velocity equals zero within the boundary. This requirement can be reasonably approximated for many cases of extracellular ion transport, but not for the case of the vibrating probe, with its attendant convection loops.

The current density can be obtained from Eq. 1 as follows:

$$I = F\Sigma_i z_i J_i = -F\Sigma_i z_i D_i \text{grad} C_i - \sigma \, \text{grad} V, \qquad (2)$$

where the summation is over all ion species, and $\sigma$ ($= \Sigma_i D_i C_i (z_i F)^2 / RT$) is the electrical conductivity of the medium. The term in $\upsilon$ drops out because of the requirement for electroneutrality ($\Sigma_i z_i C_i = 0$). The electroneutrality condition also implies that the divergence of the current density equals zero, and since the curl of a gradient equals zero we can see from Eq. 2 that the curl of the current density equals zero. Thus, the current density will have a unique solution that depends on the normal component of the current density on the boundary, but that does not depend on the convection velocity, even in the case that the convection velocity has a nonzero curl (forms closed loops).

If all but one of the ion species in the system have about the same diffusion coefficient, say $D_o$, while the other ion species is designated as species $h$ (because we may specify that it has a higher diffusion coefficient), then we can rewrite Eq. 2

$$I = -(1 - B) F z_h D_h \text{grad} C_h - \sigma \, \text{grad} V, \qquad (3)$$

where $B = D_o / D_h$, and we have used the electroneutrality condition in going from Eq. 2 to Eq. 3.

By combining Eqs. 1 and 3 we can obtain

$$J_h = -D_h[1 - (1 - B)(\sigma_h/\sigma)] \text{grad} C_h + [\sigma_h/(z_h F \sigma)] I + \upsilon C_h, \qquad (4)$$

where $\sigma_h = D_h C_h (z_h F)^2 / RT$ is the conductivity attributable to species $h$. Eq. 4 shows that, if species $h$ carries the current at steady state, if the convection velocity is low, and if $C_h$ is small relative to the total ionic concentration, then the flux of species $h$ will be driven largely by its concentration gradient. Thus, under these conditions, $I = -F z_h D_h \text{grad} C_h$. Putting this relation into Eq. 3 gives $\text{grad} V = -BI/\sigma$. So, we see that in cases where high mobility ions such as protons or hydroxyls carry the current, there can be a significant deviation from Ohm's law, since $B$ will be much less than 1 ($B = 0.17$ for protons, $B = 0.31$ for hydroxyl ions).

Eqs. 3 and 4 can also be used to show that the magnitude of the electrical potential gradient can be greater than would be expected on the basis of Ohm's law. In a situation with a flux of high mobility ions that is balanced by the flux of other ions so that the current density equals zero, and with a low convection velocity, Eq. 4 again shows that the flux of species $h$ would be largely driven by its concentration gradient. Eq. 3 then shows that the electrical potential gradient would be nonzero. This would apply, for example, to a steady state situation where a proton flux through the cell membrane was balanced by an equal but opposite potassium flux. It would also apply to the situation where there had been a steady state current carried by protons that was suddenly switched off.

Eq. 3 can also be used to investigate the theoretical effect of the vibrating probe on the electrical potential gradient. We will consider the case with an initial steady state with low convection and with current carried by a high mobility ion species. When the vibrating probe is turned on, the resulting convection loops may significantly alter the concentration gradient for species $h$. Since the vector field for current density will not be affected by the convection loops, Eq. 3 can be used to calculate the change in the electrical potential gradient that results from the alteration of the concentration gradient of the high mobility species. However, to estimate the effect of the convection loops on this concentration gradient, we must resort to a numerical computer calculation.

## METHODS

### Numerical Calculations

Because of the convection loops produced by the vibrating probe (Jaffe and Nuccitelli, 1974), the vector field for the flux of an ion species will no longer be uniquely determined by the normal component of the flux on the boundary. To calculate the effect of the convection loops on the concentration gradient of species $h$, Eq. 4 was put into difference equation form and solved on a computer (DEC 10 system; University of Toronto, Toronto, Ontario, Canada). Only the terms involving the concentration gradient and convection velocity were used, since the term with current density will be extremely small for reasonable values of $\sigma_h$. We used rectangular coordinates, with spatial elements of 10 $\mu$m dimension, and time increments of 0.25 ms. The numerical calculation was very close to steady state after 4,000 iterations.

In an attempt to simulate the convection pattern produced by the vibrating probe, the computer calculation was performed with two convection loops, which represent the main features of the pattern observed by Jaffe and Nuccitelli (1974). The magnitude of the convection

velocity and the width of the convection stream were allowed to vary around the loops. The outer boundary of each loop was assumed to be circular. For simplicity, mirror-symmetry of the loops was also assumed. It was found that the numerical results were not sensitive to the velocity used in the central region of each loop. The results reported here are with zero velocity in the central regions. The rectangular components of the convection velocity for each element in the computational grid were calculated according to their position relative to the loops as shown in Fig. 1. The direction of the current and flux of the high mobility ion species is from top to bottom of the figure.

## RESULTS

Without the convection loops, the isoconcentration lines shown in Fig. 2 would be equally spaced, straight, parallel, and horizontal. As Fig. 2 shows, these lines are significantly altered by the convection loops. The isoconcentration lines are pushed in the direction of the convection velocity. The concentration gradient is largely eliminated within each loop, but is increased between the two loops, and on the boundaries of the loops.

Using Eq. 3, the resulting electrical potential can be calculated. Fig. 3 shows the resulting equipotential lines for proton transport ($B = 0.17$). Without the convection loops, the equipotential lines would also be equally spaced, straight, parallel, and horizontal. With the convection loops, there is a greatly increased potential gradient within each loop. Near the bottom of the top loop, there is a very low potential valley. There is a very steep upward potential gradient (opposite in direction to the original potential gradient) spanning the interface between the convection loops, with a very high potential peak near the top of the bottom loop.

The concentration and electrical potential profiles along a path through the convection loops, 20 $\mu$m to the right of the centres of the loops, are shown in Fig. 4. These profiles should be close to those existing in the plane of oscillation of the vibrating probe. The profiles along parallel paths within 20 $\mu$m are similar to those shown. These results imply that, if the vibrating probe actually oscillates between the two convection loops, the measured electrical potential gradient would be smaller than, or even of opposite sign to, the potential gradient without convection. In this case, the current density would be significantly underestimated, or even taken as being of opposite direction to the actual current, if Ohm's law were used to calculate the current density. If the probe oscillates within

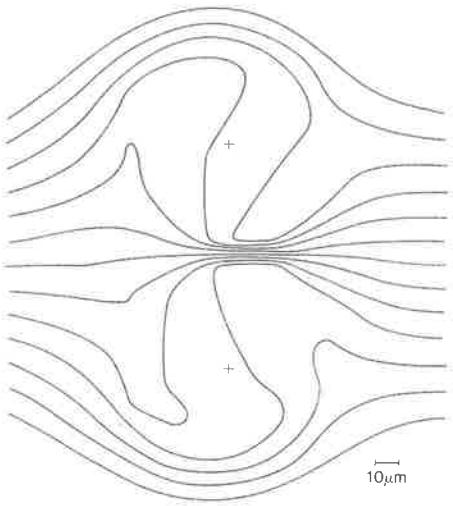


FIGURE 2 Isoconcentration lines in the presence of the convection loops. These lines are $1 \times 10^{-6}$ mol litre$^{-1}$ apart, for a current density of 10 $\mu$A cm$^{-2}$, a flux for the high mobility ion species in the absence of convection of 100 pmol cm$^{-2}$ s$^{-1}$, and $D_h = 1.0 \times 10^{-4}$ cm$^2$ s$^{-1}$. However, the concentration gradient, current density, and ion flux can all be scaled by the same factor for a given $D_h$. For example, the lines would be $1 \times 10^{-7}$ mol litre$^{-1}$ apart for a current density of 1 $\mu$A cm$^{-2}$ and a flux of 10 pmol cm$^{-2}$ s$^{-1}$. For $C_h$ much less than the total ion concentration, the concentration gradient scales inversely with $D_h$ for a given current density and ion flux, and the concentration gradient does not depend on $C_h$. The centers of the convection loops are indicated by crosses.

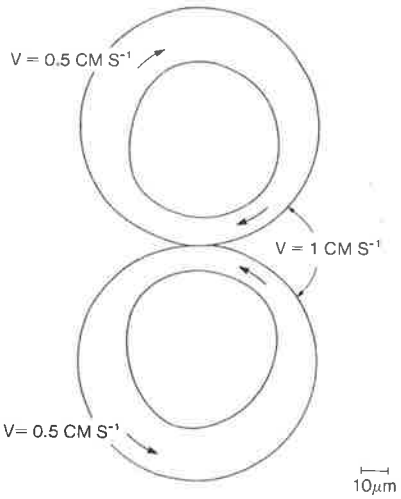


FIGURE 1 The convection loops used in the numerical calculation, showing the velocity and the width of the convection streams.

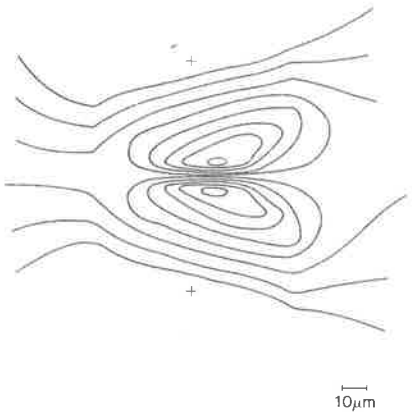


FIGURE 3 Equipotential lines in the presence of the convection loops. The lines are 20 $\mu$V apart, for a current density of 10 $\mu$A cm$^{-2}$, an electrical conductivity of $3 \times 10^{-4}$ S cm$^{-1}$, and a $B$ value of 0.17. The electrical potential gradient will scale with the same factor as the concentration gradient and the current density, for a given $B$ value. For example, the lines would be 2 $\mu$V apart for a current density of 1 $\mu$A cm$^{-2}$. The centers of the convection loops are indicated by crosses.

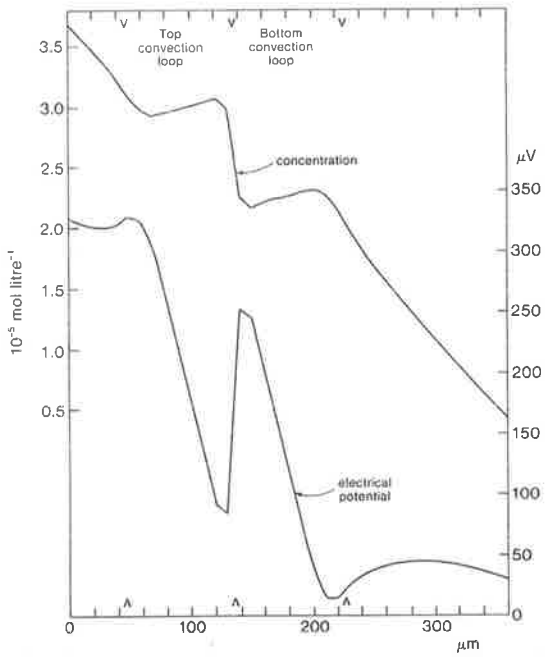


FIGURE 4 Concentration and electrical potential profiles along a path through the convection loops, 20 μm to the right of the centers of the loops, for a current density of 10 μA cm$^{-2}$, and $B = 0.17$. The gradients of concentration and electrical potential will scale with the same factor as the current density.

one convection loop, as appears to be the case from the observations of Jaffe and Nuccitelli (1974), then the measured electrical potential gradient would be greater than the potential gradient without convection. The electrical potential gradient within each loop is almost 9 times greater than the gradient without convection. In this case, the current density calculated from Ohm's law would be greater than the actual current density. For hydroxyl transport ($B = 0.31$), although the electrical potential gradient outside of the convection loops is almost twice as great as for proton transport ($B = 0.17$), the computer calculation shows that the electrical potential gradient within and between the convection loops, along the paths discussed above, is altered by <10% compared to that for $B = 0.17$.

Reducing the convection velocity in the numerical calculation by a factor of 5 results in a smaller but qualitatively similar and still significant effect on the concentration and electrical potential profiles. The potential gradient within the convection loops is still up to 3 times as great as without convection. With the velocity reduced by a factor of 50, the calculation shows only a very small perturbation of the concentration and potential profiles, with the potential gradient changing by no more than 20% compared to the gradient without convection.

## DISCUSSION

The vibrating probe has been used to evaluate the apparent current density produced by a large number of different kinds of cells and tissues (Nuccitelli, 1983). In a situation where the main ion species carrying the current at steady state has a mobility that is not much different from the average in the electrolytic medium in which the measurement is carried out, the theory presented in this paper shows that the current density calculated from the measured electrical potential gradient and the conductivity of the medium using Ohm's law should be numerically correct. In this situation, $B$ in Eq. 3 would equal 1, and Ohm's law would be numerically correct with or without the convection loops. However, Eq. 3 also shows that Ohm's law is not correct if $B$ is not close to 1. This would be the case if a high mobility ion species is involved in carrying the current at steady state. The results of the numerical computer calculations based on Eqs. 3 and 4, indicate that the convection loops produced by the vibrating probe will have a profound effect on the ion concentration gradients, and hence on the electrical potential gradients, in the case that $B$ is not close to 1. The strength of this effect will depend on the convection velocity. If the vibrating probe measures the electrical potential gradient within one of the convection loops, then the measured potential gradient will be increased relative to the gradient without convection. If the measured potential gradient is increased by a factor greater than the reciprocal of $B$, then the current density calculated using Ohm's law will be greater than the actual current density. Thus, the current density obtained with the vibrating probe depends in a complex manner on the convection velocity and on the identity of the ion species carrying the current. This latter aspect depends on the ion transport processes occurring in the cell membrane. A precise determination of the relationship between the electrical potential gradient measured by the vibrating probe and the current density will require more experimental work on the pattern and velocity of the convection loops produced by the probe, as well as studies on the nature of the underlying ion transport processes occurring in particular biological systems.

A number of experimental tests of the theory presented here are possible. In principle, the ion concentration gradients, the electrical potential gradient, and the current density can all be measured in ways that do not involve the vibrating probe. Thus, Eqs. 3 and 4 could be tested experimentally. Some preliminary experiments along these lines have been done using the giant algal cells of *Chara corallina* (Ferrier and Lucas, 1979). In these experiments, the extracellular pH gradient was measured using a small pH electrode, and the extracellular electrical potential gradient was measured using a microelectrode. These measurements showed that, near the surface of the cell, the hydroxyl chemical potential gradient between the "alkaline" and "acid" regions was ~35 times greater than the electrical potential gradient. This means that the flux of hydroxyl ions was carried almost entirely by diffusion. Current carried by diffusion of hydroxyl ions along the cell surface in the alkaline regions can be calculated to be

( current carried by $OH^-$ alone being about 3× the Ohm's law current)

about twice that driven by the electrical potential gradient. These results agree quite well with the theory underlying the present work (Ferrier, 1980, 1981*a*, 1981*b*), and with the equations developed here.

Another kind of experimental test would involve altering the convection loops during a series of measurements with the vibrating probe. One way this can be done is by changing the viscosity of the medium, thereby changing the convection velocity. An experiment of this kind has been carried out by Lucas and Nuccitelli (1980) during the course of vibrating probe measurements on *Chara corallina*. They increased the viscosity of the medium by a factor of 1,500, which should decrease the velocity in the convection loops by a factor of ~500 (Jaffe and Nuccitelli, 1974). This had the effect of reducing the measured electrical potential gradient near the alkaline regions by a factor of ~4.5. As indicated above, for hydroxyl transport the numerical calculation gives an electrical potential gradient within the convection loop that is ~4.5 times greater than the potential gradient without convection. This experimental result is, thus, in accord with the theory presented here. The measured electrical potential gradient near the acid regions was reduced by a factor of ~2, indicating that the current there may be carried partly by $HCO_3^-$, for which $B$ is close to 1, and partly by protons.

This work was supported by the Medical Research Council of Canada (Jack Ferrier) and the National Science Foundation (PCM 81-17721, William J. Lucas).

*Received for publication 26 June 1985 and in final form 28 October 1985.*

## REFERENCES

Ferrier, J. M. 1973. Junction theories of photoelectric effects at dye-semiconductor interfaces. Ph.D. thesis. Ohio State University, Columbus, OH. 88 pp.

Ferrier, J. M. 1980. Extracellular ion transport. *J. Theor. Biol.* 85:739–743.

Ferrier, J. M. 1981*a*. Time-dependent extracellular ion transport. *J. Theor. Biol.* 92:363–368.

Ferrier, J. M. 1981*b*. On a boundary condition of extracellular ion transport. *J. Theor. Biol.* 93:495–496.

Ferrier, J. 1983. A mechanism for the regulation of ligament width based on the resonance frequency of ion concentration waves. *J. Theor. Biol.* 102:477–486.

Ferrier, J. M., and W. J. Lucas. 1979. Plasmalemma transport of $OH^-$ in *Chara corallina*. II. Further analysis of the diffusion system associated with $OH^-$ efflux. *J. Exp. Bot.* 30:705–718.

Ferrier, J. M., J. Dainty, and S. M. Ross. 1985. Theory of negative capacitance in membrane impedance measurements. *J. Membr. Biol.* 85:245–249.

Jackson, W. D. 1962. Classical Electrodynamics. John Wiley & Sons, Inc., New York. 12–17.

Jaffe, L. F., and R. Nuccitelli. 1974. An ultrasensitive vibrating probe for measuring steady extracellular currents. *J. Cell Biol.* 63:614–628.

Jaffe, L. F., and R. Nuccitelli. 1977. Electrical controls of development. *Annu. Rev. Biophys. Bioeng.* 6:445–476.

Lucas, W. J., and R. Nuccitelli. 1980. $HCO_3^-$ and $OH^-$ transport across the plasmalemma of *Chara*. Spatial resolution obtained using extracellular vibrating probe. *Planta (Berl.)*. 150:120–131.

Nuccitelli, R. 1983. Transcellular ion currents: signals and effectors of cell polarity. *Mod. Cell Biol.* 2:451–481.

Wannier, G. H. 1966. Statistical Physics. John Wiley & Sons, Inc., New York. 532 pp.

Plant Physiol. (1987) 83, 163–169
0032-0889/87/83/0163/07/$01.00/0

# Photorespiration and Internal $CO_2$ Accumulation in *Chara corallina* as Inferred from the Influence of DIC and $O_2$ on Photosynthesis[1]

Received for publication June 23, 1986 and in revised form August 6, 1986

FRANÇOIS BRECHIGNAC[2] AND WILLIAM J. LUCAS*
*Botany Department, University of California, Davis, California 95616*

## ABSTRACT

**An $O_2$ electrode system with a specially designed chamber for 'whorl' cell complexes of *Chara corallina* was used to study the combined effects of inorganic carbon and $O_2$ concentrations on photosynthetic $O_2$ evolution. At pH = 5.5 and 20% $O_2$, cells grown in $HCO_3^-$ medium (low $CO_2$, pH ≥ 9.0) exhibited a higher affinity for external $CO_2$ ($K_{1/2}(CO_2)$ = 40 ± 6 micromolar) than the cells grown for at least 24 hours in high-$CO_2$ medium (pH = 6.5), ($K_{1/2}(CO_2)$ = 94 ± 16 micromolar). With $O_2$ ≤ 2% in contrast, both types of cells showed a high apparent affinity ($K_{1/2}(CO_2)$ = 50 − 52 micromolar). A Warburg effect was detectable only in the low affinity cells previously cultivated in high-$CO_2$ medium (pH = 6.5). The high-pH, $HCO_3^-$-grown cells, when exposed to low pH (5.5) conditions, exhibited a response indicating an ability to fix $CO_2$ which exceeded the $CO_2$ externally supplied, and the reverse situation has been observed in high-$CO_2$-grown cells. At pH 8.2, the apparent photosynthetic affinity for external $HCO_3^-$ ($K_{1/2}[HCO_3^-]$) was 0.6 ± 0.2 millimolar, at 20% $O_2$. But under low $O_2$ concentrations (≤2%), surprisingly, an inhibition of net $O_2$ evolution was elicited, which was maximal at low $HCO_3^-$ concentrations. These results indicate that: (a) photorespiration occurs in this alga and can be revealed by cultivation in high-$CO_2$ medium, (b) *Chara* cells are able to accumulate $CO_2$ internally by means of a process apparently independent of the plasmalemma $HCO_3^-$ transport system, (c) molecular oxygen appears to be required for photosynthetic utilization of exogenous $HCO_3^-$: pseudocyclic electron flow, sustained by $O_2$ photoreduction, may produce the additional ATP needed for the $HCO_3^-$ transport.**

The investigations dealing with the interactions between photorespiration and photosynthesis in aquatic photosynthetic organisms of the $C_3$ carboxylation type have focused mostly on microalgae. In contrast to high-$CO_2$-grown cells, microalgae cultured under low-$CO_2$ conditions appear to develop a $CO_2$-concentrating mechanism. This mechanism raises the apparent affinity of photosynthesis, for external DIC,[3] to levels far exceeding the carboxylase affinity for $CO_2$ (1–4, 11, 20, 30). Consequently, the oxygenase activity of the Rubisco enzyme in low-$CO_2$-grown cells is inhibited, and they do not exhibit the general features associated with the occurrence of photorespiration, as deduced from the effects of $O_2$ concentration (8, 21, 28, 29, 31). In addition, since most of these cells appeared to be able to photosynthetically use exogenous $HCO_3^-$, the $CO_2$ concentrating mechanism has been related to the operation of an active $HCO_3^-$ pump located either in the plasmalemma (2, 11, 18) or in the inner chloroplast envelop (20). However, this $HCO_3^-$ transport model cannot explain all the experimental data, and as a consequence, some authors have postulated the existence of a $CO_2$ transport system (1, 17).

The plasticity of the photosynthetic and photorespiratory patterns exhibited by aquatic macrophytes when grown in various culture conditions, has been recently stressed (5). Although there is a limited amount of information available on these aquatic macrophytes, it would appear that in some species, the state of reduced photorespiration may be attributed to the operation of a $HCO_3^-$ accumulation system working in association with carbonic anhydrase activity (27), in a manner similar to that in some of the microalgae.

Very little information is available concerning the macroalgae. Although *Chara corallina* has been extensively used to study the $HCO_3^-$ transport phenomenon from a photosynthetic (12) as well as an ultrastructural viewpoint (24), controversy still exists as to the actual DIC species being transported across the plasmalemma. Furthermore, experiments relating to the presence or absence of a DIC concentrating mechanism have not yet been conducted.

In the present paper we report on studies in which we examined the combined influence of DIC and $O_2$ concentration on the photosynthetic rates exhibited by high- and low-$CO_2$-grown *Chara* cells. These results establish both the occurrence of photorespiration and a putative $CO_2$ concentrating mechanism in *Chara corallina*.

## MATERIALS AND METHODS

**Plant Material and Culture Conditions.** Male cultures of *Chara corallina* Klein ex Willd., em. R. D. W. (= *Chara australis* R. Br.) were grown in 60 L containers in solutions of '*Chara* pond water' (CPW: 1.0 mM NaCl, 0.2 mM KCl, 0.2 mM $CaSO_4$). Low-$CO_2$-grown cells were cultured in the presence of 1.0 mM $NaHCO_3$, and since stagnant conditions were employed, the bulk pH value ranged from 9 to 10.5, during photosynthetic activity. High-$CO_2$-grown cells were cultured in the above-mentioned conditions, except that a 4% $CO_2$ stream (balanced with air) of approximately 1 to 2 $L \cdot h^{-1}$ was bubbled through a sintered glass in a glass exchange column (height, 60 cm; diameter, 5 cm) placed vertically in the center of the culture tank. The exchange column prevented direct contact between the $CO_2$ and the *Chara* cells and also created a gentle convection stream within the culture medium, ensuring homogeneous repartition of the high $CO_2$ concentration. Under these high $CO_2$ conditions, the culture

[1] Supported by National Science Foundation Grant DMB-85 03153,
[2] Current address: Service de Radioagronomie, Department de Biologie, CEN-Cadarache, 13108-Saint Paul lez Durance, France.
[3] Abbreviations: DIC, dissolved inorganic carbon; Rubisco, ribulose-1,5-bisphosphate carboxylase oxygenase; CPW, *Chara* pond water; RuBP, ribulose-1,5-bisphosphate.

medium was buffered with 3.0 mM Mes, and the pH value ranged from 5.5 to 6.5 during photosynthetic activity. In some experiments we also used cells obtained from short-term cultures. Here, plant material grown in control ($HCO_3^-$, low $CO_2$) cultures was cut and transferred to 4-L beakers containing solution being bubbled with 4% $CO_2$. Provided a minimum culture period of 24 h was employed, these cells exhibited the same photosynthetic behavior as those grown for long-term periods in larger containers.

Artificial light from fluorescent lamps (cool-white, Lifeline; Sylvania, Seneca Falls, NY) provided a photon flux density at the solution surface of 115 $\mu$mol photon$\cdot m^{-2}\cdot s^{-1}$ (measured using a Quantum Sensor, Licor, LI-190 SB). The photoperiod was 14 h-light and 10 h-dark.

**Preparation of *Chara* 'Whorl' Cells.** The photosynthetic pattern of *Chara* cells was found to be very sensitive to perturbation caused by improper handling and physical treatment. Such a sensitivity has already been reported (15). These perturbations were reduced to a minimum by performing the experiments immediately after removing cells from the cultures. For this purpose, apical shoot axes were carefully removed from the culture tank; the selected mature branch cell complex (whorl) attached to the 2nd to the 5th node was carefully cut from the neighboring internodal cells with sharp scissors. The peripheral (terminal) cells of each branch (5–7 branches per node) were cut in order to shape the branch complex with an approximate diameter of 5 cm, for proper loading into the measurement chamber. The excision and pruning of each whorl cell complex was carried out in freshly prepared CPW. Using this protocol, we found that freshly cut and prepared cells exhibited the fastest rates of photosynthetic $O_2$ evolution.

**DIC Solutions.** Solutions were prepared immediately before use. CPW free of $CO_2$ was first obtained by purging the CPW with $CO_2$-free air for 1 h. For experiments performed under 20% $O_2$, inorganic carbon was added to $CO_2$-free CPW via the appropriate aliquot of a recently prepared 20 mM $Na_2CO_3$ stock solution (final volume, 50 ml, in sealed glass flasks). Solution pH values were adjusted to 5.50 ± 0.15, for $CO_2$-containing solutions, and to 8.20 ± 0.15 for $HCO_3^-$ containing solutions, with $H_2SO_4$ (0.1 and 0.01 N). The correct amounts of $H_2SO_4$ were previously determined to allow for rapid pH adjustment.

For experiments performed under low $O_2$ concentrations (≤2%), 100 ml of $CO_2$-free CPW were bubbled with pure $N_2$ for 15 min. Inorganic carbon was then added and the pH adjusted as previously described; during these manipulations, the neck of the flask was continuously flushed with a stream of pure $N_2$ to minimize atmospheric $O_2$ contamination.

We stress here that in the present study, buffers were not used because of their interaction with the uptake of inorganic carbon, particularly at high pH (14, 23).

**Experimental Device.** Because of the sensitivity of *Chara* cells to perturbation, we constructed a special $O_2$ electrode system having a Plexiglas chamber designed to hold whorl cell complexes with a minimum of disturbance to the cells (Fig. 1). The experimental chamber featured a recessed magnetic stirring bar (avoiding contact between the stir bar and the *Chara* cells), a small chamber volume (12 ml) for improved $O_2$ sensitivity, overall uniform illumination of the material, and two ports to permit solution changes. Experiments were performed under fast-stirring conditions, the rate being selected in the region where polarographic $O_2$ measurements became insensitive to the stirring speed. The $O_2$ partial pressure in the chamber was measured using a YSI 4004 Clark $O_2$ probe (YSI Co., Inc., Yellow Springs, OH). Saturating illumination for photosynthesis was found to occur at 100 $\mu$mol photon$\cdot m^{-2}\cdot s^{-1}$; all experiments were then performed at 150 $\mu$mol photon$\cdot m^{-2}\cdot s^{-1}$ which did not introduce problems due to photoinhibition. The light source was a Leitz Pradovit projector (model C1500, 150 W quartz-iodide lamp, E. Leitz, Raleigh, NJ), used with neutral density filters (Balzers, type no. 106613, PTR Optics Corp., Waltham, MA). Infrared irradiation was removed using a 10 cm-long water filter and all experiments were conducted in a thermostated room at 25 ± 2°C.

**Experimental Procedures.** Two *Chara* whorl cell complexes were carefully loaded into the chamber, which was then continuously illuminated. An investigation of the DIC concentration effect on photosynthesis always began by pretreating the cells in $CO_2$-free CPW and waiting for complete depletion of available $CO_2$, a condition assumed to be reached when the rate of $O_2$ evolution approached zero. The period necessary to establish this condition ranged from 3 to 30 min at 20% $O_2$, but was longer (up to 1 h) at low $O_2$ concentrations ($O_2$ contamination, which was leaking across the Teflon membrane from the electrolyte of the probe, was probably responsible). Thereafter, the DIC concentration was increased, with the chamber being rinsed several times between each measurement, and $O_2$ evolution was recorded over a 10 to 25 min period. Steady state rates of photosynthesis were reached in this range of time, with the $O_2$ concentration being maintained either at 20 ± 2%, or between 0 and 2%.

We also conducted $CO_2$ depletion experiments. Following a DIC concentration study (at 20% $O_2$), the experimental chamber was rinsed (four times) with $CO_2$-free CPW before introducing a solution having a low $CO_2$ concentration (20–60 $\mu$M, initial pH = 5.5). The depletion of $CO_2$ was recorded by the decrease of net $O_2$ evolution for periods of up to 60 min. Relatively small amounts of $CO_2$ were used to avoid a buildup of the $O_2$ concentration in the chamber and to reach a final pH value not exceeding 6.

## RESULTS

***Chara* Photosynthetic Characteristics at pH = 5.5.** Using our new experimental system, we found that low-$CO_2$-grown *Chara* cells (stagnant alkaline pH culture conditions, 1.0 mM $HCO_3^-$) exhibited interesting photosynthetic characteristics. Figure 2 shows the influence, at pH = 5.5, of $CO_2$ concentration on the rate of net photosynthetic $O_2$ evolution. Net photosynthesis saturated at 300 $\mu$M $CO_2$, with maximal rates of approximately 200 pmol $O_2\cdot cm^{-2}\cdot s^{-1}$ (about 88 $\mu$mol $O_2\cdot$ mg $Chl^{-1}\cdot h^{-1}$). These cells exhibited a high apparent affinity for exogenous $CO_2$, as evidenced by the low $CO_2$ concentration required for half-maximal rate; the $K_{1/2}(CO_2)$ was approximately 40 $\mu$M. In contrast, high-$CO_2$-grown *Chara* cells (Fig. 3) required between 500 and 1000 $\mu$M $CO_2$ to attain saturation, with the maximal photosynthetic rate in these cells being approximately 160 pmol $O_2\cdot cm^{-2}\cdot s^{-1}$. We attribute the difference between the maximal rates in low- and high-$CO_2$-grown *Chara* cells to a slightly lower Chl concentration (on a surface basis) in the high-$CO_2$-grown cells (data not shown). However, high-$CO_2$-grown cells had a lower apparent affinity for exogenous $CO_2$; the $K_{1/2}(CO_2)$ was approximately 90 $\mu$M.

**Influence of $O_2$ Concentration on Photosynthesis at pH = 5.5.** The influence of low (≤2%) and atmospheric (20 ± 2%) concentrations of $O_2$ on the photosynthetic response curves for exogenous $CO_2$ (pH = 5.5) are shown for low-$CO_2$-grown (Fig. 4) and high-$CO_2$-grown (Fig. 5) *Chara* cells. Clearly, low-$CO_2$-grown cells were nearly insensitive to a reduction in the level of $O_2$. In contrast, photosynthesis in high-$CO_2$-grown cells was clearly stimulated when the $O_2$ concentration was lowered.

Figure 6 presents a summary of the stimulation of photosynthesis at low $O_2$, compared to atmospheric $O_2$ levels (Warburg effect), that we obtained when we investigated the effect of $CO_2$ concentration on low- and high-$CO_2$-grown cells. In high-$CO_2$-grown cells, the Warburg effect increased as the $CO_2$ concentration was reduced, except for very low $CO_2$ concentrations. The

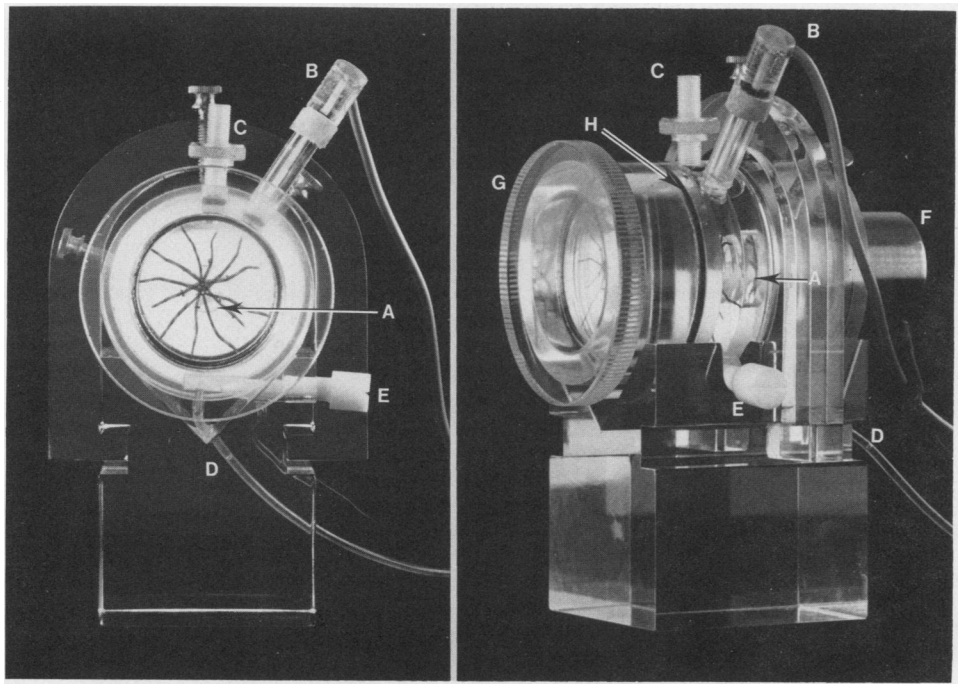


FIG. 1. Plexiglas chamber for measuring $O_2$ evolution in whorl cell complexes of *C. corallina*. This system featured a recessed magnetic stir bar (A), an $O_2$ electrode (B), an inlet (C), and outlet (D) port with a Teflon valve (E), a magnetic stirrer (F), and a removable lid (G) which hermetically closed the chamber by means of an O-ring (H).

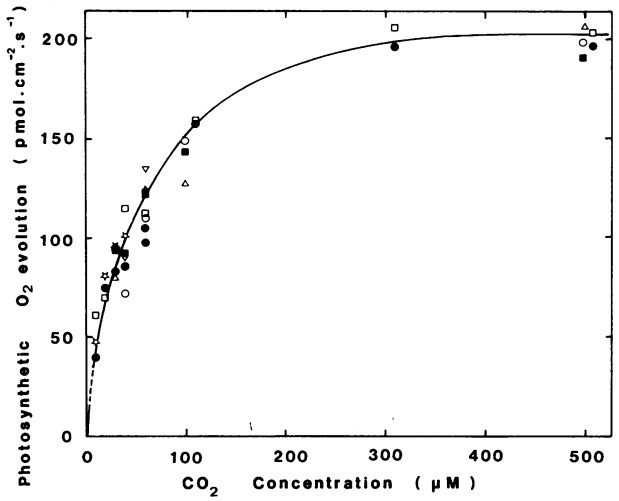


FIG. 2. Influence of $CO_2$ concentration on the rate of $O_2$ evolution in low-$CO_2$-grown cells of *C. corallina*. Each symbol represents a different experiment, conducted at pH 5.5 and over a range of $CO_2$ concentrations, on two whorl cell complexes which were grown in $HCO_3^-$ medium (low $CO_2$, pH > 9).

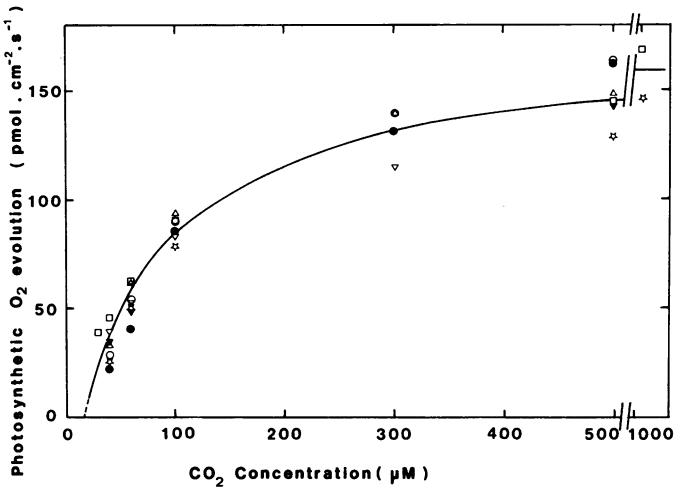


FIG. 3. Influence of $CO_2$ concentration on the rate of $O_2$ evolution in high-$CO_2$-grown cells of *C. corallina*. Details as in Figure 2.

average apparent affinities for exogenous $CO_2$, obtained under low and atmospheric $O_2$ levels, for a number of different samples of low- and high-$CO_2$-grown *Chara* cells, are presented in Table I. The difference observed in the $K_{1/2}(CO_2)$ between the low and 20% $O_2$ level experiments for low-$CO_2$-grown cells is not statistically significant.

**Photosynthetic $CO_2$ Depletion Experiments Conducted at pH = 5.5.** Photosynthetic $CO_2$ depletion of the medium (initial pH = 5.5) surrounding the cells was followed using both low- and high-$CO_2$-grown *Chara* cells. These experiments were conducted at the completion of the $CO_2$ concentration studies, and were performed in order to compare the amount of $CO_2$ externally supplied to the amount of $CO_2$ fixed photosynthetically. The $CO_2$ fixed was deduced from the integration of the rate of $O_2$ evolution as a function of time, assuming a photosynthetic ratio of 1. Figure 7 (inset) illustrates a typical exponential decrease in the rate of $O_2$ evolution *versus* time. This exponential decrease was confirmed by plotting the logarithm of the rate of $O_2$ evolution-against time (Fig. 7). From this form of analysis, we obtained the appropriate exponential functions. In this way we could calculate, on the same mathematical basis, all the integrals of each different function. Table II gives the results of these integrations, in which we estimated the amount of carbon fixed, in comparison to the amount of carbon externally supplied, along with the $K_{1/2}(CO_2)$ values which were determined in the respective preceding experiments.

We found that in low-$CO_2$-grown *Chara* cells, with high apparent affinities for exogenous $CO_2$ ($K_{1/2}[CO_2]$ = 34–40 $\mu$M), the carbon fixed always exceeded the externally supplied DIC. Consequently, some internal $CO_2$ must have been present in these cells at the beginning of the $CO_2$ depletion experiment. Alternatively, the internal $CO_2$ might have been raised by simple diffusion during the preceding investigation in which high $CO_2$ concentrations were employed. This maximal putative amount of internal DIC, which would have resulted from diffusion, can be

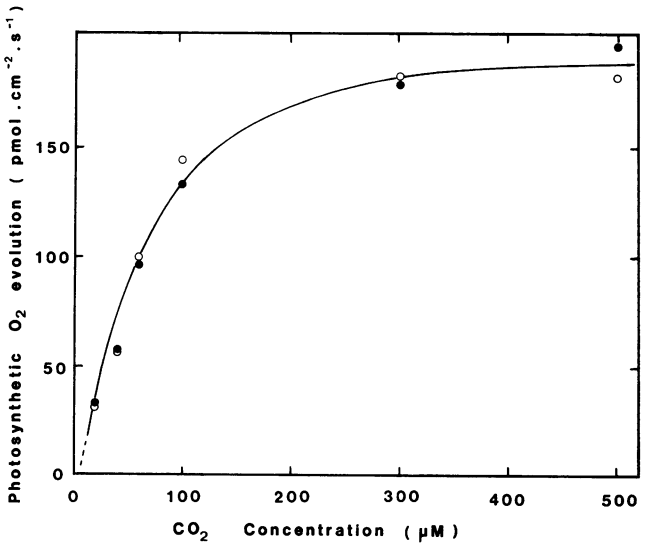


FIG. 4. Influence of $O_2$ concentration on the photosynthetic response to $CO_2$ in low-$CO_2$-grown cells of *C. corallina*. The rates of $O_2$ evolution were measured at pH ≃ 5.5 under 20% $O_2$ (●) and ≤2% $O_2$ (○).

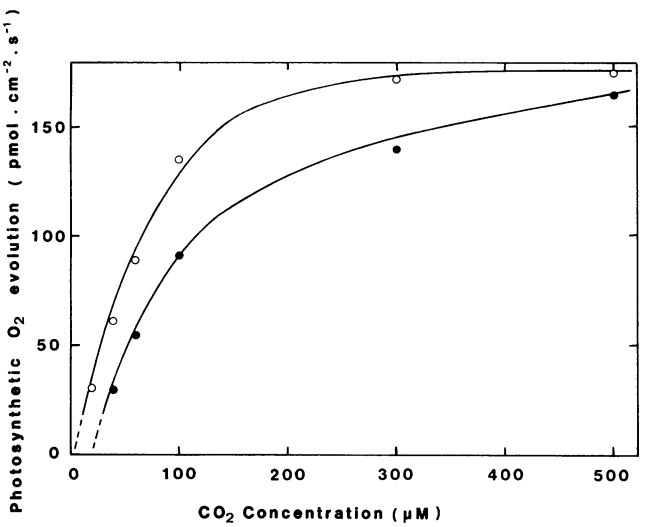


FIG. 5. Influence of $O_2$ concentration on the photosynthetic response to $CO_2$ in high-$CO_2$-grown cells of *C. corallina*. The rates of $O_2$ evolution were measured at pH ≃ 5.5 under 20% $O_2$ (●) and ≤2% $O_2$ (○).

estimated by assuming a total inefficiency of the four rinses (with $CO_2$-free CPW) in removing some internal $CO_2$ along with the external $CO_2$. However, even after deduction of the corresponding values, the internal $CO_2$ present remained significant (Table II, "internal carbon fixed," values in parentheses).

In contrast, photosynthesis by the high-$CO_2$-grown *Chara* cells (low apparent affinity for $CO_2$: $K_{1/2}[CO_2]$ = 80–98 μM) stopped before removal of all the external $CO_2$, as shown by the "unfixed external $CO_2$" values (Table II).

**Influence of $O_2$ and DIC Concentration on Photosynthesis at pH = 8.2.** Typical examples of the influence of DIC concentrations on photosynthesis at low (≤2%) and atmospheric (20%) $O_2$ levels are presented in Figure 8. At pH = 8.2, $HCO_3^-$ is the major DIC species present in solution. Thus, the observed photosynthetic response to changes in DIC concentration (pH = 8.2, 20% $O_2$) can be described as follows: $V_{max}$ ($HCO_3^-$) = 107 ± 11 pmol $O_2 \cdot cm^{-2} \cdot s^{-1}$ and $K_{1/2}(HCO_3^-)$ = 0.6 ± 0.2 mM. Surprisingly, compared to 20% $O_2$, low $O_2$ tensions caused an inhibition of photosynthesis. This inhibition was quite reproducible (Fig. 9),

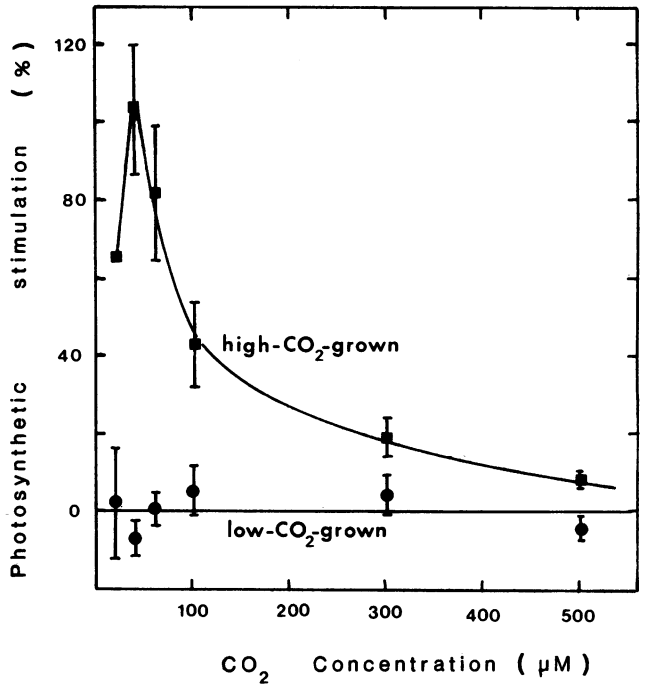


FIG. 6. Effect of low $O_2$ concentration on photosynthesis in high- and low-$CO_2$-grown cells of *C. corallina* at various concentrations. The stimulation at low $O_2$ (≤2% $O_2$) is expressed as a percentage of the rate measured under 20% $O_2$. (Values represent Mean ± SD $n \geq 3$).

Table I. *Apparent Photosynthetic Affinity for Exogenous $CO_2$ in High-$CO_2$- and Low-$CO_2$-grown Chara Cells at Atmospheric (20%) and Low (≤2%) $O_2$ Concentrations*

| | $K_{1/2}$ ($CO_2$) (μM ± SD) | |
|---|---|---|
| | ≤2% $O_2$ | 20% $O_2$ |
| High-$CO_2$-grown cells | 52 ± 9 (4)[a] | 94 ± 16 (9) |
| Low-$CO_2$-grown cells | 50 ± 6 (5) | 40 ± 6 (12) |

[a] Mean ± SD; values in parenthesis indicate number of experiments performed.

with the maximum effect being observed at low, and almost no effect at high (5.0 mM) DIC concentrations.

## DISCUSSION

**Kinetic Properties of *Chara* Photosynthesis with Exogenous DIC.** Our maximum rates of photosynthesis, obtained with *Chara* branch cells exposed to 20% $O_2$ and $CO_2$ as the main form of DIC (pH 5.5), were very close to those reported in a similar study by Price *et al.* (24). With our tissue, the apparent affinity for $CO_2$ ($K_{1/2}[CO_2]$ = 40 μM) was higher than the value reported by these workers (76 μM). Nevertheless, Price *et al.* (24) recognized that a higher affinity could probably have been obtained by using a more rapid stirring rate, which would have reduced the extent of the unstirred layer between the bulk medium and the cell surface. However, they reported no difference between the cells grown in alkaline (pH = 9.3) and those grown in slightly acidic (pH = 6.8) conditions, a feature in apparent contradiction with the clearly distinct affinity for $CO_2$ found in the present study (Table I). The probable explanation is that the *Chara* cells used by Price *et al.* (24) were all grown under low $CO_2$ conditions, corresponding to an atmosphere-equilibrated $CO_2$ concentration, at most, whereas our acid cultures were $CO_2$ enriched.

The photosynthetic characteristics of alkaline-grown cells ob-

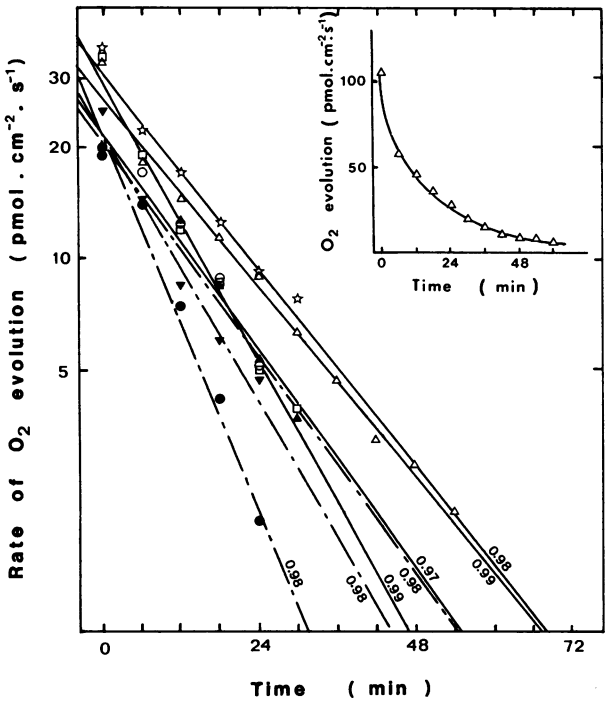


FIG. 7. Kinetics of $O_2$ evolution during photosynthetic $CO_2$ depletion studies on low- and high-$CO_2$-grown cells of *C. corallina*. The decrease in net $O_2$ evolution as a function of time (see inset) has been represented in a semilogarithmic plot for four experiments on low-$CO_2$-grown cells (open symbols, solid lines) and three experiments on high-$CO_2$-grown cells (closed symbols, broken lines). The high regression coefficients ($\geq$0.97) indicate that the decrease in $O_2$ evolution followed an exponential function.

Table II. *Comparison between the Amounts of Inorganic Carbon Supplied and Photosynthetically Fixed in Low- and High-$CO_2$-grown Chara Cells*

By assuming a photosynthetic ratio of 1, the amount of carbon fixed was calculated from the integration of the kinetics of $O_2$ evolution obtained during $CO_2$-depletion experiments (see Fig. 7). For all $CO_2$-depletion experiments, the chamber containing the *Chara* whorl cells was washed four times with $CO_2$-free CPW, and $O_2$ evolution was then initiated by addition of CPW containing 20 to 60 $\mu$M DIC (carbon supplied). In high-$CO_2$-grown cells, the carbon supplied always exceeded the carbon fixed (unfixed external carbon), whereas in low-$CO_2$-grown cells, carbon fixed always exceeded the carbon supplied. The difference between carbon fixed and that supplied externally is presented as the amount of internal carbon supplied for photosynthesis. Values in parentheses indicate the amount of internal carbon that would still exist even after deduction of the maximal $CO_2$ concentration which would have been present internally if the chamber had not been washed with $CO_2$-free CPW.

| | High-$CO_2$-Grown Cells | | | Low-$CO_2$-Grown Cells | | | |
|---|---|---|---|---|---|---|---|
| $K_{1/2}$ ($CO_2$) ($\mu$M) | 80 | 98 | 98 | 40 | 34 | 34 | |
| Carbon fixed (nmol $CO_2$) | 221 | 305 | 359 | 413 | 377 | 614 | 544 |
| Carbon supplied (nmol $CO_2$) | 720 | 480 | 480 | 360 | 240 | 480 | 480 |
| Unfixed external carbon (nmol $CO_2$) | 499 | 175 | 121 | | | | |
| Internal carbon (nmol $CO_2$) | | | | 53 (42) | 137 (89) | 134 (89) | 64 (19) |

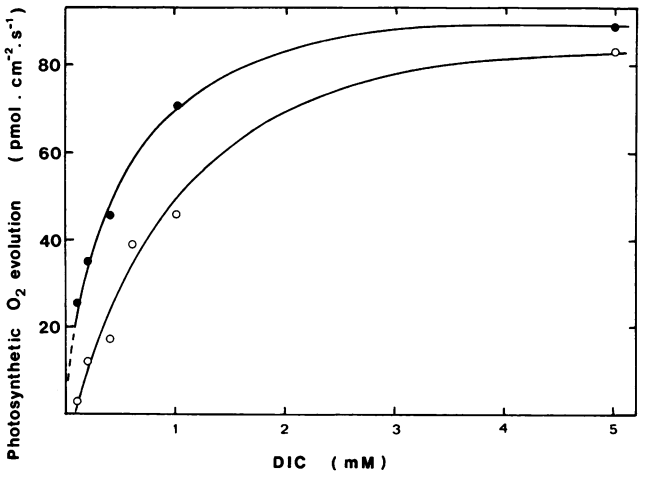


FIG. 8. Influence of $O_2$ concentration on photosynthesis in $HCO_3^-$-grown (low $CO_2$) *C. corallina*. $O_2$ evolution was measured at pH $\simeq$ 8.2 in 20% (●) and $\leq$2% $O_2$ (○).

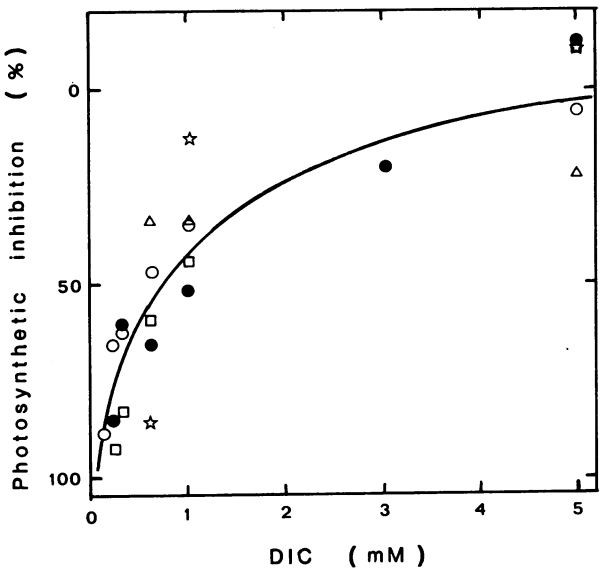


FIG. 9. Inhibition by hypoxia of $HCO_3^-$-supported photosynthesis in $HCO_3^-$-grown (low $CO_2$) *C. corallina*. The inhibition at low $O_2$ ($\leq$2%) is expressed as a percentage of the rate measured under 20% $O_2$ (at the same DIC concentration).

tained by varying the $HCO_3^-$ concentration were in agreement with those reported by Price *et al.* (24). Bicarbonate-supported photosynthesis exhibited a maximum rate (107 ± 11 pmol $O_2 \cdot cm^{-2} \cdot s^{-1}$) about half that of $CO_2$-supported photosynthesis ($\simeq$200 pmol $O_2 \cdot cm^{-2} \cdot s^{-1}$), a feature which has been attributed to the additional expense of photosynthetically generated energy involved in the uptake of exogenous $HCO_3^-$ (26).

**Involvement of Photorespiration in High-$CO_2$-Grown *Chara* Cells.** It has been well documented that the Rubisco exhibits an oxygenase activity, along with the carboxylase activity. On this enzyme, the $O_2$ and $CO_2$ substrates act as competitive inhibitors, according to the respective kinetic properties of each activity (9). Hence, the stimulation of photosynthesis when the $O_2$ concentration is decreased (Warburg effect) has been attributed to the inhibition of the oxygenase activity which gives rise to an equivalent stimulation of the carboxylase activity. Numerous workers have used this effect to establish the occurrence of photorespiration in algal systems (8, 21, 28, 31).

The clear Warburg effect observed in high-$CO_2$-grown cells of

*C. corallina* (Fig. 5) is consistent with the operation of photorespiration in this species. In accordance with the model of competitive inhibition at the Rubisco level (9): (a) the stimulation of photosynthesis by low $O_2$ tensions was $CO_2$ sensitive, being maximal at low $CO_2$ and disappearing at saturating $CO_2$ concentrations (Fig. 6); (b) the apparent affinity of photosynthesis for $CO_2$ was $O_2$-sensitive in high-$CO_2$-grown cells (Table I). Such a behavior has often been reported in high-$CO_2$ grown microalgae (2, 21, 29), or in microalgal mutants (30), both of which have a reduced ability to concentrate $CO_2$. The reduced stimulation of photosynthesis observed at 10 $\mu$M $CO_2$ may be due to the inactivation brought about by low $CO_2$ of either the catalytic site of Rubisco or the PSII complex.

**Evidence for an Internal $CO_2$ Concentrating Mechanism.** Unlike high-$CO_2$-grown cells, photosynthesis in low-$CO_2$ grown ($HCO_3^-$ medium, pH >9) *Chara* cells was $O_2$-insensitive when the experiments were performed under acidic conditions (pH = 5.5). The Warburg effect was absent (Figs. 4 and 6), and the apparent affinity of photosynthesis for $CO_2$ was high and almost not affected by $O_2$ ($K_{1/2}[CO_2]$ = 40–50 $\mu$M, Table I). In microalgae, the kinetic characteristics of the Rubisco have been shown to be similar in high- and low-$CO_2$-grown cells (4, 32). Hence, the reduced $O_2$-sensitivity of photosynthesis has been explained on the basis of an internal $CO_2$ concentrating mechanism, occurring in low-$CO_2$ grown cells, which suppresses the potential oxygenase activity of the Rubisco (2, 3, 8, 10, 11). Thus, the absence of detectable photorespiration (as deduced from $O_2$-insensitive photosynthesis) in low-$CO_2$-grown *Chara* cells appears consistent with the hypothesis that these cells can also raise their internal $CO_2$ above the external $CO_2$ concentration.

Compared with the apparent affinity of photosynthesis for $CO_2$, the lower affinity exhibited, *in vitro*, by the Rubisco extracted from some microalgae is another argument in favor of a $CO_2$ concentrating mechanism (11, 32). Yeoh *et al.* (34) reported a value of 42 ± 4 $\mu$M for the $K_m$ ($CO_2$) of Rubisco extracted from a *Chara* species, a value which was determined in the absence of $O_2$. Hence, in the absence of a $CO_2$ concentrating mechanism, intact *Chara* cells placed in 20% $O_2$ should exhibit a $K_{1/2}(CO_2)$ higher than 42 $\mu$M. Furthermore, the resistances limiting $CO_2$ diffusion between the external medium and the site of $CO_2$ fixation will also contribute to reducing the apparent photosynthetic affinity for $CO_2$. However, our $K_{1/2}(CO_2)$ for low-$CO_2$-grown *Chara* cells remained low (40 ± 6 $\mu$M, Table I), even in 20% $O_2$, a result which supports our hypothesis that a $CO_2$ concentrating mechanism exists in this alga.

The ability of low-$CO_2$-grown *Chara* cells to internally accumulate $CO_2$ is also supported by our $CO_2$-depletion experiments conducted in the presence of 20% $O_2$ (Fig. 7). The carbon fixed exceeded the carbon externally supplied, a behavior which was not observed in high-$CO_2$-grown cells (Table II). Such an excess in carbon fixed still remained even when we allowed for the maximal potential error introduced by the experimental protocol (see "Materials and Methods"). Since the investigation of the $CO_2$ effect on photosynthesis (which was performed before a $CO_2$ depletion study) began only after the cells had removed all the contaminating $CO_2$, externally as well as internally (*i.e.* when $O_2$ evolution completely stopped), these cells must have been able to accumulate some $CO_2$ from the previously used acidic (pH = 5.5) bathing medium. This ability to accumulate $CO_2$ appears to be independent of the presence of $HCO_3^-$ in the external solution.

Many reports dealing with microalgae have emphasized that the internal $CO_2$ accumulation was caused by the operation of an active $HCO_3^-$ pump located in the plasmalemma (11, 18). In *Chara* cells, the presence of a plasmalemma-mediated $HCO_3^-$ acquisition mechanism, driven by an ATP-dependent $H^+$ extrusion, is well established (for a review, see Lucas [13]). The results presented here (Fig. 7; Table II) suggest that the $CO_2$ accumulation mechanism in *Chara*, when activated, does not depend exclusively on this process.

**Oxygen Is Required for Photosynthetic Utilization of Exogenous $HCO_3^-$.** Unlike the high-$CO_2$-grown cells which exhibited a stimulation of photosynthesis at low $O_2$ concentrations, due to the reduced photorespiratory $O_2$ consumption, photosynthesis of the low-$CO_2$-grown cells was inhibited by hypoxia, when they were placed in conditions of exogenous $HCO_3^-$ assimilation (Fig. 8). The inhibition only occurred under limiting $HCO_3^-$ concentrations (Fig. 9). This indicates an $O_2$ involvement with one of the steps between the uptake of exogenous $HCO_3^-$ and the final $CO_2$ fixation step. Such an effect has already been reported in *Anacystis nidulans*, a '$HCO_3^-$-user', where the rate of $^{14}C$-fixation was enhanced at 21% $O_2$ compared with anoxic conditions (19, 21). In the work of Miyachi and Okabe (19), the stimulation only occurred under limiting $HCO_3^-$ concentrations and under high light intensities, conditions similar to those used in the present study. It should be noted that in our experiments, inhibition of photorespiration by low $O_2$ would raise the rate of $CO_2$ fixation within the chloroplasts. However, this photosynthetic enhancement is masked (or prevented) by an inhibition, via the influence of the putative $O_2$-sensitive step.

It is interesting to note that in low-$CO_2$-grown *Chara* cells we observed an $O_2$ stimulation only under exogenous $HCO_3^-$ assimilating conditions. In addition, an electrophysiological interaction between $O_2$ and the $HCO_3^-$ transport system in *Chara* has been recently demonstrated (16). Thus, it appears that the $HCO_3^-$ uptake process, *per se*, is facilitated by $O_2$. This requirement may be an evolutionary adaption to the ecological habitat occupied by *Chara*, namely stagnant water, where $HCO_3^-$ assimilation at alkaline pH values is often associated with super saturating dissolved $O_2$. $O_2$ may be involved in the biochemical process supplying energy to the transport system. It is likely that $HCO_3^-$ acquisition in *Chara* is driven by ATP, whatever the mechanism (13; see also later section). A Mehler-type $O_2$ photoreduction driving pseudocyclic photophosphorylation has been postulated to supply the $HCO_3^-$ transport systems of *Chondrus crispus* (6, 7) and *Scenedesmus* (25) with ATP, and such a process may also be involved in *Chara*. This mechanism is at variance with the model proposed by Ogawa *et al.* (22), in which it was suggested that $O_2$ interaction with ferredoxin (Fd) inhibits the DIC accumulation mechanism functioning in *Anacystis*, a process which they suggest is driven by cyclic photophosphorylation.

However, at present it is not clear why $O_2$ photoreduction should be of higher efficiency (enhanced $O_2$ stimulation of photosynthesis) when photosynthesis is $HCO_3^-$-limited. Possibly, cyclic photophosphorylation might be occurring in the presence of saturating $HCO_3^-$, when $NADP^+$ does not limit its reduction to NADPH at the reduced side of Fd. In this situation, $O_2$ is not involved and no influence on the photosynthetic rate is expected. When the level of exogenous $HCO_3^-$ limits photosynthesis, $NADP^+$ regeneration becomes limiting and would result in competition with $O_2$ for electrons at the Fd level. This may allow $O_2$ photoreduction to drive pseudocyclic photophosphorylation, in aerobic conditions, and thereby sustain a higher rate of $HCO_3^-$ uptake and fixation compared with hypoxic conditions.

**Mechanism of $HCO_3^-$ Acquisition.** It has been proposed that exogenous $HCO_3^-$ enters the cell at alkaline pH by diffusion of $CO_2$, rather than $HCO_3^-$ transport (see Lucas [13] for a review of the relevant literature). In the extracellular $CO_2$ production hypothesis, it was suggested that a plasmalemma-bound $H^+$-translocating ATPase created a high $CO_2$ partial pressure in the unstirred layer next to the wall of these giant cells (33). However, Lucas *et al.* (14) showed that fast-flowing solutions, which would remove the $CO_2$ generated in the unstirred layer, caused an increase, rather than the predicted decrease, in photosynthesis. Our present results (Fig. 8) are also inconsistent with the extra-

cellular $CO_2$ production hypothesis, in that our measured rates of $O_2$ evolution (thin boundary layer due to high stirring rate) were not lower than the $^{14}CO_2$ fixation rates obtained in stagnant solutions (12).

In a modified version of the above-mentioned hypothesis, Price *et al.* (24) and Price and Badger (23) suggested that the extracellular $CO_2$ partial pressure was created in the periplasmic space of the charasomes, a region which would be relatively insensitive to the rate of solution flow. This hypothesis does not appear to be supported by the data presented in Figure 8. In the presence of $HCO_3^-$, photosynthesis appears to saturate at about 3 mM DIC, with the maximum rate being 90 pmol $cm^{-2}s^{-1}$. From the $CO_2$-fixation data in Figure 2, we can estimate that this $V_{max}$ would require an exogenous $CO_2$ concentration in the periplasmic space of, at most, 35 $\mu$M. Clearly, this value is still below the apparent $K_m$ ($CO_2$). Unless the energy demands become too great, it seems unlikely that the periplasmic/charasome $CO_2$-production model can explain why increasing DIC does not raise the external $CO_2$ concentration (and then photosynthesis) to values higher than 35 $\mu$M.

Finally, if $CO_2$ were being supplied to the chloroplasts through an external $CO_2$ production mechanism, investigation of the DIC influence on photosynthesis should have exhibited a stimulation of photosynthesis by low $O_2$, since we have established that photorespiration occurs in *C. corallina.* However, as illustrated in Figures 8 and 9, we observed an inhibition of photosynthesis under low $O_2$ conditions.

Future experiments will utilize MS to investigate both the mechanism of $O_2$ involvement in DIC utilization and the extent to which the putative $CO_2$ concentrating mechanism raises the internal DIC level in *Chara.*

*Acknowledgment:*—We would like to express our thanks to Wes Tallon of the University of California, Physical Plant, for his excellent technical assistance in making the special *Chara* system.

## LITERATURE CITED


1. Badger MR, TJ Andrews 1982 Photosynthesis and inorganic carbon usage by the marine Cyanobacterium, *Synechococcus* sp. Plant Physiol 70: 517–523
2. Badger MR, A Kaplan, JA Berry 1980 Internal inorganic carbon pool of *Chlamydomonas reinhardtii.* Evidence for a carbon-dioxide concentrating mechanism. Plant Physiol 66: 407–413
3. Beardall J, J Raven 1981 Transport of inorganic carbon and the $CO_2$ concentrating mechanism in *Chlorella emersonii* (Chlorophyceae). J Phycol 17: 134–141
4. Berry JA, J Boynton, A Kaplan, MR Badger 1976 Growth and photosynthesis of *Chlamydomonas reinhardtii* as a function of $CO_2$ concentration. Carnegie Inst Wash Year Book 75: 423–432
5. Bowes G 1985 Pathways of $CO_2$ fixation by aquatic organisms. *In* WJ Lucas, JA Berry, eds, Inorganic Carbon Uptake by Aquatic Photosynthetic Organisms. The American Society of Plant Physiologists, Rockville, MD, pp 187–210
6. Brechignac F, M Andre 1985 Oxygen uptake and photosynthesis of the red macroalga *Chondrus crispus*, in seawater. Effects of oxygen concentration. Plant Physiol 78: 545–550
7. Brechignac F, RT Furbank 1986 On the nature of oxygen uptake in the light by *Chondrus crispus.* Effects of inhibitors, temperature and light intensity. Photosynth Res. In press
8. Coleman JR, B Colman 1980 Effect of oxygen and temperature on the efficiency of photosynthetic carbon assimilation in two microscopic algae. Plant Physiol 65: 980–983
9. Farquhar GD, S Von Caemmerer, JA Berry 1980 A biochemical model of photosynthetic $CO_2$ assimilation in leaves of $C_3$ species. Planta 149: 78–90
10. Imamura M, M Tsuzuki, D Hogetsu, S Miyachi 1981 Role of carbonic anhydrase in algal photosynthesis. *In* G Akoyunoglou, ed, Photosynthesis IV. Regulation of carbon metabolism. Balaban International Science Services, Philadelphia, pp 471–482
11. Kaplan A, MR Badger, JA Berry 1980 Photosynthesis and the intracellular inorganic carbon pool in the blue-green alga *Anabaena variabilis*: response to external $CO_2$ concentration. Planta 143: 219–226
12. Lucas WJ 1975 Photosynthetic fixation of $^{14}$carbon by internodal cells of *Chara corallina.* J Exp Bot 26: 331–346
13. Lucas WJ 1983 Photosynthetic assimilation of exogenous $HCO_3^-$ by aquatic plants. Annu Rev Plant Physiol 34: 71–104
14. Lucas WJ, DW Keifer, D Sanders 1983 Bicarbonate transport in *Chara corallina*: evidence for cotransport of $HCO_3^-$ with $H^+$. J Membr Biol 73: 263–274
15. Lucas WJ, R Nuccitelli 1980 $HCO_3^-$ and $OH^-$ transport across the plasmalemma of *Chara corallina*: spatial resolution obtained using extracellular vibrating probe. Planta 150: 120–131
16. Lucas WJ, K Ogata 1985 Hydroxyl- and bicarbonate-associated transport processes in *Chara corallina*: studies on the light-dark regulation mechanisms. J Exp Bot 36: 1947–1958
17. Marcus V, M Volokita, A Kaplan 1984 The location of the transporting system for inorganic carbon and the nature of the form translocated in *Chlamydomonas reinhardtii.* J Exp Bot 35: 1136–1144
18. Miller AG, B Colman 1980 Active transport and accumulation of bicarbonate by a unicellular Cyanobacterium. J Bacteriol 143(3): 1253–1259
19. Miyachi S, K Okabe 1976 Oxygen enhancement of photosynthesis in *Anacystis nidulans* cells. Plant Cell Physiol 17: 973–986
20. Moroney JV, NE Tolbert 1985 Inorganic carbon uptake by *Chlamydomonas reinhardtii.* Plant Physiol 77: 253–258
21. Nilsen S, O Johnsen 1982 Effect of $CO_2$, $O_2$ and diamox on photosynthesis and photorespiration in *Chlamydomonas reinhardtii* (green alga) and *Anacystis nidulans* (Cyanobacterium, blue-green alga). Physiol Plant 50: 273–280
22. Ogawa T, T Omata, A Miyano, Y Inoue 1985 Photosynthetic reaction involved in the $CO_2$ concentrating mechanism in the cyanobacterium, *Anacystis nidulans. In* WJ Lucas, JA Berry, eds, Inorganic Carbon Uptake by Aquatic Photosynthetic Organisms. The American Society of Plant Physiologists, Rockville, MD, pp 287–304
23. Price GD, MR Badger 1985 Inhibition by proton buffers of photosynthetic utilization of bicarbonate in *Chara corallina.* Aust J Plant Physiol 12: 257–267
24. Price GD, MR Badger, ME Basset, MI Whitecross 1985 Involvement of plasmalemmasomes and carbonic anhydrase in photosynthetic utilization of bicarbonate in *Chara corallina.* Aust J Plant Physiol 12: 241–256
25. Radmer R, O Ollinger 1980 Light-driven uptake of oxygen, carbon dioxide and bicarbonate by the green alga *Scenedesmus.* Plant Physiol 65: 723–729
26. Raven JA 1970 Exogenous inorganic carbon sources in plant photosynthesis. Biol Rev 45: 167–221
27. Salvucci ME, G Bowes 1983 Two photosynthetic mechanisms mediating the low photorespiratory state in submersed aquatic angiosperms. Plant Physiol 73: 488–436
28. Shelp BJ, DT Canvin 1980 Photorespiration and oxygen inhibition of photosynthesis in *Chlorella pyrenoidosa.* Plant Physiol 65: 780–784
29. Shelp BJ, DT Canvin 1981 Photorespiration in air and high-$CO_2$ grown *Chlorella pyrenoidosa.* Plant Physiol 68: 1500–1503
30. Spalding MH, RJ Spreitzer, WL Ogren 1985 Use of mutants in analysis of the $CO_2$-concentrating pathway of *Chlamydomonas reinhardtii. In* WJ Lucas, JA Berry, eds, Inorganic Carbon Uptake by Aquatic Photosynthetic Organisms. The American Society of Plant Physiologists, Rockville, MD, pp 361–375
31. Suzuki K, T Ikawa 1984 Effect of oxygen on photosynthetic $^{14}CO_2$ fixation in *Chroomonas* sp. (Cryptophyta). I. Some characteristics of the oxygen effect. Plant Cell Physiol 25: 367–375
32. Tsuzuki M, S Miyachi, JA Berry 1985 Intracellular accumulation of inorganic carbon and its active species taken up by *Chlorella vulgaris* 11 h. *In* WJ Lucas, JA Berry, eds, Inorganic Carbon Uptake by Aquatic Photosynthetic Organisms. The American Society of Plant Physiologists, Rockville, MD, pp 53–66
33. Walker NA, FA Smith, JR Cathers 1980 Bicarbonate assimilation by freshwater Charophytes and higher plants. I. Membrane transport of bicarbonate ions is not proven. J Membr Biol 57: 51–58
34. Yeoh H, MR Badger, L Watson 1981 Variations in kinetic properties of ribulose-1,5-bisphosphate carboxylases among plants. Plant Physiol 67: 1151–1155

BIOMEMBRANES
BIOLOGICAL TRANSPORT
Volumes of
METHODS IN ENZYMOLOGY
*Sidney P. Colowick and Nathan O. Kaplan, Editors-in-Chief*

Volume Editors:

SIDNEY FLEISCHER
Department of Molecular Biology
Vanderbilt University
Nashville, Tennessee 37235
Telephone: (615) 322-2132

BECCA FLEISCHER
Department of Molecular Biology
Vanderbilt University
Nashville, Tennessee 37235
Telephone: (615) 322-2574

# [75] Ion Transport in *Chara* Cells

William J. Lucas

Dept. of Botany

University of California

Davis, CA 95616, U.S.A.

and

Dale Sanders

Dept. of Biology

University of York

Heslington, York YO1 5DD

England

Running Head: Ion Transport in *Chara*

## A. INTRODUCTION

Algal cells of the family Characeae have, for many decades, provided plant cell biologists with an ideal material for studies of ion transport.[1] The size and robustness of the ecorticate giant internodal cells (diameter typically 0.4-1.0 mm, and length up to several cm) has enabled measurement of ion fluxes on single cells without the interpretational difficulties which relate to cellular heterogeneity of most multicellular higher plant tissue. The electrochemical driving forces across the plasma membrane and tonoplast for a variety of ions have been determined by direct measurement of the relevant electrical and chemical components; thus, by application of the Nernst equation, it has been possible to state which ions are actively transported, in which direction and at which membrane. In addition, single internodal cells can be perfused internally (see Beilby[2]), thereby facilitating studies on intracellular control of ion transport.

Ion transport has been most extensively investigated in the genus Chara, although Nitella, Nitellopsis and Lamprothamnium are also commonly used. Within the Chara genus, C. corallina has been the species of choice for most studies: it is easily cultured in the laboratory by rooting the thalli in river mud which is overlayed with a simple salt solution (usually termed Chara Pond Water, CPW). [By contrast, culture in axenic media of defined composition is rarely attempted, though success is possible using the formulation of Forsberg.[3,4]] Other species (e.g. C. inflata) have also been used occasionally for transport studies.[5] Substantial interspecific variation in the electrophysiological properties of Chara implies that the results of transport studies should only be extrapolated from one species to another with extreme caution.[6]

Despite the simple geometry of the internodal cells, the plasma membrane of Chara cannot be viewed as homogeneous with respect to its ion transporting properties. Zones capable of selectively acidifying or alkalinizing the medium are usually present. While the immediate effects of localized $H^+$ transport can be largely abolished with strongly-buffered media, the implications for spatial variation in the transport of other ions is not clear. Flux studies are generally expressed on the basis of cell surface area, though the possibility that this represents some sort of weighted average for the whole plasma

membrane should not be overlooked. Furthermore, Chara cells cultured in alkaline conditions possess significant membrane infoldings (charasomes[7] or plasmalemmasomes[8]). This means that the measured ion fluxes should be considered as a relative guide to the transporting capabilities of cells from a given culture rather than as a physically-interpretable and quantitative reflection of transport activity across the membrane as a whole.

## B. CELL SURGERY AND ION TRANSPORT

Ion transport studies are generally conducted with excised Chara cells bathed in CPW. One suitable formulation for CPW is $K_2SO_4$, 0.2 mM; NaCl, 1.0 mM; $CaSO_4$, 1 mM; pH adjustment via an appropriate zwitterionic buffer, 5 mM. Chara has a very high affinity electrophoretic amine uptake system in the plasma membrane[9] and in order to avoid interference from this system, via its effect on membrane potential, it is important to maintain contaminating $NH_4^+$ as low as possible. Analytical grade reagents should be used, as well as a reliable source of $H_2O$ (either freshly glass-distilled, or passed through a cation exchange column).

### 1. Obtaining Internodal Cells for Flux Measurements.

The Chara thallus assumes an upright growth habit, attaining a height of a metre or more, depending on the depth of the culture solution. The nodes which are present at the ends of the large internodal cells consist of clusters of small cells, and lateral internodes emerge from each node. For studies of ion transport at the single cell level, some degree of cell surgery is required.

Normally, the thalli are harvested from the culture by cutting with a pair of sharp dissecting scissors just above the level of the river mud. The thalli are then transferred to a large bowl of water or CPW to enable easy inspection of suitable cells for flux work. For most studies, the mature cells of the third or fourth internodes are suitable. These are commonly between 20 and 60 mm in length, which facilitates uptake of sufficient radioactivity in short periods even for ions available only at low specific activity. The adjacent internodal cells are cut away, and the lateral internodes carefully trimmed as close as possible to the node. The main axis internodes are then washed free of cell debris in CPW, placed in fresh CPW, and then divided into appropriate batches

for the particular flux experiment. Either at this time, or at the conclusion of an experiment, the surface area of the cells must be determined. This is done by measuring the cell's diameter (± 10 μm), using a binocular microscope, and length by means of tracing the shape of the cell onto paper. After these measurements, cells are placed in a large, covered Petri dish (10 ml/cell is appropriate) and left to recover overnight. Incubation periods exceeding one day should not be used, since there is a marked tendency for time-dependent reduction in transport capacity.[10]

**2. Sampling the Vacuolar Contents.**

Direct sampling of the vacuolar sap is necessary for measurement of intracellular pH with weak acids (see Section E.2.a.) and for compartmental analysis in which the tonoplast fluxes are estimated (Section C.3.b.). An isolated internodal cell (and its associated nodes) is blotted dry with a tissue and allowed to wilt slightly in air before one of the nodes is gently removed with a pair of very sharp scissors. The wilting process is essential before cutting in order to avoid explosion of the cell contents under the influence of cell turgor. The loss in cell turgor is accomplished with minimal change in cell volume—and hence minimal change in vacuolar solute concentration—because the volumetric elastic modulus of Chara is high.[11] A 100 μl Microcap (Drummond Scientific Company, USA) drawn to a fine tip in a flame is inserted into the cut end of the cell as it lies horizontally in the hand. The cell is then moved to a vertical position with the capillary uppermost. The remaining node is cut, and the vacuolar sap can be induced to emerge from the lower end by blowing gently into the capillary. The sample should appear clear: contamination by cytoplasm can be easily visualized as cloudiness or, in extreme cases, the appearance of chloroplasts. If the sample is collected on a preweighed planchet, the volume of sap can be estimated from its weight, assuming as density of unity.

The sap collected (10-20 μl) is sufficient for determination of radioactivity by scintillation counting, of osmotic pressure using an osmometer (e.g. Model 5100C, Wescor Inc., Logan, UT), or of concentration of the major inorganic ions, each measurement being possible on a single cell. The chloride concentration can be determined by electrometric titration,[12] while the $Na^+$, $K^+$ and $Ca^{2+}$ concentrations can all be measured by atomic

absorption spectroscopy (e.g. aa/ae spectrophotometer, Advanced Instrumentation Inc., Warrington, Cheshire, England).

**3. Intracellular Perfusion.**

The possibility of controlling the internal milieu is one of the fortes of using giant internodal cell for transport work.[13,14,15,16] The general technique described below is based on the work of Tazawa and coworkers for selective perfusion of the vacuolar sap,[17,18,19], as well as for perfusion of the sap and flowing cytoplasm.[20]

In order to preserve the tonoplast, it is necessary to include $Ca^{2+}$ (10 mM) in the perfusion solution; conversely, the tonoplast can be destroyed by reducing free $Ca^{2+}$ with chelators. Two sample perfusion media--for vacuolar and cytoplasmic perfusion respectively--are given in Table 1. In each case it is necessary first to measure the osmotic pressure of the intact cell by incipient plasmolysis and to match the perfusion media accordingly, since cell-to-cell variation in osmotic pressure can be considerable. Apart from the presence of $Ca^{2+}$, the actual composition of the vacuolar medium is not critical, and indeed, all other ions can be replaced with a sugar or sugar alcohol osmoticum. By contrast, the cytoplasmic perfusion medium composition is more critical to the survival of the cell. Lucas & Shimmen[21] found that incorporation of 5% Ficoll in the cytoplasmic perfusion medium enhanced the survival rate. Other recipes for cytoplasmic perfusion media have also been reported.[13,15,16,20,22,23]

Fig. 1 shows apparatus of the type commonly used for both vacuolar and cytoplasmic perfusion. Apeizon L grease is applied liberally to the Plexiglas base-plate at the prospective contact points of the three chambers. A straight internodal cell (diameter 0.7-0.9 mm, and length 40-70 mm) is selected, botted dry and 6 ligatures are tied very loosely around it. The ligatures are of waxed dental floss which has been cut to a length of about 100 mm and divided longitudinally into about 4 or 5 equal strands. The cell is placed on the elevated section of the base plate such that 3 of the ligatures reside between the eventual positions of each of the end chambers and the central chamber. The elevated section of the base-plate enables clear viewing of the cell with a binocular microscope through the cover slip which forms one side of the central chamber. The

elevated section also allows easy access to the ends of the ligatures which hang over each side. The three chambers, all pre-greased at the contact points, are then placed over the cell as indicated in Fig. 1 before turgor is lost. The chambers are each grooved (1 mm depth) at points where contact is to be made with the cell. After positioning of the chambers, CPW can be added to the central chamber in order to restore turgor, pending further manipulation of the cell. To begin perfusion, the CPW in the central chamber is removed with a pasteur pipette and the surface film blotted with a tissue. The two end chambers are then filled with an isotonic, artificial vacuolar sap. After loss of turgor, the nodes are removed with sharp dissecting scissors.

In our experience, the critical point of the operation concerns the point at which turgor is judged to have been lost sufficiently to prevent forced expulsion of the cell contents on cutting, yet insufficiently to result in physical distortion of the cell surface. If either of these conditions is exceeded, the selective permeability properties of the cell are lost. One convenient method for assessment of the time at which the nodes can be excised is to apply very gentle pressure to one end of the cell with the dissecting scissors: if a slight concavity remains in the surface, the cell can be cut without detrimental effect.

During removal of the nodes, the tap (Fig. 1) connecting the end chambers is open, thereby prohibiting the establishment of a hydrostatic pressure difference across the ends of the cell. However, as soon as excision is complete, the tap is closed, and medium is removed from one of the end chambers with a Pasteur pipette. Simultaneously, the cell is observed, with the microscope focussed on the vacuolar contents. For vacuolar perfusion, the flow rate is adjusted empirically to around 1000 μm/s. For cytoplasmic perfusion, the flow rate can be considerably faster, the sheer forces aiding the removal of the tonoplast. Actually, perfusion can be allowed to proceed driven by a 5 mm hydrostatic head. After 1-2 min of perfusion, the flow is stopped by opening the tap. The outermost pair of ligatures is tied, taking great care not to bend the cell. CPW + 100 mM sorbitol is then added to the central chamber, and the cell partially restores its turgor pressure within seconds. The middle pair of ligatures is tied, and the experimenter should now feel some

considerable resistance from the cell turgor pressure. Finally, to ensure tight sealing of the perfused cell, the cell is ligated again, this time as close as possible to the central chamber. After this, full osmotic pressure can be restored by replacement of the medium in the central chamber with CPW.

There are several variations on the above theme.[24,25] The simplest is to omit ligation altogether, in which case isotonic CPW must be added to the central chamber at the end of perfusion and the exposed cell segments covered with liquid paraffin to avoid evaporative losses. This "open vacuole" method has seen extensive use for electrophysiological studies,[2] but, despite the clear advantages of obtaining more than one flux measurement on a single cell, has not yet been applied for straightforward transport work.

For influx studies, isotope can be added to the central chamber after allowing a period of 5 min for recovery of the cell and inspection for signs of gross physical damage. An influx period of 5 min or less enables sufficient radioactivity to enter the cell, after which time the solution is removed and replaced by an identical non-radioactive solution. Cell wall exchange of radioisotopic anions is complete within 2 min (see below). The cell can then be briefly re-washed before placing in a scintillation vial for counting. Ion efflux is simply measured by sampling the external medium, which can be stirred periodically by solution withdrawal and expulsion with a Pasteur pipette.

## C. MEMBRANE FLUXES

### 1. Isotopic Influx at the Plasma Membrane.

(a) Anions

(i) Chloride. Chloride is the major anionic constituent of the Chara vacuole, and as such its transport has been more intensively studied than that of other anions. Thus, we will illustrate anion influx measurements using $Cl^-$ as the case ion. The special case of $HCO_3^-$ is dealt with in section (ii).

After overnight recovery from excision (Section B.1), and 2 h before the start of the $^{36}Cl^-$ influx measurement, the internodal cells are collected into batches of 10 cells, which are held together very loosely at one end with cotton thread. One strand of the

cotton is arranged to extend beyond the end of the batch of cells to enable subsequent manipulations with forceps. At this stage, the cells can be transferred to fresh CPW, or to some other pretreatment solution.

If influx of $Cl^-$ is to be studied in the absence of another constituent of CPW, the cells are subjected to a 5 s wash in a non-radioactive solution identical with the influx solution: this prevents contamination of the influx solution with the absent ion. Since radioactive $^{36}Cl^-$ is available only at rather low specific activity (around $10^7$ Bq $mmol^{-1}$) it is normal to use the radioisotope solution in the undiluted form. The isotopic influx solutions are made up in CPW and cells are exposed to these solutions for 5 min. Normally, influx is measured with illumination provided by two 40 W "Daylight" fluorescent tubes positioned about 50 cm above the surface of the water bath: this is sufficient to provide an intensity of photosynthetically active radiation = 12 W $m^{-2}$. If steady state dark influx is to be measured, the cells must be preincubated in darkness for at least 20 min before the start of the contact with the isotope.[26]

To terminate influx of radioisotope, the cells are removed and placed for 200 s in at least 200 ml solution identical in all other respects to the influx solution. The cotton is then removed using forceps and the cells are blotted lightly with tissue, and placed on a sheet of paper. After the cells have wilted slightly, the nodes must be removed using sharp dissecting scissors. During this operation the cell is held over a scintillation vial so that all the cell sap is retained for analysis.

A small volume of $H_2O$ (100 µl) is added to each of the vials and the vials capped after addition of scintillation cocktail. Aliquots (e.g. 50 µl) of the influx solution are also placed in vials for estimation of specific activity. [This, of course, should be identical with the specific activity of the stock radioisotope solution as no unlabelled $Cl^-$ is added, and any variation will therefore more likely reflect small concentration differences resulting from pipetting errors.] Counting efficiency is generally about 95% and can be estimated from the channels ratio on the scintillation counter after preparation of quench curves by addition of Chara cells to radioactive standards.

To calculate the flux on a surface area basis, the cell is assumed to be cylindrical

in shape. In general, fluxes of the order of 10 nmol $m^{-2}$ $s^{-1}$ are measured, which represents between 100 and 200 c.p.m./cell for the 5 min uptake period.

The cytoplasmic $Cl^-$ content has been estimated as 65 μmol $m^{-2}$ cell surface (Section C.3). This implies that the cytoplasmic specific activity will rise to a maximum of 5% of the external specific activity during the influx period. Thus the errors due to effluxing of isotope during the uptake period and the subsequent wash will be small and are insignificant in comparison with cell-to-cell variation of $Cl^-$ influx. In practice, a sizable proportion of the influxed label is also transferred to an even larger pool of $Cl^-$ in the vacuole, so that $Cl^-$ uptake proceeds at an apparently constant rate for influx periods of at least 15 min.[27] However, maintenance of a shorter influx period is generally desirable for investigation of non-steady state events such as the effects of inhibitors, since the cell is able to compensate for modulation of influx via the resulting cytosolic $Cl^-$ concentration.

If very short uptake periods are required and the expected $Cl^-$ flux is low then it may not be possible to obtain sufficient radioactivity inside the cell for unambiguous determination. In these cases, it is more convenient to use $^{82}Br^-$ as an analog for $Cl^-$. The influx system appears to have similar $K_m$ values for $Br^-$ and $Cl^-$,[14] although the maximal influx is higher by about 30% in the case of $Cl^-$.

(ii) $H^{14}CO_3^-$.

Experiments involving the use of $H^{14}CO_3^-$ require special attention because the $^{14}C$ in solution can exchange readily with the $^{12}CO_2$ in the atmosphere. Sterile $NaH^{14}CO_3$ solutions can be purchased having a specific activity of approx. 1.5 x $10^9$ Bq mmol$^{-1}$; once opened, these solutions must be stored (4°C) in sealed containers to reduce the loss of radioactivity. All stock and experimental solutions required for $H^{14}CO_3^-$ experiments are prepared just prior to their use. CPW is scrubbed with $CO_2$-free air for 1.5 hours to remove dissolved $CO_2$. A stock solution of 20 mM $Na_2CO_3$ is then prepared and kept in a sealed container. Prior to the actual experiment, a test series of solutions is prepared in which the $HCO_3^-$ concentration range and experimental pH are established using aliquots of the stock 20 mM $Na_2CO_3$ and a stock 100 mM $H_2SO_4$ solution. These solutions are used to

pretreat the Chara cells prior to the introduction of $^{14}C$.

During all treatments, cells are held in gas-tight glass vials and placed in a 25 C water bath under 20 $Wm^{-2}$ illumination. A few minutes before the end of the pretreatment period (usually 30 min duration) a second set of $HCO_3^-$ solutions is prepared. An aliquot of the $NaH^{14}CO_3$ stock is added to each of these solutions and, after mixing, two 100 ul samples are withdrawn from each solution to determine its specific activity. Although the $NaH^{14}CO_3$ solution is approx. 25 mM, its specific activity is so high that only very small aliquots are required, and thus no correction is needed to the $HCO_3^-$ concentrations. (For example, addition of 10 µl of 25 mM $NaH^{14}CO_3$ to 100 ml of a 100 µM $NaHCO_3$ solution would raise the $HCO_3^-$ level to 102.5 µM.) The $HCO_3^-$ transport system of Chara is quite labile (easily inactivated) and so the change of solutions (removal of pretreatment and introduction of $H^{14}CO_3^-$) must be carefully done. At the conclusion of the $H^{14}CO_3^-$ exposure (usually 30 min), the radioactive solutions are decanted and again sampled for specific activity as well as a final pH measurement.

After a brief wash in non-radioactive pretreatment solution to remove the excess surface radioactivity, cells are prepared for scintillation counting as described above for $^{36}Cl^-$. However, a 60 min treatment with 0.1 ml of 30% $H_2O_2$ and 0.1 ml of 7% perchloric acid is required to remove unfixed, precipitated $^{14}C$ and to digest the tissue to prevent chlorophyll quenching during scintillation counting. The digested tissue is suspended in an appropriate cocktail and radioactivity detected using a scintillation spectrometer. By knowing the specific activity of the solution, the efficiency of the scintillation counter and the cell surface area, the net flux of $H^{14}CO_3^-$ into the cell can be computed.

(b) Cations

Influx of monovalent cations can be studied essentially as detailed for $Cl^-$, with the exception that precautions must be taken to ensure that all exogenous label is removed from the negatively-charged cell wall during the wash period.[28]

## 2. Isotopic Efflux at the Plasma Membrane.

Most experimental work has focussed on $Cl^-$ efflux, and this case is therefore treated in detail. In principle, the measurement of plasma membrane efflux is quite simple, but the interpretation of data is complicated considerably by the presence of more than one intracellular compartment (especially the vacuole). The experimental methods are outlined below, and a discussion of data analysis is reserved for the section on tonoplast fluxes (Section C.3).

The vacuole of Chara has a very small rate constant for turnover of $Cl^-$, and cells therefore have to be loaded with isotope for several weeks to attain a specific activity of $Cl^-$ which approaches that of the labelling solution. The cells are loaded at room temperature in CPW containing $^{36}Cl^-$ and the solution is renewed every week to return the pH to lower levels at which $Cl^-$ influx is optimal. The light regime is 16L/8D, as constant illumination damages the chloroplasts. [If complemetary influx data are required, it is important to treat unlabelled cells similarly.[29]] Prior to the efflux experiment, the cells are bathed in non-radioactive CPW overnight, to allow the cytoplasm and its constituents to come to a constant specific activity.

Each efflux experiment is conducted with a batch of about 5 cells loosely held together with cotton thread. The cells are inserted into glass tubing (5 mm internal diameter) which is sealed at each end with a flexible compound rubber cap. Narrow bore (1 mm diameter) nylon tubing is inserted into these caps. The free end of one piece of tubing is connected to a 50 ml burette, and the other free end is positioned over a 20 ml scintillation vial. For temperature control, the efflux apparatus is immersed in a water bath.

The burette acts as a gravity-feed reservoir from which a measured volume of solution can be flowed past the cells and collected with effluxed tracer. Normally, 10 ml is collected over 30 s at the end of each 10 min efflux period. A further 30 ml over 90 s is then flushed through the apparatus and discarded. For a total chamber volume and downstream dead-space of 1.5 ml, 99.7% of the extracellular activity is flushed from the chamber by the first 10 ml: from the point of view of contamination of the succeeding

samples, the subsequent wash is therefore unnecessary. However, in many experiments the effect of rapid removal of extracellular $Cl^-$ is investigated, and the second wash is necessary to remove remaining μM levels of the ion.

Each 10 ml sample is dried in an oven at 95 C overnight, rehydrated with 1.5 ml $H_2O$ and counted by liquid scintillation. At the end of the efflux experiment, the cells are removed from the chamber and vacuolar samples obtained in order for their $Cl^-$ concentrations to be measured by electrometric titration (Section B.2). The precipitated chloride (as AgCl) can be dissolved with a drop of $NH_3$ and each sample washed into a separate scintillation vial. After counting, the specific activity of the sample can be calculated. These specific activities must be weighted in proportion to the original surface area of the cell to enable the effective overall specific activity of the sap of the 5 cells to be calculated with respect to surface area. Values of about 3 nmol $m^{-2}$ $s^{-1}$ are commonly observed in CPW with illumination, rising to 13 nmol $m^{-2}$ $s^{-1}$ in darkness.[26]

Several factors must be considered in assessing the accuracy of efflux estimates. First, the presence of the nodes must be taken into consideration, since these will also efflux label to the external medium; their contribution can be as high as 40%. Nodal fluxes can be eliminated quite simply by ligation and excision, to leave a large fragment of the internodal cell.

Second, in $Cl^-$-free media, it is possible that a significant proportion of effluxed label is reabsorbed before it diffuses through the cell wall. Tyree[30] has estimated the wall permeability to $Cl^-$ as $8 \times 10^{-10}$ $m^2$ $s^{-1}$, and, even given the higher estimates of efflux, it is unlikely that the concentration of $Cl^-$ adjacent to the membrane would exceed 1 μM--which is well below the measured $K_m$ for the uptake system. However, an alternative estimate of wall permeability is given by Mailman & Mullins[31] as $5 \times 10^{-12}$ $m^2$ $s^{-1}$, which could result in a $Cl^-$ concentration as high as 20 μM (or about half the measured $K_m$) at the external surface of the membrane.

Third, to calculate efflux it is normally assumed that the cytosolic specific activity is equal to that of the vacuole.[26,32,33] However, the true unidirectional efflux is given as:

$$\phi_{co} = \frac{r}{s_c} = \frac{s_v \phi_{vc} - s_c \phi_{cv}}{s_c} \qquad (1)$$

in which subscripts o, c and v refer to the external, cytoplasmic and vacuolar compartments respectively, $\phi_{ij}$ is the unidirectional flux from compartment i to compartment j, r is the rate of emergence of radioactivity from the cell (units: cpm $m^{-2}$ $s^{-1}$) and s is specific activity (units: cpm $nmol^{-1}$). Rearrangement of Eq. (1) shows that the true efflux, $\phi_{co}$, will be higher than the apparent efflux, $(r/s_v)$ by the factor $(\phi_{co}+\phi_{cv})/\phi_{vc}$. Thus, a crucial question concerns the magnitudes of the tonoplast fluxes. Only if these are considerably larger than the plasma membrane fluxes is an accurate estimate of efflux obtained.

### 3. Tonoplast Fluxes.

Two general strategies have been used to try to determine ion fluxes across the tonoplast of characean cells. In the first, the vacuolar specific activity is sampled at defined times after the onset of isotopic influx, and the tonoplast influx is derived from the calculated rate constant for turnover of the ion in the cytoplasm ($k_c$). In the second, the cell is loaded with isotope for a considerable time (at least $5k_c$), and $k_c$ is calculated from the washout kinetics. In both cases, it is strictly possible to carry out the analysis only for steady state conditions in which the cytoplasmic and vacuolar contents of the ion are constant during the measurement period. The theory underlying both methods is comprehensively discussed by Walker & Pitman[34] As in the case of ion effluxes, the $Cl^-$ ion has received most attention, and the accounts below treat $Cl^-$ as a case study. The same techniques are applicable to other ions.

(a) Vacuolar Fraction Method

Since its initiation in the late 1950's the vacuolar fraction method[35] has been used by a number of workers.[10,28,36,37,38,39,40] A pre-measured internodal cell is incubated in $^{36}Cl^-$ for a period during which $s_v$ is insignificant compared with $s_c$. [MacRobbie[28] set an arbitrary limit at $s_v < 0.1 s_c$, which is suggested to occur at $k_c t = 2.2$. However, this criterion is based on a high estimate of cytoplasmic $Cl^-$ concentration (see below), and for the lower estimate obtained using solid-state $Cl^-$ microelectrodes (Coster[41]) of 10 mM,

or 0.065 mmol $m^{-2}$, an incubation corresponding to $k_c t=10$ can legitimately be used before isotope backflux from the vacuole becomes problematic.]

After incubation, the cell is washed free of isotope for 100 s, blotted, rapidly wilted under the heat of a light bulb, and pinched firmly with forceps 15-20 mm from one node. This portion of the cell is removed and its length measured before trimming the node and measuring radioactive uptake, which provides an estimate of radioactive uptake by the whole cell ($Q_T^*$). A vacuolar sample is taken from the other portion of the cell and radioactivity counted in a measured aliquot. Assuming the tonoplast diameter to be 50 μm less than that of the whole cell, the fraction of intracellular isotope which has entered the vacuole ($F_v^*$) can then be established.

If the influx period is in excess of about 15 min, the cytoplasm behaves as a single kinetic compartment.[26] However, for shorter influx times, a smaller component of vacuolar transfer is apparent. Although the physical identity of this component was the subject of some controversy,[38,42,43] it now appears likely that the fast component is an artifact introduced by cutting the cell.[42] The errors arising from the presence of the fast phase can be corrected for, and $k_c$ estimated, as follows. The apparent fraction of tracer observed in the vacuole ($F_v^{*A}$) will differ from that which describes the true in vivo transfer ($F_v^{*T}$) according to the relationship:

$$F_v^{*A} = F_v^{*T} + PF_c^* \tag{2}$$

where P is the proportion of cytoplasmic isotope tranferred as a result of cutting and $F_c^*$ is the fraction of isotope in the cytoplasm. Thus:

$$F_v^{*A} = F_v^{*T} + P(1 - F_v^{*T}). \tag{3}$$

With the cytoplasm acting as a single kinetic phase, the vacuolar fraction is given as:

$$F_v^{*T} = 1 - \left[\frac{1 - \exp(-k_c t)}{k_c t}\right]. \tag{4}$$

Values of $F_v^{*A}$ measured over a range of influx times (5-75 min) are plotted as a function of time and the intercept at $t = 0$ ($F_v^{*A} = P$) is estimated assuming a smooth function.

By substituting this value of P into Eq. (3) it is possible to calculate a value of $k_c$ for each point (from a graph of $\{1-[1-\exp(-k_c t)]\}/k_c t$ vs. $k_c t$). The values of $k_c$ should be time-independent.

Using this method, $k_c$ for $Cl^-$ in Chara has been estimated as $2.9 \times 10^{-4}$ $s^{-1}$ (time constant = 57.5 min). The tonoplast flux can be calculated from the relationship:

$$\phi_{cv} = Q_c k_c - \phi_{co} \qquad (5)$$

in which $Q_c$ is the $Cl^-$ content of the cytoplasm (units: $mmol.m^{-2}$). $Q_c$ is obtained from separate measurements of cytoplasmic $Cl^-$ concentration and the volume of cytoplasm per unit cell surface area. Ion-selective electrode measurements suggest cytoplasmic $Cl^-$ concentration is 10 mM[41] and from studies in which the cytoplasm is centrifuged to one end of the cell, the volume/surface ratio is 6.5 ml $m^{-2}$ (which corresponds to a cytoplasmic thickness of 7 μm[10]).

Thus, for $Q_c$ = 0.065 mmol $m^{-2}$ and $\phi_{co}$ = 3 nmol $m^{-2}$ $s^{-1}$ (Section C.2), $\phi_{cv}$ is 15.9 nmol $m^{-2}$ $s^{-1}$. However, it has to be considered that $\phi_{co}$ itself will be underestimated if the tonoplast and plasma membrane fluxes are comparable (see Eq. (1) and discussion) so that the true fluxes by this method are more likely to be in the region $\phi_{co} \simeq 4$ nmol $m^{-2}$ $s^{-1}$ and $\phi_{cv} \simeq 15$ nmol $m^{-2}$ $s^{-1}$.

There are several potential sources of error in the vacuolar fraction method which must be considered. One arises from the assumption[28], implicit in Eq. (4), that the total measured isotope entry ($Q_T^*$) is given by $\phi_{oc} t$. However, the full expression is:

$$Q_T^* = \phi_{oc} t - \phi_{co} \int_0^t S_c \, dt \qquad (6)$$

where the cytoplasmic specific activity as a fraction of that in the loading solution is defined as:

$$S_c = \frac{\phi_{oc}}{\phi_{co} + \phi_{cv}} \left[ 1 - \exp(-k_c t) \right] . \qquad (7)$$

Integration of Eq. (7) yields

$$Q_T^* = \phi_{oc} t - \frac{\phi_{co}\phi_{oc}}{\phi_{cv} + \phi_{co}} \left\{ t - \frac{1}{k_c} \left[ 1 - \exp(-k_c t) \right] \right\} . \qquad (8)$$

The assumption is therefore valid if $\phi_{cv}$ is much greater than $\phi_{co}$. Since that does not appear to be the case, the rise of $S_c$ with time is more likely to set an upper limit on the length of influx period which can be used than is the rise in $S_v$. In practice, the time limit for loading, given by the condition $\phi_{co}\int S_c.dt < 0.1\ \phi_{oc}t$, is for $Cl^-$ in Chara equal to about 75 min.

The other uncertainties in the estimate cannot be so easily compensated. P itself contributes significantly to $F_v^{*A}$ at early times, and, with a value of 0.3, it accounts for around half of $F_v^{*A}$ even after 1 h of loading. Thus, the (1-exp) rise in $F_v^*$ has to be detected against considerable system noise.

Finally, the value of $Q_c$ has a considerable influence on the estimate of the tonoplast flux. Early measurements of $Q_c$--obtained by physical separation of the cytoplasm and vacuole[18,32,37,44]--are almost certainly erroneously high due to contamination of the cytoplasm with vacuolar sap. Estimates of $Q_c$ are therefore much more reliably obtained by the solid-state $Cl^-$ microelectrode method.[41] The effect of a high value of $Q_c$ on $\phi_{cv}$ can most simply be seen with reference to Eq. (5). Furthermore, the estimate of $\phi_{co}$ itself normally rests on the assumption that $S_c = S_v$ during efflux experiments: if $\phi_{cv}$ is comparable to $\phi_{co}$ this assumption will not hold, and the value of $\phi_{co}$ in Eq. (5) is correspondingly underestimated. Both these errors result in considerable amplification of the estimate of $\phi_{cv}$, and most published values using the vacuolar fraction method have been of the order 500-1000 nmol $m^{-2}$ $s^{-1}$.[10,28,37]

Given these difficulties, it seems more reliable to estimate tonoplast flux and $Q_c$ by a non-invasive technique such as compartmental analysis of isotope efflux.

(b) Compartmental Analysis

This technique was first applied to giant-celled algae by MacRobbie and Dainty[45], and has most recently been used to estimate steady state $Cl^-$ fluxes in Chara.[46] The theory and derivation of the rate equations is dealt with elsewhere.[34,37]

To prevent interference in the subsequent efflux studies, the nodes are either removed or coated with silicone grease. A single internodal cell is then placed in the same apparatus as that used for plasma membrane efflux measurements (Section C.2), the one

exception being that the reservoir end of the chamber is connected to a 10 ml syringe which enables faster flow rates to be established. Isotopic CPW is then introduced via the syringe for the required loading period, after which the chamber is flushed through with 10 ml unlabelled CPW. Three further aliquots of CPW are passed through the system before the first 10 ml sample is collected for counting at 140 s after the end of the loading period. Further samples are taken at 50 s intervals, decreasing in frequency to 1 sample/100 s at 500 s, 1/0.3 ks at 0.9 ks, 1/0.5 ks at 1.5 ks, 1/ks at 4 ks, 1/2 ks at 8 ks and 1/4 ks at 12 ks. This series of frequencies allows radioactivity to emerge at > 3x(background) for each sample, given a loading solution specific activity of around 16.7 Bq $nmol^{-1}$. If a separate estimate of the rate constant for vacuolar turnover is required, sampling must be continued for many days, with correspondingly reduced sampling frequency.

The samples are dried and counted as described in Section C.2. At the end of the experiment, the cell dimensions are measured and estimates of whole-cell and vacuolar isotope contents obtained as described in Section C.3.a. The vacuolar $Cl^-$ concentration can also be measured prior to determination of radioactivity (Section B.2).

Data are analysed as follows. Cell content of isotope ($Q_T^*$: units, dpm $cm^{-2}$) is plotted for each collection period logarithmically as a function of time. Isotope efflux from the cell wall dominates the exchange kinetics for the first 500 s, but at times in excess of this, it may be possible to fit the decay in isotope efflux as the sum of two exponentials[46]. Ideally, a least squares fitting routine (e.g. Marquardt[48]) should be used to facilitate an unbiased estimate of where the "break point" in the two exponentials occurs. For the steady state condition, the fluxes and contents of the two compartments can be estimated from the rate constants ($k_1$, $k_2$) and zero-time intercepts ($I_1$, $I_2$) of the two exponentials, and from the loading time (T) and specific activity of the loading solution ($s_o$) as follows[47]:

$$\phi_{oc} = \frac{I_1 k_1 [1-\exp(-k_1 T)] + I_2 k_2 [1-\exp(-k_2 T)]}{s_o}, \qquad (9)$$

$$Q_T = \frac{I_1 [1-\exp(-k_1 T)] + I_2 [1-\exp(-k_2 T)]}{s_o}, \qquad (10)$$

$$Q_c = \frac{\{I_1 k_1 [1-\exp(-k_1 T)] + I_2 k_2 [1-\exp(-k_2 T)]\}^2}{s_o \{I_1 k_1^2 [1-\exp(-k_1 T)] + I_2 k_2^2 [1-\exp(-k_2 T)]\}} , \quad (11)$$

$$Q_v = Q_T - Q_c , \quad (12)$$

$$\phi_{vc} = \frac{k_1 k_2 Q_1 Q_2}{\phi_{oc}} . \quad (13)$$

The estimates of content can then be expressed relative to volume, rather than surface area, if cytoplasmic volume is calculated from centrifugation experiments. The supplementary sampling of vacuolar $Cl^-$ concentration allows an independent verification of the estimate of $Q_v$. Jones & Walker[46] have derived the following values for $Cl^-$ fluxes and concentrations in Chara: $\phi_{oc}$ = 10.6 nmol $m^{-2}$ $s^{-1}$; $\phi_{vc}$ = 14.3 nmol $m^{-2}$ $s^{-1}$; $[Cl^-]_c$ = 1.8 mM; $[Cl^-]_v$ = 134 mM. The respective values of $k_c$ and $k_v$ were $8.5 \times 10^{-4}$ $s^{-1}$ and $1.3 \times 10^{-7}$ $s^{-1}$.

## D. NET FLUXES AT THE PLASMA MEMBRANE

In the previous sections we have outlined the methodology involved in the use of radioisotopes to obtain unidirectional fluxes crossing both the plasmalemma and the tonoplast. For influx determinations it is necessary to destroy the Chara cells in order to measure the radioactivity. As pointed out above, a second limitation associated with this method of flux analysis is that fluxes are usually expressed on the basis of total cell surface area; i.e., it is generally not possible to obtain data on localized flux densities. These limitations can be overcome by using either ion-selective electrodes,[49,50] or the extracellular vibrating probe technique.[51,52]

### 1. Ion-Selective Electrodes

In many physiological studies net $H^+$ fluxes are determined by back-titration of the medium bathing the experimental tissue. These experiments can be performed with almost any conventional glass pH electrode system. However, when information on the spatial aspect of the $H^+$, $OH^-$, $K^+$ or $Ca^{2+}$ flux is required, miniature or ion-specific microelectrodes must be employed.

In ion-specific microelectrodes, an organic solution of a neutral (or lipophilic electrolyte), ion-complexing agent(s) (ionophore[s]) acts as the ion-selective liquid "membrane." Construction and calibration of these microelectrodes is straightforward and has been discussed in detail elsewhere.[53,54,55] The only points that we wish to stress concerning the use of these microelectrodes is that they be calibrated before and after each experimental sequence, until one becomes familiar with the particular stability features of the ion-specific electrode being employed. Secondly, it is our experience that most problems in the use of these electrodes can usually be traced to the reference electrode, and so it is wise to take care in the preparation of this part of the circuit.

(a) Application to Diffusion Analysis.

In an aqueous bathing medium, the flux vector of an ionic species like $OH^-$ (or $H^+$) can be expressed as the sum of three terms, involving the activity and electric potential gradients and the convection velocity:

$$J_{OH^-} = -D_{OH} \nabla C_{OH} - (D_{OH} C_{OH} z_{OH} F/RT) \nabla E + v C_{OH} \quad (14)$$

where $D_{OH}$ is the diffusion coefficient for $OH^-$, $C_{OH}$ is the $OH^-$ concentration or activity, E is the electric potential, $\nabla$ is the gradient operator, and $-v$ is the convection velocity; R, T, z and F have their usual meanings.

By placing the Chara cell into an experimental medium that contains agar, convection is damped[49] and Eq. (14) reduces to:

$$J_{OH^-} = -D_{OH} \nabla C_{OH} - (D_{OH} C_{OH} z_{OH} F/RT) \nabla E \quad (15)$$

Under these convection-damped conditions, the light-dependent pH and electric potential profiles that develop along the surface of Chara internodal cells can be mapped. The pH values can be measured using either a commercial miniature electrode (Model MI-405; Microelectrodes Inc., Londondery, NH) in conjunction with a standard pH meter (Model 4500; Beckman, Palo Alto, CA) or an ion-specific pH microelectrode system.[56] Electric potential (external) measurements can be made using a differential amplifier (Model 750; WPI). For optimal measurements, glass microelectrodes having a tip diam. of 50 μm are filled with a solution containing 0.7% (w/v) agar and 10 mM KCl. If the system is to be thermostatted by means of a bath, spurious electrical noise can be significantly reduced by using high-

purity, low viscosity, liquid paraffin as the thermostatting fluid.[57]

A high-resolution micromanipulator must be used to move the pH and electric potential electrodes to the required position. It is relatively easy to manufacture a small holder that allows both electrodes to be held in an orientation such that the two sensing tips are very close together. This arrangement enables one to simultaneously measure the pH and electric potential profiles that develop on the surface of Chara internodal cells during photosynthetic assimilation of exogenous $HCO_3^-$.

Although the external electric potential is readily detectable, it is generally the case that $\nabla E \ll \nabla C_{OH}$, and so Eq. (15) simplifies to:

$$J_{OH^-} = -D_{OH} \nabla C_{OH} \tag{16}$$

which is Fick's First Law of Diffusion. By establishing the symmetry of the diffusion pattern, produced by the transplasmalemma $OH^-$ transport system, Eq. (16) can be used to give Fick's Second Law of Diffusion, which can be solved to give an explicit expression for $J_{OH^-}$ as a function of $C_{OH}$ and the spatial coordinates. Since the outer surface of the Chara cell acts as a boundary between the site of transport and the diffusion system, the appropriate mathematical solution usually involves "hollow" cylindrical or spherical coordinates. Lucas[49] demonstrated that the $OH^-$ or alkaline bands of Chara form spherical diffusion profiles. Thus, under steady state conditions, the flux leaving a particular $OH^-$ band can be determined using the following Eq:

$$J_{OH^-} = 4\pi D_{OH} r_1 r_2 (C_{OH(1)} - C_{OH(2)}) / r_2 - r_1 \tag{17}$$

where $C_{OH(1)}$ and $C_{OH(2)}$ are the $OH^-$ activities at the radial positions $r_1$ and $r_2$, respectively. Since the $OH^-$ bands exhibit a reasonable degree of symmetry,[49] the flux associated with each band can be determined from a single radial scan through its center of symmetry.

The accuracy of these flux determinations is high, provided the radial values employed ($r_1$, $r_2$) are larger than the physical dimensions of the miniature pH electrode. For studies on the diffusion characteristics within the region close to the Chara cell wall, where the unstirred layer (200 μm) restricts convective mixing, ion-specific microelectrodes must be employed.[56]

(b) PVC-Gelled Ion Specific Electrodes.

Intracellular ion-specific microelectrodes are not used to measure actual fluxes crossing the plasmalemma, but rather to monitor cytoplasmic (or vacuolar) pH, pCa, etc.; parameters having essential roles with respect to regulation of transmembrane fluxes. Because the plant cell is under high hydrostatic pressure (turgor), insertion into the cytosol or vacuole tends to displace the liquid membrane back from the tip of the microelectrode. This introduces the possibility of an electrical shunt between the liquid membrane and the glass surface. This problem can be overcome by mixing the liquid membrane with polyvinylchloride (PVC) in order that the sensor be gelled into the tip of the microelectrode. The basic protocol for production of these gelled tips is described below for the $Ca^{2+}$ sensor.[58]

A small quantity of PVC (1 mg, MW 200 kDa; BDH Chemicals Ltd., Dorset, England) is dissolved in tetrahydrofuran (50 µl; Sigma Chemical Co., St. Louis, MO) held in a Reactivial. The solution is kept on ice to prevent solvent evaporation. Fluka $Ca^{2+}$ cocktail (89% w/w 2-nitrophenyl octyl ether [solvent], 10% ETH 1001 and 1% sodium tetraphenylborate [functions as lipophilic anion to limit interference from anion-generated diffusion potentials]) is then mixed with the PVC solution to give a final dilution of 10% (w/w). A small quantity of this solution is back-filled into the tip region of the micropipette. A cat's whisker (or similar object) is then used to move the sensor into the tip and to remove any air bubbles that may have formed. Filled micropipettes should be stored, tips downwards, in a dessicator.

Once the PVC-$Ca^{2+}$ cocktail has gelled (leave for about 12 h) the electrode reference solution (0.1 µM $CaCl_2$) can be back-filled and air bubbles between the gelled membrane/reference solution interface removed using a cat's whisker. A reference electrode, having a similar tip diam to the $Ca^{2+}$ microelectrode, is pulled using microfiber-borosilicate glass and is filled with 100 mM KCl. After the electrodes have been connected to the high impedance amplifier, they should be given a 10-30 min preconditioning before calibration against a series of standard solutions (pCa 3 to 8). Interference characteristics for $Mg^{2+}$, $K^+$ and $H^+$ can be determined using the separate solution

method.[53]

## 2. Flux Measurements Using the Vibrating Probe

### (a) One-Dimensional Vibrating Probe

Numerous biological systems appear to generate electric fields/currents, but in many situations these fields are very small. This meant that traditional KCl-filled microelectrodes were of limited value in studying these phenomena, since the noise associated with these electrodes limits their resolution to about 10 μVolts. It was not until Jaffe and Nuccitelli[59] developed an innovative technique, called the vibrating probe, that sophisticated research became possible on the nature of these fields. Basically, this system's enhanced resolution was achieved by lowering the electrode resistance by a factor of 1,000. This was done by filling the glass micropipette (microelectrode) with solder, and the new level of resolution was 10 nVolts!

At present, several types of vibrating probes are in use. We will first describe the theory and operation of the platinum-black-tipped glass-micropipette probe, since it was the first system introduced for commercial use. This will be followed by a brief description of the very recent two-dimensional (2-D) and 3-D probes.

The important details of the 1-D probe and its housing are illustrated in Fig. 2. The small platinum-black electrode (tip diam 10 to 30 μm) can be manufactured in the laboratory or purchased commercially (Vibrating Probe Company, Davis, CA). A special alignment tool is used to hold the platinum-black electrode during its insertion into the lucite boat (see Fig. 2). A coaxial cable is then connected to the upper end of the glass micropipette. The outer portion of the cable connects to the reference on the shank of the electrode housing and is grounded in the measuring amplifier circuit. The inner portion of the cable is used to transmit the electrical signal to a phase-sensitive lock-in amplifier (Model 5101, EG & G Princeton Applied Research, Princeton, NJ).

During operation, the boat and the platinum electrode are caused to vibrate, in one plane, over a known distance (usually 20 to 25 μm) by varying the power supplied to a piezoelectric bender element via a voltage oscillator (sinusoidal signal). (The frequency at which the probe is vibrated is a function of the resonance frequencies of the specific

system. For our recent studies on Chara we routinely use approx. 290 Hz.) This vibration converts any steady potential difference between these two extremes of the probe's excursion into a sinusoidal voltage output, with a peak-to-peak amplitude equal to the D.C. voltage difference. The processing of this signal is achieved using a phase-sensitive lock-in amplifier that is driven by the same reference signal used to drive the piezoelectric bender element. Thus, it is extremely important during calibration of the probe that the phase angle of the lock-in amplifier be adjusted to that of the probe.

Phase angle adjustment, calibration and barrier artifact check can all be performed using a simple parallel plate calibration chamber. This rectangular chamber consists of two Ag/AgCl plates of fixed cross-sectional areas, separated by a solution of known conductivity (usually 60 mM NaCl). Thus, a known current can be passed between the plates (say 100 mA $m^{-2}$) to permit system calibration. Barrier artifacts, or erroneous signals not due to electric fields generated by the biological specimen, must be tested for using an inert object of approx. the same dimensions as the biological material. For Chara, a solid glass rod, 1 mm in diam. and 1 cm in length, serves this purpose adequately. If a new probe does not respond to positional changes with respect to this glass rod, then it can be used to study the extracellular ionic current patterns of Chara.[51,52]

Because of its sensitivity to spurious vibrations, the vibrating probe, the compound inverted microscope (Zeiss or Nikon) used to view the Chara cell and the micromanipulator that adjusts the position of the probe must be supported by a vibration-damped table (Model 1201, Kinetic Systems, Brighton, MA).

Chara internodal cells to be used for vibrating probe studies should be placed in a container of experimental solution so that cellular debris can be removed from the cut ends of the branch and adjoining internodal-cells; chloroplasts, in particular, tend to get caught up in the tip of the vibrating probe. Cleaning is achieved using a Pasteur pipette to which a partial vacuum has been applied. Great care should be taken during this clean procedure so that the Chara cells are not perturbed. A silk thread (type: Orizuru 9; Kanagawa Co., Kanagawa, Japan) is then attached to each end of the internodal cell (actually tied to the dead cell-wall fragment of the adjoining internodal cells).

These silk threads are then used to suspend the Chara internodal cell in the center of a Plexiglas chamber (9 mm deep, 30 mm wide and 56 mm long) filled with bathing medium. Small blocks of Plexiglas (height 4.5 mm) are placed beneath the threads, near the ends of the cell, to stabilize the cell's position.

The Plexiglas chamber containing the suspended Chara cell is placed on the stage of the inverted microscope and the cell illuminated using a bifurcated fiber optic light source (20 W m-2; Model MK II, Ehrenreigh Photo Optical Industries, Garden City, NY). The microscope is focused (200 X) on the equatorial plane of the Chara cell, and then a high resolution X-Y-Z micropositioner (Model H-2, Line-Tool, Allen Town, PA) is used to lower the vibrating probe, such that the tip is in sharp focus within this equatorial plane, and is positioned some 300 μm from the cell surface. Power to the piezoelectric bender is then switched on and adjusted to give the desired vibration amplitude (Δr). Range selection on the lock-in amplifier depends upon each individual experiment; however, a short time-constant (30 msec) should be employed to obtain the true signal amplitude. The vibrating probe is calibrated to reference, or background, at a distance of 1 cm from the cell surface before being brought into a position 50 μm from the wall.

It is best to have the microscope stage motorized (stepping motor, Model KD 3402-004; Hurst Manufacturing Corp., Princeton, IN, coupled to Model SL 10 adjustable speed controller; Minarik Electric Co., Los Angeles, CA) so that the entire length of the Chara cell can be traversed past the vibrating probe. An appropriate speed is about 1 cm of cell length per min.

The theory that underlies the conversion of the measured voltage gradient into the putative current density that would exist within the center and direction of vibration may not be as straightforward as suggest previously.[60] This issue of interpretation will be addressed shortly. In any event, Ohm's Law is invoked, and in this situation, if the amplitude of vibration (Δr in μm) is small relative to the size of the cell, the current density (I in Amps $m^{-2}$) is given by:

$$I = -\frac{1}{\rho}\frac{\Delta V}{\Delta r}\hat{a}_r \qquad (18)$$

where ΔV is the voltage difference (detected between the extremes of vibration), $\hat{a}_r$ is the

unit vector in the radial direction, and $\rho$ (Ohm-m) is the specific resistance of the bathing medium. An example of typical experimental values obtained on Chara cells within the center of an $OH^-$ band would be as follows: $\Delta V$, 120 μVolts; $\rho$, 34.7 Ohm-m; $\Delta r$, $2.0 \times 10^{-5}$ m. From Eq. (18), the current density can be calculated as:

$$I = \frac{1}{34.7 \text{ (Ohm-m)}} \times \frac{120 \times 10^{-6} \text{ (RMS Volts)} \times 2.83}{2.0 \times 10^{-5} \text{ (m)}} \text{ Amps m}^{-2}$$

$$= 0.49 \text{ Amps m}^{-2}$$

It is important to realize that the current density falls off rapidly as a function of distance from the Chara cell surface.[51] In order to determine the current density crossing the plasmalemma, it is necessary to extrapolate the measured current densities to the surface on the basis of the field's fall-off with distance from the surface. An empirical curve that fits the experimental data is generally obtained in order to determine the surface current. We should add a note of caution here, in that the fall-off profile for the inward current ($OH^-$ efflux) was found to be a function of the amplitude of vibration.[51]

If the experimental tissue is functioning normally (i.e. not perturbed by the manipulation involved in cleaning and mounting the Chara cell, nor by the vibrating probe, per se, this technique can provide much information on both the spatial distribution of membrane transport function, as well as temporal aspects of transport activation.[51,52]

(b) Two- and Three-Dimensional Vibrating Probes

The 1-D vibrating probe provides current density information only for the one vector position, that being the center and direction of vibration. If a probe could be vibrated in such a way that both the normal and tangential components of the electric field could be detected at the same time, the current density could be computed in the 2-D plane of vibration. Freeman et al.[61] developed such a 2-D probe system by using two miniature loud speakers mounted at right angles. However, this method had an undesirable side effect, in that the speaker coils produced an appreciable electromagnetic field, which complicated signal processing. This problem was avoided by using two piezoelectric bender elements

mounted at right angles and vibrated out of phase (90°) so that the platinum-black electrode moved in a circular pattern. This new 2-D approach was co-developed by Nuccitelli[62] and Freeman et al.[63] A commercially-available system has recently become available (Model NR-2000, Vibrating Probe Co., Davis, CA).

The theory and operating details of this advanced system are very similar to those described for the 1-D probe. In the 2-D system, a stationary platinum-black reference electrode is mounted on the front of the vibrator assembly, via a miniature braided wire pin. A similar pin is used to attach the measuring platinum-black electrode. These electrodes differ from those used in the 1-D system in that they are unshielded wire probes, constructed from a 90% Platinum-10% Iridium wire that has been coated with a layer of insulation (parlene, 1 μm thick; Nova Tran Corp., Clear Lake, MI). The insulation is removed from the electrode tip by local heating, and platinum-black is electroplated onto the tip until the desired size is obtained. These new electrodes are a big improvement over the glass microcapillaries. The wire electrodes can be bent to fit any application, and new platinum-black tips can be plated, in situ, using the NR 2000 system manufactured by the Vibrating Probe Company.

Signal processing involves the following:

(a) The outputs from the two electrodes are connected to a low-noise differential preamplifier.

(b) The preamplified signal is fed into a two-phase lock-in amplifier that detects both the in-phase and quadrature components of the signal.

(c) The two outputs of the lock-in amplifier are then digitized by an A-D converter (Labmaster TM40 PGH, Tekmar Co., Solon, OH) and analyzed by an IBM PCXT computer.

(d) The computer calculates the averaged current density vector, and the actual values (vectors) can be stored on hard disk as well as being displayed on a video screen for real-time experimental analysis. Associated software for the IBM PCXT is commercially available.

Further details of these new 2-D and 3-D systems can be found in the proceedings of a recent conference in which technical advances and special applications of the vibrating

probe were reviewed.[64]

(c) Effects of Probe Mixing

As mentioned above, a problem may exist in terms of extrapolating from the voltage gradient, as measured by the vibrating probe, to the physiological processes occurring at the Chara plasmalemma. In an earlier section we discussed the relative importance of $\nabla C_{OH}$ and $\nabla E$, in terms of the flux leaving an $OH^-$ band. Extracellular electric field measurements indicate that $\nabla C_{OH} \gg \nabla E$, yet when the vibrating probe is used, large extracellular "currents" can be measured.[51,57]

This problem has been recently addressed by Ferrier and Lucas,[60] who showed that when the experimental medium contains an ionic species whose diffusion coefficient is significantly greater ($D_h$) than all other ionic species present ($D_i$), a non-Ohmic condition exists. In this situation, the current density is given by:

$$I = -(1-\beta)\, Fz_h\, D_h\, \nabla C_h - \sigma\, \nabla E \qquad (19)$$

where $\beta = (D_i/D_h$ and $\sigma = (\Sigma_i D_i C_i (z_i F)^2/RT)$ is the electrical conductivity of the medium. Clearly, if $\beta \simeq 1.0$, Ohm's Law holds. However, if high mobility ions such as $H^+$ or $OH^-$ carry the current, there will be a significant deviation from Ohm's Law, since $\beta$ will be much less than 1. Under the bathing medium conditions used in our chara experiments, $\beta$ = 0.17 for protons and 0.31 for $OH^-$. Results of a computer numerical analysis study, based on Eq. (14) and Eq. (19), indicated that the convection loops produced by the vibrating probe have a profound effect on the activity gradients, and hence on the electric potential gradient, in the case where $\beta$ is not close to 1.0. If the vibrating probe measures the electric potential gradient within one of the convection loops, which appears to be the case from the observations made by Jaffe and Nuccitelli,[59] then the measured electrical gradient will be increased relative to the gradient without convection. Based on their simulation studies, Ferrier and Lucas suggested that the electrical gradient could be almost 9 times greater than the gradient present without convection.[60] Thus, the "current" density obtained with the vibrating probe depends, in a complex manner, on the convection velocity and on the specific properties of the ionic species carrying the flux ("current"). Clearly, this complexity must always be borne in mind when using this

technique.

3. Ion Fluxes During Electrophysiological Transients.

(a) Rapid Measurement of Changes in External Ion Concentration

There has been considerable interest in identifying and quantifying the ionic fluxes which occur during the characean action potential. Early studies[65,66] simply reported measurements of isotopic efflux of $K^+$ and $Cl^-$ after repetitive electrical stimulation of cells in small volumes of CPW. In most cases, conventional liquid membrane-based ion selective electrodes simply do not respond fast enough to record the changes in ion concentration. However, Oda[67] developed an apparatus which enables simultaneous estimation of $K^+$ and $Cl^-$ efflux during a single action potential, as well as giving an indication of the time course of these fluxes.

Fig. 3 is a diagrammatic representation of the apparatus used by Oda. The cell, 50 to 75 mm long, is preconditioned in CPW overnight, then for 30 min in CPW in which the $K^+$ and $Cl^-$ salts are replaced by $Na^+$ and $NO_3^-$, before being placed in the apparatus. Each of the three compartments A, B, and C are milled out of a Plexiglas block. Solution is perfused (3.6 ml/min) into A through glass tubing (3 mm I.D.), thence through a 5 mm length of 1 mm I.D. tubing to B, and out to an atomizer burner of a flame photometer (Hitachi Type-EPU) via silicon rubber tubing and glass tubing (1 mm I.D.) inserted through the plate. The $K^+$ concentration is monitored in the effluent by the flame photometer. Five Ag/AgCl electrodes are inserted in A as shown, the distance $A_1$-$A_2$ and $A_2$-$A_3$ being 25 mm. The two S electrodes are for electrical stimulation, and the three A electrodes, for recording the action potential. The electrodes labelled C are also of Ag/AgCl and are located in compartments B and C to record the change in $Cl^-$ concentration in compartment B. The solution in compartment C is static, and contact with B is made through glass tubing 10 mm long and 0.3 mm I.D. The internodal cell is positioned in compartment A.

On application of a supra-threshold stimulus (e.g. 30 μA for 10 ms) an action potential is propagated which can be recorded extracellularly by the A electrodes. The outputs from the three amplifiers (two signalling the action potential and one, the change in $Cl^-$ concentration), together with the output of the flame photometer, are recorded on a four-

channel oscillograph (Yokogawa Electric Works Type-2901 "Photocorder").

The $Cl^-$ electrode can be calibrated by perfusion of standard solutions through the apparatus, and exhibits the theoretically-predicted response:

$$E = 58\log([Cl^-]+19)/19 \quad (20)$$

where E is the electrode output in mV, $[Cl^-]$ the $Cl^-$ concentration in μM and 19 the constant derived from the solubility product of AgCl.

The operational lag in response time of the apparatus is about 1 s. The $K^+$ and $Cl^-$ concentrations appear to rise simultaneously, and to about the same extent (17.8 and 18.1 μmol $m^{-2}$ $impulse^{-1}$, respectively). More recent work,[68] using a similar method, has however indicated that the $Cl^-$ flux during an action potential is not obligatory.

(b) Transient Changes in Cytosolic Free $Ca^{2+}$

Imbalance between the $K^+$ and $Cl^-$ fluxes, as well as electrophysiological data,[69] has led to the conclusion that $Ca^{2+}$ influx might provide some of the charge compensation, for $K^+$ efflux, during the action potential. Cytoplasmic free $Ca^{2+}$ can be measured in intact or perfused Chara with either intracellular $Ca^{2+}$ microelectrodes (Section D.1.b.) or the photoprotein aequorin.[70,71] A detailed discussion of the methods for preparation of aequorin and quantification of the light signal is given elsewhere.[70,72,73] Injection into intact cells[70] is accomplished by first centrifuging the cytoplasm to one end of an internodal cell and then by reducing turgor in $Ca^{2+}$-free CPW + 200 or 250 mM sucrose. Desalted aequorin is dissolved in 150 mM KCL, 10 mM $Na_2$TES, pH 7.5 and about 50 nl of the solution is introduced into the endoplasm with a micropipette. The cell is then returned to CPW. The light emission takes a considerable time (up to 1 h) to stabilize, perhaps because of $Ca^{2+}$ entry during injection.

The resting level of cytosolic free calcium in Chara is 220 nM. During an action potential, a transient rise to 6.7 μM is observed in intact cells.[70] The major sources of error in the aequorin method are a lack of information concerning cytosolic free $Mg^{2+}$, which has a profound influence on the calibration curve, and poor mixing during cell lysis, which necessitates a large correction of the estimate for the peak emission signal.

## E. INVESTIGATION OF FACTORS REGULATING ION TRANSPORT

### 1. Adenine Nucleotide Levels in Chara.

Numerous biophysical studies on perfused Chara have indicated that the plasmalemma-bound $H^+$-translocating ATPase is strongly influenced by the cytosolic levels of ATP and ADP.[74] Several different protocols can be used to measure the adenine nucleotide levels in Chara. Until recently, the most widely used method was a modification of the luciferin-luciferase assay.[75] At present, the method of choice is the chromatography analysis of ATP, ADP, and AMP by high-performance liquid chromatography (HPLC).[76]

At the conclusion of an experimental treatment, individual Chara cells are blotted on a paper towel, to remove excess moisture, and then quickly frozen in liquid nitrogen. Frozen cells are lyophilized (Dura Dry Freeze Dryer, FTS Systems Inc., Stone Ridge, NY), weighed, and then ground in 2.0 µl of ice-cold 1.0 M $HClO_3$ using a ground-glass homogenizer. In addition, 2 mg $ml^{-1}$ of Polycar AT (Polysciences, Warrington, PA) is added to the extract. The homogenizer is rinsed with 1.0 ml of 0.05 M potassium-phosphate buffer (pH 7.5) and, after allowing 20 min for complete extraction and protein denaturation, the rinse and extract are combined. This mixture is then centrifuged at 25,000 g for 30 min at 4°C, and the supernatant adjusted to pH 7.5 with 5 N KOH. After waiting 20 min to allow for the precipitation of potassium perchlorate, the extract is again centrifuged for 30 min at 25,000 g. The supernatant can then be stored at -70°C until assayed.

Extracts are analyzed for AMP, ADP and ATP by first forming fluorescent 1,N -etheno-adenosine derivatives by reacting the nucleotides with chloroacetaldehyde and then separating them using a high-performance liquid chromatograph system. In order to maximize precision and reduce the breakdown of ATP, it is necessary to modify the procedure of Yoshioka and Tamura[77] and Preston[78] by using phosphate instead of acetate buffer. Chloroacetaldehyde (10 µl) is added to 500 µl of extract (pH 7.5) in Pyrex test tubes. The tubes are covered with glass marbles and placed in a boiling water bath for 5 min. Caution is needed with this step, as prolonged boiling results in breakdown of ATP and ADP. Nucleotide standards are handled in a similar manner, except that 100 µl of 0.1 M potassium phosphate buffer (pH 7.5) is also added prior to boiling. (Chloroacetaldehyde

is obtained by distilling a solution of chloroacetaldehyde dimethyl acetyl (100 g) (Aldrich, Milwaukee, WI) in 500 ml of 50% sulfuric acid (w/v) as described by Secrist et al.[79]

Chromatography can be performed using a standard HPLC system (Beckman Series 344 Gradient Liquid Chromatograph) equipped with an Ultrasphere IP column (4.6 mm diameter, 250 mm long). The eluting peaks are detected by using a fluorescence detector (Model 157; Beckman Instruments) and analyzed on an Altex Chromatopac C-$^{R}$1B data processor (Beckman Instruments). The etheno derivatives of AMP and ADP can be separated using a mobile phase consisting of 10% acetonitrile and 90% of a solution composed of 0.05 M tetrabutylammonium hydroxide (Fisher Scientific, Pittsburg, PA) and 0.05 M $KH_2PO_4$ (concentrated phosphoric acid is used to adjust the pH value to 2.5). ATP is analyzed separately using a 30% acetonitrile and 70% mixture of the above-detailed components. Fluorescence is measured using a 280 nm excitation filter and a 350-470 nm emission filter to eliminate detection of cytidine derivatives. A 20 µl injection volume and a flow rate of 1 ml $min^{-1}$ is suitable for all analyses.

Peaks are identified using retention times of standards. Further confirmation of the peaks in the Chara cell extracts can be obtained by enzymatic analysis. By using pyruvate kinase and adenylate kinase (Sigma, St. Louis, MO) in combination, or pyruvate kinase alone, results in the disappearance of the peaks which have been identified as AMP and ADP, respectively, on the basis of retention times. With these treatments there is a concomitant increase in the ATP peak. The putative ATP peak can be removed by addition of hexokinase or calcium phosphate to the extract. These enzymatic conversions are performed using the procedure of Kimmich et al.[80]

Using the above-mentioned procedures, the ATP, ADP and AMP levels can be determined and expressed on a pmol.mg $DW^{-1}$ basis. By weighing the Chara cells, prior to freezing in liquid nitrogen, and by assuming that the cytosol occupies 7% of the cell volume, these nucleotides can also be expressed on a mMolar basis.

## 2. Cytoplasmic pH.

Cytoplasmic pH ($pH_c$) is a crucial factor which can be shown, by intracellular perfusion, to control the activity of both the primary[81] and secondary[82] transport systems of Chara. It is therefore important that accurate estimates of $pH_c$ are available for intact cells, especially where mediation of $pH_c$ is suspected in the effect of environmental conditions on ion transport. Liquid membrane-based $H^+$ microelectrodes for intracellular use have been discussed in an earlier section (Section D.1.b.). Nevertheless, for those whose manual dexterity and patience do not extend to ion-selective electrode technology, two alternative methods are available. The principles underlying application of weak acid distribution and of $^{31}P$ nuclear magnetic resonance to measurement of intracellular pH have both been outlined in previous volumes of Methods in Enzymology:[83,84] the methods will be considered here only from the practical aspect of their use with Chara.

(a) Weak Acid Technique With 5,5-dimethyl-2,4-oxazolidinedione (DMO)

After overnight pretreatment in CPW, batches of 6-8 internodal cells are rinsed for 2 min and transferred to CPW containing $^{14}C$-DMO at 30-60 μM. After incubation for between 1.5 and 3 h, the cells are individually removed, washed for 2 min at the pH of the DMO-containing solution, to remove $^{14}C$-DMO from the cell wall, and a measured sample of vacuolar sap obtained. The sap samples and the remainder of the cell (cytplasm, plus some sap) are assayed separately for radioactivity by liquid scintillation counting. The cytoplasmic [$^{14}C$-DMO] is obtained by subtraction of the vacuolar from the whole cell concentrations, assuming the cytoplasm to occupy 7% of the intracellular space. Cytoplasmic pH can then be calculated, assuming concentration equilbrium of DMO free acid across the plasma membrane, by applying the Henderson-Hasselbalch equation as

$$pH_c = pK + \log[(C_c/U_o)-1] \qquad (21)$$

where pK is the pK for DMO (6.38), $C_c$ is the total DMO concentration in the cytoplasm and $U_o$ is the external concentration of DMO in the free acid form (given also by the Henderson-Hasselbalch equation as $C_o/[1+10^{(pH_o-pK)}]$, with $C_o$ being the total external DMO concentration and $pH_o$, the external pH).

However, the vacuolar accumulation ratio ($C_v/U_o$) is frequently observed to be < 1,

indicating net efflux of $DMO^-$ across the plasma membrane, driven by the highly negative membrane potential. Thus, $pH_c$ can also be calculated by assuming rather that DMO free acid equilibrates across the tonoplast, where the electrical potential is an order of magnitude lower than that at the plasma membrane. In that case, a relationship analogous to Eq. (21) is applied:

$$pH_c = pK + \log[(C_c/U_v)-1] \qquad (22)$$

with $U_v$ the concentration of undissociated free acid in the vacuole. A reliable determination of $U_v$ can be made, analogously with that of $U_o$, if the pH of the vacuolar sap sample is measured independently using a miniature pH electrode. However, if the vacuolar pH ($pH_v$) is 5.0 or less (as has been measured[85]), then $C_v$ can be taken as equal to $U_v$, thereby precluding the need for individual determinations of $pH_v$. However, independent spot checks of $pH_v$ are advisable before the simplification is applied. At an external pH of 6.3, a value of $pH_c$ = 7.75 is obtained by application of Eq. (21), while application of Eq. (22) yields estimates about 0.1 pH unit higher.[86] $pH_c$ falls by 0.2-0.3 units in response to darkness.

Clearly a major problem with the technique is poor time resolution: the half time for equilibration of DMO is 15-20 min and long incubation periods have to be used. Smith[87] has reported that the time resolution can be vastly improved because exchange of DMO across the tonoplast is considerably more rapid than across the plasma membrane. Thus, $pH_c$ can be calculated from Eq. (22) even before the cell achieves equilibrium with the bathing medium. This enables estimates of $pH_c$ to be obtained after as little as 5 min exposure.

(b) $^{31}$P-Nuclear Magnetic Resonance

Because of the highly vacuolate nature of Chara internodal cells, closely packed intact cells must be spun for prolonged periods (> 9 h) in order to obtain a peak for cytoplasmic $P_i$.[88] In the study conducted by Mimura and Kirino,[88] a pHc of 7.84 was obtained when cells were illuminated, with a value of 7.3 being measured in darkness. Since no provision was made for sample aeration, their cells would have been partially anaerobic in the dark, and this might be why a large drop in pHc was observed. Future

studies using this technique must incorporate aeration and utilize high fequency spectrometers.

## F. REACTION KINETIC MODELLING OF FLUXES

Cytoplasmic perfusion enables direct experimental control of solution composition on both sides of the plasma membrane, and hence the kinetics of transport can be studied in some detail with respect to variation of external and internal ligand concentrations. The aim of reaction kinetic modelling is to provide a framework within which the kinetics of transport might be interpreted, and, ultimately, to gain insight into the partial reactions of the carrier which catalyses transport.

A detailed analysis has been undertaken for $2H^+/Cl^-$ symport at the plasma membrane of Chara.[14] It is assumed that the reaction cycle of the carrier can be represented by a scheme of the type shown in Fig. 4, in which the ligand binding sites are exposed alternately to each side of the membrane. For the two ligands $H^+$ and $Cl^-$, four separate ordered binding models can be specified for influx with $Cl^-$ either binding to, and dissociating from the carrier first (First on-First off: FF, as in Fig. 4), binding first and dissociating last (First on-Last off: FL), binding last and dissociating last (Last on-Last off: LL) or binding last and dissociating first (Last on-First off: LF). Each of these variants comprises two congeners: that for which the excess positive charge carried by the second $H^+$ is carried on the loaded form of the carrier (FF+, FL+ etc.) and that for which the charge on the second $H^+$ is neutralized by the negative charge on the unloaded form of the carrier (FF-, FL- etc.).

All analyses of reaction kinetic models have been performed assuming that ligand concentration effects on the kinetics of transport are mediated solely via mass action at the appropriate binding sites for transport, and that membrane electrical potential difference influences only those reactions responsible for transmembrane charge translocation. [These assumptions appear to be the simplest which can be made, and are, of course, subject to modification if kinetic data fall outside the realm of description by all eight models.]

The kinetics of isotope transport through ordered binding models is described for initial rate measurements by a rate equation which can be derived by the method of King & Altman.[89] Since the internal concentration of isotope $([^{36}Cl^-]_i) = 0$, the influx of labelled $Cl^-$, $^*\phi_{Cl}$, is given for the FF+ model as:

$$^*\phi_{Cl} = {}^*N_1 k_{13} \tag{23}$$

where $^*N_1$ is the concentration of carrier bound to $^{36}Cl^-$ at the inner surface of the membrane (Fig. 4) and $k_{13}$ is the rate constant of the partial reaction from state $N_1$ to state $N_3$. The proportion of carrier state 1 that is isotopically labelled is not immediately known. For purposes of calculation of the isotopic flux it is therefore easier to express Eq. (23) in terms of carrier states not bound to isotope, i.e. the carrier state 6 to which $Cl^-$ binds externally. The following rate equations can then be solved for $N_6$, given steady state of the carrier:

$$\frac{d^*N_1}{dt} = 0 = {}^*N_2 k_{21} - {}^*N_1 (k_{12} + k_{13}) , \tag{24}$$

$$\frac{d^*N_2}{dt} = 0 = {}^*N_1 k_{12} + {}^*N_4 k_{42} - {}^*N_2 (k_{21} + k_{24}) , \tag{25}$$

$$\frac{d^*N_4}{dt} = 0 = {}^*N_2 k_{24} + N_6 k_{64} - {}^*N_4 (k_{42} + k_{46}) , \tag{26}$$

in which the N and k symbols have analogous meanings to those in Eq. (23). Substitution of Eqs. (24) through (26) into Eq. (23) leads to:

$$^*\phi_{Cl} = \frac{N_6 k_{64} k_{42} k_{21} k_{13}}{k_{46} k_{24} (k_{12} + k_{13}) + k_{21} k_{13} (k_{46} + k_{42})} . \tag{27}$$

It simply remains, then, to express the concentration of carrier state $N_6$ in terms of the rate constants of the cycle. The King & Altman method for expressing $N_6$ as a fraction of total carrier concentration ($N_T$) can be summarized as follows. The 6-state scheme in Fig. 4B is redrawn in Fig. 4C as 6 possible permutations of 5 contiguous partial reactions. Each diagram can be related to any of the six states as the product of the five rate constants directed towards that state. The carrier-state concentration $N_6$ can then be expressed as a proportion of $N_T$ by the ratio of the 6 King & Altman diagrams relating to

$N_6$ and the 36 diagrams describing all 6 states, i.e.

$$N_6 = N_T \frac{6KA_6}{36KA_T} \tag{28}$$

in which

$$KA_6 = k_{13}k_{35}k_{56}[k_{46}(k_{21}+k_{24}) + k_{42}k_{21}] + k_{46}k_{24}k_{12}[k_{31}(k_{53}+k_{56}) + k_{35}k_{56}] \tag{29}$$

and $36KA_T$ can be split into 21 $k_{64}$-independent terms and 15 $k_{64}$-dependent terms, respectively, as follows:

$$k_{46}(k_{24}+k_{21})[k_{65}k_{53}(k_{13}+k_{31}) + k_{13}k_{35}(k_{65}+k_{56})] +$$

$$(k_{42}k_{21}k_{13}+k_{46}k_{24}k_{12})[k_{65}(k_{35}+k_{53}) + k_{35}k_{56}] +$$

$$k_{53}k_{65}k_{12}k_{31}(k_{46}+k_{42}+k_{24}) + k_{46}k_{24}k_{12}k_{31}(k_{53}+k_{56}+k_{65}) + k_{65}k_{42}k_{21}k_{31}k_{53}$$

and

$$k_{64}\{(k_{56}+k_{53})[k_{42}k_{21}(k_{13}+k_{31}) + k_{12}k_{31}(k_{42}+k_{24})] +$$

$$k_{35}k_{56}[(k_{42}+k_{24})(k_{12}+k_{13}) + k_{42}k_{21}] + k_{21}k_{13}k_{35}(k_{42}+k_{56})\}.$$

Note that the derivation does not include the assumption that the transmembrane reactions are rate-limiting, which results in unnecessarily restictive conclusions concerning kinetic behavior. Substitution of Eq. (28) into Eq. (27) yields the full rate equation. The electrochemical gradients of the ligands are automatically incorporated in the full rate equation: concentration terms are subsumed in the ligand binding reactions, which vary linearly with concentration ($Cl^-$) or as the square of concentration ($H^+$), and the effect of membrane potential on the charge transit reactions is incorporated in the form of a symmetric Eyring barrier. Analogous equations can also be derived for the other 3 ligand binding orders.[90] The behavior of the equations can now examined with respect to variation of components of the electrochemical gradients.

The full rate equation always describes a Michaelis-Menten relationship as a function of external $Cl^-$ concentration ($[Cl^-]_o$). This can be seen quite simply because $k_{64}$, which

subsumes $[Cl^-]_o$, is present as a multiplier in the numerator, and in some, but not all, terms in the denominator. However, it is convenient to simplify the equation for the purpose of designing experiments to determine binding order, since in their complete form, the rate equations for all models can predict a wide variety of kinetic responses. Simplification can be achieved experimentally by setting some of the reaction constants to zero, and others very large. For $2H^+/Cl^-$ symport in Chara, experiments were performed at saturating external $[H^+]$ (i.e., $k_{42}$ very large) and with membrane electrical potential rather negative ($k_{21}$ large, $k_{12}$ small for the FF+ model). In these conditions, the two Michaelian parameters simplify to:

$$\phi_{max} = \frac{k_{13}k_{35}k_{56}}{(k_{31}+k_{13})(k_{53}+k_{56}) + k_{35}(k_{13}+k_{56})} \tag{30}$$

and

$$K_m = \frac{k_{53}k_{65}(k_{31}+k_{13}) + k_{13}k_{35}(k_{56}+k_{65})}{k^o_{64}[(k_{31}+k_{13})(k_{53}+k_{56}) + k_{35}(k_{13}+k_{56})]} \; . \tag{31}$$

[$k^o_{64}$ is the rate constant from $N_6$ to $N_4$ with $[Cl^-]_o$ extracted.] If intracellular chloride ($[Cl^-]_i$) is now varied in perfused cells, Eqs (30) and (31) predict linear non-competitive inhibition if $k_{31} > k_{13}$ and $k_{35}(k_{13}+k_{56})$. Similarly, in the absence of internal $Cl^-$, variation of intracellular $H^+$ ($[H^+]_i$) can result in non-competitive inhibition if $k_{53} > k_{35}$ and $k_{56}$. In both these conditions, non-competitive inhibition is observed experimentally.[14] However, none of the other orders for ligand binding, or an alternative site for charge translocation, is compatible with these kinetics. Thus, on this basis, it is possible to conclude that $Cl^-$ binds to the carrier first at the external surface, dissociates first at the inner surface, and that charge translocation is on the loaded form of the carrier. These algebraic methods therefore demonstrate the utility of the reaction kinetic modelling approach in the design of experiments on perfused Chara.

REFERENCES


1. A.B. Hope and N.A. Walker, "The Physiology of Giant Algal Cells." Cambridge University Press, London, 1975.
2. M.J. Beilby, this volume [74].
3. C. Forsberg, Physiol. Plant. 18, 275 (1965).
4. D. Sanders, Plant Physiol. 68, 401 (1981).
5. S.D. Tyerman, G.P. Findlay, and G.J. Paterson, J. Membr. Biol. 89, 139 (1986).
6. S.D. Tyerman, G.P. Findlay, and G.J. Paterson, J. Membr. Biol. 89, 153 (1986).
7. V.R. Franceschi and W.J. Lucas, Protoplasma, 104, 253 (1980).
8. G.D. Price and M.L. Whitecross, Micron, 13, 309 (1982).
9. N.A. Walker, M.J. Beilby, and F.A. Smith, J. Membr. Biol. 49, 21 (1979).
10. H.G.L. Coster and A.B. Hope, Aust. J. Biol. Sci. 21, 243 (1968).
11. U. Zimmermann and E. Steudle, Aust. J. Plant Physiol. 2, 1 (1975).
12. J.A. Ramsay, R.H.J. Brown, and P.C. Croghan, J. Exp. Biol. 32, 822 (1955).
13. D. Sanders, J. Membr. Biol. 52, 51 (1980).
14. D. Sanders and U.-P. Hansen, J. Membr. Biol. 58, 139 (1981).
15. R.J. Reid and N.A. Walker, J. Membr. Biol. 78, 157 (1984).
16. G.M. Clint, Planta in press (1987).
17. M. Tazawa, Plant Cell Physiol. 5, 33 (1964).
18. U. Kishimoto and M. Tazawa, Plant Cell Physiol. 6, 529 (1965).
19. M. Tazawa, U. Kishimoto, and M. Kikuyama, Plant Cell Physiol. 15, 103 (1974).
20. M. Tazawa, M. Kikuyama, and T. Shimmen, Cell Struct. Funct. 1, 165 (1976).
21. W.J. Lucas and T. Shimmen, J. Membr. Biol. 58, 227 (1981).
22. P.T. Smith and N.A. Walker, J Membr. Biol. 60, 221 (1981).
23. R.E. Williamson, J. Cell Sci. 17, 655 (1975).
24. T.H. Strunk, Science, 169, 84 (1970).
25. C.S. Spyropoulos, J. Membr. Biol. 76, 17 (1983).
26. D. Sanders, J. Exp. Bot. 31, 105 (1980).
27. W.J. Lucas and F.A. Smith, Aust. J. Plant Physiol. 3, 443 (1976).

28. E.A.C. MacRobbie, Aust. J. Biol. Sci. 19, 371 (1966).

29. F.A. Smith and N.A. Walker, J. Exp. Bot. 27, 451 (1976).

30. M.T. Tyree, Can J. Bot. 46, 317 (1968).

31. D.S. Mailman and L.J. Mullins, Aust. J. Biol. Sci. 19, 385 (1966).

32. A.B. Hope, A. Simpson, and N.A. Walker, Aust. J. Biol. Sci. 19, 355 (1966).

33. G.P. Findlay, A.B. Hope, M.G. Pitman, F.A. Smith, and N.A. Walker, Biochim. Biophys. Acta 183, 565 (1969).

34. N.A. Walker and M.G. Pitman, in "Encyclopedia of Plant Physiology" New Series, Vol. 2A (U. Luttge and M.G. Pitman, eds.), p. 93. Springer-Verlag, Berlin, 1976.

35. J.M. Diamond and A.K. Solomon, J. Gen. Physiol. 42, 1105 (1959).

36. E.A.C. MacRobbie, J. Gen. Physiol., 45, 861 (1962).

37. E.A.C. MacRobbie, J. Gen. Physiol., 47, 859 (1964).

38. E.A.C. MacRobbie, J. Exp. Bot., 20, 236 (1969).

39. E.A.C. MacRobbie, J. Exp. Bot., 22, 487 (1971).

40. G.P. Findlay, A.B. Hope, and N.A. Walker, Biochim. Biophys. Acta, 233, 155 (1971).

41. H.G.L. Coster, Aust. J. Biol. Sci. 19, 546 (1966).

42. E.A.C. MacRobbie, J. Exp. Bot., 26, 489 (1975).

43. N.A. Walker, in "Membrane Transport in Plants" (U. Zimmermann and J. Dainty, eds.), p. 173. Springer-Verlag, Berlin, 1974.

44. R.M. Spanswick and E.J. Williams, J. Exp. Bot. 15, 193 (1964).

45. E.A.C. MacRobbie and J. Dainty, J. Gen. Physiol. 42, 335 (1958).

46. S. Jones and N.A. Walker, in "Plant Membrane Transport: Current Conceptual Issues" (R.M. Spanswick, W.J. Lucas, and J. Dainty, eds.), p. 583. Elsevier/ North Holland, Amsterdam, 1980.

47. C.K. Pallaghy and B.I.H. Scott, Aust. J. Biol. Sci. 22, 585 (1969).

48. D.W. Marquardt, J. Soc. Indust. Appl. Math. 11, 431 (1963).

49. W.J. Lucas, J. Exp. Bot., 26, 271 (1975).

50. W.J. Lucas, J.M. Ferrier and J. Dainty, J. Membr. Biol. 32, 49 (1977).

51. W.J. Lucas and R. Nuccitelli, Planta, 150, 120 (1980).

52. W.J. Lucas, Planta, 156, 181 (1982).

53. W.J. Lucas and L.V. Kochian, in "Advanced Agricultural Instrumentation: Design and Use" (W.G. Gensler, ed.), p. 402. Nijhoff, Dordrecht, 1986.

54. D. Ammann, F. Lanter, R.A. Steiner, P. Schulthess, Y. Shijo and W. Simon, Anal. Chem, 53, 2267 (1981).

55. P.C. Meier, D. Ammann, W.E. Morf and W. Simon, in "Medical and Biological Applications of Electrochemical Devices" (J. Koryta, ed.), p. 13. Wiley, New York, 1980.

56. W.J. Lucas, D.W. Keifer and D. Sanders, J. Membr. Biol. 73, 263 (1983).

57. J.M. Ferrier and W.J. Lucas, J. Exp. Bot. 30, 705 (1979).

58. D. Sanders and A.J. Miller, in "Molecular and Cellular Aspects of Calcium in Plant Development" (A.J. Trewavas, ed.), p. 149. Plenum, New York, 1986.

59. L.J. Jaffe and R. Nuccitelli, J. Cell Biol. 56, 614 (1974).

60. J. Ferrier and W.J. Lucas, Biophys. J. 49, 803 (1986).

61. J.A. Freeman, P.B. Manis, G.J. Snipes, B.N. Mayes, P.C. Samson, J.P. Wikswo, Jr., and D.B. Freeman, J. Neurosci. Res. 13, 257 (1985).

62. R. Nuccitelli, in "Ionic Currents in Development" (R. Nuccitelli, ed.), p. 13. Alan R. Liss, New York, 1986.

63. J.A. Freeman, P.B. Manis, P.C. Samson and J.P. Wikswo, Jr., in "Ionic Currents in Development" (R. Nuccitelli, ed.), p. 21. Alan R. Liss, New York, 1986.

64. R. Nuccitelli, "Ionic Currents in Development." Alan R. Liss, New York, 1986.

65. L.J. Mullins, Nature, 196, 986 (1962).

66. A.B. Hope and G.P. Findlay, Plant Cell Physiol. 5, 377 (1965).

67. K. Oda, Plant Cell Physiol. 17, 1085 (1976).

68. M. Kikuyama, K. Oda, T. Shimmen, T. Hayama, and M. Tazawa, Plant Cell Physiol. 25, 965 (1984).

69. M.J. Beilby, Plant Cell Environ. 7, 415 (1984).

70. R.E. Williamson and C.C. Ashley, Nature, 296, 647 (1982).

71. M. Kikuyama and M. Tazawa, Protoplasma, 117, 62 (1983).

72. C.C. Ashley and A.K. Campbell, "Detection and Measurement of Free $Ca^{2+}$ in Cells." North-Holland, Amsterdam, 1979.

73. J.R. Blinks, W.G. Wier, P. Hess, F.G. Prendergast, Prog. Biophys. Molec. Biol. 40, 1 (1982).

74. M. Tazawa, T. Shimmen and T. Mimura, Ann. Rev. Plant Physiol. 38 in press (1987)

75. W. J. Lucas, C. Wilson and J.P. Wright, Plant Physiol. 74, 61 (1984).

76. C.W. Wilson, J.W. Oross and W.J. Lucas, Planta, 164, 227 (1985).

77. M. Yoshioka and Z. Tamura, J. Chromatogr. 123, 220 (1976).

78. M.R. Preston, J. Chromatogr. 275, 178 (1983).

79. J.A. Secrist, III., J.R. Barrio, N.J. Leonard and G. Weber, Biochemistry, 11, 3499 (1972).

80. G.A. Kimmich, J. Randles and J.S. Brand, Anal. Biochem. 69, 187 (1975)

81. M. Tazawa and T. Shimmen, Bot. Mag. (Tokyo) 95, 147 (1982).

82. D. Sanders, J. Membr. Biol. 53, 129 (1980).

83. H. Rottenberg, this series, Vol. 55, p. 547.

84. E. Padan and S. Shuldiner, this series, Vol. 125, p. 337.

85. J.A. Raven and F.A. Smith, J. Exp. Bot. 29, 853 (1978).

86. F.A. Smith, J. Exp. Bot. 35, 43 (1984).

87. F.A. Smith, J. Exp. Bot. in press (1986).

88. T. Mimura and Y. Kirino, Plant Cell Physiol. 25, 813 (1984).

89. E.L. King and C. Altman, J. Phys. Chem. 60, 1375 (1956).

90. D. Sanders, U.-P. Hansen, D. Gradmann, and C.L. Slayman, J. Membr. Biol. 77, 123 (1984).

**Table 1** Media for Vacuolar and Cytoplasmic Perfusion

| | Vacuolar Medium[a] (mM) | Cytoplasmic Medium[b] (mM) |
|---|---|---|
| KCl | 150 | --- |
| NaCl | 10 | --- |
| $CaCl_2$ | 10 | --- |
| HEPES | --- | 100 |
| ATP | --- | 2 |
| KOH | --- | 78 |
| $MgCl_2$ | --- | 6 |
| EGTA | --- | 5 |
| Sorbitol | --- | 50 |
| Ficoll-70 (w/v%) | --- | 5 |
| pH | 5.5 | 7.5 |
| Total osmotic pressure (kPa) | 793 | 545 |

[a]After M. Tazawa, Plant Cell Physiol. 5, 33 (1964).

[b]After W.J. Lucas & T. Shimmen, J. Membr. Biol. 58, 227 (1981)

FIGURE LEGENDS

Figure 1. Apparatus for intracellular perfusion of characean internodal cells. A cell is placed on the elevated section of the base, and is perfused with isotonic medium introduced to the two end chambers. Influx of isotope takes place in the central chamber after ligation of the cell in the two inter-chamber regions. The height of the end chambers is 5 mm, and the length of the central chamber, 20 mm.

Figure 2. A scale drawing of the 1-D vibrating probe with construction details: (1) lucite boat; (2) 6-gauge stainless steel tube; (3) bender (piezoelectric) power cable; (4) Cerrotru solder filling inside of pipette; (5) No. 9 sewing needle eye; (6) gold-plated, braided pin (Malco No. 096-0524-0000, Chicago, IL); (7) lucite boat with coverglass meniscus setter attached to bottom; (8) reference on shank of glass electrode housing (R. Nuccitelli, Modern Cell Biol. 2, 451 [1983]).

Figure 3. Apparatus for measurement of net $K^+$ and $Cl^-$ fluxes during an action potential (K. Oda, Plant Cell Physiol. 17, 1085 (1976). The cell is placed in compartment A. Ag/AgCl electrodes $A_1$, $A_2$ and $A_3$ record the action potential, which is initiated by a current pulse between electrodes $S_1$ and $S_2$. $[Cl^-]$ in compartment B is monitored by Ag/AgCl electrodes in compartments B and C. Dimensions of the compartments (length x depth x width, mm): A, 80 x 2 x 2; B, 5 x 1.5 x 1.5; C, 10 x 5 x 20).

Figure 4. Reaction kinetic model for $2H^+/Cl^-$ symport at the plasma membrane of Chara. A Carrier (X) binds to $Cl^-$ and $2H^+$ with binding sites exposed to the external surface of the membrane and undergoes a conformational change to release the ligands internally. The model (one of 8 variants of ordered ligand binding) is first-on-first-off with respect to inward transport of $Cl^-$, and carries inward current on the loaded form of the carrier (FF+). B General representation of ordered binding carriers, defining carrier state densities ($N_j$) in terms of the state number (j = 1-6). The 12 unidirectional rate constants are defined according to the reaction states participating (e.g. $k_{13}$: rate constant for the transition from State 1 to State 3). C The six King & Altman diagrams for the ordered binding models.

FIGURE 1

( Lucas and Sanders, Methods in Enzymol.)

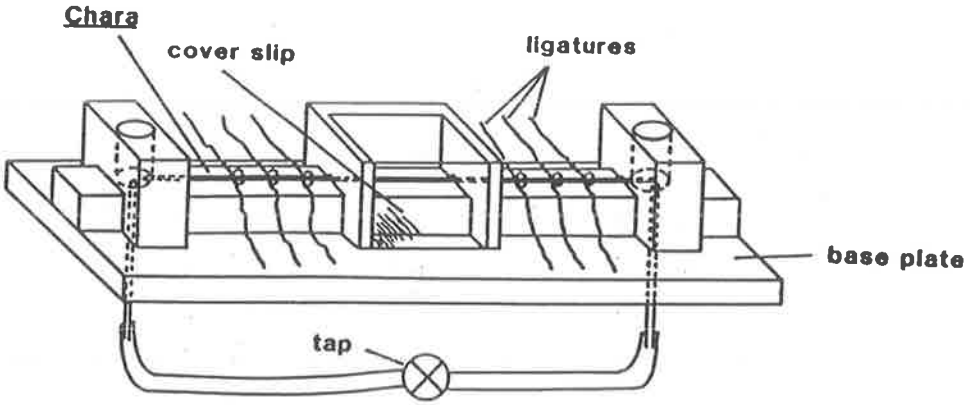


FIGURE 2

( Lucas and Sanders, Methods in Enzymol.)

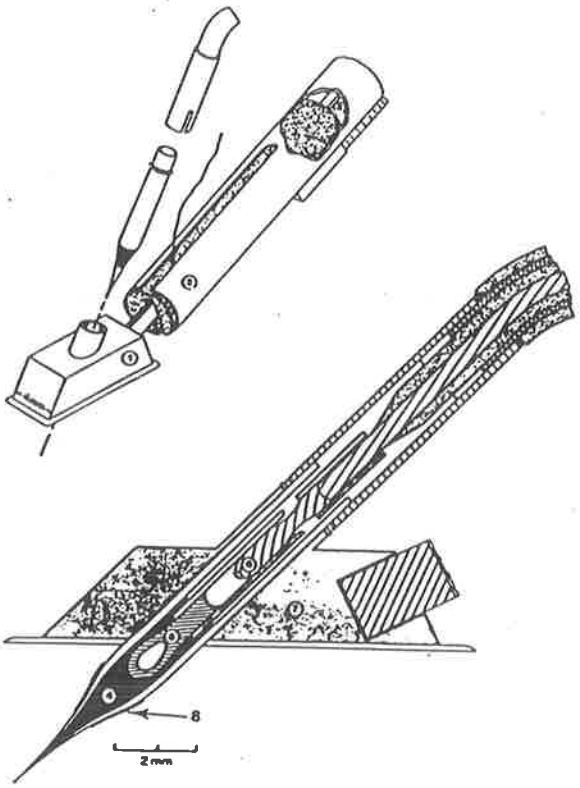

FIGURE 3

( Lucas and Sanders, Methods in Enzymol. )

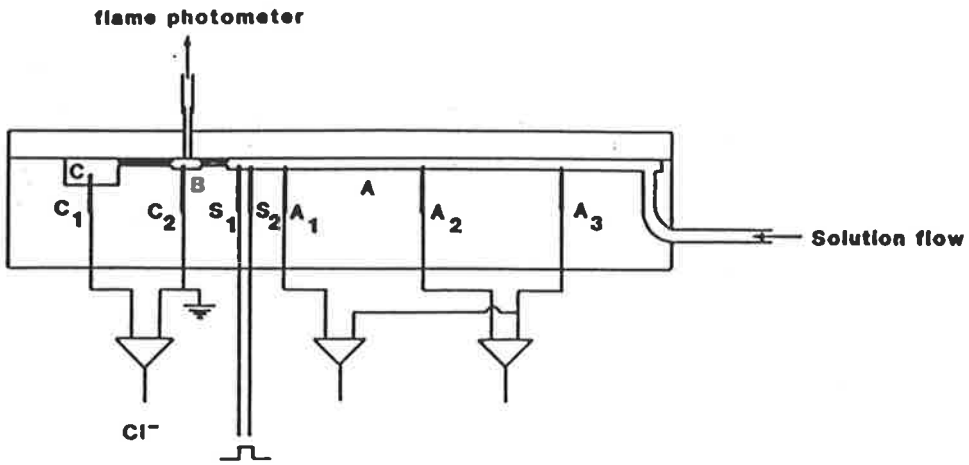


FIGURE 4
( Lucas and Sanders, Methods in Enzymol.)

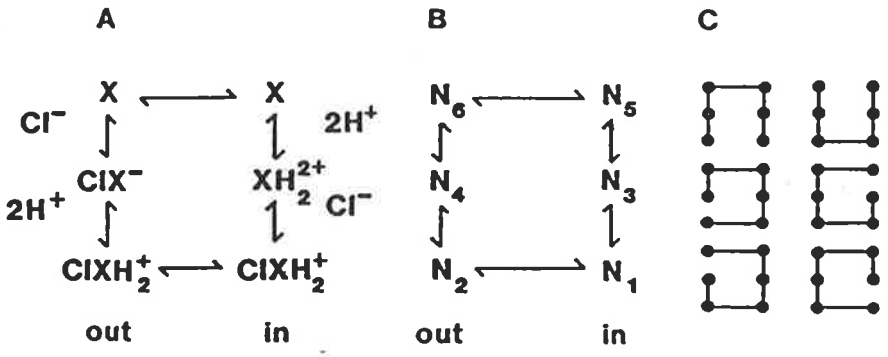

Plant Physiol. (1982) 69, 734–739
0032-0889/82/69/0734/06/$00.50/0

# A Reanalysis of the Two-Component Phloem Loading System in *Beta vulgaris*[1]

Received for publication May 13, 1981 and in revised form July 22, 1981

JULIA W. MAYNARD AND WILLIAM J. LUCAS[2]
*Department of Botany, University of California, Davis, California 95616*

## ABSTRACT

**Kinetic analysis of [$^{14}$C]sucrose loading into sugar beet leaf discs revealed the presence of two transport components. At low exogenous sucrose concentrations, a saturable component, which exhibited Michaelis-Menten characteristics, was the main mode of transport. At concentrations greater than 50 millimolar, phloem loading was dominated by a linear component which appeared to operate as a first order kinetic transport process. Over the exogenous sucrose concentrations employed, influx could be described by the equation $v = V_{max}\,S/(S + K_m) + kS$. Influx via both processes was strongly pH-dependent. Evidence is presented that the linear component was not explicable in terms of simple diffusion, or exchange diffusion, into either mesophyll or minor vein phloem tissue. Extensive metabolic conversion of sucrose was not a factor contributing to influx at high external sucrose concentrations. At present, it is believed that both components operate in parallel at the membrane bounding the sieve element-companion cell complex. The saturable component is identified with sucrose-H$^+$ cotransport. While the significance of the linear component has been established, its nature remains to be elucidated.**

The cotransport of neutral solutes with protons or ions has been well documented in animals, bacteria, fungi, and algae, as well as in higher plants (1). It has been proposed that phloem loading of sucrose in *Beta* proceeds by means of a sucrose-proton cotransport mechanism (10, 12, 13). Similar sucrose cotransport systems have been reported in castor bean cotyledons (15, 18), soybean cotyledons (20, 21), *Samanea* pulvinar organs (23), maize scutellum (14), tomato internodes (26), castor bean petiolar phloem (22), and *Vicia* minor vein phloem (5), leading Giaquinta (12) to propose that cotransport may be the general mechanism by which sucrose is transported in higher plants.

Inasmuch as this growing body of evidence supports the occurrence and importance of accumulation via cotransport, it is unfortunate that little information has been published concerning the kinetics of such uptake. The literature on uptake of neutral solutes, whether or not via cotransport, records various responses of uptake to increased substrate concentration. Biphasic saturation curves have been reported for sugar and amino acid uptake in a number of plants (8). Recently, Servaites *et al.* (24) found that the loading of leucine into soybean phloem demonstrates a triphasic saturation response and sucrose, a biphasic saturation. In contrast, uptake of sucrose by sugar beet root discs appears to be linear, with concentrations up to 100 mM (28). Uptake systems consisting of a saturable component and a nonsaturable component, operating in parallel, have been well-documented for certain animal tissues (3) but only recently have been reported in plants. Examples of such systems are the uptake of glycine by *Lemna* fronds (7) and leucine by cultured *Nicotiana* cells (2), as well as uptake of sucrose by castor bean cotyledons (18), soybean cotyledons (21), and *Vicia* leaf minor veins (6).

The present study further investigates the kinetics of phloem loading in sugar beet. Evidence is presented that sucrose transport by the phloem minor vein system proceeds by two separate transport processes, operating in parallel: a saturable process exhibiting Michaelis-Menten kinetics; and a nonsaturable process exhibiting first order kinetics. The contribution of each process to total uptake is calculated, and the nature of each discussed in the light of proposed models of phloem loading.

## MATERIALS AND METHODS

**Plant Material.** *Beta vulgaris* L. (USH10 Lot 3102) plants were grown in a controlled environment under the following conditions: 27°C day/17°C night temperatures, 45%/60% RH, and a 16-h photoperiod at 80 w m$^{-2}$. Special pots (35 cm deep, 10 cm in diameter) were constructed to accommodate the sugar beet growth habit. Plants were grown from seed in a sterilized mixture of vermiculite, peat moss, and sand (2:1:1); watered daily; and fertilized with Hoagland solution twice weekly. Experiments were performed on tissue from mature leaves of 6-week-old plants and were conducted under low laboratory lighting (1.8 w m$^{-2}$) at 23 ± 1°C.

**Uptake Kinetics Studies.** When intact leaves were used, sites were first located near the leaf tip and abraded for 15 s with a paste of carborundum-300 and $H_2O$ to disrupt the cuticle. The abraded regions were rinsed with 20 mM $CaCl_2$ and covered with plastic wrap squares to prevent evaporative drying of the tissue. These sites were then blotted; aliquots of buffered sucrose solutions were applied (65 μl; transport utilized 5% of the [$^{14}$C]sucrose), and the sites were re-covered. The tissue was given a 30-min preincubation period with nonradioactive sucrose to allow equilibration of apoplastic pH with that of the applied solution. This preincubation was followed by a 30-min exposure to [$^{14}$C]sucrose solutions. Leaves were then excised, rinsed, and passed through two 10-min washes in cold buffer to remove apoplastic label (half-time for removal of apoplastic label was approximately 2.5 min). Discs 0.2 cm$^2$ in size were cut out, taking care to exclude major veins, and placed in scintillation vials to which 0.1 ml of 7% (v/v) $HClO_4$, 0.1 ml of 30% (v/v) $H_2O_2$, and one drop of methylcellosolve were added to digest the tissue (modification of procedure used by Giaquinta [10]). After 20 min, 10 ml of a PPO-POPOP-naphthalene-dioxane cocktail were added, and the radioactivity was measured in a Beckman (LS 8000) liquid scintillation counter.

Experiments with leaf discs were similar in protocol to those with intact leaves, except that, after abrasion, discs were excised under a 20 mM $CaCl_2$ solution and floated, abraded side down, in aliquots of solution pipetted into stainless steel planchets.

[1] Supported by National Science Foundation Grant PCM-7910223 and a University of California Graduate Research Award (to J. W. M.).

[2] To whom correspondence should be addressed.

Uptake experiments performed on discs and intact leaves utilized sucrose concentrations from 5 to 200 mM. Five replicate discs were used at each concentration, and the results of three such experiments were pooled. Values of influx reported are means of 15 replicates ± SE.

All solutions used contained 20 mM $CaCl_2$. Incubation solutions were osmotically adjusted to 500 milliosmolar with mannitol. Preliminary experiments indicated that loading was unaffected by solution osmolarity over the range 160 to 800 milliosmolar. Osmotic pressures were measured using a Wescor vapor pressure osmometer (model 5130). Buffers used were citrate-phosphate (pH 4), Mes (pH 5 and 6), Mops[3] (pH 7), Tes (pH 8), and Taps (pH 9), all at 120 mM.

**Efflux Analyses.** Efflux analyses were performed using excised leaf discs. In each experiment, 12 discs were incubated in 25 mM [$^{14}$C]sucrose (pH 5) for 2 h and then transferred through a series of buffered (pH 5) and osmotically adjusted (500 milliosmolar with mannitol) wash solutions containing 0, 25, or 150 mM sucrose. Wash solutions were analyzed by scintillation counting to determine the quantity of label present. This data was used to calculate the rate at which label was lost from the tissue. After 3 h of efflux, discs were digested and counted, as described above. The total dpm lost by each batch of leaf discs, at the end of each sampling time, was added back to the dpm left in the tissue at the finish to give dpm left in the discs as a function of time.

**Alcohol Extraction.** Twenty leaf discs were pretreated and incubated as before in 200 mM unlabeled and labeled sucrose. Ten discs were digested for scintillation counting, and 10 were treated for 2 h in 80% (v/v) ethanol, in an 80°C water bath, to extract water-soluble $^{14}$C material. Aliquots of extract and the 10 cleared discs were then prepared for scintillation counting.

**Electron Microscopy.** Mature sugar beet leaf tissue was processed for transmission electron microscopy. Leaf discs, identical to those used for [$^{14}$C]sucrose experiments, were immersed in fixative solution (3% glutaraldehyde, 50 mM sodium cacodylate, 1 mM $CaCl_2$ [pH 7.2]) for 12 to 16 h at 4°C and washed for 1 h in several changes of the fixative buffer. Tissue was then postfixed in 1% osmium tetroxide (2 h, 22°C), rinsed with fixative buffer, and dehydrated in a graded acetone series. Embedded material (Spurr's resin) was sectioned (diamond knife) and stained (30 min in 2% lead citrate, then 30 min in 2% aqueous uranyl acetate) before being examined on a JEOL 100S transmission electron microscope.

## RESULTS AND DISCUSSION

**Abraded Leaf-Disc System.** The intact phloem system exhibits such complexities that it is often difficult to isolate for study one particular component of the translocation process. The need to simplify the system has led to the increasing use of leaf discs by workers in this field. After extensive investigation of intact leaf and leaf-disc systems, Giaquinta (10) concluded that sucrose uptake by source leaf discs closely resembles sucrose loading into intact leaves and is a reasonable representation of that process. Preliminary experiments verified this conclusion, showing that discs do, indeed, exhibit similar transport kinetics to those of the intact leaf. Linear time courses were obtained using abraded discs, demonstrating that pretreatment in nonradioactive sucrose had a minimal influence on the specific activity of subsequently applied radioactive solutions. This established the validity of using the pretreatments essential for experiments in which apoplastic pH was to be the controlled variable.

Use of leaf discs allowed preparation of numerous replicates from randomized tissue, and these could be handled with sufficient ease that experiments could be run simultaneously. The fact that discs represent a contained system was also advantageous, in that labeled sucrose loaded into the minor veins could not be removed from the site of uptake by translocation. (Conversely, this can be seen as a strong criticism of the system, as excision of discs destroys the normal source/sink controls operating on translocation and, presumably, on phloem loading as well.) While the main advantage of abraded discs was that possible diffusional effects on the kinetics of uptake were decreased, it should be acknowledged that some diffusion-imposed limitation (unstirred layer effect) will always be present and will influence, to some degree, the apparent kinetics of sucrose uptake (see Ref. 27) and that [$^{14}$C]sucrose is also entering non-phloem compartments.

**Dependency of Phloem Loading on Apoplastic pH.** A series of experiments was run using a range of $H^+$ concentrations (Fig. 1). At each pH, transport at sucrose concentrations above 50 mM became a linear function of concentration.

The observed pH-dependence of sucrose loading (Fig. 1) is at variance with results presented by Giaquinta (10), who found that loading in sugar beet became independent of pH at higher sucrose concentrations, and by Delrot and Bonnemain (6), who reported accumulation from exogenous 20 mM sucrose solutions to be pH-insensitive in *Vicia*. In the developing *Ricinus* cotyledon system, Komor (16) reported uptake of 30 mM sucrose to be independent of pH. However, Lichtner and Spanswick (20) found sucrose-induced membrane potential depolarizations in soybean cotyledons to be strongly pH-dependent. The discrepancies between our and Giaquinta's sugar beet leaf-disc system may have been due to

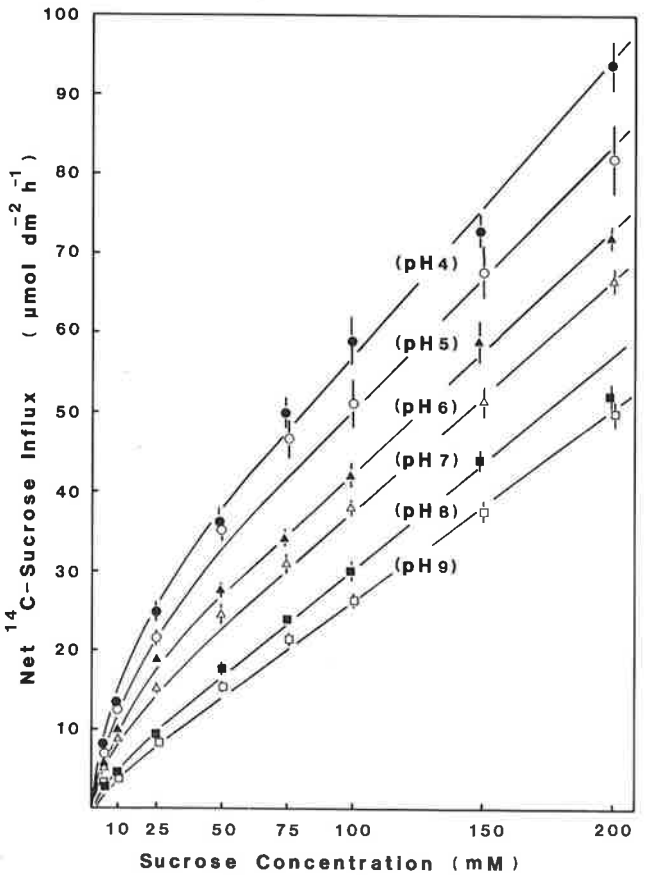


FIG. 1. Concentration dependence of sucrose influx over a range of solution pH. A 30-min preincubation with unlabeled sucrose solutions at the desired pH was followed by a 30-min incubation in [$^{14}$C]sucrose solutions. Points represent the mean ± SE for three sets of five replicate abraded leaf discs.

[3] Abbreviations: Mops, 3-(*N*-morpholino) propane sulfonic acid; Taps, tris [hydroxymethyl] methylamino-propane sulfonic acid.

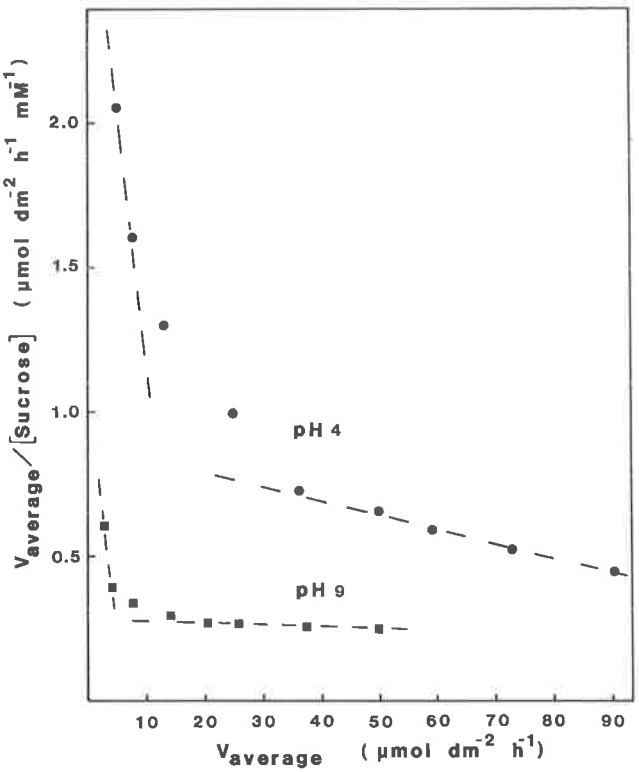


FIG. 2. Eadie-Scatchard plot of sucrose influx at pH 4 and 9. Points represent numbers estimated from the curves drawn through the experimental data presented in Figure 1.

differences in experimental protocol. Giaquinta (10) used solutions with 1 mM $CaCl_2$ and 20 mM buffering capacity and did not use a pretreatment. In our experiments, 20 mM $CaCl_2$ was used to saturate cationic binding sites that might otherwise have acted to reduce the concentration of protons available at the sites of loading. Our higher buffering capacity (120 mM) and tissue pretreatment would also establish better control of apoplastic proton concentration. However, experiments conducted under 0 to 20 mM $CaCl_2$ and 20 to 120 mM buffering capacity revealed that loading was surprisingly insensitive to these parameters (data not shown). Delrot and Bonnemain (6) used bean leaf discs that had the lower epidermis removed and used a 30-min pretreatment; hence, access to the apoplast cannot be the cause of the observed difference. Whether the reported pH responses reflect a real difference among species remains to be confirmed by further experimentation.

**Two Components of Sucrose Uptake.** Eadie-Scatchard plots of our data (Fig. 1) show a significant deviation from linearity (Fig. 2). Such deviation can be interpreted as demonstrating the presence of two separate transport components. Similar multiphasic plots (Eadie-Scatchard) have been reported for uptake of amino acids and sucrose (2, 6, 7, 12, 21, 23). According to Fischer and Lüttge (7), the vertical and horizontal parts of the plot represent active and passive components, respectively. These might be more accurately interpreted as saturable and nonsaturable components of transport. This latter interpretation seems particularly appropriate for the phloem system, where it is difficult to conceive of a passive component moving sucrose against a large concentration gradient.

For the present treatment, we will assume that two transport processes operate in parallel across the plasmalemma of the sieve element-companion cell complex. Using a modification of the basic transport concept presented by Komor and Tanner (17), the pH-dependent saturable component would conform to Michaelis-Menten kinetics, while the nonsaturable component would operate as a first order kinetic reaction. Thus, following Cohen's (4)

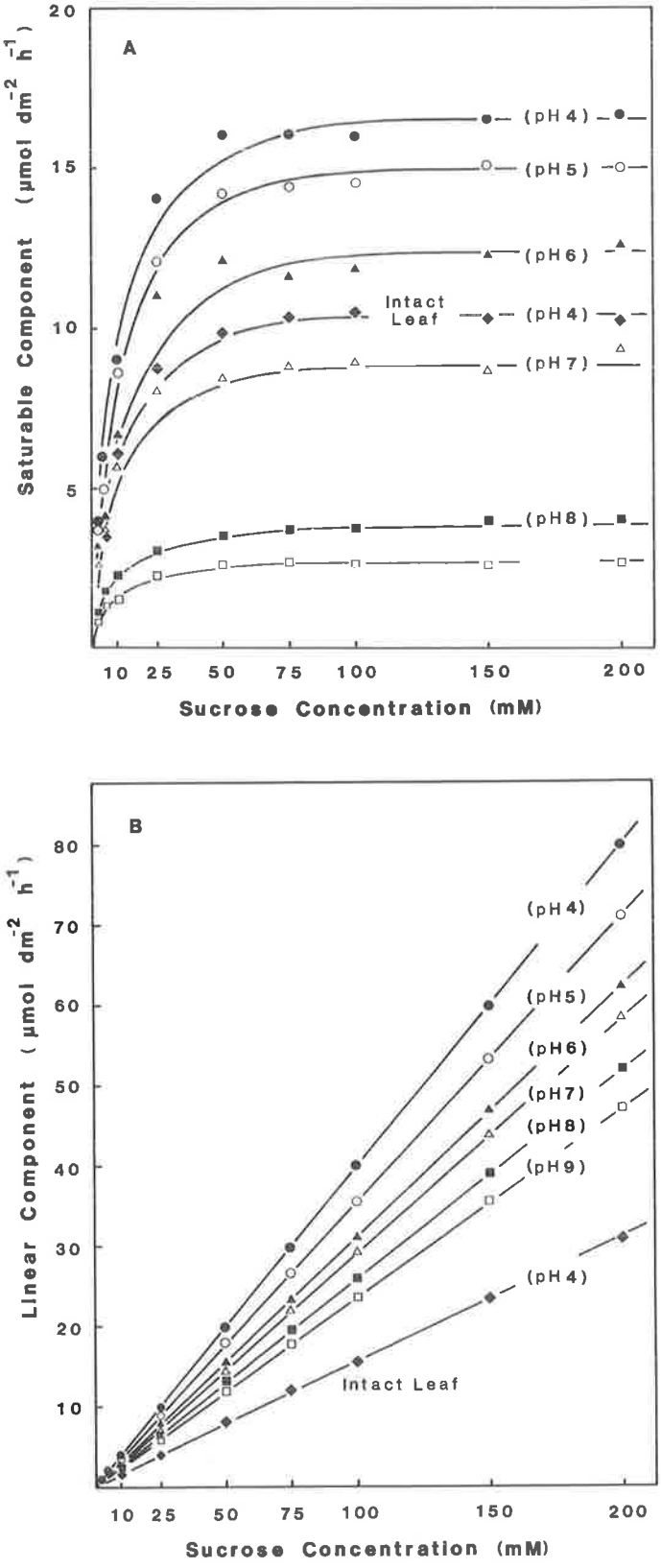


FIG. 3. Concentration dependence of the saturable component (A) and the linear component (B) of sucrose transport (influx).

formulism, the rate of total sucrose uptake would fit the equation:

$$v = V_{max}\, S/(S + K_m) + kS \qquad (1)$$

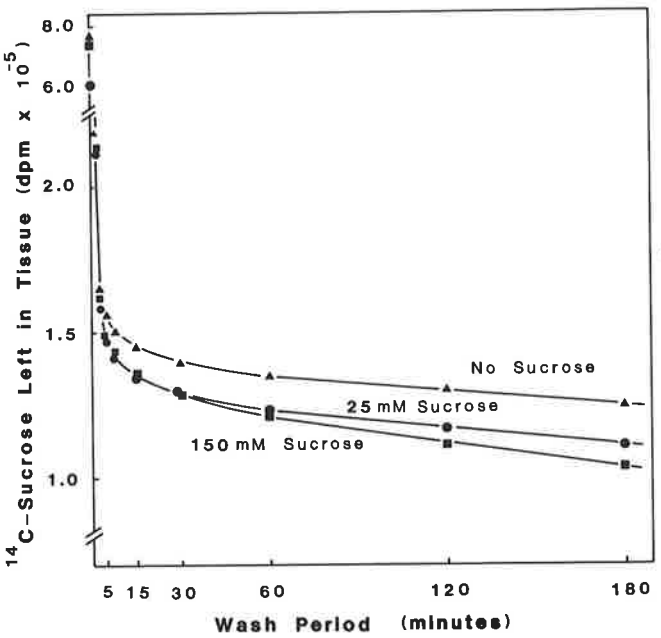


FIG. 4. Effect of sucrose concentration in the wash solutions on the efflux of accumulated sucrose. Twelve leaf discs were incubated for 2 h in 25 mM [$^{14}$C]sucrose (pH 5) and then washed in pH 5 buffered solutions containing 25 mM, 150 mM, or no sucrose. Points represent the dpm left in the tissue at a sequence of times elapsed after initiation of efflux.

where $v$ is the rate, S is the sucrose concentration, $V_{max}$ and $K_m$ are the Michaelis-Menten constants, and $k$ is the first order rate coefficient.

The contribution of the linear process to total influx can be estimated by calculating the slope of the linear portion of the kinetic profiles (Fig. 1) and by multiplying this coefficient, $k$, by the sucrose concentration at each point (Fig. 3B). Subtracting the linear component from total influx gives the rates of the saturable component (Fig. 3A). The components of influx into intact leaves are included for comparison. Inasmuch as the apoplastic concentration is thought to be near 25 mM *in vivo* (see Ref. 8), a comparison was made between the saturable and nonsaturable components to determine their relative contributions to phloem loading at that concentration; at pH 5, the values were 13 and 8 $\mu$mol dm$^{-2}$ h$^{-1}$, respectively. A similar relationship was observed at 5 mM sucrose (pH 5), where the values were 5 and 3 $\mu$mol dm$^{-2}$ h$^{-1}$ for the saturable and nonsaturable components, respectively. Intact leaf data (Fig. 3) exhibited the same general pattern. These data suggest that the nonsaturable component plays a significant role in phloem loading over the entire concentration range. The nature of this linear component remains to be elucidated. At this point, it could be hypothesized to reflect an energized, first order kinetic process driving sucrose into the sieve element-companion cell complex or phloem parenchyma, or, alternatively, it may represent simple diffusion into the mesophyll (19) or phloem parenchyma.

**Efflux Analysis.** The linear component may also indicate the operation of an exchange diffusion (counter-transport) process. Of these possibilities, counter-transport (that is, carrier-mediated exchange of exogenous labeled sucrose for previously accumulated unlabeled sucrose) will exhibit the greatest dependence of efflux on exogenous sucrose concentration.

Figure 4 represents efflux data which indicate the presence of a two-component system consisting of apoplast and symplast. Efflux was not strongly dependent upon the level of exogenous sucrose, there being less than 10% stimulation between sucrose-free and 150 mM sucrose treatments (as calculated from the slopes of the symplastic components in Fig. 4). Thus, while some [$^{14}$C] sucrose may be exchanged for unlabeled sucrose, this process alone cannot be invoked to explain the magnitude of accumulation by the linear component. However, it should be stressed that efflux analysis performed on such a complex tissue may result in a serious underestimation of the actual fluxes involved. This is due to our inability to determine the specific activity of each of the compartments that may be involved in the efflux process (mesophyll, phloem parenchyma, sieve element-companion cell complex [see Fig. 5]).

Autoradiographic investigations of sugar beet leaf discs have demonstrated that labeled sucrose is localized predominantly in the minor vein phloem (10) and that it does not accumulate significantly in the mesophyll. Similar autoradiographs have been obtained for intact sugar beet leaves (8), ruling out passive diffusion into the mesophyll as the source of the linear component. However, the possibility remains that sucrose-to-starch conversion is occurring in the phloem parenchyma, a process which would influence sucrose efflux. Transmission electron micrographs obtained from leaf discs indicate the presence of abundant starch in the phloem parenchyma tissue as well as in the companion cells (Fig. 5, A and B). (During these studies, we also noted the presence of frequent plasmodesmata interconnecting mesophyll, phloem parenchyma, and companion cell tissues [Fig. 5, B and C], as noted previously [9]. Such intercompartmental communication would further complicate any attempt to conduct accurate efflux analyses.)

It is possible that incubation of tissue in concentrations much higher than 20 to 30 mM sucrose (concentrations thought to occur in the sugar beet apoplast [25]) might accentuate the linear component by forcing sucrose into the phloem parenchyma, where it may be stored, or metabolized into starch. To ascertain whether starch synthesis was occurring under these conditions, discs were loaded in 200 mM sucrose for 30 min, and then all soluble label was extracted with ethanol. Only 4% of the label remained in the discs (data not shown). These results are in basic agreement with those of Giaquinta (11) using 5 mM sucrose. Hence, conversion of sucrose cannot be a factor contributing to the linear component.

**Kinetic Parameters: pH Dependence.** Lineweaver-Burk transformations of saturable component data yielded $V_{max}$ and $K_m$ as a function of pH (Fig. 6). The values of $k$ are also plotted for comparison. The $V_{max}$ of the saturable component was strongly dependent on pH (4-fold stimulation), while $K_m$ appears to be much less dependent. This response is consistent with the operation of a simple sucrose-$H^+$ cotransport system. The coefficient $k$ was also influenced by pH (2-fold increase); this sensitivity parallels that observed for $V_{max}$, suggesting that there may be a link, perhaps a close one, between the two processes.

While absolute values of these parameters cannot be considered significant, due to the influence of limits imposed by diffusion, it should be noted that different relative values have been reported for the sugar beet leaf-disc system by Giaquinta (10), who found $V_{max}$ to be independent and $K_m$ to be dependent on pH. These discrepancies are thought to be due to differences in tissue pretreatment and in kinetic analysis (*i.e.* a linear component was not subtracted from the observed transport data).

## CONCLUSIONS

Sucrose loading into mature sugar beet leaves occurs in a manner consistent with uptake from the apoplast into the minor vein phloem (8). This loading is accomplished through the action of two transport components. The saturable component, which exhibits a marked pH dependence ($V_{max}$), is thought to reflect the operation of a sucrose-$H^+$ cotransport system. Sucrose loading exhibits a linear component that becomes dominant at exogenous sucrose concentrations greater than those thought to be present in the apoplast but is, nonetheless, important over the entire range of

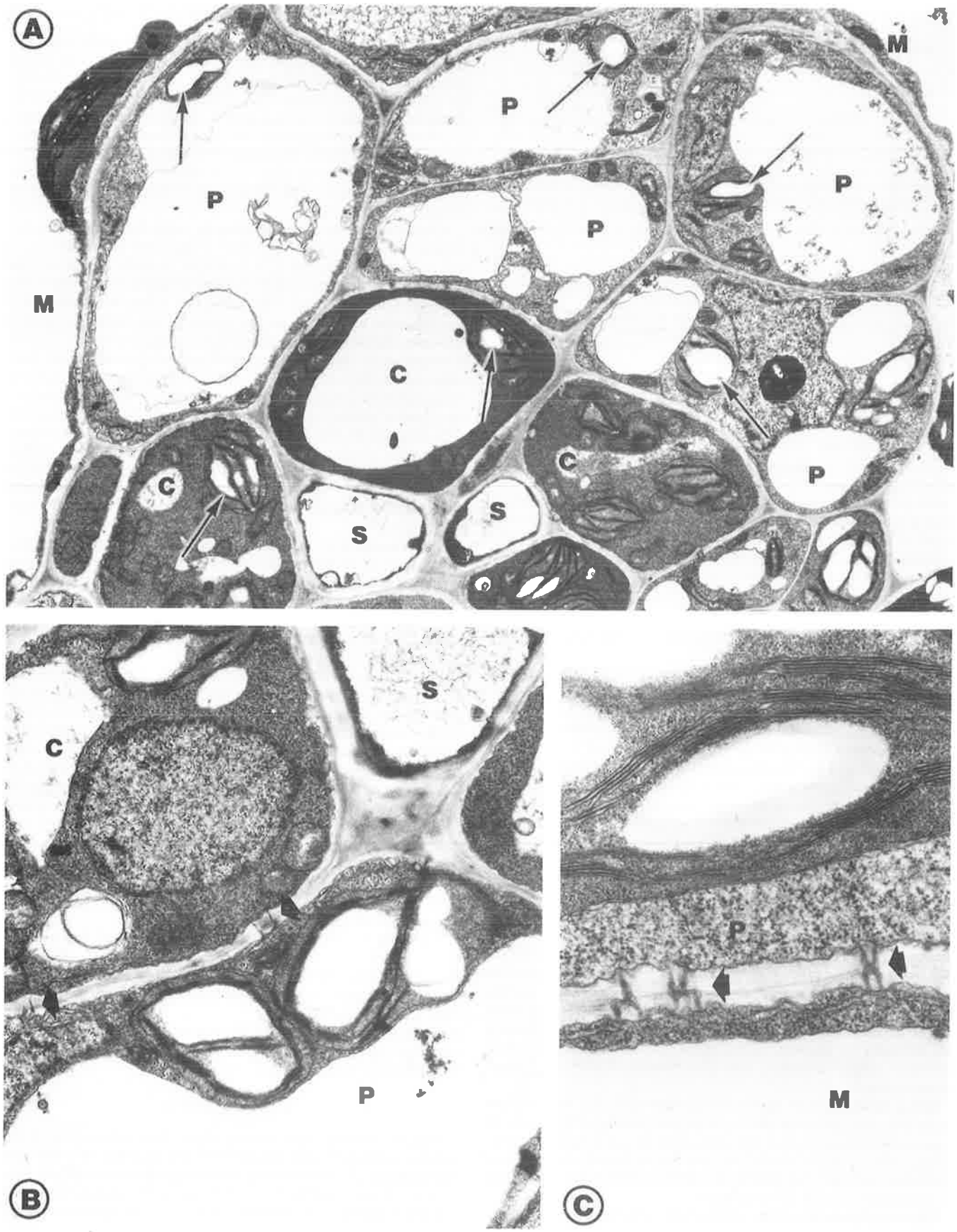


FIG. 5. Electron micrographs obtained on minor vein phloem of excised sugar beet leaf discs. A, Plastids of phloem parenchyma and companion cells contain extensive starch deposits (see arrows). Symbols are as follows: C, companion cell; M, mesophyll; P, phloem parenchyma; S, sieve element (× 7,600). B, Magnified section showing starch deposits and frequent plasmodesmatal connections (arrows) between phloem parenchyma and companion cells (× 16,000). C, Complex plasmodesmata linking mesophyll and phloem parenchyma cells (× 30,000).

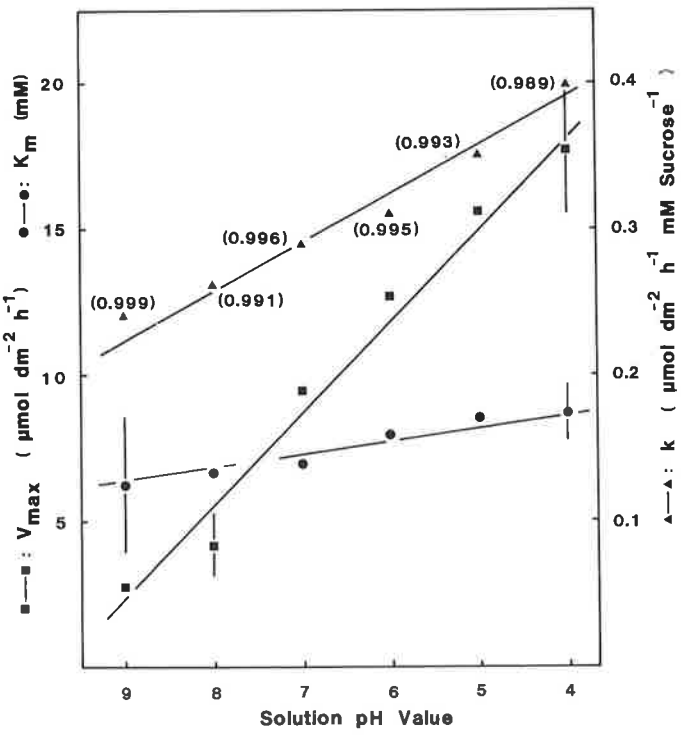


FIG. 6. Effect of apoplastic pH on the kinetic parameters. $V_{max}$ and $K_m$ are calculated from Lineweaver-Burk transformations of the sucrose influx data for the saturable component. The coefficient $k$ is the slope of the [$^{14}$C]sucrose influx *versus* sucrose concentration plots for the linear component. Values in parentheses represent correlation coefficients ($r^2$) obtained from the data presented in Figure 1.

concentrations used. This component demonstrates first order kinetics, its contribution to total sucrose uptake being given by the term $k$S (eqn 1). The comparable term for a diffusional process would be $k$ ($S_i$-$S_o$), where $S_i$ is the sucrose concentration inside the cell or tissue and $S_o$ is the exogenous concentration. This latter term could not produce a linear profile unless $S_i$ were held constant, and this would not be possible in a contained disc system, unless extensive metabolic conversion or compartmentation were occurring. Results from efflux and extraction studies, and autoradiographic investigation by previous workers (8, 10), rule out the possibility that either passive or exchange diffusion is solely responsible for the linear component.

The pH-dependence of $k$ is a phenomenon yet to be explained. Studies in this laboratory are presently investigating the nature of the linear component to determine whether it reflects the operation of a single carrier showing negative cooperativity at high sucrose concentrations (12) or, alternatively, whether the saturable ($H^+$-sucrose cotransport) and linear (first order kinetics) components represent two independent systems operating in parallel or across separate membranes within the phloem tissue. Present studies have also indicated that plasmodesmatal connections, abundant between all minor vein phloem cells, must be considered in any attempt to obtain a comprehensive analysis of the phloem-loading system.

*Acknowledgments*—We wish to thank Dr. V. R. Franceschi for providing the electron micrographs. Thanks are also due to Drs. D. W. Keifer and V. R. Franceschi and Mr. L. V. Kochian for their critical readings of the manuscript.

## LITERATURE CITED

1. BAKER DA 1978 Proton co-transport of organic solutes by plant cells. New Phytol 81: 485–497
2. BLACKMAN MS, CN MCDANIEL 1980 Amino acid transport in suspension-cultured plant cells. II. Characterization of L-leucine uptake. Plant Physiol 66: 261–266
3. COHEN SR 1975 A comparison of the rate equations, kinetic parameters, and activation energies for the initial uptake of L-lysine, L-valine, γ-aminobutyric acid, and α-aminoisobutyric acid by mouse brain slices. J Membr Biol 22: 53–72
4. COHEN SR 1980 The complete rate equation, including the explicit dependence on $Na^+$ ions, for the flux of α-aminoisobutyric acid into mouse brain slices. J Membr Biol 52: 95–105
5. DELROT S, JL BONNEMAIN 1979 Proton sugar co-transport in leaf tissues of *Vicia faba* L. Plant Physiol 63: S-244
6. DELROT S, JL BONNEMAIN 1981 Involvement of protons as a substrate for the sucrose carrier during phloem loading in *Vicia faba* leaves. Plant Physiol 67: 560–564
7. FISCHER E, U LÜTTGE 1980 Membrane potential changes related to active transport of glycine in *Lemna gibba* Gl. Plant Physiol 65: 1004–1008
8. GEIGER DR 1975 Phloem loading. *In* MH Zimmermann, JA Milburn, eds, Transport in Plants. Encyclopedia of Plant Physiology, New Series, Vol 1. Springer-Verlag, Heidelberg, pp 395–431
9. GEIGER DR, RT GIAQUINTA, SA SOVONICK, RJ FELLOWS 1973 Solute distribution in sugar beet leaves in relation to phloem loading and translocation. Plant Physiol 52: 585–589
10. GIAQUINTA RT 1977 Phloem loading of sucrose: pH dependence and selectivity. Plant Physiol 59: 750–755
11. GIAQUINTA RT 1977 Sucrose hydrolysis in relation to phloem translocation in *Beta vulgaris*. Plant Physiol 60: 339–343
12. GIAQUINTA RT 1980 Mechanism and control of phloem loading of sucrose. Ber Dtsch Bot Ges 93: 187–201
13. GIAQUINTA RT 1980 Translocation of sucrose and oligosaccharides. *In* Stumpf PK, EE Conn, eds, The Biochemistry of Plants, Vol 3. Academic Press, New York, pp 271–320
14. HUMPHREYS T 1978 A model for sucrose transport in the maize scutellum. Phytochemistry 17: 679–684
15. HUTCHINGS VM 1978 Sucrose and proton cotransport in *Ricinus communis* L. I. $H^+$ influx associated with sucrose uptake. Planta 138: 229–235
16. KOMOR E 1977 Sucrose uptake by cotyledons of *Ricinus communis* L.: characteristics, mechanism, and regulation. Planta 137: 119–131
17. KOMOR E, W TANNER 1974 The hexose-proton cotransport system of *Chlorella*: pH-dependent change in $K_m$ values and translocation constants of the uptake system. J Gen Physiol 64: 568–581
18. KOMOR E, M ROTTER, W TANNER 1977 A proton-cotransport system in a higher plant: Sucrose transport in *Ricinus communis*. Plant Sci Let 9: 153–162
19. KOMOR E, M. ROTTER, J WALDHAUSER, E MARTIN, BH CHO 1980 Sucrose proton symport for phloem loading in the *Ricinus* seedling. Ber Dtsch Bot Ges 93: 211–219
20. LICHTNER FT, RM SPANSWICK 1981 Electrogenic sucrose transport in developing soybean cotyledons. Plant Physiol 67: 869–874
21. LICHTNER FT, RM SPANSWICK 1981 Sucrose uptake by developing soybean cotyledons. Plant Physiol 68: 693–698
22. MALEK F, DA BAKER 1977 Proton cotransport of sugars in phloem loading. Planta 135: 297–299
23. RACUSEN RH, AW GALSTON 1977 Electrical evidence for rhythmic changes in the cotransport of sucrose and hydrogen ions in *Samanea* pulvini. Planta 35: 57–62
24. SERVAITES JC, LE SCHRADER, DM JUNG 1979 Energy-dependent loading of amino acids and sucrose into the phloem of soybean. Plant Physiol 64: 546–550
25. SOVONICK SA, DR GEIGER, RJ FELLOWS 1974 Evidence for active phloem loading in the minor veins of sugar beet. Plant Physiol 54: 886–891
26. VAN BEL AJE, AJ VAN ERVEN 1979 A model for proton and potassium cotransport during the uptake of glutamine and sucrose by tomato internode discs. Planta 145: 77–82
27. WALKER NA, FA SMITH, IR CATHERS 1980 Bicarbonate assimilation by freshwater Charophytes and higher plants. I. Membrane transport of bicarbonate ions is not proven. J Membr Biol 57: 51–58
28. WYSE R 1979 Sucrose uptake by sugar beet tap root tissue. Plant Physiol 64: 837–841

Plant Physiol. (1982) 70, 1436–1443
0032-0889/82/70/1436/08/$00.50/0

# Sucrose and Glucose Uptake into *Beta vulgaris* Leaf Tissues[1]

## A CASE FOR GENERAL (APOPLASTIC) RETRIEVAL SYSTEMS

Received for publication April 21, 1982 and in revised form July 30, 1982

JULIA W. MAYNARD AND WILLIAM J. LUCAS
*Department of Botany, University of California, Davis, California 95616*

### ABSTRACT

**Concentration curves for sugar and amino acid uptake by *Beta vulgaris* L. leaf tissues contained both a saturable and a linear component. Similarly shaped curves were obtained for influx of sucrose, glucose, and 3-*O*-methyl glucose by leaf discs, whole petiole slices, petiole segments containing pith tissue only, and petiole segments containing vascular bundles, although the tissues took up the various sugars via different proportions of saturable *versus* linear uptake. Two millimolar *p*-chloromercuribenzenesulfonic acid selectively inhibited the saturable component of sucrose uptake, but had almost no effect on the linear component. Uptake of glucose and 3-*O*-methyl glucose remained unaffected by *p*-chloromercuribenzenesulfonic acid treatment. Anoxia was found to inhibit the linear component of both sucrose and 3-*O*-methyl glucose influx, while the saturable component remained unaffected. The linear component of sucrose uptake was also competitively inhibited by maltose, as well as being selectively promoted by certain exposures to 5 millimolar *N*-ethylmaleimide, 2 micrograms per milliliter cycloheximide, and high levels of mannitol acting as osmoticum. These results support the proposal that the linear component is due to a process more complex than simple, or exchange, diffusion. It would also appear that the linear transport component utilizes a separate energy source than does the saturable component of sucrose influx.**

**Evidence for phloem loading from the apoplast was re-examined with respect to the present findings. Saturable sucrose uptake by minor vein tissues may represent retrieval of solute from the free space, which could explain the 'apoplastic loading' phenomenon.**

*Beta* leaves and leaf discs readily absorb [$^{14}$C]sucrose from exogenous solutions (13, 28, 31). The assumption is frequently made that such uptake predominantly represents phloem loading, the process by which assimilate is accumulated in the sieve elements prior to translocation. However, it has been well-established that exogenous sucrose does not enter phloem tissues alone (1, 7, 27). Both Geiger (9) and Giaquinta (16) have pointed out that at high external concentrations, sucrose probably enters the cells of the mesophyll and vascular parenchyma, in addition to the se-cc[2] complex. Furthermore, numerous studies report that various other organic compounds are also readily taken up when exogenously supplied to leaves. These include other sugars, both hexoses and disaccharides (1, 7), and various amino acids (30).

Previous studies have shown that absorption of exogenous sucrose by source leaf discs closely resembles sucrose uptake by intact leaves (14, 28, 31). According to Sovonick *et al.* (31), sucrose uptake into the phloem occurs via two saturable (or biphasic) systems. However, the more recent work by Maynard and Lucas (28) indicates that this interpretation is inaccurate. Typical concentration isotherms for sucrose absorption into leaf tissue consist of both a saturable and a linear component, with total sucrose uptake being represented by the equation:

$$v = V_{max}S/(S + K_m) + kS, \quad (1)$$

where $v$ is the rate, $S$ is the sucrose concentration, $V_{max}$ and $K_m$ are the Michaelis-Menten constants, and $k$ is the first-order rate coefficient (28). It is possible that the mechanisms (carriers?) responsible for the saturable and linear components of sucrose uptake are located on spatially distinct plasma membranes. For instance, the saturable process could represent the sucrose-proton cotransport that Giaquinta (14) envisions at the se-cc complex plasmalemma. The linear system may operate across the plasmalemma of the mesophyll tissue. Komor *et al.* (20) have proposed that a similar linear process in *Ricinus* seedlings may represent passive diffusion into mesophyll cells. Existing evidence does not allow an exact location of either component. Either process (or both) could conceivably operate from the apoplast at the se-cc membrane or at the phloem parenchyma cell membranes, or may represent uptake by mesophyll cells with eventual symplastic transport to the sieve elements.

Although there is a considerable body of evidence that is consistent with an apoplastic step in phloem loading (9, 16), the support is not unequivocal. The fate of exogenously supplied sucrose is, therefore, not completely clear. In the present study, we investigated whether foliar uptake of apoplastic sucrose represents a normal part of phloem loading, and not some other system. While the latter seems unlikely, it is possible that experimental conditions may exaggerate the effects of a process operating *in vivo* as, for example, a mechanism acting to retrieve solutes from the free space.

## MATERIALS AND METHODS

*Beta vulgaris* L. (USH10 Lot 3102) plants were grown as described previously (28). Experiments were performed on tissues from mature leaves of 6-week-old plants.

Leaf discs 0.2 cm$^2$ in size and slices of petiole approximately 1 mm thick were excised under 20 mM citrate-phosphate buffer (pH 5) containing 20 mM $CaCl_2$. Further separation of petiole slices into 'pith' or 'vascular bundle' pieces (Fig. 2, inset) was done by punching out the 'semicircle' of pith tissue with a modified 3 mm diameter cork borer that had been bent to the shape of the vascular tissue. Resulting pith sections were examined to ensure that vascular bundles had not been included. The basic details of the 30-min pretreatment in unlabeled sugar and subsequent 30-min incubation in $^{14}$C-sugars have been described previously (28). Briefly, all solutions contained 20 mM $CaCl_2$, Mes or citrate-

[1] Supported by National Science Foundation Grant PCM-7910223 and a University of California Graduate Research Award (to J. W. M.).

[2] Abbreviations: se-cc, sieve element-companion cell; $k$, first-order rate coefficient; PCMBS, *p*-chloromercuribenzenesulfonic acid; NEM, *N*-ethylmaleimide; DTE, dithioerythritol; DNP, dinitrophenol.

phosphate buffer (pH 5), and sufficient mannitol to attain a uniform 500 milliosmoles of osmoticum. Arginine was obtained from New England Nuclear (Boston, MA); all other radioactive isotopes were obtained from ICN (Irvine, CA). Solution specific activities were 120 $\mu$Ci/mmol for sucrose, glucose, leucine, and arginine, and 40 $\mu$Ci/mmol for 3-*O*-methyl glucose. In experiments in which petiolar material was employed, transport rates were expressed on the basis of tissue fresh weight. Pith and vascular bundle sections were given the normal rinses in ice-cold nonradioactive experimental solution, and then the tissue, used in each substrate concentration, was subdivided into 30 mg lots. A Mettler PK300 electronic microbalance with a GA23 printer was used to obtain and record tissue weights. In some experiments, leaf discs were also weighed by this method.

Kinetic constants were calculated for both components of substrate influx. The first-order rate coefficient, $k$, was calculated as the slope of the linear regression equation for points on the total influx curve at or above 10 to 25 mM substrate, depending on where the curves approached linearity. Correlation coefficients ($r^2$) for the regression equations were generally very high, usually 0.998 or above, the lowest recorded being 0.979. The contribution of the linear process to total influx was estimated as $k$ multiplied by the substrate concentration at each point, and this was subtracted from total influx at each point to give the rates due to the saturable component. The Michaelis-Menten constant, $V_{max}$, was then taken to represent the highest rate achieved by the saturable process. In order to avoid the problems associated with leaf-disc abrasion, we conducted experiments on unabraded discs. We wish to stress that because of this, the kinetic constants should be used only as indicators of relative transport components.

Sucrose and 3-*O*-methyl glucose uptake experiments were also performed in the absence of $O_2$. Anoxic conditions were established in a glove bag that was purged with a continual stream of nitrogen. Leaf discs and all experimental solutions were purged of $O_2$ and then held under anoxia for 45 min before the discs were transferred to [$^{14}$C]sucrose solutions that had also been purged of $O_2$. The subsequent 30-min incubation and two 5-min washes were also performed under anoxic conditions. Identical results were obtained under low-light conditions, (green safelight used as necessary to perform tissue manipulations) or in the dark.

In experiments in which we used various inhibitors, pretreatment in inhibitor solutions substituted for the pretreatment in unlabeled sugar solution. Except as noted, tissues were incubated in 2 mM PCMBS for 10 min (followed by two 4-min washes in citrate-phosphate buffer) or in 5 mM NEM for 5 min (followed by 5 min in 1 mM DTE to remove unreacted NEM). Further details are given in the appropriate figure legends.

Efflux analyses were performed as described previously (28). Two sets of 12 discs were incubated in 25 mM [$^{14}$C]sucrose for 2 h. One set was then transferred to 5 mM NEM solution (containing 25 mM [$^{14}$C]sucrose and 20 mM $CaCl_2$) for 5 min, and then to 1 mM DTE (also with sucrose and $CaCl_2$) for 5 min. Efflux into aliquots of $Ca^{2+}$-containing buffer was then followed for 3 h.

## RESULTS

**Kinetics of Sucrose Influx.** In the extensive minor vein network of mature *Beta* leaves, relatively small sieve elements are associated with large companion and phloem parenchyma cells (9). In the petioles, the reverse is seen; large sieve elements are associated with smaller companion and phloem parenchyma cells. Large vascular bundles within the petiole are embedded in a nondifferentiated ground parenchyma which possesses little Chl (9). Thus, it was interesting to note that kinetic profiles for sucrose influx by leaf discs and by petiole slices exhibited the same general shape (Fig. 1). The $k$ values for leaf discs and petiole slices were similar, being 0.064 and 0.057 $\mu$mol g$^{-1}$ h$^{-1}$ mM sucrose$^{-1}$, respectively, but the $V_{max}$ for the saturable component in petioles was half that

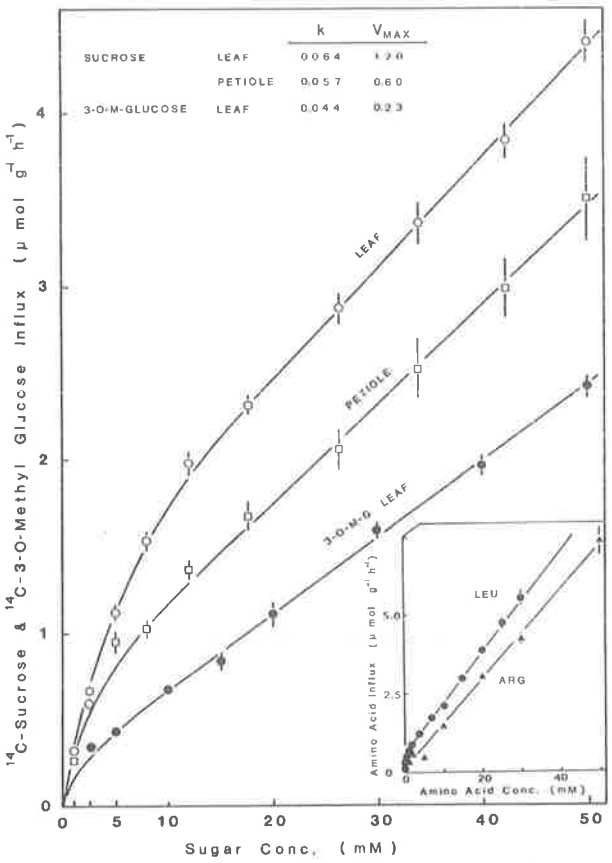


FIG. 1. Concentration dependence of sugar influx in *Beta* leaf discs and petiole slices. A 30-min preincubation in unlabeled sugar solutions was followed by 30-min in $^{14}$C-labeled media. Each point represents the mean ± SE for two sets of seven replicates. Sucrose uptake by leaf discs (○); sucrose uptake by petiole slices (□); 3-*O*-methyl glucose uptake by leaf discs (●). Values for $k$ are expressed as $\mu$mol g$^{-1}$ h$^{-1}$ mM sugar$^{-1}$ and $V_{max}$ as $\mu$mol g$^{-1}$ h$^{-1}$. Inset, Amino acid influx into *Beta* leaf discs: leucine (●); arginine (▲).

of the leaf discs. This may reflect differences in the relative amounts of undamaged vascular tissue present or differences between the minor vein absorptive tissue and the vascular bundle conducting tissue.

The glucose derivative, 3-*O*-methyl glucose, cannot generally be metabolized by plant cells, although conversion to sugar phosphate may occur in certain species (3). Exogenous 3-*O*-methyl glucose is taken up only by mesophyll tissue in *Vicia* leaf discs (1) and is not loaded into *Beta* minor veins at a significant rate (7). Thus, while sucrose may be absorbed by both minor vein and mesophyll tissues (1, 6, 7), 3-*O*-methyl glucose is presently thought to accumulate in only one tissue. Nonetheless, uptake of 3-*O*-methyl glucose into leaf discs also exhibited kinetics similar to those of sucrose (Fig. 1). This is at variance with results from the *Ricinus* seedling system, in which 3-*O*-methyl glucose uptake was entirely linear (19). We also investigated the transport of leucine and arginine into *Beta* leaf discs and found similar kinetics (Fig. 1, inset).

In further experiments, petiole sections (cut transversely) were separated into pieces containing only pith parenchyma and pieces containing both pith and vascular bundles (Fig. 2, inset). Two-component concentration profiles were generated in both segments (Fig. 2). Sucrose influx gave rise to $V_{max}$ values 3 times higher than those for uptake of 3-*O*-methyl glucose in both segments, while 3-*O*-methyl glucose influx gave rise to $k$ values twice as high. Influx of 3-*O*-methyl glucose by bundle-containing pieces

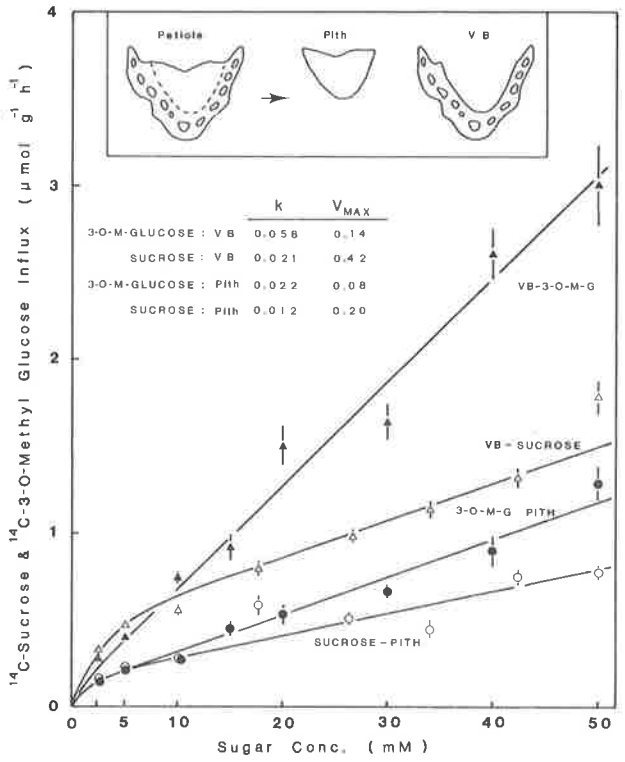


FIG. 2. Concentration dependence of sugar accumulation by dissected *Beta* petiole segments. Points represent the mean ± SE for seven replicates. Uptake of 3-*O*-methyl glucose by vascular bundle-containing (VB) segments (▲); sucrose uptake by VB segments (△); 3-*O*-methyl glucose uptake by pith parenchyma segments (●); sucrose uptake by pith segments (○) ($k$ and $V_{max}$ as in Fig. 1).

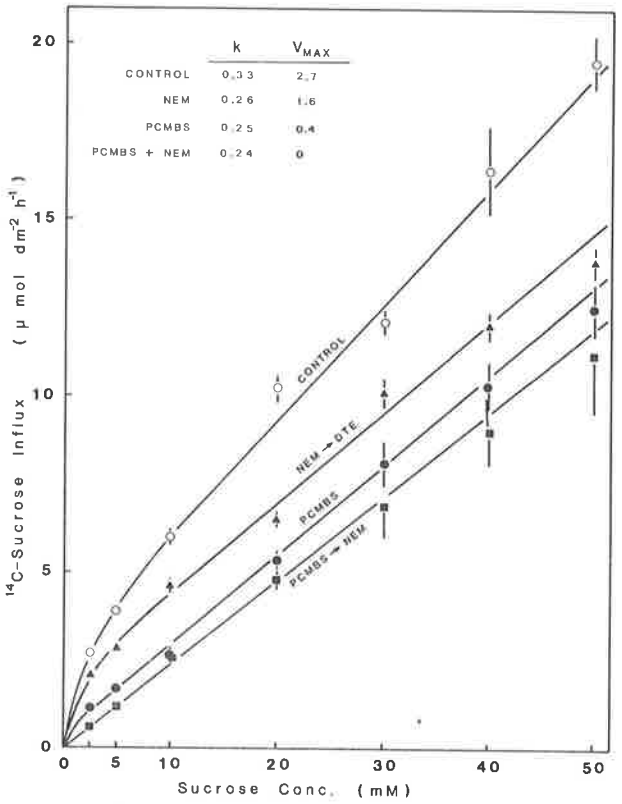


FIG. 3. Effect of sulfhydryl reagents on the concentration dependence of sucrose uptake. Control *Beta* leaf discs (○) were preincubated in citrate-phosphate buffer. PCMBS treatment (●) was for 10 min in 2 mM solutions. NEM treatment (▲) was for 5 min in 5 mM solutions followed by 5 min in 1 mM DTE. In other experiments, leaf discs were exposed to PCMBS and then NEM (■). All pretreatment solutions contained 5 mM sucrose, 1 mM $CaCl_2$, and 20 mM citrate-phosphate buffer (pH 5.0). Prior to introducing [$^{14}$C]sucrose, discs were given two 4-min washes in buffer solutions. Points represent the mean ± SE for three sets of six replicates. Values for $k$ are expressed as $\mu$mol dm$^{-2}$ h$^{-1}$ mM sugar$^{-1}$ and $V_{max}$ as $\mu$mol dm$^{-2}$ h$^{-1}$.

was essentially a linear function of concentration, while a saturable component made a large contribution to sucrose influx; the same features were observed for pith tissues. Thus, the saturable component cannot be entirely identified with the vascular bundles; however, since pith cells may be involved in sucrose storage, they could have the ability to accumulate sucrose selectively from the apoplast.

**Effects of Sulfhydryl Reagents on the Kinetics of Sucrose Uptake.** PCMBS is a nonpenetrating, reversible sulfhydryl reagent, while NEM penetrates and binds irreversibly to sulfhydryl groups. Both of these compounds have been shown to inhibit sucrose uptake into *Beta* leaves (13, 15). Five min in 5 mM NEM depressed both components of sucrose uptake below control values (Fig. 3). PCMBS-treated discs had similar $k$ values to those of NEM-treated tissue, but an additional inhibition of the saturable component was evident. In two of four experiments of this nature, PCMBS-treated discs gave rise to linear kinetic profiles, while in the remainder a small component of saturable uptake ($V_{max}$ = 0.2–0.4 $\mu$mol dm$^{-2}$ h$^{-1}$) was still evident. Treatment with PCMBS followed by NEM abolished this remaining saturable component (Fig. 3).

Sequential treatment with sulfhydryl reagents demonstrated their additive action (Fig. 4). Preincubation with PCMBS followed by NEM gave rise to a linear profile, as noted above. However, exposure of similarly treated discs to DTE (which can remove bound PCMBS but not NEM) reversed the PCMBS inhibition, restoring, in part, the saturable component. Experiments of this nature demonstrated that NEM was able to bind to additional sites that PCMBS did not affect.

In subsequent experiments with NEM, we found that its effect on sucrose influx was complex (Fig. 5). Increasing the NEM (5 mM) period of exposure from 3 to 5 min increased the degree of inhibition, but tissues given a 10-min exposure began to show a 'recovery' in sucrose accumulation. Longer exposures, such as 30 min, appeared to increase the level of accumulated [$^{14}$C]sucrose. Only the linear transport component was involved in this increase; inhibition of the saturable component increased with exposure. (Fig. 5 contains the averaged results of four experiments conducted in December 1980. In later experiments using control, 5- and 30-min treatments, we did not find promotion of the 30-min treatment above that of the control; however, $k$ values for the 30-min treated tissues were always greater than the 5-min treatment, and $V_{max}$ values were lowered. It should also be noted that the high $V_{max}$ values obtained from our earlier work, such as $V_{max}$ of 16.7 $\mu$mol dm$^{-2}$ h$^{-1}$ reported for the control curve in Fig. 5, have since declined to the 2.2–5.0 $\mu$mol dm$^{-2}$ h$^{-1}$ level reported in our other data, reflecting differences in plant material or growth conditions that we cannot explain. However, $V_{max}$ values obtained from field-grown material were within this latter range.)

NEM can also act as an inhibitor of protein synthesis (8). Cycloheximide, which is known to inhibit protein synthesis, was used in parallel experiments and was also found to selectively promote the linear component. The same effect was obtained with a 30-min treatment in cycloheximide followed by a 5-min wash as with a 5-min treatment followed by a 30-min wash, indicating that the time elapsed after exposure to cycloheximide may be the important factor, not length of treatment (Fig. 6).

It was possible, then, that long pretreatments in NEM promoted

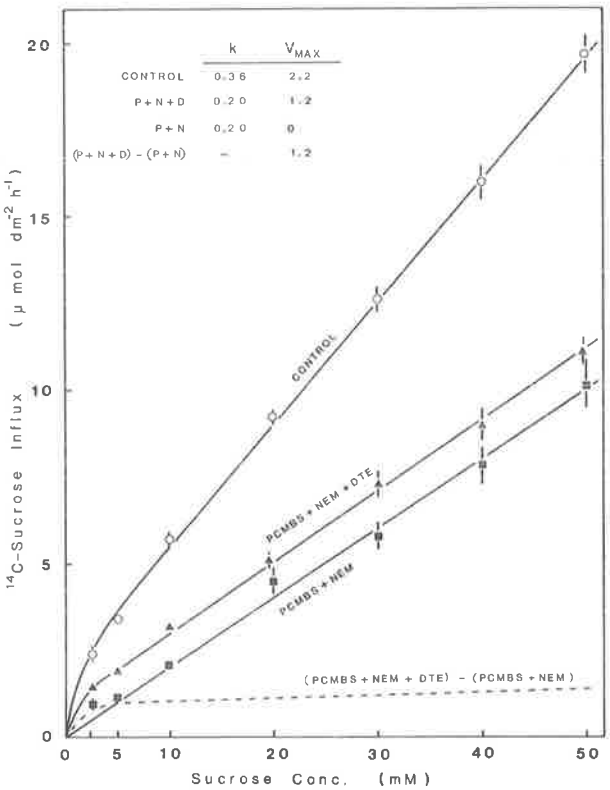


FIG. 4. Sequential addition of sulfhydryl reagents. Control *Beta* leaf discs were preincubated in 20 mM citrate-phosphate buffer (pH 5). PCMBS, NEM, and DTE treatments were as described in Figure 3. Points represent the mean ± SE for two sets of six replicates: control (○); PCMBS + NEM (■); PCMBS + NEM + DTE (▲) ($k$ and $V_{max}$ as in Fig. 3). The broken line was obtained by subtracting the PCMBS + NEM data from the values obtained in PCMBS + NEM + DTE experiments.

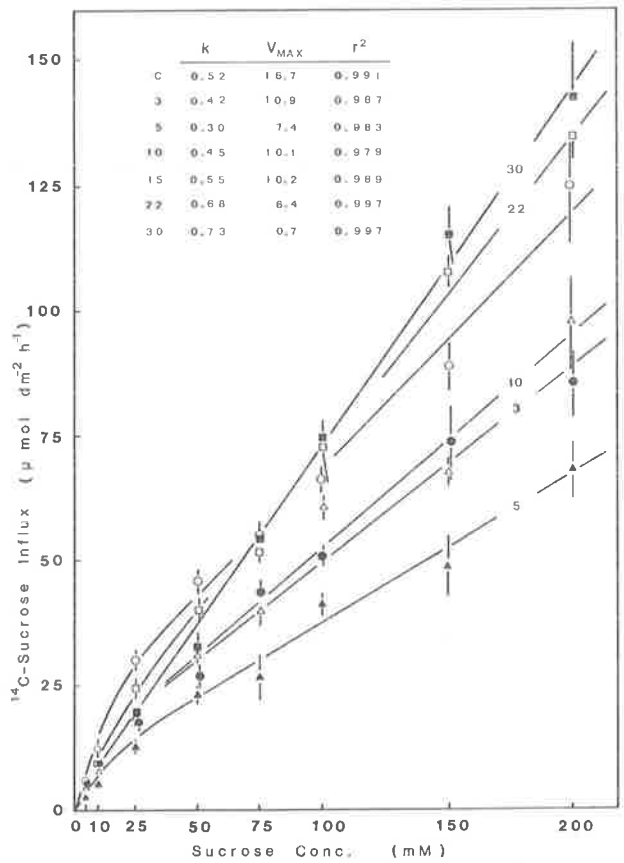


FIG. 5. Effect of increasing NEM exposure. *Beta* leaf discs were incubated in 5 mM NEM for varying times. A 5-min wash in 1 mM DTE was followed by a 30-min incubation in [$^{14}$C]sucrose. Points represent the mean ± SE for six replicate discs. Control (no exposure to NEM; ○); 3 min NEM (△); 5 min NEM (▲); 10 min NEM (●); 22 min NEM (□); 30 min NEM (■) ($k$ and $V_{max}$ as in Fig. 3).

linear uptake by allowing time for an inhibition of protein synthesis to take effect. Alternatively, long-term effects of NEM may have resulted from an increase in efflux of accumulated sugar (Table I). While both control- and NEM-treated sets of discs began the efflux period with similar dpm content, after 3 h of efflux there were significant differences in the radioactivity remaining. After the first 30 min, efflux became linear with time, with the NEM-treated discs losing about twice as much label as the control tissue.

**Effects of Sulfhydryl Reagents on Hexose Uptake.** Uptake of glucose and 3-*O*-methyl glucose by *Beta* leaf discs followed the characteristic saturable plus linear profile (Figs. 1 and 7). A comparison of the controls showed that both hexoses gave rise to similar $k$ values, but uptake of glucose showed a larger saturable component than 3-*O*-methyl glucose. Uptake of neither hexose was particularly sensitive to PCMBS, which is in agreement with the earlier studies of Giaquinta (15). However, pretreatment with NEM significantly depressed the saturable component of 3-*O*-methyl glucose uptake (see also Ref. 15).

**Further Manipulations of the Linear Component.** The disaccharide maltose, which consists of two glucose units, appeared to compete with sucrose for uptake (Fig. 8). Inclusion of 100 mM maltose in experimental solutions (pretreatment and uptake) led to inhibition of both uptake components. An increase to 400 mM maltose gave rise to further inhibition of the linear component without an additional effect on the saturable system.

The inhibitor DNP, which uncouples phosphorylation in mitochondria and chloroplasts, has been used previously to demonstrate the energy-dependence of various sucrose uptake systems (14, 15, 30, 31). Pretreatment with 0.5 mM DNP led to inhibition of both components of sucrose accumulation (Table II), with the saturable system being the more sensitive.

Under anaerobic conditions, we found that the linear component of sucrose influx was reduced, while the saturable component appeared to be completely unaffected (Fig. 9). Since anoxia affects many aspects of cellular metabolism, we examined its influence on the influx of 3-*O*-methyl glucose; this molecule is generally believed to be a nonmetabolizable analog of glucose. As shown in Figure 10, anoxia also selectively inhibited the linear component of 3-*O*-methyl glucose accumulation.

According to earlier studies on sugar beet leaf tissues (11), cells of the mesophyll, phloem parenchyma, and se-cc complex contain equivalents of 500, 300, and 1000 milliosmoles mannitol, respectively. Hence, mesophyll and phloem parenchyma cells should be well-plasmolyzed when equilibrated over solutions of 1250 milliosmoles, although collapse of cell walls may prevent the complete disruption of the symplast (12). To determine whether sucrose and 3-*O*-methyl glucose transport exhibit differential osmotic sensitivity, uptake profiles for both sugars were obtained in the presence of 250 or 1250 milliosmoles. Pretreatment solutions did not contain sugar, and incubation in $^{14}$C-sugar was shortened to 15 min in order to decrease possible effects of deplasmolysis (10). High levels of osmoticum promoted both components of sucrose uptake, with $k$ and $V_{max}$ being increased 148% and 145%, respectively. The $k$ value for 3-*O*-methyl glucose uptake was also enhanced by 145%; however, the saturable transport component remained unaffected by high osmolality.

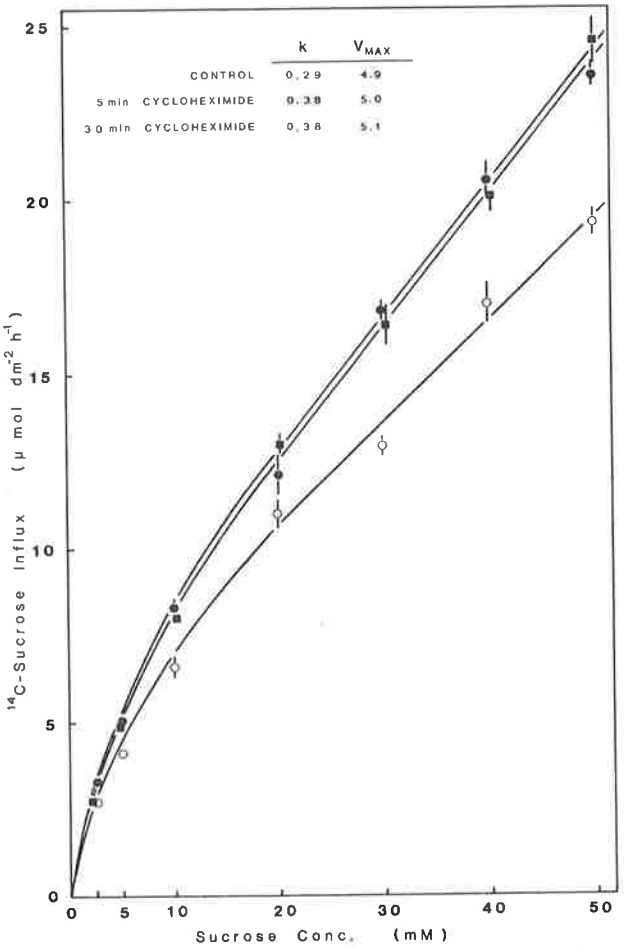


FIG. 6. Effect of cycloheximide on the concentration dependence of sucrose influx. Control sugar beet leaf discs (○) were preincubated in 20 mM citrate-phosphate buffer. Treatment in 2 μg/ml cycloheximide was for either 30 min, followed by a 5-min wash (■), or for 5 min, followed by a 30-min wash (●). Points represent the mean ± SE for seven replicates. (Units for $k$ and $V_{max}$ are as in Fig. 3).

Table I. *Effect of NEM on Efflux of Sucrose from Beta Leaf Discs*

Two sets of 12 discs were incubated in 25 mM [$^{14}$C]sucrose for 2 h. NEM-treated discs were then incubated in 5 mM NEM for 5 min, followed by 5 min in 1 mM DTE (solution details given in "Materials and Methods").

| Efflux Time | Radioactivity Remaining in Discs | |
|---|---|---|
| | Control | NEM |
| *h* | *dpm ($10^5$)* | |
| 0 | 1.83 | 1.79 |
| 0.25 | 1.19 | 1.08 |
| 0.5 | 1.09 | 1.00 |
| 1 | 1.01 | 0.88 |
| 2 | 0.89 | 0.68 |
| 3 | 0.82 | 0.51 |
| | (0.095)[a] | (0.185) |

[a] Loss of radioactivity after 1 h of efflux, in dpm h$^{-1}$.

## DISCUSSION

**Transport of Exogenous Substrates.** Phloem tissue preferentially accumulates [$^{14}$C]sucrose and, consequently, it has been the tendency to equate exogenous sucrose uptake by leaf tissues with

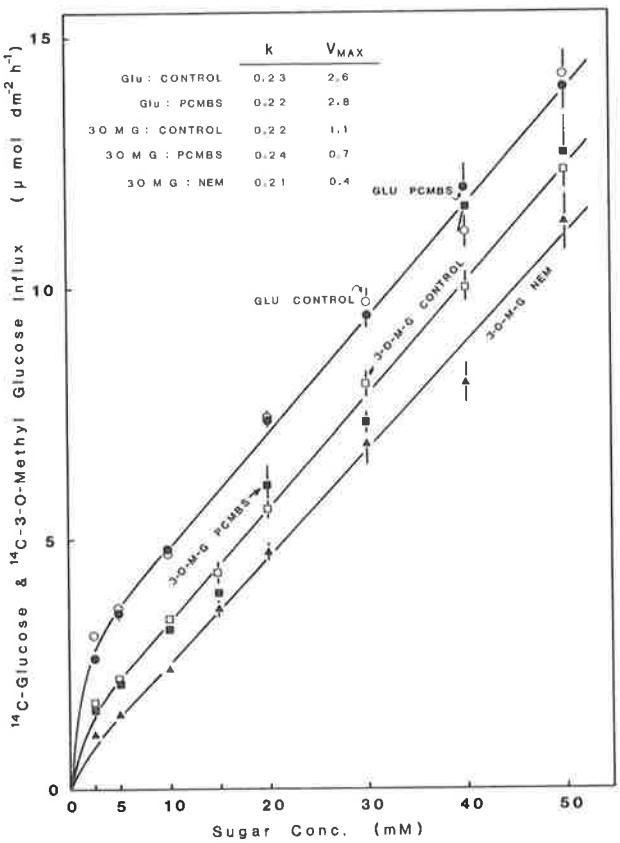


FIG. 7. Effect of sulfhydryl reagents on hexose influx in sugar beet leaf discs. Control, PCMBS, and NEM treatments are as described in Figure 3. Points for the glucose control (○), the glucose PCMBS (●), and the 3-*O*-methyl glucose control (□) represent mean ± SE for two sets of seven replicates; points for PCMBS-treated 3-*O*-methyl glucose (■) and the NEM-treated 3-*O*-methyl glucose (▲) represent the mean ± SE for seven replicates. (Units for $k$ and $V_{max}$ are as in Fig. 3.)

the actual process of phloem loading. Thus, the kinetics of [$^{14}$C] sucrose uptake have been interpreted with respect to the involvement of a $H^+$-sucrose cotransport system operating across the se-cc plasmalemma (see Refs. 9 and 16 for reviews of relevant literature). Fondy and Geiger (7) have shown, however, that in sugar beet tissue preincubated for 30 min in exogenously supplied 10 mM [$^{14}$C]sucrose, the majority of the label (60%) was found in the mesophyll tissue, with the remainder being either exported or present in the minor veins. Since our present experiments were conducted for 30 min, and we employed sucrose concentrations in the same range, it would appear that in the leaf the kinetic data represent transport of [$^{14}$C]sucrose across perhaps two different plasma membranes, those of the mesophyll and the se-cc complex.

The kinetic curve for 3-*O*-methyl glucose transport into *Beta* leaf discs was found to be identical in form to that obtained for [$^{14}$C]sucrose (Fig. 1; see also Fig. 7 for glucose); *i.e.* uptake appears to result from the operation of a saturable and a linear transport component. The similarity between these kinetic curves gains in importance when one considers that uptake of 3-*O*-methyl glucose is confined to the metabolic space of the mesophyll cells (1, 7). This line of argumentation can be extended to our results obtained on sugar beet petioles. The petiolar vascular bundles are embedded in a parenchymatous tissue, not a chlorenchymatous mesophyll, yet sucrose uptake into vascular bundle segments still exhibited both saturable and linear components (Fig. 2). Of equal importance was the finding that sucrose uptake into petiole pith segments (free of phloem tissues) exhibited the same kinetics as found using the vascular tissue. The same trends were also found for 3-

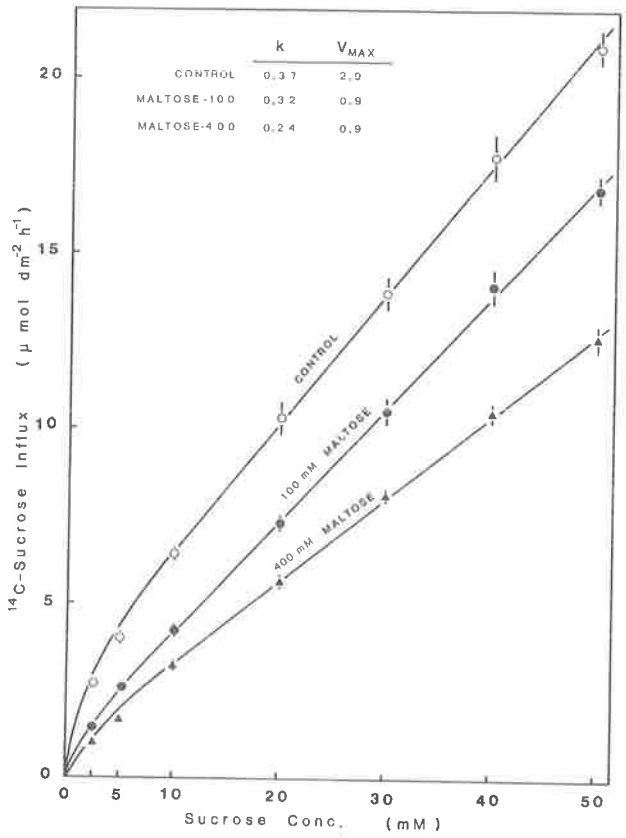


FIG. 8. Effect of maltose competition on the concentration dependence of sucrose influx. Sugar beet leaf discs were pretreated for 30 min in unlabeled sucrose and incubated for 30 min in $^{14}$C-labeled sucrose containing either no (○), 100 mM (●), or 400 mM (▲) maltose. Solutions with 100 mM maltose contained 500 milliosmoles osmoticum, while those with 400 mM maltose contained 630 milliosmoles.

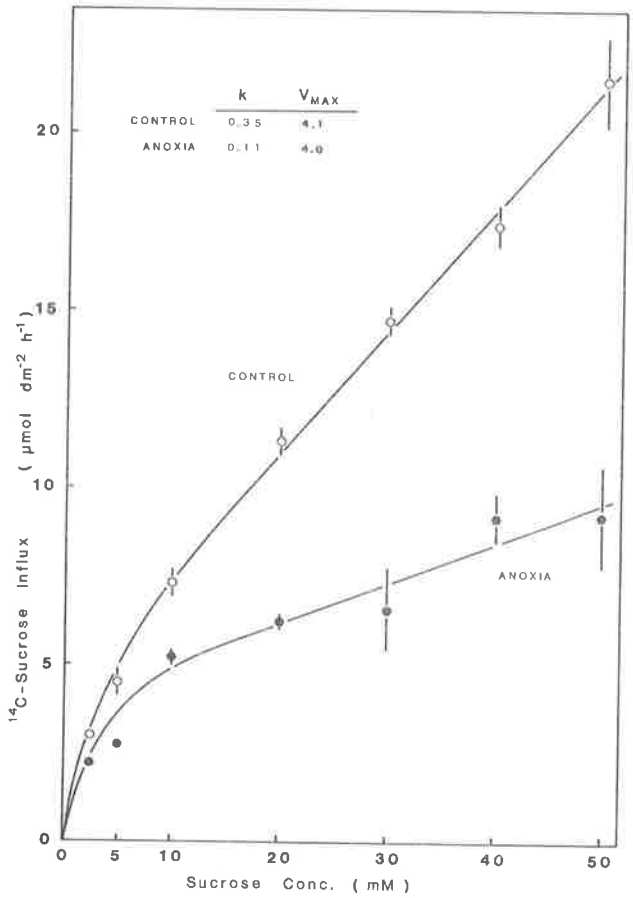


FIG. 9. Effect of anoxia on [$^{14}$C]sucrose influx. Tissue and experimental solutions were held under a nitrogen atmosphere for 45 min before the discs were transferred to [$^{14}$C]sucrose solutions. Incubation in labeled sugar for 30 min and two 5-min washes were also performed under anoxic conditions. Points represent the mean ± SE for six replicates.

Table II. *Effect of DNP on Sucrose Influx into Beta Leaf Discs*

The concentration dependence of uptake was determined for sucrose concentrations of 2.5, 5, 10, 20, 30, 40, and 50 mM, with two sets of seven replicate discs used at each concentration. Uptake curves were obtained for discs pretreated in 0.5 mM DNP for 0, 5, 10, and 60 min, and then incubated in [$^{14}$C]sucrose for 30 min. Kinetic parameters $k$ and $V_{max}$ were determined for the saturable and linear components of each curve.

| DNP Treatment | $k$ | $V_{max}$ |
|---|---|---|
| *min* | *μmol dm$^{-2}$ h$^{-1}$ mM sucrose$^{-1}$* | *μmol dm$^{-2}$ h$^{-1}$* |
| 0 | 0.51 (100)[a] | 4.8 (100) |
| 5 | 0.42 (82) | 2.4 (50) |
| 10 | 0.39 (76) | 1.8 (37) |
| 60 | 0.37 (72) | 1.5 (31) |

[a] Numbers in parentheses, percent of control values.

*O*-methyl glucose uptake into petiole vascular bundle- and pith-segments.

It seems that the presence of a saturable and a linear component of transport is a ubiquitous feature of the plasma membranes of a rather wide variety of cell types within leaf tissues. This obviously complicates the interpretation of kinetic data with respect to the importance of a particular tissue (*e.g.* the se-cc complex) in terms of its contribution to the total uptake into the leaf or petiole. We contend that this makes it very difficult to equate uptake of exogenously supplied [$^{14}$C]sucrose to the process of phloem loading.

**Nature of the Linear Component of Uptake.** Reports of uptake systems consisting of a saturable and a linear component operating in parallel are becoming numerous in the literature. Examples of such systems involved in the transport of sugars include 3-*O*-methyl glucose uptake by *Riccia* thalli (5) and sucrose uptake in soybean cotyledons (23), *Vicia* leaves (2), *Ricinus* cotyledons (19, 20), *Beta* leaves (28), and dissected vascular bundles (33).

It is important to determine the nature and the location, within the leaf tissue, of this rather ubiquitous linear component. The sulfhydryl reagent, PCMBS, inhibited 85 to 100% of the saturable component of sucrose uptake, but had far less of an effect on the linear system (Fig. 3). Autoradiographs of *Vicia* leaf discs showed that PCMBS inhibited accumulation into the minor veins (1). These results are consistent with the effect of PCMBS reported by Giaquinta (13, 15) and, collectively, may indicate that the saturable component represents uptake via a sucrose-$H^+$ cotransport system. It appears that sucrose may be absorbed by minor veins, via a saturable process, and by parenchymatous tissues, via both saturable and linear processes. A possible nonsaturable contribution to minor vein uptake of sucrose may be masked by the larger linear influx into the surrounding parenchyma. In parenchymatous tissues, 3-*O*-methyl glucose is taken up primarily by a linear process, although a saturable component does make a contribution to the total uptake in *Beta*.

Based on the assumption that sucrose uptake occurs via sucrose-proton cotransport (14), Giaquinta has proposed that PCMBS effects in *Beta* are primarily due to inhibition of a plasmalemma ATPase (15). If linear sucrose uptake is carrier-mediated, as

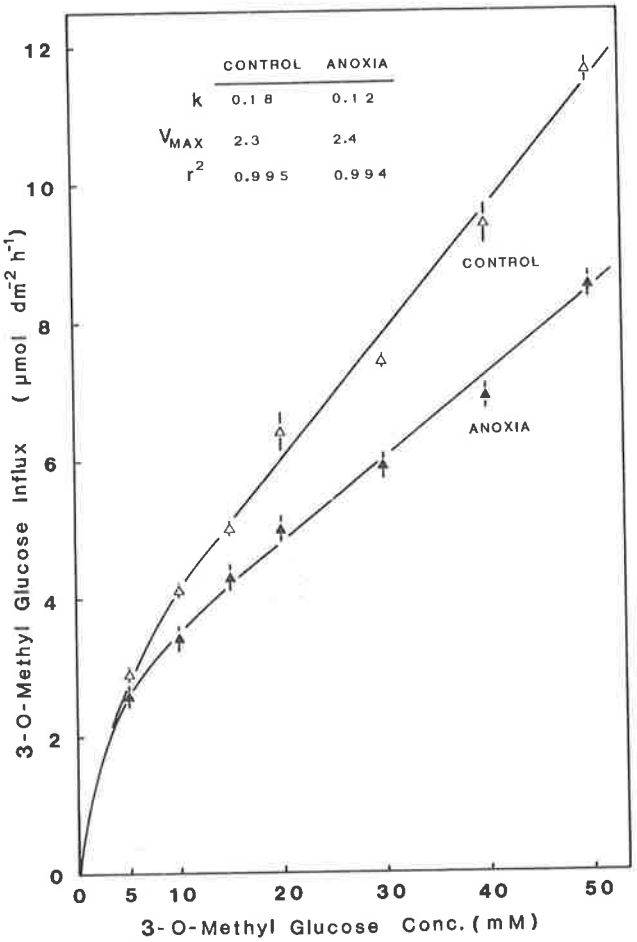


FIG. 10. Effect of anoxia on 3-*O*-methyl glucose influx. Tissue and experimental solutions were held under a nitrogen atmosphere for 45 min before the discs were transferred to [$^{14}$C]glucose solutions. Incubation in labeled sugar for 30 min and two 5-min washes were also performed under anoxic conditions. Points represent the mean ± SE for twelve replicates.

implied by maltose competition (Fig. 8), then interaction of PCMBS with the carrier system would affect both components. A relatively small degree of inhibition (20%) of *k* was seen (Fig. 3), but a much greater effect on the saturable component was observed (85–100%). Thus, if PCMBS acts on *Beta* plasmalemma ATPase activity, the linear component may utilize a different energy source compared to the saturable component (see also next section on anoxia).

The ability of NEM to enhance sucrose efflux (Table I) is not consistent with its promotion of linear uptake during long exposures, unless both phenomena represent some change in membrane permeability (22). Certain additional effects of NEM may be due to its ability to inhibit protein synthesis. In barley roots, cycloheximide treatment prevented protein synthesis but did not affect respiration, so that ATP levels actually increased, thereby causing a promotion of transport (26).

**Effect of Anaerobiosis on [$^{14}$C]Sucrose Uptake.** Selective inhibition of the linear component of sucrose uptake by anoxia is an extremely important finding (Fig. 9). Sovonick *et al.* (31) also reported an inhibitory effect of anoxia on sucrose uptake by *Beta* leaf discs. However, they analyzed their kinetic data in terms of the operation of two saturable transport components, presenting the effect of anoxia on the basis of changes in $K_m$ and $V_{max}$ of each 'saturable' system. This invalid kinetic approach led them to believe that anoxia was inhibiting both systems of transport, rather than the selective effect that we observed in the present study. We obtained the same selective inhibition of the linear uptake component of 3-*O*-methyl glucose under anaerobic conditions (Fig. 10). Since 3-*O*-methyl glucose is taken up only into mesophyll cells (7) and is not metabolized to any great extent, the similarity in effect between this molecule and that for sucrose suggests that the site of anoxia inhibition is at the plasmalemma and not at some location in the metabolic compartment(s). Thus, not only does the linear component appear to have a direct requirement for metabolic energy, but it appears to utilize a separate energy source than does the saturable component of sucrose influx. Possible energy sources include ATP from respiration, or perhaps reductant, such as NADH. Recently, a terminal oxidase which can accept electrons from exogenous NADH has been isolated from the plasmalemma of corn root protoplasts (24, 25). In this work, exogenous NADH was found to increase the $O_2$ consumption and the uptake of $K^+$ and phosphate in corn root segments. We cannot dismiss the possibility that a similar terminal oxidase may be involved in sucrose transport via the linear component.

The observation that the saturable component of sucrose (and glucose) influx was not affected by anoxia was quite unexpected. As discussed above, the saturable component of sucrose uptake is thought to represent sucrose-$H^+$ cotransport and may be operating across both phloem (se-cc complex and/or phloem parenchyma) and mesophyll plasma membranes. Due to the relatively high levels of ATP in the phloem sap (34), this tissue may not have experienced the same depletion of energy levels, under anoxia, as did the mesophyll tissue. If this were the case, the anoxia-insensitivity of the saturable component could be taken to indicate that this component resides almost entirely in the phloem. However, since the saturable component of 3-*O*-methyl glucose showed the same insensitivity to anoxia, and this sugar is only transported into mesophyll cells, this conclusion is suspect.

Anoxia, as a probe to study phloem physiology, could provide valuable insight into the operation of this complex system. Indeed there have been earlier reports that anoxic conditions inhibit phloem translocation (loading?). Leonard and Glen (21) found that a nitrogen atmosphere inhibited accumulation of label in the veins, as well as its transfer into the petioles of detached leaves of *Phaseolus vulgaris*. Similarly, Pickard *et al.* (29) reported that phloem translocation from intact moonflower leaves was stopped immediately after the imposition of anoxia. In a more extensive study on the effects of $O_2$ and phloem loading, Thorpe *et al.* (32) showed that loading in *Triticum aestivum* and *Panicum milioides* was decreased by approximately 70% within 1 to 6 min of anoxia application, but in *Zea mays* and *Panicum maximum* no reduction was observed. These authors ascribed these important differences to $C_3$ *versus* $C_4$ related properties. It will be of interest to ascertain whether species such as *Zea mays* have a linear component of sucrose uptake that is insensitive to anoxia.

**Is the Apoplastic Step in Phloem Loading an Example of General Retrieval?** Much debate has revolved around the *in vivo* movement of photosynthate from mesophyll chloroplasts into the se-cc complex. At present, an apoplastic step is favored, although the evidence in support of this is primarily from one plant: sugar beet (9, 16). If sugars normally enter the apoplast (7), then the plant must have some means of recovering this carbohydrate in order to prevent its unnecessary loss or build-up of conditions conducive to attack by pathogens. Fondy and Geiger (7) have suggested that "the mesophyll tissue may act as a collecting surface, reclaiming sucrose and hexoses which leak from the photosynthesizing cells." If this leakage does occur, and indeed there is experimental evidence showing that sugars (mainly sucrose, glucose, and fructose) do appear in the apoplast (7), then we can see no reason why sucrose would not leak from the se-cc complex. Since the sucrose concentration is high along the entire length of the translocation pathway, sucrose leakage may be a general phenomenon. Other proposals of retrieval mechanisms

have been proposed for phloem parenchyma cells (17) and certain thick-walled sieve elements in *Zea* minor veins (4). These modified cells possess an increased plasmalemma surface area, which may be set up to scavenge solutes from the apoplast and pass them on symplastically to the se-cc complex.

In experiments using exogenously applied sugar, we suggest that it is presently impossible to distinguish between 'apoplastic loading' and 'retrieval.' The distinction between the two becomes whether the mesophyll secretes sucrose only into the apoplast immediately surrounding the minor vein phloem, or whether sucrose leakage is an unavoidable phenomenon of the plasmalemma. It is possible that saturable uptake of sucrose by minor vein tissues represents the transport system that retrieves this sugar. While efflux of sugars from wheat and tobacco mesophyll protoplasts has been cited as direct support for an apoplastic step in translocation (18), this finding can also be interpreted as providing evidence for plasmalemma leakage, which may or may not be due to protoplast isolation.

Further evidence for apoplastic loading in *Beta* leaf tissues has been provided by use of the inhibitor PCMBS. Exogenous application of PCMBS inhibited uptake of [$^{14}$C]sucrose, as well as translocation of label supplied as both $^{14}CO_2$ and [$^{14}$C]sucrose, at inhibitor concentrations not affecting photosynthesis or respiration (13). If the saturable uptake seen in the present study does represent a retrieval or a loading mechanism, then its suppression would lead to the formation of a local sink at the site of inhibitor application: sieve elements would continue to leak, thus lowering their turgor, and a decrease in export would be seen from this site. Application of 10 mM PCMBS to intact *Beta* leaves led to an inhibition of [$^{14}$C]sucrose translocation from 11 to 6 $\mu$g carbon $dm^{-2}$ $min^{-1}$ after 60 min (13). Although Giaquinta (13) did not specify the sucrose concentration used, we found similar inhibition (*i.e.* approximately 50%) at lower sucrose concentrations (2.5–10 mM), and this can be explained as suppression of the saturable component (see Fig. 3).

## CONCLUSIONS

Absorption of exogenous sucrose by leaf tissues represents more than loading into the phloem. The concentration (kinetic) curves contain both a saturable and a linear component. Identification of these transport components with the plasma membrane systems of the various leaf tissues still remains to be elucidated. In the present study, we provide further evidence that the linear component of uptake is not due to simple or exchange diffusion. This contention is supported by several lines of evidence: the linear component (a) operates against a concentration gradient, at least at lower concentrations; (b) is pH-dependent (28); (c) is dependent in part on metabolic energy (Table II; Fig. 9); (d) can be competitively inhibited (Fig. 8); (e) can be selectively promoted (Figs. 5 and 6); and (f) is enhanced by water stress-related changes in turgor (J. W. Maynard and W. J. Lucas, unpublished results). Finally, it has been shown that the exogenous sucrose acquired through the operation of this linear component is available for translocation (31).

*Acknowledgments*—We wish to thank Dr. Thomas Pesacreta for helpful suggestions and assistance in some experiments. Thanks are also due to Dr. Willy Lin for making his work available prior to publication.

### LITERATURE CITED

1. Delrot S 1981 Proton fluxes associated with sugar uptake in *Vicia faba* leaf tissues. Plant Physiol 68: 706–711
2. Delrot S, JL Bonnemain 1981 Involvement of protons as a substrate for the sucrose carrier during phloem loading in *Vicia faba* leaves. Plant Physiol 67: 560–564
3. Dittrich P, K Fischer 1980 Accumulation and conversion of 3-*O*-methyl glucose in guard cells of *Commelina communis* L. Z Naturforsch 35: 832–834
4. Evert RF, W Eschrich, W Heyser 1978 Leaf structure in relation to solute transport and phloem loading in *Zea mays* L. Planta 138: 279–294
5. Felle H, FW Bentrup 1980 Electrogenic hexose transport in *Riccia fluitans*. *In* RM Spanswick, WJ Lucas, J Dainty, eds, Plant Membrane Transport: Current Conceptual Issues. Elsevier/North Holland Biomedical Press, Amsterdam, pp 549–550
6. Fellows RJ, DR Geiger 1974 Structural and physiological changes in sugar beet leaves during sink to source conversion. Plant Physiol 54: 877–885
7. Fondy BR, DR Geiger 1977 Sugar selectivity and other characteristics of phloem loading in *Beta vulgaris* L. Plant Physiol 59: 953–960
8. Fresno M, L Carrasco, D Vasquez 1976 Initiation of the polypeptide chain by reticulocyte cell-free systems. Eur J Biochem 68: 355–364
9. Geiger DR 1975 Phloem loading. *In* MH Zimmermann, JA Milburn, eds, Transport in Plants. Encyclopedia of Plant Physiology, New Series, Vol 1. Springer-Verlag, Heidelberg, pp 395–431
10. Geiger DR, BR Fondy 1980 Response of phloem loading and export to rapid changes in sink demand. Ber Dtsch Bot Ges 93: 177–186
11. Geiger DR, RT Giaquinta, SA Sovonick, RJ Fellows 1973 Solute distribution in sugar beet leaves in relation to phloem loading and translocation. Plant Physiol 52: 585–589
12. Geiger DR, SA Sovonick, TL Shock, RJ Fellows 1974 Role of free space in translocation in sugar beet. Plant Physiol 54: 892–898
13. Giaquinta RT 1976 Evidence for phloem loading from the apoplast: chemical modification of membrane sulfhydryl groups. Plant Physiol 57: 872–875
14. Giaquinta RT 1977 Phloem loading of sucrose: pH dependence and selectivity. Plant Physiol 59: 750–755
15. Giaquinta RT 1979 Phloem loading of sucrose: involvement of membrane ATPase and proton transport. Plant Physiol 63: 744–748
16. Giaquinta RT 1980 Mechanism and control of phloem loading of sucrose. Ber Dtsch Bot Ges 93: 187–201
17. Gilder J, J Cronshaw 1974 A biochemical and cytochemical study of adenosine triphosphatase activity in the phloem of *Nicotiana tabacum*. J Cell Biol 60: 221–225
18. Huber SC, DE Moreland 1980 Translocation: efflux of sugars across the plasmalemma of mesophyll protoplasts. Plant Physiol 65: 560–562
19. Komor E, M Rotter, W Tanner 1977 A proton-cotransport system in a higher plant: sucrose transport in *Ricinus communis*. Plant Sci Lett 9: 153–162
20. Komor E, M Rotter, J Waldhauser, E Martin, BH Cho 1980 Sucrose proton symport for phloem loading in the *Ricinus* seedling. Ber Dtsch Bot Ges 93: 211–219
21. Leonard OA, RK Glenn 1968 Translocation of assimilates and phosphate in detached bean leaves. Plant Physiol 43: 1380–1388
22. Lichtner FT, RM Spanswick 1981 Electrogenic sucrose transport in developing soybean cotyledons. Plant Physiol 67: 869–874
23. Lichtner FT, RM Spanswick 1981 Sucrose uptake by developing soybean cotyledons. Plant Physiol 68: 693–698
24. Lin W 1982 Responses of corn root protoplasts to exogenous reduced nicotinamide adenine dinucleotide (NADH): oxygen consumption, ion uptake, and membrane potential. Proc Natl Acad Sci USA 79: 3773–3776
25. Lin W 1982 Isolation of NADH oxidation system from the plasmalemma of corn root protoplasts. Plant Physiol 70: 326–328
26. Lüttge U, A Läuchli, E Ball, MG Pitman 1974 Cycloheximide: A specific inhibitor of protein synthesis and intercellular ion transport in plant roots. Experientia 30: 470–471
27. Martin E, E Komor 1980 Role of phloem in sucrose transport by *Ricinus* cotyledons. Planta 148: 367–373
28. Maynard JW, WJ Lucas 1982 A reanalysis of the two-component phloem loading system in *Beta vulgaris*. Plant Physiol 69: 734–739
29. Pickard WF, PEH Minchin, JH Troughton 1978 Real time studies of carbon-11 translocation in moonflower. II. The effect of metabolic and photosynthetic activity and water stress. J Exp Bot 29: 1003–1009
30. Servaites JC, LE Schrader, DM Jung 1979 Energy-dependent loading of amino acids and sucrose into the phloem of soybean. Plant Physiol 64: 546–550
31. Sovonick SA, DR Geiger, RJ Fellows 1974 Evidence for active phloem loading in the minor veins of sugar beet. Plant Physiol 54: 886–891
32. Thorpe MR, PEH Minchin, EA Dye 1979 Oxygen effects on phloem loading. Plant Sci Lett 15: 345–350
33. Turkina MV, SV Sokolova 1972 Membrane transport of sucrose in plant tissue. Sov Plant Physiol 19: 773–779
34. Ziegler H 1975 Nature of transported substances. *In* MH Zimmerman, JA Milburn, eds, Transport in Plants. Encyclopedia of Plant Physiology, New Series, Vol 1. Springer-Verlag, Heidelberg, pp 59–100

JOURNAL OF ULTRASTRUCTURE RESEARCH 81, 209–221 (1982)

# Organization of the Sieve-Element Walls of Leaf Minor Veins

W. J. LUCAS AND V. R. FRANCESCHI[1]

*Department of Botany, University of California, Davis, California 95616*

*Received May 14, 1982*

The organization of the sieve-element wall in minor veins of *Beta vulgaris* and 13 other species has been investigated at the electron microscope level using histochemical techniques. In all species examined, chemically distinct regions of the wall could be identified using the silver methenamine technique for staining carbohydrates with VIC-glycol groups and by phosphotungstic acid (PTA)/HCl poststaining. There appears to be a thin, dense layer of nonmicrofibrillar material adjacent to the sieve-element plasma membrane of most species examined. Cell-wall enzymatic digestions suggest this layer may have a high pectin content. This layer does not appear to be related to the often-reported nacreous layer of the inner sieve-element wall. Immediately surrounding this layer is a thick microfibrillar region with the microfibrils apparently transversely aligned with respect to the long axis of the cell. These two layers are interpreted as constituting the primary wall of the sieve element. The adjacent companion cell wall, which is clearly delineated by use of PTA/HCl staining, is thinner and of a different chemical composition compared with the sieve-element wall, with hemicellulose possibly predominating. Variations in cell wall structure among species are illustrated, including the wall structure of two species containing phloem transfer cells. The possible functions of the specialized wall structure are discussed.

The pathway by which photosynthate moves from mesophyll cells into the nearby minor-vein sieve tubes has been the center of much debate. It is currently believed that in mature leaf tissue this pathway contains an apoplastic step (see reviews by Geiger, 1975; Giaquinta, 1980). Phloem parenchyma cells are thought to release photosynthate (e.g., sucrose) into the apoplast and it is then transported across the plasma membranes of the neighboring sieve-element–companion cell complex. This latter process is generally referred to as phloem loading. Giaquinta (1977) and others (Delrot, 1981; Delrot and Bonnemain, 1981; Komor *et al.*; 1977; Malek and Baker, 1977) have proposed that loading of sucrose occurs via a $H^+$–sucrose cotransport system that is coupled to a plasmalemma-bound $H^+$-translocating ATPase.

In the event that phloem loading into the sieve-element–companion cell complex is via an apoplastic step, the sieve-element–companion cell wall may be expected to have special properties conducive to efficient apoplastic photosynthate transfer. In addition, the sieve-element wall might also be specialized for dealing with the high hydrostatic pressures that may develop in these cells. Sieve-element–companion cell walls have been investigated at both the light and electron microscope levels (Esau, 1969; Cronshaw, 1975, 1981; Evert, 1977, for reviews of this work). In many species the sieve-element wall has special inner thickenings that exhibit a nacreous appearance in fresh sections (Esau, 1969). Deshpande (1976) has demonstrated that in *Cucurbita* petioles the nacreous layer is comprised of very densely packed microfibrils. This characteristic may impart a high modulus of elasticity to the inner wall region, thereby making it relatively resistant to pressure-induced deformation.

In the present study we investigated mi-

[1] Present address: Department of Botany, Washington State University, Pullman, Wash. 99164.



0022-5320/82/110209-13$02.00/0

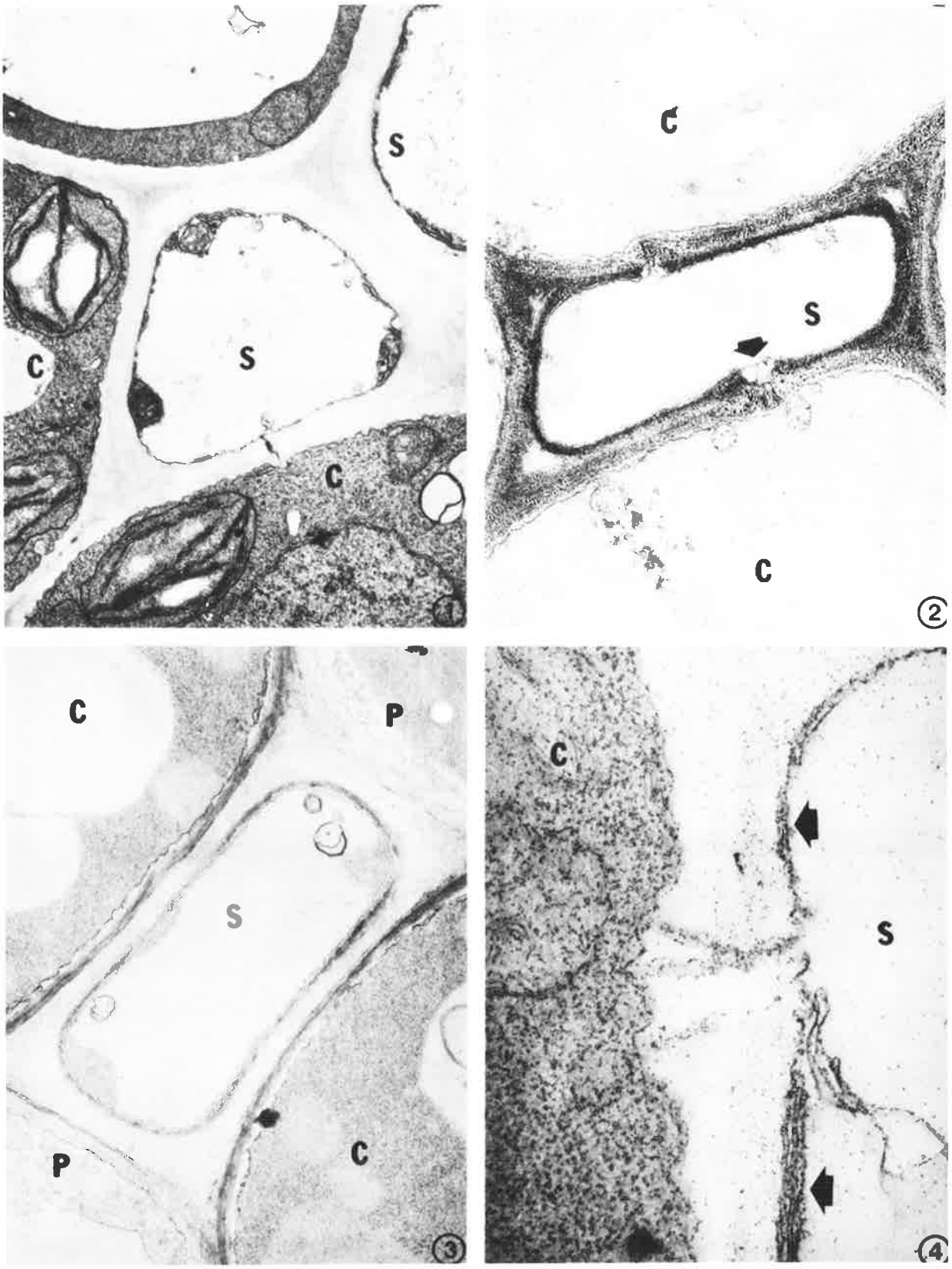


FIGS. 1–4. Sections through minor veins of mature *B. vulgaris* leaves poststained with various reagents. Companion cell (C), phloem parenchyma cells (P), sieve element (S).

FIG. 1. Uranyl acetate and lead citrate staining. × 15 000.

nor-vein sieve-element–companion cell walls of mature leaves obtained from various plant species. Cell wall structure was examined at the electron microscope level using histochemical techniques aimed at differentiating any chemically and structurally distinct regions.

## MATERIALS AND METHODS

The plants used in this study were *Beta vulgaris, Allium cepa, Phaseolus vulgaris, Gossypium hirsutum, Lycopersicon esculentum, Pisum sativum, Nicotiana tabacum, Zea mays, Glycine max, Avena sativa, Cucurbita maxima, Euphorbia celastroides, E. forbesii,* and *Claoxylon sandwicense*. *Beta vulgaris* was grown under growth-chamber conditions (see Maynard and Lucas, 1982). All other plants were cultivated in the Botany Department greenhouse facility, with the study being conducted during the early summer months (May–June). Pieces of mature leaf were fixed in 3% glutaraldehyde in 0.05 *M* sodium cacodylate buffer, pH 7.2, for 12 hr at 4°C. For histochemical purposes, after primary fixation small blocks of *B. vulgaris* leaf tissue were incubated in 1% pectinase (Sigma; in citrate–phosphate buffer, pH 4.0), 1% hemicellulase (Sigma; in citrate–phosphate buffer, pH 5.4) or 1% Cellulysin (Calbiochem; in citrate–phosphate buffer, pH 5.4), for 2.5 and 7 hr at room temperature. All tissue was then further processed as follows. The tissue was postfixed in 1% $OsO_4$ in 0.25 *M* cacodylate buffer (pH 7.2) for 2 hr at room temperature, rinsed with the same buffer, dehydrated in acetone, and embedded in Spurr's resin. Thin sections were picked up on uncoated nickel grids and stained with 2% uranyl acetate (aqueous) and 2% lead citrate (aqueous), or by histochemical techniques that will be described. All sections were examined with a JEOL (Tokyo, Japan) JEM 100S TEM operated at 80-kV accelerating voltage.

The silver methenamine technique was used to stain polysaccharides containing vicinal (*VIC*)-glycol groups (Rambourg, 1967). Sections on nickel grids were floated on 1% periodic acid for 30 min at room temperature and then stained for 60 min (unless otherwise indicated) at 60°C in the dark by floating the grids on freshly prepared stain solution (Franceschi and Lucas, 1981). The grids were then rinsed with distilled water, floated on 0.5% sodium thiosulfate for 5 min to remove nonspecific silver deposits, rinsed with distilled water, and dried for viewing in the TEM.

Sections were stained with phosphotungstic acid at low pH as follows. Sections on nickel grids were floated on 10% $H_2O_2$ for 30 min at room temperature to remove osmium, washed with distilled water, and stained for 10 min on a solution of 10% phosphotungstic acid in 10% HCl (PTA/HCl). The grids were then washed for 20 min on drops of distilled water (4 changes), dried, and examined in the TEM.

Some sections of *B. vulgaris* were stained with positively charged colloidal iron to determine negative charge distribution within the cell wall. Positively charged colloidal iron was prepared just prior to use. Ferric chloride (650 mg) was dissolved in 10 ml of distilled water, then added rapidly to 100 ml of boiling distilled water. Upon cooling, the pH was adjusted to 0.8 with HCl. This solution was diluted 1 part to 40 parts of 0.6 *M* HCl for staining. Grids were floated for 30 sec on drops of the stain, then 1 min on 0.6 *M* HCl, rinsed with distilled water, and dried.

## RESULTS

### *Beta vulgaris*

*Beta vulgaris,* which is being used in this laboratory for translocation studies, was most extensively studied, and the other species investigated will be compared with it. Various enzymatic digestions of the cell wall were only carried out on *Beta*.

The wall between sieve elements and companion cells of minor veins, when conventionally stained with uranyl acetate and lead citrate, showed no particular staining pattern (Fig. 1). When the silver methenamine technique (SM) was employed, a distinct cell wall staining pattern was observed. After SM staining, the sieve-element walls of minor veins were found to have a layer of material adjacent to the plasma membrane that stained more intensely than the rest of the cell wall (Fig. 2). The sieve-element walls of very large leaf veins and petiolar phloem are generally thicker, and

FIG. 2. Silver methenamine staining. Note darker staining layer of wall material immediately adjacent to sieve-element lumen. Callose on sieve-element side of plasmodesmata is unstained (arrow). × 15 000.

FIG. 3. PTA/HCl staining. A thin layer of stainable wall material surrounds sieve-element lumen, whereas a wider layer occurs along the companion cells. × 20 000.

FIG. 4. Cationic colloidal iron staining. Staining of the wall between sieve element and companion cell is diffuse. Membranes are also stained, with the endoplasmic reticulum (arrows) being well stained. × 50 000.

this staining pattern was not readily apparent in such walls. Other cell walls that were secondarily thickened (tracheids, fibers) were intensely stained by this technique. Such walls, however, also showed more intense staining with uranyl acetate and lead citrate.

Use of PTA/HCl, often considered a selective stain for the plasma membrane, resulted in staining of the plasma membrane of all cells of the phloem, but no other membrane systems. There was also a distinct pattern of staining within the cell wall between sieve elements and companion cells of the minor veins. The protoplasts of both sieve elements and companion cells were surrounded by a layer of PTA/HCl-stainable wall material, although that which surrounded the companion cell was always thicker (Fig. 3). The wall material between these PTA/HCl-bands remained unstained. The cell wall between companion cells and phloem parenchyma and between mesophyll cells stained evenly throughout. No layering pattern was apparent within such walls.

The cell wall, membranes, and other cytoplasmic structures within the phloem tissue, were stained to varying degrees with cationic colloidal iron (Fig. 4). Although staining of the wall between sieve elements and companion cells often occurred in layers or lines, no consistent staining pattern could be detected. Staining was heaviest along the middle lamella of mesophyll tissue, but no middle lamella could be distinguished in the wall between sieve elements and companion cells. The sieve-element reticulum was always clearly stained by the cationic colloidal iron (Fig. 4).

Our attempt at enzymatic digestion of specific wall materials was not totally successful because the commercially available enzyme preparations were contaminated with other wall hydrolytic enzymes. Nonetheless, the results do shed some light upon the chemical organization of the sieve-element wall. After enzymatic digestion, sections had to be stained for prolonged periods (2–3 hr) to make the remaining wall materials visible in the TEM.

Incubation of tissue in pectinase solution removed the material formerly found to stain with both PTA/HCl and silver methenamine (SM) (the more densely staining layer). Incubation of tissue in this solution for 7 hr, however, resulted in nearly complete hydrolysis of the wall between sieve elements and companion cells. After 2.5 hr, only a loose cellulosic network remained (Fig. 5). Seven-hour incubation in Cellulysin (cellulase) removed much of the cell wall material in the tissue. The SM-stainable layer immediately adjacent to the sieve-element plasma membrane was not removed by cellulase treatment (Fig. 6). There was also a thin, lightly staining layer that remained around the companion cells. Staining with PTA/HCl was patchy with no clear patterns occurring. Digestion of tissue with hemicellulase for 7 hr had no effect on either the SM- or PTA/HCl-staining patterns as compared with those seen in control tissues (enzyme absent). To examine hemicellulose distribution within the cell wall, thin sections (incubated 30 min in 10% $H_2O_2$ to remove $OsO_4$) were incubated on hemicellulase solution for 10, 15, and 20 hr at room temperature. After 20-hr incubation, a change in staining with SM was not-

FIGS. 5–8. Sections through minor veins of *B. vulgaris* treated with various enzymes and stained for prolonged periods (2–3 hr) with silver methenamine. Companion cell (C), phloem parenchyma cells (P), sieve element (S).

FIG. 5. Fixed tissue digested with 1% pectinase for 2.5 hr. Much of the wall has been removed leaving a diffuse cellulose network of material. × 8000.

FIG. 6. Fixed tissue digested with Cellulysin for 7 hr. A dense staining layer of material around the sieve-element lumen remains. Its thickness is accentuated in this oblique section. × 8000.

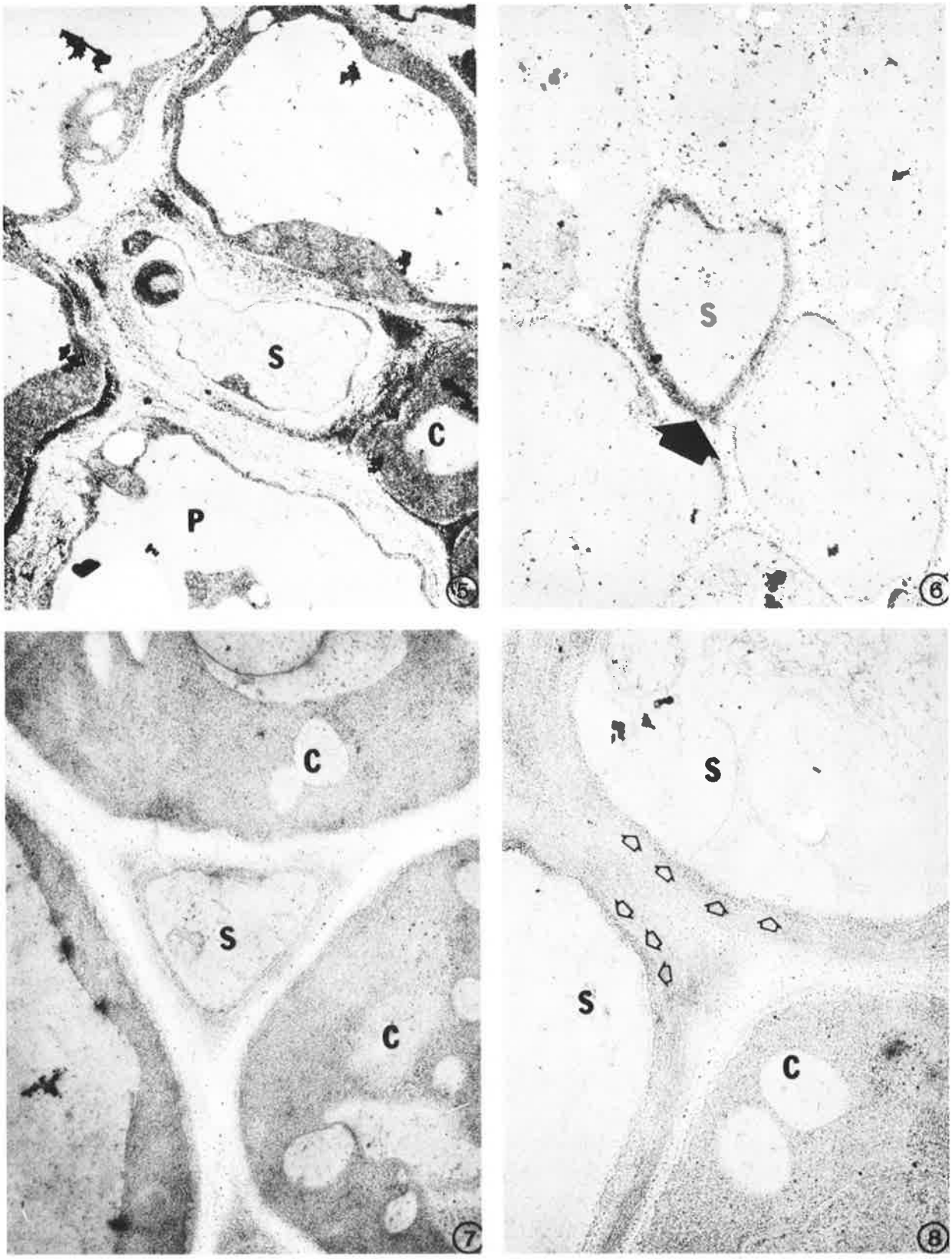


FIG. 7. Sectioned material incubated in 1% hemicellulose for 20 hr. Much of the wall material surrounding the companion cells has been removed. × 15 000.

FIG. 8. Sectioned material incubated in 1% hemicellulose for 20 hr. The central portion of the remaining wall material between sieve elements and between sieve elements and companion cells appears fibrillar whereas a slightly darker layer adjacent to the sieve-element lumen appears amorphous (arrows). × 25 000.

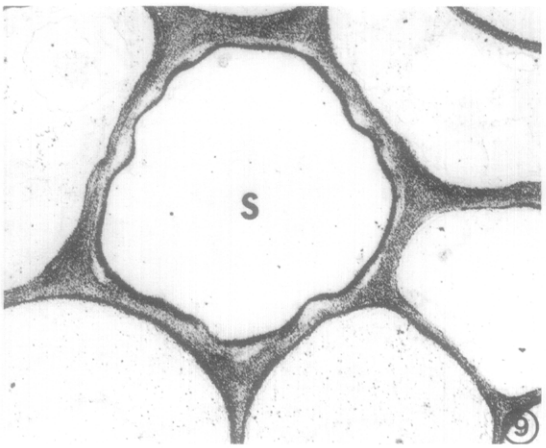
S
9

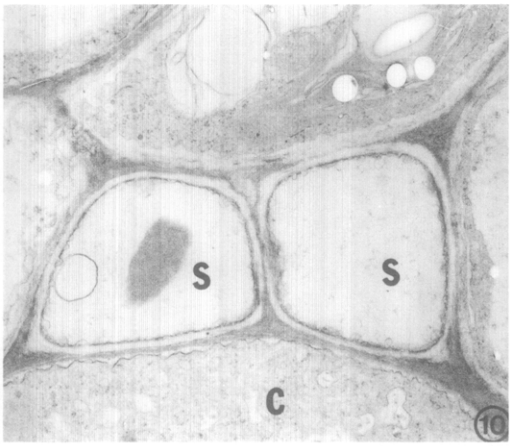
S
S
C
10

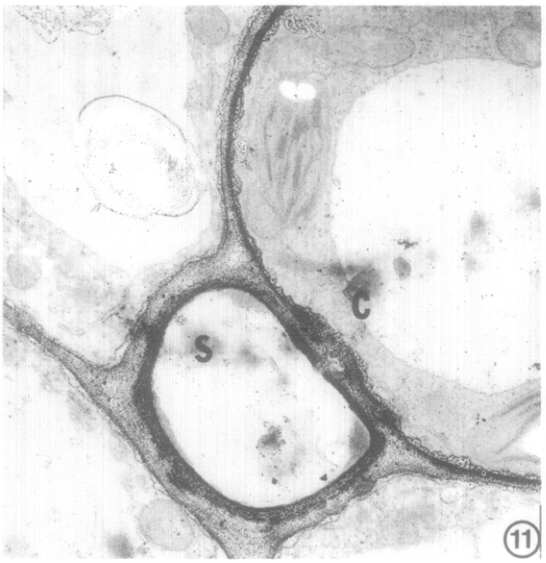
C
S
11

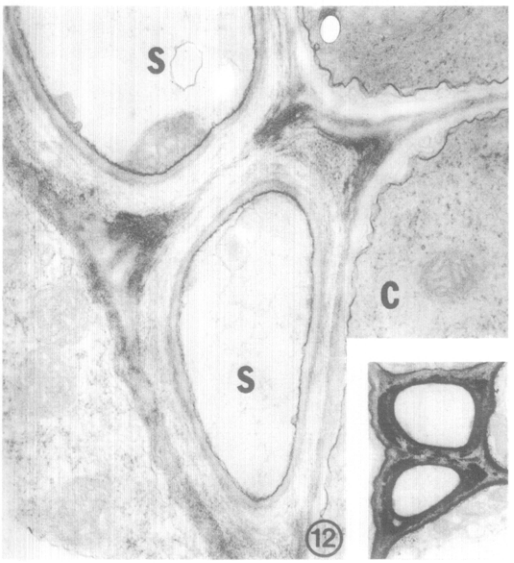
S
C
S
12

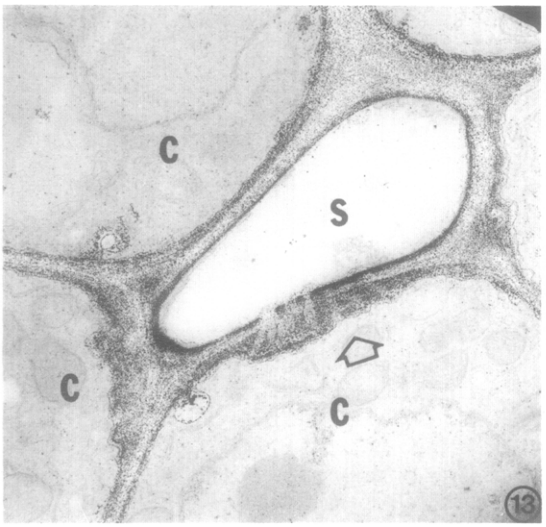
C
S
C
C
13

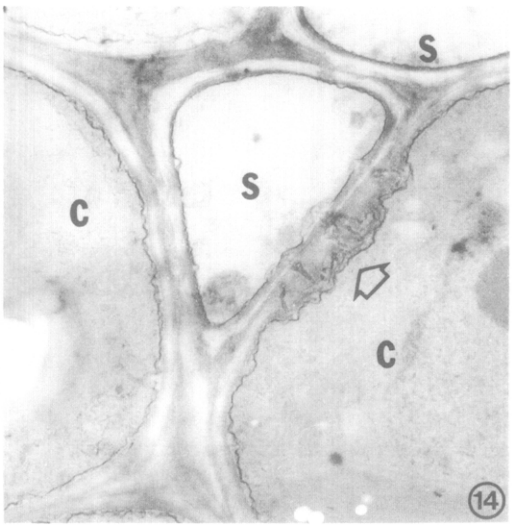
S
S
C
C
14

ed. Much of the previously stainable wall material along the periphery of the companion cells, and between companion cells, was removed by this treatment (Figs. 7 and 8). There was still a distinct layer of SM-stainable wall material around the sieve elements (Fig. 7) and the wall between sieve elements stained throughout (Fig. 8). The normally intensely staining layer of material at the sieve-element plasma membrane could still be discerned, although the staining was reduced considerably (Fig. 8). The remaining wall material between this layer and the companion cell appeared fibrillar in nature (Fig. 8). After hemicellulase treatment, the sections did not survive the treatment with harsh reagents of the PTA/HCl staining procedure. The sections would split along the walls making observations of wall staining impossible.

*Other Species*

Other species examined showed variations of the staining patterns seen in *B. vulgaris*; however, PTA/HCl staining showed the most variability. A denser, SM-stainable layer along the wall adjacent to the plasma membrane of the sieve element was a consistent feature of all species examined, although the thickness of this layer varied from species to species. *Cucurbita* sieve-element protoplasts, for example, had a distinct, darker layer at their periphery after SM staining (Fig. 9) but no definitive layer was observed after PTA/HCl staining except, of course, that associated with the plasma membrane (Fig. 10). In minor veins of *Gossypium* stained with SM there was a thick, dense-staining layer of wall material at the plasma membrane of both the sieve elements and companion cells (Fig. 11). The layer around the sieve elements was irregular in thickness and often patchy [Figs. 11 and 12 (inset)]. A very thin, even layer of wall material was seen along both the sieve elements and companion cells of *Gossypium* phloem, stained with PTA/HCl (Fig. 12). In *Claoxylon* minor veins stained with SM, a thin layer of dense-staining wall material could be observed at the periphery of both the sieve-element and companion cell protoplasts (Fig. 13). Similar sections stained with PTA/HCl had a very thin layer of stainable wall material at the sieve-element protoplast (Fig. 14).

A wall layer corresponding to the SM-stainable layer could not be discerned in sections stained with uranyl acetate and lead citrate (Figs. 15–17). This conventional staining did result in an increase of wall density, especially in the middle lamella. The PTA/HCl-staining wall layers, other than the middle lamella, could not be seen after uranyl-acetate and lead-citrate staining (compare Figs. 12 and 16). The three staining techniques used here (SM, PTA/HCl, and uranyl acetate–lead citrate) clearly show different affinities for the various wall components. The results of other species examined are given in Table I.

Some more general observations were also noted. In regions of the wall where

---

FIGS. 9–14. Sections through leaf minor veins of various species stained with silver methenamine (left) or PTA/HCl (right). Companion cell (C), sieve element (S).

FIGS. 9 and 10. *Cucurbita maxima*. × 15 000.

FIG. 11. *Gossypium hirsutum*. Both sieve elements and companion cells have a darker staining layer of wall material around their protoplasts. × 15 000.

FIG. 12. *Gossypium hirsutum*. Sieve elements and companion cells have a thin PTA/HCl stainable layer of wall material around their protoplasts. × 20 000. Inset: Same cells stained with silver methenamine showing patchy distribution of staining. × 6000.

FIG. 13. *Claoxylon sandwicense*. Sieve element has narrow darker staining layer of wall material around its protoplast. Region of wall where plasmodesmata occur also stains darker (arrow). × 15 000.

FIG. 14. *Claoxylon sandwicense*. Sieve-element wall has a narrow layer of PTA/HCl-stainable material. Region of wall where plasmodesmata occur stains intensely (arrow). × 15 000.

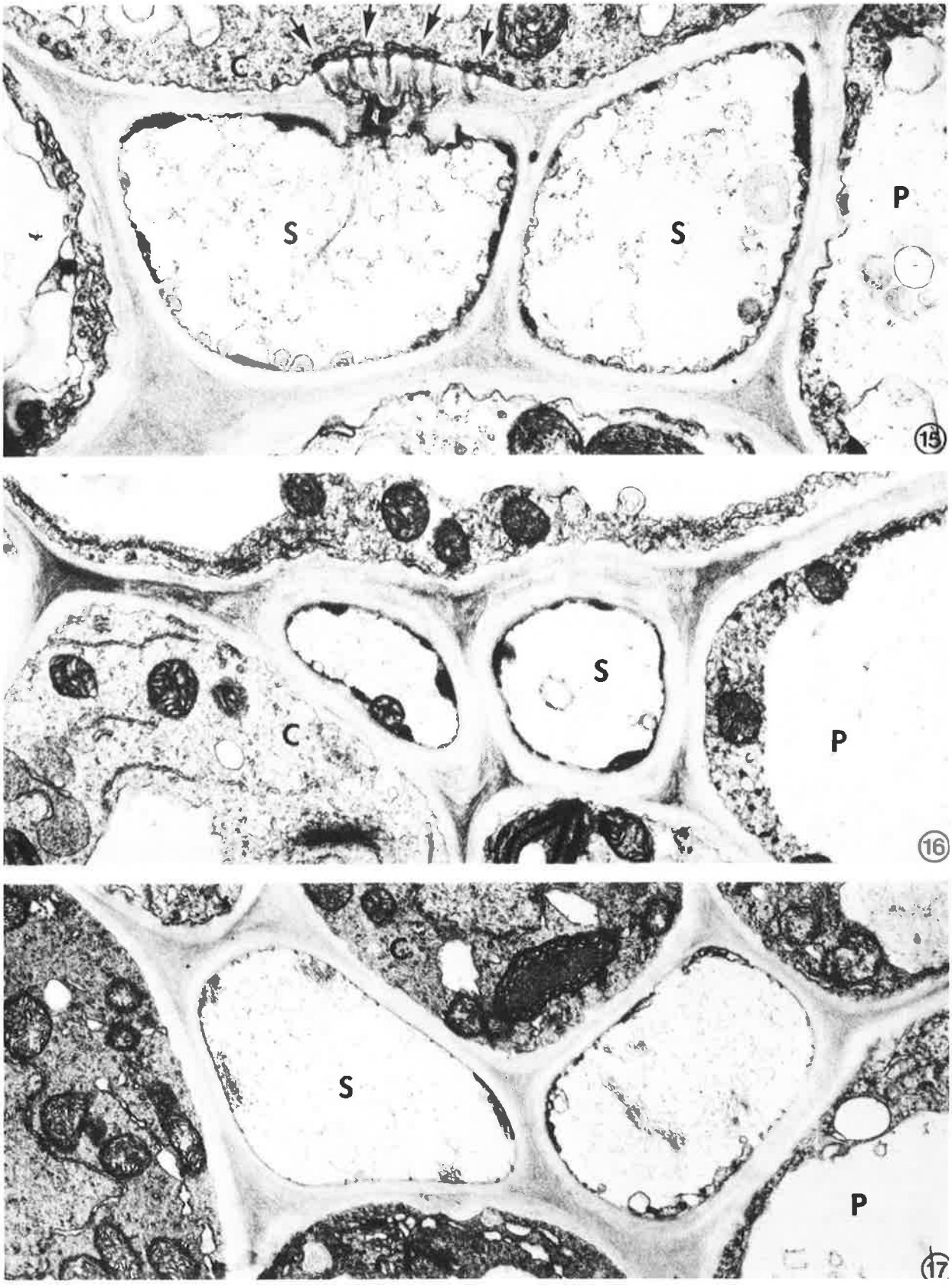


FIGS. 15–17. Leaf minor veins. Uranyl-acetate and lead-citrate staining. No trace of SM-staining layer discernable. Companion cell (C), phloem parenchyma cell (P), sieve element (S).

TABLE I

STAINING PATTERNS IN THE WALLS OF SIEVE ELEMENTS AND COMPANION CELLS OF VARIOUS PLANT SPECIES

| Species | Stain used | | | |
|---|---|---|---|---|
| | Silver methenamine | | PTA/HCl | |
| | Sieve element | Companion cells | Sieve element | Companion cell |
| *Avena sativa* | +[a] | − | + | − |
| *Euphorbia celastroides* ($C_4$) | + | + | + | + |
| *Euphorbia forbesii* ($C_4$) | + | − | + | − |
| *Glycine max* | + | − | + | + |
| *Lycopersicon esculentum* | + | + | + − | − |
| *Nicotiana tabacum* | + | − | + | + |
| *Phaseolus vulgaris* | + | − | + | + |
| *Zea mays* | + | + − | + | + |

[a] Indication of the presence (+) or absence (−) of a distinct layer of stainable wall material at the periphery of each cell type protoplast.

plasmodesmata occurred between sieve elements and companion cells, more of the cell wall stained with SM and PTA/HCl (Figs. 13 and 14). This was true of all species examined. In many species, the SM-stainable layer of the sieve-element wall was found to continue on into the sieve plate between neighboring sieve tubes (Fig. 18). This was also found to occur in the sieve area of lateral sieve plates (Fig. 19).

Two species examined, *Pisum* and *Allium,* contained transfer cells in the minor vein phloem. In *Pisum,* only the companion cells had wall ingrowths, whereas in *Allium* both companion cells and phloem parenchyma cells had vast networks of wall ingrowths. Both species had a dense SM-staining layer of wall material adjacent to the sieve-element plasma membrane (Fig. 20). In both species, the wall ingrowths also stained more intensely than the surrounding wall proper (data is only shown for *Pisum*). Very thin layers of stainable wall material could be seen along *Pisum* sieve elements and companion cells stained with PTA/HCl but no pattern could be seen in *Allium* after such staining.

## DISCUSSION

The results presented give us some insight into the structure of minor-vein sieve-element walls. Interpretation of the staining patterns observed is difficult due to the lack of knowledge concerning the specificity of the PTA/HCl stain. However, it is obvious that the silver methenamine (SM) and PTA/HCl stains have differing affinities for the various wall materials present, because little correlation was found between the layers seen with each stain.

As was found in this study, primary cell walls of mesophyll cells stain densely throughout with the PTA/HCl stain. It is fairly well documented that the primary wall of plant cells (parenchyma or mesophyll cells) contains a large amount of hemicellulose, and to a lesser degree, pectin (Northcote, 1972; Preston, 1974, 1979).

FIG. 15. *Cucurbita maxima*. Note continuity of ER and plasmodesmata at companion cell surface (arrows). × 28 000.

FIG. 16. *Gossypium hirsutum*. Same cells as Fig. 12. Thin layers stained with PTA/HCl in Fig. 12 are not discernable. × 17 500.

FIG. 17. *Claoxylon sandwicense*. × 14 000.

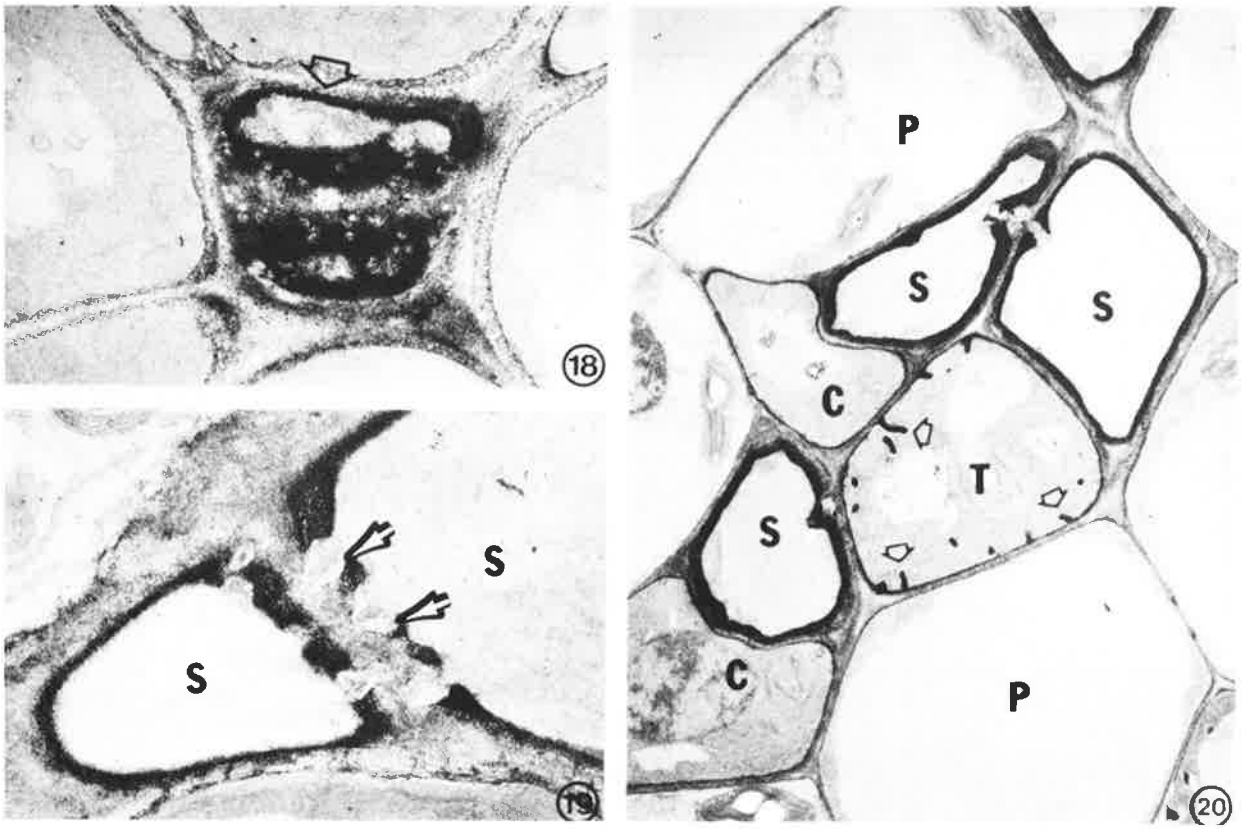


FIGS. 18–20. Sections through leaf minor veins stained with silver methenamine. Companion cell (C), phloem parenchyma cells (P), sieve element (S), transfer cell (T).

FIG. 18. Sieve plate of *E. forbesii*. The sieve plate stains more intensely than the lateral cell wall, except for the region immediately adjacent to the sieve-element lumen (arrow). The light circular areas are sieve-plate pores. × 10 000.

FIG. 19. Part of a sieve area of a lateral sieve plate of *N. tabacum*. The darker staining region of the wall continues into the sieve plate. Callose lining the sieve-plate pores does not stain (arrows). × 15 000.

FIG. 20. Minor vein of *P. sativum*. Notice intensity of staining of the wall immediately adjacent to the sieve-element and companion-cell protoplasts as compared with the parenchyma cell walls. Wall ingrowths of the companion cell modified as a transfer cell are densely stained (arrows). × 6000.

These polysaccharides are considered to be the matrix material of the wall in which cellulose is embedded. According to Hayat (1975), the basis of PTA staining may be a reaction of the stain with highly polymerized carbohydrates. Hence, it is possible that the staining of primary walls with PTA/HCl is due primarily to the presence of branched hemicelluloses and pectin. Regions of the wall that are high in cellulose content, however, may stain less intensely with PTA/HCl because the crystal lattice of the cellulose microfibrils may effectively exclude the rather large PTA molecules. This seems to be supported by the lack of staining by PTA/HCl of the outermost region of the sieve-element cell wall (Fig. 3). Silver methenamine staining, especially after hemicellulose digestion, indicates this region has a particularly high density of cellulose microfibrils (see Figs. 7 and 8). In contrast, the hemicellulose component of the wall is generally considered to be mostly amorphous in structure, and, thus, may be more accessible to the PTA molecule. The stainability of pectin by PTA/HCl may be variable because pectin molecules can become crosslinked and otherwise modified.

Silver methenamine is selective for car-

bohydrates with VIC-glycol groups, and differences in intensity of staining should indicate differences in the distribution of such carbohydrates or, rather, their density within a particular wall area. Hemicellulose, pectin, and cellulose should stain equally well with SM because of their chemical structure (all are composed of subunits having VIC-glycol groups). Thus, the darker staining layer at the periphery of the sieve-element lumen can be interpreted as an area of the wall in which the concentration of reactive carbohydrate is greater than within the rest of the wall. According to Esau and Cheadle (1958) the nacreous wall of the sieve element does not extend into the region of the sieve plate. Because the wall layer under present examination does extend into the sieve plate, we conclude that it represents a different cell wall characteristic. We suggest that this layer represents a region of the wall in which pectin predominates. The enzymatic digestion studies support this view. The SM staining in this layer was not affected by cellulose digestion and was only partially reduced by hemicellulose digestion. Pectinase digestion proved inconclusive because the enzyme preparation was highly contaminated with other wall hydrolytic enzymes. Purified enzyme preparations will have to be used to determine if the SM-staining layer is primarily pectin or a mixture of pectin and hemicellulose.

The layer of PTA/HCl stainable material surrounding the companion cell protoplast probably represents the primary cell wall. This is supported by the observation that it is continuous around the companion cell and of similar width throughout. Furthermore, it is absent, or very reduced, in the wall between adjacent sieve elements. The remaining wall can be considered the sieve-element wall, because it is likewise continuous and of equal thickness around the sieve-element protoplast. As discussed above, this wall stains differently from the companion cell wall after PTA/HCl and SM staining. The main feature of this wall appears to be that it contains a relatively thick, cellulose rich layer that is complemented by a thinner layer of noncellulosic polysaccharide material immediately adjacent to the sieve-element lumen.

There has been some controversy as to whether the sieve-element wall of minor veins represents a primary or secondary wall, especially when the nacreous thickenings are found (Cronshaw, 1975). No gross thickening of the sieve-element wall could be seen in the minor veins of species examined during this study. We have observed the development of sieve elements in *B. vulgaris* and it appears that, in the minor veins at least, the wall does not undergo any further thickening after the cell has differentiated to its functional state. Hence, the sieve-element wall of minor veins is probably a primary wall, albeit one that is very different from that of the mesophyll tissue. It is probably more similar to the "thickening primary walls" of collenchyma tissue (Majumdar and Preston, 1941).

The functional significance of this interesting wall structure is probably twofold. The function of the cellulose-rich region of the wall is undoubtedly one of structural support. Earlier studies of the sieve-element wall have examined the cellulose microfibril arrangement within the wall (Frey-Wyssling and Muller, 1957; Esau and Cronshaw, 1968; Srivastava, 1969; Behnke, 1971; Chafe and Doohan, 1972; Deshpande, 1976). The apparent transverse arrangement of microfibrils would give the wall high tensile strength and provide support against the hydrostatic pressure within the sieve element. Such an arrangement of microfibrils has been observed in sieve-element walls previously (Behnke, 1971; Deshpande, 1976; Cronshaw, 1975); however, in most instances the cells had nacreous thickenings, or were from plant tissues other than the minor veins. The layer directly adjacent to the sieve-element lumen, which appears to be rich in noncellulosic polysaccharides, may serve various functions. Pectins and

hemicellulose can become highly hydrated, and so have great compression strength. More importantly, the high degree of hydration may influence the actual concentration of solutes at the plasma membrane of the sieve element. This, in turn, could have an effect on transport processes occurring across the sieve-element plasma membrane. Additionally, pectins give rise to a large part of the Donnan charge of the cell walls and, thus, could influence movement of ions through the wall within this region. The use of cationic colloidal iron did not show a particularly high concentration of charges in the region of the wall adjacent to the plasma membrane; however, the effects on wall charge groups of the buffers, fixatives, and resin used in processing the tissue is not known, although appreciable binding of stain to membranes did occur.

The properties of the transfer cell-wall ingrowths may be similar to those proposed for the layer of material at the inner sieve-element wall. Although enzymatic digestions were not carried out on *Allium* or *Pisum,* it is likely that their transfer cell-wall ingrowths contain high concentrations of hemicellulose and pectin as indicated by the staining reaction with SM. It is often observed that the wall ingrowths of transfer cells, prepared for TEM by routine methods, are shrunken away from the plasma membrane. This suggests that this portion of the wall is highly hydrated, *in vivo,* and shrinkage occurs during tissue dehydration. An interpretation of this nature would be consistent with the above mentioned characteristics of pectins and hemicelluloses. Because transfer cells are considered sites for specialized transport (Gunning and Pate, 1974), the special properties of the wall ingrowths may reflect an essential apoplastic feature of these cells.

The use of the staining techniques presented here have allowed us to differentiate between the minor-vein sieve-element and companion cell walls, where these two walls are in contact, and have demonstrated that considerable chemical and structural differences exist between these two cell wall types. We have consistently observed a noncellulosic polysaccharide-rich cell-wall region adjacent to the plasma membrane of sieve elements and transfer cells, two different cell types considered specialized for transport processes. The chemical and physical properties of the noncellulosic polysaccharides can be expected to affect certain transport processes. The consistent presence of this feature, along sieve elements of such diverse species as have been examined here, indicates that it does have an important role in the function of this cell type. The nature of this wall material and that of the transfer cell-wall ingrowths deserve further study, because it may be related to the overall control of solute transport at these sites.

This research was supported by NSF Grant PCM-7910223 and a Sigma Xi Grant-in-Aid of Research. We thank Dr. R. W. Pearcy for making the euphorbian species available. V. R. F. gratefully acknowledges the support of a University of California Regents Fellowship.

## REFERENCES

BEHNKE, H. D. (1971) *Protoplasma* **72,** 69–78.

CHAFE, S. C., AND DOOHAN, M. E. (1972) *Protoplasma* **75,** 67–78.

CRONSHAW, J. (1975) *in* ARONOFF, S., DAINTY, J., GORHAM, P. R., SRIVASTAVA, L. M., AND SWANSON, C. A. (Eds.), Phloem Transport, pp. 129–152, Plenum, New York.

CRONSHAW, J. (1981) *Ann. Rev. Plant Physiol.* **32,** 465–484.

DELROT, S. (1981) *Plant Physiol.* **68,** 706–711.

DELROT, S., AND BONNEMAIN, J. L. (1981) *Plant Physiol.* **67,** 560–564.

DESHPANDE, B. P. (1976) *Ann. Bot. (London)* **40,** 443–446.

ESAU, K. (1969) *in* ZIMMERMANN, W., OZENDA, P., AND WULFF, H. D. (Eds.), Encyclopedia of Plant Anatomy, Vol. 5, Pt. 2, p. 505, Borntraeger, Berlin.

ESAU, K., AND CHEADLE, V. I. (1958) *Proc. Natl. Acad. Sci. U.S.A.* **44,** 546–553.

ESAU, K., AND CRONSHAW, J. (1968) *J. Ultrastruct. Res.* **23,** 1–14.

EVERT, R. F. (1977) *Ann. Rev. Plant Physiol.* **28,** 199–222.

FRANCESCHI, V. R., AND LUCAS, W. J. (1981) *J. Ultrastruct. Res.* **75,** 218–228.

FREY-WYSSLING, A., AND MULLER, H. R. (1957) *J. Ultrastruct. Res.* **1,** 38–48.

GEIGER, D. R. (1975) *in* ZIMMERMAN, M. H., AND MILBURN, J. A. (Eds.), Encyclopedia of Plant Physiology, Vol. 1, pp. 395–431, Springer-Verlag, Berlin/New York.

GIAQUINTA, R. T. (1977) *Plant Physiol.* **59,** 750–755.

GIAQUINTA, R. T. (1980) *Ber. Dtsch. Bot. Ges.* **93,** 187–201.

GUNNING, B. E. S., AND PATE, J. S. (1974) *in* ROBARDS, A. W. (Ed.), Dynamic Aspects of Plant Ultrastructure, pp. 441–480, McGraw-Hill, New York.

HAYAT, M. A. (1975) Positive Staining for Electron Microscopy, Van Nostrand–Reinhold, Princeton, N. J.

KOMOR, E., ROTTER, M.. AND TANNER, W. (1977) *Plant Sci. Lett.* **9,** 153–162.

MAJUMDAR, G. P., AND PRESTON, R. D. (1941) *Proc. R. Soc. London Ser. B.* **130,** 201–217.

MALEK, F., AND BAKER, D. A. (1977) *Planta* **135,** 297–299.

MAYNARD, J. W., AND LUCAS, W. J. (1982) *Plant Physiol.* **69,** 734–739.

NORTHCOTE, D. H. (1972) *Ann. Rev. Plant Physiol.* **23,** 113–132.

PRESTON, R. D. (1974) The Physical Biology of Plant Cell Walls, Chapman & Hall, London.

PRESTON, R. D. (1979) *Ann. Rev. Plant Physiol.* **30,** 55–78.

RAMBOURG, A. (1967) *J. Histochem. Cytochem.* **15,** 409–412.

SRIVASTAVA, L. M. (1969) *Amer. J. Bot.* **56,** 354–361.

*Journal of Experimental Botany, Vol. 35, No. 152, pp. 389–402, March 1984*

# Recovery of Cold-Inhibited Phloem Translocation in Sugar Beet

## I. EXPERIMENTAL ANALYSIS OF AN EXISTING MATHEMATICAL RECOVERY MODEL

MICHAEL A. GRUSAK AND WILLIAM J. LUCAS

*Department of Botany, University of California, Davis, California 95616, U.S.A.*

Received 30 July 1983

## ABSTRACT

Translocation studies were undertaken on a simplified single source leaf–single sink leaf sugar beet system to test various predictions of the Ferrier and Christy (1975) mathematical recovery model of translocation inhibited by cold. Experiments were performed by using a steady state $^{14}C$-labelling system for the source leaf and translocation into the sink leaf was monitored with a Geiger–Mueller system. A specially designed Peltier apparatus enabled cooling of the source petiole to 1 °C at various positions on the petiole, as well as over different lengths. Results of experiments testing changes in (1) cold block length, (2) cold block position, and (3) sink unloading rate, showed little difference in the time course of recovery. These results are at variance with the predictions of the mathematical recovery model. Additional experiments were performed to assess the potential involvement of phloem anastomoses in the recovery response. Selective petiolar incision/excision experiments showed: (1) that the monitored sink obtained $^{14}C$-labelled material via only a few of the vascular bundles within the source petiole, and (2) that anastomoses were capable of re-establishing translocation. This information was used to develop a revised model of translocation recovery following cold-induced inhibition, and this model is based on the utilization of adjoining, interconnected sieve-tubes which become integrated into the pathway that supplies this sink.

Key words: Phloem; Translocation; Cooling; Anastomoses.

## INTRODUCTION

Since the early low-temperature experimentation of Child and Bellamy (1919) numerous investigators have used various plants and techniques to study the effect of temperature on phloem translocation (Geiger and Sovonick, 1975). Much of the work has dealt with relating the observed phenomena to mechanisms of solute movement, of which the Münch pressure–flow hypothesis has received wide support. In the sugar beet system (chill-insensitive plant), Swanson and Geiger (1967) have elegantly shown that cooling a portion of the source leaf petiole to 1 °C (in a simplified one source leaf–one sink leaf and root tissue configuration) leads to an inhibition of translocation followed by a recovery to near pre-treatment rates. This recovery occurred while the petiole section was maintained at the low temperature. Subsequent work by Geiger and Sovonick (1970) demonstrated that this temporary inhibition was the result of a decrease in translocation velocity, with the recovery being due to a restoration of velocity. Coulson, Christy, Cataldo, and Swanson (1972) monitored respiration and ATP levels in control and low temperature petioles to show that

there was no correlation between the recovery response and the demand for metabolic energy in the pathway. This result suggested the involvement of a physical factor in this low temperature phenomenon. Giaquinta and Geiger (1973) working with *Phaseolus vulgaris* (a chill-sensitive plant), showed that the sieve-plate pores were occluded in the cooled petiole regions. However, in their studies, translocation did not recover following the application of a cold treatment. Although it appears that a physical process such as callose deposition or P-protein clogging could explain the inhibitory phase of the low temperature response, supporting experimental evidence is lacking.

Mathematical modelling of sieve-element function has helped to interrelate the various physical factors of phloem transport. Christy and Ferrier (1973) used this approach to analyse the Münch pressure–flow hypothesis and have subsequently applied their model to the cold inhibited recovery phenomena in sugar beet (Ferrier and Christy, 1975). Their calculations suggest that the necessary increase in pathway resistance could only be accounted for by sieve-plate pore-blockage and not by a change in viscosity of the phloem sap. According to their model, a build-up of pressure on the source side of the cold block promotes a flow of concentrated sap through this zone. Immediately below the cold block, water flows into the sieve-elements, thereby restoring the average velocity and translocation rate. Their recovery model is an interesting one which is based on a number of physiological and physical parameters. These include (1) the sink unloading rate, (2) the sucrose concentration along the translocation system, (3) the length and position of the resistance zone caused by the cold block, and (4) the hydraulic conductivity of the sieve-tube and its plasma membrane. Their model predicts that changes in these parameters will affect the overall time of recovery.

In the present study, we have experimentally tested some of the predictions of the Ferrier and Christy (1975) model. Our results did not confirm the predictions of their model. On the basis of experimental results involving selective incision/excision of the source leaf petiole, we have developed a revised model of the cold-induced recovery phenomena in sugar beet.

## MATERIALS AND METHODS

### *Materials*

Sugar beet plants (*Beta vulgaris* L. var. SSBN1, USH10, Lot 3102 or USH11 Lot 82312) were grown in a controlled environment chamber under the following conditions: 27 °C day/17 °C night temperatures, 60%/90% r. h., and a 16 h photoperiod at 265 $\mu$E $m^{-2}$ $s^{-1}$. Plants were grown from seed in a sterilized soil mixture of vermiculite, peat and sand (2:1:1), were watered daily with distilled water and fertilized twice weekly with Hoagland solution (Hoagland and Arnon, 1950). Experiments were conducted with plants at ages 28–30 d (after germination) when they had 11–12 visible emergent leaves. On days 21–23, plants were placed in a low illumination light box (5·4 $\mu$E $m^{-2}$ $s^{-1}$) for 16 h, with the remainder of the day spent under daytime conditions in the controlled environment chamber. This procedure promoted elongation of the petioles, which was necessary for manipulation of the plants in many of the experiments.

### *Experimental apparatus*

A schematic of the experimental apparatus (Fig. 1) illustrates the components of our flow-through continuous labelling system. The source leaf blade was sealed into the centre of a plexiglas chamber, where it was held flat between two layers of nylon monofilament line (Fig. 2A). A regulated stream of air ($CO_2$ concentration: 550 parts $10^{-6}$) moved through a rotameter type flowmeter (Matheson, Model 603) and into the source leaf chamber, where it was mixed by two miniature fans (Micronel, Type V361L). At the same time, a secondary circuit, linked to a bubbling cyclinder filled with distilled water, drew air out of the chamber (via a Neptune Dyna-Pump), humidified it (bubbler), and pumped it back in. Air flow out of the source chamber then passed through a column of magnesium perchlorate for drying, before entering the infrared gas analyser (IRGA) (Analytical Development Company, Model 225-2B-SS) to monitor the photosynthetic rate via the $CO_2$ concentration. Temperature within the source chamber was regulated by the movement of air past an aluminium fin system that was sealed

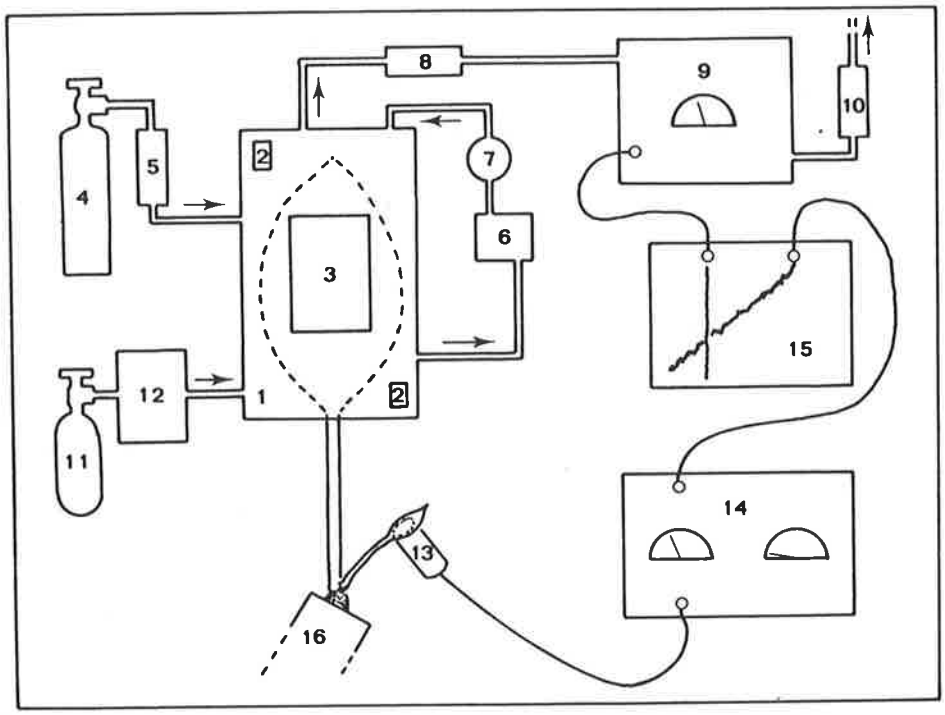


FIG. 1. Schematic diagram of continuous $^{14}C$-labelling flow-through system. A description of the integrated use of the components is presented in the text. Components are as follows: (1) plexiglas source leaf chamber; (2) fans; (3) chamber air temperature regulator; (4) unlabelled air supply; (5) flowmeter; (6) circulating pump; (7) air humidifier; (8) gas drying column; (9) infrared gas analyser; (10) $CO_2$ adsorbant column; (11) $^{14}CO_2$ supply; (12) electronic mass flow controller; (13) Geiger–Mueller tube; (14) dual ratemeter; (15) chart recorder; (16) simplified sugar beet system.

into the bottom of the chamber. The temperature of the fins was controlled by two 100 W cartridge heaters in its base, pulsing on and off against four Peltier cooling units (heat exchange rate: 50 BTU $h^{-1}$ each). The heat sink for the Peltier units was another aluminium fin system below the chamber, which received air movement from a 10 cm fan at its base. The cartridge heaters were activated by a temperature controller (Omega Engineering, Series 4200 RTD), which monitored the chamber air temperature with a ceramic platinum resistance thermometer (Omega Engineering). Source leaf temperature was monitored with a copper–constantan thermocouple appressed to its abaxial surface and coupled to a digital thermocouple thermometer (Atkins Technical, Inc., Series 497). Leaf temperature in the chamber was maintained at $25{\cdot}0 \pm 0{\cdot}5$ °C.

Labelled $CO_2$ was continuously supplied to the source leaf from a 300 $cm^3$ cylinder of $^{14}CO_2$ which was pressurized with nitrogen. A constant flow-rate of this gas was added to the chamber via an electronic mass flow controller (Matheson, Model 8240). (Gas leaving the IRGA was purged of $^{14}CO_2$ by passing through a column of soda lime.)

Accumulation of translocated $^{14}C$-assimilates in the sink leaf was measured by an end-window Geiger–Mueller tube (Picker Nuclear, Model 641401) connected to a dual ratemeter (Picker Nuclear, Model 628–046). Output from the ratemeter, operating in the 100 000 ct $min^{-1}$ range with a 30 s time constant, was recorded on a strip chart recorder (Hewlett–Packard, Model 7132A). The sink leaf was held flat against the end-window of the Geiger–Mueller tube by using two nylon monofilament line grids (Fig. 2A). The counting efficiency of this system was 1·7%.

Petiole temperature was controlled by a specially designed brass block apparatus (Figs 2A, B). An aluminium vice held two Peltier cooling units (heat exchange rate: 50 BTU $h^{-1}$ each), two brass blocks drilled to house 75 W cartridge heaters, and two milled brass blocks which fitted snugly around the petiole. A ceramic platinum resistance thermometer (Omega Engineering), positioned in a hole drilled vertically into one of the petiole blocks (near the horizontal petiole groove), signalled a second temperature controller to activate the two heater cartridges. The aluminium vice was hollowed out on the ends, and water was passed through these chambers to function as heat sinks for the Peltier cooling units. This system allowed rapid and precise changes to any desired temperature.

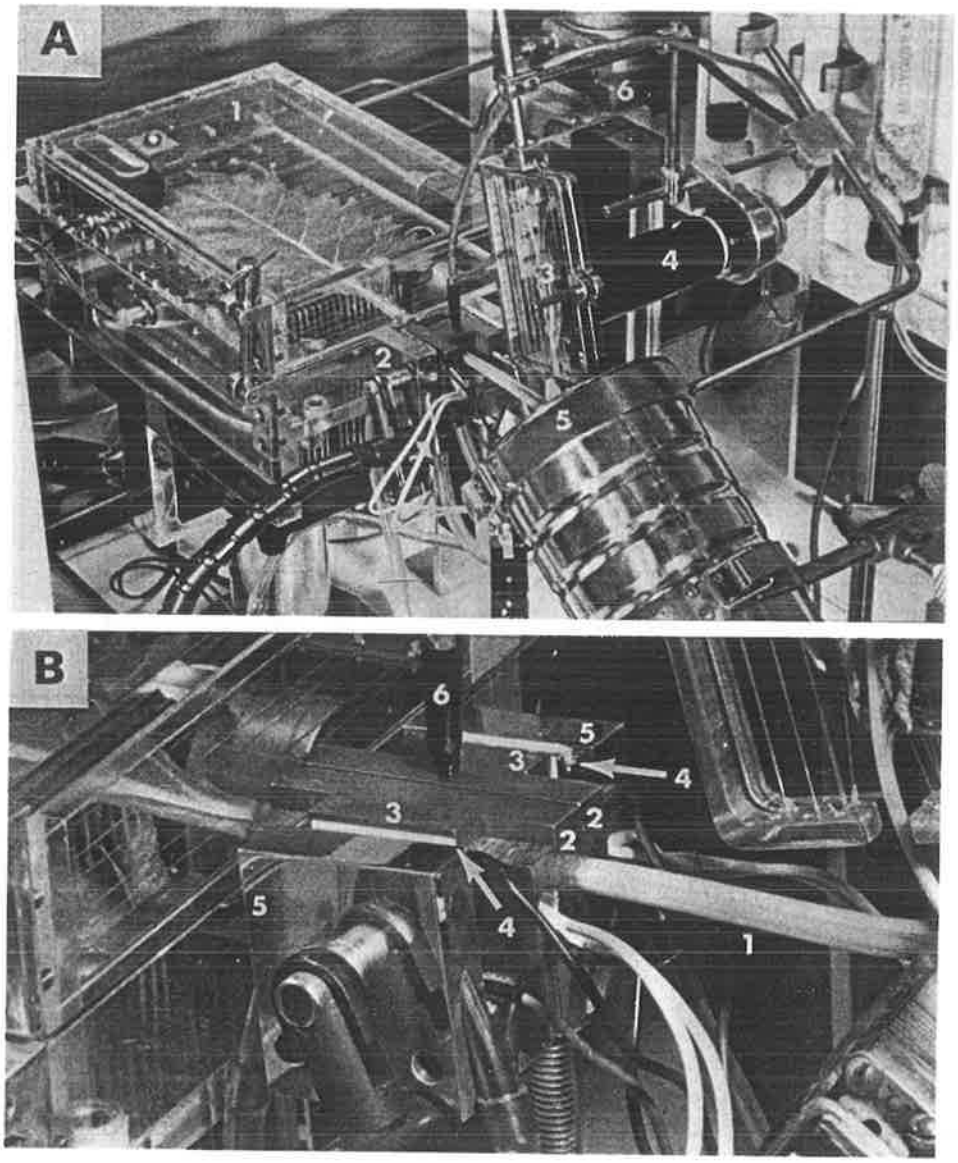


FIG. 2. Gas exchange and petiolar cold block system. (A) Components are as follows: (1) source leaf sealed within gas exchange chamber; (2) cold block system (2·0 cm brass blocks); (3) sink leaf in support (the black cloth which would normally cover the sink leaf and support, was removed for this photograph); (4) Geiger–Mueller tube appressed to leaf surface; (5) heat girdled sugar beet root in soil-filled can; (6) humidity pump. (B) Components are as follows: (1) source leaf petiole; (2) 6·0 cm brass blocks; (3) brass heating blocks with cartridge heaters; (4) Peltier system; (5) water jacket; (6) temperature probe.

*Preparation of $^{14}CO_2$*

Labelled gas was generated from $^{14}C$–$BaCO_3$ (ICN Pharmaceuticals, Inc.) in a specially designed air-tight apparatus. After generation of $^{14}CO_2$, nitrogen gas was used to sweep the $^{14}CO_2$ into a 300 $cm^3$ cylinder. This cylinder was then sealed and connected to the experimental system (Fig. 1). Counts remaining in the lactic acid were measured and subtracted from the original $^{14}C$–$BaCO_3$ activity, to determine the specific activity of the gas.

*Experimental procedures*

Preparation of each sugar beet plant was conducted the night before an experiment. The plant was reduced to a mature source leaf and one sink leaf by excising all other leaves. The source leaf was selected from the third pair of emergent leaves (average surface area 147·3 ± 15·3 $cm^2$), and the sink was from the fifth or sixth pair of emergent leaves (average surface area: 20·7 ± 5·9 $cm^2$); the two

leaves were positioned on the same side of the plant. The hypocotyl/root region was heat girdled at a position approximately 1·0 cm below the crown. This was done by looping a U-shaped length of nichrome wire around the hypocotyl and heating to redness for 2·25 min. The plant was then rotated 180° and heated again. The heated area was localized to the hypocotyl region with the aid of asbestos shielding, such that the crown, leaves, and lower root zone were unaffected. The plant was then placed into position, within the experimental apparatus, and remained in the dark for 14–16 h until the following morning.

After the overnight dark period, the sink leaf was covered with a black cloth (in most experiments), 30 min before the light was turned on. The source blade was sealed into the gas-tight plexiglas chamber and any attachments to the source petiole were put in place (brass block apparatus, tygon tubing channel). The light level was then slowly increased until steady state photosynthesis was achieved. Light was provided by a quartz–iodide lamp and was passed through a water bath to remove the infra red component. Five metal screens were sequentially removed from the light path, over a period of about one hour, until the final light intensity was reached (238 $\mu$E $m^{-2}$ $s^{-1}$). At the same time, the flow rate of unlabelled gas (550 parts $10^{-6}$ $CO_2$) was changed to attain a final chamber $CO_2$ concentration which remained constant at 330 $\pm$ 5 parts $10^{-6}$. After steady state photosynthesis was achieved, $^{14}CO_2$ was bled into the chamber and mixed with the unlabelled gas stream to yield a constant specific activity of 5·0 $\mu$Ci $mg^{-1}$ carbon.

Once the accumulation of label in the sink had reached a steady state, usually 2–3 h after the addition of $^{14}CO_2$ to the chamber, one of various experimental protocols was followed. In the cold block experiments, the temperature controller was reset for the desired temperature, with changes occurring in the following times: 25 °C to 1 °C, 2·0 cm blocks: 2·5 min, 6·0 cm blocks: 3·5 min; 1 °C to 25 °C, 2·0 cm blocks: 1·5 min, 6·0 cm blocks: 2 min. These times were obtained by running cooling and warming cycles on a number of test petioles, with copper–constantan thermocouples embedded deep into the pith tissue of the petiole. Continuous monitoring also showed that the petiole set point, at a given temperature, oscillated by no more than $\pm$0·1 °C. For any of the cutting experiments, a tygon tubing trough was sealed under the petiole with putty and filled with distilled water. All incisions were made under water with a thin, sharp scalpel blade. Depths of incisions were measured and recorded at the end of each experiment with the aid of a dissecting microscope.

Petiole clearings, following certain experiments, were performed by placing tissue sections in 5% NaOH (w/v) for 24 h in a 60 °C oven. After rinsing in distilled water, the tissues were carefully dissected under a binocular microscope to map the extent of vascular anastomoses. Only those strands containing xylem elements were visible, and it is possible that isolated phloem branches were also present, but went undetected.

*Data analysis*

The accumulation of labelled material in the sink leaf was converted, in all cases, to relative translocation rates. Smooth curves were drawn through the chart recorder tracings and the slope of the accumulation curve (over 4 min intervals) was expressed as a ratio of the control, steady state value.

## RESULTS

### *Testing the predictions of the mathematical model*

We have experimentally tested three of the predictions derived from the recovery model of Ferrier and Christy (1975). Initially, we tested the influence of cold block length on the time of recovery after cooling from 25 °C to 1 °C. Figure 3 illustrates the results from two separate plants in which 6·0 cm cold blocks were applied to the source leaf petiole. Following rewarming, 2·0 cm blocks were positioned on the petioles and a similar temperature treatment was performed. Although, for a given plant, the new steady state translocation rate attained during cooling could be higher for either the 2·0 cm or 6·0 cm length, it can be seen that similar time characteristics were obtained. Comparable experiments were also performed in which the 2·0 cm blocks were applied first, and then replaced by those of 6·0 cm. These were undertaken to alleviate any influence that the first cooling may have had on the response to the second cooling. Results similar to those presented in Fig. 3 were obtained. All results were in disagreement with the Ferrier and Christy model, which predicted a longer recovery period for the 6·0 cm cooling regime.

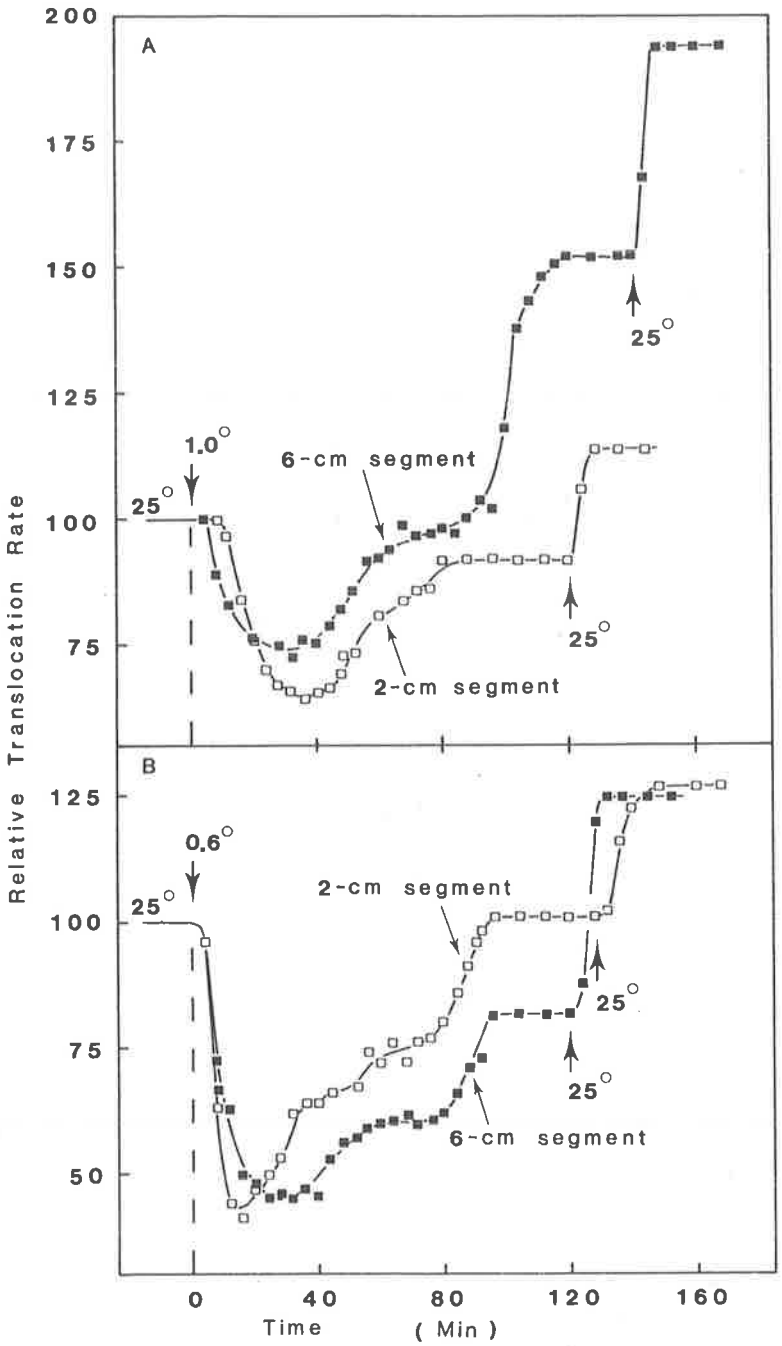


FIG. 3. Translocation profiles during cold temperature application to a 6·0 cm or 2·0 cm segment of a sugar beet source leaf petiole. A 6·0 cm brass block cooling apparatus on the source leaf petiole was cooled for the indicated time and then returned to 25 °C. These blocks were then removed and were replaced with blocks 2·0 cm in length prior to the second cooling treatment. The results from two separate plants are presented (A, B).

Positional effects of the cold block zone were also tested and typical results obtained on two plants were presented in Fig. 4. In this experimental series, the initial 2·0 cm blocks on the source leaf petiole were removed and replaced, for the second cooling, with 2·0 cm blocks at another petiole position. Again, we found that the time courses for recovery were very similar, whether the cold block was closer to the sink leaf or to the source blade. This is also

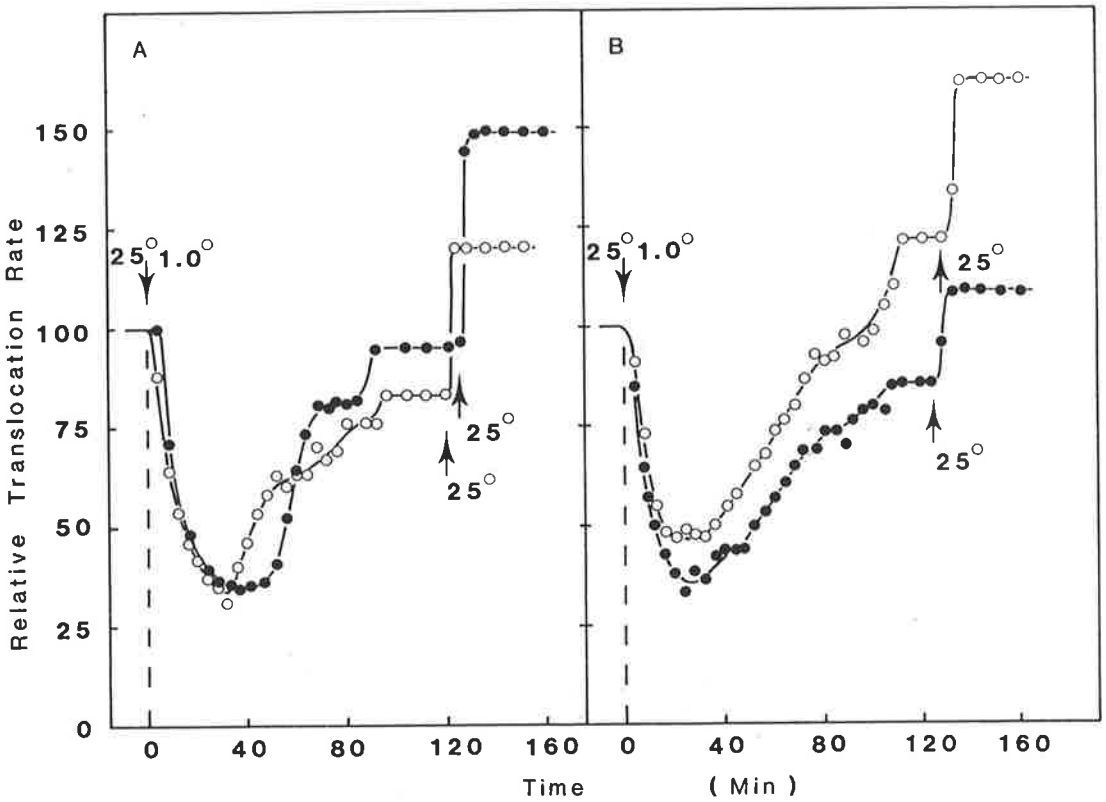


FIG. 4. Translocation profiles obtained from 2·0 cm cooling treatments at two positions on the sugar beet source leaf petiole. (A) Length of the petiole was 16·2 cm. Cooling block positions: (●)—first cooling, 8·5–10·5 cm from source blade; (○)—second cooling, 1·4–3·4 cm from source blade. (B) Length of the petiole was 13·0 cm. Cooling block positions: (●)—first cooling, 0·7–2·7 cm from source blade; (○)—second cooling, 7·0–9·0 cm from source blade.

in disagreement with the phloem model (Ferrier and Christy, 1975), which predicted a longer recovery period when the resistance zone (cold block) was further from the source (loading site).

Another consequence of the Ferrier and Christy model was that a decrease in the sink unloading rate would slow the recovery phase after cooling inhibition. Experiments were performed where a fixed-positioned 2·0 cm block was cooled with the sink leaf illuminated, and again with the sink leaf in darkness (to promote a lowered rate of sink unloading; about 2 h were allowed for the sink to reach the new translocation level before the second cooling). These experiments indicated that the recovery phenomenon was insensitive to the relative sink strength (Fig. 5). Once again we could not confirm this prediction of the Ferrier and Christy model.

In regard to all the cooling treatments, it is important to point out that rewarming the petiole to 25 °C almost always resulted in a rapid shift to a higher relative translocation rate (Figs 3, 4, 5). This increase is often considerable and the rate usually exceeds that recorded before the cooling treatment (occassionally as high as twice the original rate).

*Petiole incision/excision experiments*

During our analysis of the Ferrier and Christy recovery model, it became apparent that more information was needed on the translocation capabilities of the petiole, *per se*. The following experiments were conducted to investigate the interactive nature of the

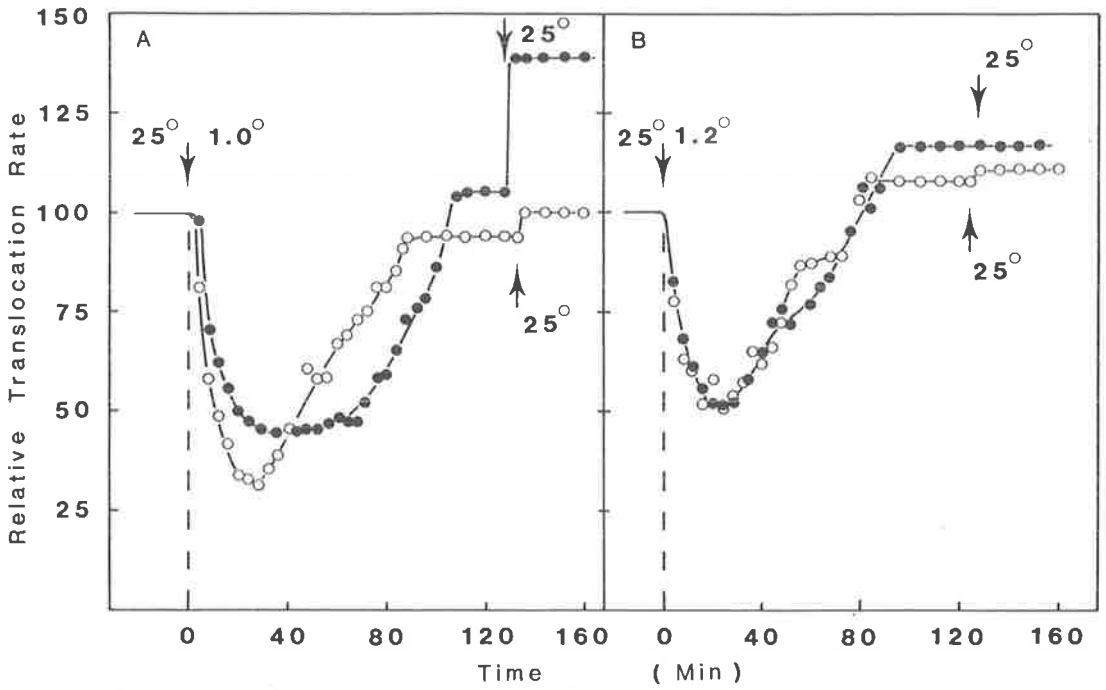


FIG. 5. Translocation profiles obtained from 2·0 cm cooling treatments at two sink unloading rates. Shading the sink leaf after the first cooling treatment lowered the unloading rate. Results are presented for two separate plants, A and B: time course of first cooling was with sink leaf illuminated, (●); sink leaf then darkened, and time course obtained after translocation rate stabilized (2 h), (○). Dark translocation rate decreased to 67% (A) and 79% (B) of value in the light.

translocation pathway within the petiole and to provide relevant information to the cold-induced recovery phenomenon.

Initially, complete excision of the source leaf blade (near the junction of blade and petiole) was undertaken, following attainment of steady state translocation. Representative results, shown in Fig. 6, reveal a very rapid drop in translocation after excision, which was then followed by a transient rise and gradual decay in translocation to the sink. This recovery suggests a storage and re-loading role for the petiole. In certain experiments a 2·0 cm cold block was applied to the excised source petiole some time after the recovery had started. A sudden drop in the translocation rate demonstrated that this flow was coming from the petiole. Presumably the limited nature of the response was due to the amount of labelled material within the sieve-tubes and surrounding tissues.

Attempts were then made to mimic the cold-induced blockage of the sieve-tubes by slicing into the side of the source petiole, to a depth of 1/3, 1/2, or 2/3 of its width, thereby disrupting flow in a portion of the sieve-tubes. A number of responses were obtained, and representative traces are presented in Fig. 7: these included (a) no change in translocation rate, (b) little inhibition with full recovery, (c) considerable inhibition with a longer recovery period. No effect of cutting implied that only a few of the vascular bundles in the source petiole were supplying assimilates to the monitored sink. Apparently, only those sieve-tubes leading to unmonitored parts of the plant (crown or hypocotyl area above the heat girdle) were severed. Similarly, when a transient decline in translocation was seen upon cutting (Fig. 7B), it was possible that none or only a small percentage of the sieve-tubes leading to the monitored sink were damaged, such that the majority of the monitored flow was only slightly perturbed.

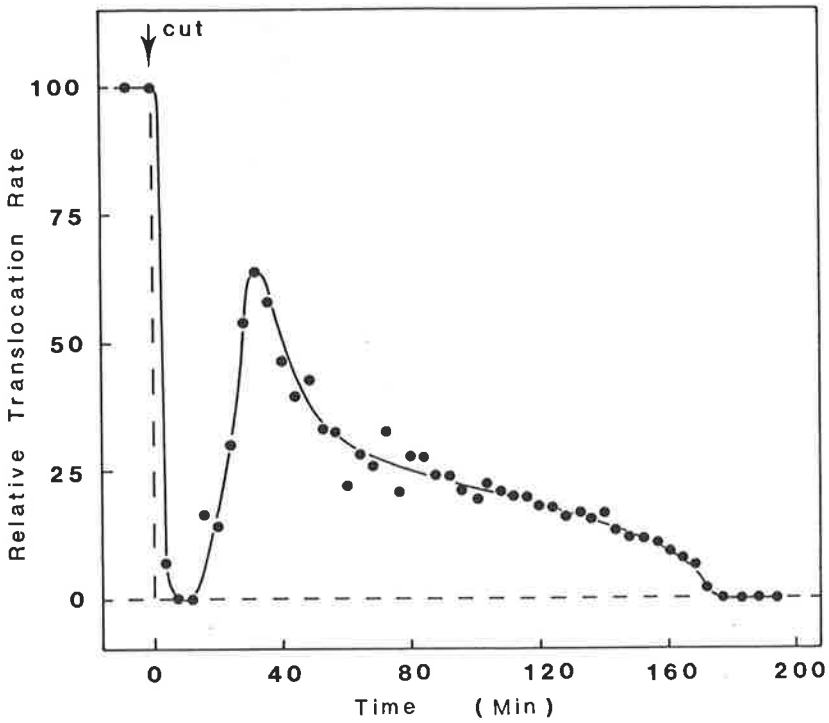


FIG. 6. Accumulation of labelled translocates after sugar beet source blade excision. Following steady state translocation, the source petiole was excised under water, near the junction of the petiole and blade.

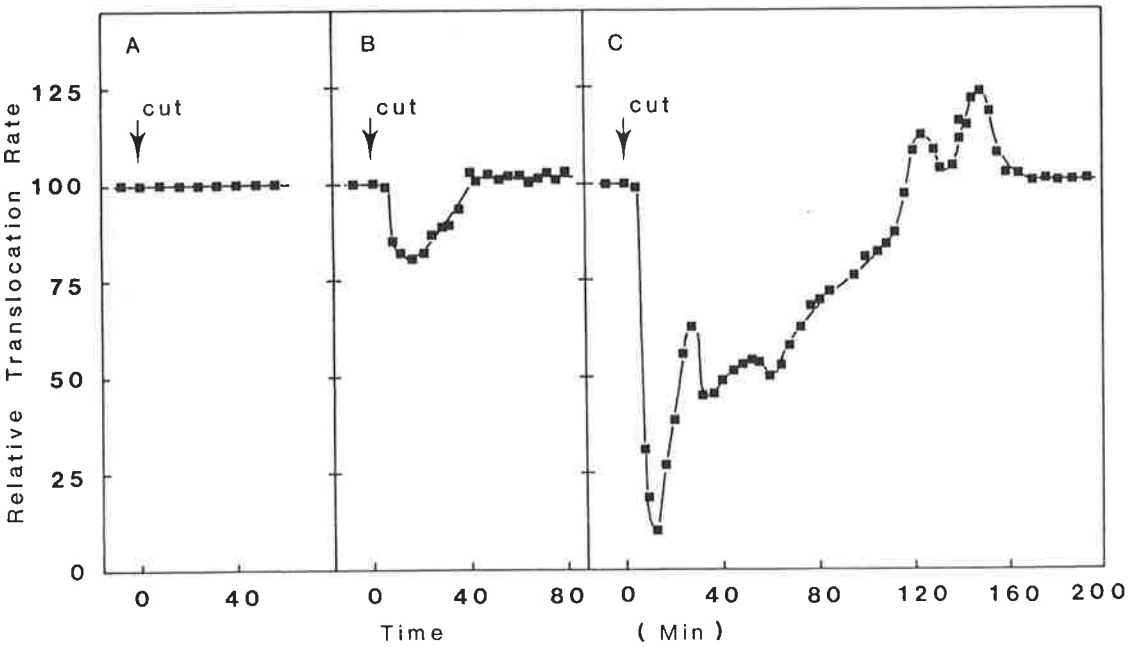


FIG. 7. Translocation profiles following sugar beet source petiole incisions. Results are presented for three plants in which transverse incisions were made into the sides of the source leaf petioles. All cuts were made under distilled water. Of the nine major bundles in the petiole, these cuts severed the following: (A) 3; (B) 5; (C) 6.

To investigate further this apparently limited utilization of the vascular system, we surgically removed longitudinal segments of the petiole. Figure 8 illustrates the results obtained when a series of excisions were made such that only two bundles remained intact over a length of 1·7 cm. Although the translocation rate showed oscillations and temporary inhibition after some of the excisions, the final rate stabilized at a level slightly higher than the control (pre-excision) value.

The third response to a single incision (Fig. 7C), with its considerable inhibition and gradual recovery, suggested that in this case the severed bundles were those directly delivering translocate to the monitored sink. Re-establishment of flow was possibly attained by re-routing transport around the incision, via anastomoses. Petiole clearings have shown that along the length of the petiole numerous vascular connections exist between adjacent bundles. To test this hypothesis, a series of experiments was carried out where two overlapping cuts were made from opposite sides of the petiole. Incisions were approximately 2·0 cm apart and were cut a distance into the peitole such that both severed the central vascular bundle. Figure 9 shows the results of one such experiment. The insets demonstrate the extent to which the cuts overlapped and the pattern of anastomoses that existed in this region. Although complete recovery was not achieved, this experiment demonstrated that a substantial level of translocation can be maintained through a minimal amount of anastomotic vascular tissue.

## DISCUSSION

### *Analysis of the Ferrier–Christy model*

The Ferrier and Christy (1975) cold block recovery model for sugar beet is not supported by the present results (Figs 3, 4, 5). Their model proposed that a zone of increased resistance along the pathway (induced by petiole cooling) would lead to an increase in sucrose concentration and sieve-tube pressure on the loading side of the blockage. This pressure

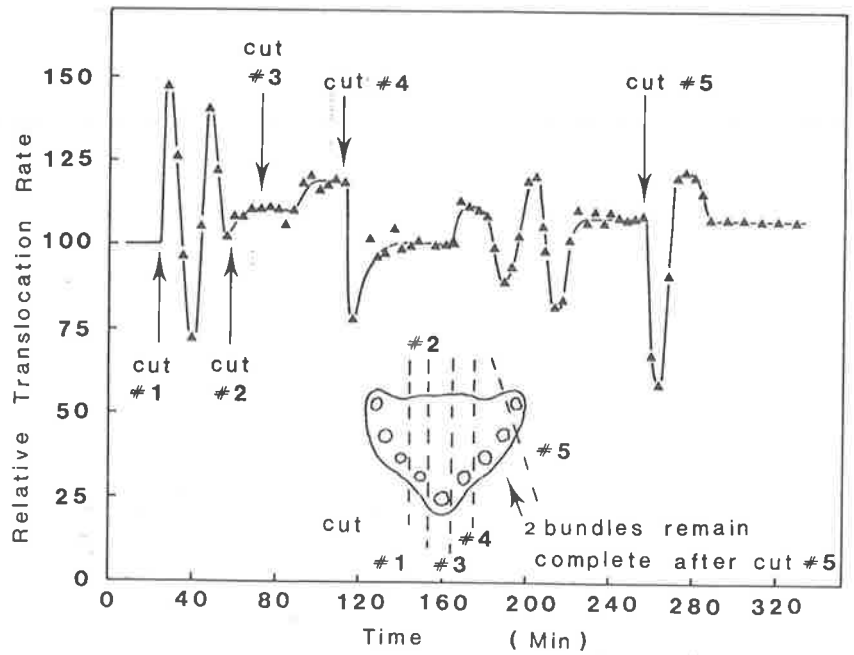


FIG. 8. Translocation profile following successive removal of sections of the sugar beet source petiole. Excisions were made to remove vascular bundles and accompanying tissues from a 1·7 cm length of source leaf petiole. Cuts were performed with the affected petiole segment immersed in distilled water.

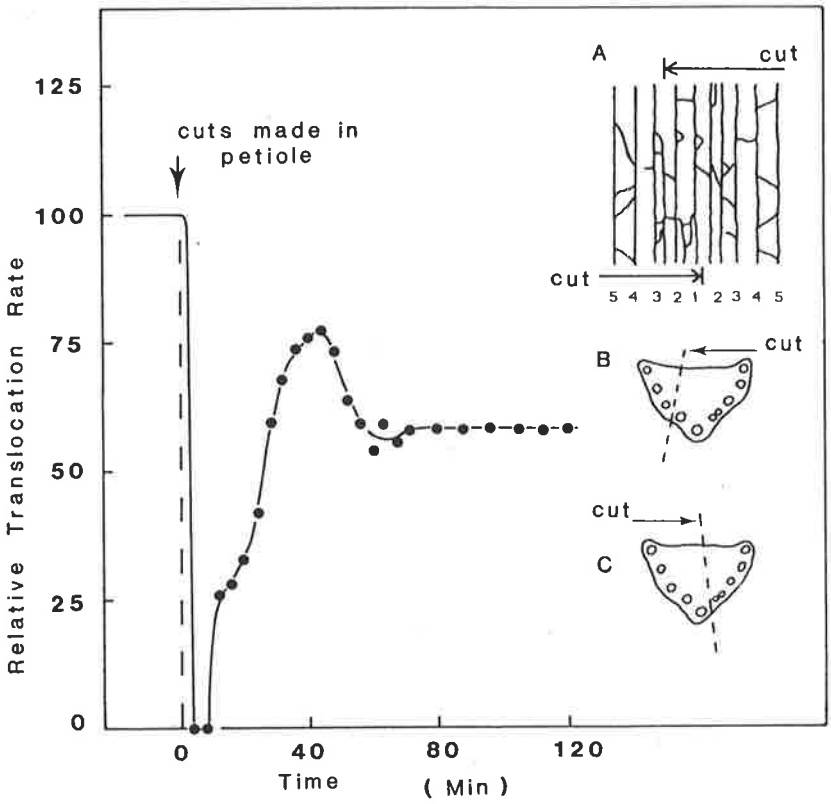


FIG. 9. Effect of two overlapping incisions made on the source petiole. After the establishment of steady-state translocation, two cuts were made from opposite sides of the petiole (1·0 cm and 4·5 cm from the source blade), such that both severed the central vascular bundle. Incisions were made with the petiole segment immersed in distilled water. Inserts: (A), Top view of major vascular bundles and anastomoses between the incisions made on the source petiole; (B and C) transverse views of source petiole, at the two sites of incision, showing the extent of cuts.

would, in time, enable a flow of concentrated sucrose solution through the blockage zone, followed by a downstream influx of water to re-establish the original translocation rate. Initially, the model suggests that the recovery would be slower for a longer cold block (4·8 cm versus 2·4 cm), since more time would be needed to generate a pressure sufficient to enable flow to return to its control value. Our results with sugar beet (6·0 cm versus 2·0 cm), as well as previous reports (8·0 cm versus 2·0 cm) (Geiger, 1969; Swanson, 1969), show that there is little difference in the time course of recovery when different lengths of petiole are cooled.

The recovery model also suggested that a cold block positioned closer to the sink would require more time to increase the upstream sieve-tube pressure, since the length and volume of upstream sieve-tubes would be increased. Figure 4 demonstrates again that similar recovery times are observed. In addition, the mathematical analysis predicts that decreasing the unloading rate in the sink would slow the recovery response by decreasing the pressure gradient from blockage to sink, and thereby slowing the movement of translocate. Our experiments with lowered sink illumination, which induced a reduction in the translocation rate, are presumed to stem from a reduced sink unloading rate. Swanson, Hoddinott, and Sij (1976) have reported that in *Phaseolus vulgaris* a lowered sink illumination resulted in a decreased translocation rate to the sink, but gave no explanation for the phenomenon. Although it is possible that a reduction in translocation could be due in part to a change in source export, Fondy and Geiger (1980) reported that changes in sink demand resulted in

only a transient change in the source export rate. We assume, therefore, that our illumination treatment reduced the sink unloading rate, and our experimental results are shown to be at variance with the unloading rate prediction of the model (Fig. 5).

It should be mentioned that we still do not know the nature of the physical (blockage) or physiological agent(s) which initiates inhibition in sugar beet. It is possible that this agent is localized within a specific section of the cooled petiole (e.g. the interface between the cold block and the downstream, uncooled petiole), such that no difference would exist, for example, in the amount of blockage produced in either a 2·0 cm or 6·0 cm cold block. If this were the case, we would expect little difference in response time between 2·0 cm or 6·0 cm cooling treatments, and this series of experiments would not be a valid test of the model (although the model would still be at variance with our other experimental tests). Giaquinta and Geiger (1973) presented evidence for blockage throughout the length of the cooled zone in the chill-sensitive plant, *Phaseolus vulgaris*. Further microscopic investigations are needed to study this aspect in the sugar beet system.

The Ferrier and Christy (1975) recovery model, although not supported by the present study on sugar beet, should not be totally discounted. It is based on a mathematical model (Christy and Ferrier, 1973) which offers some important quantitative aspects that pertain to the translocation process. One aspect of their analysis which is supported by the present study, is the observation that a resistance factor which induces inhibition cannot be due entirely to increased viscosity of the phloem contents. We can say with certainty that cooling a 6·0 cm petiole segment will tend to produce a higher resistance to flow by virtue of the greater length of sieve tubes containing high viscosity solution. Our similar results for 2·0 cm and 6·0 cm cold blocks (Fig. 3) verify that an increase in viscosity, cannot alone cause the inhibition phenomenon in sugar beet.

It should also be stressed that our results (Figs 3, 4, 5) do not invalidate the concept that there is a pressure build-up on the source side of the blockage, we have only drawn into question the model's explanation of how such a pressure increase would overcome the resistance zone. A pressure increase may occur and promote other events in the pathway which then lead to the recovery. This concept will be expanded upon in a later section.

The initial mathematical analysis of phloem translocation (Christy and Ferrier, 1973) was quite adequate for assessing Münch translocation theory and its physical/physiological parameters. However, it was based on a highly simplified sieve-tube system, composed of a source region with active loading, a path region, and an actively unloading sink region. This simplicity may have led to its inadequacy in terms of describing the cold-induced recovery phenomenon. The path region, for instance, was given the role of a passive conduit with the possibility for water influx along its length, but not for the influx or efflux of sucrose (either actively or passively). It has been suggested for some time that the long-distance pathway may serve a storage role for later re-loading and translocation of assimilates (Hill, 1963; Geiger, Saunders, and Cataldo, 1970) and our results with leaf blade excision (Fig. 6) also support this hypothesis. Geiger and Sovonick (1970) have shown that petiole cooling in bean results in a gradual decline in translocation over a number of hours. Minchin, Lang, and Thorpe (1983) suggest that this response is due to a pathway re-loading of translocates beyond the cold treated zone, such that a diminished flow is maintained for some time. Whether pathway re-loading is a factor in the sugar beet recovery phenomenon is unclear, but it should be included in any further mathematical modelling of phloem translocation.

A more serious shortcoming of the mathematical model is that it is based on a single file of sieve elements. It is clear in sugar beet (Fig. 5), as well as in other plants (Aloni and Sachs, 1973; Vogelmann, Larson, and Dickson, 1982), that the phloem network is very complex with numerous interconnections. In a source–sink study on bean, Borchers-Zampini, Glamm,

Hoddinott, and Swanson (1980) showed that shading or removal of one of the source leaves caused a re-partitioning of translocates to the various sinks. They suggested that phloem anastomoses may have facilitated these changes. Unfortunately, in the Christy and Ferrier model (1973) the simplicity of their system precluded the investigation of re-routed flow on the cold-induced recovery response.

*Petiole excision/incision results*

We have demonstrated that a limited number of vascular bundles in the source petiole function to translocate assimilates to the monitored sink leaf (Figs 7, 8). In Fig. 8 we demonstrate that translocation through a length of petiole can be maintained at the original rate, even after the cross-sectional area of the petiole has been dramatically reduced. These experiments reveal that the potential exists for higher rates of flow to the single sink leaf, when the translocation stream is re-routed.

Additionally, we have shown that with two cuts overlapping the central vascular bundle (Fig. 9), the translocation rate can recover to a substantial level (58% of the original rate). Mapping of anastomoses between the cuts revealed one vascular connection between the two separated halves of the petiole (Fig. 9). While it is possible that flow was re-established through the intervening parenchyma tissue (Thrower and Thrower, 1980), it is more likely, with the level of translocation attained, that existing connections via sieve tubes were utilized (i.e. the path of least resistance). However, in another experiment where no connections were visible, the recovery stabilized at a rate that was only 14% of the control level. It should be remembered that only visible xylem branches were mapped and it is possible that isolated phloem strands went undetected. In any event, we have demonstrated that following an obstruction to flow (induced by incision), the translocation stream can be re-routed to supply a given sink.

*A revised recovery model*

Having established this potential for flow through sieve elements previously unused by the sink leaf, we now apply this knowledge to the sugar beet recovery phenomenon. We propose that the cold-induced inhibition activates the flow of sap into adjoining sieve-tubes/vascular bundles, as an addition to the original monitored-sink translocation pathway. This process of interconnecting the adjoining sieve-tubes may involve a pressure differential, such that an increase in pressure above the cold zone would force the flow into adjacent vascular bundles via phloem anastomoses. Hence, by increasing the number of sieve-tubes involved in solution flow, the total resistance through the cooled segment would be reduced, and thus allow the recovery of the translocation rate. With the additional sieve-tubes, the potential for greater volume flow could also explain the often seen increase to rates higher than the pre-treatment values (especially when the petiole is returned to 25 °C) (Figs 3, 4, 5). Higher levels of translocation to a sink have previously been shown upon increasing the sink–source ratio in sugar beet (Fondy and Geiger, 1980). Increased translocation to one sink occurs at the expense of others (roots), rather than via an increased rate of export from the source. It appears in our system that the sink leaf is able to divert flow from other sinks (crown and hypocotyl region above the heat girdle, storage areas of source petiole), by re-routing their translocation pathways. It should be stressed, however, that this re-routing may not explain the entire recovery response, since other events such as the partial removal of a physical blockage may also occur.

Our results presented in this study suggest that the phloem translocation system is very responsive to forms of perturbation. The petiole can store assimilates and has the potential to re-load these into the transport path. More importantly, though, phloem anastomoses

between vascular bundles are capable of re-routing flow. Further investigation is needed to study the role of these connections as possible sites of regulation in the partitioning of assimilates.

## ACKNOWLEDGEMENTS

This research was supported by National Science Foundation Grant PCM-79 10223. We also wish to express our appreciation for the excellent technical assistance afforded by Ed. Young of the Physical Plant Workshop, University of California, Davis.

## LITERATURE CITED

ALONI, R., and SACHS, T., 1973. The three-dimensional structure of primary phloem systems. *Planta*, **113,** 345–53.

BORCHERS-ZAMPINI, C., GLAMM, A. B., HODDINOTT, J., and SWANSON, C. A., 1980. Alterations in source–sink patterns by modifications of source strength. *Plant Physiology*, **65,** 1116–20.

CHILD, C. M., and BELLAMY, A. W., 1919. Physiological isolation by low temperature in *Bryophyllum* and other plants. *Science*, **50,** 362–5.

CHRISTY, A. L., and FERRIER, J. M., 1973. A mathematical treatment of Münch's pressure–flow hypothesis of phloem translocation. *Plant Physiology*, **52,** 531–8.

COULSON, C. L., CHRISTY, A. L., CATALDO, D. A., and SWANSON, C. A., 1972. Carbohydrate translocation in sugar beet petioles in relation to petiolar respiration and adenosine 5′-triphosphate. Ibid. **49,** 919–23.

FERRIER, J. M., and CHRISTY, A. L., 1975. Time-dependent behaviour of a mathematical model for Münch translocation. Application to recovery from cold inhibition. Ibid. **55,** 511–14.

FONDY, B. R., and GEIGER, D. R., 1980. Effect of rapid changes in sink–source ratio on export and distribution of products of photosynthesis in leaves of *Beta vulgaris* L. and *Phaseolus vulgaris* L. Ibid. **66,** 945–9.

GEIGER, D. R., 1969. Chilling and translocation inhibition. *Ohio Journal of Science*, **69,** 356–66.

—— SAUNDERS, M. A., and CATALDO, D. A., 1969. Translocation and accumulation of translocate in the sugar beet petiole. *Plant Physiology*, **44,** 1657–65.

—— and SOVONICK, S. A., 1970. Temporary inhibition of translocation velocity and mass transfer rate by petiole cooling. Ibid. **46,** 847–9.

—— —— 1975. Effects of temperature, anoxia and other metabolic inhibitors on translocation. In *Encyclopedia of plant physiology. New Series. Volume 1: Transport in Plants. I. Phloem transport.* Eds M. H. Zimmermann and J. A. Milburn. Springer–Verlag, Berlin, Heidelberg, New York. Pp. 256–86.

GIAQUINTA, R. T., and GEIGER, D. R., 1973. Mechanism of inhibition of translocation by localized chilling. *Plant Physiology*, **51,** 372–7.

HILL, G. P., 1963. The sources of sugars in sieve-tube sap. *Annals of Botany*, **27,** 79–87.

HOAGLAND, D. R., and ARNON, D. I., 1950. The water-culture method for growing plants without soil. *California Agricultural Experiment Station Circular*, **347.**

MINCHIN, P. E. H., LANG, A., and THORPE, M. R., 1983. Dymamics of cold induced inhibition of phloem transport. *Journal of Experimental Botany*, **34,** 156–62.

SWANSON, C. A., 1969. Mechanisms of translocation of plant metabolites. In *Physiological aspects of crop yield.* Ed. R. C. Dinauer. American Society of Agronomy, Crop Sicence Society of America. Madison, Wisconsin. Pp. 167.

—— and GEIGER, D. R., 1967. Time course of low temperature inhibition of sucrose translocation in sugar beets. *Plant Physiology*, **42,** 751–6.

—— HODDINOTT, J., and SIJ, J. W., 1976. The effect of selected sink leaf parameters on translocation rates. In *Transport and transfer processes in plants.* Eds I. F. Wardlaw and J. B. Passioura. Academic Press, New York, San Francisco, London. Pp. 347–56.

THROWER, S. L., and THROWER, L. B., 1980. Translocation into mature leaves—the pathway of assimilate movement. *New Phytologist*, **86,** 145–54.

VOGELMANN, T. C., LARSON, P. R., and DICKSON, R. E., 1982. Translocation pathways in the petioles and stem between source and sink leaves of *Populus deltoides* Bartr. ex Marsh. *Planta*, **156,** 345–8.

*Journal of Experimental Botany, Vol. 36, No. 166, pp. 745–755, May 1985*

# Cold-Inhibited Phloem Translocation in Sugar Beet

## II. CHARACTERIZATION AND LOCALIZATION OF THE SLOW-COOLING RESPONSE

MICHAEL A. GRUSAK AND WILLIAM J. LUCAS[1]

*Department of Botany, University of California, Davis, California 95616, U.S.A.*

Received 23 October 1984

## ABSTRACT

Experiments were undertaken on a simplified sugar beet system to characterize the phloem translocation response to slow cooling treatments that were applied to the source leaf petiole. In these experiments the temperature was decreased by 4 °C every 16 min, such that the tissue temperature was lowered from 25 °C to 1 °C over a period of 80 min. Our results indicated that an initial slow cooling treatment, on a given test plant, caused no change in the rate of translocation. However, all subsequent slow cooling regimes that were applied to the same petiole position elicited a characteristic step-type inhibition. This inhibition averaged about 10% of the original translocation rate in all cases with no recovery being observed. The data suggest that the initial cooling treatment induced an alteration in the petiole tissue which facilitated the inhibition phenomenon during subsequent slow coolings. This alteration was shown to be localized within the upstream region of the chilled petiole segment, following an initial slow cooling, or throughout the chilled petiole segment after an initial quick cooling from 25 °C to 1 °C. Results also show that the alteration is a long-lived phenomenon that has no detectable influence on the quick-cooling induced transient inhibition of translocation.

Key words: Phloem; Translocation; Cooling response; Petiole.

## INTRODUCTION

For many years, low temperature treatment of plant tissues has been used to study the process of phloem translocation (Geiger and Sovonick, 1975). The general protocol is to quickly lower the temperature of a petiole, stem, or organ (usually from 25 °C to some temperature in the 10 °C–1 °C range), maintain the tissue at the lowered temperature, and analyse the movement of assimilates through or into this region. The common effect is an inhibition of the translocation rate followed, in certain species, by various levels of recovery. Although the exact nature of the inhibition process is still poorly understood, results of a study by Giaquinta and Geiger (1973) suggest that the stimulus for inhibition might be a threshold temperature level, which may be different for chill-sensitive and chill-insensitive species. However, recent work has questioned this idea in that it has been found that the rate of tissue cooling, *per se*, can influence the inhibition response. The slow cooling of a 4·0 cm leaf section of maize (25 °C to 1 °C in 90 min) resulted in only a slight reduction in phloem transport through the chilled region, while translocation was strongly inhibited by a quick cooling treatment (25 °C to 1 °C in approximately 5 s) (Faucher, Bonnemain, and Doffin, 1982). Similarly, when applying a cooling treatment to the stem of *Ipomea purpurea*, Minchin

[1] Address until July 31st 1985: Forstbotanisches Institute, Büsgenweg 2, D-3400 Göttingen, F.R.G.

and Thorpe (1983) found that the rate of cooling, to various temperatures, determined the degree or duration of the inhibition response.

In the present study, we have examined this cooling-rate phenomena in a simplified sugar beet system by analysing the response of translocation to the slow cooling of a source leaf petiole segment. Previous work has shown that quick cooling a petiole segment, in sugar beet, results in an inhibition and subsequent recovery of the translocation rate (Swanson and Geiger, 1967; Grusak and Lucas, 1984). The characteristic slow cooling response will be used to demonstrate, through various experimental manipulations, the actual site within the pathway where cooling-induced alterations occur.

## MATERIALS AND METHODS

### *Plant materials*

Sugar beet plants (*Beta vulgaris* L. var. SSBN1, USH11, Lot 82312) were grown in a controlled environment chamber under the conditions previously described (Grusak and Lucas, 1984). Average characteristics for the plants used in this study were as follows: source leaf surface area, $145{\cdot}7 \pm 10{\cdot}6$ cm$^2$; source leaf net carbon exchange rate, $8{\cdot}37 \pm 0{\cdot}70$ $\mu$mol $CO_2$ m$^{-2}$ s$^{-1}$; sink leaf surface area, $10{\cdot}6 \pm 1{\cdot}6$ cm$^2$; errors quoted are standard deviations.

### *Experimental apparatus and procedures*

All experiments were performed with the apparatus and experimental protocols previously described (Grusak and Lucas, 1984). In the present study, a slow sequential cooling of a source leaf petiole segment was used, in addition to the quick cooling employed in our earlier studies. Source leaves were continuously labelled with a flow of constant specific activity $^{14}CO_2$ (5·0 $\mu$Ci mg$^{-1}$ carbon) and the translocation of labelled assimilates through the chilled region was monitored at the sink leaf with a Geiger–Mueller tube. The petiole temperature, in the region of the cold block, was lowered by

TABLE 1. *Cooling and warming rates[a] for temperature changes within 2·0 cm and 6·0 cm sugar beet petiole segments*

| | Temperature change (°C) (initial to final) | $t_{1/2}$[b] (s) | |
|---|---|---|---|
| | | 2·0 cm segment | 6·0 cm segment |
| Cooling | 25–1 | 108 | 181 |
| | 25–21 | 34 | 59 |
| | 21–17 | 37 | 67 |
| | 17–13 | 40 | 72 |
| | 13–9 | 42 | 82 |
| | 9–5 | 43 | 96 |
| | 5–1 | 48 | 110 |
| Warming | 1–25 | 52 | 77 |
| | 1–5 | 25 | 46 |
| | 5–9 | 24 | 46 |
| | 9–13 | 23 | 46 |
| | 13–17 | 23 | 48 |
| | 17–21 | 25 | 46 |
| | 21–25 | 25 | 48 |

[a] Cooling rates were predetermined by placing copper-constantan thermocouples near the region of the vascular bundles in petiole segments which were surrounded by either a 2·0 cm or 6·0 cm cold block unit.

[b] Tissue temperature changes were found to be exponential, so we have reported the time taken for half of the total change in temperature ($t_{1/2}$, in seconds).

four degrees C every 16 min (25 °C to 1 °C in a total time of 80 min), with the decrease in temperature for each change occurring in the times shown in Table 1. Rewarming the tissue was performed rapidly in most studies, although in certain experiments a slow sequential warming was employed (4 °C temperature increases every 16 min). These warming rates are also shown in Table 1. Determination of these warming or cooling rates was obtained by imbedding copper-constantan thermocouples in test petioles, near the region of the vascular bundles. Plants imbedded with thermocouples were not used for translocation studies, but were prepared in an identical manner before surrounding the thermocouple-imbedded petiole segment with either a 2·0 cm or 6·0 cm cold block unit. Temperature changes were monitored with a digital thermocouple thermometer (Atkins Technical, Inc., Series 497) and recorded on a strip chart recorder (Hewlett-Packard, Model 7132A).

*Data analysis*

The accumulation of labelled material in the sink leaf was recorded by the chart recorder and then converted, in all cases, to relative translocation rates. Smooth curves were drawn through the chart recorder tracings and the slope of the accumulation curve was calculated over 4 min intervals. The relative translocation rate was expressed as the ratio of the accumulation rate at consecutive time intervals during the experiment to the steady state accumulation value prior to perturbation.

Data presented in each figure are plotted from the translocation response of a single plant obtained during one experiment and is representative of identical cooling/warming treatments performed on at least three plants.

## RESULTS

*Characteristics of the slow cooling response*

Two characteristic responses were obtained when a slow cooling regime was used on a 2·0 cm segment of the source leaf petiole of sugar beet. First, an initial slow cooling treatment to 1 °C (i.e., the first temperature perturbation for a given petiole segment) showed no change in the relative translocation rate monitored at the sink leaf (Fig. 1). Secondly, any subsequent slow cooling treatment resulted in a slight (and cumulative) inhibition of translocation (Fig. 1). This inhibition was found to be a step decrease, averaging 9·0 ± 3·9% of the original translocation rate, and we observed no recovery. Plants whose petiole segments were maintained at various temperatures for up to 3 h, following such an inhibition, showed no

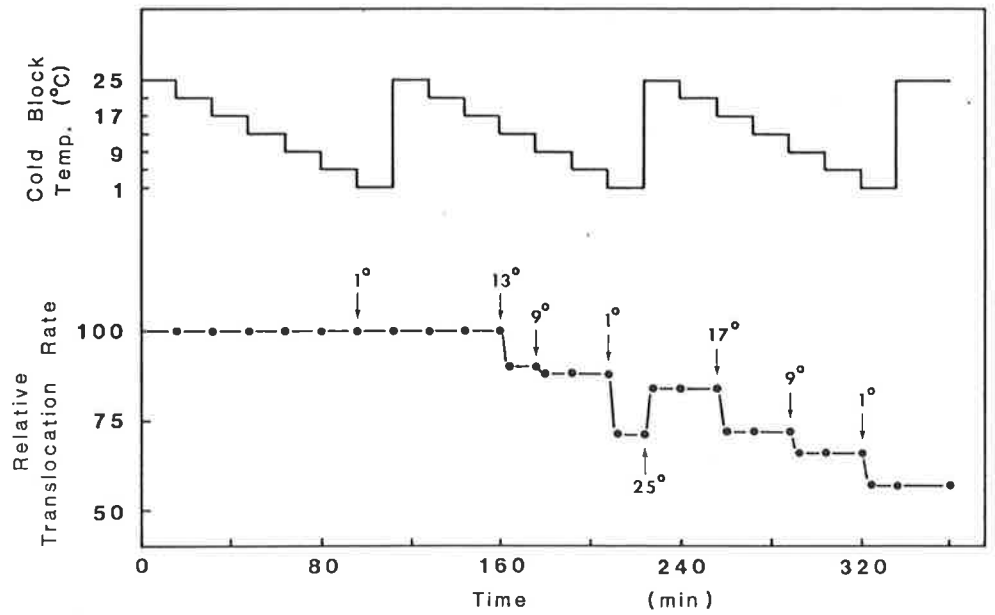


FIG. 1. Effect on translocation of repeated slow cooling treatments on a 2·0 cm segment of a sugar beet source leaf petiole. A 2·0 cm brass block cooling apparatus on the source leaf petiole was cooled or warmed to various temperatures as indicated at the top of the figure.

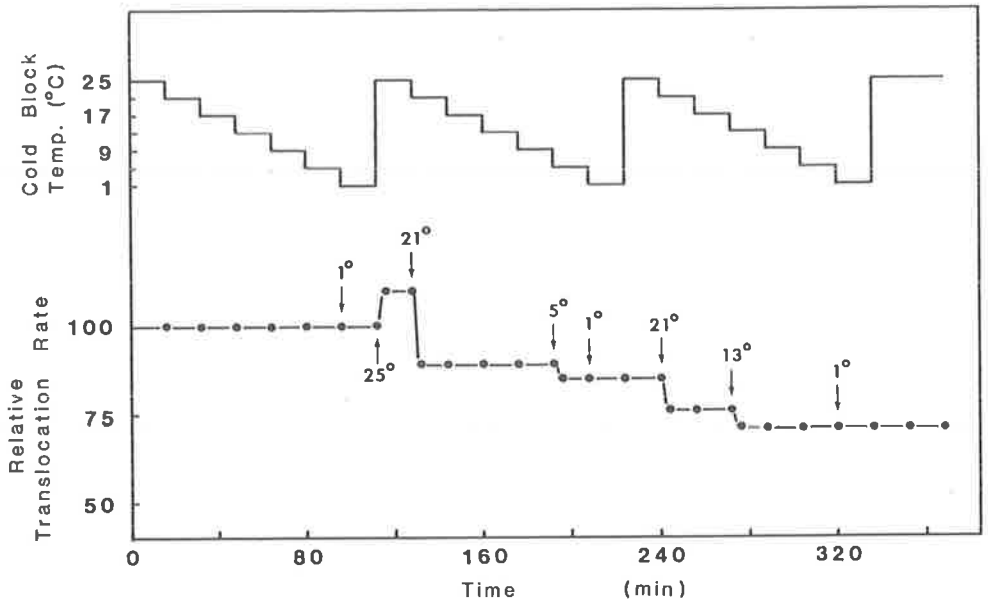


FIG. 2. Effect on translocation of repeated slow cooling treatments on a 6·0 cm segment of a sugar beet source leaf petiole. A 6·0 cm brass block cooling apparatus on the source leaf petiole was cooled or warmed to various temperatures as indicated at the top of the figure.

further change in their translocation rate (data not shown). When an inhibition occurred during a cooling treatment, the translocation response was seen to follow immediately that particular temperature change, although there appeared to be no unique temperature which promoted the inhibition response. Similar results were obtained when slow cooling treatments were applied to 6·0 cm lengths of the source petiole (Fig. 2). In addition, the degree of inhibition in the 6·0 cm length experiments was comparable to that obtained when a 2·0 cm length was used; i.e., the average step inhibition was $10{\cdot}0 \pm 2{\cdot}9\%$ of the original translocation rate.

*Influence of an initial cooling treatment on subsequent coolings*

Since it was apparent that an initial slow cooling regime influenced the translocation response during subsequent slow cooling treatments, we investigated this effect on the quick cooling response. Figure 3 reveals that when a 2·0 cm petiole segment was quickly cooled to 1 °C, following a slow cooling treatment and a rewarming to 25 °C for as short a time period as 4 min, the relative translocation rate responded with a characteristic inhibition and recovery (see Fig. 3 of Grusak and Lucas, 1984). Subsequent slow cooling treatments continued to promote step decreases in the translocation rate of the type shown in Fig. 1 (average step inhibition was $9{\cdot}3 \pm 3{\cdot}3\%$ of the original translocation rate). Similarly, if the initial cooling treatment on a petiole was a quick cooling perturbation, all subsequent slow coolings exhibited the step decrease phenomenon in the translocation rate (Fig. 4). Again, the degree of inhibition was comparable to that observed during repeated slow cooling treatments, i.e., $10{\cdot}1 \pm 4{\cdot}5\%$ of the original translocation rate.

In the experiments described above, we employed a quick rewarming step to 25 °C following the particular cooling regime. Since it was possible that this temperature manipulation, *per se*, could be influencing the slow-cooling induced inhibition, we also investigated the effect on translocation of slow rewarming cycles. Figure 5 shows that step decreases in the translocation rate were induced at various temperatures during both the

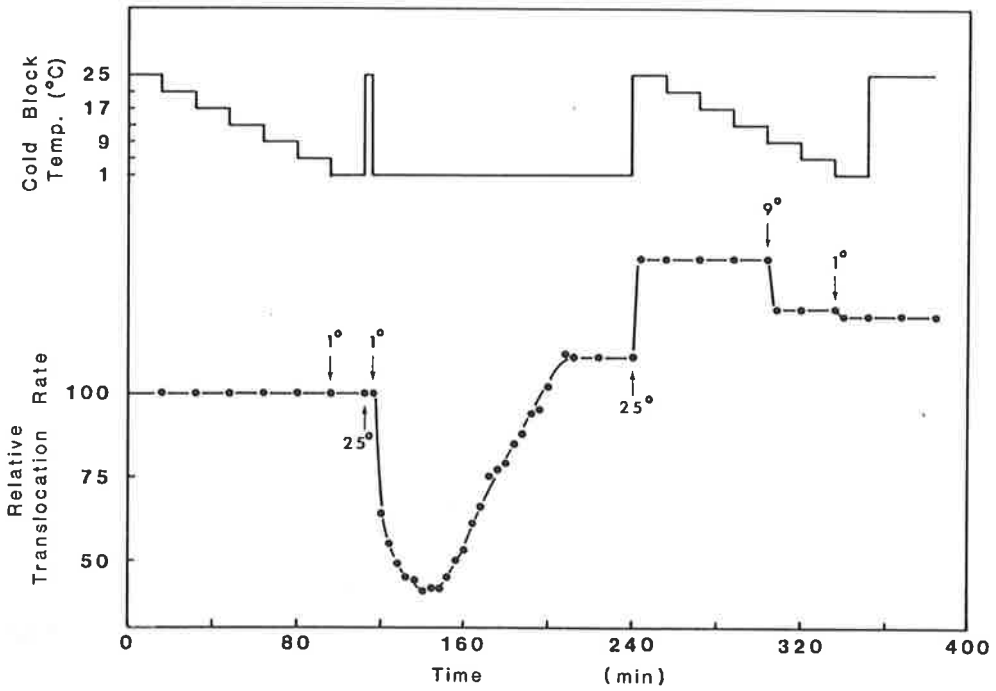


FIG. 3. Translocation rate during cooling perturbations to a 2·0 cm petiole segment of a sugar beet source leaf. A 2·0 cm brass block cooling apparatus was slowly cooled to 1 °C, was rewarmed to 25 °C for 4 min and was then quickly cooled to 1 °C. After rewarming, a subsequent slow cooling treatment was performed.

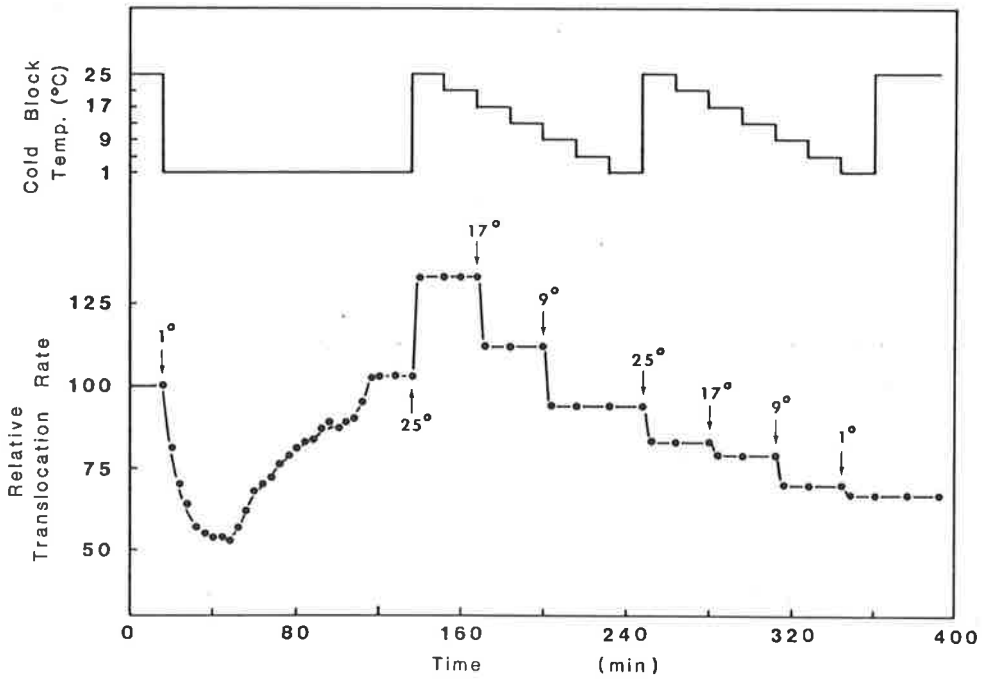


FIG. 4. Effect on translocation of quick and slow cooling treatments on a 2·0 cm petiole segment of a sugar beet source leaf. The petiole segment was quickly cooled to 1 °C and, following rewarming, was subjected to two slow cooling treatments. Temperature changes for the cold block are indicated at the top of the figure.

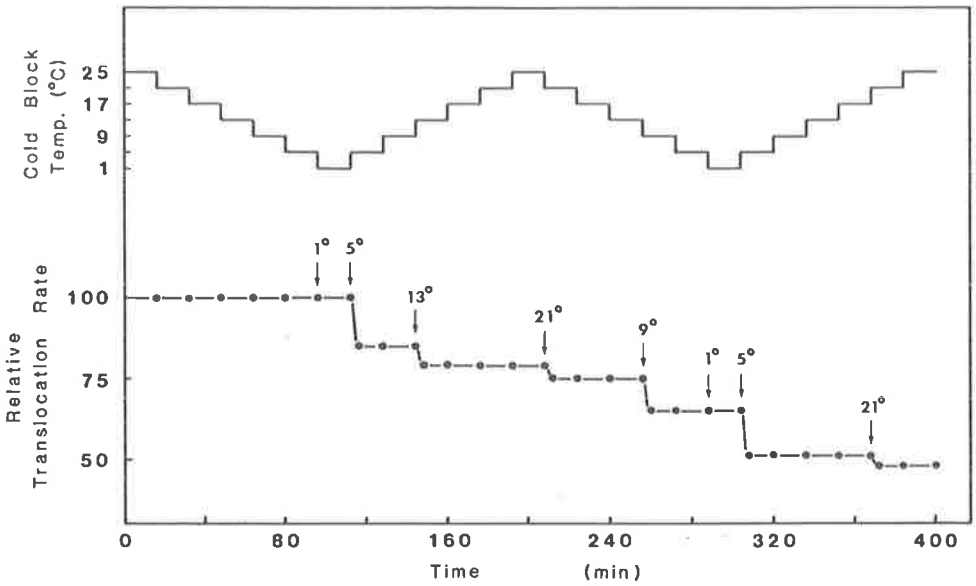


FIG. 5. Effect on translocation of slow cooling and warming treatments on a 2·0 cm petiole segment of a sugar beet source leaf. Cold block temperature changes at the top of the figure indicate that the petiole segment was slowly rewarmed to 25 °C following each slow cooling treatment.

rewarming and subsequent slow cooling cycles. Average step inhibition was 10·0 ± 4·5% and 10·0 ± 5·4% of the original translocation rate for the rewarming and cooling cycles, respectively.

*Localization of slow-cooling induced alterations*

Having characterized the translocation responses to repeated coolings, we wished to elucidate the location within the source–sink system where the tissue was being influenced by the initial cooling regime. Experiments were performed in which a cooling treatment was undertaken, with 2·0 cm blocks, at one position on the source leaf petiole and then the blocks were positioned at various new locations for subsequent slow cooling regimes. Translocation studies indicated that following an initial slow cooling, if the cold blocks were repositioned either upstream (towards the source blade) or downstream (towards the sink leaf), a distance of at least 2·0 cm from the boundaries of the initial block, the next slow cooling treatment (second cooling for the plant, first cooling at the new position) did not cause an inhibition of the translocation rate (Fig. 6). Inhibition was only observed when the slow cooling regime was repeated at the new petiole position. If the cold block was repositioned, after an initial slow cooling, such that the new downstream edge of the cold block surrounded the source petiole where the original upstream edge had previously resided, the first slow cooling treatment at the new position also promoted an inhibition of the translocation rate (Fig. 7). However, if the cold block was repositioned, after the initial slow cooling, to the downstream boundary, or was actually overlapping the original position by up to 0·7 cm on the downstream edge, no inhibition of translocation was observed until the second slow cooling treatment was applied at this new petiole location (Fig. 8).

Similar experiments involving a change in the position of the cold block were also performed following 2·0 cm quick cooling treatments. When the cold block was repositioned to *either* the upstream or downstream boundaries of the original cold block location, the step-type inhibition of translocation was observed during the first slow cooling regime in either case (Fig. 9).

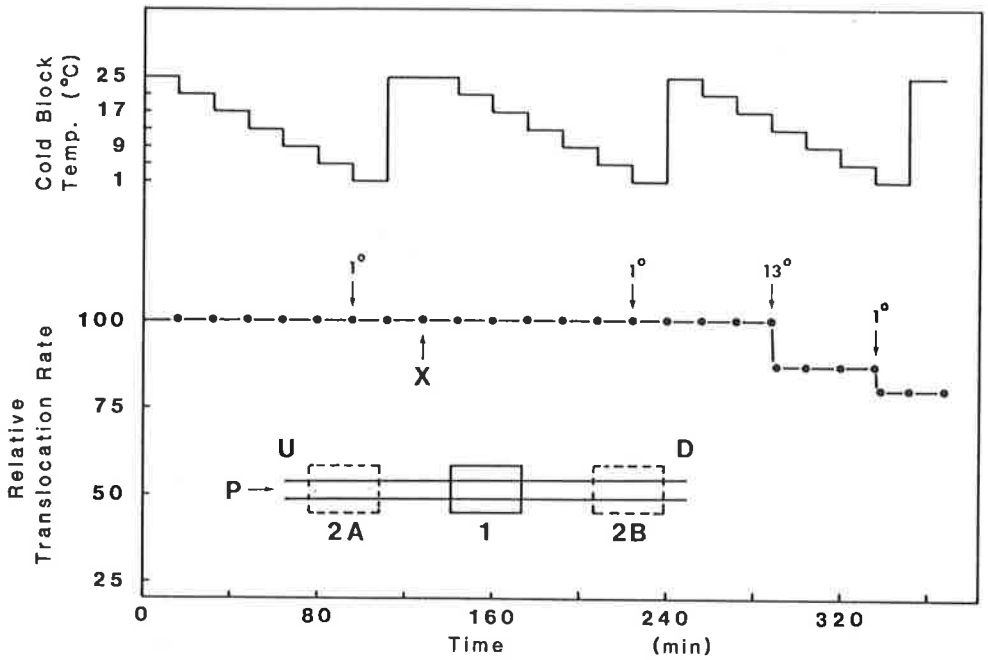


FIG. 6. Effect on translocation of slow cooling treatments at different petiole positions on a sugar beet source leaf. A 2·0 cm brass block apparatus was cooled slowly to 1 °C at one petiole position (1, see inset), and following rewarming to 25 °C was moved to a second petiole position (time of repositioning indicated by X) at least 2·0 cm from the boundaries of the original cold block. The data in this figure are representative of experiments in which the cold block was moved to either the upstream or downstream side of the first cold block position (see inset 2A or 2B, respectively). After repositioning the cold block apparatus, the petiole tissue was subjected to two additional slow cooling treatments. P: petiole; U: upstream end (towards the source blade); D: downstream end (towards the sink leaf).

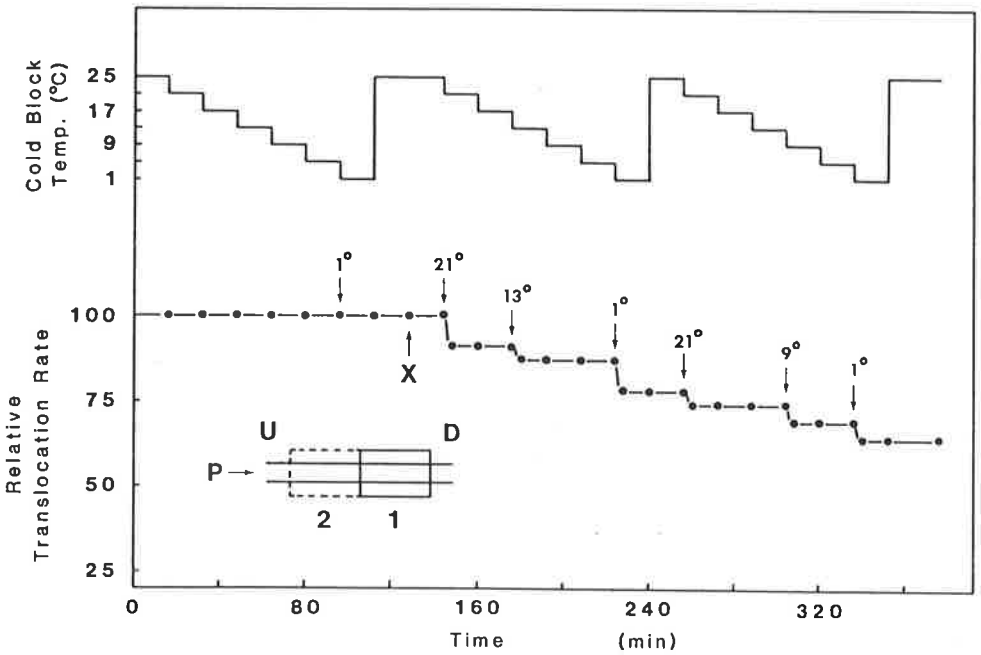


FIG. 7. Effect on translocation of slow cooling treatments at an adjacent, upstream petiole position on a sugar beet source leaf. A 2·0 cm brass block apparatus was cooled slowly to 1 °C at one petiole position (1, see inset), and following rewarming to 25 °C was moved to an upstream position (time of repositioning indicated by X) directly adjacent to the upstream boundary of the first block (2, see inset). The new petiole segment was subjected to two slow cooling treatments. Symbols are as defined in Fig. 6.

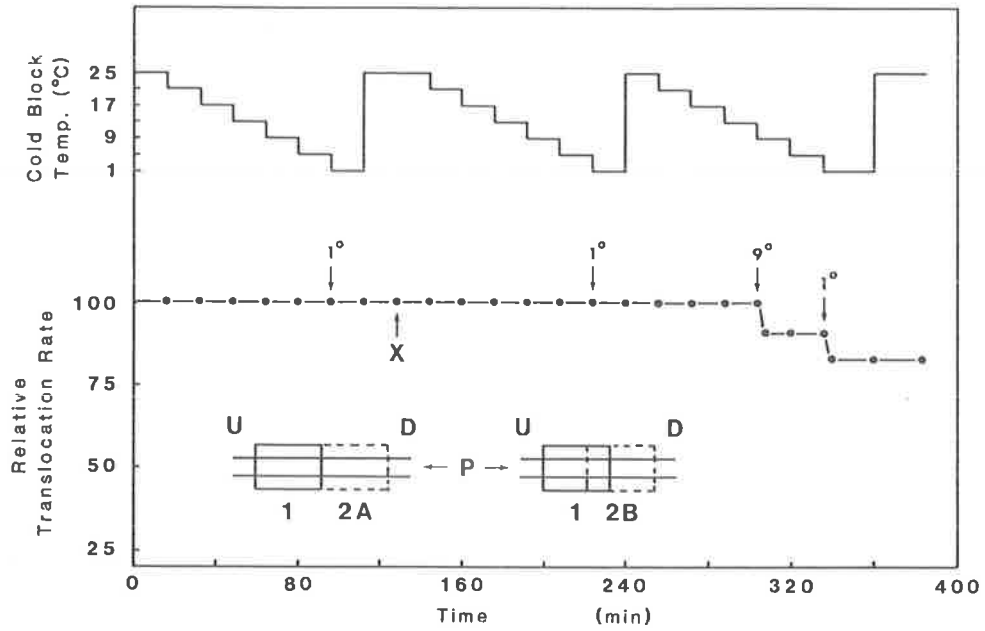


FIG. 8. Effect on translocation of slow cooling treatments at an adjacent, or overlapping downstream petiole position on a sugar beet source leaf. A 2·0 cm brass block apparatus was cooled slowly to 1 °C at one petiole position (1, see inset), and after rewarming to 25 °C was moved to a second position (time of repositioning indicated by X) on the downstream region of the first block's position. The data in this figure are representative of experiments in which the cold block apparatus was moved to either the downstream border of the first position (2A, see inset), or overlapped the downstream border by as much as 0·7 cm (2B, see inset). In all cases the new petiole segment was subjected to two slow cooling treatments. Symbols are as defined in Fig. 6.

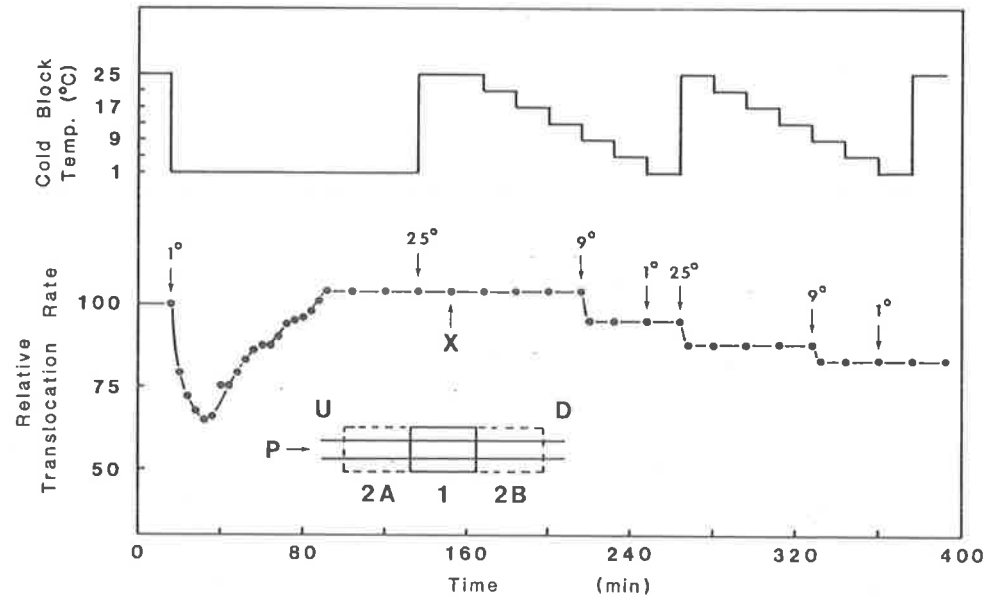


FIG. 9. Effect on translocation of quick and slow cooling treatments at adjacent petiole positions on a sugar beet source leaf. A 2·0 cm brass block apparatus was quickly cooled to 1 °C and held at that temperature for 2 h at one petiole position (1, see inset); following rewarming to 25 °C it was moved to an adjacent petiole position (time of repositioning indicated by X). The data are representative of experiments in which the cold block was moved to either the upstream (2A, see inset) or downstream (2B, see inset) border of the original cold block position. After repositioning, the new petiole segment was subjected to two slow cooling treatments. Symbols are as defined in Fig. 6.

## DISCUSSION

### *Slow-cooling induced inhibition of translocation*

Translocation studies have shown that if a slow cooling treatment is employed, the temperature of a petiole segment of a sugar beet source leaf can be cooled from 25 °C to 1 °C with no effect on the rate of translocation to the monitored sink (Figs 1, 2). This result is in agreement with previous work on maize and *Ipomoea*, in which the actual rate of cooling was found to influence the phloem translocation response (Faucher *et al.*, 1982; Minchin and Thorpe, 1983). This lack of inhibition at 1 °C, in contrast to that normally observed when a sugar beet petiole segment is quickly cooled (Swanson and Geiger, 1967; Grusak and Lucas, 1984), occurs only during the first slow cooling treatment for a given test plant. All subsequent slow coolings exhibit a characteristic step-type inhibition response following one or two temperature changes during that particular cooling treatment (Figs 1, 2). Our data suggest that during the initial cooling treatment, some form of perturbation alters the state of the tissue, such that the translocation process responds to subsequent temperature changes. The induction of this alteration is associated with the initial cooling treatment, and not with the quick rewarming used in most of these studies, since a slow rewarming also resulted in decreases in the translocation rate following various temperature changes (Fig. 5).

Previous work by Giaquinta and Geiger (1973) suggested that a threshold temperature level may exist which promotes the inhibition of translocation, and that this level may be related to a temperature-induced phase change in the fluidity of the sieve element plasmalemma. Clearly the present study does not support the existence of a threshold temperature which triggers the inhibition process in sugar beet, since (1) the slow-cooling induced inhibition can be promoted by various temperatures, and (2) the temperature of a petiole segment can be lowered, in an initial slow cooling sequence, not only to 1 °C (Fig. 1), but to as low as −4 °C (data not shown), with no effect on the rate of translocation. It appears that this lack of inhibition is not due to a slow-cooling induced change in the lipid content of the sieve element plasmalemma (which could prevent the temperature-induced lipid phase change), as rewarming to 25 °C (after an initial slow cooling) for only 4 min, followed by a quick cooling to 1 °C, shows the characteristic inhibition and recovery response (Fig. 3). This 4 min rewarming would not be a sufficient time to re-establish the original lipid composition of the membrane (Mazliak, 1973). Additionally, a recent freeze-fracture electron microscopic study on root tissue suggests that the membrane structure of either chill-sensitive or chill-insensitive plants is unaltered following a chilling treatment (Robards and Clarkson, 1984).

The slow-cooling induced alteration within the phloem tissue appears to have *no effect* on the quick cooling translocation response in sugar beet (cf. Figs 3, 4). The alteration seems to be a relatively long-lived phenomenon that would definitely be present at the time of the quick cooling treatment (Fig. 3). This long-lived nature is shown by the presence of two responses to the slow cooling regime (Fig. 1). Furthermore, if a petiole segment is maintained at 25 °C for up to 3 h following an initial slow cooling, a second slow cooling regime performed after this time still elicits the characteristic step-type inhibition response (data not shown).

### *Location of slow-cooling induced inhibition*

Having characterized the translocation response to repeated slow coolings, it was important to elucidate the location of the cooling-induced alteration within the source–sink system. Our experiments show that the alteration is localized to the chilled region of the petiole, since a second cooling treatment for a given plant, performed at a different petiole

position (at least 20 mm away from the initial block's upstream or downstream borders), has no effect on the relative translocation rate (Fig. 6). If an inhibition had been seen during this second cooling, an alteration at the loading or unloading regions of the plant would have been implicated. Further studies showed that this slow-cooling induced alteration appears to reside at the upstream boundary of the chilled petiole region (Figs 7, 8). The alteration also appears to extend upstream of the cold block's border a short distance, since an inhibition was obtained when the blocks were repositioned at this upstream border without overlapping the original position (Fig. 7). This conclusion would be consistent with our finding that no difference could be detected when the slow coolings were performed with either 2·0 cm or 6·0 cm petiole segments (cf. Figs 1, 2).

The slow-cooling induced inhibition, which in each step-type reduction averages about 10% of the original translocation rate and shows no recovery, is quite different from the response observed following a quick cooling treatment (see Fig. 3; also Grusak and Lucas, 1984). It would appear, therefore, that the cytological/biochemical/biophysical nature of the processes that give rise to the inhibition of translocation, under these two cooling regimes, are different. However, when the tissue is given a quick cooling treatment, the 'step-type' alteration is induced throughout the length of the chilled petiole segment (Fig. 9). This indicates that although the tissue has been induced by this quick cooling treatment, the 'step-type' mode of inhibition can only be manifested by the application of subsequent slow cooling treatments; repeated quick cooling treatments give rise to the previously reported inhibition and recovery phenomenon (Swanson and Geiger, 1967; Grusak and Lucas, 1984).

*Mechanisms of slow-cooling induced inhibition*

The results of this research now pose three important questions: (1) why is there no influence on the translocation rate by an initial slow cooling; (2) what is the nature of the cooling-induced alteration within the chilled petiole tissue; and (3) what activates the inhibition process during subsequent slow cooling treatments? At present, we can confidently describe the various translocation phenomena, but can offer only speculation as answers to these questions. Our present understanding of the sugar beet system does suggest, however, that the nature of the cooling-induced tissue alteration is some process intimately involved with maintaining a low resistance or optimal pressure gradient in the petiole pathway. Future work will, therefore, focus on both the ultrastructure and membrane physiology of the petiole tissues, to search for possible alterations which could account for the observed translocation responses.

## ACKNOWLEDGEMENTS

This research was supported by National Science Foundation Grants PCM 79-10223 and PCM 83-15408 to W.J.L., as well as a University of California Graduate Research Award to M.A.G.

## LITERATURE CITED

FAUCHER, M., BONNEMAIN, J.-L., and DOFFIN, M., 1982. Effets de refroidissements localisés sur la circulation libérienne chez quelques espèces avec ou sans protéines-P et influence du mode de refroidissement. *Physiologie Végétale*, **20**, 395–405.

GEIGER, D. R., and SOVONICK, S. A., 1975. Effects of temperature, anoxia, and other metabolic inhibitors on translocation. In *Encyclopedia of plant physiology. New Series. Volume 1: Transport in plants. I. Phloem transport*. Eds M. H. Zimmermann and J. A. Milburn. Springer-Verlag, Berlin, Heidelberg, New York. Pp. 256–86.

GIAQUINTA, R. T., and GEIGER, D. R., 1973. Mechanism of inhibition of translocation by localized chilling. *Plant Physiology*, **51**, 372–7.

GRUSAK, M. A., and LUCAS, W. J., 1984. Recovery of cold-inhibited phloem translocation in sugar beet. I. Experimental analysis of an existing mathematical recovery model. *Journal of Experimental Botany*, **35**, 389–402.

MAZLIAK, P., 1973. Lipid metabolism in plants. *Annual Review of Plant Physiology*, **24**, 287–310.

MINCHIN, P. E. H., and THORPE, M. R., 1983. A rate of cooling response in phloem translocation. *Journal of Experimental Botany*, **34**, 529–36.

ROBARDS, A. W., and CLARKSON, D. T., 1984. Effects of chilling temperatures on root cell membranes as viewed by freeze-fracture electron microscopy. *Protoplasma*, **122**, 75–85.

SWANSON, C. A., and GEIGER, D. R., 1967. Time course of low temperature inhibition of sucrose translocation in sugar beet. *Plant Physiology*, **42**, 751–6.

Planta (1985) 164:227-240

Planta
© Springer-Verlag 1985

# Sugar uptake into *Allium cepa* leaf tissue: an integrated approach

Clyde Wilson, John W. Oross and William J. Lucas
Department of Botany, University of California, Davis, CA 95616, USA

**Abstract.** *Allium cepa* L. leaves were subjected to enzymatic (pectolyase) and mechanical manipulation in order to ascertain the contribution made by various leaf tissues to the total sugar uptake by the leaf. In order to develop an understanding of the basic anatomy and ultrastructure of the *Allium* leaf and assess the integrity of the tissue before and after enzymatic and mechanical manipulation, a light- and transmission-electron-microscopy study was performed. One outcome of this study was the discovery that the chloroplasts of the bundle-sheath cells contain starch. The function of these inclusions in relation to carbohydrate pools and translocation is discussed. Kinetic curves for sucrose and fructose uptake by leaf discs derived from control and modified leaves are presented. In addition, kinetic curves for the tissues removed by the enzymatic treatment (inner parenchyma, bundle sheath and some vascular parenchyma) and the vascular bundles were also obtained. All tissues exhibited the same linear plus saturable profile as the dicotyledon, *Beta vulgaris*, with the exception of fructose uptake into the inner parenchyma and bundle-sheath cells; in this case the response was linear. The effect of anoxia on uptake of exogenous sucrose was also investigated. Anaerobiosis inhibited both the linear and saturable component of sucrose influx. Adenine-nucleotide levels were obtained using high-performance liquid chromatography for control (air) and anoxia-treated ($N_2$) leaf discs. A general loss of adenine nucleotides was observed. The results presented indicate that all tissues of the leaf retrieve exogenous sugar such that the kinetic curves derived from leaf discs cannot represent phloem loading, per se.

**Key words:** *Allium* (sugar uptake) – ATP – Phloem loading – Sugar uptake.

*Abbreviations:* Mes = 2-(N-morpholino)ethanesulfonic acid; E.C. = energy charge

## Introduction

Studies on the nature of phloem loading and translocation have made frequent use of sucrose uptake into leaf discs (Fellows and Geiger 1974; Giaquinta 1976, 1977; Delrot et al. 1980; Geiger and Fondy 1980; Delrot and Bonnemain 1981). Giaquinta and other workers (Sovonick et al. 1974; Giaquinta 1977) investigated the relationship between uptake of exogenous sugar into leaf discs and the intact leaf with respect to phloem translocation. Based on these studies, it was concluded that sucrose uptake into leaf discs reflects loading into the phloem and could therefore be used to study the processes involved in phloem loading (Giaquinta 1977, 1980; Delrot et al. 1980; Delrot and Bonnemain 1981). Using this system, numerous workers have investigated the kinetics of phloem loading. The inital work was interpreted in terms of two saturable systems but recent studies indicate that uptake of exogenous sucrose occurs via two different transport systems, a saturable component displaying Michaelis-Menten kinetics and a linear component obeying first-order kinetics (Komor et al. 1977; Lichtner and Spanswick 1981; Maynard and Lucas 1982a).

However, other investigators have shown that exogenously supplied sucrose may be taken up by non-phloem tissue. Geiger and co-workers (Geiger 1976; Geiger and Fondy 1980; Fondy and Geiger 1977) reported uptake of [$^{14}$C]sucrose into mesophyll tissue. They found that 60% of the sucrose absorbed by sugar-beet leaves during a 30-min incubation in 10 mM [$^{14}$C]sucrose was located in the mesophyll. Additionally, in a recent study by Maynard and Lucas (1982b) the interpretation of these kinetic data with respect to the actual site of sugar uptake was questioned. These investigators demonstrated that tissues in the petiole can take up exogenously supplied sugars. They con-

cluded that the kinetics of sucrose influx into non-phloem tissue closely resembled what previously has been regarded as representative of loading into the phloem. Therefore, it is questionable whether phloem loading can be directly equated with sugar uptake from the apoplast.

To resolve this issue, it is necessary to separate the various tissues of the leaf such that their individual contributions to sugar uptake can be determined and compared with data obtained on intact leaves. To facilitate the interpretation of such studies, a leaf which would lend itself to structural modification was sought. In the work described in this paper we used *Allium cepa* L. because its cylindrical leaf could easily be biochemically and physically manipulated. However, because of the paucity of published anatomical and ultrastructural information on *Allium*, it was necessary to perform a structural study on the onion leaf. As *A. cepa* does not possess an inner cuticle or epidermis but rather develops a lacuna, its interior tissues are highly accessible both to exogenous solutes and cell-wall-digesting enzymes that were used to help remove the various tissues. With the aid of these enzymes we were able to remove, sequentially, the parenchyma and vascular bundles. Transmission electron micrographs confirm the integrity of the leaf following enzymatic and mechanical treatment. We found that other tissues as well as the vascular bundles exhibit the familiar saturable plus linear uptake kinetics. Furthermore, to relate the present study to those previously conducted on phloem systems we utilized this method to investigate the effect of anoxia on the apoplastic retrieval of sucrose. Based on an analysis of these results, we suggest that it is necessary to reevaluate the present usage of the term phloem loading as representing the kinetics of in-vivo loading into the phloem.

## Material and methods

*Plant material. Allium cepa* L., cv. Stockton Yellow Globe (Lagomarsino Seeds, Sacramento, Cal., USA) seeds were planted in a soil mixture containing vermiculite, peat moss and sand (2:1:1, by vol.). The plants were grown under greenhouse conditions with no supplementary light or temperature control, and watered daily with distilled water supplemented with 2 mM $CaNO_3$. Experimental plants were ten weeks old.

*Kinetic studies.* Studies of uptake kinetics were performed using the method of Maynard and Lucas (1982a) with some modification. Briefly, the fifth or sixth leaf of the onion was excised at the base and was put on a rubber pad which was placed in a dish that contained a solution of 20 mM $CaCl_2$ and 60 mM 2-(N-morpholino)ethanesulfonic acid (Mes) buffer (pH 5.0). The leaf was slit longitudinally with a razor blade and leaf discs 4 mm in diameter were cut from the region 7–10 cm from the base. Once cut, the discs were given a 30-min preincubation in a solution containing 20 mM $CaCl_2$, 120 mM Mes (pH 5.0), and enough mannitol to adjust the osmolality to 200 mOsm; sugars at the concentration specified for the particular experiment were also included. Preincubation was followed by a 30-min uptake period in solution containing the appropriate radioactive sugar (D-[U-$^{14}$C]sucrose, -fructose or -glucose (International Chemical and Nuclear Corp., Irvine, Cal., USA). The specific activity of the uptake solution was $1.78 \cdot 10^7$ Bq mmol$^{-1}$. The incubation period was followed by three, 7-min washes in media containing 20 mM $CaCl_2$, 60 mM Mes and the respective sugar (40 mM). The discs were then placed in scintillation vials containing 0.1 ml of 7% $HClO_4$, 0.1 ml of 30% $H_2O_2$ and a drop of methylcellosolve (Sigma Chemical Co., St. Louis, Mo., USA). After a 15-min digestion period, 10 ml of READY-SOLV EP scintillation mixture (Beckman Instruments, Berkeley, Cal., USA) was added and the vials were counted on a Beckman LS 9800 scintillation counter. All experiments were performed at $24 \pm 1°$ C under laboratory lighting, except where noted.

For experiments in which the leaf tissue was simplified, the fifth (or sixth) leaf of an onion plant was excised and clamped such that its interior could be filled with a solution of 1 mg ml$^{-1}$ Pectolyase Y-23 (Seishin Pharmaceuticals, Chiba-Ken, Japan). The digestion by the enzyme was monitored using a binocular dissecting microscope. When the large parenchyma and interveinal parenchyma cells were digested away the leaf was emptied and rinsed with glass-distilled water. A 45-min digestion period was usually required. The resulting leaf, termed "pectolyase-treated", was either used for kinetic studies or manipulated further. The vascular bundles in the pectolyase-treated leaf were surgically removed with the use of forceps while observing the tissue under a binocular microscope. The resulting leaf was termed "stripped". These tissues were used for kinetic studies as detailed above. By subtracting the data obtained using the pectolyase-treated tissue from the data obtained using control tissue we obtained the kinetics for the tissues removed by the enzymatic treatment. The removed tissue included the large parenchyma cells next to the lacuna, interveinal parenchyma, bundle sheath, as well as some vascular parenchyma. The curve obtained by this subtraction was termed "inner parenchyma and bundle sheath". Similarly, upon subtraction of the data of pectolyase-treated tissue from that obtained using stripped tissue we derived the curve designated "vascular tissue." This represents uptake into the vascular bundles.

*Microscopy.* Control, pectolyase-treated, and pectolyase-treated and stripped leaves were fixed in 2% glutaraldehyde in 40 mM sodium-cacodylate buffer (pH 7.0) for 1 h at $24 \pm 1°$ C. The tissue samples were then postfixed in 1% osmium tetroxide in 40 mM cacodylate buffer for 2 h and dehydrated through a graded acetone series before being embedded in Spurr's resin (Spurr 1969). The samples were sectioned, observed, and photographed using a Leitz Orthoplan microscope (Leitz, Wetzlar, FRG).

Ultrathin sections for electron microscopy were prepared using conventional methods and stained with saturated aqueous uranyl acetate followed by 27 mM lead citrate (Reynolds 1963), then observed and photographed with a JEOL (Tokyo, Japan) 100S electron microscope. Periodic acid-thiocarbohydrazide-silver proteinate staining was done using the protocol reported by Roland (1978).

*Anoxia experiments.* Anoxic experiments were performed using a GLOVE BAG (Instruments for Research and Industry, Cheltenham, Pa., USA). The GLOVE BAG was purged with a con-

tinual stream of commercial nitrogen gas. All solutions were bubbled through with nitrogen prior to use. Uptake studies were performed in the dark except when tissue manipulation required the use of a green safelight (0.5 μmol $m^{-2}$ $s^{-1}$ with 95% transmission between 498 and 595 nm).

*Determination of ATP.* To obtain accurate data on adenylate levels in the leaf, tissue samples were placed under the same conditions as used in the kinetics experiments. These samples were then quickly frozen using liquid nitrogen, lyophilized, and assayed.

Lyophilized tissue samples were weighed and ground in 2.0 ml of ice-cold 1.0 M $HClO_4$ using a ground-glass homogenizer. In addition, 2 mg $ml^{-1}$ of Polyclar AT (Polysciences, Warrington, Pa., USA) was added to the extract (Kondo and Nakashima 1979). The homogenizer was rinsed with 1.0 ml of 0.05 M potassium-phosphate buffer (pH 7.5) and after allowing 20 min for complete extraction and protein denaturation, the rinse and the extract were combined. This mixture was then centrifuged at 25000 *g* for 30 min at 4° C, and the supernatant was adjusted to pH 7.5 with 5 N KOH. After waiting 20 min to allow for the precipitation of potassium perchlorate, the extract was again centrifuged for 30 min at 25000 *g*. The supernatant was stored at −70° C until assayed (2–3 d).

The extracts from *A. cepa* were analyzed for AMP, ADP and ATP by first forming fluorescent 1,$N^6$-ethenoadenosine derivatives (Kochethov et al. 1971; Barrio et al. 1972; Secrist et al. 1972a, b) by reacting the nucleotides with chloroacetaldehyde and then separating them using a high-performance liquid chromatograph system. In order to maximize precision and reduce breakdown of ATP it was necessary to modify the procedure of Yoshioka and Tamura (1976) and Preston (1983) by using phosphate instead of acetate buffer as suggested by Avigad and Damale (1972). Chloroacetaldehyde (10 μl) was added to 500 μl of extract (pH 7.5) in a Pyrex test tube. The tube was covered with a glass marble and placed in a boiling water bath for 5 min. Prolonged boiling resulted in breakdown of ADP and ATP. Nucleotide standards were handled in a similar fashion except that 100 μl of 0.1 M potassium phosphate buffer (pH 7.5) was also added prior to boiling. Chloroacetaldehyde was obtained by distilling a solution of chloroacetaldehyde dimethyl acetal (100 g) (Aldrich, Milwaukee, Wis., USA) in 500 ml of 50% sulfuric acid (w/v) as described by Secrist et al. (1972b).

The chromatography was performed using a Beckman Series 344 Gradient Liquid Chromatograph equipped with an Ultrasphere IP column (4.6 mm diameter, 250 mm long). The eluting peaks were detected by using a fluorescence detector (Beckman Model 157) and analyzed on an Altex Chromatopac C-R1B data processor (Beckman Instruments). The etheno derivatives of AMP and ADP were separated using a mobile phase which consisted of 10% acetonitrile and 90% of a solution composed of 0.05 M tetrabutylammonium hydroxide (Fisher Scientific, Pittsburg, Pa., USA) and 0.05 M $KH_2PO_4$ (concentrated phosphoric acid was used to adjust the pH value to 2.5). ATP was analyzed separately using a 30% and 70% mixture of the above-detailed components. Fluorescence was measured using a 280-nm excitation filter and a 350–470 nm emission filter to eliminate detection of cytidine derivatives. A 20-μl injection volume and a flow rate of 1 ml $min^{-1}$ was used for all analyses.

The peaks were identified by using the retention times of standards. Further confirmation of the peaks in the extracts was obtained enzymatically. The use of pyruvate kinase and adenylate kinase (Sigma) in combination, or pyruvate kinase alone, resulted in the disappearence of the peaks which were identified as AMP and ADP, respectively, on the basis of retention time. There was also a concomitant increase in the ATP peak. The addition of hexokinase or calcium phosphate to the extract resulted in a loss of the suspected ATP peak. Enzymatic conversions were performed using the procedure of Kimmich et al. (1975).

## Results

*Leaf anatomy and ultrastructure of Allium cepa.* The uniseriate *epidermis* of the leaf is composed of axially elongate cells that have thickened outer walls (Figs. 1–4) that are adcrusted with a relatively thin cuticular layer (Fig. 4). The epidermal-cell protoplast is highly vacuolate with a very thin parietal layer of cytoplasm containing few organelles (Fig. 4). Stomata were observed in most sections (Figs. 1, 12, 13, 14).

The *leaf ground tissue* not in contact with the vascular bundles may be divided into three types based on 1) relative cell size, shape and orientation; 2) volume of intercellular air space; 3) specific ultrastructural features. The first type is designated as chlorenchyma and is composed of three or four layers of palisade cells present beneath the epidermis and of one or two layers of isodiametric spongy chlorenchyma cells that subtend the palisade cells in the region of the vascular bundles. The chlorenchyma is characterized by a large volume of intercellular air space and cells containing numerous chloroplasts located almost exclusively along the walls adjoining the air spaces. Most of the cell volume is occupied by a single large vacuole which, in the outer palisade cells, contains inclusions that have a high affinity for toluidine blue (Fig. 1). The chloroplasts have a reniform shape in sectional view and contain a well-developed grana-fretwork system and many plastoglobuli (Figs. 5, 18). Reserve carbohydrate was never observed in these chloroplasts. The ends of the chloroplasts were commonly observed in close spatial association with mitochondria and microbodies (Fig. 5).

The second form of ground parenchyma is located in the interveinal regions and is characterized by a relatively small volume of intercellular air space and somewhat axially elongate cells that contain fewer chloroplasts than the chloroenchyma cells (Figs. 1, 2, 3). The chloroplasts of the interveinal parenchyma cells are similar to those of the chlorenchyma with respect to the organization of internal membranes, the lack of visible carbohydrate reserve, the location opposite intercellular air spaces, and the close association with mitochondria and microbodies. However, the chloroplast shape in sectional view is elliptical rather than reniform (Figs. 17, 19). Articulated laticifers occur at

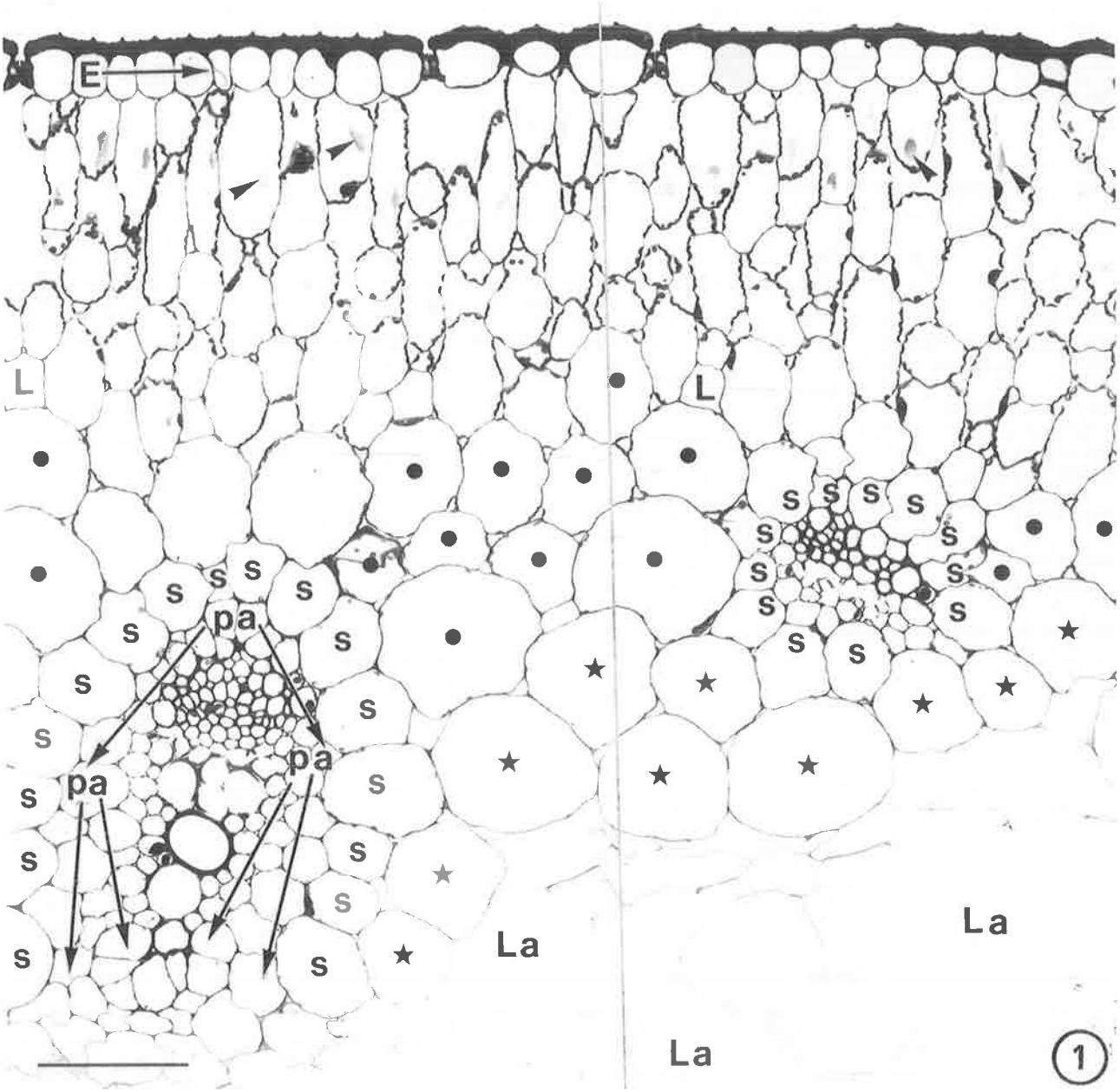
E
L
L
pa
pa
pa
s
La
La
La
1

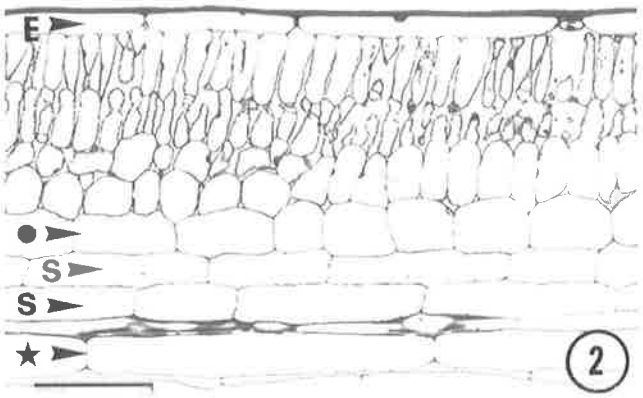
E
s
s
2

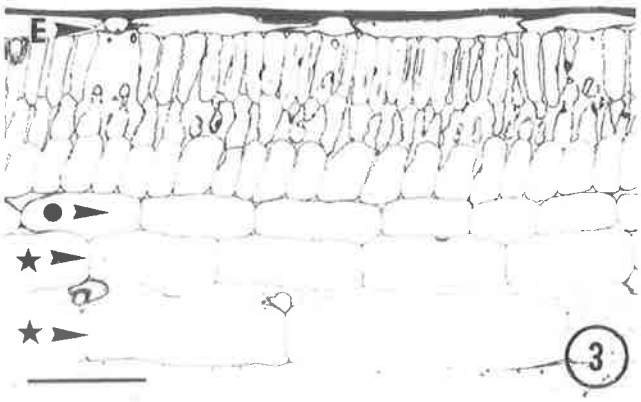
E
3

the interface between these cells and the overlying chlorenchyma (Fig. 1).

The remainder of the ground tissue not in contact with the vascular bundles is composed of very large, axially elongate cells (Figs. 1, 2, 3). Cytoplasmic organelles are less abundant than in either of the overlying cell types and not preferentially distributed in regions opposite intercellular air spaces. The chloroplasts are small in comparison to those of the more external cells and their internal membrane system is less developed. Numerous plastoglobuli are present in the stroma of these chloroplasts but no reserve carbohydrate was observed (Fig. 9).

A loosely organized layer of axially elongate cells that lack protoplasts lines the leaf lacuna (Fig. 1).

The *vascular bundles* are bounded by a uniseriate layer of compactly arranged elongate cells that comprise a bundle sheath (Figs. 1, 2). Most of the organelles in these highly vacuolate cells are located in locally thickened regions of parietal cytoplasm. Since the organelles in these regions are not closely appressed to the cell wall, cellular constituents such as dictyosomes, endoplasmic reticulum and ribosomes are more apparent. The chloroplasts can be distinguished from those of the other ground tissue cells by their spheriodal shape and irregularly shaped, electron-lucent stromal inclusions (Fig. 6). The inclusions stain reddish-brown with IKI (data not shown) and are oxidizable with periodate (Fig. 7). The starch grains in the plastids of sugar-beet phloem cells reacted similarly to these reagents (Fig. 8) and it was concluded that the inclusions in the bundle-sheath chloroplasts of *Allium cepa* are starch grains.

A limited number of observations were made on the anatomy and ultrastructure of the collateral vascular bundles. In the larger bundles, the conductive elements of the phloem are separated from the bundle sheath by a uniseriate layer of vascular-parenchyma cells that are not associated with sieve elements. This layer is continuous with a multiseriate layer of vascular parenchyma surrounding the xylem vessels (Fig. 1). In the smaller bundles, the phloem is not completely bordered by a layer of vascular parenchyma (Figs. 10, 20). The companion cells, so designated because of the presence of branched plasmodesmata between them and adjoining sieve elements, possess a relatively thick layer of parietal cytoplasm penetrated by short wall ingrowths. The companion cells, or A-type transfer cells, contain many mitochondria and a few proplastids that lack visible carbohydrate reserve (Figs. 11, 21).

*Manipulation of Allium cepa leaf tissue.* In order to ascertain the kinetic contribution of the various tissues to the intact leaf, it was necessary to dissect the onion leaf. To accomplish this we carefully controlled the concentration of the cell-wall-digesting enzyme (pectolyase) and the temperature at which the digestion was performed. We monitored the enzymatic digestion at intervals by observing sections under a microscope. Once the inner parenchyma was digested away, the tissue was either used in experiments or simplified further by using forceps to remove the vascular bundles. To determine the extent of tissue damage, plant material was examined by light and transmission-electron microscopy.

A consistent pattern of cell destruction was observed in the pectolyase-treated leaves when compared to the controls. In the ground tissue, the chlorenchyma was most commonly found to contain intact cells after wall digestion (Figs. 12–14). Only a few interveinal parenchyma cells remained intact after the enzyme treatment (Figs. 13, 14). The elongate cells nearest the leaf lacuna and the bundle-sheath cells were either completely destroyed, or contained highly disorganized protoplasts and walls that showed varying degrees of digestion (Figs. 13, 14).

Stripping of the vascular bundles from the pectolyase-treated leaves had little effect on the structure of the undamaged leaf cells, since the point of separation of the bundles from the leaves was

**Figs. 1–3.** Light micrographs of untreated leaves of *Allium cepa*. **Fig. 1.** A cross section that illustrates the histology of the leaf of *A. cepa*. Epidermal cells (*E*) are sectioned across their long axis and have a thickened outer wall. Chlorenchyma occurs between the epidermis and the cells marked with either a dot (•) or an "S". Abundant chloroplasts give a beaded appearence to the walls adjoining air spaces. Inclusions with a high affinity for toluidine blue are present in the palisade cells (*unlabelled arrows*). Transversely sectioned laticifers (*L*) are present beneath the chlorenchyma. Two additional forms of ground parenchyma not associated with the vascular bundles are indicated by dots (•) and stars (★). A bundle sheath (*S*) separates the ground parenchyma from the vascular tissue. In the larger bundle (*left*), a layer of vascular parenchyma cells (*pa*) lies between the bundle sheath and the conducting elements of the phloem (*above*) and xylem (*below*). Senescent cells are present in the leaf lacuna (*La*). ×230; bar = 100 μm. **Fig. 2.** A longitudinal section cut in a plane that intersects two files of elongate bundle-sheath cells (*S*). Elongate epidermal cells (*E*) are subtended by three to four layers of chlorenchyma cells. The files of cells indicated by dot (•) or (★) correspond to similarly labelled cells in Fig. 1. ×78; bar = 200 μm. **Fig. 3.** A longitudinal section cut in a plane approximately midway between two vascular bundles. Three layers of chlorenchyma cells are evident beneath the epidermis. Files of cells are labelled as above. ×78; bar = 200 μm

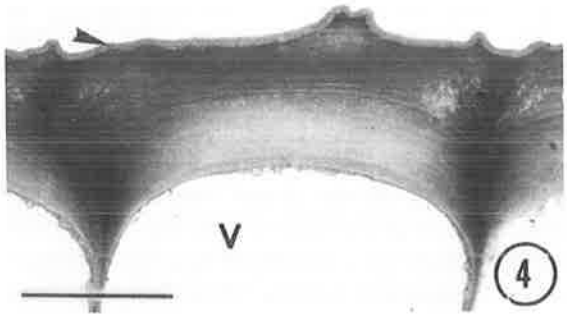
V
4

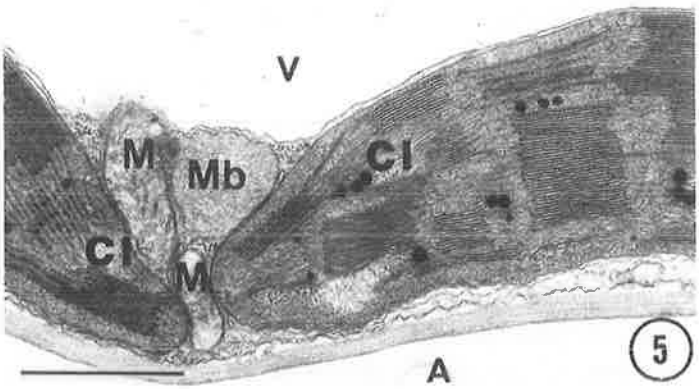
V
M
Mb
Cl
Cl
M
A
5

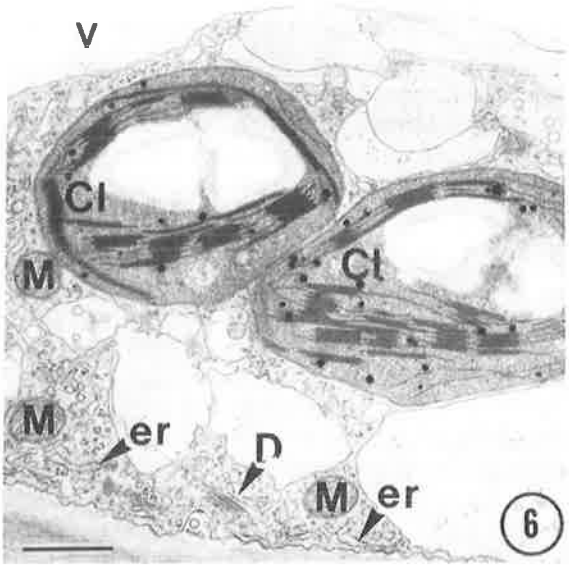
V
Cl
M
Cl
M
er
D
M
er
6

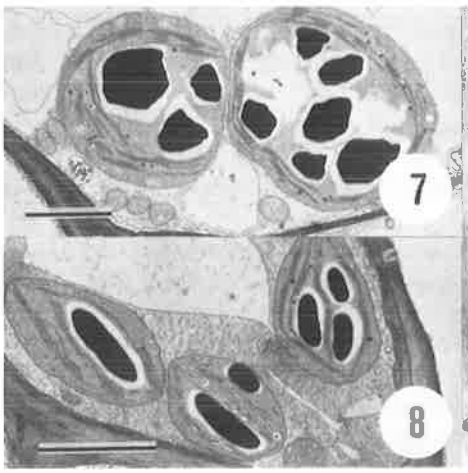
7
8

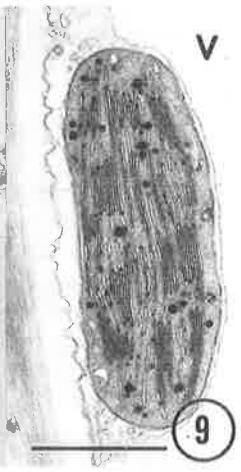
V
9

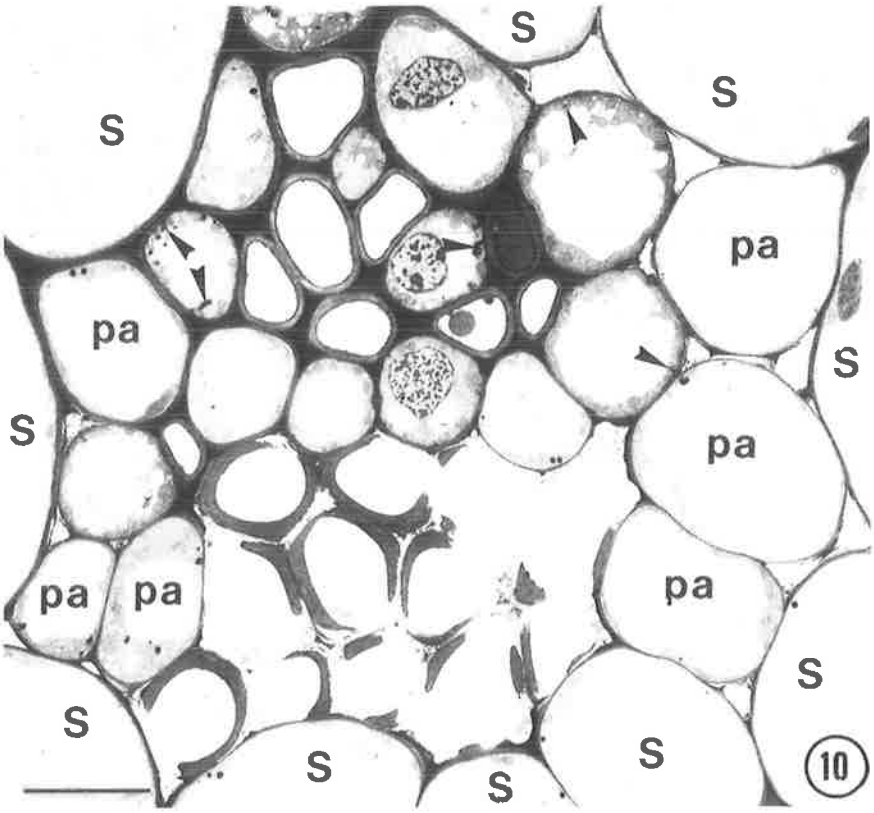
S
S
S
pa
pa
S
S
pa
pa
pa
pa
S
S
S
S
S
10

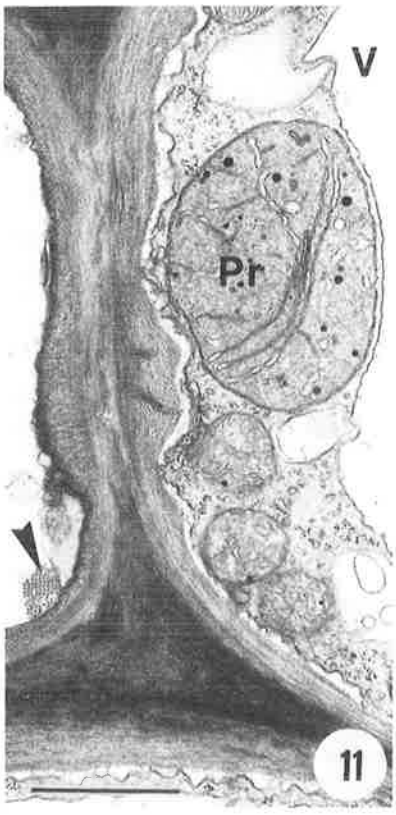
V
Pr
11

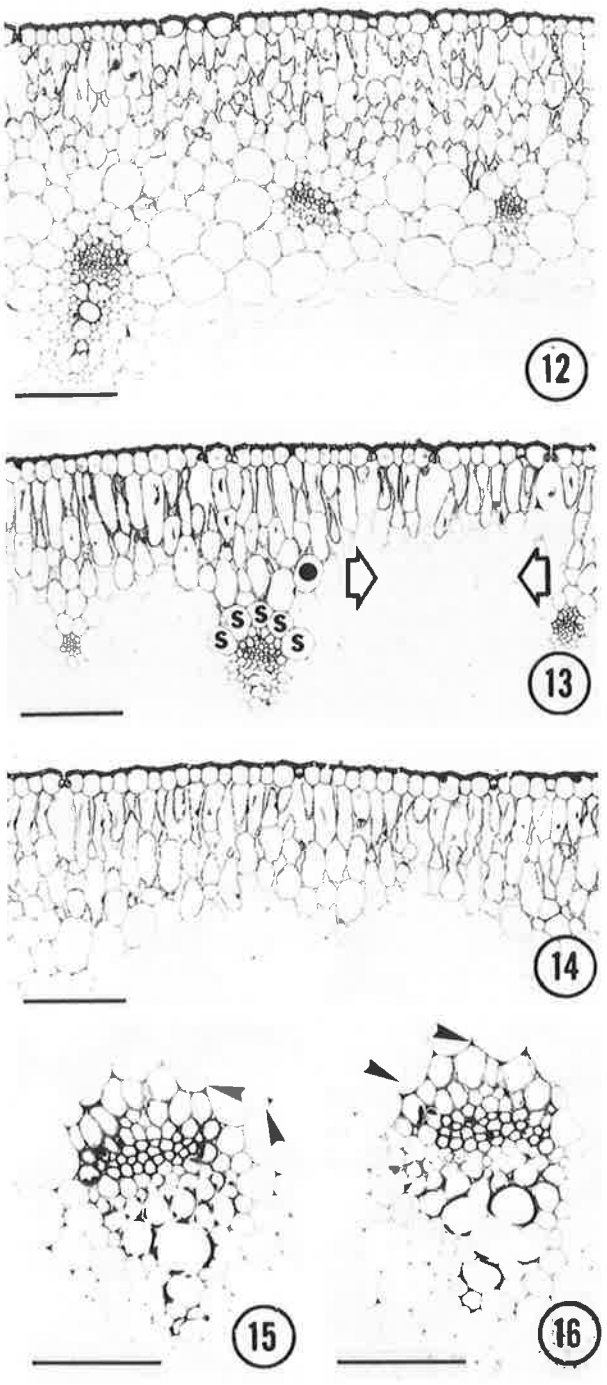


**Figs. 12–16.** Light micrographs comparing untreated (**Fig. 12**) and pectolyase-treated leaf materials of *Allium cepa* (**Figs. 13–16**). **Fig. 12.** A low-magnification micrograph of the untreated section shown in Fig. 1 that is included for comparison with the enzyme-treated materials. ×68; bar = 200 μm. **Fig. 13.** Pectolyase-treated leaf. Most of the chlorenchyma cells and also a single interveinal parenchyma cell (•) are intact after treatment. The remains of the more internal mesophyll cells are barely perceptible (*between arrows*). The vascular bundles remain attached via bundle-sheath cells (*S*) adjoining them and the spongy chlorenchyma. ×68; bar = 200 μm. **Fig. 14.** Pectolyase-treated leaf with vascular bundles removed. Somewhat more chlorenchyma and interveinal parenchyma is intact in this section. The point of detachment of the vascular bundles is at the bundle sheath. ×68; bar = 200 μm. **Figs. 15–16.** Stripped vascular bundles. Most of the cell walls are visible after digestion. The radial walls of the bundle-sheath cells broken by stripping are indicated by *arrows*. ×170; bar = 100 μm

**Figs. 4–6.** Representative electron micrographs of untreated leaf tissue of *Allium cepa*. **Fig. 4.** A cross section of the external portion of an epidermal cell that demonstrates the paucity of cytoplasm and the highly thickened outer wall characteristic of these cells. A relatively thin cuticular layer (*arrow*) adcrusts the leaf surface. ×2000; bar = 10 μm. **Fig. 5.** A portion of the parietal cytoplasm of a palisade cell showing the typical structure and organization of the vacuole (*V*), chloroplasts (*Cl*), mitochondria (*M*) and a microbody (*Mb*). The chloroplasts have a well developed internal membrane system and lack visible carbohydrate reserve. *A*, Air space. ×21500; bar = 1 μm. **Fig. 6.** A section through a locally thickened region of cytoplasm in a bundle-sheath cell. Endoplasmic reticulum (*er*), a dictyosome (*D*), and mitochondria (*M*) are prominent in the cytoplasm. The chloroplasts (*Cl*) are not appressed to the cell wall and apparently contain reserve carbohydrate. *V*, Central vacuole. ×12000; bar = 1 μm

**Figs. 7, 8.** Periodic acid-thiocarbohydrazide-silver proteinate staining of plastid inclusions for periodate oxidizable carbohydrate. **Fig. 7.** Positive staining of plastid inclusions found in the bundle-sheath cells of *Allium cepa*. ×5600; bar = 2 μm. **Fig. 8.** Positive staining of starch in companion cell plastids of *Beta vulgaris* phloem prepared for microscopy by a protocol similar to that reported for the present study. ×7800; bar = 2 μm

**Figs. 9–11.** Electron micrographs of untreated leaves of *Allium cepa*. **Fig. 9.** A chloroplast from one of the axially elongated ground parenchyma cells that line the leaf lacuna. They are smaller than those of the overlying cells and contain fewer thylakoids per granum. No reserve carbohydrate is visible. *V*, Vacuole. ×18000; bar = 1 μm. **Fig. 10.** A transection of a minor vein and a portion of the bundle sheath (*S*). Lateral parenchyma cells (*pa*) do not form a complete layer as in the larger bundles. Short wall ingrowths (*arrows*) are present in some of the phloem parenchyma cells presumed to be companion cells. ×1700; bar = 10 μm. **Fig. 11.** Interface between a sieve element (*left*) and a companion cell (*right*). An ordered array of transversely sectioned P-protein tubules is present in the lumen of the sieve element (*arrow*). The plasmalemma of the companion cell is not closely appressed to the wall and the proplastid (*Pr*) lacks visible carbohydrate reserve. *V*, Vacuole. ×19500; bar = 1 μm

the enzymatically weakened radial walls of the apparently nonviable bundle-sheath cells (Figs. 13–16).

In most respects the ultrastructural preservation of the intact cells from the pectolyase-treated leaves compared closely with that of the controls. Both had a similar distribution and morphology of organelles and an intact plasmalemma and to-

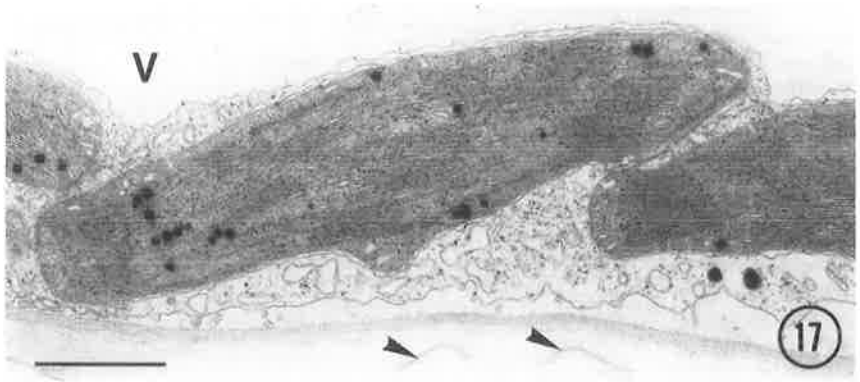
V
17

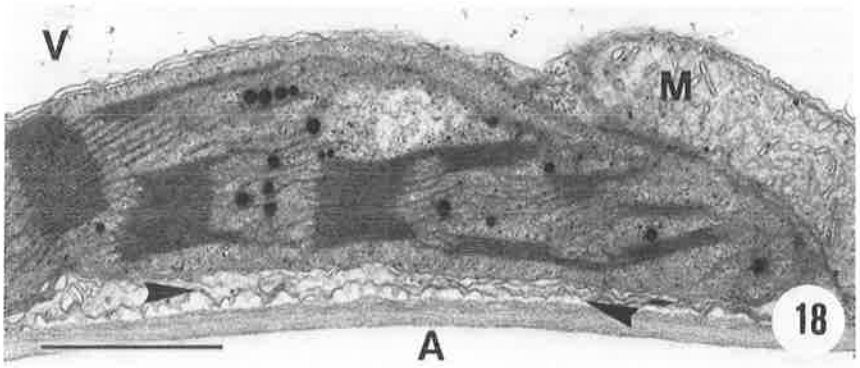
V
M
18
A

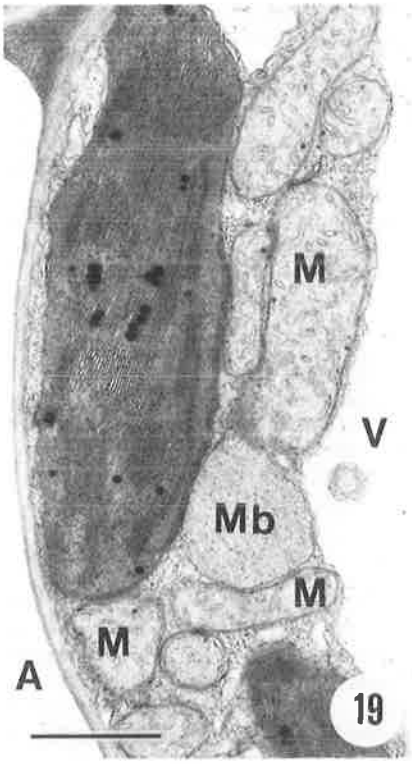
M
V
Mb
M
M
A
19

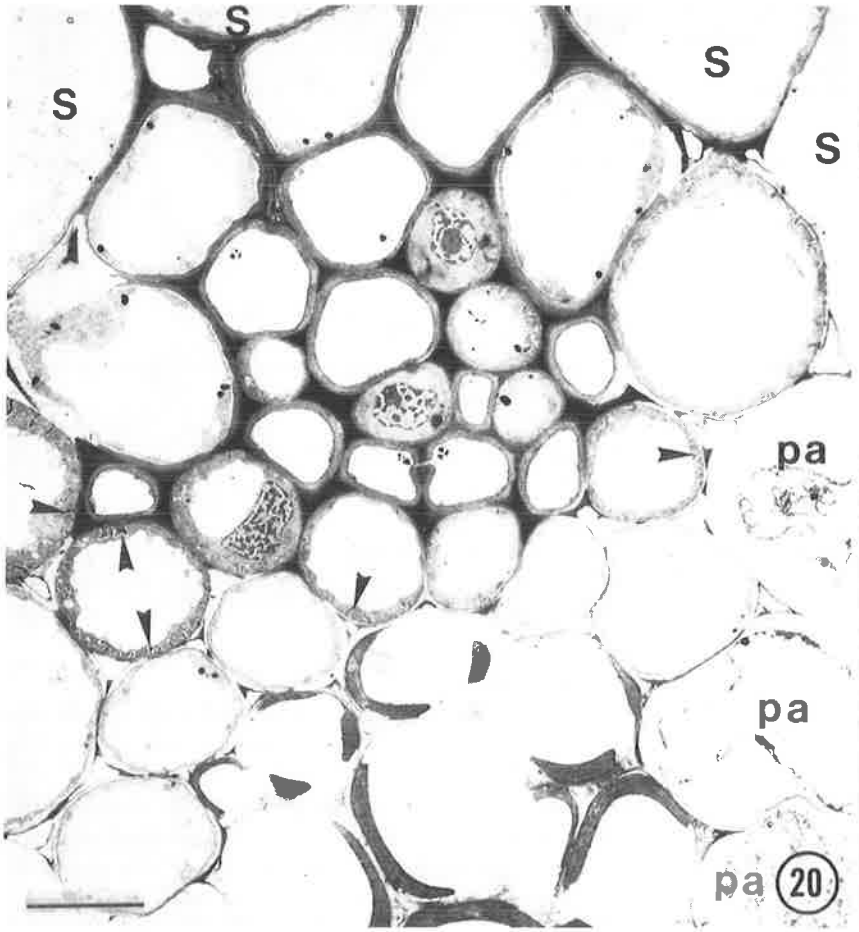
S
S
S
S
pa
pa
pa
20

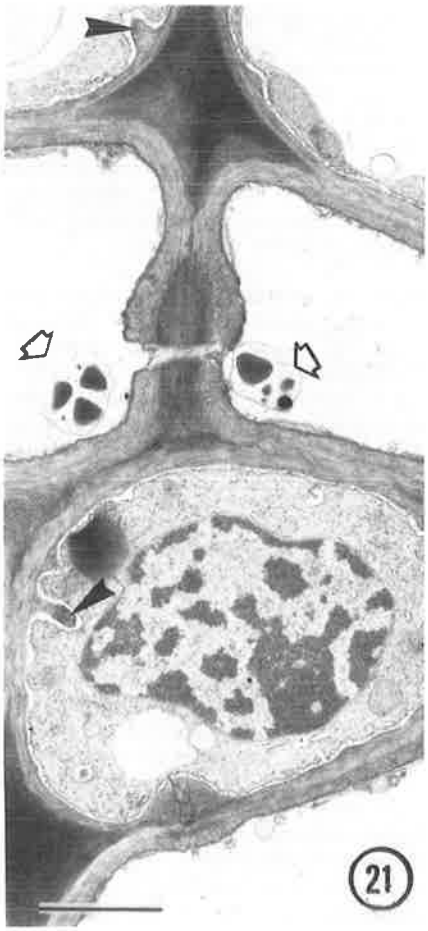
21

noplast. The only consistent difference noted between the two treatments was a varying degree of apparent plasmolysis in the mesophyll of the enzyme treated leaves. The most plasmolyzed cells were located nearest the front of cell lysis and surrounded by air spaces or lysed cells (Fig. 17). Little or no apparent plasmolysis was observed in more internally located cells (Figs. 18, 19). Within the vascular bundles of the enzyme-treated leaves, the plasmalemma of the companion cells was also separated from the cell wall (Figs. 20, 21), but this condition was also noted in the controls (Figs. 10, 11) and is assumed to be an artifact of tissue preparation.

*Kinetic studies.* Since leaf discs have been used extensively in the study of phloem loading, it was important to determine to what extent the kinetics of the intact leaf disc reflected accumulation into the phloem. Figure 22 illustrates the sucrose kinetic profiles of control and structurally manipulated tissue. These data indicate that *A. cepa* exhibited the same saturable plus linear response found previously (Maynard and Lucas 1982a) in the dicotyledon, *Beta vulgaris*, which has been used extensively in studies on phloem loading. To determine whether the two uptake components were spatially

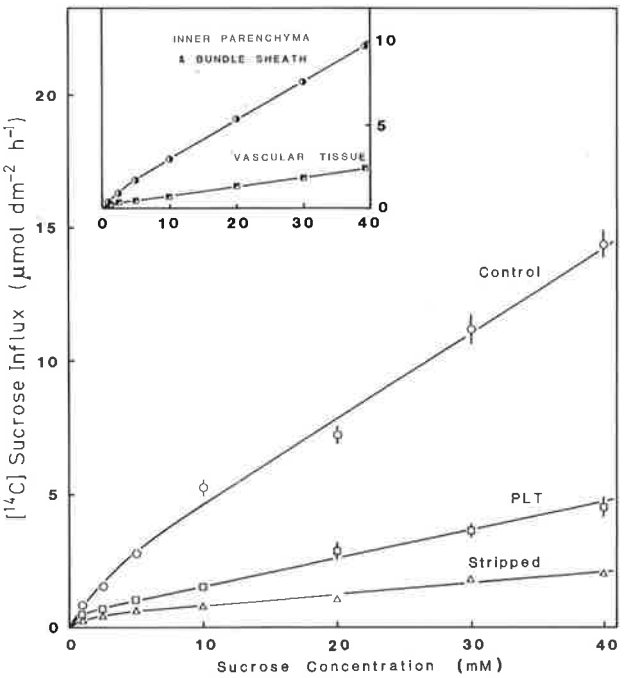


**Fig. 22.** Effect of pectolyase treatment (*PLT*) and stripping on sucrose influx into *Allium cepa* leaf discs. Cylindrical leaves were clamped at one end and filled with a solution containing 1 mg ml$^{-1}$ Pectolyase Y-23. After a 45-min digestion period the resulting leaf (*PLT*) was used for kinetic studies or manipulated further. The vascular bundles of the pectolyase-treated leaf were surgically removed with the use of forceps. A 30-min preincubation period in unlabeled sucrose was followed with a 30-min incubation in [$^{14}$C]sucrose solution. Each point represents the mean ±SE for three sets of six replicates. *Inset:* Sucrose uptake into inner parenchyma and bundle-sheath cells and vascular tissue. The inner parenchyma and bundle-sheath profile represents the area between the control (untreated) and pectolyase-treated (PLT) curves. The vascular-tissue profile represents the area between the PLT and the stripped curves

**Figs. 17–19.** Ultrastructure of ground parenchyma from pectolyase-treated leaves of *Allium cepa*. Bars = 1 µm. **Fig. 17.** The organization of the peripheral cytoplasm of an interveinal parenchyma cell surrounded mostly by air space and lysed cells. Note the degree of apparent plasmolysis which is characteristic of the cells in this location and the partially digested wall of a lysed cell (*arrows*) *V*, Vacuole. ×17500. **Fig. 18.** The cell periphery of a chlorenchyma cell one cell removed from the front of cell lysis. The plasmalemma (*arrows*) is intact, but has an irregular, dentate appearance indicating a slight degree of apparent plasmolysis. *V*, Vacuole; *A*, air space. ×24000. **Fig. 19.** Cell periphery of an interveinal parenchyma cell showing no apparent plasmolysis. Note the aggregation of mitochondria (*M*) and a microbody (*Mb*) in close proximity to the chloroplasts. *V*, Vacuole; *A*, air space. ×17500

**Figs. 20, 21.** Ultrastructure of vascular tissue from pectolyase-treated leaves of *Allium cepa*. **Fig. 20.** Section through a portion of a bundle slightly larger than the one shown in Fig. 10. Only the more internal phloem cells (*center*) appear unaffected by the enzyme treatment. The protoplasts of some of the peripheral vascular parenchyma cells (*pa*) are highly disorganized. Note that the wall ingrowths (*arrows*) of some cells appear to be more extensive than those shown in Fig. 10. ×1600; bar = 10 µm. **Fig. 21.** An enlargement of the central portion of Fig. 20 demonstrating a level of ultrastructural preservation equivalent to that of the control tissue (see Fig. 11). In both instances, the plasmalemmas of the parenchymatic elements are separated from the wall. Note the short wall ingrowths (*solid arrows*) and the sieve element plastids (*open arrows*) containing cuneate protein bodies. ×8000; bar = 2 µm

distinct or were a feature common to the plasmalemma of all cells (Maynard and Lucas 1982b), we examined the uptake curves derived from structurally simplified leaves. It should be pointed out that with regard to sucrose uptake, the curves of the inner parenchyma plus bundle sheath and the chlorenchyma have kinetic profiles that are similar to those of the vascular bundles (see Fig. 22, inset). Apparently, the combination of a saturable and linear component is not just a reflection of uptake into the vascular tissue, but may be a common feature of all cells within the leaf. It should be recognized that the various treatments which we have used to manipulate the tissue of the leaf may perturb membrane function and, consequently, sugar-related transport processes. However, if the experimental data represent an approximation of the in-vivo activity, then it can be seen that the

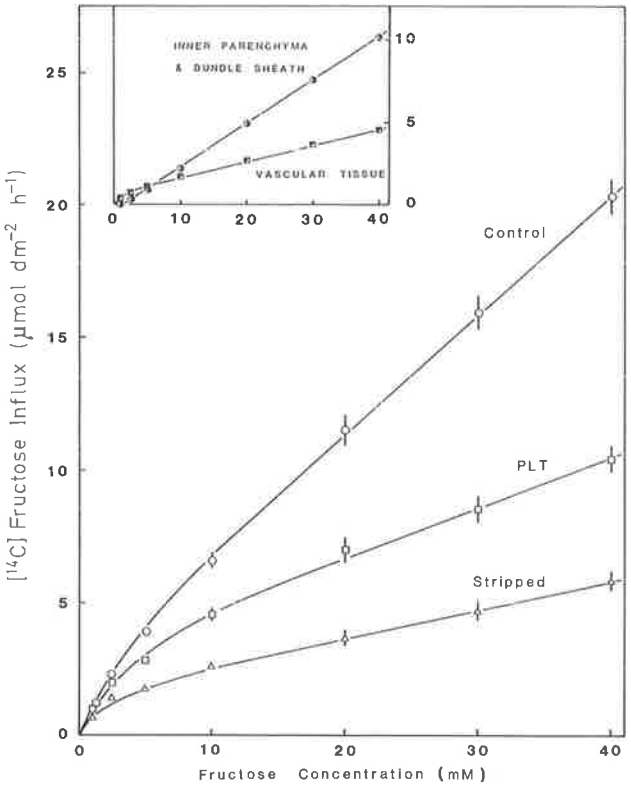


**Fig. 23.** Effect of pectolyase treatment and stripping on fructose influx into *Allium cepa* leaf discs. Experimental techniques were as described for Fig. 22. Each point represents the mean ±SE for four sets of six replicates. *Inset:* Fructose uptake into inner parenchyma and bundle-sheath cells and vascular tissue. The inner parenchyma and bundle sheath profile represents the area between the control (untreated) and pectolyase-treated (*PLT*) curves. The vascular-tissue profile represents the area between the *PLT* and the stripped curves

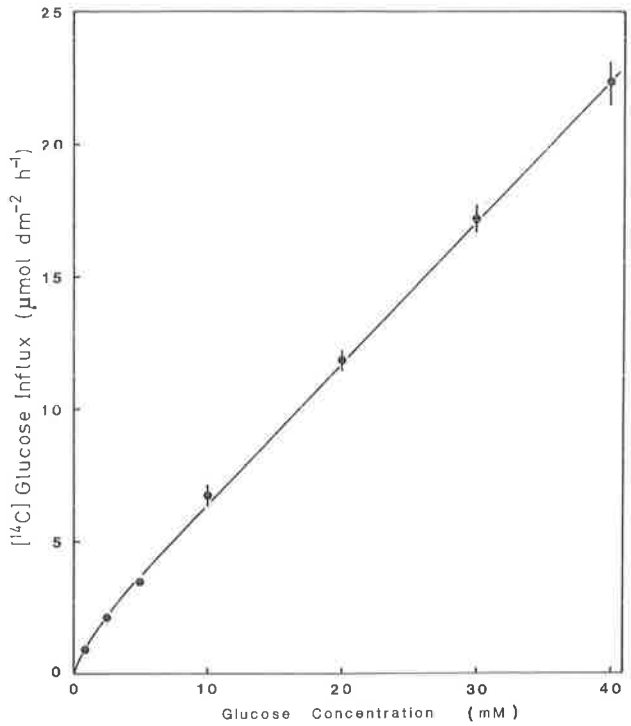


**Fig. 24.** Glucose influx into control (untreated) *Allium cepa* leaf discs. A 30-min preincubation period in unlabeled sucrose was followed with a 30-min incubation in [$^{14}$C]glucose solution. Each point represents the mean ±SE for two sets of six replicates

contribution of the vascular tissue to the total uptake of the intact leaf is small (Fig. 22).

Prior to the present study it was thought that *Allium* did not synthesize or store starch in the leaves, but rather fructan polymers (Bacon 1957; Darbyshire and Henry 1978; Darbyshire et al. 1979). Therefore, it seemed appropriate to compare the uptake kinetics of fructose with those obtained for sucrose. However, as mentioned earlier, the chloroplasts of the bundles-sheath cells contain inclusions, presumably starch, which are stained reddish brown with IKI and are oxidizable with periodate (see Figs. 6, 7). Inasmuch as *Allium* does contain large amounts of fructans it is still instructive to compare the kinetics of fructose influx with that of sucrose. Although the influx was slightly higher for fructose (see Figs. 22, 23), the general shape of the curves was similar. However, fructose influx into the inner parenchyma and bundle-sheath cells reflected the operation of only the linear component. The saturable system could well be present in this system, but the pectolyase treatment may have stimulated this system in the residual tissue such that, upon subtracting the two curves, it appears that the saturable component is missing. This interpretation is supported by the apparent increase in the $V_{max}$ observed following pectolyase treatment (Fig. 23).

Data for glucose uptake were also determined for comparative purposes (Fig. 24). The total uptake at the highest concentration tested (40 mM) was about the same as that for fructose. However, influx for glucose occurred mainly via the linear mechanism.

*Effect of anoxia on sucrose uptake.* In contrast to the work of Maynard and Lucas (1982b) on sugar beet, both the saturable and linear components of sucrose uptake in *Allium* leaf discs exhibited sensitivity to anoxia (Fig. 25). The effect was not limited to just the vascular tissue. The chlorenchyma and the inner parenchyma and bundle sheath were also inhibited (Figs. 25, 26). Comparison of apparent $V_{max}$ values obtained on control and anoxic

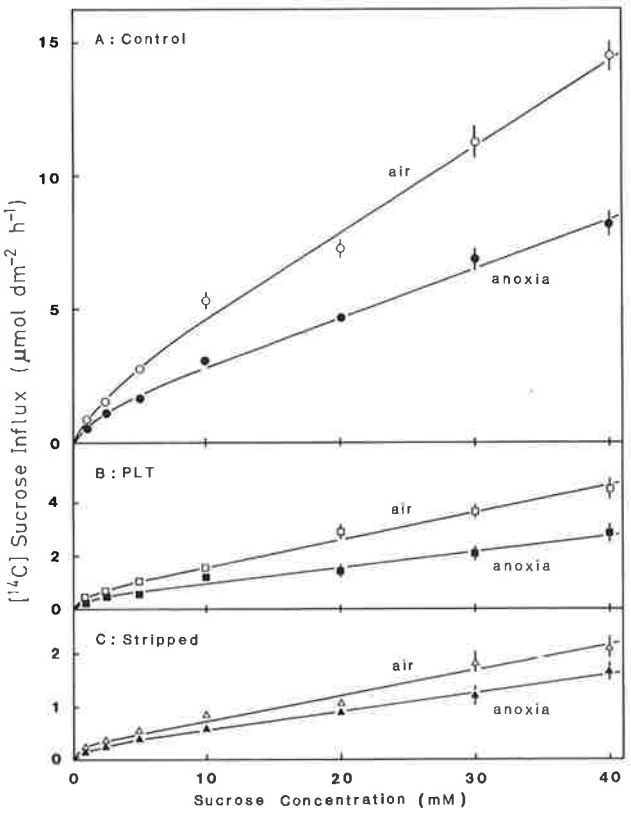


**Fig. 25.** Effect of anoxia on sucrose influx into control (untreated), pectolyase-treated (*PLT*) and stripped leaf discs of *Allium cepa*. Anoxia experiments were performed using a Glove Bag continually purged with nitrogen gas. Uptake studies were performed in the dark except when tissue manipulation required the use of a green safelight. A 30-min preincubation period in unlabeled sucrose was followed with a 30-min incubation in [$^{14}$C]sucrose solution. All solutions were bubbled through with nitrogen prior to use. Each point represents the mean ±SE for three sets of six replicates

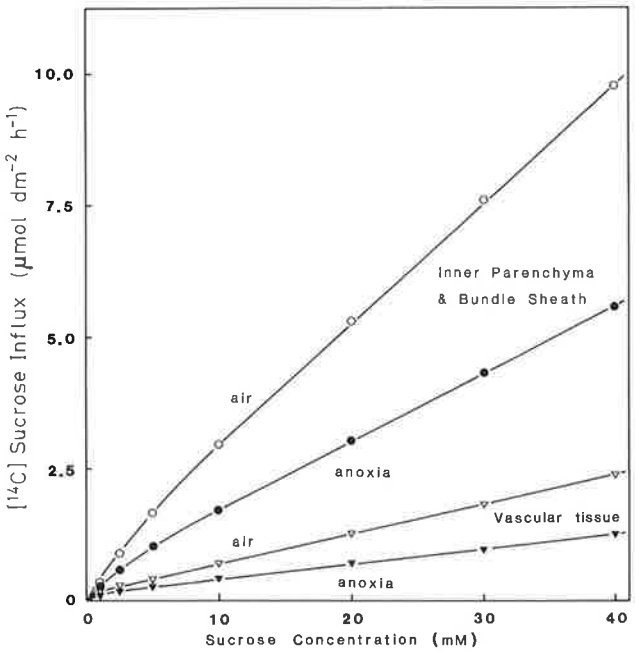


**Fig. 26.** Effect of anoxia on sucrose influx into inner parenchyma and bundle-sheath cells (○●) and vascular tissue (▽▼). The inner parenchyma and bundle sheath (air) profile represents the difference between the air-control (untreated) and air-pectolyase treated (*PLT*) curves while the inner parenchyma and bundle sheath (anoxia) profile represents the difference between the anoxia-control (untreated) and anoxia-pectolyase (*PLT*) curves in Fig. 25. Similarly, the vascular-tissue (air) curve represents the difference between the air-pectolyase (*PLT*) curve and the air-stripped curve while the vascular tissue (anoxia) curve represents the difference between the anoxia-pectolyase curve and the anoxia-stripped curve

tissues indicated that the chlorenchyma was the most sensitive (50% inhibition) and the vascular bundles the least sensitive (20%) (Table 1). Conversely, the linear component in the chlorenchyma was the least inhibited, showing only a 20% decrease while the inner parenchyma plus bundle sheath and the vascular bundles exhibited 43% and 50% inhibition, respectively.

The AMP, ADP and ATP levels for control, pectolyase-treated, and stripped leaf discs were also measured (Table 2). Low values for energy charge (E.C.), as defined by Atkinson and Walton (1967), for all nitrogen-treated tissues confirm the establishment of anoxic conditions in the kinetic experiments. Apparently, the control tissue (E.C. = 0.36) is more sensitive to anoxia than either the pectolyase-treated or stripped tissue (E.C. = 0.48 and 0.49, respectively). In addition to a lowering of the energy charge, there was a general loss of total adenylates during exposure to anaerobiosis. Other investigators have also reported a decrease in total adenine nucleotides with anoxia (Bomsel and Pradet 1967; Saglio et al. 1980). As with the E.C., the reduction in total adenylates was greater in the control tissue (60% decrease) than in the other two tissues (44% in both tissues).

It was not possible to determine the levels of adenine nucleotides in the inner parenchyma plus bundle-sheath cells or the vascular tissue as these values would be determined by subtraction. Upon subtraction, values for some of the nucleotides would be negative while others would be close to zero. Apparently, there is some interaction between these tissues and the rest of the leaf, such that their nucleotide regulation under anoxia is altered.

## Discussion

As pointed out in the Introduction, the *Allium* leaf can be easily manipulated using biochemical and

**Table 1.** Kinetic constants for sugar influx into *Allium cepa* leaf discs. Apparent $V_{max}$ refers to the Michaelis-Menten constant, and $k$ is the first-order rate coefficient

| Treatment | Apparent $V_{max}$ ($\mu$mol dm$^{-2}$ h$^{-1}$) | $k$ ($\mu$mol dm$^{-2}$h$^{-1}$mM$^{-1}$) |
|---|---|---|
| *Sucrose influx* | | |
| Control | | |
| Air | 1.40 | 0.33 |
| Anoxia | 0.78 | 0.19 |
| Pectolyase-treated | | |
| Air | 0.63 | 0.10 |
| Anoxia | 0.35 | 0.06 |
| Stripped | | |
| Air | 0.20 | 0.05 |
| Anoxia | 0.10 | 0.04 |
| Inner parenchyma + bundle sheath | | |
| Air | 0.56 | 0.23 |
| Anoxia | 0.36 | 0.13 |
| Vascular bundles | | |
| Air | 0.15 | 0.06 |
| Anoxia | 0.12 | 0.03 |
| *Fructose influx* (air only) | | |
| Control | 1.85 | 0.46 |
| Pectolyase-treated | 2.86 | 0.19 |
| Stripped | 1.36 | 0.11 |
| Inner parenchyma + bundle sheath | N.D.[a] | 0.26 |
| Vascular bundles | 0.96 | 0.09 |

[a] Not detected. Fructose influx into the inner parenchyma + bundle-sheath cells contained only the linear component

mechanical techniques. Light micrographs (see Figs. 13, 14) indicated that following such manipulation, the structural integrity of remaining leaf tissues was intact. A more detailed examination using transmission electron microscopy (see Figs. 18, 19) showed the morphology of the organelles and the condition of the plasmalemma and tonoplast to be similar to those in untreated tissue. There was, however, some plasmolysis of chlorenchyma cells nearest to the front of cell lysis. By performing uptake studies on tissues that were at different degrees of manipulation, we were able, by various subtractions, to deduce the contribution that each tissue made to the total uptake of exogenous sucrose or fructose. With the exception of fructose influx into the inner parenchyma and bundle sheath, these kinetic curves may be interpreted by using the same $v = V_{max}\ S/(S+K_m)+kS$ equation as in the dicotyledon, *Beta vulgaris*. The inner parenchyma and bundle sheath accounts for approx. 70% of the total uptake, whereas the contribution of the vascular tissue is quite small (approx. 15%). These findings provide further support for the concept, developed by Maynard and Lucas (1982b), of a general transport mechanism operating to retrieve solutes from the free space.

Anoxia caused an interesting perturbation of sugar influx. In contrast to the findings of Maynard and Lucas (1982b), anoxia inhibited both the saturable and linear components of sucrose uptake in onion tissue. These findings may represent a physiological difference in the operation of the saturable component between *A. cepa* and *B. vulgaris*. Alternatively, the energy source for the operation of the saturable component in *Allium* may differ from that in *Beta*. In order to determine the manner of anoxic inhibition of sucrose influx we analyzed the levels of AMP, ADP and ATP in the leaf discs (Table 2). Large changes in the E.C. indicate that decreases in the ATP content are affecting sucrose uptake. Presumably, decreased levels of ATP would slow the operation of the putative $H^+$-translocating ATPase in the plasmalemma. However, the levels of ATP remaining in the anoxic tissue might be sufficient to main-

**Table 2.** Effect of anoxia on adenine-nucleotide content in *Allum cepa* leaf discs

| Treatment | ATP[a] | ADP | AMP | Energy | | ADP/ATP |
|---|---|---|---|---|---|---|
| | | | | Total | Charge | |
| Control | | | | | | |
| Air | 475.9 ± 2.0 | 155.4 ± 10.1 | 59.1 ± 5.2 | 690.4 | 0.80 | 0.33 |
| Anoxia | 63.6 ± 2.7 | 76.2 ± 3.3 | 139.8 ± 12.2 | 279.6 | 0.36 | 1.20 |
| Pectolyase-treated | | | | | | |
| Air | 504.3 ± 19.1 | 189.7 ± 2.2 | 61.3 ± 6.6 | 755.3 | 0.79 | 0.38 |
| Anoxia | 133.7 ± 2.2 | 126.6 ± 6.1 | 146.6 ± 17.2 | 406.9 | 0.48 | 0.95 |
| Stripped | | | | | | |
| Air | 575.0 ± 1.0 | 145.9 ± 11.9 | 45.0 ± 4.0 | 765.9 | 0.85 | 0.25 |
| Anoxia | 137.8 ± 3.2 | 145.3 ± 2.4 | 148.5 ± 3.2 | 431.6 | 0.49 | 1.05 |

[a] All nucleotide values are expressed as pmol mg DW$^{-1}$

tain the operation of the ATPase but the system may have become sensitive to ADP, as the ADP/ATP ratio has increased under anoxia. Other researchers have previously postulated an inhibitory action by ADP on the ATPase (Smith and Walker 1981; Mimura et al. 1982; Lucas et al. 1984). Lucas and co-workers (1984), for example, found that the electrogenic component of the membrane potential of *Chara* was completely inhibited in the presence of ATP levels which were well above the postulated $K_m$ of the ATPase.

One noteworthy observation was the larger decrease in the E.C. of the control tissue under anoxia as compared with the pectolyase-treated and stripped tissue. The anatomical difference between the control and pectolyase-treated leaf is the presence of the inner parenchyma and bundle-sheath cells (including some vascular parenchyma) in the control leaf. The metabolism within these cells may be different from the remaining tissue.

Heretofore, as indicated before it has been believed that onion does not store starch in the leaves, but rather soluble fructan polymers. The appearence of inclusions within the stroma of the bundle-sheath chloroplasts is important, as these inclusions are reserve carbohydrate and they may well be targeted for later export. In addition, the large, highly vacuolated parenchyma next to the lacuna (see Fig. 1) are important structurally to the leaf since, when they are removed, the leaf loses a great deal of its mechanical strength. These cells may function to give structural support to the leaf through a turgor-related system. The large vacuoles of these cells may use sugars of osmoticum. This could account for the capacity of these cells to take up large quantities of exogenous sucrose or fructose. Geiger et al. (1983) demonstrated that in sugar beet there exists a pool of sucrose isolated from, though exchangeable with sucrose that is available for export. There may be analogous pools in the onion leaf. If so, the reserve carbohydrates in the bundle-sheath chloroplasts and in the large, vacuolated parenchyma cells may be the main sites of these pools. In further work, it will be attempted to elucidate the interrelationship between these putative carbohydrate pools and translocation.

The pathway for phloem loading, whether apoplastic, symplastic or a combination of both, is still unresolved. Much of the earlier work on the anatomy and physiology of the phloem provides a basis for defining phloem loading as "the process by which the major translocated substances are selectively and actively delivered to the sieve tubes in the source region" (Geiger 1975). However, as evidenced by our uptake experiments, many tissues are able to retrieve exogenous sugars. Therefore, the *in-vivo kinetics of phloem loading*, per se, will be extremely difficult to establish because this would require the specific inhibition of all sugar-transport mechanisms operating into non-phloem cells. Obviously, this cannot be done at the present time and may even be impossible to achieve. In this light, the present definition of the term phloem loading is of little value with respect to present-day physiological studies. Therefore, to be certain that we understand this serious limitation, the term should be modified to a broader perspective of a complex phenomenon of assimilate movement from the mesophyll cells into the sieve-element – companion-cell complex. This broader concept of phloem loading would not be limited to just the movement of the translocated species into the sieve-element – companion-cell complex but would integrate transport processes at the plasmalemma and tonoplast of a number of cell types. Furthermore, this definition would include the complex intracellular regulation and partitioning of assimilates. Thus, this proposed definition more closely matches that which is experimentally achievable.

This work was supported by National Science Foundation grant PCM 83-15408. One of us (C.W.) gratefully acknowledges the receipt of a Graduate Opportunity Fellowship and a Graduate Research Award from the Graduate Division, University of California, Davis.

## References

Atkinson, D.E., Walton, G.M. (1967) Adenosine triphosphate conversion in metabolic regulation: Rat liver citrate cleavage enzyme. J. Biol. Chem. **242**, 3239–3241

Avigad, G., Damle, S. (1972) Fluorometric assay of adenine and its derivatives. Anal. Biochem. **50**, 321–323

Bacon, J.S.D. (1957) The water-soluble carbohydrates of the onion, *Allium cepa* L. (Abstr.) Biochem. J. **67**, 5P

Barrio, J.R., Secrist., J.A. III, Leonard, N.J. (1972) Fluorescent adenosine and cytidine derivatives. Biochem. Biophys. Res. Commun. **46**, 597–604

Bomsel, J.L., Pradet, A. (1967) Étude des adénosine-5′-mono-, di- et tri-phosphates dans les tissus végétaux. II. Évolution in vivo de l'ATP, l'ADP, et l'AMP dans les feuilles de Blé en fonction de différentes conditions du milieu. Physiol. Vég. **5**, 223–236

Darbyshire, B., Henry, R.J. (1978) The distribution of fructans in onions. New Phytol. **81**, 29–34

Darbyshire, B., Henry, R.J., Melhuish, F.M., Hewett, R.K. (1979) Diurnal variations in non-structural carbohydrates, leaf extension, and leaf cavity carbon dioxide concentrations in *Allium cepa* L. J. Exp. Bot. **30**, 109–118

Delrot, S., Bonnemain, J.L. (1981) Involvement of protons as a substate for the sucrose carrier during phloem loading in *Vicia faba* leaves. Plant Physiol. **67**, 560–564

Delrot, S., Despeghel, J.P., Bonnemain, J.L. (1980) Phloem

loading in *Vica faba* leaves: effect of N-ethylmaleimide and parachloromercuribenzenesulfonic acid on $H^+$ extrusion, $K^+$ and sucrose uptake. Planta **149**, 144–148
Fellows, R.J., Geiger, D.R. (1974) Structural and physiological changes in sugar beet leaves during sink to source conversion. Plant Physiol. **54**, 877–885
Fondy, B.R., Geiger, D.R. (1977) Sugar selectivity and other characteristics of phloem loading in *Beta vulgaris* L. Plant Physiol. **59**, 953–960
Geiger, D.R. (1975) Phloem loading. In: Encyclopedia of plant physiology, N.S., vol. 1: Transport in plants I, pp. 395–431, Zimmermann, M.H., Milburn, J.A., eds. Springer, Berlin Heidelberg New York
Geiger, D.R. (1976) Phloem loading in source leaves. In: Transport and transfer processes in plants, pp. 167–215, Wardlaw, I.F., Passioura, J.B., eds. Academic Press, New York San Francisco London
Geiger, D.R., Fondy, B.R. (1980) Response of phloem loading and export to rapid changes in sink demand. Ber. Dtsch. Bot. Ges. **93**, 177–186
Geiger, D.R., Ploeger, B.J., Fox, T.C., Fondy, B.R. (1983) Sources of sucrose translocated from illuminated sugar beet source leaves. Plant Physiol. **72**, 964–970
Giaquinta, R. (1976) Evidence for phloem loading from the apoplast: chemical modification of membrane sulfhydryl groups. Plant Physiol. **57**, 872–875
Giaquinta, R. (1977) Phloem loading of sucrose: pH dependence and selectivity. Plant Physiol. **59**, 750–755
Giaquinta, R. (1980) Mechanism and control of phloem loading of sucrose. Ber. Dtsch. Bot. Ges. **93**, 187–201
Kimmich, G.A., Randles, J., Brand, J.S. (1975) Assay of picomole amounts of ATP, ADP and AMP using the luciferase enzyme system. Anal. Biochem. **69**, 187–206
Kochethov, N.K., Shibaev, V.N., Kost, A.A. (1971) New reaction of adenine and cytosine derivatives, potentially useful for nucleic acids modification. Tetrahedron Lett., 1993–1996
Komor, E., Rotter, M., Tanner, W. (1977) A proton-cotransport system in a higher plant: sucrose transport in *Ricinus cummunis*. Plant Sci. Lett. **9**, 153–162
Kondo, T., Nakashima, H. (1979) Content of adenosine phosphate compounds in a long-day duckweed, *Lemna gibba* G3, under different light and nutritional conditions. Physiol. Plant. **45**, 357–362
Lichtner, F.T., Spanswick, R.M. (1981) Sucrose uptake by developing soybean cotyledons. Plant Physiol. **68**, 693–698
Lucas, W.J., Wilson, C., Wright, J.P. (1984) Perturbation of *Chara* plasmalemma transport function by 2[4(2′,4′-dichlorophenoxy)phenoxy]propionic acid. Plant Physiol. **74**, 61–66
Maynard, J.W., Lucas, W.J. (1982a) A reanalysis of the two-component phloem loading system in *Beta vulgaris*. Plant Physiol. **69**, 734–739
Maynard, J.W., Lucas, W.J. (1982b) Sucrose and glucose uptake into *Beta vulgaris* leaf tissue: a case for general (apoplastic) retrieval systems. Plant Physiol. **70**, 1436–1443
Mimura, T., Shimmen, T., Tazawa, M. (1982) Respiration-dependent membrane hyperpolarization in tonoplast-free cells of *Nitella axilliformis*. Plant Cell Physiol. **23**, 1419–1425
Preston, M.R. (1983) Determination of adenine, adenosine and related nucleotides at the low picomole level by reversed-phase high-performance liquid chromatography with fluorescence detection. J. Chromatogr. **275**, 178–182
Reynolds, E.S. (1963) The use of lead citrate at high pH as an electron opaque stain in electron microscopy. J. Cell Biol. **17**, 208–212
Roland, J.C. (1978) General preparation and staining to thin sections. In: Electron microscopy and cytochemistry of plant cells, pp. 1–62, Hall, J.L., ed. Elsevier/North-Holland Biomedical Press, Amsterdam
Saglio, P.H., Philippe, R., Pradet, A. (1980) Metabolic activity and energy charge of excised maize root tips under anoxia: control by soluble sugars. Plant Physiol. **66**, 1053–1057
Secrist, J.A., III, Barrio, J.R., Leonard, N.J. (1972a) A fluorescent modification of adenosine triphosphate with activity in enzyme systems: 1,$N^6$-ethenoadenosine triphosphate. Science **175**, 646–647
Secrist, J.A., III, Barrio, J.R., Leonard, N.J., Weber, G. (1972b) Fluorescent modification of adenosine-containing coenzymes. Biological activities and spectroscopic properties. Biochemistry **11**, 3499–3506
Smith, P.T., Walker, N.A. (1981) Studies on the perfused plasmalemma of *Chara corallina*. I. Current-voltage curves: ATP and potassium dependence. J. Membr. Biol. **60**, 223–236
Sovonick, S.A., Geiger, D.R., Fellows, R.J. (1974) Evidence for active phloem loading in the minor veins of sugar beet. Plant Physiol. **54**, 886–891
Spurr, A.R. (1969) A low-viscosity epoxy resin embedding medium for electron microscopy. J. Ultrastruct. Res. **26**, 31–43
Yoshioka, M., Tamura, Z. (1976) Fluorimetric determination of adenine and adenosine and its nucleotides by high-performance liquid chromatography. J. Chromatogr. **123**, 220–224

Received 10 July; accepted 25 October 1984

# Phloem-Loading: A Metaphysical Phenomenon?

WILLIAM J. LUCAS

The term "phloem loading" was first used by Eschrich (5) to replace the then current term "vein loading." Since that time, numerous physiological and anatomical studies have been conducted with an aim to elucidating the mechanism and pathway of sugar (and amino acid) movement between the sites of production in the mesophyll cells and the sites of entry (loading) into the sieve elements. For reviews of this rather extensive literature, the reader is referred to Wardlaw (32), Geiger (11), Evert (6), Cronshaw (1), and Giaquinta (17). Our present treatment of phloem loading will not be encyclopedic in nature, but rather we will focus our attention on an evaluation of the experimental data relating to the specific point of the membrane transport mechanism involved in phloem loading.

Autoradiography still is one of the most important techniques used in the study of phloem loading/translocation. Application of either $^{14}CO_2$ or [$^{14}$C]-labeled sugars to mature leaf tissue indicated that the movement of radiolabeled compounds to the phloem was selective, and that the sugar, normally translocated by a particular plant, accumulated in the minor veins (8, 11). The combination of the autoradiographic image of the labeled minor veins (obtained when tissue was exposed to exogenous [$^{14}$C]-sucrose) and the demonstration that [$^{14}$C]-labeled compounds (mainly sucrose) produced by $^{14}CO_2$-mediated photosynthesis could be trapped and removed from the leaf by applying nonradioactively labeled sucrose (13), provided the basis for the hypothesis that an apoplastic stem was involved in phloem loading.

This apoplastic-step hypothesis had considerable influence on the interpretation of later work. Sovonick et al. (30) and Giaquinta (14) investigated the relationship between sugar uptake into leaf discs and the intact leaf with respect to phloem translocation. On the basis of their studies, they concluded that exogenous sucrose uptake into leaf discs reflects loading into the phloem and could, therefore, be used to study the specific mechanism involved (see also 2-4, 15, 16). Upon reflection, it is quite interesting that this concept was rarely challenged, since there were already at least two reports in the literature which showed that uptake of exogenous sucrose occurred into both the cells of the mesophyll and vascular bundles (8, 12). However, although most workers recognized that the mesophyll would act as a barrier to the penetration of exogenously supplied compounds to the phloem, it seemed that by the end of the 1970's, the general view was that phloem loading (in all tissues) could be studied via the application of [$^{14}$C]-labeled sucrose (See Fig. 1).

It was at this stage and time that our laboratory started to work on phloem physiology. Along with others working on "phloem loading," we accepted the concept of an apoplastic step and, with some slight reservations, the notion that exogenous sucrose could be used to investigate the kinetics of phloem loading, per se. In earlier studies, the kinetics of sucrose uptake were interpreted in terms of two saturable systems, both functioning to deliver sucrose into the phloem. Our initial studies, conducted on sugar beet leaf discs, simply showed that exogenous sucrose uptake occurred via two different transport systems, a saturable component displaying Michaelis-Menten kinetics and a linear component obeying first-order kinetics (26; see also 14, 21, 24). We now believe that we were incorrect in interpreting these kinetic results in terms of two transport processes operating in parallel across only the sieve element-companion cell (se-cc) complex plasma membrane (27).

## RETRIEVAL OF EXOGENOUS SUGARS

It was the sugar uptake studies of Komor et al. (23), conducted on the cotyledons of germinating Ricinus seedlings, that were instrumental in causing us to re-evaluate the interpretation of our kinetic data. In

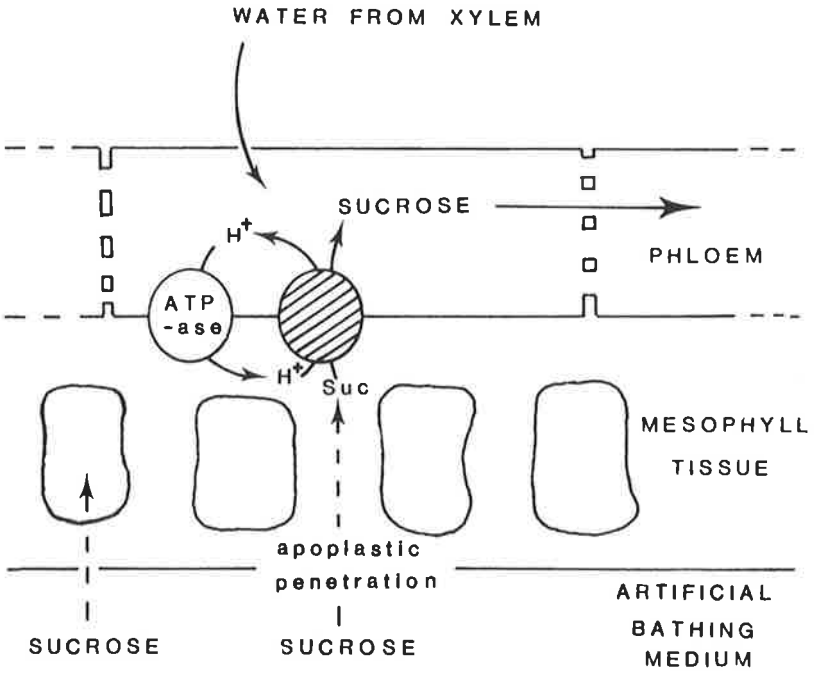


FIG 1. Schematic representation of the putative sucrose-$H^+$ cotransport system that has been proposed to function in phloem loading. The model implies that apoplastic or exogenously supplied [$^{14}C$] sucrose enters the phloem "preferentially." The broken lines depict diffusion of sucrose through the apoplast and also into the mesophyll tissue. Redrawn after Komor *et al.* (23).

their opinion, their linear component represented simple diffusion into cells of the mesophyll (see Fig. 1). However, they also claimed that "though it cannot be excluded that other tissues also can accumulate sucrose, phloem cells of cotyledons do it preferentially." But, in our sugar beet studies, the linear component made a significant contribution to the accumulation of sucrose by the leaf; at 25 mM exogenous sucrose it accounted for 43% of the uptake. Thus, either the linear component was not passive (since the sucrose concentration in the se-cc would be too high), or the linear component was occurring across the plasmalemma of the mesophyll cells, and, therefore, uptake could not be equated with phloem loading.

To investigate this question of location of the two transport components, we utilized leaf discs and petiole segments of sugar beet. Similarly-shaped kinetic curves were obtained for influx of sucrose, glucose, and 3-O-methyl glucose by leaf discs, whole petiole slices, petiole segments containing parenchyma tissue (pith) only, and petiole segments containing vascular bundles, although the tissues took up the various sugars via different proportions of the saturable versus linear uptake (see Fig. 2). These results were more consistent with the findings of Geiger (12) and Fondy and Geiger (8). They used microdensitometric techniques to examine autoradiographic plates, prepared from tissue preincubated for 30 min in exogenously supplied 10 mM [$^{14}$C] sucrose, and found that the majority of the label (60%) was in the mesophyll tissue.

The kinetic curve for 3-O-methyl glucose influx into sugar beet leaf discs was also found to be identical in form to that obtained for sucrose (see 27, Fig. 1); i.e. uptake appeared to result from the operation of a saturable and a linear transport component. This similarity was important because the uptake of 3-O-methyl glucose is thought to be confined to the metabolic space of the mesophyll cells (8). A similar situation was found in the petiole experiments. The petiolar vascular bundles are embedded in a parenchymatous tissue, not a chlorenchymatous mesophyll, yet sucrose uptake into vascular bundle segments still exhibited both a saturable and a linear component (see Fig. 2). Of equal importance was the finding that sucrose uptake into petiole "pith" segments (free of phloem tissues) exhibited the same kinetics as found when we used the

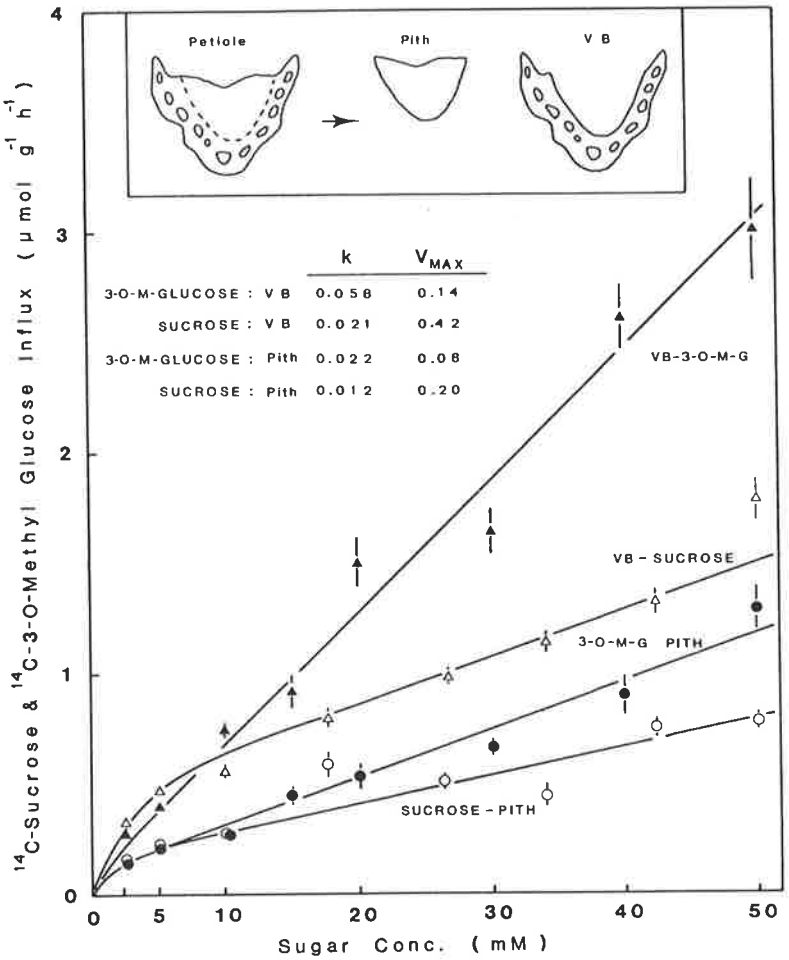


FIG. 2. Concentration dependence of sugar accumulation by dissected Beta vulgaris petiole segments. Points represent the mean ± SE for seven replicates. Uptake of 3-O-methyl glucose by vascular bundle-containing (VB) segments (▲); sucrose uptake by VB segments (Δ); 3-O-methyl glucose uptake by "pith" parenchyma segments (●); sucrose uptake by pith segments (O). The kinetic parameters for the saturable and linear components of the various substrates have been included; $V_{max}$ has the units µmol $g^{-1}$ $h^{-1}$ and k (first order rate coefficient) has units of µmol $g^{-1}$ $h^{-1}$ $mM^{-1}$ sugar. Data from Maynard and Lucas (27).

segments containing the vascular tissue. We found the same trends for 3-O-methyl glucose uptake into petiole vascular bundle--and pith--segments.

From these studies we concluded that the presence of a saturable and a linear component of transport must be a ubiquitous feature of the plasma membrane of a rather wide variety of cell types within leaf tissues. Obviously, if this were the case, it would complicate the interpretation of kinetic data with respect to the importance, etc., of a particular tissue (e.g. the se-cc complex) in terms of its contribution to the total uptake into the leaf. This, we contended, would make it very difficult to equate uptake of exogenously applied [$^{14}$C] sucrose to the process of phloem loading.

To resolve the question of whether all cell types of the leaf do actually possess the ability to transport exogenously applied sugars via both the saturable and linear systems, we sought a leaf from which the various tissues could be separated. We used mature leaves of Allium cepa, because it does not have an inner cuticle or epidermis, but rather it develops a lacuna; its interior tissues were, therefore, highly accessible both to exogenous solutes and cell wall digesting enzymes which were used to help to selectively remove the various cell types (Fig. 3). By filling the interior of an onion leaf with a solution of 1 mg ml$^{-1}$ Pectolyase Y-23, we could digest away the cell walls of the large parenchyma and interveinal parenchyma cells; a 45-min digestion period was usually required. The resulting leaf, termed "pectolyase-treated" (see Fig. 3B), was then either used for [$^{14}$C] sucrose, or fructose kinetic studies (see Figs. 4 and 5), or further manipulated. Forceps were used to remove the vascular bundles, and the resulting leaf, termed "stripped" (see Fig. 3C), was also used in uptake experiments (33).

Figure 4 illustrates the results that we obtained for [$^{14}$C] sucrose influx into control and structurally manipulated leaf tissue. Clearly the curves of the inner parenchyma plus bundle sheath and the chlorenchyma have kinetic profiles that are similar to those of the vascular bundles (see inset of Fig. 4). Also, the inner parenchyma and bundle-sheath tissue accounted for ca. 70% of the total uptake, whereas the contribution of the vascular tissue was quite small (ca. 15%). Of equal importance, all the

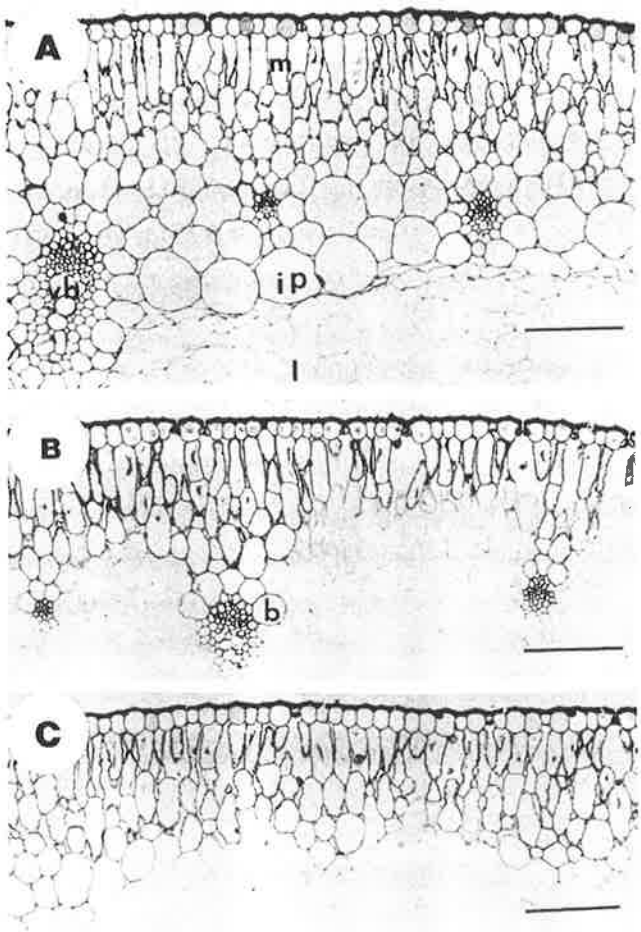


FIG. 3. Light micrographs of transverse sections taken through leaves of Allium cepa after they were subjected to various treatments. Control leaf (A) illustrates general arrangement of mesophyll (m), vascular bundles (vb), large inner parenchyma cells (ip), and central lacuna (l). Bar = 200 µm. In the pectolyase-treated tissue (B), the large inner parenchyma tissue is destroyed, as well as much of the bundle sheath (b). Bar = 200 µm. Forceps were used to remove the vascular bundles from pectolyase-treated tissue which then gave a leaf that was reduced to mesophyll cells only (c). Bar = 200 µm.

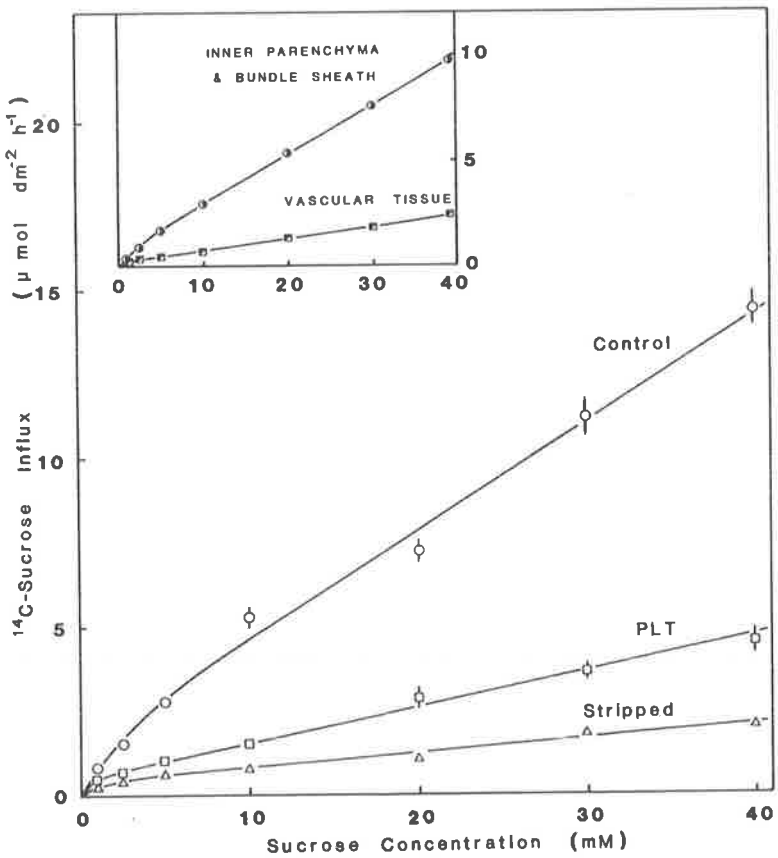


FIG. 4. Effect of pectolyase treatment (PLT) and stripping on sucrose influx into Allium cepa leaf discs. Inset: Sucrose uptake into inner parenchyma and bundle sheath cells and the vascular tissue. Data from Wilson et al. (33).

kinetic curves could be resolved into the contribution of a saturable, plus a linear (first order) component.

Similar results were obtained when we used [$^{14}$C] fructose, with the exception that influx into the inner parenchyma and bundle-sheath tissue contained only the linear component (see Fig. 5).

These findings provided strong support for our hypothesis that all cell types of the leaf have the ability to take up exogenously supplied sugars. We would suggest that, since sugars appear to leak out of mesophyll tissue (8), plant cells have developed a means of recovering this carbohydrate. Thus, we feel that the kinetics that we measure by applying exogenous sugars reflect the kinetics of sugar retrieval (27). In a more narrow sense, this concept had already been introduced by several workers; e.g. Fondy and Geiger (8) suggested that "the mesophyll tissue may act as a collecting surface, reclaiming sucrose and hexoses which leak from photosynthesizing cells." Other proposals for retrieval mechanisms have also been propounded for phloem parenchyma cells (7, 10, 18, 28).

If the mesophyll plasmalemma allows sugars to leak out, then we can see no reason why sucrose would not leak out of the se-cc complex. Indeed, since the sucrose concentration is high along the entire length of the translocation pathway, sucrose leakage may be a general phenomenon. Thus, at present we contend that it is impossible to distinguish between the operation of a transport process that loads sucrose into the phloem and the functioning of a retrieval mechanism; both processes would result in radioactivity entering the se-cc complex. However, the corollary to this statement is also true, in that the mechanism of phloem loading may represent a spatially-specialized aspect of an otherwise general retrieval process. By this we mean that in the minor veins, or in any location where loading is occurring, the phloem parenchyma cells immediately adjacent to the se-cc complex may have their sugar retrieval mechanism(s) repressed, while the se-cc complex may have an enhanced capacity.

Irrespective of the actual mechanism by which sugar is "loaded" into the se-cc complex of the phloem, the kinetic experiments conducted in our laboratory have shown that the *in vivo* kinetics of phloem loading, *per se*, will be extremely difficult to establish. To obtain these kinetic profiles on intact leaf tissue would require the specific inhibition of

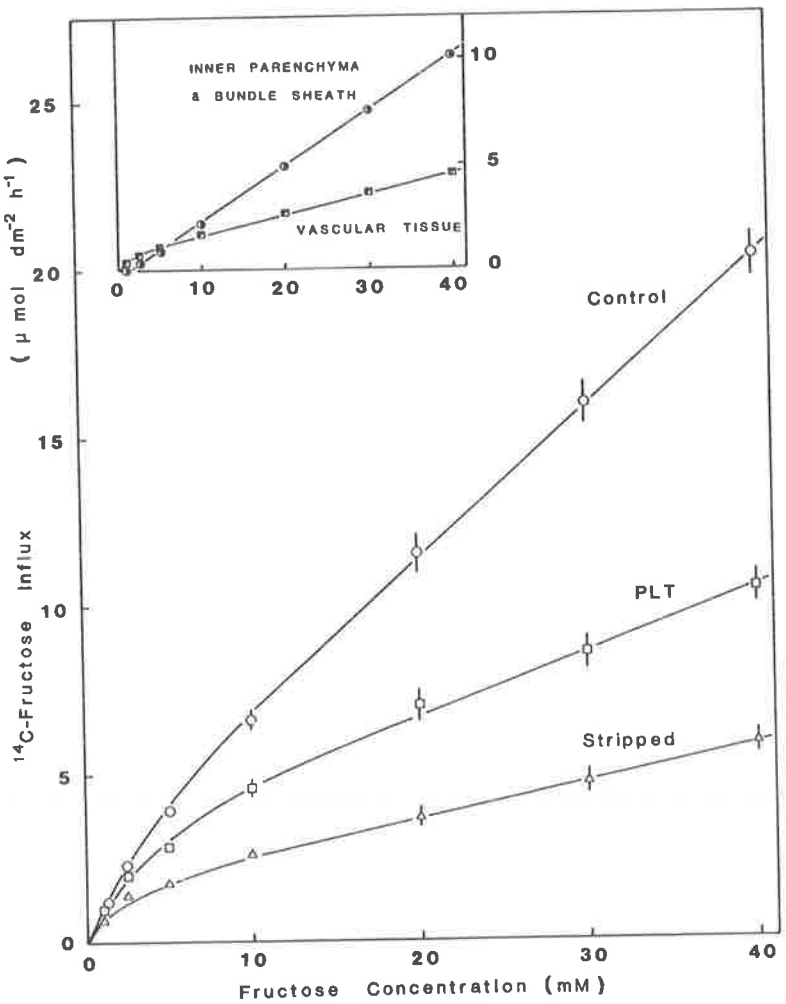


FIG. 5. Effect of pectolyase treatment (PLT) and stripping on fructose influx into Allium cepa leaf discs. Inset: Fructose uptake into inner parenchyma and bundle-sheath cells and the vascular tissue. Data from Wilson et al. (33).

all sugar retrieval (transport) systems operating into nonphloem cells. Obviously, this cannot be done at the present time and may even be impossible to achieve.

## SUCROSE-$H^+$ CO-TRANSPORT INTO THE SE-CC COMPLEX: A RE-EVALUATION

Numerous works have been published which provide circumstantial evidence in support of a sucrose-$H^+$ co-transport system operating in higher plant tissues (see 17 and 29, and references cited therein). Giaquinta (17) recently evaluated the experimental evidence pertaining to the operation of a sucrose-$H^+$ co-transport mechanism within the phloem se-cc complex plasma membrane. He states that "the most convincing evidence for a sucrose/proton co-transport mechanism of phloem loading in photosynthesizing leaves comes from Heyser's studies on corn leaves (19)." Since we now considered it impossible to elucidate the specific kinetics of the actual transport process(es) responsible for loading of sucrose into the se-cc complex, we re-evaluated some of the experimental evidence offered in support of the sucrose-$H^+$ co-transport hypothesis. In this re-evaluation, we do not seek to question the experimental data, *per se*, nor the underlying concepts, etc., of a $\Delta\mu_{H}^{-}+$-driven system, but rather the basis for ascribing the location of the co-transport system to the se-cc complex plasma membrane.

Heyser used excised leaf strips of *Zea mays*, and he mounted these strips in an ingenious device which allowed him to perfuse artificial solutions through the vessels of the xylem (see Fig. 1 of ref. 19). The pH value of the xylem perfusate could be measured as it exited the leaf strip. He found that upon introducing 25 mM sucrose, the pH of the xylem solution underwent a pronounced (0.7 pH units) alkalinization, which was transient in nature; the peak of the response was reached ca. 10-min after the sucrose was introduced. Other sugars like glucose, fructose, raffinose, etc., did not elicit a pH response. This sucrose-induced pH response is certainly consistent with the operation of a sucrose-$H^+$ co-transport system (31), but Heyser's results do not reveal the actual location of this transport process.

This question of location was addressed by Fritz *et al.* (10), who used exactly the same experimental material and system as used origin-

ally by Heyser. By using the Fritz microautoradiography technique (see ref. 9), they were able to demonstrate that after an 8- to 15-min exposure to [$^{14}$C]-labeled sucrose (fed through the xylem perfusate), the majority of the radioactivity was located in the parenchyma cells neighboring the xylem vessels (see Fig. 6A and B). Even after a 30-min exposure, little of the label in the parenchyma cells moved into the thick- or thin-walled sieve tubes (E. Fritz, personal communication). For a comparison, we have included autoradiographs of Zea mays that were prepared from tissue that was fed $^{14}CO_2$ for 5 min, with a 10-min chase, under two different light regimes of 100 (Fig. 6C) and 250 μmol photons $m^{-2}$ $s^{-1}$ (Fig. 6D). These micrographs illustrate that when sugars are produced via photosynthesis, the radioactivity enters preferentially into the sieve tubes, and this is especially true when the leaf has been exposed to low light conditions (cf. Fig. 6, C and D).

Thus, the physiological evidence which Giaquinta (17) cited as being the most convincing in support of sucrose-$H^+$ co-transport into the se-cc complex is probably not occurring at this location, but rather at the plasmalemma of the xylem (or vascular) parenchyma. We agree with the interpretation offered by Fritz et al. (10) that these cells probably function to retrieve sucrose from the xylem vessels.

A second plant tissue that has been used to study the operation of the putative sucrose-$H^+$ co-transport system in the phloem is the cotyledons of germinating Ricinus seedlings (20, 22, 23). The reader will perhaps recall that Figure 1 is an illustration of what Komor and his coworkers presented for sucrose uptake into this tissue (23). Martin and Komor (25) and Komor et al. (23) used autoradiography of entire cotyledons to correlate the presence of [$^{14}$C] sucrose with the sucrose-induced alkalinization of the experimental medium (see also Ref. 20). Although Martin and Komor (25) reported that after 5- or 10-min exposure periods the radioactive label appeared to be distributed over the entire cotyledon, they suggested that this was probably an artifact in that the minor veins could not be detected, rather than being due to label in the mesophyll cells. These authors did say that a role of the mesophyll in sucrose uptake could not be excluded, although they thought it very unlikely. However, Komor et al. (23) stated that since "phloem cells of cotyledons

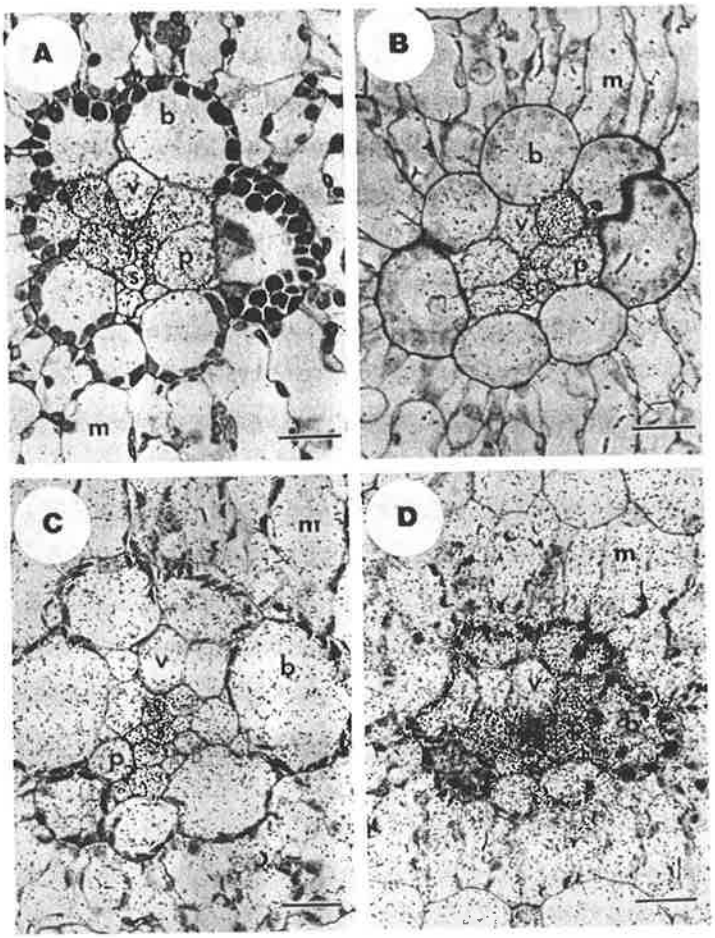


FIG. 6. Microautoradiographs of 1-µm transverse sections of Zea mays leaf strips; b, bundle-sheath cells; m, mesophyll cell; p, vascular parenchyma cell; s, thin-walled sieve tube; v, xylem vessel; all bars = 20 µm. A: leaf strip fed 2.5 mM [$^{14}$C] sucrose via the xylem (using the technique of Heyser [19]); feeding time, 8 min. B: As in A, except feeding time was 15 min. C and D: Leaf strips exposed to $^{14}CO_2$ for 5-min followed by a 10-min pulse with $^{12}CO_2$. Two light intensities were employed; C, 100 µmol photons $m^{-2}$ $s^{-1}$; D, 250 µmol photons $m^{-2}$ $s^{-1}$. (Light micrographs kindly provided by Dr. E. Fritz, der Universität Göttingen.)

do it preferentially," the "most simple assumption would be that it is direct uptake into the phloem cells which proceeds by proton symport."

In a collaborative study that is presently being conducted by Dr. Eberhardt Fritz and Dr. Ewald Komor, these workers are now applying the Fritz microautoradiographic technique to the Ricinus cotyledon. As with the work on Zea mays, Dr. Fritz is examining the distribution of the radioactivity in exactly the same system as previously used by Komor and his co-workers. The results so far obtained are extremely interesting. In tissue exposed to [$^{14}$C]-labeled sucrose for up to 30-min, i.e. the same time as needed to reach the peak of the alkalinization response, the majority of the label has been found in the mesophyll tissue (E. Fritz, personal communication). These microautoradiographic results would tend to suggest that the sucrose-$H^+$ co-transport system functions across the plasma membrane of the mesophyll cells. Thus, the contribution of the phloem cells to the measured pH transient may be quite small. Indeed, it may be impossible to detect the contribution of this tissue due to the rather long diffusion path from the se-cc complex plasma membrane to the external bathing medium.

## ELECTROPHYSIOLOGICAL STUDIES ON PHLOEM CELLS

Perhaps one of the most interesting studies on the physiology of phloem cells was that conducted by Wright and Fisher (34). These workers developed an elegant technique that allowed them to make electrophysiological measurements on phloem tissue. To achieve this, they employed aphids that probed the phloem of willow stems (bark); once the aphid had penetrated the sieve element, it was anaesthetized and in this state its stylet was cut. The cut stylet was then used to gain electrical continuity with the inner surface of the sieve element plasma membrane.

The values of the membrane potential that were measured with this technique were within the range of values normally measured on higher plant tissues. More importantly, Wright and Fisher (34) were able to show that when exogenous sucrose was introduced into their system, a transient depolarization of the membrane potential was observed; the extent of the depolarization was a function of the concentration of sucrose present in the bathing medium. These results were interpreted as

providing direct evidence for the operation of a sucrose-$H^+$ co-transport mechanism in the plasma membrane of the willow sieve element. However, there is a problem with this interpretation. Application of other sugars, like fructose, 3-0-methyl glucose and glucose, also elicited the same type of transient depolarization in the measured membrane potential. The extent of the depolarization was ca. 50 to 70% of that obtained when sucrose was employed.

Earlier autoradiographic studies on leaf tissue have shown that [$^{14}$C]glucose and $^{14}$C-3-0-methyl glucose do not enter the phloem when they are applied to the apoplast, but rather are taken up by the mesophyll cells (8). If this were also true for the willow bark system employed by Wright and Fisher, their electrical response, obtained with these non-translocatable sugars, may be located at the plasma membrane of the surrounding vascular parenchyma. Plasmodesmatal connections between the se-cc complex and the vascular parenchyma would need to exist to permit the transmission of this electrical signal from the parenchyma to the electrode inserted into the aphid stylet. If this were the case for glucose, 3-0-methyl glucose and fructose, it would make it very difficult to argue that the same situation does not also exist with respect to the sucrose-induced transients. Again, the results are consistent with the operation of a plasma membrane-bound sugar-$H^+$ co-transport mechanism, within the tissue of the phloem, but we consider that it does not provide direct evidence for the presence of such a system within the sieve element plasma membrane.

## THE QUESTION OF PHLOEM LOADING

In view of these recent findings, we are forced to ask ourselves just what do we really know about the phenomenon of phloem loading. We know that certain sugars do accumulate within the se-cc complex and the extent of this accumulation indicates that an active process seems to be required. We contend that the exact nature of this active process is yet to be elucidated. We agree that since many plant tissues (mesophyll, vascular parenchyma, scutellum, etc.) appear to contain a sucrose-$H^+$ co-transport mechanism, such a system may also function at the se-cc complex plasma membrane. But, at the present time, we cannot provide direct

evidence in support of this hypothesis. This is why we have raised the point that phloem loading may be a "metaphysical phenomenon."

The solution to this dilemma may lie in the utilization of a much wider range of plant systems than is presently being employed in studies on "phloem loading." It may be possible to utilize the biochemical variability present in the various leaf types, in combination with genetic, physiological and environmental manipulations, to establish a system that will allow us to conduct direct studies on the phloem. Whether or not this will be possible will be illustrated by future experiments.

Acknowledgments--The work conducted in our laboratory on phloem physiology has been made possible by National Science Foundation grants PCM 79-10223 and PCM 83-15408. Dr. Eberhardt Fritz generously made available his published and unpublished microautoradiographic results on Zea mays and Ricinus. Stimulating discussion with all my sabbatical colleagues in the Forstbotanisches Institut, der Universität Göttingen is gratefully acknowledged. Finally, I would like to thank Dr. John Oross for his help with the micrographs and Lyn Noah for typing the manuscript.

LITERATURE CITED

1. CRONSHAW J 1981 Phloem structure and function. Annu Rev Plant Physiol 32:465-484
2. DELROT S 1981 Proton fluxes associated with sugar uptake in Vicia faba leaf tissue. Plant Physiol 68:706-711
3. DELROT S, JL BONNEMAIN 1981 Involvement of protons as a substrate for the sucrose carrier during phloem loading in Vicia faba leaves. Plant Physiol 67:560-564
4. DELROT S, JP DESPEGHEL, JL BONNEMAIN 1980 Phloem loading in Vicia faba leaves: effect of N-ethylmaleimide and parachloromercuribenzene sulfonic acid on $H^+$ extrusion, $K^+$ and sucrose uptake. Planta 149:144-148
5. ESCHRICH W 1970 Biochemistry and fine structure of phloem in relation to transport. Annu Rev Plant Physiol 21:193-214

6. EVERT RF 1977 Phloem structure and histochemistry. Annu Rev Plant Physiol 28:199-222
7. EVERT RF, W ESCHRICH, W HEYSER 1978 Leaf structure in relation to solute transport and phloem loading in Zea mays L. Planta 138: 279-294
8. FONDY BR, DR GEIGER 1977 Sugar selectivity and other characteristics of phloem loading in Beta vulgaris L. Plant Physiol 59:953-960
9. FRITZ E 1980 Microautoradiographic localization of assimilates in phloem: problems and new method. Ber Dtsch Bot Ges 93:109-121
10. FRITZ E, RF EVERT, W HEYSER 1983 Microautoradiographic studies of phloem loading and transport in the leaf of Zea mays L. Planta 159:193-206
11. GEIGER DR 1975 Phloem loading. In MH Zimmerman, JA Milburn, eds, Transport in Plants, Encyclopedia of Plant Physiology, Vol 1, New Series. Springer-Verlag, Heidelberg, pp 395-431
12. GEIGER DR 1976 Phloem loading in source leaves. In IF Wardlaw, JB Passioura, eds, Transport and Transfer Processes in Plants. Academic Press, New York, San Francisco, London, pp 167-215
13. GEIGER DR, SA SOVONICK, TL SHOCK, RJ FELLOWS 1974 Role of free space in translocation in sugar beet. Plant Physiol 54:892-899
14. GIAQUINTA RT 1977 Phloem loading of sucrose: pH dependence and selectivity. Plant Physiol 59:750-755
15. GIAQUINTA RT 1979 Phloem loading of sucrose: involvement of membrane ATPase and proton transport. Plant Physiol 63:744-748
16. GIAQUINTA RT 1980 Mechanism and control of phloem loading of sucrose. Der Dtsch Bot Ges 93:187-201
17. GIAQUINTA RT 1983 Phloem loading of sucrose. Annu Rev Plant Physiol 34:347-387
18. GILDER J, J CRONSHAW 1974 A biochemical and cytochemical study of adenosine triphosphatase activity in the phloem of Nicotiana tabacum. J Cell Biol 60:221-225
19. HEYSER W 1980 Phloem loading in the maize leaf. Der Dtsch Bot Ges 93:221-228

20. HUTCHINGS VM 1978 Sucrose and proton cotransport in Ricinus cotyledons. I. $H^+$ influx associated with sucrose uptake. Planta 138: 229-235

21. KOMOR E 1977 Sucrose uptake by cotyledons of Ricinus communis L.: characteristics, mechanism, and regulation. Planta 137:119-131

22. KOMOR E, M ROTTER, W TANNER 1977 A proton-cotransport system in a higher plant: sucrose transport in Ricinus communis. Plant Sci Lett 9:153-162

23. KOMOR E, M ROTTER, J WALDHAUSER, E MARTIN, BH CHO 1980 Sucrose proton symport for phloem loading in the Ricinus seedling. Der Dtsch Bot Ges 93:211-219

24. LICHTNER FT, RM SPANSWICK 1981 Sucrose uptake by developing soybean cotyledons. Plant Physiol 68:693-698

25. MARTIN E, E KOMOR 1980 Role of phloem in sucrose transport by Ricinus cotyledons. Planta 148:367-373

26. MAYNARD JW, WJ LUCAS 1982 A reanalysis of the two-component phloem loading system in Beta vulgaris. Plant Physiol 69:734-739

27. MAYNARD JW, WJ LUCAS 1982 Sucrose and glucose uptake into Beta vulgaris leaf tissues: A case for general (apoplastic) retrieval systems. Plant Physiol 70:1436-1443

28. PATE JS, BES GUNNING 1969 Vascular transfer cells in angiosperm leaves. A taxonomic and morphological survey. Protoplasma 68: 135-156

29. REINHOLD L, A KAPLAN 1984 Membrane transport of sugars and amino acids. Annu Rev Plant Physiol 35:45-83

30. SOVONICK SA, DR GEIGER, RJ FELLOWS 1974 Evidence for active phloem loading in the minor veins of sugar beet. Plant Physiol 54:886-891

31. TANNER W 1980 Proton sugar cotransport in lower and higher plants. Ber Dtsch Bot Ges 93:167-176

32. WARDLAW IF 1974 Phloem transport: physical, chemical or impossible. Annu Rev Plant Physiol 25:515-539

33. WILSON CW, JW OROSS, WJ LUCAS 1985 Sugar uptake into Allium cepa leaf tissue: An integrated approach. Planta. In press

34. WRIGHT JP, DB FISHER 1981 Measurement of the sieve tube membrane pontential. Plant Physiol 67:845-848

# Sugar beet petiole structure: vascular anastomoses and phloem ultrastructure

JOHN W. OROSS AND WILLIAM J. LUCAS
*Botany Department, University of California, Davis, CA, U.S.A. 95616*

Received February 4, 1985

OROSS, J. W., and W. J. LUCAS. 1985. Sugar beet petiole structure: vascular anastomoses and phloem ultrastructure. Can. J. Bot. **63**: 2295–2304.

The vascular anatomy and phloem ultrastructure of the sugar beet petiole were studied in an attempt to evaluate the potential of petiolar phloem anastomoses to accommodate lateral movement of translocates across this structure. Clearings revealed that six of the eight interveinal regions between the nine major, axially oriented veins were connected by many anastomoses. The two interveinal areas characterized by the fewest anastomoses were located near the margin of the petiole. It was concluded that lateral translocation via anastomoses would be most efficient in the central part of the petiole. A light microscope study of the structure of the junction between anastomosing and continuous veins revealed that the sieve elements of each of the merging veins were separated from each other, for distances of up to 6 mm beyond the point of initial contact, by phloem parenchyma cells. The presence of phloem parenchyma cells in this position, and between the clusters of sieve elements that occur across the phloem of the large bundles, was taken as an indication that the parenchyma cells may have an important role in lateral translocation. An ultrastructural study of the petiolar phloem revealed that the phloem parenchyma and companion cells could be easily distinguished on the basis of the structure of the chloroplasts, dictyosomes, and endoplasmic reticulum. Microfilament bundles and spine-coated tubules and (or) vesicles were uniquely present in the parenchyma cells. The ultrastructure of the phloem parenchyma cells is discussed relative to their possible role in mediating the movement of sugars through the anastomoses.

OROSS, J. W., et W. J. LUCAS. 1985. Sugar beet petiole structure: vascular anastomoses and phloem ultrastructure. Can. J. Bot. **63**: 2295–2304.

L'anatomie vasculaire et l'ultrastructure du phloème du pétiole de la betterave à sucre ont été étudiées dans le but d'évaluer l'aptitude des anastomoses du phloème pétiolaire à assurer le mouvement latéral des substances migratrices à travers cette structure. La décoloration a montré que six des huit régions interveineuses entre les neuf nervures principales à orientation axiale étaient reliées par des anastomoses. Les deux aires interveineuses ayant le moins d'anastomoses se trouvaient près de la marge du pétiole. Nous avons conclu que le transport latéral dans les anastomoses serait le plus efficace dans la partie centrale du pétiole. Une étude au microscope photonique de la structure de la jonction entre les nervures continues et celles qui s'anastomosent a révélé que les éléments criblés de chacune des nervures ayant fusionné étaient séparés les uns des autres par des cellules de parenchyme libérien jusqu'à 6 mm au-delà du point de contact initial. Nous avons considéré que la présence de cellules de parenchyme libérien à ce niveau, et entre les massifs d'éléments criblés présents à travers le phloème des gros faisceaux, comme l'indication que les cellules de parenchyme peuvent jouer un rôle important dans le transport latéral. Une étude ultrastructurale du phloème pétiolaire a révélé que l'on pouvait facilement distinguer le parenchyme libérien des cellules compagnes en se basant sur la structure des chloroplastes, des dictyosomes et du réticulum endoplasmique. Des faisceaux de microfilaments et des tubules à revêtement épineux et (ou) des vésicules n'apparaissent que dans les cellules de parenchyme. L'ultrastructure des cellules du parenchyme libérien est discutée en liaison avec leur rôle possible de médiation dans le mouvement des sucres à travers les anastomoses.

[Traduit par le journal]

## Introduction

A recent study of assimilate translocation in the sugar beet petiole has shown that a substantial recovery in the rate of translocation can occur in a relatively short time after a large proportion of the petiolar vascular bundles is severed (Grusak and Lucas 1984). An indication of the basis for this recovery was given by another experiment in which the pattern of vascularization was mapped within the region of a surgically induced blockage in the axial translocation pathways. A number of small, laterally directed anastomosing veins, which interconnected the larger, axially oriented veins, was found in the region of the blockage. It was concluded that the commonly observed recovery in translocation was based upon a rerouting of translocational flow around localized blockages via these preexisting anastomoses.

Quick chilling of a portion of a sugar beet petiole also results in a decline in the rate of translocation, followed by a nearly complete recovery to the prechilling rates (Swanson and Geiger 1967; Grusak and Lucas 1984). In light of several experiments that provided data contradictory to certain aspects of an existing cold block recovery model (Ferrier and Christy 1975), it has been suggested that the capacity of the sugar beet petiole to reroute translocates, via laterally directed phloem anastomoses, may also be involved in this recovery response (Grusak and Lucas 1984).

While many aspects of the anatomy of the sugar beet petiole and its phloem have been documented (Artschwager 1926; Esau 1933, 1934), the structure of the lateral transport pathways in the petiole has received little attention. Information concerning the spatial distribution and frequency of anastomoses in the petiole is limited to a generalized statement, made by Artschwager (1926) in regard to mature leaves, that the petiolar bundles "anastomose freely" throughout the length of the petiole. Whether or not this generalization has relevance to the relatively young leaves used for the recent translocation studies (Grusak and Lucas 1984) remains to be established. The anatomical organization of the junction between the anastomosing and axially oriented veins has not been reported. This information, with particular reference to the way in which the phloic connections are established, is necessary for the evaluation of the junctions as a potential control point for regulating the activity of the anastomotic tissue in response to blockages in the axial pathways of the phloem.

The ultrastructure of the phloem in the petiole of the sugar

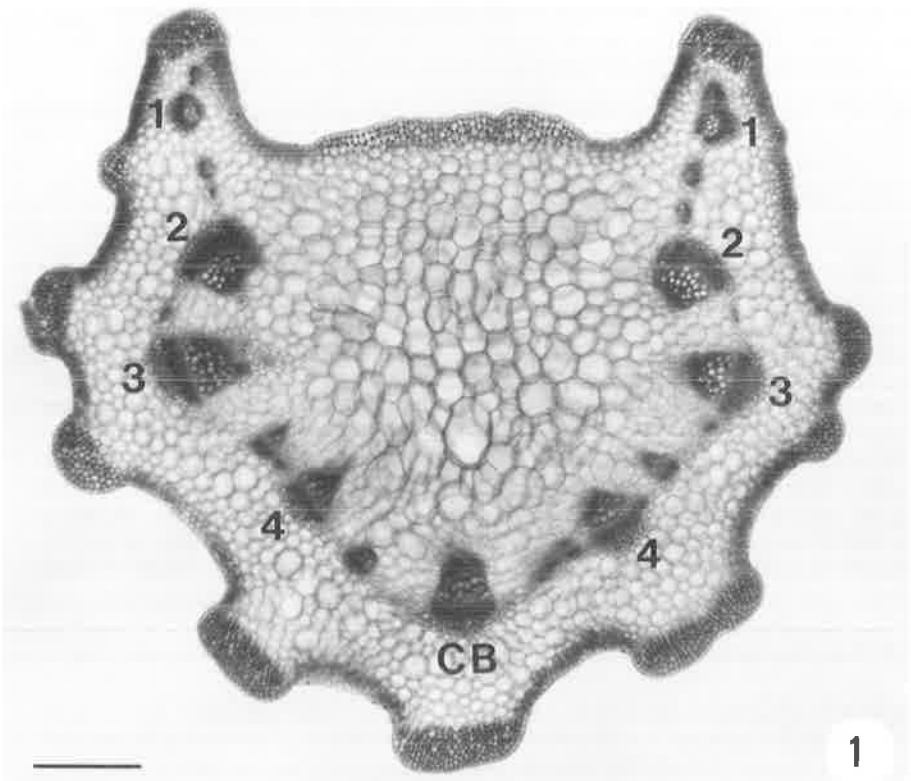


1

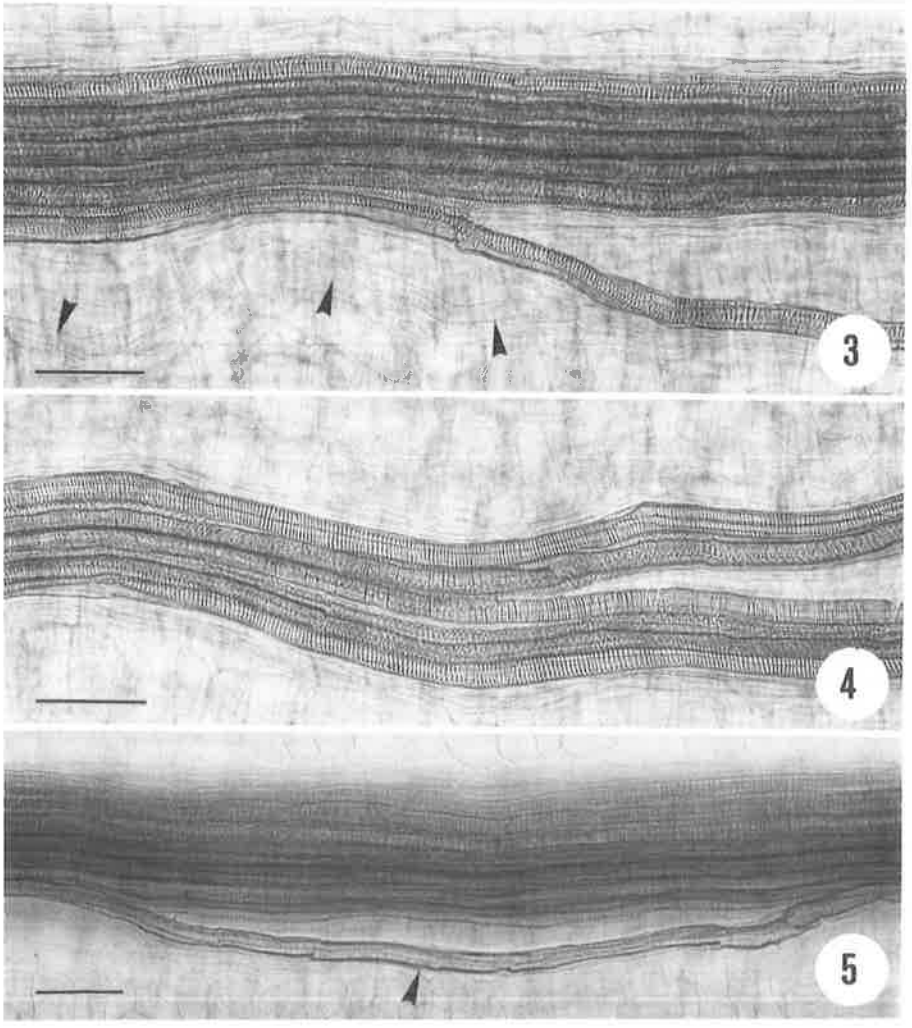


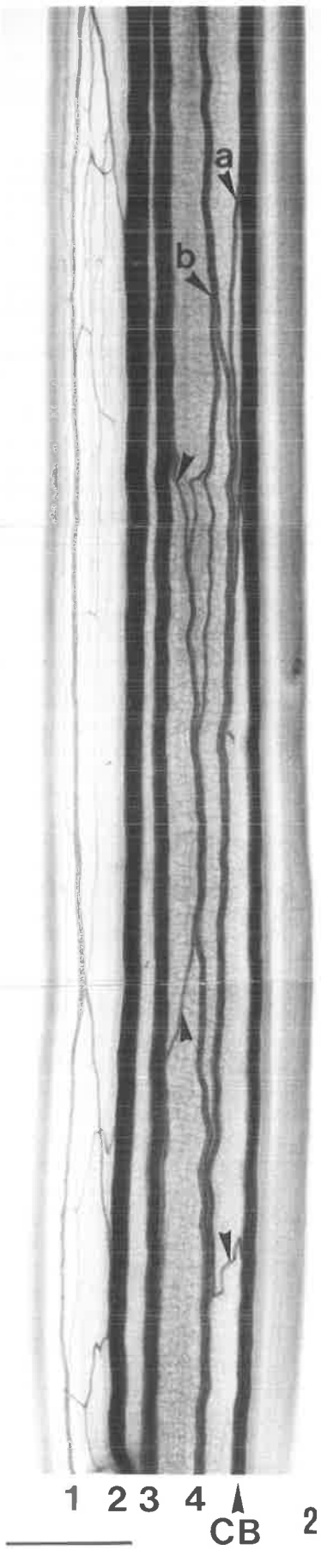


2

beet leaf has been studied only superficially (Sokolova 1968) in comparison with that of the minor veins of the blade (Esau 1967, 1972). The value of a more detailed ultrastructural study of the petiolar phloem is twofold. First, it might reveal structural specializations unique to the petiolar phloem, related to its role as a tissue specialized primarily for long distance translocation. Second, it will provide data that will be useful as a point of comparison for future ultrastructural studies of experimentally manipulated tissues.

The present study provides a detailed structural characterization of three important aspects of the petiolar vasculature of sugar beet leaves comparable to those used for recent translocation studies (see Grusak and Lucas 1984). First, the spatial distribution and frequency of anastomoses in the petiole is described from cleared material. Second, the structure of the phloem in the region of the juncture between anastomotic and continuous veins is reported. Third, the ultrastructure of the sieve element companion cell complex and the phloem parenchyma cells is described and compared with that reported for the phloem of the minor veins of the blade.

## Materials and methods

Plant material of *Beta vulgaris* L. variety SBN1, USH11, lot 82312 was grown under growth chamber conditions as previously described (Grusak and Lucas 1984). The observations reported were made only on the petioles of the third pair of leaves above the cotyledonary node from plants that were from 28–30 days old.

The clearings were done according to the Shobe and Lersten technique (Shobe and Lersten 1967) after the petioles were bisected in a dorsoventral plane and stripped of their collenchymatous ribs. A total of eight petioles was cleared and examined.

Primary fixation for light and electron microscopy employed a fixative containing 5% glutaraldehyde, 4% depolymerized paraformaldehyde, 4% dimethylsulfoxide, and 1 m*M* $CaCl_2$ in 50 m*M* sodium cacodylate buffer (pH 6.8). Before fixation, the leaf was excised near the leaf base and the blade removed. Midway between the cut ends, a longitudinally oriented trough (5 cm long and 3 mm deep) was cut into the adaxial surface of the petiole using a slightly modified Speedball No. 3 linoleum cutter (Hunt Manufacturing Co., Statesville, NC). Particular care was taken to avoid damage to the vascular bundles during the cutting of the trough, which removed most of the cortical parenchyma. The abaxial epidermis opposite the trough was then lightly abraded with coarse sandpaper (36 grit) and the entire petiole immersed in cold fixative (4°C). This temperature was maintained for 1 h and was slowly raised to 23°C during the last 4 h of primary fixation. The midregion of the petiole was then cut into 1 mm segments which were given a short buffer wash and then postfixed in buffered 1% $OsO_4$ for 5 h at 4°C.The segments were then dehydrated in a graded acetone series and embedded in Spurr's (1969) resin. Conventional techniques were used for subsequent sectioning, staining, and observation with both the light and electron microscopes. Periodic acid–thiocarbohydrazide–silver proteinate (PA–TCH–SP) staining for insoluble carbohydrates was performed using the protocol reported by Roland (1978).

## Results

Cross sections of the sugar beet petiole taken at positions along its entire length reveal the presence of 18–25 vascular bundles (Fig. 1). They range in size from large bundles composed of approximately 20 vessels and 35 sieve elements to small bundles containing a single vessel and 5 sieve elements. Occasionally, small bundles are present that contain only maturing vessels with faint secondary thickenings (Fig. 3) and five or fewer sieve elements (Fig. 10). The presence of both xylem and phloem in all of the bundles observed validated the use of safranin-stained clearings for delineating the phloic pathways in the petiole.

Of the numerous bundles present in the cross section shown in Fig. 1, only nine are traceable throughout the length of the petiole. These include the central bundle and the bundles numbered 1–4 in Figs. 1 and 2. Anastomosing bundles interconnect all of the adjoining, continuous bundles. As a result of an analysis of the entire petiolar length, the average values ± SEM determined for the number of anastomoses between veins 1 and 2, 2 and 3, and 3 and 4, and between vein 4 and the central bundles are 14.38 ± 0.71, 1.50 ± 0.36, 6.25 ± 0.49, 7.38 ± 0.71, respectively. Additionally, veins 2 and 3 are occasionally fused laterally for a distance of several millimetres near the juncture of the petiole and the lamina (not shown). Anastomoses are distributed along most of the petiole, except near its base where they are absent. Occasionally, small bundles are present that diverge from one of the continuous bundles and merge with the same large bundle at varying distances from the point of origin (Fig. 5).

The clearings also demonstrate the gross organization of the juncture between continuous and anastomosing veins. Continuity between these veins is apparently established by simple lateral apposition (Figs. 3, 4). In both instances, the vessels of the merging veins can be traced as individuals throughout the juncture.

Determination of the relationship between the phloic components required a survey of sections taken throughout the length of the juncture and beyond (Figs. 6–9, 11). Figure 7 is a micrograph of a section taken approximately 1 mm from the point of initial contact between the separate veins shown in Fig. 6. Higher magnification of the point of contact between the two veins reveals that the sieve elements associated with each of the merging veins are separated from each other by a well-defined wedge of phloem parenchyma cells (Fig. 9). Figure 8 is a micrograph of a section taken approximately 6 mm above the same juncture. Here, too, the sieve elements of the merging veins are separated by a wedge of phloem parenchyma cells (Fig. 11). Beyond this point, the parenchymatous boundary between the sieve elements of the merging bundles becomes indistinct. In this region, the phloem cells are arranged as described by Esau (1934) and others (Geiger et al. 1969)

FIG. 1. Fresh cross section of the petiole taken midway between the leaf base and the blade, illustrating the organization and size distribution of the petiolar vascular bundles. The numbering of veins corresponds with that in Fig. 2. CB, central bundle. ×14.3. Scale bar = 1 mm. FIG. 2. A clearing of a 23 mm long segment of a petiole half that demonstrates the typical pattern of vascularization in the petioles used for this study. Only the central bundle (CB) and the numbered veins extend throughout the length of the petiole. Some of the anastomosing veins are indicated by unlabeled arrows. Note that in this segment of petiole no anastomoses occur between veins 2 and 3 and that vein 4 is highly dissected near the middle of the clearing. Junctures *a* and *b* are enlarged in Figs. 3 and 4, respectively. ×9.6. Scale bar = 2 mm. FIG. 3. An enlargement of the juncture labeled *a* in Fig. 2. The vessels of the smaller vein are traceable throughout the juncture. A maturing vessel with barely perceptible secondary thickenings is indicated by arrows. ×74. Scale bar = 0.2 mm. FIG. 4. An enlargement of the juncture labeled *b* in Fig. 2. The vessels of the smaller veins to the left are traceable throughout the juncture. ×74. Scale bar = 0.2 mm. FIG. 5. A micrograph from a clearing of a segment of a large continuous vein which demonstrates the presence of a smaller vein (arrow) forming a short vascular "spur line" to the larger vein. Such spur lines were not uncommon and were most often much longer. ×58. Scale bar = 0.2 mm.

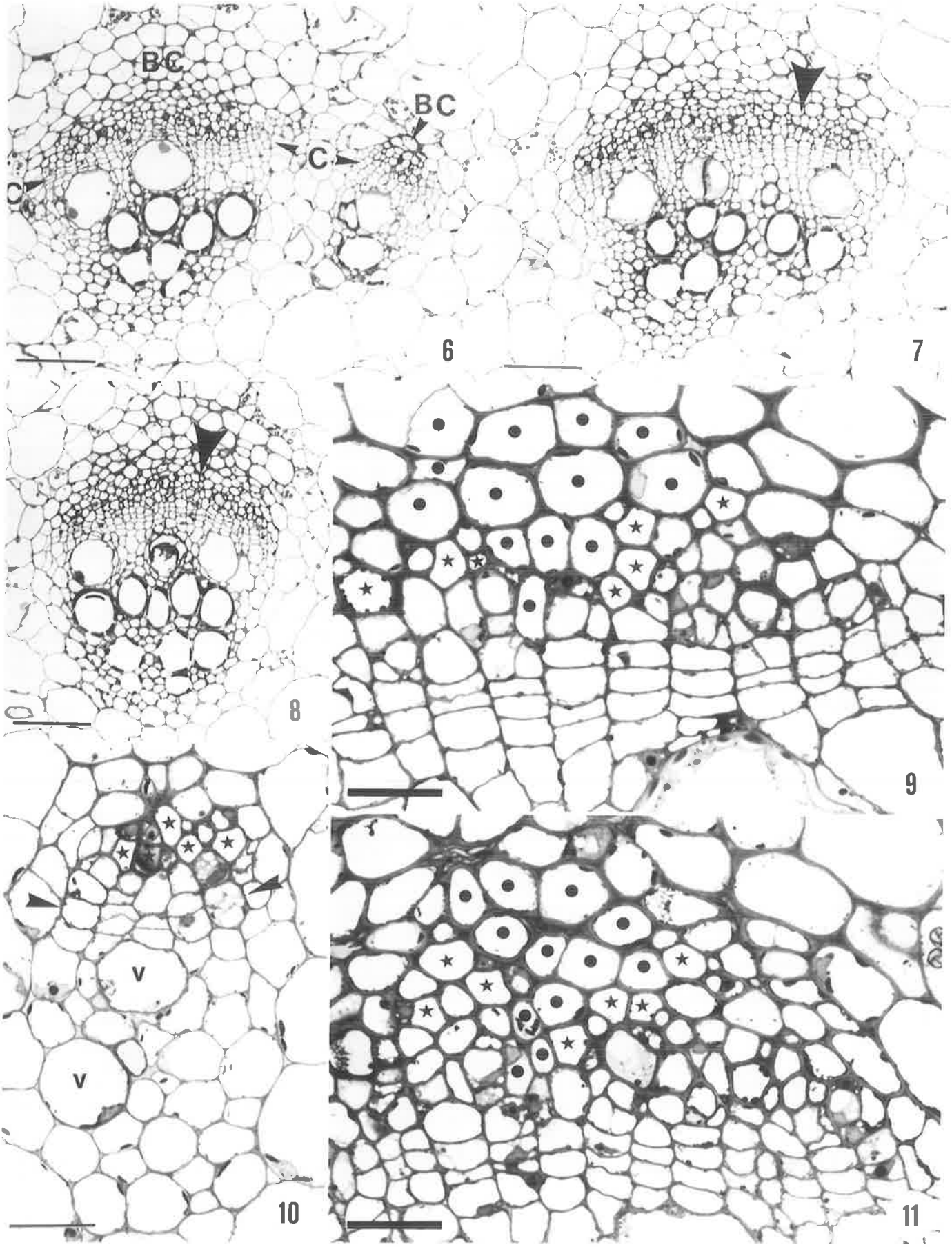
BC
BC
C
C
6
7
8
9
V
V
10
11

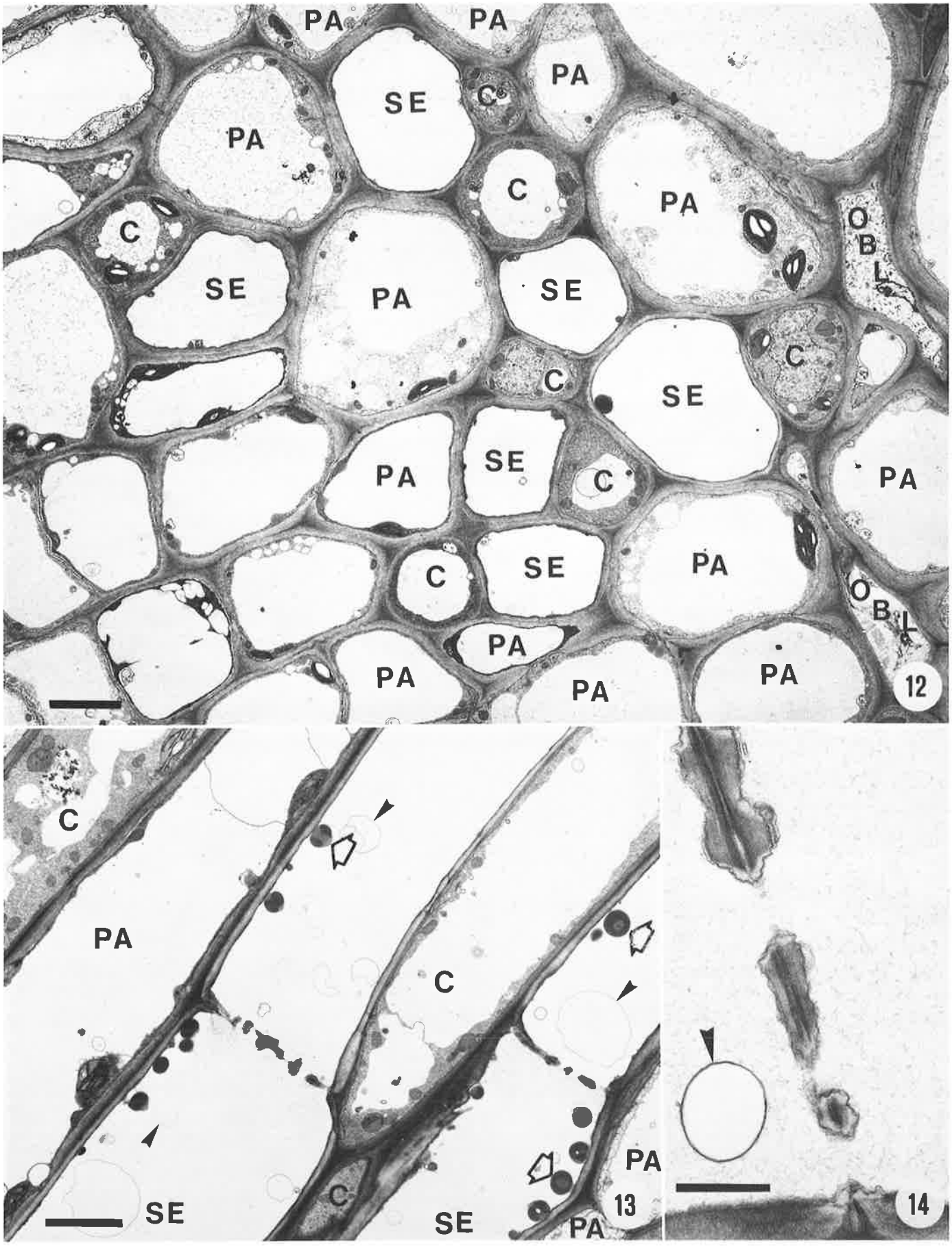
PA
PA
SE
C
PA
PA
C
C
PA
OBL
SE
PA
SE
C
C
SE
PA
SE
C
PA
C
SE
PA
PA
PA
PA
PA
OBL
12
C
PA
C
SE
C
PA
SE
13
PA
SE
C
14

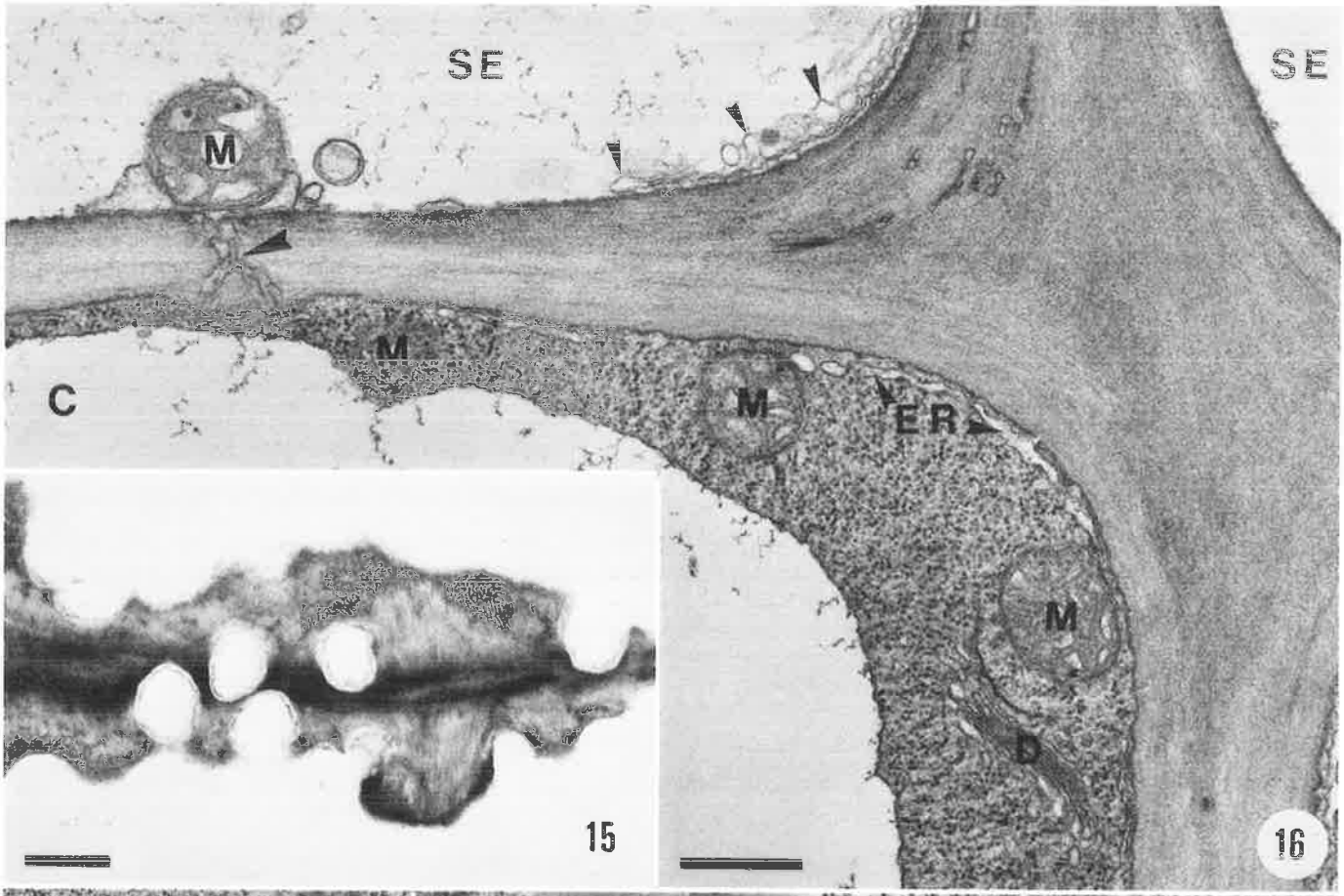
SE
SE
M
C
M
M
ER
M
D
16


15

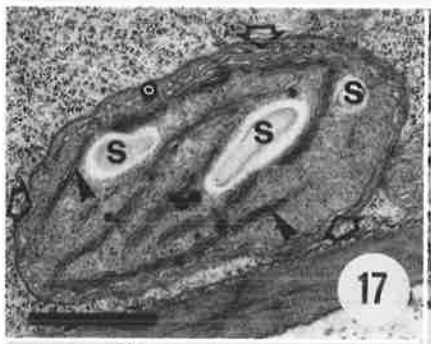
S
S
S
17

S
18

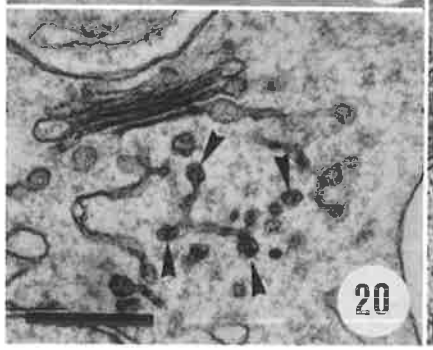
20

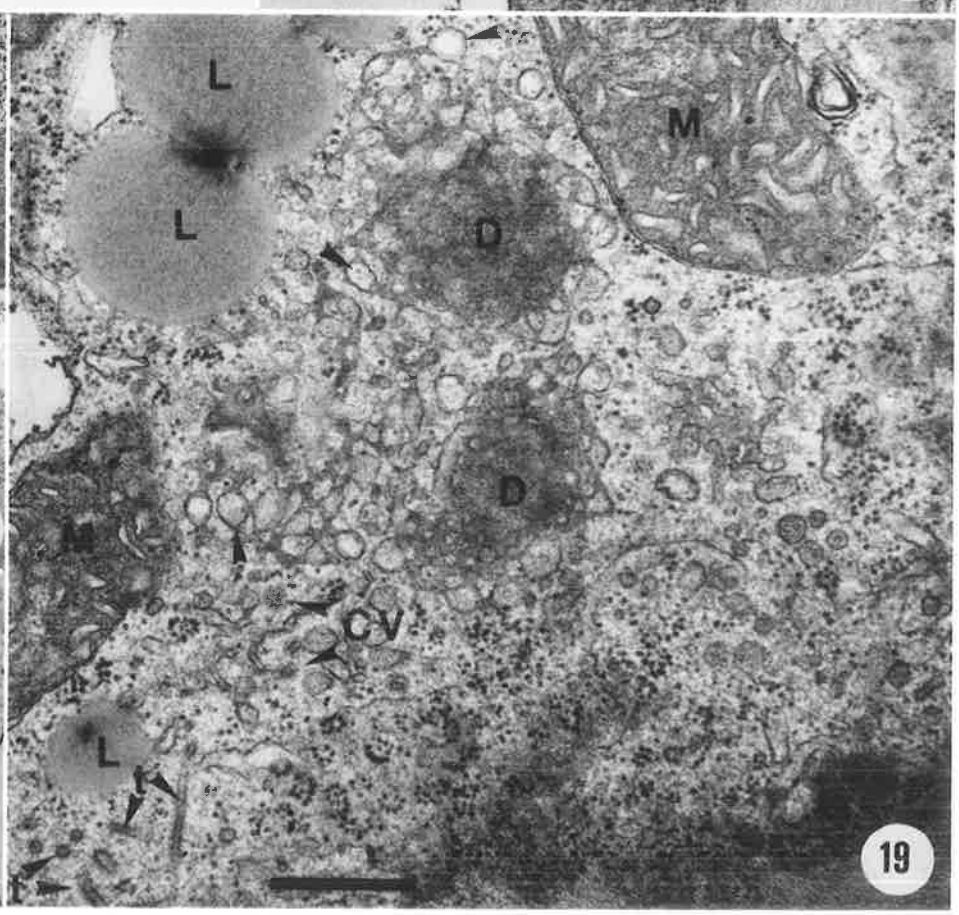
L
L
M
D
D
M
CV
L
19

where clusters of sieve elements are bounded by a combination of phloem parenchyma cells, obliterated sieve elements and companion cells, and maturing derivatives of the vascular cambium (Fig. 12). There was some variability in the length of the parenchymatous boundary separating the sieve elements of the merging veins. While it was common to find them in excess of 5 mm in length, some were found to be only 2 mm or shorter. The reason for this variation is not clear, but it may be that the longer boundaries are associated with more recently formed junctures and that the boundary shortens as a result of cambial activity occurring subsequent to the formation of the juncture.

The ultrastructural preservation of the sieve elements was generally good. Low levels of electron-lucent callose line the pores of the sieve plates (Figs. 13, 14) and those of the lateral sieve areas (Fig. 15). Phloem protein appears as a light, dispersed cloud of fibrillar material that occurs on one or both sides of the sieve plates and lateral sieve areas (Figs. 13, 14). Large vesicles with no apparent content are often present in the lumen of the sieve element (Figs. 13, 14).

Sieve element plastids of similar structure to those described by Esau (1965) for the minor veins of the lamina occur primarily near the sieve plates (Fig. 13). In sectional view, the endoplasmic reticulum (ER) usually appears as closely appressed pairs of smooth membranes that lie just inside the plasmalemma. Stacked ER cisternae are not common (Fig. 16). Slightly dilated segments of ER partially surround the small, spherical mitochondria that are characteristic of the sieve element (Fig. 16).

In cross-sectional view, the companion cells are usually of equal size or smaller than adjoining sieve elements (Fig. 12). The companion cell protoplast contains vacuoles of varying size and has a cytoplasm with a high affinity for the aqueous stains used for both light and electron microscopy. Mitochondria are present in most sections and are spherical or ovoidal in shape (Figs. 12, 13). A few chloroplasts containing weakly developed grana and a single or double layer of peripheral reticulum are also present (Fig. 17). The chloroplasts usually contain starch. Large numbers of free ribosomes are the most conspicuous feature of the companion cell cytoplasm (Fig. 16). Endoplasmic reticulum is not abundant, is primarily rough, and is most often located at the cell periphery. Dictyosomes, while not abundant, are present throughout the cytoplasm (Fig. 16).

In general, the ultrastructure of the sieve element – companion cell complex in the petiolar phloem is comparable to that reported for minor veins (Esau 1967, 1972). The only conspicuous difference is the low level of stacking of ER observed for the sieve elements of the petiolar phloem. Higher levels of stacking were occasionally observed in sieve elements that displayed evidence of surge artifacts resulting from damage during tissue preparation.

In contrast to the situation reported for the minor veins of the lamina of the sugar beet leaf (Esau 1967), the structural distinction between the companion and parenchyma cells is clear-

FIGS. 6–8. A sequential series of cross sections taken along the region of a juncture between a large continuous vein and two smaller anastomosing veins. Fig. 6. A section taken just below the juncture of the large and the small vein is shown here. The vascular bundles are composed of xylem below the cambial region (C) and phloem, containing sieve elements, between the cambial region and the bundle cap (BC). ×151. Scale bar = 0.1 mm. Fig. 7. A section taken approximately 1 mm above the juncture between the separate veins shown in Fig. 6. The interface between the veins is indicated by a solid arrow. Additionally, the small bundle shown in Fig. 10 has merged with the left side of the large composite bundle from the opposite direction, at a point approximately 2 mm above this plane of section. ×151. Scale bar = 0.1 mm. Fig. 8. A section taken approximately 6 mm above the juncture of the bundles shown in Fig. 6. The point of the juncture is indicated by a solid arrow. ×151. Scale bar = 0.1 mm. FIG. 9. A high magnification view of the interfacial area indicated in Fig. 7. The sieve elements of the merging bundles nearest the interface are indicated by stars and are separated by a wedge of phloem parenchyma cells (●). As with Fig. 11, the designation of cell types was based upon electron microscopic observations. ×727. Scale bar = 25 μm. FIG. 10. A cross section of a small bundle containing mature sieve elements (★) and immature vessels (*v*). A vascular cambium (solid arrows) is seen in an early stage of development. ×667. Scale bar = 25 μm. FIG. 11. A high magnification view of the interfacial area indicated in Fig. 8. The sieve elements of the merging bundles nearest the interface are indicated by stars and are separated by a wedge of phloem parenchyma cells (●). ×727. Scale bar = 25 μm.

FIG. 12. An electron micrograph of the central region of the phloem in a transversely sectioned large bundle. The cluster of six sieve elements (SE) and associated companion cells (C) is bordered by parenchyma cells (PA), recent derivatives of the vascular cambium (extreme left), and obliterated sieve elements and companion cells (OBL). Note the range of electron opacity exhibited by the cytoplasm of the parenchymatic elements of the phloem. ×2650. Scale bar = 5 μm. FIG. 13. An electron micrograph of a portion of four longitudinally sectioned sieve elements (SE) including their sieve plates. Phloem protein appears as a light cloud in the region of the sieve plates and has a somewhat asymmetric distribution on either side of the sieve plates. Irregularly shaped membraneous inclusions (solid arrows) are present within the sieve elements, and sieve element plastids (open arrows) containing ring-shaped proteinaceous inclusions occur primarily near the sieve plates. C, companion cell; PA, phloem parenchyma cell. ×2900. Scale bar = 5 μm. FIG. 14. A portion of a sieve plate showing the low level of electron-lucent callose present around the pores of the sieve plate. A membraneous vesicle that excludes the finely fibrillar P protein is indicated by an arrow. The pores are relatively unoccluded by the P protein. ×18 400. Scale bar = 1 μm.

FIG. 15. An oblique section through a portion of a lateral sieve area demonstrating a minimal occlusion of the sieve pores by callose and P protein. ×11 500. Scale bar = 1 μm. FIG. 16. A transverse section through a portion of two sieve elements (SE) and a companion cell (C). Endoplasmic reticulum in the sieve element at the upper left is vesiculated in some areas (arrows) and is found in close spatial association with a spherical mitochondrion (M). A branched plasmodesma (arrow) occurs between the sieve element and the companion cell. The companion cell cytoplasm is characterized by many ribosomes, mitochondria (M), short parietal elements of endoplasmic reticulum (ER), and an occasional dictyosome (D). ×33 000. Scale bar = 0.5 μm. FIG. 17. Sectional view of a companion cell plastid that contains starch (S), weakly developed grana (solid arrows), and a peripheral reticulum (open arrows) that extends around the entire periphery of the plastid. ×17 000. Scale bar = 1 μm. FIG. 18. Sectional view of a starch-containing phloem parenchyma cell plastid. The grana (solid arrows) have more thylakoids than do the companion cell plastids, but the peripheral reticulum (open arrows) does not extend around the entire periphery of the plastid. × 17 300. Scale bar = 1 μm. FIG. 19. A grazing section of a portion of a phloem parenchyma cell showing dictyosomes (D) that are associated with an elaborate system of fenestrated membranes. The fenestrations are locally dilated in many cases (unlabeled arrows). Spine-coated tubules (*t*) are present as well as a few poorly preserved coated vesicles (CV). L, cytoplasmic lipid body; M, mitochondrion. ×39 000. Scale bar = 0.5 μm. FIG. 20. Positive periodic acid – thiocarbohydrazide – silver proteinate staining of insoluble carbohydrate present within a membraneous network (arrows) close to a dictyosome. ×34 000. Scale bar = 0.5 μm.

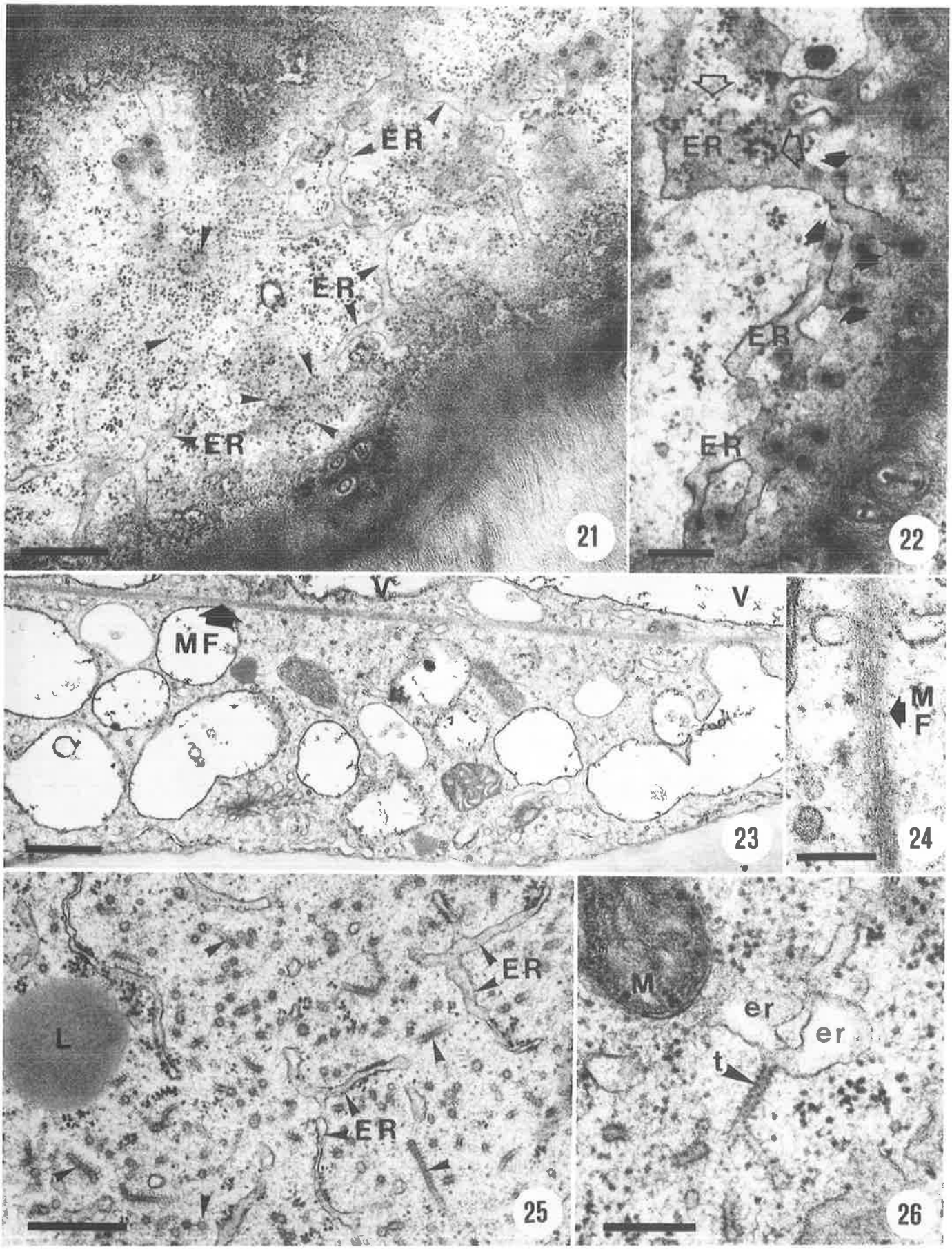
ER
ER
ER
21
ER
ER
ER
22
V
V
MF
23
MF
24
L
ER
ER
25
M
er
er
t
26

cut in the petiolar phloem. The phloem parenchyma cells are usually larger in diameter than either the sieve elements or the companion cells (Fig. 12). The staining intensity of the parenchyma cell cytoplasm is most often lighter than that of the companion cells, but some variability was often noted; this was true even between contiguous parenchyma cells of the same axial series. The phloem parenchyma cells are generally more vacuolate than the companion cells. The mitochondria appear spherical or ovoidal in some planes of section, but in others they are elongate and occasionally branched (not shown). The chloroplasts are structurally similar to those of the companion cells but often have a higher number of thylakoids per granum and a less developed peripheral reticulum (Fig. 18). Dictyosomes are a conspicuous feature of the parenchyma cells and are characterized by an elaborate array of fenestrated membranes in association with the *cis* face (Fig. 19). Additionally, membraneous vesicles and (or) tubules in the vicinity of the dictyosomes contain a fine granular material that is stainable with the PA–TCH–SP stain for insoluble carbohydrates (Fig. 20).

Endoplasmic reticulum is a prominent feature of the petiolar phloem parenchyma cells. A highly reticulate form composed of tubular and cisternal elements is present in the parietal cytoplasm that is often adorned with numerous curled chains of polyribosomes (Figs. 21, 22). In pit regions between parenchyma cells, ER tubules are associated with plasmodesmata. A limited amount of cisternal ER is also present throughout the cytoplasm and may be rough or smooth or a combination of both (Fig. 25).

A number of cytoplasmic structures not found in the companion cells are present in the phloem parenchyma cells. Microfilament bundles oriented parallel to the long axis of the cell are frequently observed near the tonoplast of the large central vacuole (Figs. 23, 24). They are approximately 0.15 μm wide and often in excess of 10.0 μm in length. The maximum number per cell was not determined. Cytoplasmic lipid bodies are also common (Figs. 19, 25). Spine-coated membraneous tubules and vesicles are present in most sections. They occur as a few isolated individuals in some cases (Figs. 19, 26), but are often found in large aggregations (Fig. 25). In the latter case, most other cytoplasmic structures are excluded, with the exception of ER and lipid bodies. Occasionally, the spine-coated membranes are continuous with irregularly shaped sacks of uncoated membranes (Fig. 26).

## Discussion

The results of the present study concerning the frequency of anastomoses between the large, continuous veins largely corroborate Artschwager's generalization that the petiolar bundles "anastomose freely" throughout the length of the petiole (Artschwager 1926). A critical exception to this generalization is the relatively low number of anastomosing bundles present between the bundles labeled 2 and 3 in the present study. The paucity of interconnections between these veins may be a feature unique to the age of the leaves used for this study. The finding of some small veins that were entirely primary in nature and others in which a vascular cambium was apparently becoming organized indicates that the vasculature of the leaves used was not completely developed, even though the leaves had apparently reached maximal size. This contention is supported by Artschwager's (1926) report that the number of petiolar bundles increases with age.

It has been postulated that the recovery in translocation, which is often observed following surgically induced blockages in the axial translocation pathways, is based upon a rerouting of translocates around the blockage via laterally directed anastomosing veins (Grusak and Lucas 1984). The relatively low number of anastomoses present between veins 2 and 3 offers a unique situation to test this hypothesis. Experiments involving a unidirectional cut severing all but veins 1 and 2 on one side of the petiole would result in a situation where a recovery in translocation would require a substantial movement of translocates between veins 2 and 3. If rerouting of translocational flow, via vascular anastomoses, is the sole basis for the observed recovery response to this sort of blockage, a severely limited recovery or no recovery at all would be expected following such an incision.

With the exception of the unique situation described above, there apparently is a sufficient number of vascular interconnections between the other continuous petiolar veins to facilitate a rerouting of translocational flow around localized obstructions of the phloem. This rerouting would not only require exchanges of translocate between anastomosing and continuous veins, but also lateral movement of solutes across the phloem of the large continuous veins. The presence of phloem parenchyma cells between the sieve elements of merging veins and between the clusters of sieve elements that occur across the phloem of the large continuous veins indicates that the lateral movement of solutes across the petiole, via direct sieve element connections, is highly restricted or precluded. This partitioning of the lateral transport pathway by phloem parenchyma cells indicates that they may be involved somehow in the regulation and maintenance of the lateral movement of translocates across the petiole.

Our ultrastructural study of the petiolar phloem revealed that the parenchyma cells were characterized by several features, not reported for those of the minor veins of the lamina, that may be related to their presumed role in lateral translocation. The

FIG. 21. A grazing longitudinal section of a portion of a phloem parenchyma cell. A highly reticulate and primarily tubular form of endoplasmic reticulum (ER) is shown which undulates in and out of the plane of section. In areas where the surface of the ER is grazed, numerous polyribosomes (unlabeled arrows) are found in close spatial association with the ER. ×34 000. Scale bar = 0.5 μm. FIG. 22. An oblique section through a portion of a pit field between two phloem parenchyma cells which demonstrates continuities (solid arrows) between the endoplasmic reticulum (ER) described in Fig. 21 and plasmodesmata. Polyribosome chains (open arrows) are found in close proximity to the ER. × 50 000. Scale bar = 0.25 μm. FIG. 23. A longitudinal section of a portion of a phloem parenchyma cell. A long segment of a microfilament bundle (MF) is present in the cytoplasm near the large central vacuole (V). ×14 800. Scale bar = 1 μm. FIG. 24. A high magnification view of a portion of a longitudinally sectioned microfilament bundle which demonstrates the filamentous substructure of the bundle. × 65 000. Scale bar = 0.25 μm. FIG. 25. A section through a cytoplasmic region of a phloem parenchyma cell which demonstrates the presence of an aggregation of spine-coated membraneous tubules and (or) vesicles (arrows). Usually only endoplasmic reticulum (ER) and lipid bodies (L) are present within the aggregations. ×38 000. Scale bar = 0.5 μm. FIG. 26. A micrograph of a portion of a phloem parenchyma cell that illustrates continuity between a spine-coated tubule (*t*) and a dilated segment of smooth membranes presumably related to endoplasmic reticulum (*er*). M, mitochondrion. × 71 000. Scale bar = 0.25 μm.

most notable among these were microfilament bundles which have been reported to occur in the phloem parenchyma cells of many other plants (Parthasarathy and Mühlethaler 1972; Esau 1973). Functionally, microfilament bundles are often considered to be associated with the phenomenon of cytoplasmic streaming (Kamiya 1981; Pesacreta et al. 1982). If cytoplasmic streaming occurs in the phloem parenchyma cells of the sugar beet petiole, as has been reported for several other species (Currier et al. 1955; Esau et al. 1963), it may enhance the symplastic movement of solutes through these cells as has been postulated in a theoretical treatment of symplastic transport (Tyree 1970).

The presence of an extended system of endoplasmic reticulum at the cell periphery, in association with numerous polyribosomes and the highly elaborated Golgi apparatus of the petiolar phloem parenchyma cells, also distinguished these cells from those of the minor vein phloem. While these structures may represent specializations associated with the lateral movement of solutes within the petiole, it is more likely that they reflect a fundamental difference in the developmental relations of these cells. In the petioles of rapidly growing leaves, cambial activity results in a displacement of functional phloem cells away from the cambium and toward the bundle cap. As these cells approach the bundle cap, the oldest sieve elements and companion cells become obliterated, and neighboring phloem parenchyma cells "merge imperceptibly" with the collenchymatously thickened cells that make up the bundle cap (Esau 1933). Thus, the phloem parenchyma cells found in the region of mature sieve elements are either about to begin or have already begun differentiation into bundle cap cells. Perietal ER of the form described in the present study has been reported for some developmentally immature cell types, such as root cells (Bonnett and Newcomb 1965). Maturing sieve elements in the sugar beet petiole were also characterized by this form of ER (J. W. Oross, unpublished observation).

The transformation of the petiolar phloem parenchyma cells into bundle cap cells also involves pronounced thickening of the cell wall (Esau 1933). The numerous dictyosomes and the dictyosome-associated membranes containing polysaccharide-positive materials may be involved in the secretion of wall materials that contribute to the wall thickening.

Spine-coated membraneous vesicles and (or) tubules have been reported in many cell types of sugar beet and tobacco, as well as phloem parenchyma cells of *Mimosa* (Esau 1973) and *Tetragonia* (Esau and Hoefert 1971). In situations where these structures are aggregated, they are often found in close spatial association with cisternae of endoplasmic reticulum, but not in actual contact (Esau and Gill 1970). Esau and Gill (1970) took this association as an indication of a functional relationship between these structures. The finding in the present study of connections between spine-coated tubules and membranes morphologically similar to endoplasmic reticulum suggests that there may also be a developmental relationship between these structures.

**Acknowledgement**

This research was supported by National Science Foundation grant PCM 83-15408 to W.J.L.

ARTSCHWAGER, E. F. 1926. Anatomy of the vegetative organs of the sugar beet. J. Agric. Res. **33**: 143–176.

BONNETT, H. T., and E. H. NEWCOMB. 1965. Polyribosomes and cisternal accumulations in root cells of radish. J. Cell Biol. **27**: 423–432.

CURRIER, H. B., K. ESAU, and V. I. CHEADLE. 1955. Plasmolytic studies of phloem. Am. J. Bot. **42**: 68–81.

ESAU, K. 1933. Pathologic changes in the anatomy of leaves of the sugar beet, *Beta vulgaris* L. affected by curlytop. Phytopathology, **23**: 679–712.

———1934. Ontogeny of phloem in the sugar beet (*Beta vulgaris* L.). Am. J. Bot. **21**: 632–644.

———1965. Fixation images of sieve element plastids in *Beta*. Proc. Natl. Acad. Sci. U.S.A. **54**: 429–437.

———1967. Minor veins in *Beta* leaves: Structure related to function. Proc. Am. Philos. Soc. **3**: 219–233.

———1972. Cytology of sieve elements in minor veins of sugar beet leaves. New Phytol. **71**: 161–168.

———1973. Comparative structure of companion cells and phloem parenchyma cells in *Mimosa pudica* L. Ann. Bot. **37**: 625–632.

ESAU, K., E. M. ENGLEMAN, and T. BISALPUTRA. 1963. What are transcellular strands? Planta, **59**: 617–623.

ESAU, K., and R. H. GILL. 1970. A spiney cell component in the sugar beet. J. Ultrastruct. Res. **31**: 444–455.

ESAU, K., and L. L. HOEFERT. 1971. Composition and fine structure of minor veins in *Tetragonia* leaf. Protoplasma, **72**: 237–253.

FERRIER, J. M., and A. L. CHRISTY. 1975. Time-dependent behaviour of a mathematical model for Münch translocation. Application to recovery from cold inhibition. Plant Physiol. **55**: 511–514.

GEIGER, D. R., M. A. SAUNDERS, and D. A. COTALDO. 1969. Translocation and accumulation of translocate in the sugar beet petiole. Plant Physiol. **44**: 1657–1665.

GRUSAK, M. A., and W. J. LUCAS. 1984. Recovery of cold-inhibited phloem translocation in sugar beet. I. Experimental analysis of an existing mathematical recovery model. J. Exp. Bot. **35**: 389–402.

KAMIYA, N. 1981. Physical and chemical basis of cytoplasmic streaming. Annu. Rev. Plant Physiol. **32**: 205–236.

PARTHASARATHY, M. V., and K. MÜHLETHALER. 1972. Cytoplasmic microfilaments in plant cells. J. Ultrastruct. Res. **38**: 46–62.

PESACRETA, T. C., W. W. CARLEY, W. W. WEBB, and M. V. PARTHASARATHY. 1982. F-actin in conifer roots. Proc. Natl. Acad. Sci. U.S.A. **79**: 2898–2901.

ROLAND, J. C. 1978. General preparation and staining of thin sections. *In* Electron microscopy and cytochemistry of plant cells. *Edited by* J. L. Hall. Elsevier/North-Holland Biomedical Press, Amsterdam. pp. 1–62.

SHOBE, W. R., and N. R. LERSTEN. 1967. A technique for clearing and staining gymnosperm leaves. Bot. Gaz. (Chicago), **128**: 150–152.

SOKOLOVA, S. V. 1968. Fine structure of petiole phloem cells of *Beta vulgaris* L. Sov. Plant Physiol. (Engl. Transl.), **15**: 631–638.

SPURR, A. R. 1969. A low viscosity epoxy resin embedding medium for electron microscopy. J. Ultrastruct. Res. **26**: 31–43.

SWANSON, C. A., and D. R. GEIGER. 1967. Time course of low temperature inhibition of sucrose translocation in sugar beets. Plant Physiol. **42**: 751–756.

TYREE, M. T. 1970. The symplast concept. A general theory of symplastic transport according to the thermodynamics of irreversible processes. J. Theor. Biol. **26**: 181–214.

ED IN CANADA IMPRIMÉ AU CANADA

0022-1554/86/$3.30
The Journal of Histochemistry and Cytochemistry
Copyright © 1986 by The Histochemical Society, Inc.
Vol. 34, No. 3, pp. 327–338, 1986
*Printed in U.S.A.*

Original Article

# Spectrophotometric and Cytochemical Analyses of Phosphatase Activity in *Beta vulgaris* L.[1]

THOMAS C. PESACRETA,[2] ALAN B. BENNETT, and WILLIAM J. LUCAS

*Departments of Botany (T.C.P., W.J.L.) and Vegetable Crops (A.B.B.), University of California, Davis, California 95616.*

Received for publication March 27, 1985 and in revised form July 5, 1985; accepted July 26, 1985 (5A0380).

**Spectrophotometric and cytochemical methods were used to investigate the localization and/or the sensitivity of phosphatase activities in aldehyde-fixed beet leaves and membrane fractions. The nonspecific acid phosphatase substrates, p-nitrophenyl phosphate and β-glycerol phosphate, each exhibited unique spectrophotometric patterns of hydrolysis as a function of pH. Additionally, β-glycerol phosphatase activity was primarily present on the tonoplast, whereas p-nitrophenyl phosphatase was present on the plasma membrane. Because of the unique pH response of each enzyme and their different localization, we conclude that they cannot be entirely "nonspecific." The spectrophotometric pattern of ATP hydrolysis differed from that of p-nitrophenol phosphate in that it decreased at pH 5.0–5.5 and was greatly inhibited by 10 mM sodium fluoride; however, both activities were on the plasma membrane. Therefore, we conclude that these activities represent either two enzymes or only one enzyme that differs in its ability to hydrolyze these two substrates. Generally, enzymatically produced lead deposits on the plasma membrane of non-vascular cells were as frequent and large as those on phloem cells; frequently, deposits on sieve element plasma membranes were relatively small. We therefore conclude that there is no evidence for the presence of relatively intense ATPase activity on the plasma membrane of phloem cells in beet leaf, in contrast to other species. Studies with membrane fractions indicated that formaldehyde could completely inhibit the inhibitor-sensitive phosphatase activities in mitochondrial and vacuolar fractions while preserving significant activity in the plasma membrane fraction.**

KEY WORDS: ATPase; Acid phosphatase; Beet; PNPase; pH response; Membrane fractions; Phloem transport.

## Introduction

Lead precipitate-based cytochemistry is a widely used technique which has been employed to study acid phosphatases (Gomori, 1952) and ATPases (Wachstein and Meisel, 1957). Several drawbacks to this technique are known to exist. For example, both glutaraldehyde and formaldehyde fixatives, which must be used to enable the cytochemical reagents to diffuse into the cells, are known to be inhibitory to many phosphatases (Anderson, 1967; Ernst and Philpott, 1970), with formaldehyde being the least inhibitory. Lead ions, which are necessary to allow localization of the phosphatase activity, are also inhibitory (Jacobsen and Jørgensen, 1969). In addition, some authors have questioned the ability of the lead precipitation technique to accurately localize phosphatase activity (Washitani and Sato, 1976). In spite of these difficulties, a careful study of factors that influence the formation of enzymatically produced lead precipitates in plant cells is still a worthwhile objective, in that it could lead to development of reliable cytochemical data about phosphatases in tissues where the physiological role of phosphatases is of interest. It should be noted here that immunological techniques alone, although suitable for localization of enzymes, completely fail to detect levels of activity.

Only a modest amount of quantitative data is available concerning the activity of plant phosphatases after or during exposure to various concentrations of formaldehyde, glutaraldehyde, and $Pb^{2+}$ and $H^+$ ions. Gilder and Cronshaw (1974) used only one relatively high concentration of both aldehyde and $Pb^{2+}$ to analyze phosphatase activity in tissue homogenates. Bentwood and Cronshaw (1976) analyzed the response of acid phosphatase (i.e., β-glycerol phosphatase) activity in tissue homogenates at different pH values. Their data showed two peaks of activity, one at pH 5.5 and another at pH 6.2. Goff and Klohs (1974) found that glutaraldehyde fixation inhibited nucleoside diphosphatase activity in onion root homogenates much more than did fixation with formaldehyde. To our knowledge, only one published report exists concerning the effects of fixation on phosphatase activities in fractionated membranes from plant cells. Al-Azzawi and Hall (1977) found that activity in a crude microsomal fraction was much more strongly inhibited by aldehyde fixation than was the activity in the mitochondrial fraction. Thus, little or no published quantitative information exists concerning the effect(s) of fixation on phospha-

[1] This research was funded by NSF Grants PCM 79-10223 and PCM 81-17721 (W.J.L.)
[2] Present address: The Biological Laboratories, Harvard University, 16 Divinity Ave., Cambridge, Massachusetts 02138

tase activities in tissues that have not been structurally perturbed following fixation and can be directly used for cytochemical investigations. This is an important point because at present we can only guess at the effect that tissue homogenization may have on enzymatic activities.

Although many articles have been published that concern the cytochemistry of phosphatases in higher plant cells at the electron microscopic level, many of these articles have dealt either with vascular tissue (Robards and Kidwai, 1969; Charvat and Esau, 1975; Evert, 1977 and references therein; Browning et al., 1980; Cronshaw, 1980 and references therein) or with interpretive questions (Van Steveninck, 1979; Hall et al., 1980). Fewer electron microscope studies have examined the cytochemistry of phosphatases in non-vascular tissues. Pyliotis et al. (1979 and references therein) examined the acid phosphatase activity of aleurone cells, Mogensen (1981) reported on the phosphatase activity in *Saintpaulia* ovules, Hall (1977) investigated the effect of washing before fixation on glucose-6-phosphatase activity in beet discs, and Sexton et al. (1971 and references therein) studied the localization of β-glycerol phosphatase activities in root tips. Little or no data are available concerning the relatively common mesophyll cell type in leaves.

Our laboratory's interest was in the comparative aspects of distribution of ATPase activity in each of the various cell types in sugar beet leaves. This interest grew out of our earlier findings that active uptake of sugars could occur in most, if not all, sugar beet leaf cell types which were incubated in media containing radiolabeled sugars (Maynard and Lucas, 1982). All of the earlier cytochemical studies that were done with *Nicotiana tabacum* (Gilder and Cronshaw, 1974; Bentwood and Cronshaw, 1976) had consistently indicated that phloem cells exhibited relatively high levels of phosphatase activity. To complement our previous physiological data, we were interested in determining cytochemically whether any particular cell type(s) in beet leaves contained a particularly active ATPase, such as that in *Nicotiana*, which had been inferentially related to the process of phloem transport.

In order to understand more fully the potential of cytochemical methods to provide meaningful information, we have extensively analyzed the ability of sugar beet leaf tissue pieces and red beet storage-organ membrane fractions to hydrolyze phosphate ester substrates after various preparatory cytochemical treatments. With cytochemical and spectrophotometric methods, we show that each of several enzymatic activities is uniquely affected by the concentration of fixative, pH, and inhibitors such as lead, molybdate, vanadate, and fluoride. In addition, we show that reliable cytochemical information can be obtained only if the very limited penetration of reagents into the tissue is taken into account. With regard to the phosphatase activity in various cell types, we show that the amount of activity on the plasma membrane of mesophyll cells appears to be similar to that in vascular cells.

## Materials and Methods

**Plant material.** Sugar beet plants (*Beta vulgaris* L. var. SSBN1, USH10, lot 3102 or USH 11 lot 82312) were grown in a growth chamber under the conditions specified in Grusak and Lucas (1984). Plants 4–6 weeks old were used. For the purpose of standardization, leaves that occupied intermediate positions in the rosette and were 14–18 cm long and 9–12 cm wide were used; in most cases, experiments conducted on a particular day were performed on a single leaf.

**Tissue preparation.** Unless otherwise noted, fixation in freshly prepared 3% formaldehyde in 50 mM sodium cacodylate buffer (pH 7) always began in the morning after the growth chamber lights had been on for 2–4 hr. Leaves were cut either by hand, using single-edge razors for no more than 10–15 strokes, or by a mechanical tissue sectioner (Mickle Laboratory Engineering Co., Gomshall, Surrey, UK, or Sorvall, Newton, CT; model TC-1). Before the leaf was cut into small pieces with the tissue sectioner, it was trimmed by hand to the shape of a disc or a square with dimensions of 5.5 cm × 5.5 cm, gently weighted, and immersed in the fixative solution (100 ml/piece) for 0.5–1 hr (this and all other solutions were at room temperature). Next, the leaf was either hand-sectioned or taped to a plastic backing and machine-sectioned at a thickness of 125–200 μm. In order to obtain large numbers of uniformly sized pieces, the leaf had to be pulled taut as part of the taping process. Each piece was then cut in half by hand, doubling the final number of pieces, and then put back into the original fixative solution for 0.5–1.0 hr. The tissue was then washed in 200 ml of 50 mM sodium cacodylate buffer, pH 7, for 0.5–1 hr, and then in 200 ml of 50 mM Tris–MES, pH 7 (if they were destined for spectrophotometric analysis) or 50 mM Tris-maleate, pH 7.25 (for most cytochemistry), for 2–3 hr. For cytochemical analysis of β-glycerol phosphate activity at pH 5.5, the tissue pieces were washed in sodium acetate buffer (pH 5.5).

Just before incubation in solution containing phosphate ester substrates, tissue pieces were placed into buffer of the appropriate pH value for 2–4 min. For incubation, eight tissue pieces were placed for 1–2 hr in 10 ml of solution in a polyethylene cup on a shaker operating at 25 rpm; each data point is the average of values obtained from four such cups, and the error bars represent SEM values. In most cases, the incubation solution contained the appropriate buffer, 5 mM substrate (i.e., either disodium adenosine triphosphate [ATP], disodium p-nitrophenyl phosphate [PNP], or disodium β-glycerol phosphate [BGP]. In addition, 10 mM $MgCl_2$ and 2 mM $Pb(NO_3)_2$ or $PbCl_2$ were added, except where noted.

**Phosphate ester hydrolysis analyses.** For spectrophotometric analyses the following procedures were used. PNP hydrolysis was stopped by removing the tissue pieces from each cup at the end of a carefully timed incubation period and then adding 2 ml of 1 N sodium carbonate per cup. These solutions were then analyzed for absorbance at 410 nm with a Zeiss PM6 spectrophotometer (Carl Zeiss, New York, NY). ATP hydrolysis was measured by using the Fiske and Subbarow (1925) reagent (Sigma Chemical Co., St. Louis, MO). BGP hydrolysis was measured using the Ames (1966) technique. In all cases, less than 5% of the total substrate was hydrolyzed during the incubation period. If solutions contained lead, they were spun on a table top centrifuge (International Equipment Co., Needham, MA; model CL operated at 180 × g) to pellet the lead precipitate which formed when the stopping solution was added in the case of incubations that analyzed PNPase activities. Control treatments were as follows:

1. Complete incubation reagents without tissue. This control detected the amount of non-enzymatic hydrolysis. In most cases the amount of such hydrolysis was very small; at pH 5.0–5.5 some non-enzymatic hydrolysis was usually present.
2. Complete incubation reagents plus tissue pieces that had been heated to 60°C for 5.0 min. This control detected the amount of hydrolysis that the inactive tissue constituents could produce. In all cases, only extremely low levels of hydrolysis were detected in these controls.
3. Complete incubation reagents plus tissue pieces which were removed after the normal period of incubation but with stopping solution not added until 1 hr had passed.

The solutions were then analyzed as usual. In all cases, the amount of inor-

ganic phosphate detected in these solutions was within 10% of the amount in test solutions to which stopping solution was added immediately after the tissue pieces had been removed. This result indicated that only a small amount of soluble activity had diffused out of the tissue pieces into the incubation solution.

If tissue pieces were to be prepared for cytochemical analysis, after the incubation period they were placed in Tris-maleate buffer for 15 min. Next, they were placed in two changes of double-distilled water for 1 hr; this was necessary to remove the Tris-maleate, which otherwise seemed to darken osmium tetroxide solutions and caused precipitates to appear in thin sections. After washing in distilled water, the pieces were placed in 1% osmium tetroxide in double-distilled water for 10–16 hr on ice. Tissues were next washed in double-distilled water, dehydrated in acetone, infiltrated, and embedded in Epon–Araldite resin, sectioned so as to have gold interference colors, and viewed on a JEOL (Tokyo, Japan), model 100S transmission electron microscope operated at 60 kV. Post-staining of sections was omitted in all cases so that the enzymatically produced lead deposits could be unambiguously identified.

**Membrane fraction preparations.** Red beet membrane fractions were prepared and analyzed as described by Bennett et al. (1984). In order to determine the effect of aldehyde fixation on phosphatase activity, the fractions were prepared in HEPES instead of Tris–MES buffer (which reacts with aldehydes) and then added to an equal volume of double-strength fixative which had been adjusted to pH 7 with MES buffer. Fixation was for 1 hr, on ice, after which the solution was diluted tenfold with HEPES buffer, pelleted by centrifugation, resuspended in Tris–MES buffer, and the membrane fractions used for ATPase analyses. With regard to membrane fractions that were analyzed to determine the effect of lead or ATPase activity, we found that the presence of lead phosphate did not influence the ability of the Ames (1966) reagents to detect phosphate in control solutions to which both lead nitrate and sodium phosphate had been deliberately added. Presumably this is the result of the solubilization of lead phosphate, which occurs as a consequence of acidification of the incubation medium during analysis (Klohs and Goff, 1973).

**Glutaraldehyde purification.** In a number of our experiments, we used glutaraldehyde as a fixative. Anderson (1967) reported that an impurity in glutaraldehyde has an inhibitory effect on various enzymatic activities. We therefore purchased Sigma Grade 1 glutaraldehyde for use in our experiments; however, even this "especially purified" preparation contained enough of the impurity to result in a purification index of 0.61 (see Anderson, 1967). To overcome this problem, we purified glutaraldehyde in a vacuum distillation apparatus; this decreased the purification index to 0.10. This purified glutaraldehyde was considered acceptable for the present study.

**Table 1.** *Effect of type and concentration of fixative on enzymatic hydrolysis of PNP in sugar beet leaf tissue pieces*

| Fixative | % Activity |
|---|---|
| 0.5% formaldehyde | 100[a] |
| 0.5% glutaraldehyde | 67 |
| 3.0% formaldehyde | 78 |
| 3.0% glutaraldehyde | 58 |
| 3.0% formaldehyde + 0.5% glutaraldehyde | 46 |
| 4.5% formaldehyde + 4.5% glutaraldehyde | 31 |
| 50 mM sodium cacodylate[b] | 17 |

[a] Activity in 0.5% formaldehyde was the highest and so was arbitrarily set as 100%.

[b] All fixatives contained 50 mM sodium cacodylate, pH 7.0.

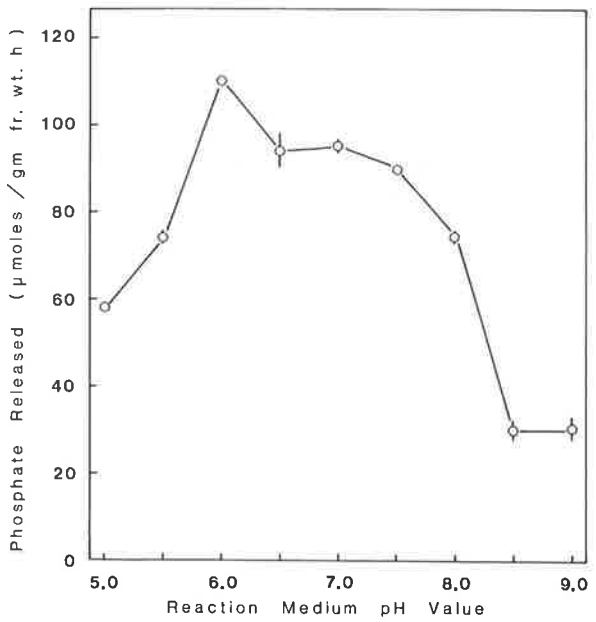


Figure 1. Hydrolysis of ATP by sugar beet leaf tissue pieces as a function of pH. Background values for the non-enzymatic hydrolysis of ATP increased as pH decreased, and all values have been adjusted accordingly. No lead present in solutions.

## Results

### *Spectrophotometric Analysis of Activity in Tissue Pieces*

Our investigations showed that the level of phosphatase activity was directly related to the concentration and type of fixative which was used to prepare the tissue (Table 1). Although the lowest concentrations of aldehyde yielded tissue pieces with the highest levels of activity, the structural preservation was relatively limited, e.g., in the chloroplasts stromal density was low, and plasma membranes appeared to be unilamellar rather than tripartite. Conversely, when the highest levels of fixative were used, structural preservation was good but enzymatic activity was low. Note that 0.5% glutaraldehyde resulted in much less activity than was present with 0.5% formaldehyde, and that adding only 0.5% glutaraldehyde to 3.0% formaldehyde also caused a noticeable reduction in the level of activity. Preparation of tissue pieces in buffer alone resulted in the lowest levels of activity. Cytochemical analysis of pieces that were prepared in buffer alone revealed that only the cut cells were reactive; apparently the intact cells were not permeable to the cytochemical reagents. Therefore, in order to permeabilize the cells adequately and also to preserve adequately both their structure and enzymatic activity, 3% freshly prepared formaldehyde (from paraformaldehyde) was used in all subsequent experiments with tissue pieces, unless otherwise noted.

By adjusting the pH of the incubation solutions, it was possible to observe pH-dependent differences in the amount of phosphate ester substrate that was hydrolyzed by tissue pieces. Three types of phosphate esters were tested, and the hydrolysis of each as a function of pH generated three unique patterns of data points with remarkably small SEM values (Figures 1–3). ATPase activity

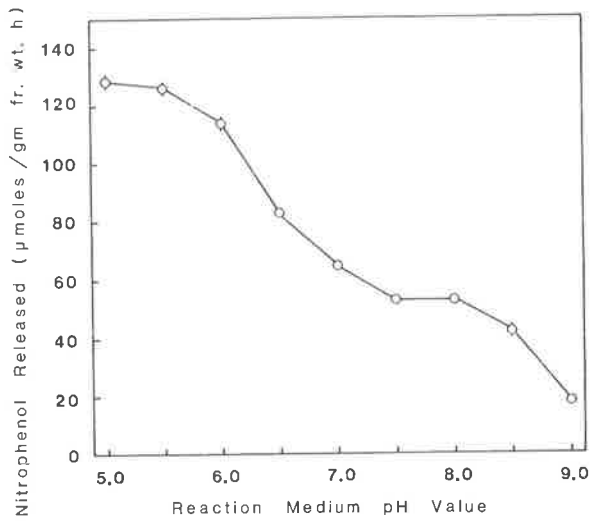


Figure 2. Hydrolysis of p-nitrophenyl phosphate by sugar beet leaf tissue pieces as a function of pH; values adjusted as in Figure 1. No lead present in solutions.

(Figure 1) peaked at pH 6.0, with lesser amounts of activity being present under more acidic or more alkaline conditions. In contrast, the PNPase activity (Figure 2) showed a broad peak at low pH values and then gradually decreased with increasing alkalinity, with a "shoulder" of activity evident between pH 7.5 and pH 8.0. BGPase activity (Figure 3) also peaked at pH 6.0; however, in contrast to both PNPase and ATPase activity, BGPase activity was almost nonexistent above pH 7.0.

ATPase activity was also shown to differ from PNPase activity by analyzing the effect of inhibitors on hydrolysis (Figure 4). PNPase was much less sensitive to fluoride than was ATPase, whereas molybdate inhibited the PNPase more than it did the ATPase. Both types of activity were equally sensitive to inhibition by vanadate. PNPase activity was not affected by either presence or absence of $MgCl_2$ in the incubation media; however, ATPase activity was almost completely dependent on the presence of $MgCl_2$ (data not shown).

Although much of the phosphatase activity could be preserved by formaldehyde fixation, in order to assay this activity cytochemically it was necessary to include lead nitrate or lead chloride in the incubation media. Although inclusion of more than 1 mM lead nitrate greatly inhibited the phosphatases (Figure 5), enzymatic activities were still sensitive to substrate concentration (Figure 5) and to pH (Figure 6).

In some experiments, the effect of including as much as 40 mM $CaCl_2$ in the fixative solution was tested. Generally, such an addition was stimulatory to phosphatase activity by as much as 15–30%; however, in some cases no increase in activity was observed. We were therefore forced to conclude that this variation was caused by some unknown factor, either in our tissue or in our preparatory technique. Addition of 50–100 mM KCl to the incubation media never significantly increased the amount of hydrolysis of either ATP or PNP.

## *Cytochemical Analysis of the Extent of Activity in Tissue Pieces*

Perhaps the most difficult aspect of our cytochemical analysis was the apparent variation in activity which we frequently noted in our initial studies. Often, mesophyll cells which were within one cell diameter (i.e., 15–25 μm) of each other would show extreme variation in the amount of lead deposition that was present as a result of enzymatic activity. This difficulty was eliminated after we realized that the penetration of our reagents into the cut tissue was quite limited. Even after incubation periods of 1.5 hr, only the outer two or three cell layers showed any enzymatically related lead deposition (Figures 7–10). Within these three layers of cells, lead deposition was not uniform but instead occurred as a gradient, with the largest amounts being present in the outermost layer; this region represents the most perturbed area of the tissue. In the first layer of intact cells, lead deposition was generally uniform, although even here the deposition was frequently more prevalent on the side of the cell that was closest to the cut surface. Further into the tissue, lead deposition was usually present only in the half of the cell that was nearest to the cut surface. Even within mature vessels that had phosphatase activity present in their cell walls, a definite deposition gradient was evident (Figure 11). Increasing

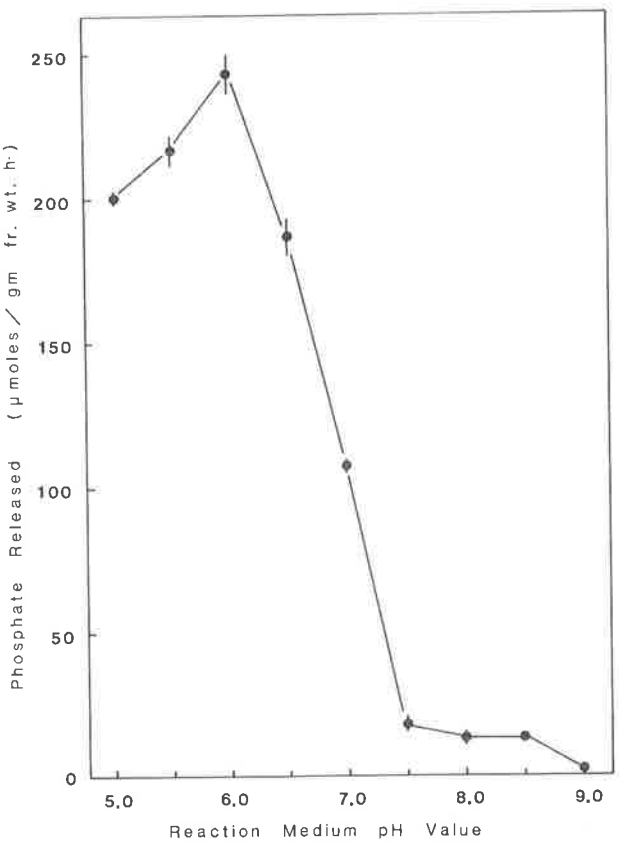


Figure 3. Hydrolysis of β-glycerol phosphate by sugar beet leaf tissue pieces as a function of pH; values adjusted as in Figure 1. No lead present in solutions.

the incubation period to 2–3 hr had the effect of slightly enhancing the extent of the lead deposition zone; however, this treatment also resulted in the production of relatively large lead deposits, which often obscured cytological features in the first layer of intact cells. If the incubation period was shortened to 0.5 hr, the lead deposits were generally restricted to the surface layer of cut cells.

The reason for the limited extent of the enzymatically related lead deposition in the leaf pieces is not understood; other experiments (Figure 18) indicated that high concentrations of lead nitrate could completely and evenly penetrate into leaf pieces within 30 min. It is therefore possible that the diffusion rate of the phosphate ester substrates into the leaves was the limiting factor for deposition. We have not directly tested the validity of this possibility, but if it is true, it could indicate that the spectrophotometric data in Figures 1–6 underestimates by as much as 50% the total ability of the leaf pieces to hydrolyze substrate.

In approximately 20% of our cytochemical experiments, partial reversal of the aforementioned deposition gradient was observed; in these cases, the cut cells at the surface of the tissue piece were relatively devoid of lead deposits (Figure 12), and the first layer of intact cells had lead deposits located primarily on the surfaces farthest from the cut surface. This phenomenon was found to occur with greatest frequency when tissue pieces were sliced to final size after relatively short periods of exposure of the rough-trimmed pieces to formaldehyde.

## *Cytochemical Analysis of Enzymatic Activities*

In several cases, tissue pieces were taken from experiments that were also spectrophotometrically analyzed. In other cases, tissue pieces were only cytochemically analyzed. We analyzed activity at pH 5.5 and 7.25 so that our results could be directly compared to the results of other authors for acid phosphatase and ATPase, respectively.

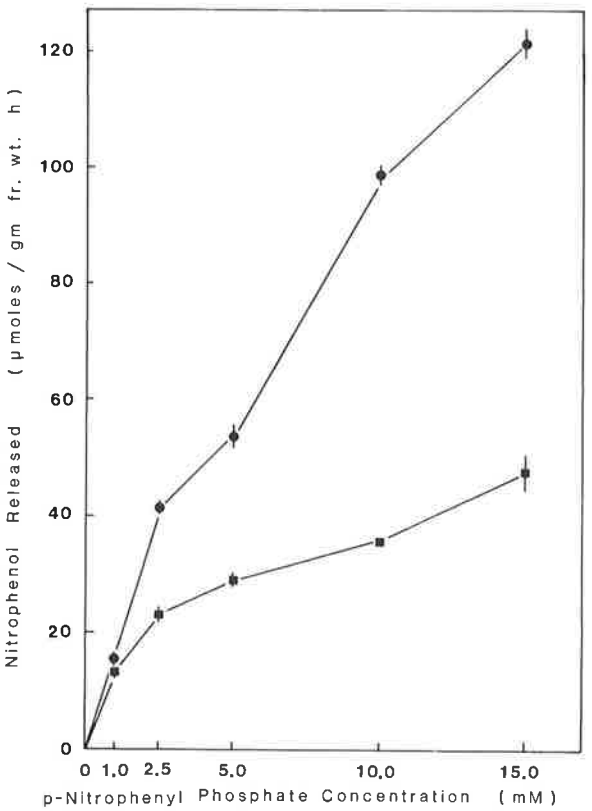


Figure 5. Hydrolysis of p-nitrophenyl phosphate by sugar beet leaf tissue pieces as a function of substrate concentration. Control (●) versus effect of 2 mM lead nitrate on hydrolysis (■).

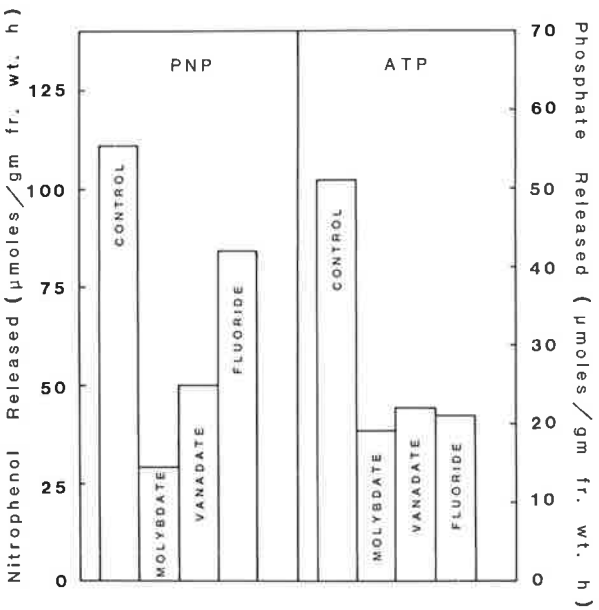


Figure 4. Comparison of the effects of three inhibitors on ATP and p-nitrophenyl phosphate hydrolysis in sugar beet leaf tissue pieces. Concentrations and inhibitors were as follows: vanadate, 100 µM; molybdate; 2 mM; fluoride, 10 mM. No lead present in solutions.

At pH 7.25, lead deposits resulting from ATPase activity were primarily found on the plasma membrane (Figure 13). This deposition was almost completely $Mg^{2+}$-dependent. Lead was also deposited on the surface of cell walls that bordered the intercellular air spaces and, less frequently, on the tonoplast; however, the frequency of deposition at these sites was sporadic in contrast to the plasma membrane. At pH 5.5 the same intracellular locations contained lead depositions, but they were much more intense than the deposits observed at pH 7.25. Without $Mg^{2+}$ in the incubation media, lead deposits were infrequent, but sometimes occurred on the plasma membrane.

Although the many mesophyll cells were the cell type we most frequently examined, we also carefully studied the patterns of lead deposition present in the cells of the vascular bundles. As noted previously, at pH 7.25 such deposits could be seen in or on the walls of mature vessels. In addition, the parenchymatous cells of the xylem and phloem contained lead deposits which appeared to be similar in size to those observed in the mesophyll cells of the same tissue pieces (Figure 14). In contrast, the mature sieve elements quite frequently contained relatively small lead deposits.

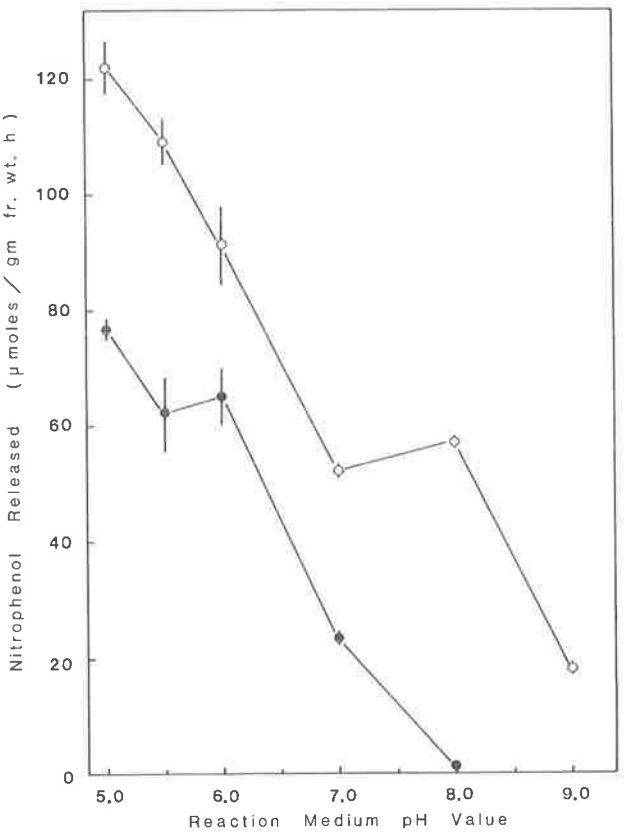


Figure 6. Hydrolysis of p-nitrophenyl phosphate by sugar beet leaf tissue pieces as a function of pH. Control (○) versus the effect of 2 mM lead nitrate on hydrolysis (●).

In some instances, the sieve elements contained lead deposits comparable in size to those in the parenchymatous vascular cells; however, in no case did we observe sieve elements and/or parenchymatous vascular cells that contained larger lead deposits than were present in the mesophyll cells of the same tissue piece.

PNPase activity at pH 7.25 appeared in the same cellular locations as did the ATPase activity (Figure 15), and was also very evident at pH 5.5. PNPase activity did not, however, seem to require $Mg^{2+}$. Occasionally the tonoplast, and more frequently the cell wall, displayed lead deposits. Lead deposits in the mesophyll cells were similar in size to those found in the vascular bundles and, as with ATP as substrate, deposits on the plasma membranes of sieve elements were only as large as, or in most cases were smaller than, those present on the plasma membranes of other adjacent cell types (Figure 16).

BGPase activity did not require $Mg^{2+}$ and was almost nonexistent at pH 7.25. At pH 5.5, BGPase activity was quite prevalent in the vacuole of all cell types (Figure 17), with some activity occurring in the cytoplasm.

## *Lead Staining in the Absence of Substrate*

Some authors (Washitani and Sato, 1976) have indicated that lead deposits may form on the cell wall and tonoplast when tissue is incubated first in lead nitrate and then washed and incubated in phosphate buffer. We performed similar experiments with sugar beet leaf tissue pieces and found that very few such deposits were present. Furthermore, we incubated tissue in very high concentrations (100 mM) of lead nitrate alone and found that many lead deposits occurred both on endomembranes and on organelles (Figure 18) but not on the plasma membrane, in the cell wall, or on the tonoplast. When tissues treated in such a manner were washed and incubated in PNP or ATP as usual and the solution was then spectrophotometrically assayed, the amount of hydrolytic activity was equal to that in the untreated tissue pieces. This result, again, indirectly indicates that lead, known to be inhibitory to phosphatases, was not retained at the site of phosphatase activity on either the plasma membrane, the cell wall, or the tonoplast.

## *Spectrophotometric Analysis of Activity in Red Beet Membrane Fractions*

Plant cells possess a number of ATPases, each of which occurs in a particular area of the cell. Red beet storage organs have been extensively studied by several investigators who have indicated that ATPases are present on the tonoplast (Leigh and Walker, 1980; Bennett et al., 1984), in mitochondria, and on the plasma membrane (Briskin and Poole, 1983). In contrast, our present cytochemical results with sugar beet leaves indicated that most of the ATPase activity was present either on the plasma membrane or in the cell wall. By using mitochondrial, vacuolar, and plasma membrane fractions from red beet storage organs, we tested the effect of cytochemical reagents on the level of ATP hydrolysis.

Figure 19 shows the effect of formaldehyde concentrations on ATPase activity. Each line represents not the total activity found in a particular fraction but rather the effect of formaldehyde on the portion of activity that was sensitive to inhibition by either vanadate, molybdate, or azide. At 3% formaldehyde (i.e., the concentration we most commonly used for cytochemistry), vanadate-

Figures 7–8. Mesophyll cells in control sugar beet leaf tissue incubated in the absence of phosphate ester substrates. Abbreviations are as follows: (CS), cut surface; (CW), cell wall; (PM), plasma membrane; (T), tonoplast. Figure 7, Original magnification × 2900. Bar = 5 μm. Figure 8, Original magnification × 13,600. Bar = 1 μm. Figure 9. Mesophyll cells in tissue incubated with p-nitrophenyl phosphate. Lead deposits (arrows) that resulted from enzymatic activity were most extensive on cells that were near the cut surface (CS). On cells located further away from the cut surface, the amount of lead deposition was much decreased (darts). Original magnification × 2900. Bar = 5 μm. Figure 10. Mesophyll cells in tissue incubated with ATP. Lead deposits formed as a result of enzymatic activity were present on the cell wall (CW), plasma membrane (PM), and tonoplast (T). Compare these deposits with the lack of such deposits in the control tissues (Figures 7 and 8). Original magnification × 13,600. Bar = 1 μm. Figure 11. Tissue incubated with ATP. Note that the lead deposits (darts) on the xylem (X) secondary wall thickenings near the cut surface (CS) are much larger than those on the thickenings in the more interior portions of the tissue piece (arrows). Bundle sheath cell (BS). Original magnification × 1600. Bar = 10 μm. Figure 12. Tissue incubated in ATP. "Reversed" deposition gradient phenomenon. Bundle sheath cells (BS) near the cut surface (CS) had larger lead deposits (arrows) on the portions of their plasma membranes furthest from the cut surface. Original magnification × 2500. Bar = 2 μm.

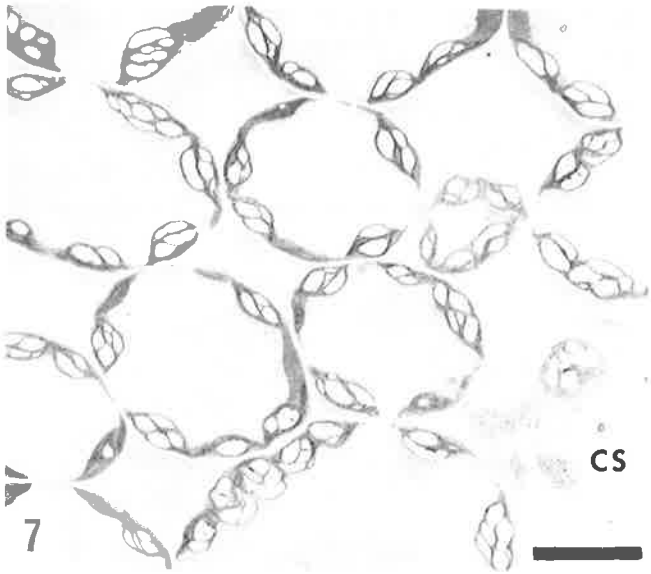
CS
7

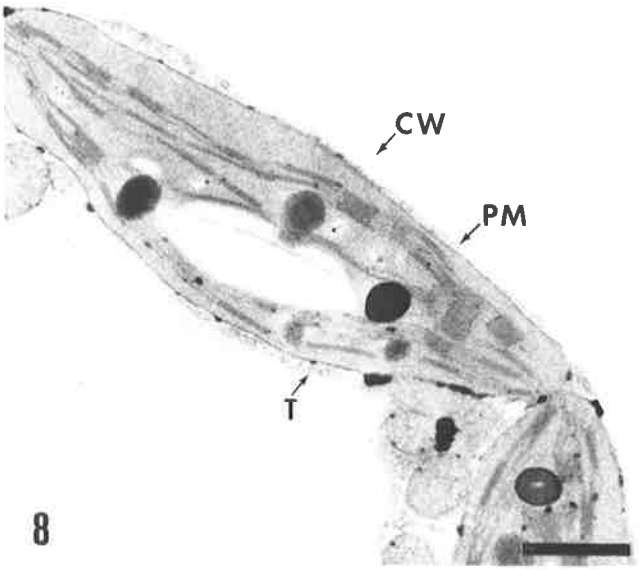
CW
PM
T
8

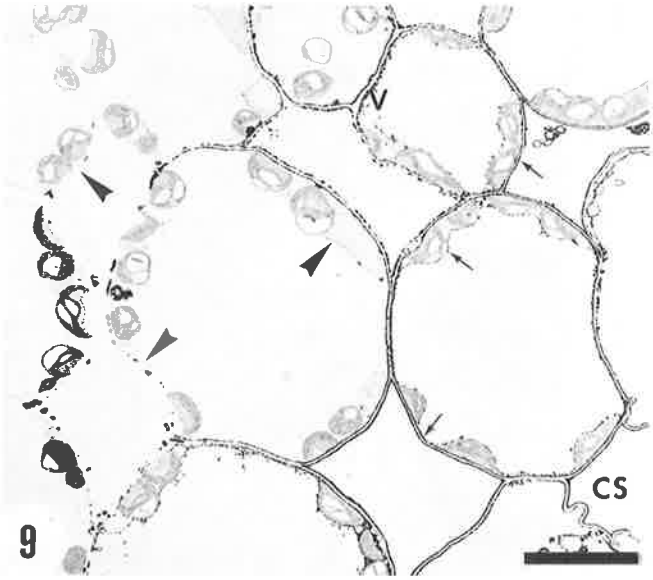
V
CS
9

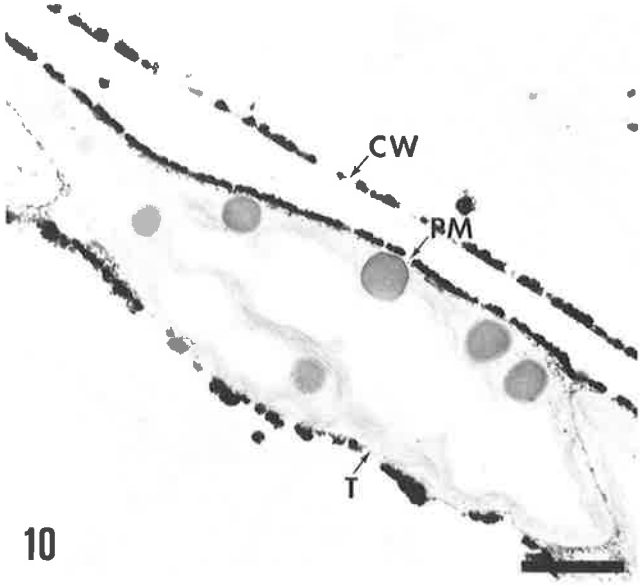
CW
PM
T
10

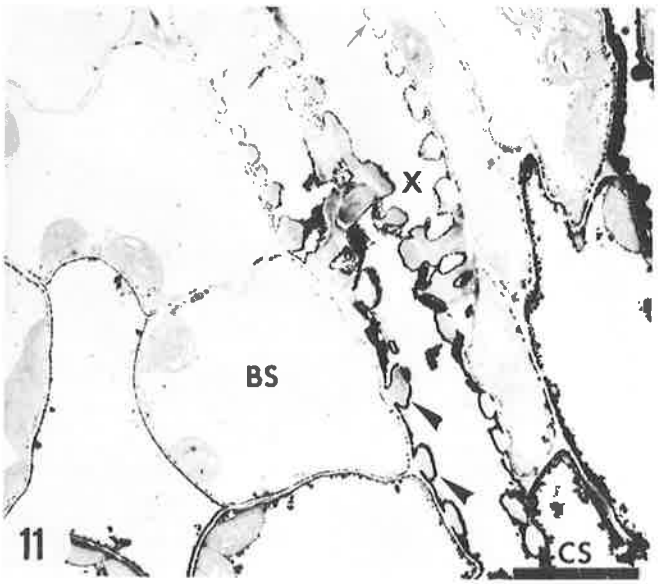
X
BS
CS
11

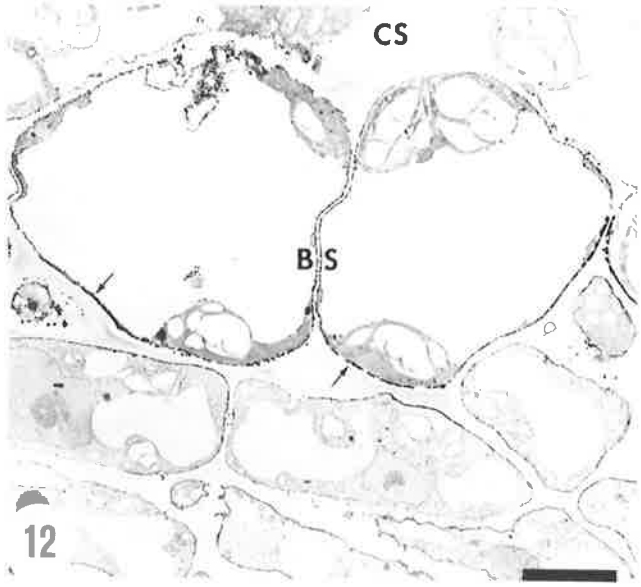
CS
BS
12

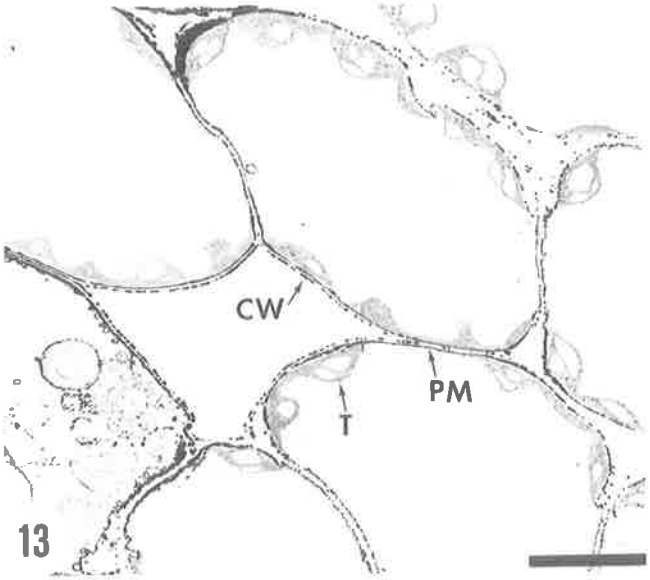
CW
PM
T
13

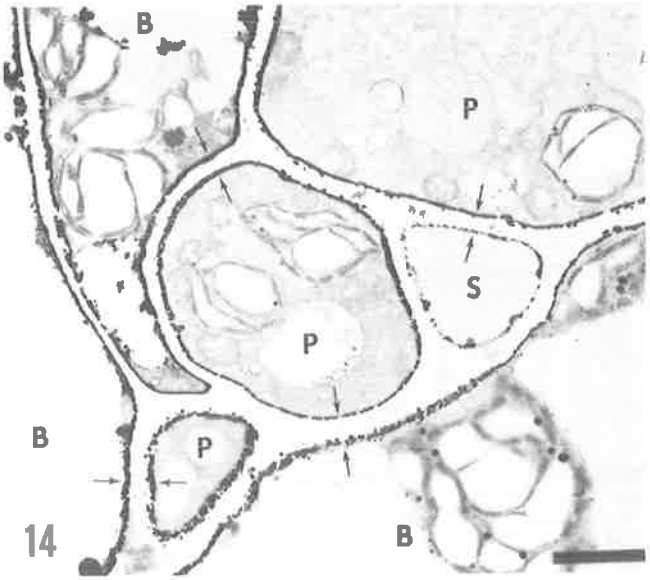
B
P
S
P
B
P
B
14

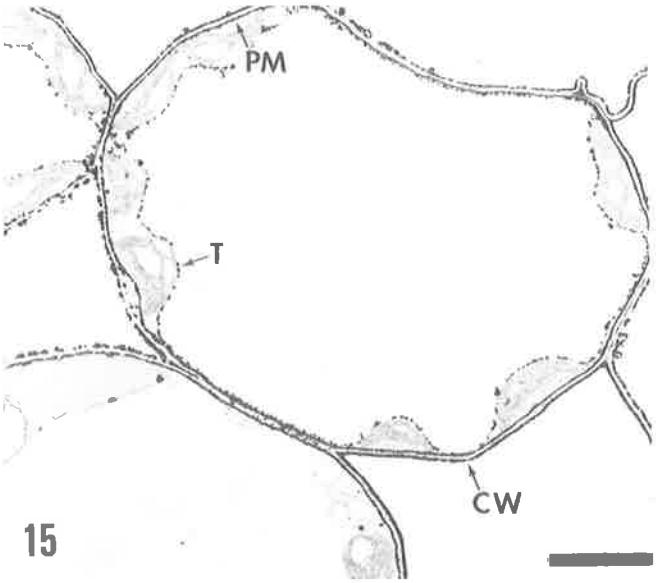
PM
T
CW
15

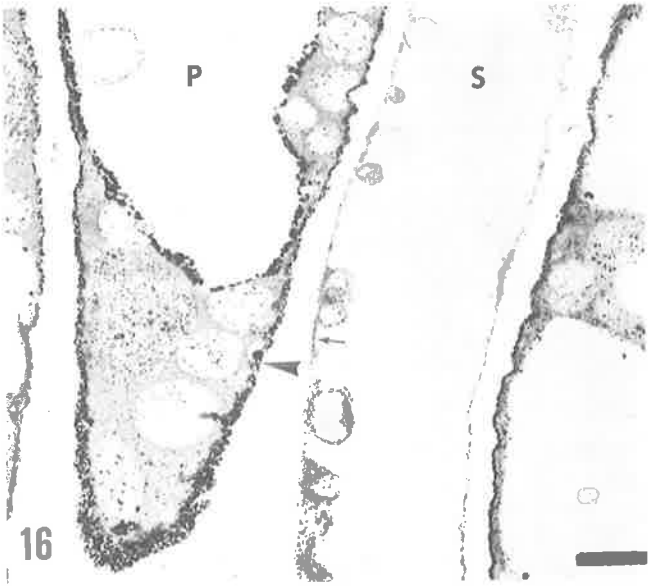
P
S
16

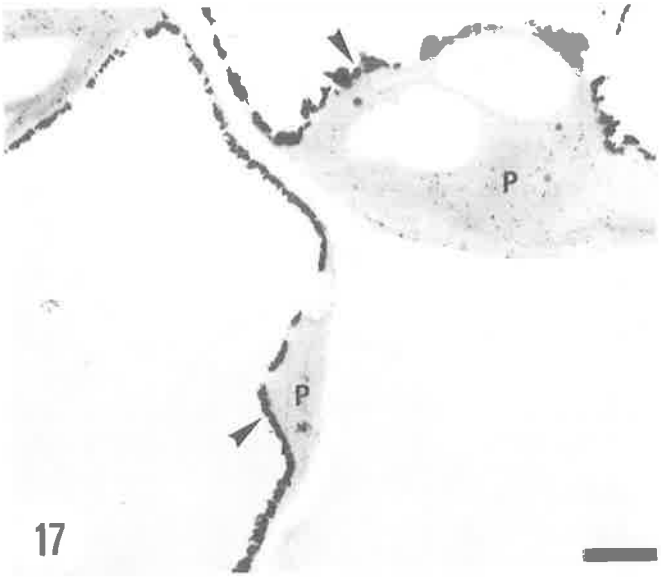
P
P
17

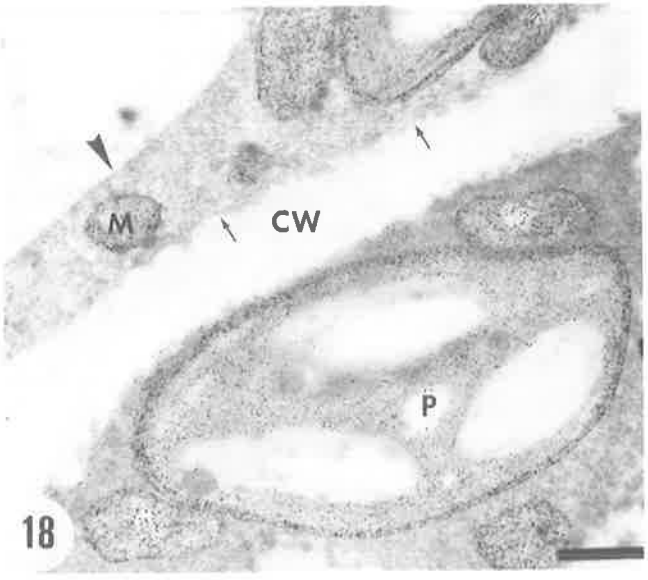
M
CW
P
18

sensitive activity in the plasma membrane fraction was still present in moderate amounts, whereas the nitrate-sensitive and azide-sensitive activities associated with the tonoplast and mitochondrial membranes, respectively, were almost undetectable. With glutaraldehyde, the results were quite different (Figure 19). All the activities had decreased to very low levels when only 0.5% glutaraldehyde was used as the fixative. In the plasma membrane fraction, a moderate amount of vanadate-sensitive activity was still present if no more than 0.1% glutaraldehyde was used. These experiments show that phosphatase activity in membrane fractions, as in leaf pieces, is by far more sensitive to glutaraldehyde than to formaldehyde. In addition, it appears likely that the previously noted lack of ATPase activity on the tonoplast at the cytochemical level is related to the relatively extreme sensitivity of these enzymes to aldehyde, as compared to that of the plasma membrane ATPases.

In addition to studying the inhibitory effect of the aldehydes, we also had to consider the effect of lead salts on activity. Because of what appeared to be a complex series of interactions between lead salts and the inhibitors we had previously used to characterize each fraction, we felt it best to present the effect of lead on the total activity in each fraction after fixation with 1% formaldehyde (Figure 20). We chose this concentration of fixative because it preserved moderate levels of all three types of activity, although the level of structural preservation in leaf pieces was marginal.

In all fractions, the effect of 0.5 mM or more of $PbCl_2$ was quite inhibitory, the activity in the plasma membrane fraction being the most sensitive. From these experiments it appeared that some ATPase activity was present in each fraction, even at the highest concentrations of $PbCl_2$ tested. Unfortunately, when we fixed leaf tissues with 1% formaldehyde and then examined them for cytochemical activity, the lead deposits in the cut cells at the surface of the tissue were quite extensive and appeared to have prevented further penetration of cytochemicals into the tissue.

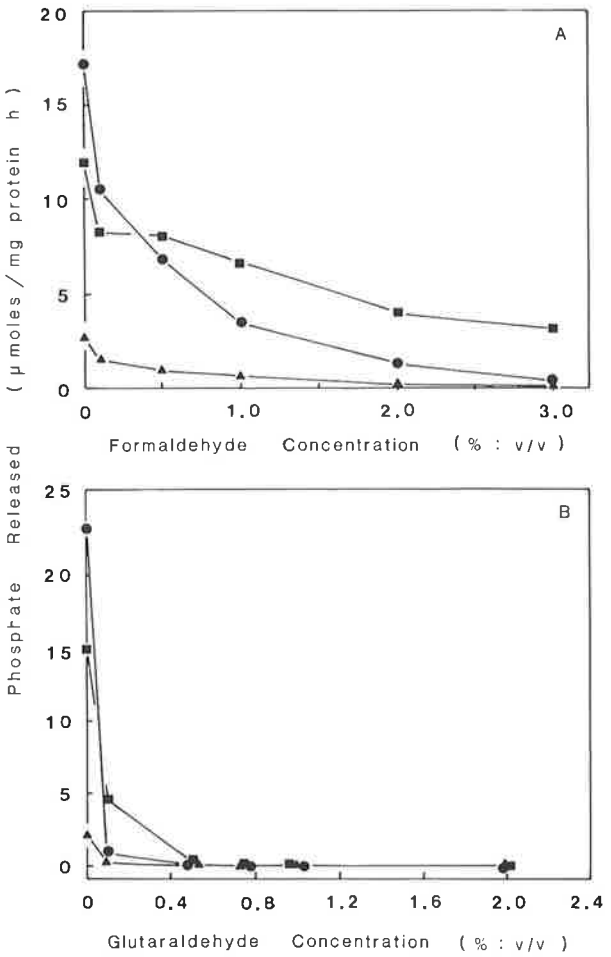


Figure 19. Hydrolysis of ATP by red beet membrane fractions following fixation with various concentrations of formaldehyde (A) and glutaraldehyde (B). Symbols are as follows: (■), vanadate-sensitive activity in the plasma membrane fraction; (●), nitrate-sensitive activity in the vacuole fraction; (▲), azide-sensitive activity in the pellet. No lead present in solutions.

## Discussion

### *Usefulness of the Pb Precipitation Technique*

A number of objections can be raised concerning the validity of the lead precipitation methods which we have used in the present study. As already mentioned, the observation by Washitani and Sato (1976) that lead deposits can occur in specific regions of the cell in the absence of phosphate ester substrates seems not to be a factor in sugar beet leaves. Recently, Price and Whitecross (1983) have further increased our confidence in the ability of the lead precipitation technique to localize ATPase activity on membranes by demonstrating ATPase activity on portions of the plasma membrane of *Chara* cells which had been prepared so as to be devoid of all other cytoplasmic contents.

With regard to our ability to localize ATPase activity within the tissue as a whole, our results closely resemble those of Van Steveninck (1979), who found that ATPase-generated, electron-dense deposits, which could be identified as lead by X-ray analysis, occurred only in the outermost two layers of cells in barley root

Figure 13. Mesophyll cells in tissue incubated in ATP. Lead deposits were primarily located on the plasma membrane (PM), with lesser amounts present on the cell wall (CW) and the tonoplast (T). Original magnification × 1700. Bar = 10 μm. Figure 14. Tissue incubated in ATP. Amount of lead deposition on the plasma membranes of bundle sheath cells (B) was generally equal to that on the plasma membranes of the parenchymatous phloem cells (P). In contrast, the lead deposits on the plasma membrane of the sieve element (S) were relatively small. Unlabeled arrows indicate the position of the plasma membrane in each cell type. Original magnification × 5600. Bar = 2 μm. Figure 15. Mesophyll tissue incubated in p-nitrophenyl phosphate. Lead deposits were located on the cell wall (CW), plasma membrane (PM) and, to a lesser extent, on the vacuole membrane (VM). Original magnification × 2600. Bar = 5 μm. Figure 16. Tissue incubated in p-nitrophenyl phosphate. Lead deposits located on the plasma membrane (dart) and tonoplast of parenchymatous phloem cell (P) were relatively large compared to those on the sieve element (S) plasma membrane (arrow). Original magnification × 9000. Bar = 1 μm. Figure 17. Tissue incubated in β-glycerol phosphate. Lead deposits (darts) were quite evident on the tonoplast (darts) of mesophyll cells. Plastid (P). Original magnification × 9000. Bar = 1 μm. Figure 18. Control tissue (no phosphate ester substrate) incubated in 100 mM (50 × normal) lead nitrate. Plastids (P) and mitochondria (M) contained large numbers of lead deposits, whereas the plasma membrane (arrows) and the tonoplast (dart) contained only a few such deposits. Original magnification × 21,000. Bar = 0.5 μm.

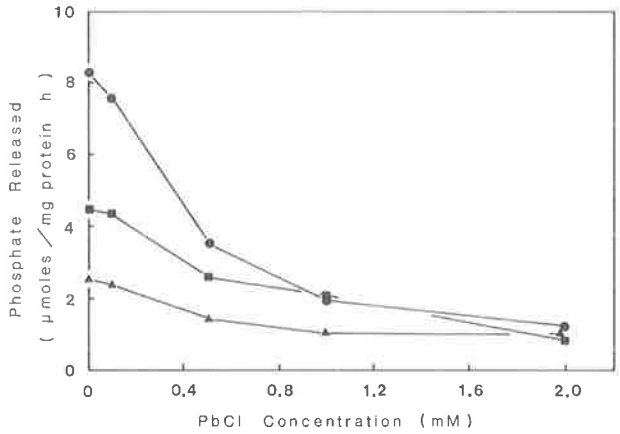


Figure 20. Hydrolysis of ATP in the presence of lead chloride by red beet membrane fractions previously fixed in 1% formaldehyde; total activity in the plasma membrane (●), vacuolar (■), and pellet/mitochondrial (▲) fractions.

tips. Our results also resemble the pattern of lead deposition in *Saintpaulia* integumentary cells (Mogensen, 1981), although the latter author apparently does not believe that permeability limitations are responsible for restriction of lead deposits to a particular zone of the tissue.

Perhaps a more serious objection to using the lead precipitation methods comes from a consideration of some results of previous investigators. For example, with regard to the sensitivity of the method, Price and Whitecross (1983) report a lack of $Mg^{2+}$ sensitivity in their cytochemical analysis of ATPases in *Chara*, while Gilder and Cronshaw (1974) report a lack of inhibition by 3.6 mM lead nitrate in fixed homogenates of *Nicotiana*. With regard to the correlative ability of the lead precipitation method, Gilder and Cronshaw (1974) report an absence of PNP-related lead deposits in the phloem of *Nicotiana*, although PNPase activity was spectrophotometrically detectable. Furthermore, they report inhibition of ATPase activity by N-ethyl maleimide at the cytochemical level but record normal levels of ATP hydrolysis at the spectrophotometric level. Although these authors have plausibly explained some of the possibilities that may have generated their results, some ambiguity remains.

In contrast, our results here have shown that sugar beet leaves, carefully prepared and sectioned, can be very consistent and sensitive cell systems for analysis of several important parameters such as $Mg^{2+}$ sensitivity, localization of various types of phosphatases, comparison of activity in different cell types, and effects of incubation media pH on phosphatase activity. This sensitivity suggests, although it does not prove, that the phosphatase activities which we have measured retain their "in vivo" characteristics to a significant extent. In addition, this system has allowed us to closely correlate cytochemistry with spectrophotometric results.

Part of the reason that we have been able to obtain this level of sensitivity may simply be due to the natural amenability of sugar beet leaves to this method of analysis. In addition, we also believe it possible that the tendency of most investigators to include glutaraldehyde as part or all of the fixative may have decreased the sensitivity of their preparations. Our spectrophometric data, of both tissue pieces and membrane fractions, clearly indicate that as little as 0.5% glutaraldehyde can inactivate significant portions of phosphatase activity. We realize that glutaraldehyde is commonly included in the fixative because it significantly increases preservation (Ernst, 1975), and we fully acknowledge the superiority of a well-preserved cell for microscopic analysis; however, if enzymatic activity located on the plasmalemma or tonoplast is the primary interest, then our present results indicate that 1–3% formaldehyde will suffice for fixation. It should be noted, however, that Goff and Klohs (1974) showed that lead salts had little effect on inosine diphosphate hydrolysis activity in formaldehyde-fixed onion root tips. It therefore seems possible that the inability of lead to inhibit some phosphatases may be a result of the characteristics of specific enzymes, rather than of the use of glutaraldehyde as a fixative.

With regard to the occasional difficulties of previous investigators in attempting to correlate closely cytochemistry and spectrophotometry, it seems possible to us that in some cases the very limited penetration of the cytochemical reagents may not have been fully appreciated, although documented evidence of this has been previously presented at the light microscopic level (Sexton et al., 1971).

### *Comparison With Studies of Membrane Fractions*

Fixation of tissue pieces with 3% formaldehyde has enabled us to make a close comparison between our spectrophometric data and results obtained on isolated plasma membrane fractions from other species. For example, our results of ATPase activity as a function of pH resemble those both for the plasma membrane fractions of corn roots (Gallagher and Leonard, 1982) and corn leaves (Perlin and Spanswick, 1980) with a distinct peak of activity being present near pH 6. In addition, our results of PNPase activity as a function of pH are similar to those of Perlin and Spanswick (1981) obtained on a corn leaf plasma membrane fraction; in their Figure 4, the data point at pH 7.5 lies above the linear portion of the activity line and may represent activity similar to the "shoulder" of activity that we observe between pH 7.5 and 8. Alternatively, it is possible that the similarity of our results to those of others is simply coincidental; however, since our cytochemical results indicate that much of the ATPase and PNPase activity is on the plasma membrane in sugar beet leaves, it seems quite valid to propose that our spectrophotometric data are also largely indicative of enzymatic activity on the plasma membrane.

Our data concerning the effect of pH and inhibitors support the conclusion that ATPase and PNPase activities represent separate enzymes. We say this in part because our results of ATPase activity as a function of pH substantially differ from that of the PNPase activity; furthermore, the results with inhibitors clearly show a major difference between the two activities with regard to their inhibition by fluoride. Obviously, our results do not prove that two enzymes are present; however, our results are in agreement with those of numerous investigators (DuPont et al., 1981; Perlin and Spanswick, 1981; Briskin and Poole, 1983) who have presented evidence from studies of membrane fractions suggesting that two enzymes, a specific ATPase and another phosphatase, are present on the plasma membrane of plant cells.

With regard to the effect of fixation on membrane fractions, our results differ from those of Al-Azzawi and Hall (1977), who

showed that aldehydes inhibited mitochondrial ATPase activity less than that of the crude microsomal fraction, and that significant activity remained after both glutaraldehyde and formaldehyde fixation. Although these differences may in part relate to interspecies differences, at least two other possibilities exist. It is possible that our membranes, fixed *after* fractionation, were more sensitive or simply more accessible to the fixatives. In addition, their microsomal fraction was relatively crude compared to ours, and therefore probably contained significant amounts of several types of membranes. This could make it impossible to compare our results directly with theirs.

### *Specificity of Acid Phosphatases*

With regard to "acid phosphatase" or "non-specific phosphatases" (Leigh and Walker, 1980; DuPont et al., 1981; Perlin and Spanswick, 1981; Briskin and Poole, 1983), our results indicate that in sugar beet leaves the PNPase and BGPase activities, both of which can be characterized as "acid phosphatase," exhibit dissimilar characteristics with regard to their intracellular localization and their activity as a function of pH. Therefore, from the combined viewpoints of biochemistry and cytochemistry, and in general accordance with the opinion of Sexton et al. (1971) concerning acid phosphatase in root tips, these two activities in beet leaves can hardly be viewed as being entirely "non-specific." Acid phosphatase in vacuoles is thought of as being primarily a digestive enzyme concerned with metabolic recycling processes (Matile, 1976), whereas, to our knowledge, the function of PNPase on the plasma membrane is unknown.

### *Vanadate and Molybdate Inhibition*

Perhaps the most frustrating aspect of our present research has been our inability to use successfully the strontium chloride technique of Ernst (1972a, b) for cytochemical detection of phosphatase activity. Our reason for wanting to use this technique was that it would have enabled us to visualize the effect of vanadate and molybdate inhibition; in our hands, lead nitrate always precipitated when combined in solution with either vanadate or molybdate, whereas strontium did not. Unfortunately, when using the strontium technique, we have never, in many tests, observed any amount of electron-dense deposition greater than that in the control tissues (without substrate). In controls the deposition was relatively intense, and closely resembled that seen in Figure 18. Therefore, although our spectrophotometric analysis revealed that either molybdate or vanadate can substantially inhibit both PNPase and ATPase activity, we are currently unable to visualize the intracellular location where this inhibition occurs. Cronshaw (1980) has reported that the strontium chloride technique can be successfully used in some plants, but obviously sugar beet is unsuitable.

### *Phosphatase Activity in the Phloem*

Several studies by other authors that have dealt with phosphatase localization at either light or electron microscopic level have indicated that vascular tissues contain relatively high amounts of various phosphatase activities (Gilder and Cronshaw, 1974; Bentwood and Cronshaw, 1976; Cronshaw, 1980 and references therein; Browning et al., 1980). If one accepts the hypothesis that phloem cells in sucrose-exporting "source" leaves are loaded with sucrose from the apoplast, the existence of intense ATPase activity on the plasma membranes of phloem cells is then consistent with theory. These ATPases would function to provide the phloem cells with an enzymatic mechanism to actively load and thereby continually replenish the high concentrations of sucrose being transported in the phloem. Although our observations do not refute the concept of apoplastic loading, we wish to reiterate that during hundreds of observations we have consistently found the level of ATPase and PNPase activity on the plasma membranes of sugar beet minor vein phloem cells to be less or, at most, similar to the level present on the plasma membranes of the nearby mesophyll cells. Why our results are qualitatively different from those of other authors is a difficult matter to decide, as our present understanding of the biochemical and physiological nature of phloem cells is imperfect. Beet vascular bundle cells could be relatively sensitive to fixation, or their structure could substantially inhibit the diffusion of cytochemical reagents; factors such as these may not have been present in the cells of the genera that other investigators have examined previously. However, given the caution that our present methods have only measured phosphate ester hydrolysis and not sucrose uptake, our results are in general agreement with Maynard and Lucas (1982), who indicated that leaf mesophyll and petiole pith parenchyma cells could actively take up significant amounts of sucrose and 3-0-methyl glucose.

### Acknowledgments

*We wish to thank Michael A. Grusak for continuously supplying us with sugar beet plants throughout the duration of this project. We also thank Dr. Benjamini for the loan of the Mickle tissue sectioner.*

## Literature Cited

Al-Azzawi MJ, Hall JL (1977): Effects of aldehyde fixation on adenosine triphosphatase and peroxidase activities in maize root tips. Ann Bot 41:431

Ames BN (1966): Assay of inorganic phosphate, total phosphate, and phosphatases. Methods Enzymol 8:115

Anderson PJ (1967): Purification and quantitation of glutaraldehyde and its effect on several enzyme activities in skeletal muscle. J Histochem Cytochem 15:652

Bennett AB, O'Neill SD, Spanswick RM (1984): $H^+$-ATPase activity from storage tissue of *Beta vulgaris*. I. Identification and characterization of an anion-sensitive $H^+$-ATPase. Plant Physiol 74:538

Bentwood BJ, Cronshaw J (1976): Biochemistry and cytochemical localization of acid phosphatase in the phloem of *Nicotiana tabacum*. Planta 130:97

Briskin DP, Poole RJ (1983): Characterization of a $K^+$-stimulated adenosine triphosphatase associated with the plasma membrane of red beet. Plant Physiol 71:350

Browning AJ, Hall JL, Baker DA (1980): Cytochemical localization of ATPase activity in phloem tissues of *Ricinus communis*. Protoplasma 104:55

Charvat I, Esau K (1975): An ultrastructural study of acid phosphatase localization in *Phaseolus vulgaris* xylem by the use of an azo-dye method. J Cell Sci 19:543

Cronshaw J (1980): Histochemical localization of enzymes in the phloem. Ber Deutsch Bot Ges Bd 93:123

DuPont FM, Burke LL, Spanswick RM (1981): Characterization of a partially purified adenosine triphosphatase from a corn root plasma membrane fraction. Plant Physiol 67:59

Ernst SA (1972a): Transport adenosine triphosphatase cytochemistry I. Biochemical characterization of a cytochemical medium for the ultrastructural localization of ouabain-sensitive, potassium-dependent phosphatase activity in the avian salt gland. J Histochem Cytochem 20:13

Ernst SA (1972b): Transport adenosine triphosphatase cytochemistry II. Cytochemical localization of ouabain-sensitive, potassium-dependent phosphatase activity in the secretory epithelium of the avian salt gland. J Histochem Cytochem 20:23

Ernst SA (1975): Transport ATPase cytochemistry: ultrastructural localization of potassium-dependent and potassium-independent phosphatase activities in rat kidney cortex. J Cell Biol 66:586

Ernst SA, Philpott CW (1970): Preservation of Na–K-activated and Mg-activated adenosine triphosphatase activities of avian salt gland and teleost gill with formaldehyde as a fixative. J Histochem Cytochem 18:251

Evert RF (1977): Phloem structure and histochemistry. Annu Rev Plant Physiol 28:199

Fiske CH, Subbarow Y (1925): The colorimetric determination of phosphorous. J Biol Chem 66:375

Gallagher SR, Leonard RT (1982): Effect of vanadate, molybdate and azide on membrane-associated ATPase and soluble phosphatase activities of corn roots. Plant Physiol 70:1335

Gilder J, Cronshaw J (1974): A biochemical and cytochemical study of adenosine triphosphatase activity in the phloem of *Nicotiana tabacum*. J Cell Biol 60:221

Goff CW, Klohs WD (1974): Nucleoside diphosphatase in the onion root tip 1. Effects of fixation and lead on enzyme activity. J Histochem Cytochem 22:945

Gomori G (1952): Microscopic Histochemistry, Principles and Practice. Chicago, University of Chicago Press

Grusak MA, Lucas WJ (1984): Recovery of cold-inhibited phloem translocation in sugar beet. I. Experimental analysis of an existing mathematical recovery mode. J Exp Bot 35:389

Hall JL (1977): Fine structural and cytochemical changes occurring in beet discs in response to washing. New Phytol 79:559

Hall JL, Browning AJ, Harvey DMR (1980): The validity of the lead precipitation technique for the localization of ATPase activity in plant cells. Protoplasma 104:193

Jacobsen NO, Jørgensen PL (1969): A quantitative biochemical and histochemical study of the lead method for localization of adenosine triphophate-hydrolyzing enzymes. J Histochem Cytochem 17:443

Klohs WD, Goff CW (1973): A characterization of nucleoside diphosphatase in the onion root tip. J Histochem Cytochem 21:417

Leigh RA, Walker RR (1980): ATPase and acid phosphatase activities associated with vacuoles isolated from storage roots of red beet (*Beta vulgaris* L.). Planta 150:222

Matile PH (1976): Vacuoles In Plant Biochemistry, 3rd Ed. Edited by J Bonner, JE Varner. Academic Press, New York, pp. 189–222

Maynard JW, Lucas WJ (1982): Sucrose and glucose uptake into *Beta vulgaris* leaf tissues. A case for general (apoplastic) retrieval systems. Plant Physiol 70:1436

Mogensen HL (1981): Ultrastructural localization of adenosine triphosphatase in the ovules of *Saintpaulia ionantha* (Gesneriaceae) and its relation to synergid function and embryo sac nutrition. Am J Bot 68:183

Perlin DS, Spanswick RM (1980): Labeling and isolation of plasma membrane from corn leaf protoplasts. Plant Physiol 65:1053

Perlin DS, Spanswick RM (1981): Characterization of ATPase activity associated with corn leaf plasma membranes. Plant Physiol 68:521

Price GD, Whitecross MI (1983): Cytochemical localization of ATPase activity on the plasmalemma of *Chara corallina*. Protoplasma 116:65

Pyliotis NA, Ashford AE, Whitecross MI, Jacobsen JV (1979): Localization of gibberellic acid-induced acid phosphatase activity in the endoplasmic reticulum of barley aleurone cells with the electron microscope. Planta 147:134

Robards AW, Kidwai P (1969): Cytochemical localization of phosphatase in differentiating secondary vascular cells. Planta 87:227

Sexton R, Cronshaw J, Hall JL (1971): A study of the biochemistry and cytochemical localization of β-glycerophosphatase activity in root tips of maize and pea. Protoplasma 73:417

Van Steveninck RFM (1979): The verification of cytochemical tests for ATPase activity in plant cells using X-ray microanalysis. Protoplasma 99:211

Wachstein M, Meisel E (1957): Histochemistry of hepatic phosphatases at a physiologic pH. With special reference to the demonstration of bile canaliculi. Am J Clin Pathol 27:13

Washitani I, Sato S (1976): On the reliability of the lead salt precipitation method of acid phosphatase localization in plant cells. Protoplasma 89:157

*Journal of Experimental Botany, Vol. 37, No. 175, pp. 277–288, February 1986*

# Cold-Inhibited Phloem Translocation in Sugar Beet

## III. THE INVOLVEMENT OF THE PHLOEM PATHWAY IN SOURCE–SINK PARTITIONING

MICHAEL A. GRUSAK AND WILLIAM J. LUCAS

*Department of Botany, University of California, Davis, California 95616, U.S.A.*

Received 24 July 1985

ABSTRACT

Grusak, M. A. and Lucas, W. J. 1986. Cold-inhibited phloem translocation in sugar beat. III. The involvement of the phloem pathway in source–sink partitioning.—J. exp. Bot. 37: 277–288.

Experiments were undertaken on sugar beet plants, reduced to one source leaf and two sink leaves, to observe the translocation response at two sinks when a slow- or quick-cooling treatment was applied to the source leaf petiole. Our results indicated that with slow-cooling treatments, both step increases and step decreases could be found in the rate of translocation to the two monitored sinks. The responses of the two sink leaves were not necessarily identical, and three classes of response were observed: (1) both sinks showed translocation increases or decreases at the same time, (2) one sink showed a translocation increase, while the other showed a concurrent decrease, or (3) one sink exhibited a translocation rate change (increase or decrease), while the other remained unchanged. Our data suggest that these translocation changes were the result of a repartitioning in the amount of flow between the two sink leaves and the unmonitored hypocotyl/crown region of the simplified plant system. We suggest that the cooling treatments induced the transmission of a rapid, physical signal along the phloem pathway to the crown region of the plant, which in turn caused alterations in the pathway and redirected the assimilate flow amongst the three terminal sinks. In addition, our results indicated that pathway repartitioning could also account for a part of the quick-cooling induced translocation recovery response.

*Key words*—Phloem translocation, cooling response, partitioning, vascular pathway.

*Correspondence to: Department of Botany, University of California, Davis, California 95616, U.S.A.*

## INTRODUCTION

The exact role of the phloem pathway in maintaining, and more importantly, partitioning source-to-sink translocation is poorly understood, due in part to the incomplete knowledge of the phloem translocation process itself. Sieve elements are involved in conducting assimilates from source(s) to sinks, but at present little information is available on how the complex organization of the sieve elements, in the vascular network of the plant, accomplishes *directed* transport to specific sinks. Although various studies have shown a *preferred* partitioning of flow from a given source (Joy, 1964; Zamski and Azenkot, 1981*b*), anastomoses which connect different vascular pathways could interconnect a particular source to almost any sink (Gifford and Evans, 1981). Indeed, by appropriate manipulations, the original partitioning pattern can be quickly altered (Joy, 1964; Fellows, Egli, and Leggett, 1979; Fondy and Geiger, 1980, 1983).

During long-distance translocation, some form of *regulation* must exist over the pathway connections of the sieve-elements that are involved in the partitioning of assimilate. A sink control of this phenomenon has been suggested, based on the utilization of sugars from

© Oxford University Press 1986

the phloem system in the sink. It has been suggested that this utilization enhances the source-to-sink pressure gradient and thereby promotes the directed flow of sugars to that particular sink (Gifford and Evans, 1981). Although this hypothesis explains the driving force for directed partitioning, it assumes that the vascular pathway passively accommodates the various source-to-sink gradients. However, it is clear that a further level of regulation exists, since it has been shown that the *resistance* of the phloem pathway is also important in the partitioning of assimilates (Patrick and Wardlaw, 1984).

In the present study, we present evidence, based on experiments involving sugar beet plants simplified to one source leaf and two sink leaves, which suggests that localized cooling treatments promote the transmission of rapid, physical signals which effect an alteration in the source–sink partitioning pattern. These results are discussed with respect to the previously described quick-cooling (Swanson and Geiger, 1967; Grusak and Lucas, 1984) and slow-cooling (Grusak and Lucas, 1985) translocation responses.

## MATERIALS AND METHODS

### *Materials*

Sugar beet plants (*Beta vulgaris* L. var. SSBN1, USH11 Lot 82312) were grown in a controlled environment chamber under the conditions previously described (Grusak and Lucas, 1984). Average characteristics for the plants used in this study were as follows: source leaf surface area, $175{\cdot}5 \pm 15{\cdot}9$ cm$^2$; source leaf net carbon exchange rate, $8{\cdot}86 \pm 0{\cdot}38$ mol $CO_2$ m$^{-2}$ s$^{-1}$; sink leaf surface areas, $10{\cdot}4 \pm 3{\cdot}4$ cm$^2$ and $6{\cdot}7 \pm 1{\cdot}2$ cm$^2$ (for first and second sink leaves); errors quoted are standard deviations.

### *Experimental apparatus and procedures*

All experiments were performed with the apparatus and experimental protocols previously described (Grusak and Lucas, 1984), except in certain experiments where two sink leaves were left on the plant, with the translocation rate into each being monitored by individual Geiger–Mueller tubes connected to a dual ratemeter. As in our earlier studies, the sink leaves were chosen from the fifth or sixth pair of emergent leaves, with either both leaves being from the fifth pair, or one leaf from the fifth and sixth pairs. Slow- or quick-cooling treatments were employed in various combinations on a 2·0 cm source leaf petiole segment of the experimental plants; specific details have been included in the text. The general procedure and specific cooling rates for these perturbations were documented in an earlier study (Grusak and Lucas, 1985).

Some experiments involved introducing solutions into the apoplast of the petiole. To facilitate the penetration of these solutions, a U-shaped trough, approximately 2·0 cm in length, was cut in the top of the source leaf petiole (adaxial surface); this incision removed the epidermal and pith parenchyma tissues. The sides and bottom of the petiole (abaxial surface) were also gently abraded with 120 grit sandpaper; this removed the epidermis and collenchyma ridges extending from the surface of the petiole. The treated petiole segment was then placed over a plexiglas tray which had U-shaped grooves cut into each end. The petiole was sealed at these grooves with stopcock grease, such that solutions could be added to the tray. Glass distilled water and a $10^3$ mol m$^{-3}$ mannitol solution were used, and were changed by aspirating one before slowly adding the other; enough solution was always added to completely cover the petiole segment.

### *Data analysis*

The accumulation of labelled material in the sink leaf (leaves) was recorded by the chart recorder and then converted, in all cases, to relative translocation rates. Smooth curves were drawn through the chart recorder tracings, and the slope of the accumulation curve was calculated over 4 min intervals. The relative translocation rate was expressed as the ratio of the accumulation rate, at consecutive time intervals during the experiment, to the steady-state accumulation value prior to the commencement of the experimental treatment.

Data presented represent the translocation response of a single plant obtained during one experiment and are representative of identical treatments performed on at least three plants.

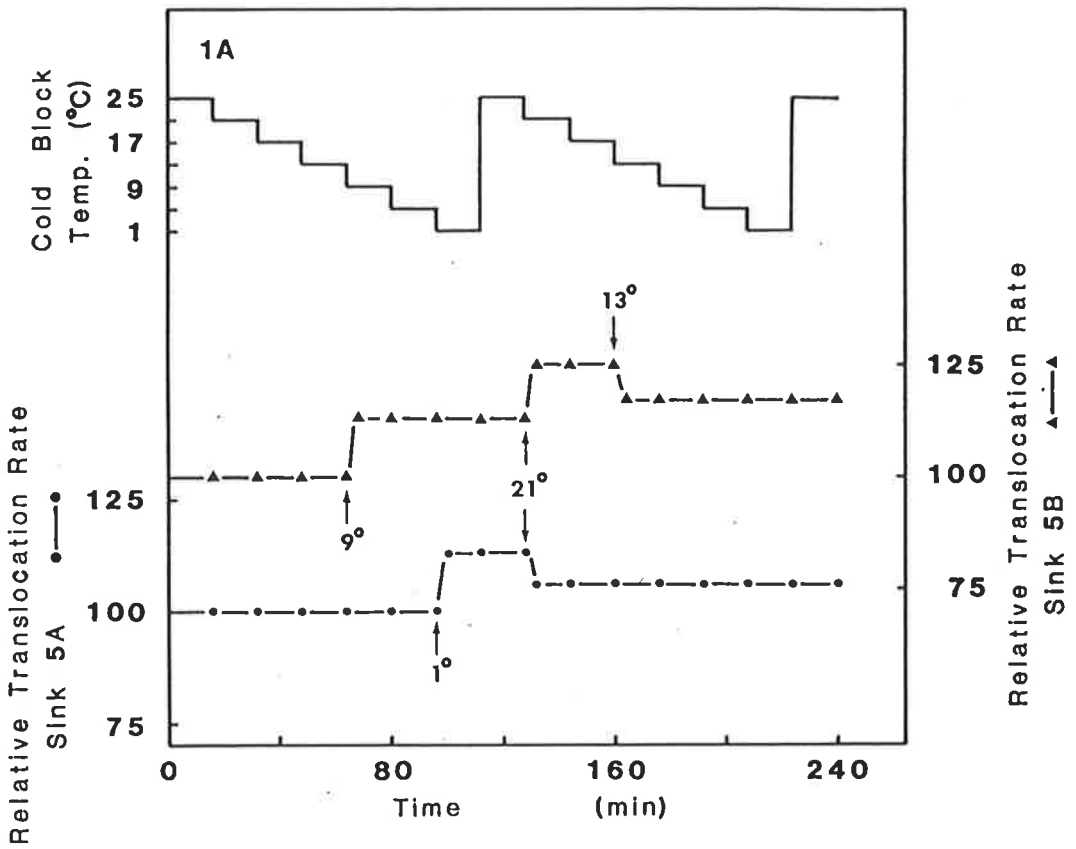


FIG. 1. Effect on translocation at two monitored sink leaves of repeated slow-cooling treatments on a 2·0 cm segment of a sugar beet source leaf petiole. A 2·0 cm brass block cooling apparatus on the source leaf petiole was cooled or warmed to various temperatures as indicated at the top of the figure. Relative translocation rates are presented for two representative plants (A and B *overleaf*) each of which contained a source leaf and two sink leaves.

## RESULTS

### *Cooling-induced translocation response with two monitored sinks*

Three patterns of translocation response were observed when slow-cooling treatments were performed on sugar beet plants simplified to one source and two sink leaves (Figs 1A, B). The translocation rate was found to decrease or increase simultaneously at the two sinks (Fig. 1B), simultaneously increase at one sink and decrease at the other (Fig. 1A), or change (increase or decrease) at one monitored sink with no concurrent change at the other sink (Figs 1A, B). The average of the absolute values of all translocation rate changes induced by the slow coolings was $10{\cdot}7 \pm 3{\cdot}7\%$ of the original rate, which is comparable to the average rate decrease reported in our previous study (Grusak and Lucas, 1985). It should be noted that contrary to the slow-cooling translocation response of a plant reduced to only *one* sink leaf (Grusak and Lucas, 1985, Fig. 1), step changes do occur during the first slow-cooling treatment when the test plant has *two* attached sink leaves (Figs 1A, B). In addition, the results of this study show both increases and decreases in the rate of translocation in response to slow-coolings, whereas only decreases in the rate were observed in the previous study.

Quick-cooling treatments were also performed on plants with one source leaf and two monitored sink leaves. The previously described inhibition and recovery response (Swanson and Geiger, 1967; Grusak and Lucas, 1984) was seen for both sink leaves (Fig. 2). However, the time course of the response and the degree of recovery were not identical for the two

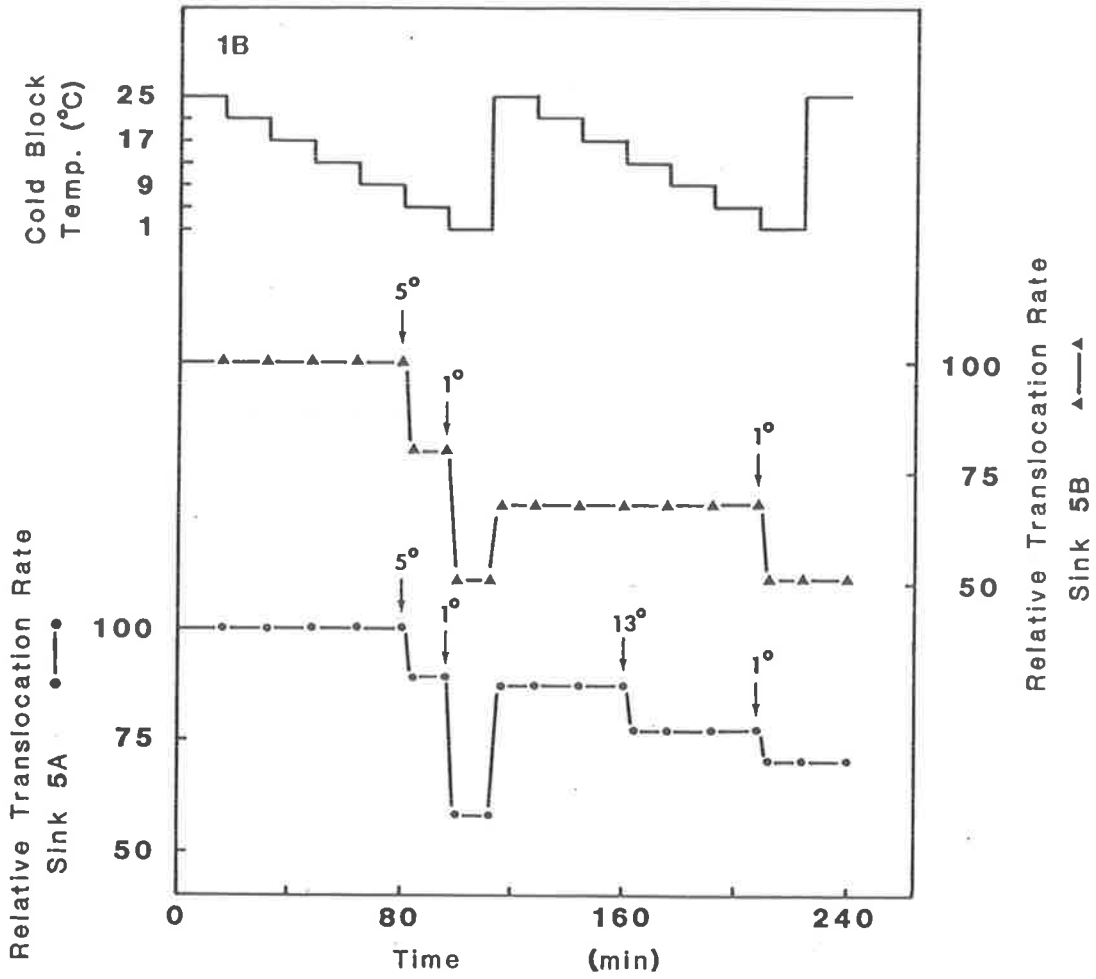


leaves. In addition, in some cases it was found that the translocation rate, observed immediately following the quick-cooling treatment, increased before beginning the usual inhibition and recovery response (sink leaf 5A, Fig. 2).

*Slow-cooling treatment following transverse petiole incisions*

In order to assess the importance of the vascular anatomy of the cooled petiole region to the step-type change in translocation rate, slow-cooling treatments were performed upstream of two incisions made on opposite sides of the petiole. Both incisions severed the central vascular bundle (inset, Fig. 3), which causes the translocation stream to be re-routed through anastomoses between the vascular bundles (Grusak and Lucas, 1984). Any re-routing of the translocation stream which might occur at the chilled petiole region, in response to the slow coolings, would be overridden by the surgically-induced re-routing that occurred within the overlapping petiole-incision zone. The data presented in Fig. 3 show that after an initial decrease and stabilization of the translocation rate following the incisions, the slow-cooling treatments still induced step changes in the translocation rate. Again, the absolute value of these changes averaged $9{\cdot}7 \pm 4{\cdot}1\%$ of the steady-state, pre-cooled value.

*Influence of apoplastically-applied mannitol*

Experiments were also performed to investigate the effect of localized apoplastic changes in the water potential within the source leaf petiole, on the relative translocation rate at two

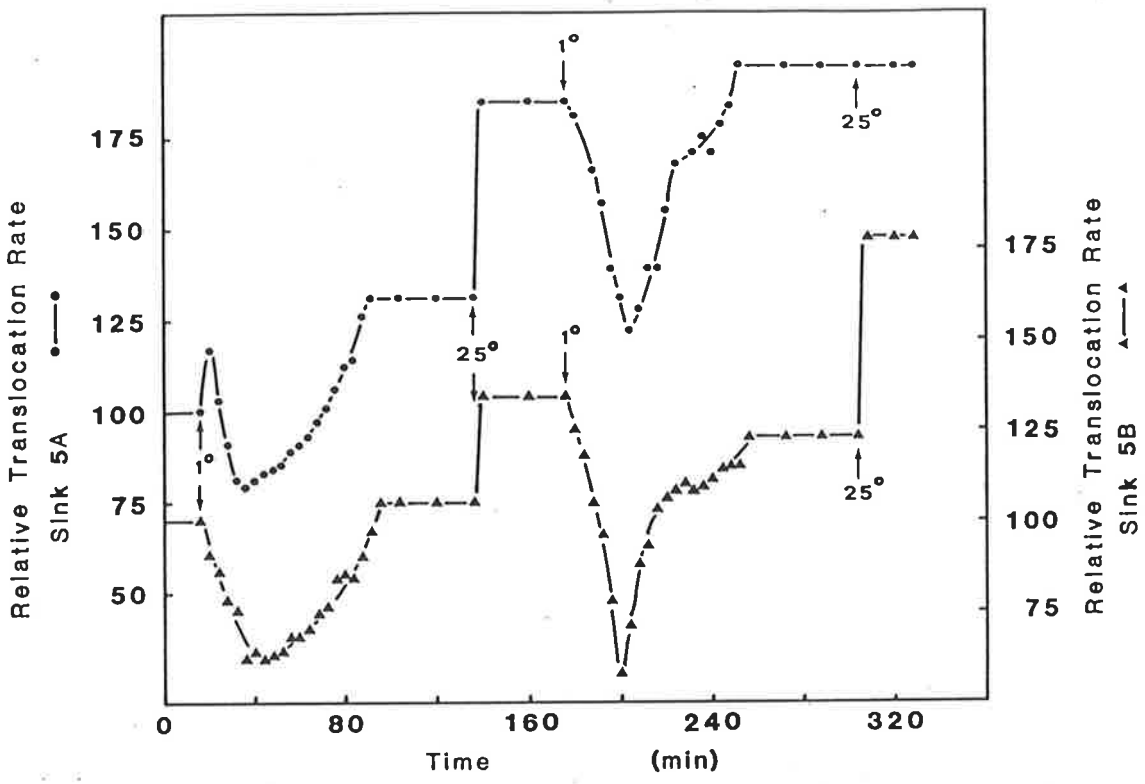


FIG. 2. Effect on translocation at two monitored sink leaves of quick-cooling treatments on a 2·0 cm segment of a sugar beet source leaf petiole. A 2·0 cm brass block cooling apparatus was quickly cooled from 25 °C to 1 °C, or quickly rewarmed from 1 °C to 25 °C as indicated on the figure. Relative translocation rates are presented for each of the two sink leaves of the simplified plant.

monitored sink leaves (Fig. 4). When the bathing solution was changed from glass-distilled water to a $10^3$ mol $m^{-3}$ mannitol solution, or vice versa, the translocation response was similar in nature to that observed when slow-cooling treatments were performed on plants with two monitored sink leaves (cf. Figs 1A, B). That is, the translocation rate was seen to decrease or increase simultaneously at one sink and decrease at the other, or change at one monitored sink with no concurrent change at the other. In these experiments, the average absolute value of all translocation rate changes was $12{\cdot}6 \pm 2{\cdot}3\%$ of the pre-treatment value. When the change in bathing solution was merely a replacement of the previous solution, no alterations in the translocation rate were observed at either sink leaf, which indicates that the act of replacing the bathing solution was not responsible for the observed rate changes. It should also be mentioned that when carefully excising a portion of the upper pith to form a trough in the top of the petiole, as well as gently abrading the outer ribs of collenchyma, both of which facilitate the entry of solutions into the apoplast, no change in the relative translocation rate was observed at either sink leaf (data not shown).

## DISCUSSION

### *Slow-cooling induced sink repartitioning*

The results of the slow-cooling experiments with two monitored sinks (Figs 1A, B) are in agreement with our previous slow-cooling investigation (Grusak and Lucas, 1985) in so far as the cooling perturbations induced sudden step changes in the rate at which radioactive material arrives at the monitored sinks. Several patterns of response were observed, including

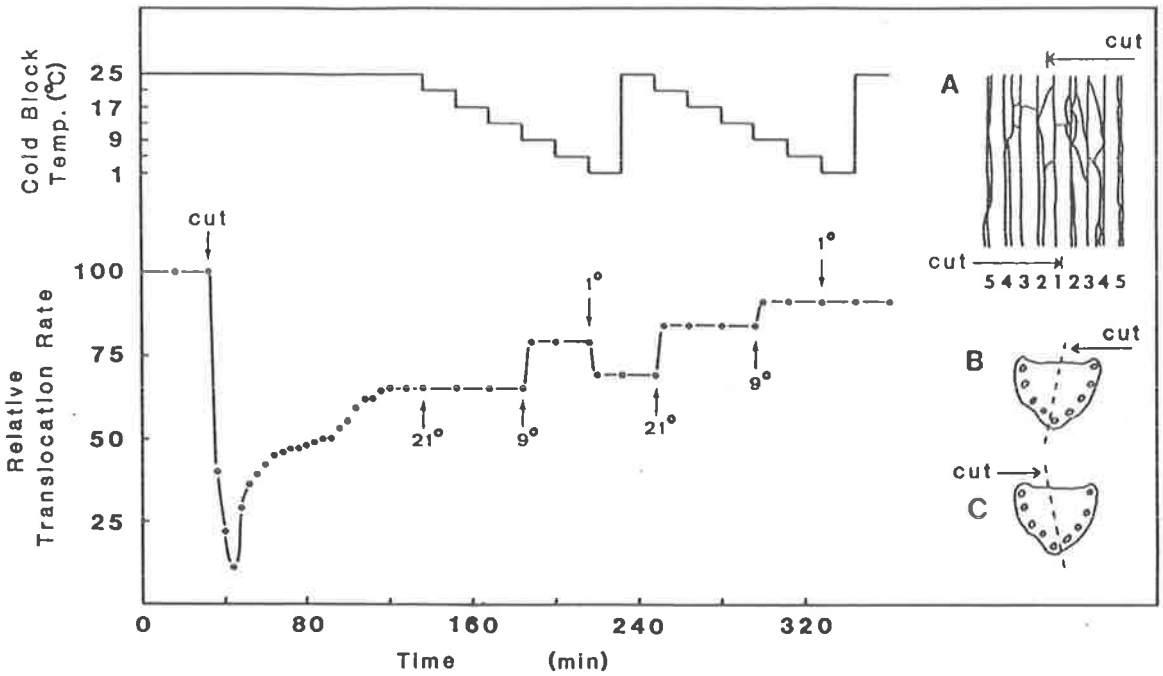


FIG. 3. Effect on translocation of overlapping petiole incisions followed by repeated slow-cooling treatments on a 2·0 cm segment of a single-source, single-sink leaf sugar beet petiole system. After the establishment of steady-state translocation, two cuts were made from opposite sides of the petiole (6·7 cm and 9·2 cm from the source blade), such that both severed the central vascular bundle. Incisions were made with the petiole segment immersed in distilled water. Slow-cooling treatments were performed on a 2·0 cm segment of the source leaf petiole at a position upstream of the overlapping cuts (2·0 cm to 4·0 cm from the source blade). Cooling and warming changes are indicated at the top of the figure. Insets: (A) Top view of major vascular bundles and anastomoses between the incisions made on the source petiole; (B and C) transverse views of the source leaf petiole, at the two sites of incision, showing the extent of cuts.

step increases and step decreases in translocation. To understand these results fully, two points must be clarified. First, it is essential to recognize that, in the present experiments, the rate of translocation is expressed on the basis of accumulation within the monitored sink(s). A change in rate at the sink leaf may not necessarily reflect a change in rate through the cooled region of the source leaf petiole. Second, the source leaf is providing assimilate to more than just the two sink leaves. The source leaf petiole can act as a sink, as well as the hypocotyl/crown region above the heat girdle.

With these points in mind, we suggest that the slow-cooling perturbations may induce a repartitioning of assimilate flow among the three terminal sinks (the two sink leaves and the hypocotyl/crown region above the heat girdle), while leaving the total translocation through the cooled source leaf petiole unaffected. A similar repartitioning among sinks, without a change in the source export rate, has been reported for soybean (Fellows *et al.*, 1979), as well as for sugar beet and *Phaseolus vulgaris* (Fondy and Geiger, 1980, 1983). In these studies, repartitioning occurred in response to alterations in the sink–source ratio. Our present results suggest that the cooling treatments induce a change in the pre-existing pathway connections which partition the available assimilates between the three terminal sinks, and alter the resistances to flow such that the percent of export to each sink is varied. When the translocation rate increases at one sink leaf and decreases at the other (Fig. 1A), we suggest that a part of the flow to one sink leaf has been transferred to the other. When the rate of translocation increases or decreases simultaneously at the two sink leaves (Fig. 1A), this

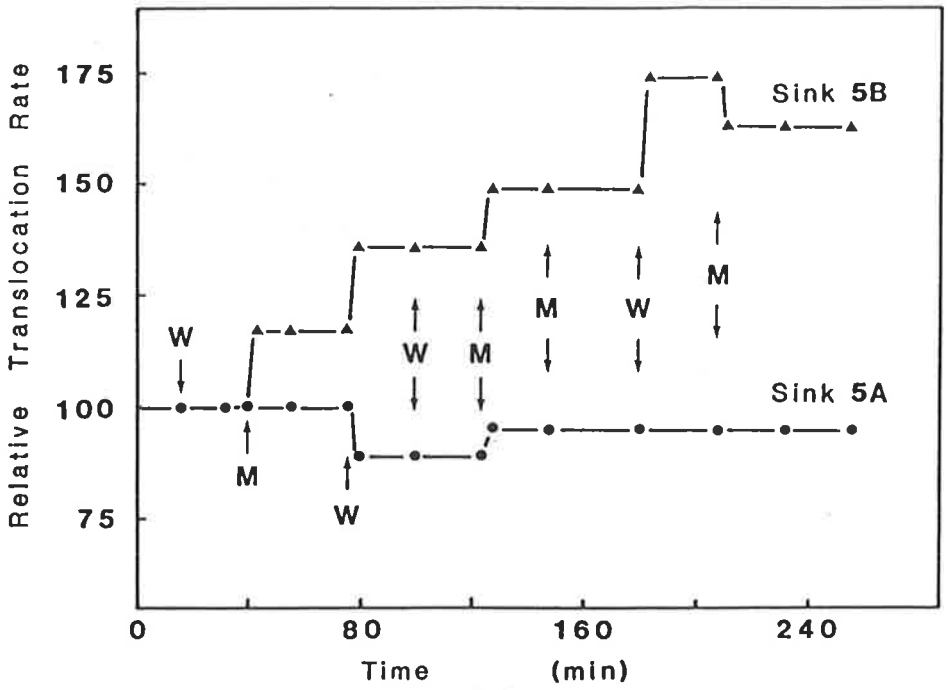


FIG. 4. Effect on translocation at two monitored sink leaves of changes in the osmotic potential within the apoplast of a sugar beet source leaf petiole segment. To facilitate access to the petiolar apoplastic space, the abaxial surface was gently abraded, and a 2·0 cm U-shaped trough of pith and epidermal tissue was removed from the top (adaxial) side of the source petiole. The petiole segment was completely submerged in either distilled water (W) or a $10^3$ mol $m^{-3}$ mannitol (M) solution, which were changed at the times indicated. The relative translocation rates at both sink leaves remained unchanged by the petiole excision or abrasion treatments, and the presented data begin after this preparation.

suggests that vascular connections are altered which transfer a percentage of the flow from the unmonitored hypocotyl/crown region to the two sink leaves, or vice versa. Finally, a change in translocation rate at one sink leaf, independent of the other (Figs 1A, B), would imply that the assimilate flow to one sink leaf alone has been repartitioned within the hypocotyl/crown region of the plant system. Similarly, the previously reported inhibitions of translocation to a single sink leaf system, following slow-cooling treatments (Grusak and Lucas, 1984), could also be explained by a transfer of flow from the single sink leaf to the unmonitored hypocotyl/crown region of the plant.

*Localization of the repartitioning event*

To account for the suggested change in sink partitioning, an alteration in phloic pathway connections would have to occur at, or prior to the point where the translocation pathways of the three sinks diverge. Either the sugar beet crown or the source leaf petiole could be the tissue involved. The sugar beet crown (which is morphologically equivalent to a compressed stem) has been shown to have a complicated vascular anatomy with numerous anastomoses connecting the vascular rings (Zamski and Azenkot, 1981*a*; Stieber and Beringer, 1984). Although the translocation flow from a given source leaf has a preferred vascular route through the crown to certain sink regions (Joy, 1964; Zamski and Azenkot, 1981*b*), export to other sinks can be induced (Joy, 1964) and the connections in the crown could serve to re-route flow. However, the source leaf petiole also contains numerous anastomoses, and apparently these can also act to re-direct the flow of assimilates (Grusak and Lucas, 1984). In order to distinguish between these two possibilities, overlapping incision experiments were

undertaken to override any cooling-induced re-routing which may have occurred within the cooled region of the petiole. If pathway alterations occurred in this region, their effect in changing flow to the monitored sinks should be cancelled by the subsequent downstream re-channelling (Grusak and Lucas, 1984) through the limited vascular connections between the overlapping incisions (inset, Fig. 3). Since cooling-induced step-changes in the translocation rate were observed with this treatment (Fig. 3), it would appear that the cooled petiole tissue is not the location of pathway alteration. In addition, sink re-partitioning has also been demonstrated in situations which involved perturbations of plant parts other than the source leaf petiole. Geiger (1966) observed an increase in translocation to the single sugar beet sink leaf when a 4·0 cm portion of the beet root was cooled to 0·5 °C. Influencing the sink–source ratio by darkening all source leaves of a sugar beet plant, other than the source leaf from which export is monitored, also induced repartitioning between the sinks (Fondy and Geiger, 1980). These investigations, in conjunction with our present results (Fig. 3), suggest that the most likely site for changes in phloic pathway connections, induced by cooling treatments, is within the complex vasculature of the crown region of the sugar beet plant.

*Influence of repartitioning on the quick-cooling induced inhibition response*

The often-seen recovery of the translocation rate to values higher than the pre-treatment level (Fig. 2) is one aspect of the quick-cooling induced inhibition response which has proven difficult to explain. In a previous study (Grusak and Lucas, 1984) we suggested that the recovery phenomenon, *per se*, may be due to a cooling-induced activation of flow into adjoining sieve elements/vascular bundles *within* the chilled region of the petiole. We suggested that this increase in the number of sieve elements participating in translocation to the monitored sink would decrease the resistance to flow through the chilled zone and, thereby, allow the translocation rate to recover. Our new understanding of the cooling-induced sink-repartitioning response now allows us to re-evaluate and extend this working hypothesis. The observed inhibition and recovery of translocation probably involves a combination of at least two separate events: a quick-cooling induced inhibition of flow in the chilled region of the petiole, with a subsequent recovery from that inhibition *to the pre-cooled translocation rate*, and a quick-cooling induced repartitioning of flow among the terminal sinks, *in the crown region of the plant*. The process of repartitioning would occur at the time of the quick cooling, and would be responsible for the final steady-state increase (or decrease) of translocation relative to the original pre-treatment value for each sink. The quick-cooling induced transient increase in translocation illustrated in Fig. 2 (sink leaf 5A) could be explicable as an integration of the rate increase, due to sink repartitioning, and the rate decreases due to the cooling-induced inhibition. In this particular sink leaf, for this cooling response, the *initial* degree of inhibition would have had to have been less than the repartitioning-induced increase.

Further understanding of the system can be achieved by separating the influence of the repartitioning and cold-induced inhibition responses. From the experimental data we know that, following the first quick-cooling treatment, leaves 5A and 5B (of Fig. 2) had different steady-state translocation values. Clearly, in this situation, the total translocation flow ($J_T$) past the crown region is equal to the sum of the flows into each sink, or

$$J_T = J_{S1} + J_{S2} + J_{S3} \quad (1)$$

where S1, S2 and S3 represent, respectively, the sink leaf 5A, sink leaf 5B, and the hypocotyl/crown region above the heat girdle for the plant in question (Fig. 2). If the quick-cooling treatment induces sink repartitioning, the new steady-state translocation

flows ($J'$), following recovery from the inhibition, would be different for each sink (although the total flow would equal that prior to cooling), such that:

$$J'_T = J_T = (J_{S1}+J_X)+(J_{S2}+J_Y)+(J_{S3}-J_X-J_Y) \quad (2)$$

$$= J'_{S1}+J'_{S2}+J'_{S3}$$

and $J_X$ and $J_Y$ represent a portion of the original flow from sink S3. If we now consider the observed time-dependent flows ($J''$) during the inhibition/recovery response, and make the assumption that the inhibition/recovery process in the source leaf petiole has an *equal* and *concurrent* effect on *all* of the sieve elements, we can designate a time-dependent inhibition factor $I$ (where $0 \leqslant I \leqslant 1$, and $I$ represents the time-dependent degree of inhibition), such that:

$$J''_T = (1-I)J'_T = (1-I)J'_{S1}+(1-I)J'_{S2}+(1-I)J'_{S3} \quad (3)$$

$$= J''_{S1}+J''_{S2}+J''_{S3}. \quad (4)$$

For any sink S, therefore, the time-dependent values of $I$ can be determined from experimental data by the equation:

$$(1-I) = \frac{J''_S}{J'_S}. \quad (5)$$

Figure 5A is a plot of $(1-I)$ versus time, determined for sink leaves 5A and 5B (of Fig. 2) from their translocation responses to the first quick-cooling treatment. The similar time dependencies of $I$ supports our concurrent-inhibition assumption made in the analysis. A similar result was also obtained when the $(1-I)$ values were compared for sink leaves 5A and 5B (Fig. 2) derived from the second quick-cooling response. Identical $(1-I)$ responses were obtained on four out of a total of five such experiments conducted on plants reduced to two sink leaves per plant. It would appear that in the fifth experiment the time-dependence of inhibition was not constant across all the veins present in the cooled petiole region.

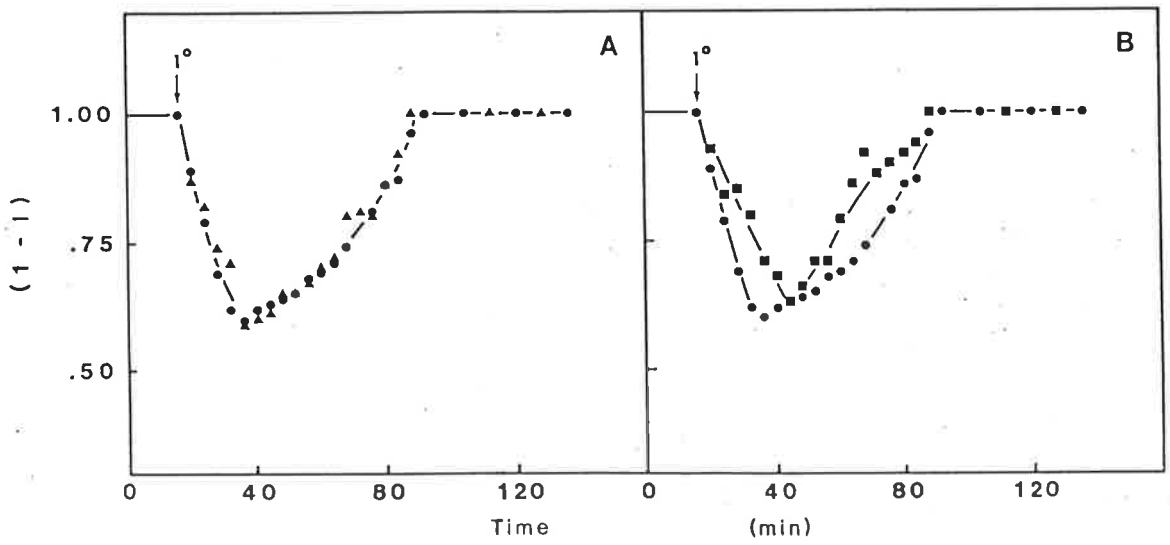


FIG. 5. Time dependency of $1-I$ ($1-$inhibition factor) calculated from the translocation responses of various sink leaves during quick-cooling treatments on a source leaf petiole segment. (A) Values calculated from the translocation responses of sink leaves 5A (●) and 5B (▲) during the first quick-cooling treatment shown in Fig. 2. (B) Values calculated from the translocation response of sink leaf 5A during the first (●) and second (■) quick-cooling treatments presented in Fig. 2.

During this analysis of translocation inhibition ($I$ versus time), we also compared the $(1-I)$ values obtained from consecutive cooling treatments on a particular sink leaf. The results of one such comparison are presented in Fig. 5 (sink leaf 5A of Fig. 2), and clearly the time-dependencies of the inhibition/recovery responses do not coincide. This disparity was observed in all experiments that we conducted and suggests that the biochemical/biophysical tissue alterations, induced by the first quick cooling, influences the response of the petiole to the second cooling treatment.

*Mechanism of the cooling-induced repartitioning event*

Having suggested that the repartitioning event occurs in the crown region of the sugar beet plant, it is necessary to consider how this may be induced by a cooling treatment on the source petiole, at a distance of some 6–10 cm away from the putative site of re-allocation. As can be seen for the translocation response to slow-cooling treatments (Figs 1A, B and 3), the rate change responds almost immediately to the change in temperature. With a volume flow of about 0·9 cm $min^{-1}$ in sugar beet (Geiger, Saunders, and Cataldo, 1969), a chemical/hormonal signal transmitted in the translocation stream could not account for the observed responses. Similar rapid changes in translocation rate at points distant from the site of perturbation have previously been observed by Webb (1971), Walding and Weatherly (1972), Pickard and Hill (1975), Watson (1976), Lang (1978), Pickard, Minchin, and Troughton (1978*a*), and Thorpe, Lang, and Minchin (1983). In these studies, it has often been suggested that a rapid physical signal, such as the transmission of a pressure change, is necessary to account for the observed results.

Ferrier (1978) used a numerical analysis model of the phloem to demonstrate that pressure waves, or as he termed them, concentration–pressure–flux (CPJ) waves, can be transmitted in both directions from any point in the long-distance translocation system. Their induction is based on a time-dependent variation of loading or unloading at the wave source, which leads to a time-dependent variation in osmotic pressure, and in turn gives rise to a time-dependent variation in hydrostatic pressure. This variation in hydrostatic pressure within the sieve elements is then propagated along the transport system at rapid velocities. In addition, Ferrier speculated that the frequency of the CPJ wave could carry information between the source and sink, with the involvement of frequency-specific membrane transport elements.

On the basis of these theoretical studies conducted by Ferrier (1978), we performed experiments on sugar beet plants which involved changing the apoplastic environment of a portion of the source leaf petiole (Fig. 4). Since it was theorized that CPJ waves are induced by time-dependent variations in sieve element hydrostatic pressure, we reasoned that changing the bathing solution from pure water to $10^3$ mol $m^{-3}$ mannitol might induce these waves and perhaps influence the rate of translocation. As can be seen from the results presented in Fig. 4, a change in the water potential (osmotic component) of the solution bathing the petiole caused translocation repartitioning to occur in a manner similar to that seen in response to slow-cooling treatments (Figs 1A, B). The results of similar apoplastic studies on moonflower (Pickard, Minchin, and Troughton, 1978*b*; see Fig. 4), in which a stem bathing solution was changed from $10^3$ mol $m^{-3}$ sucrose to water, could likewise be interpreted as a repartitioning of export from the source leaf.

At present we are unable to measure CPJ waves directly, but the results presented in Fig. 4 suggest that rapid, physical signals are induced by the osmotic changes of the bathing solution (apoplastic) and are probably transmitted to both the crown and sink regions of the plant. It is also possible that cooling treatments on a segment of the source leaf petiole may induce alterations in transport properties of the sieve element plasmalemma, such that a time-dependent alteration in the net flux of solutes is accomplished. This could then lead to a

localized change in hydrostatic pressure which may induce the propagation of a CPJ wave (Ferrier, 1978). Frequency or pressure-sensitive membrane phenomena at the juncture of sieve elements in the crown could then be induced to alter the resistance of the pathway connections (possibly via changes in the callose deposits in the sieve plate pores) and lead to a repartitioning of flow to the various sinks. However, it may also be possible that the putative signals are transmitted directly to the terminal sinks, where some type of control is exerted to alter the resistances of phloic connections in the crown region. Similar modulations in pathway resistances have similarly been suggested by Patrick and Wardlaw (1984) to explain the route of photosynthate movement in wheat. At present we are conducting a detailed electron microscopic analysis of the phloem tissue in both the crown/hypocotyl and sink leaf tissues to see if we can verify whether such structural changes actually occur in response to quick- and slow-cooling treatments.

## ACKNOWLEDGEMENTS

This research was supported by National Science Foundation Grants PCM 79-10223 and PCM 83-15408 to W.J.L., as well as a University of California Graduate Research Award to M.A.G.

## LITERATURE CITED

FELLOWS, R. J., EGLI, D. B., and LEGGETT, J. E., 1979. Rapid changes in translocation patterns in soybeans following source-sink alterations. *Plant Physiology*, **64**, 652–5.

FERRIER, J. M., 1978. Further theoretical analysis of concentration-pressure-flux waves in phloem transport systems. *Canadian Journal of Botany*, **56**, 1086–90.

FONDY, B. R., and GEIGER, D. R., 1980. Effect of rapid changes in sink-source ratio on export and distribution of products of photosynthesis in leaves of *Beta vulgaris* L. and *Phaseolus vulgaris* L. *Plant Physiology*, **66**, 945–9.

——— 1983. Control of export and of partitioning among sinks by allocation of products of photosynthesis in source leaves. *Current Topics in Plant Biochemistry and Physiology*, **2**, 33–42.

GEIGER, D. R., 1966. Effect of sink cooling on translocation of photosynthate. *Plant Physiology*, **41**, 1667–72.

——SAUNDERS, M. A., and CATALDO, D. A., 1969. Translocation and accumulation of translocate in the sugar beet petiole. Ibid. **44**, 1657–65.

GIFFORD, R. M., and EVANS, L. T., 1981. Photosynthesis, carbon partitioning, and yield. *Annual Review of Plant Physiology*, **32**, 485–509.

GRUSAK, M. A., and LUCAS, W. J., 1984. Recovery of cold-inhibited phloem translocation in sugar beet. I. Experimental analysis of an existing mathematical recovery model. *Journal of Experimental Botany*, **35**, 389–402.

——— 1985. Cold-inhibited phloem translocation in sugar beet. II. Characterization and localization of the slow-cooling response. Ibid. **36**, 745–55.

JOY, K. W., 1964. Translocation in sugar beet. I. Assimilation of $^{14}CO_2$ and distribution of materials from leaves. Ibid. **15**, 485–94.

LANG, A., 1978. Interactions between source, path and sink in determining phloem translocation rate. *Australian Journal of Plant Physiology*, **5**, 665–74.

PATRICK, J. W., and WARDLAW, I. F., 1984. Vascular control of photosynthate transfer from the flag leaf to the ear of wheat. *Australian Journal of Plant Physiology*, **11**, 235–41.

PICKARD, W. F., and HILL, III, R. L., 1975. An application of $\gamma$-scintigraphy to the observation of basipetal transport in moonflower. *Planta*, **125**, 289–301.

——MINCHIN, P. E. H., and TROUGHTON, J. H., 1978*a*. Real time studies of carbon-11 translocation in moonflower. I. The effects of cold blocks. *Journal of Experimental Botany*, **29**, 993–1001.

——— 1978*b*. Real time studies of carbon-11 translocation in moonflower. II. The effects of metabolic and photosynthetic activity and of water stress. Ibid. **29**, 1003–9.

STIEBER, J., and BERINGER, H., 1984. Dynamic and structural relationships among leaves, roots, and storage tissue in sugar beet. *Botanical Gazette*, **145**, 465–73.

SWANSON, C. A., and GEIGER, D. R., 1967. Time course of low temperature inhibition of sucrose translocation in sugar beets. *Plant Physiology*, **42**, 751–6.

THORPE, M. R., LANG, A., and MINCHIN, P. E. H., 1983. Short term interactions between flows of photosynthate. *Journal of Experimental Botany*, **34**, 10–19.

WALDING, H. F., and WEATHERLEY, P. E., 1972. The effect of cooling on translocation in *Salix viminalis*. Ibid. **23**, 338–45.

WATSON, B. T., 1976. Rapid propagation of changes in velocity of translocation along the phloem pathway of *Helianthus annuus* L. *Annals of Botany*, **40**, 659–67.

WEBB, J. A., 1971. Translocation of sugars in *Cucurbita melopepo*. VI. The reversible low temperature inhibition of $^{14}C$ movement and cold acclimation of phloem tissue. *Canadian Journal of Botany*, **49**, 717–33.

ZAMSKI, E., and AZENKOT, A., 1981*a*. Sugarbeet vasculature. I. Cambial development and the three-dimensional structure of the vascular system. *Botanical Gazette*, **142**, 334–43.

———— 1981*b*. Sugarbeet vasculature. II. Translocation of assimilates in the supernumerary phloem. Ibid. **142**, 344–6.

Phloem Transport, pages 3–15
© 1986 Alan R. Liss, Inc.

# 1. Kinetic Analysis of Sugar Transport: From Yesterday to Tomorrow

**Clyde Wilson and William J. Lucas**

*Department of Botany, University of California, Davis, California 95616*

## INTRODUCTION

According to Baker (1978), phloem loading is " . . . perhaps the most significant organic solute transport process in higher plants." Thus, a critical evaluation of the existing literature regarding the current models on phloem loading is necessary in order to determine what it is that we really know and must eventually understand so that we can proceed to unravel this important mystery of nature. In this chapter, we will trace the development of our current concepts on phloem loading and also report on our most recent laboratory findings. Through this process, we hope that new areas of inquiry will unfold that will challenge our existing dogma so we can then construct models that more closely represent in vivo events.

## BACK TO YESTERDAY: A HISTORICAL VIEW OF PHLOEM LOADING

### Apoplastic-Step Hypothesis

Do assimilates move entirely through the cytoplasm via plasmodesmata from the mesophyll cells to the phloem, or might solutes exit at some point from the mesophyll cells and then be taken up from the apoplast across the sieve element-companion cell complex (se-cc)? This question was addressed by many laboratories over a decade ago. Evidence from autoradiographic images of leaves fed $^{14}CO_2$ or $^{14}C$-labeled sugars had qualitatively demonstrated that translocated compounds accumulate in the minor veins and that this accumulation was selective (Ho and Mortimer, 1971; Fellows and Geiger, 1974; Geiger, 1976; Fondy and Geiger, 1977). However, the site of this accumulation step was not established. This question was investigated by Geiger and others. By circulating an unlabeled sucrose solution over the

abraded upper surface of a sugar beet leaf, Geiger and co-workers demonstrated that $^{14}CO_2$-produced sucrose could be intercepted, or "trapped," indicating to them that sucrose was normally present in the apoplastic space. Based on this and other data, Geiger proposed a model whereby phloem loading proceeds by uptake of solutes from the apoplast into the se-cc complex (Geiger et al., 1974). In a test of Geiger's model, Giaquinta (1976) showed that the steady-state rate of translocation (using $^{14}CO_2$) was inhibited when *p*-chloromercuribenzenesulfonic acid (PCMBS) was applied to intact leaves. The apoplastic-step hypothesis soon became established in the literature and had considerable influence on the interpretation of later work. At the time of the last International Symposium on Phloem, held in 1979 in Bad Grund, it was felt that "there is compelling evidence . . . that sucrose produced in the mesophyll travels via the symplasm to the phloem where it enters the apoplast prior to its selective and active accumulation into the sieve element-companion cell complex . . ." (Giaquinta, 1980).

### Kinetics of Phloem Loading

Initially, exogenous sucrose was viewed as being taken up by the whole leaf. However, leaf kinetics slowly became narrowed into the kinetics of phloem loading. Sovonick et al. (1974) and Giaquinta (1977) investigated the relationship between sugar uptake into leaf discs and the intact leaf. Based on these studies, uptake of exogenous sucrose into leaf discs was thought to reflect loading into the phloem and could, therefore, be used to study the specific mechanisms involved (Giaquinta, 1977, 1979, 1980; Delrot et al., 1980; Delrot, 1981; Delrot and Bonnemain, 1981). Earlier work on the kinetics of phloem loading was interpreted in terms of two saturable components, both obeying Michaelis-Menten kinetics and both delivering sucrose to the phloem. Now, many laboratories, using more recent evidence, interpret the kinetic data in terms of a saturable component follwing Michaelis-Menten kinetics, and a linear component following first-order kinetics (Komor et al., 1977; Delrot and Bonnemain, 1981; Lichtner and Spanswick, 1981; Maynard and Lucas, 1982a). We initially believed, as others, that these two transport systems were operating in parallel across the se-cc complex.

## RETRIEVAL REVISITED

Maynard and Lucas (1982b) questioned the interpretation of the kinetic results with respect to the actual site of sucrose uptake. Here the work of Komor et al. (1980) was instrumental in our challenging this concept. In Komor's model, the linear and the saturable components were spatially

distinct. The saturable component represented active uptake of sucrose into the phloem via a sucrose-$H^+$ cotransport mechanism, while the linear component represented simple diffusion into the mesophyll. But, in the work of Maynard and Lucas (1982a), the linear component accounted for 43% of the total uptake into the leaf at 25 mM exogenous sucrose. Thus, either the linear component was not simple diffusion, since the concentration in the se-cc complex would be too high, or the linear component was occurring across the plasmalemma of the mesophyll, and therefore uptake into leaf discs could not be equated with the kinetics of phloem loading. Could the mesophyll cells be taking up exogenously supplied sucrose?

There were already reports in the literature indicating that exogenously supplied sucrose can accumulate in the mesophyll (Geiger, 1976; Geiger and Fondy, 1980; Fondy and Geiger, 1977). Using quantitative grain-density scans, Geiger and Fondy found that after a 30-min incubation, in 10 mM sucrose, 60% of the radiolabel was located in the mesophyll of sugar beet leaves. In order to test the hypothesis that the linear and saturable components of sugar transport are indeed spatially distinct, Maynard and Lucas (1982b) devised an experiment using leaf discs and petiole sections from sugar beet. They reported similar sucrose and 3-0-methyl glucose kinetic profiles using leaf discs and whole petiole segments. The petiole segments were simplified by physically removing the inner-cortical-parenchyma tissue (pith), leaving behind a vascular-bundle enriched petiole system. Uptake studies performed on these simplified tissues, using sucrose and 3-0-methyl glucose, showed that these sugars were taken up by the now familiar saturable and linear components. However, previous investigations reported that 3-0-methyl glucose was taken up only by the mesophyll (Fondy and Geiger, 1977; Delrot, 1981). Consequently, Maynard and Lucas (1982b) concluded that the presence of a saturable and linear component must be a ubiquitous feature of the plasmalemma of a wide variety of cell types. It was at this time that Maynard and Lucas (1982b) reintroducted the retrieval hypothesis, meaning that the kinetic data may represent retrieval of exogenous solutes and not phloem loading (see, e.g., Pate and Gunning, 1969; Gilder and Cronshaw, 1974; Fondy and Geiger, 1977; Evert et al., 1978; Fritz et al., 1983).

In order to test this "new" hypothesis, it is necessary to separate the various tissues of the leaf so that their individual contribution to the total uptake may be compared. We sought a leaf that would lend itself both to biochemical and mechanical manipulation. We chose the mature leaf of *Allium cepa,* as it lacks an inner cuticle and epidermis and so its interior tissues are highly accessible to added solutes or cell-wall-digesting enzymes. We filled the interior with 1 mg/ml Pectolyase Y-23, and after 45 min the

inner parenchyma and part of the bundle sheath were digested away. This tissue was then either used for kinetic studies or further manipulated. As the cell walls of the bundles were weakened by enzymatic digestion we could, by using forceps and working under a high-power dissecting scope, strip away the vascular bundles. This "stripped" tissue was then used for kinetic studies (Wilson et al., 1985).

Kinetic profiles obtained using the untreated (control) leaf discs exhibited the same saturable plus linear profile as the dicotyledon, *Beta vulgaris*. With respect to sucrose influx, the curves of the inner parenchyma plus bundle sheath and the cholorenchyma are similar to those of the vascular bundles. Over most of the concentration range tested, the uptake of exogenously supplied $^{14}$C-sucrose into the *vascular tissue* was dominated by the linear component. It is indeed interesting to speculate on the significance of this observation in terms of sucrose-$H^+$ cotransport. Similar results were obtained for fructose, although this sugar is not normally considered to be loaded into the phloem. However, fructose influx into the inner parenchyma and bundle-sheath cells was strictly linear. By using existing techniques and careful tissue selection, we can now show that some tissues contain both the saturable and linear component.The interplay and regulatory processes operating remain to be elucidated.

We realize that the various treatment may have perturbed membrane function and sugar-related transport processes. However, if the experimental data reflect in vivo activity, then the contribution of the vascular tissue to overall uptake is indeed small. The pathway for phloem loading, whether apoplastic, symplastic, or both, is still unresolved. As evidenced by our uptake experiments, many tissues are able to retrieve exogenous sugars. Therefore, the in vivo kinetics of phloem loading will be difficult to ascertain, as this will require the specific inhibition of all sugar-related transport processes operating in non-phloem cells.

## EVIDENCE FOR APOPLASTIC LOADING: A RE-EXAMINATION

### Sucrose-$H^+$ Cotransport Studies

Other researchers have published circumstantial evidence in support of the sucrose-$H^+$ cotransport hypothesis. We will discuss here some of the more compelling evidence. For a review of this area, the reader is referred to the works of Giaquinta (1983) and Reinhold and Kaplan (1984). The work of Heyser (1980) has been cited as being the most convincing evidence in support of sucrose-$H^+$ cotransport into the phloem (Giaquinta, 1983). Heyser designed an ingenious experiment using leaf strips of *Zea mays*. He placed

one end of the maize leaf strip in an experimental solution, while the other end was placed in a vacuum chamber. The pH of the xylem perfusate was determined by a pH electrode placed near the tip of the leaf strip. Upon introducing 25 mM sucrose, he noted a 0.7 pH unit alkalinization of the xylem perfusate. The peak of this response occurred 10 min after the introduction of sucrose. Other sugars such as glucose, fructose, and raffinose did not stimulate the alkalinization of the xylem perfusate. These results appeared consistent with the operation of a sucrose-$H^+$ cotransport mechanism operating across the plasma membrane of the se-cc complex.

The actual location of this transport process was investigated by Fritz and Evert. They repeated Heyser's experiments, using exactly the same material and protocol (Fritz et al., 1983). Labeled $^{14}C$-sucrose was employed so that they could use the Fritz microautoradiographic technique to determine the site of uptake. They found that after an 8- to 15-min exposure, the majority of the label appeared in the vascular parenchyma. Even after 30 min, little of the label moved into the thick- or thin-walled sieve tubes. Thus, the site of Heyser's alkalinization response is probably not the se-cc complex but most likely the plasmalemma of the vascular parenchyma. Fritz et al. (1983) suggested that this may represent a retrieval function for these cells.

### Electrophysiology Studies

Additional support for the sucrose-$H^+$ cotransport hypothesis of phloem loading has come from the elegant electrophysiology investigations of Wright and Fisher (1981). They used severed aphid stylets to establish electrical continuity with the sieve elements of willow bark strips. The introduction of sucrose caused a rapid depolarization of the membrane potential, followed by a slower repolarization. These results were intepreted as the electrogenic cotransport of sucrose and $H^+$ into the sieve tubes. This interpretation needs to be examined more closely. In a part of that paper, the authors noted that other sugars such as fructose, glucose, 3-0-methyl glucose, and raffinose also produced a similar depolarization of the membrane potential, with the values ranging from 50 to 70% of those obtained with sucrose. Glucose and 3-0-methyl glucose are not thought to enter the phloem (Fondy and Geiger, 1977). Consequently, plasmodesmatal connections between the vascular parenchyma and the se-cc complex are needed to permit the transmission of the electrical signal. If the depolarization response of glucose and 3-0-methyl glucose is caused by their transport into the vascular parenchyma (or other cell types present within the bark), then the sucrose-induced depolarization may also be located at the vascular parenchyma. Again, it would appear that the site and mechanism of phloem loading remain equivocal.

## REGULATION OF APOPLASTIC RETRIEVAL

The evidence presented in this paper shows that many plant tissues are able to accumulate exogenously supplied sugars. However, this may not necessarily be regarded as phloem loading, per se. If this is not phloem loading, how may this technique be employed to investigate phloem-related events? As already mentioned, uptake of exogenous solutes may represent a retrieval function. One could then hypothesize that the activity of the plasmalemma would correlate with internal sugar levels. A prediction based on this hypothesis is that as the internal sugar levels rise, more would tend to leak out, thereby stimulating the retrieval mechanism. In order to test this hypothesis, we used mannose as a probe to alter carbohydrate partitioning. Numerous workers have used mannose to alter the partitioning of newly fixed carbon between the chloroplast and the cytosol (see Herold and Lewis, 1977; Herold et al., 1980; and the references cited therein). In the cytosol, mannose and orthophosphate are converted to mannose-6-phosphate. In some plants, such as *B. vulgaris,* mannose-6-phosphate is not further metabolized.

In an attempt to elucidate the regulatory mechanisms controlling the activity of the plasmalemma, we performed the following set of experiments. Petioles from sugar beet plants with their attached leaves were excised, underwater, at the base of the crown. The leaf-petiole complex was then either placed in water (control) or in a 10 mM mannose solution. After a specified period (3, 6, or 24 h), leaf discs were punched and used for kinetic and sugar analyses. Mannose-treated *B. vulgaris* leaves exhibited a progressive decrease in their ability to take up exogenous sucrose. After 3 h, or longer exposures, there was a decrease in both the linear and saturable components of uptake (Fig. 1). Previous researchers have demonstrated that mannose affects the partitioning of newly fixed carbon. However, upon analysis by high-performance liquid chromatography, we found that total sucrose slightly increased when the leaf was subjected to mannose, while total starch decreased. Photosynthesis, as measured by $O_2$ production, was found to decrease but was not completely inhibited.

It is possible that the effect of mannose was due to osmotic rather than biochemical interactions. To test this possibility, we substituted mannitol, a slowly penetrating sugar alcohol, for mannose. We noted that ethanol-soluble sugars increased while starch remained the same. Influx of sucrose decreased slightly but not nearly to the same extent as in the mannose treatment (Fig. 2). Evidently, mannose has effects independent of its osmotic properties. These results do not support our earlier prediction; rather, they indicate that a more complex set of regulatory mechanisms exists.

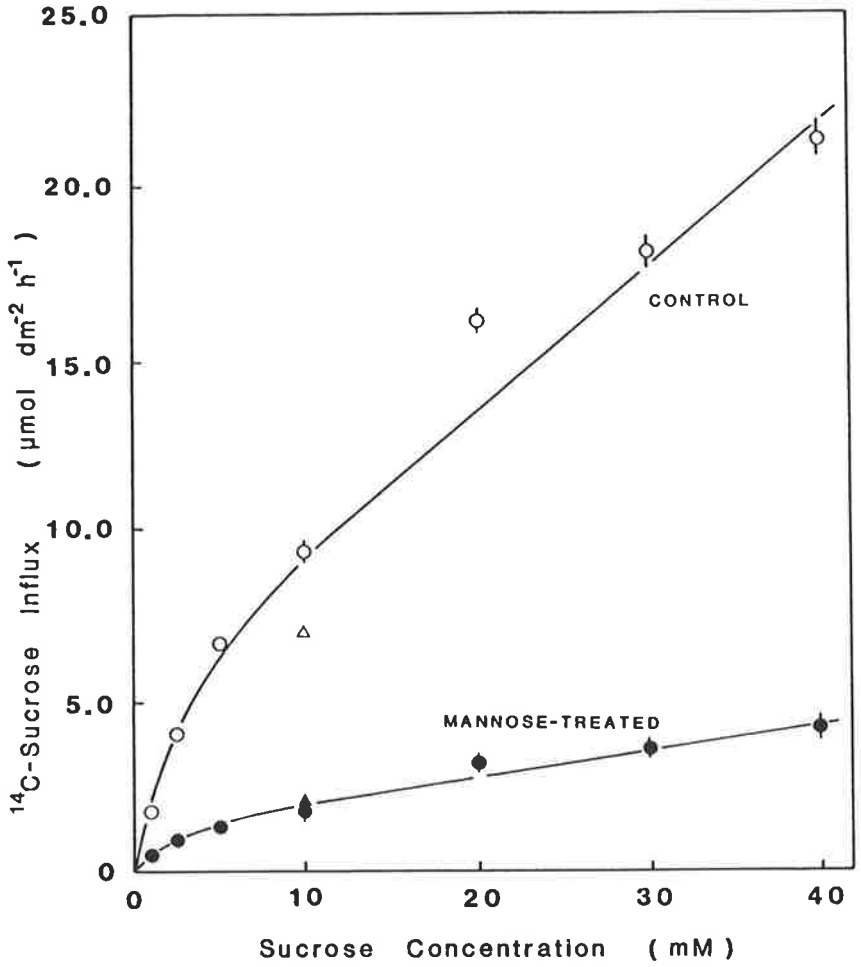


Fig. 1. Effect of mannose treatment on sucrose influx into *Beta vulgaris* leaf discs. Mannose was supplied to the leaf through the petiole. The petioles, with their attached leaves, were excised, underwater, at the base of the crown and placed in either water (control) or in a 10 mM mannose solution. The leaf-petiole complex was returned to a controlled-environment chamber. After 24 h, leaf discs were punched from the attached leaves and used for sugar and kinetic analysis. A 30-min preincubation period in unlabeled sucrose was followed with a 30-min incubation in $^{14}$C-sucrose solution. Each point represents the mean + SE for six replicates.

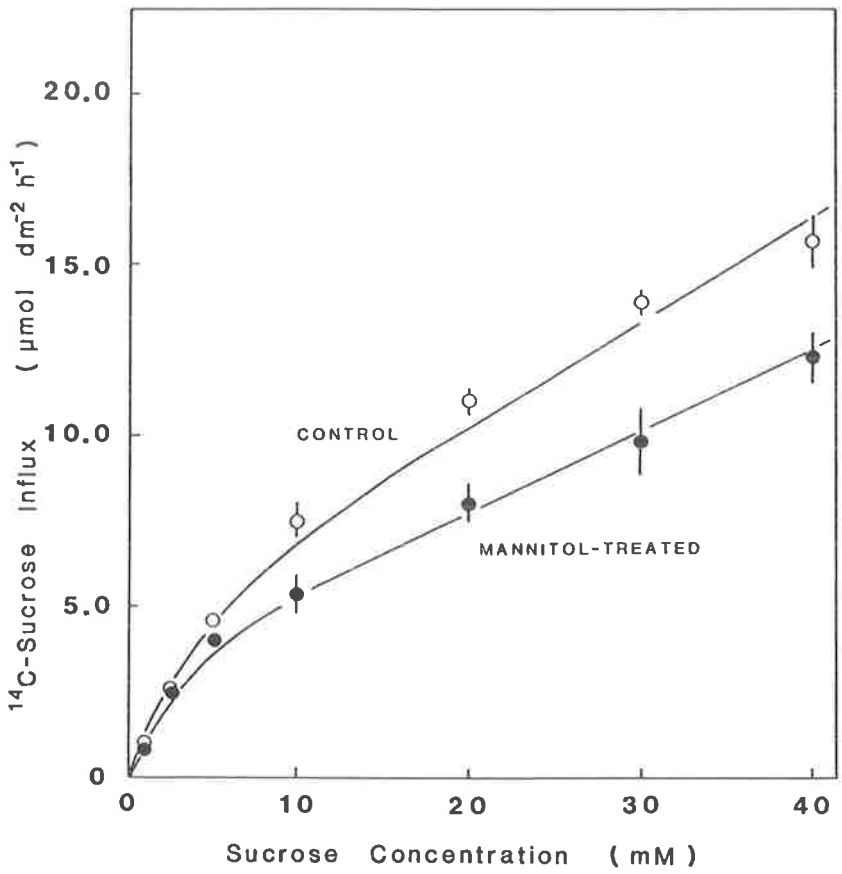


Fig. 2. Effect of mannitol treatment on sucrose influx into *Beta vulgaris* leaf discs. Mannitol substituted for mannose; otherwise, experimental techniques were as described in Figure 1. Each point represents the mean + SE for six replicates.

In addition to altering the partitioning of carbohydrate, mannose may be affecting the energy charge of the cells. Presumably, lower levels of ATP would slow the operation of the putative $H^+$-translocation ATPase in the plasmalemma. On the other hand, there may be adequate levels of ATP remaining in the mannose-treated tissue to operate the ATPase, but the system may have become sensitive to ADP. Reduced synthesis of ATP by mannose has been shown by other investigators (Garrard and Humphreys, 1969; Stenlid, 1971).

These findings necessitated a further investigation of the role of internal sugars in the control of apoplastic retrieval. We inhibited photosynthesis by the addition of 20 $\mu$m 3,4-dichlorophenyl-1-methylurea (DCMU) to the leaf in a manner similar to that described above. The DCMU treatment resulted

in a large decrease in the sucrose, fructose, glucose, and starch levels. However, our kinetic data revealed no change in the kinetic properties between DCMU-treated and control leaf discs. The lowering of internal sugars and starch did not affect the operation of the retrieval mechanisms as predicted, further indicating more complex regulation of the plasmalemma.

It also seemed important to ascertain whether the mannose effect is specific for the sucrose transport system or whether other sugar transport systems are similarly affected. As in the case of sucrose, uptake of glucose and fructose decreased in mannose-treated leaves. In contrast to sucrose, the influx of glucose and fructose in mannose-treated leaves was mediated only by the linear component (Figs. 3, 4). It is instructive to recall that these sugars are not normally loaded into the phloem. Apparently, the regulation of glucose and fructose retrieval is different from that of sucrose.

Numerous other studies conducted in our laboratory indicate that there is no correlation between simple sugar levels and the transport activity of the plasmalemma. Experiments where we preloaded the leaf with sucrose or heat-girdled the petiole failed to support our prediction. In order to test further our hypothesis, we need to know the cytosolic and vacuolar sugar levels as well as the in vivo functioning of the chloroplast and how these affect retrieval. The system is much too complicated at this stage to make any inference concerning the control of the retrieval mechanisms.

## TOMORROW: INVESTIGATING A METAPHYSICAL PHENOMENON

We have now gone from yesterday, when we thought we knew about the mechanisms and site of phloem loading, to today, when we realize that studies on the specific process of "phloem loading" may reside in the area of metaphysics. As evidenced by the work presented in this chapter, tomorrow's concepts on phloem loading must involve a much broader perspective of this complex phenomenon of assimilate movement from mesophyll cells to the se-cc complex. Our concepts must *not* be limited to the movement of the translocated species into the se-cc complex, but should integrate transport processes at the plasmalemma and tonoplast of a number of cell types. We should also include in this approach the complex intracellular mechanisms involved in regulating and partitioning assimilates.

One exciting area of investigation is the symplastic relationship between the mesophyll and the se-cc complex. New evidence by Dr. M. Madore in our laboratory indicates that the mesophyll and the sieve elements might be symplastically connected. (The reader is referred to her chapter in this volume.) Dr. Madore has been able to microinject Lucifer Yellow CH into

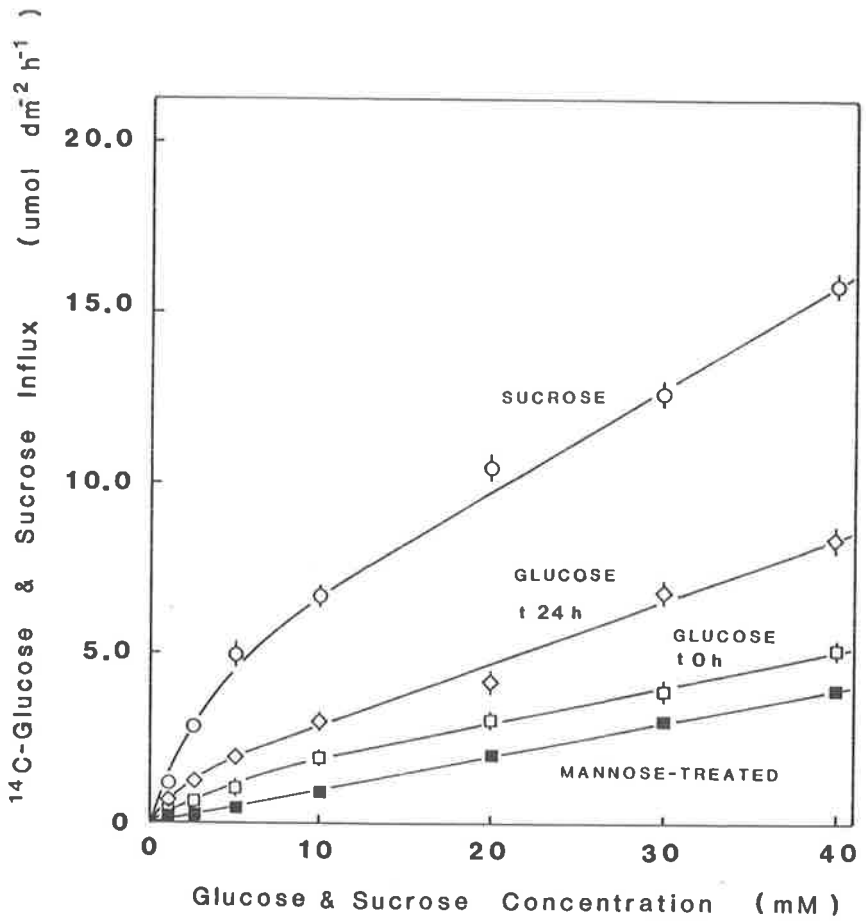


Fig. 3. Effect of mannose treatment on glucose influx into *Beta vulgaris* leaf discs. Kinetic profiles for the control tissues were established at 0 h (t 0 h) and 24 h (t 24 h) after excision of the petiole. The kinetic profile for the mannose-treated tissue was acquired after 24 h of treatment. The sucrose curve was established using leaf discs from 24-h control tissue and is included for reference. Glucose substituted for sucrose when appropriate; otherwise, experimental techniques were as described in Figure 1. Each point represents the mean + SE for six replicates.

the vacuoles of mesophyll cells of *Ipomea tricolor*. Lucifer Yellow CH is a highly fluorescent compound and is believed to be unable to cross membranes (Stewart, 1981). After 25 min, fluorescence can be detected in the minor veins. These data indicate that the se-cc complex and the mesophyll may be symplastically connected. More extensive studies, using this technique, will

provide much needed information on the relationship between plasmodesmata, the symplast of the source leaf, and *phloem loading*.

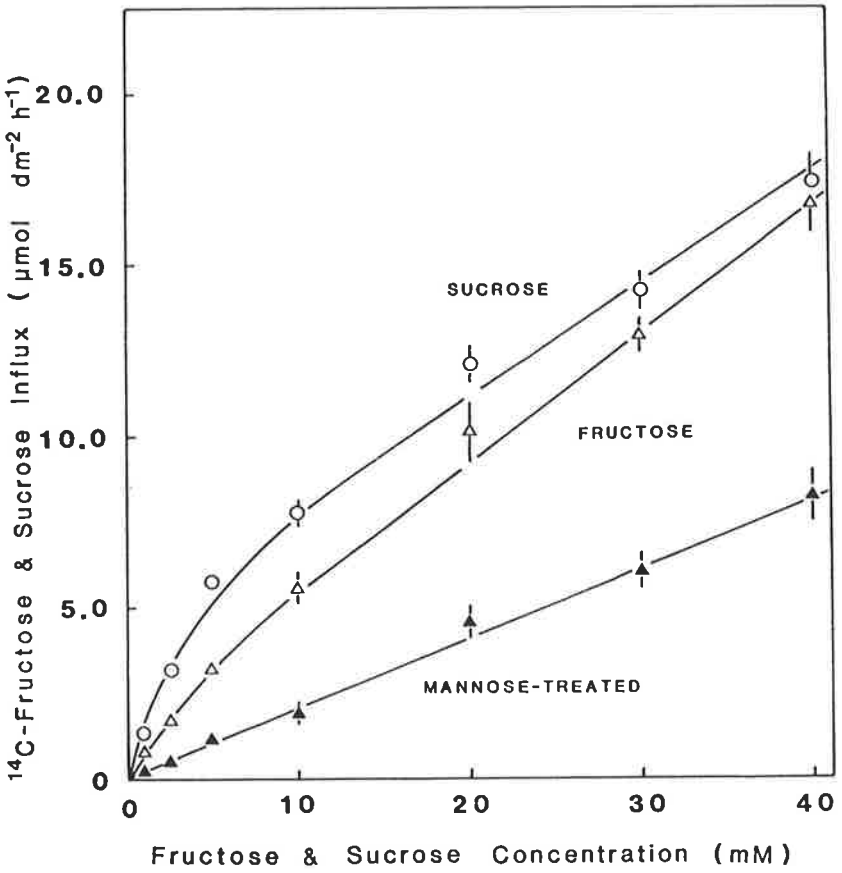


Fig. 4. Effect of mannose on fructose influx into control (untreated) and mannose-treated *Beta vulgaris* leaf discs. Sucrose profile was obtained from control tissues and is included for reference. Fructose substituted for sucrose when appropriate; otherwise, experimental techniques were as described in Figure 1. Each point represents the mean + SE for six replicates.

## ACKNOWLEDGMENTS

The work conducted in our laboratory on phloem physiology has been made possible by National Science Foundation grants PCM 79-10223 and PCM 83-15408.

## References

Baker DA (1978): Proton cotransport of organic solutes by plant cells. New Phytol 81:485–497.

Delrot S (1981): Proton fluxes associated with sugar uptake in *Vicia faba* leaf tissue. Plant Physiol 68:706–711.

Delrot S, Bonnemain JL (1981): Involvement of protons as a substate for the sucrose carrier during phloem loading in *Vicia faba* leaves. Plant Physiol 67:560–564.

Delrot S, Despeghel JP, Bonnemain JL (1980): Phloem loading in *Vicia faba* leaves: Effect of N-ethylmaleimide and parachloromercuribenzenesulfonic acid on $H^+$ extrusion, $K^+$ and sucrose uptake. Planta 149:144–148.

Evert RF, Eschrich W, Heyser W (1978): Leaf structure in relation to solute transport and phloem loading in *Zea mays* L. Planta 138:279–294.

Fellows RJ, Geiger DR (1974): Structural and physiological changes in sugar beet leaves during sink to source conversion. Plant Physiol 54:877–885.

Fondy BR, Geiger DR (1977): Sugar selectivity and other characteristics of phloem loading in *Beta vulgaris* L. Plant Physiol 59:953–960.

Fritz E, Evert RF, Heyser W (1983): Microautoradiographic studies of phloem loading and transport in the leaf of *Zea mays* L. Planta 159:193–206.

Garrard LA, Humphreys TE (1969): The effect of D-mannose on sucrose storage in the corn scutellum: Evidence for two sucrose transport mechanisms. Phytochemistry 8:1065–1077.

Geiger DR, Sovonick SA, Shock TL, Fellows RJ (1974): Role of free space in translocation in sugar beet. Plant Physiol 54:892–898.

Geiger DR (1976): Phloem loading in source leaves. In Wardlaw IF, Passioura JB (eds): "Transport and Transfer Processes in Plants." New York: Academic Press, pp 167–215.

Geiger DR, Fondy BR (1980): Response of phloem loading and export to rapid changes in sink demand. Ber Dtsch Bot Ges 93:177–186.

Giaquinta R (1976): Evidence for phloem loading from the apoplast: Chemical modification of membrane sulfhydryl groups. Plant Physiol 57:872–875.

Giaquinta R (1977): Phloem loading of sucrose: pH dependence and selectivity. Plant Physiol 59:750–755.

Giaquinta R (1979): Phloem loading of sucrose: Involvement of membrane ATPase and proton transport. Plant Physiol 63:744–748.

Giaquinta R (1980): Mechanism and control of phloem loading of sucrose. Ber Dtsch Bot Ges 93:187–201.

Giaquinta R (1983): Phloem loading of sucrose. Annu Rev Plant Physiol 34:247–387.

Gilder J, Cronshaw J (1974): A biochemical and cytochemical study of adenosine triphosphatase activity in the phloem of *Nicotiana tabacum.* J Cell Biol 60:221–235.

Herold A, Lewis DH (1977): Mannose and green plants: Occurrence, physiology and metabolism, and use as a tool to study the role of orthophosphate. New Phytol 79:1–40.

Herold A, McGee EEM, Lewis DH (1980): The effect of orthophosphate concentration and exogenously supplied sugars on the distribution of newly fixed carbon in sugar beet leaf discs. New Phytol 85:1–13.

Heyser W (1980): Phloem loading in the maize leaf. Ber Dtsch Bot Ges 93:221–228.

Ho LC, Mortimer DC (1971): The site of cyanide inhibition of sugar translocation in sugar beet leaf. Can J Bot 49:1769–1775.

Komor E, Rotter M, Tanner W (1977): A proton-cotransport system in a higher plant: Sucrose transport in *Ricinus cummunis*. Plant Sci Lett 9:153–162.

Komor E, Rotter M, Waldhauser J, Martin E, Cho BH (1980): Sucrose proton symport for phloem loading in the *Ricinus* seedling. Ber Dtsch Bot Ges 93:211–219.

Lichtner FT, Spanswick RM (1981): Sucrose uptake by developing soybean cotyledons. Plant Physiol 68:693–698.

Maynard JW, Lucas WJ (1982a): A reanalysis of the two-component phloem loading system in *Beta vulgaris*. Plant Physiol 69:734–739.

Maynard JW, Lucas WJ (1982b): Sucrose and glucose uptake into *Beta vulgaris* leaf tissue: A case for general (apoplastic) retrieval systems. Plant Physiol 70:1436–1443.

Pate JS, Gunning BES (1969): Vascular transfer cells in angiosperm leaves: A taxonomic and morphological survey. Protoplasma 68:135–156.

Reinhold L, Kaplan A (1984): Membrane transport of sugars and amino acids. Annu Rev Plant Physiol 35:45–83.

Sovonick SA, Geiger DR, Fellows RJ (1974): Evidence for active phloem loading in the minor veins of sugar beet. Plant Physiol 54:886–891.

Stenlid G (1971): The effect of some inhibitory sugars upon the content of adenosine triphosphate in wheat roots. Physiol Plant 25:397–401.

Stewart WW (1981): Lucifer dyes—highly fluorescent dyes for biological tracing. Nature 292:17–21.

Wilson C, Oross JW, Lucas WJ (1985): Sugar uptake into *Allium cepa* leaf tissue: An integrated approach. Planta 164:227–240.

Wright JP, Fisher DB (1981): Measurement of the sieve tube membrane potential. Plant Physiol 67:845–848.

Phloem Transport, pages 477–486
© 1986 Alan R. Liss, Inc.

# 64. Regulation of Long-Distance Translocation in Sugar Beet: Structural Aspects

**J.W. Oross, M.A. Grusak, and W.J. Lucas**

*Botany Department, University of California, Davis, California 95616*

## INTRODUCTION

Several studies of phloem translocation in sugar beet have shown that the rate of accumulation of translocates in a sink leaf can be affected by chilling a localized region on the source leaf petiole (Swanson and Geiger, 1967; Grusak and Lucas, 1984, 1985, 1986). These studies utilized plants that were simplified to a single source leaf, and either one or two sink leaves. Depending on the cooling rate employed, two distinct types of response have been observed with respect to the rate of translocation. A quick cooling of the source petiole, from 25 to 1°C, elicited an abrupt decline in the translocation rate into the sink leaf that was followed by a nearly complete recovery to the prechilling rate. The second type of response involved a rapid step-wise change in relative translocation that showed no recovery. This step-wise response was obtained when a specific slow-cooling regime was applied to the source leaf petiole. Our more recent studies suggest that the structure of the translocation pathway may play an important role in the manifestation of these responses. The present report describes our efforts to elucidate the relationship between these chilling-induced translocation responses and the structure of the source-to-sink phloem pathway.

## QUICK-COOLING RESPONSE

The ability of the sugar beet translocation system to recover after a quick chilling treatment clearly distinguishes this chilling response from that ob-

served when a slow-cooling treatment is applied to the source leaf petiole. Recently, Grusak and Lucas (1984) proposed that this recovery was based upon the lowering of the resistance in the region of the cold block on the source petiole by the addition of pre-existing sieve elements to the primary translocation pathway. The mechanism of this addition was suggested to involve the activation of laterally oriented vascular anastomoses that interconnect the nine large vascular bundles that run the entire length of the petiole. This proposal was based on the results of surgical experiments in which overlapping cuts were made in the petiole such that none of the axially aligned petiolar veins remained uncut (Fig. 1, insets A–C). Under these conditions, the system was able to attain approximately 60% of the precutting translocation rate (Fig. 1), which was apparently accommodated by the vascular anastomoses present between the cuts (Fig. 1, inset A).

Superficial consideration of the recovery profile obtained from this type of experiment (Fig. 1) would indicate that the activation of the anastomoses is quite rapid. However, it has been demonstrated that there are pathway sinks within the sugar beet translocation system that unload as a result of excision of the source blade (Grusak and Lucas, 1984). Consequently, a more accurate estimate of the rate at which the anastomoses are activated must involve the subtraction of this downstream unloading contribution from the total recovery response. When this is done (see Fig. 1), one sees that the activation of the anastomototic vasculature is relatively slow.

The apparent importance of anastomoses in the recovery responses of the sugar beet translocation system to surgical, as well as quick-cooling, blockages raises many important structural questions about the junction between the anastomototic and continuous veins. Clearly, the most important question relates to the elucidation of the structural basis for the regulation of flow through the anastomoses. A recent structural study that focused primarily upon this important aspect provided some interesting preliminary insights (Oross and Lucas, 1985). This study demonstrated that direct continuity between the sieve elements of the anastomosing and continuous veins was either precluded, or restricted by the presence of phloem parenchyma cells that separated the sieve elements of the merging veins (Fig. 2). This, in addition to Esau's (1934) observation that the sieve elements of the large, continuous veins are grouped into clusters that are bounded laterally by phloem parenchyma cells, indicated that these parenchyma cells are an important component of the lateral translocation pathway in the sugar beet petiole. The relative slowness of apoplastic or symplastic movement across these parenchyma cells, in comparison to the faster rate of translocation that is associated with assimilate movement through sieve tubes, perhaps explains the slowness of the activation of the anastomototic vasculature.

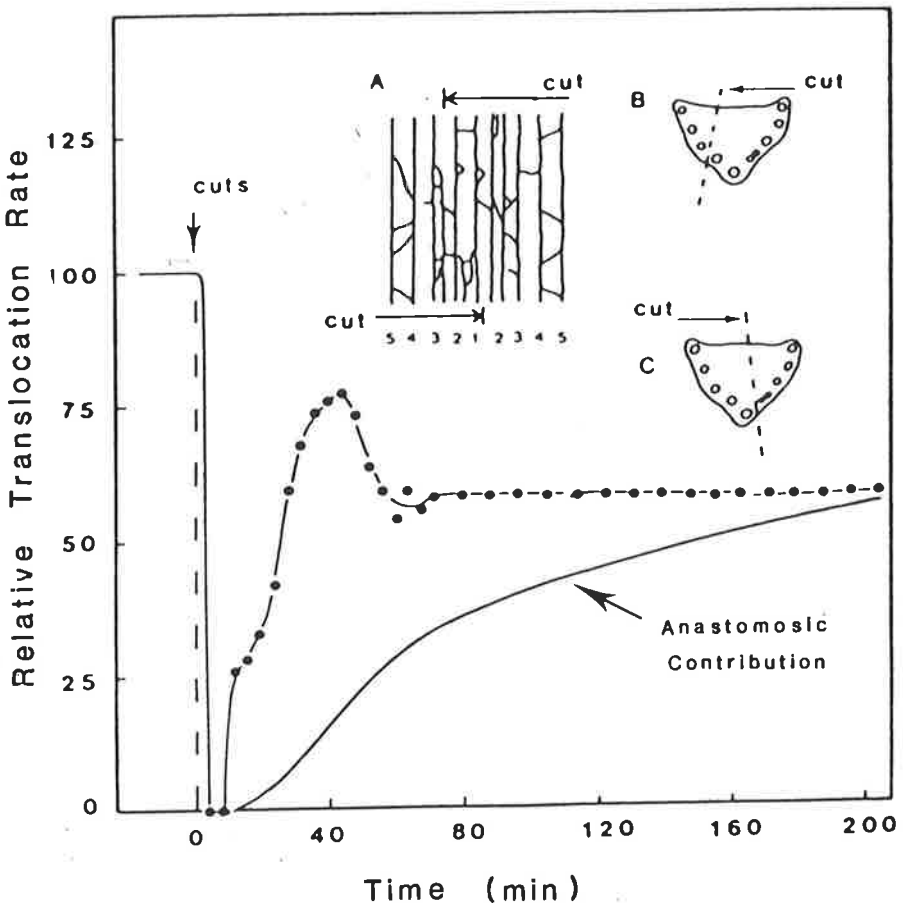


Fig. 1. Translocation profile following two overlapping cuts into the source leaf petiole of a sugar beet plant. The incisions were made under distilled water from opposite sides of the petiole such that none of the nine axially oriented veins remained uncut. A. Diagrammatic representation of the petiolar vasculature found in the region between the cuts. B and C. Cross-sectional views of the petiole showing the direction and extent of the two cuts. The line labeled "anastomosic contribution" was generated by deducting a representative translocation profile obtained after the excision of the blade of a source leaf from another plant (Fig. 6 of Grusak and Lucas, 1984). This figure is redrawn from Figure 9 of Grusak and Lucas (1984).

The involvement of petiolar phloem parenchyma in lateral translocation prompted a more detailed study of the ultrastructure of these cells. Two cytological features were found that could possibly relate to this function. The first was the presence of microfilament bundles found in the parenchyma cell cytoplasm nearest the large central vacuole that is characteristic of these cells (Fig. 3; and Oross and Lucas, 1985). These microfilament bundles may function in lateral translocation by promoting cytoplasmic streaming, which

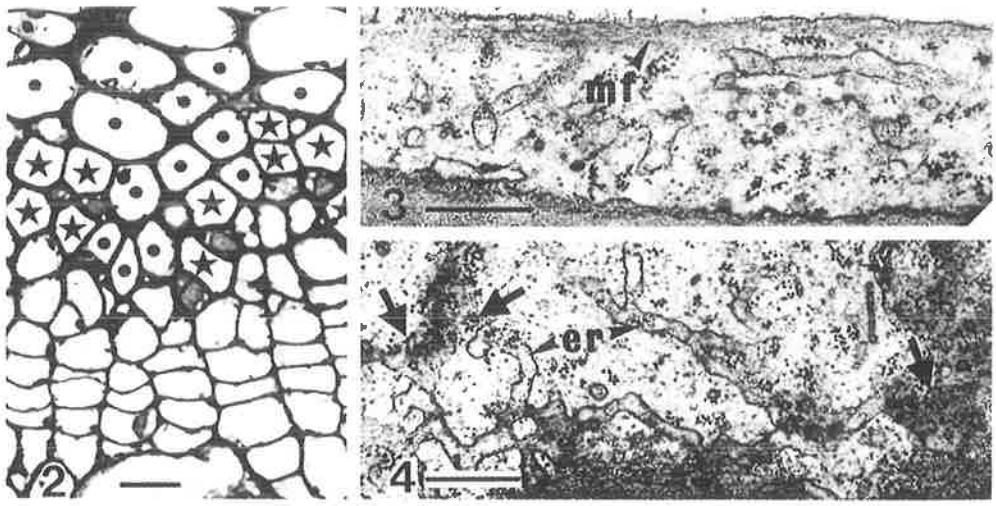


Fig. 2. A cross-section of a portion of a sugar beet petiole taken several mm above the junction between two anastomosing veins. The sieve elements of the merging veins (stars) are separated by phloem parenchyma cells (solid dots). Bar = 12.5 $\mu$m.

Fig. 3. A portion of a microfilament bundle (mf) found in a petiolar phloem parenchyma cell. Bar = 0.5 $\mu$m.

Fig. 4. Parietal endoplasmic reticulum (er) characteristic of the petiolar phloem parenchyma. Polyribosomes (arrows) are evident. Bar = 0.5 $\mu$m.

could facilitate more rapid symplastic transport. This interpretation is consistent with recent treatments of the function of microfilament bundles (Kamiya, 1981) and symplastic transport (Tyree, 1970). The other unique feature noted for the parenchyma cells was an extended system of primarily tubular endoplasmic reticulum that was located in the parietal cytoplasm, associated with the plasmodesmata interconnecting these cells and adorned with varying numbers of curled polyribosome chains (Fig. 4; and Oross and Lucas, 1986). Presently, however, a functional relationship between this endoplasmic reticulum system and lateral translocation has yet to be demonstrated. Further study of these structures, with particular emphasis on the identity and function of the translation product of the polyribosomes, is certainly warranted.

## SLOW-COOLING RESPONSE WITH ONE MONITORED SINK

The slow-cooling response described recently by Grusak and Lucas (1985) was elicited by two or more successive step-wise coolings, each of 80 min

duration, and that were separated by a rapid rewarming to the original starting temperature. This response differed from the quick-cooling response in three major aspects. First, only the second and subsequent cooling cycles effected an inhibition of the accumulation of translocates into the sink leaf. Second, the observed inhibitions occurred in an abrupt step-wise manner and immediately followed the step-wise cooling of the source petiole. Third, no translocation recovery was ever observed.

Of particular interest to the present discussion is the question as to why a preliminary cooling is required for the inhibition responses elicited by subsequent coolings. In answer to this question, Grusak and Lucas (1985) suggested that "the initial cooling treatment induced an alteration in the petiole tissue that facilitated the inhibition phenomenon during subsequent slow-coolings." Further experiments involving the movement of the cold block after the initial cooling and monitoring the effect of subsequent slow-coolings at different positions on the petiole provided evidence that the site of the tissue change, elicited by the first cooling, is immediately upstream of the site of the first cooling. This demonstration of a well defined site in the translocation pathway that has unique physiological properties prompted a comparative electron microscopic study of the regions upstream, downstream, and within the cold block of a slow-cooled petiole segment. The study employed methods published elsewhere (Oross and Lucas, 1985) and was aimed at determining whether or not there were any cytological features, localized in the region in question, that would provide information on the mechanism of the inhibition response.

The results of this investigation were disappointing. We found no variability in the structure of the phloem at the various sampling positions above, below, or within the cold block region. We also found no evidence that would suggest that the site of the slow-cooling inhibition response was localized anywhere within the region that was examined; the amount of callose and P protein localized at the sieve plates was at a comparable low level to that found in control material (i.e., the petioles of comparable leaves from intact and simplified plants).

We did, however, find two ultrastructural features unique to the sampled region in the slow-cooled petioles that may be related to the slow-cooling response. The first was a conspicuous accumulation of callose associated with the plasmodesmata that interconnect the sieve elements with adjoining companion cells (Fig. 5) and phloem parenchyma cells (Fig. 7). Figures 6 and 8 illustrate the level of callose present in control material. If these callose deposits are related to the slow-cooling response, their presence in the cold-treated region of the petiole would indicate that a portion of this petiolar

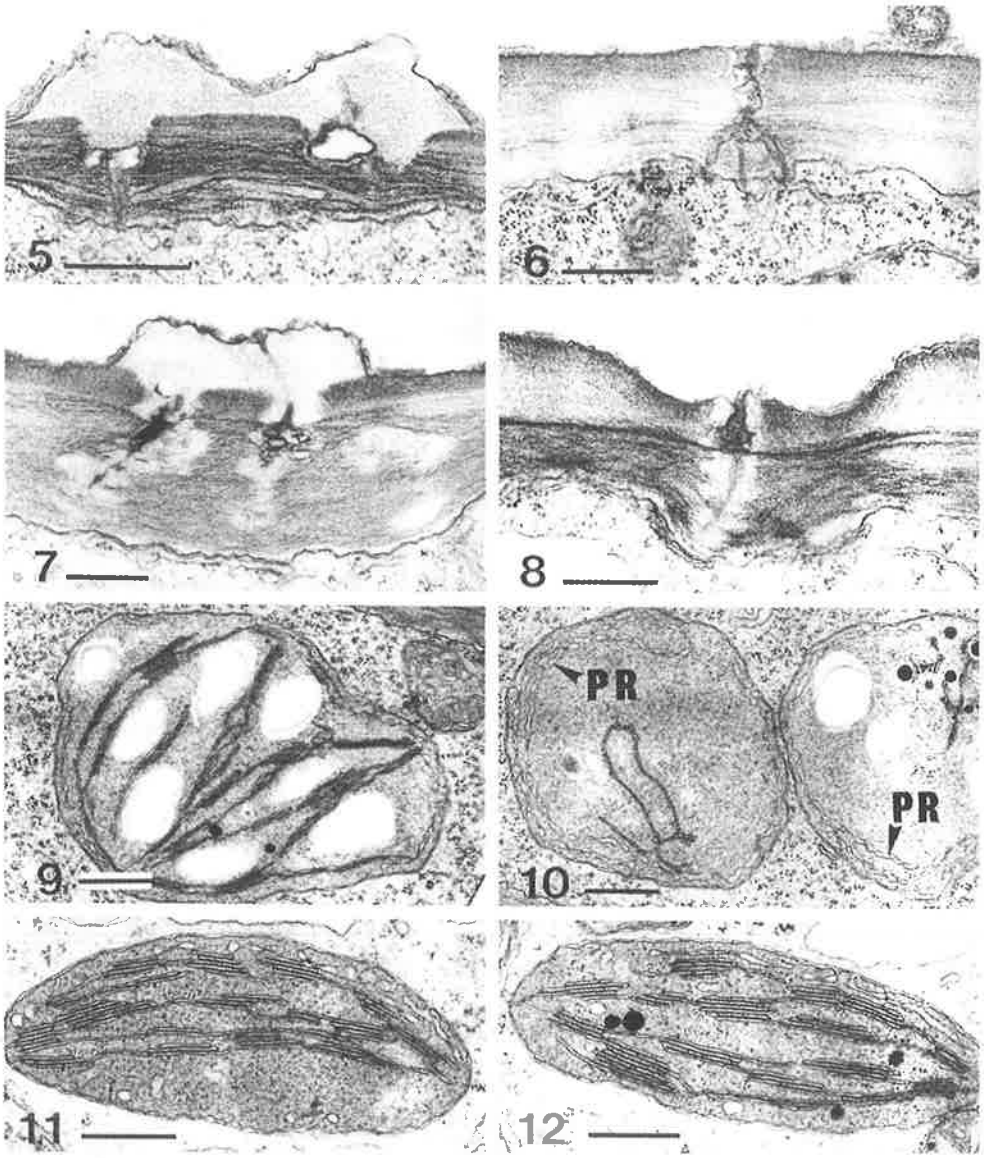
5
6
7
8
9
PR
PR
10
11
12

contribution to the slow-cooling response may be related to a blockage of metabolite or translocate flow between the pertinent cells *or* to the disruption of intercellular electrical communication. The latter possibility is derived from a recent study which indicates that plasmodesmata are involved in intercellular electrical coupling (Overall and Gunning, 1982).

The other feature noted for the slow-cooled material was a conspicuous change in the structure of the chloroplasts normally found in the companion cells of the petiolar phloem (Fig. 9). In the slow-cooled material there was a pronounced reduction in the number of photosynthetic lamellae within the plastids and a corresponding increase in the amount of membrane forming the peripheral reticulum (Fig. 10). Also, there was less starch present in the experimental material (Fig. 10). No structural changes were noted for the phloem parenchyma cell chloroplasts (cf. Figs. 11, 12). The relationship, if any, between the observed changes in the companion cell plastid structure and the slow-cooling response is unclear at present. It might be argued that this phenomenon is merely a generalized chilling effect. However, the absence of such structural changes in the chloroplasts of the phloem parenchyma cells or other petiolar tissues argues against this interpretation. If this response is related to the slow-cooling treatment, we suggest that the cooling somehow changes or disrupts the normal functional role of the companion cell chloroplasts in the total metabolism of the companion cell. Any further

---

Fig. 5. Highly callosed plasmodesmata interconnecting a sieve element (top) and a companion cell (bottom) from a slow-cooled region of a source leaf petiole. Bar = 0.5 $\mu$m.

Fig. 6. Uncallosed plasmodesmata interconnecting a sieve element (top) and a companion cell (bottom) from an uncooled, control source leaf petiole. Bar = 0.5 $\mu$m.

Fig. 7. Highly callosed plasmodesmata interconnecting a sieve element (top) and a phloem parenchyma cell (bottom) from a slow-cooled source leaf petiole. Bar = 0.5 $\mu$m.

Fig. 8. Slightly callosed plasmodesmata interconnecting a sieve element (top) and a phloem parenchyma cell (bottom) from an uncooled control source leaf petiole. Bar = 0.5 $\mu$m.

Fig. 9. Chloroplast from a companion cell of an uncooled control source leaf petiole. Bar = 0.5 $\mu$m.

Fig. 10. Simplified chloroplast structure of the companion cells from a slow-cooled source leaf petiole. PR; peripheral reticulum. Bar = 0.5 $\mu$m.

Fig. 11,12. Phloem parenchyma cell chloroplasts from control (Fig. 11) and slow-cooled source leaf petiolar material (Fig. 12). Bar = 0.5 $\mu$m.

elaboration of this possibility must await more data on the role of chloroplasts and photosynthesis in the parenchymatic elements of the petiolar phloem.

## SLOW-COOLING RESPONSE WITH TWO MONITORED SINKS

Slow-cooling experiments employing two monitored sink leaves (Grusak and Lucas, 1986) have provided data that has given a clearer understanding of the mechanism of this particular cooling response. These experiments revealed three patterns of response in which the step-change in translocation occurred simultaneously and in the same direction at both sinks (increase or decrease), the rate-change occurred simultaneously but in opposite directions at the two sinks, or the rate changed at one sink with no concurrent change at the other. It was suggested that these patterns were due to the repartitioning of assimilate flow between the individual monitored sinks *and* the unmonitored hypocotyl-crown region. We further suggested that the consistent step decline observed for plants with only one monitored sink may not reflect a decline in translocation through the source petiole but rather a preferential repartitioning of translocation from the sink leaf to the hypocotyl-crown region. This latter contention may explain our earlier mentioned inability to find any structural evidence for a blockage of the sieve elements of the source petiole that was thought, at the time, to be a likely cause for the inhibition response.

Given that the slow-cooling response is, in large part, due to a repartitioning of translocational flow, attempts were made to localize the site of the repartitioning event. In consideration of the demonstrated capacity of the source leaf petiole to regulate flow between the nine major axially oriented veins, via anastomoses (Grusak and Lucas, 1984), and that subsets of these veins are known to be connected with those of different leaves adjoining the source leaf (Zamski and Azenkot, 1981), an attempt was made to determine if the repartitioning occurred in the cold block region of the source leaf petiole. An overlapping cut experiment, similar to the one described earlier (see Fig. 1), was set up, and slow-cooling was then applied to the source petiole upstream of the cuts. The result was that step-wise changes in translocation were still observed. The lack of a "cancelling effect" that should have been caused by the downstream cutting was taken as evidence that the slow-cooling-induced repartitioning event was localized downstream of the cold block region and most probably within the hypocotyl-crown region of the plant, where the leaf traces of the different leaves form a complex interwoven network characterized by many phloic interconnections (Zamski and Azenkot, 1981; Stieber and Beringer, 1984).

If the hypocotyl-crown region is the site of the repartitioning, the question arises as to how the *rapid* signal promoting the repartitioning is transmitted from the cooled region of the source leaf petiole. Grusak and Lucas (1986) have recently presented data indicating that a pressure wave is propagated in the region of the cold block, which moves rapidly through the sieve tubes of the petiolar phloem to the repartitioning site. This form of signaling would require an unbroken sieve tube continuum from the origin of the signal to its destination. This continuum probably exists in the plants used for many of these translocation studies; but in plants that have been surgically manipulated so as to channel translocational flow through petiolar anastomoses, there is some doubt as to whether such a continuum exists (Oross and Lucas, 1985). This structural consideration and the above mentioned capacity of a surgically manipulated petiole to communicate a slow-cooling-elicited signal indicate that pressure waves are not the only signal that could promote the repartitioning event. The resolution of this question awaits an unequivocal demonstration of the junctional structure of the veins within the source-sink pathway.

## CONCLUSIONS

The preceding discussion has demonstrated that we are presently at a very elementary level in our understanding of the functional relationships between chilling-related translocation responses and the structure of the translocation pathway. However, our structural studies of a portion of this pathway, the source leaf petiole, have provided useful information for the interpretation of the results of the translocation studies we have described. In this regard, the discovery that phloem parenchyma cells are an important part of the lateral translocation pathway is particularly significant. This finding not only offers a partial explanation for the slowness of the activation of the lateral transport pathways that occurs by the imposition of localized blockages, but also identifies these cells as potential regulatory sites for lateral translocation. As to how this regulation is effected we cannot say at present, but we suggest that the translation product of the polyribosomes associated with the endoplasmic reticulum in these cells may be involved.

Our structural studies have also provided evidence that the rapid signal for the slow-cooling-elicited repartitioning may not, in all cases, be a pressure wave conducted through the sieve elements as has been suggested. This indicates the need for future studies designed to identify the nature of the signal and to determine whether or not such signals are involved in source-sink partitioning under more normal circumstances.

Finally, we feel that our attempts at discovering the structural basis for the chilling-related translocation responses have contributed greatly to our emerging understanding of their underlying mechanisms. In our assessment, closely integrated physiological and structural studies will provide the basis for future advancements in our understanding of assimilate translocation.

## ACKNOWLEDGMENTS

This research was supported by National Science Foundation grant PCM 83–15408.

## References

Esau K (1934): Ontogeny of phloem in the sugar beet (*Beta vulgaris* L.). Am J Bot 21:632–644.

Grusak MA, Lucas WJ (1984): Recovery of cold-inhibited phloem translocation in sugar beet. I. Experimental analysis of an existing mathematical recovery model. J Exp Bot 35:389–402.

Grusak MA, Lucas WJ (1985): Cold-inhibited phloem translocation in sugar beet. II. Characterization and localization of the slow-cooling response. J Exp Bot 36:745–755.

Grusak MA, Lucas WJ (1986): Cold-inhibited phloem translocation in sugar beet. III. The involvement of the phloem pathway in source-sink partitioning. J. Exp Bot 37:175 (in press).

Kamiya N (1981): Physical and chemical basis of cytoplasmic streaming. Annu Rev Plant Physiol 32:205–236.

Oross JW, Lucas WJ (1986): Sugar beet petiole structure: Vascular anastomoses and phloem ultrastructure. Can J Bot 63:12 (in press).

Overall RL, Gunning BES (1982): Intercellular communication in *Azolla* roots: II. Electrical coupling. Protoplasma 111:151–160.

Stieber J, Beringer H (1984): Dynamic and structural relationships among leaves, roots, and storage tissue in the sugar beet. Bot Gaz 145:465–473.

Swanson CA, Geiger DR (1967): Time course of low temperature inhibition of sucrose translocation in sugar beets. Plant Physiol 42:751–756.

Tyree MT (1970): The symplast concept. A general theory of symplastic transport according to the thermodynamics of irreversible processes. J Theor Biol 26:181–214.

Zamski E, Azenkot A (1981): Sugar beet vasculature. I. Cambial development and the three-dimensional structure of the vascular system. Bot Gaz 142:334–343.

Plant Physiol. (1986) 81, 171–176
0032-0889/86/81/0171/06/$01.00/0

# (1→3)-β-D-Glucan Synthase from Sugar Beet[1]

## I. ISOLATION AND SOLUBILIZATION

Received for publication October 7, 1985 and in revised form January 21, 1986

DAVID L. MORROW AND WILLIAM J. LUCAS*
*Department of Botany, University of California, Davis, California 95616*

### ABSTRACT

**A (1→3)-β-glucan synthase has been isolated from petiole tissue of sugar beet (*Beta vulgaris* L.). Enzyme activity is associated with a membrane fraction with a density of 1.03 grams per cubic centimeter when subjected to isopycnic density gradient centrifugation in Percoll. The reaction product was determined to be a linear (1→3)-β-glucan by methylation analysis and by glucanase digestion. (1→3)-β-Glucan synthase activity is markedly stimulated by $Ca^{2+}$; activation is half-maximal at about 50 micromolar $Ca^{2+}$ and is nearly saturated at 100 micromolar. Other divalent cations tested, $Mg^{2+}$, $Mn^{2+}$, and $Sr^{2+}$, also stimulate enzyme activity but are less effective. Enzyme activity was also stimulated up to 12-fold by β-glucosides. Sirofluor, the fluorochrome from aniline blue, inhibited enzyme activity 95% when included at 1 millimolar. The enzyme was solubilized in Zwittergent 3-14; 85% of total enzyme activity was solubilized in 0.03% detergent and the optimal detergent-to-protein ratio was 0.3 at 3 milligrams per milliliter protein.**

(1→3)-β-D-Glucans are common structural and/or storage polysaccharides of algae, fungi, and higher plants (14). In higher plants, (1→3)-β-D-glucan, known as callose, is an extracellular, structural polymer often associated with symplastic connections between cells, *viz.*, plasmodesmata and sieve-plate pores. Callose is deposited in the walls surrounding these structures and may be involved in the regulation of symplastic transport, particularly in the phloem, vis-a-vis regulation of sieve-plate pore diameter (9).

Deposition of callose at sieve-plate pores is induced by a number of evironmental and physiological conditions, including wounding, temperature and water stress, and infection by pathogens (9). Provided the tissue receives the correct stimulus, deposition can be very rapid, with the sieve-plates being sealed within a few min (3, 7, 12, 25, 27, 30). Under certain conditions, callose deposition is reversible (8, 28); apparently callose metabolism is well regulated.

Callose is generally considered to be synthesized by (1→3)-β-D-glucan synthase (EC 2.4.1.34). Regulation of the activity of this enzyme may be central to the control of callose metabolism in the phloem. Though there are numerous reports in the literature on β-glucan synthases (see Refs. 6 and 14 for review), only a limited number have been concerned with phloem tissues (1, 8). In the present paper, we report on the isolation of a (1→3)-β-D-glucan synthase from sugar beet petiole, and phloem-rich tissue. The enzyme is membrane-associated, activated by divalent cations, and has been solubilized in active form with the detergent, Zwittergent 3-14. We also report on a new inhibitor of (1→3)-β-D-glucan synthase, Sirofluor, the fluorochrome from aniline blue.

[1] Supported by a grant-in-aid from Chevron Chemical Company, Richmond, CA.

## MATERIALS AND METHODS

**Plant Material.** Sugar beet plants (*Beta vulgaris* L. var SSBN1, USH 11, Lot 82312) were grown in a controlled environment chamber as previously described by Grusak and Lucas (15). In brief, plants were grown from seed in a sterilized soil mixture of vermiculite, peat, and sand (2:1:1) under the following conditions: 16 h photoperiod (265 μmol $m^{-2}$ $s^{-1}$ PAR), daily maximum and minimum temperatures of 27 and 17°C, respectively, and 60/90% RH. Plants were harvested after 28 to 30 d, and petioles were excised and stored briefly in cold water.

**Isolation of Membrane Fraction.** Freshly excised petiole tissue was homogenized with a Polytron homogenizer in 2 volumes of cold buffer consisting of 50 mM Tes, 20 mM β-mercaptoethanol, 5 mM EGTA, 0.5 mM phenylmethylsulfonyl fluoride, 0.1 mM Nα-*p*-tosyl-L-lysine chloromethyl ketone, 0.1 mM *N*-tosyl-L-phenylalanine chloromethyl ketone, and 0.01 mM leupeptin, adjusted to pH 7.5 with 1 N KOH. The homogenate was filtered through eight layers of wetted cheesecloth, layered over a 60% (w/v) sucrose pad in a 30-ml Corex tube, and centrifuged for 20 min at 6000*g*. The membrane fraction banding at the homogenate/sucrose interface was removed, suspended in 10 ml of 5 mM Tes (pH 7.5) and 0.5 mM EGTA, and recentrifuged for 10 min at 8000*g*. The sedimented membranes were resuspended in 5 mM Tes (pH 7.5). The protein concentration of the resuspended membranes was about 2 mg/ml.

**Standard Assay for β-Glucan Synthase.** The standard incubation mixture contained 0.1 mM UDP-[U-$^{14}$C]glucose (200 Bq/mmol), 10 mM Tes (pH 7.5), 10 mM cellobiose, 5 mM $CaCl_2$, 5 mM $MgCl_2$, 0.1% BSA, 0.01% digitonin, and an aliquot of the suspended membrane preparation (about 10 μg protein) in a total volume of 200 μl. In assays where [$Ca^{2+}$] was varied, $Ca^{2+}$-EGTA buffers (19) were used to achieve the desired free $Ca^{2+}$ concentrations. Incubation was for 10 min at 30°C. The reaction was stopped by adding 4 ml of cold 66% (v/v) ethanol. About 10 mg of α-cellulose was added to the reaction vessel as a carrier to facilitate precipitation of ethanol-insoluble glucan. The sample was stored at −20°C for 20 min (to overnight) and then filtered through a Whatman GF/A glass fiber filter under suction. The filter was washed 3 times with 66% ethanol and dried. Radioactivity was determined by liquid scintillation counting in 10 ml of Beckman Ready-Solv cocktail using a Beckman LS 9800 liquid scintillation system. Enzyme activity was expressed as nmol of glucose incorporated into glucan/mg protein·h at 30°C.

**Purification of Fluorochrome from Aniline Blue.** Sirofluor, the fluorochrome from commercial aniline blue (Matheson, Coleman and Bell), was purified by the method of Evans and Hoyne (10). The purified fluorochrome had an absorption maximum at 376 nm (in water) and fluorescence excitation and emission

maxima at 380 and 480 nm, respectively (in ethanol), which shifted to 400 and 500 nm in the presence of laminarin (0.1% w/v in water).

**Methylation Analysis of Reaction Product.** Radioactive product was prepared with a scaled-up assay with 10 times the enzyme concentration used in the standard assay. The reaction was stopped after 10 min by immersing the reaction vessel in a boiling water bath for 5 min. Upon cooling to room temperature, ethanol (to 66%) was added to the sample to precipitate β-glucans, and centrifuged for 15 min at 8000*g*. The supernatant was discarded, and the pellet, containing radiolabeled product (about 7 nmol incorporated glucose), was suspended in cold 66% ethanol. The suspension was filtered through a Whatman GF/A filter under suction, washed with chloroform:methanol (1:1, v/v), and transferred to a 13 × 100 mm capped culture tube.

The methylation procedure of Hakamori (16) as modified by Lindberg (22) was followed. The radioactive product was dissolved in anhydrous DMSO (1 ml) and sonicated for 5 min after which 1 ml of methylsulfinyl sodium in DMSO (see below for preparation) was added. A 5 h sonication treatment was then applied, after which 0.5 ml of methyl iodide was added, at 0°C, and the sample was again sonicated for 1 h. Chloroform (2 ml) was then added, and then 4 ml of water and, after thorough mixing following each addition, the sample was centrifuged for 3 min at 3000*g*. The aqueous layer was removed and discarded; 3 ml of water was then mixed with the organic layer and the mixture was centrifuged for 30 s at 3000*g*. The washing of the organic phase was repeated 9 times before it was dried under filtered air at 40°C. This methylation procedure was repeated for each sample.

The methylated product was hydrolyzed in 1 ml of 2 M trifluoroacetic acid for 2 h at 120°C in a sealed culture tube. The resulting partially methylated derivative was reduced in 1 ml of 0.5 M $NaBH_4$ in 2 M $NH_4OH$ for 1 h at 60°C. The reduced derivative was suspended in 0.5 ml of acetone, dried at 40°C, and acetylated by adding, in order, 0.1 ml of glacial acetic acid, 0.5 ml of ethyl acetate, and 1.5 ml of acetic anhydride. The acetylation mixture was incubated for 5 min at room temperature and then cooled on ice. Water (4 ml) was added, followed by 0.1 ml of 1-methyl imidazole. After 5 min, 1 ml of DCM[2] was added, and the sample was centrifuged for 15 min at 3000*g*. The DCM layer was removed and dried under a stream of air. The residue was dissolved in 1 ml of DCM, filtered through Whatman No. 4 paper, dried, and redissolved in 0.03 ml of DCM. Derivatized sugars were separated by GC. Standards were prepared by derivatization of lichenin, a mixed-linked (1→3), (1→4)-β-glucan.

**Preparation of Methylsulfinyl Sodium.** NaH (5 g) was washed 3 times with 50 ml of hexane. The hexane was removed, 60 ml of anhydrous DMSO was added, and the mixture was brought to 40°C and incubated under a steady stream of $N_2$ for 1 h. The product was stored under $N_2$ at 4°C for up to 1 month.

**Laminarinase Digestion of the Reaction Product.** Radioactive reaction product was prepared as described above (see Methylation Analysis) and incubated at 37°C for a suitable period of time in 1 ml of 50 mM, Na-acetate buffer (pH 5.0) containing 0.05 mg (0.023 units) commercial laminarinase (Calbiochem, San Diego, CA). The reaction was stopped by immersion for 5 min in a boiling water bath. The sample was made 66% ethanol by adding 2 ml of cold absolute ethanol and then centrifuged for 15 min at 8000*g*. The pellet was resuspended in a small volume of water and assayed for radioactivity.

The products of laminarinase digestion were separated by ascending paper chromatography. Radioactive digests (about 1,500 Bq) were spotted on Whatman 3M chromatography paper (2 cm × 15 cm) and chromatographed for 6 h at 70°C with 1-propanol:ethyl acetate:water, 7:1:2 (v/v/v). The developed chromatograms were dried, cut into 0.5 cm strips, which were transferred to liquid scintillation vials filled with 10 ml of Beckman Ready-Solv cocktail, and counted. Standards of glucose, cellobiose, and laminaribiose were revealed with the silver nitrate reagent (29). Chromatograms were soaked briefly in 0.3 mM $AgNO_3$, dried, immersed in 100 mM NaOH in ethanol, and then transferred directly to photographic fixer (Kodak Rapid Fixer). After the background cleared, the chromatograms were washed for 15 min in water and dried.

**Protein Determination.** Protein (20–100 μg) was precipitated in 1 ml of cold 10% (w/v) TCA and centrifuged for 5 min at 8000*g*. The pellet was resuspended in 1 ml of cold acetone, centrifuged again for 5 min at 8000*g*, and finally suspended in 1 ml of 0.1 N NaOH. Aliquots of this suspension were assayed for protein after the method of Lowry *et al.* (23) as modified by Markwell *et al.* (26). BSA was used as standard.

**Density Gradient Centrifugation.** The 6,000*g* membrane fraction was subjected to isopycnic density gradient centrifugation in Percoll (Pharmacia). A Percoll-buffer mixture was prepared to contain Percoll:1 M sucrose:50 mM bis-trispropane:water (4:5:1:10, v/v/v/v), adjusted to pH 7.5. An aliquot of this mixture (7.2 ml) was transferred to 15 × 75 mm polyallomer tubes (Beckman, Palo Alto, CA), and then 0.8 ml of the membrane suspension (1 mg/ml) was layered on top of the mixture. The tubes were then sealed, placed in a Beckman 70.1 rotor, and centrifuged for 30 min at 60,000*g*. The Percoll gradient formed spontaneously during centrifugation; afterwards, 0.7 ml fractions were collected and assayed for β-glucan synthase activity.

**Detergent Treatment of Membrane Fraction.** Extracts of petiole tissue were prepared as described above and centrifuged for 10 min at 500 *g* to remove cell debris. The supernatant was then centrifuged for 60 min at 105,000*g*. The sedimented pellet was resuspended in 4 ml of a solubilization buffer, containing 50 mM Tes (pH 7.5), 150 mM KCl, and a suitable concentration of detergent, and incubated for 1 h at 4°C on a rotary shaker at 100 rpm. The sample was then recentrifuged for 60 min at 105,000*g*. The pellet was suspended in 4 ml of solubilization buffer containing detergent at a concentration corresponding to that present in the supernatant, and the suspended pellet and supernatant were assayed for β-glucan synthase activity.

## RESULTS

Radioactive glucose for UDP-[$^{14}$C]glucose was incorporated into an ethanol-insoluble product when incubated with a 6000*g* membrane suspension prepared from sugar beet petiole tissue. This membrane fraction was subjected to isopycnic gradient centrifugation in Percoll (Fig. 1). Most of the glucan synthase activity was recovered in a band that formed at 1.03 g/cm$^3$, with a minor peak near 1.04 g/cm$^3$. Enzyme activity was found to be optimal at pH 7.5 and at ionic strength 0.03 to 0.10. Digitonin (0.01%, w/v) stimulated enzyme activity 100% and was routinely included in the reaction mixture.

The reaction was linear with respect to time over the standard 10 min incubation period during which less than 10% of the substrate was consumed (Fig. 2A). However, in a scaled-up assay, the rate of substrate consumption quickly became nonlinear, and ceased abruptly after only 40% of the substrate was converted (Fig. 2B), although enzyme activity was stable for several hours following isolation.

The structure of the reaction product was identified by methylation analysis. The glucan product was methylated, hydrolyzed, and acetylated, and the resulting alditol acetate derivatives were separated by GC and compared with derivatized lichenin standards. A single radioactive peak was detected in the derivatized reaction product (Fig. 3). This peak corresponded with the peak for 1,3,5-tri-*O*-acetyl-2,4,6-tri-*O*-methyl glucitol, indicating a (1-

[2] Abbreviation: DCM, dichloromethane.

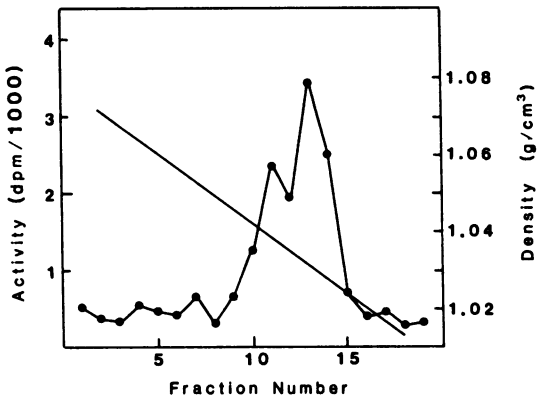


FIG. 1. Isopycnic density gradient centrifugation in Percoll of the 6,000*g* membrane fraction. An aliquot (0.8 ml) of suspended membranes (1 mg protein/ml) was layered onto 7.2 ml of Percoll-buffer mixture and centrifuged for 30 min at 60,000*g*. The gradient was determined with density gradient beads. Following centrifugation, 0.7 ml fractions were collected and assayed.

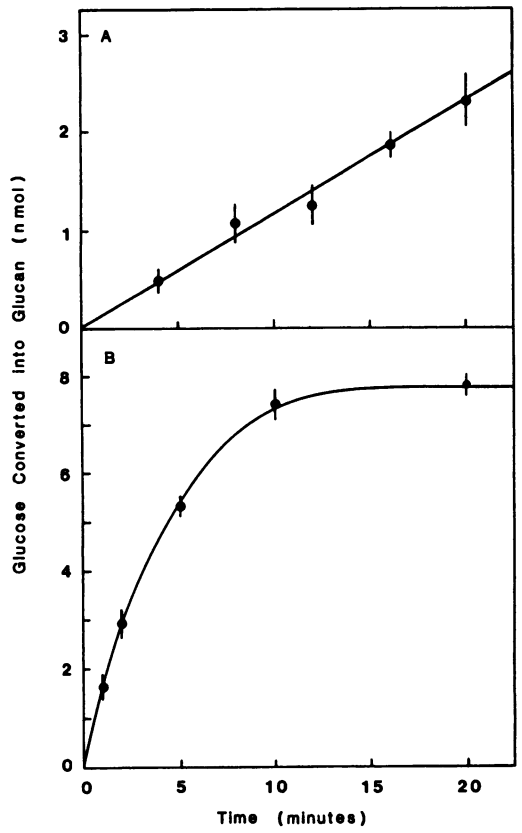


FIG. 2. Time course of β-glucan synthase reaction during a standard (A) and a 10-fold scale-up of the standard assay (B). The assay mixture contained 20 nmol of UDP-[$^{14}$C]glucose (200 Bq) in a volume of 200 μl. Suspended membranes were included at 10 μg protein per assay.

→3) glycosidic linkage. A peak corresponding to the 1,4,5-tri-*O*-acetyl-2,3,6-tri-*O*-methyl glucitol standard was not detected, though the trailing shoulder of the 2,4,6-derivative partly overlapped the peak corresponding to the 2,3,6-derivative. A small peak eluting before the 2,4,6-derivative was probably tetramethyl glucose.

The reaction product was also analyzed by enzyme digestion. Radioactive product was suspended in 1 ml of 50 mM acetate buffer (pH 5.0) containing laminarinase. The sample was incubated for 24 h after which the sugars released by hydrolase action were recovered and separated by paper chromatography. A significant portion (40%) of the reaction product was hydrolyzed after 24 h. The principal sugars released co-chromatographed with glucose and laminaribiose (Fig. 4). The abundance of glucose relative to laminaribiose in the digested reaction product was due to minor contamination of the commercial laminarinase with β-glucosidase activity (DL Morrow, WJ Lucas, unpublished data). A peak corresponding to cellobiose was not detected. Other sugars present were not identified, but probably represent higher order oligosaccharides. α-Amylase and cellobiohydrolase were also tested, but they did not degrade the reaction product.

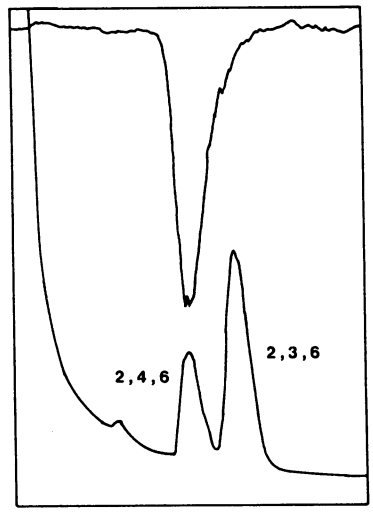


FIG. 3. Gas chromatographic separation of the alditol acetate derivatives of the radioactive glucan product. The upper curve depicts the recorder tracing of the derivatized product. The lower curve shows the tracing for the derivatized lichenin standards, 1,3,5-tri-*O*-acetyl-2,4,6-tri-*O*-methyl glucitol and 1,4,5-tri-*O*-acetyl-2,3,6,-tri-*O*-methyl glucitol. The small peak eluting before the trimethyl derivatives represents tetramethyl glucose. Standards were detected by flame ionization.

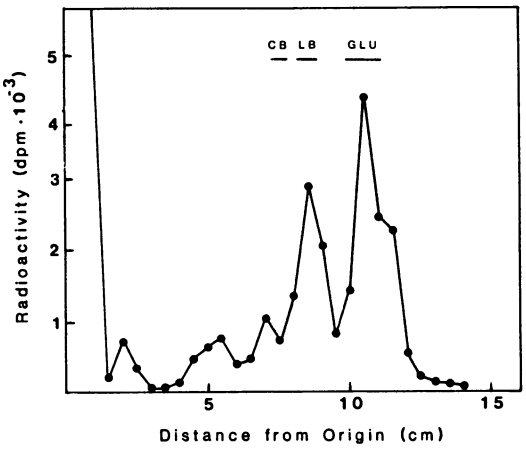


FIG. 4. Laminarinase digestion of radioactive glucan product. Digestion products were separated by ascending paper chromatography using 1-propanol:ethyl acetate:water (7:1:2) as solvent. Standards were glucose (GLU), cellobiose (CB), and laminaribiose (LB).

β-Glucan synthase activity was found to be strongly dependent on the presence of divalent cations, particularly $Ca^{2+}$ (Fig. 5). Enzyme activity was stimulated 50-fold by the addition of 1 mM $CaCl_2$; about 50 μM $Ca^{2+}$ was required for half-saturation. Other divalent cations like $Mg^{2+}$ and $Mn^{2+}$ (1 mM) were only about 30% as effective as $Ca^{2+}$; $Sr^{2+}$ was a little more effective, but still elicited only 50% of that observed in the presence of $Ca^{2+}$ (Table

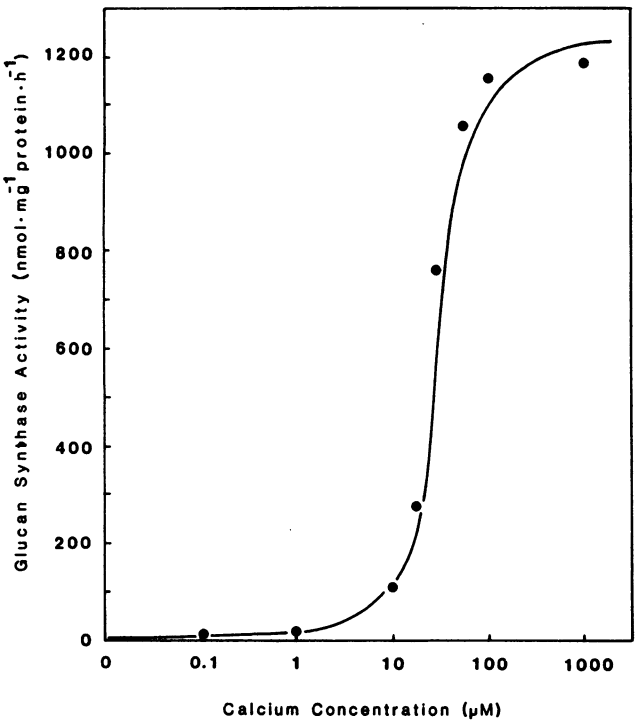


FIG. 5. Effect of $Ca^{2+}$ on β-glucan synthase activity. The reaction mixture contained 0.1 mM UDP-[$^{14}$C]glucose (200 Bq/nmol), 10 mM cellobiose, 0.1% BSA, 0.01% digitonin, 50 μl (10 μg protein) of suspended membranes, and $CaCl_2$ as indicated. $CaCl_2 \leq 10$ μM was prepared as a $Ca^{2+}$-EGTA buffer.

Table I. *Effect of Divalent Cations on β-Glucan Synthase Activity*

The reaction mixture contained 0.1 mM UDP-[$^{14}$C]glucose (200 Bq/nmol), 10 mM cellobiose, 0.1% BSA, 0.01% digitonin, and 50 μl (10 μg protein) of suspended membranes. Control assay mixtures also contained 2 mM EGTA. Values represent mean ± SE obtained from three experiments.

| Addition to Assay | β-Glucan Synthase Activity | Activation |
|---|---|---|
| | *nmol·mg⁻¹ protein·h⁻¹* | *n-fold* |
| None | 30 ± 23 | |
| KCl; 2.5 mM | 61 ± 16 | 2 |
| $MgCl_2$; 1 mM | 356 ± 21 | 12 |
| $MnCl_2$; 1 mM | 322 ± 67 | 11 |
| $SrCl_2$; 1 mM | 624 ± 38 | 21 |
| $CaCl_2$; 1 mM | 1112 ± 33 | 37 |
| $CaCl_2$ + $MgCl_2$; 1 mM | 1277 ± 29 | 43 |
| $CaCl_2$ + $LaCl_2$; 1 mM | 440 ± 42 | 15 |

I). Potassium chloride (2.5 mM) was not effective in stimulating the enzyme activity. The combined presence of $Ca^{2+}$ and $Mg^{2+}$ stimulated activity the greatest and accordingly were included in the standard assay. This was not simply an effect of ionic strength as 2.5 mM KCl added to 1 mM $CaCl_2$ actually inhibited the reaction slightly. Inclusion of $LaCl_3$ in the assay mixture with $CaCl_2$ also inhibited the activity of the enzyme.

Cellobiose, also present in the standard reaction mixture, and other sugars are known to stimulate β-glucan synthase activity (1, 4, 13, 18, 28). We have confirmed this for β-glucan synthase from sugar beet. β-Glucosides, in particular, were extremely effective in stimulating enzyme activity (Table II). Control assays contained all components of the standard assay except cellobiose. Addition of cellobiose stimulated enzyme activity over 1000%

Table II. *Effect of Glycosides on β-Glucan Synthase Activity*

The reaction mixture contained 0.1 mM UDP-[$^{14}$C]glucose (200 Bq/nmol), 5 mM $CaCl_2$, 5 mM $MgCl_2$, 0.1% BSA, 0.01% digitonin, and 50 μl (10 μg protein) of suspended membranes. Values represent mean ± SE obtained from three experiments.

| Addition to Assay (5 mM) | β-Glucan Synthase Activity | Activation |
|---|---|---|
| | *nmol·mg⁻¹ protein·h⁻¹* | *n-fold* |
| None | 155 ± 9 | |
| Cellobiose | 1830 ± 46 | 11.4 |
| Laminaribiose | 1990 ± 100 | 12.4 |
| Gentiobiose | 1520 ± 240 | 9.5 |
| Glucose | 850 ± 42 | 5.3 |
| β-Methylglucoside | 1340 ± 260 | 8.4 |
| Hydroquinone-β-glucoside | 2090 ± 150 | 13.1 |
| Maltose | 679 ± 63 | 4.4 |
| Lactose | 92 ± 14 | 0.6 |

relative to controls. Laminaribiose and gentiobiose, with (1→3)- and (1→6)-β-linkages, respectively, were also highly active. Glucose was much less effective, though addition of substituent groups to the anomeric carbon of glucose, via a β-linkage, resulted in increased activity. In fact, hydroquinone-β-glucoside equaled cellobiose and laminaribiose as an activator. Maltose, with a (1→4)-α-glycosidic linkage, was slightly less effective than glucose and only 40% as effective as cellobiose. Lactose, which differs from cellobiose only at the C-4 of the glycone, was inhibitory.

The purified fluorochrome from aniline blue, Sirofluor, was a potent inhibitor of β-glucan synthase activity. Under conditions of the standard assay, 100 μM and 1 mM Sirofluor inhibited enzyme activity to 511 ± 47 nmol·mg$^{-1}$protein·h$^{-1}$ and 111 ± 4 nmol·mg$^{-1}$ protein·h$^{-1}$, respectively. These values represent inhibition of 76 and 95% relative to controls (2150 ± 28 nmol·mg$^{-1}$ protein·h$^{-1}$).

The membrane-associated β-glucan synthase was solubilized in the detergent, Zwittergent 3-14. Membrane preparations were incubated in Tes buffer in the presence of 0.01 to 0.10% (w/v) Zwittergent 3-14 at a protein concentration of 1 mg/ml. After centrifugation at 105,000*g*, the supernatant and the resuspended pellet were assayed for β-glucan synthase activity. Solubilization of enzyme activity was maximal at 0.03% detergent (Fig. 6), both in terms of total solubilized activity (19 nmol·mg$^{-1}$ protein·h$^{-1}$) and percent of total activity solubilized (85%). Total enzyme activity decreased markedly as the detergent concentration increased from 0.1 to 1.0%. Other detergents tested, including 3-[(3-cholamidopropyl)-dimethylammonio]-1-propanesulfonate, digitonin, octylglucoside, and Triton X-100 were less effective in solubilizing the enzyme.

The optimal detergent-to-protein ratio was determined for the solubilized β-glucan synthase. Solubilization experiments were performed as described above at protein concentrations of 1 mg/ml and 3 mg/ml. At 1 mg/ml protein, the optimal detergent-to-protein ratio was 0.3, while at 3 mg/ml protein, the optimum was shifted down to 0.1 mg/ml protein.

## DISCUSSION

A (1→3)-β-D-glucan synthase has been isolated from petiole tissue of sugar beet plants. This enzyme has qualities similar to β-glucan synthases isolated from other higher plants (1, 4, 13, 20, 28), especially the enzyme from *Lolium multiflorum* (18). The enzyme is membrane-associated, activity is optimal at pH 7.5 and is stimulated by digitonin, divalent cations, and β-glucosides.

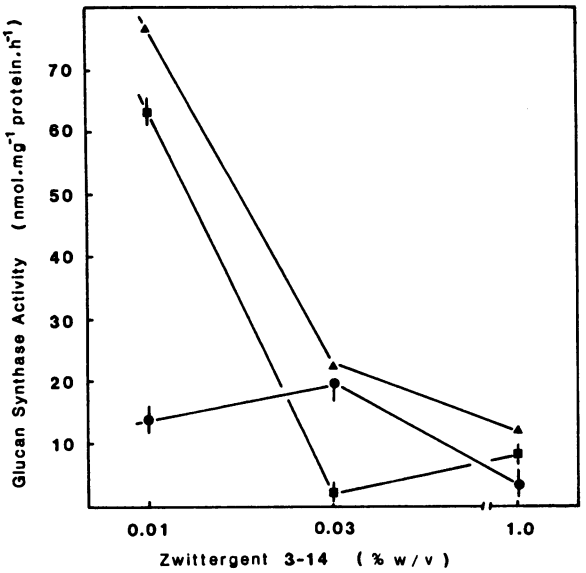


FIG. 6. Solubilization of β-glucan synthase in Zwittergent 3-14. Suspended membrane preparations (1 mg protein/ml) were incubated for 1 h at 4°C in detergent. Incubation mixtures were centrifuged 60 min at 105,000*g*; supernatants (■) and suspended pellets (●) were assayed for β-glucan synthase activity. Total activity (▲) is the sum of the supernatant and suspended pellet activities.

The ethanol-insoluble reaction product was identified as a linear (1→3)-β-glucan by methylation analysis and by glucanase digestion. Methylation analysis provides clear evidence for a (1→3)-linked glucan (Fig. 3). Degradation of the reaction product by laminarinase confirmed the presence of laminaribiosyl residues in the product (Fig. 4). Although we cannot exclude the possibility of a small number of (1→4)-linkages that went undetected, we consider it highly unlikely as (1→3)-(1→4)-β-glucans have not been found in dicotyledous plants (14).

The abrupt decline in the *in vitro* reaction rate after only 40% of the substrate was converted to insoluble product is noteworthy. The enzyme is stable for several hours following isolation, and the equilibrium constant for the reaction is large ($K_{eq}$>250). The decline in the reaction rate is likely due to a combination of substrate depletion and product inhibition, possibly by UDP. This is supported by the observation that addition of more substrate did not increase the reaction rate once 40% of the original substrate was consumed. Preliminary results have shown that 1 mM UDP inhibits the standard reaction by 93%.

Activation of β-glucan synthases by various sugars has been reported, but the mechanism of action is unknown. Several polymer biosynthetic systems require the presence of an initial acceptor molecule, or primer (2, 17), and it has been suggested that sugars such as cellobiose that markedly stimulate β-glucan synthase activity *in vitro*, may mimic an endogenous primer (24). Alternatively, stimulation of enzyme activity may be due to allosteric interactions. The striking structural requirements for activation of sugar beet (1→3)-β-D-glucan synthase by β-glucosides reported here supports a role for these sugars in chain elongation at the nonreducing end. The concentration required for optimal activation, 5 to 10 mM, is high but may reflect limited access of sugars to hydrophobic sites on an intrinsic membrane protein. This problem could be resolved through use of radioactive disaccharides as primary acceptors.

The results presented in this paper were obtained from studies with crude membrane preparations. It is likely that satisfactory answers to the questions outlined above will be attained only after the (1→3)-β-D-glucan synthase has been purified and reconstituted into lipid vesicles.

This model system will allow careful evaluation of the action of inhibitors and activators on the enzyme directly. Accordingly, as a first step toward purification, we have solubilized the sugar beet (1→3)-β-D-glucan synthase using Zwittergent 3-14. The enzyme is rather labile in the presence of detergent (Fig. 6), but stabilization should be possible with appropriate agents.

Calcium is required to achieve high rates of *in vitro* β-glucan synthase activity (Fig. 5; Table I). Other divalent cations tested, $Mg^{2+}$, $Mn^{2+}$, and $Sr^{2+}$, are much less effective than $Ca^{2+}$, though each is capable of activating the enzyme. The relatively strong effect of $Sr^{2+}$, plus the ability of $La^{3+}$ to act as an antagonist of the $Ca^{2+}$-stimulated enzyme, suggests that activation of the enzyme by divalent cations is in part $Ca^{2+}$-mediated. This has been reported for β-glucan synthases from cultured soybean cells (20) and cotton fibers (5). We have now confirmed this for β-glucan synthase from sugar beet. In addition, $Mg^{2+}$ is apparently required for maximal activity. The role of these divalent cations in activating the enzyme is not clear, although Kohle *et al.* (21) have proposed that local increases of $Ca^{2+}$ on the cytoplasmic side of the plasmalemma may activate a plasmalemma-localized β-glucan synthase.

We have found Sirofluor, the fluorochrome from aniline blue (10), to be a potent inhibitor of β-glucan synthase activity *in vitro*. Enzyme activity in the presence of 1 mM Sirofluor was only 5% that of controls. Sirofluor binds to (1→3)-β-glucans with high specificity (11), and its inhibitory action on β-glucan synthase may result from complexing with substrate, *viz.*, the nascent glucan. A Sirofluor-glucan complex may not bind effectively to the active site thereby inhibiting chain elongation.

*Acknowledgments*—The authors gratefully acknowledge the kind technical advice and assistance of Drs. Deborah Delmer and Takahisa Hayashi, ARCO Plant Cell Research Institute, Dublin, CA.

## LITERATURE CITED

1. BELTRAN JP, J CARBONELL 1978 (1,3)-β-Glucan synthase from *Citrus* phloem. Phytochemistry 17: 1531–1532
2. CORI GT, GF CORI 1939 The activating effect of glycogen on the enzymatic synthesis of glycogen from glucose-1-phosphate. J Biol Chem 131: 397–398
3. CURRIER HB 1957 Callose substance in plant cells. Am J Bot 44: 478–488
4. DELMER DP, U HEINIGER, C KULOW 1977 UDP-glucose:glucan synthetase in developing cotton fibers. I. Kinetic and physiological properties. Plant Physiol 59:713–718
5. DELMER DP, M THELEN, MPF MARSDEN 1984 Regulatory mechanisms for the synthesis of β-glucans in plants. *In* WM Dugger, S Bartnicki-Garcia, eds, Structure, Function, and Biosynthesis of Plant Cell Walls. American Society of Plant Physiologists, Rockville, MD, pp 133–149
6. DIXON RA 1985 β-(1→3)-Linked glucans from higher plants. *In* J Dey, RA Dixon, eds, Biochemistry of Storage Carbohydrates in Green Plants. Academic Press, London, pp 229–264
7. ESCHRICH W 1957 Kallosebildung in plasmolysierten *Allium cepa*-Epidermen. Planta 48: 578–586
8. ESCHRICH W 1961 Untersuchungen uber den Ab- and Aufbau der Callose. Z Botanik 49:153–218
9. ESCHRICH W 1975 Sealing systems in phloem. *In* MH Zimmermann, JA Milburn, eds, Transport in Plants. Encyclopedia of Plant Physiology, New Series, Vol 1. Springer-Verlag, Berlin, pp 39–56
10. EVANS NA, PA HOYNE 1982 A fluorochrome from aniline: blue structure, synthesis and fluorescence properties. Austr J Chem 35: 2571–2575
11. EVANS NA, PA HOYNE, BA STONE 1984 Characteristics and specificity of the interaction of a fluorochrome from aniline blue (Sirofluor) with polysaccharides. Carbohydr Polymers 4: 215–230
12. EVERT RF, WF DERR 1964 Callose substance in sieve elements. Am J Bot 51: 552–559
13. FEINGOLD DS, EF NEUFELD, WZ HASSID 1958 Synthesis of a β-1,3-linked glucan by extracts of *Phaseolus aureus* seedlings. J Biol Chem 233: 783–788
14. FINCHER GB, BA STONE 1981 Metabolism of noncellulosic polysaccharides. *In* W Tanner, FA Loewus, eds, Plant Carbohydrates. II. Extracellular Carbohydrates. Encyclopedia of Plant Physiology, New Series, Vol 13 B. Springer-Verlag, Berlin, pp 68–132
15. GRUSAK MA, WJ LUCAS 1984 Recovery of cold-inhibited phloem translocation in sugar beet. I. Experimental analysis of an existing mathematical recovery model. J Exp Bot 35: 389–402
16. HAKAMORI S 1964 A rapid permethylation of glycolipid and polysaccharide catalyzed by methylsulfinyl carbanion in dimethyl sulfoxide. J Biochem 55: 205–208

17. HANES CS 1940 The reversible formation of starch from glucose-1-phosphate catalysed by potato phosphorylase. Proc R Soc Lond B 129: 174–208
18. HENRY RJ, BA STONE 1982 Factors influencing β-glucan synthesis by particulate enzymes from suspension-cultured *Lolium multiflorum* endosperm cells. Plant Physiol 69: 632–636
19. JEWELL BR, JC RUEGG 1966 Oscillatory contraction of insect fibrillar muscle after glycerol extraction. Proc R Soc Lond B 164: 428–459
20. KAUSS H, H KOHLE, W JEBLICK 1983 Proteolytic activation and stimulation by $Ca^{2+}$ of glucan synthase from soybean cells. FEBS Lett 158: 84–88
21. KOHLE H, W JEBLICK, F POTEN, W BLASCHEK, H KAUSS 1985 Chitosan-elicited callose synthesis in soybean cells as a $Ca^{2+}$-dependent process. Plant Physiol 77: 544–551
22. LINDBERG B 1972 Methylation analysis of polysaccharides. Methods Enzymol 28: 178–195
23. LOWRY OH, NJ ROSEBROUGH, AL FARR, RJ RANDALL 1951 Protein measurement with the Folin phenol reagent. J Biol Chem 193: 265–275
24. MACLACHLAN GA 1982 Does cellulose synthesis require a primer? *In* RM Brown, ed, Cellulose and Other Natural Polymer Systems. Plenum Press, New York, pp 327–339
25. MAJUMDER SK, AC LEOPOLD 1967 Callose formation in response to low temperature. Plant Cell Physiol 8: 775–778
26. MARKWELL MAK, SM HAAS, LL BIEBER, NE TOLBERT 1978 A modification of the Lowry procedure to simplify protein determination in membrane and lipoprotein samples. Anal Biochem 87: 206–210
27. MCNAIRN RB, HB CURRIER 1968 Translocation blockage by sieve plate callose. Planta 82: 369–380
28. SOUTHWORTH D, DB DICKINSON 1975 β-1,3-Glucan synthase from *Lilium longiflorum* pollen. Plant Physiol 56: 83–87
29. TREVELYAN WE, DP PROCTER, JS HARRISON 1950 Detection of sugars on paper chromatograms. Nature 166: 444–445
30. WEBSTER DH, HB CURRIER 1968 Heat-induced callose and lateral movement of assimilates from phloem. Can J Bot 46: 1215–1220

Plant Physiol. (1986) 82, 432–442
0032-0889/86/82/0432/11/$01.00/0

# Symplastic Transport in *Ipomea tricolor* Source Leaves[1]

## DEMONSTRATION OF FUNCTIONAL SYMPLASTIC CONNECTIONS FROM MESOPHYLL TO MINOR VEINS BY A NOVEL DYE-TRACER METHOD

Received for publication January 24, 1986 and in revised form May 12, 1986

MONICA A. MADORE, JOHN W. OROSS, AND WILLIAM J. LUCAS*
*Botany Department, University of California, Davis, California 95616*

### ABSTRACT

**A novel method for the delivery of the fluorescent dye Lucifer Yellow CH to the cytosol of a source leaf mesophyll cell was devised which utilized a preencapsulation of the dye in phospholipid vesicles (liposomes). The liposomes were easily injected into the vacuoles of leaf cells of *Beta vulgaris* or *Ipomea tricolor*, where fusion with the tonoplast resulted in the release of the dye into the cytosol. Subsequent cell-to-cell movement of the dye was readily followed by fluorescence microscopy. Using this liposome technique symplastic continuity from the the mesophyll to the minor veins of the source leaf of *Ipomea tricolor* was demonstrated. This agreed with ultrastructural studies which demonstrated the presence of plasmodesmata between all cells from the mesophyll to the minor veins. The symplastic movement of dye from the injected mesophyll cell to the minor veins was unaffected by pretreatment of the leaf tissues with 2 millimolar *p*-chloromercuribenzenesulfonic acid. Pretreatment of the leaf tissues at alkaline pH (3-[*N*-morpholino] propanesulfonic acid-KOH, pH 8.0) had no apparent effect on dye movement between adjacent mesophyll cells but inhibited the movement of dye into and along the minor veins. Thus, although there were no apparent barriers to symplastic solute movement in this leaf, symplastic barriers could be imposed by the experimental conditions used.**

The transport of photosynthetically derived solutes from sites of synthesis in the source leaf mesophyll to the phloem of the minor veins has been under intensive investigation in recent years. At present, solutes are thought to move through the mesophyll symplastically, from cell to cell through plasmodesmata, but are then thought to exit into the apoplast at some point close to the sieve element/companion cell complex followed by active uptake into the phloem. This active uptake step establishes the concentration gradient that has been demonstrated to exist between the sieve element/companion cell complex and adjacent cells. The data supporting this putative apoplastic step in phloem loading have been extensively reviewed (9, 11) but are still open to question (17). The study of apoplastic transport in plant tissues therefore continues to receive considerable attention from many researchers interested in phloem transport.

In contrast, the study of symplastic transport has been relatively neglected by most investigators. This is largely due to the paucity of experimental techniques suitable for investigation of solute movement in the symplast. Most studies have been limited predominantly to the measurement of the frequency and distribution of plasmodesmata along the route from the mesophyll to the minor veins (*e.g.* 8, 15, 27). These measurements, coupled with measured rates of assimilate flux between the sites of synthesis and transport, have been used as qualitative evidence for the feasibility of symplastic transport (15, 22) but cannot prove the functionality of such a route *in vivo*.

The adaptation of neurological dye tracer techniques for use in plants has now provided a means for establishing the extent of the functional symplast in plant tissues (4–6, 12, 13, 30). A major drawback to the use of these techniques in vacuolate tissues, such as mature source leaves, is the number of injections that occur into the vacuole. Dye injected directly into the vacuole often fails to move symplastically to adjacent cells. The research reported here describes a novel method for the delivery of a fluorescent tracer to the cytosol of a source leaf mesophyll cell. Our approach involves the preencapsulation of the dye in phospholipid vesicles (liposomes) and actually exploits the ease by which vacuolar injections can be made.

We have mapped the symplastic connections in the source leaf of *Ipomea tricolor* using this liposome injection technique to introduce the fluorescent dye, Lucifer Yellow CH. In agreement with a recent report on symplastic continuity in source leaves of *Commelina cyanea* (6), we have found no apparent barrier to symplastic solute movement along the entire pathway from the mesophyll to the minor veins. More importantly, we have found that barriers to symplastic transport can be induced by certain treatments commonly used to manipulate the apoplastic uptake of sugars into leaf tissues.

## MATERIALS AND METHODS

**Plant Material.** Fully expanded source leaves from 4-week old *Ipomea tricolor* cv "Heavenly Blue" (Burpee Seeds) or 5-week old *Beta vulgaris* cv SSNB1 were used for all experiments. Plants were germinated and grown in a controlled environment chamber under conditions described previously (14).

**Chemicals.** Phosphatidylserine (beef brain), phosphatidylcholine (egg yolk), cholesterol, stearylamine, PCMBS,[2] Mes, Mops, and Lucifer Yellow CH were purchased from Sigma Chemicals. Fluorotrichloromethane (Freon 11) was obtained from Aldrich Chemicals.

**Liposome Preparation.** Liposomes were prepared by the freeze-thaw method of Pick (25). All procedures were carried out under a $N_2$ atmosphere to avoid oxidation of phospholipids. Twenty mg of phospholipid (either pure phosphatidylserine or a mixture of phosphatidylcholine:stearylamine:cholesterol in a molar ratio of 5:1:5) in chloroform was placed on ice in a 12 × 35 mm shell

[1] Supported by National Science Foundation Grant PCM 83-15408 to W. J. L. and a Natural Sciences and Engineering Research Council (Canada) Post-doctoral Fellowship to M. A. M.

[2] Abbreviations: PCMBS, *p*-chloromercuribenzenesulfonic acid; Mops, 3-(*N*-morpholino)propanesulfonic acid.

vial and taken to dryness under a stream of $N_2$ gas. To allow complete transferral of the resulting phospholipid film from the sides of the vial, the phospholipid was first redissolved in 0.5 ml ice-cold Freon 11 (29). An ice-cold solution (0.5ml, 20 mg $ml^{-1}$) of Lucifer Yellow CH was then added, and the phospholipid/dye mixture was vigorously stirred on a vortex mixer until it had reached room temperature and the Freon (b.p. 23.5°C) had boiled off. Final traces of Freon were removed by briefly placing the vial in a 300°C water bath.

Small unilamellar liposomes were generated by sonication of the phospholipid suspension for 2 min using a Branson 200 Sonifier Cell Disrupter equipped with a 3.17 mM microprobe. The preparation was frozen in liquid $N_2$ and thawed at room temperature to increase the size and trapping efficiency of the liposomes (25). After a brief 30 s resonication and filtration through a 0.2 $\mu$m membrane filter, the liposomes were separated from unencapsulated dye by gel filtration through 2 ml columns of Sephadex G-50 equilibrated with 20 mM KCl. Liposomes eluted in the void volume, which was monitored by Blue Dextran elution through similar gel columns.

**Microinjection Procedures.** Liposomes were back-loaded by capillary action into the tips of glass micropipettes of 0.5 to 1.0 $\mu$m tip diameter. The micropipettes were sealed into a micropipette holder equipped with a Luer port (model MPH-1, WPI Instruments, New Haven, CT) which was connected by a length of plastic tubing to a 1 ml gas-tight Hamilton syringe. The holder, tubing, and syringe were filled with water to provide a hydraulic system for microinjection of the liposomes. The injection pressure was controlled by a screw-driven attachment which regulated depression of the syringe plunger. The approach and impalement by the micropipette was controlled by an hydraulically driven micromanipulator (model MO-102, Narishige Scientific Instrument Laboratory, Tokyo, Japan) and cell impaler (Narishige model MM-333).

A mature source leaf, still attached to the intact plant, was fastened abaxial side up to a microscope slide with double-sided transparent tape and positioned on the microscope stage. The leaf was equilibrated for a 1 h period under a fiber-optic light source (Schott model KL1500) which provided a light intensity of 200 $\mu$mol photons $m^{-2}$ $s^{-1}$ (PAR, 400–700 nm) at the level of the microscope stage and 50 to 100 $\mu$mol photons $m^{-2}$ $s^{-1}$ over the rest of the plant. A small well of modeling clay positioned on the leaf surface was filled with a bathing medium consisting of 20 mM Mes-KOH (pH 5.0), or with distilled $H_2O$. A 5 $mm^2$ area of the leaf epidermis was peeled back to expose the injection site. The spongy mesophyll cell to be injected was localized with substage bright field illumination using a 25× long working distance objective and carefully impaled with the micropipette and injected with the liposome suspension. Liposome fusion and movement of the dye was observed by epifluorescence microscopy using a Leitz Orthoplan microscope equipped with a violet (BP 436/437) excitation filter, an RKP 475 mirror, and an LP 490 barrier filter. An additional 640 nm cut-off filter (Ditric Optics Inc., Hudson, MA) was placed between the microscope and camera to suppress Chl fluorescence. Photographs were taken on Kodak Tri-X Pan film exposed at 1000 ASA and push-processed using Acufine developer (Acufine, Chicago).

**PCMBS and pH Treatments.** For some experiments the bathing medium irrigating the injection site was changed to allow pretreatment of the leaf tissue with PCMBS or alkaline pH. For these experiments, two injection sites were prepared on each leaf to allow control and treatment experiments to be run concurrently on the same leaf tissue.

For the PCMBS pretreatment, the protocol of Giaquinta (10) was followed, and the bathing media consisted of 20 mM K-phosphate (pH 7.0) with or without 2 mM PCMBS. Both injection sites were initially pretreated for 45 min with K-phosphate (pH 7.0). The buffer was then removed and replaced with fresh buffer (control) or buffer plus 2 mM PCMBS (experimental). After 15 min the solutions in both wells were replaced with fresh buffer containing no PCMBS and injections were performed as described above. Dye movement was followed for a 1 h period after the injections.

Because the use of phosphate buffer was found to be deleterious to the movement of Lucifer Yellow in the source leaf, experiments were also run in which peeled areas were first pretreated with 2 mM PCMBS dissolved in water, followed by injection in Mes buffer as described above.

For the pH treatment, the protocol of Turgeon (31) was followed, and the bathing media consisted of 25 mM Mes-KOH plus 20 mM $CaCl_2$ (pH 5.5, control) or 25 mM Mops-KOH plus 20 mM $CaCl_2$ (pH 8.0, experimental). The injection sites were pretreated for 1 h at the selected pH, fresh buffer of the appropriate pH was placed in each well, and the injections were performed as described above. Again, dye movement was followed for a 1 h period.

**Leaf Structural and Ultrastructural Studies.** To assess the ultrastructural status of the injected leaf material, tissue preparations were made from both liposome-injected (experimental) and noninjected (control) regions of source leaves of *Ipomea*. Relatively large segments (up to 1.0 $cm^2$) of experimental and control tissues were excised and transferred to vials containing ice-cold fixative consisting of 1.6% (w/v) depolymerized paraformaldehyde, 2% (w/v) glutaraldehyde, 0.5% (w/v) tannic acid, and 2 mM $CaCl_2$ in 50 mM Na-cacodylate buffer (final pH 7.0). After 1.5 h, the leaf segments were cut into smaller pieces (approximately 20 $mm^2$) and allowed to fix for an additional 4 h at 15°C. The segments were postfixed overnight at 4°C in 1% (w/v) $OsO_4$ in 50 mM Na-cacodylate buffer (pH 7.0), then dehydrated in a graded acetone series and embedded in Spurr's resin (28). Sections were cut using conventional methods, mounted on formvar-coated slot grids and stained with aqueous uranyl acetate followed by Reynold's lead citrate (26). Sections were viewed and photographed with a JEOL 100S electron microscope operated at 80 keV.

Light micrographs of fixed tissues were obtained from semithin sections (approximately 0.75 $\mu$m) cut from plastic-embedded leaf segments prepared for EM as above. The sections were cut with glass knives and stained with 0.065% (w/v) toluidine blue in 1% (w/v) borate buffer. Sections were viewed and photographed using a Leitz Orthoplan microscope.

**Cryosectioning Techniques.** To determine the cellular location of the Lucifer Yellow following its movement in the source leaf, a section of the leaf corresponding to the injection site and the surrounding area through which the Lucifer Yellow had been seen to move was excised and thinly coated with Tissue-Tek O.C.T. compound (VWR Scientific). To allow cross-sections to be made, the tissue was inserted perpendicularly into an agar block fastened to the surface of a cryotome chuck, and then sealed in place with Tissue-Tek. The entire cryotome chuck was then dropped into a slot in a brass block held at liquid $N_2$ temperature. Following freezing, the cryotome chuck was sealed in a cylinder of aluminum foil, also held at liquid $N_2$ temperature, and then placed in a glass scintillation vial held in dry ice. The entire freezing procedure was completed within 1 min from the time of excision of the injected tissue from the intact leaf. The tissue was stored in the sealed vial in a −70°C freezer for 2 d prior to cryosectioning.

Cross-sections of 10 $\mu$m thickness were cut from the frozen leaf tissues, at −25°C using a cryostat (Damon/IEC model 3398), then mounted on formvar-coated slides, and stored for 2 d at −45°C over Drierite. The sections were then slowly warmed to room temperature, mounted in immersion oil, and viewed by

differential interference contrast and fluorescence optics with a Leitz Orthoplan microscope.

## RESULTS

**Liposome Fusion and Movement of Lucifer Yellow CH.** The effects of phospholipid composition of the microinjected liposomes on the subsequent delivery of Lucifer Yellow CH to the cytosol of source leaf mesophyll cells of *Beta vulgaris* is illustrated in Figure 1. Positively charged liposomes composed of a molar ratio of 5:5:1 phosphatidylcholine:cholesterol:stearylamine, which have been used successfully for delivery of solutes to plant cell protoplasts (2), were ineffective in delivering Lucifer Yellow to the cytosol when microinjected into the vacuole. No dye movement was seen out of the injected cell (Fig. 1a), even after 15 min following the injection (Fig. 1b). The dye instead appeared to remain inside the vacuole, indicating that liposomes of this composition were not fusing with the tonoplast. In contrast, negatively charged liposomes prepared from pure phosphatidylserine appeared to fuse readily with the tonoplast, as evidenced by the rapid delivery of the dye to the cytosol (Fig. 1, c, e, f, and g). The particular efficacy of negatively charged phosphatidylserine liposomes in the delivery of Lucifer Yellow to the cytosol is, we suspect, most probably a result of a high degree of fusion of this phospholipid under vacuolar conditions. Fusion of phosphatidylserine vesicles is known to be particularly sensitive to $Ca^{2+}$ ions, especially at a low pH (24).

Extensive movement of the dye from the injected cell to adjacent cells was recorded. In Figure 1c it can be seen that the dye had spread in a lateral direction, within 30 min, to mesophyll cells 10 cells away from the injection site (*i.e.* a distance of approximately 300 $\mu$m). Movement to cells underlying the injection site also occurred (Fig. 1e, f, and g),l but the extent to which dye movement could be visualized by light microscopy was limited, due to the compactness and thickness of the spongy mesophyll layers of the *Beta* leaf (Fig. 1d). Consequently, we could not detect movement of Lucifer Yellow into the minor veins of sugar beet source leaf tissue.

**Dye Movement in *Ipomea tricolor* Source Leaves.** Source leaves of *Ipomea tricolor* possess a much less dense mesophyll (Fig. 2 a, d and e); consequently, the minor veins were readily visible with the light microscope. In addition, the lower epidermis was easily removed, with minor damage being inflicted on the neighboring cells (Fig. 2 d and e). (During the course of these experiments, it was also found that prolonged illumination of the tissues with the epifluorescence light source could cause a further degree of tissue disruption. In this case, the damage was minimized by exposing the leaf to the light source only during the photographic exposures.) Removal of the epidermis allowed us to gain access to unperturbed spongy mesophyll cells in close proximity to minor veins (Fig. 2 a and c). Furthermore, in this leaf the space between the sieve elements and the epidermis is occupied by few cells (Fig. 2 a and b). Thus, if Lucifer Yellow were to move into the minor veins (sieve elements?), this anatomy would provide an optimal setting for its detection.

Microinjection of phosphatidylserine-encapsulated Lucifer Yellow into spongy mesophyll cells of *I. tricolor* also resulted in rapid dye release to the cytosol. Dye was evident in mesophyll cells adjacent to the injected cell 6 min after injection (Fig. 3, a and b). By 16 min, we could detect the movement of the dye into and along the minor veins of the leaf (Fig. 3, c and d). By 30 min, minor veins 1 mm away from the injection site showed considerable fluorescence, indicating a very extensive movement of dye in the symplast of this leaf (Fig. 3, e and f). Cryosections of the regions of the vasculature through which the Lucifer Yellow had moved showed that the fluorescence was confined to the bundle sheath and regions of the phloem tissue (Fig. 4). However, the specific phloem cell(s) which contained the Lucifer Yellow could not be discerned by this method.

**Symplastic Continuity in *Ipomea* Leaves.** An electron microscopic study on the mature source leaf of *I. tricolor* was conducted to ascertain the extent of symplastic continuity in this particular tissue. In addition, we sought to establish the effect(s), if any, that Lucifer Yellow, per se, might have had on the plasmodesmata.

The presence of plasmodesmata in the common walls between (a) mesophyll cells (Fig. 5, a and b), (b) mesophyll and bundle sheath cells (Fig. 5d), (c) bundle sheath and companion cells (Fig. 5f), and (d) companion cells and sieve elements (Fig. 5h). indicated symplastic continuity between all cells from the mesophyll to the sieve elements. Our fixation protocol enabled us to determine the fine structure of the various plasmodesmatal types in the *Ipomea* leaf. There were certain subtle structural differences in the plasmodesmata interconnecting mesophyll, bundle sheath, phloem parenchyma, and companion cells, but in general, the plasmodesmata shared a number of common features. Extensive median cavities, with multiple extensions to the protoplasts on either side of the wall, were frequently observed (Fig. 5, a and f). The extensions were associated with neck constrictions that occluded the cytoplasmic annulus of the plasmodesma (Fig. 5b). The axial components of these plasmodesmata were often swollen in the mid-region of the wall (Fig. 5d). ER was frequently associated with the cytoplasmic ends of the plasmodesmata (Fig. 5b). Branched plasmodesmata typical of those described for most dicotyledonous species (7) were found between companion cells and sieve elements (Fig. 5h).

Of more importance to the present study was the demonstration that movement of Lucifer Yellow through the leaf tissue had no detectable effect on plasmodesmatal ultrastructure. This is clearly shown in Figure 5 (*cf.* a, b, d, f, and h, with c, e, g, and i).

**Effects of PCMBS and Alkaline pH Pretreatments on Dye Movement.** Studies on many different leaf types have shown that uptake of exogenously supplied sugars into leaf tissues is reduced by pretreatment of the tissues with the sulfhydryl group blocking agent PCMBS or by pretreatment at alkaline pH (10, 11, 31). The effect of either of these two treatments on symplastic transport in source leaf tissues had not yet been addressed and was investigated here.

The sulfhydryl group inhibitor PCMBS had no apparent effect on the movement of Lucifer yellow in the symplast of *Ipomea* source leaves (Fig. 6). Although the movement along the veins was less extensive than that seen previously after a 30 min postinjection period (*cf.* Figs. 3e and 6, a and c), this appeared to be due to the phosphate buffer (pH 7.0) used in these experiments as dye movement was equally restricted in both the control (Fig. 6, a and b) and the PCMBS-treated (Fig. 6, c and d) tissues. Extensive dye movement following PCMBS treatment was observed if phosphate buffer was eliminated and the tissues were instead pretreated with an aqueous solution of PCMBS and then bathed in a Mes-KOH buffer at pH 5.0 for the injection and postinjection periods (Fig. 6, e and f).

In contrast to the results obtained with PCMBS, treatment of leaf tissues at an alkaline pH had a dramatic effect on the movement of Lucifer Yellow in the symplast of the *Ipomea* leaf (Fig. 7). At pH 5.5, the usual dye distribution pattern was seen between adjacent cells and then into and along the minor veins (Fig. 7, a and b). At pH 8.0, the dye still moved extensively but often only between mesophyll cells (Fig. 7, c and d). In 7 out of 11 experiments, no movement into the minor veins took place at this pH.

## DISCUSSION

Convincing evidence for a unified, operative symplastic network has now been presented for a number of plant tissues,

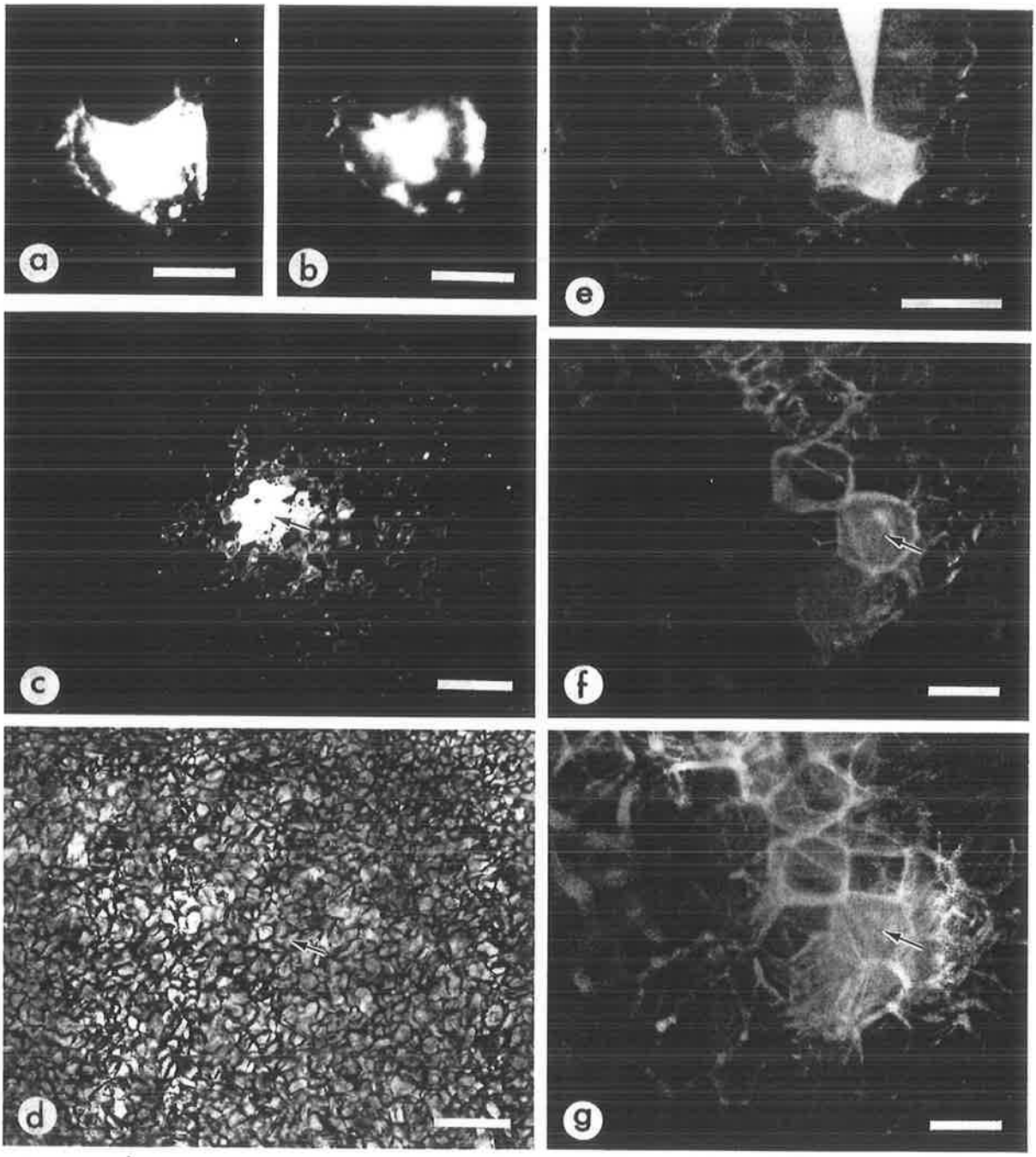


FIG. 1. Movement of Lucifer Yellow CH in the source leaf symplast of *B. vulgaris* following microinjection of liposome-encapsulated dye into a spongy mesophyll cell. Injected cells are indicated by arrows. All bars = 25 μm. Nonmovement of dye 5 min (a) and 15 min (b) after injection of Lucifer Yellow encapsulated in positively charged liposomes (phosphatidylcholine:stearylamine:cholesterol; 5:1:5 μmol). Movement of dye following injection of Lucifer Yellow encapsulated in negatively charged liposomes (phosphatidylserine): (c), 30 min after injection (×64); (d), bright field micrograph of injected area depicted in (c); (e), leaf cell during injection; (f) and (g), dye movement after 5 and 15 min, respectively.

including the leaf of *Elodea* (4), leaf and extrastelar tissues of *Egeria* (3, 5, 12) apices of *Silene* (13), leaf tissues of *Allium* (23), staminal hairs of *Setcreasea* (30), and the source leaf of *Commelina* (6). Movement of tracer dyes has been shown to be controlled by changes in cellular concentrations of ions, such as $Ca^{2+}$ and aromatic amino acids (3, 4). In addition, size exclusion limits have been established for symplastic movement in some tissues (5, 12, 13, 30) which can apparently be overcome by treatments, such as plasmolysis (4). In other studies, barriers to symplastic movement have been found even in regions where apparently normal plasmodesmata are present, suggesting the existence of symplastic "domains" within specific plant tissues (5).

The similarity of our results to those reported for symplastic movement of Lucifer Yellow in source leaves of *Commelina* (6), is convincing evidence that liposome encapsulation is a valid

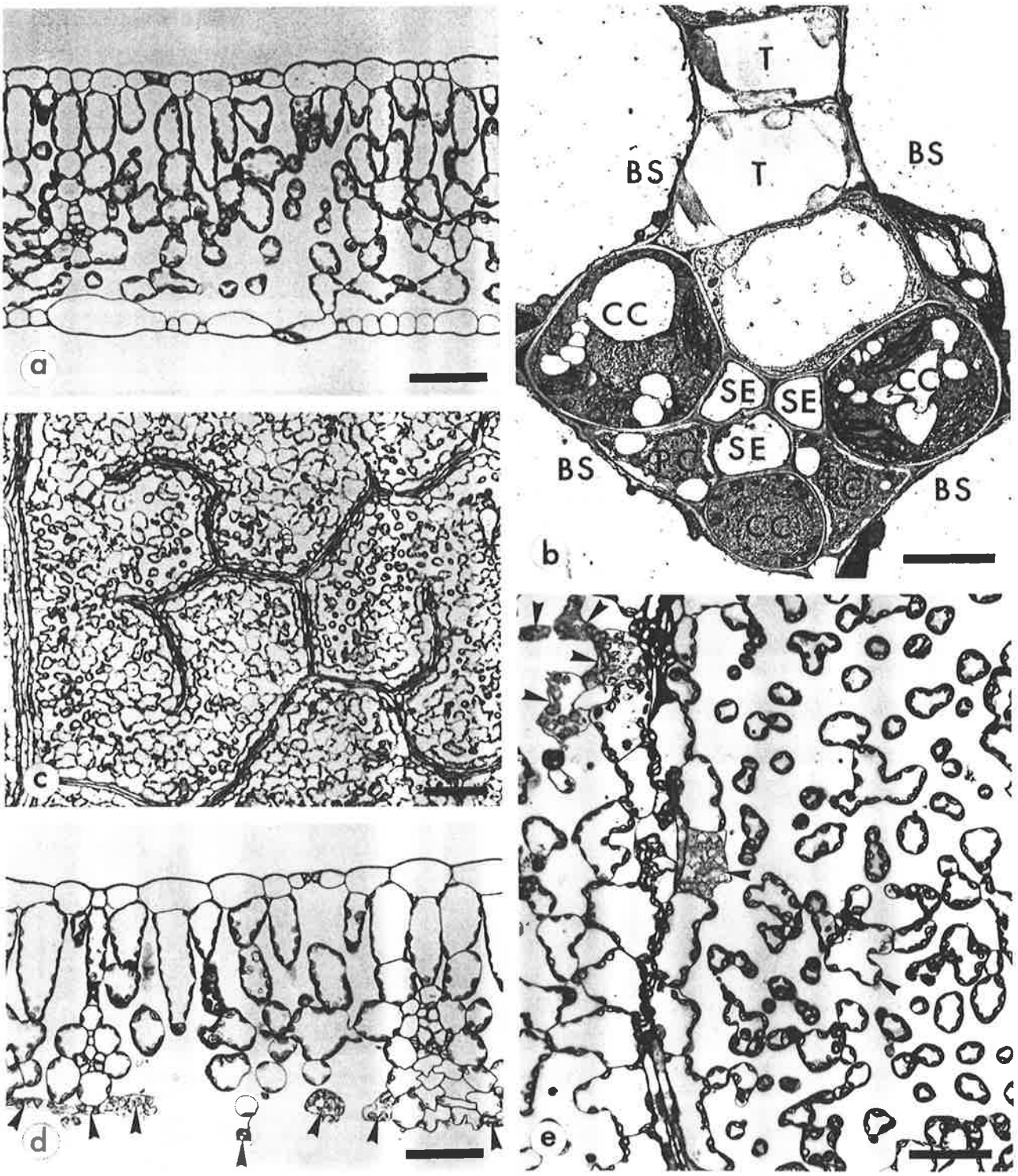


FIG. 2. Light and electron micrographs of *I. tricolor* source leaves showing the anatomical organization of the tissue used for dye tracer studies. (a) Leaf cross section. Bar = 50 $\mu$m (×270). (b), Cross-section of a minor vein and portions of the surrounding bundle sheath. Companion (CC) and phloem parenchyma cells (PC) are in contact with the bundle sheath cells (BS). (SE: sieve element, T: tracheary element). Bar = 5$\mu$m (×3300). (c), Paradermal section taken at the level of the phloem demonstrating the typical vascular pattern and the extent of lateral interconnections between the mesophyll cells at this level. Bar = 100 $\mu$m (×110). (d), Cross-section of an area of leaf injected with liposome-encapsulated Lucifer Yellow CH. Darts indicate cells damaged by removal of the lower epidermis and/or epifluorescence illumination. Bar = 5 $\mu$m (×275). (e), Paradermal section taken at the lowest level of the phloem in the injected tissue. Darts indicate cells damaged by removal of the lower epidermis and/or epifluorescence illumination. Bar = 50 $\mu$m (×300).

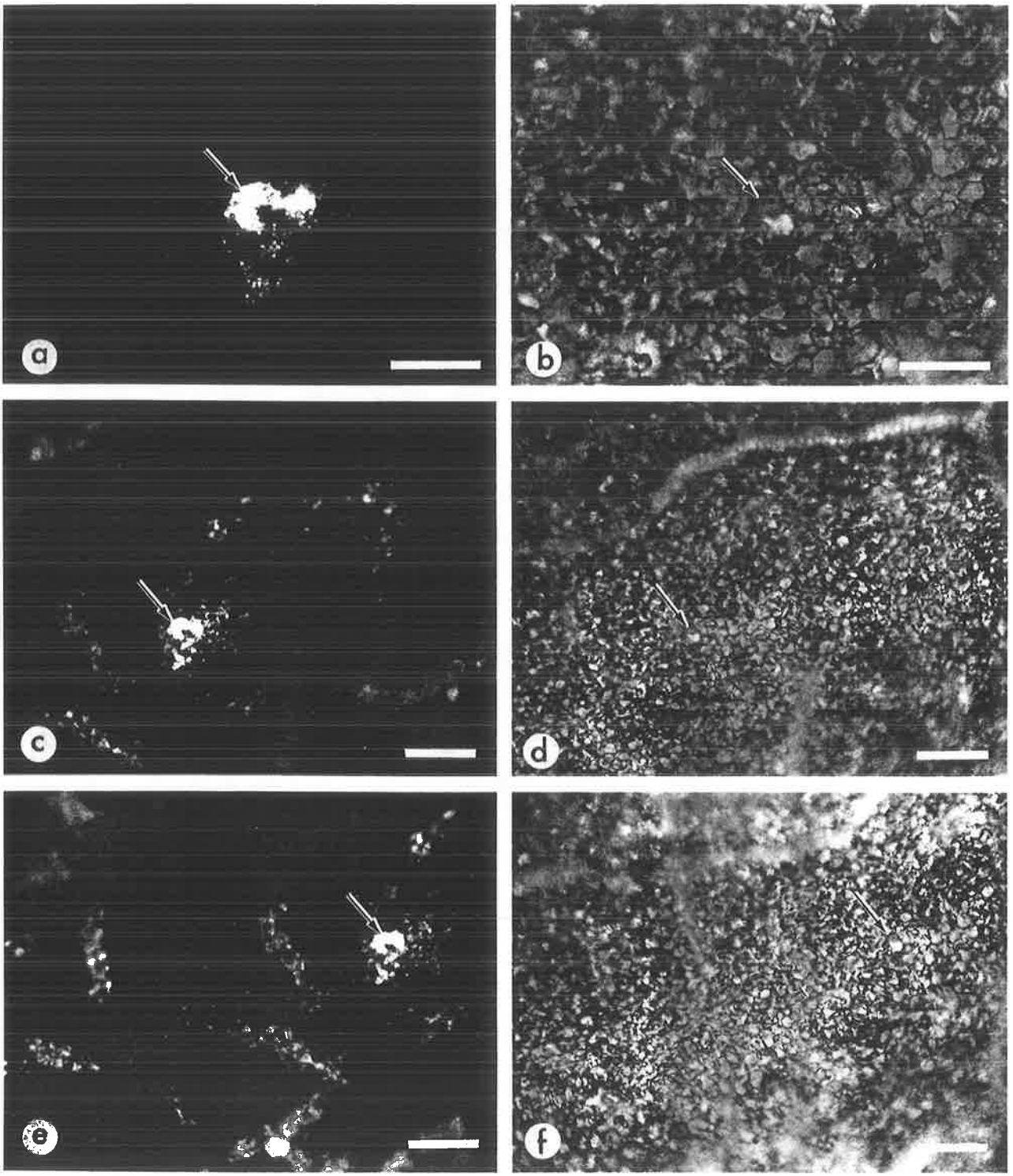


FIG. 3. Movement of Lucifer Yellow in the source leaf symplast of *I. tricolor* following microinjection of liposome-encapsulated dye into a spongy mesophyll cell. Arrows indicate the site of injection. Extent of dye movement 6 min (a), 16 min (c), and 30 min (e) after injection. Bright field micrographs (b), (d), and (f) depict regions illustrated in (a), (c), and (e), respectively. (a) and (b), Bar = 100 $\mu$m (×160); (c–f), bar = 200 $\mu$m (×64).

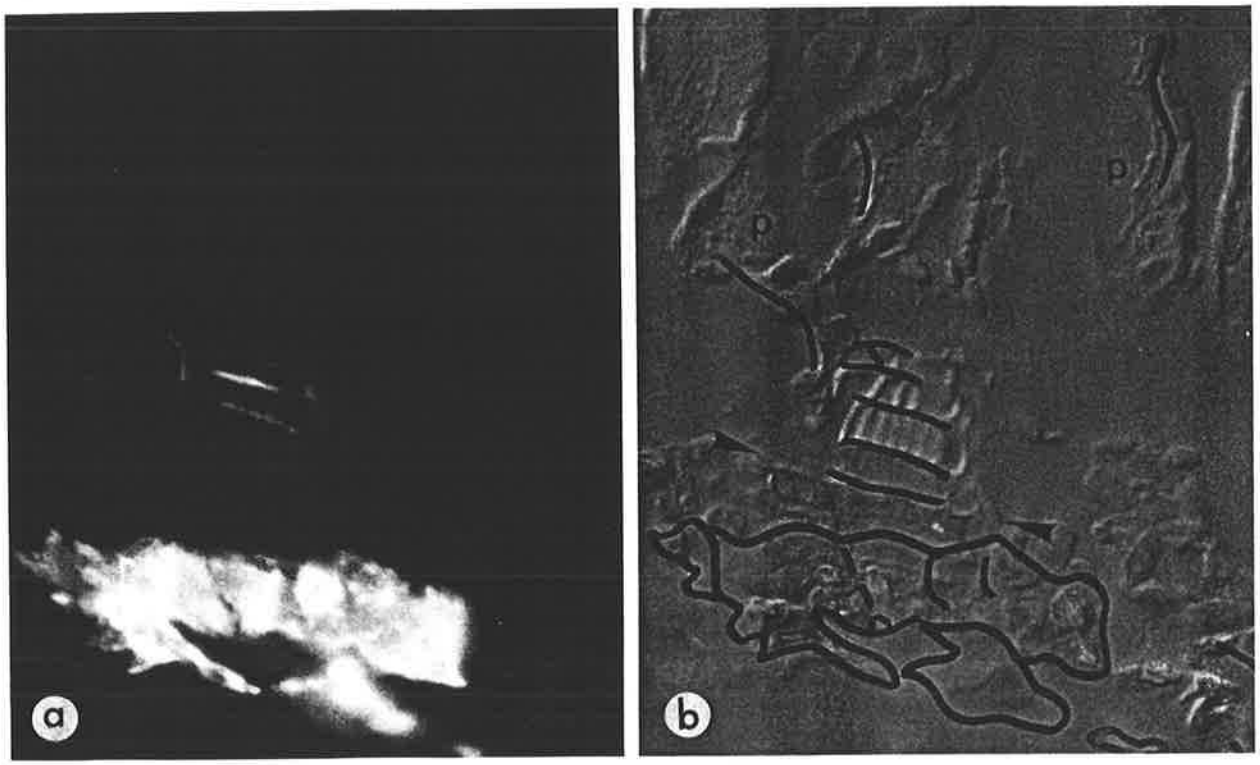


FIG. 4. Cryosection of vascular tissue of an *Ipomea* leaf through which Lucifer Yellow has moved. (a), Fluorescence micrograph; (b), differential interference contrast micrograph of the same section. Area delineated in (b) corresponds to fluorescent area depicted in (a). Darts in (b) indicate interface between xylem and phloem tissues. p, Palisade cell.

technique for the delivery of intercellular probes to the cytosol of vacuolate cells. The data presented here indicate that there are fully functional symplastic connections along the entire pathway from the mesophyll to the minor veins in the source leaf of *Ipomea*. Plasmodesmata can be found interconnecting all cell types, and there is no apparent barrier to the symplastic movement of Lucifer Yellow CH between these cells. The free permeability of the relatively small Lucifer Yellow molecule (457 D) suggests that there is no permeability barrier to the diffusion of small molecules throughout the leaf symplast. However, barriers to symplastic transport can be artifically imposed.

The image obtained of the distribution of Lucifer Yellow in the *Ipomea* leaf symplast following alkaline pH treatment is particularly interesting, especially when compared to autoradiographic images which have been reported for the distribution of exogenous [$^{14}$C]sucrose in leaf discs pretreated at high pH (31). A preferential localization of 'label', either [$^{14}$C]sucrose or Lucifer Yellow, is seen in the leaf mesophyll at high pH with little or no 'activity' in the minor veins. The effect on pH on sugar uptake is usually attributed to a reduction in sucrose-proton co-transport by the minor veins at high pH (10, 11). The data shown here for Lucifer Yellow suggest an alternative possibility; namely, that alkaline pH treatment disrupts the relay of solutes through the symplast from the mesophyll to the minor veins.

Current experimental evidence suggests that the free movement of solutes through the symplast is regulated at the level of the plasmodesmata (3–5). The actual mechanisms controlling movement through plasmodesmata are unknown at present, but modulation of intracellular Ca levels is implicated (3). The action of Ca is apparently not through its effects on cytoplasmic streaming or on callose deposition (5). Electron-dense granules with $Ca^{2+}$-ATPase activity appear at the neck region of the plasmodesma in response to $Ca^{2+}$ treatment (1). This observation has been used to implicate ATPase activity, associated with plasmodesmata, in the control of solute movement through the symplast (5), but direct experimental evidence is lacking. However, it is interesting to speculate on such a role, particularly as the plasmalemma $H^+$-ATPase is one protein thought to be metabolically regulated via phosphorylation by a $Ca^{2+}$-dependent protein kinase (33).

Regulation of symplastic solute flow at the level of the plasmodesmatal ATPase could explain the nonmovement of dye to the veins at high pH (Fig. 6). It may also explain the lack of effect of PCMBS treatment on movement of Lucifer Yellow seen in this study (Fig. 5), if, as current data appear to indicate (16, 21), the action of PCMBS is predominantly on the sucrose carrier and not on ATPase activity. The data presented here also indicate that plasmodesmata in different regions of the leaf may be regulated independently. Subsequent carbon partitioning between phloem-mobile and nontransported compounds would also be affected, as indicated in previous biochemical studies on stachyose synthesis in *Cucurbita* in response to plasmolysis (19).

The involvement of apoplastic or symplastic routes for sugar movement in source leaves appears to be much less straightforward than first envisioned in early phloem transport work (17). Most evidence now indicates that a considerable proportion of the uptake of sugar once attributed to 'phloem loading' actually represents uptake into nonphloem tissues (17, 18, 20, 32) and that the contribution of the vasculature to this uptake may, in fact, be small (32).

The data in the present study further illustrate the complexities associated with studying phloem loading. Clearly, studies based solely on structural detail are of only limited value in predicting the efficacy of the symplastic pathway in any source leaf tissue. It is essential that we now develop a better understanding of plasmodesmatal function and integrate this knowledge into stud-

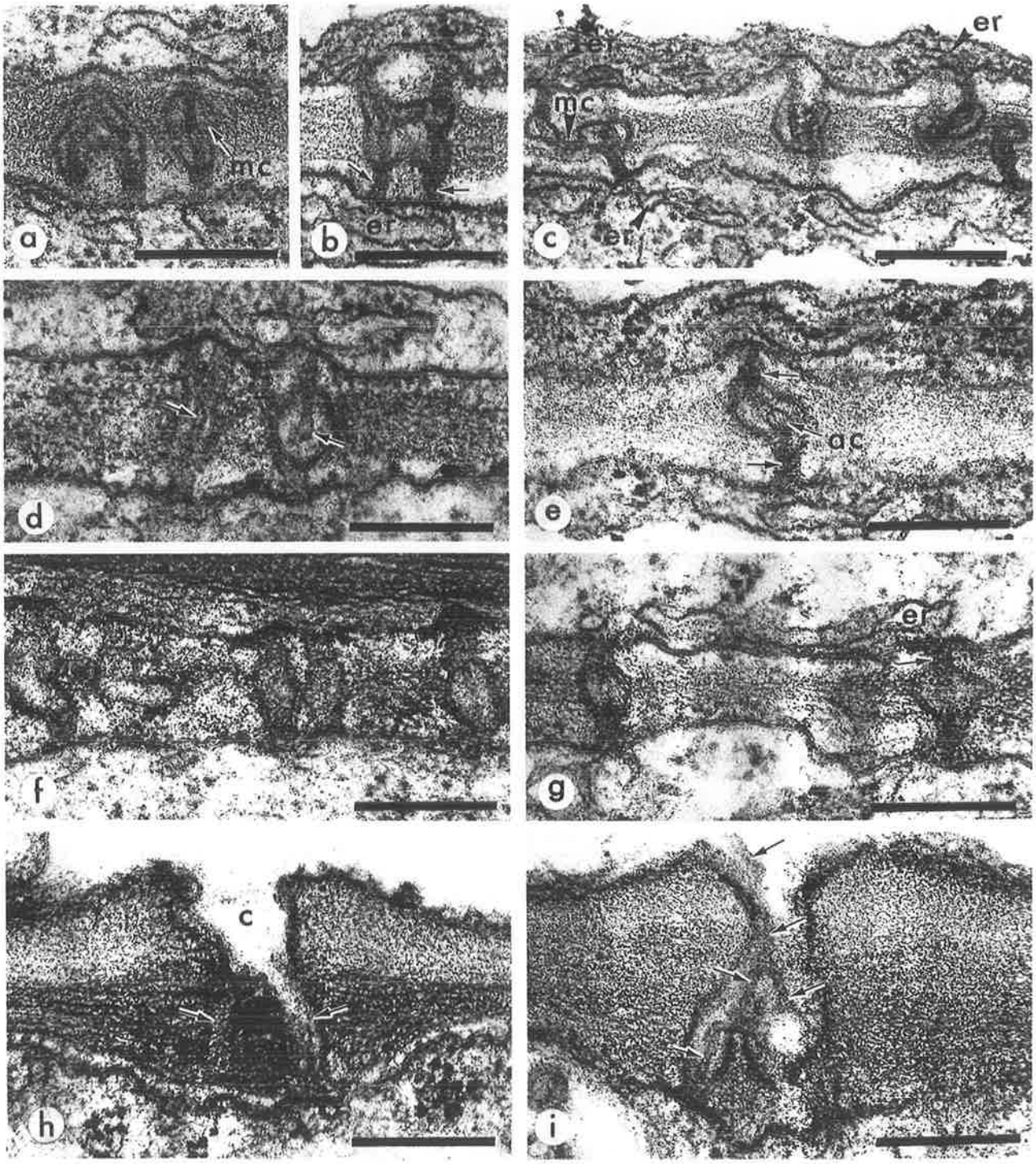


FIG. 5. Structure of plasmodesmata occurring along the pathway from mesophyll cells to the sieve elements of minor veins in the source leaf of *I. tricolor*. Representative plasmodesmata from control tissues (a, b, d, f, and h) and liposome-injected tissues through which Lucifer Yellow has moved (c, e, g, and i) are shown. All bars = 0.25 μm. (ac), Axial component (desmotubule); (er), endoplasmic reticulum; (mc), median cavity. Plasmodesmata interconnecting mesophyll cells from control (a, b) and injected (c) tissues. Arrows in (b) indicate neck constrictions; note apparent continuity between er and neck constrictions. Darts in (c) indicate horizontally oriented mc and three sites of possible contact between the elements of the ER and nearby plasmodesmata. Plasmodesmata between mesophyll (above) and bundle sheath cells (below) in control tissues (d) and injected (e) tissues. In (d), note swelling of the central part of the ac of two spatially separated plasmodesmata. In (e), note the electron opaque neck constrictions (arrows) in a plasmodesma showing a clearly defined swelling of the ac. Plasmodesmata connecting bundle sheath (above) and companion cells (below) in control (f) and injected (g) tissues. Arrow (g) indicates apparent continuity between the labeled ER element and the plasmodesmatal neck constriction. Asymmetrically branched plasmodesmata interconnecting sieve elements (above) and companion cell (below) in control (h) and injected (i) tissues. Note the large cavity or pore (c) on the side of the sieve element. Arrows indicate the extent of the ac.

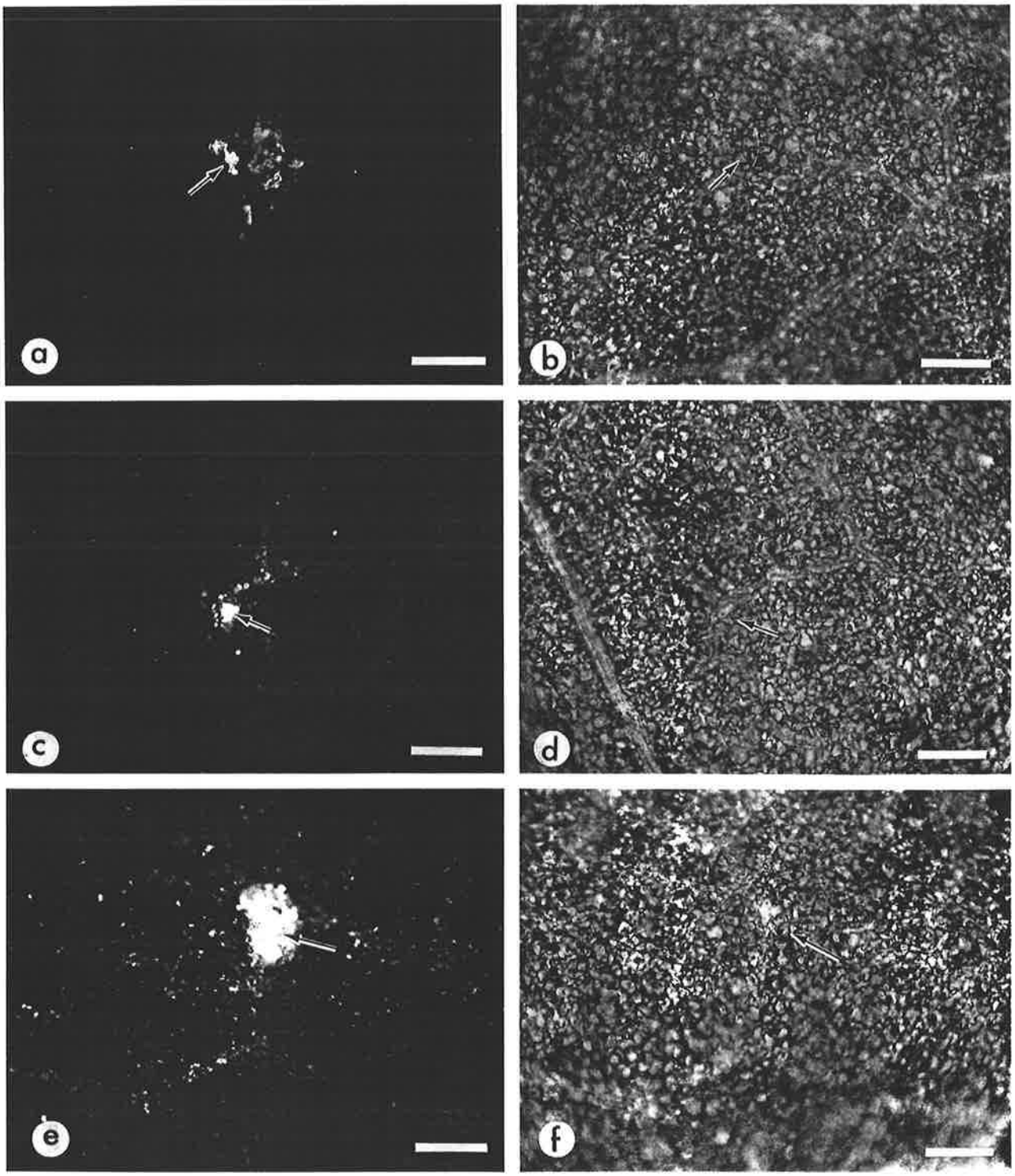


FIG. 6. Effect of PCMBS pretreatment on movement of Lucifer Yellow in the *Ipomea* source leaf symplast. Tissues were equilibrated for 60 min in K-phosphate (pH 7.0) or Mes-KOH buffer (pH 5.5). A 15 min pretreatment (±2 mM PCMBS) was then employed, and PCMBS-free buffer was reapplied. All bars = 200 μm (×64). (a), Control injection site, pretreated in K-phosphate (pH 7.0) before dye injection. (c), PCMBS injection site, pretreated in K-phosphate (pH 7.0) plus 2 mM PCMBS. (e), PCMBS injection site, pretreated with aqueous 2 mM PCMBS, then with 25 mM Mes-KOH buffer (pH 5.5) during and following the injection period. All micrographs were taken 60 min after injection. Bright field micrographs (b), (d), and (f) depict regions illustrated in (a), (c), and (e), respectively.

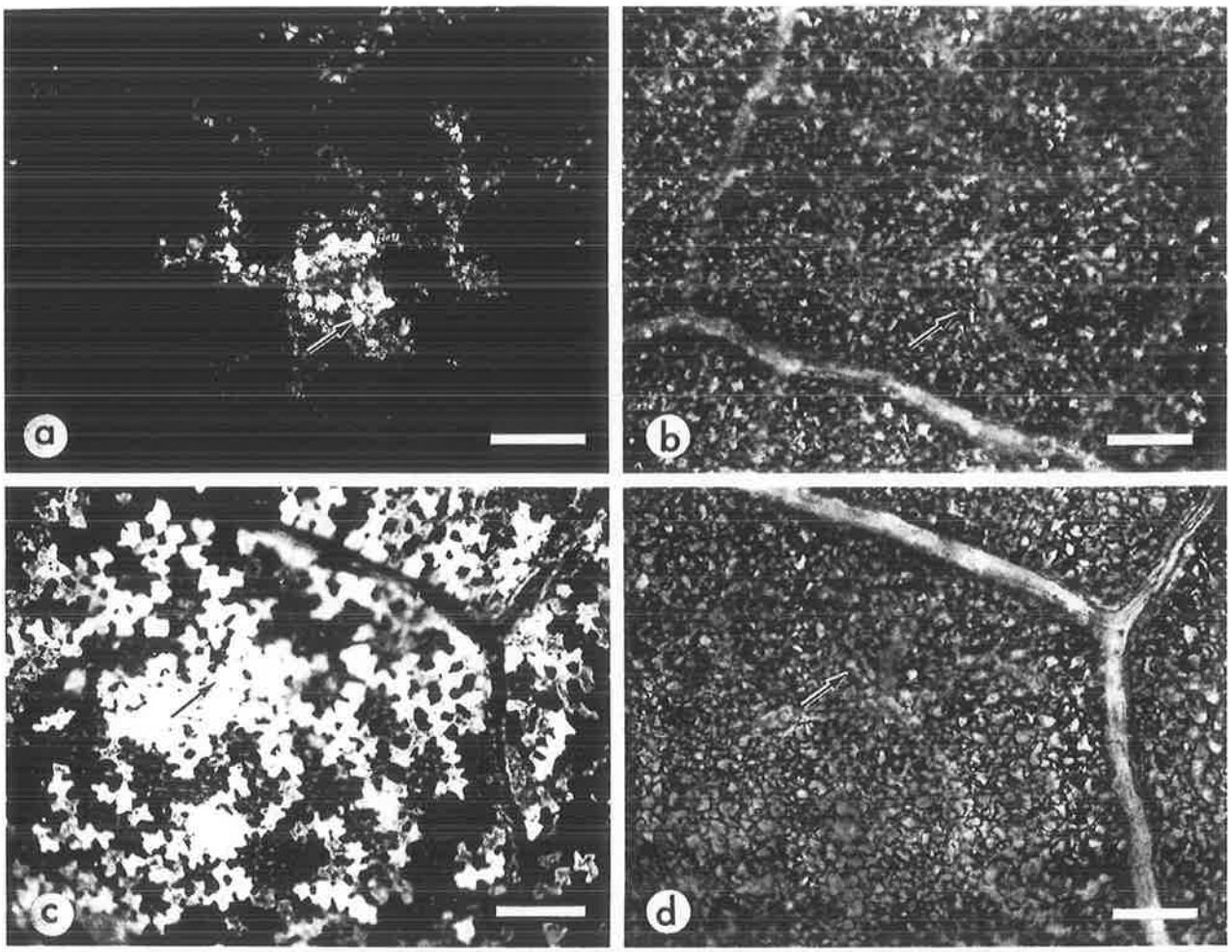


FIG. 7. Effect of bathing medium pH on movement of Lucifer Yellow in the source leaf symplast of *Ipomea*. All bars = 200 μm (×64). Pattern of dye movement 60 min after injection into tissue given a pH 5.5 (a) or pH 8.0 (c) treatment. Bright field micrographs (b) and (d) depict regions illustrated in (a) and (c), respectively.

ies on assimilate transport. The technique described in this paper provides a starting point, opening the door to the cytosol.

*Acknowledgments*—The authors wish to thank Professor T. Elliot Weier for generously allowing us the use of his cryostat for portions of the work reported here.

## LITERATURE CITED

1. BELITSER NV, GV ZAALISHVILI, NP SYTNIANSKAJA 1982 $Ca^{2+}$ binding sites and $Ca^{2+}$-ATPase activity in barley root tip cells. Protoplasma 111: 63–78
2. CUTLER AJ, PD SHARGOOL, WG KURZ, F CONSTABEL 1984 Liposomes as vehicles for transferring low molecular weight compounds into periwinkle protoplasts. J Plant Physiol 117: 29–40
3. ERWEE MG, PB GOODWIN 1983 Characterization of the *Egeria densa* Planch. leaf symplast. Inhibition of the intercellular movement of fluorescent probes by group II ions. Planta 158: 320–328
4. ERWEE MG, PB GOODWIN 1984 Characterization of the *Egeria densa* leaf symplast: response to plasmolysis, deplasmoylsis and to aromatic amino acids. Protoplasma 122: 162–158
5. ERWEE MG, PB GOODWIN 1985 Symplastic domains in extrastelar tissues of *Egeria densa* Planch. Planta 163: 9–19
6. ERWEE MG, PB GOODWIN, AJE VAN BEL 1985 Cell-cell communication in the leaves of *Commelina cyanea* and other plants. Plant Cell Environ 8: 173–178
7. ESAU K, J THORSCH 1985 Sieve plate pores and plasmodesmata, the communication channels of the symplast: ultrastructural aspects and developmental relations. Am J Bot 72: 1641–1653
8. GAMALEI YV, MV PAKHOMOVA 1981 Distribution of plasmodesmata and parenchyma transport of assimilates in the leaves of several dicots. Sov Plant Physiol 28: 649–661
9. GEIGER DR 1975 Phloem loading. *In* MH Zimmermann, JA Milburn, eds. Transport in Plants I. Springer-Verlag, Heidelberg. pp 395–450
10. GIAQUINTA RT 1977 Phloem loading of sucrose. pH dependence and selectivity. Plant Physiol 59: 750–753
11. GIAQUINTA RT 1983 Phloem loading of sucrose. Annu Rev Plant Physiol 34: 347–387
12. GOODWIN PB 1983 Molecular size limit for movement in the symplast of the *Elodea* leaf. Planta 157: 124–130
13. GOODWIN PB, RF LYNDON 1983 Synchronization of cell division during transition to flowering in *Silene* apices not due to increased symplast permeability. Protoplasma 116: 219–222
14. GRUSAK MA, WJ LUCAS 1984 Recovery of cold-inhibited phloem translocation in sugar beet I. Experimental analysis of an existing mathematical recovery model. J. Exp Bot 35: 389–402
15. GUNNING BES 1976 The role of plasmodesmata in short distance transport to and from the phloem. *In* BES Gunning, AW Robards, eds. Intercellular Communication in Plants: Studies on Plasmodesmata. Springer-Verlag, Heidelberg, pp 203–227
16. LICHTNER FT, RM SPANSWICK 1981 Electrogenic sucrose transport in developing soybean cotyledons. Plant Physiol 67: 869–874
17. LUCAS WJ 1985 Phloem-loading: a metaphysical phenomenon? *In* RL Heath, J Preiss, eds. Regulation of Carbon Partitioning in Photosynthetic Tissue. American Society of Plant Physiologists, Rockville, MD, pp 254–271
18. MADORE MA, JA WEBB 1981 Leaf free space analysis and vein loading in *Cucurbita pepo*. Can J Bot 59: 2550–2557
19. MADORE MA, JA WEBB 1982 Stachyose synthesis in isolated mesophyll cells of *Curcurbita pepo*. Can J Bot 60: 126–130

20. MAYNARD JW, WJ LUCAS 1982 Sucrose and glucose uptake into *Beta vulgaris* leaf tissues. A case for general (apoplastic) retrieval systems. Plant Physiol 70: 1436–1443
21. M'BATCHI B, D PICHELIN, S DELROT 1985 The effect of sugars on the binding of [$^{203}$Hg]-*p*-chloromercuribenzenesulfonic acid to leaf tissues. Plant Physiol 79: 537–542
22. OFFLER CE, JW PATRICK 1984 Cellular structures, plasma membrane surface areas and plasmodesmatal frequencies of seed coats of *Phaseolus vulgaris* L. in relation to photosynthate transfer. Aust J Plant Physiol 11: 79–99
23. PALEVITZ BA, PK HEPLER 1985 Changes in dye coupling of stomatal cells of *Allium* and *Commelina* demonstrated by microinjection of Lucifer Yellow. Planta 164: 473–479
24. PAPAHADJOPOULOS D, WJ VAIL 1978 Incorporation of macromolecules within large unilamellar vesicles (LUV). Ann NY Acad Sci 308: 259–267
25. PICK U 1981 Liposomes with a large trapping capacity prepared by freezing and thawing of sonicated phospholipid mixtures. Arch Biochem Biophys 212: 186–191
26. REYNOLDS ES 1963 The use of lead citrate at high pH as an electron opaque stain in electron microscopy. J Cell Biol 17: 208–212
27. RUSSIN WA, RF EVERT 1985 Studies on the leaf of *Populus deltoides* (Salicaceae): ultrastructure, plasmodesmatal frequency, and solute concentrations. Am J Bot 72: 1232–1247
28. SPURR AR 1969 A low-viscosity epoxy resin embedding medium for electron microscopy. J Ultrastruct Res 26: 31–43
29. STAEHELIN LA, SG SPRAGUE, TG DUNIHAY 1984 New methods for making chloroplast lipid liposomes and for reconstituting chlorophyll-protein complexes isolated from SDS polyacrylamide gels. Photosynth Res 5: 293–296
30. TUCKER EB 1982 Translocation in the staminal hairs of *Setcreasea purpurea*. I. A Study of cell ultrastructure and cell-to-cell passage of molecular probes. Protoplasma 113: 193–201
31. TURGEON R 1984 Efflux of sucrose from the minor veins of tobacco leaves. Planta 161: 120–128
32. WILSON C, JW OROSS, WJ LUCAS 1985 Sugar uptake into *Allium cepa* leaf tissue: an integrated approach. Planta 164: 227–240
33. ZOCCHI G, SA ROGERS, JB HANSON 1983 Inhibition of proton pumping in corn roots is associated with increased phosphorylation of membrane proteins. Plant Sci Lett 31: 215–221

Planta (1987) 171:197–204

Planta
© Springer-Verlag 1987

# Control of photoassimilate movement in source-leaf tissues of *Ipomoea tricolor Cav.*

Monica A. Madore* and William J. Lucas**
Botany Department, University of California, Davis, CA 95616, USA

**Abstract.** Autoradiographs obtained from discs from mature, peeled *Ipomoea tricolor Cav.* leaves indicated that a 15-min 2 mM *p*-chloromercuribenzene sulfonic acid (PCMBS) pretreatment did not prevent the accumulation of $^{14}CO_2$-derived $^{14}C$-photosynthate within the minor veins. However, accumulation of $^{14}C$-photosynthate within these veins was almost, or completely prevented by treatment of the leaf discs at pH 9.0. Peeled *Ipomoea* leaf discs were also used to study the kinetics of exogenously supplied [$^{14}C$]sucrose; influx occurred by the combined operation of a saturable and a first-order kinetic mechanism. Both transport mechanisms were inhibited by a 15-min 2 mM PCMBS pretreatment or by treatment at pH 9.0. An analysis of autoradiographs obtained on leaf discs that had been fed exogenous [$^{14}C$]sucrose, showed that whereas all cells of the leaf took up sucrose at pH 5.0, uptake at pH 9.0 occurred primarily into cells of the minor veins. In contrast with $^{14}C$-photoassimilate experiments, PCMBS pretreatment, at either pH 5.0 or pH 9.0, resulted in a reduction in the radioactivity within the minor veins when the label was supplied exogenously as [$^{14}C$]sucrose. Kinetic experiments conducted with mesophyll cells isolated enzymatically from peeled source-leaf discs indicated that [$^{14}C$]sucrose influx also occurred by a saturable and a first-order kinetic mechanism. Comparative studies between leaf discs and isolated mesophyll cells showed that mesophyll cells could account for 75% of the total uptake occurring into the peeled leaf discs. These results indicate that the effects of PCMBS and alkaline pH on net sucrose uptake by leaf tissues are not exerted solely on phloem tissues, and that some of the effects of these treatments may be attributable to an inhibition of symplasmic transport to the minor veins.

* *Present address:* Department of Botany and Plant Sciences, University of California, Riverside, CA 92521, USA
** To whom correspondence should be addressed

*Abbreviation:* PCMBS = *p*-chloromercuribenzene sulfonic acid

**Key words:** *Ipomoea* – Leaf (assimilate movement) – Photoassimilate movement – Sucrose uptake (leaf discs).

## Introduction

The relative importance of apoplasmic versus symplasmic routes for photoassimilate transport from the mesophyll to the minor veins in source leaves is still under debate. However, a re-evaluation of the present evidence (Lucas 1985; Lucas and Madore 1987) would indicate that uptake of exogenous sucrose into leaf discs does not necessarily represent direct uptake into the minor veins as previously postulated (Giaquinta 1983). Indeed, most evidence now indicates that a considerable proportion of the uptake of sucrose once attributed to "phloem loading" actually represents uptake into non-phloem tissues (Fondy and Geiger 1977; Madore and Webb 1981; Maynard and Lucas 1982; Wilson et al. 1985; Van Bel et al. 1986). It thus appears that not all of the carrier proteins responsible for sucrose uptake reside on the plasmalemma of the sieve-element-companion-cell complex. In fact, it is possible that the contribution of the vasculature to this uptake is actually quite small (Wilson et al. 1985; Van Bel et al. 1986).

In a recent study, we were able to map the symplasmic connections in the source leaf of *Ipomoea tricolor* by using injection of liposomes to introduce the fluorescent dye, Lucifer Yellow CH, into a mesophyll cell of a source leaf (Madore et al. 1986). Microinjected Lucifer Yellow was found to move through the symplasmically connected mesophyll cells into the neighboring minor vein, with subsequent extensive movement along the vein network. This pattern of Lucifer Yellow movement was also observed in studies on the source leaf of *Commelina cyanea* (Erwee et al. 1985).

Examination of mature *Ipomoea* leaf tissue

under the electron microscope indicated that plasmodesmata interconnected all cell types from the mesophyll to the sieve-element – companion-cell complex. Furthermore, cryosections of the vasculature, cut through regions in which Lucifer Yellow had moved, showed that the fluorescence was confined to the bundle sheath and regions of the phloem tissue (see Fig. 4 of Madore et al. 1986). Unfortunately, the specific phloem-cell type(s) which contained the Lucifer Yellow could not be identified using this cryosectioning technique. In any event, these fluorescent-dye tracer and electron-microscope studies indicated that there may be no barrier to symplasmic solute movement along the entire pathway from the mesophyll to the minor veins of the *Ipomoea* source leaf. However, during the course of this study, we discovered that barriers to symplasmic transport could be induced by treatments commonly used to manipulate the putative apoplasmic phloem-loading step.

We found that treatment of leaf tissues with *p*-chloromercuribenzene sulfonic acid (PCMBS), an impermeant sulfhydryl reagent previously shown to block the influx of exogenously supplied sucrose, had no effect on Lucifer Yellow movement throughout the symplasm of the leaf. In contrast, alkaline pH treatment, normally thought to exert its effects by inhibition of sucrose-$H^+$ co-transport into the phloem (Giaquinta 1977; 1983), actually disrupted the movement of Lucifer Yellow through the symplasm from the mesophyll to the minor veins. Apparently, movement of Lucifer Yellow between adjacent mesophyll cells was unaffected, but a blockage of the movement of this dye somewhere between these mesophyll cells and the cells of the minor vein was induced by exposing the tissues to an unphysiologically high apoplasmic pH value of 8.0.

In the present study, we examined the effects of similar treatments on the relay of photosynthetically derived solutes in source-leaf discs of *Ipomoea*. In agreement with our earlier dye-tracer results, PCMBS treatment had no effect on the movement of photoassimilates from the mesophyll to the minor veins of *Ipomoea* leaf discs, but treatment at alkaline pH strongly inhibited movement of these photoassimilates out of the mesophyll cells into the minor veins, again consistent with observations made during our Lucifer Yellow studies. These new data indicate that at least some of the effects of these treatments, previously attributed exclusively to an inhibition of an apoplasmic "phloem-loading" step, may be attributable to an inhibition of symplasmic transport to the minor veins.

## Material and methods

*Chemicals.* Dithioerythritol, 2-(N-morpholino)ethanesulfonic acid (Mes), PCMBS (Na salt) and tris-(hydroxymethyl) methylaminopropanesulfonic acid (Taps) were purchased from Sigma Chemical Co., St. Louis, Mo., USA. [U-$^{14}$C]Sucrose (specific activity = 21.9 GBq·mmol$^{-1}$) was obtained from ICN Biochemicals, Irvine, Cal., USA; Na [$^{14}$C]$HCO_3$ (specific activity = 1.76 GBq·mmol$^{-1}$) from New England Nuclear Corp., Boston, Mass., USA, and Macerase and Miracloth from Calbiochem, La Jolla, Cal., USA.

*Plant material.* Fully expanded leaves from four-week-old *Ipomoea tricolor Cav.* cv. "Heavenly Blue" (W. Atlee Burpee Co., Warminster, Pa., USA) were used for all experiments. Plants were germinated and grown in a controlled-environment chamber under the conditions described in Grusak and Lucas (1984).

Large areas of the lower epidermis of these *Ipomoea* source leaves could be peeled away by gently tearing the leaf in the regions between the major veins. Leaf discs (4 mm diameter) were then excised from the peeled areas and used for all experiments ("peeled leaf discs").

*Isolation of mesophyll cells.* Mesophyll cells were isolated from peeled leaf discs of *Ipomoea* by a method similar to that described in Madore and Webb (1982). Seventy peeled leaf discs were placed in a 100-ml Erlenmeyer flask containing 20 ml of a maceration medium consisting of 300 mM mannitol, 25 mM Mes-NaOH buffer, pH 5.0, and 1% (w/v) Macerase. The discs were infiltrated with the maceration medium by applying a gentle vacuum to the flask for 30 s, and then the flask was placed on an orbital shaker (Model 3520; Lab-Line Instruments, Melrose Park, Ill., USA) at 30 oscillations·min$^{-1}$ for a 3-h digestion period. The discs were then transferred to a centrifuge tube and gently agitated for 30 s to dissociate the mesophyll cells from the minor-vein networks. The vein networks were collected on cheesecloth and resuspended in 300 mM mannitol, while the mesophyll cells were collected on Miracloth and likewise resuspended in 300 mM mannitol.

*Kinetic studies.* Kinetic studies of [$^{14}$C]sucrose uptake into peeled *Ipomoea* leaf discs were performed as described previously (Maynard and Lucas 1982; Wilson et al. 1985). To allow recovery from wounding, leaf discs were aged for 4 h (under room light and temperature) by floating them, peeled side down, in a buffer solution at either pH 5 (25 mM Mes + 20 mM $CaCl_2$) or pH 9 (25 mM Taps + 20 mM $CaCl_2$) prior to introducing [$^{14}$C]sucrose solutions. In some experiments, a 2 mM PCMBS pretreatment (15 min) was given and the discs were then washed (15 min) in 2 mM $CaCl_2$ before the kinetic experiments were performed.

For experiments on isolated cells, the cells were suspended in 300 mM mannitol with or without 2 mM PCMBS. Following the 15-min pretreatment period, 100-µl aliquots of cell suspension were added to 150µl of uptake medium to give a final composition of 120 mM buffer (either Mes-NaOH, pH 5.0, or Taps-NaOH, pH 9.0), 20 mM $CaCl_2$, 1–40 mM [$^{14}$C]sucrose, and a total osmolality adjusted to 300 mosmol. Following a 30-min uptake period, two 100-µl aliquots were removed from each solution well and rapidly filtered through glass-wool plugs held in 1-ml plastic pipette tips. The cells were retained on the glass-wool plugs and were washed free of adhering radioactivity by rinsing the plugs five times with 1-ml volumes of 300 mM mannitol containing 20 mM $CaCl_2$. The glass-wool plugs were then transferred to scintillation vials and the radioactivity taken up by the cells was determined by liquid scintillation counting (Model LS9800; Beckman Instruments, Palo Alto, Cal., USA).

*Labelling of leaf discs with* $^{14}CO_2$. Labelling chambers for photosynthetic incorporation of $^{14}CO_2$ into peeled leaf discs were constructed from disposable plastic Petri dishes. A serum cap was inserted into the center of the dish cover through a hole made with a soldering iron. The bottom of the plate was lined with moistened (distilled water) filter paper and a small well of lactic acid was placed in the center of the dish. Aged leaf discs were then placed, peeled side up, 3 cm from the lactic-acid well, and equilibrated under a water-filtered quartz-iodide lamp (238 μmol photons·$m^{-2}$·$s^{-1}$; photosynthetically active radiation, 400–700 nm) for 5 min. The dish cover was then sealed in place with silicone grease and $^{14}CO_2$ was released inside the dish by injecting 188.5 kBq $NaH^{14}CO_3$ into the lactic-acid well. After a 5-min labelling period the dish was opened and removed from the light. The discs were refloated, five per well, on solutions of 120 mM buffer (either Mes-NaOH, pH 5.0, or Taps-NaOH, pH 9.0) and 20 mM $CaCl_2$ adjusted to 200 mosmol with mannitol. The remainder of the experiment was carried out under room light. Discs were transferred to fresh medium at 15, 30, 60, 90 and 120 min following initiation of the labelling period. Label effluxed from the leaf discs into the medium was measured by counting 0.5-ml aliquots of solution from the wells. After the efflux period, the five discs were extracted three times with 0.5 ml, of 80% ethanol heated to 70° C in a water bath. The extracts were subsequently partitioned by ion-exchange chromatography into neutral, basic and acidic fractions (Madore and Grodzinski 1984) and the radioactivity in each fraction was measured by liquid scintillation counting. The neutral fraction was further fractionated by thin-layer cellulose chromatography in *n*-propanol:ethyl acetate:water (7:1:2, by vol.) and the radioactivity in individual sugars was determined by liquid scintillation counting (Madore and Grodzinski 1984).

In some $^{14}CO_2$ experiments, discs were pretreated with 2 mM PCMBS or given a treatment at an acid or alkaline pH, as described above for kinetic studies, before being exposed to $^{14}CO_2$.

*Autoradiography*. Following a particular experimental treatment, a subsample of the discs was generally processed for autoradiography. These discs were rinsed briefly in distilled water and frozen in aluminum-foil cups that were placed on dry ice. The discs were lyophilized for 18 h in a Duradry freeze-dryer equipped with a bulk tray dryer (FTS Systems, Stone Ridge, N.Y., USA). The lyophilized discs were glued, peeled side up, to herbarium paper and exposed to Kodak Industrex M X-ray film (Eastman-Kodak, Rochester, N.Y., USA) for 0.5–7 d; the films were processed according to the manufacturer's directions.

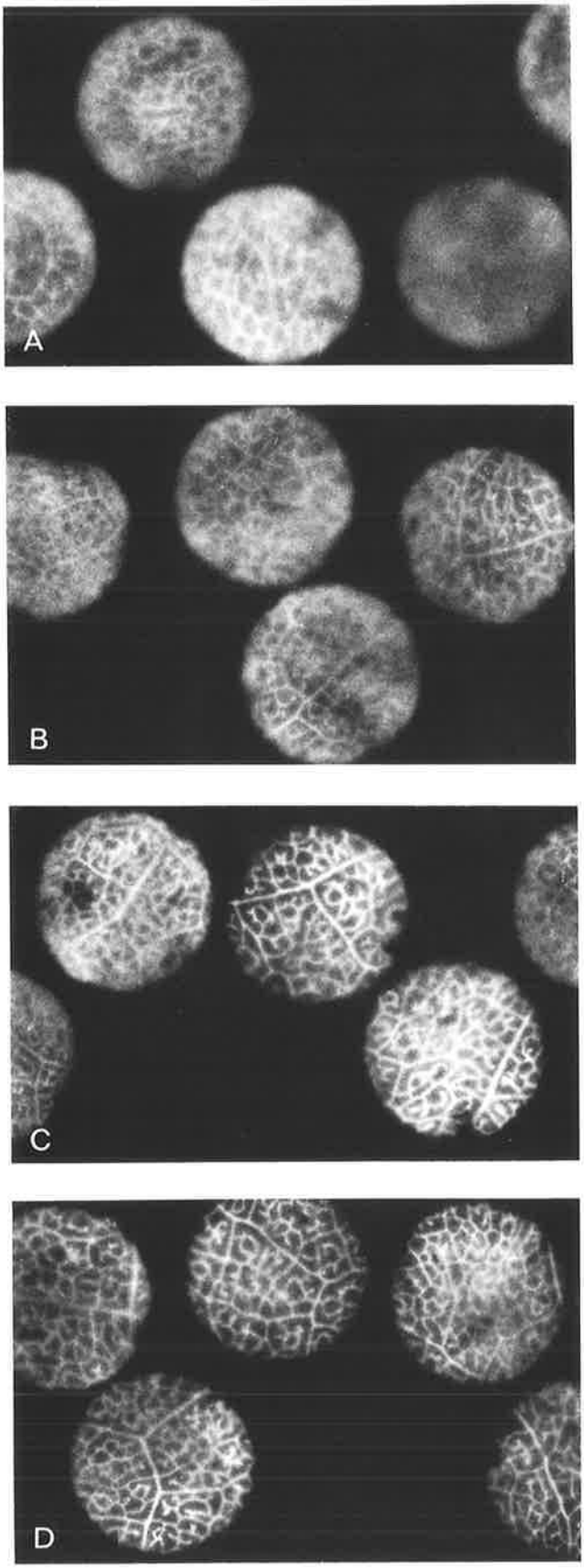


**Fig. 1 A–D.** Autoradiographs obtained from discs of peeled *Ipomoea tricolor* source leaves that were exposed, in the light, to $^{14}CO_2$ for 5 min, followed by a chase period of 10 (**A**), 25 (**B**), 55 (**C**), or 115 (**D**) min. During the chase period the discs were floated, peeled side down, on a buffered medium (pH 5.0) under room light. All discs incorporated approximately the same amount of $^{14}CO_2$ into $^{14}C$-photoassimilate

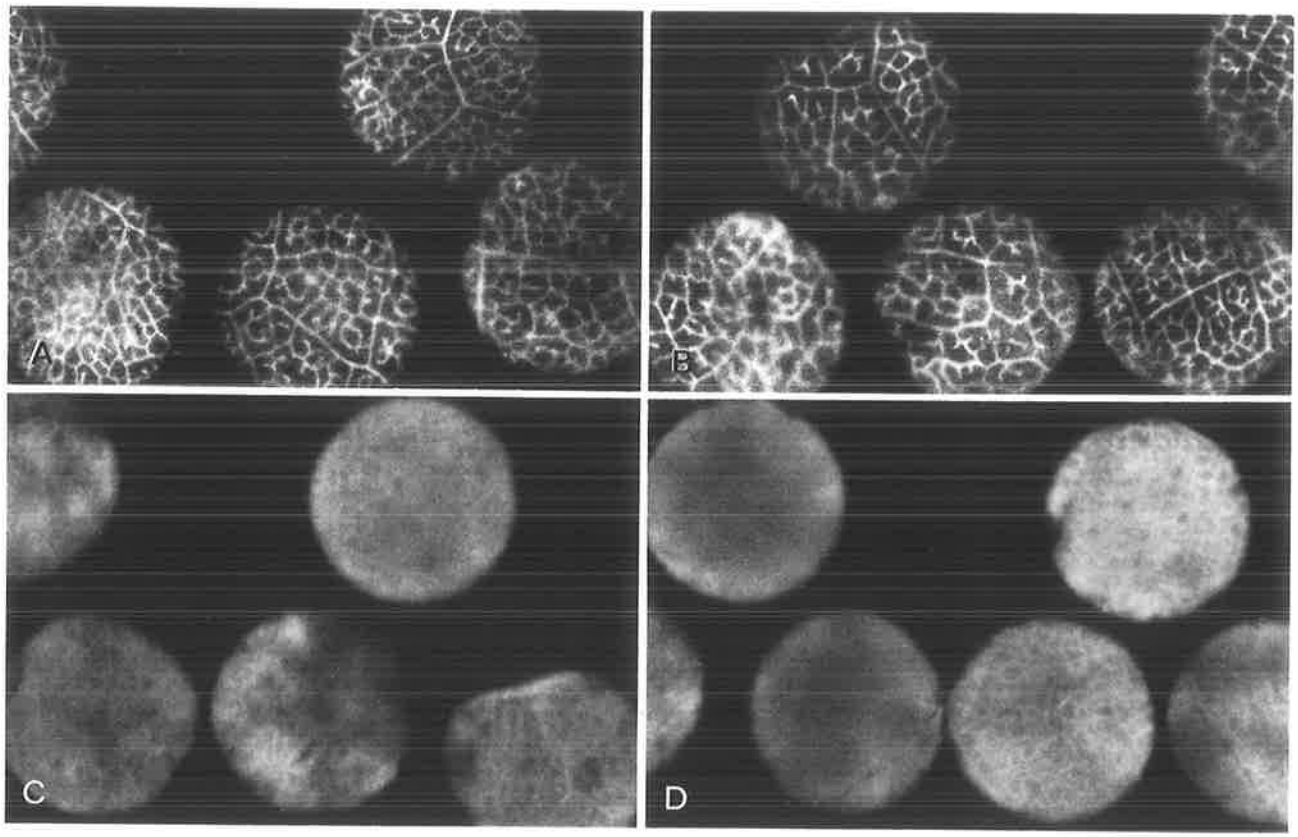


**Fig. 2A–D.** Influence of bathing medium pH and PCMBS treatment on the redistribution of $^{14}$C-photosynthate in *Ipomoea tricolor* source-leaf discs. Discs were pretreated (4 h) in bathing medium buffered at pH 5.0 (**A, B**) or pH 9.0 (**C, D**) prior to a 5-min exposure to $^{14}CO_2$; leaf discs were then given a 2-h chase period at their pretreatment-pH, before being processed for autoradiography. Discs in **B** and **D** were pretreated for 15 min in 2 mM PCMBS and then 15 min in 2 mM $CaCl_2$ prior to the $^{14}CO_2$ exposure

## Results

Autoradiographs of mature *Ipomoea* leaf discs indicated that radioactivity associated with photosynthetically produced $^{14}$C-assimilates, or from exogenously supplied [$^{14}$C]sucrose, accumulated within the minor veins. A $^{14}CO_2$ pulse-chase experiment was conducted on peeled leaf discs to determine the time course of $^{14}$C-photoassimilate movement from the mesophyll into the minor veins. Figure 1 indicates that whereas label could be discerned in the veins 10 min after a 5-min pulse with $^{14}CO_2$, considerable label remained within the mesophyll tissue even after a 25-min pulse (Fig. 1 B). Using our experimental protocol, on peeled *Ipomoea* leaf discs, we found that a 120-min chase period was required before the majority of the $^{14}$C-photoassimilates had accumulated in the minor veins (Fig. 1 D). Since we wished to examine the effects of PCMBS and apoplasmic pH on the relay of these $^{14}$C-photoassimilates into the minor veins, we chose a 2-h treatment period to ensure that sufficient time had elapsed to allow movement out of the mesophyll into the minor veins.

A 15-min pretreatment with 2 mM PCMBS (pH 5.0), prior to the 5-min $^{14}CO_2$ pulse, did not prevent the accumulation of $^{14}$C-photosynthate in the minor veins of *Ipomoea* leaf discs (see Fig. 2 A, B). We should point out that this PCMBS pretreatment had no effect on the photosynthetic incorporation of $^{14}CO_2$ within these leaf discs, irrespective of the pH value employed at the pretreatment. However, the accumulation of $^{14}$C-photosynthate in the minor veins was either almost, or completely, prevented by pH 9 treatment of the discs (Fig. 2 C, D), although this pretreatment had no effect on the photosynthetic incorporation of label or on its subsequent partitioning into sucrose (Table 1).

Uptake of exogenous [$^{14}$C]sucrose into peeled *Ipomoea* leaf discs that were bathed in a solution buffered at pH 5.0 exhibited a conventional kinetic profile that indicated the combined operation of a saturable and a first-order kinetic system (Fig. 3).

**Table 1.** Influence of bathing medium pH on the distribution of $^{14}C$-photosynthate in peeled source-leaf discs of *Ipomoea tricolor*. Leaf discs were labelled, for 5 min, with $^{14}CO_2$ then transferred to an efflux bathing medium at pH 5 or pH 9 for a further 15 or 120 min period, prior to extraction and analysis of labelled products. The values are means ± s.e.

| | Efflux period | | | |
|---|---|---|---|---|
| | 15 min | | 120 min | |
| Bathing medium pH value | 5 | 9 | 5 | 9 |
| Total $^{14}C$ fixed per disc (Bq) | 375 ±51 | 289 ±72 | 331 ±62 | 308 ±23 |
| Distribution of $^{14}C$-photoassimilates (%) | | | | |
| Neutral fraction | 45.3± 3.9 | 31.5± 3.5 | 50.2± 2.1 | 40.8±4.1 |
| Sucrose | 34.0± 3.1 | 27.1± 0.9 | 28.5± 2.1 | 25.0±1.2 |
| Hexoses | 5.6± 1.7 | 4.3± 0.1 | 14.4± 0.1 | 9.6±2.3 |
| Basic fraction | 17.7± 1.4 | 23.8± 1.9 | 11.5± 1.3 | 9.4±0.3 |
| Acidic fraction | 13.5± 1.3 | 15.4± 0.1 | 16.5± 0.8 | 16.9±0.9 |
| Ethanol-insoluble | 22.6± 1.1 | 27.0± 0.5 | 17.3± 0.7 | 24.4±0.7 |
| $^{14}C$ effluxed from discs | 1.1± 0.2 | 2.4± 0.9 | 4.5± 0.9 | 8.5±3.0 |

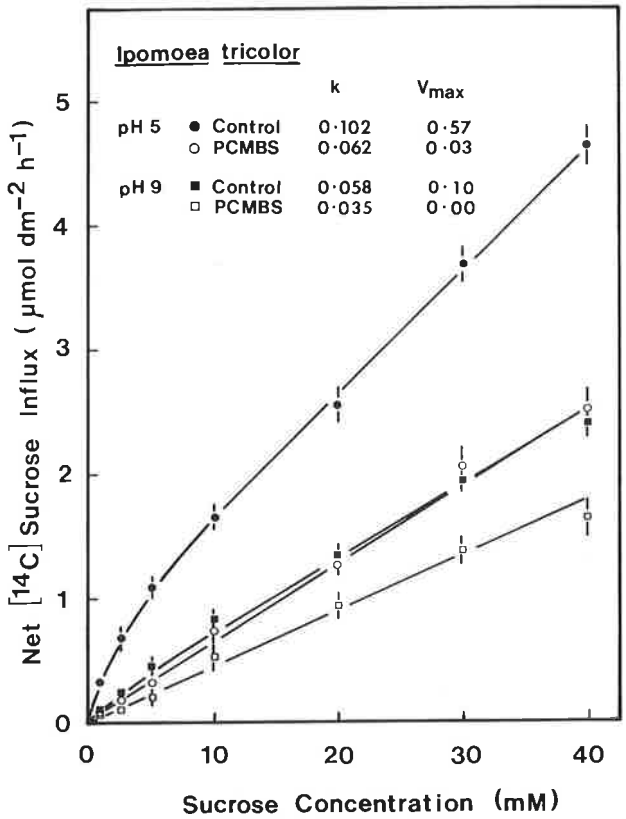


**Fig. 3.** Effect of a 15-min pretreatment with 2 mM PCMBS on the kinetic profiles of [$^{14}C$]sucrose influx at pH 5.0 or pH 9.0 in peeled source-leaf discs of *Ipomoea tricolor Cav.*

Autoradiography of these pH 5.0-treated leaf discs showed that after a 30-min labelling period, with 2.5 mM [$^{14}C$]sucrose being supplied to the apoplasm, much of the radioactivity had accumulated in the minor and major veins (Fig. 4A). However, in most cases, radioactivity could also be detected in the mesophyll tissue. A pretreatment with 2 mM PCMBS, at pH 5.0, inhibited both the saturable and the first-order kinetic systems, with the saturable system displaying the greater sensitivity, being 95% inhibited as compared to the 39% inhibition observed for the first-order kinetic system (Fig. 3). This PCMBS-mediated reduction in [$^{14}C$]sucrose uptake into the *Ipomoea* leaf discs resulted in the expected overall reduction in radioactivity discernible by autoradiography (see Fig. 4A, B). Since PCMBS pretreatment, at pH 5.0, did not prevent the relay, from the mesophyll into the phloem, of photosynthetically produced $^{14}C$-assimilates, we can extract little information concerning the site of [$^{14}C$]sucrose uptake based on the autoradiographs presented in Fig. 4B.

Treatment of peeled *Ipomoea* leaf discs with a medium buffered at pH 9.0 resulted in a substantial reduction in [$^{14}C$]sucrose uptake. Using the kinetic parameters obtained at pH 5.0 as a comparison, the saturable and first-order kinetic components were inhibited at pH 9.0 by 82% and 43%, respectively (see Fig. 3). Autoradiographs of pH 9.0-treated discs that were bathed in 2.5 mM [$^{14}C$]sucrose for 30 min indicated that much of the [$^{14}C$]sucrose had accumulated in the minor veins (Fig. 4C). Because pH 9.0 treatment prevented the relay of photosynthetically produced $^{14}C$-assimilates between the mesophyll and the minor veins (see Fig. 2C), the radioactivity present in the minor veins of pH 9.0-treated leaf discs must represent uptake of exogenous [$^{14}C$]sucrose from the apoplasm directly into the cells of the minor veins. This would indicate that the difference between the [$^{14}C$]sucrose kinetic curves obtained under pH 5.0

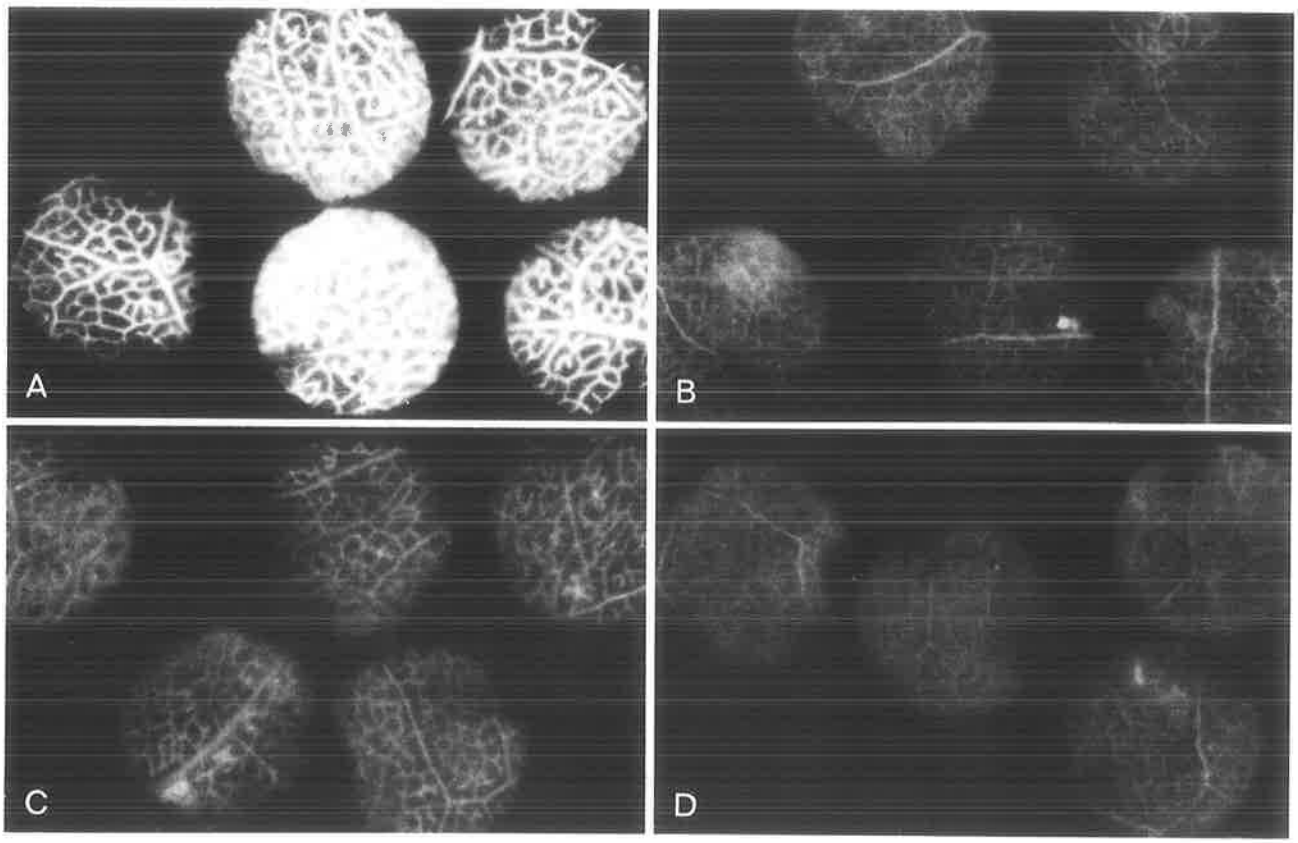


**Fig. 4A–D.** Influence of bathing medium pH and PCMBS treatment on the distribution of exogenously supplied [$^{14}$C]sucrose in discs from peeled source leaves of *Ipomoea tricolor*. Discs were pretreated (4 h) in bathing medium buffered at pH 5.0 (**A, B**) or pH 9.0 (**C, D**) prior to the introduction of 2.5 mM [$^{14}$C]sucrose for 30 min. Discs in **B** and **D** were pretreated for 15 min in 2 mM PCMBS and then 15 min in 2 mM $CaCl_2$ before the [$^{14}$C]sucrose was introduced

and 9.0 mainly reflects sucrose uptake by cells of the mesophyll.

Pretreatment of leaf discs with 2 mM PCMBS at pH 9.0 resulted in a further inhibition of [$^{14}$C]sucrose influx, with the saturable component being completely abolished and the first-order kinetic component being inhibited by 66% or 40%, compared with the respective controls (−PCMBS) conducted at either pH 5.0 or 9.0. Autoradiographs obtained from leaf discs treated with PCMBS at pH 9.0 indicated that radioactivity still appeared in the minor veins, but at a much reduced level (cf. Fig. 4A, C, D).

Experiments were also performed using mesophyll cells isolated from *Ipomoea* source leaves. The kinetic curve for [$^{14}$C]sucrose influx into isolated mesophyll cells suspended in a pH 5.0 buffered medium contained the same saturable and first-order kinetic components as present in peeled leaf discs (Fig. 5). A comparison between uptake into mesophyll cells and leaf discs (Fig. 5; ● and ◆, respectively), normalized on a chlorophyll basis, indicated that the isolated mesophyll cells could account for approx. 75% of the total uptake into peeled discs. Furthermore, [$^{14}$C]sucrose uptake into these isolated mesophyll cells displayed the same basic sensitivity to PCMBS and alkaline pH treatment as observed for leaf discs (see Figs. 3, 5); e.g. in comparison with the kinetic parameters obtained at pH 5, the saturable components that were measured at pH 9.0, using isolated mesophyll cells and leaf discs, were inhibited by 75 and 82%, respectively. A similar correlation was observed for the pH 9.0 inhibition on the first-order kinetic component; here the isolated mesophyll cells exhibited a 50% inhibition, while the inhibition for leaf discs was 43%. These results support our contention that a substantial part of the [$^{14}$C]sucrose uptake into leaf discs results from transport across the plasma membrane of the mesophyll (see also Maynard and Lucas 1982; Wilson et al. 1985).

## Discussion

The data presented here for *Ipomoea* source leaves indicate that the effects of treatments with PCMBS

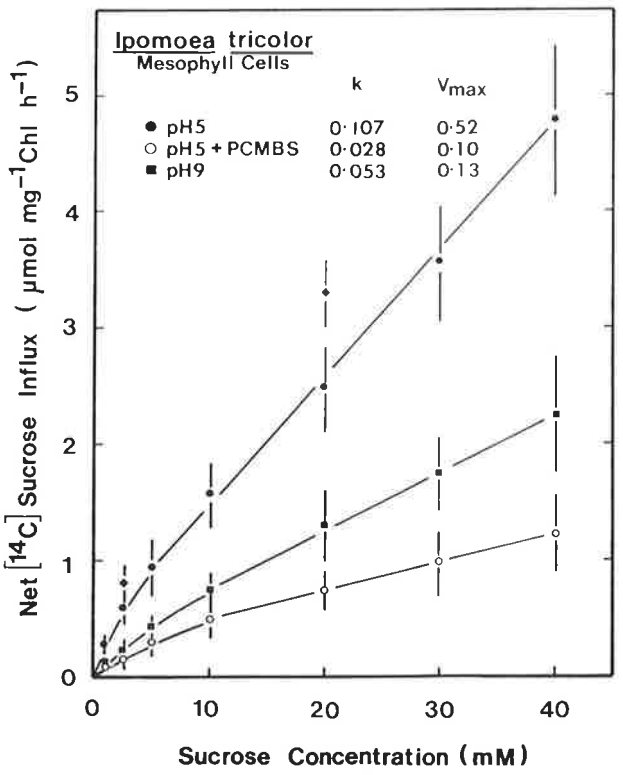


**Fig. 5.** Effect of the pH of the bathing medium and of PCMBS treatment on the kinetic profiles for [$^{14}$C]sucrose influx into enzymatically isolated mesophyll cells obtained from source leaves of *Ipomoea tricolor*. ♦ = Influx into undigested, peeled source-leaf discs at the indicated sucrose concentration

and alkaline pH on net sucrose uptake by leaf tissues are not exerted solely on phloem tissues. The image obtained of a predominantly mesophyll distribution of photosynthetically derived label in the *Ipomoea* leaf symplasm, following alkaline pH treatment, is very similar to the image obtained with Lucifer Yellow in similarly treated source leaves (Madore et al. 1986). The effect of alkaline pH on sucrose uptake is usually attributed to a reduction in sucrose-proton co-transport by the minor veins at high pH (Giaquinta 1983; Turgeon 1984). However, the data shown here for restriction of movement of photosynthetically derived solutes, taken together with those shown previously for Lucifer Yellow movement, point to an alternative possibility, namely, that the symplasmic relay of solutes from the mesophyll to the minor veins can be disrupted by treatment with an alkaline pH.

It will be very important to determine both the exact site at which this disruption occurs and the underlying mechanism responsible for this blockage in symplasmic continuity. The *Ipomoea* leaf was chosen for these studies because the minor veins have a very simple structure (see Fig. 2a, b, d in Madore et al. 1986). In these minor veins, the bundle-sheath cells are in direct contact with companion cells. Thus, if an apoplasmic transfer of sucrose is involved in "phloem loading", it would, most logically, occur at this bundle sheath-companion cell interface. If this were the case, the location of the blockage to sucrose movement would have to be at the boundary between the cells of the mesophyll and bundle sheath. Sucrose that may be lost (through leakage) from these neighboring mesophyll cells would have to diffuse through the apoplasm to enter the putative phloem-loading site at the sieve-element-companion-cell complex. The faint veination pattern seen in some of the autoradiographs obtained from discs treated at pH 9.0 may reflect the transfer of radioactivity via this pathway (see Fig. 2D).

Our current understanding of symplasmic solute movement indicates that it is regulated at the level of the plasmodesmata (Erwee and Goodwin 1983; 1984). The actual mechanisms controlling solute flux through plasmodesmata are not known but modulation of intracellular $Ca^{2+}$ levels is thought to be involved (Erwee and Goodwin 1983; 1984). It has been demonstrated that intracellular $Ca^{2+}$ levels may regulate the phosphorylation, and therefore the activity, of plasma membrane ATPases (Zocchi et al. 1983). As ATPase activity is often found associated with plasmodesmata (Belitser et al. 1982), it may be that the disruption of ATPase activity results in the inhibition of symplasmic solute movement seen at alkaline pH. In addition, the regulation of the activity of (1 − > 3)-β-D-glucan synthase by $Ca^{2+}$ (Kauss et al. 1983; Morrow and Lucas 1986) indicates that callose deposition in plasmodesmata, as well as in sieve tubes, may also be under the control of similar types of phosphorylation events. The recent demonstration that plant microsomal membranes show an inositol-1,4,5-trisphosphate-dependent release of $Ca^{2+}$ (Drobak and Ferguson 1985) indicates that the phosphoinositide signaling system that is involved in the control of cytosolic $Ca^{2+}$ levels and protein phosphorylation in animal tissues (Berridge 1984) may also be operative in plant tissues. In this context, it is interesting that lithium, a known inhibitor of that signaling system (Berridge 1984), also prevents the development of sugar-retrieval systems in leaf discs following their excision (Carlier and Thellier 1979).

Finally, it would appear from this and earlier studies that a substantial proportion of the label that appears in the minor veins following an exogenous [$^{14}$C]sucrose feeding may actually represent sucrose that was retrieved, not by the veins them-

selves, but by the mesophyll tissue (see also Leger et al. 1982; Lemoine et al. 1984; Wilson et al. 1985; Van Bel et al. 1986). Our studies conducted at pH 9.0 are important in this context, in that they establish that the cells of the minor vein can actually take up exogenously supplied [$^{14}$C]sucrose (see Fig. 4C). The question that remains is whether or not this uptake by the veins represents the true mechanism by which sucrose is accumulated (loaded) into the phloem, or whether it is the retrieval mechanism proposed to be a ubiquitous feature of all cell-types within the source leaf (Maynard and Lucas 1982). Our kinetic experiments indicate that this uptake by the minor veins occurs predominantly by the first-order kinetic mechanism, a result which is in agreement with studies on *Allium cepa* (Wilson et al. 1985) and *Commelina benghalensis* (Van Bel et al. 1986). Since a biophysical-mechanistic characterization of this first-order kinetic system is lacking, it would appear to be an appropriate target for future research.

This work was supported by National Science Foundation grant PCM 83-15408 to W.J.L. and a Natural Sciences and Engineering Research Council (Canada) Postdoctoral Fellowship to M.A.M.

## References

Belitser, N.V., Zaalishvili, G.V., Sytnianskaja, N.P. (1982) $Ca^{2+}$ binding sites and $Ca^{2+}$-ATPase activity in barley root tip cells. Protoplasma **111**, 63–78

Berridge, M.J. (1984) Inositol trisphosphate and diacylglycerol as second messengers. Biochem. J. **220**, 345–360

Carlier, G., Thellier, M. (1979) Lithium-perturbation of the induction of a methyl-glucose transport during aging of foliar leaf disks of *Pelargonium zonale* (L.) Aiton. Physiol. Vég. **17**, 13–26

Drobak, B.K., Ferguson, I.B. (1985) Release of $Ca^{2+}$ from plant hypocotyl microsomes by inositol-1,4,5-trisphosphate. Biochem. Biophys. Res. Commun. **130**, 1241–1246

Erwee, M.G., Goodwin, P.B. (1983) Characterization of the *Egeria densa* Planch. leaf symplast. Inhibition of the intercellular movement of fluorescent probes by group II ions. Planta **158**, 320–328

Erwee, M.G., Goodwin, P.B. (1984) Characterization of the *Egeria densa* leaf symplast: Response to plasmolysis, deplasmolysis and to aromatic amino acids. Protoplasma **122**, 162–168

Erwee, M.G., Goodwin, P.B., Van Bel, A.J.E. (1985) Cell-cell communication in the leaves of *Commelina cyanea* and other plants. Plant Cell Environ. **8**, 173–178

Fondy, B.R., Geiger, D.R. (1977) Sugar selectivity and other characteristics of phloem loading in *Beta vulgaris* L. Plant Physiol. **59**, 953–960

Giaquinta, R.T. (1977) Phloem loading of sucrose. pH dependence and selectivity. Plant Physiol. **59**, 750–753

Giaquinta, R.T. (1983) Phloem loading of sucrose. Annu. Rev. Plant Physiol. **34**, 347–387

Grusak, M.A., Lucas, W.J. (1984) Recovery of cold-inhibited phloem translocation in sugar beet. I. Experimental analysis of an existing mathematical recovery model. J. Exp. Bot. **35**, 389–402

Kauss, H., Kohle, H., Jablick, W. (1983) Proteolytic activation and stimulation by $Ca^{2+}$ of glucan synthase from soybean cells. FEBS Lett. **158**, 84–88

Leger, A., Delrot, S., Bonnemain, J.-L. (1982) Properties of sugar uptake by wheat leaf fragments: effects of ageing and pH dependence. Physiol. Vég. **20**, 651–659

Lemoine, R., Delrot, S., Auger, E. (1984) Development of pH sensitivity of sucrose uptake during ageing of *Vicia faba* leaf discs. Physiol. Plant. **61**, 571–576

Lucas, W.J. (1985) Phloem-loading: A metaphysical phenomenon? In: Regulation of carbon partitioning in photosynthetic tissue, pp. 254–271, Heath, R.L., Preiss, J., eds. American Society of Plant Physiologists, Rockville, Md., USA

Lucas, W.J., Madore, M.A. (1987) Recent advances in sugar transport. In: The biochemistry of plants, a comprehensive treatise, vol. 12: Carbohydrates, Preiss, J., ed. Academic Press, New York (in press)

Madore, M.A., Grodzinski, B. (1984) Effects of oxygen concentration on $^{14}$C-photoassimilate transport from leaves of *Salvia splendens* L. Plant Physiol. **76**, 782–786

Madore, M.A., Oross, J.W., Lucas, W.J. (1986) Symplastic transport in *Ipomoea tricolor* source leaves: demonstration of functional symplastic connections from mesophyll to minor veins by a novel dye tracer method. Plant Physiol. **82**, 432–442

Madore, M.A., Webb, J.A. (1981) Leaf free space analysis and vein loading in *Cucurbita pepo*. Can. J. Bot. **59**, 2550–2557

Madore, M.A., Webb, J.A. (1982) Stachyose synthesis in isolated mesophyll cells of *Cucurbita pepo*. Can. J. Bot. **60**, 126–130

Maynard, J.W., Lucas, W.J. (1982) Sucrose and glucose uptake into *Beta vulgaris* leaf tissues. A case for general (apoplastic) retrieval systems. Plant Physiol. **70**, 1436–1443

Morrow, D.L., Lucas, W.J. (1986) (1 -> 3)-$\beta$-D-Glucan synthase from sugar beet. I. Isolation and solubilization. Plant Physiol. **81**, 171–176

Turgeon, R. (1984) Efflux of sucrose from minor veins of tobacco leaves. Planta **161**, 120–128

Van Bel, A.J.E., Ammerlaan, A., Blaauw-Jansen, G. (1986) Preferential accumulation by mesophyll cells at low and high exogenous amino acid and sugar concentrations in *Commelina benghalensis* L. leaves. J. Exp. Bot. **37**, 1899–1910

Wilson, C., Oross, J.W., Lucas, W.J. (1985) Sugar uptake into *Allium cepa* leaf tissue: an integrated approach. Planta **164**, 227–240

Zocchi, G., Rogers, S.A., Hanson, J.B. (1983) Inhibition of proton pumping in corn roots is associated with increased phosphorylation of membrane proteins. Plant Sci. Lett. **31**, 215–221

Received 2 September 1986; accepted 13 February 1987

Plant Physiol. (1987) 84, 565–567
0032-0889/87/84/0565/03/01.00/0

*Communication*

# (1→3)-β-D-Glucan Synthase from Sugar Beet[1]

## II. PRODUCT INHIBITION BY UDP

Received for publication Received for publication January 27, 1987

DAVID L. MORROW AND WILLIAM J. LUCAS*
*Department of Botany, University of California, Davis, California 95616*

### ABSTRACT

**The mode of inhibition of UDP, one of the products of the reaction catalyzed by (1→3)-β-D-glucan synthase in sugar beet (*Beta vulgaris* L.) was investigated. In the absence of added UDP, the enzyme, in the presence of $Ca^{2+}$, $Mg^{2+}$, and cellobiose, exhibited Michaelis-Menten kinetics and had an apparent $K_m$ of 260 micromolar for UDP-glucose. Complex effects on the kinetics of the (1→3)-β-D-glucan synthase were observed in the presence of UDP. At high UDP-glucose concentrations, *i.e.* greater than the apparent $K_m$, UDP behaved as a competitive inhibitor with an apparent $K_i$ of 80 micromolar. However, at low UDP-glucose concentrations, reciprocal plots of enzyme activity *versus* substrate concentration deviated sharply from linearity. This unusual effect of UDP is similar to that reported for fungal (1→3)-β-D-glucan synthase. However, papulacandin B, a potent inhibitor of this fungal enzyme, had no effect on the plant (1→3)-β-D-glucan synthase isolated from sugar beet petioles. The inhibitory effect of UDP was also compared with other known inhibitors of glucan synthases.**

Callose, a noncellulosic component of primary cell walls, is ubiquitous in higher plants and is unusual for a cell wall polymer in that it can be deposited very rapidly and, in certain cases, reversibly (5). It has been implicated in the control of symplastic transport (4), the geotropic response (8), and in plant defense (9). Callose is composed primarily of (1→3)-β-D-glucan and is synthesized by a (1→3)-β-D-glucan synthase (EC 2.4.1.34), localized on the plasma membrane (2, 5). The enzyme utilizes UDP-glucose and (1→3)-β-D-glucan as substrates and is activated by β-glucosides and divalent cations (1, 12). The enzyme is under strict regulation; it is normally latent and can be activated within minutes following perturbation of plant tissue, *e.g.* in response to wounding.

The regulation of callose synthesis is an area of current interest (1, 9). One possible mechanism for regulating β-glucan synthase activity is by product inhibition. Previous studies have demonstrated that UDP, one of the products of callose synthesis, is an effective inhibitor of the reaction (7, 12). There is, however, some controversy as to the mode of inhibition by UDP. Haass *et al.* (7) reported that UDP acts as a noncompetitive inhibitor of β-glucan synthase isolated from cultured tobacco callus. The reaction products were reported to be both (1→3)-β- and (1→4)-β-D-glucan. This mode of inhibition contrasts with results from studies on fungal synthases, where inhibition by UDP has been reported to be competitive in nature (13).

In a previous paper, we reported on a highly active (1→3)-β-D-glucan synthase isolated from a membrane fraction obtained from sugar beet petioles (12). In subsequent kinetic analyses, we found that the enzyme exhibited complex kinetics in the presence of the product inhibitor UDP; at high substrate concentrations, UDP was competitive with respect to UDP-glucose while at low substrate concentrations UDP displayed anomalous inhibitory effects. We now report on these results and on the effect of other glucan synthase inhibitors on this sugar beet enzyme.

## MATERIALS AND METHODS

**Chemicals.** UDP-[U-$^{14}$C]glucose (7.4–8.1 × $10^9$ Bq/mmol; in ethanol:water, 2:8), obtained from ICN Radiochemicals (Irvine, CA), was dried under a stream of $N_2$ gas and redissolved in water. Papulacandin B was a generous gift from Ciba-Geigy (Basel, Switzerland). Other chemicals were purchased from Sigma Chemical Co. (St. Louis, MO), unless otherwise indicated.

**Plant Material.** Sugar beets (*Beta vulgaris* L. var SSBN1, USH 11, Lot 82312) were grown in a controlled environment chamber as described previously by Grusak and Lucas (6). Seeds were planted in a sterilized soil mixture of vermiculite, peat, and sand (2:1:1). Plants were grown under a 16 h photoperiod (265 μmol $m^{-2}$ $s^{-1}$ PAR), daily maximum and minimum temperatures of 27 and 17°C, respectively, and 60/90% RH. Petiolar tissue was selected from plants 28 to 30 d old.

**Preparation of Membrane Fraction.** Freshly excised petioles (10 g fresh weight) were homogenized with a Polytron homogenizer in 20 ml of 50 mM Tes, 5 mM EGTA, 20 mM β-mercaptoethanol, 0.5 mM PMSF,[2] 0.1 mM TLCK, and 0.01 mM leupeptin, adjusted to pH 7.5 with 1 N KOH. The homogenate was filtered through eight layers of wetted cheesecloth, layered over a 60% (w/v) sucrose cushion, and centrifuged at 6000*g* for 20 min. The membrane fraction banding at the buffer-sucrose interface was removed and suspended in 10 ml of 10 mM Tes, 1 mM EGTA, adjusted to pH 7.5 with 1 N KOH, and recentrifuged at 8000*g* for 10 min. The sedimented pellet was resuspended in 1 ml of 50 mM Tes-KOH (pH 7.5). This membrane suspension was used for assaying (1→3)-β-D-glucan synthase activity. Protein was determined by the method of Markwell *et al.* (10) using BSA as a standard.

**Assay of (1→3)-β-D-Glucan Synthase Activity.** Enzyme activity was determined, using a 10 min stopped reaction, as the rate of transfer of glucosyl residues from UDP-glucose to an ethanol-insoluble glucan product that we previously identified as (1→3)-β-D-glucan (12). The assay mixture contained UDP-[U-$^{14}$C]glu-

[1] Supported by National Science Foundation Grant 83-15408 to W. J. L.

[2] Abbreviations: PMSF, phenylmethylsulfonyl fluoride; DCB, 2,6-dichlorobenzonitrile; TLCK, Nα-*p*-tosyl-L-lysine chloromethyl ketone.

cose (0.1–0.5 mM, 83–200 Bq/nmol), 10 mM Tes (pH 7.5), 10 mM cellobiose, 5 mM $CaCl_2$, 5 mM $MgCl_2$, 0.1% (w/v) BSA, 0.01% (w/v) digitonin, and 50 μl (10 μg protein) of the suspended membrane preparation in a total volume of 200 μl. The reaction was initiated by the addition of enzyme and allowed to proceed for 10 min at 30°C, after which 4 ml cold 66% (v/v) ethanol was added, stopping the reaction and precipitating β-glucans. We then added 10 mg of α-cellulose to the reaction vessel to facilitate precipitation of the ethanol-insoluble glucan. Each sample was mixed thoroughly, stored at −20°C for 20 min, and then filtered through a Whatman GF/A glass fiber filter under suction. The filter was washed three times with 66% ethanol, dried, transferred to a glass vial containing 10 ml of Beckman Ready-Solv liquid scintillation cocktail, and counted on a Beckman LS 9800 liquid scintillation counter.

## RESULTS AND DISCUSSION

### (1→3)-β-D-Glucan synthase catalyzes the bisubstrate reaction

$$\text{UDP-glucose} + (1\rightarrow3)\text{-}\beta\text{-D-glucan}_n \rightarrow \text{UDP} + (1\rightarrow3)\text{-}\beta\text{-D-glucan}_{n+1}$$

in which the substrate (1→3)-β-D-glucan is also a product. Previous studies on enzymes from higher plants and fungi have shown that UDP-glucose is the preferred glucosyl donor (2, 5, and references therein) and that UDP inhibits the reaction (7, 12, 13, 15). We have compared the relative effectiveness of UDP as an inhibitor of the sugar beet enzyme with other inhibitors of glucan synthases, including glycogen synthase and cellulose synthase (Table I). With the exception of Sirofluor, UDP was the most effective inhibitor of the glucan synthase enzyme, especially over the concentration range tested, 0.1–10 mM. DCB (Aldrich Chemical Co., Inc.), an inhibitor of cellulose synthesis, caused a slight stimulation of the sugar beet petiole (1→3)-β-D-glucan synthase. Read *et al.* (14) have recently reported that DCB binds to an 18,000 mol wt polypeptide, and suggest the latter may be a regulatory protein involved in cellulose synthesis. The role, if any, of this protein in the regulation of callose synthesis remains to be investigated. Papulacandin B, a potent inhibitor of fungal (1→3)-β-D-glucan synthases (13), had no effect on the sugar beet enzyme. Nor did 2-deoxy-D-glucose, an *in vivo* inhibitor of callose synthesis (8) that presumably does not act directly on the synthase, but rather via a metabolized product, possibly UDP-2-deoxy-glucose.

Coumarin, 2′-deoxyguanosine, and caffeine, all known inhibitors of glycogen synthesis, were slightly inhibitory. δ-Gluconolactone (10 mM), a potent inhibitor of glycosidases and glycogen synthase (11), was an effective inhibitor of the sugar beet (1→3)-β-D-glucan synthase. This inhibitor structurally resembles the proposed oxonium ion transition state intermediate in glycosyl transferase reactions involving the C-1 carbon (11). This mode of inhibition seems reasonable in the case of callose synthesis, since the transfer of the glucosyl moiety from UDP-glucose to (1→3)-β-D-glucan requires the inversion of the anomeric carbon from the α to the β configuration.

Table I. *Effect of Glucan Synthase Inhibitors on (1→3)-β-D-Glucan Synthase Activity*

The reaction mixture contained 0.1 mM UDP-[U-$^{14}$C]glucose (200 Bq/nmol), 10 mM cellobiose, 5 mM $CaCl_2$, 5 mM $MgCl_2$, 0.1% BSA, 0.01% digitonin, and 50 μl (10 μg protein) of suspended membranes. Values represent the mean from three experiments.

| Inhibitor | Concentration | Relative Activity |
|---|---|---|
| | mM | % |
| None | | 100[a] |
| DCB | 0.1 | 115 |
| Papulacandin B | 0.05 | 104 |
| 2-Deoxy-D-glucose | 1.0 | 101 |
| Coumarin | 1.0 | 84 |
| 2′-Deoxyguanosine | 1.0 | 73 |
| Caffeine | 10.0 | 72 |
| δ-Gluconolactone | 10.0 | 40 |
| UDP | 1.0 | 38 |
| Sirofluor | 1.0 | 5 |

[a] 100% relative activity = 1420 nmol $h^{-1}$ $mg^{-1}$ protein.

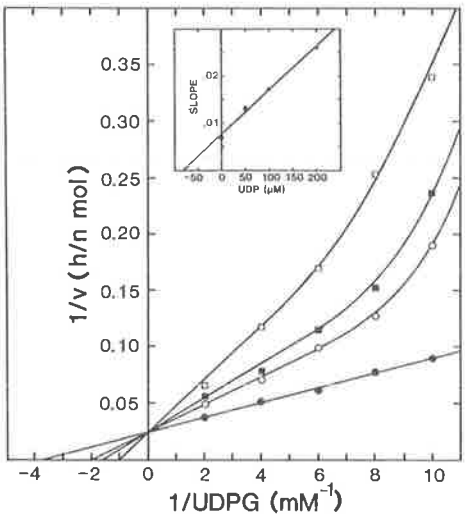


FIG. 1. Product inhibition of (1→3)-β-D-glucan synthase by UDP (double reciprocal plot). Assay mixture (200 μl) contained 50 mM Tes (pH 7.5), 10 mM cellobiose, 5 mM $CaCl_2$, 5 mM $MgCl_2$, 0.1% BSA, 0.01% digitonin, 50 μl (10 μg protein) of suspended membranes, and UDP-[U-$^{14}$C]glucose at the indicated concentration. UDP was included at 0 (●), 50 (○), 100 (■), and 200 (□) μM. Inset, secondary plot of slopes of double reciprocal plot *versus* UDP concentration.

Kinetic experiments were conducted to further investigate the mechanism(s) by which UDP inhibits the activity of the (1→3)-β-D-glucan synthase. For these kinetic experiments, standard assay conditions (including the activators $Ca^{2+}$, $Mg^{2+}$, and cellobiose) were used with varying UDP-glucose and UDP concentrations. A double reciprocal plot of enzyme activity *versus* UDP-glucose concentration is shown in Figure 1. In the absence of added UDP, the reciprocal plot is linear and the apparent $K_m$ for the enzyme was 260 μM. This value for the $K_m$ is considerably lower than those reported for other higher plant (1→3)-β-D-glucan synthases, which range from 1.74 to 5.0 mM (2). However, Dugger and Palmer (3) have described, from *in vitro* studies of intact cotton fibers, a glucan synthase with a $K_m$ of 132 μM, and Delmer *et al.* (1), also working with cotton fibers, have reported a $K_m$ of 200 to 300 μM for the enzyme extracted from tissue and assayed in the presence of cellobiose and divalent cations. Apparently, the $K_m$ of the enzyme is strongly affected by the presence of these compounds.

The addition of UDP had complex effects on the kinetics of the sugar beet (1→3)-β-D-glucan synthase (Fig. 1). At concentrations of UDP-glucose greater that the apparent $K_m$ (260 μM), UDP behaved as a competitive inhibitor, increasing the $K_m$ with no effect on the $V_{max}$. On the other hand, at low concentrations of UDP-glucose, the reciprocal plots deviated sharply from linearity. This effect became more pronounced with increasing concentrations of UDP. Tangents extrapolated from points along these portions of the curves, at a given concentration of UDP-glucose, do not intersect at a common point, suggesting mixed product/dead end inhibition. A replot of the slopes of the linear portions of the reciprocal plots *versus* UDP concentration was linear (Fig. 1); from this analysis the apparent inhibition constant

($K_i$) for UDP was calculated to be 80 μM.

These results contrast with those of Haass *et al.* (7), who reported UDP to be noncompetitive with UDP-glucose for β-glucan synthase from cultured tobacco callus. However, they used only one concentration of UDP (1 mM), which may not have been sufficient to clearly distinguish a pattern of inhibition. It should be noted that in the sugar beet system, 1 mM UDP is more than sufficient to demonstrate deviation from linearity in double reciprocal plots. Our results on the kinetics of UDP inhibition compare favorably with those of Quigley and Selitrennikoff (13) who reported on the (1→3)-β-D-glucan synthase from *Neurospora crassa*. Although this suggests a similar enzymic mechanism for (1→3)-β-D-glucan synthesis in higher plants and fungi, the lack of an effect of papulacandin B on the sugar beet enzyme does not support this hypothesis.

## LITERATURE CITED


1. DELMER DP, M THELEN, MPF MARSDEN 1984 Regulatory mechanisms for the synthesis of β-glucans in plants. *In* WM Dugger, S Bartnicki, eds, Structure, Function, and Biosynthesis of Plant Cell Walls. American Society of Plant Physiologists, Rockville, MD, pp 133–149
2. DIXON RA 1985 β-(1→3)-Linked glucans from higher plants. *In* J Dey, RA Dixon, eds, Biochemistry of Storage Carbohydrates in Green Plants. Academic Press, London, pp 229–264
3. DUGGER WM, RL PALMER 1986 Incorporation of UDP-Glucose into cell wall glucans and lipids by intact cotton fibers. Plant Physiol 81: 464–470
4. ESCHRICH W 1975 Sealing systems in phloem. *In* MH Zimmermann, JA Milburn, eds, Transport in Plants. Encyclopedia of Plant Physiology, New Series, Vol 1. Springer-Verlag, Berlin, pp 39–56
5. FINCHER GB, BA STONE 1981 Metabolism of noncelluosic polysaccharides. *In* W Tanner, FA Loewus, eds, Plant Carbohydrates II: Extracellular Carbohydrates. Encyclopedia of Plant Physiology, New Series, Vol. 13 B. Springer-Verlag, Berlin, pp 68–132
6. GRUSAK MA, WJ LUCAS 1984 Recovery of cold-inhibited phloem translocation in sugar beet. I. Experimental analysis of an existing mathematical recovery model. J Exp Bot 35: 389–402
7. HAASS D, G HACKSPACHER, G FRANZ 1985 Orientation of cell wall β-glucan synthases in plasma membrane vesicles. Plant Sci 41: 1–9
8. JAFFE MJ, AC LEOPOLD 1984 Callose deposition during gravitropism of *Zea mays* and *Pisum sativum* and its inhibition by 2-deoxy-D-glucose. Planta 161: 20–26
9. KAUSS H 1985 Callose biosynthesis as a $Ca^{2+}$-regulated process and possible relations to the induction of other metabolic changes. J Cell Sci Suppl 2: 89–103
10. MARKWELL MAK, SM HAAS, LL BIEBER, NE TOLBERT 1978 A modification of the Lowry procedure to simplify protein determination in membrane and lipoprotein samples. Anal Biochem 87: 206–210
11. MCVERRY PH, K-H KIM 1974 Purification and kinetic mechanism of rat liver glycogen synthase. Biochem 13: 3505–3511
12. MORROW DL, WJ LUCAS 1986 (1→3)-β-D-Glucan synthase from sugar beet. I. Isolation and solubilization. Plant Physiol 81: 171–176
13. QUIGLEY DR, CP SELITRENNIKOFF 1984 β-(1→3)-Glucan synthase activity of *Neurospora crassa*: kinetic analysis of negative effectors. Exp Mycol 8: 320–333
14. READ SM, M THELEN, DP DELMER 1986 Identification of polypeptides involved in cell wall β-glucan synthesis. Plant Physiol 80: S-77
15. SHEMATEK EM, JA BRATZ, E CABIB 1980 Biosynthesis of the yeast cell wall. I. Preparation and properties of β-(1→3)-glucan synthetase. J Biol Chem 255: 888–894

Plant Physiol. (1987) 84, 1088–1095
0032-0889/87/84/1088/08/$01.00/0

# Influence of Internal Sugar Levels on Apoplasmic Retrieval of Exogenous Sucrose in Source Leaf Tissue[1]

Received for publication March 10, 1987 and in revised form April 29, 1987

CLYDE WILSON AND WILLIAM J. LUCAS*
*Botany Department, University of California, Davis, California 95616*

## ABSTRACT

**Sugar levels in *Beta vulgaris* leaves were increased by heat-girdling the petiole and returning the plant to the controlled-environment chamber for 10 and 34 hours. After 10 hours, sucrose influx into the treated leaves was similar to the controls, although sucrose levels increased from 2.1 to 5.3 micromoles per milligram chlorophyll. However, after a 34-hour treatment, sucrose levels increased from 2.1 to 11.5 micromoles per milligram chlorophyll. In this instance, sucrose influx decreased relative to the untreated controls. Decreasing sugar levels by DCMU treatment resulted in a small stimulation of sucrose influx. A similar DCMU treatment applied to leaves of *Allium cepa* also resulted in an increase in sucrose influx. However, in *A. cepa* we could not attribute this increase to a lowering of sugar levels, as the kinetic profiles obtained from control leaves did not vary from each other throughout the day, despite considerable changes in sugar levels. Additionally, it appeared that sucrose uptake in onion may be set at some point and remains invariant throughout the day. Similar studies were also conducted on discs cut from mature leaves of *Spinacia oleracea* var America. Between 1 and 8 hours after the onset of the photoperiod, the sucrose content of the spinach leaves increased from 2.6 to 9.3 micromoles per milligram chlorophyll. A comparison of the kinetic profiles obtained from leaf discs, taken at these times, indicated that sucrose uptake was not influenced by these changes in internal sugar levels. The relationship between the above findings and '*trans*' inhibition of exogenous sucrose uptake is discussed. Although intermediate changes in sugar levels in sugar beet leaves did not appear to affect sucrose influx, autoradiographic studies revealed that these changes dramatically affected the partitioning of exogenously supplied [$^{14}$C]sucrose. Our results indicate that while intermediate changes in internal sugar levels have little effect on sucrose influx across the plasmalemma, they may dramatically affect partitioning between the phloem and the mesophyll vacuole.**

Phloem transport is a complex and highly regulated phenomenon which involves a variety of organelles, cell types, specialized anatomical structures, and cellular processes. An important facet of phloem transport which is in need of further study is the elucidation of the process(es) involved in the movement ('loading') of sucrose from the mesophyll into the sieve tubes. In a recent study, we proposed that this process of loading should be considered in a broader perspective than just the movement of sucrose into the sieve-element companion-cell complex (18). A working model of phloem loading must integrate not only the transport processes across the plasma membrane and tonoplast of a number of cell types, but also the biochemical and biophysical processes involved in regulating these fluxes (18).

[1] Supported by National Science Foundation Grant PCM-83-15408.

At the biochemical level, the regulatory mechanisms involved in both the partitioning of photoassimilates between the chloroplast and the cytosol, and sucrose synthesis within the cytosol is presently under intensive investigation (8, 15, 16). At the transport level, the mechanism of sugar transport across the plasmalemma has been established for some photosynthetic tissues (11). To date, it would appear that these sugars are transported into mesophyll cells via a sugar:$H^+$ cotransport mechanism at low concentrations and by a first-order kinetic process at higher concentrations. The situation at the tonoplast is less well resolved. Kaiser and Heber (9) presented data indicating that in mesophyll cells obtained from barley, sucrose transport across the tonoplast proceeds via the action of a permease. Gerhardt and Heldt (2) also concluded that sucrose transport across the tonoplast in spinach source leaves is mediated by a permease.

Little information is available concerning the regulation of sucrose transport within the tissues of the leaf. Previous workers have proposed that high internal sugar levels may inhibit sucrose influx across the plasmalemma (5, 10) possibly by a '*trans*' effect, or, if the external driver ion concentration is near saturating, by uncompetitive inhibition of sugar transport (14). Based on sugar uptake studies, putatively into the phloem of sugar beet, Giaquinta (3, 4) postulated that a *trans* effect may also operate to regulate sucrose loading into the phloem, *per se*.

The interpretation of some of these kinetic experiments is complicated because high concentrations of sucrose were used to effect the increase in internal sucrose levels, prior to conducting uptake experiments at lower sucrose concentrations. Unless the tissue was thoroughly washed after preloading treatments, the residual sucrose would change the specific activity of the uptake solution, and this would give rise to an underestimation of the true flux; *i.e.* the putative *trans* inhibition would be an artifact of the experimental design. Furthermore, kinetic data obtained using exogenously supplied $^{14}$C-sugars cannot be extrapolated to events occurring at the level of the sieve-element companion-cell complex (3, 4, 11, 18). Finally, although Komor (10) did not pretreat his *Ricinus* cotyledons with high sugar levels, he did not report using an osmoticum to standardize the osmolality of each treatment. It has recently been shown that the osmolality of the uptake solution can have a pronounced effect on the uptake kinetics of some tissues (19).

If, during the photosynthetic period, sucrose is transported across the tonoplast of mesophyll cells by a permease, then the vacuolar sucrose levels should be in near chemical potential equilibrium with the cytosol. Thus, by monitoring changes in the gross sucrose levels of the leaf, one should be able to obtain an approximate measure of the cytosolic sucrose concentration. In the present study we examined the relationship between the internal sugar levels and the uptake (retrieval) of exogenous [$^{14}$C] sucrose into leaf discs of sugar beet, onion and spinach. To this end, we manipulated the sugar levels by either supplying DCMU, or mannose, to the leaf blade through the petiole, or by means

of heat-girdling the petiole. Whereas the influx of [$^{14}$C]sucrose into the leaf exhibited little sensitivity to the internal sugar levels, our macroautoradiographic results indicated that [$^{14}$C]sucrose allocation, between the phloem and the vacuoles of the mesophyll, was influenced by changes in sugar levels. From our results, we conclude that the *in vivo* regulation of phloem loading may involve the partitioning of photoassimilates between the cytosol and vacuole such that the tonoplast and plasmodesmata might be likely targets for regulation.

## MATERIALS AND METHODS

**Plant Material.** *Allium cepa* L., cv Stockton Yellow Globe (Lagomarsino Seeds, Sacramento, CA) seeds were planted in a soil mixture containing vermiculite, peat moss, and sand (2:1:1 by volume). The plants were grown in the spring under greenhouse conditions with no supplementary light and watered daily with deionized water supplemented with $CaNO_3$. Experimental plants were 10 weeks old. *Beta vulgaris* L. (var SSBN1, USH10, Lot 3102 or USH11, Lot 82313) seeds were planted in a soil mixture described above and grown in a controlled-environment chamber under a 27°C day/17°C night temperature regime and a 16 h photoperiod (250 $\mu$mol $m^{-2}$ $s^{-1}$). Plants were watered daily and fertilized twice weekly with Hoaglands solution. The third pair of leaves (after the cotyledons) of 4-week-old sugar beet plants were used. *Spinacia oleracea* L., cv American seedlings (Burpee Seed Co., Warminster, PA) were grown under the same conditions as sugar beet, except that a 9 h photoperiod was used with 22°C day/15°C night temperatures. Experimental plants were 5 weeks old.

**Kinetic Studies.** Kinetic uptake studies were performed using the method of Maynard and Lucas (13) as modified by Wilson *et al.* (18). Briefly, for onion experiments, the fifth or sixth leaf was excised at the base, and placed on a rubber pad in a dish that contained a solution of 20 mM $CaCl_2$ and 60 mM 2-(*N*-morpholino)ethanesulfonic acid (Mes) buffer (pH 5.0). The leaf was slit longitudinally with a razor blade, and leaf discs 4 mm in diameter were cut from the region 7 to 10 cm from the base. With sugar beet and spinach, the third pair of leaves was used, and leaf discs were punched (using the system described above) from the upper one-third of the lamina.

Six leaf discs were used for each sucrose concentration, and these discs were given a 30-min preincubation on a solution containing 20 mM $CaCl_2$, 120 mM Mes (pH 5.0), and enough mannitol to adjust the osmolality to 500 mOsm for sugar beet and 200 mOsm for onion and spinach; sucrose at the concentration specified for the particular experiment was also included. Preincubation was followed by a 30-min uptake period in solution containing radioactive sucrose (D-[U-$^{14}$C]sucrose, International Chemical and Nuclear Corp., Irvine, CA). The specific activity of the uptake solution was maintained at $1.78 \times 10^7$ Bq $mmol^{-1}$. The incubation period was followed by three 7-min washes in media containing 20 mM $CaCl_2$, 60 mM Mes, and 40 mM sucrose. Leaf discs were then placed into scintillation vials containing 0.1 ml of 7% $HClO_4$, 0.1 ml of 30% $H_2O_2$ and a drop of Methyl Cellosolve (Sigma). After a 15-min digestion period, 10 ml of Beckman READY-SOLV EP scintillation mixture (Beckman Instruments) was added, and the vials were counted on a Beckman 9800 scintillation counter. Experiments were performed at 24 ± 1°C under laboratory lighting, except where noted.

**Mannose Pretreatment of Excised Leaves.** Three h into the photoperiod, the third pair of leaves was excised, at the base of the petiole, while the crown of the sugar beet plant was submerged under water. The petiole was then either placed in distilled water (control) or in 10 mM mannose, and the leaf was returned to the controlled-environment chamber. After predetermined intervals, leaf discs (4 mm diameter) were punched from the leaf and used for sugar analysis and kinetic experiments.

**Effect of DCMU on Sucrose Uptake.** A stock solution (2 mM) of DCMU (E. I. DuPont) was prepared using absolute ethanol. Two days preceding the experiment, plants were removed from the controlled-environment chamber 13 h after the start of the photoperiod, and placed in the dark for 13 h to deplete sugar and starch levels. Leaves were then excised and the petioles placed in distilled water (control) or in 20 $\mu$M DCMU. A 24-h treatment (14 h light:8 h dark:2 h light) in the controlled-environment chamber was then employed, prior to cutting leaf discs for sugar extraction and kinetic studies. Control experiments, conducted in the presence and absence of ethanol (1% v/v), showed that for all leaf types used (sugar beet, onion, and spinach) this level of ethanol had no effect on sucrose influx.

**Heat Girdling.** In order to prevent translocation out of a particular leaf, the petiole was heat-girdled; this was done at the end of the normal light period. At the beginning of the following photoperiod the kinetic properties and sugar levels were determined. Heat-girdling was accomplished by looping a U-shaped piece of Nichrome wire around the petiole at the base of the lamina; a 25 s heat pulse was used. The heated area was localized by shielding the remaining parts of the plant with asbestos sheets. The heat-girdled leaf was mechanically supported during and after the heating process. These leaves remained turgid for at least 48 h, indicating that the xylem was still functioning.

**Sugar Extraction and Starch Analysis.** Leaf tissue was sampled by punching 15 leaf discs (4 mm diameter) with a cork borer and placing these discs into a test tube. Then 0.5 ml of 80% ethanol was added, and the tube was placed in a 100°C bath for 25 to 30 s to kill the tissue. The ethanol was removed with a Pasteur pipette and collected in a second tube. An additional 0.5 ml of 80% ethanol was added to the discs. The tube was then placed in a 65 ± 5°C water bath to extract the ethanol-soluble sugars. This procedure using the 65°C bath was repeated until all the Chl was removed from the discs (usually 4 or 5 repetitions sufficed). After extraction of ethanol-soluble sugars, the discs were rinsed twice with 2.0 ml of distilled water. The ethanol-soluble extracts and rinses were combined. Then, 1 ml of distilled water was added, and the tube was placed in a water bath (100°C) for 1 h to gelatinize the starch. After the tubes were cooled, 0.5 ml of a 15 mM sodium acetate solution (pH 4.5) containing 0.5% w/v amylogucosidase (Sigma) was added and the tubes incubated at 55°C overnight. The leaf discs were stained with iodine-potassium iodide and examined under a light microscope to check for complete digestion of starch. The released glucose was analyzed with an enzymic link of hexokinase and glucose-6-phosphate dehydrogenase.

**Sugar Analysis.** Sugars were analyzed by HPLC. The chromatography was performed using a Beckman Series 344 Gradient Liquid Chromatograph equipped with a Bio-Rad HPX-87H column (7.8 mm diameter, 300 mm in length) (Bio-Rad Laboratories, Richmond, CA). The eluting peaks were detected by using an Altex Refractive Index detector and analyzed on an Altex Chromatopac C-R1B data processor. The sugars were separated using a mobile phase consisting of 0.1 N $H_2SO_4$ and a flow rate of 0.6 ml $min^{-1}$ and identified using the retention times obtained from standards. As some organic acids co-elute with sugars, it was necessary to first separate the extract into acid and neutral fractions. The ethanol-soluble extract was obtained as outlined above and fractionated by ion-exchange chromatography using DISPOSABLE POLY PREP columns (Bio-Rad Laboratories) filled to the 1 ml mark with an intermediate base anion exchange resin, Bio Rex 5, in the chloride form, 200–400 mesh. The resin columns were washed with 15 ml of distilled water before use.

The aqueous samples were prepared for fractionation by first adjusting the pH to 8 or 9 with concentrated ammonium hy-

droxide. After waiting for 10 min, the samples were passed through the resin columns, and the resin bed was washed with 2 × 1 ml of distilled water. The collected eluate contained the neutral fraction. Prior to HPLC analysis, all fractions were passed through a 0.45 μm membrane filter.

**Autoradiography.** Following a particular experimental protocol, leaf discs were rinsed briefly in distilled water and frozen in aluminum-foil cups held on dry ice. Discs were lyophilized for 18 h in a DURADRY freeze-dryer equipped with a bulk tray dryer (FTS Systems, Stone Ridge, NY) before being glued onto herbarium paper and exposed to Kodak INDUSTREX M X-ray film for 0.5 to 10 d.

## RESULTS

**Effect of Heat-Girdling on the Kinetics of Sucrose Influx.** To test whether internal sucrose levels inhibit the operation of the plasmalemma-bound sucrose carrier, we prevented translocation out of the leaf by heat-girdling the petiole at the base of the lamina. After such a treatment, the leaf remained turgid, for at least 48 h, indicating that the xylem was still functional. Heat-girdling caused an increase in the internal sugar content of the sugar beet leaf (Table I). Figure 1A illustrates the effect of an 8 h post heat-girdling period on the kinetics of sucrose uptake. Despite the increased levels of internal sugars, the kinetics of sucrose uptake of the heat-girdled and control leaves were identical. Evidently, the increased levels of sucrose (or glucose and fructose) did not influence the uptake of sucrose. Increasing the post heat-girdling period to 34 h resulted in an even greater rise in the internal levels of sucrose, glucose, and fructose (Table I). Under these conditions, both the saturable and first-order kinetic uptake systems for sucrose were reduced relative to the control (Fig. 1B). This inhibition may have been due to either an effect of internal sucrose on its influx, or to an indirect effect of the elevated glucose and fructose levels, via a perturbation of cytosolic phosphate metabolism.

**Effect of DCMU on the Kinetics of Sucrose Influx.** Since increasing internal sugar levels, *per se*, appeared to have only a limited influence on the kinetics of sucrose influx, we next investigated the effect of reduced sucrose levels on [$^{14}$C]sucrose uptake. Photosynthesis was inhibited by supplying an excised leaf with 20 μM DCMU for a 24-h period. Analysis of the ethanol-soluble extracts from the treated leaves confirmed the effectiveness of the DCMU treatment (Table II). Our analyses revealed a dramatic reduction in all sugars (sucrose, glucose, and fructose) and starch levels in these excised DCMU-treated leaves. Despite these large decreases in internal sugar levels, sucrose influx remained unaffected, or was increased slightly (Fig. 2).

The high sugar levels present in the excised control leaves (Table II) is due to the removal of the sink; *i.e.* this situation is equivalent to a heat-girdling treatment. Since, under these conditions, the fructose and glucose levels were equivalent to those found in prolonged heat-girdling experiments (*cf.* Tables I and

Table I. *Influence of Heat-Girdling on Sugar and Starch Content in Mature Leaves of B. vulgaris*

At the end of the photoperiod a U-shaped piece of Nichrome wire was looped around the base of the lamina and heated for 15 s. The heated area was localized by shielding the remaining area with asbestos sheets. The heat-girdled leaves were supported mechanically during and after the girdling process. The treated plants were returned to the controlled-environment chamber for the duration of the subsequent night period (A: 8 h) or for an additional 24 h treatment (B: 34 h total). Leaf discs were sampled 2 h into the respective light period. Data are from two experiments done in duplicate (mean ± SE).

| Treatment | Sugar Content | | | Starch |
|---|---|---|---|---|
| | Sucrose | Glucose | Fructose | |
| | *μmol mg$^{-1}$ Chl* | | | *μmol glucose equivalents mg$^{-1}$ Chl* |
| A: | | | | |
| Control | 2.1 ± 0.1 | 0.3 ± 0.1 | 0.3 ± 0.1 | 4.3 ± 1.6 |
| Heat-girdled | 5.3 ± 0.3 | 5.1 ± 0.6 | 4.9 ± 0.3 | 9.3 ± 3.2 |
| B: | | | | |
| Control | 2.1 ± 0.1 | 0.3 ± 0.1 | 0.3 ± 0.1 | 4.7 ± 0.4 |
| Heat-girdled | 11.5 ± 0.1 | 31.9 ± 0.5 | 26.7 ± 0.5 | 61.2 ± 8.5 |

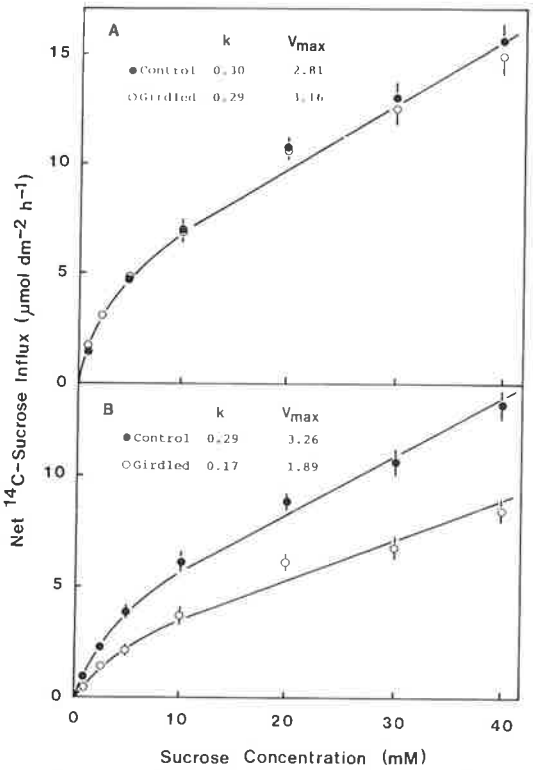


FIG. 1. Effect of heat-girdling on sucrose influx into *B. vulgaris* leaf discs. Following the heat-girdling treatment, plants were returned to the controlled-environment chamber for either the duration of the subsequent night period (A: 8 h) or a total period of 34 h (B). Kinetic studies were performed 2 h into the appropriate light period. A 30-min preincubation period in unlabeled sucrose was followed with a 30-min incubation in [$^{14}$C]sucrose solution. The points for the control (●) and heat-girdled leaves (○) represent the mean ± SE for two sets of six replicates.

Table II. *Influence of DCMU on Sugar and Starch Content in Mature Leaves of B. vulgaris*

Sugar beet leaves were excised at the base of the crown while the crown was submerged under water. The petioles of these leaves were then placed in Erlenmeyer flasks containing either distilled water (control) or 20 μM DCMU before being returned to the controlled-environment chamber for a 24-h treatment. Data are from two experiments done in duplicate (mean ± SE).

| Treatment | Sugar Content | | | Starch |
|---|---|---|---|---|
| | Sucrose | Glucose | Fructose | |
| | *μmol mg$^{-1}$ Chl* | | | *μmol glucose equivalents mg$^{-1}$ Chl* |
| Control | 5.6 ± 0.2 | 28.8 ± 3.9 | 26.6 ± 2.8 | 32.1 ± 6.6 |
| DCMU-treated | 0.9 ± 0.1 | ND[a] | ND | 2.9 ± 0.4 |

[a] ND = not detected.

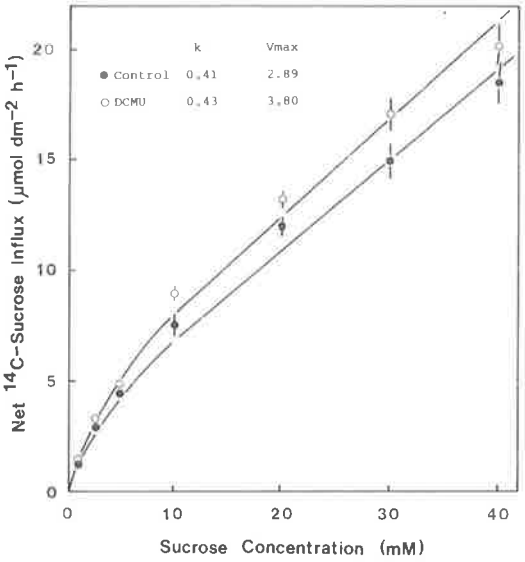


FIG. 2. Effect of DCMU pretreatment on sucrose influx in *B. vulgaris* leaf discs. Two d before the experiment, plants were removed from the controlled-environment chamber 13 h after the start of the photoperiod. They were placed in the dark for 13 h to deplete sugar and starch levels. Leaves were excised at the base of the petiole while the crown of the plants was submerged under water. Petioles were then placed into either distilled water or 20 μM DCMU before being returned to the controlled-environment chamber for a 24 h cycle consisting of 14 h light: 8 h dark: 2 h light; leaf discs were then cut for sugar extraction and kinetic studies. The points for the control (●) and the DCMU-treated leaves (○) represent the mean ± SE for two sets of six replicates.

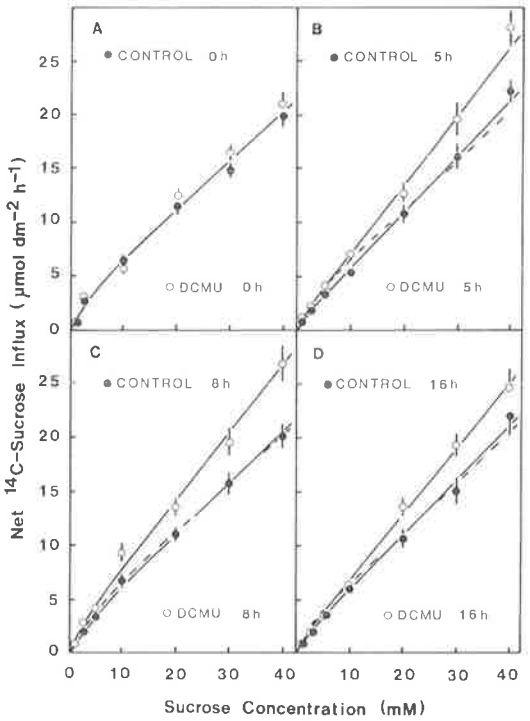


FIG. 3. Effect of DCMU pretreatment on sucrose influx into *A. cepa* leaf discs. Distilled water (control) or 20 μM DCMU was introduced into mature onion leaves (attached to the plant) via slits cut near the tops of the hollow cylindrical leaves. Solutions remained in the lacuna for 30 min and were then removed; during this period, $O_2$ was supplied by bubbling air through the solutions. This procedure was repeated with fresh solution every 3 h throughout the daylight period. Kinetic studies conducted on discs cut from these leaves were performed as in Figure 1. The uptake solutions were adjusted with mannitol to 200 mOsm. The points for the controls (●) and DCMU-treated (○) leaves represent the mean ± SE for six replicates. The dashed line represents the 0 h profile for reference.

II), the normal kinetic response observed in these controls (Fig. 2) suggests that the inhibition of sucrose influx (illustrated in Fig. 1B) may be due to the higher internal sucrose levels within the tissue. Collectively, these data obtained on heat-girdled and DCMU-treated leaves indicate that uptake of exogenously applied sucrose into sugar beet leaf discs is rather insensitive to quite large fluctuations in the internal sugar levels.

For comparison, we examined the influence of DCMU on sucrose influx in *A. cepa*. In these experiments we exploited the hollow, cylindrical architecture of the onion leaf by supplying DCMU to the leaf through a narrow slit cut near the top of the attached leaf. Plants were then analyzed for sucrose transport characteristics and carbohydrate levels at various intervals following DCMU application.

In this more physiological arrangement, with the leaves still being attached to their sinks, we found that after 5 h of DCMU treatment, sucrose uptake increased relative to the control (Fig. 3). This stimulation remained for the rest of the experimental period. By 5 h the sugar content in the DCMU-treated leaves had decreased, which suggests that sugar levels may have been affecting sucrose transport (Table III). However, a comparison of the kinetic profiles of the *control* leaves, at the predetermined time points (5, 8, and 16 h) throughout the day, with the 0 h control leaf kinetic curve, indicates a remarkable level of constancy, despite large changes in the sugar content within these same control leaves. Thus, the DCMU stimulation of sucrose uptake must be via a mechanism other than its effect on decreasing sucrose levels.

**Influence of Internal Sugar Levels on Sucrose Influx in Spinach.** Since much of our understanding regarding the regulation of sucrose synthesis is derived from studies using *Spinacia oleracea*, we included this species in the present study. In spinach, sucrose levels do not rise quickly and then remain stable throughout the day, but rather they increase continuously throughout the photoperiod (17). As with earlier experiments, spinach plants were illuminated and the kinetic curves and internal sugar levels determined at various time points. Figure 4 illustrates the kinetic profiles obtained on plants illuminated for 1 and 8 h; sucrose levels increased from 2.6 to 9.3 μmol mg $^{-1}$Chl, respectively (glucose and fructose remained at below the detection limit of our HPLC system). These data are in agreement with our experiments conducted on sugar beet and onion, and indicate that uptake of exogenously supplied sucrose is not influenced by the internal sucrose level.

**Effect of Mannose on Sucrose Influx.** Mannose has been used to decrease the cytosolic level of sucrose by altering partitioning of newly fixed carbon between the chloroplast and the cytosol (1, 6, 7). We attempted to achieve this same repartitioning in sugar beet by supplying mannose to the leaf via the petiole. As illustrated in Figure 5, this mannose pretreatment resulted in a progressive decrease in the tissue's ability to retrieve exogenously supplied sucrose. However, in contrast with reports on other leaf tissues, analysis of the ethanol-soluble extract from mannose-treated and control leaves showed that mannose did not cause a reduction in the level of sucrose (Table IV). Photosynthetic measurements under identical conditions showed that carbon fixation was inhibited by 50% (C Wilson, unpublished data), which is consistent with the observed reduction in starch levels in mannose-treated leaves.

**Autoradiography.** Macroautoradiographic studies were also conducted to determine whether our experimental treatments

Table III. *Effect of DCMU on Carbohydrate Content in A. cepa Leaves*

Just prior to sunrise, on each onion plant to be used, slits were cut near the top of two mature, hollow, cylindrical leaves. The control leaf was filled, through the slit, with distilled $H_2O$ while the test leaf was filled with a 20 $\mu$M DCMU solution. $O_2$ was supplied by bubbling air continuously through the solutions in the leaf. These solutions remained in the leaves for 30 min and were then removed. This procedure was repeated with fresh solutions every 3 h throughout the daylight period. Leaves were sampled at the times indicated.

| Carbohydrate | Time[a] | Sugar Content | |
|---|---|---|---|
| | | Control | DCMU-treated |
| | *h* | *nmol mg$^{-1}$ dry wt* | |
| Fructose | 0 | 18.8 | 18.8 |
| | 5 | 54.8 | 36.8 |
| | 8 | 19.2 | 12.7 |
| | 16 | 17.8 | 6.4 |
| Glucose | 0 | 7.1 | 7.1 |
| | 5 | 44.5 | 19.3 |
| | 8 | 7.1 | 5.8 |
| | 16 | 8.3 | 5.2 |
| Sucrose | 0 | 2.5 | 2.5 |
| | 5 | 14.9 | 11.3 |
| | 8 | 10.5 | 3.4 |
| | 16 | 4.0 | 0.7 |

[a] Experimental manipulations commenced shortly after sunrise (approximately 7:30 AM).

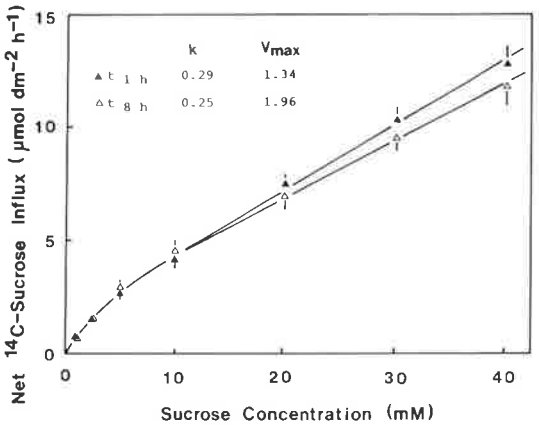


FIG. 4. Effect of increased internal sugar levels on sucrose uptake into *S. oleracea* leaf discs. Spinach plants were illuminated for 1 h (▲) and 8 h (△) prior to cutting disc from mature leaves. Over this interval sucrose levels increased from 2.6 to 9.3 $\mu$mol mg$^{-1}$Chl as determined by HPLC analysis. For kinetic studies a 30-min preincubation period in unlabeled sucrose was followed by a 30-min incubation in [$^{14}$C]sucrose solution (200 mOsm). Each point represents the mean ± SE for two sets of six replicates.

were affecting the partitioning of [$^{14}$C]sucrose between the mesophyll and the minor veins. In experiments where sugar beet leaves were cut, their petioles placed in water, and then the leaves returned to the controlled-environment chamber for 24 h, the radiolabel applied at the end of this 24 h period appeared to accumulate predominantly in the mesophyll. Rarely was label observed in the minor veins and then only in the largest veins (*cf.* Fig. 6, A and B). Under these conditions, chasing the labeled sucrose, for up to 7 h, with unlabeled sucrose did not result in movement out of the mesophyll into the minor veins (data not shown).

The change in carbohydrate partitioning illustrated in Figure 6, A and B, was used to investigate the effect on [$^{14}$C]sucrose

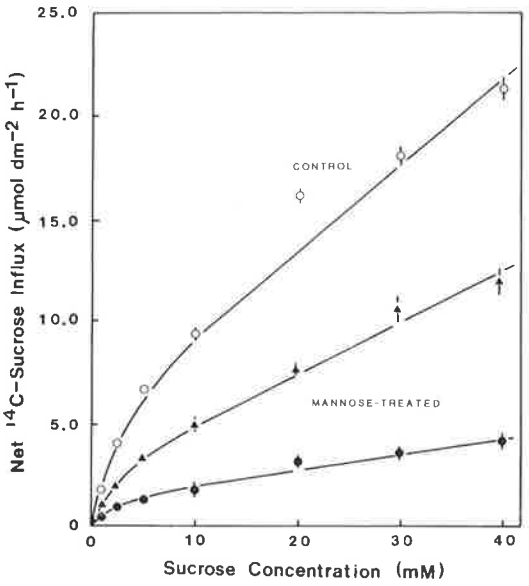


FIG. 5. Effect of mannose pretreatment on sucrose influx into *B. vulgaris* leaf discs. Leaves were excised at the base while the crown of the plant was submerged under water. Petioles were placed in either distilled water (control) or 10 mM mannose before being returned to the controlled-environment chamber for 0 h (control), 3, or 24 h. Kinetic studies were performed as described in Figure 1. The points for the control (○), 3-h mannose treated (▲), and 24-h mannose treated (●) leaves represent the mean ± SE for two sets of six replicates.

Table IV. *Influence of Mannose on Sugar and Starch Content in Mature Leaves of B. vulgaris*

Leaves were excised at the base of the petiole while the crown of the plant was submerged under water. Petioles were then either placed in distilled water (control) or 10 mM mannose before being returned to the controlled-environment chamber for 24 h. Data are from two experiments done in duplicate (mean ± SE).

| Treatment | Sugar Content | | | Starch |
|---|---|---|---|---|
| | Sucrose | Glucose | Fructose | |
| | *$\mu$mol mg$^{-1}$ Chl* | | | *$\mu$mol glucose equivalents mg$^{-1}$ Chl* |
| Control | 5.3 ± 0.3 | 16.9 ± 1.7 | 16.6 ± 2.4 | 62.3 ± 8.0 |
| Mannose-treated | 6.6 ± 0.9 | 19.9 ± 1.6 | 17.8 ± 1.8 | 29.3 ± 6.6 |

uptake by these two tissues. Figure 7A illustrates the kinetic response of leaf discs obtained from control and detached sugar beet leaves, while macroautoradiographs obtained from a subsample of these discs are presented in Figure 7B (control) and Figure 7C (detached). Whereas the distribution of the [$^{14}$C] sucrose was very different between the two treatments, the kinetic data were identical! Clearly these data reinforce our hypothesis that the kinetics of exogenously supplied [$^{14}$C]sucrose represents retrieval by the mesophyll, not the process involved in phloem loading (12, 13, 18).

Excision of the source leaf from the plant (sink removal) caused high sugar concentrations to develop within the leaf (Table II). It seemed logical to conclude that under these conditions the sucrose concentration in the phloem cells would also have increased. Such elevated sucrose concentrations might then slow the operation of the putative proton-sucrose cotransport system by a *trans* effect. In order to test this possibility, we manipulated the sugar levels within the leaf by a combination of supplying it with DCMU for increasing lengths of time during the photope-

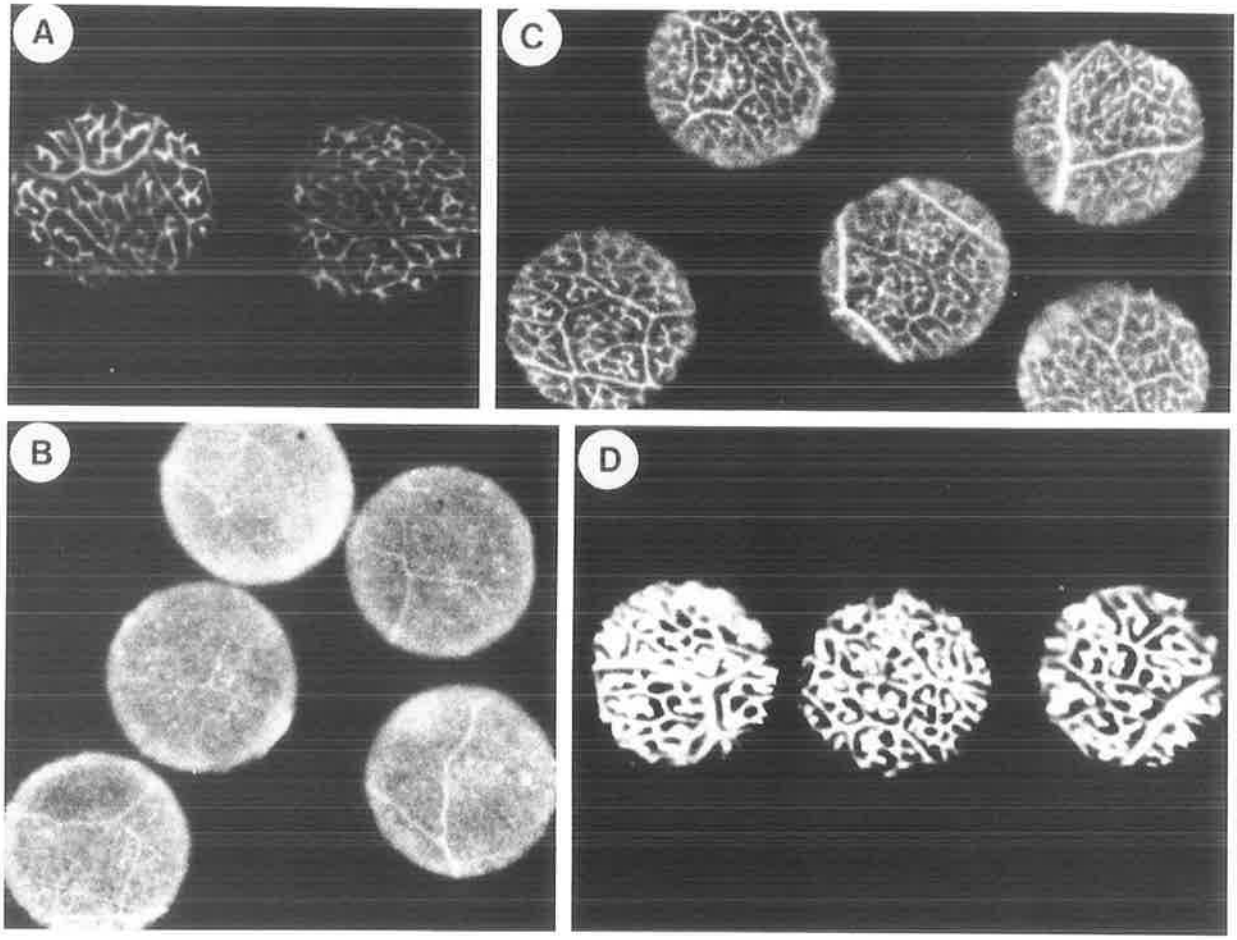


FIG. 6. Macroautoradiographs illustrating the distribution of [$^{14}$C]sucrose in peeled leaf discs from mature leaves of *B. vulgaris*. (A) Untreated (control) leaf discs were peeled by gently tearing the leaf in the regions between the major veins and removing areas of the lower epidermis. Leaf discs taken from the upper one-third area of the lamina were pretreated for 30 min on unlabeled sucrose (20 mM) followed by a 30-min [$^{14}$C]sucrose (20 mM) uptake period. This incubation period was followed by three 7-min washes (chase) in unlabeled sucrose (20 mM). (B) Leaves were cut at the base while the crown of the plant was submerged under water. Petioles were placed in distilled water before being returned to the controlled-environment chamber for 24 h. Labeled sucrose was allowed to accumulate in discs cut from the peeled leaf as described in A. Sugar levels as measured by HPLC were as follows: sucrose, 5.6 $\mu$mol mg $^{-1}$Chl; glucose, 24.1 $\mu$mol mg $^{-1}$Chl; fructose, 23.7 $\mu$mol mg $^{-1}$Chl. (C) Leaves were treated with DCMU as described in Figure 2. Labeled sucrose was allowed to accumulate in discs cut from peeled leaves as described for A. Internal sucrose level was 0.7 $\mu$mol mg $^{-1}$Chl. Glucose and fructose content were below the level of detection. (D) Leaves were treated with mannose as described in Figure 5. Labeled sucrose was allowed to accumulate in discs cut from peeled leaves as described for A. Since [$^{14}$C]sucrose influx was inhibited by mannose pretreatment, it was necessary to expose the x-ray film for longer periods of time (10 d) in order to obtain an image comparable to that presented in A (control: 1.5 d).

riod and reducing the actual photoperiod. In experiments in which excised leaves were given a normal 16 h photoperiod, during the DCMU treatment, sugars were maintained at intermediate levels between the upper values of the excised leaf control (Table II) and the leaf still attached to the plant (Table I). Under these conditions, [$^{14}$C]sucrose still accumulated predominantly within the mesophyll, *i.e.* the pattern remained equivalent to that depicted in Figure 6B. However, when the sucrose levels in the excised leaf were maintained near or below those present in an attached leaf, the veins again appeared to be able to accumulate radioactivity (Fig. 6C). Although mannose pretreatment significantly reduced [$^{14}$C]sucrose influx into the leaf discs, the radiolabel that entered the leaf still accumulated in the veins (Fig. 6D). This is a very interesting finding, especially in view of the fact that in mannose-treated leaves the sugar levels were elevated to approximately the same extent as those found in the heat-girdled or excised sugar beet leaves (Tables I, II, and IV).

## DISCUSSION

Uptake of exogenous sucrose into spinach leaves, which presumably represents transport across the mesophyll cells, is not influenced by internal sucrose levels. This insensitivity to internal sugars extended over the entire photoperiod and, over this period, the internal sucrose levels increased from 2.9 to 9.3 $\mu$mol mg $^{-1}$Chl. If transport across the tonoplast occurs via a permease (2), then the vacuolar sucrose levels should be in near chemical potential equilibrium with the cytosol, and our measurements should approximate cytosolic values. If this is indeed the case, then, in spinach, sucrose transport across the mesophyll plasmalemma does not appear to undergo *trans* inhibition.

The situation with sugar beet and onion is less certain. In the case of sugar beet, when sucrose levels were increased from 2.1 to 5.3 $\mu$mol mg $^{-1}$Chl by heat-girdling the petiole or by leaf excision, we did not detect any changes in sucrose influx into the leaf disc, which probably can be extrapolated to transport across the plasmalemma of the mesophyll cells (Fig. 7). However,

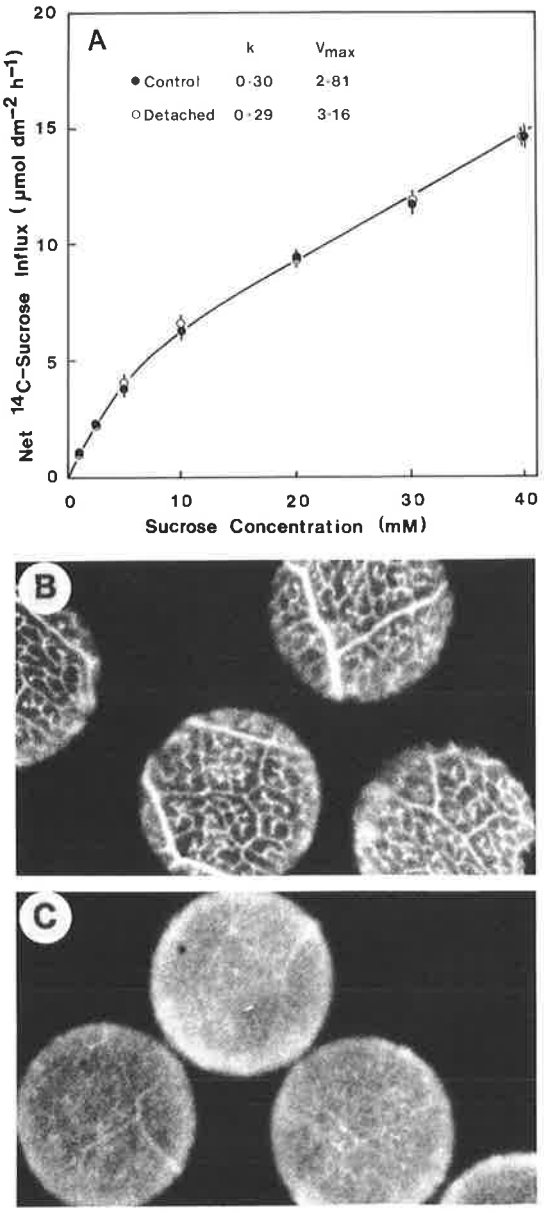


FIG. 7. Kinetic profiles and macroautoradiographic distribution of [$^{14}$C]sucrose in peeled leaf discs of *B. vulgaris* excised from attached (control) and detached leaves. Detached leaves were treated in the same manner as the controls of Figure 5, with a pretreatment period of 24 h. (A) Uptake period was 30 min, solutions containing the indicated sucrose concentrations were buffered at pH 5.0. (B) Macroautoradiographs of control discs subsampled from the 20 mM [$^{14}$C]sucrose treatment. (C) Macroautoradiographs of leaf discs cut from 24-h detached leaves and exposed to 20 mM [$^{14}$C]sucrose.

if the treatment period was extended to 34 h, sucrose levels increased from 2.1 to 11.5 μmol mg $^{-1}$Chl. Under these conditions, we found a decline in sugar uptake. Apparently, the sucrose transport system is unaffected by an intermediate increase in sucrose content but is inhibited by higher levels. Alternatively, the sugar levels in the cytosol do not reflect those of the vacuole and at some threshold level the capacity of the vacuole is exceeded, and then the cytosolic sucrose levels increase producing a concomitant inhibition of sucrose influx. Whatever the situation, it does not appear that *trans* inhibition occurs under the normal growth conditions experienced by these plants.

Another possibility is that the inhibition may result from an indirect effect of the elevated glucose and fructose levels, via a perturbation of cytosolic phosphate metabolism (Table I). However, in our control DCMU treatments with sugar beet leaves, the glucose and fructose levels rose to values equivalent to those in the prolonged heat-girdling experiment. Since, under these conditions, sucrose influx was not inhibited, it would appear that elevated glucose and fructose levels do not perturb transport.

In the case of onion, DCMU treatments resulted in an increase in sucrose influx. However, this increase cannot be attributed to decreases in sugar levels after DCMU treatment, since sucrose influx from control leaves did not vary despite changes in the sugar content throughout the day. Apparently, in onion, the sucrose influx kinetic response curve is set at some point and is generally invariant throughout the day.

In experiments in which the source leaf was removed from its sink, high sugar levels developed within the leaf (Tables I and II). The resultant change in carbohydrate partitioning, observed under these conditions, seems to be related to the increase in sugar levels, since DCMU treatment prevented this alteration from occurring. Additionally, mannose pretreatment also prevented this change in partitioning while allowing sugar levels to increase. Mannose may have interfered with some aspect of the controls employed to effect carbohydrate allocation, perhaps via its ability to sequester cytosolic phosphate.

From these results, it does not appear that the cytosolic surface of the plasmalemma is a likely target for investigation of the regulatory mechanisms operating in phloem loading. It is possible that partitioning of sucrose between cytosol and vacuole may play an important role in regulating phloem loading by modulating the quantity of sucrose available for transport. Sucrose transport into the vacuole in spinach may occur via a permease such that sucrose movement out of the vacuole may pose an interesting problem for plant physiologists and could be a likely target for regulatory signaling, as pointed out by Gerhardt and Heldt (2). During the normal photosynthetic period, sucrose entry into the vacuole may be passive, with the vacuole acting as a storage pool. However, in the dark or when conditions limit the supply of triose phosphate from the chloroplast and sucrose synthesis in the cytosol falls below the requirements of translocation, the movement of sucrose out of the vacuole may involve an active transport mechanism.

One especially intriguing aspect of this study is the partitioning of exogenously supplied [$^{14}$C]sucrose between the mesophyll and the minor veins. Figure 6 demonstrates that the transfer of exogenously supplied radiolabeled sucrose to the minor veins is inhibited in leaves removed from their sinks and kept in their normal growth environment for 24 h. Madore and Lucas (12) have recently shown that this change in partitioning occurs whether the radiolabeled carbon is supplied as $^{14}CO_2$ or [$^{14}$C] sucrose. Furthermore, we have now demonstrated that the kinetic profiles obtained with these detached leaves are indistinguishable from profiles generated from control (attached) leaves which were able to transfer radiolabeled sucrose to the minor veins (Fig. 7). These results indicate that the *in vivo* regulation of phloem loading may involve the partitioning of photoassimilates between the cytosol and vacuole such that the tonoplast and plasmodesmata might be likely targets for regulation.

*Acknowledgments*—We wish to thank Drs. J. Cronshaw, M. A. Madore, and C. R. Stocking for their valuable advice and discussion throughout the performance of this research.

## LITERATURE CITED

1. CHE-SHE S-H, DH LEWIS, DA WALKER 1975 Stimulation of photosynthetic starch formation by sequestration of cytoplasmic orthophosphate. New Phytol 74: 383–392
2. GERHARDT R, HW HELDT 1984 Measurement of subcellular metabolite levels in leaves by fractionation of freeze-stopped material in nonaqueous media. Plant Physiol 75: 542–547

3. GIAQUINTA R 1980 Translocation of sucrose and oligosaccarides. *In* PK Stumpf, EE Conn, eds, The Biochemistry of Plants, Vol 3. Academic Press, New York, pp 271–320
4. GIAQUINTA R 1980 Mechanism and control of phloem loading of sucrose. Ber Dtsch Bot Ges 93: 187–201
5. HAMPSON SE, RS LOOMIS, DW RAINS 1978 Regulation of sugar uptake in hypocotyls of cotton. Plant Physiol 62: 851–855
6. HEROLD A, DH LEWIS 1977 Mannose and green plants: occurrence, physiology and metabolism, and use as a tool to study the role of orthophosphate. New Phytol 79: 1–40
7. HEROLD A, EEM MCGEE, DH LEWIS 1980 The effect of orthophosphate concentration and exogenously supplied sugars on the distribution of newly fixed carbon in sugar beet leaf discs. New Phytol 85: 1–13
8. HUBER SC 1986 Fructose 2,6-bisphosphate as a regulatory metabolite in plants. Annu Rev. Plant Physiol 37: 233 246
9. KAISER G, U HEBER 1984 Sucrose transport into vacuoles isolated from barley mesophyll protoplasts. Planta 161: 562–568
10. KOMOR E 1977 Sucrose uptake by cotyledons of *Ricinus communis* L.: characteristics, mechanism, and regulation. Planta 137: 119–131
11. LUCAS WJ, MA MADORE 1987 Recent advances in sugar transport. *In* J Preiss, ed., The Biochemistry of Plants: A Comprehensive Treatise, Vol 12. Academic Press, New York. In press
12. MADORE MA, WJ LUCAS 1987 Control of photoassimilate movement in *Ipomoea tricolor* source leaf tissues. Planta. In press
13. MAYNARD JW, WJ LUCAS 1982 A reanalysis of the two-component phloem loading system in *Beta vulgaris*. Plant Physiol 69: 734–739
14. SANDERS D 1986 Generalized kinetic analysis of ion-driven cotransport systems. II. Random ligand binding as a simple explanation for non-michaelian kinetics. J Membr Biol 90: 67–87
15. STITT M 1985 Fine control of sucrose synthesis by fructose-2,6-bisphosphate. *In* R Heath, J Preiss, eds, Regulation of Carbon Partitioning in Photosynthetic Tissue. American Society of Plant Physiologists, Rockville, MD, pp 109–126
16. STITT M 1986 Regulation of photosynthetic sucrose synthesis: integration, adaptation, and limits. *In* J Cronshaw, WJ Lucas, RT Giaquinta, eds, Plant Biology, Vol 1: Phloem Transport. Alan R. Liss, New York, pp 331–347
17. STITT M, R GERHARDT, B KÜRZEL, HW HELDT 1983 A role for fructose 2,6-bisphosphate in the regulation of sucrose synthesis in spinach leaves. Plant Physiol 72: 1139–1141
18. WILSON C, JW OROSS, WJ LUCAS 1985 Sucrose uptake into *Allium cepa* leaf tissue: an integrated approach. Planta 164: 227–240
19. WYSE RE, E ZAMSKI, AD TOMOS 1986 Turgor regulation of sucrose transport in sugar beet taproot tissue. Plant Physiol 81: 478–481

Plant Physiol. (1987) 85, 423–429
0032-0889/87/85/0423/07/$01.00/0

# Influence of Mannose on the Apoplasmic Retrieval Systems of Source Leaves[1]

Received for publication May 8, 1987 and in revised form June 25, 1987

WILLIAM J. LUCAS* AND CLYDE WILSON
*Botany Department, University of California, Davis, California 95616*

## ABSTRACT

**Experiments were conducted in which D-mannose was supplied to mature *Beta vulgaris* L. (sugar beet) leaves, via the transpiration stream, to perturb photosynthetic carbon allocation by sequestering cytosolic Pi. Biochemical and enzymic analyses conducted on this tissue indicated that mannose 6-P was present, that it was only slowly metabolized, and that after a 24-hour pretreatment sugar metabolism was slightly perturbed. However, sucrose retrieval by the mesophyll tissue was greatly impaired in 24-hour mannose-pretreated tissue, a response which was due in part to mannose acting as an osmoticum. Inhibition of glucose, fructose, and arginine uptake into mannose-treated sugar beet leaf discs indicated that mannose may elicit a general perturbation of all membrane transport processes. This conclusion was supported by our finding that sucrose efflux was increased from mannose-treated tissue. Analysis of adenine nucleotide levels showed that whereas these levels declined over the first 3 to 6 hours of the mannose treatment, by 24 hours they had recovered to near control values. Similar experiments conducted on *Nicotiana rustica* indicated that whereas mannose 6-P was present in mature leaves, it remained at a much lower level than that found in sugar beet. Sucrose uptake into *N. rustica* was insensitive to mannose pretreatment. However, glucosamine treatment, which is also thought to sequester cytosolic Pi, inhibited sucrose uptake in both *N. rustica* and *B. vulgaris*. Further, experiments conducted on *N. tabacum* L. var Xanthii showed that mannose caused an inhibition of sucrose uptake, indicating that a range of sensitivity to mannose exists between closely related species. These results are discussed in terms of possible mechanisms of inhibition.**

In a recent study on the regulation of sucrose transport across the plasmalemma of sugar beet mesophyll cells, we used mannose to alter the partitioning of carbohydrates between the cytosol and the chloroplast. In sugar beet, mannose did not reduce the sucrose level in the manner expected from reports in the literature (5, 10, 13, 14); however, it did cause a reduction in exogenous [$^{14}$C]sucrose influx. In addition, mannose pretreatment prevented, in some way, the change in partitioning of exogenously supplied [$^{14}$C]sucrose, which was found to occur following the removal of sink activity (31). These findings suggested that further studies, using mannose as an experimental treatment, may provide information on both the regulatory mechanisms involved in transport at the plasma membrane and carbohydrate allocation in relation to 'phloem loading.'

It is generally accepted that in species lacking mannose isomerase, mannose is able to reduce cytosolic inorganic phosphate (Pi) levels by phosphorylation to mannose 6-P, which is then only slowly metabolized (10, 16, 23). Since the transport of Pi between the vacuole and cytosol is thought to be slow (23, 27; but see Ref. 16), the addition of mannose effects a sequestration of cytosolic Pi (5, 13; but *cf.* Ref. 16). Inhibition of sugar transport by mannose has been previously documented, *e.g.* glucose uptake into (15) and sucrose storage in corn scutellum (9) are both inhibited by mannose treatment. The work conducted on corn scutellum indicated that mannose treatment reduced the ATP level in this tissue, and Humphreys postulated that this may have a significant role in the inhibitory response of the tissue to mannose (see also [28]).

In the present study, we further investigated the effect of mannose on the transport of sucrose, glucose, fructose, and arginine into mature leaf tissue of sugar beet. Our results indicate that the inhibition of plasmalemma transport is not limited to sucrose as the influx of these other substrates was also reduced. Furthermore, the inhibitory aspects of mannose cannot be explained by a reduction in adenine nucleotide levels alone since, after a 24 h mannose pretreatment, these levels recovered to near-control values. Since tobacco has been reported to be able to metabolize exogenously supplied mannose (5, 12, 13, 20), we selected two species of *Nicotiana*, *N. rustica* and *N. tabacum*, to form a comparative basis for this study. We found that whereas sucrose influx into *N. rustica* was completely insensitive to mannose pretreatment, transport into *N. tabacum* was inhibited. Glucosamine pretreatment inhibited sucrose influx into *N. rustica* and sugar beet. Collectively, these studies implicate a role of cytosolic Pi in the regulation of transport across the plasmalemma.

## MATERIALS AND METHODS

**Plant Material.** *Beta vulgaris* L. (var SSBN1, USH10, Lot 3102 or USH11, Lot 82313) seeds were planted in a mixture containing vermiculite, peat moss, and sand (2:1:1 by volume) and grown in a controlled-environment chamber under a 27°C day/17°C night temperature regime and a 16 h photoperiod (250 $\mu$mol m$^{-1}$ s$^{-1}$). The plants were watered daily and fertilized twice weekly with Hoagland solution. The third pair of leaves (after the cotyledons) of 4-week-old sugar beet plants were used. *Nicotiana tabacum* L. var xanthii and *Nicotiana rustica* L., were planted in the soil mixture described above and grown under greenhouse conditions. Plants were fertilized during the third, fifth, and seventh weeks with ammonium phosphate. Experimental plants were 9 weeks old.

**Kinetic Studies.** Kinetic uptake studies on *B. vulgaris* were performed using the method of Maynard and Lucas (21) as modified by Wilson *et al.* (32) and Wilson and Lucas (31). Radioactive sugars (D-[U-$^{14}$C]sucrose, -fructose, and -glucose) were obtained from International Chemical and Nuclear Corp. (Irvine, CA). Radioactive arginine (L-[U-$^{3}$H]arginine) was obtained from NEN Research Products (Boston, MA). The specific activities of the uptake solutions for all sugar and arginine

[1] Supported by National Science Foundation Grant PCM 83-15408 to W. J. L.

experiments were $1.78 \times 10^7$ Bq $mmol^{-1}$. In *Nicotiana* experiments, a segment of the mature tobacco leaf was excised and placed on a rubber pad located in a dish containing a solution of 20 mM $CaCl_2$ and 60 mM Mes buffer (pH 5.0). Leaf discs, 4 mm in diameter, were cut and then pretreated for 30 min on a solution containing 20 mM $CaCl_2$, 120 mM Mes (pH 5.0), and enough mannitol to adjust the total osmolality to 200 mOsm; sugars at the concentration specified for the particular experiment were also included. This pretreatment was followed by a 30-min uptake period, which was terminated by using three 7-min washes in media containing 20 mM $CaCl_2$, 60 mM Mes (pH 5.0), and the appropriate sugar at 40 mM. Radioactivity within the sugar beet and tobacco leaf discs was quantitated using a Beckman 9800 scintillation spectrometer (Beckman Instruments Inc.) as previously described (22).

**ATP Extraction and Determination.** Leaf discs that had been treated using the same protocol employed for kinetic experiments were quickly frozen using liquid $N_2$. These discs were then lyophilized for 18 h in a DURADRY freeze-dryer equipped with a bulk tray dryer (FTS Systems, Stone Ridge, NY). Lyophilized samples were weighed and then ground, using a ground glass homogenizer, in 2.0 ml of ice-cold 1.0 M $HClO_4$; 2 mg $ml^{-1}$ of Polyclar AT (Polysciences, Warrington, PA) was also added to the extraction medium (18). The homogenizer was rinsed with 1.0 ml of 0.05 M phosphate buffer (pH 7.5), and after allowing 20 min for complete extraction and protein denaturation, the rinse and the extract were combined. The mixture was then centrifuged at 25,000*g* for 30 min at 4°C. The supernatant was neutralized to pH 7.5 with 5 N KOH. After waiting 20 min to allow for the precipitation of potassium perchlorate, the extract was again centrifuged for 30 min at 25,000*g*. The supernatant was stored at −70°C until assayed (2–3 d).

A modification of the procedures of Yoshioka and Tamura (33) and Preston (26) was employed to determine AMP, ADP, and ATP levels (32). Chromatography was performed using a Beckman Series 344 Gradient Liquid Chromatograph equipped with an Ultrasphere IP column (4.6 mm diameter, 250 mm long). The eluting peaks of the adenine nucleotide 1,$N^6$-ethenoadenosine-derivatives (32) were detected using a fluorescence detector (Beckman model 157) and analyzed on an Altex Chromatopac C-R1B data processor (Beckman Instruments).

Peaks were identified by using retention times of standards. Further confirmation of the peaks in the extracts was obtained enzymically. Addition of pyruvate kinase and adenylate kinase (Sigma) or pyruvate kinase alone, to extracts, resulted in the disappearance of the peaks which were identified as AMP and ADP, respectively, while the ATP peak increased. Addition of hexokinase or calcium phosphate to the extract resulted in the loss of the putative ATP peak.

**Sugar, Starch and Mannose 6-P Analysis.** Sugars and starch were extracted from leaf tissues and analyzed using the procedures and protocols described by Wilson and Lucas (31). Mannose 6-P was extracted according to the procedure of Herold *et al.* (14). The extraction procedure was similar to our sugar protocol (31), except that 20 leaf discs were used and the ethanol extractions were followed by two extractions using hot water. The extracts were evaporated to dryness under a stream of nitrogen gas and stored at −70°C until assayed (1–2 d).

To assay the extracts for mannose 6-P, the samples were first rehydrated to 0.5 ml, and 50 μl of this sample was added to a 13 × 100 mm culture tube containing 2.82 ml of 50 mM Hepes-NaOH buffer (pH 7.6), 100 μl of NADP (12 mM), and 10 μl each of glucose 6-P dehydrogenase (G6PDH, 340 units $ml^{-1}$), phosphoglucose isomerase (PGI, 580 units $ml^{-1}$), and phosphomannose isomerase (PMI, 140 units $ml^{-1}$). This mixture was incubated for 1 h by which time the stoichiometric production of 1 NADPH for each mannose 6-P molecule was complete. The resulting NADPH was measured spectrophotometrically at 366 nm against a blank containing 10 μl distilled water in place of phosphomannose isomerase. (G6PDH from Bakers yeast, PGI from Bakers yeast type III, and PMI from yeast along with NADP were obtained from Sigma.)

**Mannose and Glucosamine Pretreatments.** Three h into the photoperiod, the leaf-petiole complex of the third pair of leaves (after the cotyledons) were excised from the base of the crown while the sugar beet plant was submerged underwater. The leaf-petiole complex was then either placed in distilled water (control) or a 10 mM mannose (or glucosamine) solution before being returned to the controlled-environment chamber. After predetermined intervals, leaf discs (4 mm diameter) were punched from the leaf and used for sugar analyses and kinetic experiments (same protocol was followed for tobacco plants). When appropriate, 10 mM mannitol (or sorbitol) was substituted for mannose.

**[$^{14}$C]Sucrose Efflux Experiments.** As in sucrose uptake experiments, the third pair of leaves (after the cotyledons) from 4-week-old sugar beet plants were used in our efflux studies. Leaves were cut from the plant and submerged in a 20 mM $CaCl_2$ solution while the lower epidermis was peeled away. Leaf discs were excised and then pretreated, for 30 min, on a medium containing 20 mM mM sucrose, 120 mM Mes (pH 5.0), and mannitol added to adjust the osmolality to 500 mOsm. Discs were then transferred to an identical medium containing 20 mM [$^{14}$C]sucrose. After a 30-min loading period, the discs were transferred to fresh pretreatment medium. At predetermined times, discs were again transferred to fresh media, and aliquots of the efflux solution were analyzed for radioactivity by liquid scintillation counting. At the end of the experiment, the discs were analyzed for residual radioactivity. Efflux data were analyzed according to Pitman (25) and Cram (6), the results being interpreted in terms of an apoplasmic and two intracellular compartments (vacuole and cytosol) arranged in series. In certain instances some of the leaf discs were analyzed for ethanol-soluble sugars as previously described. Radioactivity remaining after ethanol extraction followed by cold water extraction was attributed to starch.

## RESULTS

**Inhibitory Effect of Mannose on Sugar and Amino Acid Transport.** Wilson and Lucas (31) recently showed that pretreatment of sugar beet leaves with mannose results in a progressive decline in the capacity of these leaves to retrieve exogenously supplied [$^{14}$C]sucrose. This inhibition by mannose may have been due to its osmotic rather than biochemical properties; this possibility was tested by substituting mannitol (or sorbitol) for mannose. After a 24-h mannitol treatment, the capacity of the leaves to take up [$^{14}$C]sucrose was slightly decreased, whereas a similar treatment with mannose caused a strong inhibition of sucrose influx (Fig. 1). This suggests that mannose has effects independent of its osmotic properties. (An equivalent inhibition was obtained with either sorbitol or mannitol.)

Since mannose had dramatic effects on sucrose influx, apart from a small osmotic effect, we decided to examine its influence on the transport of other sugars and amino acids. As in the case of sucrose, mannose pretreatment resulted in a decrease in the transport of both [$^{14}$C]fructose (Fig. 2A) and [$^{14}$C]glucose (Fig. 2B). However, in contrast with sucrose, the uptake of these sugars, after mannose pretreatment, was mediated solely by the first-order kinetic component.

We extended our investigation on the specificity of the mannose effect by measuring the influence of mannose on amino acid transport. Dual-label ([$^3$H]arginine and [$^{14}$C]sucrose) experiments were performed in these studies. Control experiments showed that arginine was taken up via the combined effect of a saturable and a first-order kinetic system (see also Ref. 22), with

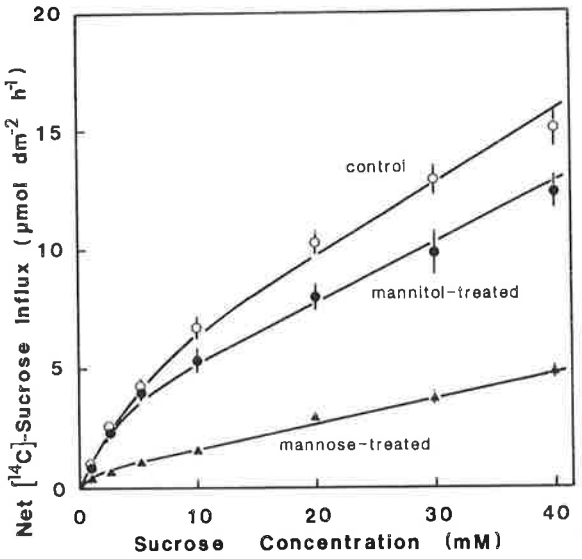


FIG. 1. Effect of mannose and mannitol on net sucrose influx into *B. vulgaris* leaf discs. Petioles were excised at the base, while the crown of the plant was submerged underwater. The petioles were then placed in either distilled water (○), 10 mM mannitol (●), or 10 mM mannose (▲) before being returned to the controlled-environment chamber. After 24 h, kinetic studies were performed. A 30-min preincubation period in unlabeled sucrose was followed by a 30-min incubation in [$^{14}$C]sucrose. Uptake solutions were adjusted to 500 mOsm with mannitol. Each point represents the mean ± SE for two sets of six replicates.

the major contribution occurring via the first-order kinetic system. As with sugar influx, mannose pretreatment resulted in an inhibition of both the first-order and saturable components of [$^{3}$H]arginine uptake (Fig. 3). Hence, the inhibitory influence of mannose appears to be related to either a general cellular- or membrane-related phenomenon.

**Adenine Nucleotide Levels Affected by Mannose Pretreatment.** It has been suggested that mannose may reduce sugar transport into cells through its sequestration of cytosolic Pi. This removal of Pi would reduce the level of ATP available for membrane transport. To investigate this hypothesis, we analyzed the levels of adenine nucleotides in mannose-treated and control tissue over a 24-h period (Table I). We found that leaves which had been pretreated with mannose for 3 h contained lower levels of AMP, ADP, and ATP compared with control leaves. However, after 24 h, the adenine nucleotide levels in the mannose-treated leaves had recovered to near-control values while, during this period, membrane transport activity continued to decline. It would appear from these data that mannose is acting by some other means to inhibit membrane transport.

**Mannose 6-P Levels in Mannose-Pretreated Leaves.** It is possible that the mannose-induced inhibition of membrane transport is related to either the sequestration of cytosolic Pi or the subsequent formation of mannose 6-P, *per se.* To examine this possibility, we sampled control and mannose-treated leaves at various intervals over a 24-h experimental period and determined the mannose 6-P levels. We were unable to detect mannose 6-P in control leaves, but in mannose-treated leaves, the mannose 6-P levels progressively increased throughout the light period and then decreased during the subsequent dark period (18 h) (Table II). During the following light period, the mannose 6-P level returned to the pre-dark value. These data indicate that *Beta vulgaris* is capable of metabolizing mannose 6-P, although the rate appears to be too low to prevent its accumulation in this tissue.

**Effect of Mannose on *Nicotiana.*** Having characterized the

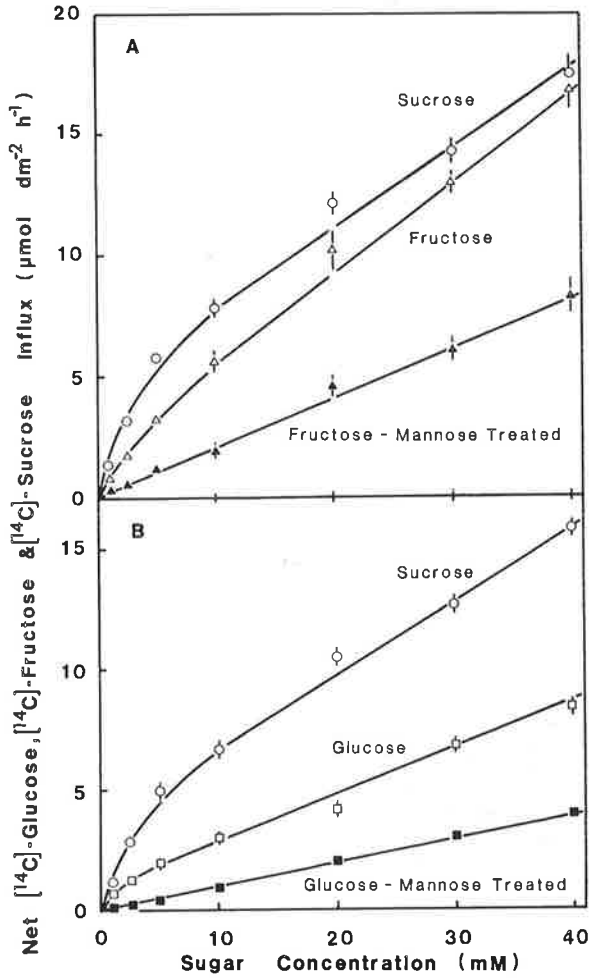


FIG. 2. Effect of mannose pretreatment on net fructose (A) and net glucose (B) influx into *B. vulgaris* leaf discs. Experimental techniques were as described in Figure 1. Points for both the fructose control (△), mannose-treated (▲), and glucose control (□), and mannose-treated (■) represent the means ± SE for two sets of six replicates. Sucrose control (○) is included for reference.

effect of mannose on sugar uptake in *B. vulgaris*, we selected two species, *N. rustica* and *N. tabacum*, for study, since *Nicotiana* has been reported to be mannose-tolerant.

In contrast to sugar beet, sucrose transport into *N. rustica* leaf discs was unaffected by mannose pretreatment (Fig. 4A). In order to determine if mannose affected leaf carbohydrate metabolism, we analyzed the starch and sugar levels within the tissue. As found in our studies with sugar beet (31), mannose-pretreatment caused the starch levels to decrease, while sugar levels increased slightly (Table III). We also measured the mannose 6-P levels in *N. rustica* leaves after 24-h control and mannose treatments (Table II). Although we could detect the presence of mannose 6-P in leaves of *N. rustica* treated with mannose, the levels were lower than those found in *B. vulgaris* after 3 h of mannose treatment. Either *N. rustica* is capable of metabolizing mannose 6-P more quickly than sugar beet, resulting in lower mannose 6-P levels, or the lower levels of mannose 6-P reflect slower uptake of mannose into tobacco mesophyll tissue. The second possibility is supported by slower uptake of sucrose (Fig. 4A). Collectively, these data indicate that in *N. rustica*, mannose can elicit biochemical responses, but that these are either insufficient in magnitude to perturb—or are tolerated more by—the sucrose transport system of this plant.

We furthered our investigations on tobacco by examining the

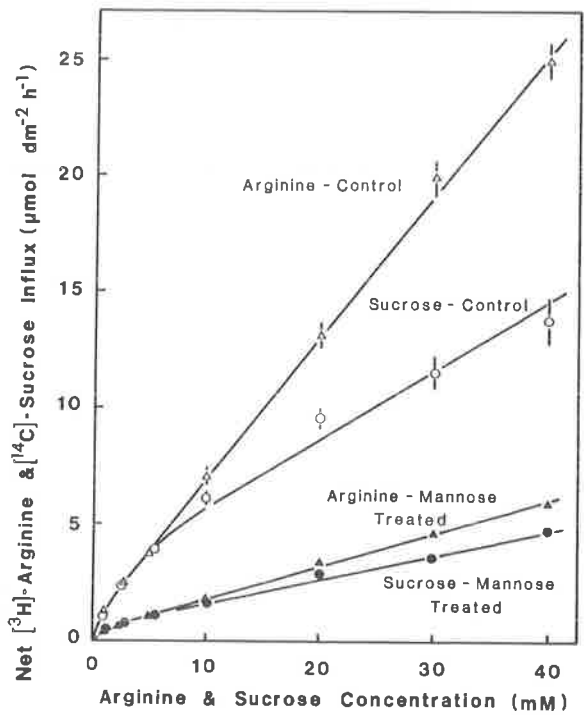


FIG. 3. Effect of mannose pretreatment on net [$^3$H]arginine influx into *B. vulgaris* leaf discs. Experimental techniques were as described in Figure 1. For kinetic studies, the preincubation media contained the appropriate concentrations of D-sucrose and L-arginine, while uptake solutions contained both [$^{14}$C]sucrose and [$^3$H]arginine. The points for the arginine and sucrose controls (△, ○), respectively, and for net arginine influx and net sucrose influx into mannose-treated leaves (▲, ●), respectively, represent the means ± SE for two sets of six replicates.

effect of mannose on another species, *N. tabacum*. Our results with this species were unexpected. A 24-h mannose pretreatment resulted in a dramatic decrease in both the first-order and saturable components of sucrose influx (Fig. 4B). This mannose response is similar to that obtained with *B. vulgaris* and indicates that there may be subtle differences among tobacco species, with respect to carbohydrate biochemistry. Since sucrose influx was also greater in *N. tabacum*, as compared with *N. rustica*, we cannot exclude the possibility that a difference in mannose transport is the basis for this discrepancy in species sensitivity to mannose.

**Effect of Glucosamine on Sucrose Influx.** If the sequestration of Pi is involved in the inhibition phenomenon, it should be possible to experimentally effect a reduction in the cytosolic Pi levels in *N. rustica* and thereby elicit a decrease in sucrose influx. Herold *et al.* (13) have suggested that glucosamine sequesters Pi in tobacco leaves. Glucosamine pretreatment of *N. rustica* leaves resulted in an inhibition of both the saturable and linear components of uptake, with the saturable system being the most affected (Fig. 5). However, the extent of glucosamine-induced inhibition was not as severe as that observed with sugar beet (Fig. 5).

**Effect of Mannose on Sucrose Efflux.** Herold (11) suggested that mannose had marked effects on the membrane permeability of spinach beet leaf tissue. We performed efflux studies in order to determine if sucrose efflux was also affected in sugar beet. The effect of a 24-h mannose pretreatment on [$^{14}$C]sucrose efflux is presented in Fig. 6. In control tissue the half-time for [$^{14}$C]sucrose exchange across the plasmalemma was 40.5 min, whereas in mannose-treated tissue this half-time was reduced to 18.8 min. Mannose also affected the distribution of [$^{14}$C]sucrose in the cytosolic and vacuolar compartments. In control leaves, only 5% of the [$^{14}$C]sucrose was present in the cytosol, while in mannose-treated tissue this value increased to about 25%. Thus, it would appear that mannose can affect intracellular transport processes in addition to perturbing the fluxes crossing the plasmalemma.

## DISCUSSION

In the present study, we used mannose and glucosamine to probe the regulatory processes involved in sugar transport into mature leaf tissues of sugar beet and tobacco. Mannose has been used in various plant systems as a tool to investigate the role of cytosolic Pi in regulating various aspects of photosynthetic carbon metabolism (8, 10, 13, 30). It is currently accepted that mannose sequesters cytosolic Pi through its reaction with Pi to produce mannose 6-P, via hexokinase. Many plant tissues either lack phosphomannoisomerase, or this enzyme is compartmentalized such that mannose 6-P is metabolized very slowly (10, 23). In our experiments, mannose pretreatment caused a dramatic perturbation of sugar influx into mesophyll tissue of sugar beet plants. Mannose pretreatment resulted in a progressive decrease in sucrose uptake over a 24-h period (31). Further studies revealed that uptake of both glucose and fructose was also reduced, indicating that the mannose effect may be a consequence of a more general phenomenon. This interpretation is supported by the observation that arginine uptake was similarly affected.

Consistent with this view is the observation that mannose also influenced sucrose efflux from sugar beet leaf discs. Our experiments indicate that both the plasmalemma and tonoplast are affected by mannose, as the half-times for sucrose efflux from both cytosolic and vacuolar compartments were decreased relative to control values. Although some caution is needed in the interpretation of the efflux data obtained in this manner (4), we

Table I. *Adenine Nucleotide Levels in Mannose-Treated Sugar Beet Leaves*

Leaves were excised at the base of the petioles while the crown of the plants was submerged underwater. The petioles were either placed in 10 mM mannose or distilled water (control) before being returned to the controlled-environment chamber for the times specified. Adenine nucleotide levels were determined by HPLC. Data are from two experiments.

| Duration | Treatment | AMP | ADP | ATP | Total |
|---|---|---|---|---|---|
| *h* | | *pmol mg$^{-1}$ dry weight* | | | |
| 0 | None | 259 | 419 | 802 | 1471 |
| 3 | Mannose | 176 | 251 | 349 | 776 |
| | Control | 314 | 329 | 832 | 1475 |
| 6 | Mannose | 223 | 235 | 368 | 826 |
| | Control | 294 | 350 | 839 | 1483 |
| 24 | Mannose | 373 | 386 | 677 | 1416 |
| | Control | 269 | 302 | 736 | 1306 |

Table II. *Mannose 6-Phosphate Levels in Mannose-Treated Sugar Beet and Tobacco Leaves*

Leaves were excised at the base of the petioles while the crown of the plants was submerged underwater. The petioles were either placed in 10 mM mannose or distilled water (control) before being returned to the controlled-environment chamber for the times specified. Experimental treatments were started 3 h into the photoperiod; the controlled-environment chamber was programmed for a 16-h light:8-h dark cycle. Mannose 6-P levels were determined by enzymic assay.

| Plant | Time | Mannose 6-P | |
|---|---|---|---|
| | | Control | Mannose-treated |
| | *h* | *μmol mg*$^{-1}$ *Chl* ± SE | |
| Sugar beet | 0 | ND[a] | ND |
| | 3 | ND | 1.3 ± 0.1 |
| | 6 | ND | 1.8 ± 0.1 |
| | 9 | ND | 1.8 ± 0.3 |
| | 12 | ND | 2.0 ± 0.3 |
| | 18 | ND | 1.1 ± 0.1 |
| | 24 | ND | 2.3 ± 0.2 |
| Tobacco (*N. rustica*) | 0 | ND | ND |
| | 24 | ND | 0.7 ± 0.1 |

[a] Not detected.

feel our interpretation of the data as representing efflux from a three-compartment model is justified (at least to a first approximation) by a comparison of plots of log $Q_t$ and log $Q_{t/dt}$ *versus* time as suggested by Cram and Laties (7) and further emphasized by Kochian and Lucas (17).

By extrapolating the efflux curves to $t = 0$, we were able to estimate the relative amounts of radiolabel present in the vacuolar and cytosolic compartments. At the end of a 30-min uptake period only 5% of the label resided in the 'cytosolic compartment' of sugar beet source leaves. This result is similar to the findings of Thom *et al.* (29) for their study of efflux of sugars from cultured sugar cane suspension cells. They reported that while most of the label was in the cytoplasm following the initial minutes of uptake, the majority of label was subsequently located in the vacuole. However, after mannose pretreatment, 25% of the [$^{14}$C]sucrose was located in the cytosolic compartment of the sugar beet leaf. Evidently, mannose may either directly or indirectly affect the partitioning of sucrose between the vacuole and the cytosol.

An important aspect of the mannose effect on sugar uptake was the difference in the pattern of inhibition displayed by sucrose, glucose, and fructose. Although uptake of sucrose was reduced by mannose pretreatment, the resulting kinetic profile demonstrated that influx was still mediated by both the first-order and saturable components. However, for fructose and glucose, mannose pretreatment completely inhibited the saturable transport component; influx was mediated solely by the first-order component. Perhaps there exists a basic difference in the regulation of the various sugar-transport systems.

Previous investigators have documented reduced synthesis of ATP upon the addition of mannose and have used this finding as a basis to explain their observations (9, 28). In the present study, we found that mannose addition reduced adenine nucleotide levels when measured after 3 h and that this correlated with decreased sugar influx. However, after 24 h, adenine nucleotide levels recovered to near control values, while sugar transport activity continued to decline. Based on this finding, we feel the explanation for our observed mannose response must lie elsewhere.

An interesting outcome of this study was the discovery that two closely related species of *Nicotiana* differed widely in their

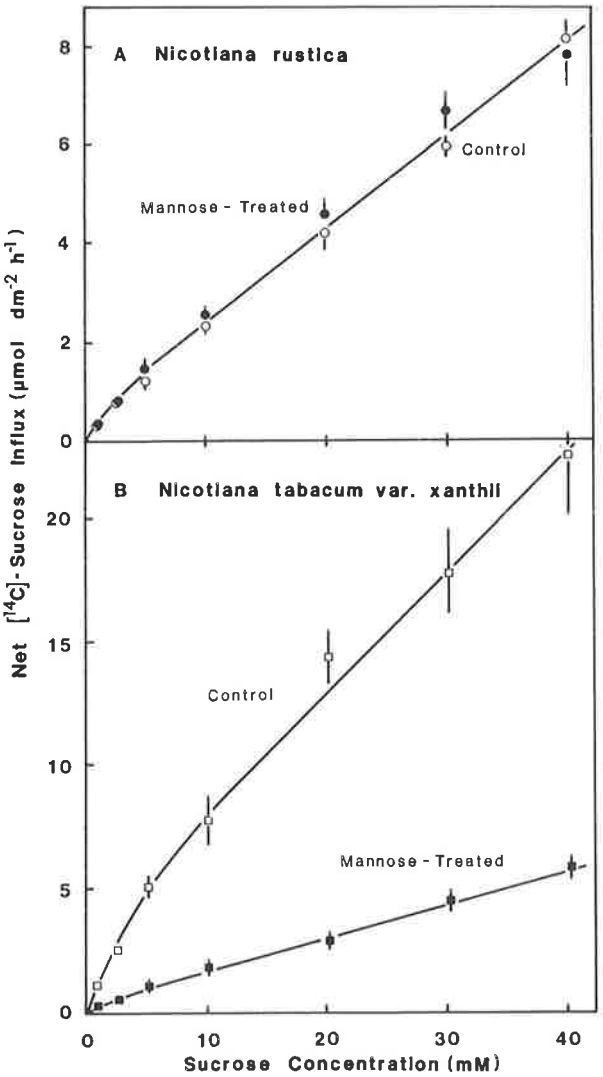


FIG. 4. Effect of mannose pretreatment on net [$^{14}$C]sucrose influx into *N. rustica* (A) and *N. tabacum* var *xanthii* (B) leaf discs. Experimental techniques were as described in Figure 1, except that the osmolality of the solution was adjusted to 200 mOsm. The points for the controls (○, □) and mannose-treated discs (●, ■) represent the means ± SE for two sets of six replicates.

response to mannose. *N. rustica* seemed very tolerant to mannose pretreatment even after 24 h, while *N. tabacum* var xanthii reacted in a manner similar to that observed with sugar beet. Differences in phosphomannoisomerase activity or compartmentalization might account for the observed differences. Although *N. rustica* appeared to be tolerant of mannose pretreatment, we were able to inhibit sucrose influx by substituting glucosamine for mannose. Since glucosamine is reported to sequester Pi in tobacco, our results imply that changing cytosolic Pi levels may be important in the regulation of sugar transport across the plasmalemma in tobacco as well as sugar beet.

On a speculative note, it may be that both mannose and glucosamine elicit a general perturbation of membrane transport by interrupting a phosphate-dependent component of the phosphatidylinositide cycle (1). Support for this hypothesis can be found in the plant literature, insofar as data is now available that the phosphatidylinositide cycle is present in plant cells (2, 24). Further, lithium, an inhibitor of phosphatidylinositide reincorporation into the plasma membrane (1), also inhibits sugar transport. Carlier and Thellier (3) reported that lithium treatment

Table III. *Influence of Mannose and Glucosamine on Sugar and Starch Content in Mature Leaves of N. rustica*

Leaf petioles were excised at the base while the crown of the plant was submerged underwater. The leaf-petiole complex was either placed in 10 mM glucosamine or 10 mM mannose when appropriate or distilled water (control) and then returned to the controlled-environment chamber for 24 h.

| Treatment | Sugar Content | | | Starch |
|---|---|---|---|---|
| | Sucrose | Glucose | Fructose | |
| | *μmol mg⁻¹ Chl ± SE* | | | *μmol glucose equivalents mg⁻¹ Chl ± SE* |
| Control (untreated) | 4.9 ± 0.3 | 4.3 ± 0.3 | 0.9 ± 0.1 | 127.6 ± 11.8 |
| Mannose-treated | 6.0 ± 0.6 | 5.6 ± 0.4 | 1.5 ± 0.3 | 87.1 ± 7.1 |
| Control | 5.4 ± 0.2 | 2.5 ± 0.3 | 0.8 ± 0.1 | 547 ± 41 |
| Glucosamine-treated | 10.5 ± 0.9 | 6.5 ± 0.5 | 6.9 ± 0.5 | 410 ± 46 |

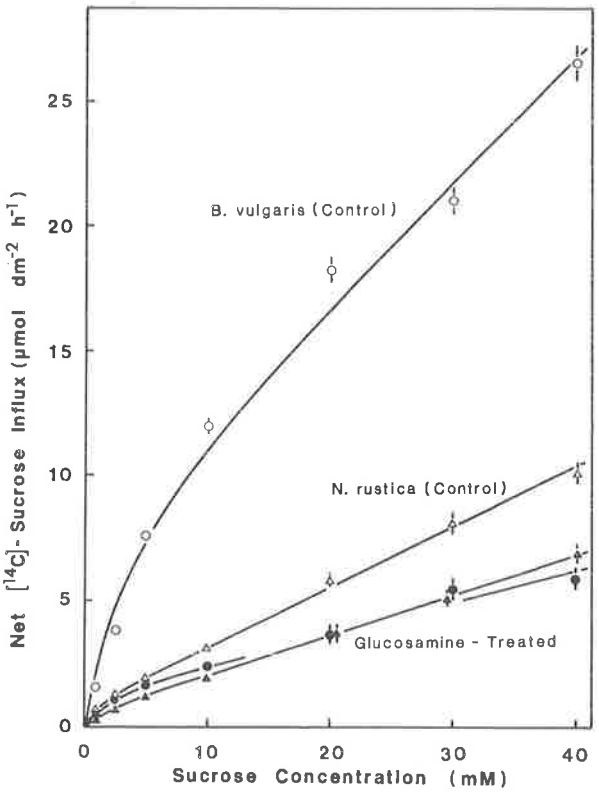


FIG. 5. Effect of glucosamine pretreatment on net [$^{14}$C]sucrose influx into *N. rustica* (▲) and *B. vulgaris* (●) leaf discs. Experimental techniques were as described in Figure 1, except 10 mM glucosamine was substituted for mannose. The points for controls (△, ○) and glucosamine-treated (▲, ●) leaves represent the means ± SE for six replicates.

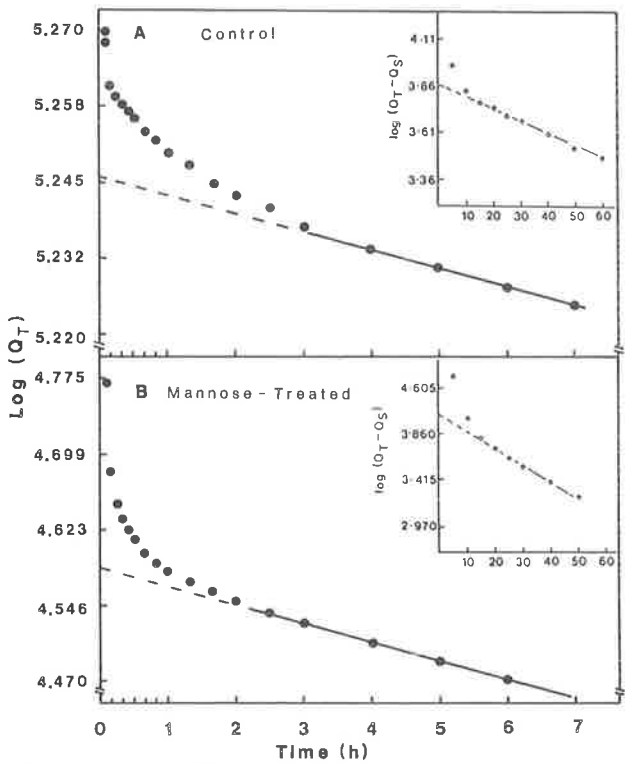


FIG. 6. Kinetics of [$^{14}$C]sucrose efflux from control (A) and mannose-treated (B) leaf discs of *B. vulgaris*. Leaf discs were loaded for 30 min in 20 mM [$^{14}$C]sucrose. The efflux solution contained 20 mM sucrose, 120 mM Mes (pH 5.0) and enough mannitol to achieve 500 mOsm. The data are plotted as the logarithm of cpm remaining in the tissue ($Q_t$) *versus* time. The slowest effluxing component (vacuole) was extrapolated to zero and subtracted from the overall curve. The insets represent cytoplasmic efflux from control (A) and mannose-treated (B) tissues. The half-times for exchange of the cytoplasmic compartment was 40.5 and 18.5 min for control and mannose-treated tissue, respectively.

prevented the induction of methyl-glucose transport into *Pelargonium* leaf discs. Application of lithium to discs that had undergone transport induction caused a large reduction in transport capability. In *Ipomoea*, the lithium inhibition of sucrose retrieval can be reversed by the addition of myo-inositol (MA Madore, personal communication). Future work will investigate the possible involvement of the phosphatidylinositide cycle in the regulation of sugar (sucrose) retrieval systems in mature mesophyll tissue, as well as the related phenomenon of wound recovery (19).

*Acknowledgments*—We wish to thank Drs. J. Cronshaw, M. A. Madore, and C. Ralph Stocking for their valuable advice and discussion throughout the performance of this research, and to Lyn Noah for typing the manuscript.

## LITERATURE CITED

1. BERRIDGE MJ, RF IRVINE 1984 Inositol triphosphate, a novel second messenger in cellular signal transduction. Nature 312: 315–321
2. BOSS WF, MO MASSEL 1985 Polyphosphoinositides are present in plant tissue culture cells. Biochem Biophys Res Commun 132: 1018–1023
3. CARLIER G, M THELLIER 1979 Lithium-perturbation of the induction of a methyl-glucose transport during aging of foliar disks of *Pelargonium zonale* (L.) Aiton. Physiol Vég 17: 13–26
4. CHEESEMAN JM 1986 Compartmental efflux analysis: an evaluation of the technique and its limitations. Plant Physiol 80: 1006–1011
5. CHEN-SHE S-H, DH LEWIS, DA WALKER 1975 Stimulation of photosynthetic

starch formation by sequestration of cytoplasmic orthophosphate. New Phytol 74: 383–392
6. CRAM WJ 1968 Compartmentation and exchange of chloride in carrot root tissue. Biochim Biophys Acta 163: 339–353
7. CRAM WJ, GG LATIES 1974 The kinetics of bicarbonate and malate exchange in carrot and barley root cells. J Exp Bot 25: 11–27
8. FOYER C, D WALKER, C SPENCER, B MANN 1982 Observations on the phosphate status and intracellular pH of intact cells, protoplasts and chloroplasts from photosynthetic tissue using phosphorus-31 nuclear magnetic resonance. Biochem J 202: 429–434
9. GARRARD LA, TE HUMPHREYS 1969 The effect of D-mannose on sucrose storage in the corn scutellum: evidence for two sucrose transport mechanisms. Phytochemistry 8: 1065–1077
10. HARRIS GC, PA GIBBS, G LUDWIG, A UN, M SPRENGNETHER, N KOLODNY 1986 Mannose metabolism in corn and its impact on leaf metabolites, photosynthetic gas exchange, and chlorophyll fluorescence. Plant Physiol 82: 1081–1089
11. HEROLD A 1978 Induction of wilting by mannose in spinach beet leaves. New Phytol 81: 299–305
12. HEROLD A, DH LEWIS 1977 Mannose and green plants: occurrence, physiology and metabolism, and use as a tool to study the role of orthophosphate. New Phytol 79: 1–40
13. HEROLD A, DH LEWIS, DA WALKER 1976 Sequestration of cytoplasmic orthophosphate by mannose and its differential effect on photosynthetic starch synthesis in $C_3$ and $C_4$ species. New Phytol 76: 397–407
14. HEROLD A, EEM MCGEE, DH LEWIS 1980 The effect of orthophosphate concentration and exogenously supplied sugars on the distribution of newly fixed carbon in sugar beet leaf discs. New Phytol 85: 1–13
15. HUMPHREYS TE, LA GARRARD 1964 Glucose uptake by the corn scutellum. Phytochemistry 3: 647–656
16. KIME MJ, RG RATCLIFFE, BC LOUGHMAN 1982 The application of $^{31}P$ nuclear magnetic resonance to higher plant tissue. J Exp Bot 33: 670–681
17. KOCHIAN LV, WJ LUCAS 1982 Potassium transport in corn roots. I. Resolution of kinetics into a saturable and linear component. Plant Physiol 70: 1723–1731
18. KONDO T, H NAKASHIMA 1979 Content of adenosine phosphate compounds in a long-day duckweed, *Lemna gibba* G 3, under different light and nutritional conditions. Physiol Plant 45: 357–362
19. LEMOINE R, S DELROT, E AUGER 1984 Development of pH sensitivity of sucrose uptake during ageing of *Vicia faba* leaf discs. Physiol Plant 61: 571–576
20. MACLACHLAN GA, HK PORTER 1959 Replacement of oxidation by light as the energy source for glucose metabolism in tobacco leaf. Proc R Soc Lond B Biol Sci 150: 460–473
21. MAYNARD JW, WJ LUCAS 1982 A reanalysis of the two-component phloem loading system in *Beta vulgaris*. Plant Physiol 69: 734–739
22. MAYNARD JW, WJ LUCAS 1982 Sucrose and glucose uptake into *Beta vulgaris* leaf tissue: a case for general apoplastic retrieval systems. Plant Physiol 70: 1436–1443
23. MIGINIAC-MASLOW M, A HOARAU 1982 Variations in the adenylate levels during phosphate depletion in isolated soybean cells and wheat leaf fragments. Z Pflanzenphysiol 107: 427–436
24. MORSE MJ, RC CRAIN, RL SATTER 1987 Phosphatidylinositol cycle metabolites in *Samanea saman* pulvini. Plant Physiol 83: 640–644
25. PITMAN MG 1963 The determination of the salt relations of the cytoplasmic phase in cells of beetroot tissue. Aust J Biol Sci 16: 647–668
26. PRESTON MR 1983 Determination of adenine, adenosine and related nucleotides at the low picomole level by reversed-phase high-performance liquid chromatography with fluorescence detection. J Chromatogr 275: 178–182
27. REBEILLE F, R BLIGNY, J-B MARTIN, R DOUCE 1983 Relationship between the cytoplasm and the vacuole phosphate pool in *Acer pseudoplatanus* cells. Arch Biochem Biophys 225: 143–148
28. STENLID G 1971 The effect of some inhibitory sugars upon the content of adenosine triphosphate in wheat roots. Physiol Plant 25: 397–401
29. THOM M, E KOMOR, A MARETZKI 1982 Vacuoles from sugarcane suspension cultures. II. Characterization of sugar uptake. Plant Physiol 69: 1320–1325
30. WALKER DA, MN SIVAK 1985 Can phosphate limit photosynthetic carbon assimilation *in vivo*? Physiol Veg 23: 829–841
31. WILSON C, WJ LUCAS 1987 Influence of internal sugar levels on apoplasmic retrieval of exogenous sucrose in source leaf tissue. Plant Physiol 84: 1088–1095
32. WILSON C, JW OROSS, WJ LUCAS 1985 Sugar uptake into *Allium cepa* leaf tissue: an integrated approach. Planta 164: 227–240
33. YOSHIOKA M, Z TAMURA 1976 Fluorimetric determination of adenine and adenosine and its nucleotides by high-performance liquid chromatography. J Chromatogr 123: 220–224

# Recent Advances in Sugar Transport

# 2

W. J. LUCAS
M. A. MADORE

I. Introduction
II. Sucrose: The Ubiquitous Transport Sugar
  A. Chemical Structure
  B. Surface Structure
  C. Carrier Recognition
III. Carrier-Mediated Sugar Transport Mechanisms
  A. Photosynthesizing Tissues
  B. Storage Tissues
IV. Group Translocator Concept for Sucrose
  A. Grape Pericarp Cells
  B. Sugarcane Tonoplast System
V. Mechanism of Phloem Loading
  A. Sucrose–$H^+$ Cotransport into the Phloem?
  B. Apoplastic versus Symplastic Pathway
VI. Sucrose Metabolism by Sink Tissues
  A. Regulation of Sucrose Supply by Source Leaf Metabolism
  B. Control by Metabolically Driven Gradients
  C. Control by Phloem Unloading
  D. Hormonally Directed Transport
VII. Turgor Sensing in Sugar Transport
VIII. Conclusions
  References

## I. INTRODUCTION

The importance of carbohydrate synthesis and translocation is clearly reflected in the degree of research activity that has occurred since this area was covered in this series (see Giaquinta, 1980b). Numerous reviews on various aspects of sugar metabolism have stressed the complexity of the

The Biochemistry of Plants, Vol. 14
Copyright © 1988 by Academic Press, Inc.
All rights of reproduction in any form reserved.

regulatory mechanisms involved in both source and sink tissues (Stitt, 1985, 1986; Huber *et al.*, 1985; Huber, 1986; Stitt *et al.*, Volume 10, Chapter 6 this treatise). Similarly, the very important agronomic aspects of carbon partitioning, with respect to crop yield, have received considerable attention (see reviews by Gifford and Evans, 1981; Geiger and Giaquinta, 1982; Ho and Baker, 1982; Gifford *et al.*, 1984; Thorne, 1985; Gifford, 1986) and here also a complex situation is emerging. Most authors have stressed the need for a greatert degree of integration of all aspects of research in this area.

Basic aspects of sugar transport have been reviewed by Komor (1982), Giaquinta (1983), and Reinhold and Kaplan (1984). A recent International Conference on "Phloem Transport" reviewed progress in this area (Cronshaw *et al.*, 1986). Because of the extensive nature of the literature pertaining to this general area of sugar transport and cognizant of the recent reviews, we have focused our attention on specific plant systems to illustrate our current understanding of the mechanistic aspects of sugar transport. Our approach has been to develop current concepts from the chemical/molecular level through the organ to the whole plant level.

## II. SUCROSE: THE UBIQUITOUS TRANSPORT SUGAR

Sucrose is the most common form in which sugar is transported in higher plants. The reasons for this are not clear but are suspected to involve its relatively unreactive chemical structure (Fig. 1). In animal systems, the more reactive monosaccharide, glucose, can be used for transport because the transport system (the blood stream) is extracellular. Blood glucose is effectively sequestered outside the cytosol and does not encounter cellular enzymes until it is taken up across a plasma membrane. In green plant cells, sugars are synthesized internally within the cytosol, but the cell also has a full complement of glycolytic enzymes for energy maintenance during the dark period. Thus, an inert molecule is an advantage, preventing a futile cycle of simultaneous carbohydrate synthesis and degradation.

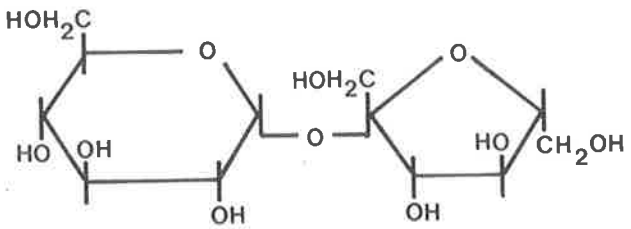


**Fig. 1.** The chemical structure of sucrose.

## A. Chemical Structure

The linkage of the glucopyranose residue through the C-1 position to the fructofuranose at the C-2 position effectively sequesters the anomeric carbons from both of the monosaccharide residues, thus imparting the chemical inertness. The presence of a fructose residue in the furanose, or envelope form, in a beta linkage with glucose, imparts an extreme lability to the fructose moiety, giving the sucrose molecule a high free energy of hydrolysis (approximately $-30$ kJ mol$^{-1}$). Thus, sucrose can be readily hydrolyzed with suitable enzymes (invertases and sucrose synthase) but is inert until coming in contact with these enzymes.

## B. Surface Structure

Space-filling models of the sucrose molecule show that it has a complex surface structure. Laterally oriented hydroxyl groups emanate from a broad internal expanse of essentially hydroxyl-free regions (Fig. 2). This results in a surface structure consisting of highly ordered hydrophilic and hydrophobic domains. Some of the hydroxyl groups are involved in intramolecular bonds reducing to some extent the hydrophilic character otherwise imparted. The hydrophilic hydroxyl groups allow the formation of hydrogen bonds, either donating a hydrogen to an acceptor or accepting a hydrogen from a donor. Additionally, the hydroxyl-free area can form bonds with other hydrophobic

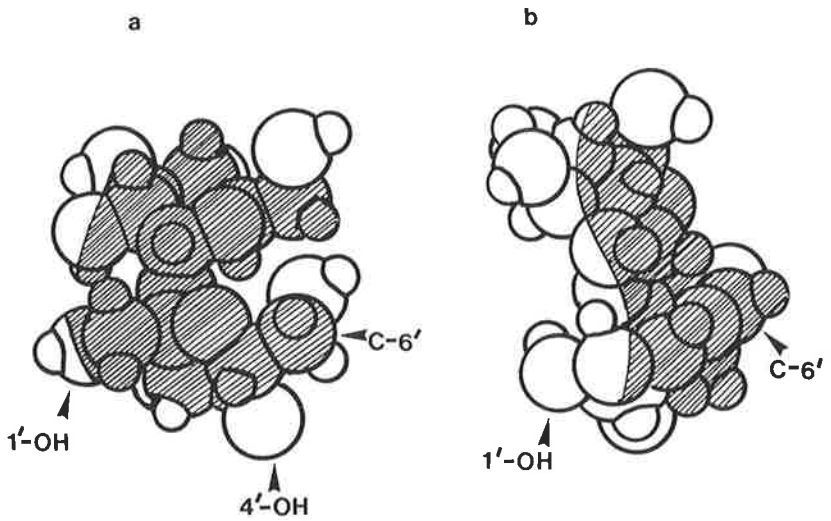


**Fig. 2.** A computer-generated space-filling model of crystalline sucrose viewed (a) toward the *b*-face of the glucose ring and the *a*-face of the fructose ring (the shaded area indicates the hydrophobic region) and (b) toward the C-2 and C-1′ regions, showing the overall wedge shape of the molecule. (From Hitz, 1986; with permission.)

groups through hydrophobic interactions. These surface properties of the sucrose molecule allow the recognition of sucrose by specific membrane proteins such as taste receptors of the tongue (Bock and Lemieux, 1982).

## C. Carrier Recognition

The role of the three dimensional surfaces of the sucrose molecule in recognition by plant membrane proteins has been addressed in an elegant series of experiments performed by Hitz and co-workers (Hitz, 1986). Using a novel approach which combined the use of specifically derivatized sucrose analogs and a readily assayed sucrose transport system, the binding characteristics of the sucrose molecule to a plasma membrane sucrose carrier were determined. The membrane carrier investigated was that found on the plasma membrane of soybean cotyledon cells. The developing soybean cotyledon is entirely reliant on the parent plant for assimilates but is symplastically isolated from the maternal tissue. Therefore, uptake of assimilates must necessarily occur from the apoplast across the plasmalemma of cotyledon cells where specific carriers for solute uptake exist for this purpose. Thorne (1985) has provided a detailed review of the soybean system.

Protoplasts can readily be prepared from cotyledons (Lin *et al.*, 1984), providing an easily studied system for assay of binding and uptake of sucrose and its derivatives. In the Hitz studies, carrier activity was measured simply by the uptake of radioactive sucrose in the presence or absence of each analog. Analogs were synthesized through various chemical reactions substituting the hydroxyl groups on a fructose molecule with chemical groups which display differing hydrophilic or hydrophobic character (Card *et al.*, 1985). These substituted fructoses were then coupled via UDP-glucose and the sucrose synthase reaction (Card and Hitz, 1984) to yield substituted sucrose molecules with varying degrees of hydrophobicity (Fig. 3).

Sucrose analogs, such as 1′-fluorosucrose, act as true competitive inhibitors increasing the apparent $K_m$ for sucrose uptake while not affecting $V_{max}$ (Fig. 4). These molecules compete with sucrose for binding sites and affect the subsequent uptake of sucrose in a manner that is dependent upon the rate of dissociation (approximated by $K_i$) of a particular analog from the carrier molecule. Thus, the more tightly an analog binds (i.e., the higher its affinity for an active site), the greater is the reduction in the rate of [$^{14}$C]sucrose uptake. Comparison of the inhibited rate ($V_i$) to the noninhibited rate ($V_0$) at various inhibitor concentrations [I] yields linear profiles from which $K_i$ can be determined, as shown in Fig. 5.

Using the soybean protoplast system, it was found that replacement of the C-1 (Fig. 3a) or C-6 (Fig. 3b) of fructose with fluorine yielded a sucrose derivative with a higher binding affinity than underivatized sucrose. Substitution at C-4 (Fig. 3c) did not affect binding, suggesting that this hydroxyl group was oriented away from the hydrophobic center of the molecule. The

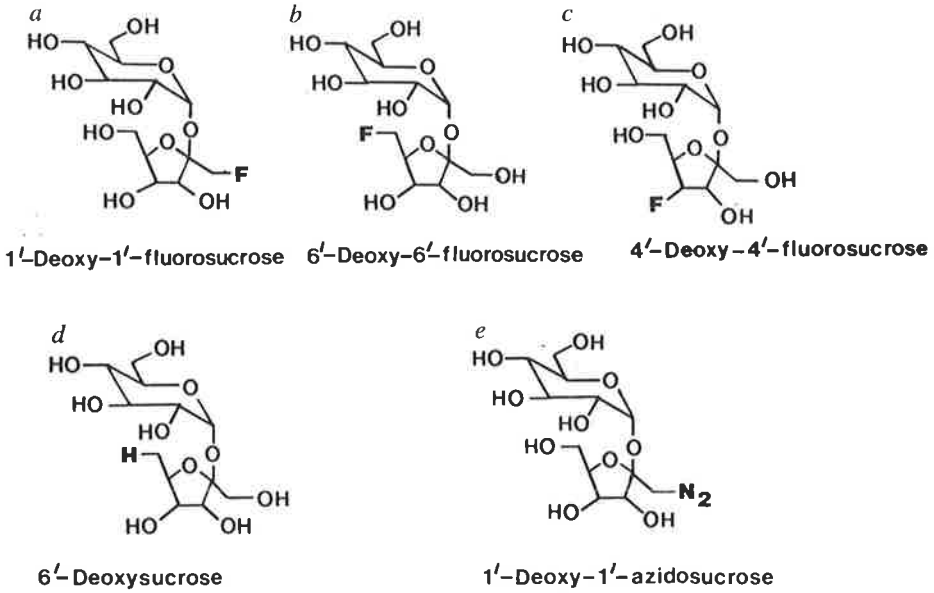


**Fig. 3.** The chemical structures of sucrose analogs used as alternate substrate inhibitors of [$^{14}$C]sucrose influx into soybean cotyledon protoplasts. (Redrawn from Hitz, 1986, with permission.)

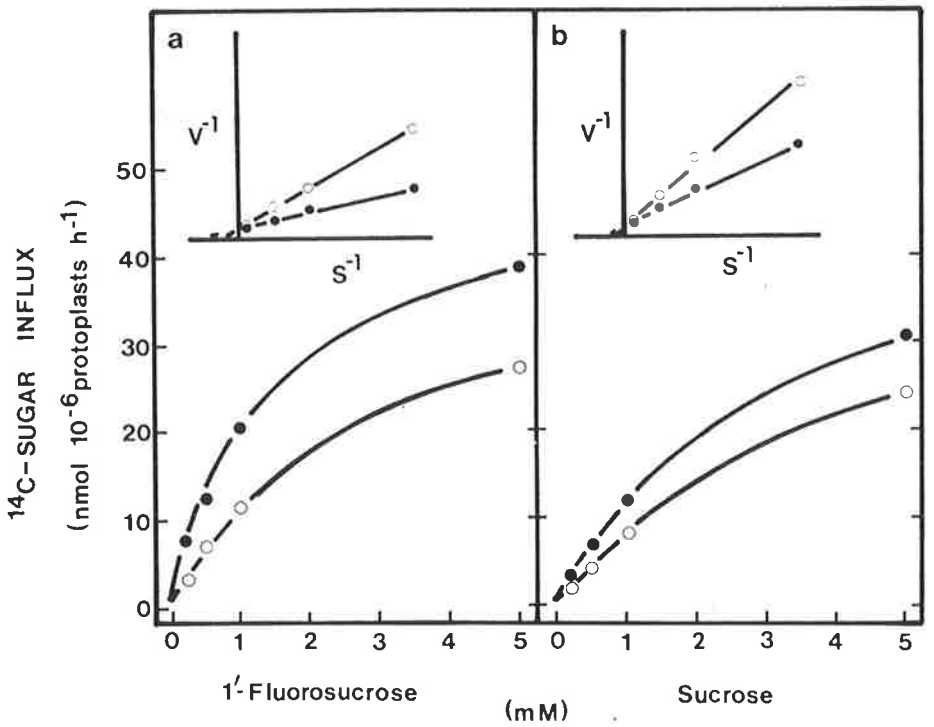


**Fig. 4.** Influx kinetics of [$^{14}$C]sucrose and of [$^{14}$C]-1′-deoxy-1′-fluorosucrose into isolated soybean cotyledon protoplasts. (From Hitz *et al.*, 1985; with permission).

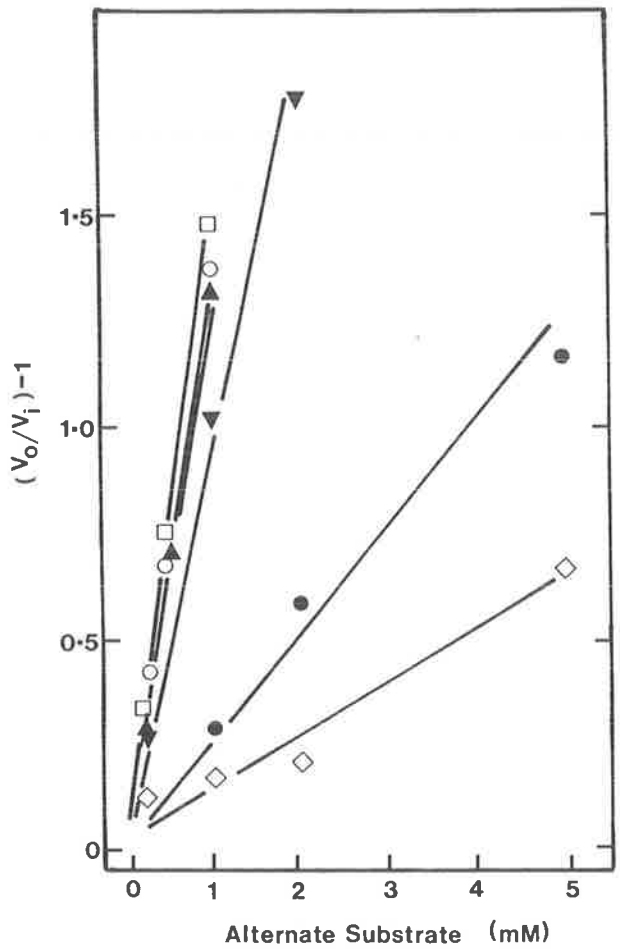


**Fig. 5.** Plots of $(V_0/V_i)^{-1}$ *vs* concentration of alternate substrate for influx of 0.2 m*M* [$^{14}$C]sucrose into soybean cotyledon protoplasts. $V_0$ is the influx in the absence of sucrose analogs, $V_i$ is the influx in the presence of sucrose analogs. Slopes of the lines are equal to $1/K_i$ for the sugar analogs ($K_m$ for sucrose = 2.4 m*M*). 1′-deoxy-1′-aminosucrose: (◇); 4′-deoxy-4′-fluorosucrose: (●); 1′-deoxy-1′-fluorosucrose: (▼); 1′-deoxy-1′-azidosucrose: (▲); 6′-deoxy-6′-fluorosucrose: (○); 6′-deoxysucrose: (□) (From Hitz, 1986, with permission.)

fluoro-derivatives were capable of forming hydrogen bonds, but also increased the hydrophobicity of the molecule. However, C-6-deoxy- (Fig. 3d) and C-1-azido- (Fig. 3e) derivatives, which were not capable of forming hydrogen bonds, also showed enhanced binding, suggesting that the hydrophobic interactions were the important factor in determining binding affinity. This was confirmed by substituting the entire fructose residue with a nonhydroxylated hydrophobic group such as phenyl-α-D-glucopyranoside or phenyl-α-D-thioglucopyranoside both of which bound more strongly than sucrose to the carrier (Card and Hitz, 1984; Hitz, 1986).

Based on these experiments it was concluded that sucrose recognition occurs by hydrophobic interactions and not by hydrogen bonding through the hydroxyl groups of the fructose residue. A recognition function for hydroxyls on the glucose residue, on the other hand, was still regarded as a possibility requiring further experimentation.

This new understanding of sucrose surface chemistry opens up entirely new avenues of approach for resolving what have been until now contentious or simply untestable issues. Already, the 1′-fluorosucrose derivative, which is not readily hydrolyzed by plant invertases, has shown potential as a tool for characterizing those tissues in which sucrose hydrolysis is a prerequisite for uptake (Hitz *et al.*, 1985). The ability to synthesize carrier-specific sugar analogs may also finally resolve the as yet unsettled question of apoplastic loading of sugars in leaves. Long hypothesized but, as discussed later, not conclusively proven, this issue could readily be resolved through the use of a tightly binding, nonpermeative sucrose analog which, when supplied to the apoplast, could be used to block the putative loading site carrier. Similarly, such an analog, if radioactively or otherwise labelled, could be used as a marker for sucrose carrier proteins, allowing their isolation for use in characterization and reconstitution experiments. The synthesis of a labelled, tightly binding sucrose analog would be invaluable for use in localization experiments, which presently rely on "markers" such as *p*-chloromercuribenzene sulfonic acid (PCMBS) (M'Batchi *et al.*, 1985) which have, at best, only dubious specificity for any one membrane protein.

The production of metabolically inert sucrose derivatives will also aid in the study of sucrose metabolism following its uptake into tissues such as occurs in developing fruits. By combining the use of sugar analogs with the traditional biochemical procedures of enzyme isolation, it should be possible to better characterize the synthesis and activation of important enzymes like sucrose synthase.

## III. CARRIER-MEDIATED SUGAR TRANSPORT MECHANISMS

Most plant tissues appear to be able to take up a wide range of exogenously applied sugars. Numerous workers have used the "exogenous sugar" technique to study the putative kinetics of sugar transport into a wide range of plant tissues. In general, these studies have indicated that the various sugars, like sucrose, glucose, 3-*O*-methyl glucose (3-*O*-MG, a nonmetabolized glucose analog), fructose, etc., are taken up via a combination of a saturable and a linear (or first-order kinetic) transport component. The interpretation of these results, especially with respect to the actual cellular location of the sugar transport process(es) and involved mechanisms has been the subject of much debate. This topic has been covered in a recent

review by Reinhold and Kaplan (1984) and we will therefore restrict our coverage to what we feel are key issues.

Four basic mechanisms have now been implicated in the carrier-mediated transport of sugars across either the plasmalemma or the tonoplast: facilitated diffusion, sugar–proton cotransport, sugar–proton antiport, and vectorial group translocation (Fig. 6a,b,c,d). In the sections that follow, we will use specific examples to illustrate both our current understanding of how these different transport mechanisms are thought to function and their location within the cell or tissue(s).

## A. Photosynthesizing Tissues

It is beyond the scope of this review to evaluate the literature pertaining to sugar metabolism in mature photosynthesizing leaves. Although considerable biochemical information is now available on the regulatory processes involved in sucrose synthesis (see Stitt, 1985, 1986; Huber, 1986; and Stitt *et al.*, Volume 10, Chapter 6 this treatise), a complete description of the relationship between synthesis and translocation of sucrose is presently unavailable. This is due, in part, to the complexity of the leaf as an organ. Sucrose synthesis occurs within the cytosol of the mesophyll tissue, a space which occupies about 2% (excluding organelles) of the entire leaf symplastic volume. The pathway followed by sucrose during its movement from the site of synthesis to the cells of the phloem remains equivocal. Furthermore, we have only recently begun to unravel the complexities associated with compartmentalization of sugars (also starch and amino acids) within the various cell types of the leaf (see, e.g., Franceschi and Giaquinta, 1983a,b; Franceschi, 1986; Gordon, 1986). Finally, it is now becoming evident that the leaves of different species can have quite dissimilar characteristics with respect to vacuolar compartmentation of sugars.

### *1. Uptake Kinetics Obtained on Leaf Tissues*

Because of the important role played by source leaves, in terms of supplying sucrose for long-distance translocation, considerable attention has been focused on sugar transport by intact and excised leaf tissues (see Giaquinta, 1983; Reinhold and Kaplan, 1984). The kinetics of sucrose uptake into such tissues was originally interpreted as representing the operation of two saturable systems (see, e.g., Geiger, 1975; Giaquinta, 1980a). More recent studies have shown that uptake occurs via the combination of a saturable and a linear, or first-order kinetic component (Maynard and Lucas, 1982a; but see Delrot and Bonnemain, 1981; M'Batchi and Delrot, 1984). Parallel experiments on sugar (sucrose) uptake and pH changes within the bathing medium indicated that the saturable component may reflect the operation of a plasma membrane-bound sucrose–$H^+$ cotransport mechanism (Giaquinta. 1977a,

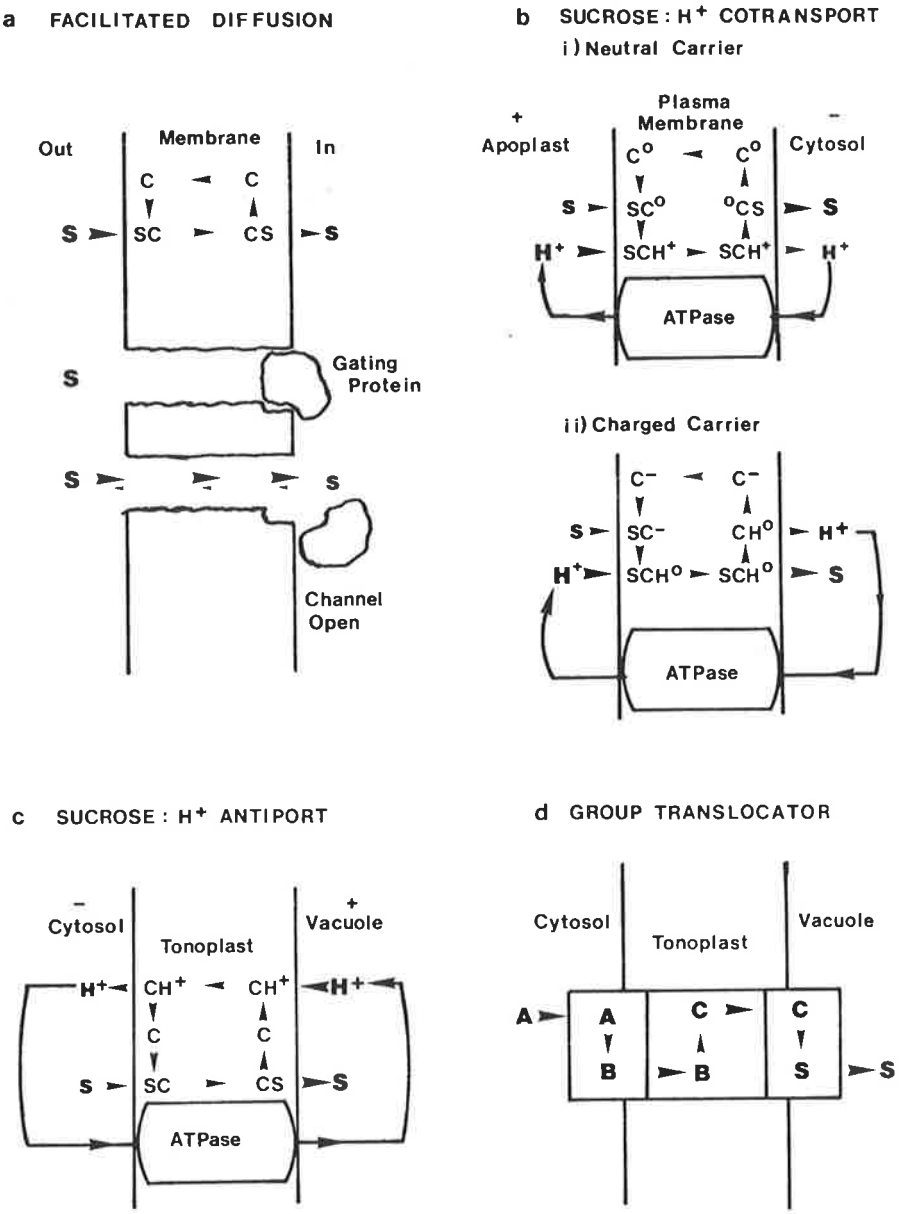


**Fig. 6.** Schematic models for sugar transport across plant cell membranes. (a) Facilitated diffusion (passive transport) as effected by carrier-mediated processes or protein-gated transport channels; (b) Sucrose–proton cotransport mechanism by (*i*) a neutral carrier or (*ii*) a charged carrier. In (*i*), the charged proton–carrier–sugar complex ($SCH^+$) moves across the membrane in response to the $H^+$ gradient established by the $H^+$-ATPase. In (*ii*) the proton gradient established by the $H^+$-ATPase is used to neutralize the charge on the carrier–sugar complex ($SC^-$). (c) Sucrose–proton antiport mechanism, as envisaged by Thom and Komor (1984), for sugar transport across the tonoplast of sugarcane suspension cells. The proton gradient established by the outwardly directed $H^+$-ATPase is used to return the carrier to the cytoplasmic face of the tonoplast. (d) A schematic group translocator system which catalyzes the vectorial synthesis through intermediates A, B, and C of a sugar molecule (S) and its transport across the tonoplast of a plant cell.

1979a, 1980a,b; Delrot, 1981; Delrot and Bonnemain, 1981; Delrot *et al.*, 1980). In photosynthetic tissues the operation of this putative sugar–$H^+$ cotransport system may be quite complicated (see, eg., Guy *et al.*, 1981).

Considerable debate has ensued as to whether these kinetics reflect sucrose transport into the phloem, *per se*, or uptake into the most readily accessible cells. During early studies, application of either $^{14}CO_2$ or $^{14}C$-labelled sugars to mature leaf tissue indicated that the movement of radiolabelled compounds to the phloem was selective, and that the sugar normally translocated by a particular plant accumulated in the minor veins (Fondy and Geiger, 1977; Geiger, 1975). The combination of the autoradiographic image of the minor veins (obtained when tissue was exposed to exogenous [$^{14}C$]sucrose) and the demonstration that $^{14}C$-labelled compounds (mainly sucrose) produced by $^{14}CO_2$-mediated photosynthesis could be trapped and removed from the leaf by applying nonradioactively labelled sucrose (Geiger *et al.*, 1974) provided the experimental basis for the hypothesis that an apoplastic step was involved in phloem loading. The higher osmotic pressure within the sieve element–companion cell complex provided indirect support for this hypothesis (Geiger *et al.*, 1973).

Sovonick *et al.* (1974) and Giaquinta (1977a) investigated the relationship between sucrose uptake into leaf discs and the intact leaf with respect to phloem translocation. Based on these studies they concluded that exogenous sucrose uptake into leaf discs reflects loading specifically into the phloem and could, therefore, be used to study the mechanism involved (see also Delrot, 1981; Delrot and Bonnemain, 1981; Delrot *et al.*, 1980; Giaquinta, 1979a, 1980a).

It is of interest that this concept was rarely challenged, since Geiger (1976) and Fondy and Geiger (1977) had obtained evidence which showed that uptake of exogenous sucrose apparently occurred into cells of both the mesophyll and vascular bundles. After a 30-min exposure to 10 m*M* $^{14}C$-sugar, approximately 60, 70 and 100% of the radioactivity was present in the mesophyll for sucrose, fructose, and 3-*O*-MG, respectively. Of equal interest was the fact that only those sugars which could be metabolized to sucrose gave rise to "phloem loading," suggesting that all of the uptake was initially into the mesophyll where exogenous sugars were used for the synthesis of sucrose. Fondy and Geiger (1977) concluded that "the mesophyll tissue may act as a collecting surface, reclaiming sucrose and hexoses which leak from the photosynthesizing cell." However, although it was generally recognized that the mesophyll would act as a barrier to the penetration of exogenously supplied compounds to the phloem, by the beginning of the 1980s the consensus was that transport characteristics deduced by application of exogenous sucrose represented those of phloem loading.

Maynard and Lucas (1982b) were the first to question the interpretation of the kinetic results with respect to the actual site of sucrose uptake. They obtained similarly shaped kinetic profiles for sucrose, glucose, and 3-*O*-MG

influx into whole sugar beet petiole slices, petiole segments containing only parenchyma tissue, and petiole segments containing vascular bundles in which many of the sieve tubes had been destroyed by tissue sectioning. The kinetic curve for 3-*O*-MG influx into sugar beet leaf discs was also found to be identical in form to that obtained with sucrose; i.e., uptake appeared to result from the operation of a saturable and a linear transport component (Fig. 7). This similarity was important because the uptake of 3-*O*-MG appears, in leaf tissue, to be almost exclusivly confined to the metabolic space of the mesophyll cells (Fondy and Geiger, 1977). Based on these studies, Maynard and Lucas (1982b) concluded that the presence of a saturable and a linear component of uptake must be a ubiquitous feature of the plasma membranes of a wide variety of cell types within the mature leaf.

Wilson *et al.* (1985) provided further experimental support for the concept that all cell types can take up exogenously supplied sugars. Mature onion leaves were chosen for their experiments because this tissue lacks an inner cuticle and so cell-wall-digesting enzymes could be used to remove various cell types. Sucrose influx into control and structurally manipulated tissues indicated similar kinetics for the inner parenchyma (plus bundle sheath), the chlorenchyma, and the vascular bundles. The inner parenchyma accounted for 70% of the total uptake, whereas the contribution of the vascular bundle was quite small (15%). Physiologic and autoradiographic studies on fresh and aged wheat (Leger *et al.*, 1982) and broad bean (Lemoine *et al.*, 1984) leaf tissues also indicated that the mesophyll can accumulate exogenously supplied sucrose. Collectively, these data support the contention that uptake kinetics, obtained on leaf tissue, represent retrieval of sugars by the various tissues and cannot be equated with the specific process of phloem loading (see also section V).

### 2. *Sugar Transport Studies on Isolated Mesophyll Cells/Protoplasts*

In an attempt to reduce the ambiguities associated with the complexities of leaf morphology, several groups have turned to isolated mesophyll cells or protoplasts to address the question of sugar transport. An important issue to determine was whether mesophyll cells, *per se,* released photosynthetically fixed carbon in the form of sucrose. Of course, this related to the conceptual issue of whether an apoplastic step was involved in loading sucrose into the phloem.

Kaiser *et al.* (1979) conducted parallel photosynthetic studies on intact leaves and isolated mesophyll cells of *Papaver somniferum* (poppy) and *Spinacea oleracea* (spinach). Analysis of the $^{14}C$-labelled products of photosynthesis showed that leakage (efflux) from the mesophyll cells into the bathing medium was minimal (less than 0.7% of the total $^{14}C$ fixed). Sucrose, glucose, and fructose were the main sugars released with sucrose accounting for 65% of the total $^{14}C$ released. However, Kaiser *et al.* (1979) claimed that since this rate of release was considerably lower than the movement of $^{14}C$-

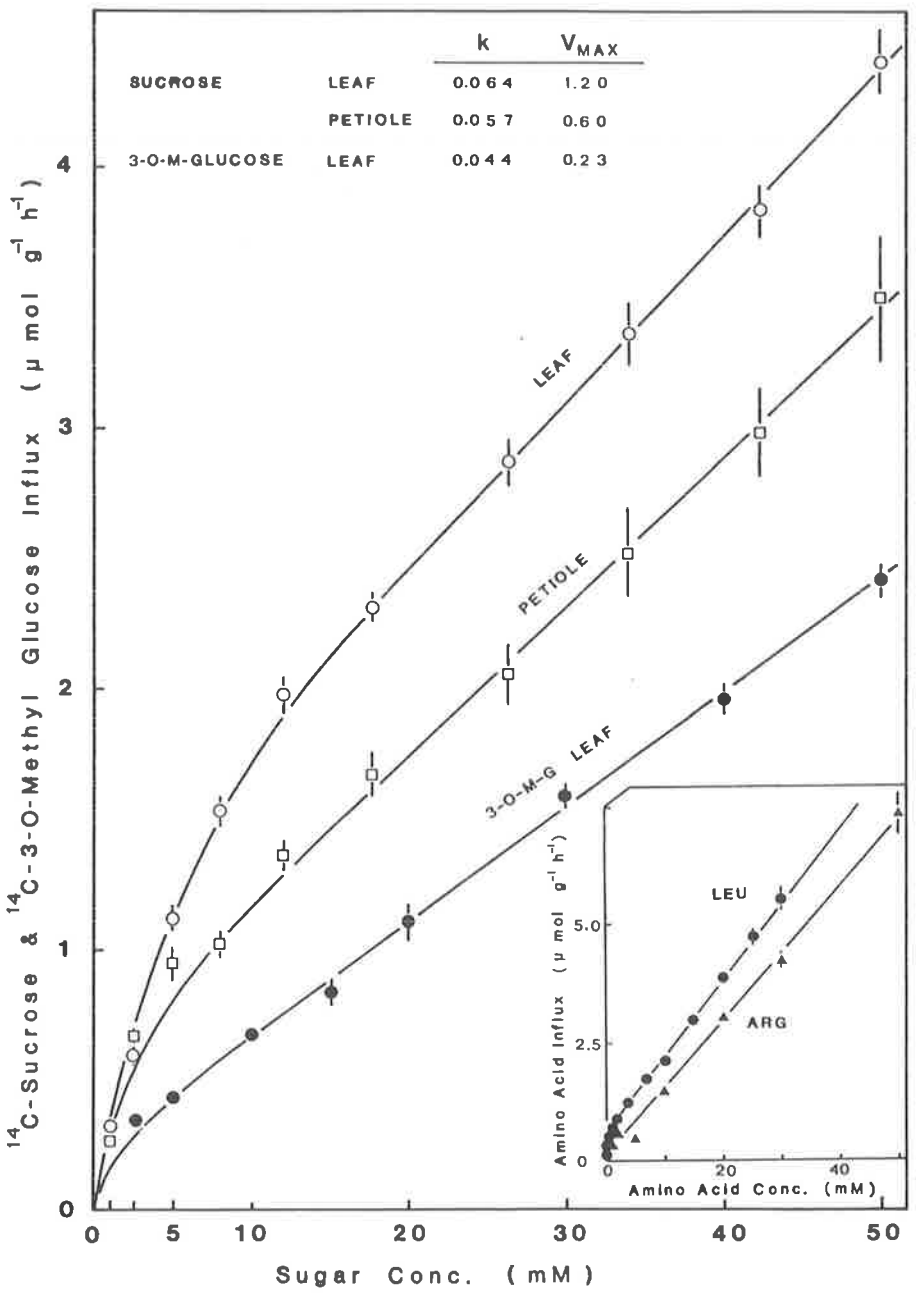


**Fig. 7.** Concentration dependence of $^{14}$C-sugar influx into sugar beet source leaf discs and petiole slices. $V_{max}$ values ($\mu$mol g$^{-1}$ h$^{-1}$) are for the saturable transport component and $k$ values ($\mu$mol g$^{-1}$ h$^{-1}$ m$M$ sugar$^{-1}$) represent the first-order rate coefficients for the linear component. Amino acid influx into this tissue shown for comparison (see Inset). (Data from Maynard and Lucas, 1982b.)

photosynthates out of the intact leaf, the mesophyll cells apparently were not involved in the apoplastic transfer of sucrose.

This issue was further examined in a study on isolated tobacco mesophyll cells (Scorer, 1984). Here, as with poppy cells, $^{14}$C-photosynthate was released very slowly from the mesophyll cells. The rate of release was reduced in the presence of $Ca^{2+}$ and enhanced when EDTA was added (see also studies on *Vicia faba* leaf discs by Anderson, 1983). Exogenously supplied [$^{14}$C]sucrose was also taken up by tobacco mesophyll cells and this influx could be inhibited by various metabolic inhibitors; under these conditions apparent efflux increased. These results were consistent with the earlier studies conducted on pea protoplasts by Guy *et al.* (1980) who demonstrated the presence of an energy-dependent 3-*O*-MG uptake mechanism at the plasmalemma. In agreement with the hypothesis forwarded by Maynard and Lucas (1982b), Scorer concluded that mesophyll cells possess energy-dependent uptake processes which recover much of the photoassimilate lost from these cells.

Protoplasts isolated from tobacco and wheat mesophyll cells appeared to behave differently from isolated mesophyll cells. Huber and Moreland (1980, 1981) reported that during photosynthesis, sugars released from tobacco protoplasts did not respond to $Ca^{2+}$, and efflux was reduced in the presence of a $H^+$-ionophore. In their studies, the rate of sugar release (mainly sucrose) was equivalent to the photosynthetic rate. In contrast, Asami *et al.* (1985) reported that photosynthesizing spinach leaf protoplasts released insignificant amounts of sucrose and hexoses.

These discrepancies highlight the problems associated with extrapolating from the *in vitro* situation back to transport processes that control the compartmentation of sucrose into transport and nontransport pools within the intact leaf. In this context, it is pertinent to note that mesophyll cells isolated from squash (Madore and Webb, 1982) or cucumber (Madore, 1984) partition almost no photosynthetically fixed carbon into stachyose, the major transport sugar in members of the Cucurbitaceae. Instead, recently fixed carbon is increasingly diverted into compounds normally assigned storage functions in these leaves (i.e., starch, sucrose, and maltose), suggesting an increased retention of assimilated carbon within the chloroplast as well as an increased diversion of photoassimilate into the vacuole. The question of altered carbon partitioning associated with the physical separation of cells or protoplasts from vascular "sinks" remains to be addressed by transport physiologists.

However, even the role of the mesophyll cell vacuole as a temporary storage compartment for sugars appears to be under debate. Kaiser *et al.* (1982) developed a silicone-oil centrifugation method that allowed them to isolate vacuoles from photosynthesizing barley mesophyll protoplasts in less than one minute. Using this technique, Kaiser and his co-workers were able to demonstrate that, following an initial lag period (12–15 min), photosynthetic products were rapidly sequestered in the vacuole. The rate of appear-

ance of [$^{14}$C]sucrose in the vacuoles was similar to its rate of synthesis within the protoplasts. Studies on isolated barley vacuoles indicated that [$^{14}$C]sucrose crosses the tonoplast by a carrier-mediated process (Kaiser and Heber, 1984). This system displayed saturation kinetics ($K_m$ of 21 m*M*) and uptake was competitively inhibited by other sugars, with maltose and raffinose being particularly effective. The sulfhydryl reagent, PCMBS, completely inhibited sucrose uptake. However, uptake into these isolated vacuoles was not dependent upon addition of ATP or pyrophosphate, nor was it reduced in the presence of carbonyl cyanide 3-chlorophenyl hydrazone (CCCP) or valinomycin.

Collectively, these results suggested that sucrose was crossing the tonoplast via a passive, nonspecific permease, or facilitated diffusion mechanism. The absence of an effect of ATP on uptake conflicts with the pioneering study of Guy *et al.* (1979) who established that 3-*O*-MG uptake into isolated pea vacuoles was stimulated by ATP. However, Guy *et al.* (1979) also discussed the likely role of facilitated diffusion in sugar transport across the tonoplast. The discrepancy may have been due to the isolation procedure employed by Kaiser and Heber (1984), in that $H^+$-translocating activity may have been absent or ineffective due to leakage or membrane damage. That this was not the case has been established by subsequent reports from this laboratory. Vacuoles isolated in the same way displayed active, ATP-dependent uptake of malate (Martinoia *et al.*, 1985) and $Cl^-$ (Kaiser *et al.*, 1986).

Boller and Alibert (1983) repeated the study conducted by Kaiser *et al.* (1982) with the intent to extend the photosynthetic period. Mature leaves of *Melilotus alba* (white clover), rather than barley, were used to prepare photosynthetically active protoplasts. A comparison of the photosynthetic rates and vacuole-to-protoplast sucrose ratios indicated close agreement between the preparations from the two different species. However, at the longer periods employed (2 h) by Boller and Alibert (1983), the sucrose level within the vacuoles continued to lag behind that in the cytosol. According to their analysis, after 2 h only 30% of the photosynthetically produced [$^{14}$C]sucrose was transferred to the vacuole, giving rise to a concentration differential of 7.5 : 70–140 m*M* (vacuole : cytosol). They concluded, therefore, that the transfer of sucrose to the vacuoles was slow and that this sugar resided preferentially in the cytosol.

The nonaqueous fractionation technique developed by Gerhardt and Heldt (1984) allowed a study of the cytosolic and vacuolar photosynthetic metabolites in "intact" spinach leaves. Vacuolar sucrose was found to increase during the day to a maximum value of 45 m*M* and during the night it decreased to approximately 1 m*M*. More importantly, Gerhardt and Heldt (1984) found that although the sucrose levels fluctuated on a diurnal basis, they could detect little difference in the concentrations within the cytosol and vacuole. But, as often seems to be the case, there is always another set of results that further confuses the issue. Asami *et al.* (1985), using proto-

plasts and vacuoles from field-grown spinach, could not detect the accumulation of [$^{14}$C]sucrose in the vacuole; nor could they detect the release of significant amounts of sucrose or hexose into the suspension medium.

Subtle differences in isolation techniques or experimental protocols may be the source of these apparent discrepancies. An alternative explanation might be that different species employ quite different strategies with respect to the compartmentation of recently fixed sugars. Indeed these "strategies" may be influenced by the photosynthetic prehistory of the leaf or plant. Analysis of the literature on $^{14}$C-translocation from intact, photosynthesizing leaves indicates that plants may differ quite widely in the times required for the equilibration of the various carbohydrate pools. In sugar beet, equilibration between the cytosolic and vacuolar pools appears to take between 4 and 6 h (Geiger *et al.*, 1983); this misled Geiger and Swanson (1965) who proposed originally that no sucrose storage pool existed in these leaves. Alternatively, for *Vicia faba*, sucrose "equilibration" across the tonoplast of the palisade parenchyma cells appears to occur quite rapidly (15–20 min; see Fisher and Outlaw, 1979). In an earlier study on *Vicia*, Outlaw and Fisher (1975) found that recently fixed $^{14}$C-sugar could be mobilized out of the mesophyll within 1 h or it could remain for prolonged periods. As pointed out by Boller and Alibert (1983), "both exclusion from and deposition in the vacuole of recently fixed solutes might occur in one and the same plant."

Since PCMBS completely prevented [$^{14}$C]sucrose efflux from preloaded wheat vacuoles (Kaiser and Heber, 1984), it is possible that the cell may also have some means of controlling this transport system. If this were the case, one could argue that causing sucrose to accumulate in the cytosol would facilitate the symplastic movement to the veins, whereas transport into the vacuoles would establish a "buffer" that could be drawn on during periods of low photosynthetic activity.

Compared with the volume of literature pertaining to the characterization of the tonoplast $H^+$-ATPase (see Sze, 1985), the information available on sugar transport across the tonoplast of mesophyll tissue is indeed meagre. Further work is needed before we can conclude whether both a passive, facilitated diffusion, and an active (possibly via a sugar–$H^+$ antiport) mechanism function at the tonoplast/vacuolar level.

At present, experimental data indicate that sugar transport (retrieval) across the plasmalemma of leaf tissues occurs by a saturable, energy-dependent process, and a first-order kinetic mechanism. The saturable process is presently considered to represent a sucrose–$H^+$ cotransport mechanism, but no concensus exists as to the underlying mechanism responsible for the linear component. A linear dependence on substrate concentration is usually interpreted as movement via a passive process. Simple diffusion through the lipid bilayer of the plasmalemma does not seem plausible since this mechanism should not show competitive inhibition (see Maynard and Lucas, 1982a,b). In addition, uptake by simple diffusion should not show drastic

differences in the rates observed between stereoisomers. A facilitated diffusion mechanism may show isomer discrimination and directionality, with the latter being imposed by metabolism or sequestration of sugars into slowly exchanging compartments (vacuoles?). However, a facilitated diffusion process should display saturation kinetics at very high substrate concentrations. To date, evidence of saturation has not been forthcoming. Thus, at present, insufficient information is available to allow a definitive statement to be made concerning the mechanism (and importance) of the linear, or first-order, mechanism in mature leaf tissues.

## B. Storage Tissues

Sucrose is ubiquitous in all higher plant species and can be isolated from all plant organs and tissues. Sucrose is normally stored in the vacuole, but in general this type of storage represents a temporary sequestration of carbon as in the case of leaf mesophyll cells. In most tissues, starch is by far the more important form of stored carbohydrate. However, certain crop species (most notably sugarcane, sugar beet, and to a lesser extent, red beet) have been specifically selected for the ability to store large amounts of sucrose in the vacuoles of the storage tissues.

### *1. Sugar Beet Taproot*

The sucrose level within a sugar beet taproot storage parenchyma cell can reach values as high as 500–800 m*M*. In this tissue, in contrast to sugarcane, the movement of sucrose from the phloem to the storage parenchyma does not appear to involve hydrolysis by an apoplastic acid invertase (Giaquinta, 1977b, 1979b). Using discs of root tissue, Wyse (1979) found that of the various sugars tested sucrose was taken up at the highest rate. However, in contrast with other studies, the kinetics of sucrose transport could be described by a first-order, or nonsaturating system; i.e., no saturable component could be detected. Based on the effects of various metabolic inhibitors, Wyse (1979) concluded that passive sucrose movement across the plasmalemma acts to rate-limit the active movement of sucrose across the tonoplast.

In a subsequent study, Saftner *et al.* (1983) found that pretreatment of sugar beet root discs in 200–250 m*M* mannitol resulted in uptake kinetics that contained both saturable and linear components. Application of 10 $\mu M$ CCCP inhibited respiratory $CO_2$ release by 99% and reduced sucrose uptake. Under these conditions the saturable component was eliminated as was a portion of the linear component. Saftner *et al.* (1983) interpreted these results as indicating the presence of two energy-dependent transport processes, a saturable and a linear (first-order) system, plus a passive system (see Fig. 8a). Efflux studies and compartmental analysis on control and CCCP-treated root discs indicated that the sucrose levels in the apoplast and cytosol were almost equal and that 10 $\mu M$ CCCP did not inhibit sucrose

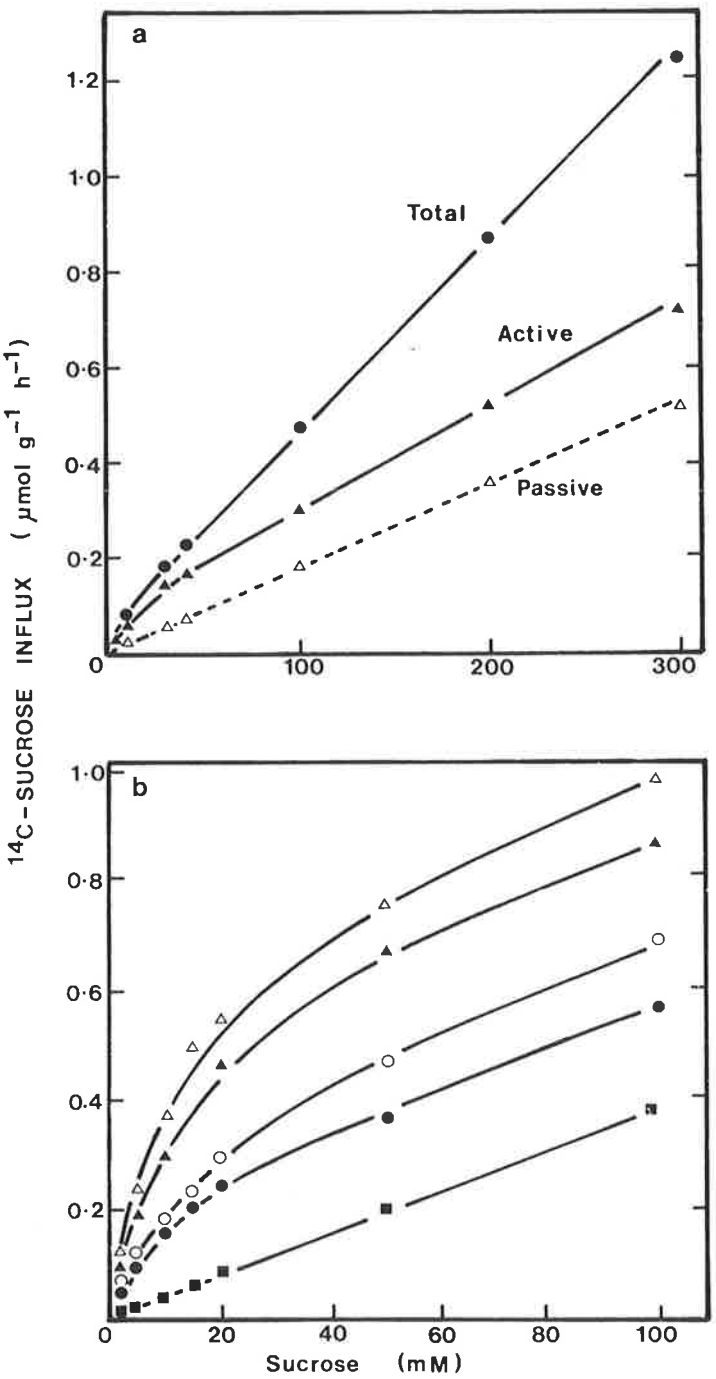


**Fig. 8.** Concentration dependence of [$^{14}$C]sucrose influx into sugar beet taproot discs. (a) Root discs were incubated without CCCP (control or total influx) or in the presence of 10 $\mu M$ CCCP (defined as passive influx). Active uptake was calculated by subtracting passive influx from the control or total influx. Discs were pretreated in 200–250 m$M$ mannitol and the experimental medium was buffered at pH 6.6. (b) as in (a), except that a range of external mannitol concentrations (0: ■; 100: ●; 200: ○; 400: ▲; 600 mM: △) was employed to examine the effects of cell turgor on [$^{14}$C]sucrose influx. (Redrawn from Saftner *et al.*, 1983, and Wyse, 1986: with permission.)

movement into the cytosol. These workers suggested that the two active components of sucrose uptake reside within the tonoplast, a conclusion consistent with Wyse's earlier work.

Recent studies by Wyse and co-workers (Wyse *et al.*, 1986) have indicated that, *in vivo*, sugar beet taproot tissues undergo turgor regulation, with the apoplast playing an important role in this phenomenon. In light of this finding, Wyse *et al.* (1986) reexamined the kinetics of sucrose transport as a function of bathing medium osmotic activity (potential). Their results were clear and dramatic: the saturable component of sucrose uptake was extremely turgor sensitive, being stimulated at lower turgor pressures (Fig. 8b). Of equal importance, sucrose efflux from the tissue increased, and the membrane potential of the parenchyma cells depolarized at high turgor pressures. These findings confirm the earlier report by Ehwald *et al.* (1980) in that leakage of sucrose was reduced as the osmotic pressure of the solution was raised.

These results also illustrate the difficulty associated with extrapolating from *in vitro* studies to physiological processes occurring within intact tissues. Clearly, the kinetic data obtained on the high-turgor root tissue need reevaluation with respect to the actual location of each component and its passive or active nature. If the apoplastic space does serve a major function in terms of tissue osmotic adjustment, the site of the turgor sensing must reside within the plasmalemma. If this were the case, it would seem unlikely that sugar transport across the plasmalemma would occur by a passive process (see also comments by Briskin *et al.*, 1985b).

Recent advances in the techniques associated with isolating plant membrane vesicles (see Sze, 1985) allowed Briskin *et al.* (1985a,b) to isolate putative tonoplast vesicles from sugar beet taproot tissue. Proton transport into these sugar beet "tonoplast" vesicles was ATP dependent and could be inhibited by $NO^{3-}$. Addition of sucrose (10 m*M*) to vesicles that had already established a pH gradient (+5 m*M* Mg·ATP) caused a transient efflux of protons. Furthermore, Briskin *et al.* (1985b) found that addition of sucrose to a vesicle preparation which did not contain charge-compensating ions caused a transient depolarization (interior going negative) of the potential. Finally, introduction of CCCP resulted in the dissipation of a preestablished sucrose gradient. Based on these results, Briskin *et al.* (1985a,b) concluded that an electrogenic $H^+$–sucrose antiport may be responsible for the active transport of sucrose across the tonoplast of sugar beet parenchyma cells.

### 2. *Sugarcane Tissues*

At maturity, storage parenchyma cells of sugarcane stalks also contain high sucrose levels [see Glasziou and Gayler (1972) for a review of the early work on this system]. In this tissue, sucrose released from the phloem is hydrolyzed by a cell-wall-bound acid invertase. To reduce the problems

associated with studying transport-related processes in complex tissues, Maretzki and co-workers began a detailed analysis of sugar transport into sugarcane cells grown in suspension culture. Maretzki and Thom (1972a,b) reported that although these suspension culture cells were grown on sucrose, the plasmalemma did not contain a specific sucrose transport mechanism. Glucose, and to a lesser extent fructose, appeared to be taken up by an energy-dependent process.

In a more extensive study, Komor *et al.* (1981) used 3-*O*-MG to elucidate the kinetics, mechanism, and regulation of hexose transport into sugarcane suspension cells. Sugar uptake into these cells occurred at rates comparable with those observed in either tissue slices or plants in the field. Kinetic data indicated that glucose is taken up by a single mechanism with a very low *K*m of 20 $\mu M$. No first-order component was reported for glucose; however, when high sucrose concentrations were employed, an apparent linear component of "sucrose uptake" was observed and a passive mechanism was invoked.

Komor *et al.* (1981) also presented evidence consistent with the operation across the plasmalemma of a glucose–$H^+$ cotransport mechanism; the observed stoichiometry was 0.87 $H^+$ per 3-*O*-MG molecule. Addition of 3-*O*-MG also caused a transient efflux of $K^+$ (0.94 $K^+$ per 3-*O*-MG molecule), a finding consistent with electrogenic glucose influx in these cells.

In a comparative study on isolated protoplasts and vacuoles (obtained from sugarcane suspension cultures), Thom *et al.* (1982a,b) found that the vacuolar level of sucrose increased with culture age; by day 14 (or stationary phase) almost all the sucrose in the protoplasts was in the vacuole. Based on these results, Thom *et al.* (1982a) concluded that "there is likely to be active transport of sugars into the vacuole, either of hexoses, or sucrose, or both." Although sucrose uptake into isolated vacuoles was reported to follow saturation kinetics with a $V_{max}$ of 0.08 nmol $min^{-1}$ $(10^6$ vacuoles$)^{-1}$, this value is an order of magnitude lower than the rate of appearance of sucrose in the vacuoles of protoplasts incubated in [$^{14}$C]glucose. A further problem with the results obtained by Thom *et al.* (1982b) and Komor *et al.* (1982a) on isolated vacuoles was that neither sugar uptake nor tonoplast potential responded to the addition of ATP. With the protocols used, the isolated vacuoles appear to have been damaged (see also Komor *et al.*, 1982). Consequently, the results presented do not establish that sucrose, *per se*, is actually synthesized within the cytosol prior to being transported across the tonoplast.

The perturbative effects of the tonoplast isolation procedures were addressed by Thom *et al.* (1983) and Thom and Komor (1984a–c, 1985). By adjusting their experimental media to reflect more realistic cytosolic conditions, these workers were able to establish that addition of Mg·ATP caused a polarization of the tonoplast (interior positive) in both isolated vacuoles and tonoplast vesicles. In addition, ATP caused an acidification of the vacu-

olar compartment with the response being specific for ATP (Thom and Komor, 1985). Experiments using 3-*O*-MG on these intact vacuolar preparations from sugarcane suspension culture cells indicated that uptake of hexoses into the vacuole appears to proceed via a hexose–$H^+$ antiport mechanism with a 1 : 1 stoichiometry (Thom and Komor, 1984b). The system would be energized by a $H^+$-translocating ATPase that establishes an outwardly directed $\Delta\tilde{\mu}_{H^+}$. The question of sucrose resynthesis and transport in this tissue remained unresolved until the concept of a sucrose group translocator was examined (see Thom and Maretzki, 1985; but c.f. Komor *et al.*, 1984). This exciting new area of membrane sugar transfer will be dealt with in Section IV.

### 3. *Seed Tissues*

Because of their economic importance, seeds have been the focus of numerous sugar/phloem transport-related studies (barley, Felker *et al.*, 1984; Lingle and Chevalier, 1984; wheat, Jenner, 1974, 1976; Sakri and Shannon, 1975; Donovan *et al.*, 1983; Ho and Gifford, 1984; rice, Oparka and Gates, 1981, 1982; *corn*, Shannon, 1972; Shannon and Dougherty, 1972; Felker and Shannon, 1980; Shannon *et al.*, 1986; bean, Patrick and McDonald, 1980; Patrick, 1983, 1984; Offler and Patrick, 1984; and soybean, Thorne, 1980, 1982; Lichtner and Spanswick, 1981a,b; Hsu *et al.*, 1984; Gifford and Thorne, 1985). Aspects of this literature have recently been reviewed (Thorne, 1985; Gifford, 1986; Shannon *et al.*, 1986) and consequently we will narrow our attention to one system, soybean, to illustrate the general concepts involved in sugar uptake by these systems. We will also return to seeds later in this review when dealing with various aspects of sink metabolism (see Section VI, C and D; VII).

**a. *In Vitro* Kinetics of Sucrose Uptake into Soybean Embryos.** During growth of the soybean seed, large quantities of photosynthate are transferred, via the phloem, to the cotyledons and embryo. Since the symplasm is discontinuous between the endothelium of the seed coat and these tissues, sucrose must first be released into and then retrieved from the apoplast (Thorne, 1981). According to Thorne (1980, 1982), the sucrose molecule does not undergo hydrolysis during this transfer process. Uptake by isolated developing embryos (cotyledons and attached embryonic axes) occurs by the combination of a saturable and a first-order kinetic component, with the latter dominating uptake at concentrations above 50 m*M* (Lichtner and Spanswick, 1981b; Thorne, 1982). Electrophysiological studies conducted on excised soybean cotyledons indicate that the membrane potential of these cells undergoes a transient depolarization upon addition of sucrose. The magnitude of this depolarization is dependent upon the sucrose concentration in the bathing medium; saturation is observed at approximately 50 m*M*.

The extent of the sucrose-induced depolarization of the potential was pH-dependent (Lichtner and Spanswick, 1981a) and, to a lesser extent, so was

[$^{14}$C]sucrose influx; both were reduced at high pH values (Lichtner and Spanswick, 1981b; Thorne, 1982). Application of $H^+$-ionophores and metabolic inhibitors also reduced sucrose uptake. These data indicated that developing soybean cotyledons also transport sucrose by means of a sucrose–$H^+$ cotransport mechanism. The slowly penetrating sulfhydryl-reactive compound, PCMBS, reduced both sucrose uptake and the sucrose-induced depolarization of the membrane potential without inhibiting the electrogenic component of the potential (Lichtner and Spanswick, 1981a). This indicated that PCMBS inhibits the putative sucrose–$H^+$ cotransport system rather than the plasmalemma $H^+$-ATPase.

The developing soybean cotyledon system was further investigated by the use of protoplasts isolated from this system (Lin *et al.*, 1984). Consistent with earlier findings, sucrose influx occurred by the combination of a saturable and a first-order component. Under these conditions (i.e., no cell walls, no compact tissue), the $K_m$ of the saturable component was approximately 2 m*M* (c.f. 8 m*M* for excised cotyledons), meaning that the system saturated at a 10-fold lower concentration of 5 m*M*. In contrast, uptake of glucose, 3-*O*-MG, and L-glucose occurred only by the first-order mechanism. Here a considerable difference in influx was observed between the different hexose molecules, an observation that needs to be accounted for when evaluating the proposal that these fluxes occur by simple diffusion.

Experiments with PCMBS and FCCP (Schmitt *et al.*, 1984) gave results similar to those reported for sugar beet (see Saftner *et al.*, 1983). The saturable component was completely inhibited by PCMBS, and the resultant linear component was identical to that observed for L-glucose. Although FCCP suppressed the saturable term, it left the linear component of sucrose uptake unaffected with rates considerably above those obtained for L-glucose. However, addition of PCMBS inhibited the FCCP-insensitive linear component, reducing it to values obtained for L-glucose. Based on this PCMBS sensitivity, Schmitt *et al.* (1984) proposed that part of the linear component is carrier-mediated.

Perhaps the most surprising result obtained on this soybean protoplast system was the finding that the sucrose-induced membrane potential depolarization exhibited a biphasic shape (Lin, 1985). The similarity between the influx of sucrose and the related depolarization is shown in Fig. 9. An examination of other studies of this kind revealed a similar response obtained on sugarcane leaf parenchyma cells (Franz and Tattar, 1981) and one purely linear response on willow bark "phloem" (Wright and Fisher, 1981). Clearly, the nature of the linear component of sucrose uptake is complex, but a mechanistic interpretation must await further careful investigation.

**b. *In Vivo* Sucrose Uptake by Embryos.** Analysis of the sucrose distribution in freshly harvested soybean cotyledons has shown that the concentration in the apoplast (37 m*M*) may be higher than that within the cotyledonary cells (7 m*M*) (Lichtner and Spanswick, 1981b). These concentrations are

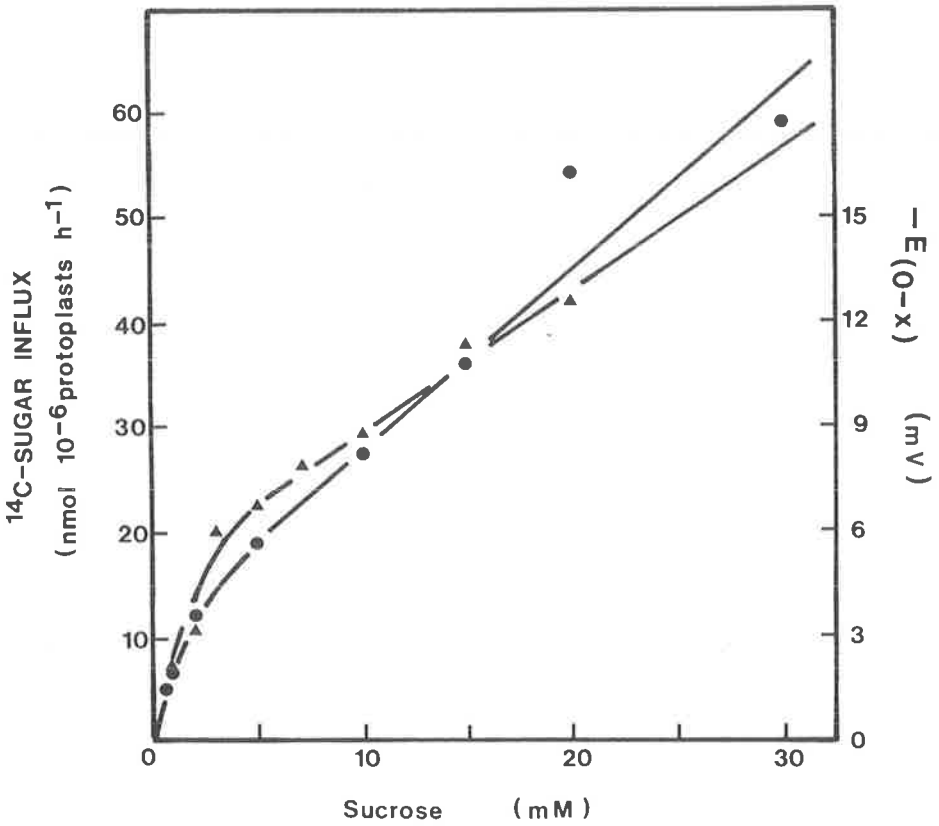


**Fig. 9.** Relationship between [$^{14}$C]sucrose influx into soybean cotyledon protoplasts (●) and the sucrose-induced membrane potential depolarization observed in these protoplasts (▲). Depolarization is expressed as the potential at a particular sucrose concentration (X) subtracted from the potential in the absence of sucrose (O). (Redrawn from Schmitt *et al.*, 1984, and Lin, 1985; with permission.)

seemingly in contradiction with the concept of an active, plasmalemma-bound sucrose transport system. Lichtner and Spanswick (1981b) resolved this conflict in their own minds by suggesting that metabolism quickly consumes the transported sucrose, thereby maintaining a low internal concentration. In this situation, sucrose transport across the plasmalemma would appear to be the rate-limiting step for its assimilation.

The apoplastic sucrose concentration within the soybean seed coat and embryo has been reexamined by two very different methods. Hsu *et al.* (1984) used the conventional compartmental efflux analysis and arrived at cotyledonary apoplastic sucrose concentrations in the range of 3.4–22.2 m*M*. Gifford and Thorne (1985) employed a novel "null-balance" technique and concluded that the apoplastic concentration was from 150 to 170 m*M*, values close to those reported for *Phaseolus vulgaris* (bean) embryos (Patrick and McDonald, 1980). If these high levels of apoplastic sucrose prove

to be correct, it would indicate that the contribution of the putative active sucrose–$H^+$ cotransport system would be insignificant. This would certainly hold in the outer cell layers of the cotyledons, and only within the central region of this organ might such a sucrose–$H^+$ cotransport mechanism be of value. The corollary to this situation would be that the first-order mechanism would be responsible for sucrose influx into the cotyledon (but see Gifford, 1986). Again we see the need to further elucidate the mechanism(s) and regulation exerted over this transport process.

## IV. GROUP TRANSLOCATOR CONCEPT FOR SUCROSE

A group translocator is basically a multienzyme complex which links a specific sequence of enzymes (Welch, 1977). The product of one enzyme is the substrate of the next in the sequence, and their close spatial proximity allows direct channelling of metabolites along the reaction sequence. The advantage of such a system is that it imposes directionality to the reaction sequence, increasing the catalytic efficiency by a relay of intermediates between subsequent enzymes. At the same time, unstable intermediates are provided some degree of protection due to sequestration within the complex. One consequence of this sequestration, which is of particular importance to physiological studies, is that the compound which initiates the reaction sequence will be a better precursor of the final product than any of the intermediate compounds. Another is that, if the enzyme complex is attached to or associated with a cell membrane, it can cause a vectorial transport of the final product across the membrane as indicated schematically in Fig. 6d.

### A. Grape Pericarp Cells

Unlike many fruits, the grape berry does not accumulate sucrose, *per se*, upon ripening; rather, it stores glucose and fructose in its vacuoles. Sucrose is the sugar supplied by the phloem; however, it is unloaded apoplastically and hydrolyzed prior to uptake into the pericarp cell (Kreidemann, 1969; Coombe, 1976). Sucrose is resynthesized inside the cell and, since accumulation of glucose and fructose in vacuoles is equimolar, the mechanism of hexose accumulation would appear intuitively to involve uptake of cytoplasmic sucrose into the vacuole followed by hydrolysis involving an invertase. Studies performed by Brown and Coombe (1982, 1984a,b), however, suggested that sucrose is synthesized not in the cytoplasm, but during the transport process itself across the tonoplast.

This hypothesis was based on experimental data which showed an unpredicted dichotomy in the labelling pattern of sugar accumulated in the vacu-

oles which was dependent on the radioactive hexose (either [$^{14}$C]glucose or [$^{14}$C]fructose) supplied to the cells. Normally, hexoses taken up would be rapidly phosphorylated by cytosolic hexokinase and the hexose phosphates in turn would be isomerized via hexose phosphate isomerase. Exogenously supplied [$^{14}$C]hexoses, whether glucose or fructose, would yield sucrose equally labelled in both hexose moieties. Sucrose accumulation from the cytoplasm, followed by hydrolysis by vacuolar invertase, would then result in the appearance of labelled glucose and labelled fructose in the vacuole, regardless of which hexose was initially supplied.

However, this only occurred when [$^{14}$C]glucose was supplied. In contrast, [$^{14}$C]fructose, although converted to glucose, did not lead to vacuolar accumulation of sugar. In addition, supply of exogeneous unlabelled fructose along with the labelled glucose had no effect on the accumulation of labelled sugar in the vacuole. Thus, only sugar derived from glucose was accumulated in the vacuole.

One explanation for these results is that hexoses are isomerized and converted to sucrose by a multistep process catalyzed by a protein complex consiting of hexose phoshate isomerase (which mediates the interconversion of glucose-6-P and fructose-6-P) and sucrose-P synthase (Fig. 10). By such a

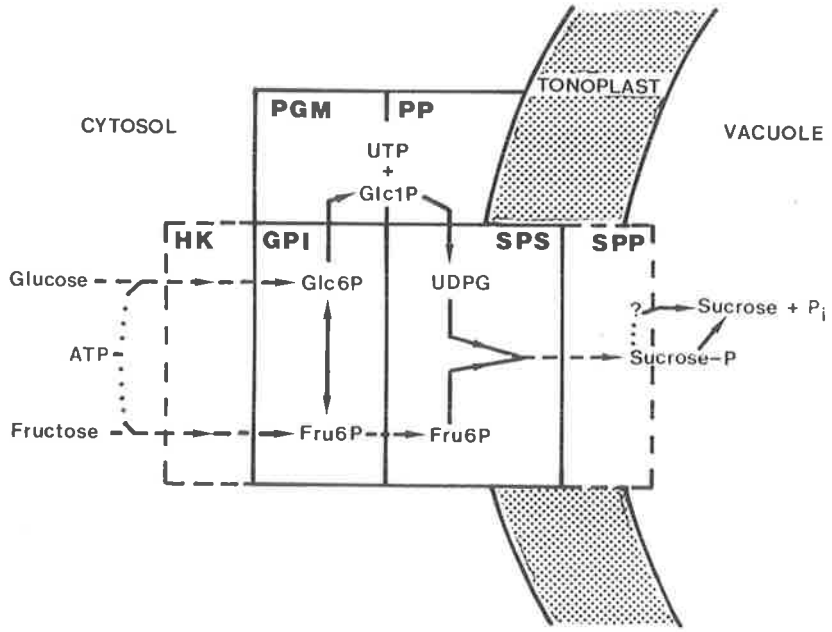


**Fig. 10.** A group translocator mechanism proposed for the tonoplast of grape pericarp cells (Brown and Coombe, 1982). The complex consists of glucose-phosphate isomerase (GPI) and sucrose-phosphate synthase (SPS) with vectorial synthesis of sucrose phosphate. Other enzymes implicated are hexokinase (HK), phosphoglucomutase (PGM), UDP-glucose pyrophosphorylase (PP) and sucrose-phosphate phosphatase (SPP). (Redrawn from Brown and Coombe. 1982 with permission.)

complex, glucose-6-P from the cytosol would provide both the glucose and fructose moieties of the transported sucrose by formation of UDP-glucose and through isomerization to fructose-6-P. These products would be immediately available for the sucrose-P synthase reaction, which would catalyze a vectorial synthesis of sucrose across the tonoplast.

## B. Sugarcane Tonoplast System

As illustrated above, early studies by Thom and co-workers indicated the operation of a $H^+$-translocating ATPase at the tonoplast which provided a $\Delta\tilde{\mu}_{H^+}$ gradient for sugar–$H^+$ antiport. Isolated vacuoles took up exogenous hexoses at the same rate as the protoplasts from which they were isolated, but did not take up appreciable amounts of sucrose (Thom *et al.*, 1982b; Komor *et al.*, 1982b). The authors first attributed this to disruption of the vacuole transport mechanisms during isolation, but recent reports (Thom and Maretzki, 1985, 1986a,b) now suggest that only hexose accumulation occurs by a sugar–$H^+$ antiport system. Sucrose accumulation, based on studies with both isolated vacuoles and tonoplast vesicles, is proposed to occur by a vectorial group translocator mechanism.

The model put forward by these workers (Thom and Maretzki, 1985) differs somewhat from that of Brown and Coombe, in that the initial substrate of the reaction sequence is thought to be UDP-glucose (UDPG). The reasoning for this was based on the finding that, of all the potential sucrose precursors tried, UDPG was the best precursor for sucrose synthesis in vacuoles and the only precursor needed in tonoplast vesicle experiments (Table I). As illustrated in the model presented in Fig. 11, UDPG provides both the glucose and fructose moieties for sucrose synthesis, and the operation of at least five enzymes working in concert at the tonoplast is required.

Extension of this model to the storage parenchyma of sugarcane is probably justified, although these sugarcane suspension cells are neither physiologically or enzymatically comparable to either mature storage parencyma cells or immature meristematic sugarcane stalk cells (Komor *et al.*, 1982b). The source of UDPG has not as yet been established, but the requirement for UDPG to supply both hexose moieties suggests that at least two of the proposed enzymes (phosphoglucomutase and hexose phosphate isomerase) must have cytosolic counterparts to allow metabolism of fructose (imported from the apoplast after sucrose hydrolysis) to UDPG. It is somewhat disturbing that at least 80% of the supplied UDPG was metabolized not to sucrose, but to hexose-P in the seven minute incubation periods used, and most of this metabolism occurred external to the vacuole. This type of result may be consistent with certain of the intermediate reactions proposed in the group translocator mechanism running at higher rates than the reactions leading to sucrose, but may also be a result of contamination and/or damage to the vacuoles and/or tonoplast vesicles. The vacuole preparations used

**TABLE I**

**Uptake of Sucrose and Its Metabolic Precursors into Isolated Vacuoles and Tonoplast Vesicles Obtained from Sugarcane Suspension Cells[a]**

| Radiolabelled substrate | Addition | Influx | |
|---|---|---|---|
| | | Isolated vacuoles (nmol $min^{-1}$ $10^6$ $vacuoles^{-1}$) | Tonoplast vesicles (nmol $min^{-1}$ mg $protein^{-1}$) |
| UDPG [glu-$^{14}$C] | — | 0.68 | 18.86 |
| UDPG [glu-$^{14}$C] | Fru-6-P | 0.67 | 18.11 |
| UDPG [Uridine-$^{14}$C] | — | 0 | 0.10 |
| Glucose | — | 0.06 | 0.10 |
| Fructose | — | 0.03 | 0.06 |
| Sucrose | — | 0.02 | 0 |
| Sucrose-P | — | 0 | 0 |
| Fru-6-P | — | 0 | 0 |
| Fru-6-P | UDPG | 0 | 0 |

[a] (Data from Thom and Maretzki, 1986b, with permission.)

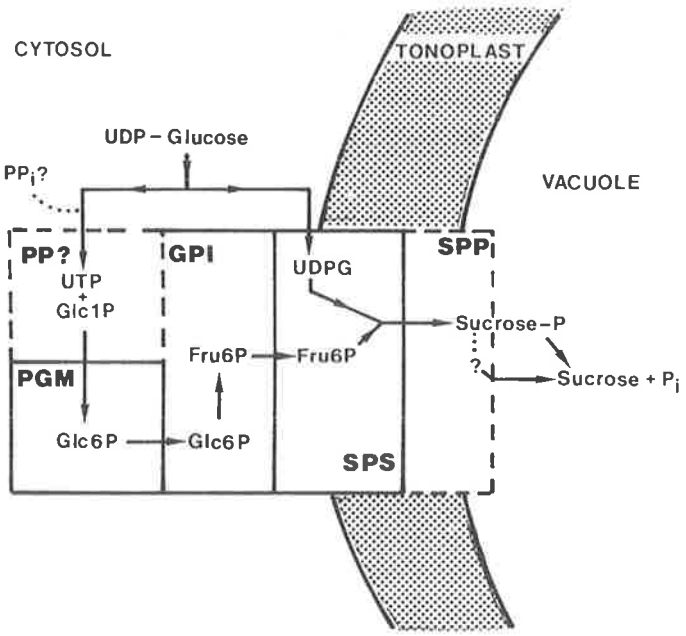


**Fig. 11.** A group translocator mechanism as proposed by Thom and Maretzki, 1985, for the tonoplast of sugarcane suspension cells. The vectorial synthesis of sucrose across the tonoplast is catalyzed by a complex of (possibly) five enzymes which convert the glucose moiety of UDP-glucose (UDPG) to the glucose and fructose moieties of sucrose. UDPG pyrophosphorylase (?) (PP?), phosphoglucomutase (PGM), glucose-phosphate isomerase (GPI), sucrose-phosphate synthase (SPS), and sucrose-phosphate phosphatase (SPP).

were contaminated by at least 11% cytoplasmic components, while the tonoplast vesicles formed sucrose at only 30% of the rate of the intact vacuoles. Clearly more study of this system needs to be undertaken to establish the true importance of this type of system in storage of sucrose in the intact sugarcane parenchyma tissue.

The group translocator mechanism is most likely to prove to be a ubiquitous transport mechanism in plant cells that store large amounts of sugar in the vacuole. This does not, however, preclude the existence of different mechanisms operating in parallel across the same membrane. Indeed, in red beet tap roots where vacuolar transport has been traditionally proposed to occur via a $\Delta\tilde{\mu}_{H^+}$-driven process (sucrose–$H^+$ antiport, Briskin *et al.*, 1985a,b; Briskin, 1986; Doll *et al.*, 1979; Willenbrink and Doll, 1979), recent advances suggest that group translocator systems may be equally important (Thom et al., 1986). The apparent adoption of different strategies or combinations of strategies for sugar uptake and storage has enormous ramifications for future studies of carbon allocation and the biochemical control of sugar synthesis in plant cells.

## V. MECHANISM OF PHLOEM LOADING

Extensive physiological and anatomical studies have been conducted in an attempt to elucidate the mechanism and pathway of sugar (usually sucrose) movement between the sites of synthesis in the mesophyll cytosol and the sites of entry into the sieve elements. This process has generally been referred to as phloem loading (see Cronshaw, 1981; Geiger, 1975; Giaquinta, 1980a, 1983).

### A. Sucrose–$H^+$ Cotransport into the Phloem?

In a previous section on sugar transport into leaf tissues (III,A,1) we discussed the complexities of evaluating [$^{14}$C]sucrose kinetics with respect to the contribution made by the phloem. In his recent review on this topic, Giaquinta (1983) summarized the situation, concluding "We now recognize that exogenously supplied sucrose can enter both the mesophyll and the phloem, so it is unlikely that kinetic analyses reflect soley the transport mechanism operating at the sieve element–companion cell complex." In this section we will deal with recent studies that address the specific question of whether a sucrose–$H^+$ cotransport mechanism does function at the plasmalemma of the sieve element–companion cell complex.

#### *1. Zea mays Leaf Strips*

According to Giaquinta (1983), Heyser's studies on corn leaves provides the most convincing evidence that phloem loading in photosynthesizing

leaves occurs via the putative sucrose–$H^+$ cotransport mechanism. Heyser (1980) used excised leaf strips of *Zea mays* and mounted these strips in an ingenious device which allowed him to perfuse artificial solutions through xylem vessels. The pH value of the xylem perfusate was measured as it exited the leaf strip. Upon introducing 25 m*M* sucrose into the perfusate, the pH value of the xylem solution underwent a transient alkalinization with the peak of the response ($\Delta$ pH = 0.75 units) being reached 10 min after the introduction of sucrose. Other sugars like glucose, fructose, raffinose, etc., did not elicit a pH response. This sucrose-induced pH response is certainly consistent with the operation of a sucrose–$H^+$ cotransport system (Tanner, 1980), but Heyser's results do not reveal the actual location of the transport process.

This question of location was addressed by Fritz *et al.* (1983). These workers used exactly the same experimental material and system as that used originally by Heyser. Application of the Fritz (1980) microautoradiography technique enabled Fritz *et al.* (1983) to demonstrate that after an 8 to 15 min exposure to [$^{14}$C]sucrose (fed by xylem perfusion), the majority of the radioactivity was located in the xylem parenchyma (see Fig. 8 of Fritz *et al.*, 1983). Even after a 30-min exposure, little of the label in the xylem parenchyma cells moved into the thick- or thin-walled sieve tubes (E. Fritz, per sonal communication).

Thus, the physiological evidence that was previously cited as being the most convincing in support of sucrose–$H^+$ cotransport at the level of the phloem must be rejected. In view of this recent data, it appears that the transient alkalinization of the xylem perfusate is due to sucrose uptake from the xylem by the surrounding xylem (vascular) parenchyma cells. Fritz *et al.* (1983) proposed that in the *in vivo* situation these cells probably function to retrieve sucrose from the xylem vessels.

### 2. *Germinating* Ricinus communis *Seedlings*

In *Ricinus* (castor bean) seedlings, the endosperm envelopes the cotyledon, but the two tissues are not symplastically connected. The endosperm functions as an oil-storing tissue and, during germination, metabolizes stored oil to sucrose through gluconeogenic processes occurring largely in a special organelle the glyoxysome (sucrose formation by the *Ricinus* endosperm has been extensively studied by Beevers; for details see Beevers, 1979). The sucrose produced by the endosperm cells is then transferred from the endosperm tissue, via the cotyledons, to the embryonic axis. The cotyledons therefore function as a sucrose retrieval system, collecting the sucrose released from the endosperm and relaying it, via phloem connections, to the developing embryo. Kreidemann and Beevers (1967a) showed that removal of the endosperm did not perturb the ability of the cotyledons to take up exogenously supplied sucrose and translocate it to the embryo. Application of asymmetrically labelled [$^{14}$C]sucrose revealed that the position of the

label was not randomized during uptake (Kreidemann and Beevers, 1969b), and so these cotyledons appeared to be an ideal system on which to study sucrose loading into the phloem.

The extensive studies by Komor and co-workers (Komor, 1977; Komor *et al.*, 1977, 1980; Martin and Komor, 1980) and Hutchings (1978) on germinating *Ricinus* cotyledons provide compelling evidence for the operation of a sucrose–$H^+$ cotransport system. Addition of sucrose caused a transient (15–30 min) alkalinization of the bathing medium and, as with *Zea* leaf strips, other sugars like glucose, fructose, and raffinose did not elicit this response. Martin and Komor (1980) and Komor *et al.* (1980) used autoradiography of entire cotyledons to correlate the presence of [$^{14}$C]sucrose with the sucrose-induced alkalinization of the medium. Although Martin and Komor (1980) reported that after a 5 or 10 min exposure to [$^{14}$C]sucrose label appeared to be distributed over the entire cotyledon, they suggested that this was probably an artifact in that the minor veins could not be detected. The more likely explanation, suggested by the physiological function of the cotyledons in this seed (i.e., that the entire surface of the cotyledon was involved in sucrose retrieval) was discounted. Rather, Komor *et al.* (1980) concluded that, with regards to sucrose uptake, since "phloem cells of the cotyledons do it preferentially," the "most simple assumption would be that it is direct uptake into the phloem cells which proceeds by proton symport."

This question of sucrose uptake specifically by phloem tissues was then further examined by Cho and Komor (1985), who compared the characteristics of sugar uptake by suspension cultures of *Ricinus* with those of intact *Ricinus* cotyledons. As earlier reports had shown, cotyledons took up sucrose without hydrolysis and hexoses (3-*O*-MG) did not competitively inhibit this process. However, the suspension cultured cells had a much higher capacity for hexose uptake. In addition, sucrose uptake into these cells was inhibited by the addition of hexoses, and hexoses appeared in the medium during incubation of the cells with sucrose. From these results, Cho and Komor (1985) claimed that sucrose is hydrolyzed prior to uptake into the suspension cells, and that these cells transport hexoses rather than sucrose. In what must be an almost unprecedented example of over extrapolation, Cho and Komor concluded that the "highly specific uptake of sucrose without hydrolysis is a special feature of certain specialized cells of the cotyledon, probably the phloem."

Our criticism of this conclusion is based, in part, on the nature of the *Ricinus* suspension culture cells used in this study. These cells, obtained from Dr. Gemmerich (see Gemmerich, 1982), were derived not from cotyledons, but from endosperm tissue (!). Since it is from the endosperm that sucrose is released for uptake by the cotyledons, it is not surprising that these cells did not retrieve sucrose. The specific cell type located in the cotyledon which is responsible for the transient alkalinization or the uptake of [$^{14}$C]sucrose was still left unresolved.

Microautoradioagraphy of [$^{14}$C]sucrose-treated *Ricinus* cotyledons revealed that after a 5–10 min incubation period, no preferential labelling pattern could be detected. Komor and Orlich (1986) reported that all cells of the cotyledon were labelled. Longer labelling periods of up to 20 min also did not reveal a preferential distribution of [$^{14}$C]sucrose in the phloem (E. Fritz, personal communication). These microautoradiographic results are inconsistent with the hypothesis that sucrose uptake by the cotyledons represents mostly phloem loading. It is likely that, as in leaf tissues, the sucrose–$H^+$ cotransport mechanism may function across the plasma membranes of all cell types within this organ.

### 3. *Electrophysiological Studies on Phloem Cells*

Perhaps one of the most interesting studies of phloem cells was that conducted by Wright and Fisher (1981). These workers developed an elegant technique that allowed them to make electrophysiological measurements on phloem tissue. To achieve this, they employed aphids that probed the phloem of willow (*Salix exigua* Nutt.) stems (bark); once the aphid had penetrated the sieve element, it was anaesthetized and in this state its sylet was cut. The cut stylet was then used to gain electrical continuity with the inner surface of the sieve element plasma membrane.

The values of the membrane potential that were measured with this technique were within the range of values normally measured on higher plant tissues. More importantly, Wright and Fisher (1981) were able to show that when exogenous sucrose was introduced into their system, a transient depolarization of the membrane potential was observed; the extent of the depolarization was a function of the concentration of sucrose present in the bathing medium. These results were interpreted as providing direct evidence for the operation of a sucrose–$H^+$ cotransport mechanism in the plasma membrane of the willow sieve tube. However, there is a problem with this interpretation. Application of other sugars, like fructose, 3-*O*-MG, and glucose also elicited the same type of transient depolarization in the measured membrane potential. The extent of the depolarization was approximately 50 to 70% of that obtained when sucrose was employed.

Earlier autoradiographic studies on leaf tissues have shown that [$^{14}$C]glucose and [$^{14}$C]3-*O*-MG *do not* enter the phloem when they are applied to the apoplast but rather are taken up by the mesophyll cells (Fondy and Geiger, 1977). Sauter (1982) has suggested that sucrose reabsorption in isolated shoots of *Salix smithiana* occurs by hexose uptake following apoplastic hydrolysis. If this were also true for the willow species employed by Wright and Fisher, their electrical response, obtained with these nontranslocatable sugars, may be located at the plasma membrane of the surrounding vascular parenchyma. In the simplest situation, plasmodesmatal connections between the se–cc complex and the vascular parenchyma would permit the transmission of this electrical signal from the parenchyma to the electrode

inserted into the aphid stylet. Alternatively, if the extracellular pathway is sufficiently restricted such that the surrounding cells are effectively electrically in series with the sieve tube plasmalemma, then it is probable that the observed electrical response will be that of these cells, rather than of the phloem (Spanswick, 1986). Consequently, if this were the case for glucose, 3-*O*-MG, and fructose it would make it very difficult to argue that the same situation does not also exist with respect to the sucrose-induced transients. Again, the results are consistent with the operation of a plasma membrane-bound sugar–$H^+$ cotransport mechanism within the tissue of the phloem, but we consider that it does not provide direct evidence for the presence of such a system within the plasma membrane of the sieve tube.

## B. Apoplastic *versus* Symplastic Pathway

In general, the question of a symplastic *versus* an apolplastic route in phloem unloading has not been controversial. As pointed out by Thorne (1986), there is ample evidence illustrating that a symplastic pathway occurs in some tissues, while in others an apoplastic step is involved. However, the same cannot be said for mature source leaves.

Although it has been known for some time that plasmodesmata interconnect all the cell types of the leaf—from the mesophyll to the sieve element–companion cell complex—it was not until recently that physiological methods were developed to allow an investigation of their function. In the absence of this information, it was generally felt that an apoplastic step in the loading process could account for the known features of the phloem translocation system, the two most important being selectivity of sugars and amino acids loaded and the often large osmotic differential between phloem and surrounding vascular and mesophyl tissues (see rationale developed by Giaquinta, 1983). But, as we have already discussed, this concept of an apoplastic step is, in itself, still a point of controversy.

### *1. Ultrastructural Studies*

One approach to this problem of the symplastic route has been to study the frequency of plasmodesmata between the various cell types (Evert *et al.*, 1977, 1978; Fisher and Evert, 1982; Gamalei, 1985; Gamalei and Pakhomova, 1981; Russin and Evert, 1985). Although this has provided valuable ultrastructural details of these leaf tissues, clearly there are problems with extrapolating from plasmodesmatal frequency to physiological processes like specific fluxes of sucrose. Frequency analysis entails the underlying implication that all plasmodesmata are more or less equal, and that they can be treated rather like pores or holes. It also ignores the complex structural diversity of the plasmodesmata that are present along the pathway from the mesophyll to the sieve elements. Consequently, the validity of the conclusion developed from such studies may not be upheld since, as Gunning and

Robards (1976) stressed, "plasmodesmata are much more complicated than mere membrane-lined holes in the cell walls."

The work of Evert and co-workers may be used to further illustrate our point. In a recent review of plasmodesmatal frequency studies on three dicot species, *Amaranthus retroflexis* ($C_4$), *Populus deltoides,* and *Beta vulgaris* (both $C_3$) Evert and Mierzwa (1986) concluded that since the frequency between cell types is lowest in sugar beet, it "must be regarded as being poorly designed for the most expeditious transport of photosynthate from the mesophyll chloroplasts to the sieve tubes." We have no argument against their analysis of leaf-type, but to make conclusions with respect to efficiency demands a complete knowledge of the mechanism(s) by which a plasmodesma functions.

### 2. *Fluorescent Dye Injection Techniques*

The adoption of neurological dye tracer techniques for use in plants recently provided a means for establishing the extent of the functional symplast. Since the dyes do not penetrate the plasmalemma, the functional status of the plasmodesmata can be ascertained by monitoring dye movement (by fluorescence microscopy) after its microinjection into the cytosol of a single cell. Convincing evidence for an operative symplastic network has now been obtained for a number of plant tissues, including the leaf and extrastelar tissues of *Egeria* (Erwee and Goodwin, 1983, 1984, 1985; Goodwin, 1983), apices of *Silene* (Goodwin and Lyndon, 1983), and leaf tissue of *Allium* (Palevitz and Hepler, 1985), *Commelina* (Erwee *et al.*, 1985; Palevitz and Hepler, 1985), *Beta vulgaris*, and *Ipomea tricolor* (Madore *et al.*, 1986).

Movement of tracer dyes has been shown to be controlled by changes in cellular concentrations of ions such as $Ca^{2+}$ and aromatic amino acids (Erwee and Goodwin, 1983, 1984). In addition, size exclusion limits have been established for symplastic movement in some tissues (Erwee and Goodwin, 1985; Goodwin, 1983; Goodwin and Lyndon, 1983; Tucker, 1982), which apparently can be overcome by treatments such as plasmolysis (Erwee and Goodwin, 1984). In other studies, barriers to symplastic movement have been found even in regions where apparently normal plasmodesmata are present, suggesting the existence of symplastic "domains" within a specific plant tissue (Erwee and Goodwin, 1985).

A major drawback to the use of these techniques in vacuolate tissues such as mature leaves is the number of injections that occurs into the vacuole. Dye injected directly into the vacuole fails to move symplastically to adjacent cells because it cannot pass the tonoplast. Madore *et al.* (1986) overcame this limitation by pre-encapsulating the dye (Lucifer Yellow CH) in small (0.2 $\mu$m diameter) phospholipid vesicles (liposomes). Liposomes were easily injected into the vacuole of mesophyll cells of sugar beet (*Beta vulgaris*) and morning glory (*Ipomoea tricolor*), where fusion with the tono-

plast resulted in the release of the dye into the cytosol. Subsequent cell-to-cell movement of the dye was followed and Madore *et al.* (1986) obtained evidence consistent with the existence of symplastic continuity from the mesophyll to the minor veins of the source leaf of *I. tricolor* (see Fig. 12). These results are similar to those obtained on *Commelina cyanea* by Erwee *et al.* (1985). Thus, the free permeability of the relatively small Lucifer Yellow molecule (457 daltons) suggests that there is no barrier to the diffusion of small molecules throughout the leaf symplast.

Using the Lucifer Yellow liposome-encapsulation microinjection technique, Madore *et al.* (1986) were able to show that barriers to symplastic transport can be artifically imposed even by quite simple physiological treatments. Turgeon (1984) reported that alkaline pH treatments favored [$^{14}$C]sucrose uptake by the mesophyll, in that under these conditions autoradiographic images of tobacco leaves showed the label in this tissue with little activity in the minor veins. Madore *et al.* (1986) found that a similar alkaline pH treatment (pH 8.0) applied to *I. tricolor* had no effect on dye movement between adjacent mesophyll cells, but inhibited the movement into and along the minor veins. These new findings offer strong support for the involvement of the symplast in movement of sucrose into the minor veins and for the retrieval role played by the mesophyll cells.

Current experimental evidence suggests that the free movement of solutes through the symplast is regulated at the level of the plasmodesmata (Erwee and Goodwin, 1983, 1984, 1985). The actual mechanisms controlling movement through plasmodesmata are unknown at present, but modulation of intracellular calcium levels is implicated (Erwee and Goodwin, 1985). Electron-dense granules with $Ca^{2+}$-ATPase activity appear at the neck regions of plasmodesmata in response to $Ca^{2+}$ treatment (Belitser *et al.*, 1982). This observation has been used to implicate ATPase activity, associated with plasmodesmata, in the control of solute movement through the symplast (Erwee and Goodwin, 1985), but direct experimental evidence is lacking. It is interesting, however, to speculate on such a role, particularly as the plasmalemma $H^+$-ATPase is one protein thought to be metabolically regulated via phosphorylation by a $Ca^{2+}$-dependent protein kinase (Zocchi *et al.*, 1983).

Recently, Schmalstig and Geiger (1985) presented evidence that the major pathway of sucrose unloading in sink leaves of sugar beet is symplastic. Turgeon (1984) considers that the sink to source transition in leaf tissues may involve a blockage of the symplast between the sieve tubes and the surrounding tissues. This hypothesis is no longer consistent with the experimental findings obtained on *Commelina* (Erwee *et al.*, 1985) or *Ipomoea* (Madore *et al.*, 1986). Mesophyll symplastic continuity was established in mature sugar beet leaves (Madore *et al.*, 1986) but the density of this tissue prevented the detection of dye movement into the minor veins. The development of cryosectioning techniques for this tissue will remove this limitation.

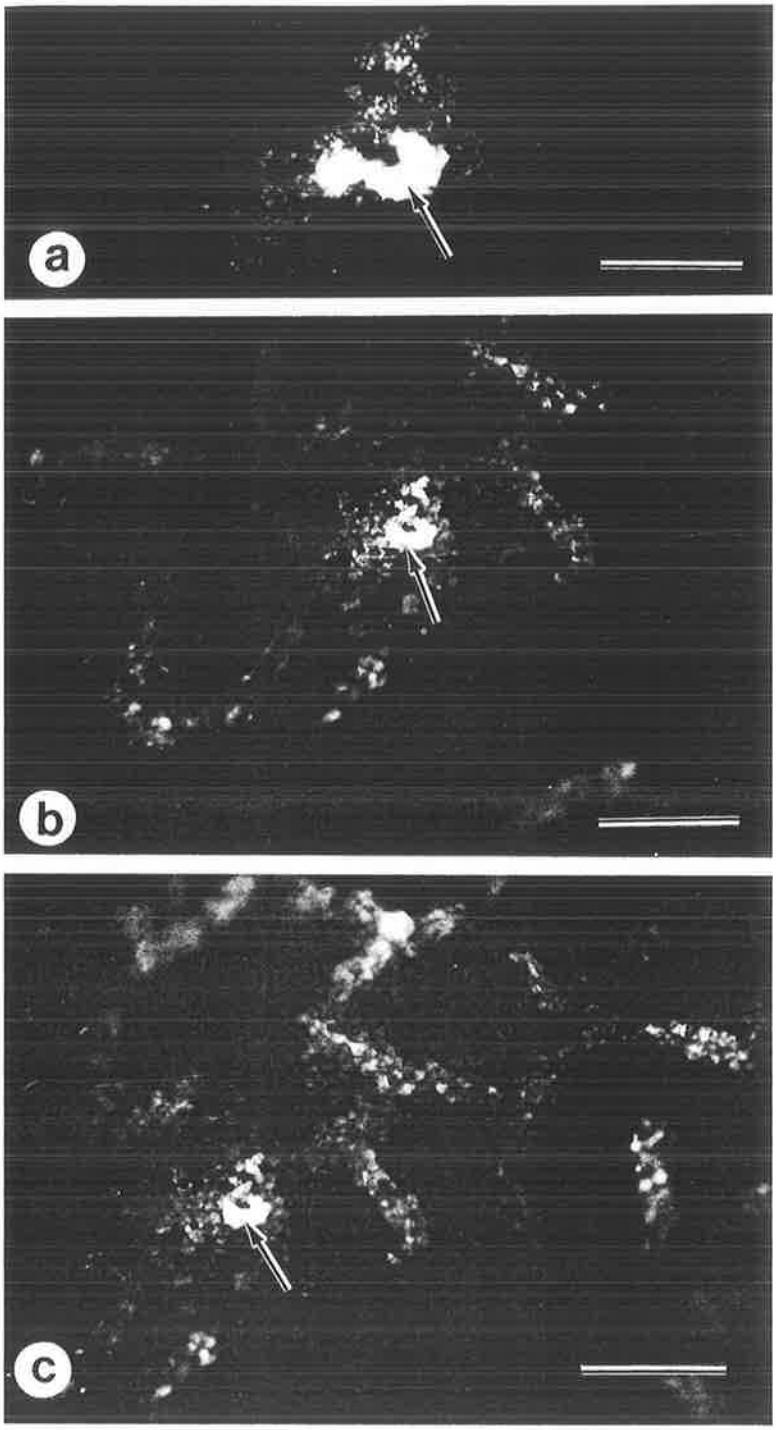


**Fig. 12.** Movement of Lucifer Yellow CH in the source leaf symplast of *Ipomoea tricolor* following microinjection of liposome-encapsulated dye into a spongy mesophyll cell. Arrows indicate the site of injection. Extent of dye movement 6 min (a), 16 min (b), and 30 min (c) after injection. (a), Bar = 100 $\mu$m (×160); (b), (c), Bar = 200 $\mu$m.

In view of the sink/source hypothesis developed by Turgeon (1984), and its intimate relationship with the concept of phloem loading, it seems imperative that these cryosectioning techniques be quickly developed. If it can be established that sugar beet behaves like *Commelina* and *Ipomoea* this would refute the hypothesis that plasmodesmata between the sieve element–companion cell complex and the surrounding cells serve a vestigial function in source leaves (see Giaquinta, 1983).

Guard cells have evolved a mechanism whereby at maturity they become symplastically isolated from the neighboring epidermal cells (Palevitz and Hepler, 1985; Wille and Lucas, 1984). Given the evolutionary importance of the phloem, one could present the argument that retention of plasmodesmata, as illustrated by cytological studies, establishes that they serve an essential role. The challenge facing phloem physiologists will be the expeditious elucidation of that role.

### 3. *Transport of Apoplastically Supplied Sugars*

One of the interesting features of the phloem is its apparent selectivity for specific (''phloem-mobile'') assimilates. This question of selectivity is an important one commercially as it determines the systemic nature of xenobiotics such as pesticides and herbicides. This selectivity has been used as an argument in support of an apoplastic loading step, as selective release of solutes to the apoplast by the mesophyll, or selective retrieval of solutes by the phloem could determine which compounds are transported (see Giaquinta, 1983). The actual mechanism that controls selectivity is still not known.

It has long been known that sugars supplied to the apoplast of leaf tissues do enter the metabolic compartment of the mesophyll (see Fondy and Geiger, 1977) where they can be extensively metabolized. The mesophyll appears to have little selectivity for uptake, with perhaps the exception of extremely large or highly charged molecules. If a sugar is supplied which is a precursor of sucrose or some other characteristic phloem-mobile compound, carbon derived from it will eventually be loaded into the phloem. This holds for sucrose as well as any nontranslocated sugar as demonstrated by Fondy and Geiger (1977), but uptake into the mesophyll for this particular sugar has largely been ignored in favor of the apoplastic loading hypothesis. As we have tried to indicate thus far in this review, uptake into nonphloem tissues creates serious problems in the interpretation of phloem transport studies, problems which are only just beginning to be addressed.

Given uptake of sucrose into the mesophyll in the *Beta* leaf, there is no adequate reason to invoke a preferential scavenging of apoplastically supplied sucrose by phloem tissues. As shown by Fondy and Geiger (1977), any sugar that can be metabolized to sucrose after uptake into the mesophyll will give rise to similar ''vein loading'' autoradiographs and phloem transport seen when [$^{14}$C]sucrose is supplied. This fact alone was sufficient to raise

questions concerning the putative "apoplastic" uptake into the phloem and prompted an investigation by Madore and Webb (1981) into the role of metabolic conversion in the transport of exogenous sugars.

As an experimental material, Madore and Webb (1981) chose to use *Cucurbita pepo*, which lends itself well to the investigation of metabolism and transport of exogenous sugars. Members of the Cucurbitaceae synthesize not one but two main transport sugars. Of these, stachyose (digalactosyl sucrose) appears to function exclusively as a transport compound (Webb and Gorham, 1964), while sucrose plays a dual role of storage and transport. In the leaf, therefore, pool sizes of sucrose will often be higher than those of stachyose (Madore and Grodzinski, 1985), while in the phloem stachyose predominates. The main advantages of *Cucurbita* is therefore that metabolism of one exogenously supplied $^{14}C$-labelled transport sugar can easily be detected, as it should result in the appearance of label in the other major transport sugar. If the transport sugar is loaded directly into the phloem, then no such conversion should occur.

As in *Beta vulgaris*, Madore and Webb (1981) found that exogenously fed [$^{14}C$]sucrose taken up into leaves of *Cucurbita pepo* was translocated from these leaves in the form of sucrose, in agreement with Fondy and Geiger's hypothesis of direct uptake into the phloem. However, in the leaf tissue stachyose and all other compounds normally found labelled following exposure of leaves to $^{14}CO_2$ had become labelled, indicating that sucrose uptake had also occurred into the mesophyll, in agreement with earlier findings by Hendrix (1973, 1977).

Interestingly, exogenously fed [$^{14}C$]stachyose (galactose-labelled) and [$^{14}C$]galactose gave rise to exactly the same labelling phenomena seen with [$^{14}C$]sucrose. Again, extensive metabolism of the fed sugar occurred in the mesophyll; but, in addition, sucrose was again the transport sugar found labelled in the phloem. There was no indication of direct uptake of stachyose into the phloem, and the similarity of uptake patterns of all three exogenous sugars suggested that none of them had been taken up to any appreciable extent by phloem tissues. This had been expected for the reducing sugar, galactose, which is not a normal component of phloem sap, but was entirely unexpected for stachyose, the major transport form in this species. The best explanation for these results was that uptake of exogenous sugar was predominantly into the mesophyll, where metabolic conversion into various photosynthetic intermediates occurred, followed by export of sucrose produced by the conversion processes.

The data presented by Madore and Webb (1981) argued equally for a symplastic route for phloem loading in *Cucurbita*, in that negligible amounts of transport sugars were normally found in the apoplast. Instead, a general leakage of various photoassimilates was indicated. In addition, stachyose was not loaded to any significant extent when supplied exogenously to the

apoplast. The synthesis of stachyose in *Cucurbita* leaf strips is strongly inhibited when the tissues are plasmolysed and is almost totally inhibited by isolation of mesophyll cells (Madore and Webb, 1982), which suggests in addition that symplastic continuity may be important for the biochemical control of assimilate partitioning.

The question of apoplastic loading needs to be further examined in view of these findings. It is quite likely that uptake of exogenous sugars represents uptake predominantly into nonphloem tissues, and that extrapolation of exogenous sugar feedings to photoassimilate transfer *in vivo* is not justified. Clearly mesophyll cells have a tremendous capacity for uptake of exogenously supplied solutes, and these solutes, or metabolic derivations of them, can be exported to sink tissues. This supports the hypothesis that sugars may leak out of mesophyll tissue, and that uptake systems may exist simply to retrieve these leaked solutes.

This is not to say the phloem tissues do not also possess retrieval mechanisms. Indeed the whole question of "selectivity," as demonstrated by Fondy and Geiger, is open to question in view of the demonstration that, given time, compounds such as L-glucose (Schmalstig and Geiger, 1985) and 3-*O*-MG (F. T. Lichtner, personal communication) can move to other tissues via the phloem. Leakage may be a general feature of plasma membranes, and in the case of the phloem, the tremendously high sugar levels may result in high leakage rates. Indeed, it has been suggested by some that a continuous passive leakage of solutes may occur through phloem membrane "pores," with a steady recapture along the path ("pump-and-leak" system) maintaining the pressure flow over a long distance (Gifford and Evans, 1981; Komor, 1983). The operation of general retrieval mechanisms in both phloem and nonphloem tissues makes it impossible at present to study preferentially the putative "phloem-loading" mechanism at the sieve element–companion cell complex.

If sucrose retrieval is a general phenomenon of the phloem, studies on isolated vascular tissues (Cataldo, 1974; van Bel and Koops, 1985; Daie, 1986) will provide information on this retrieval process rather than on the mechanism of phloem loading.

## VI. SUCROSE METABOLISM BY SINK TISSUES

It has long been assumed that the rate of export of sucrose from a source leaf is controlled by the concentration of sucrose in the leaf. This in turn has been thought to be regulated by the rate of photosynthesis and the demand for assimilates by sink tissues. Recent advances in our understanding of the regulation of chloroplast metabolite exchange and its role in photosynthetic sucrose production now indicate that this view is overly simplistic.

## A. Regulation of Sucrose Supply by Source Leaf Metabolism

Sucrose synthesis in leaves is thought to occur predominantly by the combined reactions of sucrose phosphate synthase:

$$\text{UDP-glucose} + \text{Fructose-6-P} \rightleftharpoons \text{Sucrose-P} + \text{UDP} + \text{H}^+$$

and sucrose phosphatase:

$$\text{Sucrose-P} \rightleftharpoons \text{Sucrose} + \text{P}_i$$

Since export of triose-P from the chloroplast occurs by a counterexchange of inorganic phosphate (see review by Heber and Heldt, 1981), the synthesis of sucrose, which results in the release of inorganic phosphate, is directly coupled to release of triose-P to the cytosol. However, triose-P and $P_i$ are also required inside the chloroplast for the regeneration of ribulose bisphosphate (RuBP), in order to maintain $CO_2$ fixation. A constant production and export of sucrose, in response to demand by sinks, could result in inhibition of source leaf photosynthesis through depletion of Calvin cycle metabolite pools. Sucrose synthesis itself must therefore be kept under strict metabolic control. This is attained by a number of interrelated biochemical strategies, many of which now seem to be regulated, directly or indirectly, by the metabolite fructose-2,6-bisphosphate (Fru-2,6-BP). The nature of these control mechanisms has been the subject of several recent reviews (Stitt, 1985, 1986; Huber, 1986; see Chapter 1, this volume).

According to the Münch hypothesis, the rate of transport of solutes between source and sink is regulated by the sucrose gradient created by loading of sucrose into the phloem at the source end and its removal and utilization by sinks. If, however, as proposed above, sucrose levels in the photosynthetic cells of the source leaf must obligately be tightly regulated in order to prevent inhibition of photosynthesis, the gradient between source and sink may be dictated more by the sink tissues than by the sources.

## B. Control by Metabolically Driven Gradients

The metabolic fate of imported sucrose depends largely on the type of sink. Actively growing tissues require sucrose for growth and respiratory processes, consequently sucrose imported by these tissues will be readily metabolized. In sinks which perform a storage function (e.g., taproot, stem parenchyma) sucrose is less likely to be involved in maintenance processes but may be metabolized to other storage compounds such as starch or fructans. Any of these processes will serve to reduce the effective sucrose concentration in the sink and allow the continued movement of sucrose from the source.

Control of sucrose metabolism in sink tissues is provided, at a coarse level, by restriction of the genetic expression of catabolic enzymes to specific sink tissues and organs. A further degree of regulation is attained by the

physical separation of sucrose and the enzymes involved in its breakdown in different intra- and extracellular compartments within the sink tissues (for example the vacuole). Sucrose breakdown can be catalyzed by two different mechanisms in sink tissues:

1. A reaction catalyzed by invertase ($\beta$-D-fructofuranoside fructohydrolase, EC 3.2.1.26):

$$\text{Sucrose} \rightleftharpoons \text{Glucose} + \text{Fructose}$$

Invertase isozymes with acid (pH 5) or neutral (pH 7.5) pH optima have been isolated from plant tissues. Acid invertase is often associated with the cell walls and vacuoles while neutral invertase is cytosolic.

2. A reaction catalyzed by the reversal of the sucrose synthase reaction:

$$\text{Sucrose} + \text{UDP}^- + \text{H}^+ \rightleftharpoons \text{UDP-glucose} + \text{Fructose}$$

Sucrose synthase is also thought to be cytosolic. Its appearance in sugar beet taproots is correlated with the onset of storage (Giaquinta, 1979b).

In respiring sink tissues, UDP-glucose may be further metabolized to glucose-1-P and UTP by reversal of the UDP-glucose pyrophosphorylase reaction. The source of $PP_i$ for this reversal has been hypothesized (ap Rees *et al.*, 1985) to occur through a reversal of the $PP_i$-dependent phosphofructokinase reaction that has recently been discovered in plants (Black *et al.*, 1985). (This may also prove to be an important reaction driving the group translocator mechanism proposed by Thom and Maretzki, 1985, which may also require a source of $PP_i$, see Fig. 11.) Evidence now exists for a role for Fru-2,6-BP in the control of carbohydrate metabolism in sink tissues as well (Black *et al.*, 1985; Stitt *et al.*, 1986).

## C. Control by Phloem Unloading

The pathways of unloading in sink tissues vary depending on the type of tissue and its developmental stage. In some tissues, particularly actively growing regions such as young leaves (sugar beet, Giaquinta, 1977b; Ho and Baker, 1982) and roots (pea, Dick and ap Rees, 1975; corn, Giaquinta *et al.*, 1983; barley, Farrar, 1985), unloading apparently occurs by a symplastic route. In other tissues, particularly storage organs (sugarcane, Glaziou and Gayler, 1972; sugar beet, Giaquinta, 1977b; Saftner *et al.*, 1983) and fruits (grape berry, Kreidemann, 1969; Coombe, 1976; orange, Koch, 1984) and of necessity in developing seeds (bean, Patrick and McDonald, 1980; soybean, Thorne, 1980; corn, Felker and Shannon, 1980; wheat, Cook and Oparka, 1983; Ho and Gifford, 1984; barley, Cook and Oparka, 1983; rice, Oparka and Gates, 1981), solutes are first unloaded into the apoplast. Reabsorption of apoplastic sucrose may occur with (Shannon and Dougherty, 1972; Glaziou and Gayler, 1972) or without (Giaquinta, 1977a; Jenner, 1974; Thorne, 1980) prior hydrolysis by invertase.

The study of assimilate unloading has been revolutionized by the use of empty legume ovules as experimental systems (Patrick, 1983; Thorne and Rainbird, 1983; Wolswinkel and Amerlaan, 1983; Wolswinkel *et al.*, 1983). Upon removal of the embryo, assimilates will continue to be unloaded into a bathing medium contained in the seed coat. The empty ovule is readily manipulated by metabolic inhibitors simply by replacing the bathing medium with one containing the inhibitor. Results from a number of legume species (faba bean, Wolswinkel and Amerlaan, 1983; pea, Wolswinkel *et al.*, 1983; bean, Patrick, 1983; soybean, Thorne and Rainbird, 1983) show that assimilate unloading from the seed coat is under metabolic control as release is inhibited by treatments such as azide, cyanide, CCCP, and low temperature. In addition, the process may be carrier mediated, as suggested by inhibition by sulfhydryl group modifiers. However, recent studies (Wolswinkel, 1985a) indicate that the release of sucrose into the bathing medium is a net result of release and also reabsorption by the seed coat cells. The effects of inhibitors would also be expected to affect reabsorption processes. For a more complete review of this area, see Wolswinkel (1985b).

General unloading strategies are as yet difficult to ascertain but seem to be correlated with the import physiology of the sink. Thus, symplastic unloading seems to be restricted to actively growing and respiring sinks, where direct utilization and chemical transformation of imported solutes in the cytosol can create a solute gradient. Apoplastic unloading seems to be prevalent in tissues that perform a storage role where compartmentation could drive solute flow. In this case, the apoplastic sugar concentrations are likely to be maintained at very high levels, as in the case of sugarcane stalk parenchyma (Glaziou and Gayler, 1972). As illustrated by the case study on sugar beet (Wyse *et al.*, 1986; see Section III,B,1), changes in cell turgor in response to apoplastic sugar levels is one means by which control of apoplastic uptake could be effected. Apoplastic sugar concentrations in the range of 150–200 m*M* have been obtained for the interface between the soybean seedcoat and cotyledon (Gifford and Thorne, 1985). Interestingly, in the wheat endosperm cavity, apoplastic sucrose was only 10–90 m*M*, while starch synthesis by endosperm tissues was saturated at concentrations of 200 m*M* (Gifford, 1986). This raises the intriguing possibility that the sucrose content in the apoplast may not saturate the uptake mechanism(s) of the sink tissues, such that the source tissues "do not deliver photoassimilate to the seeds fast enough for maximal growth rate" (Gifford, 1986).

### D. Hormonally Directed Transport

During plant growth, various organs and tissues undergo rather orderly transitions from sink to source metabolism. The import–export transition that occurs during leaf development is perhaps the most well-studied of these transition events, but is not the only case. A sink-to-source transition

does not necessarily involve the development of photosynthetic capacity, more often it is simply the result of remobilization of previously stored reserves in what were previously storage "sinks." This type of transition is exemplified by storage organs such as taproots, or storage tissues such as the sugarcane stalk parenchyma or the paraveinal mesophyll layer of the soybean leaf, in which mobilization of stored reserves is induced by the production of new, often reproductive, sink tissues. Mobilization of structural components by senescing leaves prior to abscision is another case in point.

It is well recognized that these transition phases during plant growth are regulated by the interaction of specific plant hormones on specific target cells or tissues. Sink tissues tend to have the highest concentrations of growth hormones and, as indicated previously, also appear to direct the flow of assimilates from the source tissues. Thus, hormonal control of assimilate partitioning has been intensively studied and much evidence has been presented implicating various plant hormones in the control of assimilate partitioning to sinks. However, as with many other aspects of transport physiology, the exact sites of action ("targets") and the mechanisms involved remain elusive.

Many hormones appear to act as strong mobilizing agents for photoassimilates. In general, gibberellins, auxins, and cytokinins appear to increase the "sink strength" of the treated tissue, while ABA can increase or decrease sink activity. Hormonal effects have been attributed to effects on "phloem loading" (Karmoker and van Steveninck, 1979; Vreugdenhil, 1983), long-distance translocation (Patrick and Wareing, 1976), and uptake by sink tissues (Mulligan and Patrick, 1979).

Correlations between ABA levels and sugar import in fruits (Düring and Alleweldt, 1980; Schussler *et al.*, 1984) have implicated this hormone in the control of assimilate partitioning. ABA has also been implicated in the control of membrane ion transport (see Morré, 1982), its effects on sugar transport may also reside in membrane transport related phenomena. However, the effects of ABA on sugar transport phenomena are often contradictory. Transport of assimilates is sometimes stimulated by ABA treatment (Karmoker and van Steveninck, 1979; Hartung *et al.*, 1980; Dewdney and McWha, 1979), is unaffected (King and Patrick, 1982), or is inhibited (Mullins, 1970; Porter 1981; Vreugdenhil, 1983). The effect observed apparently may depend on the development status of the tissue in question (Tietz *et al.*, 1981), but even this is not necessarily always true (Saftner and Wyse, 1984).

In sugar beet root discs, ABA has either no effect or greatly stimulates the uptake of exogenous [$^{14}$C]sucrose (Saftner and Wyse, 1984; Wyse, 1986). In contrast, Vreugdenhil (1983) has recently reported that ABA inhibits the uptake of exogenous [$^{14}$C]sucrose into *Ricinus* cotyledon discs, and *Beta*, *Phaseolus*, and *Petunia* leaf discs. The uptake into *Ricinus* cotyledons was apparently coupled to proton transport but the effects of ABA were not on

the proton transport system; rather, an enhanced leakage of solutes was postulated. The exact mechanism of ABA action, or its involvement in assimilate control *in vivo*, requires further investigation but may reside in control of phloem unloading processes or stimulation of uptake of unloaded solutes.

Cytokinin application often results in a mobilization of assimilates, either exogenously supplied (Mothes and Engelbrecht, 1961; Gersani and Kende, 1982) or photosynthetically produced (Quinlan and Weaver, 1969) from a remote source to the site of application. This mobilization is not limited to sugars, as $^{32}$P-labelled compounds will also be mobilized (Muller and Leopold, 1969a,b; Hatch and Powell, 1971a,b). Movement can be induced in most tissues, including leaves (Quinlan and Weaver, 1969), roots (Shindy *et al.*, 1973), and fruits (Weaver *et al.*, 1969); although young, actively growing tissues are usually more responsive (Quinlan and Weaver, 1969; Hatch and Powell, 1971a,b). Again, the mode of action is unknown, but the responsiveness of young tissues suggests activation of growth processes perhaps by meristematic or cambial induction giving rise to increased "sink strength."

In general, it would seem that most of the known plant growth regulators can be found to exert, on some experimental system at some stage of plant development, some effect on assimilate partitioning. In view of the myriad effects of growth regulators on *growth*, perhaps this is not so surprising. Present evidence would tend to support the idea that the effects of growth regulators are largely a result of their effects on sink metabolism, either delaying senescence or inducing meristematic growth. It is still difficult, however, given our present experimental systems, to separate effects of stimulation of growth on assimilate transport phenomena from the effects of stimulation of transport on growth phenomena. Direct control of assimilate transport *per se* by effects on the pathway itself, as envisaged by Patrick (1982), will be more difficult to ascertain, because once again we are faced with a highly complex system of tissues, some of which can certainly be induced experimentally to act as sinks. The whole concept of what exactly constitutes a sink is a problem that remains to be resolved before we understand the hormonal responses that are observed.

As far as hormonal mechanisms are concerned, we still know relatively little about how hormonal messages are communicated in plant tissues. One possibility that has not yet been closely examined is that, as in animal tissues, hormones may exert their activity through regulation of $Ca^{2+}$-dependent protein kinase systems. Regulation of the transport activity of $Na^+$, $K^+$, and anion-selective channels in animal tissues is achieved by phosphorylation of the channel proteins, and the degrees of phosphorylation is controlled by a variety of protein kinases modulated by $Ca^{2+}$, $Ca^{2+}$–calmodulin, and $Ca^{2+}$–phospholipid interactions (Nairn *et al.*, 1985). Protein kinases have been isolated from plant tissues (Hepler and Wayne, 1985) and have been implicated in the control of activity of plant ATPases (Zocchi *et al.*, 1984),

but their role in elicitation of hormonal responses remains to be investigated. It is interesting that the effects of one plant hormone, ethylene, can be obviated by application of $Ca^{2+}$. The demonstration that enhanced sugar uptake by aged leaf discs may be an ethylene-mediated response becomes, in this respect, a very intriguing finding (Lemoine *et al.*, 1984).

As we have already indicated earlier, the ability to take up exogenous sugars would appear to be a general feature of all plant cells; that is, all cells have the capacity to act as sinks, although they may not always be required to do so *in vivo*. However, it is not unreasonable to assume that such temporary sinks may also at times serve a source function, channelling retrieved assimilates to other sink tissues. Fluctuations between sink and source activity in certain tissues could be invoked at various intervals, perhaps diurnally in response to internal circadian rhythms, or on a short-term basis in response to environmental stress, in order to maintain a homeostatic balance of assimilate partitioning within the whole plant.

Evidence for this type of constantly shifting source–sink relationship has been shown recently by Grusak and Lucas (1986) for the crown region of the sugar beet plant. Hormonal regulation at this level, i.e., controlling the homeostasis between souce and sink activity in a single tissue, would provide a powerful mechanism for the regulation of plant growth and development in response to the fluctuating environmental conditions normally encountered by plants. The nature of the signalling mechanism by which the hormonal messages are transduced remains to be discovered but may involve a turgor sensing mechanism.

## VII. TURGOR SENSING IN SUGAR TRANSPORT

Maintenance of a turgor pressure gradient between source and sink regions is an essential correlate of the Münch pressure flow hypothesis of phloem translocation. It has been argued, therefore, that turgor sensing at the tissue level may act as a communication mechanism between source and sink, signalling the physiological status of source and sink tissues. The unloading of solutes into empty legume ovules has been shown to be sensitive to turgor (Wolswinkel and Amerlaan, 1984), which as discussed above may reflect effects on solute release and solute reabsorption processes. Sensitivity of sugar uptake to turgor has been reported for a number of tissues, notably sugar beet (see Section III,B,1; Wyse *et al.*, 1985, 1986) and also for source leaf discs (Smith and Milburn, 1980; Hagege *et al.*, 1984; Reinhold *et al.*, 1984; Daie and Wyse, 1985). Recent studies (Reinhold *et al.*, 1984) suggest that the effects of turgor changes may be mediated through changes in the proton motive force generated by $H^+$-ATPase(s) (see also Wyse *et al.*, 1986). Effects on the ATPase activities may be due to structural changes induced by membrane compression at high turgor (Coster *et al.*, 1976), but

this situation may only hold when the apoplast is involved in osmotic adjustment (see Lucas and Alexander, 1981 for a discussion of this concept).

Lang (1983) and others have also introduced the concept of turgor sensing and adjustment involving not only the source and sink regions, but also the interconnecting, or long-distance component of the phloem. This concept has important implications with respect to control over carbohydrate allocation. Grusak and Lucas (1986) recently provided preliminary experimental evidence consistent with this concept. They found that assimilate repartitioning events may be induced by turgor changes in localized areas of the long-distance transport system. This may involve the elicitation of membrane-mediated electrical and/or chemical signals, an area of obvious potential for future research.

## VIII. CONCLUSIONS

Sucrose is one of the first stable products of photosynthesis, second only to starch in importance as a major pool of photosynthetically fixed carbon in leaves. However, the conventional biochemist's view of sucrose, or even starch, as "end-products" of photosynthesis is inherently wrong from a physiological standpoint, as long- and short-distance transport processes provide a continuous spatial conversion of assimilates from one plant compartment to another. On the other hand, we are now recognizing that biochemical regulation controls many of the physiological processes involved in sugar transport.

Our current models of sugar transport and its control mechanisms are useful, but we must now recognize them as being woefully simplistic for the type of complexity that is presented at the membrane, cellular, and whole-plant level. The research advances made in the past six years since this topic was last reviewed for this series point increasingly to this conclusion. It is becoming more and more evident that plant biochemistry, physiology, and ultrastructure are (i) much more complicated than usually envisioned, and (ii) intimately linked to "transport" phenomena. Future advances in sugar transport will only come from research which does not try to minimize the complexity that we face. An integrated approach is demanded before an integrated picture can emerge of sugar transport mechanisms in plants.

## ACKNOWLEDGMENTS

Work conducted in our laboratory on phloem physiology is supported by a National Science Foundation grant PCM 83-15408. M.A.M. gratefully acknowledges the support of a Natural Sciences and Engineering Research Council (Canada) Postdoctoral Fellowship. We thank Margaret Thom and Andy Maretzki, and Jaleh Daie and Roger Wyse, for making their manuscripts

available prior to publication. We also thank those colleagues who allowed us to reproduce aspects of their work in this review.

## REFERENCES*

Anderson, R. D. (1983). *Plant Physiol.* **71,** 333–340.
ap Rees, T., Morrell, S., Edwards, J., Wilson, P. M., and Green, J. H. (1985). *In* "Regulation of Carbon Partitioning in Photosynthetic Tissue" (R. L. Heath and J. Preiss, eds.), pp. 76–92. American Society of Plant Physiologists, Rockville, MD.
Asami, S., Hara-Nishimura, I., Nishimura, M., and Akazawa, T. (1985). *Plant Physiol.* **77,** 963–968.
Beevers, H. (1979). *Annu. Rev. Plant Physiol.* **30,** 159–193.
Belitser, N. V., Zaalishvili, N. P., and Sytnianskaja, N. P. (1982). *Protoplasma* **111,** 63–78.
Black, C. C., Carnal, N. W., and Paz, N. (1985). *In* "Regulation of Carbon Partitioning in Photosynthetic Tissues" (R. L. Heath and J. Preiss, eds.), pp. 45–62. American Society of Plant Physiologists, Rockville, MD.
Bock, K., and Lemieux, R. U. (1982). *Carbohydr. Res.* **110,** 63–74.
Boller, T., and Alibert, G. (1983). *Z. Pflanzenphysiol.* **110,** 231–238.
Briskin, D. P. (1986). *In* "Phloem Transport" (J. Cronshaw, W. J. Lucas, and R. T. Giaquinta, eds.). pp. 111–123. Liss, New York.
Briskin, D. P., Thornley, W. R., and Wyse, R. E. (1985a). *Plant Physiol.* **78,** 865–870.
Briskin, D. P., Thornley, W. R., and Wyse, R. E. (1985b). *Plant Physiol.* **78,** 871–875.
Brown, S. C., and Coombe, B. G. (1982). *Naturwissenschaften* **69,** 43–45.
Brown, S. C., and Coombe, B. G. (1984a). *Biochem. Physiol. Pflanzen* **179,** 157–171.
Brown, S. C., and Coombe, B. G. (1984b). *Physiol. Veg.* **22,** 231–240.
Card, P. J., and Hitz, W. D. (1984). *J. Am. Chem. Soc.* **106,** 5348–5350.
Card, P. J., Hitz, W. D., and Ripp, K. G. (1985). *J. Am. Chem. Soc.* **108,** 158–161.
Cataldo, D. A. (1974). *Plant Physiol.* **53,** 912–917.
Cho, B. H., and Komor, E. (1985). *J. Plant Physiol.* **118,** 381–389.
Cook, H., and Oparka, K. J. (1983). *Plant Cell Environ.* **6,** 239–242.
Coombe, B. G. (1976). *Annu. Rev. Plant Physiol.* **27,** 207–228.
Coster, H. G. L., Steudle, E., and Zimmermann, U. (1976). *Plant Physiol.* **58,** 636–643.
Cronshaw, J. (1981). *Annu. Rev. Plant Physiol.* **32,** 465–484.
Cronshaw, J., Lucas, W. J., and Giaquinta, R. T. (1986). "Phloem Transport." Liss, New York, 650 p.
Daie, J. (1986). *J. Am. Soc. Hortic. Sci.* (in press).
Daie, J., and Wyse, R. E. (1985). *Physiol. Plant.* **64,** 547–552.
Delrot, S. (1981). *Plant Physiol.* **68,** 706–711.
Delrot, S., and Bonnemain, J. L. (1981). *Plant Physiol.* **67,** 560–564.
Delrot, S., Deshpegel, J. P., and Bonnemain, J. L. (1980). *Planta* **149,** 144–148.
Dewdney, S. J., and McWha, J. A. (1979). *Z. Pflanzenphysiol.* **92,** 183–186.
Dick, P. S., and ap Rees, T. (1975). *J. Exp. Bot.* **26,** 305–314.
Doll, S., Rodier, F., and Willenbrink, J. (1979). *Planta* **144,** 407–411.
Donovan, G. R., Jenner, C. F., Lee, J. W., and Martin, P. (1983). *Aust. J. Plant Physiol.* **10,** 31–42.
Düring, H., and Alleweldt, G. (1980). *Ber. Dtsch. Bot. Ges.* **93,** 339–347.
Ehwald, R., Kowallick, D., Meshcheryakov, A. B., and Kholodova, V. P. (1980). *J. Exp. Bot.* **31,** 607–620.
Erwee, M. G., and Goodwin, P. B. (1983). *Planta* **158,** 302–328.
Erwee, M. G., and Goodwin, P. B. (1984). *Protoplasma* **122,** 162–168.
Erwee, M. G., and Goodwin, P. B. (1985). *Planta* **163,** 9–19.

* Literature survey completed December 31, 1985.

Erwee, M. G., Goodwin, P. B., and van Bel, A. J. E. (1985). *Plant Cell Environ.* **8,** 173–178.
Evert, R. F., and Mierzwa, R. J. (1986). *In:* "Phloem Transport." (J. Cronshaw. W. J. Lucas, R. T. Giaquinta, eds.). pp. 419–432. Alan R. Liss, New York.
Evert, R. F., Eschrich, W., and Heyser, W. (1977). *Planta* **136,** 77–89.
Evert, R. F., Eschrich, W., and Heyser, W. (1978). *Planta* **138,** 279–294.
Farrar, J. F. (1985). *New Phytol.* **99,** 57–69.
Felker, F. C., and Shannon, J. C. (1980). *Plant Physiol.* **65,** 864–870.
Felker, F. C., Peterson, D. M., and Nelson, O. E. (1984). *Plant Physiol.* **74,** 43–46.
Fisher, D. G., and Evert, R. F. (1982). *Planta* **155,** 377–387.
Fisher, D. B., and Outlaw, W. H. (1979). *Plant Physiol.* **64,** 481–483.
Fondy, B. R., and Geiger, D. R. (1977). *Plant Physiol.* **59,** 953–960.
Franceschi, V. R. (1986). *In* "Phloem Transport" (J. Cronshaw, W. J. Lucas, and R. T. Giaquinta, eds.). pp. 399–409. Liss, New York.
Franceschi, V. R., and Giaquinta, R. T. (1983a). *Planta* **154,** 411–421.
Franceschi, V. R., and Giaquinta, R. T. (1983b). *Planta* **154,** 422–431.
Franz, S., and Tattar, T. A. (1981). *Plant Physiol.* **67,** 150–155.
Fritz, E. (1980). *Ber. Dtsch. Bot. Ges.* **93,** 109–121.
Fritz, E., Evert, R. F., and Heyser, W. (1983). *Planta* **159,** 193–206.
Gamalei, Y. V. (1985). *Sov. Plant Physiol.* **32,** 134–148.
Gamalei, Y. V., and Pakhomova, M. V. (1981). *Sov. Plant Physiol.* **28,** 649–661.
Geiger, D. R. (1975). *In* "Transport in Plants" (M. H. Zimmermann and J. A. Milburn, eds.), Vol. I, pp. 395–450. Springer-Verlag, New York.
Geiger, D. R. (1976). *In* "Transport and Transfer Processes in Plants" (I. F. Wardlaw and J. B. Passioura, eds.), pp. 167–215. Academic Press, New York.
Geiger, D. R., and Giaquinta, R. T. (1982). *In* "Photosynthesis" (Govindjee, ed.), Vol. II, pp. 345–386. Academic Press, New York.
Geiger, D. R., and Swanson, C. A. (1965). *Plant Physiol.* **40,** 942–947.
Geiger, D. R., Giaquinta, R. T., Sovonick, S. A., and Fellows, R. J. (1973). *Plant Physiol.* **52,** 585–589.
Geiger, D. R., Sovonick, S. A., Shock, T. L., and Fellows, R. J. (1974). *Plant Physiol.* **54,** 892–898.
Geiger, D. R., Ploeger, B. J., Fox, T. C., and Fondy, B. R. (1983). *Plant Physiol.* **72,** 964–970.
Gemmerich, A. R. (1982). *Plant Cell Rep.* **1,** 233–235.
Gerhardt, R., and Heldt, H. W. (1984). *Plant Physiol.* **75,** 542–547.
Gersani, M., and Kende, H. (1982). *J. Plant Growth Regul.* **1,** 161–171.
Giaquinta, R. T. (1977a). *Plant Physiol.* **59,** 750–755.
Giaquinta, R. T. (1977b). *Plant Physiol.* **60,** 339–343.
Giaquinta, R. T. (1979a). *Plant Physiol.* **63,** 744–748.
Giaquinta, R. T. (1979b). *Plant Physiol.* **63,** 828–832.
Giaquinta, R. T. (1980a). *Ber. Dtsch. Bot. Ges.* **93,** 187–201.
Giaquinta, R. T. (1980b). *Biochem. Plants* **3,** 271–320.
Giaquinta, R. T. (1983). *Annu. Rev. Plant Physiol.* **34,** 347–387.
Giaquinta, R. T., Lin, W., Sadler, N. L., and Franceschi, V. R. (1983). *Plant Physiol.* **72,** 362–367.
Gifford, R. M. (1986). *In* "Phloem Transport" (J. Cronshaw, W. J. Lucas, and R. T. Giaquinta, eds.). pp. 535–549. Liss, New York.
Gifford, R. M., and Evans, L. T. (1981). *Annu. Rev. Plant Physiol.* **32,** 485–509.
Gifford, R. M., Thorne, J. H., Hitz, W. D., and Giaquinta, R. T. (1984). *Science* **225,** 801–808.
Gifford, R. M., and Thorne, J. H. (1985). *Plant Physiol.* **77,** 863–868.
Glaziou, K. T., and Gayler, K. R. (1972). *Bot. Rev.* **38,** 471–490.
Goodwin, P. B. (1983). *Planta* **157,** 124–130.
Goodwin, P. B., and Lyndon, R. F. (1983). *Protoplasma* **116,** 219–222.
Gordon, A. J. (1986). *In* "Phloem Transport" (J. Cronshaw, W. J. Lucas, and R. T. Giaquinta, eds.). pp. 499–517. Liss, New York.

Grusak, M. A., and Lucas, W. J. (1986). *J. Exp. Bot.* **37,** 277–288.
Gunning, B. E. S., and Robards, A. W. (1976). *In* "Transport and Transfer Processes in Plants" (I. F. Wardlaw and J. B. Passioura, eds.), pp. 15–41. Academic Press, New York.
Guy, M., Reinhold, L., and Michaeli, A. (1979). *Plant Physiol.* **64,** 61–64.
Guy, M., Reinhold, L., and Rahat, M. (1980). *Plant Physiol.* **65,** 550–553.
Guy, M., Reinhold, L., Rahat, M., and Seiden, A. (1981). *Plant Physiol.* **67,** 1146–1150.
Hagege, I., Hagege, D., Delrot, S., Deshpegel, J. P., and Bonnemain, J. P. (1984). *C. R. Acad. Sci. D* **299,** 435–440.
Hartung, W., Ullrich-Eberius, C. I., Lüttge, U., Böcher, M., and Novacky, A. (1980). *Planta 148,* 256 –261.
Hatch, A. H., and Powell, A. E. (1971a). *J. Am. Soc. Hortic. Sci.* **96,** 230–234.
Hatch, A. H., and Powell, A. E. (1971b). *J. Am. Soc. Hortic. Sci.* **96,** 399–400.
Heber, U., and Heldt, H. W. (1981). *Annu. Rev. Plant Physiol.* **32,** 139–168.
Hendrix, J. E. (1973). *Plant Physiol.* **52,** 688–689.
Hendrix, J. E. (1977). *Plant Physiol.* **60,** 567–569.
Hepler, P. K., and Wayne, R. O. (1985). *Annu. Rev. Plant Physiol.* **36,** 397–439.
Heyser, W. (1980). *Ber. Dtsch. Bot. Ges.* **93,** 221–228.
Hitz, W. D. (1986). *In* "Phloem Transport" (J. Cronshaw, W. J. Lucas, and R. T. Giaquinta, eds.). pp. 27–39. Liss, New York.
Hitz, W. D., Schmitt, M. R., Card, P. J., and Giaquinta, R. T. (1985). *Plant Physiol.* **77,** 291–295.
Ho, L. C., and Baker, D. A. (1982). *Physiol. Plant.* **56,** 225–230.
Ho, L. C., and Gifford, R. M. (1984). *J. Exp. Bot.* **35,** 58–73.
Hsu, F. C., Bennett, A. B., and Spanswick, R. M. (1984). *Plant Physiol.* **75,** 181–186.
Huber, S. C. (1986). *Annu. Rev. Plant Physiol.* **37,** 233–246.
Huber, S. C., and Moreland, D. E. (1980). *Plant Physiol.* **65,** 560–562.
Huber, S. C., and Moreland, D. E. (1981). *Plant Physiol.* **67,** 163–169.
Huber, S. C., Kerr, P. S., and Kalt-Torres, W. (1985). *In* "Regulation of Carbon Partitioning in Photosynthetic Tissues" (R. L. Heath and J. Preiss, eds.), pp. 119–214. American Society of Plant Physiologists, Rockville, MD.
Hutchings, V. M. (1978). *Planta* **138,** 229–235.
Jenner, C. F. (1974). *Aust. J. Plant Physiol.* **1,** 319–329.
Jenner, C. F. (1976). *Aust. J. Plant Physiol.* **3,** 337–347.
Kaiser, G., and Heber, U. (1984). *Planta* **161,** 562–568.
Kaiser, W. M., Paul, J. S., and Bassham, J. A. (1979). *Z. Pflanzenphysiol.* **94** 377–385.
Kaiser, G., Martinoia, E., and Wiemken, A. (1982). *Z. Pflanzenphysiol.* **107,** 103–113.
Kaiser, G., Martinoia, E., Schramm, M. J., and Flugge, U. I. (1986). *In* "Phloem Transport" (J. Cronshaw, W. J. Lucas, and R. T. Giaquinta, eds.). pp. 125–127. Liss, New York.
Karmoker, J. L., and van Steveninck, R. F. M. (1979). *Planta* **146,** 25–30.
King, R. W., and Patrick, J. W. (1982). *Z. Pflanzenphysiol.* **106,** 375–380.
Koch, K. E. (1984). *Plant Cell Environ.* **7,** 647–653.
Komor, E. (1977). *Planta* **137,** 119–131.
Komor, E. (1982). *In* "Plant Carbohydrates" (F. A. Loewus and W. Tanner, eds.). Vol. 1, pp. 635–676. Springer-Verlag, New York.
Komor, E. (1983). *Prog. Bot.* **45,** 68–75.
Komor, E., and Orlich, G. (1986). *In* "Phloem Transport" (J. Cronshaw, W. J. Lucas, and R. T. Giaquinta, eds.). pp. 53–65. Liss, New York.
Komor, E., Rotter, M., and Tanner, W. (1977). *Plant Sci. Lett.* **9,** 153–162.
Komor, E., Rotter, M., Waldhauser, J., Martin, E., and Cho, B. H. (1980). *Ber. Dtsch. Bot. Ges.* **93,** 211–219.
Komor, E., Thom, M., and Maretzki, A. (1981). *Planta* **153,** 181–192.
Komor, E., Thom, M., and Maretzki, A. (1982a). *Plant Physiol.* **69,** 1326–1330.
Komor, E., Thom, M., and Maretzki, A. (1982b). *Physiol. Veg.* **20,** 277–287.

Komor, E., Cho, B. H., and Thom, M. (1984). *Ber. Dtsch. Bot. Ges.* **97,** 15–26.
Kreidemann, P. E. (1969). *Planta* **85,** 111–117.
Kreidemann, P., and Beevers, H. (1969a). *Plant Physiol.* **42,** 161–173.
Kreidemann, P., and Beevers, H. (1969b). *Plant Physiol.* **42,** 174–180.
Lang, A. (1983). *Plant Cell Environ.* **6,** 683–689.
Leger, A., Delrot, S., and Bonnemain, J. L. (1982). *Physiol. Veg.* **20,** 651–659.
Lemoine, R., Delrot, S., and Auger, E. (1984). *Physiol. Plant.* **61,** 571–576.
Lichtner, F. T., and Spanswick, R. M. (1981a). *Plant Physiol.* **67,** 869–874.
Lichtner, F. T., and Spanswick, R. M. (1981b). *Plant Physiol.* **68,** 693–698.
Lin, W. (1985). *Plant Physiol.* **78,** 41–45.
Lin, W., Schmitt, M. R., Hitz, W. D., and Giaquinta, R. T. (1984). *Plant Physiol.* **75,** 936–940.
Lingle, S. E., and Chevalier, P. (1984). *Crop Sci.* **24,** 315–319.
Lucas, W. J., and Alexander, J. M. (1981). *Plant Physiol.* **68,** 553–559.
Madore, M. A. (1984). Ph.D. dissertation, University of Guelph, Ontario, Canada.
Madore, M. A., and Grodzinski, B. (1985). *J. Plant Physiol.* **121,** 59–71.
Madore, M. A., and Webb, J. A. (1981). *Can. J. Bot.* **59,** 2550–2557.
Madore, M. A., and Webb, J. A. (1982). *Can. J. Bot.* **60,** 126–130.
Madore, M. A., Oross, J. W., and Lucas, W. J. (1986). *Plant Physiol. 82,* 432–442.
Maretzki, A., and Thom, M. (1972a). *Plant Physiol.* **49,** 177–182.
Maretzki, A., and Thom, M. (1972). *Biochem. Biophys. Res. Commun.* **7,** 44–50.
Martin, E., and Komor, E. (1980). *Planta* **148,** 367–373.
Martinoia, E., Flugge, U. I., Kaiser, G., Heber, U., and Heldt, H. W. (1985). *Biochim. Biophys. Acta* **806,** 311–319.
Maynard, J. W., and Lucas, W. J. (1982a). *Plant Physiol.* **69,** 734–739.
Maynard, J. W., and Lucas, W. J. (1982b). *Plant Physiol.* **70,** 1436–1443.
M'Batchi, B., and Delrot, S. (1984). *Plant Physiol.* **75,** 154–160.
M'Batchi, B., Pichelin, D., and Delrot, S. (1985). *Plant Physiol.* **79,** 537–542.
Morré, E. (1982). *In* "Plant Growth Substances 1982" (P. F. Wareing, ed.), pp. 407–417. Academic Press, New York.
Mothes, K., and Engelbrecht, L. (1961). *Phytochemistry* **1,** 58–62.
Muller, K., and Leopold, A. C. (1966a). *Planta* **68,** 167–185.
Muller, K., and Leopold, A. C. (1966b). *Planta* **68,** 186–205.
Mulligan, D. R., and Patrick, J. W. (1979). *Planta* **145,** 233–238.
Mullins, M. G. (1970). *Ann. Bot.* **34,** 897–909.
Nairn, A. C., Hemmings, H. C., and Greengard, P. (1985). *Annu. Rev. Biochem.* **54,** 931–976.
Offler, C. E., and Patrick, J. W. (1984). *Aust. J. Plant Physiol.* **11,** 79–99.
Oparka, K. J., and Gates, P. (1981). *Planta* **152,** 388–396.
Oparka, K. J., and Gates, P. (1982). *Protoplasma* **113,** 33–43.
Outlaw, W. H., and Fisher, D. B. (1975). *Plant Physiol.* **55,** 699–703.
Palevitz, B. A., and Hepler, P. K. (1985). *Planta* **164,** 473–479.
Patrick, J. W. (1982). *In* "Plant Growth Substances 1982" (P. F. Wareing, ed.), pp. 669–678. Academic Press, New York.
Patrick, J. W. (1983). *Z. Pflanzenphysiol.* **111,** 9–18.
Patrick, J. W. (1984). *J. Plant Physiol.* **155,** 297–310.
Patrick, J. W., and McDonald, R. (1980). *Aust. J. Plant Physiol.* **7,** 671–684.
Patrick, J. W., and Wareing, P. F. (1976). *J. Exp. Bot.* **27,** 962–982.
Porter, N. G. (1981). *Physiol. Plant.* **53,** 279–284.
Quinlan, J. D., and Weaver, R. J. (1969). *Plant Physiol.* **44,** 1246–1252.
Reinhold, L., and Kaplan, A. (1984). *Annu. Rev. Plant Physiol.* **35,** 45–83.
Reinhold, L., Seiden, A., and Volokita, M. (1984). *Plant Physiol.* **75,** 846–849.
Russin, W. A., and Evert, R. F. (1985). *Am. J. Bot.* **73,** 1232–1247.
Saftner, R. A., and Wyse, R. E. (1980). *Plant Physiol.* **66,** 884–889.
Saftner, R. A., and Wyse, R. E. (1984). *Plant Physiol.* **74,** 951–955.

Saftner, R. A., Daie, J., and Wyse, R. E. (1983). *Plant Physiol.* **72,** 1–6.
Sakri, F. A. K., and Shannon, J. C. (1975). *Plant Physiol.* **55,** 581–589.
Sauter, J. J. (1982). *Z. Pflanzenphysiol.* **111,** 429–440.
Schmalstig, J. G., and Geiger, D. R. (1985). *Plant Physiol.* **79,** 237–241.
Schmitt, M. R., Hitz, W. D., and Giaquinta, R. T. (1984). *Plant Physiol.* **75,** 941–946.
Schussler, J. R., Brenner, M. L., and Brun, W. A. (1984). *Plant Physiol.* **76,** 301–306.
Scorer, K. N. (1984). *Plant Physiol.* **76,** 753–758.
Shannon, J. C. (1972). *Plant Physiol.* **49,** 198–202.
Shannon, J. C., and Dougherty, C. T. (1972). *Plant Physiol.* **49,** 203–206.
Shannon, J. C., Porter, G. A., and Knievel, D. P. (1986). *In* "Phloem Transport" (J. Cronshaw, W. J. Lucas, and R. T. Giaquinta, eds.). pp. 265–277. Liss, New York.
Shindy, W. W., Kliewer, W. M., and Weaver, R. J. (1973). *Plant Physiol.* **51,** 345–359.
Smith, J. A. C., and Milburn, J. A. (1980). *Planta* **148,** 42–48.
Sovonick, S. A., Geiger, D. R., and Fellows, R. J. (1974). *Plant Physiol.* **54,** 886–891.
Spanswick, R. M. (1986). *In* "Phloem Transport" (J. Cronshaw, W. J. Lucas, and R. T. Giaquinta, eds.). pp. 93–101. Liss, New York.
Stitt, M. (1985). *In* "Regulation of Carbon Partitioning in Photosynthetic Tissues" (R. L. Heath and J. Preiss, eds.), pp. 109–126. American Society of Plant Physiologists, Rockville, MD
Stitt, M. (1986). *In* "Phloem Transport" (J. Cronshaw, W. J. Lucas, and R. T. Giaquinta, eds). pp. 331–347. Liss, New York.
Stitt, M., Cseke, C., and Buchanan, B. B. (1986). *Plant Physiol.* **80,** 246–248.
Sze, H. (1985). *Annu. Rev. Plant Physiol.* **36,** 175–208.
Tanner, W. (1980). *Ber. Dtsch. Bot. Ges.* **93,** 349–351.
Thom, M., and Komor, E. (1984a). *Eur. J. Biochem.* **138,** 93–100.
Thom, M., and Komor, E. (1984b). *FEBS Lett.* **173,** 1–4.
Thom, M., and Komor, E. (1984c). *Planta* **161,** 361–365.
Thom, M., and Komor, E. (1985). *Physiol. Plant.* **77,** 329–334.
Thom, M., and Maretzki, A. (1985). *Proc. Natl. Acad. Sci. U.S.A.* **82,** 4697–4701.
Thom, M., and Maretzki, A. (1986a). *Plant Physiol.* **80,** 34–37.
Thom, M., and Maretzki, A. (1986b). *In* "Phloem Transport" (J. Cronshaw, W. J. Lucas, and R. T. Giaquinta, eds.). pp. 103–110. Liss, New York.
Thom, M., Maretzki, A., and Komor, E. (1982a). *Plant Physiol.* **69,** 1315–1319.
Thom, M., Komor, E., and Maretzki, A. (1982b). *Plant Physiol.* **69,** 1320–1325.
Thom, M., Willenbrink, J., and Maretzki, A. (1983). *Physiol. Plant.* **58,** 497–504.
Thom, M., Leigh, R. A., and Maretzki, A. (1986). *Planta* **167,** 410–413.
Thorne, J. H. (1980). *Plant Physiol.* **65,** 975–979.
Thorne, J. H. (1981). *Plant Physiol.* **67,** 1016–1025.
Thorne, J. H. (1982). *Plant Physiol.* **70,** 953–958.
Thorne, J. H. (1985). *Annu. Rev. Plant Physiol.* **36,** 317–472.
Thorne, J. H. (1986). *In* "Phloem Transport" (J. Cronshaw, W. J. Lucas, and R. T. Giaquinta, eds.). pp. 211–224. Liss, New York.
Thorne, J. H., and Rainbird, R. M. (1983). *Plant Physiol.* **72,** 268–271.
Tietz, A., Ludewig, M., Dingkuhn, M., and Dörffling, K. (1981). *Planta* **152,** 557–561.
Tucker, E. B. (1982). *Protoplasm* **113,** 193–201.
Turgeon, R. (1984). *Planta* **161,** 120–128.
van Bel, A. J. E., and Koops, A. J. (1985). *Planta* **164,** 362–369.
Vreugdenhil, D. (1983). *Physiol. Plant.* **57,** 463–467.
Weaver, R. J., Shindy, W., and Kliewer, W. M. (1969). *Plant Physiol.* **44,** 183–188.
Webb, J. A., and Gorham, P. R. (1964). *Plant Physiol.* **39,** 663–672.
Welch, G. R. (1977). *Prog. Biophys. Mol. Biol.* **32,** 103–191.
Wille, A. C., and Lucas, W. J. (1984). *Planta* **160,** 129–142.
Willenbrink, J., and Doll, S. (1979). *Planta* **147,** 159–162.
Wilson, C., Oross, J. W., and Lucas, W. J. (1985). *Planta* **164,** 227–240.

Wolswinkel, P. (1985a). *Physiol. Plant.* **65,** 331–339.
Wolswinkel, P. (1985b). *J. Plant Physiol.* **120,** 419–429.
Wolswinkel, P., and Amerlaan, A. (1983). *Planta* **158,** 205–215.
Wolswinkel, P., and Amerlaan, A. (1984). *Physiol. Plant.* **61,** 172–182.
Wolswinkel, P., Amerlaan, A., and Kuyvenhoven, H. (1983). *Physiol. Plant.* **59,** 375–386.
Wright, J. P., and Fisher, D. B. (1981). *Plant Physiol.* **67,** 845–848.
Wyse, R. E. (1979). *Plant Physiol.* **64,** 837–841.
Wyse, R. E. (1986). *In* "Phloem Transport" (J. Cronshaw, W. J. Lucas, and R. T. Giaquinta, eds.). pp. 197–209. Liss, New York.
Wyse, R. E., Briskin, D., and Aloni, B. (1985). *In* "Regulation of Carbon Partitioning in Photosynthetic Tissue" (R. L. Heath and J. Preiss, eds.), pp. 231–252. American Society of Plant Physiologists, Rockville, MD.
Wyse, R. E., Zamski, E., and Tomos, A. D. (1986). *Plant Physiol.* **81,** 478–481.
Zocchi, G., Rogers, S. A., and Hanson, J. B. (1983). *Plant Sci. Lett.* **31,** 215–221.

*Journal of Experimental Botany, Vol. 39, No. 202, pp. 529–542, May 1988*

# Wounding and the Regulation of Apoplasmic Retrieval in Source Leaf Tissue of *Spinacia oleracea* L.

CLYDE WILSON AND WILLIAM J. LUCAS[1]

*Botany Department, University of California, Davis, CA 95616, U.S.A.*

Received 6 October 1987

ABSTRACT

Wilson, C. and Lucas, W. J. 1988. Wounding and the regulation of apoplasmic retrieval in source leaf tissue of *Spinacia oleracea* L.—J. exp. Bot. 39: 529–542.

Kinetic studies were performed on fresh-cut and aged leaf discs of *Spinacia oleracea* L. in order to investigate the regulatory processes involved in sugar transport across the mesophyll plasma membrane. A comparison of the kinetic profiles for fructose, glucose, sucrose and arginine obtained on freshly-cut and aged discs revealed that during wound-recovery, uptake is enhanced, but that this enhancement varies considerably for the different substrates tested. Variation in the saturable and first-order kinetic components of uptake was also observed. The involvement of a phosphoinositide-signalling mechanism in the wounding process was examined by pretreating spinach leaves with lithium. Lithium inhibited the enhancement of uptake and this effect was reversed by the addition of *myo*-inositol. However, in some experiments the tissue appeared to be insensitive to $Li^+$. Gas chromatographic analyses performed on cut discs indicated that ethylene was produced in response to wounding and that the addition of cobalt to the ageing media inhibited this ethylene production. Comparative kinetic studies of control and cobalt-treated discs indicated that ethylene was essential for the enhancement of transport across the plasma membrane. However, addition of ethylene to uncut tissue caused only a partial increase in the uptake of fructose, which indicates that some additional wound-signalling component is involved. Addition of cycloheximide to the recovery media completely inhibited this enhancement phenomenon. The cycloheximide-response was not due to an inhibition of ACC synthase synthesis nor to a reduction of ATP levels. We concluded that the effect of cycloheximide was on protein synthesis. Our results are discussed in terms of possible cellular and molecular mechanisms regulating sugar transport.

*Key words*—Sugar transport, wounding and ethylene production, spinach leaves.

*Correspondence to: Department of Botany, University of California, Davis, California 95616, U.S.A.*

## INTRODUCTION

In an earlier report (Wilson, Oross, and Lucas, 1985), we proposed that the phenomenon of phloem loading be viewed in a much broader perspective which would integrate the transport processes across the plasmalemma and tonoplast of a variety of cell types and include the biochemical and biophysical mechanisms controlling these fluxes. More recent studies from this laboratory have focused on the cellular and molecular mechanisms involved in the regulation of sucrose transport within the tissues of the leaf. We have found that the influx of $^{14}$C-sucrose into leaf discs of both *Beta vulgaris* L. and *Spinacia oleracea* L. exhibited little sensitivity to internal sugar levels, although partitioning between phloem and mesophyll vacuoles was dramatically affected (Wilson and Lucas, 1987). Additionally, we identified the tonoplast and plasmodesmata as likely sites for regulation. In a further study, we reported that mannose could perturb sugar and amino acid influx across the

[1] To whom correspondence should be addressed.

© Oxford University Press 1988

plasmalemma and suggested that cytosolic phosphate levels may be involved in the regulatory process (Lucas and Wilson, 1987). These results demonstrate that the plasmalemma-bound sucrose transport (retrieval) system is capable of being modulated. However, the exact nature of the *in vivo* regulatory processes integrating transport events at the tonoplast and plasmalemma remain to be elucidated.

One particularly intriguing and well-documented phenomenon which might provide insight into these regulatory processes is the observation that ion and organic solute uptake into plant tissues increases after wounding and subsequent recovery/ageing (Leonard and Hanson, 1972; Van Steveninck, 1975). Although many investigators have attempted to discern the exact cellular and molecular mechanisms underlying this phenomenon, the processes involved have only been partially resolved.

An examination of the electrochemical responses in *Pisum sativum* L., upon excision, led Pierce and Hendrix (1981) to suggest that a *reactivation* of an ion transport mechanism is responsible for excision-induced changes in ion accumulation. Other investigators have reported that wounding or 'shocking' of plant tissues may result in a rapid inhibition of net $H^+$ efflux (Gronewald, Cheeseman, and Hanson, 1979; Chastain and Hanson, 1981, 1982; Gronewald and Hanson, 1982); this effect on the $H^+$-ATPase would result in an inhibition of secondary active transport processes that utilize the $\Delta\mu_{H^+}$. Alternatively, Abraham and Reinhold (1980) concluded that with respect to solute uptake in *Centranthus ruber* L. leaf strips, cutting leads to tissue membrane damage and that ageing is a complex process involving lipid and protein synthesis. They suggested that wound ethylene serves as a signal which induces the *loss* of membrane function following cutting. However, Lemoine, Delrot, and Auger (1984) have argued that ethylene might also play a role in the *repair* of the membrane during the ageing process.

More recently, Madore (1987) has reported that pretreating *Ipomoea tricolor* leaf tissue with lithium inhibited the enhancement of solute uptake normally observed after ageing. Although similar results had been reported earlier by Carlier and Thellier (1979), Madore discovered that the lithium inhibition in *I. tricolor* could be relieved by the addition of *myo*-inositol. This led Madore (1987) to speculate that phosphoinositide-signalling mechanisms may be involved in the wound response phenomenon.

In the present paper, we report on experiments conducted on the ageing response in leaf discs of *S. oleracea*. Our results indicate that the enhancement of transport in spinach is not limited to sugars but also includes amino acids and thus appears to be a consequence of a more general membrane event. The involvement of a phosphoinositide-signalling mechanism(s) has been investigated using lithium and *myo*-inositol. Although we could not exclude the possibility that this system plays a role in regulating membrane transport events, we concluded that it does not serve as a major regulatory mechanism in the wound-recovery response in spinach. Whereas the enhancement of membrane transport had a limited sensitivity to lithium, it was highly sensitive to cobalt ions. Transport inhibition by cobalt could be reversed by treating the tissue with Ethrel, an ethylene-forming compound. However, the production of ethylene, *per se*, was not sufficient to induce the wound-related stimulation of membrane transport. These results are explained in terms of a model in which ethylene stimulates the synthesis of new mRNA whose ultimate expression is dependent on wounding, *per se*.

## MATERIALS AND METHODS

### *Plant material and growth conditions*

Spinach plants (*Spinacia oleracea* L. cv. America; Burpee Seed Co., Warminster, PA) were grown in a controlled-environment chamber under the following conditions: 22 °C d/15 °C night temperatures and

a 9 h photoperiod at 260 $\mu$E $m^{-2}$ $s^{-1}$. Seeds were planted in 4-inch pots and placed on a heating pad to germinate. After 3 d the seedlings were transferred to the controlled-environment chamber. Plants were watered daily with half-strength Hoagland solution (Hoagland and Arnon, 1950); ammonium phosphate (25 $cm^3$ per pot of 18·4 kg $m^{-3}$) was also applied during the third and fifth weeks. Experiments were conducted on 5- to 6-week-old plants, with the second and third leaves (after the cotyledons) being used as they represented mature source tissue.

*Chemicals*

Aminoethoxyvinylglycine (AVG), 2-(*N*-morpholino) ethanesulphonic acid (MES), cycloheximide and *myo*-inositol were obtained from Sigma Chemical Co., St. Louis, MO, U.S.A. D-[*U*-$^{14}$C]glucose, -fructose, -sucrose, and L-[*U*-$^{3}$H]arginine were purchased from International Chemical and Nuclear Corp., Irvine, CA, U.S.A. Ethrel was obtained as a gift from S. F. Yang.

*Kinetic studies*

Kinetic studies were performed using the method of Maynard and Lucas (1982) as modified by Wilson *et al.* (1985). Pre-incubation and incubation solutions contained 120 mol $m^{-3}$ MES–NaOH, pH 5·0, adjusted to 200 mOsm with mannitol. A 30 min pre-incubation period in unlabelled sugar or arginine was followed by a 30 min incubation in $^{14}$C-sugar or $^{3}$H-arginine. Uptake by micro-organisms was considered to be of minor importance in terms of the total uptake by the cut tissue, since macro-autoradiographs of the discs indicated that most of the radioactive sugars taken up could be accumulated in the phloem, after an appropriate chase period.

*Ageing studies*

The second or third leaves were excised from spinach plants and placed in a 2·0 mol $m^{-3}$ solution of $CaCl_2$. Leaf discs were then cut (using a sharpened cork borer) and floated on this same solution in a glass Petri dish, which was covered and returned to the controlled-environment chamber for the time specified. For experiments involving AVG, leaf discs were floated on a solution of either 2·0 mol $m^{-3}$ $CaCl_2$ or 2·0 mol $m^{-3}$ $CaCl_2$ plus 100 mmol $m^{-3}$ AVG. In cycloheximide experiments, 5·0 $\mu$g $cm^{-3}$ cycloheximide was included in the pretreatment medium.

In some experiments, solutions were delivered to the apoplasmic space of the mesophyll via the transpiration stream. One hour into the photoperiod, spinach leaves were excised at the base of the petiole, while the crown of the plant was submerged under water. The petiole was then placed in either distilled water (control) or the experimental solution. The leaves were then returned to the controlled-environment chamber for 24 h. The solutions used in these experiments contained either 1·0 mol $m^{-3}$ LiCl, 10 mol $m^{-3}$ *myo*-inositol, 1·0 mol $m^{-3}$ LiCl plus 10 mol $m^{-3}$ *myo*-inositol, or 1·0 mol $m^{-3}$ $CoSO_4$. In the case of studies involving the addition of ethylene, a dilute Ethrel solution containing 1·0 mol $m^{-3}$ MES–NaOH, pH 5·5, was supplied through the petiole at a concentration of 1·0 g $m^{-3}$ 2-chloroethylphosphonic acid (Ethephon).

*Ethylene measurements*

Leaf discs were cut as described above and placed into 25 $cm^3$ Erlenmeyer flasks containing 1·0 $cm^3$ of 2·0 mol $m^{-3}$ $CaCl_2$ or 2·0 mol $m^{-3}$ $CaCl_2$ plus 1·0 mol $m^{-3}$ $CoSO_4$. Each flask was then sealed with a serum stopper and after 1, 3 and 5 h, three air samples per flask were removed through the serum stopper with a 1·0 $cm^3$ gas-tight syringe attached to a 25-gauge needle. The samples were injected into a Carle 211 Analytic Gas Chromatograph equipped with an alumina column and a flame ionization detector. Nitrogen at 80 °C was used as a carrier gas. The gas chromatograph could detect ethylene at a concentration of $10^{-9}$ $cm^3$ $cm^{-3}$ in a 1·0 $cm^3$ sample with a retention time of about 28 s. Ethylene concentrations were determined by calibration against ethylene standards.

## RESULTS

*Effect of ageing on sugar and amino acid uptake*

An enhancement of sugar and amino acid influx was observed when spinach leaf discs were cut and aged for 8 h on a 2·0 mol $m^{-3}$ $CaCl_2$ solution (Fig. 1). A comparison of the kinetic parameters, $V_{max}$ of the saturable component and $k$, the first-order rate coefficient, revealed that both systems increased during the ageing process. Among the sugars tested, fructose exhibited the greatest degree of enhancement, with $V_{max}$ and $k$ increasing by 1 040% and

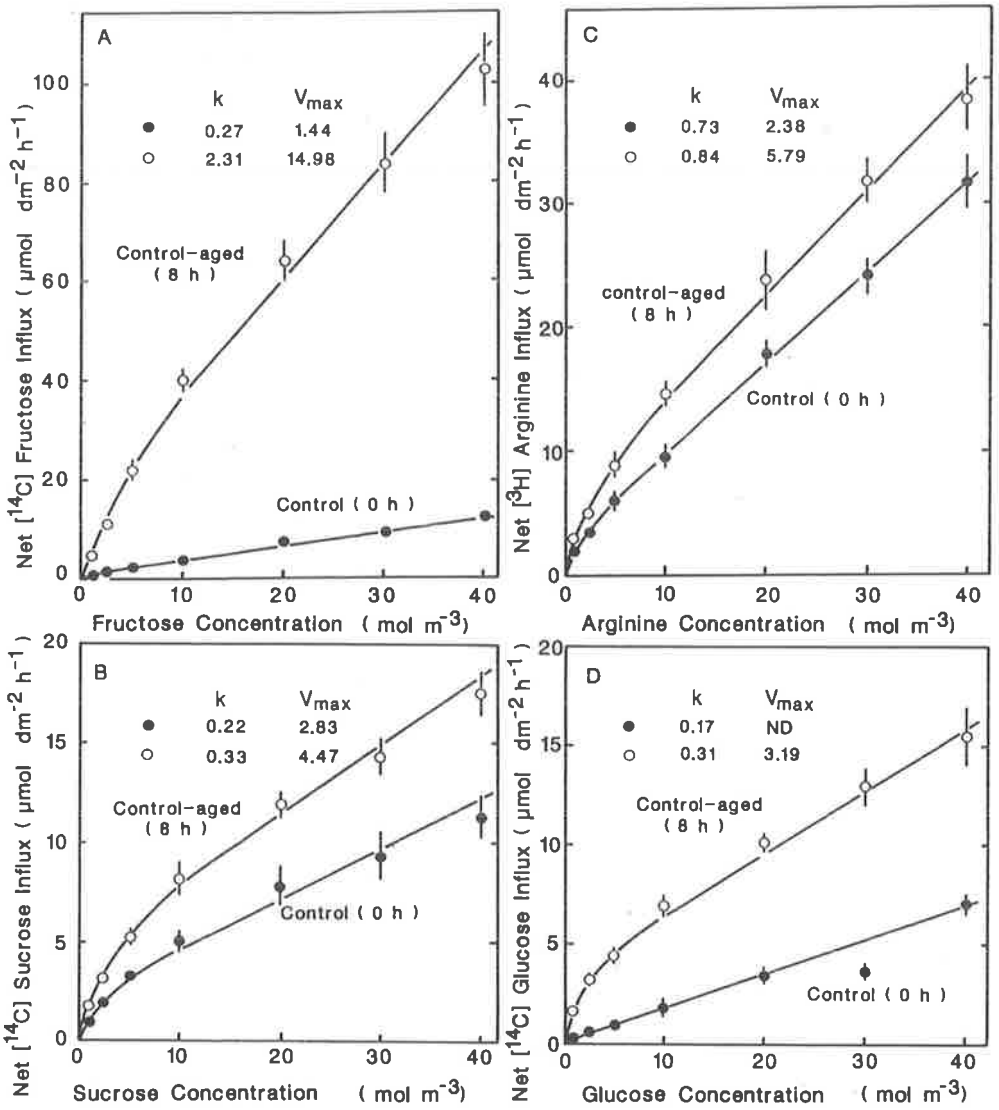


FIG. 1. Effect of ageing on sugar or amino acid uptake into leaf discs of *Spinacia oleracea* L., cv. America. Leaf discs were punched from mature leaves and either analyzed immediately for their kinetic response or aged (for 8 h) by floating the discs on 2·0 mol $m^{-3}$ $CaCl_2$ prior to kinetic analysis. A 30 min incubation in unlabelled sugar (or arginine) was followed by a 30 min incubation in $^{14}C$-sugar (or $^{3}H$-arginine) solution (200 mOsm). For fructose and glucose, each point represents the mean ± s.e. for two sets of six replicates. For sucrose and arginine, each point represents the mean ± s.e. for six replicates.

855%, respectively (Fig. 1A). Although the enhancement obtained for sucrose influx was not as dramatic, both systems (Wilson *et al.*, 1985) were stimulated to approximately the same extent (150%). The influence of ageing on glucose influx was particularly noteworthy. Ageing resulted in the development of a saturable system which was undetectable in the freshly-cut discs (Fig. 1D). In the case of arginine, the saturable system was stimulated by 240%, but the linear component showed little change (115% stimulation). This result is in contrast to the response obtained with fructose, glucose and sucrose in that both components of sugar transport demonstrated paralleled stimulation.

*Effect of $Li^+$ and* myo*-inositol on wound-induced fructose uptake*

Carlier and Thellier (1979) reported that lithium ($Li^+$) can inhibit the increase in sugar transport which occurs during the ageing process. This finding, along with the observation

that the inhibitory effect of $Li^+$ can be overcome by *myo*-inositol has led some investigators to speculate that a phosphoinositide-signalling mechanism may be operating in the wound response and recovery phenomenon (Kochian and Lucas, 1987; Madore, 1987). To examine this possibility, we investigated the effect of adding $Li^+$ to the ageing solution. Since fructose uptake displayed the greatest enhancement during the recovery period (compare Fig. 1A with B, C, and D), we focused on the effect of $Li^+$ on the transport of this substrate. Figure 2 illustrates the effect of $Li^+$ on the wound-induced enhancement of fructose influx. Added $Li^+$ produced a concentration-dependent decrease in fructose influx in a manner that is almost identical to the $Li^+$ response reported by Carlier and Thellier (1979).

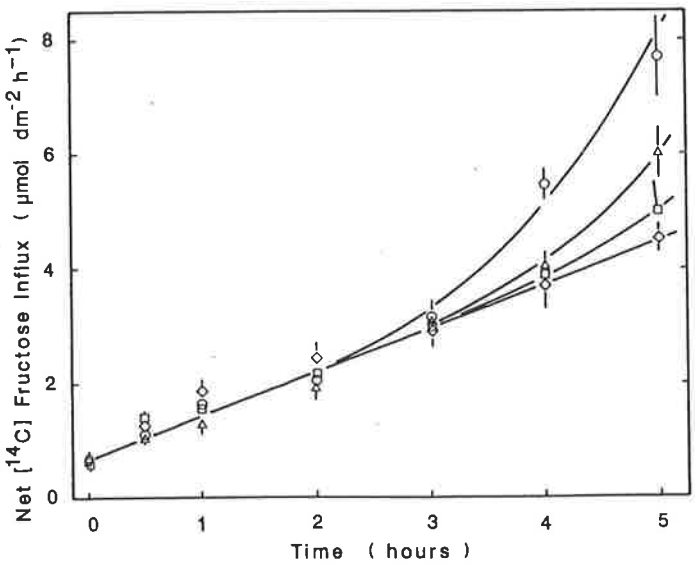


FIG. 2. Time-course on the effect of lithium chloride on fructose influx into *S. oleracea* L. leaf discs. Leaf discs were cut from mature leaves and placed into a Petri dish containing a solution of 2·0 mol $m^{-3}$ $CaCl_2$ (○), or 2·0 mol $m^{-3}$ $CaCl_2$ plus 1 (△), 5 (□), or 10 mol $m^{-3}$ LiCl (◇). At the times specified, samples were taken for kinetic analysis using 5·0 mol $m^{-3}$ fructose, as described in Fig. 1. Each point represents the mean ± s.e. for two sets of six replicates.

If lithium is acting to prevent hydrolysis of inositol-1-phosphate to *myo*-inositol and $P_i$, as hypothesized, then *myo*-inositol addition to a lithium-inhibited system should restore the enhancement of sugar uptake following wounding (Madore, 1987). Lithium supplied to the leaf blade through the petiole reduced the enhancement of uptake following wounding, while the addition of *myo*-inositol along with $Li^+$ fully restored influx to the control levels of aged discs (Fig. 3). An interesting aspect of these results was that $Li^+$ appeared to affect *only* the saturable component of fructose influx. Although these data are in agreement with the operation of a phosphoinositide-signalling mechanism, we should stress that in only four out of eight such experiments did we observe a lithium-induced inhibition. In our other experiments, uptake into leaf discs obtained from lithium-treated leaves did not vary from the distilled-water or potassium chloride controls (data not shown).

The presence of increased levels of *myo*-inositol in the cytosol, before wounding, may well decrease the cellular levels of inositol triphosphate and thus prevent, or minimize, wound signalling. To test this possibility, we fed 10 mol $m^{-3}$ *myo*-inositol to spinach leaves via the transpiration stream and then examined the tissue for its kinetic response. We found that the addition of *myo*-inositol had no effect on the uptake of fructose relative to control values (data not shown).

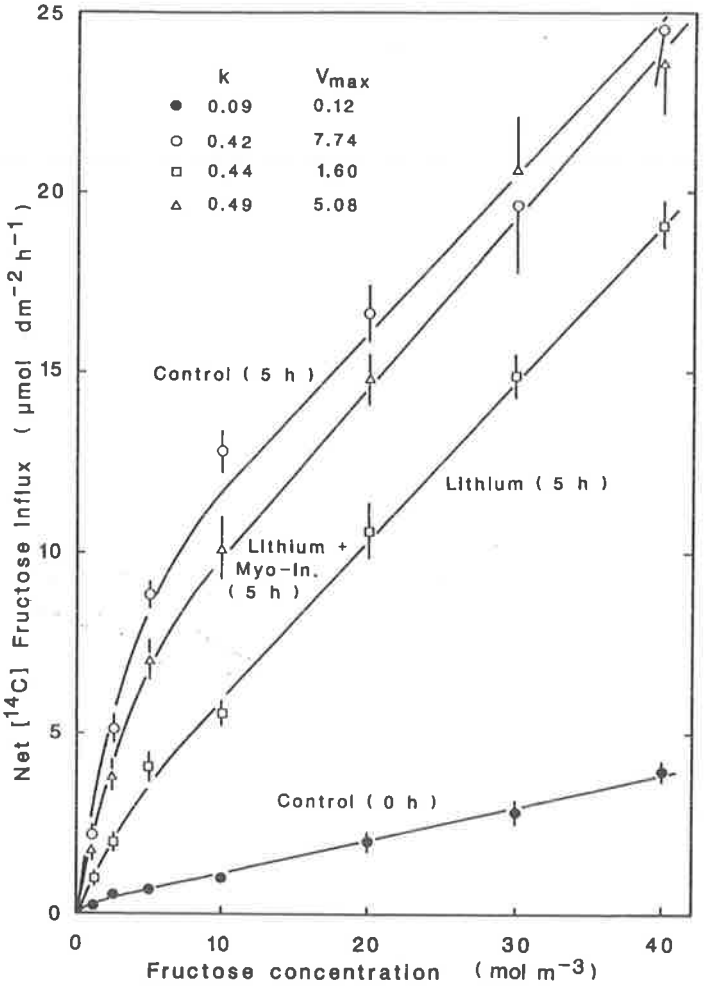


FIG. 3. Influence of *myo*-inositol in the presence of lithium chloride on the enhancement of fructose influx following wounding. One hour into the photoperiod, leaves were excised at the base of the petiole, while the crown of the plant was submerged under water. Petioles were placed into either distilled water (control), 1·0 mol $m^{-3}$ LiCl, or 1·0 mol $m^{-3}$ LiCl plus 10 mol $m^{-3}$ *myo*-inositol before being returned to the controlled-environment chamber for 24 h. Leaf discs were then cut for kinetic studies, as described in Fig. 1. All points represent the mean ± s.e. for six replicates.

TABLE 1. *Influence of ageing on ethylene production in mature leaves of* Spinacia oleracea *L.*

| Treatment | Ethylene production[a] | | | |
|---|---|---|---|---|
| | 0 h | 1 h | 3 h | 5 h |
| $CaCl_2$ (2·0 mol $m^{-3}$) | ND[b] | 0·114 ± 0·007 | 0·646 ± 0·041 | 0·766 ± 0·071 |
| $CaCl_2$ (2·0 mol $m^{-3}$) plus $CoSO_4$ (1·0 mol $m^{-3}$) | ND[b] | 0·045 ± 0·002 | 0·083 ± 0·009 | 0·077 ± 0·006 |

[a] Air samples (four replicates per treatment) were analyzed by gas chromatography and values are given as $cm^3$ of ethylene per leaf disc $\times 10^6$ (mean ± s.e.).
[b] ND = Not detected.

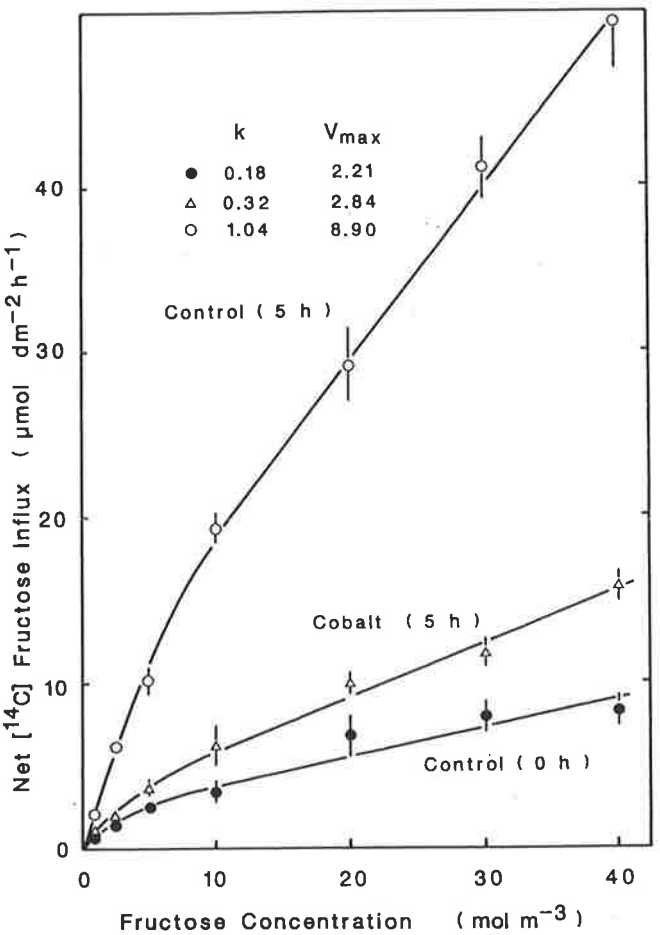


FIG. 4. Effect of $Co^{2+}$ on fructose influx into aged spinach leaf discs. Leaf discs were aged for 5 h, as described in Fig. 1, with (△) or without (○) 400 mmol $m^{-3}$ $CoSO_4$. (●) Represents time 0-h control. Kinetic studies were performed, as described in Fig. 1. Each point represents the mean ± s.e. for six replicates.

*Ethylene production in aged leaf discs*

Fuhrer, Kaur-Sawhney, Shih, and Galston (1982) have suggested that increased ethylene production may be a component of the wound phenomenon. Consistent with this hypothesis, we found that excised spinach leaf discs produced measurable amounts of ethylene within 1 h of cutting (Table 1). Cobalt has been reported to be a specific inhibitor of ethylene biosynthesis, in that it blocks the conversion of 1-aminocyclopropane-1-carboxylic acid (ACC) to ethylene (Yu and Yang, 1979). Inclusion of $Co^{2+}$ in the ageing media inhibited ethylene production from excised leaf discs (Table 1) and greatly reduced the enhancement of fructose uptake by this tissue (Fig. 4). These data further support the hypothesis that ethylene is a central constituent in the wound-recovery phenomena.

*Effect of cycloheximide on the ageing phenomenon*

The enhancement of fructose influx, following leaf disc excision, usually requires a lag period of 1 to 1·5 h (data not shown). Other investigators have reported a similar lag and have suggested that this lag period may be associated with the induction of protein synthesis (Leonard and Hanson, 1972; Abraham and Reinhold, 1980; Lemoine *et al.*, 1984). In order to determine if protein synthesis is necessary for the ageing response in spinach leaf discs, we added cycloheximide (5·0 µg $cm^{-3}$) to our ageing media (Pestka, 1977). Figure 5 indicates

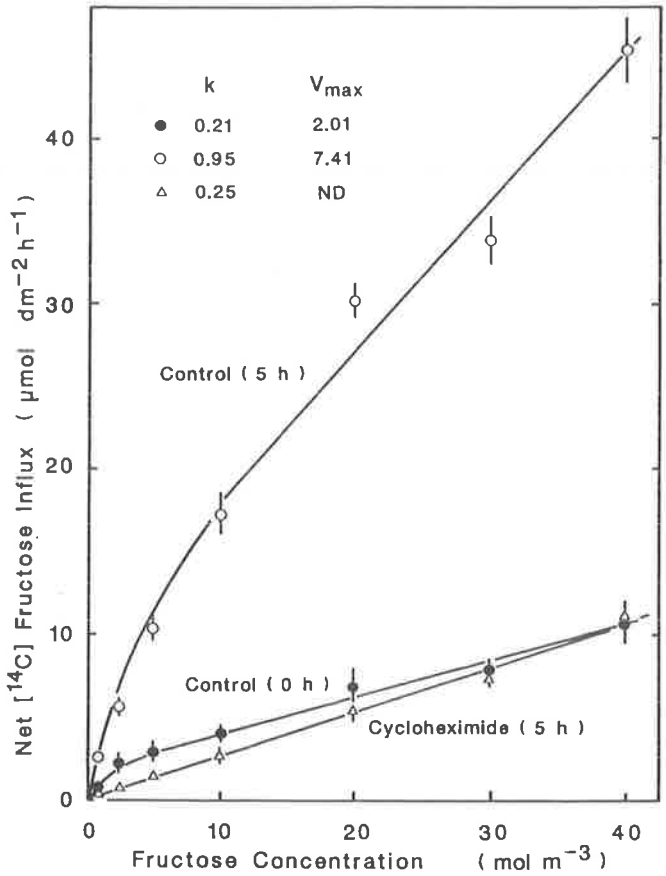


FIG. 5. Effect of cycloheximide on fructose influx into aged spinach leaf discs. Leaf discs were aged for 5 h, as described in Fig. 1, with (△) or without (○) 5·0 $\mu$g cm$^{-3}$ cycloheximide and subsequently analyzed for fructose uptake, as described in Fig. 1. (●) Represents time 0-h control. Each point represents the mean ± s.e. for six replicates.

that this concentration of cycloheximide completely inhibited the wound-induced enhancement of fructose influx. Surprisingly, cycloheximide also abolished the saturable component that was present in the freshly cut (control) tissue.

This cycloheximide effect may have been due to the inhibition of the synthesis of ACC synthase. ACC synthase catalyzes the conversion of *S*-adenosylmethionine (SAM) to ACC. Presumably, lower levels of ACC would result in decreased ethylene production. Since aminoethoxyvinylglycine (AVG) has been reported to be a specific inhibitor of SAM to ACC conversion (Adams and Yang, 1979), addition of this compound to the ageing medium should achieve the same results as cycloheximide, if the latter were acting to inhibit the synthesis of ACC synthase. That this is not the case is illustrated in Fig. 6. Although AVG did repress the stimulation of fructose influx, the effect was small and appeared to be a preferential effect on the first-order kinetic transport system.

It has also been proposed that protein synthesis inhibitors, like cycloheximide, may interfere with metabolic energy supply (Ellis and MacDonald, 1970; Kelday and Bowling, 1975; McMahon, 1975). However, other laboratories have reported that ATP levels are unaltered or slightly increased following the addition of protein synthesis inhibitors (Cocucci and Marrè, 1973; Lin and Hanson, 1974; Lado, Rasi-Caldogno, and Colombò, 1977). In our experimental tissue, cycloheximide did not influence the ATP levels. After 5 h of ageing, the ATP levels in control and cycloheximide-treated tissues were 57·7 and 52·1 pmol mg$^{-1}$ dry

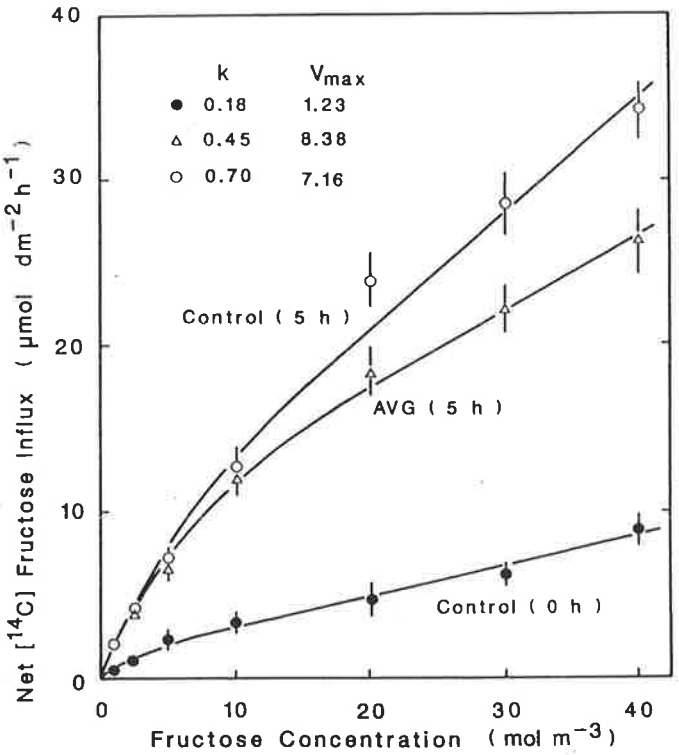


FIG. 6. Effect of AVG on fructose influx into aged spinach leaf discs. Leaf discs were aged for 5 h, as described in Fig. 1, with (△) or without (○) 400 mmol $m^{-3}$ AVG. (●) Represents time 0-h control. Kinetic studies were performed as described in Fig. 1. Each point represents the mean ± s.e. for six replicates.

weight, respectively. Thus, the observed suppression of fructose influx by cycloheximide must be due to events other than a perturbation in nucleotide levels.

*Effect of Ethrel on enhancement of fructose influx*

Based on our present results and previous work by others, it would appear that ethylene is a required component of the enhancement mechanism. If this hypothesis were correct, it should be possible to supply ethylene to uncut tissue and elicit an enhancement of fructose influx similar to that produced during a wound response. In preliminary experiments on the ageing phenomenon we found that entire leaves that were excised from the plant, at the base of the petiole, did not undergo the enhancement response (data not shown). We used such excised leaves to supply Ethrel, via the transpiration stream, to uncut mesophyll tissue.

Fructose influx into discs cut from Ethrel-treated leaves exhibited only a slight increase in transport capacity compared to the controls (Fig. 7A). This increase may be attributed to higher levels of ethylene present in the tissue at the time of cutting. If ethylene is a central component of the wound-signalling mechanism, the addition of ethylene to cobalt-treated tissue should reverse the cobalt-induced inhibition. In order to achieve minimal wound-induced ethylene levels at the time of excision, we supplied $Co^{2+}$ to the leaf blade via the petiole. Cobalt supplied alone had no effect on the 0 h (control) kinetic profiles. After 5 h of ageing in the presence of cobalt, fructose influx underwent a slight increase. However, by supplying Ethrel to the leaf blade, along with $Co^{2+}$, we found that the influence of cobalt could be almost completely reversed (Fig. 7B). Collectively, these results suggest that ethylene is necessary only after cutting and that it does not play a role in the inhibition of transport due to cutting, *per se*. In addition, exogenously supplied ethylene can substitute

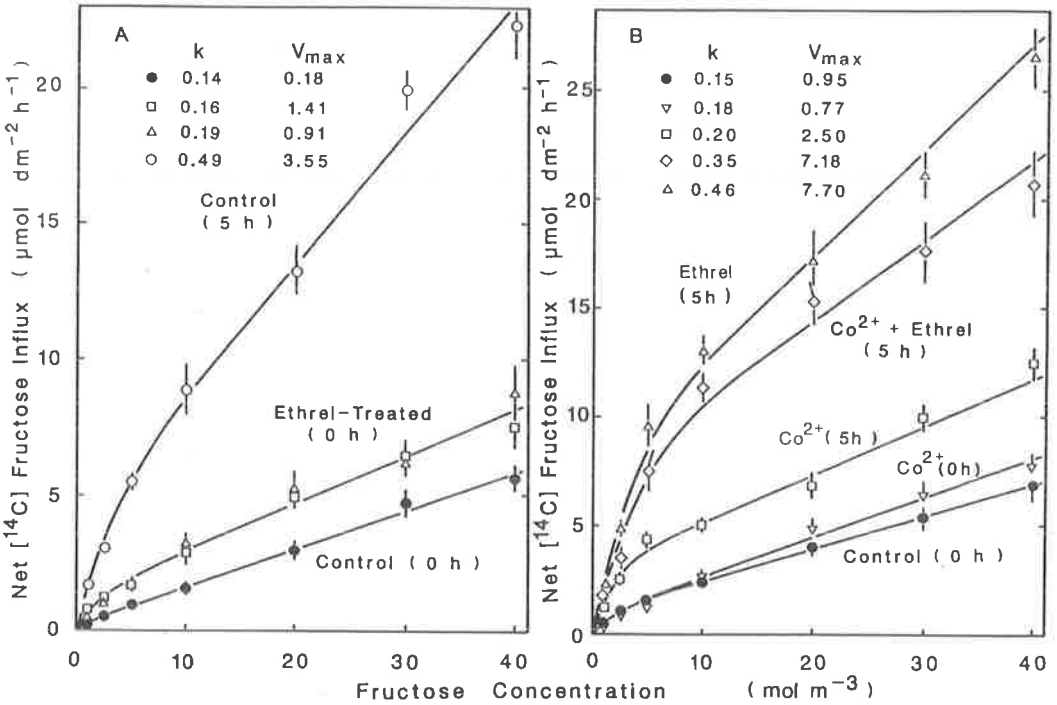


FIG. 7. Effect of Ethrel treatment on fructose influx into unaged and aged spinach leaf discs. (A) Leaves were pretreated with a dilute Ethrel solution (0·1 or 1·0 g $m^{-3}$ 2-chloroethylphosphonic acid or Ethephon) containing 1·0 mol $m^{-3}$ MES–NaOH, pH 5·5. Leaf discs were then cut for kinetic analyses. The points for time 0-h control (●), 5-h control (○), 0-h Ethrel-treated, 0·1 g $m^{-3}$ Ethephon (▲), and 0-h Ethrel-treated, 1·0 g $m^{-3}$ Ethephon (□) represent the mean ± s.e. for six replicates. (B) Petioles were placed in either distilled water, 1·0 mol $m^{-3}$ $CoSO_4$, dilute Ethrel solution (0·1 g $m^{-3}$ Ethephon), or 1·0 mol $m^{-3}$ $CoSO_4$ plus Ethrel (0·1 g $m^{-3}$ Ethephon) before being returned to the controlled-environment chamber for 24 h. Kinetic studies were performed as described in Fig. 1. All points represents the mean ± s.e. for six replicates.

for wound-ethylene in cut-tissue, allowing us to perform additional experiments on the wounding phenomenon.

## DISCUSSION

In the present study, we investigated the enhancement of solute uptake following wounding, in order to further our understanding of the cellular and molecular mechanisms involved in regulating the retrieval processes operating at the mesophyll plasma membrane. Although the transport of fructose, glucose, sucrose and arginine exhibited a stimulation following wounding, the extent of enhancement varied greatly. Furthermore, whereas the saturable and first-order kinetic components of the sugars tested underwent paralleled stimulation, the major effect for arginine transport was on the saturable component. These observations are consistent with our previous contention (Lucas and Wilson, 1987) that there may exist a basic difference in the regulation not only of the various transport systems, but also of the respective components (saturable and first-order). However, the data suggest that since all systems examined exhibit some degree of stimulation, there must also be some point in the regulatory mechanism that is common to different classes of carriers.

One possibility is that cutting stimulates the breakdown of phosphatidylinositol 4,5 *bis*phosphate (PtdIns(4,5)$P_2$). The increased breakdown of this compound would lead to higher levels of inositol 1,4,5-triphosphate ($InsP_3$) and diacylglycerol (DG), and eventually to increased cytosolic $Ca^{2+}$ levels (Berridge, 1987; Berridge and Irvine, 1984; Gill, 1985; Takai,

Kikkawa, Kaibuchi, and Nishizuka, 1984). Lithium acts to prevent hydrolysis of inositol-1-phosphate to *myo*-inositol and $P_i$ and, hence, its subsequent re-incorporation into membrane components (Berridge and Irvine, 1984). Presumably, increased cytosolic $Ca^{2+}$ would activate a protein kinase and, consequently, give rise to membrane protein phosphorylation. In addition, increased diacylglycerol concentrations resulting from PtdIns(4,5)$P_2$ breakdown may lower the sensitivity levels for protein kinase activation by calcium.

As shown in Fig. 2, inclusion of $Li^+$ in the ageing medium did result in a concentration-dependent suppression of the enhancement (or recovery) in fructose influx. Based on the kinetic data presented in Fig. 3, $Li^+$ appeared to influence only the saturable component of fructose influx and this effect could be relieved by the addition of *myo*-inositol. The problem with these $Li^+$ experiments was that we could not achieve a *consistent* inhibition of the recovery of membrane transport function. If the mesophyll of mature spinach leaves preferentially sequesters $Li^+$ into the vacuole, this might account for the limited and variable sensitivity observed in this study. Carlier and Thellier (1979) also reported that $K^+$ could reduce the $Li^+$-induced inhibition, and this suggests that the $K^+$ status of the tissue might also be an important variable in accounting for the inconsistent nature of the $Li^+$ inhibition. Thus, although this signalling/regulatory mechanism is possibly present, it does not appear to play a major regulatory role for spinach under the conditions employed in our experiments.

Our current level of understanding of the role played by ethylene in wounded or stressed tissue indicates that it can enhance the synthesis of specific mRNA (Christoffersen and Laties, 1982; Watanabe and Imaseki, 1982; Zurfluh and Guilfoyle, 1982; Nichols and Laties, 1984). It is also possible that ethylene acts as a transacting factor to initiate the synthesis of new mRNA. However, since ethylene alone could not produce the wound-induced rise in transport capacity (Fig. 7A), we suggest that the subsequent translation, or expression of translation product requires an additional signal (electrical?) produced as a consequence of cutting. Such a mechanism need not operate independently of a phosphoinositide-signalling mechanism as both mechanisms may well operate in parallel. The relative degree of control exerted by these two systems may be dependent upon environmental factors and the plant's immediate prehistory, especially with respect to stress-related events.

One other important outcome from our study was the finding that pretreatment of leaves with cobalt, prior to cutting, had no effect on fructose influx (0 h control). Abraham and Reinhold (1980) suggested that ethylene serves, at least in part, to induce the *loss* of membrane function following cutting. If ethylene were acting in this manner, with respect to fructose influx into spinach leaf discs, the presence of cobalt, prior to wound signalling, should have prevented any loss of fructose transport activity. However, when we supplied cobalt to the leaf blade for 24 h and then examined the response of the tissue to cutting, we discovered that the kinetic profiles of the cobalt-treated tissue were indistinguishable from the controls (Fig. 7B). Thus, it does not appear that ethylene is acting to induce the loss of fructose transport activity immediately after wounding, unless, of course, this response requires very low levels of ethylene.

Previous investigators have reported that cycloheximide can inhibit the ageing process in leaf discs (Lemoine *et al.*, 1984). In our experiments, cycloheximide not only inhibited the increase in uptake during ageing, but also eliminated the contribution of the saturable component of uptake. This cycloheximide effect could not be attributed to slower conversion of SAM to ACC by reduced levels of ACC synthase, nor could it be attributed to decreased levels of adenine nucleotides. We feel that the simplest explanation is that the cycloheximide effect is due to the blockage of protein synthesis, which was stimulated by ethylene. This explanation must remain tentative, as it has been suggested that cycloheximide can also have

an indirect effect on the $H^+$-ATPase. Chastain, LaFayette, and Hanson (1981) reported that protein synthesis inhibitors, including cycloheximide, can effectively block $H^+$ efflux from corn roots. The observation that cycloheximide treatment eliminated, or at least greatly reduced, the saturable component of fructose influx (Fig. 5) is interesting in this respect. If the saturable component represents fructose-$H^+$ cotransport (Maynard and Lucas, 1982), an indirect effect would explain, in part, the cycloheximide response.

The reduced transport capacity observed immediately after cutting may also result from some regulatory mechanism operating on the plasmalemma-bound $H^+$-ATPase responsible for establishing the electrochemical potential gradient needed to drive the putative sugar cotransport systems. Zocchi, Rogers, and Hanson (1983) reported that $H^+$ efflux was blocked in corn roots after wounding and suggested that this blockage may be due to phosphorylation of the $H^+$-ATPase. Furthermore, fusicoccin could by-pass the blockage of $H^+$ efflux (Chastain and Hanson, 1982). Fusicoccin has also been reported to stimulate hexose uptake (Getz, Schulte-Altedorneburg, and Willenbrink, 1987). However, when we added 20 mmol $m^{-3}$ fusicoccin to our cut leaf discs, we did not observe an increase in fructose influx into freshly-cut (0 h control) leaf discs. Evidently, in spinach, wounding inhibits the influx of sugars via some mechanism other than phosphorylation of the $H^+$-ATPase, or alternatively, for some reason fusicoccin is unable to by-pass this blockage.

Finally, although we have shown that sugar transport across the spinach mesophyll plasma membrane is insensitive to cytosolic sugar levels, we have now established that the capacity for sugar transport can be modulated by cytosolic events involving protein synthesis. We have also established that exogenously supplied ethylene (Ethrel) can substitute for wound-ethylene and this technique will be used in future experiments to elucidate both the nature of the proteins synthesized and the mechanisms by which they effect their control on sugar transport.

## ACKNOWLEDGEMENTS

This research was supported by National Science Foundation Grant DMB-87 03624. Thanks are due to Monica A. Madore for helpful discussion, Professor Shang Fa Yang and Mr T. Strike for the use of their gas chromatography equipment and William B. McCloskey for his assistance in caring for the spinach plants.

## LITERATURE CITED

ABRAHAM, G., and REINHOLD, L., 1980. Mechanism of effect of ageing on membrane transport in leaf strips of *Centranthus ruber*: possible ethylene involvement in cutting shock. *Planta*, **150**, 380–4.

ADAMS, D. O., and YANG, S. F., 1979. Ethylene biosynthesis: identification of 1-aminocyclopropane-1-carboxylic acid as an intermediate in the conversion of methionine to ethylene. *Proceedings of the National Academy of Sciences (U.S.A.)*, **76**, 170–4.

BERRIDGE, M. J., 1987. Inositol trisphosphate and diacylglycerol: Two interacting second messengers. *Annual Review of Biochemistry*, **56**, 159–228.

——and IRVINE, R. F., 1984. Inositol triphosphate, a novel second messenger in cellular signal transduction. *Nature*, **312**, 315–21.

CARLIER, G., and THELLIER, M., 1979. Lithium-perturbation of the induction of a methyl-glucose transport during ageing of foliar discs of *Pelargonium zonale* (L.) Aiton. *Physiologie Végétale*. **17**, 13–26.

CHASTAIN, C. J., and HANSON, J. B., 1981. Proton efflux from corn roots induced by tripropyltin. *Plant Physiology*, **68**, 981–2.

——— 1982. Control of proton efflux from corn root tissue by an injury-sensing mechanism. *Plant Science Letters*, **24**, 97–104.

——LAFAYETTE, P. R., and HANSON, J. B., 1981. Action of protein synthesis inhibitors in blocking electrogenic $H^+$ efflux from corn roots. *Plant Physiology*, **67**, 832–5.

Plant Physiol. (1982) 70, 1723–1731
0032-0889/82/70/1723/09/$00.50/0

# Potassium Transport in Corn Roots[1]

## I. RESOLUTION OF KINETICS INTO A SATURABLE AND LINEAR COMPONENT

Received for publication April 21, 1982 and in revised form August 27, 1982

LEON V. KOCHIAN AND WILLIAM J. LUCAS
*Department of Botany, University of California, Davis, California 95616*

### ABSTRACT

**Influx isotherms were obtained for $^{86}Rb^+$ uptake into 2-cm corn (*Zea mays* [A632 × (C3640 × Oh43)] root segments for both low- (0.2 millimolar $CaSO_4$) and high-salt (0.2 millimolar $CaSO_4$ + 5 millimolar KCl) grown roots. Unlike the discontinuous curves usually presented for $K^+$ influx, our isotherms were smooth, nonsaturating curves that approached linearity at $K^+$ ($Rb^+$) concentrations above 1 millimolar. The kinetics for $K^+$ transport could be resolved into saturable and linear components. The saturable components yielded $K_m$ values of 16 and 86 micromolar for low- and high-salt roots, respectively, while $V_{max}$ values were 5.62 and 1.85 moles per gram fresh weight per hour. Results of experiments with the penetrating sulfhydryl reagent, *N*-ethyl maleimide (NEM), and the impermeant reagent, *p*-chloromercuribenzene sulfonic acid (PCMBS) indicated that the saturable and linear components were independent mechanisms of $K^+$ transport.**

**Short-term NEM exposures (30 seconds to 5 minutes) selectively inhibited the saturable system, but had little effect on the linear component. Increasing NEM exposures resulted in further inhibition and subsequent abolition of the saturable component; the linear component exhibited limited NEM sensitivity. PCMBS elicited the same general inhibitory trends, although it was less effective as a saturable component inhibitor.**

**The effects of NEM and PCMBS on $K^+$ efflux were also studied. Short NEM exposures had no effect on cytoplasmic efflux, while inhibiting vacuolar efflux significantly. From these data, it is unclear at which site(s) NEM is acting. A more complex response was obtained with PCMBS, where a monophasic efflux curve was observed. Analysis indicated that the vacuolar efflux was stimulated, while the cytoplasmic component was abolished.**

**The nature of the linear component is discussed, and it is proposed that the mechanism may be more complex than simple facilitated diffusion.**

It is generally accepted that $K^+$ uptake isotherms for roots of higher plants are complex (11, 25). The appearance of discontinuities in influx isotherms led to Epstein's formulation of the now well-known dual-isotherm hypothesis (12), in which it was proposed that two carriers were located in the plasmalemma, each carrier having different Michaelis-Menten parameters. In opposition to this hypothesis, Nissen has argued that such kinetics are due to a single, complex transporter which undergoes transitions in response to changes in external ion concentration (29).

It has also been hypothesized that a diffusion limitation of ions exists at low external concentrations, such that their availability for uptake by root cortical cells is significantly reduced (2, 10). Göring and coworkers have argued that because of this diffusion limitation, the cells of the root periphery play a dominant role in uptake. Therefore, they propose that the commonly observed dual isotherms may be an artifact of this diffusion barrier. Uptake saturation observed at low substrate concentrations (Epstein's Mechanism I) would be due to transport into epidermal cells, while uptake at higher concentrations (Epstein's Mechanism II) would be the result of absorption by identical carriers located on cortical cells within the root. This hypothesis is supported by studies of glucose uptake by yeast cells (14). Uptake in cell suspensions yielded isotherms consisting of one saturable curve, while uptake into cells packed in an agar matrix (to approximate a tissue) yielded influx isotherms that were biphasic. Although the above results are consistent with Göring's hypothesis (14), it should be recognized that complex kinetics have been observed in a wide range of tissues (26 and references therein) and, therefore, other interpretations may be valid.

Borstlap (4) has also presented a critique of the multiphasic interpretation of uptake. He argues that many of the frequently cited discontinuous uptake isotherms could be explained by models consisting of one or more Michaelis-Menten terms plus a linear term, particularly if experimental error and biological variability are considered. The existence of this linear term has often been ignored, despite the fact that transport kinetics consisting of Michaelis-Menten and linear terms have been well documented in both plant and animal systems (3, 5, 8, 9, 13, 20, 22, 27, 28, 32). Such kinetics have generally been associated with the transport of organic solutes, the Michaelis-Menten terms are thought to represent carrier-mediated transport, while the linear term is usually considered to represent passive diffusion.

In the present study, we investigated $K^+$ ($^{86}Rb$) influx into excised root segments of *Zea mays* seedlings. Our influx isotherms were smooth and nonsaturating. Based on experiments in which sulfhydryl modifiers were employed, we present evidence that these isotherms are due to the functioning of a saturable and a linear component. Furthermore, from the results of studies on both the influx and efflux of $K^+$, we suggest that the linear component is more complex than simple facilitated diffusion.

### MATERIALS AND METHODS

**Plant Material.** *Zea mays* seeds (A632 × [C3640 × Oh43]. Crow's Hybrid Corn Co., Milford, IL) were surface sterilized in 1% NaOCl and imbibed overnight in aerated deionized $H_2O$. The seeds were then germinated on stainless steel screens placed over 4-L beakers that contained aerated solutions of either 0.2 mM $CaSO_4$ (low-salt conditions) or 0.2 mM $CaSO_4$ + 5 mM KCl (high-salt conditions). Seedlings were dark-grown in a high humidity growth chamber at 21°C. The primary root of 5-d-old seedlings was used for all influx and efflux experiments.

**Influx Experiments.** Short-term (10 or 30 min) $Rb^+$ influx experiments were performed using 2-cm-long root segments excised from the 1st through 8th cm of the primary root. Root segments were washed (4 h) in solutions of identical composition

[1] Supported by National Science Foundation Grant PCM 8117721 to W. J. L. and by a National Science Foundation predoctoral fellowship to L. V. K.

to their growth solutions to allow recovery from excision. High-salt roots were subsequently washed for 10 min in 0.2 mM $CaSO_4$ immediately before initiation of influx, to remove free space $K^+$. Root segments were then transferred to Plexiglas vials (0.1 g root segments/vial). The base of these vials consisted of stainless steel screen to allow free movement of solution (Fig. 1). The vials (with roots) were then placed into the Plexiglas uptake wells of the experimental system shown in Figure 1. These wells contained 20 ml of aerated uptake solutions which consisted of various concentrations of RbCl, plus 0.2 mM $CaSO_4$ and 1 mM Mes buffer (pH 6.50. Solution temperature was held at 23 ± 0.5°C by performing all experiments in a temperature-controlled room. The ratio of root weight to solution volume was such that isotope depletion was minimal during the 10- or 30-min uptake periods. Uptake was initiated by the addition of $^{86}Rb^+$ (as RbCl; New England Nuclear Corp.) to a final concentration of approximately 0.1 μCi/ml and terminated by the vacuum withdrawal of the radioactive solution into the chamber below the uptake wells. Free space radiolabel was removed by two 8-min washes in ice-cold 0.5 mM $CaSO_4$ + 1 mM RbCl. The Plexiglas vials (with roots) were then centrifuged for 15 s to remove surface water, and the roots weighed into scintillation vials. To rupture membranes, roots were incubated in 5 ml of 95% ethanol and then 10 ml of 5 mM ANDA[2] was added to each vial. Radioactivity was quantified via detection of Cerenkov radiation in a Beckman LS 9800 scintillation system.

To verify that transport discrimination of $Rb^+$ *versus* $K^+$ was not occurring, certain influx experiments were repeated using $^{42}K^+$ (as KCl; New England Nuclear Corp.).

**Efflux Experiments.** Roots of intact seedlings or 2-cm-long root segments were allowed to accumulate $^{86}Rb^+$ from a solution containing 0.5 mM RbCl, 0.2 mM $CaSO_4$, 1 mM Mes buffer (pH 6.5), and $^{86}$RbCl (approximately 0.25 μCi/ml) for about 24 h. Periodic additions of RbCl and $^{86}Rb^+$ were made to maintain a constant specific radioactivity. By the end of the 24-h loading period, cpm/ml of the external solution had ceased declining, indicating that isotope flux equilibrium had been achieved.

Roots were washed briefly to remove surface radioactivity and 2-cm segments were placed into experimental Plexiglas vials. The vials were placed into beakers containing 15 ml of aerated solution containing various concentrations of RbCl, 0.2 mM $CaSO_4$, and 1 mM Mes buffer (pH 6.5). At predetermined times, the vials were removed from the efflux medium, adhering solution was blotted, and the vials were placed into fresh efflux media. Aliquots of each efflux solution, at each time point, were analyzed for radioactivity. At the end of the efflux experiment, radioactivity remaining in the root segments was determined. The efflux data were analyzed according to the methods of Pitman (31) and Cram (6), and interpreted according to the model presented by these workers; *i.e.* two intracellular compartments, the vacuole and cytoplasm, arranged in series.

Efflux experiments were performed which ensured that leakage of ions from the cut ends was not occurring. The terminal 10 cm of a root preloaded with $^{86}Rb^+$ was excised, and the cut end of the root was threaded through a hole in a Plexiglas plate and sealed with vacuum grease. The cut end protruded about 0.5 cm above the surface of this plate. The 9.5 cm of root below the plate was lowered into a burette containing 10 ml of efflux solution. Therefore, efflux from the root surface could be measured without the complication of leakage from the cut end of the root.

Certain efflux experiments were repeated, monitoring the efflux of radiolabeled from $^{42}K^+$-loaded roots into solutions containing unlabeled KCl.

**Sulfhydryl Modifiers.** The effects of the permeant (NEM) and impermeant (PCMBS) sulfhydryl reagents on $Rb^+$ influx and efflux were examined. Solutions containing 0.2 mM $CaSO_4$, 1 mM Mes buffer (pH 6.5), and either 0.3 mM NEM or 2 mM PCMBS were prepared immediately before use. For experiments involving NEM, either root segments or intact roots were placed into 0.3 mM NEM for various times. The NEM solution was then aspirated and the roots were washed in an aerated solution of 1 mM DTE, 0.2 mM $CaSO_4$, and 1 mM Mes buffer (pH 6.5) for 10 min. Prior to influx or efflux experiments, roots were washed in 0.2 mM $CaSO_4$ briefly to remove DTE.

For influx experiments involving PCMBS, root segments were placed in 2 mM PCMBS for various times, PCMBS solution was then aspirated, and root segments were washed in an aerated solution of 0.2 mM $CaSO_4$ plus 1 mM Mes buffer (pH 6.5) for 10 min. PCMBS (2 mM) was often included in the experimental solution for the course of the uptake. For efflux experiments involving PCMBS, 1 mM PCMBS was added to the isotope loading solution for the last 30 min of loading; the same concentration was used throughout the course of the efflux experiment.

When it was desirable to remove any free inorganic mercury from stock PCMBS (Sigma), the method of Will and Hopfer was employed (36). Free $Hg^{2+}$ was removed by passing stock PCMBS solution through a column (0.5 × 4 cm) of Dowex chelating resin (Sigma, in $H^+$ form). The pH of eluted PCMBS was adjusted to 7.5 and the concentration was determined spectrophotometrically

[2] Abbreviations: ANDA, 7-amino-1,3-napthalene disulfonic acid; NEM, *N*-ethyl maleimide; PCMBS, *p*-chloromercuribenzene sulfonic acid; DTE, dithioerythritol.

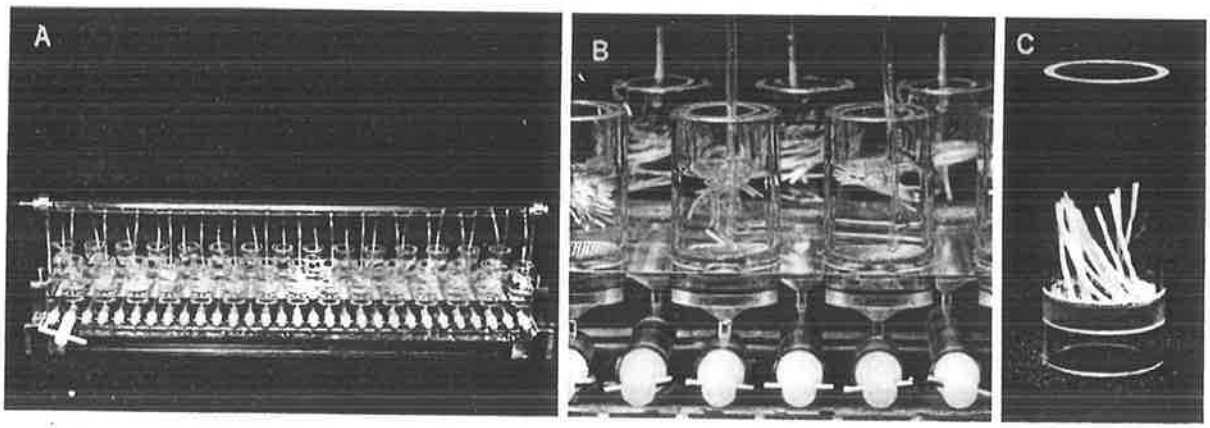


FIG. 1. Apparatus used for uptake experiments (A). Corn root segments were placed into Plexiglas vials (C) which were then placed into aerated uptake wells, as shown in B. To terminate an experiment, the Teflon valve was rotated and the uptake solution pulled, under vacuum, into the chamber below the uptake wells.

at 265 nm ($\epsilon$ = 611 $M^{-1}$ $cm^{-1}$ at pH 7.5). Purified PCMBS was prepared immediately prior to use.

## RESULTS

**$Rb^+$ Influx Isotherms.** Rubidium influx isotherms for low- and high-salt roots were smooth, nonsaturating curves (Figs. 2 and 3). As $Rb^+$ concentration increased above approximately 1 mM, the curves approached linearity; the slopes of the linear portion were almost identical for both low-salt and high-salt root isotherms. In experiments studying influx from a wider range of $Rb^+$ concentrations (0–50 mM RbCl), the observed linearity was maintained, with no evidence of discontinuities or saturation. Figure 3 focused on the concentration range associated with Mechanism I in the Epstein model. The isotherms were smooth, and although they more closely approximated Michaelis-Menten kinetics, they still did not approach saturation.

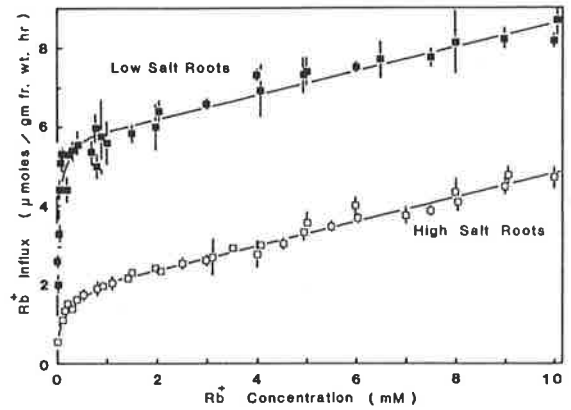


FIG. 2. $^{86}Rb^+$ influx isotherms for corn root segments grown in 0.2 mM $CaSO_4$ (low-salt status) or in 5 mM KCl + 0.2 mM $CaSO_4$ (high-salt status). All data points are the average of four replicates and error bars are ± SE. Points which lack error bars do so because the standard errors were smaller than symbols used. Linear regression performed on data points for $Rb^+$ concentrations from 1 to 10 mM yielded the first-order rate coefficient for the linear component ($k$: µmol g fresh weight$^{-1}$ $h^{-1}$ $mM^{-1}$); values in parenthesis represent correlation coefficients. Low-salt roots, $k$ = 0.30 ($r$ = 0.971); high-salt roots, $k$ = 0.31 ($r$ = 0.993).

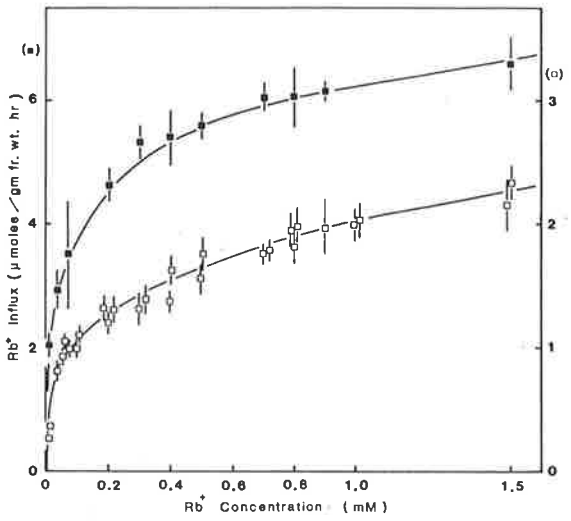


FIG. 3. $^{86}Rb^+$ influx isotherms for low salt (■) and high salt (□) corn roots, focusing on Mechanism I concentration range.

There were several problems in experimental design which had to be dealt with in these studies. Experiments were designed which generated large numbers of data points and replicates, while minimizing variability, in order to establish accurately the shapes of uptake isotherms. Through the design, construction, and subsequent use of the uptake apparatus shown in Figure 1, we were able to obtain the necessary data from our experiments. With this apparatus, we could handle large numbers of root segments rapidly with a minimum of damage, and could quickly manipulate a wide range of substrate concentrations. Reproducibility from replicate experiments was excellent.

In the present experiments, we found that uptake periods of 10 or 30 min produced isotherms that were almost identical in shape and influx value. Because a larger amount of radioisotope was accumulated during the 30-min uptake, which reduced counting variability, most experiments were run for 30 min. From efflux experiments, it was determined that the 16-min wash at 2°C removed all but about 5% of the free space $^{86}Rb^+$, while removing only 5% of the $^{86}Rb^+$ accumulated in the cytoplasm (data not shown). Thus, we thought that the 30-min uptake/16-min wash regime yielded influx values which represented transport across the plasmalemma.

The final problem concerned the potential discrimination of the transporter(s) for $K^+$ *versus* $Rb^+$. $K^+$ uptake is often measured from $^{86}Rb^+$-labeled KCl solution, with the assumption that discrimination is minor. However, in some systems, such as *Chara* (18) and *Phaseolus* leaf slices (16), significant discrimination occurs in the transport of $K^+$ *versus* $Rb^+$. Läuchli and Epstein have demonstrated that the transport discrimination between $K^+$ and $Rb^+$ in corn roots is only about 20% (21). Nonetheless, in order to have total confidence in our influx data, we studied radioisotope influx from $^{86}Rb^+$-labeled RbCl solutions. Therefore, it was necessary to repeat key flux experiments in which we followed $^{42}K^+$ uptake from KCl solutions to ensure that our interpretations derived from $Rb^+$ flux data applied to $K^+$ transport. In experiments that were the same as those of Figure 2, $K^+$ influx isotherms were nearly identical in shape and rates to those for $Rb^+$.

The kinetic profiles presented in Figure 2 can be interpreted in various ways. Because of supporting evidence which will be reported later, we have chosen to interpret these isotherms as the sum of a saturable and a linear component, which can be expressed as:

$$v = V_{max}S/(S + K_m) + kS \qquad (1)$$

where $v$ is the rate, $S$ is the cation concentration, $V_{max}$ and $K_m$ are the Michaelis-Menten constants, and $k$ is the first-order rate coefficient. Using the method of Debnam and Levin (8), the linear component ($kS$) was computed and subtracted (Fig. 4). The resulting data approximated a saturable curve. Eadie-Hofstee and Lineweaver-Burk transformations yielded identical kinetic constants for the saturable system. Apparent $K_m$ values were 16 µM for low-salt roots and 86 µM for high-salt roots, while $V_{max}$ values were 5.61 and 1.85 µmol g fresh weight$^{-1}$ $h^{-1}$, respectively, for low- and high-salt roots. The linear components were identical for isotherms from either root salt status. In order to ensure that the linear component was not an artifact of incomplete washing of radiolabel from the apoplast, the 30-min uptake 16-min wash regime was performed on root segments that had been repeatedly freeze-thawed to rupture the symplast. These roots did not accumulate any measurable radioisotope, indicating that the linear component was due to $Rb^+$ uptake into the symplast.

**Influence of Sulfydryl Reagents on Influx Isotherms.** The effect of the penetrating, covalently binding sulfhydryl reagent, NEM, on $Rb^+$ influx isotherms was studied. Increasing exposures to NEM selectively inhibited the saturable component in both low- and high-salt roots, while inhibiting the linear component much less dramatically (Fig. 5). In high-salt roots, a 10-s pulse with 0.1

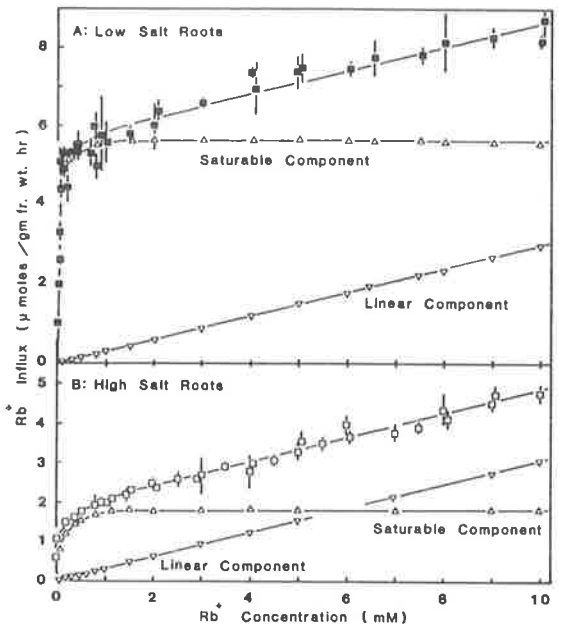


FIG. 4. Separation of influx isotherms into their saturable and linear components. Eadie-Hofstee plots for saturable curves yielded the following kinetic constants: $K_m$ values of 16 μM (low salt), 86 μM (high salt); $V_{max}$ values of 5.62 μmol g fresh weight$^{-1}$ h$^{-1}$ (low salt), 1.85 μ mol g fresh weight$^{-1}$ h$^{-1}$ (high salt). The first-order rate coefficients ($k$) for the linear components were 0.30 (low salt) and 0.31 (high salt).

mM NEM, prior to uptake, reduced the saturable component $V_{max}$ by 60%, while inhibiting the linear component only slightly. A 30-s exposure to 0.3 mM NEM totally abolished the saturable component, while reducing the linear component by 30%. Low-salt roots required longer exposures to NEM to elicit similar degrees of saturable component inhibition. A 30-s NEM pulse inhibited the saturable component $V_{max}$ by 70%, while leaving the linear component unaffected. A 5-min NEM exposure totally inhibited the saturable component. Identical responses to NEM were found for $K^+$ influx isotherms in experiments involving $^{42}K^+$ uptake from KCl solutions.

Table I summarizes the effects of different NEM exposures on both the linear and saturable components of $Rb^+$ uptake. The basic response is a selective inhibition of the saturable component with increasing NEM exposure. As NEM exposures lengthened, the linear component was also reduced, but much less significantly. It is of interest to note that increasing NEM exposures not only reduced the $V_{max}$ of the saturable component, but also increased the apparent $K_m$, indicating that the apparent affinity of the transporter for $Rb^+$ was reduced.

The influence of the impermeant sulfhydryl reagent, PCMBS, on $Rb^+$ influx was also investigated. Although the resulting kinetic curves were more complex than found for NEM experiments, the same general inhibitory trends were seen (Fig. 6). Uptake in the concentration range dominated by the saturable component (0–1 mM) exhibited a linear response to increasing $Rb^+$ concentrations, thus indicating that PCMBS caused some form of transition in the transport mechanism responsible for saturable uptake. A family of curves resulting from increasing exposure to PCMBS could be obtained (data not shown). However, even with prolonged exposure to PCMBS (40 min), it was never possible to abolish the saturable component. We also found that the linear component in low-salt root isotherms was always stimualted by PCMBS. Exposure of 1 min or longer with PCMBS (2 mM) always sitmulated the linear component by about 40% over control values.

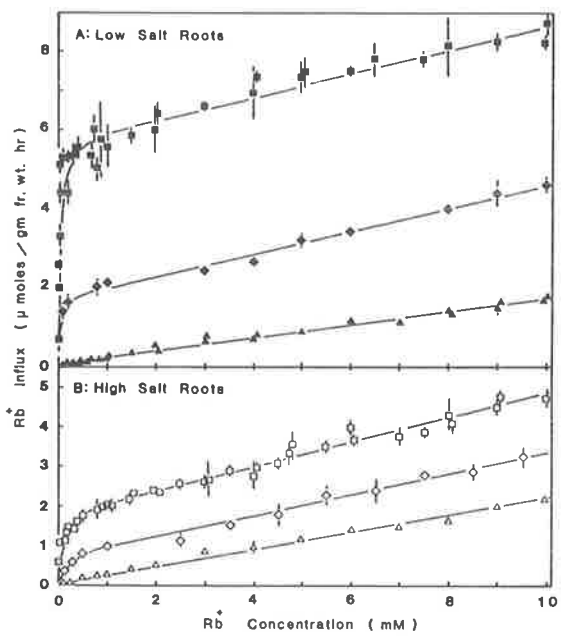


FIG. 5. Influence of various NEM exposures on $^{86}Rb^+$ influx isotherms. Corn roots were pretreated with NEM (0.3 mM except where noted) for various periods, then washed for 10 min in 1 mM DTE prior to $^{86}Rb^+$ uptake. Low-salt root NEM exposures: (◆), 30 s NEM; (▲), 5 min NEM. High-salt root NEM exposures: (◇), 10 s 0.1 mM NEM; (△), 30 s NEM. All pretreatment solutions contained 0.2 mM $CaSO_4$, 1 mM Mes (pH 6.5), in addition to NEM or DTE. Controls were pretreated in the same solution minus NEM. All NEM-treated root segments were washed with control solution prior to uptake to remove DTE.

Table I. *Effect of Various NEM Exposures on the Saturable and Linear Components of $^{86}Rb^+$ Uptake into Corn Root Segments*

Influx isotherms obtained following NEM exposures of various lengths were separated into their linear and saturable components. Except where noted, NEM concentration was 0.3 mM.

| Salt Status | Length of NEM Exposure | Saturable Component | | Linear Component ($k$)[b] |
|---|---|---|---|---|
| | | $K_m$ | $V_{max}$ | |
| | | μM | μmol g fresh wt$^{-1}$ h$^{-1}$ | |
| Low salt | 0 (control) | 16 | 5.62 | 0.30 |
| | 30 s | 29 | 1.73 | 0.29 |
| | 2 min | 81 | 0.70 | 0.20 |
| | 5 min | ND[c] | ND | 0.16 |
| High salt | 0 (control) | 86 | 1.85 | 0.31 |
| | 10 s[a] | 153 | 0.76 | 0.27 |
| | 18 s | ND | ND | 0.25 |
| | 30 s | ND | ND | 0.21 |

[a] 0.1 mM NEM.

[b] First-order rate constant for linear component of $Rb^+$ transport in mol g fresh weight$^{-1}$ h$^{-1}$.

[c] Saturable component not detectable following NEM treatment.

**$Rb^+$ Efflux Experiments.** Because sulfhydryl reagents dramatically inhibited $Rb^+$ influx, experiments were performed to determine if these modifiers also influenced efflux. Control efflux data, when plotted as the log of tissue radioactivity *versus* time, yielded curves consisting of three approximately linear components (Fig.

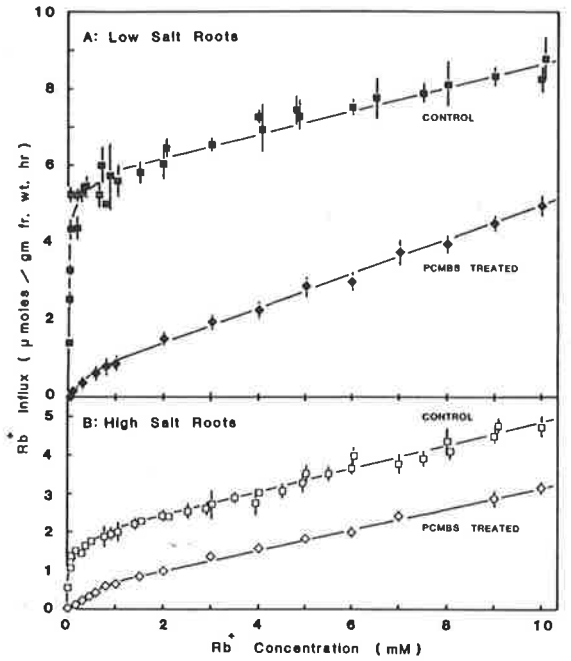


FIG. 6. Influence of PCMBS on $^{86}Rb^+$ influx isotherms. Corn root segments were given a 20-min pretreatment in 2 mM PCMBS + 0.2 mM $CaSO_4$ + 1 mM Mes (pH 6.5) prior to uptake. Two mM PCMBS was also included in the uptake solution. First-order rate coefficients following PCMBS exposure were 0.42 and 0.30 μmol g fresh weight$^{-1}$ h$^{-1}$ mM$^{-1}$, for low- and high-salt roots, respectively.

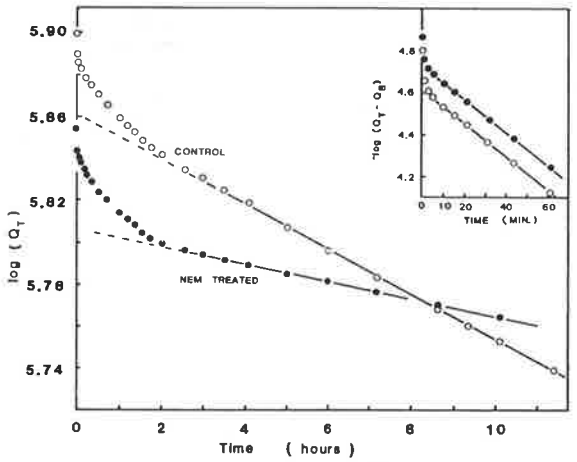


FIG. 7. Influence of NEM on efflux of $^{86}Rb^+$ from high-salt roots. Roots were loaded for 24 h with $^{86}Rb^+$ until isotopic flux equilibrium was achieved. NEM was added to the isotope loading solution (0.3 mM NEM) and roots were exposed to it for 30 s prior to commencing the $^{86}Rb$ efflux experiment. The efflux solution contained 0.2 mM RbCl + 0.2 mM $CaSO_4$ + 1 mM Mes (pH 6.5). Data was plotted as the log of cpm remaining in the tissue ($Q_t$) normalized for root weight *versus* time. The slowest effluxing component (vacuolar) was extrapolated to zero and subtracted from the overall curve. Insert shows a plot of the resulting data ($Q_s$ = cpm in slow component). These data represent cytoplasmic efflux for control (○) and NEM-treated (●) corn roots. Vacuolar half-times were 27.5 and 70 h for control and NEM-treated root tissue, respectively. Cytoplasmic half-times were 37.3 and 36 min for control and NEM-treated root tissue, respectively.

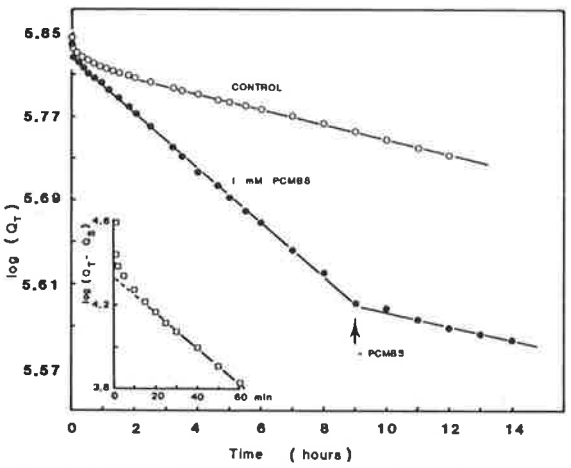


FIG. 8. Influence of PCMBS on $^{86}Rb^+$ efflux in high-salt-grown corn roots. Following a 24-h $^{86}Rb^+$ loading period, 1 mM PCMBS was added to the isotope solution for 30 min prior to initiation of efflux. One mM PCMBS was also included in the efflux solution through the first 9 h. Data was analyzed as in Figure 7. Insert depicts control cytoplasmic efflux (□). Efflux curve resulting from PCMBS exposure could not be resolved into cytoplasmic and vacuolar components. Vacuolar half-times were 42 and 11.5 h for control and PCMBS-treated root tissue, respectively. Following removal of PCMBS, the half-time increased to 48 h. The control cytoplasmic half-time was 38 min. PCMBS appeared to abolish the cytoplasmic component.

7). Each component was determined by the sequential subtraction of the slower-exchanging from the subsequent faster-exchanging component of the curve. We have chosen to interpret such curves as the product of efflux from three compartments in series, the vacuole, cytoplasm, and cell wall, while recognizing the fact that such an interpretation has been subject to some criticism (26, 35). These criticisms will be dealt with in the discussion.

The effect of a 30-s NEM pulse on $Rb^+$ efflux from high-salt roots is also shown in Figure 7, with the insert representing cytoplasmic efflux. NEM had no effect on efflux across the plasmalemma ($t_{1/2}$ [control] = 37.3 min; $t_{1/2}$ [NEM] = 36 min). However, NEM had a significant effect on vacuolar efflux, reducing it by a factor of about 2.5 ($t_{1/2}$ [control] = 27.5 h; $t_{1/2}$ [NEM] = 70 h). Similar results were obtained for $^{42}K^+$ efflux into solutions of various KCl concentration.

PCMBS had a more complex effect on $Rb^+$ efflux (Fig. 8). Following washout from the cell walls, efflux was linear throughout the remainder of the experiment, provided PCMBS was included in the efflux solution. Hence, it was impossible to separate efflux into cytoplasmic and vacuolar components. The half-time for efflux in the presence of PCMBS was 11.5 h, while in control tissue the value for the vacuole was 42 h. Thus, it appeared that the cytoplasmic component was somehow abolished, yet vacuolar efflux was stimulated. The observation that the actual flux of $^{86}Rb^+$ from PCMBS-treated roots exceeded that of control roots throughout the experiment supports the hypothesis that PCMBS stimulated vacuolar efflux. Once PCMBS was removed from the efflux solution, a rapid recovery back to control efflux values was seen (Fig. 8).

The effects of NEM and PCMBS on efflux (cytoplasmic and vacuolar half-times) are summarized in Table II. The general responses to NEM and PCMBS hold true for both low-salt and high-salt roots over a range of RbCl concentrations in the efflux solution. In efflux experiments utilizing excised root segments, the leakage of ions from the cut ends of the xylem could contribute significantly to the overall measured efflux (35). In order to ensure that the NEM effect on vacuolar efflux involved cortical tissue

Table II. *Primary Data for $^{86}Rb^+$ Efflux from Corn Root Segments or Sealed Excised Roots*

For experiments studying NEM effects on efflux, NEM was added to $^{86}Rb^+$ loading solution after a 24-h loading period. Roots were exposed to 0.3 mM NEM for either 30 s (high-salt roots) or 5 min (low-salt roots). DTE was then added (final concentration, 1 mM) to isotope loading solution for 10 min to bind up unreacted NEM. Roots were incubated briefly in fresh isotope loading solution to remove DTE prior to efflux. For PCMBS experiments, purified PCMBS (final concentration, 1 mM) was added to isotope loading solution for the last 30 min of the 24-h loading period. One mM PCMBS was included in the efflux solution for the first 9 h of efflux. Following removal of PCMBS, efflux was measured for an additional 5 h. When possible, half-times are the average of three or four experiments ± SE, otherwise results are for one experiment.

| Root Treatment | High-Salt Roots | | | | | | Low-Salt Roots | | |
|---|---|---|---|---|---|---|---|---|---|
| | Excised roots | | | Terminal 10 cm (cut end sealed) | | | Excised roots | | |
| | External [$Rb^+$] | Cyt $t_{1/2}$ | Vac $t_{1/2}$ | External [$Rb^+$] | Cyt $t_{1/2}$ | Vac $t_{1/2}$ | External [$Rb^+$] | Cyt $t_{1/2}$ | Vac $t_{1/2}$ |
| | *mM* | *min* | *h* | *mM* | *min* | *h* | *mM* | *min* | *h* |
| Control | 0.2 | 45 ± 5 | 34 ± 2.5 | 0.2 | 28 | 30 | 0.2 | 84 ± 7 | 16 ± 0.7 |
| | 5 | 36 | 29 | | | | | | |
| | 10 | 35 ± 4 | 40 ± 3 | | | | 10 | 82 ± 11 | 19 ± 1.5 |
| NEM | 0.2 | 37 ± 4 | 71 ± 3 | 0.2 | 30 | 104 | 0.2 | 70 | 73 |
| | 5 | 33 | 54 | | | | | | |
| | 10 | 32 ± 5 | 67 ± 6 | | | | 10 | 80 | 40 |
| PCMBS | 0.2 | ND[a] | 21 (+PCMBS) | | | | 0.2 | ND | 9.8 (+PCMBS) |
| | | | 53 (−PCMBS) | | | | | | 60 (−PCMBS) |
| | 10 | ND | 12 (+PCMBS) | | | | 10 | ND | 8 (+PCMBS) |
| | | | 48 (−PCMBS) | | | | | | 50 (−PCMBS) |

[a] Not detectable.

and was not due to inhibition of xylem efflux, experiments were performed with a closed system consisting of the terminal 10 cm of the root (cut end sealed and not in contact with bathing medium). The control cytoplasmic and vacuolar half-times for this system were similar to those obtained using 2-cm root segments. One possible explanation for this would be that the half-times for cytoplasmic and vacuolar xylem efflux are similar to those for cortical tissue efflux. This conclusion is supported by the observation that the kinetics of cortical and xylem $^{22}Na^+$ efflux in barley roots were similar (17). The more important observation in the sealed root system was that the NEM response was identical with that in root segments, indicating that NEM was acting on vacuolar efflux from the root cortical and epidermal cells. Another point of interest is the observation that, as the external RbCl concentration was increased from 0.2 to 10 mM there was no significant change in either cytoplasmic or vacuolar efflux in either low- or high-salt roots. Thus, it appears that exchange diffusion of $K^+$ across the plasmalemma is minimal, unlike that of $Cl^-$ (6). Finally, efflux across the plasmalemma and tonoplast appears to differ substantially in low-salt compared to high-salt roots. In high-salt roots, efflux from the cytoplasm is about twice that observed in low-salt roots, while vacuolar efflux is about twice as rapid in low-salt roots.

## DISCUSSION

In the present study, we focused on the concentration range from 0 to 10 mM to stay somewhat near the range of physiological relevance. Studies on soil $K^+$ concentrations indicate the majority of the soil $K^+$ is below 2 mM (33). As clearly shown by the results presented in Figures 2 and 3, the concentration dependence of $K^+$ influx into corn roots followed a smooth, nonsaturating profile. We were unable to detect discontinuities in the concentration region from 1 to 10 mM. These results are consistent with the recent theoretical analysis of root ion transport kinetics presented by Borstlap (4), but are at variance with the interpretations presented by many earlier workers. As is evident from Borstlap's analysis, verification of discontinuities in the kinetic profiles of other systems may require further and more detailed experimental documentation.

**Evidence for Saturating and Linear Mechanisms.** The kinetics observed for $K^+$ ($Rb^+$) influx in corn roots can be interpreted as the operation of a single complex, allosterically regulated enzyme. The binding of an effector, such as $K^+$, to a subunit of the enzyme, could induce a conformational change which would reduce the affinity of the binding site for substrate. Systems demonstrating such negative cooperativity often exhibit kinetics similar to those presented here. Hodges has argued that the kinetics observed for ion uptake in plant roots could be due to negative cooperativity, while the 'bumps' observed in most influx isotherms could be explained by an additional component exhibiting positive cooperativity (15).

An alternative interpretation would attribute the observed kinetics to the operation of a saturable mechanism in conjunction with a first-order kinetic process. The results from our sulfhydryl reagent studies offer support for this interpretation, in that it was possible to reduce, sequentially, and finally abolish, the saturable component with increasing NEM exposure. Under these conditions, the linear component was reduced much less dramatically. It would appear that as NEM exposure increased, more of the saturable carriers were titrated until they were all inhibited. Additionally, the saturable carriers which continued to function following NEM exposure exhibited a large increase in their apparent $K_m$ (see Table I), which could be the result of biochemical modification of the carrier. Alternatively, NEM could be inhibiting transport into the cells of the root periphery, while cortical cells would continue to function under the influence of diffusion limitation.

The saturable component appears to be Epstein's Mechanism I. It is dominant in the low concentration range (0–1 mM) and approximates Michaelis-Menten kinetics. Furthermore, it is sensitive to inhibitors such as the sulfhydryl reagents used for these experiments or uncouplers such as CCCP (32). $K^+$ uptake in this concentration range is believed by many workers to be active, accumulating $K^+$ against its electrochemical potential gradient,

although this is still subject to debate.

**The Linear Component: Simple Diffusion?** The nature of the linear component is intriguing, and experiments designed to characterize and identify the linear mechanism are currently being carried out in our laboratory. In the concentration range where the linear component dominates uptake, many workers feel that influx of $K^+$ is passive. It is relatively insensitive to inhibitors and shows no signs of saturation at the higher concentrations tested. There have been many examples of transport kinetics in both animals and plants in which a linear component makes a significant contribution. The linear component has usually been dismissed as either passive or exchange diffusion. However, some of our findings suggest that linear uptake may be the product of a more complex mechanism. First, a transporter accumulating radioisotope via exchange diffusion should be rate controlled by either internal or external substrate concentration. In our system, the linear component was identical in roots varying significantly in internal $K^+$ concentration (low- *versus* high-salt roots), an observation that argues against exchange diffusion. Furthermore, changes in the external $K^+$ ($Rb^+$) concentration from 0.2 to 10 mM had no effect on $K^+$ ($Rb^+$) efflux. This is in contrast to $Cl^-$ efflux, which has been shown to be stimulated by increases in external $Cl^-$, thereby leading to the postulation of a $Cl^-$ exchange diffusion system at the plasmalemma (6). Second, some of the sulfhydryl reagent effects on the linear component cannot be explained by a simple diffusion-mediated mechanism. An ionic species such as $K^+$ should permeate the lipid bilayer of biological membranes slowly; therefore, it is safe to assume that diffusive influx of $K^+$ would be carrier-mediated (*i.e.* a facilitated diffusion, possibly through a proteinaceous channel or pore). Although the linear component was relatively insensitive to sulfhydryl reagent inhibition, increasing exposures of NEM did result in a reduction of the linear component. NEM has been shown to depolarize the membrane potential to a level presumed to be the diffusion potential for $K^+$ (22, 23). This depolarization would reduce the driving force for passive $K^+$ influx. Thus, this NEM-induced reduction in the linear component is still consistent with uptake by facilitated diffusion. However, PCMBS has also been shown to depolarize the membrane potential to the $K^+$ diffusion potential (22, 23), and PCMBS had no effect on the linear component in high-salt roots, while consistently stimulating the linear component by 40% in low-salt roots.

The linear component of uptake may be due to a more complex mechanism than facilitated diffusion. Baker and Hall (1) have cytochemically detected ATPase activity on vesicles near the plasmalemma of corn root cells and have hypothesized that passive uptake in the higher concentration range could be due to endocytosis. Others have proposed vesicular transport between the plasmalemma and vacuole to account for anomalous 'shoulders' occasionally observed on efflux curves (30). Another explanation is based on the consideration that any carrier-mediated transport (including facilitated diffusion) should eventually saturate. Therefore, it is possible that what we observe as linear uptake is only the linear portion of a saturating kinetic curve for a very high $K_m$ (low affinity) transporter.

Finally, Göring and coworkers have hypothesized that multiphasic kinetics could be generated by a single carrier type operating under conditions which diffusion-limit availability of substrate for carriers located on cortical cells beneath the root surface. In a recent paper, we have shown that the 30-s NEM pulse, which abolished saturable uptake in high-salt roots while leaving the linear component unaffected, acts almost exclusively at the root periphery (19). It is possible, therefore, that saturable component uptake is due to transport into the epidermis and hypodermis, while the linear component could be transport into cortical cells within the root.

**Sulfhydryl Involvement in $K^+$ Transport.** Evidence implicating mutiple sulfhydryls comes from the differential sensitivity of $K^+$ uptake to NEM and the impermeant PCMBS. While short NEM exposures abolished the saturable component of uptake, it was never possible to totally inhibit the saturable component with PCMBS (exposures up to 50 min). Therefore, saturable $K^+$ uptake appears to involve both sulfhydryls at the exterior of the plasmalemma and within the interior of the membrane (or cytoplasm). This situation is similar to the sulfhydryl involvement in $HCO_3^-$ uptake in *Chara* (24). Purified PCMBS was a much less effective inhibitor of $HCO_3^-$ uptake than the penetrating sulfhydryl reagents, $Hg^{2+}$ or NEM.

In addition to being a less effective inhibitor of saturable component uptake than NEM, PCMBS also appears to alter the basic mechanism of saturable uptake. In the presence of PCMBS, the saturable mechanism was converted such that it responded linearly to changes in external ion concentration. It is possible that the carriers, following sulfhydryl modification, have undergone a change in conformation to some form of 'open channel' structure. Lucas and Alexander obtained similar results while studying NEM effects on $HCO_3^-$ uptake in *Chara* (24). As exposure to NEM (or $Hg^{2+}$) increased, $HCO_3^-$ uptake exhibited a reduction in the $V_{max}$, while the $K_m$ was unaffected. Further increases in NEM exposure caused a rapid transition in $HCO_3^-$ uptake to a linear mode. The authors speculated that this transition represents either a transport conversion to a facilitated diffusion system or, alternatively, influx could have continued unaffected while a change in the carrier allowed for a dramatic increase in $HCO_3^-$ efflux; thus, the transporter would be converted to a 'pump and leak' system.

Will and Hopfer (36) have reported that PCMBS can contain as much as 0.5% (by weight) inorganic mercury. Many enzyme systems are extremely sensitive to inorganic mercury, which is a potent sulfhydryl reagent and can penetrate into the cytoplasm. Lucas and Alexander (24) found that unpurified PCMBS inhibited $HCO_3^-$ uptake in *Chara* much more dramatically than purified PCMBS. However, in our experiments, purified and unpurified PCMBS had similar effects on $Rb^+$ uptake. The possibility exists that any free $Hg^{2+}$ in the PCMBS could have been bound up in the cell walls of the root, and thus was not available to influence $Rb^+$ transport.

**Efflux Analysis.** There are obvious inherent dangers in the treatment of a complex organ, such as a root, as a simple structure composed of three compartments in a series. This danger is underscored by occasional examples of efflux kinetics that deviate from the strict three compartment model (30). However, in all of our efflux experiments, the data agreed well with a system obeying first-order kinetics for efflux from a three-compartment model. Further verification of the model can be obtained by applying certain kinetic analyses to the experimental data. As Cram and Laties have shown (7), the plots of ln content *versus* time and ln efflux *versus* time should both yield curves fitted by the same number of compartments, with identical rate constants for the corresponding compartments from each plot. This can be best illustrated by the following analysis. For the sake of simplicity, the initial rapid component due to wash out from the cell walls can be ignored; thus, the radioactive content ($Q_t$) of the resulting two-compartment model would be described by the equation:

$$Q_t = A\, e^{-K_f t} + B\, e^{-K_s t} \qquad (2)$$

where $K_f$ and $K_s$ are the rate constants for the rapidly (cytoplasm) and slowly (vacuole) effluxing compartments. Plots of ln $Q_t$ *versus* time would yield curves composed of two linear phases with slopes of $K_f$ and $K_s$ and $y$ intercepts $A$ and $B$. Efflux ($dQ_t/dt$) from this system would be described by the equation:

$$dQ_t/dt = -\,[K_f A\, e^{-K_f t} + K_s B\, e^{-K_s t} \qquad (3)$$

A plot of ln $dQ_t/dt$ *versus* time would again yield curves with two linear phases. The slopes of the two linear phases would again be

$K_f$ and $K_s$. Furthermore, the intercepts of this plot, which we will call $I_f$ and $I_s$, should be related to the intercepts of the ln $Q_t$ *versus* time plot by the following equations:

$$I_f = K_f A \text{ and } I_s = K_s B \quad (4)$$

Therefore, the ratio of the intercepts from the ln $dQ_t/dt$ *versus* time plot ($I_f/I_s$) should equal the ratio of the intercepts from the ln $Q_t$ *versus* time plot multiplied by the ratio of the rate constants

$$\left(\frac{K_f}{K_s} \times \frac{A}{B}\right).$$

(We emphasize this point because of previous misinterpretations of Cram's and Laties' original work.) These tests were applied to our efflux data (Fig. 7); the rate constants from plots of log $Q_t$ and log $dQ_t/dt$ *versus* time were approximately equal. $K_s$ values were $4.20 \times 10^{-4}$ min$^{-1}$ and $6.20 \times 10^{-4}$ min$^{-1}$, and $K_f$ values were 1.93 $\times 10^{-2}$ min$^{-1}$ and $1.90 \times 10^{-2}$ min$^{-1}$. In addition, the ratio of the intercepts from the log $dQ_t/dt$ *versus* time plot ($I_f/I_s$) equaled 2.29, while

$$\frac{K_f}{K_s} \times \frac{A}{B}$$

equaled 2.10. Therefore, we feel that our efflux data represent, at least as a first-order approximation, efflux from the vacuole and cytoplasm in series, and have chosen to present our kinetic parameters as the half-time for efflux from these compartments.

**Effects of NEM and PCMBS on Efflux.** NEM influenced efflux in a much different manner than influx, while the results involving PCMBS, although difficult to interpret, seem to indicate that its effect on efflux and influx are related. NEM, which significantly inhibited plasmalemma influx, had no effect on efflux across the plasmalemma, while substantially reducing transport from the vacuole. Because NEM is a penetrating molecule, it may be acting directly at the tonoplast to inhibit vacuolar efflux. Alternatively, it could be acting at the plasmalemma to inhibit vacuolar efflux in some unknown fashion. It seems less likely that NEM is acting at a cytoplasmic site, such as the mitochondria, to reduce energy supply for transport, at least following the 30-s NEM pulses in high-salt roots. A 30-s NEM pulse had no effect on root respiration (L. V. Kochian and W. J. Lucas, unpublished results).

The experiments with purified PCMBS demonstrate the effects on efflux of a modifier acting exclusively at the plasmalemma. PCMBS had several significant effects on efflux. First, the basic shape of the efflux curve was changed from the usual biphasic (ignoring cell wall exchange) to a monophasic efflux, presumably representing efflux from one compartment (vacuole). It is difficult from these data to interpret what has happened to efflux from the cytoplasm. As we speculated for influx, it is possible that PCMBS has modified some portion of the carrier for $K^+$, so that it now functions as an open channel. Other workers have reported that long exposures to PCMBS (up to 1 h) caused transport systems to undergo dramatic structural changes. Trump *et al.* (34) have demonstrated structural changes of the plasmalemma of Ehrlich ascites tumor cells following exposure to PCMBS, and Will and Hopfer (36) found that PCMBS produced significant increases in the cation permeability of red blood cell membranes. Second, PCMBS significantly increased vacuolar efflux. Since it is acting at the plasmalemma, it appears that this membrane does exert influence on vacuolar transport processes. It is not likely that PCMBS has altered the plasmalemma structure to such a degree that it could penetrate into the cytoplasm. This follows from the observation that the removal of PCMBS from the efflux solution elicited a rapid recovery in efflux, back to approximately control values (Fig. 8).

In conclusion, our results for $K^+$ transport into corn roots are consistent with the combined operation of saturable and linear components. The saturable component, which may represent Epstein's Mechanism I, appears to be engaged in active transport of $K^+$ into the root symplast. Nonsaturation transport kinetics are widespread and have been demonstrated in uptake systems ranging all the way from single cells to brain tissue. Although generally considered to represent simple or facilitated diffusion, the first-order kinetic mechanism may be more complex in nature. Therefore, the linear component may be a fairly universal feature of transport, with definite biological significance, and warrants further study.

*Acknowledgments*—We wish to express our appreciation for the excellent technical assistance afforded by Messrs. Young and Tallon of the Physical Plant Workshop, University of California, Davis.

## LITERATURE CITED

1. Baker DA, JL Hall 1973 Pinocytosis, ATPase and ion uptake by plant cells. New Phytol 72: 1281–1291
2. Bange GGJ 1973 Diffusion and absorption of ions in plant tissue. III. The role of the root cortex cells in ion absorption. Acta Bot Néerl 22: 529–542
3. Blackman MS, CN McDaniel 1978 Amino acid transport in suspension cultured plant cells. I. Method and kinetics of L-leucine uptake. Plant Sci Lett 13: 27–34
4. Borstlap AC 1981 Invalidity of the multiphasic concept of ion absorption in plants. Plant Cell Environ 4: 189–195
5. Cohen SR 1975 A comparison of the rate equations, kinetic parameters, and activation energies for the initial uptake of L-lysine, L-valine, γ-aminobutyric acid, and α-aminoisobutyric acid by mouse brain slices. J Membr Biol 22: 53–72
6. Cram WJ 1968 Compartmentation and exchange of chloride in carrot root tissue. Biochim Biophys Acta 163: 339–353
7. Cram WJ, GG Laties 1974 The kinetics of bicarbonate and malate exchange in carrot and barley root cells. J Exp Bot 25: 11–27
8. Debnam ES, RJ Levin 1975 An experimental method of identifying and quantifying the active transfer electrogenic component from the diffusive component during sugar absorption measured in vivo. J Physiol 246: 181–196
9. Delrot S, JL Bonnemain 1981 Involvement of protons as a substrate for the sucrose carrier during phloem loading in *Vicia faba* leaves. Plant Physiol 67: 560–564
10. Ehwald R, P Sammler, H Göring 1973 Die Bedeutung der Diffusion in den "Freien Raum" für die Konzentrationsabhängigkeit der Aufnahme von Zuckern und Ionen durch pflanzliche Gewebe. Biochim Physiol Pflanzen 164: 596–613
11. Epstein E 1972 Mineral Nutrition of Plants: Principles and Perspectives. John Wiley and Sons, New York
12. Epstein E, CE Hagen 1952 A kinetic study of the absorption of alkali cations by barley roots. Plant Physiol 27: 457–474
13. Fischer E, U Lüttge 1980 Membrane potential changes related to active transport of glycine in *Lemna gibba* G1. Plant Physiol 65: 1004–1008
14. Göring H 1976 Die Bedeutung ungerührter Schichten für die Kinetik des trägervermittelten Membrantransportes in pflanzlichen Geweben. Wiss Z Humboldt-Univ Math-Naturwiss Reihe 25: 61–65
15. Hodges TK 1973 Ion absorption by plant roots. Adv Agron 25: 163–207
16. Jacoby B 1975 Light sensitivity of $^{22}$Na, $^{86}$Rb, and $^{42}$K absorption by different tissues of bean leaves. Plant Physiol 55: 978–981
17. Jeschke WD 1974 The effect of inhibitors on the $K^+$-dependent $Na^+$ efflux and the $K^+$-$Na^+$ selectivity of barley roots. *In* U Zimmermann, J Danity, eds, Membrane Transport in Plants. Springer Verlag, Berlin, pp 397–405
18. Keifer DW, RM Spanswick 1978 Activity of the electrogenic pump in *Chara corallina* as inferred from measurements of the membrane potential, conductance, and potassium permeability. Plant Physiol 62: 653–661
19. Kochian LV, WJ Lucas 1983 Studies on location and kinetics of $K^+$ fluxes in corn roots: Resolution of kinetics into saturable and linear components. Proceedings of Plant Growth Regulator Society of America, Vol 9. In press
20. Komor E, M Rotter, W Tanner 1977 A proton-cotransport system in a higher plant: sucrose transport in *Ricinus communis*. Plant Sci Lett 9: 153–162
21. Läuchli A, E Epstein 1970 Transport of potassium and rubidium in plant roots. The significance of calcium. Plant Physiol 45: 639–641
22. Lichtner FT, RM Spanswick 1981 Sucrose uptake by developing soybean cotyledons. Plant Physiol 68: 693–698
23. Lichtner FT, WJ Lucas, RM Spanswick 1981 Effect of sulfhydryl reagents on the biophysical properties of the plasmalemma of *Chara corallina*. Plant Physiol 68: 899–904
24. Lucas WJ, JM Alexander 1980 Sulfhydryl group involvement in plasmalemma transport of $HCO_3^-$ and $OH^-$ in *Chara corallina*. Plant Physiol 65: 274–280
25. Lüttge U, N Higinbotham 1979 Transport in Plants. Springer Verlag, New York, pp 125–128
26. MacRobbie EAC 1971 Fluxes and compartmentation in plant cells. Annu Rev Plant Physiol 22: 75–96
27. Maynard JM, WJ Lucas 1982 A reanalysis of the two-component phloem loading system in *Beta vulgaris*. Plant Physiol 69: 734–739

28. MUNCK BG, SG SCHULTZ 1969 Lysine transport across isolated rabbit ileum. J Gen Physiol 53: 157–182
29. NISSEN P 1974 Uptake mechanisms: inorganic and organic. Annu Rev Plant Physiol 25: 53–79
30. PALLAGHY CK, U LÜTTGE, K VON WILLERT 1970 Cytoplasmic compartmentation and parallel pathways of ion uptake in plant root cells. Z Pflanzenphysiol 62: 51–57
31. PITMAN MG 1963 The determination of the salt relations of the cytoplasmic phase in cells of beet root tissue. Aust J Biol Sci 16: 647–668
32. POLLEY LD, JW HOPKINS 1979 Rubidium (potassium) uptake by *Arabidopsis*. A comparison of uptake by cells in suspension culture and by roots of intact seedlings. Plant Physiol 64: 374–378
33. REISENAUER HM 1966 Mineral nutrients in soil solution. *In* PL Altman, DS Dittmer, eds, Environmental Biology. Federation of American Societies for Experimental Biology, Bethesda, MD, pp 507–508
34. TRUMP BF, A PENTTILA, IK BEREZESKY 1979 Studies on cell surface conformation following injury. I. Scanning and transmission electron microscopy of cell surface changes following *p*-chloromercuribenzene sulfonic acid (PCMBS)-induced injury of Ehrlich ascites tumor cells. Virchows Arch B Cell Pathol 29: 281–296
35. WALKER NA, MG PITMAN 1976 Measurement of fluxes across membranes. *In* U Lüttge, MG Pitman, eds, Encyclopedia of Plant Physiology, New Series, Vol 2A. Springer-Verlag, Berlin, pp 93–128
36. WILL PC, U HOPFER 1979 Apparent inhibition of active non-electrolyte transport by an increased sodium permeability of the plasma membrane. Mechanism of action of *p*-chloromercuribenzene sulfonate. J Biol Chem 25: 3806–3811

# What's New

# in PLANT PHYSIOLOGY

Volume 13, Number 12 December 1982


## A RE-EVALUATION OF THE CARRIER-KINETIC APPROACH TO ION TRANSPORT IN ROOTS OF HIGHER PLANTS


**Leon V. Kochian and William J. Lucas**
**Department of Botany**
**University of California**
**Davis CA 95616 USA**


Over the past quarter century, and particularly during the 1960s and early 1970s, a widely studied and controversial area of plant physiology involved kinetic studies on ion uptake into the roots of higher plants. These studies often centered on the uptake of various mineral ions ($K^+$, $Cl^-$, $Na^+$, etc) from solutions labeled with radioactive analogues (eg, $^{86}Rb^+$ or $^{42}K^+$ for potassium). Many of the early studies focused on the shapes of kinetic curves for uptake (influx *versus* substrate concentration). In fact, mechanistic interpretations of the shapes of such kinetic curves have formed a cornerstone of research in plant ion transport, and enabled early researchers to formulate the now well-known carrier theory for transport into cells. This was based on the concept that special structures existed in the plasmalemma and complexed with ions in the external solution. It was suggested that these complexes carried the ions across the membrane and released them inside the cell. When uptake from dilute solutions was studied, the kinetic curves approximated a rectangular hyperbola, a response similar to that found in classical enzyme kinetic studies [Fig 1 (see low concentration range)]. Epstein and Hagen were the first to apply Michaelis-Menten (enzyme) kinetics to ion transport and they postulated an ion-specific carrier in analogy to a substrate-specific enzyme (6).

**"Dual-Isotherms": Multiphasic Kinetics?** Epstein and coworkers (5, 7) went on to show that at higher concentrations their observed kinetics deviated from the classical Michaelis-Menten form (Fig 1). Saturation was attained at low concentrations, but then at higher concentrations the curves appeared to reach a second level of saturation. This biphasic pattern was labeled the "dual isotherm of uptake" by Epstein, and was hypothesized to be due to the operation of two separate classes of carriers, each following distinctly different Michaelis-Menten kinetics. In the low concentration range (< 0.5 mM), Mechanism I was hypothesized to be a high affinity, low velocity transporter. In the higher concentration range, Mechanism II was proposed to operate as a low affinity, high velocity transport mechanism with lower substrate specificity. Further studies in the Mechanism II range suggested that the kinetic profile was not a smooth curve, but characterized by multiple inflections.

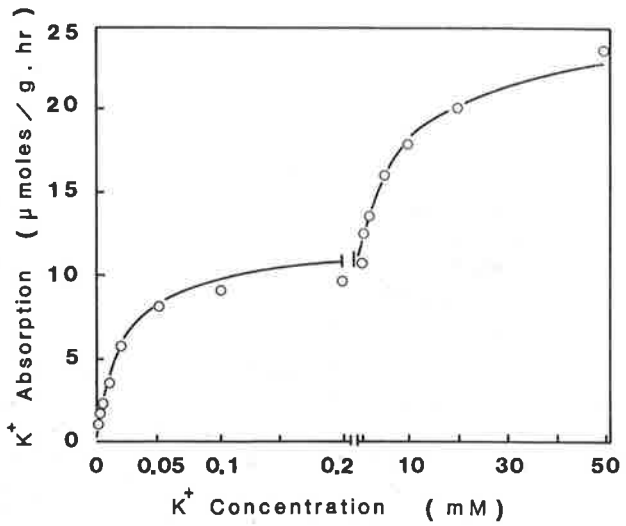


Fig 1. Rate of $K^+$ absorption in barley roots as a function of $K^+$ concentration. $CaCl_2$ is 0.5 *mM* throughout. Note that the concentration scale has been broken after 0.2 *mM* $K^+$. (Redrawn from Epstein, et al, 1963.)

This pioneering work by Epstein and his colleagues had a tremendous impact on the field, and subsequently, complex uptake kinetics was observed for many plant tissues involving a range of substrates. The great volume of published work reflected the interest and importance attached to this field. Conflicting hypotheses were presented and these focused on such aspects as the number of phases, the cellular localization of each phase, and the physiological significance of each phase within the kinetic curves (11). Despite the many controversies arising from mechanistic interpretations of uptake kinetics, a common thread tied together these conflicting views; ie, plant uptake kinetics was complex and universally characterized by curves containing kinks, bumps, or multiple inflections.

In the early 1970s, an alternative interpretation for discontinuous uptake kinetics was presented by Nissen. After reanalyzing the kinetic data of other researchers, using both logarithmic (Fig 2) and Lineweaver-Burk

transformations of the data, he hypothesized that the kinetics observed was due to the operation of a single complex transport system located in the plasmalemma (14, 15). As the external substrate concentration was increased, the transport system underwent abrupt transitions at discrete concentrations. Within each phase the system was thought to obey Michaelis-Menten kinetics, with the kinetic constants for each phase increasing in a fairly regular manner.

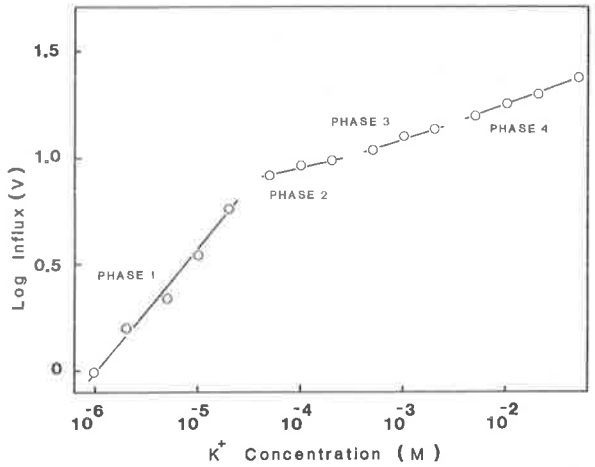


Fig 2. Uptake data from Fig 1 (Epstein, et al, 1963), replotted as log V versus log [$K^+$]. This is the form of analysis used by Nissen (14, 15) to determine the various phases associated with the multiphasic transport hypothesis.

**Criticisms of the Carrier-Kinetic Approach.** Despite the importance afforded carrier kinetics, this approach has been the subject of some fairly serious criticisms. A straightforward graphical presentation of kinetic data, ie, rate (V) *versus* substrate concentration ([S]), is easiest to interpret, but usually has a limited range on the [S] axis. To overcome this, several conventions have been followed, and each has its shortcomings. The procedure of breaking the concentration axis (see Fig 1) in order to present data both in the low and high concentration rangcs may be misleading, as it tends to suggest discontinuities where none may exist.

Alternatively, rate and concentration data have been plotted on logarithmic scales. Nissen has made considerable use of the log V *versus* log [S] plot depicted in Fig 2. However, curves resulting from such transformations do not lend themselves to straightforward analysis. The assumption that a non-linear log V *versus* log [S] plot is evidence for a transport system exhibiting discontinuous kinetics is not founded on any biochemical principle. In reality, sigmoidal log V *versus* log [S] plots are usually evidence for multiple enzymes catalyzing the same reaction (16).

The other kinetic transformation widely used is the Lineweaver-Burk plot (1/V *versus* 1/[S]). Straight line reciprocal plots are often taken as evidence for a transport mechanism following Michaelis-Menten kinetics; additionally, non-linear Lineweaver-Burk plots are often analyzed as the sum of multiple linear segments, each segment representing Michaelis-Menten kinetics. However, the Lineweaver-Burk plot is statistically suspect and can lead to distortion of the data (4, 16, 18). Equally spaced increments of [S], when plotted as 1/[S], tend to cluster close to the 1/V axis. Thus, there will be relatively fewer points at the high end of the 1/[S] scale, and these points will be quite influential in the analysis. Furthermore, small errors in V are magnified when the data are plotted as 1/V, and errors in V tend to be greatest at low [S] (16). Hence, data points that are most variable have a significant influence when analyzed using a Lineweaver-Burk plot. Dowd and Riggs (4) have studied the reliability of various linear plots using a computer to calculate the kinetic constants from each of 500 replicate experiments, which differed from one another only by the normally distributed error in V. The Lineweaver-Burk plot was found to be the least reliable kinetic transformation, and tended to give a deceptively good visual fit, even with poor data (4). Thus, unless the data clearly fit Michaelis-Menten kinetics, Lineweaver-Burk transformations are useful only as an initial form of analysis.

All of the kinetic studies discussed above were performed on a heterogenous complex tissue, the root, and not with purified enzymes. Hence, researchers have dealt with systems consisting of a multitude of cell types, each under different physiological states, with the problems of unstirred layers and diffusion limitation further confounding data interpretation. These problems have been addressed by Wyn Jones (18) and he points out the need to recognize the necessity for data replication and reproducibility. This is particularly so "if small differences, eg, Nissen's phases, are to be given any credence" (18). Unfortunately, much of the kinetic data on ion absorption has lacked any measure of variability, and reproducibility from experiment to experiment has rarely been reported. Furthermore, when standard errors have been presented, they have often been given as the average error for *all* data points and not as a measure of individual variability.

Borstlap (1) also has criticized these various kinetic approaches, and has argued that many of the multiphasic uptake curves could be explained equally well by models consisting of one or more Michaelis-Menten terms in conjunction with a linear term, particularly if biological variability and experimental error are not ignored. It becomes apparent, from the various criticisms considered in this section, that if reasonable progress is to be made, it is not sufficient to obtain kinetic data and attempt, via various mathematical manipulations, to deduce basic transport mechanisms. Primary kinetic data can only be a starting point from which various hypotheses can originate. From this point on, experiments must be designed to test the working hypothesis.

**Resolution of $K^+$ Influx Kinetics into a Saturable and First Order Component.** With these thoughts in mind, we decided to design an experimental system which would enable us to handle large numbers of root segments and uptake solutions, with a minimum of damage to the roots. We felt it imperative to generate numerous data points on the [S] axis, with enough replicates to obtain sufficiently precise values. Only then could we accurately evaluate the shapes of the kinetic curves for uptake of $K^+$ into corn roots. If abrupt discontinuities existed, the process of obtaining many data points within the concentration range of these discontinuities would enable us to study the underlying phenomenon responsible for these breaks. Through use of an uptake apparatus which could handle many root segments and solutions at one time, we were able to obtain accurate and reproducible results (9). Influx of $K^+$ ($^{86}Rb^+$ was used as the chemical

radioisotope analog because of its longer half-life of decay) in high salt-grown roots (seedlings grown on 5 *mM*KCl + 0.2 *mM* $CaSO_4$; calcium ions were included to maintain structural and transport integrity) is illustrated in Fig 3A; these kinetic curves were smooth and nonsaturating. The curves approached linearity at concentrations above 1 *mM*. In experiments in which we studied influx over a wider concentration range (0 to 50 *mM*), we observed no evidence for discontinuities or saturation.

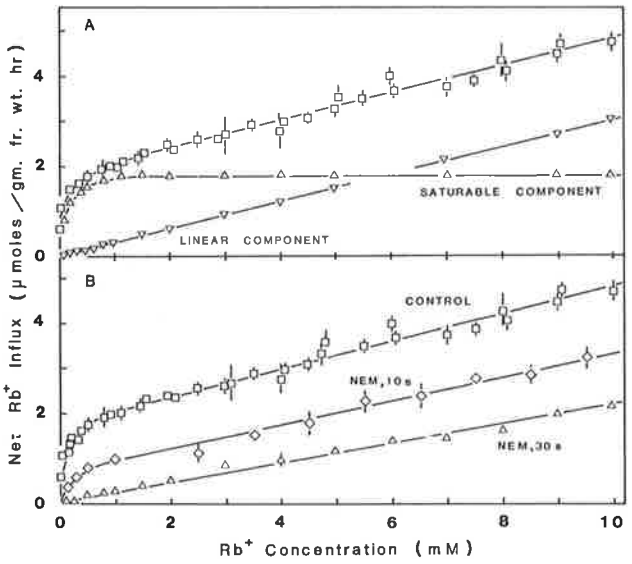


Fig 3. $^{86}Rb^+$ influx curves for corn root segments grown in 5 *mM* KCl + 0.2 *mM* $CaSO_4$ (high-salt status). All data points are the average of four replicates and error bars are ± SE. In A, the control influx curve (open squares) has been separated into its saturable and linear components. In B, the influence of NEM exposures on $^{86}Rb^+$ influx is depicted (see text). Corn roots were pretreated with NEM (0.3 *mM*) for 10 or 30 s, then washed for 10 min in 1 *mM* dithioerythritol (DTE: an -SH containing agent) prior to $^{86}Rb^+$ uptake. All uptake and pretreatment solutions contained 0.2 *mM* $CaSO_4$, 1 *mM* MES buffer (pH 6.5), in addition to RbCl, NEM, or DTE (9).

The kinetic profile presented in Fig 3A (see curve indicated by open squares) can be interpreted in several ways. (a) Göring and coworkers have argued that complex influx kinetics, whether smooth or discontinuous, could be due to the effects of diffusion-limited availability of substrate to the transport system(s) (8). Uptake at low substrate concentration would be due to transport into epidermal cells, while uptake at higher concentration would be the result of absorption by identical carriers located in cortical cells within the root. The interplay of diffusion and uptake would tend to change saturation kinetics to a more complex profile. (b) A transport system in which allosteric regulation is operating would also generate the observed kinetics. In such a system, the binding of an effector ($K^+$) to a subunit of the transporter induces a conformational change such that the affinity of other substrate binding sites is reduced (ie, negative cooperativity). (c) Finally, kinetics such as those in Fig 3A could be due to the sum of two separate transport mechanisms, one exhibiting *saturation* [$V_{max}$ S/(S + $K_m$)] and the other exhibiting *first-order* kinetics (kS). Such a model can be expressed as:

$$V = V_{max} S/(S + K_m) + kS$$

where V is the rate, S the concentration, $V_{max}$ and $K_m$ the Michaelis-Menten constants, and k the first-order rate coefficient. We computed the first-order kinetic component (kS), and its subtraction from our data yielded a saturable curve (Fig 3A).

The effects of N-ethyl maleimide (NEM) and p-chloromercuribenzene sulfonic acid (PCMBS) on $K^+$ influx were studied because they are reagents that react with -SH groups in proteins, and it has been well-documented that -SH groups are often involved at the active sites of both enzymes and transport proteins (17). NEM inhibited the saturable component, but the first-order kinetic component was almost unaffected (Fig 3B). In high-salt grown roots, a 10 s pulse with 0.1 *mM* NEM prior to uptake reduced the saturable component $V_{max}$ by 60%. A 30 s exposure to 0.3 *mM* NEM totally abolished the saturable component, while only reducing the linear component by 30%. PCMBS elicited the same general inhibitory trends; in high-salt roots the saturable component was inhibited, and again the linear component was unaffected.

These results, obtained on corn roots, offer strong support for the third hypothesis presented above. It would appear that as NEM (or PCMBS) exposure increased, more of the saturable carriers reacted with this reagent until they were all inhibited, while the linear component transport system exhibited limited -SH sensitivity. Such results argue against a single allosterically-regulated transporter, or the complex transport mechanism championed by Nissen (14, 15). It may still be argued, however, that the complex kinetics are the product of the interplay of diffusion and active uptake. Possibly, saturable component uptake may be due to absorption into epidermal cells, while linear component influx may represent diffusion-limited uptake by cortical cells. In order to test this latter possibility, we isolated protoplasts from corn root cortices. The kinetic profiles for $K^+$ influx in protoplasts were identical in shape to those obtained using root segments (10). These results clearly suggest that the observed complex, nonsaturation kinetics is due to uptake by single cells, and that the two kinetic components represent different cellular transport mechanisms.

At this point it is important to illustrate just how misleading graphical manipulations of kinetic data can be. The kinetic data presented in Fig 3 appears to be quite smooth, with no apparent discontinuities. If one takes the kinetic parameters calculated from the saturable and linear components one can generate a continuous, smooth curve, which closely fits our experimental data. Fig 4 is the result of plotting this calculated data as log V *versus* log [S]. This curve can be divided into four linear segments (phases) and deemed discontinuous, yet the original data were continuous!!

**Is the Linear Component of Physiological Importance?** The existence of a kinetically-derived mechanism that does not appear to saturate (ie, the linear component) deserves some comment. There have been many examples of transport kinetics in bacteria, animals, and plants in which a linear component makes a significant contribution (9, and references therein). The linear component has routinely been dismissed as passive diffusion or ex-

change diffusion, and not considered to be of physiological relevance. However, in our system, it would appear that linear uptake may be due to a fairly complex, carrier-mediated mechanism. First, $K^+$ uptake via the linear component is quantitatively significant. It is unlikely that an ion such as $K^+$ would rapidly diffuse across the lipid portion of plant membranes.

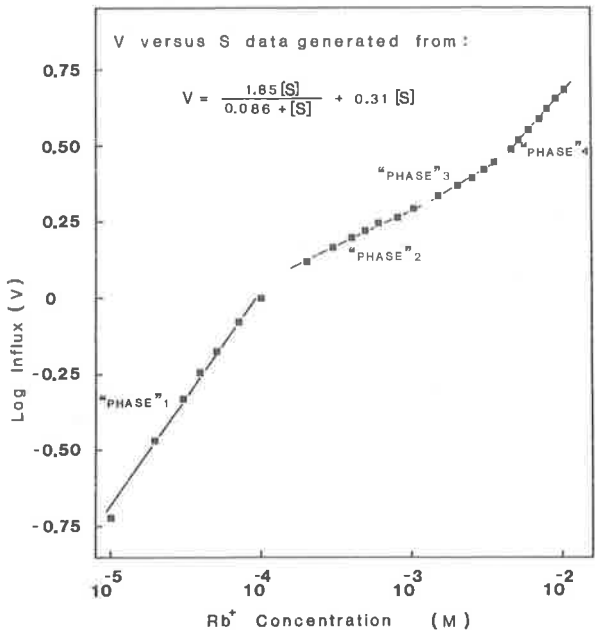


Fig 4. Log V versus log [$Rb^+$] plot for kinetic data generated from equation shown. Kinetic parameters ($K_m$, $V_{max}$, k) were calculated from the saturable and linear components illustrated in Fig 3A, and these were then used to compute this theoretical curve.

However, as stated above, the linear component may reflect the presence of a facilitated diffusion (a membrane carrier that moves substrate *passively* down the chemical or electrochemical gradient of that substrate) or exchange diffusion mechanism, which could be a transmembrane channel. Any system driven by exchange diffusion (the one-for-one exchange of internal for external substrate) should be influenced by either internal or external substrate concentrations. In our system, the linear component was identical in roots varying significantly in internal $K^+$ concentrations (low- versus high-salt roots). Also, changes in external $K^+$ from 0.2 to 10 *mM* had no effect on $K^+$ efflux. This is in contrast to $Cl^-$ efflux, which has been shown to be stimulated by external $Cl^-$, thereby leading to the postulation of a $Cl^-$ exchange diffusion system at the plasmalemma (2).

In addition, the linear component exhibited some interesting sulfhydryl interactions. NEM has been shown, in some systems, to cause a dramatic depolarization of the membrane potential (12, 13), and such a depolarization would reduce the driving force for *passive* $K^+$ influx. However, in our experiments, NEM caused only a slight reduction in the linear component. PCMBS has also been shown to depolarize the membrane potential (12, 13), and it had no effect on the linear component in high-salt roots, while consistently stimulating (by 40%) the linear component in low-salt roots. These conflicting sulfhydryl effects are interesting and difficult to interpret, but suggest a complex transport mechanism.

**Concluding Remarks.** Initially, research in the field of plant ion transport (ie, carrier-kinetics) yielded considerable insight into the physiology of transport. However, in recent years there has been an overemphasis on mathematical and graphical manipulations of primary experimental data. These studies have contributed little towards resolving the controversies concerning carrier kinetics. We have attempted to demonstrate in this article that merely plotting V *versus* [S] (in a conventional manner) or employing any of the standard kinetic transformations, is not sufficient to determine whether the kinetics is due to multiple Michaelis-Menten systems; Michaelis-Menten systems plus a linear component; or to a single, complex transport process.

If breakthroughs are to be made concerning the mechanisms by which ions are transported into and across roots, it is now necessary to integrate experimental approaches derived from a wide range of research areas, including transport kinetics, membrane biochemistry, biophysics and genetics (transport mutants). Recent advances in microelectrode technology make it possible (and necessary) to combine studies involving ion-specific microelectrodes, micro-pH electrodes, electrophysiology, and extracellular ion current mapping with the more traditional ion flux techniques. Furthermore, the time has come for the plant anatomists and researchers specializing in structure/function to join forces with the transport physiologists and biophysicists. Hence, it will be possible to utilize current innovative electron microscope technology, such as cryotechnique, X-ray microanalysis, immunocytochemistry, and high-resolution computer image analysis to gain further understanding in this area. The authors feel that only by drawing from a diverse and wide range of research areas, in an integrative and synergistic manner, will the next pieces of the puzzle involving the mechanism(s) and regulation(s) of plant ion transport fall into place.


1) Borstlap AC 1981 Plant Cell Envir 4:189-195
2) Cram WJ 1968 Biochim Biophys Acta 163:339-353
3) Debnam ES, RJ Levin 1975 J Physiol 246:181-196
4) Dowd JE, DS Riggs 1965 J Biol Chem 240:863
5) Epstein E 1972 *Mineral Nutrition of Plants: Principles and Perspectives.* John Wiley & Sons, New York
6) Epstein E, CE Hagen 1952 Plant Physiol 27:457-474
7) Epstein E, et al 1963 Proc Natl Acad Sci USA 49:684-692
8) Göring H 1976 Wiss Z. Humboldt - Univ Math - Naturwiss Reihe 25:61-65
9) Kochian LV, WJ Lucas 1982 Plant Physiol 70: 1723-1731
10) Kochian LV, WJ Lucas 1983 Plant Physiol In Press
11) Laties GG 1969 Annu Rev Plant Physiol 20:89-116
12) Lichtner FT, et al 1981 Plant Physiol 68:899-904
13) Lucas WJ, JM Alexander 1980 Plant Physiol 65:274-280
14) Nissen P 1973 Physiol Plant 28:113-120
15) Nissen P 1974 Annu Rev Plant Physiol 25:53-79
16) Segel IH 1975 *Enzyme Kinetics.* John Wiley & Sons, New York, pp 208-210
17) Webb JL 1966 *Enzymes and Metabolic Inhibitors,* Vol. III. Academic Press, New York, pp 336-365
18) Wyn Jones RC 1975 *In* DA Baker and JL Hall, eds, *Ion Transport in Plant Cells and Tissues.* North Holland Publishing Co, pp 193-229



**What's New in Plant Physiology** publishes a monthly review of up to 3,000 words on a timely topic of interest to plant scientists. **If you wish to write one in your area of expertise please consult first with the Editor, George Fritz,** Agronomy Dept/Bldg 857/Museum Rd, University of Florida, Gainesville FL 32611 USA. **1982 Prices are USA Individual $7 Foreign Individual $10, Libraries - US or Foreign $20,** (Airmail option for foreign addresses: add $5), payable by US bank draft or International Money Order to **WNPP** at th above address.


Copyright **©1982 by George Fritz. All Rights Reserved.**


1982 December issue, Volume 13, #12, printed 1983 April. USPS 414-530. ISSN 0193-0648. **Postmaster** return changes of address to What's New in Plant Physiology, Agronomy Dept/Bldg 857/Museum Rd, University of Florida, Gainesville FL 32611 USA. Second class postag paid at Gainesville FL and additional mailing offices.

Plant Physiol. (1983) 73, 208–215
0032-0889/83/73/0208/08/$00.50/0

# Potassium Transport in Corn Roots[1]

## II. THE SIGNIFICANCE OF THE ROOT PERIPHERY

Received for publication December 15, 1982 and in revised form May 7, 1983

LEON V. KOCHIAN AND WILLIAM J. LUCAS
*Department of Botany, University of California, Davis, California 95616*

### ABSTRACT

**The relative transport capabilities of the cells of the root periphery and cortex were investigated using a variety of experimental techniques. Brief (30 seconds to 1 minute) exposures with the penetrating sulfhydryl reagent, *N*-ethyl maleimide (NEM), and the impermeant reagent, *p*-chloromercuribenzene sulfonic acid (PCMBS), dramatically reduced $^{86}Rb^+$ (0.2 millimolar RbCl) uptake into 2 centimeter corn (*Zea mays* [A632 × (C3640 × Oh43)]) root segments. Autoradiographic localization studies with [$^3$H]NEM and [$^{203}$Hg]PCMBS demonstrated that, during short term exposures with either reagent, sulfhydryl binding occurred almost exclusively in the cells of the root periphery.**

**Corn root cortical protoplasts were isolated, and exhibited significant $K^+$($^{86}Rb^+$) influx. The kinetics for $K^+$ uptake were studied; the influx isotherms were smooth, nonsaturating curves that approached linearity at higher $K^+$($Rb^+$) concentrations (above 1 millimolar $K^+$). These kinetics were identical in shape to the complex kinetics previously observed for $K^+$ uptake in corn roots (Kochian, Lucas 1982 Plant Physiol 70: 1723–1731), and could be resolved into a saturable and a first order kinetic component.**

**The existence of a hypodermal apoplastic barrier was investigated. The apoplastic, cell wall binding dye, Calcofluor White M2R, appeared to be excluded from the cortex by the hypodermis. However, experiments with damaged roots indicated that this result may be an artifact resulting from the binding of dye to the epidermal cell walls. Furthermore, [$^{203}$Hg] PCMBS autoradiography demonstrated that the hypodermis was not a barrier to apoplastic movement of PCMBS.**

**These results suggest that although cortical cells possess the capacity to absorb ions, $K^+$ influx at low concentrations is limited to the root periphery. Cortical cell uptake appears to be repressed under these conditions. At higher concentrations, cortical cells may function to absorb $K^+$. Such a model may involve regulation of cortical cell ion transport capacity.**

The pathway of ion movement from the soil solution to the stele is thought to involve both the symplast and apoplast of the root cortex. Both epidermal and cortical cells may be able to absorb ions from the cell wall solution. Thus, ions are believed to move to the endodermis via either diffusion through the root free space, or by symplastic movement, presumably through the plastmodesmata, or by a combination of the two routes. Influx across the plasmalemma of any of the cells lining the free space would allow entry into the symplast; subsequent flux across the endodermis would proceed exclusively via the symplast. Although this model has general acceptance (5, 7, 15, 27), dissension does exist in the literature.

The ability of root cortical cells to absorb ions from the apoplastic solution has been questioned. Vakhimistrov (28) has suggested that the cortical cells play an insignificant role in ion uptake, with most transport occurring at the epidermal cells. Using a theoretical model for $Rb^+$ uptake in barley roots, Bange (3) found that the model only generated reasonable uptake kinetics when transport was restricted to the epidermis. The recent work of van Iren and Boers-van der Sluij (29) also supports this hypothesis. Their work was based on the assumption that plasmolysis severs plasmodesmata, and therefore would symplastically isolate each cortical and epidermal cell of a barley root. Autoradiographic localization of $^{86}Rb^+$, accumulated following plasmolysis, was generally limited to the root periphery.

Some workers have also suggested that the kinetics usually presented for ion uptake into roots may be explained as the basis of a complex interplay between diffusion and uptake within a multilayered tissue (4, 6, 10, 21, 25, 26). In the model presented by Göring and coworkers (6, 10), uptake at low concentrations would approximate the saturation kinetics of carriers located at the root periphery, whereas uptake at higher concentrations would be complicated by diffusion-limited availability of ions for carriers located within the cortex. In support of this hypothesis, Grunwaldt *et al.* (12) found that in corn roots, osmotic shock selectively damaged the cells of the root periphery. Following such a treatment, phosphate uptake was severely inhibited only at low external phosphate concentrations (13).

In the older roots of most monocots and some dicots, the presence of a hypodermis has been demonstrated (8, 9, 22). In detailed work involving fluorescence microscopy of cell walls and studies on the movement of apoplastic dyes in corn and onion roots, Peterson and coworkers have demonstrated that the hypodermis appears to be an apoplastic barrier to the diffusion of high mol wt dyes which bind to cell walls (22–24). Furthermore, they found that all radial and transverse walls of the hypodermis contained what appeared to be a Casparian band. Although most of this work has been done with the older root regions, the possibility exists that such an apoplastic barrier could be present in the regions engaged in ion uptake. Such a barrier could cause uptake to occur primarily at the root surface, even though cortical cells have the ability to absorb ions.

Any attempt to integrate anatomical and physiological evidence to produce a coherent model for ion movement through the root gives rise to a complicated scheme. In part, this complexity is due to the ambiguity which exists concerning the basic mechanism(s) by which ions are transported across the plasmalemma. In a recent study of the kinetics of $K^+$ transport into corn roots, we presented data consistent with uptake being due to the combined effect of a saturable and first order kinetic process (14). Brief exposure (30 s) of the root to sulfhydryl reagents caused a dramatic inhibition of $K^+$ uptake. This indi-

[1] Supported by National Science Foundation Grant PCM 8117721 to W. J. L. and by a National Science Foundation predoctoral fellowship and a Jastro-Shields Research Award to L. V. K.

cated that these sulfhydryl reagents could be used to further resolve the question concerning the site of entry of $K^+$ into the root symplast. In the present paper, we have used these reagents, along with a wide range of other experimental techniques, to investigate the relative contribution of the root periphery and cortex to $K^+$ uptake in corn roots. These studies indicate that individual cells of the epidermis and cortex have the ability to transport $K^+$. However, under physiological conditions, the epidermis appears to be the main site of $K^+$ entry into the root symplast.

## MATERIALS AND METHODS

**Plant Material.** *Zea mays* seeds (A632 × [C3640 × Oh43], Crows Hybrid Corn Co., Milford, IL) were imbibed, germinated, and grown by the methods previously outlined (14). Seedlings were either grown on a 0.2 mM $CaSO_4$ solution (low salt conditions) or 0.2 mM $CaSO_4$ + 5 mM KCl (high salt conditions). Primary roots of 5-d-old seedlings were used for all experiments.

**Influx Experiments.** Short term (10 or 30 min) $^{86}Rb^+$ influx experiments were performed using 2-cm root segments as detailed previously (14). Briefly, experiments were performed with 2-cm root segments cut from the 1st through 8th cm of the primary root. Uptake was initiated by the addition of $^{86}Rb^+$ (as RbCl; New England Nuclear) and terminated by the vacuum withdrawal of radioisotope solution. Free space radiolabel was removed by two 8-min washes in ice cold 0.5 mM $CaSO_4$ + 1 mM RbCl.

In experiments examining the effects of various exposures of the permeant (NEM[2]) and impermeant (PCMBS) sulfhydryl reagents on $Rb^+$ influx, the protocol was identical with that previously described (14). Additionally, $^{86}Rb^+$ uptake kinetic studies were performed on segments cut from intact low salt roots and from roots which had been split in half. A special apparatus was constructed which enabled us to position a root in place, pierce the longitudinal axis of the root with a surgical blade, and pull the root past the edge of the blade. Thus, we were able to split roots cleanly and precisely into 10-cm long half roots. These half-roots were cut into 2-cm segments prior to being used in uptake experiments.

**NEM Effects on Respiration.** Root respiration was followed by measuring $O_2$ consumption with a Clark $O_2$ electrode and monitor (Rank Bros.; Cambridge, England). Two-cm root segments were washed for 4 h and then 0.1 g of root tissue was placed in 4 ml of air-saturated solution (0.2 mM $CaSO_4$). $O_2$ consumption was measured for 20 min at 25°C. NEM was added to a final concentration of 0.3 mM, and after various exposures, DTE (1 mM final concentration) was added to bind unreacted NEM. Stable $O_2$ consumption was measured for at least 20 min following NEM treatment.

**[$^3$H]NEM Microautoradiography.** The degree of movement of NEM into the root cortex was measured by performing microautoradiography on corn roots exposed to [$^3$H]NEM. Two-cm root segments from the 3rd through 5th cm of the main root of 5-d-old low salt roots were placed in a solution consisting of 0.2 mM $CaSO_4$, 1 mM Mes (pH 6.5), and 0.3 mM [$^3$H]NEM (200 μCi/ml; New England Nuclear) for periods of 10 s, 30 s, 1, 2, or 5 min. At the end of each exposure, the roots were washed in an excess volume of 1 mM DTE. Two-mm-long sections were excised from the center of each segment and fixed in 1.25% gluteraldehyde for 5 h at 4°C. The sections were rinsed and postfixed in 1% $OsO_4$ for 2 h at 25°C. The tissue was then dehydrated in a graded acetone series and embedded in Spurr's resin. Thick sections (3 μm) were cut and glued onto glass slides. The slides were then dipped in Kodak Nuclear Track Emulsion NTB3 at 40°C, and allowed to dry. The slides were exposed for up to 17 d at −20°C and developed in Kodak Dektol developer. Control sections (no [$^3$H]NEM treatment) were processed in an identical manner.

To quantify the distribution of autoradiographic grains in the sections, the microscopic images were analyzed with an Imanco Quantimet 720 Image Analyzing Computer (Cambridge Instruments; Cambridge, England).

**[$^{203}$Hg]PCMBS Microautoradiography.** Two-cm root segments from the 3rd through 5th cm of the main root of low and high salt-grown roots were placed in a solution consisting of 0.2 mM $CaSO_4$, 1 mM Mes (pH 6.5), and 2 mM [$^{203}$Hg] PCMBS (40 μCi/ml; Amersham Corp.) for 1, 2, 10, or 20 min. At the end of each PCMBS exposure, the roots were briefly rinsed in 25 ml of 0.2 mM $CaSO_4$ + 1 mM Mes (pH 6.5), and subsequently washed (10 min) in 25 ml of identical solution. Two segments were used per treatment.

Unlike NEM, PCMBS forms reversible linkages with sulfhydryls. Therefore, it was necessary to freeze-substitute the PCMBS-treated tissue to prevent movement of radiolabel. Following the wash, root segments were rapidly frozen in slushy liquid $N_2$ and then placed into vials containing dry acetone at −70°C for 7 d to allow for dissolution of tissue ice. The vials were then warmed to 25°C, dry acetone was changed twice, and then segments were embedded in Spurr's resin. Sections were cut (1 μm) dry from the central region of the root segments and placed on a drop of ether on a glass slide. The evaporation of the ether caused the adherence of the section to the slides. The slides were then dipped in Kodak Nuclear Track Emulsion NTB2, and exposed at 4°C for up to 32 d. Slides were developed with Kodak D-19 developer and analyzed for autoradiographic grain distribution as in the preceding section. Because the freeze-substituted tissue was unstained, the outline of each cell was poorly resolved during microscopic examination. Therefore, cell walls were stained by placing a drop of 0.2% Azur-B stain in 0.1% $Na_2CO_3$ over the sections following development of the photographic emulsion. The dye was washed off after 20 s, and resulted in a light staining of cell walls.

**Investigation of Root Hypodermis.** The fluorescent, impermeant dye, Calcofluor White M2R (Polysciences, Inc., Warrington, PA), which binds to cell walls, was used to investigate the potential existence in the root periphery of an apoplastic diffusion barrier. The methods of Peterson *et al.* (23) were employed. Briefly, either (a) intact root systems, (b) roots in which the hypodermis was ruptured by scoring with a needle along the terminal 10 cm, or (c) roots with the terminal 10 cm split longitudinally (using apparatus previously described) were immersed in a solution consisting of 0.1% Calcifluor, 0.2 mM $CaSO_4$, and 2 mM Mes-Tris (pH 7.0) for 18 to 24 h. The roots were then washed in running tap water for 1 to 2 h to remove unbound dye. Freehand cross sections were taken from the region approximately 5 cm behind the root tip and placed in a drop of nonfluorescent immersion oil. The sections were immediately observed with a Zeiss photomicroscope fitted with epifluorescence optics. Zeiss UGl excitation and barrier 53 filters were used.

**Corn Root Protoplast Isolation.** Protoplasts were isolated from the cortex of *Z. mays* roots by the methods of Lin (17) and Gronewald and Leonard (11), with minor modifications to minimize the release of epidermal protoplasts. Briefly, the terminal 10 cm of 5-d-old low salt roots were used for all experiments. The root apex was removed and the stele was pulled from the root, leaving the root cortex and epidermis intact. About 12 g of root cortex was collected, cut into 2-mm sections, and placed into digestion solution consisting of 0.6 M mannitol, 1 mM $CaCl_2$, 0.1% (w/v) Pectolyase Y-23 (Seishin Pharm., Chiba-Ken, Japan),

[2] Abbreviations: NEM, *N*-ethyl maleimide; PCMBS, *p*-chloromercuribenzene sulfonic acid; DTE, dithioerythritol; ANDA, 7-amino-1,3-naphthalene disulfonic acid; PTS, trisodium, 3-hydroxy-5,8,10-pyrene-trisulfonate.

2.0% (w/v) Cellulysin (Calbiochem), 0.05% (w/v) BSA (Sigma), and 0.5 mM DTT (pH 5.5). All solutions used for isolation were sterilized by passing through a 0.45-$\mu$m Millipore filter prior to use. Root material (3 g) was incubated in 20 ml of digestion solution for 2 h at 29°C with gentle shaking (50 cycles/min).

Following digestion, the resultant mixture was filtered through two layers of cheesecloth saturated with suspension solution [0.7 M Mannitol, 25 mM Mes-Tris (pH 5.5), 0.2 mM $CaCl_2$, 0.5 mM DTT]. The undigested material was resuspended in 20 ml of suspension solution and gently agitated to release cortical protoplasts. Very gentle agitation was used to minimize release of epidermal protoplasts.

The filtrates were combined and centrifuged at room temperature for 8 min at 350$g$. The protoplast pellet was gently resuspended in suspension solution and recentrifuged (8 min, 350$g$). The pellet was again gently resuspended, in 7 ml of 10% (w/v) Ficoll (type 400; Sigma) in suspension solution, and overlaid with successive layers consisting of 7 ml of 8, 5, and 0% Ficoll in suspension solution. The step gradient was centrifuged at 360$g$ for 18 min and protoplasts collected at the interface of the 0 and 5% Ficoll layers. The protoplasts were diluted with suspension solution and pelleted at 360$g$ for 8 min. The final pellet was resuspended in a solution consisting of 0.7 M mannitol, 0.2 mM $CaCl_2$, and 2 mM Mes-Tris (pH 6.5).

The root tissue which remained following digestion was examined using Nomarski microscopy with a Zeiss Photoscope III to determine the degree to which the epidermal cells retained their protoplasts.

**$^{86}Rb^+$ Protoplast Influx Experiments.** The kinetics of $K^+(^{86}Rb^+)$ influx were studied following the methods of Mettler and Leonard (20) and Gronewald and Leonard (11), with minor modifications. Briefly, influx at 23°C was measured from solutions which contained 0.2 mM $CaCl_2$, 2 mM Mes-Tris (pH 6.5), RbCl (0.05–10 mM), and approximately 0.7 M mannitol. The osmotic concentration of each uptake solution was measured with a Wescor 5100C vapor pressure osmometer (Wescor, Inc., Logan, UT) and osmotically adjusted to 720 ± 5 mOsm/kg. Protoplasts were added to a final concentraton of 500,000/ml and uptake was initiated by the addition of $^{86}Rb^+$ (0.4 $\mu$Ci/ml). Final uptake volume was 1 ml. The protoplasts were allowed to accumulate radioisotope for 15 min with agitation (50 cycles/min). Uptake was terminated by pipetting the entire 1 ml volume onto a step gradient consisting of 5 ml of 0.7 M mannitol, 2 mM Mes-Tris (pH 6.5), 1 mM $CaCl_2$, and 10 mM KCl, laid on top of 3 ml of 2% Ficoll in 0.7 M mannitol. The step gradients were contained in 12-ml plastic conical centrifuge tubes. The protoplasts were pelleted by centrifugation at 1000$g$ for 10 min, the gradient solutions removed by vacuum aspiration, and the pellet resuspended in 1 ml of water. A 100-$\mu$l aliquot was used for Lowry protein determination; the remaining 0.9 ml were added to 10 ml of 5 mM ANDA and radioactivity determined using a Beckman LS9800 scintillation counter.

## RESULTS

**Influence of Sulfhydryl Modifiers on $K^+(^{86}Rb^+)$ Influx and Respiration.** The effect of increasing exposures of the permeant sulfhydryl reagent, NEM, on influx from a 0.2 mM RbCl solution was investigated. NEM rapidly inhibited influx; a 30-s exposure to 0.3 mM NEM inhibited $Rb^+$ uptake by 75 to 95% (Fig. 1A). Such a short NEM exposure would be expected to influence primarily the cells of the root periphery. Since NEM has been shown to inhibit a number of cellular processes, including respiration (31), we examined its effect on root respiration (Table I). The 30-s NEM pulse, which dramatically reduced $Rb^+$ uptake, had no effect on root respiration; significant inhibition was not observed until the tissue was exposed for 2 min or longer.

Because NEM can influence a number of processes, both at the plasmalemma and inside the cell, the effect of the impermeant sulfhydryl reagent, PCMBS, on $K^+(^{86}Rb^+)$ uptake was also studied (Fig. 1B). Again, a rapid inhibition of influx was observed. A 1-min exposure with 2 mM PCMBS inhibited uptake from 0.2 mM RbCl by 70 to 85%. Inhibition by sulfhydryl modification (both NEM and PCMBS) was reversed by DTE treatment (2 mM). Significant recovery occurred only after a period of 4 h: under 0.2 mM $K^+$ conditions, influx returned to 65% of the control value; a value of 80% of control was obtained for 10 mM $K^+$ conditions.

At low $K^+$ concentrations, where uptake may be limited to the epidermis because of diffusion limitations and ion depletion by the root surface, sulfhydryl modification rapidly abolished $K^+$

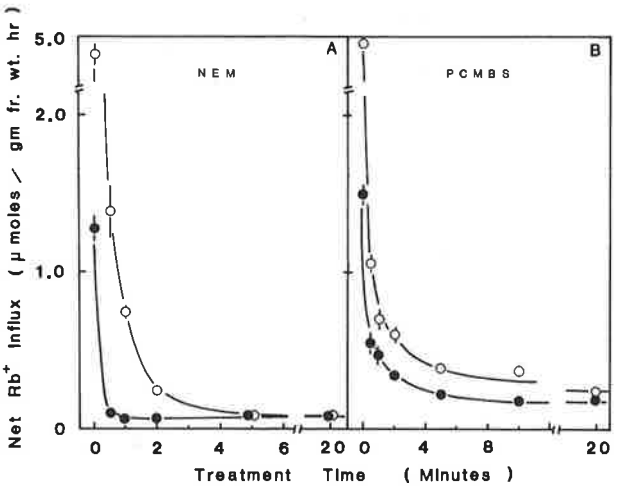


FIG. 1. NEM- and PCMBS-induced inhibition of $^{86}Rb^+$ influx (0.2 mM RbCl) for corn root segments grown in 0.2 mM $CaSO_4$ (low salt status [○]) or in 5 mM KCl + 0.2 mM $CaSO_4$ (high salt status [●]). The sequence of experimental procedures was as follows. A, Root segments were pretreated in 0.3 mM NEM for indicated time, then given a 10-min wash in 1 mM DTE. Root segments were then washed in 0.2 mM $CaSO_4$ + 1 mM Mes (pH 6.5) prior to uptake to remove DTE. B, Root segments were pretreated in 2 mM PCMBS for indicated time, then given a 10-min wash in 0.2 mM $CaSO_4$ + 1 mM Mes (pH 6.5) prior to uptake. Pretreatment solutions contained 0.2 mM $CaSO_4$ + 1 mM Mes (pH 6.5) in addition to NEM, PCMBS, or DTE. Uptake solution contained 0.2 mM RbCl, 0.2 mM $CaSO_4$, and 1 mM Mes (pH 6.5). All data points in this figure and subsequent ones (except Fig. 7) are the average of four replicates; the error bars are ± SE. Points which lack error bars do so because the SE were smaller than symbols used.

Table I. *Effect of Various NEM Exposures on Root Respiration*

Respiration was followed by monitoring $O_2$ consumption in a Clark-type $O_2$ electrode. After control root respiration was measured for 20 min, NEM was added to a final concentration of 0.3 mM. Roots were exposed to NEM for the desired length of time, and then DTE was added to a final concentration of 1 mM. After respiration stabilized at its subsequent value, $O_2$ consumption was followed for an additional 20 min. The resultant respiration values are listed as per cent of control.

| Treatment | Respiration |
|---|---|
| | *% of Control* |
| Control | 100[a] |
| Control + DTE | 100 |
| 30 s NEM + DTE | 100 |
| 1 min NEM + DTE | 96 |
| 2 min NEM + DTE | 78 |
| 5 min NEM + DTE | 57 |
| 20 min NEM | 39 |

[a] Average control respiration was 18.0 $\mu$mol $O_2$/g fresh weight·h.

uptake. The time course for NEM inhibition from more concentrated $K^+$ solutions (1 or 10 mM) was next studied. Under these conditions, diffusion of substrate into the cortex may allow these cells to contribute to $K^+$ transport into the tissue. In high salt-grown roots, maximal inhibition of uptake was achieved with an NEM exposure of approximately 30-s, irrespective of the substrate concentration (Fig. 2B). However, maximal inhibition of uptake in 10 mM RbCl was 50% of the control and exposures of up to 20 min did not result in further inhibition. This correlates with our earlier work (14) in which we showed that sulfhydryl modifiers influence the kinetics of $K^+$ uptake by abolishing what was interpreted as a saturable component of transport; the linear component was relatively insensitive to sulfhydryl inhibition. In high salt roots, the linear component was responsible for about 50% of the observed uptake when 10 mM RbCl was present. In low salt-grown roots, the inhibition was slightly different. A 30-s NEM pulse inhibited uptake from 10 mM RbCl by only 30%. Prolonging the exposure to NEM resulted in further inhibition (Fig. 2A). Maximal inhibition occurred after exposures of 6 min or longer, and resulted in a 75% inhibition. This result is also consistent with our previous data (14).

**Localization of NEM and PCMBS in the Root.** To determine if the brief NEM or PCMBS pulses were binding primarily at the root periphery, autoradiography was performed on roots exposed to [$^3$H]NEM and [$^{203}$Hg]PCMBS. Figure 3 demonstrates the spatial location of [$^3$H]NEM in the root following a 30-s or 5-min exposure. A 30-s NEM pulse produced a binding pattern localized predominantly in the epidermis, with a smaller amount of label in the hypodermis (Fig. 3A). A relatively diffuse and low level of activity was distributed throughout the rest of the root. To quantify the distribution of radiolabel, the autoradiographs were analyzed using an Imanco Quantimet 720 Image-Analyzing computer. Numerous cross-sections were analyzed and the data averaged and presented in histogram form (see fig. 3). Analysis of the 30-s NEM treatment verified that almost all of the label was localized in the root periphery. The low, fairly constant level of label throughout the rest of the root (4%) was due to computer detection of the cell walls, as verified by analysis of control sections (data not shown). By comparison, both the autoradiograph and image analysis, after a 5-min NEM pulse, showed that significant amounts of [$^3$H]NEM were bound to cells throughout the root (Fig. 3B).

Because NEM can penetrate and move within the symplast, it was necessary to repeat the autoradiographic experiments with the impermeant [$^{203}$Hg]PCMBS. Following a 1-min [$^{203}$Hg]

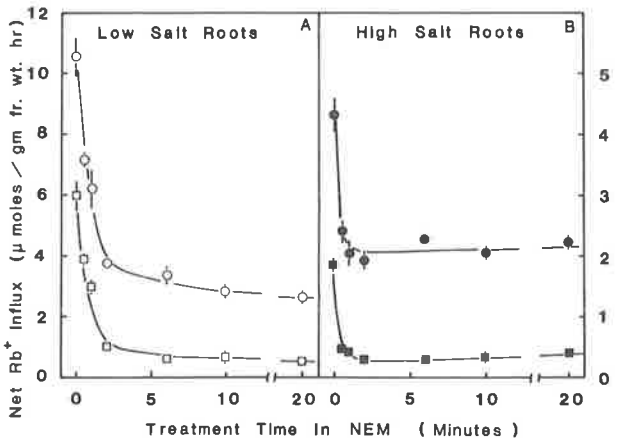


FIG. 2. NEM-induced inhibition of $^{86}Rb^+$ influx for low salt-grown and high salt-grown corn roots. A, Low salt-grown root uptake from either 1 mM RbCl (□) or 10 mM RbCl (○). B, High salt-grown root uptake from either 1 mM RbCl (■) or 10 mM RbCl (●). Experimental pretreatments and solutions are as described in Figure 1.

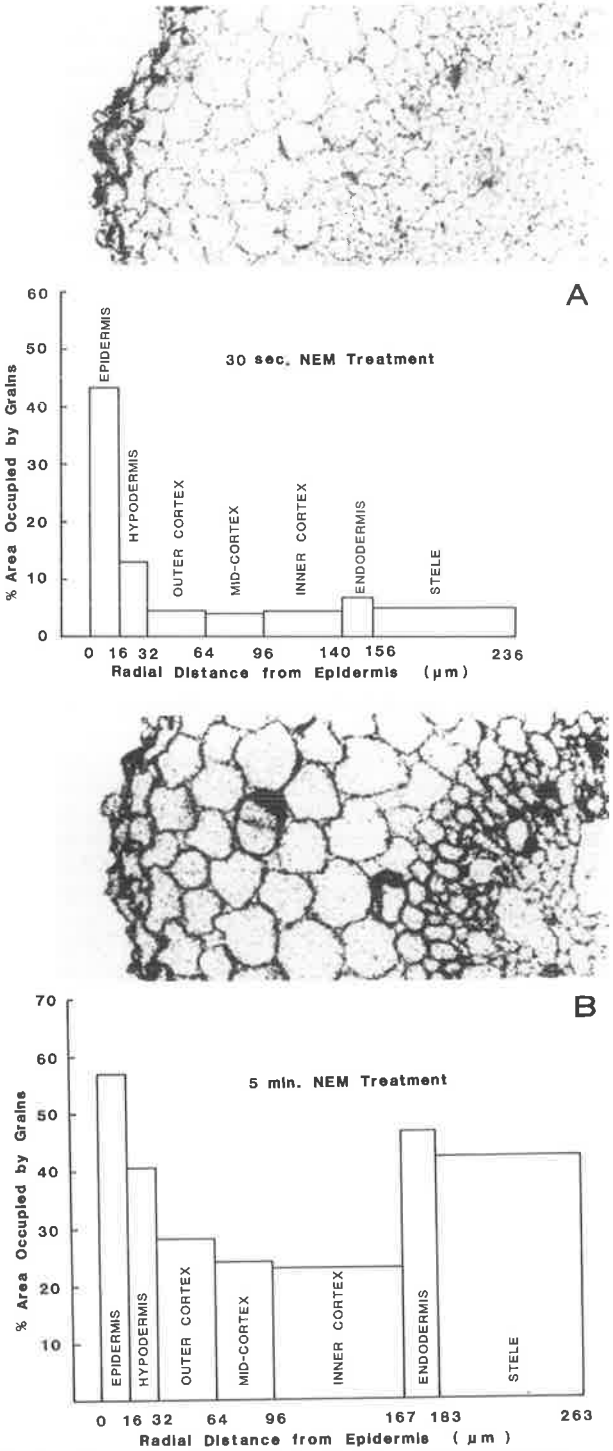


FIG. 3. Microautoradiographic localization of [$^3$H]NEM (0.3 mM) in a corn root following exposures of 30 s (A) or 5 min (B). Experimental pretreatments are as described in Figure 1. Each micrograph is representative of the grain distribution for that particular exposure. Numerous root cross-sections from each NEM treatment were analyzed for grain distribution with an Imanco Quantimet 720 Image Analyzing Computer. The data were averaged and presented in the histograms located below each micrograph. Because the histograms represent an average obtained from many cross-sections, radial distance into the root had to be normalized to account for variations in root diameter. Therefore, the labels above the histograms, which denote various root regions encountered as one moves radially into the root, do not always match exactly with the corresponding micrographs (× 470).

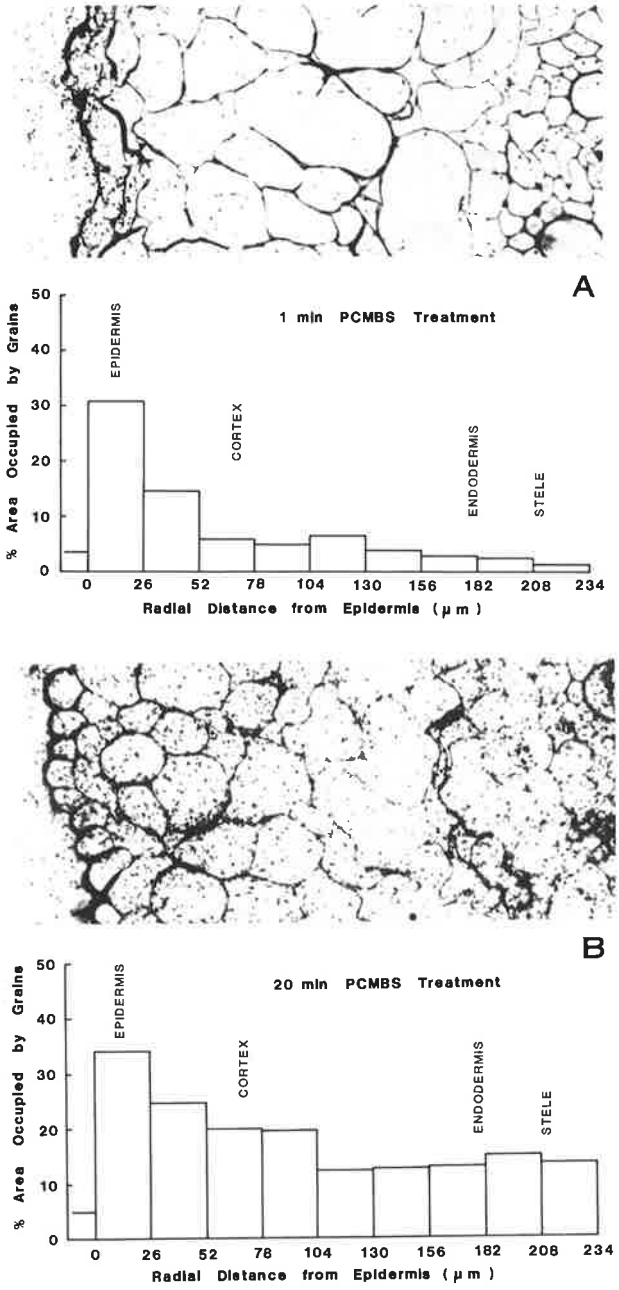


FIG. 4. Microautoradiographic localization of [$^{203}$Hg]PCMBS (2 mM) in the corn root following exposures of 1 min (A) or 20 min (B). Experimental pretreatments are as described in Figure 1. The comments concerning the micrographs and subsequent image analysis in Figure 3 also apply. Freeze substitution of the tissue following PCMBS exposure resulted in some damage as evidenced in the micrographs (× 510).

PCMBS exposure, label was bound almost exclusively to the cells of the root periphery (Fig. 4A). Unfortunately, there was tissue damage during the freeze substitution, as evidenced in both micrographs. However, the grain distribution was unaffected by this damage. The brief PCMBS exposures always resulted in label localized in the root periphery. The band of autoradiographic grain distribution was wider than we observed for [$^{3}$H]NEM. This is due to at least two factors. First, because $^{203}$Hg is a $\gamma$-emitter, exposures can occur some distance from the actual site of decay. Second, during freeze-substitution, there appears to have been some slight movement of label. These observations are supported by the appearance of label beyond the surface of

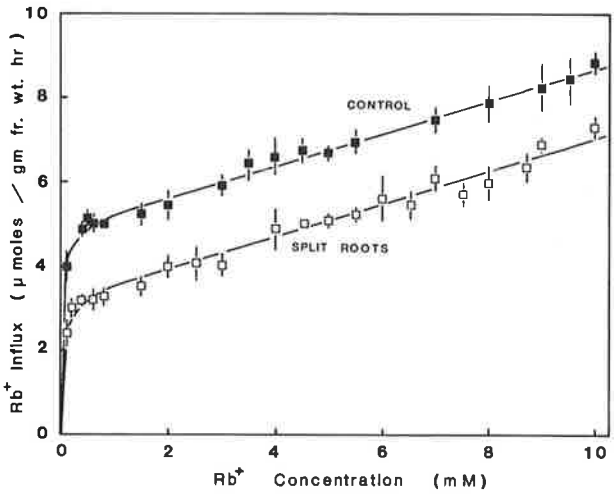


FIG. 5. $^{86}Rb^{+}$ influx isotherms for either corn root segments (■) or split-root segments (□). Five-d-old low salt-grown seedlings were used for all experiments. To obtain split-root segments, the terminal 10 cm of the main root was split longitudinally through its center with the apparatus described in "Materials and Methods." The root halves were then cut into 2-cm segments and washed prior to uptake.

the root (Fig. 4A). In comparison with the short exposure autoradiographs, a 20-min PCMBS pulse resulted in fairly heavy grain distribution throughout the entire root (Fig. 4B). Image analysis of freeze-substituted control tissue resulted in a low (5%) level of detection distributed uniformly throughout the root (data not shown).

**Kinetic Studies.** If ion uptake by cortical cells is diffusion limited, then splitting the roots longitudinally should increase the availability of substrate to cortical cells. This would be especially so if the hypodermis of the corn root does function as an apoplastic barrier to the movement of $K^{+}$ into the cortex. Furthermore, if the complex $K^{+}$ influx kinetics observed previously were due to, or at least partially influenced by, diffusion-limited availability of ions to the root cortex, they would be modified by uptake in split-roots. In Figure 5, the kinetics for $K^{+}$ uptake in intact *versus* split-roots are compared. The overall shape of the kinetic curves was identical. However, the influx values in the split-roots were consistently lower than those in whole root segments.

**Corn Root Cortical Protoplasts.** Corn root protoplasts were next studied for the following reasons. First, if a protoplast preparation could be shown to be purely cortical in origin, the capacity (or lack thereof) for cortical cell ion uptake could be demonstrated. Second, if the complex kinetics found for $K^{+}$ uptake in roots were due to two kinetically distinct mechanisms, such kinetics should also be observed in a single-cell system, where significant diffusion limitations and the problems which arise in a complex tissue do not exist.

Our protoplast preparations were free of cellular debris and bacteria and tests using vital stains indicated that the majority of the protoplasts were viable. After cell wall digestion, each root segment remained as a translucent tube. Extensive microscopic examination indicated that these tubes always consisted of intact epidermal cells (Fig. 6). As shown in Figure 6A, the epidermis and hypodermis remained undigested. Often several outer layers of cortex were also left intact. By observing the epidermal cells with Normarski optics, it was determined that they always maintained their cellular contents (Fig. 6B). Thus, since we removed the stele, and the epidermal cells always remained intact, the kinetics presented represent uptake by cortical protoplasts. Average yields of about 700,000 protoplast/g root tissue were obtained and $K^{+}$ influx values fell between those presented by

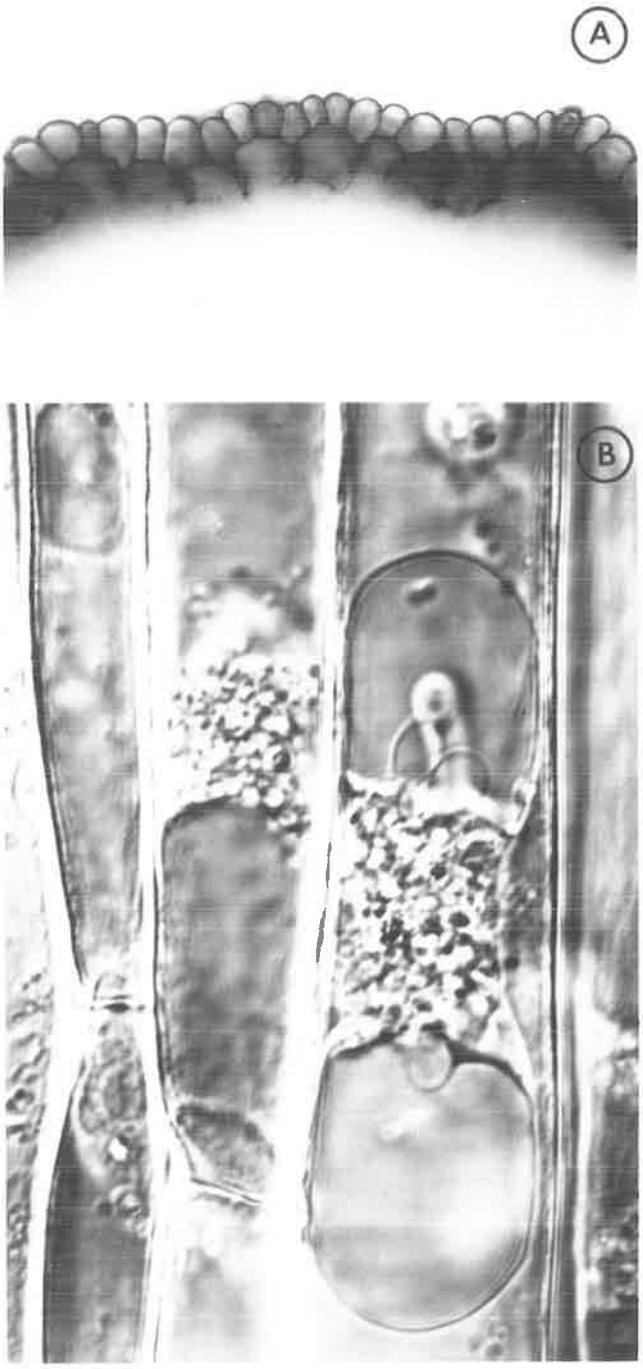


FIG. 6. Micrographs of corn root tissue which remained intact after enzymic digestion had released protoplasts from the cortex. In all sections observed, the epidermis resisted digestion and remained whole. A, Cross-section of corn root tissue observed with bright field optics. The epidermal and hypodermal cell walls were intact following enzymic treatment. Note that although the inner tangential wall of the hypodermis has undergone partial digestion, it is still continuous with the rest of the hypodermal cell wall (× 280). B, Surface view using Nomarski optics of corn root tissue observed in A. Nomarski optics were used to examine the cellular structure of the epidermis (× 1600).

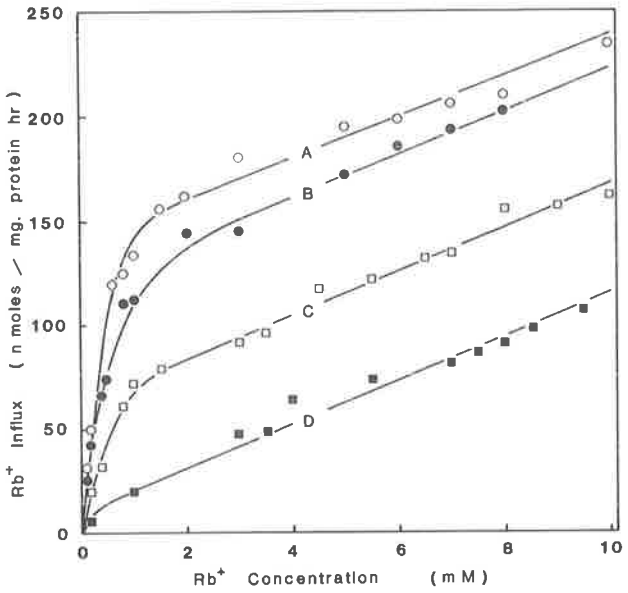


FIG. 7. $^{86}Rb^+$ influx isotherms for protoplasts isolated from the cortex of corn roots. Fifteen-min uptake experiments were run in solutions consisting of RbCl (0.05–10 mM), 0.2 mM $CaCl_2$, 2 mM Mes (pH 6.5), and approximately 0.7 M mannitol. The isotherms labeled A, B, C, and D represent replicate experiments performed on different days. Linear regression performed on data points for $Rb^+$ concentrations from 1.5 to 10 mM yielded the first order rate coefficient, $k$ (in $\mu$mol g fresh weight$^{-1}$ h$^{-1}$ mM$^{-1}$), for the linear component 9.2 (A), 10.9 (B), 10.7 (C), 10.0 (D). The $V_{max}$ values (in $\mu$mol g fresh weight$^{-1}$ h$^{-1}$) for the saturable component were 143.8 (A), 118.0 (B), 62.0 (C), and approximately 0 (D).

others (11, 17).

To minimize variability in uptake from a range of $Rb^+$ concentrations (0–10 mM), it was necessary to osmotically adjust each influx solution with mannitol. In experiments in which we examined the effect of osmotic concentration on $Rb^+$ uptake from 1 mM RbCl solutions, varying the mannitol concentration from 600 to 725 mM caused a 50% increase in $Rb^+$ influx.

The kinetic curves obtained for protoplasts were quite similar in form to those presented for $K^+$ influx in corn roots (Fig. 7). The curves presented are from four separate experiments. Unlike influx values obtained from corn roots, we found considerable variability in the measured fluxes obtained on different protoplast preparations. This does not seem unusual considering the fragile nature of the system studied. However, the linear component showed little change in replicate experiments. Note that in curve D of Figure 7, which involved uptake in protoplasts isolated from roots which appeared to be damaged, uptake was almost completely linear.

**Is the Hypodermis an Apoplastic Barrier?** Most monocots and some dicots exhibit a modification of the cell layer just beneath the root epidermis, the hypodermis, which some workers believe acts as a barrier to apoplastic movement of ions and water. Peterson and coworkers have extensively studied the hypodermis in onion and corn; they have found that it appears to exclude the apoplastic, cell wall-binding fluorescent dyes, Calcofluor and Tinopal, from the cortex (22–24). Because of the importance of such a barrier to our work on the kinetics and site of $K^+$ uptake in corn roots, it was necessary to repeat these fluorescent dye experiments with our tissue. Our results with intact roots were quite similar to those of Peterson *et al.* (22–24). Calcofluor appeared to be bound exclusively to the epidermis (data not shown). We next ruptured the hypodermis by scoring with a needle, or by longitudinally splitting the terminal 10 cm of the root, prior to a 24-h immersion in Calcofluor. Fluorescence

microscopy demonstrated that the dye penetrated only into the first cell layer along the cut surface (data not shown). We expected that during a 24-h incubation, Calcofluor should be able to diffuse into the exposed cortex of split or scored roots and bind to the cell walls of the entire cortex. Thus, the apparent dye exclusion may be due to the binding of dye to epidermal walls (or walls of cells along the cut surface), which may create a barrier retarding further penetration by free dye molecules. The observation that the apoplastic dye, PTS, which does not bind to cell walls, could penetrate freely to the endodermis of corn roots, further supports this contention (23).

Additionally, from studies concerning the penetration of $Na^+$, $HPO_4^{2-}$, and water into corn roots, various workers have concluded that the hypodermis was not an apoplastic barrier unless the oldest (>30 cm from tip) regions of the root were used (1, 2, 8, 9). Our own autoradiographic localization of the impermeant [$^{203}$Hg]PCMBS also indicated that a hypodermal apoplastic barrier does not exist. After exposures of 5 min or longer, PCMBS appeared to be distributed uniformly throughout the entire cortex.

## DISCUSSION

**Involvement of the Root Periphery in Ion Uptake.** The results of the rapid NEM and PCMBS inhibition of $Rb^+$ uptake, in conjunction with the autoradiographic localization studies, lend further support to previous work implicating the root periphery in ion uptake from solutions of low concentration. A 30-s NEM or 1-min PCMBS exposure dramatically inhibited $Rb^+$ uptake, while binding almost exclusively to the cells of the epidermis and hypodermis. The autoradiography following the 30-s NEM (0.3 mM) exposure demonstrated that almost all of the labeled NEM was bound to the root periphery. There was, however, a very low level of more diffusely distributed label throughout the rest of the root cortex and stele. It is not likely that this small amount of NEM would significantly influence ion uptake. This contention is supported by the root respiration data (Table I). A significant inhibition of root respiration was observed only after NEM exposures of 2 min or longer. After a 30-s NEM exposure, binding of NEM to epidermal cells may have resulted in an inhibition of epidermal respiration, along with $Rb^+$ influx. Longer exposures to NEM may be necessary to allow this chemical to penetrate into the cortical cells and affect respiration. Hence, the low level of NEM found in the root cortex may be insufficient to influence respiration and, quite possibly, it had little or no effect on other cortical cell processes. Furthermore, if the sparse grain distribution in the cortical cells is due to NEM being bound from the cell wall solution, it should represent an extremely low apoplastic NEM concentration. It has been demonstrated that in single cell systems, NEM concentrations of 0.1 mM or higher are usually necessary for significant inhibition of transport. For example, in *Chara*, a 30-s pulse with 0.1 mM NEM inhibited $HCO_3^-$ influx by only 25% (18).

The PCMBS autoradiography is more definitive. PCMBS has been shown to penetrate membranes quite slowly and is considered an impermeant sulfhydryl modifier (30). Therefore, the complications resulting from penetration into the symplast are alleviated. The autoradiograph following a 1-min exposure to PCMBS demonstrated that it was restricted to the root periphery. This result, in conjunction with the dramatic inhibition of $K^+$ uptake by a 1-min PCMBS exposure, clearly implicates the cells of the root periphery in ion absorption.

**Involvement of the Root Cortex in Ion Uptake.** Vakhmistrov (28), Bange (3), and Van Iren and Boers-Van der Sluij (29) have argued that ion uptake capacity is restricted to the epidermis. The strongest evidence in support of this hypothesis comes from the localization of absorbed $^{86}Rb^+$ in the epidermis and outer cortex of plasmolyzed barely roots. However, such an interpretation can be subject to criticism. First, this hypothesis is based primarily on a localization pattern obtained by ion transport under plasmolytic conditions. Plasmolysis can severely alter transport in a number of systems. For example, Lucas and Alexander (19) demonstrated in the unicellular giant alga, *Chara corallina*, that when turgor was reduced to near the plasmolytic point with an osmoticum, localized $HCO_3^-$ influx and $OH^-$ efflux were unaffected. However, if the cells were plasmolyzed, both transport systems were inhibited. Thus, it may be erroneous to base a hypothesis concerning 'normal' transport function on data obtained from a system where transport physiology may have been dramatically changed. Second, the work of Anderson and Reilly concerning fluid exudation from the xylem of excised corn roots indicated that the cortical cells do have the capacity to absorb ions (1). They found that surgical removal of the epidermis and outer cortex of excised corn roots did not prevent significant fluxes of ions and water to the xylem.

It is impossible to determine from our NEM and PCMBS experiments whether ion uptake is restricted to the root periphery under all physiological conditions. Our protoplast studies clearly demonstrate that cortical cells do have the capacity to absorb ions. We determined that the protoplasts isolated from corn roots (stele removed) were purely cortical in origin. The technique of 'pulling' the stele from corn roots has been shown to destroy the endodermis while leaving the cortex intact (16). In our preparations, care was taken to prevent liberation of epidermal cell protoplasts (see Fig. 6). Thus, the $K^+$ fluxes obtained were due to absorption by cortical cells.

Despite demonstrated $K^+$ absorption capacity by corn root cortical protoplasts, it is still unclear whether this capacity is operational in the intact tissue. The 30-s NEM and 1-min PCMBS pulses, shown to bind to the root periphery, abolished $Rb^+$ influx from a 0.2 mM solution during a 30-min uptake period. If these sulfhydryl modifiers inhibited epidermal ion uptake, then the hypothesized 'depletion layer' at the root surface would no longer exist. It would then be expected that during the 30-min uptake period a significant amount of $^{86}Rb^+$ should be able to diffuse into the cell wall solution of the cortical cells. If these cells were absorbing $K^+$, a significant influx would be expected. Inasmuch as uptake was minimal under these low substrate conditions, we suggest that the cortical cells are not functioning to absorb ions. In the presence of high substrate (10 mM RbCl), NEM caused less of an inhibition and so it may be that under these conditions the cortical cells function to absorb $K^+$. Such a model implicates regulation of cortical cell ion uptake. At low concentrations, uptake would be restricted to the root periphery, and cortical cell uptake would be repressed or 'shut off.' At higher concentrations a signal, originating within the epidermis, may function to activate existing transport mechanisms in cortical cells. However, such a system must be dynamic because we found that giving high salt-grown roots a brief (10 min) wash in 0.2 mM $CaSO_4$ solution resulted in the cells being very sensitive to NEM inhibition (cf. Figs. 1A and 2B).

**Kinetic Studies.** Our data could also be explained according to the kinetic model presented in an earlier paper (14), which would not necessarily involve cortical uptake. It was previously shown that the kinetic curves for $K^+$ influx were smooth, nonsaturating, and approached linearity at higher substrate concentrations. We proposed that the observed kinetics were the result of two separate transport mechanisms, one exhibiting saturation and the other following first order kinetics. Through the use of the sulfhydryl modifiers, NEM and PCMBS, it was possible to separate these two systems kinetically. A 30-s NEM exposure was shown to abolish the saturable component of $K^+$ influx in high salt-grown roots, while the linear component was unaffected. Approximately 50% of total influx of 10 mM $Rb^+$ was contributed by the linear component. Hence, it is possible that

the NEM-insensitive $K^+$ uptake at high $K^+$ levels may be due to a sulfhydryl-insensitive mechanism operating in the epidermis.

These studies have also enabled us to gain further understanding concerning mechanistic interpretations of ion uptake kinetics. Göring and coworkers have argued that such complex kinetics could still be the result of a single transport system following Michaelis-Menten kinetics; the kinetics would appear complex due to the influences of diffusion-limited ion availability for transport in cortical cells (6, 10, 12, 13). However, our kinetic experiments with both split-roots and protoplasts indicate that this is not the case. If ion diffusion into the cortical free space were limited, particularly by a hypodermal barrier, then the splitting of roots should increase the availability of ions for cortical cell uptake. This should significantly increase $K^+$ influx, especially at low concentrations, and cause an alteration of the kinetics. However, the kinetics observed for split roots were similar to those for intact root segments. The moderate reduction in uptake could be attributed to tissue damage resulting from the root-splitting procedure.

The $K^+$ uptake kinetics observed for cortical protoplast were quite similar to those previously detailed for roots (Figs. 5 and 7). Therefore, these results clearly indicate that such complex, nonsaturating kinetics are due to uptake by single cells. The $K^+$ influx kinetics varied from experiment to experiment only in the shape and size of the saturable component (Fig. 7). The linear component remained unchanged; in fact, in one experiment it appears that the saturating transport mechanism was not operating, while linear component uptake continued unaltered (Fig. 7, curve D). These data strongly support the contention that the linear component does indeed represent a cellular transport mechanism, which presumably operates across the plasmalemma in conjunction with a separate saturable component of uptake.

## CONCLUSIONS

The pathway for ion flux from the external solution to the stele is still not clearly defined. The root periphery appears to play an important role in ion uptake, possibly as the primary site for uptake at low ion concentration. It was clearly demonstrated that cortical cells have the capacity to absorb ions. However, in the intact tissue, it is unclear whether cortical cells express this capacity. At low ion concentrations, the uptake capacity by cortical cells appears to be repressed, whereas under higher substrate levels it is possible that the ability to absorb ions is stimulated or 'turned on.' Whether the present findings can be extended to other root systems awaits further research.

The complex kinetics obtained for $K^+$ uptake in split-roots and isolated root protoplasts strongly indicate that such kinetics are not due to diffusion-limited uptake by a complex tissue. Instead, the results support the hypothesis that $K^+$ uptake results from two kinetically distinct mechanisms. Thus, it appears that saturable and linear uptake are due to separate transport mechanisms, both located on the plasmalemma of epidermal and cortical cells of corn roots.

*Acknowledgments*—We wish to express our appreciation to Drs. V. R. Franceshi and T. C. Pesacreta for their expert advice and assistance concerning the various microscopic techniques employed in this work.

### LITERATURE CITED

1. ANDERSON WP, EJ REILLY 1968 A study of the exudation of excised maize roots after removal of the epidermis and outer cortex. J Exp Bot 58: 19–30
2. BAKER DA 1971 Barriers to the radial diffusion of ions in maize roots. Planta 98: 285–293
3. BANGE GGJ 1973 Diffusion and absorption of ions in plant tissue. III. The role of the root cortex cells in ion absorption. Acta Bot Néerl 22: 529–542
4. BOWLING DJF 1976 Uptake of Ions in Plant Roots. Chapman and Hall, London
5. CLARKSON DT 1974 Ion Transport and Cell Structure in Plants. McGraw Hill, Maidenhead, UK
6. EHWALD R, P SUMMLER, H GÖRING 1973 Die Bedeutung der Diffusion in den "freien Raum" für die Konzentrationsabhängigkeit der Aufnahme von zuckern und Ionen durch pflanzliche Gewebe. Biochim Physiol Pflanzen 164: 596–613
7. EPSTEIN E 1972 Mineral Nutrition of Plants: Principles and Perspectives. John Wiley and Sons, Inc, New York
8. FERGUSON IB, DT CLARKSON 1975 Ion transport and endodermal suberization in the roots of *Zea mays*. New Phytol 75: 69–79
9. FERGUSON IB, DT CLARKSON 1976 Ion uptake in relation to the development of a root hypodermis. New Phytol 77: 11–14
10. GÖRING H 1976 Die Bedeutung ungerührter Schichten für die Kinetik des trägervermittelten Membrantransportes in pflanzlichen geweben. Wiss Z Humboldt-Univ Berl Muth-Naturwiss Reihe 25: 61–65
11. GRONEWALD JW, RT LEONARD 1982 Isolation and transport properties of protoplasts from cortical cells of corn roots. Plant Physiol 70: 1391–1395
12. GRUNWALDT G, R EHWALD, H GÖRING 1978 Suitability of the osmotic shock procedure for the analysis of membrane transport in root tips of *Zea mays* L. J Exp Bot 29: 97–106
13. GRUNWALDT G, R EHWALD, W PIETZCH, H GÖRING 1979 A special role of the rhizodermis in nutrient uptake by plant roots. Biochem Physiol Pflanzen 174: 831–837
14. KOCHIAN LV, WJ LUCAS 1982 Potassium transport in corn roots. I. Resolution of kinetics into a saturable and linear component. Plant Physiol 70: 1723–1731
15. LÄUCHLI A, R PFLÜGER 1979 Potassium transport through plant cell membranes and metabolic role of potassium in plants. *In* Potassium Research—Review and Trends. International Potash Institute, Worblaufen, Bern/Switzerland, pp 111–163
16. LEONARD RT, G NAGAHASHI, WW THOMPSON 1975 Effect of lanthanum on ion absorption in corn roots. Plant Physiol 55: 542–546
17. LIN W 1981 Inhibition of anion transport in corn root protoplasts. Plant Physiol 68: 435–438
18. LUCAS WJ, JM ALEXANDER 1980 Sulfhydryl group involvement in plasmalemma transport of $HCO_3^-$ and $OH^-$ in *Chara corallina*. Plant Physiol 65: 274–280
19. LUCAS WJ, JM ALEXANDER 1981 Influence of turgor pressure manipulation on plasmalemma transport of $HCO_3^-$ and $OH^-$ in *Chara corallina*. Plant Physiol 68: 553–559
20. METTLER IJ, RT LEONARD 1979 Ion transport in isolated protoplasts from tobacco suspension cells. I. General characteristics. Plant Physiol 63: 183–190
21. NYE PH 1973 The relation between the radius of a root and its nutrient-absorbing power [$\alpha$]. J Exp Bot 24: 783–786
22. PETERSON CA, RL PETERSON, AW ROBARDS 1978 A correlated histochemical and ultrastructural study of the epidermis and hypodermis of onion roots. Protoplasma 96: 1–21
23. PETERSON CA, ME EMANUAL, GB HUMPHREYS 1981 Pathway of movement of apoplastic fluorescent dye tracers through the endodermis at the site of secondary root formation in corn (*Zea mays*) and broad bean (*Vicia faba*). Can J Bot 59: 618–625
24. PETERSON CA, ME EMANUAL, C WILSON 1982 Identification of a Casparian band in the hypodermis of onion and corn roots. Can J Bot 60: 1529–1535
25. PITMAN MG 1965 Sodium and potassium uptake by seedlings of *Hordeum vulgare*. Aust J Biol Sci 18: 10–25
26. PITMAN MG 1977 Ion transport into the xylem. Annu Rev Plant Physiol 28: 71–88
27. SALISBURY FB, CW ROSS 1978 Plant Physiology. Wadsworth, Belmont, CA
28. VAKHMISTROV DB 1967 On the function of the apparent free space in plant roots. A study of the absorbing power of epidermal and cortical cells in barley roots. Sov Plant Physiol 14: 103–107
29. VAN IREN F, P BOERS-VAN DER SLUIJ 1980 Symplasmic and apoplasmic radial ion transport in plant roots. Cortical plasmalemmas lose absorption capacity during differentiation. Planta 138: 130–137
30. VAN STEVENINCK J, RI WEED, A ROTHSTEIN 1965 Localization of erythrocyte membrane sulfhydryl groups essential for glucose transport. J Gen Physiol 48: 617–632
31. WEBB JL 1966 Enzymes and Metabolic Inhibitors, Vol 3. Academic Press, New York, pp 337–365

Plant Physiol. (1985) 77, 429–436
0032-0889/85/77/0429/08/$01.00/0

# Potassium Transport in Corn Roots[1]

## III. PERTURBATION BY EXOGENOUS NADH AND FERRICYANIDE

Received for publication July 24, 1984 and in revised form October 18, 1984

LEON V. KOCHIAN AND WILLIAM J. LUCAS*
*Department of Botany, University of California, Davis, California 95616*

### ABSTRACT

**It has recently been reported that plasmalemma electron transport may be involved in the generation of $H^+$ gradients and the uptake of ions into root tissue. We report here on the influence of extracellular NADH and ferricyanide on $K^+$ ($^{86}Rb^+$) influx, $K^+$ ($^{86}Rb^+$) efflux, net apparent $H^+$ efflux, and $O_2$ consumption in 2-centimeter corn (*Zea mays* [A632 × Oh43]) root segments and intact corn roots. In freshly excised root segments, NADH had no effect on $O_2$ consumption and $K^+$ uptake. However, after the root segments were given a 4-hour wash in aerated salt solution, NADH elicited a moderate stimulation in $O_2$ consumption but caused a dramatic inhibition of $K^+$ influx. Moreover, net apparent $H^+$ efflux was significantly inhibited following NADH exposure in 4-hour washed root segments.**

**Exogenous ferricyanide inhibited $K^+$ influx in a similar fashion to that caused by NADH, but caused a moderate stimulation of net $H^+$ efflux. Additionally, both reagents substantially altered $K^+$ efflux at both the plasmalemma and tonoplast.**

**These complex results do not lend themselves to straightforward interpretation and are in contradiction with previously published results. They suggest that the interaction between cell surface redox reactions and membrane transport are more complex than previously considered. Indeed, more than one electron transport system may operate in the plasmalemma to influence, or regulate, a number of transport functions and other cellular processes. The results presented here suggest that plasmalemma redox reactions may be involved in the regulation of ion uptake and the 'wound response' exhibited by corn roots.**

In plant cells, it is generally accepted that solute uptake is energized by the hydrolysis of ATP via plasmalemma-bound ATPases. In particular, it has been hypothesized that the operation of a $H^+$-translocating ATPase generates an electrochemical potential gradient for protons which is used for the uptake of both ions and organic molecules (14, 15). However, evidence has been presented that also implicates a plasmalemma-bound redox chain for the generation of $H^+$ gradients, without the direct involvement of ATP (4, 5, 9, 21, 23).

Several redox systems have been identified in the plasma membranes of bacteria and animal cells that appear to be involved in transport processes. In bacteria, it has long been recognized that amino acid uptake is coupled to electron flow (17). In animals, it is generally believed that amino acid uptake is linked to $Na^+$ influx; the $Na^+$ gradient is believed to be generated by the $Na^+$, $K^+$-ATPase. However, a redox-driven amino acid transport system has been described by Garcia-Sancho *et al.* (10). More recently, a transmembrane redox chain has been demonstrated in ascites tumor cells. This redox system appears to be involved in the generation of a $Na^+$ gradient used for amino acid uptake (30). When external NADH was used as an electron donor and phenazine methosulfate as an electron acceptor, a 2-fold increase in amino acid uptake was observed.

The involvement of a plasmalemma electron transport chain in plants has been suggested by several researchers. Novak and Ivankina (27) postulated that a redox chain exists in the plasmalemma of *Elodea* and *Vallisneria* which may function to drive uptake via the generation of a proton gradient. Craig and Crane (4, 5) have shown that cultured carrot cells reduce external ferricyanide. Furthermore, they have observed an increase in net apparent $H^+$ efflux during ferricyanide reduction. Thus, they suggested that a transmembrane electron transport chain in carrot cells may be involved in the control of cell growth via modulation of membrane transport. Recently, this group has shown that when carrot cells oxidize external NADH, a moderate stimulation of $K^+$ influx was observed (25). They postulated that a plasma membrane redox system operates in close association with the plasmalemma $H^+$-ATPase to exert an influence on $K^+$ transport.

In studies involving protoplasts isolated from corn roots, Lin (21–23) has presented evidence for a redox chain located in the plasmalemma of corn root cortical cells. He found that external NADH tripled $O_2$ consumption in corn root protoplasts, while causing a 2- to 3-fold increase in $K^+$ influx, a marked stimulation of $H^+$ efflux, and a moderate hyperpolarization of the membrane potential. Lin also reported that application of external NADH to excised corn root segments stimulated $K^+$ influx. However, the degree of stimulation of $O_2$ consumption and $K^+$ influx was much less than he reported for his corn root protoplasts. Finally, extracellular ferricyanide reduction has been observed with intact roots of both corn and oats (9, 29). Federico and Giartosio (9) found that during ferricyanide reduction by corn roots, a very mild stimulation of net apparent $H^+$ efflux was detected. Rubinstein *et al.* (29) have recently presented evidence indicating that oat roots can reduce external ferricyanide and oxidize external NADH. Furthermore, the presence of both NADH and ferricyanide resulted in redox reactions that were greater than the sum of the rates due to either reagent alone. They have speculated that several electron transport systems may be present in the plasma membrane of oat roots.

In recent studies on the kinetics of $K^+$ transport into corn roots, we have presented data consistent with uptake being due to the combined effect of a saturable and a first-order kinetic process (18, 19). We have been intrigued by the possibility that the two distinctly different $K^+$ transport systems we have been studying could be driven by separate energy-transducing mechanisms. Experiments were designed to investigate the existence of a redox chain in the plasmalemma of our corn root cells, and

[1] Supported by National Science Foundation Grant PCM 8117721 to W.J.L. and by a Graduate Research Fellowship and a Jastro-Shields Research Award to L.V.K.

its possible role in $K^+$ uptake. We found that in our experimental system either external NADH or ferricyanide caused a significant inhibition of $K^+$ influx. This effect on $K^+$ transport is at variance with previous reports (21, 23, 25). These seemingly contradictory results suggest that the interactions between cell surface redox reactions and ion transport processes are more complex than previously postulated and a caveat will be made concerning the simplistic interpretation of such results.

## MATERIALS AND METHODS

**Plant Material.** *Zea mays* seeds (A632 × Oh43, Crows Hybrid Corn Co., Milford, IL) were imbibed, germinated, and grown by the methods previously outlined (18). Seedlings were either grown on a 0.2 mM $CaSO_4$ solution (low salt conditions) or 0.2 mM $CaSO_4$ + 5 mM KCl (high salt conditions). Primary roots of 3- through 7-d-old seedlings were used.

Alternatively, corn seedlings were grown in glass trays which contained several layers of Whatman No. 1 filter paper saturated with 0.1 mM $CaCl_2$. The trays were covered with plastic food wrap that was perforated in order to allow for gas exchange. The seedlings were grown in the dark for 3 d at 23°C; additional 0.1 mM $CaCl_2$ was added to the filter paper as needed. The roots from these seedlings will be referred to as 'towel-grown' roots, in contrast to the 'solution-grown' roots that are normally used.

**$K^+$ Influx Experiments.** Short-term (15 min) $^{86}Rb^+$ influx experiments were performed using 2-cm root segments as detailed previously (18). Briefly, experiments were performed either with 2-cm root segments cut from the 1st through 8th cm of the primary root or with intact seedlings. Uptake was initiated by the addition of $^{86}Rb^+$ (as RbCl, New England Nuclear Corp.) and terminated by the vacuum withdrawal of radioisotope solution. Free space radiolabel was removed by two 8-min washes in ice-cold 0.5 mM $CaSO_4$ + 1 mM KCl. We have found that a 16-min wash in ice-cold desorption solution removed approximately 95% of the free space radiolabel while exchanging only about 5% of the intracellular label.

In experiments examining the effect of external NADH or ferricyanide on $K^+$ influx, the protocol was identical with that previously described (18). Solutions containing NADH were always freshly prepared to prevent the possible formation of enzyme inhibitors (8). During the 15-min influx period, 1.5 mM $Na_2NADH$ or 1 mM $Na_3FE(CN)_6$ was included in all uptake solutions. Additionally, 3 mM NaCl was added to the uptake media for the controls.

**$K^+$ Efflux Experiments.** Studies examining the influence of NADH and ferricyanide on $K^+(^{86}Rb^+)$ efflux from excised roots were performed as previously outlined (18). Briefly, roots of intact high salt-grown seedlings were allowed to accumulate $^{86}Rb^+$ from a solution containing 1 mM KCl, 1 mM Mes buffer (pH 6.5), 0.2 mM $CaSO_4$, and $^{86}Rb^+$ (approximately 0.2 $\mu$Ci/ml) for 24 h until isotopic flux equilibrium was achieved. The terminal 10 cm of the preloaded roots were excised. The cut ends of four roots were then threaded into narrow bore polypropylene tubes cemented into a Plexiglas plate and sealed with vacuum grease. The four roots (approximately 0.3 g) were briefly washed to remove surface radioactivity and then lowered into the efflux chamber containing 50 ml of the efflux solution. This solution consisted of 1 mM KCl, 1 mM Mes (pH 6.5), 0.2 mM $CaSO_4$, and either 1.5 mM $Na_2NADH$, 1 mM $Na_3Fe(CN)_6$, or 3 mM NaCl. The efflux solutions were continuously aerated. At predetermined times, the efflux solution was drained through a valve located in the base of the efflux chamber and 50 ml of fresh solution were added. The efflux data were analyzed according to the methods outlined previously (18).

**$O_2$ Uptake Experiments.** Root $O_2$ consumption was measured using a Clark $O_2$ electrode and monitor (Rank Bros., Cambridge, England). Approximately 0.1 g of 1-cm root segments excised from either low or high salt roots were placed in 3 ml of air-saturated solution (0.2 mM $CaSO_4$ + 1 mM Mes ([pH 6.5] ± 5 mM KCl, depending on the root-salt status) at 25°C. Stable $O_2$ consumption was monitored for 10 min prior to the addition of $Na_2NADH$ to a final concentration of 1.5 mM. Stable $O_2$ uptake was followed for 15 min following NADH treatment. Either freshly cut root segments or those washed for 4 h were used.

**Measurement of $H^+$ Efflux.** Net apparent $H^+$ efflux was determined with either 0.3 g of 4-h washed root segments (2 cm) excised from either low or high salt roots, or the roots of intact seedlings. Net $H^+$ efflux was measured in 50 ml of an aerated solution consisting of either 0.2 mM KCl, 1 mM KCl, or 10 mM KCl, 0.2 mM $CaSO_4$, and 1 mM Mes (pH 6.5). Changes in solution pH were monitored using a Beckman model 4500 digital pH meter with a model MI-405 pH electrode (Microelectrodes Inc.). After the addition of root tissue to solution, 5 min were allowed for equilibration, after which the pH was adjusted to approximately 6.5 with 20 mM NaOH. Solution pH was monitored for a prescribed period (usually 10 min), after which the pH was back titrated to 6.5 with 20 mM NaOH.

## RESULTS

**NADH-Stimulated $O_2$ Consumption in Freshly Cut and Washed Roots.** The influence of 1.5 mM $Na_2NADH$ on $O_2$ consumption by corn root segments was examined (Table I). Some variability in $O_2$ consumption was found from experiment to experiment. But after many replicate experiments were performed, a definite pattern in the response to NADH was established. In younger tissue (3–4 d), freshly cut roots exhibited little or no NADH stimulation of $O_2$ consumption. But after the usual post-excision wash (4 h) was carried out, a moderate 20 to 30% stimulation of $O_2$ uptake by NADH was always observed. In older (6–8 d) roots, a much larger stimulation of $O_2$ consumption was seen when NADH was applied to freshly cut roots. Often this stimulation exceeded 100%. However, when older

Table I. *Influence of Tissue Age and Washing on NADH-Stimulated $O_2$ Consumption*

Four- and 7-d-old low or high salt-grown roots were used for these experiments. Root segments (1 cm) were excised 1 to 7 cm from the tip and either used immediately for $O_2$ uptake studies or were washed for 4 h in an aerated solution which contained either 1 mM Mes (pH 6.5) and 0.2 mM $CaSO_4$ (low salt-grown roots) or 0.2 mM $CaSO_4$, 1 mM Mes (pH 6.5), and 5 mM KCl (high salt-grown roots). It should be noted that root salt status had no influence on the NADH and ferricyanide-associated responses presented here or in subsequent tables.

| Treatment | Seedling Age | Addition of NADH[a] | $O_2$ Consumption | |
|---|---|---|---|---|
| | *d* | | *μmol/g fresh wt·h* | *% of control* |
| Freshly cut roots | 4 | Control | 27.9 | 100 |
| | 4 | NADH | 28.2 | 101 |
| 4-h washed roots | 4 | Control | 23.0 | 100 |
| | 4 | NADH | 29.5 | 128 |
| Freshly cut roots | 7 | Control | 25.0 | 100 |
| | 7 | NADH | 47.2 | 189 |
| 4-h washed roots | 7 | Control | 24.7 | 100 |
| | 7 | NADH | 30.5 | 124 |

[a] NADH was supplied as $Na_2NADH$ to final concentration of 1.5 mM.

roots were washed for 4 h prior to measurement of $O_2$ uptake, a 20 to 30% stimulation was again observed.

During the course of these experiments, it was noted that following excision (with single-edged razor blades), the roots often appeared damaged, and the solution bathing the roots in the $O_2$ electrode often exhibited turbidity, which in all probability resulted from intracellular material leaking from the cut ends of the roots. This situation was most severe when older roots were used. These observations indicated that tissue damage was occurring and that mitochondrial fragments could have been released into the solution. If double-edged razor blades were used to excise segments from 6-d-old roots, much less apparent damage resulted. Additionally, root segments freshly cut with double-edged razor blades did not exhibit appreciable NADH stimulation of $O_2$ consumption. If root segments from older seedlings were freshly cut with double-edged blades and then squeezed gently beneath a glass slide in order to inflict very mild physical damage, a 50% stimulation in $O_2$ consumption was observed after addition of NADH.

Finally, we studied the effect that leached materials from the roots had on $O_2$ uptake. Roots were freshly cut with a single-edged blade, and a control rate for $O_2$ consumption was measured (approximately 18 $\mu$mol $O_2$ g fresh weight$^{-1}$ h$^{-1}$). The roots were then removed from the $O_2$ electrode; no apparent $O_2$ uptake was detected. If NADH was then added to the solution in the $O_2$ electrode, a very significant $O_2$ consumption was measured. In fact, the $O_2$ consumption (NADH-stimulated) without roots was about 150% of that observed with roots in the chamber. This result definitely indicated that cellular fragments, presumably originating from mitochondria, were being released from the damaged roots and were complicating the interpretation of the data. If roots were freshly cut with a single-edged razor blade, washed briefly to remove cellular debris, and then placed in the $O_2$ electrode, no stimulation of $O_2$ consumption by NADH was observed. These results indicate that in older, freshly cut roots, NADH stimulation of $O_2$ consumption is mediated by cellular fragments. However, in 4-h washed roots, the moderate stimulation in $O_2$ consumption may be due to a plasmalemma redox system.

**Influence of NADH and Ferricyanide on K+ Influx.** The influence of 1.5 mM $Na_2NADH$ on the kinetics of $K^+$ uptake in 4-h washed, high salt root segments was next examined (Fig. 1). Unlike the results of previous researchers (21, 23, 25), NADH caused a significant inhibition of $K^+$ influx at all $K^+$ concentrations examined (0.1–10 mM). Both the saturable and linear components were inhibited, the saturable component was reduced to a greater degree than the linear $K^+$ uptake system.

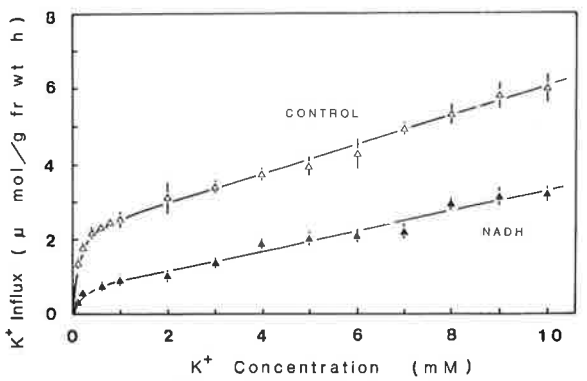


FIG. 1. Influence of 1.5 mM NADH (disodium form) on $^{86}Rb^+$ influx into 4 h washed corn root segments (high salt status). Uptake solutions contained 1.5 mM $Na_2NADH$ for NADH-treated roots, while 3 mM NaCl was included in all control uptake solutions. All data points in this and subsequent figures are the average of four replicates and error bars are ± SE. (Points which lack error bars do so because SE were smaller than symbols used.) It should be noted that root salt status had no effect on the NADH- and ferricyanide-associated responses presented in this and subsequent figures.

Thus far it is apparent that NADH was influencing $O_2$ consumption and $K^+$ influx differently in our solution-grown roots than in the corn root segments and protoplasts utilized by Lin, which were grown on paper towels saturated with dilute $CaCl_2$ solution. To investigate this difference, corn roots were grown and handled according to the published methods of Lin (21, 22). The influence of 1.5 mM $Na_2NADH$ on both $O_2$ consumption and $^{86}Rb^+$ uptake in freshly cut and 4-h washed root segments was examined (Table II). The results were nearly identical to those previously observed in our solution-grown roots. In freshly cut roots, NADH had no influence on either $O_2$ consumption or $K^+$ influx. However, after a 4-h wash, NADH elicited a moderate (30%) stimulation in $O_2$ uptake and a 60% reduction in $K^+$ influx. It is also interesting to note that in freshly cut roots, $K^+$ influx was quite low (1.2 $\mu$mol g fresh weight$^{-1}$ h$^{-1}$) in comparison to roots washed for 4 h (3.4 $\mu$mol g fresh weight$^{-1}$ h$^{-1}$). However, after addition of NADH to 4-h washed roots, $K^+$ uptake was reduced to values comparable with those observed in freshly cut roots.

Ferricyanide (as $Na_3Fe(CN)_6$; 1 mM) had a similar inhibitory effect on $K^+$ influx in 4-h washed root segments (Fig. 2). However, the kinetic profile following exposure to ferricyanide was different from that obtained after NADH treatment. The saturable component was inhibited dramatically, and exhibited a linear response in the concentration range dominated by the saturable transport system (0.1–1.0 mM). Furthermore, the linear component was unaffected by ferricyanide. A similar response was previously observed for $K^+$ uptake kinetics when corn roots were exposed to the nonpenetrating sulfhydryl reagent, PCMBS[2] (18). Finally, it was observed that ferricyanide had no effect on $K^+$ influx in freshly cut roots; a result quite similar to that presented above for NADH.

**Influence of NADH and Ferricyanide on K+ Efflux.** Because of the inhibitory effect of these redox agents on $K^+$ influx, experiments were performed to determine their influence on $K^+$ ($^{86}Rb^+$) efflux. Excised roots were loaded with $^{86}Rb^+$ for 24 h until isotopic flux equilibrium was achieved, and then efflux of $^{86}Rb^+$ was monitored for the next 9 h in solutions containing 1 mM KCl (pH 6.5) in addition to either 1.5 mM $Na_2NADH$, 1 mM $Na_3Fe(CN)_6$, or 3 mM NaCl (control). Both the efflux kinetic parameters and efflux values for various time intervals are presented in Table III. Ferricyanide and NADH had significant effects on $K^+$ ($^{86}Rb^+$) efflux at the plasmalemma and tonoplast. Both reagents stimulated plasmalemma $K^+$ efflux by approximately 25 to 35%. However, while ferricyanide elicited a significant stimulation of $K^+$ efflux across the tonoplast, NADH inhibited tonoplast efflux by approximately 75%. If both reagents were removed from the efflux solution after 4 h, a dramatic change in $K^+$ flux was immediately observed. In the case of NADH, $K^+$ efflux increased to a value similar to control efflux, while the removal of ferricyanide after 4 h caused a dramatic inhibition of $K^+$ efflux from the tissue,

**NADH, Ferricyanide, and Wounding in Roots.** The operation of these redox systems seems to require a 4-h wound recovery period. In previous studies on excision and ion uptake, it was suggested that protein synthesis during the washing period was necessary for the recovery of ion uptake (20). Therefore, cycloheximide (10 $\mu$g/ml) was included during the 4-h wash, and its effect on the NADH-mediated stimulation of $O_2$ consumption and inhibition of $K^+$ influx was examined (Table IV). Cycloheximide abolished both NADH-associated responses, thus suggest-

[2] Abbreviation: PCMBS, *p*-chloromercuribenzene sulfonic acid.

Table II. *Influence of NADH on $O_2$ Consumption and $K^+$ Influx in Towel-Grown Roots*

Seedlings were grown on absorbent paper saturated with 0.1 mM $CaCl_2$. Three-d-old seedlings were used; 0.5-cm segments were cut 0.5 to 2.5 cm from the tip and washed for 4 h in a solution consisting of 0.2 mM $KH_2PO_4$ (pH 6.0) and 0.2 mM $CaCl_2$.

| Treatment | Addition of NADH | $O_2$ Consumption | | $K^+$ Influx[a] | |
|---|---|---|---|---|---|
| | | *μmol/g fresh wt·h* | *% of control* | *μmol/g fresh wt·h* | *% of control* |
| Freshly cut roots | Control | 16.8 | 100 | 1.20 ± 0.05 | 100 |
| | NADH | 17.0 | 101 | 1.10 ± 0.04 | 92 |
| 4-h washed roots | Control | 16.0 | 100 | 3.20 ± 0.2 | 100 |
| | NADH | 21.0 | 130 | 1.31 ± 0.02 | 41 |

[a] $K^+$ influx was from a solution containing 1.0 mM KCl in addition to 0.2 mM $CaSO_4$ + 1 mM Mes (pH 6.5).

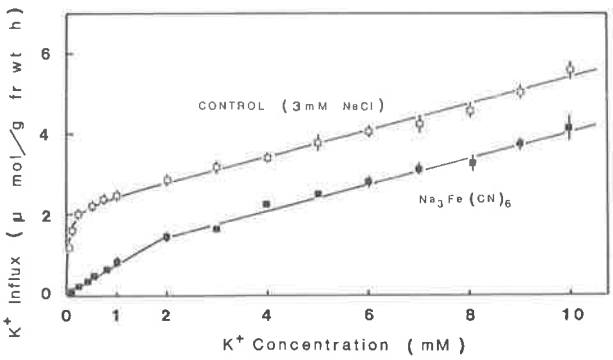


FIG. 2. Influence of 1 mM $Na_3Fe(CN)_6$ on $^{86}Rb^+$ influx into 4-h washed corn root segments (high salt status). One mM $Na_3Fe(CN)_6$ was included in all uptake solutions for ferricyanide-treated roots, while 3 mM NaCl was included in all control uptake solutions.

Table III. *Influence of NADH and $Na_3Fe(CN)_6$ on $^{86}Rb^+$ Efflux from Excised Corn Roots*

The roots from intact high salt-grown seedlings were exposed to a solution containing 1 mM KCl, 0.2 mM $CaSO_4$, 1 mM Mes (pH 6.5), and $^{86}Rb^+$ (0.1 μCi/ml) for 24 h prior to initiating the efflux experiment. After the 24-h loading period, the terminal 10 cm of the primary root was excised, rinsed briefly to remove adhering radioactive solution, and placed into chambers that allowed for the isolation of $^{86}Rb^+$ leakage out of the cut end of the root from $^{86}Rb^+$ efflux from the cells of the epidermis and cortex. Efflux was initiated by the addition of a solution containing 1 mM KCl, 1 mM Mes (pH 6.5), 0.2 mM $CaSO_4$, and either 3 mM NaCl (control), 1.5 mM $Na_2NADH$, or 1 mM $Na_3Fe(CN)_6$.

| Root Treatment | Efflux Kinetic Parameters | | $^{86}Rb^+$ Efflux at Following Periods (h) | | | |
|---|---|---|---|---|---|---|
| | Cyt $t_{1/2}$ | Vac $t_{1/2}$ | 0–0.5 | 0.5–1.0 | 1.0–1.5 | 3–4 |
| | min | h | $\times 10^{-3}$ dpm/g fresh wt·h | | | |
| Control | 62 | 44.3 | 793 | 1104 | 737 | 278 |
| NADH | 46 | 71.4 | 1131 | 853 | 560 | 151 |
| NADH removed[a] | | 48.8 | | | | |
| $Fe(CN)_6^{3-}$ | 50 | 24.9 | 1126 | 1402 | 1133 | 615 |
| $Fe(CN)_6^{3-}$ removed[a] | | 68.1 | | | | |

[a] After 4 h into the particular efflux experiment, the NADH or $Fe(CN)_6^{3-}$ was removed from the efflux solution.

Table IV. *Influence of Cycloheximide on NADH-Associated $O_2$ Consumption and $K^+$ Influx in Corn Roots*

Four-d-old high salt roots were excised into 1-cm segments from the region 1 to 7 cm from the tip and either used immediately for $O_2$ and $K^+$ uptake studies or washed for 4 h in either excision recovery solution[a] or excision recovery solution + 10 μg/ml cycloheximide. It should be noted that similar responses were obtained for low salt-grown roots.

| Treatment | Addition of NADH | $O_2$ Consumption | | $K^+$ Influx[a] | |
|---|---|---|---|---|---|
| | | *μmol/g fresh wt·h* | *% of control* | *μmol/g fresh wt·h* | *% of control* |
| Freshly cut roots | Control | 19.1 | 100 | 0.97 ± 0.10 | 100 |
| | NADH | 19.1 | 101 | 0.82 ± 0.06 | 85 |
| Excised roots washed in standard excision recovery solution[b] | Control | 16.0 | 100 | 2.00 ± 0.11 | 100 |
| | NADH | 21.1 | 132 | 0.85 ± 0.05 | |
| Excised roots washed in standard excision recovery solution + cycloheximide[c] | Control | 12.0 | 100 | 0.75 ± 0.02 | 100 |
| | NADH | 12.0 | 100 | 0.65 ± 0.02 | 80 |

[a] $K^+$ uptake was measured in a solution containing of 0.2 mM KCl + 0.2 mM $CaSO_4$ + 1 mM Mes (pH 6.5).

[b] Standard excision recovery solution for high salt roots consisted of 5 mM KCl + 0.2 mM $CaSO_4$ + 1 mM Mes (pH 6.5).

[c] 10 μg/ml cycloheximide.

ing that protein synthesis is necessary for the operation of the redox chain following excision shock. It also appeared that washing in cycloheximide prevented the increase in $K^+$ uptake normally seen during a postexcision wash, as has been previously documented (20). It should be noted that $O_2$ consumption in cycloheximide-treated roots was approximately 25 to 40% lower than that observed in freshly cut or 4-h washed roots.

If cycloheximide was included in the excision recovery solution during experiments examining the kinetics of $K^+$ uptake in high salt roots, influx was greatly reduced (*cf.* Fig. 1 and Fig. 3A). As was the case with exogenously applied NADH, both transport components were inhibited. Addition of NADH to cycloheximide-treated roots caused only a slight reduction in the values obtained for $K^+$ influx. The kinetic profiles (± NADH) obtained following cycloheximide pretreatment were quite similar to those

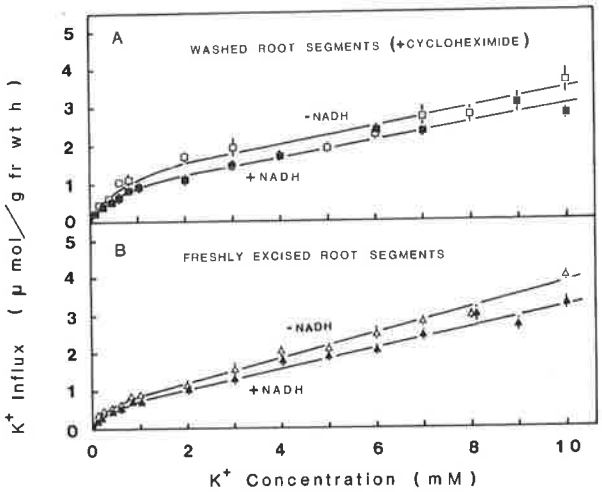


FIG. 3. Influence of 1.5 mM NADH (disodium form) on $^{86}Rb^+$ influx into excised cycloheximide-treated (A) and freshly excised (B) high salt roots. A, Following excision, root segments were given a 4-h wash in a solution containing 10 μg/ml cycloheximide in addition to 0.2 mM $CaSO_4$ + 5 mM KCl. All other experimental procedures were as detailed in Figure 1. B, Immediately following excision, roots were allowed to absorb $^{86}Rb^+$ from standard KCl uptake solutions with and without 1.5 mM $Na_2NADH$. Three mM NaCl was included in all control uptake solutions. It should be noted that the -NADH kinetic curves in A and B are not equivalent to the control curve in Figure 1. Both -NADH curves in Figure 3 are comparable in influx value to the NADH-treated kinetic curve in Figure 1.

observed when roots given a standard 4-h wash were treated with NADH (*cf.* Figs. 1 and 3A). These results suggest that NADH elicits a response in washed roots that is similar to the 'wounding response' observed when intact roots are excised.

This possibility was further examined by studying the influence of NADH on $K^+$ uptake kinetics in freshly cut, high salt roots (Fig. 3B). As illustrated above, NADH again had very little influence on $K^+$ influx in freshly cut roots. The kinetic profiles (± NADH) again exhibited reduced influx values similar to those presented for cycloheximide-treated roots and for NADH-treated roots that had been handled in the standard fashion.

It has been well documented that corn roots can be 'wounded' via a number of different perturbative treatments (excision, cold shock, mechanical pressure), which results in a rapid reduction of ion influx and $H^+$ efflux. During a subsequent 4-h wash, ion transport capacity increases to a steady state value similar to that observed in intact roots (11–13, 20). If NADH is eliciting a wound response in corn roots, then a subsequent 4-h wash following exposure of intact roots to NADH should allow for a recovery of $K^+$ influx. Figure 4 illustrates that exposure of intact roots to 1.5 mM $Na_2NADH$ inhibited $K^+$ influx from a solution containing 1 mM KCl by about 70%. Following a 4-h wash, $K^+$ influx recovered to about 95% of control (Fig. 4B). The time course for the recovery of $K^+$ influx following NADH exposure, was quite similar to that observed following root excision (Fig. 4A). It is interesting to note that when 4-h washed excised roots were then exposed to NADH, $K^+$ influx was reduced to a value comparable with that seen in freshly excised wounded roots. By comparison, the time course for recovery of $K^+$ influx following inhibition due to exposure to ferricyanide was significantly different than that observed after NADH treatment (data not shown). A rapid recovery of $K^+$ influx was observed following ferricyanide exposure, usually a total recovery of $K^+$ influx required only 30 to 60 min.

It has been previously reported that when the redox chain in corn roots (or protoplasts) was stimulated by either NADH or

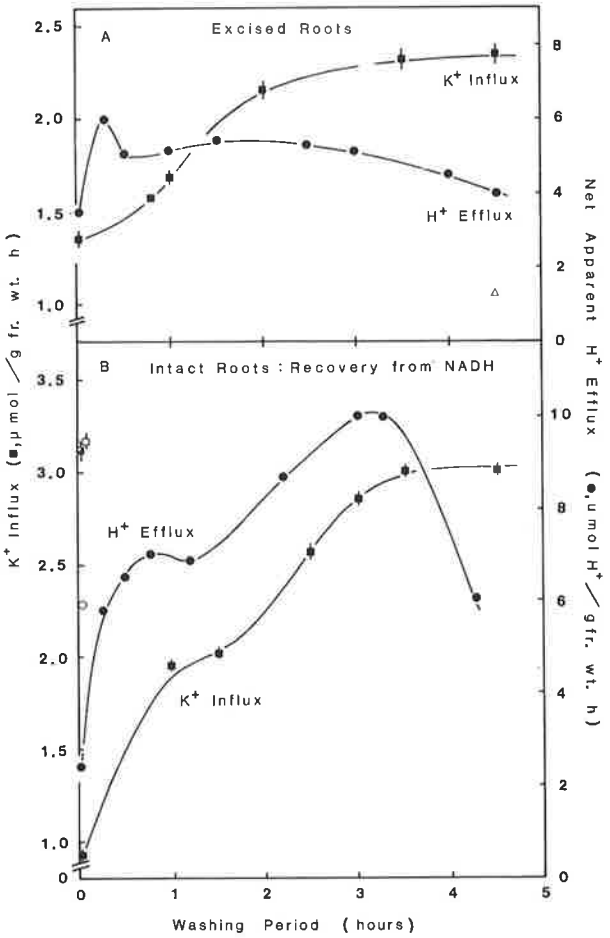


FIG. 4. Recovery of $K^+$ ($^{86}Rb^+$) influx (■) and net apparent $H^+$ efflux (●) from excision (A) and NADH treatment (B) in high salt-grown roots. The solutions used for the measurement of $K^+$ influx and $H^+$ efflux consisted of 1 mM KCl, 0.2 mM $CaSO_4$, and 1 mM Mes (pH 6.5). A, Root segments were excised and then washed in the solution described above. At the various times, root segments were removed from the wash solution and used to measure $K^+$ influx and $H^+$ efflux. After the 4-h wash, $K^+$ influx was also measured from an uptake solution that contained 1.5 mM $Na_2NADH$ (△). B, Intact roots were exposed to 1.5 mM $Na_2NADH$ (in a solution containing 1 mM KCl, 0.2 mM $CaSO_4$, and 1 mM Mes [pH 6.5]) for 15 min and then washed in the solution described for A. Experimental protocol as in A. Prior to NADH exposure, control values were obtained for $K^+$ influx (□), $K^+$ influx + 3 mM NaCl (◪), and for net $H^+$ efflux (○).

ferricyanide, a stimulation of $H^+$ efflux was observed (9, 23). However, in our experimental system NADH elicited a significant decrease in net apparent $H^+$ efflux in both washed corn root segments and intact roots (see Tables V and VI). In some cases an alkalinization of the external media resulted after NADH addition, suggesting that net apparent $H^+$ influx was occurring. It should also be noted that when roots were transferred from a solution containing NADH to fresh control solution, $H^+$ efflux recovered almost immediately to the original, pre-NADH-treated values (see Tables V and VI).

When either intact or excised corn roots were treated with ferricyanide, a moderate stimulation of net apparent $H^+$ efflux was often observed (Table VI). Generally, $H^+$ efflux was stimulated approximately 60 to 100% following exposure to 1 mM $Na_3Fe(CN)_6$. However, it is important to note that it was not possible to consistently reproduce this result. Out of every three experiments, two would result in a stimulation of $H^+$ efflux while

Table V. *Influence of External $K^+$ and 1.5 mM $Na_2NADH$ on Net Apparent $H^+$ Efflux in Corn Roots*

Net $H^+$ efflux was measured in 2 cm corn root segments excised from the region 1 to 7 cm from the tip and washed for 4 h prior to use. Roots were allowed to equilibrate in each test solution for 5 min prior to the initiation of the measurement of $H^+$ efflux (10 min).

| Conditions | $K^+$ Concn. | Net Apparent $H^+$ Efflux |
|---|---|---|
| | mM[a] | μmol/g fresh wt·h |
| 4-h washed high salt roots | 0.2 | 4.71 |
| Transfer to fresh solution + NADH | 0.2 | −14.75 |
| Transfer to fresh solution (−NADH) | 0.2 | 7.56 |
| 4-h washed high salt roots | 10.0 | 9.19 |
| Transfer to fresh solution + NADH | 10.0 | 0.62 |
| Transfer to fresh solution (−NADH) | 10.0 | 6.40 |
| 4-h washed low salt roots | 0.2 | 2.36 |
| Transfer to fresh solution + NADH | 0.2 | −0.59 |
| Transfer to fresh solution (−NADH) | 0.2 | 4.55 |
| 4-h washed low salt roots | 10.0 | 8.77 |
| Transfer to fresh solution + NADH | 10.0 | 0.73 |
| Transfer to fresh solution (−NADH) | 10.0 | 7.18 |

[a] Test solution consisted of 0.2 mM $CaSO_4$, 1 mM Mes (pH 6.5), 3 mM NaCl, and either 0.2 or 10.0 mM KCl.

Table VI. *Influence of 1.5 mM NADH and 1 mM $Na_3Fe(CN)_6$ on Net Apparent $H^+$ Efflux in Excised and Intact Corn Roots*

Either intact roots or 2-cm root segments excised from the region 1 to 7 cm from the tip were used for these measurements, and $H^+$ efflux was measured as described in Table V. Both low salt- and high salt-grown roots yielded similar responses.

| Conditions | Net Apparent $H^+$ Efflux |
|---|---|
| | μmol g fresh wt·h |
| Intact roots | 6.92 |
| Transfer roots to test solution[a] + $Na_2NADH$ | 2.91 |
| Transfer roots back to test solution | 6.20 |
| Intact roots | 4.50 |
| Transfer roots to test solution + $Na_3Fe(CN)_6$ | 9.67 |
| Transfer roots back to test solution | 4.01 |
| 4-h washed root segments | 3.60 |
| Transfer roots to test solution + $Na_3Fe(CN)_6$ | 6.08 |
| Transfer roots back to test solution | 3.80 |

[a] Test solution consisted of 1 mM KCl, 1 mM Mes (pH 6.5), 0.2 mM $CaSO_4$, and 3 mM NaCl (except for NADH and $Fe(CN)_6^{-3}$ solutions which contained 3 mM $Na^+$ from the 1.5 mM $Na_2NADH$ and 1 mM $Na_3Fe(CN)_6$, respectively).

the other would result in little or no effect following ferricyanide treatment.

Finally, in conjunction with the studies on the recovery of $K^+$ influx from excision and NADH 'perturbation', the recovery of net apparent $H^+$ efflux following the same treatments was examined (Fig. 4, A and B). In both cases, an initial increase in $H^+$ efflux was observed 15 min after the particular treatment. However, excised roots often exhibited a gradual decline in $H^+$ efflux during the subsequent 4-h wash, while in NADH-treated intact roots, $H^+$ efflux continued to increase over the next 3 h before declining to initial $H^+$ efflux values (pre-NADH). Similar results with excised corn roots have been observed (12). In light of the observation that $K^+$ influx steadily increases (recovers) over the same period, it may be suggested that $K^+$ influx and $H^+$ efflux, or at least net apparent $H^+$ efflux, are not tightly coupled. However, because several different transport and metabolic processes can contribute to root-mediated pH changes in the external solution, these data are not easily interpreted. The complexities involved in interpreting $H^+$ efflux data will be considered in more detail in the discussion. However, these mechanistic interpretations, which have been based on $H^+$ efflux data may be complicated by the fact that other processes can influence external pH, such as $CO_2$ evolution from respiration, organic acid efflux, or influx processes which consume protons (*i.e.* sugar or amino acid uptake).

## DISCUSSION

**Perturbative Effects of NADH and Ferricyanide.** The results presented here offer support for the previously developed hypothesis that corn roots can oxidize exogenous NADH and reduce ferricyanide, presumably via one or more plasmalemma-bound redox systems. It appears that the wounding induced by root excision is sufficient to 'turn off' the operation of a system that transfers electrons from NADH to $O_2$, and that protein synthesis during the subsequent recovery wash may be necessary in order for this redox chain to function. Furthermore, it appears that this system is intimately involved in ion transport across the plasmalemma. Whenever NADH oxidation was detected (increased $O_2$ consumption), a significant inhibition of both $K^+$ influx and net $H^+$ efflux was always observed. These results are difficult to interpret but suggest that plasmalemma electron transport chains may be involved in regulation of ion transport, rather than as an energy-transducing system for transport.

We were quite perplexed that our results were in direct opposition to those published by Lin (21, 23).Where we found that NADH dramatically inhibited ion uptake and $H^+$ efflux, Lin found a significant stimulation. Furthermore, Lin reported a 300% stimulation of $O_2$ consumption in protoplasts and a 100% stimulation in root segments, when NADH was added to the tissue. In our washed root segments, we never observed a stimulation of $O_2$ consumption greater than 30%. When such different results are obtained with a seemingly similar system, the obvious approach is to analyze any differences in experimental technique. One major difference was in the methods used to grow the corn seedlings. As mentioned above, the tissue Lin used was grown on paper towels saturated with dilute $CaCl_2$ solution. Three-d-old seedlings were used, and 0.5-cm segments were cut from the region 0.5 to 2.5 cm from the tip. We used seedlings grown on 4-L beakers containing aerated dilute salt solutions. For our experiments, 5-d-old seedlings were used, and 1- or 2-cm segments were excised from the region 1.0 to 9 cm from the tip. However, in experiments with corn seedlings grown and handled by techniques identical to those detailed by Lin (21, 22), we again observed a mild stimulation of $O_2$ uptake and a significant inhibition of $K^+$ influx (see Table II).

The other major difference in experimental approach concerns the use of protoplasts *versus* root segments. Most of Lin's results

were obtained with protoplasts isolated from corn roots, while we utilized corn root segments exclusively. It is possible that when corn root tissue is altered dramatically during protoplast isolation, the operation of a fairly complex plasmalemma electron transport system could be changed, and then would operate in a modified manner. Furthermore, we have shown that when protoplasts are released from corn root segments, the epidermal and hypodermal cell walls resist digestion (19). Hence, the protoplasts that Lin used must have been cortical in origin. However, when root segments are used, NADH is most likely to be interacting only with the outer two files of cells. This is the region that has been implicated as the primary site for ion uptake in corn roots (19). We cannot discard the possibility that the various regions of the root interact differentially with respect to NADH treatment. However, Lin has reported a moderate stimulation of $O_2$ consumption and $K^+$ influx in corn root segments (21). It should be noted that this observed stimulation of $K^+$ influx was only 35%, and no mention of data replication or measure of data variability were provided. This makes it extremely difficult to ascertain whether this stimulation was significant, particularly in view of the large variability often observed for ion uptake by root segments. Finally, it is important to note that Lin has recently reported to us that external NADH can elicit an inhibition of $K^+$ uptake in his corn root segments, while $H^+$ efflux is stimulated (Lin, personal communication to W.J.L.).

Our effects of external ferricyanide on ion transport further illustrate the complexity of this root system. When corn root segments were exposed to ferricyanide, a dramatic inhibition of saturable $K^+$ influx was observed. Also, following ferricyanide treatment, $K^+$ uptake in this concentration range (0–1 mM KCl) was converted to a linear profile. A similar response was observed when corn roots were treated with PCMBS, and it was speculated that such a change could represent conversion of a saturable carrier transport system to an open channel mode (18).

The complex and different responses for both $K^+$ influx and efflux, and $H^+$ efflux following NADH and ferricyanide exposure make it difficult to generate a single model for the interaction of cell surface redox reactions and ion transport in plant cells. NADH stimulated $O_2$ consumption and inhibited $K^+$ influx and net $H^+$ efflux in 4-h washed excised roots, while having little effect on these processes in freshly cut roots. Ferricyanide also inhibited $K^+$ influx in a similar manner, while it either stimulated or had no influence on $H^+$ efflux. The effect of these redox reagents on $K^+$ efflux further complicate the picture. Both reagents stimulated plasmalemma $K^+$ efflux, while NADH inhibited and ferricyanide stimulated vacuolar efflux (Table III). These results are interesting because they indicate that these relatively impermeant chemicals, which presumably act at the plasmalemma, have a significant influence on fluxes across the tonoplast. A similar result was observed when corn roots were treated with the impermeant sulfhydryl modifier, PCMBS (18). It would appear that the plasmalemma exerts control over tonoplast transport processes, either through one or more signals, or through the modification of the cytoplasmic $K^+$ pool. When NADH and ferricyanide were removed from the efflux solution midway through the experiment (4 h), dramatic changes in the efflux characteristics were observed. Removal of NADH resulted in an almost immediate increase in $K^+$ ($^{86}Rb^+$)efflux back to control values, while removal of ferricyanide caused a strong inhibition of efflux, with the resulting flux being significantly lower than that observed in the controls.

These different responses to NADH and ferricyanide suggest that redox systems do operate in the plasmalemma to influence ion transport and are much more complex than previously believed. Furthermore, these data suggest that more than one electron transport system may be present in the plasmalemma. Further support for the existence of multiple redox systems in the plasmalemma of corn root cells come from the work examining the relationship between NADH oxidation, ferricyanide reduction, and the wound response in corn roots. The inhibition of $K^+$ influx and $H^+$ efflux by NADH, and the similarities of the time courses for recovery of these transport processes following NADH exposure and excision strongly suggest that NADH elicits a wound response in corn roots. However, the rapid recovery of $K^+$ influx following ferricyanide exposure suggests that fericyanide reduction, unlike NADH oxidation, does not cause a wound response in roots. Hence, inhibition of $K^+$ influx by ferricyanide must be mediated by a different process. Recently, Rubinstein *et al.* (29) have identified three different redox activities at the surface of oat roots that involve NADH and ferricyanide. They speculated that reduction of exogenous ferricyanide by endogenous reductant is mediated by a separate redox system that appears to be associated with proton secretion. This system may be involved in the reduction of extracellular iron, as it has been recently suggested that extracellular iron is reduced by a plasma membrane redox system prior to iron uptake (28). Furthermore, Rubinstein *et al.* (29) tentatively suggest that the other redox activities, *i.e.* the transfer of electrons from either NADH to ferricyanide or $O_2$ involves a separate redox system. This system may alter ion transport processes possibly by altering the redox state at the plasmalemma.

It is possible that one or more of the redox chains examined in the present study are not involved in the generation of a proton gradient, as previously believed. Oxidation-reduction reactions and changes in cellular redox potential have been implicated in a number of cellular processes. Löw and Crane (24) have speculated that plasmalemma redox components could be involved in altering the oxidation-reduction state at the plasmalemma, and thus could help to modulate cellular functions. Additionally, evidence has been presented for the existence of a flavin Cyt protein complex in plant plasma membranes that has an absorption spectrum similar to that for phototropism (1, 16, 26). This flavo-protein also appears to be responsible for NADH oxidase activity in the plasmalemma. These results suggest that the blue light response observed in plants may be mediated by an electron transport chain in the plasmalemma of plant cells. Thus, we presently believe that the available experimental evidence is consistent with the hypothesis that cell surface redox reactions are involved in the regulation of ion transport, and may mediate the wound response that has been so well documented for uptake into excised roots.

**Relationship between $H^+$ Efflux and $K^+$ Uptake.** Because $H^+$ efflux is often directly linked to $K^+$ influx, we were surprised by our findings that although ferricyanide always inhibited $K^+$ influx, net apparent $H^+$ efflux was either unaffected or moderately stimulated. Other researchers have detected ferricyanide reduction in yeast, carrot suspension cells, and corn roots, and in each case have observed a mild stimulation of $H^+$ efflux (4, 7, 9). These workers have speculated that a plasmalemma redox system may operate to transfer both $e^-$ and $H^+$ across the plasmalemma, thus generating a $H^+$ gradient which can be used to drive other transport processes. A further inconsistency in the stoichiometry between $H^+$ efflux and $K^+$ influx was found when we conducted experiments under different levels of $K^+$. Increasing the external $K^+$ from 0.2 to 10 mM resulted in a doubling of $H^+$ efflux from 4.71 to 9.19 $\mu$mol/g fresh weight·h (Table V), while $K^+$ influx nearly quadrupled from 1.70 to 6.30 $\mu$mol/g fresh weight·h.

An even more striking discrepancy between $K^+$ influx and $H^+$ efflux can be found in Lin's (23) work with corn root protoplasts. In this study, control $H^+$ efflux was 880 nmol/$10^6$ protoplasts·h, while $K^+$ influx was only 25 nmol/$10^6$ protoplasts·h. After the addition of NADH, $H^+$ efflux increased to 2610 nmol/$10^6$ protoplasts·h, while $K^+$ influx only increased to 65 nmol/$10^6$ protoplasts·h. The tremendous differences in the values for $H^+$

efflux and $K^+$ influx make mechanistic interpretations tenuous.

**Wounding Phenomenon.** An additional level of complexity exists when one must consider the interaction of wounding with ion transport. When experiments were conducted on freshly excised wounded roots, no NADH stimulation of $O_2$ uptake or inhibition of $K^+$ influx was detected. Only when roots were allowed to recover from excision were these responses observed. It has been well documented in the literature that root excision and other perturbations, such as cold shock or mechanical pressure, cause a reduction in ion influx and $H^+$ efflux, and during a subsequent washing period, uptake capacity increases to a steady state value similar to that observed in intact roots (2, 3, 11–13, 20). It has been shown that this recovery from excision requires RNA and protein synthesis (20). In the work presented here, we have demonstrated that protein synthesis was also necessary for the recovery of NADH-stimulated $O_2$ consumption following root excision. Apparently, excision leads to a wounding response of unknown origin, which causes an inhibition of both ion transport and exogenous NADH oxidation. Additionally, the similarities in the inhibition of both $K^+$ influx and $H^+$ efflux following either excision or exposure to NADH, and the similar time courses for recovery of these transport processes following excision or NADH exposure, strongly suggest that NADH elicits a wound response similar to that caused by excision in intact roots or 4-h washed root segments. The nature of these responses is yet to be elucidated, but it is possible that this putative plasmalemma redox system may be involved in the wound response. If NADH is added to roots that have been allowed to recover from excision, $K^+$ influx and $H^+$ efflux are again inhibited to levels comparable to those observed in wounded tissue. In future studies we will attempt to elucidate the mechanism by which this wound response is effected.

*Acknowledgments*—We wish to express our appreciation to Drs. W. Lin and B. Rubinstein for their helpful discussions and to Drs. B. Rubinstein, A. I. Stern, and R. G. Stout for providing us with their manuscript prior to publication.

## LITERATURE CITED

1. Brain RD, JA Freeberg, CV Weiss, WR Briggs 1977 Blue light-induced absorbance changes in membrane fractions from corn and *Neurospora*. Plant Physiol 59: 948–952
2. Chastain CJ, PR LaFayette, JB Hanson 1981 Action of protein synthesis inhibitors in blocking electrogenic $H^+$ efflux from corn roots. Plant Physiol 67: 832–835.
3. Chastain CJ, JB Hanson 1982 Control of proton efflux from corn root tissue by an injury-sensing mechanism. Plant Sci Lett 24: 97–104
4. Craig TA, FL Crane 1980 Evidence for a trans-plasma membrane electron transport system in plant cells. Proc Indiana Acad Sci 90: 150–155
5. Craig TA, FL Crane 1981 Hormonal control of a transplasmamembrane electron transport system in plant cells. Proc Indiana Acad Sci 91: 150–154
6. Crane FL, H Goldenberg, DJ Morré 1979 Dehydrogenases of the plasma membrane. *In* DB Rodyn, ed, Subcellular Biochemistry, Vol 6. Plenum Press, New York, pp 345–399
7. Crane FL, H Roberts, AW Linnane, H Löw 1982 Transmembrane ferricyanide reduction by cells of the yeast *Saccharomyces cerevisiae*. J Bioenerg Biomembr 14: 191–205
8. Fawcett CP, MM Ciotti, NO Kaplan 1961 Inhibition of dehydrogenase reactions by a substance formed from reduced diphosphopyridine nucleotide. Biochim Biophys Acta 54: 210–212
9. Federico R, CE Giartosio 1983 A transplasmamembrane electron transport system in maize roots. Plant Physiol 73: 182–184
10. Garcia-Sancho J, A Sanchez, ME Handlogten, HN Christensen 1977 Unexpected additional mode of energization of amino-acid transport into Ehrlich cells. Proc Natl Acad Sci USA 74: 1488–1491
11. Glass ADM 1978 Influence of excision and aging upon $K^+$ influx into barley roots. Recovery or enhancement? Plant Physiol 61: 481–483
12. Gronewald JW, JB Hanson 1980 Sensitivity of the proton and ion transport mechanisms of corn roots to injury. Plant Sci Lett 18: 143–150
13. Gronewald JW, JM Cheeseman, JB Hanson 1979 Comparison of the responses of corn root tissue to fusicoccin and washing. Plant Physiol 63: 255–259
14. Higinbotham N 1973 Electropotentials of plant cells. Annu Rev Plant Physiol 24: 25–46
15. Hodges TK 1976 ATPases associated with membranes of plant cells. *In* U Lüttge, MG Pitman, eds, Encyclopedia of Plant Physiolgy, New Series, Vol 2A. Springer-Verlag, Berlin, pp 260–283
16. Jesaitis AJ, PR Heners, R Hertel, WR Briggs 1977 Characterization of a membrane fraction containing a *b*-type cytochrome. Plant Physiol 59: 941–947
17. Kaback HR 1972 Transport across isolated cytoplasmic membranes. Biochim Biophys Acta 265: 367–416
18. Kochian LV, WJ Lucas 1982 Potassium transport in corn roots. I. Resolution of kinetics into a saturable and linear component. Plant Physiol 70: 1723–1731
19. Kochian LV, WJ Lucas 1983 Potassium transport in corn roots. II. The significance of the root periphery. Plant Physiol 73: 208–215
20. Leonard RT, JB Hanson 1972 Induction and development of increased ion absorption in corn root tissue. Plant Physiol 49: 430–435
21. Lin W 1982 Responses of corn root protoplasts to exogenous reduced nicotinamide adenine dinucleotide: Oxygen consumption, ion uptake, and membrane potential. Proc Natl Acad Sci USA 79: 3773–3776
22. Lin W 1982 Isolation of NADH oxidation system from the plasmalemma of corn root protoplasts. Plant Physiol 70: 326–328
23. Lin W 1984 Further characterization on the transport property of plasmalemma NADH oxidation system in isolated corn root protoplasts. Plant Physiol 74: 219–222
24. Löw WH, FL Crane 1978 Redox function in plasma membranes. Biochim Biophys Acta 515: 141–161
25. Misra PC, TA Craig, FL Crane 1984 A link between transport and plasma membrane redox system(s) in carrot cells. J Bioenerg Biomembr 16: 143–152
26. Munoz V, WL Butler 1975 Photoreceptor pigment for blue light in *Neurospora crassa*. Plant Physiol 55: 421–426
27. Novak VA, NG Ivankina 1978 Nature of electrogenesis and transport of ions in plant cells. Doklady Biophys 242: 1229–1232
28. Römheld V, II Marschner 1983 Mechanism of iron uptake by peanut plants. I. $Fe^{III}$ reduction, chelate splitting, and release of phenolics. Plant Physiol 71: 949–954
29. Rubinstein B, AI Stern, RG Stout 1984 Redox activity at the surface of oat root cells. Plant Physiol 76: 386–491
30. Yamamoto, T Kawasaki 1981 The involvement of the membrane oxidoreduction system in stimulating amino acid uptake in Ehrlich ascites tumor cells. Biochim Biophys Acta 644: 192–200

Plant Physiol. (1985) 79, 771–776
0032-0889/85/79/0771/06/$01.00/0

# Potassium Transport in Corn Roots[1]

## IV. CHARACTERIZATION OF THE LINEAR COMPONENT

Received for publication January 27, 1985 and in revised form July 22, 1985

LEON V. KOCHIAN, JIAO XIN-ZHI[2], AND WILLIAM J. LUCAS*
*Department of Botany, University of California, Davis, California 95616*

### ABSTRACT

**A detailed examination was conducted on the linear, or first-order kinetic component for $K^+$($^{86}Rb^+$) influx into root segments of both low- and high-salt grown corn seedlings (*Zea mays* [A632 × Oh 43]). In tissue from both low- and high-salt grown roots, replacement of $Cl^-$ in the uptake solution by either $SO_4^{2-}$, $H_2PO_4^-$, or $NO_3^-$ caused a significant (50–60%) and specific inhibition of the linear component of $K^+$ influx. The anion transport inhibitor, 4,4′-diisothiocyano-2,2′-disulfonic acid, was found to abolish saturable $Cl^-$ influx in corn roots while causing a significant (50–60%) and specific inhibition of the linear $K^+$ uptake system; this inhibition was identical to that observed when $Cl^-$ was replaced by other anions in the $K^+$ uptake solution. Additionally, the quaternary ammonium cation, tetraethylammonium, which has been shown to block $K^+$ channels in nerve axons, also caused a dramatic (70%) and specific inhibition of the linear component of $K^+$ influx, but this was obtained only in high-salt roots. The reasons for this difference are discussed with respect to the differing abilities of low- and high-salt roots to absorb tetraethylammonium.**

**Our present results indicate that the linear component of $K^+$ influx may occur by a passive process involving transmembrane $K^+$ channels. Fluxes through these $K^+$ channels may be partly coupled to a saturating $Cl^-$ influx mechanism.**

In studies involving the kinetics of uptake for various plant tissues, the majority of the work has focused on the generation of discontinuous isotherms, via either the operation of multiple Michaelis-Menten transport systems, or by complex, multisite carriers. In many of these studies, the presence of a linear component was either ignored or considered to reflect diffusion across the plasma membrane (13 and references therein).

Recently there has been a growing interest in nonsaturating transport kinetics for organic solutes and ions. In contrast to earlier investigations, the more recent literature suggests that the nonsaturating or linear transport component may be a relatively complex process (2, 6, 7, 13–15, 20, 21, 31). Consistent with these results, we have previously demonstrated that in corn roots, the kinetics for $K^+$ influx could be resolved into saturable and linear components (13, 14). Sulfhydryl reagents either had no effect on the linear component, or, in the case of PCMBS[3], caused a significant stimulation, while resulting in complete inhibition of the saturable system.

In the present work, we document a more detailed characterization of the linear component. We were able to selectively inhibit linear component $K^+$ uptake either by varying the accompanying anion, inhibiting $Cl^-$ influx, or by the application of $K^+$ channel-blocking agents. These results are discussed with respect to possible transport mechanisms and the relationship between cation and anion fluxes across the plasmalemma of corn root tissue.

## MATERIALS AND METHODS

**Plant Material.** *Zea mays* seeds (A632 × Oh 43, Crows Hybrid Corn Co., Milford, IL) were imbibed, germinated, and grown by the methods previously outlined (13). Seedlings were either grown on a 0.2 mM $CaSO_4$ solution (low-salt conditions) or 0.2 mM $CaSO_4$ and either 5 mM KCl, $KNO_3$, $KH_2PO_4$, or 2.5 mM $K_2SO_4$ (high-salt conditions). Primary roots of 4-d-old seedlings were used for all uptake experiments.

**$K^+$ and $Cl^-$ Influx Experiments.** Short-term (10 min) $^{86}Rb^+$ and $^{36}Cl^-$ influx experiments were performed using 2-cm root segments as previously described (13). Briefly, experiments were performed with 2-cm root segments cut from the 1st through 8th cm of the primary root. Root segments were washed (4 h) in solutions of identical composition to their growth solutions to allow for recovery from excision. Uptake was initiated by the addition of $^{86}Rb^+$ (as RbCl, New England Nuclear, Boston) or $^{36}Cl^-$ (as NaCl, ICN Biochemicals, Irvine, CA) and terminated by the vacuum withdrawal of radioisotope solution. Free space radiolabel was removed by either two 8-min washes for $^{86}Rb^+$ or two 5-min washes for $^{36}Cl^-$ in ice-cold 0.5 mM $CaSO_4$ + 1 mM KCl. We have found that these desorption regimes removed approximately 95% of the free space radiolabel while exchanging only about 5% of the intracellular label. Following desorption, root segments were centrifuged (300*g*) for 15 s to remove surface water, and then the roots were weighed into scintillation vials. In order to quantify $^{86}Rb^+$ absorbed by roots, they were incubated (15 min) in 5 ml of 95% ethanol and then 10 ml of 5 mM ANDA were added to each vial. We have found this treatment quite effective in releasing $^{86}Rb^+$ from root segments. Radioactivity was quantified via detection of Cerenkov radiation in a Beckman LS 9800 scintillation counter. For $^{36}Cl^-$ influx studies, root segments were weighed into scintillation vials and then 10 ml of Beckman Ready Solve Hp/b scintillation cocktail (Beckman Industries, Fullerton, CA) was added. Radiocactivity was also

[1] Supported by National Science Foundation Grant PCM 8117721 to W. J. L. and by a University of California, Davis Graduate Fellowship and a Jastro-Shields Research Award to L. V. K.

[2] On leave from Laboratory of Plant Nutrition, Shanghai Institute of Plant Physiology, Academia Sinica, Shanghai, China.

[3] Abbreviations: PCMBS, *p*-chloromercuribenzene sulfonic acid; ANDA, 7-amino-1,3-naphthalene disulfonic acid; CCCP, carbonyl cyanide *m*-chlorophenylhydrazone; DIDS, 4,4′-diisothiocyano-2,2′-disulfonic acid stilbene; NEM, *N*-ethylmaleimide; TEA-Cl, tetraethylammonium chloride.

quantified using a Beckman LS 9800 scintillation counter.

The effect of the amino-reactive anion transport inhibitor, DIDS (Calbiochem-Behring, Fullerton, CA), on $K^+$ and $Cl^-$ influx in excised root segments was studied. Roots were pretreated for 15 min prior to $^{36}Cl^-$ or $K^+$ ($^{86}Rb^+$) influx with either 1 or 2 mM DIDS in a solution containing 0.2 mM $CaSO_4$ + 5 mM Mes (pH 6.0). DIDS was included in all uptake solutions. Buffer concentration was increased to 5 mM in all uptake solutions in order to maintain the appropriate pH value.

We have previously shown that in our corn root system, $^{86}Rb^+$ is a suitable radiotracer for $K^+$ influx experiments (13).

**$K^+$ Channel-Blocking Agents.** Experiments were performed to investigate the influence of the quaternary ammonium salt, TEA-Cl (Aldrich Chem. Co.), on $K^+$ influx. During the last 30 min of the 4-h wound recovery wash, either high- or low-salt roots were transferred to an identical wash solution containing 10 mM TEA-Cl for pretreatment. Additionally, 10 mM TEA-Cl was included in the uptake solutions.

For experiments investigating the absorption of TEA by low- and high-salt roots, 2-cm root segments were handled as previously described for $K^+$ and $Cl^-$ influx studies. Root segments were placed into 20 ml of aerated uptake solution which consisted of various concentrations of TEA-Cl (1–20 mM). Uptake was initiated by the addition of [$^{14}$C]TEA (as TEA-Br, New England Nuclear Corp.) to a final concentration of approximately $3.7 \times 10^3$ Bq/ml. The subsequent experimental protocol was as previously described for $K^+$ ($^{86}Rb^+$) influx studies.

## RESULTS

**Anion Involvement in Linear $K^+$ Influx.** Early work by Epstein *et al.* (8) demonstrated that in barley roots, Mechanism II $K^+$ influx was dramatically inhibited when $Cl^-$ was replaced by $SO_4^{2-}$ in the uptake solution. Since our linear $K^+$ uptake component functions primarily in the Mechanisms II concentration range, we examined the influence of $Cl^-$ replacement by other anions, on the uptake of $K^+$ in both low-salt and high-salt grown roots. Replacement of $Cl^-$ with $SO_4^{2-}$, $NO_3^-$, or $H_2PO_4^-$ in the uptake solution resulted in a 60% reduction in linear component $K^+$ influx and a 20% reduction in the $V_{max}$ for saturable uptake in low salt roots (Fig. 1). In these roots, the $K_m$ ($K^+$) for the saturable system exhibited no discernible change in response to changes in the accompanying anion (Table I).

To perform $Cl^-$ replacement studies on high-salt grown roots, we cultivated the tissue on solutions containing 2.5 mM $K_2SO_4$, instead of the usual 5 mM KCl so that contamination of the uptake solution, via chloride leakage from the tissue, was minimized. Using this tissue, we found that $Cl^-$ replacement resulted in an even more selective inhibition of the linear component. When $Cl^-$ was replaced by $SO_4^{2-}$, $NO_3^-$, or $H_2PO_4^-$, a 60% reduction in the linear component was again seen, while the $V_{max}$ of the saturable component remained totally unaffected (Fig. 2). It should be noted that the apparent $K_m$ ($K^+$) of the saturating system increased from approximately 100 to 145 $\mu$M when $Cl^-$ was replaced (Table I).

To determine whether linear component $K^+$ uptake was linked to $Cl^-$ influx, $^{36}Cl^-$ uptake studies were performed. As shown in Figure 3, the kinetics for $Cl^-$ uptake into low-salt roots exhibited both the saturable and linear components. A comparison between the flux data presented in Figures 1 and 3 indicate that the value for $K^+$ ($^{86}Rb^+$) influx is almost double that for $^{36}Cl^-$.

The membrane-impermeable, amino-reactive reagent, DIDS, has been shown to irreversibly inhibit anion uptake in red blood cells. More recently, DIDS has been used to inhibit $Cl^-$ and $SO_4^{2-}$ uptake in corn root protoplasts (16) and was shown to be a reversible inhibitor of $Cl^-$ influx in *Chara corallina* (12). To investigate the effect of DIDS on the kinetics of both $Cl^-$ and $K^+$ influx in low-salt grown corn roots, the following experiments were performed. DIDS, at 1 mM, was sufficient for maximal inhibition of $Cl^-$ influx (data not shown). Furthermore, a pretreatment in 1 mM DIDS for 15 min was necessary to elicit this inhibition. Additionally, as with *Chara*, DIDS inhibition of $Cl^-$ influx was reversible; a 15-min wash without DIDS (in 1 mM $Cl^-$) was sufficient to reverse the inhibition caused by a 60-min DIDS pretreatment. Consequently, all DIDS experiments consisted of a 15-min pretreatment with 1 mM DIDS, followed by the inclusion of 1 mM DIDS in all uptake solutions.

The results of such a DIDS treatment on $Cl^-$ influx are presented in Figure 3. The saturable component for $Cl^-$ influx

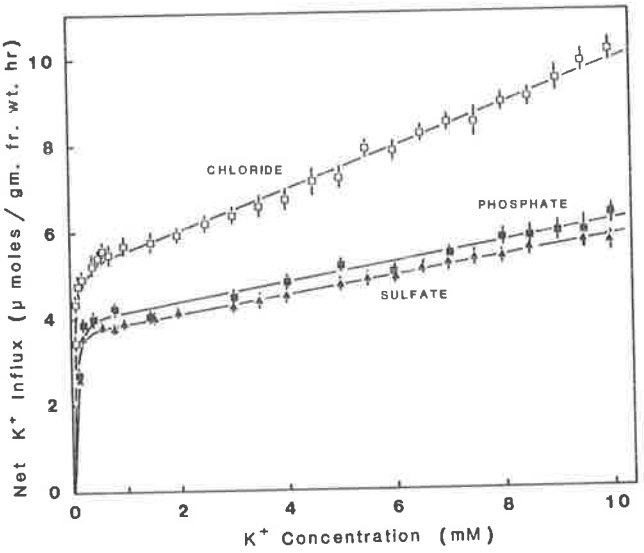


FIG. 1. Influence of the accompanying anion on $K^+$ ($^{86}Rb^+$) influx for corn root segments grown in 0.2 mM $CaSO_4$ (low-salt status). The first order rate coefficients, k, (in $\mu$mol g fresh weight$^{-1}$ h$^{-1}$ mM$^{-1}$), for the linear component, were as follows: 0.50 ($Cl^-$), 0.21 ($SO_4^{2-}$), 0.24 ($H_2PO_4^-$). To ensure clarity, the isotherm obtained with $NO_3^-$ as the accompanying anion was omitted. All data points in this figure and subsequent ones are the average of eight replicates and error bars are SE. Points which lack error bars do so because standard errors were smaller than symbols used.

Table I. *Influence of Various Experimental Treatments on the Saturable and Linear Components of $K^+$ ($^{86}Rb^+$) Uptake into Corn Root Segments*

Influx isotherms were separated into their saturable and linear components. Eadie-Hofstee plots for saturable curves yielded the following $K_m$ and $V_{max}$ values. Linear regression performed on data points for $K^+$ concentrations from 1.5 to 10 mM yielded the first order rate coefficient (k).

| Salt Status | Experimental Treatment | Saturable Component | | Linear Component (k) |
|---|---|---|---|---|
| | | $K_m$ | $V_{max}$ | |
| | | $\mu M$ | $\mu$mol g fresh wt$^{-1}$ h$^{-1}$ | $\mu$mol g fresh wt$^{-1}$ h$^{-1}$ mM$^{-1}$ |
| Low-Salt | $Cl^-$ | 57 | 5.10 | 0.51 |
| | $SO_4^{2-}$ | 50 | 4.05 | 0.21 |
| | $H_2PO_4^-$ | 55 | 4.15 | 0.24 |
| Low-Salt | Control | 50 | 5.25 | 0.40 |
| | 1 mM DIDS | 54 | 4.30 | 0.20 |
| High-Salt | $Cl^-$ | 112 | 2.85 | 0.54 |
| | $SO_4^{2-}$ | 114 | 2.75 | 0.24 |
| | $H_2PO_4^-$ | 150 | 2.70 | 0.25 |
| | $NO_3^-$ | 147 | 2.75 | 0.30 |

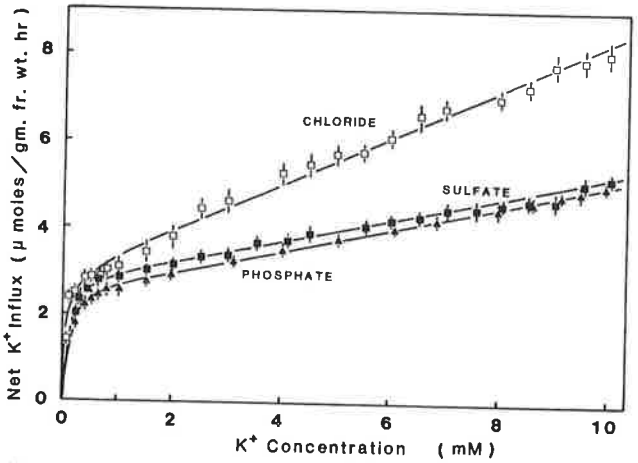


FIG. 2. Influence of the accompanying anion on $K^+$ ($^{86}Rb^+$) influx for corn root segments grown in 0.2 mM $CaSO_4$ + 2.5 mM $K_2SO_4$ (high-salt status). The first order rate coefficients, k (in $\mu$mol g fresh weight$^{-1}$ $h^{-1}$ $mM^{-1}$), for the linear component were as follows: 0.53 ($Cl^-$), 0.24 ($SO_4^{2-}$), 0.25 ($H_2PO_4^-$), 0.30 ($NO_3^-$). To ensure clarity, the isotherm obtained with $NO_3^-$ as the accompanying anion was omitted.

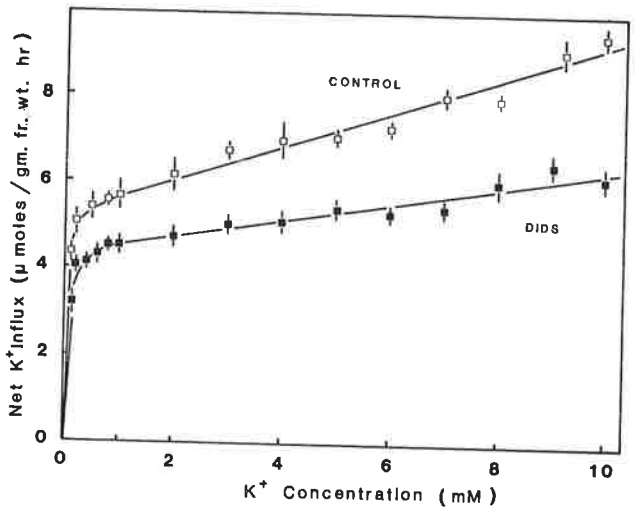


FIG. 4. Influence of 1 mM DIDS on $K^+$ ($^{86}Rb^+$) influx for low-salt roots. See Figure 3 for the experimental conditions. The first order rate coefficients, k, for the linear component, were as follows: 0.40 (control), 0.19 (DIDS).

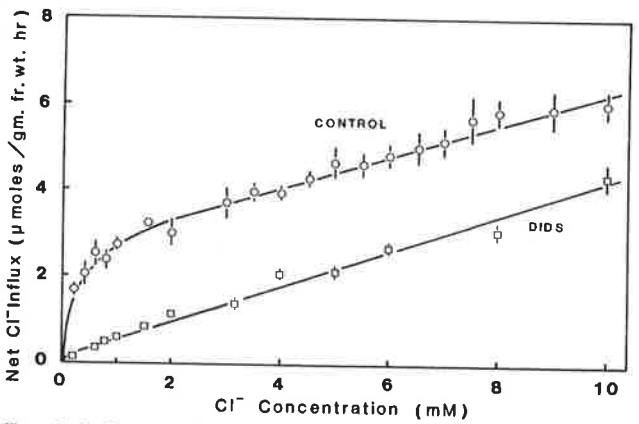


FIG. 3. Influence of 1 mM DIDS on $^{36}Cl^-$ influx for low salt roots. Roots were pretreated with a solution consisting of 1 mM DIDS, 5 mM Mes (pH 6.0), and 0.2 mM $CaSO_4$ for 15 min prior to uptake and 1 mM DIDS was included in all uptake solutions. The first-order rate coefficients, k, for the linear component were as follows: 0.37 (control), 0.41 (DIDS).

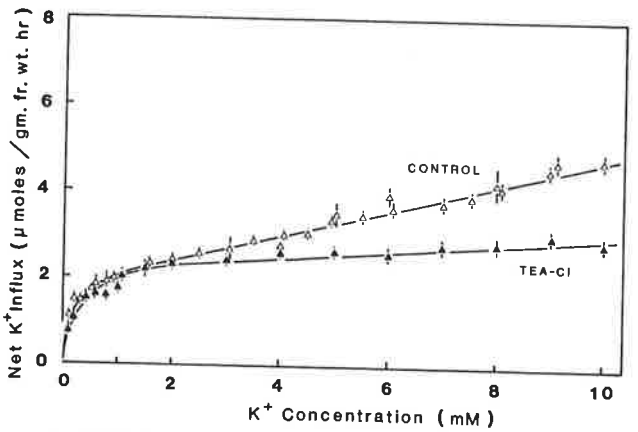


FIG. 5. Influence of 10 mM TEA-Cl on $K^+$ ($^{86}Rb^+$) influx for high-salt roots. Roots were pretreated with a solution containing 10 mM TEA-Cl, 5 mM KCl, and 0.2 mM CaSO4 for 30 min prior to uptake and 10 mM TEA-Cl was included in all uptake solutions. The first order rate coefficients, k, for the linear component were as follows: 0.31 (control); 0.09 (TEA-Cl).

was abolished following DIDS exposure, while the linear component was left unchanged. In Figure 4, the influence of this same DIDS treatment on $K^+$ ($^{86}Rb^+$) uptake into low-salt roots is illustrated; a significant inhibition (60%) of the linear component for $K^+$ influx was observed. The $V_{max}$ ($K^+$) was only moderately reduced (20%), while the $K_m$ was unaffected (Table I). The $K^+$ uptake kinetics in DIDS-treated roots were almost identical to the kinetics observed when $Cl^-$ was removed from the uptake solution (Fig. 1).

**$K^+$ Channel-Blocking Agents.** In studies involving $K^+$ uptake in *E. coli*, it has been suggested that the linear component for $K^+$ uptake is due to the operation of $K^+$ channels in the plasma membrane (27). It has long been established that the membrane of giant nerve fibers support both $K^+$ and $Na^+$ currents that are mediated via ion-specific channels. It is also well documented that quaternary ammonium salts, such as TEA, cause a specific decrease in $K^+$ conductance in these tissues (30).

To further elucidate the relationship between $Cl^-$ uptake and the linear component of $K^+$ influx, we investigated the effect of the $K^+$ channel-blocking agent, TEA-Cl, on the kinetics of $K^+$ influx for both low- and high-salt roots. Roots were pretreated in 10 mM TEA-Cl for 30 min, and then 10 mM TEA-Cl was included in all uptake solutions. In high-salt roots, TEA caused a dramatic (75%) and specific inhibition of the linear component (Fig. 5); consistent with our earlier findings for anion replacement and DIDS experiments, the saturable component remained unaffected. The TEA results suggest that $K^+$ channels may be involved in linear component $K^+$ uptake into high-salt roots. However, although low-salt roots possess a similar linear component for $K^+$ influx, in the present studies this component was insensitive to TEA (data not shown).

In an attempt to resolve the discrepancy between the linear component TEA-sensitivity in these tissues, we measured [$^{14}C$] TEA influx into high- and low-salt roots. We found that over a TEA concentration range of 1 to 20 mM, influx into high-salt roots was approximately twice that obtained on low-salt roots (Fig. 6). This observed difference in TEA transport capability may result in higher TEA cytoplasmic levels in high-salt roots. These elevated cytoplasmic TEA levels may be sufficient to block $K^+$ channels in high-salt roots, while the reduced TEA influx in

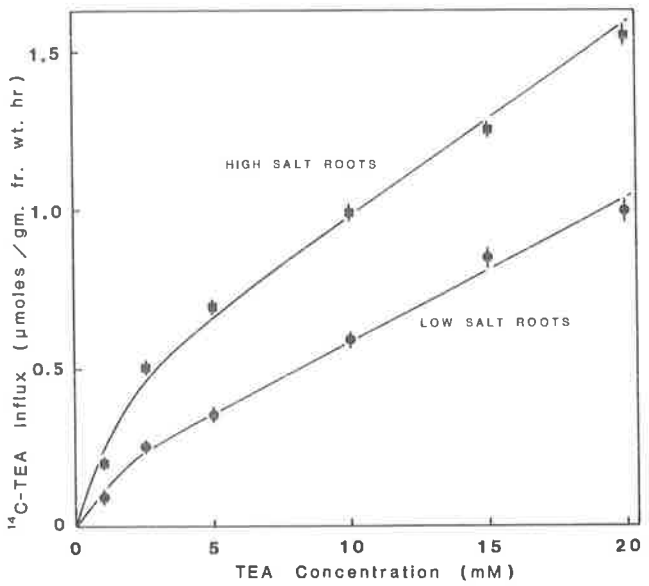


FIG. 6. Uptake of [$^{14}$C]TEA-Cl in low-salt (●) and high salt (■) corn root segments. Experimental protocol was identical to that used for $K^+$ ($^{86}Rb^+$) uptake studies (see "Materials and Methods").

low-salt roots may result in cytoplasmic TEA concentrations that are not high enough to influence $K^+$ channels. Of course, this situation is predicated on the condition that TEA would have to act at the cytoplasmic face of the plasmalemma in order to block $K^+$ channels in corn roots.

**Influence of $Na^+$ on Linear Component $K^+$ Influx.** Epstein *et al.* (8) demonstrated that in low-salt roots, Mechanism I for $K^+$ influx was quite specific for $K^+$ or $Rb^+$, while Mechanism II could be competitively inhibited by $Na^+$. We therefore investigated the influence of 3 mM NaCl on the $K^+$ uptake kinetics in both low- and high-salt roots. In low-salt roots, 3 mM $Na^+$ caused a significant reduction (50%) in linear component $K^+$ uptake, while having little effect on the saturable component (data not shown); this result is in agreement with previous studies conducted in barley roots (8). However, in high-salt roots, 3 mM $Na^+$ had absolutely no effect on either the linear or saturable components of $K^+$ influx (data not shown). These results are similar to those previously obtained by Pitman *et al.* (23–25), who found that in the Mechanism II concentration range, high-salt roots showed a much greater selectivity for $K^+$ over $Na^+$ than did low-salt roots. Therefore, in our low-salt grown roots, linear uptake may be mediated by a general cation channel; however, in high-salt roots, linear uptake appears to be due to a more specific $K^+$ channel.

## DISCUSSION

**Relationship between Anion Transport and Linear $K^+$ Fluxes.** The linear component dominates $K^+$ uptake in the concentration range where most researchers feel uptake occurs via a thermodynamically passive process. This feature, in conjunction with the linear concentration dependence for uptake, has caused numerous workers to dismiss the linear component for solute uptake as a physiologically insignificant process, *i.e.* the result of diffusion into either the apoplast of plant tissues, or across the plasmalemma.

However, in the present study, we have shown that it is possible to selectively inhibit the linear component for $K^+$ uptake, either by inhibiting $Cl^-$ influx, or by the application of $K^+$ channel-blocking agents. The results from the $Cl^-$ replacement experiments suggest that there is a coupling between the presence of $Cl^-$ in the uptake solution and linear $K^+$ influx. It has been documented previously that $K^+$ influx from solutions containing $K_2SO_4$ is significantly lower than from KCl solutions (8, 23). Anion uptake may co-limit cation influx, and since $Cl^-$ is absorbed more rapidly than $SO_4^{2-}$, $K^+$ influx should be greater from KCl solutions. However, the similarity between $Cl^-$ (Fig. 3) and $NO_3^-$ (9) influx values obtained on corn roots suggests that a more complex situation may exist. We have shown that substitution of either $SO_4^{2-}$ or $NO_3^-$ for $Cl^-$ resulted in a similar reduction in the linear component of $K^+$ influx (Figs. 1 and 2), which suggests that the observed response may be specific for $Cl^-$ rather than a general coupling to anion transport.

The results of the experiments examining the influence of DIDS on the kinetics of $^{36}Cl^-$ and $K^+$ ($^{86}Rb^+$) influx offer additional support for the involvement of $Cl^-$ with linear $K^+$ uptake. The kinetics for $K^+$ influx following DIDS treatment (which abolished saturable $Cl^-$ influx) were almost identical to the kinetics observed when $Cl^-$ was removed from the uptake solution (Figs. 1 and 3). These results strongly suggest that linear component $K^+$ influx is linked to saturable $Cl^-$ uptake. It has been proposed that $Cl^-$ influx in plants is mediated by a proton-$Cl^-$ co-transport system (10, 19, 28). Hence, it seems reasonable to speculate that saturable $Cl^-$ influx is due to a proton-$Cl^-$ symport which is inhibited by DIDS, and is coupled, in some manner, to a linear $K^+$ transport system.

**Nature of the Linear Component.** Our TEA experiments allow us to speculate on the molecular nature of the transport system involved in nonsaturating (linear) $K^+$ influx in corn roots. The observation that 10 mM TEA caused a dramatic and specific inhibition of linear $K^+$ influx in high-salt roots (Fig. 5) clearly suggests that $K^+$ channels are involved. However, we were intrigued by the lack of TEA sensitivity observed for low-salt root linear $K^+$ influx. It is possible that, as in *Chara* (11, 18), the exposure to higher external levels of $K^+$ experienced by high-salt roots, causes a conformational change at the outer surface of the $K^+$ channels, which facilitates TEA binding (blockage).

An alternative explanation for the TEA insensitivity found in low-salt roots is that this tissue behaves in a similar manner to nerve axons, where it is necessary to inject TEA into the axoplasm to block $K^+$ channels (1, 30). A transport system for the uptake of the quaternary ammonium salt, choline, has been demonstrated in the roots of higher plants (22). Hence, the different TEA responses exhibited by high- and low-salt roots could be explained on the basis of the greater [$^{14}$C]TEA influx into high-salt roots (Fig. 6), which would develop higher levels of cytoplasmic TEA. If this were the case, $K^+$ channels could be involved in linear $K^+$ influx in both low- and high-salt roots; only in high-salt roots would the cytoplasmic TEA concentration rise to a level high enough to block $K^+$ channels at the cytoplasmic face of the plasmalemma.

The involvement of channels in linear $K^+$ influx, as opposed to enzyme-like carriers, would provide the most straightforward explanation for a carrier-mediated transport process that is difficult to saturate. A water-filled protein channel could incorporate such properties as specific radius, electrostatic properties at its mouth, and chemical- or voltage-induced conformational changes (gating), in such a way as to impart to it substrate specificity and control.

As Cohen (7) has pointed out, such a channel-mediated process may eventually saturate at high substrate concentrations. However, in his system (amino acid uptake into mouse brain slices), at high substrate levels, the medium changes from isotonic-buffered saline to hypertonic-buffered amino-acid saline. Any observed changes in transport kinetics may therefore be due to changes in media composition. The same applies for $K^+$ influx into corn roots. We have followed $K^+$ influx from a range of KCl concentrations up to 50 mM. At these high $K^+$ levels, we still saw no evidence for saturation, although the slope of the linear

component did decrease slightly. We were reluctant to study uptake from solutions of higher concentration, because we felt that at such ionic and osmotic levels, possible alterations in the membrane lipid/protein structure would make data interpretation doubtful.

**Relationship between $K^+$ Influx and $E_m$.** An important fact that is often ignored when analyzing $K^+$ influx kinetics is the relationship between changes in external $K^+$, $K^+$ influx, and cell membrane potential ($E_m$). It is generally accepted that $E_m$ comprises a large component of the driving force for $K^+$ influx, particularly at higher external $K^+$ levels (3, 4). It has also been well documented that as external $K^+$ concentrations are increased, depolarization of $E_m$ occurs, and the driving force for passive $K^+$ influx through the $K^+$ channel would be reduced (3, 4). Thus, the influence of $E_m$ on channel-mediated $K^+$ influx must be considered. The most detailed study to date concerning $K^+$ influx in plant roots from an electrophysiological viewpoint was conducted by Cheeseman *et al.* (3–5). They investigated the influence of anoxia, proton ionophores, and ATPase inhibitors on $K^+$ influx and $E_m$ over a range of $K^+$ concentrations. Based on their studies, they proposed that over low $K^+$ concentrations, uptake was an active and electrogenic process linked to a $H^+$-ATPase. At $K^+$ levels above approximately 1 mM (*i.e.* the range where the linear component dominates), they suggested that $K^+$ influx occurs via a passive electrophoretic uniport mechanism. This system mediates passive $K^+$ influx and is insensitive to ATPase inhibitors. It is quite possible that this second system described by Cheeseman *et al.* is the putative $K^+$ channel system responsible for linear $K^+$ uptake.

**Physiological Role for the Linear Component?** It has been noted that linear substrate influx often occurs over a concentration range which exceeds the levels normally experienced by roots in the soil, and so it is difficult to assign a physiological role to this system. For example, in corn roots, the linear component for $K^+$ influx becomes significant at $K^+$ levels above 1 mM. Reisenauer (26) has pointed out that the majority of soil $K^+$ is below 2 mM. What then would be the significance of a transport mechanism that operates at substrate levels rarely experienced by the plant? The answer to this question may come from transport studies conducted on *E. coli* and *Neurospora*. In both organisms, it has been well documented that multiple carrier systems are often involved in the transport of a single solute. These organisms tend to combine constitutive, low affinity, high capacity transport systems with derepressible high affinity systems; phospate or glucose uptake into *N. crassa* are excellent examples of this strategy (17, 29). These systems give the organism the adaptive advantage to most effectively obtain nutrients whose concentrations may vary considerably over a period of time. A root growing through the soil may often experience extermely low $K^+$ levels. Therefore, a high affinity system may be necessary in order for the plant to satisfy its requirements for this essential nutrient. However, if the growing root encounters a localized region of high soil $K^+$, the high affinity system may not have the capacity to utilize the excess $K^+$. In such a situation a low affinity system, represented by the linear component, would allow the plant to effectively utilize these pockets of high soil $K^+$. In this way, the plant may maintain a relatively efficient method of dealing with its varying environment.

## CONCLUSIONS

We have previously shown that it is possible to selectively inhibit the saturable component for $K^+$ influx into corn roots through the application of sulfhydryl modifiers (13, 14). Based on our earlier studies, we proposed that the complex $K^+$ uptake kinetics we observed were due to the combined operation of two transport systems, one saturable and one exhibiting linear, or first-order kinetics. In the present study, we have conducted a more detailed characterization of the linear component for $K^+$ influx. The selective inhibition of the linear component by either inhibiton of saturable $Cl^-$ uptake, or by the application of $K^+$ channel-blocking agents, suggests that this tranport process may represent flux through $K^+$ channels. It would also appear that these putative $K^+$ channels are coupled, in some way, to a saturable $Cl^-$ transport system.

## LITERATURE CITED


1. Armstrong CM 1969 Inactivation of the potassium conductance and related phenomena caused by quaternary ammonium ion injection in squid axons. J Gen Physiol 54: 553–575
2. Bennett AB, RM Spanswick 1983 Derepression of amino acid-$H^+$ cotransport in developing soybean embryos. Plant Physiol 72: 781–786
3. Cheeseman JM, JB Hanson 1979 Mathematical analysis of the dependence of cell potential on external potassium in corn roots. Plant Physiol 63: 1–4
4. Chesseman JM, JB Hanson 1979 Energy-linked potassium influx as related to cell potential in corn roots. Plant Physiol 64: 842–845
5. Cheeseman JM, PR LaFayette, JW Gronewald, JB Hanson 1980 Effect of ATPase inhibitors on cell potential and $K^+$ influx in corn roots. Plant Physiol 65: 1139–1145
6. Christensen HN, M Liang 1966 On the nature of the non-saturable migration of amino acids into Ehrlich cells and into rat jejunum. Biochim Biophys Acta 112: 524–531
7. Cohen SR 1975 A comparison of the rate equations, kinetic parameters, and activation energies for the initial uptake of L-lysine, L-valine, γ-aminobutyric acid, and α-aminoisobutyric acid by mouse brain slices. J Membr Biol 22: 53–72
8. Epstein E, DW Rains, OE Elzam 1963 Resolution of dual mechanisms of potassium absorption by barley roots. Proc Natl Acad Sci USA 49: 684–692
9. Jackson WA, D Flesher, RH Hageman 1973 Nitrate uptake by dark-grown corn seedlings. Some characteristics of apparent induction. Plant Physiol 51: 120–127
10. Jacoby B, B Rudich 1980 pH-gradient dependent $Cl^-$ flux in ATP depleted root cells, *In* RM Spanswick, WJ Lucas, J Dainty, eds, Plant Membrane Transport: Current Conceptual Issue. Elsevier Press, Amsterdam, pp 497–498
11. Keifer DW, WJ Lucas 1982 Potassium channels in *Chara corallina*. Control and interaction with the electrogenic $H^+$ pump. Plant Physiol 69: 781–788
12. Keifer DW, VR Franceschi, WJ Lucas 1982 Plasmalemma chloride transport in *Chara corallina*. Inhibition by 4,4′-diisothiocyano-2,2′-disulfonic acid stilbene. Plant Physiol 70:1327–1334
13. Kochian LV, WJ Lucas 1982 Potassium transport in corn roots. I. Resolution of kinetics into a saturable and linear component. Plant Physiol 70: 1723–1731
14. Kochian LV, WJ Lucas 1983 Potassium transport in corn roots. II. The significance of root periphery. Plant Physiol 73: 208–215
15. Lichtner FT, RM Spanswick 1981 Sucrose uptake by developing soybean cotyledons. Plant Physiol 68: 693–698
16. Lin W 1981 Inhibition of anion transport in corn root protoplasts. Plant Physiol 68: 435–438
17. Lowendorf HS, CL Slayman, CW Slayman 1974 Phosphate transport in *Neurospora*. Kinetic characterization of a constitutive, low affinity transport system. Biochim Biophys Acta 373: 369–382
18. Lucas WJ, RM Spanswick, J Dainty 1978 $HCO_3^-$ influx across the plasmalemma of *Chara corallina*. Physiological and biophysical influence of 10 mM $K^+$. Plant Physiol 61: 487–493
19. Marrè, E 1977 Effects of fusicoccin and hormones on plant cell membrane activities: Observations and hypothesis. *In* E Marrè, O Ciferri, eds. Regulation of Cell Membrane Activities in Plants. Elsevier Press, Amsterdam, pp 185–202
20. Maynard JM, WJ Lucas 1982 A reanalysis of the two-component phloem loading system in *Beta vulgaris*. Plant Physiol 69: 734–739
21. Maynard JW, WJ Lucas 1982 Sucrose and glucose uptake into *Beta vulgaris* leaf tissues. A case for general (apoplastic) retrieval systems. Plant Physiol 70: 1436–1443
22. Michaelis G, R Ehwald, H Göring 1976 Kinetik der Aufnahme von 2-Chlor-cholin-Ionen durch isolierte Wurzelspitzen von *Zea mays* L. Biochem Physiol Pflanzen 169: 241–247
23. Pitman MG 1964 Effect of divalent cations on the uptake of salt by beet-root tissue. J Exp Bot 15: 444–456
24. Pitman MG 1970 Active $H^+$ efflux from cells of low salt barley roots during salt accumulation. Plant Physiol 45: 787–790
25. Pitman MG, AC Courtice, B Lee 1968 Comparison of potassium and sodium uptake by barley roots at high- and low-salt status. Aust J Biol Sci 21: 871–881
26. Reisenauer HM 1966 Mineral nutrients in soil solution. *In* PL Altman, DS Dittmer, eds, Environmental Biology. Federation of American Societies for Experimental Biology, Bethesda, MD, pp 507–508
27. Rhoads DB, FB Waters, W Epstein 1976 Cation transport in *Escherichia coli*. VIII. Potassium transport mutants. J Gen Physiol 67: 325–341

28. SANDERS D 1980 The mechanism of $Cl^-$ transport at the plasma membrane of *Chara corallina*. I. Cotransport with $H^+$. J Membr Biol 53: 129–141
29. SCARBOROUGH GA 1970 Sugar transport in *Neurospora crassa*. II. A second glucose transport system. J Biol Chem 245: 3985–3987
30. TASAKI I, S HAGIWARA 1957 Demonstration of two stable potential states in the squid giant axon under tetraethylammonium chloride. J Gen Physiol 40 859–885
31. VAN BEL AJE, AC BORSTLAP, A VAN PINXTEREN-BAZUINE, A AMMERLAAI 1982 Analysis of valine uptake by *Commelina* mesophyll cells in a biphasi active and diffusional component. Planta 155: 335–341

Plant Physiol. (1987) 84, 1177–1184
0032-0889/87/84/1177/08/$01.00/0

# Fluxes of $H^+$ and $K^+$ in Corn Roots[1]

## CHARACTERIZATION AND STOICHIOMETRIES USING ION-SELECTIVE MICROELECTRODES

Received for publication February 23, 1987 and in revised form May 6, 1987

IAN A. NEWMAN, LEON V. KOCHIAN, MICHAEL A. GRUSAK, AND WILLIAM J. LUCAS*
*Physics Department, University of Tasmania, Hobart, Tasmania 7001, Australia* (I.A.N.); *United States Plant, Soil, and Nutrition Laboratory, United States Department of Agriculture, Agricultural Research Service, Cornell University, Ithaca, New York 14853* (L.V.K.); *and Botany Department, University of California, Davis, California 95616* (M.A.G., W.J.L.)

### ABSTRACT

**We report here on an experimental system that utilizes ion-selective microelectrodes to measure the electrochemical potential gradients for $H^+$ and $K^+$ ions within the unstirred layer near the root surface of both intact 4-day-old corn seedlings and corn root segments. Analysis of the steady state $H^+$ and $K^+$ electrochemical potential gradients provided a simultaneous measure of the fluxes crossing a localized region of the root surface. Net $K^+$ influx values obtained by this method were compared with unidirectional $K^+$ ($^{86}Rb^+$) influx kinetic data; at any particular $K^+$ concentration, similar values were obtained by either technique. The ion-specific microelectrode system was then used to investigate the association between net $H^+$ efflux and net $K^+$ influx. Although the computed $H^+$:$K^+$ stoichiometry is dependent upon the choice of diffusion coefficients, the values obtained were extremely variable, and net $K^+$ influx rarely appeared to be charge-balanced by $H^+$ efflux. In contrast to earlier studies, we found the cortical membrane potential to be highly $K^+$ sensitive within the micromolar $K^+$ concentration range. Simultaneous measurements of membrane potential and $K^+$ influx, as a function of $K^+$ concentration, revealed similar $K_m$ values for the depolarization of the potential ($K_m$ 6–9 micromolar $K^+$) and net $K^+$ influx ($K_m$ 4–7 micromolar $K^+$). These data suggest that $K^+$ may enter corn roots via a $K^+$-$H^+$ cotransport system rather than a $K^+$/$H^+$ antiporter.**

A significant proportion of the research on both intact and excised roots has been based on techniques such as radioisotope flux analysis, quantification of the ionic content of bulk root tissue following ion absorption, or studies monitoring the depletion of a particular ion in the solution surrounding the root. While these approaches have provided data that have led to the development of a general understanding of the mechanism(s) and regulation of ion transport processes in roots, these techniques possess similar shortcomings. First, all of these techniques tend to average ion uptake over the entire root surface, and second, they time-average ion uptake over the course of the uptake period, which can range from several minutes to many hours. Thus, these techniques cannot be employed to study transients, or transport events associated with a small number of cells at the root surface.

Recent improvements in ion-selective microelectrode technology now allow the routine construction of neutral, carrier-based, liquid membrane microelectrodes for $H^+$ and $K^+$ (14, 15). We report here on a system which utilizes these microelectrodes to measure the extracellular electrochemical potential gradients for $H^+$ and $K^+$ ions along intact roots of 4-d-old corn seedlings. Using this system, we have been able to simultaneously determine the 'instantaneous' net $H^+$ and $K^+$ fluxes associated with a localized region on the corn root. Whereas it has generally been accepted that $K^+$ uptake in roots is coupled to the efflux of $H^+$, either directly through the action of a $H^+$/$K^+$ ATPase (8, 18), or indirectly via electrical coupling to a $H^+$ translocating ATPase (1, 6, 17), we obtained no experimental support for this putative coupling. Based on our instantaneous flux and electrophysiological data, we propose that $K^+$ influx into corn roots occurs via a $H^+$-$K^+$ cotransport mechanism.

## MATERIALS AND METHODS

**Plant Material.** *Zea mays* seeds (3377 Pioneer) were imbibed, germinated, and grown under low salt (0.2 mM $CaSO_4$) conditions as previously described (11, 12). Seedlings (4-d-old) having straight primary roots, 12 to 16 cm long, were used. In some experiments, 7 cm long root segments were employed. These segments were obtained by cutting the primary root at 1 cm and 8 cm from the tip and were washed for 4 h in aerated 0.2 mM $CaSO_4$ before experimental use.

**Experimental Chamber and Conditions.** The root was placed horizontally along the center of a Plexiglas chamber that was 20 cm long, 3 cm deep, and 4 mm wide. The seed and other roots, when present, were housed in an adjoining chamber. Support for the root was provided by fine stainless steel pins, positioned 5 mm above the floor of the chamber, with the surface of the bathing solution being 1.5 cm above the root. Because the corn root is slightly less dense than water, the tip was held in position by a soft plastic wedge located 5 mm from the root tip. When root segments were used, the proximal end was held down by a silk thread, looped around the root and under a stainless steel pin; attachment to the seed provided adequate anchorage for intact roots. The root was centered within the chamber by means of vertical Plexiglas guides glued to the lateral walls of the chamber.

Solutions were unbuffered to allow maximum $H^+$ gradients to develop. Changing of the experimental solution within the chamber was achieved either by flowing new solution through the chamber (1 min) or by draining and refilling (3 times). Solution temperatures were held at 24 ± 1°C.

**Microelectrode Techniques.** We used a Ag/AgCl/3 M KCl (in 0.7% agar) combination as the grounded reference electrode. In our initial experiments this reference electrode was located in the experimental chamber. However, diffusion of KCl from the

[1] Supported by National Science Foundation grant DMB 8503153 to W. J. L.

agar resulted in a slow rise in $K^+$ concentrations (see Fig. 2). To prevent this contamination from occurring, the reference was located at the end of a 3 cm tube which extended from the base of the chamber and contained the same bathing solution as the chamber.

Extracellular electric potential measurements near the root surface were made using standard microelectrode techniques, except that the micropipette (0.5 $\mu$m tip diameter) was filled with 0.2 M $Na_2SO_4$ to avoid local changes in $K^+$ and $Cl^-$ concentrations. Potentials near the root were measured with respect to the background bathing medium; the amplifier used allowed a precision of 10 $\mu$V.

Liquid membrane-type neutral carrier-based ion-selective microelectrodes were constructed as previously detailed (15). Proton and $K^+$ electrodes were prepared using Fluka cocktails ($H^+$: 82500 and $K^+$: 60031; Fluka Chemical Co.). For extracellular ion-selective microelectrode measurements, the micropipettes were initially broken back to a diameter of 5 $\mu$m. Later experiments employed microelectrodes without broken tips (tip diameter = 0.5 $\mu$m). Microelectrodes of both tip diameters yielded similar responses. Electrodes prepared from these micropipettes had tip resistances of approximately 3 Gohms and gave fast, stable responses to concentration changes. Each ion-specific microelectrode was calibrated against a known set of pH buffers or standard $K^+$ solutions before and after each experiment, to ensure against electrode drift.

Microelectrodes were mounted in pressure-relieved holders (type MEH-1S, WP Instruments, Inc., New Haven, CT) on preamplifiers of a $10^{15}$ Ohm input resistance dual electrometer (model FD No. 223, WP Instruments, Inc.). The preamplifiers holding the $H^+$ and $K^+$ microelectrodes were mounted on a dual micromanipulator (model 520143, E. Leitz Inc., Rockleigh NJ) which allowed the two tips to be placed very close together (10 $\mu$m). This micromanipulator was mounted on a combination of Narishige manipulators which were affixed to the stage of a Zeiss compound microscope. A third Narishige micromanipulator was used to hold the extracellular electric potential electrode. With this combination, all three microelectrode tips could be placed together, within a 15 to 20 $\mu$m horizontal separation, and lowered into the solution to reach chosen radial distances from the axis of the root (Fig. 1).

The root and vertically positioned microelectrodes were viewed under high magnification (×100–320) by the Zeiss compound microscope whose optical axis was both horizontal and at right angles to the root axis. The manipulator for the microelectrodes was affixed to the (vertical) stage of the microscope. The experimental chamber containing the root was attached to the laterally moving slide holder on the stage so that the entire length of the root could be scanned, the microelectrode tips remaining fixed within the field of view. Observations were generally made at positions 2, 3, 4, 5, and 6 cm from the root tip. These were chosen to be within mature tissue behind the elongation region but before the region of developing root hairs, or lateral roots. Most data were obtained from positions at 3 or 5 cm from the tip of intact roots, there being no consistent difference between the responses at those two positions. Measurements of electric potential, $H^+$, and $K^+$ concentrations were made at radial positions 15, 80, 230, and 620 $\mu$m from the root surface. Measurements were made by advancing the electrodes inwards from 620 $\mu$m down to 15 $\mu$m and then out again to 620 $\mu$m, making seven measurements of the three variables. Average values were used in the flux calculations; measurements at the 620 $\mu$m position approximated that of the 'bulk solution.'

**Electrophysiological Studies.** Membrane potentials were measured using a WPI model 750 amplifier (WP Instruments) and microelectrodes (tip diameter = 0.5 $\mu$m) made from single-barrelled borosilicate glass tubing (Catalog No. 1B100F-4; WP

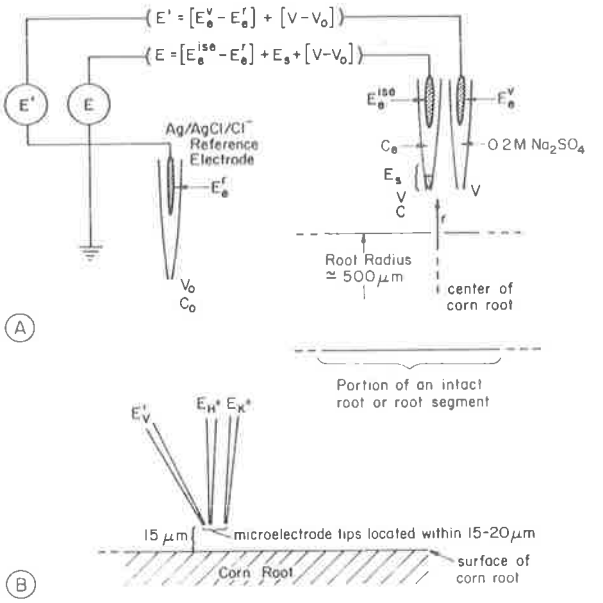


FIG. 1. Schematic representation of the ion-specific microelectrode system used to measure the $K^+$ and $H^+$ electrochemical potential gradients which develop at the surface of corn roots. The individual voltage components are shown in (A): $E_e^r$ and $E_e^{ise}$ represent the EMF of the half cells for the reference and ion-specific electrode, respectively (in the text we refer to $[E_e^{ise} - E_e^r]$ as $E_e$); $E_e^v$ is the EMF of the half cell for the extracellular electric potential electrode; $E_s$ is the potential developed across the liquid ion-exchange resin (stippled area); $V$ and $V_0$ are the extracellular potentials near the root surface and in the background bathing solution, respectively, $E$ and $E'$ are the electrometers used to measure the voltages generated by the ion-specific and extracellular potential electrodes, respectively. A scaled representation of the relative positions of $K^+$ ($E_{K^+}$), $H^+$ ($E_{H^+}$) and extracellular potential ($E_v'$) electrodes is given in (B). Here we show the microelectrodes (tip diameter = 0.5 $\mu$m) at their closest position to the root surface.

Instruments). The microelectrodes were filled with 3 M KCl (adjusted to pH 2 to reduce tip potentials). Cells of the root cortex were impaled using the Narishige micromanipulator that was normally used to position the extracellular electric potential microelectrode.

For experiments in which membrane potentials and net $K^+$ fluxes were simultaneously measured, two microelectrodes were affixed to the Narishige micromanipulators and positioned 15 and 80 $\mu$m from the root surface. The second Narishige micromanipulator was then used to impale the root for measurements of membrane potential. This system was used to allow us to continuously monitor $K^+$ fluxes and membrane potentials without moving the micromanipulators.

**Radioisotope Influx Experiments.** Short-term (10 min) $^{86}Rb^+$ influx experiments were performed using 2 cm root segments as detailed previously (11, 12). These experiments were conducted in order to provide a comparison between the net $K^+$ influx values obtained by the microelectrode-diffusion analysis method and $K^+$ influx obtained with radioisotopes. Briefly, experiments were performed with 2-cm root segments cut from the second through fourth cm of the primary root. Uptake was initiated by the addition of $^{86}Rb^+$ (as RbCl; New England Nuclear) and terminated by the vacuum withdrawal of radioisotope solution. Free space radiolabel was removed by two 8-min washes in an ice-cold solution of 5 mM $CaCl_2$ + 1 mM KCl. The uptake solutions were identical to those used in the $K^+$ microelectrode flux studies and consisted of unbuffered solutions of various concentrations of $K_2SO_4$ + 0.2 mM $CaSO_4$. The initial pH of the unbuffered solutions was approximately 5.7 and usually fell to

about 5.5 by the end of the 10-min uptake period.

**Theory Underlying Flux Calculations.** In an experimental system in which convection is minimal, and in which the coordinates of cylindrical symmetry apply (which we established for $K^+$ and $H^+$ by experimental measurement), the radial net flux density, $J$, of an ion is given by:

$$J = -(D/RT)C(d\bar{\mu}/dr) \qquad (\text{mol}\cdot\text{m}^{-2}\cdot\text{s}^{-1}) \qquad (1)$$

where $D$ is the diffusion coefficient for the ion, and $C$ its concentration at the radial position $r$ (measured from the center of the root), and $\bar{\mu}$ is the electrochemical potential for the ion of interest (of valency $z$) and is given by:

$$\bar{\mu} = \bar{\mu}_0 + RT\ln(C/C_0) + zF(V - V_0) \qquad (2)$$

In this expression, we have set $\bar{\mu}_0$ as the electrochemical potential at a distant point where the electric potential is $V_0$ and the concentration is $C_0$. The electric potential at the radial position $r$ is represented by $V$ ($F$, $R$, and $T$ have their usual meanings).

In order to compute the ionic flux, and to examine the relative importance of the electric and concentration gradients, in terms of the driving force on the flux, it is necessary to develop the relationship between the flux equation and the voltage measured by the electrometer. As illustrated in Figure 1, the actual voltage measured by the electrometer is a complex parameter given by:

$$E = E_e = E_s + (V - V_0) \qquad (3)$$

Here, $E_e$ is a constant contribution from the reversible Ag/AgCl/$Cl^-$ half cells whose junction potentials are constant but not necessarily equal. $E_s$ is the potential difference across the sensor in the microelectrode tip, through which the ion is in electrochemical potential equilibrium. In practice, the ion may not behave ideally across the sensor, and so we introduce a factor $g$, constant for a particular ion and usually near unity, and write the appropriate Nernst expression as:

$$E_s = g\frac{RT}{zF}\ln(C/C_e) \qquad (4)$$

where $C_e$ is the constant concentration of the ion within the electrode filling solution.

It is convenient to write $(C/C_e) = (C/C_0)(C_0/C_e)$ and to define $\beta = gRT/(zF)$. Then equation 4 becomes:

$$E_s = \beta\ln(C/C_0) + \beta\ln(C_0/C_e) \qquad (5)$$

The second term on the right of equation 5 is constant for all measurements in a given solution and thus it may be combined with $E_e$ to form a parameter $E_0$ which depends on the reference concentration $C_0$ in the solution:

$$E_0 = E_e + \beta\ln(C_0/C_e) \qquad (6)$$

The electrometer reading is then expressed as:

$$E = E_0 + \beta\ln(C/C_0) + (V - V_0) \qquad (7)$$

When the microelectrode and the reference electrode are in a standard solution of known, uniform concentration, $C = C_0$ and $V = V_0$. In this case, equation 7 reduces to $E = E_0$ and provides the reference value of $E_0$ needed for that concentration, $C_0$. The difference between the $E$ values measured in two known solutions allows the factor $\beta$, and hence $g$, to be calculated. If $g = 1$, then $\beta$ has its Nernst value of 25.6 mV per $e$-fold concentration change, at 24°C.

To calculate the flux, we use equation 7 to substitute for the $\ln(C/C_0)$ term in equation 2. Hence,

$$\bar{\mu} = \bar{\mu}_0 + (E - E_0)RT/\beta - (V - V_0)RT/\beta + zF(V - V_0) \qquad (8)$$

*i.e.*

$$\bar{\mu} - \bar{\mu}_0 = (RT/\beta)([E - E_0] + [g - 1][V - V_0]) \qquad (9)$$

Substituting equation 9 into equation 1, and noting that $E_0$, $V_0$, and $\bar{\mu}_0$ are constant, we obtain:

$$J = -(DC/\beta)([dE/dr] - [1 - g][dV/dr]) \qquad (10)$$

This flux density depends on the radial position. We wish to know the total flux, $\phi$, emerging radially from unit length of root. This is:

$$\phi = 2\pi rJ \qquad (\text{mol}\cdot\text{m}^{-1}\cdot\text{s}^{-1}) \qquad (11)$$

If we divide by $A\rho$, where $A$ is the cross-sectional area of the root and $\rho$ is the density in $SI$ units, and scale by $3.6 \times 10^6$, we obtain the flux, $\phi$, in the usual units:

$$\phi = 3.6 \times 10^6(2\pi r/A\rho)J \qquad (\mu\text{mol}\cdot\text{g}^{-1}\cdot\text{h}^{-1}) \qquad (12)$$

Substituting for $J$, from equation 10, into equation 12 and defining the constant $\kappa = 7.2 \times 10^6\pi D/(A\rho\beta)$, we obtain:

$$\phi = -\kappa Cr([dE/dr] - [1 - g][dV/dr]) \qquad (13)$$

Integration of equation 13 between two closely spaced radii, $r_1$ to $r_2$, and making the assumption that $C$ is nearly constant and can be replaced by the mean of the concentrations at those two radii, $\frac{1}{2}(C_2 + C_1)$ yields:

$$\phi = \tfrac{1}{2}\kappa(C_2 - C_1)([E_2 - E_1] - [1 - g]\cdot[V_2 - V_1])/\ln(r_1/r_2) \qquad (14)$$

The concentrations $C_1$ and $C_2$ can be established with sufficient accuracy from equation 7, which may be rewritten as:

$$C = C_0\exp([E - E_0]/\beta)\cdot\exp([V_0 - V]/\beta) \qquad (15)$$

In the present work for both $K^+$ and $H^+$, the value of $V_0 - V$, measured independently of $E$ via the extracellular electric potential electrode, was rarely as much as 1 mV. Since the value of $\beta$ is about 25 mV, the term $\exp([V_0 - V]/\beta)$ is at most 4% different from unity, so it was treated as unity. Hence, from equation 15, the sum of the two values of $C$ can be given by:

$$C_2 + C_1 = C_0\exp[(E_2 - E_0)/\beta] + \exp[(E_1 - E_0)/\beta])$$

Substituting into equation 14 gives the final equation to be used for the net flux:

$$\phi = \tfrac{1}{2}\kappa C_0(\exp[(E_2 - E_0)/\beta] + \exp\cdot[(E_1 - E_0)/\beta])(E_2 - E_1)/\ln(r_1/r_2) \qquad (16)$$

In equation 16, the term in $(1 - g)(V_2 - V_1)$ has been neglected because in the present work the difference in the electric field is small compared with $(E_2 - E_1)$, and $(g - 1)$ is near zero ($g = 0.97$ for $H^+$, and $g = 0.92$ for $K^+$). However, the term should be included for electrodes that have smaller values of $g$ or when $\Delta V$ is significant.

As detailed above, electrochemical potential gradients were calculated from measurements at two close points on a radius, so that the concentration difference and electrical potential differences between them were both small. The two points chosen were those at 15 and 80 $\mu$m from the root surface. These points were at about 500 $\mu$m from the axis of a typical root. The following values of the diffusion coefficients *D° were used: for $H^+$, $9.17 \times 10^{-5}$ cm$^2\cdot$s$^{-1}$, and for $K^+$, $1.9 \times 10^{-5}$ cm$^2\cdot$s$^{-1}$. These values represent the modified self diffusion coefficients that appear to be applicable to conditions of low ionic strength (19). Calculations based on these self-diffusion coefficients generated the maximum possible $H^+$ efflux; the limiting diffusion coefficients would reduce the $H^+/K^+$ flux ratio by a factor of 2.75. Finally, we employed self diffusion coefficients, rather than limiting equivalent ionic conductances, because our preliminary

studies revealed that in the presence of 0.2 mM $CaSO_4$ and 0.1 mM $K_2SO_4$, the electrical component of the electrochemical potential gradient was very small in comparison with the concentration component.

## RESULTS

**Net $H^+$ Efflux in the Presence of Low $K^+$.** In our initial experiments we wished to characterize net $H^+$ efflux that occurred in the presence of very low concentrations of transportable cations. To this end, we conducted experiments on intact and excised roots bathed in 0.2 mM $CaSO_4$; since this solution also contained 0.2 $\mu$M $K^+$ as a contamination, we also made parallel measurements of net $K^+$ influx. With intact roots, large fluctuations in net $H^+$ efflux were observed (Fig. 2A); efflux from root segments appeared to be more stable (Fig. 2B). Although we generally observed a net $H^+$ efflux along the root, there were times when $H^+$ influx was detected (Fig. 2A). These regions of net $H^+$ influx were generally associated with a region on the root where the radial $H^+$ activity gradient was consistent with net $H^+$ influx. However, we occasionally observed a situation where the outer radial $H^+$ activity gradient was declining, indicating general $H^+$ efflux, but the radial gradient near the root surface was reversed. Such a situation was found for the 28 and 99 min measurements made at the 2 cm position illustrated in Figure 2A. We suggest that these unusual profiles are the result of $H^+$ influx, localized to a few adjacent cells on the root, occurring against a general background of net $H^+$ efflux.

A substantial variation of $H^+$ efflux, with position along the root, was found at any one time. For a sample of 7 intact roots we found no consistent trend with position from the 2 to 5 cm position (measured from the root apex). However, based on measurements made on four root segments, the $H^+$ efflux at 5 cm was twice the efflux at 3 cm, the difference being statistically significant at the 3% level.

Associated with the reduced variability of proton efflux along excised roots (as compared with intact roots), there was also a reduction in $H^+$ efflux. For example, for measurements made at the 3 cm position (Fig. 2B), $H^+$ efflux declined from an initial value of 0.82 $\mu$mol $g^{-1}$ $h^{-1}$ to near zero after 40 min, and remained at this value for the rest of the experiment. This result suggests that some care should be exercised with root segments that have been removed from the intact plant for long periods of time, which in the case presented in Figure 2B was about 7 h (4-h wash followed by 3 h for flux measurements).

A representative time-course for $K^+$ influx into intact roots and root segments bathed in 0.2 mM $CaSO_4$ is shown in Figure 2, A and B, respectively. The gradual increase in net $K^+$ influx, over time, was due to the import of $K^+$, into the experimental chamber, by diffusion from the reference electrode; the initial concentration was generally 0.2 $\mu$M $K^+$ and this rose to approximately 20 $\mu$M over a 2-h period. These simultaneous measurements of net $H^+$ efflux and net $K^+$ influx revealed that the base-level of $H^+$ efflux did not increase as the $K^+$ influx rose, due to the increasing level of $K^+$ available in the medium. For excised root segments, a negative correlation was observed in that as the $K^+$ influx increased, net $H^+$ efflux declined (see Fig. 2B).

**Localized Net $H^+$ and $K^+$ Fluxes.** We next conducted experiments in which intact roots were pretreated, in 0.2 mM $CaSO_4$, for 130 min before 0.2 mM $K^+$ was introduced as $K_2SO_4$. (By relocating the reference electrode, we prevented the previous rise in $K^+$ concentration.) During the pretreatment period, we monitored the fluxes of $H^+$ and $K^+$, as in Figure 2.

Typical data of the intact root response to a step-wise increase in $K^+$, from <1.0 $\mu$M to 0.2 mM, is presented in Figure 3. Net $K^+$ influx increased rapidly from less than 0.03 to about 2 $\mu$mol $g^{-1}$ $h^{-1}$, which was followed by a slower increase towards a steady state value of 2.5 $\mu$mol $g^{-1}$ $h^{-1}$ (average obtained from six experiments). The introduction of 0.2 mM $K^+$ appeared to elicit a biphasic transient in net $H^+$ efflux, there being an initial decrease, followed by a recovery phase. At the end of this recovery phase, net $H^+$ efflux generally underwent a small increase to a value (1.81 $\mu$mol $g^{-1}$ $h^{-1}$, $n = 6$) slightly above that measured in the absence of $K^+$ (1.30 $\mu$mol $g^{-1}$ $h^{-1}$, $n = 6$), and the root did not respond to an application of fresh $K_2SO_4$ solution (Fig. 3). Thus, also under high $K^+$ concentrations, we did not find a close correlation between the large increase in net $K^+$ influx and the small change in net $H^+$ efflux.

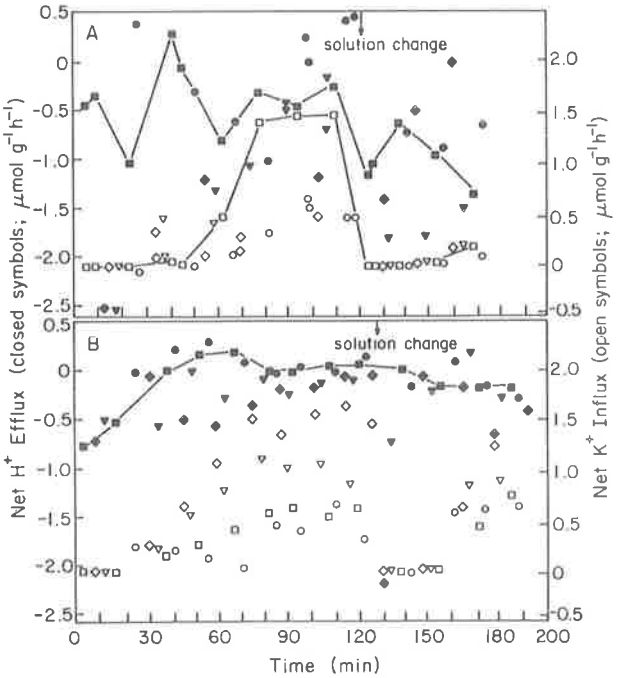


FIG. 2. Net apparent fluxes of $H^+$ (closed symbols), and $K^+$ (open symbols) for (A) an intact corn root and (B) a 7-cm-long root segment (washed for 4 h following excision). The bathing solution consisted of 0.2 mM $CaSO_4$. The $K^+$ concentration in the bathing solution rose with time from an initial value of near 0.2 $\mu$M, to about 20 $\mu$M (in A) or about 80 $\mu$M (in B) after 2 h. At this time the solution was replaced with fresh 0.2 mM $CaSO_4$. Measurements were made at the following distances back from the root apex: 2 cm (○), 3 cm (□), 4 cm (△), and 5 cm (◇). A line has been drawn through the data points obtained at the 3 cm position to give an idea of trends and variability of the data. For the *Y* axis labeled $H^+$ efflux, a negative value indicates net $H^+$ efflux, while a positive value for $K^+$ flux indicates net $K^+$ influx.

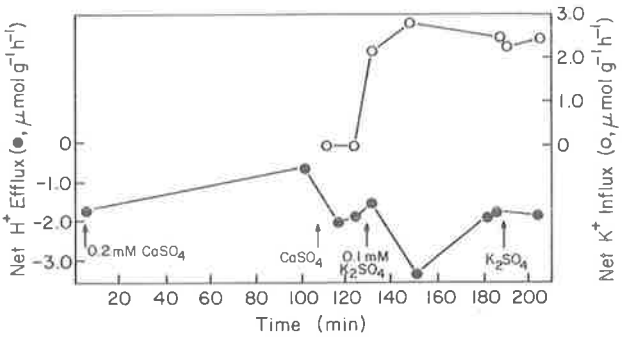


FIG. 3. Measurements of $H^+$ efflux (●) and $K^+$ influx (○) are shown at representative times following the application of a 0.2 mM $CaSO_4$ solution, and then solution containing $CaSO_4$ + 0.1 mM $K_2SO_4$. (Before the application of $K_2SO_4$ solution at 130 min, the $K^+$ concentration in solution was <1 $\mu$M).

Experiments of this type were also conducted on excised root segments and similar results were obtained (data not shown).

**Kinetics of $K^+$ Influx.** In order to compare the net $K^+$ influx values obtained by diffusion analysis, with influx values, measured by radioisotopic methods, we conducted a $^{86}Rb^+$ experiment. We deemed this necessary because the present experiments were performed on a Pioneer cultivar of *Zea mays*, while our earlier kinetic studies were conducted on a cultivar (A632×OH 43) from Crows Hybrid Corn Co. (11–13). The kinetic parameters obtained from this $^{86}Rb^+$ study (Fig. 4) were as follows: $V_{max}$ = 2.91 $\mu$mol $g^{-1}$ $h^{-1}$, apparent $K_m$ = 22 $\mu$M. These unidirectional $K^+$ influx values were very similar to the computed net $K^+$ influx values obtained with our $K^+$ microelectrode system. Michaelis-Menten analysis of the net $K^+$ influx *versus* $K^+$ concentration data, that were obtained from the data presented in Figure 2, yielded $V_{max}$ values of 3.5 and 1.5 $\mu$mol $g^{-1}$ $h^{-1}$ for intact roots and root segments, respectively, and apparent $K_m$ values of 10.4 $\mu$M (intact roots) and 4.2 $\mu$M (root segments). (These values were obtained by measuring the time-dependent increase in $K^+$ influx as the bathing solution $K^+$ concentration rose from 0.2–20 $\mu$M.) These low apparent $K_m$ values, obtained from microelectrode experiments, reflect the increased accuracy of determining the $K^+$ concentration at the root surface. We will pursue this advantage further in a later section.

**Influence of $Cl^-$ on $H^+$ and $K^+$ Fluxes.** In comparison to the introduction of $K^+$ as $K_2SO_4$, 0.2 mM KCl caused a transient dramatic reduction in $H^+$ efflux. For the example shown in Figure 5 (curve HA), it can be seen that after addition of $Cl^-$ to the bathing solution, net $H^+$ efflux was reduced within the first few minutes from its pretreatment value of 2.06 $\mu$mol $g^{-1}$ $h^{-1}$ to an actual transient $H^+$ influx (Fig. 5, curve HA). This decline in $H^+$ efflux was found to occur irrespective of the prior presence of $K^+$. Following this initial transient, $H^+$ efflux returned to a steady state value that was about one-half the $H^+$ flux that was measured in $K_2SO_4$ (Fig. 5, curve HB, dotted line). Again, this occurs whether or not the root has been previously exposed to $K_2SO_4$.

The increase in $K^+$ influx, in response to the application of KCl, was similar to the increase observed following the introduction of $K_2SO_4$ (Fig. 5, curves KA and KB). Although in the experiment presented in Figure 5, net $K^+$ influx in the presence

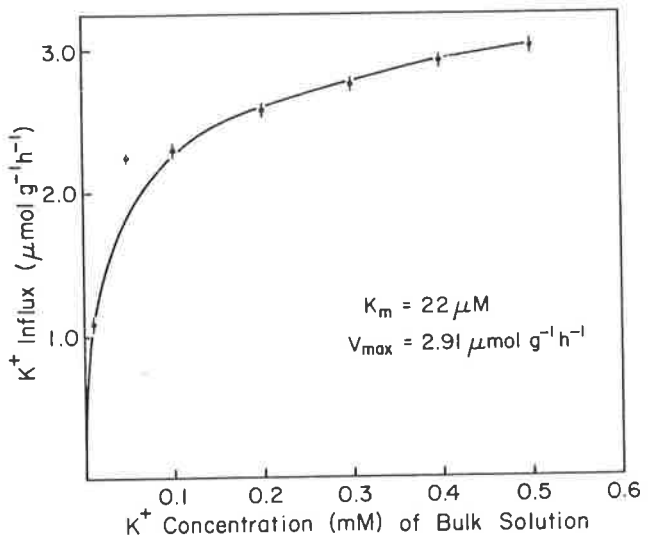


FIG. 4. Kinetic curve for $K^+$ ($^{86}Rb^+$) influx into 4 h-washed corn root segments excised from the 2 to 4 cm region behind the root apex. Uptake solution consisted of various concentrations of $K_2SO_4$ plus 0.2 mM $CaSO_4$. Solution pH was initially approximately 5.7 and dropped to about 5.5 during the 10 min uptake period.

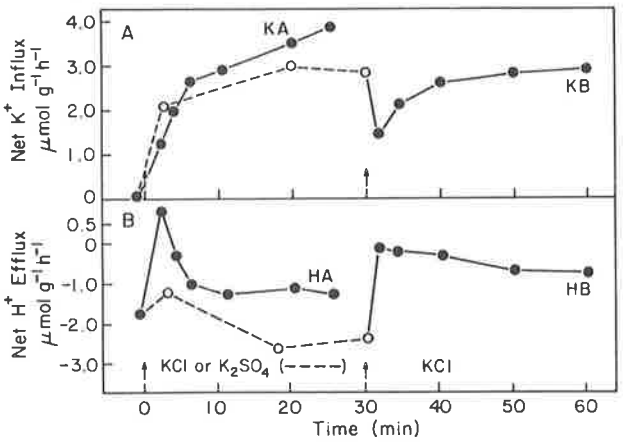


FIG. 5. Influence of 0.1 mM $K_2SO_4$ or 0.2 mM KCl on net fluxes of $K^+$ (A) and $H^+$ (B) into intact corn roots. A pretreatment of 90 min in 0.2 mM $CaSO_4$ was employed prior to commencing the KCl or $K_2SO_4$ treatments. $K^+$ and $H^+$ fluxes measured initially in KCl solution are labeled KA and HA, respectively (——). The dotted lines drawn through the data points for $H^+$ and $K^+$ fluxes measured over the first 30 min (○) depict fluxes determined in $K_2SO_4$ solution. At 30 min, the solution bathing these roots was changed to a 0.2 mM KCl solution, and these traces are labeled KB and HB for the subsequent $K^+$ and $H^+$ fluxes, respectively (——, ●).

of $Cl^-$ was slightly higher than the flux in $K_2SO_4$, we found that when a number of such experiments were compared this difference was not statistically significant. However, it is important to note that in these experiments, again the steady state net $K^+$ fluxes greatly exceeded net $H^+$ efflux.

**Electrophysiological Studies.** The response of the cortical root cell membrane potential to changes in $K^+$ level in the bathing solution has been investigated by several workers. A detailed study on corn roots was conducted by Cheeseman and Hanson (3, 4), who reported that the plasmalemma of corn root cells was sensitive to changes in external $K^+$, once the concentration reached approximately 20 $\mu$M. An increase in the $K^+$ concentration from 20 $\mu$M to 0.2 mM elicited a 30 mV depolarization of the membrane potential from −150 to −120 mV. This sensitivity of the membrane potential is above the apparent $K_m$ of the high-affinity $K^+$ transport mechanism described in the present study.

In our preliminary electrophysiological studies on corn roots, we were surprised to find that in our system the corn root membrane potential was extremely sensitive to low levels of $K^+$. Increasing the $K^+$ concentration from <0.2 to 20 $\mu$M (as 10 $\mu$M $K_2SO_4$) caused a 70 mV depolarization of the membrane potential, from −190 to −120 mV (Fig. 6). Following this depolarization, the membrane potential remained stable at approximately −120 mV. A further increase in the $K^+$ concentration to 0.2 mM $K^+$ (as $K_2SO_4$) only elicited a further 7 mV depolarization (Fig. 6). Similar responses were observed when $Cl^-$ was used as the accompanying anion for $K^+$ (data not shown).

In view of the high-$K^+$ sensitive state of the membrane potential, we conducted experiments in which we simultaneously monitored the response of the membrane potential to changes in external $K^+$ and measured the net $K^+$ influx occurring at these concentrations. This was accomplished by utilizing a three-microelectrode system; one microelectrode was impaled into a cortical cell of the root, to monitor changes in the membrane potential, while two $K^+$ microelectrodes were positioned 15 and 80 $\mu$m from the root surface, in order to continuously record the extracellular $K^+$ activity gradient and, hence, allow us to compute net $K^+$ fluxes. The response of the membrane potential to sequentially increasing (closed circles) and then decreasing (open circles) the external $K^+$ concentration is presented in Figure 7.

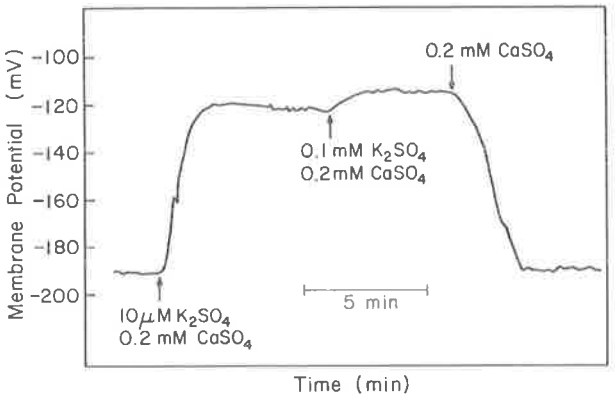


FIG. 6. Response of the cortical membrane potential of intact low-salt-grown corn roots to changes in the concentration of external $K^+$ (as $K_2SO_4$). ($CaSO_4$ was present at 0.2 mM in all solutions.)

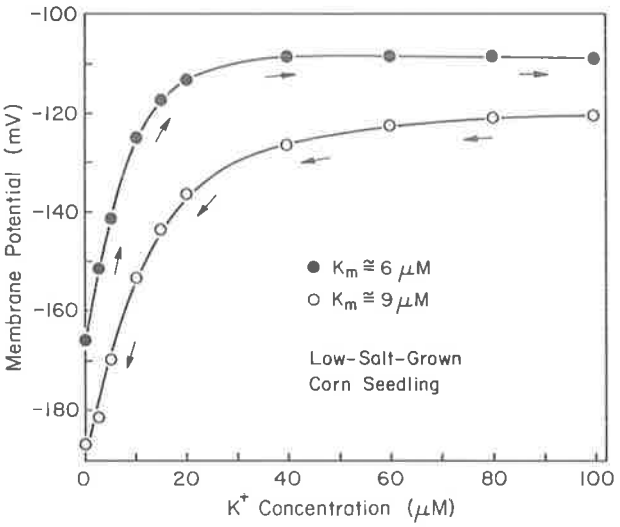


FIG. 7. Response of the membrane potential, measured in intact low-salt-grown corn roots, to either sequentially increasing (●) or decreasing (○) the external $K_2SO_4$ concentration. $CaSO_4$ (0.2 mM) was included in all solutions. Experimental solution containing the required $K^+$ concentration was flowed rapidly past the root; at the time a measurement was to be taken, flow was stopped and a steady state diffusion profile near the root surface was allowed to develop (approximately 5 min). Subsequently, both the membrane potential and the external $K^+$ concentration in the unstirred layer at 15 and 80 $\mu$m from the root surface, were measured.

Analysis of the depolarization revealed an 'apparent $K_m$' of 6 $\mu$M $K^+$, while a value of 9 $\mu$M $K^+$ was computed for the reverse, repolarization phase. It is interesting to note that all of the values obtained during the repolarization sequence were more negative (by about 20 mV), than those obtained when the external $K^+$ concentration was increased for the first time. When the external $K^+$ concentration was again increased sequentially, the values obtained for the membrane potential were found to lie on this lower, more negative curve (data not shown). It appears that the initial exposure of these low-salt-roots to $K^+$ causes a permanent change in the electrical properties of the corn root cortical plasma membrane.

The $K^+$ fluxes that were recorded simultaneously during these changes in membrane potential are presented as a kinetic response curve in Figure 8. Only the $K^+$ fluxes obtained over the low $K^+$ concentrations are presented, since these data reflect the region of highest experimental accuracy. Using the data presented in Figure 8, we performed a kinetic analysis which yielded a $K_m$

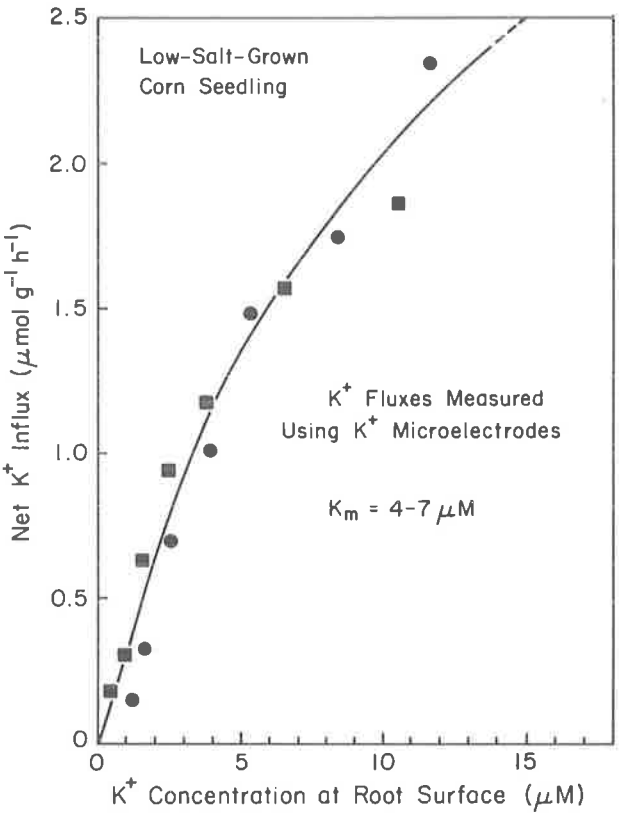


FIG. 8. Kinetic curve for net $K^+$ influx (measured with $K^+$-specific microelectrodes) as a function of the $K^+$ concentration present at the root surface. Flux experiments were conducted simultaneously with the measurement of membrane potential, as described in Figure 7.

value in the range of 4 to 7 $\mu$M. This value is very close to the $K_m$ obtained for the membrane potential response to changing $K^+$ concentration and again underscores the sensitivity of these cells to $K^+$ changes in the $\mu$M concentration range. The results of these combined electrophysiological and ion-selective electrode studies indicate that corn roots possess a very high-affinity $K^+$ uptake system and, based on the dramatic depolarization of the membrane potential by $\mu$M $K^+$ levels, it would appear that this transport system must be highly electrogenic.

## DISCUSSION

**$H^+$ Efflux.** In view of the small tip diameter of the ion-selective microelectrodes, our present study presumably relates to fluxes that are associated with several cells at the root surface, rather than the entire organ. Hence, it is not surprising that we observed some rather dramatic fluctuations in fluxes measured at any one location over a period of time. This is particularly true for the $H^+$ fluxes, which can change quite significantly with time (Fig. 2). Indeed, we often observed changes in $H^+$ flux at any one point that varied from a moderately large efflux (approximately 1.65 $\mu$mol $g^{-1}$ $h^{-1}$) to zero flux, and even in some cases a moderate $H^+$ influx was observed.

It is difficult to explain these endogenous variations at this time, but these phenomena indicate that proton fluxes are probably involved in a number of associations such as various symports, antiports, and possibly current loops. In particular, $H^+$ flux must be accompanied by other ionic fluxes in order to maintain charge balance. It is also possible that fluxes into other parts of the root may be carried by ions other than protons. Ion current loops were proposed by Scott and Martin to fit their observations concerning electric fields surrounding broad bean

roots (23). Additionally, it should be noted that any calculation of proton fluxes based on changes in the pH of the unstirred layer can be complicated by the possibility that other processes can influence external pH, such as $CO_2$ evolution from respiration, or organic acid efflux, which could not only provide protons but also modify the buffering capacity of the external solution.

There are several other observations concerning $H^+$ fluxes that warrant attention. First, a net $H^+$ efflux of 1.65 $\mu$mol $g^{-1}$ $h^{-1}$ was measured in $CaSO_4$ alone or after 1 h in 0.2 mM $K^+$ (Fig. 2). This value is lower than the values obtained by other workers using techniques based on bulk solution pH measurements (2, 7, 13). These previous studies used experimental solutions that had other ions present and, in particular, a higher pH value (in the range of 6.0–6.5). The lower pH of the present study (5.0–5.6) would be expected to result in a lower net $H^+$ efflux. Second, it was mentioned earlier that we occasionally observed an apparent $H^+$ flux reversal in measurements made within 75 $\mu$m from the root surface. Our explanation for this unusual behavior was that $H^+$ influx was occurring in a localized region associated with a few adjacent cells on the root surface, which was proceeding against a background of general $H^+$ efflux from the rest of the root. This observation provides circumstantial evidence that the efflux is located predominantly in cells in, or close to, the epidermis. This adds further support for a similar conclusion that we made in an earlier study of $K^+$ fluxes in corn roots (12).

**$K^+$ Influx.** By using $^{86}Rb^+$ as a radioactive analog for $K^+$, we were able to compare the net $K^+$ influx values computed from our $K^+$ extracellular electrochemical potential measurements, with measurements of unidirectional $K^+$ influx into 4 h-washed corn root segments, using $^{86}Rb^+$-labeled $K_2SO_4$ solutions. The influx of $K^+$ ($^{86}Rb^+$) from a 0.1 mM $K_2SO_4$ solution was 2.6 $\mu$mol $g^{-1}$ $h^{-1}$. This agrees well with the value of 2.5 $\mu$mol $g^{-1}$ $h^{-1}$ for net $K^+$ influx obtained using $K^+$ microelectrodes (Fig. 3). Although the cancelling effect of experimental errors may be involved, it is pleasing to have such agreement between a direct measurement of net $K^+$ flux and the measurement of unidirectional flux of $K^+$ using $^{86}Rb^+$ as a tracer.

In the present study, KCl diffusing from the reference electrode into the 0.2 mM $CaSO_4$ solution bathing the root produced a rising $K^+$ concentration, which allowed for an assessment of the kinetic parameters, $K_m$ and $V_{max}$, for $K^+$ uptake. It is interesting to note that the representative $V_{max}$ value of 3.5 $\mu$mol $g^{-1}$ $h^{-1}$ for intact roots is relatively close to the value of 2.91 $\mu$mol $g^{-1}$ $h^{-1}$ obtained from the kinetic curve for $K^+$ ($^{86}Rb^+$) uptake in 2 cm root segments (Fig. 4). The data from the microelectrode studies on 7 cm root segments yielded a significantly lower $V_{max}$ (1.5 $\mu$mol $g^{-1}$ $h^{-1}$). Because we often had difficulties securing these segments into the microelectrode chamber, it is possible that the reduced flux values obtained with segments was the result of mechanical perturbation or 'wounding' of the root segment during handling.

The $K_m$ values for $K^+$ uptake obtained from the $K^+$ microelectrode studies presented in Figure 2 and the more detailed kinetic study utilizing two $K^+$ microelectrodes (Fig. 8) were considerably lower than the value of 22 $\mu$M determined from $K^+$ ($^{86}Rb^+$) experiments (Fig. 4). In our kinetic analysis of the $^{86}Rb^+$ data we had to use the bathing medium $K^+$ concentrations and this must result in an overestimation of the $K_m$ for $K^+$ uptake. This is supported by our observation that at low $K^+$ concentrations (up to about 100 $\mu$M), the steady state $K^+$ concentration in the unstirred layer next to the root was about one-half that of the bulk solution. For example, if the root was placed in a solution containing 50 $\mu$M $K^+$, the $K^+$ concentration at the root surface was rapidly reduced to a steady state value of about 25 $\mu$M. These steady state values were used for the kinetic analysis of the data in Figure 8, and resulted in a more accurate assessment of the kinetic parameters for transport. This is another example of how the microelectrode system made it possible to obtain more accurate information than could be obtained from studies based on bulk tissue or solution measurements.

The results of our electrophysiological studies (Figs. 6 and 7) are important in that previous studies have not provided evidence for such a highly sensitive $K^+$ state of the membrane potential. The similarity in the $K_m$ values for the depolarization of the membrane potential (Fig. 7), and for the dependence of net $K^+$ influx on the external $K^+$ concentration, suggests that $K^+$ uptake is involved in the depolarizing event. Hence, it appears that the $K^+$ uptake system operating at low $K^+$ concentrations, which is presumed to be active and coupled to $H^+$ efflux (3–6, 8, 16–18), is a highly electrogenic process. There are difficulties in reconciling an uptake process that transports a large number of positive charges into a cell, with a transport system that is involved in $K^+/H^+$ exchange. This will be discussed further in the next section.

**$H^+$ Efflux and $K^+$ Influx: A Coupled System?** It has generally been accepted that $K^+$ uptake is coupled, either directly or electrophoretically, to $H^+$ efflux. In their evaluation of the literature pertaining to this hypothesis, Glass and Siddiqi (6) argued that the experimental data did not support either form of coupling. Our results also support their contention. During the course of simultaneous $K^+$ and $H^+$ flux measurements, there were many occasions in which $H^+$ efflux was near zero and $K^+$ influx was 'normal;' the converse was also occasionally observed. Additionally, when repeated measurements were made over a period of time at the same location, both $K^+$ influx and $H^+$ efflux could vary significantly, and quite often the variation of the two fluxes did not show any correlation.

It was never possible to determine a fixed stoichiometry for the two fluxes. Generally, net $K^+$ uptake was significantly larger than $H^+$ efflux; the $K^+/H^+$ flux ratio was found to range from 3.6:1 through 2.2:1 to 1:2.75 (see Fig. 5). Clearly, this stoichiometry is dependent on the type of diffusion coefficient used in calculating net $H^+$ fluxes. However, if the smaller limiting diffusion coefficients were used in place of the self-diffusion coefficients, net $K^+$ uptake would exceed net $H^+$ efflux by an even greater amount, and the lack of correlation between the endogenous variations in the two fluxes would be amplified. Not surprisingly, the $K^+/H^+$ flux ratios were influenced significantly by the ionic composition of the bathing solution. If a relatively impermeant anion such as $SO_4^{2-}$ was used, $H^+$ efflux was larger than when the fluxes were measured in a KCl solution (Fig. 5). These results, which have been previously observed (9, 17), could be due to either the response of the $H^+$-ATPase to excess cation uptake ($K_2SO_4$ conditions), or to a diminution of the proton gradient, as protons are consumed via the $H^+/Cl^-$ cotransport system that has been shown to operate in *Chara corallina* and is believed to function in higher plants (10, 21, 22).

This situation is illustrated in Figure 5, where upon changing the solution from $K_2SO_4$ to KCl, $H^+$ efflux declined from a steady state value of about 1.1 down to 0.55 $\mu$mol $g^{-1}$ $h^{-1}$, while $K^+$ influx remained steady at about 3 $\mu$mol $g^{-1}$ $h^{-1}$. Furthermore, during the first few minutes following the change to KCl, the $H^+$ flux dropped to zero, with the $H^+$ efflux being reestablished after about 30 minutes. It is possible that immediately following the change to KCl solution, the transient reduction in $H^+$ flux (occasionally $H^+$ influx is observed) could be due to the cotransport of protons and $Cl^-$ into the root. The subsequent $H^+$ efflux would probably represent a reestablishment of the $H^+$ gradient by the proton pump. No matter what explanation is presented for these data, the ability of the microelectrode system to detect such transients again illustrates the utility of this sytem for the study of root transport processes.

The results of the electrophysiology experiments also raise questions concerning the coupling between $H^+$ efflux and $K^+$

uptake. The large depolarization of the membrane potential following exposure to low levels of $K^+$ (20 $\mu$M), indicates that the majority of the $K^+$-induced depolarization occurs at extremely low $K^+$ levels, where $K^+$ uptake has been thought to occur by a stoichiometrically balanced $K^+/H^+$ antiport system. It would not be expected that this system would be strongly electrogenic. Our results indicate that $K^+$ uptake at low $K^+$ levels is highly electrogenic; the 70 mV depolarization after exposure to 20 $\mu$M $K^+$ suggests that other cations could be transported into the cell along with $K^+$ ions. Because these are simple salt solutions (10 $\mu$M $K_2SO_4$ + 0.2 mM $CaSO_4$), protons are one of the likely candidates for cotransport with $K^+$. Although this possibility is quite speculative at this time, there is support for a $K^+$-$H^+$ cotransport from work on $K^+$ transport in *Neurospora* conducted by Slayman and coworkers (20, 24). Based on current-voltage experiments, they obtained strong evidence for $K^+$-$H^+$ cotransport into *Neurospora* that is coupled to the proton translocating ATPase (20, 24). The complex structure of the corn root precludes us from conducting similar current-voltage experiments on intact roots. However, we plan to test this $K^+$-$H^+$ co-transport hypothesis using the patch clamp technique on corn root cortical protoplasts.

**Conclusion.** Recent advances in various microanalytical techniques now provide a number of noninvasive/nondestructive approaches that can be used to study ion transport processes with increased resolution and sensitivity. Application of this technology was made to corn roots to investigate the putative coupling between $H^+$ efflux and $K^+$ influx. Our investigations did not yield any evidence in support of a stoichiometric coupling between these two fluxes. Indeed, our simultaneous flux and membrane potential studies suggest that $K^+$ influx occurs via a highly electrogenic process which, speculatively, may involve a $K^+$-$H^+$ cotransport system.

## LITERATURE CITED


1. Bellando M, A Trotta, A Bonetti, R Colombo, P Lado, E Marré 1979 Dissociation of $H^+$ extrusion from $K^+$ uptake by means of lipophilic cations. Plant Cell Environ 2: 39–47
2. Chastain CJ, JB Hanson 1982 Control of proton efflux from corn root tissue by an injury-sensing mechanism. Plant Sci Lett 24: 97–104
3. Cheeseman JM, JB Hanson 1979 Mathematical analysis of the dependence of cell potential on external potassium in corn roots. Plant Physiol 63: 1–4
4. Cheeseman JM, JB Hanson 1979 Energy-linked potassium influx as related to cell potential in corn roots. Plant Physiol 64: 842–845
5. Cheeseman JM, JB Hanson 1980 Does active $K^+$ ion influx to roots occur? Plant Sci Lett 18: 81–84
6. Glass ADM, MY Siddiqi 1982 Cation stimulated $H^+$ efflux by intact roots of barley. Plant Cell Environ 5:385–393
7. Gronewald JW, JM Cheeseman, JB Hanson 1979 Comparison of the responses of corn root tissue to fusicoccin and washing. Plant Physiol 63: 255–259
8. Hanson JB 1977 Energy coupling in ion and water fluxes across plant membranes. *In* AM Jungreis, TK Hodges, A Kleinzeller, SG Schultz, eds, Water Relations in Membrane Transport in Plants and Animals. Academic Press, New York, pp 277–290
9. Jackson PC, HR Adams 1963 Cation-anion balance during potassium and sodium absorption by barley roots. J Gen Physiol 46: 369–386
10. Jacoby B, B Rudich 1980 pH-dependent $Cl^-$ flux in ATP-depleted root cells. *In* RM Spanswick, WJ Lucas, J Dainty, eds, Plant Membrane Transport: Current Conceptual Issues. Elsevier Press, Amsterdam, pp 497–498
11. Kochian LV, WJ Lucas 1982 Potassium transport in corn roots. I. Resolution of kinetics into a saturable and linear component. Plant Physiol 70: 1723–1731.
12. Kochian LV, WJ Lucas 1983 Potassium transport in corn roots. II. The significance of the root periphery. Plant Physiol 73: 208–215
13. Kochian LV, WJ Lucas 1985 Potassium transport in corn roots. III. Perturbation by exogenous NADH and ferricyanide. Plant Physiol 77: 429–436
14. Kochian LV, IA Newman, WJ Lucas 1987 Ion transport in corn roots: localized stoichiometries for $H^+$, $K^+$, and $Cl^-$. *In* Proceedings of Seventh International Workshop on Plant Membrane Transport. Australian Academy of Science, Sydney. In press
15. Lucas WJ, LV Kochian 1986 Ion transport processes in corn roots: an approach utilizing microelectrode techniques. *In* WG Gensler, ed, Advanced Agricultural Instrumentation. Design and Use. Martinus Nijhoff, Dordrecht, pp 402–425
16. Pitman MG 1970 Active $H^+$ efflux from cells of low-salt barley roots during salt accumulation. Plant Physiol 45: 787–790
17. Pitman MG, N Schaefer, RA Wildes 1975 Relation between permeability to potassium and sodium ions and fusicoccin-stimulated hydrogen-ion efflux in barley roots. Planta 126: 61–73
18. Poole RJ 1974 Ion transport and electrogenic pumps in storage tissue cells. Can J Bot 52: 1023–1028
19. Robinson RA, RH Stokes 1959 Electrolyte Solutions. Butterworths, London, pp 286–296
20. Rodriguez-Navarro A, MR Blatt, CL Slayman 1986 A potassium-proton symport in *Neurospora crassa*. J Gen Physiol 87: 649–674
21. Sanders D 1980 The mechanism of $Cl^-$ transport at the plasma membrane of *Chara corallina*. I. Cotransport with $H^+$. J Membr Biol 53: 129–141
22. Sanders D, U-P Hansen 1981 The mechanism of $Cl^-$ transport at the plasma membrane of *Chara corallina*. II. Transinhibition and the determination of $H^+/Cl^-$ binding order from a reaction kinetic model. J Membr Biol 58: 139–153
23. Scott BIH, DW Martin 1962 Bioelectric fields of bean roots and their relation to salt accumulation. Aust J Biol Sci 15: 83–100
24. Slayman CL, A Rodriguez-Navarro, MR Blatt 1987 Potassium-proton symport: a major pathway for active transport of potassium. *In* Proceedings of Seventh International Workshop on Plant Membrane Transport. Australian Academy of Science, Sydney. In press

Reprinted from Root Development and Function eds. Gregory, Lake & Rose. SEB Sem Series 30. ©Cambridge University Press 1987. Printed in Great Britain.

# FUNCTIONAL ASPECTS OF CELLS IN ROOT APICES

William J. Lucas

## *INTRODUCTION*

To survive and function within the physically harsh environment of the soil, roots of terrestrial plants have developed a range of important anatomical and physiological features. The root system of a particular plant species may well encounter a range of soils, all with differing structural and chemical properties as well as biotic composition, thus the root system must also be capable of adapting to these changes in soil properties. In this chapter we shall examine selected examples to illustrate both the function of these cells within the root apex and their interactive nature.

## *ACQUISITION OF MINERAL NUTRIENTS*

Although cells of the root apex can take up macronutrients like $K^+$, $Cl^-$, etc., from the soil solution (Torii & Laties, 1966), these ions are generally supplied to the shoot by cells that are much further removed from the apex. On the other hand, certain essential micronutrients like Fe seem to be taken up by cells within the first few millimeters of the root tip (Ambler, Brown & Gauch, 1971; Brown & Ambler, 1974; Clarkson & Sanderson, 1978; Römheld & Marschner, 1981b). We will use the example of Fe nutrition to illustrate the point that in many plants, the cells of the root apex have the capability to respond to changes in the levels of available nutrient ion within the microenvironment of the soil. At the outset, we must stress that not all plants respond in the same way when challenged with Fe deficiency.

When an Fe-efficient plant like *Helianthus* (sunflower) is transferred to Fe-deficient culture conditions, the development of the root apex is dramatically changed. The cortex thickens considerably and root hair development is enhanced in comparison with that in plants supplied with adequate Fe. Kramer *et al.* (1980) conducted a cytological investigation on *Helianthus* roots obtained from plants that had been transferred to nutrient solutions free of Fe. They found that within 24-48 hours of Fe deficiency

most of the peripheral cells within the root tips had differentiated into transfer cells (for a description of the characteristics of these cells, see Gunning, 1977). The interesting feature of this cytological response was that the wall labyrinths that developed were always located on the peripheral walls facing the external medium. Kramer *et al.* (1980) proposed that these rhizodermal transfer cells are in some way responsible for the Fe-efficient response of sunflower.

Kramer (1983) and Römheld & Kramer (1983) further investigated the role of rhizodermal transfer cells in terms of a response to Fe deficiency. They found that Fe deficiency-induced transfer cells were present in all dicotyledonous species examined, but in the monocots, only two *Allium* (onion) species developed these characteristics; in these species the wall labyrinths were quite limited in comparison to sunflower. Iron-efficient plants, like *Zea mays* (maize), did not develop transfer cells in their root apices. These studies provide the basis for interesting future research, especially in terms of elucidating the genetic determinant for, and the basic physiological mechanism by which these transfer cells are induced.

Other physiological processes that are also influenced by Fe deficiency include an enhancement in both the rate of net $H^+$ efflux from the root apex (Römheld & Marschner, 1981b), and the capability of the root tip to reduce $Fe^{3+}$ (Bienfait, van der Bliek & Bino, 1982; Marschner, Römheld & Ossenberg-Neuhaus, 1982). Both processes may increase the supply of available Fe to the root, and that in association with the rhizodermal transfer cells, could account for the enhanced capacity for Fe absorption, a phenomenon observed in Fe-efficient plants (see, for example, Römheld & Marschner, 1981a).

Experimental data consistent with the presence of a regulatory mechanism involved in Fe uptake (by the root tips) were obtained by Römheld & Marschner (1981a). They used both hydroponic- and soil-cultured sunflower plants grown under *suboptimal* Fe conditions. As illustrated in Figs. 1 and 2, they detected a distinct rhythm in $^{59}Fe$ uptake under both culture conditions. The rhythmic changes in $^{59}Fe$ occurred every 2-4 days, simultaneously in roots, shoots and in the exudate collected from the excised sunflower stems (Fig. 1). The rhythm in $^{59}Fe$ uptake observed in plants grown in calcareous soil (Fig. 2) is very important because it represents both ecological and agronomic situations where the soil is low in available Fe. Based on these studies, Römheld & Marschner (1981a) suggested that, "the iron nutritional status of the sunflower plant is transformed into a 'signal' which

induces distinct biochemical and morphological changes within the root tips and causes a fine regulation of iron supply to the plant." A general scheme of this regulation of Fe uptake is presented in Fig. 3.

In an integrated ultrastructural and physiological study of the roots of *Helianthus annuus*, *Cucumis sativus*, *Solanum tuberosum*, *Allium porrum*, *Coleus blumei* and *Zea mays*, Römheld & Kramer (1983) failed to find the expected correlation between the induction of transfer cells and the

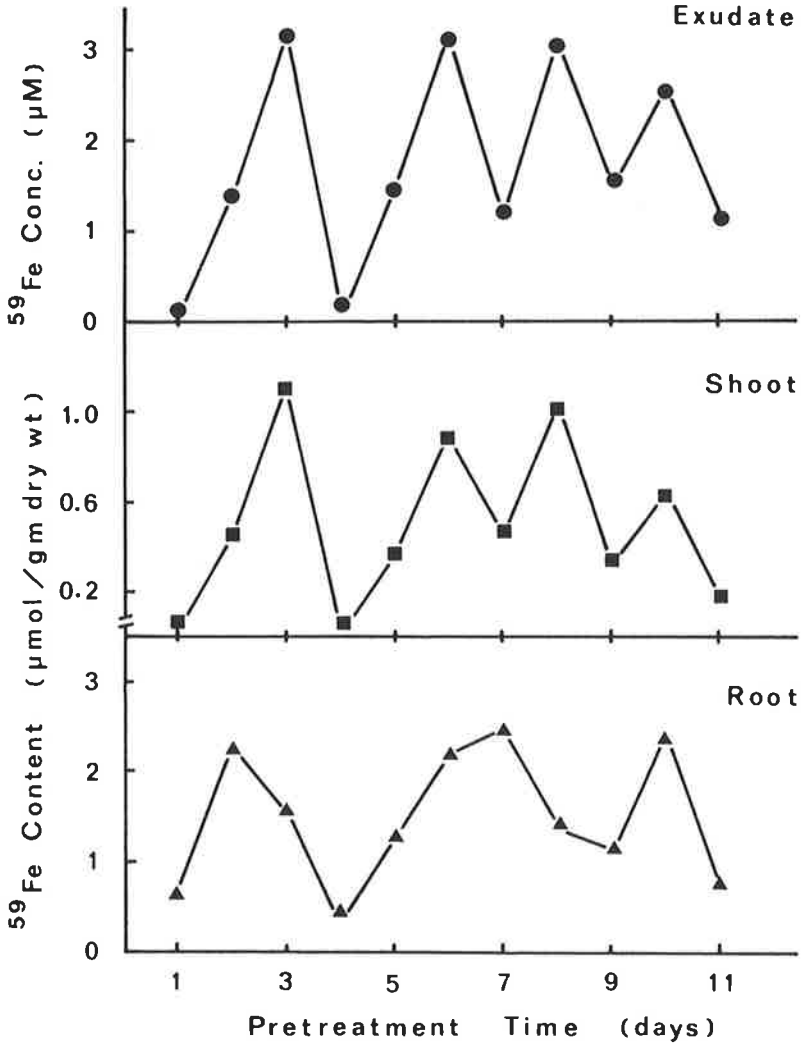


Figure 1. $^{59}$Fe content in roots, shoots and exudate of hydroponically-grown sunflower plants (*Helianthus annuus*) pretreated with 2 x $10^{-6}$ M ferric ethylenediaminedi(O-hydroxyphenylacetic acid)(FeEDDHA unlabelled) for 1 to 11 days. Every day two plants were supplied with 2x$10^{-5}$ M $^{59}$FeEDDH . (Redrawn from Römheld & Marschner, 1981a).

enhanced ability both to reduce $Fe^{3+}$ and secrete protons. What they did find was a good correlation between the formation (and extent) of rhizodermal transfer cells and the rate of net proton efflux induced by Fe deficiency. The poor correlation between the observed increased capacity for Fe absorption and the extent of rhizodermal transfer cell development is perplexing. Until more information is available about the properties of the wall labyrinth that develops in the transfer cells of different species, we cannot conclude that transfer cells are not directly involved in the process of Fe uptake.

Much remains to be learnt about the mechanism involved in regulating Fe uptake. Debate also continues as to how roots reduce $Fe^{3+}$. In some plants, low molecular weight reductants are thought to be involved, while in others, a plasmalemma-bound NADH- (or NADPH) dependent electron transport system may be involved in $Fe^{3+}$ reduction (Beinfait *et al.*, 1983); Sijmons & Bienfaith, 1983). Similarly, little is known about the mechanism of Fe transport across the plasmalemma. Until these issues have been resolved, it will be impossible to elucidate the molecular events which

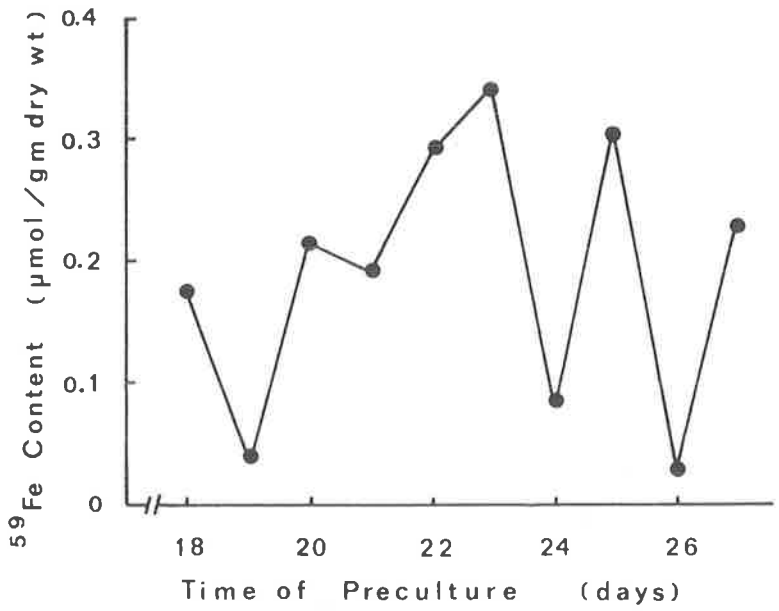


Figure 2. $^{59}$Fe content in shoots of sunflower plants precultured on calcareous soil for 18 to 27 days. After different times $^{59}$FeEDDHA ($2x10^{-5}$M) was percolated through the pots and the plants harvested after 24 hours. (Redrawn from Römheld & Marschner, 1981a).

regulate the iron nutritional status of a plant.

*ROOT PENETRATION*

*Soil physical properties: influence on root growth*

It is common knowledge among agriculturalists that the physical characteristics of the soil influence the development of roots, modifying both the growth rate and the distribution within the soil. Root penetration through the soil may be greatly influenced by the size of the pores between the soil particles and the degree of compaction (i.e., compacted soils would need greater pressures to enlarge the soil pores). Thus, the physical

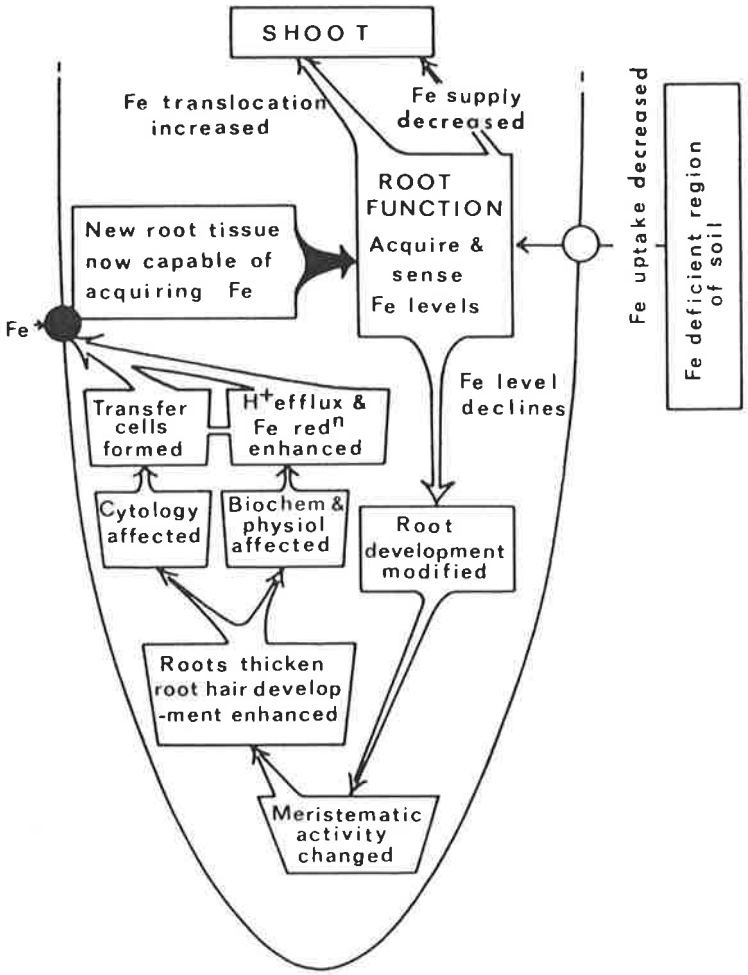


Figure 3. Schematic representation of the dicot root response to changing levels of available Fe in the soil. The mechanism by which the tissue of the root tip actually 'senses' the change in tissue Fe is yet to be elucidated.

properties of the soil can modify root diameter, development of root hairs and the branching pattern of lateral roots. These responses show some similarities to those observed in plants responding to Fe deficiency; again the site of perception and response is thought to be located in the root tip (see Feldman, 1984 and references therein).

Numerous workers have studied the relationship between the characteristics of the soil and the response of various plant root systems. Goss and coworkers used an ingenious experimental chamber which allowed them to vary, independently, the pore size and the applied pressure within the root zone. With this system, Goss (1977) found that in many agriculturally important crops (barley, wheat, maize and sugar beet), the rate of root elongation was considerably decreased (to about one-half) by rather small mechanical stresses (20 to 50 kPa). An anatomical study conducted on barley plants, grown in this experimental chamber, provided valuable details on the root's response to mechanical impedance (Wilson, Robards & Goss, 1977). Wilson *et al.* (1977) found that the increase in the diameter of the barley roots resulted largely from an increased thickness of the cotex; the number of cells in the transverse section increased and the diameter of the outer cells was greater. However, surprisingly, the diameter of the inner cells was decreased. The organization of the vascular tissue of the root was also modified by these low levels of physical impedance. Near the apex the diameter of the stele, in impeded roots, exceeded that of the control roots, with the greatest difference (22 percent) being found 0.5 cm from the apex.

These complex reactions of the barley root to rather small physical constraints (about 20 kPa) indicate that the effect of mechanical impedance cannot be explained in terms of the increased external pressure causing a reduction in the rate of cell expansion (Wilson *et al.*, 1977; see also Feldman, 1984).

Perhaps the most interesting aspect of the root's response to mechanical impedance and soil pore size is its ability to modify the pattern of lateral branching. Goss (1977) showed that, in barley, 50 kPa of applied pressure shortened the region of initiation of laterals from a zone of about 30 mm (control) to a zone only 4 mm from the apex! In many cases the increased growth in the length of the lateral roots compensated for the reduction in length of the primary axes.

Goss & Russell (1980) further found that when a barley root was forced to grow around a glass bead, the site of lateral root initiation occurred preferentially on the outer (convex) side, whereas root hairs

developed on the inner (concave) side of the root. This level of developmental complexity along with the examples cited above, clearly illustrate the high level of morphological and anatomical "plasticity" present within the cells of the root apex. This "plasticity" will be important during the life of the plant, but may be paramount in the early stages of germination, where the establishment of an adequate water supply is crucial.

Finally, given the obvious importance of these root characteristics, it is disappointing that at present "it is not possible to advance a detailed interpretation of the way root development is subsequently affected... Present uncertainty reflects the incompleteness of information on many aspects of the processes whereby growth is coordinated (Goss & Russell, 1980)."

*Mucilage and the rhizosphere*

According to Rougier (1981), Haberlandt originally proposed that root cap slime functions both as a lubricant and a protectant for the newly-forming root tip. These slime-, or mucilage-producing cells are found at the periphery of the root cap. In addition to their secretory functions, these cells are continually being sloughed off, so that the surface of the growing root becomes covered by a very heterogeneous material. This gelatino material, which ensheaths roots growing in normal non-sterile soil, contains in addition to soil particles, substances of both plant and microbial origin as well as living plant and microbial cells, and is generally termed mucigel (Rovira, Foster & Martin, 1979).

Over the ensuing seventy years since Haberlandt made his observations, considerable research effort has been expended in an attempt to elucidate the composition, properties and biological functions of this very interesting material. Several excellent reviews are available and the reader is referred to these for an extensive analysis of this literature (see Oades 1978; Rovira *et al.* 1979; Rougier, 1981 and Northcote, 1982). I will briefly describe the site of synthesis of root cap slime and then discuss some of the more controversial functions attributed to the mucigel.

Although most research on slime production has been conducted on a few hydroponically grown plants, chiefly *Zea mays*, the details are generally applicable to most root systems. Cells produced by the root cap meristem develop into statocytes, containing numerous starch-filled amyloplasts (see next section for role played by these cells). Continued meristematic activity displaces these cells towards the root periphery and, at

maturation, their cytoplasm undergoes marked changes (see Juniper, Gilchrist & Robins, 1977; Moore & McClelen, 1983). The starch reserves within the amyloplasts become degraded and the carbohydrate that they contained is processed via the endoplasmic reticulum and Golgi apparatus. Exocytosis of the secretory vesicles produced by the Golgi delivers the complex polysaccharides (or slime) into either the space between the cell wall and the plasmalemma, or into the wall proper, if the polysaccharide is small enough to pass through the interstices of the wall (Morré, Jones & Mollenhauer, 1976; Paull & Jones, 1975; Rougier, 1981).

The slime produced by various hydroponically-grown plants has been analyzed by several laboratories. However, as pointed out by Rougier (1981) and Chaboud (1983), the roots used were usually not grown under sterile conditions, so just what originated from the root cap cells was difficult to distinguish from metabolic products of the microbial flora. However, these analyses indicate that slime consists, in part, of a central β-1, 4-linked glucan that is rendered soluble by a coating of hydrophilic polysaccharides that are linked both covalently and non-covalently. The covalently-linked polysaccharides are thought to be relatively rich in galaturonic acid and fucose in regions near the central glucan (Wright & Northcote, 1976; Rougier, 1981).

The presence of fucose in this high molecular weight polysaccharide is a characteristic feature of the slime produced by the root cap. Vermeer & McCully (1981, 1982) used this feature to develop a lectin label that allowed them to follow the polysaccharide distribution in axenic (hydroponic) and field-grown maize plants. Other studies have been based on the detection of various chemical groups by more standard cytochemical methods (see examples cited in Rougier, 1981). Collectively, these studies reveal that the rhizosphere of the root is a more complex mucigel than previously envisaged. For example, Miki, Clarke & McCully (1980) found that in maize, wheat, barley, oats and sorghum the root surface is covered by two types of mucilage. A gelatinous material originates from the root cap and a firm, uniformly thick mucilage overlies the columnar epidermal cells. The epidermal mucilage has a thin outer and thicker inner layer distinct from the epidermal cell wall; periodic acid-Schiff staining indicated that the outer layer and the cell wall contain carboxyl groups which are absent from the thick inner layer. The root cap mucilage of these plants had an inner region with histochemical properties resembling those of the inner epidermal mucilage.

In a further study on field-grown maize plants, Vermeer & McCully (1982) observed that the rhizodermal sheath of the root is permeated by extracellular mucilage which is histochemically distinct from that present at the epidermal surface. This mucilage appears to originate from the root cap.

Finally, Foster (1981) conducted histochemical tests on root material of *Paspalum notatum* and *Triticum aestivum* that had been fixed, *in situ*, in the soil. He reported that he could distinguish, via various histochemical tests, between the polysaccharides secreted by the epidermis and those produced by soil fungi and bacteria. He also found that the nature of the mucilage and the boundaries between the cell wall and the soil depended on the age of the epidermal cells. In this context, a cuticle could be detected on the surface of the younger regions of the root (Foster, 1982). This level of chemical and spatial heterogeneity within the rhizosphere must surely reflect various roles of the mucigel in the physiological functioning of the root.

Numerous phenomenological observations have been reported that tend to support the hypothesis that mucigel production by the root tip (both root cap and epidermal cells) can respond interactively to changes within the immediate physical environment of the root. The production of mucigel is thought to be important in protecting younger parts of roots from desiccation during short periods of drought (see Greenland, 1979; Rougier, 1981). In an interesting study using fucose-specific lectins, Baldo, Reid & Bonifac (1983) demonstrated that, in developing (maturing) wheat grains, a fucose-containing mucilage is already present around the root prior to germination. Such results support the claim that root cap mucilage functions as a protectant/lubricant.

The relationship between mucigel production and water stress is of particular interest, because crop plants are almost continuously exposed to varying levels of water stress. Recent work on axenic cultures of *Zea mays* (Chaboud, 1983) and *Oryza sativa* (rice)(Chaboud & Rougier, 1984) is important in this context. Their analyses of the root cap mucilage from these two root systems revealed a high content of galactose, arabinose and xylose. They suggested that the mucilage polymers could be related to, or could contain arabinogalactans; these compounds possess such properties as adhesiveness, water holding capacity and the ability to associate with other macromolecules (see Clarke, Anderson & Stone, 1979).

If a constituent of the mucigel does possess arabinogalactan-like properties this would certainly aid in the aggregation of soil particles around the root (see Oades, 1978). In addition, the strong water holding/binding properties would help to maintain the continuity of the water column from the soil to the root surface. Thus, under the development of water stress, the root may secrete more mucilage not only to facilitate its penetration into soil, but also to prevent its desiccation and to attempt to maintain the continuity of the contact between root and soil water.

Limited support is available in the literature for this role of the mucigel as an adaptation to water stress. Martin (1977) used an interesting experimental system to study the relationship between water stress and organic carbon release in soil-grown wheat roots. Individual wheat plants were grown in soil columns that had varying soil moisture content in the upper half, while the lower half of the column was saturated. By supplying $^{14}CO_2$ to the leaves, Martin could follow the release of organic carbon into the various regions of the soil. Although released organic carbon was reported as the summation of carbon secreted as mucilage and by cell lysis, the amount increased in zones of water stress, even though other sections of the root had adequate available water.

It has often been speculated that the carboxyl groups within the mucigel influence ion uptake into the root (Rougier, 1981; Chaboud & Rougier, 1984). In calcareous soils the high divalent cation binding affinity of the mucigel may protect the root tip from $Ca^{2+}$ toxicity. In addition, the bound $Ca^{2+}$ may form $Ca^{2+}$-galacturonic acid bridges between the different polysaccharide units, thereby modifying the physical characteristics of the mucigel (Cortez & Billes, 1982).

Aluminium toxicity in plants, which is often observed in acid soils, may be alleviated by the production of sufficient mucigel to protect the root meristem. In hydroponic experiments on *Vigna unguiculata* (cowpea) removal of the root cap mucliage resulted in an enhanced Al sensitivity of root elongation (Horst, Wagner & Marschner, 1982). Because mucilage has a high binding affinity for polyvalent cations (see Clarkson & Sanderson, 1969), Horst *et al*. (1982) suggested that mucilage may have an important ecological role in providing Al tolerance to plants growing in acid mineral soils. This hypothesis should be further investigated in field-based studies.

Attention has also been focused on the microbial utilization of

the organic carbon released by cells of the root tip. Nitrogen fixing bacteria like *Azospirillum lipoferum* appear to be specifically attracted to certain plants, like maize (Baldani & Dobereiner, 1980), and these bacteria are associated with the mucigel (Umali-Garcia *et al.*, 1980). However, whether these nitrogen fixing bacteria are important in terms of supplying organic nitrogen to the roots remains uncertain (see Beck & Gilmer, 1983; Whipp & Lynch, 1983). In any event, the quantity of the organic carbon released by the roots can be a large proportion of the total amount translocated into the tip (see chapter 6 for more discussion of this point). Thus this area should remain active in future research. The statement made by Chaboud & Rougier (1981) that "a greater understanding of the nature of the mucigel, i.e., of its diverse components, would be of use in analyzing potential extracellular recognition phenomena of both benevolent and pathogenic microorganisms", seems to identify an important area for future studies. Elucidation of the mechanism(s) by which the plant root system may recognize and respond to pathogenic attack could be of value in developing a complete picture of the way the root system responds to stress phenomena in general.

## *GRAVITROPISM IN ROOTS*

### *General background*

Gravity is an important component of the root's physical environment and in general a positive response is observed at the root tip. Excellent reviews of plant gravitropism have been provided by Audus (1975), Jackson and Barlow (1981), Juniper (1976), Volkmann & Sievers (1979), and Wilkins (1984). We shall examine the gravitropic phenomenon in detail because it represents an excellent system in which to study regulation in a complex organ, the root. And of course, these regulatory events involve modulation of physiological processes occurring in the cells of the root apex.

At the beginning of the 1980s there appeared to be a consensus that roots responded to gravity in the following manner. The statenchyma, situated within the centre of the root cap, functions as the site of graviperception. In these cells specialized plastids, called amyloplasts, contain large starch granules. Because of their greater density in comparison with the surrounding cytosol, the amyloplasts, the presumed statoliths, sediment under the influence of gravity. In a vertically oriented root, the amyloplast

rest near the lower surface of the cell; i.e., the end of the cell nearest to the actual tip of the root cap, and the rate of cell elongation within the growth zone of the root conformed to circumferential symmetry. However, displacement of the root away from this orientation results in a redistribution of the amyloplasts. Although the mechanism of transduction is uncertain, this movement of the amyloplasts was thought to result in the release of an inhibitory plant growth substance (hormone, IAA, ABA or?) from the root cap. An asymmetric distribution of this putative substance, in the region of cell elongation (i.e., more in the lower than in the upper half of the root), would elicit root curvature. This is a summary of the Cholodny-Went hypothesis (see Went & Thimann, 1937). Unfortunately, to demonstrate the phenomenon of root gravitropism has been easier than to test the prediction of the Cholodny-Went hypothesis.

*Hormone involvement: ABA, IAA or ?*

Jackson & Barlow (1981) provided an excellent analysis of the literature on the role of plant growth regulators in root gravitropism. Since their review several important findings have been published. Pilet & Ney (1981) have now answered one of the questions raised by Jackson & Barlow. As illustrated in Fig. 4, curvature of the maize root, in response to gravity, is obtained by an initial marked decrease in growth rate on the lower side and a slight stimulation in growth rate on the upper side. However, the mechanism responsible for this modulation in growth remains controversial. That a concentration gradient of the hormone indole-3-acetic acid (IAA) can elicit a stimulation of growth at low concentrations and an inhibition at slightly higher levels, is clearly illustrated by experiments with segments of maize roots (Pilet, Elliott & Moloney, 1979). The important question is whether these experiments with excised segments of root can be extrapolated to the intact root system.

Using a very sensitive enzyme immunoassay and radioimmunoassay for IAA and abscisic acid (ABA), Mertens & Weiler (1983) studied the distribution of these two growth regulators in gravistimulated maize roots. Although they could detect endogenous IAA and ABA, they could not detect the predicted increased concentrations on the lower side of the gravitropic root. This result suggests that either these hormones are not involved in the gravitropic response, or the technique used does not differentiate between total hormone present and its actual distribution within active and nonactive pools.

It is important to point out that the immunoassay results are in contradiction to the results of Pilet & Rivier (1981), who used gas chromatography-mass spectroscopy to analyze for endogenous ABA levels. However, as will be discussed shortly, present consensus is that ABA may not be directly involved in gravitropism.

The recent work of Lee, Mulkey & Evans (1984) also implicates IAA in the graviresponse mechanism. Treatment of maize or pea roots with inhibitors of auxin transport (morphactin, naphthylphthalamic acid, and

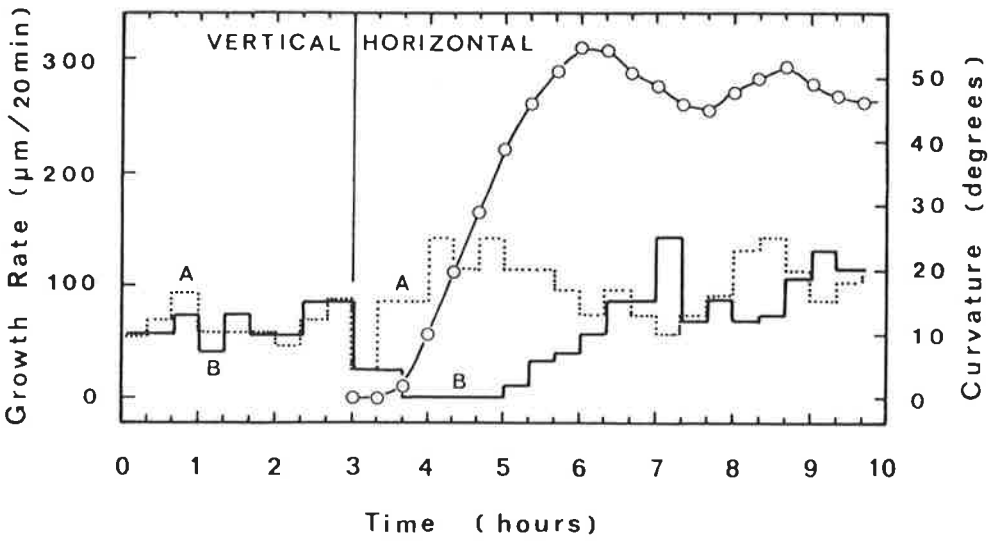


Figure 4. Growth rate of the two sides of a primary maize root that was first kept for 3 hours in the vertical position, and then placed horizontally for 7 hours. The gravitropic response (downward curvature) is plotted in degrees of deflection from the horizontal (O). A, upper side, B, lower side of maize root (Redrawn from Pilet & Ney, 1981).

2,3,5-triodobenzoic acid) prevented the gravitropic response. This is consistent with their earlier finding, in that these auxin transport inhibitors also suppressed the asymmetric acid efflux that appears to be a characteristic of gravistimulated maize roots (Mulkey & Evans, 1982). However, in their recent work, Lee *et al.* (1984) reported that these auxin transport inhibitors also prevented the gravity-induced polar movement of $Ca^{2+}$ across the *root tip*. Thus, the question of IAA involvement remains to be resolved.

Jackson & Barlow (1981) presented a thorough examination of the experimental results concerning the role of ABA in gravitropism, and they concluded that "the evidence that ABA is the inhibitor seems poor at present." Several recent studies support their conclusion (see, for example, Mulkey, Evans & Kuzmanoff, 1983). Perhaps the most definitive results were those obtained by Moore & Smith (1984). ABA is thought to be synthesized via the carotenoid pathway and so Moore & Smith investigated the effect of Fluridone, an inhibitor of this pathway, on maize roots. Fluridone was found to completely inhibit ABA synthesis. However, primary roots of treated and untreated plants were strongly graviresponsive, with no significant differences being found between the curvatures or the growth rates of the Fluridone-treated and control plants. Clearly these results show that ABA is not necessary for positive gravitropism in primary roots of maize.

The possibility that some other plant hormone may have a role in gravitropism has been raised by the work of Feldman (1981). By using a cultivar of maize whose roots require light, in addition to gravity, to cause root curvature, he was able to demonstrate that the root cap, *per se*, produces a root cap inhibitor substance which causes dark-grown roots to respond to gravity. In these experiments $10^{-9}$ M IAA was necessary for optimal root cap inhibitor (RCI) production, but *in vivo* this hormone would probably be supplied from its site of synthesis in the meristematic zone of the apex (Feldman, 1980).

In subsequent studies on this light-dependent maize cultivar, Feldman (1983) and Feldman & Gildow (1984) showed that light stimulates protein synthesis (but not DNA synthesis) that is necessary for the gravitropic response of the maize root. Using electrophoretic techniques, they were able to single out specific proteins whose levels within the root cap were influenced by light. Interestingly, several of these proteins, for which synthesis was stimulated by light, appeared to turn over rapidly. It will be very interesting to follow the developments on this RCI substance.

*Role of $Ca^{2+}$ in root gravitropism*

Although $Ca^{2+}$ has long been known to be important in polar auxi transport (see de la Fuente & Leopold, 1973), more recent studies indicate that this divalent cation may be involved in the early stages of transductic of the regulatory signal(s), from the root cap, to the zone of elongation, where curvature occurs.

If the statoliths (amyloplasts), in the statocytes of the root cap, are involved in the initial perception of a change in the gravitational field, the first transduction step must occur within these cells. At present no consensus exists as to the nature of this signal, but a change in cytosol $Ca^{2+}$ may be involved. For a long time it has been proposed that the amyloplasts may form some special contact with the endoplasmic reticulum (ER) in the statenchyma (see Sievers & Volkmann, 1972; Hensel, 1984; and also Barlow Hawes & Horne, 1984; and Olsen *et al.*, 1984, for a differing viewpoint). The physical change in location of the amyloplasts, in response to gravity, may elicit a $Ca^{2+}$ response from either the amyloplasts, or the ER. Chandra *et al.* (1982) used an ion microscope to show that $Ca^{2+}$ is present in the root cap statoliths of maize, pea and lettuce. In addition, Buckhout, Heyder Caspers & Sievers (1982) and Buckhout (1983) have developed a technique that allows them to isolate the ER from the root cap region. They found that the vesicles in this putative ER fraction took up $Ca^{2+}$ via an ATP-dependent process that appeared to be a direct $CA^{2+}$-translocating ATPase. There are also several reports for plant tissues, other than root cap cells, which indicate that a $Ca^{2+}$ efflux system is probably present in the plasmalemma (see Dieter & Marme, 1983; Dieter, 1984).

Since Biro *et al.* (1982) found that chlorpromazine, an inhibitor of the $Ca^{2+}$-activated form of calmodulin, significantly inhibited the negative gravitropic response of the oat coleoptile, it seems plausible to suggest that a calmodulin-mediated signal(s) may well be involved in the earliest stages of graviperception. We know of no reports on the effects of calmodulin inhibitors on the gravitropic response in roots. However, Buckhou (1984) found that calmodulin seems not to be involved in regulating $Ca^{2+}$ transport across ER membrane vesicles prepared from *Lepidium sativum* roots. This area of research should be pursued to test the $Ca^{2+}$-calmodulin hypothesis.

An alternative $Ca^{2+}$ signalling system in animal tissues, involving Inositol 1,4,5-triphosphate ($InsP_3$), has recently received considerable attention (see Nishizuka, 1984). In this system, hormone bindin

to a receptor site in the plasma membrane is presumed to activate an inositol diesterase and this eventually leads to the production of $InsP_3$ (Berridge, 1983). Prentki *et al.* (1984) showed that this $InsP_3$ causes the rapid release of $Ca^{2+}$ from a microsomal fraction of rat insulinoma but not from mitochondria, and they propose that $InsP_3$ functions as a cellular messenger inducing the mobilization of $Ca^{2+}$ from the endoplasmic reticulum. An interesting study on $InsP_3$, which illustrates a way in which this system may function in the statocytes, is that conducted on ventral photo-receptors. A single photon can cause approximately 1,000 ionic channels to open in the receptor of the eye. This must require an internal transmitter and Fein *et al.* (1984) demonstrated that injection of $InsP_3$ excited and adapted ventral photoreceptors in a manner similar to light.

On a speculative note, sedimenting amyloplasts may cause a perturbation in the microtubular arrangement in the statocytes and so move plasma membrane-bound, or associated, receptors that activate the $InsP_3$ system. This $InsP_3$ may also be involved in opening ionic ($Ca^{2+}$?) channels in plant cells or it may mediate in the ER release of $Ca^{2+}$.

Evans and his coworkers have shown that the gravitropic response in roots of maize and pea can be modified by adjusting the exogenous $Ca^{2+}$ level. Lee, Mulkey & Evans (1983a) found that application of $Ca^{2+}$ chelating agents, like EDTA or EGTA (held in small agar blocks), to the tips of maize roots caused a loss of gravitropic sensitivity. Non-specific effects cannot be discounted, because an extremely high concentration (50 mM) was used. But, since replacing the chelating agent with $CaCl_2$ restored the root's gravitropic sensitivity, the results are probably valid. Placement of agar blocks containing $CaCl_2$ on one side of the root cap of a vertically oriented root caused curvature towards the $Ca^{2+}$, whereas application of a block containing EDTA caused curvature away from the EDTA or $Ca^{2+}$-diminished side of the root. However, application of $CaCl_2$ to the tips of decapped maize roots, which in this state are insensitive to gravity, did not restore this ability. Thus, $Ca^{2+}$, *per se*, cannot be a direct signal, but seems rather to be one of the factors necessary for the transduction of the growth regulating signal.

Further work by this group illustrated that $^{45}Ca^{2+}$ movement across the root tip depends strongly on the position of the root. When oriented horizontally the maize root cap showed a strong asymmetry to the movement of $^{45}Ca^{2+}$; movement from top to bottom increased, while that from the bottom to the top decreased (Lee, Mulkey & Evans, 1983b). Similar

results were obtained on the graviresponsive roots of pea, but no such asymmetry was detected on onion roots which do not respond to gravity (Lee *et al.*, 1984). A further finding was that pretreatment of maize and pea roots with auxin transport inhibitors prevented both the gravitropic response and the polar movement of $^{45}Ca^{2+}$ across the root cap. These results suggest that in some way $Ca^{2+}$ plays a key role in linking gravistimulation to the gravitropic growth response in roots. Lee *et al.* (1984) suggest that the increased level of $Ca^{2+}$ on the lower side of the root cap "may lead to enhanced acropetal movement of auxin into the elongation zone on the lower side of the root", i.e., they still favour the Cholodny-Went hypothesis.

*Geoelectric phenomena in roots*

The role of electric currents has recently been invoked in terms of mediating the graviperceptive response of roots. We will examine both the old concept of the geoelectric response of roots and the recent electrical data to ascertain whether a biophysical mechanism is involved in the transduction phase of graviperception.

The original geoelectric theory was based on the early observations of Bose (1907) and Brauner (1927), who found that coleoptiles and roots, when placed in the horizontal position, developed an electric polarity across the organ. In roots, the lower side was positively charged. Thus since auxin is a weak acid, it would be present as an anion at pH 5 to 6, and so the then presumed growth-active hormone would be attracted to the positively charged lower surface where it would inhibit cell elongation.

A difficulty in these early electrical studies was to make good electrical contacts with the tissue. The problem was solved by Grahm & Hertz (1962) and Grahm (1964), who developed an ingenious vibrating-reed electrode that could detect the surface electric field of gravistimulated coleoptiles without making contact with the surface of the organ. Using this technique they were able to show that indeed an asymmetric electric potential is established following gravistimulation, however, the time course was much slower than the almost immediate response reported by Brauner (1927). Grahm (1964) clearly showed that the electrical phenomenon had a lag phase of 15 minutes which was almost exactly the same as the observed latent period for curvature response in the coleoptile. In view of this, Grahm concluded that "the geoelectric effect is a secondary phenomenon of asymmetric auxin distribution", and thus cannot be the factor responsible for auxin movement.

The concept of electrical events being involved in gravistimulation in roots received no further attention until the work of Behrens, Weisenseel & Sievers (1982). These workers used the *Lepidium sativum* root system and applied the external vibrating electrode technique to study the influence of gravistimulation on the electric fields that are normally present around roots (see Scott, 1967). Although their experimental system was not set up for making optimal measurements, Behrens *et al.* (1982) found that the electric field, in the region of the root tip, underwent a rapid change (within 30 seconds), in response to a change in the gravitational field (see Fig. 5). Gravitropic curvature was first visible approximately 10 minutes after placing the root in the horizontal position. Thus, since the change in current pattern in the root cap region precedes root curvature, Behrens *et al.* (1982) suggested that the current may be involved in the transduction of information from the root cap to the elongation zone, following graviperception in the cap.

Sievers *et al.* (1984) and Behrens, Gradmann & Sievers (1985) pursued this concept further by making electrophysiological measurements on the cells of the *Lepidium* root cap. Their findings were indeed very interesting. As illustrated in Fig. 6, the membrane potential of statocytes on the upper and lower surface of the gravistimulated root responded in an asymmetric manner. In statocyte cells on the lower surface the membrane potential was transiently depolarized, while cells on the upper surface responded by developing a more negative potential across the plasmalemma. Sievers *et al.* (1984) developed a model to relate cytological changes, induced by a change in gravistimulation, to extracellular current and membrane potential (Fig. 7).

As discussed in an earlier section (4.3), there are numerous ways in which the initial events of perception could be transduced into a membrane depolarizing signal ($Ca^{2+}$-calmodulin or $Ca^{2+}$-$InsP_3$ may be involved). But we do not know what ionic fluxes are responsible for the transient depolarization or what new transmembrane ion flux pattern is responsible for the change in extracellular current at the root cap (see Fig. 5). Finally, if these electrical changes are part of the early perception-transduction phase of graviperception (and the data are certainly compelling), how do these current changes elicit the necessary modulation in growth rates in the far removed zone of elongation?

*CONCLUSIONS*

Roots, functioning not in laboratory culture but in the soil, must be capable of making a wide range of adjustments in response to their changing physical environment. Many of the examples cited to illustrate both the functional aspects of the cells of the root apex, and how these cells may respond to environmental changes, have been drawn from laboratory-

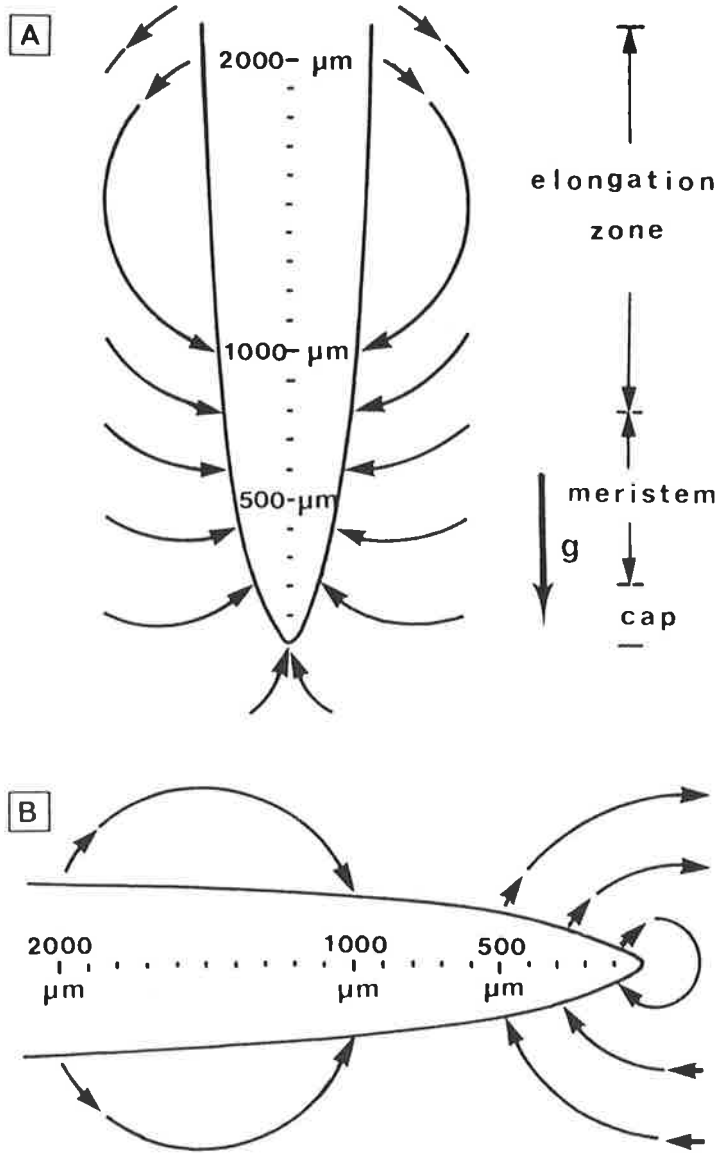


Figure 5. Current pattern associated with the root tip of *Lepidium*. A: Symmetrical pattern during vertical growth. B: Asymmetric pattern established in the root cap 3 minutes after placing root in the horizontal position. (By courtesy of H.M. Behrens.)

based studies. This is a consequence of the difficulty of designing experiments on soil-grown root systems when so much basic information on the functional aspects of root cells is still lacking. When such knowledge becomes available and soil-grown plants become widely used, we will gain greater appreciation of the biochemical/biophysical control systems that must function within the root to allow it to survive.

*ACKNOWLEGMENTS*

I thank the Forstbotanisches Institut der Universitat Gottingen, and the Deutsche Forschungsgemeinschaft for generous support provided during my sabbatical leave. I would also like to thank Prof. A. Sievers and his

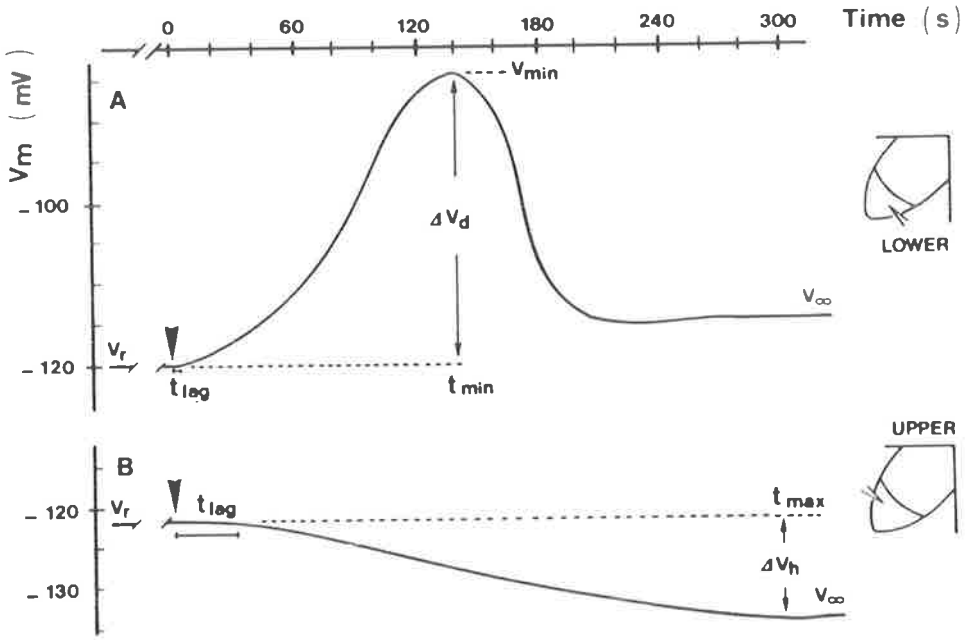


Figure 6. Membrane potential recordings from representative *Lepidium* roots growing vertically ($V_r$) and at 45° to the vertical direction. A: Glass microelectrode inserted into statocyte on the lower (A) and upper (B) side of the root prior to tilting the micromanipulator platform through 45°. Statocytes in the vertically growing root had typical resting potentials of -120 mV. Following tilting (V), the statocytes on the lower side of the root transiently depolarized to approx. -84 mV ($V_{min}$) and then repolarized back to a value of approx. -115 mV ($V_\infty$). The statocytes on the upper side of the root hyperpolarized their membrane potential, to a new table value of approx. -134 mV, upon tilting. (From Sievers *et al.*, 1984).

colleagues for providing their manuscripts prior to publication. This work would not have been possible without the "long-range" support of my laboratory in Davis, and especially the efforts of Clyde Wilson and Dr. Leon Kochian. Finally I would like to thank Frau Wehr and Lyn Noah for their assistance in preparing the manuscript.

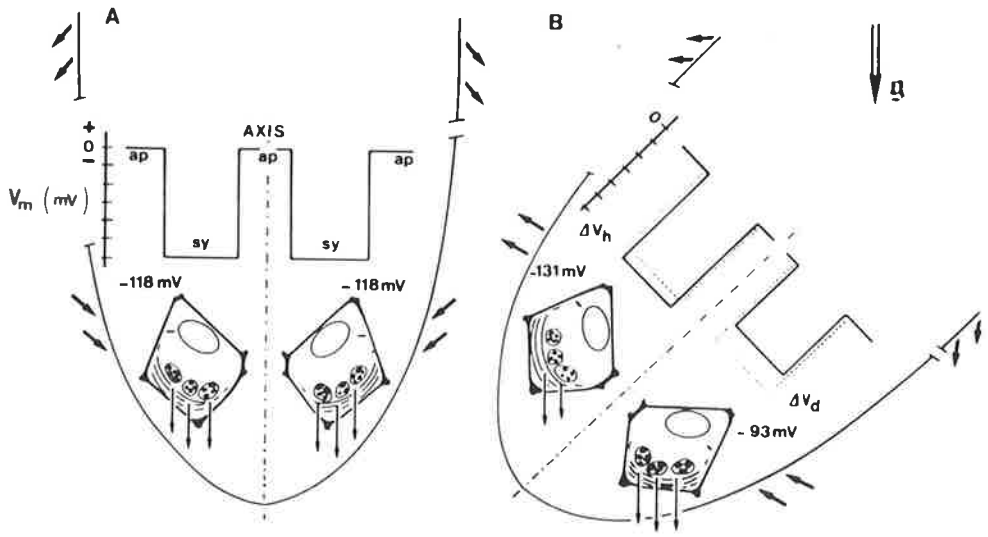


Figure 7. Synopsis of early graviresponses in *Lepidium* root tips. A: In vertically growing roots, three symmetrical patterns are observed; sedimentation of the amyloplasts on the ER complex (thin arrows in the g direction), the potential profiles through the symplast (sy) and apoplast (ap) and the direction of external current flow (thick arrows). B: Following tilting at 45° from the vertical direction, these patterns become asymmetric; the ER complex is differentially compressed by the sedimenting amyloplasts (thin arrows) and a potential depolarization ($\Delta V_d$) in the physically lower and hyperpolarization ($\Delta V_h$) in the upper statocytes. These changes generate a net asymmetrical current pattern across the root cap, the site of graviperception (From Sievers *et al.*, 1984).

*REFERENCES*

Ambler, J.E., Brown, J.C. & Gauch, H.G. (1971). Sites of iron reduction on soybean plants. *Agronomy Journal*, 63, 95-7.

Audus, L.J. (1975). Geotropism in roots. In *The Development and Function of Roots*, ed. J.G. Torrey & D.T. Clarkson, pp.327-63. London: Academic Press.

Baldani, V.L. & Dobereiner, D.J. (1980). Host-plant specificity in the infection of cereals with *Azospirillum* spp. *Soil Biology and Biochemistry*, 12, 443-9.

Baldo, B.A., Reid, A.L. & Boniface, P.A. (1983). Lectins as cytochemical probes of the developing wheat grain. IV. Demonstration of mucilage containing L-fucose associated with roots in ungerminated grain. *Australian Journal of Plant Physiology*, 10, 459-70.

Barlow, P.W., Hawes, C.R. & Horne, J.C. (1984). Structure of amyloplasts and endoplasmic reticulum in the root caps of *Lepidium sativum* and *Zea mays* observed after selective membrane staining and by high-voltage electron microscopy. *Planta*, 160, 363-71.

Beck, S.M. & Gilmour, C.M. (1983). Role of wheat root exudates in associative nitrogen fixation. *Soil Biology and Biochemistry*, 15, 33-8.

Behrens, H.M., Gradmann, D. & Sievers, A. (1985). Membrane-potential responses following gravistimulation in roots of *Lepidium sativum* L. *Planta*, 163, 463-72.

Behrens, H.M., Wiesenseel, M.H. & Sievers, A. (1982). Rapid changes in the pattern of electric current around the root tip of *Lepidium sativum* L. following gravistimulation. *Plant Physiology*, 70, 1079-83.

Berridge, M.J. (1983). Rapid accumulation of inositol trisphosphate reveals that agonists hydrolyse polyphosphoinositides instead of phosphatidylinositol. *Biochemical Journal*, 212, 849-58.

Bienfait, H.F., Bino, R.J., van der Bliek, A.M., Duivenvoorden, J.F. & Fontaine, J.M. (1983). Characterization of ferric reducing activity in roots of Fe-deficient *Phaseolus vulgaris*. *Physiologia Plantarum*, 59, 196-202.

Bienfait, H.F., van der Bliek, A.M. & Bino, R.J. (1982). Different regulations on ferric reduction and acidification of the medium by roots of Fe-stressed plants in a "rhizostat". *Journal of Plant Nutrition*, 5, 447-50.

Biro, R.L., Hale II, C.C., Wiegand, O.F. & Roux, S.J. (1982). Effects of chlorpromazine on gravitropism in *Avena* coleoptiles. *Annals of Botany*, 50, 737-45.

Bose, J.C. (1907). *Comparative Electrophysiology*. London: Longmans and Green.

Brauner, L. (1927). Untersuchungen uber das geoelektrische Phanomen. I. *Jahrbucher fur wissenschaftliche Botanik*, 66, 381-428.

Brown, J.C. & Ambler, J.E. (1974). Iron-stress response in tomato *(Lycopersicon esculentum)*. I. Sites of iron reduction, absorption and transport. *Physiologia Plantarum*, 31, 221-4.

Buckhout, T.J. (1983). ATP-dependent $Ca^{2+}$ transport in endoplasmic reticulum isolated from roots of *Lepidium sativum* L. *Planta*, 159, 84-90.

Buckhout, T.J. (1984). Characterization of $Ca^{2+}$ transport in endoplasmic reticulum membrane vesicles from *Lepidium sativum* L. roots. *Plant Physiology*, 76, 962-7.

Buckout, T.J., Heyder-Caspers, L. and Sievers, A. (1982). Fractionation and characterization of cellular membranes from root tips of garden cress (*Lepidium sativum* L.). *Planta*, 156, 108-16.

Chaboud, A. (1983). Isolation, purification and chemical composition of maize root cap slime. *Plant and Soil*, 73, 395-402.

Chaboud, A. and Rougier, M. (1981). Secretions racinarier mucilagineuses et role dans la rhizosphere. *Annals of Biology*, 20, 313-26.

Chaboud, A. and Rougier, M. (1984). Identification and Localization of sugar components of rice (*Oryza sativa* L.) root cap mucilage. *Journal of Plant Physiology*, 116, 323-30.

Chandra, S., Chabot, J.F., Morrison, G.H. and Leopold, A.C. (1982). Localization of calcium in amyloplasts of root-cap cells using ion microscopy. *Science*, 216, 1221-3.

Clarke, A.E., Anderson, R.L. & Stone, B.A. (1979). Form and function of arabinogalactans and arabinogalactan-proteins. *Phytochemistry*, 18, 521-40.

Clarkson, D.T. and Sanderson, J. (1969). The uptake of a polyvalent cation and its distribution in the root apices of *Allium cepa*: Tracer and autoradiographic studies. *Planta*, 89, 136-54.

Clarkson, D.T. and Sanderson, J. (1978). Sites of absorption and translocation of iron in barley roots. *Plant Physiology*, 61, 731-6.

Cortez, J. and Billes, G. (1982). Role of calcium ions in formation of mucilage in the root cap of *Zea mays*. *Acta Oecologica* Serie 3, *Oecologia Plantarum*, 3, 67-78.

dela Fuente, R.K. and Leopold, A.C. (1973). A role for calcium in auxin transport. *Plant Physiology*, 51, 845-7.

Dieter, P. (1984). Calmodulin and calmodulin-mediated processes in plants. *Plant, Cell and Environment*, 7, 371-80.

Dieter, P. & Marme, D. (1983). The effect of calmodulin and far-red light on the kinetic properties of the mitochondrial and microsomal calcium-ion transport system for corn. *Planta*, 159, 277-81.

Fein, A., Payne, R., Corson, D.W., Berridge, M.J. and Irvine, R.F. (1984). Photoreceptor excitation and adaptation by inositol 1,4,5-trisphosphate. *Nature*, 311, 157-60.

Feldman, L.J. (1980). Auxin biosynthesis and metabolism in isolated roots of *Zea mays*. *Physiologia Plantarum*, 49, 145-50.

Feldman, L.J. (1981). Root cap inhibitor formation in isolated root caps of *Zea mays*. *Journal of Experimental Botany*, 323, 779-88.

Feldman, L.J. (1983). Light-enhanced protein synthesis in gravitropically stimulated root caps of corn. *Plant Physiology*, 72, 833-6.

Feldman, L.J. (1984). Regulation of root development. *Annual Review of Plant Physiology*, 35, 223-42.

Feldman, L.J. & Gildow, V. (1984). Effects of light on protein patterns in gravitropically stimulated root caps of corn. *Plant Physiology* 74, 208-12.

Foster, R.C. (1981). The ultrastructure and histochemistry of the rhizosphere. *New Phytologist*, 89, 263-73.

Foster, R.C. (1982). The fine structure of epidermal cell mucilages of roots. *New Phytologist*, 91, 727-40.

Goss, M.J. (1977). Effects of mechanical impedance on root growth in barley (*Hordeum vulgare* L.). I. Effects on the elongation and branching of seminal root axes. *Journal of Experimental Botany*, 31, 577-88.

Grahm, L. (1964). Measurements of geoelectric and auxin-induced potentials in coleoptiles with a refined vibrating reed electrode technique. *Physiologia Plantarum*, 17, 231-61.

Grahm, L. & Herz, C.H. (1962). Measurements of the geoelectric effect in coleoptiles by a new technique. *Physiologia Plantarum*, 15, 96-114.

Greenland, D.J. (1979). The physics and chemistry of the soil-root interface: some comments. In *The Soil-Root Interface*, ed. J.L. Harley & R.S. Russell, pp. 83-98. London: Academic Press.

Gunning, B.E. (1977). Transfer cells and their roles in transport of solutes in plants. *Science Progress, Oxford*, 64, 539-68.

Hensel, W. (1984). A role of microtubules in the polarity of statocytes from roots of *Lepidium sativum* L. *Planta*, 162, 404-14.

Horst, W.J., Wagner, A. & Marschner, H. (1982). Mucilage protects root meristem from aluminium injury. *Zeitschrift für Pflanzenphysiologie*, 105, 435-44.

Jackson, M.B. & Barlow, P.W. (1981). Root gravitropism and the role of growth regulators from the cap: a re-examination. *Plant, Cell and Environment*, 4, 107-23.

Juniper, B.E. (1976). Geotropism. *Annual Review of Plant Physiology*, 27, 385-406.

Juniper, B.E., Gilchrist, A.J. & Robins, R.J. (1977). Some features of secretory systems in plants. *Histochemistry Journal*, 9, 659-80.

Kramer, D. (1983). Genetically determined adaptations in roots to nutritional stress: correlations of structure and function. *Plant and Soil*, 72, 167-73.

Lee, J.S., Mulkey, T.J. & Evans, M.L. (1983a). Reversible loss of gravitropic sensitivity in maize roots after tip application of calcium chelators. *Science*, 220, 1375-6.

Lee, J.S., Mulkey, T.J. & Evans, M.L. (1983b). Gravity-induced polar transport of calcium across root tips of maize. *Plant Physiology*, 73, 874-6.

Lee, J.S., Mulkey, T.J. & Evans, M.L. (1984). Inhibition of polar calcium movement and gravitropism in roots treated with auxin-transport inhibitors. *Planta*, 160, 536-43.

Marschner, H., Romheld, V. & Ossenberg-Neuhaus, H. (1982). Rapid method for measuring changes in pH and reducing processes along roots of intact plants. *Zeitschrift fur Pflanzenphysiologie*, 105, 407-16.

Martin, J.K. (1977). Effect of soil moisture on the release of organic carbon from wheat roots. *Soil Biology and Biochemistry*, 9, 303-4.

Mertens, R. & Weiler, E.W. (1983). Kinetic studies on the distribution of endogenous growth regulators in gravireacting plant organs. *Planta*, 158, 339-48.

Miki, N.K., Clarke, K.J. & McCully, M.E. (1980). A histological and histochemical comparison of the mucilages on the root tips of several grasses. *Canadian Journal of Botany*, 58, 2581-93.

Moore, R. & McClelen, C.E. (1983). Ultrastructural aspects of cellular differentiation in the root cap of *Zea mays*. *Canadian Journal of Botany*, 61, 1566-72.

Moore, R. & Smith, J.D. (1984). Growth, graviresponsiveness and abscisic-acid content of *Zea mays* seedlings treated with Fluridone. *Planta*, 162, 342-4.

Morré, D.J., Jones, D.D. & Mollenhauer, H.H. (1967). Golgi apparatus mediated polysaccharide secretion by outer root cap cells of *Zea mays*. I. Kinetics and secretory pathway. *Planta*, 74, 386-301.

Mulkey, T.J. & Evans, M.L. (1982). Suppression of asymmetric acid efflux and gravitropism in maize roots treated with auxin transport inhibitors or sodium orthovanadate. *Journal of Plant Growth Regulators*, 1, 259-65.

Mulkey, T.J., Evans, M.L. & Kuzmanoff, K.M. (1983). The kinetics of abscisic acid action on root growth and gravitropism. *Planta*, 157, 150-7.

Northcote, D.H. (1982). The synthesis and transport of some plant glycoproteins. *Philosophical Transactions of the Royal Society, London*, Series B, 300, 195-206.

Nishizuka, Y. (1984). The role of protein kinase C in cell surface signal transduction and tumor promotion. *Nature*, 308, 693-8.

Oades, J.M. (1978). Mucilages at the root surface. *Journal of Soil Science* 29, 1-16.

Olsen, G.M., Mirze, J.I., Maher, E.P. & Iversen, T-H. (1984). Ultrastructure and movements of cell organelles in the root cap of agravitropic mutants and normal seedlings of *Arabidopsis thaliana*. *Physiologia Plantarum*, 60, 523-31.

Paull, R.E. & Jones, R.L. (1975). Studies on the secretion of maize root-cap slime. II. Localization of slime production. *Plant Physiology*, 56, 307-12.

Pilet, P.E., Elliott, M.C. & Moloney, M.M. (1979). Endogenous and exogenous auxin in the control of root growth. *Planta*, 146, 405-8.

Pilet, P.E. & Rivier, L. (1981). Abscisic acid distribution in horizontal maize root segments. *Planta*, 153, 453-8.

Prentki, M., Biden, T.J., Janjie, D., Irvine, R.F., Berridge, M.J. & Wollheim, C.B. (1984). Rapid mobilization of $Ca^{2+}$ from rat insulinoma microsomes by inositol-1,4,5-triphosphate. *Nature*, 309, 562-4.

Römheld, V. & Kramer, D. (1983). Relationship between proton efflux and rhizodermal transfer cells induced by iron deficiency. *Zeitschri fur Pflanzenphysiologie*, 113, 73-83.

Römheld, V. & Marschner, H. (1981a). Rhythmic iron stress reactions in sunflower at suboptimal iron supply. *Physiologia Plan* 53, 347-53.

Römheld, V. & Marschner, H. (1981b). Iron deficiency stress induced morphological and physiological changes in root tips of sunflower. *Physiologia Plantarum*, 53, 354-60.

Rougier, M. (1981). Secretory activity of the root cap. In *Encyclopedia of Plant Physiology*, New Series, Volume 13 B, Plant Carbohydrate II, ed. W. Tanner and F.A. Leowus, pp. 542-74. Berlin: Springer-Verlag.

Rovira, A.D., Foster, R.C. & Martin, J.K. (1979). Origin, nature and nomenclature of the organic materials in the rhizosphere. In *The Soil-Root interface*, ed. J.L. Harley and R.S. Russell, pp. 1-4. London: Academic Press.

Scott, B.I.H. (1967). Electric fields in plants. *Annual Review of Plant Physiology*, 18, 409-18.

Sievers, A., Behrens, H.M., Buckhout, T.J. & Gradmann, D. (1984). Can a $Ca^{2+}$ pump in the endoplasmic reticulum of the *Lepidium* root be the trigger for rapid changes in membrane potential after gravistimulation? *Zeitschrift fur Pflanzenphysiologie*, 114, 195-200.

Sievers, A. & Volkmann, D. (1972). Verursacht differentieller Druck der Amyloplasten auf ein komplexes Endomembran-system die Geoperzepti in Wurzeln? *Planta*, 102, 160-72.

Sijmons, P.C. & Bienfait, H.F. (1983). Source of electrons for extracellular Fe(III) reduction in iron-deficient bean roots. *Physiologia Plantarum*, 59, 409-15.

Torii, K. & Laties, G.G. (1966). Dual mechanisms of ion uptake in relation to vacuolation in corn roots. *Plant Physiology*, 41, 863-70.

Umali-Garcia, M., Hubbell, D.H., Gaskins, M.H. & Dazzo, F.B. (1980). Association of *Azospirillum* with grass roots. *Applied Environmental Microbiology*, 39, 219-26.

Vermeer, J. & McCully, M.E. (1981). Fucose in the surface deposits of axenic and field grown roots of *Zea mays* L. *Protoplasma*, 109, 233-48.

Vermeer, J. & McCully, M.E. (1982). The rhizosphere in *Zea*: new insight into its structure and development. *Planta*, 156, 45-61.

Volkmann, D. & Sievers, A. (1979). Graviperception in multicellular organisms. In *Encyclopedia of Plant Physiology*, New Series, Volume 7, Physiology of Movements, ed. W. Haupt and M.E. Feinleib, pp. 573-600. Berlin: Springer-Verlag.

Went, F.W. & Thimann, K.V. (1937). *Phytohormones*. London: Macmillan.

Whipps, J.M. & Lynch, J.M. (1983). Substrate flow and utilization in the rhizosphere of cerials. *New Phytologist*, 95, 605-23.

Wilkins, M.B. (1984). Gravitropism. In *Advanced Plant Physiology*, ed. M.B. Wilkins, pp. 163-200. London: Pitman.

Wilson, A.J., Robards, A.W. & Goss, M.J. (1977). Effects of mechanical impedance on root growth in barley, *Hordeum vulgare* L. II. Effects on cell development in seminal roots. *Journal of Experimental Botany*, 28, 1216-27.

Wright, K. & Northcote, D.H. (1976). Identification of β-1,4-glucan chains as part of a fraction of slime synthesized within the dictyosomes of maize root caps. *Protoplasma*, 88, 225-39.

# Potassium Transport in Roots

LEON V. KOCHIAN[a] and WILLIAM J. LUCAS[b]

[a] *U.S. Plant, Soil and Nutrition Laboratory, USDA-ARS, Cornell University, Ithaca, New York, USA*
[b] *Department of Botany, University of California, Davis, California, USA*

I. Introduction . . . . . 94

II. Plasma Membrane Transport of $K^+$ in Roots . . . . . 94
A. Early Work: the Carrier-Kinetic Approach . . . . . 94
B. Are Root $K^+$ Fluxes Coupled to $H^+$? . . . . . 99
C. Uptake at High $K^+$ Concentrations: the Linear Component . 120
D. Summary . . . . . 128

III. Redox-coupled Plasmalemma Transport of $K^+$ . . . . . 129
A. Influence of Exogenous NADH on $K^+$ Influx . . . . . 130
B. Membrane Transport and the Wound Response . . . . . 131
C. Development of an Integrated NADH Model . . . . . 132

IV. Radial $K^+$ Transport to the Xylem . . . . . 136
A. Site of $K^+$ Entry into the Symplasm . . . . . 137
B. Radial Pathway . . . . . 140
C. Lag Phase in Xylem Loading . . . . . 143
D. $K^+$ Transport into the Xylem . . . . . 145

V. Regulation of $K^+$ Fluxes within the Plant . . . . . 151
A. Allosteric Regulation of $K^+$ Transport . . . . . 152
B. $K^+$ Cycling within the Plant: an Integration of Regulatory Mechanisms . . . . . 163

VI. Future Research and Prospects . . . . . 169

Advances in Botanical Research Vol. 15
ISBN 0-12-005915-0

Copyright © 1988 Academic Press Limited
All rights of reproduction in any form reserved.

# I. INTRODUCTION

The involvement of $K^+$ in a number of plant functions (enzyme activation, maintenance of turgor, protein synthesis, etc.), along with the relatively high permeability of plant cell membranes to $K^+$, has been the basis for the study of $K^+$ transport as a model system for plant ion transport. Numerous investigations have been conducted over the past 40 years, aimed at furthering our understanding of the mechanism(s), energetics, and cellular location of $K^+$ transport systems in roots. Despite the surfeit of literature in these areas, it can be said with some confidence that the processes by which $K^+$ ions are transported into and across the root are still far from being fully resolved. This is due, in part, to the complex nature of the root, with its various cell types and tissues. Additional complications arise from the fact that the individual cells are coupled (both electrically and physiologically) via plasmodesmata, and also simply from the complex nature of individual cells, with their multiple compartments and subcompartments. In the first part of this chapter, we will outline and summarize what is known (or at least thought to be known) concerning mechanistic aspects of $K^+$ transport in roots. Once this background has been established, the regulation of these transport processes can be discussed in the context of the integration of these cellular processes at the organ and whole plant level.

# II. PLASMA MEMBRANE TRANSPORT OF $K^+$ IN ROOTS

## A. EARLY WORK: THE CARRIER-KINETIC APPROACH

Over the past half century, most of the studies that have been conducted concerning ion absorption by plants have generally utilized three basic types of plant material: the giant algae such as *Chara*, *Nitella*, and *Valonia*, slices cut from storage tissue of beet, potato, and carrot, and either intact roots or roots excised from seedlings. The use of excised roots as research material can be traced to the classical paper of Hoagland and Broyer (1936). They found that the roots of barley seedlings grown in dilute salt solutions exhibited extremely high initial rates of ion accumulation. Because radioisotopes had not yet been introduced, the ability of these roots to maintain high rates of accumulation made them very useful experimental material. Hence, the now well-known "low-salt roots" characterized by low salt content, high sugar content, and a large capacity for ion transport, became widely used in research.

It was during this era that many of the basic concepts of membrane transport were developed. Much of the work conducted with low-salt roots concerned the absorption of $K^+$ and other alkali cations (for the reasons discussed above). Although the concept of the lipid bilayer nature of the plasmalemma had not yet been fully developed, many researchers were

beginning to realize that plant (and animal) cells were bounded by a non-aqueous layer that was relatively impermeable to electrolytes (Osterhout, 1931). Furthermore, the rapid absorption of $K^+$ by plant cells led a number of investigators to hypothesize that special structures must exist that would facilitate $K^+$ uptake across this outer boundary (Jacobsen and Overstreet, 1947; Jacobsen *et al.*, 1950; Osterhout, 1950, 1952).

The concept that, in the plasmalemma, specific carriers were involved in $K^+$ uptake was developed further by Epstein and co-workers. When $K^+(^{86}Rb^+)$ uptake from dilute solutions into excised barley roots was studied, the kinetic profile approximated a rectangular hyperbola. This response was quite similar to that found in classical enzyme kinetic studies [Fig. 1 (see low concentration range)]. Epstein and Hagen (1952) were the first to apply Michaelis-Menten enzyme kinetics to ion transport. They postulated that specific alkali cation transport systems operated in a fashion analogous to substrate-specific enzymes. They went on to show, for the uptake of $K^+$ and other alkali cations, that at higher external concentrations their observed kinetics deviated from classical Michaelis-Menten form (Leggett and Epstein, 1956; Epstein *et al.*, 1963). Saturation was attained at low external $K^+$ concentrations, but then at higher concentrations the curves appeared to reach a second level of saturation (Fig. 1). This biphasic pattern was labelled the "dual isotherm of uptake" by Epstein, and was hypothesized to be due to the operation of two separate classes of carriers in the plasmalemma. In the low $K^+$ concentration range (<0.5 mM), mechanism I was hypothesized to be a $K^+$ transport system with a high affinity for $K^+$

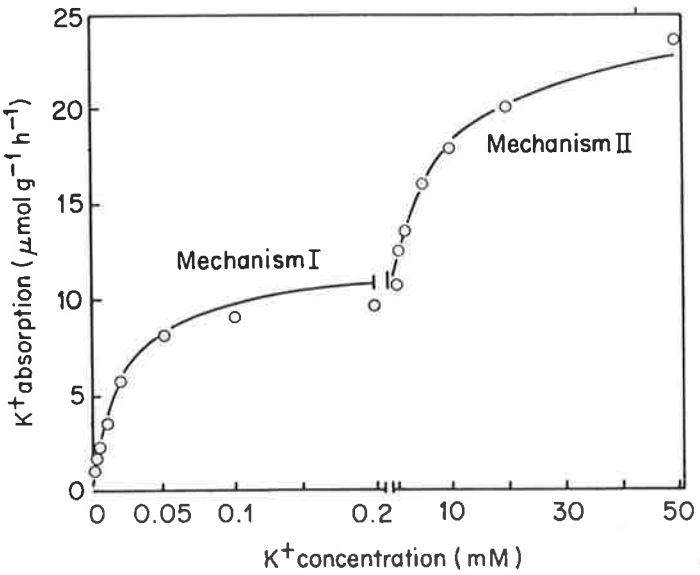


Fig. 1. Rate of $K^+$ absorption in barley roots as a function of $K^+$ concentration. Note that the concentration scale has been changed after 0.2 mM $K^+$. Data from Epstein *et al.* (1963).

(particularly with respect to $Na^+$). In the higher concentration range, mechanism II was proposed to operate as a low-affinity, high-velocity transport mechanism that was less specific for $K^+$. Further studies in the mechanism II range suggested that the kinetic profile was not a smooth curve, but was characterized by multiple inflections (Elzam *et al.*, 1964; Epstein and Rains, 1965).

This pioneering work by Epstein and his colleagues had a significant influence on the field of plant membrane transport. Subsequently, publications emerged from many laboratories indicating that the uptake of a number of inorganic and organic solutes in most plant tissues followed complex kinetics. These complex kinetics were, for the most part, interpreted to be the result of two or more transport systems. Subsequent kinetic analyses suggested that each transport system (for a particular solute) exhibited distinctly different Michaelis-Menten kinetics. The great volume of published work reflected the interest and importance associated with this field. A number of controversies arose concerning the kinetic aspects of $K^+$ absorption (and the uptake of other solutes). Conflicting hypotheses were presented concerning such aspects as the number of phases and the cellular and subcellular localization of each phase (for a review see Laties, 1969; Epstein, 1976).

The most direct challenge to Epstein's "dual isotherm" hypothesis was introduced in the early 1970s by Nissen, who presented an alternative interpretation for multiphasic uptake kinetics (Nissen, 1971, 1973, 1974). Nissen's approach was to analyse both his own and other researcher's kinetic data for solute uptake (uptake versus solute concentration) by performing various kinetic transformations of the primary data. These transformations (usually Lineweaver-Burk reciprocal plots) yield linear relationships for uptake kinetics that followed Michaelis-Menten relationships. Because the kinetics for solute uptake in plants are almost always complex, the reciprocal plots, quite naturally, yielded non-linear transformations. Nissen has fitted the transformed data by means of a statistical computer program and has found that the best fit, generally, for uptake of $K^+$ and any other solutes that he and others have studied, is a series of adjacent linear segments (e.g. Nissen and Nissen, 1983; Nissen, 1987).

Nissen claims that this type of analysis is strong evidence for the operation of a single complex transport system located in the plasmalemma. As external $K^+$ concentration is increased, this putative transport system is thought to undergo abrupt transitions at discrete external $K^+$ concentrations. Within each phase, the transport system is thought to obey Michaelis-Menten kinetics, with the kinetic constants for each phase usually increasing in a fairly regular manner. This approach is somewhat controversial and has been subjected to some fairly strong criticisms (Walker, 1974; Wyn Jones, 1975; Borstlap, 1981a,b, 1983; Kochian and Lucas, 1982b).

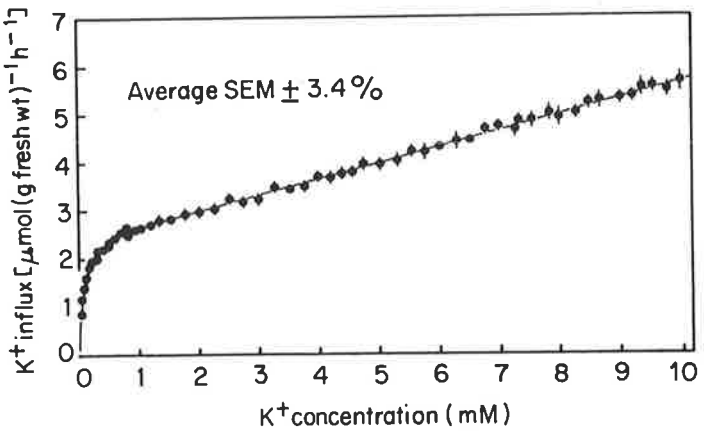


Fig. 2. Potassium ($^{86}Rb^+$) influx as a function of $K^+$ concentration in the experimental medium, obtained on corn root segments that were grown in 5 mM KCl + 0.2 mM $CaSO_4$ (high-salt status). Flux determinations were performed using the apparatus developed by Kochian and Lucas (1982a). Data points represent the mean ± SE (points which lack error bars do so because the standard errors were smaller than symbols used). Linear regression performed on data points for $K^+$ concentrations from 1.0 to 10 mM gave a value of 0.334 $\mu$mol (g fresh weight)$^{-1}$ h$^{-1}$ for the first-order rate coefficient of the linear component (the regression coefficient was 0.999).

Some of these criticisms, and an overall critique of the carrier-kinetic approach to $K^+$ transport in roots, will be discussed in a later section.

Most of the work of this era centred around the deduction of ion transport mechanisms from either the shapes of kinetic curves (influx versus concentration) or from the shapes of curves resulting from various mathematical transformations of the kinetic data. Many of these published data are of limited value because, in many cases, the kinetic profiles lack a sufficient number of data points for the concentration ranges tested. Also, data replication was often lacking.

Kochian and Lucas (1982a) addressed this problem by developing an experimental apparatus which enabled them to generate large numbers of data points on the [S] axis, with enough replicates to obtain sufficiently precise values. As illustrated in Fig. 2, no abrupt discontinuities were observed for $K^+$ transport into corn roots. Kinetic curves for $K^+$ influx into roots of both low- and high-salt-grown corn seedlings were found to be smooth and nonsaturating; the curves approached linearity at concentrations above 1 mM and exhibited no tendency towards saturation at concentrations up to 50 mM. The kinetics for $K^+$ transport could be resolved into saturable and nonsaturating, or first-order kinetic components. The saturable component could be specifically inhibited by application of sulphhydryl reagents (Fig. 3), whereas the nonsaturating component could be specifically inhibited by either the application of $K^+$ channel-blocking

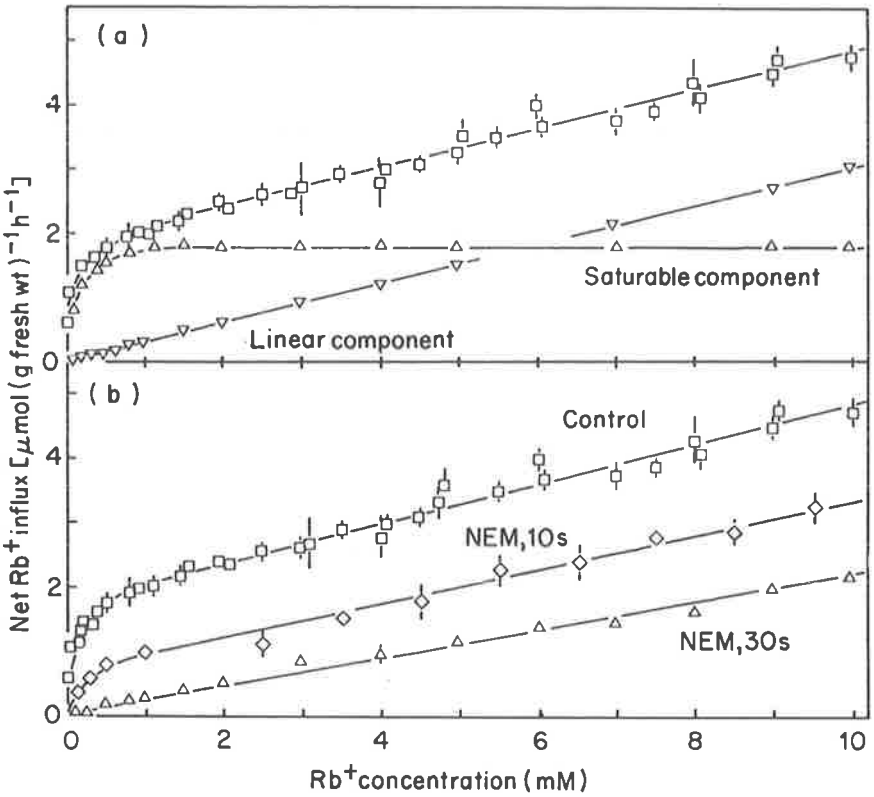


Fig. 3. Kinetic curves for $^{86}Rb^+$ influx into high-salt-grown corn root segments. In (a), the control curve (□) has been separated into its saturable and linear components. In (b), the influence of *N*-ethyl maleimide (NEM) exposures on $^{86}Rb^+$ influx is depicted. Corn root segments were pretreated with 0.3 mM NEM for 10 or 30 s, then washed for 10 min in 1 mM dithioerythritol (DTE) prior to $^{86}Rb^+$ uptake. Data from Kochian and Lucas (1982a).

agents, or by substituting $Cl^-$ in the uptake solution with other anions (Kochian *et al.*, 1985). The discrepancy between Epstein's mechanism II and the first-order kinetic component observed in corn roots, will be addressed in Section II.C.

Although the carrier-kinetic approach has provided important information on the mechanisms of ion transport, clearly there are limitations associated with this approach. In studying root ion transport, one is dealing with a system consisting of many cell types, each potentially in a different physiological state, with the problems of unstirred layers and diffusion limitation further confounding data interpretation. In studying the concentration dependence of uptake, the bulk solution ion concentration is generally taken as representing the substrate level available for transport, despite the knowledge that the cation and anion concentrations at the surface of the plasmalemma are probably considerably different from those in the bulk solution. This point is highlighted by the recent work of Newman *et al.* (1987), in which ion-selective microelectrodes were utilized to analyse the

electrochemical gradients for $H^+$ and $K^+$ in the unstirred layer near the surface of corn roots. Newman *et al.* (1987) found that in the presence of low levels of $K^+$ (less than 50 $\mu$M), the steady-state concentration at the root surface was about one-half that of the bulk solution, due to depletion arising from net $K^+$ uptake into the root. This considerable difference may be *magnified* further within the cell walls and at the surface of the plasmalemma, where additional diffusion limitation and ionic effects may have a dramatic influence on cation and anion activities. These points are of particular significance when mechanistic models, such as those presented by Nissen, are based solely on small differences between and within uptake kinetic curves.

### B. ARE ROOT $K^+$ FLUXES COUPLED TO $H^+$?

It has long been accepted that $K^+$ influx into roots is either coupled to the transport of $H^+$ or, at the very least, influenced by $H^+$ activities (or activity gradients) associated with the $K^+$ transport system. Like most areas of plant membrane transport, the concept that $K^+$ and $H^+$ fluxes are coupled has been controversial. Over the past 40 years, various models have been presented to explain the mechanism(s) by which $K^+$ uptake is coupled to $H^+$ efflux. The earliest models proposed that $H^+$ efflux was *dependent* upon $K^+$ uptake, or more specifically, depended upon cation uptake that was in excess of anion absorption. The $H^+$ excreted by the root had a *compensatory* role; that is, they were involved in maintaining charge balance across the plasmalemma. Organic acid metabolism and cytoplasmic pH regulation were also involved in this model (Ulrich, 1941; Jacobsen *et al.*, 1950; Jackson and Adams, 1963; Torii and Laties, 1966; Hiatt, 1967a,b).

More recent models have reversed the dependency between $K^+$ and $H^+$ fluxes. The influence of Mitchell's chemiosmotic hypothesis (Mitchell, 1970) has led some researchers to hypothesize that active $H^+$ efflux is the primary event (and driving force) for the subsequent (and dependent) $K^+$ uptake. Although most plant transport physiologists now generally accept that $K^+$ uptake is dependent on $H^+$ efflux, controversy still exists concerning the degree of this dependence. There appear to be two groups of adherents, with some researchers subscribing to a direct chemical coupling (Poole, 1974; Hanson, 1977; Leonard and Hanson, 1972; Lin and Hanson, 1976; Cheeseman and Hanson, 1979a,b; Cheeseman *et al.*, 1980), and others arguing that the two fluxes are indirectly coupled, through the electrical component of the protonmotive force generated by the electrogenic, plasmalemma $H^+$-ATPase (e.g. Pitman *et al.*, 1975; Marrè, 1977, 1979; Bellando *et al.*, 1979; Bellando and Trotta, 1980).

Glass and co-workers have severely questioned the existence of either a direct or an electrical coupling of the two fluxes, and have again suggested that the maintenance of charge balance may be the primary role for $H^+$ fluxes in relation to $K^+$ uptake (Glass and Siddiqi, 1982; Siddiqi and Glass,

1984). However, recent studies with *Neurospora* (Rodriguez-Navarro and Ramos, 1986; Rodriguez-Navarro *et al.*, 1986; Blatt and Slayman, 1987; Slayman *et al.*, 1988) and *Zea mays* roots (Kochian and Lucas, 1987; Kochian *et al.*, 1987, 1988; Newman *et al.*, 1987) have provided evidence consistent with the hypothesis that a $K^+$–$H^+$ co-transport system may operate in the plasmalemma of fungal and higher plant cells. The evidence supporting the various models based on different modes of coupling between $K^+$ and $H^+$ fluxes will now be considered in more detail.

*1. Unequal Cation/Anion Uptake Charge Balanced by $H^+$*

It has long been recognized that both intact and excised roots can maintain disparate rates of cation and anion absorption, depending on the composition of the salt solution bathing the roots. Even in early studies on root ion absorption, it was observed that, for example, excess cation absorption could occur from a solution containing $K_2SO_4$, while excess anion uptake was often seen in solutions containing $CaCl_2$ or $Ca(NO_3)_2$ (Brooks, 1929; Hoagland and Broyer, 1940). Uptake from KCl solutions usually results in a balance between cation and anion fluxes. During these early studies, it was recognized that the processes which transport net charge across the plasmalemma could not continue indefinitely, due to the axiom that electroneutrality must be maintained within living cells. (Additionally, we now realize that such processes could not continue in an uncompensated fashion due to the dielectric properties and limited capacitance of biological membranes.) Therefore, compensatory reactions must occur, in order to maintain charge balance both across membranes and within cells. Ulrich (1941) was the first to propose an interrelationship between unequal cation/anion uptake, cytoplasmic pH, and organic acid metabolism. He found that under conditions of excess cation uptake, organic acid content increased in proportion to the cation excess; the converse was found for uncompensated anion absorption. Ulrich hypothesized that under conditions of excess cation (usually $K^+$) absorption, $H^+$ were exchanged for $K^+$ ions. This could give rise to an alkalinization of the cell sap, stimulating the synthesis of organic acids which would help to buffer internal pH.

Subsequent work from a number of laboratories extended these initial speculations. Several researchers dealt with the mechanism of $K^+$ (and other cation) uptake in terms of a $K^+$–$H^+$ exchange and anion absorption as an anion–$OH^-$ antiport. Both processes would result in a trend towards electroneutrality (Jacobsen *et al.*, 1950; Jackson and Adams, 1963). It was also amply established that during excess $K^+$ uptake, the pH and buffering capacity of expressed root sap increased, as did dark $CO_2$ fixation and organic acid (usually malate) synthesis (Jacobson and Ordin, 1954; Jacobson, 1955; Torii and Laties, 1966; Hiatt, 1967a; Hiatt and Hendricks, 1967; Jacoby and Laties, 1971). It is still not clearly understood how excess $K^+$ absorption stimulates organic acid synthesis in the root. It has been proposed

that the $K^+$–$H^+$ exchange involved in charge balance should increase cytoplasmic pH, and such a pH shift has been suggested from pH measurements of total expressed root sap. This pH shift would "turn on" carboxylating enzymes in the cytoplasm (PEP carboxylase + malate dehydrogenase) and result in the synthesis of malic acid. Subsequent dissociation of the malic acid carboxyl groups would yield $H^+$ that could both help maintain cytoplasmic pH and permit continued $K^+$–$H^+$ exchange (Hiatt, 1967a,b). This model has been promoted as a regulatory mechanism involved in the maintenance of cytoplasmic pH (Davies, 1973; Raven and Smith, 1974; Smith and Raven, 1976). Alternatively, other models have been proposed which involve alterations in the levels of substrate ($CO_2$ versus $HCO_3^-$) available for organic acid synthesis (Jacoby and Laties, 1971), feedback regulation of PEP carboxylase by cytosolic malate levels (Osmond, 1976), and ionic effects on carbon metabolism (Osmond, 1976; Osmond and Greenway, 1972; Schnabl, 1987).

The above discussion has dealt more directly with regulatory aspects of $K^+$ (and general cation) uptake, and not specifically with mechanisms of $K^+$ absorption. It was important to introduce this topic in this section because this area of research was instrumental in developing the concept that $K^+$ and $H^+$ fluxes were, in some fashion, correlated. For a more detailed consideration of the interactions of ion absorption, carbon metabolism, and cytoplasmic pH regulation, the reader is referred to reviews by Osmond (1976), Smith and Raven (1976, 1979), and Davies (1979).

### 2. *Direct Coupling: $K^+$–$H^+$ Antiport*

It has been well documented that plant cells accumulate $K^+$ in the cytoplasm and generally maintain electrochemical potential gradients for $K^+$ across the plasmalemma (Läuchli and Pflüger, 1979; Leonard, 1984, 1985). Numerous studies have demonstrated that $K^+$ uptake into root tissue is extremely sensitive to metabolic inhibitors. Uptake is energy-dependent, and a close correlation with cellular levels of ATP (modified through the application of metabolic inhibitors) has been demonstrated (Petraglia and Poole, 1980). However, the problems of elucidating underlying mechanisms on the basis of such studies is all too obvious. Nevertheless, by combining electrophysiological, kinetic, and inhibitor studies, it has been possible to demonstrate that at least at low external $K^+$ levels, uptake is a thermodynamically active process (see Pitman, 1976; Cheeseman and Hanson, 1980).

Additionally, compelling evidence has been accumulated over the past 20 years that electrogenic transport processes operate across both the plasmalemma and tonoplast of lower and higher plant cells. Further, it is now well accepted that these transport systems are membrane-bound ATPases that are involved (at the very least) in the active transport of $H^+$ (for reviews see Poole, 1978; Spanswick, 1981; Leonard, 1982; Serrano, 1984; Marrè and Ballarin-Denti, 1985; Sze, 1985). During this same period, the chemiosmotic

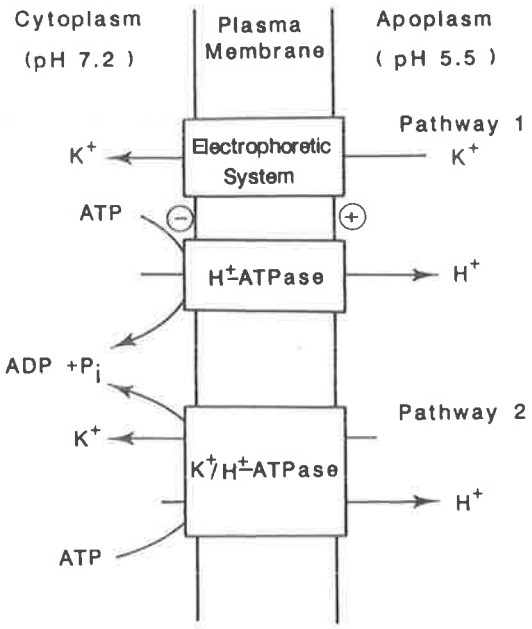


Fig. 4. Possible mechanisms for $K^+$ transport into plant cells. The plasma membrane $H^+$-ATPase produces a pH gradient and a membrane potential during ATP hydrolysis. $K^+$ transport can be either driven by the electrical component of the membrane potential with movement occurring through a membrane protein (pathway 1) or by direct transport via a $K^+/H^+$-ATPase (pathway 2). It is also possible that both pathways can occur. Modified from Briskin (1986), with permission.

hypothesis, developed by Mitchell (1970) to explain energy transduction in mitochondria and chloroplasts, had alerted plant physiologists to the possibility that $H^+$ gradients could be coupled to other ion fluxes. Because plant transport scientists already had observed associations between $K^+$ uptake and $H^+$ efflux, it was only natural that all of these factors would influence thinking about active $K^+$ influx. Hence, a number of mechanistic models were developed that coupled $H^+$ to $K^+$ fluxes. As mentioned previously, two types of coupling were hypothesized, and these are detailed in Fig. 4.

For a number of different root tissues it has been demonstrated that as external pH is increased, a concomitant increase in $K^+$ influx occurs (e.g. Poole, 1966, 1974; Lin, 1979; Glass and Siddiqi, 1982). This apparent pH dependency for washed corn root segments and intact barley roots is shown in Fig. 5. Poole (1974), working with slices from red beet roots, observed that as external pH was increased from 5.5 to 8.0, there were parallel stimulations of $H^+$ efflux and $K^+$ uptake, and a hyperpolarization of the $E_m$. He was probably the first to suggest that the plasmalemma electrogenic proton pump of plant cells was actually a $K^+$–$H^+$ exchange ATPase, facilitating $K^+$ uptake in response to active $H^+$ efflux.

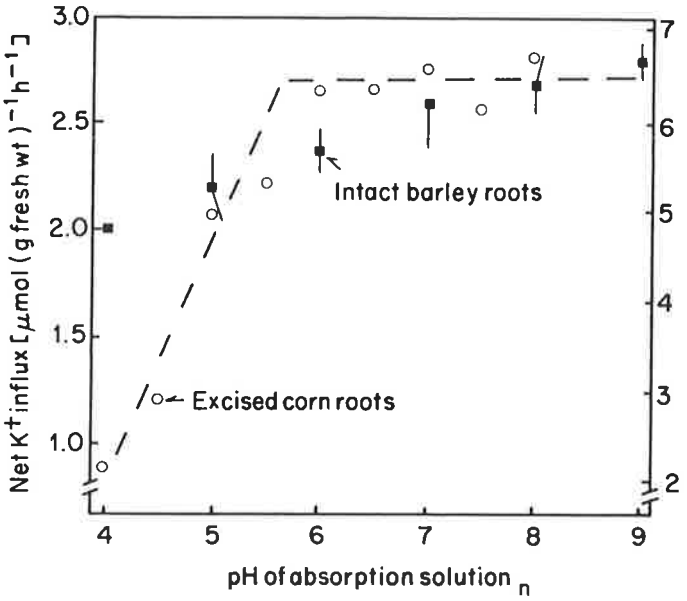


Fig. 5. Effect of external pH on $K^+$ ($^{86}Rb^+$) influx into 4-h-washed corn root segments (○) and intact barley roots (■). Where present, error bars represent ±SE. Note the apparent pH insensitivity from pH 6–9. (Scale on right-hand side for intact barley roots.) ○: Data replotted from Lin (1979). ■: Data replotted from Glass and Siddiqi (1982).

Hanson and co-workers, working with intact and excised corn root segments, have been among the more vocal proponents of a direct $K^+$–$H^+$ exchange mechanism (Hanson, 1977). Lin and Hanson (1976) demonstrated that the sulphhydryl-containing compound dithioerythritol (DTE) could "activate" a passive and stoichiometric (1:1) $K^+$–$H^+$ exchange system. However, as they note, in their experiments this antiporter was involved in the release of $K^+$ from corn root cells. They speculated that this passive antiport mechanism could be involved in $K^+$ uptake under conditions where the thermodynamic gradients favoured $K^+$ influx ($K^+$ directed inwardly and/or $H^+$ out). However, this seems to be unlikely for the thermodynamic gradient for $H^+$ would rarely be directed *out* of the cell. Lin and Hanson presented a model in which an active $K^+/H^+$-ATPase (for which *no evidence* was presented) was coupled to the observed DTE-induced passive $K^+$–$H^+$ exchange system as well as to an active anion uptake system (anion–$OH^-$ antiport). An alternative function could exist for the passive $K^+$–$H^+$ antiport system, if it is physiologically significant. As the authors mention, this system could be involved in osmotic regulation and/or control of internal $K^+$ under conditions of high $K^+$ status. A precedence exists for such a situation. Active $K^+$ uptake into the photosynthetic bacterium, *Chromatium vinosum*, is mediated via a $K^+$-ATPase that exhibits a high affinity for $K^+$, while a low-affinity $K^+$–$H^+$ antiport system (which mediates $K^+$ efflux) is involved

in osmotic balance and cytoplasmic pH regulation under conditions of high internal $K^+$ (Davidson and Knaff, 1981, 1982).

In a subsequent paper investigating ion transport ($K^+$ and $P_i$) in corn root segments, the differential effects of pH and several chemical modifiers on $K^+$ and $P_i$ transport were shown and used to support the existence of separate (and active) $K^+$–$H^+$ and $P_i$–$OH^-$ exchange systems (Lin, 1979). The apparent stimulation of $K^+$ uptake at high pH values (Fig. 5) was correlated with increased values of $H^+$ efflux. These results were considered to be consistent with an active exchange system whose $H^+$ efflux activity was increased in response to a reduction in the $\Delta\bar{\mu}_H$ opposing $H^+$ extrusion as the pH was increased. Lin found that the fungal toxin, fusicoccin, which has been shown to stimulate both $H^+$ efflux and cation uptake, and to hyperpolarize the $E_m$ of plant cells (Marrè, 1979), rapidly stimulated $K^+$ uptake while having little influence on phosphate transport. Additionally, the ATPase inhibitor diethylstilbestrol (DES) and the $H^+$ ionophore carbonyl cyanide 4-(trifluoromethoxy)hydrazone (FCCP) both immediately inhibited $K^+$ uptake while having an apparently less direct effect on $P_i$ uptake. These results were taken by Lin as *further* evidence that $K^+$ uptake occurs by an active, electrogenic $K^+$–$H^+$ exchange (even though no evidence for such a mechanism was presented in earlier papers). It should be noted that these results are quite circumstantial, and can be used to support other models for $K^+$ transport, as will be discussed later.

Cheeseman and Hanson (1979a,b) conducted a detailed study investigating the influence of anoxia and uncouplers on $K^+$ influx and $E_m$ over a range of $K^+$ concentrations. They analysed their data using the Goldman equations [used to describe passive ionic fluxes (Goldman, 1943; Hodgkin and Katz, 1949; Hodgkin and Huxley, 1952)] in order to determine the contributions of passive flux to the total $K^+$ influx. They proposed the model illustrated in Fig. 6, which indicates that at low external $K^+$ concentrations, active $K^+$ influx is coupled to the $H^+$-translocating ATPase. As $K^+$ concentrations are increased in the mechanism I range, saturation of this carrier occurs and the increasing inward $K^+$ current would have a depolarizing effect. As external $K^+$ increases into the mechanism II range, $K^+$ influx occurs via a passive electrophoretic uniport. However, in this concentration range, external $K^+$ is thought to have a stimulatory effect on the ATPase.

Cheeseman and Hanson originally suggested that both $K^+$ transport functions were carried out by the same system, utilizing a single type of $H^+$-ATPase. However, in a later publication (Cheeseman *et al.*, 1980) they revised their model. After analysing the influence of ATPase inhibitors on $E_m$ and $K^+$ influx, they hypothesized that at low $K^+$ levels an electrogenic system dominates that is sensitive to ATPase inhibitors, and is associated with active $K^+$ influx and $H^+$ efflux. A second electrogenic system was proposed which operates at all external $K^+$ concentrations and becomes dominant at higher $K^+$ concentrations. This system drives passive $K^+$ influx,

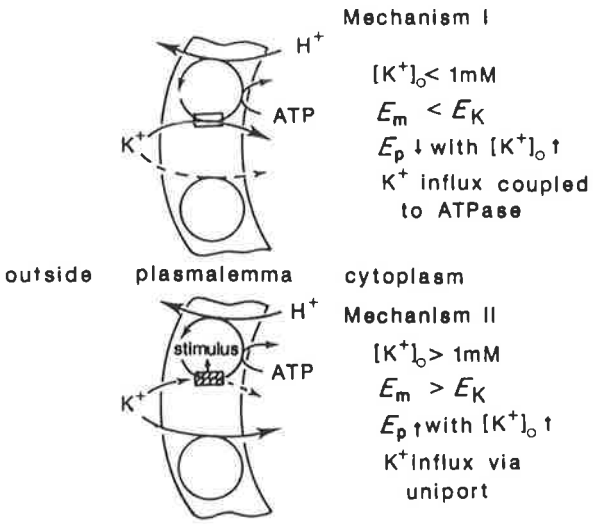


Fig. 6. Schematic model developed by Cheeseman and Hanson (1979b) to explain the role of the electrogenic $H^+$-ATPase in $K^+$ transport across the corn root plasmalemma when the external $K^+$ concentration is within the mechanism I and II range. Note that within the mechanism II $K^+$ concentration range, it is proposed that external $K^+$ has a stimulatory effect on the rate at which $H^+$ are pumped out by the ATPase. $E_p$ is the electrogenic component of the $E_m$ contributed by the $H^+$-ATPase.

and is insensitive to ATPase inhibitors. Essentially, what Cheeseman and co-workers were proposing was a model that incorporates both types of coupling illustrated in Fig. 4. At low external $K^+$ levels, active $K^+$ uptake would occur via a $K^+$–$H^+$ exchange ATPase (pathway 2 of Fig. 4). At higher external $K^+$ concentrations, passive $K^+$ uptake would be mediated by a $K^+$ channel, with the driving force arising primarily from the electrical potential difference developed across the plasmalemma by a $H^+$-ATPase. Recently, evidence in support of this model was presented following a re-evaluation of the electrogenic nature of $K^+$–$H^+$ fluxes in corn roots (Thibaud *et al.*, 1986). It should be noted that if $K^+$ uptake is active at low $K^+$ levels, then the $K^+$ transport system *must* be coupled either directly to an ATPase ($K^+$-ATPase or $K^+$–$H^+$ exchange ATPase), or to the transmembrane proton electrochemical gradient (PMF) via a $K^+$–$H^+$ co-transport system. Indirect coupling (pathway 1, Fig. 4) can only be invoked for the passive $K^+$ uniport.

Early evidence for the existence of a $K^+$-transporting ATPase came from work which correlated $K^+$ influx in corn, wheat, oat, and barley roots with $K^+$-stimulated ATPase activity located in a microsomal membrane preparation isolated from these roots (Fisher and Hodges, 1969; Fisher *et al.*, 1970). The putative plasmalemma ATPase was further characterized in subsequent studies (Hodges *et al.*, 1972; Leonard and Hodges, 1973; Leonard and Hotchkiss, 1976). The enzyme showed an acidic pH optimum for activity, and a requirement for $Mg^{2+}$, and was further stimulated by

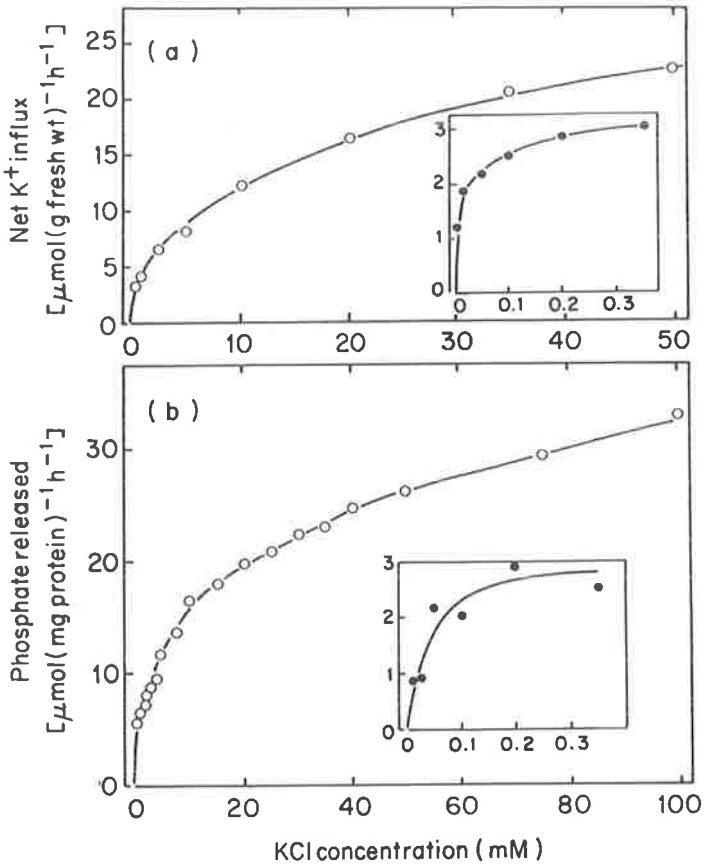


Fig. 7. Correlation between the kinetics of $^{42}K^+$ influx into excised oat roots (a) and the stimulation of a microsomal ATPase activity as a function of $K^+$ present in the reaction medium (b). ATPase activity was determined by the amount of $P_i$ released. Insets show $^{42}K^+$ influx and $P_i$ released over the concentration range of 0.01–0.35 mM KCl. Data from Leonard and Hodges (1973).

monovalent cations, particularly $K^+$ and $Rb^+$. Leonard and Hodges (1973) showed that the complex kinetics for $K^+$ absorption, in oat roots, were quite similar to the kinetics observed for $K^+$ stimulation of ATPase activity (Fig. 7). It seemed appropriate, therefore, to correlate $K^+$ transport in plants with the $H^+/K^+$-ATPase of the gastric mucosa and the $Na^+/K^+$-ATPase of animal cells, since these systems all exhibited cation-induced stimulation and transported $K^+$ directly (Hodges, 1976; Cantley, 1981; Faller *et al.*, 1982; Leonard, 1984; Briskin, 1986a).

The correlation between plasma membrane-associated, $K^+$-stimulated ATPase activity and $K^+$ influx, and the similarity between the sequence for monovalent cation stimulation of ATPase activity ($K^+ > NH_4^+ > Rb^+ > Cs^+ > Li^+$) and the specificity of monovalent cation uptake into roots (Sze and Hodges, 1977), has been used as further evidence that this ATPase is involved in $K^+$ uptake, putatively as a $K^+$–$H^+$ exchange system. It has also been demonstrated that microsomal membrane vesicles isolated from

tobacco callus, and believed to be plasmalemma in origin, exhibited a stimulation of $K^+$-ATPase activity in the presence of nigericin (which facilitates electroneutral $K^+$–$H^+$ exchange), or valinomycin plus a protonophore (Sze, 1980). These results again suggest that the plasmalemma ATPase may be involved in $K^+$–$H^+$ exchange.

Recent work with isolated plasma membranes from corn roots (Briskin and Leonard, 1982a,b), oat roots (Vara and Serrano, 1983), and red beet storage tissue (Briskin and Poole, 1983a,b), has demonstrated that the plasmalemma ATPase forms a covalently bound, phosphorylated intermediate during the course of ATP hydrolysis. Briskin and Leonard (1982a,b) showed that $K^+$ mildly stimulated the breakdown of this phosphorylated intermediate, using a crude preparation from corn roots, and concluded that this stimulation is further evidence for a $K^+$ transport function by the ATPase. An analogy was again drawn with the reaction mechanism for the $Na^+/K^+$-ATPase of animal cells, which also exhibits a $K^+$ stimulation of dephosphorylation, and transports $K^+$ directly (Cantley, 1981). However, it should be noted that the $Na^+/K^+$-ATPase phosphoenzyme intermediate has a much higher turnover rate, and the influence of $K^+$ on the rate of dephosphorylation is considerable. Similar $K^+$ effects on the dephosphorylation step were obtained with the plasmalemma ATPase isolated from red beet (Briskin and Poole, 1983a,b; Briskin and Thornley, 1985; Briskin, 1986b). However, in these studies the authors appear to place less emphasis on ascribing a $K^+$ transport function for the ATPase.

In contrast to the above studies, Vara and Serrano (1983) could find no effect of $K^+$ on the phosphorylation and dephosphorylation of the plasmalemma ATPase from oat roots. This result led Serrano (1984) to propose that the ATPase is *not* a $K^+$-dependent enzyme involved in $K^+$ transport. As he points out, this interpretation is supported by the observation that, in the studies of the corn root microsomal membranes, the turnover of the phosphoenzyme was quite slow, and the $K^+$ stimulation of the phosphoenzyme breakdown was much too small to support the concept of a direct role for $K^+$ in the reaction kinetic scheme for this enzyme. Recently, Spanswick and Anton (1988) presented a model describing the kinetic characteristics of a $H^+$-translocating ATPase purified from isolated plasmalemma vesicles of tomato roots (Fig. 8). They observed that the kinetics for the ATPase were similar to those for other cation-transporting ATPases that form phosphorylated intermediates. Their model does not ascribe a $K^+$ transport role to the ATPase. Instead, stimulation of the breakdown of the phosphorylated intermediate by cytoplasmic $K^+$ appears to be sufficient to explain the $K^+$-stimulation of ATPase activity, without invoking a $K^+$ transport role for the ATPase. It was proposed that $K^+$ transport occurs by a separate mechanism operating in conjunction with the $H^+$-ATPase.

There are additional criticisms that can be directed at the work published in support of a $K^+$ transport function for the plant plasmalemma ATPase.

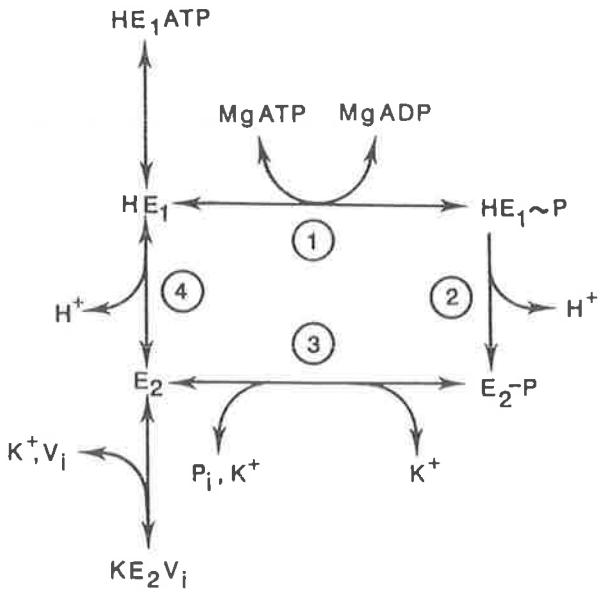


Fig. 8. A reaction scheme for the plasma membrane ATPase proposed by Spanswick and Anton (1988). The binding of $H^+$ at the cytoplasmic face of the plasma membrane occurs via reaction 4 to give $HE_1$, subsequent hydrolysis of ATP via reaction 1 produces $HE_1 \sim P$ and from this state the $H^+$ is released to the outer surface of the plasma membrane, via reaction 2. Potassium is proposed to act from the cytoplasmic face of the membrane to accelerate the dephosphorylation of $E_2$–P, to return the ATPase to the state in which it can again bind $H^+$. ($V_i$ stands for inorganic vanadate which acts as a competitive inhibitor on the $E_2$ complex.)

First, the degree of $K^+$ stimulation of ATPase activity is quite low when compared with total ATPase activity, and the $K^+$ concentrations often used to achieve this stimulation are excessively high (50 mM) when considering $K^+$ concentrations likely to be present in the soil solution or root apoplasm. These results again suggest that the $K^+$ effect may be a general salt effect, or activation by cytoplasmic $K^+$, and not evidence for $K^+$ requirement by a $K^+$ transporting ATPase. Additionally, $K^+$ stimulation is observed only at pH values below 7 (Leonard and Hodges, 1973; Leonard and Hotchkiss, 1976). These considerations led Serrano (1984), in his quite comprehensive review of fungal and higher plant plasmalemma ATPases, to state, "Thus, the plasma membrane ATPase is not a potassium-dependent enzyme although it is specifically stimulated by this ion".

An alternative view can be taken which would fit both mechanistic views. The dominant transport protein in the plant plasmalemma could be the $H^+$-translocating ATPase, which might not be expected to exhibit $K^+$-stimulated activity. However, a $K^+$-ATPase could also be present, at much lower levels. This could explain the small $K^+$ stimulation of ATPase activity and phosphoenzyme turnover, which would be measured against a large background of activity due to the $H^+$-ATPase. It is not unrealistic, in the light of work from animal and bacterial systems, to suggest that a number of

different ATPases might be contained in the various plant membranes, operating in response to different signals and participating in various cell functions.

The resolution of this controversy may ultimately come from demonstrations of ATP-dependent $K^+$ and $H^+$ transport in purified and reconstituted systems (Briskin, 1986a). Much of the early work on plasma membrane ATPases shared the rather common problem of contamination by other membranes. For example, it was only recently that ATP-dependent transport was demonstrated with membrane fractions isolated from plant roots. Using microsomal membranes isolated from corn, several different groups have now been able to demonstrate the existence of an ATP-dependent proton pump (Sze and Churchill, 1981; Churchill and Sze, 1983; DuPont *et al.*, 1982; Mettler *et al.*, 1982; Stout and Cleland, 1982; Bennett and Spanswick, 1983). However, it was unclear at the time whether the membrane vesicles exhibiting $H^+$ transport originated from the plasmalemma. It appears that much of the early examples of ATP-dependent $H^+$ pumping were being conducted with tonoplast vesicles (Mettler *et al.*, 1982; Serrano, 1984). It has now been amply demonstrated that at least two distinct ATPases were contained in these microsomal membrane preparations: a $K^+$-stimulated, vanadate-sensitive, $NO_3^-$-insensitive ATPase that is plasma membrane in origin, and a $Cl^-$-stimulated, vanadate-insensitive, $NO_3^-$-inhibited ATPase that is located in the tonoplast (Marrè and Ballarin-Denti, 1985). ATP-dependent $H^+$ pumping has been demonstrated with both types of membrane vesicles.

Recent improvements in plant membrane fractionation techniques have allowed for the isolation of fairly pure membrane fractions. Hence, it is now possible to reconstitute partially purified preparations of plasmalemma ATPases into proteoliposomes (Vara and Serrano, 1982; O'Neill and Spanswick, 1984). However, an unequivocal demonstration of ATP-dependent $K^+$ transport is still lacking. When partially purified oat root (Vara and Serrano, 1982) and red beet storage tissue plasmalemma ATPases (O'Neill and Spanswick, 1984) were reconstituted into liposomes, only $H^+$ transport was observed. Vara and Serrano demonstrated ATP-dependent $H^+$ pumping with inverted liposomes containing $K^+$-free solutions (Fig. 9), which suggested to them that the ATPase did not mediate $K^+$–$H^+$ exchange. Additionally, it can also be seen in Fig. 9 that introducing $K^+$ produced an *instantaneous* stimulation of $H^+$ transport, which would be expected if $K^+$ was acting on the active site of the ATPase facing the external medium (cytoplasmic side of inverted vesicles). They interrupted this result as further evidence against a $K^+$–$H^+$ transport function, since a lag in the stimulation by $K^+$ would be expected as $K^+$ diffused into the vesicle and became available for transport.

Because of the demonstrated $H^+$-pumping capacity of these membranes, and a lack of $K^+$ transport ability, the present consensus of most researchers

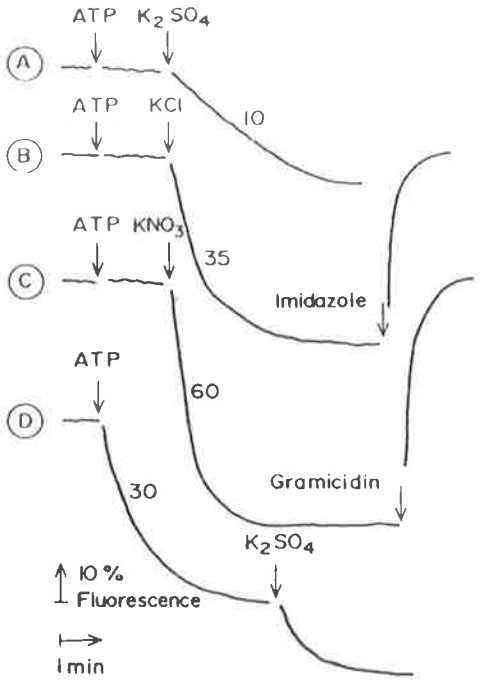


Fig. 9. Changes in 9-amino-6-chloro-2-methoxyacridine fluorescence upon energization of $K^+$-free proteoliposomes prepared from oat root plasma membrane ATPase. Assay medium contained either 25 mM $MgSO_4$ (A, B and C), or 25 mM $Mg(NO_3)_2$ (D). Tris-ATP (1.25 mM), $K_2SO_4$ (25 mM), KCl (50 mM), $KNO_3$ (50 mM), imidazole-HCl (pH 6.5, 20 mM), and gramicidin D (5 $\mu$g $ml^{-1}$) were added as indicated. The initial rate of quenching expressed as per cent of total fluorescence $min^{-1}$ is indicated. Data from Vara and Serrano (1982).

in this area appears to be that the plant plasmalemma ATPase acts as an electrogenic $H^+$ transport system rather than a $K^+/H^+$-ATPase.

However, this is an area of research in which rapid progress is being made, and it may well be that this consensus will be modified in the near future. Very recently, evidence suggesting ATP-dependent $K^+$ transport in plasmalemma vesicles isolated from red beet storage tissue has been presented (Giannini *et al.*, 1987). In this study, inverted plasmalemma vesicles were loaded with $^{86}Rb^+$-labelled $K^+$ solutions by a freeze-thaw technique. Although these vesicles were leaky for $K^+$, the addition of ATP stimulated $K^+$ efflux over and above that observed in the absence of ATP. The ATP-dependent efflux was completely inhibited by vanadate, but only partially inhibited by carbonyl cyanide *N*-chlorophenylhydrazone (CCCP), which should have abolished the $H^+$ electrochemical gradient. Giannini *et al.* suggest that $K^+$ transport may be mediated by two systems; one system would be indirectly coupled to the $H^+$ gradient, while the other would be directly coupled to the ATPase, as a $K^+$-translocating ATPase.

It should be noted that the results of Giannini *et al.* do not support the $K^+$–$H^+$ exchange hypothesis. As noted by Serrano (1984), $H^+$ ionophores

should not influence the transport function of ATPases that directly transport $K^+$, either as a $K^+$-ATPase or as a $K^+/H^+$-ATPase. However, since $H^+$ ionophores dissipate *both* the chemical and electrical components of the protonmotive force generated by a $H^+$-ATPase, any indirect coupling of $K^+$ transport to a $H^+$-ATPase would be significantly inhibited. This would include $K^+$ uniports driven by the electrical component of the PMF *and* $H^+$–$K^+$ co-transport. Evidence for the co-transport of $K^+$ with $H^+$ will be discussed in Section II.B.4.

*3. Indirect Coupling: Electrophoretic $K^+$ Uniport*

A number of researchers have argued that $K^+$ uptake is not directly coupled to the $H^+$-translocating ATPase, but is associated indirectly with the activity of the $H^+$ pump through a $K^+$ transport system driven by the electrical component of the PMF (Pitman *et al.*, 1975; Marrè, 1979 and references therein). Pitman and co-workers were the first to propose this type of electrophoretic coupling, following studies on the effects of fusicoccin (FC) on $K^+$ and $H^+$ fluxes in low-salt and salt-saturated barley roots (Pitman *et al.*, 1975). Their studies were generally conducted at high external $K^+$ levels (5 mM). In low-salt roots, the FC-stimulated $H^+$ efflux was similar, whether the roots were exposed to 5 mM KCl or 5 mM NaCl. However, in salt-saturated roots, which have a greater passive permeability to $K^+$ than $Na^+$ (in relation to low-salt roots), $H^+$ efflux was stimulated to a greater degree in KCl solutions. Hence, they suggested that FC acted to stimulate passive $K^+$ influx, through the increased electrical gradient created when $H^+$ extrusion was enhanced by FC.

Subsequent studies, which further support the hypothesis of an electrical coupling between the $H^+$ efflux and $K^+$ influx, are based on the application of FC to various plant tissues at $K^+$ concentrations (>1 mM) where uptake is considered to be passive (Marrè, 1977, 1979). It has been consistently observed that under these conditions FC stimulates both $H^+$ efflux and $K^+$ uptake, and elicits a hyperpolarization of $E_m$. A large body of circumstantial evidence has been accumulated, indicating that FC acts directly on the plasmalemma $H^+$-ATPase to stimulate $H^+$ translocation (Marrè, 1979). Since, in either the direct or indirect mode of coupling, a stimulation of $H^+$ efflux should enhance $K^+$ uptake, it is not possible to differentiate between the two models simply through the application of FC. Obviously, other approaches must be used in conjunction with FC experiments.

Marrè (1979), in his review on FC, has summarized the observations in support of indirect (electrophoretic) coupling. They are as follows:

1. The stoichiometry of the FC-stimulated $K^+$–$H^+$ exchange is often quite close to 1:1 (at least for corn roots and pea stem segments), particularly when corrections are made to account for $H^+$ consumption during anion uptake. Although this observation can be used in support of either mode of

coupling, it appears to support indirect coupling when considered in conjunction with the following observations.

2. Under the conditions in which FC-stimulated fluxes are generally studied, $K^+$ is in passive equilibrium across the plasmalemma (Pitman *et al.*, 1975; Cocucci *et al.*, 1976). Hence, any stimulation of net $K^+$ influx would involve an increase in passive uptake.

3. It has been demonstrated that lipophilic cations, such as tributylbenzylammonium and tetraphenylphosphonium, can substitute for $K^+$ in its role in promoting FC-stimulated $H^+$ efflux (Bellando *et al.*, 1979; Bellando and Trotta, 1980). Presumably, these cations cross the plasmalemma nonspecifically, by permeating the lipid bilayer. When this occurs, it has been shown that $E_m$ is depolarized and $H^+$ efflux is stimulated. Therefore, it has been argued that the apparent dependency of $H^+$ efflux on $K^+$ is due to a $K^+$ influx-induced depolarization of $E_m$, which would activate the electrogenic $H^+$-translocating ATPase. Conversely, chemical modifiers that stimulate the proton pump (such as FC) would hyperpolarize the membrane potential and increase the driving force for passive, electrophoretic $K^+$ influx.

Interpretation of FC experiments is based on the premise that FC acts specifically on the plasma membrane ATPase to increase its activity. The rapidity of the FC effects on plasmalemma ion transport, and the similar inhibitions of FC-stimulated $K^+$ and $H^+$ fluxes, and ATPase activity, by known plasmalemma ATPase inhibitors, are often used in support of this premise (Marrè *et al.*, 1974a,b). Additionally, [$^3$H]-FC has been shown to bind specifically to a protein component of the plasmalemma-enriched fraction isolated from corn coleoptiles (Dohrmann *et al.*, 1977), and FC is known to stimulate ATPase activity associated with plasmalemma-enriched membrane fractions (Beffagna *et al.*, 1977). However, caution must be exercised when interpreting these data. Several groups have solubilized the putative FC-binding protein from plasmalemma-enriched membrane fractions of corn coleoptile (Pesci *et al.*, 1979; Tognoli *et al.*, 1979) and oat roots (Stout and Cleland, 1980). In each case, it has been shown that the FC-binding protein can be separated from the $K^+$-stimulated plasmalemma $H^+$-translocating ATPase. Although it has been suggested in each of the above studies that the FC-binding protein could be a subunit of a multisubunit ATPase, the possibility exists that FC may act at sites totally separate from the $H^+$-ATPase. In a recent electrophysiological study on *Vicia faba* guard cells, Blatt (1987) obtained evidence that FC *may not* act on the pump, but via an effect on the related co-transport processes. Additionally, his current-voltage data indicated that FC may act to *block* a $K^+$ channel involved in $K^+$ efflux from guard cells. Such a mode of action could also explain the FC effects on other plant cell membranes, and it may be necessary to conduct a complete re-evaluation of these FC data.

The use of the electrophoretic coupling model to explain $K^+$ uptake over *all* $K^+$ concentrations is subject to a number of criticisms, some of which

have been rather eloquently summarized (Glass and Siddiqi, 1982; Siddiqi and Glass, 1984). They point out that $K^+$ influx often greatly exceeds $H^+$ efflux, an observation that we have also stressed (Kochian *et al.*, 1987, 1988; Newman *et al.*, 1987). This is a feature which has been presented in work dealing with $K^+$ and $H^+$ fluxes, although it has often gone unmentioned in the texts of these papers (e.g. Poole, 1974; Pitman *et al.*, 1975; Lado *et al.*, 1976; Lin and Hanson, 1976). It is difficult to reconcile a model where $K^+$ influx is energetically dependent on the membrane potential (which, in turn, is dependent primarily on $H^+$ efflux), when the $H^+$ fluxes are usually much smaller than the associated $K^+$ fluxes. Sometimes this disparity has been explained on the basis that the measured, "apparent" net $H^+$ efflux is considerably smaller than the true unidirectional efflux, due to processes that also consume $H^+$. These processes might include anion–$H^+$ co-transport, passive "leaks" that would tend to return $H^+$ into the cell, and $H^+$ captured by the cell wall. However, Glass and Siddiqi (1982) conducted a careful assessment of the contribution of these processes to the underestimation of "true" $H^+$ efflux, and concluded that for their system (low-salt barley roots) the measured net $H^+$ efflux is a good approximation of the unidirectional flux.

Furthermore, the data presented in Fig. 10 indicate that $H^+$ efflux may be dependent upon external $K^+$, or $K^+$ influx, *per se*. Clearly, as stressed by Glass and Siddiqi (1982), this is the converse of what would be expected if $K^+$ uptake were dependent upon $H^+$ extrusion. They also noted that at

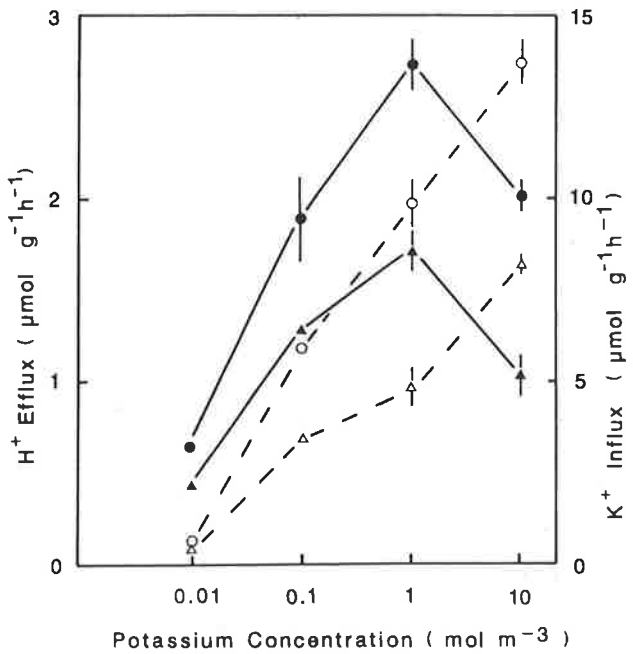


Fig. 10. Potassium influx (○, △) and $H^+$ efflux (●, ▲) as a function of $K^+$ ($K_2SO_4$) in the bathing medium. Experiments were conducted on two varieties of barley, var. Fergus (○, ●) and var. Conquest (△, ▲). Data from Glass and Siddiqi (1982).

higher $K^+$ levels (>1 mM), $H^+$ efflux often levels off or declines slightly (see Fig. 10). This saturation is somewhat surprising, considering earlier published reports which specifically linked $K^+$ and $H^+$ fluxes at higher $K^+$ concentrations (Pitman, 1970; Marrè, 1977). Because it was found that anion influx [$SO_4^{2-}$ in the case of Glass and Siddiqi (1982)] was greatly increased at higher substrate levels (>0.5 mM $K_2SO_4$), these potentially anomalous results could be explained by a reduction in net $H^+$ efflux due to the consumption of $H^+$ during $SO_4^{2-}$ influx, if uptake were mediated by an anion–$H^+$ co-transport. However, these data, and most of the results used in support of models coupling $K^+$ and $H^+$ fluxes, could be explained equally well by a $H^+$ extrusion mechanism involved in the maintenance of charge balance (Glass and Siddiqi, 1982), as originally suggested by Ulrich (1941).

The constraints of charge balance are most evident when low-salt roots are transferred from a $CaSO_4$ medium to one containing various inorganic ions, whence they begin to increase their internal salt levels. The roots would then be in a transition between two regulatory states. Pitman (1970) proposed that the stimulated $K^+$ uptake, $H^+$ efflux, and excess cation absorption exhibited as salt status is increased, would be a reflection of this transitional stage. Siddiqi and Glass (1984) have extended this hypothesis, by suggesting that these transitional changes are the result of a concerted effort, by the root, to maintain electrical neutrality during the alteration of salt status. This attempt to maintain electroneutrality does not appear to be specific for $H^+$ efflux. Under certain conditions, plants can use other ion transport processes in order to effect charge balance (Siddiqi and Glass, 1984). For example, both $K^+$-stimulated $Na^+$ efflux and $NH_4^+$-stimulated $K^+$ efflux have been observed in plant roots. Thus, the apparent coupling of $K^+$ and $H^+$ fluxes may reflect a more general feature of plants, i.e. that cation exchanges ($H^+$, $K^+$, $Na^+$, $Ca^{2+}$ etc.) may be needed to maintain charge balance during times when high rates of cation uptake occur (i.e. during the transition from low-salt to high-salt status).

Finally, it seems unlikely that a single type of mechanism, or coupling mode, will suffice to account for $K^+$ uptake in higher plants. This is particularly apparent when one considers the potentially wide range of soil $K^+$ concentrations that a root may experience. There are many examples in the literature for plant, bacterial, and animal transport systems, where the uptake of a particular solute is mediated by two or more types of transport mechanisms. Since it appears that $K^+$ uptake in higher plants is active at low $K^+$ levels, and thermodynamically passive at higher concentrations, it seems plausible to speculate that two different $K^+$ transport systems might exist. The existence of $K^+$ channels has been known for many years in animal and bacterial membranes, and increasingly strong evidence for $K^+$ channels in higher plants has been accumulating (Schroeder *et al.*, 1984, 1987; Bentrup *et al.*, 1985; Kochian *et al.*, 1985; Kolb *et al.*, 1987). Hence, it is quite possible that $K^+$ channels in the plasmalemma facilitate passive $K^+$ uptake (or release) at higher (>0.5 mM) concentrations. The direction and magnitude

of these fluxes would depend upon the value of the membrane potential and on any voltage-dependent characteristics that these channels may possess. However, at low $K^+$ concentrations, where active $K^+$ uptake most probably occurs, a different type of transport system must operate. Uptake must either be directly coupled to an ATPase, as a $K^+$-ATPase (or the less likely case of a $K^+/H^+$-ATPase), or active $K^+$ uptake may be coupled to the $H^+$ gradient, via a $K^+$–$H^+$ co-transport system. The $K^+$–$H^+$ co-transport hypothesis will be considered in the next section.

*4. Other Modes of Coupling: $K^+$–$H^+$ Co-transport?*

Another approach that has been taken in order to *simultaneously* study $K^+$ and $H^+$ transport in roots involves the use of ion-selective microelectrodes for $K^+$ and $H^+$ (Kochian and Lucas, 1987; Kochian *et al.*, 1988; Newman *et al.*, 1987). An ion-selective microelectrode system was developed that could quantify and map the extracellular electrochemical potential gradients for $K^+$, $H^+$, and $Cl^-$ along the roots of 4-day-old corn seedlings. From an analysis of the extracellular ion gradients, it is possible to simultaneously determine and monitor the net $H^+$ and $K^+$ fluxes associated with a few cells at the root surface (due to the small electrode tip diameter of 0.5–1.0 $\mu$m). Because this system provides a high degree of spatial (and temporal) resolution, it has proven to be a useful method for studying the coupling of $K^+$ and $H^+$ fluxes at the *cellular* level. A diagrammatic representation of the system used in these studies is shown in Fig. 11.

Data collected with this system indicated that at any point along the root, large fluctuations in the fluxes (particularly $H^+$ fluxes) occurred with time. On many occasions, $H^+$ efflux was near zero while $K^+$ influx was "normal"; the converse was also occasionally observed. Additionally, when repeated measurements were made at the same location on the root, both $H^+$ efflux and $K^+$ influx could vary significantly, and usually the variation of the two fluxes did not show any correlation. The data presented in Table I illustrate

TABLE I

*Measurement of net $H^+$ and $K^+$ influx in low-salt-grown corn roots*

| Time (min) | $H^+$ Efflux ($\mu$mol (g fresh wt)$^{-1}$ h$^{-1}$) | $K^+$ Influx ($\mu$mol (g fresh wt)$^{-1}$ h$^{-1}$) |
|---|---|---|
| 0 | 1.87 | 2.92 |
| 3 | 0.76 | 3.18 |
| 8 | 0.00 | 2.52 |
| 12 | 0.00 | 2.89 |
| 20 | 1.12 | 2.27 |

Measurements were made with pH and $K^+$ microelectrodes at a position 3.0 cm from the root apex at distances of 50 and 125 $\mu$m from the root surface. Bathing solution consisted of 0.1 mM $K_2SO_4$ + 0.2 mM $CaSO_4$. Data taken from Kochian and Lucas (1987).

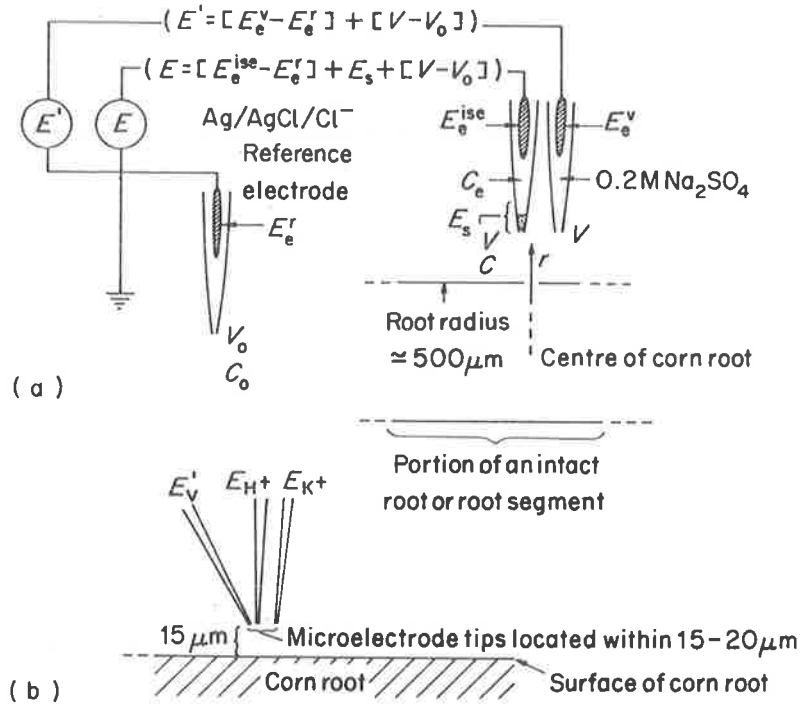


Fig. 11. Schematic representation of the ion-specific microelectrode system used by Newman *et al.* (1987) to measure the $K^+$ and $H^+$ electrochemical potential gradients which develop at the surface of intact corn roots. Individual voltage components are shown in (a): $E_e'$ and $E_e^{ise}$ represent the EMF of the half-cells for the reference and ion-selective electrode, respectively; $E_e^v$ is the EMF of the half-cell for the extracelluar electric potential electrode; $E_s$ is the EMF developed across the ion-exchange resin; $V$ and $V_o$ are the extracellular potentials near the root surface and in the background bathing solutions, respectively. A scaled representation of the relative positions of $K^+$, $H^+$ and extracellular potential ($E_v'$) microelectrodes is shown in (b). Here the microelectrodes (0.5 μm tip diameter) ae shown at their closest position to the corn root surface.

this point. Here, five separate measurements of $K^+$ influx and $H^+$ efflux were made over a 20-min period, and it can be seen that $H^+$ efflux varied rather dramatically, while $K^+$ uptake was relatively stable. From these studies no fixed stoichiometry was found for the two fluxes. Generally, net $K^+$ uptake was significantly larger than $H^+$ efflux; the $K^+$:$H^+$ flux ratio ranged from 3.6:1 to 1:2.75.

A similar lack of correlation between $K^+$ and $H^+$ fluxes was observed in barley roots (Glass and Siddiqi, 1982). Increasing the bathing medium pH resulted in a gradual, but small, increase in $K^+$ influx (see Fig. 5). However, $H^+$ efflux did not exhibit a similar pH dependency, but rather appeared to vary independently of the pH value. In this situation, the $K^+$:$H^+$ flux stoichiometries varied from 1:1 to 12:1, again with no apparent pH dependency.

The response of the cortical cell membrane potential to changes in

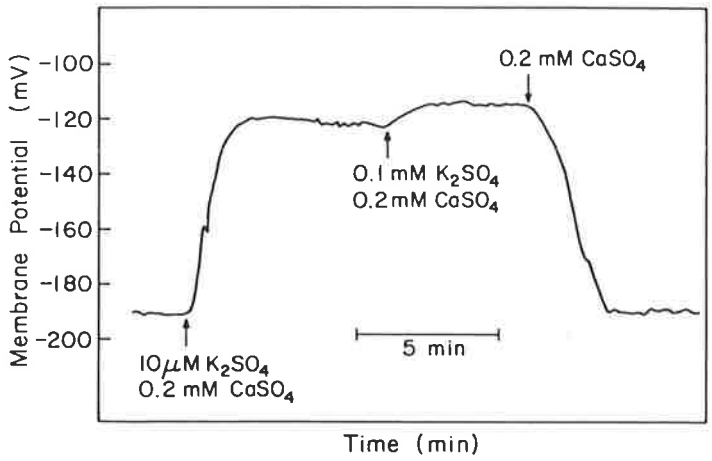


Fig. 12. Response of the cortical membrane potential of intact low-salt-grown corn roots to changes in the concentration of external $K^+$ (as $K_2SO_4$). ($CaSO_4$ was present at 0.2 mM in all solutions.) Data from Newman *et al.* (1987).

external $K^+$ was also investigated in these studies. Unlike the case in earlier studies (Cheeseman and Hanson, 1979a,b), the low-salt corn root membrane potential was extremely sensitive to external $K^+$. Increasing the $K^+$ concentration from 0.2 to 20 $\mu$M caused a rapid 70 mV depolarization, from $-190$ mV to $-120$ mV (see Fig. 12). A further increase in $K^+$ to 200 $\mu$M only elicited a further 7 mV depolarization. Newman *et al.* (1987) made simultaneous measurements of $E_m$ and $K^+$ fluxes in response to changes in external $K^+$, using a three-microelectrode system (one to measure $E_m$, and two $K^+$ microelectrodes for $K^+$ flux measurements). Both the kinetics (dependence on external $K^+$) for $K^+$ influx and the depolarization of the membrane potential yielded similar (and quite low) apparent $K_m$ values in the 6–9 $\mu$M range. These results indicated that low-salt corn roots possess a very high affinity $K^+$ uptake system that is extremely electrogenic (Newman *et al.*, 1987). In view of the highly electrogenic nature of this system, it is possible that other cations may be transported into the cell with $K^+$. Since these measurements were made in simple salt solutions (10 $\mu$M $K_2SO_4$ + 0.2 mM $CaSO_4$), $H^+$ appears to be the most likely candidate for co-transport with $K^+$. In such a situation, active $K^+$ influx would be achieved using the energy gained from the movement of $H^+$ down their $\Delta\bar{\mu}_H$.

Strong evidence for the existence of a $K^+$–$H^+$ co-transport system in fungi has been recently provided by work on *Neurospora* (Rodriguez-Navarro and Ramos, 1986; Rodriguez-Navarro *et al.*, 1986; Blatt and Slayman, 1987; Slayman *et al.*, 1988). Slayman and co-workers have described a high-affinity ($K_m$ = 1–10 $\mu$M) $K^+$ uptake system, in $K^+$-starved *Neurospora* cells, that is highly electrogenic, as demonstrated by the response presented in Fig. 13. Measurements of internal and external $K^+$, and $E_m$, suggested that this uptake system may mediate active $K^+$ uptake, and the system appears to be

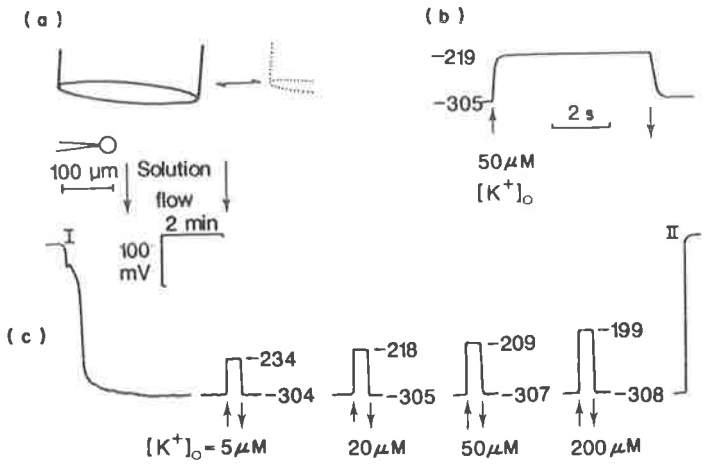


Fig. 13. Effect of added extracellular $K^+$ on the membrane potential measured in low-$K^+$ spherical cells of *Neurospora crassa*. (a) Diagram of the arrangement of the cell, the impaling electrode and a $K^+$-flooding pipette for rapid introduction and removal of $K^+$. (b) Depolarization of the $E_m$ with 50 $\mu$M $K^+$. (c) Condensed record from a single cell, showing the $E_m$ response to four different $K^+$ concentrations. Symbols I and II indicate cell impalement and electrode removal, respectively. Data from Rodriguez-Navarro *et al.* (1986).

coupled to the very active plasmalemma $H^+$-ATPase of *Neurospora*. A net stoichiometry of one $H^+$ out for one $K^+$ in was demonstrated, which could be taken as evidence for $K^+$–$H^+$ exchange. However, current-voltage analysis conducted by Slayman's group indicated that the $K^+$-associated inward current was twice that of the net $K^+$ influx (see Fig. 14). Thus, one additional positive charge enters with every $K^+$. In addition, the following points must be considered: (1) the $H^+$-ATPase operates in parallel with the $K^+$ uptake system; (2) almost every charge absorbed must be balanced by an extruded $H^+$; and (3) only a single $H^+$ is measured (released to the external solution) for every $K^+$ taken up. Hence, the second charge coming in with the $K^+$ must be a $H^+$, which indicates that the high-affinity $K^+$ uptake system operates as a $K^+$–$H^+$ symport (Rodriguez-Navarro *et al.*, 1986; Slayman *et al.*, 1988). Slayman and co-workers speculate that the data presented for higher plants could also be explained by this type of co-transport system coupled to the plasmalemma $H^+$-ATPase.

As discussed previously, it has been proposed that a similar co-transport system exists in the plasmalemma of corn root cells (Newman *et al.*, 1987). Further support for this hypothesis comes from the observed similarities between the $K^+$ uptake system seen in $K^+$-starved *Neurospora* cells and that described above for low-salt corn roots (Kochian *et al.*, 1987, 1988; Newman *et al.*, 1987). Both are very high affinity $K^+$ uptake systems with almost identical $K_m$ values for $K^+$. Furthermore, $K^+$ uptake through both systems is

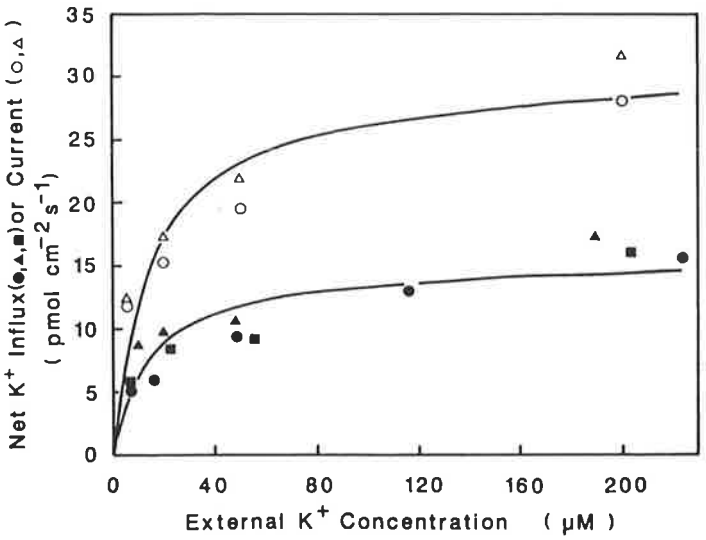


Fig. 14. Stoichiometry of the $K^+$–$H^+$ co-transport system of *Neurospora crassa*. The smooth curves are Michaelis-Menten functions fitted to the two sets of data, using a common value of 14.9 $\mu$M $K^+$ for the apparent $K_m$. Separate values of $V_{max}$ are 15.3 ± 1.0 pmol $cm^{-2}$ $s^{-1}$ for the flux, and 30.1 ± 1.6 pmol $cm^{-2}$ $s^{-1}$ for the measured current. The stoichiometric ratio of the current to net $K^+$ flux is very close to two. Data from Rodriguez-Navarro *et al.* (1986).

highly depolarizing (compare Figs 12 and 13). The similarities between the two systems, taken in conjunction with the lack of evidence, in low-salt corn roots, for a coupling between $K^+$ influx and $H^+$ efflux, strongly suggest that such a co-transport system could be operating in higher plants.

On a kinetic basis, it can be reasoned that a $K^+$–$H^+$ co-transport system should reflect a sensitivity to changes in both extracellular and cytoplasmic pH values. Previous reports of increasing $K^+$ influx, in response to decreasing $H^+$ concentrations in the bathing medium, appear to be somewhat at variance with this prediction. However, in these reports, $K^+$ influx was insensitive to external pH values from 6 to 9 (see Fig. 5). To further investigate this hypothesis for $K^+$ influx into corn roots, Kochian *et al.* (1987) used $K^+$-selective microelectrodes and $^{86}Rb^+$ to measure $K^+$ influx as a function of pH. Varying the external pH from 4 to 8 had *no effect* on either net $K^+$ influx (measured with $K^+$ microelectrodes) or unidirectional $K^+$($^{86}Rb^+$) influx. Additionally, Kochian *et al.* found that the $K^+$-induced depolarizations of $E_m$ (with solution of 50 $\mu$M $K^+$) also exhibited absolutely no pH dependence from pH 4 to 8. These results suggest that the $K^+$–$H^+$ co-transport system may have an extremely high affinity for $H^+$. However, an alternative interpretation is that $K^+$ influx is mediated by a different molecular mechanism, e.g. a $K^+$-ATPase, which would not, *a priori*, show a sensitivity to external pH values.

### C. UPTAKE AT HIGH $K^+$ CONCENTRATIONS: THE LINEAR COMPONENT

As discussed in Section II.A, studies on the kinetics of $K^+$ uptake, for various plant tissues, have generally focused on the generation of complex and often discontinuous kinetic curves, via either the operation of multiple Michaelis-Menten transport systems (such as Epstein's mechanisms I and II), or by complex, multisite carriers. However, there are numerous examples, particularly in association with studies involving animal and bacterial systems, of complex transport kinetics that appear to be due to the parallel operation of one or more saturable transport mechanisms *plus* a system that exhibits nonsaturating, or first-order uptake kinetics (linear component). For example, a linear transport component has been demonstrated for the uptake of amino acids and sugars in animal cells (Akedo and Christensen, 1962; Christensen and Liang, 1966; Munck and Schultz, 1969; Cohen, 1975, 1980; Debnam and Levin, 1975), and for the uptake of lactose (Maloney and Wilson, 1973), $K^+$ (Rhoads *et al.*, 1976; Epstein and Laimins, 1980) and amino acids (Wood, 1975; Iaccarino *et al.*, 1978) in *E. coli.*

In many of these studies, nonsaturating solute uptake was dismissed as a physiologically insignificant process, because it was considered to reflect passive diffusion across the lipid portion of the plasma membrane. However, in work on $K^+$ uptake in *E. coli*, linear $K^+$ uptake was hypothesized to be mediated by a transport protein, which was presumably a $K^+$ channel (Rhoads *et al.*, 1976; Epstein and Laimins, 1980). Furthermore, Christensen and Liang (1966) demonstrated that nonsaturating amino acid uptake in Ehrlich tumour cells was substrate-specific, and exhibited considerable sensitivity to pH and temperature. Thus, passive diffusion was discounted in favour of a more complex system involving a transport protein.

In recent years, there has been an increasing interest in linear, nonsaturating solute uptake kinetics from studies involving plant tissues. First-order kinetics have been observed for the uptake of $Fe^{2+}$ in rice roots (Kannan, 1971), sucrose and 3-*O*-methylglucose in *Ricinus* cotyledons (Komor, 1977; Komor *et al.*, 1977), sucrose in sugar beet leaf and petiole sections (Maynard and Lucas, 1982a,b), soybean cotyledons (Lichtner and Spanswick, 1981), *Vicia* leaves (Delrot and Bonnemain, 1981) and red beet vacuoles (Willenbrink and Doll, 1979), and sucrose, fructose, and glucose in *Allium* leaf discs (Wilson *et al.*, 1985), and for amino acid transport in *Lemna* (Fischer and Lüttge, 1980), and suspension-cultured tobacco cells (Blackman and McDaniel, 1978).

Separation of the contribution made by the linear transport component from the saturable mechanisms has been achieved through the use of various inhibitors (Debnam and Levin, 1975; Polley and Hopkins, 1979; Maynard and Lucas, 1982b; Van Bel *et al.*, 1982). For $K^+$ uptake into corn roots, Kochian and Lucas (1982a,b, 1983) have shown that the complex kinetics

could be resolved into saturable and first-order kinetic components, through the use of sulphhydryl modifiers. When corn root segments were subjected to a series of increasing *N*-ethyl maleimide (NEM) exposures (e.g. 0, 10, and 30 s NEM exposures for the data illustrated in Fig. 3b), saturable $K^+$ uptake was specifically inhibited and subsequently abolished, while linear uptake was relatively unaffected. Hence, it was suggested that the saturable and linear kinetic components represented separate $K^+$ transport systems. Saturable $K^+$ uptake would be analogous to Epstein's mechanism I; however, nonsaturating $K^+$ uptake, which dominates uptake in the concentration range associated with Epstein's mechanism II, appears to be distinctly different from the transport system described by Epstein and co-workers. Therefore, subsequent work was carried out in order to characterize this linear component for $K^+$ uptake (Kochian and Lucas, 1984; Kochian *et al.*, 1985); certain features of this transport system will now be discussed.

### 1. *Anion Involvement in Nonsaturating $K^+$ Uptake*

Early work by Epstein *et al.* (1963) demonstrated that in barley roots $K^+$ uptake by mechanism II was dramatically inhibited when $Cl^-$ was replaced by $SO_4^{2-}$ in the uptake solution. Similarly, it was shown that linear $K^+$ uptake in corn roots was partially dependent on the presence of $Cl^-$ in the uptake solution (Kochian *et al.*, 1985). As shown in Fig. 15, replacing $Cl^-$ in the

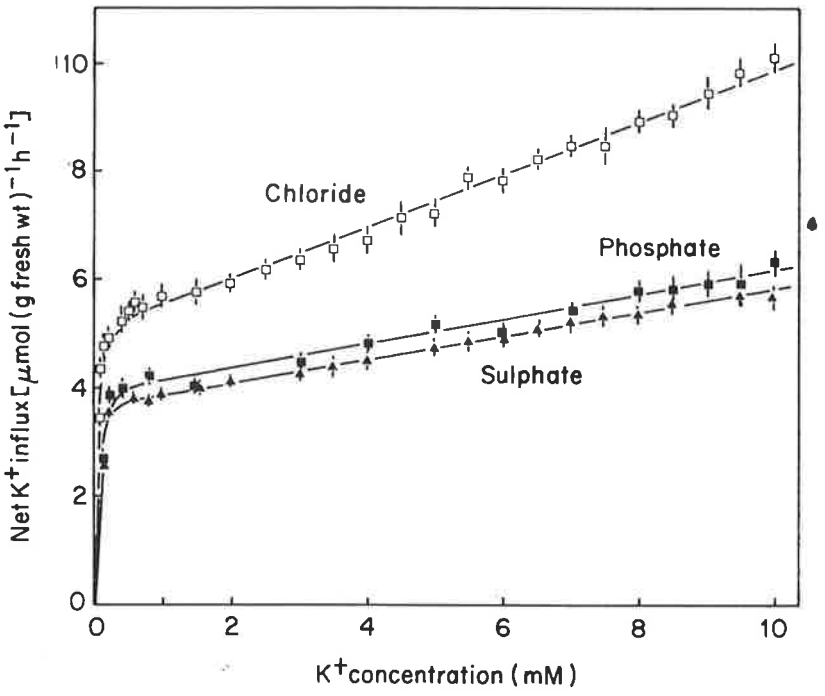


Fig. 15. Influence of the accompanying anion on $K^+$ ($^{86}Rb^+$) influx into corn root segments grown in 0.2 mM $CaSO_4$ (low-salt status). The first-order rate coefficients, $k$, in μmol (g fresh wt)$^{-1}$ h$^{-1}$ mM$^{-1}$, for the linear component of $K^+$ influx were as follows: 0.5 ($Cl^-$), 0.21 ($SO_4^{2-}$), and 0.24 ($H_2PO_4^-$). Data from Kochian *et al.* (1985).

uptake solution with $SO_4^{2-}$, $H_2PO_4^-$ or $NO_3^-$ resulted in a 60% reduction in $K^+$ uptake by the linear component in low-salt roots, while causing only a 15% reduction in the $V_{max}$ for the saturable system. In high-salt roots (grown on 5 mM KCl), a similar reduction in linear $K^+$ uptake was seen, while saturable uptake was unaffected.

This association between the linear component for $K^+$ uptake and the presence of $Cl^-$ was shown to be related to a coupling via the saturable $Cl^-$

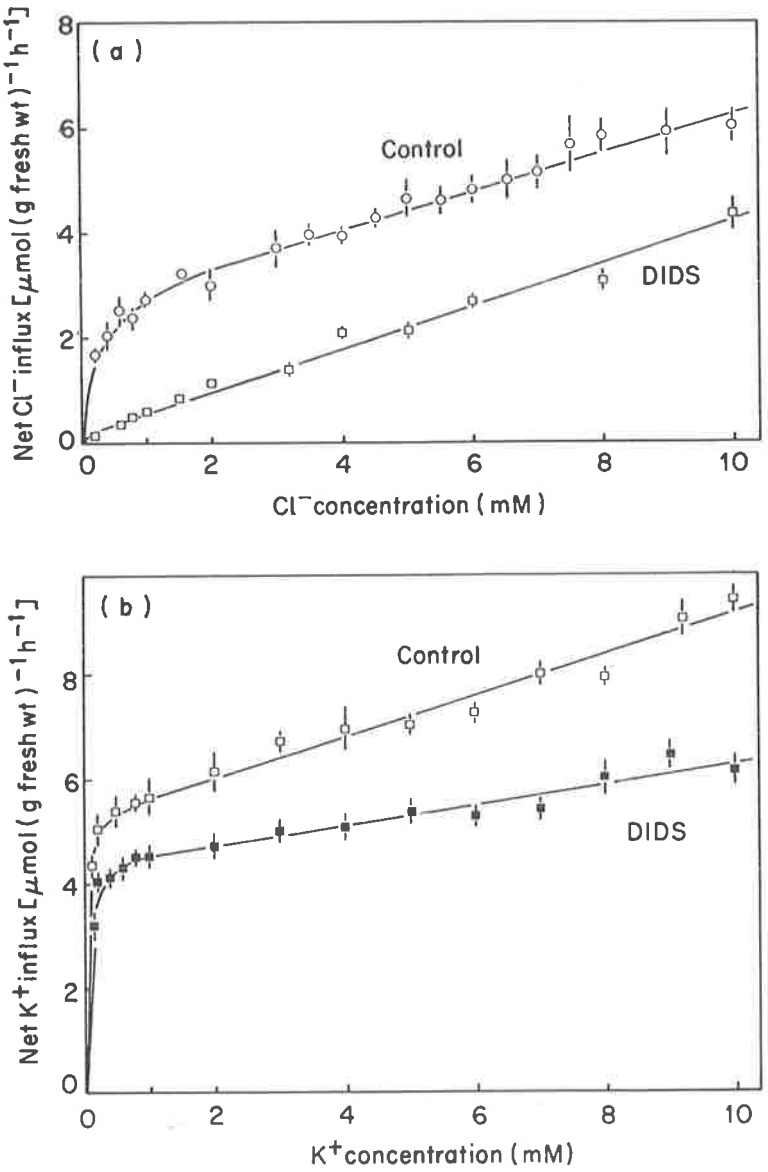


Fig. 16. Effect of the anion transport inhibitor DIDS on the influx of $^{36}Cl^-$ (a) and $K^+$ ($^{86}Rb^+$) (b) into low-salt corn root segments. For $K^+$ influx, $k$ had values of 0.40 and 0.19 μmol (g fresh wt)$^{-1}$ h$^{-1}$ mM$^{-1}$ for the control and DIDS treatment, respectively. Data from Kochian *et al.* (1985).

influx process. Application of 1 mM 4,4-diisothiocyano-2,2′-disulphonic acid stilbene (DIDS), which has been shown to be an anion transport inhibitor in red blood cells (Cabantchik *et al.*, 1978), corn roots (Lin, 1981) and *Chara* (Keifer *et al.*, 1982), abolished the saturable component for $Cl^-$ influx into low-salt corn roots (Fig. 16a). In the presence of this inhibitor, the linear component of $K^+$ uptake was suppressed to an identical degree to that seen when $Cl^-$ was replaced in the uptake solution by other anions (compare Figs 15 and 16b). These results strongly suggest that the linear component of $K^+$ influx in corn roots is, in some way, linked, at least partially, to saturable $Cl^-$ uptake.

*2. Involvement of $K^+$ Channels?*

The effect of the quaternary ammonium salt, tetraethylammonium chloride (TEA), which has been shown to block $K^+$ channels in excitable membranes, such as the plasma membrane of nerve fibres (Tasaki and Hagiwara, 1957; Armstrong, 1969), and in *Chara* (Keifer and Lucas, 1982), was studied on $K^+$ uptake in low- and high-salt corn roots. In high-salt roots, TEA caused a dramatic (75%) and specific inhibition of the linear component of $K^+$ influx (Fig. 17), which suggests that $K^+$ channels may be involved. However, although low-salt roots possess a similar linear component for $K^+$ influx, it was found to be insensitive to TEA, which seems at variance with the above interpretation. Uptake studies with [$^{14}$C]-TEA indicated that high-salt corn roots exhibited much higher rates of TEA accumulation than did low-salt roots, presumably via a transport system for quaternary ammonium salts

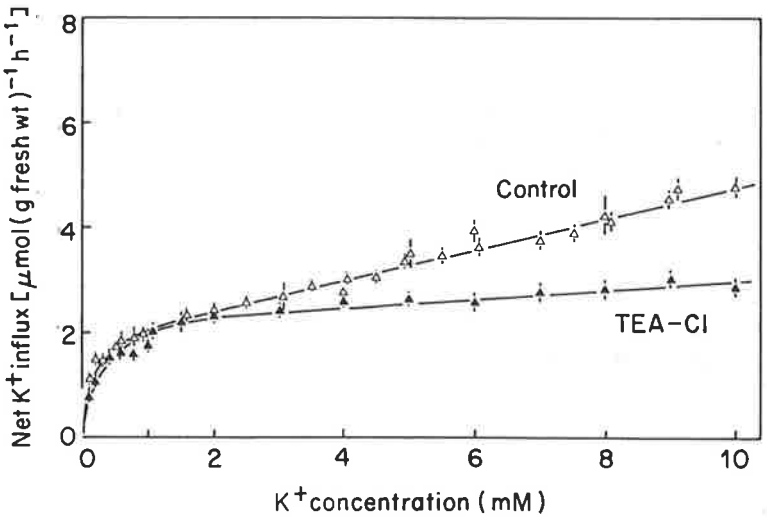


Fig. 17. Influence of 10 mM TEA-Cl on $K^+$ ($^{86}Rb^+$) influx into high-salt-grown corn roots. Roots were pretreated with a solution containing 10 mM TEA-Cl, 5 mM KCl, and 0.2 mM $CaSO_4$ for 30 min prior to $K^+$ ($^{86}Rb^+$) uptake (10 mM TEA-Cl was included in the uptake solutions). The first-order rate coefficients, $k$, for the linear component were 0.31 and 0.09 μmol (g fresh wt)$^{-1}$ h$^{-1}$ mM$^{-1}$ for the control and TEA-Cl, respectively. Data from Kochian *et al.* (1985).

that has been demonstrated in higher plants (Michaelis *et al.*, 1976). Hence, it was proposed that corn root tissue behaves in a similar manner to nerve axons, where it is necessary to inject the TEA into the axoplasm in order to block $K^+$ channels (Tasaki and Hagiwara, 1957; Armstrong, 1969). High-salt roots may be able to accumulate more TEA in the cytoplasm relative to low-salt roots. If this were the case, then $K^+$ channels could be involved in nonsaturating $K^+$ influx in both low- and high-salt roots; but only in high-salt roots would the cytoplasmic TEA concentration rise to a level high enough to block the putative $K^+$ channels at the cytoplasmic face of the channel.

In recent years, the application of the patch-clamp technique to plant cell membranes has provided direct evidence for the existence of $K^+$ channels in higher plant cell membranes. For example, $K^+$ channels have been demonstrated in the plasmalemma of guard cells (Schroeder *et al.*, 1984, 1987), *Samanea* pulvinar cells (Moran *et al.*, 1987) and corn root cells (Ketchum *et al.*, 1987), and in the tonoplast of *Chenopodium* suspension cells (Bentrup *et al.*, 1985) and barley mesophyll cells (Kolb *et al.*, 1987). Therefore, it seems reasonable to speculate that one or more classes of $K^+$ channels could operate in the plasmalemma of root cells, in order to facilitate passive $K^+$ uptake at high external levels of $K^+$.

Although it is axiomatic that any transport system should have a finite transport capacity, it is possible that a system like an ion channel would not exhibit saturation kinetics under physiological conditions. As Cohen (1975) has pointed out, such a channel-mediated process should eventually saturate at high substrate concentrations. However, in his system (amino acid uptake into mouse brain slices), at high substrate levels, the medium changes from isotonic buffered saline to hypertonic buffered amino acid saline. Thus, any changes in transport kinetics may be due to changes in media composition. The same applies for $K^+$ influx in corn roots. Potassium uptake has been studied from a range of concentrations up to 50 mM. At these high $K^+$ levels, there was no significant change in nonsaturating $K^+$ uptake (Kochian and Lucas, 1982a). Uptake was not studied from solutions of higher concentration, because it was felt that ionic and osmotic effects could alter membrane lipid/protein structure and make data interpretation tenuous.

### 3. *Root Salt Status and Nonsaturating $K^+$ Uptake*

Uptake into low-salt barley roots, at low external $K^+$ levels, is highly specific for $K^+$, while at higher $K^+$ concentrations (>0.5 mM), $Na^+$ can competitively inhibit $K^+$ influx (Epstein *et al.*, 1963). A similar response was also observed with low-salt corn roots. Inclusion of 3 mM NaCl in the uptake solution ($K^+$ concentration was from 0.1 to 10 mM) caused a 50% inhibition of the linear component for $K^+$ uptake, while saturable uptake was unchanged (Kochian *et al.*, 1985). The interesting feature is that within the mechanism II concentration range, high-salt corn roots exhibit a much higher selectivity for $K^+$ influx over other cations (Pitman, 1967, 1970; Pitman *et al.*, 1968; Kochian *et al.*, 1985). If we accept that the linear component represents the

operation of a $K^+$ channel, these data indicate that some aspect of tissue salt status modifies the channel characteristics from relatively nonspecific to highly $K^+$-specific in high-salt roots. It will be interesting to see whether this prediction can be confirmed using the patch-clamp technique.

*4. Alternative Explanation for the Linear Component*

Sanders (1986) has developed a generalized model to explain biphasic or otherwise complex transport kinetics, based on the co-transport of a solute with a driver ion. For $K^+$ influx into roots, a $K^+$–$H^+$ co-transport system would be driven by the inwardly directed $\Delta\bar{\mu}_H$ generated by the $H^+$-ATPase. In Sander's reaction kinetic model, the assumption is made that both solute ($K^+$) and driver ion ($H^+$) can bind randomly to the carrier, and the limitation is made that the carrier can cross the membrane only as the fully loaded complex (influx) and can return to the outside free of ligand. The reaction kinetic scheme for this model is shown in Fig. 18. Numerical analysis

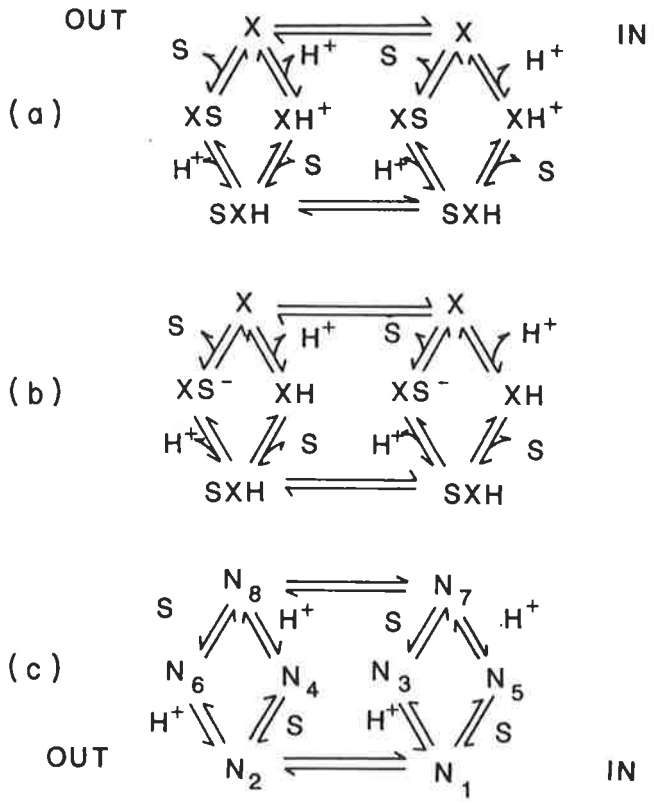


Fig. 18. Membrane transport modelled on the basis of a reaction kinetic scheme. (a) Reaction kinetic scheme for random binding of solute (S) and $H^+$ to a membrane-bound carrier (X) which catalyses the transport of S across the membrane. Carrier is represented as transporting positive charge in the loaded form. (b). As in (a), but with loaded carrier being neutral and charge transfer occurring on the unloaded form of the carrier. (c) Generalized reaction kinetic scheme for the charged and uncharged models. Concentration (density) of carrier state "j" is designated as $N_j$, with rate constants (not shown) from carrier state i to state j designated $k_{ij}$. Redrawn from Sanders (1986), with permission.

simulation of this model demonstrated that it generates biphasic kinetics under conditions resembling those present in many uptake experiments. The utility of this model is that it makes a number of predictions that are experimentally testable. These predictions are (in terms of a $K^+$–$H^+$ co-transport system):

1. As $[H^+]_o$ is increased to saturating levels, the kinetics for $K^+$ uptake should change from a complex biphasic to a monophasic profile.
2. At saturating $[H^+]_o$, increasing levels of internal $K^+$ should result in an uncompetitive inhibition of $K^+$ influx.

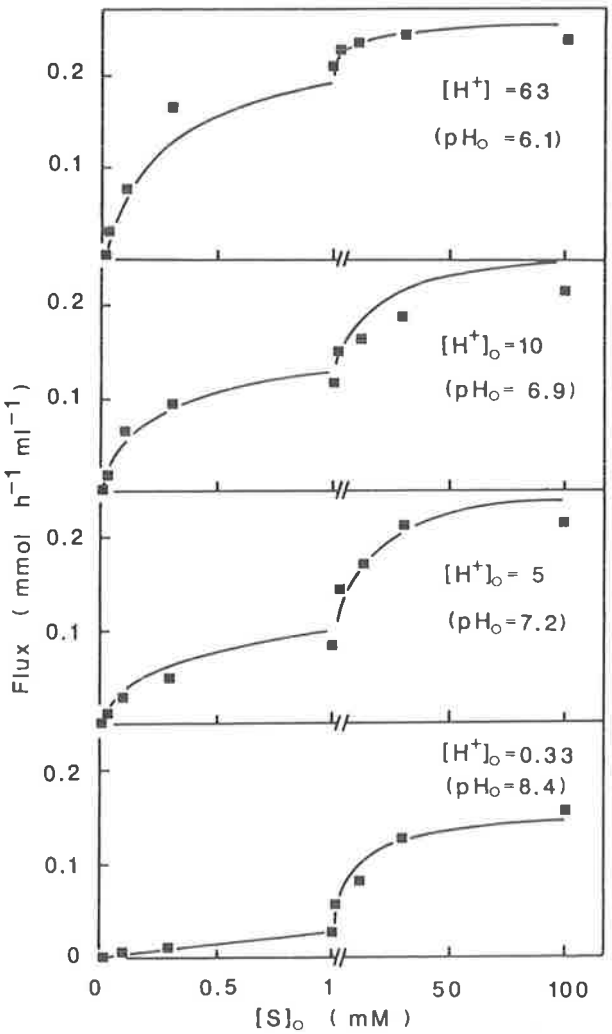


Fig. 19. Comparison between the experimental data (■) obtained for 6-deoxyglucose influx into *Chorella*, as a function of bathing medium pH (Komor and Tanner, 1975), and the theoretical simulation of Sanders' (1986) reaction kinetic model. The solid lines represent a simulation of the charged carrier model, simplified for very negative $E_m$ and internal 6-deoxy-glucose concentration set at zero. Data from Sanders (1986).

3. As $[H^+]_o$ is *decreased*, the relative contribution to the uptake isotherm made by the "apparent" low-affinity $K^+$ transport should increase.

As Sanders (1986) noted, there are few published examples of data concerning pH effects on complex isotherms for solute uptake in plants that permit his predictions to be properly tested. However, such kinetic isotherms do exist for the $H^+$–sugar co-transport system of *Chlorella* (Komor and Tanner, 1975). As shown in Fig. 19, these data give a reasonable fit to the first prediction of the Sanders model. However, if one then examines the pH dependency of the detailed kinetics for sucrose uptake into sugar beet leaves obtained by Maynard and Lucas (1982a), it is apparent that as the external pH is decreased from 9.0 to 4.0, both the saturable and nonsaturable components of sucrose uptake are stimulated. Clearly, these data do not fit the first prediction of the Sanders (1986) model.

Furthermore, it is difficult to reconcile $K^+$ uptake into high-salt corn roots with this Sanders model, since, in this system, it was possible to *specifically* abolish saturable $K^+$ uptake with NEM, while leaving nonsaturable uptake relatively unaffected (Fig. 3b). Conversely, it was possible to specifically inhibit the linear transport component either by replacing $Cl^-$ in the uptake solution with other anions (Fig. 15), or by treating the roots with the $K^+$ channel blocking agent, TEA (Fig. 17). At present it is not obvious how these perturbations, which appear to specifically resolve the complex kinetics for $K^+$ uptake into separate kinetic components, can be explained by the Sanders reaction kinetic model.

### 5. *Physiological Role for Nonsaturating $K^+$ Uptake?*

It has been noted that nonsaturating solute uptake often occurs over a concentration range which exceeds the levels normally experienced by roots in the soil, and so it is difficult to assign a physiological role for such a transport system. Reisenauer (1966) has pointed out that the majority of soil $K^+$ is below 2 mM; yet, in corn roots, nonsaturating $K^+$ uptake becomes significant above 1 mM external $K^+$. What then would be the physiological relevance of a transport system that operates at substrate levels rarely experienced by the plant? The answer to this question may come from transport studies conducted on *E. coli* and *Neurospora*. In both organisms, it has been well documented that multiple carrier systems are often involved in the transport of a single solute. These organisms tend to combine constitutive, low-affinity, high-capacity transport systems with derepressible high-affinity systems; glucose and phosphate uptake into *N. crassa* are excellent examples of this strategy (Lowendorf *et al.*, 1974; Scarborough, 1970). These systems give the organism the adaptive advantage of most effectively obtaining nutrients whose concentrations may vary considerably over a period of time.

A root growing through the soil may often experience extremely low $K^+$ levels. Therefore, a high-affinity system may be necessary in order for the

plant to satisfy its requirements for this essential nutrient. However, if the growing root encounters a localized region of high soil $K^+$, the high-affinity system may not have the capacity to utilize excess $K^+$. In such a situation, a low-affinity, high-velocity system would allow the plant to effectively utilize these pockets of high soil $K^+$. Furthermore, as soil water content (potential) declines, the root system must respond in terms of osmotic adjustment. If only a high-affinity $K^+$ transport system were present, the root would not be able to take advantage of the *increase* in the $K^+$ concentration of the soil solution that would occur along with the decline in soil moisture. The presence of a high-velocity system may provide the plant with an advantage in terms of its response to water stress. In this way, the plant may maintain relatively efficient methods of dealing with its varying environment.

## D. SUMMARY

A summary of the mechanisms by which $K^+$ may enter the symplasm of the root is given in Fig. 20. Uptake at low external $K^+$ levels is facilitated by a

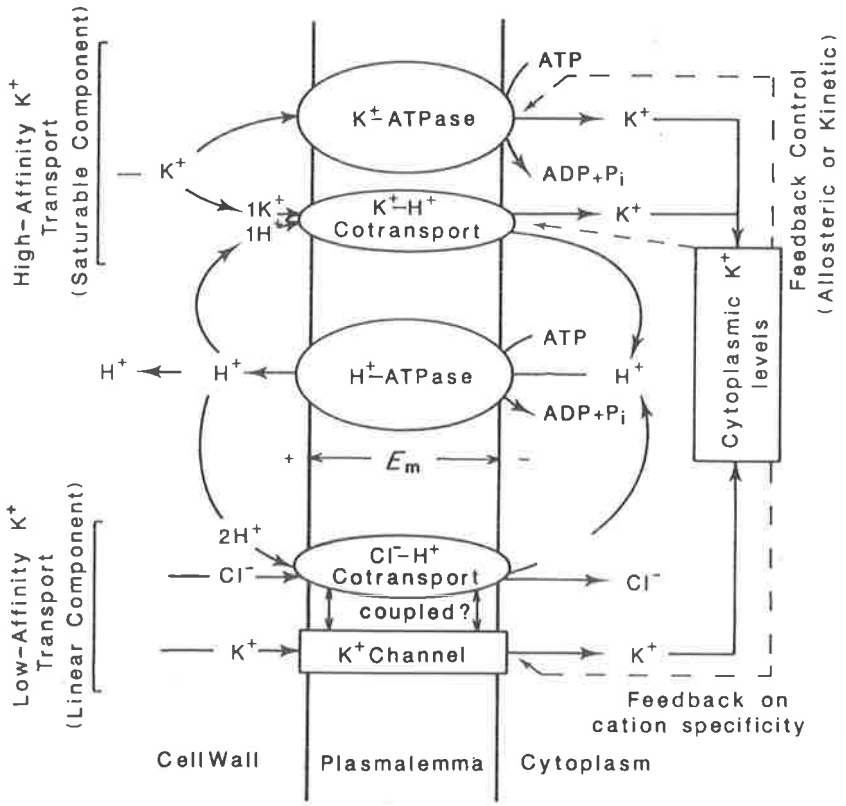


Fig. 20. Schematic representation of possible $K^+$ transport systems operating at the plasmalemma to facilitate $K^+$ uptake at both low and high external $K^+$ concentrations. At low $K^+$ levels, a high-affinity system is hypothesized to be either a $K^+$-ATPase, or a $H^+$–$K^+$ co-transport system, coupled to the $H^+$-ATPase. Both systems would be subject to feedback control by internal $K^+$. Under high $K^+$ levels, nonsaturating $K^+$ uptake involves a $K^+$ channel which is, in some way, coupled to anion ($Cl^-$) transport. The degree of $K^+$ specificity exhibited by this channel may be influenced by cytoplasmic $K^+$ levels.

very high affinity transport system that is strongly depolarizing, and can transport $K^+$ against its electrochemical potential gradient. Several possible models appear to fit the published data equally well. In our evaluation, the most likely candidates would either be a $K^+$-translocating ATPase or, as in *Neurospora*, a $K^+$–$H^+$ symport coupled to the $H^+$-translocating ATPase. The possibility exists that *both* types of active transport could be functioning in parallel. This transport system would appear to be subject to kinetic and thermodynamic control, and would also be subject to feedback (allosteric) regulation from $K^+$ contained in an internal compartment (see Section V.A).

Potassium uptake at higher external levels would be due to a lower-affinity transport system that would transport $K^+$ passively, down its electrochemical potential gradient. This system could be a $K^+$ channel, or a less specific cation channel, which is coupled, in some way, to a saturable $Cl^-$ uptake system which may function as a $H^+$–$Cl^-$ co-transport system (Sanders, 1980b; Jacoby and Rudich, 1980). This system does not appear to be subject to feedback regulation by internal $K^+$ levels, but does exhibit changes in substrate specificity as internal salt levels are altered.

## III. REDOX-COUPLED PLASMALEMMA TRANSPORT OF $K^+$

The influence of exogenous electron donors and acceptors has been studied in a variety of plant cell types (Bienfait, 1985; Lin, 1985; Lüttge and Clarkson, 1985; Møller and Lin, 1986). Although much of this work has concerned the role of plasmalemma electron transport (redox) systems in $Fe^{3+}$ reduction at the root surface (Lüttge and Clarkson, 1985; Møller and Lin, 1986), several studies have addressed the more general topic of the involvement of plasma membrane redox systems in the energetics of solute transport into plant cells. Crane and co-workers (Craig and Crane, 1980, 1981; Misra *et al.*, 1984) investigated the effects of exogenous NADH and ferricyanide on membrane transport and cell growth in suspension cells of carrot. They reported that carrot suspension cells can oxidize exogenous NADH with a concomitant increase in $O_2$ consumption (30% stimulation), and that this oxidation results in a stimulation (~60%) of $K^+$ influx. Misra *et al.* (1984) postulated that a plasma membrane redox system operates in close association with the $H^+$-translocating ATPase of this membrane to exert an influence on $K^+$ transport.

In experiments conducted on corn root cortical protoplasts, Lin (1982a,b; 1984) reported that addition of NADH tripled $O_2$ consumption, and caused a two- to three-fold *increase* in $K^+$ influx, a marked stimulation of $H^+$ efflux and a moderate (20 mV) hyperpolarization of the $E_m$. Although the extent of the NADH influence was less, Lin reported that similar results were obtained on excised corn root segments. Consistent with the results of earlier workers, Lin (1984) proposed a model in which the oxidation of

exogenous NADH would result in the establishment of a transplasma membrane $H^+$ gradient. The relationship between this $H^+$ gradient and $K^+$ influx remains to be established (but see Rubinstein and Stern, 1986).

### A. INFLUENCE OF EXOGENOUS NADH ON $K^+$ INFLUX

Almost all of the above-mentioned NADH studies were conducted at one particular $K^+$ concentration, usually 0.2 or 1.0 mM. However, Lin (1984) showed that the addition of 1.5 mM NADH to corn root protoplasts had its main effect on $K^+$ influx within the mechanism I range. In these protoplast experiments the apparent $K_m$ for $K^+$ influx (0.3 mM) was not affected by NADH, but the $V_{max}$ underwent a four-fold stimulation. Uptake of $K^+$ over the higher concentration range did not appear to be affected by exogenous NADH.

Although in some cases a stimulatory effect of exogenous NADH has been observed on $K^+$ uptake, a clear discrepancy exists between these reports and the findings of Kochian and Lucas (1985) and Thom and Maretzki (1985). Figure 21 illustrates the inhibitory effect that 1.5 mM NADH had on $K^+$ influx into corn root segments (Kochian and Lucas, 1985). At low external $K^+$ concentrations (<0.5 mM)) influx was inhibited by 80%, and a similar degree of inhibition of $K^+$ influx into protoplasts, prepared from sugar cane suspension cells, was reported by Thom and Maretzki (1985). (Leucine, arginine and 3-*O*-methyl glucose influx into

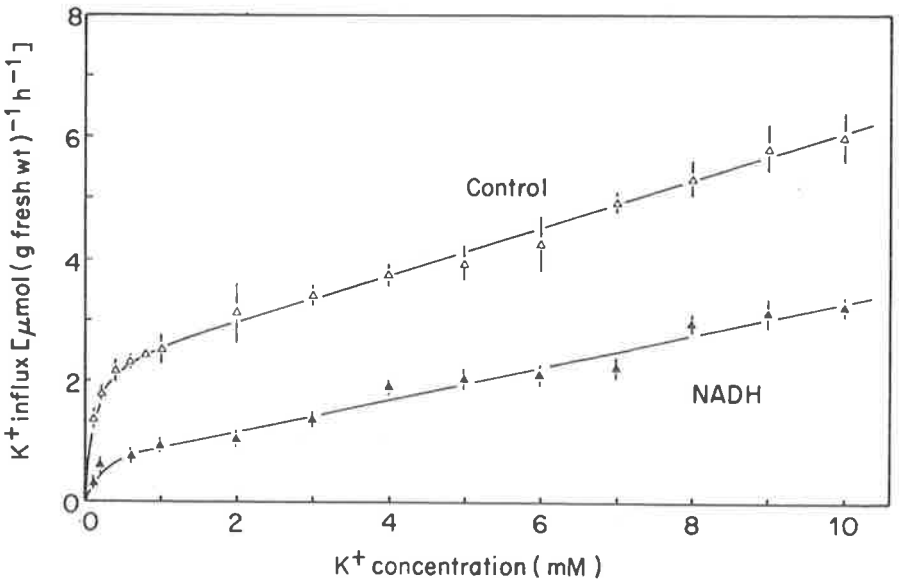


Fig. 21. Influence of 1.5 mM NADH on $^{86}Rb^+$ influx into high-salt-grown corn root segments. (A similar response was observed in NADH experiments conducted on low-salt corn roots.) Data from Kochian and Lucas (1985).

these protoplasts were similarly inhibited by NADH.) Interestingly, $K^+$ influx into corn roots was *also* inhibited by the electron acceptor ferricyanide (Kochian and Lucas, 1985; Rubinstein and Stern, 1986). It has been suggested that these two chemicals elicit this inhibition by separate mechanisms, based on the different $K^+$ influx kinetics elicited after exposure to NADH or ferricyanide, and the different time courses for recovery from inhibition.

### B. MEMBRANE TRANSPORT AND THE WOUND RESPONSE

Kochian and Lucas (1985) proposed that exogenous NADH reacts with the outer surface of the plasmalemma to signal a tissue wound response. Hanson and co-workers have shown that corn roots are a particularly sensitive tissue, and that physical handling of the roots, imposition of cold shock etc., can elicit a wound response (Leonard and Hanson, 1972; Gronewald and Hanson, 1980; Chastain and Hanson, 1982; Zocchi and Hanson, 1982). This response is generally characterized by a reduction in $K^+$ influx and a stimulation of efflux, a reduction in $H^+$ efflux, and a depolarization of the $E_m$. A recovery period of about 4 h is usually required before the "wounded" tissue returns to control levels of physiological functioning.

It was shown that NADH does *not* affect $K^+$ influx if the corn root segments have not yet recovered from excision-associated wounding (Kochian and Lucas, 1985). Additionally, if cycloheximide is included in the recovery medium, $K^+$ influx does not return to the control level, and again NADH has no effect on $K^+$ influx. These results indicate that activation of a wound response blocks the NADH effect. Kochian and Lucas (1985) demonstrated that in this state no NADH-stimulated $O_2$ consumption can be detected. Only in the *recovered* state could they measure a 30% stimulation of $O_2$ uptake upon addition of 1.5 mM NADH. Interestingly, although addition of NADH perturbed $K^+$ influx (and efflux), it continued to be oxidized by these perturbed root segments.

As mentioned earlier, when the redox system in corn roots (or protoplasts) is stimulated by NADH, net *apparent* $H^+$ efflux was reported to increase (Lin, 1984). However, Kochian and Lucas (1985) found that NADH elicited a significant decrease in $H^+$ efflux in both washed corn root segments and intact roots (see also Lucas and Kochian, 1987). In some cases an alkalinization of the external medium was observed after addition of NADH. which implies net *apparent* $H^+$ influx. A similar situation has also been reported for sugar cane protoplasts (Thom and Maretzki, 1985).

Transferring NADH-treated roots to fresh control solution (minus NADH) resulted in an almost immediate recovery of net apparent $H^+$ efflux to pretreatment values (Kochian and Lucas, 1985). This imbalance between recovery of $H^+$ efflux and $K^+$ influx has also been observed with roots that

are recovering from excision wounding (Gronewald and Hanson, 1982; Kochian and Lucas, 1985). Wounding the root elicits a depolarization of the $E_m$, a response which is in direct contrast to the NADH-induced hyperpolarization of the potential reported by Lin (1982a). In recent studies conducted by Lucas and Kochian (1987), NADH was found to cause a significant depolarization of the corn root $E_m$. In some cases the potential remained in this depolarized state, while in others it repolarized very slowly towards the pre-NADH resting potential. However, consistent with the response of $H^+$ efflux discussed above, removal of NADH always resulted in a repolarization of the potential. Certainly, then, the NADH influence on $K^+$ influx, $H^+$ efflux, and the $E_m$ is consistent with the hypothesis that *exogenous* application of this redox reagent elicits some form of wound response in corn root tissue, while in protoplasts and suspension-cultured cells its application appears to stimulate these physiological processes.

### C. DEVELOPMENT OF AN INTEGRATED NADH MODEL

Although there is a clear conflict concerning the reported effects of exogenous NADH on plasmalemma transport of $K^+$, there is little doubt that bona fide redox systems are located within this membrane (De Luca *et al.*, 1984; Rubinstein *et al.*, 1984; Buckhout and Hrubec, 1986; Böttger and Lüthen, 1986; Macri and Vianello, 1986; Pupillo *et al.*, 1986; Luster *et al.*, 1987). The challenge is to develop a working model of the way in which these putative redox systems interact with the various transport systems functioning within the plasmalemma of plant cells. Such a model would have to account for these reported *extremes* in tissue response to NADH. In the present context, we will confine our attention to the effects of NADH on $H^+$ and $K^+$ fluxes and the membrane potential.

Firstly, the inability of freshly cut, or wounded, corn roots to *oxidize* exogenous NADH must be explained in terms of the inability of NADH to further inhibit $K^+$ influx, once the $K^+$ transport system has received the wound response "signal(s)". In analysing the NADH response we have, perforce, assumed that $K^+$ transport occurs via a $K^+$–$H^+$ *co-transport* system.

Zocchi *et al.* (1983) have shown that cold shock treatment of corn roots increased the phosphorylation of microsomal membrane proteins. These changes were correlated with a decrease in ATPase activity and, since the major changes in phosphorylated proteins occurred within the 92 to 100 kDa range, they concluded that one effect of injury is the blockage of $H^+$ efflux via phosphorylation of the plasma membrane $H^+$-ATPase. This hypothesis is consistent with the observed changes in adenine nucleotide content of corn roots during the injury recovery period (Zocchi *et al.*, 1983). The critical step is the mechanism by which tissue injury is "sensed" by the cells and transduced into protein phosphorylation.

Several possible control systems appear to be tenable. Calcium influx has been shown to increase upon wounding (Zocchi and Hanson, 1982; De Quintero and Hanson, 1982), and the resultant change in the cytosolic $Ca^{2+}$ level may activate a $Ca^{2+}$–calmodulin system. One consequence of this activation could be the stimulation of a specific protein kinase. Alternatively, the turnover of phosphatidylinositol may function as a biochemical signal transduction system in roots in a manner analogous to its function in animal tissues (Berridge, 1983; Berridge and Irvine, 1984; Nishizuka, 1984). In animal cells, various *external* stimuli activate a phospholipase C on the inner plasma membrane surface, which then hydrolyses phosphatidylinositol 4,5-bisphosphate to release myoinositol 1,4,5-triphosphate ($IP_3$) into the cytosol and diacylglyceride (DG) which remains within the membrane. $IP_3$ can stimulate numerous biochemical and biophysical processes, including the release of internally sequestered $Ca^{2+}$ and activation of certain kinase systems.

Recent studies on plant tissues have demonstrated the presence and metabolic turnover of $IP_3$ (Boss and Massel, 1985; Morse *et al.*, 1986; Sandelius and Sommarin, 1986; Rincon and Boss, 1987). These reports, along with the central role played by $IP_3$ in regulatory phenomena in animal tissues, provided the impetus to incorporate the $IP_3$ cycle as a central component in our NADH "wound" model outlined in Fig. 22. When the alternative agonist membrane receptor (MR) has been stimulated by a wound "signal", the membrane transmitter (MT) activates the signal transduction system (STS; phospholipase C), and this produces an increase in the level of $IP_3$. The consequences of this increase in $IP_3$ are:

1. Activation of a protein kinase which results in phosphorylation of a protein subunit of the $H^+$-ATPase near the $P_i$ release site. This causes a reduction in $H^+$ efflux; the effect will depend on the extent of phosphorylation and the dephosphorylation capability of the cell.
2. $Ca^{2+}$ release, which may or may not exert its effects on cellular metabolism via $Ca^{2+}$–calmodulin (CaCM).
3. Direct or indirect effects of $IP_3$ on the gating (G) of ionic channels in both the plasma membrane and tonoplast.

An important consequence of this wound activation of MT is that in this state the transmission system is incapable of accepting alternative stimuli. As indicated in Fig. 22, we suggest that an external NADH-oxidizing site can function to stimulate the MT system. Evidence for the presence of this NADH oxidation system comes from a reinterpretation of Lin's trypsin data (Lin, 1982b; see also Buckhout and Hrubec, 1986). Although the SDS-polyacrylamide gel electrophoretogram of the TCA-precipitated protein obtained from the supernatant of trypsin-treated corn root protoplasts indicates a high level of endogenous protease activity, Lin (1982b) was able to show that the supernatant was capable of NADH oxidation. If endomem-

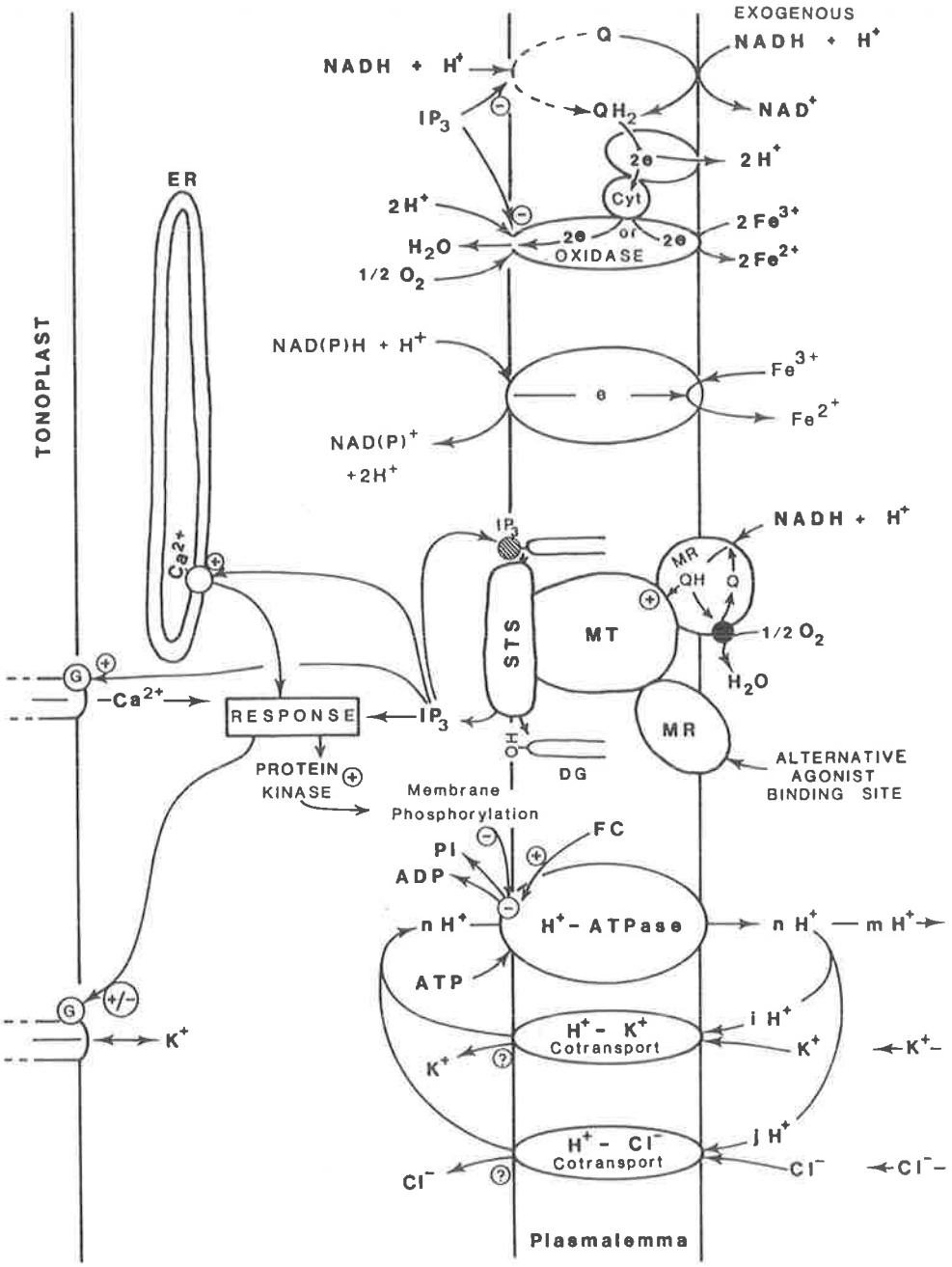
TONOPLAST
ER
Ca2+
G
−Ca2+
RESPONSE
IP3
PROTEIN KINASE
G
+/−
K+
NADH + H+
Q
QH2
IP3
2e
2H+
Cyt
2H+
H2O
2e or 2e
OXIDASE
1/2 O2
2 Fe3+
2 Fe2+
NAD(P)H + H+
e
Fe3+
Fe2+
NAD(P)+
+2H+
EXOGENOUS
NADH + H+
NAD+
IP3
STS
MT
MR
QH
Q
NADH + H+
1/2 O2
H2O
MR
ALTERNATIVE AGONIST BINDING SITE
HO
DG
Membrane Phosphorylation
FC
PI
ADP
n H+
H+ - ATPase
n H+
m H+
ATP
H+ - K+ Cotransport
i H+
K+
K+−
K+
H+ - Cl− Cotransport
j H+
Cl−
Cl−−
Cl−
Plasmalemma

Fig. 22.

brane contamination (mitochondria and endoplasmic reticulum) was absent (but see Komor *et al.*, 1987), this NADH oxidation may be attributed to the presence of a 42 kDa polypeptide released by mild trypsin action (Lin, 1982b, 1984). This protein appears to be able to oxidize NADH and reduce $O_2$ (provided that $O_2$ is present); these properties are inconsistent with the NADH redox model proposed by Lin (1984). Note that in the model presented in Fig. 22, exogenous NADH will result in the following:

1. A stimulation of the MT and STS, with the consequences outlined above.
2. A continued stimulation of $O_2$ consumption, even though the cell has received a wound signal.
3. Proton consumption at the outer surface of the plasmalemma; depending on the degree to which the total $H^+$-ATPase system is inhibited, this may give rise to alkalinization of the root surface.
4. Continual exogenous NADH oxidation is required to maintain the enhanced $IP_3$ level; removal of the exogenous NADH results in a decline in $IP_3$ with the rate being dependent on the levels and/or activation states of the enzymes involved in its breakdown and resynthesis to phosphatidylinositol 4,5-biphosphate.

These properties would account for all of our experimental observations on the perturbative influence of exogenous NADH on $K^+$ fluxes in corn roots and corn root segments (Kochian and Lucas, 1985; Lucas and Kochian, 1987). How, then, is it possible to explain the NADH-mediated stimulation of $K^+$ influx observed in corn root segments, corn root protoplasts (Lin, 1982a, 1984) and carrot suspension cells (Misra *et al.*, 1984)? Based on recent reports of plasmalemma-bound electron transport systems, we have included two forms of NADH redox systems in our model (Fig. 22). We propose that these systems would function only when the protoplast, cell or tissue is not in a "wound" state. The protoplast is the easiest system to

Fig. 22. Model summarizing the various effects of NADH on $K^+$ influx into corn roots (or protoplasts). Two transplasmalemma NADH redox systems are shown. The Lin (1984) model (top) utilizes endogenous or exogenous NADH and transports both electrons and $H^+$. The Rubinstein and Stern (1986) model transfers only electrons across the plasmalemma. In this model, generation of the $H^+$ in the cytoplasm, by the oxidation of NAD(P)H, is compensated for by transport out of the cell by the $H^+$-ATPase. In both models, stimulation of $K^+$ uptake would occur by $H^+$–$K^+$ co-transport. We propose that the NADH-induced "wound response" exhibited by corn, is mediated by the coupling of a membrane-bound signal transduction system (STS) to the $IP_3$ cycle. Two agonist membrane receptors (MR) are postulated, one being an NADH oxidase [the 44 kDa protein from Lin (1984)], and the other being an alternative receptor mediating other types of wound response. Binding to the MR activates the STS (phospholipase C) via a membrane transmitter (MT). The resultant release of $IP_3$ acts via the activation of protein kinases and/or the release of $Ca^{2+}$, to modify transport proteins ($H^+$-ATPase, cation channels) at the plasmalemma and tonoplast. Redrawn from Lucas and Kochian (1988).

rationalize, because lysis during preparation could release proteases that actually remove the NADH MR protein. Buckhout and Hrubec (1986) also reported that washing their isolated plasmalemma preparation (with or without salt) resulted in a partial loss of NADH reductase as well as oxidase activity. In this state, the protoplasts may oxidize NADH (either exogenously supplied or via the cytosol) to cause an increase in the $\Delta\bar{\mu}_H$ across the plasmalemma by direct transport of $H^+$ (Lin, 1984; Böttger and Lüthen, 1986) or by coupling to the $H^+$-ATPase (Rubinstein and Stern, 1986).

The $IP_3$ recycling system may also vary from cell to cell, or from one tissue to another, as a consequence of the physiological prehistory of the plant system. Since lithium acts as an inhibitor of $IP_3$ conversion to inositol and hence its resynthesis to phosphatidylinositol 4,5-bisphosphate, growing cultures in the presence of lithium may reduce the sensitivity of the $IP_3$ regulatory system, thereby allowing the NADH redox system to function. Introduction of myoinositol should re-establish the wound response. A further test of the $IP_3$-regulation/wounding hypothesis may be achieved using FC. Chastain and Hanson (1982) have shown that in wounded corn roots FC can override the endogenous control mechanism that inhibits the plasmalemma $H^+$-ATPase. It will be of interest to see whether FC can negate the perturbative influence that exogenous NADH has on $K^+$ influx into roots.

Purification of these putative redox systems of the plasmalemma should greatly assist the elucidation of their function. Questions of sidedness, direction of electron transport, and natural substrates (donors and acceptors) are all important issues that need to be resolved. Reconstitution of these proteins into liposomes may provide an unambiguous answer to the question of whether or not they are important in energizing $K^+$ transport into roots.

## IV. RADIAL $K^+$ TRANSPORT TO THE XYLEM

A symplasmic pathway for $K^+$ movement, from the epidermis to the xylem parenchyma, was first proposed by Crafts and Broyer (1938). In their hypothesis, the cortex was the site where nutrients, like $K^+$, were taken up into the symplasm by active, $O_2$-dependent processes. Movement to the stele was via plasmodesmata, and release into the xylem vessels was by diffusion, or leakage, since the compact tissue of the stele was thought to be low in oxygen.

Some 38 years later, Anderson (1976), in his review on solute transport across the root, concluded that, "In the stele, the most *common* proposal is that the parenchyma either leaks or secretes solutes which then diffuse or are swept along into the vessels." Figure 23 is a diagrammatic representation of the pathway discussed by Anderson (1976). Based on Anderson's reviews, it

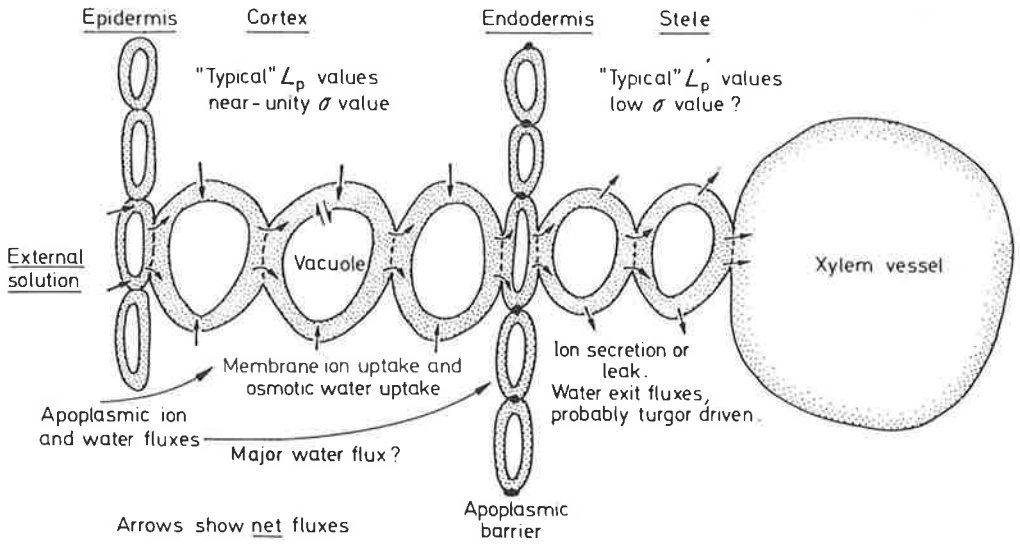


Fig. 23. Diagrammatic sketch of the root in cross-sectional view showing what Anderson (1976) considered to be the "usually accepted mechanisms of ion and water through-put to the xylem vessels." Stippled areas represent the cytosol which, in this Anderson model, also extends in the xylem vessel. From Anderson (1976).

would appear that over the period from 1938 to 1976 the only improvement to the Crafts and Broyer hypothesis was the concept that solutes might be secreted into the xylem vessels. However, the mechanistic basis for this "secretion" remained poorly defined. Note also that Fig. 23 suggests that the xylem vessels may be symplasmically connected to the surrounding parenchyma and contain parietal cytoplasm. For those who are quick to be critical of this concept, we should point out that the controversy of whether living xylem vessels are engaged in the release of $K^+$ to the translocation stream is still unresolved (Läuchli *et al.*, 1978; McCully *et al.*, 1987).

Clearly, the complexity of the root has made it difficult to obtain a rigorous test of the Crafts and Broyer hypothesis. However, experiments of the past decade have provided some new insights.

## A. SITE OF $K^+$ ENTRY INTO THE SYMPLASM

### *1. Epidermis or Cortex?*

Most current textbooks on ion transport and plant physiology discuss $K^+$ movement into the cortex in terms of two parallel pathways, namely the apoplasmic and symplasmic routes. However, there is still some question as to the relative importance of each component (Anderson, 1976; Läuchli, 1976; Van Iren and Boers-van der Sluijs, 1980; Kochian and Lucas, 1983). Using a theoretical model for $Rb^+$ uptake into barley roots, Bange (1973) found that the model only generated reasonable profiles when transport was

restricted to the epidermis. The studies of Van Iren and Boers-van der Sluijs (1980) offered experimental support for this hypothesis. These workers investigated $K^+$ uptake by applying the assumption that plasmolysis would sever plasmodesmata, thereby symplasmically isolating each cortical and epidermal cell of a barley root. Autoradiographic localization of $^{86}Rb^+$, accumulated by the root following plasmolysis, was generally limited to the root periphery. These results suggested that when roots are exposed to low $K^+$ concentrations (<1 mM), transport into the symplasm occurs at the epidermis; i.e. the apoplasmic pathway and subsequent uptake by the cortical cells is of little significance.

The criticism which must be levelled at this work is that it may be erroneous to base a hypothesis concerning "normal" transport function on data obtained from a system where transport physiology may have been dramatically changed by plasmolytic treatment. Furthermore, the work of Anderson and Reilly (1968) concerning fluid exudation from the xylem of corn roots indicated that the cortical cells *do* have the capacity to absorb ions. They found that surgical removal of the epidermis and outer cortex of excised corn roots did not prevent significant fluxes of ions and $H_2O$ to the xylem.

Kochian and Lucas (1983) examined this issue by using radioactively labelled sulphhydryl reagents, [$^3$H]*N*-ethyl maleimide (NEM) and [$^{203}$Hg]*p*-chloromercuribenzenesulphonic acid (PCMBS). A brief (30–60 s) exposure of corn roots to either NEM or PCMBS dramatically reduced $K^+$ influx into the root, without affecting root respiration. Autoradiographic localization studies revealed that sulphhydryl binding occurred almost exclusively in the cells of the root periphery (see Fig. 24). However, protoplasts isolated from corn root cortical tissue exhibited significant $^{86}Rb^+$ influx, the kinetics of which were identical in shape to those obtained on corn roots (Kochian and Lucas, 1982a, 1983). These results suggest that although cortical cells possess the capacity to absorb ions at the low concentrations likely to be present in normal soils, $K^+$ influx into the root symplasm most probably occurs at the root periphery.

*2. Aerenchyma Induction*

The role of the cortex in $K^+$ uptake and radial movement into the stele has been investigated by the induction of aerenchymatous tissue (Drew *et al.*, 1980; Drew and Saker, 1986; Deacon *et al.*, 1986). Drew *et al.* (1980) showed that an $O_2$-stress treatment of young corn roots induced aerenchyma in the developing, adventitious roots (Fig. 25). Microscopic examination of this root tissue revealed extensive breakdown of cells within the mid-cortex, while the epidermis, endodermis and stele remain unaffected. A comparison of this aerenchymatous tissue with control roots revealed that the volume of the cortex was reduced by 36% and that there was an 80% reduction in the symplasmic pathway available for $K^+$ movement from the epidermis to the stele. Thus, if the cortex were involved in $K^+$ uptake, the flux into these

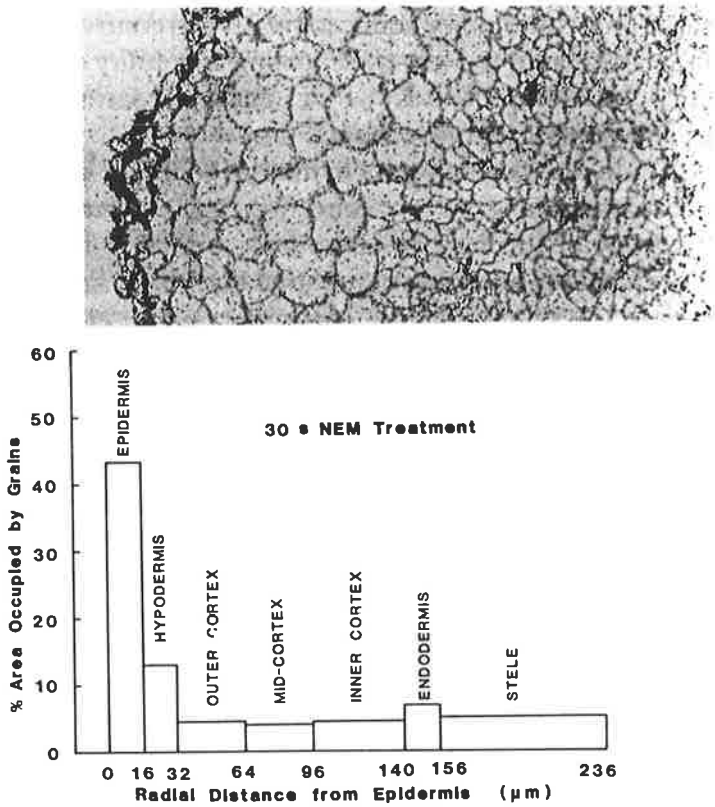


Fig. 24. Microautoradiographic localization of [$^3$H]*N*-ethyl maleimide (NEM) following a 30-s exposure of corn root segments to 0.3 mM NEM. Numerous cross-sections were analysed for grain distribution with an Imanco Quantimet 720 Image Analysing Computer. These data have been averaged and presented in the histogram below the micrograph. Data from Kochian and Lucas (1983).

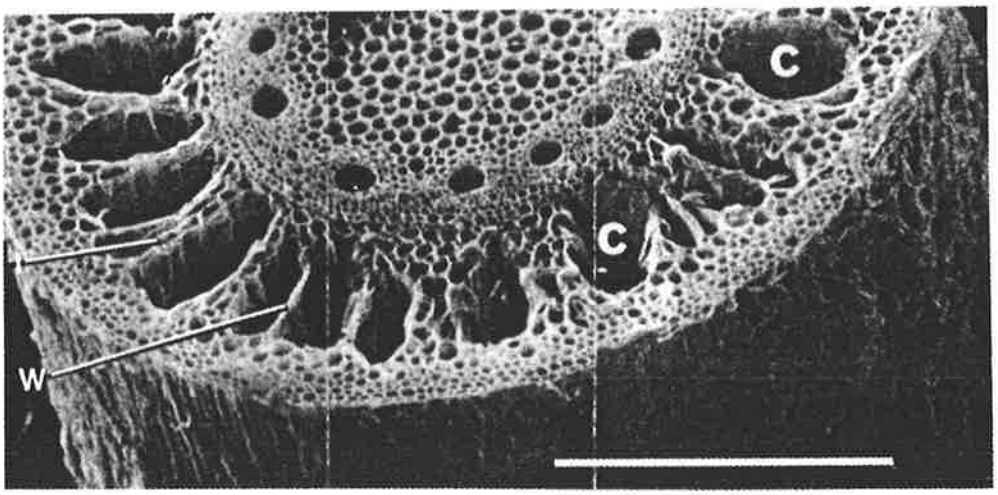


Fig. 25. Scanning electronmicrograph illustrating the aerenchyma that develops in nodal, adventitious roots of corn grown in non-aerated culture solution. Root sections were cut from the region 8–10 cm from the root tip and lyophilized before being viewed in the electron microscope. Symbols are as follows: C, cortical air spaces; W, wall residues of collapsed cells; I, intact cells linking inner and outer cortex. (Bar represents 500 μm.) From Drew *et al.* (1980), with permission.

aerenchymatous roots should be reduced relative to control roots. Drew and Saker (1986) investigated the ion-transporting capability of such corn roots and found that, with respect to $K^+$, $PO_4^{2-}$ and $Cl^-$, aerenchymatous roots were at least as effective as control roots.

These results obtained using aerenchymatous roots are consistent with the hypothesis that ion uptake, at low concentrations, occurs primarily at the epidermis. In view of this lack of effect of a reduction in the symplasmic pathway, it would also appear that the radial flux to the stele is rate-limited by transport into the symplasm (see Anderson, 1976). However, a note of caution is needed in the interpretation of these flux data. The experimental system used by Drew *et al.* (1980) and Drew and Saker (1986) imposed a relatively thick unstirred layer at the surface of both control and aerenchymatous roots. It is possible that the equivalent performance of the two root types was due to a limitation in the supply of nutrients to the actual root surface. This possibility should be investigated using a well-mixed bathing medium. Alternatively, flux analysis using the technique of Newman *et al.* (1987) might be informative.

## B. RADIAL PATHWAY

### *1. Symplasmic Route*

Although the symplasmic pathway is the currently accepted route for $K^+$ movement from the epidermis to the stele, there have been only a few studies on plasmodesmatal structure, frequency and function in root tissues. Spanswick (1972) was the first to demonstrate that corn root cortical cells are electrically connected via plasmodesmata. Clarkson and Robards (1975) showed that plasmodesmatal connections exist between cortical, endodermal and stelar parenchyma cells in the mature, transporting region of the root. The elegant work by Overall *et al.* (1982) and Overall and Gunning (1982) provided important information on the substructure of the plasmodesma in *Azolla* roots but, unfortunately, this work focused on the root apex. Consequently, their findings with respect to symplasmic coupling cannot be extended to the mature region of terrestrial root systems.

Plasmodesmatal frequency distribution studies have been conducted on the root apex of corn (Juniper and Barlow, 1969), and this work indicated that as the cells matured, the number of plasmodesmata per unit area decreased. However, this study also focused on developing tissue. Perhaps the most interesting study, from the viewpoint of radial transport, is the electrical systems analysis of *Lipidium sativum* roots reported by Behrens and Gradmann (1985). By employing a combination of microelectrodes located at various positions along the root, it was possible to detect electrical anisotropy within the root, there being a preference for longitudinal over transverse (or radial) coupling. These results suggest that further studies are

needed on the spatial distribution of plasmodesmata within the cortical tissue of mature roots. It seems almost inconceivable that the concept of symplasmic $K^+$ transport is so well entrenched, in view of the almost complete absence of supporting cytological data obtained on mature root tissue.

*2. Compartmentation and the Endoplasmic Reticulum?*

In the Robards (1971, 1975) model of the plasmodesma, there is continuity between the endoplasmic reticulum (ER) of neighbouring cells, via the desmotubule. Läuchli and others have extended this concept of an ER continuum in terms of providing a specialized $K^+$ transport compartment in roots (see Fig. 26). Much of the justification for this special compartment comes from X-ray microprobe analysis and cytohistochemical precipitation data.

Läuchli *et al.* (1971) analysed the radial distribution of $K^+$ within the roots of 8-day-old corn seedlings. Roots were pretreated for 4 h in 0.2 mM KCl plus 0.5 mM $CaSO_4$, before the terminal 1 cm was removed and subsequent 1 mm sections cut and immediately frozen in liquid $N_2$. Following freeze-substitution and embedding in Spurr's resin, anhydrous sections were cut (1–2 $\mu$m) and analysed for $K^+$ distribution using X-ray microprobe. The reported line scan indicated a high level of $K^+$ in the epidermis and within the cells of the stele; the xylem parenchyma appeared to contain the highest levels of $K^+$.

Clearly, there are problems in evaluating these X-ray microprobe data, the question of artefacts generated during tissue preparation being the most serious. Of course, there is also the problem of spatial resolution, with the possibility of contamination from the vacuole and, to a lesser extent, the cell walls. To circumvent these problems, Läuchli *et al.* (1977) used the bulk-tissue frozen-hydrated specimen protocol developed by Läuchli (1975). Barley root segments, obtained from a position 1–2 cm from the apex of soil-grown tissues, were frozen in liquid $N_2$ and then fractured under liquid

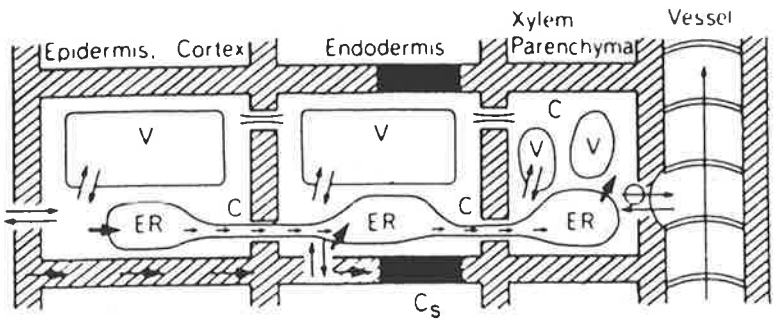


Fig. 26. Pathways of ion ($K^+$) transport in roots, involving the endoplasmic reticulum (ER) as a special compartment of the symplasmic route. Symbols: C, cytoplasm; $C_s$, Casparian strip; V, vacuole. From Läuchli (1976), with permission.

$N_2$. This tissue was then quickly transferred to an SEM cryostage (held at −150°C). A comparison of the X-ray spectra collected from epidermal and xylem parenchyma *cells* again revealed that $K^+$ was higher in the xylem parenchyma. However, the $K^+$ level in the metaxylem vessels was suspiciously high, perhaps indicating the presence of developing vessel elements (McCully *et al.*, 1987).

Although one might have more confidence in the $K^+$ distribution determined on frozen-hydrated tissue, one must not lose sight of the fact that barley roots are still quite thick and so ice crystal artefacts cannot be discounted, especially deep within the root where the rate of cooling would be the slowest. Spatial resolution on bulk frozen-hydrated tissue is also a serious limitation, especially when the SEM is operated at 10 keV. Since the cytosolic compartment in the barley xylem parenchyma cells was less than 0.5 $\mu$m [see Fig. 5 of Läuchli *et al.* (1977)], it is highly unlikely that the system could resolve $K^+$ within the cytosol. Thus, provided that ice crystal artefacts are not seriously affecting the $K^+$ concentrations, the above data establish that the $K^+$ level in the *vacuole* of the xylem parenchyma is higher than elsewhere in the root.

The problem of spatial resolution on frozen-hydrated root tissue was further investigated by Echlin *et al.* (1981) and Pitman *et al.* (1981). In these studies, and especially in the latter, it is clear that the SEM system was operating at the limit of resolution. Additionally, the images showed clear evidence of ice crystal artefacts and so X-ray microprobe data on such tissue must be interpreted with caution. Finally, Pitman *et al.* realized that their data on relative distributions of $K^+$ and $Na^+$ were of a preliminary nature with respect to assigning valid concentrations. The problem of chemical activities versus "bulk" concentrations remains a formidable problem.

Even with the above-mentioned limitations of the X-ray microprobe technique, data collected on root tissues by several groups show that variations in $K^+$, $Na^+$ and $Cl^-$ distributions, among individual cells of the root, do not correlate with their spatial position in the root (Läuchli *et al.*, 1977; Echlin *et al.*, 1981; Pitman *et al.*, 1981; Chino, 1981; Harvey, 1985). As stressed by Pitman *et al.* (1981), these spatial inhomogeneities in ionic distribution draw into question one of the most basic assumptions underlying radioisotope flux analysis, namely, a homogeneous distribution of the label. Finally, at present, it is our assessment that statements made about $K^+$ concentration gradients across the root must be interpreted in terms of vacuolar changes. It is anticipated that X-ray microprobe studies, conducted with more advanced systems capable of higher spatial resolution and lower accelerating voltages, will provide the much needed information on cytosolic versus vacuolar concentrations at all sites across the root. Without such data, it will be difficult to make progress in elucidating the role played by the xylem parenchyma in $K^+$ transport into the xylem.

A final comment on the putative role of the ER in $K^+$ transport is

necessary. Although no unique model of the plasmodesma is accepted at present, the model proposed by Overall *et al.* (1982) (see also Lopez-Saez *et al.*, 1966) appears to be consistent with most studies on symplasmic permeability (Erwee and Goodwin, 1983, 1984; Erwee *et al.*, 1985; Madore *et al.*, 1986; Terry and Robards, 1987). In this model, the "desmotubule" is presented as a solid phospholipid rod, not an open tubule as in the Robards model. Movement through the plasmodesma is considered to occur via the "cytoplasmic annulus" and not via the ER-associated desmotubule. Hence, the role of the ER in intercellular $K^+$ transport should be viewed as being entirely speculative and perhaps at variance with the current view of the structure of the plasmodesma.

### C. LAG PHASE IN XYLEM LOADING

An extensive literature exists on the application of compartmental flux analysis to $K^+$ movement across the root. Theoretical aspects of this work have been reviewed by Walker and Pitman (1976). For a broad description of compartmental flux analysis, as it pertains to ion transport across the root, the reader is referred to Jeschke (1980) and Pitman (1982). For the present, we will focus on the phenomenon of the lag phase in $K^+$ transport into the xylem, to illustrate the complex nature of the processes controlling $K^+$ movement into the various compartments of the root (see also Section V).

When low-salt-grown plants are transferred from their $CaSO_4$ medium to a solution containing $K^+$ (or $^{86}Rb^+$), there is immediate uptake into the symplasm of the root. However, as shown by the data presented in Fig. 27, transport into the xylem translocation stream is delayed, or lags behind root uptake by a period of 1–4 h (Hooymans, 1976; Bange, 1977; Glass, 1978; Van Iren *et al.*, 1981). Van Iren *et al.* (1981) showed that this lag was not due to a time-dependent penetration of $K^+$ into the stele. Also, the extent of the lag phase was independent of both the amount of $K^+$ in the bathing medium and the extent of $K^+$ uptake by the root (Fig. 27). However, it would appear that the *abrupt* transition from root accumulation to transport to the xylem is influenced by the rate at which the root is taking $K^+$ into the symplasm (see Fig. 27c).

In subsequent studies, Bange (1977, 1979) has shown that during this lag phase, $^{86}Rb^+$ accumulation into the vacuole starts slowly, even though the cytoplasmic "compartment" seems to fill quite rapidly. Consequently, the difference between the lack of $K^+$ accumulation in the barley roots bathed in 5 and 10 $\mu$M $K^+$ (Fig. 27a,b) and the accumulation found in 1.0 mM $K^+$ (Fig. 27c), must reflect the operation of a regulatory mechanism that in some way senses the $K^+$ requirement for xylem translocation. When this requirement is exceeded, vacuolar transport of $K^+$ appears to be activated [but see Glass (1978) for an alternative explanation]. At present no informa-

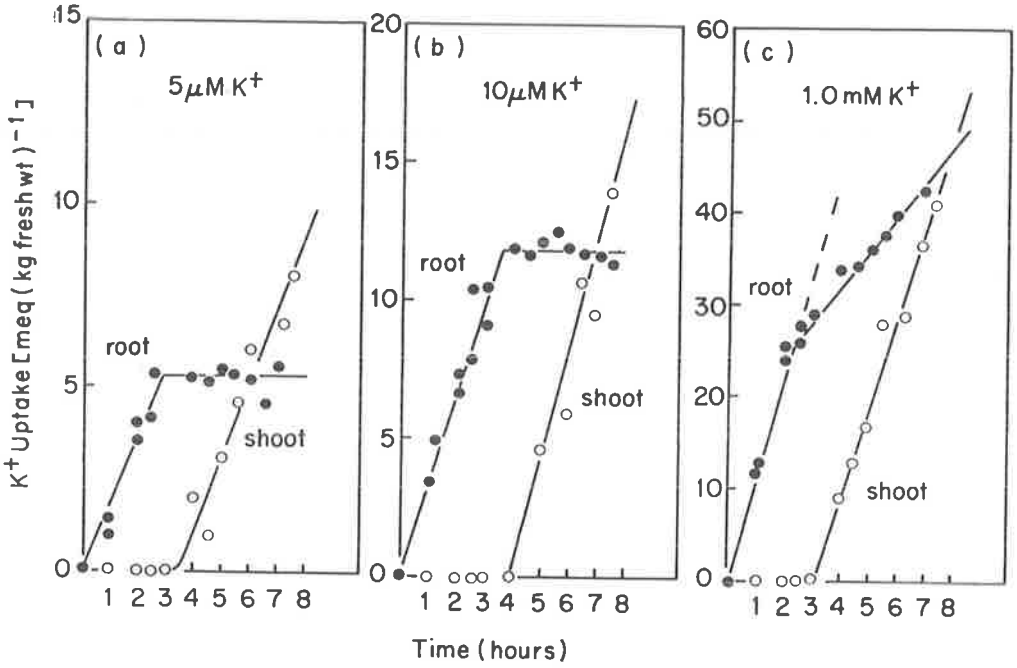


Fig. 27. Influence of extracellular $K^+$ levels on $K^+$ uptake into intact barley roots (●) and subsequent translocation to the shoot (○) as a function of time after roots were introduced to $K_2SO_4$. Experimental solutions contained 5 mM $CaCl_2$, 0.1 mM $Ca(HCO_3)_2$ and 5, 10 or 1000 μM $K^+$ in (a), (b) and (c), respectively. Note the pronounced lag in the supply of $K^+$ to the shoot. Data from Hooymans (1976).

tion exists as to the nature of this putative sensing mechanism (see Section V for a further discussion on regulation of $K^+$ transport within the root).

Hooymans (1976) argued that the insensitivity of the lag phase to both external and bulk root $K^+$ concentration supported the hypothesis that a specialized compartment or "organelle" was involved in $K^+$ transport to the xylem. Glass (1978) offered a seemingly more plausible hypothesis that the lag phase reflected an inductive period associated with establishing the conditions necessary for $K^+$ transport into the xylem. Induction by high symplasmic $K^+$ concentration (Glass, 1978) would be inconsistent with Hooymans' (1976) data; consequently, a threshold $K^+$ concentration may be involved in the induction process.

Van Iren *et al.* (1981) attempted to test this induction hypothesis by giving low-salt-grown barley plants a brief exposure to $K^+$. They argued that this brief treatment would allow sufficient $K^+$ to enter the symplast to activate the induction process. If this were correct, the lag would be either absent or considerably shortened when these pretreated plants were resupplied with $K^+$. In experiments where a 5-min $K^+$ pretreatment was employed there was no observable reduction in the lag period. It is unfortunate that Van Iren *et al.* did not investigate the effect of longer pretreatment periods.

Another approach to studying the nature of this lag phase would be to employ *p*-fluorophenylalanine (FPA), an analogue of the amino acid phenylalanine, which produces abnormal or defective proteins. A review of the effect of this compound on transport across the root is given by Pitman (1977). When high-salt barley roots are treated with FPA, transport into the root remains unaffected, whereas transport into the xylem becomes inhibited (Schaefer *et al.*, 1975). The response to FPA is quite rapid, which indicates that the essential "transport" protein(s) involved in the release of $K^+$ or $Cl^-$ to the xylem turns over quite rapidly. Low-salt-grown roots could be pretreated with FPA, for various times, prior to introducing $K^+$ to commence the induction phenomenon. Roots pretreated in FPA should not commence transport into the xylem, but upon FPA removal transport should commence almost immediately if a threshold level of cytoplasmic $K^+$ is involved.

Studies by Jeschke (1984) also implicate a role for the phloem in the duration of the lag period. On a speculative note, it may be that the induction of transport to the xylem may be affected by the level of $K^+$ recirculating to the root via the phloem. In any event, the abrupt transition to xylem loading (Fig. 27) is at variance with loading via $K^+$ leakage (see Fig. 23), and at first sight seems inconsistent with $K^+$ release into the translocation stream by late-maturing xylem elements (McCully *et al.*, 1987).

### D. $K^+$ TRANSPORT INTO THE XYLEM

Roots grown in a full nutrient medium (high-salt status) take up $K^+$ and transport a major part of this influx to the shoot. By contrast, in low-salt-grown roots a definite lag period exists between $K^+$ entering the root and its transfer to the xylem (see Fig. 27). Numerous studies have contributed to this type of phenomenological characterization of the transport of mineral nutrients from the soil solution to the shoot (Pitman, 1977, 1982). Although it was necessary to utilize a flux compartmental analysis approach in many of these studies, the data could be evaluated without the assignment (or knowledge) of specific transport mechanisms. The active or passive nature of these specific fluxes (to the symplasm and the xylem vessels) was deduced from studies involving various metabolic inhibitors and chemical agents, as well as from frustratingly difficult attempts at determining the electrochemical potential gradients for the various ions (Läuchli, 1976; Bowling, 1981; Pitman, 1982).

Although it may come as a surprise to the reader, it was not until 1978 that Mitchell's chemiosmotic hypothesis was applied to solute transport at *both* boundaries of the symplasm; i.e. at the plasmalemma of the epidermal and xylem parenchyma cells. Hanson (1978) developed a "speculative" model in which he placed two "opposing" $H^+$-translocating ATPases in the plasma

membranes of the outer cortex and the stelar parenchyma. The impermeable nature of the Casparian strip of the endodermis separated the apoplasmic solutions of the cortex and stele, with the symplasm operating as a "bridging" osmotic unit. Transport of cations and anions was proposed to occur by various uniport and antiport systems. It is worth stressing that $K^+$ transport into the xylem was hypothesized to take place by a $K^+$–$H^+$ antiporter with the flux being dependent on the $\Delta\bar{\mu}_H$.

An important prediction of the Hanson (1978) hypothesis was that the transroot potential, measured between the apoplasm of the xylem and the bathing medium, should have two opposing (or "antagonistic") electrogenic components. Although many electrophysiological studies had been conducted on the nature of the transroot potential, no study indicated the presence of an electrogenic component at the xylem parenchyma plasma membrane (Shone, 1968, 1969; Davis and Higinbotham, 1969; Ansari and Bowling, 1972; Bowling and Ansari, 1972). In general, these studies suggested that the transroot potential (measured from the xylem with respect to the bathing medium) could be interpreted based on the transmembrane potential difference equivalent to that of a single cell.

Although their experiments were conducted on an excised hypocotyl–root system from *Vigna sesquipedalis*, Okamoto *et al.* (1978, 1979) were able to demonstrate the existence of opposing electrogenic pumps between the surface of the hypocotyl and the xylem vessels. De Boer *et al.* (1983) constructed a similar experimental system to investigate the transroot potential of two *Plantago* species. The elegant system developed by De Boer *et al.* (1983) is illustrated in Fig. 28 (the reader is directed to the original paper for important technical details).

An investigation of the response of excised *Plantago* roots to changes in $O_2$ partial pressure revealed three classes of transroot potentials. One class, having transroot potentials of approximately −100 mV, was comparable to the earlier reports of Davis and Higinbotham (1969) and Shone (1968, 1969). The second and third class of roots had transroot potentials from 0 to −20 mV and −50 to −70 mV, respectively, with the latter class being the less frequently observed of the three classes. The response of the second class of *Plantago* roots to changes in the $O_2$ partial pressure is illustrated in Fig. 29. Anoxia, and recovery from anoxia, elicited a transient change in the transroot potential (Fig. 29a), while exposure of the root to 10% oxygen resulted in a shift in the transroot potential from −20 mV to −60 mV (Fig. 29b).

An electrical analogue of Hanson's (1978) model is presented in Fig. 29c. As discussed by De Boer *et al.* (1983), this model can readily account for the observed responses in the transroot potential when the excised *Plantago* root undergoes changes in oxygen status. If the two opposing electrogenic components are functioning and almost equal, their net effect on the transroot potential will be small, and the value of the potential will depend

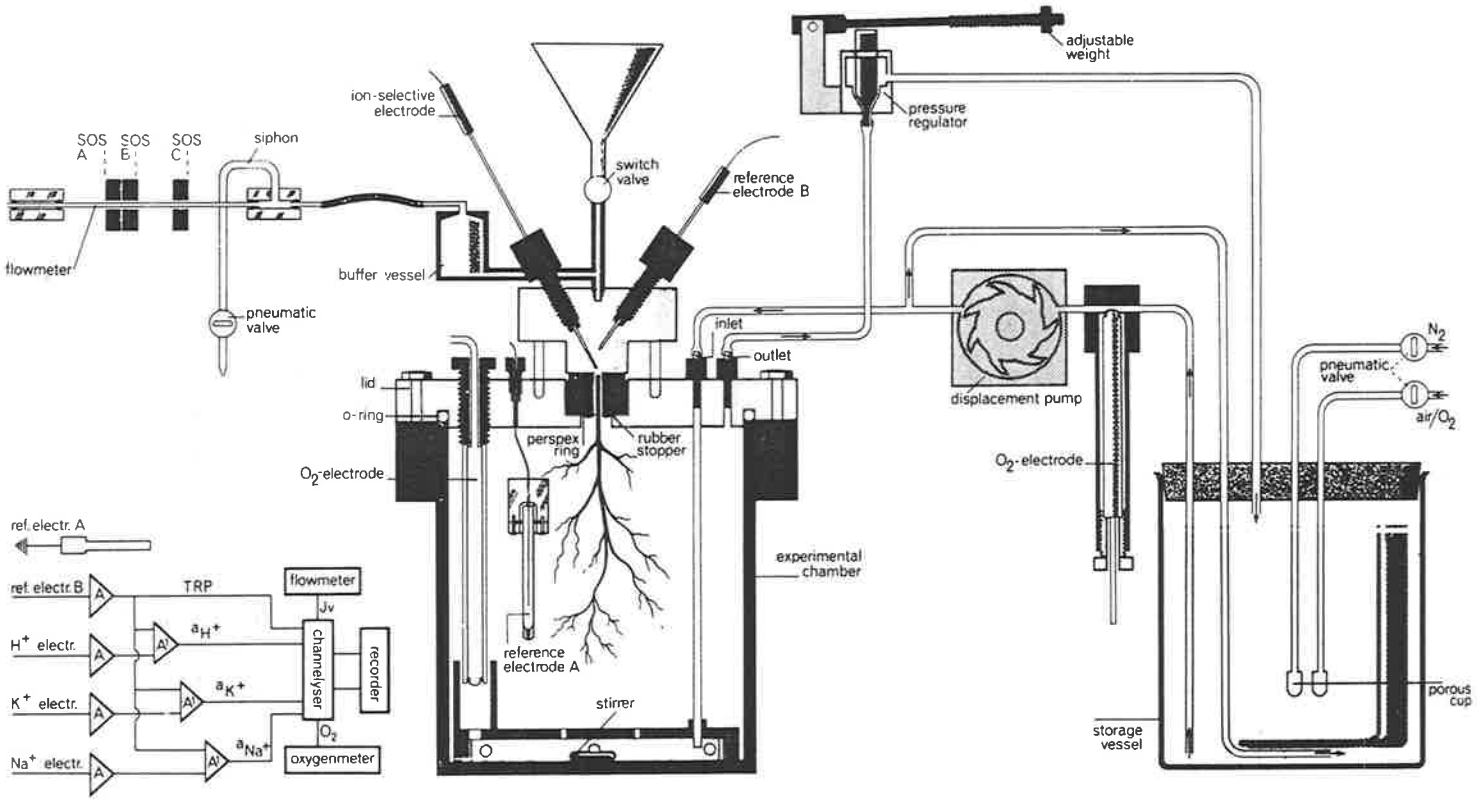


Fig. 28. Experimental system used by De Boer *et al.* (1983) to simultaneously measure the transroot potential (TRP), ionic activities for $H^+$, $K^+$ and $Na^+$, and the xylem sap flow rate ($J_v$) on an excised *Plantago* root. Symbols: A, amplifier; $A^1$, precision intrumentation amplifier; SOS, slotted optical switch. From De Boer *et al.* (1983), with permission.

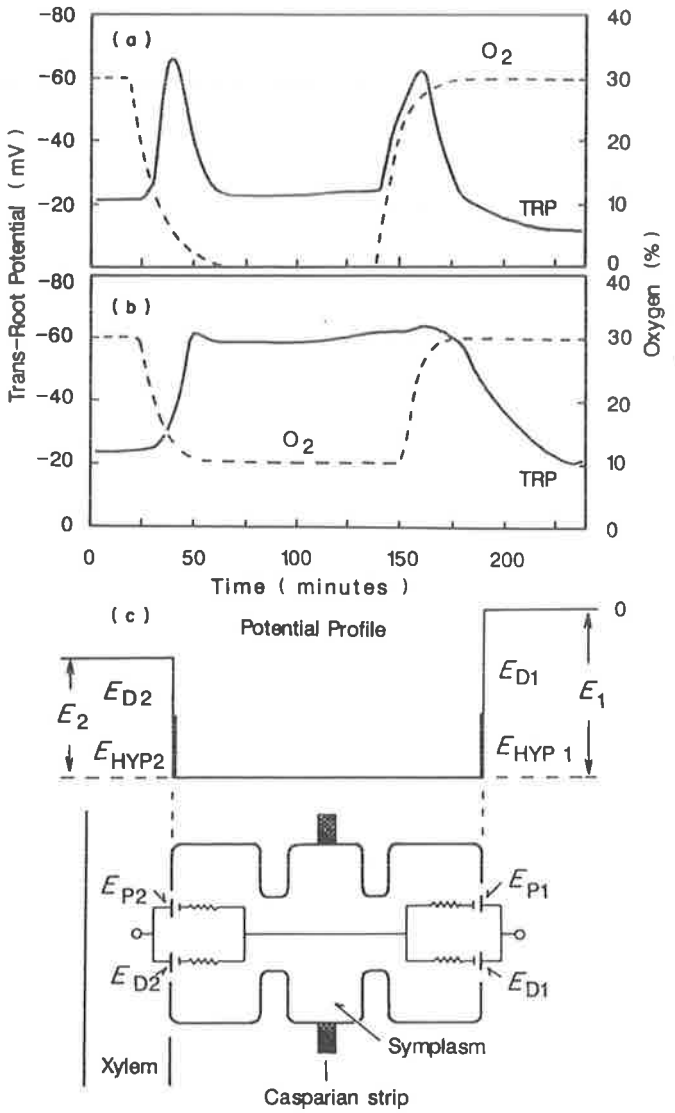


Fig. 29. Response of the transroot potential of *Plantago* to changes in the $O_2$ tension of the medium bathing the roots. (a) Roots brought under anoxia and then returned to 30% $O_2$. (b) Oxygen tension reduced from 30% to 10% and then subsequently returned to 30%. (c) Schematic representation of the electrophysiological organization of the *Plantago* root. The $E_m$ of the epidermal/cortical cells ($E_1$) and the xylem parenchyma cells ($E_2$) result from the combined EMF of the passive diffusion potential ($E_{D1}$ and $E_{D2}$, respectively) and the electrogenic pump ($E_{P1}$ and $E_{P2}$, respectively). The hyperpolarization produced by the electrogenic pumps ($E_{HYP1}$ and $E_{HYP2}$) will depend upon the EMF and conductances ($g$) of the pump and passive diffusion systems. The transroot potential is given by: $TRP = E_1 - E_2 = (E_{HYP1} + E_{D1}) - (E_{HYP2} + E_{D2})$. Data from De Boer *et al.* (1983).

upon the difference between the diffusion potentials generated at the boundary of the cortex and the xylem parenchyma. When the $O_2$ level in the bathing solution is lowered from 30 to 10% (Fig. 29b), the $O_2$ supply to the inner regions of the root will be reduced, causing a decline in the available ATP level, and so the activity of the electrogenic pump on the xylem parenchyma plasmalemma will be decreased. The outer region of the root will still have an adequate $O_2$ supply, and so the continued operation of the outwardly directed $H^+$-ATPase will cause the transroot potential to shift to a more negative value (Fig. 29b). Anoxia eventually reduces the activity of both $H^+$-ATPases, but the differing time courses of the decline in ATP give rise to the observed transient change in the transroot potential (Fig. 29a).

The electrophysiological data obtained on *Plantago* roots (De Boer *et al.*, 1983; De Boer and Prins, 1984, 1985) and the related measurements conducted on *Vigna* hypocotyls (Okamoto *et al.*, 1978, 1979) provide support for the most important aspect of the Hanson model for ion transport into the xylem. Further support is also offered by the xylem perfusion studies of Clarkson *et al.* (1984) and Clarkson and Hanson (1986). Using a special xylem perfusion system, these workers introduced unbuffered solutions of different pH values into excised roots of *Allium cepa*. Irrespective of whether the initial pH value was acidic (pH 3.9) or basic (pH 9.3), the pH value of the perfusate leaving the root was adjusted to within a range of pH 5.5–6.5. Furthermore, the extent of $H^+$ efflux into the xylem perfusate could be increased greatly by buffering the medium at alkaline pH values. It is also interesting to note that malate has been reported to be a normal constituent of the xylem sap in some roots (Butz and Long, 1979); the $pK_a(2)$ of malate is ~5.3. These pH shift data were interpreted in terms of pH regulation of the xylem sap, *in situ*; a process which would be essential if $K^+$ transport into the xylem were to occur via a $K^+$–$H^+$ antiporter as suggested by Hanson (1978).

Figure 30 represents a synthesis of current data on $K^+$ transport into the symplasm of the root and its efflux across the xylem parenchyma to the xylem vessel. Unfortunately, the complexity of the root, and especially that of the stele, has made it extremely difficult to conduct the necessary biophysical experiments to gain further data in support of the Hanson model. Although various attempts have been made to determine electrochemical gradients across the cells of the root (Dunlop and Bowling, 1971; Bowling, 1972; Dunlop, 1973, 1982; Davis and Higinbotham, 1976), these studies generally involved making successive electrode impalements through cells of the epidermis, cortex and stele. As stressed by Anderson and Higinbotham (1975), great caution should be used when evaluating these data. Thus, with the spatial resolution of the X-ray microprobe system(s) used to examine $K^+$ distribution across the root being such that only vacuolar estimates can be deemed reliable, and the microelectrode studies on the stelar tissue being

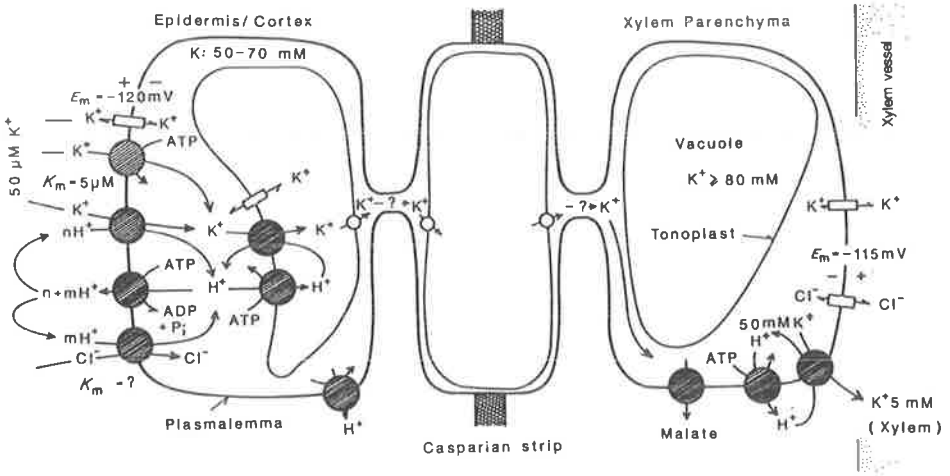


Fig. 30. Schematic representation of the transport processes thought to be involved in the acquisition of $K^+$ from the soil solution and in its subsequent transport from the symplasmic compartment of the root into the xylem vessels. This model has been developed on the basis of the chemiosmotic scheme originally proposed by Hanson (1978) and later refined by Clarkson and Hanson (1986). (Open "arrowed" circles on tonoplast represent regulation of $K^+$ movement between the cytoplasm, vacuole and radial transport "pools", and rectangles represent channels.)

somewhat dubious, precious little information is currently available concerning the $K^+$ gradients across the root. The only reliable data concerns the $K^+$ concentrations within the xylem vessels, and even here one must be concerned with extrapolation from *in vitro* measurements to the intact root.

As a consequence of these limitations, we can only make general comments on the thermodynamic nature of the $K^+$ fluxes at the two boundaries of the root symplasm. Provided that the Donnan charges within the epidermal cell wall do not result in a significant increase in the $K^+$ concentration at the outer surface of this plasma membrane, the typical gradients illustrated in Fig. 30 indicate that net $K^+$ influx into the symplasm is clearly an active process. Our comments concerning the situation at the xylem parenchyma plasmalemma cannot be made with the same degree of certainty. If the $K^+$ concentration in the cytoplasm is within the range expected for normal physiological functioning ($\geq$50 mM), and the steady-state level in the xylem vessels is approximately 5 mM, the thermodynamic status of $K^+$ efflux will depend very much on the magnitude of the potential across this membrane. If the value is similar to that deduced for the *Plantago* root system, then $K^+$ efflux would necessarily occur by an active process. Although the $K^+$–$H^+$ antiport hypothesis is still purely speculative, if $K^+$ were to be transported by such a mechanism, with a 1 : 1 stoichiometry, the $E_m$ would not influence the thermodynamics of the situation, but it could have a significant influence on $K^+$ efflux through its effect on the kinetic parameters of the putative transport system.

It is perhaps indicative of the complexity of the root that hypotheses like the Crafts and Broyer (1938) and Hylmö (1953) models have been so difficult to disprove. It is interesting to note that the Hylmö model was recently resurrected by McCully *et al.* (1987). The Hylmö model proposes that ion accumulation in the root involves uptake into the vacuoles of living xylem vessels, which upon maturation release their contents into the translocation stream. Although this model received some degree of support in the mid-1970s (Davis and Higinbotham, 1976), Läuchli *et al.* (1978) provided irrefutable evidence that ion transport occurs across the stele into mature xylem vessels. However, in the recent report by McCully *et al.* (1987), X-ray microprobe was used on bulk, frozen-hydrated tissue, to examine the $K^+$ concentrations within the late-maturing xylem vessels of field-grown corn plants. Surprisingly, $K^+$ values in the range of 150–400 mM were detected; the microprobe system was "calibrated" against known KCl standards that were vacuum-infiltrated into the mature xylem vessels. Clearly, these levels of $K^+$ could only be established by transport across the tonoplast of these maturing vessels. In view of these findings, McCully *et al.* claim that since the living, late-maturing xylem elements contain the highest $K^+$ concentrations of any cells in the root, they "represent the end point of potassium accumulation from the soil before it is released as a slug of concentrated solution to the transpiration stream in the mature vessel". In view of all the available data, it seems to us that a combination of the two routes may not be completely unrealistic.

## V. REGULATION OF $K^+$ FLUXES WITHIN THE PLANT

In contrast to the situation in animal cells where homeostasis is mediated primarily at the tissue or organ level, plants *must* be able to regulate their metabolism at the cellular level. This is particularly true for the cells of a root growing in the soil, which can be exposed to a wide range of environmental conditions. Glass and Siddiqi (1984) suggest that two primary priorities for the regulation of inorganic nutrients in the plant are the maintenance of ionic composition of the cytoplasm and nutrient allocation to the shoot. These priorities are particularly applicable to $K^+$. Although the levels of $K^+$ do not appear to be precisely regulated, the cytoplasmic values seem to be constrained within certain limits. In glycophytic plants, cytoplasmic $K^+$ concentrations range from 100 to 200 mM (Leigh and Wyn Jones, 1984). It has been suggested that maintenance of $K^+$ within these limits is important because of its roles in activating a number of cytoplasmic enzymes and in protein synthesis (Läuchli and Pflüger, 1979; Wyn Jones *et al.*, 1979).

Unfortunately, direct measurements of cytoplasmic $K^+$ have been difficult to accurately obtain. However, it has been well documented that "bulk" $K^+$ concentrations are generally maintained at fairly constant levels, even in the

face of widely varying $K^+$ supply to the root. For example, Asher and Ozanne (1967) studied the growth and $K^+$ content of 14 plant species grown at external $K^+$ concentrations held constant at levels varying from 1 to 1000 $\mu$M. They found that at 24 $\mu$M $K^+$, eight of the species reached maximum yield, while at 95 $\mu$M $K^+$, the remaining species reached maximum yield, and increases in external $K^+$ above 95 $\mu$M had little further effect on $K^+$ content or root : shoot ratios.

Although our knowledge of ion transport regulation is far from complete, most of the work that has been conducted has been directed at the cellular level. A large portion of this work has focused on the regulation of $K^+$ uptake across the plasmalemma of higher plant roots, undoubtedly because of the important metabolic and osmotic roles played by this ion. An examination of the pathway of $K^+$ movement from the root surface to the shoot indicates a number of potentially important regulatory sites. These include the plasmalemma of epidermal cells, the tonoplast of epidermal and cortical cells, the plasmodesmata hypothesized to be involved in maintaining symplasmic continuity along this pathway, and the xylem parenchyma, which may form the site of $K^+$ transfer into the xylem translocation stream. The location where ions are transported into the xylem vessels appears to be an important focal point for root–shoot interaction, in terms of regulatory signals moving between the shoot and root. We will advance the concept that there is a hierarchy of regulatory mechanisms operating to regulate $K^+$ within the plant which extend from the subcellular to the whole plant level. These various levels of regulation are thought to establish a feedback system which influences $K^+$ uptake across the plasmalemma of root epidermal cells. We will deal with regulation of $K^+$ transport at the level of the plasmalemma. Regulation of transport across the root will then be examined in terms of the importance of the shoot in the regulation of root $K^+$ fluxes.

## A. ALLOSTERIC REGULATION OF $K^+$ TRANSPORT

A number of studies that have involved either bulk tissue $K^+$ measurements, or indirect measurements of cytoplasmic $K^+$ (i.e. compartmental analysis), have suggested that cytoplasmic $K^+$ is maintained at fairly constant levels, while vacuolar $K^+$ concentrations can vary more dramatically (e.g. Glass and Siddiqi, 1984; Leigh and Wyn Jones, 1984; Memon *et al.*, 1985). Hence, a number of researchers have sought to uncover the regulatory mechanisms involved in the maintenance of cytoplasmic $K^+$ levels. Certainly the most widely discussed and studied model involves allosteric regulation of the plasmalemma $K^+$ transport system by cytoplasmic $K^+$ concentration.

### *1. Feedback by Internal $K^+$*

A negative correlation between $K^+$ uptake and internal $K^+$ concentration ($[K]_i$) has been reported for a number of plant tissues (Johansen *et al.*, 1970;

Young and Sims, 1972; Glass, 1975, 1976, 1977; Jensen and Pettersson, 1978; Cram, 1980; Kochian and Lucas, 1982a). In many of these studies, $K^+$ influx was correlated with bulk tissue $K^+$ levels. However, in the work of Young and Sims (1972) and Glass (1977), the adjustment of $K^+$ influx and $[K]_i$ following either an increase or decrease in the external $K^+$ concentration was quite rapid and correlated with known half-times for the turnover of cytoplasmic $K^+$. These results provide circumstantial evidence in support of the hypothesis that a regulatory feedback loop exists between cytoplasmic $K^+$ levels and $K^+$ influx across the plasmalemma. The $K^+$ transport protein(s) may possess both catalytic (transport) and regulatory (allosteric) sites (Cram, 1976; Glass, 1975, 1976, 1977, 1978; Jensen and Pettersson, 1978; Pettersson and Jensen, 1978, 1979). Binding of cytoplasmic $K^+$ to internal *allosteric* sites on the transporter may induce a conformational change in the protein which would result in a reduction of $K^+$ influx.

Further evidence in support of the allosteric regulation hypothesis for $K^+$ influx into roots has been provided by the work of Glass and co-workers (for reviews see Glass, 1983; Glass and Siddiqi, 1984). Glass (1975) observed that when low-salt barley roots were being exposed to high exogenous $K^+$ levels, in order to increase $[K]_i$, $K^+$ influx was inversely related to the square of $[K]_i$, a result previously reported for *Lemna* (Young and Sims, 1972). Subsequently, the kinetics for $K^+$ influx at low external $K^+$ concentrations (<0.5 mM) were obtained on barley root tissue in which different $[K]_i$ levels had been established (Glass, 1976). As shown in Fig. 31a, as $[K]_i$ increased from 26.3 $\mu$mol $g^{-1}$ to 130.5 $\mu$mol $g^{-1}$, the $V_{max}$ for the saturable component of $K^+$ influx decreased, and the related $K_m$ increased. Replotting these data

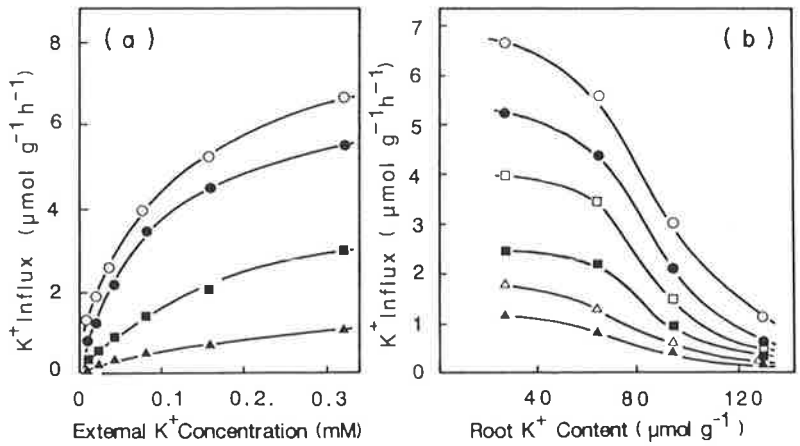


Fig. 31. Evidence for allosteric control of $K^+$ influx into barley roots. (a) Influence of pretreatment in 50 mM KCl upon the influx kinetics obtained on low-salt-grown barley roots. Symbols: ○, 0 h; ●, 3 h; ■, 6 h; ▲, 12 h duration in 50 mM KCl. (b) Relationship between influx values from solutions containing various KCl concentrations as a function of $[K]_i$. Symbols (mM KCl): ○, 0.32; ●, 0.16; □, 0.08; ■, 0.04; △, 0.02; ▲, 0.01. Data taken from Glass (1976).

as a function of $[K]_i$ indicated that a sigmoidal relationship exists between $K^+$ influx and $[K]_i$ (Fig. 31b).

Glass (1976) noted that these observations are characteristic of an enzyme exhibiting allosteric regulation. He applied a transformation of the Hill equation to these kinetic data to determine the number of allosteric binding sites [a description of the use of the Hill equation can be found in Segel (1975)]. Linear Hill plots were obtained from which Glass deduced that four allosteric sites were operational on each transport protein. Glass has quite cautiously suggested (due to the dangers inherent in extrapolating from simple enzyme kinetics to a complex tissue such as a root) that in low-salt barley roots the $K^+$ carrier possesses one binding site for external $K^+$ and four allosteric binding sites for $[K]_i$. Similar results have been subsequently obtained for $K^+$ influx into the roots of a number of different plants (Jensen and Pettersson, 1978; Pettersson and Jensen, 1979).

In low-salt-grown roots, the reduction in net $K^+$ influx, by internal $K^+$, was not due to a change in $K^+$ efflux (Glass and Siddiqi, 1984). This is not surprising, since it is well established that in low-salt roots net $K^+$ uptake is equivalent to unidirectional $K^+$ influx, indicating that $K^+$ efflux is quite small (Johansen *et al.*, 1970; Glass and Siddiqi, 1982; Newman *et al.*, 1987). It had been previously reported that as excised barley roots were loaded with KCl, $K^+$ influx remained constant but efflux increased (Jackson and Edwards, 1966). However, the fluxes in this study were measured in 10 mM KCl, which is in the range of passive $K^+$ uptake that we suggest is mediated by $K^+$ channels. In this concentration range, $K^+$ influx does not respond significantly to $[K]_i$ (Glass and Dunlop, 1978). It would appear that only the high-affinity $K^+$ uptake system ($K^+$–$H^+$ symport or $K^+$-ATPase?) is subject to feedback control by internal $K^+$ (see Fig. 20).

### 2. *Involvement of Protein Synthesis and/or Degradation?*

The response of the $K^+$ transport system to changes in $[K]_i$ can be quite rapid, which indicates a direct control on the transport system, as opposed to regulation via synthesis or degradation of transport carriers, or regulatory proteins (Glass, 1977; Glass and Siddiqi, 1984). Glass (1977) found that the reduction in $K^+$ influx, in response to increasing $[K]_i$, showed no lag and appeared to be independent of RNA, DNA and protein synthesis. Pettersson and Jensen (1979), on the other hand, have hypothesized that a combination of both allosteric regulation and carrier synthesis occurs either simultaneously or sequentially during the period of adjustment following a perturbative treatment.

Unfortunately, for higher plants, techniques have not been available that allow for the demonstration of transport regulation through carrier synthesis/degradation. As Glass and Siddiqi (1984) point out, even though direct evidence is lacking, a realistic model for transport regulation would involve short-term adjustments involving rapid responses of transport systems to

changes in internal ion levels, in conjunction with long-term adaptations (hours or days) involving control of carrier synthesis and degradation. In this context, recent work by Fernando *et al.* (1987) indicated that $K^+$ deprivation in barley roots resulted in an increase of both a 34 and a 44 kDa plasmalemma protein, as well as $K^+$ uptake. However, the increase in $K^+$ uptake occurred before any changes in the plasmalemma protein complement could be detected. Fernando *et al.* (1987) speculated that allosteric regulation occurs *prior* to a stimulation in the synthesis of specific plasmalemma proteins (in response to $K^+$ deprivation). Clearly, further studies in this area are needed to confirm this hypothesis.

*3. Regulation of Tonoplast $K^+$ Transport?*

The complex structure of the root makes it difficult to measure tonoplast fluxes and vacuolar content. In general, only approximate values can be obtained through radioisotope compartmental analysis studies. Glass and Siddiqi (1984) have analysed this literature and conclude that as the root is loaded with $K^+$, *both* plasmalemma and tonoplast $K^+$ fluxes are reduced, with the greater reduction being observed at the tonoplast. Leigh and Wyn Jones (1984) have also proposed that a coupling exists between the cytoplasmic and vacuolar $K^+$ pools. They developed a model which attempts to explain the relationship between growth and tissue $K^+$ levels. The model is based on the observations that: (1) $K^+$ is not replaceable in the cytoplasm; (2) $K^+$ salts in the vacuole that are involved in turgor generation can be replaced by other solutes like $Na^+$, $Mg^{2+}$, $Ca^{2+}$ and organic molecules, during periods of $K^+$ deficiency; and (3) $K^+$ is often unequally distributed between the vacuole and cytoplasm. They propose that as the $K^+$ concentration in a plant tissue declines (during periods of $K^+$ deficiency), cytoplasmic $K^+$ concentrations are initially maintained while vacuolar $K^+$ is depleted and replaced by other solutes. A minimum vacuolar $K^+$ level (usually around 20 mM) is envisaged; when the vacuolar $K^+$ reaches this minimum, cytoplasmic $K^+$ begins to decline and metabolism and growth become negatively affected.

Support for the Leigh and Wyn Jones (1984) model was provided by the $K^+$-use efficiency study of Memon *et al.* (1985). In this work three barley varieties were examined and one was found to exhibit "typical" $K^+$ deficiency symptoms when grown at 10 $\mu$M $K^+$. The important point is that this same variety was capable of accumulating $K^+$ to higher levels, in the root and shoot, than the other varieties used in this study. Using a compartmental analysis approach, it was shown that the variety which exhibited $K^+$ deficiency symptoms retained more of its $K^+$ in the vacuole. This failure to transport vacuolar $K^+$ to the cytoplasm resulted in a depletion of cytoplasmic $K^+$, which then caused the onset of $K^+$ deficiency symptoms.

These studies suggest that the relative levels of cytoplasmic and vacuolar $K^+$ must, in some fashion, be integrated. Furthermore, these concepts can be extended to indicate that the transport systems at both membranes must

share some common controls. Observations have been made of membrane perturbations acting specifically at the outer face of the plasmalemma (applications of PCMBS, NADH, ferricyanide) that have resulted in significant alterations in tonoplast $K^+$ fluxes (Kochian and Lucas, 1982a, 1985). In these studies, it was suggested that signalling mechanisms operate between the two membranes.

The mechanism(s) of $K^+$ transport at the tonoplast is poorly developed, and information concerning regulation of transport across the tonoplast is essentially nonexistent. Recent studies with tonoplast vesicles purified from roots and storage tissue have shown that the tonoplast contains two $H^+$-translocating enzymes, an ATPase and a pyrophosphatase (Blumwald, 1987). Both function to generate an electrochemical gradient for $H^+$ across the tonoplast. This gradient is dominated by the activity component, which is considered to be approximately two pH units (the vacuole being acidic), while a small electrical component is also thought to exist. A number of $H^+$-associated antiport mechanisms have recently been described for the tonoplast. Examples include $Ca^{2+}$ uptake into the vacuole of oat roots (Schumaker and Sze, 1985) and $Na^+$ uptake into the vacuole of red beet storage tissue (Blumwald and Poole, 1985). Evidence consistent with a $K^+$–$H^+$ antiport for tonoplast vesicles from red beet was recently presented (Sarafian and Poole, 1987).

In terms of mechanisms for the transport of $K^+$ into and out of the vacuole, one could speculate that $K^+$ uptake may be mediated by a $K^+$–$H^+$ antiport, while $K^+$ efflux from the vacuole could be facilitated by gated $K^+$ channels, where the driving force for $K^+$ efflux would be derived from the small (interior-positive) membrane potential. Of course these speculations do not describe potential regulatory processes for the tonoplast $K^+$ transport systems, or offer explanations for how the plasmalemma and tonoplast might "communicate". Answers to these questions must be sought in future studies.

### 4. *Criticisms of the Allosteric Model*

The major criticism of the allosteric regulation model is based on our inability, due to technical limitations, to make accurate measurements of cytoplasmic $K^+$ concentrations. As Sanders (1980a) has pointed out, it is impossible to demonstrate a direct interaction between cytoplasmic $K^+$ and the plasmalemma, since changes in root tissue content reflect primarily those occurring within the vacuole. Furthermore, according to the model of Leigh and Wyn Jones (1984), changes in vacuolar $K^+$ content may not necessarily reflect what is occurring in the cytoplasm. Conversely, alterations in the cytoplasmic concentration of an ion can occur without corresponding changes in vacuolar concentration, as has been observed for $Cl^-$ in perfused *Chara* cells (Sanders, 1980a). Consequently, caution must be exercised when attempting to generate models dealing with ionic levels of cytoplasmic compartments from data based on average (or bulk) tissue content.

This cautionary note is supported by the occasional observation that at times $K^+$ fluxes can be altered even though *no* change in $[K]_i$ was recorded. An excellent example of this type can be found in the article by Pettersson and Jensen (1978). These workers attempted to alter the internal $K^+$ content of barley roots (grown in full nutrient solution that contained either 0.1 or 10 mM $K^+$) by placing the low-$K^+$ seedlings in 10 mM KCl solution and the high-$K^+$ seedlings in 0.1 mM $KNO_3$ solution; these pretreatments were applied for up to 80 min. Pettersson and Jensen found that $K^+$ fluxes either decreased or increased significantly, while root $K^+$ content did not change (Fig. 32). The authors argued that this was evidence for allosteric regulation,

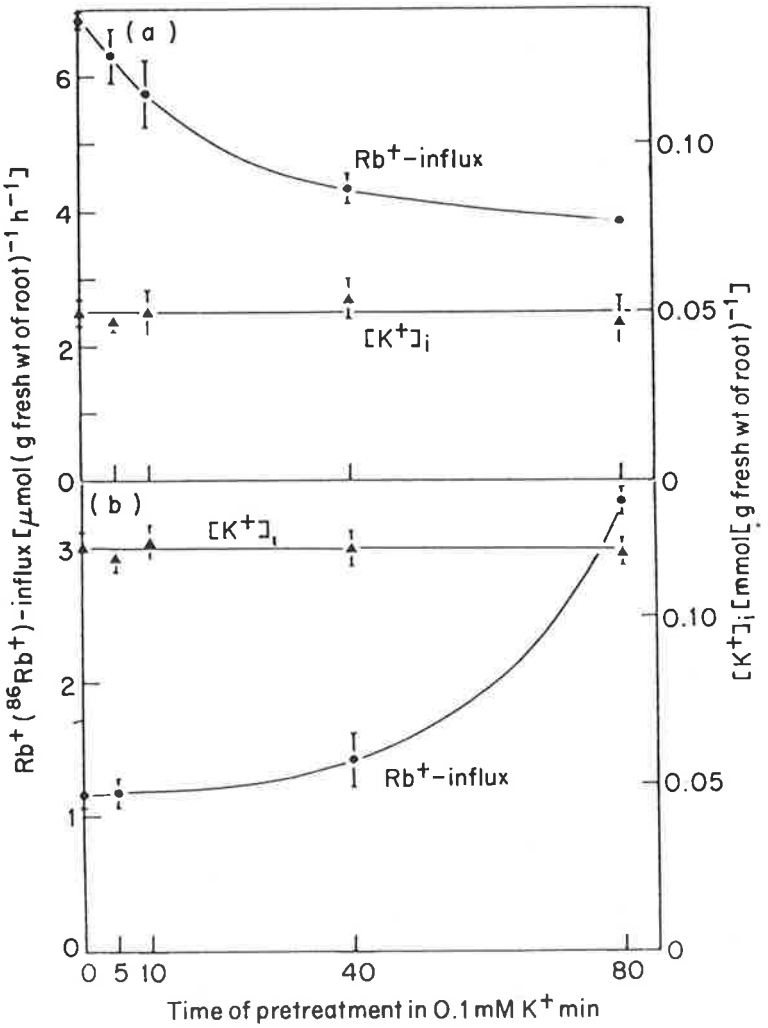


Fig. 32. Investigation of the apparent relationship between $[K]_i$ and $Rb^+(^{86}Rb^+)$ influx into barley roots. (a) Roots grown in the presence of 0.1 mM $K^+$ in the cultivation medium and then transferred to a 10 mM $K^+$ pretreatment solution for the times indicated. (b) As in (a), except 10 mM $K^+$ in cultivation medium and 0.1 mM $K^+$ in pretreatment solution. $Rb^+(^{86}Rb^+)$ uptake (●) was measured from a complete nutrient medium containing 1.0 mM $Rb^+$. At each pretreatment time internal $K^+$ ($[K]_i$) was also determined (▲). Data from Pettersson and Jensen (1978).

because it indicated (to them) that the cytoplasm was filling rapidly and thus influencing allosteric sites, while bulk $K^+$ concentration, which represented the vacuole, remained constant. Unfortunately, although these events could be occurring, there is no possible way to extrapolate from the data to the conclusions drawn by Pettersson and Jensen. Obviously, precise measurements of cytoplasmic $K^+$ concentrations must be made before such extrapolations can be accepted.

Certainly those who have championed the allosteric model are aware of this criticism, and some have attempted to deal with it via indirect measurements of cytoplasmic $K^+$. However, direct measurements are required. Hopefully, recent technological advances in ion-selective microelectrodes may enable routine (?) measurements of cytoplasmic $K^+$ (Felle and Bertl, 1986). Furthermore, the ability to measure $K^+$ influx while making instantaneous changes in the $K^+$ concentration at the cytoplasmic face of the plasmalemma, as has been done for perfused *Chara* cells, would be a powerful technique in the study of allosteric regulation. The use of the patch-clamp technique to study plasmalemma (and tonoplast) $K^+$ currents, while controlling the ionic environment on each side of a membrane, in either the "patch" or "whole cell" ("whole vacuole") mode, may be the answer to this technical problem. However, because the patch-clamp technique, of necessity, involves the use of protoplasts and isolated vacuoles, the regulatory aspects of transport involved in the integration of cells and subcellular compartments at the tissue level will be lost.

Many of the studies concerning both regulatory and mechanistic aspects of $K^+$ uptake have utilized low-salt-grown roots. As we previously indicated, low-salt roots are in a transitional stage between two regulatory states. Glass and Siddiqi (1984) have defined uptake experiments in which plants are grown under one set of conditions and then exposed to uptake media that differ from the growth solutions, as a perturbation technique. The use of low-salt roots for the generation of kinetic curves for $K^+$ influx is a prime example of a perturbation technique. As they have noted, this technique has been useful for the elucidation of transport mechanisms, but its utility as an approach for studying transport regulation is limited, primarily because this technique is incapable of documenting long-term adaptations.

Glass and Siddiqi (1984) illustrate their point with a comparison of two kinetic curves for $K^+$ influx (over identical external $K^+$ concentrations) for barley plants grown under different growth regimes. The fluxes measured via the perturbation technique were obtained by using intact plants that had been grown in a balanced inorganic nutrient solution containing 40 $\mu$M $K^+$. A kinetic profile for $K^+$ influx was determined by transferring these plants to new solutions containing from 1 to 100 $\mu$M $K^+$ (10 min uptake). Steady-state $K^+$ influx, on the other hand, was determined by growing barley plants under conditions of continuous $K^+$ supply at the same concentrations used to obtain the $K^+$ fluxes. For example, plants grown in 10 $\mu$M $K^+$ solution were

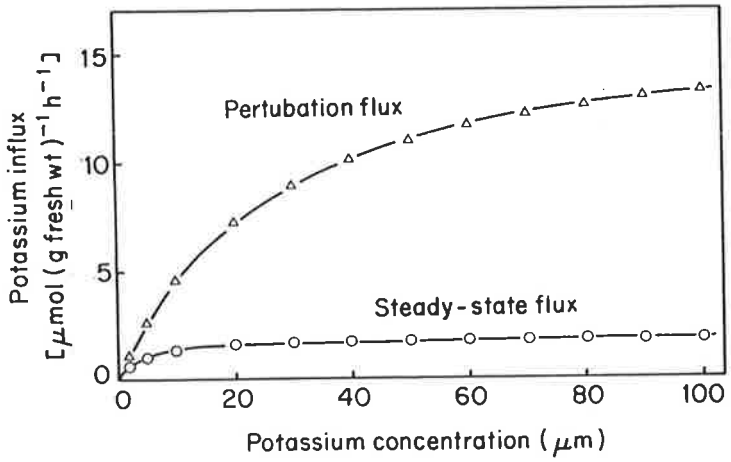


Fig. 33. Comparison between "steady-state" and "perturbation" kinetic profiles obtained for $K^+$ influx. Steady-state experiments were conducted on barley roots that were grown at the concentration used in the $K^+$ influx experiment (○). Perturbation experiments were conducted on barley plants that were grown in 40 μM $K^+$ and then transferred to the indicated $K^+$ concentrations to determine the "perturbation flux" (△). Data from Glass and Siddiqi (1984).

used only for flux determinations from an uptake solution containing 10 μM $K^+$. As shown in Fig. 33, the two kinetic profiles are dramatically different. The curve obtained using the perturbation technique yielded a $V_{max}$ and $K_m$ of 16.8 μmol $g^{-1}$ $h^{-1}$ and 26 μM, respectively, while the steady state fluxes were considerably smaller and were independent of external concentrations above about 10 μM $K^+$. The differences in the two kinetic curves graphically illustrate the influence that growth conditions can have on $K^+$ fluxes.

Although their point is well taken, there are some inconsistencies in the data presented by Glass and Siddiqi (1984). At an external $K^+$ concentration of 40 μM, one would expect that the fluxes obtained from both techniques would be quite similar, since the seedlings used for this particular concentration were grown at that concentration. However, the data in Fig. 33 indicate that the perturbation flux at 40 μM $K^+$ is approximately 10 times the steady-state flux. If one examines the original paper from which these data originate, the apparent discrepancy is explained. Siddiqi and Glass (1983) obtained the data for the perturbation fluxes from 8-day-old barley seedlings, while the steady-state fluxes were obtained with seedlings grown for 18 days. Therefore, a significant portion of the reduction seen in the steady-state fluxes was due to an increase in $[K]_i$. For example, the root $K^+$ content of the 8-day-old seedlings grown in 40 μM $K^+$ solution and used for the perturbation flux determinations was 13.7 μmol $g^{-1}$, while the roots used for steady-state fluxes that were grown in 10–50 μM $K^+$ solutions for 18 days contained between 35 to 68 μmol $K^+$ $g^{-1}$. Although we still agree with the ideas that were proposed, a better choice of data could have been made in order to illustrate the concept.

Another *caveat* concerning the use of low-salt roots for studies on ion transport regulation was made by Cheeseman (1985) in his study on the influence of $Na^+$ on $K^+$ uptake in both low-salt corn seedlings and corn seedlings grown in full nutrient solution. In an earlier study on excised roots from 3-day-old low-salt corn roots, Cheeseman (1982) found that inclusion of $Na^+$, over a concentration range from 0.02 to 20 mM, had no effect on $K^+$ uptake from solutions containing 2 $\mu$M to 20 mM $K^+$. However, when Cheeseman (1985) conducted his experiments using the roots of 8-day-old corn seedlings that had been grown on a full nutrient solution (containing 1 mM $K^+$) he found that the inclusion of $Na^+$ in the uptake solution caused a marked stimulation of $K^+$ influx. When the kinetics for $K^+$ uptake were determined from solutions containing from 0.05 to 2 mM KCl and $Na^+$ at 45 times the $K^+$ concentration, influx values quite similar to those for low-salt roots were obtained. On the basis of these results, Cheeseman proposed that transport regulation in full-nutrient-grown plants may be qualitatively different from that operating in low-salt roots. This idea is similar to those expressed earlier by Pitman (1970) and Siddiqi and Glass (1984) concerning transitions between different regulatory modes as a low-salt root alters its salt status.

It should be noted that with respect to this $Na^+$ response, there are some differences in terms of $K^+$ uptake between the low-salt seedlings used by Cheeseman (1982) and those used by other laboratories. The lack of inhibition of $K^+$ influx, at high external $K^+$ concentrations (>1 mM), by $Na^+$ in Cheeseman's investigation is rather surprising, considering the measurements made by Epstein *et al.* (1963). In this work conducted on low-salt barley roots, mechanism II $K^+$ uptake was inhibited by $Na^+$. Additionally, Kochian *et al.* (1985) have demonstrated, for low-salt corn roots, that the inclusion of 3 mM $Na^+$ in the uptake solution inhibits the linear component for $K^+$ uptake by approximately 50%. The possibility exists that, in addition to the existence of qualitative differences between Cheeseman's low-salt and full-nutrient-grown roots, there may be some qualitative differences between his low-salt roots and those grown by other laboratories.

It is clear that in studies involving regulation of root ion transport, the various growth conditions used to produce experimental material may have a significant influence on the results obtained and the models generated from these data. Therefore, particularly when work is conducted with the relatively non-physiological low-salt roots, special care must be taken when evaluating the data. However, this does not mean that earlier work with low-salt roots is invalid, or that they are not still a useful research material. In fact, the use of nutrient-starved roots may be necessary in order to unmask transport mechanisms that would otherwise not be detected in nutrient-rich roots. For example, the high-affinity $K^+$ uptake system recently observed in low-salt corn roots (Newman *et al.*, 1987) could not be detected in high-salt-grown roots. The same is true for the high-affinity $K^+$ transport

system operating in *Neurospora*. Earlier $K^+$ uptake studies by Slayman and Tatum (1965) were carried out with $K^+$-replete cells, and were conducted in the absence of extracellular $Ca^{2+}$. In these cells, $K^+$ uptake occurred via a low-affinity, high-velocity transport system. However, if $K^+$-starved *Neurospora* cells were grown (analogous to low-salt roots), and $K^+$ uptake studied in the presence of $Ca^{2+}$, the high-affinity $K^+$ transport system ($K^+$–$H^+$ symporter) was revealed (Rodriguez-Navarro and Ramos, 1986; Rodriguez-Navarro *et al.*, 1986).

### 5. *Alternatives to the Allosteric Model*

Although most of the root work concerned with feedback control of $K^+$ uptake by $[K]_i$ has centred on allosteric models, other models can also account for regulation of ion transport in plants. At the cellular level, control of $K^+$ uptake by cytoplasmic $K^+$ could also be explained on the basis of a reaction kinetic model (see Fig. 18). Here, feedback inhibition by high cytoplasmic $K^+$ levels can be accounted for in terms of a reduction in $K^+$ dissociation from the cytoplasmic face of the carrier; i.e. in an analogous way to that proposed for the $H^+$–$Cl^-$ co-transport system of *Chara* (Sanders, 1980a,b; Sanders and Hansen, 1981). Unfortunately, due to technical limitations, it has not yet been possible to conduct the appropriate experiments, in roots, that would enable a differentiation between these two models.

Recently, a regulatory model was presented which suggested that under conditions of increased shoot demand, allosteric regulation of $K^+$ transport at the root epidermal and cortical cell level is superseded by a more complex regulatory mechanism that focuses on ion transport to the xylem as a key point for root–shoot interactions. Drew *et al.* (1984) and Drew and Saker (1984) investigated the effects of $K^+$ deficiency (along with $PO_4^{3-}$ and $Cl^-$) on $K^+$ uptake and translocation. In their initial study, they determined the kinetic parameters for $K^+$ uptake into barley roots by monitoring rates of depletion of labelled ions from dilute $K^+$ solutions (Claassen and Barber, 1974). By this means, they were able to measure $K^+$ fluxes over a full range of concentrations (as the roots depleted external $K^+$ from the initial value of 100 $\mu$M) on the same sets of plants.

With 14-day-old plants, they found that 1 day of $K^+$ starvation caused the $K_m$ to decline dramatically (from 53 to 11 $\mu$M), while the $V_{max}$ remained unaffected. Further $K^+$ starvation (4 or 7 days) had no influence on the $K_m$, while the $V_{max}$ increased two-fold. Bulk $K^+$ content of the roots and shoots declined significantly after each period of starvation (1, 4 and 7 days). Drew *et al.* (1984) proposed that the initial rapid decrease in $K_m$ reflected allosteric regulation of the carriers by decreasing $[K]_i$. For the starvation periods longer than 1 day, they speculated that the increase in $V_{max}$ was the result of protein synthesis which increased the number of available transport proteins with a high affinity for $K^+$.

In the accompanying work, Drew and Saker (1984) conducted divided-root experiments with young barley plants. These plants were grown such that one seminal root was segregated from the remaining four or five seminal roots. This single root was continuously supplied with full nutrient solution (including $K^+$), while the remaining roots were supplied with the same solution (controls), or with the same solution minus $K^+$ for either 2 or 4 days. Using $^{42}K^+$ in the compartment containing the single root, net uptake of $^{42}K^+$ into the root was monitored, as well as $^{42}K^+$ translocation to both the shoot and the $K^+$-starved roots. Additionally, bulk $K^+$ concentration of the single absorbing root, the other roots, and the shoot were determined at the end of the experimental period. The results of this study are presented in Table II. Following $K^+$ starvation of the other roots, for either 2 or 4 days, there was a marked stimulation in $K^+$ uptake into the single fed root, as well as dramatic stimulations of $K^+$ translocation to the shoot and other roots (compared with controls). However, the bulk $K^+$ concentration of the fed root remained unchanged following either 2 or 4 days of $K^+$ starvation of the other roots. The bulk $K^+$ concentrations of the other roots declined significantly after both 2 and 4 days of starvation, while the shoots exhibited a significant decline in $K^+$ content only after 4 days.

Drew and Saker (1984) concluded that the marked stimulation of $K^+$ uptake and translocation to the shoot that occurred during the period of $K^+$

TABLE II

*Potassium uptake and internal ion concentration in barley plants with roots divided between $K^+$-free (−K) and $K^+$-containing (+K) nutrient solution*

| | Control (single root +K, other roots +K) | Potassium-deficient (single root +K, other roots −K) | |
|---|---|---|---|
| | | 2 day | 4 day |
| Net uptake of $^{42}$K-labelled $K^+$ by single root ($\mu$mol (g dry wt root)$^{-1}$ day$^{-1}$) | | | |
| Single root | 452[a] | 634[b] | 826[c] |
| Shoots | 481[a] | 1280[b] | 1830[c] |
| Other roots | 53[a] | 188[b] | 252[c] |
| Total translocated | 533[a] | 1470[b] | 2090[c] |
| Tissue $K^+$ concentration ($\mu$mol (g dry wt)$^{-1}$) | | | |
| Single root | 1730[a] | 1700[a] | 1600[a] |
| Shoots | 1550[a] | 1430[a] | 1280[b] |
| Other roots | 1590[a] | 970[b] | 500[c] |

Values across the table followed by a different letter are significantly different from each other ($P < 0.05$, $N = 8$). Data taken from Drew and Saker (1984).

deprivation, without any detectable change in $K^+$ concentration within the absorbing root, was incompatible with the operation of an allosterically regulated transport mechanism. They suggested that allosteric regulation had been overriden by an alternative mechanism involving transport across the root; i.e. $K^+$ uptake into the root was regulated by transport to the xylem. The implications of such a model are that allosteric regulation will be the primary regulatory mechanism when $K^+$ flux to the xylem is not significant. An example of such a situation would be during the lag in $K^+$ transport to the shoot which is characteristic of low-salt roots undergoing the transition to salt saturation. Furthermore, such a model suggests the integration of regulatory mechanisms (and signals) over the entire plant, because it indicates that increased nutrient demand on a root would influence the uptake characteristics of that root.

This type of transport regulation would involve a hierarchy of regulatory mechanisms ranging from control at the cellular or membrane level, which might include allosteric and/or kinetic control, to transport across the root, which might involve a feedback loop from the xylem parenchyma to the epidermis. At yet a higher level, signals from the shoot might influence root ion transport processes via the $K^+$ transport systems involved in releasing $K^+$ into the xylem (presumably at the plasmalemma of the xylem parenchyma).

Siddiqi and Glass (1987) have challenged the concept that shoot demand directly controls root $K^+$ levels. Various combinations of experimental protocols were used in order to manipulate barley root and shoot $K^+$ levels. Usually, the trends in changing root and shoot $K^+$ levels were similar; i.e. root and shoot $K^+$ increased or decreased in concert. However, some of their experimental conditions resulted in situations where alterations in the $K^+$ content of shoots and roots did not correlate. In these cases, the kinetic parameters for $K^+$ influx were always correlated with root $K^+$. Based on such analyses, Siddiqi and Glass proposed that although other types of transport regulation may operate, in addition to allosteric control, negative feedback from root $K^+$ content is the primary effector in terms of regulating $K^+$ uptake *into* the root.

### B. $K^+$ CYCLING WITHIN THE PLANT: AN INTEGRATION OF REGULATORY MECHANISMS

When one considers the complexities involved in nutrient cycling within the plant, particularly for a highly mobile and important nutrient such as $K^+$, it seems reasonable to hypothesize a multicomponent regulatory system for the uptake and translocation of $K^+$. This would particularly apply to the fully autotrophic plant growing in the field, which would encounter a wide range of different environmental variables for the root versus the shoot, and would also impose the constraints of shoot and root growth upon the regulation of

$K^+$ uptake and partitioning. Hence, a regulatory model which simply involves the control of $K^+$ influx across the plasmalemma of the epidermis/cortex appears to lack the level of integration necessary to achieve a balance of $K^+$ between the shoot and root (Drew and Saker, 1984; Jeschke *et al.*, 1985; Cheeseman and Wickens, 1986a,b).

A number of reports have shown that alterations in root $K^+$ uptake are not negatively correlated with root $K^+$ content (e.g. Jensen and Pettersson, 1978; Pettersson and Jensen, 1978; Wild *et al.*, 1979; Drew and Saker, 1984; Jeschke, 1984; Pettersson, 1986; Cheeseman and Wickens, 1986a,b). Generally, non-allosteric regulation has been observed when environmental conditions have been manipulated in order to change factors such as relative growth rate (RGR) or shoot:root ratio. As Siddiqi and Glass (1987) have argued, it is possible that an alteration of factors such as environmental conditions or shoot parameters *indirectly* influences regulation, by changing the quantitative relationship between root $[K]_i$ and $K^+$ influx. That is, the magnitude of the change in $K^+$ influx in response to a particular incremental change in $[K]_i$ could be altered in response, for example, to a change in shoot growth. This explanation would still be based on the premise that only root $K^+$ levels *directly* control $K^+$ transport in the plant.

Alternatively, a model that relates the needs of the shoot to the root, via signals directed to the site of $K^+$ transfer into the xylem, with subsequent changes in transport activity then feeding back (ultimately) to $K^+$ uptake at the root surface, would appear to be better suited to the needs of the entire plant. Such a model would still be ultimately based on feedback control of root $K^+$ uptake by root $[K]_i$, but in a more complex manner.

Unfortunately, few studies have addressed the relationship between growth and $K^+$ uptake specifically in terms of transport regulation. Pitman (1972) looked at the influence of shoot growth rate (modified through variations in the photoperiod) on root $K^+$ uptake and translocation to the shoot. He found that under conditions of low shoot growth, $K^+$ uptake and translocation were decreased in relation to the situation observed under conditions of rapid shoot growth. These results suggested that "shoot demand" for $K^+$ could override regulatory processes operating in the root. Pitman suggested that phytohormones, such as ABA and cytokinins, could be participating in feedback control of $K^+$ transport. Although hormones are often considered as likely candidates for the signal between the shoot and root, the available data appears contradictory. Thus, we can only conclude that hormones may play a role in the regulation of ion transport within the plant and that this area of research awaits further clarification (for review, see van Steveninck, 1976).

Jeschke (1982) has examined the effect of shoot:root ratios on $K^+$ and $Na^+$ fluxes in intact barley seedlings. The shoot:root ratio was increased by excising all but one seminal root. This resulted in an increase in plasmalemma $K^+$ influx, net $K^+$ uptake, transport to the xylem, *and* cytoplasmic

$K^+$. The positive correlation that was observed between $K^+$ influx and cytoplasmic $K^+$ levels again suggests a situation where allosteric regulation has been overriden. Based on this work, Jeschke proposed that increasing the shoot : root ratio (which would be analogous to increasing shoot demand) altered the feedback control of root ion fluxes by the shoot, possibly through the participation of hormonal signals.

In a subsequent study, Jeschke (1984) studied the influence of increased transpiration on $K^+$ fluxes in barley seedlings in which the root system had been reduced. It was found that accelerated water flow stimulated $K^+$ uptake and translocation to the shoot, while root $K^+$ content decreased. These observations appear to be consistent with the allosteric model. However, compartmental analysis performed under these conditions indicated that *vacuolar* $K^+$ declined, while cytoplasmic $K^+$ remained constant, or increased slightly. These results further underscore the need for measurements of cytoplasmic $K^+$.

In terms of transport regulation, Jeschke has commented on the marked similarities between the effects of increased transpiration and increased shoot : root ratio on $K^+$ fluxes and compartmentalization within the plant. He speculated that water flow and $K^+$ recycling within the plant could play a role in regulatory interactions between the shoot and root. This would be particularly true for seedlings where the root system has been reduced to a single root. In this situation very high rates of phloem translocation are maintained from the shoot to the root (Passioura and Ashford, 1974). The participation of recycled $K^+$ as a signal between the shoot and root is discussed below.

Cheeseman and Wickens (1986a,b) conducted a detailed study on the relationships between $K^+$ uptake, tissue $K^+$ content, root : shoot ratios, and growth in intact, vegetative *Spergularia marina* plants grown under full nutrient conditions. Potassium uptake into *S. marina* was negatively correlated with root weight (or root : shoot ratio), but positively correlated with root $K^+$ content. Again, these results are incompatible with the concept that allosteric regulation of uptake functions as the prime regulatory mechanism.

In all of the studies relating ion transport to growth, the focus has been placed, quite logically, on the needs of the shoot. However, there are situations where root nutrient demands may change the way a regulatory network might operate. It is well documented that nutrient deficiency often results in an increase in root growth and, therefore, a decrease in shoot : root ratio (Clarkson and Hanson, 1980). Any regulatory scheme for $K^+$ transport in the whole plant must take into account growth factors of both the shoot and root.

In terms of an integrated regulatory scheme for $K^+$ transport throughout the plant, one logical choice for the signal between the root and shoot would be $K^+$ recirculated from the shoot to the root, via the phloem. At least three important sites need to be considered when developing a regulatory model

for $K^+$ transport. These include the site of entry for $K^+$ (the root surface), the site of transfer to the shoot (the xylem parenchyma), and the site of $K^+$ recirculation (the shoot). The critical "fulcrum" for such a model would be the xylem parenchyma, which would be the point of signal reception from the shoot, and also the site from which root $K^+$ uptake would be modulated, presumably through the feedback control that exists between root $[K]_i$ and plasmalemma $K^+$ influx. As Drew and Saker (1984) have proposed, $K^+$ recirculated to the root via the phloem could be the signal that would affect xylem $K^+$ transport, and, ultimately, root $K^+$ uptake.

Potassium recirculation within the plant, via the phloem, has been well documented (Greenway and Pitman, 1965; Pate, 1975; Armstrong and Kirkby, 1979; Jeschke *et al.*, 1983). Although cytological studies within the root, detailing the relationship between various cells of the phloem and the xylem parenchyma, are lacking (and much needed), the close proximity of the xylem parenchyma to the phloem does make it possible that $K^+$ released from the phloem could influence $K^+$ transport by these cells. Recently, elegant studies on ion recirculation ($K^+$, $Mg^{2+}$, $Ca^{2+}$, and $Na^+$) throughout

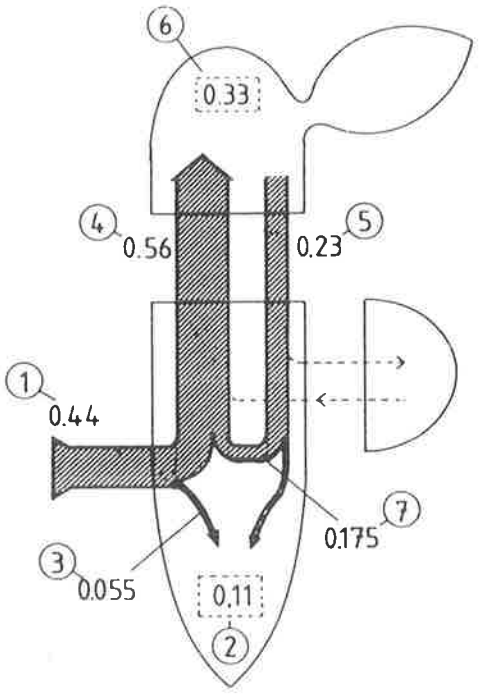


Fig. 34. Model of $K^+$ transport and accumulation in nodulated *Lupinus albus* plants. Rates of ion flows (figure at arrows) and of accumulation during growth (figures in boxes) are given in $\mu$mol (g fresh wt)$^{-1}$ h$^{-1}$. Arrow thicknesses relate to net uptake (1) into the root of 100%. Numbers represent: accumulation in the root (2) and shoot (6); (3) "direct" accumulation from the external medium; transport via xylem (4) and phloem (5); phloem to xylem transfer in the root (7). Data from Jeschke *et al.* (1985).

the plant have been conducted by Jeschke and co-workers on both nodulated white lupin and barley (Jeschke *et al.*, 1985, 1987; Wolf and Jeschke, 1987).

Initially, Jeschke and co-workers chose white lupin because of its ability to bleed from both the xylem and phloem. Xylem and phloem sap was collected, and rates of ion flow and cycling between the shoot and root were calculated from the measured carbon : ion weight ratios in the xylem and phloem streams. These determinations were based on an empirical model previously developed for carbon and nitrogen partitioning in lupin (Pate *et al.*, 1979). The model for $K^+$ circulation in lupin is shown in Fig. 34. The data indicate that 52% of the absorbed $K^+$ is recirculated back to the root, and that 76% of the phloem-borne $K^+$ returning to the root re-enters the xylem stream and is transported *again* to the shoot! Clearly, since a large portion of the $K^+$ moving in the xylem transpiration stream is supplied by the phloem, the concept gains strength that $K^+$ transfer, from the phloem, influences the ionic environment of the root xylem parenchyma.

An even more detailed study of $K^+$ and $Na^+$ recirculation in barley has been developed to take into account the interactions between older and younger leaves (Wolf and Jeschke, 1987). The Wolf and Jeschke model is presented in Fig. 35, and from this the complexities involved in $K^+$ partitioning within the plant are clearly evident. A number of points are brought out by this model:

1. The older leaves were the major sinks for xylem-borne $K^+$. Subsequently, most of this imported $K^+$ was re-exported out of the older leaves via the phloem.
2. Most of the $K^+$ supplied to the young leaves came from the older leaves, via the phloem. However, the oldest leaves retranslocated their $K^+$ primarily to the root, with a smaller proportion going to the younger leaves.
3. A large portion of the shoot $K^+$ was recirculated to the root, and subsequently returned to the shoot via the xylem. It was estimated that 43% of the $K^+$ absorbed by the root was recirculated back from the shoot to the root.

From these models, it is apparent that the $K^+$ flows are strongly influenced by photoassimilate partitioning, as evidenced by the large proportion of $K^+$ that is conducted in the phloem. When the details of such complicated flow schemes are examined in the context of $K^+$ transport regulation within the whole plant, it becomes apparent that regulatory models based on the control of a single $K^+$ transport system (i.e. allosteric regulation of root $K^+$ uptake) are inadequate to account for the control that would be necessary to direct these flows. Instead, it should be recognized that feedback control of $K^+$ uptake, at the cellular level, is probably the most critical component of a multicomponent, hierarchical regulatory system that would integrate $K^+$ fluxes at the cellular, organ, and whole plant level. It should be made clear that, at this time, such a speculative regulatory model is only a conceptual

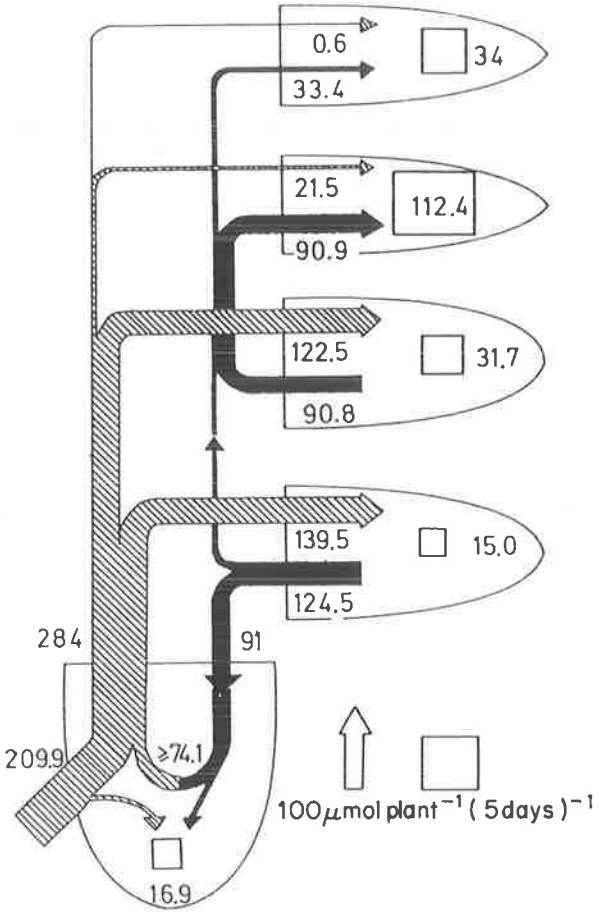


Fig. 35. Rates of $K^+$ flow between single leaves and the root of barley plants. Figures represent ion movements and increments in individual organs [$\mu$mol plant$^{-1}$ (5 days)$^{-1}$] for the period 14–19 days after germination (four-leaf stage). Arrow thicknesses are drawn proportional to transport rates, with striped arrow indicating flows in the xylem and solid arrows flows in the phloem. Squares in leaves or roots represent ion increments due to growth and/or to increases in tissue ion concentrations; areas are drawn in proportion to ion increments. The indicated rate of phloem to xylem transfer within the root represents a minimum estimate. Data from Wolf and Jeschke (1987).

framework from which future work can be directed. Certainly almost nothing is known, for example, about how alterations in the activity of $K^+$ transport systems in the plasmalemma of the xylem parenchyma might feed back upon $K^+$ uptake systems in the root epidermal plasmalemma. Obviously, as Cheeseman and Wickens (1986a,b) noted earlier, future research must be directed at the elucidation of the physiological basis for the signals and transduction systems operating within the plant, and also the mechanisms by which the plant integrates these components into an interactive and coherent system.

## VI. FUTURE RESEARCH AND PROSPECTS

We began this chapter by noting the lack of understanding and knowledge concerning the mechanisms and regulatory aspects of $K^+$ transport in roots. It can certainly be said that progress in this area has not been rapid, primarily because of the complexities of the processes being studied. However, our examination of the literature indicates that over the past 10 years significant insight has been gained into both the mechanisms of $K^+$ transport across the root and the control processes involved. Progress has come primarily through the application of a range of recent technological advances. In order to maintain this progress, we must not only continue to take advantage of new technologies as they become available, but we must also apply them in an integrated manner.

In terms of mechanisms of plasmalemma and tonoplast $K^+$ transport, a combination of biophysical, biochemical and molecular techniques should prove extremely fruitful. The application of patch-clamp studies (both whole cell and vacuole, and excised patch) will enable the investigation of the coupling and stoichiometry of $K^+$ and $H^+$ fluxes. In this way, it should be possible to study the putative $K^+$–$H^+$ co-transport system in the most rigorous of ways. Additionally, we are pleased to note that the study of $K^+$ channels with the patch-clamp technique has already begun and should yield important information on mechanisms and control of passive $K^+$ transport systems. Recent improvements in cell fractionation and purification techniques should also enable researchers to obtain purified preparations of transport proteins (at least the more ubiquitous ones) which can be used for further reconstitution and transport studies. This approach should complement patch-clamp and traditional electrophysiological techniques in discriminating between $K^+$-ATPases, $K^+$–$H^+$ co-transport systems, and $K^+$–$H^+$ exchange ATPases. Furthermore, the combination of membrane purification techniques with immunology and molecular genetics is enabling researchers to obtain the gene sequences for some transport proteins. Further progress in this exciting field will allow for the molecular characterization of various transport proteins. By integrating these new techniques into existing programmes, plant transport physiologists should be able to study the different $K^+$ transport systems at the mechanistic/molecular level.

The future prospects for research into $K^+$ transport regulation, at the cellular, root, and whole plant level, are very exciting. At the cellular level, the patch-clamp technique should again be very useful. This approach will enable researchers to study $K^+$ transport while carefully controlling the ionic environment on both sides of the plasmalemma (or tonoplast). Hence studies into kinetic and allosteric control can be conducted. Additionally, this technique can be used to study the interactions between membrane-associated redox systems, $K^+$ transport, and the control of growth. Recent

advances in ion-selective microelectrode technology should enable researchers to use $K^+$ and $H^+$-selective microelectrodes to obtain direct measurements of cytoplasmic and vacuolar pH and $K^+$ activities, and to monitor changes in these activities as the root absorbs and translocates $K^+$.

Finally, the application of high-resolution SEM X-ray microprobe analysis should prove to be a powerful tool in the investigation of $K^+$ compartmentalization within the various cells of the root, especially during alterations in the status of this ion. The integration of $K^+$ transport across the root with root–shoot interactions is an important area of research that is gaining the attention of a number of plant physiologists. Studies must be focused on the roles of the xylem parenchyma in $K^+$ transport to the shoot and $K^+$ recirculation within the plant. Furthermore, possible modes of coupling between the xylem parenchyma and root epidermis, in terms of regulating $K^+$ transport across the root, should be investigated. This will require the integration of cell cytology, biophysics, biochemistry and whole plant physiology. In view of the models indicating that $K^+$ recirculation from the shoot to the root may play an important role in regulating $K^+$ transport in the plant, it is obvious that an extensive cytological study is needed to establish whether symplasmic continuity exists between the phloem and xylem tissues of the stele.

Additionally, the use of detopped roots for the study of both transroot electrical potentials and ion transport to the xylem, using combinations of various nutritional regimes and chemical probes directed at the xylem parenchyma, are needed to further characterize $K^+$ transport across the root. Finally, further whole plant studies quantifying $K^+$ flows within the plant, particularly under conditions where $K^+$ concentrations and flow in the phloem are artificially modified, should prove of particular value.

In conclusion, it is apparent that as we gain further understanding and insights concerning $K^+$ transport within the plant, we also gain a growing appreciation of the complexities involved in this highly regulated physiological system. In the future, it will often be necessary to dissect the system into its cellular, subcellular and molecular components, even down to the gene level. However, we should take every opportunity to integrate these new findings to yield a highly cohesive approach to the study of $K^+$ transport in the plant. We feel that only in this way will we be able to build upon the knowledge that has been yielded up so grudgingly by our beloved plant!

## ACKNOWLEDGEMENTS

Work on $K^+$ transport conducted in our laboratories has been supported by grants from the United States National Science Foundation (W.J.L.) and the United States Department of Agricultural Research Service (L.V.K.). We also wish to thank Lyn Noah and Cheryl Redlich for their help in typing

the manuscript and the many scientists who provided us with reprints/preprints of their work. We offer special thanks to Drs Glass, Drew and Jeschke for valuable discussion. Finally, we would like to thank Diana Lucas for her patience and encouragement throughout the preparation of this manuscript.

## REFERENCES

Akedo, H. and Christensen, H. N. (1962). *J. Biol. Chem.* **237**, 118–122.
Anderson, W. P. (1976). *In* "Encyclopedia of Plant Physiology" (U. Lüttge and M. G. Pitman, eds), New Series, Vol. 2B, pp. 129–156. Springer-Verlag, Berlin.
Anderson, W. P. and Higinbotham, N. (1975). *J. Exp. Bot.* **26**, 533–535.
Anderson, W. P. and Reilly, E. J. (1968). *J. Exp. Bot.* **19**, 19–30.
Ansari, A. Q. and Bowling, D. J. F. (1972). *J. Exp. Bot.* **23**, 641–650.
Armstrong, C. M. (1969). *J. Gen. Physiol.* **54**, 553–575.
Armstrong, M. J. and Kirkby, E. A. (1979). *PBefflant Physiol.* **63**, 1143–1148.
Asher, C. J. and Ozanne, P. G. (1967). *Soil Sci.* **103**, 155–161.
Bange, G. G. J. (1973). *Acta Bot. Neerl.* **22**, 529–542.
Bange, G. G. J. (1977). *Acta Bot. Neerl.* **26**, 53–62.
Bange, G. G. J. (1979). *Physiol. Plant.* **46**, 179–183.
Beffagna, N., Cocucci, S. and Marrè, E. (1977). *Plant Sci. Lett.* **8**, 91–98.
Behrens, H. M. and Gradmann, D. (1985). *Planta* **163**, 453–462.
Bellando, M. and Trotta, A. (1980). *Plant Sci. Lett.* **17**, 467–472.
Bellando, M., Trotta, A., Bonetti, A., Colombo, R., Lado, P. and Marrè, E. (1979). *Plant Cell Environ.* **2**, 39–47.
Bennett, A. B. and Spanswick, R. M. (1983). *J. Membr. Biol.* **71**, 95–107.
Bentrup, F. W., Hoffmann, B., Gogarten-Boekels, M. and Gogarten, J. P. (1985). *Z. Naturforsch* **40**, 886–890.
Berridge, M. J. (1983). *Biochem. J.* **212**, 849–858.
Berridge, M. J. and Irvine, R. F. (1984). *Nature* **312**, 315–321.
Bienfait, H. F. (1985). *J. Bioenerg. Biomembr.* **17**, 73–83.
Blackman, M. S. and McDaniel, C. N. (1978). *Plant Sci. Lett.* **13**, 27–34.
Blatt, M. R. (1987). "Abstracts of XIV International Botanical Congress", 1-16-9, Berlin, West Germany.
Blatt, M. R. and Slayman, C. L. (1987). *Proc. Natl Acad. Sci. USA* **84**, 2737–2741.
Blumwald, E. (1987). *Physiol. Plant.* **69**, 731–734.
Blumwald, E. and Poole, R. J. (1985). *Plant Physiol.* **78**, 163–167.
Borstlap, A. C. (1981a). *Plant Cell Environ.* **4**, 189–195.
Borstlap, A. C. (1981b). *Naturwiss.* **68**, 41–43.
Borstlap, A. C. (1983). *Plant Cell Environ.* **6**, 407–416.
Boss, W. F. and Massel, M. (1985). *Biochem. Biophys. Res. Commun.* **132**, 1018–1023.
Böttger, M. and Lüthen, H. (1986). *J. Exp. Bot.* **37**, 666–675.
Bowling, D. J. F. (1972). *Planta* **108**, 147–151.
Bowling, D. J. F. (1981). *Physiol. Plant.* **53**, 392–397.
Bowling, D. J. F. and Ansari, A. Q. (1972). *J. Exp. Bot.* **23**, 241–246.
Briskin, D. P. (1986a). *Physiol. Plant.* **68**, 159–163.
Briskin, D. P. (1986b). *Arch. Biochem. Biophys.* **248**, 106–115.
Briskin, D. P. and Leonard, R. T. (1982a). *Proc. Natl Acad. Sci. USA* **79**, 6922–6926.
Briskin, D. P. and Leonard, R. T. (1982b). *Plant Physiol.* **70**, 1459–1464.
Briskin, D. P. and Poole, R. J. (1983a). *Plant Physiol.* **71**, 507–512.

Briskin, D. P. and Poole, R. J. (1983b). *Plant Physiol.* **71**, 969–971.
Briskin, D. P. and Thornley, W. R. (1985). *Phytochemistry* **24**, 2797–2802.
Brooks, S. C. (1929). *Protoplasma* **8**, 389–412.
Buckhout, T. J. and Hrubec, T. C. (1986). *Protoplasma* **135**, 144–154.
Butz, R. G. and Long, R. C. (1979). *Plant Physiol.* **64**, 684–689.
Cabantchik, Z. I., Knauf, P. A. and Rothstein, A. (1978). *Biochim. Biophys. Acta* **515**, 239–302.
Cantley, L. C. (1981). *Curr. Top. Bioenerg.* **11**, 201–237.
Chastain, C. J. and Hanson, J. B. (1982). *Plant Sci. Lett.* **24**, 97–104.
Cheeseman, J. M. (1982). *J. Membr. Biol.* **70**, 157–164.
Cheeseman, J. M. (1985). *Physiol. Plant.* **64**, 243–246.
Cheeseman, J. M. and Hanson, J. B. (1979a). *Plant Physiol.* **63**, 1–4.
Cheeseman, J. M. and Hanson, J. B. (1979b). *Plant Physiol.* **64**, 842–845.
Cheeseman, J. M. and Hanson, J. B. (1980). *Plant Sci. Lett.* **18**, 81–84.
Cheeseman, J. M. and Wickens, L. K. (1986a). *Physiol. Plant.* **67**, 7–14.
Cheeseman, J. M. and Wickens, L. K. (1986b). *Physiol. Plant.* **67**, 15–22.
Cheeseman, J. M., LaFayette, P. R., Gronewald, J. W. and Hanson, J. B. (1980). *Plant Physiol.* **65**, 1139–1145.
Chino, M. (1981). *Soil Sci. Plant Nutr.* **27**, 487–503.
Christensen, H. N. and Liang, M. (1966). *Biochim. Biophys. Acta* **112**, 524–531.
Churchill, K. A. and Sze, H. (1983). *Plant Physiol.* **71**, 610–617.
Claassen, N. and Barber, S. A. (1974). *Plant Physiol.* **54**, 564–568.
Clarkson, D. T. and Hanson, J. B. (1980). *Ann. Rev. Plant Physiol.* **31**, 239–298.
Clarkson, D. T. and Hanson, J. B. (1986). *J. Exp. Bot.* **37**, 1136–1150.
Clarkson, D. T. and Robards, A. W. (1975). *In* "The Development and Function of Roots" (J. G. Torrey and D. T. Clarkson, eds), pp. 425–436. Academic Press, London.
Clarkson, D. T., Williams, L. and Hanson, J. B. (1984). *Planta* **162**, 361–369.
Cocucci, M., Marrè, E., Ballarin-Denti, A. and Scacchi, A. (1976). *Plant Sci. Lett.* **6**, 143–156.
Cohen, S. R. (1975). *J. Membr. Biol.* **22**, 53–72.
Cohen, S. R. (1980). *J. Membr. Biol.* **52**, 95–105.
Crafts, A. S. and Broyer, T. C. (1938). *Am. J. Bot.* **25**, 529–535.
Craig, T. A. and Crane, F. L. (1980). *Proc. Indiana Acad. Sci.* **90**, 150–155.
Craig, T. A. and Crane, F. L. (1981). *Proc. Indiana Acad. Sci.* **91**, 150–154.
Cram, W. J. (1976). *In* "Encyclopedia of Plant Physiology" (U. Lüttge and M. G. Pitman, eds), New Series, Vol. 2A, pp. 284–316. Springer-Verlag, Berlin.
Cram, W. J. (1980). *Aust. J. Plant Physiol.* **7**, 41–49.
Davidson, V. L. and Knaff, D. B. (1981). *Photobiochem. Photobiophys.* **3**, 167–174.
Davidson, V. L. and Knaff, D. B. (1982). *Arch. Biochem. Biophys.* **213**, 358–362.
Davies, D. D. (1973). *Symp. Soc. Exp. Biol.* **27**, 513–529.
Davies, D. D. (1979). *Ann. Rev. Plant Physiol.* **30**, 131–158.
Davis, R. F. and Higinbotham, N. (1969). *Plant Physiol.* **44**, 1383–1392.
Davis, R. F. and Higinbotham, N. (1976). *Plant Physiol.* **57**, 129–136.
Deacon, J. W., Drew, M. C. and Darling, A. (1986). *Ann. Bot.* **58**, 719–727.
Debnam, E. S. and Levin, R. J. (1975). *J. Physiol.* **246**, 181–196.
De Boer, A. H. and Prins, H. B. A. (1984). *Plant Cell Physiol.* **25**, 643–655.
De Boer, A. H. and Prins, H. B. A. (1985). *Plant Cell Environ.* **8**, 579–586.
De Boer, A. H., Prins, H. B. A. and Zanstra, P. E. (1983). *Planta* **157**, 259–266.
Delrot, S. and Bonnemain, J. L. (1981). *Plant Physiol.* **67**, 560–564.
De Luca, L., Bader, U., Hertel, R. and Pupillo, P. (1984). *Plant Sci. Lett.* **36**, 93–98.
De Quintero, M. R. and Hanson, J. B. (1982). *Plant Physiol.* **76**, 403–408.
Dohrmann, U., Hertel, R., Pesci, P., Cocucci, S. M., Marrè, E., Randazzo, G. and Ballio, A. (1977). *Plant Sci. Lett.* **9**, 291–299.

Drew, M. C. and Saker, L. R. (1984). *Planta* **160**, 500–507.
Drew, M. C. and Saker, L. R. (1986). *J. Exp. Bot.* **37**, 22–33.
Drew, M. C., Chamel, A., Garrec, J.-P. and Fourcy, A. (1980). *Plant Physiol.* **65**, 506–511.
Drew, M. C., Saker, L. R., Barber, S. A. and Jenkins, W. (1984). *Planta* **160**, 490–499.
Dunlop, J. (1973). *J. Exp. Bot.* **24**, 995–1002.
Dunlop, J. (1982). *J. Exp. Bot.* **33**, 910–918.
Dunlop, J. and Bowling, D. J. F. (1971). *J. Exp. Bot.* **22**, 445–452.
DuPont, F. M., Giorgi, D. L. and Spanswick, R. M. (1982). *Plant Physiol.* **70**, 1694–1699.
Echlin, P., Lai, C. and Hayes, T. L. (1981). *Scan. Electron Microsc.* **2**, 489–498.
Elzam, O. E., Rains, D. W. and Epstein, E. (1964). *Biochem. Biophys. Res. Commun.* **15**, 273–276.
Epstein, E. (1976). *In* "Encyclopedia of Plant Physiology" (U. Lüttge and M. G. Pitman, eds), New Series, Vol. 2B, pp. 70–94. Springer-Verlag, Berlin.
Epstein, E. and Hagen, C. E. (1952). *Plant Physiol.* **27**, 457–474.
Epstein, E. and Rains, D. W. (1965). *Proc. Natl Acad. Sci. USA* **53**, 1320–1324.
Epstein, E., Rains, D. W. and Elzam, O. E. (1963). *Proc. Natl Acad. Sci. USA* **49**, 684–692.
Epstein, W. and Laimins, L. (1980). *TIBS* **5**, 21–23.
Erwee, M. G. and Goodwin, P. B. (1983). *Planta* **158**, 320–328.
Erwee, M. G. and Goodwin, P. B. (1984). *Protoplasma* **122**, 162–168.
Erwee, M. G., Goodwin, P. B. and Van Bel, A. J. E. (1985). *Plant Cell Environ.* **8**, 173–178.
Faller, L., Jackson, R., Malinowska, D., Mukidjam, E., Rabon, E., Saccomani, G., Sachs, G. and Smolka, A. (1982). *Ann NY Acad. Sci.* **402**, 146–163.
Felle, H. and Bertl, A. (1986). *J. Exp. Bot.* **37**, 1416–1428.
Fernando, M., Siddiqi, M. Y. and Glass, A. D. M. (1987). *Plant Physiol.* **83**, S-164.
Fischer, E. and Lüttge, U. (1980). *Plant Physiol.* **65**, 1004–1008.
Fisher, J. and Hodges, T. K. (1969). *Plant Physiol.* **44**, 385–395.
Fisher, J., Hansen, D. and Hodges, T. K. (1970). *Plant Physiol.* **46**, 812–814.
Giannini, J. L., Gildensoph, L. H., Ruiz-Cristin, J. and Briskin, D. P. (1987). *Plant Physiol.* **83**, S-55.
Glass, A. D. M. (1975). *Plant Physiol.* **56**, 377–380.
Glass, A. D. M. (1976). *Plant Physiol.* **58**, 33–37.
Glass, A. D. M. (1977). *Aust. J. Plant Physiol.* **4**, 313–318.
Glass, A. D. M. (1978). *Can. J. Bot.* **56**, 1759–1764.
Glass, A. D. M. (1983). *Ann. Rev. Plant Physiol.* **34**, 311–326.
Glass, A. D. M. and Dunlop, J. (1978). *Planta* **141**, 117–119.
Glass, A. D. M. and Siddiqi, M. Y. (1982). *Plant Cell Environ.* **5**, 385–393.
Glass, A. D. M. and Siddiqi, M. Y. (1984). *In* "Advances in Plant Nutrition" (P. B. Tinker and A. Läuchli, eds), Vol. 1, pp. 103–147. Praeger Publishers, New York.
Goldman, D. E. (1943). *J. Gen. Physiol.* **27**, 37–60.
Greenway, H. and Pitman, M. G. (1965). *Aust. J. Biol. Sci.* **18**, 235–247.
Gronewald, J. W. and Hanson, J. B. (1980). *Plant Sci. Lett.* **18**, 143–150.
Gronewald, J. W. and Hanson, J. B. (1982). *Plant Physiol.* **69**, 1252–1256.
Hanson, J. B. (1977). *In* "Water Relations in Membrane Transport in Plants and Animals" (A. M. Jungreis, T. K. Hodges, A. Kleinzeller and S. G. Schultz, eds), pp. 277–290. Academic Press, New York.
Hanson, J. B. (1978). *Plant Physiol.* **62**, 402–405.
Harvey, D. M. R. (1985). *Planta* **165**, 242–248.
Hiatt, A. J. (1967a). *Plant Physiol.* **42**, 294–298.

Hiatt, A. J. (1967b). *Z. Pflanzenphysiol.* **56**, 223–245.
Hiatt, A. J. and Hendricks, S. B. (1967). *Z. Pflanzenphysiol.* **56**, 220–232.
Hoagland, D. R. and Broyer, T. C. (1936). *Plant Physiol.* **11**, 471–507.
Hoagland, D. R. and Broyer, T. C. (1940). *Am. J. Bot.* **27**, 173–185.
Hodges, T. K. (1976). *In* "Encyclopedia of Plant Physiology" (U. Lüttge and M. G. Pitman, eds), New Series, Vol. 2A, pp. 260–283. Springer-Verlag, Berlin.
Hodges, T. K., Leonard, R. T., Bracker, C. E. and Keenan, T. W. (1972). *Proc. Natl Acad. Sci. USA* **69**, 3307–3311.
Hodgkin, A. C. and Huxley, A. F. (1952). *J. Physiol.* **117**, 500–544.
Hodgkin, A. C. and Katz, B. (1949). *J. Physiol.* **108**, 37–77.
Hooymans, J. J. M. (1976). *Z. Pflanzenphysiol.* **79**, 182–186.
Hylmö, B. (1953). *Physiol. Plant.* **6**, 333–405.
Iaccarino, M., Guardiola, J. and DeFelice, M. (1978). *J. Membr. Sci.* **3**, 287–302.
Jackson, P. C. and Adams, H. R. (1963). *J. Gen. Physiol.* **46**, 369–386.
Jackson, P. C. and Edwards, D. G. (1966). *J. Gen. Physiol.* **50**, 225–241.
Jacobsen, L. and Overstreet, R. (1947). *Am. J. Bot.* **34**, 415–420.
Jacobsen, L., Overstreet, R., King, H. and Handley, R. (1950). *Plant Physiol.* **25**, 639–647.
Jacobson, L. (1955). *Plant Physiol.* **30**, 264–269.
Jacobson, L. and Ordin, L. (1954). *Plant Physiol.* **29**, 70–75.
Jacoby, B. and Laties, G. G. (1971). *Plant Physiol.* **47**, 525–531.
Jacoby, B. and Rudich, B. (1980). *In* "Plant Membrane Transport: Current Conceptual Issues" (R. M. Spanswick, W. J. Lucas and J. Dainty, eds), pp. 497–498. Elsevier/North-Holland Biomedical Press, Amsterdam.
Jensen, P. and Pettersson, S. (1978). *Physiol. Plant.* **42**, 207–213.
Jeschke, W. D. (1980). *In* "Plant Membrane Transport: Current Conceptual Issues" (R. M. Spanswick, W. J. Lucas and J. Dainty, eds), pp. 17–31. Elsevier/North-Holland Biomedical Press, Amsterdam.
Jeschke, W. D. (1982). *J. Exp. Bot.* **33**, 601–618.
Jeschke, W. D. (1984). *J. Plant Physiol.* **117**, 267–285.
Jeschke, W. D., Stelter, W., Reising, B. and Behl, R. (1983). *J. Exp. Bot.* **34**, 964–979.
Jeschke, W. D., Atkins, C. A. and Pate, J. S. (1985). *J. Plant Physiol.* **117**, 319–330.
Jeschke, W. D., Pate, J. S. and Atkins, C. A. (1987). *J. Plant Physiol.* **128**, 77–93.
Johansen, C., Edwards, D. G. and Lonergan, J. F. (1970). *Plant Physiol.* **45**, 601–603.
Juniper, B. E. and Barlow, P. W. (1969). *Planta* **89**, 352–360.
Kannan, S. (1971). *Planta* **96**, 262–270.
Keifer, D. W. and Lucas, W. J. (1982). *Plant Physiol.* **69**, 781–788.
Keifer, D. W., Franceschi, V. R. and Lucas, W. J. (1982). *Plant Physiol.* **70**, 1327–1334.
Ketchum, K. A., Cooper, E., Shrier, A. and Poole, R. J. (1987). *Plant Physiol.* **83**, S-112.
Kochian, L. V. and Lucas, W. J. (1982a). *Plant Physiol.* **70**, 1723–1731.
Kochian, L. V. and Lucas, W. J. (1982b). *What's New in Plant Physiol.* **13**, 45–48.
Kochian, L. V. and Lucas, W. J. (1983). *Plant Physiol.* **73**, 208–215.
Kochian, L. V. and Lucas, W. J. (1984). *In* "Membrane Transport in Plants" (W. J. Cram, R. Rybova and K. Sigler, eds), pp. 410–411. Academia, Prague.
Kochian, L. V. and Lucas, W. J. (1985). *Plant Physiol.* **77**, 429–436.
Kochian, L. V. and Lucas, W. J. (1987). *In* "Redox Functions of the Eukaryotic Plasmalemma" (J. Ramirez, ed.), pp. 155–173. CSIC, Madrid.
Kochian, L. V., Xin-Zhi, J. and Lucas, W. J. (1985). *Plant Physiol.* **79**, 771–776.

Kochian, L. V., Shaff, J. E. and Lucas, W. J. (1987). *Plant Physiol.* **83**, S-111.
Kochian, L. V., Newman, I. A. and Lucas, W. J. (1988). *In* "Proceedings of 7th International Workshop on Plant Membrane Transport", Australian Academy of Science, Canberra. (In press.)
Kolb, H.-A., Kohler, K. and Martinoia, E. (1987). *J. Membr. Biol.* **95**, 163–169.
Komor, E. (1977). *Planta* **137**, 119–131.
Komor, E. and Tanner, W. (1975). *Planta* **123**, 195–198.
Komor, E., Rotter, M. and Tanner, W. (1977). *Plant Sci. Lett.* **9**, 153–162.
Komor, E., Thom, M. and Maretzki, A. (1987). *Planta* **170**, 34–43.
Lado, P., DeMichelis, M. I., Cerana, R. and Marrè, E. (1976). *Plant Sci. Lett.* **6**, 5–20.
Laties, G. G. (1969). *Ann. Rev. Plant Physiol.* **20**, 89–116.
Läuchli, A. (1975). *J. Microscopie Biol. Cell.* **22**, 433–440.
Läuchli, A. (1976). *In* "Transport and Transfer Processes in Plants" (I. F. Wardlaw and J. B. Passioura, eds), pp. 101–112. Academic Press, New York.
Läuchli, A. and Pflüger, R. (1979). *In* "Potassium Research—Review and Trends", pp. 111–163. International Potash Institute, Worblaufen, Bern/Switzerland.
Läuchli, A., Spurr, A. R. and Epstein, E. (1971). *Plant Physiol.* **48**, 118–124.
Läuchli, A., Kramer, D., Sluiter, E. and Gullasch, J. (1977). *Colloque du CNRS Echanges Ioniques Transmembranaires chez les Vegetaux* **258**, 469–476.
Läuchli, A., Pitman, M. G., Lüttge, U., Kramer, D. and Ball, E. (1978). *Plant Cell Environ.* **1**, 217–223.
Leggett, J. E. and Epstein, E. (1956). *Plant Physiol.* **31**, 222–226.
Leigh, R. A. and Wyn Jones, R. G. (1984). *New Phytol.* **97**, 1–13.
Leonard, R. T. (1982). *In* "Membranes and Transport" (A. N. Martonosi, ed.), Vol. 2, pp. 633–637. Plenum Press, New York.
Leonard, R. T. (1984). *In* "Advances in Plant Nutrition" (P. B. Tinker and A. Läuchli (eds), Vol. 1, pp. 209–240. Praeger Scientific, New York.
Leonard, R. T. (1985). *In* "Potassium in Agriculture" (R. O. Munson, ed.), pp. 327–335. Am. Soc. Agron., Madison, WI.
Leonard, R. T. and Hanson, J. B. (1972). *Plant Physiol.* **49**, 430–435.
Leonard, R. T. and Hodges, T. K. (1973). *Plant Physiol.* **52**, 6–12.
Leonard, R. T. and Hotchkiss, C. W. (1976). *Plant Physiol.* **58**, 331–335.
Lichtner, F. T. and Spanswick, R. M. (1981). *Plant Physiol.* **68**, 693–698.
Lin, W. (1979). *Plant Physiol.* **63**, 952–955.
Lin, W. (1980). *Plant Physiol.* **66**, 550–554.
Lin, W. (1981). *Plant Physiol.* **68**, 435–438.
Lin, W. (1982a). *Proc. Natl Acad. Sci. USA* **79**, 3773–3776.
Lin, W. (1982b). *Plant Physiol.* **70**, 326–328.
Lin, W. (1984). *Plant Physiol.* **74**, 219–222.
Lin, W. (1985). *Physiol. Plant.* **65**, 102–108.
Lin, W. and Hanson, J. B. (1976). *Plant Physiol.* **58**, 276–282.
Lopez-Saez, J. F., Giminez-Martin, G. and Risueno, M. C. (1966). *Protoplasma* **61**, 81–84.
Lowendorf, H. S., Slayman, C. L. and Slayman, C. W. (1974). *Biochim. Biophys. Acta* **373**, 369–382.
Lucas, W. J. and Kochian, L. V. (1987). *In* "Redox Functions of the Eukaryotic Plasmalemma" (J. M. Ramirez, ed.), pp. 176–193. CSIC, Madrid.
Luster, D. G., Hrubec, T. C. and Buckhout, T. J. (1987). *Plant Physiol.* **83**, S-54.
Lüttge, U. and Clarkson, D. T. (1985). *Prog. Bot.* **47**, 73–86.
Macri, F. and Vianello, A. (1986). *Plant Sci.* **43**, 25–30.
Madore, M. A., Oross, J. W. and Lucas, W. J. (1986). *Plant Physiol.* **82**, 432–442.
Maloney, P. C. and Wilson, T. H. (1973). *Biochim. Biophys. Acta* **330**, 196–205.

Marrè, E. (1977). *In* "Regulation of Cell Membrane Activities in Plants" (E. Marrè and O. Ciferri, eds), pp. 185–202. Elsevier/North Holland, Amsterdam.
Marrè, E. (1979). *Ann. Rev. Plant Physiol.* **30**, 273–288.
Marrè, E. and Ballarin-Denti, A. (1985). *J. Bioenerg. Biomembr.* **17**, 1–21.
Marrè, E., Colombo, R., Lado, P. and Rasi-Caldogno, F. (1974a). *Plant Sci. Lett.* **2**, 139–150.
Marrè, E., Lado, P., Ferroni, A. and Ballarin-Denti, A. B. (1974b). *Plant Sci. Lett.* **2**, 257–265.
Maynard, J. M. and Lucas, W. J. (1982a). *Plant Physiol.* **69**, 734–739.
Maynard, J. M. and Lucas, W. J. (1982b). *Plant Physiol.* **70**, 1436–1443.
McCully, M. E., Canny, M. J. and Van Steveninck, R. F. M. (1987). *Physiol. Plant.* **69**, 73–80.
Memon, A. R., Saccomani, M. and Glass, A. D. M. (1985). *J. Exp. Bot.* **36**, 1860–1876.
Mettler, I. J., Mandala, S. and Taiz, L. (1982). *Plant Physiol.* **70**, 1738–1742.
Michaelis, G., Ehwald, R. and Göring, H. (1976). *Biochem. Physiol. Pflanzen* **169**, 241–247.
Misra, P. C., Craig, T. A. and Crane, F. L. (1984). *J. Bioenerg. Biomembr.* **16**, 143–152.
Mitchell, P. (1970). *Symp. Soc. Gen. Microbiol.* **20**, 121–166.
Møller, I. M. and Lin, W. (1986). *Ann. Rev. Plant Physiol.* **37**, 309–334.
Moran, N., Iwasa, K., Ehrenstein, G., Mishke, C., Bare, C. and Satter, R. (1987). *Plant Physiol.* **83**, S-112.
Morse, M. J., Crain, R. C. and Satter, R. L. (1986). *Plant Physiol.* **80**, S-92.
Munck, B. G. and Schultz, S. G. (1969). *J. Gen. Physiol.* **53**, 157–182.
Newman, I. A., Kochian, L. V., Grusak, M. A. and Lucas, W. J. (1987). *Plant Physiol.* **84**, 1177–1184.
Nishizuka, Y. (1984). *Nature* **308**, 693–698.
Nissen, P. (1971). *Physiol. Plant.* **24**, 315–324.
Nissen, P. (1973). *Physiol. Plant.* **28**, 113–120.
Nissen, P. (1974). *Ann. Rev. Plant Physiol.* **25**, 53–79.
Nissen, P. (1987). *Plant Cell Environ.* **10**, 475–485.
Nissen, P. and Nissen, Ø. (1983). *Physiol. Plant.* **57**, 47–56.
Okamoto, H., Ichino, K. and Katou, K. (1978). *Plant Cell Environ.* **1**, 279–284.
Okamoto, H., Katou, K. and Ichino, K. (1979). *Plant Cell Physiol.* **20**, 103–114.
O'Neill, S. D. and Spanswick, R. M. (1984). *J. Membr. Biol.* **79**, 231–243.
Osmond, C. B. (1976). *In* "Encyclopedia of Plant Physiology" (U. Lüttge and M. G. Pitman, eds), New Series, Vol. 2A, pp. 347–372. Springer-Verlag, Berlin.
Osmond, C. B. and Greenway, H. (1972). *Plant Physiol.* **49**, 260–263.
Osterhout, W. J. V. (1931). *Biol. Rev.* **6**, 369–411.
Osterhout, W. J. V. (1950). *Biol. Bull.* **90**, 308–309.
Osterhout, W. J. V. (1952). *J. Gen. Physiol.* **35**, 579–594.
Overall, R. L. and Gunning, B. E. S. (1982). *Protoplasma* **111**, 151–160.
Overall, R. L., Wolfe, J. and Gunning, B. E. S. (1982). *Protoplasma* **111**, 134–150.
Passioura, J. B. and Ashford, A. E. (1974). *Aust. J. Plant Physiol.* **1**, 521–527.
Pate, J. S. (1975). *In* "Encyclopedia of Plant Physiology" (M. H. Zimmermann and J. A. Milburn, eds), New Series, Vol. 1, pp. 451–473. Springer-Verlag, Berlin.
Pate, J. S., Layzell, D. B. and McNeil, D. L. (1979). *Plant Physiol.* **63**, 730–738.
Pesci, P., Tognoli, L., Beffagna, N. and Marrè, E. (1979). *Plant Sci. Lett.* **15**, 313–322.
Petraglia, T. and Poole, R. J. (1980). *Plant Physiol.* **65**, 967–972.
Pettersson, S. (1986). *Physiol. Plant.* **66**, 122–128.
Pettersson, S. and Jensen, P. (1978). *Physiol. Plant.* **44**, 110–114.

Pettersson, S. and Jensen, P. (1979). *Physiol. Plant.* **45**, 83–87.
Pitman, M. G. (1967). *Nature* **216**, 1343–1344.
Pitman, M. G. (1970). *Plant Physiol.* **45**, 787–790.
Pitman, M. G. (1972). *Aust. J. Biol. Sci.* **25**, 243–257.
Pitman, M. G. (1976). *In* "Encyclopedia of Plant Physiology" (U. Lüttge and M. G. Pitman, eds), New Series, Vol. 2B, pp. 95–128. Springer-Verlag, New York.
Pitman, M. G. (1977). *Ann. Rev. Plant Physiol.* **28**, 71–88.
Pitman, M. G. (1982). *Q. Rev. Biophys.* **15**, 481–554.
Pitman, M. G., Courtice, A. C. and Lee, B. (1968). *Aust. J. Biol. Sci.* **21**, 871–881.
Pitman, M. G., Schaefer, N. and Wildes, R. A. (1975). *Planta* **126**, 61–73.
Pitman, M. G., Läuchli, A. and Stelzer, R. (1981). *Plant Physiol.* **68**, 673–679.
Polley, L. D. and Hopkins, J. W. (1979). *Plant Physiol.* **64**, 374–378.
Poole, R. J. (1966). *J. Gen. Physiol.* **49**, 551–563.
Poole, R. J. (1974). *Can. J. Bot.* **52**, 1023–1028.
Poole, R. J. (1978). *Ann. Rev. Plant Physiol.* **29**, 437–460.
Pupillo, P., Valenti, V., De Luca, L. and Hertel, R. (1986). *Plant Physiol.* **80**, 384–389.
Raven, J. A. and Smith, F. A. (1974). *Can. J. Bot.* **52**, 135–148.
Reisenauer, H. M. (1966). *In* "Environmental Biology" (P. L. Altman and D. S. Dittmer, eds), pp. 507–508. Federation of American Societies for Experimental Biology, Bethesda, MD.
Rhoads, D. B., Waters, F. B. and Epstein, W. (1976). *J. Gen. Physiol.* **67**, 325–341.
Rincon, M. and Boss, W. F. (1987). *Plant Physiol.* **83**, 395–398.
Robards, A. W. (1971). *Protoplasma* **72**, 315–323.
Robards, A. W. (1975). *Ann. Rev. Plant Physiol.* **26**, 13–29.
Rodriguez-Navarro, A. and Ramos, J. (1986). *Biochim. Biophys. Acta* **857**, 229–237.
Rodriguez-Navarro, A., Blatt, M. R. and Slayman, C. L. (1986). *J. Gen. Physiol.* **87**, 649–674.
Rubinstein, B. and Stern, A. I. (1986). *Plant Physiol.* **80**, 805–811.
Rubinstein, B., Stern, A. I. and Stout, R. G. (1984). *Plant Physiol.* **76**, 386–391.
Sandelius, A. and Sommarin, M. (1986). *FEBS Lett.* **201**, 282–286.
Sanders, D. (1980a). *J. Membr. Biol.* **52**, 51–60.
Sanders, D. (1980b). *J. Membr. Biol.* **53**, 129–141.
Sanders, D. (1986). *J. Membr. Biol.* **90**, 67–87.
Sanders, D. and Hansen, U.-P. (1981). *J. Membr. Biol.* **58**, 139–153.
Sarafian, V. and Poole, R. J. (1987). *Plant Physiol.* **83**, S-55.
Scarborough, G. A. (1970). *J. Biol. Chem.* **245**, 3985–3987.
Schaefer, N., Wildes, R. A. and Pitman, M. G. (1975). *Aust. J. Plant Physiol.* **2**, 61–73.
Schnabl, H. (1987). "Abstracts of XIV International Botanical Congress," 1-16-1, Berlin, West Germany.
Schroeder, J. I., Hedrich, R. and Fernandez, J. M. (1984). *Nature* **312**, 361–362.
Schroeder, J. I., Raschke, K. and Neher, E. (1987). *Proc. Natl Acad. Sci. USA* **84**, 4108–4112.
Schumaker, K. S. and Sze, H. (1985). *Plant Physiol.* **79**, 1111–1117.
Segel, I. H. (1975). "Enzyme Kinetics." John Wiley and Sons, New York.
Serrano, R. (1984). *Curr. Top. Cell Regul.* **23**, 87–126.
Shone, M. G. T. (1968). *J. Exp. Bot.* **19**, 468–485.
Shone, M. G. T. (1969). *J. Exp. Bot.* **20**, 698–716.
Siddiqi, M. Y. and Glass, A. D. M. (1983). *Can. J. Bot.* **61**, 1551–1558.
Siddiqi, M. Y. and Glass, A. D. M. (1984). *Plant Sci. Lett.* **33**, 103–114.
Siddiqi, M. Y. and Glass, A. D. M. (1987). *J. Exp. Bot.* **38**, 935–947.
Slayman, C. L. and Tatum, E. L. (1965). *Biochim. Biophys. Acta* **102**, 149–160.

Slayman, C. L., Rodriguez-Navarro, A. and Blatt, M. R. (1988). *In* "Proceedings of 7th International Workshop on Plant Membrane Transport". Australian Academy of Science, Canberra. (In press.)
Smith, F. A. and Raven, J. A. (1976). *In* "Encylopedia of Plant Physiology" (U. Lüttge and M. G. Pitman, eds), New Series, Vol. 2A, pp. 317–346. Springer-Verlag, Berlin.
Smith, F. A. and Raven, J. A. (1979). *Ann. Rev. Plant Physiol.* **30**, 289–311.
Spanswick, R. M. (1972). *Planta* **102**, 215–227.
Spanswick, R. M. (1981). *Ann. Rev. Plant Physiol.* **32**, 267–289.
Spanswick, R. M. and Anton, G. E. (1988). *In* "Proceedings of 7th International Workshop on Plant Membrane Transport". Australian Academy of Science, Canberra. (In press.)
Stout, R. G. and Cleland, R. E. (1980). *Plant Physiol.* **66**, 353–359.
Stout, R. G. and Cleland, R. E. (1982). *Plant Physiol.* **69**, 798–803.
Sze, H. (1980). *Proc. Natl Acad. Sci. USA* **77**, 5904–5908.
Sze, H. (1985). *Ann. Rev. Plant Physiol.* **36**, 175–208.
Sze, H. and Churchill, K. A. (1981). *Proc. Natl Acad. Sci. USA* **78**, 5578–5582.
Sze, H. and Hodges, T. K. (1977). *Plant Physiol.* **59**, 641–646.
Tasaki, I. and Hagiwara, S. (1957). *J. Gen. Physiol.* **40**, 859–885.
Terry, B. R. and Robards, A. W. (1987). *Planta* **171**, 145–157.
Thibaud, T.-B., Soler, A. and Grignon, C. (1986). *Plant Physiol.* **81**, 847–853.
Thom, M. and Maretzki, A. (1985). *Plant Physiol.* **77**, 873–876.
Tognoli, L., Beffagna, N., Pesci, P. and Marrè, E. (1979). *Plant Sci. Lett.* **16**, 1–14.
Torii, K. and Laties, G. G. (1966). *Plant Cell Physiol.* **7**, 395–403.
Ulrich, A. (1941). *Am. J. Bot.* **28**, 526–537.
Van Bel, A. J. E., Borstlap, A. C., Van Pinxteren-Bazuine, A. and Ammerlaan, A. (1982). *Planta* **155**, 335–341.
Van Iren, F. and Boers-van der Sluijs, P. (1980). *Planta* **138**, 130–137.
Van Iren, F., Joolen, M. L., Gerritsen, A. F. C., Noordervliet, M. A. W. and Boers-van der Sluijs, F. P. (1981). *Physiol. Plant.* **52**, 15–22.
Van Steveninck, R. F. M. (1976). *In* "Encyclopedia of Plant Physiology" (U. Lüttge and M. G. Pitman, eds), New Series, Vol. 2A, pp. 307–342. Springer-Verlag, Berlin.
Vara, F. and Serrano, R. (1982). *J. Biol. Chem.* **257**, 12826–12830.
Vara, F. and Serrano, R. (1983). *J. Biol. Chem.* **258**, 5334–5336.
Walker, N. A. (1974). *In* "Membrane Transport in Plants" (U. Zimmerman and J. Dainty, eds), p. 348. Springer-Verlag, Berlin.
Walker, N. A. and Pitman, M. G. (1976). *In* "Encyclopedia of Plant Physiology" (U. Lüttge and M. G. Pitman, eds), New Series, Vol. 2A, pp. 93–126. Springer-Verlag, Berlin.
Wild, A., Woodhouse, P. J. and Hopper, M. J. (1979). *J. Exp. Bot.* **30**, 697–704.
Willenbrink, J. and Doll, S. (1979). *Planta* **147**, 159–162.
Wilson, C., Oross, J. W. and Lucas, W. J. (1985). *Planta* **164**, 227–240.
Wood, J. M. (1975). *J. Biol. Chem.* **250**, 4477–4485.
Wolf, O. and Jeschke, W. D. (1987). *J. Plant Physiol.* **128**, 371–386.
Wyn Jones, R. G. (1975). *In* "Ion Transport in Plant Cells and Tissues" (D. A. Baker and J. L. Hall, eds), pp. 193–229. American Elsevier, New York.
Wyn Jones, R. G., Brady, C. J. and Speirs, J. (1979). *In* "Recent Advances in the Biochemistry of Cereals" (D. L. Laidman and R. G. Wyn Jones, eds), pp. 63–103. Academic Press, London.
Young, M. and Sims, A. P. (1972). *J. Exp. Bot.* **23**, 958–969.
Zocchi, G. and Hanson, J. B. (1982). *Plant Physiol.* **70**, 318–319.
Zocchi, G., Rodgers, S. A. and Hanson, J. B. (1983). *Plant Sci. Lett.* **31**, 215–221.